Third Edition

Donald School Textbook of ULTRASOUND IN OBSTETRICS & GYNECOLOGY

Asim Kurjak
Frank A Chervenak

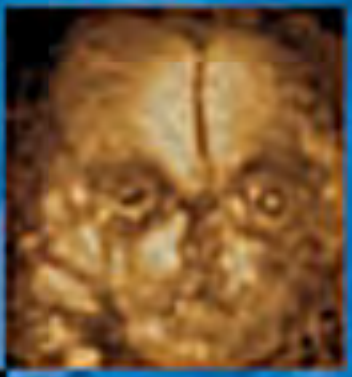

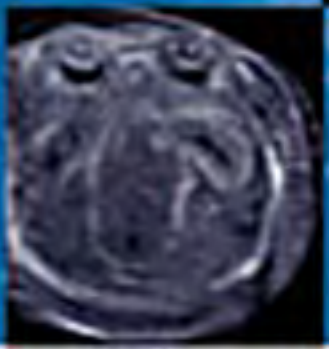

JAYPEE

Donald School
Textbook of Ultrasound in Obstetrics and Gynecology

Donald School
Textbook of Ultrasound in Obstetrics and Gynecology

THIRD EDITION

Editors

Asim Kurjak MD PhD
Professor and Chairman
Department of Obstetrics and Gynecology
Medical School University of Zagreb
Sveti Duh Hospital
Zagreb, Croatia

Frank A Chervenak MD PhD
Professor and Chairman
Department of Obstetrics and Gynecology
The New York Weill Hospital-Cornell Medical Center
New York, USA

JAYPEE BROTHERS MEDICAL PUBLISHERS (P) LTD

New Delhi • Panama City • London

Published by
Jaypee Brothers Medical Publishers (P) Ltd

Corporate Office

4838/24, Ansari Road, Daryaganj, **New Delhi** 110 002, India
Phone: +91-11-43574357, Fax: +91-11-43574314
Website: www.jaypeebrothers.com

Offices in India

- **Ahmedabad**, e-mail: ahmedabad@jaypeebrothers.com
- **Bengaluru**, e-mail: bangalore@jaypeebrothers.com
- **Chennai**, e-mail: chennai@jaypeebrothers.com
- **Delhi**, e-mail: jaypee@jaypeebrothers.com
- **Hyderabad**, e-mail: hyderabad@jaypeebrothers.com
- **Kochi**, e-mail: kochi@jaypeebrothers.com
- **Kolkata**, e-mail: kolkata@jaypeebrothers.com
- **Lucknow**, e-mail: lucknow@jaypeebrothers.com
- **Mumbai**, e-mail: mumbai@jaypeebrothers.com
- **Nagpur**, e-mail: nagpur@jaypeebrothers.com

Overseas Offices

- **Central America Office, Panama City, Panama**, Ph: 001-507-317-0160
  e-mail: cservice@jphmedical.com, Website: www.jphmedical.com
- **Europe Office, UK**, Ph: +44 (0) 2031708910
  e-mail: info@jpmedpub.com

Donald School Textbook of Ultrasound in Obstetrics and Gynecology

First Edition: 2004
Second Edition: 2008

Third Edition: **2011**

ISBN 978-93-5025-259-8

Typeset at JPBMP typesetting unit

Printed in India

To
Ian Donald
(Our Teacher and Friend)

CONTRIBUTORS

Badreldeen Ahmed
Head
Feto-Maternal Unit
Department of Obstetrics and Gynecology
Women's Hospital
Hamad Medical Corporation
Doha, State of Qatar

Juan Luis Alcázar
Department of Obstetrics and Gynecology
University Clinic of Navarra
School of Medicine
University of Navarra
Pamplona, Spain

Cristian Andrei
Department of Obstetrics and Gynecology
Elias University Hospital
Carol Davila University of Medicine
Bucharest, Romania

Aris Antsaklis
Head
1st Department of Obstetrics and Gynaecology
"Alexandra" Maternity Hospital
University of Athens
Medical School
Athens, Greece

Silvia Arevalo
Fetal Medicine Unit
Hospital Vall d'Hebron
Barcelona, Spain

Guillermo Azumendi Pérez
Clinica Gutenberg
Malaga, Spain

Kazunori Baba
Center for Maternal, Fetal and Neonatal Medicine
Saitama Medical Center, Saitama Medical University
Saitama, Japan

María J Barco
Gynecologic Centre "Bolonia"
Zaragoza, Spain

Jill Beithon
Ultrasound Services Sanford Health
Fargo, ND, USA

Isaac Blickstein
Department of Obstetrics and Gynecology
Kaplan Medical Center
Rehovot, and
Hadassah-Hebrew University
School of Medicine
Jerusalem, Israel

Tatjana Bozanovic
School of Medicine
Belgrade University, and
Institute for Obstetrics and Gynecology
Clinical Center of Serbia
Belgrade, Serbia

Lluis Cabero
Department of Obstetrics and Gynecology
Hospital Vall d'Hebron
Barcelona
Spain

José M Carrera
Senior Member
Department of Obstetric and Gynaecology
University Institute Dexeus
Autonomous University of Barcelona
Barcelona, Spain

Elena Carreras
Fetal Medicine Unit
Obstetrics and Gynecology Department
Hospital Vall d'Hebron
Barcelona, Spain

Romina Castagno
Hospital Vall d´ Hebron
Barcelona, Spain

Gabriele Centini
Prenatal Diagnosis Unit
University of Siena
Siena, Italy

Giovanni Centini
Prenatal Diagnosis Unit
University of Siena
Siena, Italy

Aleksandar Cetkovic
Clinical Center of Serbia
Belgrade, Serbia

Stephen T Chasen
Weill Medical College of Cornell University, New York, USA

Frank A Chervenak
Chairman
Department of Obstetrics and Gynecology
Joan and Sanford I Weill Medical College of Cornell University
The New York Presbyterian Hospital, New York, USA

Judith L Chervenak
New York University School of Medicine
New York, USA

Carmina Comas Gabriel
Fetal Medicine Unit
Department of Obstetrics and Gynecology
University Institute Dexeus
Barcelona, Spain

Antonella Cromi
Department of Obstetrics and Gynecology
University Medical School of Insubria, Varese, Italy

Vincenzo D'Addario
Department of Obstetrics and Gynecology, University of Bari
Bari, Italy

Luca Di Cagno
Fetal Medicine Unit
Department of Obstetrics and Gynecology, University of Bari
Bari, Italy

Edoardo Di Naro
III Obstetrics and Gynecology Unit
University Medical School of Bari
Bari, Italy

Marko Dosen
Department of Reproductive Medicine and Gynecologic Endocrinology
University Clinical Center Maribor
Maribor, Slovenia

Alaa Ebrashy
Director
Fetal Medicine Unit
Kasr El Aini Hospital
Faculty of Medicine
Cairo University
Cairo, Egypt

A Kubilay Ertan
Head
Department of Obstetrics and Gynecology
Hospital of Leverkusen
Leverkusen,
Germany

Francesc Figueras
Service of Fetal Medicine
Clinical Institute of Gynecology Obstetrics and Neonatology
University of Barcelona
Barcelona,
Spain

Biserka Funduk Kurjak
Department of Obstetrics and Gynecology
Medical School
University of Zagreb
Zagreb, Croatia

Alessandra Giocolano
Department of Obstetrics and Gynecology
III Obstetrics and Gynecology Unit
University Medical School of Bari
Bari, Italy

Teresa Higueras
Fetal Medicine Unit
Hospital Vall d'Hebron
Barcelona
Spain

Ulrich Honemeyer
Head
Department of Obstetrics and Gynecology
Welcare Hospital
Dubai, UAE

Jon Hyett
Head
High Risk Obstetrics
RPA Women and Babies
Royal Prince Alfred Hospital
Central Clinical School
University of Sydney
Sydney, Australia

Shigenori Iwagaki
Department of Maternal and Fetal Medicine
National Hospital Organization
Nagara Medical Center
Nagara Gifu, Japan

Robin B Kalish
Division of Maternal-Fetal Medicine
Department of Obstetrics and Gynecology
Weill Medical College of Cornell University, New York, USA

Ichiro Kawabata
Department of Maternal and Fetal Medicine
National Hospital Organization
Nagara Medical Center
Nagara Gifu, Japan

Ashok Khurana
The Ultrasound Lab
New Delhi, India

Sanja Kupesic Plavsic
Department of Medical Education
Paul L Foster School of Medicine
Texas Tech University
El Paso, Texas, USA

Asim Kurjak
Department of Obstetrics and Gynecology
Medical School
University of Zagreb
Zagreb, Croatia

Mario Lituania
Centro di Fisiopatologia Preconcezionale e Prenatale.
Ospedali Galliera Genova
Genova, Italy

Aleksandar Ljubic
School of Medicine
University of Belgrade, and
Institute for Obstetrics and Gynecology
Clinical Center of Serbia
Belgrade, Serbia

Kazuo Maeda
Department of Obstetrics and Gynecology (Professor Emeritus)
Tottori University Medical School
Yonago, Japan

Jaideep Malhotra
Malhotra Nursing and Maternity Home (P) Ltd
Agra, India

Narendra Malhotra
Malhotra Nursing and Maternity Home (P) Ltd
Agra, India

Neharika Malhotra
Malhotra Nursing and Maternity Home (P) Ltd
Agra, India

Alexandra Matias
Department of Obstetrics and Gynecology
Porto Medical Faculty of Medicine
Hospital of S João
Porto, Portugal

Eva Meler
Department of Obstetrics and Gynaecology
University Institute Dexeus
Autonomus University of Barcelona, Barcelona, Spain

Luis T Mercé
CENEGO (National Center of Gynecology and Obstetrics US) and Assisted Reproduction Unit
International Ruber Hospital
Madrid, Spain

Eberhard Merz
Chairman
Department of Obstetrics and Gynecology
Krankenhaus Nordwest
Frankfurt/Main, Germany

Srboljub Milicevic
Institute for Obstetrics and Gynecology
Clinical Center of Serbia
Belgrade, Serbia

Berivoj Miskovic
Head
Department of Obstetrics and Gynecology
Clinical Hospital Sveti Duh
Zagreb, Croatia

Giovanni Monni
Head
Department of Obstetrics and Gynecology
Prenatal and Preimplantation Genetic Diagnosis
Microcitemico Hospital
Cagliari, Sardinia, Italy

Nuno Montenegro
Porto Medical Faculty of Medicine
Department of Obstetrics and Gynecology, Hospital of S João
Porto, Portugal

Ajlana Mulic-Lutvica
Department of Women's and Children's Health
Obstetrics and Gynaecology
Uppsala University
Uppsala, Sweden

Zehra Nese Kavak
Director
Fetal Medicine Unit
Department of Obstetrics and Gynecology
Marmara University Teaching and Research Hospital, Pendik
Istanbul, Turkey

Agnieszka Nocun
Gynecology and Oncology Clinic
University Hospital in Krakow
Krakow, Poland

Aleksandra Novakov
School of Medicine
University of Novi Sad
Clinical Center of Vojvodina
Novi Sad, Serbia

Zoltán Papp
Maternity Private Clinic
Semmelweis University
Budapest, Hungary

George A Partsinevelos
1st Department of Obstetrics and Gynaecology
University of Athens
Medical School
Athens, Greece

Bhargavi Patham
Department of Medical Education
Paul L Foster School of Medicine
Texas Tech University
El Paso, Texas, USA

Vincenzo Pinto
Department of Obstetrics and Gynecology
University of Bari
Bari, Italy

Armando Pintucci
Department of Obstetrics and Gynecology
University of Bari
Bari, Italy

Branko M Plavsic
Department of Radiology
Paul L Foster School of Medicine
Texas Tech University
El Paso, Texas, USA

Ritsuko K Pooh
Director
CRIFM Clinical Research Institute of Fetal Medicine PMC
Osaka, Japan

KyongHon Pooh
Department of Neurosurgery
Kagawa National Children's Hospital, Zentsuji,
Japan

Maja Predojevic
Department of Physiology
Medical School
University of Zagreb
Zagreb, Croatia

Luigi Raio
Department of Obstetrics and Gynecology, University of Bern
Bern, Switzerland

Jai Prakash Rao
Malhotra Nursing and Maternity Home (P) Ltd
Agra, India

Frederico Rocha
Division of Maternal Fetal Medicine
Department of OB/GYN and Women's Health
John A Burns School of Medicine
University of Hawaii
Honolulu, Hawaii,
USA

Carlota Rodó
Fetal Medicine Unit
Hospital Vall d'Hebron
Barcelona, Spain

Lucia Rosignoli
Prenatal Diagnosis Unit
P Palagi Hospital
Florence, Italy

Cristina A Rossi
Fetal Medicine Unit
Department of Obstetrics and Gynecology, University of Bari
Bari, Italy

Aida Salihagic Kadic
Department of Physiology, and
Croatian Institute for Brain
Research Medical School
University of Zagreb
Zagreb, Croatia

Cihat Şen
Chairman
Department of Perinatology
Cerrahpasa Medical School
University of Istanbul
Istanbul, Turkey

Geeta Sharma
Weill Medical College of Cornell
University
New York, USA

Kohei Shiota
Department of Anatomy and
Developmental Biology and
Congenital Anomaly Research
Center
Kyoto University Graduate School
of Medicine
Kyoto, Japan

Daniel W Skupski
Director
Maternal-Fetal Medicine
Associate Chairman
Department of Obstetrics and
Gynecology
The New York Hospital of Queens
Flushing, New York, USA

Jiri Sonek
Department of Obstetrics and
Gynecology
Wright State University
President
Fetal Medicine Foundation of
the United States of America
Dayton, Ohio, USA

Yuichiro Takahashi
Department of Maternal and Fetal
Medicine
National Hospital Organization
Nagara Medical Center
Nagara Gifu, Japan

András Tankó
Department of Obstetrics and
Gynecology
County Hospital
Kecskemét, Hungary

H Alper Tanriverdi
Head
Maternal-Fetal Medicine Unit
Department of Obstetrics and
Gynecology
Adnan Menderes University
Faculty of Medicine
Aydin, Turkey

Sakshi Tomar
Malhotra Nursing and Maternity
Home (P) Ltd
Agra, India

Nuria Toran
Department of Pediatric Pathology
Hospital Vall d'Hebron
Barcelona
Spain

Zoltán Tóth
Department of Obstetrics and
Gynecology
Debrecen University
Debrecen, Hungary

Boris Ujevic
Department of Obstetrics and
Gynecology
Clinical Hospital Sveti Duh
Zagreb, Croatia

Martina Ujevic
Polyclinic "Vili"
Zagreb, Croatia

Gino Varga
Polyclinic "Nemetova"
Zagreb, Croatia

Oliver Vasilj
Department of Obstetrics and
Gynecology
Clinical Hospital Sveti Duh
Zagreb, Croatia

Radu Vladareanu
Chairman
Department of Obstetrics and
Gynecology
Elias University Hospital
Carol Davila University of
Medicine
Bucharest, Romania

Veljko Vlaisavljevic
Department of Reproductive
Medicine and Gynecologic
Endocrinology
University Clinical Center Maribor
Maribor, Slovenia

Marcin Wiechec
Obstetrics and Perinatology Clinic
University Hospital in Krakow
Krakow, Poland

Tevfik Yoldemir
Department of Obstetrics and
Gynecology
Marmara University Teaching and
Research Hospital, Pendik
Istanbul, Turkey

Nadah B Zafar
Department of Medical Education
Paul L Foster School of Medicine
Texas Tech University
El Paso, Texas, USA

Ivica Zalud
Chief,
Division of Maternal Fetal
Medicine
Department of OB/GYN and
Women's Health
John A Burns School of Medicine
University of Hawaii
Honolulu, Hawaii, USA

Mona Zvanca
Department of Obstetrics and
Gynecology
Elias University Hospital
Carol Davila University of
Medicine
Bucharest, Romania

PREFACE TO THE THIRD EDITION

The Ian Donald International School of Ultrasound bears testament to globalization in its most successful and worthwhile form. The school was founded in Dubrovnik in 1981; in the preface of the first edition in 2004 we were proud to announce that the School had grown to 8 branches. Since then, the growth has been meteoric and now consists of 55 branches in almost every corner of the globe. The reason for this success has been the tireless and selfless efforts of the world's leading authorities in ultrasound who are willing to dedicate their valuable time without reimbursement to teach sonologists and sonographers throughout the world. Our teachers put national, religious, political, and other parochial considerations aside as they strive to improve the care of all women and fetal patients. Politicians in the countries represented by our School have much to learn from the purity of spirit that exists throughout our international family. We believe that Ian Donald is smiling down from heaven at the School that bears his name.

In the educational efforts of the 55 branches of the Ian Donald School, there is clearly a need for a textbook to complement and supplement lectures and didactic sessions. The first and second textbooks were successful in this endeavor, but with the explosion of knowledge, it was clear that an expanded and updated third edition would be invaluable. For the sake of simplicity, our book is divided into three sections. Section One deals with a variety of topics that lay the foundation for the rest of the book. Section Two addresses the myriad subtopics in obstetric ultrasound that optimize the care of pregnant women and fetal patients. The last section addresses the essential role that ultrasound plays in the many dimensions of clinical gynecology.

A special word of thanks to Jadranka, our tireless secretary for her hundreds of dedicated hours of quality work.

We are grateful to many course directors and lecturers of the Ian Donald School who have enabled its growth and have selflessly contributed to this volume. In order to maximize the reach of this textbook by minimizing its price, all contributors have waived any honorarium or royalty. Their dedication to the dream of globalized quality ultrasound has enabled its reality.

Asim Kurjak
Frank A Chervenak

PREFACE TO THE FIRST EDITION

Ultrasound is the backbone of modern obstetric and gynecology practice. For those of us old enough to remember the dark ages of clinical practice prior to ultrasound, this is not an overstatement. Younger physicians may find it hard to imagine the clinical realities of doctors who delivered undiagnosed twins presenting at delivery, who performed unnecessary surgeries for the clinical suspicion of a pelvic mass that was not present, and who consoled anguished parents when an anomalous infant was born unexpectedly. Recent technological breakthroughs in diagnostic ultrasound, including the advent of color Doppler, power Doppler, three-dimensional and four-dimensional imaging, have led ultrasound to surpass the expectations of Ian Donald, its visionary father.

The Ian Donald School was founded in 1981 and is devoted to international education and research cooperation concerning all aspects of diagnostic ultrasound. The first chapter was founded in Dubrovnik at that time and has now expanded to 7 additional national branches.

To facilitate the educational efforts of the Ian Donald School we believed a textbook would be of value. The text is divided into three parts general aspects, obstetrics, and gynecology. All contributors are either present or former teachers in the 8 branches of the Ian Donald School. We believe this comprehensive text with state-of-the-art images will be of value for both new learners and experienced practitioners.

We are grateful to all of the teachers in the School and especially to all of the contributors to this textbook for their tireless efforts to enhance the quality of ultrasound practice throughout the world.

Asim Kurjak
Frank A Chervenak

CONTENTS

SECTION 1: GENERAL ASPECTS

SECTION 2: OBSTETRICS

SECTION

1

General Aspects

CHAPTER 1

Safety of Ultrasound in Obstetrics and Gynecology

Kazuo Maeda

INTRODUCTION

Although no adverse effects of ultrasound diagnosis have been reported, bioeffect and safety issues have been studied and discussed by various medical ultrasound organizations.[1-9] It is emphasized that, for safe use, ultrasonic examinations are only performed when medically indicated. Secondly, the users are responsible for safety and should recognize that biological tissues of developing embryos and fetuses may be damaged by intense ultrasound.[6] The main biological effect is the thermal effect due to the temperature rise induced by ultrasound absorption, because teratogenicity was reported in fetal animals exposed to high temperature.[2]

Non-thermal effects of ultrasound are inertial cavitation and other mechanical effects. Diagnostic ultrasound users are requested to know the ultrasonic intensity of their devices, the mechanisms of ultrasound bio-effects and usage of their instruments prudently. No hazardous thermal effects are expected when the temperature rise in exposed tissue is less than 1.5ºC and local temperature is lower than 38.5ºC,[1] the fetus was tolerable to 50 hours exposure up to 2ºC rise,[5] while 5 minutes at 41ºC can be hazardous to the tissue.[1] No hazardous thermal effects are expected in common B-mode imaging devices because there is minimum heat production due to low ultrasound intensity. World Federation of Ultrasound in Medicine and Biology (WFUMB) concluded that the use of simple imaging equipment is not contraindicated on thermal grounds.[1]

Simple transvaginal B-mode, simple three dimensional (3D) and four dimensional (4D) imaging are included in this category. The International Society of Ultrasound in Obstetrics and Gynecology (ISUOG) also stated the safe use of Doppler ultrasound.[7] More practical plans on the safe use of Doppler ultrasound from the user's view is discussed in this chapter. Direct subject heating with transvaginal transducer is avoided where the transducer should be lower than 41ºC.

Ultrasound bioeffects are estimated by thermal effect with thermal index (TI), mechanical effects with mechanical index (MI) and also by output ultrasound power, e.g. the safety of fetal heart detector and simple B-mode equipments was established by the Japanese Industrial Standard regulating the output power below spatial peak temporal average (SPTA) 10 mW/cm^2 in 1980, where the level was 1/100 of hazardous threshold of continuous wave ultrasound, which was SPTA 1 W/cm^2 in our study.[8,10-11] However, ultrasound safety has been discussed again after introduction of Doppler flow velocity measurements which definitely needed higher ultrasound intensity than simple B-mode.

DIAGNOSTIC ULTRASOUND INSTRUMENTS AND ULTRASOUND INTENSITY

Ultrasonic imaging devices and Doppler blood flow studies utilize pulsed wave (PW) ultrasound while continuous wave (CW) ultrasound is applied in fetal functional tests **(Table 1.1)**. The ultrasound intensity differs between PW and CW machines **(Fig. 1.1)**, i.e. temporal peak intensity is large in PW and weak in CW ultrasound, while temporal average intensity is almost

TABLE 1.1

Diagnostic ultrasound	
Pulsed wave (PW) for imaging and blood flow studies	Continuous wave (CW) for the functional tests
Real-time B-mode	Fetal heart Doppler detector
3D/4D ultrasound	Fetal heart rate tracing
Pulsed Doppler flow velocity wave	Fetal movement record (actocardiogram)
Color/power Doppler flow mapping	CW Doppler flow velocity wave
High peak and low temporal average intensities in simple B-mode and 3D/4D ultrasound	Low peak and temporal average intensities
High peak and average intensities in pulsed Doppler flow velocity wave	
High peak intensity and medium average intensity in color/power Doppler flow mapping	

identical in simple PW B-mode imaging device and CW machines **(Table 1.1)**. However, pulsed Doppler flow velocity measurement needs high peak and average intensity due to its long pulse and high repetition frequency **(Figs 1.1A and B)**. The temporal average intensity of color and power Doppler flow mapping is lower than pulsed Doppler but higher than simple B-mode machine.

ULTRASOUND INTENSITY OF DOPPLER ULTRASOUND

The maximum intensity of adult Doppler ultrasound was 1–3 W/cm^2, which was as high as the ultrasonic physiotherapy for the tissue heating, where the transducer was always moved on the bone and young patient's bone and pregnant woman were contraindicated from the concern on ultrasound safety. The difference between therapeutic ultrasound and pulsed Doppler device is the exposure duration, which is short in Doppler flow measurement. Thermal effect is therefore a big concern in Doppler ultrasound. Temperature rises not only at the sample volume but also in all tissues passed by the ultrasound beam. Ultrasound intensity is lower in color/power Doppler flow mapping than pulsed Doppler because of the scanning motion of Doppler ultrasound beam in the region of interest (ROI). Temporal average intensity of color Doppler is lower than adult Doppler devices and within the limit of non-hazardous FDA regulation which is 720 mW/cm^2. Thermal effect is discussed in the first place in pulsed

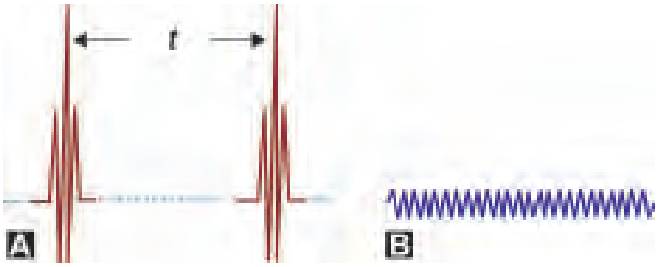

Figures 1.1A and B: Two types of diagnostic ultrasound waves. (A) Pulse wave (PW): 1/t is repetition frequency; (B) Continuous wave (CW)

Doppler, where the safety is determined by ultrasound intensity and exposure duration.

THE EFFECT OF HEATING ON MAMMAL FETUSES

Teratogenic effects were reported by biologists in the exposure of mammal animal embryos and fetuses to experimental high temperature of 39–50°C in various mammals. The results are summarized in the National Council for Radiation Protection and Measurement (NCRP) report 2 in 1992, where a discrimination line clearly separates hazardous and non-hazardous areas.

There is no hazard in the area under the line determined by connecting high temperature/short exposure and low temperature/long exposure points. Non-hazardous exposure is as short as one minute in 43°C and infinite in physiological body temperature. Absolute temperature is studied when the temperature rise derived from TI is added 37°C in ultrasound exposure because TI is calculated in the worst case of temperature elevation by the exposure to standard tissue model.

NON-HAZARDOUS EXPOSURE TIME OF THE FETUS TO THE HEAT

The revised safety statement on diagnostic ultrasound of American Institute of Ultrasound in Medicine (AIUM)[5] published in 1998, is based on the NCRP report[2] in 1992, where inverse relation is found between hazardous temperature level and exposure time. They stated that the fetus tolerated 50 hours at 2°C rise (absolute temperature was 39°C) and 1 min at 6°C rise (43°C). They showed the relation of the temperature rise (T) above 37°C and the non-hazardous exposure time (t min) by the equation 1. The author modified the equation 1 and obtained non-hazardous time (t min) from the temperature rise with the equation 2;

TABLE 1.2

Non-hazardous exposure time (t min) to the temperature rise above 37°C and body temperature is estimated by the equation 2

Temperature rise (°C)	*Body temperature (°C)*	*Non-hazardous exposure time; t (t min)*	*Log t*
1	38	1000.0	3.00
2	39	251.8	2.40
3	40	63.10	1.80
4	41	15.85	1.20
5	42	3.98	0.60
6	43	1.0	0

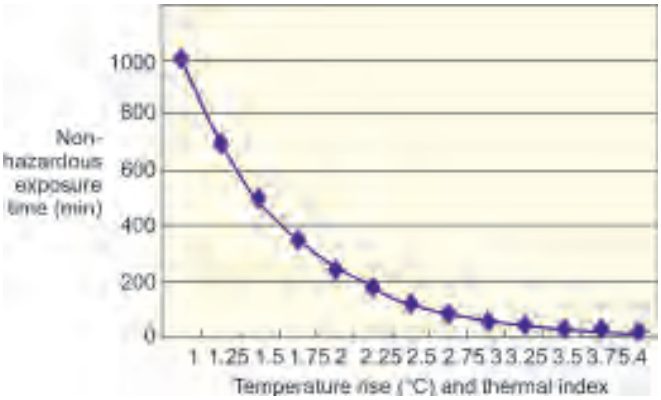

Figure 1.2: Tolerable exposure time of animal fetuses to the temperature rise and TI.
From the equation 2 in the text $t = 10^{(3.6-0.6T)}$
T: temperature rise = thermal index (TI)
t: non-hazardous time (min)

$$T\ (°C) = 6 - \{(\log_{10} t)/0.6\} \text{ - - - - - - - - } (1)$$

$$t = 10^{(3\ 6-0\ 6T)} \text{ - - - - - - - - - - - - - - - - - } (2)$$

Relations of non-hazardous exposure time, temperature rise and body temperature are known by the equation 2 **(Table 1.2 and Fig. 1.2)**. The thermal safety of ultrasound is known by the TI which is theoretically equal to the temperature rise.

STRATEGY FOR THE SAFETY OF DIAGNOSTIC ULTRASOUND EQUIPMENTS

The safety to electrical and mechanical impacts is proved in ultrasound devices by the manufacturer under international and domestic guidelines. In a Doppler scanner, the TI, MI, transducer temperature and other related indices are displayed on the monitor screen when they are excessively high values[3], making the users to keep the safety of ultrasound diagnosis. Obstetric setting should be confirmed before Doppler flow velocity measurements during pregnancy, in order to keep the safety of Doppler ultrasound. Ultrasonic examinations should be done only by medical indications. Although ISUOG safety statement[7] reported that there is no reason to withhold the use of scanners that have received current FDA clearance in the absence of gas bodies, AIUM[5] stated that for the current FDA regulatory limit at 720 mW/cm^2, the best available estimate of the maximum temperature increase can exceed 2°C. Pulsed ultrasound intensity threshold to suppress cultured cell-growth curve was 240 mW/cm^2 in our studies.[10] The FDA regulation may be still controversial from the opinions and reports.

Prevention of Thermal Damage due to Ultrasound Exposure

The TI is a useful index of the temperature rise by ultrasound exposure. Standard tissue models are used in the TI determination in the worst case, i.e. TI is determined by the highest temperature rise. One TI stands for one degree celsius temperature elevation, e.g. temperature rises for 3°C and absolute temperature is 40°C if TI is 3. Since local temperature rise is estimated only by TI at present, TI is the index to estimate tissue temperature in ultrasound examination, to study ultrasonic thermal effect and to avoid possible thermal damage of intense ultrasound. Soft tissue TI (TIS) is used in case of embryo of no bone before 10 weeks of pregnancy and bone TI (TIB) is applied in the fetus with bone.

No hazardous thermal effect is expected when the temperature rise of exposed tissue is less than 1.5°C. An ultrasound examination is totally safe with the TI less than one in daily practice, particularly in the screening of pregnancy and research works. The output power is reduced if the displayed TI is higher than one, until the TI is lower than one. Revised safety statement AIUM[5] stated that equal or less than 2°C temperature rise above 37°C was tolerated up to 50 hours and that the upper limit of safe exposure duration was 16 min at 4°C rise and 1 min at 6°C rise above normal, respectively. The AIUM opinion on the effect of high temperature is similar to the report of NCRP.[2]

Although the statement[5] is useful in a retrospective criticism after the ultrasound exposure, fetal exposure with the temperature rise for 4–6°C may be medically

controversial because absolute temperature is 41–43°C. Non-hazardous exposure time at such temperature higher than 40°C is critically short,[2,5] where remained safe margin is very narrow, excess heating may not be completely avoided in the highest temperature. The author proposes practically applicable safe exposure time in the prospective situation before a Doppler ultrasound diagnosis.

Two Modes in Ultrasonic Exposure Duration

Two modes can be used in the Doppler ultrasound. The mode of TI lower than one (AIUM) or the temperature rise below 1.5°C (WFUMB) after temperature equilibrium can be adopted for the infinite exposure in the research work or pregnancy screening where the exposure time is hardly expected before the study.

Diagnostic pulsed Doppler study is another situation where users require improved Doppler flow wave by the higher TI than one. Some ultrasound lecture showed us higher TI than one in Doppler studies where the safety is proved by short exposure time. The technique was the same as the NCRP report, where short exposure to high temperature was nonhazardous. Doppler examinations with higher TI than one can be permitted by short exposure.

Non-hazardous exposure time to high temperature, temperature rise and high TI is obtained by the application of the equation 2 **(Table 1.2 and Fig. 1.2)**. Exposure time is 250 min when TI is 2 and temperature is 39°C, it is 1hr if TI is 3 and temperature 40°C and 15 min when TI is 4 and the temperature is 41°C. The fetus is tolerable for 4min if the TI is 5 and absolute temperature is 42°C, and finally, one min' exposure time is allowed, if TI is 6 and temperature is 43°C, in the revised safety statement of AIUM.[5] The statement is useful in the confirmation of Doppler ultrasound safety in the past examination. On the other hand, however, the setting of exposure time is required in prospective situation before examination.

Prospective Setting of Exposure Time before Examination

Exposure time is preset before the Doppler examination in the case of higher TI than one with the intention to improve Doppler flow wave. The author recommends to determine actual exposure time by dividing the non-hazardous time of NRCP with the "safety factor" at 50 before every examination with high TI **(Tables 1.2 and 1.3, Fig. 1.2)**. The method was similar to the past regulation of simple B-mode devices in Japan, where threshold intensity was divided by 100 and the output power was regulated to be lower than 10 mW/cm^2 and the safety was generally accepted before the Doppler flow studies. As ultrasound intensity may increase for about three times if standing wave is present, three is the lowest safety factor. In addition, the intensity may increase by the distortion of ultrasonic wave measured by A/B ratio and possible estimation error of TI.[9] These situations are added up to the safety factor and therefore, the author proposes the safety factor up to 50.

TABLE 1.3

Thermal index (TI), tissue temperature, non-hazardous exposure time based on the NCRP report 2, the safety factors and exposure time to ultrasound are listed. Although the user can voluntarily set the safety factor and exposure time, the author recommends to choose the safety factor at 50 and exposure time at 5 min when TI is 2

TI	*Absolute temperature (°C)*	*Non-hazardous exposure time of NCRP report 2 (min)*	*Exposure time (min) obtained by dividing non-hazardous exposure time of NCRP report 2 by various safety factors* Safety Factor			
			3	*10*	*50*	*100*
6	43	1	0.3	0.1	0.02	0.01 (no use)
4	41	16	5	0.2	0.03	0.02 (no use)
3	40	64	21	6	***1***	0.6
2	39	256	85	25	***5***	2.5

For example, non-hazardous exposure time limit is 252 min at 39°C in AIUM statements **(Table 1.2)**, where the temperature rises for 2°C and corresponding TI is 2. In author's recommendation, 252 min are divided by 50 and actual exposure time is 5 min. By the same manner, 1 min exposure time is preset when TI is 3 **(Table 1.3)**.

Higher TI than 3 is not recommended because absolute temperature is higher than 40°C that will be medically controversial. The author's setting is close to the BMUS safety statement 11 where the exposure time is 4 min when TI is 2 and 1 min if TI is 2.5.

Other Thermal Issues

Caution should be paid for the temperature of the tissue exposed to Doppler ultrasound in febrile patients, where the basic temperature is higher than 37°C.[1] For example, if TI is 2 in 38°C febrile patient, the temperature rise above physiologic condition is 3°C, the situation is the same as TI 3 in nonfebrile normal temperature case, and

therefore, 1 minute's exposure time is appropriate. Surface temperature of transvaginal transducer should not be 41°C or more.[1] The user should concern the direct heating of attached tissues and pelvic organs.

Animal fetal skull was heated and the temperature elevation was more than 4°C by the exposure to intense ultrasound.[6] Thermal damage of the brain surface can not be denied. Therefore, maximal intensity of Doppler ultrasound is inadvisable in intracranial flow studies even in late pregnancy. Exposure duration and TI should be documented in patient records in the study where TI is higher than one. The safety indices including TI and MI are documented in the "Methods" of Doppler ultrasound study reports.

The Safety of 3D Ultrasound

Simple B-mode imaging is not concerned for the thermal effect, because of its very low output intensity, e.g. the output of B-mode machine is regulated in Japan[10] to be lower than SPTA 10 mW/cm^2. The gray level data is acquired in 3D imaging by repeated scan of real-time B mode array transducer, the scans are completed within a few seconds, the image data are stored in the computer memory and the unique 3D images are processed in the computer after the ultrasound exposure. A point of fetal body would be exposed to ultrasound infrequently in whole scans. Therefore, 3D ultrasound exposure at a point of the fetus or embryo and possible heating caused by ultrasound would be the same as a simple B-mode.

Accordingly, possible temperature rise and thermal effect in 3D ultrasound are almost the same as simple B-mode, therefore 3D technique will be as safe as the simple B-mode ultrasound in its thermal effect. Doppler flow study accompanied by 3D ultrasound is regulated by its own thermal effects. The mechanical effect of pulsed ultrasound in 3D is equal to the simple B-mode and it is determined by its temporal peak (TP) intensity, sound pressure or mechanical index (MI). The 3D ultrasound is safe in mechanical effects if the MI is lower than one, as commonly recommended.

The Safety of 4D Ultrasound

Although the 4D ultrasound image is obtained by computer processing of 10–24 frames of fetal 3D pictures in a second, most fetal parts are expected not to be exposed to ultrasound repeatedly, because the fetus is moving and therefore a fetal part continuously changes its position. Thermal effect of ultrasound will not be concerned in 4D, despite large number of ultrasound scan is repeated, because simple B-mode is the base of 3D and 4D imaging and thermal effect is not concerned in the B-mode. The 4D ultrasound is considered to be long scan of simple B-mode scan. Therefore, there will be no problem caused by ultrasonic thermal effect in 4D surface imaging. Although, theoretically, there is no limit of B-mode ultrasound examination if the thermal index (TI) is less than one, the duration of 4D fetal studies would be limited in diagnostic or scientific purposes. Doppler study accompanied by 4D ultrasound is regulated by its own thermal effects. As for the safety of mechanical effect of pulsed ultrasound, 4D ultrasound is safe to the fetus or embryo when the MI is less than one and the duration is prudent.

MECHANICAL EFFECTS OF DIAGNOSTIC ULTRASOUND

Mechanical index (MI) is used for the estimation of mechanical bioeffect where MI is rarefactional sound pressure (Pr) expressed in Mega-Pascal (MPa), divided by square root of ultrasound frequency in MHz, e.g. MI is 2 when Pr is 2 MPa and the US frequency is 1 MHz. MI indicates non-thermal effect of ultrasound particularly for the cavitation in the presence of gas bubbles in liquids. Although gas containing contrast medium is still infrequent in OB/GY, its common use in adult circulation should be carefully studied. It is also taken into account that common B-mode is weak in thermal effect, while its pulse peak intensity is not much different from Doppler machines. However, the free radical formed by the inertial cavitation hardly reaches floating cells in the fluid due to short life span and no cavitation may occur within the cell due to high viscosity of cell plasma. Effects of acoustic streaming, capillary blood cell stasis by standing waves or the positive ultrasound pressure require further basic studies. Since hemorrhages are found in neonatal animal lung by the exposure to intense ultrasound, lower MI than one should be used in neonatal lung examination. Although recently the failure of neuronal cell migration in fetal mouse brain was reported after exposure of pregnant mouse to real time B-mode transducer with high pulse average intensity, the report needed 30 minutes or more exposure time to develop the effect.[12] AIUM stated that fetal mice exposed to ultrasound were found to have small but detectable effects only after extended duration of ultrasound exposure, conditions beyond those commonly used in diagnostic ultrasound imaging. The whole brain exposure in the rapidly developing mouse brain used in this study differs significantly from the short duration of diagnostic ultrasound imaging to selected sites in the human fetus.

Similar opinions were stated by the Japan Society of Ultrasound in Medicine and Japan Society of Biomedical Engineering in Obstetrics and Gynecology.

NON-MEDICAL USE OF DIAGNOSTIC ULTRASOUND

Although the use of diagnostic ultrasound should be limited for medical purposes and users are responsible to the safety of ultrasound, i.e. users must keep the knowledge on possible ultrasound bioeffect and use the ultrasound under the ALARA (as low as reasonably achievable) principle, nonmedical ultrasound in entertainment or keepsake ultrasound, fetal portrait studios or prenatal boutiques which record intrauterine fetal 3D/4D ultrasound on DVD are recent problems concerning ultrasound safety. There are also ethical concerning and false reassuring problem in the topics.[13-16]

The WFUMB[13] disapproves of the use of ultrasound for the sole purpose of providing souvenir images of the fetus. Because the safety of an ultrasound examination cannot be assured, the use of ultrasound without medical benefit should be avoided. Furthermore, ultrasound should be employed only by health professionals who are well trained and updated in ultrasound clinical usage and bioeffects. The use of ultrasound to provide keepsake images or video of the fetus may be acceptable if it is undertaken as part of normal clinical diagnostic ultrasound examination, provided that it does not increase exposure to the fetus. Ultrasound imaging for nonmedical reasons is not recommended unless carried out for education, training or demonstration purposes. Live scanning of pregnant models for equipment exhibition at ultrasound congresses is considered a nonmedical practice that should be prohibited since it provides no medical benefit and afford potential risk to the fetus. When using ultrasound for nonmedical reasons, the ultrasound equipments display should be used to ensure that TI<0.5 and MI<0.3.[13]

The safe obstetric ultrasound intensity level was reported to be one thermal index (1TI) and one mechanical index (1MI) in general opinions of medical ultrasound authorities **(Fig. 1.2)**. There can be possible biological hazardous effects in the ultrasound intensity above the levels. In particular case where the user's knowledge is abundant on the ultrasound safety, the TI may be allowed to be 2 but the exposure time should be limited less than 5 mins **(Table 1.3).**

In our detailed ultrasound radiation experiments insulating the heating of the transducer in the thermostat water, the cultured fetal amniotic origin cell line floated in the culture medium held in ultrasound translucent container was exposed quantitative ultrasound 20–30 mins and the cell growth curve was compared to the sham of no radiation in the same thermostat water. The cell growth curve showed no difference to the sham below the SPTA 240 mW/cm^2 (SPTP 20 W/cm^2) of pulsed ultrasound, while the growth curve was suppressed after the exposure to the output intensity ultrasound above the threshold output intensity.[11] Since Japan Society of Ultrasonics in Medicine authorized the results, Japan Industrial Standard (JIS)[10] regulated medical ultrasound output intensity at the level lower than SPTA 10 mW^2, afterwards the medical ultrasound safety was generally recognized.

Although the regulated intensity is low level, the standing wave in case of ultrasound reflection may increase the intensity and the deformed pulsed ultrasound waves may further increase the intensity. The prudent JIS setting will contribute the safety of medical ultrasound even in its accidental increase, while possible increase of output intensity to get further clear fetal image in nonmedical entertainment will easily exceed the safe threshold intensity level. The risk should be prevented by the skilful medical staff with rich safety knowledge and prudent use of diagnostic ultrasound equipment.

In summary of the opinion of ultrasound safety specialists, the non-medical use of diagnostic ultrasound for solely entertainment is not recommended or not permitted from the standpoint of diagnostic ultrasound.[13-16]

CONCLUSION

The strategies to keep the safety of each diagnostic ultrasound equipments depends on their system, because the thermal effect estimated by TI has been the main criteria in the safety. Simple B-mode, 3D and 4D ultrasound, fetal heart detector and fetal monitor, are not contraindicated due to thermal effect because of their low temporal average intensity. Pulsed Doppler machines are the main target in the safety due to its high temporal average intensity. Non-hazardous exposure time of NCRP/AIUM criteria and the temperature rise estimated by TI are useful in retrospective criticism on the past examination. The principle of safe diagnostic ultrasound in daily practice is to keep the TI below one, where obstetrical setting is useful. Research works and pregnancy screening strictly follow the

principle. Moderately higher TI is allowed when more improved Doppler flow wave is required, where the author recommends the exposure time less than 5 min if TI is 2 and 1 min if TI is 3. Higher TI than 3 is not used. Attention should be paid to the decreased safety in febrile patient. Transvaginal transducer temperature should be lower than 41°C. Although 3D and 4D ultrasound are safe, the study duration should be prudent in 4D. The MI is recommended to be less than one, particularly in the studies on air containing neonatal lung. Fetal mice brain effects detected after extended duration of ultrasound exposure were conditions beyond the short exposure in common clinical imaging.

REFERENCES

1. Barnett SB, Kossoff G. WFUMB Symposium on Safety and Standardisation in Medical Ultrasound. Issues and recommendations regarding thermal mechanisms for biological effects of ultrasound. Hornbaek, 1991. Ultrasound in Med Biol. 1992;18(9):731-810.
2. National Council on Radiation Protection and Measurements; Exposure Criteria for Medical Diagnostic Ultrasound: I. Criteria Based on Thermal Mechanisms. NCRP Report No.113, 1992.
3. American Institute of Ultrasound in Medicine/ National Electrical Manufacturers Association; Standard for Real Time Display of Thermal and Mechanical Acoustic Output Indices on Diagnostic Ultrasound Equipment, 1992.
4. Barnett SB, ter Haar GR, Ziskin MC, et al. Current status of research on biophysical effects of ultrasound. Ultrasound in Med Biol. 1994;20(3):205-18.
5. AIUM Official Statement Changes; Revised statements; Clinical safety, AIUM Reporter. 1998;154(Issue 1):6-7.
6. Barnett SB, Rott HD, ter Haar GR, et al. The sensitivity of biological tissue to ultrasound. Ultrasound Med Biol. 1997;23(6):805-12.
7. ISUOG Bioeffects and Safety Committee; Safety statement, 2000 (reconfirmed 2002). Ultrasound Obstet Gynecol. 2002;19:105.
8. Ide M. Japanese policy and status of standardisation. Ultrasound in Med Biol. 1986;12:705-8.
9. The Safety Group of the British Medical Ultrasound Society. Guidelines for the safe use of diagnostic ultrasound equipment. BMUS Bulletin. 2000;3:29-33.
10. Maeda K, Ide M. The limitation of the ultrasound intensity for diagnostic devices in the Japanese Industrial standards. IEEE Trans Ultrasonics, Ferroelectrics and Frequency Control, 1986; UFFC-33:241-4.
11. Maeda K, Murao F, Yoshiga T, et al. Experimental studies on the suppression of cultured cell growth curves after irradiation with CW and pulsed ultrasound. IEEE Trans Ultrasonics Ferroelectr Freq Control. 1986;33(2):186-93.
12. Ang ESB Jr, Gluncic V, Duque A, et al. Prenatal exposure to ultrasound waves impacts neuronal migration in mice. Proceedings of the National Academy of Science of the United States of America (PNAS). 2006;103(34):12909.
13. Barnett S, Abramowicz JS, Ziskin MC, et al. WFUMB Symposium on Safety of Nonmedical Use of Ultrasound. Ultrasound in Med Biol. 2010;36:1209-12.
14. Abramowicz JS. Nonmedical use of ultrasound: bioeffects and safety risk. Ultrasound Med Biol. 2010;36:1213-20.
15. Phillips RA, Stratmeyer ME, Harris GR. Safety and US Regulatory considerations in the nonclinical use of medical ultrasound devices. Ultrasound in Med Biol. 2010;36(8): 1224-8.
16. Brezinka C. Nonmedical use of ultrasound in pregnancy: ethical issues, patients' rights and potential misuse. Ultrasound in Med Biol. 2010;36:1233-6.

CHAPTER 2

Development of 3D Ultrasound

Kazunori Baba

INTRODUCTION

Short History of 3D Ultrasound

Szilard developed a mechanical three-dimensional (3D) display system to see a fetus three-dimensionally in 1974.[1] Brinkley and colleagues invented a 3D position sensor for a probe. They took many tomographic images of a stillborn baby underwater, traced its outline manually and showed its wire-framed 3D images in 1982.[2]

A modern 3D ultrasound system was first developed by Baba and colleagues in 1986 and a live fetus *in utero* was depicted three-dimensionally.[3,4] The system was comprised of an ultrasound scanner, position sensor and computer. An imaging technology, named surface rendering, was used for 3D image construction. This system was also applied to placental blood flows (by combining 3D ultrasound with color Doppler) and breast ducts and cysts (by using so-called inversion mode).[5]

A 3D probe and an ultrasound scanner, that displayed three orthogonal planes on a screen, were developed and became commercially available in 1989. In the early 1990s, clinical applications of the 3-orthogonal-plane display in obstetrics were reported.[6,7] Sohn reported translucent display by using volume rendering in 1991.[8] Since 1994, the number of reports on fetal 3D images has been increasing rapidly because a 3D ultrasound scanner, that could construct and display a 3D image as well as three orthogonal planes, became commercially available.

Two unique 3D ultrasound technologies were also developed. One was defocusing lens method[9,10] and the other was real time ultrasonic beam tracing.[11] In the former method, only by using a probe with a defocusing lens a fetal volume image was obtained. In the latter method, construction of a 3D image and 3D scanning were performed simultaneously and a complete 3D image could be obtained just when a 3D scanning was completed without any delay.

The first world congress on 3D ultrasound in obstetrics and gynecology was held in Mainz, Germany in 1997 and also the first English book on it got published in the same year.[12] Development of 3D ultrasound has been accelerated afterwards and all major manufacturers of ultrasound scanners now provide 3D ultrasound scanners.

WHAT CAN 3D ULTRASOUND DO?

Three-dimensional ultrasound handles 3D data, whereas conventional 2D ultrasound can take care of only 2D data **(Figs 2.1A and B)**. Some functions that only 3D ultrasound can perform are:

- Display of a 3D image
- Display of an arbitrary section
- Measurement in 3D space (including volume measurement)
- Display of a 3D blood flow image

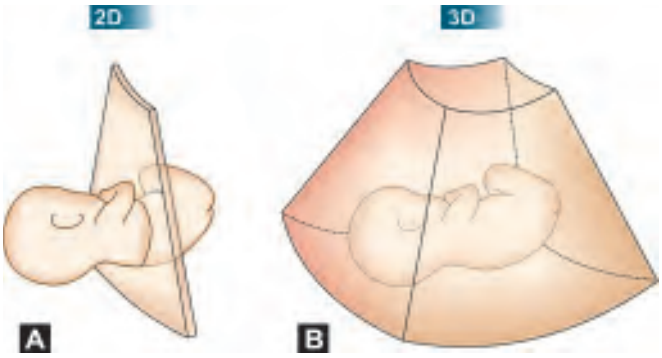

Figures 2.1A and B: (A) Two-dimensional data for conventional 2D ultrasound; (B) 3D data for 3D ultrasound[13]

- Saving, copying and transmission of all information in 3D space
- Re-examination with a saved 3D data set, without the patient.

TECHNICAL ASPECTS OF 3D ULTRASOUND

Various images are obtained through the following processes in 3D ultrasound **(Fig. 2.2)**:

- Acquisition of 3D data (3D scanning)
- Construction of a 3D data set
- Volume visualization.

Acquisition of 3D Data

Three-dimensional data is usually acquired as a large number of consecutive tomographic images through movements of an ultrasound transducer array (conventional 2D ultrasound probe). The most popular way is to use a 3D probe because of its easiness for scanning. A 3D probe has a built-in transducer array (2D ultrasound probe), which tilts in the 3D probe and 3D data are obtained automatically **(Fig. 2.2)**.

There are some other 3D scanning methods for wide scanning area **(Figs 2.3A to C)**. Each tomographic image should be acquired with its positional information for construction of a 3D data set. Accurate positional information can be obtained through an electromagnetic position sensor, an electric gyro attached to the probe **(Fig. 2.4)** or a mechanical position sensor.

Ultrasound travels in a soft tissue at an average speed of 1540 m/s. This speed limits 3D scanning speed. Parallel receiving technique is a method to overcome the limitation. In this technique, one broad ultrasonic beam is transmitted and its echoes are received as plural ultrasonic beams. In a 2D array probe **(Fig. 2.5)**, a high

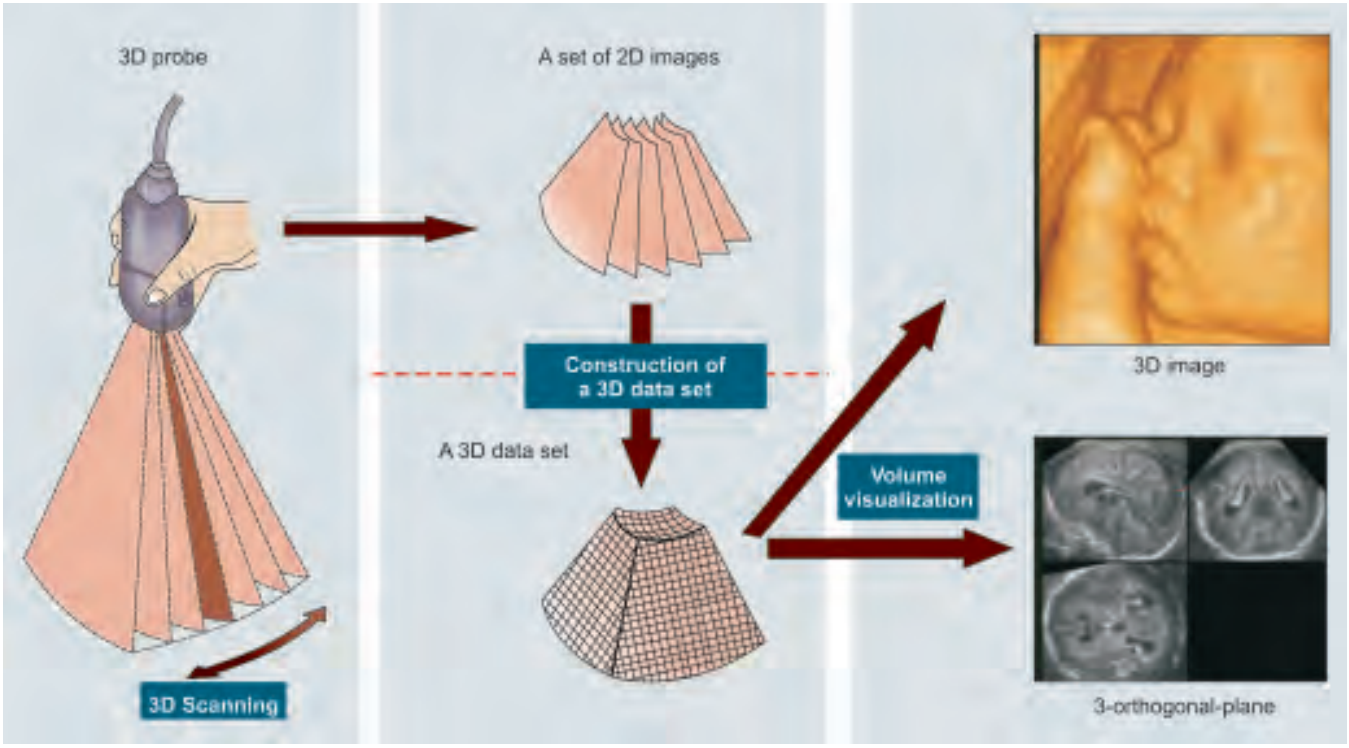

Figure 2.2: Basic processes in 3D ultrasound[14]

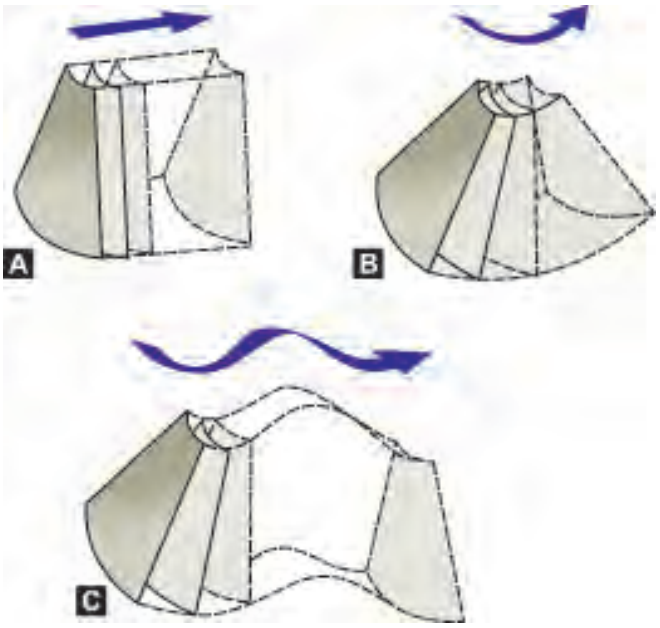

Figures 2.3A to C: 3D scanning methods. (A) Parallel scanning; (B) Fan-like scanning; (C) Free surface scanning[15]

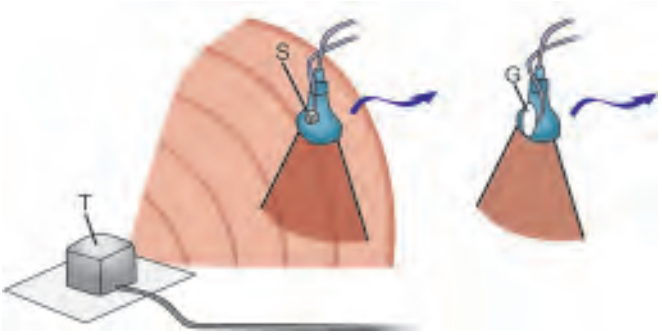

Figure 2.4: A position sensor or an electric gyro attached to a probe detects a relative position of the probe. T: transmitter; S: electromagnetic sensor; G: electric gyro[16]

degree of parallel receiving (at least 1:16) is used and high-speed 3D scanning is possible.[17,18]

Construction of a 3D Data Set

A set of tomographic images obtained through 3D scanning must be constructed three-dimensionally into a 3D data set for further computer processing **(Fig. 2.6)**. This construction process involves interpolation and improvement of data quality by filtering.[15] A 3D data set is composed of a set of voxels (volume elements). Each voxel has a gray value (and color information in 3D color Doppler ultrasound).

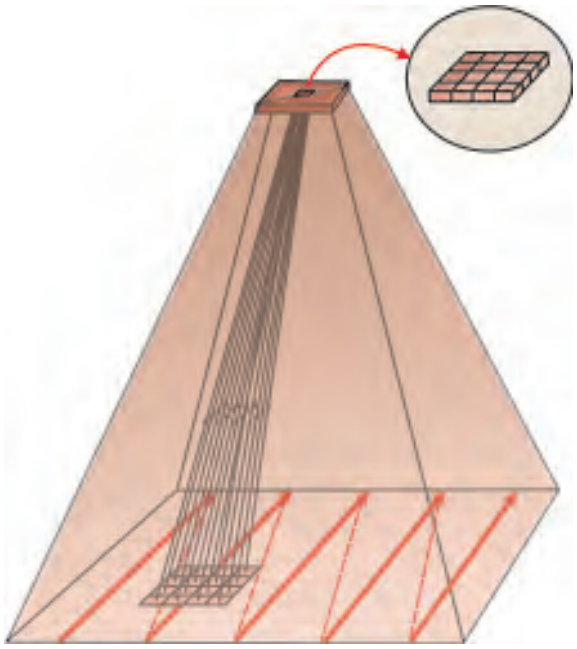

Figure 2.5: 3D scanning by a 2D array probe. A large number of tiny transducers are arranged two-dimensionally and 3D scanning is performed electrically. High-speed 3D scanning is possible by 1:16 parallel receiving[13]

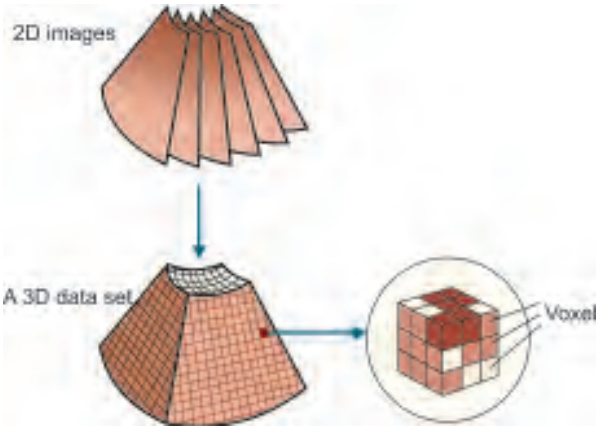

Figure 2.6: Construction of a 3D data set[16]

For scanning of the heart, a gated technique (so called STIC: spatiotemporal image correlation) is applied[19,20] to avoid distortion of a 3D data set due to movement. Tomographic images are rearranged according to the phase of the cardiac cycle and a 3D data set is constructed with only tomographic images at the same phase of the cardiac cycle **(Fig. 2.7)**. The heart can be seen beating three-dimensionally by constructing many 3D data sets in a single cardiac cycle.

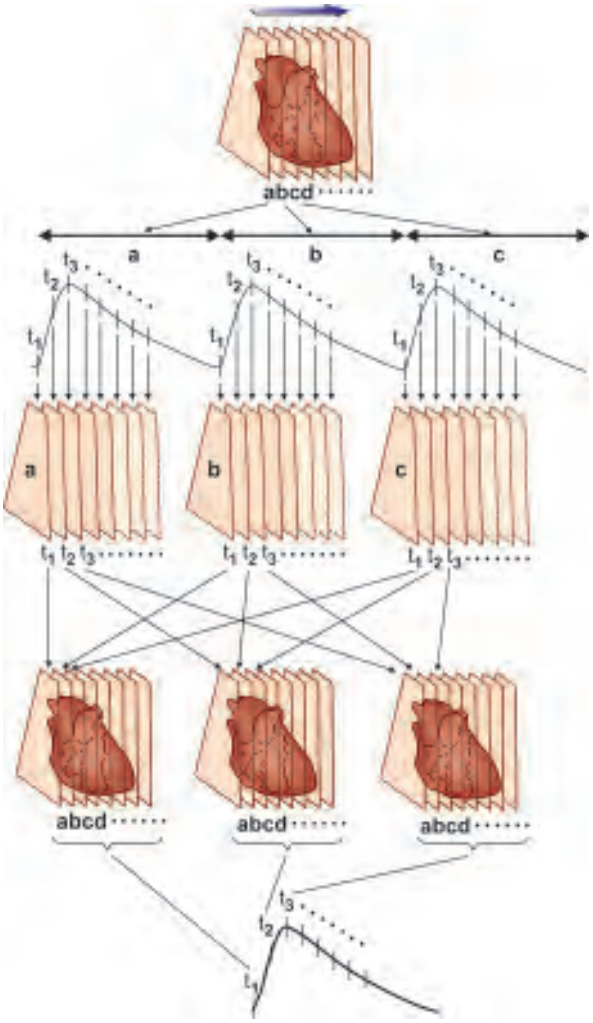

Figure 2.7: A gated technique for 3D scanning of the fetal heart[13]

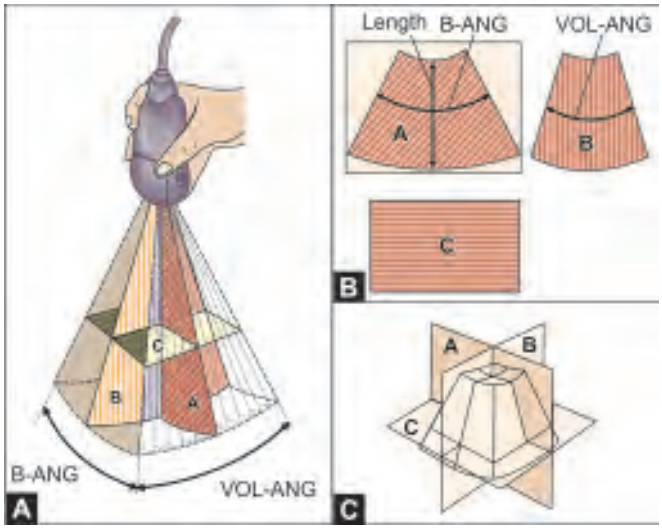

Figures 2.8A to C: (A) Relation between a 3D probe; (B) Initial three orthogonal planes on the screen; (C) 3D data set[14]

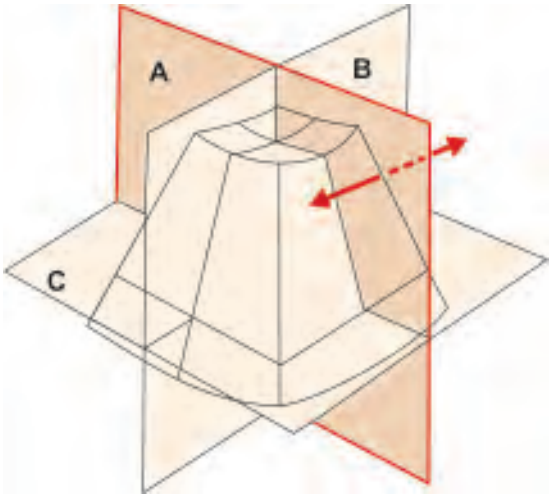

Figure 2.9: Arbitrary section display by translating. Not only plane A but also B and C planes can be translated individually[14]

Volume Visualization

A 3D data set is processed by a computer to be displayed on a 2D screen. This process is called volume visualization. These three methods are usually used for volume visualization in 3D ultrasound:

1. Section reconstruction
2. Volume rendering
3. Surface rendering.

Section Reconstruction

Three orthogonal planes are displayed on a screen immediately after 3D scanning in most of 3D ultrasound scanners **(Figs 2.8A to C)**. An arbitrary section can be selected and displayed through translation **(Fig. 2.9)** and rotation **(Figs 2.10A and B)** of the 3D data set. This means that re-examination can be done after the patient has left, only if 3D data sets are saved.

Usually, 3-orthogonal-plane display **(Figs 2.11A to C)** or parallel-plane display **(Fig. 2.12)** are used for better understanding of the position and orientation of each section in 3D space. These reconstructed sections, some of which cannot be obtained by conventional 2D ultrasound, are very useful for diagnosis in some cases. Three orthogonal sections may also be allocated three-dimensionally **(Figs 2.13A to C)**.

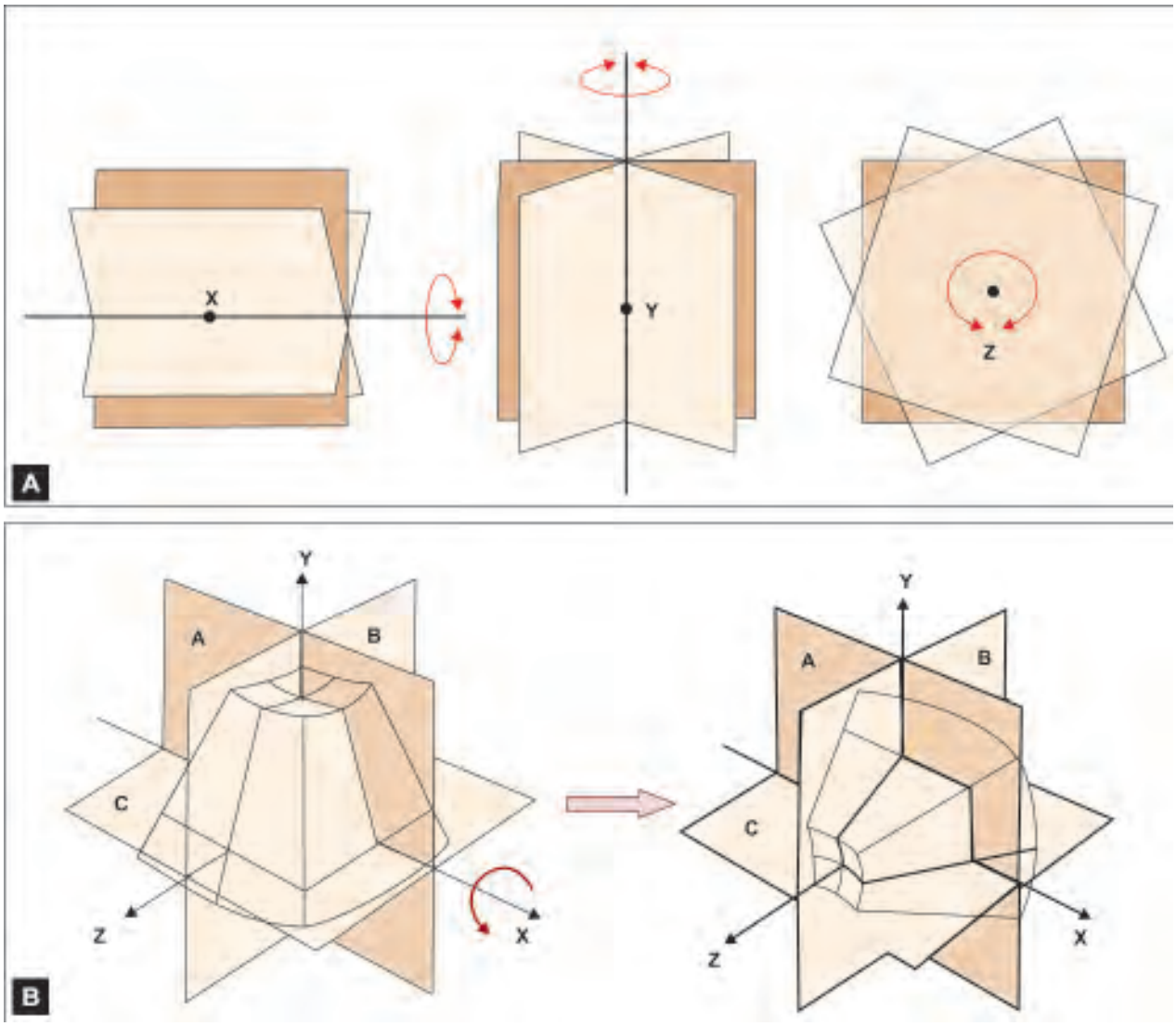

Figures 2.10A and B: Arbitrary section display by rotating the 3D data set. One of 3 axes (X, Y, Z) is selected for rotation[14]

Volume Rendering

Three-dimensional images are obtained by an algorism called volume rendering. A smaller 3D data set for rendering (3D image generation) is extracted first from the original 3D data set to eliminate unnecessary parts around the object as much as possible **(Fig. 2.14)**. A 3D data set for rendering is projected directly on a projection plane **(Fig. 2.15)** in volume rendering. Rays are assumed from each pixel on the projection plane into the 3D data set. Brightness of each pixel is determined based on gray values of voxels on each corresponding ray. **Figure 2.16** illustrates how brightness is calculated through voxels in the original volume rendering.[22]

A fetal surface image **(Fig. 2.17)** is obtained through volume rendering. Boundaries of the object do not need to be outlined strictly in volume rendering because low level noises around the object become transparent and do not affect the final 3D image much. An inside view of the heart can be also depicted three-dimensionally by using a 3D data set constructed with a gated technique **(Figs 2.18A and B)**.

Some other kinds of 3D images can be obtained by volume rendering. A fetal skeletal image is obtained when only the maximum gray values on each ray are displayed on the projection plane (maximum intensity projection) **(Fig. 2.19)**. A 3D image of cystic parts and blood vessels is obtained when only the minimum gray

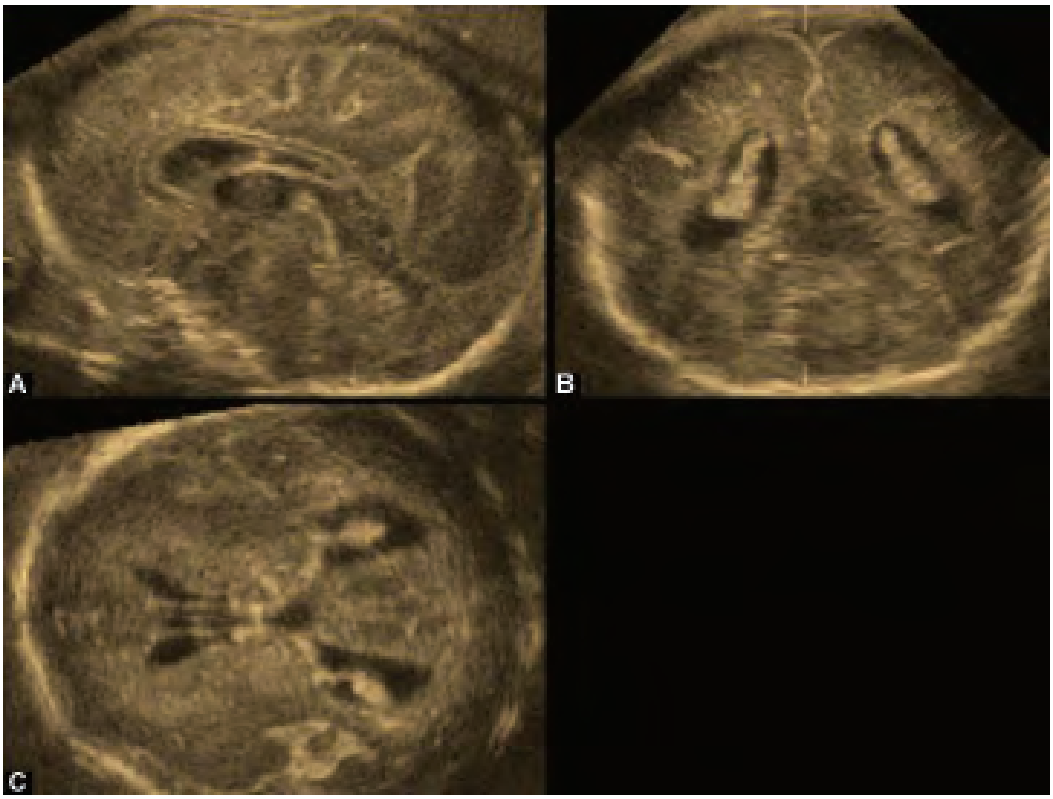

Figures 2.11A to C: Three-orthogonal-plane display of a fetal head. (A) Midsagittal plane; (B) Coronal plane; (C) Axial plane are displayed on a screen simultaneously

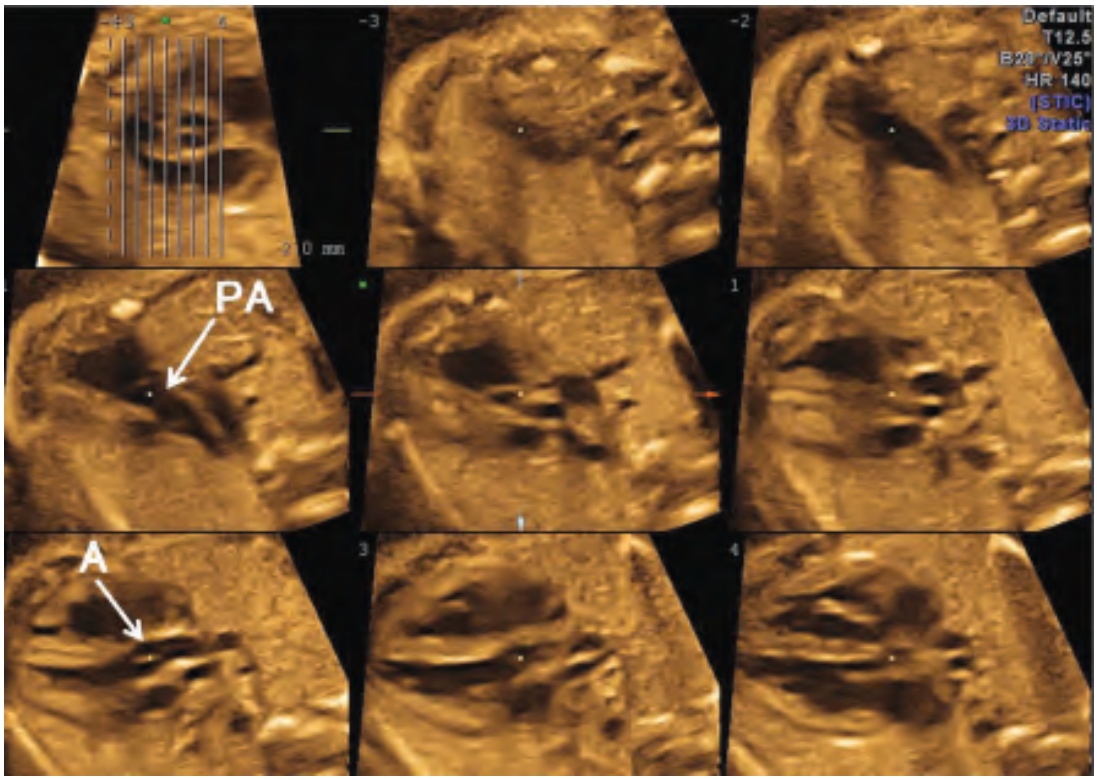

Figure 2.12: Parallel-plane display of a fetal heart. Both pulmonary artery (PA) and aorta (A) are depicted on an image

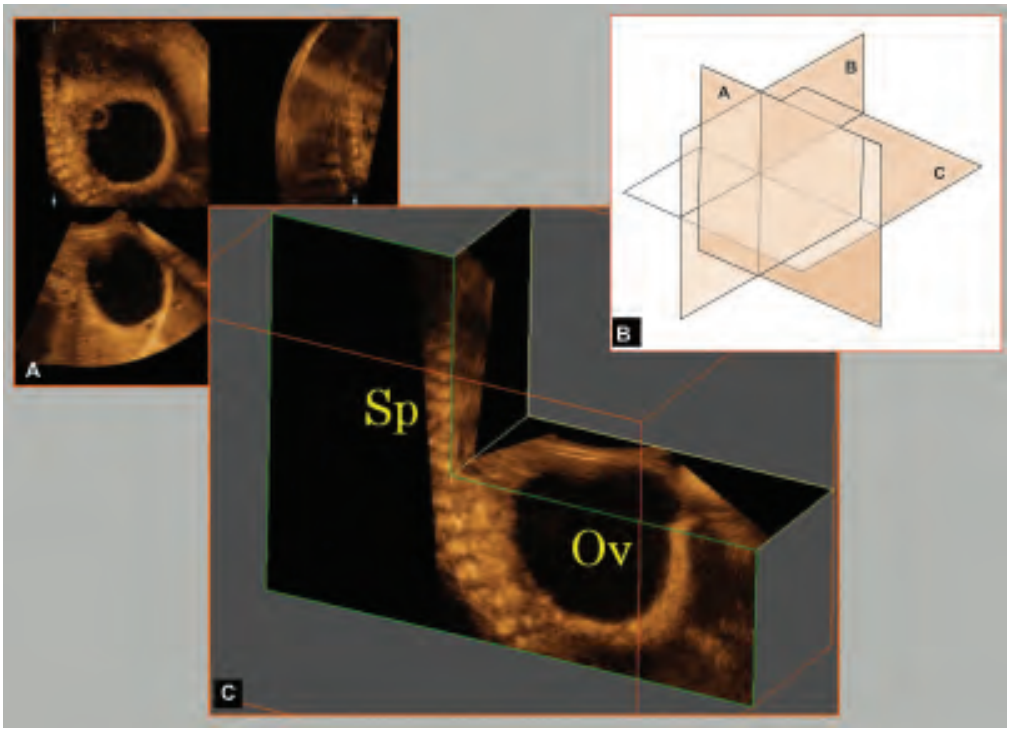

Figures 2.13A to C: A fetal ovarian cyst at 36 weeks of gestation. (A) Three-orthogonal-plane display; (B) A display in which three orthogonal planes are allocated three-dimensionally; (C) As shown in the schema. Sp: spine. Ov: ovarian cyst

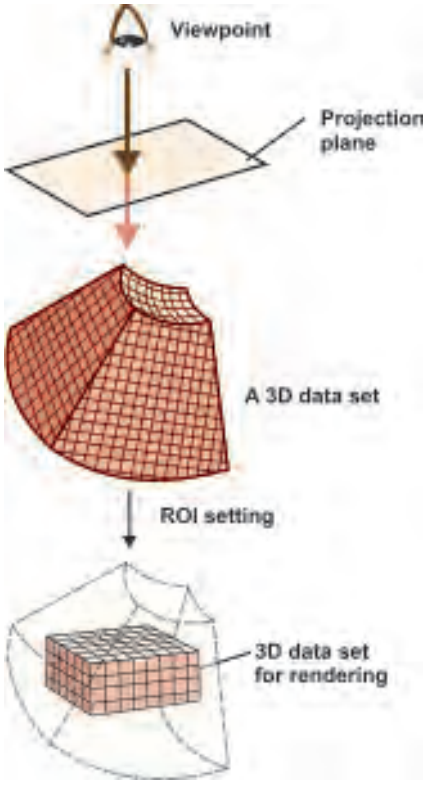

Figure 2.14: Settings of a viewpoint and ROI (region of interest) for a 3D data set for rendering[16]

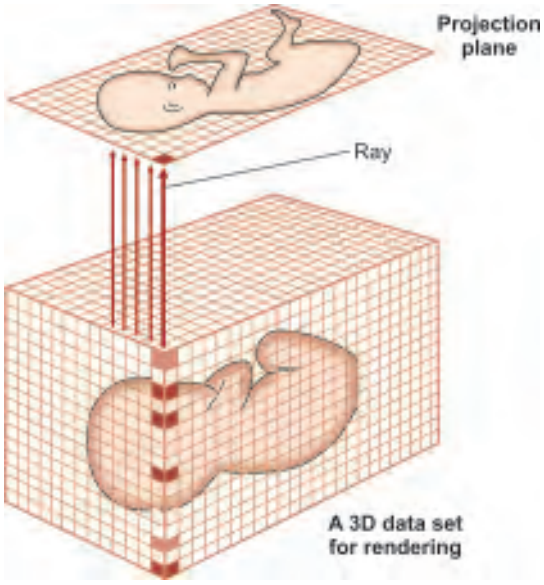

Figure 2.15: Volume rendering[16]

values on each ray are displayed on the projection plane (minimum intensity projection) **(Figs 2.20A to D)**. However, a 3D image shows only silhouettes in this way. A surface rendered 3D image of cystic parts is obtained by inverting black and white and processing

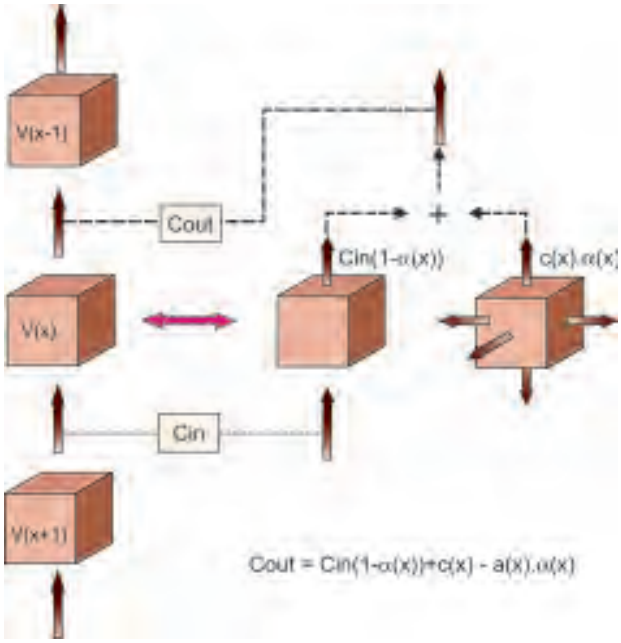

Figure 2.16: The original method of calculation in volume rendering[15]

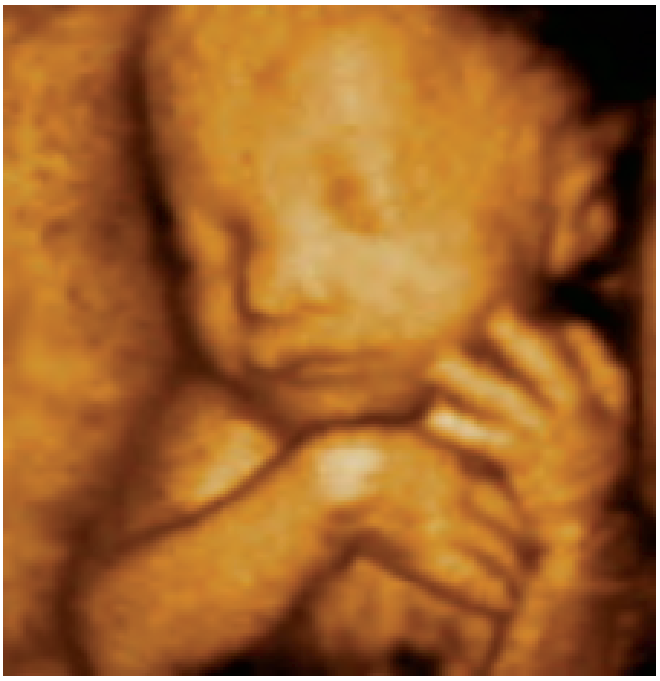

Figure 2.17: A surface-rendered image of a fetus at 33 weeks of gestation by volume rendering

cystic parts as solid parts (so-called inversion mode).[5] **Figures 2.21A to C** shows the difference between images by so-called minimum mode (minimum intensity projection) and by inversion mode.

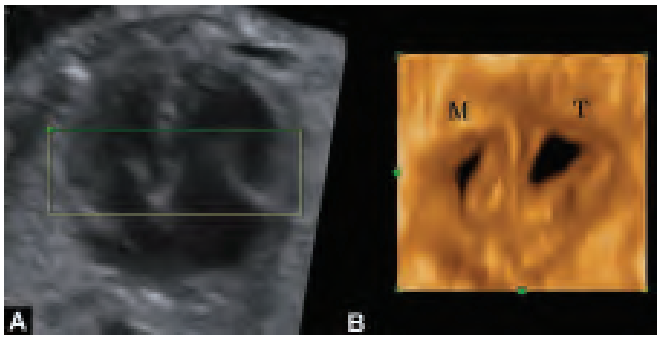

Figures 2.18A and B: (A) A tomographic image for ROI setting; (B) A 3D image of openings of mitral (M) and tricuspid (T) valves. A normal fetus at 28 weeks of gestation

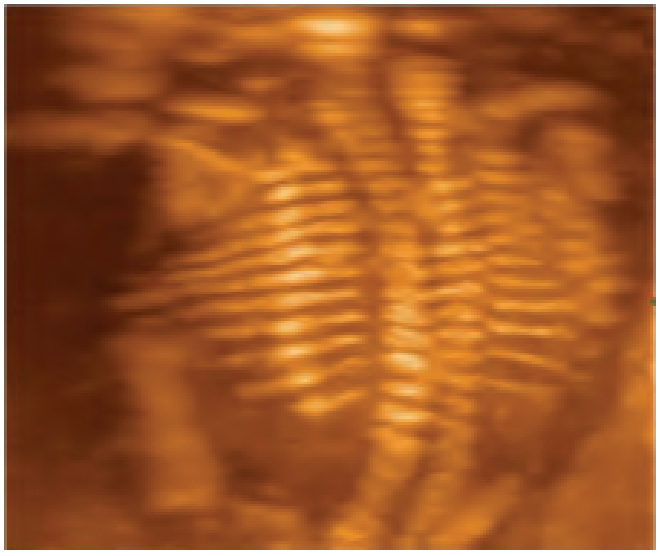

Figure 2.19: A 3D image of the fetal skeleton by maximum intensity projection

Speckle noises are accumulated in volume rendering and a higher contrasted and clearer image than a sectional image can be obtained in some cases **(Figs 2.22A and B)**. A 3D image of blood flows (blood vessels) is obtained by using color Doppler or power Doppler images instead of B-mode images **(Fig. 2.23)**. Volume rendering is a good rendering method for observation but not for volume measurement.

Surface Rendering

Three-dimensional surface images are also obtained by an algorism called surface rendering. **Figure 2.24** illustrates the principle of surface rendering. The object is extracted from a 3D data set, transformed to a set of intermediate geometrical data and projected on a 2D plane. Intermediate geometrical data is composed of small cubes or small polygons **(Figs 2.25A and B)**. A

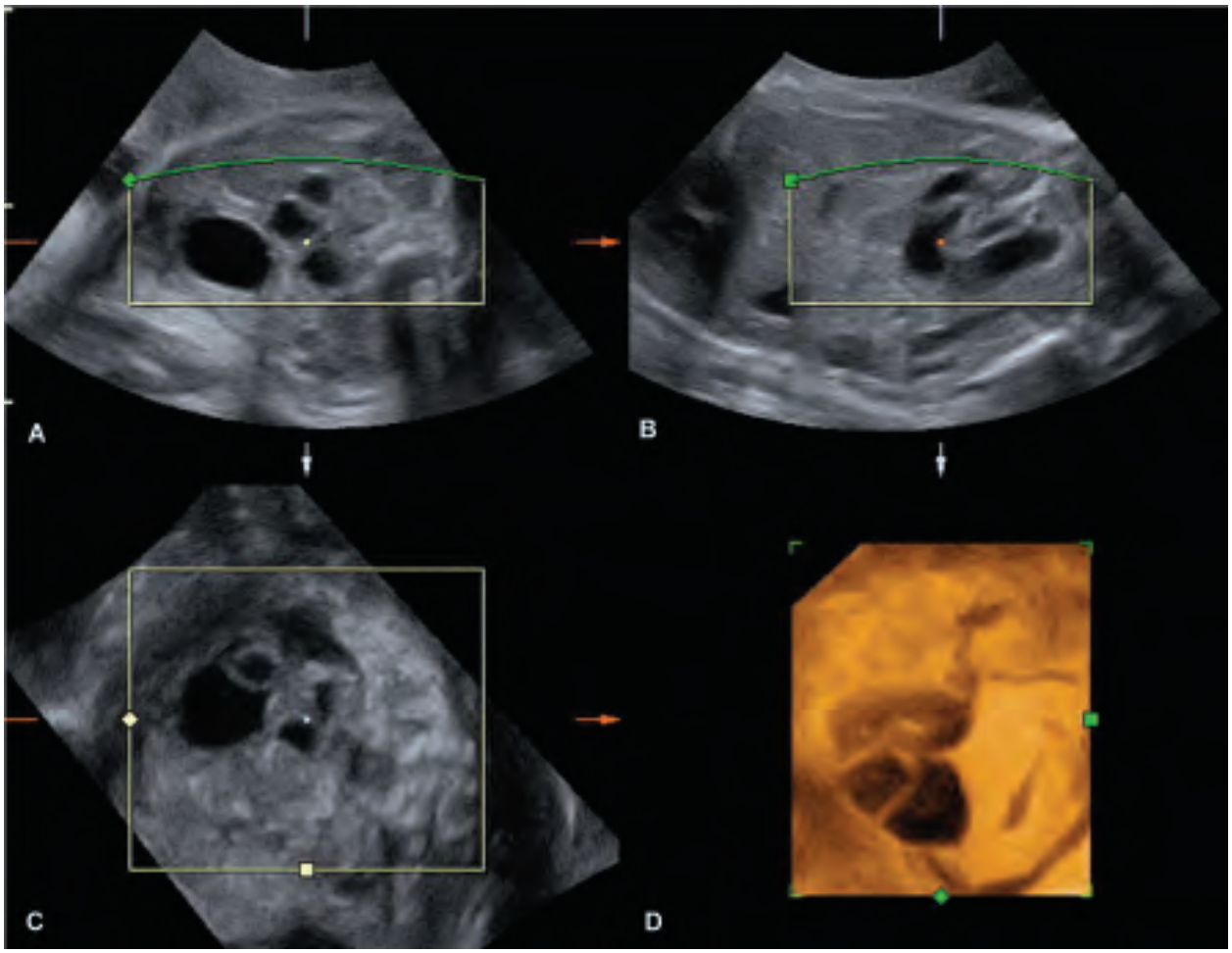

Figures 2.20A to D: (A to C) Three orthogonal planes; (D) A 3D image of a hydroureter by minimum intensity projection[14]

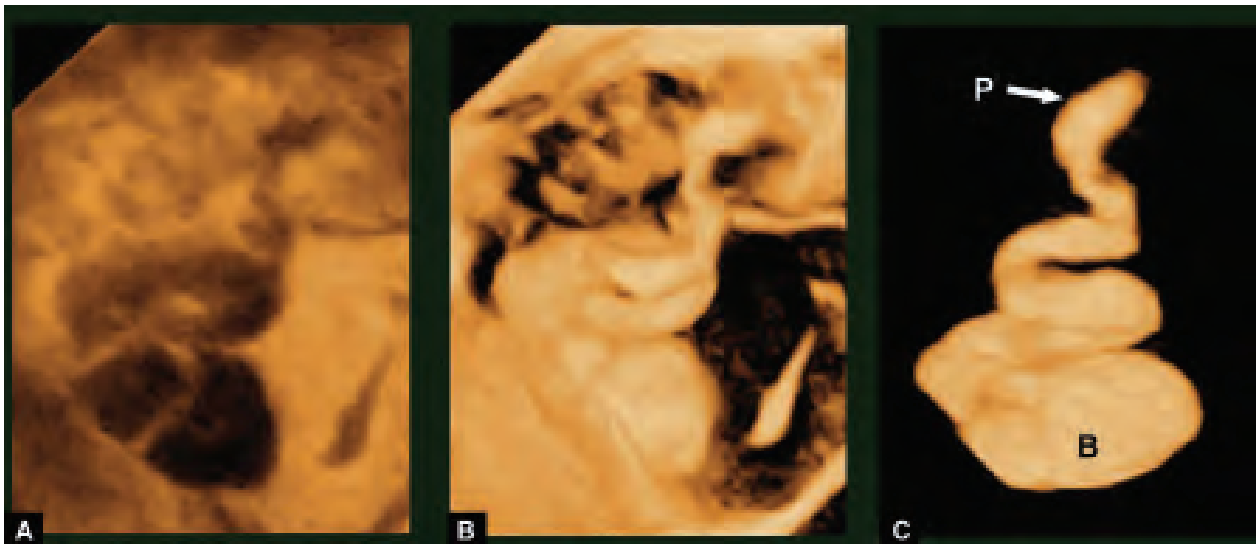

Figures 2.21A to C: (A) A 3D image of a hydroureter by minimum intensity projection (same image in Figure 2.20); (B) A 3D surface image of the hydroureter by inversion mode; (C) A 3D surface image of the hydroureter by inversion mode after removal of surrounding unnecessary parts. P: pelvis; B: bladder[14]

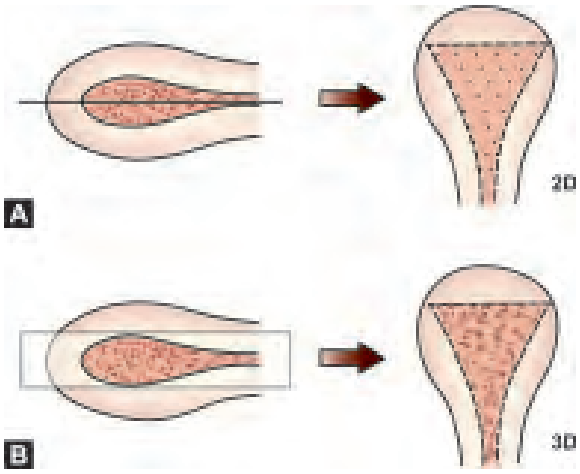

Figures 2.22A and B: (A) A plane image of a coronal section of the uterus; (B) A 3D image (lower right). A higher contrasted image can be obtained by volume rendering

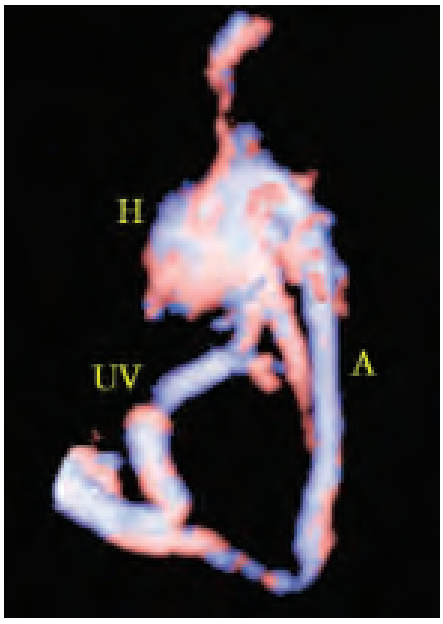

Figure 2.23: A 3D image of fetal circulation. The heart (H), the aorta (A) and the umbilical vein (UV). A normal fetus at 19 weeks of gestation

3D image can be modeled by shading **(Figs 2.26A and B)**.[15]

Extraction of the object may be performed by setting an appropriate threshold **(Fig. 2.27)**. But in most of the cases, extraction is done by manual tracing **(Figs 2.28A and B)** because boundaries of the object should be outlined strictly in surface rendering. Thus, surface rendering is more troublesome than volume rendering. But once the object is extracted, not only 3D image is displayed but also its volume can be calculated **(Figs 2.29A to E)**.

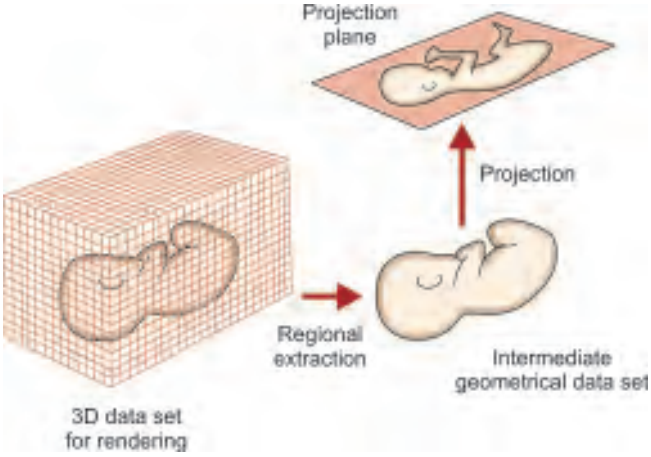

Figure 2.24: Surface rendering[16]

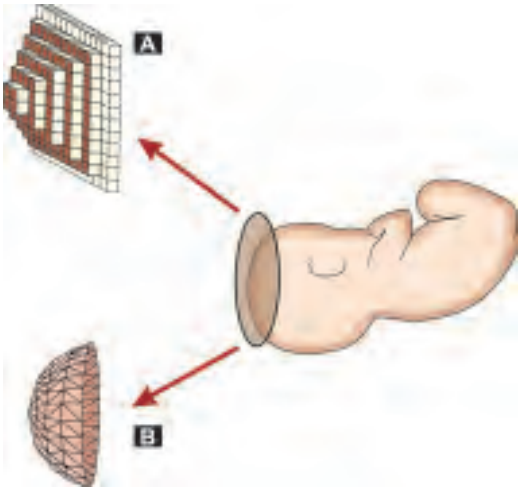

Figures 2.25A and B: (A) Intermediate geometrical data set composed of small cubes; (B) Small polygons[16]

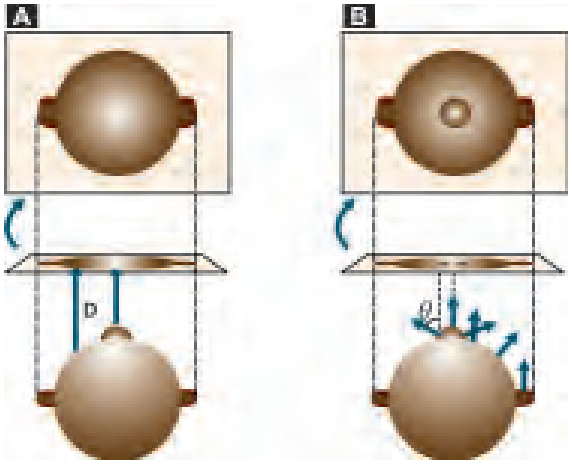

Figures 2.26A and B: Shading makes a 3D image more realistic. (A) Depth-only shading; (B) Shading with the orientation of the object surface[16]; D: depth; θ: angle of orientation

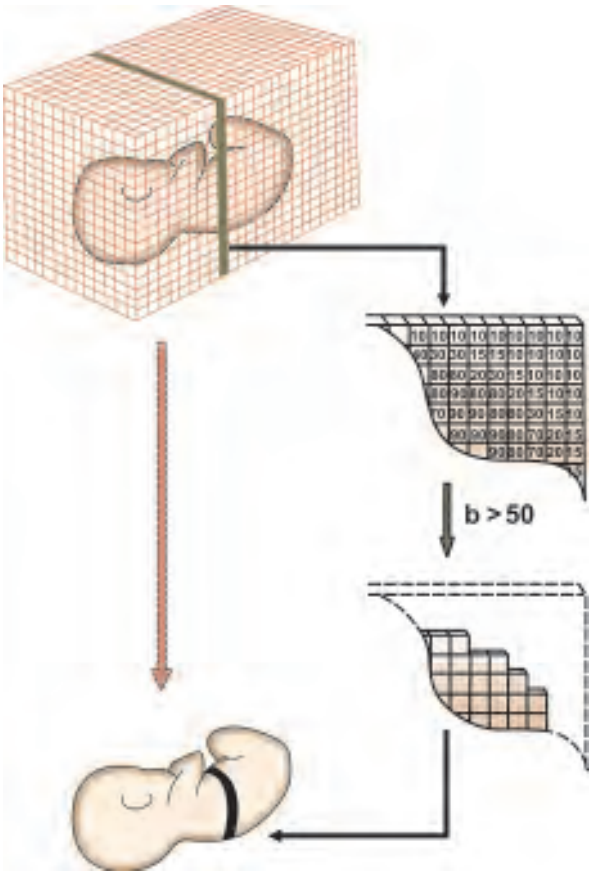

Figure 2.27: Extraction of the object (segmentation) may be performed by setting a threshold properly[16]

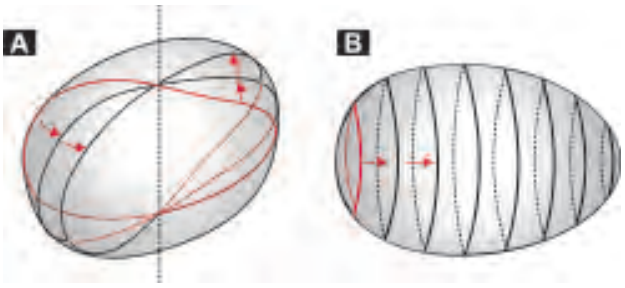

Figures 2.28A and B: Manual extraction of the object (segmentation) is done on several sections. The sections are selected by (A) Rotating or; (B) Translating the 3D data set[14]

Real Time Ultrasonic Beam Tracing

In this method, each ultrasonic beam is regarded as a ray in volume rendering. Calculation for each ultrasonic beam is performed immediately after the beam is received **(Fig. 2.30)**. This means that 3D scanning and volume rendering are performed simultaneously. This method does not require construction of a 3D data set, but a 3D image is always displayed as seen from the probe.

Defocusing Method

This method is referred to as volume imaging or thick slice 3D imaging. A thick slice by defocusing lens attached to the surface of a conventional probe captures

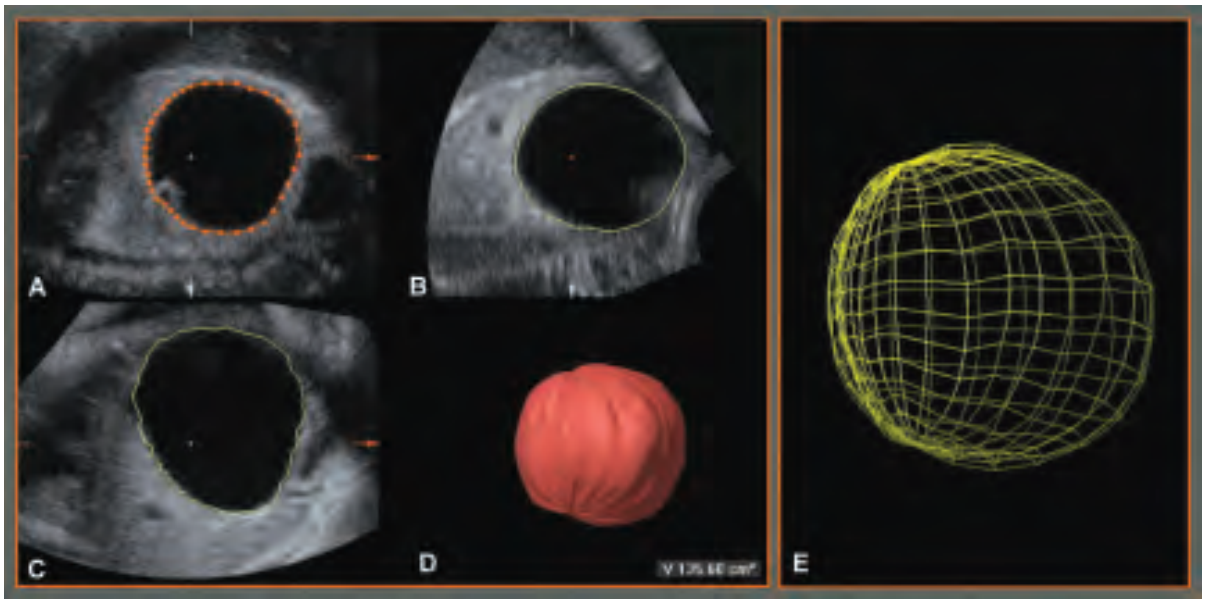

Figures 2.29A to E: (A to C) Surface rendering and measurement of the volume of a fetal ovarian cyst at 36 weeks of gestation. The outlines of the cyst were traced manually on three orthogonal planes like "A" in Figure 2.28; (D) A 3D image by surface rendering is displayed; (E) The 3D image is based on a set of small polygons and the volume is calculated automatically with the polygon data

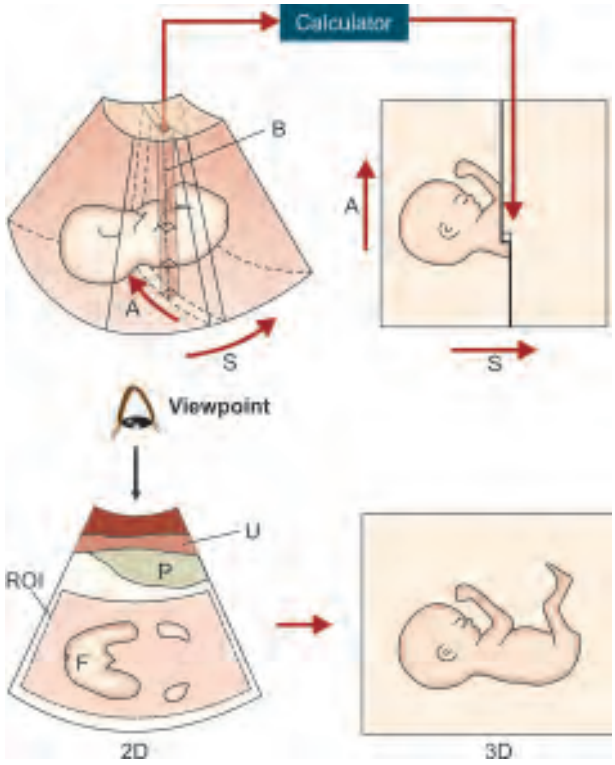

Figure 2.30: 3D image generation by real time ultrasonic beam tracing[16]

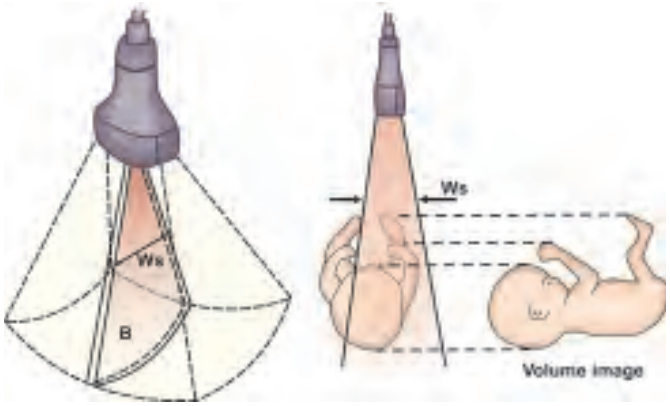

Figure 2.31: Volume imaging. Slice width (Ws) is widened by a defocusing lens attached to the surface of a conventional probe[16]

an object three-dimensionally **(Fig. 2.31)**. Real time observation is possible, but the clinical application of this method is very limited.

PRACTICAL TIPS

3D Scanning

The first point is to find a proper probe position and orientation for 3D scanning. For a fetal surface image, a position and orientation where a sufficient amount of amniotic fluid is seen over the fetus should be selected.

The second point is to consider the direction of 3D scanning. An ultrasonic beam is converged electrically in the direction of transducer array. In the direction perpendicular to the tomogram (the direction of slice width), only an acoustic lens is used for converging the beam **(Fig. 2.32)**. But convergence by an acoustic lens is not good enough and the object in the 3D data set tends to be expanded in the direction of slice width or in the direction of 3D scanning **(Fig. 2.33)**. Consequently, the width of the object on a 3D image **(Figs 2.34A and B)** and resolution of a 3D image **(Figs 2.35A and B)** varies on the direction of 3D scanning.

Region of Interest

Figure 2.36 illustrates the relation between three orthogonal planes and a 3D image. A 3D data set for

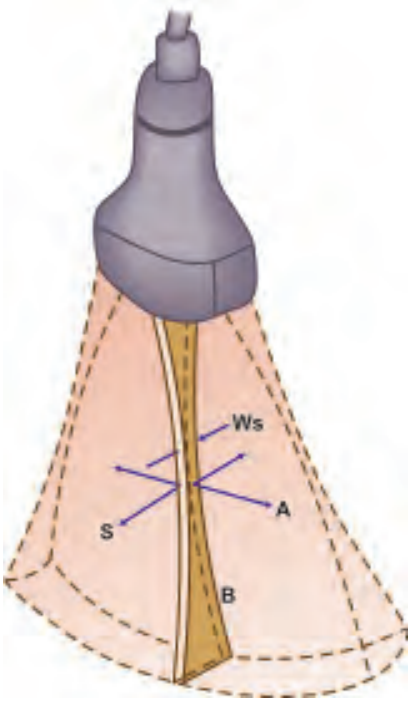

Figure 2.32: Widths of an ultrasonic beam (B). The width (Ws) in the direction of slice width (S) is much wider than the width in the direction of transducer array (A)[16]

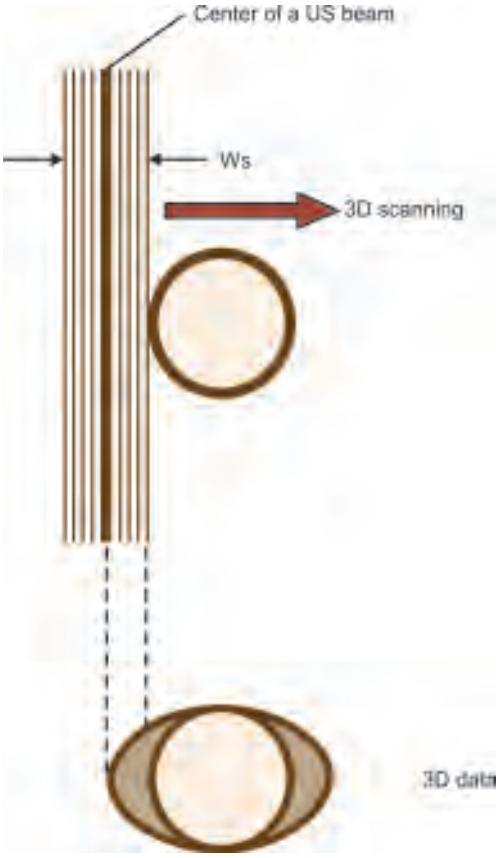

Figure 2.33: Influence of slice width (Ws) on 3D data. The 3D data of the object is expanded in the direction of 3D scanning[15]

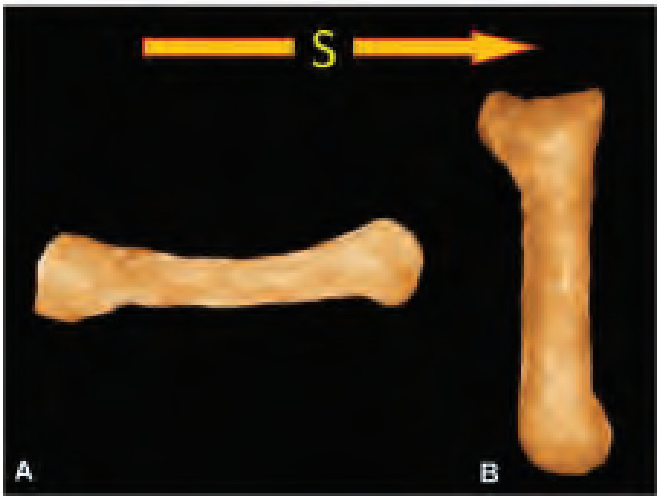

Figures 2.34A and B: An example of influence of slice width on a 3D image. The same fetal femur was scanned in different directions. The femur looks thicker in B than in A. S: direction of 3D scanning

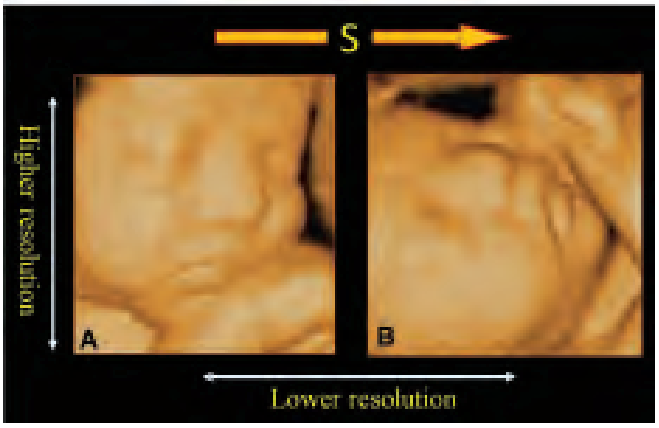

Figures 2.35A and B: An example of influence of slice width on a 3D image. The same fetal face was scanned in different directions. A gap between eyelids is seen clearer in A than in B. S: direction of 3D scanning

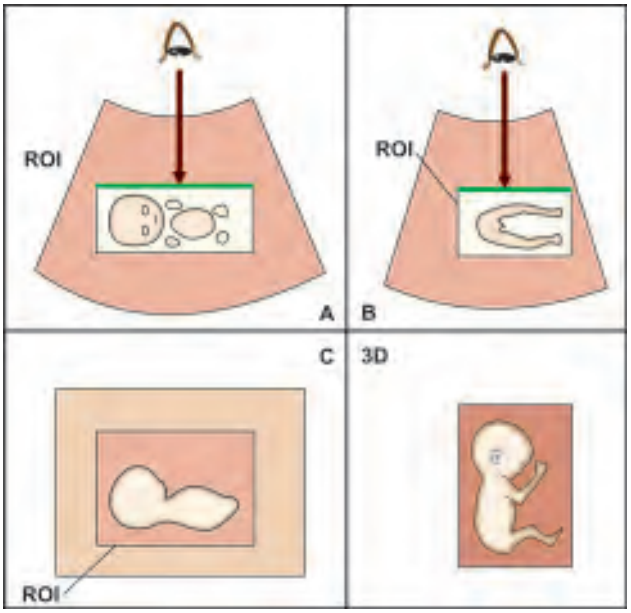

Figure 2.36: The relation between three orthogonal planes and a 3D image. Objects under the green line are depicted on the 3D image.[14] ROI: Region of interest

rendering is extracted by setting a region of interest (ROI) on the three orthogonal planes. The point is to fit the ROI to the object as much as possible, by translating and rotating the original 3D data set and by selecting ROI size **(Figs 2.37A and B)**.

Threshold

Setting the threshold properly is also very important to obtain a good 3D image. By doing so, unnecessary weak noises around the object can be removed **(Fig. 2.27)** and

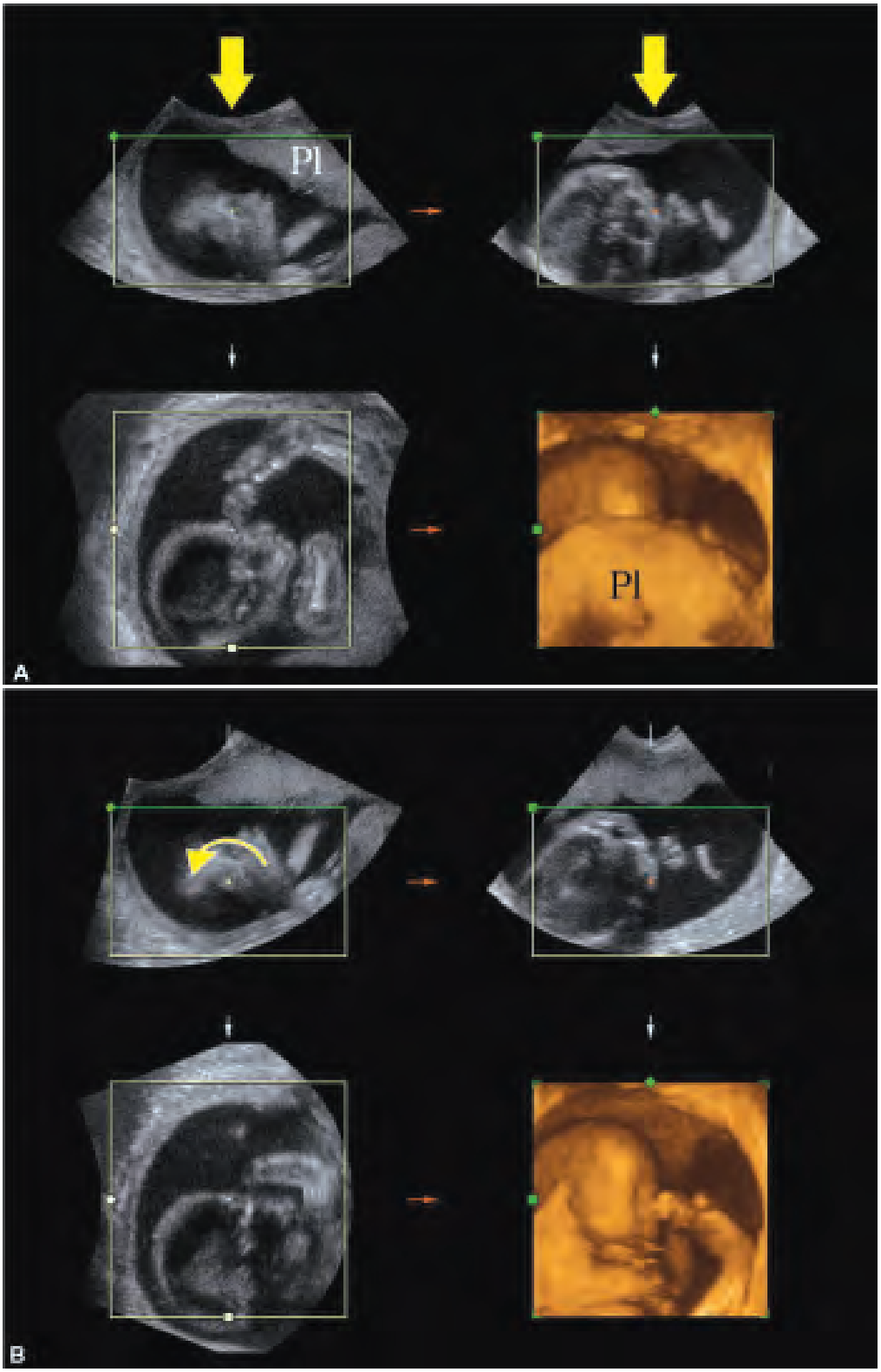

Figures 2.37A and B: (A) The placenta (P) hides a part of a fetus on the 3D image; (B) By rotating upper left plane counterclockwise around Z axis, hidden parts can be seen on the 3D image

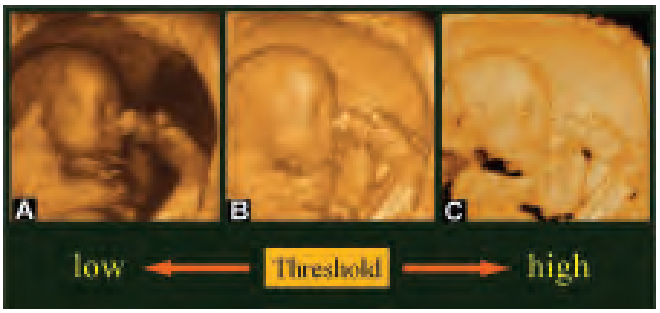

Figures 2.38A to C: Three-dimensional images of the same fetus as in Figure 2.37. (A) Left leg cannot be seen with a low threshold; (B) It can be seen with increasing the threshold; (C) Parts of the fetus are also eliminated when the threshold is set too high

a clear 3D image can be obtained. When the threshold is too low, weak noises around the object hide it. When the threshold is too high, parts of the object get eliminated **(Figs 2.38A to C)**.

Electrical Scalpel

Even when unfavorable images remain around a 3D image of the object after proper settings of ROI and threshold, unnecessary parts in the 3D data set can be removed in the computer and unfavorable images can be eliminated **(Figs 2.39A to F)**. This function is called electrical scalpel or 3D cutting. Even a separated fetal bone can be displayed by this function **(Fig. 2.34)**.

CONCLUSION

Three-dimensional ultrasound has many functions and possibilities that are not involved in conventional 2D ultrasound. Both volume rendering and surface rendering give a 3D image. Volume rendering provides various kinds of 3D images as well as a surface-rendered image. In surface rendering, the intermediate geometrical 3D data set can be easily used for volume measurement of the object as well as 3D image

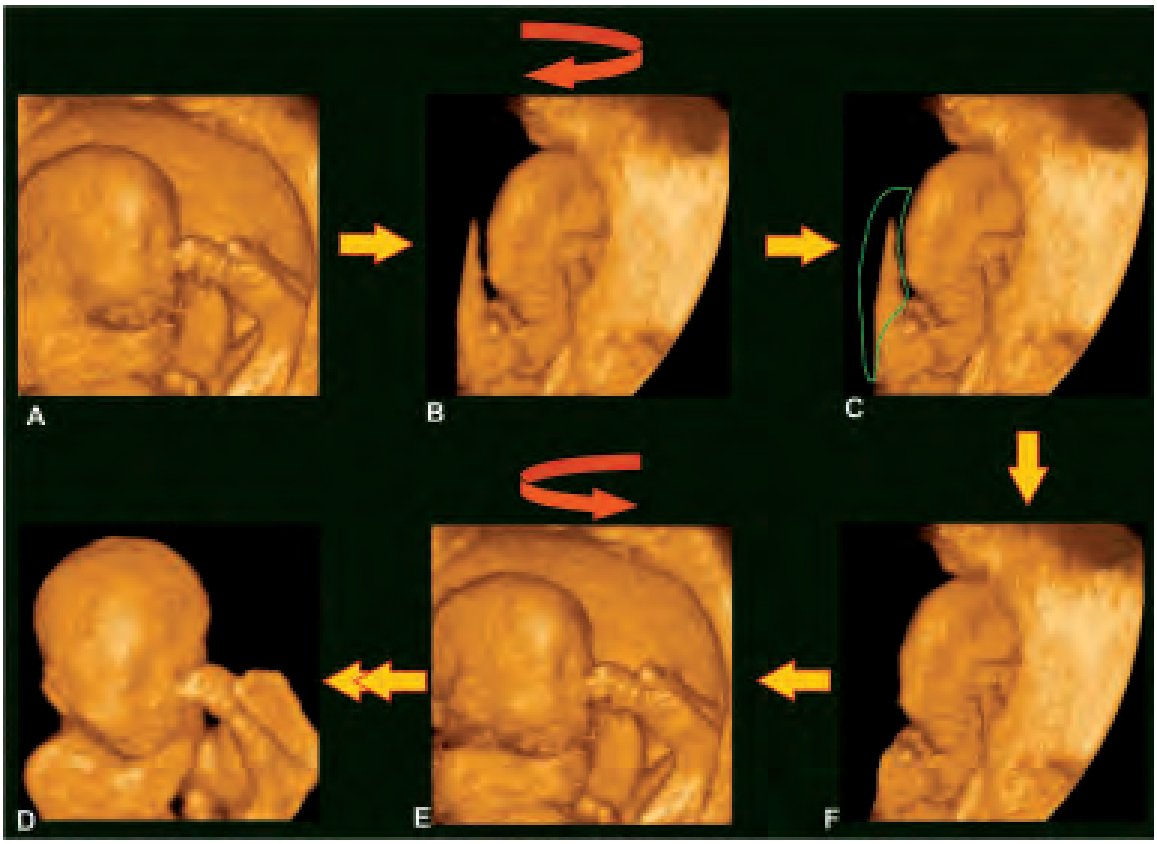

Figures 2.39A to F: Removal of unfavorable parts around a fetus. (A) The fetus is partially covered by the uterine wall; (B to E) The uterine wall over the right shoulder is eliminated after rotating the 3D image and surrounding the uterine wall with green line. The remaining uterine wall and umbilical cord around the fetus can also be eliminated in the same manner; (F) A 3D image after removal of all unfavorable parts around the fetus

generation. Some considerations are required in 3D scanning, ROI setting, threshold setting and electrical scalpel to obtain a clearer 3D image.

REFERENCES

1. Szilard J. An improved three-dimensional display system. Ultrasonics. 1974;12(6):273-6.
2. Brinkley JF, McCallum WD, Muramatsu SK, et al. Fetal weight estimation from ultrasonic three-dimensional head and trunk reconstructions: evaluation in vitro. Am J Obstet Gynecol. 1982;144(6):715-21
3. Baba K, Satoh K. Development of the system for ultrasonic fetal three-dimensional reconstruction. Acta Obst Gynaec Jpn. 1986;38:1385.
4. Woo J. A short history of the development of ultrasound in obstetrics and gynecology. [online]. Available from http://www.ob-ultrasound.net/history3.html [Accesed on February, 2011].
5. Baba K. Leaps of obstetrics and gynecology by ultrasonography – from transabdominal to transvaginal, from 2-dimensinoal to 3-dimensional – Osaka, Japan: Nagai Shoten, 1992.
6. Merz E, Macchiella D, Bahlmann F, et al. Fetale Fehlbildungsdiagnostik mit Hilfe der 3D-Sonographie. Ultraschall Klin Prax. 1991;6:147.
7. Kuo HC, Chang FM, Wu CH, et al. The primary application of three-dimensional ultrasonography in obstetrics. Am J Obstet Gynecol. 1992;166(3):880-6.
8. Sohn C, Stolz W, Nuber B, et al. Three-dimensional ultrasound diagnostics in gynaecology and obstetrics. Geburtsh u Frauenheilk. 1991;51:335-40.
9. Chiba Y, Yamazaki S, Takamizawa K, et al. Real-time three-dimensional effect using acoustic wide-angle lens for the view of fetuses. Jpn J Med Ultrasonics. 1993;20(suppl.1): 611-2.
10. Kossoff G, Griffiths KA, Warren PS. Real-time quasi-three-dimensional viewing in sonography, with conventional gray-scale volume imaging. Ultrasound Obstet Gynecol. 1994;4(3):211-6.
11. Baba K, Okai T, Kozuma S. Real-time processable three-dimensional fetal ultrasound. Lancet. 1996;348(9037):1307.
12. Baba K, Jurkovic D (Eds). Three-dimensional Ultrasound in Obstetrics and Gynecology. Carnforth, UK: Parthenon Publishing, 1997.
13. Baba K. Introduction to three- and four-dimensional ultrasound. In: Kurjak A, Jackson D, (Ed.). An Atlas of Three- and Four-Dimensional Sonography in Obstetrics and Gynecology. New York, USA: Taylor and Francis; 2004. pp. 3-18.
14. Baba K. Basis of 3D ultrasound. In: Baba K (Ed.). Ultrasound in Obstetrics and Gynecology. Tokyo, Japan: Tokyo Igaku Publishing; 2010. pp. 27-37.
15. Baba K, Okai T. Basis and principles of three-dimensional ultrasound. In: Baba K, Jurkovic D (Eds). Three-dimensional Ultrasound in Obstetrics and Gynecology. Carnforth, UK: Parthenon Publishing; 1997. pp. 1-19.
16. Baba K. Basis and principles of three-dimensional ultrasound. In: Takeuchi H, Baba K (Eds). Master three-dimensional ultrasound. Tokyo, Japan: Medical View; 2001. pp. 12-29.
17. Smith SW, Trahey GE, vonRamm OT. Two-dimensional array ultrasound transducers. Ultrason Imaging. 1992;14(3):213-33.
18. von Ramm OT, Smith SW, Carroll BA. Advanced real-time volumetric ultrasound scanning. J Ultrasound Med. 1995;14(suppl):S35.
19. Nelson TR, Pretorius DH, Hagan-Ansert S. Fetal heart assessment using three-dimensional ultrasound. J Ultrasound Med. 1995;14(suppl):S30.
20. Deng J, Gardener JE, Rodeck CH, et al. Fetal echocardiography in three and four dimensions. Ultrasound Med Biol. 1996;22:979-86.
21. Baba K, IO Y. Three-dimensional ultrasound in obstetrics and gynecology. Tokyo, Japan: Medical view, 2000.
22. Levoy M. Display of surfaces from volume data. IEEE Computer Graphics and Applications. 1988;8(3):29-37.

CHAPTER 3

Artifacts, Pitfalls and Normal Variants

Ivica Zalud, Frederico Rocha

INTRODUCTION

Artifacts in ultrasound are common problem in everyday clinical practice. Differentiating real findings and deceptive artifacts is very important. A good understanding of the physical principles of ultrasound waves, equipment and their interaction with anatomy being examined is essential in distinguishing reality, normal variants and artifacts.

What is the Problem?

- What gives the multiple appearance of an intrauterine contraceptive device?

Answer: Reverberation

- Why does an early single intrauterine pregnancy sometimes look like a twin gestation?

Answer: Duplication artifact

- Why is a large cyst-like structure occasionally seen in the pelvis when it does not exist?

Answer: Mirror image artifact

- Why does a simple cyst sometimes appear to contain a sludge-like layer?

Answer: Slice thickness artifact

- Why are dermoids, even large ones, sometimes not detectable sonographically?

Answer: Shadowing (tip of the iceberg phenomenon)

- What does it all mean?

Answer: In this chapter, these intriguing artifacts are described and explained. Advice on how to recognize and in some cases, how to minimize them is also given. On the other hand, the presence of artifacts can sometimes even be helpful in clinical practice and give additional information.

DEFINITION

Artifacts in ultrasound imaging occur as structures that are one of the following:

- Not real
- Missing
- Of improper brightness
- Of improper shape
- Of improper size.

Some artifacts are produced by improper equipment operation (e.g. improper transducer location and orientation information sent to the display) or settings (e.g. incorrect receiver compensation settings). Some are caused by improper scanning technique (e.g. allowing

patient or organ movement during scanning). Other as inherent in the ultrasound diagnostic method and can occur even with proper equipment and technique.

MECHANISM

Artifacts are merely errors in presentation that result from the following assumptions:

Echoes come from interfaces that are:

- Directly in front of the transducer
- At a depth equal to half the time of flight of the sound pulse multiplied by a constant velocity (1,540 m/s).

In other words, if the pulse is reflected, refracted or otherwise affected in the body, the ultrasound machine has no way of knowing that. A blip that does not correspond to an actual interface at a corresponding point in the body may appear on the screen. The blip always appears on the screen at a point corresponding to the time since the production of the pulse and from the direction that the transducer was pointing.

CLASSIFICATION

Commonly encountered artifacts include:

- Reverberation and ring-down (comet tail)
- Shadowing
- Enhancement
- Mirror (multipath) artifacts
- Refraction and side lobes
- Curved and oblique reflector
- Propagation speed error
- Resolution
- Doppler artifacts
- Three-dimensional artifacts.

These artifacts are seen daily. Although some of these artifacts are more pronounced in the upper abdomen, chest or neck, the examples chosen are mainly those encountered in obstetric and gynecologic ultrasound examinations.

REVERBERATION

Reverberation results in reflectors that are not real, being placed on the image. They will be placed behind the second real reflector at separation intervals equal to the separation between the first and second real reflectors. Each subsequent reflection will be weaker than prior ones. This can occur from the anterior wall of the urinary bladder, especially in an obese person **(Fig. 3.1)**. The

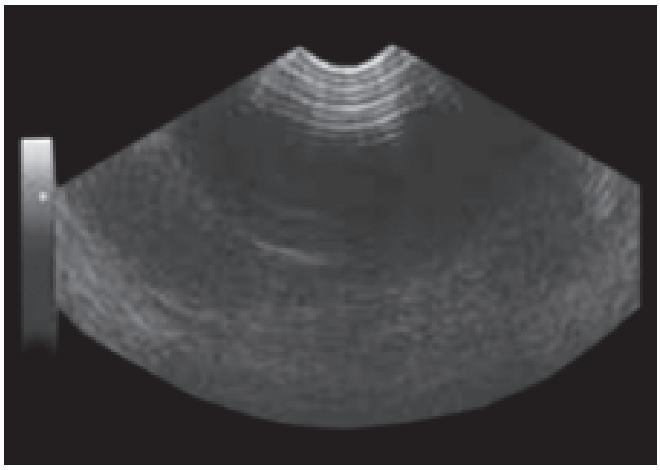

Figure 3.1: Reverberation: Anterior wall of the urinary bladder in an obese person

sound pulse is reflected back from the anterior wall of the bladder to the transducer face. As the transducer has to produce the true echo, it absorbs some of the pulse. However, some of that sound is reflected from the transducer-skin interface back into the body. It again hits the anterior bladder interface and is reflected back for a second time to the transducer. This produces a first reverberation artifact on the image. The ultrasound equipment assumes (incorrectly) that the signal has returned from a point in the body that is twice the distance from the transducer, as it is aware only of the time taken for the signal to return and not of the path actually travelled. This artifact is seen as a blip on the screen at twice the depth of the true echo. This is because the time taken for the first reverberation artifact is the same time taken for the pulse to travel the original distance and back. This same reverberation can occur a second and third time to give the second or third reverberation artifact. This is commonly known as "near-field" artifact, especially in obese patients. The echoes may be more diffuse and fuzzy if they bounce around in various directions in the subcutaneous fat before returning to the transducer.[1] Occasionally, care must be taken not to confuse this artifact for an anterior placenta.

Ring-down is another type of reverberation artifact. It occurs when the sound hits a metallic structure, such as a metallic surgical clip or a group of small gas bubbles. In this situation, the sound bounces back and forth numerous times within the structure, each time sending some of the sound back to the transducer. This, therefore, appears on the screen as numerous tiny parallel echoes deep to the structure. This artifact has also been called a "comet tail". Certain situations are

there, where there are only one or two reverberations deep to a structure. This can occur with intrauterine device (IUD) in the uterus.

Since reverberation artifacts are produced by sound bouncing back and forth within the body, it is virtually impossible to adjust the machine to get rid of them. Although one can turn down the near gain, the real echoes will be lost along with the artifactual ones. The presence of a ring-down artifact enables the identification of gas. When this is found in an abnormal, extraluminal location, it may indicate that the patient has an abscess. In other situations, a ring-down artifact indicates that there is gas and therefore, the "mass" seen deep to it is likely to be an artifact. When needle biopsies are done under ultrasound guidance, the needle also produces a ring-down artifact, which is particularly helpful in identifying the location of the needle on the image.

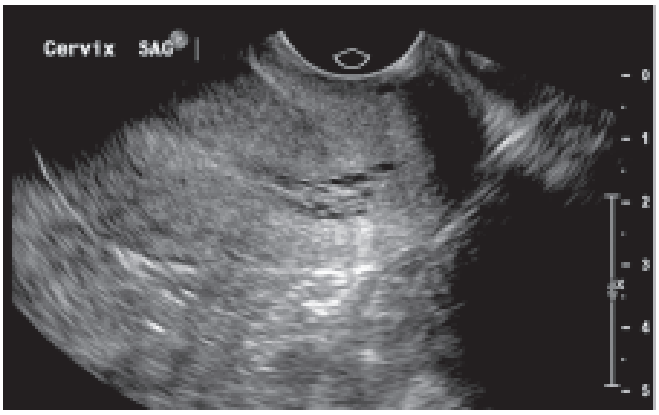

Figure 3.2: Shadowing artifacts on transvaginal ultrasound caused by air in the condom. Portion of the cervix and cul-de-sac are "in the dark"

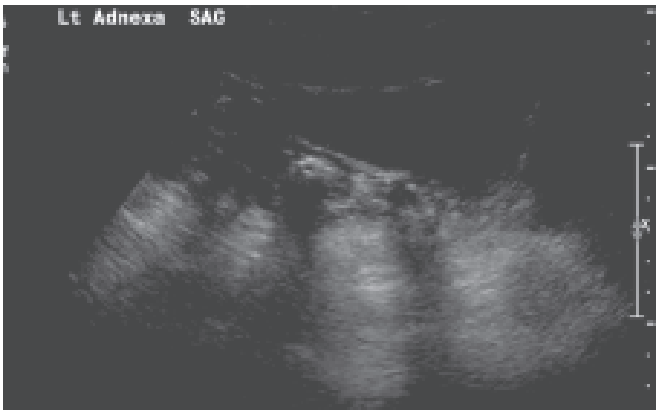

Figure 3.3: Another example of shadowing caused by air in the bowels

SHADOWING

Shadowing is the reduction in reflection amplitude from reflectors that lie behind a strongly reflecting or attenuating structure. Shadows in ultrasound may be due to reflection, absorption or refraction. The reflective or absorptive shadows are entirely analogous to the shadow cast by a tree in the sun. All of the light is reflected and/or absorbed by the tree trunk, so that there is a relative shadow on the tar side. With ultrasound, all of the sound beam must be blocked by a calcification to produce a shadow. There should be an echo from the near side of the structure as well. It is possible to produce an echo without a shadow if the structure only impinges on part of the sound beam without being large enough to block it completely. It is therefore possible to have small clumps of calcification that do not produce a shadow. One cannot change the size of the calcified structure. However, one can choose the correct transducer or the correct focal level to maximize the chance of identifying the shadow. The narrowest beam and narrowest portion of the beam are necessary to identify a shadow. If the focal depth of a transducer is adjusted either too close or too far, the echoes may be identified but not the shadows. If shadowing is not present, the calcified nature of a lesion or structure may be missed.

Air can also cause shadowing **(Figs 3.2 and 3.3)**. Most of the time, this causes great interference on the ultrasound examination by obscuring the deeper structures. For this reason, patients have to be examined with a full bladder to displace the air-containing bowel from the pelvis. The shadow deep to gas is different from the shadow deep to a calcified structure. With the latter, although some of the sound is reflected, much of it is absorbed. With gas, the acoustic mismatch is so great that virtually all of the sound is reflected. This sound bounces around in the tissues between the transducer and the gas, and can cause numerous reverberations and other mirror image artifacts, which on the image appear deep to the echo from the gas interface. This has been called a "dirty" shadow as opposed to the "clean" shadow deep to bone or other calcified (sound-absorbing) structures. This distinction does not always hold true but most of the shadows due to gas are easily differentiated from shadows due to hard and/or calcified structures. As previously mentioned, the presence of ring-down is of further value in recognizing gas. Another type of shadowing is associated particularly with dermoid cysts. This is a peculiar situation in which there is a strong "dirty" shadow that is likely due to the inhomogeneous

structures within a dermoid. These include hair, cartilage, fat and so on. This appearance of strong shadowing can cause a difficulty in diagnosing dermoids because they can look very similar to gas and stool in the bowel, in both transverse and longitudinal scans. This is the so-called tip of the iceberg sign.[2] The stool-filled rectum can mimic a dermoid or a dermoid can be overlooked by assuming that it is the rectum. When there is a clinical suspicion, a digital examination or water enema during ultrasound visualization may help differentiate between the two.

Another kind of shadow occurs at the edge of structures when the sound beam passes through an oblique interface. When the sound beam passes through a curved or oblique interface, some of the sound beam can be refracted away from the central line. This can result in a defocusing of the sound beam deep to the oblique interface and can be seen at the edge of the fetal skull, especially when the beam passes through the placenta. Occasionally, these can be at the edges of cysts in the ovaries. Refractive shadowing can also cause a drop-out of echoes deep to the bladder in the lower uterine segment or in the region of the cervix. This is especially true in patients with leiomyomas.

ENHANCEMENT

Enhancement is the opposite of shadowing. It is the increase in reflection amplitude from reflectors that lie behind a weakly attenuating structure **(Figs 3.4 and 3.5)**. Shadowing and enhancement result in reflectors being placed on the image with amplitudes that are too low and too high, respectively. In this situation, the echoes returning from structures deep to cysts appear more intense than if the cyst were not interposed. There are two explanations for this phenomenon. One is that the fluid replaces normal soft tissue in the intervening space, decreasing its attenuation.[3] The time gain compensation (TGC) is set to expect tissue between the transducer and the deepest echoes. If there is fluid instead, especially if the fluid occupies only the central portion of the image, the echoes returning from deep to the fluid collection will be more intense than expected.[3] This appears as a posterior enhancement of the beam and this finding indicates that a lesion is truly cystic, even if there are internal echoes within the cyst. Occasionally, enhancement will be noted deep to a very small cystic structure, more than what can be explained by a lack of attenuation. The small cyst acting as a lens and refocusing the sound beam may cause this enhancement.[4] This is the opposite of refractive shadowing where the oblique interface defocusses the beam. Often the two co-exist.

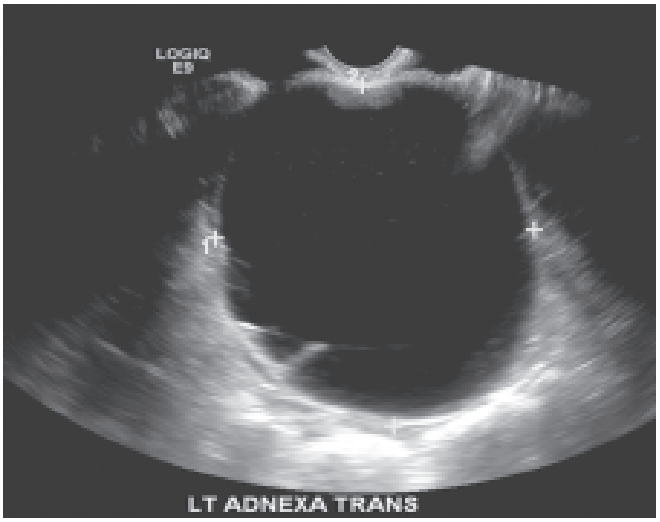

Figure 3.4: Enhancement: The echoes returning from structures deep to the cyst appear more intense than if the ovarian cyst was not interposed

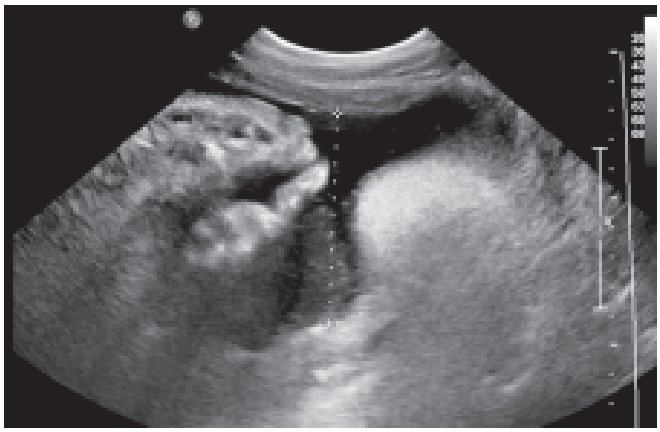

Figure 3.5: Enhancement caused by amniotic fluid. Bright edges are clearly seen

MIRROR ARTIFACTS

The term mirror or multipath artifact describes the situation in which the paths to and from a reflector are different. This artifact results in improper reflector image positioning. If separation is not sufficient, two reflectors are seen as one (missing-reflector artifact). Whereas reverberations and ring-downs are reflections that occur back and forth within the direction of the original sound beam, a mirror image artifact is one in which the sound beam is deflected away from the transducer. The reflected sound may hit a strong

interface, be bounced back to the "mirror" and then back to the transducer. The machine will therefore receive an echo and display a blip on the screen in the direction that the transducer was pointing and at a distance corresponding to the time taken. However, this will be a phantom echo since there is no interface in that position. It can also cause significant trouble when it produces a mirror image of the bladder deep to the rectum or sigmoid colon. In this situation, the phantom can closely resemble a cyst, ovarian tumor or leiomyoma.[1] This kind of artifact can fool even the most experienced sonologists. Differentiating between a true lesion and a mirror image artifact can be difficult. However, the phantom cyst frequently has an unusual, somewhat triangular shape on the longitudinal scan. The back wall is often very ill defined, whereas true cystic lesions invariably have a good, clear posterior wall. It is important to realize that this artifact is seen on both transverse and longitudinal scans. One can have the patient partially empty the bladder. This will cause the phantom mass to become proportionately smaller. It is, however, important that the patient does not empty the bladder completely as real lesions can then be missed. Transvaginal scanning can be very useful in difficult cases.

REFRACTION (DUPLICATION) AND SIDE LOBES

This most interesting artifact occurs uniquely when the transducer is held in a transverse plane over the linea alba. The sound is refracted toward the midline when the transducer is pointing to the medial edge of the rectal muscle on either side. This makes small midline structures appear duplicated on the screen. This phenomenon can cause an erroneous appearance of early twins due to duplication of a single small gestational sac. In addition, intrauterine device can appear duplicated. One could similarly diagnose a bicornuate uterus erroneously. This artifact does not occur in a sagittal or transverse section once the transducer is moved to either side of the midline.[5,6] Not only is the beam not as narrow as anticipated, but also there is a phenomenon called "side lobes." Due to refraction, there are relatively strong beams of sound outside the main beam. If one of these "side lobes" strikes an interface and especially if that interface is concave toward the transducer, an echo is received by the transducer. Once again, the transducer and machine have no way of knowing that this came from outside the main beam and it will be displayed as though it were an interface directly in front of the transducer. These artifacts generally appear as curved lines that can be followed back to their origin. They are commonly seen in the bladder, coming off the concave surface anterior to the fundus of the uterus. Occasionally, they come from a loop of bowel that indents the bladder slightly. Refraction can cause a reflector to be improperly positioned on the display. A similar occurrence can be caused by reflections from side lobes. Refraction and propagation speed error can also cause a structure to be displayed with incorrect shape.

OTHER ARTIFACTS

A curved reflector can produce a reflection low in amplitude because some of the reflection is missed by the transducer. Oblique reflection can produce a reflection low in amplitude or the reflection may be completely missed by the transducer. Resolution also increases the apparent size of a reflector on a display. Propagation speed error occurs when the assumed value for propagation speed in the range equation is incorrect. Diagnostic instrumentation assumes a speed of 1,540 m/s. If the propagation speed that exists over a path traveled is greater than 1,540 m/s, the calculated distance to the reflector is too small and the display will place the reflector too close to the transducer. If the actual speed is less than 1,540 m/s, the reflector will be displayed too far from the transducer. The minimum displayed lateral and longitudinal dimensions will be the beam diameter and one-half the spatial pulse length, respectively.

DOPPLER ULTRASOUND ARTIFACTS

Aliasing

Aliasing is the most common artifact encountered in Doppler ultrasound.[7] There is an upper limit to Doppler shift that can be detected by pulsed instruments. If the Doppler shift frequency exceeds one half the pulse repetition frequency (normally in the 1–30 kHz range), aliasing occurs and improper Doppler shift information (improper direction and improper value) results. Higher pulse repetition frequencies permit higher Doppler shifts to be detected but also increase the chance of the range ambiguity artifact **(Figs 3.6 and 3.7)**. Aliasing in a color flow system is exposed in a spatial two-dimensional plane in which the aliased flow is shown in reversed color surrounded by non-aliased flow **(Fig. 3.8)**. This pattern mimics the color flow appearance of separate streams in differing directions. The two patterns are, however, clearly distinguishable. In an

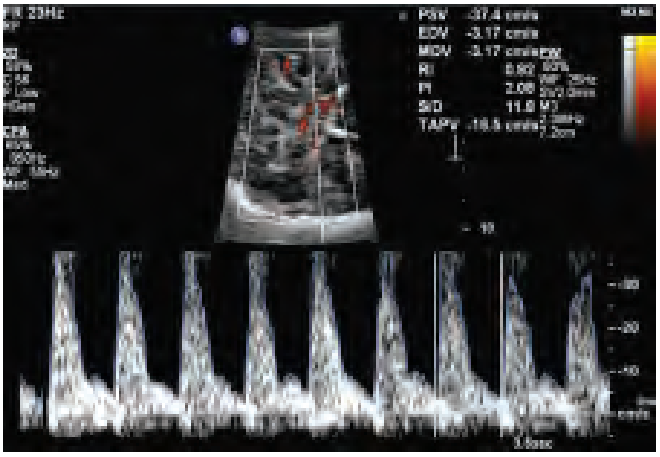

Figure 3.6: Aliasing: Higher pulse repetition frequencies (PRF) permit higher Doppler shifts to be detected but also increase the chance of the range ambiguity artifact

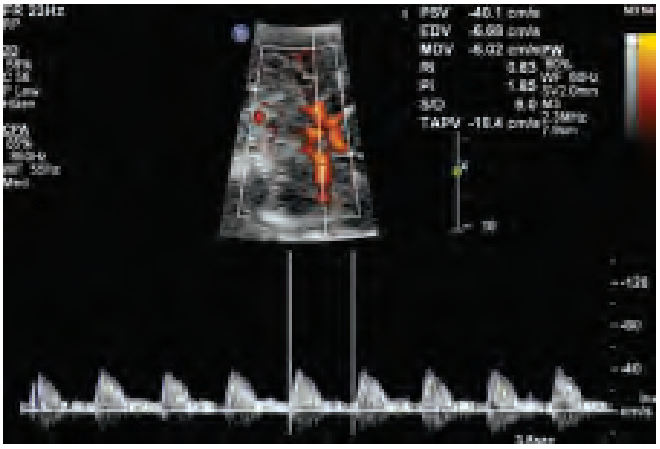

Figure 3.7: Appropriate PRF setting to avoid aliasing in pulsed Doppler waveform analysis

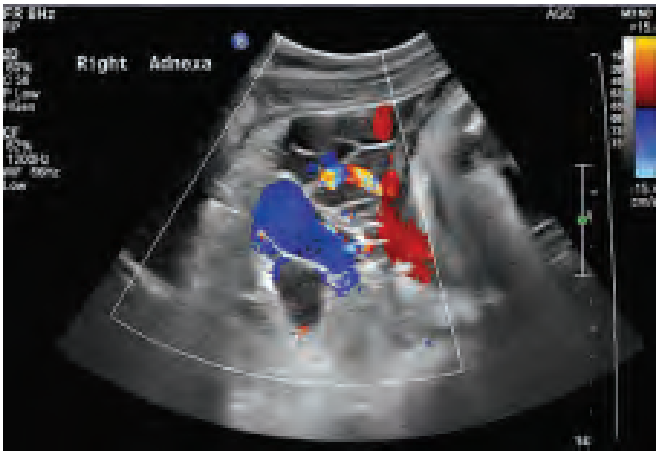

Figure 3.8: Right complex, mostly cystic adnexal mass. Color Doppler aliasing shown in the middle of the mass (neovascularization) with normal red (uterine vein) and blue color (internal iliac vein) displayed on side

aliased flow, the higher velocity generates a higher Doppler shifted frequency that is depicted with greater brightness. The higher the frequency shifts, the brighter the color. The brightest level in the color calibration bar (the uppermost for the flow toward the transducer and lowermost for the flow away from the transducer) represents the Nyquist limit. As the velocity and therefore, the frequency shift exceeds this limit, the color wraps around the calibration bar and appears at the other end as the most luminous color of the opposite direction. For example, a flow toward the transducer with an increasing velocity is depicted with an increasingly bright red color changing to yellow. As the Nyquist limit is reached, the color flow shows brightest yellow in the color bar and as the limit exceeds, flow is shown in the brightest blue. Thus in an aliased flow, bright or pale color of one direction is juxtaposed against bright color of the opposite direction. In contrast, in genuine flow separation the distinct flow streams are depicted in the directionally appropriate colors that are separated by a dark margin. It should be noted that the hue that demarcates an aliased flow would depend on the choice of the color-mapping scheme.

Aliasing can be eliminated by increasing pulse repetition frequency, increasing Doppler angle (which decreases the Doppler shift for a given flow) or by baseline shifting. The latter is an electronic "cut and paste" technique that moves the misplaced aliasing peaks over to their proper location. It is a successful technique as long as there is no legitimate Doppler shifts in the region of the aliasing. If there are, they will get moved over to an inappropriate location along with the aliasing peaks. Other approaches to eliminating aliasing include changing to a lower frequency Doppler transducer or changing to a continuous-wave instrument. Aliasing occurs with the pulsed system because it is a sampling system.[8] If samples are taken often enough, the correct result is achieved. Sufficient sampling yields the correct result. Insufficient sampling yields an incorrect result.

Range Ambiguity

In an attempt to solve the aliasing problem by increasing pulse repetition frequency, the range ambiguity problem can be encountered.[9] This occurs when a pulse is emitted before all the echoes from the previous pulse have been received. When this happens, early echoes from the last pulse are simultaneously received with late echoes from the previous pulse. This causes difficulty with the ranging process. The instrument is unable to determine whether an echo is an early one (superficial) from the last pulse or a late one (deep) from the previous pulse.

To avoid this difficulty, it simply assumes that all echoes are derived from the last pulse and that these echoes have originated from some depth. As long as all echoes are received before the next pulse is sent out, this will be true. However, with high pulse repetition frequencies, this may not be the case. Doppler flow information may, therefore, come from locations other than the assumed one (the gate location). In effect, multiple gates or sample volumes are operating at different depths. Instruments often increase pulse repetition frequency (to avoid aliasing) into the range where range ambiguity occurs. Multiple sample gates are shown on the display to indicate this condition. Range ambiguity in color-flow Doppler, as in sonography, places echoes (color Doppler shifts in this case) that have come from deep locations after a subsequent pulse was emitted in shallow locations where they do not belong. In practice, however, most Doppler color flow devices prevent this problem by automatically reducing the depth when the pulse repetition frequency is increased to the threshold of range ambiguity.

Temporal Ambiguity

Temporal ambiguity occurs when Doppler color flow mapping fails to depict hemodynamic events with temporal accuracy. Specifically, such a situation arises when the frame rate for color flow is too slow relative to the circulatory dynamics. As discussed earlier, the basic unit of color flow depiction is a single frame which when completed shows the average mean frequency shifts color coded and superimposed on the gray scale tissue image. The flow dynamics are, therefore, summarized for the duration of one frame. As we have noted above, the frame rate is inversely proportional to the number of scan lines and the number of samples per scan line. The slower the frame rates the better the color image quality in terms of both spatial resolution and Doppler sensitivity. Herein lies the paradox as a slower rate means longer duration of a frame. As the frame duration increases, there is a progressive loss of the ability to recognize discrete hemodynamic events.

Angle of Insonation

Angle dependency of the Doppler shifted frequencies is also a critical factor in blood-flow analysis. In sector scanning, multiple scan lines spread out from the transducer in a fan-like manner. When the sector scanner is used to interrogate a circulatory system in which the direction of flow is across these scan lines in a color window, the angle of insonation between the flow axis and the ultrasound beam changes. The angle is smallest when the flow stream enters in the sector field and progressively rises to 90° as the flow approaches the center of the field. Concurrently, the Doppler shifted frequencies progressively decline and may become undetectable at the center of the color field. A sector scanner may also create apparently contradictory directional information in a vessel traversing across the color field. As the flow approaches the midline of the field, the flow is depicted in color encoding for flow toward the transducer which usually is red; as the flow moves away, it will be encoded blue. Thus, the same vessel will show bidirectional flow. This paradox actually highlights the basic concept of representation of flow directionality by any Doppler system.

Doppler Mirror Artifact

The mirror image artifact can also occur with Doppler systems. This means that an image of a vessel and a source of Doppler shifted echoes can be duplicated on the opposite side of a strong reflector (such as a bone). The duplicated vessel containing flow could be misinterpreted as an additional vessel. It will have a spectrum similar to that for the real vessel **(Fig. 3.9)**. A mirror image of a Doppler spectrum can appear on the opposite side of the baseline when, indeed, flow is unidirectional and should appear only on one side of the baseline.[10] This is an electronic duplication of the spectral information. It can occur when receiver gain is set too high (causing overloading in the receiver and cross talk between the two flow channels) or with low gain (where the receiver has difficulty determining the sign of the Doppler shift). It can also occur when Doppler angle is near 90°. Here the duplication is

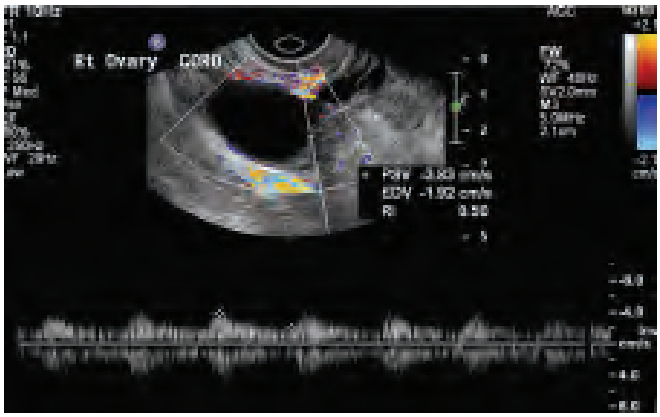

Figure 3.9: Mirror effect: A mirror image of a Doppler spectrum appeared on the opposite side of the baseline when blood flow was unidirectional and should appear only on one side of the baseline

usually legitimate and this is because beams are focused and not cylindrical in shape. Thus, portions of the beam can experience flow toward while other portions can experience flow away.

3D ULTRASOUND ARTIFACTS

Three-dimensional (3D) ultrasonography is a rapidly developing area with increased application in obstetrics and gynecology. Unfortunately, its technology is not only susceptible to artifacts, but the volume acquisition also can present unique artifacts. The images obtained are usually acquired by a series of 2D image planes that are rendered to a volume 3D image. Motion or vibration of the targeted organ during the acquisition of a volume introduces a motion artifact into the volume. The motion artifact affects the overall quality of a volume and is particularly relevant in obstetric imaging because of the movement of the fetus.[11] Shadowing from adjacent structures can reproduce, for example, an apparent limb defect or cleft lip and palate **(Fig. 3.10)**.[12]

Technical aspects of imaging must be considered as this new technology is learned by practitioners in our field. Not only are there artifacts inherent to 2D imaging present in 3D ultrasound but additional artifacts specific to volume imaging have also emerged. Such acoustic artifacts as dropout and shadowing which are well known to the ultrasound community are present in 3D imaging, although more difficult to recognize due to different and unfamiliar displays. Color and power Doppler artifacts relating to gain and flash may also be confusing in rendered images. Three-dimensional volume sets are hampered by fetal movement, cardiac motion, as well as movement of adjacent structures. Acoustic shadowing and other artifacts look very different when displayed in 3D volumes and may be more difficult to recognize than on standard 2D due to lack of specific training of personnel. Acquiring data from multiple orientations may avoid artifacts of this type.

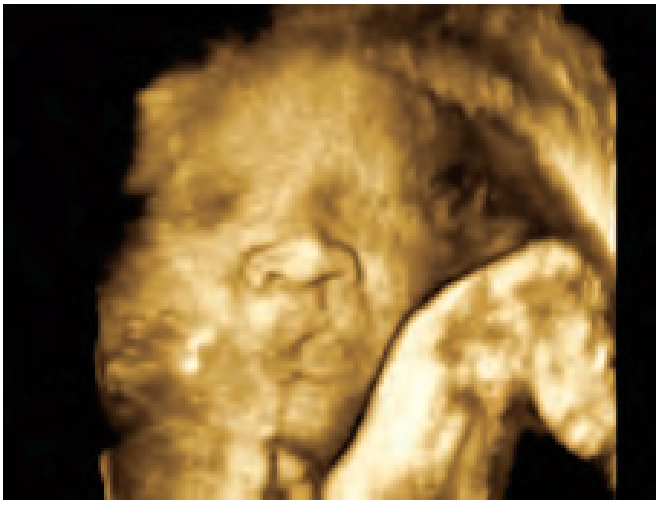

Figure 3.10: 3D artifact: Shadowing from adjacent structures reproduced an apparent cleft lip and palate

CONCLUSION

A prerequisite for optimal utilization of ultrasound in obstetrics and gynecology is an in-depth knowledge of the principles and limitations of this dynamic technique. It is important to appreciate that the appearance of Doppler images is influenced by the operational setting of the equipment that must be taken into account for any reliable interpretation. Only persons with sufficient training and education should perform diagnostic ultrasound. One of the major reasons for so many conflicting and controversial results in the ultrasound literature originates from technique complexity and rather limited education in physics and technique. With all artifacts, but especially with mirror image artifacts, it is important not to let a superficial knowledge cause trouble. Once the cause and nature of an artifact are understood, it is important not to misinterpret a real lesion as an artifact and miss the true pathology. This can happen, particularly with pelvic masses such as leiomyomas with poor through transmission in which the deep wall is not well seen. If there is also an artifact situated near where the deep wall would be, the actual mass might be dismissed as simply an artifact. One must pay attention at all times not only to identify artifacts, but also not to let them interfere with the identification of true lesions. While the more common artifacts seen on ultrasound images frequently are ignored and appreciated as such, it is certainly interesting to know why they occur. On the other hand, the usefulness of artifacts cannot be underestimated. Occasionally, the identification of an artifact may prevent the novice from making an important error in diagnosis or management. An appreciation and understanding of how to avoid artifacts can help even the more experienced practitioner decide whether a structure is real. It is also important not to ignore real pathology under the assumption that it is caused by an artifact.

REFERENCES

1. Laing FC, Brown DL, DiSalvo DN. Gynecologic ultrasound. Radiol Clin North Am. 2001;39(3):523-40.

2. Guttman PH. In search of the elusive benign cystic ovarian teratoma: application of the ultrasound "tip of the iceberg" sign. J Clin Ultrasound. 1977;5(6):403-6.
3. Filly RA, Sommer FG, Minton MJ. Characterization of biological fluids by ultrasonic computed tomography. Radiology. 1980;134(1):167-71.
4. Robinson DE, Wilson LS, Kossoff G. Shadowing and enhancement in ultrasonic echograms by reflection and refraction. J Clin Ultrasound. 1981;9(4):181-6.
5. Buttery B, Davison G. The ghost artifact. J Ultrasound Med. 1984;3(2):49-52.
6. Sauerbrei EE. The split image artifact in pelvic ultrasonography: the anatomy and physics. J Ultrasound Med. 1985;4(1):29-34.
7. Zalud I, Kurjak A, Maulik D, et al. Transvaginal Doppler: measurements and errors. In: Kurjak A, Kupesic S (Eds): An Atlas of transvaginal color Doppler. New York-London, Parthenon Publishing. 2000;255-62.
8. Mitchell DG. Color Doppler imaging: principles, limitations, and artifacts. Radiology. 1990;177(1):1-10.
9. Kremkau FW. Doppler color imaging: principles and instrumentation. Clin Diagn Ultrasound. 1992;27:7-60.
10. Burns PN. Principles of Doppler and color flow. Radiol Med. 1993;85(5 Suppl 1):3-16.
11. Nelson TR, Pretorius DH, Hull A, et al. Sources and impact of artifacts on clinical three-dimensional ultrasound imaging. Ultrasound Obstet Gynecol. 2000;16(4):374-83.
12. Hull AD, Pretorius DH, Lev-Toaff A, et al. Artifacts and the visualization of fetal distal extremities using three-dimensional ultrasound. Ultrasound Obstet Gynecol. 2000;16(4):341-4.

4

CHAPTER

Routine Use of Obstetric Ultrasound

Geeta Sharma, Stephen T Chasen, Frank A Chervenak

INTRODUCTION

Ultrasound examination of the fetus became integrated into prenatal care soon after its introduction in the late 1950s. The past four decades have seen further improvements in ultrasound technology and advances in its utility, as well as the promotion of respect for patient's autonomy and involvement in medical care. There is concomitant support for and opposition to the routine use of ultrasound in pregnancy. Questions remain regarding the benefits and harms of routine obstetric ultrasound. How often should a "routine" ultrasound be performed? When should the "routine" ultrasound be performed? Who should receive an ultrasound? Who should perform the ultrasound? How should the results be interpreted? Many of these questions do not have a clear answer. These answers gain importance as ultrasound burgeons with the dynamic field of obstetrics and gynecology research unveils a multitude of applications for this remarkable tool.

BASIC ULTRASOUND

The real-time obstetric ultrasound examination is usually performed with the pregnant patient in the supine position. A distended bladder aids in displacing bowel loops and can facilitate visualization with the transabdominal approach.[1] Sonogram gel is applied to the transabdominal or transvaginal transducer. The gel simulates a liquid interface that permits optimum travel of the sound waves.

Ultrasound consists of high frequency sound waves that encounter a tissue interface and are reflected, refracted, attenuated or absorbed. The mechanical vibration required for the most obstetric imaging ranges between 3–7 MHz (megahertz), million cycles per second. A transducer or ultrasound probe contains piezoelectric material and a crystal that together generate ultrasound waves. The crystal resonates when electrical current traverses the piezoelectric ceramic.[2]

The ultrasound beam is emitted radially and transmits through tissue as a longitudinal wave influenced by the velocity of the ultrasound between interacting particles and density of particles encountered. Therefore, ultrasound penetration is dependent on the tissue particles' elasticity and mass, which both contribute to the tissue's acoustic impedance. The velocity of ultrasound in soft tissue is relatively constant, except in adipose tissue where the speed is reduced by approximately 20%. In most of the soft tissues, changes in acoustic impedance are dependent on changes in tissue density. When the ultrasound beam contacts large differences in tissue interfaces, reflection of the beam can occur. Only 2–10% reflection occurs between soft tissues, permitting most of the ultrasound waves to travel deeper to distant structures. However, interfaces such as air-tissue or bone/calculus-tissue allow 100% and 67% reflection of the incident ultrasound beam, respectively, creating a distal acoustic shadow.[2]

After processing the reflected beams received by the transducer, an image is constructed and displayed on a monitor. Most obstetric ultrasound imaging uses the pulse-echo method that measures the time delay

between the insonant beam to the echo reflected by the tissue back to the transducer. An image is recreated from these echoes and reflected waves. Real-time ultrasound relies on a continual sweep of pulsed waves. With rapid repetition, the transducer sweeps the area being scanned approximately 30 times in one second.[3]

Other ultrasound wave behaviors include refraction, attenuation and absorption. In addition to reflecting the insonant beam, tissue can refract or scatter the normally coherent waves. Ultrasound energy is lost by refraction, resulting in diminished energy returned to the transducer. Thus, the received signal is attenuated. Further attenuation can occur from the conversion of acoustic energy to thermal energy by tissues and energy is absorbed. A larger degree of absorption is seen with tissue containing larger molecules, greater viscosity and with higher frequency ultrasound. Although higher frequency ultrasound, with its shorter wavelengths, allows for greater resolution, its transabdominal use can be limited due to absorption. Conversely, endovaginal ultrasound minimizes both the distance between the transducer and the area being scanned and contact with tissue with high acoustic impedence, i.e. bone. The frequencies employed in diagnostic ultrasound do not generate significant thermal energy as is possible and often desired with therapeutic ultrasound.[2]

Ultrasound intensity is a temporal measure of energy (watts) exposure over a surface (cm^2). The special peak temporal average intensity represents the peak intensity. Devices for fetal heart auscultation use continuous wave ultrasound with a special peak temporal average intensity ranging between 0.6–80 mW/cm^2. The range for pulse echo imaging is between 1–200 mW/cm^2. The fetal dose depends on both intensity and exposure time, which are influenced by maternal habitus and operator skill.[4,5] It is prudent to minimize the number and duration of ultrasound examinations in order to keep the *in utero* exposure as low as reasonably achievable, i.e. the ALARA principle.[5]

SAFETY

Diagnostic ultrasound of the developing fetus has largely been considered safe without apparent deleterious effects. Greater image resolution and pulsed Doppler mode are possible with greater acoustic output. With this technological innovation, the fetal intensity may be increased up to eight fold. The potential teratogenicity of sound energy conversion to thermal energy and mechanical bioeffects of cavitation have not been proven or ascribed to diagnostic ultrasound.[6] These effects are associated with the higher intensities of continuous wave therapeutic ultrasound. Cavitation refers to the escape of dissolved gases in tissues due to localized low pressure created by very high intensity ultrasound.[2]

The American Institute of Ultrasound in Medicine (AIUM) 1998 conference on mechanical bioeffects encouraged continued research regarding ultrasound safety, especially in tissues with known gas bodies, i.e. lung and intestine. The conference did conclude "there is no known risk of lung or intestinal hemorrhage in the fluid-filled human fetal lung or intestine that is exposed to diagnostic ultrasound during a routine obstetrical examination."[7] In 2002, the AIUM stated "although there are no confirmed biological effects from ultrasound at the present time, the possibility exists that such biological effects may be identified in the future."[8]

In order to monitor the potential bioeffects, newer ultrasound equipment can display the acoustic output, measured by the thermal and mechanical indices. The thermal index measures the temperature absorption; a value below 1.0 is not considered concerning. The mechanical index measures the likelihood of cavitation by measuring the decompressive and compressive forces of ultrasound pulses. Some machines will display one index; the thermal index will be shown for Doppler imaging and the mechanical index for imaging.[5]

Long-term follow up of randomized controlled studies of routine versus selected ultrasound in Norway[9,10] and in Sweden[11,12] do not show a significant affect on subsequent childhood neurological development **(Fig. 4.1)**. In addition, a meta-analysis of childhood malignancies and birth weight showed, overall, no significant negative effects from antenatal ultrasound.[13] An association has been described between left-handedness in a retrospective cohort study of males enlisting in the military. Their exposure or nonexposure to ultrasound was assumed in accordance to local practices based on their place of birth.[14] However, follow-up in the aforementioned randomized controlled trials did not show an increase in non-right-handedness in children randomized to routine ultrasound when subgroup gender analysis was not performed and intention to treat maintained.[15] A provocative study from Yale School of Medicine showed a dose (duration of exposure) – response effect at 7.5 MHz in neuronal migration in mice exposed to ultrasound waves. As the gestational period and alignment of mice fetuses in the U-shaped mouse uterus differs greatly from human gestations, it is difficult to extrapolate this study to significant clinical effects in human fetuses.[16] In addition, the aforementioned long-term studies show that routine ultrasound does not have deleterious effects in humans.

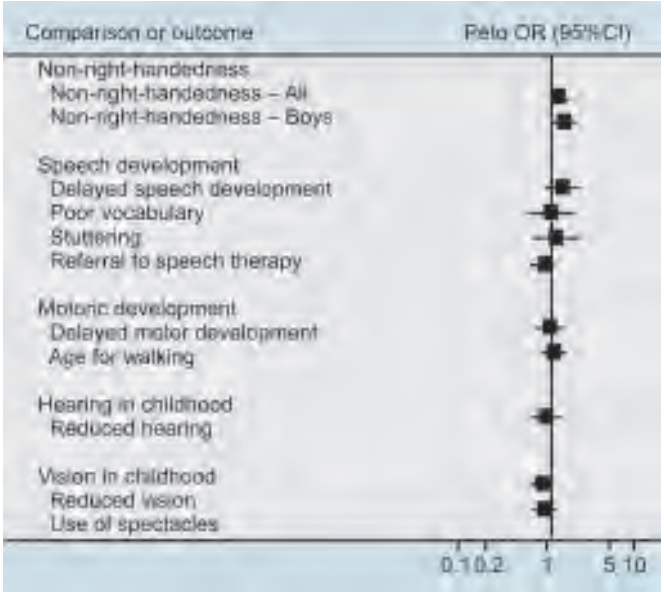

Figure 4.1 Meta-analysis of Nordic and Swedish studies on routine ultrasound during pregnancy and childhood neurological development

Note: Meta-analysis from ultrasound during pregnancy and birthweight, childhood malignancies and neurological development. Ultrasound in Med. and Biol. 1999;25(7):1028. Reproduced with permission

GUIDELINES FOR THE USE OF OBSTETRIC ULTRASOUND

The 1984 National Institutes of Health (NIH) Consensus Development Conference on Diagnostic Ultrasound Imaging in Pregnancy called for studies to evaluate the efficacy of antenatal ultrasound and its affect on perinatal morbidity and mortality.[17,18] The consensus statement suggested 28 scenarios that may benefit from ultrasound evaluation **(Box 4.1)**. However, "this document is no longer viewed by NIH as guidance for current medical practice."[17] In 1993 and 1997, the AIUM and Royal College of Obstetricians and Gynecologists, respectively, set forth standards for the "antepartum obstetrical ultrasound examination" **(Box 4.2 and Fig. 4.2)**.[19] Further detail for performing the anatomical survey is found in **Table 4.1**.[20] The AIUM has also delineated guidelines for ultrasound accreditation to ensure proper technique and expertise.[21]

Responsible utilization of this technology obligates expert training in performance and interpretation of antenatal sonography to minimize false positive and false negative diagnoses.

Routine obstetric ultrasound has been implemented in the United Kingdom, Sweden (1976), Germany (1980), Denmark, Norway (1986), Iceland (1987) Austria (1988), Greece, France, Canada and Australia.[22-26] The rate of antenatal ultrasound performance in the United States by women with live births has steadily increased from 47.7% in 1989 to more than 67% in 2001. Since data was acquired from birth certificate information, this percentage is underestimated, as it does not include spontaneous fetal losses and abortions.[27] The American College of Obstetrics and Gynecology (ACOG) now

TABLE 4.1

Fetal measurements and anatomic features visualized on the routine scan between 18 to 22 weeks

1. Standard fetal measurements:
   - Biparietal diameter
   - Head circumference
   - Abdominal circumference
   - Femoral length

2. Fetal anatomic features and measurements:
   - Brain
     - a. Ventricular section: anterior and posterior horns of the cerebral ventricles; measurement: anterior and posterior ventricle-hemisphere ratio
     - b. Posterior fossa section: cerebellum, vermis, cisterna magna and nuchal skinfold; measurement: trans-cerebellar diameter, and nuchal skinfold
   - Skull
     - Shape
   - Face
     - Orbits (and both lenses) measurement: interorbital, external orbital diameters
     - Nose, lips, palate and mandible
   - Spine
     - "Anterior" view of spinous processes down to tip of sacrum; clear view of skin margin throughout length of spine
   - Chest
     - Heart: 4-chamber view, aortic root and arch, pulmonary artery and ductus
   - Abdomen
     - Diaphragm
     - Cord insertion
     - Liver, stomach and intestines
     - Both kidneys for parenchyma and renal pelvis size
     - Bladder
     - Genitalia
   - Limbs
     - Femur, tibia, fibula, foot and toes (both limbs)
     - Humerus, radius, ulna, hand and fingers (both limbs)
   - Placenta
     - Morphology and site
   - Cord
     - Number of vessels
   - Amniotic Fluid
     - Volume assessment

Reproduced with permission from Campbell S. The obstetric ultrasound examination. In: Chervenak FA, Isaacson GC, Campbell S, (Eds). Ultrasound in Obstetrics and Gynecology. Boston: Little Brown, 1993: p188.

Box 4.1: 1984 NIH indications for ultrasound assessment
(No longer viewed by NIH as guidance for current medical practice)

1. **Estimation of gestational age for patients with uncertain clinical dates, or verification of dates for patients who are to undergo scheduled elective repeat cesarean delivery, indicated induction of labor, or other elective termination of pregnancy:** Ultrasonographic confirmation of dating permits proper timing of cesarean delivery or labor induction to avoid premature delivery.
2. **Evaluation of fetal growth** (e.g. when the patient has an identified etiology for uteroplacental insufficiency, such as severe preeclampsia, chronic hypertension, chronic renal disease, severe diabetes mellitus or for other medical complications of pregnancy where fetal malnutrition, i.e. IUGR or macrosomia, is suspected): Following fetal growth permits assessment of the impact of a complicating condition on the fetus and guides pregnancy management.
3. **Vaginal bleeding of undetermined etiology in pregnancy:** Ultrasound often allows determination of the source of bleeding and status of the fetus.
4. **Determination of fetal presentation:** When the presenting part cannot be adequately determined in labor for the fetal presentation is variable in late pregnancy. Accurate knowledge of presentation guides management of delivery.
5. **Suspected multiple gestation:** Based upon detection of more than one fetal heartbeat pattern, or fundal height larger than expected for dates, and/or prior use of fertility drugs. Pregnancy management may be altered in multiple gestations.
6. **Adjunct to amniocentesis:** Ultrasound permits guidance of the needle to avoid the placenta and fetus, to increase the chance of obtaining amniotic fluid, and to decrease the chance of fetal loss.
7. **Significant uterine size/dates discrepancy:** Ultrasound permits accurate dating and detection of such conditions as oligohydramnios and polyhydramnios, as well as multiple gestation, IUGR and anomalies.
8. **Pelvic mass detected clinically:** Ultrasound can detect the location and nature of the mass and aid in diagnosis.
9. **Suspected hydatidiform mole:** On the basis of clinical sign of hypertension, proteinuria and/or the presence of ovarian cysts felt on pelvic examination or failure to detect fetal heart tones with a Doppler ultrasound device after 12 weeks. Ultrasound permits accurate diagnosis and differentiation of this neoplasm from fetal death.
10. **Adjunct to cervical cerclage placement:** Ultrasound aids in timing and proper placement of the cerclage for patients with incompetent cervix.
11. **Suspected ectopic pregnancy:** When pregnancy occurs after tuboplasty or prior ectopic gestation. Ultrasound is a valuable diagnostic aid for this complication.
12. **Adjunct to special procedures,** such as fetoscopy, intrauterine transfusion, shunt placement, *in vitro* fertilization, embryo transfer or chorionic villi sampling. Ultrasound aids instrument guidance, which increases safety of these procedures.
13. **Suspected fetal death:** Rapid diagnosis enhances optimal management.
14. **Suspected uterine abnormality** (e.g. clinically significant leiomyomata, or congenital structural abnormalities, such as bicornuate uterus or uterus didelphys, etc.). Serial surveillance of fetal growth and state enhances fetal outcome.
15. **Intrauterine contraceptive device localization:** Ultrasound guidance facilitates removal, reducing chances of IUD-related complications.
16. **Ovarian follicle development surveillance:** This facilitates treatment of infertility.
17. **Biophysical evaluation for fetal well being** after 28 weeks of gestation. Assessment of amniotic fluid, fetal tone, body movements, breathing movements and heart rate patterns assists in the management of high-risk pregnancies.
18. **Observation of intrapartum events** (e.g. version/extraction of second twin, manual removal of placenta, etc.). These procedures may be done more safely with the visualization provided by ultrasound.
19. **Suspected polyhydramnios or oligohydramnios:** Confirmation of the diagnosis is permitted, as well as identification of the cause of the condition in certain pregnancies.
20. **Suspected abruptio placentae:** Confirmation of the diagnosis and extent assists in clinical management.
21. **Adjunct to external version from breech to vertex presentation:** The visualization provided by ultrasound facilitates performance of this procedure.
22. **Estimation of fetal weight and/or presentation in premature rupture of membranes and/or premature labor:** Information provided by ultrasound guides management decisions on timing and method of delivery.
23. **Abnormal serum alpha-fetoprotein value** for clinical gestational age when drawn. Ultrasound provides an accurate assessment of gestational age for the AFP comparison standard and indicates several conditions (e.g. twins, anencephaly) that may cause elevated AFP values.
24. **Follow-up observation of identified fetal anomaly:** Ultrasound assessment of progression of lack of change assists in clinical decision making.
25. **Follow-up evaluation of placenta location for identified placenta previa.**
26. **History of previous congenital anomaly:** Detection of recurrence may be permitted or psychological benefit to patients may result from reassurance of no recurrence.
27. **Serial evaluation of fetal growth in multiple gestation:** Ultrasound permits recognition of discordant growth, guiding patient management and timing of delivery.
28. **Evaluation of fetal condition in late registrants for prenatal care:** Accurate knowledge of gestational age assists in pregnancy management decisions for this group.

Box 4.2: 1993 AIUM Standards reproduced from AIUM

Equipment

These studies should be conducted with real-time equipment, using an abdominal and/or vaginal approach. A transducer of appropriate frequency should be used. Fetal ultrasound should be performed only when there is a valid medical reason. The lowest possible ultrasonic exposure setting should be used to gain the necessary diagnostic information.

Documentation

Adequate documentation of the study is essential for quality patient care. This should include a permanent record of the ultrasound images, incorporating whenever possible the measurement parameters and anatomical findings proposed [herein]. Images should be appropriately labeled with the examination date, patient identification, and, if appropriate, image orientation. A report of the ultrasound findings should be included in the patient's medical record. Retention of the ultrasound examination should be consistent both with clinical need and with relevant legal and local healthcare facility requirements.

Standards for First Trimester Sonography

1. The uterus and adnexa should be evaluated for the presence of a gestational sac. If a gestational sac is seen, its location should be documented. The presence or absence of an embryo should be noted and the crown-rump length recorded.
2. Presence or absence of cardiac activity should be reported.
3. Fetal number should be documented.
4. Evaluation of the uterus, adnexal structures and cul-de-sac should be performed.

Standards for Second and Third Trimester Sonography

1. Fetal life, number, presentation and activity should be documented.
2. An estimate of amniotic fluid volume (increased, decreased, normal) should be reported.
3. The placental location, appearance and its relationship to the internal cervical os should be recorded. The umbilical cord should be imaged.
4. Assessment of gestational age should be accomplished at the time of the initial scan using a combination of cranial measurement such as biparietal diameter or head circumference and limb measurement such as the femur length.
   A. The standard reference level for the measurement of the biparietal diameter is an axial image that includes the thalamus.
   B. Head circumference is measured at the same level as the biparietal diameter, around the outer perimeter of the calvarium.
5. Fetal weight should be estimated in the late second and in the third trimesters and requires the measurement of abdominal diameter of circumference.
   A. Abdominal circumference should be determined on a true transverse view, preferably at the level of the junction of the left and right portal veins.
   B. If previous fetal biometric studies have been performed, an estimate of the appropriateness of interval growth should be given.
6. Evaluation of the uterus (including the cervix) and adnexal structures should be performed.
7. The study should include, but not necessarily be limited to, assessment of the following fetal anatomy: cerebral ventricles, posterior fossa (including cerebellar hemispheres and cisterna magna), four-chamber view of the heart (including its position within the thorax), spine, stomach, kidneys, urinary bladder, fetal umbilical cord insertion site and intactness of the anterior abdominal wall. While not considered part of the minimum required examination, when fetal position permits, it is desirable to examine other areas of the anatomy.

recommends routine ultrasound for the general population as their 2007 Practice Bulletin supports first trimester nuchal translucency measurement as part of a combined first trimester risk assessment for fetal aneuploidy.[28]

RANDOMIZED CONTROLLED TRIALS OF ROUTINE ULTRASOUND

The wide acceptance of antenatal ultrasound by physicians and patients precludes the fulfillment of a study that adequately and accurately evaluates the impact of ultrasound on prenatal care and perinatal outcomes. In addition, in the setting of uncertainty where benefits outweigh potential risks, respect for a patient's autonomy obligates the physician to offer obstetric ultrasound where available.[29]

Antecedent ultrasound studies randomized patients to routine versus selective antenatal sonography, but were of insufficient power to detect a reduction in perinatal mortality or morbidity. An early prospective randomized trial of routine obstetric ultrasound was performed by Bennet et al. in London.[30] In this study, 1,062 women underwent routine ultrasound at 16 weeks

The minimum standard for a "20 week" anomaly scan:

Gestational age can be established by measurement of biparietal diameter, head circumference and femur length. The inclusion of abdominal circumference would be optional.

Fetal Normality

- Head shape + internal structures cavum pellucidum cerebellum ventricular size at atrium (<10 mm)
- Spine: longitudinal and transverse
- Abdominal shape and content at level of stomach
- Abdominal shape and content at level of kidneys and umbilicus
- Renal pelvis (< 5 mm AP measurement)
- Longitudinal axis—Abdominal-thoracic appearance (diaphragm/bladder)
- Thorax at level of 4 chamber cardiac view
- Arms—Three bones and hand (not counting fingers)
- Legs—Three bones and foot (not counting toes)

The *optimal standard* for the "20 week" anomaly scan. If resources allow, the following could be added to the features listed above:

- Cardiac outflow tracts
- Face and lips.

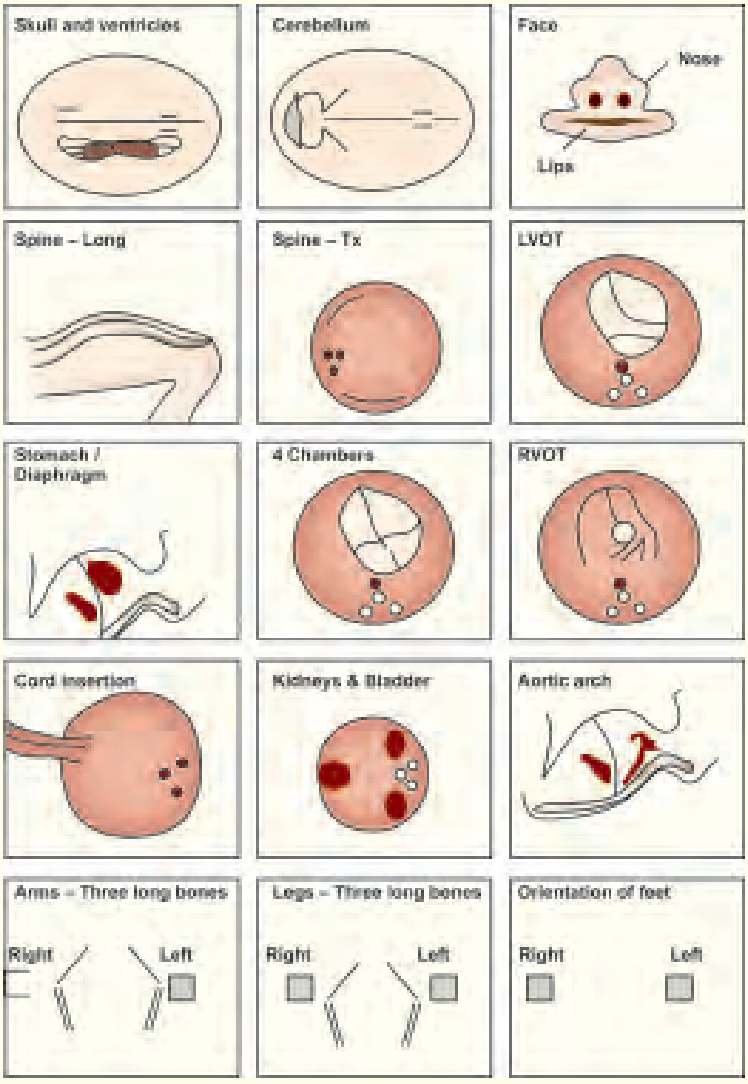

Figure 4.2 Baseline examination views – 20 week anomaly scan

Reproduced with permission from: 2000: Routine Ultrasound Screening in Pregnancy - Protocol, Standards and Training Supplement to Ultrasound Screening for Fetal Abnormalities Report of the RCOG Working Party *http://www.rcog.org.uk/mainpages.asp?PageID=439*

menstrual age. The fetal biparietal diameter (BPD) was measured and dates corrected in 25% of the patients, mostly due to an overestimation from the last menstrual period. Patients were then randomized to one of two groups, using the last digit of the patients' hospital number. In the study group, the BPD information was shared with the clinician while it was withheld in the control group. However, the authors conceded BPD results were revealed, due to ethical obligations, in 30% (161/531) of the patients in the control group in which there was a high degree of clinical concern. Intention to treat analysis between the two groups did not show a difference in fetal outcome (birth weight centile, Apgar score at 1 minute and perinatal mortality) or rate of labor induction. Subgroup analysis demonstrated a significantly greater labor induction rate for suspected growth retardation in the revealed control group, 34.8% (56/161) than in either the concealed control group, 13.8% (51/370) or the study group, 19.6% (104/531). The study did not look at differences in neonatal morbidity; therefore, the clinical significance of the ultrasound information could not be completely assessed. The authors concluded that accurate dating information was critical in assessment for growth retardation and the ultrasound findings were of obstetric value in 25% of the patients. This study illustrates the difficulty of performing a randomized controlled trial of ultrasound utility, as concern surrounding the information generated from ultrasound obligated disclosure of the BPD in 15% of the population.

In another study designed to investigate early detection of growth restriction and perinatal outcome, Neilson et al.[31] in Glasgow, Scotland, conducted a practice-based randomized controlled trial between 1979–1981 of 877 (90%) low risk women without prior risk of growth restriction. All patients had gestational age confirmed by ultrasound prior to 24 weeks gestation and underwent crown-rump length and trunk area measurements at 34–36.5 weeks. Patients were randomized by hospital number to a study group or control group. The study group comprised of 433 patients whose results were shared with the obstetricians, while the results of 455 patients in the control group were concealed with the exception of breech presentation (nine cases) or placenta previa (one case). The control group information was made available by clinician request; no requests were made. The two-stage ultrasound approach was 94% sensitive and 90% specific for the detection of birth weight below the 5th percentile. There were no differences noted between the two groups. The groups were compared with respect to many parameters, including number of labor inductions overall and for suspicion of growth restriction, number of emergency cesarean sections, unfavorable Apgar scores, mean gestational age at delivery, mean birth weight and number of small-for-dates neonates.

Bakketeig et al.[32] investigated the use of a two-stage ultrasound regimen in patients randomly selected for ultrasound examination compared to a control group of patients that did not undergo antenatal ultrasound. This randomized controlled practice-based trial was conducted between 1979–1980 in Trondheim, Norway. A total of 1,009 patients were enrolled. The 510 women in the screened group underwent ultrasound examination at 18 weeks and 32 weeks gestation. When compared to the background rate of low birth weight, 4.2%, the rate in the study population, 3.9%, suggested that the study population was biased towards being more low risk and may not have accurately reflected the populace. A power analysis to assess perinatal mortality was not provided. There were no statistical differences between the screened and control groups, except for an unexplained greater number of antenatal admissions, mostly for pre-eclampsia, in the screened group. There was a trend towards earlier detection of twin gestations, fewer post-date inductions and fewer low birth weight neonates in the screened group.

With regards to routine ultrasound specifically after 24 weeks gestation, the 2009 Cochrane review,[33] a meta-analysis of eight trials, including a total of 27,024 women from unselected population, showed no difference in neonatal outcome but did show a trend towards a higher cesarean delivery rate in the screened group.

Another Norwegian trial was conducted from 1979–1980 in Ålesund. Eik-Nes et al. reported preliminary results in 1984 and subsequently published a complete analysis in 2000.[34] This prospective randomized trial involved 1,628 patients. Routine ultrasound screening at 18 and 32 weeks gestation was performed in the study group (n=825) and ultrasound examinations were performed upon clinician request in 34% of the control group (n=803). The screened group had significantly less post-term inductions, fewer neonates with five minutes Apgar scores below eight and fewer neonates that required positive pressure ventilation for more than one minute. Also, twins were detected earlier in the screened group, but there were no significant differences in twin outcome between the groups. The study lacked power to assess perinatal mortality (PNM), but did show a trend towards improved perinatal outcomes in the ultrasound screened group for both singleton and twin pregnancies.

In Copenhagen, Denmark, Secher et al.[35] recruited patients between 1980–1983 and studied a low-risk population that underwent ultrasound gestational age assessment before 22 weeks gestation and subsequently underwent third trimester screening for growth retardation. All patients were screened at 32 and 37 weeks gestation. An additional ultrasound was performed at 34 weeks if the estimated fetal weight was at or less than the 15th percentile at 32 weeks. There were 184 fetuses suspected to be at or less than the 15th percentile at one or more third trimester ultrasound examinations. These patients were randomized to a treatment (n=96) or control (n=88) group. The ultrasound results were withheld from the control group, but were revealed in 28 cases due to clinical concern. The treatment group was followed with weekly non-stress tests (NST) and serum estradiol and human placental lactogen. There were no differences between the two groups with respect to the number of neonates weighing <2,500 grams and maternal and neonatal complications. There were statistically more labor inductions in the treatment group, although the indications for induction were not detailed. There was suggestion of a marginal, not statistically significant, benefit of a reduced occurrence of neonatal hypoxia, measured by arterial cord pH < 7.15, in the treatment group. The authors acknowledge that there was insufficient power in the study and was further weakened by the 32% of the control group whose results were revealed.

The first randomized controlled trial in the United States included enrolled patients from 1984–1986. Ewigman et al.[36] randomized 42% (915/2171) patients presenting for prenatal care to a study group that received an ultrasound at 10–12 weeks gestation or to a control group that received indicated ultrasonography; 23.9% of the control group underwent ultrasound scans. The strict inclusion and exclusion criteria of the study still did not ensure minimum control group exposure to ultrasound and the demographics of this study's population was not reflective of the general United States. Patient recruitment was practice-based, not population-based, with Caucasians representing over 90% of the patients. The power calculations permitted a 64% chance of detecting a 50% reduction in post-term inductions and a 70% chance of detecting a 50% reduction in adverse perinatal outcome. Adverse perinatal outcome was defined as perinatal death, neonatal intensive care unit (NICU) admission of or more days or Apgar score at five minutes less than 6. The groups did not differ in the number of post-term inductions, total inductions or adverse perinatal outcomes. Ultrasound was beneficial in both groups for adjustment of estimated date of confinement.

Waldenström et al.[37] in Stockholm, Sweden randomized 4,997 women without clinical indication for ultrasound into a screening group (n=2482) and a control group (n=2511). Patients were recruited between 1985–1987 from all local antenatal clinics. The screening group underwent an ultrasound at 15 weeks gestation. Subsequent ultrasound examinations were performed in either group at the request of the clinician. Excluding the initial screening ultrasound in the screening group, the 31.8% of unscreened group that underwent ultrasound, utilized more ultrasound examinations after 19 weeks than the screened group, 1,279 and 736, p=0.039, respectively. Gestational age estimation by ultrasound prior to 19 weeks had been performed in 103 patients in the control group. Compared to the control group, the screening group had significantly fewer inductions for post-term pregnancy (9.1% versus 5.9% p < 0.0001), greater average birth weight (3497 ± 557, 3521± 527 p=0.008) and fewer low birth weight neonates (4% versus 2.5% p=0.005). There were 48 sets of twins between the two groups. All 24 sets of twins in the screening group were identified by 24 weeks and the 20 sets of twins in the control group were identified by 32 weeks. There were no significant differences in twin pregnancy outcomes, i.e. gestational age at delivery, birth weight, Apgar scores and perinatal death, between the two groups.

The largest European randomized controlled trial assessing routine versus selective antenatal ultrasound screening was also the first to compare systematically the detection of fetal abnormalities. The study took place in Helsinki, Finland and patients were recruited from 1986–1987. Saari-Kemppainen et al.[38] randomized 9,310 patients into a study group (n=4691) that routinely underwent ultrasonography between 16–20 weeks and a control group (n=4619) that selectively underwent ultrasonography. In the latter group, 77% of patients received an ultrasound during the course of the pregnancy, while most ultrasound examinations were performed prior to 20 weeks in the study group. The large number of controls exposed to ultrasound could account for the lack of significant difference in labor inductions and mean birth weights between the two groups. The study group utilized less antenatal care outpatient visits than the control group (2.3 versus 2.6, p < 0.0001) and had improved detection of twins by 24 weeks (100% versus 76.3%). Most importantly, the perinatal mortality of singletons was reduced by 49.2% in the study group (4.6/1000) as compared to the control group (9.0/1000). This difference was attributed to the detection of severe fetal abnormalities and the participants' acceptance of pregnancy termination. The rate of fetal abnormality detection varied according to

ultrasound site. The detection rate at the City Hospital was less than that of the University Hospital, 36.0% versus 76.9%. The overall perinatal mortality rate was reduced, but the small number of twins restricted further analysis between the two groups; though it appeared that the perinatal mortality rate for twins was less in the study group than in the control group, 27.8/1000 versus 65.8/1000. The reduction in overall perinatal mortality rate was impressive as Finland already exhibited one of the lowest perinatal mortality rates in the world confirming the impact of congenital malformations on perinatal mortality.

Geerts et al.[39] in South Africa, assessed the utility of a single screening ultrasound in a developing country. After randomization, 8% of patients were excluded; 909 patients remained with 457 in the routine ultrasound group and 452 in the selective ultrasound group. Patients were recruited from 1991–1992 and study patients received a screening ultrasound between 18–24 weeks gestation. As seen in other similar studies, ultrasound examinations were performed in 25% of the control group. Compared to the study group, the control group had a greater degree of suspected post-dates pregnancies (9 versus 38, p=0.00002) and more ultrasounds (3 versus 23, p=0.0001) and inductions (1 versus 14, p=0.002) were performed for this indication. Five patients in the control group required confirmation of lung maturity by amniocentesis while no patients in the study group underwent fetal lung maturity testing, p=0.03. There were no differences seen in adverse pregnancy outcomes (perinatal mortality, NICU admission or long-term morbidity) in singletons between the two groups. The routine group did have a greater proportion of low birth weight infants (p=0.007, or 1.61; 95% CI 1.13-2.30), but the numbers were too small for statistical comparison of perinatal outcome. Similarly, as there were only a total of 6 sets of twins, perinatal outcomes for multiple gestations could not be compared. More major congenital anomalies were detected in the routine group (n=8) than in the control group (n=3). Within each group, there were two pregnancy terminations due to these fetal abnormalities. The authors concluded that the selective use of ultrasound did not increase adverse pregnancy outcomes and that the results did not support the additional cost accrued by routine ultrasound.

In response to the 1984 NIH Consensus Conference, the Routine Antenatal Diagnostic Imaging with Ultrasound (RADIUS)[40] trial was created as the largest prospective randomized controlled trial of routine versus selective antenatal ultrasound. The RADIUS trial was a practice-based study that attempted to evaluate the effect of two-stage routine ultrasound screening in a low-risk population on perinatal morbidity and mortality. Patients were recruited from 1987–1991 from 109 private practices in five Midwestern states and one New England state. A total of 55,744 patients registered for prenatal care in the participating clinics. Ignoring patients that were lost to follow-up, 61% (32,317/53,367) of screened registrants were deemed ineligible or were excluded. Another 26% were then lost to follow-up or declined screening. The remaining 15,530 patients, representing 28% of the original registrants, were randomized. The study group (n=7,812) underwent sonography at 15–22 weeks and again at 31–35 weeks. Power calculations were performed but did not state the percent chance of detecting their primary goal of a 20% reduction in adverse perinatal outcomes (fetal or neonatal death or moderate or severe neonatal morbidity). Secondary outcome measures included the incidence neonates born small for gestational age or post-term and rate of labor induction in presumed post-term pregnancies. Multiple gestations were analyzed separately according to birth weight and rate of premature births.

The RADIUS trial did not demonstrate significant differences between the routine and selective screening groups with respect to maternal and perinatal morbidity and perinatal mortality.[40] However, there were significant differences in the detection of fetal anomalies and multiple gestation, use of tocolysis and diagnosis of post-date pregnancy.[41,42] Prior to 24 weeks gestation, 4.9% (8/163) of fetal anomalies in the control group were detected, as opposed to the three-fold increase in the detection of fetal anomalies, 16.6% (31/187), seen in the routine screening group. Subgroup analysis revealed a 35% (19/54) detection rate of fetal anomalies at the tertiary centers while nontertiary centers detected 13% (8/64). Twin pregnancies were detected by 24 weeks in 98.5% (67/68) of patients in the study group. The one missed patient was noncompliant with the screening regimen. Conversely, 37% (23/61) of twin pregnancies were detected by 24 weeks in the control group. Tocolysis was utilized by 3.4% (260/7617) patients in the study group versus 4.2% (318/7534) in the control group. The study group had significantly less pregnancies past 41 weeks and past 42 weeks than the control group, 19.1% versus 21.4%, $p < 0.001$, 3.2%, 4.6%, $p < 0.001$, respectively.

CRITIQUE OF RADIUS TRIAL

Although the magnitude of the RADIUS trial is impressive, there are four important points to consider regarding its conclusions.[43]

Applicability of Results

An extremely low-risk population was enrolled in the RADIUS trial. Selection bias commenced with enrollment in prenatal care and in private clinics. Most patients were whites (93%), English speaking (100%), had ideal body weight (90%) had received college level education (70%)[44] and were indifferent to pregnancy termination. The stringent exclusion criteria removed 60% of patients at initial enrollment and 45% of the remaining 40% of patients considered low risk subsequently underwent ultrasonography.[45] Therefore, the conclusions of the trial are applicable to less than 40% of low-risk private patients, who are deemed low risk after extensive scrutiny.[43]

Outcomes Emphasized

Although a power analysis was performed, the number of participants was insufficient to draw definitive conclusions on the lack of effect of a single technology, ultrasound, on perinatal morbidity and mortality. Therefore, the potential for improvement in perinatal morbidity and mortality cannot be dismissed. Published estimated power calculations show a minimum of 6,250 patients in each group to demonstrate a 50% decrease in perinatal mortality (from 10/1000–5/1000).[46] Ultrasound screening could possibly predict approximately half of the congenital malformations or intrauterine growth restriction cases that lead to fetal or neonatal demise. Thus, a more realistic reduction from 10 to 8 per 1,000 perinatal deaths would require 46,820 patients in each group.[47]

The RADIUS trial also ascribed therapeutic properties to ultrasound examination, which serves purely a diagnostic role. Romero asserted it is unreasonable to expect ultrasound to reduce the rate of prematurity and small for gestational age neonates without the combination of an effective treatment modality.[48]

There were significant findings in the RADIUS trial that deserve emphasis. Routine ultrasound examination led to an increased detection of fetal anomalies, earlier diagnosis of twin pregnancies, fewer cases of tocolysis and induction of labor for post-dates.[49] With larger numbers, the benefits of these significant findings may have translated into improved perinatal morbidity and mortality.

Ultrasound Quality

The non-uniform detection rate of fetal anomalies between tertiary and non-tertiary centers highlights a critical issue regarding the quality of the ultrasound examinations performed in the study. The detection rate prior to 24 weeks gestation of 16.6% was much lower than that seen in European studies. Romero compared the sensitivity of the RADIUS trial with a series of European trials for which a combined sensitivity was generated, 16.6% versus 50.9%, $p<0.00001$.[48] Proper and frequent ultrasound accreditation, training and auditing is required in any ultrasound setting to maximize the full potential of ultrasonography and to minimize harm.

Cost Analysis

According to the cost analysis proposed by the RADIUS trial, the additional 1.6 ultrasound scans at $200/scan would incur an increased cost of $500 million. However, DeVore illustrated that the cost per fetal anomaly detected in tertiary centers is 48% below the RADIUS trial's projected cost and also less than the cost of universal screening with maternal serum alpha-fetoprotein.[50] The RADIUS trial also did not address the financial cost of caring for infants with severe congenital anomalies.[49]

META-ANALYSES OF RANDOMIZED CONTROLLED TRIALS

Thacker summarized the first four randomized controlled trials of routine ultrasound in 1983.[30-32,34] The combined results did not show a significant difference in frequency of low Apgar score at one minute or in the rate of perinatal mortality between the pooled study and control groups. However, a significant reduction in labor induction for incorrectly presumed post-dates was seen.[46]

Bucher and Schmidt also analyzed four randomized control trials with a combined total of 15,935 pregnancies.[32,36-38] This meta-analysis demonstrated a significant reduction in perinatal mortality, largely due to the contribution of the Helsinki study. The Helsinki study achieved a reduction in perinatal mortality due to their reasonable early detection rate of fetal abnormalities that permitted the option of induced abortion.[51]

A Cochrane review in 2002 concluded, "routine ultrasound in early pregnancy appears to enable better gestational age assessment, earlier detection of multiple pregnancies and earlier detection of clinically unsuspected fetal malformation at a time when termination of pregnancy is possible. However, the benefits for other substantive outcomes (perinatal mortality) are less clear."[52] The use of routine ultrasound, overall, significantly improved detection of twin pregnancies by 20 and 24 weeks gestation, reduced the rate of post-term labor inductions and led to a greater proportion of pregnancy terminations. The meta-analysis did not

show a difference in antenatal hospital admissions, Apgar score below 7 at 1 or 5 minutes, low birth weight or special care admissions for singletons or in perinatal mortality (twins and singletons). The follow-up studies of ultrasound safety also did not show a difference between routine and unscreened groups in school related oral reading, reading comprehension, spelling, arithmetic, overall performance, dyslexia, reduced vision, reduced hearing, spectacle use, non-right-handedness, left-handedness and ambidexterity.[52] The 2009 Cochrane review of routine ultrasound after 24 weeks gestation did not show a difference in neonatal outcome, but did not assess long-term outcomes of neurological development. The cesarean delivery rate was slightly higher in the group that received routine ultrasound after 24 weeks gestation, but trend was not significant.[33]

DIAGNOSTIC ABILITY OF ROUTINE ULTRASOUND

One of the pioneer programs integrating routine ultrasound in prenatal care began in Malmö, Sweden in 1973 in order to improve the diagnosis of twin pregnancies. A retrospective study of their screening program from 1973–1978 revealed most (94.4%) twin pregnancies were diagnosed by 19–20 weeks gestation. The benefit of early diagnosis of twins, compared to prior diagnosis by 27 weeks was seen in the reduction of premature births (from 33–10%) and perinatal mortality (from 6–0.6%).[53] In addition, placenta previa was better identified and greater accuracy of gestational age led to a reduction in post-term induction of labor from 8–2.6%. The authors estimated that the improved outcomes reduced the use of hospital care resources by 10%.[54]

Another early site for routine ultrasound, Barcelona, Spain, reported 22 years, 1970–1991, of ultrasound screening for fetal abnormalities in a mixed high and low-risk population. As expected, the improving skill and technology led to better detection rates of major fetal abnormalities in the second decade of examination, 19.75–96.4%; detection rates prior to 22 weeks increased from 8.63–84.8%. The specificity remained 99%. Overall, 59.4% (598/1006) fetal anomalies were detected early in pregnancy. Termination of pregnancy procedures paralleled the increase in fetal anomaly detection and the perinatal mortality rate declined from 8.4/1000 in 1981–1985 to 5.5/1000 in 1986–1990. Although the population included many high-risk referrals, the majority of fetal abnormalities, 85–90%, were detected in low-risk patients.[25]

In Finland, Rosendahl and Kivinen[55] performed routine ultrasonography on 9,012 patients between 1980–1988. For the first two years, a routine scan was completed at 18 weeks, subsequently; a second scan was added at 34 weeks. The additional third trimester survey increased the sensitivity of major malformations to 63.8% from 41.7%. The sensitivity of structural anomaly detection prior to 24 weeks was 39.4%. Fetal abnormality detection correlated with clinical suspicion of an abnormality in only 25.8% of cases; therefore, the authors "emphasized the necessity for ultrasound examination of all pregnancies."[55]

In Belgium, Levi et al.[56] described a multicenter experience of ultrasonography performed in each trimester from 1984–1989. In this unselected population, a total of 16,361 fetuses were evaluated. Between 12–22 weeks, 62.1% (259/417) of fetal malformations were scanned with a 21% (59/259) sensitivity, 100% specificity and 100% positive predictive value. The sensitivity rose to a 40% (154/318) detection rate of abnormal fetuses with additional sonograms later in pregnancy. There were 66 false negative and 8 false positive cases. Anomaly detection was analyzed according to type, gestational age at detection, gestational age-based probability of detection and severity. Eighty-five percent of lethal anomalies were correctly diagnosed antenatally. The authors evaluated the appropriateness of ultrasound as a screening test and found it to be suitable in their population.

In a similar analysis, Gonçalves et al.[57] conducted a retrospective case-control study of congenital anomaly detection from 1987–1991. Participants were referred for indicated ultrasound examination. Infants and fetuses were selected based upon hospital discharge diagnoses. The study and control groups each contained 287 women. There were 152 true positives for 287 cases, yielding an overall sensitivity of 53%. Congenital anomalies were also analyzed according to diagnostic category and gestational age at detection. Advanced gestational age, lethality of the anomaly and high-risk categorization of the pregnancy all increased sensitivity. From 20–23 weeks, the sensitivity was 59% while it reached 68% after 24 weeks. A high percentage, 89%, of lethal anomalies was detected. Sensitivity of detecting an anomaly was higher in high-risk patients as compared to low or unknown risk patients, 71%, 36%, 46%, respectively. Since the study did not have a reference population and many false-negative cases may have been omitted.[58]

In another retrospective trial, Chitty et al.[59] correctly identified 93 of 125 fetal anomalies in 8,342 fetuses prior to 24 weeks gestation for a sensitivity of 4%. The study

was conducted between 1988–1989. All patients who registered early for prenatal care underwent ultrasonography prior to 24 weeks gestation. There were 14 trisomies that were not included in the calculation of sensitivity; their inclusion would reduce the sensitivity to 63%. The authors were able to demonstrate the utility of ultrasonography for antenatal fetal anomaly detection in a low-risk population. They also addressed problems encountered with routine ultrasonography in this population. These problems are:

- Technical problems such as maternal obesity, fetal position and multiple gestations hindered diagnosis of some structural anomalies
- Uncertain outcomes of recognizable anomalies such as mild ventriculomegaly
- Late presentation of some findings such as duodenal atresia
- The abnormality may not be detectable, i.e. tracheoesophageal fistula
- Evolving data on minor markers such as choroids plexus cysts, mild pyelectasis
- Late registration for prenatal care.

Shirley et al.[60] performed a combined retrospective and prospective study in an unselected pregnant population. The study evaluated 6,183 (96%) infants delivered from 1989–1990 who had been scanned in the second trimester. Of the 84 abnormal fetuses scanned prior to 22 weeks gestation, 51 had fetal anomalies detected yielding a sensitivity of 60.7%. The sensitivity for detecting lethal anomalies by 22 weeks gestation was 73% (41/56). There was one false-positive diagnosis of omphalocele that was a hemangioma at birth. The specificity was 99.98%. The authors supported a routine screening program that allowed patients the opportunity to adapt to or to consider termination of an abnormal fetus and acknowledged its potential to reduce perinatal mortality.

Papp et al.[61] prospectively studied two-stage routine sonography in 51,675 women between 1988–1990. Of the 63,794 patients offered screening, 81% participated. Sensitivity of maternal serum alpha fetoprotein (MSAFP) was compared with the sensitivity of ultrasound scanning at 18–24 weeks and at 28 weeks. Of the 496 severe anomalies detected, 317 were detected by ultrasonography between 18–20 weeks. The sensitivity of ultrasound screening of major fetal anomalies was 63.9% and significantly exceeded that of MSAFP screening. The efficiency of prenatal detection in this study supports the contention of perinatal mortality reduction by offering patients the option of pregnancy termination.

Luck[62] examined the impact of routine ultrasonography at 19 weeks gestation in an unselected population. All pregnant women from 1988–1991 were offered to participate and 96% (8523/8849) accepted. There were 160 fetal anomalies of which 140 were detected at 19 weeks gestation. According to Luck, the majority of anomalies occur in low-risk pregnancies and thus routine screening of pregnant women by trained and skilled ultrasonographers is advocated. Additional benefits of early anomaly detection included appropriate and timely tertiary care referrals and emotional preparation for parents with a fetal anomaly. A cost analysis demonstrated cost effectiveness of termination of pregnancy for lethal, crippling deformities detected with expert ultrasonography.

The Multicentric Eurofetus Study[63] investigated the sensitivity of fetal anomaly detection in a large unselected population involving 14 European countries. Routine ultrasound examination was performed between 18–22 weeks gestation from 1990–1993. Fetal abnormalities occurred in 3,686 fetuses, 44% of all these cases were detected prior to 24 weeks while 55% of severe anomalies were identified. The information from this study supports the use of routine ultrasound performance and enhances physician–patient discussion regarding pregnancy options, limitations of ultrasonography (i.e. a negative test cannot provide absolute assurance) and areas to focus on to improve detection.

Routine obstetric ultrasonography in low-risk patients was assessed by Skupski et al.[64] from 1990–1994. A retrospective review of 860 fetuses revealed a 1.2% (10/860) incidence of major anomalies. Considering only diagnoses identifiable by ultrasound, a 75% (3/4) sensitivity for major anomaly detection was reported. As the incidence of major fetal anomalies detectable sonographically was 0.5%, the authors analogize amniocentesis performance for a similar incidence of aneuploidy. With early prenatal diagnosis patients received nondirective counseling and 2 out of 3 patients with ultrasound detected major anomalies opted for pregnancy termination; thereby, availing themselves of autonomy enhancing facets of prenatal care.

Quisser-Luft et al.[65] performed a retrospective case control analysis of patients with and without antenatally detected fetal anomalies. Cases from 1990–1994 were reviewed and 298 malformed cases were identified from 20,248 livebirths, stillbirths and abortuses; 30.3% (95/298) were identified antenatally. As per standard policy in Germany, each patient underwent a minimal of three ultrasounds. Specific detection rates for anomalies

TABLE 4.2

High-risk characteristics identified from anamnestic data

	Statistically significant increased odds ratios		
Risk Factors	*OR*	*CI*	*P value*
Anamnestic risk factors			
Sibling with malformation	4.6	1.3-16	0.02
Mother/father with malformation	4.1	1.3-13	0.01
Consanguinity	3.1	1.4-6.6	0.004
Neonatal death/stillbirth	1.9	1.1-3.6	0.001
Alcohol abuse (mother)	2.4	1.1-6.3	0.04
Maternal age > 35	1.3	1.1-1.7	0.007
Drug exposure (first trimester)	1.2	1.1-1.3	0.008
Clinical signs:			
Polyhydramnios*	13.5	9.5-19.0	0.001
Oligohydramnios*	8.7	5.2-14.0	0.001
Premature labor•	4.7	3.8-4.9	0.001
Placental insufficiency*	1.9	1.1-2.7	0.01
Growth retardation*	1.8	1.3-2.6	0.001
Vaginal bleeding*	1.5	1.2-1.8	0.001
Pre-eclampsia*	1.3	1.1-1.6	0.003

* (< 32 weeks)
• (< 28 weeks)
Reproduced with permission from Queisser-Luft A, Stopfkuchen H, Stolz G, et al. Prenatal diagnosis of major malformations: quality control of routine ultrasound examinations based on a five-year study of 20,2248 newborn fetuses and infants. Prenat Diag 1998;18:573.

detectable with ultrasound were described. The detection rates improved during the course of the study and with increasing gestational age with 38% sensitivity for ultrasound examinations prior to 24 weeks gestation and 50% after 24 weeks. Anamnestic data was collected for the 298 cases and high-risk criteria developed retrospectively to identify women with abnormal fetuses **(Table 4.2)**.[65] Retrospective application of the risk factors identified 22% (4,525/20,248) of the population as high risk of which 3.2% (145/4,525) newborns had detectable anomalies as opposed to 0.9% (142/15,723) in the remainder of the population. However, the absolute number of detectable anomalies between the two groups remained the same, i.e. scanning for indications would potentially miss the opportunity to detect half of the anomalies.

In a six year retrospective analysis of antenatal fetal anomaly detection with ultrasound, Boyd et al.[66] demonstrated an increase in sensitivity over time from 1991–1997. Cases (n=725) were selected from an ongoing birth and malformations registry (n=33,376) and matched with antenatal ultrasound data. In the first three years, 42% of fetal anomalies were detected versus 68% in the latter half. However, there was a concomitant twelve-fold increase in false-positive diagnoses largely attributed to the incorporation of soft markers in screening. This study emphasized the cautious use of soft markers as isolated anomalies and respect for autonomy enhancing practices of non-directive counseling and offering of abortion. An estimated 23% reduction in congenital malformations occurred due to pregnancy termination.

Sprigg et al.[67] conducted a prospective trial from 1992–1994 comparing routine versus selective ultrasound practices for the detection of fetal anomalies. The detection of fetal malformations from the year prior to establishing routine ultrasound surveillance was compared with the new policy. The incidence of major anomalies remained the same between the two scanning regimens. However, the routine scan permitted ultrasound detection of 29 anomalies of which 17 were true positives. There were 11 severe anomalies and 7 patients opted for pregnancy termination that led to a significant estimated cost savings. Weighing the benefit burden calculus of screening, the authors found the use of routine screening justified.

A large difference in detection of fetal anomalies between women screened routinely versus based on indication was seen in the prospective trial conducted by VanDorsten et al., 47.6% versus 75.0%, p = 0.001.[68] From 1993–1996, 2,031 patients enrolled for prenatal care at a tertiary care center. The indicated scans were primarily performed at a maternal-fetal medicine unit whereas the screening ultrasounds took place in a

primary care center. There were 15 anomalous fetuses that were not detected antenatally, 73% (11/15) were in the screening group. These false negative diagnoses included eight missed cardiac anomalies, five ventricular septal defects, one atrial septal defect, one valvular incompetence and one atrioventricular canal defect. Detection rates of specific anomalies were analyzed. VanDorsten supported routine ultrasound as a screening test as it potentially can improve patients' healthcare with respect to morbidity, mortality, disfigurement and anxiety. He acknowledged that more experience and better equipment promotes antenatal ultrasound and that "low risk for adverse perinatal outcome does not confer low risk for anomalies."[68]

Routine prenatal ultrasound prior to 22 weeks for the detection of congenital anomalies was strongly supported by the Euroscan study.[69] Included were 709,030 unselected pregnancies from 12 European countries. A total of 20 Congenital Malformation Registries participated from 1993 to 1996; 18 registries were population-based and 16 collaborated with the EUROCAT program. Congenital malformations existed in 8,126 cases and 44.3% (3,601/8,126) were detected with antenatal ultrasound screening. All categories of major congenital anomalies capable of prenatal detection were detected less frequently in countries without a routine antenatal ultrasound policy and in Eastern Europe. These findings suggest that operator experience, equipment and gestational age at examination are important factors affecting the sensitivity of congenital anomaly detection. From the results of this largely population based trial, the authors recommend single-stage routine ultrasound screening for fetal anomalies as the majority occur in pregnancies without ascertainable risks.[69,70]

A compilation of studies yielded a combined sensitivity of 50.9% for ultrasound detection of fetal anomalies before 24 weeks gestation **(Table 4.3)**.[48] In this analysis, Romero proposed if prenatal care should encompass detection of fetal anomalies, then routine ultrasound screening by experts can achieve this goal. Clementi also supported the use of routine ultrasound as the detection of congenital anomalies continues to improve concomitant with experience and advances in ultrasound technology. In addition, congenital malformations impact heavily on perinatal morbidity and mortality and their detection can be amendable to secondary and tertiary prevention.[70]

In order to maximize visualization of fetal anatomy and minimize follow-up ultrasound examinations, the ideal time to perform the second trimester ultrasound is between 20–22 weeks gestation. Schwärzler et al.[24] determined this optimum gestational age by randomizing 1,206 women who were available for follow up and had undergone normal first trimester ultrasonography. Three groups were established; group 1 was scanned between 18 weeks–18 weeks 6 days, group 2 was scanned between 20 weeks–20 weeks 6 days and group 3 was scanned between 22 weeks–22 weeks and 6 days. The anatomy scan was more likely to be completed and

TABLE 4.3

Comparison of sensitivity of fetal anomaly detection

Reference	*Period*	*n*	*Gestational age (weeks)*	*Prevalence of anomalies*	*Sensitivity*	*Specificity*	*PPV*	*NPV*
Saari-Kamppainen[38]	1986-87	4073	16-20	0.99%	40% (18/45)	99.8% (4636/4646)	64.3% (18/28)	99% (4636/4663)
Levi[56]	1984-89	16072	12-20	1.61%	20.8% (54/259)	100% (15972/15972)	100% (54/54)	98.7% (15972/16177)
Rosendahl[55]	1980-88	9012	< 24	1.03%	39.8% (37/93)	*	*	*
Shirley[60]	1989-91	6183	19	1.36%	60.7% (51/84)	99.9% (6098/6099)	98.1% (51/52)	99.5% (6098/6131)
Chitty[59]	1988-89	8432	< 24	1.48%	74.4% (93/125)	99.9% (8305/8307)	97.9% (93/95)	99.6% (8305/8337)
Luck[62]	1988-91	8523	19	1.95%	84.3% (140/166)	99.9% (8355/8357)	98.6% (140/142)	99.7% (8355/8381)
Overall	**1980-91**	**52295**	**< 24**		**52.9%** (393/772)	**99.9%** (43366/43381)	**95.9%** (356/371)	**99.26%** (43366/43689)

Reproduced with permission from Romero R. Routine obstetric ultrasound. Ultrasound Obstet Gynecol. 1993;306.

within a shorter time period between 20–22 weeks than at 18 weeks, 88–90% versus 76%, (p=0.001).

FIRST TRIMESTER ULTRASONOGRAPHY

The benefits of antenatal ultrasound examination can proceed from assessment in the first trimester. Determination of risk assessment of aneuploidy in singleton and multiple gestations, fetal viability, accurate gestational age, multiple gestations, and chorionicity and amnionicity[71] and detection of fetal anomalies have been described with first trimester ultrasonography. Fetal nuchal translucency measurement has emerged as a valuable tool for aneuploidy screening and fetal nasal bone assessment is gaining importance.[72] Although the first trimester scan continually advances its ability to detect fetal anomalies, it does not currently substitute for the second trimester sonogram.[73,74]

Crowther et al.[75] demonstrated the utility of first trimester sonography performed at the first prenatal visit. There were 648 eligible patients randomized to ultrasound versus no ultrasound prior to routine screening at 18–20 weeks. Patients presented for prenatal care at mean gestational ages of 10.7±2.7 and 10.6±2.6 weeks, respectively. The study group who underwent early sonography had more accurate estimation of gestational age and expressed more positive feelings towards their pregnancy. There was a trend towards earlier detection of twins in the study group compared to the control group. Earlier diagnosis of twins and accurate gestational age determination are important factors in maternal biochemical screening.

Studies evaluating first trimester sonographic detection of structural anomalies demonstrate sensitivities similar to those reported for second trimester ultrasonography. Economides et al.[74] assessed first trimester fetal anomaly detection in 1,632 low-risk pregnancies. The incidence of anomalous fetuses was 1% (17/1632) of which 64.7% (11/17) were detected in the first trimester. The routine second trimester ultrasound identified an additional three anomalous fetuses for a combined trimester sensitivity of 82.3% (14/17). The specificity at each screening ultrasound was greater than 99%. Analysis by the time of detection and specific anomaly revealed similar disparities in the detection rates of central nervous system and cardiac anomalies in first and second trimester ultrasound examinations in low-risk populations. However, with nuchal translucency screening, the first trimester ultrasound can potentially identify those fetuses at increased risk of cardiac anomalies.[76,77] Whitlow et al.[77] expanded the aforementioned study to include an additional 4811 viable pregnancies (n=6443). There were 92 abnormal fetuses yielding an incidence of 1.4% that included 63 fetuses with prenatally detected structural anomalies of which 43 were aneuploid. There were three false-positive initial diagnoses of exopthalmos that were cancelled upon subsequent rescanning. First trimester sensitivities for the detection of structural anomalies and chromosomal abnormalities were 59% (37/63) and 78% (31/40). Chromosomal abnormalities, except for three cases of Klinefelter's syndrome, were suspected by fetal structural anomalies and/or nuchal translucency greater than the 99th percentile for crown-rump length. Combining first and second trimester scans, increased the sensitivity for structural anomaly detection to 81% (51/63). The authors concluded that most structural and chromosomal abnormalities can be detected by fetal ultrasound examination between 11–14 weeks, ideally at 13 weeks, but should not replace second trimester ultrasound.

Carvalho et al.[78] evaluated 2,853 pregnancies with first trimester transabdominal and transvaginal ultrasound, median gestational age 12 weeks and 4 days. Patients enrolled in antenatal care at a tertiary referral center. There were a total of 130 fetal anomalies during the study period, 93 (71.5%) of which were detected with antenatal ultrasound. First trimester ultrasonography detected 29 out of 130 (22.3%) fetal anomalies representing 31.2% (29/93) of the prenatally detected fetal anomalies. Of the structural anomalies, 50.8% major anomalies (66/130) were noted and 78.8% (52/66) detected antenatally. The first trimester scan detected 37.8% (25/66) of all major anomalies.

With an increasing proportion of pregnant women of advanced maternal age, the incidence of trisomy 21 in the second trimester increased from 1/740 in 1974 to 1/504 in 1997.[73] Early detection of aneuploidy allows women to consider invasive diagnostic testing and termination of pregnancy in the first trimester or early second trimester. However, many of these aneuploid fetuses may result in spontaneous fetal demise. The advent of nuchal translucency screening in the first trimester has facilitated earlier detection of fetal aneuploidy. Nicolaides et al.[79] in 1992 described an association between increased first trimester nuchal translucency thickness and aneuploidy and introduced first trimester nuchal translucency screening for abnormal karyotypes. He reported a sensitivity of 64% for aneuploidy using a nuchal translucency cutoff of $\geq$ 3 mm. Snijders et al.[80] in 1998 reported a detection rate of 82%, false positive rate 8.3%, for trisomy 21 fetuses. This multicenter European trial involved 22 centers, 306 sonographers and 96,127 fetuses. Each

fetus had a nuchal translucency measurement obtained from which a gestational age (by crown-rump length) related likelihood ratio was used to combine the maternal age and nuchal thickness-related risks to estimate an adjusted risk. Nuchal translucency measurements vary normally with gestational age and a single cutoff should not be used to adjust risk since it will lead to a lower sensitivity than if nuchal translucency is treated as a continuous variable. Studies using nuchal translucency screening as a continuous, not dichotomous, variable, demonstrate similar detection rates for trisomy 21 and other abnormal karyotypes as reported by the Fetal Medicine Foundation.[81-84] After the introduction of a nuchal translucency screening protocol, Zoppi et al.[85] compared the rate of declining an invasive diagnostic procedure in women of advanced maternal. Prior to the initiation of such a screening program, the incidence of declined invasive procedures was 22% and detection of aneuploidy by transabdominal chorionic villi sampling was 31.5%. However, 30% of women who underwent nuchal translucency screening declined invasive procedures, yet the fewer number of chorionic villi samples revealed a higher rate, 65%, of chromosomal abnormalities. Therefore, nuchal translucency screening in a high-risk population was able to influence a reduction in the number of invasive diagnostic procedures.[85,86] This reduction was also seen in the work of Chasen et al.[86]

Nuchal translucency screening for aneuploidy has been used successfully in unselected populations. Economides et al.[87] retrospectively investigated first trimester anatomy and nuchal translucency screening for detecting chromosomal abnormalities in 2,281 consecutive, unselected gravidas. Of the 16 chromosomal abnormalities, 44% (7/16) were diagnosed between 11–14 weeks due to a nuchal translucency measurement at or greater than the 99th percentile for gestational age. Of the eight cases of trisomy 21, 63% (5/8) were detected by nuchal translucency screening. The sensitivity of detection improved when combined with evaluation of first trimester anatomy. The combined sensitivities were 81% for all chromosome abnormalities and 75% for trisomy 21. Schwärzler et al.[88] investigated the applicability of nuchal translucency screening in an unselected population of 4,523 consecutive, viable fetuses. There were 230 patients (5.1%) that were screen-positive for fetal aneuploidy. Patients were screen-positive, if the nuchal translucency measurement translated to an adjusted risk greater than 1:270. Chromosomal abnormalities were found in 23 (0.51%) cases. The sensitivity of nuchal translucency screening for the detection of an abnormal karyotype was 78%, with a false-positive rate of 4.7%, specificity of 95.3%, positive and negative predictive values of 7.8% and 99.9%, respectively.

The First Trimester Maternal Serum Biochemistry and Ultrasound Fetal Nuchal Translucency Screening Study (BUN)[89] found this test to be efficacious. In this prospective observational trial, the detection rate of trisomy 21 in 7,668 patients based on maternal age and nuchal translucency measurement was 84.2% with a false positive rate of 12.0%. With the same sensitivity, the false positive rate was reduced to 9.4% with the advent of combined screening—the addition of first trimester maternal serum screening with pregnancy-associated plasma protein A (PAPP-A) and free β – human chorionic gonadotropin (fBHCG). The BUN trial also assessed the feasibility of widespread implementation of nuchal translucency screening. Quality sonographic images for assessment was possible with interventions such as diligent individual feedback and occasional equipment tuning.[89]

The credibility, greater sensitivity and acceptability[90,91] of first trimester combined (nuchal translucency measurement plus PAPP-A and fBHCG) screening has been supported by large international trials.[89,91-95] Large prospective trials assessing first and second trimester biochemical and sonographic screening for aneuploidy were completed in North America and in the United Kingdom. In North America, the FASTER[95] (First and Second Trimester Evaluation of Risk for aneuploidy) trial and in the United Kingdom, the SURUSS (Serum Urine and Ultrasound Screening Study) trial addressed comparisons between and among these screening modalities.[92]

ETHICAL DIMENSIONS

Controversy exists surrounding the practice of routine obstetric ultrasound with objections to its use, inadequately addressing the central ethical principles of beneficence and respect for autonomy.

Beneficence

Beneficence, the oldest principle of medical ethics dating back to Hippocrates, obligates physicians to seek greater good than harm for patients. Using sound clinical judgment, physicians should seek clinical treatments that engender a greater balance towards good. Health-related interests should be promoted and protected rather than harmed. Therefore, the concept of nonmaleficence is subordinate to beneficence in obstetric ethics as avoiding harm for one patient in the mother-

fetus unit, may portend worse harm for the other.[43] A beneficence-based discussion regarding routine obstetric ultrasound centers on potential benefits and harms from application of this technique.[96] Arguments against ultrasound screening wrongly assume its benefits are diminutive with respect to its harms. The reported benefits include decreased postdatism, decreased labor induction and use of tocolytics and improved detection of multiple gestations.[52] Additional benefits of ultrasonography develop from continued research. In the case of multiple gestations, which are known to have an increased risk of anomalies, preventing the birth of an anomalous twin can be advantageous to decreased morbidity of the surviving co-twin. This tertiary prevention approach requires the early detection of multiple gestations, an accurate determination of chorionicity and a thorough evaluation of fetal anatomy.[49] The putative harms involve the theoretical risk of fetal damage from ultrasound exposure and false positive diagnoses yielding unnecessary interventions and maternal anxiety. No *in vivo* data exist to suggest that diagnostic two-dimensional ultrasound, performed adeptly and within reasonable time constraints is harmful.[6,21,52,97] It is the sonologist's integrity centered responsibility to ensure quality ultrasound performance. Expert quality ultrasonography can detect many lethal and disabling anomalies during a routine 18–20 week scan, even in low-risk pregnancies. Quality of ultrasound performance underlies the wide range of rates of detection of anomalies.[98] Poor quality ultrasound can lead to a higher incidence of false-positive and false-negative diagnoses. These circumstances can lead to more harm than good incurring additional interventions such as invasive diagnostic testing with chorionic villi sampling, amniocentesis, and cordocentesis and procedure-related fetal loss.[99] Minor ultrasound markers of aneuploidy may cause maternal anxiety, especially in low-risk populations.[99] However, one is unable to discern with certainty for an individual whether a specific minor marker occurs as a normal variant or as a sign of aneuploidy. Careful scrutiny to reduce false positive diagnoses is reasonable and achievable. In order to maximize the potential benefits of ultrasound and to minimize false positive prenatal diagnoses, serial and composite screening modalities have evolved.[91,100-102] First trimester serum analyte testing coupled with nuchal translucency screening can reach 90% sensitivity and 5% false-positive rate for aneuploidy detection.[91] As seen with the introduction of nuchal translucency screening, improved sensitivity for aneuploidy with decreasing frequency of false-positive diagnoses can reduce both the number of invasive prenatal testing procedures and resulting fetal losses.[85,86] Nuchal translucency measurement also offers patients the ability to decline invasive prenatal testing or to decide whether to undergo chorionic villi sampling versus amniocentesis. The former may have slightly higher miscarriage and mosaicism rates and does not permit simultaneous screening for neural tube defects with amniotic fluid α-fetoprotein determination.[103] Since beneficence-based clinical judgment supports routine obstetric ultrasound practice, when quality ultrasound is available, patients should not be denied access to its use just as their autonomy should not be disrespected.[43,104,105]

Autonomy

The physician's role of patient advocate is supported by beneficence and autonomy-based ethical principles. The physician's perspective on the patient's interests provides the basis for beneficence-based obligations owed to her; the patient's perspective on those interests provides the basis for autonomy-based obligations owed to her.[43] Respect for patient autonomy underlies medical, and therefore, obstetric ethics. Autonomy-based practice warrants careful discussion with patients regarding the use of antenatal ultrasound as well as relevant antenatal diagnostic and therapeutic alternatives and acknowledgment by the physician of the patient's preferences and values. Eliciting a patient's views is integral in respecting one's autonomy since these views may influence management, barring any compelling contstraints.[106] Chervenak et al.[29] stated "the standard of care demands that prenatal informed consent for sonogram be accepted as an indication for the prudent use of obstetric ultrasonography performed by qualified personnel." Implementing autonomy-based principles requires a three step process:

1. Adequate information transfer regarding the patient's condition and management.
2. Patient comprehension of the information.
3. Voluntary action by the patient to either accept or decline clinical management.[43]

Diagnostic and therapeutic alternatives should be discussed with the patient as a central component of prenatal care and autonomy enhancing practice. Non-disclosure of alternatives, such as not routinely offering obstetric ultrasound, impairs the patient's exercise of autonomy and may preclude options of diagnosis of severe anomalies and pregnancy termination.

The fetus, prior to viability, does not directly posses autonomy, unless proscribed by the mother. Therefore, autonomy-based obligations to the fetus must be balanced with maternal autonomy and beneficence

principles and practices.[43] Autonomy-based obligation to the gravida seeking obstetric ultrasound is not diminished by controversy regarding lack of benefit or excess cost. Studies that did not show improvement in perinatal morbidity and mortality were limited by insufficient power[46-48,51] and exclusive definition of benefits. Beneficence-based clinical judgment would not condone ignoring outcomes that could reduce or prevent harm in a small but important subset of patients.[104] Regarding excessive cost, the argument to strip away autonomy due to financial concerns falls short of both cost-effective and cost-beneficial analysis. Cost-effectiveness of routine ultrasound was demonstrated by Devore[50] in California where the cost of anomaly detection with ultrasound was less than that detected by serum screening. Cost-benefit analysis incorporates long-term emotional and financial benefits that are often ignored in discussions of implementation costs across a population. The costs to an individual and to the society are harder to measure with regards to care of a child with severe malformation.

CONCLUSION

Routine first trimester ultrasound for nuchal translucency measurement in conjunction with maternal serum analyses is an effective tool for adjusting risk for aneuploidy.[27,89-95] Routine midtrimester ultrasound is an effective diagnostic tool. Establishment of accurate gestational age, detection of fetal anomalies and multiple gestations, and reduction in postdate pregnancies and labor inductions are proven benefits of routine ultrasound. The benefit burden calculus of routine antenatal ultrasonography support its use and fulfillment of ethical principles of beneficence and respect for patient's autonomy.

REFERENCES

1. Fleischer AC. Ultrasound in obstetrics and gynecology. In: Grainer and Allison's Diagnostic Radiology: A Textbook of Medical Imaging, 4th edition. Churchill Livingstone; 2001. pp. 2177-85.
2. Cosgrove DO. Ultrasound: general principles. In: Grainer and Allison's Diagnostic Radiology: A Textbook of Medical Imaging, 4th edition. Churchill Livingstone; 2001. pp. 43-57.
3. Woo J. Obstetric Ultrasound: A comprehensive guide. Available at www.ob-ultrasound.net. Accessed on February 2011.
4. NIH Consensus Conference. The use of diagnostic ultrasound imaging during pregnancy. JAMA. 1984;252(5):669-72.
5. American College of Obstetricians and Gynecologists. New Ultrasound Output Display Standard. ACOG Committee Opinion No. 180. Washington, DC: ACOG, 1996.
6. Reece EA, Assimakopoulos E, Zheng XZ. The safety of obstetric ultrasonography: concern for the fetus. Obstet Gynecol. 1990;76(1):139-46.
7. AIUM Bioeffects Report. Mechanical bioeffects from diagnostic ultrasound: AIUM consensus statements. J Ultrasound Med. 2002;29:73-6.
8. AIUM News Release: AIUM opposes use of ultrasound for entertainment. Laurel, MD: November 5, 2002.
9. Salvesen KÅ, Bakketeig LS, Eik-Nes SH, et al. Routine ultrasonography in utero and school performance at 8-9 years. Lancet 1992;339:85-9.
10. Salvesen KÅ. Routine ultrasonography in utero and development in childhood – a randomized controlled follow-up study. Acta Obstet Gynecol Scand. 1995;74:166-7.
11. Kieler H, Haglund B, Waldenström U, et al. Routine ultrasound screening in pregnancy and the children's subsequent growth, vision and hearing. Br J Obstet and Gynaecol. 1997;104:1267-72.
12. Kieler H, Ahlesten G, Haglund H, et al. Routine ultrasound screening in pregnancy and the children's subsequent neurologic development. Obstet Gynecol. 1998;91(5 Pt 1):750-6.
13. Salvesen KÅ, Eik-Nes SH. Ultrasound during pregnancy and birthweight, childhood malignancies and neurological development. Ultrasound Med Biol. 1999;25(7):1025-31.
14. Kieler H, Cnattingius S, Halund B, et al. Sinistrality – a side-effect of prenatal sonography: a comparative study of young men. Epidemiology. 2001;12:618-23.
15. Salvesen KÅ, Eik-Nes SH. Ultrasound during pregnancy and subsequent childhood non-right handedness: a meta-analysis. Ultrasound Obstet Gynecol. 1999;13:241-6.
16. Ang ES, Gluncic V, Duque A, et al. Prenatal exposure to ultrasound waves impacts neuronal migration in mice. Proc Natl Acad Sci USA. 2006;103(34):12903-10.
17. National Institute Health Consensus Development Conference Consensus Statement. 1984;5(1):17. Available at http://hstat.nlm.nih.gov/hq/Hquest/screen/HquestHome/s/45672 . Accessed on February, 2011.
18. Ultrasound Screening: Implications of the RADIUS Study [draft summary]. NIH Technol Assess Statement Online. 1993;12:1-5.
19. American Institute of Ultrasound In Medicine. Standards for Performance of the Antepartum Obstetrical Examination. J Ultrasound Med.1996;29:185-7. Available at www.aium.org. Accessed on February 2011.
20. Campbell S. The obstetric ultrasound examination. In: Chervenak FA, Isaacson GC, Campbell S (Eds). Ultrasound in Obstetrics and Gynecology. Boston: Little Brown; 1993. pp. 187-98.
21. American Institute of Ultrasound in Medicine (2002). Standards and Guidelines for the Accreditation of Ultrasound Practices (online). Available at www.aium.org/consumer/statement_selected.asp?statement=27. Accessed February 2011.
22. Marinac-Dabic D, Krulewitch CJ, Moore RM. The safety of prenatal ultrasound exposure in human studies. Epidemiology. 2002;13:S19-22.

23. Anderson G. Routine prenatal ultrasound screening. In: Canadian Task Force on the Periodic Health Examination. Canadian Guide to Clinical Preventive Health Care. Ottawa: Health Canada; 1994. pp. 4-14.
24. Royal College of Obstetricians and Gynaecologists. Ultrasound Screening for Fetal Abnormalities Report of the RCOG Working Party. London, UK: RCOG; 1997.
25. Schwarzler R, Senat M-V, Holden D, et al. Feasibility of the second-trimester ultrasound examination in an unselected population at 18, 20 or 22 weeks of pregnancy: a randomized controlled trial. Ultrasound Obstet Gynecol. 1999;14(2):92-7.
26. Carrera JM, Torrents M, Mortera C, et al. Routine prenatal ultrasound screening for fetal abnormalities: 22 years' experience. Ultrasound Obstet Gynecol. 1995;5(3):174-9.
27. Martin JA, Hamilton BE, Ventura SJ, et al. Births: Final data for 2001. National vital statistics reports; Hyattsville, MD: National Center for Health Statistics. 2002; 51.
28. American College of Obstetricians and Gynecologists. Screening for fetal chromosomal abnormalities. ACOG Practice Bulletin No. 77. Washington, DC: ACOG; 2007.
29. Chervenak FA, McCullough LB, Chervenak JL. Prenatal informed consent for sonogram: an indication for obstetric sonography. Am J Obstet Gynecol. 1989;161(4):857-60.
30. Bennett MJ, Little G, Dewhurst J, et al. Predictive value of ultrasound measurement in early pregnancy: a randomized controlled trial. British J Obstet Gynaecol. 1982;89(5):338-41.
31. Neilson JP, Munjanja SP, Whitfield CR. Screening for small for dates fetuses: a controlled trial. Br Med J. 1984; 289(6453):1179-82.
32. Bakketeig LS, Eik-Nes SH, Jacobsen G, et al. Randomised controlled trial of ultrasonographic screening in pregnancy. Lancet. 1984;2(8396):207-11.
33. Bricker L, Neilson JP, Dowswell T. Routine ultrasound in late pregnancy (after 24 weeks' gestation). Cochrane Database of Systematic Reviews [1469-493X]. 2008;4: CD001451.
34. Eik-Nes SH, Salvesen KÅ, Økland O. Routine ultrasound fetal examination in pregnancy: the 'Ålesund' randomized controlled trial. Ultrasound Obstet Gynecol. 2000; 15(6):473-8.
35. Secher NJ, Kern Hansen P, Lenstrup C, et al. A randomized study of fetal abdominal diameter and fetal weight estimation for detection of light-for-gestation infants in low-risk pregnancies. Br J Obstet Gynaecol. 1987;94(2):105-9.
36. Ewigman B, LeFevre M, Hesser J. A randomized trial of routine prenatal ultrasound. Obstet Gynecol. 1990;76:189-94.
37. Waldenström U, Axelsson O, Nilsson S, et al. Effects of routine one-stage ultrasound screening in pregnancy: a randomized controlled trial. Lancet. 1988;2(8611):585-8.
38. Saari-Kemppainen A, Karjalainen O, Ylöstalo P, et al. Ultrasound screening and perinatal mortality: controlled trial of systemic one-stage screening in pregnancy. Lancet. 1990;336:387-91.
39. Geerts L, Brand E, Theron G. Routine obstetric ultrasound examinations in South Africa: cost and effect on perinatal outcome – a prospective randomized controlled trial. Br J Obstet Gynaecol. 1996;103(6):501-7.
40. Ewigman BG, Crane JP, Frigoletto FD, et al. Effect of prenatal ultrasound screening on perinatal outcome. RADIUS Study Group. N Engl J Med. 1993;329(12):821-7.
41. LeFevre ML, Bain RP, Ewigman BG, et al. A randomized trial of prenatal ultrasonographic screening: impact on maternal management and outcome. RADIUS (Routine Antenatal Diagnostic Imaging with Ultrasound) Study Group. Am J Obstet Gynecol. 1993;169(3):483-9.
42. Crane JP, LeFevre ML, Winborn RC, et al. A randomized trial of prenatal ultrasonographic screening: Impact on the detection, management, and outcome of anomalous fetuses. The RADIUS Study Group. Am J Obstet Gynecol. 1994; 171(2):392-9.
43. Skupski DW, Chervenak FA, McCullough LB. Is routine ultrasound screening for all patients? Clin Perinatol. 1994;21(4):707-22.
44. Berkowitz RL. Should every pregnant woman undergo ultrasonography? New Eng J Med. 1993;329(12):874-5.
45. Gunderson EW. Cost of routine ultrasonography. Am J Obstet Gynecol. 1994;171(2):581-2.
46. Thacker SB. Quality of controlled clinical trials. The case of imaging ultrasound in obstetrics: a review. Br J Obstet Gynaecol. 1985;92(5):437-44.
47. Lilford RJ, Chard T. The routine use of ultrasound. Br J Obstet Gynaecol. 1985;92:434-6.
48. Romero R. Routine obstetric ultrasound. Ultrasound Obstet Gynecol. 1993;3(5):303-7.
49. Chasen ST, Chervenak FA. What is the relationship between the universal use of ultrasound, the rate of detection of twins, and outcome differences? Clin Obstet Gynecol. 1998;41(1):66-77.
50. DeVore GR. The routine antenatal diagnostic imaging with ultrasound study: another perspective. Obstet Gynecol. 1994;84(4):622-6.
51. Bucher HC, Schmidt JG. Does routine ultrasound scanning improve outcome in pregnancy? Meta-analysis of various outcome measures. BMJ. 1993; 307(6895):13-7.
52. Neilson JP. Ultrasound for fetal assessment in early pregnancy (Cochrane Review). In: The Cochrane Library, Issue 4, 2002. Oxford: Update Software.
53. Grennert L, Persson PH, Gennser G. Benefits of ultrasonic screening of a pregnant population. Acta Obstet Gynecol Scand. 1978; Suppl 78: 5-14.
54. Persson PH, Kullander S. Long-term experience of general ultrasound screening in pregnancy. Am J Obstet Gynecol. 1983;146(8):942-7.
55. Rosendahl H, Kivinen S. Antenatal Detection of Congenital Malformations by Routine Ultrasonography. Obstet Gynecol. 1989;73(6):947-51.
56. Levi S, Hyjazi Y, Schaapst JP, et al. Sensitivity and specificity of routine antenatal screening for congenital anomalies by ultrasound: the Belgian multicentric study. Ultrasound Obstet Gynecol. 1991;1(2):102-10.
57. Gonçalves LF, Jeanty P, Piper JM. The accuracy of prenatal ultrasonography in detecting congenital anomalies. Am J Obstet Gynecol 1994; 171(6):1606-12.
58. Boyle JG. The accuracy of prenatal ultrasonography in detecting congenital anomalies (letter). Am J Obstet Gynecol. 1995;173(2):667-8.

59. Chitty LS, Hung GH, Moore J, et al. Effectiveness of routine ultrasonography in detecting fetal structural abnormalities in a low risk population. BMJ. 1991;303(6811):1165-9.
60. Shirley IM, Bottomley F, Robinson VP, et al. Routine radiographer screening for fetal abnormalities by ultrasound in an unselected low risk population. Br J Radiol. 1992;65(775):564-9.
61. Papp Z, Tóth-Pál E, Papp C, et al. Impact of prenatal mid-trimester screening on the prevalence of fetal structural anomalies: a preospective epidemiological study. Ultrasound Obstet Gynecol. 1995;6(5):320-6.
62. Luck CA. Value of routine ultrasound scanning at 19 weeks: a four year study of 8849 deliveries. BMJ. 1992;304 (6840):1474-8.
63. Grandjean H, Larroque D, Levi S, et al. The performance of routine ultrasonographic screening of pregnancies in the Eurofetus Study. Am J Obstet Gynecol. 1999;181(2):446-54.
64. Skupski DW, Newman S, Edersheim T, et al. The impact of routine obstetric ultrasonographic screening in a low-risk population. Am J Obstet Gynecol. 1996;175(5):1142-5.
65. Queisser-Luft A, Stopfkuchen H, Stolz G, et al. Prenatal diagnosis of major malformations: quality control of routine ultrasound examinations based on a five-year study of 20,248 newborn fetuses and infants. Prenat Diag. 1998;18:567-76.
66. Boyd PA, Chamberlain P, Hicks NR. 6-year experience of prenatal diagnosis in an unselected population in Oxford, UK. Lancet. 1998; 352(9140):1577-81.
67. Long G, Sprigg A. A comparative study of routine versus selective fetal anomaly ultrasound scanning. J Med Screen. 1998;5(1):6-10.
68. VanDorsten JP, Hulsey TC, Newman RB, et al. Fetal anomaly detection by second-trimester ultrasonography in a tertiary center. Am J Obstet Gynecol. 1996;178:742-9.
69. Stoll C, Tenconi R, Clementi M, et al. Detection of congenital anomalies by fetal ultrasonographic examination across Europe. Community Genet. 2001;4(4):225-32.
70. Clementi M, Stoll C. The Euroscan Study. Ultrasound Obstet Gynecol. 2001;18(4):297-300.
71. Sepulveda W, Odibo A, Sebire NJ, et al. The lambda sign at 10-14 weeks of gestation as a predictor of chorionicity in twin pregnancies. Ultrasound Obstet Gynecol. 1996;7(6):421-3.
72. Cicero S, Curcio P, Papageorghiou A, et al. Absence of nasal bone in fetuses with trisomy 21 at 11-14 weeks of gestation: an observational study. Lancet. 2001; 358(9294):1665-7.
73. Souter VL, Nyberg DA. Sonographic screening for fetal aneuploidy: first trimester. J Ultrasound Med. 2001;20(7): 775-90.
74. Economides DL, Braithwaite JM. First trimester ultrasonographic diagnosis of fetal structural abnormalities in a low risk population. Br J Obstet Gynaecol. 1998; 105(1):53-7.
75. Crowther CA, Kornman L, O'Callaghan S, et al. Is ultrasound assessment of gestational age at the first antenatal visit of value? A randomized clinical trial. Br J Obstet Gynaecol. 1999;106(12):1273-9.
76. Hyett JA, Perdu M, Sharland GK, et al. Using fetal nuchal translucency to screen for major congenital cardiac defects at 10-14 weeks of gestation: population based cohort study. BMJ. 1999;318(7176):81-5.
77. Whitlow BJ, Chatzipapas IK, Lazanakis ML, et al. The value of sonography in early pregnancy for the detection of fetal abnormalities in an unselected population. Br J Obstet Gynaecol. 1999;106(9):929-36.
78. Carvalho MHB, Brizot ML, Lopes LM. Detection of fetal structural abnormalities at the 11-14 weeks ultrasound scan. Prenat Diagn. 2002; 22:1-4.
79. Nicolaides KH, Azar G, Byrne D, et al. Fetal nuchal translucency: ultrasound screening for chromosomal defects in first trimester of pregnancy. BMJ. 1992;304(6831): 867-9.
80. Snijders RJ, Noble P, Sebire N, et al. UK multicentre project on assessment of risk of trisomy 21 by maternal age and fetal nuchal-translucency thickness at 10-14 weeks of gestation. Fetal Medicine Foundation First Trimester Screening Group. Lancet. 1998;352(9125):343-6.
81. Fukada Y, Takizawa M, Amemiya A, et al. Detection of aneuploidy with fetal nuchal translucency and maternal serum markers in Japanese women. Acta Obstet Gynecol Scand. 2000;79(12):1124-5.
82. Acacio GL, Barini R, Pinto Junior W, et al. Nuchal translucency: an ultrasound marker for fetal chromosomal abnormalities. Sao Paulo Med J. 2001;119(1):19-23.
83. Comas C, Torrents M, Munoz A, et al. Measurement of nuchal translucency as a single strategy in trisomy 21 screening: should we use any other marker? Obstet Gynecol. 2002;100(4):648-54.
84. Sharma G, Chasen ST, Kalish RB, et al. Aneuploidy screening with nuchal translucency: performance in a single institution. Am J Obstet Gynecol. 2002;187 part 2:S177.
85. Zoppi MA, Ibba RM, Putzolu M, et al. Nuchal translucency and the acceptance of invasive prenatal chromosomal diagnosis in women aged 35 or older. Obstet Gynecol. 2001;97:916-20.
86. Chasen ST, McCullough LB, Chervenak FA. Is nuchal translucency screening associated with different rates of invasive testing in an older obstetric population? Am J Obstet Gynecol. 2004;190:769-4.
87. Economides DL, Whitlow BJ, Kadir R, et al. First trimester sonographic detection of chromosomal abnormalities in an unselected population. Br J Obstet Gynaecol. 1998;105(1):58-62.
88. Schwärzler P, Carvalho JS, Senat MV, et al. Screening for fetal aneuploidies and fetal cardiac abnormalities by nuchal translucency thickness measurement at 10-14 weeks of gestation as part of routine antenatal care in an unselected population. Br J Obstet Gynaecol. 1999;106(10):1029-34.
89. Snijders RJM, Thom EA, Zachary JM, et al. First trimester trisomy screening: nuchal translucency measurement training and quality assurance to correct and unify technique. Ultrasound Obstet Gynecol. 2002;19:353-9.
90. Sharma G, Gold HT, Chervenak FA, et al. Patient preference regarding first-trimester aneuploidy risk assessment. Am J Obstet Gynecol. 2005;193(4):1429-36.
91. Nicolaides KH, Chervenak FA, McCullough LB, et al. Evidence-based obstetric ethics and informed decision-making by pregnant women about invasive diagnosis after

first-trimester assessment of risk for trisomy 21. Am J Obstet Gynecol. 2005;193(2):322-6.
92. Bindra R, Heath V, Liao A, et al. One-stop clinic for assessment of risk for trisomy 21 at 11-14 weeks: a prospective study of 15,030 pregnancies. Utrasound Obstet Gynecol. 2002;20:219-25.
93. Wald NJ, Rodeck C, Hackshaw AK, et al. First and second trimester antenatal screening for Down's syndrome: the results of the Serum, Urine and Ultrasound Screening Study (SURUSS). Health Technol Assess. 2003;7(11):1-77.
94. Wapner R, Thom E, Simpson JL, et al. First-trimester screening for trisomies 21 and 18. N Engl J Med. 2003;349:1405-13.
95. Malone FD, Canick JA, Ball RH, et al. First- and Second-Trimester Evaluation of Risk (FASTER) Research Consortium. First-trimester or second-trimester screening, or both, for Down's syndrome. N Engl J Med. 2005;353(19):2001-11.
96. McCullough LB, Chervenak FA. Ethics in Obstetrics and Gynecology. New York, NY: Oxford University Press; 1994.
97. Salvesen, KÅ. Ultrasound and left-handedness: a sinister association? Ultrasound Obstet Gynecol. 2002;19(3):217-21.
98. Chitty LS. Utrasound screening for fetal abnormalities. Prenat Diag. 1995;15:1241-57.
99. Smith-Bindman R, Hosmer W, Feldstein V, et al. Second-trimester ultrasound to detect fetuses with Down syndrome. A meta-analysis. JAMA. 2001;285(8):1044-55.
100. Nyberg DA, Luthy DA, Resta RG, et al. Age-adjusted risk assessment for fetal Down's syndrome during the second trimester: description of the method and analysis of 142 cases. Ultrasound Obstet Gynecol. 1998;12(1):8-14.
101. Wald NJ, Watt HC, Hackshaw AK. Integrated screening for Down's syndrome based on tests performed during the first and second trimesters. New Engl J Med. 1999; 341(7):461-7.
102. Spencer K. Accuracy of Down syndrome risks produced in a first-trimester screening program incorporating fetal nuchal translucency thickness and maternal serum biochemistry. Prenat Diag. 2002;22:244-6.
103. Chasen ST, Skupski DW, McCullough LB, et al. Prenatal informed consent for sonogram – the time for first-trimester nuchal translucency has come. J Ultrasound Med. 2001;20:1147-52.
104. Skupski DW, Chervenak FA, McCullough LB. A clinical and ethical evaluation of routine obstetric ultrasound. Curr Opin Obstet Gynecol 1994;6(5):435-9.
105. Sharma G, McCullough LB, Chervenak FA. Ethical considerations of early (first vs second trimester) risk assessment disclosure for trisomy 21 and patient choice in screening versus diagnostic testing. Am J Med Genet Part C Semin Med Genet. 2007; 145C(1):99-104.
106. Chervenak FA, McCullough LB, Ledger WJ. Advocacy for routine obstetric ultrasound. ACOG Clinical Review. 1996;1:1-4.

CHAPTER 5

Medicolegal Issues in Obstetric and Gynecologic Ultrasound

Frank A Chervenak, Judith L Chervenak

INTRODUCTION

Ultrasound has revolutionized the practice of Obstetrics and Gynecology in one generation more than any other innovation. However, practitioners should be aware of the medicolegal risks.

Obstetric ultrasound plays a vital and increasingly frequent role in legal actions, either as the focus in a case alleging wrongful birth in which an anomaly was not diagnosed and the mother was deprived of a chance to terminate her pregnancy; or as a significant or contributing factor in a case alleging negligent obstetric care with resulting damage to the infant-plaintiff or mother.

This chapter will focus upon the general aspects of a medical negligence case as they relate to the performance of the obstetric ultrasound examination, summarize the recommendations of both the American College of Obstetrics and Gynecology (ACOG) and the American Institute of Ultrasound in Medicine (AIUM), regarding the performance of these examinations, and outline potential areas of negligence and discuss ways to avoid them.

MEDICAL NEGLIGENCE

In order to establish negligence, the plaintiff must show that there was:

- A duty recognized by the law
- A breach of that duty, in that there was a failure on the part of the physician to meet what was considered to be the standard of care at the time the treatment was rendered
- A causal relationship between the treatment and the resulting injury, and
- Actual loss or damage to the plaintiff.[1]

Obstetric ultrasound cases may include allegations of a failure on the part of the maternal-fetal medicine specialist performing the ultrasound to fully advise the obstetric patient regarding the medical aspects of her case, given his specialized training in the field of high-risk obstetrics. The maternal-fetal medicine specialist has a duty to the patient and should clearly define the extent of his role in the patient's care, whether he or she is co-managing a patient, rendering consultative services or only performing antenatal diagnoses.

Generally, damages are easily established, granting either or both the departure from the accepted standards of care and the causal connection between that breach and the damages as the major focus of the litigation. Standard of care is most commonly established by the testimony of an expert witness whose knowledge, training or experience qualifies him to testify as to the standard of care.[2] These experts are limited by the state of medical knowledge and standards of practice at the time of the alleged negligence.[2] While these standards were previously limited to local legal requirements, they have expanded to those practiced nationally, given the recent advances in communication and dissemination of medical information.

Although guidelines promulgated by various organizations do not establish the standard of care introduced at trial, the obstetric ultrasound practitioner should be aware of the recommendations of ACOG and

the AIUM. These organizations have published recommendations regarding guidelines, instrumentation and safety, documentation, indications, examination content and quality control. They periodically issue clinical recommendations. These guidelines are designed to inform the practitioner so that he or she is aware of currently suggested practices in this ever-evolving discipline.

GUIDELINES

ACOG's recent publications include a Practice Bulletin entitled *Ultrasonography in Pregnancy* issued in December of 2004[3] and a *Committee Opinion on Guidelines for Diagnostic Imaging During Pregnancy* in September of 2004.[4] In 2003, the AIUM published a *Practice Guideline for the Performance of an Antepartum Obstetric Ultrasound Examination* in conjunction with ACOG and the American College of Radiology (ACR).[5] The AIUM guidelines were originally published in 1985 and are now in their fourth revision.

INSTRUMENTATION AND SAFETY

While acknowledging that manufacturers offer machines with 3D capability, the practice bulletin indicates that proof of a clear advantage over 2D imaging has not yet been demonstrated.[3] ACOG also recommends that practitioners should have a method of storing images and equipment should be serviced on a regular basis.[3]

The US Food and Drug Administration has arbitrarily limited energy exposure from ultrasonography to 94mW/cm^2.[4] In the 2004 *Committee Opinion on Guidelines for Diagnostic Imaging During Pregnancy*, ACOG noted that there had been no documented reports of adverse fetal effects from diagnostic ultrasound procedures, including duplex Doppler imaging.[4] The AIUM concurs and emphasizes the "as low as reasonably achievable" (ALARA) principle, which means that the lowest possible ultrasonic exposure setting should be used to gain the necessary information.[5]

DOCUMENTATION

The AIUM has published a standard for documentation of an ultrasound exam which can be obtained from the AIUM's website, www.aium.org.[6] These guidelines recommend that a permanent record of both the images and the interpretation of the ultrasound be recorded in a retrievable format and should be kept in accordance with the relevant requirements of local legal and healthcare facilities. The AIUM suggests that the documentation include the patient's name and identifying numbers, such as a social security or medical record number, the date of ultrasound exam and image orientation on all recorded images. Additionally, the healthcare provider's name, type of ultrasound examination and identification of the sonographer/sonologist should be included on the accompanying report.[6]

A preliminary report of the findings may be provided and a final report should be included in the patient's medical record. Within the final report, limitations of the examination should be noted, biometric data, including variations from normal size, should be accompanied by measurements and a final report should be completed, and transmitted to the patient's healthcare provider. Depending on the circumstances, the results may need to be directly conveyed to the patient's referring health care provider and documentation of this communication is recommended.[6]

ACOG has noted "Absence of visual image documentation eliminates the possibility of future review or clinical reintegration and weakens the defense against an allegation that an incomplete or inadequate study was performed."[3]

INDICATIONS

The AIUM has published indications for first and second obstetric ultrasound examinations, which are listed in **Tables 5.1 and 5.2**.[5] When there is no indication,

TABLE 5.1

First trimester ultrasound examination

Indications: A sonographic examination can be of benefit in many circumstances in the first trimester of pregnancy, including, but not limited to, the following indications:

- To confirm the presence of an intrauterine pregnancy
- To evaluate a suspected ectopic pregnancy
- To define the cause of vaginal bleeding
- To evaluate pelvic pain
- To estimate gestational (menstrual*) age
- To diagnose or evaluate multiple gestations
- To confirm cardiac activity
- As an adjunct to chorionic villus sampling, embryo transfer, and localization and removal of an intrauterine device (IUD)
- To evaluate maternal pelvic masses and/or uterine abnormalities
- To evaluate suspected hydatidiform mole.

*For the purpose of this document, the terms "gestational age" and "menstrual age" are considered equivalent.

AIUM Practice Guideline for the performance of an antepartum obstetric ultrasound examination. J Ultrasound Med. 2003;22(10): 1116-25. Permission obtained.

TABLE 5.2

Second- and third-trimester examination

Indications: Sonography can be of benefit in many situations in the second and third trimesters, including, but not limited to, the following circumstances: (adapted from National Institutes of Health. Diagnostic Ultrasound Imaging in Pregnancy: Report of a Consensus. NIH Publication 84-667. Washington, DC: US Government Printing Office; 1984).

- Estimation of gestational age
- Evaluation of fetal growth
- Vaginal bleeding
- Abdominal/pelvic pain
- Incompetent cervix
- Determination of fetal presentation
- Suspected multiple gestation
- Adjunct to amniocentesis
- Significant discrepancy between uterine size and clinical dates
- Pelvic mass
- Suspected hydatidiform mole
- Adjunct to cervical cerclage placement
- Suspected ectopic pregnancy
- Suspected fetal death
- Suspected uterine abnormality
- Evaluation of fetal well-being
- Suspected amniotic fluid abnormalities
- Suspected placental abruption
- Adjunct to external cephalic version
- Premature rupture of membranes and/or premature labor
- Abnormal biochemical markers
- Follow-up evaluation of a fetal anomaly
- Follow-up evaluation of placental location for suspected placenta previa
- History of previous congenital anomaly
- Evaluation of fetal condition in late registrants for prenatal care.

In certain clinical circumstances, a more detailed examination of fetal anatomy may be indicated.

AIUM Practice Guideline for the performance of an antepartum obstetric ultrasound examination. J Ultrasound Med. 2003;22(10): 1116-25. American Institute of Ultrasound in Medicine, publisher. Permission obtained.

ACOG has commented that, while it is reasonable to honor a patient's request for an ultrasound, based upon the limitations of the various studies analyzing the benefits of routine screening and their equivocal results, a physician is not obligated to perform an ultrasound in a low-risk patient without indications.[3] The authors have argued that all pregnant women should be offered a quality second trimester ultrasound examination in clinical settings where it is available.[7] Further, it has been argued that pregnant women should also be offered a quality first trimester ultrasound examination in clinical settings where it is available.[8] Currently, ACOG has recommended that all pregnant women, regardless of their age, should be offered screening for Down Syndrome in a quality manner.[9]

EXAMINATION CONTENT

The AIUM has published a practice guideline for the performance of an antepartum obstetric ultrasound examination in conjunction with ACOG and the American College of Radiology (ACR).[5] The components of a first trimester ultrasound examination and second and third trimester examinations are listed in **Tables 5.3 and 5.4**. The AIUM and ACOG use the terms "standard," "limited" and "specialized" to describe the types of obstetric ultrasound performed during the second and third trimesters. Standard and limited examinations are defined by their components and the components of a specialized exam are determined on a case by case basis.[3,5]

Standard examinations include an evaluation of fetal presentation, amniotic fluid volume, cardiac activity, placental position, biometry and an anatomic survey. An examination of the uterus and adnexa is also suggested if technically feasible.[3,5]

Limited exams are performed for a specific indication such as identification of fetal presentation, evaluation of fetal cardiac activity or amount of amniotic fluid and are appropriate when a standard examination has already been performed. In such cases, an anatomic survey is not necessary.

Specialized examinations include the biophysical profile, fetal Doppler studies, fetal echocardiography and those examinations that are done when it is necessary to evaluate a specific question or to evaluate a specific or suspected fetal anomaly or maternal biochemical screening test. These examinations should be performed by operators with specific experience in the relevant area.[3,5]

TABLE 5.3

Contents of first trimester ultrasound examination

- Scanning in the first trimester may be performed either transabdominally or transvaginally. If a transabdominal examination is not definitive, a transvaginal scan or transperineal scan should be performed whenever possible.
- The uterus and adnexa should be evaluated for the presence of a gestational sac. If a gestational sac is seen, its location should be documented. The gestational sac should be evaluated for the presence or absence of a yolk sac or embryo and the crown-rump length should be recorded, when possible.
- Presence or absence of cardiac activity should be reported.
- Fetal number should be reported.
- Evaluation of the uterus, adnexal structures, and cul-de-sac should be performed.

Adapted from: AIUM Practice Guideline for the performance of an antepartum obstetric ultrasound examination. J Ultrasound Med. 2003:22(10):1116-25. Permission obtained.

TABLE 5.4

Contents of a standard second and third trimester obstetric ultrasound examination

- Fetal cardiac activity, number and presentation should be reported.
- A qualitative or semiquantitative estimate of amniotic fluid volume should be reported.
- The placental location, appearance, and relationship to the internal cervical os should be recorded. The umbilical cord should be imaged and the number of vessels in the cord should be evaluated, when possible.
- Gestational age assessment.
- Fetal weight estimation.
- Maternal anatomy. Evaluation of the uterus and adnexal structures should be performed.
- Fetal anatomic survey.
- The following areas of assessment represent the essential elements of a standard examination of fetal anatomy. A more detailed fetal anatomic examination may be necessary if an abnormality or suspected abnormality is found on the standard examination.
  - Head and neck
    - Cerebellum
    - Choroid plexus
    - Cisterna magna
    - Lateral cerebral ventricles
    - Midline falx
    - Cavum septi pellucidi
  - Chest
    - The basic cardiac examination includes a 4-chamber view of the fetal heart.
    - If technically feasible, an extended basic cardiac examination can also be attempted to evaluate both outflow tracts.
  - Abdomen
    - Stomach (presence, size and sinus)
    - Kidneys
    - Bladder
    - Umbilical cord insertion site into the fetal abdomen
    - Umbilical cord vessel number
  - Spine
    - Cervical, thoracic, lumbar and sacral spine
  - Extremities
    - Legs and arms (presence or absence)
  - Gender
    - Medically indicated in low-risk pregnancies only for evaluation of multiple gestations.

Adapted from: AIUM Practice Guideline for the Performance of an Antepartum Obstetric Ultrasound Examination. J Ultrasound Med. 2003:22(10):1116-25. Permission obtained.

QUALITY CONTROL

Following the results of the Routine Antenatal Diagnostic Imaging with Ultrasound trial (RADIUS) published in 1993[10] and other studies which indicated that the detection of anomalies was dependent on the experience of the operator, the AIUM began to offer voluntary medical facility accreditation for ultrasound practices. This process reviews the qualifications of the facility's practitioners, the type of equipment and its maintenance, including the proper methods of antimicrobial cleaning and/or chemical sterilization and storing of transducers to prevent contamination between patients, and methods of reporting and storage.[11]

The acquisition and maintainance of such accreditation ensures compliance with current organizational standards, is recommended and is often required for reimbursement for obstetric ultrasound studies by various insurance companies. A recent study in which practices that sought and received accreditation were re-evaluated three years later, found that these practices had improved compliance within accepted standards, and therefore concluded that this improvement would translate into an enhancement of the quality of practice.[11]

LITIGATION RELATED TO ULTRASOUND

Sanders had tracked litigation related to ultrasound. Since there is no reliable system of tabulating legal cases that are filed, many cases are dropped following the review of a competent expert, the majority of cases settle out of court and not all of those that do go to court are reported, this task has been made especially difficult. In 2003, Sanders published his latest series documenting the types of cases he reviewed that were filed between 1997–2002.[12]

When categorizing suits by specialty, predictably those relating to obstetric ultrasound were the most common of all those involving ultrasound examinations, followed by gynecologic examinations. Suits relating to obstetric ultrasound can be expected to have large economic damages because damages are based upon the life-expectancy of the infant-plaintiff, thereby rewarding plaintiff's attorneys with large contingency fees. Sanders found that the missed fetal anomalies are now the most common reason for litigation, comprising over half of the cases in his most recent series.[13] **Table 5.5** documents Sander's tabulation of the possible ways to be sued when performing ultrasound.[13]

NON-MEDICAL USE OF ULTRASONOGRAPHY

The AIUM has published the following "prudent use" statement, endorsed by ACOG.

"The AIUM advocates the responsible use of diagnostic ultrasound. The AIUM strongly discourages the non-medical use of ultrasound for psychosocial or

TABLE 5.5

Nineteen possible ways to get sued for ultrasound

1. Missing the sonographic finding.
2. Misinterpretation of the sonographic finding.
3. Failure to compare findings with previous ultrasound.
4. Failure to properly communicate the sonographic report to the referring physician or the patient.
5. Failure to personally examine the patient or take a proper history.
6. Incorrect sonographic approach for a specific condition.
7. Incomplete examination.
8. Inadequate quality of films.
9. Slip and fall injuries.
10. Complications from puncture techniques under ultrasound control.
11. Failure to obtain informed consent.
12. Complications of ultrasound such as induced vaginal bleeding or abortion.
13. Equipment complications (e.g. electric shocks).
14. Failure to recommend additional sonographic or radiologic studies or biopsy.
15. Failure to order a sonographic examination.
16. Inclusion of sinologist in a shotgun suit.
17. Loss of films, inadequate filing system, misplacement of films or reports.
18. Abuse of patient by sonologist or sonographer (sexual, physical or mental).
19. Miscellaneous anxiety produced by misdiagnosis, invasion of privacy, etc.

From: Sanders RC. The Effect of the Malpractice Crisis on Obstetrics and Gynecologic Ultrasound. In: Ultrasound in Obstetrics and Gynecology, (Eds). Frank A. Chervenak, Glenn C. Isaacson, et al. Boston: Little, Brown and Company; 1993. pp. 263-7.

entertainment purposes. The use of either two-dimensional or three-dimensional ultrasound only to view the fetus, obtain a picture of the fetus or determine the fetal gender without a medical indication is inappropriate and contrary to responsible medical practice. Although there are no confirmed biological effects on patients caused by exposures from present diagnostic ultrasound instruments, the possibility exists that such biological effects may be identified in the future. Thus, ultrasound should be used in a prudent manner to provide medical benefit to the patient."[14] This position has been ethically defended.[15]

CONCLUSION

Physicians who perform obstetric ultrasound can expect to be subjected to increasing legal risk. While knowledge of and comportment with the published recommendations and guidelines of ACOG and the AIUM does not offer complete protection from legal risk, they help to both avoid and to defend oneself. Failure to comply with such standards has the potential to make any subsequent legal case more difficult to defend.

REFERENCES

1. Prosser W, Keeton WP, Dobbs DB, et al. Prosser and Keeton on the Law of Torts, 5th Ed. Minnesota:West Publishing Group; 1984, p.187.
2. Moore T, Gaier M. Medical Malpractice. New York Law Journal;2004:1.
3. Ultrasonography in Pregnancy. ACOG Practice Bulletin(58), 2004. www.acog.org.
4. Guidelines for Diagnostic Imaging During Pregnancy. ACOG Committee Opinion, 2004. 299. www.acog.org.
5. AIUM Practice Guideline for the performance of an antepartum obstetric ultrasound examination. J Ultrasound Med. 2003;22(10):1116-25.
6. American standard for documentation of an ultrasound examination. American Institute of Ultrasound in Medicine. J Ultrasound Med. 2002:21(10):1188-9.
7. Chervenak FA, McCullough LB, Chervenak JL. Prenatal informed consent for sonogram (PICS): An indication for obstetric ultrasound. Am J Obstet Gynecol. 1989;161:857-60.
8. Chasen S, Skupski DW, McCullough LB, Chervenak FA. Prenatal consent for sonogram: the time for first trimester nuchal translucency has come. J Ultrasound Med. 2001;20:1147-52.
9. Laurie Barclay. Screening for Fetal Chromosomal Abnormalities. Obstet Gynecol. 2007.
10. Ewigman BG, Crane JP, Frigoletto FD, et al. Effect of prenatal ultrasound screening on perinatal outcome. RADIUS Study Group. N Engl J Med. 1993; 329(12):821-7.
11. Abuhamad AZ, Benacerraf B, Woletz P, et al. The accreditation of ultrasound practices-impact on compliance with minimum performance guidelines. J Ultrasound Med. 2004:23(8):1023-9.
12. Sanders RC. Changing patterns of ultrasound-related litigation: a historical survey. J Ultrasound Med. 2003: 22(10):1009-15.
13. Sanders RC. The effect of the malpractice crisis on obstetrics and gynecologic ultrasound. In: Frank A Chervenak, Glenn C Isaacson, Stuart Campbell (Eds). Ultrasound in Obstetrics and Gynecology. Boston: Little Brown and Company; 1993. pp:263-76.
14. Non-medical Use of Obstetric Ultrasonography. ACOG Committee Opinion, Non-medical Use of Obstetric Ultrasonography 2004;297.
15. Chervenak FA, McCullough LB. An Ethical Critique of Boutique Fetal Imaging: A case for the medicalization of fetal imaging. Am J Obstet Gynecol. 2005; 192(1):31-3.

SECTION

2

Obstetrics

6

CHAPTER

Fetal and Maternal Physiology and Ultrasound Diagnosis

Aida Salihagic Kadic, Maja Predojevic, Asim Kurjak

INTRODUCTION

Human life does not begin with birth. Normal development of the human being lasts 280 days before parturition. In prenatal growth and development, the placenta plays a key role. It has numerous functions essential for maintaining the pregnancy and promoting normal fetal development. During intrauterine period, the fetus gradually begins to perform many vital physiological functions. Furthermore, through nine months of gestation, a repertoire of fetal functions and activities constantly expands. Development of modern imaging methods has revealed the existence of a full range of fetal movement patterns, even facial movements similar to emotional expressions in adults. Indeed, the world *in utero* is fascinating. Therefore, the birth is not the beginning, but only a new chapter in the story of human life.

PLACENTA

"The vessels join to the uterus like the roots of plants, and through them the embryo receives its nourishment." Aristotle, De Generatione Animalium, Book II.

DEVELOPMENT OF THE PLACENTA

The placenta is an organ that is indispensable for the transfer of nutrients and gases from the mother to the fetus and the removal of fetal waste products. Placenta can be defined as a fusion of fetal membranes with the uterine mucosa. The development of the placenta starts with the implantation, in the moment when the blastocyst begins the invasion of the endometrium, about the 6th day after conception.[1] Prior to implantation in the uterine lining, blastocyst consists of an external, single-layer, cellular component named the trophoblast and the inner cell mass, embryoblast. After the trophoblast has attached to the endometrial epithelium, rapid cellular proliferation occurs and the trophoblast differentiates into two layers consisting of the inner cytotrophoblast and an outer syncytiotrophoblast, a multinucleated mass without cellular boundaries. Syncytial trophoblast processes extend through the endometrial epithelium to invade the endometrial stroma. Stromal cells surrounding the implantation site become laden with lipids and glycogen, develop into polyhedral shape, and are referred to as decidual cells. These decidual cells degenerate in the region of the invading syncytiotrophoblast and provide nutrition to the developing embryo.[2] At day 7–8 after conception, the blastocyst has completely crossed the epithelium and is embedded within the endometrium. At day 8–9 postconception, the syncytiotrophoblast generates a number of fluid-filled spaces within its mass. These spaces flow together forming larger lacunae and are finally separated by parts of the syncytiotrophoblast (trabeculae) that cross the syncytial mass from the embryonic to the maternal side. The development of the lacunar system leads to the division of the placenta into several compartments. The embryonically oriented part of the trophoblast will become the chorionic plate, the lacunae will develop into the intervillous space **(Fig. 6.1)**, while the trabeculae will become the anchoring villi, with the growing branches developing into floating

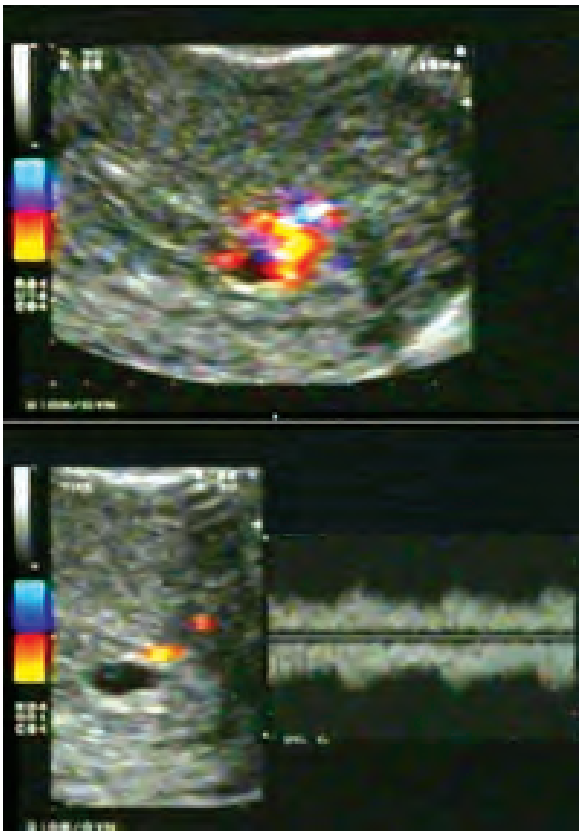

Figure 6.1: Image recorded by 2D color Doppler sonography, showing intervillous blood flow

villi. Finally, the maternally oriented part of the trophoblast will develop into the basal plate.[3]

At day 12 after conception, the process of implantation is completed. The developing embryo with its surrounding extraembryonic tissues is totally embedded in the endometrium and the syncytiotrophoblast surrounds the whole surface of the conceptus. Mesenchymal cells derived from the embryo spread over the inner surface of the trophoblast, thus generating a new combination of trophoblast and mesoderm, termed chorion. Starting on day 12 postconception, proliferation of cytotrophoblast pushes trophoblast cells to penetrate into the syncytial trabeculae, reaching the maternal side of the syncytiotrophoblast by day 14. Further proliferation of trophoblast cells inside the trabeculae (day 13) stretches the trabeculae resulting in the development of syncytial side branches filled with cytotrophoblast cells (primary villi). Shortly after, the mesenchymal cells from the extraembryonic mesoderm too follow the cytotrophoblast and penetrate the trabeculae and the primary villi, thus generating secondary villi. At this stage there is always a complete cytotrophoblast layer between the penetrating

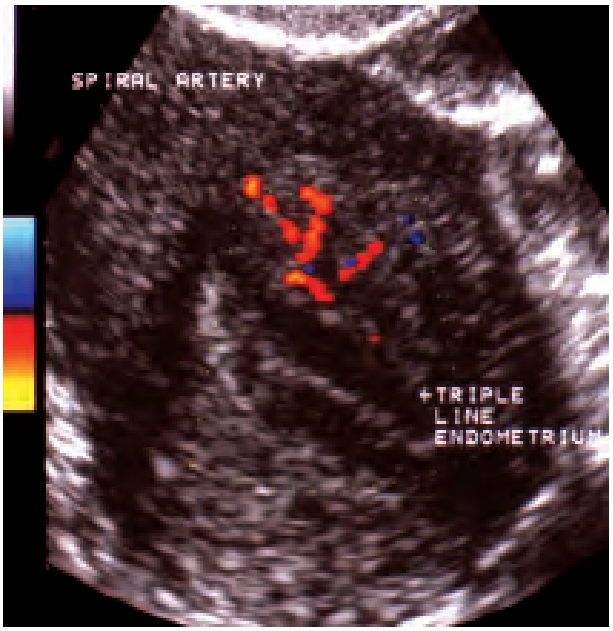

Figure 6.2: Image recorded by 2D color Doppler sonography showing blood flow in spiral arteries

mesenchyme and syncytiotrophoblast. Around day 20–21, vascularization within the villous mesenchyme gives rise to the formation of the first placental vessels (tertiary villi). Only later, the connection to the fetal vessel system will be established. The villi are organized in villous trees that cluster together into a series of spherical units known as lobules or placentones. Each placentone originates from the chorionic plate by a thick villous trunk stemming from a trabecula. Continuous branching of the main trunk results in daughter villi mostly freely ending in the intervillous space.[3]

In normal pregnancies, decidual and myometrial segment of the spiral arteries **(Fig. 6.2)**, undergo changes to convert them into large vessels of low resistance **(Figs 6.3 and 6.4)**. Two types of migratory cytotrophoblast cause this—endovascular and interstitial cytotrophoblast. Endovascular cytotrophoblast invades spiral arteries on the decidua and myometrium and replaces arterial endothelium, destroying muscle and elastic tissues in the tunica media. Interstitial cytotrophoblast destroys the ends of decidual blood vessels, promoting the flow of blood into the lacunae. The maternal arteries are opened up and functionally denervated so that they are completely dilated and unresponsive to circulatory pressor substances or autonomic neural control. Behind this, at uterine radial artery level, local prostacyclin maintains vasodilatation.[1] Free transfer of maternal blood to the intervillous space is established at the end of the first trimester of pregnancy.[3]

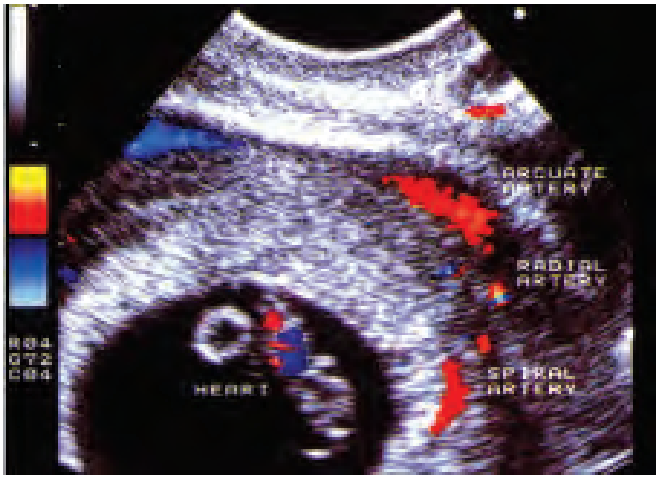

Figure 6.3: Image recorded by 2D color Doppler sonography showing blood flow in part of uteroplacental circulation (arcuate, radial and spiral arteries). The terminal segments of spiral arteries will be remodelated by trophoblast cell invasion

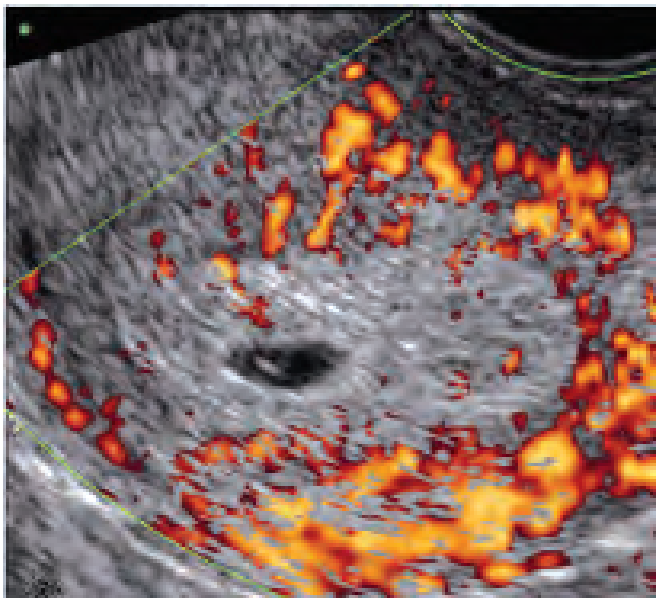

Figure 6.4: Image recorded by 2D power Doppler sonography showing increased blood flow that surrounds the gestational sac as a direct consequence of the spiral arteries dilation

ABNORMAL PLACENTAL DEVELOPMENT AND ULTRASOUND

Trophoblast invasion is a key process during human placentation. Failure of trophoblast invasion and spiral artery transformation leads to reduced perfusion of the placenta and fetus, and inadequate fetal nutrition and oxygenation. This condition is called uteroplacental insufficiency because the metabolic demands of the fetus and placenta exceed the uteroplacental transport capacity. It is considered that there are two phases of trophoblast invasion. The first wave of trophoblastic invasion converts the decidual segments of the spiral arteries between 6–10 weeks of the pregnancy. The second wave converts the myometrial segments between 14–16 weeks of the pregnancy.[2] As a result of these physiological changes, the diameter of the spiral arteries increase from 15–20 mm to 300–500 mm, reducing impedance to flow and optimizing feto-maternal exchange in the intervillous space.[4] In pregnancies complicated by preeclampsia and IUGR, trophoblast invasion is limited to the decidualized endometrium, which results in failure of the spiral arteries to become low-resistance vessels.[5] Using Doppler ultrasound, uteroplacental and fetal vessels conversion of the uterine spiral arteries and placental development may be assessed.

Successful trophoblast invasion results in loss of early diastolic notching in the uterine artery Doppler waveform by the end of the first trimester.[6,7] The failure to undergo physiological trophoblastic vascular changes is reflected by the high impedance to the blood flow at the level of the uterine arteries and with the characteristic waveform of early diastolic notching **(Fig. 6.5)**. In normal pregnancies, due to progressive maturation of the placenta, impedance to flow in the umbilical artery decreases and end-diastolic velocity establishes by the end of the first trimester. Doppler indices continue to fall towards term as umbilical blood flow resistance decreases[6-8] **(Fig. 6.6)**. In cases of placental

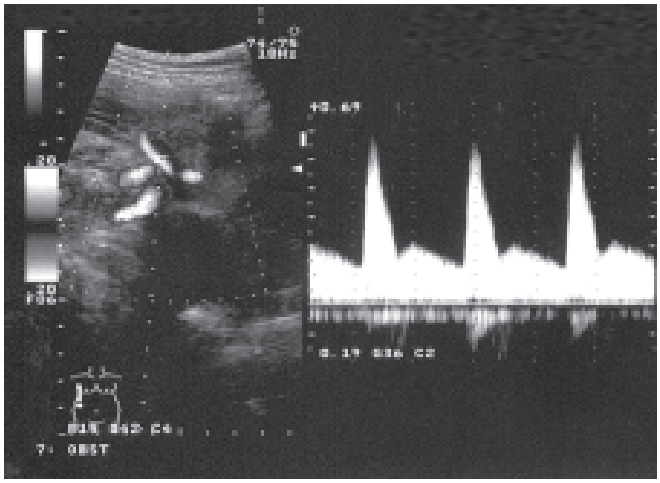

Figure 6.5: Image recorded in the 30th week of gestation showing increased impedance to flow in the uterine artery with early diastolic notching

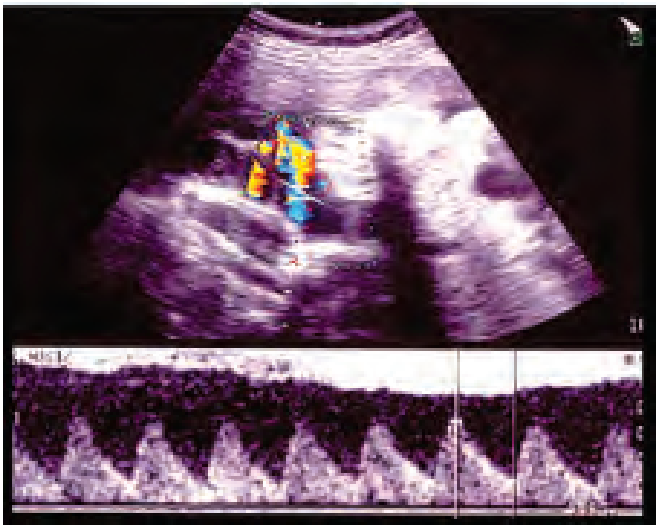

Figure 6.6: Normal Doppler waveforms from the umbilical artery

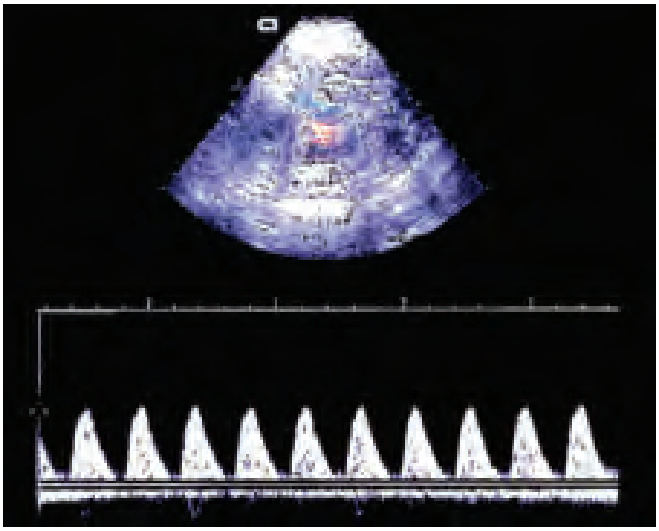

Figure 6.7: Increased impedance to flow in the umbilical artery with an absent end-diastolic flow

insufficiency, because of inadequate ramification of villi and increased degradation due to degenerative processes, surface of the capillary network is reduced and blood flow resistance in the placenta is elevated. These conditions reflect in the abnormal umbilical artery blood velocity waveforms. However, pathological studies have demonstrated that increased impedance in the umbilical arteries becomes evident only when at least 60% of the placental vascular bed is obliterated.[9] In pregnancies with reversed or absent end-diastolic flow in the umbilical artery, compared to those with normal flow, mean placental weight is reduced and the cross-sectional diameter of terminal villi is shorter.[10] Absent diastolic velocity or retrograde diastolic velocity in the umbilical artery indicate extremely increased placental vascular impedance **(Fig. 6.7)**.

Endangered by placental insufficiency, fetus activates compensatory mechanisms. Fetal response to placental dysfunction evolves from early compensatory reactions to late decompensation in multiple organ systems.[11] Fetal hypoxia activates a range of biophysical, cardiovascular, endocrine and metabolic responses. Fetal cardiovascular responses to hypoxia, which include modification of the heart rate, an increase in arterial blood pressure and redistribution of the cardiac output towards vital organs, are probably the most important adaptive reactions responsible for maintaining fetal homeostasis.[12] The redistribution of blood flow towards the fetal brain is known as the 'brain-sparing effect' **(Figs 6.8 and 6.9)**. Doppler assessment of the fetal cerebral and umbilicoplacental circulations can detect fetal blood flow redistribution towards the

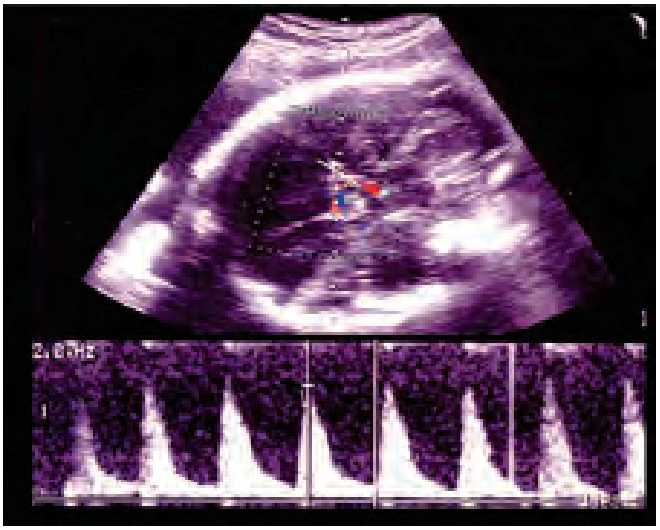

Figure 6.8: Normal flow of the middle cerebral artery in the third trimester

brain during hypoxia and quantify the degree of this redistribution using the C/U ratio.[12-14] In normal pregnancies, cerebral vascular resistance remains higher than placental vascular resistance. Therefore, the cerebroumbilical (C/U) ratio, expressed as the cerebral resistance index/the umbilical remains resistance index, remains higher than 1. This ratio becomes less than 1 in case of blood flow redistribution in favor of the fetal brain.[13] Previous experimental studies on animal models have shown that the C/U ratio decreases in proportion to fetal pO_2 [12,15]

Although the brain-sparing effect attempts to compensate for the reduced oxygen delivery to the fetal

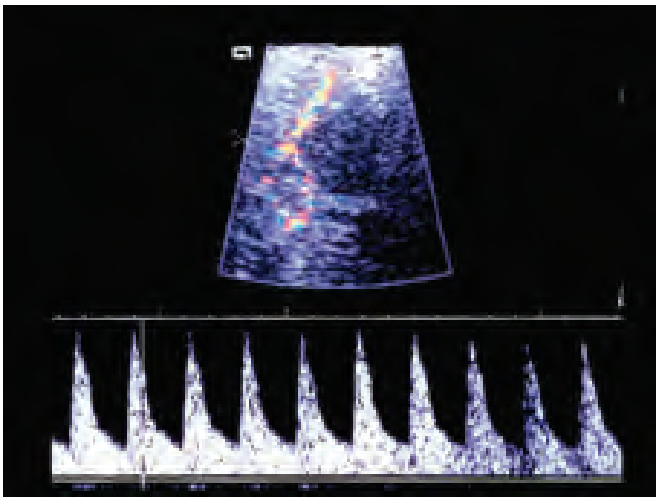

Figure 6.9: Decreased impedance to flow in the middle cerebral artery ('brain-sparing effect')

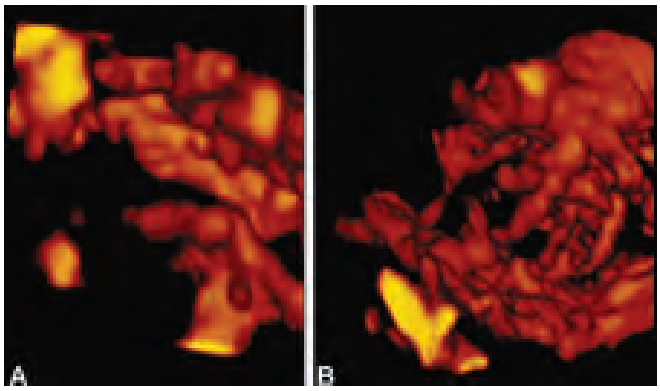

Figures 6.10A and B: 3D power Doppler angiography of the placental vascular tree at the (A) 16th week of pregnancy and at the (B) 36th week of pregnancy

brain, it has recently become clear that this phenomenon cannot always prevent the development of brain lesions.[15-17] Our studies have demonstrated the existence of several phases in the hemodynamic response of the fetal brain to chronic hypoxia. During the early phase of Doppler surveillance, cerebrovascular variability was still observed; this was followed by a loss of cerebrovascular variability and finally an increase in cerebrovascular resistance with a reduction in brain perfusion. Maximal redistribution of blood flow in favor of the fetal brain was reached 5–8 days prior to the onset of fetal heart rate abnormalities.[16,18]

FUNCTIONS OF THE PLACENTA

The placenta has multiple roles in fetal metabolism and growth. The major function of the placenta is to provide diffusion of nutrients and oxygen from the mother's blood into the fetus's blood and diffusion of excretory products from the fetus back into the mother.[19] The placenta also produces hormones that affect fetal growth. The placenta is usually fully formed and functional as a nutritive, respiratory, excretory and endocrine organ by the end of the third month of pregnancy. However, well before this time, oxygen and nutrients are diffusing from maternal to embryonic blood, and embryonic metabolic wastes are passing in the opposite direction.[20] Most of the early nutrition is due to trophoblastic digestion and absorption of nutrients from the endometrial deciduas. This is the only source of nutrients for the embryo during the first week after implantation. The embryo continues to obtain at least some of its nutrition in this way for another eight weeks, although the placenta also begins to provide nutrition after about the 16th day after fertilization (a little more than one week after implantation).[19] Molecules of low molecular weight such as blood gases, sodium, water, urea, fatty acids, nonconjugated steroids, pass through placental membrane by simple diffusional exchange between the circulations. Hexose sugars, conjugated steroids, amino acids, nucleotides, water-soluble vitamins, plasma proteins, cholesterol will not gain access to the fetal circulation unless either special transport mechanisms exist or the integrity of the barrier is breached.[21] In the early months of pregnancy, the placental membrane is still thick because the placenta is not fully developed. Therefore, its permeability is low. Further, the surface area is small because significant placental growth has not occurred yet. In later pregnancy, the permeability increases due to the thinning of the membrane diffusion layers and the multiple expansion of the surface area, giving way to a tremendous increase in placental diffusion **(Figs 6.10A and B)**.[19] In addition to the placental thickness, the factors that will influence exchange between the mother and the fetus include the maternal and the fetal blood flow; the fetal and the maternal concentrations of the substances to be transported; and the types of transport mechanisms available. The exchange of more freely diffusible molecules such as O_2 is to a larger extent dependent on the blood flow than placental thickness.[21]

Fetal Growth and Metabolism

As soon as within the 1st month following the fertilization of the ovum, all the organs of the fetus have already begun to develop and in the next 2–3 months, the fine anatomic structures of the organs will be formed. After the 4th month, the organs of the fetus,

including the majority of their substructures, are for the most part the same as those of the neonate. However, the development of the cells in the structures is still far from complete and will require the remaining five months of pregnancy to complete development.[19]

Normal fetal growth requires macronutrients—carbohydrates, lipids, proteins and micronutrients—vitamins and minerals. Also, other factors influence growth, like growth factors and hormones. The main ingredient of the fetal diet is carbohydrate. The fetus has a low capacity for gluconeogenesis, largely because the necessary enzymes, although present, are inactive due to a low fetal arterial pO_2. The fetus must therefore obtain its glucose from the maternal blood.[21] The growing fetus requires approximately 87 kcal/kg/per day.[22] About half of the calories needed for fetal growth and metabolism come from the mother's glucose, and the other half from her amino acids and placental lactate.[21] The fetus has a high ability of storing proteins and fats.[19] Protein accumulation occurs early in fetal development, to reach its maximum by week 35. Protein deposition precedes fat deposition.[21] Fetal fat content is low at 26 weeks. Fat acquisition starts sometime between the 26–32 weeks and continues intensively thereafter, being a result of glucose utilization rather than placental fatty acid uptake.[22] By term, about three times as much energy is stored as fats than as proteins. In addition, glucose is also stored as glycogen in the fetal liver. Glycogen is an important nutrient in the period immediately after birth, before nutrients from breast milk are used.[21]

Fetal metabolism shows some particularity in relation to calcium, phosphate, iron, and some vitamins. About 22.5 grams of calcium and 13.5 grams of phosphorus are accumulated in an average fetus during gestation. About one-half of these accumulate during the last four weeks of gestation, which is coincident with the period of rapid ossification of the fetal bones and with the period of rapid weight gain of the fetus. Iron accumulates in the fetus even more rapidly than calcium and phosphate. Most of the iron is in the form of hemoglobin, which begins to be formed as early as in the third week after fertilization of the ovum. Small amounts of iron are concentrated in the mother's uterine progestational endometrium even before implantation of the ovum. This iron is used to form the early red blood cells. About one-third of the iron in a fully developed fetus is normally stored in the liver. Interestingly, the fetus needs an equal intake of vitamins as the adult. The B vitamins, especially vitamin B_{12} and folic acid, are necessary for formation of red blood cells and the nervous tissue, as well as for the overall growth of the fetus. Vitamin C is necessary for appropriate formation of intercellular substances, especially the bone matrix and fibers of connective tissue. Vitamin D is needed for normal bone growth in the fetus. The mother needs it for adequate absorption of calcium from her gastrointestinal tract. If the mother has plenty of this vitamin in her body fluids, large quantities of the vitamin will be stored by the fetal liver to be used by the neonate for several months after birth. Vitamin E, although the mechanisms of its functions are not clear, is necessary for normal development of the early embryo. In its absence in laboratory animals, spontaneous abortion usually occurs at an early stage of pregnancy. Vitamin K is used by the fetal liver for formation of blood coagulation factors. Prenatal storage in the fetal liver of vitamin K derived from the mother is helpful in preventing fetal hemorrhage, particularly hemorrhage in the brain when the head is traumatized by squeezing through the birth canal.[19]

The fetus actively participates in endocrine regulation of its metabolism and growth by synthesis and secretion of hormones. For instance, the rate at which glucose is utilized by growing fetal tissues is probably determined largely by the actions of fetal insulin. The storage of glucose as fat is also regulated primarily by fetal insulin. Fetal adrenocorticotropic hormone (ACTH) and glucocorticoids stimulate the storage of glucose as glycogen.[21] Hormonal regulation of fetal growth differs from hormonal regulation of growth during postnatal life. Furthermore, fetal growth hormone (GH) has a small role in stimulating fetal growth. Although pituitary begins to produce and secrete GH during the 5th week of gestation, fetal GH does not significantly affect fetal growth, possibly due to the lack of functional GH receptors on fetal tissues.[23] Data have shown that pituitary aplasia and congenital hypopituitarism do not cause severe IUGR.[24,25] On the contrary, fetal insulin significantly stimulates fetal growth. It is a known fact that pancreatic agenesis is associated with severe growth restriction[26] and that fetal hyperinsulinemia leads to fetal mass overgrowth. It is believed that insulin-like growth factors (IGFs or somatomedins) produced by a large range of fetal cell types and particularly by the fetal liver, provide a major endocrine stimulus to fetal growth.[21] They have the potent effect of increasing all aspects of bone growth in postnatal life.[19] IGFs are present in human fetal tissue extracts after 12 weeks gestation.[22] IGF-1 has the most important role in stimulation of fetal growth.[21] Its levels in fetal and cord circulation directly correlate with the fetal length and mass.[27] Reduced plasma concentration of IGF-1 has been reported in intrauterine growth

restriction (IUGR).[28] Furthermore, maternal starvation leads to a rapid decrease in fetal plasma IGF-1 concentration, which is generally associated with the cessation of intrauterine growth.[29] It is considered that glucose is the major regulator of fetal IGF-1 secretion.[30] Maternal IGF-1, IGF-2 and insulin do not cross the placenta, and do not have a direct effect on fetal growth, but may have an effect on placental function, thus altering the nutrient exchange between the placenta and the fetus.[31] It has been found that maternal plasma IGF-1 concentration correlates with fetal growth.[32] Production of fetal IGFs is stimulated by prolactin, insulin and human chorionic somatomammotropin (HCS).[33] In the fetus, HCS acts via lactogenic receptors to stimulate growth, regulate intermediary metabolism and stimulate the production of IGFs, insulin, adrenocorticotropic hormones and pulmonary surfactant.[23] Fetal thyroid hormones also stimulate growth, especially in the later stage of pregnancy, but their most significant role is the one they have in the central nervous system development.[21]

Additional factors that affect birth weight include parity (primiparous mothers have smaller babies than multiparous mothers), maternal size, multiple pregnancy.[21] Maternal nutrition is also of great significance for fetal growth and the adverse effects of severe malnutrition on fetal well-being and neonatal survival have been long known. Recent data have confirmed a great impact of maternal diet during pregnancy on fetal growth and development, as well as on postnatal development and health.[34-43] It is during intrauterine life that the diet has significant effect on the brain development. It has been known for some time that folic acid plays a protective role in neurodevelopmental processes. Periconceptional use of folic acid has been proven to significantly reduce the risk of neural tube birth defects.[34] Such birth defects can cause death or permanent physical disability. Periconceptional use of folic acid decreases the occurrence of anencephaly and spina bifida by at least 50%.[35] Hence, some countries (USA, Canada) have decided to fortify food with folic acid. A recent study on the prevalence of congenital abnormalities following folic acid fortification of grain in the United States found a modest, yet statistically significant decrease in prevalence of transposition of the great arteries, cleft palate, pyloric stenosis and omphalocele.[35] Yet, other studies provide no evidence of folate being an important factor in the prevention of birth defects other than neural tube defects.[36] Furthermore, a significant protective effect was seen with large doses of folic acid (approximately 6 mg/d) and iron (150-300 mg/d of ferrous sulfate) during the first gestational month against Down's syndrome.[37]

Numerous findings have shown a favorable impact of essential fatty acids on prenatal development.[38-40,42,43] Omega-3 and omega-6 fatty acids are necessary for human growth and development. Since their endogenous synthesis is impossible, they need to be taken into the body through diet. The arachidonic (AA) and docosahexanoic acids (DHA) are the key components of all membranes and are incorporated into the structural lipids of the developing brain. Fetal demand for essential fatty acids is at its peak during the third trimester of pregnancy.[21] A recent study has demonstrated that DHA supplemented during pregnancy plays a role in the maturation of the visual system and benefits infant visual acuity at four but not six months of age.[38] Also, results of a recent study indicate that DHA consumption in pregnancy significantly affects problem solving abilities at the age of nine months, but does not affect memory processes.[39] Additionally, children's mental processing scores at 4 years of age correlated significantly with maternal intake of DHA during pregnancy.[40] Seafood (especially sardine and tuna) is a rich source of omega-3 fatty acids. Essential fatty acids can be also found in linseed oil, walnut oil and soy. In the USA, women are advised to limit their seafood intake during pregnancy to 340 g per week. According to a recent study published in an esteemed journal, maternal seafood consumption should be more than 340 g per week. A lower seafood intake during pregnancy was in the study associated with an increased risk of suboptimum developmental outcome.[41] Further, the findings suggest a protective effect of fish intake during pregnancy against the risk of atopy and asthma.[42] Consumption of apples during pregnancy may also have a protective effect against the development of childhood asthma and allergic diseases.[43]

Healthy and varied diet during pregnancy is required for normal fetal growth and development. Most pregnant women need 2200–2900 kcal a day.[44] If appropriate nutritional elements are not present in a pregnant woman's diet, a number of maternal deficiencies can occur, especially in calcium, phosphates, iron and vitamins.[19]

Fetal Cardiovascular System

The cardiovascular system is the first embryonic system to start functioning. The need for substrates which facilitate fast growth and development of the embryo requires an early development of the mechanism that supplies the cells with nutrients and removes the metabolic products from them. Cardiovascular development begins when the process of diffusion becomes inadequate to supply the fetus with nutrients and oxygen. Blood circulation can be observed in the "body"

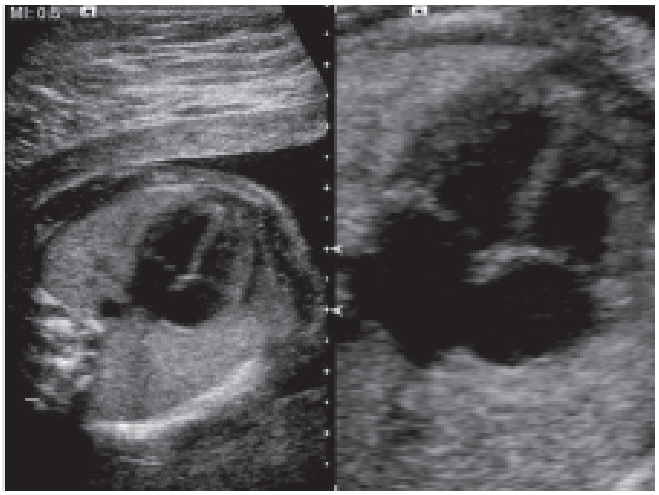

Figure 6.11: Four chamber view of the fetal heart

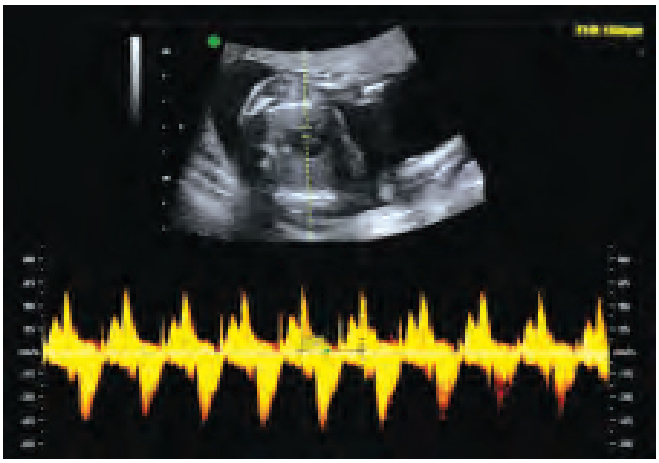

Figure 6.12: Fetal cardiac activity with a heart rate of 150 bpm

of the embryo as early as at the end of the third week of the intrauterine life.[45]

Between the 27–35th day of intrauterine life, during which the embryo grows from 5 mm in length to about 16–17 mm, cardiac septum and endocardial cushions begin to form. The endocardial cushions will give rise to mitral and tricuspid valves. By the end of 7th week, they are short and thick, but over the next few weeks they are becoming longer and thinner, and achieve their final shape. Impairments in cardiac septum development lead to the existence of pathological communication between the heart chambers **(Fig. 6.11)**, which can be more or less life-threatening condition for newborn child. Some of these anomalies, such as ventricular septal defect, are among common congenital anomalies and can occur independently or as a part of different syndromes.[46,47] Fetal echocardiography is a powerful tool and many cardiac malformations can be successfully diagnosed before birth.

The human heart starts beating between the 21–23rd day after fertilization, at a heart rate of 65 beats/min.[48] In that period, the heart is a tube-like structure with a single lumen. Between the 5–9th week of gestation the heart rate accelerates from 80 beats/min to 165 beats/min.[49,50] It has been shown that a continuous decrease in the heart rate during this period is associated with miscarriages occurring in the first trimester.[50] By the 10th week after fertilization, the heart rate has reached its highest value (approximately 170/min), it starts decreasing **(Fig. 6.12)**. Before birth, the human heart contracts at a rate of about 140 beats/min.

The fetal circulatory system operates much differently than the circulatory system of the newborn baby, which is not surprising considering the specific features of fetal environment. After the birth, the individual components of the circulatory system are in serial connection. However, the fetal circulatory system is organized in parallel circle.[51] Further, fetal values of cardiac output and blood pressure are significantly different from values in adults.

During intrauterine life, blood returning from the placenta through the umbilical vein passes through the ductus venosus, mainly bypassing the liver. Then most of the blood entering the right atrium from the inferior vena cava is directed in a straight pathway across the posterior aspect of the right atrium and through the foramen ovale directly into the left atrium. Thus, the well-oxygenated blood from the placenta enters mainly the left side of the heart, rather than the right side and is pumped by the left ventricle mainly into the arteries of the head and forelimbs. The blood entering the right atrium from the superior vena cava is directed downward through the tricuspid valve into the right ventricle. This blood is mainly deoxygenated blood from the head region of the fetus and it is pumped by the right ventricle into the pulmonary artery. Since the pressure in the pulmonary artery is about 0.7 kPa higher than the pressure in the aorta, almost all the blood from the pulmonary artery goes through the arterial duct (ductus Botallijev) into the descending aorta, then through the two umbilical arteries into the placenta, where the deoxygenated blood becomes oxygenated. Only a small portion of blood from the descending aorta portion goes to the visceral organs and lower extremities.[19]

Blood carrying the highest oxygen saturation goes to the fetal heart, the brain, the upper extremities while the other parts of fetal body receive blood with lower

oxygen saturation. Also, fetal blood pO_2 is much lower than maternal blood pO_2. At term pO_2 of fetal blood after the oxygenation in the placenta amounts 30 mm Hg.[2] Such low pO_2 levels can be observed in adults at altitudes between 6000–8000 meters, at which human life is barely possible. Therefore, fetal environment has long been considered «the Mount Everest *in utero*».[52] Despite the low pO_2 in the fetal blood, the fetus does not live in hypoxic environment. Due to adaptive mechanisms, the amount of oxygen delivered to the fetal tissue is similar to the amount of oxygen delivered to maternal tissue by maternal blood.[19] In addition, the hemoglobin concentration of fetal blood is about 50% greater than that of the mother. Furthermore, fetal hemoglobin can carry more oxygen at a low than it can at a high PCO_2. The fetal blood entering the placenta carries large amounts of carbon dioxide, but much of this carbon dioxide diffuses from the fetal blood into the maternal blood. Loss of the carbon dioxide makes the fetal blood more alkaline, whereas the increased carbon dioxide in the maternal blood makes it more acidic. These changes cause the capacity of fetal blood to combine with oxygen to increase and that of maternal blood to decrease. This forces more oxygen from the maternal blood, while enhancing oxygen uptake by the fetal blood. Thus, the Bohr shift operates in one direction in the maternal blood and in the other direction in the fetal blood. These two effects make the Bohr shift twice as important here as it is for oxygen exchange in the lungs; therefore, it is called the double Bohr effect. These mechanisms, as well as a large cardiac output, ensure adequate supply of oxygen of fetal tissues, despite its low partial pressure.[19]

Maintenance of normal cardiovascular function, blood pressure, heart rate and the flow distribution through the placenta and fetal tissue are influenced by the local vascular and reflex mechanisms. Further, the autonomic nervous system and hormones also have an effect on the fetal heart and circulation. The potential regulators can be identified by measuring their concentration and dynamics of secretion in states in which a redistribution of the blood flow occurs, such as fetal hypoxia. The first line of supervision over the circulation of the fetus are the carotid chemoreceptors, but not the aortic chemoreceptors. They mediate the fetal cardiovascular response (redistribution of circulation in favor of vital organs like the heart, brain and adrenal glands to acute hypoxemia).[53] Slower regulators, the second line of control, are hormones antidiuretic hormone (ADH), angiotensin II, catecholamines and cortisol.[54-56] ADH and angiotensin II are released independently of the carotid chemoreceptors, whereas the secretion of cortisol and catecholamines is partially under the control of these neural mechanisms. After carotid sinus denervation or splanhic blockade, rapid secretion of cortisol in response to hypoxia or a sudden drop in blood pressure, is decreased. While the secretion of ACTH does not change and occurs about 15 minutes after stimulation.[57,58] Thus, the rapid rise in cortisol secretion is the result of neural mechanisms and not as a result of ACTH stimulation. However, the role and purpose of such regulation is unclear. Medullary, hypothalamic and cerebral cortical activity also affect fetal cardiovascular function.[59] Furthermore, in control of fetal circulation autocrine and paracrine mechanisms play important role. Some of the possible regulators of the peripheral resistance, at least in the sheep fetuses, are endothelin-1 and nitrogen-(II)-oxide (NO).[60,61] They allow an increase of cerebral flow in fetal hypoxia. Several other factors such as sleeping of the fetus or uterine contractions, can also have a temporary influence on the cardiovascular system.[62]

One of the most important events after the delivery is the adjustment of the circulation of new conditions. The transitional period of circulation, which lasts 4–12 hours after birth, is characterized by a large increase of the blood flow through the lungs and by the establishment of the pulmonary circulation. The primary change in the circulation at birth is loss of the tremendous blood flow through the placenta, which approximately doubles the systemic vascular resistance at birth. This increases the aortic pressure as well as the pressures in the left ventricle and left atrium. Furthermore, in the unexpanded fetal lungs, the blood vessels are compressed because of the small volume of the lungs. After birth, the pulmonary vascular resistance greatly decreases as a result of expansion of the lungs. Also, in fetal life, the hypoxia of the lungs causes considerable tonic vasoconstriction of the lung blood vessels but when aeration of the lungs eliminates the hypoxia, the capillary endothelial cells produce vasoactive substances such as NO and prostaglandin I2, which have a strong vasodilatory effect and vasodilation takes place.[19] All these changes together reduce the resistance to blood flow through the lungs as much as fivefold, which reduces the pulmonary arterial pressure, right ventricular pressure and right atrial pressure. Changes in pulmonary and systemic resistances at birth cause blood now to attempt to flow from the left atrium into the right atrium, through the foramen ovale. Consequently, the small valve that lies over the foramen ovale on the left side of the atrial septum closes over this opening, thereby preventing further flow through the foramen ovale. Arterial ductus begins to close

around four hours after birth and is usually completely closed after 24 hours. Its closing marks the end of the transitional period of the newborn circulation. After birth, blood begins to flow backward from the aorta into the pulmonary artery through the ductus arteriosus, rather than in the other direction as in fetal life. However, after only a few hours, the muscle wall of the ductus arteriosus constricts markedly. This is called functional closure of the ductus arteriosus. Then, during the next 1–4 months, the ductus arteriosus ordinarily becomes anatomically occluded by growth of fibrous tissue into its lumen. The cause of ductus arteriosus closure relates to the increased oxygenation of the blood flowing through the ductus. In fetal life, the PO_2 of the ductus blood is only 15–20 mm Hg, but it increases to about 100 mm Hg within a few hours after birth. Furthermore, many experiments have shown that the degree of contraction of the smooth muscle in the ductus wall is highly related to this availability of oxygen.[19] The reason for the closure of the venous duct is still unknown. Immediately after birth, blood flow through the umbilical vein ceases, but most of the portal blood still flows through the ductus venosus, with only a small amount passing through the channels of the liver. However, within 1–3 hours the muscle wall of the ductus venosus contracts strongly and closes this avenue of flow. As a consequence, the portal venous pressure rises from near 0 to 6 to 10 mm Hg, which is enough to force portal venous blood flow through the liver sinuses. Although the ductus venosus rarely fails to close, we know almost nothing about what causes the closure. Knowing the characteristics of this transitional phase of circulation is very important because the postnatal increase of the resistance in the pulmonary capillaries, for example caused by hypoxia or respiratory distress syndrome, if exceeds the value of systemic resistance, can restore conditions as they existed in the fetal life, greater resistance in the pulmonary circulation than in systemic and pulmonary-aortic or right-left flow of blood through the arterial duct.[19]

Fetal Gastrointestinal System, Development of Appetite and Satiety Mechanisms

The primitive gut forms during the fourth week of the embryonic development. The primitive gut is divided into three parts: the foregut, midgut and hindgut. The derivatives of the foregut are the pharynx and its derivatives, the lower respiratory tract, the esophagus, the stomach, the duodenum, proximal to the common bile duct, and the liver, biliary tract, gallbladder, and pancreas. The derivatives of the midgut are the small intestines [except for the duodenum from the stomach **(Fig. 6.13)** to the entry of the common bile duct], cecum and appendix, ascending colon, and proximal one-half to two-thirds of the transverse colon. The derivatives of the hindgut are the distal one-third to one-half of the transverse colon, descending colon, sigmoid colon, rectum and upper portion of the anal canal, and part of the urogenital system.[63] Activity of the gastrointestinal system begins during an early stage of pregnancy. By 10 weeks, peristalsis begins in the large intestine[64] and by 11 weeks in the small intestine.[65] Also, fetal swallowing activity was observed from the 11th week of gestation.[66]

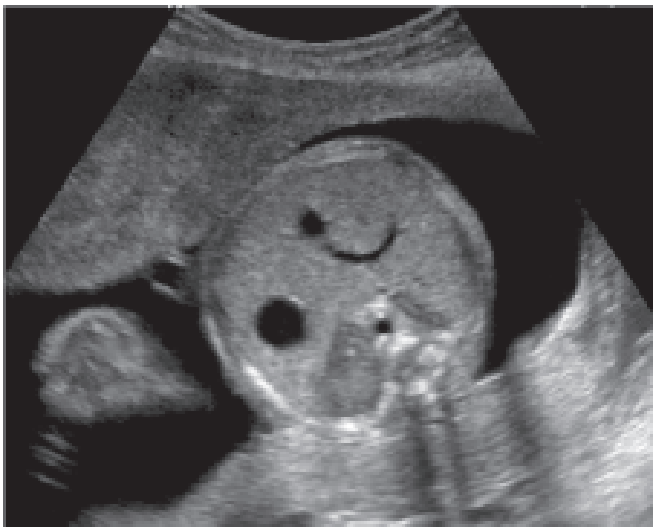

Figure 6.13: Transverse scan of the fetal abdomen showing the stomach, liver, and intrahepatic part of the umbilical vein

Swallowing amniotic fluid reflects fetal CNS maturation and has numerous, although not entirely understood roles **(Fig. 6.14)**. Fetal swallowing activity contributes to somatic growth, development and maturation of the fetal gastrointestinal tract. It has been estimated that swallowing of amniotic fluid proteins provides 10–15% of nitrogen requirements in the normal fetus. Upper gastrointestinal tract obstructions in human fetuses are associated with significantly greater occurrence of fetal growth restriction as compared with lower gastrointestinal obstructions. Studies have demonstrated that impairment of fetal swallowing in rabbits near term induces weight decrease. Esophageal ligation of ovine fetuses during midgestation induces a 30% decrease of small intestine villus height and a reduction in the liver, pancreas and intestinal weight.[67] Fetal swallowing is an important, yet not the only mechanism of amniotic fluid volume regulation. Altered

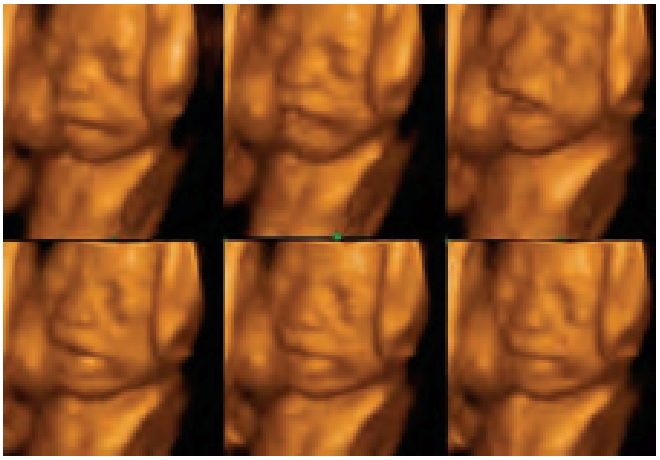

Figure 6.14: A sequence of images of the fetus recorded by 4D sonography showing swallowing movements

fetal swallowing has been associated with both a decrease and an increase in the amniotic fluid volume.[68] These conditions are associated with a higher risk of perinatal morbidity and mortality. Furthermore, in some fetuses with esophageal atresia, the volume of amniotic fluid is increased. It is important to note that this is the case in some, but not all fetuses with esophageal atresia. Namely, this anomaly is often accompanied by tracheo-esophageal fistula, a shortcut to the gastrointestinal tract. Therefore, intake of liquid during the respiratory movements might explain the nonappearance of polyhydramnios in some of these cases.[67] Polyhydramnios sometimes, although not always, develops in anencephalic fetuses. Some of these fetuses have an intact swallowing reflex. Cases of a normal amniotic fluid volume and reduced fetal swallowing have also been described. Assessment of fetal swallowing using gray-scale and color Doppler sonography has demonstrated that there is a fetal trend towards the development of more coordinated swallow-related movements and more functional nose-mouth flow with the advancement of gestational age. These investigators have postulated that knowledge of the physiologic mechanism involving swallowing development could contribute to identification of altered swallow-related movements in fetuses with malformations of the gastrointestinal tract or with neurological disorders.[69] Our recent investigation, performed by 4D ultrasound, has shown that swallowing pattern displays a peak frequency at the end of the second trimester. At the beginning of the third trimester, a decreasing incidence of this pattern was recorded.[70] Some studies have shown that fetal swallowing activity may be modulated in accordance with neurobehavioral state alterations (stimulation of swallowing with shifts from quiet to active sleep). Furthermore, fetal swallowing is influenced by the volume of amniotic fluid, hypoxia, hypotension and plasma osmolality changes.[67] Experiments in fetal lambs have indicated that dipsogenic mechanisms begin to regulate swallowing during intrauterine life. Swallowing and arginine–vasopressin (AVP) secretion increase, following the central administration of hypertonic saline solution and angiotensin II.[71,72] However, the fetus seems to have an extensively reduced sensitivity to osmotic stimuli when compared to the adult[73-75], despite the intact dipsogenic nuclei. The fetus swallows about six times more liquid in comparison to the adult. Mechanisms underlying the high rate of human fetal swallowing are regulated, in part, by tonic activity of central angiotensin II, glutamate N-methyl-D-aspartate receptors and neuronal production of the nitric oxide.[68] A reduced NMDA receptor expression within the forebrain dipsogenic neurons contributes to observed differences in drinking activities between the fetus/neonate and the adult.[76] Reduced swallowing activity during the systemic hypotension, despite elevated renin levels in plasma, provides further evidence that the fetal dipsogenic response is markedly different from that of the adult.[77] It is possible that dipsogenic responses develop *in utero* in the human fetus to provide thirst stimulation for appropriate water intake during the immediate neonatal period.[67] According to some studies, altered intrauterine osmotic environment may modulate not only fetal swallowing activity, but also the development of adult sensitivities for thirst, AVP secretion and AVP responsiveness.[67,68,78] An animal study demonstrated that extracellular dehydration during pregnancy (commonly observed during pregnancy after vomiting or diarrhea) can enhance the natriophilic propensity in offspring and suggested that vomiting during pregnancy may contribute to the epidemiological factors of hypertension.[78] Furthermore, mothers consuming excessive amounts of salt and water during pregnancy increase salt preference in adult offspring.[79] Similar to dipsogenic mechanisms, peripheral and central fetal orexic mechanism also develop during intrauterine life. Prenatal ingestive behavior is manifested as swallowing and intake of amniotic fluid. By swallowing amniotic fluid, the fetus explores a wide variety of tastes even before birth. By the 7th week of gestation, taste buds develop in human embryos.[80] Fetal taste bud cells are spread over a wider surface than in the neonate or the adult.[81] It has been shown that sweet taste, such as that of a low-concentration sucrose solution, stimulates swallowing in the human fetus, whereas the incidence of swallowing

movements decreases following the injection of Lipiodol—a bitter extract of poppy seeds used as a contrast—into the amniotic fluid.[81] Sweet taste is already *in utero* the favorite taste. It has been found that although oral sucrose significantly stimulates near term ovine fetal ingestive behavior, sweet taste adaptation or habituation does not occur, in contrast to that observed in adult animals and humans. Absence of taste adaptation in the fetus/newborn may facilitate increased neonatal food intake and accelerated growth.[82] Increased or decreased glucose level in the serum does not affect the swallowing activity.[81] The main feeding regulatory factors, neuropeptide Y (NPY) and leptin, are secreted in the human fetuses as early as at 16–18 weeks, respectively.[83-85] NPY is the most potent known inducer of food intake and leptin is a satiety factor. In some animal experiments, increased fetal swallowing has been demonstrated upon central NPY administration.[86] The role of leptin in regulating ingestive behavior is interesting because, as opposed to its function in adults, leptin does not suppress fetal ingestive behavior.[68] Fetal swallowing was significantly increased following the injection of leptin.[87] Therefore, some investigators have postulated that the absence of leptin-inhibitory response potentiates feeding and facilitates weight gain in newborns, despite high body fat levels.[88] Some findings suggest a possible role of leptin in the development of the fetal gastrointestinal tract.[89] Apart from determined high leptin concentration in amniotic fluid and in the gastrointestinal mucosa at the time when the fetus starts swallowing an early presence of Ob-Rb (functional receptor of leptin) has been found in mucosa. This suggests a possible role for leptin, exerted endoluminally and in a paracrine pathway, in the developmental process (growth and/or maturation) of the human digestive tract.[89] According to some other studies, the potential *in utero* imprinting of appetite and satiety mechanisms may affect infant, childhood and ultimately adult appetite "set-points". An adverse intrauterine environment, with altered fetal orexic factors, could change the normal set-points of appetitive behavior and potentially lead to programming of adulthood hyperphagia and obesity.[68,88] In a recent paper, prenatal exposure to over or undernutrition, rapid growth in early infancy, an early adiposity rebound in childhood and early pubertal development have all been implicated in the development of obesity.[90] Further investigations are needed to delineate precisely the relationship between the intrauterine environment and the development of the set-points of adult appetite and thirst.

It is important to note that the function of the fetal digestive system also begins at an early stage of pregnancy. Water, electrolytes and other small molecules, such as glucose are absorbed through the small bowel.[21] By 13 weeks, the intestine starts to absorb glucose and water swallowed by the fetus.[65] Salivary amylase activity was found in the amniotic fluid in the late first trimester pregnancies. Enzyme activity breaking down peptone is present in the small intestine of 7–10 week old fetuses and rises slightly after the 14th week of gestation. Lipase was found in the stomachs of fetuses in the 4th month of gestation, its activity increased with subsequent development. In addition, the pH of the gastric fluid in newborns is usually neutral or slightly acidic and the acidity increases shortly after birth, within several hours. The first traces of gastric acidity appear in four month old fetuses.[91] Generally, during the last 2–3 months, fetal gastrointestinal function approaches that of the normal neonate. However, if the infant is more than two months premature, the digestive and absorptive systems are almost always inadequate. The absorption of fat is so poor that the premature infant must have low-fat diet.[19] Insufficient fat absorption can cause problem to newborns that were fed milk that contains more fat than breast milk, such as undiluted cow milk.[81]

Fetal Respiratory System

Fetal lungs begin to develop in the 4th week after fertilization. At this time, the respiratory diverticulum (lung bud) appears ventrally to the caudal portion of the foregut. Angiogenesis in the lungs begins at the 5th week after fertilization. From the 16–26th week of pregnancy, formation of early respiratory units occurs and pneumocytes types II appear. From 26th week until birth, thinning of the respiratory membrane takes place, primitive alveoli dilate and establish close relationship with the capillaries. From 36th week onwards, secondary alveolar septa, with rich capillary network, develop. Hence, respiratory surface enlarges. Further thinning of the respiratory membrane happens.[46] Mature neonate has 50% lower number of alveoli than an adult. Final number of alveoli is reached at 2nd year of postnatal life.[92] Normal fetal lung development requires the presence of lung liquid as well as fetal movements, like breathing. In the regulation of the lung liquid volume fetal breathing-like movements have a very important role. Other functions of breathing-like movements **(Fig. 6.15)** during intrauterine life are the development of respiratory muscles, widening of the alveolar spaces, maintenance of the lung liquid volume and lung organogenesis.[93-95] Animal investigation has shown that absence of respiratory movements (due to destruction of the brainstem nuclei above the phrenic

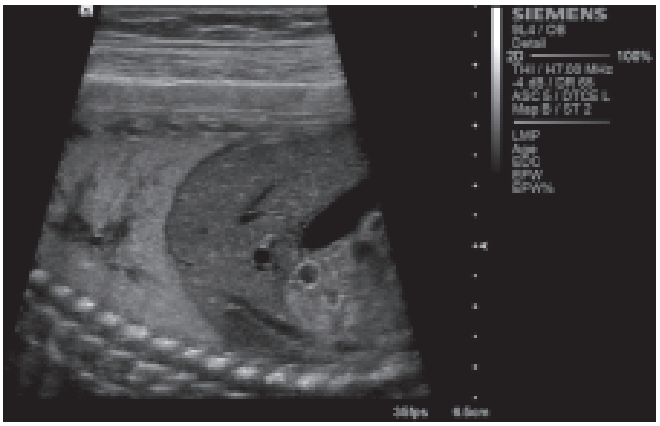

Figure 6.15: Image of the fetus recorded by 2D sonography showing fetal lung and liver

nucleus) leads to hypoplasia of the lungs.[96] Breathing-like movements appear at the 10th week.[97] Early in gestation, fetal breathing activity is variable and isolated event but the frequency and complexity of the breathing patterns change over the following weeks and months. Changes in breathing-like patterns are consequences of the maturation of the fetal lungs as well as the respiratory and sleep centers in the CNS. During the 38–39th week of gestation, the frequency of movements decrease to 41 respirations per minute and the movements become as regular as in the postnatal period.[98] A number of internal and external factors can influence fetal breathing-like movements during the second half of pregnancy. At 24–28 weeks, the fetal respiratory rate can rise as high as 44 inhale/exhale cycles per minute.[99] This rate changes according to maternal carbondioxide (CO_2) levels, strongly suggesting that respiratory center in the brainstem of the fetus already detects and responds to changes in CO_2 levels in the blood. This respiratory response to CO_2 is similar to that seen in newborns and adults.[100] Furthermore, an increased number of fetal respiratory movements following the elevation of the glucose concentration in the maternal blood have been observed at the 34th week of gestation.[101,102] Recent investigation has shown that intermittent maternal fasting is connected with a considerable alteration in the frequency and pattern of fetal breathing-like movements from the 30th week of gestation onwards.[103] Following premature rupture of membranes,[104,105] during the three days prior to the initiation of labor, a decrease in fetal breathing-like has been recorded.[106,107] However, similar maturation patterns in breathing and spontaneous fetal body movements were demonstrated among low-and high-risk fetuses threatening to deliver prematurely, which suggests normal functional development in the high-risk fetal group.[108] Some studies have shown that maternal consumption of alcohol, methadone, as well as cigarette smoking decrease the incidence of breathing-like movements.[109-111] On the contrary, aminophylline, conjugated estrogens and beta-methasone are responsible for an increase in its frequency.[112,113]

One of the most important events in the lung development is production and secretion of surfactant. At the end of 6th month, alveolar cells pneumocytes type II appear and begin to secrete surfactant. These cells differ from pneumocytes type I by the presence of numerous surfactant containing granules, lamellar bodies. By adsorbing to the air-water interface of alveoli during the first breath, with the hydrophilic head-groups in the water and the hydrophobic tails facing towards the air, the main lipid component of surfactant, dipalmitoyl-phosphatidyl-choline, reduces surface tension. In this way, surfactant prevents the closure of the alveoli, with each expiration.[46] The composition of surfactant changes during fetal life. Mature surfactant, rich with dipalmitoyl-phosphatidyl-choline, is detectable after 35 weeks of gestation and indicates the functional maturity of fetal lungs. It is important to emphasize that the secretion of pulmonary surfactant in the lung liquid occurs only in the last weeks of fetal life.[114] Besides phospholipids, surfactant contains proteins. Four types of surfactant-associated proteins have been described, SP-A, SP-B, SP-C and SP-D. They differ in structure, as well as in the function. SP-A and SP-D are hydrophilic molecules, they stimulate the secretion and removal of phospholipids and participate in maintaining of the homeostasis of surfactant. SP-B and SP-C are hydrophobic molecules as they enable the spreading of the phospholipid bilayer along the alveoli and improve the stability of surfactant. However, most important role of all proteins is the defense as they are participating in innate immune defense of the lung. In addition, they bind and react with many micro-organisms, allergens and mitogens, and their receptors have been detected in alveolar macrophages.[115] Various hormones and inflammatory mediators affect the synthesis and secretion of surfactant. There are convincing data to support the use of antenatal corticosteroids in improving the respiratory outcome of newborn infants, especially those at greatest risk of developing respiratory failure. The current data suggest that this improvement may be due to enhanced expression of proteins and phospholipids of the surfactant system and enzymes of the antioxidant systems. Nevertheless, caution is needed, as the scanty data that are available

in animal models suggest that lung growth, especially the development of capillary network and secondary alveolar septa, as well as somatic growth may be adversely affected.[116] The existence of receptors for triiodothyronine, thyroid hormone in the fetal lung, as well as certain studies conducted in animal models, suggest that this hormone also participates in the development of the fetal lung. Data have shown that thyroid hormones promote morphogenesis of lung histotypic structures but have a negative effect on surfactant synthesis.[117,118] However, it seems that the role of prolactin, which increases in the serum of fetuses just before birth, is important for lung maturation.[119] It is known that children of mothers who are heroin abusers have lower incidence of neonatal respiratory distress syndrome and heroin stimulates prolactin secretion.[120] Studies conducted on experimental animals have shown that estrogen also stimulates the synthesis of surfactant in the fetal lungs too.[121,122] Insulin and androgens play a role in inhibition of surfactant secretion. Higher incidence of neonatal respiratory distress in children of diabetic mother and in normal male neonates has been confirmed. Insulin and androgens inhibit synthesis of the surfactant. Chronic hyperglycemia with hyperinsulinemia have been connected with the delayed appearance of surfactant in the fetal lung tissue.[123] The hypothesis that insulin achieves its inhibitory effect primarily by disruption of protein synthesis of surfactant was confirmed by studies on cell cultures of human pneumocytes type II.[124] However, it is interesting, that insulin, administered together with cortisol stimulates the synthesis of surfactant more than cortisol alone.[124] Respiratory distress syndrome of newborn is more common in male than in female children, possibly due to later start of surfactant production in male fetuses. This difference could be influenced by androgen effects, but definitely genetic factors have a certain role in it.[125,126] Further, powerful modulators of lung maturation are inflammatory mediators, particularly interleukin 1, tumor necrosis factor-á and bacterial endotoxin. Maternal chorioamnionitis, in which the fetus is exposed to inflammatory agents, is a common cause of premature birth. However, these children, rarely suffer from respiratory distress syndrome. Still, although these cytokines enhance the maturation of the lungs and allow the survival of the child, their long-term effect is negative because they affect lung growth and development, especially vascularization.[127] Therefore, in these children the respiratory surface is decreased. In addition, due to insufficient vascularization, vascular resistance in the lungs remains high after birth. This prevents the increase in flow through the lungs and leads to pulmonary arterial hypertension.[128]

Although the fetal lungs are functionally inactive during the entire period of intrauterine life, respiratory function becomes essential for survival of the infant immediately after birth. Breathing is initiated by sudden exposure to the exterior world and it is a consequence of slightly asphyxiated state due to the birth process and sensory impulses that originate from the suddenly cooled skin. If an infant doesn't begin to breathe immediately, progressive hypoxia and hypercapnia develop, and additionally stimulate the respiratory center. At birth, the walls of alveoli are collapsed due to the viscid fluid that fills them. More than 25 mm Hg of negative inspiratory pressure is required to oppose the effect of surface tension. First inspirations of the neonate are extremely powerful and capable of creating as much as 60 mm Hg negative pressure in the intrapleural space. During first inspiration, about 40 milliliters of air enters the lungs. To deflate the lungs, considerable positive pressure is required because of viscous resistance offered by the fluid in the bronchioles. Expansion of the alveoli and increased concentration of oxygen in them stimulates the release of vasodilatator substances from the endothelium of capillaries. This, together with the mechanical stretching of the alveoli, leads to the dilatation of the lung capillaries and the resistance to blood flow in the pulmonary circulation decreases several fold. Development of a nearly normal compliance curve and normal postnatal breathing establishes within 40 minutes after birth.[19]

In addition to allowing gas exchange, increased blood flows through the lungs probably accelerate reabsorption of the lung liquid. Although the existence of lung liquid is necessary for the development of the lung, it must be quickly removed during delivery to allow normal breathing of the newborn. Most of the lung liquid reabsorbs in the pulmonary circulation and only a small part of it removes through the upper airway during passage through the birth canal. Infusions of norepinephrine in concentrations, similar to those present at the delivery, prevent the lung liquid secretion. Hormones and factors that facilitate the removal of liquid from the lungs are arginine–vasopressin, catecholamine, prostaglandin-E_2, prolactin, surfactant, some growth factors and increase of the concentration of oxygen in the lungs, originating from the first breath.[19]

Fetal Urinary System

At the beginning of the fourth week, the intermediate mesoderm forms the nephrogenic cords. From the

nephrogenic cords, three successive sets of excretory organs develop: the pronephros, the mesonephros and the metanephros. The first two, i.e. the pronephros and mesonephros, persist over a period of time and then regress, while the third, the metanephros, forms the definitive kidney. The permanent adult kidney, the metanephros, begins to develop early in the fifth week and is functional 2–3 weeks later. The ureteric bud develops as an outgrowth from the mesonephric duct. The ureteric bud forms the ureter, renal pelvis, calyces and collecting tubules. The nephrons are derived from the metanephric blastema.[63] First nephrons appear in the kidney medulla, around 20–22 weeks of gestation, later they can be found in the periphery of the kidney. Formation of nephrons ends around the 35th week of gestation and further development occurs due to the growth of existing nephrons.[129] At birth, the nephrons, approximately one million in each kidney, are formed but are still short. No new nephrons are formed after birth. During infancy, the nephrons complete their differentiation and increase in size until adulthood.[63] Enlargement of the glomeruli, enlargement and elongation of the tubules, as well as enlargement of the vascular and connective tissue contribute to the growth of kidneys.[130] Failure in the maturation of the primitive kidneys can lead to the abnormal development of the genital system, adrenal glands and lungs.[129] Various anomalies of the urinary tract can be caused by developmental disorders of pronephros and mesonephros. Developmental anomalies of the urinary tract account for about 40% of all anomalies. Frequent occurrence of the urinary tract anomalies is due to complicated ontogenesis of this system.[130] Recently, attention has been given to less noticeable but potentially very harmful consequences of impaired kidney development, such as a congenital nephron deficit. Since the lack of nephrons after birth is unrecoverable, numerous studies have been conducted to detect factors that in some way may impair the process of nephrogenesis.[131] Studies conducted on the cell cultures of the fetal kidney showed that retinoids, metabolites of vitamin A, have a significant impact on the number of nephrons and that this effect is dose-dependent. Vitamin A deficiency in pregnant women is rare in developed countries but is more frequently observed in underdeveloped countries as a result of insufficient food intake. Even in a healthy population, concentrations of vitamin A and retinoids in the plasma considerably vary. Habits that are most commonly associated with its low plasma values are cigarette smoking, alcoholism and unbalanced diets.[131] Unfortunately, lack of vitamin A is not the only factor that can lead to a nephron deficit. Experiments on animals have proved that fetal growth retardation[132], maternal hyperglycemia[133] and some medications, such as gentamicin[134], cause a reduced number of nephrons, which cannot be fully compensated for after birth. If we remember that nephrogenesis in the humans ends before birth, we can assume that the harmful effects of these factors on the human fetus may be even more dangerous. Even a slight deficit of nephrons, often unrecognized after the birth, could be associated with diseases that occur later in the life, such as renal failure or hypertension. Therefore, more and more scientists believe that congenital nephron deficit could be a "missing link" in understanding of the etiology of essential hypertension.[131]

For many years, data on fetal renal function have been insufficient and indirect. Investigations were carried out mainly in experimental animals and aborted fetuses. The insertion of a catheter into the fetal blood vessels and bladder allowed the testing under physiological conditions, and brought new insights about the function of the fetal kidneys, and the application of ultrasonic methods, enabled the non-invasive and easy way to study the physiology and pathophysiology of fetal urinary tract. Glomerular filtration rate in term-fetuses, measured by ultrasound and biochemical measurements, is 0.73–5.25 mL/min, which amounts to 1/29–1/4 values in adults. After birth, during the first four days of life, glomerular filtration rate rapidly increases.[135] It was found that the time of umbilical cord ligation influences on the value of glomerular filtration rate. In the newborns in which umbilical cord ligation was performed relatively late after the birth, a circulating blood volume and glomerular filtration was 40–50% greater than in the newborns in which the umbilical cord ligation was done immediately after birth.[129] Further, values of tubular re-absorption in fetal kidneys at term range between 55–97% of the adult values.[135,136] Although histologically, kidney tubules seem well developed, at the time of delivery, the surface of transporting cells and the number of transporters is small. Reabsorption and excretory function are not completely developed. Immature cells tubules have low concentration of Na^+/K^+ ATP-ase, an enzyme that provides energy for active transport of sodium.[137,138] Therefore, capacity of renal tubular cells for sodium transport is limited. Consequently, reabsorption of bicarbonates, glucose and phosphates is also limited.[139-141] Due to low glucose threshold, tendency of excretion of glucose and consequently of the water and sodium is increased. Because of that in neonate, dehydration can develop more rapidly than in an adult. Further, it was found that term-fetus is not capable to

respond on dehydration or hypertonic solution by creating concentrated urine, like adult. Sodium overload of the mature newborn and increase of plasmatic concentration of sodium can cause increase of the body mass due to generalized edema. If the newborn gets a cow's milk, which contains four times more sodium, protein and phosphate than mother's breast milk, signs of salt and fluid retention may occur.[129] The fetus usually produces hypotonic urine and in case of dehydration, ability to concentrate urine does not exceed the limit of 600–700 mOsm/L. Antidiuretic hormone (ADH), whose role is to preserve water in the body by concentrating the urine, the fetus begins to produce in the 11th week of pregnancy and its concentration in fetal blood is almost equal to the concentration in adults. Infusion of hypertonic NaCl solution, hypoxia or hypovolemia can increase concentration of ADH in fetal plasma.[142,143] Therefore, we cannot talk about lack of ADH, as a cause of low osmolarity of fetal urine. However, it is possible to assume that the kidney is insensitive to ADH. The fetus cannot concentrate urine before appearing of specific water channels called aquaporin. They occur in human fetuses in the 12–15th week of pregnancy but their expression in the fetus and newborn is much lower than in adults.[142] Insensitivity of the fetal kidney to ADH could be explained by the slow emergence of these water channels.[81] Further, hydrogen ion secretion in the fetus and newborn is sufficient to allow bicarbonate reabsorption and excretion of metabolic acids. Filtered phosphate and synthesized ammonia are in quantities sufficient for buffering excessive hydrogen ions.[81] However, it is important to note that the fetal kidneys do not play a major role in the regulation of acid-base balance. Even in fetuses with renal agenesis, acid-base balance may be normal.[129] In fetus, the acid-base balance is regulated by maternal lungs and kidneys. CO_2 is quickly removed through the placenta into the mother's bloodstream and then mother exhaled it.[144] Large amounts of CO_2 can be effectively removed if the mother's respiration, the uteroplacental flow and the umbilical flow are normal. Somewhat, more slowly, metabolic acids are transferred through the placental barrier and they are excreted through the mother's kidneys.[145] Thus, regulation of fetal acid-base balance depends on many interrelated factors, which include state of the mother, placenta and the fetus.

Fetal kidneys **(Fig. 6.16)** excrete urine from the 3rd month of pregnancy. This can be confirmed by the existence of urine in the bladder of the fetus **(Fig. 6.17)**.[146,147] Urine extracted from the fetal kidney is hypotonic and that is not surprising because the main excretion

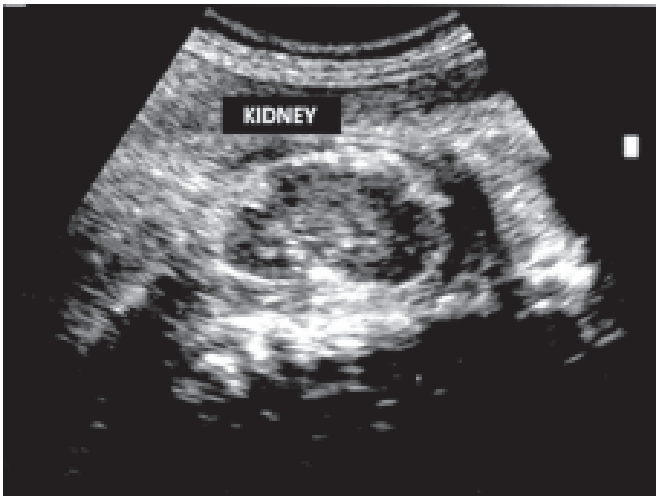

Figure 6.16: 2D ultrasound image showing fetal kidney

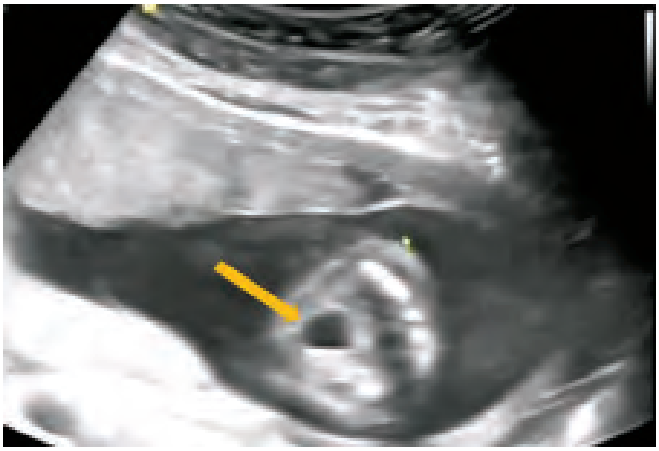

Figure 6.17: 2D ultrasound image showing fetal bladder

function is performed by the placenta. Due to this fact, electrolyte composition of fetal urine is poor.[146-148] The pH of fetal urine is about 6.[149] By the mid-gestation, fetal urine becomes the main source of amniotic fluid and swallowing the main way of its removal. These two processes are essential elements in the production and regulation of amniotic fluid in the middle trimester. The term-fetus excretes in the amniotic fluid about 400–1200 ml of urine daily. The fact that fetal urine is the main component of the amniotic fluid in the second half of pregnancy, allows us to determine the concentrations of electrolytes, creatinine, protein or glucose. Further, recording of their changes enables us to study the functional development and maturation of the fetal kidney during this period.[81] After birth, the kidneys are still immature, more accurately, their functional capacity is limited. Due to this, disorders in the maintenance of homeostasis can easily develop.

Exchange of fluid in the newborn is very large and the intensity of metabolism and acid production are higher than in the adult. Taking into account immaturity of the kidney, we can easily understand that in this period acidosis, dehydration and sometimes excessive hydration frequently develop. The disruption in the maintenance of homeostasis is more often if the child is born before term, in hypoxia or infection. Fetal kidneys and kidneys of newborn do not perform their functions poorly, indeed, they work impressively, but they need time to achieve the perfect harmony of their functions.

Fetal Central Nervous System

Development of the human CNS begins in the early embryonic period and proceeds through a sequence of very complicated processes long after delivery. CNS develops from the embryonic ectoderm. Cells that will become neurons and glial cells originate from the neural plate, which is located within the ectoderm and contains about 125,000 cells. The neural plate is formed in the early third week of pregnancy. Its lateral edges are gradually rising and approaching one another, forming first a concave area known as the neural groove and then the neural tube. Cranial and caudal opening of the neural tube are closing between the 25–27th day of pregnancy.[150] Failure of these openings to close contributes a major class of neural abnormalities. Further development is characterized by changes in size, shape and internal structure of the neural tube wall, which reflect the complex histogenetic processes. Since some parts of the neural tube grow and develop at different speeds and intensities, it bends and changes its shape, forming the major subdivisions of the CNS. There are three subdivisions of the cranial part of the neural tube: prosencephalon, the mesencephalon, and the rhombencephalon. They will each eventually develop into distinct regions of the central nervous system: the forebrain (the cerebral cortex and basal ganglia), midbrain and posterior brain (the cerebellum, pons and medulla oblongata). From the caudal part of the neural tube develops the spinal cord.[46]

Early embryonic development is characterized by its immobilization. Prerequisite for fetal movements is the existence of interneuronal and neuromuscular connections. The earliest interneuronal connections—the synapses, can be detected in the spinal cord shortly before the onset of embryonic motility, at 6–7 weeks of gestation.[151] Therefore, the neural activity leading to the first detectable movements is considered to originate from the spinal motoneurons.[152] Another important prerequisite for the motility is the development and innervation of muscular fibers. It is well known that primitive muscle fibers (myotubes) are able to contract as soon as they are innervated by motor neurons.[153] Between 6–8 weeks of gestation, muscle fibers have formed by fusion of myoblasts, efferent and afferent neuromuscular connections have developed, and spontaneous neural activity causing motility can begin. The first spontaneous embryonic movements are gross body movements and they can be observed at the 7–7.5th weeks of gestation. They consist of slow flexion and extension of the fetal trunk, accompanied by the passive displacement of arms and legs.[154] These, so called, "vermicular" movements appear in irregular sequences.[155] Simultaneously, with the onset of spontaneous movements, at the 7.5th week of gestation, the earliest motor reflex activity can be observed, indicating the existence of the first afferent–efferent circuits in the spinal cord.[156] The first reflex movements are massive and indicate a limited number of synapses in a reflex pathway. General movements are the first complex, well-organized movement pattern, which involve head, trunk and limb movements. This pattern has been interpreted as the first sign of a supraspinal control on motor activity[157,158] and can be recognized from 8–9 weeks of gestation onwards **(Fig. 6.18)**.[158,159]

The brainstem is fashioned around the 7th week of gestation[157] and basic structures of the diencephalon and cerebral hemispheres are formed by the end of the 8th

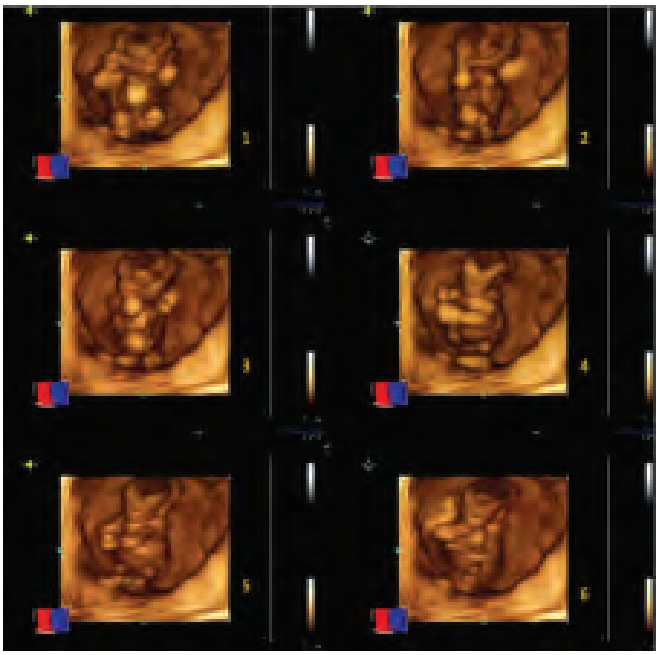

Figure 6.18: A sequence of images of the fetus at nine weeks of gestation recorded by 4D sonography, showing general movements

gestational week.[159] The remarkable expansion of the cerebral hemispheres follows during the remainder of gestation. The development of synapses in the human cerebral cortex begins after the formation of the cortical plate, at the end of the 10th week of gestation.[160,161] The brainstem consists of the medulla oblongata, pons and midbrain. It forms and matures in a caudal to rostral direction. That means that the fillogenetically older structures, such as the medulla oblongata, will form and mature earlier in the gestation. In addition to its many subnuclei, the medulla gives rise to a variety of descending spinal motor tracts which reflexively trigger limb and body movements. It also hosts the five cranial nerves (VIII–XII), which exert tremendous influences on gross body movements, heart rate, respiration and the head turning. As the medulla matures in advance of more rostral structures of the brainstem, reflexive movements of the head, body, extremities, as well as breathing movements and alterations in heart rate, appear in advance of other functions.

The formation of pons begins almost simultaneously, but its maturation is more prolonged. The structures of the pons include the V-VIII cranial nerves (vestibular nuclei of the nerve VIII) and the medial longitudinal fasciculus (MLF), pontine tegmentum, raphe nucleus and locus coeruleus, which exert widespread influences on arousal, including the sleep-wake cycles. Facial movements, which are also controlled by V and VII cranial nerve, appear around 10–11 weeks.[157] The brain stem gradually begins to take the control over fetal movements and behavioral patterns during the first trimester and continues its maturation in the second trimester, resulting in expansion and complexity of the behavioral repertoires.[157]

From 10 weeks onwards, the number and frequency of fetal movements increase and the repertoire of movements begins to expand. Qualitative changes in general movements can be also observed. These movements, which are slow and limited amplitude during 8–9 weeks, become more forceful at 10–12 weeks. After the 12th week, they become more variable in speed and amplitude.[162] Using four dimensional (4D) sonography, Kurjak and collaborators have found that from 13 gestational weeks onwards, a "goal orientation" of hand movements appears and a target point can be recognized for each hand movement.[163] According to the spatial orientation, they classified the hand movements into several subtypes: hand to head, hand to mouth **(Fig. 6.19)**, hand near mouth, hand to face, hand near face, hand to eye and hand to ear. Our recent longitudinal study, performed by 4D ultrasound in 100

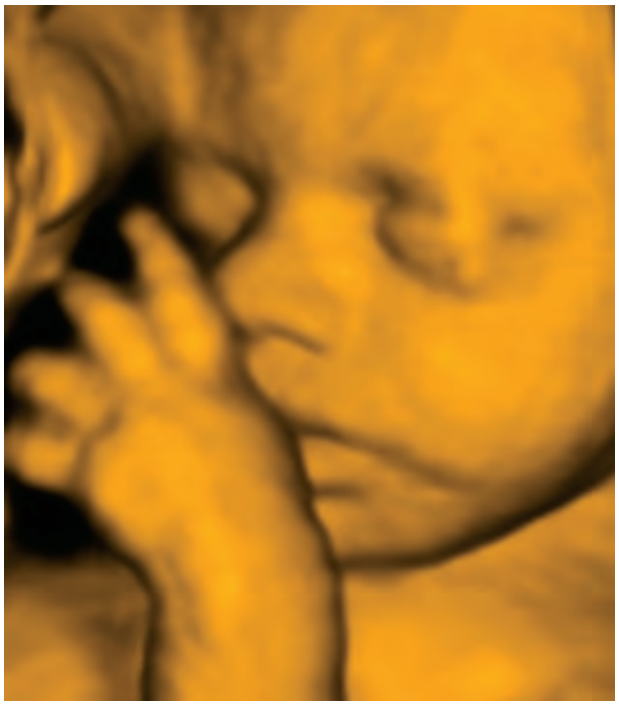

Figure 6.19: Image of the fetus recorded by 3D/4D sonography, showing hand-to-mouth movement

fetuses from all trimesters of normal pregnancies, has shown increasing frequency of various movement patterns, such as general movements, isolated arm and leg movements, stretching, as well as head movements, during the first trimester.[164] Using 4D sonography, general movements were found to be the most frequent movement pattern between 9–14 weeks of gestation.[165] From 14–19 weeks of gestation, fetuses are highly active and the longest period between movements last only 5–6 minutes. In the 15th week, 16 different types of movements can be observed. Besides the general body movements and isolated limb movements, retroflection, anteflection and rotation of the head can be easily seen. Moreover, facial movements such as mouthing **(Fig. 6.20)**, yawning, hiccups, suckling and swallowing, can be added to the wide repertoire of fetal motor activity in this period.[158] The earliest eye movements appear as sporadic movements with a limited frequency, at 16–18 weeks of gestation.[166,167] The delayed onset of eye movements can be explained with later onset of midbrain maturation.

Although the midbrain begins to form at almost the same time as the pons, its maturation does not even begin until the second trimester. It consists of the dopamine producing substantia nigra, the inferior-auditory and superior-visual colliculus, and cranial

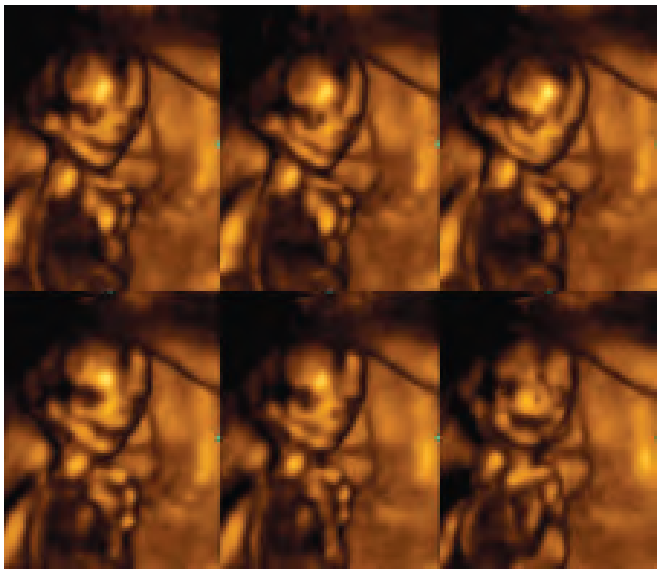

Figure 6.20: A sequence of images recorded by 4D sonography showing fetal mouth opening movements at 16 weeks of gestation

nerves III–IV, which, together with MLF and cranial nerve VI, control eye movements.[166,167]

Fetal human brain has a number of transitory structures, which cannot be observed in the adult human brain. One of the very important zone in the developing cortex is the subplate zone, that is a site for transient synapses and neuronal interactions. The development of subplate zone, between the 15–17th week of gestation, is accompanied with an increase in the number of cortical synapses, which probably form the substrate for the earliest cortical electric activity at 19 weeks of gestation.[168] Subplate zone can play a major role in the developmental plasticity following perinatal brain damage.[169]

The second half of pregnancy is characterized by organization of fetal movement patterns and increase in complexity of movements. The periods of fetal quiescence begin to increase and the rest-activity cycles become recognizable. Hardly any new movement pattern emerges in this period. The number of general body movements, which tends to increase from the 9th week onwards, gradually declines during the last 10 weeks of the pregnancy.[170-172] Although this decrease was first explained as a consequence of the decrease in amniotic fluid volume, it is now considered to be a result of cerebral maturation processes. As the medulla oblongata matures, myelinates and stabilizes, these spontaneous movements are less easily triggered, and begin to be controlled by more stable intrinsic activities generated within the brainstem.[157] It is very important to point out that general movements are characterized by large variation and complexity in the third trimester.[173] Revolutionary improvement in the study of fetal facial movements came with the development of 3D and 4D sonography. Our results confirmed the potential of 3D/4D sonography for the investigation of structural and functional development of the fetal face.[174] The application of 4D sonography in the examination of fetal facial movements has revealed the existence of a full range of facial expressions, including smiling, crying and eyelid movements,[164,175] similar to emotional expressions in adults, in the 2nd and 3rd trimesters. Other facial movements, such as yawning, suckling, swallowing and jaw opening can also be observed in this period by 4D ultrasound. Recent study demonstrated that the most frequent facial movement patterns in the 2nd trimester were isolated eye blinking, grimacing, suckling and swallowing, whereas mouthing, yawning, tongue expulsion and smiling could be seen less frequently. Mouthing was the most frequent facial movement during early third trimester[176] **(Figs 6.21A and B)**. Our longitudinal analysis of the frequencies of different facial movements in the 2nd and 3rd trimester revealed some interesting results. Contrary to the declining trend of head movement and hand movement patterns from the beginning of the second trimester to the end of the third trimester, a constant increase in the frequencies of almost all facial movement patterns was observed during the 2nd trimester. Various types of facial expression patterns displayed a peak frequency at the end of 2nd trimester, except eye blinking pattern **(Fig. 6.22)**, which displayed a peak frequency at 28 weeks of gestation. During the remainder of pregnancy, decreasing or stagnant incidence of facial expression patterns was noted.[164] Obviously, this

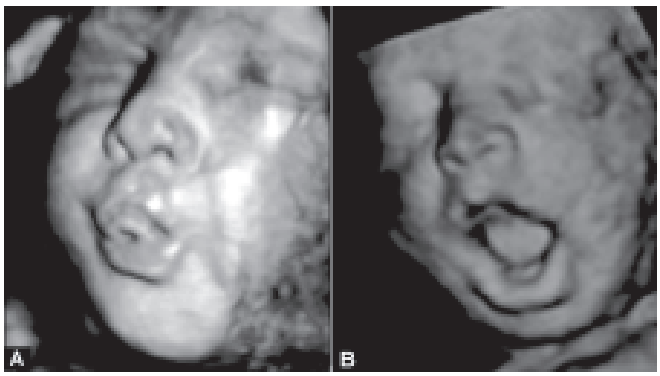

Figures 6.21A and B: Images of the fetus in the 3rd trimester recorded by 3D/4D sonography, exhibiting mouthing movements

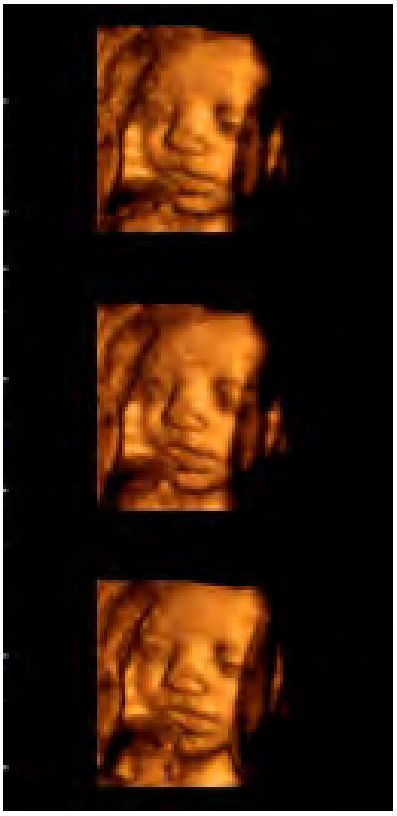

Figure 6.22: A sequence of images of the fetus in the 3rd trimester recorded by 4D sonography, showing eye blinking

developmental trend provides yet another example of the maturation of the medulla oblongata, pons and midbrain, or perhaps even the establishment of control of more cranial structures. The facts that even in the embryonic period same inductive forces that cause the growth and reshaping of the neural tube influence the development of facial structures and that many genetic disorders affecting the CNS are also characterized by dysmorphology and dysfunction of facial structures, emphasize the importance of structural and functional evaluation of the fetal face.[159,177] Our recent study has demonstrated that there were no movements observed in fetal life that were not present in neonatal life. Furthermore, prenatal—neonatal continuity exists even in subtle, fine movements such as facial mimics.[178]

In addition to morphological studies of the development of the central nervous system and studies about fetal behavior that provide insight into the functional development of central nervous system of fetuses, attention of researchers attracts the development of the fetal senses. For a long time, experts from different fields of science debate about whether the fetus feels pain. In humans, it is possible to distinguish several different reactions to pain. The simplest is reflex motor reaction, removal of stimulated body parts from painful stimuli. Next unconscious reaction involves the secretion of the so-called stress hormones—cortisol and catecholamines. The most complex reaction is conscious perception of pain and emotional reaction to it. We can claim with certainty that the first two are already present in the fetal period. The earliest reactions to painful stimuli are motor reflexes, resembling withdrawal reflexes. They appear early in gestation. Reflex threshold is remarkably low and various kinds of stimuli may induce very holistic and unspecific reactions. It is important to emphasize that these reactions are completely reflexive, directed by the spinal cord, and higher perception or processing of painful sensation does not exist at this stage.[179] Further, as early as 16–18 weeks of gestation, fetal cerebral blood flow increases during invasive procedures.[180,181] This increase of blood flow towards the brain may be mediated by the sympathetic system or by other undetermined mechanisms.[181] With regard to the autonomic and endocrine responses to pain, an elevation of noradrenaline, cortisol and beta-endorphin plasma levels, in response to needle pricking of the innervated hepatic vein for intrauterine transfusion, was registered in a 23-week-old fetus. Pricking of the noninnervated placental cord insertion for the same purpose had no effect.[182,183] Obviously, painful stimuli trigger a wide spectrum of reactions, such as activation of the hypothalamo-hypophysial axis or autonomic nervous system, without reaching the cortex. It has been suggested that neither motor reflexes nor hormonal stress responses to invasive procedures prove the existence of fetal pain.[184] It is unknown whether and when the fetus begins consciously to feel pain. Functional thalamocortical connections are required for fetal awareness of noxious stimuli. Thalamocortical path is formed between 22–26 weeks and after this period, the fetus is probably capable of consciously perceiving painful stimuli. Evidence for conscious pain perception during intrauterine life is indirect, but evidence for the subconscious incorporation of fetal pain into neurological development and plasticity is incontrovertible.[185] Despite the great interest in conscious experience and memory of pain, unconscious reactions like the secretion of stress hormones and their far-reaching detrimental effect, are probably more dangerous for the development of fetus than terrifying memories.

Reflex arcs involving the brainstem, such as vestibular, auditory and olfactory, mature early in fetal life. Vestibular nerve cells mature earlier than neurons of the lateral and inferior vestibular nuclei, which begin to function during the 9th week of pregnancy. It is

believed that vestibular stimulation has a role in the emerging fetal movements. Nearly weightless state of the fetus in the uterus provides a particularly convenient medium for the vestibular reflexes. According to electrophysiological examinations of evoked potentials in prematurely delivered healthy infants, cochlear function develops between 22–25 weeks of gestation and its maturation continues during the first six months after delivery.[186-188] However, fluid in the fetal ear as well as the immaturity of the cochlea, complicate the sound transmission, so that only strong acoustic stimuli can be registered by the fetus.[157] Due to this reason and because of the immaturity of the cochlea, a very strong stimuli is needed for fetus to notice it. Maternal heartbeats and motility of gastrointestinal tract during digestion appear to generate 60–90 decibels of sound *in utero*, which is comparable to noise of the busiest street.[189] During the last weeks of pregnancy, from the 36th gestational week onwards, the fetus reacts to extremely loud sounds and even the mother's voice with reflex movements of the body, by turning his head, and increased heart rate. More fascinating is the notion that a fetus at this age not only hears sounds but also can discriminate between different sounds. This finding is explained by the tonotopic organization of the cochlear nuclei and by the maturation of the brainstem during the last weeks of pregnancy. It was noted that the development of the auditory system can be disrupted by the influence of adverse factors (cigarette consumption) and also in some pathological conditions (intrauterine growth retardation, maternal hypertension).[190–192] It is important to mention also that development of the auditory system affects the subsequent learning of speech and language acquisition.

Animal experiments have indicated that the intrauterine environment is not completely deprived of light. Although the developing fetus cannot distinguish objects clearly, the intensity of light is equal to the splendor that occurs through the cheek when mouth is highlighted by the powerful batteries. Furthermore, according to some experimental results, the development of visual and auditory organs could not be possible without any light or auditory stimulation.[193,194] The structural development of sensory pathways is a prerequisite for functional development, but the final organization of the brain circuitries depends mainly on guidance from external inputs.[169] A histological study of the human visual pathway has shown that thalamic projections reach the visual cortex between 23–27 weeks of gestation.[195] The primary visual cortex can be clearly delineated in the occipital lobe by immunohistochemical staining even before the 25th week. In this cortical area, synaptogenesis persists between 24 weeks of gestation and 8 months after delivery,[193] while myelination of the optical tract begins at 32 weeks of gestation.[194] Cortical visual evoked potentials indicate the development and maturation of the primary visual cortex. Maturation of the visual cortex is characterized by the appearance of surface-positive evoked potentials, which occurs between the 36–40th weeks.[169] New data have shown that the amplitude of visual evoked responses can be used in the assessment of fetal and neonatal habituation to light stimuli.[196] Flash stimuli over the maternal abdomen can cause the visual evoked brain activity in the human fetus, recorded by magnetoencephalography. The latency of the fetal response falls with increasing gestational age and begins to approach the adult latency near term.[197] Recent experimental findings have demonstrated the importance of fetal eye motility in retinal (neuronal) cell differentiation, as well as eye functional maturation.[198]

Fetal life *in utero* is organized in cyclical patterns. From the midgestation onwards, periods of activity begin to alternate with the periods of rest. Between 30–38 weeks of pregnancy the difference between quiet and paradoxical, "active" sleep can be seen. In advanced pregnancy, the fetus usually sleeps at the same time as the mother. In fetal animals, simultaneous measurements of fetal electrocortical activity, eye and body movements have shown that deep sleep, characterized by high-voltage waves and decreased fetal activity, occurred during 54% of a day. The total length of the REM sleep period, characterized by low-voltage waves and rapid eye movements, lasted 40% of a day. The wakeful state (6% of a day) is characterized by low-voltage waves.[199] In human premature newborns, born four weeks prior to term, 60–65% of the total sleeping period is REM sleeping, whereas in term-newborns, the REM sleeping period includes 50% of the total 16 hours of sleep.[200] During delivery, fetal EEG shows waves characteristic for quiet sleep, active sleep and wakefulness of the newborn.[201] It is thought that REM sleep plays a role in the development of the nervous system, similar as physical activity helps to develop muscles. REM sleep is probably caused by intense activity of neural circuits and thus participates in the development of the central nervous system.[202]

The human brain is intricately designed to execute cognitive functions, such as perception, attention, memory and learning. Psychobiologic investigations inspired the hypothesis that the acoustically rich environment in the uterus contributes to fetal learning.[203] The intrauterine origin of learning and memory processes has been investigated extensively employing

habituation methods, classical conditioning or exposure learning to assess fetal learning.

It was also found that the fetus has the ability to remember tastes to which it was exposed during the intrauterine period. Flavors from the mother's diet during pregnancy are transmitted to amniotic fluid and are swallowed by the fetus. Consequently, the type of food eaten by the mother during pregnancy is experienced by the infants before their first exposure to solid food. For instance, garlic ingestion by pregnant women significantly alters the odor of their amniotic fluid, barely 45 minutes after ingestion.[204] Prenatal experience of taste greatly affects the newborn child. It prepares it for the taste of the mother's milk, whose taste also depends on the mother's diet. Prenatal and early postnatal exposure to a flavor enhances the infant's enjoyment of that flavor in solid foods during weaning.[205] A study has shown that the infants who have been exposed to the flavor of carrots in either amniotic fluid or breast milk behaved differently in response to that flavor in food than did the nonexposed control infants. Specifically, previously exposed infants exhibited fewer negative facial expressions while being fed the carrot-flavored cereal compared to the plain cereal, whereas control infants whose mothers drank water during pregnancy and lactation exhibited no such difference.[205] According to recent data, the neonate strongly reacts to fragrant signals of mother's breasts.[206,207] In the close proximity of mother's breasts, in the first minutes after birth, the newborn spontaneously turns towards the breast and starts making the movement of sucking even before coming in the direct contact with the breast.[208] In the first days of life, it demonstrates a similar reaction to its own amniotic fluid.[209] To some extent, the chemical profile of breast secretions overlaps with that of amniotic fluid. Therefore, early postnatal attraction to odors associated with the nipple/areola may reflect prenatal exposure and familiarization.[210]

The development of human brain is not completed at the time of delivery. Only subcortical formations and primary cortical areas are well developed in a newborn. Associative cortex, barely visible in a newborn, is scantily developed in a six months old infant. Postnatal formation of synapses in associative cortical areas, which intensifies between the 8th month and the 2nd year of life, precedes the onset of first cognitive functions, such as speech. Following the 2nd year of life, many redundant synapses are eliminated. Elimination of synapses begins very rapidly and continues slowly until puberty, when the same number of synapses as seen in adults is reached.[211]

Fetal Stress

A large number of environmental factors can trigger the fetal stress response. For instance, maternal undernutrition or placental insufficiency can alter the intrauterine environment, causing fetal stress.[212] Painful stimuli also lead to the fetal stress response.[213] Even severe maternal emotional stress or stressful life events, according to some investigations, may influence the fetal environment.[214-216] The primary role of stress is the protection of organism but fetal exposure to stress may affect neurodevelopment, as well as the development of many other organ systems and have lifelong consequences. Many adaptive changes induced by fetal stress increase the chance of fetal survival by creating a short-term protection. However, these changes can leave profound alterations in the structure and functions of the organism.[212] It is a known fact that fetal cardiovascular adaptation to hypoxia is manifested by the redistribution of blood flow primarily towards the fetal brain. However, our latest investigations have shown that severe brain damage can develop despite the fetal blood flow redistribution and increased brain perfusion, even earlier than it was previously thought.[217] The neuroendocrine stress axis includes the production of the corticotropin releasing hormone (CRH), adrenocorticotropic hormone (ACTH) and cortisol. Fetal CRH has been shown to influence the timing of birth. These findings have pointed to an active role of the fetus in the initiation of parturition.[81] Furthermore, ACTH impairs motor coordination and muscle tonicity, reduces attention span and increases irritability.[212] Recently, epidemiological and experimental investigations have shown that chronic exposure to high levels of cortisol during intrauterine life, occurring either as a result of its exogenous application or the fetal stress, has a very adverse effect in the long run. Unfortunately, it has been recently established that cortisol, which accelerates lung and brain maturation and enables survival of premature infants, may have an adverse effect on growth of the lungs, development of the secondary alveolar septa and even on the growth of the whole organism.[218] Accelerated maturation of the brain is also associated with the structural as well as behavioral changes. Stress induces structural changes of the hippocampus[219-222] that are associated with memory impairment and learning disabilities. Behavioral changes associated with accelerated maturation of the brain include hyperalertness and impaired fetal responsiveness to novel stimuli.[223] Retrospective studies on children whose mothers experienced severe psychological stress or adverse life events during their pregnancy have

suggested long-term neurodevelopment effects on the infant.[224-227] Such children exhibited symptoms of attention deficit hyperactivity disorder, sleep disorders, unsociable and inconsiderate behavior, as well as psychiatric disorders, including schizophrenic episodes, depressive and neurotic symptoms, drug abuse and anxiety.[228] Increased maternal stress during pregnancy seems to influence infant temperament and cognitive functions.[229,230] Moreover, stressful maternal life events measured during the first part of pregnancy negatively affected the child's attention/concentration index measured at the age of six.[231] The adverse health effects of stress may also include an increased risk of certain birth defects (cleft palate, cleft lip with or without cleft palate, d-transposition of the great arteries and tetralogy of Fallot).[214] Chronic high glucocorticoid exposure *in utero* is associated with adult hypertension and according to some data with coronary disease. Impaired glucose tolerance has also been noticed.[232-234] We can conclude that some of the most common diseases of the modern society may have their origins in prenatal life.

CONCLUSION

Fetal developmental potential is determined at the moment of conception by genetic inheritance. However, this development is modulated by environmental factors. Basic and clinical researches into fetal life present us with ever deeper understandings of important role that the environment plays in prenatal and postnatal life. It is important to recognize that both, the mother and the fetus, actively participate in the maintenance of the physiological intrauterine environment. Unfortunately, the fetus is not entirely protected from harmful influences of the external factors. By altering the intrauterine environment, these factors can have a long-term effect on fetal health. Finally, physiological fetal growth and development is the precondition for optimal child development.

REFERENCES

1. Stables D. Physiology in childbearing with anatomy and related biosciences. Edinburgh: Bailliere Tindall;1999. pp. 73-148.
2. Wong KHH, Adashi EY. Early conceptus growth and immunobiologic adaptations of pregnancy. In: Reece EA, Hobbins JC, Gant NF (Eds). Clinical obstetrics: the fetus and mother. Oxford: Blackwell Publishing Ltd; 2007. pp. 3-19.
3. Huppertz B, Kingdom JCP. The placenta and fetal membranes. In: Edmonds KD (Ed). Dewhurst's Textbook of Obstetrics and Gynaecology. Oxford:Blackwell Publishing Ltd; 2007. pp. 19-28.
4. http://www.centrus.com.br/DiplomaFMF/SeriesFMF/doppler/capitulos-html/chapter_03.htm
5. Kahn BF, Hobbins JC, Galan HL. Intrauterine Growth Restriction. In: Gibbs RS, Karlan BY, Haney AF, Nygaard (Eds). Danforth's Obstetrics and Gynecology. Philadelphia: Lippincott Williams and Wilkins; 2008. pp. 198-220.
6. Baschat AA. Fetal growth restriction—from observation to intervention. J Perinat Med. 2010;38(3):239-46.
7. Harrington K, Goldfrad C, Carpenter RG, et al. Transvaginal uterine and umbilical artery Doppler examination of 12-16 weeks and the subsequent development of pre-eclampsia and intrauterine growth retardation. Ultrasound Obstet Gynecol. 1997;9(2):94-100.
8. Rizzo G, Arduini D, Romanini C. Umbilical vein pulsations: a physiologic finding in early gestation. Am J Obstet Gynecol. 1992;167(3):675-7.
9. Giles WB, Trudinger BJ, Baird PJ. Fetal umbilical artery flow velocity waveforms and placental resistance: pathological correlation. Br J Obstet Gynaecol. 1985;92(1):31-8.
10. Karsdorp VH, Dirks BK, van der Linden JC, et al. Placenta morphology and absent or reversed end diastolic flow velocities in the umbilical artery: a clinical and morphometrical study. Placenta. 1996;17(7):393-9.
11. Baschat AA. Fetal responses to placental insufficiency: an update. BJOG. 2004;111(10):1031-41.
12. Arbeille P, Maulik D, Fignon A, et al. Assessment of the fetal PO_2 changes by cerebral and umbilical Doppler on lamb fetuses during acute hypoxia. Ultrasound Med Biol. 1995;21(7):861-70.
13. Arbeille P, Roncin A, Berson M, et al. Exploration of the fetal cerebral blood flow by duplex Doppler linear array system in normal and pathological pregnancies. Ultrasound Med Biol. 1987;13(6):329-37.
14. Gramellini D, Folli MC, Raboni S, et al. Cerebral-umbilical Doppler ratio as predictor of adverse perinatal outcome. Obstet Gynecol. 1992;79:416-20.
15. Arbeille P, Maulik D, Salihagić A, et al. Effect of long-term cocaine administration to pregnant ewes on fetal hemodynamics, oxygenation, and growth. Obstet Gynecol. 1997;90(5):795-802.
16. Fignon A, Salihagic A, Akoka S, et al. Twenty-day cerebral and umbilical Doppler monitoring on a growth retarded and hypoxic fetus. Eur J Obstet Gynecol Reprod Biol. 1996;66(1):83-6.
17. Laurini RN, Arbeille B, Gemberg C, et al. Brain damage and hypoxia in an ovine fetal chronic cocaine model. Eur J Obstet Gynecol Reprod Biol. 1999;86(1):15-22.
18. Salihagic A, Georgescus M, Perrotin F, et al. Daily Doppler assessment of the fetal hemodynamic response to chronic hypoxia: a five case report. Prenat Neonat Med. 2000;5:35-41.
19. Guyton i Hall. Medicinska fiziologija. 11. Izdanje. Zagreb: Medicinska naklada; 2006. pp. 1042-52, 1027-41, 918-30.
20. Marieb EN. Human Anatomy and Physiology. 5th Edition. San Francisco:Benjamin Cummings; 2000. pp. 1118-48.
21. Johnson MH, Everitt BI. Essential Reproduction. 5th edition. Oxford:Blackwell Science; 2000. pp. 203-22.

22. Ross MG, Ervin MG, Novak D. Fetal Physiology. In: Gabbe SG, Niebyl JR, Simpson JL (Eds). Obstetrics Normal and Problem Pregnancies. Philadelphia:Churchill Livingston Elsevier; 2007. pp. 26-54.
23. Handwerger S, Freemark M. The role of placental growth hormone and placental lactogen in the regulation of human fetal growth and development. J Pediatric Endocrinol Metabol. 2000; 13(4):343-56.
24. Lovinger RD, Kaplan SL, Grumbach MMJ. Congenital hypopituitarism associated with neonatal hypoglycemia and microphallus: four cases secondary to hypothalamic hormone deficiencies. Pediatr. 1975;87(6 Pt 2):1171-81.
25. Goodman HG, Grumbach MM, Kapaln SL. Growth and growth hormone. II. A comparison of isolated growth hormone deficiency and multiple pituitary hormone deficiencies in 35 patients with idiopathic hypopituitary dwarfism. N Eng J Med. 1968;278(2):57-68.
26. Lemons JA, Ridenour R, Orsini EN. Congenital absence of the pancreas and intrauterine growth retardation. Pediatr. 1979;64(2):255-7.
27. Lassare C, Hardouin S, Daffos F, et al. Serum insulin-like growth factors and insulin-like growth factors binding protein in the human fetus. Relationships with growth in normal subjects and in subjects with intrauterine growth retardation. Pediatr Res. 1991;29(3):219-25.
28. Ashton IK, Zapf J, Einschenk I, et al. Insulin-like growth factors IGF 1 and 2 in human fetal plasma and relationship to gestational age and fetal size during mid pregnancy. Acta Endocrinol. 1985;110:558-63.
29. Basset NS, et al. The effect of maternal starvation on plasma insulin-like growth factor I concentration in the late gestation ovine fetus. Pediatr Res. 1990;27:401-4.
30. Oliver MH, et al. Glucose but not a mixed amino acid infusion regulates insulin like growth factor-I concentration in fetal sheep. Pediatr Res. 1993;34:62-5.
31. Prada JA, Tsang RC. Biological mechanisms of environmentally induced causes of IUGR. Eur J Clin Nutr 1998;52 Suppl 1:S21-7;discussion S27-8.
32. Mirlesse V, et al. Placental growth hormone levels in normal pregnancy and in pregnancies with intrauterine growth retardation. Pediatr Res. 1993;34:439-42.
33. Gluckman PD, Grumbach MM, Kaplan SL. The human fetal hypothalamus and pituitary gland. U: Tulchinsky D, Ryan KJ, ur. Maternal-fetal endocrinology. Philadelphia: WB Saunders Company 1980; str 196.
34. Czeizel AE. Folic acid in the prevention of neural tube defects. J Pediatr Gastroenterol Nutr. 1995;20(1):4-16.
35. Canfield MA, Collins JS, Botto LD, et al. Changes in the birth prevalence of selected birth defects after grain fortification with folic acid in the United States: findings from a multi-state population-based study. Birth Defects Res A Clin Mol Teratol. 2005;73(10):679-89.
36. Bower C, Miller M, Payne J, Serna P. Folate intake and the primary prevention of non-neural birth defects. Aust N Z J Public Health. 2006;30(3):258-61.
37. Czeizel AE, Puhó E. Maternal use of nutritional supplements during the first month of pregnancy and decreased risk of Down's syndrome: case-control study. Nutrition. 2005;21(6):698-704.
38. Judge MP, Harel O, Lammi-Keefe CJ. A docosahexaenoic acid-functional food during pregnancy benefits infant visual acuity at four but not six months of age. Lipids. 2007;42(2):117-22.
39. Judge MP, Harel O, Lammi-Keefe CJ. Maternal consumption of a docosahexaenoic acid-containing functional food during pregnancy: benefit for infant performance on problem-solving but not on recognition memory tasks at age 9 mo. Am J Clin Nutr. 2007;85(6):1572-7.
40. Helland IB, Smith L, Saarem K, et al. Maternal supplementation with very-long-chain n-3 fatty acids during pregnancy and lactation augments children's IQ at 4 years of age. Pediatrics. 2003;111(1):e39-44.
41. Hibbeln JR, Davis JM, Steer C, et al. Maternal seafood consumption in pregnancy and neurodevelopmental outcomes in childhood (ALSPAC study): an observational cohort study. Lancet. 2007;369(9561):578-85.
42. Romieu I, Torrent M, Garcia-Esteban R, et al. Maternal fish intake during pregnancy and atopy and asthma in infancy. Clin Exp Allergy. 2007;37(4):518-25.
43. Willers SM, Devereux G, Craig LC, et al. Maternal food consumption during pregnancy and asthma, respiratory and atopic symptoms in 5-year-old children. Thorax. 2007;62(9):773-9.
44. Kaiser L, Allen LH. Position of the American Dietetic Association: nutrition and lifestyle for a healthy pregnancy outcome. J Am Diet Assoc. 2008;102(10):553-61.
45. Tucker Blackburn S, Lee Loper D. Maternal, fetal and neonatal physiology. A clinical perspective. Philadelphia-London-Toronto-Montreal-Sydney-Tokyo: WB Saunders Company; 1992. pp. 228-47.
46. Sadler TW. Langmanova Medicinska embriologija. Zagreb:Školska knjiga; 1996. pp. 183-231, 232-41,272-311, 374-415.
47. Sutton MJ, Gill T, Plappert P. Functional anatomic development in the fetal heart. In: Polin RA, Fox WW (Eds). Fetal and neonatal physiology. Philadelphia-London-Toronto-Montreal-Sydney-Tokyo: WB Saunders Company; 1992. pp. 598-607.
48. Sutton MJ, Gill T, Plappert P. Functional anatomic development in the fetal heart. In: Polin RA, Fox WW (Eds). Fetal and neonatal physiology. Philadelphia-London-Toronto-Montreal-Sydney-Tokyo:WB Saunders Company; 1992. pp. 598-607.
49. Schats R, Jansen CAM, Wladimiroff JW. Embryonic heart activity: appearance and development in early human pregnancy. Br J Obstet Gynecol. 1990,97(11):989-94.
50. Merchiers EH, Dhont M, De Sutter PA, et al. Predictive value of early embryonic cardiac activity for pregnancy outcome. Am J Obstet Gynecol. 1991,165(1):11-4.
51. Berne RM, Levy MN. Fiziologija. 3. izd. Zagreb:Medicinska naklada; 1996. pp. 489-91,831-63, 879-907,908-48.
52. Bancroft J. Researches in prenatal life. Oxford:Blackwell; 1946.
53. Bartelds B, van Bel F, Teitel DF, et al. Carotid, not aortic, chemoreceptors mediate the fetal cardiovascular response to acute hypoxemia in lambs. Pediatr Res. 1993;34(1):51-5.
54. Jones CT, Robinson RO. Plasma catecholamines in fetal and adult sheep. J Physiol. 1975; 248:15-33.

55. Guissani DA, Mc Grrigle HHG, Spencer JA, et al. Effect of carotid denervation on plasma vasopressin level during acute hypoxia in late gestation sheep fetus. J Physiol. 1994;477(1):81-7.
56. Green LR, McGarrigle HHG, Bennet L, et al. The effect of acute hypoxaemia on plasma angiotensin II in intact and carotid sinus-denervated fetal sheep. J Physiol. 1994;470(P):81P.
57. Richardson B, Korkola S, Assano H, et al. Regional blood flow and the endocrine response to sustained hypoxaemia in the preterm ovine fetus. Ped Res. 1996;40(2):337-43.
58. Myers DA, Robertshow D, Nathanielsz PW. Effect of bilateral splanchnic nerve section on adrenal function in the ovine fetus. Endocrinology. 1990;127:2328-35.
59. Tucker Blackburn S, Lee Loper D. Maternal, fetal and neonatal physiology. A clinical perspective. Philadelphia-London-Toronto-Montreal-Sydney-Tokyo: WB Saunders Company; 1992. pp. 228-47.
60. Green LR, Mc Grrigle HHG, Bennet L, et al. Effect of carotid sinus denervation on plasma endothelin-1 during acute isocapnic hypoxaemia im the late gestation ovine fetus (sa•etak). J Soc Gynaecol Inv. 1995;2(2):159.
61. Green LR, Bennet L, Hanson MA. The role of nitric oxide synthesis in cardiovascular response to acute hypoxia in the late gestation sheep fetus. J Physiol. 1996;497(Pt 1):271-7.
62. Heymann MA. Fetal cerebrovascular physiology. U: Creasy RK, Resnik R. Maternal-fetal medicine: principles and practice. 2 izd. Philadelphia-London-Toronto-Montreal-Sydney-Tokyo: WB Saunders Company; 1989. pp. 288-300.
63. Trivedi VN, Hay P, Hay JC. Normal embryonic and fetal development. In: Reece EA, Hobbins JC, Gant NF (Eds). Clinical obstetrics: the fetus and mother. Oxford:Blackwell Publishing Ltd; 2007. pp. 19-35.
64. Grand RJ, Watkins JB, Torti FM. Development of the human gastrointestinal tract. A review. Gastroenterology. 1976;70(5 PT. 1):790-810.
65. Cunningham FG, MacDonald PC, Gant NF, et al. Williams Obstetrics, 20th Edition. Stamford;Appleton and Lange; 1997.
66. Diamant NE. Development of esophageal function. Am Rev Respir Dis. 1985;131:S29-32.
67. Ross MG, Nijland JM. Development of ingestive behavior. Am J Physiol. 1998;274:R879-93.
68. El-Haddad MA, Desai M, Gayle D, et al. In utero development of fetal thirst and appetite: potential for programming. J Soc Gynecol Investig. 2004;11(3):123-30.
69. Grassi R, Farina R, Floriani I, et al. Assessment of fetal swallowing with gray-scale and color Doppler sonography. AJR Am J Roentgenol. 2005;185(5):1322-7.
70. Kurjak A, Andonotopo W, Hafner T, et al. Normal standards for fetal neurobehavioral developments—longitudinal quantification by four-dimensional sonography. J Perinat Med. 2006; 34(1):56-65.
71. Ross MG, Kullama LK, Ogundipe OA, et al. Ovine fetal swallowing response to intracerebroventricular hypertonic saline. J Appl Physiol. 1995;78(6):2267-71.
72. Ross MG, Kullama LK, Ogundipe OA, et al. Central angiotensin II stimulation of ovine fetal swallowing. J Appl Physiol. 1994;76(3):1340-5.
73. Davison JM, Gilmore EA, Dürr J. Altered osmotic thresholds for vasopressin secretion and thirst in human pregnancy. Am J Physiol. 1984;246:105-9.
74. Ross MG, Sherman DJ, Schreyer P, et al. Fetal rehydration via amniotic fluid: contribution of fetal swallowing. Pediat Res. 1991;29(2):214-7.
75. Nijland MJ, Kullama LK, Ross MG. Maternal plasma hypo-osmolality: effects on spontaneous and stimulated ovine fetal swallowing. J Mater-Fetal Med. 1998;7(4):165-71.
76. El-Haddad MA, Chao CR, Ross MG. N-methyl-D-aspartate glutamate receptor mediates spontaneous and angiotensin II-stimulated ovine fetal swallowing. J Soc Gynecol Investig. 2005; 12(7):504-9.
77. Ross MG, Sherman DJ, Ervin MG, et al. Fetal swallowing: response to systemic hypotension. Am J Physiol. 1990;257:R130-4.
78. Nicolaidis S, Galaverna O, Meltzer CH. Extracellular dehydration during pregnancy increases salt appetite of offspring. Am J Physiol. 1990;258(1 Pt 2):R281-3.
79. Vijande M, Brime JI, López-Sela P, et al. Increased salt preference in adult offspring raised by mother rats consuming excessive amounts of salt and water. Regul Pept. 1996;66(1-2):105-8.
80. Bradley RM, Mistretta CM. The developing sense of taste. U: Olfaction and Taste V.D.A. Denton and J.P.Coghlan. New York:Academic; 1975. pp. 91-8.
81. Salihagić A, Kurjak A, Medić M. Novije spoznaje o fiziologiji fetusa. In: Kurjak A, Đelemiš J (Eds). Ginekologija i perinatologija II. Vara•din:Tonomir; 2003. pp. 112-52.
82. El-Haddad MA, Jia Y, Ross MG. Persistent sucrose stimulation of ovine fetal ingestion: lack of adaptation responses. J Matern Fetal Neonatal Med. 2005;18(2):123-7.
83. Kawamura K, Takebayashi S. The development of noradrenaline-, acetylcholinesterase-, neuropeptide Y- and vasoactive intestinal polypeptide-containing nerves in human cerebral arteries. Neurosci Lett. 1994;175(1-2):1-4.
84. Cetin I, Morpurgo PS, Radaelli T, et al. Fetal plasma leptin concentrations: relationship with different intrauterine growth patterns from 19 weeks to term. Pediatr Res. 2000;48(5):646-51.
85. Jaquet D, Leger J, Levy-Marchal C, et al. Ontogeny of leptin in human fetuses and newborns: effect of intrauterine growth retardation on serum leptin concentrations. J Clin Endocrinol Metab. 1998;83(4):1243-6.
86. Roberts TJ, Caston-Balderrama A, Nijland MJ, et al. Central neuropeptide Y stimulates ingestive behavior and increases urine output in the ovine fetus. Am J Physiol Endocrinol Metab. 2000;279:E494-500.
87. Roberts TJ, Nijland MJ, Caston-Balderrama A, et al. Central leptin stimulates ingestive behavior and urine flow in the near term ovine fetus. Horm Metab Res. 2001; 33(3):144-50.
88. Ross MG, El-Haddad M, Desai M, et al. Unopposed orexic pathways in the developing fetus. Physiol Behav. 2003;79(1):79-88.
89. Aparicio T, Kermorgant S, Darmoul D, et al. Leptin and Ob-Rb receptor isoform in the human digestive tract during fetal development. J Clin Endocrinol Metab. 2005;90(11): 6177-84.

90. Adair LS. Child and adolescent obesity: epidemiology and developmental perspectives. Physiol Behav. 2008;94(1):8-16.
91. Cunningham FG, Gant NF, Leveno KJ, et al. Williams Obstetrics. 21st Edition. New York: McGraw-Hill; 2001.
92. Kotecha S. Lung growth: implications for the newborn infant. Arch Dis Child Neonatal Ed. 2000;82(1):F69-74.
93. Dawes GS. Breathing before birth in animals and man. An essay in developmental medicine. N Engl J Med. 1974;290(10):557-9.
94. Olver RE, Strang LB. Ion fluxes across the pulmonary epithelium and the secretion of lung liquid in the fetal lamb. J Physiol. 1974;241(2):327-57.
95. Jain L. Alveolar fluid clearance in developing lungs and its role in neonatal transition. Clin Perinatol. 1999;26(3):585-99.
96. Wigglesworth JS, Desai R. Effects on lung growth of cervical cord section in the rabbit fetus. Early Hum Dev. 1979;3(1):51-65.
97. de Vries JI, Visser GH, Prechtl HF. The emergence of fetal behavior. In: Qualitative aspects. Early Human Dev. 1982;7(4):301-22.
98. Patrick J, Campbell K, Carmichael L, et al. A definition of human fetal apnea and the distribution of fetal apneic intervals during the last 10 weeks of pregnancy. Am J Obstet Gynecol. 1978;136(4):471-7.
99. Natale R, Nasello-Paterson C, Connors G. Patterns of fetal breathing activity in the human fetus at 24 to 28 weeks of gestation. Am J Obstet Gynecol. 1988;158(2):317-21.
100. Connors G, Hunse C, Carmichael L, et al. Control of fetal breathing in the human fetus between 24 and 34 weeks gestation. Am J Obstet Gynecol. 1989;160(4):932-8.
101. Natale R, Patrick J, Richardson B. Effects of maternal venous plasma glucose concentrations on fetal breathing movements. Am J Obstet Gynecol. 1978;132(1):36-41.
102. Patrick J, Natale R, Richardson B. Patterns of human fetal breathing activity at 34 to 35 weeks gestational age. Am J Obstet Gynecol. 1978;132(5):507-13.
103. Mirghani HM, Weerasinghe SD, Smith JR, et al. The effect of intermittent maternal fasting on human fetal breathing movements. Obstet Gynaecol. 2004;24(6):635-7.
104. Roberts AB, Goldstein I, Romero R, et al. Fetal breathing movements after preterm premature rupture of membranes. Am J Obstet Gynecol. 1991;164(3):821-5.
105. Kivikoski A, Amon E, Vaalamo PO, et al. Effect of third-trimester premature rupture of membranes on fetal breathing movements: a prospective case-control study. Am J Obstet Gynecol. 1988;159(6):1474-7.
106. Richardson B, Natale R, Patrick J. Human fetal breathing activity during induced labor at term. Am J Obstet Gynecol. 1979;133(3):247-55.
107. Besinger RE, Compton AA, Hayashi RH. The presence or absence of fetal breathing movements as a predictor of outcome in preterm labor. Am J Obstet Gynecol. 1987;157(3):753-7.
108. Kisilevsky BS, Hains SMJ, Low JA. Maturation of body and breathing movements in 24-33 week-old fetuses threatening to deliver prematurely. Early Hum Dev. 1999;55(1):25-38.
109. Fox HE, Steinbrecher M, Pessel D, et al. Maternal ethanol ingestion and occurrence of human breathing movements. Am J Obstet Gynecol. 1978;132(4):354-61.
110. Richardson B, O'Grady JP, Olsen GD. Fetal breathing movements in response to carbon dioxide in patients on methadone maintenance. Am J Obstet Gynecol. 1984;150(4):400-4.
111. Manning FA, Wym Pugh E, Boddy K. Effect of cigarette smoking on fetal breathing movements in normal pregnancy. Br Med J. 1975;1(5957):552-8.
112. Ishigava M, Yoneyama Y, Power GG, et al. Maternal teophylline administration and breathing movements in late gestation human fetus. Obstet Gynecol. 1996;88(6):973-8.
113. Cosmi EV, Cosmi E, La Torre R. The effect of fetal breathing movements on the utero-placental circulation. Early Pregnancy. 2001;5(1):51-2.
114. Jobe A. Development of the fetal lung. U: Creasy RK, Resnik R. Maternal- fetal medicine: principles and practice. 2 izd. Philadelphia-London-Toronto-Montreal-Sydney-Tokyo: WB Saunders Company; 1989. pp. 288-300.
115. Haagsman HP, Demiel RV. Surfactant associated proteins: functions and structural variations. Comp Biochem A Mol Integr Physiol. 2001;129(1):91-108.
116. Vyas JR, Kotecha S. The effect of antenatal and postnatal corticosteroids on the preterm lung. Arch Dis Child Fetal Neonatal Ed. 1997;77:F147-50.
117. Hundertmark S, Ragosch V, Zimmermann B, et al. Effect of dexametasone, triiodothyronine and dimetyl-isopropyl-thyronine on the maturation of the fetal lung. J Perinat Med. 1999;27(4):309-15.
118. Chan L, Miller TF, Yuxin J, et al. Antenatal triiodothyronine improves neonatal pulmonary function in preterm lambs. J Soc Gynecol Investig. 1998;5(3):122-6.
119. Debieve F, Beerlandt S, Hubinot C, et al. Gonadotropines, prolactin, inhibin A, inhibin B, and activin A in human fetal serum from midpregnancy and term pregnancy. J Clin Endocrin Metab. 1997;85(1):270-4.
120. Glass L, Rajegowda BK, Evans HE. Absence of respiratory distress syndrome in premature infants of heroin-addicted mothers. Lancet. 1971;2(7726):685-6.
121. Thuresson-Klein A, Moawad AH, Hedqvust P. Estrogen stimulates formation of lamellar bodies in the rat fetal lung. Am J Obstet Gynecol. 1985;151(4):506-14.
122. Adamson IY, Bakowska J, Mc Millan E, et al. Accelerated fetal lung maturation by estrogen is associated with an epithelial-fibroblast interaction. In Vitro Cell Dev Biol. 1990;26 (8):784-90.
123. Warburton D. Chronic hyperglycemia reduces surface active maternal flux in tracheal fluid of fetal lambs. J Clin Invest. 1983;71(3):550-5.
124. Dekowski SA, Snyder JM. The combined effect of insulin and cortisol on surfactant protein mRNA levels. Pediatr Res. 1995;38(4):513-21.
125. Klein JM, Nielsen HC. Androgen regulation of epidermal growth factor receptor binding activity during rabbit fetal development. J Clin Invest. 1993;91(2):425-31.
126. Hallman M, Glumoff V, Ramet M. Surfactant in respiratory distress syndrome and lung injury. Comp Biochem Physiol A Mol Integr Physiol. 2001;(1):287-94.

127. Jobe AH, Ikegami M. Antenatal infection/inflammation and postnatal lung maturation and injury. Resp Res. 2001;2(1):27-32.
128. Mardešić D i sur. Pedijatrija. 6. izd. Zagreb:Školska knjiga; 2000. pp. 303-94.
129. Kleinmann LI. The kidney. In: Stave U (Ed). Perinatal physiology. New York-London: Plenum Medical Book Company; 1978. pp. 589-616.
130. Čvorić A. Razvoj bubrega i bubre•nih funkcija. In: Koraè D. Pedijatrija. Beograd. Zagreb: Medicinska knjiga; 1983. pp. 441-3.
131. Gilbert T, Merlet-Bénichou C. Retinoids and nephron mass control. Pediatr Nephrol. 2000; 14(12):1137-44.
132. Merlet-Benichou C, Gilbert M, Muffet-Joly M, et al. Intrauterine growth development leads to a permanent nephron deficit in the rat. Pediatr Nephrol. 1994;8(2):175-80.
133. Amri K, Freund N, Vilar J, et al. Adverse effects of hyperglycemia on kidney development in rats: in vivo and in vitro studies. Diabetes. 1999;48(11):2240-5.
134. Gilbert T Gaonach S, Moreau E, et al. Defect of nephrogenesis induced by gentamicin in rat metanephric organ culture. Lab Invest. 1994;70(5):656-66.
135. Kurjak A, Kirkinen P, Latin V, et al. Ultrasonic assessment of fetal kidney function in normal and complicated pregnancies. Am J Obstet Gynecol. 1981;141(3):266-70.
136. Wladimiroff JW. Effect of furosemide on fetal urine production. Br J Obstet Gynaecol. 1975;82(3):221-4.
137. Aperia A, Larsson L, Zetterström R. Hormonal induction of Na+/K+ ATPase in developing proximal tubular cells. Am J Physiol. 1981;241(4): F356-60.
138. Schmidt U, Horster M. Na+ -K+ - activated ATPase: Activity maturation in rabbit nephron segments dissected in vitro. Am J Physiol. 1977; 233: F55-61.
139. Arant BS Jr. Developmental patterns of renal function maturation compared in the human neonate. J Pediatr. 1978;92(5):705-12.
140. Karlen J, Paeria A, Zetterström R. Renal excretion of calcium and phosphate in preterm and fullterm infants. J Pediatr. 1985;106:814-9.
141. Schwartz GJ, Evan AP. Development of solute transport in rabbit proximal tubule. In: HCO_3^- and glucose absorption. Am J Physol. 1983;245:F382-6.
142. Battaglia FC, Meschia IG. An introduction to fetal physiology. Orlando: Academic Press; 1986. pp. 154-67, 184-5.
143. Devuyst O, Burrow CR, Smith BL, et al. Expression of aquaporins -1 and -2 during nephrogenesis and in autosomal dominant poycystic kidney disease. Am J Physiol. 1996;271(1 Pt 2):F169-83.
144. Boylan PC, Parisi VM. Fetal acido-base balance. In: Creasy RK, Resnik R (Eds). Maternal-fetal medicine: principles and practice. Philadelphia-London-Toronto-Montreal-Sydeny-Tokyo: WB Saunders Company; 1989. pp. 362-73.
145. Winkler CA, Kittelberger AM, Watkins RH. Maturation of carbonic anchidrase IV expression in rabbit kidney. Am J Physiol Renal Physiol. 2001;280(5):F895-903.
146. McCance RA, Widdowson EM. Renal function before birth. U: Widdowson EM. Studies in perinatal physiology. 1. izd. Bath:Pitman press; 1980. pp. 94-103.
147. McGroy WW. Development of renal function in utero. Cambridge:Harvard University Press; 1972. pp. 51-78.
148. McCance RA, Young WF. The secretion of urine by newborn infants. U: Widdowson EM. Studies in perinatal physiology. 1. izd. Bath:Pitman press; 1980. pp. 45-50.
149. McCance RA, Von Fimck MA. The titratable acidity, pH, ammonia and phosphates in the urine of very young infants. U: Widdowson EM. Studies in perinatal physiology. 1. izd. Bath:Pitman press; 1980. pp. 81-8.
150. Judaš M, Kostović I. Temelji neuroznanosti. 1. izd. MD Zagreb;1997. pp. 24-31,622-42,353-60.
151. Okado N, Kakimi S, Kojima T. Synaptogenesis in the cervical cord of the human embryo: sequence of synapse formation in a spinal reflex pathway. J Comp Neurol. 1979;184(3):491-518.
152. Okado N, Kojima T. Ontogeny of the central nervous system: neurogenesis, fibre connection, synaptogenesis and myelination in the spinal cord. In: Prechtl HFR (Ed). Continuity of neural function from prenatal to postnatal life. Oxford:Blackwell Science; 1984. pp. 31-5.
153. Landmesser LT, Morris DG. The development of functional innervation in the hind limb of the chick embryo. J Physiol. 1975;249(2):301-26.
154. Prechtl HFR. Ultrasound studies of human fetal behaviour. Early Hum Dev. 1985;12(2): 91-8.
155. Ianniruberto A, Tajani E. Ultrasonographic study of fetal movements. Semin Perinatol. 1981;4:175-81.
156. Okado N. Onset of synapse formation in the human spinal cord. J Comp Neurol. 1981;201 (2):211-9.
157. Joseph R. Fetal brain and cognitive development. Dev Rev. 1999;20:81-98.
158. de Vries JIP, Visser GHA, Prechtl HFR. The emergence of fetal behavior. I. Qualitative aspects. Early Human Dev. 1982;7(4):301-22.
159. Pomeroy SL, Volpe JJ. Development of the nervous system. In: Polin RA, Fox, WW (Eds): fetal and neonatal physiology. Philadelphia: London-Toronto-Montreal-Sydney-Tokyo: WB Saunders Company; 1992. pp. 1491-509.
160. Kostović I, Judas M. Transient patterns of cortical lamination during prenatal life: do they have implications for treatment? Neurosci Biobehav Rev. 2007;31(8):1157-68.
161. Molliver ME, Kostovic I, Van der Loos H. The development of synapses in cerebral cortex of the human fetus. Brain Res. 1973;50(2):403-7.
162. Lüchinger AB, Hadders-Algra M, van Kan CM, et al. Fetal onset of general movements. Pediatr Res. 2008;63(2):191-5.
163. Kurjak A, Azumendi G, Vecek N, et al. Fetal hand movements and facial expression in normal pregnancy studied by four-dimensional sonography. J Perinat Med. 2003;31(6):496-508.
164. Kurjak A, Andonotopo W, Hafner T, et al. Normal standards for fetal neurobehavioral developments—longitudinal quantification by four-dimensional sonography. J Perinat Med. 2006; 34(1):56-65.
165. Andonotopo W, Medic M, Salihagic-Kadic A, et al. The assessment of fetal behavior in early pregnancy: comparison between 2D and 4D sonographic scanning. J Perinat Med. 2005;33 (5):406-14.
166. Awoust J, Levi S. Neurological maturation of the human fetus. Ultrasound Med Biol. 1983; Suppl 2:583-7.

167. Inoue M, Koyanagi T, Nakahara H. Functional development of human eye-movement in utero assessed quantitatively with real-time ultrasound. Am J Obstet Gynecol. 1986;155(1):170-4.
168. Kostović I, Rakic P. Developmental history of the transient subplate zone in the visual and somatosensory cortex of the macaque monkey and human brain. J Comp Neurol. 1990;274(3):441-70.
169. Kostović I, Judas M, Petanjek Z, et al. Ontogenesis of goal-directed behavior: anatomo-functional considerations. Int J Psychophysiol. 1995;19(2):85-102.
170. D'Elia A, Pighetti M, Moccia G, et al. Spontaneous motor activity in normal fetus. Early Human Dev. 2001;65(2):139-44.
171. Natale R, Nasello-Paterson C, Turlink R. Longitudinal measurements of fetal breathing, body movements, and heart rate accelerations, and decelerations at 24 and 32 weeks of gestation. Am J Obstet Gynecol. 1985;151(2):256-63.
172. Eller DP, Stramm SL, Newman RB. The effect of maternal intravenous glucose administration on fetal activity. Am J Obstet Gynecol. 1992;167(4 Pt 1):1071-4.
173. Haddres-Algra M. Putative neural substrate of normal and abnormal general movements. Neurosci Biobehav Rev. 2007;31(8):1181-90.
174. Kurjak A, Azumendi G, Andonotopo W, et al. Three- and four-dimensional ultrasonography for the structural and functional evaluation of the fetal face. Am J Obstet Gynecol. 2007;196(1):16-28.
175. Kozuma S, Baba K, Okai T, et al. Dynamic observation of the fetal face by three-dimensional ultrasound. Ultrasound Obstet Gynecol. 1999;13(4):283-4.
176. Yan F, Dai SY, Akther N, et al. Four-dimensional sonographic assessment of fetal facial expression early in the third trimester. Int J Gynaecol Obstet. 2006;94(2):108-13.
177. Merz E, C Weller. 2D and 3D Ultrasound in the evaluation of normal and abnormal fetal anatomy in the second and third trimesters in a level III center. Ultraschall Med. 2005;26(1):9-16.
178. Kurjak A, Stanojevic M, Andonotopo W, et al. Behavioral pattern continuity from prenatal to postnatal life: a study by four-dimensional (4D) ultrasonography. J Perinat Med. 2004;32(4):346-53.
179. Vanhatalo S, van Nieuvenhuizen O. Fetal pain? Brain Dev. 2000;22(3):145-50.
180. Teixeira JM, Glover V, Fisk NM. Acute cerebral redistribution in response to invasive procedures in the human fetus. Am J Obstet Gynecol. 1999;181(4):1018-25.
181. Smith RP, Gitau R, Glover V, et al. Pain and stress in the human fetus. Eur J Obstet Gynecol Reprod Biol. 2000;92(1):161-5.
182. Giannakoulopoulos X, Sepulveda W, Kourtis P, et al. Fetal plasma cortisol and beta endorphin response to intrauterine needling. Lancet. 1994;344(8915):77-81.
183. Giannakoulopolous X, Teixeira J, Fisk N, et al. Human fetal and maternal noradernaline responses to invasive procedures. Pediatr Res. 1999;45(4 Pt 1):494-9.
184. Lee SJ, Ralston HJ, Drey EA, et al. Fetal pain: a systematic multidisciplinary review of the evidence. JAMA. 2005; 294(8):947-54.
185. Lowery CL, Hardman MP, Manning N, et al. Neurodevelopmental changes of fetal pain. Semin Perinatol. 2007;31(5):275-82.
186. Morlet T, Collet L, Salle B, et al. Functional maturation of cochlear active mechanisms and of the medial olivocochlear system in humans. Acta Otolaryngol. 1993;113(3):271-7.
187. Morlet T, Collet L, Duclaux R, et al. Spontaneous and evoked otoacustical emissions in preterm and full term neonates, Is there a clinical application? Int J Ped OtoRhinoLaryngol. 1995; 33(3):207-11.
188. Leader LR, Baille P, Martin B, et al. The assessment and significance of habituation to a repeated stimulus by the human fetus. Early Human Dev. 1982;7(3):211-9.
189. Liley AW. Fetus as a person. Speach held at the 8th meeting of the psychiatric societies of Australia and New Zealand. Fetal therapy. 1986;1:8-17.
190. Sun W, Hansen A, Zhang L, et al. Neonatal nicotine exposure impairs development of auditory temporal processing. Hear Res. 2008;245(1-2):58-64.
191. Kiefer I, Siegel E, Preissl H, et al. Delayed maturation of auditory-evoked responses in growth-restricted fetuses revealed by magnetoencephalographic recordings. Am J Obstet Gynecol. 2008;199(5):503.e1-7.
192. Lee CT, Brown CA, Hains SM, et al. Fetal development: voice processing in normotensive and hypertensive pregnancies. Biol Res Nurs. 2007;8(4):272-82.
193. Huttenlocher PR, de Courten CH. The development of synapses in striate cortex of man. Human Neurobiol. 1987;6(1):1-9.
194. Magoon EH, Robb RM. Development of myelin in human optic nerve tract. A light and electron microscopic study. Arch Ophtalmol. 1981;99(4):655-9.
195. Kostovic I, Rakic P. Development of prestriate visual projections in the monkey and human fetal cerebrum revealed by transient cholinesterase staining. J Neurosci. 1984;4(1):25-42.
196. Sheridan CJ, Preissl H, Siegel ER, et al. Neonatal and fetal response decrement of evoked responses: A MEG study. Clin Neurophysiol. 2008;119(4):796-804.
197. Eswaran H, Wilson J, Preissl H, et al. Magnetoencephalographic recordings of visual evoked brain activity in the human fetus. Lancet. 2002;360(9335):779-80.
198. Kablar B. Determination of retinal cell fates is affected in the absence of extraocular striated muscles. Dev Dyn. 2000;226(3):478-90.
199. Ruckenbush Y, Gaujoux M, Eghbali B. Sleep cycles and kinesis in the fetal lamb. Electroenceph Clin Neurophysiol. 1977;42(2):226-37.
200. Kelly DD. Sleep and dreaming. In: Kandell ER, Schwartz JH (Eds). Principles of neural science. 2nd Edition. New York-Amsterdam-Oxford:Elsevier Science Publishing; 1985. p. 651.
201. Rosen MG, Scibetta JJ, Chik L, et al. An approach to the study of brain damage: the principles of fetal FEEG. Am J Obstet Gynecol. 1973;115:37-47.
202. Roffag HP, Muzio JN, Dement WC. Ontogenetic development of the human sleep-dream cycle. Science. 1966;152(3722):604-19.
203. Abrams RM, Gerhardt KJ. The acoustic environment and physiological responses of the fetus. J Perinatol. 2000;20(8 Pt 2):S31-6.

204. Mennella JA, Johnson A, Beauchamp GK. Garlic ingestion by pregnant women alters the odor of amniotic fluid. Chem Senses. 1995;20(2):207-9.
205. Mennella JA, Jagnow CP, Beauchamp GK. Prenatal and postnatal flavor learning by human infants. Pediatrics. 2001;107(6):E88.
206. Varendi H, Porter RH, Winberg J. Does the newborn baby find the nipple by smell? Lancet. 1994;334(8928):989-90.
207. Varendi H, Porter RH, Winberg J. Natural odour preference of newborn change over time. Acta Pediatrica. 1997;86:985-90.
208. Widstrom AM, Ransjö-Arvidson AB, Christensson K, et al. Gastric suction in healthy newborn infant. Effects on circulation and developing feeding behavior. Acta Paediatr Scand. 1987;76(4):556-72.
209. Varendi H, Porter RH, Winberg J. Attractiveness of amniotic fluid odor: evidence of prenatal olfactory learning? Acta Paediatr. 1996;85(10):1223-7.
210. Porter RH, Winberg J. Unique salience of maternal breast odors for newborn infants. Neurosci Biobehav Rev. 1999;23(3):439-49.
211. Kostovic I. Prenatal development of nucleus basalis complex and related fiber system in man: a histochemical study. Neuroscience. 1986;17(4):1047-77.
212. Salihagic Kadic A, Medic M, Kurjak A. Recent advances in neurophysiology. In: Kurjak A, Azumendi G (Eds). The fetus in three dimensions. London: Informa Healtcare; 2007. pp. 411-33.
213. Anand KJ. Clinical importance of pain and stress in preterm neonates. Biol Neonate. 1998;73(1):1-9.
214. Carmichael SL, Shaw GM, Yang W, et al. Maternal stressful life events and risks of birth defects. Epidemiology. 2007;18(3):356-61.
215. Monk C, Fifer WP, Myers MM, et al. Maternal stress responses and anxiety during pregnancy: effects on fetal heart rate. Dev Psychobiol. 2000;36(1):67-77.
216. DiPietro JA, Hilton SC, Hawkins M, et al. Maternal stress and affect influence fetal neurobehavioral development. Dev Psychol. 2002;38(5):659-68.
217. Jugović D, Tumbri J, Medić M, et al. New Doppler index for prediction of perinatal brain damage in growth-restricted and hypoxic fetuses. Ultrasound Obstet Gynecol. 2007;30(3):303-11.
218. Hundertmark S, Ragosch V, Zimmermann B, et al. Effect of dexamethasone, triiodothyronine and dimethyl-isopropyl-thyronine on lung maturation of the fetal rat lung. J Perinat Med. 1999;27(4):309-15.
219. Uno H, Lohmiller L, Thieme C, et al. Brain damage induced by prenatal exposure to dexamethasone in fetal rhesus macaques. I. Hippocampus. Brain Res Dev Brain Res. 1990;53(2): 157-67.
220. Barbazanges A, Piazza PV, Le Moal M, et al. Maternal glucocorticoid secretion mediates long-term effects of prenatal stress. J Neurosci. 1996;16(12):3943-9.
221. Hayashi A, Nagaoka M, Yamada K, et al. Maternal stress induces synaptic loss and developmental disabilities of offspring. Int J Dev Neurosci. 1998;16(3-4):209-16.
222. Rees S, Harding R. Brain development during fetal life: influences of the intra-uterine environment. Neurosci Lett. 2004;361(1-3):111-4.
223. Sandman CA, Wadhwa PD, Chicz-Demet A, et al. Maternal corticortropin-releasing hormone and habituation in human fetus. Dev Psychobiol. 1999;34(3):163-73.
224. Glover V. Maternal stress or anxiety in pregnancy and emotional development of the child. Br J Psychiatry. 1997;171:105-6.
225. Graham YP, Heim C, Goodman SH, et al. The effects of neonatal stress on brain development: implications for psychopathology. Dev Psychopathol. 1999;11(3):545-65.
226. Weinstock M. Does prenatal stress impair coping and regulation of hypothalamic-pituitary-adrenal axis. Neurosci Biobehav Rev. 1997;21(1):1-10.
227. Weinstock M. Alterations induced by gestational stress in brain morphology and behavior of the off-spring. Prog Neurobiol. 2001;65(5):427-51.
228. Amiel-Tison C, Cabrol D, Denver R, et al. Fetal adaptation to stress: Part II. Evolutionary aspects; stress induced hippocampal damage; long-term effects on behavior; consequences on adult health. Early Human Dev. 2004;78(2):81-94.
229. Buitelaar JK, Huizink AC, Mulder EJ, et al. Prenatal stress and cognitive development and temperament in infants. Neurobiol Aging. 2003;24 Suppl 1:S53-60; discussion S67-8.
230. Davis EP, Glynn LM, Schetter CD, et al. Prenatal exposure to maternal depression and cortisol influences infant temperament. J Am Acad Child Adolesc Psychiatry. 2007;46(6):737-46.
231. Gutteling BM, de Weerth C, Zandbelt N, et al. Does maternal prenatal stress adversely affect the child's learning and memory at age six? J Abnorm Child Psychol. 2006;34(6):789-98.
232. Benediktsson R, Lindsay RS, Noble J, et al. Glucocorticoid exposure in utero: a new model of adult hypertension. Lancet. 1993;341(8841):339-41.
233. Edward CR, Benediktsson R, Lindsay RS, et al. Dysfunction of placental glucocorticoid barrier: link between fetal environment and adult hypertension? Lancet. 1993; 341(8841):355-7.
234. Hales CN, Barker DJ, Clark PM, et al. Fetal and infant growth and impaired glucose tolerance at age 64. BMJ. 1991;303(6809):1019-22.

7

CHAPTER

Ultrasound Markers of Implantation

Luis T Mercé, Maria J Barco, Asim Kurjak

INTRODUCTION

Implantation is the penetration of the embryo in the uterine endometrium. This process is characterized by taking place only during a very specific period called "implantation window". Between days 19 to 22 of the menstrual cycle, synchronization between the embryo development blastocyst stage and endometrium receptivity occurs.

Current assisted reproduction techniques (ART), especially *in vitro* fertilization (IVF), makes possible to know the implantation process and the best conditions to achieve a successful outcome. Today we know that obtaining a pregnancy after embryo transfer is closely related to the embryo quality, endometrium receptivity and the transfer technique.

Currently, it is firmly believed that to increase pregnancy rates and decrease multiple gestations through ART, a better knowledge of implantation markers is required. Ultrasonography, color Doppler, the recently introduced 3D ultrasonography and power Doppler angiography offer the possibility to assess the uterine and ovarian markers of implantation to be able to use them in our clinical practice. As it is described below, endometrial ultrasound and Doppler parameters give us the information related to endometrial receptivity and can be used as implantation markers.

ULTRASOUND IMPLANTATION MARKERS

Real-time ultrasonography allows us the study of two main implantation markers: endometrial thickness and endometrial morphological patterns.[1] Pulsed and color Doppler assessment is applied to the study of different variables of uterine and endometrial perfusion that are also used as receptivity factors.[2] Three-dimensional ultrasound and power Doppler angiography (3D US-PDA) have the advantage of simultaneous assessment of endometrial volume and endometrial blood flow.[3]

Endometrial Thickness and Volume

Endometrial thickness is defined as the maximal distance between the echogenic interfaces of the myometrium and the endometrium when measured on the longitudinal plane of the uterus **(Fig. 7.1A)**. Significant differences of this thickness have not been observed between spontaneous and stimulated cycles even using different stimulation protocols.[4] This finding suggests that there is a maximal endometrial response induced by estrogens that is achieved during the natural ovulatory cycle.[5] A significant correlation between the endometrial thickness and endometrial histopathological dating has not been found either.[6]

In IVF stimulated cycles, the endometrium increases 1.9 mm between days 7–9 of the stimulation treatment, 0.9 mm between days 9–11 and 0.6 mm between the latter and the day of human chorionic gonadotropin (hCG) administration.[7] The endometrial thickness increases 0.5 mm per day[8] or does not change until the embryo transfer day.[7] Significant differences have not

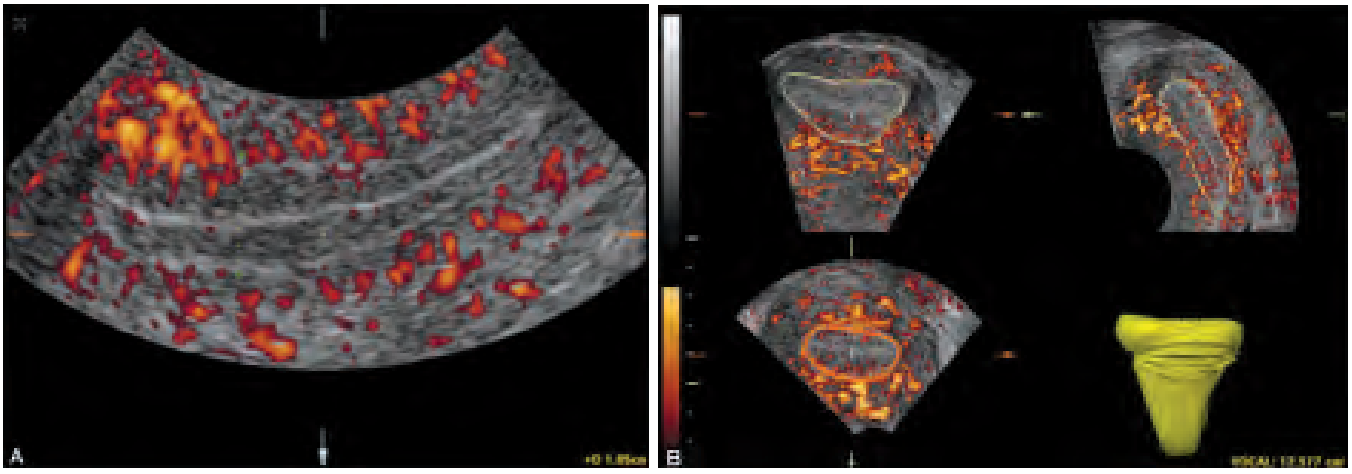

Figures 7.1A and B: (A) Endometrial thickness measured on the longitudinal plane of the uterus; (B) Endometrial volume assessed by three-dimensional ultrasound

been observed in endometrial thickness between hCG day and the day of embryo transfer[9], which clearly has practical implications to choose the timing for the measurement.

There is not enough data to demonstrate if a linear relationship exists between endometrial thickness and the probability of pregnancy after an ART.[10] Endometrial thickness in a great number of cycles studied shows similar ranges in conception cycles (n = 514; 8.6–11.8 mm) as well as the ones that did not conceive (n = 1110; 8.6–11.9 mm).[10] However, in the conception cycles there is an accelerated increase in the endometrial thickness during the luteal phase that reaches significant differences regarding to that in nonconception cycles 14 days after the day of oocyte retrieval.[8,11]

As an implantation marker, endometrial thickness is characterized by its significant sensitivity (95–100%), but also shows a high number of false positives (78–97%);[10] therefore, the main advantage is a high negative predictive value (87–100%) **(Table 7.1)**. An endometrial thickness lower than 7 mm on the day of hCG administration is considered an acceptable marker for nonreceptive endometrium. It has also been reported that implantation and pregnancy rates are negatively affected by the endometrium being thicker than 14 mm,[12] although data from recent studies do not support this finding.[13,14] On the other hand, a very thin (< 6 mm) or very thick (> 13 mm) endometrium has also been associated with an increase in early miscarriages.[15]

In a donor oocyte program with hormone replacement therapy (HRT) it is proven that pregnancy rates and endometrial thickness decrease at the same time.[16] When endometrial thickness is equal or greater than 9 mm a pregnancy rate of 68% is achieved, diminishing to 20% when endometrial thickness is less than 6 mm.[16] Although it is possible to achieve pregnancies with a thin endometrium,[17] this is always a bad predictive factor that requires further study of the endometrium.[16] In a retrospective study of 1,228 IVF/ICSI (Intracytoplasmic sperm injection) cycles, endometrial thickness

TABLE 7.1

Predictive values of sonographic and Doppler parameters to achieve pregnancy with assisted reproduction techniques

Parameters[1]	*Se*	*Sp*	*PPV*	*NPV*
Endometrial thickness[2]	95-100	3-22	26-45	87-100
Endometrial pattern[3]	79-100	9-43	32-48	86-100
Uterine Doppler[4]	96-100	13-35	44-56	88-100

[1]All the values are percentages;[2] According to different authors, techniques and limits of endometrial thickness, between 6–10 mm;[3] According to different authors and techniques;[4] For a pulsatility index of uterine arteries between 3 and 3.3 according to different authors and techniques. Se: Sensitivity; Sp: Specificity; PPV: Positive predictive value; NPV: Negative predictive value.

on the day of embryo transfer was positively associated with pregnancy rates. Improved pregnancy rates were found when the endometrium reached at least 10 mm and rates further improved with additional increases in endometrial thickness between 10–14 mm. Nevertheless, these authors did not find any significant difference in endometrial thickness between ongoing pregnancies and the ones resulting in a first-trimester loss.[18] After a retrospective analysis of 897 IVF-ET cycles, an increased endometrial thickness on the hCG day administration is associated with an improved outcome, but this relationship also depends on patient age, length of ovarian stimulation and embryo quality. A thin endometrium is associated with reduced pregnancy rates only for the transfers of less good quality embryos.[14] More recently, it was evaluated that the relationship between endometrial thickness and embryo implantation by a retrospective study on 1,294 IVF cycles with transfer of two blastocyst-stage embryos.[19] The authors demonstrated a significant relationship between both variables. Pregnancy rates increased gradually with increasing endometrial thickness. This relationship is independent of the patient age, the number and quality of embryos transferred. Nevertheless, good pregnancy rates can be achieved with endometrial lines of only 6–7 mm, when good-quality blastocysts are transferred.[19]

Three-dimensional technology has added to our daily practice in reproduction the use of endometrial volume as an implantation marker **(Fig. 7.1B)**.[3] Our team has recently demonstrated an excellent intra- and inter-observer reproducibility of this measurement.[20,21] The best intraclass correlation indices to obtain the endometrial volume and endometrial vascularity indices with the virtual organ computer-aided analysis (VOCAL) program are achieved working in the coronal or "C" plane with a rotational angle of 9° **(Table 7.2)**.[21]

During spontaneous menstrual cycles, the changes in uterine/endometrial volume ratio proved a good correlation with the day of menstrual cycle.[22] Endometrial volume increased significantly during the follicular phase, reaching a plateau around the time of ovulation and remaining relatively stable throughout the luteal phase.[23,24] Parous women showed endometrial volumes significantly larger than nulliparous women.[23] According to our results, basal endometrial volumes after pituitary suppression with a long gonadotropin-releasing hormone (GnRH) protocol are significantly smaller than preovulatory endometrial volumes after ovarian simulation with single or multiple preovulatory follicles and midluteal endometrial volumes **(Fig. 7.2A)**.

A pioneering study[25] demonstrated that endometrial volume at the time of ET is related to pregnancy achievement. An endometrial volume larger than 2 ml

TABLE 7.2

Intraobserver repeatability of measurements of endometrial volume (EV), vascularization index (VI), flow index (FI), vascularization flow Index (VFI) according to acquisition plane (A and C) and rotation step (9º and 15º angle) for endometrium

Parameter	*Plane*	*Rotation step*	*Datasets (n)*	*Mean difference**	*SD*	*ICC*	*95%-CI ICC*
EV	A	15º	80	-0.04	0.85	0.99	0.98-1.00
		9º	80	0.29	1.72	0.97	0.95-0.99
	C	15º	80	0.25	1.44	0.98	0.96-0.99
		9º	80	-0.22	1.20	0.98	0.97-0.99
VI	A	15º	80	-0.77	4.34	0.95	0.91-0.97
		9º	80	-0.97	3.54	0.96	0.93-0.98
	C	15º	80	-1.07	4.27	0.95	0.91-0.97
		9º	80	-1.07	3.62	0.97	0.94-0.98
FI	A	15º	80	-0.38	1.84	0.91	0.83-0.95
		9º	80	-0.07	1.85	0.91	0.83-0.95
	C	15º	80	-0.07	1.70	0.91	0.84-0.95
		9º	80	-0.27	1.82	0.90	0.82-0.95
VFI	A	15º	80	-0.21	1.38	0.95	0.91-0.98
		9º	80	-0.31	1.17	0.96	0.93-0.98
	C	15º	80	-0.30	1.42	0.95	0.92-0.98
		9º	80	-0.27	1.23	0.97	0.94-0.98

***** Mean of difference between both measurements. ICC: intraclass correlation coefficient; 95%-CI: 95% confidence interval for ICC; SD: standard deviation

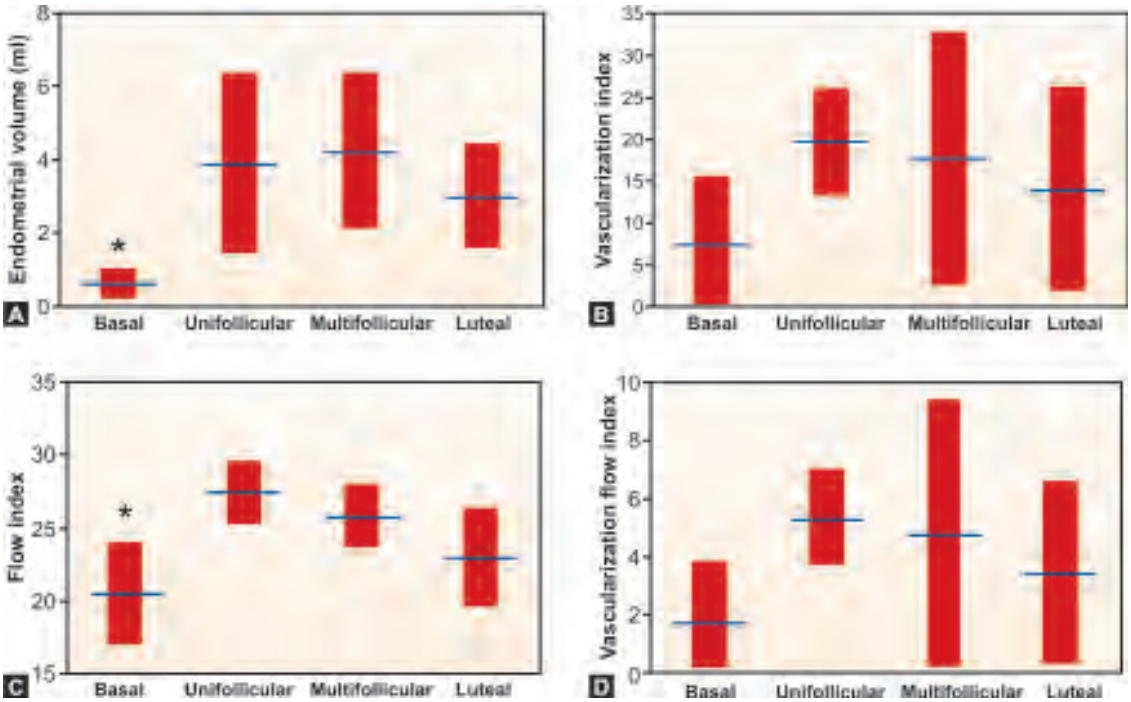

Figures 7.2A to D: (A) Endometrial volume; (B) Vascularization index; (C) Flow index; (D) Vascularization flow index according to ovarian functional status. Basal (12 cases): on the day of pituitary suppression confirmation after a standard long GnRH protocol; Unifollicular (11 cases): on the day of hCG administration after low doses of FSH ovarian stimulation getting a single follicle development; Multifollicular (14 cases): on the day of hCG administration after standard doses for ovarian stimulation and multifollicular development; Luteal (10 cases): on mesoluteal phase in normal ovulatory cycles. * P < 0.05

TABLE 7.3

Endometrial thickness, volume, vascularization index, flow index and vascularization flow index on the hCG day in an IVF/ICSI program according to outcome

	Pregnant (n = 38)	*Nonpregnant (n = 39)*	*P*
Endometrial thickness (mm)	12.29 ± 2.71	12.15 ± 2.31	0.81
Endometrial volume (ml)[a]	5.63 (2.67-16.64)	4.82 (2.05-9.24)	0.02
Vascularization index	21.19 ± 8.91	16.05 ± 9.84	0.02
Flow index	28.12 ± 3.90	24.27 ± 3.71	<0.001
Vascularization flow index	6.30 ± 4.46	3.64 ± 2.75	0.01

Data are presented as mean ± standard deviation or n (%) or [a] median (range).

could be a prerequisite for good endometrial receptivity given that pregnancy and implantation rates were significantly lower with a smaller endometrial volume.[25] More recently, an endometrial volume of 2.5 ml on the day of ET has been proposed as a reliable threshold value to predict pregnancy after ET in IVF/ICSI cycles.[26] The analysis of the endometrium on the hCG day by 3D ultrasonography in 80 infertile women undergoing a first IVF-ICSI cycle, proved that endometrial volume is significantly greater in women that got pregnant, whereas endometrial thickness is unchanged **(Table 7.3)**. Other studies have not demonstrated that endometrial volume is predictive for pregnancy.[27-31] This could be explained by methodological differences in volume calculation. Whereas we perform VOCAL program in plane C with a 9° rotational steps, some

authors use a nonrotational method [27-29] or apply the VOCAL program but delineating and measuring an inferior number of planes.[30,31] In addition, endometrial volumes evaluated in different cycle day, such as the day of hCG administration, the day of oocyte retrieval or the day of embryo transfer, might be difficult to compare. Comparing endometrial volume before hCG administration with that on the day of oocyte retrieval, it significantly decreased after hCG injection in women who conceived but not in those who did not conceive.[30] Our group has recently published a prospective clinical study in eighty women who underwent IVF cycle.[32] Endometrial volume was significantly increased in the pregnant group (38 cycles) comparatively with non-pregnant group (39 cycles). On the contrary, endometrial thickness and triple-line pattern did not show significant differences between both groups. According to our results, endometrial volume measured with 3D ultrasound is a useful parameter in predicting outcome cycle in IVF and ET procedure.[32]

Other parameters have been assessed, such as the length and the width of the endometrium[7] or the endometrial area,[33] although no advantage over endometrial thickness or volume in using these parameters has been demonstrated.

Endometrial Pattern

The endometrial pattern is the relative echogenicity that the endometrium presents with respect to the adjacent myometrium. Its importance as an implantation marker lies in that it reflects the degree of histological development.[34]

During the proliferative phase of the menstrual cycle, the endometrium achieves a "triple line" morphology **(Fig. 7.3A)** where the echogenic central line represents the uterine cavity and the outer echogenic lines reflect the basal layer of the endometrium or the interface between the endometrium and, the myometrium. The hypoechogenic zones between the outer and central line are the functional layers of the endometrium. This image is attributed to the glandular disposition, reduced secretion and scarce stromal edema.[35]

During the secretory phase of the menstrual cycle, the endometrium acquires a hyperechogenic morphology **(Fig. 7.3C)** that is due to stromal edema, spiralization and secretion of the endometrial glands caused by the action of progesterone.[2,7,11,36] However, since a correlation between echogenicity and progesterone has not been demonstrated,[9,37] other factors, such as androgen and gonadotropin effects, could explain these changes.[38,39]

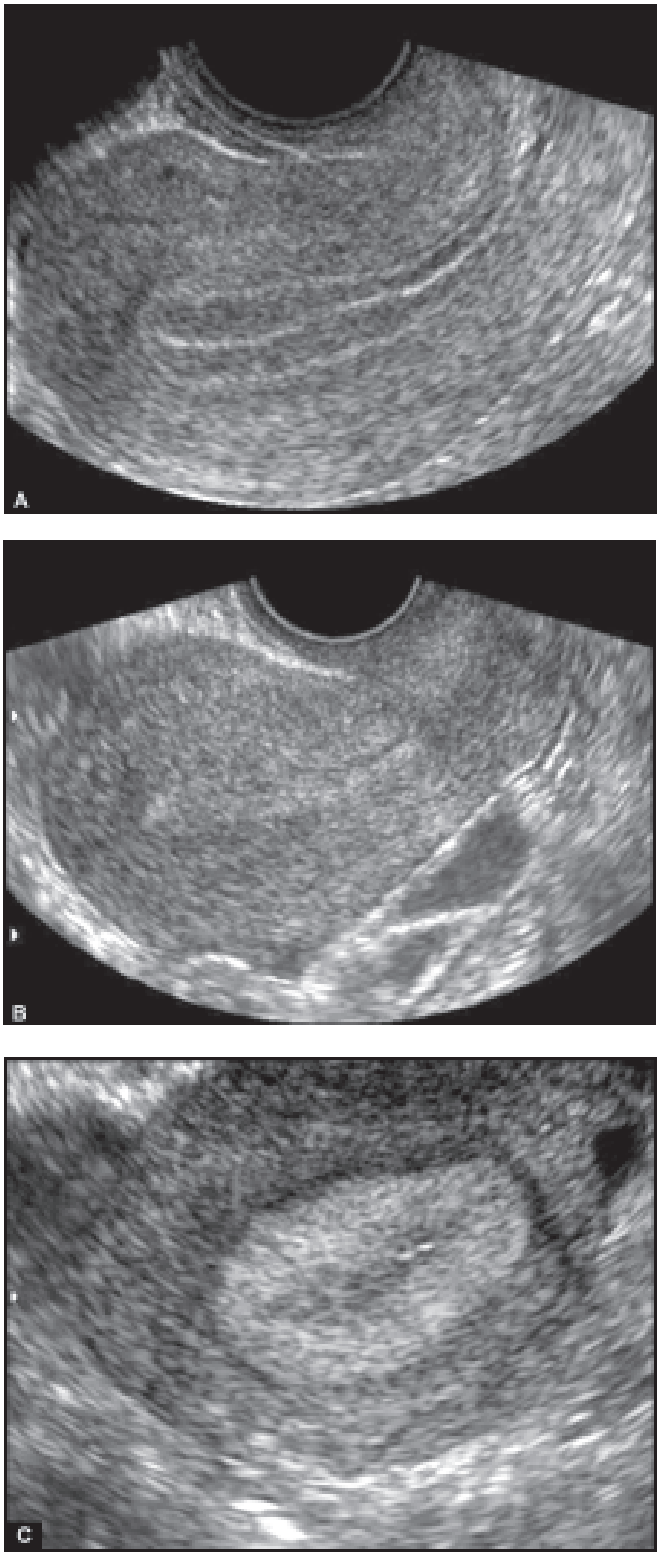

Figures 7.3A to C: Endometrial echogenicity patterns: (A) Multilayered proliferative endometrium or "triple line" pattern; (B) Nonmultilayered endometrium; (C) Secretory endometrium

The subendometrial halo or uterine junctional zone between the endometrium and the myometrium is a distinct compartment of the myometrium comprising tightly packed muscle cells and an increased vascularity.[40]

Although initially four different myometrial echogenicity patterns were described[41] it were lately reduced to three[42], because a "triple line" pattern as the only positive implantation marker results more predictive[43] **(Fig. 7.3B)**. The endometrial pattern does not appear to be influenced by the ovarian stimulation protocol and it is also present when hormonal replacement for frozen ET is carried out.[5] Significant differences of the endometrial morphological pattern between hCG day and the transfer day have not been observed either.[9]

A "triple line" endometrium is the ultrasound marker that most accurately reflects endometrial receptivity, while the "non-triple-line" pattern is frequently associated with nonconception cycles, although the possibility of implantation must never be excluded.[10] Just as with thickness, the "triple line" endometrial pattern has high sensitivity (79–100%) but an elevated percentage of false positives (57–91%) also, subsequently it has an additional interest by its high negative predictive value (75–100%) **(Table 7.1)**. Although achieving a pregnancy with a "non-triple-line" pattern is possible, its frequency is low.[5]

Since the increase in echogenicity during the follicular phase is the best endometrial parameter to indicate low receptivity, an attempt has been made to evaluate this characteristic by computerized analysis of endometrial morphology.[2,11,36,44] During the menstrual cycle, myometrial echogenicity increases significantly in both spontaneous and stimulated cycles,[11,44] but the most important fact is that implantation and pregnancy rates decrease progressively as myometrial echogenicity increases on the day of hCG administration.[11,36] Therefore, there is an inverse relationship between the extent of endometrial echogenicity transformation and the possibility of pregnancy. More recently it has been also demonstrated a positive relationship between trilaminar pattern with successful implantation and ongoing pregnancy in IVF/ICSI cycles using antagonists.[45] Nevertheless, some authors think that combined analysis of endometrial thickness and pattern on the day of hCG administration is a better predictor of the outcome of IVF/ICSI-ET and may be more helpful for patient counseling than the separate analyses.[46]

The normal luteal endometrial pattern has been also implied as an implantation marker. A nonhomogenous hyperechogenic pattern three days after ET has been associated with lower pregnancy rates.[47] In addition, the midluteal endometrial pattern of women with unexplained infertility is related to the chance of pregnancy. The pregnancy rate is significantly higher when the endometrium displays a homogenous hyperechogenic pattern comparatively with nonhomogeneous pattern.[48] Endometrial pattern and thickness were not predictive of pregnancy outcomes in oocyte donation cycles, both prior and following progesterone administration.[49] However, in frozen embryo transfers, it was showed that an increase in progesterone dosage when there is not a mid luteal nonhomogeneous pattern could lead an increased pregnancy rate.[50]

Uterine Doppler

Doppler studies have demonstrated that the resistance of uterine and endometrial arteries decreases significantly during the mesoluteal phase, i.e. in the period of embryo implantation.[51-57] It is probable that these vascular changes play a significant role in the implantation process because they are present from the beginning of the embryo nidation. In rodents, it has been proven an increase of the capillary permeability 24 hours before the blastocyst endometrium contact that takes place at the invasion site due to the local mediation of prostaglandins.[58] Between the 6–12 postovulatory days the endometrium capillaries experience a progressive dilation acquiring a sinusoidal appearance, while the syncytiotrophoblast invades the endometrium. Around the 11th–12th day, the uteroplacental circulation is fully established when maternal blood flows into syncytiotrophoblast lacunae.[59]

Goswany, Williams and Steptoe[60] demonstrated that the blood flow in the uterine arteries determines IVF success and that the uterine receptivity improved by increasing the vascular perfusion with HRT. Despite of the many studies that have been published since, there is no consensus on the importance of Doppler studies of these arteries in ART **(Fig. 7.4)**. A substantial group of authors found significant differences in uterine arteries resistance between cycles with or without pregnancy, yet another important group does not observe this.[61] These contradictory results are due to significant methodological variations, such as the ovarian stimulation protocol used, the cycle's day when the Doppler study was carried out or the sonographic examination route.[61]

Optimal uterine receptivity seems to occur when the mean pulsatility index of both arteries ranges between 2–3,[62-64] the implantation and pregnancy rates significantly decreasing when pulsatility is over three or four[62-70] or when diastolic flow is absent in the Doppler waveform.[69,70] These limits have been proposed

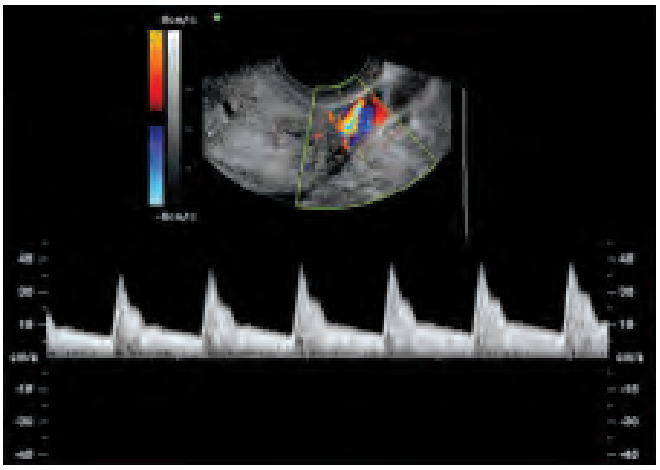

Figure 7.4: Flow velocity waveform of uterine artery on the day of hCG administration

as a clinical marker to indicate the convenience to transfer or not the embryo. In doing so, its ability to predict uterine receptivity presents high sensitivity (96–100%) and a high negative predictive value (88–100%) although it has low specificity (13–35%) and positive predictive value (44–56%).[10] **(Table 7.1)**. Inadequate blood flow would thus prevent implantation, although optimal uterine perfusion does not always imply pregnancy. In addition to this, high uterine resistance is observed in less than 10% of nonconception cycles, suggesting that this parameter is responsible for implantation failure in very few cases.[71]

The relationship between uterine Doppler, endometrial and subendometrial blood flow assessed by 3D power Doppler angiography during stimulated and natural cycles has been evaluated. Several authors conclude that uterine Doppler is a poor reflection of subendometrial blood flow and its measurement cannot represent endometrial blood flow during stimulated cycles.[72]

2D and 3D Endometrial Doppler

Endometrial Doppler should reflect more appropriately the endometrial perfusion and uterine receptivity because the endometrium is the place where implantation occurs. Uterine and endometrial blood flows perform in a similar way during the menstrual cycle. Nevertheless, they show a weak correlation when evaluated by velocimetric indices.[73] During the luteal phase, the vascular endothelial growth factor (VEGF) expression is increased in the endometrium[74,75] and there is a greater angiogenic activity.[76] Recently, a close relationship between a strong VEGF expression in the endometrium and a successful outcome of implantation has been demonstrated.[77]

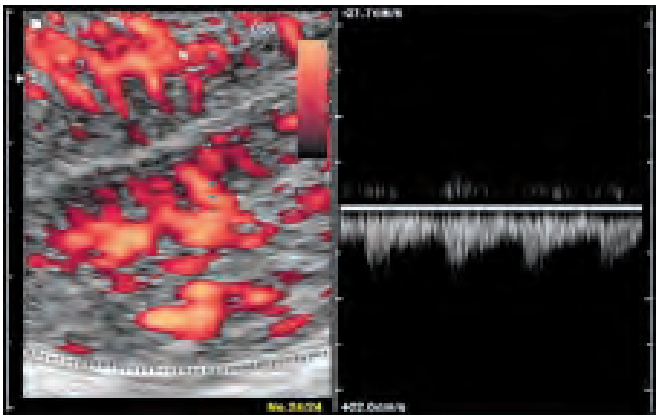

Figure 7.5: Flow velocity waveform of subendometrial-endometrial arteries on hCG administration day

Doppler study allows us to evaluate endometrial blood flow by means of analyzing flow velocity waveforms of subendometrial and endometrial arteries[78-85] and the color mapping by 2D[79,81,86-89] or 3D ultrasound.[28-32,90-92]

Vascular resistance in the endometrial spiral arteries or the subendometrial radial arteries **(Fig. 7.5)**, also called intramyometrial subendometrial arteries,[56,61,80] is found to be decreased on the day of oocyte retrieval or ET in patients who achieve pregnancy,[28,81,84,85] although every author cannot find it.[79,82,83] In an intrauterine insemination program,[80] we observed that the peak systolic velocity of the dominant uterine artery was significantly higher in the midluteal phase in the cycles in which pregnancy was achieved. Moreover, subendometrial radial arteries pulsatility was the only parameter that improved in those cycles where pregnancy was achieved after a previous nonconceptional cycle, except when implantation failed and subsequently a miscarriage or ectopic pregnancy was diagnosed.[61,80]

Color mapping of endometrial vascularity can be classified in various types according to the degree of penetration into the endometrial thickness, using conventional color[79,81,87] or power Doppler.[86,87] In this way we differentiate four types of endometrial blood flow:

- Type 0 or negative flow, when only the surrounding myometrial vessels are seen non-reaching the endometrium
- Type I or peripheral flow, if the color signal reaches the hyperechogenic outer layer of the endometrium
- Type II or intermediate, when color mapping fills in the outer half of the endometrial hypoechogenic thickness; and
- Type III or central flow, if the vessels reach the endometrial cavity invading the entire endometrial thickness **(Figs 7.6A and B)**.

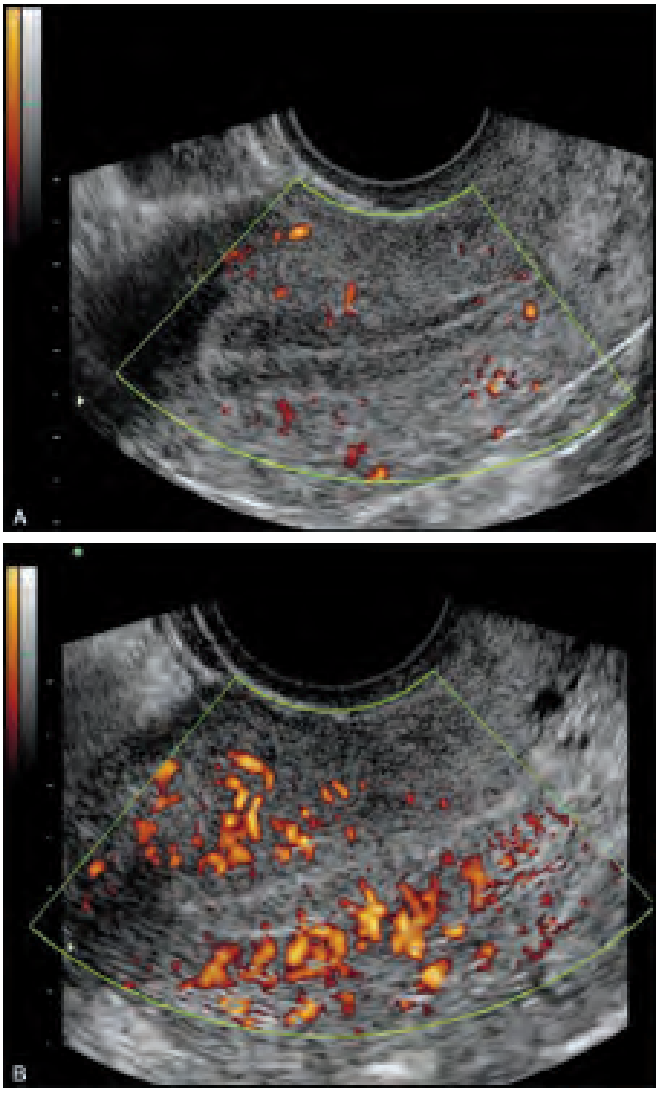

Figures 7.6A and B: (A) Endometrial power Doppler mapping type 0 in which only myometrial vessels can be seen without reaching the subendometrial halo; (B) Endometrial amplitude mapping type II when color signal reaches the endometrial cavity

It has been proposed that the endometrial and subendometrial area should be taken as a unity when the uterine perfusion is assessed by color Doppler, since there is no difference between the endometrial and subendometrial blood flow regarding to the possibility of achieving pregnancy.[88] Nevertheless, color mapping is directly related to the sensitivity of the equipment and the adequate angle of insonation applied, so it is very important to always use the same characteristics, especially when recording the minimum velocity. For this reason, power Doppler is more reliable because signal amplitude mapping detects lower blood flow velocities and is unaffected by the angle of insonation. In general, endometrial color mapping has been evaluated in a subjective way although the color area can also be quantified.[89]

The absence of color mapping of the endometrium and subendometrial areas means an absolute implantation failure[79,85] or a significant decrease[88] of the implantation rate. Conversely, the pregnancy rate increases when the vessels reach the subendometrial halo and endometrium.[79,88] The presence of vessels within the endometrium is associated with a thicker endometrium, which suggests a correlation between the endometrial perfusion and endometrial growth.[88] On the other hand, the absence of endometrial-subendometrial blood flow is accompanied by a high uterine artery resistance.[88] Women with a higher endometrial flow area by power Doppler study have a greater probability of pregnancy, whereas below 5 mm^2 it is difficult that implantation will take place even with an adequate endometrial thickness.[89] We have not found significant differences in endometrial thickness, uterine and endometrial blood flow between conception and nonconception cycles after intrauterine insemination. On the contrary, all these parameters present higher values on the day of hCG administration in these cycles that achieve pregnancy by IVF. Nevertheless, only endometrial thickness and the uterine implantation index combining ultrasound and Doppler parameters show significant differences **(Table 7.4)**. When pregnancy is achieved but endometrial–subendometrial flow on the day of ET cannot be seen, more than a half of these pregnancies will end in spontaneous miscarriage.[88] This suggests that the development of the endometrial vascular network should be important for the support of the first stages of pregnancy.

As mentioned above, three-dimensional ultrasound allows studying not only the endometrial volume but also the complete endometrial perfusion **(Fig. 7.7A)**. A specific software named VOCAL performs an automatic quantification of endometrial vascularization by three 3D power Doppler indices.[93] The vascularization index (VI) estimates the number of color voxels inside the endometrial volume, thus expressing the number of endometrial blood vessels as a percentage. The flow index (FI) is the average color value from all the color voxels, depicting the mean intensity of the endometrial blood flow. The vascularization flow Index (VFI) is the average color value out of all the color and gray voxels, meaning the vascularization as well as the blood flow, in other words, the perfusion inside the endometrium **(Fig. 7.7B)**.[93]

TABLE 7.4

Uterine receptivity parameters on the day of hCG administration in an intrauterine insemination and IVF cycles[1]

Parameters	*IIU*		*P*	*IVF*		*P*
	Pregnant (n = 10)	*Nonpregnant (n = 40)*		*Pregnant (n = 10)*	*Nonpregnant (n = 22)*	
ET	10.0 ± 2.8	10.3 ± 2.3	ns	14.4 ± 3.1	12.1 ± 2.0	0.02
UPI	2.18 ± 0.81	2.65 ± 0.93	ns	2.18 ± 0.49	2.21 ± 0.44	ns
EF	1.4 ± 0.9	1.5± 1.3	ns	3.1 ± 1.2	2.2 ± 1.4	ns
UMI	17 ± 15	18 ± 17	ns	46 ± 18	29 ± 17	0.01

(1) Values indicate mean ± SD; ET: Endometrial thickness in mm; UPI: Mean pulsatility index of both uterine arteries; EF: Endometrial blood flow evaluated by power Doppler mapping according to the following "scoring system": absent, only miometrial (Type 0) = 0 ; Peripheral (Type I) = 1; Intermediate (Type II) = 2; Central (Type III) = 4; UMI: Uterine implantation index according to formula (ET x EF) + [EMP/UPI-notch], where ET is the endometrial thickness in mm, EF: endometrial flow according to the explained scoring system; EMP endomiometrial pattern, whose value is calculated by adding the endometrial pattern score (triple line = 3; other types = 0) and miometrial pattern (homogeneous = 1; nonhomogeneous = 0); UPI value is the mean pulsatility index of both uterine arteries and uterine "notch" is pointed as present (0) or absent.[1]

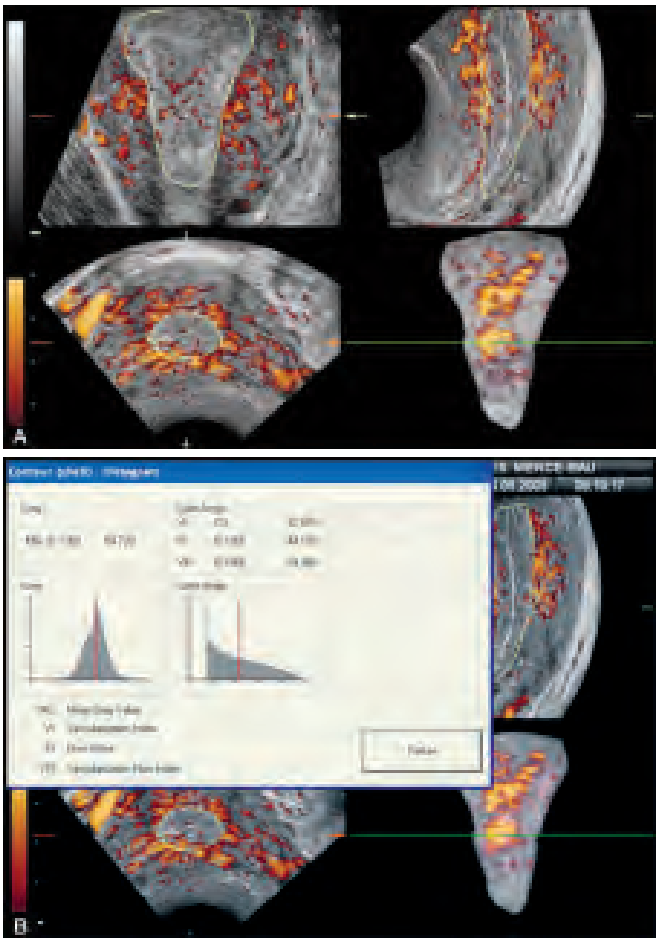

Figures 7.7A and B: (A) Three-dimensional power Doppler acquisition of endometrial vascularity on hCG administration day in an IVF cycle; (B) Power Doppler indices quantification by VOCAL software

Endometrial 3D power Doppler indices change significantly during the normal menstrual cycle. These vascularity indices increase during the proliferative phase reaching a maximum 2–3 days before ovulation. From this peak, vascularity indices decrease to reach a nadir 2–5 days after ovulation. Afterwards, endometrial vascular indices increase progressively along the rest of the luteal phase. Subendometrial blood flow experiences parallel changes but shows higher values of the vascularity indices.[24,94] A reduced endometrial blood flow after ovulation could be related to an increased uterine contractility[95] and may lead to endometrial hypoxia during the implantation period.[96]

Endometrial and subendometrial blood flows assessed in the same patients by 3D power Doppler indices are significantly lower in stimulated than in natural cycles.[97] It has also been reported that endometrial and subendometrial blood flows are negatively affected by serum estradiol concentrations, but they are not affected by other factors, such as women age, smoking habits, or types of infertility or parity, during IVF treatment.[98] This fact could explain that ovarian hyper-responders tend to have lower endometrial and subendometrial blood flows during the early luteal phase (+2 hCG day).[99] We have observed that endometrial FI is significantly decreased after pituitary suppression with a long GnRH protocol. Endometrial vascularity indices on the day of hCG administration do not show statistical differences between single and multifollicular ovarian development. Midluteal endometrial blood flow is found to be lower than preovulatory endometrial blood flow but differences do not reach statistical significance

TABLE 7.5

ROC analysis of 3D endometrial volume and power Doppler indices for predicting pregnancy in IVF/ICSI cycles according to number of Grade 1 embryos transferred

Parameters	*No G1 or 1 G1 embryos transferred (n = 43)*			*> 1 G1 embryos transferred (n = 34)*		
	Area under curve	*95% CI**	*P*	*Area under curve*	*95% CI**	*P*
Endometrial volume (ml)	0.75	0.60-0.90	0.01	0.60	0.38-0.81	0.38
Vascularization index	0.72	0.56-0.89	0.02	0.42	0.21-0.63	0.47
Flow index	0.83	0.68-0.97	0.001	0.65	0.43-0.86	0.19
Vascularization flow index	0.80	0.65-0.95	0.002	0.34	0.16-0.53	0.15

* 95% confidence interval

(Figs 7.2B to D). Small intramural fibroids do not seem to affect the endometrial and subendometrial blood flow;[100] on the other hand, patients with hydrosalpinx show a decreased endometrial and subendometrial blood flow.[101]

Even though most authors assess both endometrial and subendometrial vascularization as a pregnancy predictor,[28-31,90,91] we prefer to calculate only the 3D power Doppler indices of the endometrium.[32] There are three reasons that account for this decision:

1. The endometrium is the actual place where implantation occurs
2. Subendometrial vascularization experiences the same changes as the endometrial one but with higher vascularity indices
3. It is not possible to determine the subendometrial space accurately as it has been defined as an outer shell surrounding the endometrium with many different thicknesses—10 mm,[30] 5 mm [28,29] or 1 mm.[31]

The uterine wall thickness varies from patient to patient, so if we apply the same shell thickness, the vessels in the subendometrial zone will vary greatly from patient to patient, diminishing the reliability of the results. The only way to accurately define the subendometrial space would be applying a single percentage for the various thicknesses of the uterine wall. Furthermore, the endometrial vascularization is well defined as it is, within the limits of the myoendometrial junction.

Some authors have proved that subendometrial vascularity indices may behave as predicting factors for pregnancy on the transfer day[28] and the day of hCG administration.[29,32] Others cannot prove 3D power Doppler indices to be good predictors for pregnancy after follicle-stimulating hormone (FSH) stimulation[30] or in the oocyte retrieval day.[31] Recently it has been proposed the day of hCG administration as the best day to evaluate the uterine receptivity.[84] In frozen-thawed ET cycles, endometrial and subendometrial vascularity measured by 3D power Doppler ultrasound is not a good predictor of pregnancy if measured at one time point only.[90,92] On the contrary, endometrial and subendometrial power Doppler indices are significantly higher in pregnant patients with live following stimulated IVF and frozen thawed-ET transfer than those who suffered miscarriage.[91]

Our results out of 80 infertile women undergoing a first IVF-ICSI cycle show significantly increased endometrial indices of **v**ascularization flow on the hCG day in the pregnant group **(Table 7.3)**.[32] In addition, the ability of 3D parameters for pregnancy prediction seems to depend on the quality of the embryos transferred. When two or three grade embryos were transferred, the area under the receiver operating characteristic (ROC) curve of the endometrial volume and the endometrial vascularity indices was inferior to 0.65, although with no statistical significance. On the other hand, when none or only one grade 1 embryo was transferred, the ROC curve showed a significant area for all the parameters, being slightly greater for FI. A FI greater than or equal to 26.1 predicted gestation with a sensitivity of 85.7% and a 27.6% false-positive rate **(Table 7.5)**. The ROC analysis also demonstrated that the endometrial volume and 3D power Doppler indices predict significantly which pregnancies will carry on normally; however, no relationship with the possibility of multiple gestations has been found.

According to our results it can be assumed that the 3D sonographic and power Doppler implantation markers are specially related to pregnancy when the quality of the transferred embryos is not good enough or only one top embryo can be transferred. Therefore, in order to achieve a pregnancy, a good endometrial receptivity, as assessed by ultrasound markers, seems

essential when only one top quality embryo is available for transfer. The majority of ET policies propose a reduced number of embryos to be transferred[102,103] and the amount of cycles where only one embryo is transferred is progressively increasing.[104,105] At this point, we believe that the new 3D markers of endometrial receptivity could be useful to select the more suitable cycle for the transfer of a single embryo.

REFERENCES

1. Mercé LT. Ultrasound markers of implantation. Ultrasound Rev Obstet Gynecol. 2002;2(2):110-23.
2. Fanchin R. Assessing uterine receptivity in 2001: ultrasonographic glances at the New Millennium. Ann N Y Acad Sci. 2001;943:185-202.
3. Mercé LT. Ultrasound markers of implantation. In: Kurjak A, Chervenak FA (Eds). Donald School Textbook of Ultrasound in Obstetrics and Gynecology. New Delhi: Jaypee Brothers medical publishers; 2004. pp. 691-700.
4. Imoedemhe DA, Shaw RW, Kirkland A, et al. Ultrasound measurement of endometrial thickness on different ovarian stimulation regimens during in vitro fertilization. Hum Reprod. 1987;2(7):545-7.
5. Tan SL, Biljan MM. Selection of candidates for in vitro fertilization based on color Doppler findings. In: Kupesic S, De Ziegler D (Eds). Ultrasound and Infertility. London: The Parthenon publishing group; 2000. pp. 155-68.
6. Li TC, Nuttall L, Klentzeris L, et al. How well does ultrasonographic measurement of endometrial thickness predict the results of histological dating? Hum Reprod. 1992;7(1):1-5.
7. Bassil S. Changes in endometrial thickness, width, length and pattern in predicting pregnancy outcome during ovarian stimulation in in vitro fertilization. Ultrasound Obstet Gynecol. 2001;18(3):258-63.
8. Rabinowitz R, Laufer N, Lewin A, et al. The value of endometrial measurement in the prediction of pregnancy following in vitro fertilization. Fertil Steril. 1986;45(6):824-8.
9. Khalifa E, Brzyski RG, Oehninger S, et al. Sonographic appearance of the endometrium: the predictive value for the outcome of in vitro fertilization in stimulated cycles. Hum Reprod. 1992;7(5):677-80.
10. Friedler S, Schenker JG, Herman A, et al. The role of ultrasonography in the evaluation of endometrial receptivity following assisted reproduction treatments: a critical review. Hum Reprod Update. 1996;2(4):323-35.
11. Leibovitz Z, Grinin V, Rabia R, et al. Assessment of endometrial receptivity for gestation in patients undergoing in vitro fertilization, using endometrial thickness and the endometrium-myometrium relative echogenicity coefficient. Ultrasound Obstet Gynecol. 1999;14(3):194-9.
12. Weissman A, Gotlieb L, Casper RF. The detrimental effect of increased endometrial thickness on implantation and pregnancy rates and outcome in an in vitro fertilization program. Fertil Steril. 1999;71(1):147-9.
13. Dietterich C, Check JH, Choe JK, et al. Increased endometrial thickness on the day of human chorionic gonadotropin (hCG) injection does not adversely effect pregnancy or implantation rates following in vitro fertilization-embryo transfer (IVF-ET). Fertil Steril. 2002;77(4):781-6.
14. Zhang X, Chen CH, Confino E, et al. Increased endometrial thickness is associated with improved treatment outcome for selected patients undergoing in vitro fertilization-embryo transfer. Fertil Steril. 2005;83(2):336-40.
15. Dickey RP, Olar TT, Curole DN, et al. Endometrial pattern and thickness associated with pregnancy outcome after assisted reproduction technologies. Hum Reprod. 1992;7(3):418-21.
16. Noyes N, Hampton BS, Berkeley A, et al. Factors useful in predicting the success of oocyte donation: a 3-year retrospective analysis. Fertil Steril. 2001;76(1):92-7.
17. Remohí J, Ardiles G, García-Velasco, et al. Endometrial thickness and serum oestradiol concentrations as predictors of outcome in oocyte donation. Hum Reprod. 1997;12(10):2271-6.
18. Kovacs P, Matyas S, Boda K, et al. The effect of endometrial thickness on IVF/ICS outcome. Hum Reprod. 2003;18(11):2337-41.
19. Richter KS, Bugge KR, Bromer JG, et al. Relationship between endometrial thickness and embryo implantation, based on 1,294 cycles of in vitro fertilization with transfer of two blastocyst-stage embryos. Fertil Steril. 2007;87(1):53-9.
20. Alcázar JL, Mercé LT, García-Manero M, et al. Endometrial volume and vascularity measurements by transvaginal 3-dimensional utrasonography and power Doppler angiography in stimulated and tumoral endometria. An interobserver reproducibility study. J Ultrasound Med. 2005;24(8):1091-8.
21. Mercé LT, Alcázar JL, Engels V, et al. Endometrial volume and vascularity measurements by transvaginal three-dimensional ultrasonography and power Doppler angiography in stimulated and tumoral endometria: intraobserver reproducibility. Gynecol Oncol. 2006;100(3):544-50.
22. Lee A, Sator M, Ktatochwil A, et al. Endometrial volume change during spontaneous menstrual cycles: volumetry by transvaginal three-dimensional ultrasound. Fertil Steril. 1997;68(5):831-5.
23. Raine-Fenning N, Campbell BK, Clewes JS, et al. Defining endometrial growth during the menstrual cycle with three-dimesnional ultrasound. Br J Obstet Gynaecol. 2004;111(9):944-9.
24. Jokubkiene L, Sladkevicius P, Rovas L, et al. Assessment of changes in endometrial and subendometrial volume and vascularity during the normal menstrual cycle using three-dimensional power Doppler ultrasound. Ultrasound Obstet Gynecol. 2006;27(6):672-9.
25. Raga F, Bonilla-Musoles F, Casan EM, et al. Assessment of endometrial volume by three-dimensional ultrasound prior to embryo transfer: clues to endometrial receptivity. Hum Reprod. 1999;14(11):2851-4.
26. Zollner U, Zollner KP, Specketer MT, et al. Endometrial volume as assessed by three-dimensional ultrasound is a

predictor of pregnancy outcome after in vitro fertilization and embryo transfer. Fertil Steril. 2003;80(6):1515-7.
27. Schild Rl. Indefrei D, Eschweiler S, et al. Three-dimensional endometrial volume calculation and pregnancy rate in an in vitro fertilization programme. Hum Reprod. 1999;14(5):1255-8.
28. Kupesic S, Bekavac I, Bjelos D, et al. Assessment of endometrial receptivity by transvaginal color Doppler and three-dimensional power Doppler ultrasonography in patients undergoing in vitro fertilization procedures. J Ultrasound Med. 2001;20(2):125-34.
29. Wu HM, Chiang CH, Huang HY, et al. Detection of the subendometrial vascularization flow index by three-dimensional ultrasound may be useful for predicting the pregnancy rate for patients undergoing in vitro fertilization-embryo transfer. Fertil Steril. 2003;79(3):507-11.
30. Järvelä IY, Sladkevicius P, Nelly S, et al. Evaluation of endometrial receptivity during in vitro fertilization using three-dimensional power Doppler ultrasound. Ultrasound Obstet Gynecol. 2005;26(7):765-9.
31. Ng EH, Chan CC, Tang OS, et al. The role of endometrial and subendometrial blood flows measured by three-dimensional power Doppler ultrasound in the prediction of pregnancy during IVF treatment. Hum Reprod. 2006;21(1):164-70.
32. Mercé LT, Barco MJ, Bau S, et al. Are endometrial parameters by three-dimensional ultrasound and power Doppler angiography related to in vitro fertilization/embryo transfer outcome? Fertil Steril. 2008;89(1):111-7.
33. Turnbull LW, Rice CF, Horsman A, et al. Magnetic resonance imaging and transvaginal ultrasound of the uterus prior to embryo transfer. Hum Reprod. 1994;9(12):2438-43.
34. Grunfeld L, Walker B, Bergh PA, et al. High-resolution endovaginal ultrasonography of the endometrium: a non-invasive test for endometrial adequacy. Obstet Gynecol. 1991;78(2):200-4.
35. Parsons AK, Parada C, Parsons M, et al. Ultrasound correlation with endometrial histology. Gynecologic investigation, 38th Annual Meeting, San Antonio, Texas, March 20-23, 1991; Abstract 560, p. 378.
36. Fanchin R, Righini C, Ayoubi JM, et al. New look at endometrial echogenicity: objective computer-assisted measurements predict endometrial receptivity in in vitro fertilization-embryo transfer. Fertil Steril. 2000;74(2):274-81.
37. Bakos O, Lundvist O, Bergh T. Transvaginal sonographic evaluation of endometrial growth and texture in spontaneous ovulatory cycles a descriptive study. Hum Reprod. 1993;8(6):799-806.
38. Tang B, Gurpide E. Direct effect of gonadotropins on decidualization of human endometrial stroma cells. J Steroid Biochem Mol Biol. 1993;47(1-6):115-21.
39. De Ziegler D, Fanchin R. Endometrial receptivity in controlled ovarian hyperstimulation (COH): the hormonal factor. In: Bulletti C, Gurpide E, Flagmini C (Eds). The Human Endometrium. Ann N. Y. Acad. Sci. 1994;734:209-20.
40. Tetlow RL, Richmond I, Manton DJ, et al. Histological analysis of the uterine junctional zone as seen by transvaginal ultrasound. Ultrasound Obstet Gynecol. 1999;14(3):188-93.
41. Smith B, Porter R, Ahuja K, et al. Ultrasonic assessment of endometrial changes in stimulated cycles an in vitro fertilization and embryo transfer program. J In Vitro Fert Embryo Transf. 1984;1(4):233-8.
42. Gonen Y, Casper RF. Prediction of implantation by the sonographic appearance of the endometrium during controlled ovarian stimulation for in vitro fertilization (IVF). J In Vitro Fert Embryo Transf. 1990;7(3):146-52.
43. Sher G, Herbert C, Maassarani G, et al. Assessment of the late proliferative phase endometrium by ultrasonography in patients undergoing in-vitro fertilization and embryo transfer (IVF/ET). Hum Reprod. 1991;6(2):232-7.
44. Leibovitz ZS, Degani R, Rabia R. Endometrium-to-myometrium relative echogenicity coefficient. A new sonographic approach for the quantitative assessment of endometrial echogenicity. Gynecol Obstet Invest. 1998;45(2):121-5.
45. Detti L, Yelian FD, Krugger ML, et al. Endometrial thickness dynamics and morphologic characteristics during pituitary downregulation with antagonists in assisted reproductive technology cycles. J Ultrasound Med. 2008;27(11);1591-6.
46. Chen SL, Wu FR, Luo C, et al. Combined analysis of endometrial thickness and pattern in predicting outcome of in vitro fertilization and embryo transfer: a retrospective cohort study. Reprod Biol Endocrinol. 2010;24(8):30.
47. Check JH, Dietterich C, Lurie D. Non-homogenous hyperechogenic pattern 3 days after embryo transfer is associated with lower pregnancy rates. Hum Reprod. 2000;15(5):1069-74.
48. Check JH, Gandica R, Dietterich C, et al. Evaluation of a nonhomogeneous endometrial echo pattern in the midluteal phase as a potential factor associated with unexplained infertility. Fertil Steril. 2003;79(3):590-3.
49. Barker MA, Boehnlein LM, Kovacs P, et al. Follicular and luteal phase endometrial thickness and echogenic pattern and pregnancy outcome in oocyte donation cycles. J Assist Reprod Genet. 2009;26:243-9.
50. Check JH, Dietterich C, Cohen R, et al. Increasing the dosage of progesterone (P) supplemention from mid-luteal phase in women not attaining a mid-luteal homegenous hyperechogenic (HH) pattern with sonography improves pregnancy rates (PRS) following frozen embryo transfer. Clin Exp Obstet Gynecol. 2010;37(1):13-4.
51. Scholtes MCW, Wladimiroff JW, Van Rijen HJM, et al. Uterine and ovarian flow velocity waveforms in the normal menstrual cycle: a transvaginal study. Fertil Steril. 1989;52(6):981-5.
52. Sladkevicius P, Valentin L, Marsál K. Blood flow velocity in the uterine and ovarian arteries during the normal menstrual cycle. Ultrasound Obstet Gynecol. 1993;3(3):199-208.
53. Tan SL, Zaidi J, Campbell S, et al. Blood flow changes in the ovarian and uterine arteries during the normal menstrual cycle. Am J Obstet Gynecol. 1996;175(3 Pt 1):625-31.
54. Bourne TH, Hagström HG, Granberg S, et al. Ultrasound studies of vascular and morphological changes in the

human uterus after a positive self-test for the urinary luteinizing hormone surge. Hum Reprod. 1996;11(2):369-75.
55. Agrawal R, Conway GS, Sladkevicius P, et al. Serum vascular endothelial growth factor (VEGF) in the normal menstrual cycle: association with changes in ovarian and uterine Doppler blood flow. Clin Endocrinol (Oxf). 1999;50(1):101-6.
56. Mercé LT. Doppler de los cambios ováricos y endometriales preimplantatorios. In: Kurjak A, Carrera JM (Eds). Ecografía en Medicina Materno-Fetal. Barcelona: Masson; 2000. pp. 87-104.
57. Kupesic S, Mercé LT, Zodan T, et al. Normal and abnormal corpus luteum function. In: Kupesic S, de Ziegler D (Eds). Ultrasound and Infertility. Lancs: The Parthenon publishing group; 2000.pp.67-76.
58. Psychoyos A, Martel D. Embryo-endometrial interactions at implantation. In: Edwards RG, Purdy JM, Steptoe PC (Eds). Implantation of the Human Embryo. London: Academic Press;1985. pp.197-219.
59. Czyba JC, Montella A. Les deux premieres semaines du developpemnet embryonnaire. In: Czyba JC, Montella A (Eds). Biologie De La Reproduction Humaine. Montpellier: Sauramps medical; 1993. pp. 217-28.
60. Goswany RK, Williams G, Steptoe PC. Decreased uterine perfusion-a cause of infertility. Hum Reprod. 1988;3(8):955-9.
61. Mercé LT. Estudio Doppler de la implantación y placentación inicial. In: Kurjak A, Carrera JM (Eds). Ecografía en Medicina Materno-Fetal. Barcelona: Masson; 2000. pp. 113-36.
62. Steer CV, Campbell S, Tan SL, et al. The use of transvaginal color flow imaging after in vitro fertilization to identify optimum uterine conditions before embryo transfer. Fertil Steril. 1992;57(2):372-6.
63. Zaidi J, Pittrof R, Shaker A, et al. Assessment of uterine artery blood flow on the day of human chorionic gonadotropin administration by transvaginal color Doppler ultrasound in an in vitro fertilization program. Fertil Steril. 1996;65(2):377-81.
64. Tsai YC, Chang JC, Tai MJ, et al. Relationship of uterine perfusion to outcome of intrauterine insemination. J Ultrasound Med. 1996;15(9):633-6.
65. Coulam CB, Bustillo M, Soenksen DM, et al. Ultrasonographic predictors of implantation after assisted reproduction. Fertil Steril. 1994;62(5):1004-10.
66. Coulam CB, Stern JJ, Soenksen DM, et al. Comparison of pulsatility indexes on the day of oocyte retrieval and embryo transfer. Hum Reprod. 1995;10(1):82-4.
67. Bustillo M, Krysa LW, Coulam CB. Uterine receptivity in an oocyte donation programme. Hum Reprod. 1995;10(2): 442-5.
68. Favre R, Bettahar K, Grange G, et al. Predictive value of transvaginal uterine Doppler assessment in an in vitro fertilization program. Ultrasound Obstet Gynecol. 1993;3(5):350-3.
69. Tekay A, Martikainen H, Jouppila P. The clinical value of transvaginal colour Doppler ultrasound in assisted reproductive technology procedures. Hum Reprod. 1996;11:1589-91.
70. Deichert U, Albrand-Thielman C, Van de Sandt M. Doppler-sonographic pelvic blood flow measurements and their prognostic value in terms of luteal phase and implantation. Hum Reprod. 1996;11(8):1591-3.
71. Caccitore B, Simberg N, Fusaro P, et al. Transvaginal Doppler study of uterine artery blood flow in in-vitro fertilization-embryo transfer cycles. Fertil Steril. 1996;66(1):130-4.
72. Ng EHY, Chan CCW, Tang OS, et al. Relationship between uterine blood flow and endometrial and subendometrial blood flows during stimulated and natural cycles. Fertil Steril. 2006;85(3):721-7.
73. Dickey RP. Doppler ultrasound investigation of uterine and ovarian blood flow in infertility and early pregnancy. Hum Reprod Update. 1997;3(5):467-503.
74. Torry DS, Holt VJ, Keenan JA, et al. Vascular endothelial growth factor expression in cycling human endometrium. Fertil Steril. 1996;66(1):72-80.
75. Shifren JL, Tseng JF, Zaloudek CJ, et al. Ovarian steroid regulation of vascular endothelial growth factor in the human endometrium; implications for angiogenesis during the menstrual cycle and in the pathogenesis of endometriosis. J Clin Endocrinol Metab. 1996;81(8):3112-8.
76. Rogers P, Abberton K, Susil B. Endothelial cell migratory signal produced by human endometrium during the menstrual cycle. Hum Reprod. 1992;7(8):1061-6.
77. Jinno M, Ozaki T, Iwashita M, et al. Measurement of endometrial tissue blood flow: a novel way to assess uterine receptivity for implantation. Fertil Steril. 2001;76(6):1168-74.
78. Achiron R, Levran D, Sivan E, et al. Endometrial blood flow response to hormone replacement therapy in women with premature ovarian failure: a transvaginal Doppler study. Fertil Steril. 1995;63(3):550-4.
79. Zaidi J, Campbell S, Pittrof R, et al. Endometrial thickness, morphology, vascular penetration and velocimetry in predicting implantation in an in vitro fertilization program. Ultrasound Obstet Gynecol. 1995;6(3):191-8.
80. Mercé LT, Moreno C, Bau S. Assessment of luteal and peri-implantation blood flow with color Doppler in A.I.H. In: Abstract Book of ESHRE Symposium on Reproductive Medicine. Valencia; 1995. p. 12.
81. Battaglia C, Artini PG, Giulini S, et al. Colour Doppler changes and thromboxane production after ovarian stimulation with gonadotrophin-releasing hormone agonist. Hum Reprod. 1997;12(11):2477-82.
82. Yuval Y, Lipitz S, Dor J, et al. The relationships between endometrial thickness, and blood flow and pregnancy rates in in-vitro fertilization. Hum Reprod. 1999;14(4):1967-71.
83. Schild RL, Knobloch C, Dorn C, et al. Endometrial receptivity in an in vitro fertilization program as assessed by spiral artery blood flow, endometrial thickness, endometrial volume, and uterine artery blood flow. Fertil Steril. 2001;75(2):31-6.
84. Dechaud H, Bessueille E, Bousquet PJ, et al. Optimal timing of ultrasonographic and Doppler evaluation of uterine receptivity to implantation. Reprod Biomed Online. 2008;16(3):368-75.
85. Wang L, Qiao J, Li R, et al. Role of endometrial blood flow assessment with color Doppler energy in predicting

pregnancy outcome. Reprod Biol Endocrinol. 2010;18(8): 122.
86. Mercé LT. Aplicaciones del Doppler color en Reproducción. IV Curso Teórico-Práctico sobre Doppler en Ginecología, Obstetricia y Ecocardiografía fetal. Barcelona, 2-4 de mayo;2002.
87. Applebaum M. The menstrual cycle, menopause, ovulation induction, an in vitro fertilization. In: Copel JA, Reed KL (Eds). Doppler Ultrasound In Obstetrics And Gynecology. New York:Raven Press; 1995. pp. 71-86.
88. Chien LW, Au HK, Chen PL, et al. Assessment of uterine receptivity by the endometrial-subendometrial blood flow distribution pattern in women undergoing in vitro fertilization-embryo transfer. Fertil Steril. 2002;78(2):245-51.
89. Yang JH, Wu MY, Chen CD, et al.Association of endometrial blood flow as determined by a modified colour Doppler technique with subsequent outcome of in-vitro fertilization. Hum Reprod. 1999;14(6):1606-10.
90. Ng EH, Chan CC, Tang OS, et al.The role of endometrial and subendometrial vascularity measured by three-dimensional power Doppler ultrasound in the prediction of pregnancy during frozen-thawed embryo transfer cycles. Hum Reprod. 2006;21(6):1612-7.
91. Ng EH, Chan CC, Tang OS, et al. Endometrial and subendometrial vascularity is higher in pregnant patients with livebirth following ART than in those who suffer a miscarriage. Hum Reprod. 2007;22(4):1134-41.
92. Zácková T, Järvelä IY, Tapanainen JS, et al. Assessment of endometrial and ovarian characteristics using three dimensional power Doppler ultrasound to predict response in frozen embryo transfer cycles. Reprod Biol Endocrinol. 2009;7:151.
93. Mercé LT, Barco MJ, Alcázar JL, et al. Mediciones con la ecografía tridimensional y el programa VOCAL: cálculo de volúmenes e índices de la angiografía power Doppler. In: Mercé LT (Ed). Manual MISUS: Teoría y Práctica de la Ecografía y Angiografía Doppler Tridimensional en Obstetricia y Ginecología. Madrid: HABE; 2006. pp. 43-57.
94. Raine-Fenning NJ, Campbell BK, Kendall NR, et al. Quantifying the changes in endometrial vascularity throughout the normal menstrual cycle with three-dimensional power Doppler angiography. Hum Reprod. 2004;19(2):330-8.
95. Hauksson A, Akerlund M, Melin P. Uterine blood flow and myometrial activity at menstruation, and the action of vasopressin and a synthetic antagonist. Br J Obstet Gynaecol. 1988;95(9):898-904.
96. Fischer B, Bavister BD. Oxygen tension in the oviduct and uterus of rhesus monkeys, hamsters and rabbits. J Reprod Fertil. 1993;99(2):673-9.
97. Ng EHY, Chan CCW, Tang OS, et al. Comparison of endometrial and subendometrial blood flow measured by three-dimensional power Doppler ultrasound between stimulated and natural cycles in the same patients. Hum Reprod. 2004;19(10):2385-90.
98. Ng EHY, Chan CCW, Tang OS, et al. Factors affecting endometrial and subendometrial blood flow measured by three-dimensional power Doppler ultrasound during IVF treatment. Hum Reprod. 2006;21(4):1062-9.
99. Ng EHY, Chan CCW, Tang OS, et al. Endometrial and subendometrial blood flow measured during early luteal phase by three-dimensional power Doppler ultrasound in excessive ovarian responders. Hum Reprod. 2004;19(4):924-31.
100. Ng EHY, Chan CCW, Tang OS, et al. Endometrial and subendometrial blood flow measured by three-dimensional power Doppler ultrasound in patients with small intramural uterine fibroids during IVF treatment. Hum Reprod. 2005;20(2):501-6.
101. Ng EHY, Chan CCW, Tang OS, et al. Comparison of endometrial and subendometrial blood flows among patients with and without hydrosalpinx shown on scanning during in vitro fertilization treatment. Fertil Steril. 2006;85(2);333-8.
102. American Society of Reproductive Medicine. Practice Committee Report. Guidelines on number of embryos transferred. Release May 2004.
103. ESHRE Task Force on Ethics and Law. Ethical issues related to multiple pregnancies in medically assisted procreation. Hum Reprod. 2003;18(9):1976-9.
104. Saldeen P, Sundström P. Would legislation imposing single embryo transfer be a feasible way to reduce the rate of multiple pregnancies after IVF treatment? Hum Reprod. 2005;20(1):4-8.
105. De Neubourg D, Gerris J. What about the remaining twins since single-embryo transfer? How far can (should) we go? Hum Reprod. 2006;21(4):843-6.

8

CHAPTER

Normal and Abnormal Early Pregnancy

Ulrich Honemeyer, Asim Kurjak, Giovanni Monni

The first trimester is characterized by many important landmarks with regard to the ultimate outcome of pregnancy and is mostly defined by the first 100 days of pregnancy. Woman becomes aware of her pregnancy after missing her last period and in that time she is already at least four weeks pregnant.[1] A positive pregnancy test opens Pandora's box, offering more questions than answers. Although, a positive pregnancy test most likely suggests an intrauterine pregnancy, production of human chorionic gonadotropin (hCG) occurs also by tumors (dysgerminoma, choriocarcinoma) or maldevelopment of pregnancy (ectopic pregnancy or mola hydatidosa).[2] Falsely positive results are mainly obtained in the case of proteinuria, erythrocyturia or some drug intake (e.g. tranquilizers). The role of the ultrasonographer in these situations is to help the practicing clinician to evaluate pregnancy and determine the exact pregnancy status.

INTRODUCTION

Ultrasonographic evaluation of pregnancy during the first trimester has no longer the limited purpose of confirmation of viability and gestational age. The amazing improvement of technical equipment and deepened knowledge of embryonic and early fetal development, have brought sonomorphologic exploration of pregnancy forward into 1st trimester and changed the agenda of ultrasound examinations in this pregnancy section. Sonographic assessment during 1st trimester targets now ovulation, conceptus, embryo and early fetus. It is obvious that diagnosis of abnormal early pregnancy, pregnancy failure and fetal abnormalities should be ascertained as early as possible to enable timely decisions about management. However, newly gained insights have also pointed out the limitations of early ultrasound diagnosis. The sonoanatomic survey of the fetus after 11 weeks gestation is more likely to produce usable information than before 11 weeks, simply because physiologic structural alterations of the embryo, such as herniation of bowel into the proximal umbilical cord, have disappeared. Moreover, advanced ossification after 11 weeks permits assessment of cranial vault and nasal bone. The introduction of 3D, real time 3D (4D), color-and power Doppler and their attachment to transvaginal scanning has boosted our knowledge of early pregnancy ever more. Reports of new findings arrive almost monthly. All this should not let sonographers forget about safety of ultrasound in embryonic and early fetal diagnosis.

NORMAL EARLY PREGNANCY

Events Following Implantation

Discriminatory zone: At a serum beta-hCG level of 1500 mIU/ml, which is reached at day 10–14 pc in a normal gravidity, an intrauterine chorionic sac can be detected by TVS probe with minimum 5 MHz frequency. In transabdominal US, serum beta-hCG values may have to be as high as 6500 mIU/ml before an intrauterine gestational sac is detected. These serum beta-hCG levels mark the so-called discriminatory zone in which

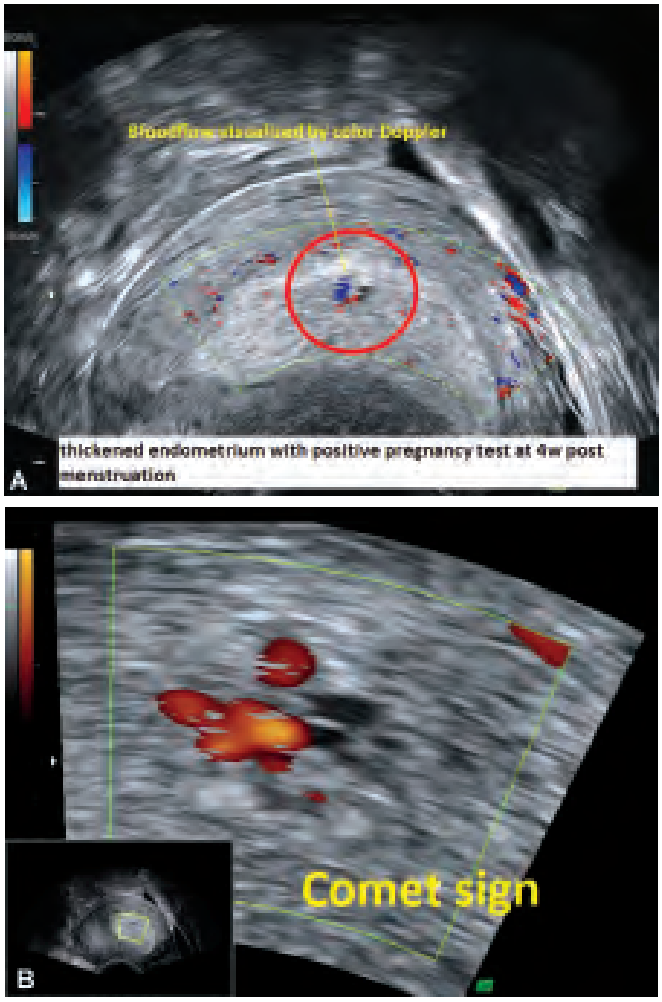

Figures 8.1A and B: Comet sign (A) Color Doppler and (B) Power Doppler

discrimination of a normal intrauterine chorionic sac should be possible. In a normal intrauterine pregnancy, a chorionic sac is visible at 4.5–5 weeks gestation presenting a double echogenic ring around a hypoechoic GS, with eccentric embedding in the decidua. The "Comet sign" **(Figs 8.1A and B)** of intervillous flow in PD assessment of the decidua around the double echogenic ring and visualization of a yolk sac at 5w+, confirm the impression of an intrauterine implantation.

Conversely, in patients with beta-hCG of 1500 mIU/ml and more, an empty uterine cavity visualized by TVS with specifications as above, can be taken as indirect proof for ectopic pregnancy. An ectopic pregnancy can occur as pregnancy with viable embryo in 10%, as blighted ovum in 40% and as questionable adnexa in 50% of cases. Color and power Doppler demonstrate randomly dispersed multiple small vessels within the adnexa, with pulsed wave (PW)-Doppler showing resistance to- flow as low as RI <0.42. Color coded flow signals of the ectopic pregnancy are clearly separated from ovarian tissue and corpus luteum. The extent of vascularity reflects trophoblastic vitality and invasiveness (neoangiogenesis), enhanced by vasodilatation of the fallopian vessels under the influence of maternal progesterone.[3]

5th week: Gestational sac (GS) visible eccentric within the endometrium, appears as hypoechoic oval structure, surrounded by a hyperechoic ring.

Maternal uterine unit: Gradual decrease of uterine artery resistance index (RI) during the 1st trimester, leveling of the protodiastolic notch, increasing diastolic flow velocities.

These changes are consequence of decrease in total peripheral resistance-to-flow, caused by progressive conversion of spiral arteries into nonmuscular dilated tortuous channels after trophoblast invasion (1st wave of trophoblast invasion). Dilated spiral arteries are easily detected with color- or power Doppler close to the chorion, near the placental implantation site and are well recognizable with relatively lower RI and higher peak systolic velocities followed by turbulent flow (Comet sign).

Placental unit: Primary chorionic villi appear during the 4th week of gestation and mark the beginning of placental development. At five weeks gestation, chorionic villi have branched and mesenchymal cells within the villi have differentiated into capillaries and started to form an arteriovenous capillary network. Until eight weeks, chorionic villi have covered the entire GS. In the 9th week, on the side of the chorion which has the connecting stalk and embryo, the villi proliferate towards the decidua basalis and form the chorion frondosum, whereas they begin to degenerate on the opposite side, in the area of the decidua capsularis which then transforms into an avascular shell. Normal placentation is characterized by progressive change of spiral arteries into wide channels. The trophoblast carries these changes deep into the inner third of the myometrium, until at the end of 20 weeks gestation all spiral arteries are transformed into wide blood channels (2nd wave of trophoblast invasion). Disturbance of 1st and 2nd trophoblast invasion is suspected to be leading cause of early pregnancy failure and pre-/eclamsia.

Pulsed Doppler analysis of intervillous placental flow demonstrates two types of waveforms:

1. Pulsatile arterial-like flow
2. Continuous venous-like flow.

Fetal unit

5th week: Transvaginal approach

Embryo has an attenuated tail and deep neural groove is visible. Heart prominence is recognizable.

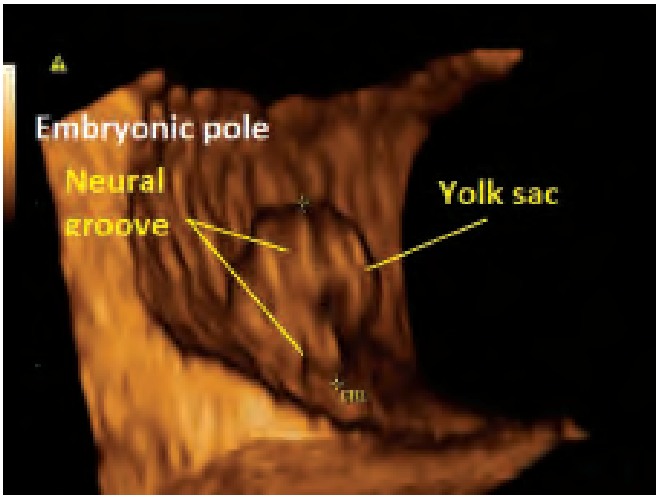

Figure 8.2: Embryo 5-6 weeks 3D surface rendered GS with embryo and yolk sac

3D. Gestational sac (GS) visible as small anechoic vesicle placed in one of the endometrial leafs. 3D ultrasound with multiplanar mode at the end of 5th week **(Fig. 8.2)**, at a GS-diameter of 8 mm and above, allows easy discrimination of yolk sac and embryonic pole of 2–3 mm length, which appears 24–48 hours after visualization of the yolk sac, at approximately 33rd postmenstrual day.

3D Power Doppler: Intense vascularity around the chorionic shell. The hyperechoic chorionic ring is interrupted by color sprouts of the early intervillous and spiral artery blood flow (comet sign).

6th week: Transvaginal approach
C-shaped embryo with dominating head. Physiological midgut herniation begins. Embryonic erythropoietic stem cells, produced at first in the yolk sac and para-aortic mesoderm (aorto-gonad-mesonephros region), have colonized the liver, where erythropoiesis now continues.[4]

3D. Rounded bulky head due to developing forebrain and thinner body, umbilical cord and ductus Vitellini discernable. Surrounding the embryo, amniotic membrane with extraamniotic yolk sac visible. Limb buds rarely seen at this stage. Ductus omphalo-entericus present, with up to four times the length of the embryo.

3D Power Doppler. Fetal heart from 5 weeks 4 days onwards, at crown-rump-length (CRL) 3–4 mm, with heartbeat visible, as well aorta and umbilical cord to placental insertion. Proof of embryonic viability.

7th week: Transvaginal approach
GS occupies about one-third of the uterus. The main landmark is now an echogenic embryonic pole adjacent to a cystic yolk sac. The embryonic head is much larger than the trunk and bent forward over the cardiac prominence. Hand and foot plates are formed, digital rays start to appear. The Vitelline duct as part of the Vitelline circulation undergoes complete obliteration during the 7th week (in about 2% of cases its proximal part persists as a diverticulum from the small intestine, Meckel's diverticulum, which is situated about 60 cm proximal to the Bauhin's valve (ileocoecal valve) and may be attached by a fibrous cord to the abdominal wall at the umbilicus.[4]

3D chorion frondosum distinguishable from chorion leave. Amnion visible as spherical hyperechoic membrane, still close to the embryo. The head has become the dominant embryonic structure. Using 3D planar mode, the rhombencephalon (hindbrain), at this stage the largest of the developing vesicles of the brain, can be found at the top of the head (vertex).

3D power Doppler: At the end of the 7th week, cerebral blood flow becomes apparent at the base of the embryonic skull, with discrete pulsations of the carotid arteries. Venous and arterial blood flow signals from the intervillous space have become more intense.

8th week: Transvaginal approach
Transabdominal approach possible (except in retroverted uterus).

CRL 10-16 mm. The embryo has developed a skeleton, though still mostly cartilaginous. The head begins to erect **(Fig. 8.3A)** from the anterior flexion due to the expansion of the lateral, third and midbrain ventricles. Vertex of the embryo now shifted to the midbrain (mesencephalon).

3D. The most impressive change is the complete visualization of the limbs with thickening of the ends where hands and feet develop. The distinction of facial forms is still rather vague, due to insufficient ultrasonographic resolution and because of persisting cranial pole flexion. Umbilical cord insertion is visible **(Fig. 8.3C)**.

3D power Doppler. At this stage of pregnancy, 3D power Doppler allows the visualization of the entire embryonic circulation **(Fig. 8.3B)**.

9–10th week: End of embryonic period. Transvaginal approach still most accurate, transabdominal approach possible.

The head constitutes now almost half of the fetus. Upper limbs develop faster than lower limbs, formation of fingers complete at the end of 9th week. The rapid growth of the liver and intestine before closure of the abdominal wall may cause herniation into the proximal

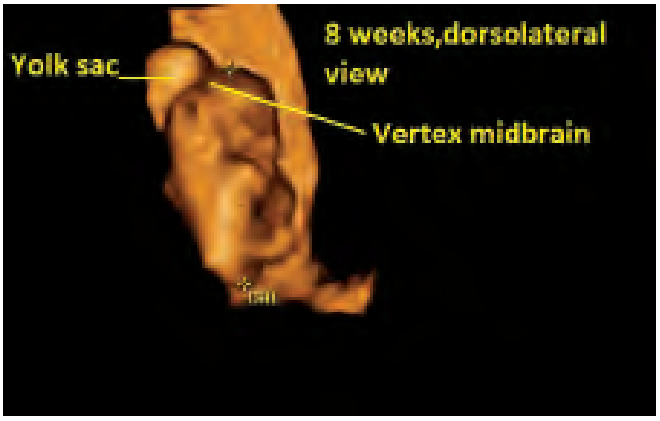

Figure 8.3A: Embryo 8 weeks, beginning erection of the head, foot-and hand plates

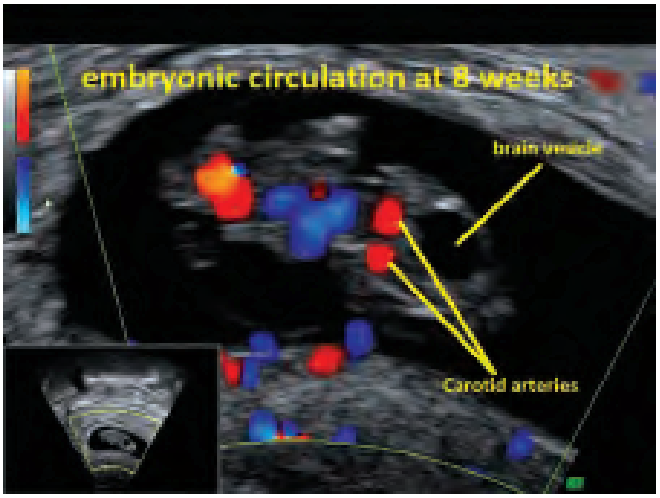

Figure 8.3B: Fetal circulation at 8 weeks with carotid arteries

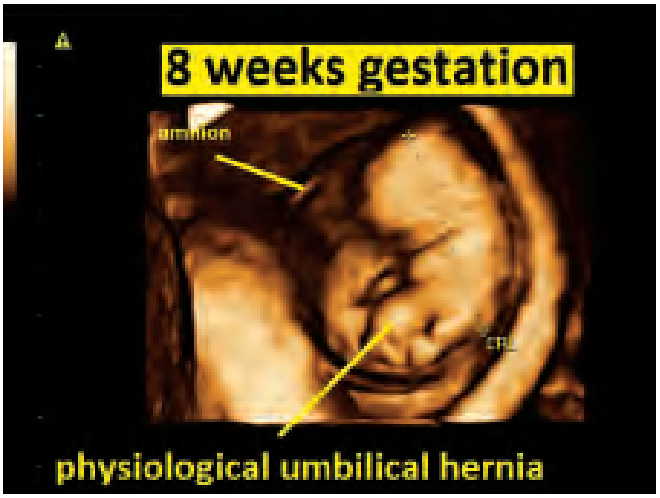

Figure 8.3C: 8 weeks 5 days physiologic umbilical hernia

umbilical cord in most fetuses (physiological midgut herniation). At 10 weeks, when the abdominal wall finishes its development with closure, the bowel undergoes two turns of 180° with final return to its original position[4] **(Figs 8.4A to D)**.

3D. Physiological midgut herniation visible. The dorsal column (early spine) characterized by two echogenic parallel lines **(Fig. 8.5)**, can be examined in whole length. The arms with elbows and legs with knees are visible. Head is clearly divided from the body by the neck. At this gestational age, images of the fetal face can be obtained. The lateral ventricles in the brain are seen, containing the hyperechoic choroid plexus.

3D power Doppler. From the 9th week, the circle of Willis and its major branches are visible.

11th week: Transvaginal and transabdominal approach.

Physiological midgut herniation disappears. Fetal kidneys start to produce urine, fetal bladder is visible.

3D. Planar mode enables visualization of the entire fetal body, with differentiation of fetal stomach and urinary bladder. Kidneys become visible. Detailed 3D analysis of the fetal skeleton using maximum mode is possible, the spine is seen in detail. Facial details such as nose, maxilla, mandibles and orbits can be differentiated.

3D power Doppler. Depiction of major aortic branches like renal and common iliac arteries is achievable.

12th week: Transvaginal and transabdominal approach. The fetal neck is well defined, the face is broad, with wide distance between the eyes. Structural development of the heart is complete (four chamber view). Erythropoiesis shifts from liver to spleen. Fetal gender can be distinguished.

3D. Depiction of fetal anatomy has reached a degree of accuracy which allows counting of fingers and toes. The growing cerebellum is clearly visible, the lateral ventricles with choroid plexus dominate the brain. From now on, differentiated visualization of vertebral anatomy is feasible using maximum mode: the medullar channel, each vertebra, intervertebral disks and the ribs can be measured.

3D power Doppler. Fetal vascular system is now part of detailed anatomic survey of cerebrum, digestive and urinary tract. The middle cerebral artery with its pulsations can be differentiated within the circle of Willis. Until the end of the first trimester, the absence of end-diastolic flow in fetal circulation including umbilical arteries is a normal finding.[5]

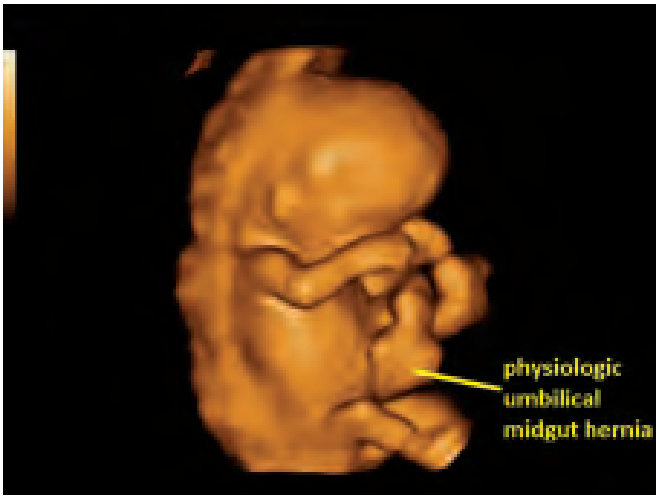

Figure 8.4A: Physiologic umbilical hernia at 10 weeks 5 days

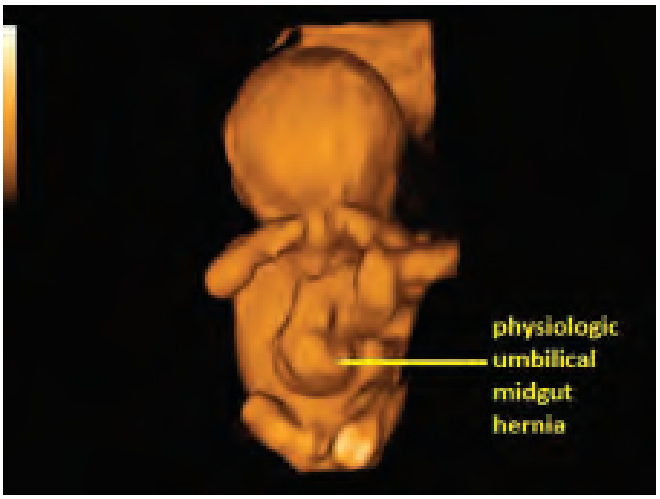

Figure 8.4B: Physiologic umbilical hernia at 10 weeks 5 days

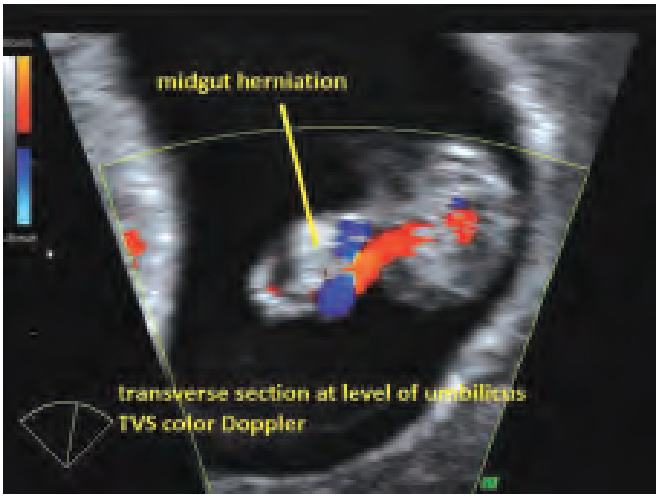

Figure 8.4C: Physiologic umbilical hernia: gray scale color Doppler

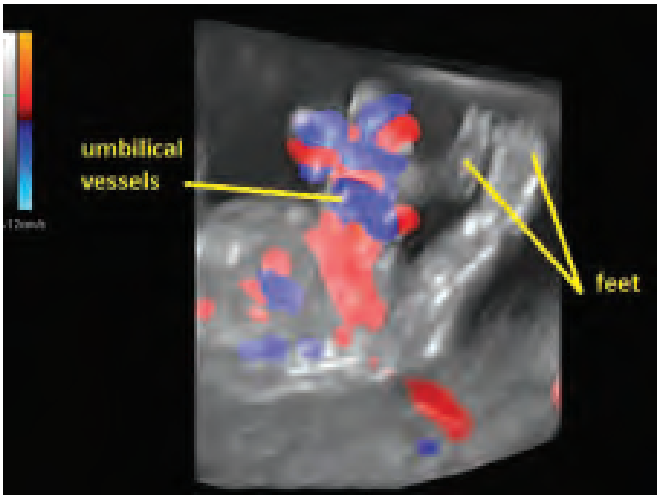

Figure 8.4D: Physiologic umbilical hernia 10 weeks 5 days glass body CD

Figure 8.5: Spinal column at 10 weeks 5 days, characterized by two echogenic lines

The Yolk Sac

The microscopic structure of the primary yolk sac is visible in an implanted nine days human blastocyst and extends as a cavity surrounded by the exocoelomic (Heuser's) membrane and the cytotrophoblast layer towards the not yet completely closed surface defect of the endometrium at the site of implantation. At the base (embryonic pole) of the primary yolk sac is the inner cell mass, the embryoblast. Beyond the embryoblast and the small half-moon shaped early amniotic cavity, towards deeper layers of the endometrium, follows a thicker cell layer of cytotrophoblast and the syncytiotrophoblast. Here is the future location of the embryonic stem and the chorion frondosum as the main area of trophoblast invasion into maternal spiral arteries.

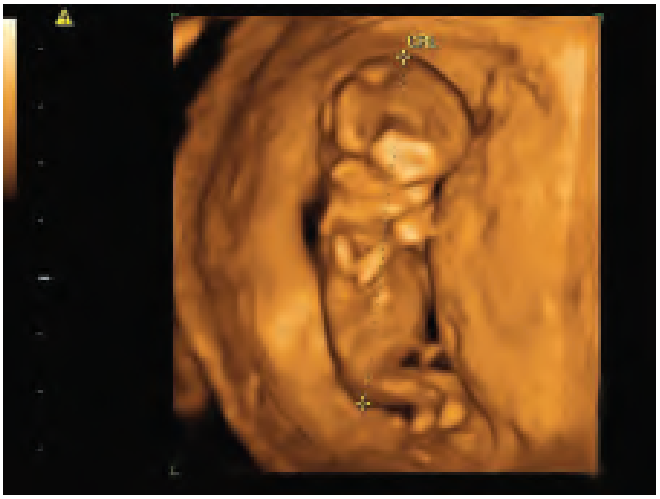

Figure 8.6A: Early fetal circulation at 12 weeks 3 days 3D surface rendered fetus

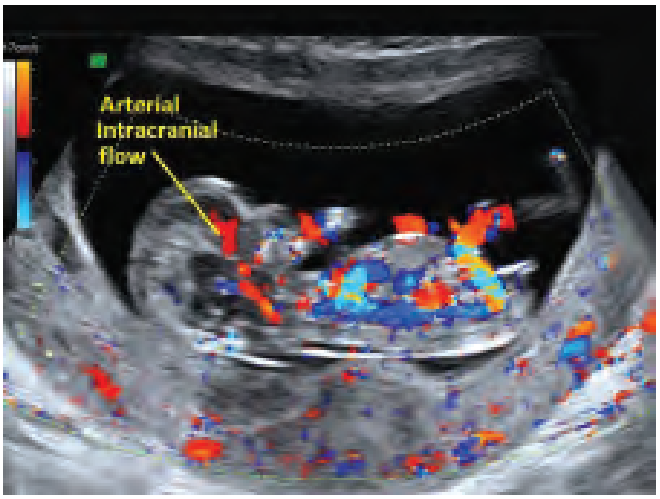

Figure 8.6B: Early fetal circulation color Doppler

Between the exocoelomic membrane (Heuser's) and the cytotrophoblast develops, until day 12 post conception, a surrounding layer of fluid creating the extra-embryonic celom, also called chorionic cavity. The primary yolk sac—being now surrounded by the extra-embryonic celom—has hence become the secondary yolk sac, visible until about 12 weeks of gestation. The secondary yolk sac is by origin embryonic tissue and ultrasonographically the first visible embryonic structure in the GS at 5 weeks: it appears as circular, well defined, echo free area, diameter 3–4 mm, within the GS which measures at this time about 8–10 mm. The yolk sac grows slowly until it reaches a maximum diameter of approximately 5–6 mm at 10 weeks. Its stalk (Vitelline duct) can be followed from the origin into the embryonic abdomen. The Vitelline duct is a tubular elongation connecting yolk sac and embryonal midgut which had developed during progressive separation of the yolk sac from the embryo through formation of the intraembryonic body cavity, with the embryonic stalk as remaining opening. The yolk sac is the source of omnipotent stem cells including the gametes, which are formed from primordial germ cells in the embryoblast and which later move into the wall of the yolk sac. From here they migrate through the Vitelline duct into the embryo. As the gestational sac grows and the amniotic cavity (the yolk sac was always extra-amniotic!) quickly expands, the yolk sac as "extraembryonic embryonic" structure is gradually separated from the embryo.[4]

Multiple Pregnancy

Determination of chorionicity and amnionicity in multiples is one of the important goals of early pregnancy ultrasound because of its prognostic value in regards to subsequent development of discordant growth or/and twin-to-twin transfusion syndrome (TTTS). 3D surface rendering of multiple gestation **(Fig. 8.6A)** is an excellent tool because the "off-line" evaluation of the sweep volume will give quick evidence of the number of embryos **(Fig. 8.6B)**, their spatial relation and lambda- or T-sign of separating membranes (chorionicity) **(Figs 8.7A,B and 8.8)**.

Abnormalities in twins can be classified in those specific for monochorionicity and malformations equally affecting multiple and singleton pregnancies, such as cardiac- or neural tube defects. Conjoined twins in monochorionic pregnancies occur when the division of the zygote is delayed until day 13–16 post conception **(Figs 8.9A and B)**.

Ultrasound Evaluation of Abnormal Early Pregnancy

Ultrasound evaluation of an early pregnancy includes detection of the pregnancy location (extrauterine or intrauterine), the type of pregnancy (one-fetus pregnancy, multiple pregnancy, molar pregnancy), the viability of the pregnancy and establishment of the gestational age. Evaluating pregnancy, the ultrasonographer also recognizes the complications that may occur in first trimester. Ultrasound examination has become the "golden standard" in follow-up of the development and complications of early pregnancy. With introduction of transvaginal sonography (TVS), the quality of early possibility for early morphological and biometrical ultrasound examinations has been significantly improved. Application of color Doppler ultrasound has enabled functional hemodynamic presentation and evaluation, soon after implantation.

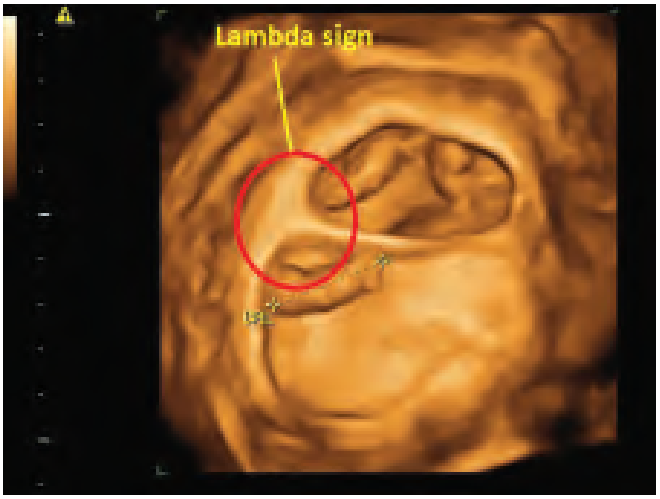

Figure 8.7A: Lambda sign in triplets

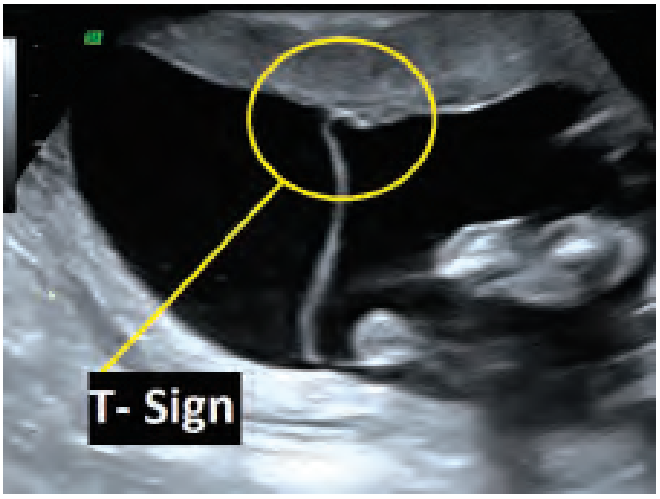

Figure 8.7B: T-sign in monochorionic twins

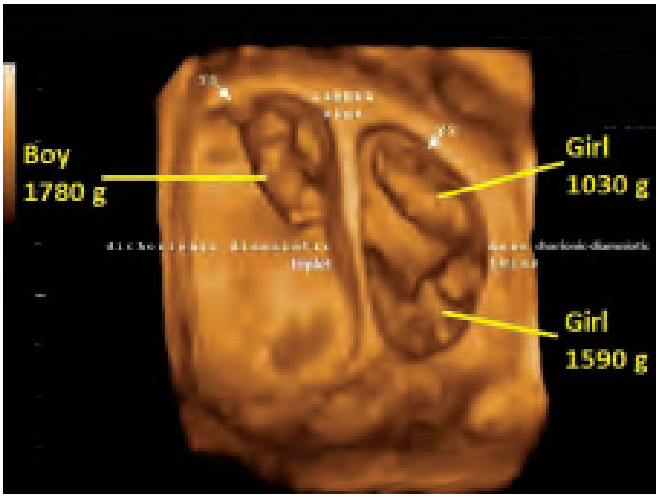

Figure 8.8: Dichorionic–diamniotic and monochorionic triplets and their birth-weights at 35 weeks

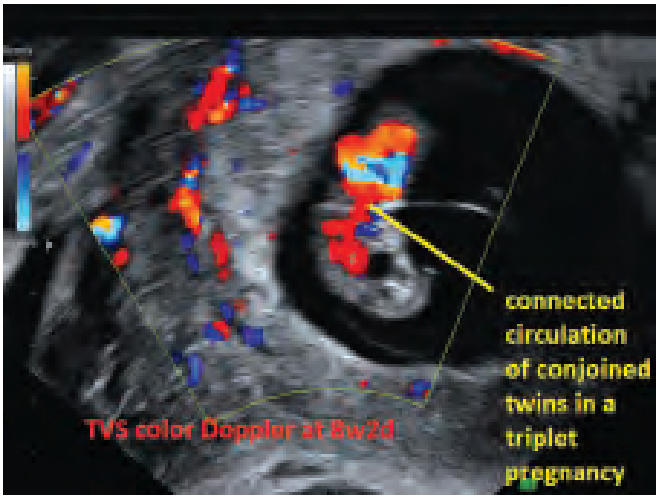

Figure 8.9A: Conjoined twins in a triplet pregnancy

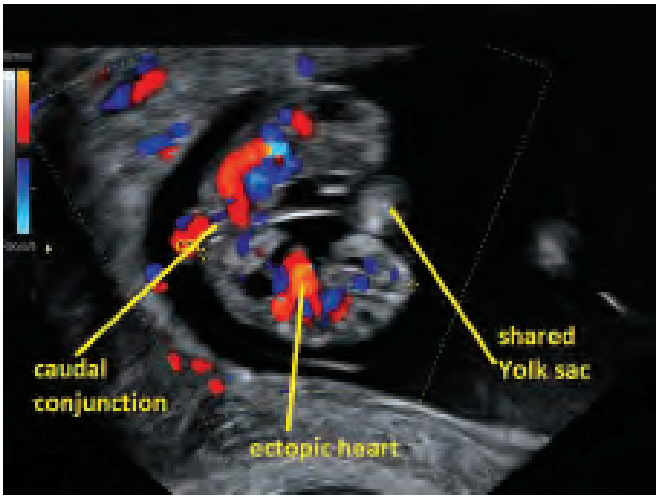

Figure 8.9B: Conjoined twins in triplet pregnancy, ectopia cordis

Basic ultrasound markers for normal pregnancy are intrauterine gestational sac, morphologically normal embryo and its heart action **(Flow chart 8.1)**. Normal embryonic echo, in 90% of the cases suggests normal pregnancy.

The possibility of early pregnancy loss is very high and can be related to fetal biometry **(Table 8.1)**.[6] There is discordance between the clinicians' and embryolo-

TABLE 8.1

The risk of early pregnancy loss in relation to CRL values

CRL (mm)	*Possibility for pregnancy loss (%)*
< 5	8
6-10	3-4
> 10	below 1

Adapted from ref. 6

Flow chart 8.1: Basic ultrasound markers for normal intrauterine pregnancy

gists' statements in determining the gestational age. Clinicians define gestational age from the first day of the last menstrual period. However, embryologists define the gestational age from the time of conception. Therefore, when talking about embryonic period embryologists define it as a period of organogenesis from the 3–8th week after conception, while obstetricians define it as a period from 5–10th week after first day of the last menstrual period.[7]

Fetal period begins after 8th week according to embryologists, i.e. after 10th week according to clinicians. As the onset of marrow formation in the humerus (the end of embryonic period according to the embryologists that occurs 56–57 day after ovulation)[8] is not visible by ultrasound, Blass[9] suggests that disappearance of the physiological midgut herniation could be sonographic orientation for the end of embryonic period. The physiological midgut herniation is a macroscopically visible process, which starts after seven completed weeks. The retraction of the bowel into the abdominal cavity occurs between approximately 10.5–12 completed weeks.[10] Application of 3D and 4D ultrasound seems to be advantageous in determining the points for differentiation of embryonic and fetal period.

EARLY PREGNANCY FAILURE AND VAGINAL BLEEDING

Early pregnancy failure is defined as a pregnancy that ends spontaneously before the embryo is detected by ultrasound at the gestational age, in which visualization of viable embryo should be possible. The most common pathological symptom of the early pregnancy failure is vaginal bleeding.

One of the main problems in diagnosis of early pregnancy failure is why vaginal bleeding occurs.

Several questions that can radically alter the management are:

- Is the patient pregnant?
- Is the embryo viable or not?
- What is the gestational age?
- Is there any evidence to suggest that the pregnancy is ectopic?
- If an abortion occurs, is it complete or incomplete?
- Is there any associated pelvic mass?

Only accurate evaluation of pregnancy status and embryo/fetus make it possible to find appropriate therapeutic measures in cases where a normal outcome of the pregnancy can be expected. At this moment, ultrasonography is considered to be the best diagnostic method for detection of early pregnancy complications. For these patients the skill of the ultrasonographer is very important, since accurate diagnosis of pregnancy failure will often result in surgical intervention.

Clinical presentation of symptoms such as vaginal bleeding and abdominal pain, with or without the expulsion of products of conception[11] should arouse suspicion of spontaneous abortion. For ultrasound evaluation, it is important to distinguish threatened, complete and incomplete abortion.

Threatened Abortion (Abnormal Vaginal Bleeding)

Threatened abortion is the clinical term used to describe symptom such as vaginal bleeding during the first 20 weeks of pregnancy in women who, on the basis of clinical evaluation, are considered to have a potentially living embryo/fetus. The main problem in the management of these patients is to confirm the accurate diagnosis. The threatened and spontaneous abortions together present the most common complications of early pregnancy. Sometimes, we are not even aware that a woman has been pregnant and that she aborted. If we take into consideration these cases also, incidence of spontaneous abortions is estimated up to 70%.[12] Only 1/3 of embryos continue further development and 50% of abortions occur before the time of expected menstruation.[9,10] These types of abortion usually cause the symptoms of sterility rather than infertility because it seems that a woman is not even able to conceive. Thirty to forty percent of pregnancies fail after implantation and only 10–15% manifest with clinical symptoms.[13,14]

In patients with a normal intrauterine pregnancy, bleeding from the chorion frondosum is undoubtedly the most common source of vaginal bleeding during the first trimester.

The development of transvaginal sonography allowed improved assessment of patients presenting vaginal bleeding during the first half of pregnancy, clarifying the differential diagnosis of missed abortion, ectopic pregnancy, blighted ovum and threatened abortion with a living embryo. Embryo vitality can be established reliably by documenting cardiac activity on real-time, B-mode or color Doppler ultrasonography.

Sonography can identify perigestational hemorrhage in 5–22% as the cause of vaginal bleeding in women with threatened abortion. However, some precautions must be taken because perigestational hemorrhage is occasionally difficult to distinguish from a blighted twin. The prognostic significance of identifying perigestational hemorrhage during the first trimester remains uncertain. Most of the small hemorrhages resolve without clinical sequelae, while in some cases spontaneous abortion may occur.

Incomplete and Complete Spontaneous Abortion

As per definition, *incomplete abortion* is the passage of some, but not all fetal or placental tissue through the cervical canal. In *complete abortion*, all products of conception are expelled through the cervix.[15] In incomplete abortion, the uterine debris may consist of a combination of products of conception, blood and decidua.[16]

Transvaginal ultrasonography plays important role in evaluating uterine cavity in spontaneous abortion due to detection of the retained products of conception. Retained products of conception after abortion may cause bleeding or chorioamnionitis.[17] An echogenic and vascularized mass within the uterine cavity supports the diagnosis of retained products of conception.[18] Wong and coworkers[19] reported 100% sensitivity and 80% specificity of transvaginal sonographic examination in differentiation of the complete from incomplete spontaneous abortions. The sonographic definition of incomplete abortion is a bilayer endometrial thickness of more than 8 mm. In 29% of patients with incomplete abortion, transvaginal sonography obviated the need for surgical intervention, but in 30% of patients with complete abortion detected retained products of conception. Adding color Doppler examination to basic transvaginal 2D ultrasound examination increases detection rate of the retained trophoblastic tissue.[20-23] In their recent paper, Alcázar and co-workers[23] suggested that transvaginal color Doppler is a helpful method for detecting retained trophoblastic tissue in patients with first-trimester spontaneous abortion. They analyzed 62 patients with positive urine pregnancy test and history of heavy vaginal bleeding whose gestational age was less than 14 weeks. In each patient, transvaginal ultrasound (TV US) and β-hCG serum measurements were performed at the time of admission to the hospital. Retained trophoblastic tissue was suspected in the presence of low resistance flow (RI <0.45) within the myometrium or just beneath the endometrial–myometrial interface. In 29% of women retained trophoblastic tissue was suspected and in 88.9% of these patients pathological analysis was positive for retained trophoblastic tissue. The authors suggested to perform B-mode and color Doppler examination when there is suspicion on retained trophoblastic tissue **(Figs 8.10A and B).**

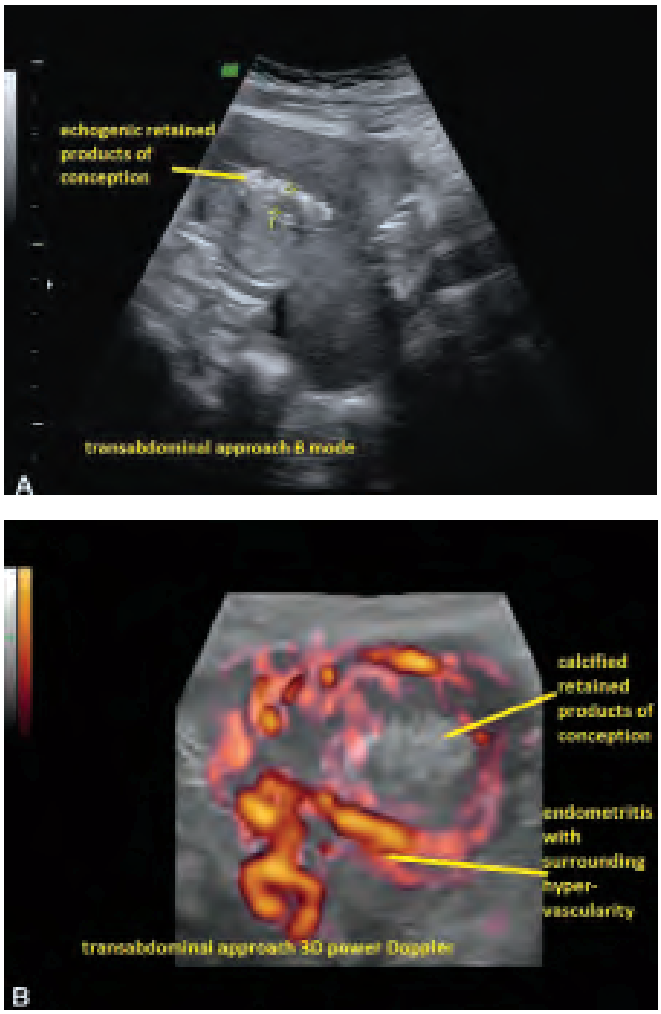

Figures 8.10A and B: Transvaginal power Doppler image of an irregular uterine cavity. Note abundant vascularity around calcified residual placental tissue

Recent studies demonstrate that risk for repeated spontaneous abortion depends exclusively on the number of previous spontaneous abortions and their cause. Even though, many different risk factors have been thoroughly researched, around 60% of unsuccessful pregnancies remain a "causa ignota".[24] The important criteria for evaluation of pregnancy loss are:[25]

- Always to keep in mind that the risk of spontaneous miscarriage is higher in older women
- Try to uncover causes for repetitive first- trimester miscarriages. Karyotyping of couples will reveal that 3 to 8% have some abnormality, most frequently balanced chromosomal rearrangement, a translocation (other abnormalities: sex chromosome mosaicism, chromosome inversions or ring chromosomes). Besides spontaneous miscarriages, these abnormalities are associated with high risk of malformations and mental retardation. Karyotyping is especially vital if the couple has had a malformed infant or fetus in addition to miscarriages in previous pregnancies.
- Smoking, alcohol, and heavy coffee consumption have been reported to be associated with an increased risk of recurrent pregnancy losses[26]
- Patients with thyroid disease or uncontrolled diabetes mellitus may suffer spontaneous miscarriages although these diseases are not causes of recurrent miscarriages
- Uterine abnormalities can result in impaired vascularization of a pregnancy, limited space for a fetus due to distortion of the uterine cavity and incoordinate uterine contractility (See the chapter: Sonographic imaging in infertility)
- Looking at the first trimester miscarriage, a firm correlation with bacterial vaginosis-associated micro-organisms was found in the study of Donders and colleagues[27]
- The major cause of thrombosis in pregnancy is an inherited predisposition for clotting, especially the factor V Leiden mutation.

Immunological problems can be classified into two groups: autoimmunity (self antigens) and alloimmunity (foreign antigens). In the autoimmunity, a humoral or cellular response is directed against a specific component of the host. The lupus anticoagulant and anticardiolipin antibodies are antiphospholipid antibodies, which arise as the result of an autoimmune disease. Several series demonstrated that 10–16% of women with recurrent miscarriages have had antiphospholipid antibodies.[12,28] These antibodies are also associated with growth retardation and fetal death in addition to recurrent miscarriages. Preferred treatment for significant titers of antiphospholipid antibodies consists of the combination of low-dose aspirin (80 mg daily) and low-dose heparin as soon as pregnancy is diagnosed.[29,30] Unfortunately, treatment is not always successful. Alloimmunity refers to all causes of pregnancy losses related to an abnormal maternal immune response to antigens on placental or fetal tissues.

MISSED ABORTION

The diagnosis of missed abortion is determined by the ultrasound identification of an embryo/fetus without any heart activity. It is relatively easy to make this diagnosis by means of transvaginal color Doppler ultrasound. The main parameter is the absence of the heart beats and the lack of color flow signals at its expected position after the 6th gestational week **(Figs 8.11A to E)**.

With the aid of sensitive color Doppler equipment, it is possible to demonstrate two types of blood flow velocity waveforms from the intervillous space[31] (pulsatile arterial-like and continuous venous-like patterns) in both, normal and abnormal early pregnancies. Studies did not show any difference in terms of RI and PI of the intervillous arterial blood flow between women with missed abortion and those with normally developing pregnancy. In long-standing demise, the cessation of the embryonic portion of placental circulation leaves the fluid pumping action of the trophoblast unaffected, as it remains nourished by the maternal side of circulation. As a consequence, the embryonic circulation no longer drains a trophoblast-conveyed fluid in the villous stroma. Progressive accumulation of the fluid may result in a significant reduction of the intervillous blood flow impedance. Lower impedance to blood flow, observed in spiral arteries, indicates that a massive and continuous congestion with maternal blood without effective drainage causes further disruption of the maternal embryonic interface resulting in abortion. These changes can be effectively studied by 2D and 3D power Doppler. In spontaneous abortions, the feto-maternal interface shows as well dysfuntional changes: histological studies of the material obtained after spontaneous abortions demonstrated insufficient trophoblastic invasion into the spiral arteries. Such findings suggest defective transformation of spiral arteries as a possible cause of spontaneous abortion in these cases. Being aware that chromosomal abnormalities are one of the most important factors for spontaneous abortion occurring in more than 50%, it is not surprising that Doppler studies do not demonstrate any significant difference

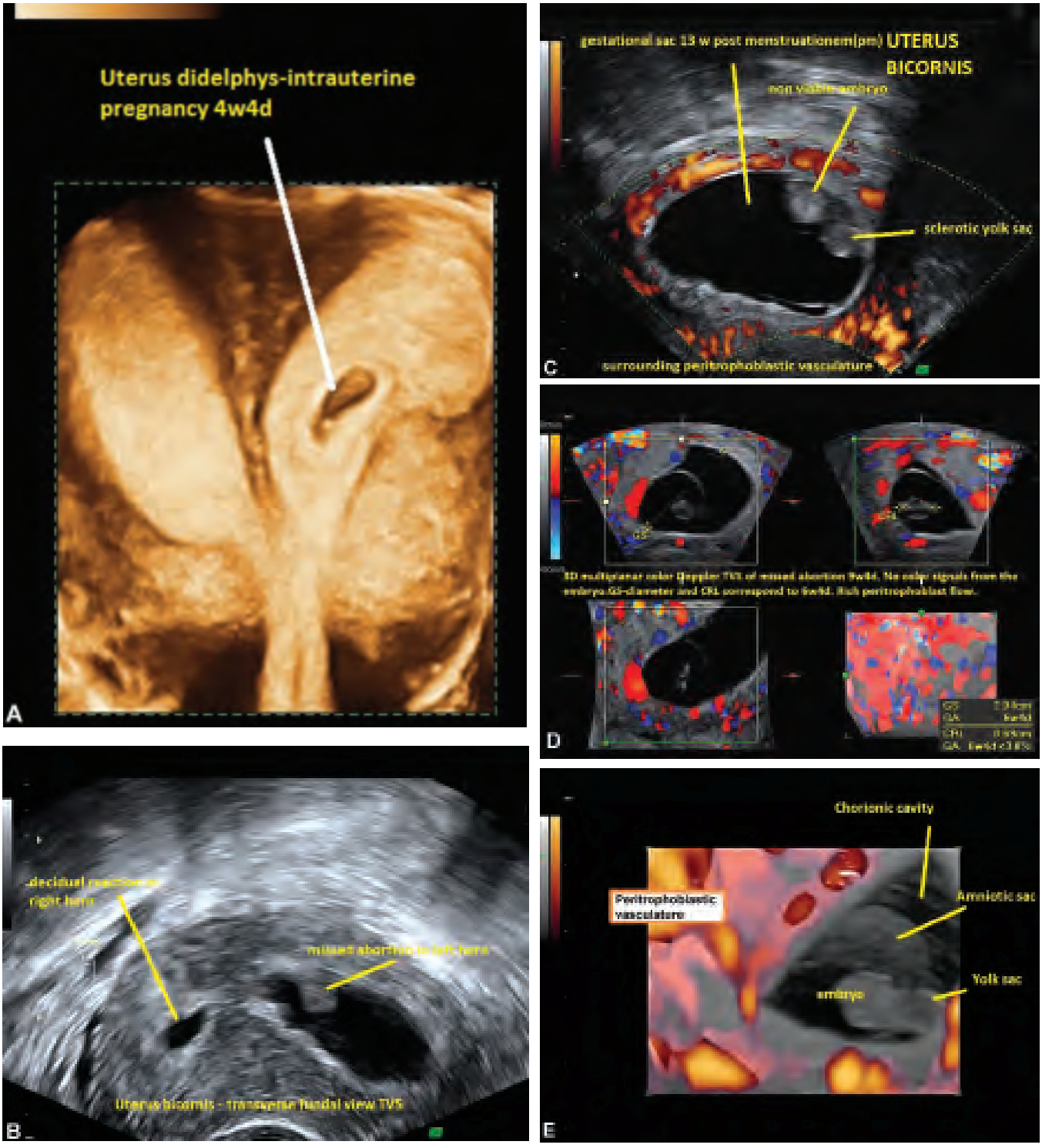

Figures 8.11A to E: Transvaginal color Doppler scan of a missed abortion. Prominent blood flow signals are obtained from the spiral arteries, while absence of heart activity is noted by color Doppler

in terms of vascular resistance between normal pregnancies and those with missed abortions. Pellizzari and coworkers[32] pointed out that blood flow analysis of uterine artery does not have any clinical role in the management of early pregnancies complicated by uterine bleeding.

Acharya and Morgan[33] compared 2D and 3D ultrasound findings in the first trimester of normal and abnormal pregnancies. 3D ultrasound volume measurements of intrauterine contents in normal and failed pregnancies correlated well with conventional 2D ultrasound. 3D volumetric assessment does not improve the diagnosis of abortion, but it can help in predicting pregnancies that will fail and gives possibility to determine the appropriate management regimen.

BLIGHTED OVUM (ANEMBRYONIC PREGNANCY)

Blighted ovum (anembryonic pregnancy) refers to a gestational sac in which the embryo either failed to develop or died at a stage too early to be visualized. The diagnosis of anembryonic pregnancy is based on the absence of embryonic echoes within a gestational sac, whose size is large enough to suggest a pregnancy age at which such structures should be visible, independent of the clinical data or menstrual cycle. Advances in transvaginal sonography allow us to detect this kind of abnormality at a mean sac diameter of 1.5 cm **(Figs 8.12A to C)**.[34] If the volume of the sac is less than 2.5 ml and is not increasing in size by at least 75% over a period of one week, the definition of this pathological condition in early pregnancy is a blighted ovum. A large empty sac usually measures between 12–18 mm in mean diameter. To confirm the diagnosis, these findings should be correlated with other clinical and sonographic data including the presence of a yolk sac.

Transvaginal sonography can clearly detect an existing, but nonviable embryo (embryonic demise) in some cases that undoubtedly would have been diagnosed as a blighted ovum if transabdominal sonography was the only examination performed. What the ultrasonographer would detect on his screen depends on gestational age and when the resorption process began.

In anembryonic pregnancy, a fertilized ovum develops into a blastocyst, but the inner cell mass and resultant embryonic pole never develops. The gestational sac with the syncytiotrophoblast invade the endometrium and act partly like a normally developing pregnancy, producing human chorionic gonadotropin.

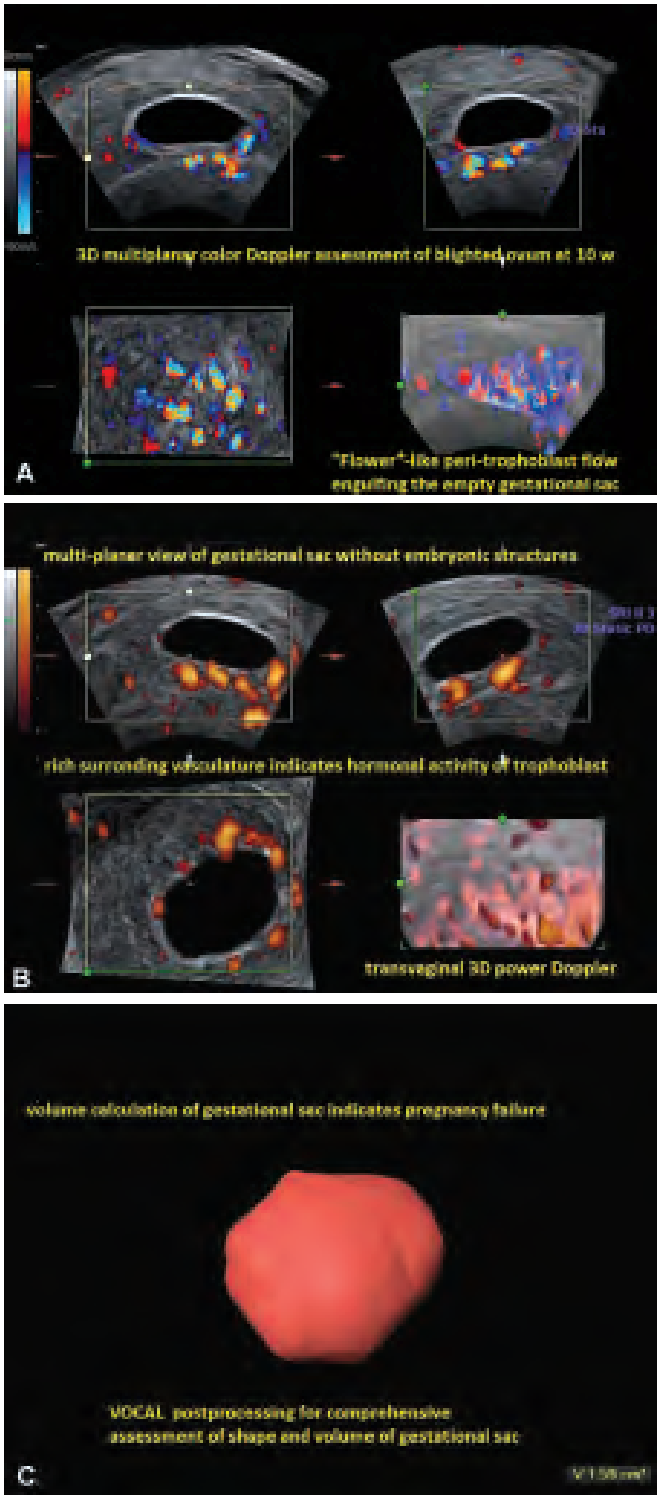

Figures 8.12A to C: Transvaginal sonogram of an anembryonic pregnancy. Note the absence of the living embryo and the yolk sac indicative of an anembryonic pregnancy. Color Doppler image presents signals obtained from the spiral arteries and other maternal vessels

The syncytiotrophoblast invades the endometrium and produces human chorionic gonadotropin. Therefore, pregnancy tests are positive and clinical signs of the pregnancy occur. But, the gestational sac fails to grow and develop normally, and the uterus fails to develop as expected. In this condition, the incidence of chromosomal abnormality is high. Generally, one can estimate that about 15–20% of all human pregnancies diagnosed before the end of the first trimester terminate in spontaneous abortion.

With falling levels of human chorionic gonadotropin, progesterone and estrogen, the feeling of being pregnant and the associated clinical signs of pregnancy that occurred earlier are lost. The diagnosis of a blighted ovum is in 100% of cases by 2D real-time ultrasonography examinations when performed a week apart after absence of embryo development has been confirmed.

Using color Doppler ultrasound in evaluation of normal and abnormal pregnancies, Kurjak and Kupesic[31] hypothesized that lower PI from the intervillous space of the anembryonic pregnancy may reflect changes in the placental stroma, where individual villi are prone to edema. Sometimes even embryos that measure 1 cm by transvaginal sonography may be absorbed totally after prolonged retention. Consequently, in absence of embryonic fluid drainage, edema of villous stroma develops, resulting in disruption of the maternal-embryonic interface and finally abortion **(Figs 8.12A to C)**.

Analyzing intervillous circulation as one of the first ultrasonographic signs of the pregnancy, studies demonstrated lower vascular resistance of the arterial-like signals in patients with blighted ovum when compared with the normal pregnancies.

Flow chart 8.2 offers way of management for women presenting with vaginal bleeding.

Flow chart 8.2: Ultrasound evaluation of women with vaginal bleeding and positive pregnancy test

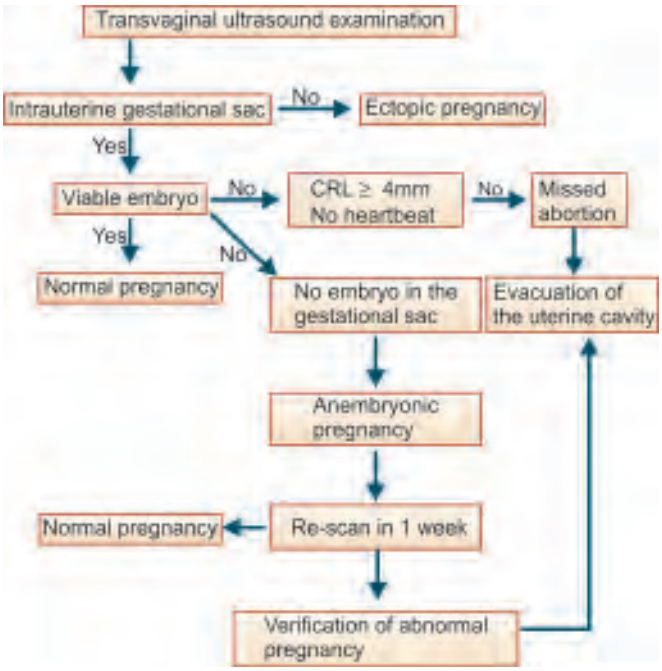

INTRAUTERINE HEMATOMAS

Intrauterine hematomas are defined as sonolucent crescent or wedge-shaped structures between chorionic tissue and uterine wall, or fetal membranes.[35] By localization we can divide them into retroplacental, subchorionic,marginal and supracervical. The most severe are large, central, retroplacental hematomas in which separation of chorionic tissue from basal decidua occurs by mechanism similar to the mechanism of abruption of the placenta.

The most common causes of intrauterine hematoma are:

- Disturbed trophoblast invasion and defect in spiral arteries transformation
- Infection
- Mechanical factors
- Autoimmune factors
- Hematological factors.

It is important to stress that findings of an intrauterine hematoma does not immediately indicate the likelihood of a spontaneous abortion. As the measure of precaution we would rather classify this pregnancy into a high-risk group with additional necessity for further intensive monitoring. Prognostically, there are two main elements, which determine the pregnancy outcome. First one is the location of the hematoma. According to Kurjak and associates, location is more predictive sign than the volume of hematoma.[35,36] It is likely that if the bleeding occurs at the level of the definitive placenta (under the cord insertion), it may result in placental separation and subsequent abortion.[37] Conversely, in a subchorionic hematoma **(Fig. 8.13B)** detaching only a membrane opposite to the cord insertion could probably reach a significant volume before it affects normal pregnancy development.[38] Supracervical hematoma has much better prognosis because it is easily drained into the vagina and for this reason it does not represent mechanical factor for compression of the uteroplacental vessels. Higher incidence of spontaneous abortions has been reported in the cases where hematoma was localized in the fundal or corporal region, which could be attributed to placental

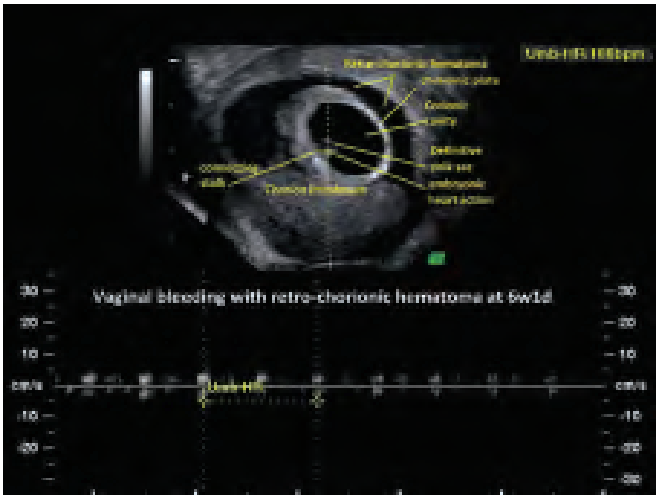

Figure 8.13A: Transvaginal sonogram of a large-volume hematoma located in fundal–corporeal region. Note M-mode detection of embryonic heartbeat inspite of large hematoma

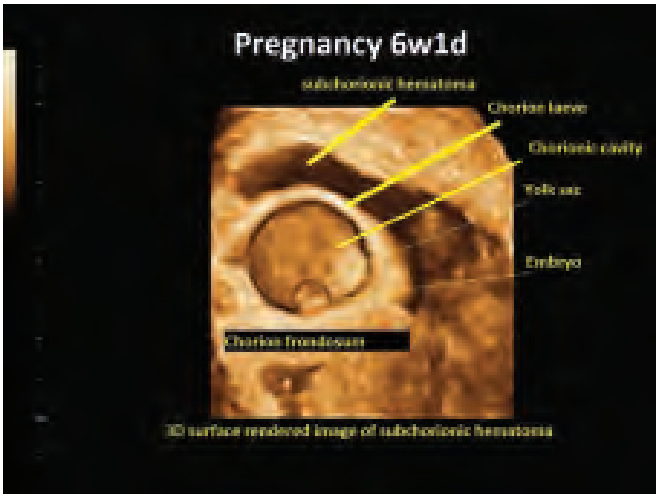

Figure 8.13B: Three-dimensional transvaginal sonogram of the subchorionic hematoma in a close proximity to the gestational sac

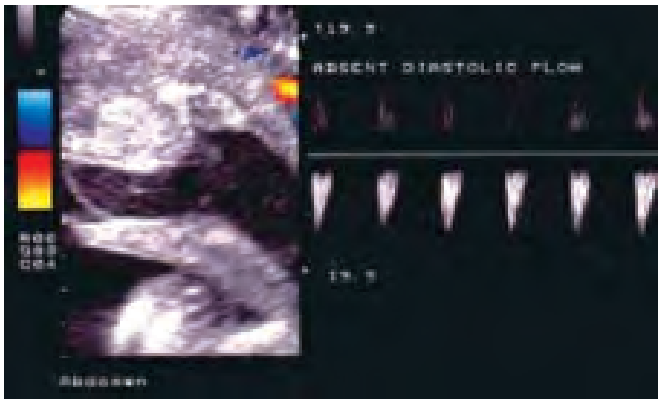

Figure 8.13C: Transvaginal color Doppler scan of a hematoma. Note the absence of diastolic flow (RI=1.0) detected in spiral arteries close to the perigestational hemorrhage

TABLE 8.2

Hematoma site and pregnancy outcome

Hematoma site	*Spontaneous abortion*			*Preterm delivery*	
Site	*N*	*n*	*%*	*n*	*%*
Supracervical	30	2	6.7	2	6.7
Fundus-corpus	29	8	27.5	1	3.4
Total	59	10	17.5	3	5

Fisher exact test: one-tail P = 0.01, two-tail P = 0.03.
From ref. 35, with permission

location in that area.[36] Retroplacental or central hematomas have the worst prognosis because they cause the largest impact on the uteroplacental circulation and placental tissue (**Fig. 8.13A**).[39] The pathological mechanism is probably placental abruption, in which retroplacental clots are located between the placenta and myometrium, and preplacental clots are found between the amniotic fluid and the placenta later in the second trimester.

Table 8.2 presents data on hematoma site and pregnancy outcome.[35] Kurjak and coworkers reported on increased resistance to blood flow and decrease in velocity through spiral arteries on the side of subchorionic hematoma, which is a consequence of mechanical compression of hematoma itself.[35,40] With the progression of pregnancy and growth of the trophoblastic tissue most of the hematomas gradually disappear, and circulation normalizes, but the pregnancy remains in the high-risk group with necessity for intensive monitoring.

Second element in diagnosis of intrauterine hematoma is its size. The modern ultrasonographic machines with transvaginal approach enable accurate evaluation of the size of the intrauterine hematoma. Intrauterine hematoma should be analyzed in relation to the trophoblast tissue, and its distance from the internal cervical os.[41]

Furthermore, software of the newest machines makes possible the spatial three-dimensional image of hematomas and surrounding structures as well as measuring their volume and dynamic follow-up of biometric changes. At the same time, Doppler measurements can evaluate compression effect on adjacent uteroplacental circulation.[35,36]

Kupesic and coworkers[42] used color Doppler to visualize the spiral arteries in the patients affected with intrauterine hematoma. Blood flow velocity waveforms were analyzed by means of pulsed Doppler. Parameters used in the study were the resistance index (RI) and peak-systolic velocity (PVS). **Table 8.3** presents the effect

TABLE 8.3

Clinical outcome of pregnancies complicated by subchorionic hematoma

	Correlation among variables			
Variable	*Gestational weeks*	*Resistance index*	*Peak systolic velocity*	*Volume*
GW	1.000			
RI	–0.304	1.000		
PS	0.702	–0.791	1.000	
V	0.157	0.527	–0.276	1.000

From ref. 42, with permission.
GW—Gestational weeks; RI—Resistance index; PS—Peak systolic; V—Volume

of the subchorionic hematoma on the local hemodynamics.[42]

The essential finding is that in the presence of hematomas, RI in the ipsilateral spiral arteries was increased and blood flow was decreased. Doppler measurements showed lack of the diastolic flow (RI=1.0) in most of the patients **(Fig. 8.13C)**. The subchorionic hematoma compresses the spiral arteries and reduces the peak-systolic velocity. With continuation of pregnancy and reabsorption of the hematoma, impedance to blood flow returns to normal values. This statistical relationship suggests that the changes in blood flow velocity are secondary and not the cause of subchorionic hematoma. It means that the improvement of blood flow is predictive for normal pregnancy outcome, while decreased spiral artery perfusion indicates increased risk of first and early second trimester loss. Since no increased risk for preterm delivery was found in patients with subchorionic hematoma, it is expected that the elevated impedance to blood flow is a transitory consequence of a compression of the arterial walls by the hemorrhage itself.

ECTOPIC PREGNANCY

When the endometrium is abnormally thick or has irregular echogenicity and intrauterine sac is not detected in the patient with the positive urinary or serum pregnancy test, one should always think of an ectopic pregnancy. An interested reader can find more about this entity in a separate chapter.

EARLY PREGNANCY LOSS

Nowadays, there is possibility to determine pregnancy outcome or to detect possible maldevelopment of the embryo by evaluating early pregnancy ultrasound signs. As a result of an abnormal development of an early pregnancy structures, early pregnancy loss could occur. Evaluation should include analysis of structures by the time of their expected ultrasound appearance **(Fig. 8.14)**:

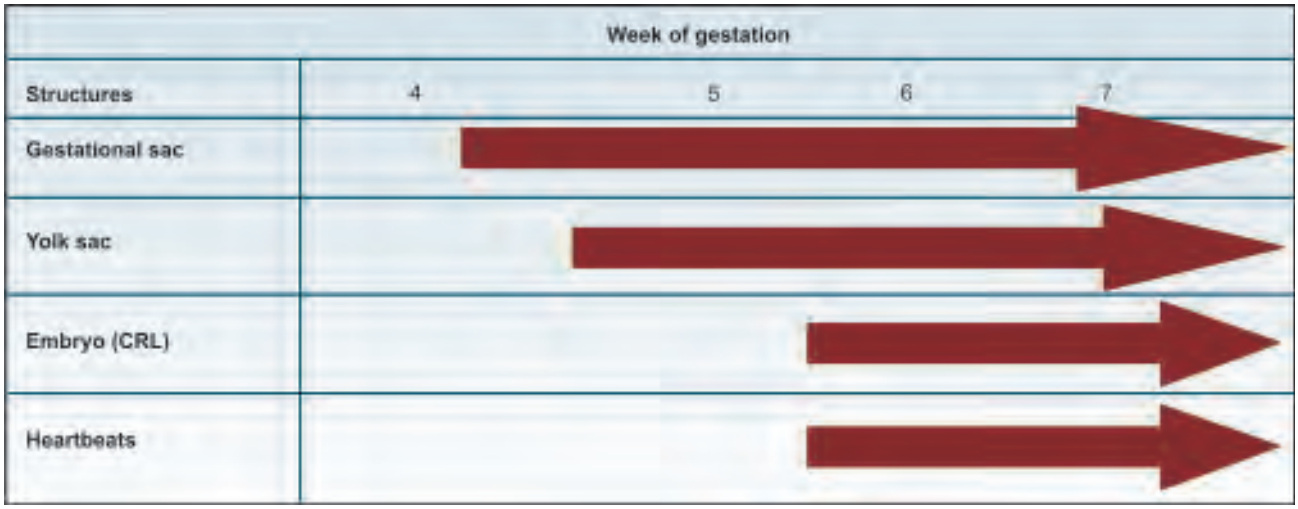

Figure 8.14: Time of appearance of important developing structures in first trimester as assessed by transvaginal ultrasound

- Gestational sac
- Yolk sac
- Crown-rump length
- Embryonic heart rate
- Amnion.

Gestational Sac

The first visible structure within the uterus is a gestational sac. During the 5th gestational week, it measures 2–3 mm in diameter[43,44] as estimated by transvaginal ultrasound. The measurement should be obtained from the inner-to-inner part of the gestational sac. The gestational sac grows approximately 1-2 mm in size per day.[45]

Biometric and morphological characteristics of gestational sac and embryonic echo can be used as a predictive factor in diagnosis of abnormal early pregnancy. Decreased values of gestational sac diameter and/or its irregular shape can suggest upcoming incident and may be used as a marker for chromosomopathies. For example, early spontaneous abortion as one of the complications in early pregnancy usually connected with triploidy and trisomy is preceded by abnormal gestational sac growth.[46,47]

By transabdominal approach, abnormal gestational sac criteria include:

- Impossibility to detect double decidual sac when sac diameter is 10 mm or greater
- Impossibility to detect yolk sac when sac diameter is 20 mm or greater, and/or
- Impossibility to detect an embryo with cardiac activity when sac diameter is 25 mm or greater.[48,49]

By transvaginal approach abnormal gestational sac criteria include:

- Impossibility to detect yolk sac when sac diameter is 8 mm or greater
- Impossibility to detect cardiac activity when sac diameter is 16 mm or greater.[50]

When growth rate fails to increase by at least 0.7 mm/day, abnormal sac and early embryo failure should be considered.[51]

Color Doppler evaluation of the supposed gestational sac is important for obtaining additional information and differentiation between pseudogestational sac and intrauterine gestational sac. Pseudogestational sac is characterized by either absent flow around it or very low velocity flow (< 8 cm/s peak systolic velocity) and moderate resistance to blood flow (RI > 0.50).[52]

Normal or abnormal intrauterine gestational sac is characterized by high velocity and low resistance pattern (RI< 0.45) (**Fig. 8.15A**). As mentioned, there is no difference in blood flow between normal and abnormal gestational sac.[53,54]

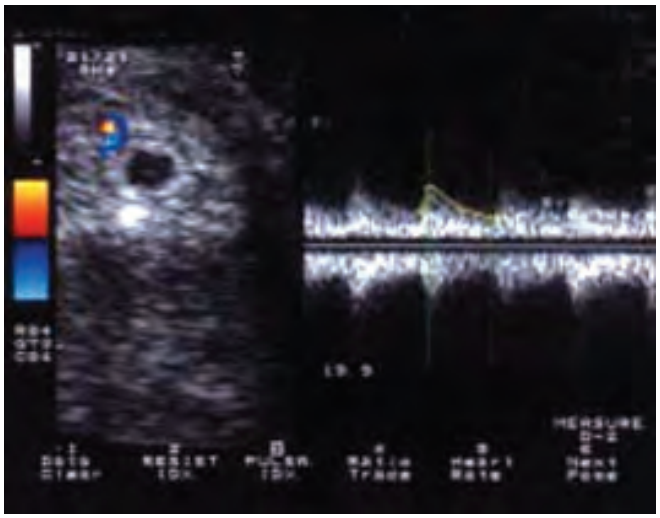

Figure 8.15A: Transvaginal color Doppler image of an early gestational sac. Blood flow signals derived from spiral arteries demonstrate low vascular resistance (PI=0.77)

Measurement of the gestational sac volume by 3D US can be used for estimation of gestational age in early pregnancy. An abnormal measurement of gestational sac could potentially be used as a prognostic marker for pregnancy outcome.[55]

Yolk Sac

Yolk sac is the first recognizable structure inside the gestational sac and should be visualized as a regularly rounded extraamniotic structure when gestational sac reaches 8–10 mm.[56] Normal biometric values of yolk sac diameter during the first trimester are 3–6 mm (inner diameter) **(Fig. 8.15B).**

Following changes assessed by 2D US are related to spontaneous abortion prediction:[56]

- Absence of the yolk sac
- Too large—more than 6 mm (over 2SD, sensitivity 16%, specificity 97%, PPV60%)
- Too small—less than 3 mm (below 2SD, sensitivity 15%, specificity 95%, PPV 44%)
- Irregular shape—mainly wrinkled with indented walls
- Degenerative changes—abundant calcifications with decreased translucency of the yolk sac (**Fig. 8.15C**)
- Number of yolk sacs—has to be equal to the number of the embryos.

It is, nowadays, assumed that yolk sac abnormalities are rather the consequence than the cause of

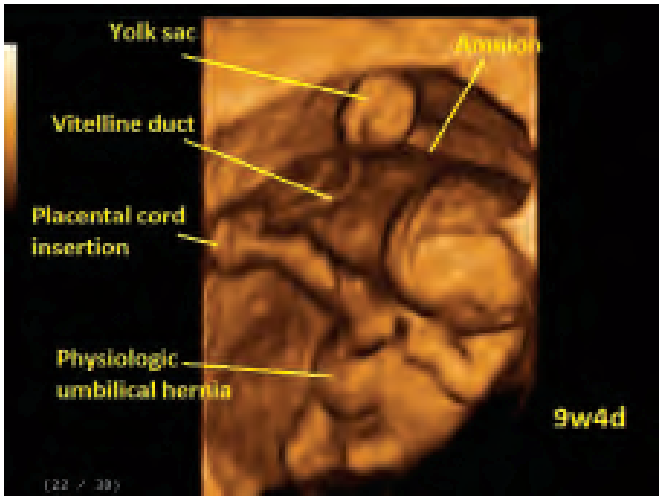

Figure 8.15B: Three-dimensional transvaginal imaging at 9 weeks 4 days of gestation by surface mode. Note regular shape of the yolk sac

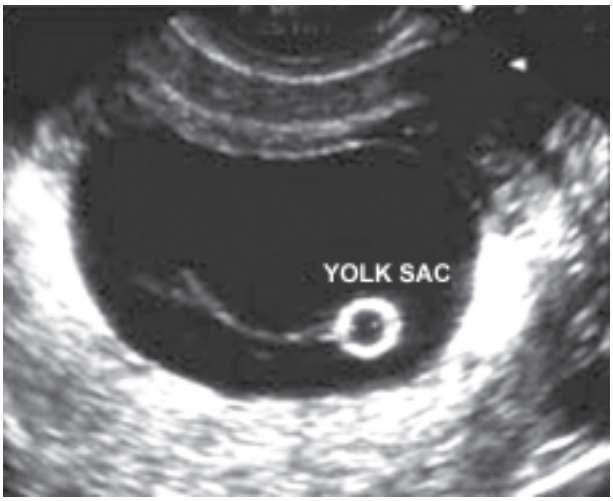

Figure 8.15C: Transvaginal sonogram of vitelline duct and yolk sac characterized with increased echogenicity

TABLE 8.4

Yolk sac diameter and vascularity between 6 and 10 weeks of gestation in normal pregnancies

Gestational	*N*	*Yolk sac diameter*		*N*	*Yolk sac vascularity age(weeks)*	
		Mean (range) (mm)	*Significance*		*%*	*Significance*
6	9	3.1 (2.5-3.8)		3	33.33	
7	15	3.6 (2.9-4.4)	p<0.05	12	80.00	p<0.005
8	19	4.1 (3.6-5.1)	p<0.05	17	89.47	p<0.05
9	18	4.5 (4.1-5.9)	p<0.05	15	83.33	p<0.05
10	14	5.3 (4.3-6.0)	p<0.001	8	57.14	p<0.001
11	12	5.0 (4.1-5.9)	p<0.05	3	25.00	p<0.005
12	10	4.3 (3.4-4.9)	p<0.001	0	0	p<0.001
Total	97	4.2 (2.5-6.0)		58	66.67	

From refernce 57, with permission

altered embryonic development [57,58] **Table 8.4** refers on yolk sac diameter and vascularity between 6–12 weeks of gestation in normal pregnancies.[57]

The ultrasound appearance of the yolk sac has already been proposed as a prognostic parameter for the outcome of pregnancy. Kurjak and coworkers[35] established sonographic criteria for distinguishing between "normal" and "abnormal" yolk sac appearance. In their experience, yolk sac should always be visible before the viable embryo; yolk sac measures 4.0–5.0 mm in diameter until 7–8 weeks of gestation and reaches 6.0–6.5 mm by the end of the 9th week. After that period

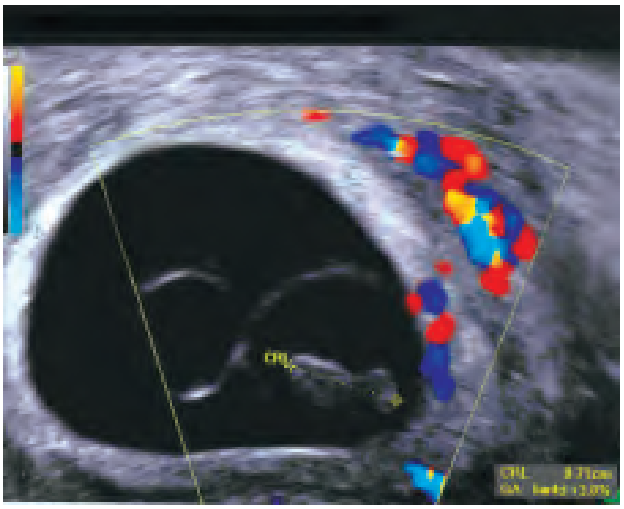

Figure 8.15D: Abnormal YS diameter, spontaneous abortion two weeks later

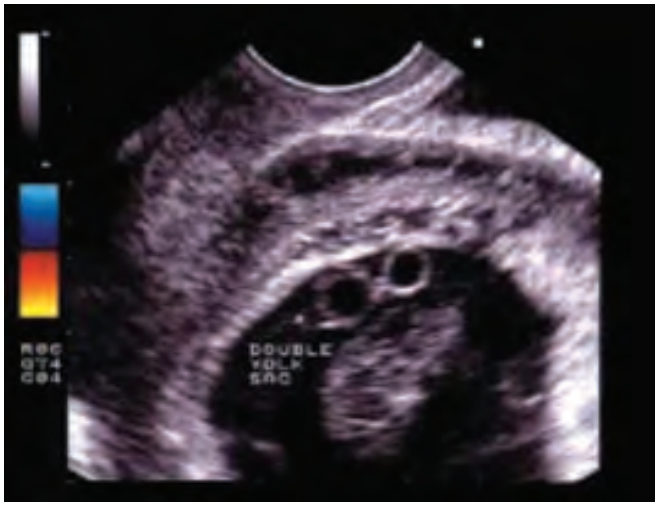

Figure 8.16: Transvaginal color Doppler scan of an 8-week embryo. Note the double yolk sac close to the embryonic body

yolk sac starts its regression and disappears at 12 weeks of gestation[59] **(Fig. 8.15D)**.

The sonographic detection of abnormal yolk sac morphology may predict abnormal fetal outcome. Attempts have been made to identify abnormal parameters. Parameters of abnormal yolk sac findings listed above are predictive indicators of early pregnancy failure. All these parameters should be defined and assessed prior to 10 gestational weeks.

Abnormal yolk sac size may be the first sonographic indicator of associated failure. Primarily, the presence of an embryo without visible yolk sac before the 10th gestational week is mostly an abnormal finding. According to some authors, the inner diameter of the yolk sac is always less than 5.6 mm in a normal pregnancy before the 10th week of gestational age. Lyons[60] established that for a mean gestational sac diameter of less than 10 mm, the yolk sac diameter should be less than 4 mm. In 15 patients who had abnormally large sacs, six had no embryo, five aborted spontaneously and only one conceptus survived. Out of nine others with embryo and large yolk sac, eight patients aborted and in one patient trisomy 21 was detected at the 24th gestational week.

The yolk sac can be too small, and this is accepted as a marker of poor pregnancy outcome. Green and Hobbins[61] analyzed a group of patients between 8–12 weeks' gestational age, and found out that a yolk sac diameter of less than 2 mm was associated with adverse pregnancy outcome.

Most often, the shape of the yolk sac is changed when compressed by a growing fetus after the 10th gestational week. The normal spherical shape of the yolk sac could be distorted even earlier, requiring intensive follow-up within the next few weeks. The most difficult diagnostic puzzle is the double yolk sac **(Fig. 8.16)**. Each singleton pregnancy should have a single yolk sac. A double yolk sac is an extremely rare finding. The diagnostic puzzle includes the morphological differentiation of a delayed disappearance of physiological midgut herniation or an early abdominal wall defect.

It is unknown whether abnormalities of the yolk sac are related primarily to the yolk sac or secondary to embryonic maldevelopment. According to the present data, is seems that the yolk sac plays an important role in materno-embryonal transportation in early pregnancy. Changes in size and shape could indicate or reflect significant dysfunction of this system and therefore could influence early embryonic development. Currently, the major benefits of sonographic evaluation of the yolk sac are:

- Differentiation of potentially viable and nonviable gestations
- Confirmation of the presence of an intrauterine pregnancy vs. a decidual cast, and
- Indication of a possible fetal abnormality.

Kurjak and associates[57] performed a transvaginal color Doppler study of yolk sac vascularization.

They examined 105 patients whose gestational age ranged from 6–10 weeks from the last menstrual period. Transvaginal color and pulsed Doppler examination was performed before the termination of pregnancy for psychosocial reasons. The overall visualization rate for yolk sac vessels was 72.38%. A characteristic waveform profile included low velocity (5.8 ± 1.7 cm/s) and the absence of diastolic flow was found in all examined yolk

sacs. The pulsatility index showed a mean value of 3.24 ± 0.94 without significant changes between the subgroups.

Kurjak and coworkers[62,63] also analyzed the vascularization of yolk sac in abnormal pregnancies. Study included 48 patients with missed abortion between 6–12 weeks' gestation. Yolk sac blood flow was detected in 18.54% of missed abortions. Three types of abnormal vascular signals were obtained from the yolk sac:

1. Irregular blood flow
2. Permanent diastolic flow
3. Venous blood flow signals.

Changes in vascularization of the yolk sac noticed in missed abortions in this study are probably a consequence of embryonic death and reabsorption of the embryo through the vitelline duct. Abnormal patterns of the yolk sac vascularity can be related to decreased vitelline blood flow, which may cause progressive accumulation of nutritive secretions not utilized by the embryo. This process ends with enlargement of the yolk sac indicative of an early pregnancy failure. In 28.57% of missed abortions, yolk sac vascularity was detected with large diameter of the yolk sac and 20% with normal yolk sac diameter.

Yolk sac calcification was reported to result from the typical dystrophic changes that occur in nonviable cellular material.[64] Recognition of a calcified yolk sac without blood flow signals suggests long-standing demise in the first trimester, which directs the clinician to further diagnostic work-up.

Kurjak and Kupesic[63] presented data indicating that there is an interaction between the yolk sac vascularity and intervillous circulation in patients with missed abortion. In patients with long-standing demise, vascular signals could not be extracted from the hyperechoic walls of the yolk sac. Parallel assessment of the intervillous circulation demonstrated numerous color-coded areas within the intervillous space indicating low mesenchymal turgor and progressive disruption of the maternoembryonic interface. Therefore, the changes in the intervillous circulation noticed in some missed abortions are rather the consequence of embryonic death and inadequate drainage than being the primary cause of early pregnancy failure. Independent Doppler studies from three institutions using sensitive conventional and power Doppler velocimetry found that continuous and pulsatile blood flow can be extracted from intervillous space in both normal pregnancies and those with adverse outcome.[65-67]

Data presented by Kurjak and Kupesic[60] support the concept that establishment of the intervillous circulation is a progressive process during the first trimester of pregnancy. Between the 6–10th week of gestation, clear blood flow signals are derived from the walls of the yolk sac supporting the hypothesis that yolk sac is responsible for optimal delivery of nutrients and oxygen to the developing embryo up to 10 weeks of gestation. Later on, intervillous circulation becomes more prominent, indicating a possible switch from the vitelline towards intervillous circulation.

Three-dimensional ultrasound (3D US) significantly contributes to *in vivo* observation of the yolk sac surface pattern, enabling reduced scanning time and observation of the honeycomb surface pattern of the yolk sac. Automatic volume calculation allows us to estimate precise relationship between the yolk sac and gestational sac volumes, as well as to obtain the correlation between yolk sac volume and CRL measurements.[68] Distinguishing the yolk sac and embryo in 6th and 7th week of gestation decreases possibility of CRL measurement error **(Fig. 8.10)**.

Table 8.5 reveals normal and abnormal yolk sac features.[69]

TABLE 8.5
Normal and abnormal yolk sac characteristics

	Normal yolk sac	*Abnormal yolk sac*
Size	5-6 mm up to 9th week of gestation	< 2 mm in 8 to 12 weeks (too small) > 6 mm after 10th week (too large)
Shape	Round	Oval, distorted
Ultrasound finding	Echoic rim, hypoechoic center	Hyperechoic
Doppler	Absence of diastolic flow	Irregular blood flow Permanent diastolic flow Venous blood flow

From ref. 69, with permission

Crown-rump Length (CRL)

Crown-rump length is used to estimate growth of the embryo and define exact gestational age. Measurement of CRL is performed in midsagittal section from the top of the head (crown) to the end of the rump of embryo by transvaginal probe.

Reliability of CRL measurements depends on embryo size and the fact that the measurements are only precise when the greatest long axis reaches 18–22 mm. In smaller embryos, a mistake in few millimeters means a large deviation. In embryos over 18 mm, when the real CRL is measured and the anatomic structures are visible, the possibility of a mistake is smaller.

The median CRL in fetuses with trisomies 21 and 13 or sex chromosome aneuploidies is not significantly different from normal fetuses as reported by Kuhn and coworkers.[70] This is the reason why routine pregnancy dating should be based on measurement of CRL, like the risk-calculation of combined nuchal translucency — or biochemical screening for aneuploidies.

However, some results suggest that the measurement of fetal CRL may be useful predictor of spontaneous miscarriage and SGA in pregnancies with threatened abortion.[71]

Embryonic Heart Rate

The cutoff CRL for detecting cardiac activity by transvaginal probe is 4 mm,[72] and by transabdominal approach 9 mm.[73] Heart rate progressively increases to 120–160 beats/minute after 6–7 weeks.[74]

Embryonic heart rate demonstrates certain physiologic variability within its normal range of frequencies which is 150–190 beats/minute for embryos bigger than 10 mm at 8–12 weeks of gestation. An embryonic heart rate less than 100 beats per minute (bpm) at 7 weeks is recognized as embryonic bradycardia.[75] An embryonic heart rate less than 70 bpm has been reported to result in a fetal demise in 100% patients.[76] Bradycardia or arrhythmia could be considered as predictors of heart action cessation. In these cases, an early hemodynamic heart failure was noticed with subsequent gestational sac enlargement, yolk sac enlargement (more than 6 mm) and initial generalized hydrops. This type of hemodynamic disturbances can occur in patients presenting with massive intrauterine hematomas prior to fetal demise.[77] Doubilet[78] reported that pregnancies in which the embryos have a slow heart rate at or before seven weeks of gestation and which continue beyond the first trimester, have a high likelihood (90%) of congenital anomalies, compared to pregnancies with normal embryonic heart rates. Reduced body movements of the embryo during first and second trimester are also considered as possible predictors of early pregnancy complications.[77]

Amnion Evaluation

At 6–8 weeks of gestation by transvaginal probe, amniotic membrane is visualized as a thin rounded structure encircling the embryo. It could appear before 6th week of gestation as a linear echogenic interface projected within the gestational sac in proximity to the embryo.[44]

When the amniotic membrane is clearly visualized or its thickness and echogenicity approach that of yolk sac, abnormal amnion development should always be suspected.[79] Mean amniotic sac diameter is approximately equal to the CRL in normal early pregnancy. Enlarged amniotic cavity in relation to CRL measurement suggests early pregnancy abnormality.[79]

Horrow[80] presented data on the difference between the CRL and amniotic cavity diameter and stated that in normal pregnancies was approximately 1 mm but reached almost 9 mm in abnormal pregnancies. Their results suggest that an amniotic cavity that is enlarged relative to the CRL and the size of the chorionic cavity correlates with subsequent embryonic death.

In a normal pregnancy,the embryo is usually detected earlier than the amniotic membrane. Cases of "empty amnion" with gestational sac greater than 16 mm are highly suggestive of abnormal pregnancy and require further analysis.[81]

CONCLUSION

Ultrasound examination has become the "golden standard" in follow-up of the development and complications in early pregnancy. With introduction of transvaginal sonography, the quality of early morphological and biometrical ultrasound examinations has been significantly improved. The essential aim of an early pregnancy ultrasound is not only to diagnose a pregnancy, but also to differentiate between normal and abnormal pregnancy. Application of color Doppler ultrasound has enabled functional hemodynamic assessment, soon after implantation.

Early pregnancy failure is defined as a pregnancy that ends spontaneously before the embryo is detected by ultrasound at the gestational age in which visualization of viable embryo should occur. The most common pathological symptom of early pregnancy failure is vaginal bleeding. Accurate evaluation of pregnancy dates, gestational sac and embryo assist in

finding therapeutic measures for cases where a normal outcome of the pregnancy can be expected.

The development of transvaginal sonography has improved assessment of the patients presenting vaginal bleeding during the first half of pregnancy, clarifying the differential diagnosis of missed abortion, ectopic pregnancy, blighted ovum and threatened abortion with a living embryo. Embryo vitality can be established reliably by documenting cardiac activity in real-time, B-mode and/or color Doppler ultrasonography.

Threatened abortion is the clinical term used to describe vaginal bleeding during the first 20 weeks of pregnancy in women who, on the basis of clinical evaluation, are considered to have the potential of delivering a viable fetus. With a normal intrauterine pregnancy, bleeding from the chorion frondosum is undoubtedly the most common source of vaginal bleeding during the first trimester and should be considered in the diagnosis of threatened abortion.

As per definition, incomplete abortion is the passage of some, but not all fetal or placental tissue through the cervical canal. In complete abortion, all products of conception are expelled through the cervix. Transvaginal ultrasonography plays an important role in evaluating uterine cavity in spontaneous abortion, since it enables detection of retained products of conception. Retained products of conception after abortion may cause bleeding or endometritis. Recent studies demonstrate that the risk for repeated spontaneous abortion depends exclusively on the number of previous spontaneous abortions, their cause, maternal age, chromosomal abnormalities, uterine anomalies, etc. Though many different risk factors have been thoroughly researched, around 60% of unsuccessful pregnancies remain unexplained.

When spontaneous abortion is suspected, we suggest to perform not only 2D but also color Doppler sonographic evaluation of the retained trophoblastic tissue.

The diagnosis of missed abortion is confirmed by the ultrasound identification of an embryo/fetus without any heart activity. It is relatively easy to make this diagnosis by means of transvaginal color Doppler ultrasound. The main parameter is the absence of the heart beats and the lack of color flow signals at its expected position after the sixth gestational week.

Blighted ovum (anembryonic pregnancy) refers to a gestational sac in which the embryo either failed to develop or died at a stage too early for sonographic visualization. The diagnosis of anembryonic pregnancy is based on the absence of embryonic echoes within a gestational sac large enough for such structures to be visualized independent of the clinical data or menstrual cycle. Advances in transvaginal sonography allow us to detect this kind of abnormality at a mean sac diameter of 1.5 cm. To confirm the diagnosis, these findings should be correlated with other clinical and sonographic data including the presence of a yolk sac.

Intrauterine hematomas are defined as sonolucent crescent or wedge-shaped structure between chorionic tissue and uterine wall or fetal membranes. By localization intrauterine hematomas can be divided into retroplacental, subchorionic, marginal and supracervical. The most severe are large, central, retroplacental hematomas. Prognostically, there are two main elements which determine the pregnancy outcome: location and the size of the hematoma. The essential color Doppler finding is that in the presence of hematomas, vascular resistance in the ipsilateral spiral arteries is increased and blood flow is decreased. Doppler measurements showed lack of diastolic flow in most of hematomas resulting in RI of 1.0. Since no increased risk for preterm delivery was found in patients with subchorionic hematoma, it is expected that the elevated impedance to blood flow is a transitory consequence of a compression of the spiral arterial walls by the hemorrhage itself.

Biometric and morphological characteristics of gestational sac and embryonic echo can be used as predictive factors in diagnosis of abnormal early pregnancy. Decreased values of gestational sac diameter and/or its irregular shape can suggest upcoming incident and could be used as markers for chromosomopathies. When growth rate fails to increase by at least 0.7 mm/d an early embryo failure should be considered.

Yolk sac is the first recognizable embryonic structure inside the gestational sac in early pregnancy. Following changes assessed by 2D US are related to the prediction of spontaneous abortion: absence of yolk sac, too large yolk sac (more than 6 mm), too small yolk sac (less than 3 mm), irregular shape of the yolk sac (mainly wrinkled with indented walls), degenerative changes of the yolk sac (abundant calcifications with decreased translucency of yolk sac) and number of yolk sacs (has to be equal to the number of embryos).

Crown–rump length (CRL) is used to estimate growth of the embryo and define exact gestational age. The median CRL in fetuses with trisomies 21 and 13 or sex chromosome aneuploidies is not significantly different from that of normal fetuses. An embryonic heart rate less than 100 beats per minute (bpm) before seven weeks is recognized as embryonic bradycardia. Bradycardia of arrhythmia could be considered as predictors for heart action cessation. In these cases, an

early hemodynamic heart failure is usually noticed with subsequent gestational sac enlargement, yolk sac enlargement (more than 6 mm) and initial generalized hydrops.

Mean amniotic sac diameter is approximately equal to the CRL in normal early pregnancy. Enlarged amniotic cavity compared with CRL suggests early pregnancy abnormality.

Increased NT thickness at 10–14 weeks of gestation is associated with fetal chromosomal defects, many genetic syndromes and abnormalities. Because of the change of the value of NT with CRL, each measurement of the NT should be compared with adequate CRL value.

The interested reader will find detailed explanation of combined NT screening in special chapter.

REFERENCES

1. Kurjak A. Ultrasound in early pregnancy. In: Kurjak A (Ed). Diagnostic Ultrasound in Developing Countries. Mladost. Zagreb; 1986. pp. 65-75.
2. Jukic S. Pathology of women's reproductive system. AGML:Zagreb; 1999.
3. Kurjak A, Zalud I, Schulman H. Ectopic pregnancy: transvaginal color Doppler of trophoblastic flow in questionable adnexa. J Ultrasound Med. 1991;10(12):685-9
4. Sadler TW. Langman's Medical Embryology. 9th Edition. Lippincott Williams and Wilkins. 2(5):102.
5. Azumendi G, Kurjak A. Three–dimensional Sonoembryology. Donald School Journal of Ultrasound in Obstetrics and Gynecology. 2008;2(2):62-86.
6. Goldstein SR. Embryonic death in early pregnancy: a new look at the first trimester. Obstet Gynecol. 1994;84(2):294-7.
7. Sadler TW. Langman's Medical Embriology. 7th edition. Williams and Wilkins: 1994.
8. Streeter GL. Developmental horizons in human embryo: a review of the histogenesis of cartilage and bone. Contr Embryol Carneg Inst. 1949;220(4):150-73.
9. Blaas HG. The examination of the embryo and early fetus: how and by whom? Ultrasound Obstet Gynecol. 1999;14(3):153-8.
10. Blaas HG, Eik-Nes SH, Kiserud T, et al. Early development of the abdominal wall, stomach and heart from the 7 to 12 weeks of gestation: a longitudinal study. Ultrasound Obstet Gynecol. 1995;6(4):240-9.
11. Cetin A, Cetin M. Diagnostic and therapeutical decision-making with transvaginal sonography for first trimester spontaneous abortion, clinically thought to be complete or incomplete. Contraception. 1998;57(6):393-7.
12. Edmonds DK, Lindsky KS, Miller JF. Early embryonic mortality in women. Fertil Steril. 1982;38(4):447-53.
13. Hakim RB, Gray RH, Zacur H. Infertility and early pregnancy loss. Am J Obstet Gynecol. 1995;172(5):1510-7.
14. Alberman E. The epidemiology of repeated abortion. In: Beard RW, Bishop F (Eds). Early pregnancy loss: mechanism and treatment. New York: Springer- Verlag; 1988. pp.9-17.
15. Kurtz AB, Shlansky-Goldberg BB. Detection of retained products of conception following spontaneous abortion in the first trimester. J Ultrasound Med. 1991;10:387-95.
16. Chung TKH, Cheung LP, Sahota DS, et al. Evaluation of the accuracy of transvaginal sonography for the assessment of retained products of conception after spontaneous abortion. Gynecol Obstet Invest. 1998;45(3):190-3.
17. Kaakaji Y, Nghiem HV, Nodel C, et al. Sonography of obstetric and gynecologic emergencies: Part I, Obstretic emergencies. AJR Am J Roentgenol. 2000;174(3):641-9.
18. Moore L, Wilson SR. Ultrasonography in obstetric and gynecologic emergencies. Radiol Clin North Am. 1994;32(5):1005-22.
19. Wong SF, Lam MO, Ho LC. Transvaginal sonography in the detection of retained products of conception after first-trimester spontaneous abortion. J Clin Ultrasound. 2002;30(7):428-32.
20. Achiron R, Goldenberg M, Lipitz S, et al. Transvaginal duplex Doppler sonography in bleeding patients suspected on having residual trophoblastic tissue. Obstet Gynecol. 1993;81(4):507-11.
21. Dillon EH, Case CQ, Ramos IM, et al. Endovaginal US and Doppler findings after first-trimester abortion. Radiology. 1993;186(1):87-91.
22. Tal J, Timor-Tritsch I, Degani S. Accurate diagnosis of postabortal placental remnant by sonohysterography and color Doppler sonographic studies. Gynecol Obstet Invest. 1997;43(2):131-4.
23. Alcázar JL, Ortiz CA. Transvaginal color Doppler ultrasonography in the management of first-trimester spontaneous abortion. Eu J Obstet Gynecol Reprod Biol. 2002;102(1):83-7.
24. Kos M, Kupesic, S Latin V. Diagnostics of spontaneous abortion. In: Kurjak A (Ed). Ultrasound in Gynecology and Obstetrics. Zagreb: Art Studio Azinovic 2000. pp. 314-21.
25. Reccurrent early pregnancy loss. In: Speroff L, Glass RH, Kase NG (Eds). Clinical gynecologic endocrinology and infertility. London:Williams and Wilkins; 1999. pp. 1043-55.
26. Windham GC, Von Behren J, Fenster L, et al. Moderate maternal alcohol consumption and risk of spontaneous abortion. Epidemiology. 1997;8(5):509-14.
27. Donders GGG, Odds A, Veercken A, et al. Abnormal vaginal flora in the first trimester, but not full blown bacterial vaginosis, is associated with preterm birth. Prenat Neonat Med. 1998;3:558-93.
28. Kupesic S, Kurjak A, Chervenak F. Doppler studies of subchorionic hematomas in early pregnancy. In: Chervenak F, Kurjak A (Eds). Current perspectives on the fetus as a patient. Carnforth, UK: Parthenon Publishing; 1996. pp. 33-9.
29. Cowchock FS, Reece EA, Balaban D, et al. Repeated fetal losses associated with anti- phospholipid antibodies: a collaborative randomized trial comparing prednizone with low-dose heparin treatment. Am J Obstet Gynecol. 1992;166(5):1318-23.
30. Rai R, Cohen H, Dave M, et al. Randomized controlled trial of aspirin and aspirin plus heparin in pregnant women

with recurrent miscarriage associated with phospholipid antibodies. BMJ. 1997;314(7076):253-7.
31. Kurjak A, Kupesic S. Doppler assessment of the intervillous blood flow in normal and abnormal early pregnancy. Obstet Gynecol. 1997;89(2):252-6.
32. Pellizari P, Pozzan C, Marchiori S, et al. Assessment of uterine artery blood flow in normal first-trimester pregnancies and those complicated by uterine bleeding. Ultrasound Obstet Gynecol. 2002;19(4):366-70.
33. Acharya G, Morgan H. First-trimester, three- dimensional transvaginal ultrasound volumetry in normal pregnancies and spontaneous miscarriages. Ultrasound Obstet Gynecol. 2002;19(6):575-9.
34. de Crepigni LC. Early diagnosis of pregnancy failure with transvaginal sonography. Am J Obstet Gynecol. 1988;159(2):408-9.
35. Kurjak A, Schulman H, Kupesic S, et al. Subchorionic hematomas in early pregnancy: clinical outcome and blood flow patterns. J Matern Fetal Med. 1996;5(1):41-4.
36. Kurjak A, Chervenak F, Zudenigo D, et al. Early pregnancy hemodynamics assessed by transvaginal color Doppler. In: Chervenak F, Kurjak A (Eds). The Fetus as a Patient. Carn forth UK: Parthenon Publishing; 1994. pp. 435-55.
37. Jauniaux E, Gavril P, Nicolaides KH. Ultrasonographic assessment of early pregnancy complication. In: Jurkovic D, Jauniaux E (Eds). Ultrasound and early pregnancy. Carn forth, UK:Parthenon Publishing; 1995. pp. 53-64.
38. Kurjak A, Kupesic S. Blood flow studies in normal and abnormal pregnancy. In: Kurjak A, Kupesic S (Eds). An Atlas of Transvaginal Color Doppler. London: Parthenon Publishing;2000. pp. 41-51.
39. Laurini RN. Abruptio placentae: From early pregnancy to term. In: Chervenak F, Kurjak A (Eds). The fetus as a patient. Carnfor th UK: Parthenon Publishing; 1996. pp. 433-44.
40. Mantoni M, Pedersen JF. Intrauterine hematoma. An ultrasonic study of threatened abortion. Br J Obstet Gynaecol. 1981;88(1):47-51.
41. Falco P, Milano V, Pilu G, et al. Sonography of pregnancies with first- trimester bleeding and a viable embryo: a study of prognostic indicators by logistic regression analysis. Ultrasound Obstet Gynecol. 1996;7(3):165-9.
42. Kupesic S, Kurjak A. Physiology of uteroplacental and embryonic circulation. In: Kurjak A (Ed). Textbook of Perinatal Medicine. Parthenon Publishing; 1998. pp. 482-90.
43. Timor-Tritsch IE, Farine D, Rosen MG. A close look at the embryonic development with the high frequency transvaginal transducer. Am J Obstet Gynecol. 1988;159(3):676-81.
44. de Crespigny LC, Cooper D, McKenna M. Early detection of intrauterine pregnancy with ultrasound. 1988;7(1):7-10.
45. Fleischer AC, Kepple DM. Transvaginal sonography of early intrauterine pregnancy. In: Fleischer AC, Manning FA, Jeanty P, et al (Eds). Sonography in obstetrics and gynecology: Principles and Practice. 6th edition. The McGraw-Hill Companies;2001. pp. 61-88.
46. Bromley B, Harlow BL, Laboda LA, et al. Small sac size in the first trimester: a predictor of poor fetal outcome. Radiology. 1991;178(2):375-7.
47. Dickey RP, Gasser R, Oltar TT, et al. Relationship of initial chorionic sac diameter to abortion and abortus karyotype based in new growth curves for the 16th to 49th post-ovulation day. Hum Reprod. 1994;9(3):559-65.
48. Nyberg DA, Laing FC, Filly RA. Threatened abortion: sonographic distinction of normal and abnormal gestational sac. Radiology. 1986;158(2):397-400.
49. Nyberg DA, Laing FC, Filly RA, et al. Ultrasonographic differentiation of the gestational sac of early intrauterine pregnancy and pseudogestational sac of ectopic pregnancy. Radiology. 1983;146(3):755-9.
50. Levi CS, Lyons EA, Lindsay DJ. Early diagnosis of normal pregnancy with transvaginal ultrasound. Radiology. 1988;167:383-5.
51. Nyberg DA, Mack LA, Laing FC, et al. Distinguishing normal from abnormal gestational sac growth in early pregnancy. J Ultrasound Med. 1987;6:23-7.
52. Dillon EH, Feyock AL, Taylor KJ. Pseudogestational sacs: Doppler US differentiation from normal or abnormal intrauterine pregnancies. Radiology. 1990;176(2):359-64.
53. Kurjak A, Zalud I, Predanic M, et al. Transvaginal color and pulsed Doppler study of uterine blood flow in the first and early second trimesters of pregnancy: normal versus abnormal. J Ultrasound Med. 1994;13(1):43-7.
54. Jaffe R, Warsof SL. Color Doppler imaging in the assessment of uteroplacental blood flow in the abnormal first trimester intrauterine pregnancies. An attempt to define etiologic mechanisms. J Ultrasound Med. 1992;11(1):41-4.
55. Benoit B, Hafner T, Bekavac I, et al. Three- dimensional sonoembryology. Ultrasound Rev Obstet Gynecol. 2001;1:111-9.
56. Lindsay DJ, Lovett IS, Lyons EA. Endovaginal appearance of the yolk sac in pregnancy: normal growth and usefulness as a predictor of abnormal pregnancy. Radiology. 1992;183:115-8.
57. Kurjak A, Kupesic S, Kostovic Lj. Vascularization of yolk sac and vitelline duct in normal pregnancy studied by transvaginal color Doppler. J Perinat Med. 1994;22(5):433-40.
58. Kurjak A, Kupesic S, Kos M, et al. Ultrasonic and Doppler studies of human yolk sac. In: Chervenak F, Kurjak A (Eds). The fetus as a patient. Carnforth UK: Parthenon Publishing; 1996. pp. 345-7.
59. Jauniaux E, Moscoso JG. Morphology and significance of the human yolk sac. In: Barnea E (Ed). The first twelve weeks of gestation. Heidelberg: Springer; 1992. pp. 192-216.
60. Lyons EA. Endovaginal sonography of the first trimester of pregnancy. Proceedings of the 3rd International Perinatal and Gynecological Ultrasound Symposium Ottawa, Ontario; 1994. pp. 1-25.
61. Green JJ, Hobbins JC. Abdominal ultrasound examination of the first trimester fetus. Am J Obstet Gynecol. 1988; 159(1):165-75.
62. Kurjak A, Kupesic S. Parallel Doppler assessment of yolk sac and intervillous circulation in normal pregnancy and missed abortion. Placenta. 1998;19(8):619-23.
63. Kurjak A, Kupesic S, Kos M. Early hemodynamics studied by transvaginal color Doppler. Prenatal and neonatal medicine. 1996;1:38-49.

64. Harris RD, Vincent LM, Askin FB. Yolk sac calcification: a sonographic finding associated with intrauterine embryonic demise in the first trimester. Radiology. 1988;166(1 Pt 1):109-10.
65. Mercé LT, Barco MJ, Bau S. Color Doppler sonographic assessment of placental circulation in the first trimester of normal pregnancy. J Ultrasound Med. 1996;15(2):135-42.
66. Valentin L, Sladkevicius P, Laurini R, et al. Uteroplacental and luteal circulation in normal first-trimester pregnancies: Doppler ultrasonographic and morphologic study. Am J Obstet Gynecol. 1996;174(2):768-75.
67. Kurjak A, Dudenhausen JW, Hafner T, et al. Intervillous circulation in all three trimesters of normal pregnancy assessed by color Doppler. J Perinat Med. 1997;25(4):373-80.
68. Kurjak A, Kupesic S, Kos M. Three-dimensional sonography for assessment of morphology and vascularization of the fetus and placenta. J Soc Gynecol Investig. 2002;9(4):186-202.
69. Kurjak A, Kupesic S. Blood flow studies in early pregnancy. In: Kurjak A, Kupesic S (Eds). Color Doppler in obstetrics, gynecology and infertility. Art Studio Azinovic-Medison Zagreb-Seoul; 1999. pp. 87-108.
70. Kuhn P, Brizot M, Pandya PP, et al. Crown-rump length in the chromosomally abnormal fetuses at 10 to 13 weeks' gestation. Am J Obstet Gynecol. 1995;172(1 Pt 1):32-5.
71. Reljic M. The significance of crown-rump length measurement for predicting adverse pregnancy outcome of threatened abortion. Ultrasound Obstet Gynecol. 2001;17(6):510-2.
72. Levi CS, Lyons EA, Zheng XH. Transvaginal US: demonstration of cardiac activity in embryos less than 5.0 mm in crown-rump length. Radiology. 1990;176:71-4.
73. Pennell RG, Needelman L, Pajak T. Prospective comparison of vaginal and abdominal sonography in normal early pregnancy. J Ultrasound Med. 1991;10(2):63-7.
74. Laboda LA, Estroff JA, Benacerraf BR. First trimester bradycardia. A sign of impending fetal loss. J Ultrasound Med. 1989;8(10):561-3.
75. Albayram F, Hamper UM. First-trimester obstetric emergencies: spectrum of sonographic findings. J Clin Ultrasound. 2002;3(3):161-77.
76. Benson CB, Doubilet PM. Slow embryonic heart rate in early first trimester: indicator of poor pregnancy outcome. Radiology. 1994;192(2):343-4.
77. Birnholz JC, Kent FB. The embryo as a patient: early pregnancy loss. In: Chervenak F, Kurjak A (Eds). The fetus as a patient. Carnforth UK: Parthenon Publishing; 1996. pp. 345-7.
78. Doubilet PM, Benson CB, Chow JS. Long term prognosis of pregnancies complicated by slow embryonic heart rates in early first trimester. J Ultrasound Med. 1999;18(8):537-41.
79. Laing FC, Frates MC. Ultrasound evaluation during the first trimester of pregnancy. In: Callen PW (Ed). Ultrasound in Obstetrics and Gynecology. 4th edition. Saunders Company. 2000;105-45.
80. Horrow MM. Enlarged amniotic cavity: a new sonographic sign of early embrionic death. AJR Am J Roentgenol. 1992;158(2):359-62.
81. McKenna KM, Feldstein VA, Goldstein RB, et al. The empty amnion: a sign of early pregnancy failure. J Ultrasound Med. 1995;14(2):117-21.

9

CHAPTER

Ectopic Pregnancy: Diagnosing and Treating the Challenge

Sanja Kupesic Plavsic, Nadah Zafar, Ulrich Honemeyer

INTRODUCTION

Ectopic pregnancy represents implantation of the fertilized ovum outside the uterine cavity. In 95% of the cases, it is localized in the fallopian tube (95%). Other sites such as the abdominal cavity, ovary, intraligamentous location, cornual, intramural or cervical sites are not unusual.[1-4] The exact cause of blastocyst implantation and development outside the endometrial cavity is not fully understood. The increased incidence of ectopic pregnancy found during the last decades[5,6] are mainly attributed to the greater degree of socially acceptable sexual behavior, which has led to an increased incidence of pelvic inflammatory disease (PID). Fortunately, fatal outcomes have been reduced by up to 75% due to early diagnosis and less invasive treatment techniques. The mechanical factors predisposing towards pathomorphological sites of implantation include low-grade pelvic infection (the main cause for the faulty implantation), peritubal adhesions (resulting from a previous history of PID) and salpingitis with the partial or total destruction of the tubal mucosa. It has been reported that ectopic pregnancies do occur in totally normal tubes, suggesting that abnormalities of the conceptus or maternal hormonal changes may act as etiological factors.[7,8]

Risk factors for ectopic pregnancy are STD–PID (sexually transmitted diseases–pelvic inflammatory disease),[9,10] assisted reproductive techniques, abnormalities of the conceptus, maternal hormonal changes, surgical procedures in pelvis,[11] intrauterine device (IUD),[12,13] previous ectopic pregnancy, fibroids, uterine malformations, cigarette smoking, etc. It is essential to identify risk factors so we can provide patients with adequate information to diagnose and treat an ectopic pregnancy early and in addition, possibly develop preventive strategies.[14-16] The main challenge of an ectopic pregnancy is the clinical presentation.[17] Symptoms can vary from vaginal spotting to vasomotor shock with hemoperitoneum.[18] The classic triad of delayed menses, irregular vaginal bleeding and abdominal pain is not commonly encountered and the exact frequency of these clinical symptoms and signs is hard to assess.[1] Both the typical and atypical clinical presentations can mimic various diseases. These diseases may have no connection with the pathology of reproductive system, e.g. appendicitis, diverticulitis, nonspecific mesenterial lymphadenitis or diseases of the urinary system. Most commonly an ectopic pregnancy is confused with an early spontaneous abortion because of similar symptoms in both processes (delayed menses, enlarged and softened uterus and bleeding). Other conditions that should be considered in the differential diagnosis of an ectopic pregnancy are normal intrauterine pregnancy, salpingitis, torsion or rupture of the ovarian cyst, adnexal torsion, bleeding corpus luteum, endometriosis, appendicitis, gastroenteritis, diverticulitis, conditions affecting urinary tract, etc.[19] Therefore, early and reliable diagnosis of an ectopic pregnancy is a major challenge for every clinician.[20] Significance of the early diagnosis renders the possibility of conservative methods of treatment. This is crucial for preserving further reproductive capability and in severe cases life itself. Diagnostic procedures are divided into two groups:

1. *Noninvasive:* History, general clinical and gynecological examination, hormonal and other laboratory markers and ultrasound diagnostics.
2. *Invasive:* Culdocentesis,[21] curettage[22] and laparoscopy.

ROLE OF BIOCHEMICAL MARKERS IN ECTOPIC PREGNANCY

Beta hCG (human chorionic gonadotropin) is the glycoprotein hormone released into circulation as soon as implantation occurs. Beta hCG is produced by the human placental trophoblastic cells from the 8th day post conception. Its blood concentration rises 1.7 times every 24 hours.[23] The commonly used urine beta hCG tests react at concentrations equal to or higher than 1000 IU/l of urine, which means that they become positive 10–14 days after conception.[1] False-positive results are mainly obtained in the case of proteinuria, erythrocyturia, gynecological tumors, tubo-ovarian abscess[24] or some drug intake (e.g. tranquilizers). In cases of an ectopic pregnancy, the embryo usually disappears by getting resorbed. In such cases, the ultrasound visualizes an empty gestational sac, which produces smaller amounts of beta hCG. Normal levels of beta hCG can only be found only in the cases of a live embryo. This occurs in 5–8% of ectopic pregnancies.[23] Because of the low concentrations of hCG, only 40–60% of ectopic pregnancies have a positive urine test. Therefore, the more sensitive blood test should be performed, which becomes positive 10 days after conception.[23] In an ectopic pregnancy, the absolute values of beta hCG levels in circulation are much lower than in normal intrauterine pregnancies of the same gestational age.[25,26] The dynamics of the titer show a slower increase of circulating concentrations and a prolonged time for the doubling values. The most important use of the quantitative beta hCG determination is in conjunction with ultrasonography in order to understand the value of "the discriminatory zone" of beta hCG. The discriminatory zone represents that level of beta hCG above which all normal intrauterine chorionic sacs will be detected by ultrasound. There is now almost a consensus in considering the discriminatory zone to be about 1000 mIU/ml with the use of transvaginal probe of at least 5 MHz.[27-30]

ROLE OF ULTRASOUND IN THE DIAGNOSIS OF AN ECTOPIC PREGNANCY

With recent technological development, ultrasonography (but more precisely, transvaginal sonography) has become the "gold standard" diagnostic modality for the effective and fast detection of an ectopic pregnancy. An important advantage of most currently used transvaginal transducers is the ability to perform simultaneous and spectral Doppler studies, allowing easy identification of the ectopic peritrophoblastic flow. In comparison to transvaginal sonography, transabdominal ultrasound, as a method for detecting ectopic gestation is restricted to a very small number of oddly located ectopic pregnancies, mainly high up in the pelvis—outside the effective reach of 5 MHz vaginal probe.[31]

Transabdominal Ultrasound

The absence of a gestational sac inside the intrauterine cavity at 6 weeks' gestation raises the suspicion of an ectopic pregnancy. Transabdominal ultrasonography cannot reliably diagnose ectopic pregnancy, except when a live fetus is demonstrated in the abdominal cavity. In only 3–5% of the cases an ectopic gestational sac with embryonic echoes and clear heart activity can be demonstrated.[32] A probe with frequency of 3.5 MHz and large contact area is used for transabdominal ultrasonographic imaging. A full bladder plays the role of an acoustic window. Resolution of this probe is somewhat lower but the penetration is much deeper than one of the transvaginal probe.

The best results in confirming the intrauterine pregnancy are achieved using following criteria:

- Normal size, shape and location of the gestational sac in the uterine cavity
- Double ring surrounding the gestational sac
- Embryonic parts with an eventual heart action
- Heart action.

Signs of an ectopic pregnancy can be divided into uterine and extrauterine, some of which are just suggestive or diagnostic.

Diagnostic signs include the absence of the intrauterine gestational sac surrounded by a double ring, absence of the yolk sac and/or fetal structures inside the gestational sac and presence of extraovarian adnexal structure.

Suggestive signs include uterine enlargement with a thickened endometrium and blood or coagulum in the retrouterine space.[32]

Low sensitivity, specificity, positive and negative predictive values for the detection of an ectopic pregnancy are shortcomings of transabdominal ultrasound.[33,34] This modality still has some value in successful detection of a small proportion of ectopic pregnancies with bizarre location such as the high pelvis.

Transvaginal Ultrasound

In comparison with the transabdominal approach, the transvaginal ultrasound enables a much better image

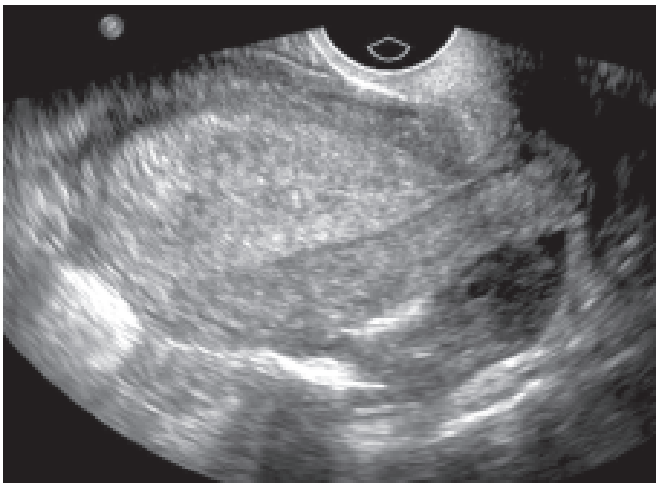

Figure 9.1A: Key to the diagnosis of ectopic pregnancy is determination of the presence or absence of an intrauterine gestational sac correlated with quantitative serum beta-subunit hCG (ß-hCG) levels. An ectopic pregnancy should be suspected if transvaginal ultrasonography does not show an intrauterine gestational sac when the beta hCG level is higher than 1.500 mIU/mL. Here is an example of a thickened endometrium and empty uterus in a patient with ectopic pregnancy

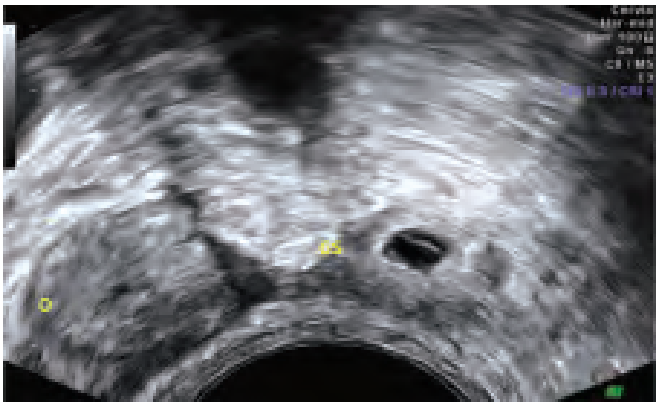

Figure 9.1B: Transvaginal ultrasound of ectopic pregnancy. Gestational sac (GS) is visualized adjacent to the ovary (O)

of the morphological features in pelvis thanks to the higher frequencies and probe location in the immediate vicinity of the examined area. The sensitivity of transvaginal sonography was found to be 96%, the specificity reached 88%, the positive predictive value 89% and the negative predictive value is 95%.[35] An intrauterine gestational sac surrounded by a double ring with clear embryonic echo is considered to be strong evidence against an ectopic pregnancy because a heterotopic pregnancy (intrauterine and ectopic), rarely coincide. This must be taken into consideration, especially in patients undergoing some of the methods of assisted reproduction.[36]

Intrauterine sonographic findings in women with ectopic pregnancy are variable **(Fig. 9.1A)**. These include:

- Empty uterus, with or without increased endometrial thickness
- Central hypoechoic area or a sac-like structure inside the cavity—the so-called pseudogestational sac
- Concurrent intrauterine pregnancy.

Early intrauterine pregnancy and recent spontaneous abortion may present themselves on transvaginal sonography with an empty uterus and an endometrial layer of variable thickness.[3] Therefore, they are considered to be suggestive signs. A pseudogestational sac can be demonstrated in 10–20% of patients with an ectopic pregnancy[3] as a mixed echo pattern of endometrium that results from a decidual reaction, fluid or both. Careful examination of the uterine cavity usually allows a reliable distinction to be made between the pseudogestational sac and a normal gestational sac. The pseudogestational sac is detected in the middle of the uterine cavity, with a changing shape, due to myometrial contractions. In differentiating a real gestational sac from a pseudogestational one, transvaginal color and pulsed Doppler ultrasound proved to be very useful.

Adnexal sonographic findings in women with ectopic pregnancy are variable. A gestational sac located inside adnexa with a clear embryonic echo and heart activity directly proves an ectopic pregnancy. This is seen in only 15–28% of the cases. Less rare is the visualization of an adnexal gestational sac with or without embryonic echo (without heart activity)[37] **(Fig. 9.1B)**. Such a finding is detected in 46–71% of reported cases if the tube is unruptured.[38] The most common finding is an unspecific adnexal tumor. Free fluid in the retrouterine space is seen in 40–83% of cases.

Accurate ultrasound diagnosis of ectopic pregnancy depends strongly on the examiner's experience. Adnexal abnormalities may be difficult to identify because of confusion with loops of bowel or other pelvic structures.[39]

There are four adnexal structures that may resemble an ectopic pregnancy and should be correctly identified.[40] One is the corpus luteum, which is eccentrically located within the ovary, surrounded by ovarian tissue and possibly creating the impression of a sac-like structure. About 85% of ectopic pregnancies are formed on the same side as the corpus luteum.[41] This is important to bear in mind while trying to distinguish a tubal pregnancy from the ipsilateral corpus

luteum. When the corpus luteum is found in the ovary, its echogenicity is slightly (or at times even substantially) lower than that of trophoblastic tissue of the tubal ring.

Furthermore, the hemorrhagic corpus luteum usually shows a hypoechoic rather than a cystic central region.[42] Three other conditions that need to be correctly differentiated from an ectopic gestation are a thick-walled ovarian follicle, the small intestine and pathological tubal conditions, such as hydrosalpinx containing fluid.

Using the protocol of a combination of clinical examination, serum beta hCG assay and transvaginal ultrasound examination, it is possible to diagnose ectopic pregnancy with a sensitivity of 100% and specificity of 99%.[43]

Another problem in the detection of an ectopic pregnancy in the adnexal region arises in patients undergoing assisted reproductive procedures or simple hormonal superovulation. Besides the increased risk for ectopic pregnancy in these patients, a large number of artificial corpora lutea will be seen that resemble the tubal ring of an ectopic pregnancy. Sometimes cystic adnexal masses (ovarian cystadenoma, cystadenofibroma, endometrioma, teratoma and pedunculated fibroids) may also raise differential diagnostic problems.

Although free intraperitoneal fluid is seen in 40–83% of women with an ectopic pregnancy, it can also be seen in up to 20% of normal intrauterine pregnancies.[38] In a case of tubal abortion, echogenic echoes suggesting the presence of blood clots are demonstrated, while tubal rupture is associated with a homogeneous, hypoechoic retrouterine echo that represents blood collection. The possibility of an ectopic pregnancy increases if the amount of fluid is moderate to large, but the absence of blood does not exclude its diagnosis.

A serial serum beta hCG assay may raise the suspicion of an ectopic pregnancy at a very early gestational age, when the transvaginal ultrasound scan may not be able to demonstrate the site of the pregnancy. Under these circumstances, sometimes it is necessary to perform a laparoscopic examination to exclude the possibility of an ectopic pregnancy. However, even laparoscopic examination may not be able to achieve a precise diagnosis, especially when the ectopic pregnancy is very small or when there are co-existing pathologies such as hydrosalpinges, adhesions or fibroids. Some reports demonstrated that a laparoscopic ultrasound can facilitate the diagnosis of the site of an ectopic pregnancy intraoperatively, even if it is as small as 3.9 mm.[44] The number of negative laparoscopies can be decreased and a repeat laparoscopy avoided. Therefore, laparoscopic ultrasound should be used when the site of the ectopic pregnancy cannot be determined or is obscured by other pathologies during the laparoscopic examination.

Color Doppler Ultrasound

The ultrasound machine with color Doppler facility is an excellent guide to search for blood flow signals within the entire pelvis. The color flow pattern associated with an ectopic pregnancy is variable. It usually presents as randomly dispersed multiple small vessels within the adnexa **(Fig. 9.2A)**, showing high-velocity and low impedance signals (RI = 0.36–0.45), which are clearly separated from the ovarian tissue and corpus luteum **(Fig. 9.2B)**. The sensitivity of the transvaginal color and pulsed Doppler in the diagnosis of an ectopic pregnancy has been reported by several studies and ranges from 73–96% and the specificity ranges from 87–100%.[3,4,38,45]

Visualization of the ipsilateral corpus luteum blood flow may aid in the diagnosis of an ectopic pregnancy **(Fig. 9.2C)**. The resistance index (RI) of luteal flow in cases of ectopic pregnancy has been reported to be 0.48 ± 0.07, which is between the values of a non-pregnant women (0.42 ± 0.12) and those with normal early intrauterine pregnancy (0.53 ± 0.09).[46] In majority of patients with a proven ectopic pregnancy, luteal flow is detected on the same side as the ectopic pregnancy. This observation could be used as a guide when searching for an ectopic pregnancy **(Fig. 9.2D)**.

The between-side difference in the tubal artery blood flow was also documented. There was a significant increase in the tubal artery blood flow on the side of the tubal gestation. The mean reduction of the RI on the side with the ectopic pregnancy compared to the opposite side was 15.5%. These changes appear to be due to trophoblastic invasion, and showed no dependence on the gestational age. A bright color when visualized on the screen while using the pulsed Doppler facility is due to the very high speed of the peritrophoblastic blood flow and low impedance **(Fig. 9.3)**. It should be stressed that patients with tubal abortion demonstrate significantly higher vascular impedance of peritrophoblastic flow (RI > 0.60) and less prominent color signals **(Fig. 9.4)**.

The main diagnostic importance of transvaginal color and pulsed Doppler is in differentiating the nature of a nonspecific adnexal mass. Doppler blood flow indices in the uterine, spiral arteries and corpus luteum arteries in ectopic and intrauterine pregnancies showed that the mean uterine and spiral artery RI decreased with an increased gestational age of the intrauterine

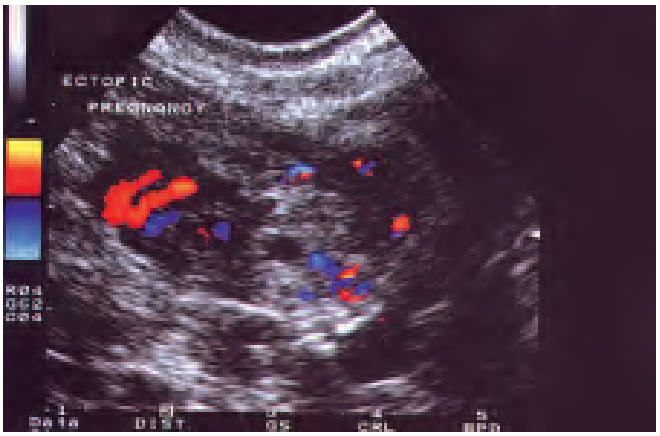

Figure 9.2A: Transvaginal color Doppler scan of a small gestational sac in the adnexal region measuring 8–10 mm. Note the dilated tubal vessels, indicating the pathophysiological site of the pregnancy (within the tube)

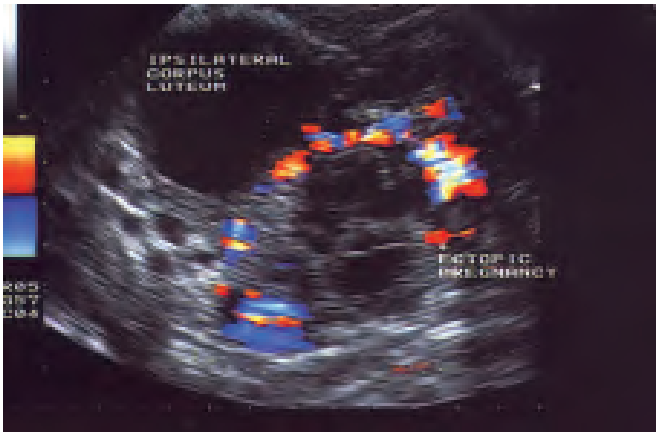

Figure 9.2D: Color Doppler facilitates visualization of randomly dispersed tubal arteries indicating prominent trophoblastic vitality and invasiveness. Note the ipsilateral corpus luteum

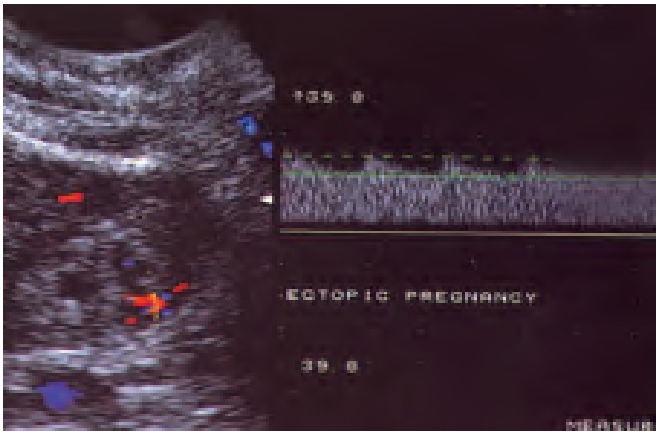

Figure 9.2B: The same patient as in previous figure. Blood flow velocity waveforms depicted from the area of peritrophoblastic flow show high velocity (23.3 cm/s) and low vascular resistance (RI = 0.25)

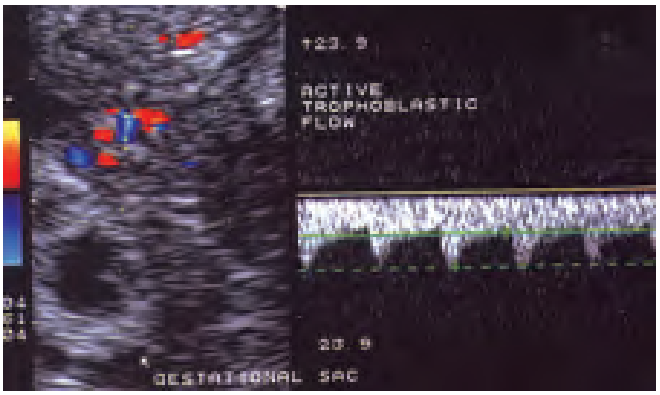

Figure 9.3: Transvaginal color Doppler imaging of a left-sided ectopic pregnancy. Note the color signals indicative of invasive trophoblast (left). Pulsed Doppler waveform analysis (right) demonstrates low resistance index (RI = 0.43)

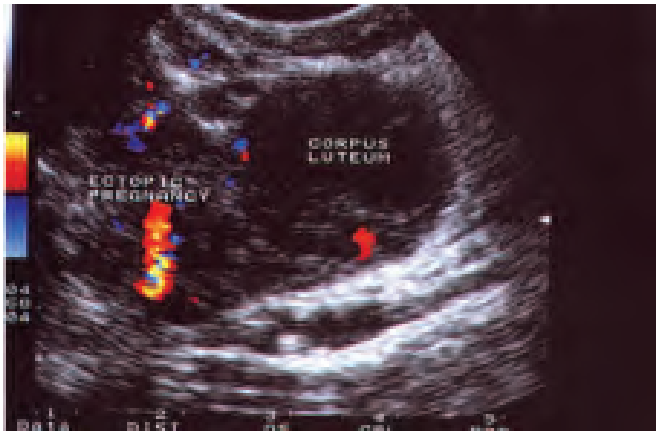

Figure 9.2C: The same patient as in images 9.2A and 9.2B. An ipsilateral corpus luteum is demonstrated laterally to the ectopic gestational sac

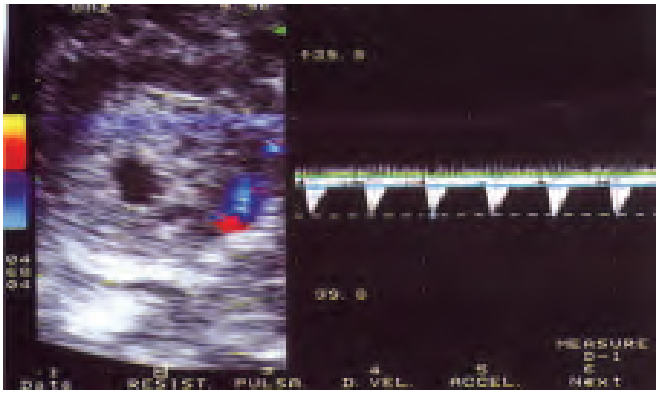

Figure 9.4: Gestational sac measuring 12 mm in the left adnexal region. Color Doppler depicts a small area of angiogenesis characterized by a high resistance index (RI = 0.73). This finding is indicative of tubal abortion

pregnancies, but remained constantly high in ectopic pregnancies.[47] The peak systolic blood flow velocity in the uterine artery increased with an increasing gestational age in intrauterine pregnancies and the values were significantly higher than in ectopic pregnancies.[48] The difference in peak systolic velocity reflects a decreased blood supply to the ectopic pregnancy. An intrauterine gestational sac shows prominent peritrophoblastic vascular signals (RI = 0.44–0.45), while pseudogestational sacs do not demonstrate increased blood flow (RI > 0.55). It has been suggested that velocities below 21 cm/s are diagnostic for pseudogestational sac and can successfully rule out trophoblastic flow of a normal intrauterine pregnancy.[49]

The intravascular ultrasound contrast agent has a recognizable effect on Doppler ultrasonographic examination of the adnexal circulation **(Figs 9.5A and B)**. It appears to be helpful when the finding in the color flow imaging is ambiguous. The use of the contrast agent may also facilitate localization of trophoblastic tissue in hemorrhagic adnexal lesions.[50]

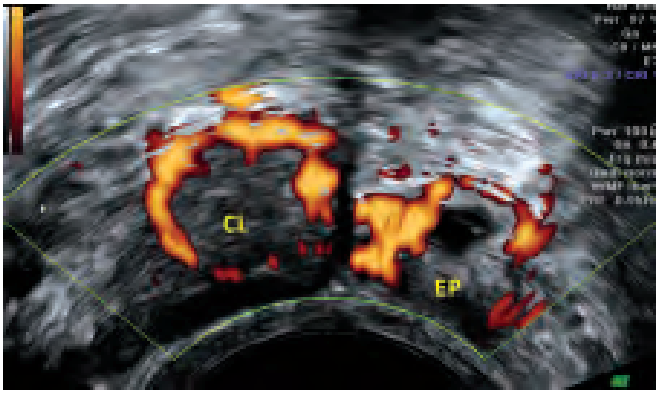

Figure 9.5A: Transvaginal power Doppler of tubal ectopic pregnancy (EP) and ipsilateral corpus luteum (CL)

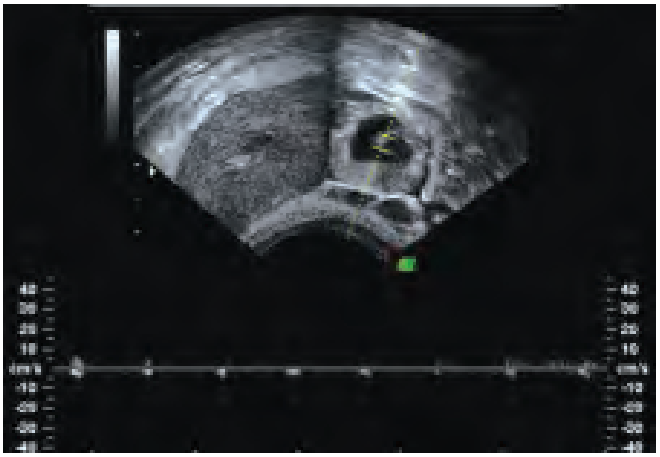

Figure 9.5B: The same patient as in Figure 9.5A. Irregular heart activity is obtained from the ectopic gestational sac

As with other diagnostic methods, transvaginal color and pulsed Doppler studies include both, false-positive and false-negative findings. A false-positive diagnosis arises predominantly from the corpus luteum, but in exceptional cases some adnexal lesions may mimic an ectopic pregnancy. A false-negative result may arise from technical inadequacy, lack of experience or the patients' noncompliance. The other possibility of a faulty diagnosis is a nonvascularized ectopic gestation, as these are associated with low beta hCG values.

Some authors compared technical errors with improper setting of color flow parameters.[51] The color velocity scale, color priority, color gain, color sensitivity and color wall filter should be adjusted to optimize color flow information. Technical errors may result in the false diagnosis of an ovarian torsion, malignancy and an ectopic pregnancy.

The diagnosis of ectopic pregnancy still remains a challenge to the clinician despite advances in ultrasound and biochemical technology. Frequently, the diagnosis remains uncertain until a laparoscopy or D & C are performed. With the increasing tendency towards conservative therapy, the distinction between ectopic pregnancies that will resolve spontaneously and those that will rupture is essential.[52] Usually patients without any acute symptoms and with declining beta hCG values are treated conservatively.[53] However, secondary ruptures have been reported in patients with low initial beta hCG concentrations.[54] The differentiation between viable ectopic pregnancies with trophoblastic activity and dissolving tubal abortions could facilitate the decision to proceed with conservative or operative treatment.

After implantation in the mucosa of endosalpinx, the lamina propria and then the muscularis of the oviduct, the blastocyst grows mainly between the lumen of the tube and its peritoneal covering.[55] Growth occurs both parallel to the long axis of the tube and circumferentially around it. As the trophoblast invades surrounding vessels, intensive blood flow and/or intraperitoneal bleeding occur **(Figs 9.6A and B)**. The intensive ring of vascular signals could be a criterion for the viability of an ectopic pregnancy that can be determined rapidly and easily and seems to be independent of beta hCG values.[56] In patients with a viable ectopic pregnancy, especially in those cases where beta hCG levels slowly normalize who demand a conservative treatment, this method could provide an aid in addition to beta hCG values for supervising the efficiency of treatment. This way the duration of the

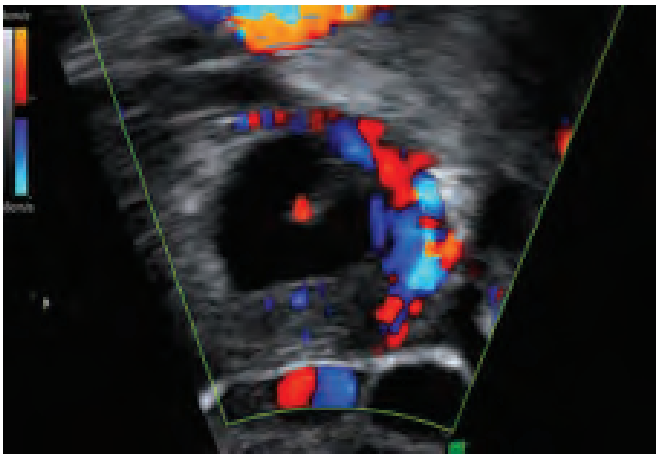

Figure 9.6A: Prominent blood flow signals indicate vital trophoblast. In addition to peritrophoblastic flow, color Doppler can depict embryonic cardiac activity

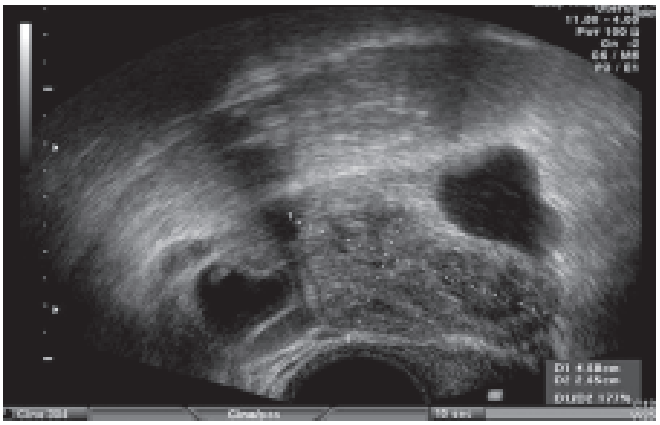

Figure 9.7A: Transvaginal ultrasound of a complex adnexal mass in a patient with positive pregnancy test. Note tubular structure with solid part measuring 4.6 x 2.7 cm

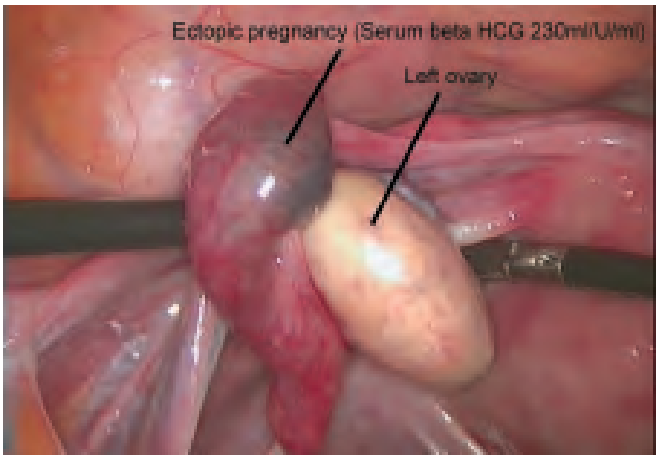

Figure 9.6B: Laparoscopic image of ectopic pregnancy. Note ipsilateral corpus luteum

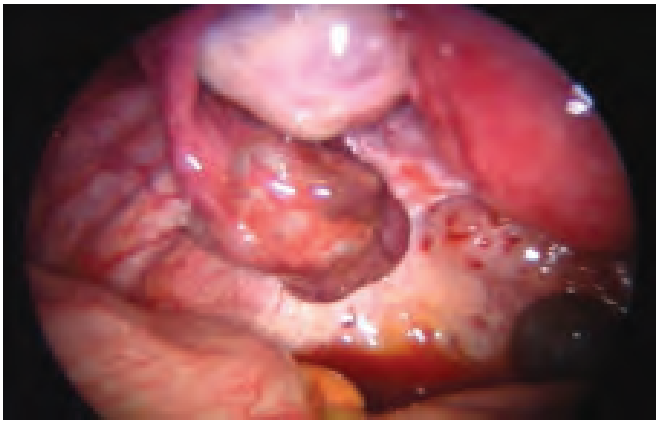

Figure 9.7B: Laparoscopy revealed chronic tubal pregnancy and free fluid in the cul-de-sac

hospitalization could be shortened, the patients' uncertainty diminished and the cost of the treatment reduced. In the cases of persistent high beta hCG levels after operative removal of the ectopic pregnancy, color Doppler sonography can provide evidence for the presence of viable trophoblast remnants **(Figs 9.7A and B)**. On the contrary, in asymptomatic patients with hypoperfused and/or avascular ectopic gestational sac and decreased values of beta hCG, expectant treatment can be established.

3D Ultrasound in the Assessment of Tubal Ectopic Pregnancy

Three-dimensional (3D) ultrasound technology offers some advantages over conventional two-dimensional (2D) sonographic imaging.[57,58] Modern systems are capable of generating surface and transparent views depicting the sculpture-like reconstruction of surfaces or the transparent images structure's content.

Planar mode tomograms are helpful in distinguishing the early intraendometrial gestational sac from a collection of the fluid between the endometrial leaves (pseudogestational sac).

A prospective follow-up study was conducted in order to evaluate the potential utility of 3D ultrasound to differentiate the intrauterine from ectopic gestations.[59] Fifty-four pregnancies with a gestational age < 10 weeks and with an intrauterine gestational sac < 5 mm in diameter formed the study group. The configuration of the endometrium in the frontal plane of the uterus was correlated with pregnancy outcome. After exclusion of three patients with a poor 3D image

quality, the endometrial shape was found to be asymmetrical with regard to the median longitudinal axis of the uterus in 84% of intrauterine pregnancies, whereas endometrium showed symmetry in the frontal plane in 90% of ectopic pregnancies. Intrauterine fluid accumulation may distort the uterine cavity, thus being responsible for false-positive, as well as false-negative results. The evaluation of the endometrial shape in the frontal plane appeared to be a useful additional means of distinguishing intrauterine from ectopic pregnancies, especially when a gestational sac was not clearly demonstrated with the conventional ultrasound. Similarly, preliminary data of other authors suggested that 3D sonography is an effective procedure for early diagnosis of ectopic pregnancy in asymptomatic patients before six weeks of amenorrhea.[60]

The possible use of 3D power Doppler is the monitoring of the vascularity (VI) of an ectopic pregnancy. The hypoperfusion, quantified by indices of and flow (FI) could indicate that the ectopic pregnancy is spontaneously being resolved and that laparoscopy should be postponed. This way, the conservative approach to an ectopic pregnancy would rely on more precise and easily obtainable data. In case of hyperperfusion, the patients should be subjected to laparoscopy or medical treatment immediately.

Shih and colleagues[61] described the use of 3D color/power angiography in two cases in which an arteriovenous malformation of the mesosalpinx was diagnosed following involution of an anembryonic ectopic gestation. The diagnosis of arteriovenous malformations has traditionally been made by arteriography. Recently, it has also been diagnosed by noninvasive methods such as contrast enhanced CT, MRI and color Doppler ultrasound. The advantage of 3D reconstruction of color/power angiography images is a better spatial and anatomic orientation and a quick demonstration of the vessels, usually within one minute, especially in the areas where complex structures are present. Therefore, unlike MRI, digital subtraction angiography or contrast enhanced CT, 3D color/power angiography allows the physician to examine vascular anatomy immediately and without radiation exposure.

Most tubal gestations are not ongoing viable gestations. They are usually in the involutional phase of abortion within a confined area, which results in the extrusion of products of conception through a ruptured site or fimbriae. In the two reported cases, the serum assays of beta hCG in both patients increased to significant levels, which precluded intrauterine missed abortion.[61] Besides, there were neither retained products of conception *in utero* nor heavy vaginal bleeding (indicating process of abortion in progress) prior to the diagnosis of arteriovenous malformation. Therefore, the authors speculated that there might be an ectopic gestation occurring somewhere, although they could only find a pelvic arteriovenous malformation rather than an adnexal gestational sac.

The major difference between uterine implantation and tubal gestation is that endosalpingeal stroma usually fails to undergo decidualization. The chorionic villi of the tubal implantation may then invade into the tubal wall and mesentery (mesosalpinx) more directly and rapidly. The vascularization within the ectopic pregnancy is an analog of placenta increta.[62] In such situations, cytotrophoblast may invade the contiguous artery and vein of the mesosalpinx with destruction of these vessels' walls and thus may induce an arteriovenous malformation *in situ* or nearby. Possibly, the secretion of angiogenic factors (by trophoblast) and the increasing afterload of an arterioventricular shunt existing in the tubal gestation can induce the rapid growth of a small pre-existing congenital arteriovenous malformation. However, two unusual cases of adnexal arteriovenous malformations associated with "vanishing" ectopic gestation where congenital etiology seemed unlikely have also been reported.[61] B-mode ultrasound and color Doppler provided information on the hemodynamics of the vascular tumor and led to the diagnosis of the arteriovenous malformation. Three-dimensional color/power angiography further improved the understanding of the complex vascular anatomy and refined the diagnosis.

Even though the exact role of 3D ultrasound in the pathology of early pregnancy is yet to be established, promising results in already published papers are encouraging. Unlimited numbers of sections are easily obtained without the need for excessive manipulation of the probe. Additional progress has been made, owing to the permanent possibility or repeated analysis of previous stored 3D volumes and Cartesian elimination of surrounding structures and artifacts. A 3D reconstruction of stored images without any degradation is the most impressive benefit of 3D scanning.

OTHER SITES OF IMPLANTATION

About 5% of ectopic pregnancies implant in sites other than the tubes.[1] These are at times more difficult to detect and some, owing to their specific sites of implantation, may cause rupture, significant bleeding and higher morbidity and mortality than the tubal gestations.

Interstitial (Cornual) Pregnancy

Occurs in 1.1–6.3% of all ectopic pregnancies.[1,63] This location of the ectopic pregnancy usually occurs following *in vitro* fertilization (IVF) and previous salpingectomy,[63] but in most cases there are no apparent risk factors. Interstitial pregnancy clinically presents with abdominal pain and a tender asymmetrically enlarged uterus. The major problem of this location lies in late diagnosis because it is commonly diagnosed after the rupture of the cornu has occurred and this may result in massive hemorrhage. Previously, interstitial pregnancies were diagnosed only at laparotomy following the rupture. For the reason of major hemorrhage, hysterectomy rate was as high as 40%.[60] In recent years, the routine use of ultrasound for the assessment of women with early pregnancy complications has enabled a noninvasive diagnosis of interstitial pregnancy to be made. Earlier diagnosis made before serious complications, allows the use of more conservative management, such as medical treatment or laparoscopic surgery.

A viable interstitial pregnancy may occasionally be misinterpreted as a normal intrauterine pregnancy. Therefore, it is important that strict diagnostic criteria are used in every case:[64]

- Empty uterine cavity **(Fig. 9.8)** and
- A chorionic sac that is seen separately and more than 1 cm from the most lateral edge of the uterine cavity and surrounded by a thin myometrial layer **(Fig. 9.8)**.

It is worth mentioning that approximately 15% of patients with interstitial pregnancy have heterotopic pregnancy.[64] In these cases, intrauterine findings may be misleading and should be interpreted with caution, rather than being used as primary diagnostic criterion. Visualization of the interstitial part of the tube in close proximity of the endometrium and depiction of the trophoblastic tissue improves the diagnosis of interstitial pregnancy.[65] It also confirms that the pregnancy is located outside the uterine cavity, facilitating the differential diagnosis between an interstitial pregnancy and unusual forms of intrauterine pregnancy such as angular pregnancy or pregnancy in the cornu of an anomalous uterus. This sign is particularly helpful in women with small intramural fibroids located in the vicinity of the interstitial part of the tube, which may be misinterpreted as a solid interstitial pregnancy.[66] In women with fibroids, the intramural part of the tube is displaced and can be visualized bypassing the mass, thus preventing the false-positive diagnosis of the interstitial pregnancy. Color Doppler facilitates the diagnosis of a cornual pregnancy by exposing low resistance peritrophoblastic flow **(Fig. 9.9)**.

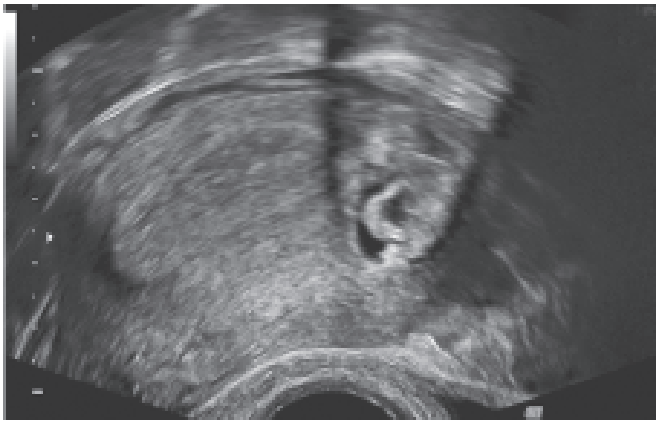

Figure 9.8: Transvaginal ultrasound demonstrates empty uterine cavity and a chorionic sac seen separately and more than 1 cm from the most lateral edge of the uterine cavity and surrounded by a thin myometrial layer

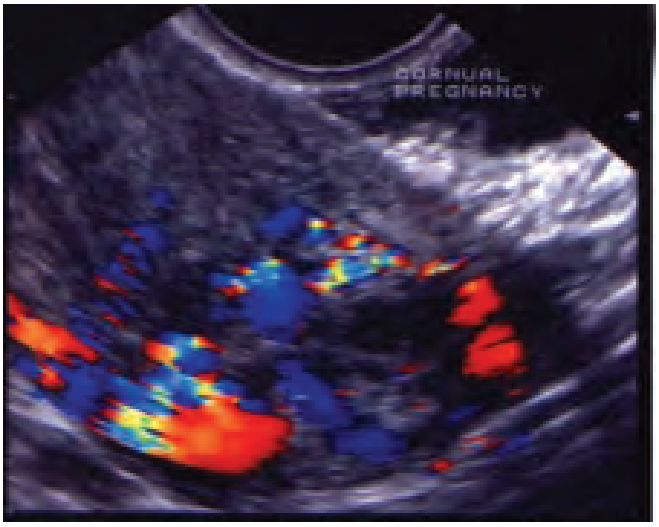

Figure 9.9: Transvaginal color Doppler scan of interstitial pregnancy. Color signals facilitate early diagnosis of this ectopic pregnancy location by exposing low resistance peritrophoblastic flow

Three-dimensional ultrasound has the advantage of providing views of the uterus, which can rarely be obtained by conventional 2D ultrasound scan.[67] In the coronal section, the position of the interstitial pregnancy in relation to the uterine cavity can be studied in detail **(Fig. 9.10A)**. Visualization of the proximal section of the interstitial tube is also facilitated, which increases the diagnostic confidence.[67] It is believed that 3D ultrasound is a helpful diagnostic tool in women with suspected interstitial pregnancy and should be considered in the cases where the diagnosis is not certain on conventional 2D transvaginal ultrasound scan.[65,68] It has been demonstrated that 3D color and/or power Doppler may aid in the early diagnosis of cornual/interstitial pregnancy **(Fig. 9.10B)**.

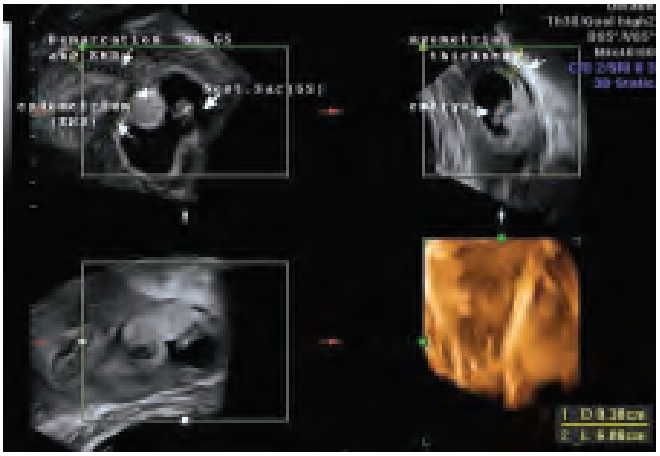

Figure 9.10A: Three-dimensional ultrasound provides views of the uterus, which cannot be obtained by conventional 2D ultrasound scan. Coronal section (upper left image) and surface rendering (lower right image) enable visualization of the cornual ectopic pregnancy

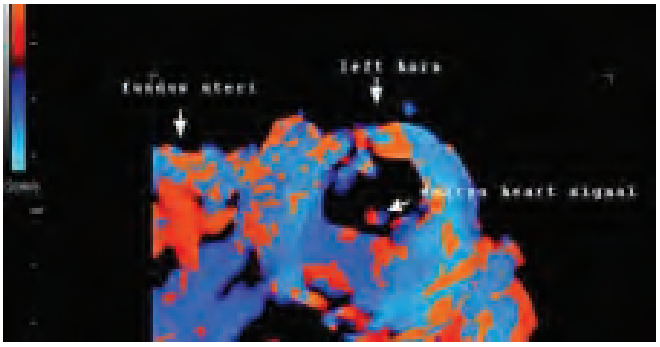

Figure 9.10B: Three-dimensional color Doppler ultrasound of cornual pregnancy. Prominent peritrophoblastic flow indicates vital trophoblast

Most cornual/interstitial ectopic pregnancies are treated by laparoscopy and laparotomy using various surgical procedures (excision, suturing, etc.) **(Figs 9.11A to E)**. Lately, transvaginal sonographic puncture and local injection of methotrexate, has been used to treat both viable and nonviable interstitial pregnancies.[64] There have been very few reported side-effects after treatment with low-dose local injection of methotrexate.[69] Data reported in the literature suggest the superiority of local therapy, with regard to both the safety aspect and the success rates. In general, a likely explanation for the increased effectiveness of local injection is a higher concentration of therapeutic agent achieved at the target tissue. Although absorption of methotrexate into the circulation occurs after both local and systemic administration, a lower dose of methotrexate is used locally, leading to lower systemic levels and therefore fewer side-effects.[70] Color Doppler plays an extremely important role providing an aid in approaching the cornual pregnancy from the medial aspect and traversing the thicker myometrial layer and so rupture or bleeding are less likely to occur.[71] In these cases, color Doppler guidance during the instillation of methotrexate enables better visualization of blood vessels and avoidance of intraprocedural complications.

Viable heterotopic/interstitial pregnancies are often treated by local injection of potassium chloride, as this is not teratogenic. All six reported cases of heterotopic pregnancies in the literature were successfully treated in this way, with three (50%) intrauterine pregnancies progressing normally to full term.[4]

Expectant management of the interstitial pregnancy has also been reported.[64,66] All three nonviable interstitial pregnancies managed in this way were resolved spontaneously without any need for intervention. Expectant management can therefore be a useful option in selected cases.

Cervical Pregnancy

It is defined as the implantation of the conceptus below the level of the internal os. Cervical pregnancy is the rare condition that occurs in one in 50,000.[4] Intrauterine adhesions, uterine anomalies, previous cesarean sections, fibroids, previous therapeutic abortions and IVF treatment have all been associated with cervical implantation. Traditionally, the diagnosis of cervical pregnancy was based solely on clinical findings and history reports after hysterectomy. Therefore, it is likely that only the most severe cases were diagnosed and a number of cervical pregnancies went undiagnosed or were treated as incomplete miscarriages. In the past two decades, ultrasound has become the method of choice for the diagnosis of early pregnancy disorders and certainly contributed to the recent increase in the number of reported cervical pregnancies.

The diagnosis of cervical pregnancy can be made using the following criteria:

- No evidence on intrauterine pregnancy
- An hourglass uterine shape with ballooned cervical canal
- Presence of a gestational sac or placental tissue within the cervical canal and a closed internal os **(Fig. 9.12A)**.

Early diagnosis may also explain the milder clinical symptoms and better prognosis of cervical pregnancy today as compared to preultrasound era.

Transvaginal ultrasound approach has become the accepted standard for the examination of patients with suspected early pregnancy abnormalities. Apart from providing superior images of pelvic anatomy, the addition of color Doppler enables simultaneous visualization of the pelvic blood vessels and embryonic

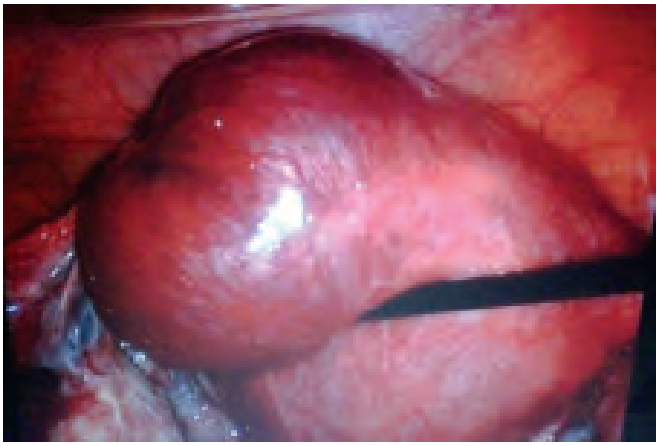

Figure 9.11A: Laparoscopic view of cornual pregnancy. Note swelling and hypervascularity of the cornual area

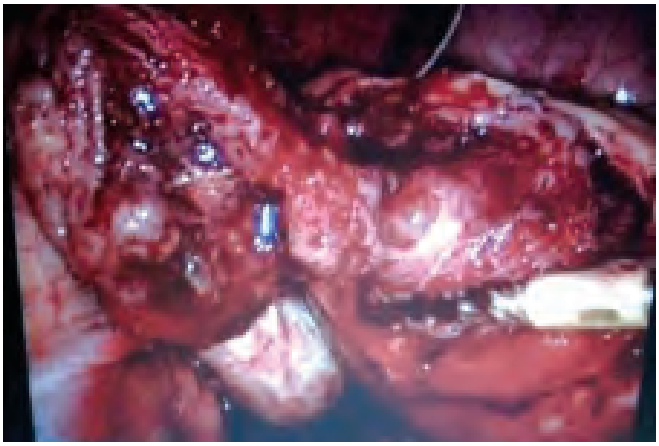

Figure 9.11D: Cornual pregnancy at the time of excision

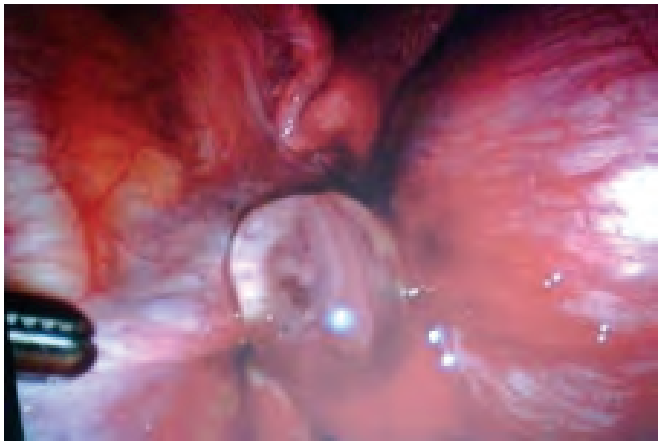

Figure 9.11B: Laparoscopic image demonstrates the gestational sac with an embryo at the site of cornual pregnancy rupture

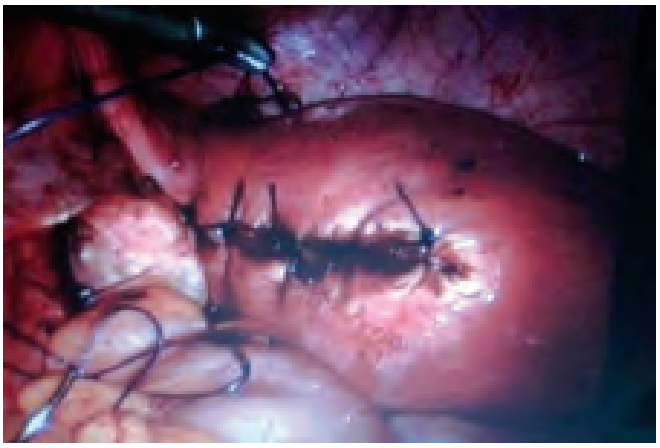

Figure 9.11E: Closure of the cornual region with sutures

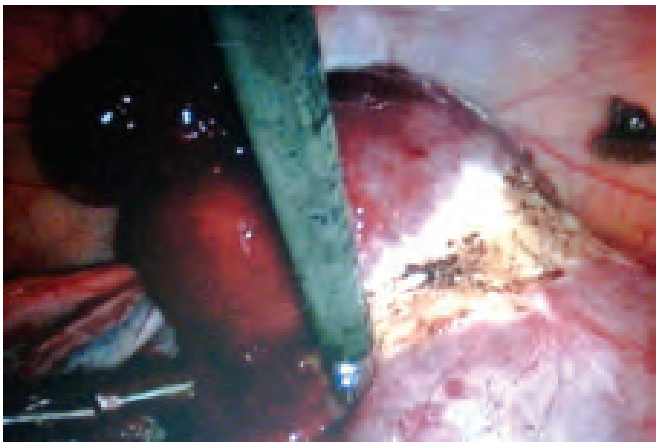

Figure 9.11C: Resection of the cornual pregnancy after infiltration with vasopressin

heart action **(Figs 9.12B and C)**. The level of the insertion of the uterine arteries should be used to identify the internal os and thus facilitate the diagnosis of a cervical pregnancy.[71] The extensive vascular blood supply to the trophoblastic tissue originating from the adjacent maternal arteries at the implantation site (within the cervix) is easily visualized by transvaginal color Doppler. The products of conception in transit through the cervix after the failure of a normally implanted pregnancy are detached from their implantation site and maternal vascular supply. It is therefore impossible to detect any peritrophoblastic blood flow in these cases.[72] Conversely, even a small amount of placental tissue in a true cervical pregnancy remains highly vascularized on color Doppler examination.[73] This facilitates the differential diagnosis between the cervical pregnancy and incomplete miscarriage. Color Doppler analysis may also improve selection of the patients for primary

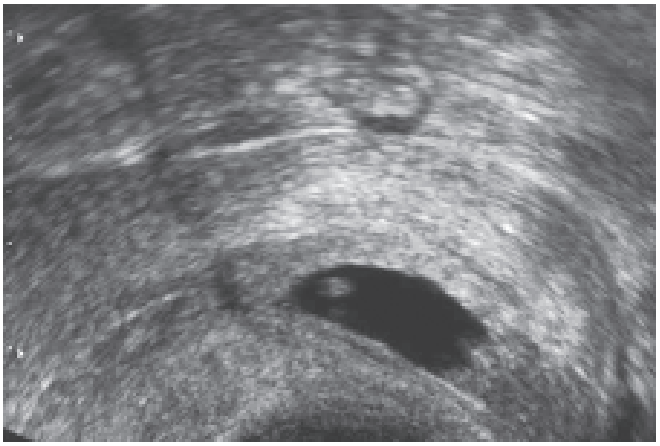

Figure 9.12A: Transvaginal ultrasound demonstrates a cervical pregnancy. Both internal and external cervical os are closed

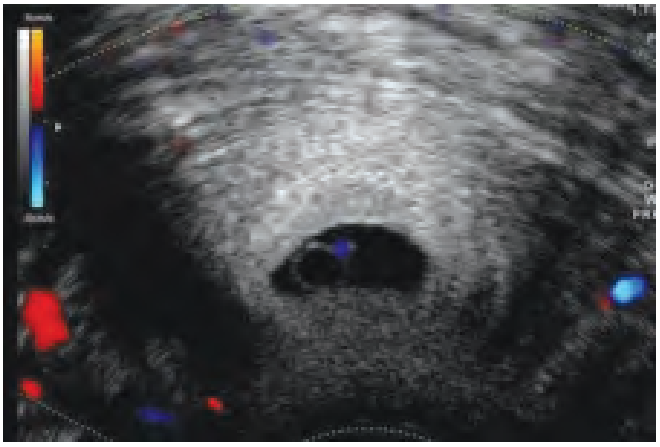

Figure 9.12B: Transvaginal color Doppler scan of a cervical pregnancy. Note yolk sac and embryonic heart activity

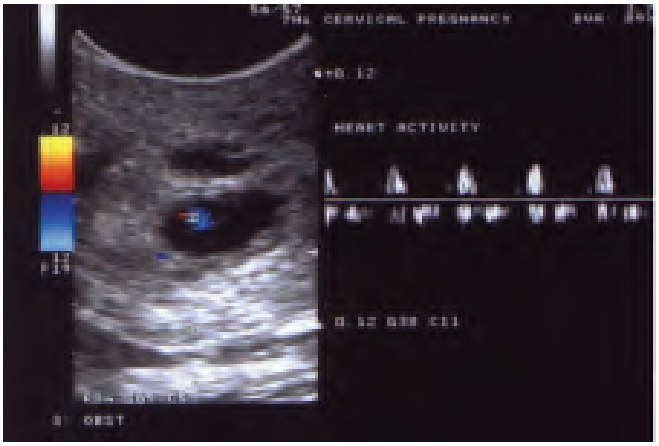

Figure 9.12C: Transvaginal color Doppler scan of a cervical pregnancy. Blood flow signals are derived from the fetal heart and demonstrate regular heart action

surgical removal of cervical pregnancy and assist in planning dilation and curettage (D & C) following medical treatment. It is necessary to stress the potential of 3D sonography in the diagnosis of cervical gestation and include the better anatomic orientation and multiplanar sections of the investigated area.

Local injection of methotrexate or potassium chloride appears to be the most effective way of treating an early viable cervical pregnancy regardless of the gestational age. There are no data on the use of local injection in nonviable pregnancies and it is uncertain whether the treatment would be as effective as in viable pregnancies. Systemic use of methotrexate in nonviable pregnancies is simple and highly effective.

The regimens and dosages of methotrexate used for systemic therapy have varied considerably. There is no clear correlation between the dose and therapeutic success and it is therefore logical to use as little methotrexate as possible to minimize side effects. The usual regimen should be two intramuscular injections of 1 mg/kg methotrexate followed by folic acid. For local injection, 25 mg methotrexate into gestation sac appears to be sufficient. Potassium chloride 3–5 mEq is equally successful and less likely to cause side effects.[4]

The place of surgery should be limited to those cases where medical treatment has failed. Dilatation and curettage in combination with cervical cerclage or the insertion of a Foley catheter is probably the best choice for a general gynecologist and is as effective as more complicated and expensive methods for the prevention of uncontrollable hemorrhage.[71]

The sonographic diagnosis of an ovarian pregnancy is extremely difficult to establish. It has been calculated that ovarian pregnancy accounts for less than 3% of ectopic pregnancies.[1,2] The sonographic diagnosis is made upon the finding of a hyperechoic trophoblastic ring detected within the ovarian tissue **(Figs 9.13A to C)**) and the fact that it is impossible to separate the ectopic gestational sac from the ovary by transabdominal pressure from either the examiner's hand or the transvaginal ultrasound probe.[2] Color Doppler facilitates detection of the peritrophoblastic flow, which can speed up the entire diagnostic procedure.

Intra-abdominal Pregnancy

It is a rare condition, constituting only 1% of all ectopic gestations.[74] Its complications, however, can be devastating. These include massive hemorrhage due to disseminated intravascular coagulation (DIC) and placental separation complicating fetal demise or infection with abscess formation. The outlook for the fetus is even worse, and perinatal mortality may reach

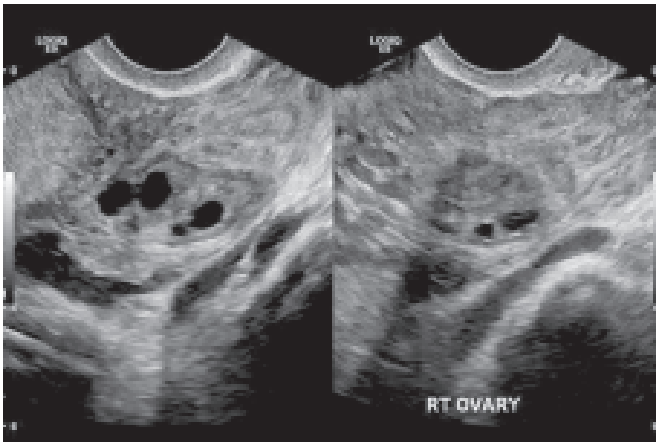

Figure 9.13A: Transvaginal ultrasound scan of a complex ovarian mass in a patient with positive pregnancy test and no evidence of intrauterine pregnancy

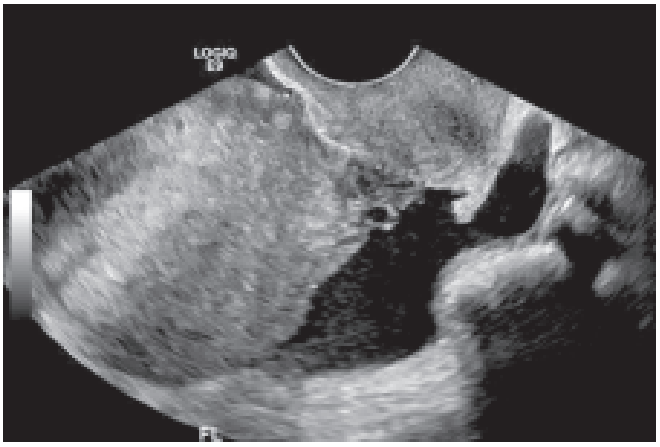

Figure 9.13B: The same patient as in Figure 9.13A. Free fluid is visualized in the cul-de-sac

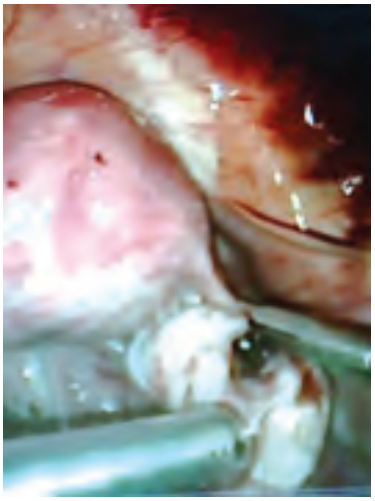

Figure 9.13C: The same patient as in figures 9.13A and 9.13B. Laparoscopy confirmed the diagnosis of ovarian pregnancy

75%, with up to 90% of the surviving infants having serious malformations.[75] The diagnosis of the abdominal pregnancy is not easy, especially in the early stages. Characteristically, patients present with abdominal pain, vaginal bleeding and gastrointestinal complaints. Ultrasonography combined with beta hCG estimations have made early diagnosis easier. The problem still exists, because as a patient subgroup, an ambiguous clinical presentation still remains.[76]

Ultrasound seems to be the most valuable diagnostic tool to localize this rare type of ectopic pregnancy.[2] Primary abdominal pregnancy is a condition where fertilized egg implants itself directly into the peritoneal surface of abdominal cavity. If, however, an early tubal pregnancy dislodges and aborts into the pelvis, adhering to peritoneal surface, it is termed a secondary abdominal pregnancy through the secondary nidation. The sonographic presentation of abdominal pregnancy is not different from any other ectopic pregnancy, i.e. showing no evidence of intrauterine pregnancy **(Fig. 9.14A)**, presence of a hyperechoic ectopic gestational sac containing embryonic/fetal structures and extra-embryonic structures with or without active heart beats **(Figs 9.14B and C)**. Oligohydramnion is the rule and there is no uterine mantle around the fetus.

Surgery is a time-honored treatment for abdominal pregnancy following its diagnosis, with placenta left *in situ* **(Figs 9.14D and E)**. This is mainly because, in many instances, the placenta is attached to vital organs or vascular sites, which could be seriously damaged during placental separation. No serious complications occur when it's left *in situ*.[77] An additional important factor is that most abdominal pregnancies are diagnosed relatively late in pregnancy, when the placenta and its area of attachment are larger. Recently, abdominal pregnancies have been diagnosed earlier and in one case the diagnosis was made at six weeks of amenorrhea.[74] This made it possible for these pregnancies to be removed laparoscopically. The possible advantages of such therapeutic approach include lower morbidity and mortality, as well as better fertility outcome. However, only a limited number of cases of abdominal pregnancy have been reported early in pregnancy and the safety of operative laparoscopy can be guaranteed only in appropriately selected cases.[74] Similar cases demonstrate the further importance of first-trimester ultrasound examination in diagnosing early pregnancy complications. The importance of sonographic imaging in cases of acute abdomen in pregnancy cannot be overstressed.[78]

Although there are no available data on the use of color Doppler and 3D ultrasound in this field, we believe that these modalities may add additional information on the implantation site and attachment of the placenta to the surrounding structures.

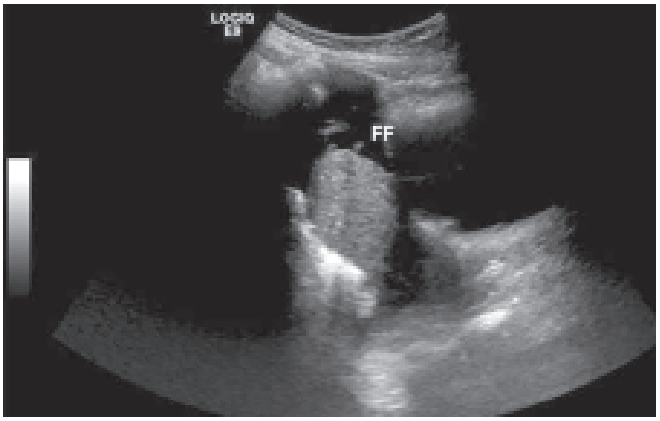

Figure 9.14A: Transabdominal utrasound shows empty uterus and free fluid in the pelvis. Patient presented with abnormal genital tract bleeding and abdominal/pelvic pain at 15 weeks gestation

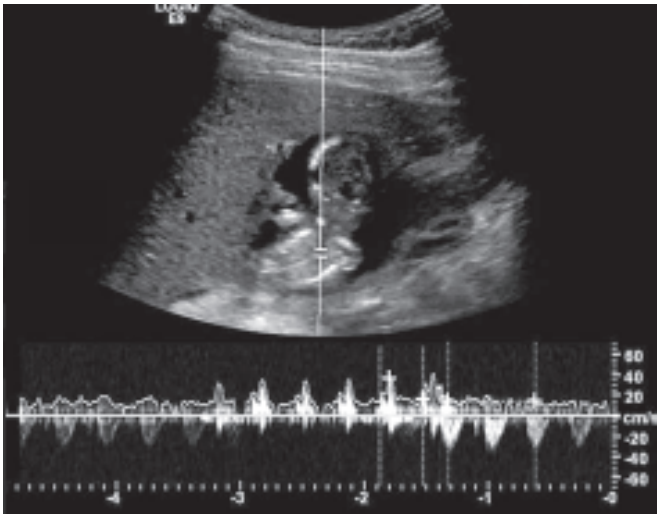

Figure 9.14B: Transabdominal pulsed Doppler ultrasound demonstrates regular heart activity with frequency of 171 beats per minute

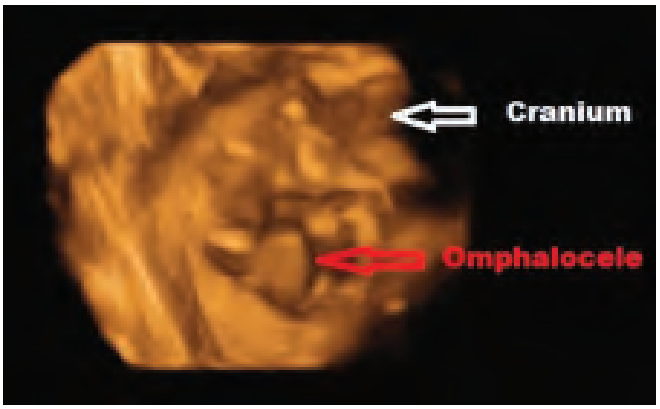

Figure 9.14C: Three-dimensional ultrasound of the same fetus demonstrates an omphalocele

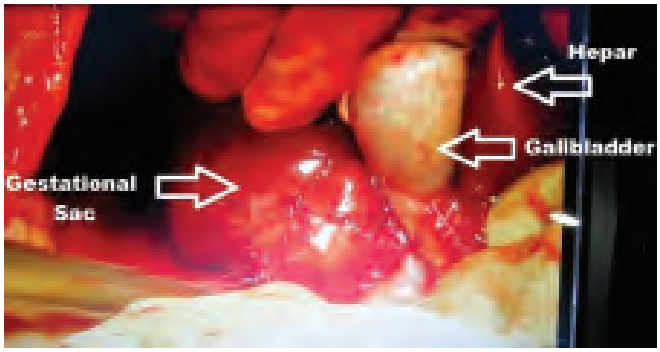

Figure 9.14D: Laparoscopy revealed abdominal pregnancy. Gestational sac was implanted below the liver and gallbladder

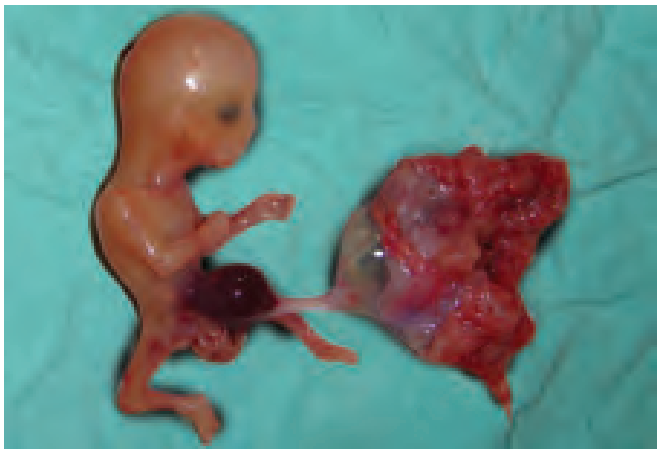

Figure 9.14E: Gross anatomy of the fetus with evidence of an omphalocele. Compare the image with Figure 9.14C

THERAPY

Throughout the years, the treatment of ectopic pregnancy has been emergency laparotomy, including salpingectomy. In order to preserve fertility, alternatives to laparotomy and salpingectomy include observation, laparoscopic removal of ectopic pregnancy and systemic or local use of methotrexate or other feticidal agents. As medical therapy for ectopic pregnancy becomes a common practice, familiarity with its side effects may lead to greater success rates. The decision to abandon medical treatment and proceed with surgery should be based on defined guidelines, such as development of peritoneal signs, decreasing hemoglobin levels or hemodynamic instability.[79]

Methotrexate may be administered systemically,[80] locally[81,82] or in combination. Local application is performed either laparoscopically or transvaginally under ultrasound needle puncture.[40] In the latter approach, methotrexate is injected directly into the gestational sac. The success rate of systemic, single-dose

methotrexate (83–96%) is similar to that of local administration under laparoscopic guidance (89–100%), but the success rate of methotrexate under ultrasound guidance seems to be lower (70–83%).[83] Local injection of methotrexate under control of color Doppler imaging may increase the success rate.[4] The use of color and pulsed Doppler enables visualization of the trophoblastic adnexal flow with high-velocity and low impedance pulsed Doppler (RI<0.40). The needle can be inserted into the area of maximum color signal, which marks trophoblastic invasiveness and vitality.

Pharmacological management of an unruptured, size-appropriate ectopic pregnancy is now an established standard of care. The present protocol recommends systemic use of methotrexate in a single-dose.[84] This form of methotrexate has proven to be successful and cost-effective alternative to traditional surgical management of ectopic pregnancy.[85] In view of the risk of standard therapy and the patients' desire for fertility, methotrexate treatment may be a therapeutic alternative in cervical pregnancy as well. Recent reports have affirmed that ectopic pregnancy has become, a medical rather than a surgical disease.[2,4,69,72,79,83,84,86]

Puncture injections are valid and reasonable alternative to a traditional surgical approach, especially in patients with an interstitial, cervical or heterotopic pregnancy. In these particular cases, puncture procedures guided by transvaginal ultrasound can efficiently replace surgical treatment and save the patient from unnecessary hysterectomy.

Early diagnosis is the key to effective nonsurgical treatment. Diagnostic algorithms using serial beta hCG measurements and transvaginal ultrasound examinations make definitive diagnosis possible without laparoscopy **(Fig. 9.15A)**. As stated before, with the help of color Doppler, it is possible to identify the activity, invasiveness and vitality of trophoblasts **(Fig. 9.15B)**.

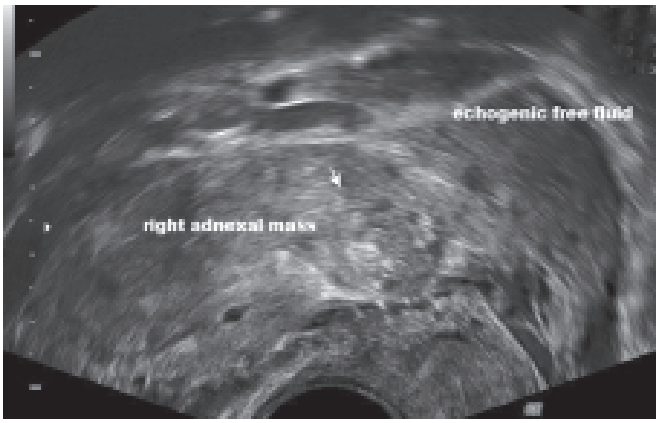

Figure 9.15A: Transvaginal ultrasound scan demonstrates a complex adnexal mass in a patient presenting with amenorrhea, pelvic pain and positive pregnancy test

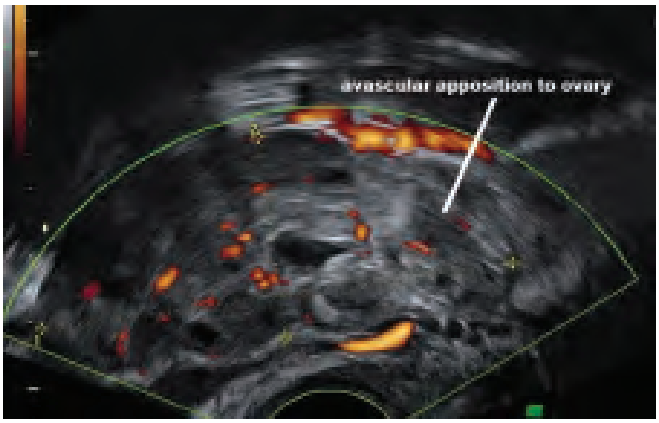

Figure 9.15B: Color Doppler ultrasound demonstrates increased vascularity suggestive of ectopic pregnancy with vital trophoblast

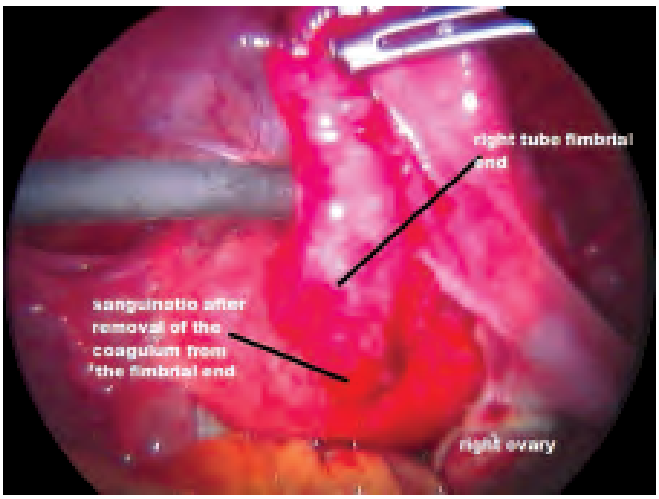

Figure 9.15C: Laparoscopy revealed ectopic pregnancy in the ampular part of the tube, hematosalpinx and bleeding from the fimbrial end

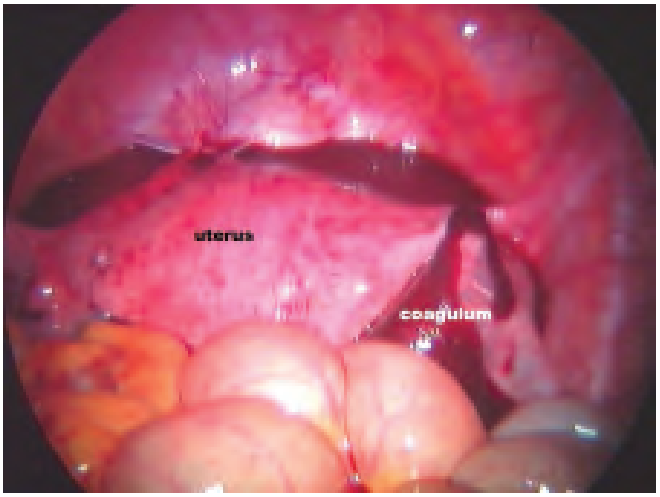

Figure 9.15D: Free fluid and coagulum in the cul-de-sac

These represent the most important characteristics for making the decision for more selective management of an ectopic pregnancy. Three-dimensional ultrasound seems to be an even more effective procedure for the early diagnosis of ectopic pregnancy in asymptomatic patients, even before six weeks of amenorrhea.[59]

Laparoscopic salpingostomy, the surgical gold standard, is an effective therapy in patients who are hemodynamically stable and wish to preserve their fertility **(Figs 9.15C and D)**. The reproductive performance after salpingostomy appears to be equal to, or better than salpingectomy, but the recurrent ectopic pregnancy rate is slightly higher.[3] A variable systemic dose of methotrexate produces outcomes close to those of laparoscopic salpingostomy in similar patients.[87] Methotrexate treatment is recommended in the asymptomatic patient with serum beta hCG levels of less than 2000 IU/ml, a tubal diameter of < 2 cm, and absence of fetal heart activity. The patient's understanding of her condition and compliance are mandatory. However, in many cases, the ectopic pregnancy does not meet suitable medical criteria and still requires surgery. In cases suspicious of tubal abortion with a high impedance signal (RI>0.55) and beta hCG below 1000 IU/ml, local administration of methotrexate is not advised. A recent paper assessed the protocol of a single dose methotrexate for the treatment of ectopic pregnancy and confirmed that 15% decrease in serum hCG between day 4–7 is a very good predictor of the likely success of medical treatment.[88] A recent meta-analysis, including data from 26 trials, demonstrated the success with the single-dose regimen to be 88.1%, while the success with the multiple dose regimen was 92.7%.[89] A small randomized clinical trial also demonstrated the single-dose regimen to have a slightly higher failure rate.[90] Barnhart et al. more recently reported that the minimum rise in beta hCG for a potentially viable pregnancy in women who present with vaginal bleeding or pain is 53% per two days (up to 5,000 IU/L).[91] A hybrid protocol, involving two equal doses of methotrexate (50 mg/m^2) given on days 1 and 4 without the use of leucovorin has been shown to be an effective and convenient alternative to the existing regimens.[92]

CONCLUSION

With the use of beta hCG testing and transvaginal ultrasound our approach to the patient suspected of ectopic pregnancy has been vastly improved. An important advantage of the most currently used transvaginal transducers is the ability to perform simultaneous color and spectral Doppler studies, allowing easy identification of the ectopic peritrophoblastic flow. Therefore, color should be applied whenever a finding is suggestive of ectopic pregnancy.

Further progresses in diagnostic procedures were made when 3D ultrasound was introduced. Transvaginal 3D ultrasound enables the clinician to perceive the true spatial relations and thus easily distinguish the origin of an adnexal mass, while 3D power Doppler allows detailed analysis of the vascularization.

Transvaginal color and pulsed Doppler imaging may be potentially used for detection of the patients with less prominent tubal perfusion, suitable for the expectant management of an ectopic pregnancy. It is expected that the increased sensitivity of the serum beta hCG immunoassay and the quality of transvaginal B-mode, color Doppler ultrasound and more recently 3D with color and power Doppler facilities will allow even earlier detection and conservative management of ectopic pregnancies. Furthermore, it seems that the fertility outcomes and the number of women attempting to conceive after an ectopic pregnancy will increase even more.

REFERENCES

1. Ectopic pregnancy. In: Speroff L, Glass RH, Kase NG (Eds). Clinical gynecologic endocrinology and infertility. London: Williams and Wilkins; 1999. pp. 1149-67.
2. Timor-Tristch IE, Monteagudo A. Ectopic pregnancy. In: Kupesic S, de Ziegler D (Eds). Ultrasound and infertility. UK: Partenon Publishing Group; 2000. pp. 215-39.
3. Kurjak A, Kupesic S. Ectopic pregnancy. In: Kurjak A (Ed.). Ultrasound in Obstetrics and Gynecology. Boston: CRC Press; 1990. pp. 225-35.
4. Kupesic S, Kurjak A. Color Doppler assessment of ectopic pregnancy. In: Kurjak A, Kupesic S (Eds). An atlas of transvaginal color Doppler. London: Parthenon Publishing; 2000. pp. 137-47.
5. Boufous S, Quartararo M, Mohsin M, et al. Trends in the incidence of ectopic pregnancy in New South Wales between 1990-1998. Aust N Z J Obstet Gynaecol. 2001;41(4):436-8.
6. Rajkhowa M, Glass MR, Rutherford AJ, et al. Trends in the incidence of ectopic pregnancy in England and Wales from 1966 to 1996. BJOG. 2000;107(3):369-74.
7. Nederlof KP, Lawson HW, Saftlas AF, et al. Ectopic pregnancy surveillance. Morbid Mortal Weekly Rep. 1990;39:9.
8. Strandell A, Thorburn J, Hamberger L. Risk factors for ectopic pregnancy in assisted reproduction. Fertil Steril. 1999;71(2):282-6.
9. Kamwendo F, Forslin L, Bodin L, et al. Epidemiology of ectopic pregnancy during a 28 year period and the role of pelvic inflammatory disease. Sex Transm Infect. 2000;76(1):28-32.

10. Barlow RE, Cooke ID, Odukoya O, et al. The prevalence of Chlamydia trachomatis in fresh tissue specimens from patients with ectopic pregnancy or tubal factor infertility as determined by PCR and in-situ hybridisation. J Med Microbiol. 2001;50(10):902-8.
11. Brown WD, Burrows L, Todd CS. Ectopic pregnancy after cesarean hysterectomy. Obstet Gynecol. 2002;99(5 Pt 2):933-4.
12. Bouyer J, Rachou E, Germain E, et al. Risk factors for extrauterine pregnancy in women using an intrauterine device. Fertil Steril. 2000;74(5):899-908.
13. Bouyer J, Coste J, Fernandez H, et al. Sites of ectopic pregnancy: a 10 year population-based study of 1800 cases. Hum Reprod. 2002;17(12):3224-30.
14. Mol BW, van der Veen F, Bossuyt PM. Symptom-free women at increased risk of ectopic pregnancy: should we screen? Acta Obstet Gynecol Scand. 2002;81(7):661-72.
15. Kalinski MA, Guss DA. Hemorrhagic shock from a ruptured ectopic pregnancy in a patient with a negative urine pregnancy test result. Ann Emerg Med. 2002;40(1):102-5.
16. Mertz HL, Yalcinkaya TM. Early diagnosis of ectopic pregnancy. Does use of a strict algorithm decrease the incidence of tubal rupture? J Reprod Med. 2001;46(1):29-33.
17. Sagaster P, Zojer N, Dekan G, et al. A paraneoplastic syndrome mimicking extrauterine pregnancy. Ann Oncol. 2002;13(1):170-2.
18. Hick JL, Rodgerson JD, Heegaard WG, et al. Vital signs fail to correlate with hemoperitoneum from ruptured ectopic pregnancy. Am J Emerg Med. 2001;19(6):488-91.
19. Birkhahn RH, Gaeta TJ, Bei R, et al. Shock index in the first trimester of pregnancy and its relationship to ruptured ectopic pregnancy. Acad Emerg Med. 2002;9(2):115-9.
20. Wong E, Suat SO. Ectopic pregnancy-a diagnostic challenge in the emergency department. Eur J Emerg Med. 2000;7(3):189-94.
21. Dart R, McLean SA, Dart L. Isolated fluid in the cul-de-sac: how well does it predict ectopic pregnancy? Am J Emerg Med. 2002;20(1):1-4.
22. Barnhart KT, Katz I, Hummel A, et al. Presumed diagnosis of ectopic pregnancy. Obstet Gynecol. 2002;100(3):505-10.
23. Sheppard RW, Patton PE, Novy MJ, et al. Serial beta hCG measurements in the early detection of ectopic pregnancy. Obstet Gynecol. 1990;75(3 pt 1):417-20.
24. Levsky ME, Handler JA, Suarez RD, et al. False-positive urine beta-HCG in a woman with a tubo-ovarian abscess. J Emerg Med. 2001;21(4):407-9.
25. Dumps P, Meisser A, Pons D, et al. Accuracy of single measurements of pregnancy-associated plasma protein-A, human chorionic gonadotropin and progesterone in the diagnosis of early pregnancy failure. Eur J Obstet Gynecol Reprod Biol. 2002;100(2):174-80.
26. Poppe WA, Vandenbussche N. Eur Postoperative day 3 serum human chorionic gonadotropin decline as a predictor of persistent ectopic pregnancy after linear salpingotomy. J Obstet Gynecol Reprod Biol. 2001;99:249-52.
27. Timor-Tristch IE, Rottem S, Thale I. Review of transvaginal ultrasonography: description with clinical application. Ultrasound Q. 1988;6:1-32.
28. Peisner DB, Timor-Tritsch IE. The discriminatory zone of beta hCG for vaginal probes. J Clin Ultrasound. 1990;18:280-5.
29. Fossum GT, Davajan V, Kletzky OA. Early detection of pregnancy with transvaginal ultrasound. Fertil Steril. 1988;49(5):788-91.
30. Bernascheck G, Rudelstorfer R, Csaicsich P. Vaginal sonography versus serum human chorionic gonadotropin in early detection of pregnancy. Am J Obstet Gynecol. 1988;158(3 Pt 1):608-12.
31. Albayram F, Hamper UM. First-trimester obstetric emergencies: spectrum of sonographic findings. J Clin Ultrasound. 2002;30(3):161-77.
32. Kurjak A, Zalud I, Volpe G. Conventional B-mode and transvaginal color Doppler in ultrasound assessment of ectopic pregnancy. Acta Med lugosl. 1990;44(2):91-103.
33. Rubin GL, Petersin HB, Dorfman SF. Ectopic pregnancy in the United States 1970-1978. J Am Med Assoc. 1983;249:1725-9.
34. Bolton G, Cohen F. Detecting and treating ectopic pregnancy. Contemp Obstet Gynecol. 1981;18:101-4.
35. Hopp H, Schaar P, Entezami M. Diagnostic reliability of vaginal ultrasound in ectopic pregnancy. Geburtshilfe Frauenheilkd. 1995;55(12):666-70.
36. Hertzberg BS, Kliewer MA. Ectopic pregnancy: ultrasound diagnosis and interpretive pitfalls. South Med J. 1995;88(12):1191-8.
37. Thoma ME. Early detection of ectopic pregnancy visualizing the presence of a tubal ring with ultrasonography performed by emergency physicians. Am J Emerg Med. 2000;18(4):444-8
38. Nyberg D. Ectopic pregnancy. In: Nyberg DA, Hill LM, Bohm-Velez M (Eds). Transvaginal Sonography. St. Louis: Mosby Year Book; 1992. pp. 105-35.
39. Wojak JC, Clayton MJ, Nolan TE. Outcomes of ultrasound diagnosis of ectopic pregnancy. Dependence on observer experience. Invest Radiol. 1995;30(2):115-7.
40. Timor-Tritsch IE, Yeh MN, Peisner DB, et al. The use of transvaginal ultrasonography in the diagnosis of ectopic pregnancy. Am J Obstet Gynecol. 1989;161(1):157-61.
41. Pellerito JS, Taylor KJW, Quedens-Case C. Ectopic pregnancy: evaluation with endovaginal color flow imaging. Radiology. 1992;183:831-3
42. Fleischer AC, Pennell RG, McKee MS. Ectopic pregnancy: features at transvaginal sonography. Radiology. 1990;174:375-8.
43. Bernhart K, Mennuti MT, Benjamin I, et al. Prompt diagnosis of ectopic pregnancy in an emergency department setting. Obstet Gynecol. 1994;84(6):1010-5.
44. Leung TY, Ng PS, Fung TY. Ectopic pregnancy diagnosed by laparoscopic ultrasound scan. Ultrasound Obstet Gynecol. 1999;13(4):281-2.
45. Kurjak A, Zalud I, Schulman H. Ectopic pregnancy: transvaginal color Doppler of trophoblastic flow in questionable adnexa. J Ultrasound Med. 1991;10(12):685-9.
46. Zalud I, Kurjak A. The assessment of luteal blood flow in pregnant and non-pregnant women by transvaginal color Doppler. J Perinat Med. 1990;18(3):215-21.
47. Jurkovic D, Bourne TH, Jauniaux E, et al. Transvaginal color Doppler study of blood flow in ectopic pregnancies. Fertil Steril. 1992;57(1):68-73.

48. Wherry KL, Dubinsky TJ, Waitches GM, et al. Low-resistance endometrial arterial flow in the exclusion of ectopic pregnancy revisited. J Ultrasound Med. 2001;20(4):335-42.
49. Dillon EH, Feyock AL, Taylor KJW. Pseudogestational sacs: Doppler US differentiation from normal or abnormal intrauterine pregnancies. Radiology. 1990;176:359-64.
50. Orden MR, Gudmundsson S, Helin HL, et al. Intravascular contrast agent in the ultrasonography of ectopic pregnancy. Ultrasound Obstet Gynecol. 1999;14(5):348-52.
51. Pellerito JS, Troiano RN, Quedens-Case C, et al. Common pitfalls of endovaginal color Doppler flow imaging. Radiographics. 1995;15(1):37-47.
52. Lurie S, Katz Z. Where a pendulum of expectant management of ectopic pregnancy should rest? Gynecol Obstet Invest. 1996;42(3):145.
53. Stovall TG, Link WF. Expectant management of ectopic pregnancy. Obstet Gynecol Clin North Am. 1991;18(1):135-44.
54. Laurie S, Insler V. Can the serum beta hCG level reliably predict likelihood of a ruptured tubal pregnancy? Isr J Obstet Gynecol. 1992;3:152-544.
55. Budowick M, Johnson TR, Genadry R. The histopathology of developing tubal ectopic pregnancy. Fertil Steril. 1980;34(2):169-71.
56. Kemp B, Funk A, Hauptmann S, et al. Doppler sonographic criteria for viability in symptomless ectopic pregnancies. Lancet. 1997;349(9060):1220-1.
57. Baba K, Satoh K, Sakamoto S, et al. Development of an ultrasonic system for three dimensional reconstruction of the fetus. J Perinat Med. 1989;17(1):19-24.
58. Fredfeldt KE, Holm HH, Pedersen JF. Three-dimensional ultrasonic scanning. Acta Radiol Diagn. 1984;25(3):237-41.
59. Rempen A. The shape of the endometrium evaluated with three-dimensional ultrasound: an additional predictor of extrauterine pregnancy. Hum Reprod. 1998;13(2):450-4.
60. Harika G, Gabriel R, Carre-Pigeon F, et al. Primary application of three-dimensional ultrasonography to early diagnosis of ectopic pregnancy. Eur J Obstet Gynecol Reprod Biol 1995;60(2):117-20.
61. Shih JC, Shyu MK, Cheng WF, et al. Arteriovenous malformation of mesosalpinx associated with a vanishing ectopic pregnancy: diagnosis with three-dimensional color power angiography. Ultrasound Obstet Gynecol. 1999;13(1):63-6.
62. Mazur MT, Kurman RJ. Disease of the fallopian tube. In: Kerman RJ (Ed.). Blaustein's Pathology of the Female Genital Tract, 4th edition. New York: Springer – Verlag; 1994. pp. 541-3.
63. Agarwal SK, Wisot AL, Garzo G, et al. Cornual pregnancies in patients with prior salpingectomy undergoing in vitro fertilization and embryo transfer. Fertil Steril. 1996;65(3):659-60.
64. Timor-Tritsch IE, Monteagudo A, Matera C, et al. Sonographic evaluation of cornual pregnancies treated without surgery. Obstet Gynecol. 1992;79:1044-9.
65. Honemeyer U, Kupesic Plavsic S, Kurjak A. Interstitial ectopic pregnancy: the essential role of ultrasound diagnosis. Donald School Journal of Ultrasound in Obstetrics and Gynecology. 2010;4(3):321-5.
66. Hafner T, Aslam N, Ross JA, et al. The effectiveness of non-surgical management of early interstitial pregnancy: a report of ten cases and review of the literature. Ultrasound Obstet Gynecol. 1999;13(2):131-6.
67. Jurkovic D, Geipel A, Gruboeck K, et al. Three-dimensional ultrasound for the assessment of uterine anatomy and detection of congenital uterine anomalies. A comparison with hysterosalpingography and two dimensional sonography. Ultrasound Obstet Gynecol. 1995;5(4):233-7.
68. Lawrence A, Jurkovic D. Three-dimensional ultrasound diagnosis of interstitial pregnancy. Ultrasound Obstet Gynecol. 1999;14(4):292-3.
69. Ben-Sholmo I, Eliyahu S, Yanai N, et al. Methotrexate as a possible cause of ovarian cyst formation: experience with women treated for ectopic pregnancies. Fertil Steril. 1997;67(4):786-8.
70. Schiff E, Shalev E, Bustan M, et al. Pharmacokinetics of methotrexate after local tubal injection for conservative treatment of ectopic pregnancy. Fertil Steril. 1992;57(3):688-90.
71. Timor-Tritsch IE, Monteagudo A, Mandeville EO, et al. Successful management of viable cervical pregnancy by local injection of methotrexate guided by transvaginal ultrasonography. Am J Obstet Gynecol. 1994;170(3):737-9.
72. Jurkovic D, Hacket E, Campbell S. Diagnosis and treatment of early cervical pregnancy: a review and a report of two cases treated conservatively. Ultrasound Obstet Gynecol. 1996;8(6):373-80.
73. Jauniaux E, Zaidi J, Jurkovic D, et al. Comparison of color Doppler features and pathological findings in complicated early pregnancy. Hum Reprod. 1994;9(12):2432-7.
74. Morita Y, Tsutsumi O, Kurmochi K, et al. Successful laparoscopic management of primary abdominal pregnancy. Hum Reprod. 1996;11(11):2546-7.
75. Ahmed B, Fawzi HW, Abushama M. Advanced abdominal pregnancy in the developing countries. J Obstet Gynecol. 1996;16:400-5.
76. Angtuaco TL, Shah HR, Neal MR, et al. Ultrasound evaluation of abdominal pregnancy. Crit Rev Diagn Imaging. 1994;35(1):1-59.
77. Bajo JM, Garcia FA, Huertas MA. Sonographic follow-up of a placenta left in situ after delivery of the fetus in abdominal pregnancy. Ultrasound Obstet Gynecol. 1996;7(4):285-8.
78. Zaki ZM. An unusual presentation of ectopic pregnancy. Ultrasound Obstet Gynecol. 1998;11(6):456-8.
79. Thoen LD, Crenin MD. Medical treatment of ectopic pregnancy with methotrexate. Fertil Steril. 1997;68:727-30.
80. Lipscomb GH, Meyer NL, Flynn DE, et al. Oral methotrexate for treatment of ectopic pregnancy. Am J Obstet Gynecol. 2002;186(6):1192-5.
81. Haimov-Kochman R, Sciaky-Tamir Y, Yanai N, et al. Conservative management of two ectopic pregnancies implanted in previous uterine scars. Ultrasound Obstet Gynecol. 2002;19(6):616-9.
82. El-Lamie IK, Shehata NA, Kamel HA. Intramuscular methotrexate for tubal pregnancy. J Reprod Med. 2002;47(2):144-50.
83. Yao M, Tulandi T. Current status of surgical and non-surgical management of ectopic pregnancy. Fertil Steril. 1997;67:421-33.

84. Powell MP, Spellman JR. Medical management of the patient with an ectopic pregnancy. J Perinat Neonatal Nurs. 1996;9(4):31-43.
85. Luciano AA, Roy G, Solima E, et al. Ectopic pregnancy from surgical emergency to medical management. Ann N Y Acad Sci. 2001;943:235-54.
86. Morlock RJ, Lafata JE, Eisenstein D. Cost-effectiveness of single-dose methotrexate compared with laparoscopic treatment of ectopic pregnancy. Obstet Gynecol. 2000;95(3): 407-12.
87. Tulandi T, Sammour A. Evidence-based management of ectopic pregnancy. Curr Opin Obstet Gynecol. 2000;12(4): 289-92.
88. Stovall TG, Ling FW, Carson SA, et al. Serum progesterone and uterine curettage in differential diagnosis of ectopic pregnancy. Fertil Steril. 1992;57(2):456-7.
89. Kirk E, Condous G, van Calster B, et al. A validation of the most commonly used protocol to predict the success of single dose metotrexate in the treatment of ectopic pregnancy. Hum Reprod. 2007;22(3)858-63.
90. Van Den Eeden SK, Shan J, Bruce C, et al. Ectopic pregnancy rate and treatment utilization in a large managed care organization. Obstet Gynecol. 2005;105(5 Pt 1):1052-7.
91. Barnhart KT, Sammel MD, Hummel A, et al. A novel "two dose" regimen of methotrexate to treat ectopic pregnancy. Fertil Steril. 2005;84(Suppl):S130.
92. Alleyassin A, Khademi A, Aghahosseini M, et al. Comparison of success rates in the medical management of ectopic pregnancy with single-dose and multiple-dose administration of methotrexate: a prospective, randomized clinical trial. Fertil Steril. 2006;85(6):1661-6.

CHAPTER 10

Sonographic Determination of Gestational Age

Robin B Kalish

INTRODUCTION

Importance of Accurate Gestational Age Assessment

Accurate assessment of gestational age is fundamental in managing both low and high risk pregnancies. In particular, uncertain gestational age has been associated with adverse pregnancy outcomes including low birth weight, spontaneous preterm delivery and perinatal mortality, independent of maternal characteristics.[1] Making appropriate management decisions and delivering optimal obstetric care necessitates accurate appraisal of gestational age. For example, proper diagnosis and management of preterm labor and post-term pregnancy requires an accurate estimation of fetal age. Many pregnancies considered to be preterm or post-term are wrongly classified. Unnecessary testing, such as fetal monitoring and unwarranted interventions, including induction for supposed post-term pregnancies may lead to an increased risk of maternal and neonatal morbidity. In addition, pregnancies erroneously thought to be preterm may be subject to avoidable and expensive hospitalization stays as well as excessive and potentially dangerous medication use including tocolytic therapy. In one study by Kramer et al. that assessed over 11,000 pregnant women who underwent early ultrasound, one-fourth of all infants who would be classified as premature and one-eighth of all infants who would be classified as post-term by menstrual history alone would be misdiagnosed.[2] Accurate pregnancy dating may also assist obstetricians in appropriately counseling women who are at imminent risk of a preterm delivery about likely neonatal outcomes.

Precise knowledge of gestational age is also essential in the evaluation of fetal growth and the detection of intrauterine growth restriction. During the third trimester, fundal height assessment may be helpful in determining appropriate fetal growth by comparing the measurement to a known gestational age. In addition, dating a pregnancy is imperative for scheduling invasive diagnostic tests, such as chorionic villus sampling (CVS) or amniocentesis, as appropriate timing can influence the safety of the procedure. Certainty of gestational age is also important in the interpretation of biochemical serum screening test results and may help avoid undue parental anxiety from miscalculations and superfluous invasive procedures, which may increase the risk of pregnancy loss. Assessment of gestational age is also crucial for counseling patients regarding the option of pregnancy termination.

ASSESSMENT OF GESTATIONAL AGE BY LAST MENSTRUAL PERIOD (LMP)

Traditionally, the first day of the LMP has been used as a reference point, with a predicted delivery date 280 days later. The estimated date of confinement (EDC) can also be calculated by Nägele's rule by subtracting three months and adding seven days to the first day of the last normal menstrual period. However, there are inherent problems in assessing gestational age using the

menstrual cycle. One obstacle in using the LMP is the varying length of the follicular phase and the fact that many women do not have regular menstrual cycles. Walker et al. evaluated 75 ovulatory cycles using luteinizing hormone levels as a biochemical marker and found that ovulation occurred within a wide range of 8–31 days after the LMP.[3] Similarly, Chiazze et al. collected over 30,000 recorded menstrual cycles from 2,316 women and found that only 77% of women have average cycle lengths between 25–31 days.[4] Another barrier in using a menstrual history is that many women do not routinely document or remember their LMP. Campbell et al. demonstrated that of more than 4,000 pregnant women, 45% were not certain about their LMP as a result of poor recall, irregular cycles, bleeding in early pregnancy or oral contraceptive use within two months of conception.[5]

Clinical Methods for Determining Gestational Age

Other methods used to assess gestational age have included uterine size assessment, time at quickening and fundal height measurements. However, these clinical methods are often suboptimal. Robinson noted that uterine size determination by bimanual examination produced incorrect assessments by more than two weeks in over 30% of patients.[6] Similarly, fundal height estimation does not provide a reliable guide to predicting gestational age. Beazly et al. found up to eight weeks variation in gestational age for any particular fundal height measurement during the second and third trimesters.[7] In addition, quickening or initial perception of fetal movement can vary greatly among women. While these modalities may be useful adjuncts, they are unreliable as the sole tool for the precise dating of a pregnancy.

Ultrasound Assessment of Gestational Age

In recent years, ultrasound assessment of gestational age has become an integral part of obstetric practice.[8] Correspondingly, prediction of gestational age is a central element of obstetric ultrasonography. Fetal biometry has been used to predict gestational age since the time of A-mode ultrasound.[9] Currently, the sonographic estimation is derived from calculations based on fetal measurements and serves as an indirect indicator of gestational age. Over the past three decades, numerous equations regarding the relationship between fetal biometric parameters and gestational age have been described and have proven early antenatal ultrasound to be an objective and accurate means of establishing gestational age.[10-15]

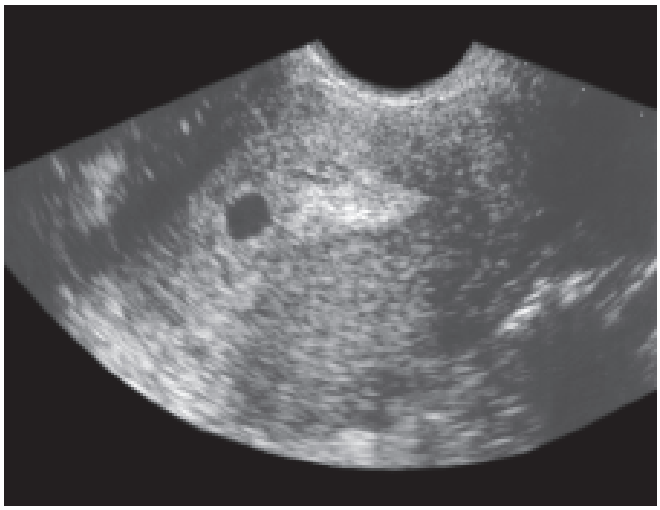

Figure 10.1: Transvaginal ultrasound image demonstrating an early gestational sac prior to the visualization of a fetal pole

First Trimester Ultrasound

Ultrasound assessment of gestational age is most accurate in the first trimester of pregnancy.[16] During this time, biological variation in fetal size is minimal. The gestational sac is the earliest unequivocal sonographic sign of pregnancy.[17-20] Historically, gestational sac size and volume had been used as a means to estimate gestational age.[21,22] This structure sonographically resembles a fluid filled sac surrounded by a bright echogenic ring, the developing chorionic villi, within the endometrial cavity **(Fig. 10.1)**. This sac can be visualized as early as five menstrual weeks using transvaginal sonography.[23-25] More recently, studies have shown that fetal age assessment by gestation sac measurement is not reliable, with a prediction error up to two weeks.[6,26] Another imprecise yet often used modality is the sonographic visualization of distinct developing structures.[27] During the fifth menstrual week, the yolk sac—the earliest embryonic structure detectable by sonography, can be visualized prior to the appearance of the fetal pole. And, by the end of the sixth menstrual week, a fetal pole with cardiac activity should be present **(Fig. 10.2)**. Subsequently, the presence of limb buds and midgut herniation can be seen at approximately eight weeks gestation. However, these developmental landmarks can only provide rough estimates to the actual fetal age.

In 1973, Robinson reported using the CRL for determining gestational age.[28] Since that time, ultrasound equipment, techniques and prediction formulas have substantially improved and allow for more rapid and precise measurement of the CRL and determination of

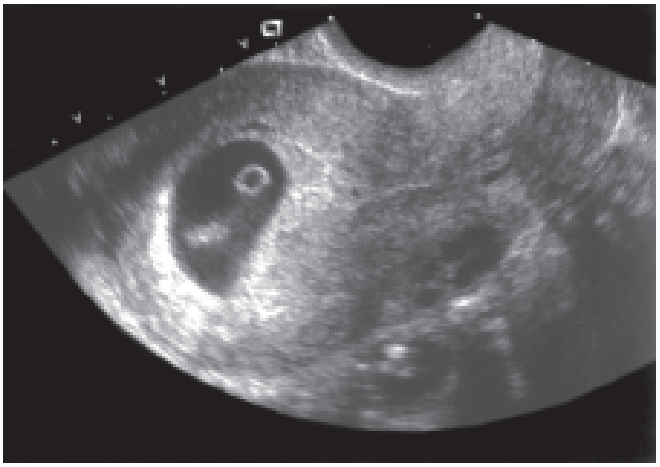

Figure 10.2: Transvaginal ultrasound image demonstrating an early embryo with a visible yolk sac at approximately seven weeks gestation

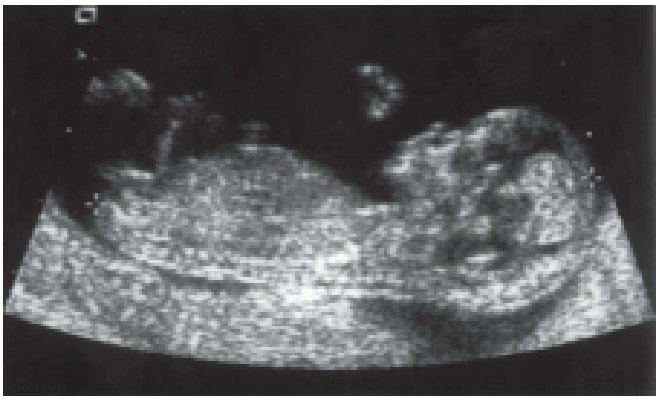

Figure 10.3: Ultrasound image demonstrating the fetal crown-rump length measurement in the first trimester

gestational age.[29,30] For the best results, the fetus should be imaged in a longitudinal plane. The greatest embryonic length should be measured by placing the calipers at the head and rump of the fetus **(Fig. 10.3).** Three adequate CRL measurements should be taken and the average used for gestational age determination.[31] The accuracy of the CRL measurement has been well documented in the medical literature. Specifically, gestational age can be estimated safely with a maximal error of 3–5 days in the first trimester.[6,16,32,33]

In summary, first trimester ultrasound is a useful and reliable tool in the assessment of gestational age. In particular, sonographic measurement of the CRL during the first trimester is the best parameter for estimating gestational age and is accurate within five days of the actual conception date.[16,32]

Second Trimester Ultrasound

Although routine ultrasonography at 18–20 weeks gestation historically has been controversial,[34] it is currently practiced by most obstetricians in the United States.[35] In addition to screening for fetal anomalies, sonographic gestational age assessment may be of clinical value in that it has been shown to decrease the incidence of post-term as well as preterm diagnoses and thus the administration of tocolytic agents.[36,37] In addition, uncertain gestational age has been associated with higher perinatal mortality rates and an increase of low birth weight and spontaneous preterm delivery.[1]

Ultrasound Parameters

When choosing the optimal parameter for estimating gestational age, it is essential that the structure has little biologic variation, is growing at a rapid pace and can be measured with a high degree of reproducibility.[38] In the past, the biparietal diameter (BPD) had been described as a reliable method of determining gestational age.[9,12] While the BPD was the first fetal parameter to be clinically utilized in the determination of fetal age in the second trimester, more recent studies have evaluated the use of several other biometric parameters including head circumference (HC),[39] abdominal circumference (AC),[40] femur length (FL),[41] foot length,[42] ear size,[43] orbital diameters,[44,45] cerebellum diameter[46,47] and others. In a large study by Chervenak et al. that evaluated pregnancies conceived by IVF and thus had known conception dates, HC was found to be the best predictor of gestational age compared with other commonly used parameters **(Table 10.1)**.[48] This finding is in agreement with that of Hadlock,[10] Ott[11] and Benson[49] who compared the performance of HC, BPD, FL and AC in different populations.

The HC should be measured in a plane that is perpendicular to the parietal bones and traverses the third ventricle and thalami **(Fig. 10.4)**.[31] The image should also demonstrate smooth, symmetrical calvaria and the presence of a cavum septum pellucidum. The calipers should be placed on the outer edges of the calvaria and a computer-generated ellipse should be adjusted to fit around the fetal head without including the scalp. The BPD can be taken in the same plane by placing the calipers on the outer edge of the proximal calvarium wall and on the inner edge of the distal calvarium wall.[50] The BPD, while highly correlated with HC, is less accurate as a predictor of gestational age as a result of variation in head shape.[48]

Multiple parameters have been shown to improve the accuracy of gestational age assessment.[48] Along with HC,

TABLE 10.1

Comparison of stepwise multiple linear regression in estimation of fetal age for singletons using different second trimester biometric parameters by Chervenak et al.[47]

Biometric parameters	*Random error (days)*
HC	3.77
AC	3.96
BPD	4.26
FL	4.35
HC+AC	3.44
HC+FL	3.55
HC+AC+FL	3.35

[Adapted from Chervenak FA, Skupski DW, Romero R, et al. How accurate is fetal biometry in the assessment of fetal age? Am J Obstet Gynecol. 1998;178(4):678-87.]

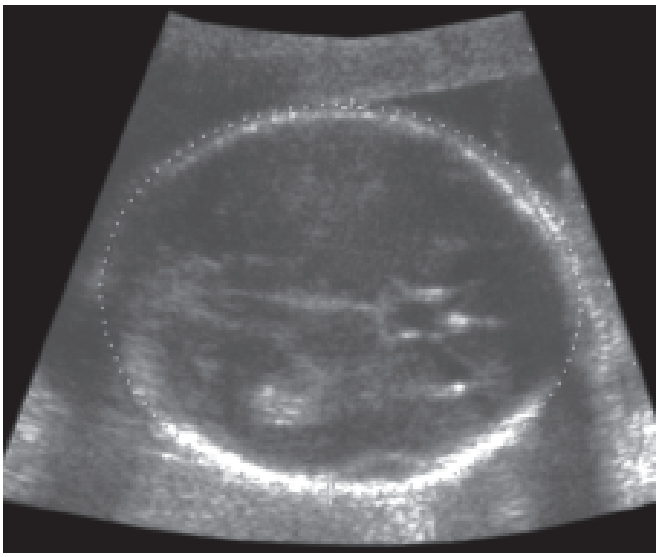

Figure 10.4: Ultrasound image demonstrating the head circumference measurement in a second trimester fetus

the addition of one parameter (AC or FL) or two parameters (AC and FL) is slightly superior to HC alone in the prediction of fetal age. **Table 10.1** demonstrates the relative error associated with the use of different biometric parameters. The use of multiple parameters also reduces the effect of outliers caused by biologic phenomena (i.e. congenital anomalies or growth variation) or technical error in measurement of a single structure. Still, with multiple parameters, it is important to take the images in the proper plane and place the calipers appropriately. For example, when assessing FL, the long axis of the femur should be aligned with the transducer measuring only the osseous portions of the diaphysis and metaphysis of the proximal femur. While not included in the FL measurement, the proximal epiphyseal cartilage (future

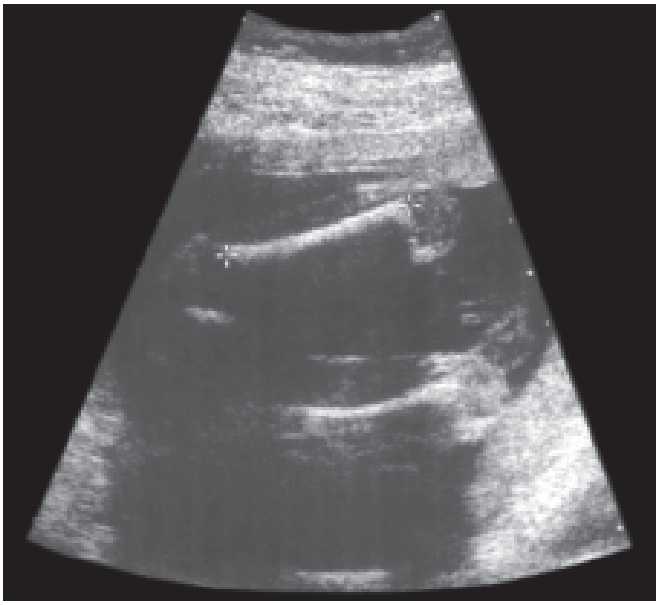

Figure 10.5: Ultrasound image demonstrating the femur length measurement in a second trimester fetus

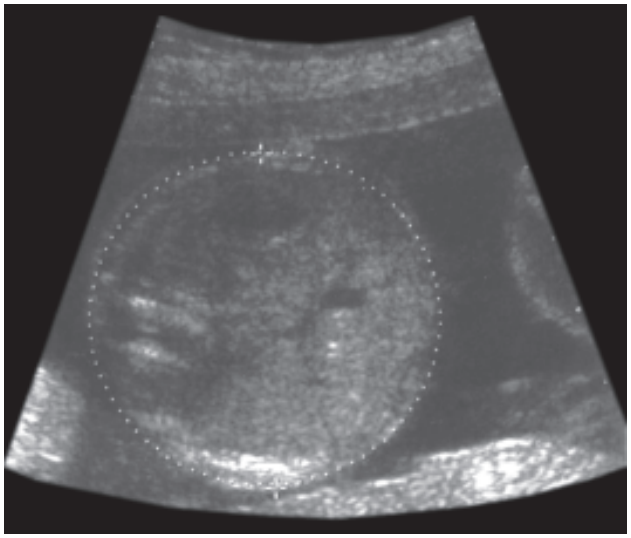

Figure 10.6: Ultrasound image demonstrating the abdominal circumference measurement in a second trimester fetus

greater trochanter) and the distal femoral epiphyseal cartilage (future distal femoral condyle) should be visualized to assure that the entire osseous femur can be measured without foreshortening or elongation **(Fig. 10.5)**.[31,51] Similarly, the AC must be measured appropriately in order to obtain an accurate estimate. The image should be taken in a plane slightly superior to the umbilicus at the greatest transverse abdominal diameter, with the liver, stomach, spleen and junction of the right and left portal veins visualized **(Fig. 10.6)**.[31]

Most modern ultrasound machines are equipped with computer software that will automatically calculate the estimated gestational age based on the entered measurements. Using a large singleton IVF population from 14–22 weeks, Chervenak et al. derived an optimal gestational age prediction formula using stepwise linear regression with a standard deviation (SD) of 3.5 days between the predicted and true gestational age.[48] This formula was compared to 38 previously published equations. Nearly all equations produced a prediction within one week demonstrating that fetal biometry in the midtrimester for assessment of gestational age is applicable and accurate across populations and institutions. Clinically, when a discrepancy greater than seven days (2SD) exists between the menstrual and ultrasound dating in the second trimester, the biometric prediction should be given preference.

Recently, we published a study evaluating and comparing the accuracy of first- and second-trimester ultrasound assessment of gestational age using pregnancies conceived with IVF.[16] Our data showed that first- and second-trimester estimates of gestational age had small differences in the systematic and random error components for an estimated gestational age that was based on fetal CRL or biometry. On the basis of this data derived from pregnancies with known conception dates, ultrasound scanning can determine fetal age to within less than five days in the first trimester and less than seven days in the second trimester in more than 95% of cases. This data further confirms the findings of Wisser et al.[32] and Chervenak et al.[48] regarding the precision of ultrasound scans to assess gestational age in the first and second trimester, respectively.

Third Trimester Ultrasound

While ultrasound has proven to be useful in the assessment of gestational age in the first and second trimesters, accuracy in the third trimester is not as reliable. Biologic variation can be a major factor that affects accuracy in gestational age prediction, and this variability greatly increases with advancing pregnancy. Doubilet and Benson evaluated late third-trimester ultrasound examinations of women who had also received a first-trimester exam and found the disparity in gestational age assessments to be three weeks or greater.[52] Thus, third-trimester sonographic estimates of gestational age should be used with caution, if at all.

MULTIFETAL PREGNANCIES

Dating equations generated for singletons can be applied to twins and triplets in order to accurately predict fetal age. Chervenak et al. used multiple linear regression to determine an optimal dating formula for multiple gestations.[48] In twin pregnancies, a single averaged prediction of the gestational age of each fetus is appropriate and was found to yield the most accurate results. This approach of averaging the two fetal age estimates is reasonable as the combined biologic and measurement variability among twins is larger than the decrease in average size of twins relative to singletons. In contrast, using the maximum or minimum estimate in a twin set yielded a slightly larger systematic error than an averaged prediction **(Table 10.2)**. In the case of triplets, one day can be added to the average of the largest and shortest gestational age prediction among these fetuses for the most accurate gestational age assessment.

Slightly larger deviations in the predictions are not unexpected for individual twins or triplets as the formulae have been derived from a singleton population. However, this imprecision is partially compensated for by the fact that multiple pregnancy predictions are based on more information, namely two or three times as many measurements as for singletons. As singleton and multiple gestations grow at similar rates during the second trimester, the difference in the uncertainty of the prediction for gestational age is small using a singleton gestation formula. Indeed, using IVF pregnancies with known conception dates, we have published data confirming that gestational age predictions for twin and triplet gestations have similar accuracy as singleton gestations **(Table 10.3)**.[16]

TABLE 10.2

Application of a singleton multiple linear regression formula for estimation of fetal age to multiple gestations by Chervenak et al.

Pregnancy type	*Prediction type*	*Mean error (days)*
Twins	GA of larger twin	0.8
	GA of smaller twin	-1.3
	Mean GA of both fetuses	-0.3
	GA of larger twin-GA of smaller twin	2.2
Triplets	GA of largest triplet	0.8
	GA of smallest triplet	-3.4
	Mean GA of all fetuses	-1.3
	GA of largest triplet-GA of smallest triplet	4.2

GA = gestational age

[Adapted from Chervenak FA, Skupski DW, Romero R, et al. How accurate is fetal biometry in the assessment of fetal age? Am J Obstet Gynecol. 1998;178(4):678-87.]

TABLE 10.3

Discrepancies between ultrasound estimates and true gestational age for the first and second trimester in singleton, twin, and triplet pregnancies

	Systematic Error[a]		*Random Error*[b]		*Absolute Error*[a]		
	First Trimester	*Second Trimester*	*First Trimester*	*Second Trimester*	*First Trimester*	*Second Trimester*	*Second|– |First|*[c]
Singleton	+1.3 ± 0.2 days	-0.1 ± 0.4 days	2.4 days	3.5 days	2.3 ± 0.1 days	2.8 ± 0.2 days	0.5 ± 0.3 days
Twin	+1.4 ± 0.2 days	-0.6 ± 0.3 days	1.7 days	2.7 days	1.8 ± 0.1 days	2.1 ± 0.2 days	0.3 ± 0.3 days
Triplet	+0.8 ± 0.4 days	-0.6 ± 0.5 days	2.1 days	2.8 days	1.7 ± 0.2 days	2.2 ± 0.3 days	0.5 ± 0.3 days

Systematic error, average difference between estimated and true gestational age; Random error, residual standard deviation between estimated and true gestational age; Absolute error, average absolute value of the discrepancy between estimated and true gestational age

[a] mean ± standard error of the mean

[b] standard deviation

[c] for gestations with both assessments

[Adapted from Kalish RB, Thaler HT, Chasen ST, Gupta M, et al. First- and second-trimester ultrasound assessment of gestational age. Am J Obstet Gynecol. 2004;191(3):975-8.]

CHOOSING A DUE DATE

When the date of conception is unequivocal, as in cases of IVF, the estimated date of confinement should not be changed based on ultrasound. However, more often than not, this is not the case. In the first trimester, an estimated date of confinement (EDC) based on the LMP that is greater than five days different from the CRL measurement should be changed to the sonographically derived EDC **(Fig. 10.7)**.[28,32,33] In the second trimester, a combination of biometric parameters that includes the HC should be used to predict the EDC. In the face of a discrepancy of more than seven days in the second trimester, the sonographic biometric prediction should be given preference, provided there is no anomaly or severe growth delay **(Fig. 10. 8)**.[48] In fact, some authors argue that biometric prediction in the first and second trimesters should be given preference in every case.[53-56]

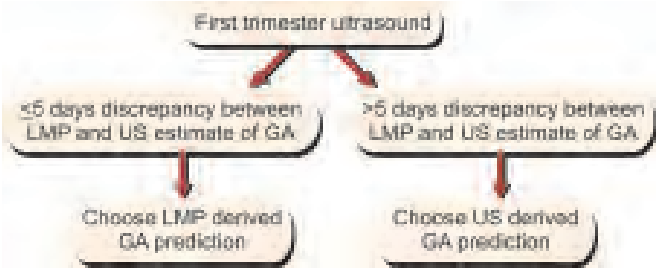

Figure 10.7: Gestational age assessment using first trimester ultrasound (LMP = Last menstrual period, US = Ultrasound, GA = Gestational age)

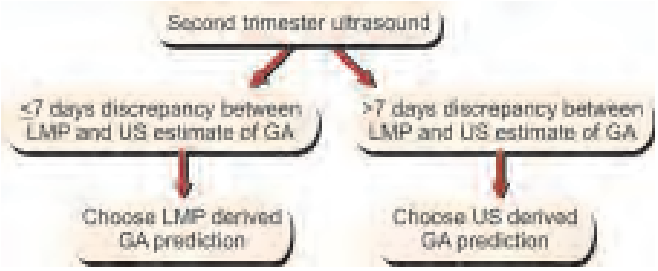

Figure 10.8: Gestational age assessment using second trimester ultrasound (LMP = Last menstrual period, US = Ultrasound, GA = Gestational age)

One of the most common and serious mistakes made when determining gestational age is changing the due date based on a second or subsequent ultrasound exam. The inaccuracy of ultrasound dating increases with gestational age. If the LMP and clinical findings suggest a gestational age within five days of a first trimester scan or within seven days of a second trimester scan, no further investigation is necessary. If the initial first or second trimester sonographically determined gestational age is outside these ranges, the due date should be changed. However, as the pregnancy progresses, revision of a due date that was based on a previous ultrasound is never warranted. If there is a discrepancy between the gestational age assessments of two ultrasound examinations, considering explanations such as intrauterine growth restriction (IUGR), macrosomia or other pathological conditions may be appropriate.

ULTRASOUND PITFALLS

Recent advances in ultrasound image quality and the wide availability of accurate biometric formulas have greatly improved physicians' ability to calculate gestational age. However, properly dating a pregnancy sonographically still depends on adherence to good ultrasound technique. Obtaining a clear and precise image of each biometric indicator is essential. Errors in estimation may arise from technical difficulties including obtaining the proper axis for measurement, movement of the mother or fetus, machine sensitivity settings or caliper placement. If a certain biometric indicator is not well visualized or is difficult to measure, it is better to use an alternative indicator rather than include a suboptimal measurement. In addition, it is helpful to obtain several measurements of each indicator and use an average to ensure a more precise calculation of fetal age.

CONCLUSION

Knowledge of gestational age is of great importance in obstetric practice. Optimal assessment requires good judgment by the obstetrician caring for the patient. Since clinical data such as the menstrual cycle or uterine size are often not reliable, the most precise parameter for pregnancy dating should be determined by the obstetrician early in the pregnancy. Ultrasound is an accurate and useful modality for the assessment of gestational age in the first and second trimester of pregnancy and, as a routine part of prenatal care, can greatly impact obstetric management and improve antepartum care.

REFERENCES

1. Hall MH, Carr-Hill RA. The significance of uncertain gestation for obstetric outcome. Br J Obstet Gynaecol. 1985; 92(5):452-60.
2. Kramer MS, McLean FH, Boyd ME, et al. The validity of gestational age estimation by menstrual dating in term, preterm and post-term pregnancies. JAMA. 1988;260(22):3306-8.
3. Walker EM, Lewis M, Cooper W, et al. Occult biochemical pregnancy: fact or fiction? Br J Obstet Gynaecol. 1988;95(7): 659-63.
4. Chiazze L Jr, Brayer FT, Macisco JJ Jr, et al. The length and variability of the human menstrual cycle. JAMA. 1968; 203(6):377-80.
5. Campbell S, Warsof SL, Little D, et al. Routine ultrasound screening for the prediction of gestational age. Obstet Gynecol. 1985;65(5):613-20.
6. Robinson HP. Gestational age determination: first trimester. In: Chervenak FA, Isaacson GC, Campbell S (Eds). Ultrasound in Obstetrics and Gynecology. Boston: Little, Brown and Company; 1993. pp. 295-304.
7. Beazley JM, Underhill RA. Fallacy of the fundal height. Br Med J. 1970;4(5732):404-6.
8. Kalish RB, Chervenak FA. Ultrasound assessment of gestational age. Optimal Obstetrics. 2002;1:1-6.
9. Campbell S. The prediction of fetal maturity by ultrasonic measurement of the biparietal diameter. J Obstet Gynaecol Br Commonw. 1969;76(7):603-6.
10. Hadlock FP, Deter RL, Harrist RB, et al. Estimating fetal age: computer assisted analysis of multiple fetal growth parameters. Radiology. 1984;152(2):497-501.
11. Ott WJ. Accurate gestational dating revisited. Am J Perinatol. 1994;11(6):404-8.
12. Kurtz AB, Wapner RJ, Kurtz RJ, et al. Analysis of biparietal diameter as an accurate indicator of gestational age. J Clin Ultrasound. 1980;8(4):319-26.
13. Mul T, Mongelli M, Gardosi J. A comparative analysis of second-trimester ultrasound dating formulas in pregnancies conceived with artificial reproductive techniques. Ultrasound Obstet Gynecol. 1996;8(6):397-402.
14. Campbell S, Newman GB. Growth of the fetal biparietal diameter during normal pregnancy. J Obstet Gynaecol Br Commonw. 1971;78(6):513-9.
15. Persson PH, Weldner BM. Reliability of ultrasound fetometry in estimating gestational age in the second trimester. Acta Obstet Gynecol Scand. 1986;65(5):481-3.
16. Kalish RB, Thaler HT, Chasen ST, et al. First- and second-trimester ultrasound assessment of gestational age. Am J Obstet Gynecol. 2004;191(3):975-8.
17. Goldstein I, Zimmer EA, Tamir A, et al. Evaluation of normal gestational sac growth: appearance of embryonic heartbeat and embryo body movements using the transvaginal technique. Obstet Gynecol. 1991;77(6):885-8.
18. Yeh HC, Rabinowitz JG. Amniotic sac development: ultrasound features of early pregnancy-the double bleb sign. Radiology. 1988;166:97-103.
19. Selbing A. Gestational age and ultrasonic measurement of gestational sac, crown-rump length and biparietal diameter during the first 15 weeks of pregnancy. Acta Obstet Gynecol Scand. 1982;61(3):233-5.
20. Bernaschek G, Rudelstorfer R, Csaicsich P. Vaginal sonography versus human chorionic gonadotropin in early detection of pregnancy. Am J Obstet Gynecol. 1988;158(3 Pt. 1):608-12.
21. Kohorn EI, Kaufman M. Sonar in the first trimester of pregnancy. Obstet Gynecol. 1974;44(4):473-83.
22. Donald I, Abdulla U. Ultrasonics in obstetrics and gynaecology. Br J Rad. 1967;40:604-11.
23. Hellman LM, Kobayashi M, Fillitri L, et al. Growth and development of the human fetus prior to the twentieth week of gestation. Am J Obstet Gynecol. 1969;103(6):789-800.
24. Nyberg DA, Filly RA, Mahony BS, et al. Early gestation: correlation of HCG levels and sonographic identification. AJR. 1985;144(5):951-4.
25. De Crispigny LC, Cooper D, McKenna M. Early detection of intrauterine pregnancy with ultrasound. J Ultrasound Med. 1988;7(3):7-10.
26. Warren WB, Timor-Tritsch I, Peisner DB, et al. Dating the early pregnancy by sequential appearance of embryonic structures. Am J Obstet Gynecol. 1989;161(3):747-53.

27. Steinkampf MP, Guzick DS, Hammond KR, et al. Identification of early pregnancy landmarks by transvaginal sonography: analysis by logistic regression. Fertility and Sterility.1997;68(1):168-70.
28. Robinson HP, Fleming JE. A critical evaluation of sonar "crown-rump length" measurements. Br J Obstet Gynaecol. 1975;82(9):702-10.
29. Daya S. Accuracy of gestational age estimation by means of fetal crown-rump length measurement. Am J Obstet Gynecol. 1993;168(3 Pt. 1):903-8.
30. MacGregor SN, Tamura RK, Sabbagha RE, et al. Underestimation of gestational age by conventional crown-rump length curves. Obstet Gynecol. 1987;70(3 Pt. 1):344-8.
31. Filly RA, Hadlock FP. Sonographic determination of menstrual age. In: Callen PW (Ed). Ultrasonography in Obstetrics and Gynecology. Philadelphia: WB Saunders; 2000. pp. 146-70.
32. Wisser J, Dirschedl P, Krone S. Estimation of gestational age by transvaginal sonographic measurement of greatest embryonic length in dated human embryos. Ultrasound in Obstetrics and Gynecology. 1994;4(6):457-62.
33. Drumm JE, Clinch J, MacKenzie G. The ultrasonic measurement of fetal crown-rump length as a method of assessing gestational age. Br J Obstet Gynaecol. 1976;83(6): 417-21.
34. Ewigman BG, Crane JP, Frigoletto FD, et al. Effect of prenatal ultrasound screening on perinatal outcome. N Engl J Med. 1993;329(12):821-7.
35. Chervenak FA, McCullough LB. Should all pregnant women have an ultrasound examination? Ultrasound Obstet Gynecol. 1994;4(3):177-9.
36. Whitworth M, Brisker L, Neilson JP, et al. Ultrasound for fetal assessment in early pregnancy. Cochrane Database Syst Rev. 2010;(4):CD007058. (PMID 20393955).
37. Taipale P, Hiilesmaa V. Predicting delivery date by ultrasound and last menstrual period in early gestation. Obstet Gynecol. 2001;97(2):189-94.
38. Campbell S. Gestational age determination: second trimester. In: Chervenak FA, Isaacson GC, Campbell S (Eds). Ultrasound in Obstetrics and Gynecology. Boston:Little, Brown and Company; 1993. pp. 305-10.
39. Hadlock FP, Deter RL, Harrist RB, et al. Fetal head circumference: relation to menstrual age. Am J Radiol. 1982;138(4): 649-53.
40. Hadlock FP, Deter RL, Harrist RB, et al. Fetal abdominal circumference as a predictor of menstrual age. Am J Radiol. 1982;139(2):367-70.
41. O'Brien G, Queenan JT, Campbell S. Assessment of gestational age in the second trimester by real-time ultrasound measurement of the femur length. Am J Obstet Gynecol. 1981;139(5):540-5.
42. Mercer BM, Sklar S, Shariatmadar A, et al. Fetal foot length as a predictor of gestational age. Am J Obstet Gynecol. 1987;156(2):350-5.
43. Chitkara U, Lee L, El-Sayed YY, et al. Ultrasonographic ear length measurement in normal second- and third-trimester fetuses. Am J Obstet Gynecol. 2000;183(1):230-4.
44. Mayden KL, Tortora M, Berkowitz RL, et al. Orbital diameters: a new parameter for prenatal diagnosis and dating. Am J Obstet Gynecol. 1982;144(3):289-97.
45. Goldstein I, Tamir A, Zimmer EZ, et al. Growth of the fetal orbit and lens in normal pregnancies. Ultrasound Obstet Gynecol. 1998;12(3):175-9.
46. Davies MW, Swaminathan M, Betheras FR. Measurement of the transverse cerebellar diameter in preterm neonates and its use in assessment of gestational age. Australasian Radiology. 2001;45(3):309-12.
47. Smith PA, Johansson D, Tzannatos C, et al. Prenatal measurement of the fetal cerebellum and cisterna cerebellomedullaris by ultrasound. Prenat Diagn. 1986;6(2):133-41.
48. Chervenak FA, Skupski DW, Romero R, et al. How accurate is fetal biometry in the assessment of fetal age? Am J Obstet Gynecol. 1998;178(4):678-87.
49. Benson CB, Doubilet PM. Sonographic prediction of gestational age: accuracy of second- and third-trimester fetal measurements. AJR. 1991;157(6):1275-7.
50. Manning FA. General principles and applications of ultrasonography. In: Creasy RK, Resnik R (Eds). Maternal-Fetal Medicine. Philadelphia: WB Saunders Company; 1999. pp. 169-206.
51. Goldstein RB, Filly RA, Simpson G. Pitfalls in femur length measurements. J Ultrasound Med. 1987;6(4):203-7.
52. Doubilet PM, Benson CB. Improved prediction of gestational age in the late third trimester. J Ultrasound Med. 1993;12(11):647-53.
53. Geirsson RT. Ultrasound: the rational way to determine gestational age. Fetal and Maternal Medicine. 1997;9(3):133-46.
54. Geirrson RT, Have G. Comparison of actual and ultrasound estimated second trimester gestational length in in-vitro fertilized pregnancies. Acta Obstet Gynecol Scand. 1993;72(5):344-6.
55. Geirrsson RT. Ultrasound instead of last menstrual period as the basis of gestational age assignment. Ultrasound Obstet Gynecol. 1991;1(3):212-9.
56. Mul T, Mongelli M, Gardosi J. A comparative analysis of second trimester ultrasound dating formulas in pregnancies conceived with artificial reproductive techniques. Ultrasound Obstet Gynecol. 1996;8(6):397-402.

11
CHAPTER

Trophoblastic Diseases

Kazuo Maeda, Asim Kurjak, Gino Varga, Ulrich Honemeyer

INTRODUCTION

Although trophoblastic diseases were frequent in East Asia in the past, choriocarcinoma is rare at present after the introduction of effective chemotherapy and postmolar management in Japan. Molar pregnancy is also decreased, possibly due to ultrasound diagnosis and termination in early pregnancy. Outcome of disease has greatly improved by ultrasound diagnosis including real-time B-mode, color/power Doppler flow images and pulsed Doppler tumor blood flow studies.

CLASSIFICATION, DEVELOPMENT AND PATHOLOGY

Trophoblastic diseases are grossly classified into gestational trophoblastic disease and nongestational choriocarcinoma. Gestational diseases are pathologically classified[1] into hydatidiform mole, choriocarcinoma and placental site trophoblastic tumor (PSTT) and epithelioid trophoblastic tumor (ETT). There is also persistent trophoblastic disease that is a particular clinical entity. Hydatidiform mole is subdivided into complete mole, partial mole and invasive mole. There is definite outcome difference between choriocarcinoma and invasive mole which are classified by pathological changes in spite of their symptomatic resemblance. There are also clinical NCL (National Cancer Institute)/NIH (National Institute of Health) classification and FIGO (Federation internatiole de gynecolgoe et d' obstetrique) staging **(Table 11.1)**.

TABLE 11.1

Pathological classification of trophoblastic diseases[1]

- Gestational trophoblastic disease
- Hydatidiform mole
- Complete hydatidiform mole
- Partial hydatidiform mole
- Invasive hydatidiform mole
- Choriocarcinoma
- Placental site trophoblastic tumor (PSTT)
- Persistent trophoblastic disease (PTD)
- Nongestational choriocarcinoma

COMPLETE HYDATIDIFORM MOLE

Complete (total) hydatidiform mole is an abnormal pregnancy, where placental villi change into molar vesicles, there is neither embryo or fetus, nor umbilical cord **(Fig. 11.1)**. Amnion is, however, found in some cases.[2] No capillary vessel is found in molar vesicles covered by proliferated trophoblasts. With an intravascular mole the vesicles spread into blood vessels. The metastasis rarely appears in distant organs.

The chromosome is usually diploid 46, XX, where the XX are both of male origin (androgenesis) and the mechanism is two X sperms fertilized in a vacant ovum without a nucleus[3] or single X is fertilized and divided into two after the fertilization. The chromosome is rarely 46, XY, where X and Y are of male origin.[4] Complete

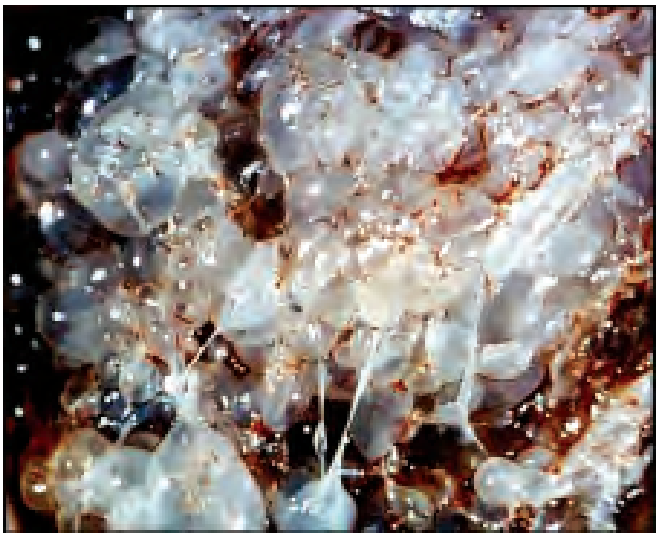

Figure 11.1: Molar vesicles in a complete hydatidiform mole *in situ* in the uterus

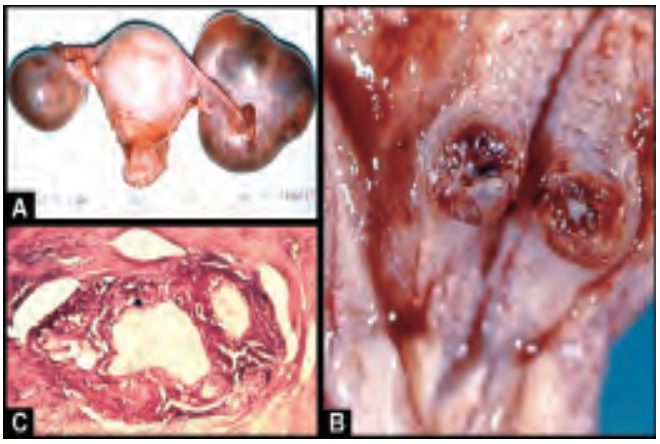

Figures 11.3A to C: (A) A case 01 invasive mole in removed uterus and theca lutein cysts before 1960; (B) Invaded molar vesicle was found in the myometrium and (C) Histology was invasive—mole surrounded by proliferated trophoblasts

mole can also develop in one of the twins or triplets. The risk of repeated mole is less than 1%, while it is not indicated for chemotherapy.[5] Telomerase activity in complete mole may progress to an invasive mole or choriocarcinoma.[6]

Ovarian theca lutein cysts are frequent in developed complete mole and invasive moles **(Figs 11.3A to C)**, while its incidence is low in the first trimester.[7] Since the lutein cyst is not a trophoblastic disease and disappears after remission, surgical removal is not appropriate.

PARTIAL HYDATIDIFORM MOLE

A partial hydatidiform mole is partial change of placental villi into molar vesicles, associated with embryo, fetus or fetal parts **(Figs 11.2A and B)**. Fetal anomalies are common. Chromosomes are usually triploids, 69, XXX, 69, XXY or 69, XYY.[8] DNA analysis confirmed the androgenic mechanism.[9] Capillary vessels are found in the interstitium of molar vesicles.

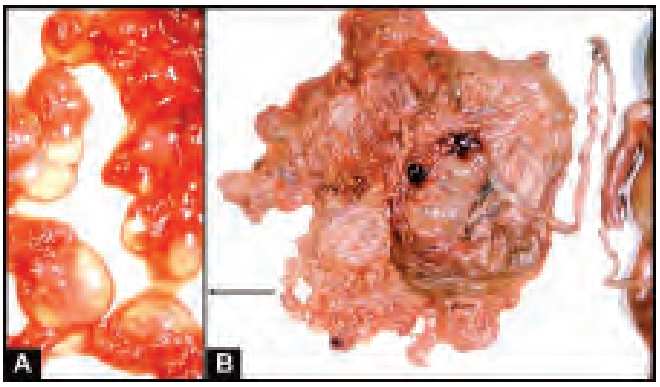

Figures 11.2A and B: Partial hydatidiform mole in the placenta with an anomalous fetus in six months of pregnancy. Left enclosed figure is of enlarged molar vesicles

INVASIVE HYDATIDIFORM MOLE

Invasive hydatidiform mole is the invasion of molar vesicles into the myometrium with destruction and hemorrhage. The lesion is found either in total or partial moles, usually after molar evacuation. The change is visually noted in a surgical specimen and microscopically confirmed, where the trophoblasts proliferate, hemorrhage and necrosis occur in the myometrium **(Figs 11.3A to C)**. An invasive mole rarely metastasized and has low malignancy, e.g. pulmonary focus spontaneously disappeared after hysterectomy in an invasive mole case. The outcome is more favorable than choriocarcinoma.

CHORIOCARCINOMA

Choriocarcinoma is solid trophoblastic tumor developed primarily in the myometrium **(Figs 11.4A to D)** or in distant organs and tissues,[10-15] usually after the removal of a complete or partial hydatidiform mole and also infrequently after abortion or normal delivery. They are defined as gestational choriocarcinoma or trophoblastic disease (GTD). Nongestational choriocarcinoma develops from germ cells in the ovary[10] or testis, or from other cancer cells. Primary choriocarcinomas are also reported in reproductive as well as in nonreproductive organs, e.g. vulva,[11] uterine cervix,[12] lung, stomach,

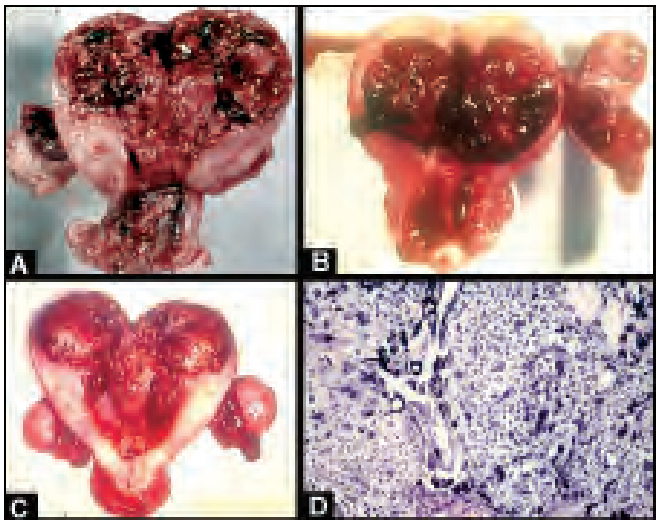

Figures 11.4A to D: (A to C) Three cases of choriocarcinoma surgically removed around at 1960 before the introduction of effective chemotherapy. The color of intrauterine tumor was dark red characteristic in the choriocarcinoma; (D) Histology of choriocarcinoma where syncytio and cytotrophoblasts actively proliferated but no villus pattern was detected

pancreas,[13,14] gallbladder[15] and urinary bladder.[16] Uterine cervical choriocarcinoma was also experienced.[17] Choriocarcinoma is constructed of syncytia and cytotrophoblasts and shows no villus pattern at all **(Figs 11.4A to D)**. Since the villus pattern is a characteristic sign of an invasive mole **(Figs 11.3A to C)** and its outcome is less ominous than choriocarcinoma, microscopic studies should be detailed on the whole specimen if the uterus is removed.

Widespread distant metastases of choriocarcinoma was common before the introduction of effective chemotherapy. The interval of diagnosis and metastasis was about half to one year. Early metastases were dark red tumors on the external genitalia and vaginal wall. Subsequent frequent spread was the lung, where typical radiographic foci showed round shapes of various sizes **(Figs 11.5A to G)**, while a diffuse pulmonary shadow is found in multiple trophoblast emboli in pulmonary arterioles. Organs or tissues were affected after pulmonary metastasis, e.g. skin,[18] subcutaneous tissue, intestine, liver, spleen, kidney, heart,[19,20] spinal cord, coronary artery[21] and finally in brain **(Figs 11.5A to G)**. Every organ is damaged by the trophoblasts and hemorrhage. Patients died from brain and multiple

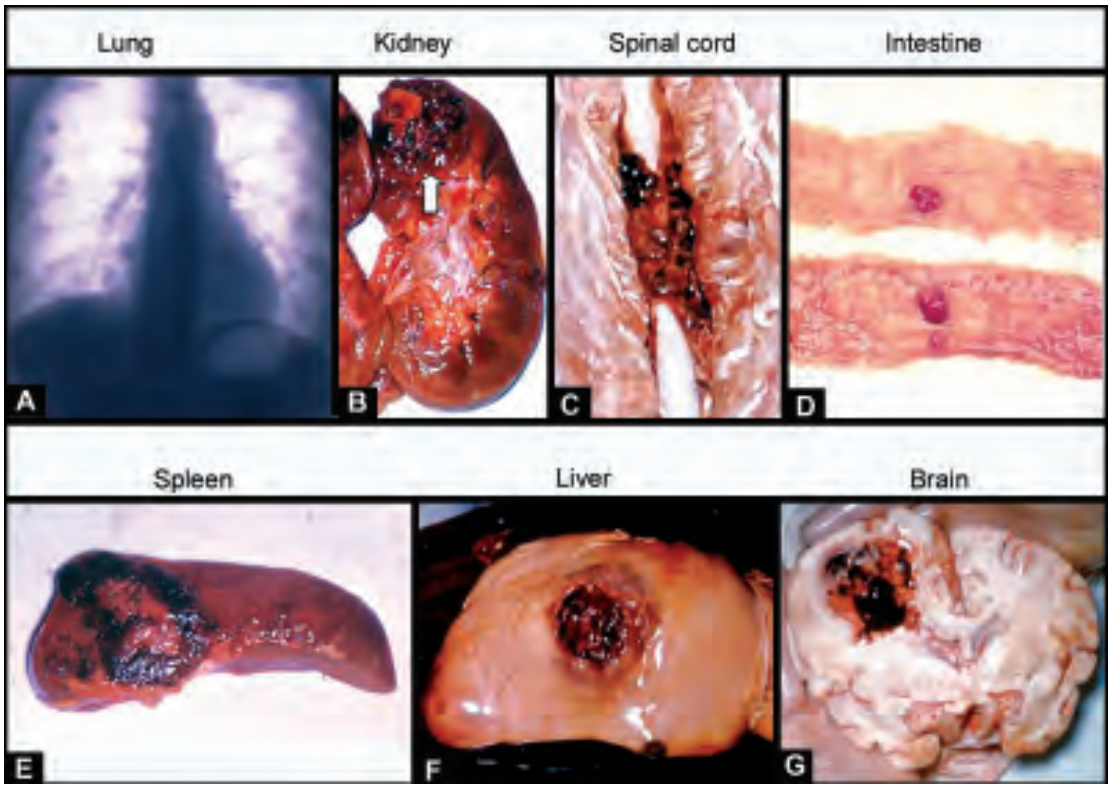

Figures 11.5A to G: Radiogram shows typically round foci of choriocarcinoma metastases. Dark red choriocarcinoma metastases in the lung, kidney, spinal cord, intestine, spleen, liver and brain (photographed after autopsies)

metastases due to damage and dysfunction occurring before effective chemotherapy.

Choriocarcinomas are divided into three subtypes:

1. Gestational choriocarcinoma
2. Nongestational choriocarcinoma
3. Unclassified choriocarcinoma.

1. Gestational choriocarcinoma is related to pregnancy and three categories are further classified:
   a. Uterine choriocarcinoma is the most common, which develops in the uterus after a hydatidiform mole and rarely after abortion or normal delivery. Choriocarcinoma with an intact pregnancy has been reported.[22]
   b. Extrauterine choriocarcinoma develops primarily at the place of ectopic pregnancy; there is no tumor in the uterus.
   c. Intraplacental choriocarcinoma is found in the placenta mainly after delivery. These cases were reported to be associated with viable pregnancy.[23]
2. Nongestational choriocarcinoma is divided into two categories:
   a. Choriocarcinoma of germ cell origin is a subtype of the germ cell tumor which develops in the ovary of the woman before marriage or the testis of an adult male. This tumor is more resistant to chemotherapy than a gestational tumor.
   b. Choriocarcinoma derived from other carcinomas involves choriocarcinomatous change of other cancers that may excrete human chorionic gonadotropin (hCG).
3. Unclassified choriocarcinoma is unclassified into gestational or nongestational.

PLACENTAL SITE TROPHOBLASTIC TUMOR

The placental site trophoblastic tumor (PSTT) is a rare uterine tumor of proliferated intermediate trophoblasts.[24] The tumor is preceded by a hydatidiform mole, abortion or delivery. The levels of hCG arc low and the human placental lactogen (HPL) is higher than β-hCG.[25] Final diagnosis is made by histological study. Metastasis and recurrence are commonplace.[24-28] A case of PSTT was reported in both mother and child.[29] PSTT produces less β-hCG and is less sensitive to chemotherapy. More than half of patients present with disease confined in the uterus and the remainder present with disease extension beyond the uterus. Simple hysterectomy is the mainstay of treatment. The outcome of patients with disease confined in the uterus is usually excellent, while most patients with the extension beyond the uterus experience progression of disease and die despite surgery and intense chemotherapy. Other adverse prognostic factors are, interval from gestational events is more than two years, age is more than 40 years and mitotic count is higher than 5 mf/10 HPF. The EP/EMA regimen seems to be the most effective chemotherapy.[30] In another report[31] of 55 PSTT cases, statistically significant adverse survival factors were over 35 years of age, interval since the last pregnancy over two years, deep myometrial invasion, stage III or IV, maximum hCG level more than 1000 mIU/ml, extensive coagulative necrosis, high mitotic rate and the presence of cells with clear cytoplasm.

EPITHELIOID TROPHOBLASTIC TUMOR

The epithelioid trophoblastic tumor (ETT) is rare trophoblastic disease which represented vaginal bleeding, associated with a gestational event. Serum hCG was elevated. Two out of fourteen presented extrauterine lesions in the uterus. ETT was presented as a discrete, hemorrhagic solid and cystic lesion. Microscopically, it was composed of intermediate trophoblastic cells forming nests and solid masses; typically islands of trophoblastic cells were surrounded by necrotic masses; mean mitosis was 2/10 HPF; it was immunohistochemically positive for inhibin-alpha, cytokeratin, hPL, placental alkaline phosphatase and Mel-CAM(CD- 148),[32] its monomorphic growth pattern was more close to PSTT than choriocarcinoma. ETT grows in a nodular fashion compared to the infiltrative pattern of PSTT; it appears to be less aggressive than choriocarcinoma, more closely resembling to the behavior of PSTT, where histological and immunohistochemical features were characteristic of EPTT,[33] although a report[34] included ETT in the category of PSTT.

PERSISTENT TROPHOBLASTIC DISEASE

The persistent trophoblastic disease (PTD) is a postmolar metastatic mole, disseminated trophoblasts in tissues, invasive mole or choriocarcinoma; no specimen has been obtained and a pathological finding is unknown.

Postmolar Persistent hCG

It shows abnormal type II hCG regression pattern after the hydatidiform mole, i.e. urinary hCG greater than 100 mlU/ml after 5 weeks, serum hCG greater than 100 mlU/ml after 8 weeks, or serum hCG greater than

β 1.0 mIU/ml (hCG β CTP 0.5 mIU/ml) after 20 weeks, where the focus is unknown.

Clinical Invasive Mole or Metastatic Mole

It is estimated by the modified Ishizuka[1] scoring system or by the suspected focus.

Clinical Choriocarcinoma

It is estimated from the Ishizuka scoring system, suspected focus or by the postmolar state where hCG levels elevate again after complete remission; this is confirmed by lower than cut-off hCG level, except for new pregnancies.

SYMPTOMS OF GESTATIONAL TROPHOBLASTIC DISEASE

Complete Hydatidiform Mole

Typical symptoms of well-developed complete hydatidiform moles are hyperemesis, hypertension, no fetal movement, no fetal heart beat with Doppler detector, larger uterus than in normal pregnancy, abdominal pain, hemorrhage after amenorrhea, expelled molar vesicles and urinary hCG levels usually higher than 100,000 mIU/ml. Typical symptoms are infrequently detected by ultrasonic screening in the first trimester of pregnancy; with transvaginal scan, an early stage hydatidiform mole can be detected and evacuated before its development. Ovarian theca lutein cysts are also detected by ultrasound.

Partial Hydatidiform Mole

Symptoms of the mole associated with living fetus are similar to common pregnancy except for hyperemesis, enlarged uterus and high titer hCG. Ultrasonic screening of pregnancy detects partial molar changes of the placenta with the embryo, fetus or fetal particles being present. Twenty percent of complete moles are followed by sequelae and choriocarcinoma develops in 2% of cases with a complete mole, whereas partial moles show sequelae in 5% of cases and rarely progress to choriocarcinoma.[25]

Invasive Hydatidiform Mole

An invasive mole is found after a mole and presents with vaginal bleeding, enlarged uterus, bilaterally enlarged ovaries and high urinary or serum hCG levels. The symptoms resemble those of choriocarcinoma and differential diagnosis is needed. The interval from antecedent molar pregnancy is usually within half a year and it is shorter than choriocarcinoma. Urinary hCG is continuously elevated after molar curettage, but the titer is lower than choriocarcinoma. Ultrasonic study discloses the presence of molar vesicles in the myometrial mass.

Choriocarcinoma

Gestational choriocarcinoma is usually preceded by a molar pregnancy and rarely by abortion or term delivery. The interval from antecedent pregnancy can be longer than 1 year and longer than with an invasive mole. There may be a period of partial remission and it can exist for more than 10 years as an extrauterine choriocarcinoma. The symptoms are vaginal bleeding, enlarged uterus, high hCG titer, ovarian masses and irregular basal body temperature (BBT). Choriocarcinoma is often diagnosed by the presence of metastasis. Multiple pulmonary foci show the progress of malignancy. The hCG titer should be checked even in nongynecological cases when pulmonary round foci are found in the female patient. The symptoms resulting from distant metastases suggest choriocarcinoma, e.g. abdominal pain and hemorrhage in hepatic lesion, or persistent headache and vomiting followed by unconciousness and apnea in the brain metastasis.

Placental Site Trophoblastic Tumor

It can be preceded by any gestational process. Enlarged uterus and vaginal bleeding are the clinical symptoms. Metastasis is frequent. The disease often recurs after treatment. PSTT is malignant and can be fatal.[25]

Persistent Trophoblastic Disease

It includes postmolar hCG persistence, clinically invasive or metastatic moles choriocarcinoma. Although the focus is unknown, all three show persistence of abnormally high hCG titers.

DIAGNOSIS OF GESTATIONAL TROPHOBLASTIC DISEASE

Complete Hydatidiform Mole

Complete hydatidiform mole is diagnosed by symptoms, such as high urinary and serum hCG titers, and particularly by ultrasonic B-mode, color Doppler and Doppler flowmetry. Transvaginal scan is useful in the first trimester. Ultrasonic B-mode detects molar vesicles in the uterine cavity without detecting a fetus or embryo or its particles **(Figs 11.6A and B)**. Amniotic membrane and fluid are, however, occasionally detected by the B-

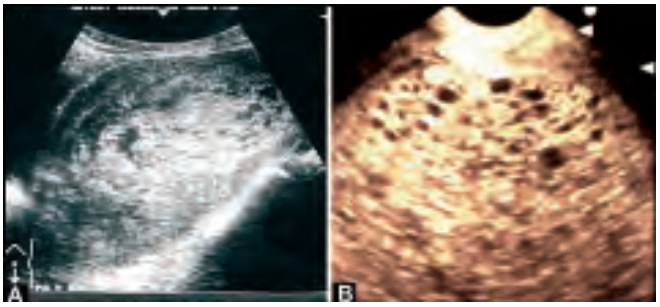

Figures 11.6A and B: Typical vesicular images in grown-up complete moles imaged by real-time B-mode
Courtesy: (A) M Utsu Seirei Mikatahara Hospital, Japan (11 weeks of pregnancy); (B) S Kupesic, University of Zagreb, (Croatia)

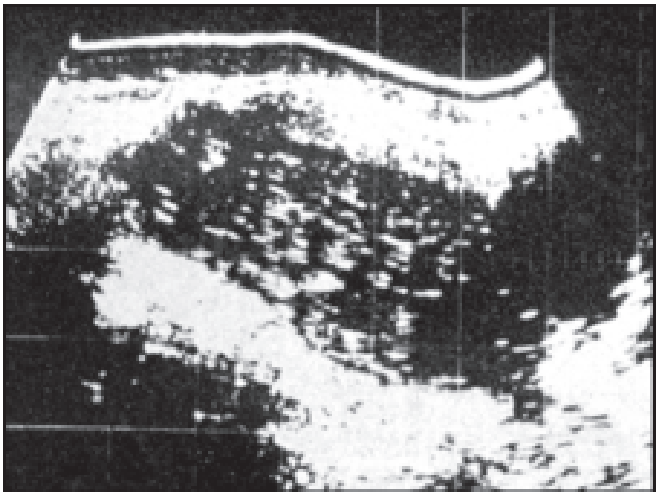

Figure 11.7: Erroneous artifact of complete hydatidiform mole imaged by contact-compound scan B-mode in old time. It was called "snow-storm pattern" which was thought typical image of complete mole in old time but a heavy artifact caused by bad resolution of old transducer of single unit without suitable focusing. Modern real-time scanner does not produce snow-storm pattern but round vesicular images in the mole

mode. A characteristic molar pattern is composed of multiple small cysts, but not a snowstorm pattern **(Fig. 11.7)** with a modern real-time B-mode device.

Characteristic changes are found in complete hydatidiform moles by various ultrasonic imaging techniques.

Real-Time B-Mode

A complete hydatidiform mole is detected in its early stages by screening during the first trimester. An empty gestational sac, where the wall showed small cystic changes without an embryo was ultrasonically detected before typical growth of the complete hydatidiform

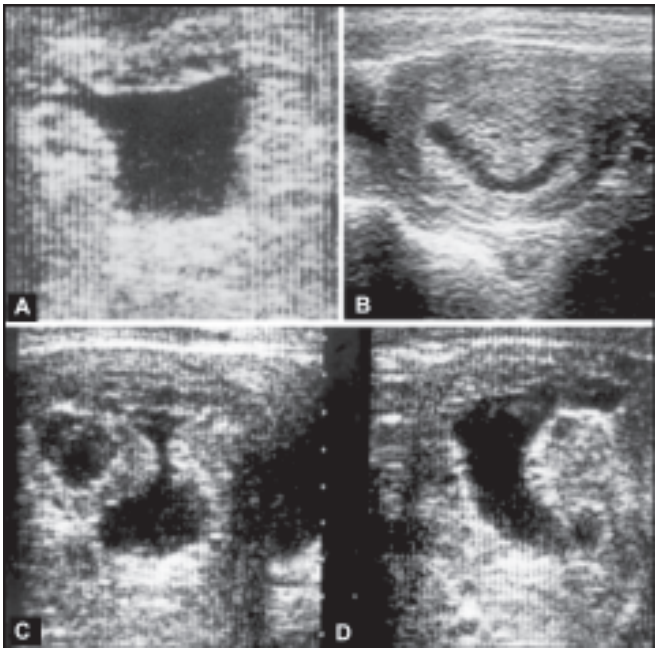

Figures 11.8A to D: (A and B) Complete molar images detected by real-time 8-mode in early first trimester resembled a blighted ovum. Empty but thick gestational sac without embryo nor yolk sac was characteristic; (C and D) The chorion became thick and irregular, then produced molar vesicles in the irregular mass 2–3 weeks later.

The specimen of atypical blighted ovum should be carefully examined by histology after currettages and suspicious cases should be monitored by urinary hCG and transvaginal scan 8-mode

mole **(Figs 11.8A to D)**. An early complete mole resembles a blighted ovum, whereas vomiting and high urinary hCG titer of molar case are contradictory to the presence of a blighted ovum. The chorionic plate thickness increases and typical molar cysts develop within 1–2 weeks in early pregnancy. Complete hydatidiform mole develops in one of the twins or triplets. It is diagnosed by the septum that has originated from the fetus **(Figs 11.9 and 11.10)**. A partial mole in a singleton pregnancy is differentiated from the complete mole of a multiple pregnancy by the partial molar change of the placental villi without separating the septum, or by the presence of triploid chromosome.

Color and Power Doppler Flow Mapping

The diagnosis of molar pregnancy is difficult with simple B-mode when the uterine cavity is filled with homogeneous image without typical vesicular changes. The difficulty may be caused by identical ultrasonic density of molar vesicles to that of intervesicular blood. The two materials, molar vesicles and the blood are

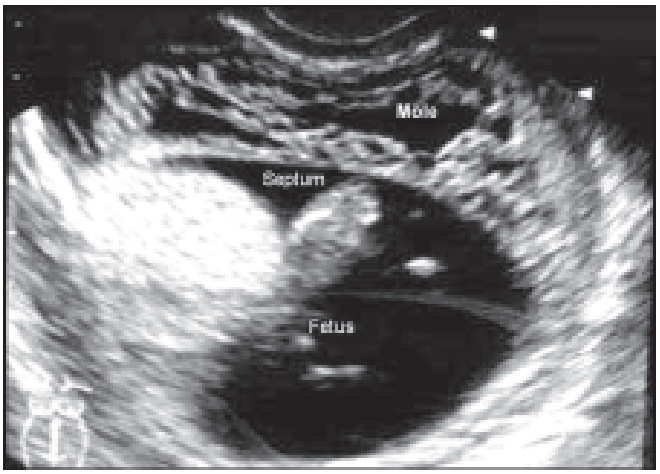

Figure 11.9: Complete mole of a twin is differentiated from partial mole by the clear formation of the septum between the fetus and molar vesicles in the 8-mode examination of twin pregnancy
Courtesy: M Utsu, Japan

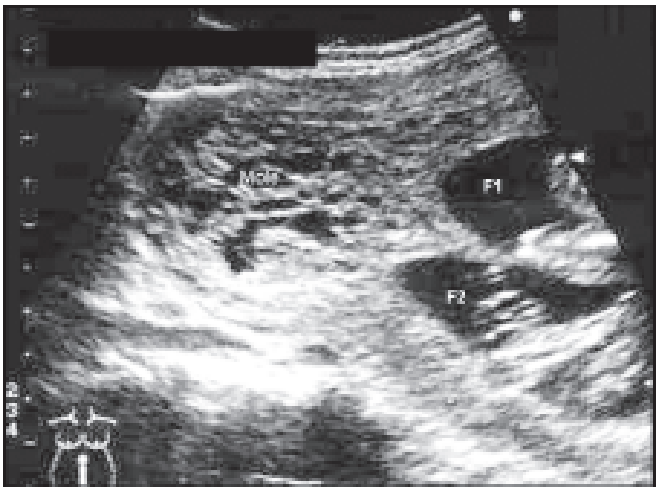

Figure 11.10: The complete mole in a triplet pregnancy was also determined by the clear septum between the mole and other fetuses
Courtesy: M Utsu, Japan

unable to be differentiated in the case. The detection of blood flow in the uterine cavity in complete molar pregnancy is the answer to the difficult diagnosis with real-time B-mode. A complete hydatidiform mole was studied by 2D color Doppler, power Doppler, pulsed Doppler flow wave with flow impedance and by 3D power Doppler flow mapping.

The static color Doppler flow mapping visualized rich color flow pattern of various direction in the uterine cavity without detecting fetal or placental blood flow. The color pattern was almost stable in the repeated color

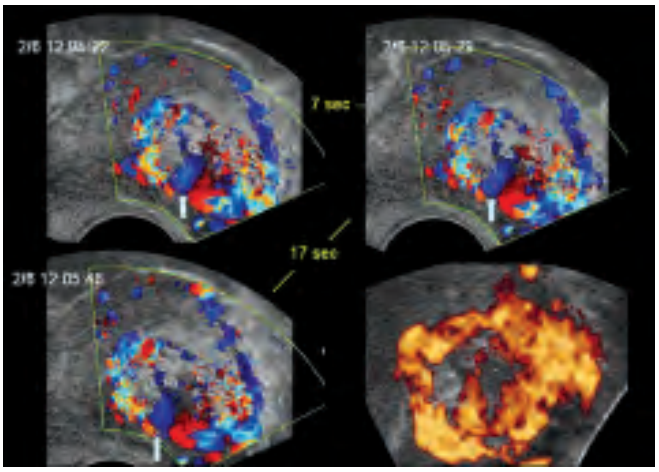

Figure 11.11: Three static color Doppler and power Doppler images were recorded in a complete hydatidiform mole. Color Doppler images were almost identical in spite of time differences, i.e. particular blood flow existed in the uterus. Red and blue color images suggested blood streams taking opposite directions, i.e. arterial jet stream into intervesicular spaces and venous drainage. Multiple small round images in the images can be molar vesicles. Power Doppler also showed rich intrauterine blood flow. The blue color flow (arrows) beated about 80 times per minute in the real-time color images. These findings are new diagnostic marker of complete hydatidiform mole
Courtesy: G Varga

Doppler images of which interval was 7 and 17 seconds, when ultrasound probe was held at fixed position. The fixed blood flow was confirmed in the uterus by the color images which probably show jet streams of spiral arteries located at the uterine wall and the draining of the blood into the vein located at the other part **(Fig. 11.11)**. Round low-intensity images found among the blood flow images indicated the presence of molar vesicles floated among maternal intrauterine blood flow. The real-time color Doppler flow mapping visualized a jet blood flow streaming into the uterine cavity of which pulse rate was about 80 beats/min. It was confirmed by pulsed Doppler arterial flow velocity wave, of which pulse rate was 83 beats/min **(Fig. 11.12)**.

Power Doppler now mapping detected molar vesicles more clearly and furthermore, 3D power Doppler image revealed rich intrauterine blood now **(Fig. 11.13)**. From these results, it was confirmed that 2D color and power Doppler flow image and 3D power Doppler image are new diagnostic technique of complete hydatidiform mole. Further, progress is expected in the flow characters of a hydatidiform mole by 4D ultrasound images.

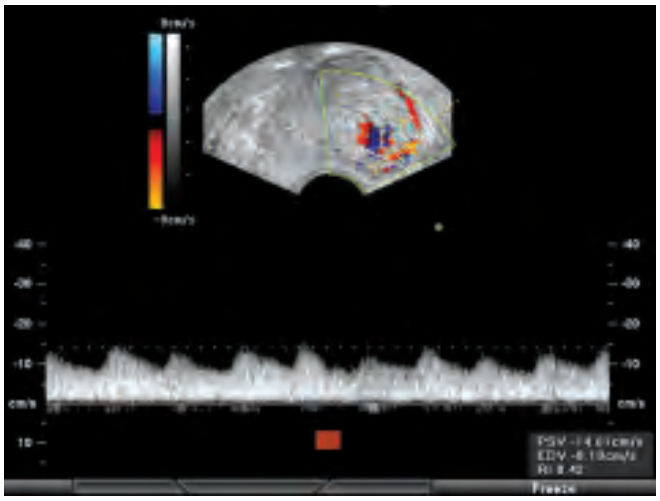

Figure 11.12: Pulsed Doppler flow velocity wave in the complete mole showed 83 beats/min flow which coincided with the real-time color Doppler observation. RI was as low as 0.42 and systolic flow velocity was as slow as 14 cm/sec *Courtesy:* G Varga

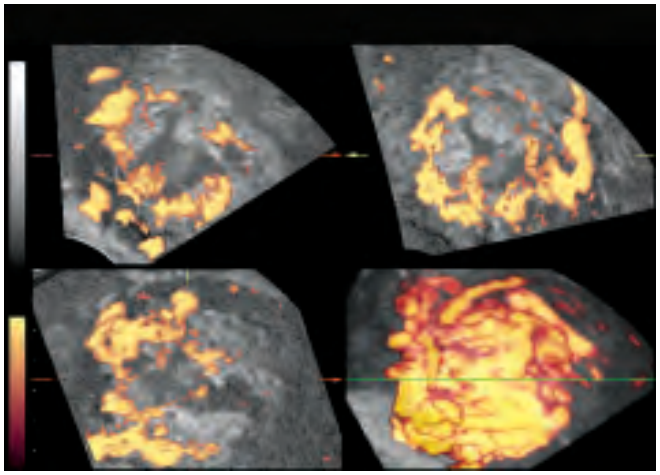

Figure 11.13: Orthogonal three planes of 2D power Doppler showed clear molar vesicles and the 3D power Doppler showed rich intreuterine blood flow of various directions. There was no image of the fetus or fetal blood flow or any fetal particle through all images of these Doppler studies *Courtesy:* G Varga

Pulsed Doppler Flow Wave and Flow Impedance

Diastolic flow is larger and the resistance index (RI) was lower in uterine, arcuate, radial and spiral arteries in the mole than in normal pregnancy.[35] Also, RI was low in the molar fIow.[36] In the present study, in the intervesicular space of the complete mole, peak systolic velocity of maternal arterial blood is as slow as 14 cm/sec and the RI is as low as 0.42 **(Fig. 11.12)**. Theoretically, fetal blood flow is not recorded, because there is no fetal capillary in the complete mole vesicle.

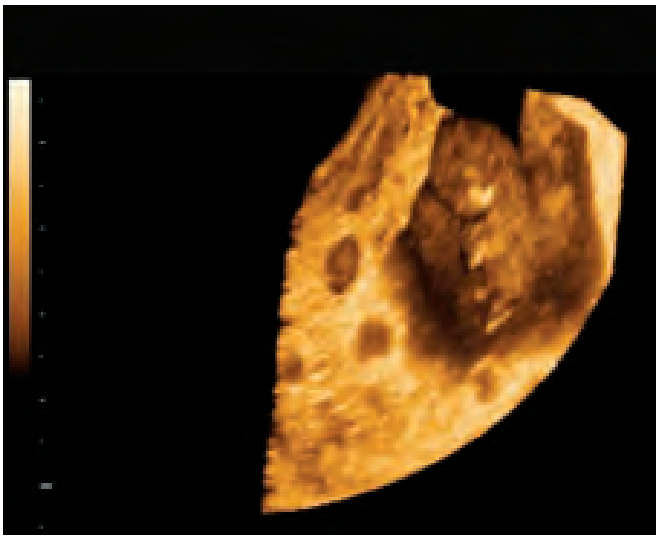

Figure 11.14: A partial hydatidiform mole was diagnosed by placental molar vesicles and a fetus by the 3D ultrasound *Courtesy:* JR Benitez, Clinics Gutenberg, Spain

hCG and Other Diagnostic Methods

Complete hydatidiform mole is estimated when urinary or serum hCG levels are higher than 10,000 mIU/ml, which is within the higher normal range of early pregnancy. A complete mole can, however, be present with lower hCG levels. The postmolar state is monitored every 1–2 weeks by hCG levels, ultrasound and local conditions after the mole removal by repeated curettages, until the hCG reaches a low cut-off level. Abnormal regression of hCG or persistent trophoblastic disease is treated with chemotherapy for the prophylaxis of choriocarcinoma.[37] Chromosomal diploidy and DNA analysis reports androgenic origin.

Partial Hydatidiform Mole

Partial hydatidiform mole is diagnosed by symptoms, such as high urinary hCG and presence of fetus, or the partial image of the fetus and partial changes of the placenta into molar vesicles. 3D ultrasound shows the diagnosis of a particle mole in early pregnancy **(Fig. 11.14)**. Anomalies are frequent in the fetus. Chromosomal examination shows triploidy. Postmolar changes of urinary and serum hCG are the same as with a complete hydatidiform mole. Chemotherapy in the case of abnormal regression and persistent trophoblastic disease is also the same as for a complete hydatidiform mole.

Invasive Hydatidiform Mole

Invasive hydatidiform moles are mainly found within half a year after the termination of a complete or partial

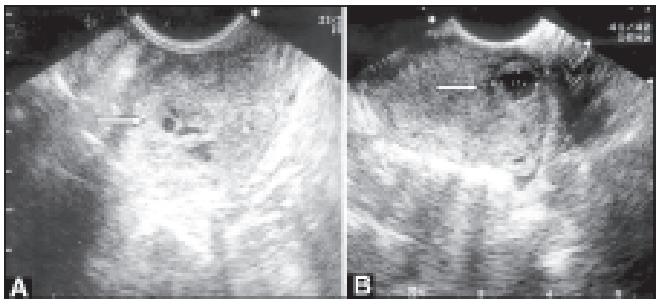

Figures 11.15A and B: Invasive mole was confirmed by the detection of cystic villus pattern-arrows—imaged by real-time B-mode ultrasound. Focus size was 1.23 × 0.88 cm in the right sonogram
Courtesy: S Yoshida, Tottori University Hospital, Japan

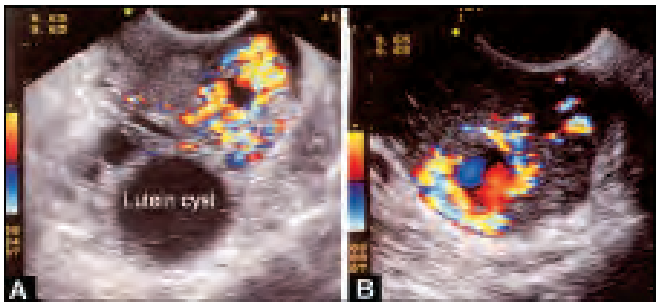

Figures 11.16A and B: Rich blood flow was detected by color Doppler flow mapping around the villus patterns of invasive mole. A theca lutein cyst was confirmed to be avascular in Figure 11.16A
Courtesy: S Yoshida

molar pregnancy, although the molar tissue can invade the myometrium during pregnancy. Myometrial invasion may be detected by detailed and hard study with B-mode and color or power Doppler flow mapping of the uterine wall before the termination.

The symptoms of invasive mole are similar to those of choriocarcinoma, i.e. postmolar development, vaginal bleeding, enlarged uterus and possible metastasis. Urinary or serum hCG is positive, but the levels are lower than with choriocarcinoma. Ultrasound B-mode shows a uterine mass. An invasive mole is usually diagnosed if molar cysts are imaged in the tumor **(Figs 11.15A and B)**. Rich blood flow is found by color flow mapping **(Figs 11.16A and B)** and power Doppler imaging. Flow impedance is low with an invasive mole. In contrast, flow impedance is high in the wall artery of a theca lutein cyst.

Gestational Choriocarcinoma

Gestational choriocarcinoma develops after a hydatidiform mole, abortion or normal delivery. Clinical symptoms are vaginal bleeding, enlarged uterus, ovarian masses, high hCG titer and is similar to an early stage invasive mole before metastasis. The interval of its development is usually more than half a year after the mole, and longer than that of an invasive mole which is mainly within half a year. Metastases are found in external genitalia and the vaginal wall in its early stage, and then in the lung. An invasive mole rarely develops the metastasis.

TABLE 11.2
Clinical differentiation of choriocarcinoma and invasive mole

	Choriocarcinoma	*Invasive mole*
Antecedent pregnancy	Mole, abortion, term delivery	Mole
Vaginal bleeding	Yes	Yes
Enlarged uterus	Yes	Yes
High hCG titer	Yes	Yes
Postmolar period	> 6 months, years, > 10 years	Usually < 6 months
Metastasis	Frequent and wide, until brain	Rare
Uterine B-mode image	Solid mass	Villus pattern
Pelvic angiography	Pooling focus	Villus pattern
Distr bution	Whole body, systemic disease	Local in the uterus
Outcome	Fatal without chemotherapy	Less malignant

Differential diagnosis of choriocarcinoma from an invasive mole is important, because the outcome is ominous in the former and less risky in the latter, in spite of the similarity of clinical symptoms **(Table 11.2)**. Ultrasonic detection of a cystic pattern in the focus **(Figs 11.15 and 11.16)** is decisive evidence for an invasive mole, while a cystic villus pattern is not detected by various ultrasound imaging techniques in a choriocarcinoma, while color Doppler flow mapping shows a rich blood flow **(Figs 11.17A and B)**. Flow impedance is usually low in both diseases, but it is lower in choriocarcinoma than in an invasive mole.[38] The RI of uterine artery is significantly lower in a choriocarcinoma than in a hydatidiform mole.[38] A differential gene expression pattern is reported between normal trophoblast and choriocarcinoma cells.[39] Although the risk was clinically suspected by FIGO staging, NIC/NIH classification, Ishizuka's and WHO's scoring tables, it is important to examine the trophoblastic disease with

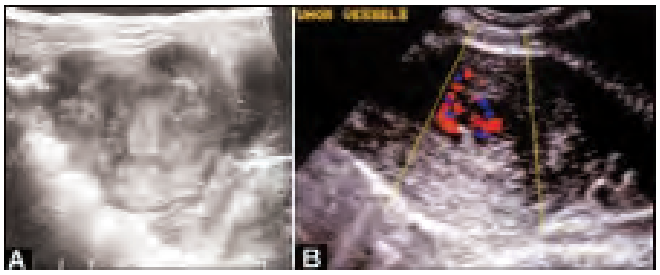

Figures 11.17A and B: There is no villus pattern in ultrasound images of choriocarcinoma
Courtesy: (A) B-mode—M Terahara, Imakyurei Hospital, Japan; (B) Color Doppler—S Kondo, Saitama University Hospital, Japan

objective imaging techniques, particularly with various ultrasound methods. Pelvic angiography has been used in the past, but ultrasound is an alternative to the angiography at present.

Nongestational Choriocarcinoma

Nongestational choriocarcinoma of germ cell origin develops in the ovary or testis without precedence of gestation. Urinary and serum hCG levels are positive and palpation and ultrasound imaging reveal the tumor. DNA polymorphism analysis is reported in pure nongestational choriocarcinoma.[40] Metamorphosed cancer to choriocarcinoma is diagnosed by its own symptoms and findings associated with hCG excretion.

Persistent Trophoblastic Disease

Since the persistent trophoblastic disease (PTD) patients receive chemotherapy that may lead to complete remission without surgical removal of the foci, no histological diagnosis is made and the clinical diagnosis is final in the case of complete remission.

Placental Site Trophoblastic Tumor

The long interval after antecedent gestation and symptoms including vaginal bleeding and enlarged uterus and the lack of high hCG titer, suggest the presence of the disease. Differential diagnosis from other malignant trophoblastic disease is required. Also, due to its rarity, the diagnosis tends to be incorrect. Final diagnosis is made by histology of the removed specimen. Other than common examination and B-mode, color Doppler documents indicated uterine vascularity that is characterized by low resistance flow, its persistence after the chemotherapy and negative plasma β-hCG. Serial transvaginal color Doppler is useful for monitoring chemotherapy and residual tumor.[41] Savelli, et al (2009)[42] reported a PSTT case who was 34-year-old woman who complained persistent vaginal bleeding and raised β-hCG (308–546 mIU/ml) 6 months after the 2nd cesarean section showed enlarged uterus, presence of inhomogeneous lesion with 3 cm diameter and ill defined outer borders by transvaginal ultrasound (TVS) and several blood vessels within the mass by power Doppler imaging. The RI imaging revealed similar intramyometrial mass. Histological diagnosis of violet colored tissue obtained by an operative hysteroscopy was PSTT. The patient underwent total laparoscopic hysterectomy and peritoneal washing which revealed no malignancy. The final diagnosis was PSTT confined within the uterus (FIGO stage I). No adjuvant chemotherapy was performed. The diagnosis on TVS was largely determined by the inhomogeneous mass with undefined borders. Power Doppler imaging strengthened the diagnosis by showing irregularly dispersed blood vessels within the mass.

Our case reported by U Honemeyer, a 32-year-old woman who received C-section for the 1st pregnancy in March 2009, complained intermittent vaginal bleeding in February and 5 months amenorrhea since March, 2010. She was suspected to be suffering from choriocarcinoma but β-hCG was low at 64 mIU/ml. Her uterus had enlarged to the size of 12 weeks pregnancy, and normal cervix and adnexal region. Transvaginal ultrasound (TVS) disclosed 6.09 x 6.68 cm tumor with multiple lacunae and undistinct margin within the uterus **(Figs 11.18 and 11.19)**. Color flow was remarkable surrounding the tumor and in the lacunae by color Doppler flow mapping and the flow signal was

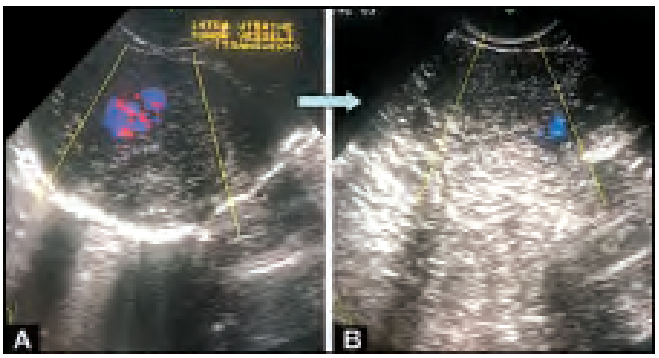

Figures 11.18A and B: Chemotherapy of choriocarcinoma with MTX. (A) Adriamycin and cyclophosphamide was monitored by hCG, B-mode ultrasound, color Doppler and pulsed Doppler flow indices; (B) Tumor flow RI and PI sharply increased in the first course of chemotherapy. Color Doppler image and hCG decreased after two chemotherapeutic courses and complete remission was achieved. The flow indices can be useful for early estimation of choriocarcinoma sensitivity to chemotherapy
Courtesy: S Kondo[21]

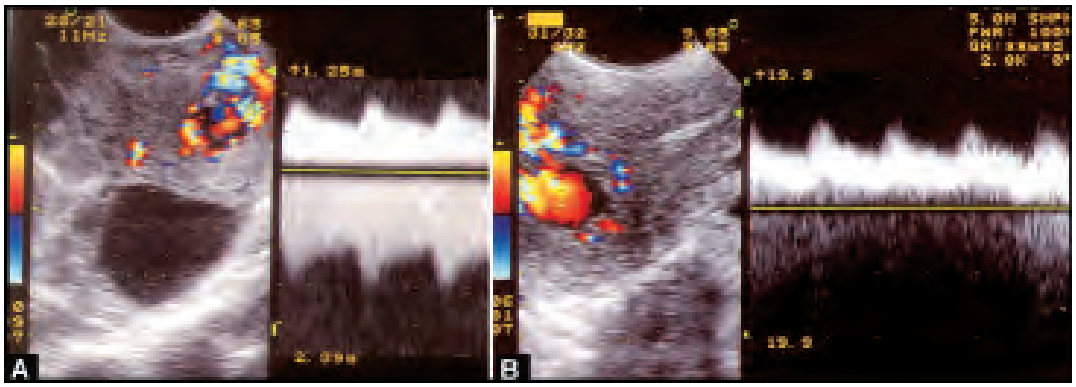

Figures 11.19A and B: Pulsed Doppler RI and color Doppler did not significantly change in an invasive mole refractory to chemotherapy. (A) Tumor flow RI was 0.23 before MTX chemotherapy; (B) 0.36 after two MTX courses
Courtesy: S Yoshida

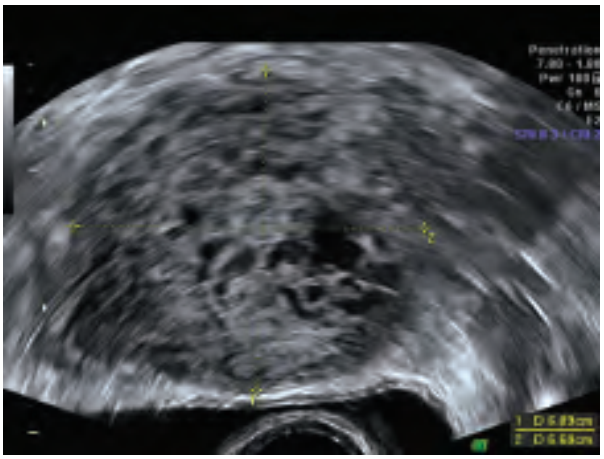

Figure 11.20: 2D B-mode of Honemeyer's case shows intrauterine tumor with multiple lacunae and indistinct border of the tumor
Courtesy: U Honemeyer

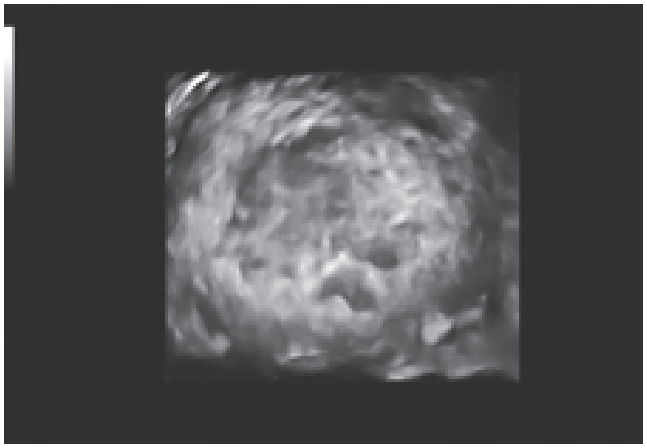

Figure 11.21: 3D multiple section image of Figure 11.20 tumor. Many lacunae and moderately distinct border of the tumor are revealed
Courtesy: U Honemeyer

surrounding the surface of the tumor **(Figs 11.20 to 11.25)**. Tumor malignancy was supposed due to the very low resistance index of pulsed Doppler flow velocity wave **(Fig. 11.23)**, but the tumor seemed not to invade the myometrium and surrounding tissues. No distant metastasis was found outside the uterus. She was sent to the other hospital and received surgery to excise the tumor of about 4 x 4 cm from the posterior uterine wall which was supposed to be a PSTT. The uterine and abdominal walls were closed in layers. The uterus and vagina was packed with ribbon gauges. No active bleeding was seen. The patient was treated in ICU after the surgery. β-hCG level was 54, and the patient received 50 mg methotrexate injection. The tumor microscopically examined by a pathologist showed in two sections myometrial smooth muscle bundles infiltrated by tumor cells (morphologically intermediate cells)

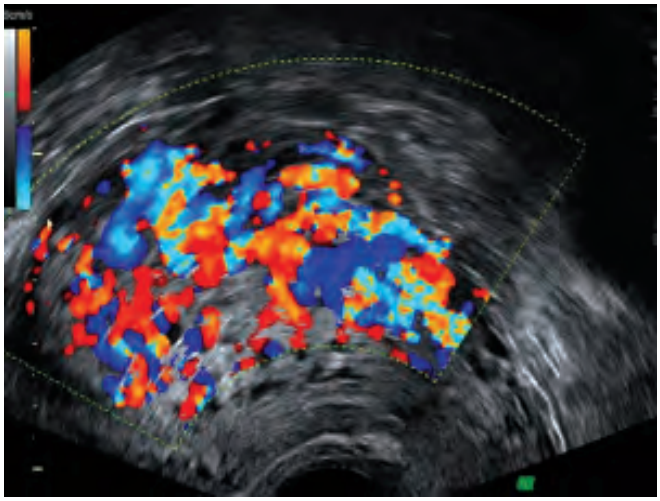

Figure 11.22: 2D color-Doppler flow mapping of the tumor shown in Figure 11.20. Rich blood flow is recognized in the tumor and its lacunae
Courtesy: U Honemeyer

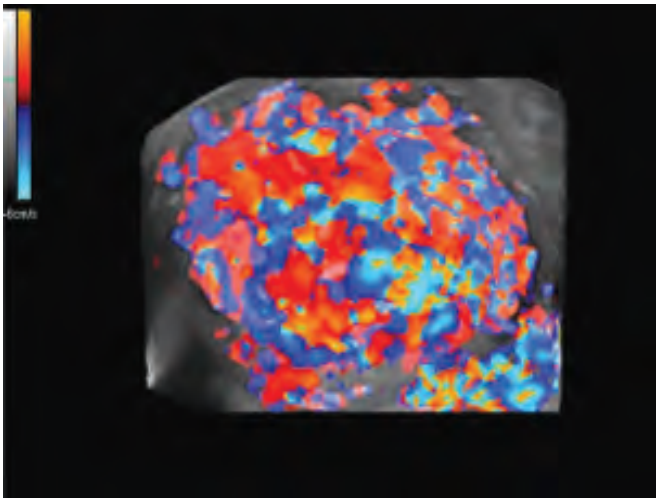

Figure 11.23: 3D color-Doppler flow mapping of figure 11.20 tumor which shows rich blood flow covering the surface of tumor
Courtesy: U Honemeyer

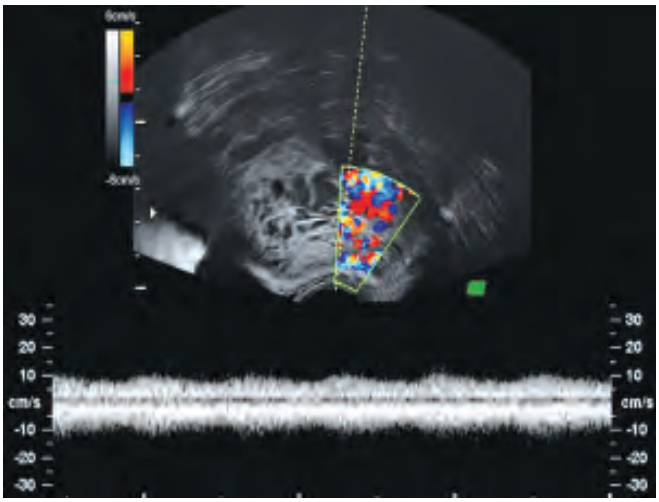

Figure 11.25: The pulsed Doppler blood flow velocity wave of Figure 11.20 tumor. The resistance index is very small because of rich blood flow in the diastolic phase. Malignant feature of tumor was supposed from the flow velocity curve
Courtesy: U Honemeyer

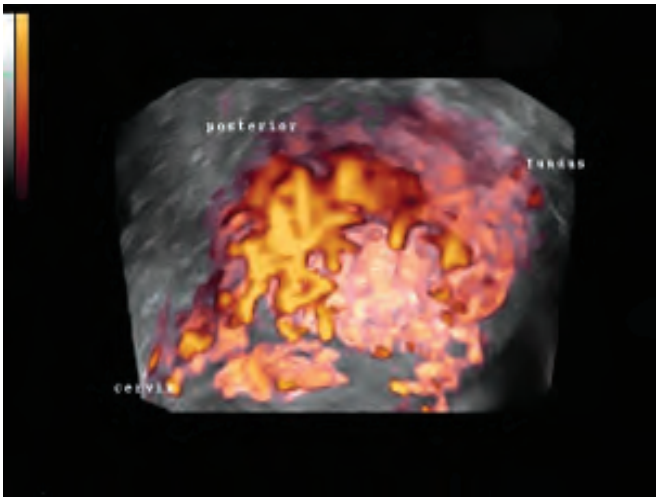

Figure 11.24: 3D power-Doppler flow mapping of the figures 11.20 and 11.21 tumor. The surface of tumor is covered by the blood flow
Courtesy: U Honemeyer

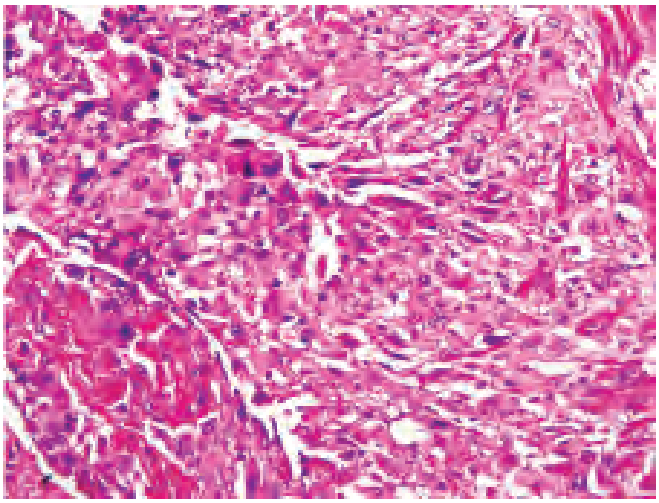

Figure 11.26: The H-E stain histology of excised uterine tumor of which pathological diagnosis was "Feature are of placental site trophoblastic tumor"

which had pleomorphic and hyperchromatic nucleus with multiple prominent nucleoli, cytoplasm was eosinophilic, tumor giant cells were invading blood vessels also seen on areas of necrosis and hemorrhage. The impression was "Features are of placental site trophoblastic tumor **(Fig. 11.26)**". Advised immunohistochemistry was hPL and hCG. The serum β-hCG level was dropping and about 20 mIU/ml two months after the surgery when color Doppler still revealed intrauterine tumor.

Epithelioid Trophoblastic Tumor

An epithelioid trophoblastic tumor (ETT) case was reported by Okumura, et al[43] with its transvaginal sonogram and color flow mapping, where rich color flow revealed surrounding intrauterine tumor with multiple lacunae.

Vaginal bleeding, uterine tumor and serum β-hCG were improved by the combination chemotherapy with MTX, actinomycin D, etoposide and cysplatin, and later the patient received hysterectomy. Its histology was

intermediate trophoblasts with epithelioid appearance and nuclear pleomorphism.

THERAPY OF TROPHOBLASTIC DISEASES

Complete Hydatidiform Mole

Complete hydatidiform mole is treated primarily by curettage, where the well-developed massive mole should be carefully treated, i.e. the cervix is slowly dilated and uterine contraction is induced by prostaglandin before expulsion and curettage to prevent excessive hemorrhage and uterine damage. Ultrasonically diagnosed early stage evacuation is easier than treating the developed mole in later stages. Curettage is repeated for complete evacuation. Ultrasound monitoring of intrauterine maneuver is useful for successful curettage and the prevention of uterine damage.

Partial Hydatidiform Mole

In the treatment of a partial hydatidiform mole, labor is induced by prostaglandin, followed by curettage for expulsion of the fetus and removal of the mole.

Postmolar Monitoring

Postmolar monitoring is indispensable for the detection of any sequelae and prevention of malignant trophoblastic disease. After ultrasonically confirmed complete evacuation of the uterus, ultrasonic transvaginal scan and urinary or serum hCG are studied every 1–2 weeks until hCG decreases to normal cut-off levels, then every 1–2 months for a year.[25] An X-ray image is studied when there is any suspicion of pulmonary change. Clinical care, however, lasts for three years, because 85% of choriocarcinomas develop at three years after the mole.

It is type I when the postmolar hCG regression pattern is normal and when urinary hCG is decreased to 1000 mlU/ml or less after 5 weeks, serum hCG is 100 mlU/ml or less after 8 weeks and serum hCG is 1 mlU/ml or less with an hCG β-CTP system 0.5 mlU/ml which is the cut-off level after 20 weeks. Type II is abnormal regression, where the hCG level is higher than type I regression. Type II or hCG relevation after transient remission should be treated by prophylactic chemotherapy[44] for prevention of the development of choriocarcinoma, where the use of methotrexate (MTX) is common. Prophylactic chemotherapy was tried in our controlled study,[37] where significantly less choriocarcinoma (actually zero) developed in the study group than in the control group.

Choriocarcinoma

Choriocarcinoma is treated by primary chemotherapy, which means the first choice of treatment for choriocarcinoma is chemotherapy, because choriocarcinoma is not a local tumor but systemic disease and the tumor is sensitive to chemotherapy. Hysterectomy was common in the old ages, but was frequently followed by metastases. Radiation was also a local therapy. MTX was the first primary chemotherapy in 1960s. It was systemic chemotherapy because choriocarcinoma was recognized as a systemic disease, the effect is further improved by combined chemotherapy, which is EMA (Etoposide, MTX, Actinomycin-D),[45] or further combination of CO (cyclophosphamide and vincristine), forming the EMA/CO regimen.[46,47] The most intensive therapy may be salvage chemotherapy including etoposide or cisplatine.[48] Chemotherapy-resistant metastasis or recurrence is associated with surgery, e.g. pulmonary lobectomy or craniotogy,[49] and when severe vaginal bleeding accompanies uterine removal. Active combination of hysterectomy[50] or endoscopic surgery[51] and chemotherapy resulted in favorable remission.

Serum hCG level should be lower than the cut-off level for complete remission, i.e. disappearance of primary and metastatic foci and lower hCG levels than the cut-off level. Since there is cross-sensitivity of hCG antibody to pituitary luteinizing hormone (LH), hCG β or hCG β-CTP antibody that is more specific for hCG is in common use in trophoblastic disease, particularly low-level hCG. However, recent studies reported the presence of false positive tests in some hCG antibodies including hCG β and hCG β-CTP.[52,53] The reports suggested repeated tests, urine test instead of serum, serial dilution test or removal of interfering substances if there is any discrepancy among clinical condition and the test results.

The systemic side effects of intensive chemotherapy are stomatitis, skin eruption, hair-fall, fever, reduced granulocytes, bone marrow damage, hepatic lesion, gastrointestinal tract damage, etc. Heavily life threatening is bone marrow damage and its expression is leucopenia in peripheral blood. Mild leukopenia is cured by steroids, while severe damage is treated by bone marrow transplantation and stem cell support.[50]

Intra-arterial infusion chemotherapy was used in the treatment of liver metastases, which decreased by using this treatment.[54] We[17] tried internal iliac arterial infusion in the chemotherapy of uterine cervical choriocarcinoma, followed by tumor regression and necrotic change. Pregnancy outcome after complete remission obtained by intensive chemotherapy was favorable and the treatment showed minimal impact.[55] As for further

long-term influence of chemotherapy treatment, menopause was three years earlier than in control women.[56]

The Role of Ultrasound in the Chemotherapy of Choriocarcinoma

Tumor size and blood flow are effectively monitored in chemotherapy by various ultrasound techniques. Primary or metastatic tumor reduces the size of the ultrasound image and the tumoral blood flow reduces by color or power flow imaging when chemotherapy is effective **(Figs 11.18 and 11.19)**. Early estimation of the tumor sensitivity to systemic chemotherapy is requested in actual chemotherapy.

Pulsed Doppler for the Early Detection of Sensitivity to Chemotherapy

Impedance to flow in the tumor, e.g. RI and PI, clearly elevated immediately after initiation of chemotherapy in the first course, when the choricarcinoma was sensitive to chemotherapy,[21] before later reduction of hCG and color Doppler flow image and tumor reduction. The changes of flow indices may be caused by tumor shrinkage by the effective chemotherapy. In contrast, a chemotherapy-resistant invasive mole showed no change of RI and PI in tumor flow.[21] Another chemotherapy resistant invasive mole also showed only mild increase of RI at the end of systemic chemotherapy. Therefore, tumor blood flow impedance can be the indicator of tumor sensitivity in the early period of chemotherapy. This method can also be tried in other malignancy chemotherapy treatments.

Germ cell origin choriocarcinoma is treated by its original therapy, usually resection followed by adjuvant chemotherapy. Metastasis surgically removed and followed by chemotherapy. Resistive cases receive multiple adjuvant therapy, usually EMA/CO therapy. Cancer which has metamorphosed to choriocarcinoma may receive its own therapy and chemotherapy.

Persistent Trophoblastic Disease

Postmolar hCG persistence receives prophylactic chemotherapy for the choriocarcinoma, usually single MTX. The courses are repeated until hCG reaches normal levels. Clinical choriocarcinoma receives common chemotherapy treatment as described previously. Clinically, invasive mole also receive chemotherapy treatment, but hysterectomy when it is refractory.

Invasive Mole

Invasive moles are treated by systemic chemotherapy, although they tend to be refractory. An invasive mole is a molar vesicle which is more differentiated than choriocarcinoma. A higher local dose of agents may be needed for invasive moles than choriocarcinomas. Local therapy before hysterectomy in the future may be tumor resection or laser evaporation in the open uterus, or possibly less invasive focused ultrasound hyperthermia.

Placental Site Trophoblastic Tumor

The PSTT was treated by hysterectomy when it was limited in the uterus, while chemotherapy was used when it was spread further than the uterus, although clinical outcome was poor when the precedent pregnancy was more than two years before the PSTT.[57] Janni et al.[58] recommended a cytostatic-surgical approach for metastatic PSTT. Furthermore, Tsuji et al.[59] reported that resection of tumor and EMA/CO chemotherapy could achieve long-term remission and save the fertility of young patients. Other reports[60-64] also obtained favorable results mainly by EMA/CO chemotherapy and further use of the etoposide-cisplatin cycle.[64] The outcome of patients with FIGO stage I-II disease were excellent after hysterectomy, but for III-IV stage patients the survival rate was only for 30%.[62] In these reports, PSTT responds to chemotherapy, and complete remission can be expected.

Other Reported Treatment

Wantanebe et al.[65] reported choriocarcinoma in the pulmonary artery which needed treatment with emergency pulmonary embolectomy under cardiopulmonary bypass. Kohyama et al.[66] reported the stereotactic radiation therapy of the choriocarcinoma in the cranium followed by conventional craniospinal irradiation. Bohlmann et al.[19] reported intracardiac resection of a metastatic choriocarcinoma. Brain metastasis is usually treated in intensive chemotherapy.[67] We also experienced massive MTX treatment in a case of brain metastasis; the patient was successfully treated and has survived for more than 20 years.

CONCLUSION

Classification, clinical course, pathological change, diagnosis and chemotherapy of trophoblastic disease were studied, particularly ultrasound diagnosis with real-time B-mode, 3D image, color/power Doppler flow mapping and 3D power Doppler was analyzed.

Complete hydatidiform mole in the first trimester and in multiple pregnancy were diagnosed by real-time B-mode. It was new discovery that 2D and 3D color/power Doppler detected a characteristic blood flow pattern in the complete hydatidiform mole. 3D ultrasound was used in the diagnosis of partial mole. Ultrasound imaging was important in the postmolar monitoring. Invasive mole and choriocarcinoma were differentiated by real-time B-mode and color Doppler images. Effective primary chemotherapy and preventive chemotherapy for choriocarcinoma were proposed. The sensitivity of choriocarcinoma to chemotherapy was proved by elevated RI and PI in pulsed Doppler flowmetry. Ultrasound was useful in the diagnosis of trophoblastic disease and also for the monitoring of its treatments.

REFERENCES

1. Japan Society of Obstetrics and Gynecology and Japanese Pathological Society. The general rules for clinical and pathological management of trophoblastic diseases. 2nd edition.Tokyo: Kanehara Shuppan,1995.
2. Weaver DT, Fisher RA, Newlands ES, et al. Amniotic tissue in complete hydatidiform moles can be androgenetic. J Pathol. 2000;191:67-70.
3. Kajii T, Ohama K. Androgenetic origin of hydatidiform mole. Nature. 1977;268(5621):633-4.
4. Ohama K, Kajii T, Okamoto E, et al. Dispermic origin of XY hydatidiform mole. Nature. 1981;292(5823):551-2.
5. Lorigan PC, Sharma S, Bright N, et al.Characteristics of women with recurrent molar pregnancies. Gynecol Oncol. 2000;78(3 pt. 1):288-92.
6. Bae SN, Kim SJ. Telomerase activity in complete hydatidiform mole. Am J Obstet Gynecol. 1999;180(2 Pt. 1):328-33.
7. Lazarus E, Hulka C, Siewert B, et al. Sonographic appearance of early complete molar pregnancy. J Ultrasound Med. 1999;18:589-94.
8. Szulman AE. Philippe E, Boue JG, et al. Human triploidy association with partial hydatidiform moles and nonmolar conceptuses. Hum Pathol. 1981;12(11):1016-21.
9. Hirose M, Kimura T, Mitsuno N, et al. DNA flow cytometric quantification and DNA polymorphism analysis in the case of ,a complete mole with a coexisting fetus. J Ass Reprod Genet. 1999;16(5):263-7.
10. Suita S, Sono K, Tajiri T, et al. Malignant germ cell tumors: clinical characteristics, treatment and outcome. A report from the study group for pediatric solid malignant Tumors in the Kyushu area, Japa J Pediatr Surg. 2002;37:1703-6.
11. Weiss S, Amit A, Schwarz MR, et al. Primary choriocarcinoma of the vulva. lnt J Gynecol Cancer. 2001;11(3): 251-4.
12. Yahata T, Kodama S, Kase H, et al. Primary choriocarcinoma of the uterine cervix: clinical, MRI, and color Doppler ultrasonographic study. Gynecol Oncol. 1997; 64(2):274-8.
13. Coskun M, Agildere AM, Boyvart F,et al. Primary choriocarcinoma of the stomach and pancreas: CT findings. Eur Radiol. 1988;8(8):1425-8.
14. Liu Z,Mira JL,Cruz-Caudilo JC. Primary gastric choriocarcinoma:a case report and review of the literature. Arch Pathol Lab Med. 2001;125(12):1601-4.
15. Wang JC, Angeles S, Chak P, et al.Choriocarcinoma of the gallbladder: treated with cisplatine-based chemotherapy. Med Oncol 2001;18:165-9.
16. Sievert K, Weber EA, Herwig R, et al. Pure primary choriocarcinoma of the urinary bladder with long-term survival. Urology. 2000;56(5):856.
17. Koga K, Izuchi S, Maed K, et al. Treament of chorionepithelioma of uterine cervix with hypogastric arterial infusion of amethopterin. J Jpn Obstet gynecol Soc. 1966;13:245-9.
18. Chama CM, Nggada HA, Nuhu A. Cutaneous metastasis of gestational choriocarcinoma. Int J gynecol Obstet. 2002;77(3):249-50.
19. Bohlmann MK, Eckstein FS, Allemann Y, et al. Intracardiac, resection of a metastatic choriocardinoma. Gynecol Oncol. 2002;84 157-80.
20. Gersak B, Lakic N, Gorjup V, et al. Right ventricular metastatic, choriocarcinoma obstructing inflow and outflow tract. Ann Thorac. Surg. 2002;73(5):1631-3.
21. Kondo S. Personal communication. In: Maeda K (Ed). Gestational trophoblastic disease, Lecture in the Ian Donald Inter-University School of Medical Ultrasound, Dubrovnik, 1995.
22. Steigrad SM, Cheung AP, Oshborn RA. Choriocarcinoma coexistent with and intact, pregnancy: case report and review of the literature. J Obstet Gynecol Res. 1999;25:197-203.
23. Jacque SM, Quershi F, Doss BJ, et al. Intraplacental choriocarcinoma associated with viable pregnancy: pathologic features and implications for the mother and infant. Pediatr Dev Pathol. 1998;1(5):380-7.
24. Feltmate CM, Genset DR, Goldstein DP, et al. Advances in the understanding of placental site trophoblastic tumor. J Reprod Med. 2002;47:337-41.
25. Santoso JT, Coleman RI (Eds). Handbook of Gyn Oncology. New York: Mcgraw Hill, 2001.
26. Mangili G, Garavaglia E, De Marzi P, et al. Metastatic placental site trophoblastic tumor. Report of a case with complete response to chemotherapy. J Reprod Med. 2001;46(3):259-62.
27. Remadi S, Lifschita-Mercer B, Ben-Hur H, et al. Metastasizing placental site trophoblastic tumor: immunohistochemical and DNA analysis. 2 case reports and a review of the literature. Arch gynecol Obstet. 1997;259(2):97-103.
28. Feltmate CM, Genest DR, Wise L, et al. Placental site trophoblastic tumor: a 17-year experience at the New England Trophoblastic Disease Center. Gynecol Oncol. 2001;82(3):415-9.
29. Monclair T, Abeler VM, Kren J, et al. Placental site trophoblastic tumor (PSTT) in mother and child: first report of PSTT in infancy. Med Pediatr Oncol. 2002;38(3):187-91.
30. Piura B. Placental site trophoblastic tumor: a challenging rare entity. Eur J Gynaecol Oncol. 2006;27(6):545-51.

31. Baergen RN, Rutgers JL, Young RH, et al. Placental site trophoblastic tumor: a study of 55 cases and review of the literature emphasizing factors of prognostic significance. Gynecol Oncol. 2006;100(3):511-20. Epub 2005 Oct 21.
32. Allison KH, Love JE, Garcia RL. Epithelioid trophoblastic tumor: review of a rare neoplasma of the chorionic-type intermediate trophoblast. Arch Pathol Lab Med. 2006;130(12):1875-7.
33. Shih IM, Kurman RJ. Epithelioid trophoblastic tumor: a neoplasm distinct from choriocarcinoma and placental site trophoblastic tumor simulating carcinoma. Am J Surg Pathol. 1998;22(11):1393-403.
34. Sebire NJ, Lindsay I. Current issues in the histopathology of gestational trophoblastic tumors. Fetal Pediatr Pathol. 2010;29(1):30-44.
35. Kurjak A, Zalud I, Predanic M, et al. Transvaginal color and pulsed Doppler study of uterine blood flow in the first and early second trimesters of pregnancy: normal versus abnormal. J Ultrasound Med. 1994;13(1):43-7.
36. Kurjak A, Zalud L, Salihagic A, et al. Transvaginal color Doppler in the assessment of abnormal early pregnancy. J Perinat Med. 1991;19(3):155-65.
37. Koga K, Maeda K. Prophylactic chemotherapy with amethopterin for the prevention if choriocarcinoma following removal of hydatidiform mole. Am J Obstet Gyncol. 1968;100:270-5.
38. Gungor T, Ekin M, Dumanli H, et al. Color Doppler ultrasonography in the earlier differentiation of benign molehydatidiform from malignant gestational trophoblastic disease. Acta Obstet Gynecol Scand. 1998;77(8):860-2.
39. Vegh GL, Fulop V, Liu Y, et al. Differential gene expression pattern between normal human trophoblast and choriocarcinoma cell lines: downregulation of heat shock protein-27 in choriocarcinoma *in vitro* and *in vivo*. Gynecol Oncol. 1999;75:(3)391-6.
40. Shigematsu T, Kamura T, Wake N, et al. DNA polymorphism analysis of a pure polymorphism non-gestational choriocarcinoma of the ovary: case report. Eur J Gynecol Oncol. 2000;21:153-4.
41. Bettencourt E, Pinto E, Abreul E, et al. Placental site trophoblastic tumor: the value of transvaginal colour and pulsed Doppler sonography (TV-CGS) in its diagnosis: case report. Eur J Gynecol Oncol. 1997;18:461-4.
42. Savelli L, Pollastri P, Mabrouk M, et al. Placental site trophoblastic tumor diagnosed on transvaginal sonography. Ultrasound Obstet Gynecol. 2009;34(2):235-6.
43. Okumura M, Fushida K, Rezende WW, et al. Sonographic appearance of gestational trophoblastic disease evolving into epithelioid trophoblastic tumor. Ultrasound Obstet Gynecol. 2010;36(2):249-51.
44. PMK TK, Kim SN, Lee SK. Analysis of risk factors for postmolar trophoblastic disease: categorization of risk factors and effect of prophylactic chemotherapy. Yonsei Med J. 1996;37:412-9.
45. Soto-Wright V, Goldstein DP, Bernstein MR, et al. The management of gestational trophoblastic tumors with etoposide, methotrexate, and actinomycin D. Gynecol Oncol. 1997;64(1):156-9.
46. Newlands ES, Oaradubas FJ, Fisher RA. Recent, advances in gestational trophoblast disease. Hematol Oncol Clin. North Am. 1999;13(1):225-44.
47. Nozue A, Ichikawa Y, Minami R, et al. Postpartum choriocarcinoma complicated by brain and lung metastases treated successfully with EMA/CO regimen. BJOG. 2000;107(9):1171-2.
48. Okamoto T, Goto S. Resistance to multiple agent chemotherapy including cisplatin after chronic low-dosage oral etoposide. Administration in gestational choriocarcinoma. Gynecol Obstet Invest. 2001;52(2):139-41.
49. Kang SB, Lee CM, Kim JW, et al. Chemoresistant choriocarcinoma cured by pulmonary lobectomy and craniotomy. Int J Gynecol Cancer. 2000;10(2):165-9.
50. Knox S, Brooke SE, Wog-You cheong J, et al. Choriocarcinoma and epithelial trophoblastic tumor: successful treatment of relapse with hysterectomy and high dose chemotherapy with peripheral stem cell support: a case report. Gynecol Oncol. 2002;85(1):204-8.
51. Chou HH, Lai CH, Wang PN, et al. Combination of high-dose chemotherapy, autologous bone marrow/peripheral blood stem cell transplantation, and thoracoscopic surgery in refractory nongestational choriocarcinoma of a 45XO/46XY female: a case report. Gynecol Oncol. 1997;64(3):521-5.
52. Cole LA, Butler S. Detection of hCG in trophoblastic disease. The USA hCG reference service experience. J Reprod Med. 2002;47(6):433-44.
53. ACOG Committee opinion. Avoiding inappropriate clinical decisions based on false-positive human chorionic gonadotropin test results. Obstet Gyecol. 2002;100(5 Pt 1):1057-9.
54. Tanase K, Tawada M, Moriyama N, et al. Intra-arterial infusion chemotherapy for liver metastases of testicular tumors: report of two cases. Hinyokika Kiyo. 2000;46(11):823-7.
55. Woolas RP, Bower M, Newlands ES, et al. Influence of chemotherapy for gestational trophoblastic disease on subsequent pregnancy outcome. Br J Obstet Gynaecol. 1998;105(9):1032-5.
56. Bower M, Rustin GJ, Newlands ES, et al. Chemotherapy for gestational trophoblastic tumours hastens menopause by 3 years. Eur J Cancer. 1998;34(8):1204-7.
57. Newlands ES, Bower M, Fisher RA, et al. Management of placental site trophoblastic tumors. J Reprod Med. 1995;43(1):53-9.
58. Janni W, Hantschmann P, Rehbock J, et al. Successful treatment of malignant placental site trophoblastic tumor with combined cytostatic-surgical approach: case report and review of literature. Gynecol Oncol. 1999;75(1):164-9.
59. Tsuji Y, Tsubamoto H, Hori M, et al. Case of PSTT treated with chemotherapy followed by open uterine tumor resection to preserve fertility. Gynecol Oncol. 2002;87(3):303-7.
60. Twigs LB, Hartenbach E, Saltzman AK, et al. Metastatic placental site trophoblastic tumor. Int J Gynecol Obst. 1998;60(Suppl. l):S51-5.
61. Swisher E, Drescher CW. Metastatic placental site trophoblastic tumor: long-term remission in a patient

treated with EMA/CO chemotherapy. Gynecol Oncol. 1998;68(1):62-5.
62. Chang YL, Chang TC, Hsuen KG, et al. Prognostic factors and treatment for placental site trophoblastic tumor report of 3 cases and analysis of 88 cases. Gynecol Oncol. 1999;73(2):216-22.
63. Manili G, Garavaglia E, De Marzi P, et al. Metastatic placental site trophoblastic tumor. Report of a case with complete response to chemotherapy. J Reprod Med. 2001;46(3):259-62.
64. Randall TC, Coukos G, Wheeler JE, et al. Prolonged remission of recurrent, metastatic placental site trophoblastic tumor after chemotherapy. Gynecol Oncol. 2000;76(1):115-7.
65. Watanbe S, Shimokawa K, Sakasegawa K, et al. Choriocarcinoma in the pulmonary artery treated with emergency pulmonary embolectomy. Chest. 2002;121(2):654-6.
66. Kohyama S, Uematsu M, Ishihara S, et al. An experience of stereotactic radiation therapy for primary intracranial choriocarcinoma. Tumori. 2001;87(3):162-5.
67. Landanio G, Sartore-Bianchi A, Giannetta L, et al. Controversies in the management of brain metastases: the role of chemotherapy. Forum (Genova). 2001;11(1): 59-74.

CHAPTER 12

First-Trimester Ultrasound Screening for Fetal Anomalies

Jon Hyett, Jiri Sonek

INTRODUCTION

The utility of the first-trimester ultrasound examination of the gravid uterus and its contents continues to expand. Improvements in the resolution of ultrasound equipment and better understanding of normal and abnormal fetal development now enables us to perform a highly reliable fetal anatomic evaluation even at a relatively early gestational age (11–13+6 weeks). Furthermore, first trimester evaluation of the fetus, maternal pelvic vasculature and maternal serum in conjunction with maternal history and physical examination may be used to establish the risk of fetal aneuploidy and certain pregnancy complications that do not become clinically evident until later in gestation. In this chapter, we will discuss current information regarding the benefits and limitations of this approach.

Gray-scale examination of the fetal head and neck yields a great amount of information regarding the risk of trisomy 21 and other aneuploidies. Many of the ultrasound markers that are used in the first trimester to establish the risk of trisomy 21 have their equivalents in the postnatal phenotype. In 1866, Langdon Down[1] described individuals with a syndrome that later came to bear his name as “having skin that appears to be too large for their bodies” [recognized as increased nuchal translucency (NT) thickness],[2] having a “small nose” [recognized as an absent or hypoplastic nasal bone (NB)][3] and having a “flat face” [recognized as a shallow frontomaxillary facial (FMF) angle].[4]

Gray-scale examination of the fetal heart in the first trimester may yield evidence of a cardiac defect, which is the most common structural anomaly seen in individuals with trisomy 21.[5] However, even in the absence of an overt structural defect, the function of the heart may be altered. There is ample evidence that the microscopic and ultrastructural anatomy of the myocardium and valve leaflets is abnormal in trisomy 21.[6-8] These findings were exploited to develop a second type of ultrasound marker through Doppler evaluations of the cardiovascular system. Cardiac function can be assessed through evaluation of blood flow across the tricuspid valve (TCV)[9-11] or through the ductus venosus (DV).[12-19] Additionally, a measure of fetal heart rate (FHR) may also be helpful. Whilst this marker is of marginal benefit in screening for trisomy 21, it has significant value when screening for other types of aneuploidy.[2,20]

Pregnancy and the development of the placenta, is associated with the appearance of novel proteins in maternal blood, and alteration in the levels of already extant proteins. Through empirical observation followed by prospective studies, it has been noted that the concentration of some proteins differs between aneuploid and chromosomally normal pregnancies. At 12 weeks’ gestation, two proteins have significant discriminative power between populations of trisomic and chromosomally normal fetuses: free beta-human chorionic gonadotropin (free β-hCG) and pregnancy associated plasma protein-A (PAPP-A).[21] It should be stressed that it is the free β-hCG rather than other forms of hCG that has been tested most rigorously and performs best.[22]

First-trimester screening has been shown to be useful not only for trisomy 21 but for other types of aneuploidy (trisomies 18 and 13, monosomy X, other aneuploidies involving the sex chromosomes and triploidy).[2,3,22-24] Some of these conditions are associated with median nuchal translucencies that are even thicker than that seen with trisomy 21 and are also more likely to have other major or minor structural defects. As a result, in some cases detection rates are even higher than for trisomy 21.[2,22]

Another first-trimester marker called intracranial translucency (IT) has been recently described.[25] This marker appears to be useful in screening for open neural tube defects. Additionally, FMF angle measurements appear to be significantly smaller in fetuses with open neural tube defects than in those with an intact spine.[26] Further prospective studies are needed to determine whether this marker is as powerful as the Chiari type II malformation and biparietal scalloping seen in virtually all fetuses with open spina bifida in the second trimester.

First-trimester Doppler evaluation of the maternal uterine arteries and measurement of certain maternal serum markers along with maternal blood pressure measurement, have been shown to be useful in estimating the risk of preeclampsia.[27-30] This is especially true for early and severe preeclampsia, which is frequently associated with growth restriction. The utility of this approach is limited by the fact that currently there is no proven method for the prevention of either of these conditions. However, identification of the truly high-risk patients early in pregnancy may in the future lead to methods that improve pregnancy outcome.

The Fetal Medicine Foundation played an active role in the development and implementation of these additional first trimester markers. They are included in the current Fetal Medicine Foundation's algorithm for first-trimester pregnancy evaluation.

AN ARGUMENT FOR SCREENING IN THE FIRST TRIMESTER

Evaluating pregnancies formally in the first trimester has a number of potential benefits. The combination of ultrasound (NT) and maternal serum markers (PAPP-A and free β-hCG) provides the best method of screening for fetal aneuploidy with a high (approximately 90%) detection rate and positive predictive value.[31] Ultrasound measurements are helpful in establishing the risk of a number of fetal disorders in addition to aneuploidy.[32-79] Fetal anatomy can be systematically examined even at this early gestation and the majority of major structural anomalies can be detected at this stage.[80-91]

The majority of women have a normal pregnancy and can be appropriately reassured, relieving the anxiety that many feel about the risk of fetal abnormality. In the minority of cases where a problem is detected, first trimester diagnosis preserves maximum privacy and autonomy as well as safety with regards to reproductive choices. An added advantage of first trimester ultrasound evaluation lies in accurate pregnancy dating through measurement of the crown-rump length (CRL).[92] Accurate gestational age is one of the most important pieces of information in the management of both high-risk and normal pregnancies.

First-trimester ultrasound is particularly valuable in multiple gestations as chorionicity can be determined most accurately at an early stage.[93-95] A distinct thickening of the dividing membrane ("lambda" or "twin peak" sign) as it approaches the placental surface indicates that the pregnancy is dichorionic (DC) whereas a thin, "T-shaped" insertion of the membrane into the placental surface is indicative of monochorionic placentation. The accurate determination of chorionicity is fundamental for successful management of twin pregnancies: monochorionicity is associated with a risk of adverse perinatal outcome that is higher than in dichorionic pregnancies.[96] Therefore, monochorionic pregnancies merit a significantly increased level of antenatal surveillance.

Algorithms used to calculate risks for aneuploidy vary in monochorionic and dichorionic pregnancies. This is to account for the fact that the monochorionic twins are monozygous as well as the fact that biochemical parameters vary according to the type of placentation.[97-99] Unlike maternal serum biochemistries, the use of ultrasound markers in multiple gestations allows risk to be assigned to each individual fetus, rather than establishing a risk for the pregnancy overall. Maternal serum markers in higher order multiple gestations (triplets and greater) are unreliable and first trimester ultrasound screening is the best option.

In monochorionic/diamniotic gestations, the risk of developing twin-to-twin transfusion syndrome (TTTS) later in pregnancy may be estimated by measuring the NT's (the likelihood of TTTS increases with increasing

difference in the NT measurements between the two fetuses),[100] and by evaluating the ductus venosus with Doppler (presence of reversed a-wave increases the risk of TTTS).[101]

An Argument For Confining The First-Trimester Ultrasound Exam to 11–13+6 Weeks' Gestation

The benefits of a first trimester ultrasound examination are best realized between 11 and 13+6 weeks' gestation. Visualization of normal anatomical structures is easier after the process of embryonic development is more complete,[102] allowing the identification of anomalies that are not necessarily visible at an earlier stage. For example; physiologic extra-abdominal herniation of the bowel continues to 11 weeks' gestation making the diagnosis of an omphalocele difficult prior to this time.[103-105] The cranial vault is not ossified prior to 11 weeks' gestation, which reduces the accuracy of first trimester diagnosis of exencephaly/anencephaly sequence.[106] Finally, aside from NT measurement, the effectiveness of first trimester markers prior to 11 weeks' gestation is likely reduced. For example, the NB is not normally ossified prior to 11 weeks' gestation[107] and almost 50% of normal fetuses have an incompetent TCV at 10 weeks' gestation.[108]

The effectiveness of NT measurement as a marker of aneuploidy diminishes beyond 13+6 weeks'—a gestation where image acquisition also becomes more difficult due to fetal lie.[109-111] Estimation of gestational age by measurement of CRL becomes inaccurate beyond this gestational age and the potential benefits of early diagnosis with regard to complications of interrupting the pregnancy are reduced.

ELEMENTS OF FIRST-TRIMESTER FETAL SCREENING

General Principles of Screening

The development of a credible screening protocol has a number of essential components. Firstly, a marker (ultrasound or maternal serum) needs to be identified. A marker for aneuploidy is defined as an observation that has a different prevalence in euploid and aneuploid populations. Each marker can be ascribed a specific mathematical value, known as a likelihood ratio, which is based on the ratio of prevalence of the observation in the two populations. For any individual, the absolute risk of having aneuploidy is then calculated by multiplying the background risk of the disease by this likelihood ratio.

Likelihood ratios can be calculated to reflect the presence or absence of the observation—positive and negative likelihood ratios, respectively. Both are important as the negative likelihood ratio also impacts on the overall risk for aneuploidy. The strength of a marker depends on the degree of difference in the prevalence of the observation in normal and aneuploid fetuses. Some markers are affected by other maternal and fetal factors (e.g. the effect of maternal weight, smoking and ethnicity on maternal serum biochemistry).[2] These effects need to be accounted for mathematically when generating likelihood ratios. Similarly, if more than one marker is used it needs to be established whether or not they are interdependent. A weak association between markers usually may be compensated for mathematically. If the association is strong, it may be best not to use them together. The manner in which the marker is examined must be standardized, so that it is reproducible and may be implemented in more than one center.

The implementation of a credible screening protocol also has a number of essential components. Above all, only those operators that have the appropriate background and training should be involved in the performance of screening. It is equally important to establish a quality assurance system that reviews the performance of the screening on an ongoing basis.

General Principles of the Use of Ultrasound and Biochemical Markers

Two techniques are used to generate likelihood ratios for the markers used in first trimester screening: by the use of continuous variables and categorical variables.

Nuchal translucency thickness, maternal serum free β-hCG and PaPP-A, the FMF angle and FHR are all continuous variables. Generally, normal ranges of continuous variables change with gestational age in both euploid and aneuploid populations. The likelihood ratio is based on the measurement itself while taking into account any changes associated with gestational age. Small variations in measurement lead to small changes in the likelihood ratio and in the calculated risk for aneuploidy. This contrasts with markers like the absent NB, tricuspid regurgitation, an abnormal ductus venosus a-wave and other structural anomalies that are categorical: they are either present or not—and the likelihood ratio is either positive or negative. The result of the assessment (positive or negative) is generally associated with a large change in risk.

The final risk for Down syndrome is calculated by multiplying an "a priori risk" by these likelihood ratios.

The "a priori" risk is based on maternal age but must also take into account gestational age and any history of a previous affected pregnancy.[112,113] Of note is that while the history of a previous affected pregnancy is a categorical variable, the 'a priori' risk based on maternal and gestational age is a continuous variable. Therefore, the addition of either categorical or continuous type of markers results in a continuous spectrum of risks across the screened population.

The final risk can be viewed in two ways: from an individual's perspective and from the public health perspective. From the individual perspective, the value of risk assessment is to help the patient with the decision whether or not to proceed with diagnostic testing. However, the decision to proceed with diagnostic testing depends on a number of other factors including the individual's attitude towards having an affected child, the stress that a miscarriage would create, and whether or not termination of pregnancy is an acceptable option. Even though the patient is provided with numerical risks of aneuploidy based on the individual risk assessment and procedure-related loss rate, the significance that she attaches to these adverse events varies from individual to individual. Non-directive counseling and honoring patient autonomy is paramount.

From a public health perspective, it is the detection and false-positive rates that are important. To that end, it is necessary to define a "risk cut-off," which divides the population into "high" and "low-risk" groups, i.e. those that are screen positive and those that are screen negative. Generally, it is only those women that fall into the "high-risk" category that are offered an invasive diagnostic test. However, in accordance with the dictum of patient autonomy, even patients who are in the low-risk category and who understand the risks of an invasive procedure may choose to have an invasive procedure done. The cut-off is somewhat arbitrary but over the past 30 years, it has been set so the false-positive rate is 5%. Recently, due to the effectiveness of combined first-trimester screening, some programs have adjusted this cut-off to reduce the false-positive rate while maintaining the high levels of detection.[114] Reduction in the false-positive rate results in a reduction of invasive procedures. This in turn decreases the overall cost and the number of normal fetuses lost as a result of invasive procedures.

In order to appropriately compare screening algorithms and programs, it is critical to evaluate them while holding either the false-positive rate or the detection rate constant (e.g. holding the FP rate at 5% and looking at the detection rates that two or more separate screening approaches produce or holding the detection rate at 90% and looking at the various false-positive rates).

Crown-rump Length (CRL)

The background prevalence of Down syndrome, normal ranges of continuously variable markers, (NT and FMF angle measurements, serum free β-hCG and PaPP-A) and prevalence of categorical markers (NB absence, tricuspid regurgitation and abnormal DV a-wave) are all dependent on gestational age. Consequently, it is critical to establish the gestational age as accurately as possible in order for the correct 'a priori' risk and likelihood ratios to be used.[92] Measurement of fetal CRL appears to be the most reliable method for determining gestational age.[115] To measure the CRL, a midline longitudinal view of the fetus is obtained and the image is magnified so that the fetus fills the screen. The fetus is measured from the top of the head to the rump. The measurement should be done with the fetus in a neutral position, i.e. not hyperflexed or extended. Salomon et al. developed a model, which simulates the effect of inaccurate CRL measurements on Down syndrome risks based on the combination of first-trimester NT and second-trimester biochemical markers.[116] They showed that even small (5 mm) changes in CRL led to significant changes in risk and concluded that quality assurance of CRL measurements may be as important as methods currently used to standardize measurements of NT. At the present time, development of a CRL measurement quality assurance program is hampered by the fact that there is no gold standard that can be used for comparison of acquired datasets.

Nuchal Translucency

Nuchal translucency describes a sonographically echolucent space beneath the skin at the nape of the neck.[113] This sonolucent area can be seen in all fetuses between 11 and 13+6 weeks of gestation. As NT thickness increases, there is an increasing chance of the fetus being affected by a chromosomal or structural abnormality, a genetic syndrome or intrauterine death.[53] Despite this, a proportion of fetuses with increased NT will be normal, underscoring the fact that this finding is not diagnostic and serves merely as a marker for a potential fetal anomaly.[117]

Possible Mechanisms for Increased NT

A number of mechanisms for increased NT have been proposed: structural cardiovascular abnormalities and/or abnormalities of myocardial performance,[6,118-121]

abnormalities of connective tissue composition,[7,8,122-124] abnormalities or delay in lymphatic system formation,[66,67,125,126] increase in intrathoracic pressure,[48,55-61] decrease in fetal movement,[51,70-72] fetal hypoproteinemia,[69,127] fetal anemia,[73-76] and fetal infection.[77-79,128] It is likely that under different clinical circumstances, different mechanisms are in effect. It is also likely that in many cases, especially in fetuses with chromosomal defects, the thickened NT is caused by more than one mechanism. The latter is exemplified by trisomy 21 where abnormalities of the connective tissue and lymphatic system along with cardiovascular defects are commonly seen in the same fetus.

Nuchal Translucency Measurement

A standardized method for measurement of NT thickness has been described by the Fetal Medicine Foundation **(Fig. 12.1 and Box 12.1)**. The software that has been developed by the foundation to generate likelihood ratios and to provide individual risk assessment is based on this method of assessment.[129] Nuchal measurements are made at 11–13+6 weeks' gestation, corresponding to a CRL measurement of 45–84 mm. The fetus is assessed in a midsagittal section with the head and neck in a neutral position. There are a number of anatomic landmarks that help to establish that the ultrasound plane is in the midline: delineation of the fetal profile with echogenic lines representing the skin over the nasal bridge and nasal tip being visible in the same view (only if the fetus is facing the transducer) and the intracranial hypoechoic regions of the thalamus, the pons and the medulla oblongata (if the fetus is either facing towards or away from the transducer). Extension of the neck artificially increases the NT measurement and hyperflexion decreases it.[130] The image should be magnified such that the fetal head and the upper thorax occupy the majority of the image, so that caliper measurements are accurate to an interval of 0.1 mm. Square calipers should be used to measure the NT at its widest point, placing the calipers so that the inner aspect of the caliper cross hatch is flush with the inner aspect of the echodense lines bracketing the nuchal fluid. The ultrasound settings should be adjusted so that these lines are as thin and sharply delineated as possible. This view is optimized by keeping the face of the transducer parallel to the longitudinal axis of the fetus, i.e. insonating the nuchal skin at 90°. The NT must be clearly differentiated from the amniotic membrane, which has a similar ultrasound appearance to the skin line. The measurement should be repeated on at least three separate images and the largest measurement that meets the criteria should be used for risk assessment.

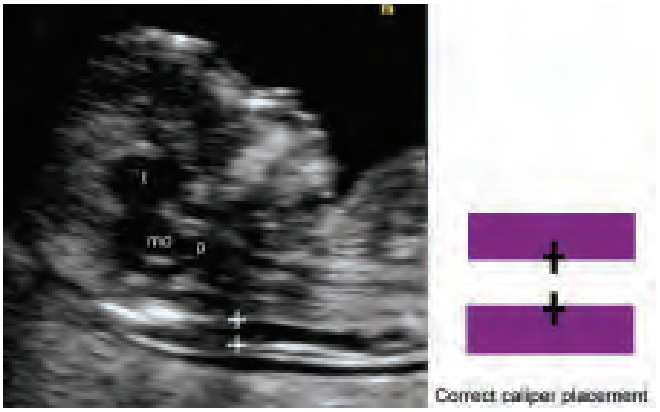

Figure 12.1: Nuchal translucency measurement that meets Fetal Medicine Foundation criteria (t=thalamus, mo=medulla oblongata, p=pons). The correct caliper placement is "on-to-on"

Box 12.1: The Fetal Medicine Foundation criteria for the measurement of nuchal translucency

- CRL: 45-84 mm (11+0 to 13+6 weeks' gestation)
- Midsagittal view (fetus may either be facing towards or away from the transducer)
- Landmarks of the profile: skin over the nasal bridge and the nasal tip
- Intracranial structures: thalamus, pons, medulla oblongata
- Image size: head and upper thorax occupies most of the screen (measurement degree of precision—1 mm)
- Neutral fetal position (avoid neck extension or flexion)
- Skin line needs to be seen separately from the amnion
- Nuchal cord (5% of the cases measure NT above and below the nuchal cord and average the measurements)
- "On-to-on" caliper placement
- Motivated sonographer

In approximately 5% of cases, a nuchal cord is identified.[131] The initial suspicion of a nuchal cord being present is often raised when a segment of NT cannot be clearly visualized or an indentation in the NT is noted. Commonly, faint echodense lines are seen in this region, which represent walls of the tortuous umbilical vessels in cross section. The presence of a nuchal cord is best confirmed with color Doppler. In this circumstance, the NT should be measured both above and below the nuchal cord and risk assessment is based on the average of these two measurements.

Risk assessment is based on NT thickness alone, not the subjective appearance of this region. On close inspection, septations may be seen in all thickened nuchal translucencies; attempting to differentiate between simple NT and a "cystic hygroma" is not useful.[132] Assigning different risks based on the appearance of NT was proposed as a part of the FASTER

study.[133] The statistical analysis used in this article was questioned by some.[134] Additionally, subsequent analysis of the same data by the FASTER group did suggest that NT size rather than appearance is the most important.[135]

Nuchal Translucency and Fetal Aneuploidy

The prevalence of chromosomal defects increases with increasing NT thickness.[136,137] The relation between fetal NT and chromosomal defects was initially derived from a multicenter screening study involving[96,127] singleton pregnancies.[136] The distribution of NT measurements has changed since that time due to minor adjustments in measurement technique and improvements in ultrasound equipment. The distribution of normal measurements that is currently used for risk estimation is based on 37,078 fetuses examined in a standardized fashion at the Fetal Medicine Centre in London between 1999 and 2005.[109]

The mathematical descriptions of the NT measurement distribution and the manner in which the likelihood ratios are generated have evolved over the past 15 years. Recently, a mixture model of the NT measurement distributions has been introduced.[109] This model is based on the observation that the NT measurement distributions in both euploid and aneuploid fetuses follow two distinct patterns. In a certain population of fetuses, NT measurement ranges increase between 11 and 13+6 weeks' gestation, whereas in a second population, NT measurements are independent of gestational age and remain constant over this time period. The percentage of fetuses that fit into these two categories varies according to the chromosomal complement. Recent changes to the statistical methodology used for risk assessment have improved both the sensitivity and specificity of screening for chromosomal abnormality—particularly for trisomies 13 and 18.

When measured correctly, NT is arguably the most robust single marker for chromosomal abnormality.[31] The NT measurement is therefore the "foundation stone" of any screening protocol that includes first trimester ultrasound examination. Using just the combination of maternal age and NT measurement, the detection rates for a 5% false-positive rate are about 75% for trisomies 21, 18 and 13, and are 90% and 60% for monosomy X and triploidy, respectively.[136,138,139]

The maternal serum analytes that have been shown to be most effective in first-trimester screening for aneuploidy are free β-hCG and PAPP-A. As NT measurements and the serum analytes are independent of one another, they can all be used to adjust the "a priori" maternal age-related risk (combined first trimester screen) without the need for additional mathematical manipulation.[21,140-144] Combined screening improves the detection rate for trisomies 21, 18 and 13, monosomy X and triploidy to 90% or more for a 5% false-positive rate.[2,145,146]

Nasal Bone

The logic behind using the prenatal NB evaluation in screening for trisomy 21 is based on the characteristic facial features found in individuals with Down syndrome and on anthropometric, radiological and histological studies.[147-151] All of these studies demonstrate a significant difference in either the size of the NB or in the degree of ossification between euploid individuals and those with trisomy 21.[152]

This phenomenon is also apparent on prenatal ultrasound,[153] and a number of studies have been published indicating that absence of the NB is highly associated with trisomy 21 in both the first and the second trimesters.

Mechanism for the NB Absence in Trisomy 21

The exact mechanism leading to the NB abnormalities seen in trisomy 21 is unknown. However, it is likely that the changes in connective tissue known to exist in trisomy 21 are at least in part responsible.[122-124,150,151]

Ultrasound Evaluation of the Fetal NB

In the first trimester, the nasal bridge is evaluated only for the presence or absence of the NB.[152,154-159] Measuring the NB does not appear to improve screening performance at this gestational age.[152,160]

The protocol for ultrasound evaluation of the NB is shown in **Figures 12.2A and B and Box 12.2**. A midline section of the fetal profile is obtained by visualizing the following fetal structures: the hypoechoic region of the thalamus, pons and medulla oblongata, the echogenic line over the nasal bridge representing the skin, and an echogenic line that is located anteriorly and slightly superiorly to the nasal bridge, which represents the skin over the nasal tip. If the NB is present, an echogenic line is also seen within the substance of the nasal bridge. This line is approximately parallel to the line representing the nasal bridge skin. These two lines form a so-called "equal sign". The echogenicity of the NB needs to be greater than that of the skin in order for the NB to be identified as present. The reason for this requirement is that even if the NB is not ossified (i.e. sonographically absent), a very faint echodense line may be seen within the nasal bridge.

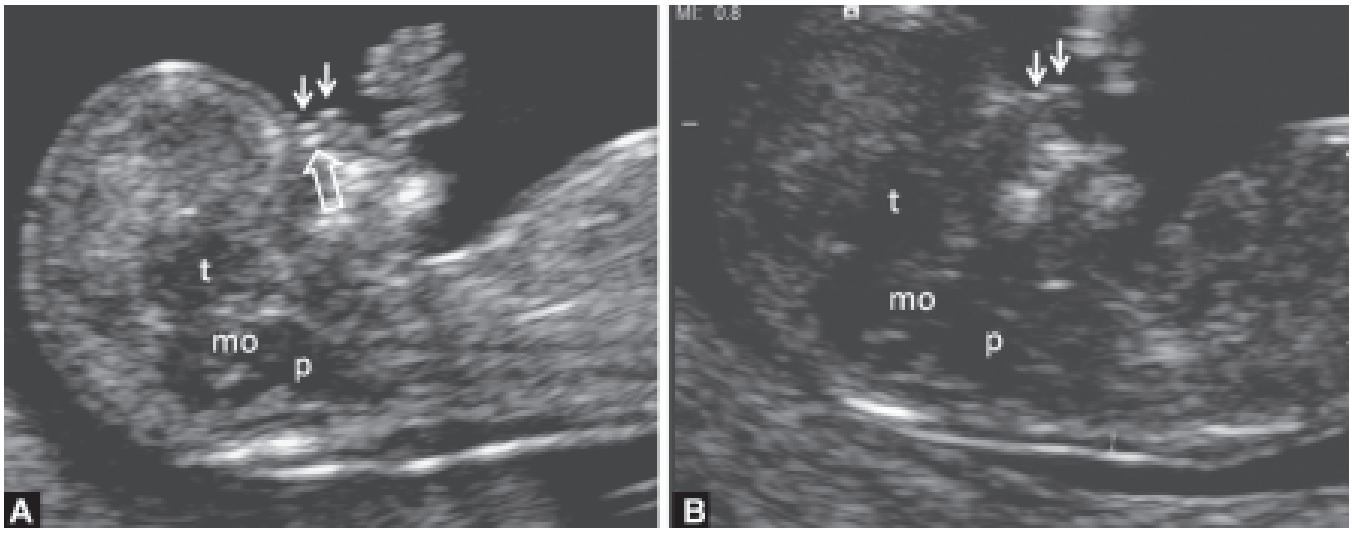

Figures 12.2A and B: Nasal bone evaluation that meets Fetal Medicine Foundation criteria (t=thalamus, mo=medulla oblongata, p=pons, solid arrows=skin over the nasal bridge and the tip of the nose, open arrow=nasal bone) (A) The nasal bone is present (note the "equal sign" formed by the echogenic lines of the skin of the nasal bridge and the nasal bone; (B) The nasal bone is absent (note the absence of the "equal sign")

Box 12.2: The Fetal Medicine Foundation criteria for evaluation of the nasal bone

- CRL - 45-84 mm (11+0 to 13+6 weeks' gestation)
- Midsagittal view (fetus must be facing towards the transducer)
- Image size: head and upper thorax occupies most of the screen
- The face of the transducer is parallel to the long axis of the nasal bone and the skin over the nasal bridge
- Fetal profile must include an echogenic line representing the skin over nasal bridge and an echogenic line in front of it representing the skin over the nasal tip
- Intracranial structures: hypoechoic areas representing the region of the thalamus, pons, and the medulla oblongata
- If the nasal bone is present, a line that is more echogenic than the skin is seen within the nasal bridge. This line is approximately parallel to the skin over the nasal bridge; the two lines form the so called "equal sign"

In order to visualize these anatomic landmarks and identify the NB as a separate structure from the nasal skin, the image needs to be magnified so that the fetal head and upper thorax occupy the majority of the screen. The angle of insonation is extremely important in evaluation of the NB. The face of the transducer should be parallel to the longitudinal axis of the nasal bridge and the NB (90º angle of insonation). The NB may become sonographically invisible if there is a significant deviation from this angle. This is due to the fact that the NB is an extremely thin structure and the lateral resolution of ultrasound equipment is insufficient to visualize the NB if it is viewed "end-on" (close to 0º angle of insonation). Nasal bone evaluation may be done only if the fetus is facing the transducer.

Three-dimensional ultrasound does not appear to significantly improve the success of examination of the NB.[161] However, one advantage that it holds over the two-dimensional (2D) examination is that it can reliably identify unilateral absence of the NB.[161] The exact likelihood ratio associated with this finding has not been established. However, since it has been seen in association with trisomy 21, unilateral absence of the NB has been assigned the same significance as the bilateral finding.

Nasal Bone and Fetal Aneuploidy

A review of several major studies including approximately 50,000 fetuses found that the NB was absent in 2% of euploid and 65% of trisomy 21 fetuses.[152] The prevalence of an absent NB is also increased in trisomy 18 (55%), trisomy 13 (34%), monosomy X (11%) but not in triploidy.[162] The presence or absence of the NB is independent of the maternal serum free β-hCG and PAPP-A levels.[3,154,163,164] However, likelihood ratios do need to be adjusted for gestational age, ethnicity and NT thickness.[162] A higher proportion of euploid fetuses have an absent NB at early (11 weeks) gestation and the prevalence of this marker is higher in Africans than Asians and Caucasians with resultant changes in the likelihood ratios. The relationship between an absent NB and NT measurement is not significant until the NT measurement exceeds the 99th percentile (equating to

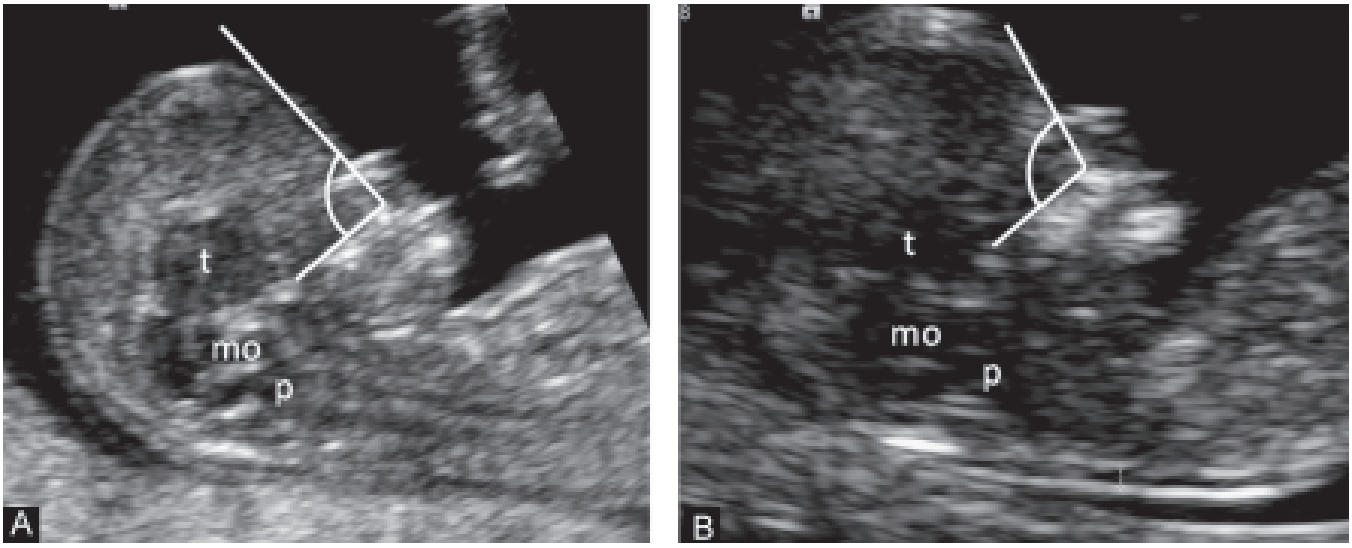

Figures 12.3A and B: Frontomaxillary angle measurement that meets Fetal Medicine Foundation criteria (t = thalamus, mo = medulla oblongata, p = pons). Note the absence of the frontal process of the maxilla between the hard palate and the nasal bone, which helps to assure that plane of insonation is precisely in the midline. (A) The frontomaxillary angle is acute and within normal limits; (B) The frontomaxillary angle is obtuse and is above the normal range

approximately 3.5 mm at any point between 11 and 13+6 weeks' gestation).[162] The consequence of this is that in most circumstances, the likelihood ratio for an absent NB does not have to be adjusted for the NT measurement.

A study of 19,614 fetuses demonstrated that the addition of NB evaluation to traditional combined first trimester screening led to a decrease in the false-positive rate (to 3%) and increase in the detection rate (92%) of trisomy 21. In this series, inclusion of the NB in the screening algorithm gave a 100% detection rate for trisomies 18, 13, and for monosomy X.[3]

Frontomaxillary Facial Angle

Flat faces is recognized as a common dysmorphic feature in individuals with Down syndrome. This may be subjectively assessed even on prenatal ultrasound by examining the fetal profile. However, in order for this facial feature to be exploited for screening purposes, a method had to be developed to evaluate it using a standardized measurement. The FMF angle measurement is an objective way to estimate mid-face hypoplasia; the deeper the location of the front edge of the maxilla is with respect to the forehead, the shallower the FMF angle.[165] The reason for mid-face hypoplasia in trisomy 21 also appears to be the presence of abnormal connective tissue. Theoretically, abnormal bone modeling due to hypotonia of the tongue may also be a contributing factor.

Box 12.3: Fetal Medicine Foundation criteria for measurement of the frontomaxillary angle

- CRL : 45-84 mm (11+0 to 13+6 weeks' gestation)
- Midsagittal view (fetus must be facing towards the transducer)
- Image size: head and upper thorax occupies most of the screen
- Face of the transducer is approximately parallel to the long axis of the nasal bone
- Fetal profile must include an echogenic line representing the skin over nasal bridge and an echogenic line in front of it representing the skin over the nasal tip
- Intracranial structures: hypoechoic areas representing the region of the thalamus, pons, and the medulla oblongata
- Space between the upper palate and the nose should be devoid of echogenic structures (frontal process of the maxilla)
- FMF angle: first ray is drawn along the upper edge of the hard palate, apex of the angle is at the anterior edge of the maxilla, second ray from the apex upwards resting on the echogenic line beneath the skin (the non-calcified metopic suture)

Frontomaxillary Facial Angle Measurement

The image requirements for FMF angle measurement **(Figs 12.3A and B and Box 12.3)** are very similar to those for NB evaluation. The head and the upper thorax should fill the majority of the image and the fetus needs to be facing the transducer. The greatest of care must be taken to obtain a precise midline section, as the smallest deviation has a significant effect on measurement.[166] The landmarks used to determine this are the same as those used for NB evaluation: echogenic skin over the nasal bridge and nasal tip seen in the same

view on the surface of the profile and the intracranial hypoechoic regions of the thalamus, pons and the medulla oblongata.[166] Additionally, in the precise midline view, the area between the upper edge of the hard palate and the NB is relatively echo free. As the plane of insonation deviates slightly from the midline, an echogenic structure comes into view. This represents the frontal process of the maxilla, a finding that should be absent in the correct view. The use of 3D ultrasound may be helpful in establishing the precise midline section.[166]

The angle of insonation is also similar to the one required for NB evaluation: the face of the transducer should be roughly parallel to the long axis of the NB and the skin over the nasal bridge. The hard palate, which is composed of the maxilla and the vomer bones, is seen as a roughly trapezoid echogenic structure with the posterior portion being slightly thicker than the anterior one.

In order to measure the frontomaxillary angle, the following lines are generated: The first one runs along the upper edge of the hard palate. The vertex of the angle is at the anterior-most portion of the maxilla. The second line of the angle runs upwards from the vertex towards the forehead. It is positioned so its inner edge rests upon the metopic suture, which lies a short distance beneath the skin. In the first trimester, the metopic suture is not yet ossified. Therefore, it is seen as a line of similar echogenicity as the skin.

The deep position of the front edge of the maxilla in fetuses with trisomy 21 may be due to maxillary hypoplasia, dorsal displacement of the maxilla or a combination of the two. **Figures 12.3A and B** illustrate the difference between FMF measurements in a fetus with trisomy 21 and in an euploid fetus.

In the first trimester, the division between the vomer bones and the maxilla is usually difficult to see. However, towards the end of the first trimester, this division may become evident as an oblique hypoechoic line running from the upper edge of the hard palate anteriorly to the lower edge of the hard palate posteriorly.[167] This line should not be used to form the lower boundary of the FMF angle.

Frontomaxillary Angle and Fetal Aneuploidy

The normal range of frontomaxillary angle measurements decreases with advancing gestational age.[168] They are independent of NT measurements, presence or absence of the NB and maternal serum biochemistries.[4,165]

Shallow FMF angles are seen not only in trisomy 21 but also in trisomies 18 and 13. Fetuses with trisomies 21, 18 and 13 have FMF angle measurements that are above the 95th percentile in 45%, 58% and 48% cases, respectively.[4,169,170] In a study, which included 782 euploid fetuses and 108 fetuses with trisomy 21, a 92% detection rate for a 3% false-positive rate was achieved by adding FMF angle measurement to the combined screen.[4]

Doppler Evaluations of Fetal Blood Flow as Markers for Aneuploidy

The fetal cardiovascular system has a number of structural and functional features that differentiate it from the cardiovascular system *ex utero*. The arrangement of the myocytes within the fetal heart is less well organized and there are fewer sarcomeres per unit mass.[6] The fetal myocardium has lower compliance resulting in a higher intraventricular pressure at any cardiac volume. Early in pregnancy, placental vascular resistance is relatively high, placing additional strain on the heart. As a consequence, the fetal heart functions at the upper limits of the Frank-Starling curve. In the first trimester, abnormalities of cardiac structure and/or performance may lead to detectable changes in blood flow through certain structures. The two structures that have been investigated the most and hold promise in screening for aneuploidy are the TCV[171] and the DV.[172] The DV is strictly a fetal structure that carries 50% of the oxygenated blood from the umbilical vein and empties into the inferior vena cava at a point that is very close to the right atrium. Its proximity to the right side of the heart makes it susceptible to changes in cardiac function.[173-184] Tricuspid valve flow is considered abnormal in the presence of regurgitation and DV flow is considered abnormal if the a-wave is reversed (see below). The temporal relationship between Doppler flow patterns (normal and abnormal) across the TCV and DV are demonstrated in **Figure 12.4**.

Tricuspid Valve Regurgitation

The exact reason for the increased prevalence of TCV regurgitation in fetuses with trisomy 21 is not completely clear. However, it is likely that it is related to the structural and ultrastructural changes in the heart that are known to be associated with trisomy 21: decreased number of myocytes, abnormal orientation of myocytes and myofibrils and abnormal connective tissue.[6,8,122-124] It may be that these changes result in a relative dilatation of the right ventricle. It is also recognized that dilatation of the right ventricle may lead to tricuspid regurgitation by dilating the TCV annulus. Finally, the connective tissue abnormalities that affect the myocardium are also present in the valve itself.[8] It

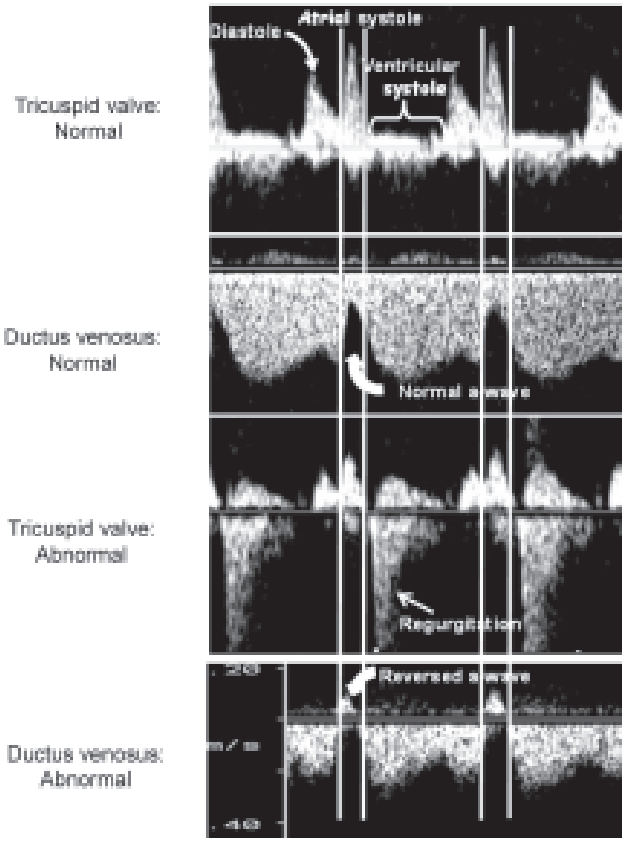

Figure 12.4: Tricuspid valve and ductus venosus Doppler waveforms demonstrating temporal relationship between normal and abnormal findings during the cardiac cycle. (reproduced with permission from ref. 228)

may be that both of these mechanisms are involved in causing TCV incompetence and regurgitation.

Pulsed Doppler Evaluation of Blood Flow across the TCV

The protocol for TCV evaluation using pulsed Doppler is shown in **Figures 12.5A and B and Box 12.4**. A magnified transverse section of the fetal thorax containing a four-chamber view is obtained. The angle of insonation is important. The heart view should be apical so that the angle of insonation with respect to the ventricular septum is less than 30°. The Doppler gate is placed across the TCV. The gate should be relatively large (2–3 mm) to make certain that it covers both sides of the valve. It should be kept in mind that not all of the leaflets of the TCV are necessarily incompetent. Therefore, at least three Doppler evaluations should be obtained. It is also helpful to interrogate the TCV flow in real-time sweeping through the valve to make sure that it is interrogated in its entirety. If tricuspid regurgitation is present, color Doppler may occasionally demonstrate a small discrete jet within the right atrium.

The normal TCV waveform demonstrates a biphasic pattern of blood flow into the right ventricle. The first peak represents filling during ventricular diastole and the second peak represents filling in atrial systole **(Figs 12.4 and 12.5)**. If the TCV is competent, there should be no flow during ventricular systole. Since the size of the first trimester heart is quite small and a relatively large Doppler gate is used, the waveform may

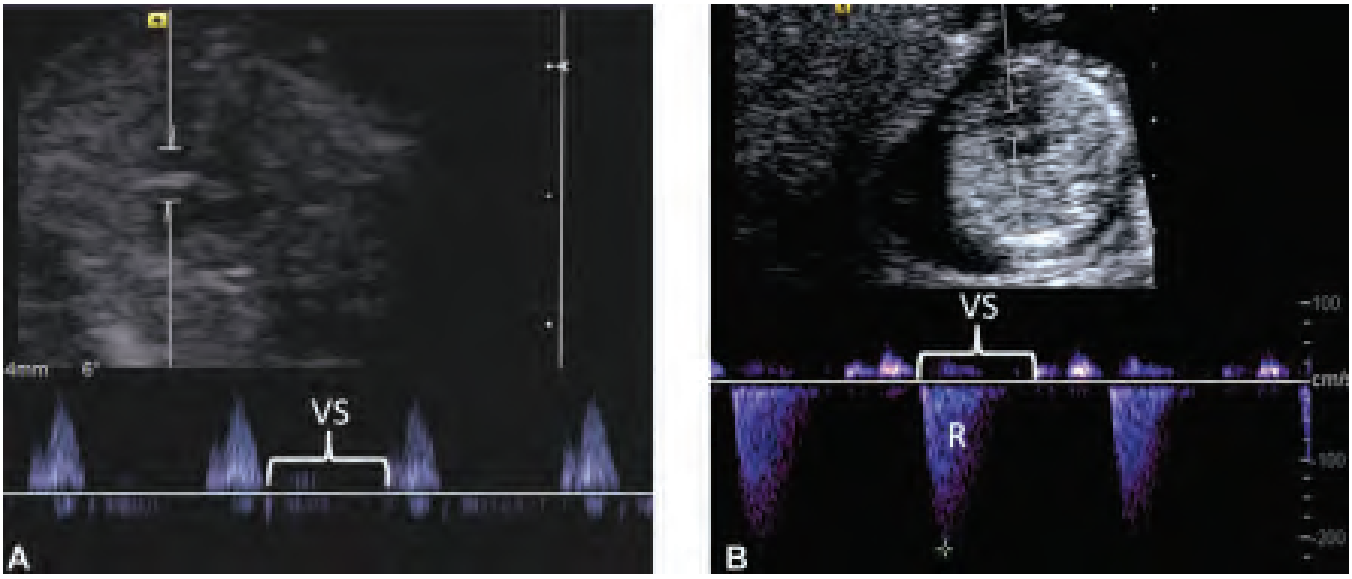

Figures 12.5A and B: Evaluation of the flow across the tricuspid valve (TCV) using Doppler; (A) Normal flow pattern across the TCV with no regurgitant flow during ventricular systole (VS); (B) Abnormal flow pattern across the TCV with regurgitant flow (R) present during ventricular systole (VS)

Box 12.4: The Fetal Medicine Foundation criteria for the evaluation of flow across the tricuspid valve using Doppler

- CRL : 45-84 mm (Gestation ~ 11+0 to 13+6 wks)
- Apical four-chamber heart view (fetus may be facing towards or away from the transducer)
- Image size: thorax occupies most of the screen
- Pulsed-wave Doppler: the sample gate should be large (2-3mm in width) and is positioned across the tricuspid valve, the angle formed by the ventricular septum and Doppler beam must be < 30°
- True tricuspid regurgitation (R): 1. velocity > 60 cm/sec (in order to differentiate from a great vessel waveform where the velocity is generally ≤ 50 cm/sec). 2. duration ≥30% of the ventricular systole (VS)
- At least three sample volumes need to be obtained as the insufficiency may not be present in all three cusps

be contaminated by flow through the left ventricular outflow tract. The direction of blood flow through the aortic root is the same as that of the regurgitant jet and they are seen at the same point in the cardiac cycle: therefore, it is imperative to be able to differentiate between the two. There are two consistent differences in their flow pattern. Firstly, the velocity in the great vessel is typically < 40 cm/sec whereas the velocity of the regurgitant jet is always > 60 cm/sec. Therefore, in order to diagnose TCV regurgitation, the blood flow velocity has to be in excess of 60 cm/sec. Secondly, unlike flow through the left ventricular outflow tract, the regurgitant jet has a distinctive high-pitched hissing sound on Doppler. Indeed, it is often this sound that first alerts the sonographer to the presence of TCV regurgitation. Since a signal from a closing TCV and trivial tricuspid regurgitation are fairly common findings and are of no clinical significance, regurgitation must last at least 30% of the ventricular systole to be defined as an abnormal finding.

Tricuspid Valve Doppler and Fetal Aneuploidy

Tricuspid regurgitation is more prevalent in aneuploid than euploid fetuses. The prevalence in fetuses with trisomies 21, 18 and 13 and monosomy X is 56%, 33%, 30%, and 38%, respectively. The prevalence of tricuspid regurgitation in euploid fetuses is 1%.[11] In a study of 19,614 fetuses where TCV evaluation was added to combined first trimester screening, a 96% detection rate for trisomy 21 was achieved while maintaining a 3% false-positive rate. The detection rates for trisomies 18 and 13 and monosomy X were 92%, 100% and 100%, respectively.[11]

The prevalence of tricuspid regurgitation decreases with advancing gestational age and increases with NT thickness.[11] These associations are factored into the risk algorithm developed by the Fetal Medicine Foundation. It should be noted that tricuspid regurgitation is also associated with an increased risk of congenital heart defects.[10] A careful examination of the fetal heart should be performed at the time when TCV regurgitation is noted and repeated in the mid-second trimester.

Reversed A-Wave in the Ductus Venosus

The exact reason for a reversal of the a-wave in the DV in association with trisomy 21 is also not clear. However, it is likely that this abnormality is not a result of a change in the DV itself but rather due to a change in the fetal heart performance. Therefore, the ultrastructural changes in the cardiac anatomy described earlier in the "TCV regurgitation" section may also be responsible for this phenomenon.[6,8,122-124] However, the a-wave abnormality is likely to be the result of decreased compliance of the ventricular walls rather than ventricular dilatation. The mechanical explanation for a-wave reversal may be that the atrial wall is contracting against a relatively stiffer wall and has to generate more pressure to push the blood across the TCV. The increased back pressure, which would be inevitably generated in this situation, may be sufficient to either stop or reverse the blood flow during atrial systole (absent or reversed a-wave). In the current FMF algorithm, the DV flow is considered abnormal only if the a-wave is actually reversed.

Pulsed Doppler Evaluation of Blood Flow through the Ductus Venosus

The fetus is examined in right parasagittal section **(Figs 12.6A and B and Box 12.5)**. The DV is seen as a short continuation of the hepatic portion of the umbilical vein (UV) and is best identified using color Doppler. The DV is distinguishable from the UV as it has a distinctly higher velocity and aliasing of flow can be seen. The pulsed Doppler gate is placed within the lumen of the DV. The gate needs to be small (0.5–1 mm) to minimize contamination of the signal by venous structures such as the hepatic veins and the inferior vena cava, which are in close proximity. The magnification should be such that the fetal abdomen and thorax fill the majority of the image. The angle of insonation of the Doppler beam should be < 30° with respect to the longitudinal axis of the DV.

On pulsed Doppler, a normal DV waveform demonstrates forward blood flow throughout the cardiac cycle. There are two adjoining peaks of increased flow representing ventricular systole and the diastole.

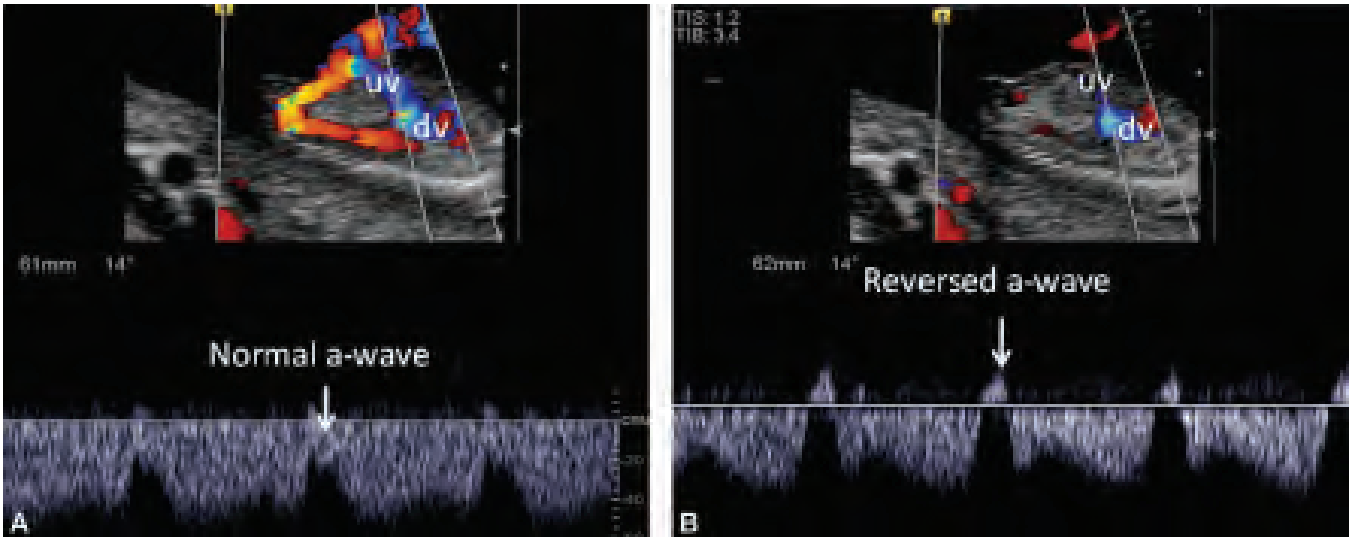

Figures 12.6A and B: Evaluation of the ductus venosus (DV) flow using Doppler (uv=hepatic portion of the umbilical vein). (A) Normal DV flow pattern with antegrade flow during the entire cardiac cycle, including during the atrial contraction (a-wave); (B) Abnormal DV flow pattern with reversed flow during the atrial contraction (a-wave)

Box 12.5: The Fetal Medicine Foundation criteria for the evaluation of ductus venosus flow using Doppler

- CRL : 45-84 mm (11+0 to 13+6 weeks' gestation)
- Right ventral midsagittal view
- Image size: thorax and abdomen occupy most of the screen
- Color flow Doppler is used to identify the hepatic portion of the umbilical vein and the ductus venosus, which appears as a continuation of the umbilical vein. Since the flow velocity in the ductus venosus is significantly higher than in the rest of the venous system, aliasing will be seen on color Doppler
- Pulsed-wave Doppler: angle of insonation with respect to the longitudinal axis of the DV must be < 30° and the sample gate must be small (0.5-1mm).
- The filter should be set at a low frequency (50-70 Hz) so the a-wave is not obscured
- The sweep speed should be high (2-3cm/sec); the spreading of the waveforms allows better assessment of the a-wave

Normally, blood flow is diminished during atrial systole but forward flow is maintained **(Figs 12.4 and 12.6)**.

Ductus Venosus Doppler Flow and Fetal Aneuploidy

A reversed a-wave is seen not only in fetuses affected by trisomy 21 but also in those with trisomies 18 and 13 and monosomy X. The prevalence of reversed flow in the a-wave of the DV in fetuses with trisomies 21, 18 and 13 and monosomy X is 66%, 58%, 55% and 75%, respectively. The prevalence of a reversed a-wave in euploid fetuses is 3%.[17] In a study of 19,614 fetuses where evaluation of the DV was added to combined first-trimester screening, 96% of fetuses affected by trisomy 21 were detected while maintaining a 3% false-positive rate. The detection rates for trisomies 18 and 13 and monosomy X were 92%, 100% and 100%, respectively.[17]

The prevalence of a-wave reversal decreases with advancing gestational age and increases with NT thickness. These associations are mathematically accounted for in the FMF risk algorithm.[17] A-wave abnormalities are also associated with an increased risk of cardiac anomalies.[18,19,182] A careful examination of the fetal heart should be performed at the time when the reversed a-wave is noted and be repeated in the mid-second trimester.

Fetal Heart Rate in Screening for Aneuploidy

It has been noted that aneuploid fetuses tend to have different heart rates from euploid fetuses at the time of first-trimester screening.[2,20] The largest difference is seen in trisomy 13 and monosomy X where the heart rate is >95th percentile in 69% and 53% of cases, respectively. The heart rate also tends to be increased in trisomy 21 but much less so (14% are >95th percentile). Both trisomy 18 and triploid fetuses tend to be bradycardic (19% and 36% <5th percentile, respectively). If FHR is included in first-trimester screening, it needs to be adjusted for gestational age as the normal ranges decrease between 11 and 13+6 weeks of gestation.[2,20]

QUALITY ASSURANCE IN FIRST-TRIMESTER ULTRASOUND

All the ultrasound markers for aneuploidy listed above can be used to generate likelihood ratios in risk assessment for trisomy 21 and other chromosomal abnormalities. The likelihood ratios are based on the described prevalence of these anomalies in normal and aneuploid populations. It is therefore extremely important to standardize techniques for measurement to ensure that accurate risks are produced. Sonographers must have adequate opportunity for training and to develop experience in first-trimester ultrasound before they begin to employ any of the ultrasound markers for risk assessment. It is equally important to have a method of audit in place that provides operators with feedback about their performance. The Fetal Medicine Foundation provides sonographers with an opportunity to complete an annual audit cycle to review their performance. This involves comparison of an individual's NT measurement data with the internationally established normal ranges. Undermeasurement of NT has the potential to decrease both the false-positive rate and the detection rate of screening while overmeasurement will lead to an increase in both of these parameters.[185]

For example, review of the audit process in Australia, using the methods described by the FMF, has shown that while the national range of NT measurements is almost identical to that described in a UK population, there is a significant minority of operators who under and overmeasure NT.[186] This process of review of the audit system has allowed the NT accreditation program to identify operators that have widely differing NT distributions and provide them with additional education and assist them with development of practical skills in first-trimester ultrasound.

Studies examining the introduction of additional markers, such as examination of the NB and of the DV have shown that a sonographer needs to perform approximately 60–80 ultrasound examinations in order to be able to evaluate each of the first trimester markers correctly on a consistent basis.[187-189] These markers are categorical, i.e. they are either present or absent, and their prevalence is high in the aneuploid population and low in the euploid population. Consequently, the likelihood ratios (positive and negative) are large and have a significant effect on risk evaluation. This underscores the fact that adequate training and experience before employing these markers is critical. Methods for auditing categorical markers on an ongoing basis are less well developed. One approach currently available is to monitor the overall screen positive rate as this is a reflection of the false-positive rate. If the false-positive rate deviates significantly from that reported in the reference population, one of the explanations may be inappropriate examination of the additional ultrasound markers. This is especially true if the sonographer's distribution of NT measurements is adequate. Evaluating first-trimester ultrasound markers in a manner that is not in accordance with the standard method not only affects the performance of the screening program overall but also provides individual patients with inaccurate risk assessments.

First-Trimester Screening for Aneuploidy Using Multiple Ultrasound Markers

Assessment of these additional ultrasound markers is best performed within the context of an overall risk algorithm rather than independently as the latter approach risks increasing the false-positive rate. The ultrasound and maternal serum biochemical markers described above are sufficiently independent of each other to be used in combination. This can be either done by evaluating and using all markers in the calculation of risks for every fetus or on a contingent basis. The latter approach includes the use of three categories: high, intermediate and low risk. It begins by calculation of the risk for aneuploidy from a more limited combination of markers. Evaluation of additional markers is done only in fetuses that fall into the intermediate risk group, i.e. it is contingent on the initial findings. The contingent approach allows the extra markers to be used selectively but still increases the detection rate whilst maintaining a low false-positive rate. Furthermore, mathematical modeling predicts that the detection and false-positive rates are identical whether the contingent approach is used or if all markers are examined in every fetus.

An algorithm using ultrasound markers for aneuploidy on a contingent basis in the first trimester was developed by the Fetal Medicine Foundation.[143] The first step taken in using this approach is to perform the combined screen (maternal age, NT measurement, free β-hCG level and PAPP-A level) in every patient. Based on the results of the combined screen, the patients are divided into the three categories described above: high risk (trisomy 21 risk of $\geq$1:50), intermediate risk (trisomy 21 risk of 1:51 to 1:1,000) and low-risk category (trisomy 21 risk <1:1,000). The patients that fall into the high-risk category are offered an invasive diagnostic procedure without any additional screening. This category constitutes only 1.3% of the total screened

population but contains 82% of the fetuses with trisomy 21. The low-risk group constitutes the majority of the screened population (86.7%) but contains only 4% of fetuses with trisomy 21. These patients are reassured and invasive diagnostic testing is limited to women requesting it, despite the screening result. The intermediate risk category constitutes 12% of the screened population and includes 14% of trisomy 21 fetuses. Women in this group undergo additional screening by evaluating the additional ultrasound markers (NB, FMF angle, TCV and DV). If the resultant risk of trisomy 21 exceeds 1:100, an invasive diagnostic test is offered. If it is less than that, they are treated in the same way as the low-risk group. A careful mid-second trimester ultrasound examination is indicated for patients who reach that point in all three categories. For a 2% false-positive rate, the detection rate for trisomy 21 using one, two, three or four additional marker are 90%, 94%, 95% and 96%, respectively. These detection rates are the same whether the contingent approach is used or if all additional markers are used in every patient.[3,4,11,17,142]

Structural Abnormalities as Markers of Aneuploidy

Some structural anomalies, seen on first-trimester ultrasound also increase the risk of aneuploidy. As such they play a dual role: they serve as markers and they are of clinical significance even in the absence of aneuploidy. Structural abnormalities that have well-defined fixed risks associated with them include holoprosencephaly (risk of 1 in 2 for trisomy 13), diaphragmatic hernia (risk of 1 in 4 for trisomy 18), atrioventricular septal defect (risk of 1 in 2 for trisomy 21), omphalocele (risk of 1 in 4 for trisomy 18 and risk of 1 in 10 for trisomy 13), megacystis defined as bladder length of $\geq$ 7 mm (risk of 1 in 10 for either trisomy 18 or 13).[190-193] The fixed risks associated with these anomalies are included in the FMF risk algorithm.

"Soft" Ultrasound Markers for Aneuploidy

Some ultrasound markers that have been shown to increase the risk of fetal aneuploidy in the second trimester appear to do so in the first trimester as well. "Soft" or "pure" ultrasound markers are defined as those findings that, in the absence of aneuploidy, have no clinical significance. These include choroid plexus cysts (>1.5 mm), echogenic intracardiac foci, hyperechogenic bowel and hydronephrosis (anteroposterior diameter of the renal pelvis >1.5 mm).[194] These markers are also included in the FMF algorithm in screening for trisomy 21. The presence of these markers should be interpreted in the context of the presence/absence of other markers or anomalies: an isolated minor marker probably does not increase the risk of aneuploidy as the absence of other markers acts as a counterbalance and decreases the risk sufficiently to negate the effect of the presence of a single marker.[194]

SCREENING MULTIPLE PREGNANCIES FOR DOWN SYNDROME

The calculation of the risk of aneuploidy in a twin pregnancy is complicated by a number of factors. Ultrasound is very effective at determining chorionicity. Monochorionic twins can be defined as being monozygotic, which almost universally have the same karyotype. Dichorionic twins, on the other hand may be either dizygotic (majority) or monozygotic (minority). In dizygotic twins, development of abnormalities in one or the other fetus is an essentially independent event. The result is that if an abnormality is present, it generally affects only one fetus. Both fetuses may also be affected, though the statistical chance of this happening is invariably very small. In the small proportion of dichorionic twins that are monozygotic, if aneuploidy is present, generally both the fetuses are affected.

Placentation also affects the performance of biochemical markers, as the presence of a "normal" twin placenta partially masks any changes in serum markers seen in the placenta of the affected co-twin. The situation becomes more complex in higher order multiples and currently there is no data to support the use of serum screening in these groups. Due to these difficulties, it is tempting to rely on markers for aneuploidy that are expressed by the fetus, namely those that can be assessed with ultrasound: NT thickness, the NB, FMF angle and the hemodynamic markers.

In singleton pregnancies, the calculation of risks generated by combined first-trimester screening first involves defining a background risk based on maternal age, gestational age and taking account of a previous history of a pregnancy affected by aneuploidy. Maternal age-related risks for twins have been calculated and published and suggest that the presence of two fetuses compounds the risk for the mother.[195,196] The first consequence of this is that a 32-year-old woman carrying twins effectively has the same background risk as a 35-year-old woman pregnancy. Therefore, maternal age potentially has a greater impact on the final risk generated through screening in twins and may lead to an increase in the false-positive rate for any age group compared to singleton pregnancies. There is a little

prospective data to support this proposed increase in risk and some concern over the methodology by which these risks were calculated and it has been suggested that the overall level of risk in a dizygotic twin pregnancy is in fact similar to that seen in a singleton pregnancy.[197]

Gestational age, which also affects the background level of risk, may be harder to calculate in a twin pregnancy. Since it is rare to find both twins that have the same CRL measurement, a decision must be made as to which CRL should be used for gestational age assessment. It is likely that if a pathologic process affects fetal growth in the first trimester, it will do so by restricting it. Therefore, it appears to be sensible to use the larger CRL measurement for dating purposes. It should be remembered that likelihood ratios for all ultrasound and biochemical findings are generated on the basis of CRL and relatively small changes in CRL can affect risks significantly.[116] Similarly, large CRL discrepancies are associated with poor pregnancy outcome[198,199] and include pathologies, which may also impact the markers being assessed for aneuploidy.

There is some evidence that points to an association between the NT measurements in twin pairs. Interestingly, this appears to be present in both monochorionic and dichorionic twin pregnancies. Therefore, it has been suggested that likelihood ratio generated in one twin should be based not only on its own NT measurement but be also adjusted by a correction factor based on the co-twin's NT measurement.[200,201]

Most importantly, there is a good evidence to suggest that NT measurements in monochorionic twins may be affected by an early form of twin-to-twin transfusion syndrome (TTTS).[100,202] It is thought that the inequity in the circulating blood volumes of the twins results in nuchal thickening in the recipient. Since this condition affects up to 15% of monochorionic twins, a significant discordance in fetal NT's is more likely an early sign of TTTS than of aneuploidy.[100] Vandencrus et al. examined a number of options for the incorporation of NT in risk assessment in monochorionic twins.[203] The method that appears to produce the best result is to calculate risks based on CRL and NT for each individual fetus and assign the overall risk for the whole pregnancy by averaging the two. This is, however, likely associated with an increase in the screen positive rate of screening.

There are a few studies that have examined the incorporation of additional ultrasound markers in a screening strategy for twins. Matias et al. have shown that the hemodynamic marker of an absent or reversed a-wave in the DV is strongly associated with TTTS.[184] To date there is no data on the performance of TCV regurgitation in this cohort of pregnancies. The NB is an attractive and potentially powerful marker in twins–as pathologies related to fetal growth and/or TTTS are unlikely to affect the presence of the NB. Sepulveda et al. have demonstrated that the technical difficulties the sonographer faces in assessing twins can be overcome and that the NB can be assessed effectively in 95% of cases.[204] Early data examining the effectiveness of a variety of screening combinations suggests that using NT and NB may be more effective than using NT and biochemistry.[205] Effective screening of twins appears to be possible. However, limitations inherent to the calculation of risk under these circumstances and the potential influence by pathologies other than aneuploidy need to be recognized.

FIRST TRIMESTER SCREENING FOR FETAL ANOMALIES OTHER THAN CHROMOSOMAL DEFECTS

Nuchal Translucency Measurement as a Marker for Fetal Abnormalities in Chromosomally Normal Fetuses

Nuchal translucency thickening is associated with an increase in poor pregnancy outcome even if the fetus is chromosomally normal.[206-215] This increase does not become statistically significant until the NT measurement exceeds the 99th percentile. Conveniently, the 99th percentile cutoff remains constant at 3.5 mm across the 11–13+6 weeks' gestation period.[216]

A number of different fetal conditions may result in NT thickening making this measurement a useful test across a broad range of fetal anomalies.

Nuchal Translucency Thickening and Fetal Structural Defects

The prevalence of major fetal abnormalities increases exponentially as the NT measurement increases beyond the 99th percentile (> 3.5 mm). The prevalence is approximately 2.5% for an NT of 3.5 mm and reaches 45% for an NT of 6.5 mm or more.[51,217]

One of the most important areas where NT screening appears to offer an advantage is the prenatal diagnosis of cardiac defects. Cardiac defects are some of the most common congenital structural anomalies but their prenatal diagnosis is in many cases challenging. However, if an accurate prenatal diagnosis of CHD is made, the overall outcome is improved by allowing for the fetus to be delivered in a setting where appropriate

neonatal treatment is available. Combined data from a number of screening studies demonstrates that the prevalence of major cardiac defects is 1–2% in fetuses with a < 3.5 mm NT measurement. A significant increase in the prevalence of CHD is noted with NT measurements ≥ 3.5 mm: 3% (3.5–4.5 mm), 7% (4.5–5.4 mm), 20% (5.4–6.4 mm), 30% (≥6.5 mm).[36,39,41-43,206]

A meta-analysis of screening studies showed a detection rate of 31% for CHD using an NT measurement of 3.5 mm as the cutoff. It is estimated that fetal echocardiography in all chromosomally normal fetuses with NT above the 99th percentile would identify one major cardiac defect in every 16 patients examined.[46] Furthermore, this analysis showed that increased NT measurements increase the risk of a variety of heart defects. Results of another study arrived at the same conclusion.[218] In this multicenter study, nuchal thickening was found to be present in all types of heart defects: left as well as right heart lesions, septal defects, outflow tract disorders, laterality disorders and complex heart lesions.

With improvements in the resolution of ultrasound equipment, a detailed fetal cardiac evaluation may be performed even in the first trimester of pregnancy. Many of the major cardiac defects may now be diagnosed at the time of the 11–13+6 week scan.[37,52,89,219,220] Even if a specific diagnosis cannot be made, the cardiac examination often indicates whether or not a cardiac structural defect is present.

There are a number of other types of fetal defects that are seen more commonly in fetuses with NT measurements of > 3.5 mm than in fetuses with normal NT measurements.[52-54,201] These include diaphragmatic hernia,[49] omphalocele,[48] body stalk anomaly,[50] skeletal defects[55-65] and certain genetic syndromes such as congenital adrenal hyperplasia,[68] fetal akinesia deformation sequence,[70] Noonan syndrome,[66] Smith-Lemli-Opitz syndrome[221] and spinal muscular atrophy.[71,72] There are many additional disorders that have been reported in association with a thickened NT that are quite rare. Because of their rarity, a definite association with a thickened NT is difficult to prove in many of these.[53]

Finally, the prevalence of fetal demise is increased in chromosomally normal fetuses in which the NT measurement ≥ 3.5 mm even if a specific fetal defect cannot be diagnosed. An analysis of 4,540 fetuses categorized based on the NT measurement showed an increase in intrauterine loss from 1.3% in the 95th–99th percentile group to 20% in those that had NT measurements ≥ 6.5 mm.[52,217] The majority of fetal losses occur by 20 weeks' gestation. In fetuses that survive to the mid-second trimester and in which a targeted ultrasound fails to reveal any anomalies or increased nuchal fold thickness, the risk for perinatal or long-term morbidity and mortality does not appear to be increased.[211,212,222-226]

Screening For Open Neural Tube Defects

One of the major failings of the first-trimester fetal ultrasound examination had been the inability to consistently diagnose open neural tube defects (ONTD) other than the exencephaly/anencephaly sequence. However, a recently described intracranial marker [intracerebral translucency (IT)] may overcome this deficiency.[25] The fetal image required to evaluate the IT is identical to those needed for the NT, NB and FMF angle evaluation. A magnified midline view of the fetal head and upper thorax is obtained and the following intracranial structures need to be visualized: hypoechoic regions of the thalamus, the pons (brainstem) and the medulla oblongata **(Fig. 12.7 and Box 12.6)**. Intracranial translucency represents the fluid-filled fourth ventricle, which is located posterior to the pons. The combination of the posterior border of the pons and the floor of the fourth ventricle is seen as a single, thin echogenic line, which forms the anterior border of the IT. The posterior border of the IT is the roof of the fourth ventricle. This is also seen as a relatively thin echogenic line accentuated by the choroid plexus of the fourth ventricle.

The IT was consistently visualized and was found to be normal at the 11–13+6 week scan in the 200 consecutive fetuses that were subsequently shown not to have an ONTD.[25] In the same study, each of the four fetuses that were diagnosed with an ONTD in the second trimester had an absent first trimester IT (i.e. the fourth ventricle was obliterated).[25] The proposed mechanism for this finding is similar to that of the Chiari type II malformation ("banana sign") seen in second trimester fetuses with spina bifida aperta: decreased pressure in the subarachnoid spaces leading to the caudal displacement of the brain. In the initial study dealing with IT, it appeared that measuring the IT does not provide additional information. However, this needs to be evaluated in prospective studies.

Another recent publication looked at the difference in FMF angle measurements in 20 fetuses with ONTD and 100 fetuses with a normal spine at 11 and 13 weeks' gestation. Ninety percent of the fetuses with ONTD had a FMF angle measurement below the 5th percentile. The FMF angle measurements in the fetuses with ONTD were on average 10° smaller than in fetuses with normal spine.

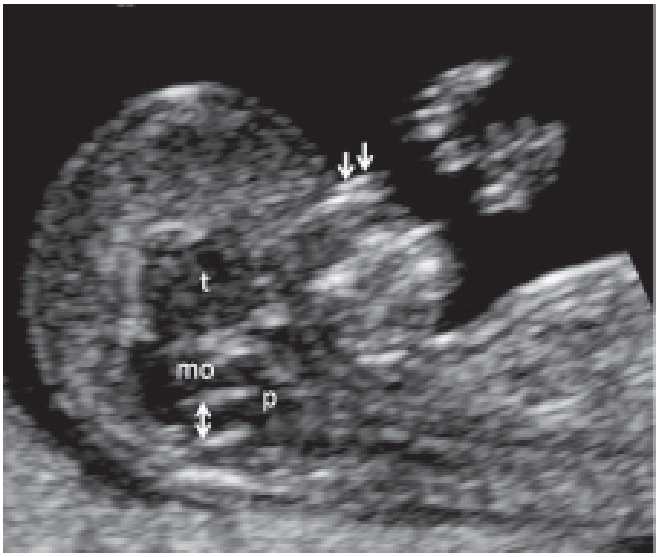

Figure 12.7: Evaluation of the intracranial translucency (double arrow) that meets Fetal Medicine Foundation criteria (t = thalamus, mo = medulla oblongata, p = pons, solid arrows = skin of the nasal bridge and the tip of the nose)

Box 12.6: The Fetal Medicine Foundation criteria for evaluation of the intracranial translucency (IT)

- CRL : 45-84 mm (11+0 to 13+6 weeks' gestation)
- Midsagittal view (fetus may either be facing towards or away from the transducer but the IT is more difficult to see with the fetus facing away from the transducer due to shadowing from the occipital bone)
- Intracranial structures: thalamus, pons, medulla oblongata
- Image size: head and upper thorax occupies most of the screen
- The IT represents fluid within the developing fourth ventricle. The anterior echogenic line is formed by the combination of the posterior border of the pons and the floor of the fourth ventricle. The posterior echogenic line is the roof of the fourth ventricle accentuated by the presence of the choroid plexus

It would be premature to state that obliteration of IT and/or an unusually small FMF angle measurement have the same predictive value as the Chiari type II malformation or the bifrontal scalloping in the second trimester. However, detection of either one of these findings at the time of the first trimester ultrasound should lead to an extremely careful ultrasound evaluation of the spine. If the appearance of the spine is normal on the initial scan, the fetus should be re-examined at approximately 16 weeks. A 20-week scan should also be performed if the 16 week scan is normal.

First-Trimester Screening for Preeclampsia

Preeclampsia is associated with vascular problems within the placental bed. Even though the diagnosis of preeclampsia is not made until the second-half of the pregnancy, maldevelopment of the placental bed vessels occurs well before that time.[227] Vascular resistance to the placenta and placental bed normally decreases as the pregnancy progresses. This process is inhibited in many of those patients who are destined to develop preeclampsia. Different degrees of severity of placental insufficiency appear to be associated with various pregnancy-associated hypertensive disorders, including early-onset preeclampsia [< 34 weeks' gestation, very often associated with intrauterine growth restriction (IUGR)], late-onset preeclampsia (≥ 34 weeks' gestation) and gestational hypertension.[228]

Pulsed Doppler Evaluation of Blood Flow through the Uterine Arteries

The impedance of the maternal blood supply to the placental bed may be estimated by measuring the pulsatility index (PI) of the uterine arteries using Doppler ultrasound. It has been shown that the risk of developing preeclampsia increases with uterine artery PI.[27-30]

First-trimester Doppler examination of the uterine artery involves obtaining a sagittal view of the cervix and the lower uterine segment where the cervical canal and the endocervix are identified. The transducer is then tilted from side-to-side to locate the uterine arteries at the level of the endocervix with the aid of color Doppler **(Fig. 12.8 and Box 12.7)**. The PI is measured using pulsed Doppler with the sample gate set at 2 mm. The angle of insonation with respect to the longitudinal axis of the uterine artery should be < 30°. Magnification needs to be such that the uterine artery can be identified with confidence and the Doppler may be placed accurately within the lumen. In addition to identifying the artery in its proper location, there are two main ways to confirm that the vessel being interrogated with Doppler is the uterine artery. Firstly, the direction of the blood flow should be towards the transducer (i.e. towards the uterine fundus) when the transabdominal approach is used; this assures that the cervical branches are not being insonated. Secondly, the peak velocity of the insonated vessel should be > 60 cm/sec. This assures that the main uterine artery is being insonated rather one of its branches. At least three waveforms similar in shape should be obtained and the PI should be measured in both uterine arteries. The lowest PI is used for risk assessment.

Uterine Artery Doppler and Preeclampsia

Based on a recent publication that included 7,797 patients, it appears that the most efficient method of screening for

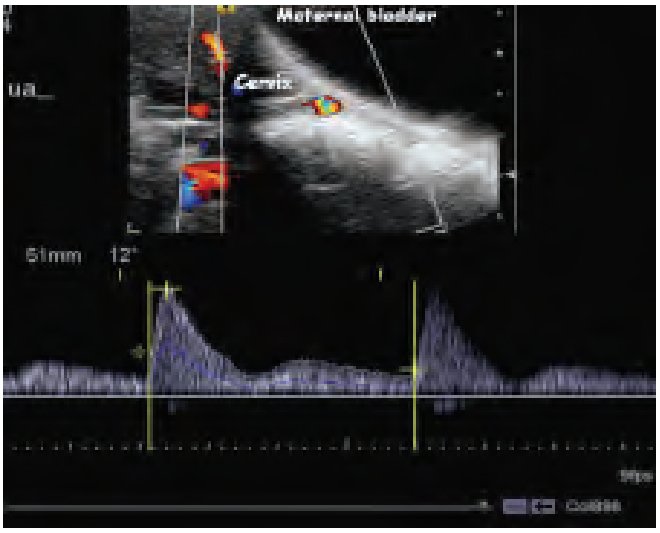

Figure 12.8: Evaluation of the uterine artery blood flow using Doppler

Box 12.7: The Fetal Medicine Foundation criteria for the evaluation of uterine artery blood flow using Doppler

- Location of the uterine artery: just lateral to the cervix at the level of the endocervix
- Doppler gate: 2 mm
- Angle of insonation: < 30°
- Direction of flow: towards the uterine fundus
- Peak systolic velocity > 60 cm/sec
- The lowest PI is used for risk assessment

preeclampsia in the first trimester is based on the following parameters: maternal history, uterine artery pulsatility index (increased PI increases the risk of preeclampsia), mean arterial pressure (increased MAP increases the risk of preeclampsia), pregnancy-associated plasma protein-A (decreased PAPP-A increases the risk of preeclampsia) and placental growth factor (decreased PIGF increases the risk of preeclampsia).[27] Factors in the maternal history that appear to make a significant independent contribution to preeclampsia risk assessment include maternal BMI, age, ethnicity, smoking and parity. For a 5% false-positive rate, combining all these risk factors was shown to predict 90% of early preeclampsia, 35% of late preeclampsia and 20% of gestational hypertension.[27] This compares favorably with screening based on maternal history alone where only 30% of early and 20% of late preeclampsia are predicted for a 5% false-positive rate.

CONCLUSION

Over the past 40 years, ultrasound has become established as an invaluable tool in obstetric management. There has been a steady increase in our understanding of normal and abnormal fetal physiology along with an improvement in the quality of ultrasound equipment. This has not only lead to our ability to diagnose an ever increasing number of fetal conditions but has also moved the point of diagnosis to an earlier gestation. This benefits the patient in a number of ways not the least of which is maintaining the maximum level of privacy and preservation of reproductive choices.

Advances in the screening capabilities of the first trimester scan have lead to an improved detection of fetal abnormalities, especially aneuploidy and resulted in a decreased false-positive rate. The latter has two very important benefits: fewer women have to go through the stress of being told that they fall into the "increased risk" category and fewer women undergo invasive diagnostic procedures. The decrease in the number of invasive diagnostic procedures being performed in turn leads to a decrease in both miscarriage and cost related to invasive procedures.

As our understanding of risk assessment improves, we are able to screen pregnancies for complications other than those caused by the genetic makeup of the fetus. This includes the use of ultrasound assessment of maternal uterine artery flow which can be combined with other clinical and biochemical parameters to accurately estimate the risk of developing preeclampsia and fetal growth restriction later in pregnancy. By improving the selection of high-risk patients, we may be able to manipulate placental development therapeutically and reduce the prevalence of this disease in the future.

As the utility of ultrasound expands and this tool is used in predictive models, our responsibility to perform a quality assured examination increases. This can be achieved only with proper training followed by an ongoing and rigorous quality assurance program. A factor that is difficult to quantify but is none-the-less crucial in performing a high quality ultrasound examination is the level of commitment on the part of each individual sonographer.

REFERENCES

1. Down LJ. Observations on an ethnic classification of idiots. Clin Lectures and Reports, London Hospital. 1866;3:259-62.
2. Kagan KO, Wright D, Valencia C, et al. Screening for trisomies 21,18 and 13 by maternal age, fetal nuchal translucency, fetal heart rate free beta-hCG and pregnancy-associated plasma protein-A. Human Reprod. 1968;23:57.
3. Kagan KO, Cicero S, Staboulidou I, et al. Fetal nasal bone in screening for trisomy 21, 18, 13 and Turner syndrome at

11-13 weeks of gestation. Ultrasound in Obstet Gynecol. 2009;33:259-64.
4. Borenstein M, Persico N, Kagan KO, et al. Frontomaxillary facial angle in screening for trisomy 21 at 11+0 to 13+6 weeks. Ultrasound Obstet Gynecol. 2008;32(1):5-11.
5. Vis JC, Duffels MGJ, Winter, et al. Down syndrome: a cardiovascular perspective. J Intellect Disabil Res. 2009; 53(5):419-25. Epub 2009 Feb 18.
6. Recalde AL, Landing BH, Lipsey AI. Increased cardiac muscle size and reduced cell number in Down syndrome: heart muscle cell number in Down syndrome. Pediatric Pathol. 1986;6(1):47-53.
7. Gittenberger-De Groot AC, Bartram U, Oosthoek PW, et al. Collagen type VI expression during cardiac development and in human fetuses with trisomy 21. Anat Rec A Discov Mol Cell Evol Bio. 2003;275(2):1109-16.
8. Carvalhaes LS, Gervásio OL, Guatimosim C, et al. Collagen XVIII/endostatin is associated with the epithelial-mesenchymal transformation in the atrioventricular valves during cardiac development. Dev Dynamics. 2006;235(1): 132-42.
9. Huggon IC, DeFigueiredo DB, Allan LD. Tricuspid regurgitation in the diagnosis of chromosomal anomalies in the fetus at 11-14 weeks of gestation. Heart. 2003;89(9): 1071-3.
10. Faiola S, Tsoi E, Huggon IC, et al. Likelihood ratio for trisomy 21 in fetuses with tricuspid regurgitation at the 11 to 13+6 week scan. Ultrasound Obstet Gynecol. 2005;26(1): 22-7.
11. Kagan KO, Valencia C, Livanos P, et al. Tricuspid regurgitation in screening for trisomies 21, 18 and 13 and Turner syndrome at 11+0 to 13+6 weeks of gestation. Ultrasound Obstet Gynecol. 2009;33(1):18-22.
12. Maiz N, Valencia C, Emmanuel EE, et al. Screening for adverse pregnancy outcome by ductus venosus Doppler at 11-13+6 weeks of gestation. Obstet Gynecol. 2008;112(3): 598-605.
13. Mavrides E, Sairam S, Hollis B, et al. Screening for aneuploidy in the first trimester by assessment of blood flow in the ductus venosus. BJOG. 2002;109(9):1015-9.
14. Murta CG, Moron AF, Avila MA, et al. Application of ductus venosus Doppler elocimetry for the detection of fetal aneuploidy in the first trimester of pregnancy. Fetal Diagn Ther. 2002;17(5):308-14.
15. Zoppi MA, Putzolu M, Ibba RM, et al. First-trimester ductus venosus velocimetry in relation to nuchal translucency thickness and fetal karyotype. Fetal Diagn Ther. 2002;17(1): 52-7.
16. Borrell A, Martinez JM, Seres A, et al. Ductus venosus assessment at the time of nuchal translucency measurement in the detection of fetal aneuploidy. Prenat Diagn. 2003; 23(11):921-6.
17. Maiz N, Valencia C, Kagan KO, et al. Ductus venosus Doppler in screening for trisomies 21, 18, and 13 and Turner syndrome at 11-13 weeks of gestation. Ultrasound Obstet Gynecol. 2009;33(5):512-7.
18. Bilardo CM, Müller MA, Zikulnig L, et al. Ductus venosus studies in fetuses at high risk for chromosomal or heart abnormalities: relationship with nuchal translucency measurement and fetal outcome. Ultrasound Obstet Gynecol. 2001;17(4):288-94.
19. Maiz N, Plasencia W, Daklis T, et al. Ductus venosus Doppler in fetuses with cardiac defects and increased nuchal translucency thickness. Ultrasound Obstet Gynecol. 2008;31(3):256-60.
20. Liao AW, Snijders R, Geerts L, et al. Fetal heart rate in chromosomally abnormal fetuses. Ultrasound Obstet Gynecol. 2000;16(7):610-3.
21. Spencer K, Souter V, Tul N, et al. A screening program for trisomy 21 at 10–14 weeks using fetal nuchal translucency, maternal serum free beta-human chorionic gonadotropin and pregnancy-associated plasma protein-A. Ultrasound Obstet Gynecol. 1999;13(4):231-7.
22. Spencer K. Aneuploidy screening in the first trimester. Am J Med Genet C Semin Med Genet. 2007;145C(1):18-32.
23. Borenstein M, Persico N, Dagklis T, et al. Frontomaxillary facial angle in fetuses with trisomy 13 at 11+0 to 13+6 weeks. Ultrasound Obstet Gynecol. 2007;30(6):819-23.
24. Borenstein M, Persico N, Strobl I, et al. Frontomaxillary and mandibulomaxillary facial angles at 11+0 to 13+6 weeks in fetuses with trisomy 18. Ultrasound Obstet Gynecol. 2007;30(7):928-33.
25. Chaoui R, Benoit B, Mitkowska-Wozniak K, et al. Assessment of intracranial translucency (IT) in the detection of spina bifida at the 11-13 week scan. Ultrasound Obstet Gynecol. 2009;34(3):249-52.
26. Lachmann R, Picciarelli J, Moratalla N, et al. Fronto-maxillary facial angle in fetuses with spina bifida at 11-13 weeks' gestation. Ultrasound Obstet Gynecol. 2010; 36(3):268-71.
27. Poon LCY, Kametas NA, Chelemen T, et al. Maternal risk factors for hypertensive disorders in pregnancy: a multivariate approach. J Hum Hypertens. 2010;24(2):104-10.
28. Poon LC, Staboulidou I, Maiz N, et al. Hypertensive disorders in pregnancy: screening by uterine artery Doppler at 11-13 weeks. Ultrasound Obstet Gynecol. 2009;34(2):142-8.
29. Poon LC, Stratieva V, Piras S, et al. Hypertensive disorders in pregnancy: combined screening by uterine Doppler, blood pressure and serum PAPP-A at 11-13 weeks. Prenat Diagn. 2010;30(3):216-23.
30. Poon LC, Karagiannis G, Leal A, et al. Hypertensive disorders in pregnancy: screening by uterine artery Doppler and blood pressure at 11-13 weeks. Ultrasound Obstet Gynecol. 2009;34(5):497-502.
31. Cuckle H, Benn P, Wright D. Down syndrome screening in the first and/or second trimester: model predicted performance using meta-analysis parameters. Semin Perinatol. 2005;29(4):252-7.
32. Hyett J, Moscoso G, Papapanagiotou G, et al. Abnormalities of the heart and great arteries in chromosomally normal fetuses with increased nuchal translucency thickness at 11-13 weeks of gestation. Ultrasound Obstet Gynecol. 1996;7(4):245-50.
33. Schwarzler P, Carvalho JS, Senat MV, et al. Screening for fetal aneuploidies and fetal cardiac abnormalities by nuchal translucency thickness measurement at 10-14 weeks of gestation as part of routine antenatal care in an unselected population. Br J Obstet Gynaecol. 1999;106(10):1029-34.

34. Bahado-Singh RO, Wapner R, Thom E, et al. Elevated first-trimester nuchal translucency increases the risk of congenital heart defects. Am J Obstet Gynecol. 2005;192(5):1357-61.
35. Moselhi M, Thilaganathan B. Nuchal translucency: a marker for the antenatal diagnosis of aortic coarctation. Br J Obstet Gynaecol. 1996;103(10):1044-5.
36. Hyett JA, Perdu M, Sharland GK, et al. Increased nuchal translucency at 10-14 weeks of gestation as a marker for major cardiac defects. Ultrasound Obstet Gynecol. 1997;10(4):242-6.
37. Zosmer N, Souter VL, Chan CSY, et al. Early diagnosis of major cardiac defects in chromosomally normal fetuses with increased nuchal translucency. Br J Obstet Gynaecol. 1999;106(8):829-33.
38. Ghi T, Huggon IC, Zosmer N, et al. Incidence of major structural cardiac defects associated with increased nuchal translucency but normal karyotype. Ultrasound Obstet Gynecol. 2001;18(6):610-4.
39. Lopes LM, Brizot ML, Lopes MA, et al. Structural and functional cardiac abnormalities identified prior to 16 weeks' gestation in fetuses with increased nuchal translucency. Ultrasound Obstet Gynecol. 2003;22(5):470-8.
40. Galindo A, Comas C, Martinez JM, et al. Cardiac defects in chromosomally normal fetuses with increased nuchal translucency at 10-14 weeks of gestation. J Matern Fetal Neonatal Med. 2003;13(3):163-70.
41. McAuliffe F, Winsor S, Hornberger LK, et al. Fetal cardiac defects and increased nuchal translucency thickness. Am J Obstet Gynecol. 2003;189, Abstract 571.
42. Hyett J, Perdu M, Sharland G, et al. Using fetal nuchal translucency to screen for major congenital cardiac defects at 10-14 weeks of gestation: population based cohort study. BMJ. 1999;318(7176):81-5.
43. Mavrides E, Cobian-Sanchez F, Tekay A, et al. Limitations of using first trimester nuchal translucency measurement in routine screening for major congenital heart defects. Ultrasound Obstet Gynecol. 2001;17(2):106-10.
44. Orvos H, Wayda K, Kozinszky Z, et al. Increased nuchal translucency and congenital heart defects in euploid fetuses. The Szeged experience. Eur J Obstet Gynecol Reprod Biol. 2002;101(2):124-8.
45. Hafner E, Schuller T, Metzenbauer M, et al. Increased nuchal translucency and congenital heart defects in a low-risk population. Prenat Diagn. 2003;23(12):985-9.
46. Makrydimas G, Sotiriadis A, Ioannidis JP. Screening performance of first-trimester nuchal translucency for major cardiac defects: a meta-analysis. Am J Obstet Gynecol. 2003;189(5):1330-5.
47. Hyett J, Moscoso G, Papapanagiotou G, et al. Abnormalities of the heart and great arteries in chromosomally normal fetuses with increased nuchal translucency thickness at 11-13 weeks of gestation. Ultrasound Obstet Gynecol. 1996;7(4):245-50.
48. Schemm S, Gembruch U, Germer U, et al. Omphalocele-exstrophy-imperforate anus-spinal defects (OEIS) complex associated with increased nuchal translucency. Ultrasound Obstet Gynecol. 2003;22(1):95-7.
49. Sebire NJ, Snijders RJM, Davenport M, et al. Fetal nuchal translucency thickness at 10–14 weeks of gestation and congenital diaphragmatic hernia. Obstet Gynecol. 1997;90(6):943-6.
50. Smrcek JM, Germer U, Krokowski M, et al. Prenatal ultrasound diagnosis and management of body stalk anomaly: analysis of nine singleton and two multiple pregnancies. Ultrasound Obstet Gynecol. 2003;21(4):322-8.
51. Monteagudo A, Mayberry P, Rebarber A, et al. Sirenomelia sequence: first-trimester diagnosis with both two- and three-dimensional sonography. J Ultrasound Med. 2002; 21(8):915-20.
52. Souka AP, Snidjers RJM, Novakov A, et al. Defects and syndromes in chromosomally normal fetuses with increased nuchal translucency at 10-14 weeks of gestation. Ultrasound Obstet Gynecol. 1998;11(6):391-400.
53. Souka A, Heath V. Increased nuchal translucency with normal karyotype. In: Sebire NJ, Snijders RJM, Nicolaides KH (Eds). The 11-14 week scan: diagnosis of fetal abnormalities. Carnforth, UK: Parthenon Publishing; 1999. pp. 67-88.
54. Souka AP, Von Kaisenberg CS, Hyett JA, et al. Increased nuchal translucency with normal karyotype. Am J Obstet Gynecol. 2005;192(4):1005-21.
55. Ben Ami M, Perlitz Y, Haddad S, et al. Increased nuchal translucency is associated with asphyxiating thoracic dysplasia. Ultrasound Obstet Gynecol. 1997;10(4):297-8.
56. Soothill PW, Vuthiwong C, Rees H. Achondrogenesis type 2 diagnosed by transvaginal ultrasound at 12 weeks of gestation. Prenat Diagn. 1993;13(6):523-8.
57. Makrydimas G, Souka A, Skentou H, et al. Osteogenesis imperfecta and other skeletal dysplasias presenting with increased nuchal translucency in the first trimester. Am J Med Genet. 2001;98(2):117-20.
58. Meizner I, Barnhard Y. Achondrogenesis type I diagnosed by transvaginal ultrasonography at 13 weeks' gestation. Am J Obstet Gynecol. 1995;173(5):1620-2.
59. den Hollander NS, van der Harten HJ, Vermeij-Keers C, et al. First trimester diagnosis of Blomstrand lethal osteochondrodysplasia. Am J Med Genet. 1997;73(3):345-50.
60. Souka AP, Raymond FL, Mornet E, et al. Hypophosphatasia associated with increased nuchal translucency: a report of three consecutive pregnancies. Ultrasound Obstet Gynecol. 2002;20:294-5.
61. Eliyahu S, Weiner E, Lahav D, et al. Early sonographic diagnosis of Jarcho-Levin syndrome: a prospective screening program in one family. Ultrasound Obstet Gynecol. 1997;9(5):314-8.
62. Souter V, Nyberg D, Siebert JR, et al. Upper limb phocomelia associated with increased nuchal translucency in a monochorionic twin pregnancy. J Ultrasound Med. 2002;21(3):355-60.
63. Petrikovsky BM, Gross B, Bialer M, et al. Prenatal diagnosis of pseudothalidomide syndrome in consecutive pregnancies of a consanguineous couple. Ultrasound Obstet Gynecol. 1997;10(6):425-8.
64. Percin EF, Guvenal T, Cetin A, et al. First-trimester diagnosis of Robinow syndrome. Fetal Diagn Ther. 2001;16(5): 308-11.

65. Hill LM, Leary J. Transvaginal sonographic diagnosis of short-rib polydactyly dysplasia at 13 weeks' gestation. Prenat Diagn. 1998;18(11):1198-201.
66. Achiron R, Heggesh J, Grisaru D, et al. Noonan syndrome: a cryptic condition in early gestation. Am J Med Genet. 2000;92(3):159-65.
67. Souka AP, Krampl E, Geerts L, et al. Congenital lymphedema presenting with increased nuchal translucency at 13 weeks of gestation. Prenat Diagn. 2002;22(2):91-2.
68. Fincham J, Pandya PP, Yuksel B, et al. Increased first-trimester nuchal translucency as a prenatal manifestation of salt-wasting congenital adrenal hyperplasia. Ultrasound Obstet Gynecol. 2002;20(4):392-4.
69. Souka AP, Skentou H, Geerts L, et al. Congenital nephrotic syndrome presenting with increased nuchal translucency in the first trimester. Prenat Diagn. 2002;22(2):93-5.
70. Hyett J, Noble P, Sebire NJ, et al. Lethal congenital arthrogryposis presents with increased nuchal translucency at 10–14 weeks of gestation. Ultrasound Obstet Gynecol. 1997;9(5):310-3.
71. Rijhsinghani A, Yankowitz J, Howser D, et al. Sonographic and maternal serum screening abnormalities in fetuses affected by spinal muscular atrophy. Prenat Diagn. 1997;17(2):166-9.
72. de Jong-Pleij EA, Stoutenbecek P, van der Mark-Batseva NN, et al. The association of spinal muscular atrophy type II and increased nuchal translucency. Ultrasound Obstet Gynecol. 2002;19(3):312-3.
73. Lam YH, Tang MH, Lee CP, et al. Nuchal translucency in fetuses affected by homozygous a-thalassemia-1 at 12-13 weeks of gestation. Ultrasound Obstet Gynecol. 1999;13(4):238-40.
74. Souka AP, Bower S, Geerts L, et al. Blackfan-Diamond anemia and dyserythropoietic anemia presenting with increased nuchal translucency at 12 weeks of gestation. Ultrasound Obstet Gynecol. 2002;20(2):197-9.
75. Pannier E, Viot G, Aubry MC, et al. Congenital erythropoietic porphyria (Gunther's disease): two cases with very early prenatal manifestation and cystic hydroma. Prenat Diagn. 2003;23(1):25-30.
76. Tercanli S, Miny P, Siebert MS, et al. Fanconi anemia associated with increased nuchal translucency detected by first-trimester ultrasound. Ultrasound Obstet Gynecol. 2001;17(2):160-2.
77. Petrikovsky BM, Baker D, Schneider E. Fetal hydrops secondary to human parvovirus infection in early pregnancy. Prenat Diagn. 1996;16(4):342-4.
78. Markenson G, Correia LA, Cohn G, et al. Parvoviral infection associated with increased nuchal translucency: a case report. J Perinatol. 2000;20(2):129-31.
79. Smulian JC, Egan JF, Rodis JF. Fetal hydrops in the first trimester associated with maternal parvovirus infection. J Clin Ultrasound. 1998;26(6):314-6.
80. Becker R, Wegner RD. Detailed screening for fetal anomalies and cardiac defects at the 11-13 week scan. Ultrasound Obstet Gynecol. 2006;27(6):613-8.
81. Green JJ, Hobbins JC. Abdominal ultrasound examination of the first trimester fetus. Am J Obstet Gynecol. 1988;159(1):165-75.
82. Rottem S, Bronshtein M, Thaler I, et al. First trimester transvaginal sonographic diagnosis of fetal anomalies. Lancet. 1989;1(8635):444-5.
83. Johnson P, Sharland G, Maxwell D, et al. The role of transvaginal sonography in the early detection of congenital heart disease. Ultrasound Obstet Gynecol. 1992;2(4):248-51.
84. Braithwaite JM, Armstrong MA, Economides DL. Assessment of fetal anatomy at 12 to 13 weeks of gestation by transabdominal and transvaginal sonography. Br J Obstet Gynaecol. 1996;103(1):82-5.
85. Hernadi L, Torocsik M. Screening for fetal anomalies in the 12th week of pregnancy by transvaginal sonography in an unselected population. Prenat Diagn. 1997;17(8):753-9.
86. Economides DL, Braithwaite JM. First trimester ultrasonographic diagnosis of fetal structural abnormalities in a low risk population. Br J Obstet Gynaecol. 1998;105(1):53-7.
87. Carvalho MH, Brizot ML, Lopes LM, et al. Detection of fetal structural abnormalities at the 11-14 week ultrasound scan. Prenat Diagn. 2002;22(1):1-4.
88. Souka AP, Pilalis A, Kavalakis I, et al. Screening for major structural abnormalities at the 11- to 14-week ultrasound scan. Am J Obstet Gynecol. 2006;194(2):393-6.
89. Gembruch U, Knöpfle G, Bald R, et al. Early diagnosis of fetal congenital heart disease by transvaginal echocardiography. Ultrasound Obstet Gynecol. 1993;3(5):310-7.
90. Achiron R, Rotstein Z, Lipitz S, et al. First-trimester diagnosis of fetal congenital heart disease by transvaginal ultrasonography. Obstet Gynecol. 1994;84(1):69-72.
91. Smrcek JM, Gembruch U, Krokowski M, et al. The evaluation of cardiac biometry in major cardiac defects detected in early pregnancy. Arch Gynecol Obstet. 2003;268(2):94-101.
92. Wisser J, Dirschedl P, Krone S. Estimation of gestational age by transvaginal sonographic measurements of greatest embryonic length in dated human embryos. Ultrasound Obstet Gynecol. 1994;4(6):457-62.
93. Monteagudo A, Timor-Tritsch I, Sharma S. Early and simple determination of chorionic and amniotic type in multifetal gestations in the first 14 weeks by high frequency transvaginal ultrasound. Am J Obstet Gynecol. 1994;170(3):824-9.
94. Sepulveda W, Sebire NJ, Hughes K, et al. The lambda sign at 10-14 weeks of gestation as a predictor of chorionicity in twin pregnancies. Ultrasound Obstet Gynecol. 1996;7(6):421-3.
95. Selpuveda W, Sebire NJ, Hughes K, et al. Evolution of the lambda or twin/chorionic peak sign in dichorionic twin pregnancies. Obstet Gynecol. 1997;89(3):439-41.
96. Sebire NJ, Snijders RJ, Hughes K, et al. The hidden mortality of monochorinic twin pregnancies. Br J Obstet Gynaecol. 1997;104(10):1203-7.
97. Noble PL, Snijders RJ, Abraha HD, et al. Maternal serum free beta-hCG at 10 to 14 weeks in trisomic twin pregnancies. Br J Obstet Gynaecol. 1997;104(6):741-3.
98. Spencer K. Screening for trisomy 21 in twin pregnancies in the first trimester using free beta-hCG and PAPP-A,

combined with fetal nuchal translucency thickness. Prenat Diagn. 2000;20(2):91-5.
99. Spencer K, Nicolaides KH. Screening for trisomy 21 in twins using first trimester ultrasound and maternal serum biochemistry in a one-stop clinic: a review of three years experience. BJOG. 2003;110(3):276-80.
100. Kagan KO, Gassoni A, Selpuveda-Gonzalez G, et al. Discordance in nuchal translucency thickness in the prediction of severe twin-to-twin transfusion syndrome. Ultrasound Obstet Gynecol. 2007;29(5):527-32.
101. Maiz N, Staboulidou I, Leal AM, et al. Ductus venosus Doppler at 11 to 13 weeks of gestation in the prediction of outcome in twin pregnancies. Obstet Gynecol. 2009;113(4): 860-5.
102. Souka AP, Pilalis A, Kavalakis Y, et al. Assessment of fetal anatomy at the 11-14 week ultrasound examination. 2004;24(7):730-4.
103. van Zalen-Sprock RM, van Vugt JMG, van Geijn HP. First-trimester sonography of physiological midgut herniation and early diagnosis of omphalocele. Prenat Diagn. 1997;17(6):511-8.
104. Snijders RJ, Sebire NJ, Souka A, et al. Fetal exomphalos and chromosomal defects: relationship to maternal age and gestation. Ultrasound Obstet Gynecol. 1995;6(4):250-5.
105. van Zalen-Sprock RM, van Vugt JMG, van Geijn HP. First-trimester sonography of physiological midgut herniation and early diagnosis of omphalocele. Prenat Diagn. 1997;17(6):511-8.
106. Johnson SP, Sebire NJ, Snijders RJ, et al. Ultrasound screening for anecephaly at 10-14 weeks of gestation. Ultrasound Obstet Gynecol. 1997;9(1):14-16.
107. Sandikcioglu M, Molsted K, Kjaer I. The prenatal development of the human nasal and vomeral bones. J Craniofac Genet Dev Biol. 1994;14(2):124-34.
108. Makikallio K, Jouppila P, Rasanen J. Human fetal cardiac function during the first trimester of pregnancy. Heart. 2005;91(3):334-8.
109. Wright D, Kagan KO, Molina FS, et al. A mixture model of nuchal translucency thickness in screening for chromosomal defects. Ultrasound Obstet Gynecol. 2008;31(4):376-83.
110. Whitlow BJ, Economides DL. The optimal gestational age to examine fetal anatomy and measure nuchal translucency in the first trimester. Ultrasound Obstet Gynecol. 1998;11(4): 258-61.
111. Mulvey S, Baker L, Edwards A, et al. Optimizing the timing for nuchal translucency measurement. Prenat Diagn. 2002;22(9):775-7.
112. Nicolaides KH, Brizot ML, Snijders RJ. Fetal nuchal translucency: ultrasound screening for fetal trisomy in the first trimester. Br J Obstet Gynaecol. 1994;101(9):782-6.
113. Uehara S, Yaegashi N, Maeda T, et al. Risk of recurrence of fetal chromosomal aberration: analysis of trisomy 21, trisomy 18, trisomy 13, and 45 X, in 1,076 Japanese mothers. J Obstet Gynaecol Res. 1999;25(6):373-9.
114. UK National Screening Committee Policy. Down's Syndrome Screening. Compiled by the National Screening Committee, 2006. http://www.library.nhs.uk/screening. (Accesed on February 2011)
115. Chalouhi GE, Bernard JP, Ville Y, et al. A comparison of first trimester measurements for prediction of delivery date. J Matern Fetal Neonatal Med. 2011;24(1):51-7.
116. Salomon LJ, Bernard M, Amarsy R, et al. The impact of crown-rump length measurement error on combined Down syndrome screening: a simulation study. Ultrasound Obstet Gynecol. 2009;33(5):506-11.
117. Nicolaides KH, Azar G, Byrne D, et al. Fetal nuchal translucency: ultrasound screening for chromosomal defects in first trimester of pregnancy. BMJ. 1992;304(6831): 867-9.
118. Simpson JM, Sharland GK. Nuchal translucency and congenital heart defects: heart failure or not? Ultrasound Obstet Gynecol. 2000;16(1):30-6.
119. Rizzo G, Muscatello A, Angelini E, et al. Abnormal cardiac function in fetuses with increased nuchal translucency. Ultrasound Obstet Gynecol. 2003;21(6):539-42.
120. Hyett JA, Brizot ML, von Kaisenberg CS, et al. Cardiac gene expression of atrial natriuretic peptide and brain natriuretic peptide in trisomic fetuses. Obstet Gynecol. 1996;87(4):506-10.
121. Tsuchimochi H, Kurimoto F, Leki K, et al. Atrial natriuretic peptide distribution in fetal and failed adult human hearts. Circulation. 1988;78(4):920-7.
122. von Kaisenberg CS, Krenn V, Ludwig M, et al. Morphological classification of nuchal skin in fetuses with trisomy 21, 18 and 13 at 12–18 weeks and in a trisomy 16 mouse. Anat Embryol (Berl). 1998;197(2):105-24.
123. von Kaisenberg CS, Brand-Saberi B, Christ B, et al. Collagen type VI gene expression in the skin of trisomy 21 fetuses. Obstet Gynecol. 1998;91(3):319-23.
124. Böhlandt S, von Kaisenberg CS, Wewetzer K, et al. Hyaluronan in the nuchal skin of chromosomally abnormal fetuses. Hum Reprod. 2000;15(5):1155-8.
125. Chitayat D, Kalousek DK, Bamforth JS. Lymphatic abnormalities in fetuses with posterior cervical cystic hygroma. Am J Med Genet. 1989;33(3):352-6.
126. von Kaisenberg CS, Nicolaides KH, Brand-Siberi B. Lymphatic vessel hypoplasia in fetuses with Turner syndrome. Hum Reprod. 1999;14(3):823-6.
127. Nicolaides KH, Rodeck CH, Lange I, et al. Fetoscopy in the assessment of unexplained fetal hydrops. Br J Obstet Gynaecol. 1985;92(7):671-9.
128. Sohan K, Carroll S, Byrne D, et al. Parvovirus as a differential diagnosis of hydrops fetalis in the first trimester. Fetal Diagn Ther. 2000;15(4):234-6.
129. Pandya PP, Snijders RJ, Johnson SP, et al. Screening for fetal trisomies by maternal age and fetal nuchal translucency thickness at 10 to 14 weeks of gestation. Br J Obstet Gynaecol. 1995;102(12):957-62.
130. Whitlow BJ, Chatzipapas IK, Economides DL. The effect of fetal neck position on nuchal translucency measurement at 10-14weeks. Br J Obstet Gynaecol. 1998;105:872-6.
131. Shaefer M, Laurichesse-Delmas H, Ville Y. The effect of nuchal cord on nuchal translucency measurement at 10-14 weeks. Ultrasound Obstet Gynecol. 1998;11(4):271-3.
132. Molina F, Avgidou K, Kagan K, et al. Cystic hygromas, nuchal edema, and nuchal translucency at 11-14 weeks of gestation. Obstet Gynecol. 2006; 107(3):678-83.

133. Malone FD, Ball RH, Nyberg DA, et al. First-trimester septated cystic hygroma: prevalence, natural history, and pediatric outcome. Obstet Gynecol. 2005;106(2):288-94.
134. Sonek J, Croom C, McKenna D, et al. Letter to the Editor. Obstet Gynecol. 2006; 107:424.
135. Comstock CH, Malone FD, Ball RH, et al. Is there a nuchal translucency millimeter measurement above which there is no added benefit from first trimester serum screening? Am J Obstet Gynecol. 2006;195:843-7.
136. Snijders RJ, Noble P, Sebire N, et al. UK multicentre project on assessment of risk of trisomy 21 by maternal age and fetal nuchal translucency thickness at 10–14 weeks of gestation. Lancet. 1998;352(9125):343-6.
137. Hewitt BG, de Crespigny L, Sampson AJ, et al. Correlation between nuchal thickness and abnormal karyotype in first trimester fetuses. Med J Aust. 1996;165(7):365-8.
138. Snijders RJ, Johnson S, Sebire NJ, et al. First-trimester ultrasound screening for chromosomal defects. Ultrasound Obstet Gynecol. 1996;7:216-26.
139. Pajkrt E, van Lith JM, Mol BW, et al. Screening for Down's syndrome by fetal nuchal translucency measurement in a general obstetric population. Ultrasound Obstet Gynecol. 1998;12:163-9.
140. Spencer K, Spencer DE, Power M, et al. Screening for chromosomal abnormalities in the first trimester using ultrasound and maternal serum biochemistry and in a one-stop clinic: a review of three years prospective experience. Br J Obstet Gynaecol. 2003;110(3):281-6.
141. Kagan KO, Wright D, Baker A, et al. Screening for trisomy 21 by maternal age, fetal nuchal translucency thickness, free beta human chorionic gonadotropin and pregnancy-associated plasma protein-A. Ultrasound Obstet Gynecol. 2008;31(6):618-24.
142. Kagan KO, Etchegaray A, Zhou Y, et al. Prospective validation of first-trimester combined screening for trisomy 21. Ultrasound Obstet Gynecol. 2009;34(1):14-8.
143. Nicolaides KH, Spencer K, Avgidou K, et al. Multicenter study of first-trimester screening for trisomy 21 in 75, 821 pregnancies: results and estimation of the potential impact of individual risk-orientated two-stage first-trimester screening. Ultrasound Obstet Gynecol. 2005;25(3):221-6.
144. Avgidou K, Papageorghiou A, Bindra R, et al. Prospective first-trimester screening for trisomy 21 in 30,564 pregnancies. Am J Obstet Gynecol. 2005;192(6):1761-7.
145. Kagan KO, Anderson JM, Anwandter G, et al. Screening for triploidy by the risk algorithms for trisomies 21, 18 and 13 at 11-13weeks and 6 days of gestation. Prenat Diagn. 2008;28(13):1209-13.
146. Kagan KO, Wright D, Maiz N, et al. Screening for trisomy 18 by maternal age, fetal nuchal translucency, free beta-human chorionic gonadotropin and pregnancy-associated plasma protein-A. Ultrasound Obstet Gynecol. 2008;32(4): 488-92.
147. Farkas LG, Katic MJ, Forrest CR, et al. Surface anatomy of the face in Down's syndrome: linear and angular measurements in the craniofacial regions. J Craniofac Surg. 2001;12(4):373-9.
148. Keeling JW, Hansen BF, Kjaer I. Pattern of malformation in the axial skeleton in human trisomy 21 fetuses. Am J Med Genet. 1997;68(4):466-71.
149. Stempfle N, Huten Y, Fredouille C, et al. Skeletal abnormalities in fetuses with Down's syndrome: A radiologic postmortem study. Pediatr Radiol. 1999;29:682-8.
150. Tuxen A, Keeling JW, Reintoft I, et al. A histological and radiological investigation of the nasal bone in fetuses with Down syndrome. Ultrasound Obstet Gynecol. 2003;22(1): 22-6.
151. Minderer S, Gloning KP, Henrich W, et al. The nasal bone in fetuses with trisomy 21: sonographic versus pathomorphological findings. Ultrasound Obstet Gynecol. 2003;22(1):16-21.
152. Sonek J, Cicero S, Neiger R, et al. Nasal bone assessment in prenatal screening for trisomy 21. Am J Obstet Gynecol. 2006;195:1219-30.
153. Sonek J, Nicolaides K. Prenatal ultrasonographic diagnosis of nasal bone abnormalities in three fetuses with Down syndrome. Am J Obstet Gynecol. 2002;186(1):139-41.
154. Cicero S, Curcio P, Papageorghiou A, et al. Absence of nasal bone in fetuses with Trisomy 21 at 11-14 weeks of gestation: an observational study. Lancet. 2001:358(9294):1665-7.
155. Otano L, Aiello H, Igarzabal L, et al. Association between first trimester absence of fetal nasal bone on ultrasound and Down's syndrome. Prenat Diagn. 2002;22(10):930-2.
156. Zoppi MA, Ibba RM, Axinan C, et al. Absence of fetal nasal bone and aneuploidies at first-trimester nuchal translucency screening in unselected pregnancies. Prenat Diagn. 2003;23(6):496-500.
157. Viora E, Masturzo B, Errante G, et al. Ultrasound evaluation of fetal nasal bone at 11 to 14 weeks in a consecutive series of 1906 fetuses. Prenat Diagn. 2003;23(10):784-7.
158. Wong SF, Choi H, Ho LC. Nasal bone hypoplasia: is it a common finding amongst chromosomally normal fetuses of southern Chinese women? Gynecol Obstet Invest. 2003;56(2):99-101.
159. Cicero S, Longo D, Rembouskos G, et al. Absent nasal bone at 11-14 weeks of gestation and chromosomal defects. Ultrasound Obstet Gynecol. 2003;22(1):31-5.
160. Cicero S, Bindra R, Rembouskos G, et al. Fetal nasal bone length in chromosomally normal and abnormal fetuses at 11-14 weeks of gestation. J Matern Fetal Neonatal Med. 2002;11(6):400-2.
161. Rembouskos G, Cicero S, Longo D, et al. Assessment of the fetal nasal bone at 11-14 weeks of gestation by three-dimensional ultrasound. Ultrasound Obstet Gynecol. 2004;23(3):232-6.
162. Cicero S, Rembouskos G, Vandecruys H, et al. Likelihood ratio for trisomy 21 in fetuses with absent nasal bone at the 11-14 weeks scan. Ultrasound Obstet Gynecol. 2004;23(3):218-23.
163. Cicero S, Bindra R, Rembouskos G, et al. Integrated ultrasound and biochemical screening for trisomy 21 using nuchal translucency, absent fetal nasal bone, free beta-hCG, and PAPP-A at 11 to 14 weeks of gestation. Prenat Diagn. 2003;23(4):306-10.

164. Cicero S, Avgidu K, Rembouskos G, et al. Nasal bone assessment in prenatal screening for trisomy 21. Am J Obstet Gynecol. 2006;195(1):109-14.
165. Sonek J, Borenstein M, Dagklis T, et al. Fronto-maxillary facial angle in fetuses with trisomy 21 at 11-13 (+6) Weeks'. Am J Obstet Gynecol. 2007;196(3):271.e1-4.
166. Plasencia W, Dagklis T, Pachoumi C, et al. Frontomaxillary facial angle at 11+0 to 13+6 weeks: effect of plane of acquisition. Ultrasound Obstet Gynecol. 2007;29(6):660-5.
167. Sonek J, Borenstein M, Downing C, et al. Frontomaxillary facial angles in screening for trisomy 21 at 14-23 weeks' gestation. Am J Obstet Gynecol. 2007;197(2):160.e1-5.
168. Borenstein M, Persico N, Kaihura C, et al. Frontomaxillary facial angle in chromosomally normal fetuses at 11+0 to 13+6 weeks. Ultrasound Obstet Gynecol. 2007;30(7):737-41.
169. Borenstein M, Persico N, Dagklis T, et al. Frontomaxillary facial angle in fetuses with trisomy 13 at 11+0 to 13+6 weeks. Ultrasound Obstet Gynecol. 2007;30(6):819-23.
170. Borenstein M, PersicoN, Strobl I, et al. Frontomaxillary and mandibulomaxillary facial angles at 11+0 to 13+6 weeks in fetuses with trisomy 18. Ultrasound Obstet Gynecol. 2007;30(7):928-33.
171. Falcon O, Auer M, Gerovassili A, et al. Screening for trisomy 21 by tricuspid regurgitation, nuchal translucency and maternal serum free β-hCG and PAPP-A at 11+0 to 13+6 weeks. Ultrasound Obstet Gynecol. 2006;27(2):151-5.
172. Antolin E, Comas C, Torrents M, et al. The role of ductus venosus blood flow assessment in screening for chromosomal abnormalities at 10-16 weeks of gestation. Ultrasound Obstet Gynecol. 2001;17(4):295-300.
173. Kiserud T, Eik-Nes SH, Blaas HG, et al. Ductus venosus blood velocity and the umbilical circulation in the seriously growth-retarded fetus. Ultrasound Obstet Gynecol. 1994;4(2):109-14.
174. Hecher K, Campbell S, Doyle P, et al. Assessment of fetal compromise by Doppler ultrasound investigation of the fetal circulation: arterial, intracardiac, and venous blood flow velocity studies. Circulation. 1995;91(1):129-38.
175. Hecher K, Ville Y, Snijders R, et al. Doppler studies of the fetal circulation in twin-twin transfusion syndrome. Ultrasound Obstet Gynecol. 1995;5(5):318-24.
176. Huisman TW, Bilardo CM. Transient increase in nuchal translucency thickness and reversed end-diastolic ductus venosus flow in a fetus with trisomy 18. Ultrasound Obstet Gynecol. 1997;10(6):397-9.
177. Montenegro N, Matias A, Areias JC, et al. Ductus venosus revisited: a Doppler blood flow evaluation in the first trimester of pregnancy. Ultrasound in Med and Biol. 1997;23:171-6.
178. Kiserud T. In a different vein: the ductus venosus could yield much valuable information. Ultrasound Obstet Gynecol. 1997;9(6):369-72.
179. Borrell A, Antolin E, Costa D, et al. Abnormal ductus venosus blood flow in trisomy 21 fetuses during early pregnancy. Am J Obstet Gynecol. 1998;179(6 Pt 1):1612-7.
180. Matias A, Gomes C, Flack N, et al. Screening for chromosomal abnormalities at 10-14 weeks: the role of ductus venosus blood flow. Ultrasound Obstet Gynecol. 1998;12(6):380-4.
181. Matias A, Montenegro N, Areias JC, et al. Anomalous fetal venous return associated with major chormosomopathies in the late first trimester of pregnancy. Ultrasound Obstet Gynecol. 1998;11(3):209-13.
182. Matias A, Huggon I, Areias JC, et al. Cardiac defects in chromosomally normal fetuses with abnormal ductus venosus blood flow at 10-14 weeks. Ultrasound Obstet Gynecol. 1999;14(5):307-10.
183. Matias A, Montenegro N, Areias JC, et al. Haemodynamic evaluation of the first trimester fetus with special emphasis on venous return. Hum Reprod Update. 2000;6(2):177-89.
184. Matias A, Ramalho C, Montenegro N. Search for hemodynamic compromise at 11-14 weeks in monochorionic twin pregnancy: Is abnormal flow in the ductus venosus predictive of twin-twin transfusion syndrome? J Matern Fetal Neonatal Med. 2005;18(2):79-86.
185. Kagan KO, Wright D, Etchegaray A, et al. Effect of deviation of nuchal translucency measurements on the performance of screening for trisomy 21. Ultrasound Obstet Gynecol. 2009;33(6):657-64.
186. Nisbet DL, Robertson AC, Schluter PJ, et al. Auditing ultrasound assessment of fetal nuchal translucency thickness: a review of Australian National Data 2002-2008. Aust N Z J Obstet Gynaecol. 2010;50(5):450-5.
187. Braithwaite JM, Kadir RA, Pepera TA, et al. Nuchal translucency measurement: training of potential examiners. Ultrasound Obstet Gynecol. 1996;8(3):192-5.
188. Cicero S, Dezerega V, Andrade E, et al. Learning curve for sonographic examination of the fetal nasal bone at 11-14 weeks. Ultrasound Obstet Gynecol. 2003;22(2):135-7.
189. Maiz N, Kagan KO, Milovanovic A, et al. Learning curve for Doppler assessment of ductus venosus flow at 11-13+6 weeks' gestation. Ultrasound Obstet Gynecol. 2008;31:503-6.
190. Nicolaides KH, Snijders RJ, Gosden CM, et al. Ultrasonographically detectable markers of fetal chromosomal abnormalities. Lancet. 1992;340(8821):704-7.
191. Liao A, Sebire N, Geerts L, et al. Megacystis at 10-14 weeks of gestation: chromosomal defects and outcome according to bladder length. Ultrasound Obstet Gynecol. 2003;21(4): 338-41.
192. Sebire NJ, Von Kaisenberg C, Rubio C, et al. Fetal megacystis at 10-14 weeks of gestation. Ultrasound Obstet Gynecol. 1996;8(6):387-90.
193. Liao AW, Sebire NJ, Geerts L, et al. Megacystis at 10-14 weeks of gestation: chromosomal defects and outcome according to bladder length. Ultrasound Obstet Gynecol. 2003;21(4):338-41.
194. Dagklis T, Plasencia W, Maiz N, et al. Choroid plexus cyst, intracranial echogenic focus, hyperechoic bowel and hydronephrosis in screening for trisomy 21 at 11+0 to 13+6 weeks. Ultrasound Obstet Gynecol. 2008;31:132-5.
195. Rodis JF, Egan JF, Craffey A, et al. Calculated risk of chromosomal abnormalities in twin gestations. Obstet Gynecol. 1990;76(6):1037-41.
196. Odibo AO, Elkousy MH, Ural SH, et al. Screening for aneuploidy in twin pregnancies: maternal age- and race-specific risk assessment between 9-14 weeks. Twin Res. 2003;6(4):251-6.

197. Cuckle H. Down's syndrome screening in twins. J Med Screen. 1998;5(1):3-4.
198. Bartha JL, Ling Y, Kyle P, et al.Clinical consequences of first-trimester growth discordance in twins. Eur J Obstet Gynecol Reprod Biol. 2005;119(1):56-9.
199. Kalish RB, Gupta M, Perni SC, et al. Clinical significance of first-trimester crown rump length disparity in dichorionic twin gestations. Am J Obstet Gynecol. 2004;191(4):1437-40.
200. Wøjdemann KR, Larsen SO, Shalmi AC, et al. Nuchal translucency measurements are highly correlated in both mono- and dichorionic twin pairs. Prenat Diagn. 2006;26(3):218-20.
201. Cuckle H, Maymon R. Down syndrome risk calculation for a twin fetus taking account of the nuchal translucency in the co-twin. Prenat Diagn. 2010;30(9):827-33.
202. Sebire NJ, D' Ercole C, Hughes K, et al. Increased nuchal translucency thickness at 10–14 weeks of gestation as a predictor of severe twin-to-twin transfusion syndrome. Ultrasound Obstet Gynecol. 1997;10(2):86-9.
203. Vandecruys H, Faiola S, Auer M, et al. Screening for trisomy 21 in monochorionic twins by measurement of fetal nuchal translucency thickness. Ultrasound Obstet Gynecol. 2005;25(6):551-3.
204. Sepulveda W, Wong AE, Casasbuenas A. Nuchal translucency and nasal bone in first-trimester ultrasound screening for aneuploidy in multiple pregnancies. Ultrasound Obstet Gynecol. 2009;33(2):152-6.
205. Cleary-Goldman J, Rebarber A, Krantz D, et al. First-trimester screening with nasal bone in twins. Am J Obstet Gynecol. 2008;199(3):283.e1-3.
206. Ville Y, Lalondrelle C, Doumerc S, et al. First-trimester diagnosis of nuchal anomalies:significance and fetal outcome. Ultrasound Obstet Gynecol.1992;2(5):314-6.
207. Brady AF, Pandya PP, Yuksel B, et al. Outcome of chromosomally normal live births with increased fetal nuchal translucency at 10-14 weeks' gestation. J Med Genet. 1998;35(3):222-4.
208. Souka AP, Krampl E, Bakalis S, et al. Outcome of pregnancy in chromosomally normal fetuses with increased nuchal translucency in the first trimester. Ultrasound Obstet Gynecol. 2001;18(1):9-17.
209. Mangione R, Guyon F, Taine L, et al. Pregnancy outcome and prognosis in fetuses with increased first-trimester nuchal translucency. Fetal Diagn Ther. 2001;16(6):360-3.
210. Bilardo CM, Pajkrt E, de Graaf I, et al. Outcome of fetuses with enlarged nuchal translucency and normal karyotype. Ultrasound Obstet Gynecol.1998;11(6):401-6.
211. Michailidis GD, Economides DL. Nuchal translucency measurement and pregnancy outcome in karyotypically normal fetuses. Ultrasound Obstet Gynecol. 2001;17(2):102-5.
212. Shulman LP, Emerson DS, Grevengood C, et al. Clinical course and outcome of fetuses with isolated cystic nuchal lesions and normal karyotypes detected in the first trimester. Am J Obstet Gynecol. 1994;171(5):1278-81.
213. Cheng C, Bahado-Singh RO, Chen S, et al. Pregnancy outcomes with increased nuchal translucency after routine Down syndrome screening. Int J Gynaecol Obstet. 2004;84(1):5-9.
214. Senat MV, De Keersmaecker B, Audibert F, et al. Pregnancy outcome in fetuses with increased nuchal translucency and normal karyotype. Prenat Diagn. 2002;22(5):345-9.
215. Cha'Ban FK, van Splunder P, Los FJ, et al. Fetal outcome in nuchal translucency with emphasis on normal fetal karyotype. Prenat Diagn. 1996;16(6):537-41.
216. Michalaides GD, Econdomides DL. Nuchal translucency measurement and pregnancy outcome in karyotypically normal fetuses. Ultrasound Obstet Gynecol. 2001;17(2):102-5.
217. Souka AP, Krampl E, Bakalis S, et al. Outcome of pregnancy in chromosomally normal fetuses with increased nuchal translucency at 10-14 weeks of gestation. Ultrasound Obstet Gynecol. 2001;18(1):9-17.
218. Makrymidas G, Sotiradis A, Huggon IC, et al. Nuchal translucency and fetal cardiac defects: a pooled analysis of major fetal echocardiography centers. Am J Obstet Gynecol. 2005;192(1):89-5.
219. Carvalho JS, Moscoso G, Ville Y. First trimester transabdominal fetal echocardiography. Lancet. 1998;351(9108): 1023-7.
220. Simpson JM, Jones A, Callaghan N, et al. Accuracy and limitations of transabdominal fetal echocardiography at 12-15 weeks of gestation in a population at high risk for congenital heart disease. Br J Obstet Gynaecol. 2000;16:30-6.
221. Hyett JA, Clayton PT, Moscoso G, et al. Increased first trimester nuchal translucency as a prenatal manifestation of Smith-Lemli-Opitz syndrome. Am J Med Genet. 1995;58(4):374-6.
222. Nadel A, Bromley B, Benaceraff BR. Nuchal thickening or cystic hygromas in first- and second- trimester fetuses: prognosis and outcome. Obstet Gynecol. 1993;82:43-8.
223. Brady AF, Pandya PP, Yuksel B, et al. Outcome of chromosomally normal livebirths with increased fetal nuchal translucency at 10-14 weeks' gestation. J Med Genet. 1998;35(3):222-4.
224. Adekunle O, Gopee A, El-Sayed M, et al. Increased first-trimester nuchal translucency: pregnancy and infant outcomes after routine screening for Down's syndrome in an unselected antenatal population. Br J Radiol. 1999; 72(857):457-60.
225. Maymon R, Jauniaux E, Cohen O, et al. Pregnancy outcome and infant follow-up of fetuses with abnormally increased first trimester nuchal translucency. Hum Reprod. 2000;15(9):2023-27.
226. Hiippala A, Eronen M, Taipale P, et al. Fetal nuchal translucency and normal chromosomes: a long-term follow-up study. Ultrasound Obstet Gynecol. 2001;18(1):18-22.
227. Khong TY, De Wolf F, Robertson F, et al. Inadequate maternal vascular response to placentation in pregnancies complicated by preeclampsia and by small-for-gestational age infants. Brit J Obstet Gynaecol. 1986;93:1049-59.
228. Sonek JD, Glover M, Zhou M, et al. First trimester ultrasound screening: an update. Donald School Journal of Ultrasound in Obstetrics and Gynecology. 2010;4:97-116.

CHAPTER 13

Fetal Anatomical Survey during Second-Trimester Screening Examination

Vincenzo D' Addario, Vincenzo Pinto, Luca Di Cagno, Armando Pintucci

INTRODUCTION

Screening for fetal malformations is one of the main aims of ultrasonography during pregnancy. In most cases, fetal anomalies occur as an unexpected event in not at risk patients: for this reason the only way to rule out congenital malformations is to screen every pregnant patient with a systematic evaluation of the fetal anatomy.

Fetal organogenesis is a complex and evolutive process that cannot be squeezed in a single ultrasonic examination;[1] an accurate evaluation, which would take in account the complex fetal morphological evolution, should require multiple ultrasonic examinations during pregnancy. In the clinical practice, however, a so complicated screening program cannot be applied to the general population of the pregnant women due to the elevated cost and the unjustified use of medical resources. For this reason, the ultrasonic screening of fetal malformations has to be based on a single examination that has to be planned at a gestational age which is advanced enough to visualize most fetal anomalies and early enough to plan further diagnostic tests and allow the termination of pregnancy in the case of severe malformation. The gestational age that constitutes the best compromise between the need of an early diagnosis and the natural history of most congenital malformations is the period ranging from 19 to 21 weeks of gestation. This ultrasonic examination is known as "fetal anomaly scan" or "fetal morphology scan".

In order to obtain a systematic evaluation of the fetal anatomy it is essential to establish:

- The orientation of the ultrasonic images on the screen in regard to the patient lie (i.e. the left border of the screen corresponds to the left side of the patient abdomen in the axial scans and to the cephalic pole in the longitudinal ones)
- The fetal lie in the uterus.

To obtain the latter goal it is necessary to correlate the three-dimensional movements of the probe on the maternal abdomen to the bidimensional images appearing on the screen and to reconstruct a mental three-dimensional model from the pool of images seen. Once the idea of the fetal lie in uterus is obtained, the probe can be quickly oriented on the correct plane to visualize the desired fetal anatomical structure.[2]

The fetal anatomical figures, which can be visualized by ultrasound, are innumerable and the expert sonographer may carry out a detailed evaluation of the complex fetal anatomy.

HEAD AND BRAIN

The measurements of biparietal diameter (BPD) and head circumference are obtained on an axial scan of the fetal head showing the thalami, the cavum septi pellucidi and the frontal horns of the lateral ventricles (transthalamic scan) **(Fig. 13.1)**.

By slightly tilting the probe caudally (towards the base of the skull), the atrium of the lateral ventricle filled by the echogenic choroid plexus and continuing in the

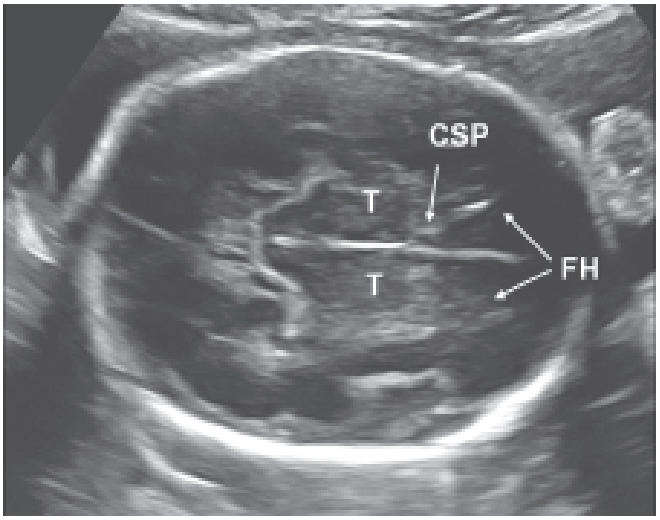

Figure 13.1: Transthalamic scan for measurement of BPD and HC. T = thalami; CSP = cavum septi pellucidi; FH = frontal horns

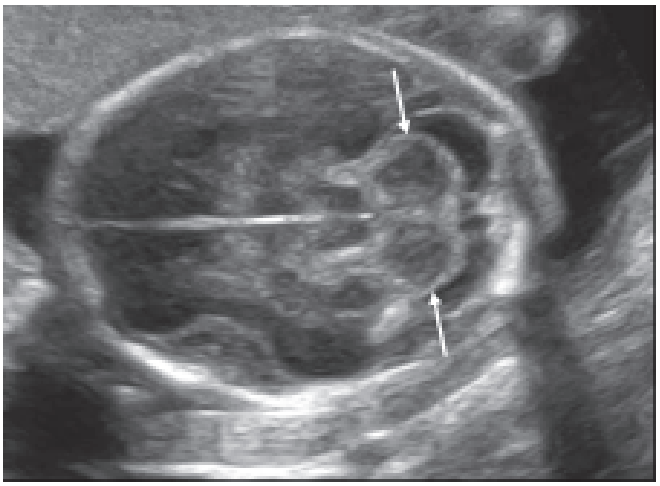

Figure 13.3: Transcerebellar scan for measurement of the transverse cerebellar diameter (arrows). The cerebellum is contourned by the cisterna magna

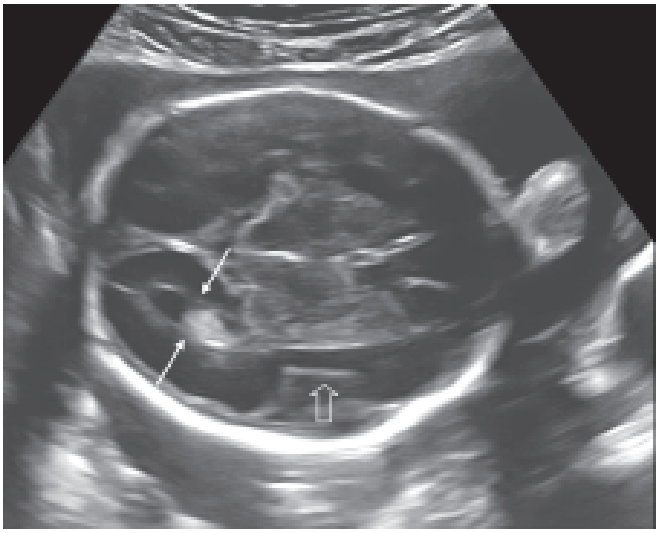

Figure 13.2: Transventricular scan for measurement of the atrial width. Arrows point to the atrium of the lateral ventricle. Arrowhead = insula

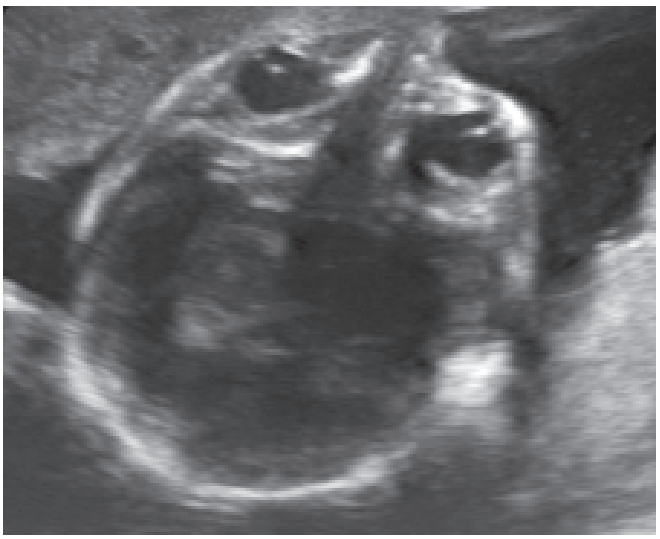

Figure 13.4: Transverse scan on the orbits. The lenses can be recognized

posterior occipital horn is shown (transventricular scan) **(Fig. 13.2)**; at this level the atrial width is measured: its normal value is less than 10 mm independently from the gestational age. During the second trimester, the surface of the cerebral hemispheres is still smooth, since the development of the gyri and sulci is a late event, and the Sylvian fissure is wide, such allowing to recognize the lobe of the insula.

By further tilting the probe caudally, the posterior fossa is shown with the cerebellum and the cisterna magna (transcerebellar scan) **(Fig. 13.3)**. At this level the transverse cerebellar diameter is measured. By tilting the probe on the opposite side, the orbits can be visualized (transorbitary scan) **(Fig. 13.4)**.

These four simple scans allow an accurate evaluation of the brain anatomy and the recognition of the majority of the brain anomalies. However, further scans can be obtained allowing a more detailed evaluation of the finest brain structures. Particularly when the fetus is in breech presentation or in transverse lie, sagittal and coronal scans can be obtained. A midsagittal scan shows the corpus callosum above the cavum septi pellucidi as

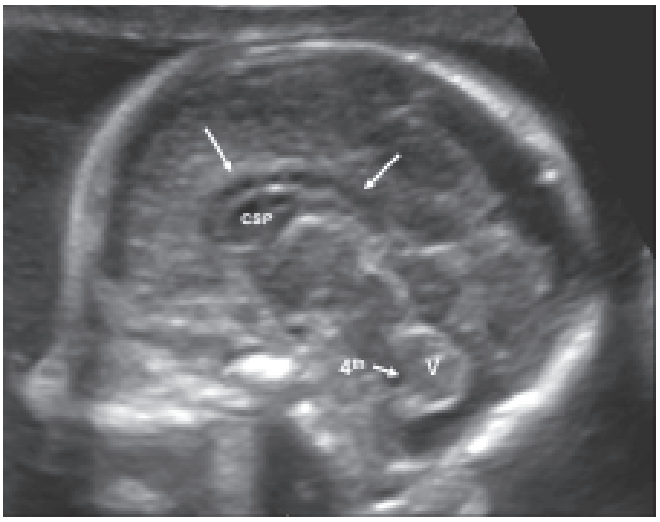

Figure 13.5: Midsagittal scan of the brain showing the corpus callosum (arrows), the cavum septi pellucidi (CSP), the posterior fossa with the cerebellar vermis (V) and the fourth ventricle (4th)

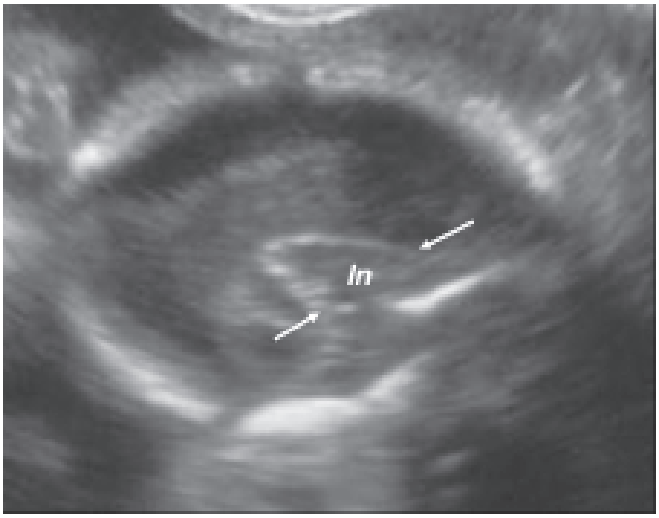

Figure 13.7: External parasagittal scan showing the smooth surface of the brain, the wide insula (In) and the opercula (arrows)

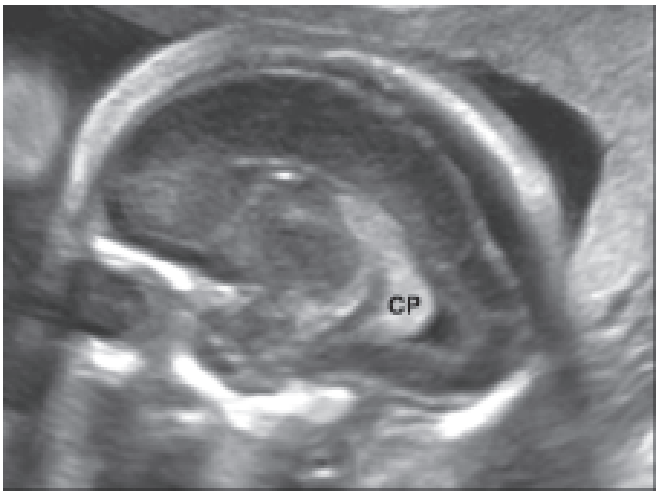

Figure 13.6: Parasagittal scan of the brain showing the "three horns view" of the lateral ventricle with the choroid plexus inside (CP)

well as the posterior fossa, where the cerebellar vermis and the fourth ventricle can be recognized **(Fig. 13.5)**. A parasagittal scan shows the different components of the lateral ventricle (so called "three horns view") **(Fig. 13.6)**. A more external parasagittal scan shows the smooth surface of the brain with the wide insula delimited by the opercula **(Fig. 13.7)**. The coronal scans will show the lateral ventricles with a different appearance, depending on the level of the scan: the most anterior one will show the frontal horns in the frontal hemispheres (transfrontal plane) **(Fig. 13.8A)**; moving behind the cavum septi pellucidi and corpus callosum may be seen interposed between the frontal horns above the caudate nuclei (transcaudate plane) **(Fig. 13.8B)**; then the thalami may be seen below the bodies of the lateral ventricles (transthalamic plane) **(Fig. 13.8C)** and finally the occipital horns with their typical round appearance

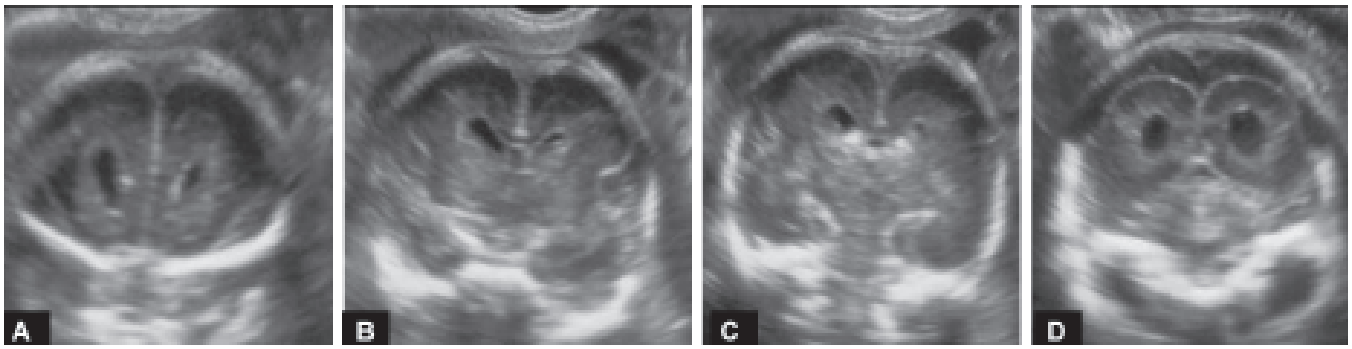

Figures 13.8A to D: Coronal planes of the brain from the anterior to the posterior aspect. (A) Transfrontal; (B) Transcaudate; (C) Transthalamic; (D) Transcerebellar

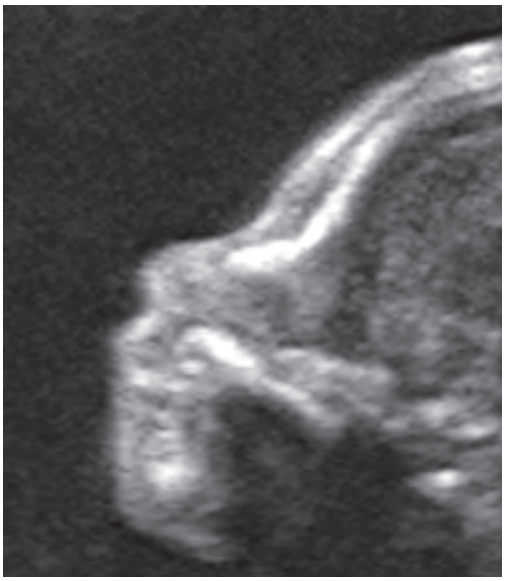

Figure 13.9: Fetal profile

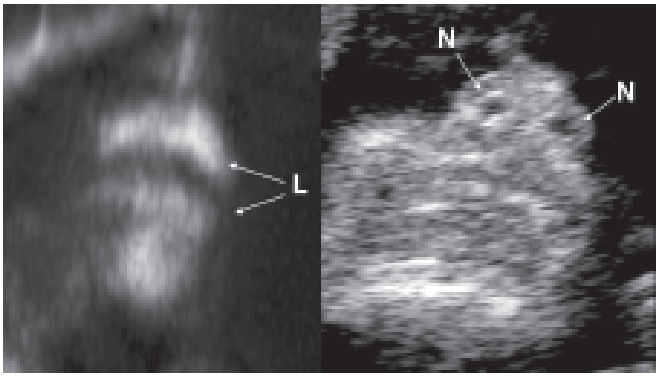

Figure 13.10: Coronal scan of the lips (L) and nostrils (N)

above the cerebellum may be seen in the most posterior plane (transcerebellar plane) **(Fig. 13.8D)**.

The fetal face can be evaluated both by midsagittal scan, showing the profile **(Fig. 13.9)** and by coronal scan, showing the lips and nostrils **(Fig. 13.10)**.

Axial scans at the level of the mouth show the maxilla in the upper level and the tongue with the pharynx at the lower level **(Figs 13.11A and B)**.

SPINE

The spine can be evaluated in longitudinal, coronal and axial scans. The longitudinal scan passing through the spinal canal may also show the chest and ribs which produce sharp acoustic shadows **(Fig. 13.12)**. An alternative way to visualize the spinal canal is the coronal scan passing through the laminae **(Fig. 13.13)**.

In the axial scan, the vertebrae show three ossification centers independently from the level, one generating the body and two generating the laminae, which will fuse posteriorly in the spinous process. According to the level of the section, the axial view may show the clavicle, the ribs or the kidneys **(Figs 13.14A to C)**.

Close to the spine, further bony structures can be seen such as the scapulae and the iliac wings **(Figs 13.15A and B)**.

CHEST

It is important to establish the correct fetal position *in utero* in order to confirm the normal "situs solitus" (both stomach and apex of the heart on the left side of the fetus).

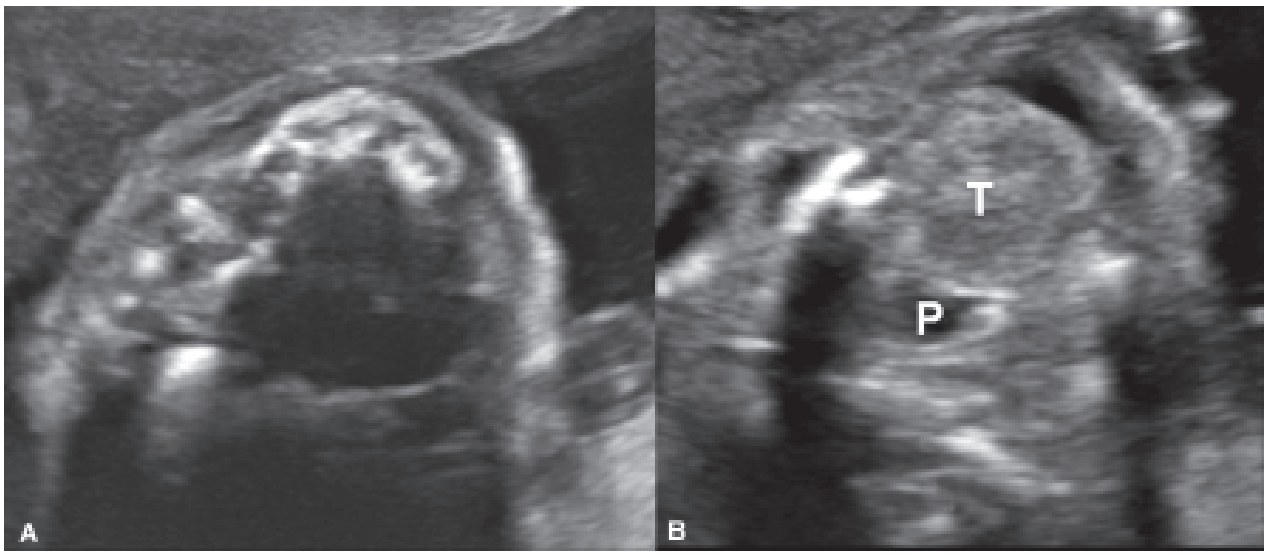

Figures 13.11A and B: Axial scan of the mouth. (A) At the upper level, the maxilla can be seen; (B) At the lower level, the tongue (T) and the pharynx (P) are shown

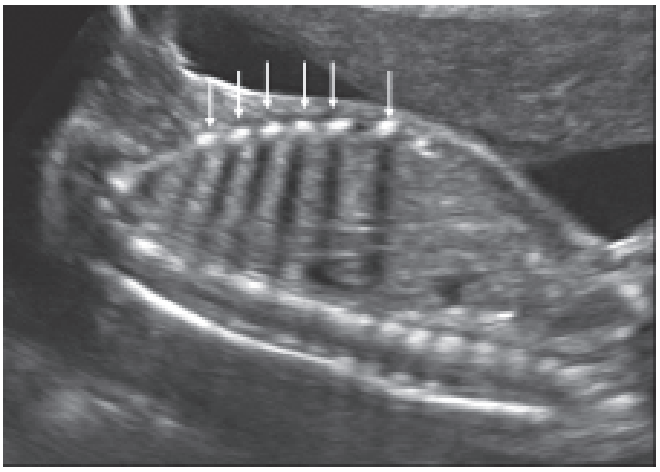

Figure 13.12: Longitudinal scan of the spine. The ribs (arrows) produce sharp acoustic shadows

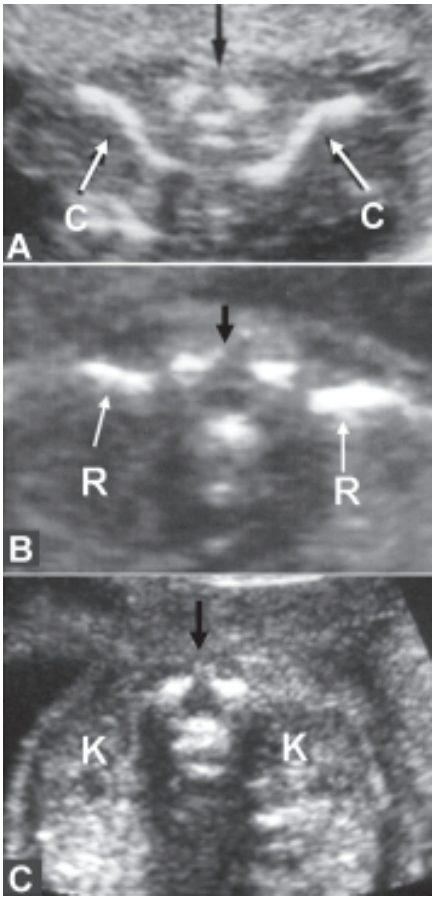

Figures 13.14A to C: Transverse scan of the vertebrae at different levels. (A) Cervical level, where the clavicles (C) can be seen; (B) Dorsal level, where the ribs (R) can be seen; (C) Lumbar level where the kidneys (K) can be seen. Independently from the level, the vertebrae (black arrows) show three ossification centers referring to the body and the laminae

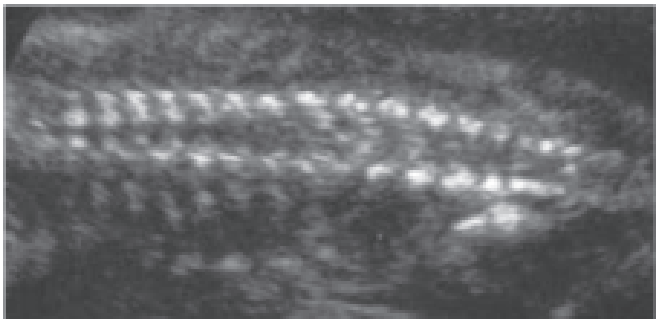

Figure 13.13: Coronal scan of the spine passing through the laminae and showing the spinal canal

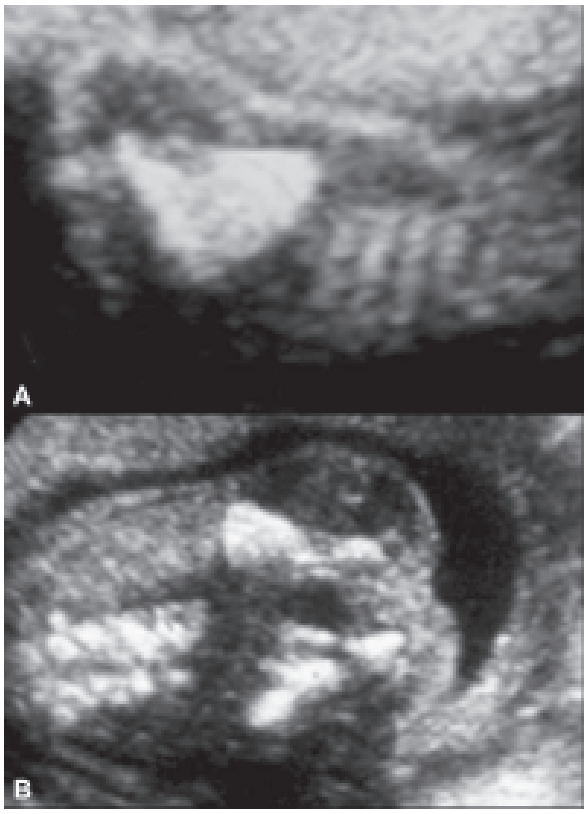

Figures 13.15A and B: The scapula and the iliac wings can be seen close to the spinal canal

The best section to evaluate the chest structures is the axial one at the level of the heart: this scan shows the hyperechoic lungs "embracing" the cardiac area. In this axial scan, the four-chambers view of the heart is looked for. In order to obtain a correct four-chambers view, the first step is to localize the stomach in an axial scan on the abdomen and then moving the transducer cranially without tilting it; in such a way, a confirmation of a normally left-sided heart as well as a correct heart section are easily obtained. The four-chamber view can

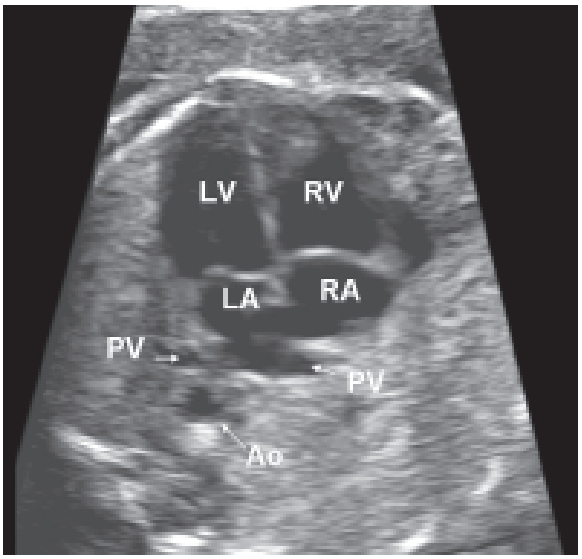

Figure 13.16: "Four-chambers" apical view of the heart. LV = left ventricle; RV = right ventricle; LA = left atrium; RA = right atrium; PV = pulmonary veins; Ao = descending aorta

be "apical" when the ultrasonic beam is parallel and "transverse" when it is perpendicular to the interventricular septum. It is better to try to obtain both scans, since the "apical" is optimal for evaluating the atrioventricular valves and the "transverse" for evaluating the interventricular and interatrial septa.

In the "four-chambers" view, the following cardiac structures can be seen **(Fig. 13.16)**:

- The atria: They have approximately the same size; the left one is closer to the spine and contains the foramen ovale's valve
- Two of the pulmonary veins opening in the left atrium
- The interatrial septum with the interruption due to the foramen ovale
- The atrioventricular valves: The tricuspid has a slightly lower septal insertion than the mitral valve
- The ventricles: They have approximately the same size but a different shape; the right one is more roundish and contains the "moderator band" close to the apex
- The interventricular septum.

Once the "four-chambers" view has been obtained, by slight movements of the transducer, it is possible to visualize the outflow tracts and the subaortic part of the interventricular septum.

The left outflow tract (also called left long axis) is obtained from the "four-chambers" view, by rotating the transducer towards the right fetal shoulder.

In the left long axis, the following structures can be evaluated **(Fig. 13.17)**:

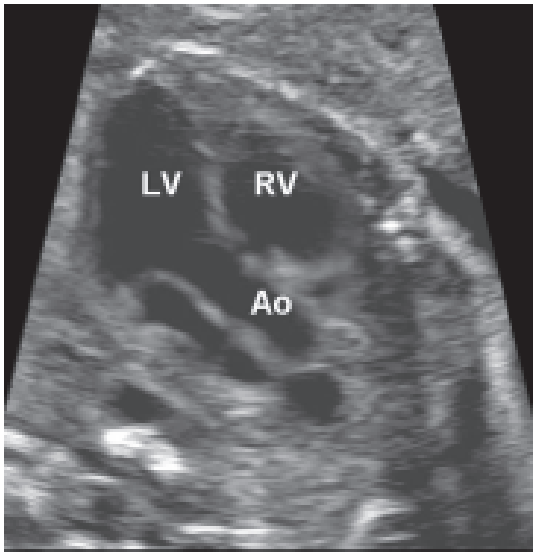

Figure 13.17: Left long axis of the heart showing the emerging aorta. RV = right ventricle; LV = left ventricle; Ao= aorta

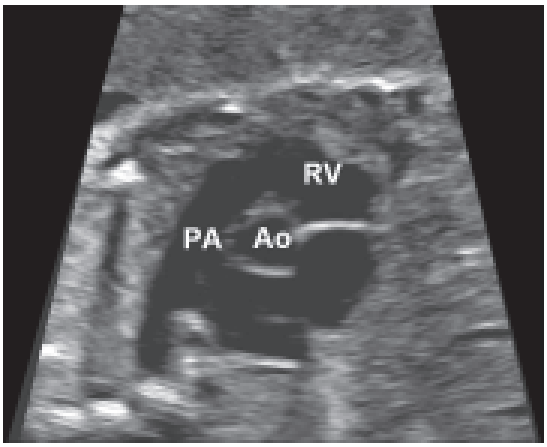

Figure 13.18: Right short axis of the heart showing the pulmonary artery (PA) emerging from the right ventricle (RV) and crossing the aorta (Ao)

- The connection between the left ventricle and the aorta
- The integrity of the subaortic part of the interventricular septum
- The presence and function of the aortic valve.

By rotating the transducer from the long axis view towards the fetal head, the right short axis view can be obtained showing the right outflow tract.

In the right short axis view, the following structures can be seen **(Fig. 13.18)**:

- The connection between the right ventricle and the pulmonary artery
- The crossover of the pulmonary artery
- The presence and function of the pulmonary valve.

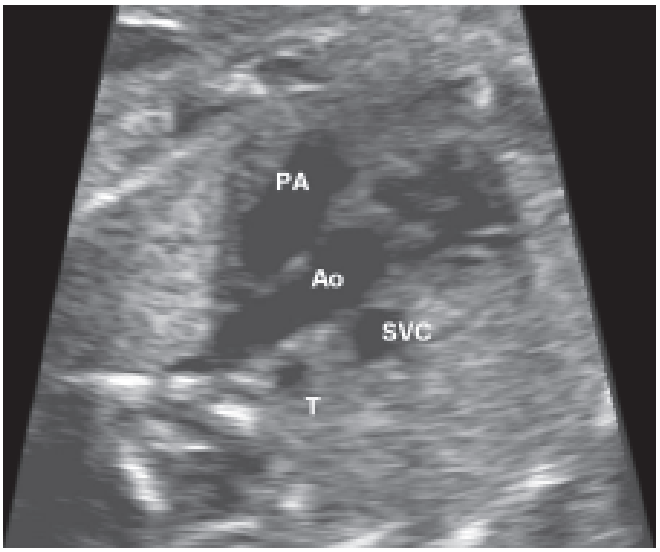

Figure 13.19: Three vessels-trachea view, showing the superior vena cava (SVC), the aortic arch (Ao), the pulmonary artery (PA) continuing in the ductal arch and the trachea (T)

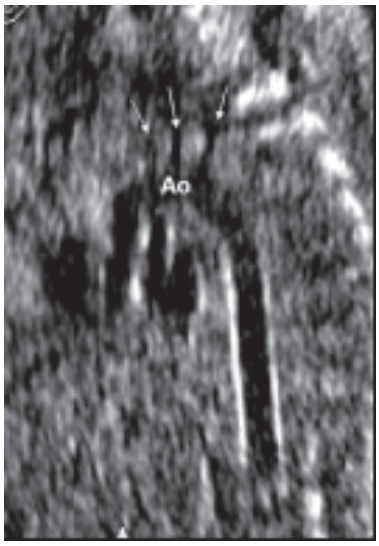

Figure 13.20: Longitudinal scan of the aortic arch (Ao). The arrows point to the brachiocephalic vessels

An alternative way to evaluate the heart and large vessels is to obtain a correct four-chambers apical view and then to move the transducer upward to the head: the emerging aorta and the crossover of the pulmonary artery can be seen during such a movement. At the end of this excursion, the so-called "three vessels-trachea view" (3VT view) can be obtained **(Fig. 13.19)** showing from the right to the left the superior vena cava, the aortic arch and the pulmonary artery progressing in the ductal arch; the trachea appears as a small anechoic area on the right side of the aorta and posterior to the superior vena cava.

Longitudinal scans may show the aortic arch with the brachiocephalic vessels **(Fig. 13.20)** and the superior and inferior vena cava opening in the right atrium **(Fig. 13.21).**

A complete bidimensional echocardiographic evaluation is reported in **Figures 13.22A to F**.

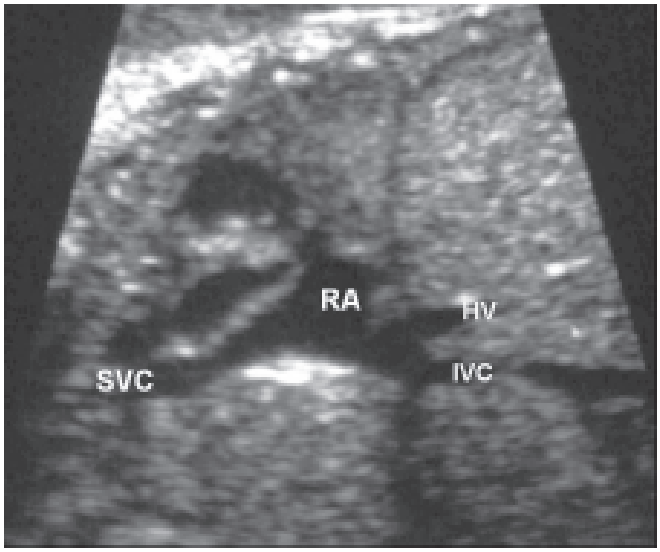

Figure 13.21: Longitudinal scan showing the superior (SVC) and inferior vena cava (IVC) opening in the right atrium (RA). HV = hepatic vein

ABDOMEN

The best scan to visualize the fetal abdomen is the transverse one at the level where the abdominal circumference is measured; at this level the following structures can be recognized: the intrahepatic tract of the umbilical vein on the anterior aspect, the stomach on the left side, the spine and the transverse section of the abdominal aorta on the posterior aspect **(Fig. 13.23)**.

The gallbladder appears as a pear-shaped anechoic structure located in the right side of the abdomen immediately below the right lobe of the liver **(Fig. 13.24)**.

The bowel during the second trimester appears as an echogenic area with irregular borders in the lower part of the abdomen **(Fig. 13.25)**.

Longitudinal section of the abdomen and chest show the diaphragm as a thin hypoechoic curve line dividing the liver from the lung **(Fig. 13.26)**.

Following the course of the umbilical vein, the insertion of the umbilical cord on the abdominal wall is seen **(Fig. 13.27).**

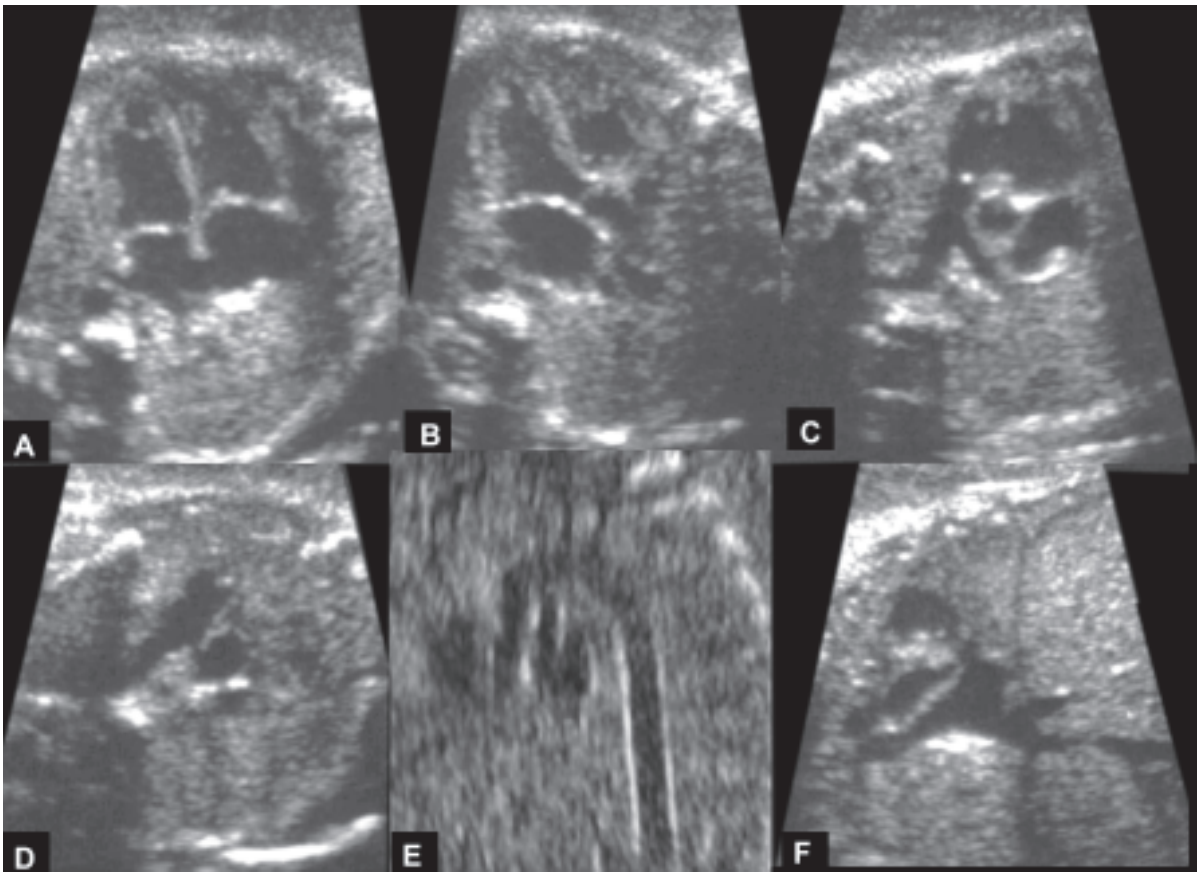

Figures 13.22A to F: Complete bidimensional echocardiography. (A) Four-chamber view; (B) Left ventricle outflow tract; (C) Right ventricle outflow tract; (D) Three vessels-trachea view; (E) Aortic arch; (F) Superior and inferior vena cava

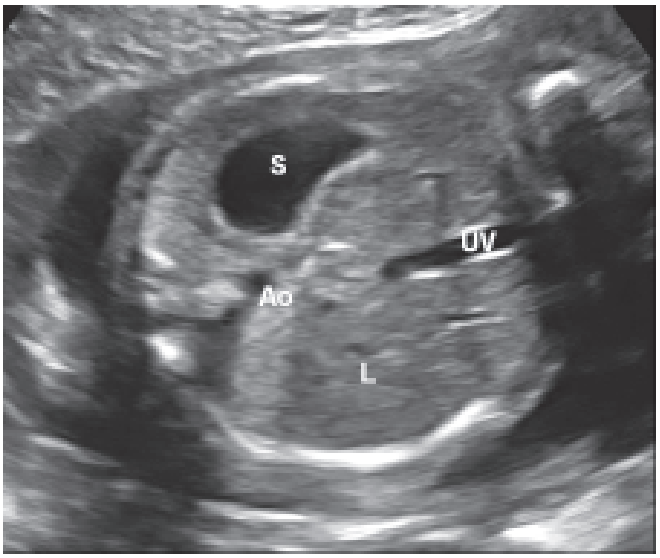

Figure 13.23: Transverse scan of the abdomen for measurement of the abdominal circumference: the intrahepatic tract of the umbilical vein (UV) crossing the liver (L), the stomach (S) and the transverse section of the abdominal aorta (Ao) can be recognized

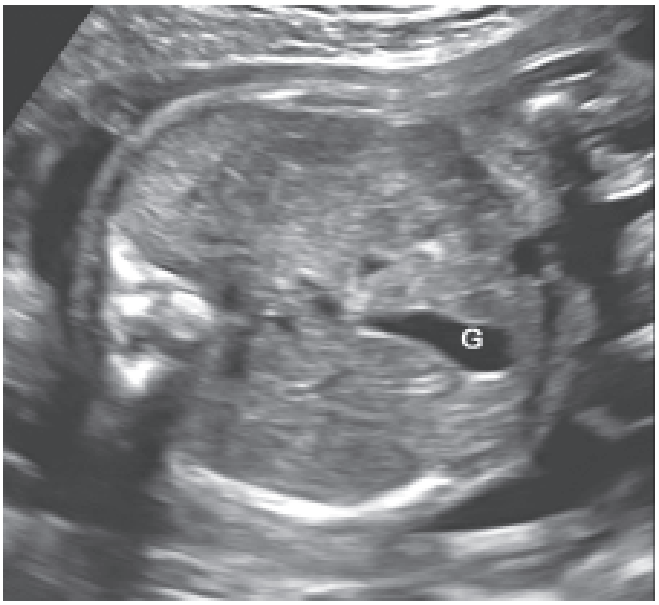

Figure 13.24: The gallbladder (G) appears as a pear-shaped anechoic structure in the right side of the liver

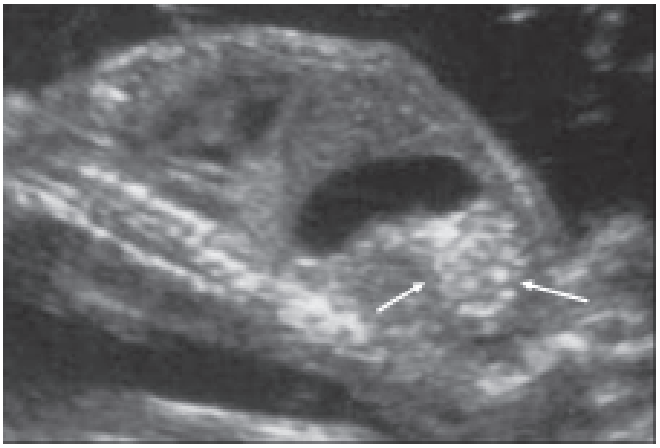

Figure 13.25: The bowel appears as an echogenic area in the lower part of the abdomen (arrows)

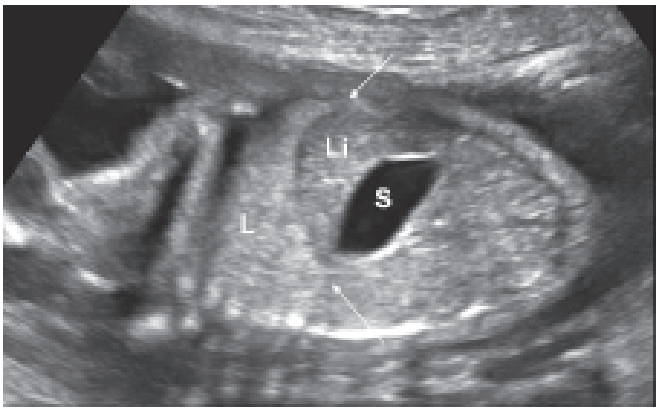

Figure 13.26: The diaphragm appears as a thin curve hypoechoic line dividing the liver from the lung

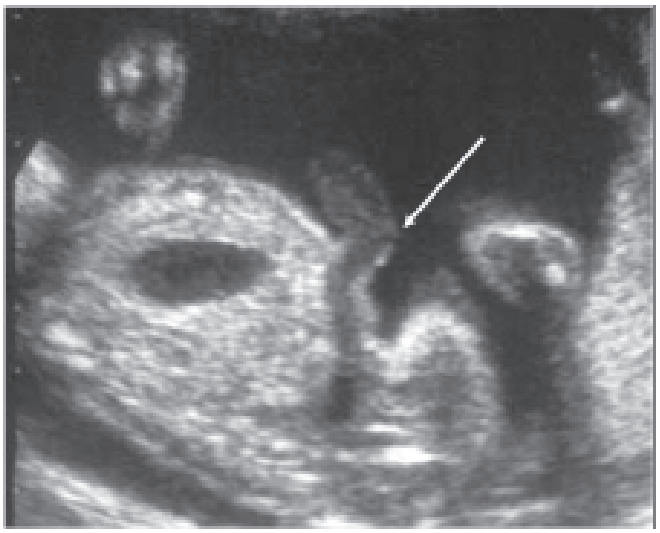

Fig 13.27: Abdominal insertion of the umbilical cord

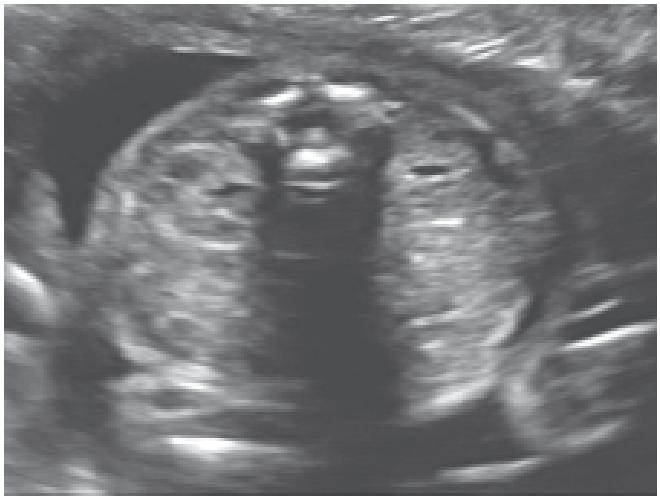

Figure 13.28: Transverse section of the kidneys: they appear as two roundish moderately echogenic structure. A slight dilatation of the pelvis is frequently seen

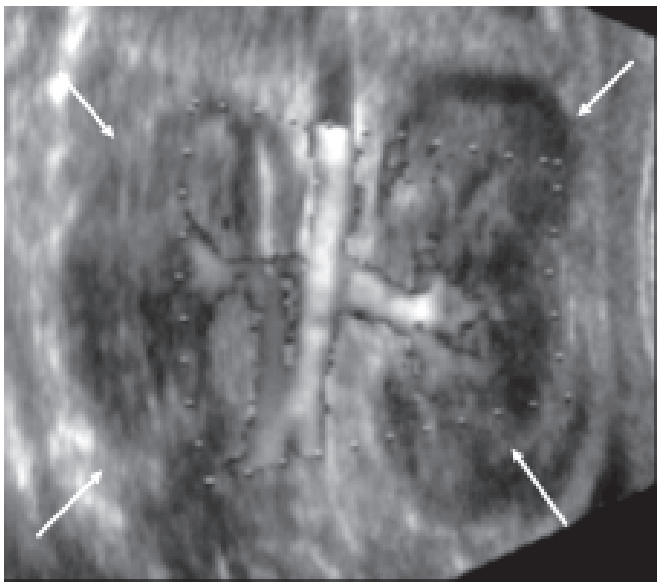

Figure 13.29: Coronal section of the kidneys showing their typical bean-shaped appearance

The examination of the fetal abdomen also includes the visualization of kidneys and bladder. The kidneys are visible on the high axial scan of the abdomen and appear as two echogenic structures on both sides of the spine **(Fig. 13.28)**. The capsule and the pelvis show an echogenicity higher than the renal tissue; a mild physiological dilatation of the renal pelvis can sometimes be seen. In the coronal scan, the kidneys show their typical "bean" shape appearance **(Fig. 13.29)**. The visualization of the bladder is easy: It appears as a cystic median structure in the lower abdomen **(Fig. 13.30)**.

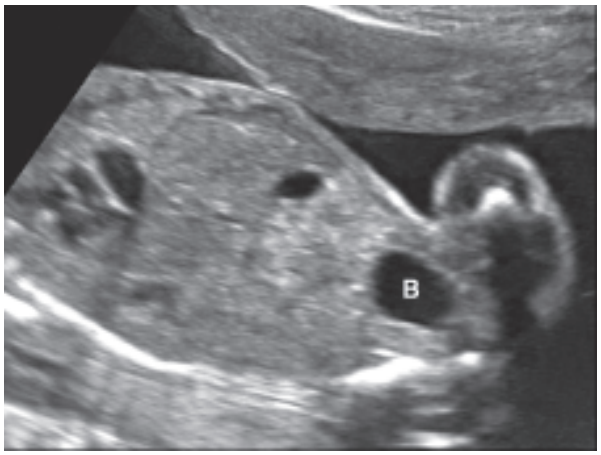

Figure 13.30: The bladder (B) is easily recognized as a roundish cystic structure in the fetal pelvis

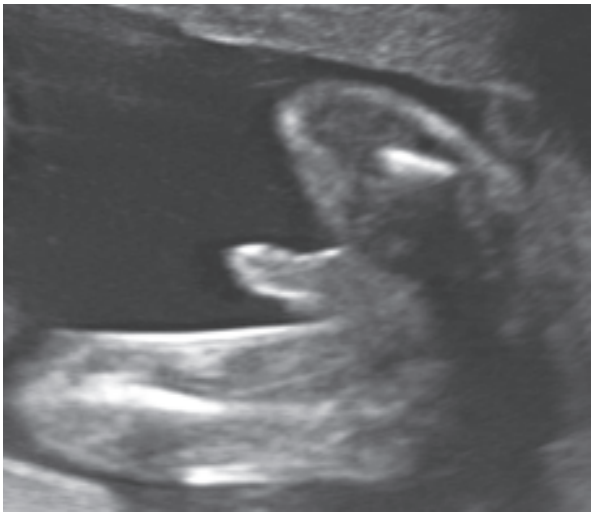

Figure 13.31: Male genitalia

Above the bladder and between the legs the penis in the male fetus **(Fig. 13.31)** and the labia majora in the female **(Fig. 13.32)** may be seen.

LIMBS

The visualization of the limbs requires a correct understanding of the fetal lie in uterus and some skill in following their movements. The amount of amniotic fluid is very important: In case of oligohydramnios, the recognition of the limbs becomes difficult. The long bones of the four arms may be recognized **(Figs 13.33 and 13.34)**.

The hands and feet should also be visualized but only to define whether they are present or absent. The count of the fingers on the open hand is not always possible since the fetus usually has the hands in the closed position.

The fetal anatomical features described so far are only a part of the innumerable fetal structures that can

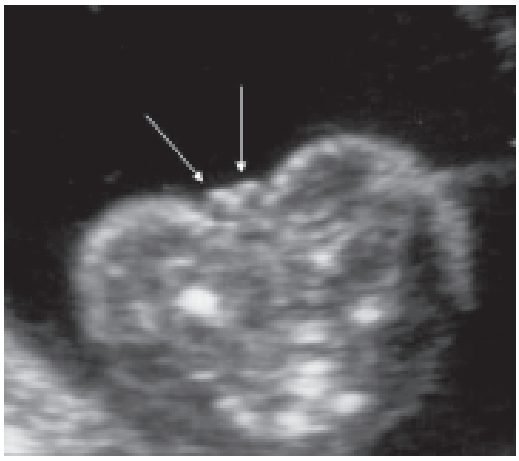

Figure 13.32: Female genitalia. The arrows point to the labia majora

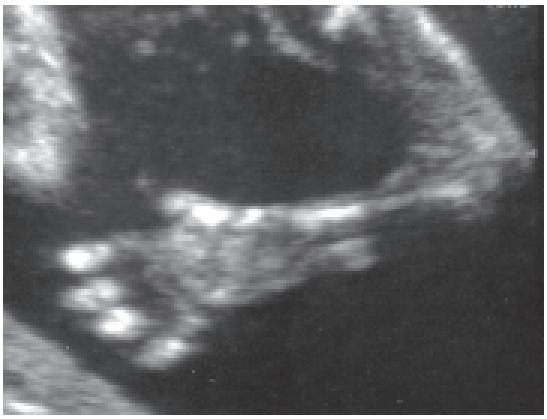

Figure 13.33: Upper limb

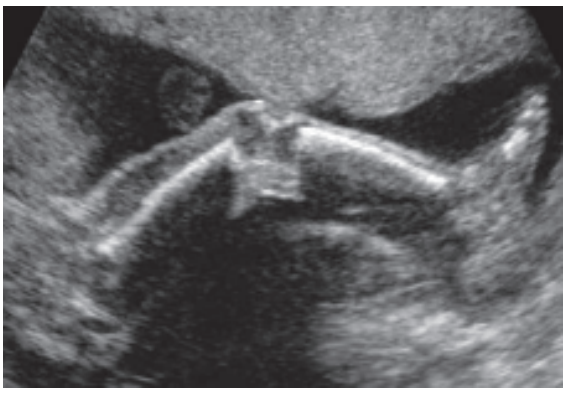

Figure 13.34: Lower limb

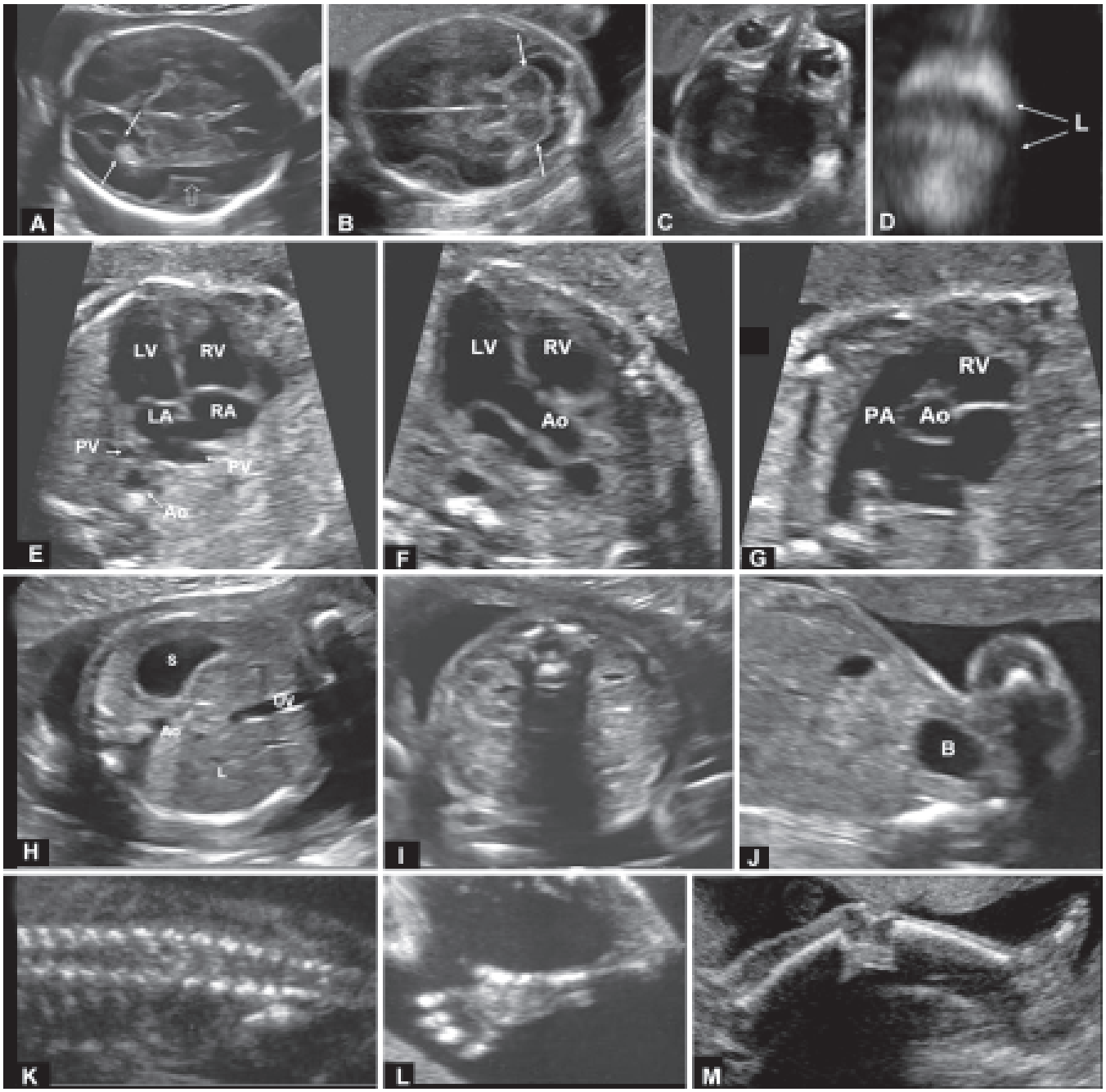

Figures 13.35A to M: Minimal standards for fetal anatomical survey during the second trimester required by the Guidelines of the Italian Society of Ultrasound in Obstetrics and Gynecology. (A) Transventricular view; (B) Transcerebellar view; (C) Transorbital view; (D) Upper lip; (E) Four-chambers view; (F) Left outflow tract; (G) Right outflow tract; (H) Transabdominal view with the stomach; (I) Transverse view of the kidneys; (J) Bladder; (K) Longitudinal view of the spine; (L) Upper limb; (M) Lower limb

be visualized and that will be reported in detail in another section of this book regarding the malformations of the different anatomical systems.

In order to standardize the fetal morphological examination, several scientific societies have suggested guidelines reporting the minimal standards of the fetal structures, which should be visualized during a routine scan performed during the second trimester.[3-5]

The guidelines of the Italian Society of Ultrasound in Obstetrics and Gynecology (SIEOG) suggest the visualization and measurement of the following structures[3] **(Figs 13.35A to M)**:

Head and Face

- Measurement of the BPD and head circumference (it means that a correct scan of the skull and brain has been obtained showing the integrity of the calvarium, the cavum septi pellucidi, the thalami, the falx, the symmetry of the two cerebral hemispheres)
- Measurement of the atrial width (it means that the lateral ventricles have been evaluated)
- Measurement of the transverse cerebellar diameter (it means that the normality of the posterior fossa has been checked)
- Visualization of the orbits
- Visualization of the upper lip.

Spine

- Longitudinal view of the spine.

Chest

- Visualization of the lungs on a transverse scan
- Situs cardiacum
- Four-chambers view
- Left outflow tract
- Right outflow tract.

Abdomen

- Measurement of the abdominal circumference
- Visualization of the stomach and the anterior abdominal profile
- Visualization of the kidneys and bladder.

Limbs

- Visualization of the long bones of the four limbs
- Visualization of the hands and feet (present/absent) without counting the fingers
- Measurement of the femur length.

The guidelines of the American Institute of Ultrasound in Medicine (AIUM)[4] suggest the visualization of the following structures:

Head, Face and Neck

- Cerebellum
- Choroid plexus
- Cisterna magna
- Lateral cerebral ventricles
- Midline falx
- Cavum septi pellucidi
- Upper lip.

Comment

A measurement of the nuchal fold may be helpful during a specific age interval to suggest an increased risk of aneuploidy.

Chest

- The basic cardiac examination includes a four-chamber view of the fetal heart
- If technically feasible, views of the outflow tracts should be attempted as part of the cardiac screening examination.

Abdomen

- Stomach (presence, size and situs)
- Kidneys
- Bladder
- Umbilical cord insertion site into the fetal abdomen
- Umbilical cord vessel number.

Spine

Cervical, thoracic, lumbar and sacral spine.

Extremities

Legs and arms: presence or absence.

Sex

Medically indicated in low-risk pregnancies only for the evaluation of multiple gestations.

Minimum requirements for the basic fetal anatomic survey during the midtrimester of pregnancy according to the guidelines of the International Society of Ultrasound in Obstetrics and Gynecology (ISUOG)[5] are the following:

Head

Skull

Size, shape, integrity and bone density of the skull are visualized at the time of the head measurements and when the brain is evaluated for anatomic integrity.

Brain

Two axial planes permit visualization of the cerebral structures relevant to the anatomic integrity of the brain. These planes are commonly referred to as the transventricular and transthalamic planes. A third axial transcerebellar plane can be added to evaluate the posterior fossa. The following brain structures should be evaluated:

- Lateral ventricles (including choroid plexi)
- Cavum septi pellucidi
- Thalami
- Cerebellum
- Cisterna magna.

Face

Suggested views for minimum evaluation of the fetal face include the presence of both orbits, evaluation of the nose/nostrils and presence of the mouth. If technically feasible, a median facial profile view can be obtained.

Neck

Detailed neck anatomy is not part of the screening examination, although this region can be evaluated in transverse and sagittal planes. This structure should be cylindrical with no protuberances, masses or fluid collections.

Thorax

The shape should be regular with a smooth transition to the abdomen**.** The ribs should have normal curvature without deformities. Both lungs should appear homogenous and without evidence for mediastinal shift or the presence of masses. The diaphragmatic interface can often be visualized as a hypoechoic dividing line between the thoracic and abdominal content (e.g. liver and stomach).

Heart

Basic cardiac examination: The basic cardiac screening examination is interpreted from a four-chamber view of the fetal heart. A normal regular rate ranges from 120 to 160 beats per minute. The heart should be located in the left chest (same side as the fetal stomach) if the situs is normal. A normal heart is usually no larger than one-third the area of the chest and without pericardial effusion. The heart is normally deviated about 45 ± 20° (2 SD) towards the left side of the fetus.

Extended basic cardiac examination: This includes the aortic and pulmonary outflow tracts and can increase the detection rate for major cardiac malformations above those achievable by the four-chamber view alone. These additional views to the basic examination are more likely to identify conotruncal anomalies. Normal great vessels are approximately equal in size and should cross each other as they exit from their respective ventricular chambers.

Some investigators have described an optional "three-vessels and trachea view" that may also be useful for evaluating the pulmonary artery, ascending aorta and right superior vena cava in terms of their relative sizes and anatomic relationships.

Abdomen

The situs of abdominal organs should be determined. The fetal stomach should be identified in its normal position on the left side.

The following should be routinely imaged:

- Stomach
- Bowel
- Umbilical cord insertion and intact abdominal wall
- 3-vessel cord.

Kidneys and Bladder

The fetal bladder and both kidneys should be identified. If either the bladder or renal pelvis appear enlarged, a measurement should be documented. Persistent failure to visualize the bladder should prompt a referral for a more detailed assessment.

Spine

The detailed examination of the fetal spine requires expertise and meticulous scanning, and the results are heavily dependent upon the fetal position. Therefore, a full detailed evaluation of the fetal spine from every projection is not a part of the basic examination. The most frequent of the severe spinal abnormalities, open spina bifida, is usually associated with abnormal intracranial anatomy such as a no visualized cisterna magna. However, a longitudinal section of the fetal spine should always be obtained because it may reveal at least in some cases, other spinal malformations including vertebral abnormalities and sacral agenesis.

Limbs and Extremities

The presence or absence of both arms/hands and both legs/feet should be documented using a systematic approach. Counting fingers or toes is not required as part of the basic scan.

Genitalia

Characterization of external genitalia, to determine fetal gender, is not considered mandatory in the context of a midtrimester routine scan. Reporting of gender should be considered only with parental consent and in the context of local practices.

Although many countries have already developed local guidelines for the practice of fetal ultrasonography, there are still many areas of the world where they have not been implemented. This can be related to the availability of qualified examiners and equipment, local practices, legal considerations and costs related to reimbursement. Nonetheless, a WHO Study Group[6] stated: "Worldwide, it is likely that much of the ultrasonography currently performed is carried out by individuals with in fact little or no formal training." It is desirable, therefore, that the use of guidelines in performing midtrimester anomaly scan becomes a common worldwide practice. It in fact allows the performance of a good level basic examination with the correct selection of patients which should be referred to a second level center.

REFERENCES

1. Kalousek DK, Lau AE. Development of the embryo, fetus and placenta. In: Dimmick JE, Kalousek DK (Eds). Developmental pathology of the embryo and fetus. New York: JB Lippincott Co;1992. pp. 1-25.
2. Staudach A. Fetal echo-anatomy. Berlin:Springer-Verlag; 1989.
3. SIEOG. Linee Guida 2010. www.sieog.it.
4. 2007. AIUM practice guidelines for the performance of obstetric ultrasound examination. www.aium.org.
5. 2010. ISUOG practice guidelines for performance of the routine mid-trimester fetal ultrasound examination. www.isuog.org.
6. World Health Organization. Training in diagnostic ultrasound: essentials, practice, and standards. Geneva, World Health Organization (WHO Technical Report Series, No. 875);1998.

CHAPTER 14

Fetal Biometry

Frederico Rocha, Ivica Zalud

INTRODUCTION

It is important to understand some definitions applied to fetal biometry. Conceptional age is the age of the fetus from the day of fertilization. In obstetrics, we conventionally use the term gestational age as the fetal age. However, gestational age is the conceptional age plus fourteen days and it is also called menstrual age. For clinical and ultrasound purposes, we use the term gestational age when referring to the measurements of the embryo or fetus.

Ultrasound permits an accurate determination of gestational age and is also an important tool for the assessment of fetal growth and diagnosis of fetal growth disorders. When the gestational age is established, the pregnancy should not be redated.[1]

Accurate dating is essential for the proper timing of chorionic villi sampling and nuchal translucency (NT) assessment in the first trimester, amniocentesis in the second trimester as well as relating the various maternal blood serum levels to risk factors and timing for elective cesarean section.[1]

The focus of this chapter is to review the methods of biometric measurements and estimation of gestational age and fetal growth.

FIRST TRIMESTER MEASUREMENTS

Gestational Sac

The first definitive sonographic sign to suggest early pregnancy is visualization of the gestational sac **(Fig. 14.1)**. Gestational sac size measurement should be determined by calculating the mean sac diameter (MSD). This value is obtained by adding the three orthogonal sac diameter dimensions of the chorionic cavity and dividing by three. To correctly measure sac diameter, the cursors should be placed on the sac itself and should not include the echogenic region surrounding the gestational sac.[2] Gestational sac grows 1–2 mm in early pregnancy, but it is less accurate when the embryonic or fetal pole is identified.[2] Gestational sac measurements have only moderate accuracy in establishing gestational age. Intraobserver variability is significant and alternative measurements (e.g. CRL) are more superior. We use gestational sac measurements only in the case when the embryo is not visualized and the last menstrual period is unknown.

Crown-Rump Length

The crown-rump length (CRL) is considered the standard biometric measurement of the embryo in the first trimester.[3] By definition, the crown-rump length is the longest straight-line measurement of the embryo measured from the outer margin of the cephalic pole to the rump **(Fig. 14.2)**. Tables have been formulated to estimate gestational age for each numeric measurement of CRL up to 120 mm.[3-5] In general, when the CRL is under 25 mm, the GA (in days) is CRL+42.[4]

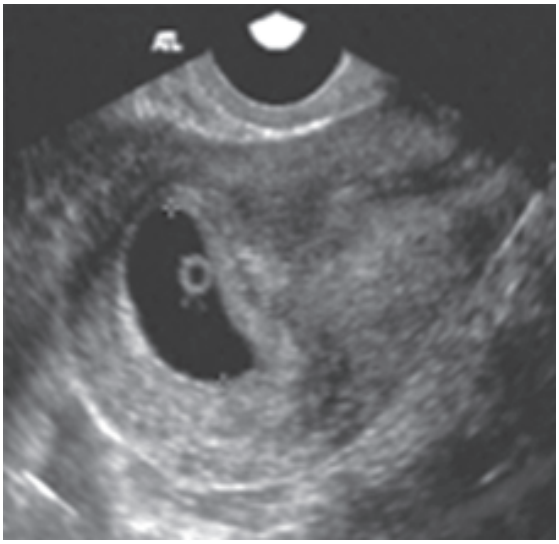

Figure 14.1: Gestational sac measurements. Yolk sac is also visible

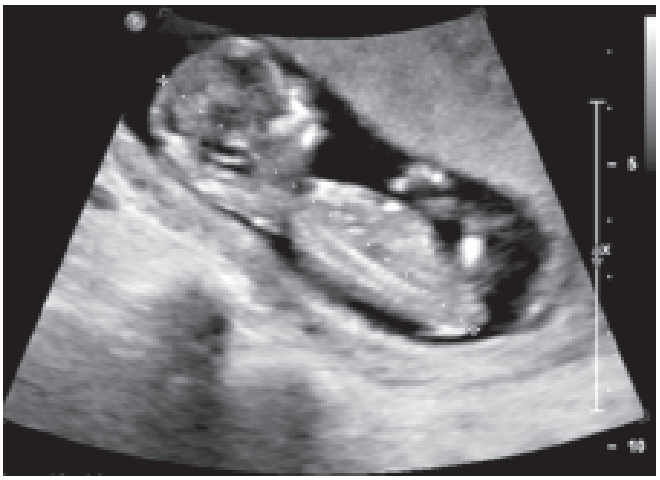

Figure 14.2: Crown-rump length measurement in a 13 weeks 1 day fetus

Standard practice for determining gestational age is to take the mean of three CRL measurements.[6] When CRL is measured between 7 and 10 weeks, this method is accurate within three days.[3,6] However, accuracy wanes as the gestation progresses. Estimation of gestational age by CRL between 10 and 14 weeks is accurate within ± 5 days.[7,8] The CRL remains the standard biometric measurement for first-trimester estimation of gestational age up to 14 weeks. In our practice, if CRL is more than 5 mm, embryonic cardiac activity has to be documented. Otherwise, the diagnosis of missed abortion is made.

Nuchal Translucency

Nuchal translucency is the subcutaneous collection of fluid behind the fetal back and neck. This hypoechoic space is presumed to represent mesenchymal edema and is often associated with distended jugular lymphatic.[9] An NT > 95th percentile is strongly associated with fetal chromosomal abnormalities, isolated heart defects, intrauterine fetal demise, structural malformations and rare genetic syndromes.[10] The optimal gestational age for measurement of fetal NT is 11 weeks to 13 weeks and 6 days. The minimum fetal crown–rump length should be 45 mm and the maximum 84 mm.[11,12] This gestational time frame might vary between different clinical practices and genetic laboratories. In our practice, we use NT measurement as a part of the sequential screen in the risk assessment for aneuploidy. Genetic counseling is integrated in evaluation process. The optimal time for NT assessment is between 10 weeks 3 days and 13 weeks and 6 days of gestation or CRL 39–84 mm. The use of NT measurements in assessment of aneuploidy has been studied excessively. In order to perform NT measurements, individuals need to possess ultrasound proficiency certified by appropriate authority or society with constant quality assurance and improvement processes in place. The NT measurements in combination with serum analytes is excellent screening test for aneuploidy.

Only the fetal head and upper thorax should be included in the image for the measurement of NT **(Figs 14.3 and 14.4)**. A sagittal section of the fetus, as for measurement of fetal crown–rump length, should be obtained and the NT should be measured with the fetus in the neutral position. The maximum thickness of the subcutaneous translucency between the skin and

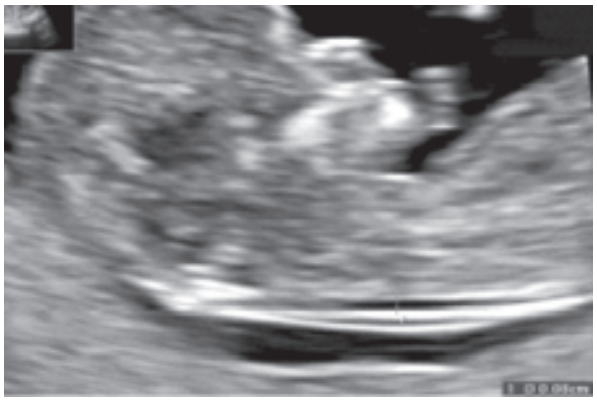

Figure 14.3: Nuchal translucency measurement

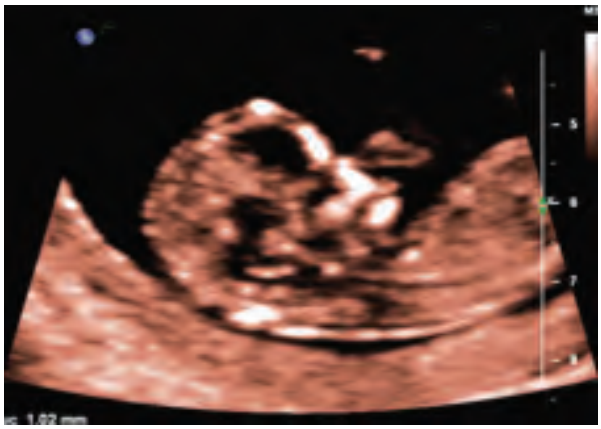

Figure 14.4: Another normal nuchal translucency measurement

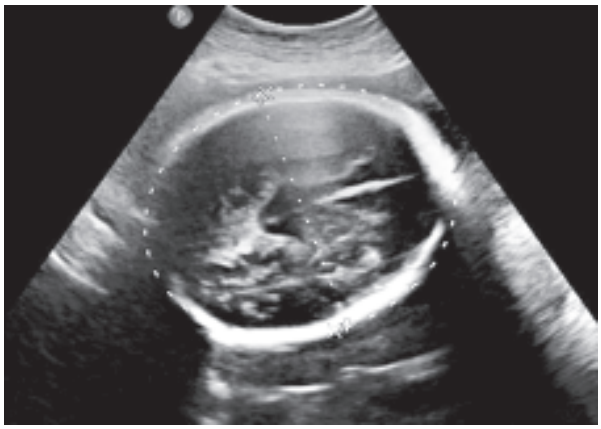

Figure 14.5: Head circumference and biparietal diameter measurement

the soft tissue overlying the cervical spine should be measured. The calipers should be placed on the lines that define the NT thickness from its inner-to-inner borders. Care must be taken to distinguish between fetal skin and amnion because, at this gestation, both structures appear as thin membranes.[11,12]

SECOND-TRIMESTER MEASUREMENTS

The four standard biometric parameters commonly used to estimate gestational age and/or fetal weight in the second and third trimesters are: biparietal diameter (BPD), head circumference (HC), abdominal circumference (AC) and femur length (FL).

Biparietal Diameter

Biparietal diameter is measured at the level of the thalami and cavum septum pellucidum (CSP) **(Fig. 14.5)**. The cerebellar hemispheres should not be visible in this scanning plane. The measurement is taken from the outer edge of the proximal skull to the inner edge of the distal skull.[11] It is the best studied biometric parameter because it is highly reproducible and can predict gestational age within ±7 days when measured between 14 and 20 weeks of gestation.[13-15] By the mid to late third trimester, the margin of error is 3–4 weeks. This significant variation is likely due to a large normal biological variation in fetal shape and size near term.[13-15]

In late pregnancy, it can be difficult to obtain the ideal imaging plane due to the head lying low in the pelvis. A change in head shape due to molding can cause dolichocephaly (flattened and elongated) or brachycephaly which can affect the BPD measurement.[16,17] When this occurs the cephalic index (CI) should be measured. Cephalic index refers to the ratio of the BPD and the occipitofrontal diameter (OFD) multiplied by 100 [CI = (BPD/OFD) x 100%].[16-18]

The standard CI range for normal shaped craniums approximates one standard deviation from the mean (>74 or <83). Therefore, if the CI measurement approaches the outer limits of the normal range, the use of the BPD for estimation of gestational age is not accurate.[16-18]

Head Circumference

Head circumference is measured at the same level as the biparietal diameter, around the outer perimeter of the calvarium **(Figs 14.5 and 14.6)**. This measurement is not affected by shape of the head. It is important to avoid measuring the outer margin of the skin overlying the scalp, since doing so will falsely increase the HC.[11]

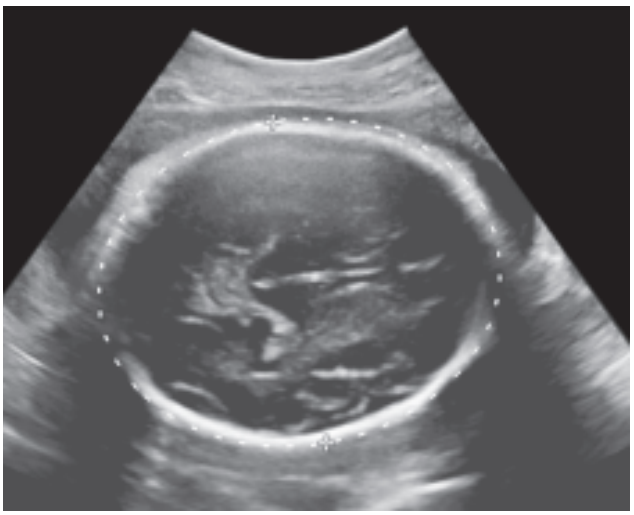

Figure 14.6: Head circumference measurement

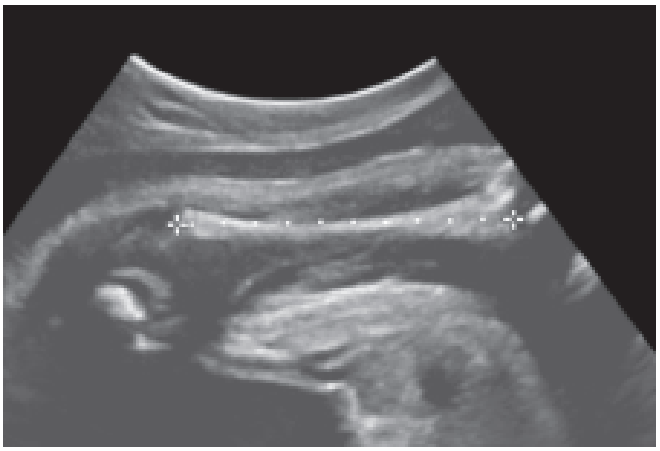

Figure 14.7: Femur length measurement

Femur Length

Femoral diaphysis length can be reliably used after 14 weeks' gestational age **(Fig. 14.7)**. The long axis of the femoral shaft is most accurately measured with the beam of insonation being perpendicular to the shaft, excluding the distal femoral epiphysis.[11]

Abdominal Circumference

Abdominal circumference or average abdominal diameter should be determined at the skin line on a true transverse view at the level of the junction of the umbilical vein, portal sinus and fetal stomach when visible **(Fig. 14.8)**.[11] Several studies have stated that this imaging plane is the most difficult to obtain, especially in late pregnancy and yet is one of the most essential for inclusion in a fetal weight formula.[11]

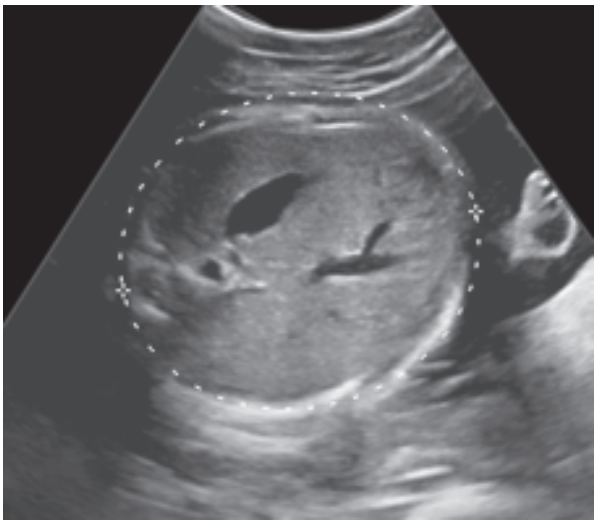

Figure 14.8: Abdominal circumference

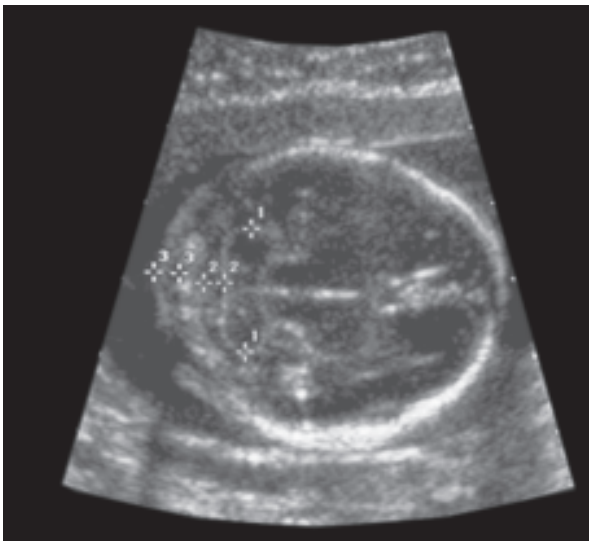

Figure 14.9: Measurement of the cerebellum, posterior fossa and nuchal fold

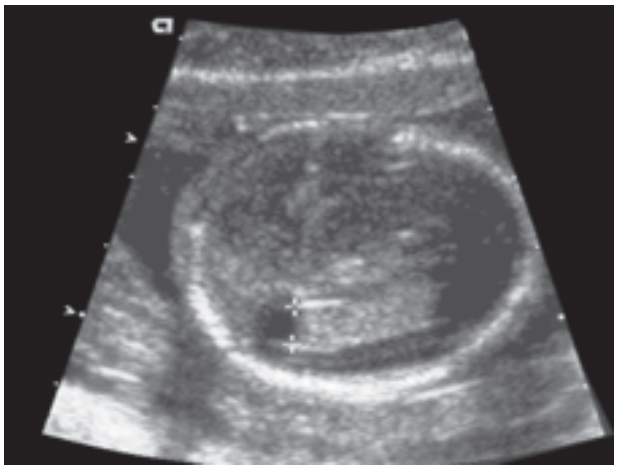

Figure 14.10: Posterior horn of the lateral ventricles

Other Measurements

Ultrasound evaluation and measurements of cerebellum, posterior fossa, nuchal fold, posterior horn of the lateral ventricle and renal pelvis are part of detailed anatomical survey **(Figs 14.9 to 14.11)**. Those measurements have role in anatomical integrity and aneuploidy assessment and are not routinely used for gestational age or fetal growth evaluation. For more details please see other chapters in the book.

Estimating Fetal Age Using Multiple Markers

A number of combinations of fetal parameters, including the combination of head circumference and femur length, provided age estimates that were

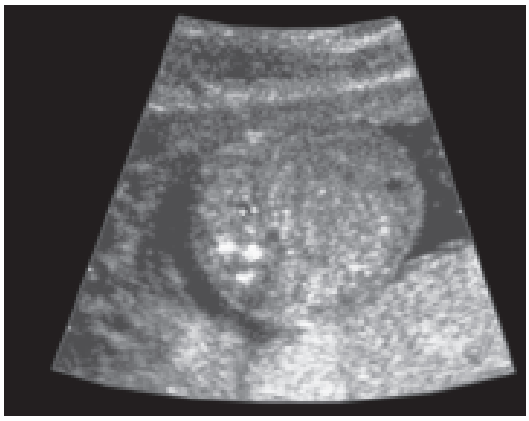

Figure 14.11: Anterior-posterior diameter of the renal pelvis

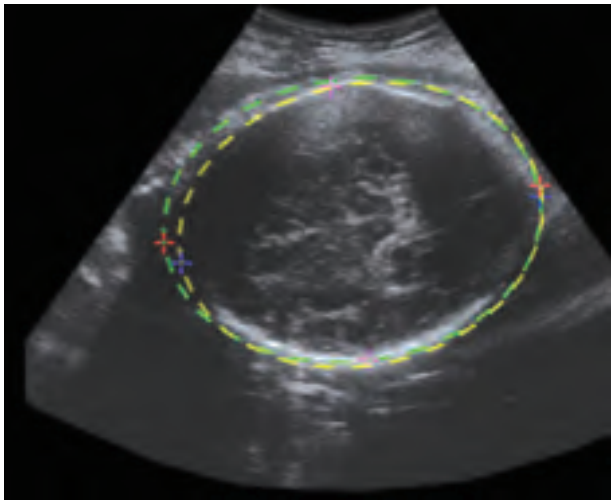

Figure 14.12: Automatic measurements of the head circumference generated by pattern recognition software

significantly better than those using any single parameter alone.[19,20] Hadlock and colleagues showed that in 177 normal pregnancies, there was significant improvement in the ultrasound estimation of estimated date of delivery when two or more parameters were used to make that estimate, rather than just BPD alone.[19] Before 36 weeks' gestation, the optimal combination of parameters included the BPD, AC and FL. However, after 36 weeks, the HC, AC and FL gave the best estimate with significant reduction in the mean errors, standard deviation, and size of maximum error.

Chervenak et al. published a large study of patients conceived by IVF, to assess the accuracy of fetal biometry in the second trimester of pregnancy for assignment of fetal age. Results showed that head circumference was the best individual predictor of fetal age. The addition of abdominal circumference and femur length to head circumference improved the overall accuracy of dating compared with any individual measurement. The study concluded that the use of fetal biometry in the second trimester is also an accurate means of establishing gestational age within 7 days.[21]

Third-trimester sonographic estimation of gestational age has been proven to be an inaccurate method with median error of plus or minus three weeks after 30 weeks gestation.[21,22] The imprecision of the measurements occur primarily because of the normal variability among fetuses. The accuracy of third-trimester biometric measurements is also impaired by fetal crowding, shadowing from other fetal bony parts, diminished amniotic fluid volumes and descent of the presenting part into the pelvis.[23]

Other non-traditional methods of biometry have been attempted as an alternative to aid in the determination of the gestational age in late gestation. Those include transverse cerebellar diameter, fetal foot length epiphyseal ossification centers.[24] Among those the transverse cerebellar diameter in millimeters correlates well with the gestational age up to 22–24 weeks.[24-26]

Ultrasound fetal biometry requires training and it can be time consuming. A new concept that could improve efficiency and limit the measurement errors by inexperienced sonographers is the automatic fetal measurements by the pattern recognition **(Fig. 14.12)**. This approach could reduce keystrokes and therefore reduce repetitive stress injuries. It could also improve everyday work-flow to increase patient productivity.[22]

Estimating Fetal Weight

A variety of formulas are used for prediction of fetal weight. Not all authorities agree on any formula derived from fetal parts measurements.[27] Fetuses from different populations may show different growth patterns. Race and parity are important parameters to consider when applying general population growth curves.[28-31] Birth weight standards vary from one population to another, depending upon ethnicity and environmental and socioeconomic circumstances.[28,30] Fetal growth formulas provide weight estimates with errors of up to 20% when compared with actual birth weights.[11,13-15] A study reported a general tendency to underestimate the weight in fetuses with high birth weight (>4000 gm).[32-34]

Three-Dimensional Biometry

The introduction of three-dimensional (3D) ultrasound imaging has allowed the accurate and reliable calculation of fetal organ volumes. Some authors have

demonstrated that the prediction of birth weight using fetal limb volumetry is more precise than that obtained using conventional 2D ultrasound parameters.[29] Different organ volumes have been used, including kidneys, adrenal gland, brain, cerebellum and fetal thigh. The 3D ultrasound techniques require technically advanced and expensive equipment, special operator training and skills, and are time consuming.[35] At present, it does not seem reasonable to abandon the 2D ultrasound methods in favor of 3D ultrasound imaging for fetal weight estimation.[35]

CONCLUSION

The application of fetal biometric measurements in routine obstetrical care has definitely become part of the standard of care. Ultrasound evaluation is essential to confirm or establish gestational age. In the first trimester, its use has optimized the establishment of an accurate pregnancy dating and also as an important tool in the screening for chromosomal anomalies. Later in gestation, the biometric measurements of a fetus help to estimate fetal weight and follow the growth. The use of customized growth curves appropriate for local population may help improve the accuracy of the biometric estimates for the fetus.

REFERENCES

1. ACOG Practice Bulletin No. 101: Ultrasonography in pregnancy. Obstet Gynecol. 2009;113(2 Pt 1):451-61.
2. Laing FC, Frates MC. Ultrasound evaluation during the first trimester of pregnancy. In: Ultrasonography in obstetrics and gynecology. 4th Edition. Callen PW (Ed). WB Saunders: Philadelphia; 2000.
3. Robinson HP, Fleming JE. A critical evaluation of sonar "crown-rump length" measurements. Br J Obstet Gynaecol. 1975;82(9):702-10.
4. Goldstein SR, Wolfson R. Endovaginal ultrasonographic measurement of early embryonic size as a means of assessing gestational age. J Ultrasound Med. 1994; 13(1):27-31.
5. Daya S. Accuracy of gestational age estimation by means of fetal crown-rump length measurement. Am J Obstet Gynecol. 1993;168(3):903-8.
6. Kalish RB. Sonographic determination of the gestational age. In: Donald School Textbook of Ultrasound in Obstetrics and Gynecology, 2nd Edition. Asim Kurjak (Ed). Jaypee Brothers Medical Publishers: New Delhi; 2008.
7. Hadlock FP, Shah YP, Kanon DJ, et al. Fetal crown-rump length: reevaluation of relation to menstrual age (5-18 weeks) with high-resolution real-time US. Radiology. 1992;182(2):501-5.
8. MacGregor SN, Tamura RK, Sabbagha RE, et al. Underestimation of gestational age by conventional crown-rump length dating curves. Obstet Gynecol. 1987; 70(3 Pt 1):344-8.
9. Bekker MN, Haak MC, Rekoert-Hollander M, et al. Increased nuchal translucency and distended jugular lymphatic sacs on first-trimester ultrasound. Ultrasound Obstet Gynecol. 2005;25(3):239-45.
10. Haak MC, van Vugt JM. Pathophysiology of increased nuchal translucency: a review of the literature. Human Reproduction Update. 2003;9(2):175-84.
11. AIUM Practice Guideline for the Performance of Obstetric Ultrasound Examinations. AIUM 2007 http://www.aium.org/publications/guidelines/obstetric.pdf (Accessed October 31, 2010).
12. Sebire NJ, Snijders RJM, Hughes K, et al. Screening for trisomy 21 in twin pregnancies by maternal age and fetal nuchal translucency thickness at 10-14 weeks of gestation. BJOG. 1996;103(10):999-1003.
13. Hadlock FP, Harrist RB, Martinez-Poyer J. How accurate is second trimester fetal dating? J Ultrasound Med. 1991;10(10):557-61.
14. Rossavik IK, Fishburne, JI. Conceptional age, menstrual age, and ultrasound age: a second-trimester comparison of pregnancies of known conception date with pregnancies dated from the last menstrual period. Obstet Gynecol. 1989;73(2):243-9.
15. Hadlock FP, Deter RL, Harrist RB, et al. Fetal biparietal diameter: rational choice of plane of section for sonographic measurement. AJR A J Roentgenol. 1982; 138(5):871-4.
16. O'Keeffe DF, Garite TJ, Elliott JP, et al. The accuracy of estimated gestational age based on ultrasound measurement of biparietal diameter in preterm premature rupture of the membranes. Am J Obstet Gynecol. 1985;151(3):309-12.
17. Hadlock FP, Deter RL, Carpenter RJ, et al. Estimating fetal age: effect of head shape on BPD. AJR Am J Roentgenol. 1981;137(1):83-5.
18. Gray DL, Songster GS, Parvin CA, et al. Cephalic index: a gestational age-dependent biometric parameter. Obstet Gynecol. 1989;74(4):600-3.
19. Hadlock FP, Deter RL, Harrist RB, et al. Estimating fetal age: computer assisted analysis of multiple fetal growth parameters. Radiology. 1984;152(2):497-501.
20. Hadlock FP, Harrist RB, Shah YP, et al. Estimating fetal age using multiple parameters: a prospective evaluation in a racially mixed population. Am J Obstet Gynecol. 1987;156(4):955-7.
21. Chervenak FA, Skupski DW, Romero R, et al. How accurate is fetal biometry in the assessment of fetal age? Am J Obstet Gynecol. 1998;178(4):678-87.
22. Zalud I, Good S, Carneiro, et al. Fetal biometry: a comparison between experienced sonographers and automated measurements. J Matern Fetal Neonat Med. 2009;22(1): 43-50.
23. Platz E, Newman R. Diagnosis of IUGR: traditional biometry. Semin Perinatol. 2008;32(3):140-7.
24. Gottlieb AG, Galan HL. Nontraditional sonographic pearls in estimating gestational age. Semin Perinatol. 2008:32(3): 154-60.
25. Doubilet PM, Benson CB. Improved prediction of gestational age in the late third trimester. J Ultrasound Med. 1993;12(11):647-53.

26. Goldstein I, Reece EA, Pilu G, et al. Cerebellar measurements with ultrasonography in the evaluation of fetal growth and development. Am J Obstet Gynecol. 1987:156(5):1065-9.
27. Degani S. Fetal biometry: clinical, pathological, and technical considerations. Obstet Gynecol Surv. 2001;56(3): 159-67.
28. Brenner WE, Edelman DA, Hendricks CH. A standard of fetal growth for the United States of America. Am J Obstet Gynecol. 1976;126(5):555-64.
29. Raju TNK, Winegar A, Seifert L, et al. Birth weight and gestational age standards based on regional perinatal network data: an analysis of risk factors. Am J Perinatol. 1987;4(3):253-8.
30. Mongelli M, Gardosi J. Reduction of false-positive diagnosis of fetal growth restriction by application of customized fetal growth standards. Obstet Gynecol. 1996;88(5):844-8.
31. Zhang J, Bowes WA. Birth-weight-for-gestational-age patterns by race, sex, and parity in the United States population. Obstet Gynecol. 1995:86(2):200-8.
32. Miller JM Jr, Korndorf FA 3rd, Gabert HA. Fetal weight estimates in late pregnancy with emphasis on macrosomia. J Clin Ultrasound. 1986;14(6):437-42.
33. Bennini JR et al. Birth-weight prediction by two- and three-dimensional ultrasound imaging. Ultrasound Obstet Gynecol. 2010;35(4):426-33.
34. Dudley NJ. A systematic review of the ultrasound estimation of fetal weight. Ultrasound Obstet Gynecol. 2005;25(1):80-9.
35. Lindell G, Marsál K. Sonographic fetal weight estimation in prolonged pregnancy: comparative study of two- and three-dimensional methods. Ultrasound Obstet Gynecol. 2009;33(3):295-300.

CHAPTER 15

Ultrasound and Doppler Management of Intrauterine Growth Restriction

José M Carrera, Francese Figueras, Eva Meler

INTRODUCTION

Intrauterine growth restriction (IUGR) undoubtedly is one of the most challenging areas of research for obstetricians today. It is considered as a major contributor to perinatal morbidity and mortality, and has been described as etiologically responsible of about a 50% of perinatal deaths occurring preterm and 20% at term.[1] In addition, growth restriction is associated with intrapartum distress and metabolic acidosis, which are in turn contributors to hypoxic encephalopathy and cerebral palsy.[2] Furthermore, there is increasing evidence of the association between fetal growth restriction and infant death[3] and metabolic syndrome in adulthood.[4] Despite marked progress made over the past two decades in both diagnostic procedures and management strategies, the question of what causes growth restriction still remains unanswered in 30–40% of all cases of IUGR.

DEFINITIONS

It is necessary to make a difference between three different concepts: growth, development and maturity. "Growth" is usually defined as the process whereby the body mass of a living being increases in size as a result of the increase in number and/or size of its cells. "Development" should be understood as the process by which the organs acquire their particular anatomy and their specific functions in living beings, and consequently the progressive anatomical and functional "Maturity" of all of them, as well as its physiological regulations. Thanks to these three processes, that are going on in a parallel way, the fetus reach at the gestation terminus maturity enough to face the extra uterine life.

Regarding the fetal weight anomalies, a clear distinction should be made between the meanings of three different terms: Low-birth weight (LBW), small-for-gestational age (SGA), and intrauterine growth restriction (IUGR). The LBW refers only to newborn infants weighing less than 2,500 grams independently of gestational age. Some of these newborns will be premature and others will be newborns with a growth restriction. The SGA is a term based on a statistical definition, which includes all newborn infants found below the lower range limit of normal weight by gestational age. Hence, is a term that comprises a heterogeneous group of fetuses and newborns with several etiologic conditions. The IUGR theoretically refers to any process that is capable of limiting intrinsic fetal growth potential *in utero*, but is mainly used to define those cases in which a placental insufficiency is responsible for the growth deficit.

Unfortunately, in literature, the terms IUGR and SGA are frequently considered as synonymous. This confusion was increased even more when the National Institute of Child Health and Human Development in the USA stated that for "both medical and research purposes, IUGR should be defined as a situation which results in a newborn weight that is lower than 10th percentile for its gestational age."

CLASSIFICATION

Most Fetal Medicine Units classify SGA in three main categories according to what Soothill published in a breaking editorial.[5] Firstly, the "IUGR", that is limited to those fetuses in which a reduction in their growth potential is believed to be due to placental insufficiency. Secondly, the "Normal-SGA", which includes those SGA fetuses, which are believed to be constitutionally small. And, finally, the "Abnormal-SGA", which comprises other pathological causes of SGA as infections, congenital malformations, chromosomopathies, etc. Despite that in the past, SGA fetuses and neonates were classified according to the relationship between abdominal and cephalic biometries as symmetrical or asymmetrical, this classification has demonstrated to be poorly correlated with the underlying etiological condition,[6] with the gasometric status of the fetus at cordocentesis[7] or with any of the perinatal events that define an adverse perinatal outcome,[8-9] and, therefore, is no longer recommended as a primary tool in managing SGA fetuses.

INCIDENCE

While the incidence of SGA depends upon the used threshold for normality (10th, 5th or 2.5th centile) resulting in a 10%, 5% or 2.5%, respectively, the incidence of IUGR varies greatly in the literature, with reports of figures ranging from 1–12%. The reason for this may be found in different factors, including the social and economic status of the population studied, different criteria used for discrimination (10th percentile, 5th percentile, etc.), different ways in which standard curves are drawn, data obtained from transverse or longitudinal studies, etc.[10] Approximately, only a 20–30% of all SGA fetuses are true growth-restricted fetuses,[11] whereas only a 10-20% are pathological-SGA.[12] Hence, most of the cases of SGA are constitutionally small, i.e. normal-SGA.

SCREENING

"Traditional" maternal serum screening have proved disappointing for IUGR: elevated levels of alphafetoprotein and human chorionic gonadotrophin are associated with IUGR but are very poor screening tests (sensitivity about 5%).[13] For the time being, the biochemical markers that are more promising candidates for antenatal screening are FMS-like tyrosine kinase 1 and placental growth factor. Despite that, there exists evidence of the association between the plasmatic maternal levels of these markers and the occurrence of preeclampsia and growth-restriction,[14] new clinical studies are required before its clinical application.

Since IUGR is caused by uteroplacental insufficiency and it shares some common physiopathological paths with preeclampsia leading to a poor trophoblast invasion, IUGR has been associated with an increased resistance in the uterine arteries. Doppler evaluation of this vessel constitutes the main screening method for IUGR. Evaluation of this tool has been hampered by different criteria for growth-restriction and for abnormal Doppler waveform, by discrepancies in the targeted population and by differences in instrumentation (use of color Doppler, transvaginal versus transabdominal approach) among the studies. Nevertheless, a multicentric and massive-population-based study[15] aimed to evaluate the role of transvaginal uterine artery at 23 weeks, has demonstrated an overall sensitivity for growth-restriction of 16%. Nevertheless, when the event of interest is the occurrence of disease requiring delivery before 32 weeks (which represents the subgroup with significant perinatal morbidity and mortality), the sensitivity for preeclampsia-associated and no-preeclampsia-associated growth restriction is 93% and 56%, respectively, with specificities of 95%. It would be appealing to move the screening into early pregnancy, but despite the fact that it seems a promising strategy for preeclampsia, the sensitivity of uterine artery Doppler evaluation in early second trimester for growth restriction requiring delivery before 32 is only of 28% (12% for growth restriction without preeclampsia).[16] Hence, it seems that uterine artery evaluation identifies a subgroup with an increased risk for developing severe growth-restriction.

Screening strategies which combine epidemiological, biochemical and Doppler parameters are being tested to enhance the low sensitivity of each individual parameter.

DIAGNOSIS

The antenatal detection of IUGR is of utmost importance and constitutes a major challenge for modern obstetrics. SGA neonates not antenatally detected had a 4-fold risk of adverse outcome.[17] Furthermore, it has been reported that a suboptimal antenatal management is the most common finding in cases of unexplained stillborns.[18]

Anamnesis

Antenatal risk factors include a previous history of SGA or stillbirth, toxic substances such as tobacco, alcohol

and other drugs, fetal infections (CMV and Rubeola are the most associated ones) and maternal diseases (mainly renal and vascular). Other risk factors are preeclampsia related such as thrombophilic conditions, obesity and chronic hypertension. Although these risk factors are multiple and not always well defined, a correct anamnesis remains a key step to select a population of high-risk on which a close follow-up may be warranted. Nevertheless, only 10% of this high-risk group will develop IUGR.

Fundal Height Measurement

Both the fundal height measurement and the abdominal palpation have sensitivities of about 30% to detect SGA[19] and therefore, could not be recommended. Nevertheless, it has been reported that customized standards for fundal height, which adjust for parity, maternal height and weight, ethnicity and fetal gender, and a longitudinal evaluation allow sensitivities of about 50%,[20] comparable to the detection rate of routine third trimester fetal biometry in low-risk pregnancies. In settings where a policy of third-trimester ultrasound is not in place, fundal height measurements remain common practice.

Ultrasound Diagnosis

An accurate antenatal detection of SGA fetuses remains the key process to subsequently detect and manage IUGR. This ultrasound assessment require three consecutive steps:

1. Pregnancy dating
2. Biometric evaluation
3. Assessing growth as normal or abnormal.

Pregnancy Dating

Pregnancy dating based upon the last menstrual period provides inaccurate estimates of the gestational age, since up to a 20% of women with regular cycles ovulate later than expected.[21] Hence, in clinical settings where a policy of first or early second trimester scan is in place, it seems to be more appropriate to systematically use the fetal biometries to date the pregnancy and ensure a reliable fetal age assessment for most purposes, for example Down's syndrome screening. There are several formulae to date the pregnancy from early biometries, with low systematic and random errors. Crown-rump length (CRL) is a biometric parameter that can be measured in the early stages of gestation. Technically, the main limitation is the progressive bending of the embryo, which makes measurements less reliable beyond 12–13 weeks of gestation (or 60–70 mm). Normal reference ranges to date the pregnancy are published elsewhere.[22] If possible, below the 14 weeks, all obstetric ultrasound units are currently recommended to adopt this method of assessing gestational age from crown-rump length. From then on, it seems conceptually more appropriate to use cephalic (head circumference) and/or femur (femur length) biometries. Series in which different formulas have been tested in pregnancies conceived with artificial reproductive techniques provide comprehensive recommendations on this matter.[23] Once the pregnancy has been dated by an early scan, further adjustments must not be performed.

Biometric Evaluation

Initially and still in many places, the biparietal diameter (BPD) was the only measurement that was routinely taken for the assessment of fetal growth. When pregnancy is normal, this parameter falls within the normal range and can be considered as a representative indicator of the growth of other fetal organs and tissues, but when pregnancy is abnormal it may still fall within the normal range (head size is rarely affected in many cases of IUGR) although in this case, it is not representative indicator of the growth of other fetal structures. On the other hand, misdiagnoses have been on many occasions in fetuses with marked brachycephalism or dolichocephalism in association with normal development of the rest of the body. In addition, measurement of the BPD does not permit determination of fetal weight with acceptable reliability. The substitution of BPD by head circumference or cephalic area does not substantially improve the sensitivity of the method. With the purpose of improving the screening method, measurement of the length of the femur was introduced. It has the advantage that it measures a component of fetal longitudinal growth and does not suffer the sudden flattening out characteristic of cephalic parameters at term, although it has the disadvantage of not being a useful parameter for establishing the diagnosis of IUGR early stages. Abdominal circumference (AC) is the most accurate single biometry to predict SGA at birth.[24] In high-risk women, AC at less than the tenth centile has sensitivities of 72.9–94.5% and specificities of 50.6–83.8% in the prediction of fetuses with birth weight at less than the tenth centile. The use of cross-sectional reference charts for each biometry with the closest distribution to that of the screened population remains the gold standard and some studies alert to the impact of choice of reference charts in the assessment of fetal biometry. In that sense they recommend to use Z-scores in order to choose the most appropriate chart.[25] Moreover, many charts require the average of at least

three repeated measurements in order to control random error. By increasing the number of measurements to four, the 95% error span is reduced to half.

Fetal biometries could be used to estimate the fetal weight. The estimated fetal weight (EFW) predicts the occurrence of SGA at birth with sensitivities of 33.3–89.2% and specificities of 53.7–90.9%.[24] A prospective study[26] comparing several formulas concluded that Shepard formula[27] have the best interclass correlation coefficient, with smallest mean difference from actual birth weight. Nevertheless, for fetuses weighting less than 2,000 gm, this formula has not been validated. The Hadlock formula[28] may be more appropriate when the fetus is expected to be very small.[29]

Controversy exists regarding using AC or EFW for the antenatal assessment of fetal growth. Whereas AC, the simplest method, has in high-pregnancies higher sensitivities, EFW has a stronger association with birthweight below the 10th centile.[24] We prefer using EFW since it is more consistent with the neonatal assessment, which is mainly performed by weight. In addition, the accuracy of the individual fetal parameters cannot be checked as there is no gold standard. On the contrary, estimated fetal weight could be assessed against birth weight and has a random error of about 8%.[28]

Since growth is a dynamic process, it seems logical that its quantification requires the evaluation of serial measurements. In fact, serial measurements of AC and EFW are superior to single estimates in the prediction of neonatal growth restriction defined by ponderal index or skin-fold thickness[30] and in the prediction of adverse outcome.[31] Nevertheless, from our point of view, there are major concerns regarding the use of serial measurements. Firstly, there is a scarcity of published normal ranges for growth velocity and is common practice to use normal ranges derived from transversal series to evaluate serial measurements, and use of standards across population may be misleading. Secondly, there is no agreement regarding the optimal methodology. Theoretically, conditional centiles, whereby the EFW or AC of each individual fetus at a first ultrasound examination is extrapolated to give a range of normal ranges (expressed as centiles) at a later scan, appears to be the most appropriate method for longitudinal growth assessment.[32] Compared to the ranges for the entire population, the conditional ranges for small fetus would be narrower and skewed in the direction of the initial measurement.[32] However, this approach has not demonstrated to be superior to other methodologically more straightforward alternatives, such as z-velocity.[34] In addition, the interval between scan is of paramount importance since two-week intervals are associated with false-positive rates for growth restriction in excess of 10%, increasing to much higher rates late in the third trimester.[35] A four-week interval, which is a too long interval for clinical purposes in high-risk pregnancies, has been reported to optimize the prediction.[36]

Individualized growth standards could be inferred in a forward direction on the basis of ultrasound biometry in early pregnancy. The Rossavik model[37] calculates an expected growth curve from two scans at about 18 and 24–26 weeks. In addition to have failed to demonstrate an improvement in the prediction of fetal weight,[38] there are several concerns regarding its conceptual framework. First, ultrasound error at each of the sequential scans can lead to substantial variation when forward projecting the growth curve that has been calculated from these measurements. Second, the fetus could already be affected by early-onset growth restriction, especially at the latter of the two scans, which would result in depressed values being projected as a "norm".

Assessing Growth

The normal ranges used when evaluating fetal growth is a question of utmost importance. When evaluating single measurements, such as AC, it is recommended to use local standards since differences between populations could be a source of unaccuracy. Nevertheless, strict methodological requirements are needed for normal ranges: a transversal design (each fetus is measured only once), reliable dating, enough sample size at the extremes of the gestational age and correct exclusion criteria. With regard to the question of selection criteria for the development of fetal size, only conditions for which information is available at the time of scanning for fetal growth should be excluded, such as fetal malformations and maternal diseases frequently associated with IUGR.[39] A comprehensive review of several reference ranges is provided elsewhere.[40]

For AC, a systematic review[24] found that a threshold of the tenth centile had better sensitivities and specificities than other commonly used centiles.

Regarding normal ranges for fetal weight, neonatal weight is frequently used as a proxy for fetal weight. Nevertheless, due to the fact that an epidemiological association exists between IUGR and preterm delivery, the birth weight distribution in preterm gestations is negatively skewed, while the distribution of fetal weight at the same gestation is close to normal.[41] As a consequence, population-based standards fail to identify a significant proportion of cases of preterm intrauterine SGA.[42]

For EFW, a systematic review[24] found that a threshold of the tenth centile had better sensitivities and specificities than other commonly used centiles.

Due to the fact that several maternal (height, weight, race, age, parity) and fetal (number, gender) variables play a significant role in fetal growth both in low and high risk pregnancies, population-based birth weight standards result in misclassification of a large proportion of cases.[43] Individually adjusted or customized growth charts aim to optimize the assessment of fetal growth by taking individual variation into account and by projecting an optimal curve which delineates the potential weight gain in each pregnancy. The use of customized birth weight standards, which take these factors into account, has demonstrated to improve the definition of SGA and the prediction of abnormal five-minute Apgar score, hospital stay length, admission to the intensive care unit, hypoglycemia, need for neonatal resuscitation and perinatal death, both in high-risk[44] and low-risk[45-48] populations. On the other hand, those neonates with a normal customized birth weight have been found to have a perinatal outcome comparable to the general population, regardless of being SGA according population-based centiles.[44-47] The inference of these findings is that SGA according to customized standards and growth restriction are equivalent, and it has been claimed that customized SGA could be used as reliable proxy of growth restriction.[43]

Regarding the customized fetal weight assessment, it has been found that a threshold of the tenth centile had better sensitivities and specificities than other used centiles for the prediction of adverse outcome.[44]

Three-dimensional Fetal Growth Assessment

The advent of three-dimensional sonography has allowed a new insight into fetal growth.

The upper arm[49] or thigh[50] volumes are parameters for detecting IUGR,[49] but need further validation. Calculation of organ volumes could also be made reliably and in a noninvasive way using this new technology. Interestingly, the fetal brain/liver volume ratio has been described[51] as a predictor of fetal outcome in the growth-restricted fetus. An inverse relationship exists in small-for-gestational-age fetuses between brain/liver volume ratio and fetal weight-related umbilical venous blood flow. The benefit of prospectively assessing organ values also requires further studies and could not be recommended.

DIAGNOSIS OF THE TYPE OF SGA

Following the diagnosis of a SGA fetus, further evaluation is warranted to determine the type of SGA.

Abnormal-SGA

- *Anatomical ultrasound:* An anatomical study is mandatory to rule out the presence of malformations (up to 25% of malformed fetuses are SGA) or the presence of signs of fetal infection (ventriculomegaly, microcephalia, brain or intraabdominal calcifications, placentomegaly, hydramnios). Most cases of congenital cytomegalovirus infection have oligohydramnios and therefore should be considered in the differential diagnosis.
- *Karyotyping:* Up to 15% of the abnormal SGA fetuses have some associated syndrome,[47] being either aneuploidy and nonaneuploidy syndromes. Some of them are recognized to be related to imprinting/methylation defects, e.g. the Silver Rusell, a clinically heterogeneous syndrome characterized by intrauterine and postnatal growth retardation with spared cranial growth, dysmorphic features and frequent body asymmetry. The risk of association is greater when there are associated structural abnormalities, a normal liquor volume or a normal uterine or umbilical artery Doppler. Therefore, it may also be appropriate to offer some genetic studies in selected cases.
- *Infectious study:* Although less than 5% of the cases are associated with infection, a TORCH serology seems reasonable to rule out this etiology. In most of the developed countries, the most prevalent infectious etiology of SGA is the cytomegalovirus. In cases, where an early infection is suspected, an amniotic fluid PCR determination for cytomegalovirus may be useful even in the presence of a negative maternal IgM.

IUGR versus Normal-SGA

The differentiation between growth-restricted and constitutionally small fetuses is essential for clinical practice: whereas the former are those who have failed to reach its genetically endowed growth potential, the latter are considered to represent one end of the normal size spectrum. The benchmark for this differentiation is the Doppler evaluation.

Umbilical Artery Doppler

Vasoconstriction phenomena of the tertiary stem villi[52] are considered responsible for the up river modifications in the normal wave flow velocity of the umbilical artery with a decrease in the diastolic velocities and an increase in the resistance and impedance indices. From the pioneering research in Doppler, it has been clearly demonstrated that abnormal umbilical Doppler

correlates with histological evidence of placental vascular pathology. As a result, Doppler umbilical artery indices correlate with fetal levels of glucose, amino acids and blood gases[53,54] and therefore, it could be considered as a surrogate measurement of the placental functionality. Moreover, a decreased flow in the umbilical vein has also been demonstrated in an asymptomatic stage of the disease related to a decrease of the placental volume. SGA with abnormal umbilical artery Doppler are smaller.[55-57] There is an extensive body of evidence that those SGA fetuses with abnormal umbilical artery flow are at higher risk of adverse perinatal outcome than those with normal flow.[31,45,55-60] Even when controlling for gestational age at delivery some series have reported a significant association between the abnormal umbilical artery flow and the perinatal results.[31,55,60] In addition, the occurrence of perinatal death in the presence of a normal umbilical flow is very uncommon.[55,57,61] Thus, Doppler of the umbilical artery flow could be considered as a risk-discriminator tool in the management of SGA fetuses. Evidence supports those SGA fetuses with normal Doppler benefit from a nonintensive follow-up.[62] As a consequence of this evidence, SGA fetuses with normal Doppler have been claimed normal SGA fetuses, representing the lowest spectrum of healthy fetuses and to manage them accordingly .[6,63] Some recent studies would suggest that even those normal-SGA would have a suboptimal perinatal and neurodevelopmental outcome,[64,66] suggesting that a proportion of these SGA fetuses are, in reality, late-onset mild IUGR cases.

Cerebroumbilical Ratio

It has been claimed that the relationship between the umbilical and cerebral flow provides a more sensitive tool to discriminate between constitutional SGA and IUGR as it may be decreased even when UA and MCA are very close to normal. In fact, animal models have demonstrated that this ratio is better correlated with hypoxia than its individual components.[64] Furthermore, it has also been extensively reported that the prediction of adverse outcome is improved using umbilical and cerebral parameters in a combined ratio,[66-72] with sensitivities of about 70%.[68,74] This initial redistribution would also be reflected in an impaired flow in the fetal aorta.

Uterine Artery

A defective trophoblast invasion is a common pattern in early and severe cases of growth restriction,[75] and this phenomenon is responsible for the presence of abnormal flow patterns in the uterine artery.

It has been suggested that uterine artery Doppler provide additional value to the umbilical and cerebral arteries to predict the occurrence of adverse outcome media,[76,77] and some management protocols consider this parameter as a criteria for IUGR independently to the fetal Doppler parameters. Nevertheless, a systematic review with meta-analysis[78] found that uterine artery Doppler had limited accuracy in predicting IUGR and perinatal death, and, therefore, its use needs to be evaluated further in studies.

STUDY OF FETAL DETERIORATION

Assessment of fetal well-being and delivery when the risks of leaving the fetus in an intrauterine hostile environment are considered to be greater than the risks of prematurity, remains the main management strategy for IUGR fetuses. Fetal well-being tests could be classified as chronic or acute. Whilst the former become progressively abnormal due to increasing hypoxemia and/or hypoxia, the latter correlate with acute changes occurring in advanced stages of fetal compromise, characterized by severe hypoxia and metabolic acidosis, and usually precede fetal death in few days. Since there does not exist a fixed sequence of fetal deterioration, integration of several well-being tests into comprehensive management protocols seems to be warranted.

Chronic Tests

Umbilical Artery

Vasoconstriction changes of the tertiary stem villi[52] are considered responsible for the upriver modifications in the wave flow velocity of the umbilical artery with a decrease in the diastolic velocities and an increase in the resistance and impedance indices. In advanced stages of placental histological and functional damage, diastolic velocities will become absent or even reversed. It has not been demonstrated qualitative differences in placental histological changes between the cases of IUGR with abnormal but positive diastolic flow and cases with reversed end-diastolic flow,[52] and therefore, the latter is considered the end of the spectrum of placental damage and is associated with an increased risk of perinatal death. As suggested by animal[79] and mathematical[80] experimental models of chronic placental embolization, it is required the obliteration of more than a 50% of the placental vessels before absent or reversed end-diastolic velocities appear.

Studies where IUGR fetuses were followed longitudinally[81] have reported that up to 80% of the fetuses have abnormal umbilical artery indices two weeks before the fetal acute deterioration, and, therefore, this

parameter could be considered a chronic marker. End-diastolic velocities have been reported to be present on an average one week before the acute deterioration.[81] Up to 40% of fetuses with acidosis show this umbilical flow pattern.[81] Despite the fact that an association exists between the presence of reversed end-diastolic flow in the umbilical artery and adverse perinatal outcome (with a sensitivity and specificity of about 60%), it is not clear whether this association is due to the confounding effect of prematurity and abnormal precordial venous flows.[82] Recent series[83-84] of severely compromised IUGR suggest an independent value of this pattern to predict perinatal morbidity and mortality, with a relative risk of 4.0 and 10.6 for those fetuses with absent or reversed end-diastolic flow, respectively. In addition to increased fetal and neonatal mortality, this finding is also associated with increased risk of long-term abnormal neurodevelopment.

However, a multicenter randomized trial,[85] the Growth Restriction Intervention Trial (GRIT), found that early delivery prompted by umbilical artery reversed end-diastolic flow does not improve the mortality rate or the neurological outcome in preterm IUGR fetuses, supporting the concept that a safe interval of 24–48 hours exists to allow for corticoid administration for lung maturation.

Middle Cerebral Artery

The reduction in the number of functional arterioles in the tertiary villi leads to a decrease in the PO_2 in the fetal blood. This event sets into motion a phenomena of circulatory redistribution principally characterized by the redistribution and centralization of blood flow. The better oxygenated blood goes towards the most vital organs (brain, heart, adrenals), whilst vasoconstriction limits the blood supply at the organs considered less indispensable (digestive system, lungs, skin, skeleton, etc.). As a consequence, a vasodilatation in the cerebral arteries occurs, known as a "brain-sparing" effect. This vasodilatation leads to an increase in the diastolic velocities and a decrease in the resistance and impedance indices in these vessels. The middle cerebral artery has become the standard for the clinical evaluation of the centralization of flow in IUGR fetuses. MCA pulsatility index steadily decrease through gestational age in preterm IUGR fetuses, suggesting a progressive redistribution.[86]

Moreover, longitudinal studies on deteriorating IUGR fetuses have reported that the pulsatility index in the MCA progressively becomes abnormal.[86] Up to a 80% of fetuses have vasodilatation 2 weeks before the acute deterioration,[81] although other series have found this figure to be less than 50%.[83] Preliminary findings of an acute loss of the MCA vasodilatation in advanced stages of fetal compromise have not been confirmed in more recent series,[81,83,86,87] and therefore, this sign does not seems to be clinically relevant for management purposes.

The value of cerebral Doppler to predict adverse outcome in the overall population of SGA fetuses is limited, with low sensitivities.[68,74] It has been suggested[88,89] that in near term SGA fetuses, the MCA could be useful to predict adverse outcome, independently of the umbilical artery Doppler. In addition, controversy exists whether cerebral vasodilatation is a merely protective mechanism or on the contrary is associated with suboptimal neurological development.[70] In a longitudinal cohort of infants born preterm (26–33 weeks), accelerated visual maturation was found using visual evoked cortical potentials at 3 years. At 5 years, these series demonstrated that both the changes in cerebral Doppler and the acceleration of visual maturation were associated with a deficit in cognitive scores. Recently, studies in the same cohort confirmed that brain sparing was associated with impaired visual function and visual motor capabilities at 11 years of age.[70-71] In consequence, further evidence is required before recommending its use as an isolated surveillance tool.

Amniotic Fluid

The pathways leading to oligohydramnios in fetuses with IUGR is not well understood. A renal hypoperfusion caused by redistribution phenomena and resulting in a decrease in the urinary production explains only partially this finding. A meta-analysis[90] of 18 randomized studies demonstrated that an amniotic fluid index less than 5 is associated with abnormal 5-minute Apgar score, but failed to demonstrate an association with acidosis.

Longitudinal studies IUGR fetuses have shown that the amniotic fluid index progressively decrease.[83-84,86] Nowadays, amniotic fluid volume in believed to be a chronic parameter. In fact, among the components of biophysical profile, it is the only one that is not considered acute. One week before the acute deterioration, a 20–30% of cases have oligohydramnios.[84,87]

Acute Markers

Precordial Veins (Ductus Venosus, Inferior Vena Cava and Umbilical Vein)

There is a growing evidence that the fetal heart contributes to the hemodynamic redistribution by

shifting the main cardiac output to the left ventricle, maximizing the oxygen supply to the brain. Animal studies have confirmed this adaptative mechanism.[91] Nevertheless, with increasingly adverse condition, these cardiac adaptive mechanisms have been suggested to become overburdened and a progressive impairment of cardiac function has been reported in longitudinal studies.[91] Secondary to severe tissue hypoxia, anerobic metabolism is required for energy production. Chronically, this anerobic metabolism leads to metabolic acidemia and acidosis. The fetal myocardium responds to this acidosis with myocardial cell necrosis phenomena, with replacement by fibroid tissue, which affects the myocardial compliance and therefore increase telediastolic pressure at both ventricles. The increased concentrations of troponin-T in neonates with pulsatile umbilical vein[92] suggests that myocardial cell destruction is the underlying cause of precordial veins flow abnormalities, with a decrease in velocities during atrial contraction and a consequent increase in pulsatility indices.

The association between abnormal precordial veins flows and adverse perinatal outcome has been extensively reported and has been demonstrated to be independent of the gestational age at delivery.[82] It has also been shown a correlation with acidosis by cordocentesis.[93]

The ductus venosus would allow the diversion of highly oxygenated blood from the umbilical vein into the right atria. This preferential blood flow crosses the foramen ovale to the left cavities and hence to irrigate the fetal brain. There are two possible mechanisms for abnormal venous blood flow waveforms in severe hypoxemia. Firstly, the flow redistribution in the umbilical venous blood towards the DV at the expense of hepatic blood flow, and secondly, there may be a myocardial failure. Whereas ductus venous pulsatility index above the 95th centile is an earlier sign, reversed velocities during atrial contraction represents the end of the spectrum of abnormal flow. It has been reported[94] that in these preterm fetuses, a 3SD cut-off optimize the combination of sensitivity and specificity. Moreover, a recent multicentric prospective study demonstrated that ductus venosus Doppler parameters emerge as the primary cardiovascular factor in predicting neonatal outcome in those preterm early-onset IUGR fetuses below 28 weeks. The perinatal mortality when there an absent or reversed flow in the a-wave was present ranged from 60–100%.[94] However, its sensitivity for perinatal death is still 40–70%.

Although each precordial vein correctly predicts acid-base status in a significant proportion of IUGR neonates, combination, rather than single vessel assessment provides the best predictive accuracy. Doppler abnormality in either vessel identified about a 90% of newborns with acidosis.[96]

Longitudinal studies have demonstrated that precordial vein flow waveforms become abnormal in advanced stages of fetal compromise.[81,83,86,87] The temporal relation with other acute markers are variable: whereas in about a 50% of cases, abnormal ductus venosus precedes the loss of short-term variability in the fetal heart rate, this later sign is the first to become abnormal in the other cases.[86] In about a 90% of cases, the ductus venosus become abnormal only 48–72 hours before the biophysical profile shows changes.[87] Debate exists regarding the advantages of DV Doppler investigation over the biophysical profile. However, observational studies suggest that to integrate both DV Doppler investigation and biophysical profile in the management of preterm IUGR seems to more effectively stratify IUGR fetuses into risk categories. Further research is warranted to investigate how they are best combined.

Other Cardiac Doppler Parameters

The aortic isthmus is a link between the right and left ventricles which perfuse the lower body and placental circulation, and upper body, respectively. Consequently, its blood flow pattern reflects the balance between both ventricular outputs and the existence of differences in the vascular impedance in either vascular system. The clinical use of aortic isthmus waveforms for monitoring fetal deterioration in IUGR has been limited, but preliminary work suggests that abnormal AoI impedance indices are an intermediate step between placental insufficiency-hypoxemia and cardiac decompensation.[96-97] A prospective study in severe early-onset IUGR demonstrated that a retrograde flow in the AoI in growth-restricted fetuses correlated strongly with adverse perinatal outcome.[98]

Hypoxemia and acidosis may also impair cardiac contractility directly. The myocardial performance index (MPI) is a novel method in fetal medicine that assesses both systolic and diastolic functions by including the measurement of isovolumetric and ejection times and would be useful in assessing the progressive hemodynamic deterioration. It has been recently reported to be independently associated with perinatal mortality, mainly in very preterm IUGR fetuses,[99] although its role as a surveillance tool needs to be further elucidated.

Fetal Heart Rate

Due to severe hypoxemia, signal from peripheral chemoreceptors and baroreceptors triggers a parasympathetic response that results in fetal heart decelerations. In advanced stages of fetal compromise, the direct effect of acidosis on the nervous system and on the myocardium results in a loss of the fetal heart rate variability as well as deceleration.

Early studies on high risk demonstrated that though highly sensitive, a 50% rate of false positive hampers its clinical usefulness. In addition, a meta-analysis[100] on high-risk pregnancies failed to demonstrate any beneficial effect in reducing perinatal mortality. Hence, there is no evidence to support the use of traditional fetal heart rate in IUGR fetuses.

Computerized fetal heart rate analyses has provided new insight into the pathophysiology of IUGR. It has been demonstrated by cordocentesis that the short-term variability closely correlates with acidosis and severe hypoxia. Despite the fact that Bracero et al[101] demonstrated non-significant perinatal outcome differences between visual and computerized FHR, more recent longitudinal series pointed out a potential role as acute marker.[86] Short-term variability becomes abnormal coinciding with the ductus venosus: whereas in about a 50% of cases abnormal ductus venosus precedes the loss of short-term variability in the fetal heart rate, this later sign is the first to become abnormal in the other cases.[86] Both parameters are considered acute responses to fetal acidosis.

Biophysical Profile

Among the components of the Manning[102] biophysical profile, amniotic fluid volume is the more chronic parameter. With increasing fetal compromise, the amniotic fluid volume progressively decreases.[83,86] In advanced stages of hypoxia, a decrease in the breathing movements is observed and finally, mainly acidosis accounts for the loss of fetal tone and gross body movements.

Observational studies demonstrated an association between abnormal biophysical profile and perinatal mortality and cerebral palsy.[103] Studies in which a cordocentesis was performed demonstrated a good correlation with acidosis,[104] being the fetal tone and gross motor movements the best correlated components. However, similarly to the fetal heart rate, although highly sensitive, a 50% rate of false positive limits the clinical usefulness of the biophysical profile.[105] A meta-analysis[106] showed no significant benefit of biophysical profile in high-risk pregnancies, but more recent series[107] on IUGR have suggested that both Doppler and BPS effectively stratify IUGR fetuses into risk categories. Since fetal deterioration appears to be independently reflected by both tests, further studies are warranted to prove the usefulness of combined both testing modalities. The above mentioned study uses a cut-off of 4 (or 6 if oligohydramnios exists), for the time being these are the more comprehensive criteria for decision-making.

Longitudinal series[87] have demonstrated that except for the amniotic fluid volume and the fetal heart rate, the other components of the biophysical profile become abnormal in advanced stages of fetal compromise: In about 90% of cases, the ductus venosus become abnormal only 48–72 hours before the biophysical profile.[87]

OBSTETRIC MANAGEMENT

Despite clear guidelines supported by strong evidence cannot be provided, protocols for management of SGA fetus may be developed according to current knowledge. It is evident that an integrated approach seems most appropriate when using any Doppler algorithm in management. Our protocol is as follows:

- Normal-SGA (estimated fetal weight below the 10th centile with normal cerebroplacental ratio and normal uterine artery Doppler flow): Excluding infectious and genetic causes, the perinatal results are good. Fortnightly Doppler and biophysical profile are performed. Delivery should only be indicated for obstetrics or maternal factors. A vaginal delivery with continuous fetal monitoring is recommended. Delivery should not be postponed more than 40 weeks of gestation.
- The IUGR with normal fetal well-being tests (estimated fetal weight below the 10th centile with abnormal cerebroplacental ratio but no presence of vasodilation or uterine artery Doppler flow): Weekly Doppler and biophysical profile are performed. Delivery beyond 37 weeks or when pulmonary maturity is proven, could be considered. A vaginal delivery with continuous fetal monitoring is recommended.
- The IUGR (estimated fetal weight below the 10th centile with abnormal cerebroplacental ratio or uterine artery Doppler flow) with significant placental insufficiency (absent end-diastolic flow in the umbilical artery) or centralization (persistent vasodilatation of middle cerebral artery):
  a. Beyond 34 weeks: A vaginal delivery is accepted. A cesarean section would be required in absent end-diastolic umbilical flow.

b. Between 32 and 34 weeks:
   i. Reversed end-diastolic flow: Steroids and delivery in 24-48 hours by cesarean section
   ii. Absent end-diastolic flow: Steroids, daily Doppler and biophysical profile until 34 weeks.
c. Below 32 weeks: Steroids, daily Doppler and biophysical profile until 34 weeks.

- The IUGR (estimated fetal weight below the 10th centile with abnormal cerebroplacental ratio or uterine artery Doppler flow) with suspected fetal compromise (persistent increased ductus venosus waveforms pulsatility, low short-term variability, abnormal biophysical profile):
  a. Beyond 32 weeks: Delivery by cesarean section
  b. Below 32 weeks: Hospital admission, steroids, daily Doppler and biophysical profile/12 hours until 32 weeks.
- The IUGR (estimated fetal weight below the 10th centile with abnormal cerebroplacental ratio or uterine artery Doppler flow) with fetal decompensation (persistent absent or reversed a-wave in the ductus venosus or persistent pulsatile umbilical vein or persistent abnormal biophysical profile or decelerative cardiotocography): delivery by cesarean section at a tertiary care center. In the subgroup under 28 weeks, each case should be evaluated by a multidisciplinary committee composed by an obstetrician and a neonatologist with experience in those case, and taking into account the opinion of the parents: expectant management could be an option in these extremely preterm and compromised fetuses.

REFERENCES

1. Kady S, Gardosi J. Perinatal mortality and fetal growth restriction. Best Pract Res Clin Obstet Gynaecol. 2004;18(3):397-410.
2. Jarvis S, Glinianaia SV, Torrioli MG, et al. Cerebral palsy and intrauterine growth in single births: European collaborative study. Lancet. 2003;362(9390):1106-11.
3. Smith GC, Wood AM, Pell JP, et al. Sudden infant death syndrome and complications in other pregnancies. Lancet. 2005;366(9503):2107-11.
4. Godfrey KM, Barker DJ. Fetal nutrition and adult disease. Am J Clin Nutr. 2000;71(5 Suppl):1344S-52S.
5. Todros T, Plazzotta C, Pastorin L. Body proportionality of the small-for-date fetus: is it related to aetiological factors? Early Hum Dev. 1996;45(1-2):1-9.
6. Soothill PW, Bobrow CS, Holmes R. Small for gestational age is not a diagnosis. Ultrasound Obstet Gynecol. 1999. 13(4):225-8.
7. Blackwell SC, Moldenhauer J, Redman M, et al. Relationship between the sonographic pattern of intrauterine growth restriction and acid-base status at the time of cordocentensis. Arch Gynecol Obstet. 2001;264(4):191-3.
8. Lin CC, Su SJ, River LP. Comparison of associated high-risk factors and perinatal outcome between symmetric and asymmetric fetal intrauterine growth retardation. Am J Obstet Gynecol. 1991;164(6 Pt 1):1535-41; discussion 1541-2.
9. Kramer MS, Olivier M, McLean FH, et al. Impact of intrauterine growth retardation and body proportionality on fetal and neonatal outcome. Pediatrics. 1990;86(5):707-13.
10. Carrera J. Definitions, etiology and clinical implications. Ultrasound and Fetal Growth. London: The Parthenon Publish; 1999. pp. 17-34.
11. Wilcox AJ. Intrauterine growth retardation: beyond birthweight criteria. Early Hum Dev. 1983;8(3-4):189-93.
12. Snijders RJ, Sherrod C, Gosden CM, et al. Fetal growth retardation: associated malformations and chromosomal abnormalities. Am J Obstet Gynecol. 1993;168(2):547-55.
13. Yaron Y, Ochshorn Y, Heifetz S, et al. First trimester maternal serum free human chorionic gonadotropin as a predictor of adverse pregnancy outcome. Fetal Diagn Ther. 2002;17(6):352-6.
14. Levine RJ, Lam C, Qian C, et al. Soluble endoglin and other circulating antiangiogenic factors in preeclampsia. N Engl J Med. 2006;355(10):992-1005.
15. Papageorghiou AT, Yu CK, Bindra R, et al. Multicenter screening for pre-eclampsia and fetal growth restriction by transvaginal uterine artery Doppler at 23 weeks of gestation. Ultrasound Obstet Gynecol. 2001;18(5):441-9.
16. Martin AM, Bindra R, Curcio P, et al. Screening for pre-eclampsia and fetal growth restriction by uterine artery Doppler at 11-14 weeks of gestation. Ultrasound Obstet Gynecol. 2001;18(6):583-6.
17. Lindqvist PG, Molin J. Does antenatal identification of small-for-gestational age fetuses significantly improve their outcome? Ultrasound Obstet Gynecol. 2005;25(3):258-64.
18. European comparison of perinatal care—the Euronatal Study. Maternal and Child Health Consortium. CESDI 8th Annual Report: Confidential Inquiry of Sitllbirth and Deaths in Infancy. 2001.
19. British College of Obstetricians and Gynaecologist. The Investigation and Management of The Small-for-Gestational Age Fetus. Geen-Top Guidelines 2002 (Guideline No.31).
20. Gardosi J, Francis A. Controlled trial of fundal height measurement plotted on customised antenatal growth charts. Br J Obstet Gynaecol. 1999;106(4):309-17.
21. Mongelli M, Wilcox M, Gardosi J. Estimating the date of confinement: ultrasonographic biometry versus certain menstrual dates. Am J Obstet Gynecol. 1996;174(1 Pt 1):278-81.
22. Robinson HP, Fleming JE. A critical evaluation of sonar "crown-rump length" measurements. Br J Obstet Gynaecol. 1975;82(9):702-10.
23. Mul T, Mongelli M, Gardosi J. A comparative analysis of second-trimester ultrasound dating formulae in pregnancies conceived with artificial reproductive techniques. Ultrasound Obstet Gynecol. 1996;8(6):397-402.

24. Chang TC, Robson SC, Boys RJ, et al. Prediction of the small for gestational age infant: which ultrasonic measurement is best? Obstet Gynecol. 1992;80(6):1030-8.
25. Chien PF, Owen P, Khan KS. Validity of ultrasound estimation of fetal weight. Obstet Gynecol. 2000;95(6 Pt 1):856-60.
26. Salomon LJ, Bernard JP, Duyme M, et al. The impact of choice of reference charts and equations on the assessment of fetal biometry. Ultrasound Obstet Gynecol. 2005;25(6):559-65.
27. Shepard MJ, Richards VA, Berkowitz RL, et al. An evaluation of two equations for predicting fetal weight by ultrasound. Am J Obstet Gynecol. 1982;142(1):47-54.
28. Hadlock FP, Harrist RB, Sharman RS, et al. Estimation of fetal weight with the use of head, body, and femur measurements—a prospective study. Am J Obstet Gynecol. 1985;151(3):333-7.
29. Kaaij MW, Struijk PC, Lotgering FK. Accuracy of sonographic estimates of fetal weight in very small infants. Ultrasound Obstet Gynecol. 1999;13(2):99-102.
30. Chang TC, Robson SC, Spencer JA, et al. Identification of fetal growth retardation: comparison of Doppler waveform indices and serial ultrasound measurements of abdominal circumference and fetal weight. Obstet Gynecol. 1993;82(2):230-6.
31. Chang TC, Robson SC, Spencer JA, et al. Prediction of perinatal morbidity at term in small fetuses: comparison of fetal growth and Doppler ultrasound. Br J Obstet Gynaecol. 1994;101(5):422-7.
32. Royston P, Altman DG. Design and analysis of longitudinal studies of fetal size. Ultrasound Obstet Gynecol. 1995;6(5):307-12.
33. Kiserud T, Lian S. Biometric assessment. Best practice and Research Clinical Obstetrics and gynecology. 2009;23:819-31.
34. Owen P, Donnet ML, Ogston SA, et al. Standards for ultrasound fetal growth velocity. Br J Obstet Gynaecol. 1996;103(1):60-9.
35. Mongelli M, Ek S, Tambyrajia R. Screening for fetal growth restriction: a mathematical model of the effect of time interval and ultrasound error. Obstet Gynecol. 1998;92(6):908-12.
36. Mondry A, Pengbo L, Loh M, Mongelli M. Z-velocity in screening for intrauterine growth restriction. Ultrasound Obstet Gynecol. 2005;26(6):634-8.
37. Deter RL, Rossavik IK, Harrist RB, et al. Mathematic modeling of fetal growth: development of individual growth curve standards. Obstet Gynecol. 1986;68(2):156-61.
38. Shields LE, Huff RW, Jackson GM, et al. Fetal growth: a comparison of growth curves with mathematical modeling. J Ultrasound Med. 1993;12(5):271-4.
39. Altman DG, Chitty LS. Charts of fetal size: 1. Methodology. Br J Obstet Gynaecol. 1994;101(1):29-34.
40. Figueras F, Torrents M, Munoz A, et al. References intervals for fetal biometrical parameters. Eur J Obstet Gynecol Reprod Biol. 2002;105(1):25-30.
41. Wilcox M, Gardosi J, Mongelli M, et al. Birth weight from pregnancies dated by ultrasonography in a multicultural British population. BMJ. 1993;307(6904):588-91.
42. Gardosi JO. Prematurity and fetal growth restriction. Early Hum Dev. 2005;81(1):43-9.
43. Gardosi J. Customized fetal growth standards: rationale and clinical application. Semin Perinatol. 2004;28(1):33-40.
44. De Jong CL, Francis A, Van Geijn HP, et al. Customized fetal weight limits for antenatal detection of fetal growth restriction. Ultrasound Obstet Gynecol. 2000;15(1):36-40.
45. McCowan LM, Harding JE, Stewart AW. Customized birthweight centiles predict SGA pregnancies with perinatal morbidity. BJOG. 2005;112(8):1026-33.
46. Clausson B, Gardosi J, Francis A, et al. Perinatal outcome in SGA births defined by customised versus population-based birthweight standards. BJOG. 2001;108(8):830-4.
47. Ego A, Subtil D, Grange G, et al. Customized versus population-based birth weight standards for identifying growth restricted infants: a French multicenter study. Am J Obstet Gynecol. 2006;194(4):1042-9.
48. Sciscione AC, Gorman R, Callan NA. Adjustment of birth weight standards for maternal and infant characteristics improves the prediction of outcome in the small-for-gestational-age infant. Am J Obstet Gynecol. 1996;175(3 Pt 1):544-7.
49. Chang CH, Yu CH, Ko HC, et al. Fetal upper arm volume in predicting intrauterine growth restriction: a three-dimensional ultrasound study. Ultrasound Med Biol. 2005;31(11):1435-9.
50. Chang CH, Yu CH, Ko HC, et al. The efficacy assessment of thigh volume in predicting intrauterine fetal growth restriction by three-dimensional ultrasound. Ultrasound Med Biol. 2005;31(7):883-7.
51. Chang CH, Yu CH, Chang FM, et al. The assessment of normal fetal liver volume by three-dimensional ultrasound. Ultrasound Med Biol. 2003;29(8):1123-9.
52. Sebire NJ. Umbilical artery Doppler revisited: pathophysiology of changes in intrauterine growth restriction revealed. Ultrasound Obstet Gynecol. 2003;21(5):419-22.
53. Nicolaides KH, Bilardo CM, Soothill PW, et al. Absence of end diastolic frequencies in umbilical artery: a sign of fetal hypoxia and acidosis. BMJ. 1988;297(6655):1026-7.
54. Karsdorp VH, van Vugt JM, Jakobs C, et al. Amino acids, glucose and lactate concentrations in umbilical cord blood in relation to umbilical artery flow patterns. Eur J Obstet Gynecol Reprod Biol. 1994;57(2):117-22.
55. Trudinger BJ, Cook CM, Giles WB, et al. Fetal umbilical artery velocity waveforms and subsequent neonatal outcome. Br J Obstet Gynaecol. 1991;98(4):378-84.
56. James DK, Parker MJ, Smoleniec JS. Comprehensive fetal assessment with three ultrasonographic characteristics. Am J Obstet Gynecol. 1992;166(5):1486-95.
57. Burke G, Stuart B, Crowley P, et al. Is intrauterine growth retardation with normal umbilical artery blood flow a benign condition? BMJ. 1990;300(6731):1044-5.
58. Gaziano EP, Knox H, Ferrera B, et al. Is it time to reassess the risk for the growth-retarded fetus with normal Doppler velocimetry of the umbilical artery? Am J Obstet Gynecol. 1994;170(6):1734-41; discussion 1741-3.
59. Reuwer PJ, Sijmons EA, Rietman GW, et al. Intrauterine growth retardation: prediction of perinatal distress by Doppler ultrasound. Lancet. 1987;2(8556):415-8.

60. Yoon BH, Lee CM, Kim SW. An abnormal umbilical artery waveform: a strong and independent predictor of adverse perinatal outcome in patients with preeclampsia. Am J Obstet Gynecol. 1994;171(3):713-21.
61. McCowan LM, Harding JE, Stewart AW. Umbilical artery Doppler studies in small for gestational age babies reflect disease severity. BJOG. 2000;107(7):916-25.
62. McCowan LM, Harding JE, Roberts AB, et al. A pilot randomized controlled trial of two regimens of fetal surveillance for small-for-gestational-age fetuses with normal results of umbilical artery doppler velocimetry. Am J Obstet Gynecol. 2000;182(1 Pt 1):81-6.
63. Bobrow CS, Soothill PW. Fetal growth velocity: a cautionary tale. Lancet. 1999;353(9163):1460.
64. Arbeille P, Maulik D, Fignon A, et al. Assessment of the fetal PO_2 changes by cerebral and umbilical Doppler on lamb fetuses during acute hypoxia. Ultrasound Med Biol. 1995;21(7):861-70.
65. Figueras F, Eixarch E, Meler E, et al. Small-for-gestational-age fetuses with normal umbilical artery Doppler have suboptimal perinatal and neurodevelopmental outcome. Eur J Obstet Gynecol Reprod Biol. 2008;136(1):34-8.
66. Leitner Y, Fattal-Valevski A, Geva R, et al. Neurodevelopmental outcome of children with intrauterine growth retardation: a longitudinal, 10-year prospective study. J Child Neurol. 2007;22(5);580-7.
67. Arias F. Accuracy of the middle-cerebral-to-umbilical-artery resistance index ratio in the prediction of neonatal outcome in patients at high risk for fetal and neonatal complications. Am J Obstet Gynecol. 1994;171(6):1541-5.
68. Bahado-Singh RO, Kovanci E, Jeffres A, et al. The Doppler cerebroplacental ratio and perinatal outcome in intrauterine growth restriction. Am J Obstet Gynecol. 1999;180(3 Pt 1):750-6.
69. Gramellini D, Folli MC, Raboni S, et al. Cerebral-umbilical Doppler ratio as a predictor of adverse perinatal outcome. Obstet Gynecol. 1992;79(3):416-20.
70. Scherjon S, Briet J, Oosting H, et al. The discrepancy between maturation of visual-evoked potentials and cognitive outcome at five years in very preterm infants with and without hemodynamic signs of fetal brain-sparing. Pediatrics. 2000;105(2):385-91.
71. Kok JH, Prick L, Merckel E, et al. Visual function at 11 years of age in preterm-born children with and without fetal brain sparing. Pediatrics. 2007;119(6):e1342-50.
72. Devine PA, Bracero LA, Lysikiewicz A, et al. Middle cerebral to umbilical artery Doppler ratio in post-date pregnancies. Obstet Gynecol. 1994;84(5):856-60.
73. Makhseed M, Jirous J, Ahmed MA, et al. Middle cerebral artery to umbilical artery resistance index ratio in the prediction of neonatal outcome. Int J Gynaecol Obstet. 2000;71(2):119-25.
74. Odibo AO, Riddick C, Pare E, et al. Cerebroplacental Doppler ratio and adverse perinatal outcomes in intrauterine growth restriction: evaluating the impact of using gestational age-specific reference values. J Ultrasound Med. 2005;24(9):1223-8.
75. Madazli R, Somunkiran A, Calay Z, et al. Histomorphology of the placenta and the placental bed of growth restricted foetuses and correlation with the Doppler velocimetries of the uterine and umbilical arteries. Placenta. 2003;24(5):510-6.
76. Severi FM, Bocchi C, Visentin A, et al. Uterine and fetal cerebral Doppler predict the outcome of third-trimester small-for-gestational age fetuses with normal umbilical artery Doppler. Ultrasound Obstet Gynecol. 2002;19(3):225-8.
77. Vergani P, Roncaglia N, Andreotti C, et al. Prognostic value of uterine artery Doppler velocimetry in growth-restricted fetuses delivered near term. Am J Obstet Gynecol. 2002;187(4):932-6.
78. Chien PF, Arnott N, Gordon A, et al. How useful is uterine artery Doppler flow velocimetry in the prediction of pre-eclampsia, intrauterine growth retardation and perinatal death? An overview. BJOG. 2000;107(2):196-208.
79. Morrow RJ, Adamson SL, Bull SB, et al. Effect of placental embolization on the umbilical arterial velocity waveform in fetal sheep. Am J Obstet Gynecol. 1989;161(4):1055-60.
80. Thompson RS, Trudinger BJ. Doppler waveform pulsatility index and resistance, pressure and flow in the umbilical placental circulation: an investigation using a mathematical model. Ultrasound Med Biol. 1990;16(5):449-58.
81. Ferrazzi E, Bozzo M, Rigano S, et al. Temporal sequence of abnormal Doppler changes in the peripheral and central circulatory systems of the severely growth-restricted fetus. Ultrasound Obstet Gynecol. 2002;19(2):140-6.
82. Schwarze A, Gembruch U, Krapp M, et al. Qualitative venous Doppler flow waveform analysis in preterm intrauterine growth-restricted fetuses with ARED flow in the umbilical artery—correlation with short-term outcome. Ultrasound Obstet Gynecol. 2005;25(6):573-9.
83. Cosmi E, Ambrosini G, D'Antona D, et al. Doppler, cardiotocography, and biophysical profile changes in growth-restricted fetuses. Obstet Gynecol. 2005;106(6):1240-5.
84. Valcamonico A, Danti L, Frusca T, et al. Absent end-diastolic velocity in umbilical artery: risk of neonatal morbidity and brain damage. Am J Obstet Gynecol. 1994;170(3): 796-801.
85. Thornton JG, Hornbuckle J, Vail A, et al. Infant wellbeing at 2 years of age in the Growth Restriction Intervention Trial (GRIT): multicentred randomised controlled trial. Lancet. 2004;364(9433):513-20.
86. Hecher K, Bilardo CM, Stigter RH, et al. Monitoring of fetuses with intrauterine growth restriction: a longitudinal study. Ultrasound Obstet Gynecol. 2001;18(6):564-70.
87. Baschat AA, Gembruch U, Harman CR. The sequence of changes in Doppler and biophysical parameters as severe fetal growth restriction worsens. Ultrasound Obstet Gynecol. 2001;18(6):571-7.
88. Hershkovitz R, Kingdom JC, Geary M, et al. Fetal cerebral blood flow redistribution in late gestation: identification of compromise in small fetuses with normal umbilical artery Doppler. Ultrasound Obstet Gynecol. 2000;15(3):209-12.
89. To WW, Chan AM, Mok KM. Use of umbilical-cerebral Doppler ratios in predicting fetal growth restriction in near-term fetuses. Aust N Z J Obstet Gynaecol. 2005;45(2):130-6.

90. Chauhan SP, Sanderson M, Hendrix NW, et al. Perinatal outcome and amniotic fluid index in the antepartum and intrapartum periods: a meta-analysis. Am J Obstet Gynecol. 1999;181(6):1473-8.
91. Gilbert RD. Fetal myocardial responses to long-term hypoxemia. Comp Biochem Physiol A Mol Integr Physiol. 1998;119(3):669-74.
92. Makikallio K, Vuolteenaho O, Jouppila P, et al. Association of severe placental insufficiency and systemic venous pressure rise in the fetus with increased neonatal cardiac troponin T levels. Am J Obstet Gynecol. 2000;183(3):726-31.
93. Hecher K, Snijders R, Campbell S, et al. Fetal venous, intracardiac, and arterial blood flow measurements in intrauterine growth retardation: relationship with fetal blood gases. Am J Obstet Gynecol. 1995;173(1):10-5.
94. Bilardo CM, Wolf H, Stigter RH, et al. Relationship between monitoring parameters and perinatal outcome in severe, early intrauterine growth restriction. Ultrasound Obstet Gynecol. 2004;23(2):119-25.
95. Bashat AA, Cosmi E, Bilardo C, et al. Predictors of neonatal outcome in early-onset placental dysfunction. Obstet Gynecol. 2007;109(2 Pt 1):253-61.
96. Baschat AA, Guclu S, Kush ML, Gembruch U, Weiner CP, Harman CR. Venous Doppler in the prediction of acid-base status of growth-restricted fetuses with elevated placental blood flow resistance. Am J Obstet Gynecol 2004;191(1):277-84.
97. Kennelly MM, Farah N, Turner MJ, et al. Aortic isthmus Doppler velocimetry: role in assessment of preterm fetal growth restriction. Prenat Diagn. 2010;30(5):395-401.
98. Del Río M, Martínez JM, Figueras F, et al. Doppler assessment of the aortic isthmus and perinatal outcome in preterm fetuses with severe intrauterine growth restriction. Ultrasound Obstet Gynecol. 2008;31(1):41-7.
99. Hernandez-Andrade E, Crispi F, Benavides-Serralde A, et al. Contribution of the modified myocardial performance index and aortic isthmus blood flow index to refine prediction of mortality in preterm intrauterine growth restricted fetuses. Ultrasound Obstet Gynecol. 2009;34(4):430-6.
100. Pattison N, McCowan L. Cardiotocography for antepartum fetal assessment. Cochrane Database Syst Rev. 2000(2): CD001068.
101. Bracero LA, Morgan S, Byrne DW. Comparison of visual and computerized interpretation of nonstress test results in a randomized controlled trial. Am J Obstet Gynecol. 1999;181(5 Pt 1):1254-8.
102. Manning FA, Platt LD, Sipos L. Antepartum fetal evaluation: development of a fetal biophysical profile. Am J Obstet Gynecol. 1980;136(6):787-95.
103. Manning FA, Bondaji N, Harman CR, et al. Fetal assessment based on fetal biophysical profile scoring. VIII. The incidence of cerebral palsy in tested and untested perinates. Am J Obstet Gynecol. 1998;178(4):696-706.
104. Manning FA, Snijders R, Harman CR, et al. Fetal biophysical profile score. VI. Correlation with antepartum umbilical venous fetal pH. Am J Obstet Gynecol. 1993;169(4):755-63.
105. Miller DA, Rabello YA, Paul RH. The modified biophysical profile: antepartum testing in the 1990s. Am J Obstet Gynecol. 1996;174(3):812-7.
106. Alfirevic Z, Neilson JP. Biophysical profile for fetal assessment in high risk pregnancies. Cochrane Database Syst Rev. 2000(2):CD000038.
107. Baschat AA, Galan HL, Bhide A, et al. Doppler and biophysical assessment in growth restricted fetuses: distribution of test results. Ultrasound Obstet Gynecol. 2006; 27(1):41-7.

16
CHAPTER

Fetal Central Nervous System

Ritsuko K Pooh, Kyong Hon Pooh

INTRODUCTION

Transvaginal Neurosonography

Imaging technologies have been remarkably improved and contributed to prenatal evaluation of fetal central nervous system (CNS) development and assessment of CNS abnormalities *in utero*.

Conventional transabdominal ultrasonography, by which it is possible to observe fetuses through maternal abdominal wall, uterine wall and sometimes placenta, has been most widely utilized for antenatal imaging diagnosis. By transabdominal approach, whole CNS of fetuses can be well demonstrated, for instance, the brain in the axial section and the spine in the sagittal section. However, transabdominal approach to the fetal CNS, has several obstacles, such as maternal abdominal wall, placenta and fetal cranial bones, and it is difficult to obtain clear and detailed images of fetal CNS structure.

Introduction of high-frequency transvaginal transducer has contributed to establishing "sonoembryology"[1] and recent general use of transvaginal sonography in early pregnancy enabled early diagnoses of major fetal anomalies.[2] In the middle and late pregnancy, fetal CNS is generally evaluated through maternal abdominal wall. The brain, however, is three-dimensional (3D) structure and should be assessed in basic three planes of sagittal, coronal and axial sections. Sonographic assessment of the fetal brain in the sagittal and coronal section, requires an approach from fetal parietal direction. Transvaginal sonography of the fetal brain opened a new field in medicine, "neurosonography."[3] Transvaginal approach to the normal fetal brain during the second and third trimester was introduced in the beginning of 1990s. It was the first practical application of 3D CNS assessment by two-dimensional (2D) ultrasound.[4] Transvaginal observation of the fetal brain offers sagittal and coronal views of the brain from fetal parietal direction[5-8] through the fontanelles and/or the sagittal suture as ultrasound windows. Serial oblique sections[3] via the same ultrasound window reveal the intracranial morphology in detail. This method has contributed to the prenatal assessment of congenital CNS anomalies and acquired brain damage *in utero.*

BASIC ANATOMICAL KNOWLEDGE OF THE BRAIN

As described above, the brain should be understood as a 3D structure. It is generally believed that the brain anatomy is complicated and there must be lots of terms to remember. However, in order to demonstrate the brain structure and evaluate fetal CNS disorders, it is not necessary to remember all of detailed structure. Here, essential anatomical structures are selected for neuroimaging and comprehension of fetal CNS diseases. **Figures 16.1A and B** show the basic brain anatomy in the axial and sagittal sections and **Figure 16.2** shows anterior coronal and posterior coronal sections.

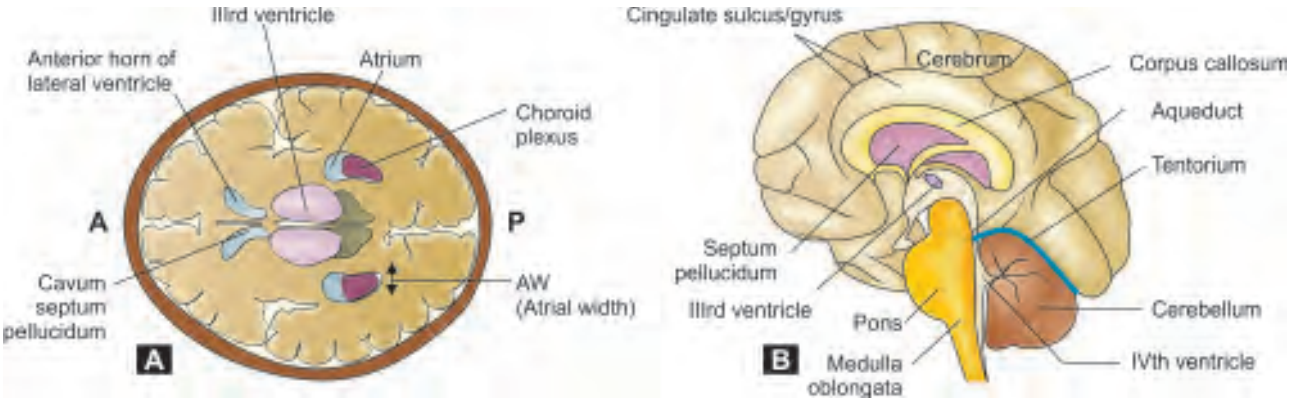

Figures 16.1A and B: Basic anatomy of the fetal brain (Axial and sagittal section)

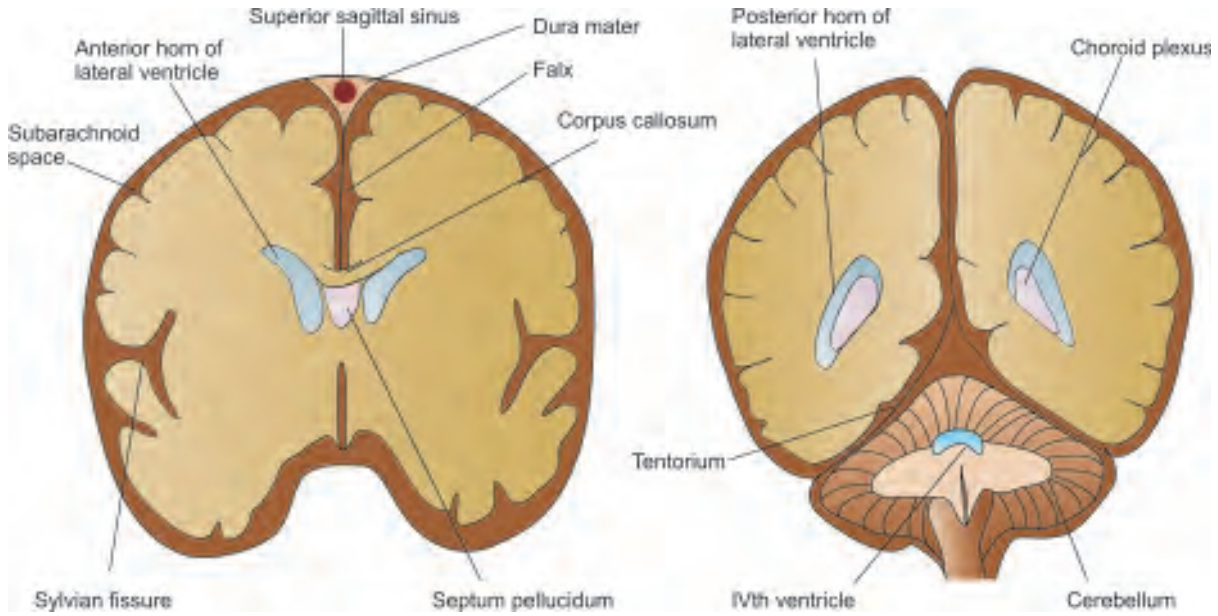

Figure 16.2: Basic anatomy of the fetal brain (Coronal section)

Transvaginal 3D Sonographic Assessment of Fetal Central Nervous System

The 3D ultrasound is one of the most attractive modality in the field of fetal ultrasound imaging. There are two scanning methods of free-hand scan and automatic scan. Automatic scan by dedicated 3D transducer produces motor driven automatic sweeping and is called as a fan scan. With this method, a shift and/or angle-change of the transducer is not required during scanning and scan duration needs only several seconds. After acquisition of the target organ, multiplanar imaging analysis and tomographic imaging analysis are possible. Combination of both transvaginal sonography and 3D ultrasound[9-12] may be a great diagnostic tool for evaluation of 3D structure of fetal CNS. Recent advanced 3D ultrasound equipments have several useful functions as follows:

- Surface anatomy imaging
- Bony structural imaging of the calvaria and vertebrae
- Multiplanar imaging of the intracranial structure
- Tomographic ultrasound imaging of fetal brain in the any cutting section
- Thick slice imaging of the intracranial structure

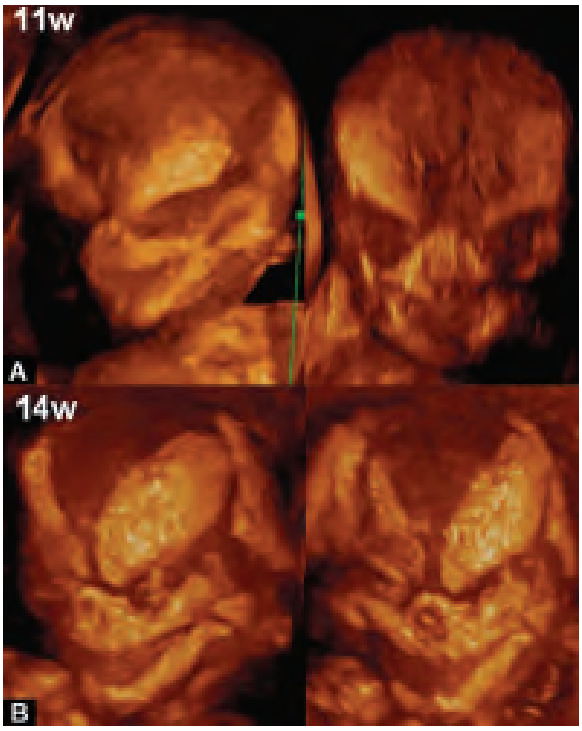

Figures 16.3A and B: Fetal craniofacial skeletal structure at 11 and 14 weeks of gestation. Craniofacial bony structure rapidly develops in the first half of pregnancy. (A) At 11 weeks, premature cranial bones (frontal and parietal bones) and facial bone (nasal bone, maxilla and mandible) are demonstrated; (B) At 14 weeks, metopic suture and coronal sutures are well formed according to development of cranial bones

- Simultaneous volume contrast imaging of the same section or vertical section of fetal brain structure
- Volume calculation of target organs, such as intracranial cavity, ventricle, choroid plexus and intracranial lesions
- The 3D sono-angiography of the brain circulation (3D power Doppler or 3D color Doppler).

It is well known that 3D ultrasound demonstrates the surface anatomy. In cases of CNS abnormalities, facial abnormalities and extremities anomalies are often complicated. Therefore, surface reconstructed images are helpful. Bony structural imaging of the calvaria **(Figs 16.3A and B)** and vertebrae **(Figs 16.4 and 16.5)** are useful in cases of craniosynostosis and spina bifida. The vertebral level of spina bifida may provide important information to prospect postnatal neurological deficits. In multiplanar imaging of the brain structure, it is possible to demonstrate not only the sagittal and coronal sections but also the axial section of the brain, which cannot be demonstrated from parietal direction by a conventional 2D transvaginal sonography **(Figs 16.6A to C)**. Transvaginal 3D ultrasound is the

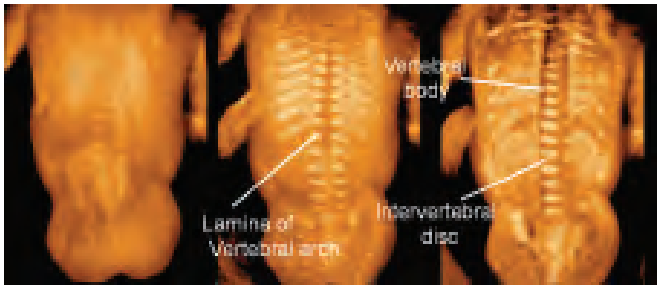

Figure 16.4: 3D image of normal vertebral structure at 16 weeks of gestation. 3D reconstructed image of the surface level (left), vertebral arch level (middle) and vertebral body level (right). Intervertebral disk spaces are well demonstrated

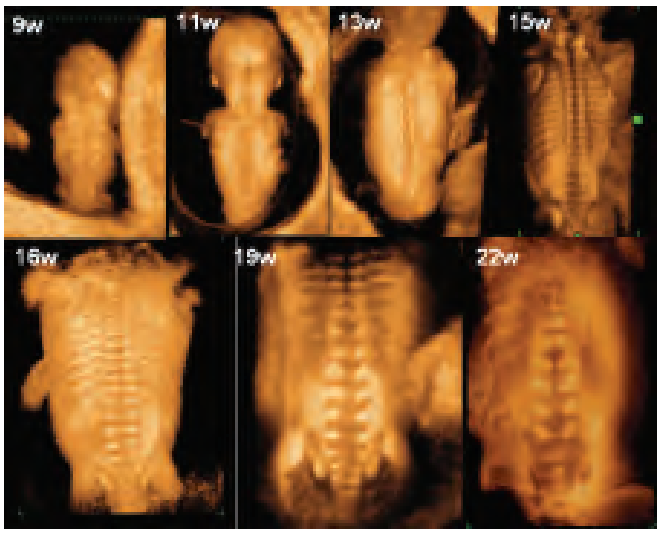

Figure 16.5: Fetal vertebral development by 3D US from 9 to 22 weeks of gestation. Approaching stage of bilateral vertebral lamina according to neural tube closure is visible with advanced gestational weeks

first modality during the first and early second trimesters. In the late second and third trimester, magnetic resonance imaging (MRI) is occasionally utilized as a prenatal diagnostic tool.[13] As shown in **Figure 16.7**, images obtained by tomographic ultrasound imaging (TUI) are quite similar to pictures of MRI. The superior point of TUI to MRI is that it is easily possible to change slice width, to rotate the images, to magnify images and to rotate images to any directions. This function is extremely useful for detailed CNS assessment and also for consultation with neurosurgeons and neurologists. Thick slice imaging of the intracranial structure **(Figs 16.8A and B)** and simultaneous volume contrast imaging (VCI) of the same plane or vertical plane of conventional 2D image are often convenient to observe the gyral formation and inside lateral ventricles.[14] The

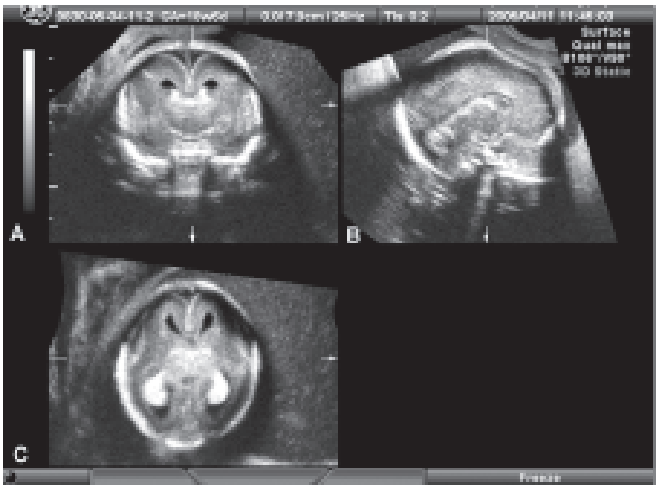

Figures 16.6A to C: 3D orthogonal view of normal brain at 18 weeks of gestation. Three orthogonal view is useful to obtain orientation of the brain structure. (A) Coronal; (B) Sagittal; (C) Axial images can be visualized on a single screen. Any rotation of the brain image around any (x,y,z) axis is possible

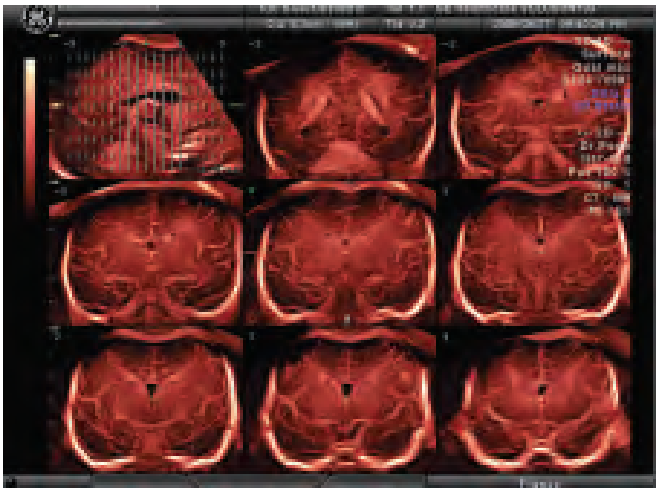

Figure 16.7: Tomographic ultrasound imaging (TUI) of the fetal brain. Normal brain in the coronal cutting section at 31 weeks of gestation. Intracranial structure including gyral formation is clearly demonstrated

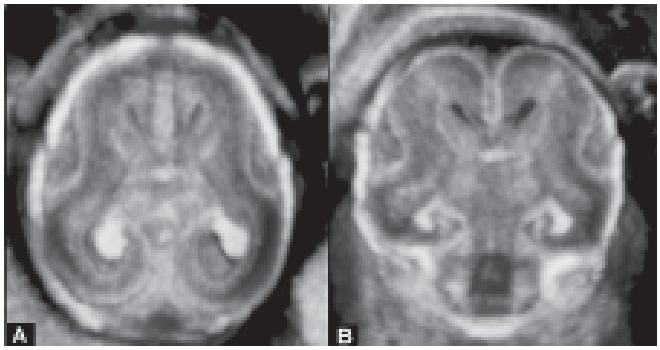

Figures 16.8A and B: 3D thick slices of the brain (20 weeks of gestation). (A) Axial thick slice; (B) Coronal thick slice of the premature brain. Observation by those 3D thick slices, anatomy of cortical structure and inside of ventricles become comprehensive

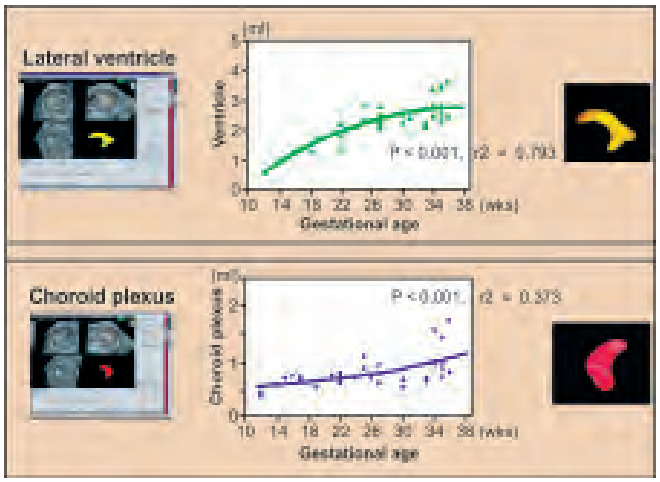

Figure 16.9: 3D volume extraction and volumetric analysis of lateral ventricle and choroid plexus. On three orthogonal sections, the target organ can be traced automatically or manually with rotation of volume imaging data. After tracing, volume extracted image (right) is demonstrated and volume calculation data is shown. Middle graphs show normograms of ventricular size (upper) and choroid plexus size (lower) during pregnancy

premature brain image obtained by use of VCI clearly demonstrates anatomical CNS structure.

Volume extracted image and volume calculation of the fetal brain in early pregnancy was reported in 1990s.[15,16] In our institute, VOLUSON 730 Expert (GE Medical Systems, Milwaukee, USA) with transvaginal 3D transducer and 3D View or 4D View software (Kretztechnik AG, Zipf, Austria) has been used for volume extraction and volume estimation of the brain structure.[17-19] On three orthogonal images, the target organ can be traced automatically or manually with rotation of volume imaging data. After tracing, volume extracted image is demonstrated and volume calculation data is shown **(Fig. 16.9)**. 3D fetal brain volume measurements have a good intraobserver and inter-observer reliability[20,21] and could be used to determine estimated gestational age.[20] Volume analysis by 3D ultrasound provides exceedingly informative imaging data. Volume analysis of the structure of interest provides an intelligible evaluation of the brain structure

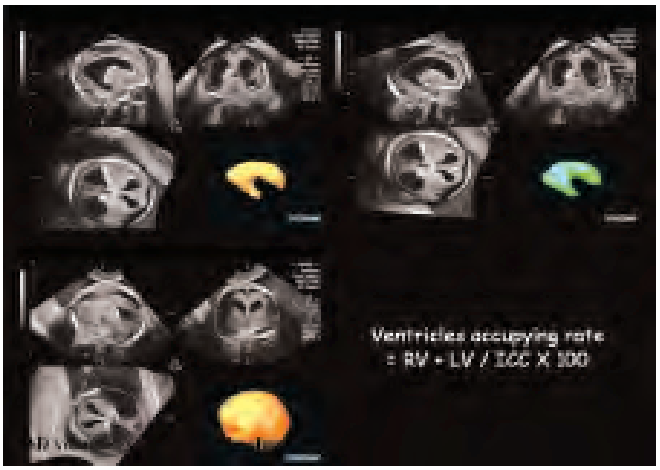

Figure 16.10: 3D volume extraction and volumetric analysis of lateral ventricle and intracranial cavity. Each volume of right (RV) and left ventricles (LV) and intracranial cavity volume can be calculated by 3D volumetry. Total ventricular volume / intracranial cavity (ICC) volume shows ventricles occupying rate and it is useful for longitudinal assessment of ventriculomegaly cases

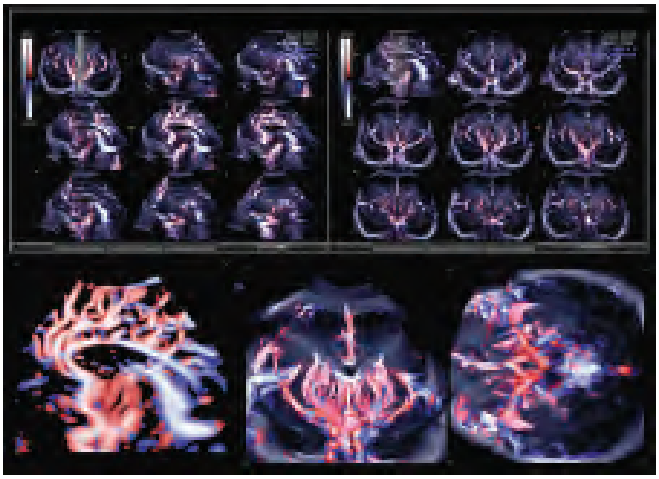

Figure 16.12: Tomographic ultrasound imaging and reconstructed 3D angiography of normal cerebral circulation at 31 weeks. (upper) Tomographic directional power Doppler imaging of sagittal (left upper), coronal (right upper) sections. Anterior cerebral arteries and their branches are seen on the sagittal plane, middle cerebral arteries and their branches on the coronal plane. (lower) 3D sonoangiogram of sagittal, coronal and axial sections from left

in total and longitudinal and objective assessment of enlarged ventricles and intracranial occupying lesions **(Fig. 16.10)**. Any intracranial organ can be chosen as a target for volumetry no matter how distorted its shape and appearance may be. In new method of inversion mode, the cystic portions within the volume are displayed in their entirety as an echogenic area, while the gray scale portions of the image are rendered as transparent[22] and recently it has been applied in fetal diagnosis.[23,24] **Figure 16.11** shows inversion-mode images of enlarged ventricles seen at 19 weeks of gestation.

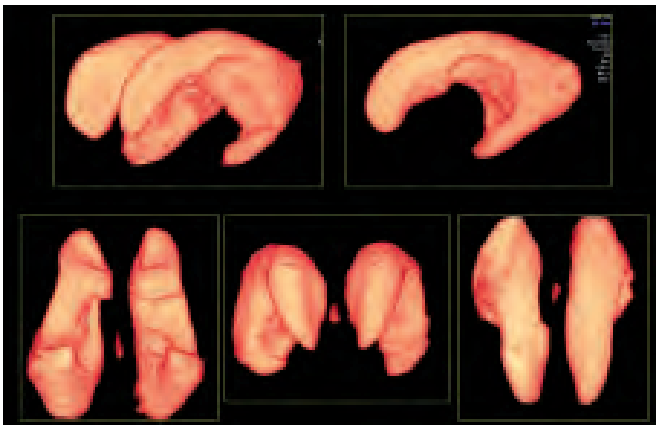

Figure 16.11: 3D extraction volume imaging of bilateral ventricles by inversion mode. Ventricle appearance is objectively demonstrable by inversion mode. Those images were from ventriculomegaly case at 19 weeks of gestation

The brain circulation demonstrated by transvaginal 2D power Doppler was first reported in 1996.[25] Thereafter, transvaginal 3D power Doppler assessment of fetal brain vascularity was successful.[18,26] Recently, by advanced technology of directional power Doppler, 3D angiostructural image has become furthermore sophisticated **(Fig. 16.12)**. Recent high-frequent transvaginal neuroscan has been able to demonstrate the medullary veins from the cortex towards subependymal area **(Figs 16.13A to C)**. The three primary brain vesicles of forebrain (prosencephalon), midbrain (mesencephalon) and hindbrain (rhombencephalon) are formed in early embryonal period. At 7–8 weeks of gestation, those three primary brain vesicles are demonstrated on the midsagittal plane. The forebrain partly divides into two secondary brain vesicles of the telencephalon and diencephalon and the hindbrain partly divides into the metencephalon and myelencephalon. The five secondary brain vesicles are consequently formed. The telencephalon forms derivatives of cerebral hemisphere and lateral ventricles.[27] At 9 weeks of gestation, those secondary vesicles are detected by sonography. Thereafter, the premature brain vesicles rapidly develop during the first half of pregnancy. The choroid plexuses develop in the roof of the third ventricle, in the medial walls of the lateral ventricles and in the roof of the fourth

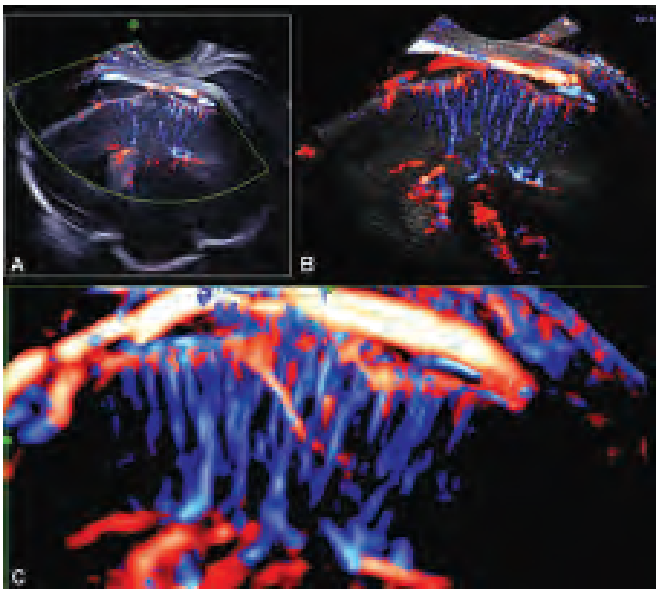

Figures 16.13A to C: Normal medullary veins at 28 weeks. (A) Intracerebral peripheral vessels by 2D directional power Doppler; (B) Parasagittal plane from 3D orthogonal view. Upper large vessel is the superior sagittal sinus. Cerebral superficial vessels are on the surface of cerebrum. Numerous linear vessels run down from the cortex towards subependymal region are medullary veins; (C) 3D reconstructed image

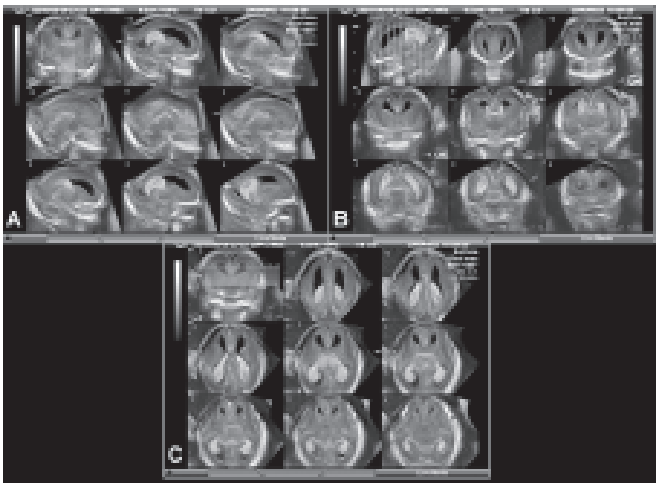

Figures 16.14A to C: Normal brain at 17 weeks. (A) Tomographic ultrasound imaging of sagittal; (B) Coronal; (C) Axial sections. Choroid plexus (echogenic part) shifts its position to posterior half of the lateral ventricles

ventricle.[27] The choroid plexuses secrete ventricular fluid, which becomes cerebrospinal fluid (CSF). The choroid plexuses are high echogenic structure, detectable from ninth gestational week and conspicuous during the first trimester. From the beginning of the second trimester, the choroid plexuses of lateral ventricle gradually change its location backward. As the cerebral cortex develops, the commissures connect corresponding areas of the cerebral hemispheres with one another. The largest cerebral commissure is the corpus callosum, connecting neocortical areas. The corpus callosum initially lies in the lamina terminalis, but fibers are added to it as the cortex enlarges, as a result it gradually extends beyond the lamina terminalis. The rest of the lamina terminalis lies between the corpus callosum and the fornix. It becomes stretched to form the thin septum pellucidum, a thin plate of brain tissue. The corpus callosum extends over the roof of the diencephalon.[27] The corpus callosum is detectable by ultrasound from around 16 weeks of gestation in some cases and at 18 weeks in most cases. **Figures 16.14A to C** shows normal 17 weeks brain. Neuroimaging in the third trimester, gyral formation is a main change of the brain development **(Fig. 16.7)**. Initially the surface of the hemispheres is smooth, however, as growth proceeds, sulci (grooves or furrows) and gyri (convolutions or elevations) develop. The sulci and gyri permit a considerable increase in the surface area of the cerebral cortex without requiring an extensive increase in cranial size. As each cerebral hemisphere grows, the cortex covering the external surface of the corpus striatum grows relatively slowly and is soon overgrown. This buried cortex, hidden from view in the depths of the lateral sulcus (fissure) of the cerebral hemisphere, is the insula.[27]

3D/4D Sonography and Magnetic Resonance Imaging: Alternatives or Complementaries

In multiplanar imaging of the brain structure, it is possible to demonstrate not only the sagittal and coronal sections but also the axial section of the brain, which cannot be demonstrated from parietal direction by a conventional 2D transvaginal sonography. Parallel slicing provides a tomographic visualization of internal morphology similar to MRI. Parallel slices used to be obtained on translating the cutting plane, however, recent advanced technology can produce tomographic ultrasound images and demonstrate a series of parallel cutting slices on a single screen as well as an MRI does.[14] As described above, images obtained by TUI are quite similar to pictures of MRI. The superior point of TUI to MRI is easy off-line analysis, with changing slice width, magnifying images and rotating images to any directions. This function is extremely useful for detailed CNS assessment and also for consultation to neurosurgeons and neurologists. As shown in **Figure 16.15**

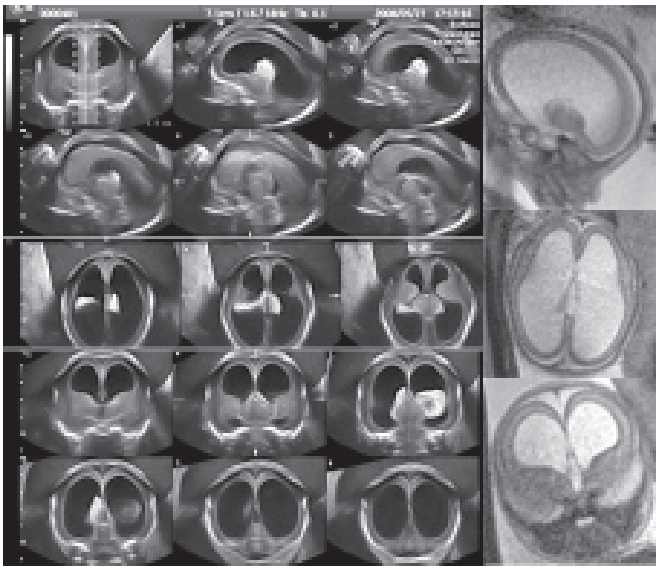

Figure 16.15: Tomographic ultrasound imaging (TUI) and MR imaging of hydrocephalus at 21 weeks of gestation. (left) Sagittal, axial and coronal parallel cutting sections by sonography well demonstrate ventriculomegaly. Partial agenesis of the corpus callosum is detected in the midsagittal section. (right) MRI images of the same case. No significant difference between sonography and MRI

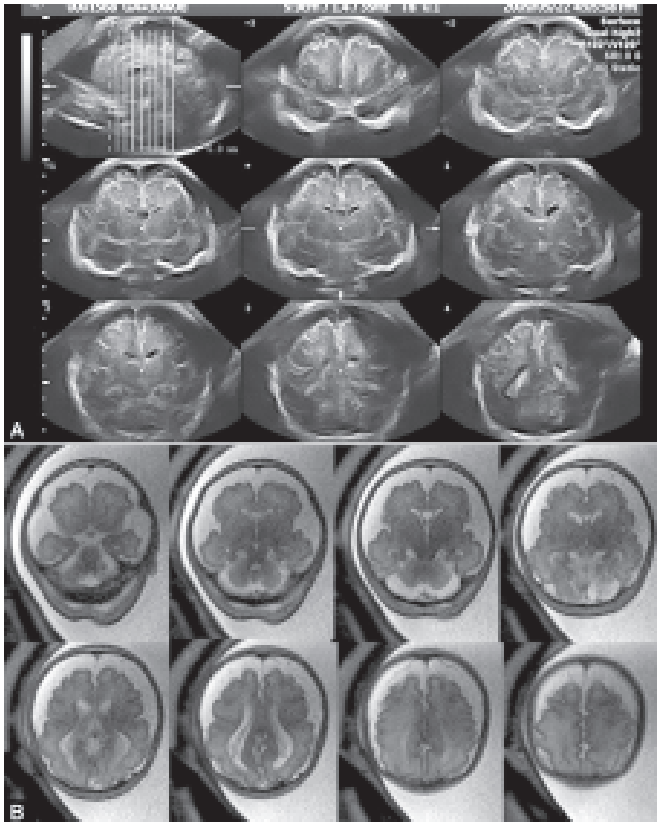

Figures 16.16A and B: Tomographic ultrasound imaging (TUI) and MR imaging of hydrocephalus *ex vacuo* at 30 weeks of gestation. (A) TUI coronal image of the brain. Note the conspicuous external subarachnoid/subdural space around hemispheres; (B) MR images of the same case. The cause of this phenomenon was unknown and this space spontaneously disappeared three weeks later. Array CGH of amnio cells was normal but postnatal neurological prognosis has been progressively deteriorated

(hydrocephalus at 21 weeks of gestation, ultrasound and MRI) and **Figures 16.16A and B** (hydrocephalus ex-vacuo, ultrasound and MRI), the transvaginal 3D TUI demonstrates the detailed intracranial structures and seems not to require the further imaging modality.

Fetal neuroimaging with advanced 3D ultrasound technology is easy, noninvasive and reproducible methods. It not only produces comprehensible images but also objective imaging data. Easy storage/extraction of raw volume data set enables easy off-line analysis and consultation to neurologists and neurosurgeons. 3D technology also provides us a longitudinal study of maldevelopment of CNS diseases by a serial neuroscan through a whole gestational period. Dedicated transvaginal 3D ultrasound is no doubt the first modality suitable for visualization and assessment of fetal CNS. Although the first introduction of transvaginal fetal neurosonography, which has revolutionized the visualization of the fetal brain, was almost 20 years ago, this approach has still not gained popularity in the world. Malinger et al.[28] described that this fact may be due to the relatively complex brain anatomy and pathology that is usually not familiar enough to most obstetricians and the reluctance to use transvaginal sonography in many countries.

Recent advances in fast MRI technology has remarkably improved the T2-weighted image resolution despite a short acquisition time and minimized artifacts due to fetal movement and/or maternal respiratory motion. The MRI is not influenced by physical factors, such as fetal location, fetal head position and ossification of fetal cranial bones, which sometimes obstruct transvaginal ultrasound approach. The MRI is playing an increasingly prominent role in depicting brain maturation, especially cortical formation that follows a temporospatial pattern and in detecting developmental abnormalities of the cortex and other brain sectors.[29] The MRI of fetal CNS possesses less abilities in detecting bony structure and angioarchitectonics and in volumetric assessment, compared with transvaginal 3D ultrasound imaging. However, in multiplanar imaging, MRI has much superiority in the assessment of a whole intracranial structure including the brainstem **(Figs 16.17 and 16.18)**, posterior fossa and gyral formation

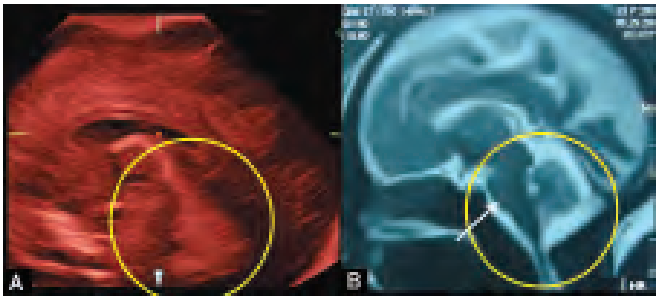

Figures 16.17A and B: Comparison of transvaginal 3D US and MRI in demonstrating the brainstem and posterior fossa. Median cutting section images of normal fetal brain by (A) Transvaginal sonography; (B) MRI at 30 weeks of gestation.

Inside circles, the brainstem and posterior fossa are demonstrated. Although ultrasound image shows the cerebellum and fourth ventricle, MR image reveals much clearer appearance of brainstem (arrow) and detailed cerebellar structure than sonogram, because of MR feature of higher contrast between different tissues

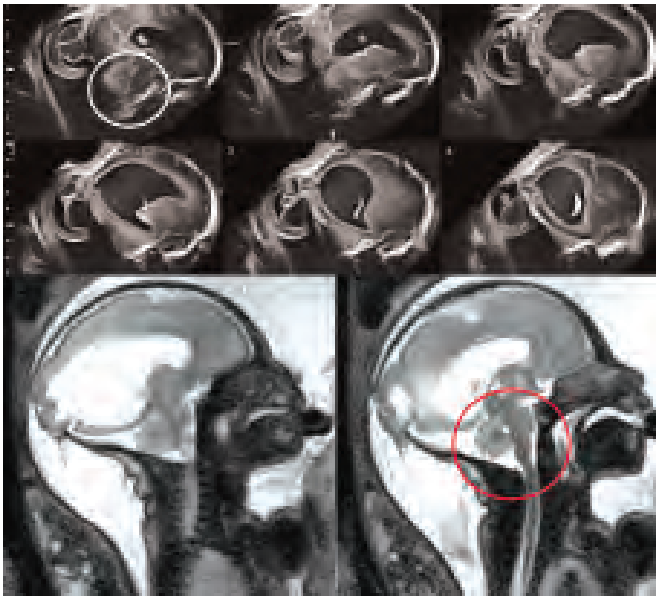

Figure 16.18: Tomographic ultrasound imaging (TUI) and MR imaging of the brain in a case of encephalomeningocele at 28 weeks of gestation. Prolapsed cerebral tissue with meninges are well demonstrated by both TUI (upper) and MRI (lower), but MRI indicates that the amount of cerebral tissue inside encephalomeningocele is quite little. Furthermore, in cases with encephalocele, the existence of Chiari malformation is important, and the brainstem and posterior fossa is more clearly depicted by MRI (red circle) than sonography (white circle). This case had no Chiari malformation

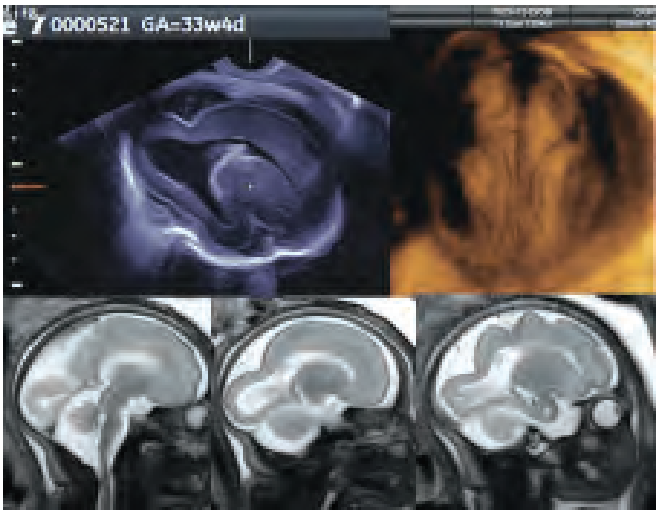

Figure 16.19: Cortical development by sonography and MRI in a case of pachygyria at 33 weeks of gestation. Cortical development with gyral/sulcal formation should be remarkably demonstrated after 29 weeks by parasagittal plane. In this case, sonography shows less gyri/sulci on the parasagittal sonographic image (upper left) and 3D sonographic surface anatomical view (upper right). (lower) MRI images of midsagittal and parasagittal sections. In late pregnancy, transfontanelle/transsutural sonography is getting more difficult because of cranial ossification. MRI greatly helps in demonstration of cortical development after 30 weeks of gestation

(Fig. 16.19) with better contrast between different tissue. In cases of microcephaly, with difficulty of obtaining ultrasound windows of fontanelles and sutures, intracranial observation by MRI is much more helpful than transfontanelle ultrasound neuroscan.

It has been controversial whether ultrasound or MRI is more practical and effective in prenatal assessment of fetal CNS abnormalities. Several previous studies[30-33] on MRI in diagnosis of fetal brain anomalies have reported that MRI added more valuable information than ultrasound. Kubic-Huch et al.[34] published the statistical analysis study with the result finding no statistically significant difference between sonography and MRI for the detection of abnormality in any organ system. Malinger et al.[28] criticized that the past reports describing superiority of MRI over ultrasound may have been biased because a comparison had been done with routine transabdominal ultrasound exams, without insistence on an additional confirmatory tertiary level ultrasound examination, especially by transvaginal sonography. Their opinion seems to be right to the point. In their other article, they described that dedicated

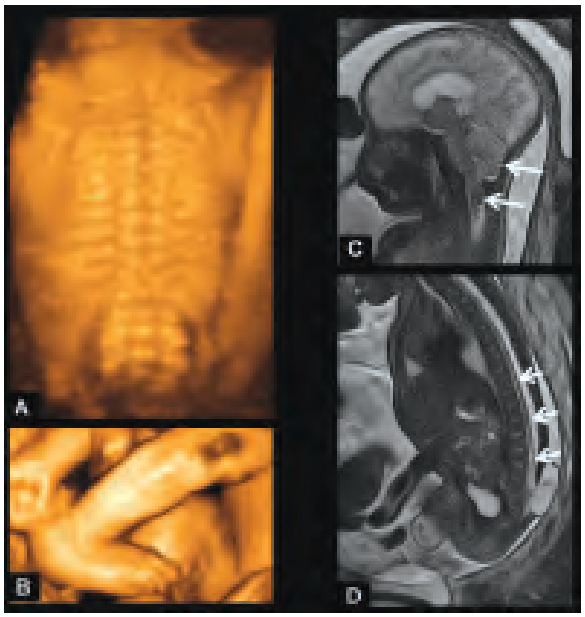

Figures 16.20A to D: Features of 3D sonography and MRI in cases of myelomeningocele. In cases of myelomeningocele, 3D ultrasound can demonstrate the accurate vertebral level of (A) Spina bifida; (B) Affected foot joint appearance. MRI can demonstrate the condition of (C) Chiari type II malformation (arrows); (D) Spinal cord inside the spinal canal (arrows) in detail. In late pregnancy, cerebrospinal region and intravertebral structure cannot be depicted by sonography because of cranial/vertebral ossification, therefore, MR imaging is more reliable in demonstrating those structures

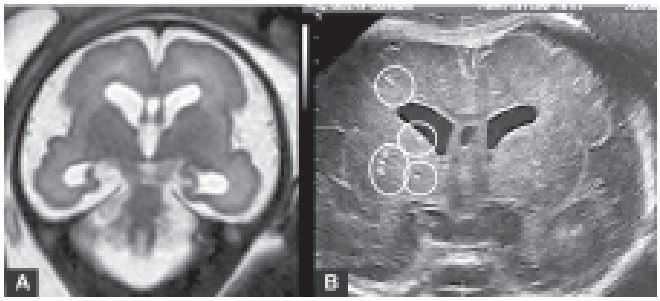

Figures 16.21A and B: Comparison of MR and sonographic images in a case of cytomegalovirus infection. Cytomegalovirus infection often affects the brain development and representative features of the affected brain are ventriculomegaly, cortical maldevelopment and intracranial calcification. (A) MR image at 34 weeks well shows ventriculomegaly and cortical maldevelopment; (B) Sonographic image at the same gestation add the information of multiple intracranial calcification (inside circles), which is never demonstrable by MRI

TABLE 16.1

Advantages of magnetic resonance imaging and dedicated 3D transvaginal sonography in central nervous system assessment

MRI	*3D-TVS*
Whole brain assessment	Intracranial calcification
Brainstem development	Vascular anomaly
Posterior fossa assessment	Intratumoral vascularity
Cortical development	Bony structure assessment
	Extra CNS abnormality detection

neurosonography by transvaginal sonography is equal to MRI in the diagnosis of fetal brain anomalies, in most cases MRI confirmed the ultrasonographic diagnosis and in a minority of cases, each modality provided additional/different information.[35] They also concluded that the major role of MRI was in reassurance of the parents regarding the presence or absence of brain anomalies. This is an easily acceptable observation for sonographers with expertise.

In fact, as shown in **Figures 16.15 and 16.16**, there is no significant difference between dedicated neurosonography and MRI in detection of intracranial structure. In late pregnancy with developed calvarium and vertebrae, MRI is superior in detection of the spinal cord inside the spinal canal and cerebellar herniation with Chiari malformation **(Figs 16.20C and D)**, however detection of the accurate vertebral level of spina bifida and associated lower limb abnormality can be easily assessed by 3D ultrasound **(Figs 16.20A and B)**. In cases with cytomegalovirus (CMV) infection, intracranial calcification can be detected only by dedicated neurosonography **(Figs 16.21A and B)**, not visualized by MRI. The vascular anomaly, such as Galen's aneurysmal malformation or intratumoral vascularity, **(Fig. 16.22)** is much more clearly detectable by using 3D power Doppler or 3D blood flow (B flow) images. Additional advantage of 3D sonography is demonstration of extra CNS anomalies strongly associated with CNS abnormalities, such as fetal face and extremities **(Fig. 16.23)**. The advantages of both MRI and dedicated sonography are summarized in **Table 16.1**.

Regarding objectives of accurate prenatal diagnosis for proper management, any less-invasive modalities can be used. For CNS anomaly screening scan, ultrasound is no doubt the first modality and once CNS abnormality is suspicious, after considering each advantage and disadvantage of transvaginal 3D ultrasound and MRI, it is suggested to use those different technologies according to what is to be detected and evaluated in each abnormal CNS case. Of course, those

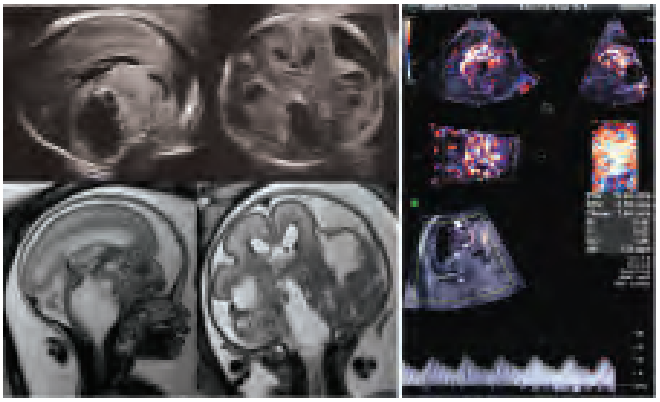

Figure 16.22: Comparison of MR and sonographic images in a case of brain tumor at 26 weeks of gestation (upper left and middle) Sonographic median and anterior-coronal images. (lower left and middle) MR median and anterior-coronal images. Note the huge tumor below the oppressed bilateral hemispheres and oppressed brainstem. (upper right) Three orthogonal view and reconstructed image by 3D bidirectional power Doppler. (lower right) Intratumoral blood flow with low resistance is demonstrated. Intracranial morphology is more comprehensive by MRI than sonography due to MR feature of more contrast between different tissues, however, sonography is much more helpful in assessment of intratumoral vasculature and blood flow analysis

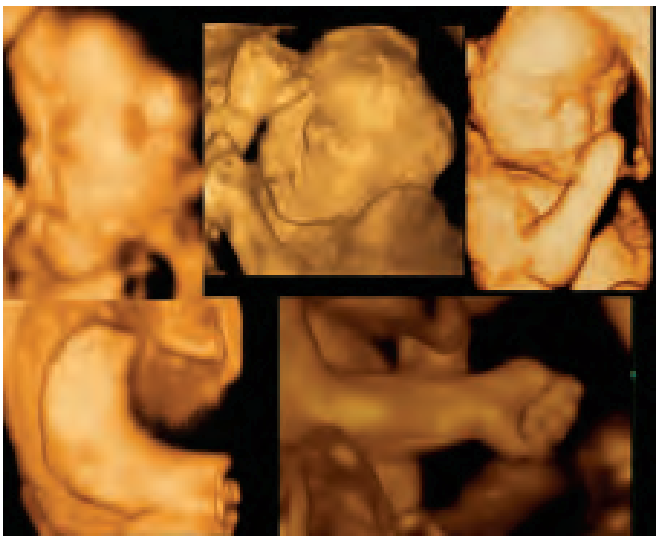

Figure 16.23: 3D sonographic feature of extra CNS abnormality assessment. 3D sonographic surface anatomy can demonstrate extra CNS abnormalities which are strongly associated or affected with brain anomalies, such as facial abnormalities and limb abnormalities (upper left) Facial anomaly with exophthalmos and prominent forehead in a case of Apert syndrome. (upper middle) Exophthalmos, nasal aplasia and cleft lip in a case of holoprosencephaly. (upper right and lower left) Syndactyly in a case of Apert syndrome. (lower right) Adducted thumb in a case of X-linked hydrocephalus

two technologies should be utilized as alternatives and complementaries as well.[36]

VENTRICULOMEGALY AND HYDROCEPHALUS

"Hydrocephalus" and "ventriculomegaly" are both the terms used to describe dilatation of the lateral ventricles. However, those two should be distinguished from each other. Hydrocephalus signifies dilated lateral ventricles resulting from increased amount of CSF inside the ventricles and increased intracranial pressure, while ventriculomegaly is a dilatation of lateral ventricles without increased intracranial pressure, due to cerebral hypoplasia or CNS anomaly such as agenesis of the corpus callosum.[8,37] Of course, ventriculomegaly can sometimes change into hydrocephalic state. In sonographic imaging, these two intracranial conditions can be differentiated by visualization of subarachnoid space and appearance of choroid plexus. In normal condition, subarachnoid space, visualized around the both cerebral hemispheres is well preserved during pregnancy **(Figs 16.24A and B)**. Choroid plexus is a soft tissue and easily affected by external pressure. Obliterated subarachnoid space and dangling choroid plexus are observed in the case of hydrocephalus. In contrast, the subarachnoid space and choroid plexus are well preserved in cases of ventriculomegaly **(Fig. 16.25)**. It is difficult to evaluate subarachnoid space in the axial plane because the subarachnoid space is observed in the parietal side of the hemispheres. Therefore, transabdominal approach may not differentiate accurately hydrocephalus with increased intracranial pressure from ventriculomegaly without pressure. It is suggested that the evaluation of enlarged ventricles should be done in the parasagittal and coronal views by transvaginal approach to the fetal brain or 3D multidimensional analysis. As a screening examination, the

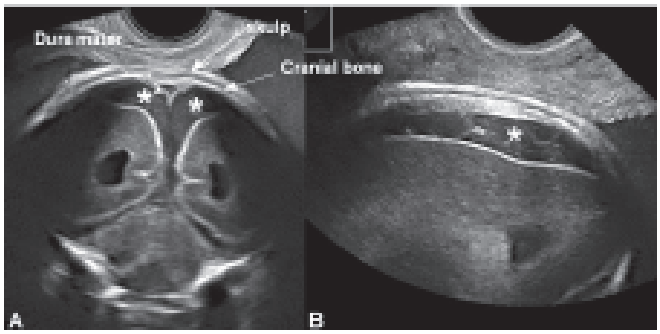

Figures 16.24A and B: Subarachnoid space in normal 25-week-brain. (A) Posterior coronal image. Asterisks indicate subarachnoid space; (B) Parasagittal image

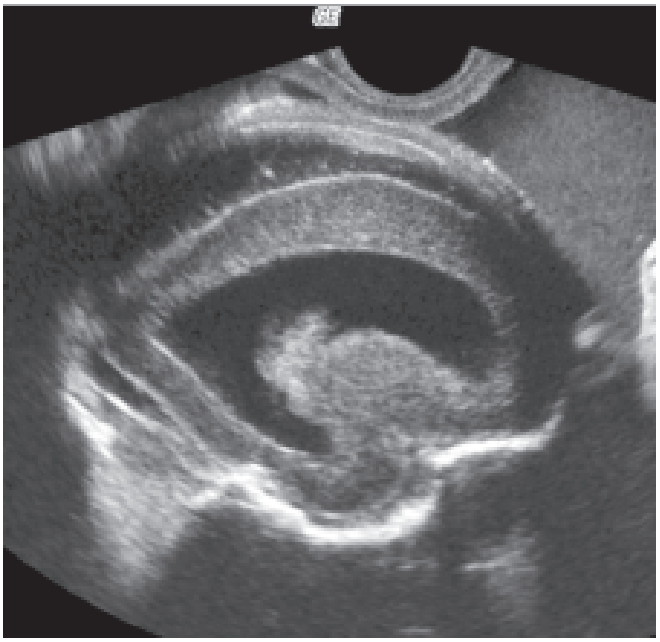

Figure 16.25: Ventriculomegaly due to cerebral hypoplasia at 29 weeks of gestation. Enlarged ventricle exists but subarachnoid space is well preserved and no dangling choroid plexus is seen. From those findings, non-increased intercranial pressure (ICP) is estimated. This condition should be differentiated from hydrocephalus with increased ICP

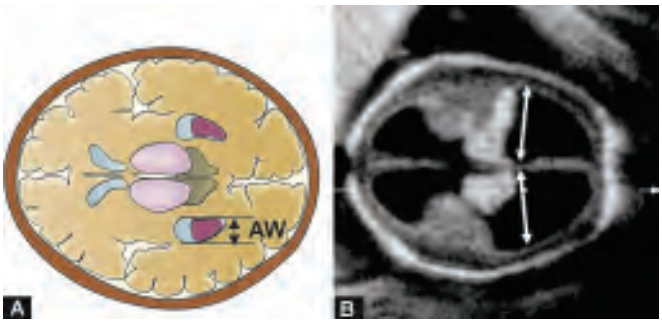

Figures 16.26A and B: Atrial width measurement

measurement of atrial width (AW) **(Figs 16.26A and B)** is useful with a cut-off value of 10 mm[38,39] although isolated mild ventriculomegaly with AW of 10–12 mm may be normal variant.[40] In normal fetuses, blood flow waveforms of dural sinuses, such as the superior sagittal sinus, vein of Galen and straight sinus, have pulsatile pattern.[41] However, in cases with progressive hydrocephalus, normal pulsation disappears and blood flow waveforms become flat pattern.[41] Intracranial venous blood flow may be related to increased intracranial pressure.

TABLE 16.2

Cases of ventriculomegaly with atrial width of 10–15 mm	
With additional abnormality	*13/23 cases (56.5%)*
Chromosomal/genetic abnormality	31%
Other brain abnormality	69%
Extra CNS abnormality	31%
MR, CP, neurological deficits	40%
No neurological deficit (<2 years)	30%
IUFD, TOP	30%
Ventriculomegaly during pregnancy	
Resolved	31%
Remain stable	31%
Progressive	23%
Uncertain	15%
No other abnormality	*10/23 cases (43.5%)*
Cerebral palsy	10%
Epilepsy	10%
No neurological deficit (<2 years)	80%
Ventriculomegaly during pregnancy	
Resolved	70%
Remain stable	20%
Progressive	10%

Variety of Mild Ventriculomegaly with Atrial Width 10-15 mm

Mild ventriculomegaly is defined as a width of the atrium of the lateral cerebral ventricles of 10–15 mm. It has been reported that mild ventriculomegaly with atrial width 10–15 mm resolves in 29%, remains stable in 57%, progresses in 14% of the cases during pregnancy.[42] **Figures 16.27 to 16.30** show the prenatal diagnostic imaging of the cases with mild ventriculomegaly and associated abnormalities such as craniosynostosis, micrognathia, vein of Galen aneurysmal malformation and multiple intracerebral bleeding. These cases were referred due to ventriculomegaly and atrial width was 10–13 mm at referral. Various outcomes and prognosis followed according to complicated abnormalities.

Table 16.2 summarizes 23 cases of ventriculomegaly with atrial width 10–15 mm, 13 cases with additional anomaly and 10 cases without other abnormality. More than 30% of cases with other abnormalities had chromosomal aberration or genetic disorder. However, among the cases with other complications, 30% of them have had no neurological deficit in short-term. It is difficult to estimate postnatal prognosis simply by intrauterine progression or resolution of ventricular enlargement during pregnancy. Normalization of

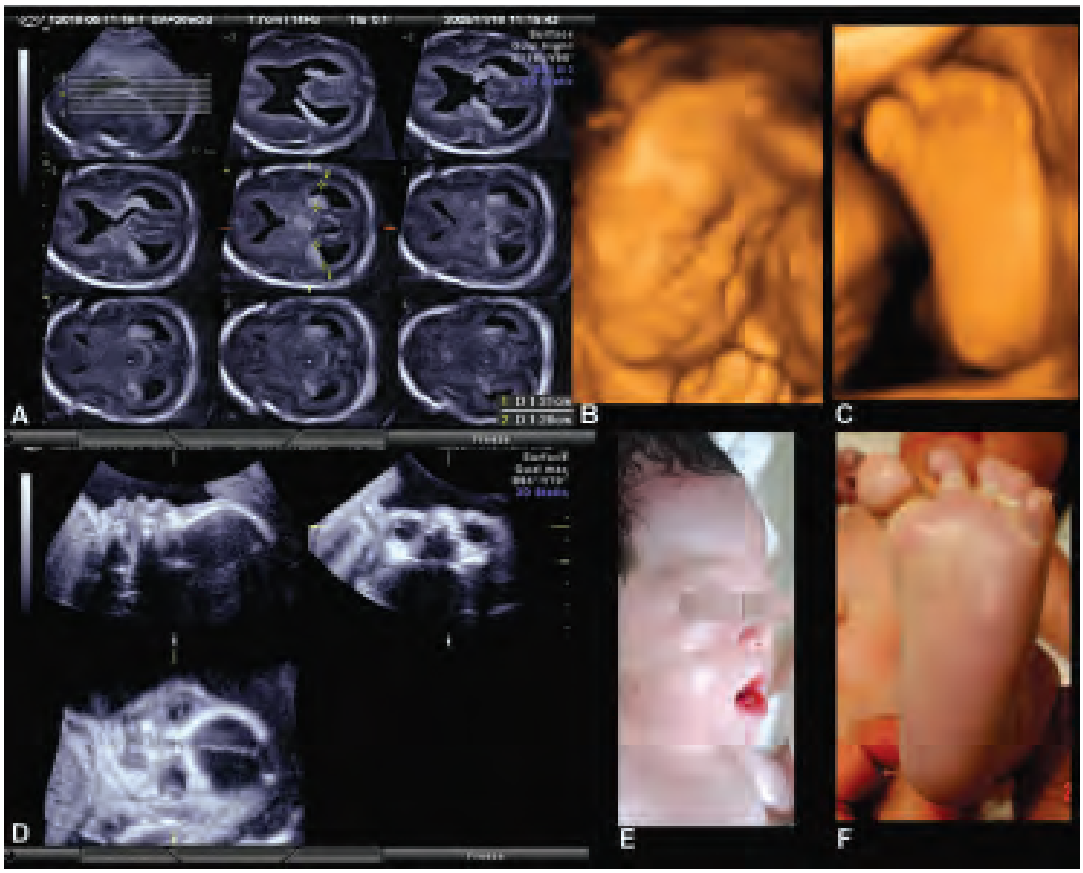

Figures 16.27A to F: Mild ventriculomegaly due to craniosynostosis (Pfeiffer syndrome). (A) Tomographic ultrasound imaging of the brain at 26 weeks. Fused ventricle with mild enlargement is demonstrated. Atrial width measurement shows 12 to 13 mm; (B and C) 3D surface images of fetal face and foot. Exophthalmos with flat face and large thumb are seen; (D) Three orthogonal view of fetal face; (E and F) Abnormal facial expression and foot appearance after birth

ventricular enlargement during fetal period was seen in 70% of cases with no other complications. In our series, all cases with both no complications and spontaneous resolution of enlargement have had favorable prognosis in short-term.

Generally, in cases of mild fetal ventriculomegaly with a normal karyotype and an absence of malformations, the outcome appears to be favorable.[43] Pilu and his colleagues[44] reviewed 234 cases of borderline ventriculomegaly including an abnormal outcome in 22.8% and concluded that borderline ventriculomegaly carries an increased risk of cerebral maldevelopment, delayed neurological development and possibly, chromosomal aberrations. Isolated mild ventriculomegaly with atrial width of 10–12 mm may be normal variation. Signorelli and colleagues[40] described that their data of normal neurodevelopment between 18 months and 10 years after birth in cases of isolated mild ventriculomegaly (atrial width of 10–12 mm), should provide a basis for reassuring counseling. Ouahba and colleagues[45] recently reported the outcome of 167 cases of isolated mild ventriculomegaly and concluded that in addition to associated anomalies, three criteria are often associated with an unfavorable outcome:

1. Atrial width greater than 12 mm
2. Progression of the enlargement
3. Asymmetrical and bilateral ventriculomegaly.

Moderate to Severe Ventriculomegaly with Atrial Width More Than 15 mm

Hydrocephalus

The term *'Hydrocephalus'* does not identify a specified disease, but is a generic term which means a serial pathologic condition because of abnormal circulation of CSF. Treatment method of hydrocephalus should be

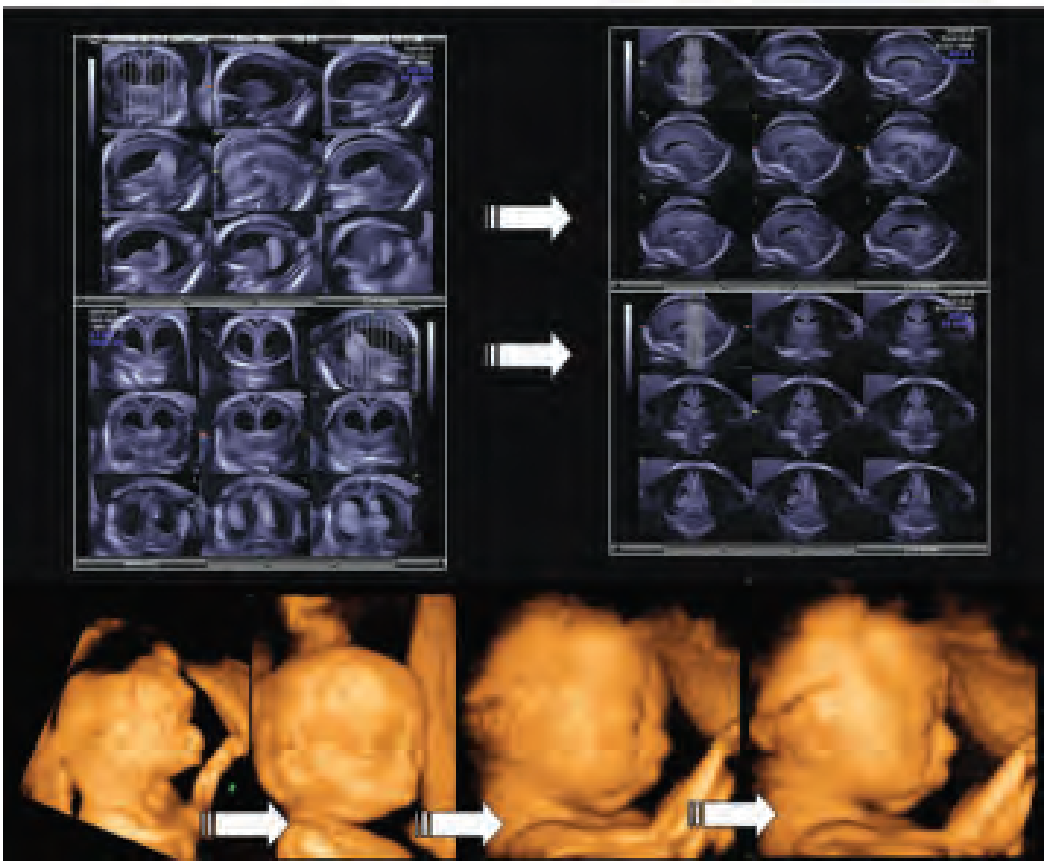

Figure 16.28: Mild ventriculomegaly and micrognathia with spontaneous resolution (Pierre Robin syndrome). (left upper) Tomographic ultrasound imaging of the brain at 17 weeks. Atrial width measurement shows 10–11 mm. (upper right) Tomographic brain imaging at 25 weeks. Spontaneous resolution of ventriculomegaly is seen. (lower) Slow mandibular development between 17 and 28 weeks of gestation was demonstrated by 3D reconstructed images

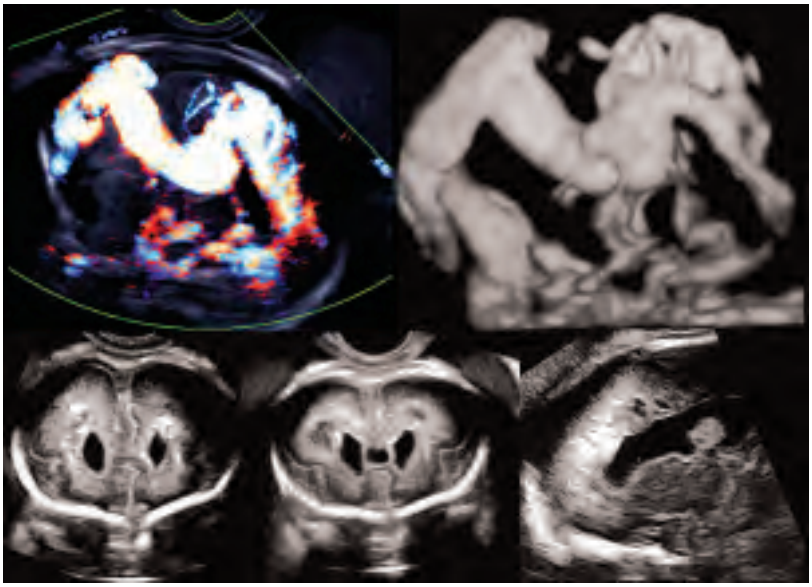

Figure 16.29: Mild ventriculomegaly and brain damage due to vein of Galen aneurysmal malformation (28 weeks). (left upper) Bidirectional power Doppler image of sagittal section. Enlarged sinus is seen. (upper right) 3D B-flow image of vascular structure. Many arteries run directly towards aneurysmal sac. (lower) Anterior coronal slices and parasagittal sections of the brain. Note multiple brain damage with low and high echogenicity around mildly enlarged ventricles. Atrial width measurement was just 10 mm at this stage

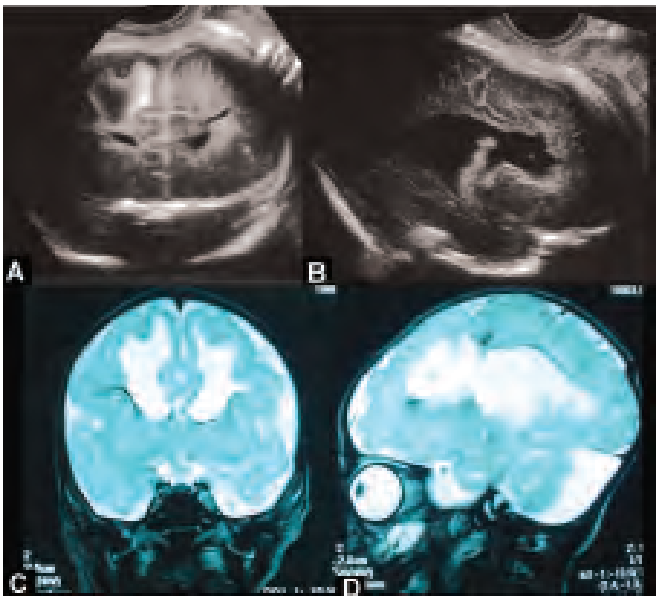

Figures 16.30A to D: Mild ventriculomegaly to postnatal porencephaly due to multiple cerebral hemorrhage. (A) Anterior coronal section at 36 weeks. Note the low echogenic parts inside high echogenicity, which indicate brain hemorrhage; (B) Parasagittal section. Note the irregular ventricular wall indicating the beginning of porencephaly. At this stage, atrial width measurement was 10–12 mm; (C) MR coronal image at 17th postnatal day. Conspicuous bilateral porencephalic parts fused with lateral ventricles are seen; (D) Parasagittal section of MRI. Porencephalic cyst was clearly formed for 4 weeks

selected according to age of onset and symptoms. Congenital hydrocephalus is classified into three categories by causes which disturb CSF circulation pathway: simple hydrocephalus, dysgenetic hydrocephalus and secondary hydrocephalus.[37]

Simple Hydrocephalus

Simple hydrocephalus caused by developmental abnormality which is localized within CSF circulation pathway includes aqueductal stenosis, atresia of foramen of Monro and maldevelopment of arachnoid granulation.

Dysgenetic Hydrocephalus

Dysgenetic hydrocephalus indicates hydrocephalus as a result of cerebral developmental disorder in early developmental stage and includes hydranencephaly, holoprosencephaly, porencephaly, schizencephaly, Dandy-Walker malformation, dysraphism, and Chiari malformation.

Secondary Hydrocephalus

Secondary hydrocephalus is a generic term indicating hydrocephalus caused by intracranial pathologic condition such as brain tumor, intracranial infection and intracranial hemorrhage.

In cases with progressive hydrocephalus, there may be seven stages of progression:

1. Increased fluid collection of lateral ventricles
2. Increased intracranial pressure
3. Dangling choroids plexus
4. Disappearance of subarachnoid space
5. Excessive extension of the dura and superior sagittal sinus
6. Disappearance of venous pulsation and finally
7. Enlarged skull.[37]

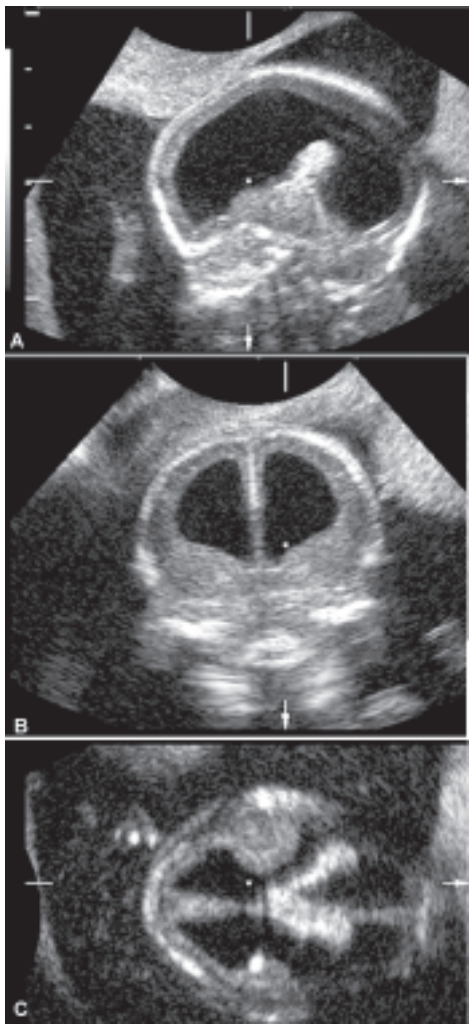

Figures 16.31A to C: Hydrocephalus due to myelomeningocele and Chiari type II malformation at 17 weeks. Severe hydrocephalus with dangling choroid plexus and disappearing subarachnoid space

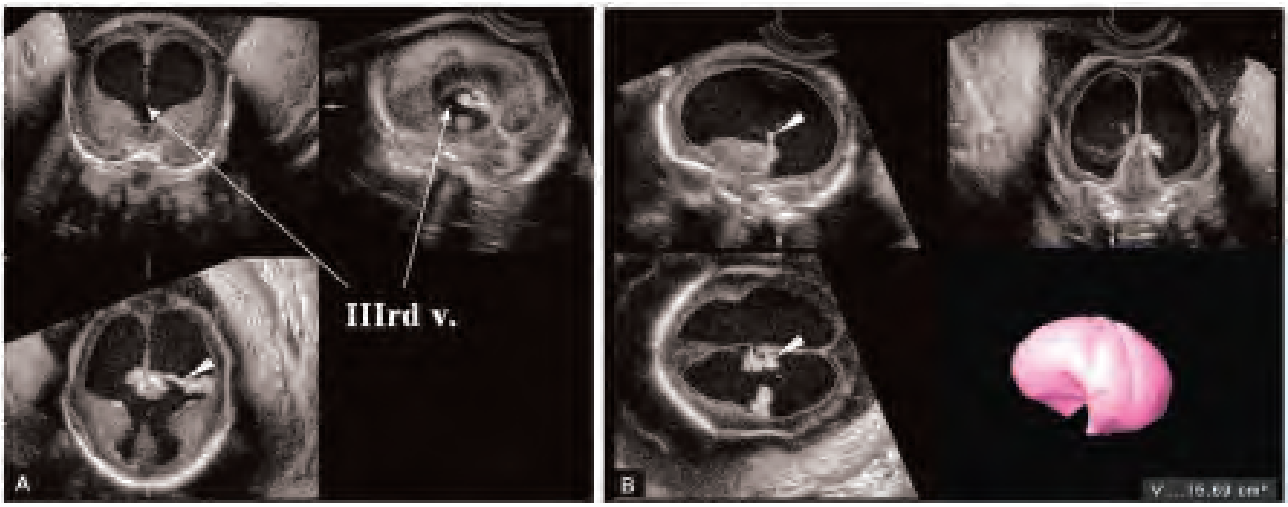

Figures 16.32A and B: Hydrocephalus due to aqueductal obstruction at 19 weeks of gestation. (A) Three orthogonal views with anterior coronal (upper left) and median sagittal (upper right) and axial (lower left) slices. Bilateral ventriculomegaly and third ventriculomegaly (IIIrd v.) are seen. No enlargement of fourth ventricle indicates obstruction of the aqueduct; (B) Three orthogonal views with parasagittal (upper left) and posterior coronal (upper right) and axial (lower left) slices. Subarachnoid space is already obliterated and dangling choroid plexus (arrowheads) is seen. Lower right pink figure shows extracted 3D ventricular image by VOCAL mode. Ventricle in this case was tenfold size of normal 19-week-ventricle

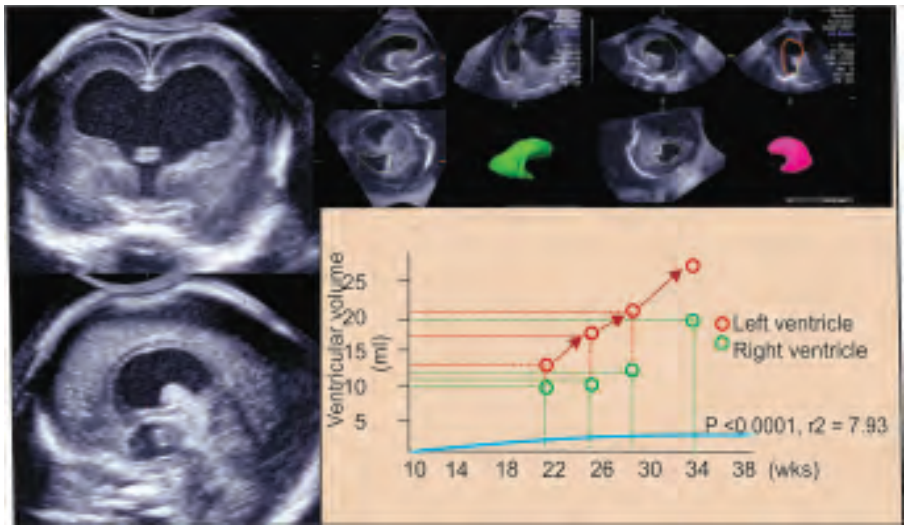

Figure 16.33: Moderate ventriculomegaly (21 weeks). (left) Ultrasound images in the coronal and sagittal sections. Fused ventriculomegaly, enlarged foramen of Monro, mild IIIrd ventriculomegaly are demonstrated in the coronal section, and no enlargement of IVth ventricle was seen in the sagittal section. Therefore, aqueductal stenosis and cerebral hypoplasia were suspected. (right upper) 3D images with volume calculation of bilateral ventricles. (right lower) Longitudinal study of ventricular size was on the graph. This case shows moderate increase of ventricular size during pregnancy

In general, both hydrocephalus and ventriculomegaly are still evaluated by the measurement of biparietal diameter (BPD) and AW in transabdominal axial section. As described above however, hydrocephalus and ventriculomegaly should be differentiated from each other and hydrocephalic state should be assessed by changing appearance of intracranial structure. To evaluate enlarged ventricles, examiners should carefully observe the structure below and specify causes of hydrocephalus:

- Choroid plexus, dangling or not
- Subarachnoid space, obliterated or not
- Ventricles, symmetry or asymmetry
- Visibility of third ventricle
- Pulsation of dural sinuses
- Ventricular size (3D volume calculation, if possible)
- Other abnormalities.

Figures 16.31 to 16.34 show prenatal sonographic imaging of fetal ventriculomegaly with AW of over 15 mm. Although all cases have similar ventricular

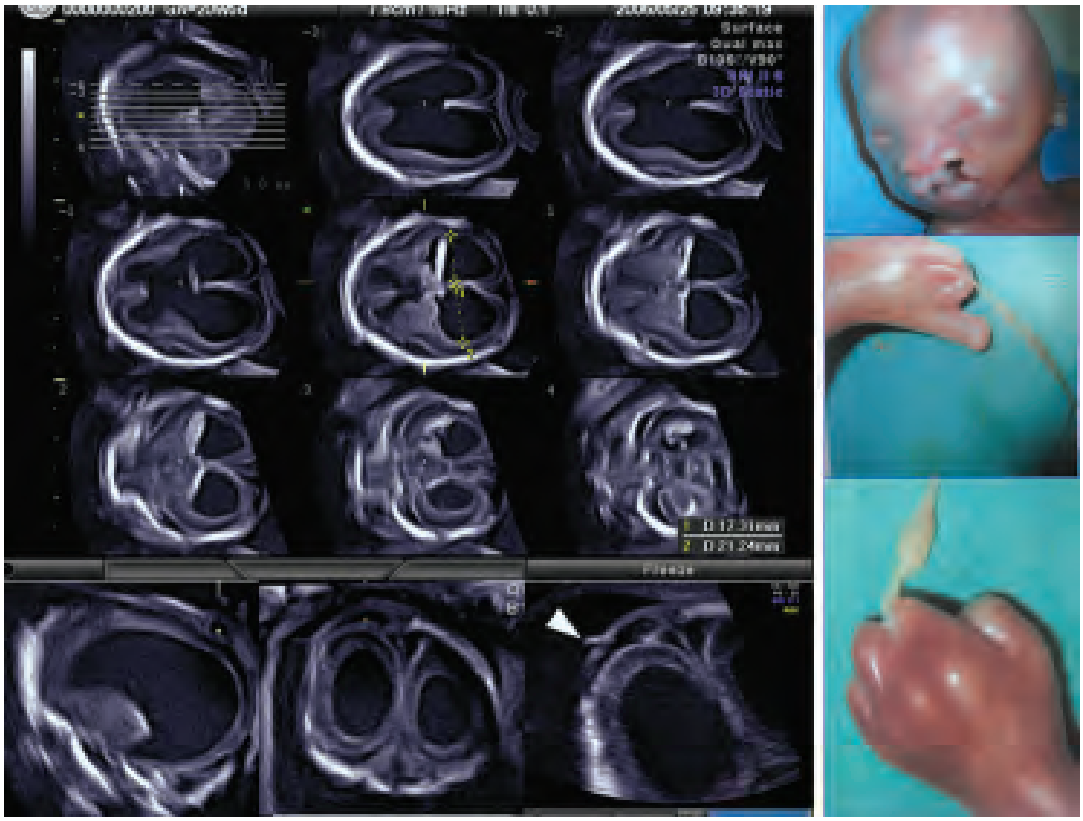

Figure 16.34: Hydrocephalus due to amniotic band syndrome (20 weeks). (left upper) Tomographic ultrasound imaging in the axial section of fetal brain at referral. Bilateral atrial width was 17 and 21 mm respectively. From the observation of enlarged ventricles, simple hydrocephalus due to Monro obstruction was suspected. However, the fetus was complicated with cleft lip, amputation of fingers and amniotic band was detected by extra CNS scan. (lower) Small cephalocele (arrows) were seen with remnant of the amniotic band (arrowhead). (right) Macroscopic view of the face and extremities after termination of pregnancy

TABLE 16.3

Twenty-three cases of ventriculomegaly of atrial width more than 15 mm	
Isolated ventriculomegaly	9
– normal karyotypes	7
– abnormal	2
Holoprosencephaly	5
Myelomeningocele	5
Dandy-Walker syndrome	1
Agenesis of CC	1
ACC + IHC	1
Multiple porencephaly	1
Total	23

appearance, the causes of ventriculomegaly vary such as Chiari type II malformation **(Fig. 16.31)**, aqueductal obstruction **(Fig. 16.32)**, aqueductal stenosis and cerebral hypoplasia **(Fig. 16.33)**, and amniotic band syndrome (ABS) **(Fig. 16.34)**. In the case of ABS, amniotic band attached to the skull resulted in partial cranial bone defect and a small cephalocele, which may have caused Monro obstruction and enlarged ventricles.

Table 16.3 shows the summary of 23 ventriculomegaly cases with atrial width more than 15 mm.

Nine cases (39.1%) had no other CNS abnormality but two out of those nine were complicated with chromosomal aberration. Among the rest of 14 cases, holoprosencephaly was detected in 5 cases and myelomeningocele in 5 cases. Four cases out of 7 without any complication had favorable postnatal prognosis after ventricular-peritoneal shunting procedure.

CONGENITAL CENTRAL NERVOUS SYSTEM ANOMALIES

During fetal period, the embryonal premature CNS structure rapidly develops into the mature structure

TABLE 16.4
Developmental stages and major disorders

Developmental stages	*Disorders*
Primary neurulation (3-4 weeks' gestation)	Spina bifida aperta, Cranium bifidum
Caudal neural tube formation (secondary neurulation, from 4 weeks' gestation)	Occult dysraphic states
Prosencephalic development (2-3 months' gestation)	Holoprosencephaly, Agenesis of the corpus callosum, Agenesis of the septum pellucidum, Septo-optic dysplasia
Neuronal proliferation (3-4 months' gestation)	Micrencephaly, Macrencephaly
Neuronal migration (3-5 months' gestation)	Schizencephaly Lissencephaly, Pachygyria Polymicrogyria
Organization (5 months' gestation – years postnatal)	Idiopathic mental retardation
Myelination (Birth – years postnatal)	Cerebral white matter hypoplasia

with gyral formation. Within this rapid change of development, various developmental disorders and/or insults result in various phenotypes of fetal CNS abnormalities. For understanding fetal CNS diseases, basic knowledge of the development of the nervous system is essential. The developmental stages and their major disorders are described in **Table 16.4**.

Cranium Bifidum

Prevalence

Anencephaly; 0.29/1,000 births,[46] overall neural tube defect (NTD);0.58–1.17/1000 births.[47-49] Many reported remarkable reduction of prevalence of NTDs after using folic acid supplementation and fortification,[46-49] although some reported no decline of anencephaly rate.[50]

Definition

As in spina bifida, cranium bifidum is classified into four types of encephaloschisis (including anencephaly and exencephaly):

1. Meningocele
2. Encephalomeningocele
3. Encephalocystocele
4. Cranium bifidum occultum

Encephalocele occurs in the occipital region in 70–80%. Acrania, exencephaly and anencephaly are not independent anomalies. It is considered that dysraphia (absent cranial vault, acrania) occurs in very early stage and disintegration of the exposed brain (exencephaly) during the fetal period results in anencephaly.[51]

Etiology

Multifactorial inheritance, single mutant genes, specific teratogens (valproic acid), maternal diabetes, environmental factors, predominant in females.

Pathogenesis

Failure of anterior neural tube closure or a restricted disorder of neurulation.

Associated Anomalies

Open spina bifida (iniencephaly), Chiari type III malformation, bilateral renal cystic dysplasia and postaxial polydactyly with occipital cephalocele (Meckel-Gruber syndrome), hydrocephalus, polyhydramnios.

Prenatal Diagnosis

Acrania in **Figures 16.35A and B**, anencephaly in **Figures 16.36A to D**, encephalocele in **Figures 16.37A to D** and early detection of iniencephaly in **Figures 16.38A to D**.

Differential Diagnosis

Amniotic band syndrome (ABS): In cases of ABS, cranial destruction occurs secondarily to an amniotic band, similar appearance is observed. However, ABS has completely different pathogenesis from acrania/exencephaly.

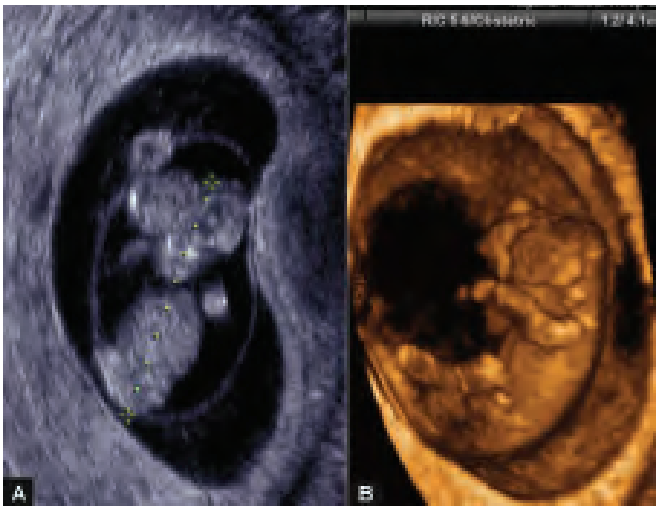

Figures 16.35A and B: Acrania at 10 weeks of gestation. (A) US coronal image at 10 weeks. Note the normal appearance of amniotic membrane, which indicates that this condition is not amniotic band syndrome; (B) 3D US image of the same fetus

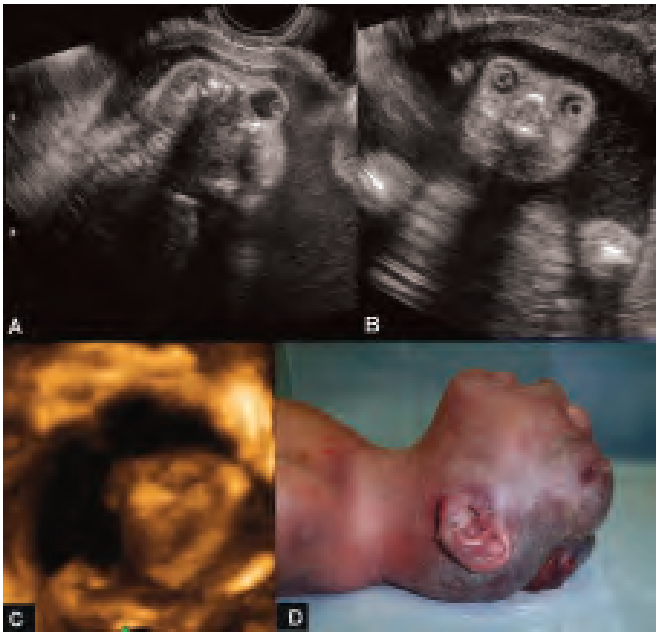

Figures 16.36A to D: Anencephaly in middle gestation (same case as Fig. 16.25). (A) US sagittal image at 23 weeks of gestation; (B) US coronal image; (C) 3D US image; (D) External appearances of stillborn fetus at 25 weeks of gestation. It is clear that exencephalic brain tissue which had existed at 10 weeks scattered in the amniotic space

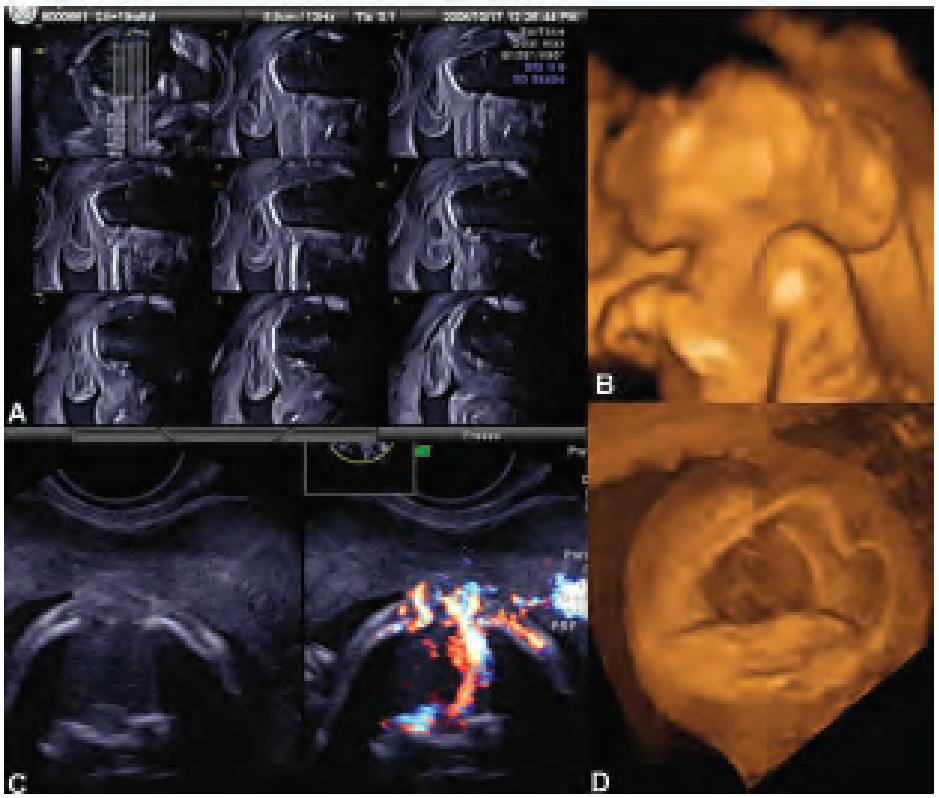

Figures 16.37A to D: Encephalocele at 18 weeks of gestation. (A) Tomographic sagittal imaging of encephalocele; (B) 3D reconstructed image. Microcephaly and occipital encephalocele are demonstrated; (C) Gray scale mode and bidirectional power Doppler image of connection between intracranial brain and extracranial brain. Cerebral vessels between them are clearly visualized; (D) 3D maximum mode of the occipital bone defect

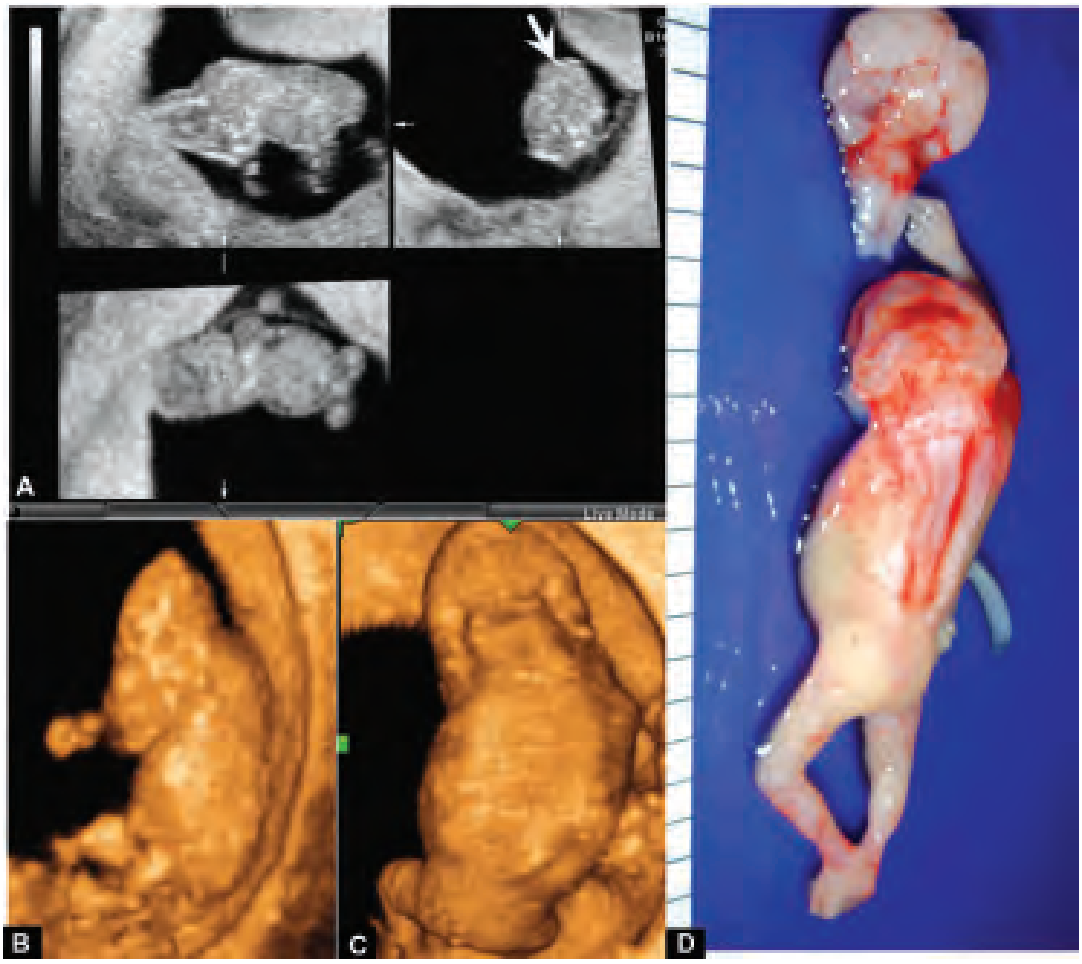

Figures 16.38A to D: 3D detection of a fetus with iniencephaly and acrania at 10 weeks of gestation. (A) Three orthogonal views of the fetus. Spina bifida (arrow) was demonstrated in the coronal section; (B and C) 3D images show the fetal lateral and dorsal views; (D) External appearance of aborted fetus at the end of 11 weeks of gestation. The brain and a part of spinal cord was detached at delivery

Prognosis

Anencephaly is a uniformly lethal anomaly. Other types of cranium bifidum, various neurological deficits may occur, depending on types and degrees.

Recurrence Risk

Used to be high recurrence risk of 5-13%, however, recently declined by use of folic acid supplementation and fortification.

Obstetrical Management

Termination of pregnancy can be offered in cases with anencephaly.

Neurosurgical Management

For other cranium bifidum, surgical operation aims at transposition of cerebral tissue into the intracranial cavity. Ventriculoperitoneal shunt for hydrocephalus.

Spina Bifida

Prevalence

0.22/1000 births,[46] overall NTD, 0.58–1.17/1000 births.[47-49] Many reported remarkable reduction of prevalence of NTDs after using folic acid supplementation and fortification.[46-49]

Definition

Spina bifida aperta—manifest form of spina bifida is classified into four types:

1. Meningocele
2. Myelomeningocele
3. Myelocystocele
4. Myeloschisis.

Spina bifida occulta is a generic term of spinal diseases covered with normal skin tissue and does not indicate spinal diseases which cannot be diagnosed by external appearance, cutaneous abnormalities near the spinal lesion are found; skin bulge (subcutaneous lipoma), dimple, hair tuft, pigmentation, skin appendage and hemangioma. In case with thickened film terminale, dermal sinus, or diastematomyelia (split cord malformation), abnormal tethering and fixation of the spinal cord occur.

Etiology

Multifactorial inheritance, single mutant genes, autosomal recessive, chromosomal abnormalities (trisomy 18, 13), specific teratogens (valproic acid), maternal diabetes, environmental factors, predominant in females.

Pathogenesis

Spina bifida aperta; an impairment of neural tube closure.

Spina bifida occulta; caudal neural tube malformation by the processes of canalization and retrogressive differentiation.

Associated Anomalies

Chiari type II malformation, hydrocephalus, scoliosis (above L2), kyphosis, polyhydramnios, additional non-CNS anomalies.

Prenatal Diagnosis

Figures 16.39 to 16.42.

Differential Diagnosis

Sacrococcygeal teratoma.

Prognosis

Disturbance of motor, sensory and sphincter function. Depends on lesion levels. Below S1; unable to walk unaided, above L2; wheelchair dependent, variable at intermediate level.

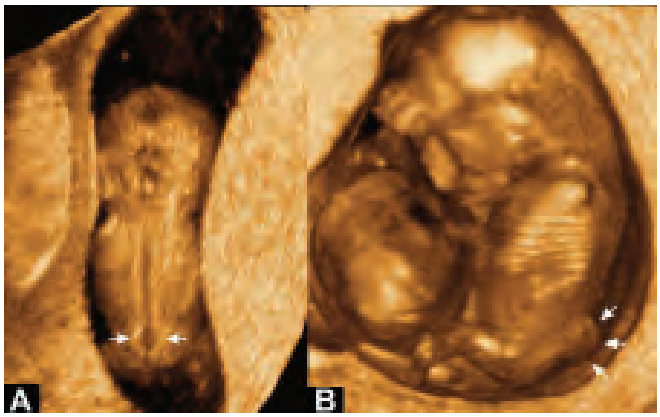

Figures 16.39A and B: Myelomeningocele in the first trimester. (A) Three dimensional dorsal view at 9 weeks, clearly demonstrates a neural tube defect at the lower lumbar and sacral level (arrows); (B) The same fetus at 12 weeks of gestation. Arrows indicate the lumbosacral myelomeningocele

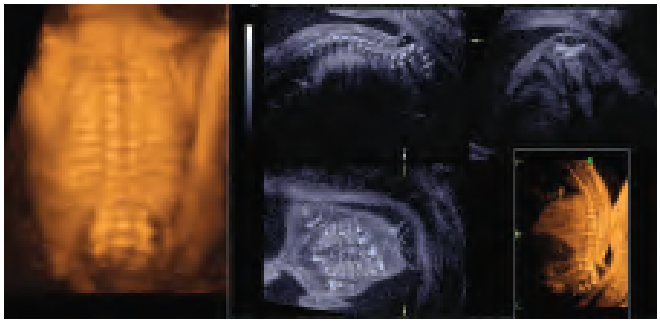

Figure 16.40: Myelomeningocele with severe kyphosis at 20 weeks of gestation. (left) 3D surface reconstruction image shows the large myelomeningocele from T12. Black and white pictures show three orthogonal view of vertebral structure and myelomeningocele with severe kyphosis. Right lower image demonstrates the 3D thick slice of vertebral structure

Recurrence Risk

Decreased, almost no recurrence rate[52] by use of folic acid supplementation and fortification.

Obstetrical Management

In case with spina bifida aperta, especially with defect of skin, cesarean section is preferable to protect the spinal cord and nerves and prevent infection.

Neurosurgical Management

Spina bifida aperta: In cases with defect of normal skin tissue, immediate closure of spina bifida after birth reduces spinal infection. Spinal cord reconstruction is

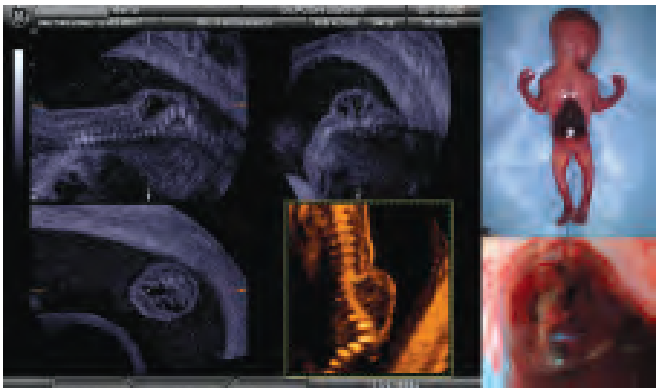

Figure 16.41: 3D US image of myelomeningocele with kyphosis at 16 weeks of gestation. Three orthogonal views and surface reconstruction image. (upper left) Sagittal US image. Spinal cord completely protrude into the sac surface from spinal canal and severe kyphosis are seen. (upper middle) Axial US view. (lower left) Coronal US view of myelomeningocele. Lower middle figure demonstrates the sagittal vertebral bony structure by 3D thick slice. Right figures show aborted fetus at 17 weeks. Right lower picture shows tortuous structure of spinal cord

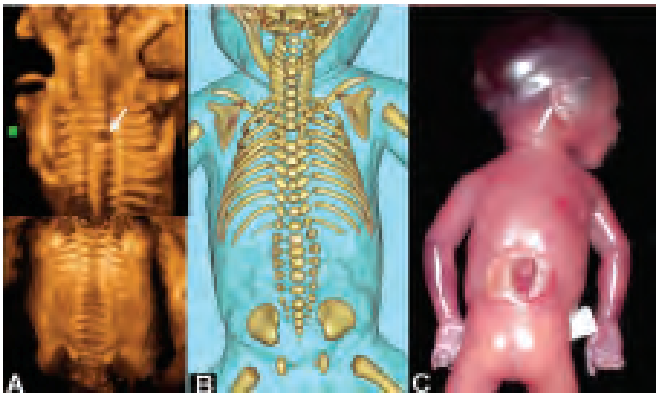

Figures 16.42A to C: Myelomeningocele with vertebral body defect at 17 weeks. (A) Left upper image demonstrates vertebral body defect of T4 and T5 (arrow). Left lower image demonstrates spina bifida from T11 level; (B) 3D-CT image of aborted fetus at 20 weeks of gestation. L4 and L5 vertebral body defect and spina bifida are well demonstrated; (C) The myelomeningocele of aborted fetus

the most important role of operation. Miniature Ommaya reservoir placement and subsequent ventriculoperitoneal shunt are required for hydrocephalus. For symptomatic Chiari malformation, posterior fossa decompressive craniectomy and/or tonsillectomy is performed.

Spina bifida occulta: The aim of surgical treatment is decompression of the spinal cord and cutting off tethering to the spinal cord.

Chiari Malformation (Figs 16.43A and B)

Prevalence

Depends on prevalence of spina bifida (Chiari type II malformation). According to recent remarkable reduction of prevalence of NTDs after using folic acid supplementation and fortification, prevalence has declined. Other types are rare.

Definition

Chiari classified anomalies with cerebellar herniation in the spinal canal into three types by contents of herniated tissue; contents of type I is a lip of cerebellum, type II part of cerebellum, fourth ventricle and medulla oblongata, pons, and type III is a large herniation of the posterior fossa. Thereafter, type IV with just cerebellar hypogenesis was added. However, this classification occasionally leads to confusion in neuroimaging diagnosis. Therefore, at present the classification as below is advocated.

Type I: Herniation of only cerebellar tonsil, not associated by myelomeningocele

Type II: Herniation of cerebellar tonsil and brainstem. Medullary kink, tentorial dysplasia, associated with myelomeningocele **(Figs 16.43A and B)**

Type III: Associated with cephalocele or craniocervical meningocele, in which cerebellum and brainstem herniated

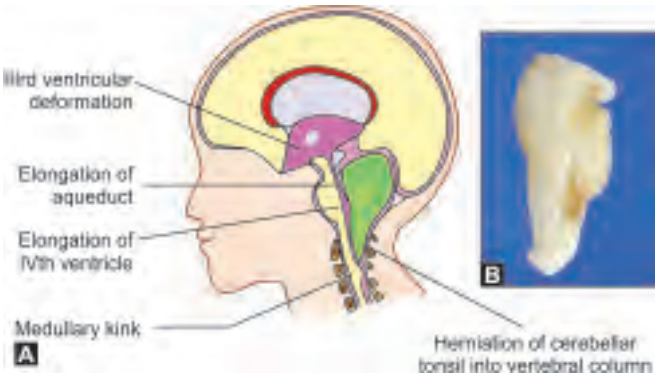

Figures16.43A and B: (A) Schema and macroscopic finding of Chiari type II malformation. Chiari type II malformation is characterized by inferior displacement of the lower cerebellum through the foramen magnum with obliteration of the cisterna magna, inferior displacement of the medulla into the spinal canal, and elongation of the fourth ventricle and aqueduct; (B) The macroscopic view of the elongated aqueduct, IVth ventricle and cerebellum from the specimen of an aborted fetus at 21 weeks of gestation

Type IV: Associated with marked cerebellar hypogenesis and posterior fossa shrinking.

Synonyms

Arnold-Chiari malformation.

Etiology

Depends on the types.

Pathogenesis

Chiari malformation occurs according to:

- Inferior displacement of the medulla and the fourth ventricle into the upper cervical canal
- Elongation and thinning of the upper medulla and lower pons and persistence of the embryonic flexure of these structures
- Inferior displacement of the lower cerebellum through the foramen magnum into the upper cervical region
- A variety of bony defects of the foramen magnum, occiput, and upper cervical vertebrae.[53]

Associated Anomalies

Hydrocephalus caused by obstruction of fourth ventricular outflow or associated aqueductal stenosis. Myelomeningocele or myeloschisis (type II), cephalocele or craniocervical meningocele (type III), cerebellar hypogenesis (type IV) and syringomyelia (type I).

Prenatal Diagnosis

Prenatal ultrasound diagnosis by features, lemon sign which indicates deformity of the frontal bone, banana sign which indicates abnormal shape of cerebellum without cisterna magna space **(Figs 16.44A to C)**, medullary kink, small clivus-supraocciput angle.[54] Lemon and banana signs are circumstantial evidences of Chiari malformation. Sonographic detection of Chiari malformation itself is occasionally possible **(Figs 16.45A and B)**.

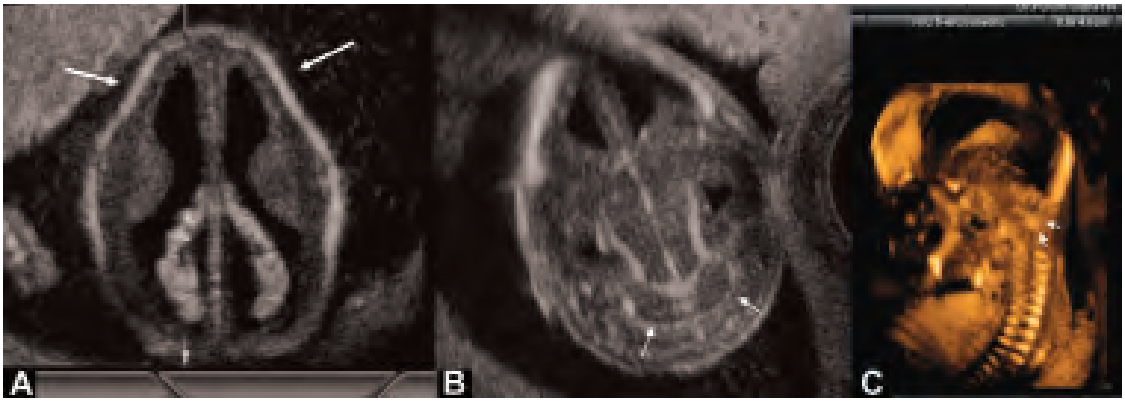

Figures 16.44A to C: Chiari type II malformation at 16 weeks of gestation. Chiari type II malformation is observed in most cases with myelomeningocele and myeloschisis. (A) Typical lemon sign (arrows); (B) Typical banana sign (arrows); (C) 3D reconstruction internal image of Chiari type II malformation (arrows)

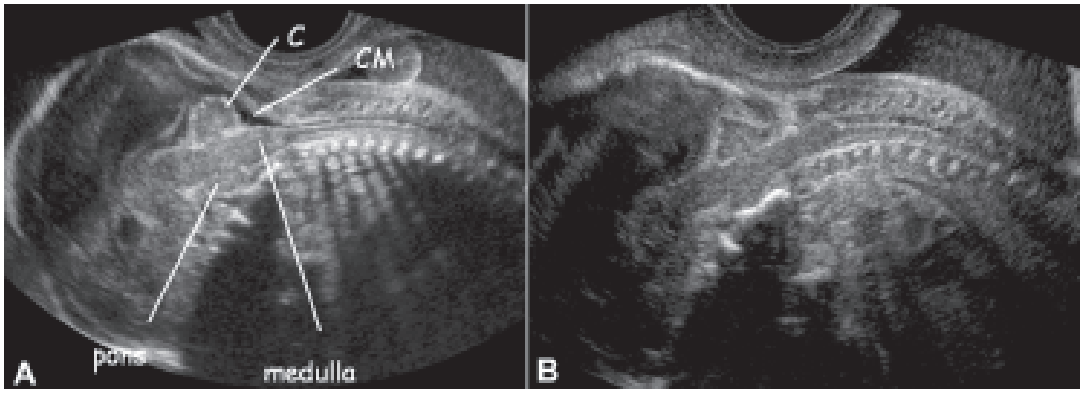

Figures 16.45A and B: Ultrasound imaging of Chiari II malformation at 20 weeks of gestation. (A) Normal sagittal section of cerebrospinal region at 20 weeks. The brainstem (pons and medulla) and cerebellum (C) are well demonstrated. Cisterna magna (CM) is well preserved; (B) The same cutting section of Chiari II malformation. Herniation of the cerebellum and medulla into spinal canal is demonstrated. Posterior fossa including cisterna magna is compressed

Differential Diagnosis

Craniosynostosis.

Prognosis

Nearly every case of myelomeningocele is accompanied morphological Chiari II malformation. Many cases with Chiari II are asymptomatic. However, clinical features due to Chiari malformation, such as feeding disturbances, laryngeal stridor or apneic episode, are found in approximately 9–30% of cases. In cases with these clinical features, vital prognosis is often poor.

Recurrence Risk

Depends on types of Chiari malformation. Decreased according to decline of NTD recurrence rate by use of folic acid supplementation and fortification.

Neurosurgical Management

Neurosurgical decompression of foramen magnum (FMD) for any types of Chiari malformation. Syringo-subarachnoid shunt for Chiari type I.

Holoprosencephaly

Incidence

One in 15,000–20,000 live births, however, initial incidence may be more than sixty fold greater in aborted human embryos.[55,56]

Classification

Holoprosencephalies are classified into three varieties:

1. *Alobar type:* A single-sphered cerebral structure with a single common ventricle, posterior large cyst of third ventricle (dorsal sac), absence of olfactory bulbs and tracts and a single optic nerve.
2. *Semilobar type:* With formation of a posterior portion of the interhemispheric fissure.
3. *Lobar type:* With formation of the interhemispheric fissure anteriorly and posteriorly but not in the midhemispheric region. The fusion of the fornices is seen.[57]

Etiology

Seventy five percent of holoprosencephaly has normal karyotype, but chromosomes 2, 3, 7, 13, 18 and 21 have been implicated in holoprosencephaly.[47] Particularly, trisomy 13 has most commonly been observed. Autosomal dominant transmission is rare.

Pathogenesis

Failure of cleavage of the prosencephalon and diencephalon during early first trimester (5–6 weeks) results in holoprosencephaly.

Associated Anomalies

Facial abnormalities, such as cyclopia, ethmocephaly, cebocephaly, flat nose, cleft lip and palate, are invariably associated with holoprosencephaly. Extracerebral abnormalities are also invariably associated, such as renal cysts/dysplasia, omphalocele, cardiac disease and/or myelomeningocele.

Prenatal Diagnosis

Alobar type in the first trimester and at 15 weeks of gestation are shown in **Figures 16.46** and **16.47**, and semilobar type in late pregnancy in **Figures 16.48A to E**. **Figure 16.49** shows facial appearance in cases of holoprosencephaly.

Differential Diagnosis

Hydrocephalus, hydranencephaly.

Prognosis

Extremely poor in alobar holoprosencephaly. Uncertain in lobar type. Various but poor in semilobar type.

Recurrence Risk

Six percent,[58] but much lower in sporadic or trisomy cases, much higher in genetic cases.

Management

Chromosomal evaluation is offered.

Agenesis of the Corpus Callosum

Prevalence

Uncertain, but 3–7:1,000 in the general population is estimated.

Definition

Absence of the corpus callosum, which may be divided into (complete) agenesis, partial agenesis or hypogenesis of the corpus callosum.

Complete agenesis: Complete absence of the corpus callosum.

Partial agenesis (hypogenesis): Absence of splenium or posterior portion in various degrees.

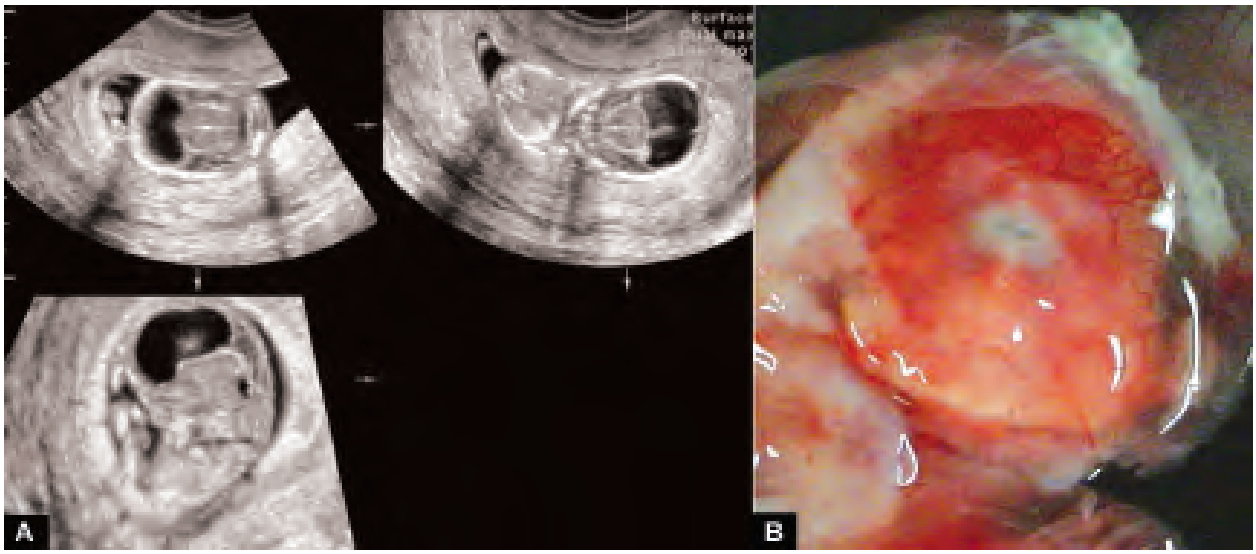

Figures 16.46A and B: Alobar holoprosencephaly in the first trimester. (A) Three orthogonal views demonstrate holoprosencephaly at 13 weeks. CRL was compatible to 10 weeks of gestation; (B) The face of aborted fetus with cyclopia, arhinia and small mouth

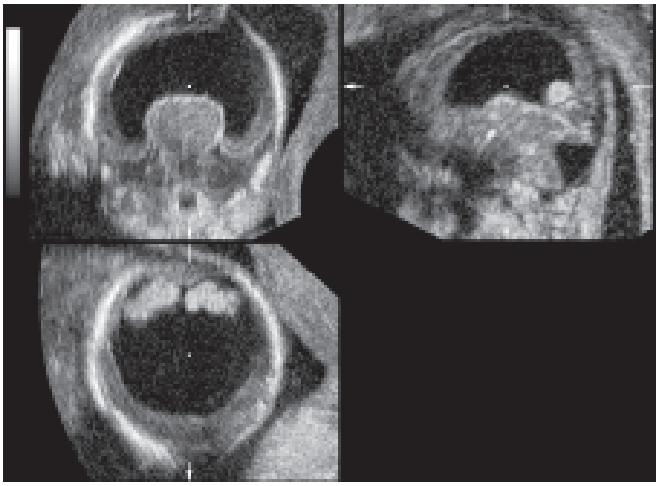

Figure 16.47: Alobar holoprosencephaly at 15 weeks of gestation. Three orthogonal images of intracranial structure show a complete single ventricle within a single-sphered cerebral structure

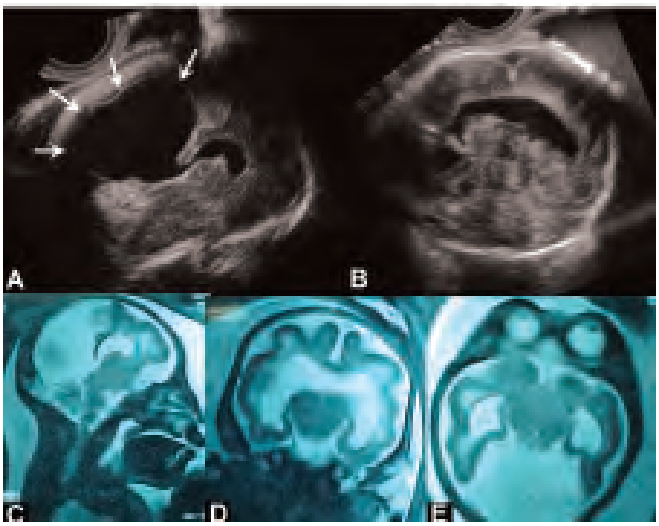

Figures 16.48A to E: Semilobar holoprosencephaly at 33 weeks of gestation.(A) Dorsal sac (arrows) in the median section; (B) Demonstrates the fused ventricle; (C to E) Fetal MR images. Sagittal (C), coronal (D) and axial (E) sections. A blind end of nasal cavity and hypotelorism are seen in the sagittal and axial MR images respectively

Etiology

Chromosomal abberation in 20% of affected cases such as trisomy 18, 8 and 13. Autosomal dominant, autosomal recessive, X-linked recessive, part of mendelian syndrome such as Walker-Warburg syndrome, and X-linked dominant such as Aicardi syndrome.

Pathogenesis

Uncertain, but callosal formation may be associated with migration disorder.

Associated Anomalies

Colpocephaly (ventriculomegaly with disproportionate enlargement of trigones, occipital horns and temporal horns, not hydrocephaly), superior elongation of the third ventricle, interhemispheric cyst, lipoma of the corpus callosum.

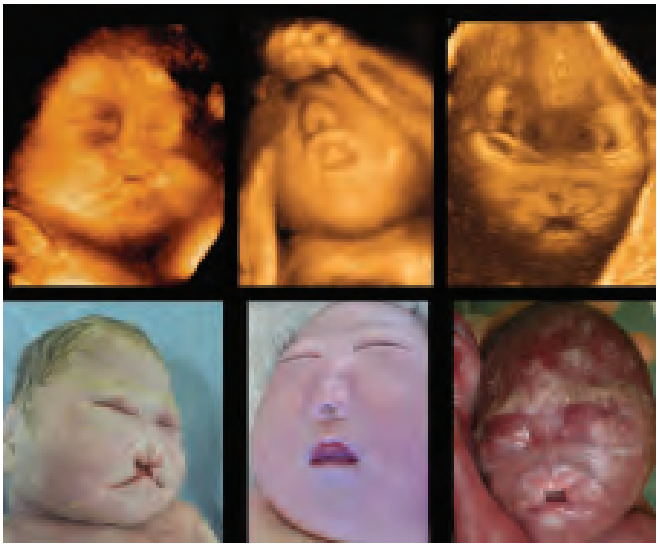

Figure 16.49: Facial abnormality in cases of holoprosencephaly. Upper figures are prenatal 3D facial images and lower figures show postpartum face appearance of each baby. Left: alobar holoprosencephaly at 20 weeks, Middle and right: semilobar type in late pregnancy. Hypotelorism, exophthalmos are common. Left and middle cases had cleft lip and palate and obstruction of the nasal cavity. Right case had a single and obstructed nasal cavity

Prenatal Diagnosis

Median sonographic images of complete agenesis and hypogenesis of the corpus callosum and fetal MRI are shown in **Figures 16.50A to H**. Abnormal brain vessels in a case of agenesis of the corpus callosum is demonstrated in **Figure 16.51**.

Diagnosis

As the corpus callosum is depicted after 17 or 18 weeks of gestation by ultrasound, it is impossible to diagnose agenesis of the corpus callosum prior to this age.[59]

Prognosis

Various; depends on associated anomalies. Most cases with isolated agenesis of the corpus callosum without other abnormalities are asymptomatic and prognosis is good. Complete agenesis has a worse prognosis than partial agenesis.[60] Epilepsy, intellectual impairment or psychiatric disorder[61] may occur later on.

Recurrence Risk

Depends on etiology. Chromosomal; 1%, autosomal recessive; 25%, X-linked recessive male; 50%.

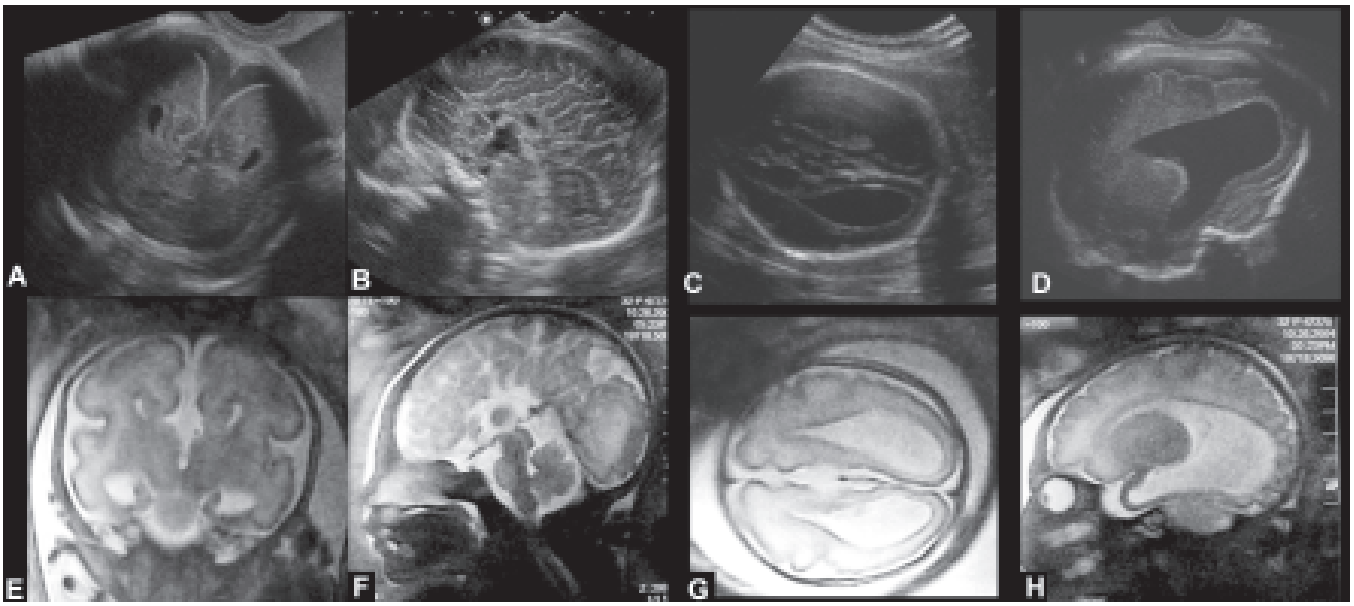

Figures 16.50A to H: Fetal US and MR images of complete agenesis of the corpus callosum. (A to D) Sonographic images and (E to H) MR. Anterior coronal, midsagittal, axial and parasagittal sections from the left. (right) No communicated bridge is between bilateral hemispheres. Note the bull's horn-like appearance of the anterior horns of lateral ventricle in the coronal image. Typical ventricular shape of colpocephaly is demonstrated on the axial and parasagittal sections

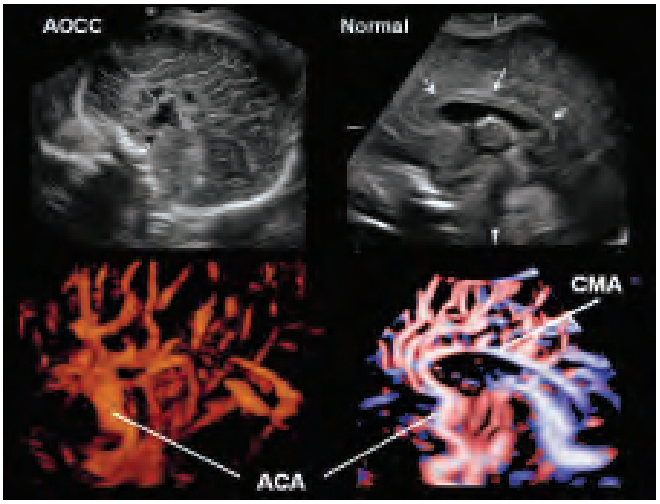

Figure 16.51: Agenesis of the corpus callosum (AOCC). (left upper) Midsagittal section in a case of AOCC. Typical radial sulcus formation is seen instead of normal cingulate sulcus and gyrus formed with normal development of the corpus callosum (arrows) seen in the upper right figure. (lower left) Angiostructure by 3D power Doppler. Normal callosomarginal artery (CMA, lower right) does not exist and radial formation of the branches of anterior cerebral arteries (ACA) is seen

Management

Standard obstetrical care. Chromosomal evaluation is offered. In cases with interhemispheric cyst, postnatal fenestration or shunt procedure may be performed.

Absent Septum Pellucidum, Septo-optic Dysplasia

Incidence

Unknown, rare.

Definition

Absent septum pellucidum: Absence of the septum pellucidum with or without associated anomalies. The septum pellucidum can be destroyed by concomitant hydrocephalus or by contiguous ischemic lesions such as porencephaly. An isolated absent septum pellucidum[62] exists but rare.

Septo-optic dysplasia: Absence of the septum pellucidum and unilateral or bilateral hypoplasia of the optic nerve.

Synonyms

De Morsier syndrome (septo-optic dysplasia).

Etiology

Maternal drug (multidrug, valproic acid,[63] cocaine[64]), autosomal recessive, HESX1 homeodomain gene mutation.[65]

Pathogenesis

May occur as a vascular disruption sequence, with other prosencephalic or neuronal migration disorders.

Associated Anomalies

Schizencephaly, gyral abnormalities, heterotopias, hypotelorism, ventriculomegaly, communicating lateral ventricles, bilateral cleft lip and palate, hypopituitarism.

Differential Diagnosis

Dysgenesis of the corpus callosum, lobar holoprosencephaly.

Prognosis

Depends on associated anomalies. Variable degree of mental deficit, multiple endocrine dysfunction. In cases with isolated absence of septum pellucidum, prognosis may be good.

Recurrence Risk

Unknown.

Management

Confirmation of diagnosis after birth is important for genetic counseling. Endocrine dysfunction should be searched and corrected. Shunt procedure in cases with progressive ventriculomegaly.

Migration Disorder

Incidence

Rare.

Definition

Arise specifically from defective formation of the central nervous system.

Etiology

Thought to be genetic in cause.

Pathogenesis

The abnormal migration of neurons in the developing brain and nervous system. In the developing brain, neurons must migrate from the areas where they are born to the areas where they will settle into their proper neural circuits. Neuronal migration, which occurs as early as the second month of gestation, is controlled by a complex assortment of chemical guides and signals. When these signals are absent or incorrect, neurons do not end up where they belong. This can result in

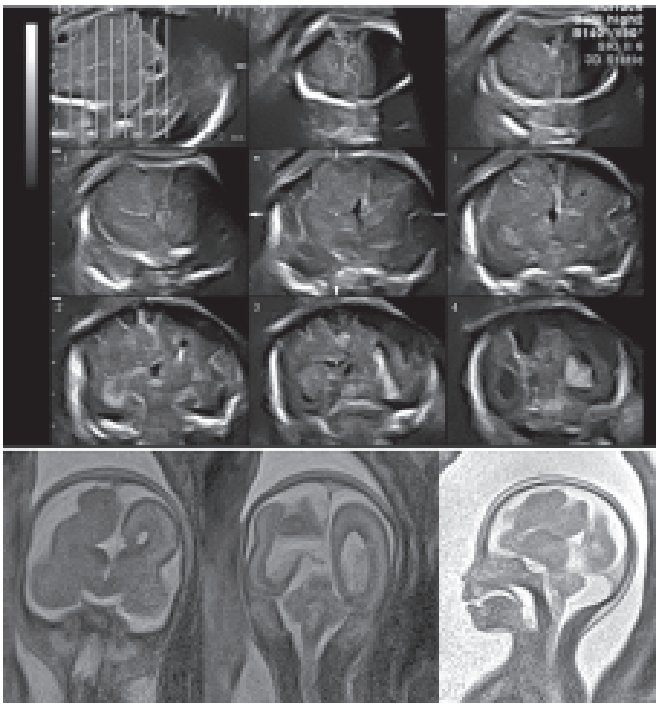

Figure 16.52: Migration disorder at 18 weeks of gestation. (upper) Tomographic coronal image of the brain. Note the different development between bilateral hemispheres. (lower) MR images. Anterior-coronal, posterior-coronal and sagittal sections from the left. Unilateral abnormal brain development was caused according to migration disorder

structurally abnormal or missing areas of the brain in the cerebral hemispheres, cerebellum, brainstem, or hippocampus, including schizencephaly, porencephaly, lissencephaly, agyria, macrogyria, pachygyria, microgyria, micropolygyria, neuronal heterotopias (including band heterotopia), agenesis of the corpus callosum and agenesis of the cranial nerves.

Differential Diagnosis

Brain tumor.

Prenatal Diagnosis

Unilateral maldevelopment caused by migration disorder detected by ultrasonography and MRI is shown in **Figure 16.52**.

Prognosis

Symptoms vary according to the specific disorder and the degree of brain abnormality and subsequent neurological losses, but often feature poor muscle tone and motor function, seizures, developmental delays, mental retardation, failure to grow and thrive, difficulties with feeding, swelling in the extremities, and a smaller than normal head. Most infants with a neuronal migration disorder appear normal, but some disorders have characteristic facial or skull features.

Recurrence Risk

Unknown.

Treatment

Treatment is symptomatic and may include anti-seizure medication and special or supplemental education consisting of physical, occupational and speech therapies.

Lissencephaly

Incidence

Unknown, rare.

Definition

Characterized by a lack of gyral development and conventionally divided into two types:

1. *Lissencephaly type I:* A smooth surface of the brain. Cerebral wall is similar to that of an approximately 12-week-old fetus.[66]
2. *Lissencephaly type II:* Cobblestone appearance.

Walker-Warburg syndrome with macrocephaly, congenital muscular dystrophy, cerebellar malformation, retinal malformation. Fukuyama congenital muscular dystrophy with microcephaly and congenital muscular dystrophy.

Recently many of responsible genes were clarified and classification has been changed by etiology **(Table 16.5)**.

Synonyms

Agyria, Pachygyria, Walker-Warburg syndrome was known as HARD±E syndrome (*h*ydrocephalus, *a*gyria, *r*etinal *d*ysplasia, with or without *e*ncephalocele).

Etiology

Isolated lissencephaly is linked to chromosome 17p13.3 and chromosome Xq24-q24. Miller-Dieker syndrome is also linked to chromosome 17p13.3. Walker-Warburg syndrome is autosomal recessive inheritance. Fukuyama congenital muscular dystrophy is linked to chromosome 9q31, fukutin.[67]

Pathogenesis

Defective neuronal migration with four rather than six layers in the cortex.

TABLE 16.5

Classification of lissencephaly	
Category	*Types*
Classic (or Type 1) lissencephaly	• LIS1 (17p13.3): lissencephaly due to PAFAH1B1 gene mutation, which subdivides into: type 1 isolated lissencephaly Miller-Dieker syndrome • LISX1: lissencephaly due to doublecortin (DCX) gene (Xq23) mutation • lissencephaly, type 1, isolated, without other known genetic defects
Cobblestone (or Type 2) lissencephaly	Walker-Warburg syndrome, also called HARD(E) syndrome Fukuyama syndrome Muscle-eye-brain disease (MEB)
X-linked lissencephaly	ARX gene (Xq22.13) mutation
Lissencephaly with cerebellar hypoplasia	Norman-Roberts syndrome (reelin gene (7q22.1) mutation)
Microlissencephaly	Lissencephaly + Microcephaly

Associated Anomalies

Polyhydramnios, less fetal movement, colpocephaly, agenesis of the corpus callosum, Dandy-Walker malformation, In Miller-Dieker syndrome, micrognathia, flat nose, high forehead, low-set ears, cardiac anomalies, genital anomalies in male are often observed.

Prenatal Diagnosis

A few reports of prenatal diagnosis of lissencephaly have been published.[68-70] Without previous history of an affected child, probably cannot be reliably made until 26–28 weeks' gestation.

Prognosis

Type I: Hypotonia, paucity of movements, feeding disturbance, seizures. The prognosis is poor, and death occurs.

Type II: Severe seizures, mental disorders, severe muscle disease with hypotonia. Death in the first year is common.

Recurrence Risk

Depends on etiology.

Management

Karyotyping is recommended to detect the chromosomal defect.

Schizencephaly

Incidence

Rare.

Definition

A disorder characterized by congenital clefts in the cerebral mantle, lined by pia-ependyma, with communication between the subarachnoid space laterally and the ventricular system medially. Sixty three percent is unilateral and thirty seven percent is bilateral. Frontal region in 44% and frontoparietal 30%.[66]

Etiology

Uncertain. In certain familial case, a point mutation in the homeobox gene, EMX2 was found.[71,72] Cytomegalovirus infection was also related in some cases.[73]

Pathogenesis

Neuronal migration disorder.

Associated Anomalies

Ventriculomegaly, microcephaly, polymicrogyria, gray matter heterotopias, dysgenesis of the corpus callosum, absence of the septum pellucidum and optic nerve hypoplasia.

Differential Diagnosis

Porencephaly, arachnoid cyst or other intracranial cystic masses. The MRI is useful in diagnosis of schizencephaly.[74]

Prognosis

Variable. Generally suffer from mental retardation, seizures, developmental delay and motor disturbances.

Recurrence Risk

Unknown.

Management

Ventriculoperitoneal shunt for progressive hydrocephalus.

Dandy-Walker Malformation, Dandy-Walker Variant, Megacisterna Magna

Incidence

Dandy-Walker (DW) malformation has an estimated prevalence of about 1:30,000 births and is found in 4–12% of all cases of infantile hydrocephalus.[75] Incidence of Dandy-Walker variant and megacisterna magna is unknown.

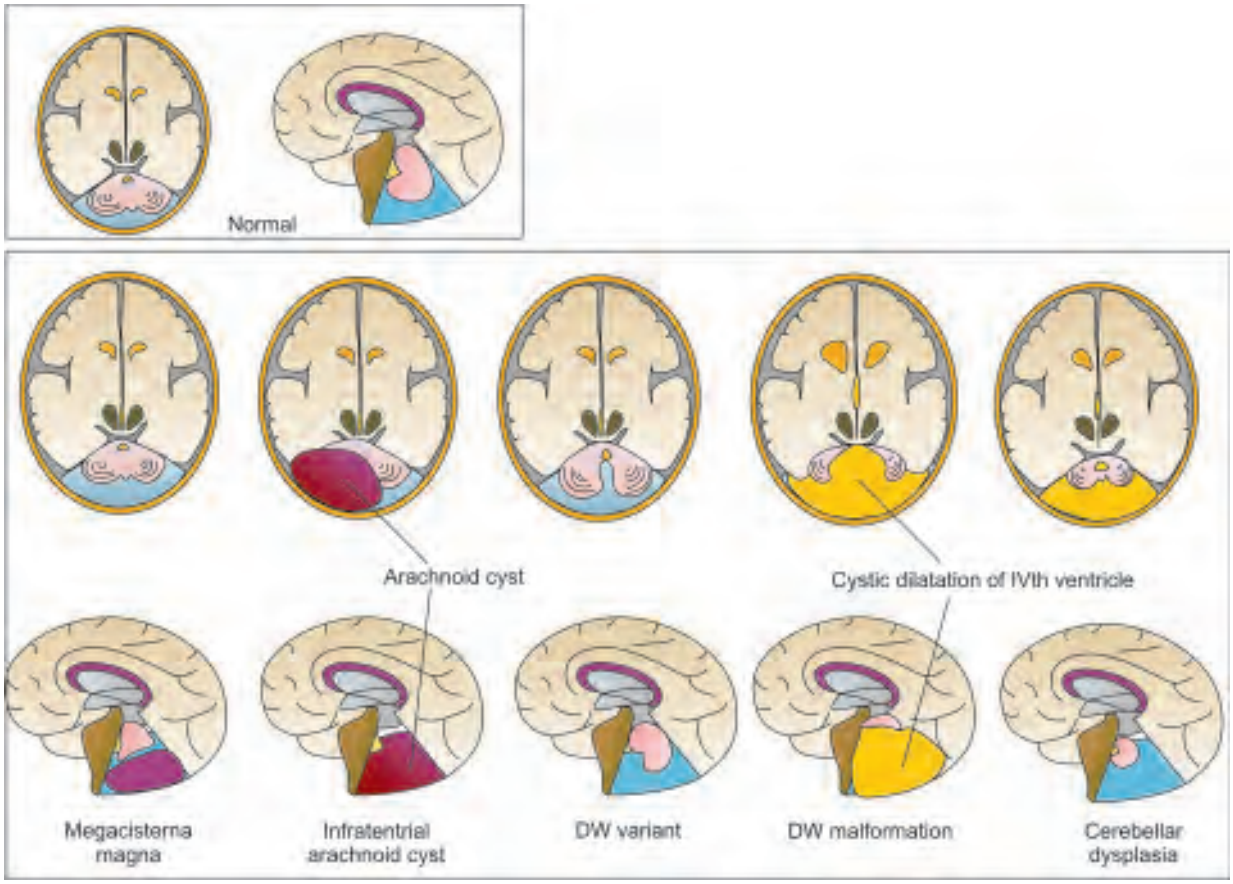

Figure 16.53: Differential diagnosis of hypoechoic lesion of the posterior fossa

Definition

At present, the term Dandy-Walker complex[76] is used to indicate a spectrum of anomalies of the posterior fossa that are classified by axial CT scans as it follows. Dandy-Walker malformation, Dandy-Walker variant and megacisterna magna seem to represent a continuum of developmental anomalies of the posterior fossa.[76] **Figure 16.53** shows the differential diagnosis of hypoechoic lesion of the posterior fossa.

Dandy-Walker Malformation (Classic)

Cystic dilatation of fourth ventricle, enlarged posterior fossa, elevated tentorium and complete or partial agenesis of the cerebellar vermis.

Dandy-Walker Variant

Variable hypoplasia of the cerebellar vermis with or without enlargement of the posterior fossa.

Megacisterna Magna

Enlarged cisterna magna with integrity of both cerebellar vermis and fourth ventricle.

Etiology

Mendelian disorders, such as Warburg, chromosomal aberration including 45,X, partial monosomy/trisomy, viral infections and diabetes.

Pathogenesis

During development of the fourth ventricular roof, a delay or total failure of the foramen of Magendie to open occurs, allowing a buildup of CSF and development of the cystic dilation of the fourth ventricle. Despite the subsequent opening of the foramina of Luschka (usually patent in Dandy-Walker malformation), cystic dilatation of the fourth ventricle persists and CSF flow is impaired.

Associated Anomalies of Dandy-Walker Malformation

Hydrocephalus. Other midline anomalies, such as agenesis of the corpus callosum, holoprosencephaly and occipital encephalocele. Extracranial abnormalities, such as congenital heart diseases, neural tube defects and cleft lip/palate. A frequency of additional anomalies ranges between 50 and 70%.

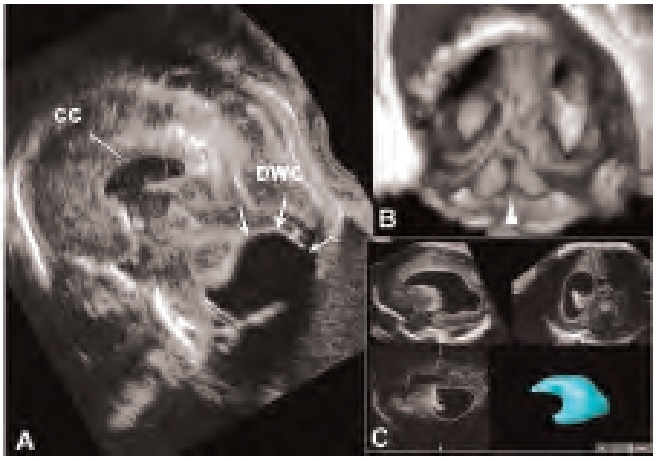

Figures 16.54A to C: Dandy-Walker malformation at 28 weeks of gestation. (A) The median section of the brain. Corpus callosum (CC) is normally demonstrated and Dandy-Walker cyst (DWC, arrows) is seen in the posterior fossa; (B) 3D view in the posterior coronal section. Hypoplastic vermis of the cerebellum (arrowhead) is seen; (C) Three orthogonal views and an extracted ventricular appearance, demonstrate moderate ventriculomegaly in this case

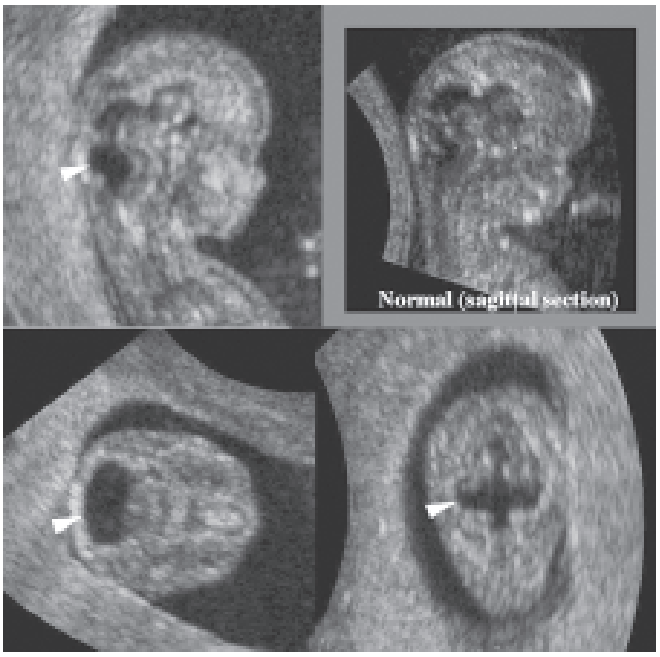

Figure 16.55: Early stage of Dandy-Walker malformation or variant at 11 weeks of gestation. Abnormal dilatation of the posterior fossa (arrowheads). Upper right figure is a sagittal image at the same gestational age in a normal case. Amniocentesis revealed trisomy 9 mosaicism and the fetus died *in utero* at 19 weeks

Prenatal Diagnosis

Dandy-Walker malformation in **Figures 16.54A to C**, and DW variant in **Figures 16.55 and 16.56**. To observe the agenesis of the cerebellar vermis, axial cutting

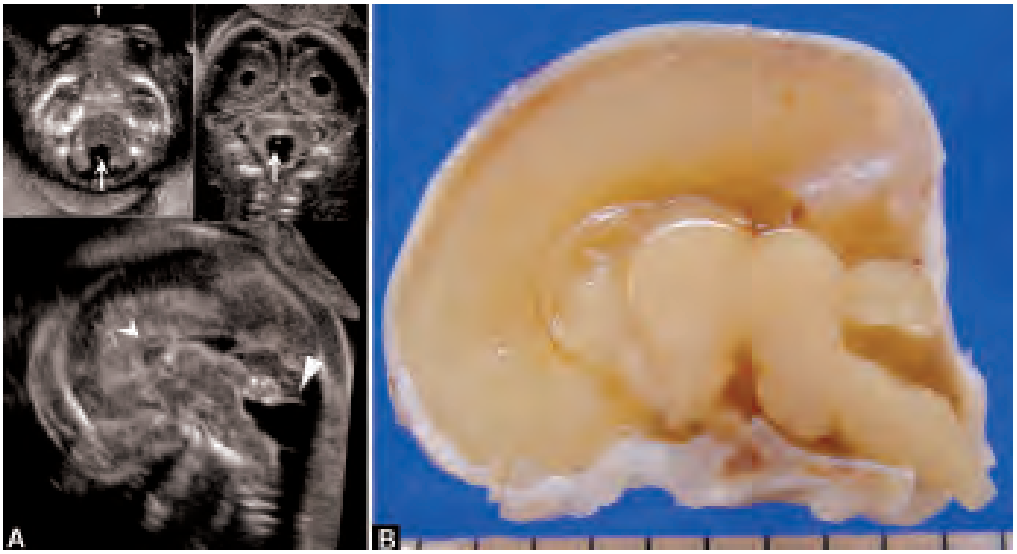

Figures 16.56A and B: Dandy-Walker variant at 20 weeks of gestation. (A) Upper figures show the 2D axial, 2D posterior coronal, 3D thick slices of oblique coronal and axial sections from the left. Hypoplasia of the vermis (arrows) is demonstrated and no marked ventriculomegaly was seen. Lower left figure shows the median section. Partial agenesis of the corpus callosum (arrowhead), floated celebellum and cystic formation of the posterior fossa (triangle arrowhead) are seen; (B) The median cutting section of the specimen of an aborted fetus at 21 weeks of gestation. This case had other complicated anomalies and the karyotype was partial trisomy of chromosome 10

section is preferable. To observe the elevated tentorium, sagittal section is preferable.

Differential Diagnosis

Infratentorial arachnoid cyst, other intracranial cystic tumor, hydrocephalus, cerebellar dysplasia.

Prognosis

Progressive hydrocephalus, not observed in neonates but often progressive during the first one month. Cases diagnosed *in utero* or neonatal period, outcome is generally unfavorable. Nearly 40% die, and 75% of survivors exhibit cognitive deficits. Prognosis of Dandy-Walker variant is good. Clinical significance of megacisterna magna is uncertain.

Recurrence Risk

Depends on etiology. Generally 1–5% (Dandy-Walker malformation).

Management

Cystoperitoneal shunt, cystoventriculoperitoneal shunt.

Arachnoid Cyst, Interhemispheric Cyst

Prevalence

One percent of intracranial masses in newborns.

Definition

Congenital or acquired cyst, lined by arachnoid membranes, and filled with fluid collection which is the same character as the cerebrospinal fluid. The number of cysts is mostly single, but two or more cysts can be occasionally observed. Location of arachnoid cyst is various; approximately 50% of cysts occur from the Sylvian fissure (middle fossa), 20% from the posterior fossa and 10–20% each from the convexity, suprasellar, interhemisphere, and quadrigeminal cistern. Interhemispheric cysts are often associated with agenesis or hypogenesis of the corpus callosum.

Etiology

Unknown.

Pathogenesis

Congenital arachnoid cyst is formed by maldevelopment of the arachnoid membrane. CSF accumulation in the subarachnoid space or intraarachnoid layers from a choroid plexus-like tissue within the cyst wall, leads to a progressive distension of the lesion.

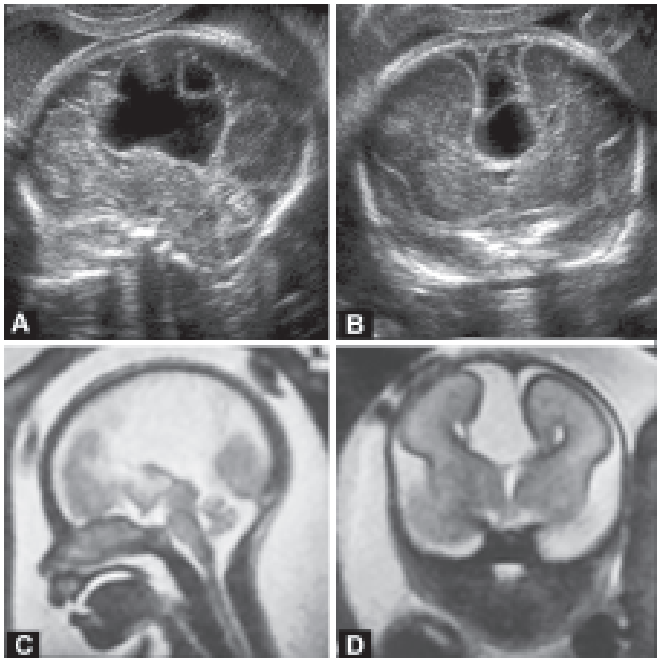

Figures 16.57A to D: US and MR images of interhemispheric cyst at 24 weeks of gestation. (A) US median section; (B) US anterior coronal section; (C) MR median section; (D) MR anterior coronal section. Cystic lesion exists between hemispheres. Intracystic cyst is visible on US images

Associated Anomalies

Unilateral or bilateral hydrocephalus, macrocrania.

Prenatal Diagnosis

Interhemispheric cyst in **Figures 16.57A to D**, suprasellar arachnoid cyst in **Figures 16.58A to F**. Intrauterine spontaneous resolution or changing cyst size are often detected. Detection in the first trimester was reported.[77]

Differential Diagnosis

Porencephaly, schizencephaly, third ventriculomegaly, intracranial cystic type tumor, vein of Galen aneurysm, Dandy-Walker malformation, large cisterna magna, external hydrocephalus.

Prognosis

Generally good. Postnatally, many are asymptomatic and remain quiescent for years, although others expand and cause neurological symptoms by compressing adjacent brain, ventriculomegaly and/or expanding the overlying skull.

Recurrence Risk

Unknown.

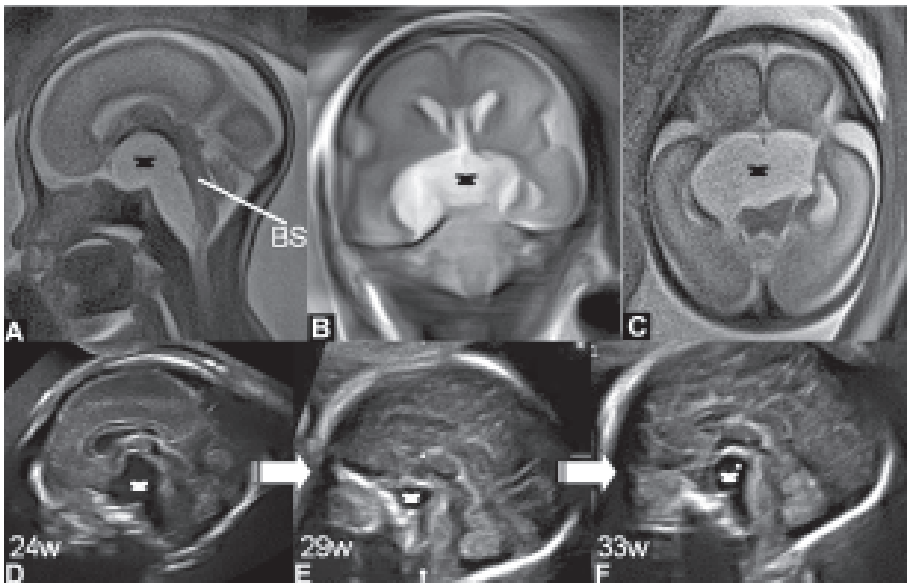

Figures 16.58A to F: MR images and serial US scan images of suprasellar arachnoid cyst. (A to C) MRI at 24 weeks of gestation. Sagittal, coronal and axial planes from the left. Suprasellar arachnoid cyst opressing the brainstem (BS) and bilateral hemispheres; (D to F) Serial scan images of the midsagittal section. Spontaneous size decrease from 24 to 29 weeks and increase from 29 to 33 weeks are well demonstrated. Asterisks indicate the arachnoid cyst

Obstetrical Management

Arachnoid cysts may increase or decrease its size. Therefore, expectant management of antenatally diagnosed cases is suggested.[78] In cases with accompanied hydrocephalus, mode and timing of delivery may be modified.

Postnatal Management

In cases with those symptoms or with prospects of neurological symptoms, treatment should be considered. Operation methods include:

- Cyst fenestration by craniotomy
- Cyst fenestration by neuroendoscopy
- Cystoperitoneal shunt.

Craniotomy, shunting or neuroendoscopic method has been still controversial.[79,80]

Craniosynostosis

Incidence

Unknown.

Definition

Premature closure of cranial suture, which may affect one or more cranial sutures. Simple sagittal synostosis is most common. Various cranial shapes depend on affected suture(s) **(Table 16.6)**.

Etiology

Crouzon (AD, variable), Apert (AD, usually new mutation), Pfeiffer (AD), Antley-Bixler (AR). In five autosomal dominant craniosynostosis syndromes (Apert, Crouzon, Pfeiffer, Jackson-Weiss and Crouzon syndrome with acanthosis nigricans) result from mutations in FGFR genes.[81] Abnormalities caused by various syndromes is given in **Table 16.7**.

TABLE 16.6

Cranial shape on the basis of affected suture	
Suture	*Abnormal cranial shape*
Sagittal suture	Scaphocephaly or dolichocephaly
Bilateral coronal suture	Brachycephaly
Unilateral coronal suture	Anterior plagiocephaly
Metopic suture	Trigonocephaly
Lambdoid suture	Acrocephaly
Unilateral lambdoid suture	Posterior plagiocephaly
Coronal/lambdoid/metopic or squamous/sagittal suture	Cloverleaf skull
Total cranial sutures	Oxycephaly

Pathogenesis[82]

- Cranial vault bones with decreased growth potential
- Asymmetrical bone deposition at perimeter sutures
- Sutures adjacent to the prematurely fused suture compensate in growth more than those sutures not contiguous with the closed suture
- Enhanced symmetrical bone deposition occurs along both sides of a nonperimeter suture continuing prematurely closed suture.

TABLE 16.7
Abnormalities caused by various syndromes

Syndromes	*Abnormalities*
Crouzon syndrome	Acrocephaly, synostosis of coronal, sagittal and lambdoid sutures With ocular proptosis, maxillary hypoplasia
Apert syndrome	Brachycephaly, irregular synostosis, especially coronal suture With midfacial hypoplasia, syndactyly, broad distal phalanx of thumb and big toe
Pfeiffer syndrome	Brachycephaly, synostosis of coronal and/or sagittal sutures With hypertelorism, broad thumbs and toes, partial syndactyly
Antley-Bixler syndrome	Brachycephaly, multiple synostosis, especially of coronal suture With maxillary hypoplasia, radiohumeral synostosis, choanal atresia, arthrogryposis

Associated Anomalies

Hypertelorism, syndactyly, polydactyly, exophthalmos.

Prenatal Diagnosis

Facial abnormality and intracranial structure with abnormal shape of ventricles in a case of Pfeiffer syndrome are demonstrated in **Figures 16.17A and B**. Abnormal craniofacial appearance can be detected by 2D/3D ultrasound.[83,84]

Prognosis

Various. In some of trigonocephaly and syndromic types, prognosis is poor.

Recurrence Risk

Depends on etiology.

Management

Operative aim of cranioplasty is improvement of intracranial pressure and cosmetic change.

Vein of Galen Aneurysm

Incidence

Rare.

Definition

Direct arteriovenous fistulas between choroidal and/or quadrigeminal arteries and an overlying single median venous sac.

Synonym

Vein of Galen malformation.

Etiology

Unknown.

Pathogenesis

Venous sac most probably represents persistence of the embryonic median prosencephalic vein of Markowski, not the vein of Galen, per se.[85]

Associated Anomalies

Cardiomegaly, high cardiac output, secondary hydrocephalus, macrocrania, cerebral ischemia (intracranial steal phenomenon), subarachnoid/cerebral/intraventricular hemorrhages.

Prenatal Diagnosis

2D and 3D color/power Doppler and 3D B-flow detection of VGAM and brain damage caused by cerebral ischemia or hemorrhage with mild ventriculomegaly are shown in **Figure 16.19**.

Differential Diagnosis

Arachnoid cyst, porencephalic cyst, intracranial teratoma. Color/power Doppler is helpful for differential diagnosis.

Prognosis

According to earlier review, outcome did not differ between treated and nontreated group and over 80% of cases died.[86] However, recent advances in treatment have improved outcome, such that 60–100% survive and over 60% have a good neurological outcome.[87,88]

Recurrence Risk

Unknown.

Management

Evaluation of the fetal high-output cardiac state for the proper obstetrical management. Percutaneous embolization by microcoils is recent main postnatal treatment and remarkably improved outcome.

Choroid Plexus Cysts

Incidence

0.61–2.89% of all fetuses scanned.[89-95]

Definition

Cysts with fluid collection within the choroid plexus, which may exist unilaterally or bilaterally. They are depicted in the second trimester and usually resolve by the 24th week.

Etiology

Normal variant.

Pathogenesis

Choroid plexus is located within the ventricular system and produces cerebrospinal fluid. Within the choroidal villi, choroid plexus cysts exist, surrounded by the loose stroma of the choroid plexus.[92] Choroid plexus cysts probably result from entrapment of cerebrospinal fluid within angled villi of the fetal ventricular system.[96]

Associated Anomalies

In cases of trisomy 18, associated anomalies include growth retardation, congenital heart diseases such as ventricular septum defect and double outlet right ventricle, overlapping finger, facial anomaly, cerebellar dysplasia and others.

Prenatal Diagnosis

It is impossible to distinguish normal from abnormal karyotypes only by location and appearance of choroid plexus cyst. Detection of additional anomalies is important for differential diagnosis.

Differential Diagnosis

Intraventricular hemorrhage.

Prognosis

Choroid plexus cysts, per se, are usually asymptomatic and benign, but rarely, symptomatic and disturb CSF flow.[97,98] Isolated choroid plexus cysts may be normal variation.

Recurrence Risk

Unknown.

Management

An isolated choroid plexus cyst is an indication to perform a detailed and accurate examination of other markers of aneuploidy. If the choroid plexus cyst is an isolated finding, there is no reason to perform amniocentesis.[93]

ACQUIRED BRAIN ABNORMALITIES *IN UTERO*

In terms of encephalopathy or cerebral palsy, 'timing of brain insult, antepartum, intrapartum or postpartum' is one of the serious controversial issues including medicosociolegal-ethical problems.[37] Although brain insults may relate to antepartum events in a substantial number of term-infants with hypoxic-ischemic encephalopathy, the timing of insult cannot always be clarified. It is a hard task to give antepartum evidences of brain injury predictive of cerebral palsy. Fetal heart rate monitoring cannot reveal the presence of encephalopathy, and neuroimaging by ultrasound and MRI is the most reliable modality for disclosure of silent encephalopathy. In many cases with cerebral palsy with acquired brain insults, especially, term-delivered infants with reactive fetal heart rate tracing and good Apgar score at delivery, are not suspected having encephalopathy and often overlooked for months or years. Recent imaging technology has revealed brain insult *in utero*.

Brain Tumors

Incidence

Extremely rare.

Definition

Tumors located in the intracranial cavity.

Histological Types

Brain tumors are divided into teratoma, most commonly reported and nonteratomatous tumor. Nonteratomatous tumors include neuroepithelial tumor, such as medulloblastoma, astrocytoma, choroid plexus papilloma, choroid plexus carcinoma, ependymoma, ependymoblastoma and mesenchymal tumor, such as craniopharyngioma, sarcoma, fibroma, hemangioblastoma, hemangioma and miningioma and others of lipoma of the corpus callosum, subependymal giant-

cell astrocytoma associated with tuberous sclerosis (often accompanied by cardiac rhabdomyoma).[99,100]

Location of Tumor

Supratentorial predominance in neonatal tumor. Infratentorial predominance in medulloblastoma. Choroid plexus papilloma is located within the lateral ventricles.

Associated Abnormalities

Macrocrania or local skull swelling, epignathus, secondary hydrocephalus, intracranial hemorrhage, intraventricular hemorrhage, polyhydroamnios, heart failure by high-cardiac output[101] and/or hydrops.

Diagnosis

Intracranial masses with solid, cystic or mixture pattern with or without visualization of hypervascularity by ultrasound and fetal MRI. Brain tumor should be considered in cases with unexplained intracranial hemorrhage.

Prenatal Diagnosis

Prenatal diagnosis of intracranial tumor and its vascularization by 3D power Doppler is shown in **Figure 16.59**, glioma at 18 weeks in **Figure 16.60**.

Differential Diagnosis

Arachnoid cyst, vein of Galen aneurysm, porencephaly, schizencephaly, periventricular leukomalacia, subdural hemorrhage.

Prognosis

Fetal demise, stillborn may occur. Prognosis in neonates is generally poor, but depends on timing of diagnosis and the histological type of tumor. Choroid plexus papilloma has minimal mortality rate and high

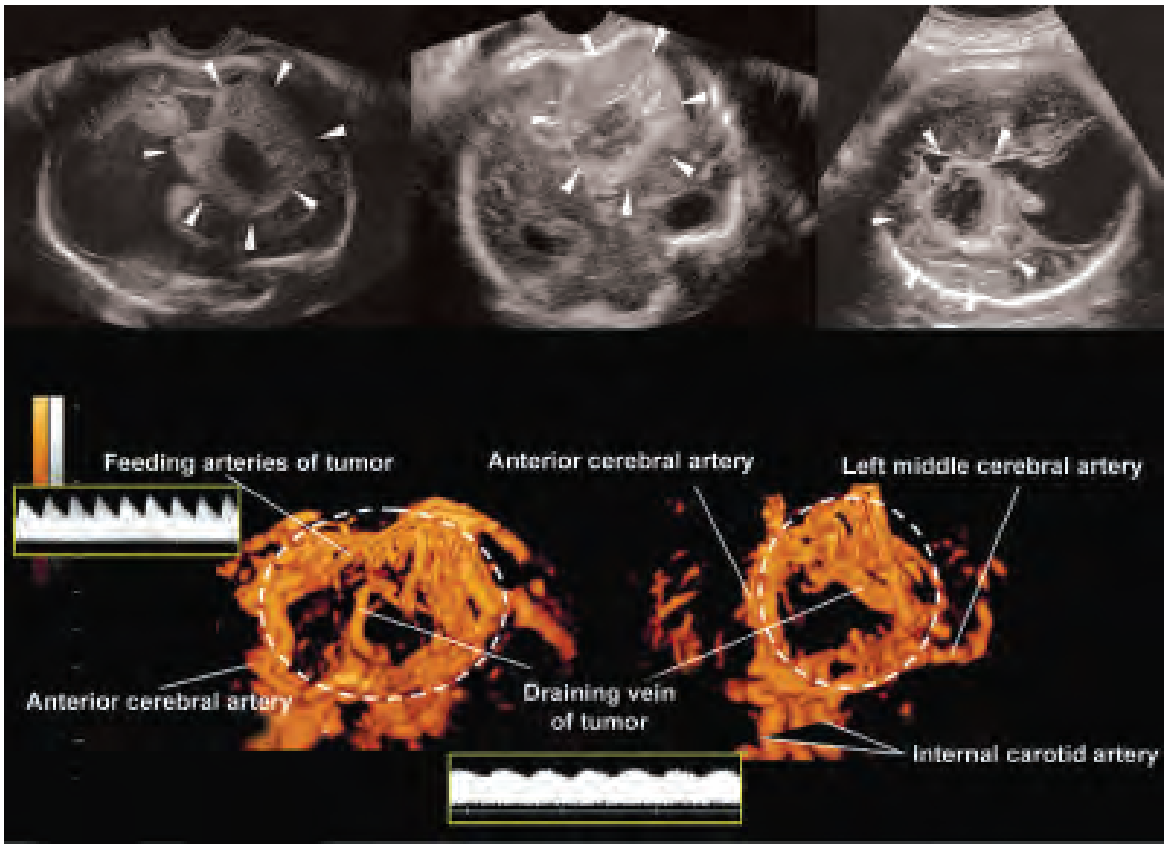

Figure 16.59: Ultrasound images and tumoral vascular visualization by 3D power Doppler in a fetus of intracranial tumor with interventricular hemorrhage (35 weeks and 5 days of gestation). (upper) Sagittal, coronal and axial US images. Huge tumor (arrowheads) with hemorrhage within the tumor in the frontoparietal lobe complicated with unilateral hydrocephalus with intraventricular hemorrhage (arrow). (left lower) Oblique sagittal view from fetal left side. (right lower) Oblique coronal view from fetal frontal side. Tumor is fed by numerous feeding arteries from anterior cerebral artery. Feeder arteries have low resistant flow waveform. One large vein which drains blood from tumor is visible. The draining vein has pulsatile flow

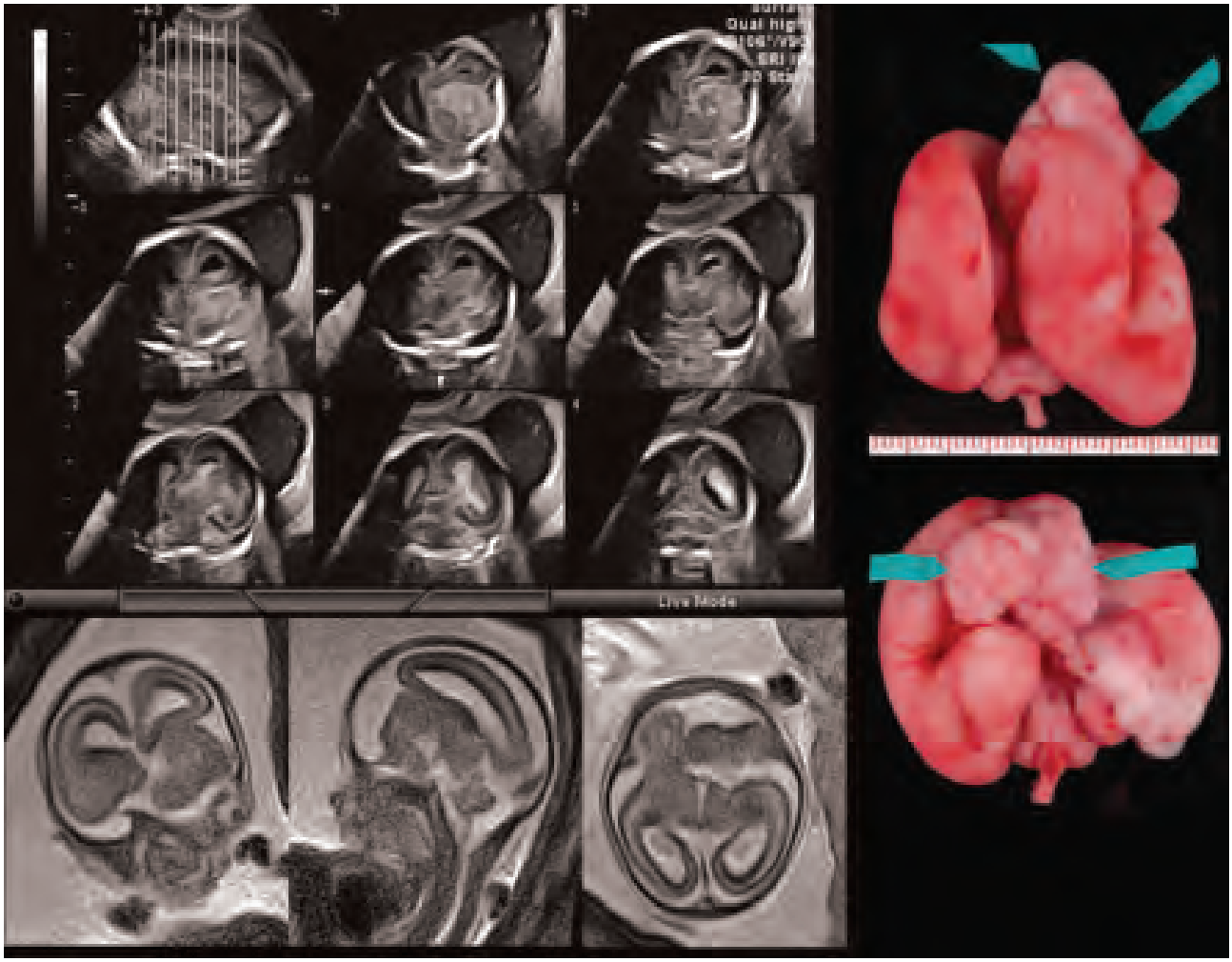

Figure 16.60: Brain tumor at 18 weeks of gestation. (upper left) Tomographic coronal image of the brain. Unilateral hemisphere is opressed by echogenic mass. (lower left) MR images. Coronal, sagittal and axial planes from the left. (upper right) Brain specimen from the parietal direction. The tumor is indicated by green arrows. (lower right) View from the bottom. The tumor was easily detachable from the brain

likelihood of neonatal outcome. Mortality rate of teratomas is over 90%, medulloblastoma over 80%. Other tumors have various prognosis.

Recurrence Risk

Unknown.

Management

Cesarean section may be considered. Neurosurgical tumor resection including subtotal hemispherectomy by craniotomy and chemotherapy are possible treatments for neonatal tumors. Radiation therapy is usually not indicated in neonates.

Subependymal Pseudocysts

Prevalence

2.6–5% of all neonates, 1% of premature newborns, unknown in fetuses.

Definition

Cystic formation, which is located in the caudothalamic groove or in the caudate nucleus, lateral to the wall of the anterior horns of lateral ventricles.

Synonym

Periventricular pseudocysts.[102,103]

Etiology

Infection (cytomegalovirus, rubella), subependymal hemorrhage, metabolic diseases, chromosomal deletions (del q6, del p4), cocaine exposure and others.

Pathogenesis

Cystic cavity is lined by a pseudocapsule, consisting of aggregates of germinal cells and glial tissue, but no epithelium can be found. Origin of pseudocysts is uncertain. May be cystic matrix regression or germinolysis.

Associated Anomalies

Congenital infection such as cytomegalovirus, congenital heart diseases, associated CNS abnormalities.

Prenatal Diagnosis

Often detectable by transvaginal sonography in the sagittal and anterior-coronal sections.

Differential Diagnosis

Periventricular leukomalacia.

Prognosis

Good in cases with isolated subependymal pseudocysts. In cases with accompanied abnormalities, such as cardiac disease, cytomegalovirus infection, other intracranial abnormalities, or cases with atypical pseudocysts, prognosis may be poor.[102-104]

Recurrence Risk

Unknown.

Management

In many cases, cysts regress in several months after birth. Normal obstetrical/neonatal care.

Porencephaly

Incidence

Unknown.

Definition

Fluid filled spaces replacing normal brain parenchyma and may or may not communicate with the lateral ventricles or subarachnoid space.

Synonym

Porencephalic cyst.

Etiology

Ischemic episode, trauma,[105] demise of one twin, intercerebral hemorrhage, infection.

Pathogenesis[106]

Easy to occur when immature cerebrum has some factors with propensity of dissolution and cavitation (high content of water, myelinated fiber bundles, deficient astroglial response). Timing of ischemic injury (maybe as early as second trimester) is strongly related to porencephaly, hydranencephaly.

Associated Anomalies

Intercerebral hemorrhage, interventricular hemorrhage, hydrocephalus.

Prenatal Diagnosis

Figures 16.61A to F show porencephaly after intracerebral hemorrhage at 25 weeks. Some cases *in utero* have been reported.[107,108]

Differential Diagnosis

Schizencephaly, arachnoid cyst, intracranial cystic tumor, other cysts. Porencephalic cyst never causes a mass effect, which is observed in cases with arachnoid cyst or other cystic mass lesions. This condition is acquired brain insult and differentiated from schizencephaly of migration disorder.

Prognosis

Various; depends on timing and size of lesion. Seizures, neurological deficits, cerebral palsy often occur.[109]

Recurrence Risk

Unknown.

Management

Ventriculoperitoneal shunt if hydrocephalus progresses.

Hydranencephaly

Incidence

1–2.5:10,000 births.

Definition

Absence of the cerebral hemispheres and a sac-like structure containing cerebral spinal fluid surrounding the brainstem and basal ganglia.

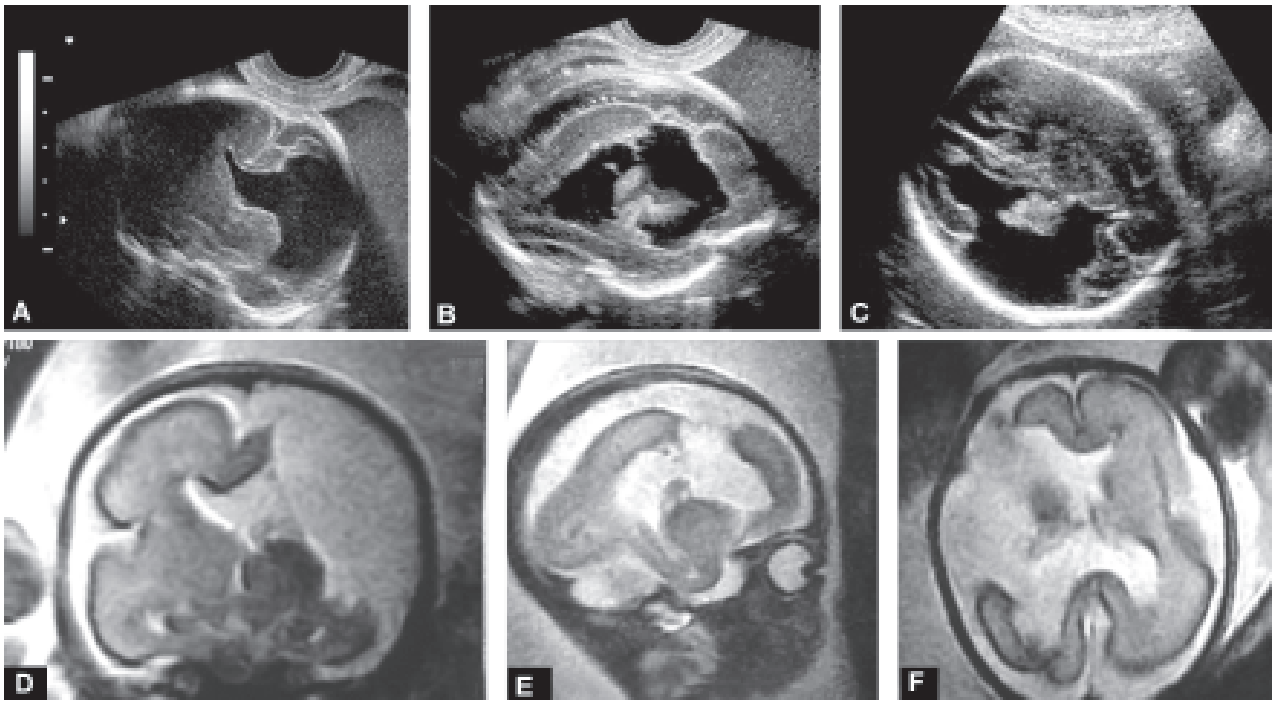

Figures 16.61A to F: Fetal US and MR images of porencephaly at 25 weeks of gestation. (A) Transvaginal US coronal image. Defect of parietolateral part of the unilateral cerebrum. This case has also absent septum pellucidum; (B) Parasagittal US image. Porencephalic part is fused with the unilateral ventricle. Echogenicity of inside ventricular wall indicates intraventricular hemorrhage; (C) Transabdominal US axial image; (D to F) Fetal MR images at the same day. Coronal, parasagittal and axial sections from the left side

Etiology

Ischemic episode, trauma, demise of one twin, intercerebral hemorrhage, infection. There are several theories but bilateral occlusion of the supraclinoid segment of the internal carotid arteries[110] or of the middle cerebral arteries is one of the cause of subtotal defects of cerebral hemisphere.

Pathogenesis

Easy to occur when immature cerebrum has some factors with propensity of dissolution and cavitation (high content of water, myelinated fiber bundles, deficient astroglial response). Timing of ischemic injury (maybe as early as second trimester) is strongly related to porencephaly and hydranencephaly.

Prenatal Diagnosis

Recently hydranencephaly from 11 weeks of gestation has been reported.[111]

Differential Diagnosis

Massive hydrocephalus, alobar holoprosencephaly, porencephaly.

Prognosis

Extremely poor.

Recurrence Risk

Unknown.

Management

No active treatment. Shunt procedure for progressive increase of infant's head.

Intracranial Hemorrhage

Incidence

Unknown, rare *in utero.*

Definition

Hemorrhage, bleeding inside of the cranium. Intracranial hemorrhage includes subdural hemorrhage, primary subarachnoid hemorrhage, intracerebellar hemorrhage, intraventricular hemorrhage and intraparenchymal hemorrhage other than cerebellar hemorrhage.[112]

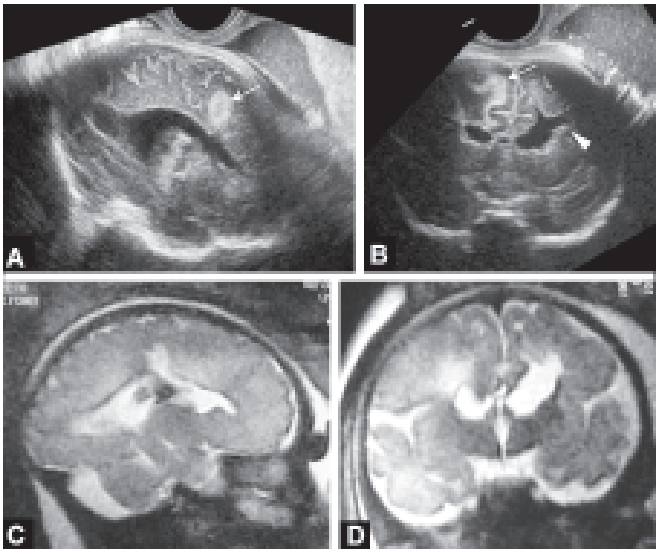

Figures 16.62A to D: US and MR images in a fetus with cerebral hemorrhage and mild ventriculomegaly at 35 weeks of gestation. (A) Ultrasound parasagittal; (B) Anterior coronal images of the brain. Arrows indicate intracerebral hemorrhage. Arrowhead shows a porencephalic part fused with the lateral ventricle; (C and D) MR images showing the same cutting sections as upper US images

Etiology

Trauma, alloimmune and idiopathic thrombocytopenia, von Willebrand's disease, specific medications (warfarin) or illicit drug (cocaine) abuse, seizure, fetal conditions including congenital factor-X and factor-V deficiencies, intracranial tumor, twin-twin transfusion, demise of a co-twin, vascular diseases, or fetomaternal hemorrhage, extracorporeal membrane oxygenation (ECMO).[113]

Associated Anomalies

Hydrocephalus, hydranencephaly, porencephaly, or microcephaly.

Prenatal Diagnosis

Figures 16.62A to D show multiple intracerebral hemorrhage at 35 weeks.

Differential Diagnosis

Intracranial tumor.

Prognosis

Poor in premature infants. Apnea, seizures, and other neurological symptoms.

Recurrence Risk

Depends on etiology.

Management

Ventriculoperitoneal shunt if hydrocephalus progresses.

Fetal Periventricular Leukomalacia

Incidence

Twenty five to seventy five percent of premature infants at autopsy are complicated with periventricular white matter injury. However, clinically, incidence may be much lower. The 5–10% of infants less than 1500 gm birth weight. In at term infants, periventricular leukomalacia (PVL) is very rare.

Definition

Multifocal areas of necrosis found deep in the cortical white matter, which are often symmetrical and occur adjacent to the lateral ventricles. The PVL represents a major precursor for neurological and intellectual impairment, and cerebral palsy in later life.

Etiology

Birth trauma, asphyxia and respiratory failure, cardiopulmonary defects, premature birth/low birth weight, associated immature cerebrovascular development and lack of appropriate autoregulation of cerebral blood flow in response to hypoxic-ischemic insults.[114]

Pathogenesis

Distinctive and consists primarily of both focal periventricular necrosis and more diffuse cerebral white matter injury. Two most common sites are at the level of the cerebral white matter near the trigone of the lateral ventricles and around the foramen of Monro. Volpe[106] described three factors, such as:

1. Periventricular, vascular, anatomical and physiological factors
2. Cerebral ischemia
3. Intrinsic vulnerability of cerebral white matter of premature newborn, are strongly related to PVL.

Differential Diagnosis

Subarachnoid (periventricular) pseudocysts, porencephaly, other intracranial cystic formation.

Prognosis

Neurological features of PVL in neonatal period is probable lower limb weakness and as features of long-

term sequelae, spastic diplegia, intellectual deficits and visual deficits are observed.[106]

Recurrence Risk

Unknown.

Management

Early rehabilitation.

Microcephaly

Incidence

Rare.

Definition

A head circumference that is more than two standard deviations below the normal mean for age, sex, race, and gestation (Some authorities define microcephaly as more than three standard deviations below the mean).

Etiology

Infections such as with rubella, CMV, varicella (chicken pox) virus and toxoplasmosis, radiation, medications, chromosome abnormalities and genetic diseases. It is part of many chromosomal abnormalities and other syndromes including:

Chromosome abnormalities: Trisomy 18 (Edwards syndrome), trisomy 13 (Patau syndrome), the Wolf-Hirschhorn syndrome, the cat cry syndrome and partial deletion of long arm of chromosome 13.

Contiguous gene syndromes: Miller-Dieker syndrome. Langer-Giedion syndrome, Prader-Willi syndrome and the Aniridia-Wilms tumor syndrome.

Genetic disorders: Johanson-Blizzard syndrome, Seckel syndrome and the Smith-Lemli-Opitz syndrome.

Environmental insults: Maternal phenylketonuria (PKU) (mothers who have poorly controlled PKU during pregnancy) and the fetal alcohol syndrome.

Pathogenesis

May be caused by a disturbance in the proliferation of nerve cells. Abnormalities of neurocranial architecture occur in approximately two-thirds of cases.[115]

Differential Diagnosis

Craniosynostosis.

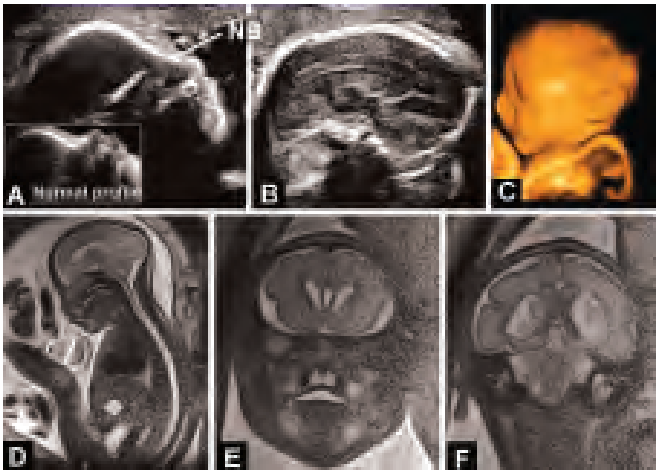

Figures 16.63A to F: Microcephaly at 28 weeks of gestation. (A) Fetal face in the sagittal section.Note the flat face with the frontal bone and nasal bone (NB) on a single line, comparing to the normal face in the yellow box; (B) Sagittal section of the brain. Microcephaly and microbrain are detectable; (C) 3D reconstruction image of fetal craniofacial expression. (D to F) MR image in the sagittal, anterior-coronal and posterior-coronal sections

Prenatal Diagnosis

Ultrasonograms and MRI images of typical microcephaly are shown in **Figures 16.63A to F**. Occasionally, microcephaly occurs with late onset during pregnancy.[116]

Prognosis

Development of motor functions and speech may be delayed. Hyperactivity and mental retardation are common occurrences, although the degree of each varies. Convulsions may also occur. Motor ability varies, ranging from clumsiness in some to spastic quadriplegia in others.

Recurrence Risk

Unknown.

Treatment

No specific treatment for microcephaly. Treatment is symptomatic and supportive.

FUTURE ASPECT

Neurological prognosis should be longitudinally and carefully evaluated according to precise diagnosis. In Japan, Research Committee for Intractable Fetal Brain

Malformation in Research of Intractable Disease Health and Labor Science Research Grants in 2009 by Ministry of Health, Labor and Welfare in Japan was organized including pediatric neurosurgeons, obstetrician (the author), radiologists and others specializing fetal neurology and neurodiagnosis, and published a book of 'Fetal Hydrocephalus Guideline for Diagnosis and Management (1st edition)' in 2005 and 2nd edition in 2010. The research committee has been involved with online registration systems on fetal CNS abnormalities and investigating neurological prognosis/outcome of fetuses with accurate prenatal diagnoses by clear neuroimaging which is well-discussed and examined among neurospecialists members.

REFERENCES

1. Timor-Tritsch IE, Peisner DB, Raju S. Sonoembryology: an organ-oriented approach using a high-frequency vaginal probe. J Clin Ultrasound. 1990;18(4):286-98.
2. Pooh RK. B-mode and Doppler studies of the abnormal fetus in the first trimester. In: Chervenak FA, Kurjak A (Eds). Fetal Medicine. Carnforth: Parthenon Publishing; 1999. pp. 46-51.
3. Timor-Tritsch IE, Monteagudo A. Transvaginal fetal neurosonography: standardization of the planes and sections by anatomic landmarks. Ultrasound Obstet Gynecol. 1996;8(1):42-7.
4. Monteagudo A, Reuss ML, Timor-Tritsch IE. Imaging the fetal brain in the second and third trimesters using transvaginal sonography. Obstet Gynecol. 1991;77(1):27-32.
5. Monteagudo A, Timor-Tritsch IE, Moomjy M. In utero detection of ventriculomegaly during the second and third trimesters by transvaginal sonography. Ultrasound Obstet Gynecol. 1994;4(3):193-8.
6. Monteagudo A, Timor-Tritsch IE. Development of fetal gyri, sulci and fissures: a transvaginal sonographic study. Ultrasound Obstet Gynecol. 1997;9:222-8.
7. Pooh RK, Nakagawa Y, Nagamachi N, et al. Transvaginal sonography of the fetal brain: detection of abnormal morphology and circulation. Croat Med J. 1998;39(2):147-57.
8. Pooh RK, Maeda K, Pooh KH, et al. Sonographic assessment of the fetal brain morphology. Prenat Neonat Med. 1999;4:18-38.
9. Pooh RK. Three-dimensional ultrasound of the fetal brain. In: Kurjak A (Ed). Clinical application of 3D ultrasonography. Carnforth: Parthenon Publishing; 2000. pp. 176-80.
10. Pooh RK, Pooh KH, Nakagawa Y, et al. Clinical application of three-dimensional ultrasound in fetal brain assessment. Croat Med J. 2000;41(3):245-51.
11. Timor-Tritsch IE, Monteagudo A, Mayberry P. Three-dimensional ultrasound evaluation of the fetal brain: the three horn view. Ultrasound Obstet Gynecol. 2000;16(4):302-6.
12. Monteagudo A, Timor-Tritsch IE, Mayberry P. Three-dimensional transvaginal neurosonography of the fetal brain: 'navigating' in the volume scan. Ultrasound Obstet Gynecol. 2000;16(4):307-13.
13. Pooh RK, Nagao Y, Pooh KH. Fetal neuroimaging by transvaginal 3D ultrasound and MRI. Ultrasound Rev Obstet Gynecol. 2006;6:123-34.
14. Pooh RK, Pooh KH. Fetal neuroimaging with new technology. Ultrasound Review Obstet Gynecol. 2002;2:178-81.
15. Blaas HG, Eik-Nes SH, Kiserud T, et al. Three-dimensional imaging of the brain cavities in human embryos. Ultrasound Obstet Gynecol. 1995;5(4):228-32.
16. Blaas HG, Eik-Nes SH, Berg S, et al. In-vivo three-dimensional ultrasound reconstructions of embryos and early fetuses. Lancet. 1998;352(9135):1182-6.
17. Pooh RK. Fetal Brain Assessment by Three-Dimensional Ultrasound. In: Kurjak A, Kupesic S (Eds). Clinical Application of 3D Sonography. Carnforth,UK:Parthenon Publishing; 2000. pp. 171-9.
18. Pooh RK, Pooh KH. Transvaginal 3D and Doppler ultrasonography of the fetal brain. Semin Perinatol. 2001;25(1):38-43.
19. Pooh RK, Pooh KH. The assessment of fetal brain morphology and circulation by transvaginal 3D sonography and power Doppler. J Perinat Med. 2002;30(1):48-56.
20. Endres LK, Cohen L. Reliability and validity of three-dimensional fetal brain volumes. J Ultrasound Med. 2001;20(12):1265-9.
21. Roelfsema NM, Hop WC, Boito SM, et al. Three-dimensional sonographic measurement of normal fetal brain volume during the second half of pregnancy. Am J Obstet Gynecol. 2004;190(1):275-80.
22. Benacerraf BR. Inversion mode display of 3D sonography: applications in obstetric and gynecologic imaging. AJR Am J Roentgenol. 2006;187(4):965-71.
23. Kusanovic JP, Nien JK, Gonçalves LF, et al. The use of inversion mode and 3D manual segmentation in volume measurement of fetal fluid-filled structures: comparison with Virtual Organ Computer-aided AnaLysis (VOCAL). Ultrasound Obstet Gynecol. 2008;31(2):177-86.
24. Hata T, Dai SY, Kanenishi K, et al. Three-dimensional volume-rendered imaging of embryonic brain vesicles using inversion mode. J Obstet Gynaecol Res. 2009;35(2):258-61.
25. Pooh RK, Aono T. Transvaginal power Doppler angiography of the fetal brain. Ultrasound Obstet Gynecol. 1996;8(6):417-21.
26. Pooh RK. Two-dimensional and three-dimensional Doppler angiography in fetal brain circulation. In: Kurjak A (Ed). 3D Power Doppler in Obstetrics and Gynecology. Carnforth: Parthenon Publishing; 1999. pp 105-11.
27. Moore KL, Persaud TVN. The developing human; clinically oriented embryology. 7th edition. Pennsylvania: Saunders; 2003.
28. Malinger G, Lev D, Lerman-Sagie T. Is fetal magnetic resonance imaging superior to neurosonography for detection of brain anomalies? Ultrasound Obstet Gynecol. 2002;20(4):317-21.

29. Girard N, Chaumoitre K, Confort-Gouny S, et al. Magnetic resonance imaging and the detection of fetal brain anomalies, injury, and physiologic adaptations. Curr Opin Obstet Gynecol. 2006;18(2):164-76.
30. Levine D, Barnes PD, Madsen JR, et al. Central nervous system abnormalities assessed with prenatal magnetic resonance imaging. Obstet Gynecol. 1999;94(6):1011-9.
31. Simon EM, Goldstein RB, Coakley FV, et al. Fast MR imaging of fetal CNS anomalies in utero. Am J Neuroradiol. 2000;21(9):1688-98.
32. Sonigo PC, Rypens FF, Carteret M, et al. MR imaging of fetal cerebral anomalies. Pediatr Radiol. 1998;28(4):212–22.
33. Wagenvoort AM, Bekker MN, Go ATJI, et al. Ultrafast scan magnetic resonance in prenatal diagnosis. Fetal Diagn Ther. 2000;15(6):364-72.
34. Kubik-Huch RA, Huisman TAGM, Wisser J, et al. Ultrafast MR imaging of the fetus. AJR. 2000;174(6):1599-606.
35. Malinger G, Ben-Sira L, Lev D, Ben-Aroya Z, et al. Fetal brain imaging: a comparison between magnetic resonance imaging and dedicated neurosonography. Ultrasound Obstet Gynecol. 2004;23(4):333-40.
36. Pooh RK, Kurjak A. 3D and 4D sonography and magnetic resonance in the assessment of normal and abnormal CNS development: alternative or complementary. J Perinat Med. 2010;39(1):3-13.
37. Pooh RK, Maeda K, Pooh KH. An Atlas of Fetal Central Nervous System Disease. Diagnosis and Management. New York: Parthenon CRC Press London; 2003.
38. Alagappan R, Browning PD, Laorr A, et al. Distal lateral ventricular atrium: reevaluation of normal range. Radiology. 1994;193(2):405-8.
39. Almog B, Gamzu R, Achiron R, et al. Fetal lateral ventricular width: what should be its upper limit? A prospective cohort study and reanalysis of the current and previous data. J Ultrasound Med. 2003;22(1):39-43.
40. Signorelli M, Tiberti A, Valseriati D, et al. Width of the fetal lateral ventricular atrium between 10 and 12 mm: a simple variation of the norm? Ultrasound Obstet Gynecol. 2004;23(1):14-8.
41. Pooh RK, Pooh KH, Nakagawa Y, et al. Transvaginal Doppler assessment of fetal intracranial venous flow. Obstet Gynecol. 1999;93(5 Pt. 1):697-701.
42. Kelly EN, Allen VM, Seaward G, et al. Mild ventriculomegaly in the fetus, natural history, associated findings and outcome of isolated mild ventriculomegaly: a literature review. Prenat Diagn. 2001;21(8):697-700.
43. Goldstein I, Copel JA, Makhoul IR. Mild cerebral ventriculomegaly in fetuses: characteristics and outcome. Fetal Diagn Ther. 2005;20(4):281-4.
44. Pilu G, Falco P, Gabrielli S, et al. The clinical significance of fetal isolated cerebral borderline ventriculomegaly: report of 31 cases and review of the literature. Ultrasound Obstet Gynecol. 1999;14(5):320-6.
45. Ouahba J, Luton D, Vuillard E, et al. Prenatal isolated mild ventriculomegaly: outcome in 167 cases.BJOG. 2006;113(9): 1072-9.
46. Martinez de Villarreal L, Perez JZ, Vazquez PA, et al. Decline of neural tube defects cases after a folic acid campaign in Nuevo Leon, Mexico. Teratology. 2002;66(5):249-56.
47. Ray JG, Meier C, Vermeulen MJ, et al. Association of neural tube defects and folic acid food fortification in Canada. Lancet. 2002;360(9350):2047-8.
48. Persad VL, Van den Hof MC, Dube JM, et al. Incidence of open neural tube defects in Nova Scotia after folic acid fortification. CMAJ. 2002;167(3):241-5.
49. Mathews TJ, Honein MA, Erickson JD. Spina bifida and anencephaly prevalence—United States, 1991-2001. MMWR Recomm Rep. 2002;51(RR-13):9-11.
50. Green NS. Folic acid supplementation and prevention of birth defects. J Nutr. 2002;132:2356S-2360S.
51. Monteagudo A, Timor-Tritsch IE. Fetal Neurosonography of congenital brain anomalies. In: Timor-Tritsch IE, Monteagudo A, Cohen HL (Eds). Ultrasonography of the Prenatal and Neonatal Brain, 2nd edition. New York: McGraw-Hill; 2001. pp. 151-258.
52. Stevenson RE, Allen WP, Pai GS, et al. Decline in prevalence of neural tube defects in a high-risk region of the United States. Pediatrics. 2000;106(4):677-83.
53. Volpe JJ. Neural tube formation and prosencephalic development. Neurology of the Newborn, 4th edition. Philadelphia: WB Saunders; 2001. pp. 3-44.
54. D'Addario V, Pinto V, Del Bianco A, et al. The clivus-supraocciput angle: a useful measurement to evaluate the shape and size of the fetal posterior fossa and to diagnose Chiari II malformation. Ultrasound Obstet Gynecol. 2001;18(2):146-9.
55. Matsunaga E, Shiota K. Holoprosencephaly in human embryos: epidemiologic studies of 150 cases. Teratology. 1977;16(3):261-72.
56. Cohen MM Jr. Perspectives on holoprosencephaly. I. Epidemiology, genetics and syndromology. Teratology. 1989;40(3):211-35.
57. Pilu G, Ambrosetto P, Sandri F, et al. Intraventricular fused fornices: a specific sign of fetal lobar holoprosencephaly. Ultrasound Obstet Gynecol. 1994;4(1):65-7.
58. Cohen MM. An update on the holoprosencephalic disorders. J Pediatr. 1982;101(5):865-9.
59. Pilu G, Porelo A, Falco P, et al. Median anomalies of the brain. In: Timor-Tritsch IE, Monteagudo A, Cohen HL (Eds). Ultrasonography of the Prenatal and Neonatal Brain, 2nd edition. New York: McGraw-Hill; 2001. pp. 259-76.
60. Goodyear PW, Bannister CM, Russell S, et al. Outcome in prenatally diagnosed fetal agenesis of the corpus callosum. Fetal Diagn Ther. 2001;16(3):139-45.
61. Taylor M, David AS. Agenesis of the corpus callosum: a United Kingdom series of 56 cases. J Neurol Neurosurg Psychiatry. 1998;64(1):131-4.
62. Schmidt-Riese U, Zieger M. Ultrasound diagnosis of isolated aplasia of the septum pellucidum. Ultraschall Med. 1994;15(6):286-92.
63. McMahon CL, Braddock SR. Septo-optic dysplasia as a manifestation of valproic acid embryopathy. Teratology. 2001;64(2):83-6.
64. Dominguez R, Aguirre Vila-Coro A, Slopis JM, et al. Brain and ocular abnormalities in infants with in utero exposure to cocaine and other street drugs. Am J Dis Child. 1991; 145(6):688-95.

65. Dattani MT, Martinez-Barbera JP, Thomas PQ, et al. Mutations in the homeobox gene HESX1/Hesx1 associated with septo-optic dysplasia in human and mouse. Nat Genet. 1998;19(2):125-33.
66. Volpe JJ. Neuronal proliferation, migration, organization and myelination. In: Volpe JJ (Ed). Neurology of the Newborn. 4th edition. USA: W.B. Saunders; 2001. pp. 45-99.
67. Kobayashi K, Nakahori Y, Miyake M, et al. An ancient retrotransposal insertion causes Fukuyama-type congenital muscular dystrophy. Nature. 1998 23;394(6691):388-92.
68. McGahan JP, Grix A, Gerscovich EO. Prenatal diagnosis of lissencephaly: Miller-Dieker syndrome. J Clin Ultrasound. 1994;22(9):560-3.
69. Greco P, Resta M, Vimercati A, et al. Antenatal diagnosis of isolated lissencephaly by ultrasound and magnetic resonance imaging. Ultrasound Obstet Gynecol. 1998;12(4):276-9.
70. Kojima K, Suzuki Y, Seki K, et al. Prenatal diagnosis of lissencephaly (type II) by ultrasound and fast magnetic resonance imaging. Fetal Diagn Ther. 2002;17(1):34-6.
71. Granata T, Farina L, Faiella A, Cardini R, et al. Familial schizencephaly associated with EMX2 mutation. Neurology. 1997;48(5):1403-6.
72. Brunelli S, Faiella A, Capra V, et al. Germline mutations in the homeobox gene EMX2 in patients with severe schizencephaly. Nat Genet. 1996;12(1):94-6.
73. Iannetti P, Nigro G, Spalice A, et al. Cytomegalovirus infection and schizencephaly: case reports. Ann Neurol. 1998;43(1):123-7.
74. Denis D, Maugey-Laulom B, Carles D, et al. Prenatal diagnosis of schizencephaly by fetal magnetic resonance imaging. Fetal Diagn Ther. 2001;16(6):354-9.
75. Osenbach RK, Menezes AH. Diagnosis and management of the Dandy-Walker malformation: 30 years of experience. Pediatr Neurosurg. 1991;18:179-85.
76. Barkovich AJ, Kjos BO, Norman D, et al. Revised classification of the posterior fossa cysts and cystlike malformations based on the results of multiplanar MR imaging. AJR. 1989;153(6):1289-300.
77. Bretelle F, Senat MV, Bernard JP, et al. First-trimester diagnosis of fetal arachnoid cyst: prenatal implication. Ultrasound Obstet Gynecol. 2002;20(4):400-2.
78. Elbers SE, Furness ME. Resolution of presumed arachnoid cyst in utero. Ultrasound Obstet Gynecol. 1999;14(5):365-6.
79. Ciricillo SF, Cogen PH, Harsh GR, et al. Intracranial arachnoid cysts in children. A comparison of the effects of fenestration and shunting. J Neurosurg. 1991;74(2):230-5.
80. Nakamura Y, Mizukawa K, Yamamoto K, et al. Endoscopic treatment for a huge neonatal prepontine-suprasellar arachnoid cyst: a case report. Pediatr Neurosurg. 2001;35(4):220-4.
81. Hollway GE, Suthers GK, Haan EA, et al. Mutation detection in FGFR2 craniosynostosis syndromes. Hum Genet. 1997;99(2):251-5.
82. Delashaw JB, Persing JA, Broaddus WC, et al. Cranial vault growth in craniosynostosis. J Neurosurg. 1989;70(2):159-65.
83. Benacerraf BR, Spiro R, Mitchell AG. Using three-dimensional ultrasound to detect craniosynostosis in a fetus with Pfeiffer syndrome. Ultrasound Obstet Gynecol. 2000;16(4):391-4.
84. Pooh RK, Nakagawa Y, Pooh KH, et al.Fetal craniofacial structure and intracranial morphology in a case of Apert syndrome. Ultrasound Obstet Gynecol. 1999;13(4):274-80.
85. Raybaud CA, Strother CM, Hald JK. Aneurysms of the vein of Galen: embryonic considerations and anatomical features relating to the pathogenesis of the malformation. Neuroradiology. 1989;31(2):109-28.
86. Hoffman HJ, Chuang S, Hendrick EB, et al. Aneurysms of the vein of Galen. Experience at The Hospital for Sick Children, Toronto. J Neurosurg. 1982;57(3):316-22.
87. Campi A, Rodesch G, Scotti G, et al. Aneurysmal malformation of the vein of Galen in three patients: clinical and radiological follow-up. Neuroradiology. 1998;40(12):816-21.
88. Friedman DM, Verma R, Madrid M, et al. Recent improvement in outcome using transcatheter embolization techniques for neonatal aneurysmal malformations of the vein of Galen. Pediatrics. 1993;91(3):583-6.
89. Kupferminc MJ, Tamura RK, Sabbagha RE, et al. Isolated choroid plexus cyst(s): an indication for amniocentesis. Am J Obstet Gynecol. 1994;171(4):1068–71.
90. Reinsch R. Choroid plexus cysts—association with trisomy: prospective review of 16,059 patients. Am J Obstet Gynecol. 1997;176(6):1381–3.
91. Snijders RJ, Shawa L, Nicolaides KH. Fetal choroid plexus cysts and trisomy 18: assessment of risk based on ultrasound findings and maternal age. Prenat Diagn. 1994;14(12):1119–27.
92. Nadel AS, Bromley BS, Frigoletto FD Jr, et al. Isolated choroid plexus cysts in the second-trimester fetus: is amniocentesis really indicated? Radiology. 1992;185(2):545–8.
93. Coco C, Jeanty P. Karyotyping of fetuses with isolated choroid plexus cysts is not justified in an Unselected Population. J Ultrasound Med. 2004;23(7):899-906.
94. Morcos CL, Platt LD, Carlson DE, et al. The isolated choroid plexus cyst. Obstet Gynecol. 1998;92(2):232–6.
95. Geary M, Patel S, Lamont R. Isolated choroid plexus cysts and association with fetal aneuploidy in an unselected population. Ultrasound Obstet Gynecol. 1997;10(3):171–3.
96. Kennedy KA, Carey JC. Choroid plexus cysts: significance and current management practices. Semin Ultrasound CT MR. 1993;14(1):23–30.
97. Lam AH, Villanueva AC. Symptomatic third ventricular choroid plexus cysts. Pediatr Radiol. 1992;22(6):413-6.
98. Parizek J, Jakubec J, Hobza V, et al. Choroid plexus cyst of the left lateral ventricle with intermittent blockage of the foramen of Monro, and initial invagination into the III ventricle in a child. Childs Nerv Syst. 1998;14(12):700-8.
99. Wakai S, Arai T, Nagai M. Congenital brain tumors. Surg Neurol. 1984;21(6):597-609.
100. Volpe JJ. Brain tumors and vein of Galen malformation. Neurology of the Newborn. 4th edition Philadelphia: WB Saunders; 2001. pp. 841-56.
101. Sherer DM, Abramowicz JS, Eggers PC, et al. Prenatal ultrasonographic diagnosis of intracranial teratoma and

massive craniomegaly with associated high-output cardiac failure. Am J Obstet Gynecol. 1993;168(1 Pt. 1):97-9.
102. Lu JH, Emons D, Kowalewski S. Connatal periventricular pseudocysts in the neonate. Pediatr Radiol. 1992;22(1):55-8.
103. Malinger G, Lev D, Ben Sira L, et al. Congenital periventricular pseudocysts: prenatal sonographic appearance and clinical implications. Ultrasound Obstet Gynecol. 2002;20(5):447-51.
104. Bats AS, Molho M, Senat MV, et al. Subependymal pseudocysts in the fetal brain: prenatal diagnosis of two cases and review of the literature. Ultrasound Obstet Gynecol. 2002;20(5):502-5.
105. Eller KM, Kuller JA. Porencephaly secondary to fetal trauma during amniocentesis. Obstet Gynecol. 1995;85(5 Pt. 2):865-7.
106. Volpe JJ. Hypoxic-Ischemic Encephalopathy: Neuropathology and pathogenesis. Neurology of the Newborn. 4th edition. Philadelphia: WB Saunders;2001. pp. 296-330.
107. Meizner I, Elchalal U. Prenatal sonographic diagnosis of anterior fossa porencephaly. J Clin Ultrasound. 1996;24(2): 96-9.
108. de Laveaucoupet J, Audibert F, Guis F, et al. Fetal magnetic resonance imaging (MRI) of ischemic brain injury. Prenat Diagn. 2001;21(9):729-36.
109. Scher MS, Belfar H, Martin J, et al. Destructive brain lesions of presumed fetal onset: antepartum causes of cerebral palsy. Pediatrics. 1991;88(5):898-906.
110. Stevenson DA, Hart BL, Clericuzio CL. Hydranencephaly in an infant with vascular malformations. Am J Med Genet. 2001;104(4):295-8.
111. Lam YH, Tang MH. Serial sonographic features of a fetus with hydranencephaly from 11 weeks to term. Ultrasound Obstet Gynecol. 2000;16(1):77-9.
112. Sherer DM, Anyaegbunam A, Onyeije C. Antepartum fetal intracranial hemorrhage, predisposing factors and prenatal sonography: a review. Am J Perinatol. 1998;15(7): 431-41.
113. Hardart GE, Fackler JC. Predictors of intracranial hemorrhage during neonatal extracorporeal membrane oxygenation. J Pediatr. 1999;134(2):156-9.
114. Rezaie P, Dean A. Periventricular leukomalacia, inflammation and white matter lesions within the developing nervous system. Neuropathology. 2002;22(3):106-32.
115. Persutte WH. Microcephaly—no small deal. Ultrasound Obstet.Gynecol. 1998;11(5):317-8.
116. Schwarzler P, Homfray T, Bernard JP, et al. Late onset microcephaly: failure of prenatal diagnosis. Ultrasound obstet. Gynecol. 2003;22(6):640-2.

CHAPTER 17

Pathology of the Fetal Neck

Radu Vladareanu, Mona Zvanca, Cristian Andrei

INTRODUCTION

Embryological Development

The development of the fetal neck starts between the fourth and the fifth week with the presence of four pairs of branchial arches. These represent bars of mesenchymal tissue that are separated by four paired clefts and pouches. At the end of the fourth week, the stomodeum (rudimentary mouth) is formed at the center of the face and is surrounded by the first pair of branchial arches.

The first pharyngeal pouch gives rise to the eustachian tube, middle ear and mastoid cells, as part of the temporal bone, the maxilla and the mandible, including the premaxilla and zygoma.

The second pouch forms the supratonsillar fossa.

The third pouch develops into the thymus gland and upper parathyroid glands.

The fourth pouch gives rise to the lower parathyroid gland and part of the thyroid gland.

Each arch contains neural crest cells, which contribute to the skeletal development. The mesoderm of the arches results in the musculature of the face and neck.

ABNORMAL DEVELOPMENT OF FETAL NECK

Hygroma

The latin word *hygroma* is translated as moist tumor. Cystic hygroma, as it is often called, represents not a tumor, but an anomaly of the lymphatic drainage into the venous system, which leads to the accumulation of lymph in the jugular lymphatic sacs of the cervical region. The anomaly is visible from the first trimester and it represents the end of the spectrum of the increased nuchal translucency. Cystic hygroma was divided into nonseptated (simple) and septated, with a presumably worse prognosis in the latter case.[1] However, with the improving resolution and the increasing quality of the image offered by the advance of the ultrasound machines, it has become clear that all nuchal translucencies have visible septations.[2] Therefore, this classification has been abandoned.

Abnormal lymphatic development in the fetal neck could lead to distension of the jugular venous sacs, an accumulation of fluid in the nuchal region and retrograde increase in venous pressure. This hypothesis is supported by the observation that reversed or absent ductus venosus flow during atrial contraction is observed in these fetuses.[3] Eventual recanalization or formation of collaterals may explain the transient nature of abnormal ductus venosus waveforms and nuchal edema.

Enlarged nuchal translucency is also an important marker for congenital heart disease. Although nuchal edema in fetuses with heart defects was initially thought to be related to impaired atrial contraction, reduced myocardial compliance or cardiac failure, studies have not supported these mechanisms.[4] No differences in intracardiac flow velocities in normal fetuses and those with enlarged nuchal translucency have been identified.[5] Changes in the carotid artery, jugular vein

or ductus venosus Doppler velocimetry are also not significantly related to nuchal translucency.[6] Pericardial, pleural and peritoneal fluid (ascites) are frequent findings in fetuses with cardiac decompensation, but are rare in fetuses with enlarged nuchal translucency.

Enlarged nuchal translucency is often associated with aneuploidy, particularly trisomy 21 and Turner syndrome (Monosomy X).[7] The pathophysiology is different for the two aneuploidies. In trisomy 21, the collagen content of the dermis is abnormal; its hydrophilic properties may lead to the accumulation of subcutaneous fluid. By comparison, fetuses with Turner syndrome often have lymphatic dysplasia. These fetuses are also at risk for narrowing of the aortic isthmus and widening of the ascending aorta, which may lead to overperfusion of the head and neck, thus contributing to the development of subcutaneous edema. Nuchal translucency may regress, if these connections are established later in gestation.

Incidence

Even though it cannot be considered pathology in itself, cystic hygroma is the most common cervical mass detected antenatally. The incidence varies with gestational age. In the first trimester, the overall prevalence of cystic hygromas is about 1 in 100 fetuses.[1]

Diagnosis

Cystic hygromas consist of large single or multilocular fluid-filled cavities, which are usually, easily identified during first-trimester ultrasound examination. They tend to be largest in the nuchal region, but may extend along the entire length of the fetus. Multiple internal septae or trabeculae may be detected when imaging a cystic hygroma in multiple planes **(Figs 17.1A to E)**. The distended jugular lymph sacs can sometimes be visualized on either side of the fetal neck.

With improvements in first trimester imaging, the distinction between simple cystic hygroma and increased nuchal translucency has become less clear. Possible distinguishing features of cystic hygromas are that they tend to be larger, extend along the entire length of the fetus and are more likely to contain multiple septae, whereas nuchal translucency is often confined to the nuchal region between the occiput, and upper spine. Regardless of the etiology, size appears to be the significant determinant of outcome for all nuchal fluid collections, irrespective of whether there are internal septations or the fluid envelops the entire length of the fetus.[7]

Associated Anomalies

About 50% of first trimester septated cystic hygromas occur in fetuses with trisomies, most commonly

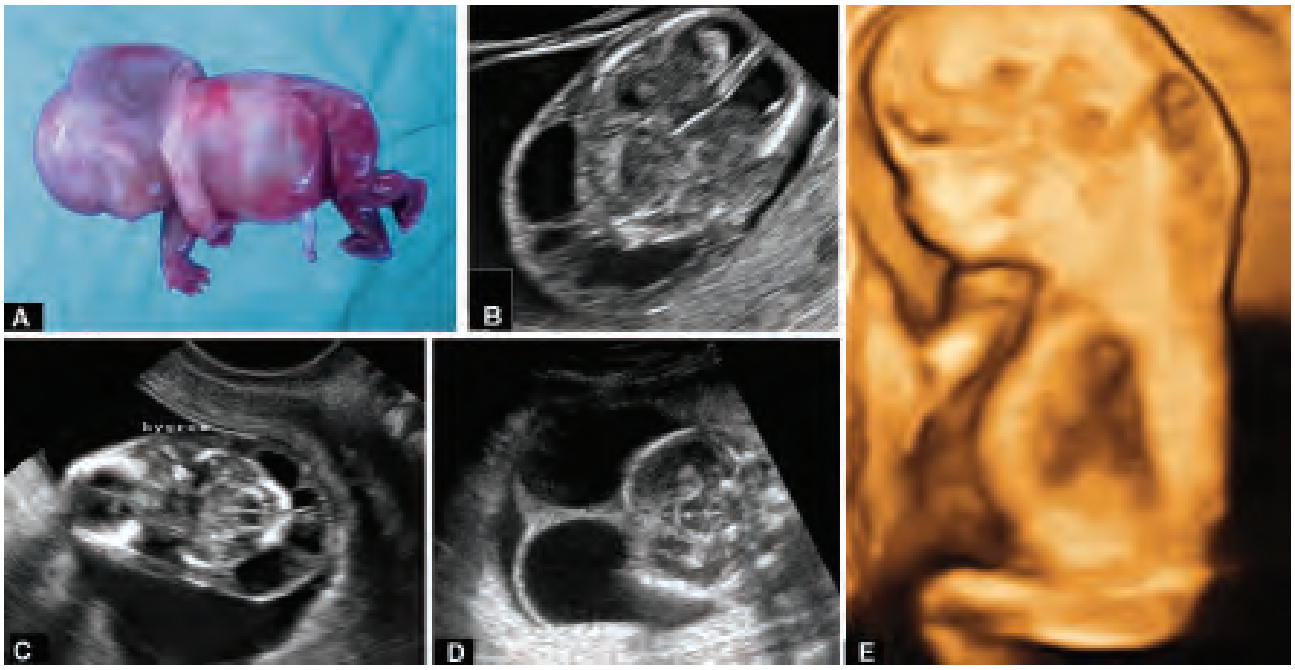

Figures 17.1A to E: Cystic hygroma in a 16 weeks fetus with Turner syndrome. (A) Postabortum specimen; (B to D) Transverse section showing septations; (E) 3D rendering

trisomy 21. First-trimester cystic hygromas are often associated with trisomies, whereas second-trimester cystic hygromas are often associated with Monosomy X.[8-9]

About one-third of euploid fetuses with first-trimester septated cystic hygromas have major structural anomalies.[9] In contrast, structural anomalies are detected in only 4–10% of euploid fetuses with enlarged nuchal translucency.[10] Associated malformations include cardiac defects, diaphragmatic hernia, renal anomalies, body stalk disruption and abdominal wall defects.

A significant discordance between nuchal translucency measurements in monochorionic twins is also predictive of twin-to-twin transfusion. About 25% of monochorionic twins will have an intertwined discordance in nuchal translucency measurement of greater than 20%; this subset of twins is more likely to develop twin-to-twin transfusion syndrome and experience early fetal demise.[11]

Differential Diagnosis

Other defects in the differential diagnosis of cystic hygroma include neural tube defects, such as a posterior encephalocele or cervical meningocele and cystic teratoma or hemangioma. These diagnoses can usually be excluded on high resolution transvaginal ultrasonography if an intact skull and spine are visualized, no solid component is seen in the cystic space, color-flow mapping shows a limited vascular supply, and internal septae are identified in the cystic mass.

Prognosis

Normal pediatric outcomes occur in 15–30% of fetuses with first-trimester cystic hygromas, but the prognosis for a specific fetus depends upon the presence or absence of associated findings.

In the absence of aneuploidy or structural anomalies, the size of the first trimester cystic hygroma appears to be the most important determinant of outcome. The larger the measurements of the nuchal translucency, the higher the risk of associated structural anomalies or intrauterine fetal demise. Even with a normal karyotype the possibility of an underlying rare genetic disorder should always be considered and a detailed anatomical survey should be carried out, including a specialist echocardiography.

Some studies have reported an increased prevalence (up to 8.7%) of neurodevelopmental delay in children with a fetal history of increased nuchal translucency; however others have found no excess risk of developmental delay in children with normal karyotype and no congenital malformations in whom first-trimester nuchal thickening is resolved.[12] Additional standardized pediatric evaluations and long-term neurodevelopmental follow-up studies are needed to better define these risks. Some genetic syndromes and conditions associated with developmental delay do not have any features amenable to prenatal diagnosis by ultrasound.

Management

Although the clinical implications may differ, the initial management of a pregnancy with a cystic hygroma and increased nuchal translucency is the same, which are as follows:

- Fetal karyotyping
- Comprehensive fetal anatomic survey
- Fetal echocardiography
- Serial assessment of fetal status.

Considering that cystic hygroma is a large nuchal translucency and the risk for associated chromosomal anomalies is about 50%, it is reasonable to offer invasive testing in all the cases.

Early fetal anatomic evaluations can be performed using a combined approach, starting with an abdominal survey and assessing details through high-resolution transvaginal ultrasound; experienced ultrasonographers can detect many major malformations in the first trimester.

Fetal echocardiography may be attempted as early as the first trimester. According to the quality of image and the ultrasound findings, fetal heart may be reassessed at 14, 16, 18 or 20 weeks.

Fetal Goiter

Enlargement of fetal thyroid gland is accompanied by increased or decreased level of thyroid hormones (hyper or hypothyroidism), but the thyroid function may also be normal. The incidence of fetal goiter is better quantified for congenital hypothyroidism, which occurs in 1 out of 2,000–4,000 births, according to different statistics.[13]

Fetal production of thyroid hormones starts at 11–12 weeks, but the function of the hypothalamic-pituitary-thyroid system is under maternal influence and it relies exclusively on the maternal supply of iodine, which is transferred into fetal circulation via a placental sodium-iodide (Na^+/I^-) symporter. A maternal iodine deficit will cause fetal goiter, but an iodine excessive diet may have the same effect. Fetal thyroid-stimulating hormone (TSH) receptors become responsive to TSH and TSH antibodies at 20 weeks.

TABLE 17.1

Causes of fetal goiter	
Inborn errors of thyroid hormone production	*Dyshormonogenesis*
Transplacental passage of maternal ant bodies	TSH-receptor blocking antibodies TSH-receptor stimulating antibodies
Maternal ingestion of anti-thyroid drugs and other goitrogens	Propylthiouracil Methimazole or carbimazole Iodine and iodine-containing drugs
Activating mutations of the TSH receptor	Congenital nonimmune hyperthyroidism
Activating mutations of the G protein alpha subunit	McCune-A bright syndrome
Thyroid hemiagenesis	
Thyroid tumors	

Therefore, fetal thyroid dysfunction can be detected only after this stage. Whereas maternal (thyroxine) T4 usually crosses the placenta in only minimal (but crucial for fetal development) amounts and TSH does not cross the placenta at all, maternal TSH receptor antibodies freely cross the placenta and may stimulate or, more rarely, inhibit fetal thyroid function. A normal fetal level of thyroid hormones is essential in the development of the brain and fetal hypothyroidism is the most common treatable cause of mental retardation. The IQ level tends to be inversely correlated to the age of the diagnosis of hypothyroidism. Fetal hyperthyroidism is equally dangerous, exposing the fetus to the risk of *in utero* death due to thyrotoxicosis or to long-term sequelae of an impaired thyroid function.

The physiopathology of fetal and neonatal goiter is complex. In 85% of cases, it is sporadic and in the remaining 15%, it has hereditary causes **(Table 17.1)**.

Inborn Errors of Thyroid Hormone Production

Genetic defects in each step of thyroid hormone production (dyshormonogenesis) have been described. These defects are inherited as autosomal recessive traits. All result in varying degrees of hypothyroidism, and may be detected by newborn screening.[14]

The defects include the following:

- A defect in iodine transport because of a mutation in the Na^+/I^- symporter gene.[15]
- Iodine organification and coupling defects because of deficiency in the quantity or activity of thyroid peroxidase or in hydrogen peroxide generation.
- Pendred's syndrome is characterized by both goiter and sensorineural deafness (not caused by hypothyroidism). These children have a mutation in a transport protein (pendrin) on chromosome 7q, which transports iodide into the exocytotic vesicles in which thyroid hormone is synthesized. This chloride-iodide transport protein functions in both the thyroid gland and inner ear.[16]
- Defects in thyroglobulin biosynthesis in which thyroglobulin production is decreased or the molecule is truncated or has amino-acid substitutions within it. The result is decreased formation of T4 and triiodothyronine (T3) within the thyroglobulin.[17]
- Defects in iodotyrosine deiodinase result from mutations in the iodotyrosine dehalogenase 1 (DEHAL1) gene, so that the iodine contained in the iodotyrosine residues of thyroglobulin is lost.

These disorders account for approximately 10–15% of cases of congenital hypothyroidism. Elucidation of specific defects requires thyroid radionuclide imaging or ultrasonography, measurements of serum thyroglobulin and iodothyronines, and gene analysis.

Transplacental Passage of Maternal Thyroid-reactive Antibodies

Women with chronic autoimmune thyroiditis or Graves' disease may produce antibodies that cross the placenta, resulting in fetal and neonatal goiter and thyroid dysfunction, depending upon the type of antibody.

TSH-receptor blocking antibodies: Transplacental passage of TSH-receptor antibodies that block the action of TSH can cause fetal hypothyroidism, which is occasionally accompanied by goiter. These antibodies are detected in approximately 1:100,000 newborn infants. This disorder is confirmed by laboratory testing showing elevated thyrotropin-binding inhibitory immunoglobulin (TBII). The hypothyroidism and goiter in these infants are transient, typically resolving in 3–6 months, as the transplacentally acquired antibodies are cleared.[18]

TSH-receptor stimulating antibodies: Transplacental passage of TSH-receptor antibodies that mimic the action of TSH cause fetal and neonatal Graves' hyperthyroidism and goiter. The mother may have had hyperthyroidism during the pregnancy, or she may have had it in the past and have been treated by thyroidectomy or radioactive iodine.

Neonatal Graves' disease occurs in approximately 1:25,000 neonates. Laboratory testing showing elevated thyroid stimulating immunoglobulin (TSI) in mother or neonate will confirm Graves' disease. Neonatal Graves' hyperthyroidism and goiter resolve in 3–6 months as the antibodies are cleared.

Maternal Ingestion of Antithyroid Drugs and Other Goitrogens

The antithyroid drugs propylthiouracil, methimazole and carbimazole all cross the placenta and can cause fetal hypothyroidism and goiter. Other compounds that can cross the placenta and cause fetal hypothyroidism and goiter are iodine-rich drugs such as expectorants, amiodarone and skin disinfectants.

Activating Mutations of the TSH-receptor (Congenital Nonimmune Hyperthyroidism)

Germline mutations of the TSH-receptor gene that result in constitutive activation of the receptor are a rare cause of diffuse goiter and hyperthyroidism, which may be present at birth or first become evident, years or even decades later.[19] These mutations are inherited as autosomal dominant traits; as a result, there may be a family history of hyperthyroidism and goiter.

McCune-Albright Syndrome

Somatic mutations in the alpha subunit of the guanine nucleotide-binding protein (G protein) are present in the thyroid gland in infants and children with the McCune-Albright syndrome.[20] They are activating mutations and therefore result in thyroid hyperplasia or formation of nodules and, ultimately, in toxic nodular goiters. Other features of the syndrome, such as café-au-lait skin pigmentation, precocious puberty or polyostotic fibrous dysplasia, are usually present and provide clues to the underlying diagnosis. The hyperthyroidism is permanent and some form of thyroid ablation is indicated.

Thyroid Hemiagenesis

Thyroid hemiagenesis may cause unilateral goiter in neonates because of compensatory hypertrophy of the contralateral lobe.

Diagnosis

Detection of the fetal goiter is facilitated by the associated maternal history, present in most of the cases. Even though it is not part of the routine second-trimester examination, there are nomograms for the size of the thyroid gland starting with 16 weeks.[21,22] This is particularly useful in fetuses with mild enlargement of the gland. Both the volume and the circumference of the gland have proven to have good correlations with the gestational age and biparietal diameter and there is a constant ratio between the thyroid volume and the estimated fetal weight throughout the gestation (0.163 +/– 0.079 cm^3/kg).[22] Assessment of the thyroid gland size and structure should be done using both sagittal and transverse sections of the fetal neck **(Figs 17.2A to C)**.

By definition, goiter means enlargement of the thyroid gland above the 95th centile of the normal range, irrespective of the considered parameter, volume or linear size. The sonographic appearance is solid, hypoechoic, but it may also have a cystic component. Previous studies have described an association between the pattern of the blood flow inside the thyroid gland and the level of the fetal thyroid hormones.[23,24] By using color-flow mapping at a velocity of 13 cm/sec the authors described that a Doppler signal that is detected throughout the entire gland is suggestive of fetal hyperthyroidism, whereas a blood flow confined to the periphery is indicative of fetal hypothyroidism. There are reports of glandular blood flow quantification using the vascularization indices and the vocal software.[25]

In the situation of a very large fetal goiter, the neck is usually hyperextended and it may be associated polyhydramnios. In such cases, there should be considered the possibility of airway obstruction with serious perinatal consequences.

Functional assessment of the fetal thyroid gland may be done through invasive methods, either amniocentesis or cord blood sampling. Indirect information about the

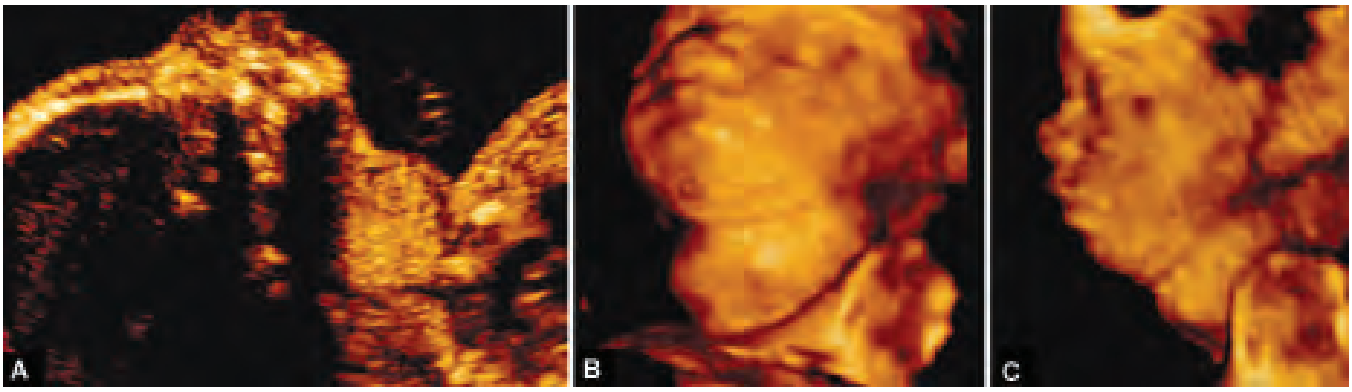

Figures 17.2A to C: Twenty-eight weeks fetus with goiter. (A) Fetal profile compared to; (B and C) 3D surface rendering mode show a clearly visible goiter

status of the fetal metabolism may be given by the bone maturation and the fetal heart rate and heart function. The distal femoral ossification center is undetectable before 28 weeks; it is dot-size at 32 weeks, smaller than 3 mm at 33 weeks. Accelerated bone maturation was defined as the presence of the distal femoral ossification center before 31 weeks of gestation, and delayed bone maturation was defined as the absence of the center after 33 weeks of gestation.[26] Accelerated bone maturation is associated with an excessive amount of thyroid hormones.

Reliable and objective data about fetal thyroid function involve an invasive testing. Measurement of the TSH, free T3 and free T4 should be performed only using cord blood, as there is a poor correlation between the amniotic levels and the fetal metabolic status. The amniotic fluid may be, however, a good transport for therapeutic drugs.[27]

Differential Diagnosis

The goiter should be distinguished from other cervical pathologies as follows:

- Cervical teratoma: Rapidly growing tumor, mixed structure, solid-cystic, no association with maternal thyroid dysfunction
- Hemangioma/lymphangioma: Usually lateral mass of the neck, with a dominant cystic component.

Associated Anomalies

Congenital hypothyroidism appears to be associated with an increased risk of additional congenital malformations affecting the heart, kidneys, urinary tract, gastrointestinal and skeletal systems.[28] Infants with congenital hypothyroidism and cleft palate may have a TTF-2 (FOXE1) gene mutation.[29] Infants with persistent neurologic problems, including ataxia, are suspect for a NKX2-1 gene mutation.[30]

Management

Fetal hypothyroidism: The following instructions can be useful in the prevention, diagnosis and management of fetal hypothyroidism.[31]

- Adequate iodine intake should be ensured for all pregnant women (250 gm daily)
- For women with a personal or family history of thyroid disease, measure plasma TSH and free T4 levels before, at the beginning and during pregnancy
- On ultrasonography between 22 and 32 gestational weeks, measure fetal thyroid diameter and circumference: if above the 95th centile for gestational week, consider fetal thyroid disorder
- If thyroxine treatment is given to a pregnant woman, ensure adequate increase in dose throughout pregnancy
- If fetal goiter is documented, consider cordocentesis and fetal blood T4 and TSH level measurement, and intra-amniotic thyroxine injections, if severe hypothyroidism is diagnosed.

Fetal hyperthyroidism: It may be treated safely and effectively by means of antithyroid drugs administered to the mother.[32] The therapeutic level in fetal blood may induce maternal hypothyroidism. This is easily corrected by the addition of thyroxine. In pregnant women, propylthiouracil is preferred to methimazole or carbimazole because the latter has been associated with aplasia cutis congenita and other malformations.[33]

In pregnant women who are taking antithyroid therapy and/or who have positive results for TSI, monthly ultrasound imaging might be justified after 20 weeks of gestation to monitor whether evidence of thyroid dysfunction, including goiter, is developing in the fetus.

Teratoma/Sarcoma

Teratomas are large mixed tumors arising from the neck region. They are very rare, accounting for less than 0.1% of all neonatal neoplasms.[34] The incidence varies from 1 in 20,000 to 1 in 40,000 live births, according to different studies.[35] Even though they are benign tumors, the associated mortality is, however, high because of immediate neonatal respiratory distress due to tracheal compression or compression of other critical structures of the neck. Some of these tumors may be malignant or may develop later into adult life.

Teratomas are cystic, semicystic or solid tumors. They develop from all three germ cell layers. Histologically, most of these tumors are composed of neural tissue (68%). Thyroid tissue may be found inside the tumor mass or as a pseudocapsule. Malignant characteristics, invasive growth and metastatic spread are found more often in tumors developing in teenagers and adults.[36]

They may develop in the anterior or posterior triangle of the neck and they were subclassified into thyroid or cervical teratomas. This classification has no clinical significance and was abandoned. In almost all anteriorly located teratomas, a close relationship with the thyroid gland was observed.[37]

Diagnosis

Cervical teratomas are detected antenatally in most cases, as they are large sized tumors. When located in

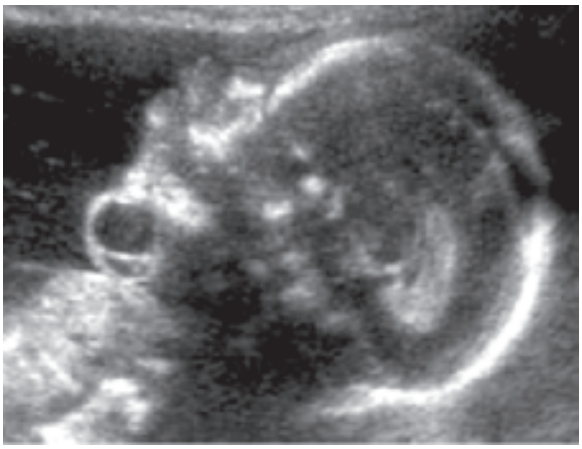

Figure 17.3: Cervical teratoma located in the anterolateral region, with a mainly cystic component. The extended position of the neck is to be noted

the anterior region they hyperextend in the fetal neck. Like most tumors of this type, due to the important blood supply, they have a fast growth rate. The mixed, semicystic structure is clearly visible on the antenatal ultrasound and makes the diagnosis easy **(Fig. 17.3)**. Sometimes calcifications may be seen inside the tumor mass, which suggest the presence of high-density tissue such as cartilage. The diagnosis may be as early as the first trimester.[38]

Associated Anomalies

Polyhydramnios may be associated due to esophageal obstruction and interference with the fetal deglutition. Deviation of the larynx and trachea results in compression of the esophagus and inhibits fetal swallowing. Hypoglossal nerve compression by the expanding tumor mass may add to the deglutition problem.

Pulmonary insufficiency may develop due to compression of a very large tumor on the thorax.

Chondromalacia is also reported as a result of the mass effect.

Differential Diagnosis

Teratomas should be distinguished from other cervical masses as:

- Hemangiomas
- Lymphangiomas
- Goiter.

The sonographic and developmental characteristics of a teratoma make the distinction very easy **(Table 17.2)**.

TABLE 17.2
Differential diagnosis of cervical teratoma

Tumor	*Characteristics*
Hemangioma	Homogeneously echogenic or mixed cystic and solid appearance with typical blood flow distribution
Goiter	Bilobed anterior neck mass adjacent to the midline, solid-mixed-cystic-l ke appearance
Teratoma	Well-defined, broad-based mass of the antero-lateral portion of the neck, hyperextension of the neck, partially cystic, partially solid with echogenic reflections, polyhydramnios

Prognosis

The main factors that influence the immediate fetal prognosis are as follows:

- Preterm birth, due to polyhydramnios or iatrogenic
- Perinatal death, due to failure in establishing airway at birth.

Even when anticipated by the ultrasound, the procedure may be extremely difficult, as there is an important degree of tracheal deviation. The size of the teratoma is not necessarily predictive of this complication, as small tumors may be associated with an important alteration of the upper airway anatomy.

Management

The anterior localization and the semisolid appearance of these tumors can provoke an upper airway obstruction, which is the most urgent neonatal emergency, requiring immediate intervention. When anticipated by ultrasound, the necessary equipment can be mobilized at the time of the cesarean section to deal with these respiratory difficulties.

In small tumors, emergency tracheotomy may secure adequate ventilatory support.

Recurrence risk is absent. These tumors are strictly sporadic.

In **Figures 17.4A to C**, the authors show a recent case of a large cervical teratoma (ultrasound and postnatal image). The baby died because the maternity unit was not aware of the diagnosis prior to delivery.

Hemangioma/Lymphangioma

Hemangiomas and lymphangiomas are tumors derived from the endothelial tissue of blood vessels or lymphatic vessels. They may develop anywhere in the body, but in the antenatal life and the first years they show a predisposition for the head, neck and axillary area. Even

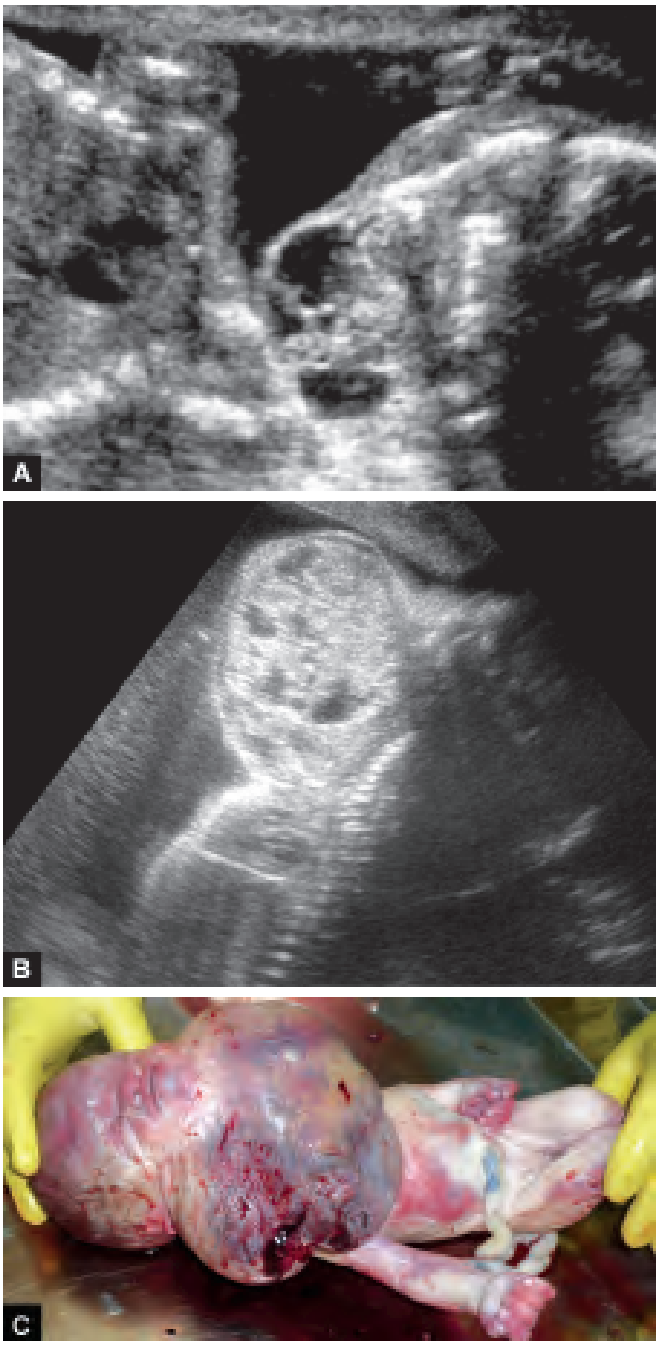

Figures 17.4A to C: Large teratoma. Ultrasound with hyperextended body and immediate postnatal aspect
Courtesy Dr Cringu Lonescu

though hemangiomas and lymphangiomas originate from different vascular structures, they have common pathological and sonographic features, which explain why they are discussed together.

These vascular tumors are the most common tumors in the first three years of life, most of them (90%) being present at birth or in the first days/months and some of them are diagnosed antenatally.[39]

They affect up to 5% of infants, with a threefold higher rate for girls. It is difficult to estimate the true incidence of hemangiomas and the reported numbers vary from 15 to 10%.[40]

The incidence of hemangiomas is increased in preterm infants. The most significant risk factor appears to be low-birth-weight.[41]

Multiple hemangiomas more commonly occur in products of multiple gestations.[41]

Pathology

Hemangiomas are the result of vascular endothelial proliferation. They have a predilection for the head and neck, although they can occur anywhere in the skin, mucous membranes, or internal organs. Hemangiomas range in size from a few millimeters to many centimeters in diameter. They may be superficial, deep or combined (compound hemangiomas).

Superficial hemangiomas present as a red papule, nodule, or plaque elevated above clinically normal skin. They are not detected antenatally. These are also called strawberry or capillary hemangiomas.

Cavernous hemangiomas are deep, subcutaneous tumors and their structure consists of vascular lakes, blood collections with low velocity flow. The hemangioma is typically a raised, skin-colored nodule, which often has a bluish hue with or without central telangiectatic patch. The name "cavernous" hemangiomas, is erroneously used to describe venous malformations and is thus best avoided.

Hemangiomas characteristically undergo a growth (proliferative) phase that is generally rapid for the first several months. Slow proliferation can continue for the first 6–12 months.

The proliferative phase is followed by a spontaneous involution phase that typically begins after one year and lasts a variable number of years. Superficial hemangiomas typically enter the involution stage earlier than deep hemangiomas.

Lymphangiomas originated from the lymphatic vessels and develop in the axilla and neck. As for cavernous hemangiomas, it is difficult to say, if lymphangiomas are a lymphatic tumor or, more likely, a lymphatic drainage malformation.

Diagnosis

Both hemangiomas and lymphangiomas may be large size tumors, which makes the prenatal diagnosis easy. There are reports of first-trimester detection.[42]

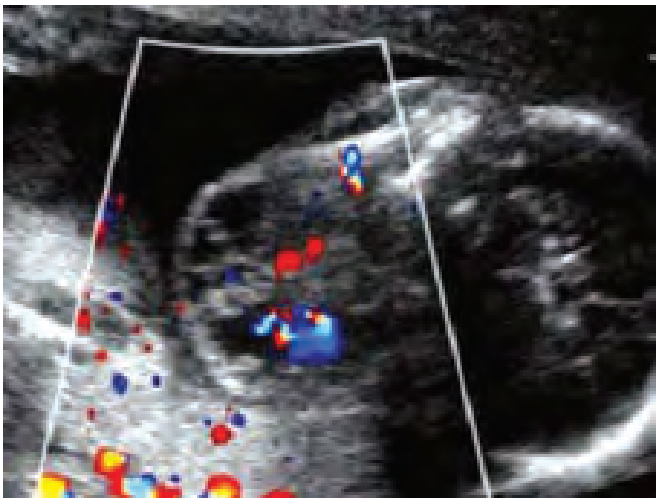

Figure 17.5: Cervical hemangioma: a mixed solid-cystic tumor with marked vascularization

Hemangiomas are solid or mixed solid and cystic tumors, with important vascularization **(Fig. 17.5)**. Due to the low velocity of the blood flow, power Doppler may be more useful than color Doppler. Even though the lesion is benign it may be fatal in cases with large tumors where congestive heart failure and hydrops may occur.

Associated Anomalies

The examiner has to be aware that in many cases the lesions are multiple. The presence of superficial hemangiomas may herald associated, visceral tumors. Multifocal hepatic hemangiomas most commonly occur in the presence of multiple skin hemangiomas and are probably most often asymptomatic. Rarely, multifocal hepatic hemangiomas can have large vessel shunts that result in heart failure.

The Klippel-Trenaunay-Weber syndrome is an association between vascular anomalies, such as lymphangiomas and limb hypertrophy.

Posterior fossa malformations, Hemangiomas, Arterial anomalies, Coarctation of the aorta and other cardiac defects and Eye abnormalities (PHACE) syndrome (MIM 606519) is defined by the presence of a large, segmental hemangioma, usually on the face, in association with one or more congenital malformations, most commonly structural or cerebrovascular anomalies of the brain.

Management

Involution is part of the natural history and only a limited number of cases will require further intervention. The involution rate is about 10% per year, so that about 90% of the hemagiomas will have disappeared by the age of 9 years.[43] The parents have to be aware, though, that complete involution may be associated with lesions of the overlying skin such as scarring, atrophy, redundant skin, discoloration and telangiectasias.

Medical treatment consists of corticosteroids and interferon.

Persisting hemangiomas and lymphangiomas may require laser ablation or surgical removal.

Recurrence

Although most hemangiomas occur sporadically, familial transmission in an autosomal dominant fashion has been reported.

Cervical Chondrocutaneous Branchial Remnants

Branchial remnants are developmental anomalies of the four pairs of branchial arches. These remnants may be cysts, fistula and skin tags, chondrocutaneous vestiges. Cervical chondrocutaneous branchial remnants are usually embedded in the anterior border of the sternocleidomastoid muscle and appear as skin tags. They probably originate from the second branchial arch.

Diagnosis

Depending on the size of the lesion, the brachial remnants may be visible antenatally. Skin tags are detected by ultrasound, as they are echogenic and elongated.

A clinical study following 20 children over a period of 13 years[44] found that these lesions are more commonly found on the left side than the right and in boys rather than the girls.

Associated Anomalies

Associated anomalies are common, found in 70–80% of the cases.

They include anomalies of the auditory, respiratory, gastrointestinal, genitourinary, cardiovascular, musculoskeletal and visual systems. Therefore, it is essential that the detection of a skin tag, especially when located in the cervical region, should prompt for a detailed anatomical survey.

Differential Diagnosis

- Branchial cyst/fistula
- Thyroglossal cyst/fistula
- Hemangioma
- Dermoid tumor
- Goldenhar syndrome.

Regarding the occipital encephalocele and iniencephaly, even though they represent major anomalies that affect the cervical and cephalic area, from a developmental point of view they are part of the neural tube defects spectrum and should be considered as such especially from a prognosis point of view.

REFERENCES

1. Malone FD, Ball RH, Nyberg DA, et al. First-trimester septated cystic hygroma. Prevalence, natural history, and pediatric outcomes. Obstet Gynecol. 2005;106(2):288-94.
2. Molina FS, Avgidou K, Kagan KO, et al. Cystic hygromas, nuchal edema, and nuchal translucency at 11-14 weeks of gestation. Obstet Gynecol. 2006;107(3):678-83.
3. Haak MC, Twisk JW, Bartelings MM, et al. Ductus venosus flow velocities in relation to the cardiac defects in first-trimester fetuses with enlarged nuchal translucency. Am J Obstet Gynecol. 2003;188(3):727-33.
4. Simpson JM, Sharland GK. Nuchal translucency and congenital heart defects: heart failure or not? Ultrasound Obstet Gynecol. 2000;16(1):30-6.
5. Haak MC, Twisk JW, Bartelings MM, et al. First-trimester fetuses with increased nuchal translucency do not show altered intracardiac flow velocities. Ultrasound Obstet Gynecol. 2005;25(3):246-52.
6. Martinez JM, Echevarria M, Gomez O, et al. Jugular vein and carotid artery blood flow in fetuses with increased nuchal translucency at 10-14 weeks' gestation. Ultrasound Obstet Gynecol. 2003;22(5):464-9.
7. Nicolaides KH. First-trimester screening for chromosomal abnormalities. Semin Perinatol. 2005;29(4):190-4.
8. Malone FD, Ball RH, Nyberg DA, et al. First-trimester septated cystic hygroma. Prevalence, natural history, and pediatric outcomes. Obstet Gynecol. 2005;106(2):288-94.
9. Bronshtein M, Zimmer EZ, Blazer S. A characteristic cluster of fetal sonographic markers that are predictive of fetal Turner syndrome in early pregnancy. Am J Obstet Gynecol. 2003;188(4):1016-20.
10. Graesslin O, Derniaux E, Alanio E, et al. Characteristics and outcome of fetal cystic hygroma diagnosed in the first trimester. Acta Obstet Gynecol Scand. 2007;86(12):1442-6.
11. Mangione R, Guyon F, Taine L, et al. Pregnancy outcome and prognosis in fetuses with increased first-trimester nuchal translucency. Fetal Diagn Ther. 2001; 16(6):360-3.
12. Kagan KO, Gazzoni A, Sepulveda-Gonzalez G, et al. Discordance in nuchal translucency thickness in the prediction of severe twin-to-twin transfusion syndrome. Ultrasound Obstet Gynecol. 2007;29(5):527-32.
13. Senat MV, Bussieres L, Couderc S, et al. Long-term outcome of children born after a first-trimester measurement of nuchal translucency at the 99th percentile or greater with normal karyotype: a prospective study. Am J Obstet Gynecol. 2007;196(1):53e1-6.
14. Mehta PS, Mehta SJ, Vorherr H. Congenital iodide goiter and hypothyroidism: a review. Obstet Gyncol Surv. 1983;38:237-47.
15. Muir A, Daneman D, Daneman A, et al. TI. Thyroid scanning, ultrasound, and serum thyroglobulin in determining the origin of congenital hypothyroidism. Am J Dis Child. 1988;142:214-6.
16. Pohlenz J, Rosenthal IM, Weiss RE, et al. Congenital hypothyroidism due to mutations in the sodium/iodide symporter. Identification of a nonsense mutation producing a downstream cryptic 3' splice site. J Clin Invest. 1998;101:1028-35.
17. Everett LA, Morsli H, Wu DK, et al. Expression pattern of the mouse ortholog of the Pendred's syndrome gene (Pds) suggests a key role for pendrin in the inner ear. Proc Natl Acad Sci USA. 1999;96:9727–32.
18. van de Graaf SA, Ris-Stalpers C, Veenboer GJ, et al. A premature stopcodon in thyroglobulin messenger RNA results in familial goiter and moderate hypothyroidism. J Clin Endocrinol Metab. 1999;84:2537-42.
19. Brown RS, Bellisario RL, Mitchell E, et al. Detection of thyrotropin binding inhibitory activity in neonatal blood spots. J Clin Endocrinol Metab. 1993;77:1005-8.
20. Paschke R, Ludgate M. The thyrotropin receptor in thyroid diseases. N Engl J Med. 1997;337(23):1675-81.
21. Mastorakos G, Mitsiades NS, Doufas AG, et al. Hyperthyroidism in McCune-Albright syndrome with a review of thyroid abnormalities sixty years after the first report. Thyroid. 1997;7:433-9.
22. Ranzini AC, Ananth CV, Smulian JC, et al. Ultrasonography of the fetal thyroid: nomograms based on biparietal diameter and gestational age. J Ultrasound Med. 2001;20:613-7.
23. Ho SS, Metreweli C. Normal fetal thyroid volume. Ultrasound Obstet Gynecol. 1998;II:118-22.
24. Luton D, Fried D, Sibony O, et al. Assessment of fetal thyroid function by colored Doppler echography. Fetal Diagn Ther. 1997;12(1):24-7.
25. Polak M, Le Gac I, Vuillard E, et al. Fetal and neonatal thyroid function in relation to maternal Graves' disease. Best Pract Res Clin Endocrinol Metab. 2004;18:289-302.
26. Marín RC, Bello-Muñoz JC, Martínez GV, et al. Use of 3-Dimensional Sonography for Prenatal Evaluation and Follow-up of Fetal Goitrous Hypothyroidism. J Ultrasound Med. 2010;29:1339-43.
27. Goldstein I, Lockwood C, Belanger K, et al. Ultrasonographic assessment of gestational age with the distal femoral and proximal tibial ossification centers in the third trimester. Am J Obstet Gynecol. 1988;158:127-30.
28. Ribault V, Castanet M, Bertrand AM, et al. Experience with intraamniotic thyroxine treatence with intraamniotic thyroxine treatroidism in 12 cases. J Clin Endocrinol Metab. 2009;94(10):3731-9.
29. Olivieri A, Stazi MA, Mastroiacovo P, et al. A population-based study on the frequency of additional congenital malformations in infants with congenital hypothyroidism: data from the Italian Registry for Congenital Hypothyroidism (1991-1998). J Clin Endocrinol Metab. 2002;87(2): 557-62.
30. Castanet M, Park SM, Smith A, et al. A novel loss-of-function mutation in TTF-2 is associated with congenital hypothroidism, thyroid agenesis, and cleft palate. Hum Mol Genet. 2002;11(17):2051-9.

31. Doyle DA, Gonzalez I, Thomas B, et al. Autosomal dominant transmission of congenital hypothyroidism, neonatal respiratory distress, and ataxia caused by a mutation of NKX2.1. J Pediatr. 2004;145(2):190-3.
32. Polak M, Van Vliet G. Therapeutic Approach of Fetal Thyroid Disorders. Horm Res Paediatr. 2010;74(1):1-5.
33. Luton D, Le Gac I, Vuillard E, et al. Management of Graves' disease during pregnancy: the key role of fetal thyroid gland monitoring. J Clin Endocrinol Metab. 2005;90(11):6093-8.
34. Foulds N, Walpole I, Elmslie F, et al. Carbimazole embryopathy: an emerging phenotype. Am J Med Genet. 2004;132A:130-5.
35. Isaacs H. Perinatal neoplasms: a report of 110 cases. Pediatr Pathol. 1985;3:165-216.
36. Teal LN, Antuaco TL, Jimenez JF, et al. Fetal teratomas: antenatal diagnosis and clinical management. J Clin Ultra sound. 1988;16(5):329-36.
37. Catte LD, De Backer A, Goosens A, et al. In: Teratoma, neck. Jeanry P. (Ed). Available at: http://www.thefetus.net. Accessed September 3, 2002.
38. Jordan RB, Gauderer MW. Cervical teratomas: an analysis. Literature review and proposed classification. J Pediatr Surg. 1988;23:583-91.
39. Clavelli A. Lymphangioma, case of day. Jeanty P. Available at: http://www.thefetus.net. Accessed August 1999.
40. Kilcline C, Frieden IJ. Infantile hemangiomas: how common are they? A systematic review of the medical literature. Pediatr Dermatol. 2008;25(2):168-73.
41. Haggstrom AN, Drolet BA, Baselga E, et al. Prospective study of infantile hemangiomas: demographic, prenatal, and perinatal characteristics. J Pediatr. 2007;150(3):291-4.
42. Viora E, Grassi Pirrone P, Comoglio F, et al. Ultrasonographic detection of fetal craniofacial hemangioma: case report and review of the literature. Ultrasound Obstet Gynecol. 2000;15:431-4.
43. Metry DW, Hebert AA. Benign cutaneous vascular tumors of infancy: when to worry, what to do? Arch Dermatol. 2000;136:905.
44. Atlan G, Egerszegi EP, Brochu P, et al. Cervical chrondrocutaneous branchial remnants. Plast Reconstr Surg. 1997;100(1):32-9.

CHAPTER 18

Detection of Limb Malformations—The Role of 3D/4D Ultrasound

Eberhard Merz

INTRODUCTION

The 3D/4D ultrasound has evolved into a powerful and effective adjunct to conventional 2D ultrasound and has become a part of daily clinical routine in prenatal diagnosis. Once a suspicious finding has been detected in a 2D examination of the fetus, 3D/4D ultrasound is applied as a helpful adjunct in establishing the final diagnosis. Particularly in the diagnosis of fetal limb/skeletal anomalies, which increasingly involves the detection of different surface and bone abnormalities, the various display options offered by 3D ultrasound provide an excellent means of detecting these defects. The 4D ultrasound additionally provides a real-time three-dimensional display of normal and abnormal fetal movements of the extremities. The sequentially stored volumes allow a detailed examination from the memory, similar to a 2D cine loop. The operator can thus rapidly locate the volume which gives the best 3D view of a particular movement phase or anatomical area. In cases with a high recurrence risk of a particular malformation, 3D/4D rendered images of the normal anatomy give worried parents a greater degree of reassurance than 2D images can provide.

INCIDENCE OF LIMB ANOMALIES

Anomalies of the limbs occur in approximately 2.2% of all newborns.[1]

Etiology

Limb abnormalities are characterized by a heterogeneous etiology. Possible defects include genetic defects, defects due to exposure to exogenous agents or an amniotic band syndrome or defects due to a severe reduction in amniotic fluid (oligohydramnios). A number of the abnormalities are associated with specific genetic syndromes or chromosomal aberrations.

Different Types of Limb Malformations

Fetal limb malformations can generally be divided into the following three groups:

1. Abnormalities representing a generalized disorder of bone and cartilage growth (osteochondrodysplasias)
2. Abnormalities confined to individual bones or limb segments (e.g. peromelia)
3. Limb malformations impairing fetal mobility (e.g. arthrogryposis multiplex congenita).

3D ULTRASOUND APPEARANCE OF THE LIMBS/FETAL SKELETON

In contrast to 2D ultrasound, which permits images to be displayed in one plane only, 3D ultrasound offers various display options.

Multiplanar View

This view demonstrates the three orthogonal planes at the same time on the monitor **(Figs 18.1A to C)**.[2] All planes can be translated or rotated, allowing the operator to conduct a detailed survey of the stored volume. Any arbitrary 2D plane can be reconstructed from a stored volume and displayed.

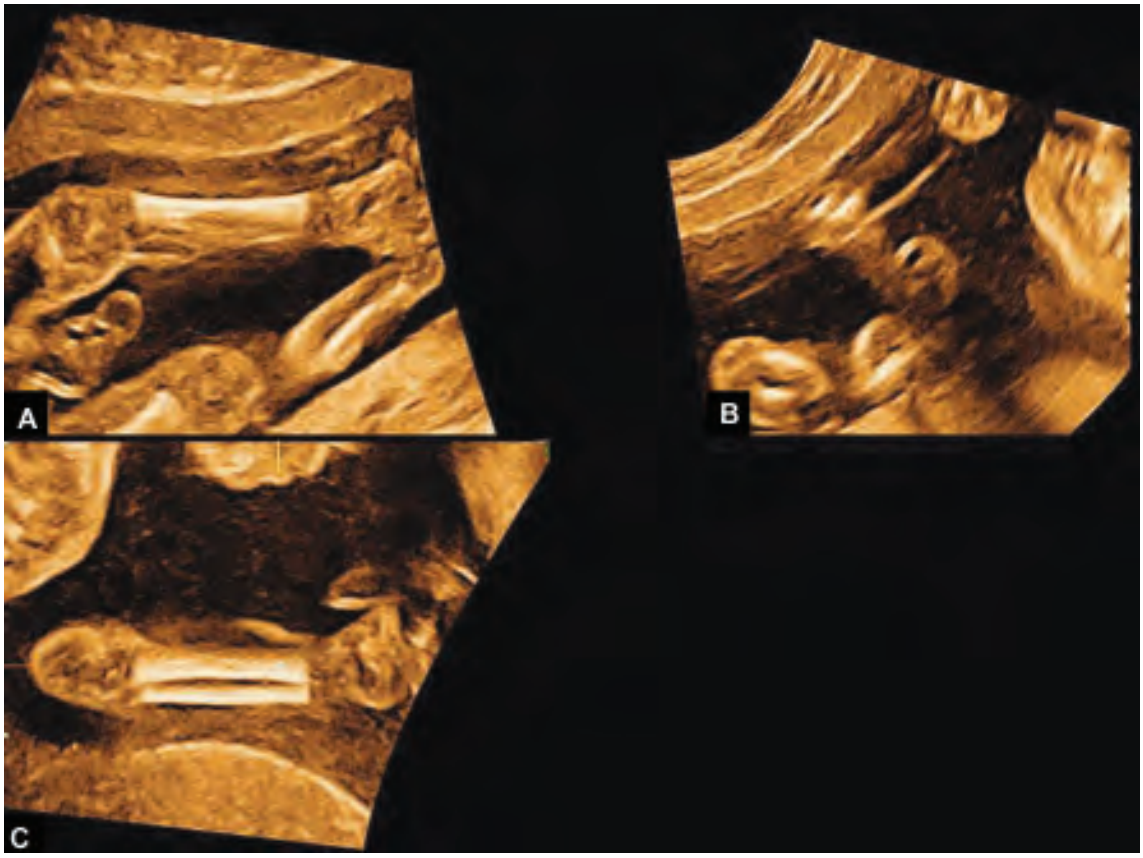

Figures 18.1A to C: Multiplanar (triplanar) display of the right lower limb (20 weeks of gestation). (A) Sagittal scan plane, showing tibia;(B) Transverse scan plane, showing tibia and fibula; (C) Coronal scan plane, demonstrating tibia and fibula

Tomographic View

This view demonstrates a certain volume in parallel planes as in CT or MRI **(Fig. 18.2)**.[3,4] The distance between the parallel slices as well as the direction of the slices can be chosen by the operator.

Surface View

Surface imaging is used to demonstrate fetal body surfaces **(Figs 18.3A and B)**.[2] One basic requirement of all 3D surface rendering is the presence of an adequate fluid pocket in front of the region of interest (ROI) and the absence of overlying or abutting structures. All structures obscuring the ROI have to be removed electronically using an electronic scalpel.[5]

Surface imaging can further be used to reconstruct surfaces of the long bones **(Figs 18.4A to D)**. For this purpose the desired subvolume has to be outlined in all three planes.

Transparent View

The maximum mode preferentially displays hyperechoic structures like bones, while markedly attenuating less echogenic structures, such as the soft tissue **(Figs 18.5A and B)**.[2] The transparent view is capable of displaying all ossified regions of the fetal skeleton.

Animated Rotating Display

Entire series of images can be reconstructed within a few seconds with both the surface and the transparent mode or from an isolated vascular display. This enables viewing the object of interest from multiple angles in the form of an animated rotating display.[2]

4D ULTRASOUND APPEARANCE OF THE LIMBS/FETAL SKELETON

In contrast to a 3D ultrasound, which can acquire only static pictures, the 4D ultrasound can depict fetal

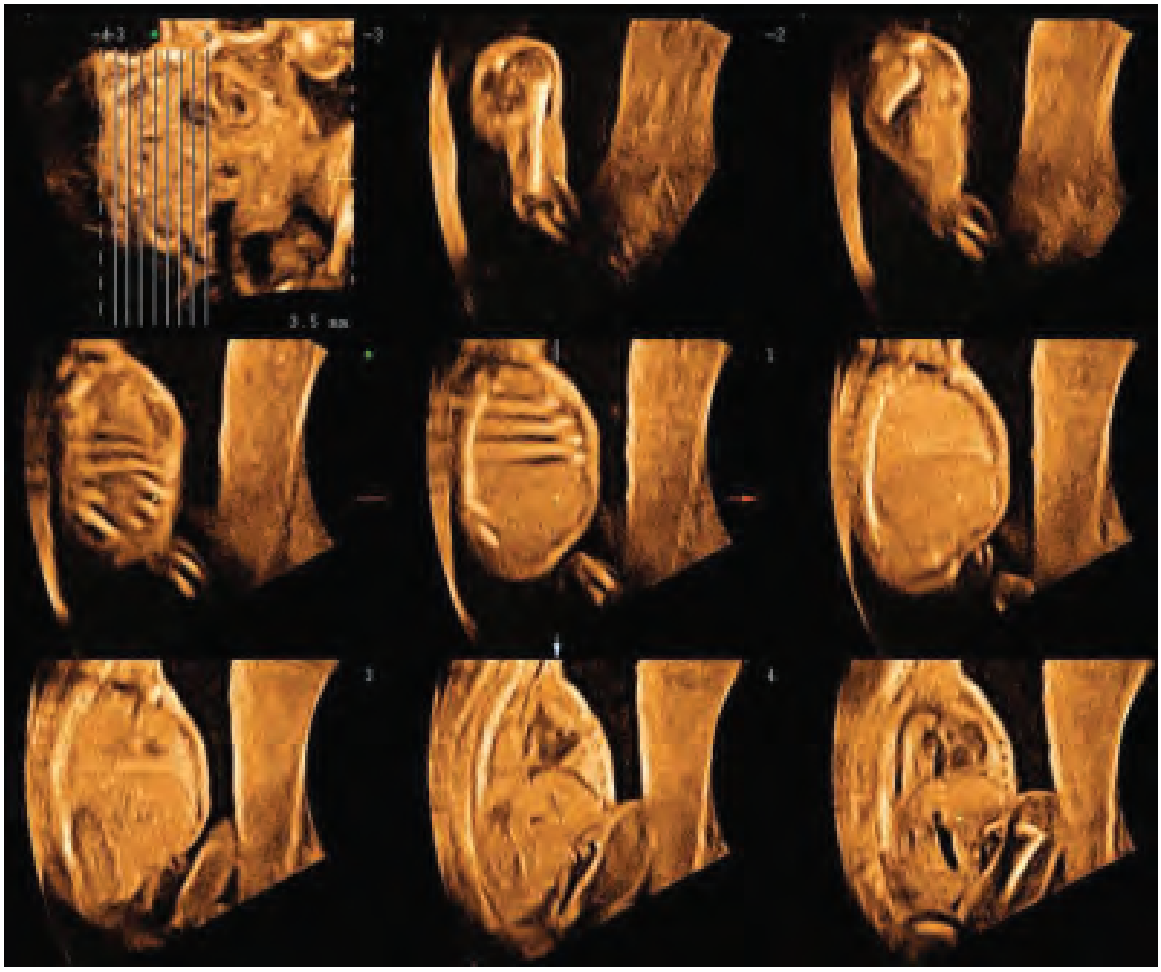

Figure 18.2: Tomographic views of the right arm and the right half of the thorax (sagittal planes with a distance of 3.5 mm) (20 weeks)

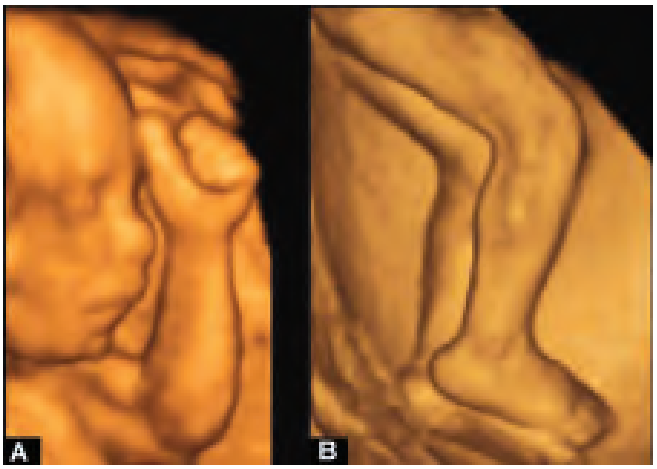

Figures 18.3A and B: Surface-rendered views. (A) Lateral view of a fetal face and left forearm (20 weeks); (B) Lateral view of fetal legs (21 weeks)

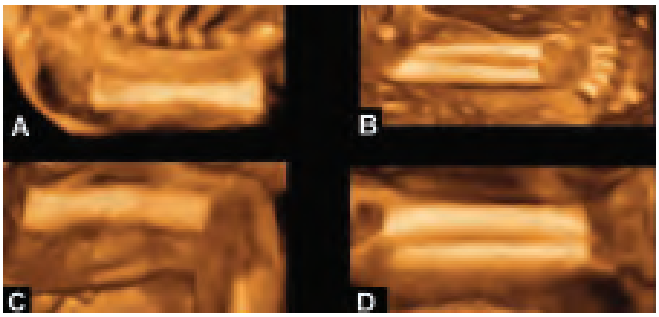

Figures 18.4A to D: Rendered views of cut surfaces revealing the normal long bones at 20 weeks of gestation. (A) Humerus; (B) Radius and ulna; (C) Femur; (D) Tibia and fibula

movements in real time **(Figs 18.6A to D)**.[6,7] This provides an excellent opportunity to observe limb movements in the surface and the transparent mode.

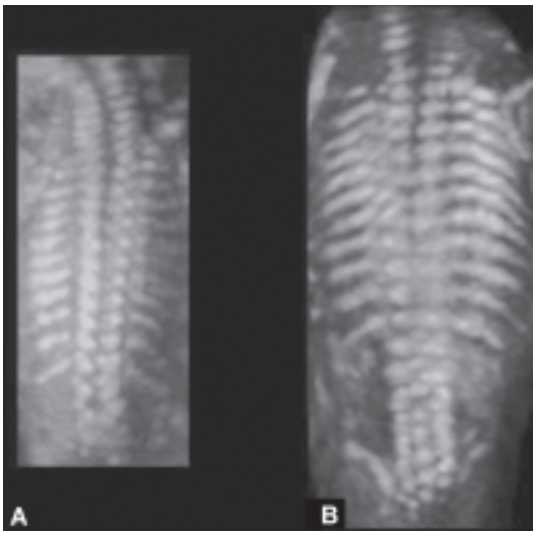

Figures 18.5A and B: Transparent (maximum mode) view of normal fetal skeletons. (A) 16 weeks; (B) 20 weeks

TRANSVAGINAL/TRANSABDOMINAL ULTRASOUND EXAMINATION OF THE LIMBS/FETAL SKELETON

All phases of embryologic limb development during the first trimester can be depicted with transvaginal 3D/4D ultrasound.[8,9] A targeted search for severe limb anomalies can already be conducted at this stage. However, most of the antenatal diagnoses will be done using transabdominal 3D/4D ultrasound starting at approximately 13 weeks of gestation.

GENERAL ASPECTS OF THE SONOGRAPHIC DETECTION OF LIMB MALFORMATIONS

During the second trimester, a large number of fetal malformations are detectable by conventional two-dimensional ultrasound.[10,11] This technology can, however, provide only two-dimensional sectional views of the fetus, while individual sectional planes of the region of interest cannot be achieved in the presence of an unfavorable position of the fetus. Furthermore, complex anomalies require an evaluation not only in one, but in multiple planes.[2]

The 3D/4D ultrasound technology with its different display modes facilitates the demonstration of skeletal/limb malformations.[12-26] In particular, surface anomalies can be communicated to the parents or the pediatric surgeon. Conversely, in cases where fetal surface defects have been excluded, a key advantage of 3D ultrasound may be seen in its ability to give the worried parents a greater degree of reassurance than 2D images can provide.[27]

In a study comparing 2D and 3D ultrasound for the diagnosis of limb malformations, Merz and colleagues reported an advantage of 3D over 2D ultrasound in 90.3% of cases.[19]

The fact that the majority of skeletal anomalies occur in a low-risk population makes a thorough prenatal ultrasound examination a precondition for the detection of limb malformations. A definitive diagnosis of a limb malformation requires not only the measurement of the fetal head, abdomen and femur but of all long bones. All data should be plotted on nomograms to obtain a

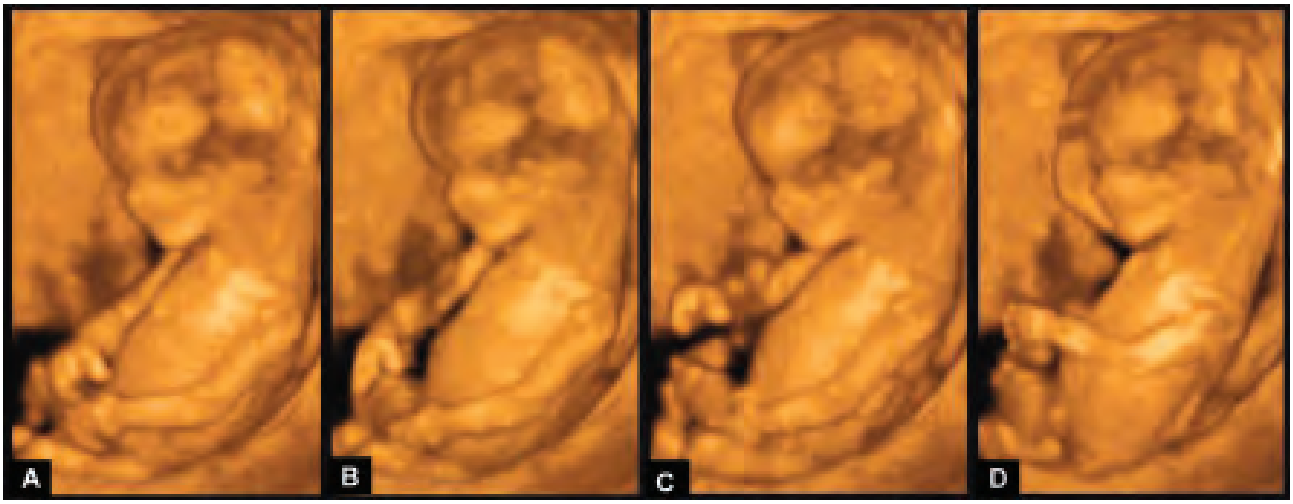

Figures 18.6A to D: A 4D rendering: Surface demonstration of limb movements (12 weeks)

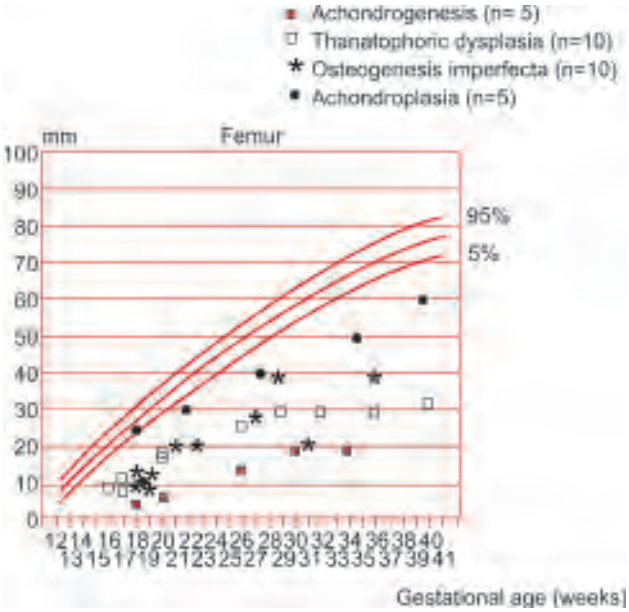

Figure 18.7: Femur length in various osteochondrodysplasias. The degree of bone shortening is highest in achondrogenesis and smallest in achondroplasia (Adapted from Merz E[11])

TABLE 18.1

Bone parameters for the differential diagnosis of limb anomalies
Bone length
Pattern of bone shortening (rhizomelia, mesomelia, micromelia)
Absence or hypoplasia of a bone (e.g. radial or fibular aplasia)
Abnormal bone structure (diaphysis, metaphysis)
Degree of bowing
Detection of bone fractures

(Adapted from Merz E[11])

precise profile of the fetal growth and to determine the severity of bone shortening **(Fig. 18.7 and Table 18.1)**. In cases where bone length cannot be accurately interpreted due to uncertain data, it can be helpful to compare the length of the femur and the foot. Since, at least during the second trimester, the femur and the foot have similar antenatal lengths, a femur which is considerably shorter than the foot is always suspicious for skeletal dysplasia.[11]

In all cases of suspected bone dysplasia, additional anatomic details have to be checked to enable a differential diagnosis **(Table 18.2)**.

TABLE 18.2

Parameters for the differentiation of skeletal anomalies	
Head	Head size (macrocephaly) Abnormal head shape (cloverleaf) Ossification of calvaria Deformable calvaria Hypertelorism Abnormal facial profile (flat profile, frontal bossing, depressed nasal bridge, cleft lip and palate, retrognathia)
Spinal column	Abnormal curvature Hypomineralization
Clavicle	Aplasia, hypoplasia
Scapula	Aplasia, hypoplasia
Thorax	Thoracic shape (champagne-cork thorax, bell-shaped) Hypoplasia of the bony thorax Pulmonary hypoplasia Cardiac anomaly
Pelvic bones	Absent or delayed ossification
Gender	Ambiguous gender
Hands	Polydactyly
Feet	Foot length, pes equinovarus, polydactyly
Movement pattern	Decreased motor activity

(Adapted from Merz E[11])

Osteochondrodysplasias

The incidence of skeletal dysplasias is approximately 1:4,100 newborns, including stillbirths.[28] The incidence of lethal osteochondrodysplasias is approximately 1:19,000 live births.[29]

The most common skeletal dysplasias are:

- Thanatophoric dysplasia
- Achondroplasia
- Achondrogenesis
- Osteogenesis imperfecta.

All of these dysplasias are characterized by severe limb shortening. The degree and type of shortening as well as the demonstration of fractures or bowing of the long bones are used to differentiate between the different osteochondrodysplasias **(Table 18.3)**.

The lethal group of skeletal dysplasias is characterized by short limb bones, a narrow thorax and hypoplastic lungs **(Table 18.4)**.[11,30]

The photorealistic view of the fetus in the surface display provides valuable opportunities for the detection of disproportional growth of short limbs **(Fig. 18.8)**, frontal bossing **(Fig. 18.9)**, narrow thorax

TABLE 18.3

Patterns of limb shortening	
Rhizomelia	Shortening of the proximal long bones (femur, humerus)
Mesomelia	Shortening of the distal long bones (tibia, fibula, radius, ulna)
Acromelia	Shortening of the distal segments (hands, feet)
Micromelia	Shortening of the proximal and distal long bones

(Adapted from Merz E[11])

TABLE 18.4

Fatal osteochondrodysplasias with narrow thorax
Achondrogenesis **(Figs 18.8 and 18.11)**
Hypochondrogenesis
Thanatophoric dysplasia **(Figs 18.9 and 18.11)**
Osteogenesis imperfecta II **(Figs 18.10 and 18.12)**
Camptomelic dysplasia **(Fig. 18.13)**
Homozygous achondroplasia
Short rib polydactyly syndrome I-VII **(Fig. 18.14)**

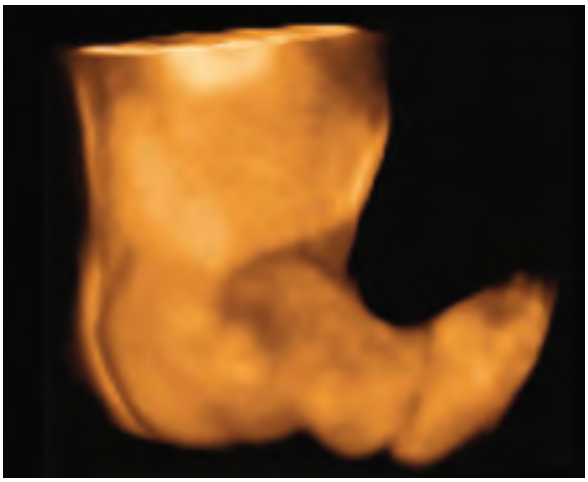

Figure 18.8: Surface-rendered view of a fetus with achondrogenesis (22 weeks)

(Fig. 18.9) or axis deviation of the limbs **(Fig. 18.10)**. The transparent display facilitates the detection of ossification defects involving the long limb bones, the skull, the bony thorax and the spine, scapula and pelvis. Not only shortening but also bowing or the presence of fractures can be observed in the long bones **(Figs 18.11 to 18.13)**.

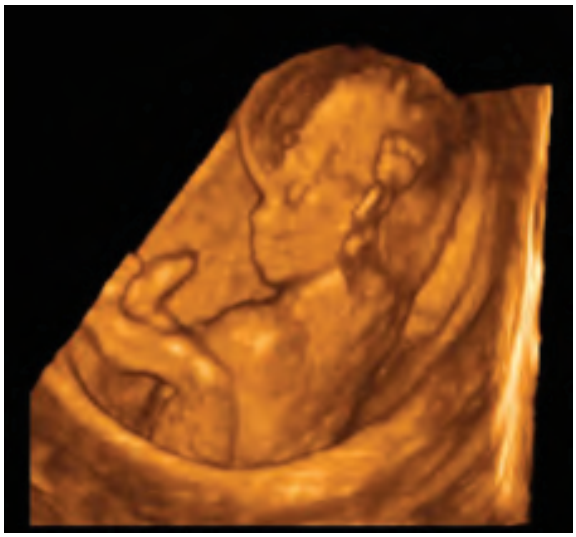

Figure 18.9: Surface-rendered view of thanatophoric dysplasia with short limbs, frontal bossing and narrow thorax (16+2 weeks)

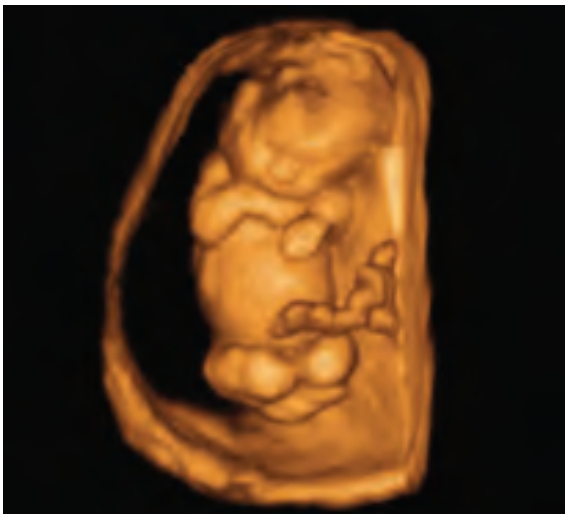

Figure 18.10: Surface-rendered view of a fetus with osteogenesis imperfecta II. Severe bowing of the limbs due to several fractures of the long bones (20 weeks)

The interactive shift from one display mode to the other is particularly useful for the detection or exclusion of specific abnormalities, making it possible to identify even subtle fetal abnormalities and to define the extent of a defect in all dimensions.

An essential aim of prenatal diagnosis is the early detection or exclusion of lethal forms of skeletal dysplasia. However, it has to be taken into account that some osteochondrodysplasias, in particular non-lethal dysplasias such as heterozygous achondroplasia **(Figs 18.11A to C)**, are not detectable before 20 weeks of gestation.

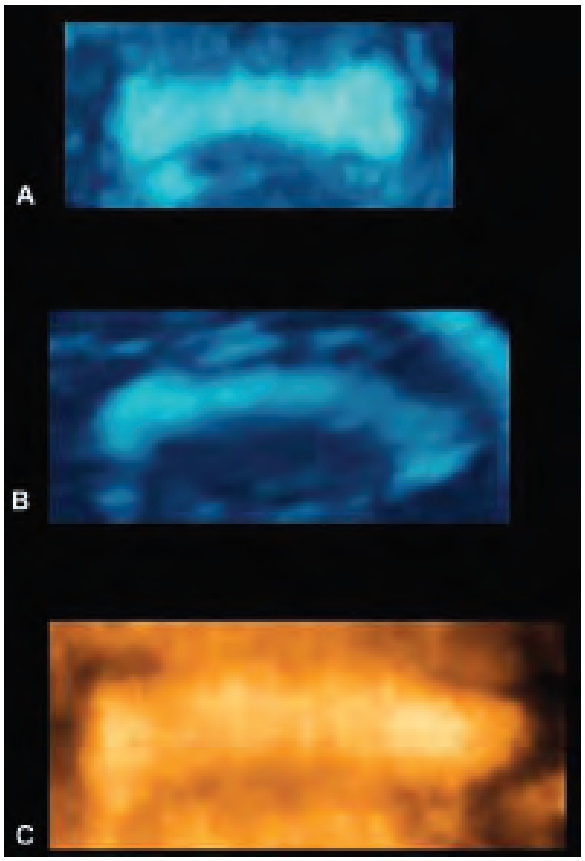

Figures 18.11A to C: Transparent views of different femurs. (A) Very short femur in a fetus with achondrogenesis; (B) Short and bowed femur in a fetus with thanatophoric dysplasia; (C) Slightly shortened femur in a fetus with achondrogenesis

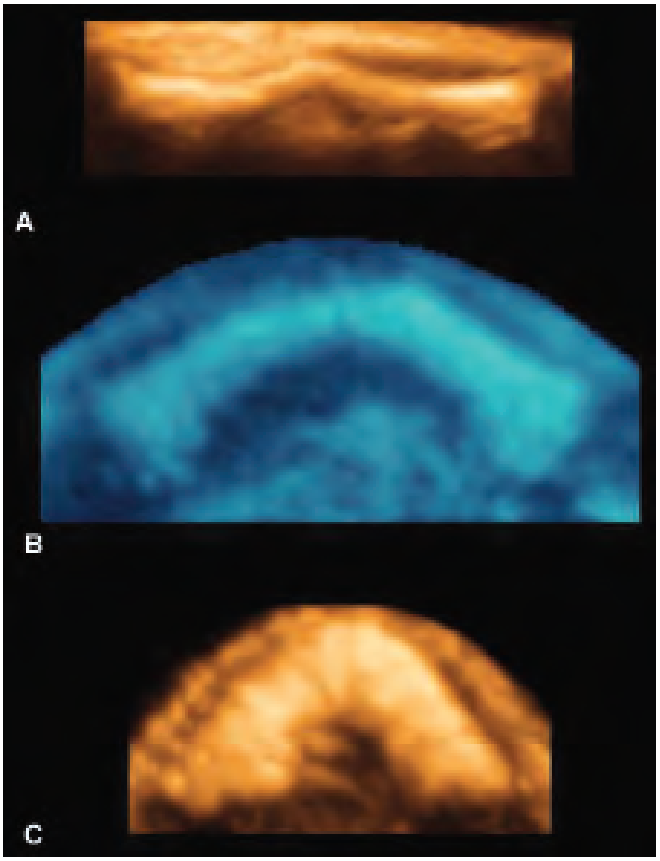

Figures 18.12A to C: Transparent views of different femurs with deviation of the bone axis due to fractures (osteogenesis imperfecta II). (A) Angulation; (B) Moderate bowing; (C) Severe bowing

Limb Anomalies Involving Specific Segments Only

Isolated limb defects can be detected only by critical comparison of the right and left limb.

Surface rendering has created new capabilities in the diagnosis of limb anomalies which involve specific segments only **(Table 18.5)**. Since the examination is not performed on a live, moving fetus but on a digitally stored limb that can be rotated freely in space, isolated limb defects such as amelia **(Figs 18.15A and B)** or peromelia **(Fig. 18.16)** can be readily detected. Nevertheless, the examiner needs to be very careful in establishing the diagnosis. If the arm or the leg is not completely within the volume box, the distal part of the limb will be electronically cut by the volume box and may thus falsely be interpreted as a malformation, e.g. peromelia **(Figs 18.17A and B)**. In all cases of uncertainty the false-positive defect can be excluded in an animated rotating image display.

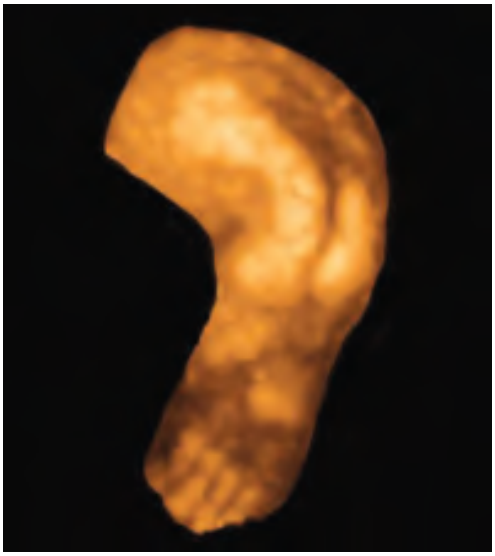

Figure 18.13: Severe bowing of the lower limb bones in camptomelic dysplasia (20 weeks)

TABLE 18.5

Nomenclature for limb abnormalities	
Amelia	Absence of one or more limbs
Peromelia	Absence or deformity of the terminal part of a limb or limbs
Hemimelia	Absence of the distal portion of one limb (form of peromelia)
Meromelia	Partial absence of a limb
Acheira	Absence of one or both hands
Apodia	Absence of one or both feet
Acheiropodia	Absence of hands and feet
Adactyly	Absence of fingers or toes
Phocomelia	A malformation in which the proximal portions of the extremities are poorly developed or absent. Hands and feet are directly attached to the trunk.
Ectromelia	Hypoplasia of the long bones of the limbs
Oligodactylia	Subnormal number of fingers or toes
Polydactyly • preaxial • postaxial	Condition of having supernumerary fingers or toes • Extra digit on radial or tibial side • Extra digit on ulnar or fibular side
Brachydactylia	Abnormal shortness of the fingers or toes
Ectrodactylism	Absence of all or part of a digit (split hand, lobster claw)
Sirenomelia	Anomaly in which the lower extremities are fused
Syndactylism	A fusion of two or more fingers or toes
Clinodactyly	Permanent medial or lateral deflection of one or more fingers
Camptodactylia	Permanent flexion of fingers or toes
Talipes • valgus • varus	Clubfoot Heel and foot are turned outward Heel and foot are turned inward

Axis deviations of the limbs **(Figs 18.18A and B)** are always suspicious of fractures in the long bones or aplasia of one bone (e.g. radius aplasia). The absence of radius and angular deviation of the hand serve as an indication of a Holt-Oram syndrome **(Figs 18.18A and B)**. Surface demonstration of the fetal hand further permits the detection of ectrodactylism **(Fig. 18.19)**, oligodactylia, brachydactylia or syndactylism **(Fig. 18.20)**. Moreover, the 3D surface analysis of the stored hand can conclusively demonstrate the presence of

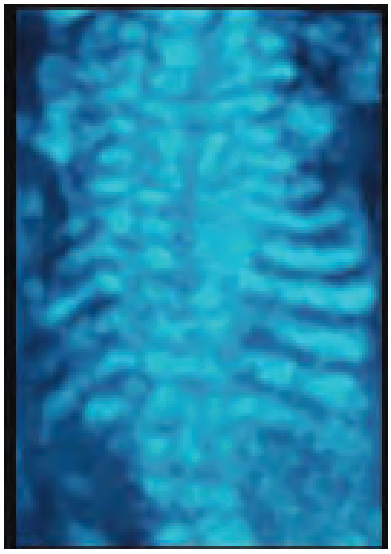

Figure 18.14: Short rib polydactyly syndrome. The maximum mode reveals the poorly ossified short ribs (22 weeks)

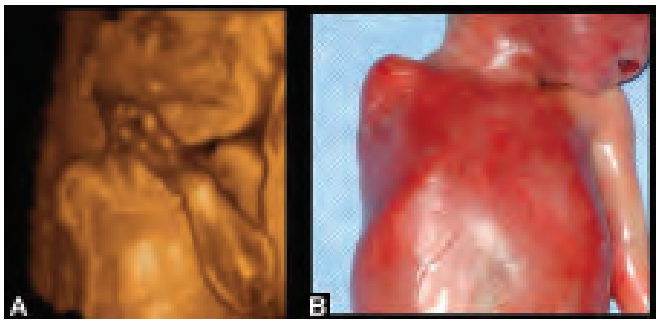

Figures 18.15A and B: (A) Surface-rendered view of amelia on the right side (22 weeks); (B) Specimen after abortion

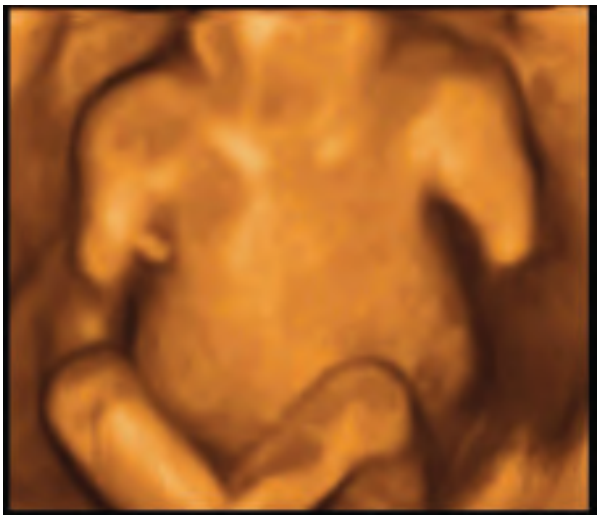

Figure 18.16: Surface-rendered view of bilateral peromelia (17+1 weeks)

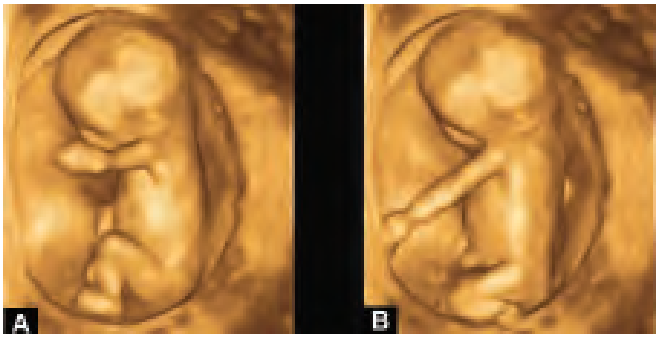

Figures 18.17A and B: (A) Surface-rendered view mimicking a peromelia due to the placement of the distal forearm outside the volume box; (B) Same fetus with demonstration of the entire arm inside the volume box (17+4 weeks)

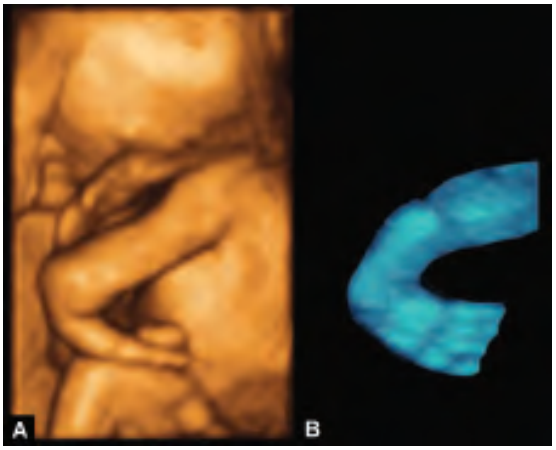

Figures 18.18A and B: Fetus with Holt-Oram syndrome (19 weeks). (A) Surface-rendered view of the left arm with severe deviation of the forearm; (B) Transparent view of the same arm showing radial aplasia and severe angulation of the hand with only four fingers

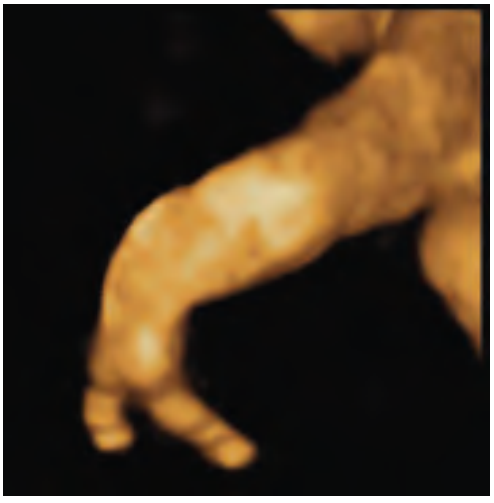

Figure 18.19: Surface-rendered view of a fetus with ectrodactylism (22 weeks)

Figure 18.20: Surface-rendered view of syndactylism between finger 4 and 5 (21+6 weeks)

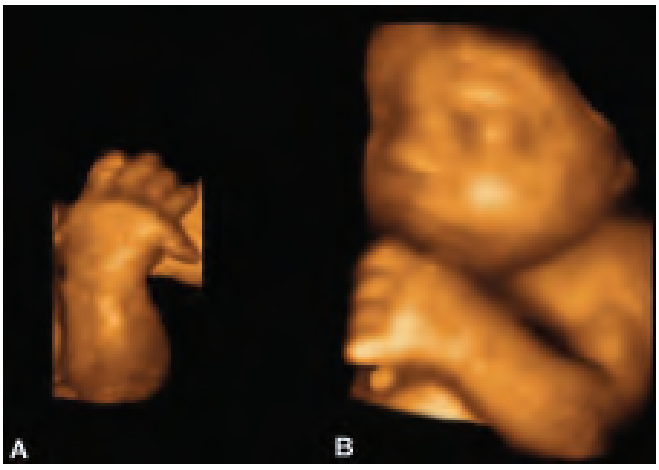

Figures 18.21A and B: Surface-rendered views of hexadactyly. (A) Postaxial hexadactyly right (31 weeks); (B) Postaxial hexadactyly left (31 weeks)

polydactylia, such as pre- or postaxial hexadactyly **(Figs 18.21A and B)**. Clinodactyly, camptodactylia or overlapping fingers **(Fig. 18.22)** are also easily detectable.

This also applies to a detailed examination of the foot. Angular deformities such as club foot **(Figs 18.23A and B)** or oligodactylia of the foot **(Figs 18.23A and B)** can be readily demonstrated.[12,15]

In all limb anomalies involving only specific segments of the foot, the use of the transparent mode is mandatory to display the bone defects **(Fig. 18.18B).**

A number of limb anomalies such as, radius aplasia or overlapping fingers **(Fig. 18.22)**, are indicators of chromosomal aberrations and should serve as an indication for karyotyping.

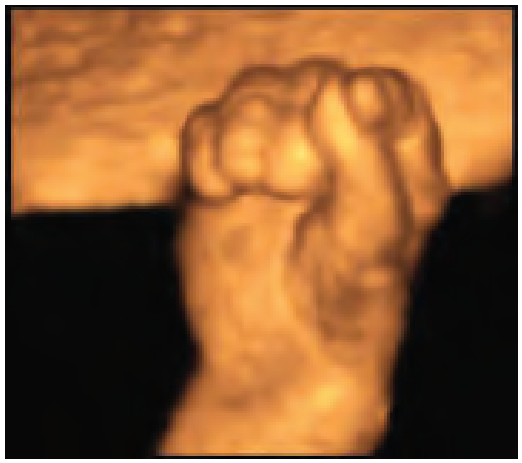

Figure 18.22: Overlapping fingers, indicating the presence of a chromosomal defect (here trisomy 18) (29 weeks)

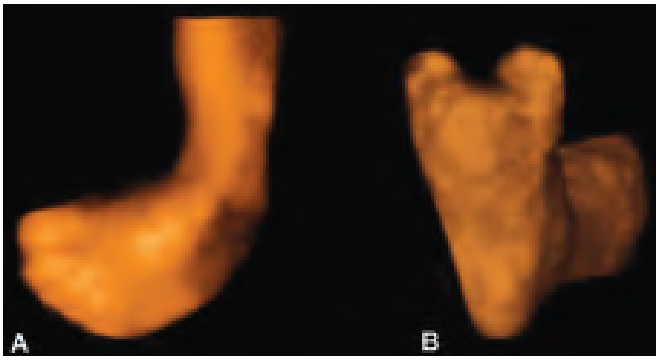

Figures 18.23A and B: (A) Surface-rendered view of a club foot (31+6 weeks); (B) Split foot with only two toes (21+2 weeks)

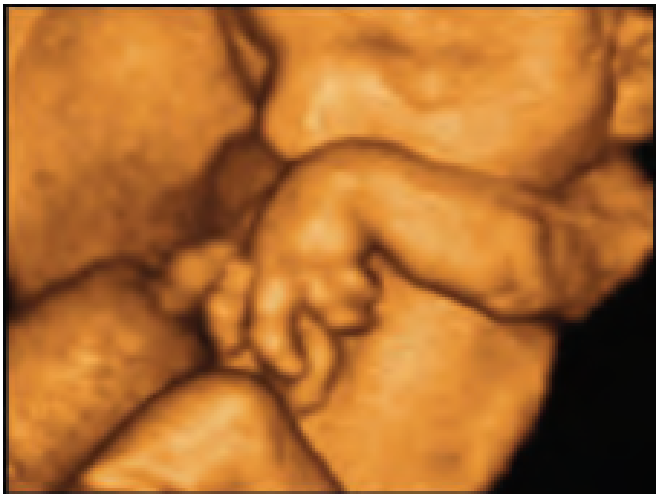

Figure 18.24: Surface-rendered view of a fetus with arthrogryposis multiplex congenita (21+6 weeks). Despite the acute polyhydramnios, the fetus shows no arm movement due to contractures of the wrist and fingers

Limb Malformations which Impair Fetal Mobility

The 4D ultrasound with its acquisition rate up to 35 volume/s provides an excellent means of detecting abnormal fetal movement patterns.[27] All grades of intrauterine flexion or extension contractures affecting a variable number of joints can occur in arthrogryposis multiplex congenita (AMC) **(Fig. 18.24)**. Polyhydramnios combined with the absence of fetal movement and clubfeet invariably gives rise to the suspicion of AMC with CNS involvement.[11] The combination of AMC with pulmonary hypoplasia serves as an indication of a Pena-Shokeir syndrome[11] with a grave prognosis.

A neural tube defect has to be excluded in all cases of abnormal movement patterns of the fetal limbs.

REFERENCES

1. Schaller A. Geburts medizinische Teratologie: Extremitätenfehlbildungen. Urban and Schwarzenberg. München; 1975. p. 138.
2. Merz E. 3D Ultrasound in prenatal diagnosis. In: Merz E (Ed). Ultrasound in Obstetrics. Stuttgart-New York: Thieme; 2005. pp. 516-28.
3. Kalache KD, Bamberg C, Proquitte H, et al. Three-dimensional multi-slice view: new prospects for evaluation of congenital anomalies in the fetus. J Ultrasound Med. 2006;25(8):1041-9.
4. Merz E. Tomographic ultrasound imaging. Ultraschall in Med. 2006;27(4):307-8.
5. Merz E, Miric-Tesanic D, Welter C. Value of the electronic scalpel (cut mode) in the evaluation of the fetal face. Ultrasound Obstet Gynecol. 2000;16(6):564-8.
6. Kurjak A, Carrera J, Medic M, et al. The antenatal development of fetal behavioral patterns assessed by a four-dimensional sonography. J Matern Fetal Neonatal Med. 2005;17(6):401-16.
7. Hata T, Kanenishi K, Tanaka H, et al. Four-dimensional ultrasound evaluation of fetal neurobehavioral development. Donald School Journal of Ultrasound in Obstetrics and Gynecology. 2010;4:233-48.
8. Benoit B. The value of three-dimensional ultrasonography in the screening of the fetal skeleton. Childs Nerv Syst. 2003;19(7-8):403-9.
9. Benoit B, Hafner T, Kurjak A, et al. Three-dimensional sonoembryology. J Perinat Med. 2002;30(1):63-73.
10. Goncalves L, Jeanty P. Fetal biometry of skeletal dysplasias: a multicentric study. J Ultrasound Med. 1994;13(12):977-85.
11. Merz E. Anomalies of the extremities. In: Merz E (Ed). Ultrasound in Obstetrics. Stuttgart - New York: Thieme; 2005.pp.336-58.
12. Steiner H, Spitzer D, Weiss-Wichert PH, et al. Three-dimensional ultrasound in prenatal diagnosis of skeletal dysplasia. Prenat Diagn. 1995;15(4):373-7.
13. Lee A, Kratochwil A, Deutinger J, et al. Three dimensional ultrasound in diagnosing phocomelia. Ultrasound Obstet Gynecol. 1995;5(4):238-40.

14. Merz E, Bahlmann F, Weber G. Volume (3D)-scanning in the evaluation of fetal malformations: a new dimension in prenatal diagnosis. Ultrasound Obstet Gynecol. 1995; 5(4): 222-7.
15. Dyson RL, Pretorius DH, Budorick NE, et al. Three-dimensional ultrasound in the evaluation of fetal anomalies. Ultrasound Obstet Gynecol. 2000;16(4):321-8.
16. Kos M, Hafner T, Funduk-Kurjak B, et al. Limb deformities and three-dimensional ultrasound. J Perinat Med. 2002; 30(1):40-7.
17. Krakow D, Williams J 3rd, Poehl M, et al. Use of three-dimensional ultrasound imaging in the diagnosis of prenatal-onset skeletal dysplasias. Ultrasound Obstet Gynecol. 2003;21(5):467-72.
18. Ruano R, Molho M, Roume J, et al. Prenatal diagnosis of fetal skeletal dysplasias by combining two-dimensional and three-dimensional ultrasound and intrauterine three-dimensional helical computer tomography. Ultrasound Obstet Gynecol. 2004;24(2):134-40.
19. Merz E, Welter C. 2D and 3D Ultrasound in the evaluation of normal and abnormal fetal anatomy in the second and third trimesters in a level III center. Ultraschall Med. 2005;26(1):9-16.
20. Chen CP, Chang TY, Su YN, et al. Prenatal two- and three-dimensional ultrasound diagnosis of limb reduction defects associated with homozygous alpha-thalassemia. Fetal Diagn Ther. 2006;21(4):374-9.
21. David AL, Turnbull C, Scott R, et al. Diagnosis of Apert syndrome in the second-trimester using 2D and 3D ultrasound. Prenat Diagn. 2007;27(7):629-32.
22. Kennelly MM, Moran P. A clinical algorithm of prenatal diagnosis of radial ray defects with two and three dimensional ultrasound. Prenat Diagn. 2007;27(8):730-7.
23. Lin IW, Chueh, HY, Chang SD, et al. The application of three-dimensional ultrasonography in the prenatal diagnosis of arthrogryposis. Taiwan J Obstet Gynecol. 2008;47(1):75-8.
24. Kang A, Visca E, Bruder E, et al. Prenatal diagnosis of a case of ectrodactyly in 2D and 3D ultrasound. Ultraschall Med. 2009;30(2):121-3.
25. Tsai PY, Chang CH, Yu CH, et al. Thanatophoric dysplasia: role of 3-dimensional sonography. J Clin Ultrasound. 2009;37(1):31-4.
26. Bashiri A, Sheizaf B, Burstein E, et al. Three dimensional ultrasound diagnosis of caudal regression syndrome at 14 gestational weeks. Arch Gynecol Obstet. 2009;280(3):505-7.
27. Merz E. 3-D and 4-D ultrasonography. In: Twining P, McHugo JM, Pilling DW (Eds). Textbook of fetal abnormalities. Churchill Livingstone: Elsevier; 2007. pp. 483-93.
28. Camera G, Mastroiacovo P. Birth prevalence of skeletal dysplasias in the Italian multicentric monitoring system for birth defects. In: Papadatos CJ, Bartsocas CS (Eds). Skeletal Dysplasias. New York: Alan R Liss; 1982. pp. 441-9.
29. Curran JP, Sigman BA, Opitz JM. Lethal forms of chondrodysplastic dwarfism. Pediatrics. 1974;53(1):76-85.
30. Merz E, Miric-Tesanic D, Bahlmann F, et al. Prenatal sonographic chest and lung measurements for predicting severe pulmonary hypoplasia. Prenat Diagn. 1999;19(7):614-9.

19
CHAPTER

The Fetal Thorax

Aleksandar Ljubic, Aleksandra Novakov, Aleksandar Cetkovic

INTRODUCTION

Although relatively uncommon, congenital abnormalities in the thorax are important because of the potential effect on lung growth as well as the effect of the intrinsic abnormality.

DEVELOPMENTAL ANATOMY AND ULTRASONOGRAPHIC CORRELATIONS

The ossification of the thoracic cage/ribs begins at the end of the first trimester.[1] The lower aperture of the thorax with the lower ribs is one of the landmarks for the measurement of the abdomen. The thoracic transverse diameter, the mean abdominal diameter and the abdominal circumference are measurements taken at virtually the same level of the fetal body. Measurement of the thoracal length in a long axis of the midline section is done from the superior end of the sternum to the level of the diaphragm.

The rib length is measured by tracing the lateral edge of a rib at the level of the four-chamber view. It's size correlates well with the fetal age, thus this parameter can be useful in the management of a pregnancy with fetal skeletal dysplasia.[2]

The sternum shows extremely individual variation in its development: the number of sonographically visible ossification centers varies (up to 6) and the first 2–3 ossification centers appear at the 19 weeks of gestation, a fourth center during weeks 22–23 and five ossification centers are usually visible from 29 weeks onwards.[1]

The main structures in the fetal thorax that are subjected to examination are the heart, the lungs and eventually the esophagus. The anatomy of the heart is of interest because it can be influenced by extracardiac anomalies within thorax, e.g. unilateral pulmonal hypoplasia or cystic adenomatoid lung malformation. While the heart occupies approximately half of the size of the thorax during the embryonic period it occupies one-third of the thoracic area positioned in the middle of the thorax with the apex pointing towards the left during the second and third trimester.[2] Because of its complex anatomy and importance, the detailed anatomy and anomalies of the heart are discussed in a different chapter.

Diaphragm

The borderline between the thorax (lungs, heart) and the abdominal content is the diaphragm. Sonographically, the diaphragm appears as a thin, dark, arched line. It usually shows a dome on each side, where the right side seems higher than the left side. However, recent anatomical studies[3] did not find any difference between the height of the left and the right diaphragmatic dome. The costodiaphragmatic recess is most commonly located at the level of the ninth rib.[3] The function of the diaphragm, namely breathing, has been the subject of extensive ultrasound research. As early as the 1970s, ultrasound studies of fetal breathing movements (FBM) in human fetuses showed that their presence was indicative of well-being, while the absence of FBM, though less reliably, was a sign of pregnancy

disorder. Movements of the diaphragm start as early as 9–10 weeks.[4] Hiccups can be registered first, followed by breathing movements during week 10.

At 8 weeks' gestation, clear identification of the difference between thoracic and abdominal content is already possible, especially in those cases with a mild fluid accumulation in the thorax or pericardial cavity, however, at that stage the pleuroperitoneal canals are still open. The diaphragm, or rather the dividing line between the thoracic and abdominal content, becomes detectable at approximately 10–11 weeks.

Lungs

The development of the vertebrate lung has been subdivided into five distinct periods based on the anatomical changes that occur in lung architecture: embryonic (3–7 weeks), pseudoglandular (7–17 weeks), canalicular (17–29 weeks), saccular (24–36 weeks) and alveolar (36 weeks to maturity). Initially, the tracheobronchial tubules are formed from the pulmonary diverticulum that forms at the medial tracheolaryngeal sulcus in the ventral wall of the foregut. Branching of the trachea produces two lobar bronchi on the left and three on the right side, defining the lobar anatomy of the human lung. The esophagus and trachea separate, bronchial tubules subdivide to form the bronchial pulmonary segments and the splanchnic mesenchyme undergoes differentiation and organization to form blood vessels, lymphatics and other supporting structures. In the pseudoglandular period (7–17 weeks), there is a rapid expansion of the conducting airways and peripheral lung tubules, which continue to branch and bud to form acinar tubules. The expansion of these small tubules in the periphery of the lung produces a glandular appearance. The peripheral lung mesenchyme thins and becomes increasingly vascularized. Neuroendocrine bodies, nerves and organized smooth muscle are observed in the developing areas. Cartilage rings form around the segmental bronchi. The pleura and peritoneal cavity closes, the diaphragm thickens and becomes increasingly muscularized.[5]

The echogenicity of the lungs usually appears somewhat brighter than the echogenicity of the liver; this becomes clearer by applying harmonic imaging[6] **(Figs 19.1A and B)**. Tekesin and co-workers tried to quantify this subjective assessment of the tissue appearance by quantitative ultrasonic tissue characterization.[6] They concluded that the echogenicity of the fetal lung showed a particular changing pattern during pregnancy: The mean gray value of the lungs was almost the same as that of the liver at 22–23 weeks gestation, decreased between 23 and 31 weeks and increased again later in pregnancy. They thought that these changes of echogenicity coincided with the saccular and alveolar phases of fetal lung development. Normal data for the pulmonal size are important to assess lung development in a fetus at risk for pulmonary hypoplasia such as congenital diaphragmatic hernia, cystic adenomatoid lung malformation or pleural effusions.

During the recent 10 years, two-dimensional (2D) ultrasound[7,8] and three-dimensional (3D) ultrasound assessment[6,9,10] of normal and abnormal lungs has been studied *in extenso*. The significance of 3D ultrasound volumetry versus 2D measurements in the prenatal assessment of lung hypoplasia still remains to be

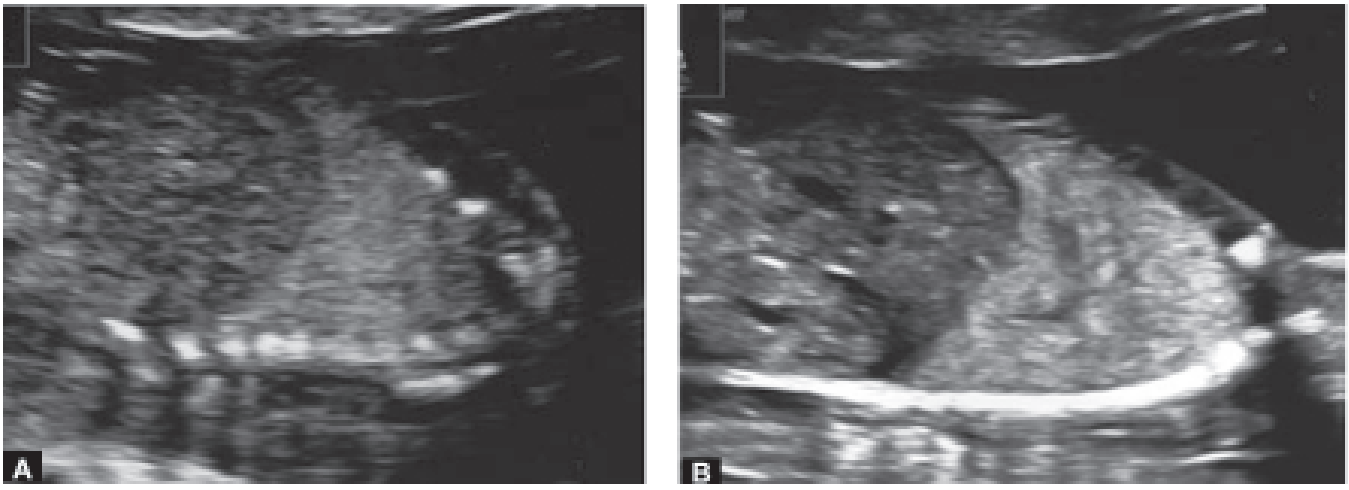

Figures 19.1A and B: Sagittal section through right lung, diaphragm, liver and bowel at 18 weeks. (A) Standard gray scale; (B) By using harmonic imaging a better distinction between liver and lungs is achieved

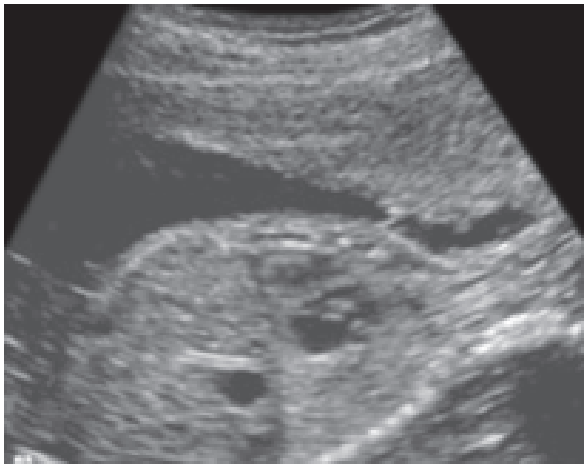

Figure 19.2: Normal appearance of heart and lungs

evaluated in studies on a larger scale. For example, in diaphragmatic hernia, the identification of the lung contours is very difficult, especially on the side of the diaphragmatic defect. The potential of lung volumetry in the prenatal assessment of fetal lung anomalies has already been indicated **(Fig. 19.2).**[10,11]

Esophagus

The examination of the fetal esophagus has received little attention in the medical literature. The esophagus is a tube permitting the passage of fluid to the stomach during the process of swallowing. The esophagus is usually empty except in pathological conditions such as duodenal obstruction, when an increased fluid volume dilates the duodenum, the stomach and in several cases the esophagus as well. The esophagus has a tubular echogenic appearance consisting of four parallel echogenic lines and can be seen in the thorax in close contact with the posterior aspect of the heart.[2] These lines represent the outer and luminal borders of the esophageal wall. In early pregnancy, these echogenic lines melt together on the ultrasound screen into two or one echogenic line.

Malinger et al.[12] examined 60 fetuses between 19 and 25 weeks to demonstrate luminal patency and peristaltic waves of the esophagus. They obtained complete anatomical visualization of the entire esophagus throughout its course in 87% of the cases and at least partial visualization was possible in 97%. Passage of fluid through the esophageal lumen was recorded during five minutes of examination in 90% of the fetuses. Thus, it is possible to evaluate the esophagus in fetuses with suspected obstruction.[13]

SCANNING TECHNIQUES

The fetus is usually scanned with a 3.5–5.0 MHz probe. The thorax is scanned in a transaxial plane, supplemented by sagittal and coronal planes as needed. The four-chamber heart scan is useful to assess chest size and lung status. Color flow Doppler is a valuable adjunct to assess vascular structures and their connections.

Before doing the detailed examination of the thoracic contents, an overall view of the whole trunk should be obtained to make sure that the relative proportions are correct.

At the transverse section, the thoracic circumference at the level of the heart, should be roughly similar to the abdominal circumference at the level of umbilical vein.

The ribs should enclose about two-thirds of the thorax, which should be almost circular in transverse section.

The major thoracic contents are the heart and great vessels and the lungs. The heart occupies about one third of the chest and is situated with the apex towards the left side, the left ventricle lying posterolaterally and the right anteromedially.

The left lung lies behind the heart and is smaller than the right. The continuity of the diaphragm should be checked in sagittal and coronal views, thus confirming that liver and bowels are separated from heart and lungs.

PATHOLOGY

Diaphragmatic Hernia

Diaphragmatic hernia represents herniation of the abdominal contents into the chest through a defect in the diaphragm. The defect in diaphragm exists from the tenth week of gestation, but the herniation of the gut into the chest in about 50% of the cases may not occur before the 24th week and this is probably the cause of the relatively low detection rate at the 18–20 weeks scan, though the evidence suggests that the marker for those cases where the prognosis is likely to be poor is increased NT at the 11–14 weeks scan.[14]

The incidence of diaphragmatic hernia on birth is 1/2500–4000. There are three types of hernias **(Figs 19.3A to C)**:

1. Posterolateral defect or Bochdalek's hernia, which accounts for about 90% of cases found in the neonatal period. It occurs on the left side in 80% of cases, on the right in 15% and may be bilateral in

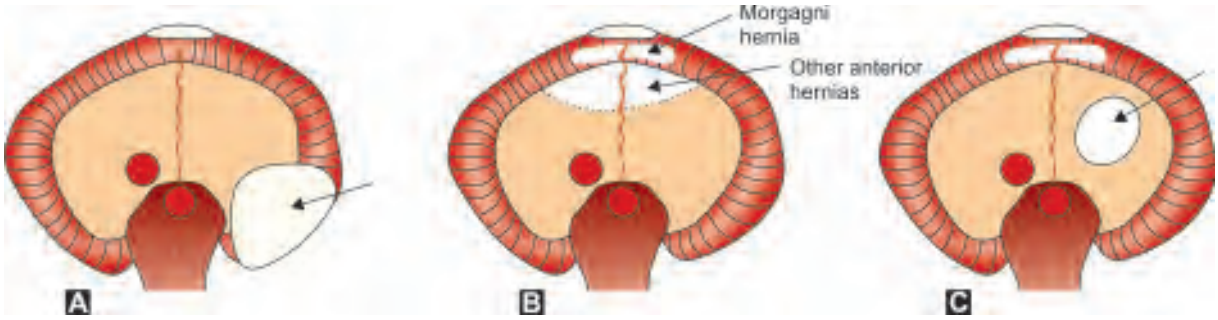

Figures 19.3A to C: Anatomic descriptions of diaphragmatic defects. (A) Bochdalek hernia; (B) Morgagni hernia and other anterior hernias; (C) Central hernia

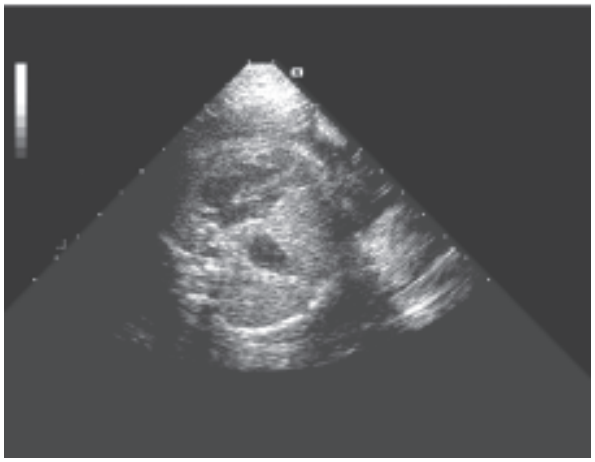

Figure 19.4: Right-sided diaphragmatic hernia

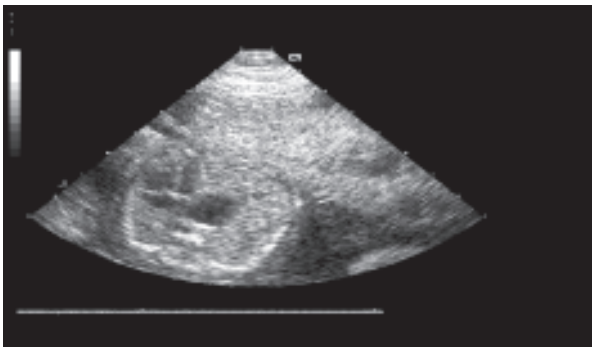

Figure 19.5: Diaphragmatic hernia with the stomach in the thoracal cavity

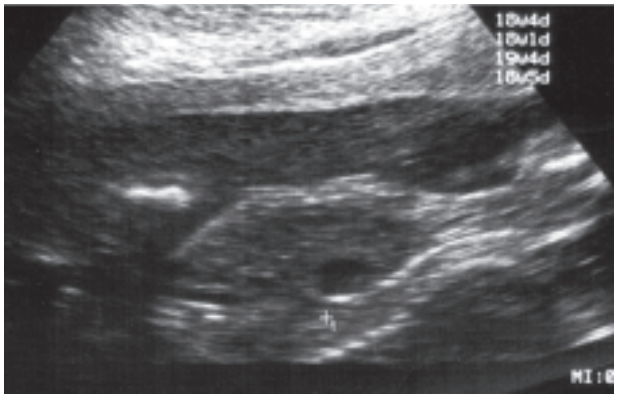

Figure 19.6: Diaphragmatic hernia with the stomach in the thoracal cavity—oblique sagittal

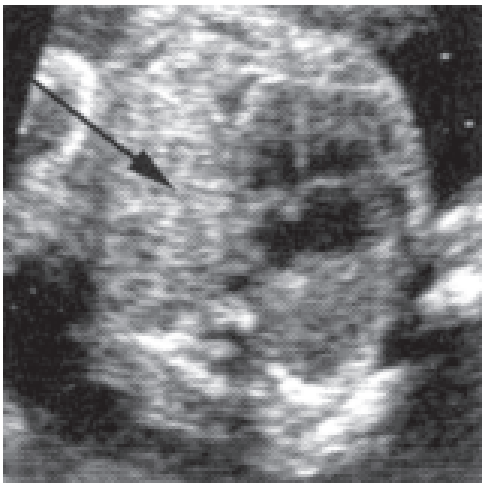

Figure 19.7: Diaphragmatic hernia (arrow) with the intestines in the thoracal cavity

approximately 5%. The most common contents of a left-sided hernia are stomach, bowel and spleen. If the defect is right-sided the usual intrathoracic organs are liver and gallbladder.

2. Parasternal defect, or Morgagni's hernia—It accounts for 1–2% of cases and is more often right sided or bilateral. It usually contains liver.
3. Eventration of the diaphragm occurs in 5% of cases and it is more commonly reported on the right.

Prenatal diagnosis by ultrasound **(Figs 19.4 to 19.7)** is based on:

- Demonstration of abdominal organs within the thoracic cavity. On longitudinal scanning, a defect in the posterior aspect of the diaphragm may be seen, at least for the most common Bochdalek type

of hernia. For left-sided congenital diaphragmatic hernia (CDH), mediastinal shift and rightwards displacement of the heart can be seen, and in most cases, a fluid-filled stomach or bowels are later on present within the thoracic cavity. An important feature to look for is the presence of (a portion of) the liver in the thorax. Doppler interrogation of the umbilical vein and hepatic vessels may be helpful in this respect. With right-sided CDH, the right lobe of the liver usually herniates into the chest, combined with mediastinal shift to the left.

- Shift in the position of the heart or cardiac compression
- Polyhydramnion is a commonly associated finding. It is rarely observed before 24 weeks' gestation and is thought to be due to either esophageal compression or reduced absorption of fluid by the hypoplastic lungs.

A right-sided hernia may be harder to diagnose because of the similar echogenicity of the lung and liver tissue, but the condition should be suspected by the presence of mediastinal shift or hydrothorax.

Differential Diagnosis

The differential diagnosis includes other cystic chest lesions such as cystic adenomatoid malformation, bronchogenic cysts or tumors of the chest.

Associated Anomalies

In prenatal series, about 50% of fetuses have an isolated diaphragmatic defect and in the rest a chromosomal abnormality may be found, usually trisomy 18, as well as a major defect, including congenital heart disease, exomphalos, renal anomalies, brain anomalies and spinal abnormalities.

Management of Pregnancy

When diaphragmatic hernia is diagnosed antenatally, fetal karyotyping and detailed ultrasound examination of the fetus (in particular the heart) should be undertaken. Fetal echocardiogarphy should be arranged as well as consultation with pediatric surgeon.

Prediction of Outcome

In neonates with isolated diaphragmatic hernia, the primary determinant of survival is the presence of pulmonary hypoplasia and hypertension. The mortality has remained high despite optimal postnatal management and the introduction of extracorporal membrane oxygenation.

Antenatal prediction of pulmonary hypoplasia is difficult and it is the most important part in counseling parents and selecting those cases that may benefit from prenatal surgery. In isolated cases of CDH, prognosis is poor when the liver is intrathoracic[15] and the lung-to-head ratio (LHR) is less than 1.[16]

When making a measurement of the LHR, a transverse section of the chest is taken at the level of the four-chamber view. The contralateral lung is measured—the longest axis is measured and multiplied by the longest measurement perpendicular to it. It is divided by the head circumference, which is measured at the standard biparietal view, typically showing two equal hemispheres, the septum cavum pellucidum, one-third of the way from the front to the back and the posterior horns of the lateral ventricles.[17]

Recent research shows that in isolated congenital diaphragmatic hernia, fetal lung volume measurement by 3D ultrasound may be a potential predictor for pulmonary hypoplasia and postnatal outcome.[11,18]

CYSTIC ADENOMATOID MALFORMATION

Cystic adenomatoid malformation (CAM) of the lung is a developmental abnormality of the lung characterized by a cystic mass of disordered pulmonary parenchyma with the proliferation of terminal respiratory bronchioles and a lack of normal alveoli.[19] The CAM usually arise from a single pulmonary lobe and multilobar or bilateral lung involvement is rare. The prenatal natural history of CAM is quite variable, forming a spectrum in severity extending from cases that present *in utero* as a rapidly growing intrathoracic mass resulting in nonimmune hydrops and *in utero* demise to lesions, which despite achieving a significant size, spontaneously regress and "disappear" during the third trimester.[20] As many as 40% of CAMs will progress to hydrops and without fetal surgery this is almost uniformly fatal while, as many as 15% of CAMs will regress and may disappear completely.[20] Unfortunately, no predictor has been available to determine into which category a particular fetus will fall. Studies of large CAMs that were resected *in utero* because they resulted in nonimmune hydrops have shown a higher rate of cellular proliferation and lower rate of apoptosis than normal fetal lung of equivalent gestational age.[21,22] The rapid growth of some CAMs during the late second and early third trimesters may be caused by disregulation of mesenchymal platelet-derived growth factor gene expression driving cellular proliferation.[19]

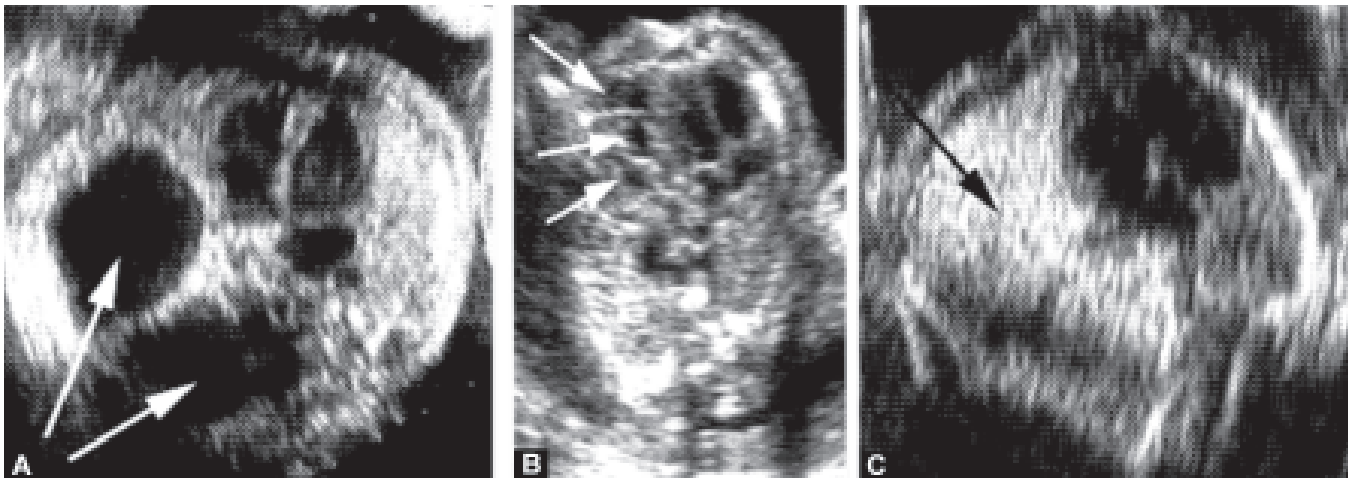

Figures 19.8A to C: Three different subtypes of cystic adenomatoid malformation (CAM) according to the size of the cysts. (A) CAM I; (B) CAM II; (C) CAM III

The diagnosis of CAM relies on the demonstration of a solid or cystic, nonpulsatile intrathoracic tumor.

Stocker et al. proposed a classification of CAM into three subtypes **(Figs 19.8A to C)** according to the size of the cysts—type I has large cysts, type II has multiple small cysts of less than 1.2 cm in diameter and type III consists of a noncystic lesion producing mediastinal shift. The worst prognosis is seen in type III lesions. Associated anomalies are frequently present in type II. Prenatally, the more useful characterization is to identify CAM as either cystic or solid as these provide more useful categories for determining options and prognosis.[23]

Unilateral lesions are often associated with the deviation of the mediastinum in the contralateral side. In bilateral disease, the heart may be severely compressed and this is usually associated with ascites from venocaval obstruction or cardiac compression.

In about 85% of cases, CAM is unilateral and approximately half are microcystic and the other half macrocystic **(Figs 19.9A to C)**. During the third trimester polyhydramnios may develop, which is likely to be due to decreased fetal swallowing, the consequence of esophageal compression by the mass or there may be increased fetal lung fluid production by the abnormal tissue.

Associated Anomalies

The condition is usually isolated but in about 10% of cases there are additional malformations, usually renal, abdominal wall or central nervous system. There is no significant association with chromosomal defects.

Prognosis

Bilateral CAM is a lethal condition while unilateral CAM is associated with a good prognosis which is as follows:

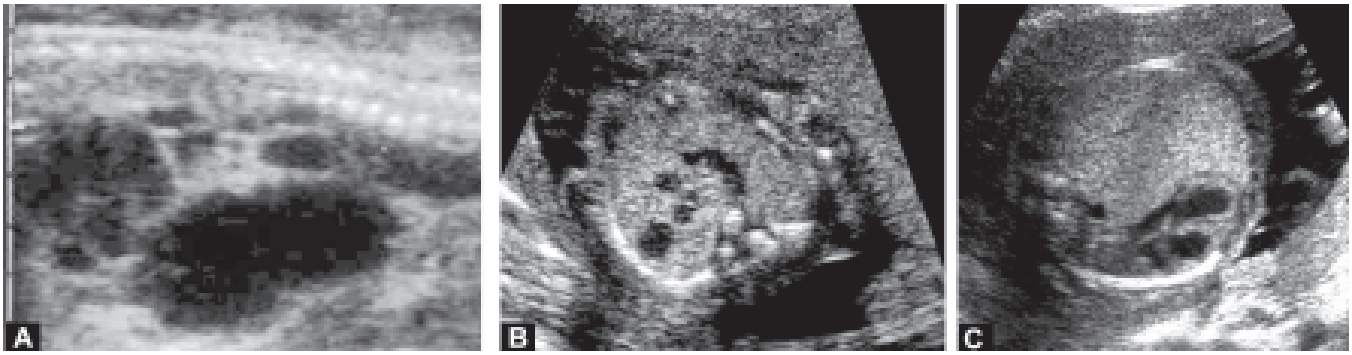

Figures 19.9A to C: (A) Microcystic (cysts < 5 mm in diameter); (B) Mixed; (C) Macrocystic (cysts > 5 mm in diameter) form of cystic adenomatoid malformation (CAM)

- In about 40% of cases there is apparent spontaneous antenatal resolution of the lesion
- In 50%, it remains the same
- In 10%, it enlarges.

In majority of cases, it either remains the same in size or there is an apparent spontaneous antenatal resolution and in a minority of cases it enlarges. Good prognosis has been shown in recent studies, with about half of cases in pregnancies that were allowed to continue resulting in spontaneous regression.[24,25]

In the majority of cases with antenatal resolution, postnatal investigation with chest X-ray, computed tomography (CT) and magnetic resonance imaging (MRI) will demonstrate residual lung disease.

FETAL PLEURAL EFFUSIONS

Fetal pleural effusions can be primary or secondary, with an estimated incidence of 1:10,000–15,000 pregnancies. Primary pleural effusions, correctly termed "hydrothorax" antenatally are due to lymphatic leakage and can be unilateral or bilateral. Secondary pleural effusions are usually part of a generalized picture of fluid retention in nonimmune hydrops and their prognosis is mainly dependent on the underlying pathology. Pleural effusions were first reported antenatally in 1977.[26]

Their optimal antenatal management is controversial because some fetuses are not significantly compromised, whereas others either die *in utero* from secondary hydrops or at birth from pulmonary hypoplasia.

The first step on detecting a fetal pleural effusion should be to determine whether it is primary or secondary. Primary fetal hydrothorax is a diagnosis of exclusion and the work-up is similar to that for hydrops; maternal serology to exclude congenital infections (toxoplasmosis, rubella, cytomegalovirus, syphilis, herpes and parvovirus B195); blood type and antibody screen to rule out immune hydrops; Kleihauer–Betke test to exclude fetomaternal hemorrhage and Doppler evaluation of the peak systolic velocity (PSV) in the middle cerebral artery (MCA) to exclude fetal anemia. Fetal anemia will always present with ascites before a pleural effusion appears. Fetal karyotype is recommended because aneuploidy (predominantly trisomy 21 and 45, X) has been reported in 6–17% of fetuses with hydrothorax, the vast majority of which are hydropic.[27]

The fact that pleural effusions are associated with structural fetal malformations in 25% of cases highlights the importance of meticulous ultrasound and echocardiographic evaluations.[28] Pulmonary causes of secondary hydrothorax, such as congenital cystic adenomatoid malformation (CCAM), bronchopulmonary sequestration (BPS) or congenital diaphragmatic hernia (CDH), should be excluded.

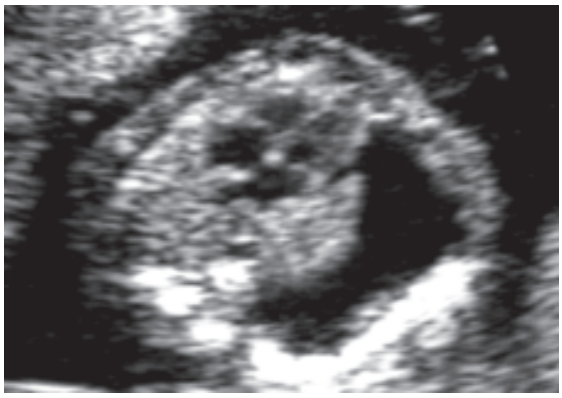

Figure 19.10: Ultrasound appearances of pleural effusion

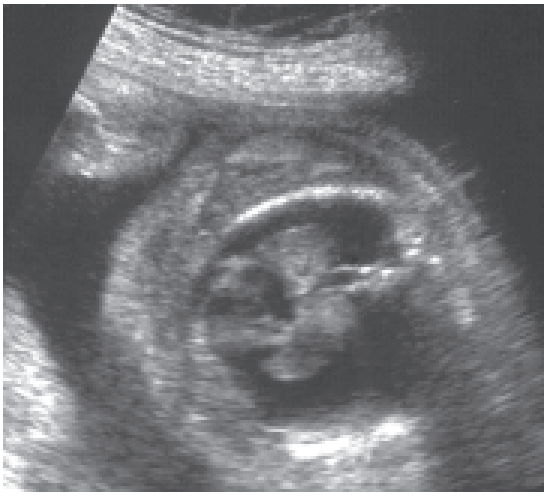

Figure 19.11: Thoracic shunting of pleural effusion. Shunt can be seen at the posterior paraspinal site

Ultrasound appearances of pleural effusion is shown in **Figures 19.10 and 19.11**.

Prognosis

Irrespective of the underlying cause, infants affected by pleural effusions usually present in the neonatal period with severe, and often fatal, respiratory insufficiency. This is either a direct result of pulmonary compression caused by the effusions or due to pulmonary hypoplasia secondary to chronic intrathoracic compression. The overall mortality of neonates with pleural effusions increases from low in infants with isolated pleural effusions to very high in those with gross hydrops.[26]

Chromosomal abnormalities, mainly trisomy 21, are found in about 5% of fetuses with apparently isolated pleural effusions.

Isolated fetal pleural effusions may resolve spontaneously antenatally, or they may persist. In some cases, postnatal thoracocentesis may be sufficient but in others the chronic compression of the fetal lungs can result in pulmonary hypoplasia and neonatal death. Additionally, mediastinal compression may lead to the development of fetal hydrops and polyhydramnios, which are associated with a high risk of premature delivery and subsequent perinatal death.[26]

Parameters associated with a better prognosis include later gestational age at diagnosis, spontaneous resolution of the effusion prior to delivery, lack of hydrops, isolated effusion and unilateral effusion.

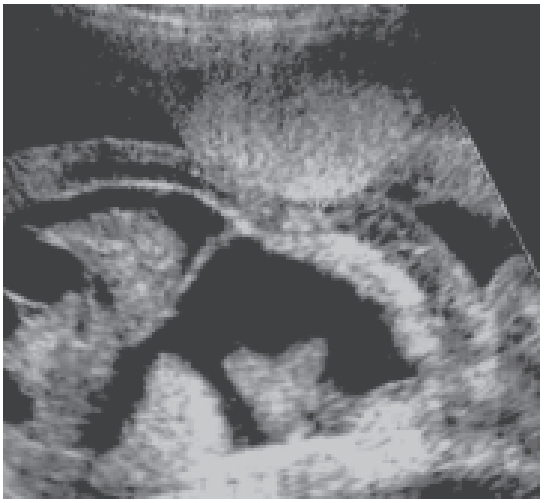

Figure 19.12: Sagittal scan of the fetal thorax demonstrating bilateral hydrothorax and the sequestered lung. Note also evidence of ascites and subcutaneous edema

LUNG SEQUESTRATION

Pulmonary sequestration is a rare developmental abnormality in which a segment of lung parenchyma is isolated from the normal lung tissue. It usually does not communicate with an airway and receives its blood supply from the systemic circulation, rather than the pulmonary artery.

The sequestered lung tissue may either be adjacent to the normal lung and covered by the same pleura (intralobar sequestration) or it may have its own pleura (extralobar sequestration). Intralobar sequestration typically affects the lower lobes.[29] In extralobar sequestration, the lung is most commonly located between the lower lobe and diaphragm but it can also be found below the diaphragm in the abdomen.

Ultrasonically, the abnormal lung appears as an echogenic intrathoracic or intra-abdominal mass. In about 50% of cases there is an associated pleural effusion. Polyhydramnios is a frequent complication **(Fig. 19.12).**

Associated Anomalies

Extrapulmonary anomalies are found in about 60% of cases with extralobar sequestration and 10% of those with intralobar sequestration. The commonest abnormalities are diaphragmatic hernia and cardiac, renal, cerebral or vertebral defects **(Figs 19.13A to D)**.

Prognosis

The condition carries a very poor prognosis, due to pulmonary hypoplasia or the associated malformations. Some cases may not become apparent until later in life, the individual complaining of repeated chest infections or hemorrhage.[29]

Syndromic Associations with Congenital Anomalies of the Fetal Thorax

Conditions to Consider in the Presence of a Diaphragmatic Hernia

Pallister-Killian syndrome (Tetrasomy 12p): In addition to diaphragmatic hernia, polyhydramnios, rhizomelic limb shortening and an abnormal facial profile with prominent philtrum are found in association with fetal somatic overgrowth. These features are variable and may even be absent. Pallister-Killian syndrome is a chromosomal abnormality with mosaicism for an isochromosome of 12p, which is an extra chromosome comprising the two short arms of 12. Thus, the fetus has four copies of 12p in some cell lines. In the neonate, this chromosome abnormality is usually present in skin fibroblasts but not usually in blood. For this reason, the cytogenetic abnormality may not be detected in either chorionic villi or fetal blood, the latter being the least indicated method because of the low frequency of the isochromosome in lymphocytes. In cases thought to have a normal karyotype following CVS, amniocentesis should be considered if this diagnosis is suspected, as this is the most likely to reveal the mosaicism, particularly if fluorescent *in situ* hybridization (FISH) and especially interphase FISH on noncultured cells is performed.[29]

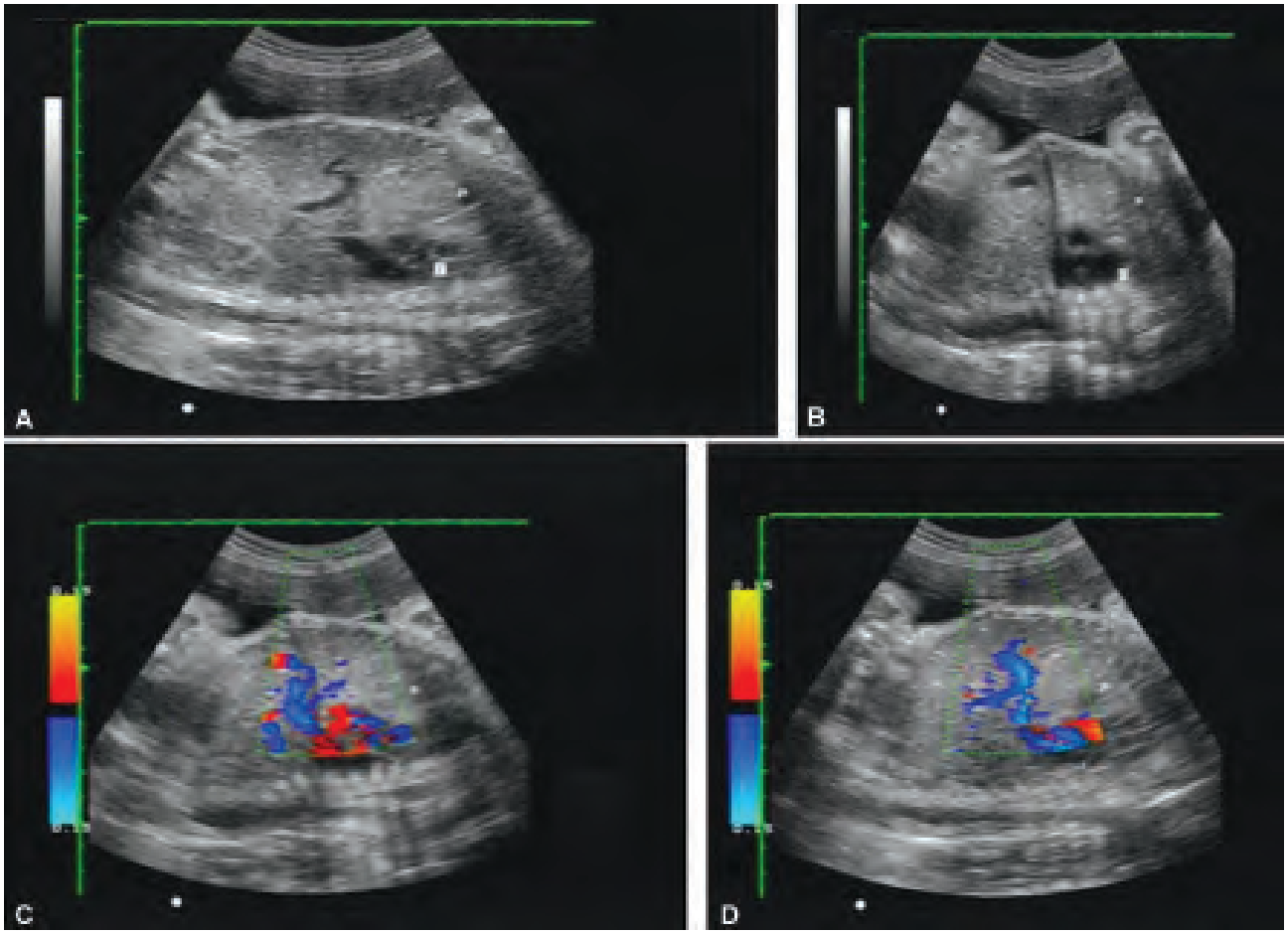

Figures 19.13A to D: Nonfunctioning pulmonary parenchyma, separated from normal lung, blood supply from the systemic circulation, has its own pleura

Fryns syndrome: Fryns syndrome is a rare autosomal recessive disorder of multiple congenital abnormalities, but can occur in around 4% of fetuses with CDH and multiple anomalies with normal chromosomes. Major diagnostic criteria include CDH, distal limb and nail hypoplasia and abnormal facies.[30] Prenatally, suspicion of this condition is raised in fetuses with a CDH, IUGR and an increased nuchal fold. Cataracts may be detected later in gestation.

Simpson-Golabi-Behmel syndrome: This X-linked recessive disorder is due to mutations in *glypican 3* (Xq26). There is overlap with the features of Pallister-Killian syndrome and BWS, with overgrowth of prenatal onset that continues postnatally. The birth weight and birth occipital-frontal circumference (OFC) of affected males are usually both > 97th centile. They may have cardiac and gastrointestinal malformations and polydactyly.

Maternal AFP is elevated. Unless there are life-threatening malformations, this is not a lethal condition with most boys presenting at later age with other manifestations of the syndrome such as learning difficulties and overgrowth.[31]

Cornelia de Lange syndrome: Cornelia de Lange (de Lange) syndrome is a rare sporadic syndrome with a birth incidence of about 1 in 50,000 and is caused by new mutations in Nipped-B homolog (Drosophila) (NIPBL).[31] The fetus has IUGR (often developing in the third trimester), with upper limb anomalies ranging from short forearms with small hands and tapering fingers to oligodactyly and severe limb reduction defects. Diaphragmatic herniae are recognized but a relatively rare feature, although may be more frequently represented in cases presenting prenatally.

There are distinctive craniofacial features (microbrachycephaly, depressed nasal bridge with anteverted nares, long smooth overhanging philtrum and micrognathia) which may be recognized with prenatal ultrasound and are clearly seen at birth.[32]

Maternal serum pregnancy-associated plasma protein-A is reported to be significantly reduced in de Lange syndrome.

CONGENITAL CYSTIC LUNG LESIONS

If a cystic lung lesion is isolated and unilateral karyotyping is not indicated. "Bilateral" lesions may represent laryngeal/tracheal atresia, thus consideration should be given to the autosomal recessive Fraser-crytophthalmos syndrome where the likely mechanism for pulmonary hyperplasia is retention of fetal lung fluid by laryngeal or tracheal obstruction.

Fraser Syndrome (Fraser-cryptophthalmos Syndrome)

Fraser syndrome is inherited in an autosomal recessive fashion and can be caused by mutation in the FRAS1 gene or in the FREM2 gene and there may be yet further unidentified genes. The classic features are a combination of cryptophthalmos, laryngeal stenosis, syndactyly, renal agenesis and genital abnormalities (fused labia and enlarged clitoris).[32] It is now recognized that not all infants with Fraser syndrome have cryptophalmos. Some authors observed pulmonary hyperplasia and laryngeal stenosis in two siblings with Fraser syndrome. Markedly enlarged echogenic lungs may be demonstrable on ultrasound in this condition.

Esophageal/Tracheoesophageal Atresia

Tracheoesophageal atresia results from incomplete separation of the foregut into the trachea and esophagus and 85% of cases are associated with esophageal atresia. About half the number of infants with a tracheoesophageal atresia will have other malformations, in particular anomalies of the heart, limbs and vertebrae. Chromosomal anomalies, including trisomy 21, trisomy 18 and deletion of 22q11, developmental and genetic syndromes are relatively frequent and need to be carefully considered and investigated.[33] If the pregnancy is terminated, a detailed postmortem examination should be performed to establish if the malformation is isolated or part of a syndrome or association. This should include cytogenetic testing and consent for tissue/DNA storage.

REFERENCES

1. Zalel Y, Lipitz S, Soriano D. The development of the fetal sternum: a cross-sectional sonography. Ultrasound Obstet Gynecol. 1999;13(3):187-90.
2. Harm-Gerd K, BlaasSturla H, Eik-Nes. Sonographic development of the normal foetal thorax and abdomen across gestation. Prenat Diagn. 2008;28(7):568-80.
3. Malas MA, Evcil EH, Desdicioglu K. Size and location of the fetal diaphragma during the fetal period in human fetuses. Surg Radiol Anat. 2007;29(2):155-64.
4. de Vries JIP, Fong BF. Normal fetal motility: an overview. Ultrasound Obstet Gynecol. 2006;27(6):701-11.
5. Whitsett JA, Wert SE, Trapnell BC. Genetic disorders influencing lung formation and function at birth. Human Mol Genet. 2004;13:207-15.
6. Kalache KD, Espinoza J, Chaiworapongsa T. Three-dimensional ultrasound fetal lung volume measurement: a systematic study comparing the multiplanar method with the rotational (VOCAL) technique. Ultrasound Obstet Gynecol. 2003;21(2):111-8.
7. Peralta CF, Cavoretto P, Csapo B, et al. Assessment of lung area in normal fetuses at 12–32 weeks. Ultrasound Obstet Gynecol. 2005;26(7):718-24.
8. Jani J, Peralta CFA, Benachi A, et al. Assessment of lung area in fetuses with congenital diaphragmatic hernia. Ultrasound Obstet Gynecol. 2007;30(1):72-6.
9. Chang CH, Yu CH, Chang FM, et al. Volumetric assessment of normal fetal lungs using three-dimensional ultrasound. Ultrasound Med Bio. 2003;29(7):935-42.
10. Peralta CF, Cavoretto P, Csapo B, et al. Lung and heart volumes by three-dimensional ultrasound in normal fetuses at 12–32 weeks' gestation. Ultrasound Obstet Gynecol. 2006;27(2):128-33.
11. Osada H, Iitsuka Y, Masuda K, et al. Application of lung volume measurement by three-dimensional ultrasonography for clinical assessment of fetal lung development. J Ultrasound Med. 2002;21(8):841-7.
12. Malinger G, Levine A, Rotmensch S. The fetal esophagus: anatomical and physiological ultrasonographic characterization using a high-resolution linear transducer. Ultrasound Obstet Gynecol. 2004;24(5):500-5.
13. Brantberg A, Blaas HG, Haugen SE, et al. Esophageal obstruction-prenatal detection rate and outcome. Ultrasound Obstet Gynecol. 2007;30(2):180-7.
14. Variet F, Bousquet F, Clemenson A, et al. Congenital diaphragmatic hernia. Two cases with early prenatal diagnosis and increased nuchal translucency. Fetal Diagn Ther. 2003;18(1):33-5.
15. Kitano Y, Nakagawa S, Kuroda T, et al. Liver position in fetal congenital diaphragmatic hernia retains a prognostic value in the era of lung-protective strategy. J Pediatr Surg. 2005;40(12):1827-32.
16. Jani J, Benachi A, Favre R, et al. Lung-to-head ratio and liver position to predict outcome in early diagnosed isolated left sided diaphragmatic hernia fetuses: a multicenter study. Am J Obstet Gynecol. 2004;191:176-82.
17. Deprest J, Jani J, Van Schoubroeck D, et al. Current consequences of prenatal diagnosis of congenital diaphragmatic hernia. Journal of Pediatric Surgery. 2006;41(2):423-30.
18. Ruano R, Benachi A, Joubin L, et al. Three-dimensional ultrasonographic assessment of fetal lung volume as prognostic factor in isolated congenital diaphragmatic hernia. BJOG. 2004;111(5):423-9.

19. Crombleholme T, Coleman B, Hedrick H, et al. Cystic adenomatoid malformation volume ratio predicts outcome in prenatally diagnosed cystic adenomatoid malformation of the lung. J Pediatric Surg. 2002;37(3):331-8.
20. Winters WD, Effmann EL, Nghiam HV, et al. Disappearing fetal lung masses: Importance of postnatal imaging studies. Pediatr Radiol. 1997;27(6):535-9.
21. Cass DL, Quinn TM, Yang EY, et al. Increased cell proliferation and decreased apoptosis characterizes congenital cystic adenomatoid malformation of the lung. J Pediatr Surg. 1998;33:1043-7.
22. Stocker JT, Madewell JE, Drake RM. Congenital cystic adenomatoid malformation of the lung. Classification and morphologic spectrum. Hum Pathol. 1977; 8(2):155-71.
23. Gilbert-Barness E, Debich-Spicer D. Respiratory system. In: Gilbert-Barness E, Debich-Spicer D (Eds). Embryo and fetal pathology. Cambridge, UK: Cambridge University Press. pp. 470-89.
24. Duncombe GJ, Dickinson JE, Kikiros CS. Prenatal diagnosis and management of congenital cystic adenomatoid malformation of the lung. Am J Obstet Gynecol. 2002;187(4):950-4.
25. Laberge JM, Flageole H, Pugash D, et al. Congenital cystic adenomatoid malformation of the lung: prognosis when diagnosed in utero. Saudi Med J. 2004;24(5 Suppl):S33.
26. Yinon Y, Kelly E, Rzan G. Fetal pleural effusions. Best Practice and Research. Clin Obstet and Gynecol. 2008;22(1):77-96.
27. Waller K, Chaithongwongwatthana S, Yamasmit W, et al. Chromosomal abnormalities among 246 fetuses with pleural effusions detected on prenatal ultrasound examination: factors associated with an increased risk of aneuploidy. Genet Med. 2005;7(6):417-21.
28. Frazier AA, Dosado DE, Cristenson ML, et al. Intralobar seqestration: radiologic-pathologic correlation. Radiographics 1997; 17(3):725-45.
29. Doray B, Girard-Lemaire F, Gasser B, et al. Pallister-Killian syndrome: difficulties of prenatal diagnosis. Prenat Diagn. 2002;22(6):470-7.
30. Slavotinek AM. Fryns syndrome: a review of the phenotype and diagnostic guidelines. Am J Med Genet. 2004;124A(4): 427-33.
31. Slavotinek AM. Single gene disorders associated with congenital diaphragmatic hernia. Am J Med Genet C Semin Med Genet. 2007;145C(2):172-83..
32. Hurst J, Firth H, Chitty L. Syndromic associations with congenital anomalies of the fetal thorax and abdomen. Prenat Diagn. 2008;28:676-84.
33. Shaw-Smith C. Esophageal atresia, tracheo-esophageal fistula, and the VACTERL association: review of genetics and epidemiology. J Med Genet. 2006;43(7):545-54.

CHAPTER 20

Three- and Four-dimensional Evaluation of the Fetal Heart

Carmina Comas Gabriel

INTRODUCTION

During the past 25 years, two-dimensional (2D) imaging of the fetal heart has evolved into a sophisticated and widely practiced clinical tool, but most heart diseases still go prenatally undetected despite routine fetal ultrasound evaluations. Over the next few years, tremendous advances in fetal cardiac imaging, including three-dimensional (3D) imaging, promise to revolutionize both the prenatal detection and diagnosis of congenital heart diseases. Image resolution continues to improve year after year, allowing earlier and better visualization of cardiac structures. This chapter reviews the possibilities of the 3D and four-dimensional (4D) fetal echocardiography. Three-dimensional imaging of the fetal heart may improve the detection of outflow tract abnormalities and facilitate comprehension of complex forms of congenital heart diseases (CHDs). This review highlights the potential of acquiring a digital volume data set of a heart cycle for later offline examination, either for an offline diagnosis, a second opinion (e.g. via Internet link) or for teaching fetal echocardiography to trainees and sonographers. On the other hand, other imaging modalities, such as Doppler tissue imaging and magnetic resonance imaging, continue to evolve and to complement two- and three-dimensional sonographic imaging of the fetal heart. As a result of these ongoing advances in prenatal detection and assessment of CHD, this is an exciting and promising time for the field of fetal cardiac imaging.[1]

IMPACT OF CONGENITAL HEART DISEASES: EPIDEMIOLOGY AND POPULATION AT RISK

Prenatal detection of fetal congenital heart defects remains the most problematic issue of prenatal diagnosis.[2] Major CHDs are the most common severe congenital malformations, with an incidence of about five in a thousand live births, whenever complete ascertainment is done and minor lesions are excluded.[2,3] Congenital heart anomalies have a significant effect on affected children's life with up to 25–35% mortality rate during pregnancy and the postnatal period, and it is during the first year of life, when the 60% of this mortality occurs. Moreover, major CHDs are responsible for nearly 50% of all neonatal and infant deaths due to congenital anomalies, and it is likely to be significantly higher if spontaneous abortions are considered. Although CHDs used to appear isolated, they are frequently associated with other defects, chromosomal anomalies and genetic syndromes. Their incidence is six times greater than chromosomal abnormalities and four times greater than neural tube defects.[2-4] Nonetheless, structural cardiac defects are among the most frequently missed abnormalities by prenatal ultrasound.[5] Although, the at-risk population-based approach has been crucial in decreasing disease, prenatal diagnosis of CHD remains largely a scenario of too much effort for too few diagnoses. Clinicians need to re-examine the reasons for this shortfall and redefine new strategies to improve the efficacy of our effort.

It must be remembered that 90% of congenital heart defects occur in low-risk mothers. The way forward to

increase detection of CHD is to improve the effectiveness of screening programs so that a higher number of cases from low-risk populations are referred for a specialized scan. The positive aspect of screening for cardiac defects compared with other anomalies (e.g. Down syndrome, neural tube defects) is that it does not automatically result in the termination of pregnancy in most cases. It is one of the anomalies where optimizing management of the neonate in the perinatal period could improve outcome. Improved morbidity/mortality has been clearly shown as a result of prenatal diagnosis in the outcome of all forms of CHD, which are dependent on the patency of the arterial duct in the immediate postnatal period, being the transposition of the great arteries, the single most important lesion to diagnose prenatally.[6]

All these reasons emphasize the role of sonography in prenatal diagnosis of congenital heart abnormalities.

PRENATAL DIAGNOSIS OF CONGENITAL HEART DISEASES: CURRENT SITUATION

Screening Techniques

Most major CHDs can be prenatally diagnosed by detailed transabdominal second-trimester echocardiography at 20–22 weeks' gestation.[2,4,7-9] The identification of pregnancies at high risk for CHD needing referral to specialist centers is of paramount importance in order to reduce the rate of overlooked defects.[9,10] However, the main problem in prenatal diagnosis of CHD is that the majority of cases take place in pregnancies with no identifiable risk factors. Therefore, there is wide agreement that cardiac ultrasound screening should be introduced as an integral part of the routine scan at 20–22 week. In the 1990s, the American Institute of Ultrasound in Medicine and the American College of Radiology incorporated the four-chamber view into their formal guidelines for the screening fetal ultrasound.[11,12] Although early investigators found the four-chamber view to have a high sensitivity for the prenatal detection of CHD, subsequent studies have found this view to be far less sensitive. Even in the best hands, this plane may fail to detect significant percentage of major frequently ductal-dependent CHD. Many investigators have demonstrated an incremental value of adding outflow tracts to the routine screening fetal ultrasound.[13,14] When applied to low-risk population, scrutiny of the four-chamber view allows only the detection of 40% of the anomalies while additional visualization of the outflow tracts and the great arteries increase the rate up to 60–70%.[4,7,8] The systematic incorporation of the four–chamber view and outflow tracts into the routine screening, fetal ultrasound represents an important advance in fetal cardiac image.

The Standard Fetal Cardiac Examination Protocol

The basic fetal cardiac screening examination entails an analysis of the four-chamber view, obtained from an axial plane across the fetal thorax. If technically feasible, optional views of the outflow tracts can be obtained as a part of an extended cardiac screening examination. The systematic incorporation of the four-chamber view and outflow tracts into the routine screening fetal ultrasound represents an important advance in fetal cardiac image. Summarizing the data from screening studies, a detection rate of less than 10% can be expected if the heart is not explicitly examined, a rate of 10–40% detection if the four-chamber view is visualized and a rate of 40–80% if the visualization of the great vessels is added.[4,7,8]

In a high-risk pregnancy, in addition to the information provided by the basic screening exam, a detailed analysis of cardiac structure and function may further characterize visceroatrial situs, systemic and pulmonary venous connections, foramen ovale mechanism, atrioventricular connections, ventriculoarterial connections, great vessels relationships and sagittal views of the aortic and ductal arches. Additional sonographic techniques can be used for this purpose, as Doppler ultrasonography or M-mode modality.

Color Doppler is an essential tool for the fetal cardiologist, but is not considered standard of care for a routine obstetric scan. Color Doppler findings can substantially increase the likelihood of prenatal diagnosis and decrease the incidence of false-positive diagnosis. Spectral power Doppler can also add important information to normal and abnormal color flow patterns.

Recently, a sequential segmental approach for the complete evaluation of fetal heart disease as a screening technique has been described using five or six short-axis views from the fetal upper abdomen to the mediastinum.[15,16] The transverse view of the fetal upper abdomen is obtained to determine the arrangement of the abdominal organs, which, in most cases, provides the important clues to the determination of the atrial arrangement. The four-chamber view is obtained to evaluate the atrioventricular junctions. The views of the left and right ventricular outflow tracts are obtained to evaluate the ventriculoarterial junctions. The three-vessel view and the aortic arch view are obtained for

the evaluation of the arrangement and size of the great arteries, which provides the additional clues to the diagnosis of the abnormalities involving the ventriculo-arterial junctions and the great arteries.

Suggestions to Improve Detection Rate of Congenital Heart Defects

Inadequate examination is likely to be the most common cause of heart defects being overlooked in the four-chamber view. Chaoui have suggested some hints to improve visualization of the heart.[17] Examination of the fetal heart should be carried out at every second-trimester screening examination. This should ideally be performed at 20–22 weeks' gestation, using a 5-MHz transducer. Optimal analysis of the heart may be achieved by magnification of the image, using the zoom function, so that the heart fills a third to half of the screen and by the use of the cine-loop to assess the different phases of the cardiac cycle. Established ultrasound screening programs also increase detection rates.[5] They have to focus on equivocal prenatal signs of the heart abnormality, so called borderline findings, which should raise suspicion for referral to a specialist, as echogenic foci, small pericardial effusions, mild discrepancy in ventricular size, tricuspid regurgitation or deviation of the cardiac axis. Since heart anomalies developing *in utero* can be missed at second-trimester scan, fetal heart should be examined if third-trimester scanning is performed. The use of color Doppler during cardiac scanning will also improve detection rates, increasing the speed and the accuracy of the fetal cardiac scan, although it is controversial to use this modality for screening purposes.

Finally, introduction of 3D technology in the field of the prenatal diagnosis has allowed a better evaluation of the static anatomical structures. Nevertheless, its application in the study of the fetal heart has not involved a significant advance up to now, since being the fetal heart a structure in rapid movement, the conventional 3D image appeared distorted without providing significant diagnostic information.

HISTORY OF FETAL ECHOCARDIOGRAPHY

The birth of fetal echocardiography occurred in the late 1970s, when fetal heart movements were first visualized by primitive A-scan ultrasound or by M-mode techniques. Since then, different technologies and modalities have been incorporated in order to improve the diagnostic accuracy and possibilities in this field. We review the diagnostic tools that are available and the potential roles of fetal echocardiography in the field of fetal medicine.[18]

Real-time ultrasound is still the gold standard for the structural evaluation of the fetal heart. In the most sophisticated ultrasound machines, there is an ideal setting for fetal heart evaluation which is based on a high image resolution, a high frame rate and good penetration. Two main features have facilitated the prenatal assessment of the fetal heart: the use of transducers with a high frequency (5–7MHz transducers) and the incorporation of the cine-loop, and the zoom functions. Tissue harmonic imaging (THI) has recently been introduced to enhance diagnostic performance in individuals with limited acoustic window mainly due to obesity or abdominal scarring.[19] Their different behavior from the fundamental frequency ultrasound, the energy of which decreases linearly with depth, is the reason why the use of THI has been shown to improve image quality in some circumstances, particularly in obese individuals.

Time motion (M-mode) was a revolutionary tool in fetal cardiology when simultaneous real-time visualization became available. First used for cardiac biometry, it was soon relegated to a second line since such measurements became easier using the cine-loop techniques to selectively image diastole and systole. Two main fields of interest are still in the domain of M-mode: the assessment and classification of fetal arrhythmias (where this mode can document the atrioventricular conduction by putting the cursor simultaneously in an atrial and ventricular structure) and to assess myocardial contractility (calculating indices such as shortening fraction, ejection fraction, etc.).

The acquisition of flow velocity waveforms from different fetal cardiac structures and vessels by using *pulsed or continuous wave Doppler* ultrasound enables a noninvasive quantification of perfusion: Evaluation of peak velocities in different sites of the circulatory system, measurement of contractility indices, stroke volume, and the recent incorporation of the assessment of coronary and venous system are some examples. The pathological conditions investigated are no longer confined to fetal heart defects but have expanded to include other fetal conditions involving the cardiovascular system. Investigation of intracardiac flow in severe intrauterine growth restriction, diabetes or fetal anemia represents some examples of the big potential of this technical modality.

In addition to grayscale examination of the fetal heart, *color Doppler* is now considered to be a second-line investigation for cardiac evaluation. This method

allows rapid orientation within the fetal heart and completes the evaluation supplied by grayscale information. Once abnormal flow is suspected, quantification by Doppler flow velocities waveforms becomes mandatory.

Color Doppler is an essential tool for the fetal cardiologist, but is not considered standard of care for a routine obstetric scan.

Power Doppler ultrasound is a technique introduced in the early 1990s using the information from the amplitude of the Doppler signal rather than the frequency shift and direction, opening the possibility of displaying flow independently of its velocity and direction. Since this technique is significantly more sensitive than conventional color Doppler, it has been applied in regions with low flow and small vessels. This technique can be used in fetal cardiology, facilitating the detection of some CHD (such as small ventricular septal defects) and enabling spatial orientation of the great vessels. On the other hand, we cannot be informed about the blood direction or turbulences. However, these characteristics make it suitable for the 3D power Doppler evaluation of the cardiovascular system.

In *tissue Doppler echocardiography (TDE)*, color-coding is used to visualize wall movements rather than blood flow. Tissue Doppler echocardiography has only recently been applied to the fetus, with promising preliminary results.[20,21] Color and power Doppler mapping could be applied on a regular high-resolution ultrasound machine by sampling the relatively high reflected acoustic energy from cardiac walls. Fetal TDE is a new technique that can provide additional insights into fetal cardiac function that are not available with the conventional approach.

Although *fetal 3D* imaging currently faces important image resolution concerns, the technique has the potential to improve markedly both the prenatal detection and diagnosis of CHD. Already demonstrated to improve the diagnosis of CHD in infants, children and adults, 3D imaging of the fetal heart offers important potential advantages over conventional 2D imaging. By acquiring volumetric data within a few seconds from a single window, 3D imaging may reduce scanning time and operator dependence. For screening the low-risk pregnancy, 3D imaging may facilitate visualization of the four-chamber view and outflow tracts, particularly when 2D imaging fails because of time constraint, limited window or sonographer inexperience. Volume data sets could be transmitted electronically to experts for further evaluation. For teaching purposes, the volumetric data sets could be sent to a remote virtual scanning station. Finally, quantitative measurements using 3D imaging promise to be more accurate and reproducible than those derived from 2D imaging. Sophisticated volume processing algorithms that allow quantitative measurements of volume and function may offer additional insights into cardiac function and development. Recently, *spatiotemporal image correlation (STIC)* has been introduced as a new 3D technique allowing the automatic acquisition of a volume of data from the fetal heart, being displayed as a cineloop of a single cardiac cycle. This technique allows dynamic multiplanar slicing and surface rendering of heart anatomy. Spatiotemporal imaging correlation, in combination with color or power Doppler ultrasound, is a promising new tool for multiplanar and 3D/4D rendering of the fetal heart, making possible the assessment of hemodynamics changes throughout the cardiac cycle. Since its commercial introduction in 2002, some foreign authors have published their experience in the management and application of this new technology. In the following section, we deeply review this topic and present the first study on a nationwide scale with the introduction of the new technology in our environment.

Telemedicine represents an emerging but potentially critical advance in prenatal screening for CHD.[22,23] Telemedicine, like 3D ultrasound, may enable fetuses to be scanned in remote sites, with their respective studies reviewed instantaneously or within minutes at more centrally located, highly specialized centers, avoiding the need to transport the pregnant patient.

NEW PERSPECTIVES IN THREE- AND FOUR-DIMENSIONAL FETAL ECHOCARDIOGRAPHY

Rapid advances in graphics computing and microengineering have offered new techniques for prenatal cardiac imaging. Some of them can be noninvasively applied to both clinical and laboratory settings, including dynamic 3D echocardiography, myocardial Doppler imaging, harmonic ultrasound imaging and B-flow sonography. Appropriate use of these new tools will not only provide unique information for better clinical assessment of fetal cardiac disease but also offer new ways to improved understanding of cardiovascular development and pathogenesis.[24] This improvement in imaging technology combined with new sophisticated computer processing systems promise to revolutionize both prenatal detection and diagnosis of CHD.[25] Even 2D imaging still remains the principal diagnostic modality to confirm normal cardiac development and in cases of congenital heart abnormalities, new

techniques (dynamic 3D color Doppler ultrasound, Doppler-gated 3D fetal echocardiography and 3D multiplanar time-motion ultrasound) are now technically feasible for a wide range of lesions, and may provide additional information of clinical value in some selected cases. In this sense, new terms have been recently incorporated in our practice, for describing various multidimensional imaging features, including "three-dimensional", "four-dimensional", "real-time", "cardiac gating", "online" or "offline".[26] This chapter reviews the possibilities of 3D and 4D fetal echocardiography, where a volume data set can be acquired as a static volume, as a real-time 3D volume or as an offline 4D volume cine using STIC software.[27] Spatial-temporal image correlation is explained and the potentials of this modality are particularly emphasized in the next section.

Fetal Cardiac Screening

As current methods to screen the fetus for cardiac abnormalities continue to miss most CHD, a more effective approach to screening the low-risk population for fetal heart disease would represent an important clinical advance. In this sense, preliminary results suggest that 3D and 4D technologies applied to prenatal diagnosis have the potential to function as a screening tool for fetal heart diseases. Investigators are trying to demonstrate the feasibility and applications of different modalities, such as real-time,[28] gated reconstructive 3D imaging[29] or fetal real-time 3D echocardiography (RT3DE).[30]

Feasibility to Obtain Greater Number of Cardiac Views

Three-dimensional ultrasonography permits a greater number of cardiac planes to be extracted from volume data than does 2D standard ultrasonography. Bega's study compares the percentage of cardiac planes obtained by conventional 2D or 3D ultrasonography, demonstrating higher successful view by the latter technique for the left and right outflow tracts and ductal and aortic arches.[31]

Improvement of Basic Cardiac Views in Unfavorable Fetal Positions

Among the basic cardiac views in fetuses in anterior spine positions, 3D ultrasound improves the visualization of pulmonary outflows tracts and provides reliable alternate technique for clinical use.[32]

Evaluation of Fetal Cardiac Function

Three-dimensional echocardiography can provide estimates of ventricular volume and function.[33] Particularly, 3D imaging can provide estimates of ventricular volume changes in fetal hearts with abnormal ventricular morphology that cannot be easily performed by 2D echocardiography.[34] This technique is a promising tool for the evaluation of fetuses with CHD and cardiac dysfunction, and it may provide insight into evolving CHDs.

Dynamic Three-Dimensional Color Doppler Ultrasound

By using simultaneously two ultrasound machines, one grayscale and color Doppler echocardiography and another one for spectral Doppler ultrasound, a novel technique has made possible the prenatal visualization of the spatial distribution and the true direction of intracardiac flow of blood in 4D in the absence of motion artifacts. This technique suggests that diagnosis of cardiac malformations can be made on the basis of morphological and hemodynamics changes throughout the entire cardiac cycle, offering significant information complementary to conventional techniques.[35]

Doppler-Gated Three-Dimensional Fetal Echocardiography

Even 2D imaging remains the principal diagnostic modality to confirm normal or abnormal cardiac development, Doppler-gated 3D fetal echocardiography is technically feasible for a wide range of lesions and may provide additional information of clinical value in some selected cases.[36] Gated 3D fetal echocardiography provides significantly better visualization and comprehension of cardiac anatomy than nongated 3D fetal echocardiography. The superiority of gated over nongated 3D fetal echocardiography appears to come from both improved image quality and the anatomic clues that derive from the ability to view cardiac motion.[29]

Real-Time Three-Dimensional Echocardiography

Conventional prenatal screening for CHD involves a time-consuming and highly operator-dependent acquisition of the four-chamber view and outflow tracts. In response, many investigators have demonstrated the potential for gated, reconstructive 3D echocardiography to evaluate the fetal heart. Reconstructive 3D echo-

cardiography has been shown to simplify and shorten the acquisition component of fetal cardiac imaging. However, reconstructive 3D fetal cardiac imaging reconstructs a volume of data following the sequential acquisition of a series of planes. As a result, reconstructive approaches suffer from artifacts related to cardiac gating and random fetal and maternal motion. In contrast, RT3DE acquires a volume of data virtually instantaneously, without the need for cardiac gating and with less potential for artifacts. By acquiring the entire fetal heart instantaneously as a single volume, RT3DE may facilitate fetal cardiac screening. In this sense, preliminary studies suggest a high sensitivity for detecting CHD (93%), although specificity is low (45%), with a high rate of "cannot determine" responses and false-positive artifacts.[30] These preliminary results suggest that RT3DE has the potential to function as a screening tool for fetal heart disease. However, artifacts must be recognized and minimized, resolution must improve, and substantial training will be necessary prior to widespread clinical use.

Three-Dimensional Power Doppler Ultrasound

In the recent years few reports and studies demonstrated that the 3D power Doppler ultrasound (3D-PDU) helps in the reconstruction of the vessels of interest and thus improves the understanding of the spatial appearance of the vascular tree.[37]

Three-Dimensional Multiplanar Time-Motion Ultrasound

This new technique enables the easy acquisition of optimal M-mode traces from different heart structures. Because offline plane positioning is possible on 3D multiplanar reconstruction, M-mode traces can be obtained from different stored cardiac structures independently of the fetal position.[38]

Spatiotemporal Image Correlation

Spatiotemporal image correlation is a new approach for clinical assessment of the fetal heart. This feature offers an easy-to-use technique to acquire data from the fetal heart and its visualization in a 4D sequence. The acquisition is performed in two steps. First, data is acquired by a single, automatic volume sweep. In the second step, the system analyzes the data according to their spatial and temporal domain and processes a 4D sequence. This sequence presents the heart beating in real-time in a multiplanar display. The examiner can navigate within the heart, re-slice and produce all the standard planes necessary for comprehensive diagnosis.

The acquisition of the 3D volume information is based on initial application of 2D imaging techniques including grayscale, Doppler, Power Doppler and B-flow modalities. Once the cardiac volume is obtained, a combination of postprocessing tools such as surface mode, minimal mode, transverse rendering, inversion and glass body modes allow preferential display of various features of the fetal heart. Motion display modes including cineloop and STIC in combination with automated and semi-automated display of examination planes opens a whole new array of diagnostic possibilities in clinical practice.[39]

New Reconstructive Approaches

Real-time 3D echocardiography with instantaneous volume-rendered displays of the fetal heart represents a new approach to fetal cardiac imaging with tremendous clinical potential.[28] New plans and views, not visualized in conventional fetal 2D echocardiography, can be generated with minimal processing of rendered image displays.

Virtual Echocardiography by Internet Link

A complete virtual cardiological examination can be achieved in stored 3D volumes of the fetal heart and transmitted to a tertiary fetal cardiology center via the Internet. Previous experiences have demonstrated that 3D virtual cardiac examination is possible.[40,41] The use of the internet link has major implications, particularly for situations in which the scanning center is geographically remote from the tertiary center, or facilitating a second opinion diagnosis.

CLINICAL APPLICATION OF 3D or 4D IN FETAL CARDIOVASCULAR SYSTEM

The clinical application of 3D or 4D in prenatal visualization of the fetal cardiovascular system is closely related to the regions of interest known from the application of color and power Doppler ultrasound: vessels of the placenta, umbilical cord, abdomen, kidneys, lung, brain and fetal tumors as well as the heart and great vessels.[37]

Peripheral Vascular System in 3D

Umbilical Cord and Placenta

From Chaoui experience, it seems to be the structure most easily accessible to 3D throughout pregnancy. Intraplacental vessel network architecture can be visualized with this method. Abnormalities such as

placenta previa, vasa previa or velamentous insertion can be demonstrated as well as single umbilical artery or less important conditions as the connecting vessels in twin pregnancies, nuchal cord or true or false knot.[37,42]

Intra-abdominal Vessels

The vessels of interest are the umbilical vein, the ductus venosus, the portal vein, the hepatic veins, splenic vessels, inferior vena cava and abdominal aorta. Since the application of color Doppler and the recent intensive study of the ductus venosus, abnormalities of intrahepatic venous system were detected to be more common as expected. Conditions to study by 3D power Doppler could involve the abnormal cord insertion on the abdomen (omphalocele, gastroschisis), abnormal umbilical vein size (varix or ectasia) and absence of the ductus venosus or abnormal course of vessels in isomerism conditions.

Renal Vessels

The visualization of renal vessels is known to increase the accuracy of the diagnosis of kidney malformations in the fetus. The renal vascular tree is well visualized in a coronal plane with the descending aorta showing a horizontal course. Conditions with possible benefit of 3D-PDU application are agenesis of one or both kidneys, arteries in duplex kidney, horseshoe or pelvic kidney.

Intracerebral Vessels

A transversal insonation easily allows the reconstruction of the circulus of Willis, whereas a more sagittal approach enables the visualization of the pericallosal artery with its ramifications. Choosing a lower velocity scale flow, the cerebral veins and sagittal sinus can be imaged as well. Main fields of interest are the abnormal anterior cerebral artery in agenesis of corpus callosum, the aneurysm of the vein of Galen and disturbed vascular anatomy in cerebral malformations.

Lung Vessels

Fields of interest are the analysis of the 3D vessel architecture in cystic lung malformation, congenital diaphragmatic hernia and bronchopulmonary sequestration. The role of color or power Doppler in predicting pulmonary hypoplasia failed and it is not expected that the 3D demonstration of the vessels could be in this field of great interest in the near future.[37]

Fetal Tumors or Aberrant Vessels

Aberrant vessels can be visualized in the presence of several malformations like lung sequestration, chorioangioma, lymphangioma or in sacrococcygeal teratoma, acardiac twin, etc. In this sense, fetal tumors can be of interest to be visualized not only for their risk of cardiac failure due to the presence of arteriovenous fistulae, but also to assess compression of shifting of neighboring organs.

The Fetal Heart in 3D and 4D

In the last decade, 3D and 4D fetal echocardiography was investigated intensively in laboratories using external work stations, static volume sweep, matrix transducers and recently a new ultrasound equipment with integrated software (STIC™) was introduced allowing a reliable 3D and 4D fetal echocardiography.[39]

SPATIOTEMPORAL IMAGING CORRELATION: A NEW APPROACH TO THREE- AND FOUR-DIMENSIONAL EVALUATION OF THE FETAL HEART

In 2002, Voluson Expert 730 (GE Medical Systems, Kretz Ultrasound, Zipf, Austria) introduced a new technological concept called Spatiotemporal Image Correlation (STIC). This technology enables to review, handle and store digitally volume data of the fetal heart in a looped cine sequence. The aim for the development of the STIC technique was to create a useful screening tool that is easy to use and facilitates the detection of the fetal heart anomalies during the routine obstetrical scan. In several studies, 4D fetal echocardiography proves to offer a more comprehensive assessment of the fetal heart morphology and relationship of the great vessels,[29,36,43] even if the fetus is in an unfavorable scanning position.[32]

Spatiotemporal image correlation basically displays three different imaging modalities, in a grayscale, in color Doppler and in Power Doppler **(Figs 20.1A to C)**. Each of them can display two possible formats, multiplanar (showing perpendicular planes to each other) or rendered (reconstruction of the plane A) **(Figs 20.2A to D)**. The rendered format can be displayed in different algorithms (gray, color and glass body) **(Figs 20.3A to D)**. The multiplanar format is the first system that allows a simultaneous and dynamic multiplanar evaluation of several 2D planes. The volumetric format is a technique process in which the 3D structures of the scanned volume are transferred to a 2D image.

TECHNICAL BASES

The main aspects that have to be considered when evaluating a 3D imaging system are the volume data

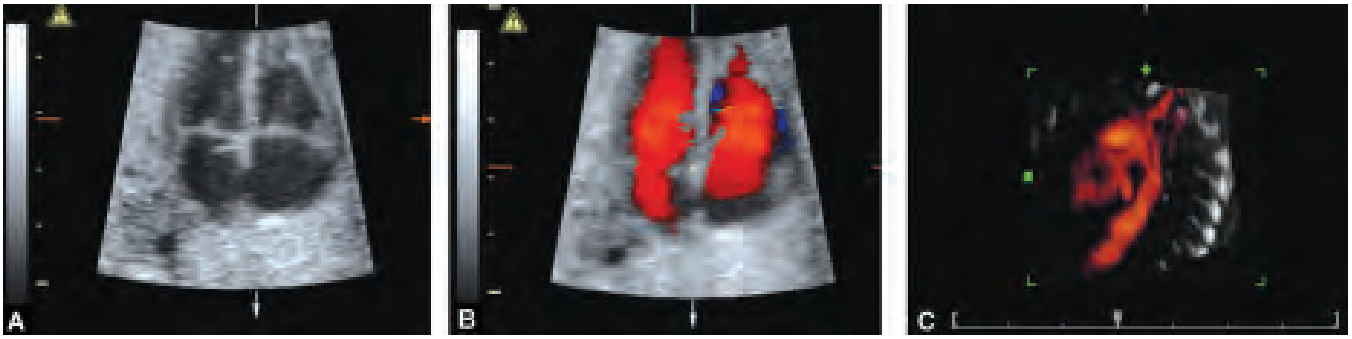

Figures 20.1A to C: Spatiotemporal image correlation technique offers different display formats, in grayscale or combined with color and power Doppler. (A) Display format in grayscale; (B) Display format in grayscale combined with color Doppler; (C) Display format in grayscale combined with power Doppler

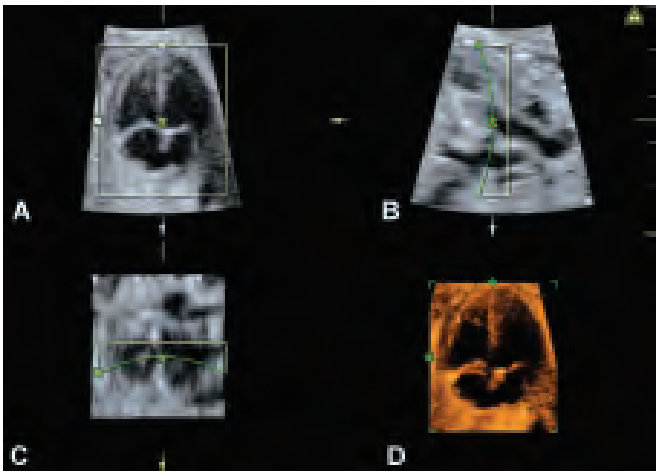

Figures 20.2A to D: (A) Plane A demonstrates the acquired image obtained during the STIC sweep; (B) Plane B is the orthogonal plane vertical to the plane A (sagittal plane); (C) Plane C is the orthogonal plane horizontal to the plane A (coronal plane); (D) Volume rendering image

acquisition and the image rendering display. The acquisition can be achieved either in 3D static mode (a volume consisting of series of still images) or in 4D mode (which reflects the beating character of the heart). The latter can be acquired either in live real-time 3D or as offline 4D, which is possible by the recent advent of the new software of STIC. In these acquisitions heart and vessels can be visualized either in grayscale mode or in combination with color Doppler,[44] Power Doppler or B-flow.[37] Image rendering is the process of creating a 3D visual representation of the parameters of interest.

The STIC technology enables the automatic and sequential acquisition of 2D images in a volume digitally stored, performing a single sweep in slow motion over a limited area of interest, which provides a high-resolution image (150 frames/second). It is possible to optimize the image changing the acquisition time (between 7, 5 and 15 seconds, with intervals of 2, 5 seconds) and the sweep angle (from 15 to 40°, with intervals of 5°). The steps are defined as follows:

1. Acquisition

Automatic volume acquisition: It means the array inside the transducer housing performs an automatic slow single sweep, recording one single 3D data set. This volume consists of a high number of 2D frames, one behind the other. Due to the small region of interest, the B-mode frame rate during the volume scan is very high, in the range of approximately 150 frames per second, which means that 2D images are stored in high resolution.

2. Post Processing

After the volume scan is acquired, the system runs a spatial and temporal correlation of the recorded data. This technology identifies the rhythmical movements and depending on their periodicity, the fetal heart rate can be calculated. Based on the exact timing of the systolic peak and the time fraction between one systole and the next, the system rearranges the 2D images, obtaining consecutive volumes presenting a complete and "synchronized" cardiac cycle (it correlates the images of different cardiac cycles obtained in the slow sweep rearranging the events according to their spatial and temporal domain).

3. Visualization

These volumes are displayed in an endless cine sequence (showing the heart cycle in real-time in cine loop), which can be played in different possibilities (slow motion, frame-by-frame, stopped at any stage during the cycle, rotation in the three planes of the space

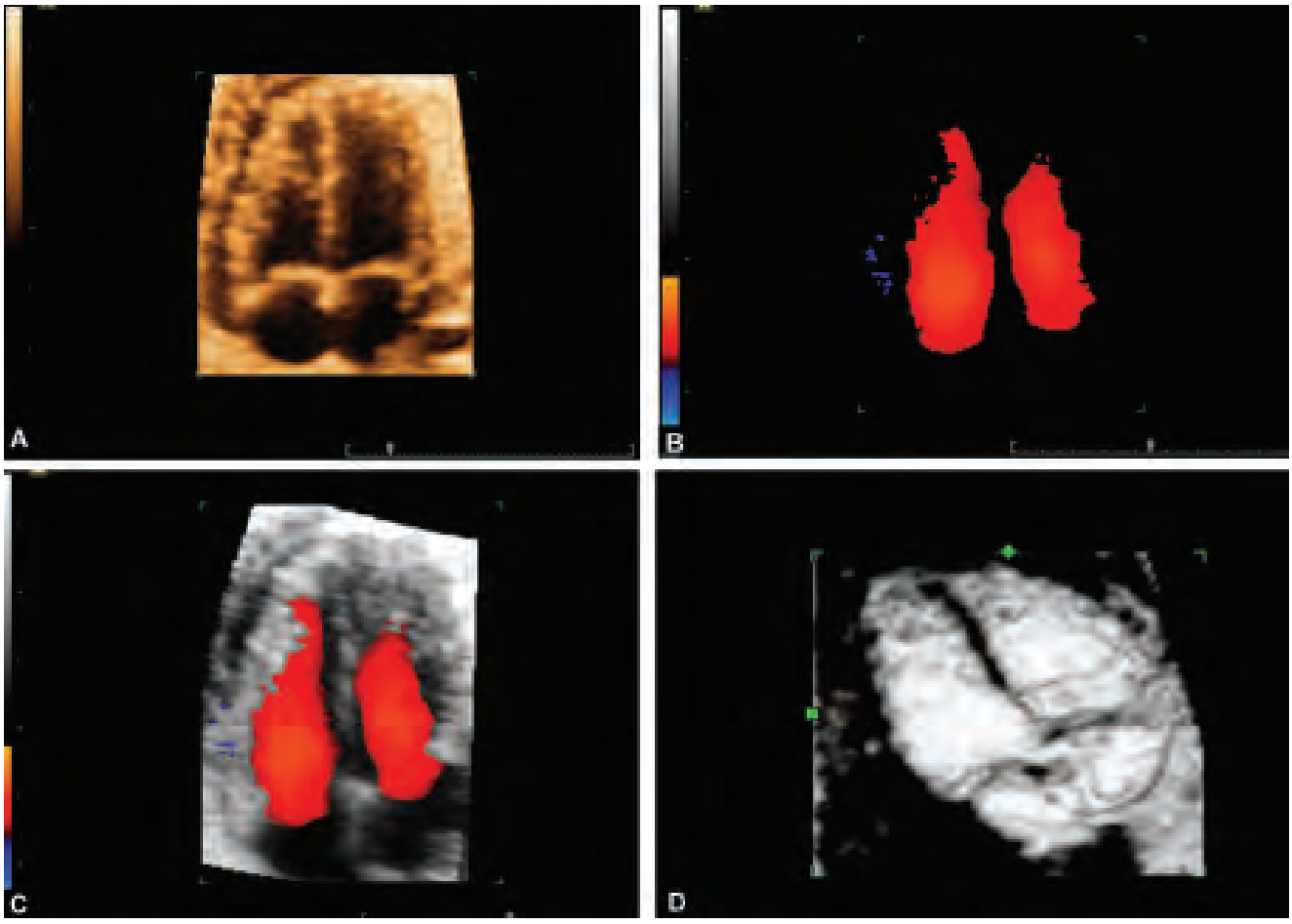

Figures 20.3A to D: The heart volume dataset can be displayed as a single image of a 3D/4D surface or a transparent volume, in which grayscale or color Doppler information or both can be demonstrated (so called "glass body" mode). Inversed mode has been recently described as a new rendering algorithm that transforms echolucent structures into echogenic voxels. (A) Gray rendering volume; (B) Color rendering volume; (C) Glass body rendering volume; (D) Inversed mode rendering volume

(x, y and z planes), multiplanar view, single plane, volumetric reconstruction, etc). Similarly, it is possible to perform postprocessing adjustments, such as the gamma curve correction to optimize the contrast resolution, the modification of color threshold (balance to control and modify the color intensity over the grayscale) or grayscale threshold, etc.

Summarizing, thanks to this algorithm, following a dynamic acquisition of a volume dataset including the fetal heart, a single cardiac cycle is virtually reconstructed according to heart rate with fundamental section planes being displayed in multiplanar fashion or integrated into a moving volume (4D echocardiography). In this sense, STIC can be defined as an "online" system with an "indirect volume scan" and "post-3D/4D-acquisition correlation".[44] Thanks to this technique, a more comprehensive investigation of fetal heart is feasible since all structures are amenable to exploration along any view angle, irrespective of fetal position.

ADVANTAGES

Improved Temporal Resolution

Due to the increased number of frames acquired for a specific anatomical region using STIC technique, this method results in improved temporal resolution of the online dynamic 3D image sequence that is displayed in the multiplanar or the rendered display.[45] As a result, the difficult or not identifiable cardiac images in the conventional 2D mode can improve with this new approach.

Dynamic Evaluation of the Four-Chamber View

It enables a dynamic evaluation of the four-chamber view. It doesn't examine a single static four-chamber plane at a time but it allows a dynamic study of this view in the three planes, in anteroposterior sense as well as laterolateral and superoinferior, letting in this way the planes rotate around a 360° axis.

Evaluation of the Outflow Tracts

The 2D evaluation of the outflow tracts may be difficult due to an inadequate fetal orientation or the own fetal movement. The STIC technology facilitates the assessment of the outflow tracts since it enables the rotation of the data volume around a single reference point.[32,44]

Multiplanar Dynamic Display and Navigation

The volume acquired by 3D ultrasonography can be displayed on a monitor in three orthogonal planes, representing the transverse, sagittal and coronal planes of a representative 2D plane within the volume. Such a display of three orthogonal planes from the 3D volume acquisition is termed "multiplanar display". Spatiotemporal imaging correlation is the first system with a simultaneous dynamic multiplanar view in the three planes.[45,46] Using multiplanar slicing, examiners can dynamically visualize the heart in three orthogonal planes at the same time. The reference dot can be employed to "navigate" the volume in any direction, placing the reference dot at any location in planes a, b or c and observing the corresponding plane changes in their respective images **(Figs 20.4 to 20.6)**.

Reconstruction of a Three-Dimensional Rendered Image

It enables the reconstruction of a 3D rendered image that contains depth and volume which may provide additional information that is not available from the multiplanar image slices.[44,46] Thanks to multiplanar volume rendering of the cardiac structures, some CHDs, traditionally proven inaccurate in prenatal diagnosis, can be accurately documented, such as small ventricular defects[47] or abnormal venous connections.[48]

Online Acquisition (Patient in the Room)

It reduces the online exploration time. Moreover, acquisition is less operator-dependent compared to 2D conventional sonography.

Offline Analysis

This technique allows recreating again the examination of the heart. Through the 2D mode, the static images or videotapes can only be reviewed in a retrospective way. Undoubtedly, this is one of the most promising applications of this technique, opening up new opportunities for consultation, clinical diagnoses or new screening strategies.[45,49]

Timing

It can be theoretically applied at any time during the gestation. However, some limitations may be found later in gestation in fetuses with large hearts and early in gestation as a result of low discrimination of signals.[44]

New Anatomical Planes

It presents new anatomical planes, which can be difficult or impossible to obtain through the conventional 2D mode. Such views could focus on demonstrating the AV-valves, the so called "en face view" of the atrioventricular valves",[44] or the interventricular or atrial septum. The future will show which views are appropriate for clinical application.

New Promising Technology

New promising technology can be introduced, in combination with STIC technique, such as Speckle Reduction System or Tomographic Ultrasound Imaging. Speackle Reduction System allows us to improve image resolution, particularly in difficult scan conditions **(Fig. 20.7)**. Tomographic Ultrasound Imaging (TUI) allows the diagnosis in one unique screen of multiples images **(Fig. 20.8)**.

High Intra- and Interobserver Repeatability

Cardiac examination from 4D-STIC volumes has showed a high repeatability between and within observers in each trimester of pregnancy.[50]

Volume Measurements

Four-dimensional ultrasonography with STIC is a feasible and accurate method for calculating volumes of 0.30 mL upwards. In an *in vitro* model, the 3D slice method proved accurate, was the least time consuming, had the best reliability and had the smallest LOA. This method may prove useful when applied to *in vivo* investigations.[51]

Telestic

It lends itself to storage and review of volume data by the examiner or by experts at remote sites. Volume datasets can be transmitted to remote sites via Internet in order to facilitate the access to the reference experts located in difficult geographical areas with the

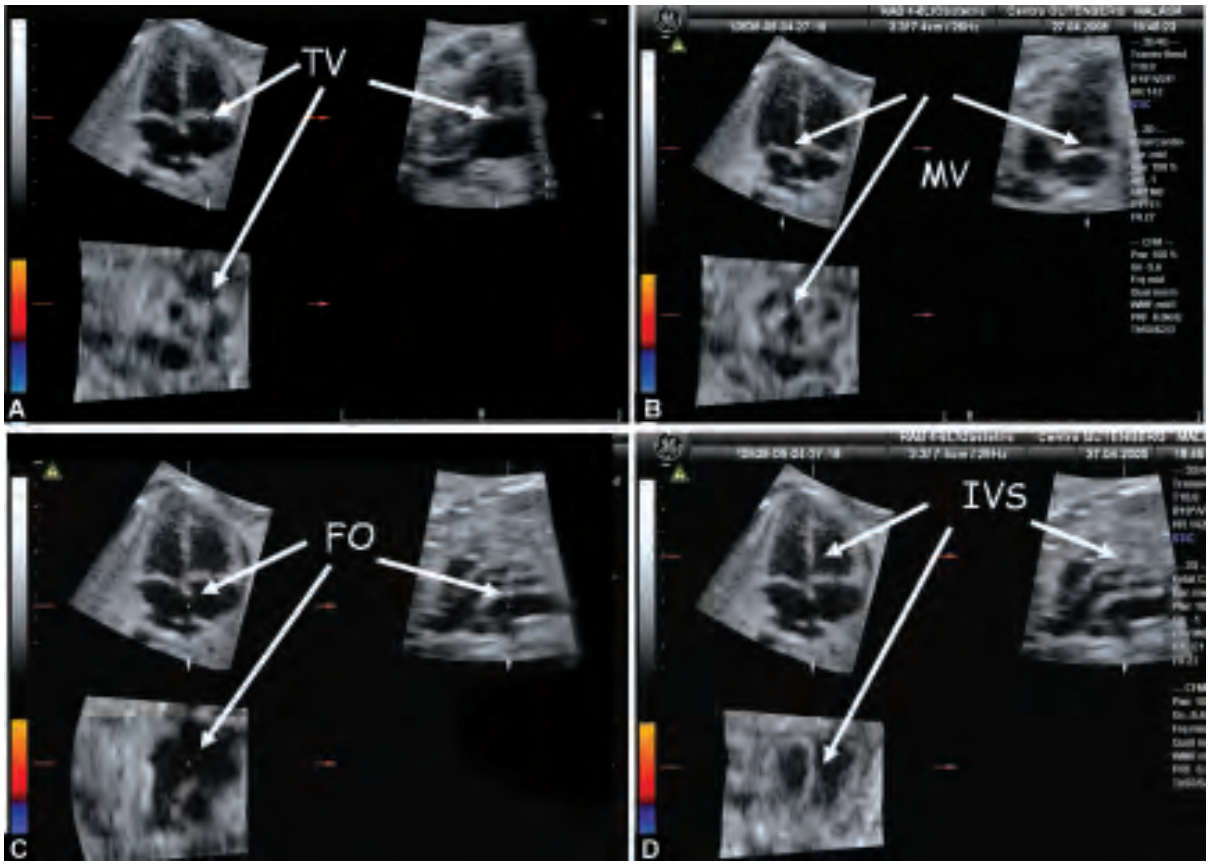

Figures 20.4A to D: Three-dimensional multiplanar slicing of the four-chamber view. The examiner can place the reference dot at any location in planes A, B or C and observe the corresponding plane change their respective images. By using the cineloop the examiner can choose within the volume the heart cycle phase of interest. (A) The reference dot is positioned at the level of the tricuspid valve during systole. The valves can be visualized simultaneously in the three orthogonal planes: transverse (left upper panel), sagittal (right upper panel) and coronal (left lower panel); (B) The reference dot is positioned at the level of the mitral valve, during systole. The valves can be visualized simultaneously in the three orthogonal planes: transverse (left upper panel), sagittal (right upper panel) and coronal (left lower panel); (C) The reference dot is positioned at the level of the foramen ovale. Both atria can be visualized in the coronal plane (left lower panel) and a sagittal view of the foramen ovale is provided on the right upper panel; (D) The reference dot is positioned at the level of the interventricular septum. A sagittal view of the interventricular septum can be visualized simultaneously in the right upper panel. TV: tricuspid valve; MV: mitral valve; FO: foramen ovale; IVS: interventricular septum

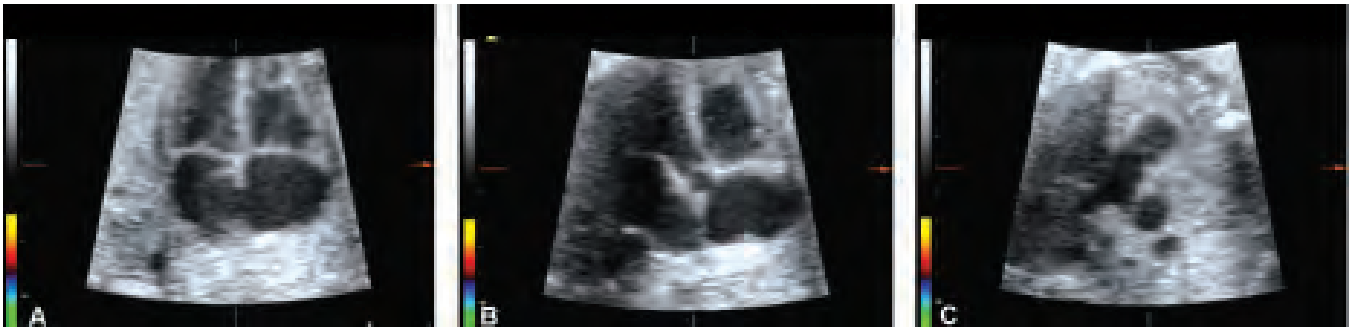

Figures 20.5A to C: The examiner can magnify and visualize the plane A in a single format. By scrolling through the volume we can visualize any plane. In this case, the most important planes are presented: (A) the four-chamber view; (B) the five-chamber view; (C) The three vessels and trachea view. By using the cineloop, the examiner can choose within the volume the heart cycle phase of interest

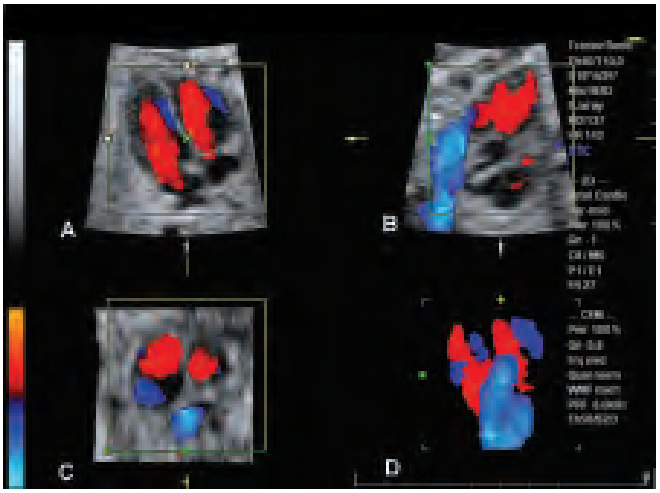

Figures 20.6A to D: Color Doppler spatiotemporal image correlation (STIC) volume of a 27-week fetus displayed in multiplanar and render mode. By scrolling through the cineloop the different phases of the cardiac cycle can be visualized as the diastolic filling of the ventricles, the beginning of the systole with blood flow streaming in the outflow tracts, and late systole with blood still recognizable in both great vessels. In this view the criss-crossing of the great vessels can be appreciated in a way not seen before in prenatal diagnosis. Due to the presetting of color persistence the volume in D plane shows simultaneously late diastole and early systole. Additionally, in C plane we can appreciate a new anatomical view, the en-face view of the AV valves, with both mitral and tricuspid valve demonstrated during diastolic flow (red)

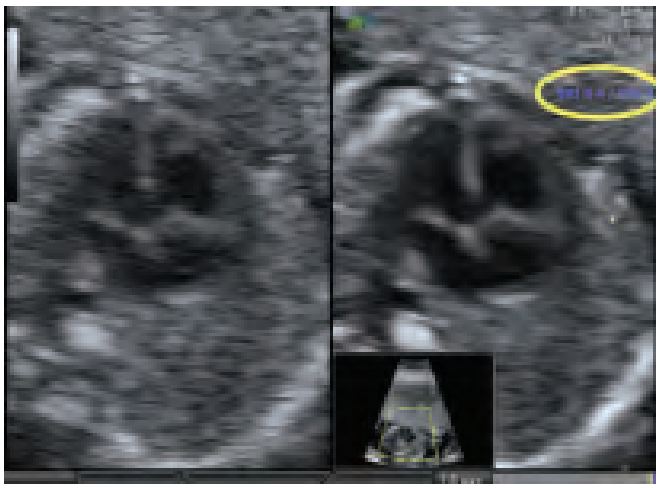

Figure 20.7: The speckle reduction system (SRI II) may reduce the artifacts, improving the image resolution, particularly in difficult quality image cases

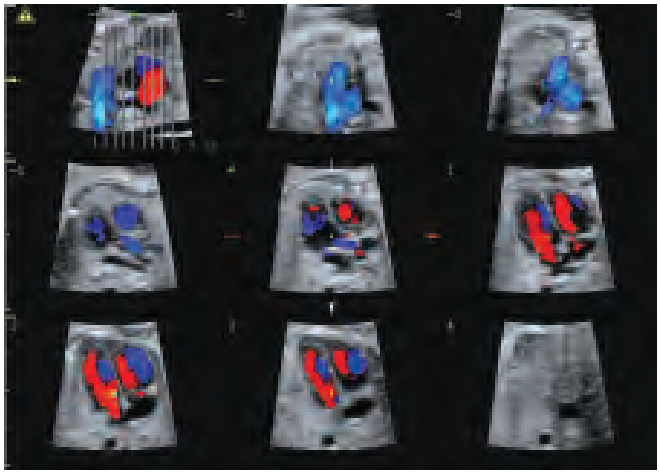

Figure 20.8: Tomographic ultrasound imaging (TUI) in a normal fetal heart at 20 weeks of gestation. TUI allows the diagnosis in one unique screen of multiples images

possibility of seeking advice from them. TELESTIC facilitates asking them for a second diagnostic opinion. Moreover, TELESTIC can be used as a filter in order to relieve the workload in these reference centers. Likewise, this modality offers a wide range of possibilities and new applications in the teaching field.[40,41,52]

LIMITATIONS

There are potential limitations to this technique. Some factors are inherent to conventional ultrasonography, some others are specifically dependent on 3D technology, some of them are inherent to Color Doppler technology and a few ones are related to STIC method.

Specific Limitations of Two-Dimensional Technology

- Resolution limitations typical of 2D image
- Low resolution of the reconstructed planes (planes B and C)
- Low resolution of the image, especially at early gestational ages.

Specific Limitations of Three-Dimensional Technology

- During the volume acquisition time, the maternal and fetal movements produce artifacts, especially in B and C planes. Whenever possible, acquisition must be performed in the absence of maternal and fetal movements.

Specific Limitations of Color Doppler Technology

- Lack of color signal when the region of interest is perpendicular to the ultrasounds (in these cases it is advisable to modify the angle of insonation).
- Adding the color, as it happens in conventional 2D modality, the resolution is reduced, in comparison with the image on a grayscale.

Specific Limitations of STIC Technology

- The fetal arrhythmias are the main limitation of this technology, since a synchronization of the cardiac cycle is not permitted in these cases. When important changes are detected in the fetal heart rate during the volume acquisition, the calculation of such rate may not be accurate or valuable enough with the appearance of artifacts caused by the difficulty in synchronizing the 2D images at the right time within the cycle.
- Learning curve required managing this technology as well as the extra-time involving the image post-processing.
- Economical expenses and current commercial monopoly of this technology. It is expected that in the near future other companies will provide new software with new possibilities of 3D/4D acquisition and rendering.

CURRENT APPLICATIONS AND NEW PERSPECTIVES

Nowadays, different work groups have published their initial experience with this new technology. The current lines of research are focused in the following points:

- *Clinical application in unselected population and also in population at risk*: Preliminary studies suggest that real-time 3D echocardiography has the potential to function as a screening tool for fetal heart disease, by introducing new screening strategies and new concepts, such as "offline echocardiography" or "screening echocardiography" or "tele-echocardiography".[30,49] Some studies of 4D echocardiography using STIC have focused on the acquisition of volume data sets by operators with limited experience in echocardiography and subsequent analysis by an expert.[49]
- *Systematization of the multiplanar technique*: Some studies of 4D echocardiography using STIC have focused on the development of a multiplanar technique to systematically examine the four-chamber view and the outflow tracts.
  - In this sense, Gonçalves has recently described a four-step technique to simultaneously display the right and left ventricular outflow tracts.[46] By the use of the four-chamber view as the starting point, the heart is rotated approximately 45° around the z-axis and the reference dot placed at the center of the interventricular septum. Next, the volume is rotated clockwise around the y-axis until the left ventricular outflow tract is visualized. The reference dot is repositioned at the center of the outflow tract, above the aortic valve. A short-axis view of the right ventricular outflow tract is displayed simultaneously in the right upper panel **(Fig. 20.9A to D)**.
  - With the same purpose, DeVore describes a new technique using 3D multiplanar imaging that allows the examiner to identify the outflow tracts within a few minutes of acquiring the 3D volume dataset by rotating the volume dataset around the x- and y- axes.[53] It is called "the spin technique". The full length of the main pulmonary artery, ductus arteriosus, aortic arch and superior vena cava can be easily identified in the normal fetus by rotating the volume dataset along the x- and y- axes. Three-dimensional multiplanar evaluation of the fetal heart allows the examiner to identify the outflow tracts using a simple and reproducible technique that requires only rotation around x- and y- axes from reference images obtained in a transverse sweep through the fetal chest **(Figs 20.10A and B)**.
- *Reproducibility study*: In this sense, recent studies suggest the reproducibility of this technique, in the terms of intraobserver and interobserver variability, although these studies are still referred to as small series[50]. Gonçalves, including a series of 20 volume datasets acquired from fetuses with normal cardiac anatomy, concludes that STIC can be reproducibly used to evaluate fetal cardiac outflow tracts by independent examiners.[54]
- *Assessment of the diagnosis ability referred to as heart diseases*: Thanks to multiplanar volume rendering of the cardiac structures, some congenital heart diseases, traditionally proven inaccurate in prenatal diagnosis, can be accurately documented, such as small ventricular defects,[47] abnormal venous connections[48] or right aortic arch. Additionally, Color Doppler STIC has the potential to simplify visualization of the outflow tracts and may improve the diagnosis of some congenital heart abnormalities[43,44] **(Figs 20.11 to 20.14A to D)**.
- *Specific applications in the prenatal diagnosis of congenital heart diseases*: Four-dimensional grayscale

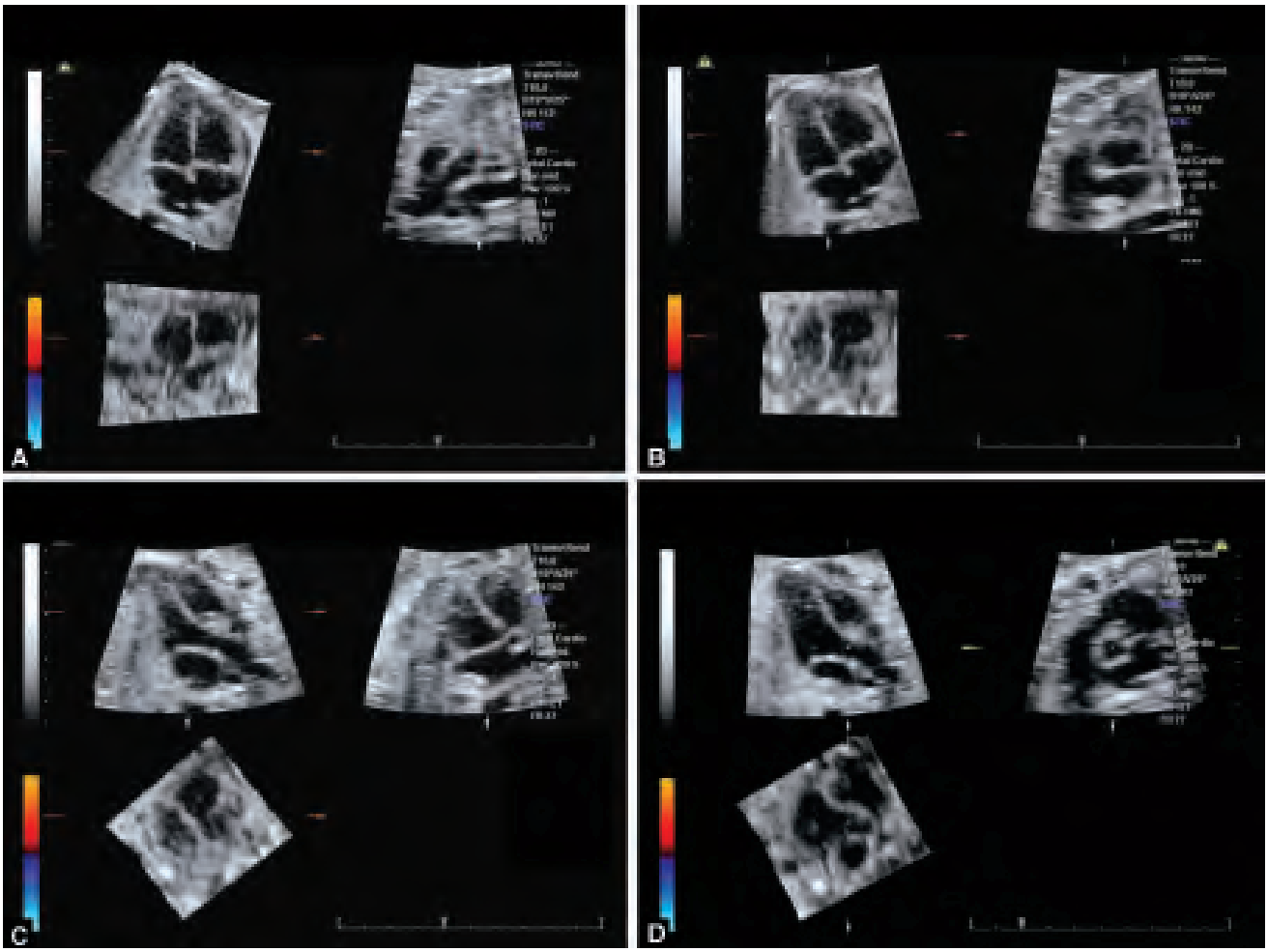

Figures 20.9A to D: Systematization of the multiplanar technique: Four-step technique. Some studies of four-dimensional echocardiography using STIC have focused on the development of a multiplanar technique to systematically examine the four-chamber view and the outflow tracts. Gonçalves has recently described a four-step technique to simultaneously display the right and left ventricular outflow tracts.[46] (A) By the use of the four-chamber view as the starting point; (B) The heart is rotated approximately 45° around the z-axis and the reference dot placed at the center of the interventricular septum; (C) Next, the volume is rotated clockwise around the y-axis until the left ventricular outflow tract is visualized. The reference dot is repositioned at the center of the outflow tract, above the aortic valve; (D) A short-axis view of the right ventricular outflow tract is displayed simultaneously in the right upper panel

and power Doppler STIC can be used to systematically visualize the abnormal relationship of the outflow tracts in fetuses with transposition of the great arteries (TGA)[44,55] **(Figs 20.13A and B)**. The detection rate of TGA by standard obstetrical scan evaluation is low and this disappointing performance has been attributed to issues related to technical difficulties in consistently imaging the outflow tracts. In this sense, 4D ultrasonography may overcome technical limitations related to the skills required to obtain appropriate planes of section. Recently, a new sign seems to help to identify additional cases of TGA. The en-face view of both AV valves and great vessels in fetuses with TGA displayed the main pulmonary artery situated side-by-side with the aorta ("big-eyed frog" sign). In contrast, fetuses with normal hearts did not have this characteristic sonographic sign. This novel sonographic sign may prove helpful in the prenatal diagnosis of TGA.[56] Finally, the "starfish" sign has been described as a novel sonographic finding with B-flow imaging and spatiotemporal image correla-

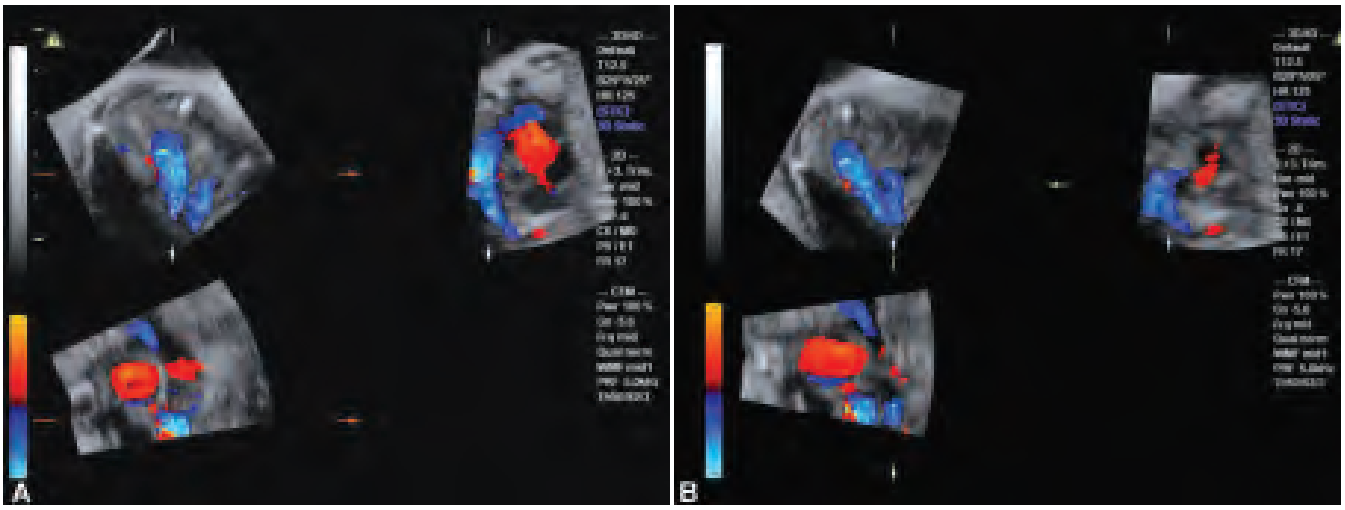

Figures 20.10A and B: Systematization of the multiplanar technique: The spin technique. Some studies of four-dimensional echocardiography using spatiotemporal image correlation have focused on the development of a multiplanar technique to systematically examine the four-chamber view and the outflow tracts. DeVore described a new technique using 3D multiplanar imaging that allows the examiner to identify the outflow tracts within a few minutes of acquiring the three-dimensional volume dataset by rotating the volume dataset around the x- and y-axes.[53] It is called "the spin technique". (A) The full length of the main pulmonary artery and ductus arteriosus, and (B) Aortic arch can be easily identified in the normal fetus by rotating the volume dataset along the x- and y-axes

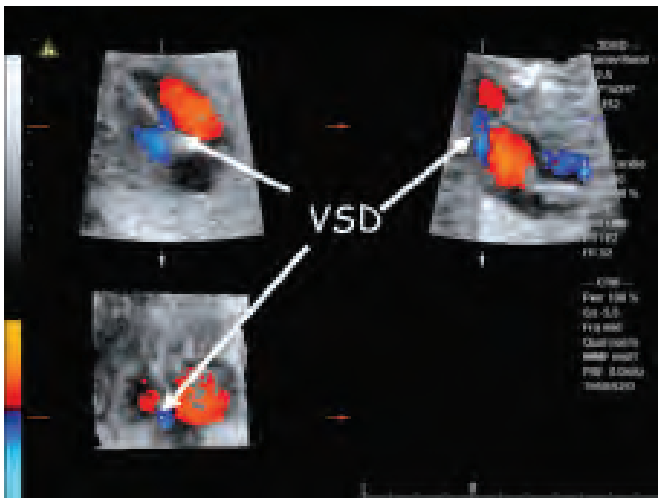

Figure 20.11: One application of the multiplanar mode is demonstrated in this fetus of 22 weeks' gestation with a ventricular septal defect (VSD) showing shunting from the left to the right ventricle (blue color crossing the septum). The arrows point to the dot present in all three planes, which shows the intersection point of these planes. The examiner can place the dot in the region of interest (here in the plane A) and see its position in both the other planes

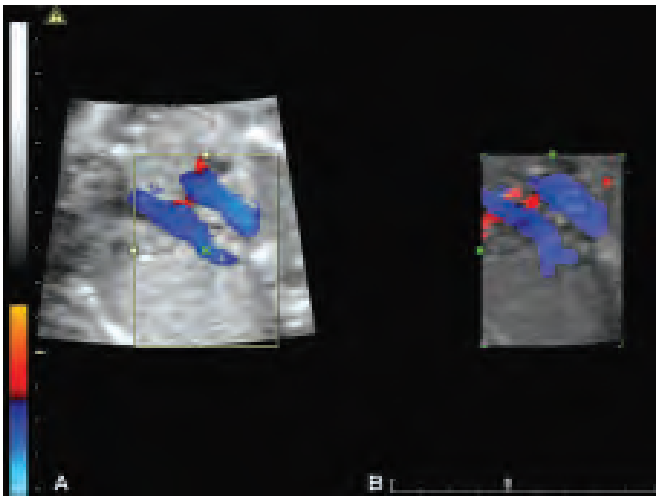

Figures 20.12A and B: A 22 weeks' gestation fetus with a right aortic arch. Two simultaneous image displays. (A) The axial plane, the plane of the acquired image obtained during the spatiotemporal image correlation sweep, corresponding to an axial plane at the level of upper mediastinum; (B) Glass-body rendered image corresponding to the acquisition plane. In both images, we can appreciate the anechoic area representing the trachea surrounded by the ductal arch (on the left side of the trachea) and the aortic arch (on the right side of the trachea)

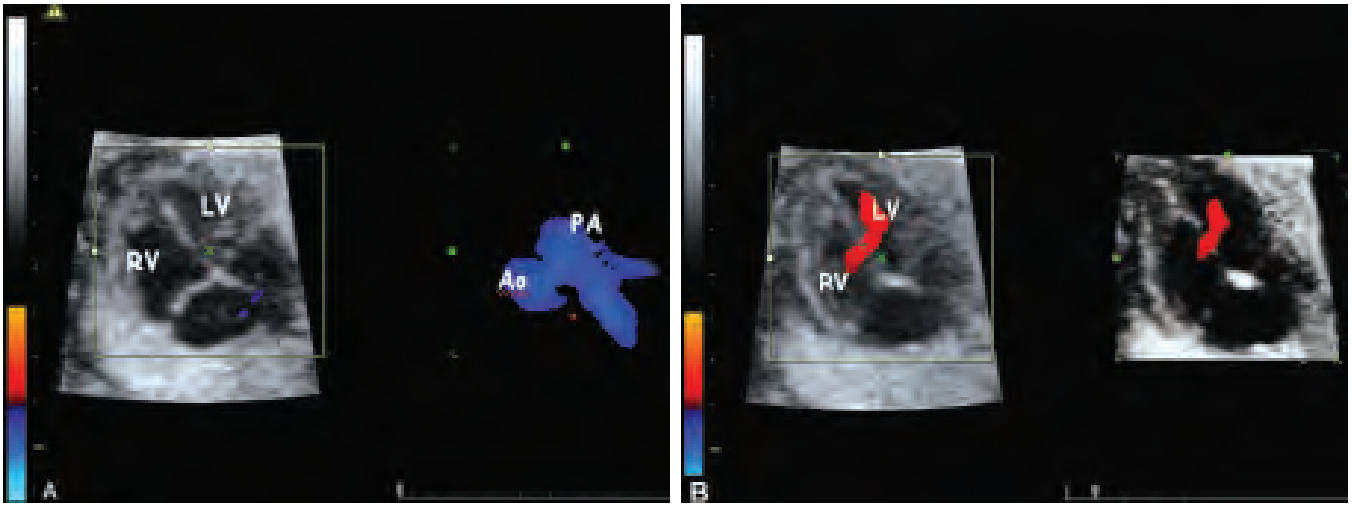

Figures 20.13A and B: A fetus with transposition of the great arteries and interventricular septum defect at 22 weeks of gestation. (A) Note the parallel course of both ventricles. The three-dimensional color rendering demonstrates the bifurcation of the pulmonary artery connecting to the left ventricle; (B) Note the additional ventricular septal defect (red color crossing the septum), in both two-dimensional four-chamber view and glass body rendered image, LV: left ventricle; RV: right ventricle; PA: pulmonary artery; Ao: aorta

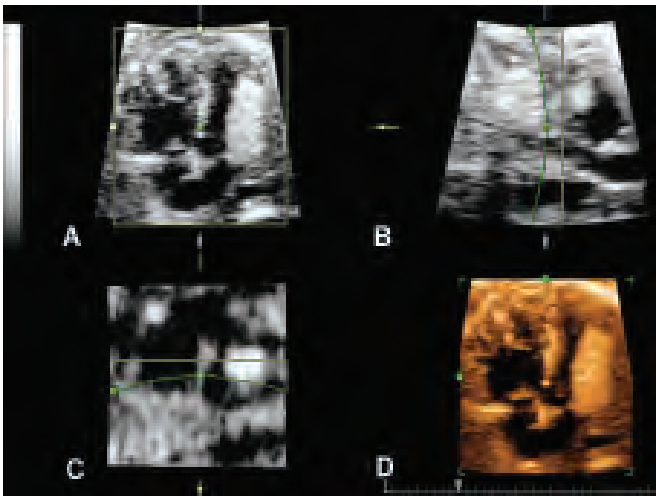

Figures 20.14A to D: A fetus with multiple solid cardiac tumors at 29 weeks of gestation, postnatally diagnosed as sclerosis tuberosa. Four simultaneous image displays. (A) The axial plane, the plane of the acquired image obtained during the spatiotemporal image correlation sweep; (B) The orthogonal plane vertical to the plane A (the sagittal plane); (C) The orthogonal plane horizontal to the plane a (coronal plane); (D) Gray rendered image

tion in a fetus with total anomalous pulmonary venous return.[57]

- *Estimation of volumes and masses in animal experimental models*: Estimation of ventricular volume and mass is important for baseline and serial evaluation of fetuses with normal and abnormal hearts. Direct measurement of chamber wall volumes and mass can be made without geometric assumptions by 3D fetal echocardiography. Recent studies have established the feasibility of fetal ventricular mass measurements with 3D ultrasound technology and have developed normal values from 15 weeks' gestation to term.[51,58] Non-gated fast 3D fetal echocardiography is an acceptable modality for determination of cardiac chamber wall volume and mass with good accuracy and acceptable interobserver variability. This method should be especially valuable as an objective serial measurement in clinical fetal studies with structurally or functionally abnormal hearts **(Figs 20.14A to D)**.
- *Algorithms for the automated obtaining of the standard anatomical slices from the stored volume*: It is anticipated that algorithms developed to image specific cardiac structures with 3D or 4D volume datasets may eventually become automated by computer software.[59-61] Despite the recent advances in ultrasonographic imaging, the acquisition, display and manipulation of 3D volumes is a technique that requires a substantial learning curve. It is theoretically possible to obtain a volume of a specific organ, such as the fetal heart, and to allow an automatic program to display out of this volume all the 2D planes that are required for a complete anatomic evaluation of this organ. Abuhamad termed this new concept as automatic multiplanar imaging (AMI). Once a 3D volume of the fetal heart is obtained from the level of a standardized plane, such

as the four-chamber view, for instance, AMI will automatically generate all other standardized planes from the acquired volume in an operator-independent method, improving the reproducibility of AMI-generated ultrasonographic images. Automatic multiplanar imaging allows for a complete evaluation of anatomically complex organs with a standardized and operator-independent approach. A software with this purpose, called Sonography-based Volume Computer Aided Diagnosis (Sono VCAD) has been recently commercialized. By standardizing the approach to image acquisition and display and by substantially reducing the possibility of human error and reducing scan time, SonoVCAD will improve the diagnostic acumen of ultrasound imaging and thus prove advantageous to clinical practice.

- *Application of this technology in the telemedicine field (TELESTIC)*: Preliminary studies suggest that a telemedicine link via Internet combined with STIC technology (TELESTIC) is technically feasible.[40,41,52,62] TELESTIC permits a second diagnostic opinion and also generates a link between different centers resultant in a new virtual tool for teaching and training in fetal heart.
- *Application in early fetal echocardiography*: Offline evaluation of 4D-STIC acquired volumes of the fetal heart in the first and early second trimester of pregnancy is reliable not only for early reassurance of normal cardiac anatomy but also to diagnose most major structural heart defects.[50,62,63]
- *New diagnostic algorithms* (Minimum Projection Mode, Inversed mode, B-flow).
  - The Minimum Projection Mode (MPM) is a rendering algorithm available in some 3D and 4D ultrasonography systems that, in one image, allows the visualization of vessels and cystic anatomic structures located in different scanning planes. This algorithm is an alternative rendering modality that facilitates visualization of normal and abnormal vascular connections to the fetal heart particularly at the level of the three-vessel view.[64] This technique may be useful in prenatal diagnosis of conotruncal abnormalities and in the assessment of the spatial relationships of abnormal vascular connections in the upper mediastinum.
  - The "inversion mode" algorithm has been recently introduced in fetal imaging as a new tool for 3D rendering of fluid-filled structures.[47,65,66] This novel 3D post-processing algorithm enables any fetal structure with an anechoic content to be converted into an echogenic volume. Numerous fetal disorders have been accurately described using inversion mode 3D ultrasound, such as urinary tract anomalies, gastrointestinal obstructions, hydrocephalus, cysts, and more recently, the inversion mode has been employed to display the fetal heart. Using this approach the beating heart is dynamically transformed into a hyperechogenic 3D structure due to signal conversion of the blood flowing within the cardiac structures. Since this technique does not use color or power Doppler sonography as a "digital contrast" to highlight the blood vessels, it does not have the inherent limitations to image reconstruction related to the angle of insonation, temporal resolution or intensity of the Doppler signal. This new rendering modality allows a better documentation of some cardiac defects, traditionally proven inaccurate in prenatal diagnosis, such as small ventricular defects,[47] or abnormal systemic venous connections,[48] as well as prenatal evaluation of complex disorders requiring precise definition of visceral situs, such as heterotaxy syndromes.[65]
  - Recently, B-flow imaging and STIC have been demonstrated to improve the visualization of small vessels with low-flow velocity. In fact, when applied to 3D fetal echocardiography, the B-flow modality is a direct volume non-gated scanning method that is able to show blood flow in the heart and in the vessels in real time, without color Doppler flow. When compared with color and power Doppler sonography, B-flow sonography has a higher frame rate and better spatial resolution. It allows angle-independent detection of weak blood reflectors from vessels. Consequently, this approach theoretically has the potential to facilitate the prenatal diagnosis of TAPVC, and might be especially important in identifying and tracking the route of thin vessels with low blood flow velocity.[57,67,68]

FIRST SPANISH STUDY IN SPATIOTEMPORAL IMAGE CORRELATION TECHNOLOGY

Introduction

Since the origin of the fetal echocardiography at the end of 1970, new techniques and applications have been appearing forming a field whose present situation and future perspectives are widely different from the

original ones. The recent introduction of the 3D and 4D ultrasonography opens a promising perspective in prenatal diagnosis, especially in certain types of surface pathologies. Nevertheless, the application of this technology is complex in echocardiography considering the movement and the dynamics itself in the cardiovascular system, being this the main limitation in the 3D and 4D reconstruction. Nowadays, this limitation has been overcome with the incorporation of a new technological appliance called STIC.

Objective

To assess the use and performance of the STIC technique in order to perform a "basic and extended cardiac fetal evaluation", with an online acquisition of the cardiac volume during the morphological scan by a general sonographer and offline analysis by an expert in fetal cardiology.

Methods and Material

A number of 58 volumes are prospectively obtained during the routine morphological scan, by a general sonographer, in 28 patients randomly selected among the ones attending our unit. Afterwards, an experimented examiner in fetal echocardiography proceeds to their offline analysis. The acquisition is made from a four-chamber view on a gray scale in an automated single sweep in a slow motion, by standardizing the acquisition time in 10 seconds (7,5–12,5) and the sweep angle in 25° (20–30), depending on the gestational age. The criteria defining a "basic" cardiac fetal study are the evaluation of the inflow tracts (four-chamber view) and the evaluation of the outflow tracts (five-chamber view, three-vessel view or three-vessel view and traquea). The criteria defining an "extended" cardiac fetal study are the evaluation of the inflow tracts, the evaluation of the outflow tracts and the situs visceral. The successful rate of volume acquisition and analysis is evaluated, as well as the percentage of cases in which it is possible a "basic" or "extended" cardiac evaluation, through the single sweep and multiplanar navigation. Cases with normal morphological scan at 20–22 weeks' gestation are included, excluding those cases with chromosomal anomalies or extracardiac malformations.

Results

Cases with gestational ages ranging between 17 and 35 weeks are included. A "basic" cardiac examination according to set criteria was achieved in 100% of cases, while an "extended" cardiac examination was achieved in 86% of them. Multiplanar study improved the visualization of those structures not identifiable through the initial acquisition single plane in all cases.

Conclusion

We present the first study on a nationwide scale about the introduction and applications of the STIC technology. The introduction of this new technique, surpassing the limitation of the cardiac movement in the volumetric reconstruction, enables a fast and easy online acquisition of a cardiac volume, during the routine morphological scan, suggesting the possibility of carrying out a more complete offline analysis of the cardiovascular structures. Spatiotemporal image correlation volumes can be obtained by operators inexperienced in fetal echocardiography and their offline analysis enables recognition of most of the structures and views necessary to assess fetal cardiac anatomy. It is emphasized that the high rate of success in the volume acquisition and offline analysis, allowing the possibility of an extended cardiac evaluation, in what we would call "SCREENING OFFLINE EXTENDED CARDIAC EXAMINATION" or "BASIC OFFLINE ECHOCARDIOGRAPHY".

Methodology

Cardiac volumes were prospectively stored according to the STIC technology[52] during the screening morphological ultrasound examination, by a general sonographer, in an aleatory selection of obstetric patients attending our unit in the period between December 2004 and February 2005 (Gutenberg Centre, Malaga, Spain). A number of 28 fetal explorations were included, all of them randomly distributed in our program, depending on the pressure attendance and the availability of ultrasound machine equipped with the STIC technology. Only fetal explorations considered as normal were included, excluding those cases with cardiac, extracardiac or chromosomal anomalies. A number between 1 and 4 volumes were acquired per patient on a grayscale (online acquisition). Afterwards, a second examiner expert in fetal echocardiography assessed the collected volumes in order to make a cardiac "basic" evaluation and an "extended" evaluation, in a limited time of 15 minutes per patient (offline analysis).

Firstly, only the initial acquisition single plane is examined, followed by a multiplanar study in order to improve the visualization of those structures not identifiable through the initial acquisition plane. The offline analysis includes the assessment of the situs visceral, the cardiac size, the cardiac axis, the myocardial contractility, the symmetry of cavities, the cardiac crux,

the insertion of the atrioventricular (AV) valves and the opening of these ones, the moderator band, the foramen ovale, the crossing of great arteries, the outflow tracts of both ventricles and the pulmonary and aortic valves. These structures are assessed in the four-chamber view (4C view), five-chamber view (5C view), three-vessel view (3VV) and the three-vessel view including trachea (3VVT). The criteria defining the assessment of the situs visceral are the abdominal identification of the position and location of the stomach, abdominal aorta and inferior vena cava and the identification of the thoracic aorta and the cardiac atrial cavities. The criteria defining a "basic" fetal cardiac study are both the evaluation of the inflow tracts view (4C view) and the evaluation of the outflow tracts view (5C view and 3VV or 3VVT) **(Figs 20.5A to C)**. The criteria defining an "extended" cardiac fetal study are the following: the evaluation of the inflow tracts (4C view), the evaluation of the outflow tracts (5C view and 3VV or 3VVT) and the situs visceral evaluation.

In our study we standardized the volume acquisition in a time of 10 seconds, with a sweep angle of 25°, modifying these variables according to the cardiac size and the conditions in the exploration (fetal movements). The acquisition was achieved from the 4C view, apical (preferable), basal or lateral depending on the fetal position, in a sweep covering the initial slice, going under and over it (including superior abdomen and thorax). Offline analysis was performed by a single investigator using the 4D View Software Version 2.1 (GE Medical Systems, Kretz Ultrasound, Zipf, Austria).

TABLE 20.1

Methodological data from our study. The characteristics of the patients and volumes in our study are reported in this table

Period of study	December 2004 to February 2005
Number of patients (n)	28
Number of analyzed volumes	58
GA (average and range)	23 weeks (17-35)
Acquisition conditions: • **time (average and range)** • **angle (average and range)**	 10 seconds (7´5-12´5) 25° (20-30)
Acquisition plane • **apical 4C** • **lateral 4C** • **basal 4C**	 68% 14% 18%
Offline analysis (average time)	15 minutes/ patient

n: number of cases in the serial
GA: gestational age in completed weeks
4C: Four-chamber view

Results

A total amount of 58 explorations of fetal cardiac volumes in 28 patients have been included, with gestational ages ranging between 17 and 35 weeks. The characteristics of the patients and volumes are reported in **Table 20.1**. The mean visualization scores for the different structures and views are shown in **Tables 20.2 and 20.3**. We evaluate the successful rate in visualizing

TABLE 20.2

Visualization rate of the cardiac structures (STIC). Success rate of visualizing different cardiac structures and plans using spatiotemporal image correlation (STIC)

Cardiac structures checklist	*Visualization rate %*
Situs visceral	86
Cardiac size	100
Cardiac axis	100
Myocardiac contractility	100
Cavities symmetry	100
Cardiac crux	96
AV valves insertion	93
AV valves opening	100
Moderator band	100
Foramen ovale	100
Crossing of great arteries	100
Outflow tract LV	100
Outflow tract RV	100
Pulmonary valve	100
Aortic valve	100
4C **5C** **3VV** **3VVT**	100 100 100 64
Extended cardiac study*	86

AV: Atrioventricular
LV: Left ventricle
RV: Right ventricle
4C: Four-chamber view
5C: Five-chamber view
3VV: Three-vessel view
3VVT: Three-vessel and trachea view
* The extended cardiac study includes the evaluation of the inflow tracts, the outflow tracts and the situs visceral

TABLE 20.3

Contribution of the multiplanar study. Contribution of the multiplanar study in visualizing different cardiac structures and plans using spatiotemporal image correlation (STIC)

Multiplanar contribution	*%*
4-step technique GA	71
IVC-RA	93
SVC-RA	79
Ao arch (sagittal)	54
Ductal arch (sagittal)	71
Additional contribution*	100

4-step technique: A four step technique to evaluate the outflow tracts from the four-chamber view
GA: Great arteries
IVC-RA: Inferior vena cava to right atrium
SVC-RA: Superior vena cava to right atrium
Ao arch: Aortic arch
* Percentage of cases in which the multiplanar examination has contributed to get some additional information

the fetal cardiac structures through the single sweep and the multiplanar format view.

COMMENT

The detection of CHD is still considered as one of the most problematic areas in the prenatal diagnosis field. Inspite of being the most frequent and severe congenital malformation in neonates, nowadays it is still one of the least diagnosed pathologies during fetal life. Besides, it is well known that the prognosis of most of them, particularly the ductus-dependent anomalies, is meaningfully better in terms of morbidity and mortality when the anomaly is prenatally detected. Their prevalence and impact are the essential factors motivating the interest to improve the prenatal detection strategies.

In this sense, the incorporation of the 4C view during the morphological scan at 20weeks' gestation, in the so called "basic" cardiac scan, has improved the prenatal detection of CHD.[11,12] Recently, the inclusion of the outflow tracts evaluation in the so-called "extended" cardiac scan has been highly recommended in order to improve the detection of conotruncal abnormalities.[13,14] Nevertheless, conventional prenatal screening for congenital heart disease still involves a time-consuming and highly operator-dependent acquisition of the four-chamber view and outflow tracts. As routine prenatal screening in the general obstetric setting is unsatisfactory, the main objective of this technique is to propose a method that is able to identify or exclude major CHD in a screening policy. It has been recently demonstrated that STIC acquisition of the fetal heart is feasible with high success rates in visualizing the heart structures. According to our experience and a few published studies,[46,49,52] the anatomy of the fetal heart can be confidentially demonstrated by the means of STIC acquisition carried out by an operator unskilled in fetal cardiology. We point out the high success rate for visualizing the structures and views included in our checklist, suggesting that most of the relevant ultrasonographic data of the fetal heart can be obtained in one STIC volume. By acquiring the entire fetal heart instantaneously as a single volume, STIC technology may facilitate fetal cardiac screening. The STIC data volume acquired by a non-expert sonographer or general obstetrician can be subsequently be used by a fetal echocardiologist for prenatal confirmation of a normal heart anatomy or exclusion of major cardiac defects.[49] That could be particularly true if the dataset volume for analysis is automatically acquired, thus reducing the need for technical skills and expertise from the sonographers. In this sense, artifacts must also be recognized and minimized, resolution must improve, and substantial training will be necessary prior to widespread clinical use. Real-time 3D examination of the fetal heart with the use of matrix phased-array probes may help to overcome such difficulties in the future.

In summary, the introduction of the STIC technology, surpassing the limitation of the cardiac movement in the volumetric reconstruction, provides a fast and easy online acquisition of the cardiac volume in the context of a routine ultrasound examination with the possibility of carrying out a more complete offline analysis of the cardiovascular structures. Potential advantages include the possibility of offline analysis in the patient's absence, remote diagnosis, novel scanning planes and new approaches for medical education. It has emphasized on the high rate of success in the volume acquisition and offline analysis, allowing the possibility of an extended cardiac evaluation, in what we would call "*Screening offline extended cardiac scan" or "Basic offline echocardiography*". This concept can be introduced as a new promising strategy that can be implemented in the general population in order to improve the prenatal detection rate of congenital heart abnormalities.

REFERENCES

1. Sklansky M. Advances in fetal cardiac imaging. Pediatr Cardiol. 2004;25(3):307-21.
2. Allan L, Benacerraf B, Copel JA, et al. Isolated major congenital heart disease. Ultrasound Obstet Gynecol. 2001;17(5):370-9.
3. Mitchell SC, Korones SB, Berendes HW. Congenital heart disease in 56,109 births. Incidence and natural history. Circulation. 1971;43(3):323-32.
4. Allan L, Sharland G, Milburn A, et al. Prospective diagnosis of 1,006 consecutive cases of congenital heart disease in the fetus. J Am Coll Cardiol. 1994;23(6):1452-8.
5. Garne E, Stoll C, Clementi M; Euroscan Group. Evaluation of prenatal diagnosis of congenital heart diseases by ultrasound: experience from 20 European registries. Ultrasound Obstet Gynecol. 2001;17(5):386-91.
6. Bonnet D, Coltri A, Butera G, et al. Detection of transposition of the great arteries in fetuses reduces neonatal morbidity and mortality. Circulation. 1999;99(7):916-8.
7. Allan LD. Fetal cardiology. Curr Opin Obstet Gynecol. 1996;8(2):142-7.
8. Gembruch U. Prenatal diagnosis of congenital heart disease. Prenat Diagn. 1997; 17(13):1283-98.
9. Todros T. Prenatal diagnosis and management of fetal cardiovascular malformations. Curr Opin Obstet Gynecol. 2000;12(2):105-9.
10. Levi S, Schaaps JP, De Havay P, Coulon R, Defoort P. End result of routine ultrasound screening for congenital anomalies. The Belgian Multicentric study 1984-92. Ultrasound Obstet Gynecol. 1995;5(6):366-71.
11. Lee W. Performance of the basic fetal cardiac ultrasound examination. J Ultrasound Med. 1998;17(9):601-7.
12. Royal College of Obstetricians and Gynaecologists. Ultrasound Screening. Royal College of Obstetricians and Gynaecologists 2000. [online] Available from: http://www.rcog.org.uk/mainpages.asp?PageID=439#20week. [Accessed in February, 2011]
13. Carvalho JS, Mavrides E, Shinebourne EA, et al. Improving the effectiveness of routine prenatal screening for major congenital heart defects. Heart. 2002;88(4):387-91.
14. Kirk JS, Riggs TW, Comstock CH, et al. Prenatal screening for cardiac anomalies: the value of routine addition of the aortic root to the four-chamber view. Obstet Gynecol. 1994;84(3):427-31.
15. Yagel S, Cohen SM, Achiron R. Examination of the fetal heart by five short-axis views: a proposed screening method for comprehensive cardiac evaluation. Ultrasound Obstet Gynecol. 2001;17(5):367-9.
16. Yoo SJ, Lee YH, Cho KS, et al. Sequential segmental approach to fetal congenital heart disease. Cardiol Young. 1999;9(4):430-44.
17. Chaoui R. The four-chamber view: four reasons why it seems to fail in screening for cardiac abnormalities and suggestions to improve detection rate. Ultrasound Obstet Gynecol. 2003;22(1):3-10.
18. Chaoui R. Fetal echocardiography: state of art. Ultrasound Obstet Gynecol. 2001;17(4):277-84.
19. Paladini D, Vasallo M, Tartaglione A, et al. The role of tissue harmonic imaging in fetal echocardiography. Ultrasound Obstet Gynecol. 2004;23(2):159-64.
20. Tutschek B, Zimmermann T, Buck T, et al. Fetal tissue Doppler echocardiography: detection rates of cardiac structures and quantitative assessment of the fetal heart. Ultrasound Obstet Gynecol. 2003;21(1):26-32.
21. Paladini D, Lamberti A, Teodoro A, et al. Tissue Doppler imaging of the fetal heart. Ultrasound Obstet Gynecol. 2000;16(6):530-5.
22. Sharma S, Parness IA, Kamenir SA, et al. Screening fetal echocardiography by telemedicine: efficacy and clinical acceptance. J Am Soc Echocardiogr. 2003;16(3):202-8.
23. Nelson TR, Pretorius DH, Lev-Toaff A, et al. Feasibility of performing a virtual patient examination using three-dimensional ultrasonographic data acquired at remote locations. J Ultrasound Med 2001;20(9):941-52.
24. Deng J, Rodeck CH. New fetal cardiac imaging techniques. Prenat Diagn. 2004;24(13):1092-103.
25. Sklansky M. New dimensions and directions in fetal cardiology. Curr Opin Pediatr. 2003;15(5):463-71.
26. Deng J. Terminology of three-dimensional and four-dimensional ultrasound imaging of the fetal heart and other moving body parts. Ultrasound Obstet Gynecol. 2003;22(4):336-44.
27. Chaoui R, Heling KS. New developments in fetal heart scanning: three- and four-dimensional fetal echocardiography. Semin Fetal Neonat Med. 2005;10(6):567-77.
28. Sklansky MS, DeVore GR, Wong PC. Real-time 3-dimensional fetal echocardiography with and instantaneous volume-rendered display: early description and pictorial essay. J Ultrasound Med. 2004;23(2):283-9.
29. Sklansky MS, Nelson TR, Pretorius DH. Three-dimensional fetal echocardiography: gated versus nongated techniques. J Ultrasound Med. 1998;17(7):451-7.
30. Sklansky M, Miller D, DeVore G, et al. Prenatal screening for congenital heart disease using real-time three-dimensional echocardiography and a novel 'sweep volume' acquisition technique. Ultrasound Obstet Gynecol. 2005;25(5):435-43.
31. Bega G, Kuhlman K, Lev-Toaff A, et al. Application of three-dimensional ultrasonography in the evaluation of the fetal heart. J Ultrasound Med. 2001;20(4):307-13.
32. Wang PH, Chen GD, Lin LY. Imaging comparison of basic cardiac views between two- and three-dimensional ultrasound in normal fetuses in anterior spine positions. Int J Cardiovasc Imaging. 2002;18(1):17-23.
33. Esh-Broder E, Ushakov FB, Imbar T, et al. Application of free-hand three-dimensional echocardiography in the evaluation of fetal cardiac ejection fraction: a preliminary study. Ultrasound Obstet Gynecol. 2004;23(6):546-51.
34. Meyer-Wittkopf M, Cole A, Cooper SG, et al. Three-dimensional quantitative echocardiographic assessment of ventricular volume in healthy human fetuses and in fetuses with congenital heart disease. J Ultrasound Med. 2001;20(4):317-27.
35. Deng J, Yates R, Sullivan ID, et al. Dynamic three-dimensional color Doppler ultrasound of human fetal intracardiac flow. Ultrasound Obstet Gynecol. 2002;20(2):131-6.

36. Meyer-Wittkopf M, Cooper S, Vaughan J, et al. Three-dimensional (3D) echocardiographic analysis of congenital heart disease in the fetus: comparison with cross-sectional (2D) fetal echocardiography. Ultrasound Obstet Gynecol. 2001;17(6):485-92.
37. Chaoui R. Three-dimensional ultrasound of the blood flow in the fetal cardiovascular system. In: Kurjak A (Ed). Textbook of Perinatal Medicine. New Delhi, India: Jaypee Brothers Medical Publishers; 2005. pp. 644-53.
38. Jürgens J, Chaoui R. Three-dimensional multiplanar time-motion ultrasound or anatomical M-mode of the fetal heart: a new technique in fetal echocardiography. Ultrasound Obstet Gynecol. 2003;21(2):119-23.
39. Turan S, Turan O, Baschat AA. Three- and four-dimensional fetal echocardiography. Fetal Diagn Ther. 2009;25(4):361-72.
40. Michailidis GD, Simpson JM, Karidas C, et al. Detailed three-dimensional fetal echocardiography facilitated by an Internet link. Ultrasound Obstet Gynecol. 2001;18(4): 325-8.
41. Viñals F, Mandujano L, Vargas G, et al. Prenatal diagnosis of congenital heart disease using four-dimensional spatiotemporal image correlation (STIC) telemedicine via an Internet link: a pilot study. Ultrasound Obstet Gynecol. 2005;25(1):25-31.
42. Lee W, Kirk JS, Comstock CH, et al. Vasa previa: prenatal detection by three-dimensional ultrasonography. Ultrasound Obstet Gynecol. 2000;16(4):384-7.
43. Gonçalves LF, Romero R, Espinoza J, et al. Four-dimensional ultrasonography of the fetal heart using color Doppler spatiotemporal image correlation. J Ultrasound Med. 2004;23(4):473-81.
44. Chaoui R, Hoffmann J, Heling KS. Three-dimensional (3D) and 4D color Doppler fetal echocardiography using spatiotemporal image correlation (STIC). Ultrasound Obstet Gynecol. 2004;23(6):535-45.
45. DeVore GR, Falkensammer P, Sklansky MS, et al. Spatiotemporal image correlation (STIC): new technology for evaluation of the fetal heart. Ultrasound Obstet Gynecol. 2003;22(4):380-7.
46. Gonçalves LF, Lee W, Chaiworapongsa T, et al. Four-dimensional ultrasonography of the fetal heart with spatiotemporal image correlation. Am J Obstet Gynecol. 2003;189(6):1792-802.
47. Ghi T, Cera E, Segata M, et al. Inversion mode spatiotemporal image correlation (STIC) echocardiography in three-dimensional rendering of fetal ventricular septal defects. Ultrasound Obstet Gynecol. 2005;26(6):679-80.
48. Espinoza J, Gonçalves LF, Lee W, et al. A novel method to improve prenatal diagnosis of abnormal systemic venous connections using three- and four-dimensional ultrasonography and 'inversion mode'. Ultrasound Obstet Gynecol. 2005;25(5):428-34.
49. Viñals F, Poblete P, Giuliano A . Spatio-temporal image correlation (STIC): a new tool for the prenatal screening of congenital heart defects. Ultrasound Obstet Gynecol. 2003;22(4):388-94.
50. Bennasar M, Martínez JM, Olivella A, et al. Feasibility and accuracy of fetal echocardiography using four-dimensional spatiotemporal image correlation technology before 16 weeks' gestation. Ultrasound Obstet Gynecol. 2009;33(6): 645-51.
51. Uittenbogaard LB, Haak MC, Peters RJ, et al. Validation of volume measurements for fetal echocardiography using four-dimensional ultrasound imaging and spatiotemporal image correlation. Ultrasound Obstet Gynecol. 2010;35(3):324-31.
52. Viñals F, Mandujano L, Vargas G, et al. Prenatal diagnosis of congenital heart disease using four-dimensional spatiotemporal image correlation (STIC) telemedicine via an Internet link: a pilot study. Ultrasound Obstet Gynecol. 2005;25(1):25-31.
53. DeVore GR, Polanco B, Sklansky MS, et al. The 'spin' technique: a new method for examination of the fetal outflow tracts using three-dimensional ultrasound. Ultrasound Obstet Gynecol. 2004;24(1):72-82.
54. Gonçalves LF, Espinoza J, Romero R, et al. Four-dimensional fetal echocardiography with spatiotemporal image correlation (STIC): a systematic study of standard cardiac views assessed by different observers. J Matern Fetal Neonatal Med. 2005;17(5):323-31.
55. Gonçalves LF, Espinoza J, Romero R, et al. A systematic approach to prenatal diagnosis of transposition of the great arteries using 4-dimensional ultrasonography with spatiotemporal image correlation. J Ultrasound Med. 2004;23(9):1225-31.
56. Shih JC, Shyu MK, Su YN, et al. 'Big-eyed frog' sign on spatiotemporal image correlation (STIC) in the antenatal diagnosis of transposition of the great arteries. Ultrasound Obstet Gynecol. 2008;32(6):762-8.
57. Lee W, Espinoza J, Cutler N, et al. The 'starfish' sign: a novel sonographic finding with B-flow imaging and spatiotemporal image correlation in a fetus with total anomalous pulmonary venous return. Ultrasound Obstet Gynecol. 2010;35(1):124-5.
58. Bhat AH, Corbett V, Carpenter N, et al. Fetal ventricular mass determination on three-dimensional echocardiography: studies in normal fetuses and validation experiments. Circulation. 2004;110(9):1054-60.
59. Abuhamad A. Automated Multiplanar Imaging. A novel approach to Ultrasonography. J Ultrasound Med. 2004;23(5):573-6.
60. Abuhamad A, Falkensammer P, Reichartseder F, et al. Automated retrieval of standard diagnostic fetal cardiac ultrasound planes in the second trimester of pregnancy: a prospective evaluation of software. Ultrasound Obstet Gynecol. 2008;31(1):30-6.
61. Tutschek B, Sahn DJ. Semi-automatic segmentation of fetal cardiac cavities: progress towards an automatic fetal echocardiogram. Ultrasound Obstet Gynecol. 2008;32(2): 176-80.
62. Viñals F, Ascenzo R, Naveas R, et al. Fetal echocardiography at 11 + 0 to 13 + 6 weeks using four-dimensional spatiotemporal image correlation telemedicine via an Internet link: a pilot study. Ultrasound Obstet Gynecol. 2008;31(6):633-8.
63. Turan S, Turan OM, Ty-Torredes K, et al. Standardization of the first-trimester fetal cardiac examination using

spatiotemporal image correlation with tomographic ultrasound and color Doppler imaging. Ultrasound Obstet Gynecol. 2009;33(6):652-6.
64. Espinoza J, Gonçalves LF, Lee W, et al. The use of the minimum projection mode in 4-dimensional examination of the fetal heart with spatiotemporal image correlation. J Ultrasound Med. 2004;23(10):1337-48.
65. Gonçalves LF, Espinoza J, Lee W, et al. Three- and four-dimensional reconstruction of the aortic and ductal arches using inversion mode: a new rendering algorithm for visualization of fluid-filled anatomical structures. Ultrasound Obstet Gynecol. 2004;24(6):696-8.
66. Lee W, Gonçalves LF, Espinoza J, et al. Inversion mode: a new volume analysis tool for 3-dimensional ultrasonography. J Ultrasound Med. 2005;24(2):201-7.
67. Zhang M, Pu DR, Zhou QC, et al. Four-dimensional echocardiography with B-flow imaging and spatiotemporal image correlation in the assessment of congenital heart defects. Prenat Diagn. 2010;30(5):443-8.
68. Volpe P, Campobasso G, De Robertis V, et al. Two- and four-dimensional echocardiography with B-flow imaging and spatiotemporal image correlation in prenatal diagnosis of isolated total anomalous pulmonary venous connection. Ultrasound Obstet Gynecol. 2007;30(6):830-7.

21
CHAPTER

Application of Spatial and Temporal Image Correlation in the Fetal Heart Evaluation

Marcin Wiechec, Agnieszka Nocun, Jill Beithon

INTRODUCTION

From the beginning of the new millennium attempts were made to apply the use of three-dimensional (3D) ultrasound in fetal echocardiography. In 2001, a study was published which utilized Doppler-gated 3D fetal echocardiography on 22 abnormal cardiac cases.[1] It was proven that fetal cardiac 3D was feasible and provided examiners with additional information. Later, Bega and coworkers compared the number of cardiac views and structures obtained from two-dimensional (2D) ultrasound to images acquired from static 3D volume datasets.[2] The same time limits (scan duration of 10 minutes) were utilized in both groups of images as was the same machine, a Voluson 530D, one of the first volume ultrasound machines. In this study, it was proven that better results were achieved by means of the 3D approach. Bega showed for the first time the advantages of volume ultrasound in fetal echocardiography, including the utilization of independent volume review, teleconsultation and operator training. A breakthrough in 3D fetal echocardiography took place in 2003, when a spatial and temporal image correlation (STIC) algorithm was introduced, which is dedicated for detailed fetal echocardiography.[3] This is one of the newest volume ultrasound modalities, which provides 3D reconstruction of a tiny organ whose walls contract at a fast frequency of about 150 beats per minute. In classic 2D echocardiography, the examiner evaluates the fetal heart by manually moving the transducer through particular cardiac views imagining a 3D reconstruction. The information gained is dependent on the examiner's image optimization and scanning skills, the examiner's knowledge of cardiac anatomy and anomalies, and the spatial imagination of the interpreting physician. The STIC technique permits replacing this subjective reconstruction by actual spatially and temporally correct cardiac ultrasound images.

TECHNICAL CONSIDERATIONS

The concept of STIC consists of a very slow static 3D acquisition of the fetal heart, encompassing approximately 25 cycles.[4] During the process of acquisition, the beam is swept through the heart capturing diastole and systole in tiny subphases,[5] e.g. as the beam sweeps into the four chamber view it is recorded in the phase of early then mid and late diastole, then early mid and late systole. As the sweep continues into the five chamber view, it is also captured in the phase of early mid and late diastole, then early mid and late systole, and so on, until the sweep reaches the most superior part of the heart, the transverse section of the aortic arch. The result is one large static volume block. Each individual subphase of the cardiac cycle is then rearranged temporally and grouped into new separate volume blocks. Eventually, approximately 20–40 blocks come into being.[5] The quality of the final product depends on the speed of the acquisition sweep. A slower sweep allows for more subphases of the cardiac cycle to be obtained, grouped together and rearranged, which adds spatial information to the final product. The final product is presented in the form of an orderly dynamic

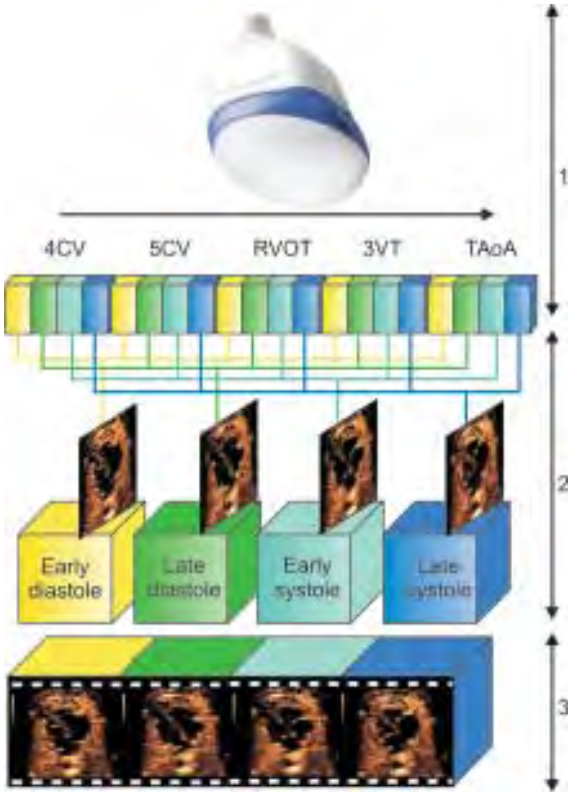

Figure 21.1: STIC acquisition and processing. One slow 3D sweep. The machine detects the location and timing of each systolic beat and calculates the heart rate. Then the system determines the time frame between each beat, which allows for rearranging of the B-mode frames into a new order depending on their temporal event within the heart cycle. Since the machine knows the length of the sweep and the heart rate, it can calculate the location of each peak systolic frame and other points in the cardiac cycle and combine the information in it with all the other frames of the corresponding times. Because many frames at the exact time reference are averaged together, the temporal resolution compares to a high frame rate B-mode image. The rearranging results in a final product of one heart cycle replayed in a continuous cine loop

sequence, a clip, which is arranged into one full cardiac cycle, from the early phase of diastole to the late phase of systole in all planes, from the four chamber view to the transverse section of the aortic arch **(Fig. 21.1)**.

THE PROCESS OF FETAL HEART ASSESSMENT IN STIC MODE

The fetal heart evaluation by using STIC technology can be divided into the following stages:

- The preparation of the 2D image and the STIC volume acquisition

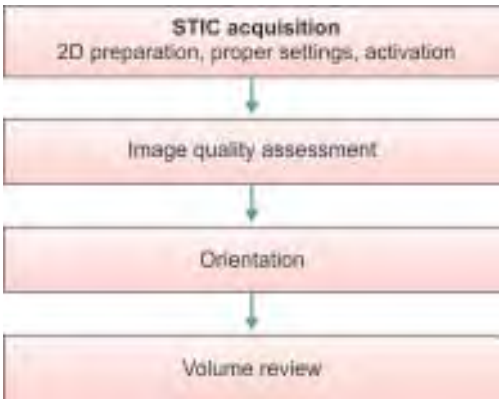

Figure 21.2: Stages of fetal cardiac evaluation by using STIC mode

- Assessing the quality of an acquired volume dataset
- The orientation of the STIC volume
- Reviewing the acquired STIC information **(Fig. 21.2)**.

THE PREPARATION OF THE 2D IMAGE AND THE STIC VOLUME ACQUISITION

The STIC acquisition is a process of rewriting 2D information into a 3D volume dataset. An acquisition sweep takes from 7.5 to 15 seconds depending on selected adjustments. Adequate preparation of the 2D image before the acquisition and proper STIC settings however is more time consuming. This is the basis of what will result in the best quality volume dataset allowing for the most accurate diagnoses.

Probe Selection

Selection of an appropriate probe is one of the key issues before the STIC acquisition is started. A transabdominal probe with a frequency range of 4–8MHz is optimal for the first and second trimesters until about 24 weeks of gestation. After this period ossified ribs generate shadowing which obscure cardiac views and affect the quality of volume acquisition. After 24 weeks of gestation, a transabdominal transducer with a frequency range of 2–5 MHz is generally more usable due to better penetration capabilities. After 30 weeks of gestation a 2–5 MHz probe is necessary for successful STIC acquisitions. One must also consider the patients' body mass index (BMI) in selecting a probe and in cases of obesity the probe with better penetration is the one of choice. It is ideal to have both of the aforementioned probes available. In 2009, a new matrix array transducer was introduced with a frequency range covering the mid ranges of the two above mentioned probes. This

probe is a good alternative. For transvaginal STIC acquisitions the most suitable probe has a frequency range of 5–9 MHz, but a probe providing 6–12 MHz frequency range can provide especially high resolution for some selected cases between 11 and 12 weeks of gestation.

An Appropriate Acoustic Window

Every STIC acquisition should be preceded by the proper probe selection and 2D image optimization. The next step is the selection of a suitable acoustic window which will assure the examiner of the proper amount of information to be acquired into the volume block. Several practical considerations are described below.

Fetal Position

In order to avoid shadowing from the fetal spine and ribs, it is necessary to move the probe to a position where the beam will insonate the fetus from an anterior approach if at all possible. The examiner maneuvers the probe on the abdomen of the patient to effectively create the impression of the fetus being turned by the examiner **(Figs 21.3A to F)**.

Selection of Acquisition Plane

In the STIC mode, the most popular way of acquiring the volume dataset is by evaluating the heart from transverse sections through the fetal chest.[6] The acquisition plane A then becomes transverse cross-sections beginning at the level of the upper abdomen to include the fetal stomach (this aids in situs determination). Proceeding superiorly are the four-chamber and five-chamber views, the right outflow tract view and the three vessels and trachea view. Planes B and C are the reconstructed views, which are orthogonal planes to A, that is to say sagittal and coronal. It is very important to make sure that the transverse section of plane that you are identifying as your start of acquisition is a true transverse plane and not oblique. Watch carefully for the ribs in the fetal chest to appear similar on both the right and left sides and that the fetal abdomen and chest are round and not elongated. Keep your image angle wide enough to view the entire width of the fetus so

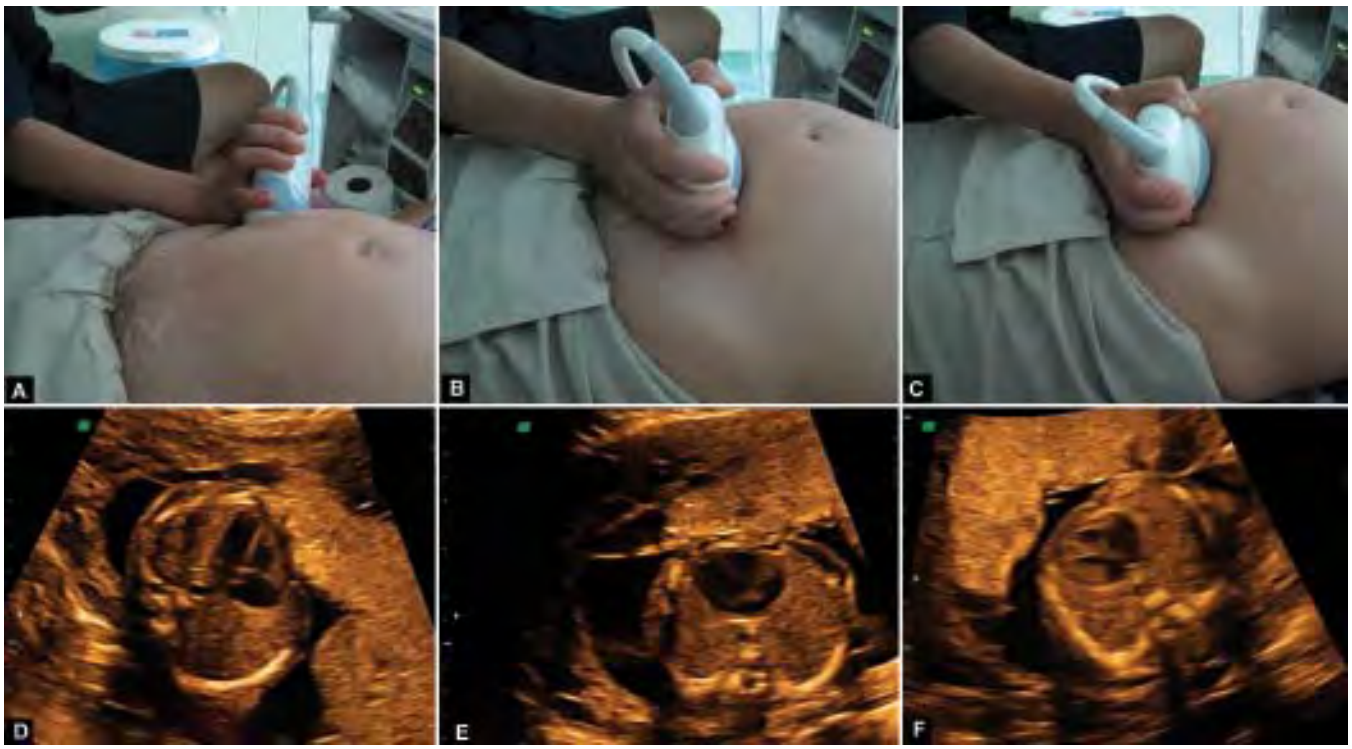

Figures 21.3A to F: Translation technique is shown, which is actually nothing more than changing the application point of the transducer. At the time of translation the same section through the fetal chest is displayed on the monitor, but the relationship between the transducer and the target changes. Translation is used for identifying the most suitable insonation angle. (A to C) Movements with the probe on the patient's abdomen; (D to F) Effect of translation on the image

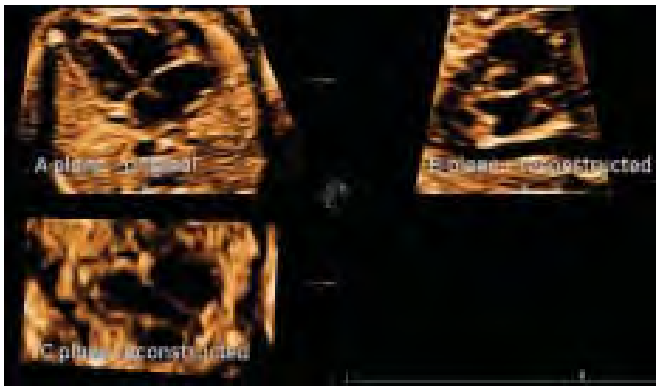

Figure 21.4: Transverse volume acquisition. The A plane is the original acquisition plane; the B plane is a sagittal plane, which is reconstructed from the A plane; the C plane is a coronal plane, which is reconstructed from the A plane

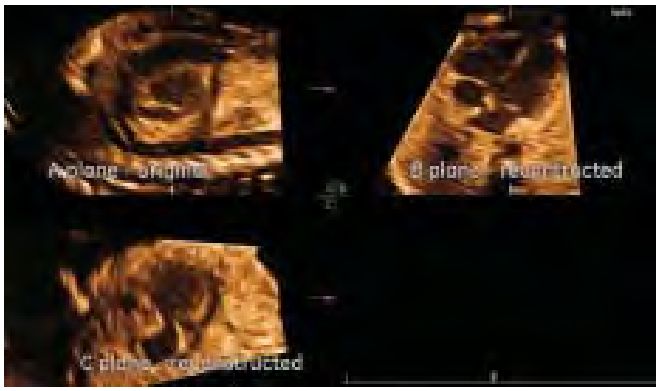

Figure 21.5: Sagittal volume acquisition. The A plane is the original acquisition plane; the B plane is a transverse plane, which is reconstructed from the A plane; the C plane is a coronal plane, which is reconstructed from the A plane

you can easily identify structures that will help you to recognize that you are in a true transverse section of the fetus **(Fig. 21.4)**.

Of note: It is also possible to obtain a STIC acquisition from a sagittal section through the fetal chest.[6] The acquisition plane A then has sagittal sections, plane B reconstructed transverse sections and plane C reconstructed coronal sections **(Fig. 21.5)**.

Selection of Insonation Angle

An optimal insonation angle should simultaneously assure the correct visualization of the chambers of the heart, outflow tracts and the interventricular septum. This is best done by assuring an angle between the beam and the interventricular septum of approximately 45°.[6] This may entail a sweep, which begins at the apex of the heart and sweeps towards the base or vice versa **(Fig. 21.6)**.

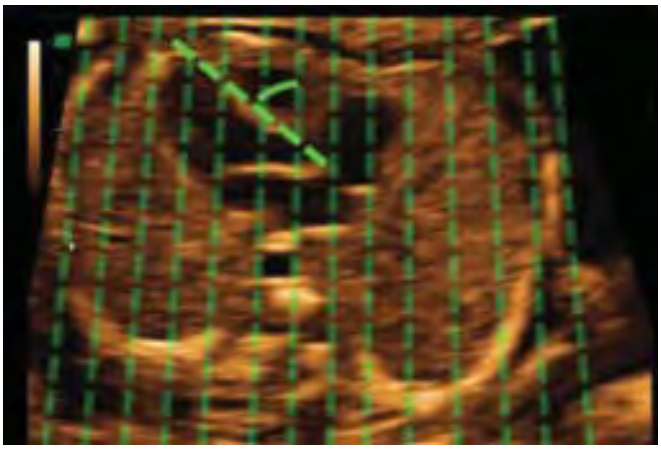

Figure 21.6: The optimal insonation angle to the interventricular septum is 45°

Selecting an Acoustic Window Free of Shadowing

"Escaping" from acoustic shadows is of utmost importance and every sonologist must assure that shadows are not encountered in any section of the heart. Before the STIC acquisition is initiated, it is prudent to make a 2D sweep through the heart imitating the STIC acquisition. If on some sections shadows are visible, one should seek a better acoustic window. Shadows from 2D images will always be rewritten on the 3D dataset.

Selecting Suitable Image Zooming and Framing

The image area which is to be utilized in the STIC acquisition should always be properly framed. Beginners at STIC should frame the image so that the acquisition area includes not only the fetal heart but also the chest in transverse section, including the fetal ribs and spine. Including this additional information into the STIC volume will allow for easier manipulation of the dataset as the spine and ribs will serve as landmarks for the examiner. In experienced hands, the frame can be limited to the heart and the transverse section through the descending aorta. The image should also be zoomed to an appropriate level so that the structures can be easily seen **(Figs 21.7A and B).**

STIC Adjustments

Now that you have chosen an appropriate probe and selected a proper acoustic window it is time to make decisions regarding two important STIC parameters, the STIC volume angle and the STIC acquisition time.

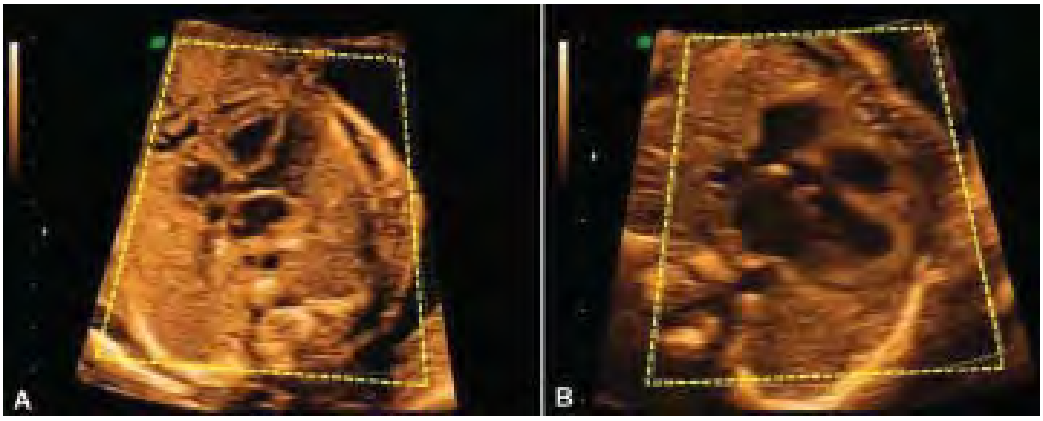

Figures 21.7A and B: The 2D image preparation for STIC acquisition—framing and zooming. (A) A frame covers the whole chest with small magnification; (B) A frame covers only the heart and includes the descending aorta and the spine, high magnification

The STIC volume angle refers to the length of the sweep. You must determine how large of an area that you want to acquire information within. The decision to set the volume angle is dependent on the size of the heart. The greater the size of the heart (gestational age of the fetus) the greater volume angle you will need. A rule of thumb for setting the degree of the angle coincidently coincides with the gestational age in weeks of the fetus.

When acquiring your volume from a transverse plane pick a volume angle that is the same as the gestational age in weeks. For example, an angle of 20° is a good choice for a 20 week fetus. Use a 30° angle for a 30 week fetus.

When acquiring your volume from a sagittal plane pick a volume angle that is the same as the gestational age in weeks plus 5°. For example, an angle of 25° is a good choice for a 20 week fetus. Use a 35° angle for a 30 week fetus.

Of course these numbers need to be adjusted larger in cases of cardiomegaly. A minimum angle size which is acceptable for use is 15° and a maximum angle size is 40°.

The STIC acquisition time determines the length of the duration of the acquisition. Your choice in setting the acquisition time should depend on how active the fetus is at the time that you are trying to do your STIC acquisition. A longer time will create a sweep, which has more time to obtain information, thus adding to the quality of the volume dataset. However, with a longer time there comes more opportunity for the fetus to move creating motion artifacts. Always choose the longest acquisition time that you think the fetus will cooperate with. You of course will have the opportunity to delete the volume and try again if the fetus moves during the acquisition. A minimum time for a STIC acquisition is 7.5 seconds and a maximum time is 15 seconds.

Finding the Optimal Original Plane of Acquisition (OPA) for a STIC Acquisition

The term original plane of acquisition or OPA refers to the center point of the volume of information, which you are trying to create. It is the midpoint of the volume angle. The OPA is the place on the image that you locate from which the sweep will back up half the distance of the angle that you have decided on and begin the sweep. The sweep will begin, come to the midpoint (the OPA) and continue past the OPA for another half of the sweep angle. This is the same way in which classic 3D volume acquisition is performed (**Fig. 21.8**).

The recommended OPA location for acquisitions done in the transverse plane is the five-chamber view. The five-chamber view is optimal because it is at the midpoint of the manual sweep across the fetal heart that one should acquire for a STIC volume dataset. The five-chamber view is not to be confused with the left ventricular outflow tract (LVOT) view, which is actually an oblique view of the heart and if used as an OPA it will not assure a suitable amount of information, which is included in the STIC dataset. It was proposed by some authors to use the four-chamber view as the OPA in the transverse plane however, if used, the aortic arch may not be included in the volume dataset **(Figs 21.9A and B)**.[2,3,6]

The recommended OPA for acquisitions done in the sagittal plane is the ventricular short axis view just below the level of the atrioventricular valves **(Figs 21.10A and B)**.

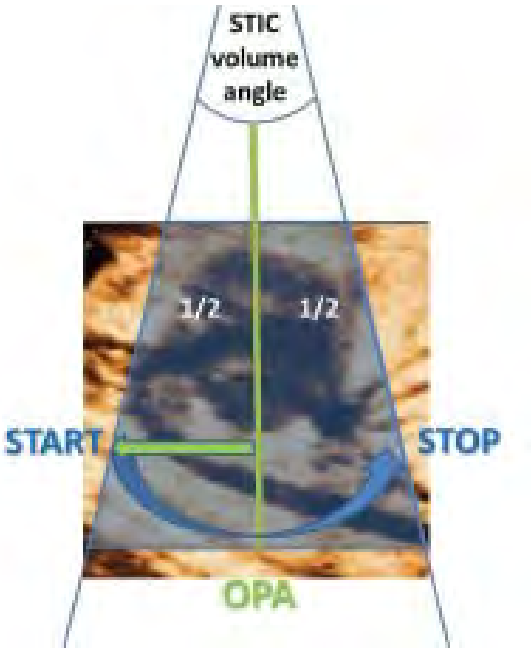

Figure 21.8: Volume acquisition. The original plane of acquisition (OPA) is the midpoint of the selected volume angle and thus the central section of the volume dataset. The OPA is chosen and the transducer automatically sweeps 50% of the chosen volume angle away from the OPA. The sweep then begins acquiring information towards the OPA, the sweep continues past the OPA and ends at the equidistance away from the OPA at which it began

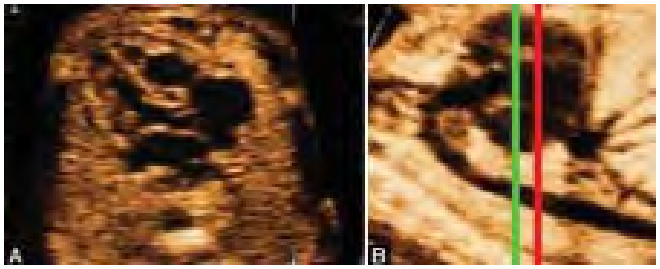

Figures 21.9A and B: The original plane of acquisition (OPA) in transverse STIC technique. (A) The five-chamber view; (B) A reconstructed image of the heart in the sagittal plane. The green line demonstrates the level of the OPA for the transverse STIC acquisition, which is the level of the five-chamber view. The red line demonstrates the level of the four-chamber view. As you can see, the green line (the five-chamber view) depicts the midpoint of the information which we would like to include in the sweep. The red line (the four-chamber view) is located too inferior

IMAGE QUALITY ASSESSMENT

After the acquisition you have to make a decision on whether or not you will save this volume of information

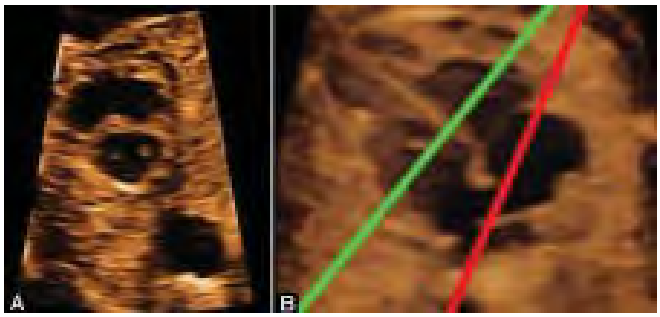

Figures 21.10A and B: The original plane of acquisition (OPA) in sagittal STIC technique. (A) Ventricular short axis view just below the atrioventricular valves; (B) A reconstructed image of the heart in the transverse plane. The green line demonstrates the level of the OPA for the sagittal STIC acquisition, which is at the level of the ventricular short axis view. The red line demonstrates the level of the aortic arch which would be too far to the right for an optimal STIC acquisition

to the machine hard drive for later review and manipulation or discard it and start over. There are three things for you to review in order to make this decision. The first is the preview of the information during the acquisition. The next is checking to see if the machine has made a correct assessment of the fetal heart rate (FHR). The third is a quick review of the volume data block to check for artifacts.

Acquisition Preview

During the acquisition you can watch as the sweep moves through the different levels of the heart. The acquisition is conveniently played at a slow speed so you can watch to make sure the sweep encompassed the stomach on one end and the transverse section of the aortic arch on the other end. You can also watch to see that the fetus did not move and that the proper positioning was maintained to visualize the common views. The experienced eye can detect even the smallest movements of the fetus such as hiccups or respiratory movements, which can cause artifacts **(Figs 21.11 and 21.12)**.

Verifying the Machine's Calculation of the Heart Rate

The machine detects the location and timing of each systolic beat and calculates the heart rate. After the acquisition of the volume, a box will appear telling you the machine's calculation of the estimated fetal heart rate. The heart rate is used by the machine in order to calculate an algorithm by which to separate the B-mode frames into a new order depending on their temporal

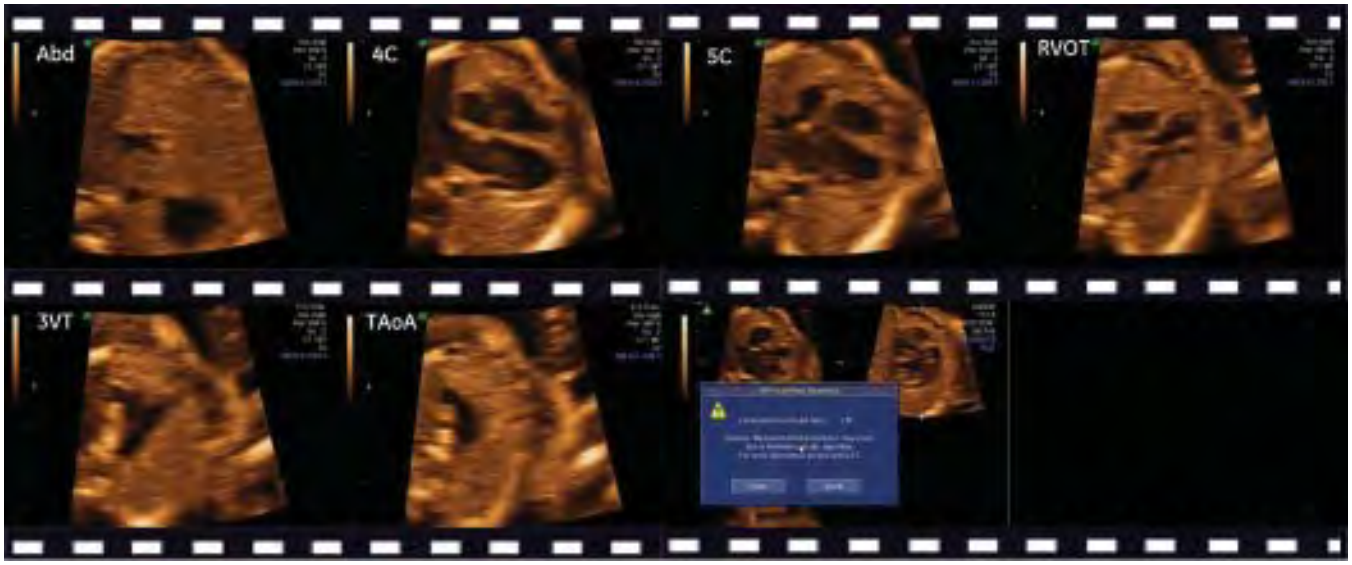

Figure 21.11: The static illustration of the preview in progress of the transverse, transabdominal STIC acquisition. The viewing permits the examiner to watch each transverse section of the fetal heart during the acquisition and to check whether or not artifacts occurred. (Abd) upper abdominal view; (4C) four-chamber view; (5C) five-chamber view; (RVOT) right outflow tract; (3VT) three vessels and trachea view; (TAoA) the transverse section through the aortic arch

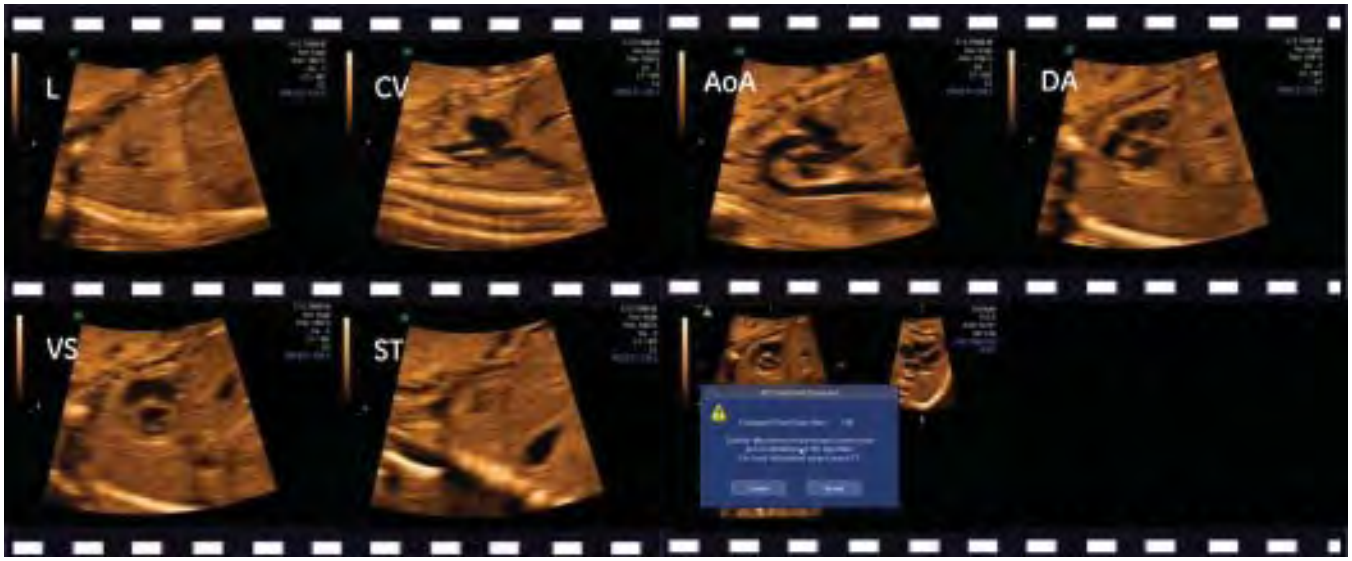

Figure 21.12: The static illustration of the preview in progress of the sagittal, transabdominal STIC acquisition. The viewing permits the examiner to watch each sagittal section of the fetal heart during the acquisition and to check whether or not artifacts occurred. (L) section through right lung; (CV) long axis caval view; (AoA) aortic arch; (DA) ductal arch; (VS) ventricular short axis view; (ST) sagittal section through the fetal trunk at the level of the stomach

event within the heart cycle. The box which appears after the acquisition will ask you to accept or cancel the machine's calculation. If the machine's estimated heart rate is not consistent with what you observed while imaging the heart you must cancel the acquisition and try again **(Fig. 21.13)**.

Initial Review of the Volume Dataset

A third and last element of the estimation of the quality of a newly acquired dataset is the quick review of the volume block. You will be looking for any reason to reject this particular volume dataset or to decide

Figure 21.13: This box will appear after the acquisition asking you to accept the machine's estimation of the fetal heart rate

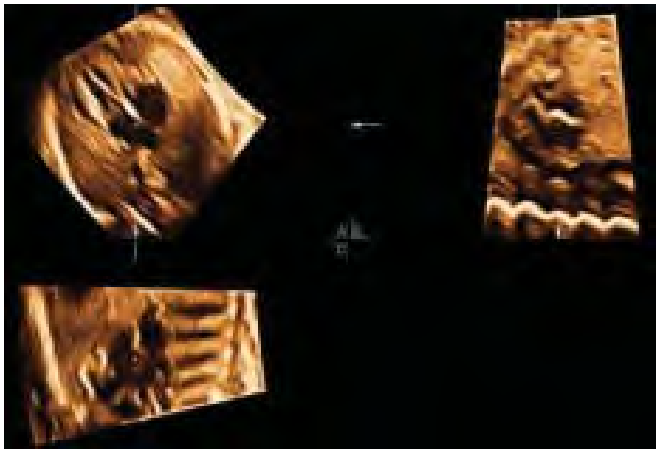

Figure 21.14: Quality rating of a new STIC dataset—motion artifacts. The multiplanar view of the fetal heart. Reference images B and C demonstrate numerous breaks in the reconstruction signifying motion of the fetus during the progress of acquisition

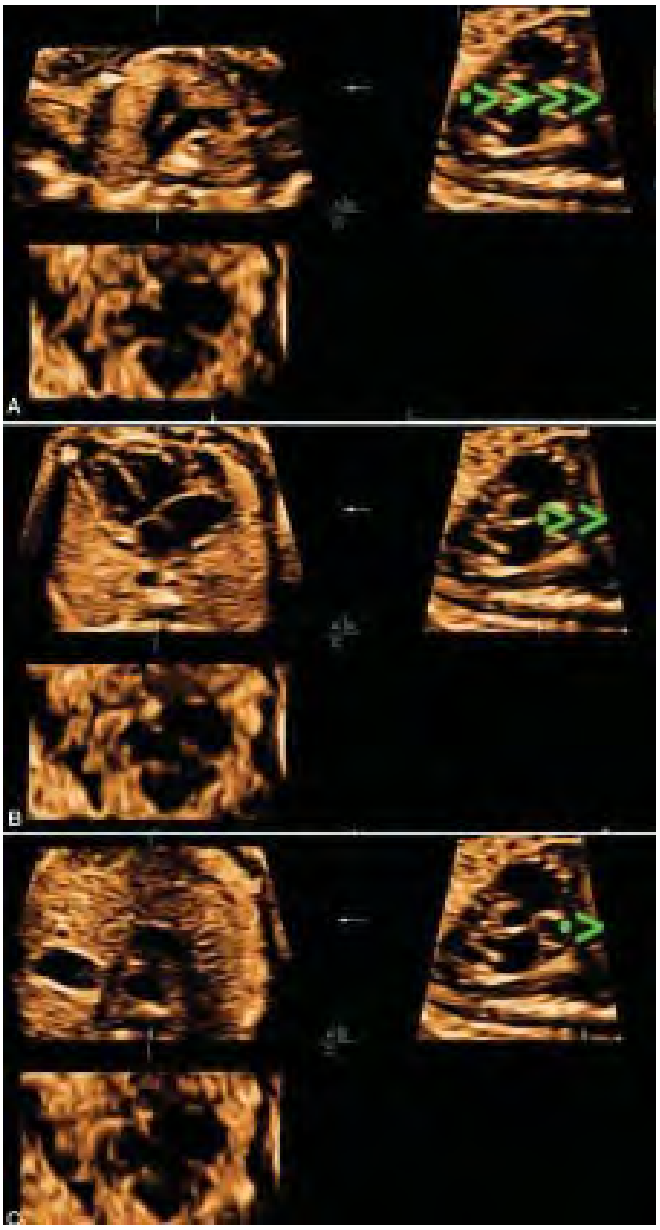

Figures 21.15A to C: Quality rating of a new acquired STIC volume—The series of multiplanar images illustrate the horizontal movement of the pivot point in reference image B and the visualization in the A plane of all recommended cardiac views. The ideal block contains sections from the upper abdominal view to the transverse section of the aortic arch

whether or not you will save it to the machine hard drive for later review and manipulation. The most obvious reasons for rejection of the dataset are motion and/or shadowing artifacts. This quick review is easily done by using the multiplanar imaging option. Here you will want to activate the reference image B and look for breaks in the reconstruction, which signify motion by the fetus during the acquisition **(Fig. 21.14)**.

Then, within the same reference image B, which is the sagittal plane, one can move the pivot point horizontally, to the right and left, while watching the A plane. Each of the recommended views from the transverse aortic arch to the level of the stomach in the abdomen will come into view and can be evaluated for motion or shadowing artifacts, or any other undesirable quality **(Figs 21.15A to C)**.

If after previewing the quality of the volume dataset and verifying that the fetal heart rate is correct then the

STIC volume dataset should be stored to the hard drive of the ultrasound machine. If you forget to store the volume, this information will be unavailable later for review and manipulation.

ORIENTATION

Orientation of a STIC Volume

Similarly as in 2D, 3D fetal echocardiography is based on standardized cardiac sections.[2,6-8] An innovation and advantage in STIC is the ability to always review the STIC images in the identical orientation from one exam to the next, one institution to the next and even one country to the next. This is possible due to the ability to manipulate the images by means of rotational knobs, which are standardized among equipment manufactures. This takes away the variability of fetal lie and promotes a continuity and unification of the prenatal diagnoses of congenital heart disease by the use of STIC.

The orientation of STIC volumes is a completely new sonographic skill.[9] It exists in the consistent anatomical arrangement of every heart, stored in STIC mode, according to the same repeatable rules, so as to prepare the volume block for review in a well organized and reproducible manner.

Foundations of the 3D orientation of the fetal heart were laid in 2001 by Bega and co-authors on static 3D volumes.[2] In the following years it was refined by other authors.[3-6,8]

For the correct orientation of STIC volumes, knobs are available, which rotate images on the x, y and z axis. Coupled with the parallel shift control knob virtually any acquired position of the fetal heart can be manipulated into standard orientations. The image below represents a correctly oriented volume data block of the heart, ready for review and interpretation **(Fig. 21.16)**.

Above is a multiplanar view of a STIC volume dataset. The examiner has arranged the anatomy in the standard viewing planes first described by Bega and co-workers, which is in the A plane, with the apex of the heart to the left of the screen.[2] If the heart is normal, the B plane will show the aortic or ductal arch to the left of the image also. Some others have proposed orientating STIC images with the apex of the heart to the right rather than the left. We believe that orientation with the apex to the left of the image is a good standard and will use this orientation throughout the remainder of this chapter.

Orientating a STIC volume is the process of image orientation in which the operator utilizes the x, y and z knobs and the parallel shift knob on the machine to twist, rotate or flip the images until they end up in a standardized viewing layout whereas the A plane is a transverse four-chamber image of the heart with the

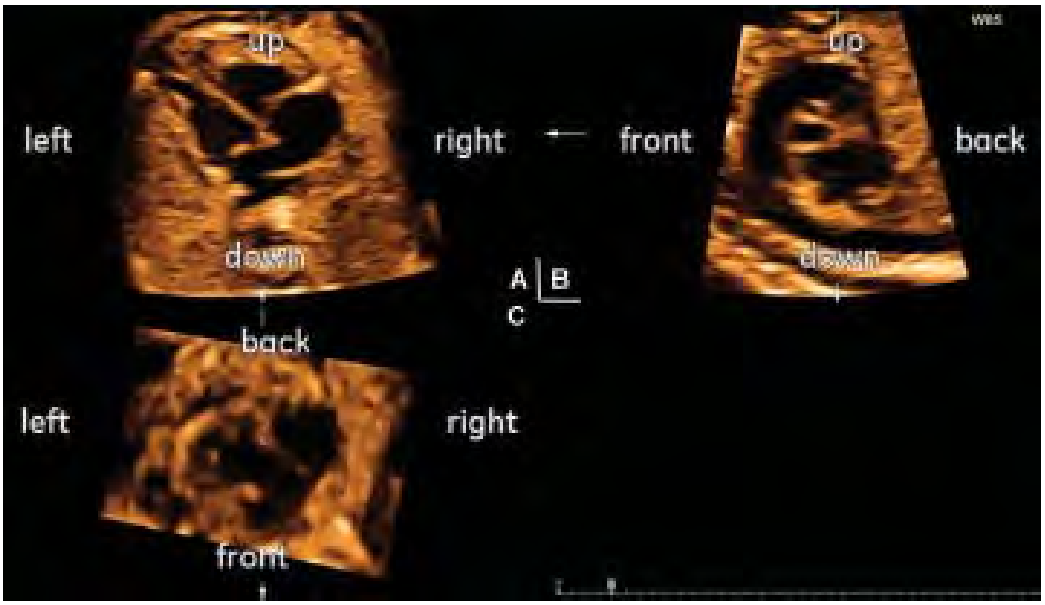

Figure 21.16: The multiplanar view of the fetal heart with the correct arrangement of viscera (situs solitus). This is a properly oriented volume dataset. In the A plane (upper left image) the axis of the heart is directed to the left. In the B plane, the section is through the ductal arch

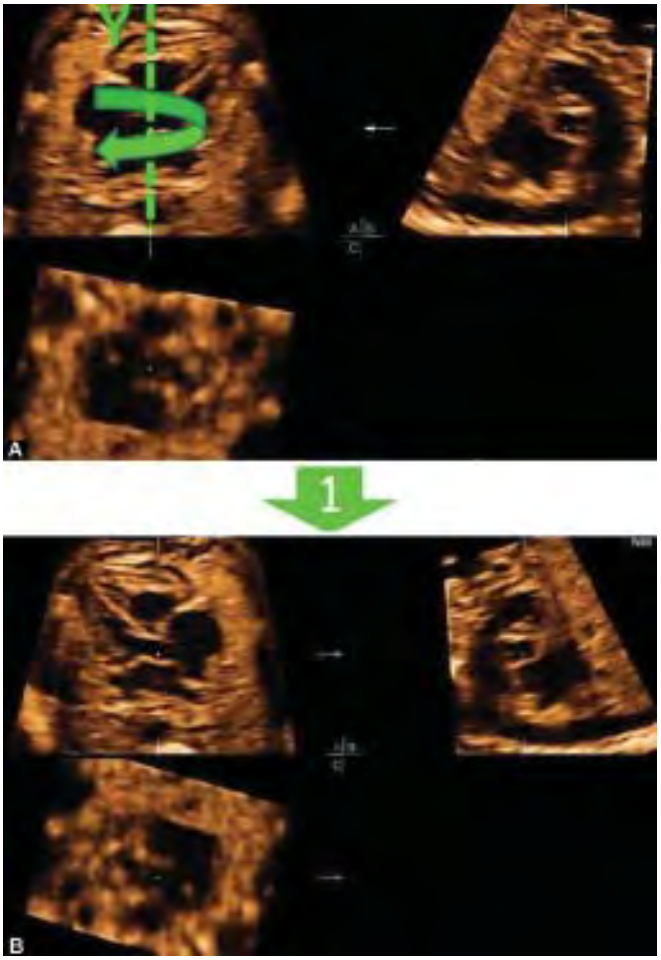

Figures 21.17A and B: (A) The dataset in the top picture was acquired with the apex of the heart to the right of the image. Since we always want to view our volumes with the apex to the left, one must turn the image of 4CV in the reference plane A by 180 degrees using the Y-axis rotation knob; (B) The result is the bottom picture

apex to the left of the image. The B plane is a reconstructed sagittal image showing superior to the left and inferior to the right and the C plane is a reconstructed coronal image. This will place the images in planes, which will make review and manipulation easy and predictable.

There are several ways to arrive at this standard orientation of the apex to the left in the A plane. These methods are based on the utilization of linear structures, situated in the anatomical neighborhood of the heart. These structures include the spine, the descending aorta, the interventricular septum and the ductal arch. The orientation should be always performed in the multiplanar view. In multiplanar mode each image has a small dot, which is called the pivot point. By utilizing

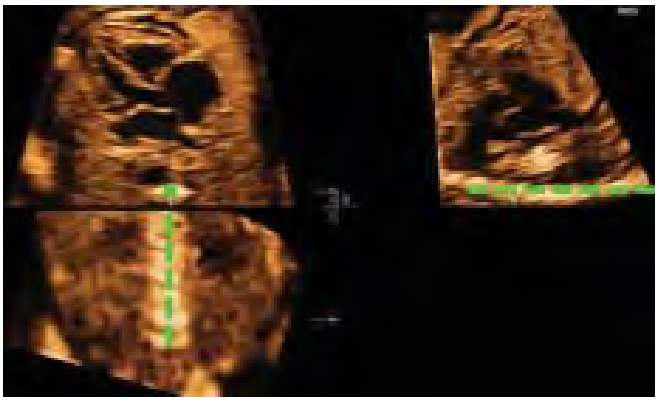

Figure 21.18: The pivot point in the A plane on the spine. The spine was used in the B and C planes to line up the images horizontally in B and vertically in C. This resulted in an optimal orientation of the volume, which can now be reviewed

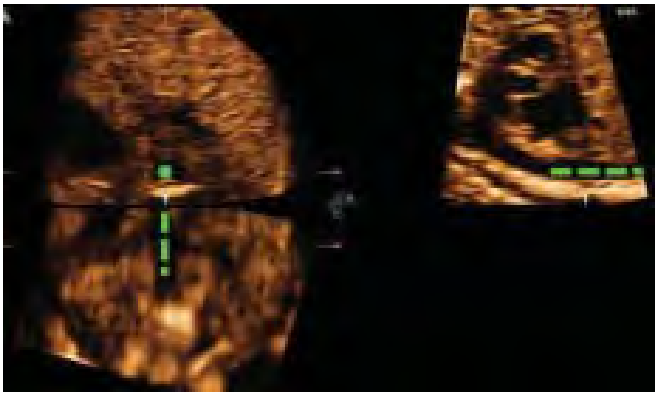

Figure 21.19: The descending aorta was used in like manner as the spine

the x, y and z knobs, the image will rotate on this pivot point allowing you to align structures within the image to a standardized orientation.

In Figures **21.17 to 21.21** manipulation of the images into a standard viewing orientation is shown.

Any of the above methods will work to manipulate the volume into the standard viewing orientation in which the apex of the heart is on the left in the A plane.

REVIEW

STIC Volume Review and the Spectrum of Viewing Options

Once proper orientation of the volume is obtained, it is ready for review and interpretation. When the volume is put into motion in the format of a clip, it represents one full heart cycle played over and over again. It is

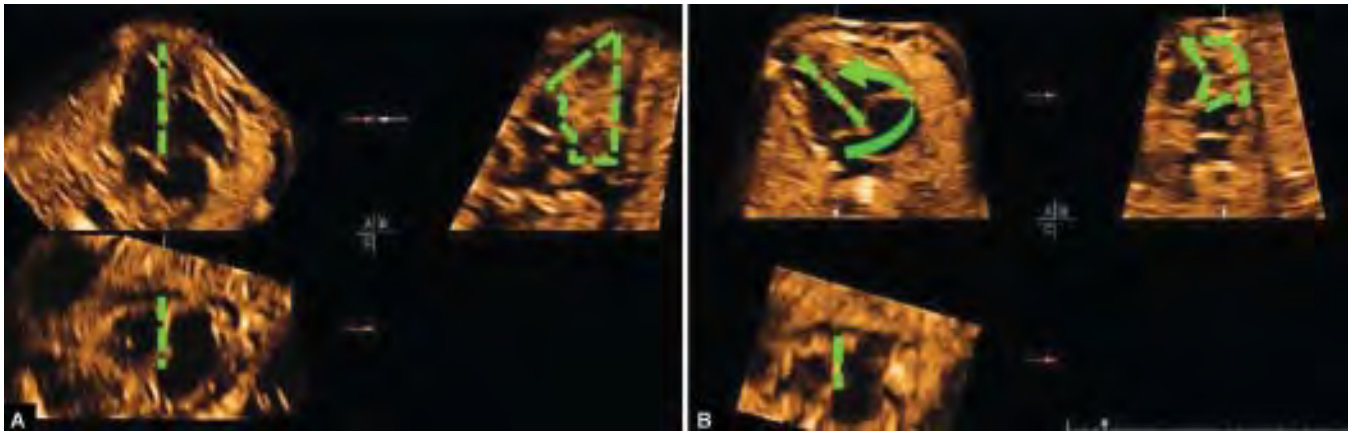

Figures 21.20A and B: (A) Orientation of the volume by using the interventricular septum placed along Y-axis in the A plane, the B plane shows the 'IVS in-plane view' and in the C plane the 'ventricular short axis view' comes into plane; (B) A z rotation is used to again turn the axis of the heart to the left in the A plane

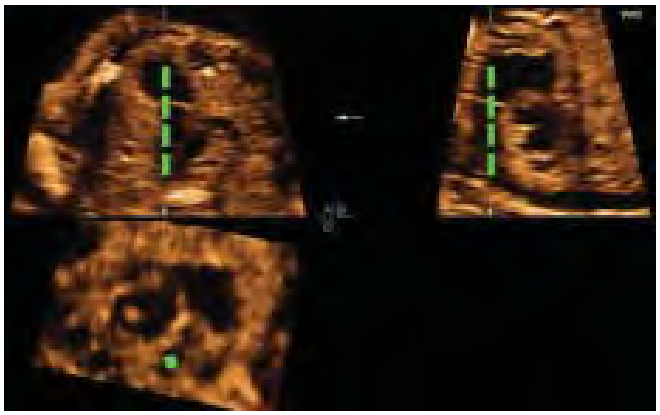

Figure 21.21: The ductal arch was aligned vertically along the Y-axis in the A plane

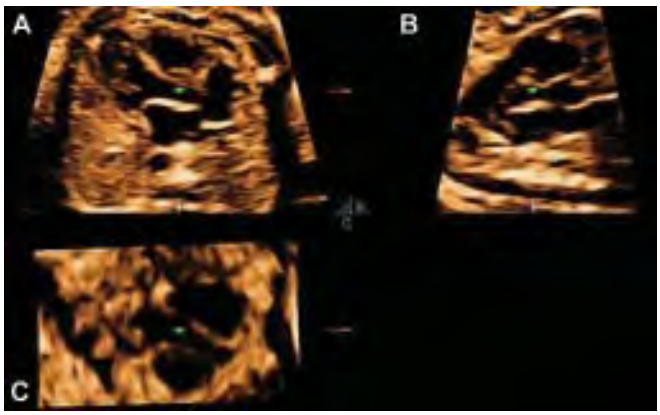

Figures 21.22A to C: (A) Multiplanar view showing the pivot point in the aortic root in the A plane; (B) This same geographic location is represented again by the pivot point in the aortic root, now in a sagittal view, in the B plane; (C) The coronal view of the aortic root is represented again in the C plane

possible to slow down the speed of the clip to about 50%, which creates superb spatial orientation for review. It is also possible to utilize the frame-after-frame review option. There are many STIC volume 3D viewing options available. These will be discussed below.

Multiplanar View

Perhaps the most important and most basic of all viewing options is the multiplanar view.[2,5,6,10,11] In this view three planes are shown, which are perpendicular to each other. They have in common one point, i.e. the pivot point, which is represented on the screen by a dot. The location of this point in the reference image of plane A, e.g. the root of the aorta, identifies the same structure in the B and C planes. Important tools in the multiplanar view are a parallel shift control, which allows for navigating through the image in a layer-after-layer manner in any of the three planes. Other tools are the x, y and z axis rotational knobs used for volume manipulation **(Figs 21.22A to C)**.

In the picture below a clinical example of the use of the multiplanar imaging is shown. The anomaly in this case is a congenital aneurysm of the right aortic Valsalva sinus which during the two-dimensional investigation imitated the root of the aorta. The detailed multiplanar evaluation gave the clear picture of this rare abnormality. With two-dimensional imaging it is not possible to obtain this type of spatial correlation in three orthogonal planes **(Figs 21.23 and 21.24)**.

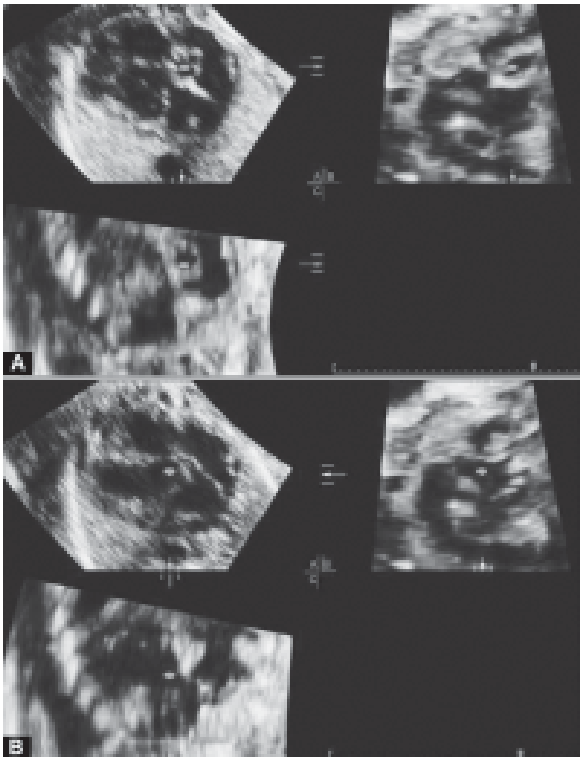

Figures 21.23A and B: (A) An aneurysm of the right aortic Valsalva sinus (green dot) appears to be the aortic root, however this structure is actually at the level of the right atrium; (B) The true aortic root is found at a more anterior level in its normal position

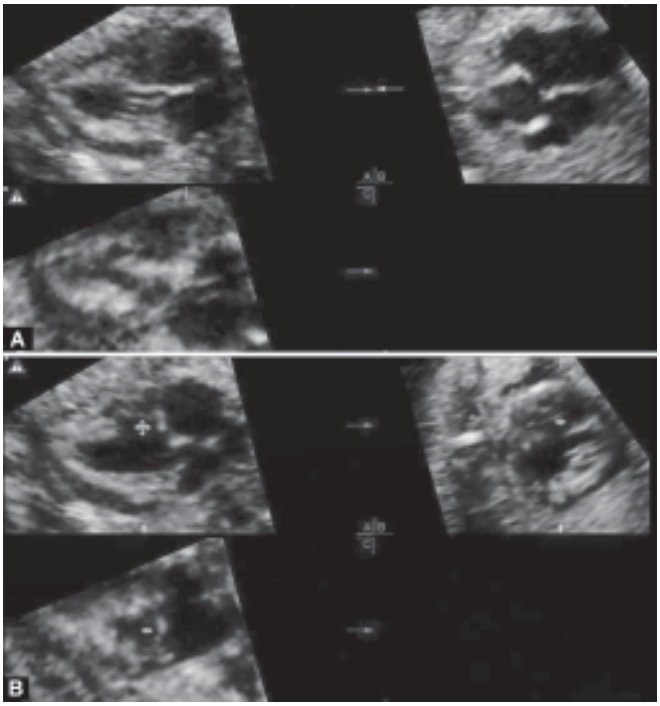

Figures 21.24A and B: A case with a large ventricular septal defect. (A) The pivot point is placed at the level of the crux; in the A plane, a papillary muscle mimics the presence of an intact IVS; (B) By moving the pivot point in the C plane more to the front it becomes clear that there is a large septal defect

Tomographic Ultrasound Imaging

Another viewing option for a STIC volume is ultrasound tomography. It has many advantages and is utilized often by many examiners.[7,12-14] Tomography allows for the viewing of multiple slices of the same image, by means of 1, 3, 5, 8, 11 or 15 sections on one screen along with a reference image, which is perpendicular to the tomographic sections with an overlay of the tomographic lines of slices. The distance between the slices can be set with equal or any distances. The mid slice is represented on the overlay by an asterisk. Slices to the left of the center line are described by negative slice numbers and slices to the right of the center line are represented by positive slice numbers. This makes identification of the slices in comparison to the reference image easy. By using three standardized tomographic planes, the plane of the four-chamber view, the plane of the five-chamber view and the right ventricular outflow tract view, most of the abnormalities of the heart can be recognized. In cases of complex defects of the heart, ultrasound tomography is an excellent way to illustrate the margins of the defect on one screen. As shown in the picture both a normal heart and a heart with Tetralogy of Fallot is illustrated with the use of tomographic imaging **(Figs 21.25 to 21.29)**.

OmniView

OmniView (GE) or Oblique View (Medison) technique allows for drawing arbitrary straight or curved sections from the reference image and displaying those sections next to the reference image **(Figs 21.30 and 21.31)**.

Rendering

A completely different kind of volume viewing option, which can be utilized in STIC is rendering. This is a technique of 3D reconstruction from flat multiplanar images.[6,14-17] Surface rendering gives the impression of depth, causing the final images to resemble autopsy sections. The surface which one wishes to examine can be chosen and applied by the use of a rendering box. Because we are using volumes of information a direction that one wishes to look from can be chosen from any plane. The thickness of the box determines the "depth" of tissue that one wants to see in the rendered image **(Fig. 21.32)**.

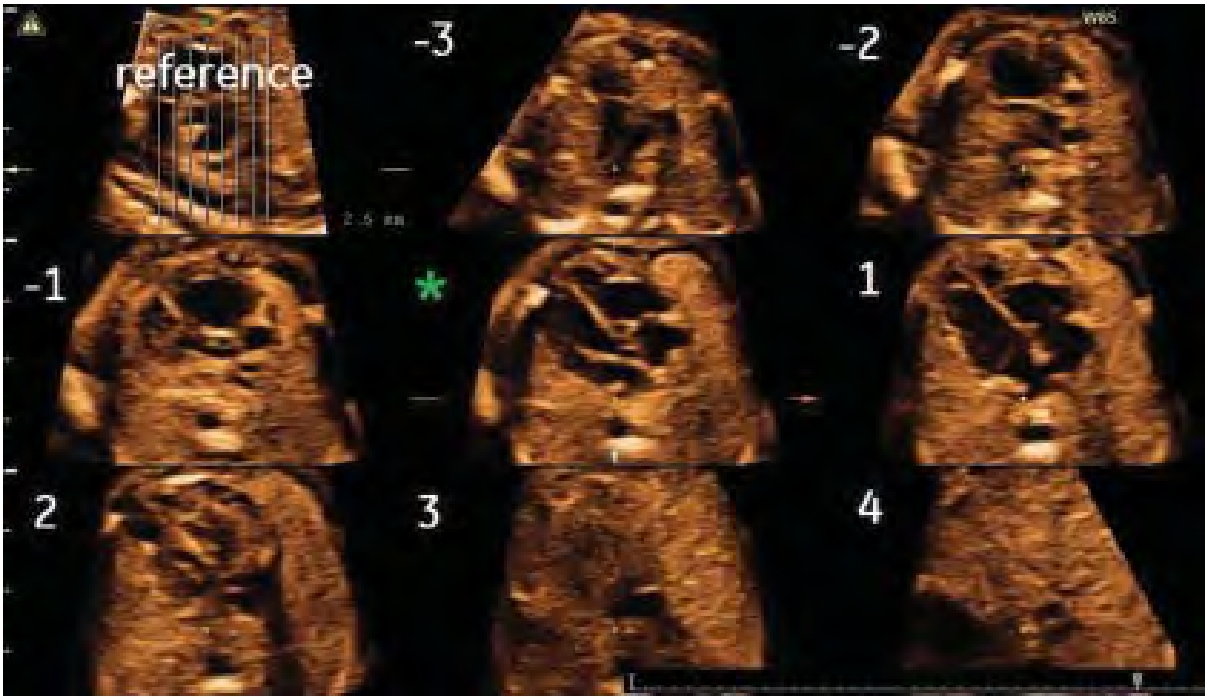

Figure 21.25: Tomographic ultrasound imaging in a STIC volume in diastole in a normal heart. In the top left section, the overlay image is presented, which is perpendicular to the tomographic layers, demonstrating section levels

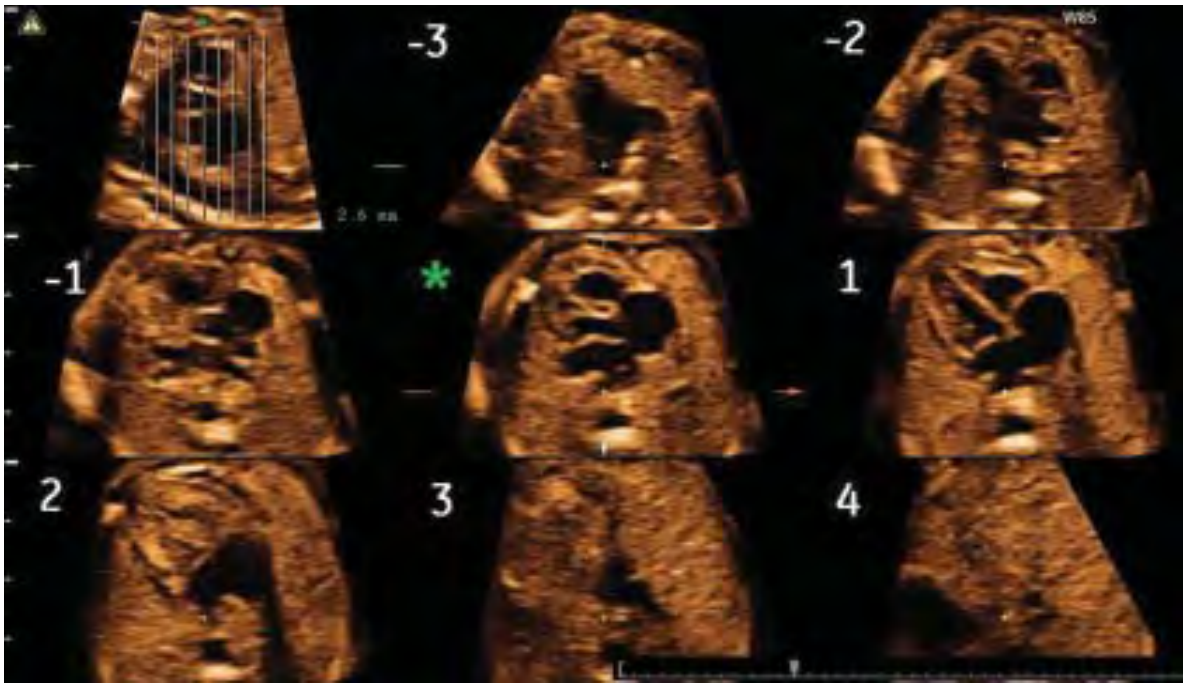

Figure 21.26: Ultrasound tomography in systole in a normal heart

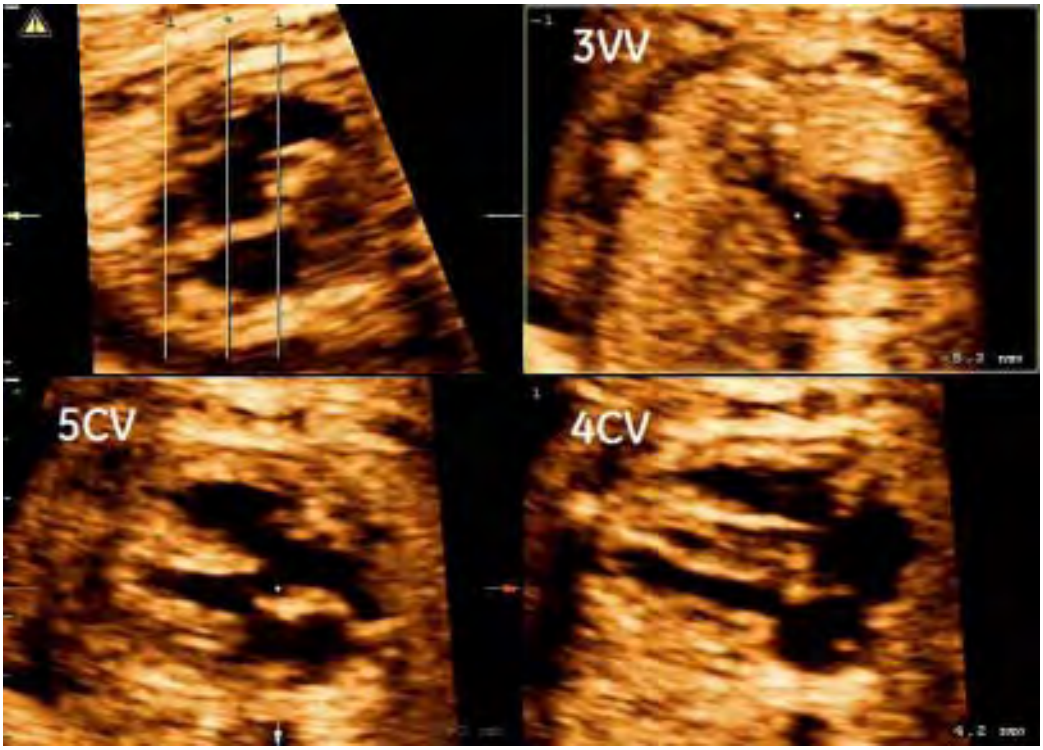

Figure 21.27: Tetralogy of Fallot in tomographic ultrasound imaging. Levels of four-chamber view (4CV); five-chamber view (5CV) and three vessel view (3VV) are presented

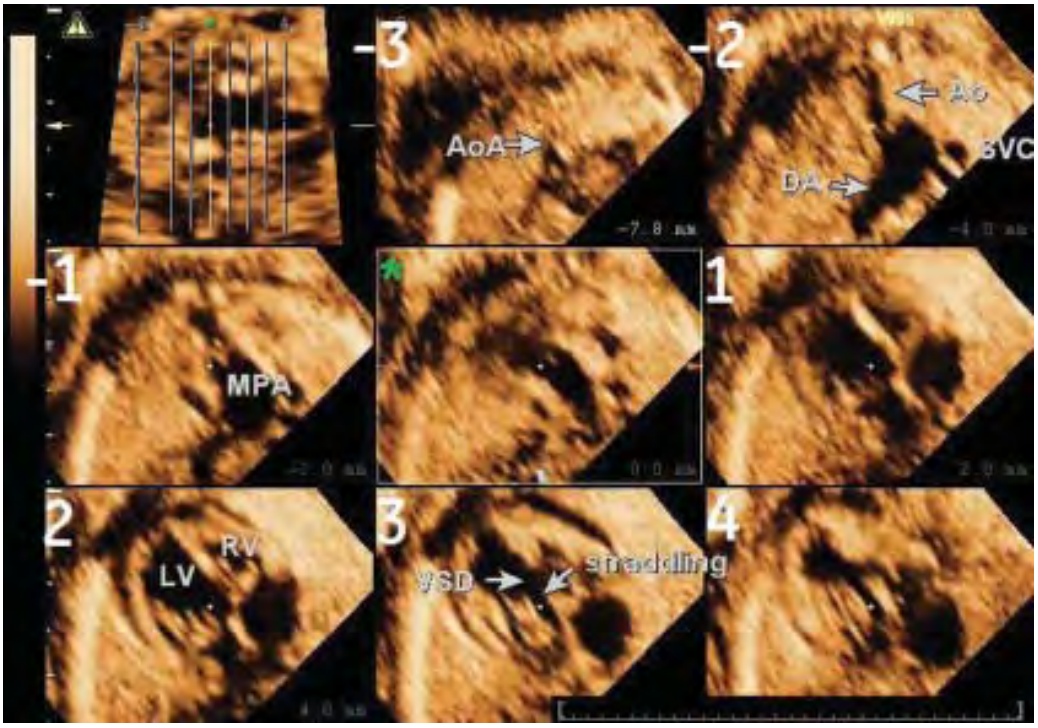

Figure 21.28: Presentation of a complex congenital heart defect (d-transposition of great arteries + large ventricular septal defect + hypoplastic aortic arch) in systolic tomographic sections

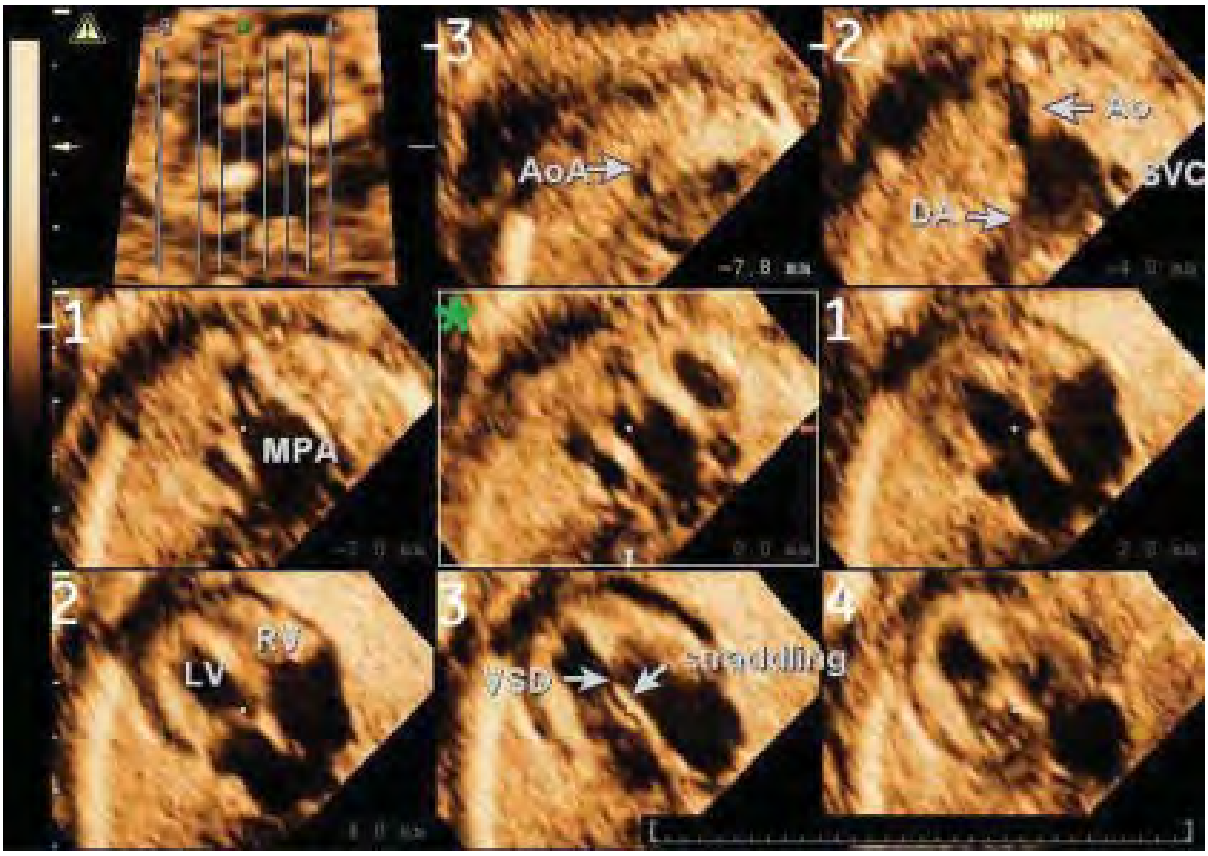

Figure 21.29: Presentation of a complex congenital heart defect (d-transposition of great arteries + ventricular septal defect + hypoplastic aortic arch) in tomographic ultrasound at the phase of diastole. Section (3): Ventricular septum defect and straddling of the tricuspid valve; section (-1): Broad vessel arising from the left ventricle and bifurcating; section (-2): Triangular arrangement at the level of three vessel view with a narrow and anteriorly positioned aorta (Ao); section (-3): Hardly visible transverse section through aortic arch

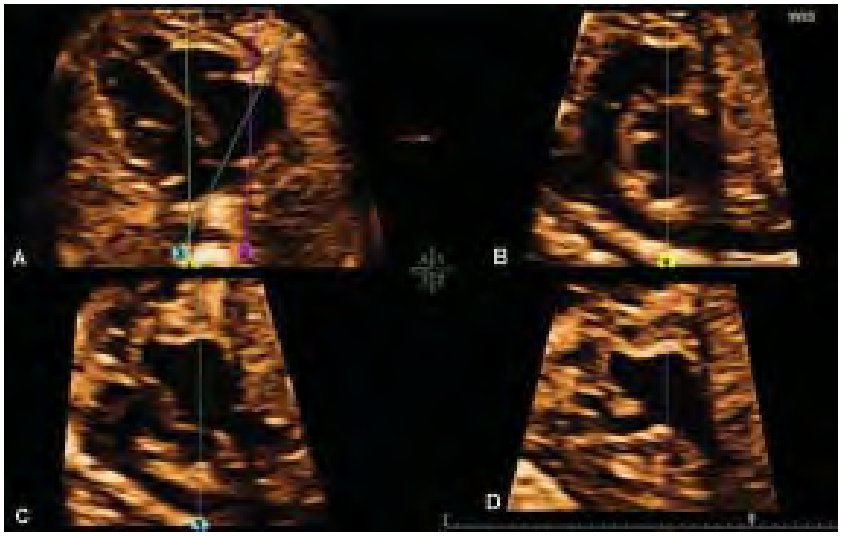

Figures 21.30A to D: OmniView imaging in a normal fetal heart. (A) Colored lines are arbitrarily placed on the reference image; (B) A perpendicular plane to the yellow line on the reference image (the ductal arch sagittal view); (C) A perpendicular plane to the purple line on the reference image (the long axis caval view); (D) A perpendicular plane to the blue line on the reference image (the aortic arch view)

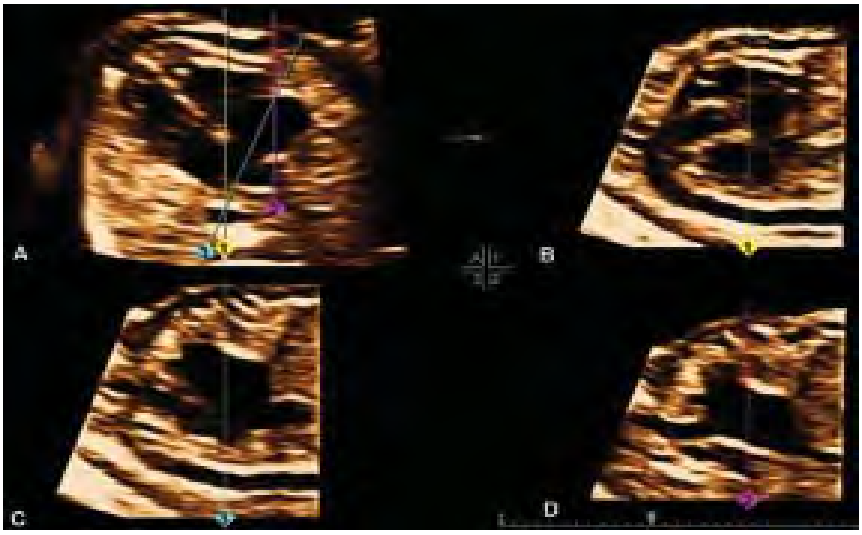

Figures 21.31A to D: (A) OmniView imaging of a heart with d-transposition of great arteries; colored lines are arbitrarily placed on the reference image; (B) A perpendicular plane to the yellow line on the reference image (the parallel course of the great arteries is seen here); (C) A perpendicular plane to the blue line on the reference image (in this case a nondiagnostic image); (D) A perpendicular plane to the purple line on the reference image (the long axis caval view)

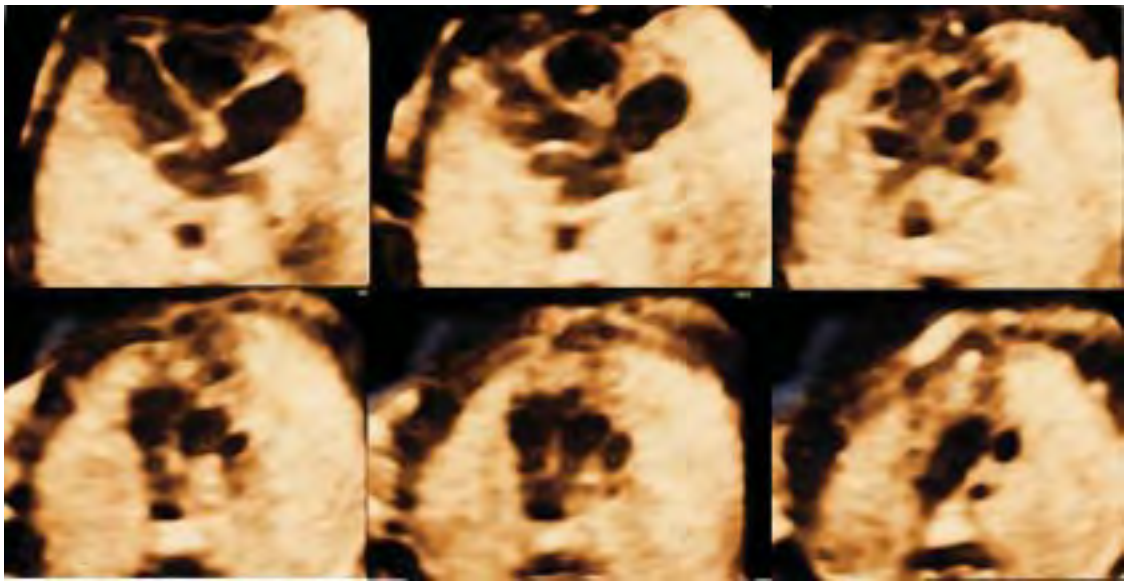

Figure 21.32: Surface rendering of the fetal heart from a STIC volume obtained at 21 weeks of gestation. Rendering direction which was applied is front to back. Subsequent cardiac views are represented starting from the four-chamber view through the five-chamber view, the three vessel view, the transverse section through ductal arch, the three vessel and trachea view and the transverse section through aortic arch. In all the presented images, the effect of depth is clearly seen

Surface rendering takes place on comparatively narrow thicknesses of the region of interest **(Fig. 21.33)**.

Most of the rendering directions can be applied in the STIC mode from the volumes obtained by a transverse acquisition technique **(Figs 21.34 to 21.37)**.

In surface rendering of the fetal heart, the options available for optimization are very important. We have found excellent results with the use of gradient light mode mixed with surface with very low levels of threshold low and transparency **(Figs 21.38 to 21.42)**.

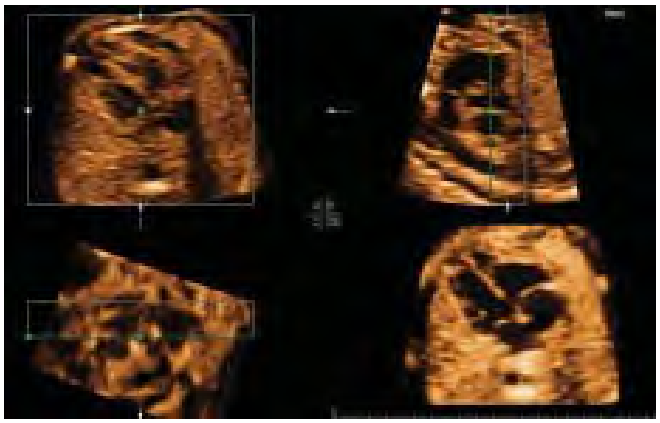

Figure 21.33: Multiplanar view of the fetal heart along with 3D rendering. In the B and C reference images a narrow region of interest is chosen, which is essential for surface rendering of the heart

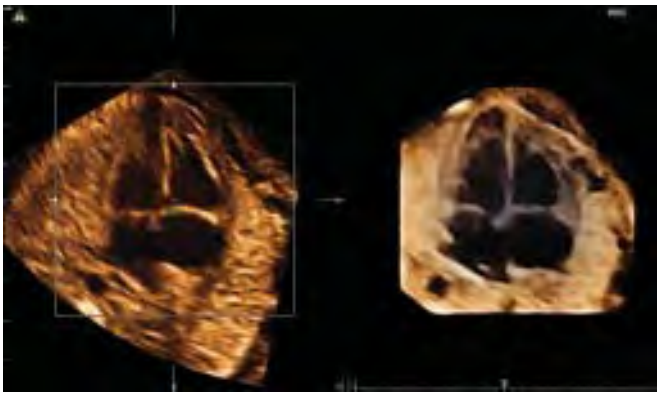

Figure 21.34: Rendering directions in surface rendering of the fetal heart: a four-chamber rendered view using a front-to-back render direction

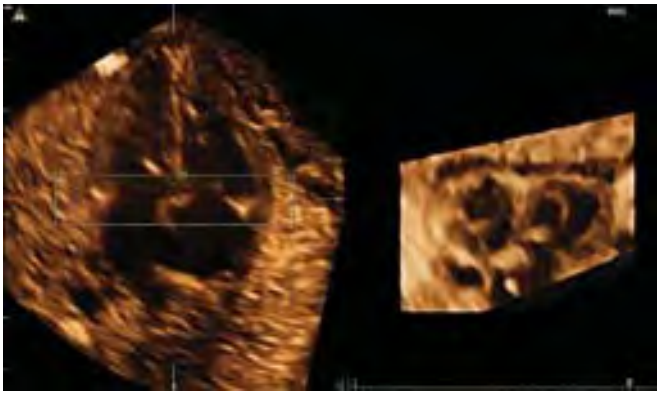

Figure 21.35: Rendering directions in surface rendering of the fetal heart: a rendering direction of up-to-down is used here for the evaluation of the atrioventricular valves

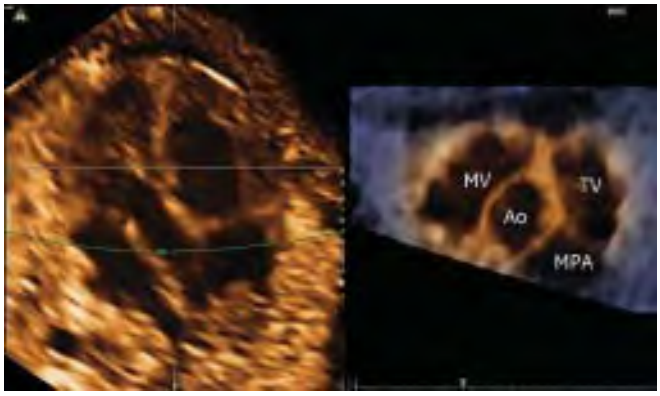

Figure 21.36: Rendering directions in surface rendering of the fetal heart: analyses of the base of the heart is rendered here from a down-to-up direction

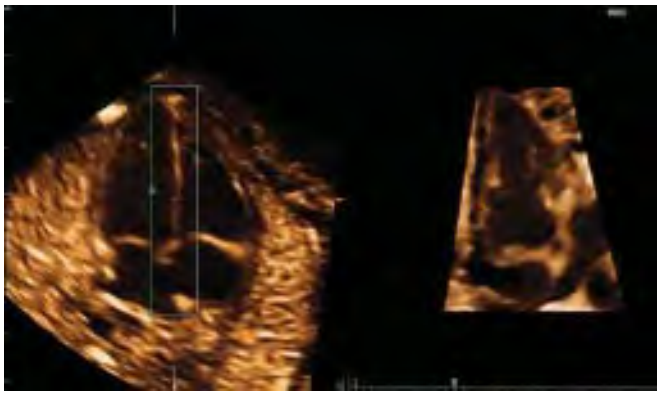

Figure 21.37: Rendering directions in surface rendering of the fetal heart: a unique view of the interventricular septum is shown here from the left-to-right direction

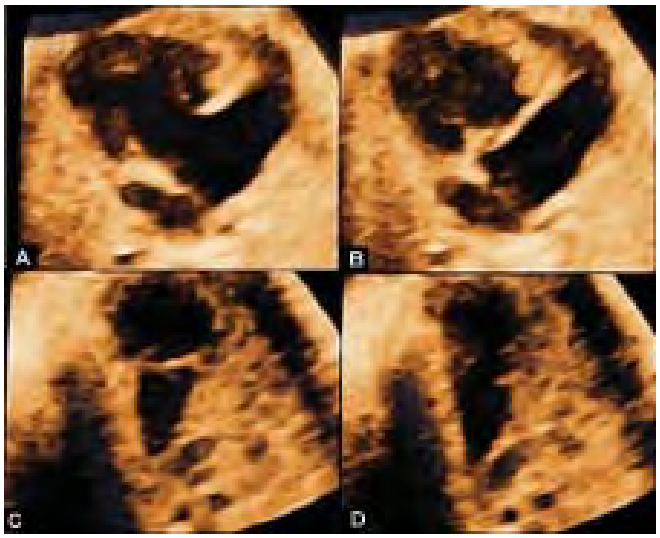

Figures 21.38A to D: Hypoplastic left heart syndrome (HLHS) shown in render mode. (A) Four-chamber view in diastole; (B) Four-chamber view in systole; (C) Three vessel view and trachea in diastole; (D) Three vessel view and trachea in systole

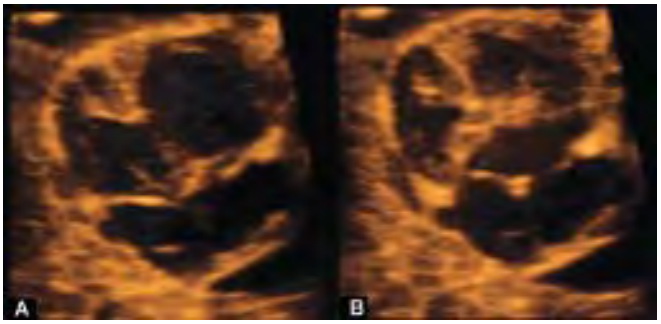

Figures 21.39A and B: Atrioventricular septal (AVSD) in render mode. (A) Systole; (B) Diastole

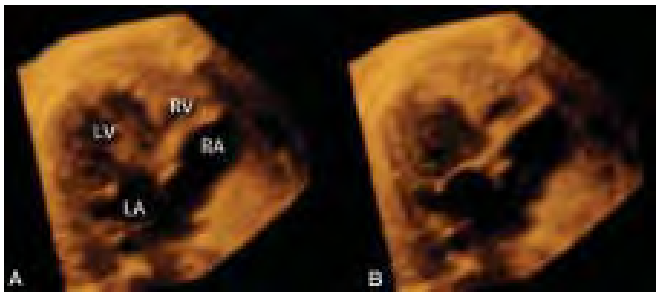

Figures 21.40A and B: Tricuspid atresia with ventricular septum defect in render mode. (A) Diastole; (B) Systole

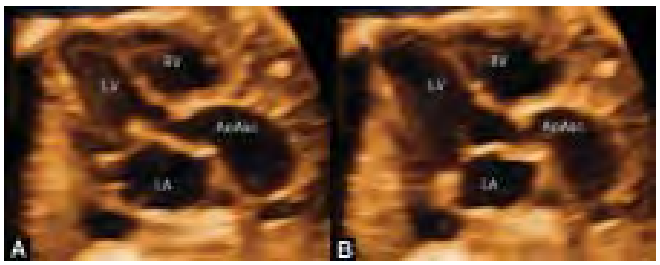

Figures 21.41A and B: Valvular aortic stenosis in render mode. (A) Diastole; (B) Systole

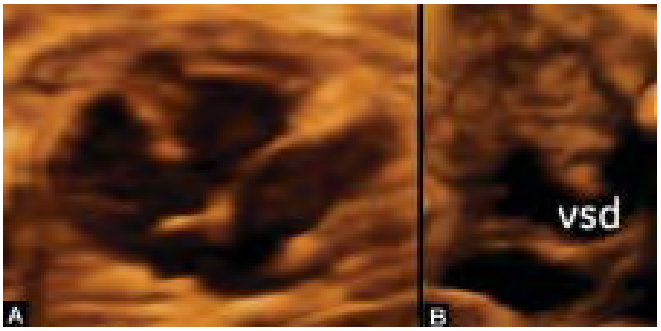

Figures 21.42A and B: Large ventricular septum defect (VSD), which involves the inlet and outlet portions of the septum. (A) The VSD is not clear by using a rendering direction of front-back; (B) But is doubtless when a direction of left-right is applied

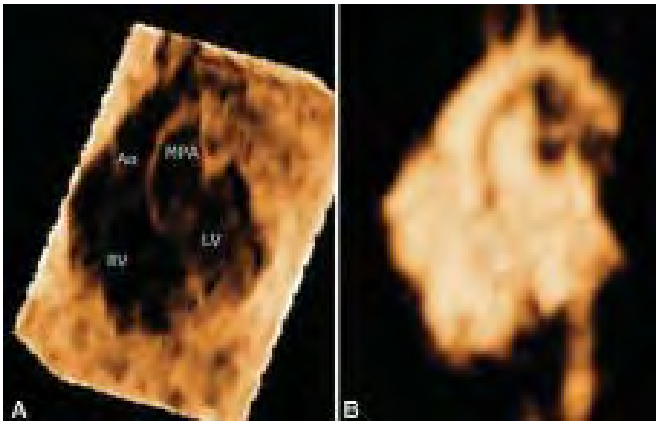

Figures 21.43A and B: Surface rendering of transposed great arteries. (A) Shows minimum mode; (B) Utilizes inversion mode

For the evaluation of the relationships of the great arteries and evaluation of cardiac chambers minimum transparent mode or inversion mode rendering can be utilized.[18,19] **Figures 21.43A and B** show an example of these modes in a case of transposed great arteries. Here the region of interest box has been enlarged so that all of the essential anatomical elements can be seen. The inversion rendering seen in **Figure 21.43B** uses the gradient light mode and an increase of lower threshold and transparency. This is a particularly good combination when utilized with a sagittal acquisition as seen in **Figures 21.45 and 21.46**. Multiplanar view coupled with inversion mode rendering is shown in **Figure 21.44**.

In the inversion mode, it is also possible to use a narrow region of interest box, encompassing only the cardiac chambers. This focuses on the relation of the size of the ventricles, their contractility, the cross of the heart, the interventricular septum, the composition of the atrioventricular valves or the relationship of the outflow tracts **(Figs 21.47 and 21.48)**.

The same viewing options accessible with STIC gray scale datasets are also accessible when using gray scale plus color mapping **(Figs 21.49 and 21.50)**.[20,21]

A rendering modality called "glass body" imaging writes the color information on the background of the grayscale information **(Figs 21.51 to 21.53)**.

A STIC acquisition can be done in gray scale with B-mode alone or with the addition of color, power or bidirectional power Doppler mapping (HD flow). Below are the examples of vascular mapping with STIC **(Figs 21.54A to D)**.

An option available with STIC imaging is the use of B-flow imaging. B-flow imaging is an exceptionally sensitive form of coding of the blood flow, allowing visualization of extremely small vessels.[22] It is a Doppler

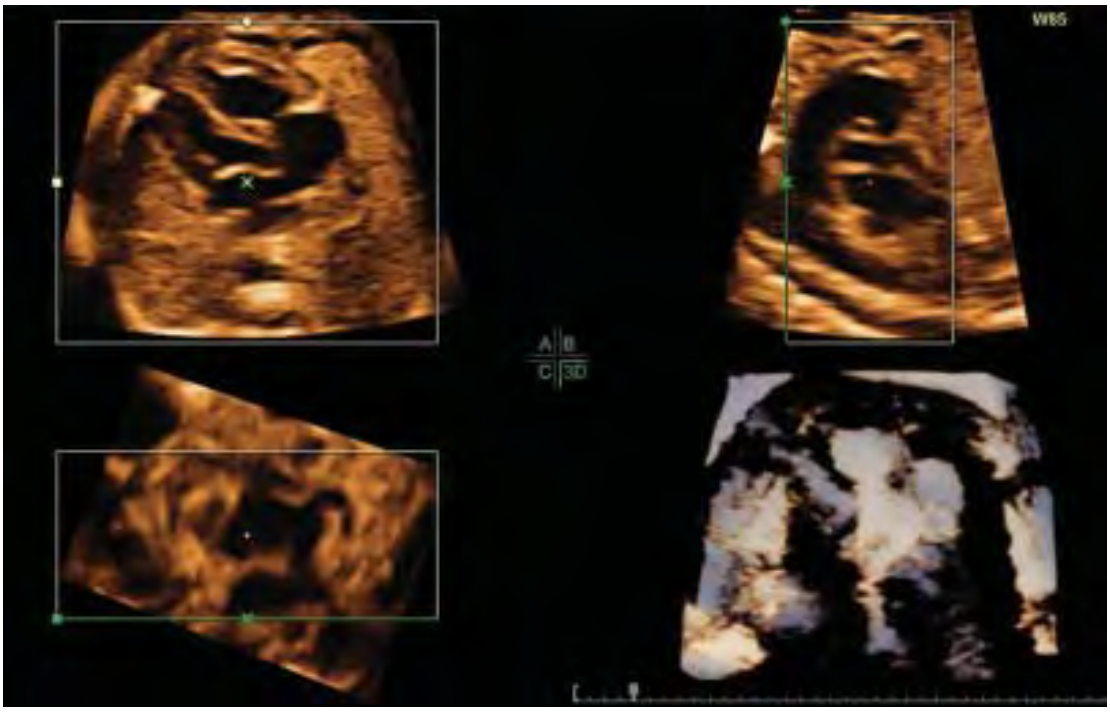

Figure 21.44: Multiplanar view coupled with inversion mode rendering (volume obtained by transverse technique of acquisition). Note the use of a large region of interest box, which can be helpful when using inversion mode

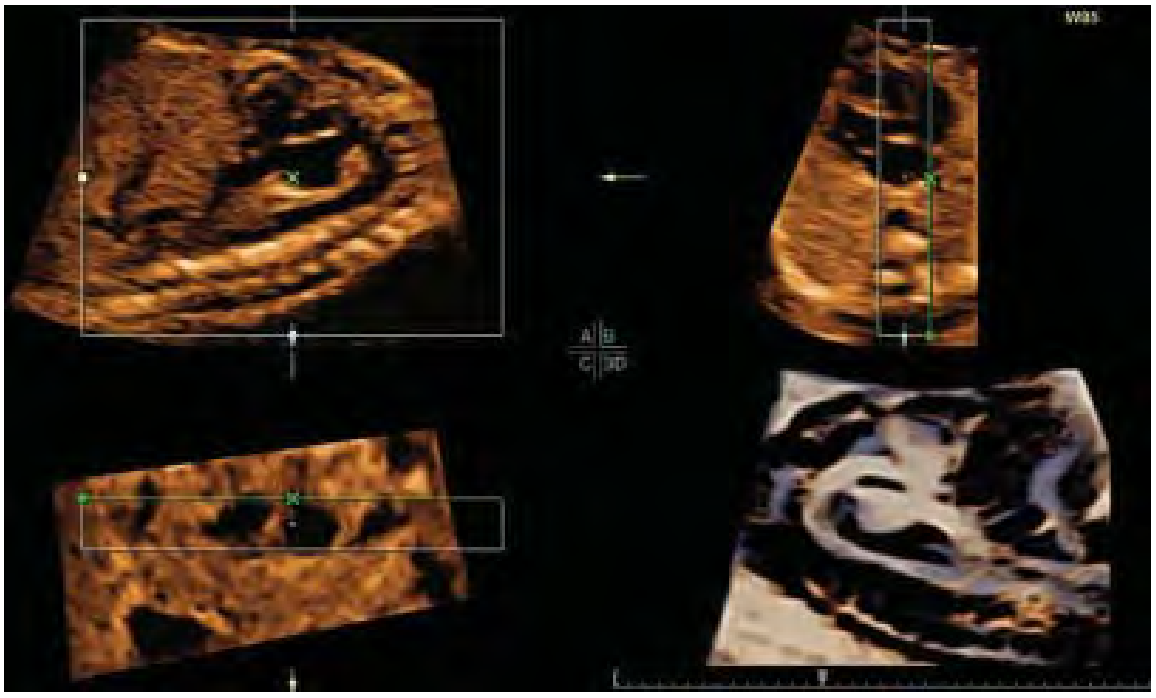

Figure 21.45: Multiplanar view coupled with inversion mode rendering from a STIC volume obtained by a sagittal technique of acquisition

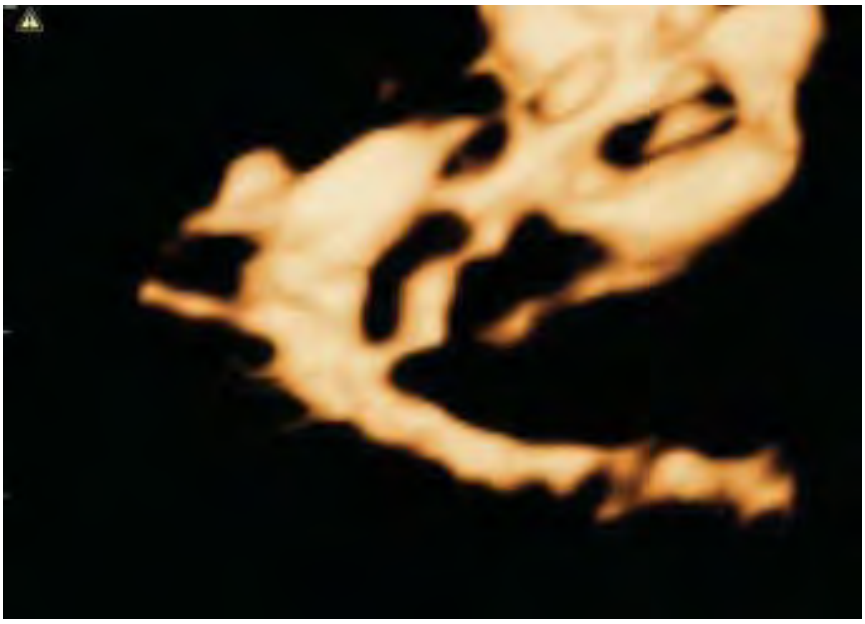

Figure 21.46: Tetralogy of Fallot—aortic arch in inversion mode. Notice the tortuous course of the ductus arteriosus, which attaches to the ventral part of the aorta

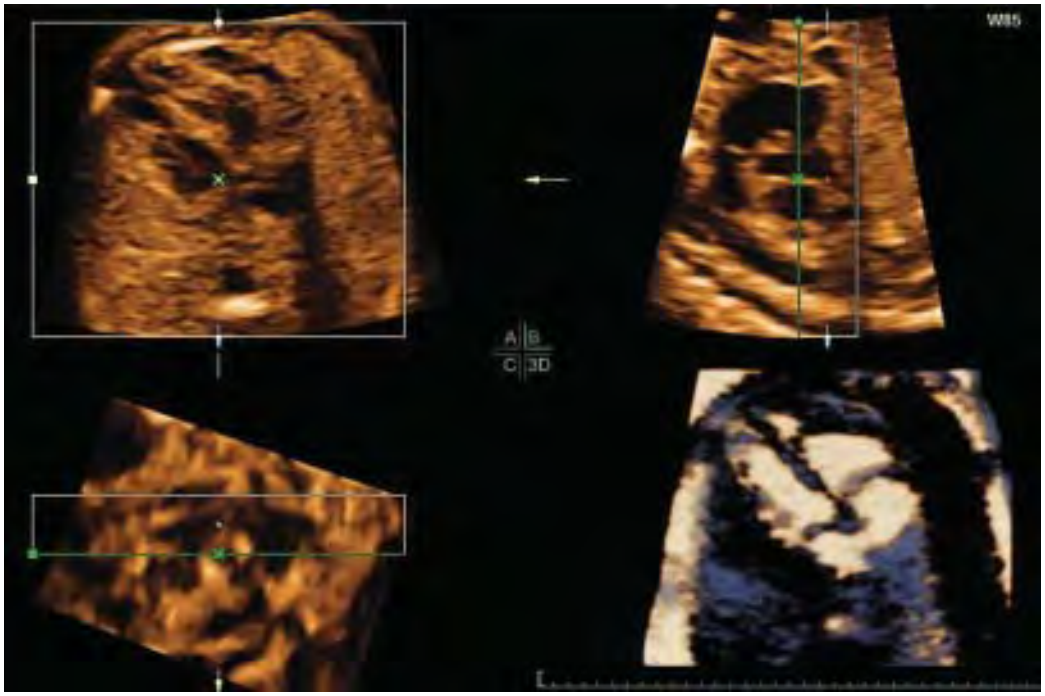

Figure 21.47: Multiplanar view coupled with inversion mode rendering from a STIC volume obtained by a transverse technique of acquisition. A narrow region of interest is utilized in the B and C planes. The relationship between cardiac chambers is clearly demonstrated

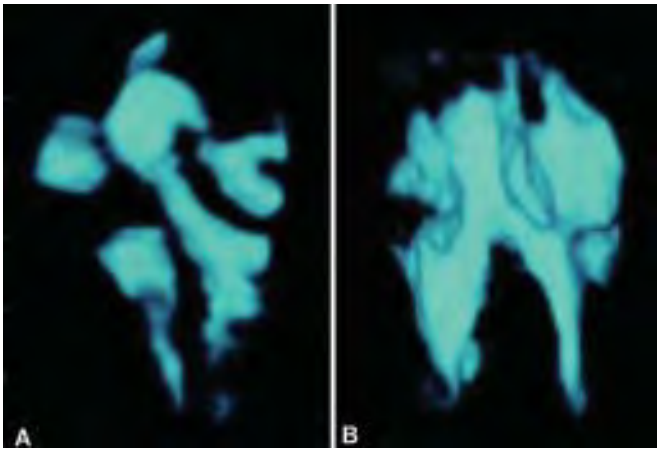

Figures 21.48A and B: Inversion mode rendering with the application of a narrow region of interest box focused on the left outflow tract. (A) A normal left outflow; (B) An overriding aorta

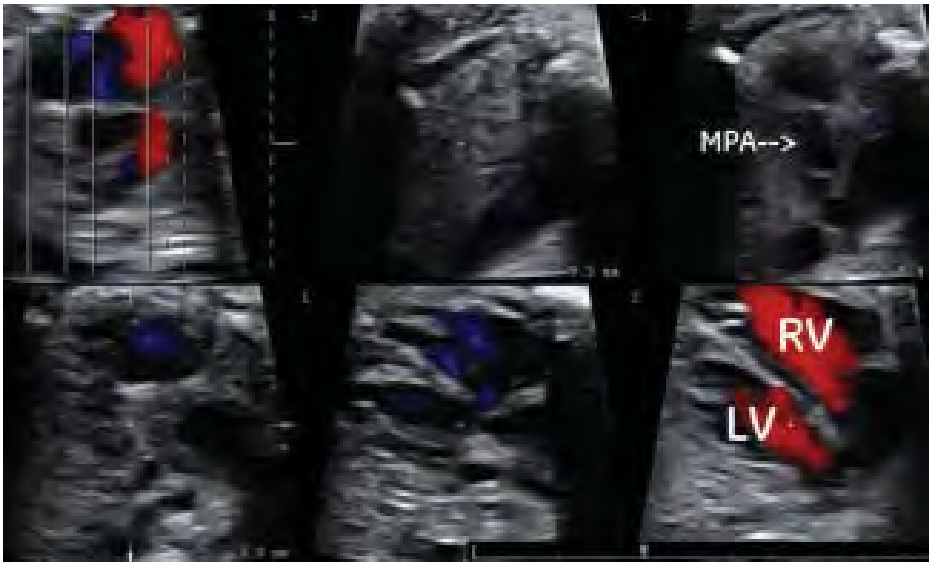

Figure 21.49: Pulmonary atresia with ventricular septum defect in tomographic ultrasound imaging in diastole (LV=left ventricle; RV=right ventricle; MPA=main pulmonary artery)

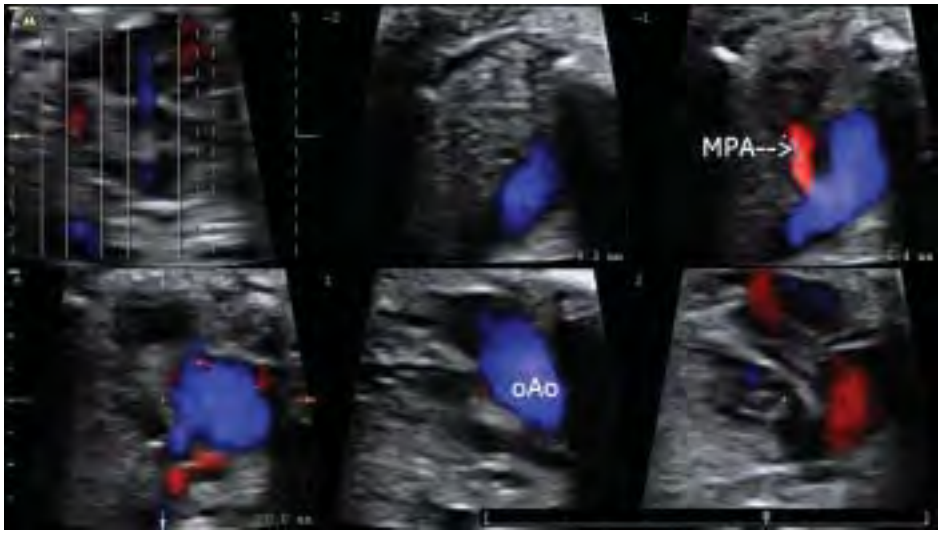

Figure 21.50: Pulmonary atresia with ventricular septum defect in tomographic ultrasound imaging in systole (MPA=main pulmonary artery; oAo=overriding aorta)

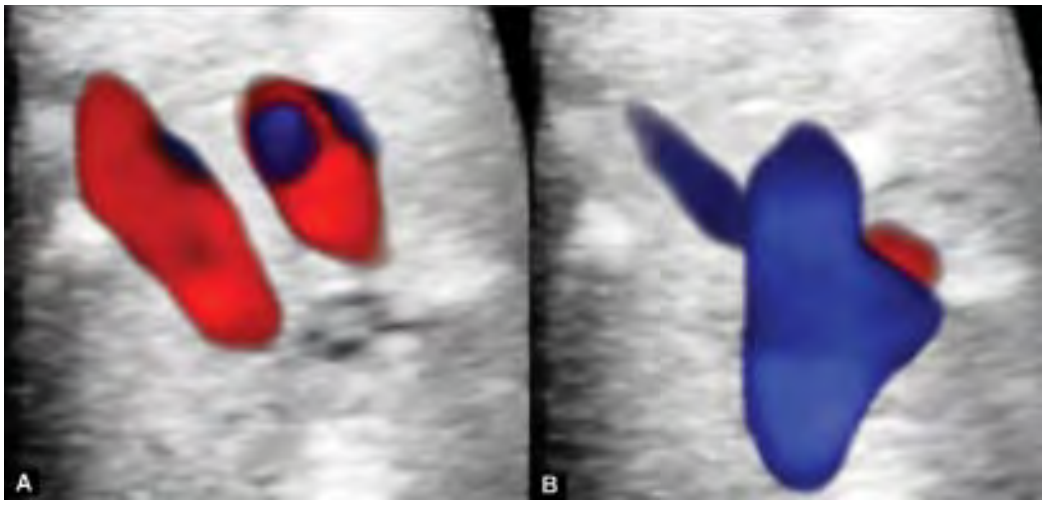

Figures 21.51A and B: Glass body rendering using a deep region of interest box

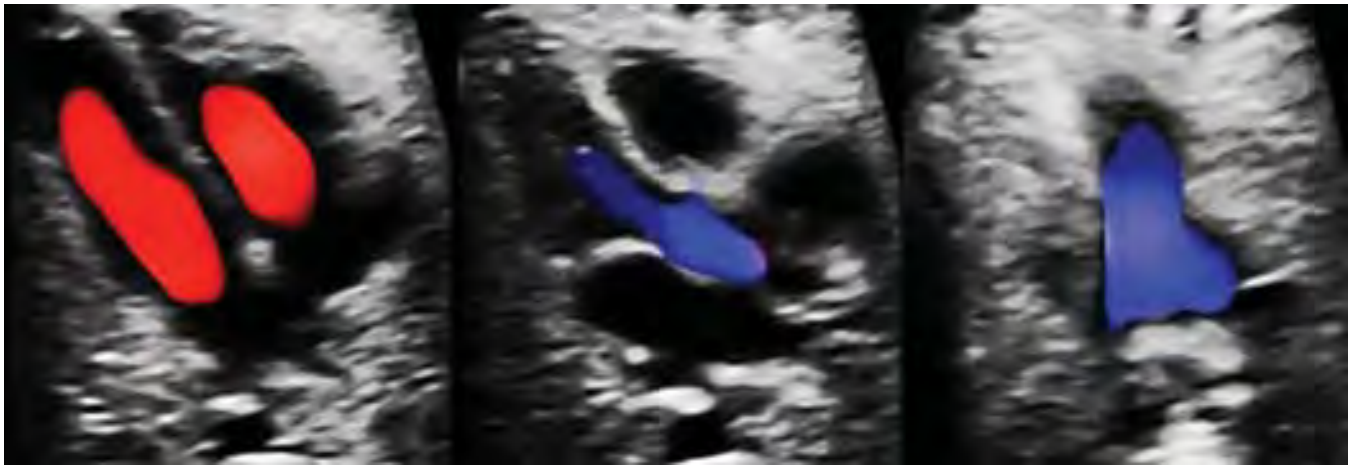

Figure 21.52: Glass body rendering using a shallow region of interest box

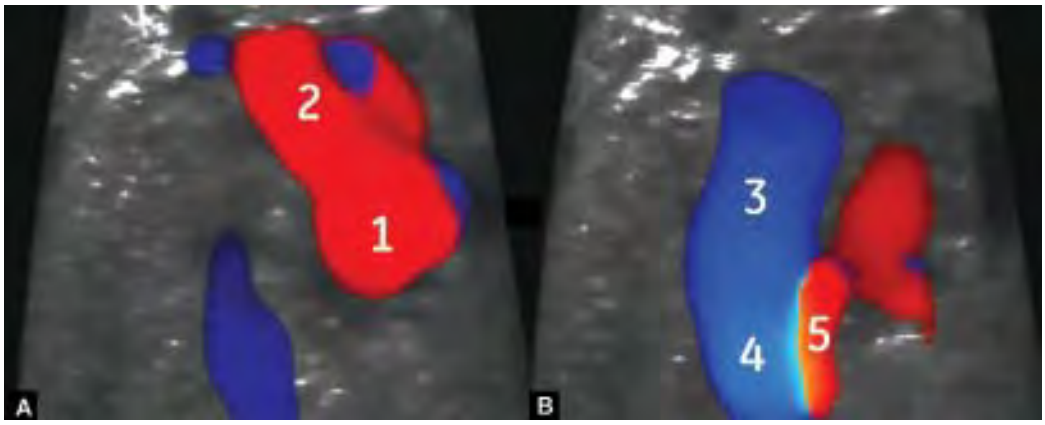

Figures 21.53A and B: Hypoplastic left heart in glass body rendering mode. (A) Diastole—no inflow to the left ventricle is noted (1: right atrium; 2: right ventricle); (B) Systole (3: main pulmonary artery; 4: ductus arteriosus; 5: transverse section through aortic arch demonstrating retrograde flow)

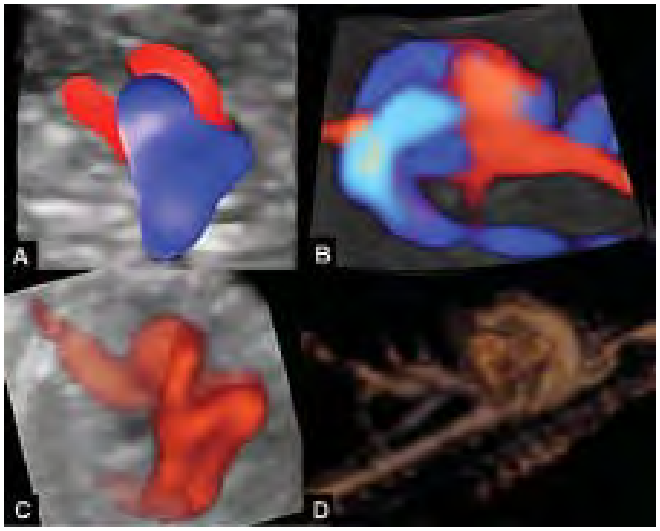

Figures 21.54A to D: Three-dimensional images of the fetal heart showing the variety of flow mapping modalities. (A) Spatial and temporal image correlation (STIC) color Doppler; (B) STIC HD flow (bidirectional Power Doppler) displayed in transparent glass body rendering mode; (C) STIC Power Doppler displayed in transparent glass body rendering mode; (D) STIC B-flow

independent B-mode option based on the use of the highest frequencies transmitted by the probe allowing for the enhancement of signals representing blood flow while simultaneously ignoring signals from stationary tissue. This allows for the visualization of vascular information independent of tissue information **(Figs 21.55A and B)**.

VOCAL, SonoAVC

Vocal and SonoAVC are both methods, which are available for volumetric calculations with STIC.[23,24] An application of this is to assess cardiac chamber volumes in various phases of the cardiac cycle. The calculations

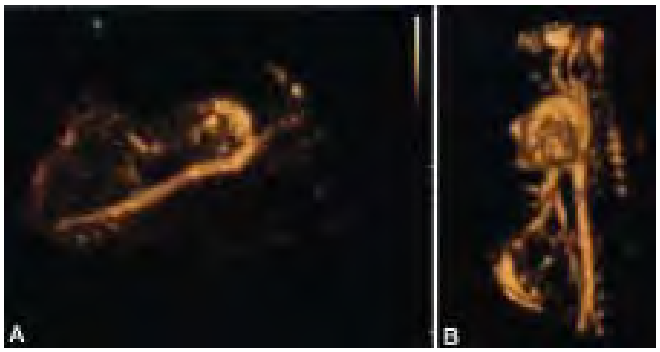

Figures 21.55A and B: B-flow imaging. (A) A fetal heart and surrounding vessels in two-dimensional B-flow mapping during the process of STIC acquisition; (B) Three-dimensional image of the same fetal heart after acquisition of a STIC volume dataset

of these algorithms have been validated on artificial models. The use of the VOCAL method requires mechanical tracing by the examiner of whatever structure one wishes to perform a volumetric measurement of. SonoAVC is also utilized for volume calculation, however it is a machine-derived volume, which can only be used for volume measurements of fluid structures. When volumetric measurements are performed in both systole and diastole, calculations of cardiac stroke volume can be easily derived **(Figs 21.56A and B)**.

Z-scores

Measurements can be made from STIC volumes in the same manner as classic 2D measurements. Since 2006, Z-score measurements have been available for use in relating cardiac measurements to gestational age. This method simplifies the expression of measurements providing the examiner with calculations in standard deviations rather than in millimeters in relation to any given gestational age and measured biparietal diameter

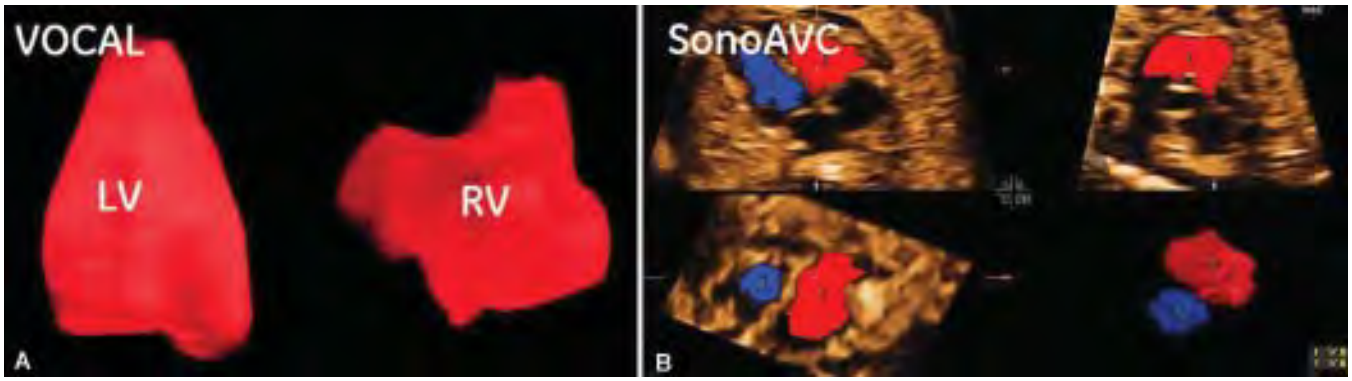

Figures 21.56A and B: Volume calculations of cardiac ventricles. (A) Done with VOCAL; (B) Uses SonoAVC

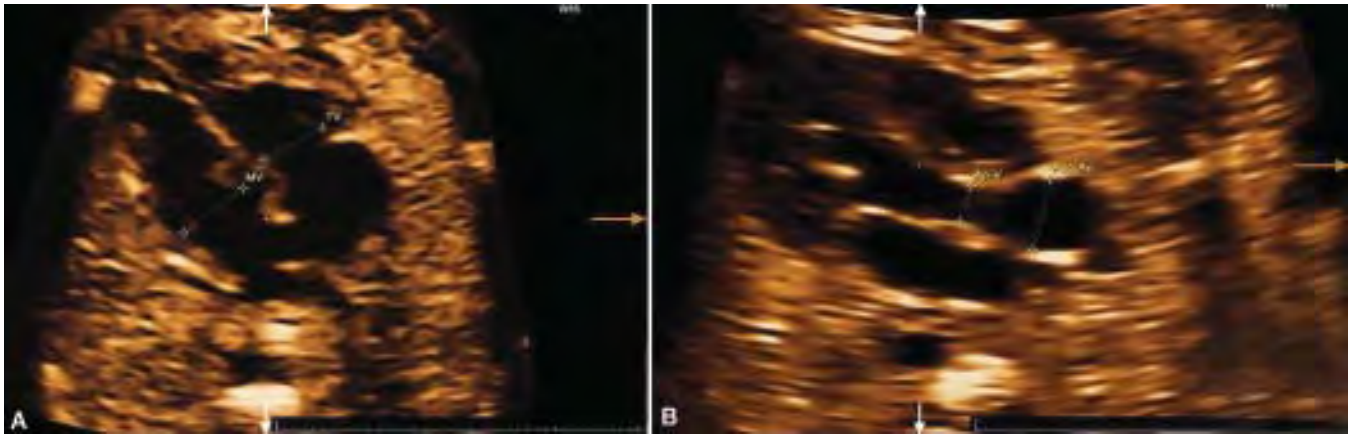

Figures 21.57A and B: Z-score measurement technique performed in a STIC volume. (A) Normal standard deviations at the level of the atrioventricular valves; (B) Dilatation of the ascending aorta (measurements indicate approximately + 3SD) in a case of valvular aortic stenosis

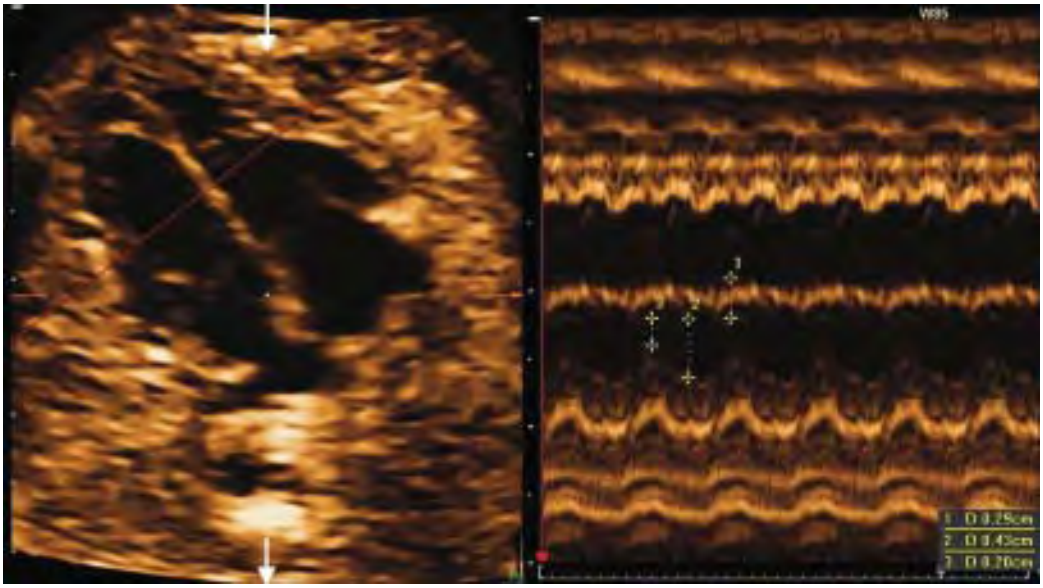

Figure 21.58: STIC M-mode technique has the capability of placing arbitrary anatomic lines allowing for M-mode measurements to be taken from positions that are not available by two-dimensional imaging

(BPD) and femur length (FL). It simplifies the precise quantification of the size of fetal cardiac structures **(Figs 21.57A and B)**.[25]

STIC M-mode

In 2009, STIC M-mode was introduced into clinical practice allowing for the capability of placing arbitrary M-mode lines into the volume dataset allowing for M-mode measurements to be taken from positions that are not available by 2D imaging **(Fig. 21.58)**.

Volume Computer-Aided Diagnosis (VCAD)

In 2006, the STIC VCAD technique was introduced for use with fetal heart imaging between 18 and 23 weeks of gestation. In this timeperiod, the heart increases in size as the whole but relationships of the sizes of the main cardiac structures remain similar. Because of this fact an automated system can be used during this time to aid in the identification of basic cardiac views.[26] After a volume is achieved, the examiner must orient the A plane so that the four-chamber view is showing and

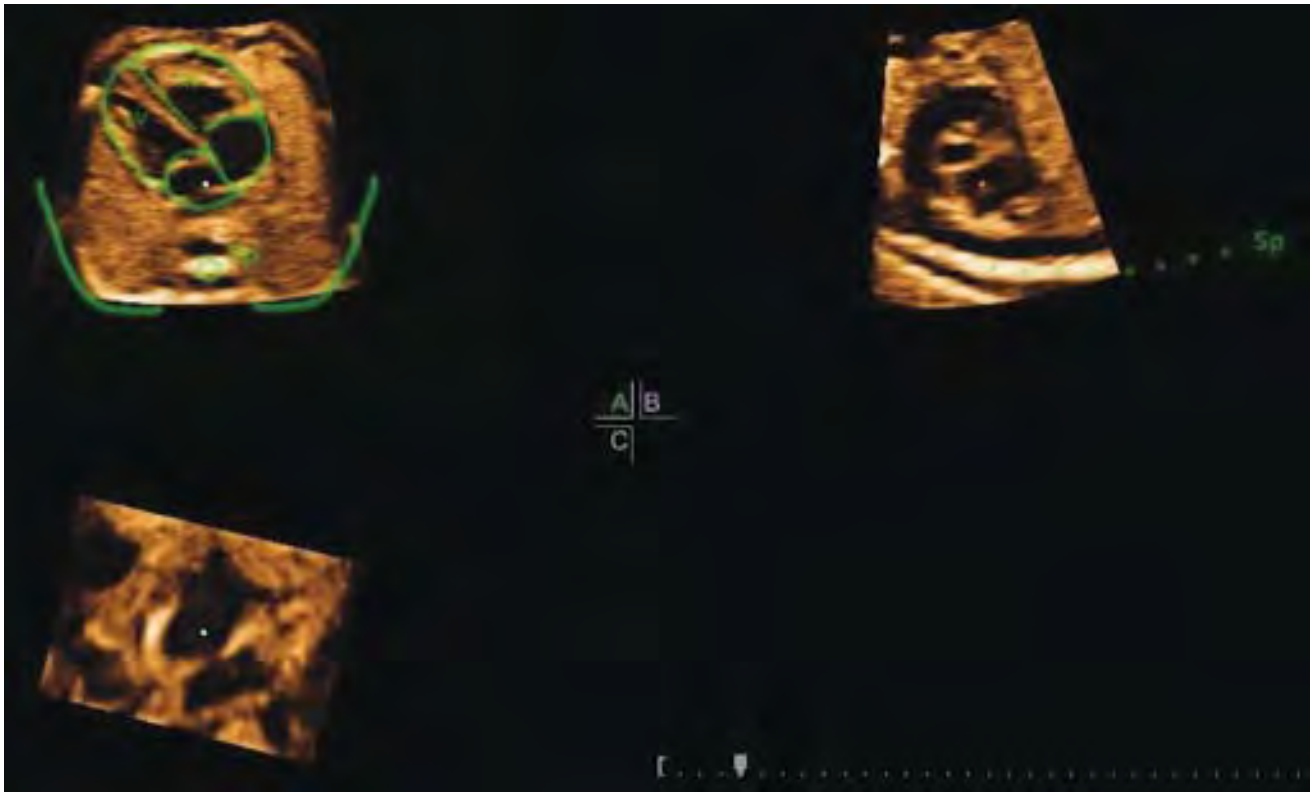

Figure 21.59: Volume computer-aided diagnosis modality. Initial stage after simplified orientation according to templates marked with green line (in reference images A and B)

the apex of the heart is to the left. When VCAD is enabled, a green template of a heart, ribs and spine appears overlying the A plane image and a green dotted line appears on the B plane representing the sagittal spine. The examiner lines up the volume in the A and B planes with the green templates, which essentially orientates the volume into an optimum position **(Fig. 21.59)**.

Because the volume is now in a standardized position, the VCAD algorithm can automatically identify the following cardiac views: left outflow tract (Cardiac 1); right outflow tract (Cardiac 2); upper abdominal (Cardiac 3); long-axis caval (Cardiac 4); ducal arch (Cardiac 5); and aortic arch (Cardiac 6).

The VCAD cannot identify and align views correctly in the cases of cardiac malformations or mediastinal shift **(Figs 21.60A to F)**.

CONCLUSION

Spatial and temporal image correlation is one of the newest diagnostic tools in fetal echocardiography. It adds, both figuratively and literally, another dimension in the prenatal diagnostics of congenital heart disease.

STIC has a number of advantages over 2D fetal echocardiography, some of which are listed below:

- The spatial evaluation of cardiac structures in multiplanar, tomographic imaging and rendering
- The ability to store spatial images of the fetal heart in a dynamic form, cine loop, accessible for unlimited evaluation from many angles
- Access to the acquisition preview: meaning demonstration of the cardiac views, which are being acquired in real-time presented in slow motion. The preview allows volume acquisition quality assessment
- The ability for multiple consultations without the presence of the patient, including internet and teleconsultations
- STIC is a good method for image archiving and retrieval
- STIC is an exceptional teaching tool.[4,5,27]

Like every modality, STIC also has its limitations. STIC is not useful in the evaluation of fetal arrhythmias. This is because of the algorithm that STIC uses.

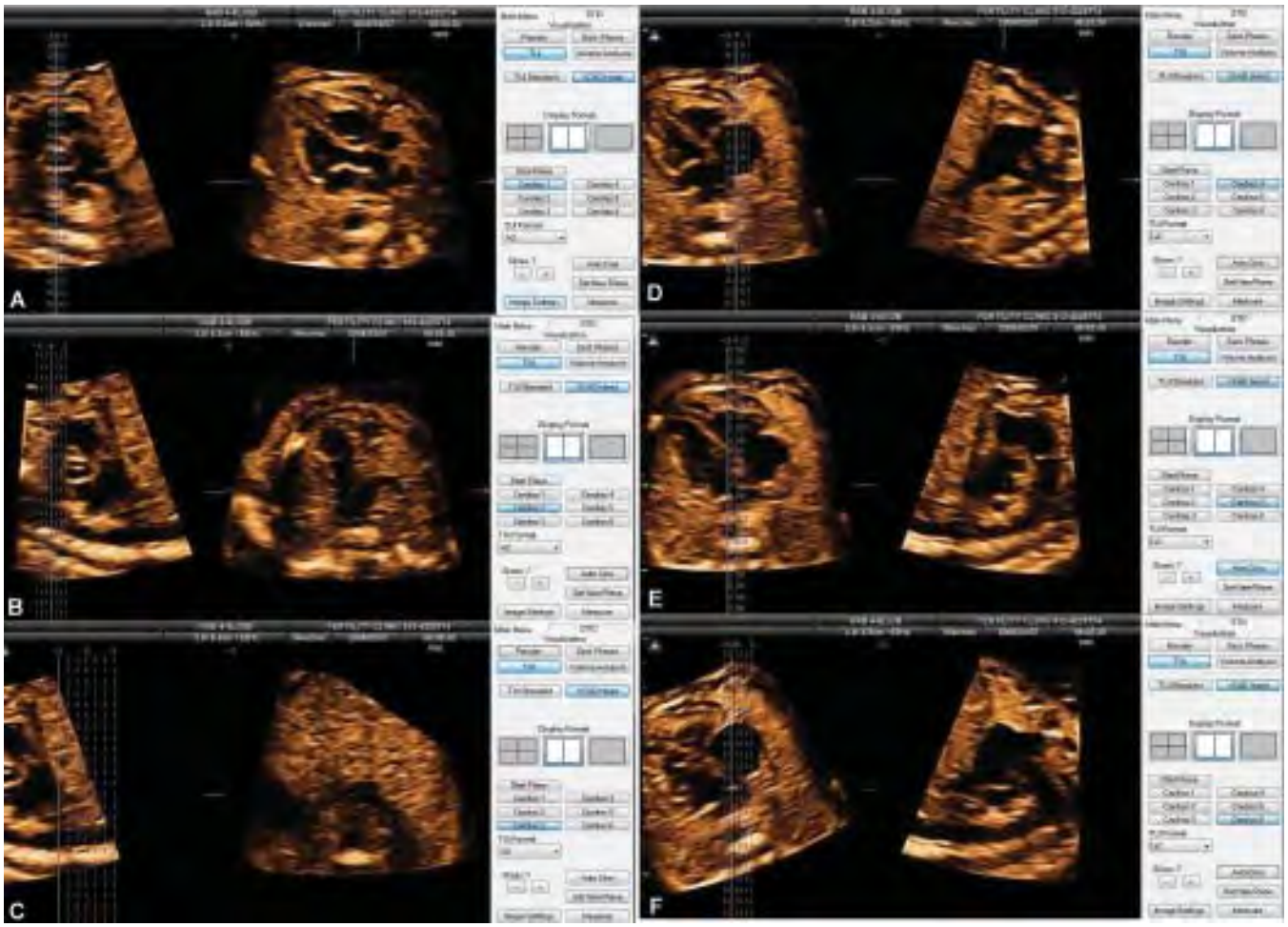

Figures 21.60A to F: Volume computer-aided diagnosis modality in the final stage. Automated identification of cardiac views. (A) Left outflow tract; (B) Right outflow tract; (C) Upper abdominal view; (D) Long axis caval view; (E) Ductal arch; (F) Aortic arch

Technical limitations include a very active fetus, as STIC has a long acquisition time. Motion artifacts from fetal movements may cause volume datasets to become nondiagnostic. The examiner's patience and experience can overcome some of these limitations by an understanding of appropriate acquisition planes. Training in STIC acquisition should begin with normal cases and only in good scanning conditions. Two-dimensional image optimization and learning how to avoid motion artifacts and shadowing from the ribs and limbs are the basics of training. Unsuccessful acquisitions should be repeated and volume datasets reviewed individually or among team members.

Cardiac 3D imaging and STIC technology have made a great contribution in modern fetal echocardiography. They allow for a detailed segmental evaluation of the fetal heart. A sequential 2D plane-by-plane analysis of the fetal heart was initially proposed by Yoo in 2D imaging.[28] Development of this 2D concept is now similar to the number of publications on STIC.[7,12,29,30] Good quality STIC volumes are ideal for segmental analysis of the fetal heart when the examiner is skilled in this modality. A good example is a publication by Vinals and co-workers, which summarized and simplified an approach to the diagnosis of d-transposition of the great arteries based on the planes of the four-chamber, five-chamber, three-vessel, and three vessels and trachea views obtained from a STIC volume.[28] Before the segmental technique, oblique sections were commonly used for prenatal cardiac diagnosis, which was confusing in some cases as it was highly operator dependent. For most congenital heart defects, a sequential segmental analysis is now recommended. In one of the first studies on STIC, 94.2% of various fetal cardiac

views and structures were identified in the datasets.[3] Our discussion on STIC however would not be complete without reporting that one article did not find STIC to be helpful. Wanitpongpan and co-workers showed inferior quality of STIC volumes and poor measurement accuracy of great vessel diameters acquired by a general obstetrician when compared with 2D fetal echocardiography performed by a pediatric cardiologist.[31] Conclusions from this study may have come from the use of large acquisition angles of 30° in STIC mode for fetal hearts between 17 and 21 weeks of gestation and preacquisition 2D settings. The introduction of STIC widened the horizons of fetal echocardiography, improved the detection of congenital heart defects and increased the education in cardiac scanning. To conclude, STIC, like other 3D techniques, is nothing more than the rewriting of 2D information into volume datasets. The better the 2D imaging, the better the quality of STIC volumes. We encourage the use of STIC as a routine element of the standard fetal cardiac evaluation.

REFERENCES

1. Meyer-Wittkopf M, Cooper S, Vaughan J, et al. Three-dimensional (3D) echocardiography analysis of congenital heart disease in the fetus: comparison with cross-sectional (2D) fetal echocardiography. Ultrasound Obstet Gynecol. 2001;17(6): 485-92.
2. Bega G, Kuhlman K, Lev-Toaff A, et al. Application of three-dimensional ultrasonography in the evaluation of the fetal heart. J Ultrasound Med. 2001;20(4):307-13.
3. Viñals F, Poblete P, Giuliano A. Spatio-temporal image correlation (STIC): a new tool for the prenatal screening of congenital heart defects. Ultrasound Obstet Gynecol. 2003;22(4):388-94.
4. DeVore GR, Falkensammer P, Sklansky MS, et al. Spatio-temporal image correlation (STIC): new technology for evaluation of the fetal heart. Ultrasound Obstet Gynecol. 2003;22(4):380-7.
5. Yagel S, Cohen SM, Shapiro I, et al. 3D and 4D ultrasound in fetal cardiac scanning: a new look at the fetal heart. Ultrasound Obstet Gynecol. 2007;29(1):81-95.
6. Goncalves LF, Lee W, Chaiworapongsa T, et al. Four-dimensional ultrasonography of the fetal heart with spatio-temporal image correlation. Am J Obstet Gynecol. 2003; 189(6):1792-802.
7. Espinoza J, Romero R, Kusanovic JP, et al. Standardized views of the fetal heart using four-dimensional sonographic and tomographic imaging. Ultrasound Obstet Gynecol. 2008;31(2):233-42.
8. Paladini D. Standardization of on-screen fetal heart orientation prior to storage of spatio-temporal image correlation (STIC) volume datasets. Ultrasound Obstet Gynecol. 2007;29(6):605-11.
9. Abuhamad A. Automated multiplanar imaging: a novel approach to ultrasonography. J Ultrasound Med. 2004; 23(5):573-6.
10. Goncalves LF, Espinoza J, Romero R, et al. Four-dimensional fetal echocardiography with spatiotemporal image correlation (STIC): a systematic study of standard cardiac views assessed by different observers. J Matern Fetal Neonatal Med. 2005;17(5):323-31.
11. DeVore GR, Polanco B, Sklansky MS, et al. The 'spin' technique: a new method for examination of the fetal outflow tracts using three-dimensional ultrasound. Ultrasound Obstet Gynecol. 2004;24(1):72-82.
12. Paladini D, Vassallo, Sglavo G, et al. The role of spatio-temporal image correlation (STIC) with tomographic ultrasound imaging (TUI) in the sequential analysis of fetal congenital heart disease. Ultrasound Obstet Gynecol. 2006;27(5):555-61.
13. Rizzo G, Capponi A, Vendola M, et al. Role of tomographic ultrasound imaging with spatiotemporal image correlation for identifying fetal ventricular septal defects. Ultrasound Med. 2008;27:1071-5.
14. Goncalves LF, Espinoza J, Romero R, et al. Four-dimensional ultrasonography of the fetal heart using a novel tomographic ultrasound imaging display. J Perinat Med. 2006;34(1):39-55.
15. Chaoui R, Heling KS. New developments in fetal heart scanning: three- and four-dimensional fetal echocardiography. Seminars in Fetal and Neonatal Medicine. 2005; 10:567-77.
16. Yagel S, Benachi A, Bonnet D, et al. Rendering in fetal cardiac scanning: the intracardiac septa and the coronal atrioventricular valve planes. Ultrasound Obstet Gynecol. 2006;28(3):266-74.
17. Vinals F, Pacheto V, Giuliano A. Fetal atrioventricular valve junction in normal fetuses and in fetuses with complete atrioventricular septal defect assessed by 4D volume rendering. Ultrasound Obstet Gynecol. 2006;28(1):26-31.
18. Goncalves LF, Espinoza J, Lee W, et al. Three- and four-dimensional reconstruction of the aortic and ductal arches using inversion mode: a new rendering algorithm for visualization of fluid-filled anatomical structures. Ultrasound Obstet Gynecol. 2004;24(6):696-8.
19. Espinoza J, Goncalves LF, Lee W, et al. The use of the minimum projection mode in 4-dimensional examination of the fetal heart with spatiotemporal image correlation. J Ultrasound Med. 2004;23(10):1337-48.
20. Chaoui R, Hoffmann J, Heling KS. Three-dimensional (3D) and 4D color Doppler fetal echocardiography using spatio-temporal image correlation (STIC). Ultrasound Obstet Gynecol. 2004;23(6):535-45.
21. Goncalves LF, Romero R, Espinoza J, et al. Four-dimensional ultrasonography of the fetal heart using color Doppler spatiotemporal image correlation. J Ultrasound Med. 2004; 23(4):473-81.
22. Volpe P, Campobasso G, Stanziano A, et al. Novel application of 4D sonography with B-flow imaging and spatio-temporal image correlation (STIC) in the assessment of the anatomy of pulmonary arteries in fetuses with pulmonary atresia and ventricular septal defect. Ultrasound Obstet Gynecol. 2006;28(1):40-6.
23. Messing B, Cohen SM, Valsky DV, et al. Fetal cardiac ventricle volumetry in the second half of gestation assessed by 4D ultrasound using STIC combined with inversion mode. Ultrasound Obstet Gynecol. 2007;30(2):142-51.

24. Tutschek B, Sahn DJ. Semi-automatic segmentation of fetal cardiac cavities: progress towards an automated fetal echocardiogram. Ultrasound Obstet Gynecol. 2008; 32(2):176-80.
25. Devore GR. The use of Z-scores in the analysis of fetal cardiac dimensions. Ultrasound Obstet Gynecol. 2005;26(6): 596-8.
26. Rizzo G, Capponi A, Cavicchioni O, et al. Application of automated sonography on four-dimensional volumes of fetuses with transposition of the great arteries. J Ultrasound Med. 2008;27(5):771-6.
27. Vinals F, Mandujano L, Vargas G, et al. Prenatal diagnosis of congenital heart disease using four-dimensional spatio-temporal image correlation (STIC) telemedicine via an Internet link: a pilot study. Ultrasound Obstet Gynecol. 2005;25(1):25-31.
28. Yoo SJ, Lee YH, Cho KS, et al. Sequential segmental approach to fetal congenital heart disease. Cardiol Young. 1999;9(4): 430-44.
29. Viñals F, Ascenzo R, Poblete P, et al. Simple approach to prenatal diagnosis of transposition of the great arteries. Ultrasound Obstet Gynecol. 2006;28(1):22-5.
30. Goncalves LF, Lee W, Espinoza J, Romero R. Examination of the fetal heart by four-dimensional (4) ultrasound with spatio-temporal image correlation (STIC). Ultrasound Obstet Gynecol. 2006;27:336-48.
31. Wanitpongpan P, Kanagawa T, Kinugasa Y, et al. Spatio-temporal image correlation (STIC) used by general obstetricians is marginally clinically effective compared to 2D fetal echocardiography scanning by expert. Prenat Diagn. 2008;28:923-8.

22
CHAPTER

Malformations of the Gastrointestinal System

Vincenzo D' Addario, Cristina A Rossi, Luca Di Cagno

INTRODUCTION

The ultrasonic appearance of the fetal gastrointestinal system changes according to the different gestational ages and, as regards the gut, to the physiologic peristalsis secondary to fetal swallowing of amniotic fluid. A correct ultrasonic examination of the fetal gastrointestinal tract in the second and third trimesters includes the visualization of the following different segments.

- *Lips and tongue*: The lips are best seen in a coronal view of the face **(Fig. 22.1A)**; the tongue and the hypopharynx in an axial view of the mouth **(Fig. 22.1B)**.
- *Esophagus*: In sagittal section of the chest, it appears as a linear echogenic structure made by four parallel lines anterior to the spine **(Fig. 22.2)**; this structure however cannot be seen routinely.
- *Diaphragm*: It appears in the parasagittal section on the thorax and abdomen as a thin anechoic line dividing the lung from the liver **(Fig. 22.3)**.
- *Stomach*: It is best seen in the left side of the upper axial plane of the abdomen, anterior to the spleen **(Fig. 22.4)**.
- *Liver*: In the same upper axial plane of the abdomen the right lobe of the liver with the intrahepatic portion of the umbilical vein can be visualized **(Fig. 22.4)**.
- *Gallbladder*: When filled it appears in the right upper axial plane of the abdomen as a pear-shaped anechoic structure below the right hepatic lobe **(Fig. 22.5)**.
- *Small bowel (ileum and jejunum)*: It appears in the lower axial or in the sagittal scan of the abdomen as an echogenic structure with irregular borders **(Fig. 22.6)**. Its sonographic appearance changes with the frequency of the ultrasonic beam: high frequencies (6–7 MHz) and the use of second harmonic produce an increased echogenicity.
- *Colon*: It is best seen in the third trimester when it is partially filled by meconium, both in lower axial and in the sagittal planes of the abdomen **(Fig. 22.7)**.
- *Rectum*: It is best seen in the lowest axial scan of the abdomen as a hypoechoic cystic structure posterior to the bladder **(Fig. 22.8)**.
- *Abdominal wall and the insertion of the umbilical cord*: They are best seen in the midsagittal section of the abdomen **(Fig. 22.9)**.

The systematic evaluation of the above mentioned structures allows the recognition of several congenital anomalies of the gastrointestinal system. The reported sensitivity of ultrasound in diagnosing gastrointestinal malformations varies from 24–72%, according to the results of various authors.[1-5] This wide variation in results is due to the different study designs (mainly the numbers of scans performed during pregnancy), inclusion criteria and the levels of examination. Since many gastrointestinal malformations, due to their natural history, appear late in pregnancy, the best results are obtained when the screening design includes a scan also in the third trimester.

The malformations of gastrointestinal tract and abdominal wall can be divided into four groups:
1. Anterior abdominal wall defects
2. Diaphragmatic defects
3. Bowel disorders
4. Non-bowel masses.

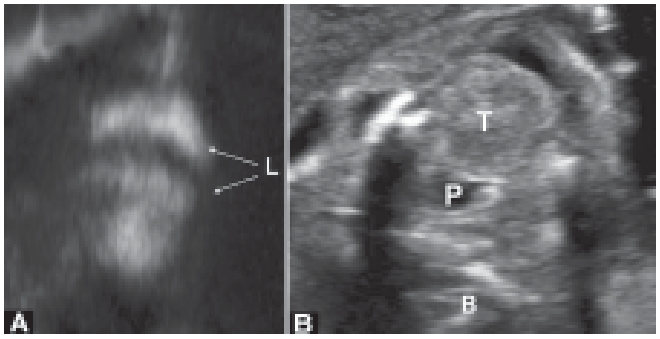

Figures 22.1A and B: (A) Coronal view on the lips; (B) Axial view on the mouth. T: Tongue; P: Pharynx

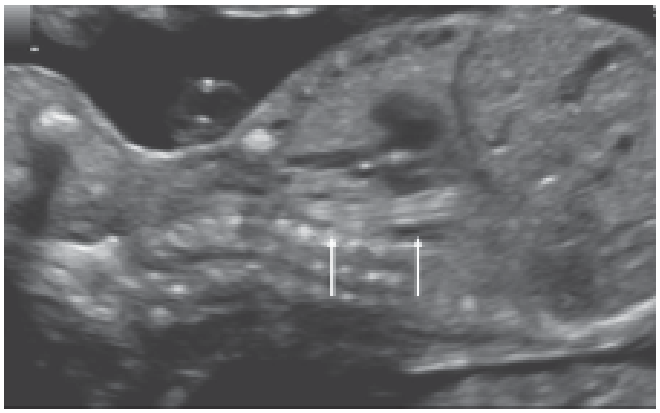

Figure 22.2: Sagittal view of the thorax showing the esophagus as a multilinear echogenic structure anterior to the spine (arrow)

ANTERIOR ABDOMINAL WALL DEFECTS

The congenital abdominal wall defects include gastroschisis, omphalocele and body stalk anomaly. The ultrasonic prenatal diagnosis of these defects is relatively simple and possible in the first half of pregnancy. However, it must be remembered that there is a physiological herniation of the small intestine outside the abdominal cavity between 5th and 11th weeks of gestation **(Fig. 22.10)** and therefore a prenatal diagnosis of abdominal wall defect cannot be made in the earliest stage of pregnancy.[6]

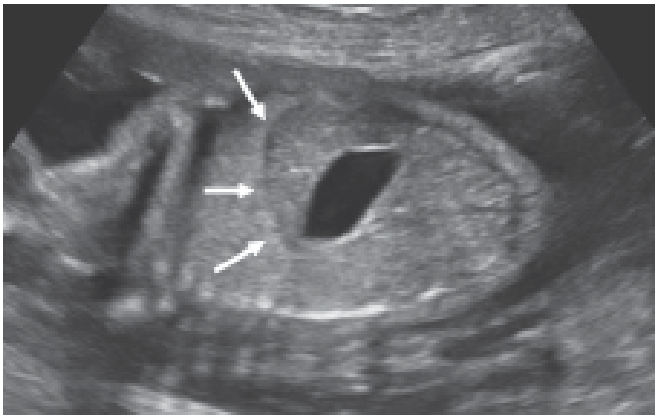

Figure 22.3: Parasagittal scan on the fetal chest and abdomen showing the diaphragm (arrows) between the lung and the liver

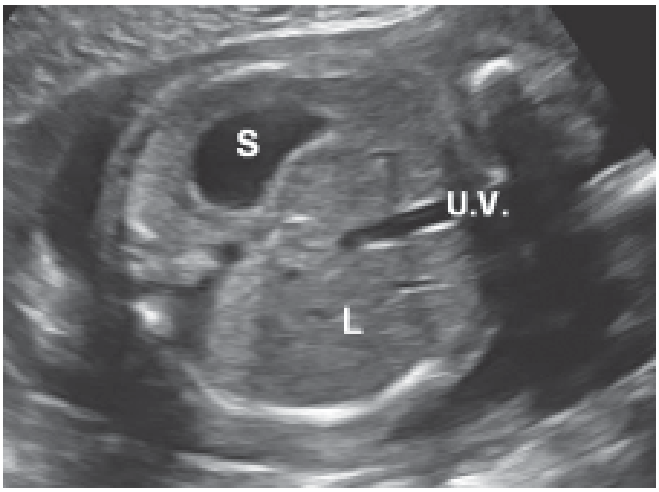

Figure 22.4: Axial view of the upper abdomen showing the stomach (S) located on the left side anterior to the spleen, the right lobe of the liver (L) and the intrahepatic portion of the umbilical vein (U.V.)

Gastroschisis

Incidence: Rare (1:10,000/15,000 live births)

US diagnosis: Free floating bowels loops in the amniotic fluid

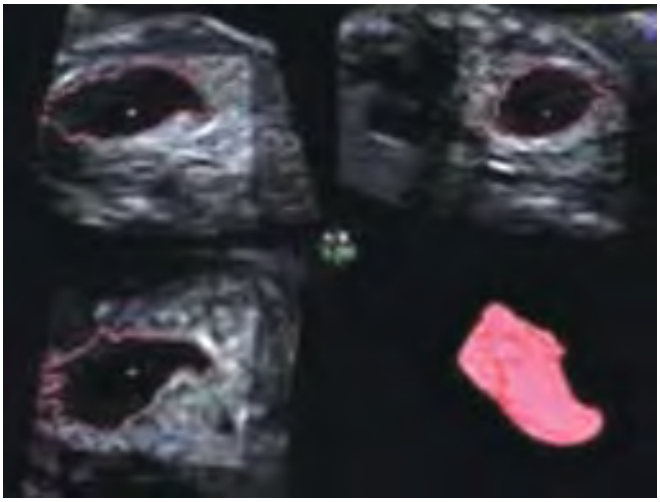

Figure 22.5: Three-dimensional multiplanar view and volume calculation of the stomach

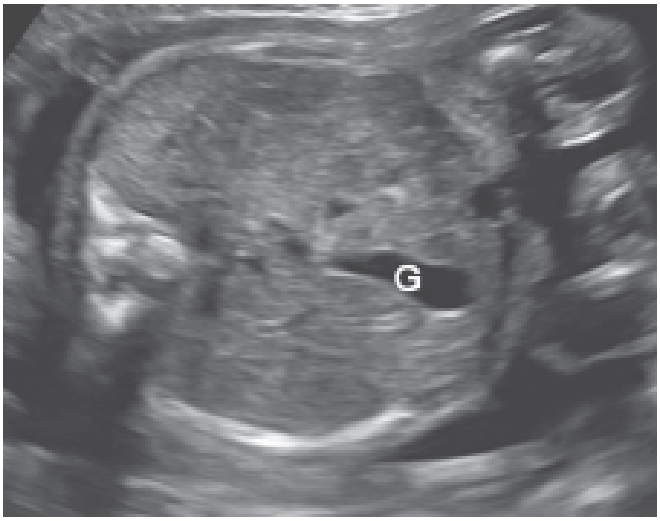

Figure 22.6: Axial view of the upper abdomen showing the gallbladder (G)

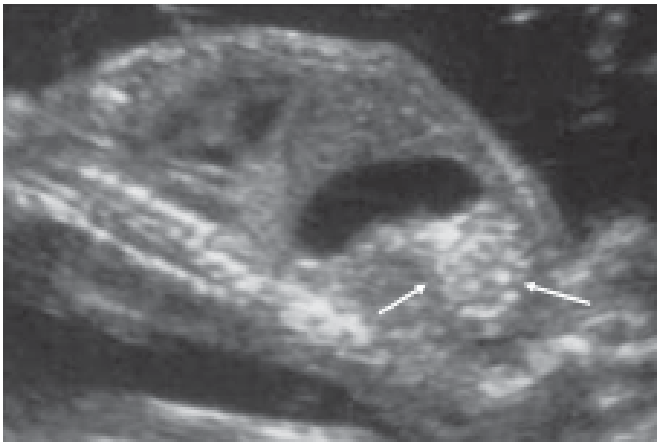

Figure 22.7: The echogenic bowel (arrows) is seen below the stomach

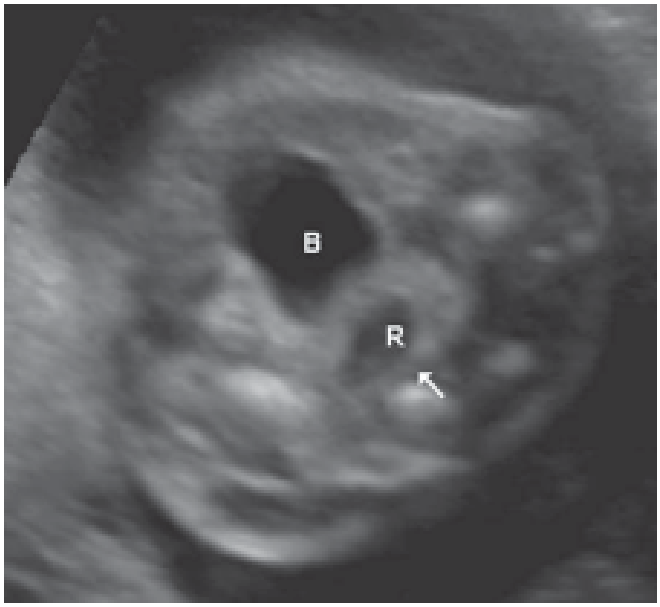

Figure 22.8: The rectum appears as a hypoechoic cystic structure (arrow) posterior to the bladder

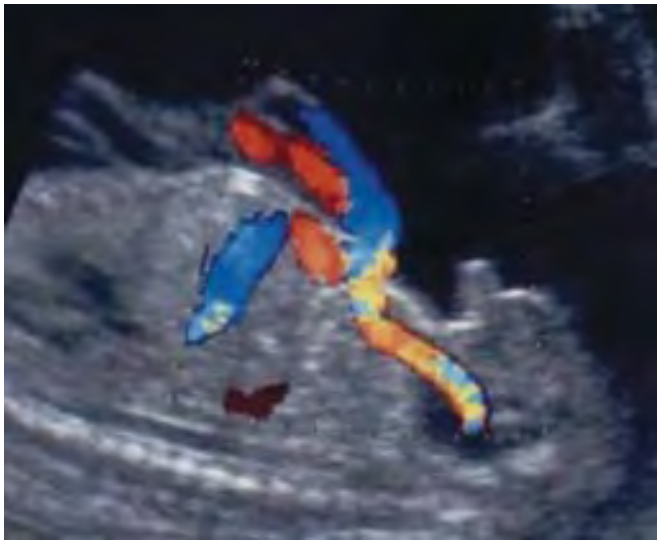

Figure 22.9: Insertion of the umbilical cord into the abdominal wall

Associated anomalies: Rare

Outcome: Good after surgery. Mortality rate ranging from 8–28%.

This malformation consists of a paraumbilical full thickness defect in the anterior abdominal wall, which is usually located to the right side of the umbilical cord insertion and is associated with evisceration of intestinal loops, rarely of the stomach.

The incidence ranges from 1:10,000–1:15,000 live births.

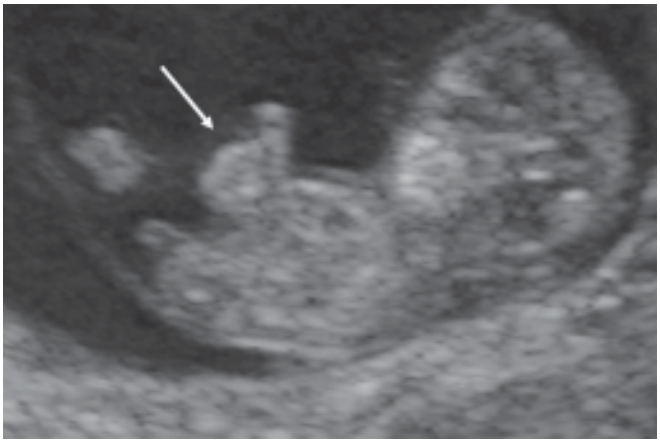

Figure 22.10: Physiological herniation of the midgut at 10 weeks of gestation (arrow)

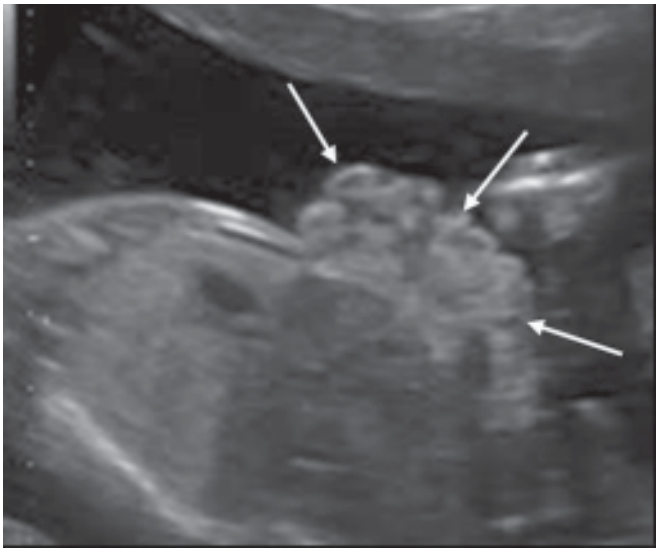

Figure 22.11: Gastroschisis: a cauliflower-like mass protrudes from the abdominal cavity into the amniotic fluid (arrows)

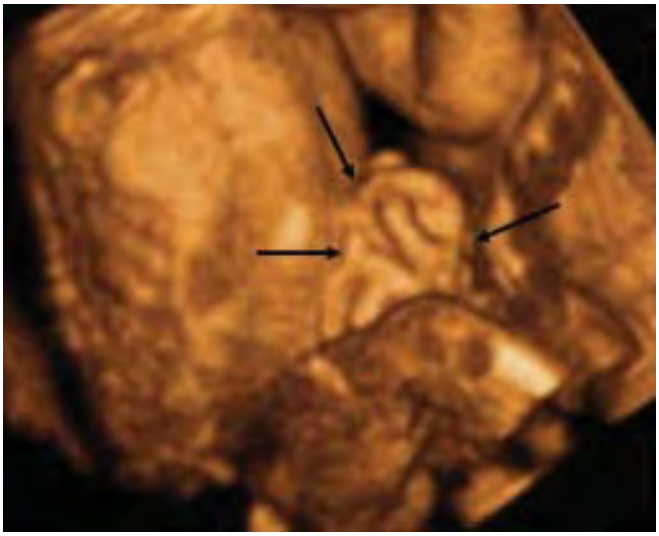

Figure 22.12: Gastroschisis: 3D visualization of the intestinal loop protruding from the abdominal wall (arrows)

Gastroschisis is considered a sporadic event with a multifactorial etiology, but cases of familiar occurrence have been reported. Young maternal age, maternal cigarette use and vasoactive drugs consumption during first trimester are considered as possible etiological factors.

The pathogenesis may be referred to an anomalous regression of the right umbilical vein or to a vascular accident of the omphalomesenteric artery with consequent failed closure of the abdominal wall. The abdominal wall defect is generally small but the amount of bowel protruding from the defect and floating freely in the amniotic fluid may be disproportionately large. The herniated organs include mainly bowel loops, rarely stomach that are not protected by a membrane but usually covered by inflammatory exudates, possibly resulting from chemical irritation by exposure to amniotic fluid.

The ultrasonographic diagnosis of gastroschisis is suggested by the finding of a partly solid, partly cystic mass adjacent to the anterior abdominal wall and freely floating in the amniotic fluid with a typical cauliflower-like appearance **(Figs 22.11 and 22.12).** Bowel dilatation can be seen both in the herniated and endoabdominal loops as a consequence of the bowel obstruction with associated polyhydramnios. In severe cases dilatation may disappear as a consequence of ischemia and necrosis of the intestinal walls ("vanishing gut").

The differential diagnosis is mainly with omphalocele and is based on the presence of a normal insertion of the umbilical cord, the lateral location of the mass and the absence of a membrane covering the herniated mass.

In contrast to omphalocele, gastroschisis is rarely associated with other malformations and chromosomal anomalies, but additional gastrointestinal abnormalities (malrotation, atresia, volvulus, and infarction) may occur in 20–40% of the cases.[3,4] A high percentage of fetuses with gastroschisis (77%) present intrauterine growth restriction and preterm labor occur in one-third of cases. The extent of bowel damage is variable and strictly affects the prognosis. Most of the bowel damage is caused by constriction at the site of the abdominal wall defect: the sonographic evidence of small bowel dilatation and mural thickening correlates with severe intestinal damage and poor clinical outcome.

The mode of delivery of fetuses affected by gastroschisis is still controversial: although there is no striking evidence for cesarean section (CS) over vaginal delivery, the former may be preferred in order to avoid trauma and infection of the herniated bowel during the vaginal delivery. Maternal transfer before delivery to a tertiary care center is recommended in order to plan prompt surgical treatment. The mortality rate ranges from about 8–28%. The most common causes of the neonatal death are sepsis, prematurity and complications related to the intestinal ischemia.

Omphalocele

Incidence: Ratio of 1:4,000–7,000 live births; higher *in utero.*

US diagnosis: Mass protruding from the abdomen, covered by a membrane, containing bowels loops or liver; umbilical cord inserted on the protruding mass.

Associated anomalies: Present in 50–70% of the cases: chromosomopathies in 30% of the cases; present in different syndromes.

Outcome: Good in isolated cases. Poor in the presence of associated anomalies, chromosomopathies and syndromes.

Omphalocele is a ventral wall defect characterized by an incomplete development of abdominal muscles, fascia and skin and the herniation of intra-abdominal organs (bowel loops, stomach and liver) into the base of umbilical cord, with a covering amnioperitoneal membrane. The defect is thought to be caused by an abnormality in the process of body infolding. The classic omphalocele is a mid-abdominal defect although there is also a high or epigastric omphalocele (typical of the pentalogy of Cantrell) and a low or hypogastric omphalocele (as seen in bladder or cloacal exstrophy), due to cephalic and caudal folding defects respectively.

The incidence of omphalocele ranges from 1:4,000–1:7,000 live births. It is more frequent in older women; most cases are sporadic, although a familial occurrence with a sex-linked or autosomal pattern of inheritance has been reported.

The ultrasonographic appearance of omphalocele varies according to the severity of the defect and to the organs herniated. Small omphalocele contains only omentum and some bowel loops **(Fig. 22.13)**. In a large omphalocele also the liver can be herniated **(Fig. 22.14)**. 3D sonography may offer a better evaluation of the size of the lesion **(Fig. 22.15)**. A common finding is the presence of a membrane covering the herniated mass where the insertion of the umbilical cord can be recognized. Sometimes ascites can be associated. Polyhydramnios is present in one-third of the cases as a consequence of bowel obstruction.

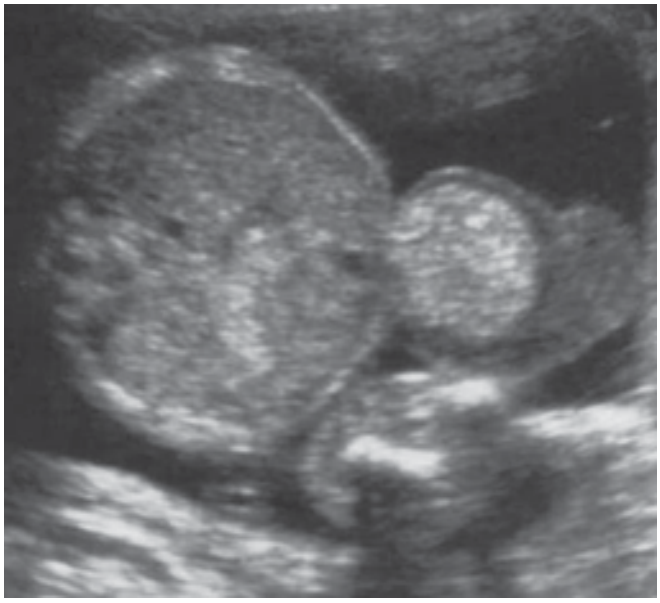

Figure 22.13: Omphalocele: an echogenic mass protruding at the level of the cord insertion, covered by an amnioperitoneal membrane

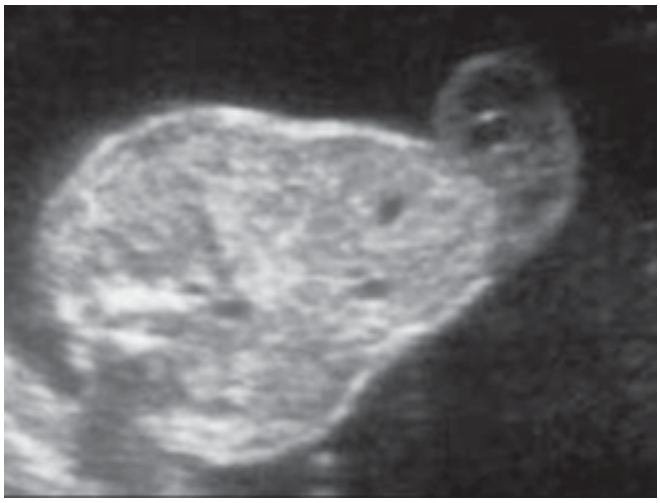

Figure 22.14: Large omphalocele containing the liver

The differential diagnosis is mainly with gastroschisis. The presence of a covering amnioperitoneal membrane and the insertion of the umbilical cord on the protruding mass easily allow making the correct diagnosis. However, the covering membrane may occasionally disrupt, thus making the differential diagnosis with gastroschisis more difficult.

There are different syndromes that include omphalocele, such as pentalogy of Cantrell (midline

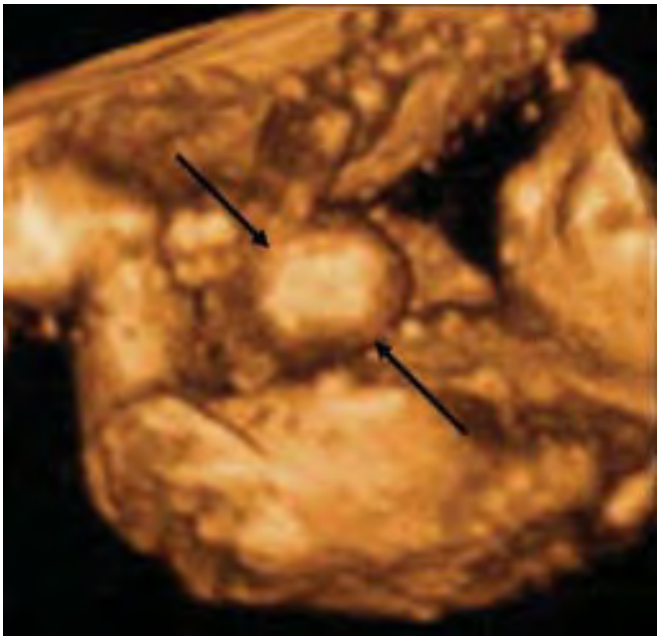

Figure 22.15: A 3D rendering of a fetus with omphalocele

supraumbilical abdominal defect, lower sternum defect, deficiency of diaphragmatic pericardium, anterior diaphragm defect, cardiac abnormality) and Beckwith-Wiedemann syndrome (macroglossia, visceromegaly, omphalocele). Although most cases of omphalocele are sporadic, a familial occurrence of this anomaly with a sex-linked or autosomal pattern of inheritance has been reported.

The most important prognostic variable is the presence of associated malformations (50–70% of cases) or chromosomal abnormalities (30% of cases).[5,6] Some authors have demonstrated that small defects containing only bowel, are associated with an increased risk of chromosomal abnormalities, as opposed to large defects that have exposed liver. The main associated malformations are cardiac anomalies (up to 47% of cases), genitourinary abnormalities (40% of cases) and neural tube defects (39% of cases).

The mode of delivery of fetuses with omphalocele has been debated in literature. The goal in the management is to deliver the fetus as close to term as possible in tertiary care centers. The CS may be necessary to avoid dystocia or sac rupture in large omphalocele. In the case of small defects vaginal delivery is recommended. The neonatal mortality after surgery mainly depends on the associated anomalies. In isolated small omphalocele the prognosis is good particularly in small omphalocele. In large omphalocele with herniated liver, respiratory distress may be the cause of failure.

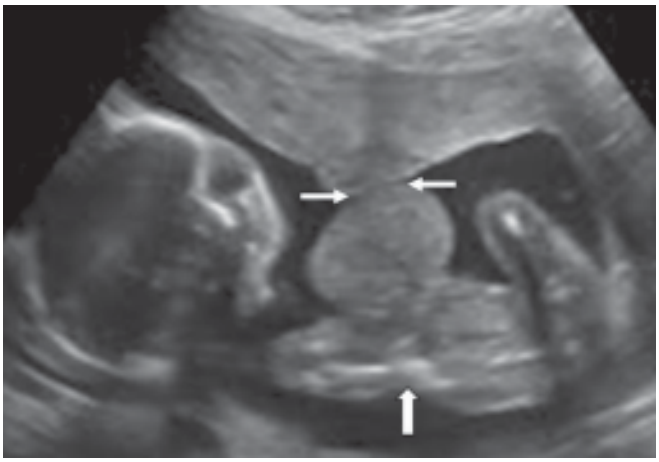

Figure 22.16: Body stalk anomaly: a large anterior abdominal wall defect attaches the fetus directly to the placenta (arrows) with subsequent deformity of the spine (large arrow)

Body Stalk Anomaly

Incidence: Rare (1:14,000).

US diagnosis: Large anterior wall defect attaching the fetus to the placenta or uterine wall with absence of umbilical cord.

Associated anomalies: Scoliosis, kyphosis, multiple malformations.

Outcome: Fatal.

The body stalk anomaly is a severe abdominal wall defect[7] caused by the failure of formation of the body stalk; it is characterized by the absence of umbilical cord and umbilicus and the fusion of the placenta to the herniated viscera. The incidence is 1:14,000 births. This malformation is caused by a developmental failure of the cephalic, caudal and lateral embryonic folds.

The ultrasonographic diagnosis is suggested by the finding of a large anterior wall defect attaching the fetus to the placenta or uterine wall, the absence of umbilical cord and the visualization of abdominal organs in a sac outside the abdominal cavity **(Fig. 22.16)**.[8] The position of the fetus may lead to scoliosis and kyphosis. Multiple malformations such as neural tube defects, gastrointestinal and genitourinary anomalies, may be associated. The body stalk anomaly is a uniformly fatal condition.

DIAPHRAGMATIC DEFECTS

Incidence: 1:3,000 live births

US diagnosis: Presence of stomach or bowel loops or liver in the thorax with lateral displacement of the heart.

Associated anomalies: Chromosomopathies (5–15%); Syndromes (20–30%); other malformations.

Outcome: Poor in syndromic cases; 40–50% survival rate in isolated cases.

A diaphragmatic hernia is a defect in the diaphragm, due to failure of the pleuroperitoneal canal to close between 9–10 weeks of gestation, thus determining the protrusion of the abdominal organs into the thoracic cavity.

The classification of these malformations is based on the location of the diaphragmatic defect:

- Diaphragmatic hernia (Bochdalek and Morgagni types)
- Septum transversum defects (defect of the central tendon)
- Hiatal hernia (congenital large esophageal orifice)
- Eventration of the diaphragm
- Agenesis of the diaphragm.

The incidence of congenital diaphragmatic hernia is 1:3,000 live births. The most common type of diaphragmatic hernia is the Bochdalek type which is a posterolateral defect mostly located on the left side (80% of cases), less frequently on the right side (15%) or bilaterally (5%). Stomach, spleen and colon are the most frequently herniated organs. When the hernia is on the right side, the main organs involved are the liver and the gallbladder.

The Morgagni type is usually a very small hernia which occurs in 1–2% of cases. It is a parasternal defect located in the anterior portion of the diaphragm; it contains liver, which may limit the degree of herniation.

Eventration of the diaphragm consists of an upward displacement of abdominal organs into the thoracic cavity secondary to a congenitally weak diaphragm which has the aspect of an aponeurotic sheet. It occurs in 5% of diaphragmatic defects and it is more common on the right side.

Diaphragmatic hernia can be either a sporadic or a familiar disorder and although the etiology is unknown this abnormality has been described in association with maternal ingestion of drugs such as thalidomide, quinine and anticonvulsivants. There are two hypotheses to explain the mechanism responsible for the origin of a diaphragmatic defect: a delayed fusion of the diaphragm or a primary diaphragmatic defect.

Another classification as mentioned below takes into account the time of onset of the malformation in relation to the lung development:

- Herniation occurring early during bronchial branching causing a severe bilateral pulmonary hypoplasia and lately death

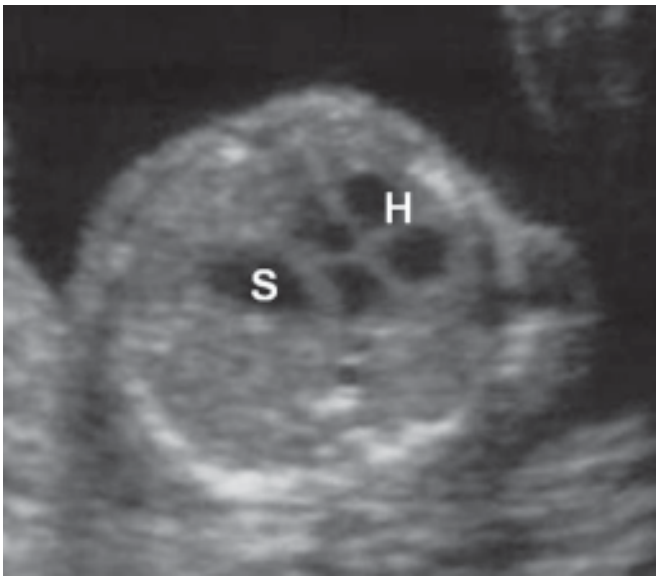

Figure 22.17: Transverse section of the fetal chest in a case of posterolateral left diaphragmatic hernia: the heart (H) is displaced to the right side by the presence of the stomach (S) and bowel loops in the thoracic cavity

- Herniation at the stage of distal bronchial branching leading to unilateral hypoplasia, with survival depending on a balance between pulmonary vascular and ductal resistances
- Late herniation in pregnancy which causes a compression of otherwise normal lung and carries a good prognosis
- Postnatal herniation without pulmonary pathology and with good chances of viability.

The prenatal sonographic diagnosis of diaphragmatic hernia is mainly based on the visualization of abdominal organs at the same level of the four chamber view of the heart in the transverse section of the fetal chest. The sonographic signs are different according to the location of the defect. In the most common case (posterolateral left defect) the heart is shifted to the right by the herniated stomach **(Fig. 22.17)**. Sometimes only bowel loops and the left lobe of the liver are herniated: in these cases the heart displacement to the right and the irregular echogenicity of the left hemithorax are the signs suggesting the diagnosis. In the sagittal view of the chest and abdomen the stomach may be recognized in the mediastinic cavity **(Fig. 22.18)**.

Polyhydramnios is common and is secondary to the bowel obstruction.

In the less common cases of right defects, the diagnosis is more difficult, since the stomach is not herniated: suspicious signs are the left rotation of the

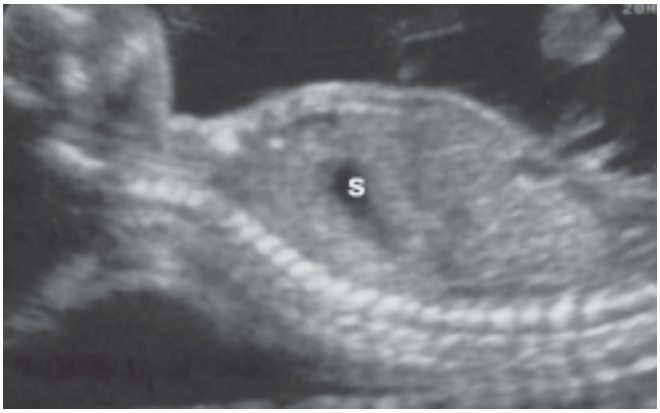

Figure 22.18: Longitudinal section of the fetal chest and abdomen in a fetus with diaphragmatic hernia, showing the stomach (S) in the mediastinic cavity

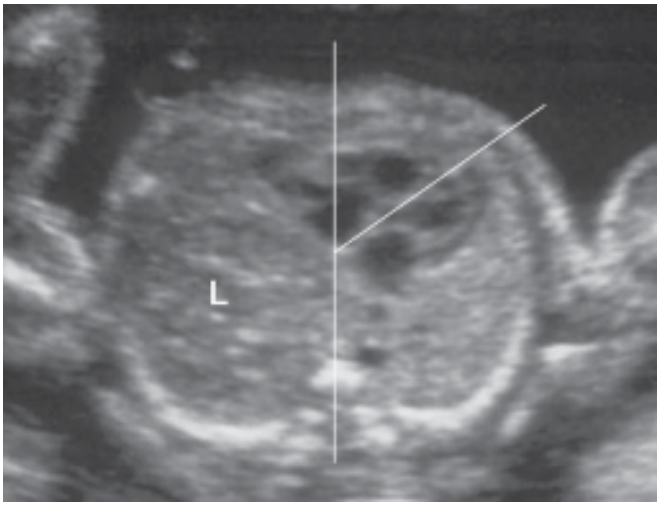

Figure 22.19: Right diaphragmatic hernia. The cardiac axis is left rotated by the herniated liver (L)

cardiac axis and upper displacement of the liver **(Fig. 22.19)**. In this case the coronal view of the chest is more useful **(Figs 22.20A and B)**.

It must be stressed that due to the possible late onset of the herniation, the prenatal diagnosis of diaphragmatic hernia may be missed in up to 40% of the cases.

The differential diagnosis is with other conditions such as cystic adenomatoid malformation of the lung, bronchogenic cysts, mediastinal cysts and pulmonary sequestration. The peristalsis of the stomach and bowel is a useful sign to differentiate them from other cystic structure.

The rate of associated anomalies is 25–75% increasing to 95% in stillborns. Such anomalies include central nervous system, cardiac and chromosomal abnormalities, omphalocele and oral cleft.

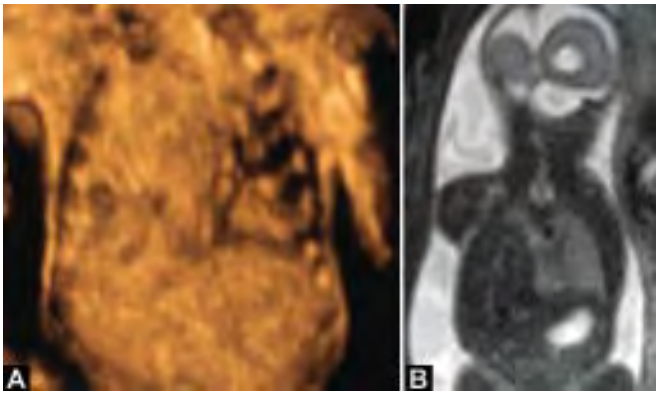

Figures 22.20A and B: A 3D rendering of the fetal chest in a fetus with right diaphragmatic hernia

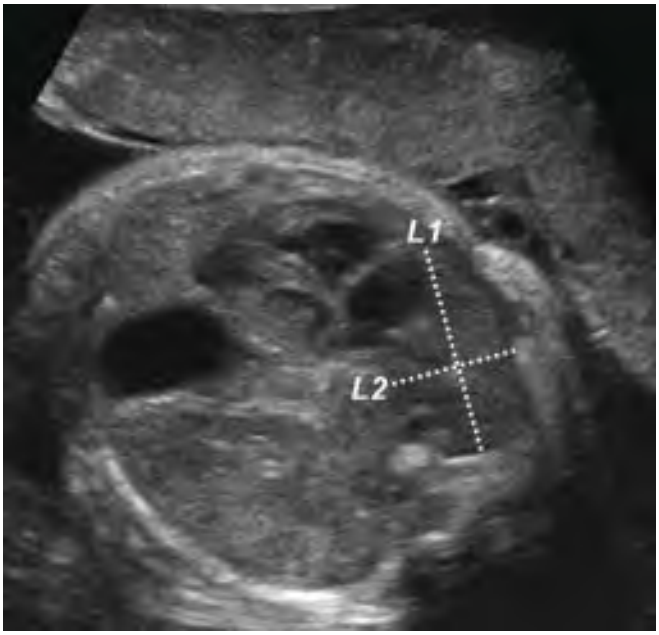

Figure 22.21: Technique of measurement of the LHR. The product of the two orthogonal diameters of the collapsed lung, contralateral to the side of herniation, is divided by the head circumference (L1xL2/HC)

The prognosis for this malformation is still very poor and becomes poorer if other malformations are associated. The poor prognosis mainly depends on the severity of pulmonary hypoplasia and hypertension induced by the prolonged compression of the lungs by the herniated viscera. Different sonographic techniques have been suggested in order to evaluate the risk of lung hypoplasia. The "lung to head ratio" (LHR) is the ratio between the product of the two orthogonal diameters of the collapsed lung, contralateral to the side of herniation and the head circumference (L1xL2/HC) **(Fig. 22.21)**. LHR values less than 0.6 are associated with

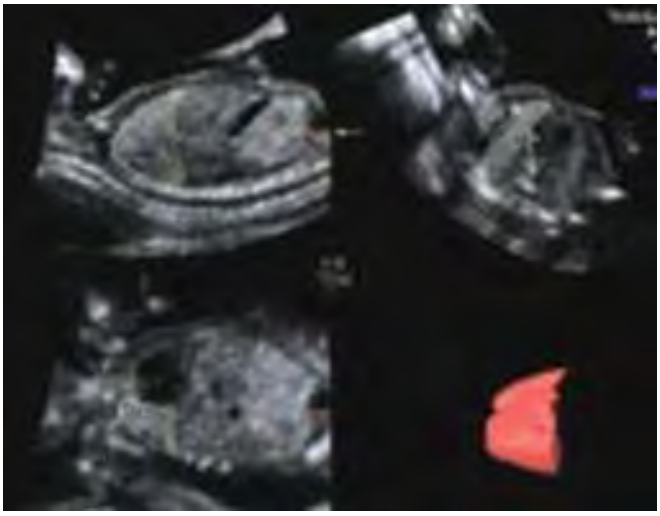

Figure 22.22: Technique of the 3D calculation of the lung

neonatal death; values greater than 1.35 are associated with good outcome and the values between 0.6 and 1.35 have a 60% survival rate.[9] The presence of "liver up" (herniation of the liver in the thorax) reduces the percentage of survival from 93 to 43% and doubles the need of ECMO (Extra Corporeal Membrane Oxygenation).[10] The results of these techniques, however, are not uniformly confirmed by different authors;[11] the main limitation is the dependency from the gestational age. For this reason alternative techniques have been suggested: one is the ratio between the observed and expected LHR (O/E LHR%), which has the advantage of being independent from the gestational age. The values less than 15% are indicative of extreme pulmonary hypoplasia, values 15–25% of severe pulmonary hypoplasia, values 25–45% of moderate pulmonary hypoplasia and values greater than 45% of mild hypoplasia. The 3D evaluation of the lung volumes **(Fig. 22.22)** and the observed/expected lung volume ratio (O/E LVR%) has also been suggested, but this measurement is technically limited in the third trimester. Better results in the third trimester may be obtained with the use of MRI.

Management of fetus with diaphragmatic hernia relies on protecting the contralateral lung hoping that it is normally formed, which depends on the gestational age at diagnosis. If the fetus is less than 24 weeks' gestation, parents may choose to terminate the pregnancy, to continue the pregnancy with postnatal care or even to consider repair of the defect *in utero*. Between 24 and 32 weeks, parents may choose between conventional postnatal therapy and fetal surgery. Anytime when a diaphragmatic defect is diagnosed, the prenatal karyotyping and detailed ultrasound examination to detect associated anomalies are recommended. There are no indications for preterm delivery or for CS. The delivery should be planned in a tertiary care center. Prenatal treatment is proposed in highly selected centers with the aim to prevent lung hypoplasia. The first approach was open fetal surgery with hysterotomy during pregnancy, but this technique is carrying several complications. An alternative invasive technique now used is the endotracheal application of a balloon catheter, following the observation that in cases of laryngeal atresia an overgrowth of the lung is observed. The balloon is introduced with endoscopically guided procedure of fetal endoscopic tracheal occlusion (FETO) and removed at delivery.[12] The first results seem to be encouraging.[13]

The prognosis after neonatal surgery mainly depends on the severity of lung hypoplasia and hypertension. In isolated left diaphragmatic hernia the average survival rate is 50–60%. In some surviving infants, however, neurological sequels by brain hypoxia have been reported.

BOWEL DISORDERS

Esophageal Atresia

Incidence: 1:2,500/4,000 live births

US diagnosis: Absent stomach bubble, polyhydramnios, dilated esophagus.

Associated anomalies: Frequent association to other malformations, chromosomopathies, syndromes (VACTERL).

Outcome: Depending on the severity of the defect and associated anomalies.

This anomaly consists in the absence of a segment of the esophagus and is often associated with a tracheoesophageal fistula (86–90% of cases). Five types of esophageal atresia may be distinguished, according to the Gross classification:

1. Isolated (type A: 8% of the cases)
2. Associated with a fistula connecting only the proximal part of the esophagus and the trachea (type B: 1% of the cases)
3. Associated with a fistula connecting the lower part of the esophagus and the trachea (type C: 88% of the cases)
4. Associated with proximal and distal fistulas (type D: 1% of the cases)
5. Tracheoesophageal fistula without esophageal atresia (type E: 2% of the cases).

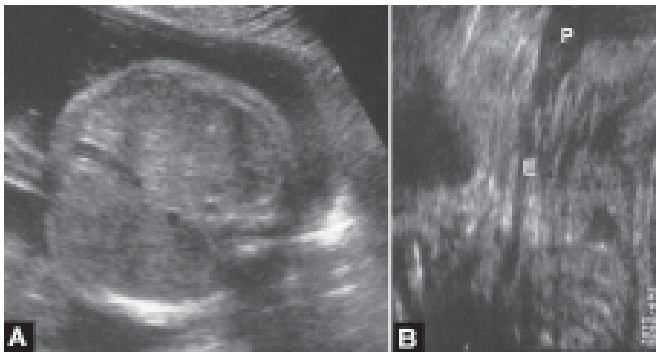

Figures 22.23A and B: Esophageal atresia. (A) The diagnosis is suspected by the association of absent stomach; (B) Dilatation of the proximal tract of the esophagus in the coronal scan of the neck (P: pharynx, E: esophagus)

The incidence varies between 1:2,500 and 1:4,000 live births. The etiology is unknown. The anomaly derives from the failed division at 8 weeks of gestation of the primitive intestine in the ventral tracheobronchial portion and in the dorsal intestinal portion.

The prenatal diagnosis is possible in only 10% of the cases and should be suspected in the presence of polyhydramnios with absent stomach bubble in several and repeated ultrasound examinations; sometimes the dilated proximal tract of the esophagus with absent stomach can also be seen **(Figs 22.23A and B)**; the former sign, however, is transient, requires a prolonged examination and usually appears late in gestation. In the remaining 90% of the cases, the presence of a tracheoesophageal fistula allows the amniotic fluid to reach and fill the stomach thus making the diagnosis impossible.[14] The differential diagnosis is with other conditions characterized by failed visualization of the stomach: diaphragmatic hernia, congenital highway obstruction syndrome (CHAOS), fetal akinesia sequence, anhydramnios with consequent failed swallowing of amniotic fluid.

Associated anomalies are present in 50–70% of the cases, including cardiac, genitourinary, chromosomal (trisomy 21), additional gastrointestinal and musculoskeletal anomalies. Characteristic associations are the "VACTERL" (vertebral, anorectal anomalies, cardiac anomalies, tracheoesophageal fistula, esophageal atresia, renal anomalies, limb anomalies) and the "CHARGE" (coloboma of the eye, heart anomaly, choanal atresia, mental retardation, microphallus, ear abnormalities). Fetal karyotyping is suggested. The prognosis depends on the associated malformations and on the severity of polyhydramnios, which can facilitate preterm delivery. The delivery should be planned in a tertiary center for the prompt intensive therapy and surgical treatment.

Duodenal Atresia or Stenosis

Incidence: 1:2,500/10,000

US diagnosis: Double bubble, polyhydramnios.

Associated anomalies: Frequent association to other malformations and chromosomopathies (mainly trisomy 21).

Outcome: Good after neonatal surgery in isolated cases.

The incidence of this malformation is 1:2,500/10,000 live births. In most cases the etiology is unknown and its genesis goes back to the 11th week of gestation due to a failure of canalization of the primitive bowel. Another possible cause is focal ischemia with consequent segmental infarction. The obstruction may also be due to external factors, such as intestinal malrotation and volvulus. Atresia is more common than stenosis (70% of cases) and could be associated with chromosomal abnormalities (trisomy 21), skeletal defects and other anomalies.

The most typical sonographic finding is the characteristic "double bubble" sign caused by the simultaneous dilatation of the stomach and the proximal duodenum **(Fig. 22.24)**. The diagnosis is usually made in the late second trimester.[15] The differential diagnosis is with other cystic lesions of the upper abdomen, such as duplication cysts, coledocal and hepatic cysts. A useful sign is the visualization of the continuity of the

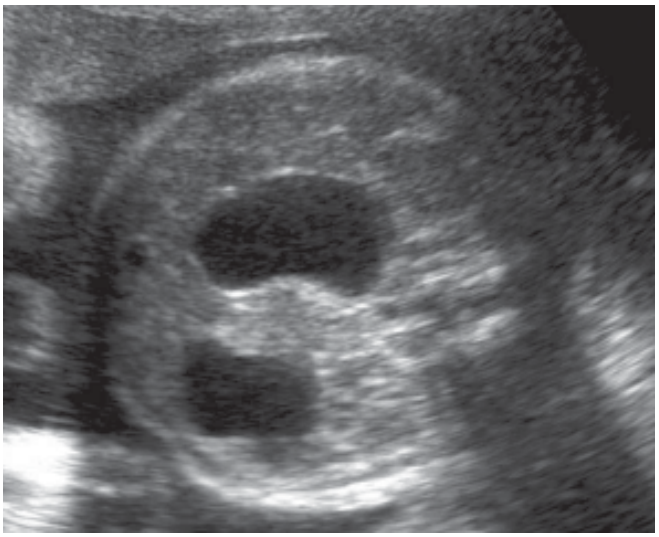

Figure 22.24: Duodenal atresia: the dilated stomach and proximal duodenum are clearly recognized with the typical "double bubble" sign

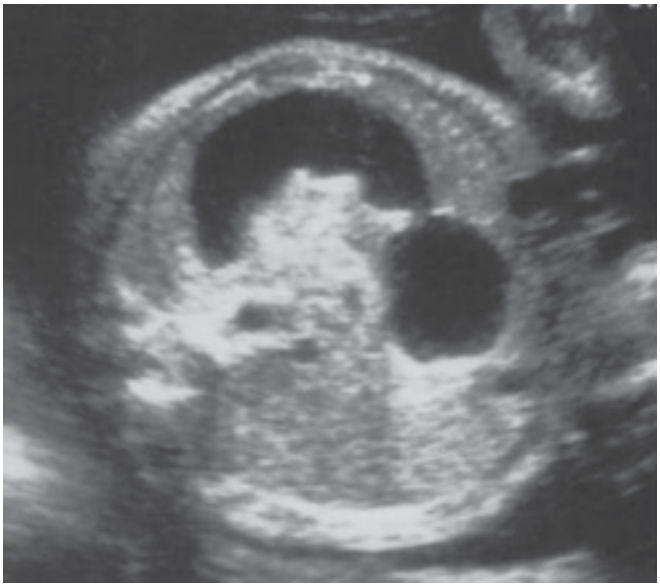

Figure 22.25: Duodenal atresia: the continuity of the lumen between the stomach and the duodenum separated by the pylorus can be seen

lumen between the stomach and the duodenum **(Fig. 22.25)**.

Up to half of duodenal atresia cases are complicated by polyhydramnios and this can contribute to preterm labor, but the main cause of death is the associated anomalies. These include gastrointestinal (26–35% of the cases), cardiac (20–30%), genitourinary (5–8%) and skeletal (4–8%). In 40–50% of the cases, the trisomy 21 is associated. Particularly the association of duodenal atresia and atrioventricular canal is highly suspicious for trisomy 21.

The neonatal outcome after surgery is good in 90% of the cases without associated anomalies. Late minor complications such as megaduodenum and gastric reflux may occur.[16] The delivery should be planned in a tertiary center for the prompt surgical treatment.

Bowel Obstruction

Incidence: 1:2,500/5,000

US diagnosis: Multiple dilated bowels loops and late polyhydramnios in ileojejunal atresia; distended sigma-rectum with normal amniotic fluid in anorectal malformations.

Associated anomalies: Rare in ileojejunal atresia; chromosomopathies in anorectal malformations.

Outcome: Usually good in isolated cases.

The incidence of bowel stenosis and atresia is 2–3:10,000 births.

These defects are usually sporadic, although familial cases have been described.

According to the site of the obstruction the defects are divided in: (1) jejunoileal atresia and stenosis, (2) colonic atresia and (3) imperforate anus.

In jejunoileal atresia the location of the defect is at proximal jejunum in 31% of the cases, distal jejunum in 20%, proximal ileum in 13% and distal ileum in 36%. In 6% of the cases the atresia interests different intestinal segments. Atresia and stenosis are thought to be a consequence of an ischemic event at the level of the mesenteric artery.

There are four types of jejunoileal atresia:

1. *Type I:* Presence of a single or multiple transverse diaphragm of mucosa or submucosa, with regular external intestinal walls and normal mesentery (32%).
2. *Type II:* Presence of blind ends of bowel loops connected by fibrous bands with regular mesentery (25%).
3. a. *Type IIIa:* Complete separation of blind ends with a corresponding "V" shaped mesenteric defect (15%).
   b. *Type IIIb:* "Apple peel" or "christmas-tree" appearance of the blind ended ileum wrapped around the ileocolic artery with loss of the superior mesenteric artery (11%).
4. Type IV: Multiple atresias of the small intestine (17%).

Colon atresia usually occurs proximal to the splenic flexure with a significant segment of absent colon with distal microcolon.

Anorectal malformations regard the terminal portion of the intestinal lumen and may be divided in high and low level malformations in relation to the elevator ani muscle. The high level anomalies are usually more complex and complicated with genitourinary perineal fistulas as well as urinary and vertebral malformations. They derive from an anomalous division of the cloaca by the urorectal septum. The low level malformations are more common and less severe and are usually represented by the imperforate anus occasionally associated with perineal fistula.

The sonographic prenatal appearance of the bowel obstruction varies according to the level of the defect. In the case of jejunoileal atresia multiple dilated bowel loops in the fetal abdomen may be seen in association with polyhydramnios **(Fig. 22.26)**.[16,17] An active peristalsis can be seen.[18] These signs usually appear in the late second or even third trimester. The first sign may be the presence of a single bowel loop with a

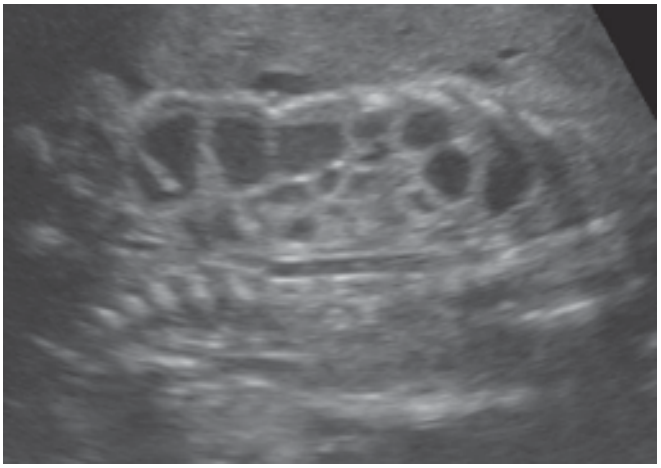

Figure 22.26: Jejunal atresia: multiple dilated bowel loops are present in the fetal abdomen

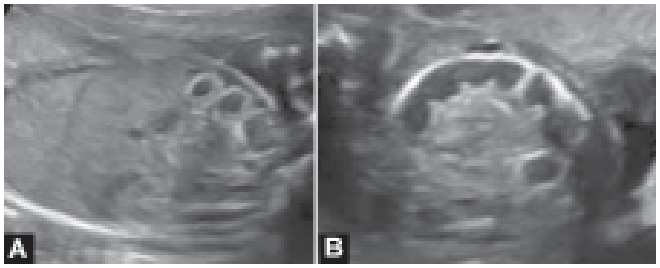

Figures 22.27A and B: Early sign of bowel dilatation

diameter above 7 mm and with hyperechoic walls **(Figs 22.27A and B)**.

In colon atresia, the sonographic finding is similar to distal ileal occlusion and the differential diagnosis may not be possible. In cases of distal occlusion, dilated intestinal loops with increased peristalsis may be seen as well as intraluminal echogenic material in the distended colon referring to meconium **(Fig. 22.28)**.[19]

The diagnosis of bowel obstruction is usually made in the third trimester: the lower is the obstruction the later is the appearance of the sonographic signs.

The prognosis of these malformations mainly depends on the level of obstruction (the lower the obstruction, the better the outcome), the length of remaining intestine and birth weight. Other important prognostic factors are the presence of associated malformations (especially gastrointestinal anomalies including bowel malrotation, esophageal atresia, microcolon and intestinal duplication), meconium peritonitis and intrauterine growth restriction.

The delivery should be planned in a tertiary center for the prompt neonatal surgery.

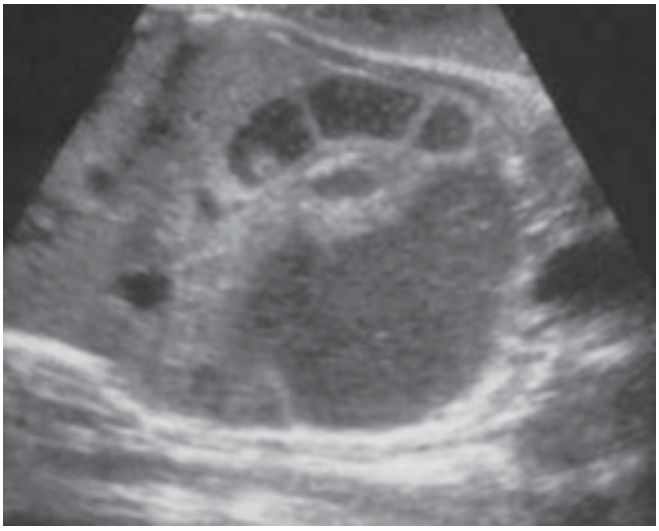

Figure 22.28: Colon obstruction in a third-trimester fetus: a dilated distal colon is seen containing echogenic material referring to meconium

Meconium Peritonitis

Incidence: 1:20,000/30,000 live births

US diagnosis: Intra-abdominal diffuse hyperechogenicity, calcifications, ascites and bowel dilatation.

Associated anomalies: Cystic fibrosis frequently associated.

Outcome: Usually poor.

This condition is the consequence of *in utero* perforation of the bowel with spread of meconium into the peritoneal cavity leading to a local sterile chemical peritonitis. The peritonitis may be localized, with the development of a dense calcified mass or fibrous tissue or diffuse with a fibrous reaction leading to bowel adhesions and pseudocyst formation. Inflammatory reaction leads to an exudative process and ascites. Its incidence is 1:20,000/30,000 live births. The most common cause of the bowel perforation is cystic fibrosis: in this disease the highly proteic meconium causes obstruction, dilatation and subsequent bowel perforation. Other causes of perforation are bowel obstructions.

The prenatal sonographic appearance of meconium peritonitis varies according to the underlying anatomical finding: main signs are intra abdominal diffuse hyperechogenicity and calcifications (85% of cases) **(Figs 22.29A and B)** and/or fetal ascites caused by exudate and bowel dilatation.[20-25]

The prognosis is usually poor since multiple intestinal resections may be required and cystic fibrosis is frequently associated.

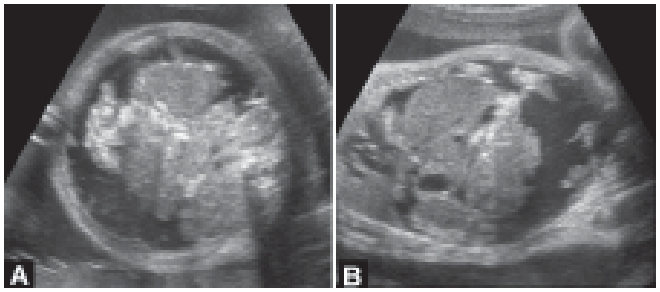

Figures 22.29A and B: Meconium peritonitis: diffuse hyperechogenicity of the abdominal cavity

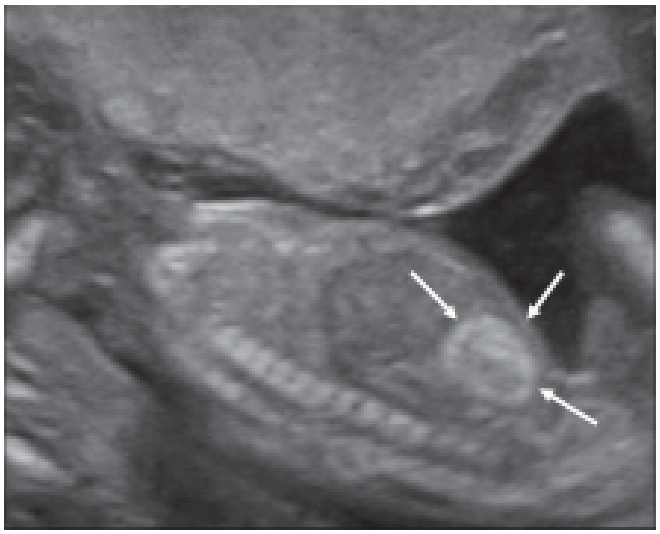

Figure 22.30: Echogenic bowel

Echogenic Bowel

Sonographically, "echogenic bowel" is defined as echogenicity of the bowel loops equal to or greater than the density of the iliac wing[26] **(Fig. 22.30)**. This feature might depend on a slow or delayed transit of the meconium along the bowel. The reported incidence of "echogenic bowel" in the midtrimester fetuses is 0.2–2%.

In up to 75% of the cases "echogenic bowel" is a normal finding with no pathological significance. It must also be stressed that the use of high frequencies (6–7 MHz) and second harmonic imaging produce an increased echogenicity. In the remaining cases it can be associated to the following pathological conditions:

- Chromosomopathies, mainly trisomy 21: however the increased risk of chromosomopathies[27] in the presence of such an isolated marker is low (3–5% in the second trimester)
- Congenital infections (mainly cytomegalovirus (CMV), toxoplasmosis, Parvovirus B19)
- Cystic fibrosis and meconium ileum
- Intestinal malformations (atresia, volvulus, enteric duplication)
- Fetal growth restriction
- Intra-amniotic bleeding.

In the presence of "echogenic bowel" the following management is suggested:

- Fetal karyotyping: only if additional markers of chromosomopathies are present
- Maternal test for infection
- Parental screening for cystic fibrosis
- Accurate evaluation of fetal growth and well-being
- Rule-out of possible intra-amniotic bleeding (previous bleeding in pregnancy, previous invasive procedures).

In the case of normal results, the fetus should be accurately monitored in the third trimester to rule out late onset intestinal anomalies of growth restriction.[28]

NON-BOWEL CYSTIC MASSES

Choledocal Cysts

Choledocal cyst is a rare congenital cystic dilatation of the common bile duct.[29] The incidence is about 1:2,000. The cysts can be single or in rare cases, multiple involving the intrahepatic or extrahepatic portion of the biliary tree. Choledocal cysts are classified into four types as mentioned below:

1. Fusiform dilatation of the common bile duct
2. Diverticular dilatation of the common bile duct
3. Intramural dilatation of the common bile duct
4. Intrahepatic biliary duct dilatation.

The sonographic appearance[30] is that of a cystic structure located in the upper right abdomen with dilated proximal ducts **(Fig. 22.31)**. Differential diagnosis includes duodenal atresia, hepatic cyst, dilated gallbladder, mesenteric cysts and ovarian cyst. The cystic size and the association with biliary obstruction affect the prognosis.

Mesenteric and Omental Cyst

These benign malformations consist in cystic structures located in the small or large bowel mesentery or in the omentum filled with serous or chylous fluid. Its sonographic appearance is that of a thin-walled, unilocular or multilocular cystic mass **(Fig. 22.32)**. It is difficult to make a differential diagnosis with other intra-abdominal cystic conditions such as choledocal, ovarian and hepatic cysts. The prognosis is usually good and no surgical treatment is required in cysts of small size.

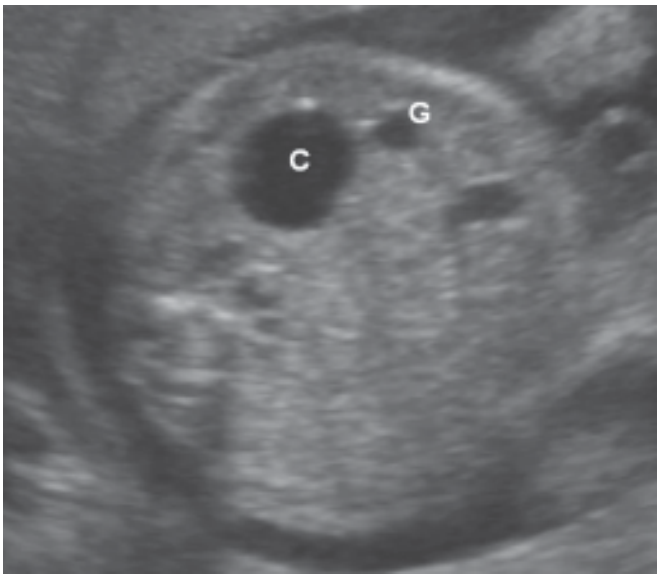

Figure 22.31: Choledocal cyst (C = cyst; G = gallbladder)

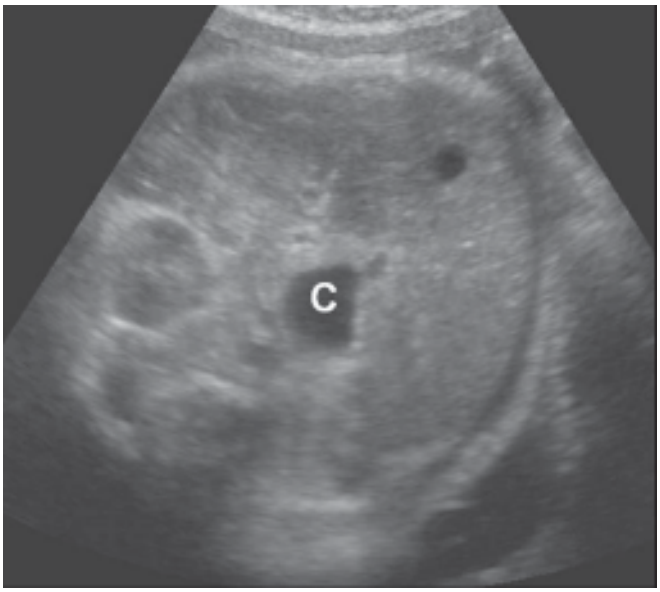

Figure 22.32: Mesenteric cyst (C)

Hepatic Masses

Hepatic masses might origin from an obstruction of the hepatic biliary system or might have a tumoral origin (hemangioma, hamartoma, etc.).

Their sonographic appearance changes depending on the origin: cysts are usually isolated and anechoic with regular borders; mesenchymal hamartoma usually appears as irregular hyperechoic areas[31] **(Fig. 22.33)**, while hemangioma appears hypoechoic, hyperechoic or mixed depending on the degree of fibrosis and stage of involution. Hepatoblastomas and adenomas have a solid appearance. Polyhydramnios may be associated; many cases of reduction in volume or even disappearance *in utero* have been described.

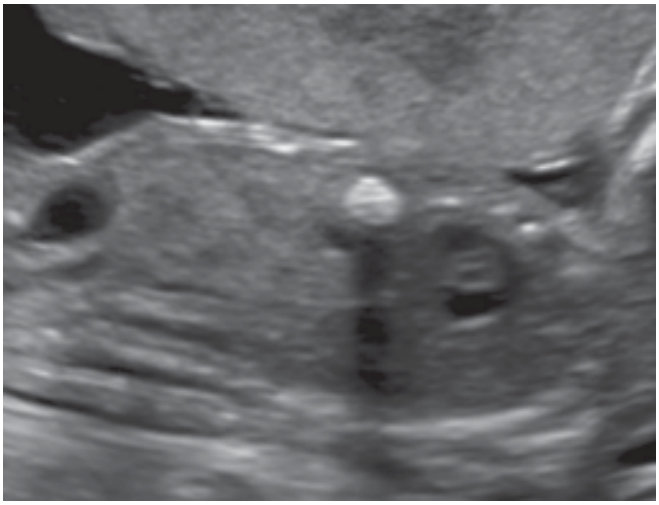

Figure 22.33: Hepatic hamartoma appearing as an isolated intrahepatic echogenic area

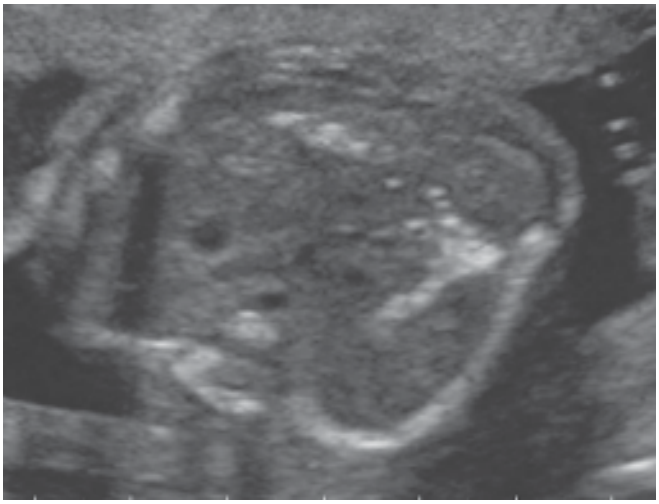

Figure 22.34: Multiple hepatic calcifications

Multiple intrahepatic calcifications **(Fig. 22.34)** may be due to congenital infection (CMV, Parvovirus B19, Herpes, Rubella, Toxoplasmosis, Varicella) or vascular accidents, such as thrombosis or ischemic disorders.

The management is expectant in terms of monitoring the size and evolution of the lesions.

REFERENCES

1. Anderson N, Boswell O, Duff G. Prenatal sonography for the detection of fetal anomalies: results of a prospective study and comparison with prior series. AJR Am J Roentgenol. 1995;165(4):943-50.

2. Bernaschek G, Stuempflen I, Deutinger J. The value of sonographic diagnosis of fetal malformations: different results between indication-based and screening-based investigations. Prenat Diagn. 1994;14(9):807-12.
3. Grandjean H, Larroque D, Levi S. The performance of routine ultrasonographic screening of pregnancies in the Eurofetus Study. Am J Obstet Gynecol. 1999;181(2):446-54.
4. Luck CA Value of routine ultrasound scanning at 19 weeks: a four year study of 8849 deliveries. BMJ. 1992;304(6840): 1474-8.
5. Queisser-Luft A, Stopfkuchen H, Stolz G, et al. Prenatal diagnosis of major malformations: quality control of routine ultrasound examinations based on a five-year study of 20,248 newborn fetuses and infants. Prenat Diagn. 1998;18(6):567-76.
6. Martin RW. Screening for fetal abdominal wall defects. Obstet Gynecol Clin North Am. 1998;25(3):517-26.
7. Kurkchubasche AG. The fetus with an abdominal wall defect. Med Health RI. 2000;84(5):159-61.
8. Oguniemy D. Gastroschisis complicated by midgut atresia, absorption of bowel and closure of the abdominal wall defect. Fetal Diagn Ther. 2001;16(4):227-30.
9. Brantberg A, Blaas HG, Salvesen KA, et al. Surveillance and outcome of fetuses with gastroschisis. Ultrasound Obstet Gynecol. 2004;23(1):4-13.
10. Brantberg A, Blaas HG, Haugen SE, et al. Characteristics and outcome of 90 cases of fetal omphalocele. Ultrasound Obstet Gynecol. 2005;25:427-37.
11. Blazer S, Zimmer EZ, Gover A, et al. Fetal omphalocele detected early in pregnancy: associated anomalies and outcomes. Radiology. 2004;232(1):191-5.
12. Lakasing L, Cicero S, Davenport M, et al. Current outcome of antenatally diagnosed exomphalos: an 11 years review. J Pediatr Surg. 2006; 41(8):1403-6.
13. Cadkin A, Strom C. Prenatal diagnosis of body stalk anomaly in the first trimester of pregnancy. Ultrasound Obstet Gynecol. 1997;10(6):419-21.
14. Metkus AP, Filly RA, Stringer MD, et al. Sonographic predictors of survival in fetal diaphragmatic hernia. J Pediatr Surg. 1996;31:148-51.
15. Geary MP, Chitty LS, Morrison JJ, et al. Perinatal outcome and prognostic factors in prenatally diagnosed congenital diphragmatic hernia. Ultrasound Obstet Gynecol. 1998;12(2):107-11.
16. Heling KS, Wauer RR, Hammer H, et al. Reliability of the lung-to-head ratio in predicting outcome and neonatal ventilation parameters in fetuses with congenital diaphragmatic hernia. Ultrasound Obstet Gynecol. 2005;25(2):112-8.
17. Harrison MR, Keller RL, Hawgood SB, et al. A randomized trial of fetal endoscopic tracheal occlusion for severe fetal congenital diaphragmatic hernia. N Engl J Med. 2003;349(20):1916-24.
18. Deprest J, Jani J, Gratacos E, et al. FETO Task Group. Fetal intervention for congenital diaphragmatic hernia: the European experience. Semin Perinatol. 2005;29(2):94-103.
19. Shulman A, Mazkereth R, Zalel Y, et al. Prenatal identification of esophageal atresia: the role of ultrasonography for evaluation of functional anatomy. Prenat Diagn. 2002;22(8):669-74.
20. Lawrence MJ, Ford WD, Furness ME, et al. Congenital duodenal obstruction: early antenatal ultrasound diagnosis. Pediatr Surg Int. 2000;16(5-6):342-5.
21. Shawis R, Antao B. Prenatal bowel dilatation and the subsequent postnatal management. Early Hum Dev. 2006;82(5):297-303.
22. Haeusler MC, Berghold A, Stoll C, et al. EUROSCAN Study Group. Prenatal ultrasonographic detection of gastrointestinal obstruction: results from 18 European congenital anomaly registries. Prenat Diagn. 2002;22(7):616-23.
23. Has R, Gunay S. 'Whirlpool' sign in the prenatal diagnosis of intestinal volvulus. Ultrasound Obstet Gynecol. 2002;20(3):307-8.
24. Chaubal N, Dighe M, Shah M, et al. Calcified meconium: an important sign in the prenatal sonographic diagnosis of cloacal malformation. J Ultrasound Med. 2003;22(7):727-30.
25. Chan KL, Tang MH, Tse HY, et al. Meconium peritonitis: prenatal diagnosis, postnatal management and outcome. Prenat Diagn. 2005;25(8):676-82.
26. Al-Kouatly HB, Chasen ST, Streltzoff J, et al. The clinical significance of fetal echogenic bowel. Am J Obstet Gynecol. 2001;185(5):1035-8.
27. Berlin BM, Norton ME, Sugarman EA, et al. Cystic fibrosis and chromosome abnormalities associated with echogenic fetal bowel. Obstet Gynecol. 1999;94(1):135-8.
28. Slotnik RN, Abuhamad AZ. Study of fetal echogenic bowel (FEB) and its implications. J Ultrasound Med. 1999;18(1):88.
29. Chen CP, Cheng SJ, Chang TY. Prenatal diagnosis of choledochal cyst using ultrasound and magnetic resonance imaging. Ultrasound Obstet Gynecol. 2004;23(1):93-4.
30. Macken MB, Wright JR, Lau H, et al. Prenatal sonographic detection of congenital hepatic cyst in third trimester after normal second-trimester sonographic examination. J Clin Ultrasound. 2000;28(6):307-10.
31. Laberge JM, Patenaude Y, Desilets V, et al. Large hepatic mesenchymal hamartoma leading to mid-trimester fetal demise. Fetal Diagn Ther. 2005;20(2):141-5.

CHAPTER 23

Diagnostic Sonography of Fetal Urinary Tract Anomalies

Zoltán Tóth, András Tankó, Zoltán Papp

INTRODUCTION

Over the course of embryogenesis, fetal kidneys and the urinary tract develop from intermediate mesoderm. Following the formation of the pronephros, the mesonephric (or Wolffian) duct gives rise to the ureteric bud, which grows into the tissue of the metanephros, induced by the transiently developing and then progrediating mesonephros. After 15 division-generations, it give rise to the ureter, the renal pelvis, the minor and major calyces, and the collecting ducts. Until 15 weeks of gestation, the formation of the collecting ducts takes place at fast pace and thereafter it is somewhat slower. By 20 weeks, however, nearly all ducts are present. The collecting ducts induce the arising of nephrons, juxtamedullar glomeruli and the definitive kidney from the metanephric blastema. Development of nephrons is intensive during the first 15 weeks, but at that time merely one-third of nephrons have developed, whereas the final nephron number is reached by 32 week. The kinetics of nephrogenesis is also marked by the changing amount of amniotic fluid. Agenesis of the pronephros, the mesonephric duct or the ureteric bud as well as disorders of the interactions between the ureteric bud, and the metanephric blastema lead to a totally or partially absent permanent kidney.[1,2]

The urorectal septum divides the cloaca into two sinuses: (1) the urogenital and (2) the anorectal sinus. The distal segment of the mesonephric duct forms part of the wall of the urogenital sinus called the trigone. The upper, wider part of the urogenital sinus gives rise to the urinary bladder; the middle segment forms the prostatic and membranous urethra, and the lower part forms the definitive urogenital sinus (phallic portion). The hydrostatic pressure of the urine produced, can result in opening of the membrane between the ureter and the urinary bladder at 9th week and if this step does not take place, ureterovesical obstruction or ureterocele develops. At 9th week, the membrane of the urogenital sinus is absorbed and from then onward, urine is excreted into the amniotic space. Problem with this step is that it can lead to obstruction of valve of the urethra.[3]

Over the course of embryogenesis, transient pronephros does not produce any urine; the mesonephros, however, more or less can produce it; the permanent kidneys are developed from the metanephros, which produces real urine. Following the conjoining of the ureter and the bladder, urinary bladder filling begins at 9th week. With the development of the urethral orifice at 10th week, urine is excreted into the amniotic fluid, thus from that time onward, the amount and composition of the amniotic fluid is also determined by the urine produced by the active kidney. Oligohydramnios due to abnormal functioning of kidneys and absence of urine excretion can be visualized from 15th week of gestation. Elimination of fetal waste products and maintenance of fetal electrolyte balance are primarily carried out by the placenta. After birth, maintaining homeostasis becomes a role of the kidneys, and 15% of glomerular filtration rate at birth is doubled in the first two weeks of life and reaches the adult rate at 1–2 years of age. This process starts from a smaller value in case of premature babies.[4,5]

During ultrasound imaging, anomalies of the fetal kidney and urinary tract can be recognized based on the differences in comparison to the normal images. The importance of recognizing these anomalies is that some of these anomalies are severe and incompatible with life, in these cases continuing pregnancy may be pointless, while other anomalies can be asymptomatic in 80% of newborns, thus absence of prenatal recognition makes early and successful treatment, aimed at saving the kidney, impossible.

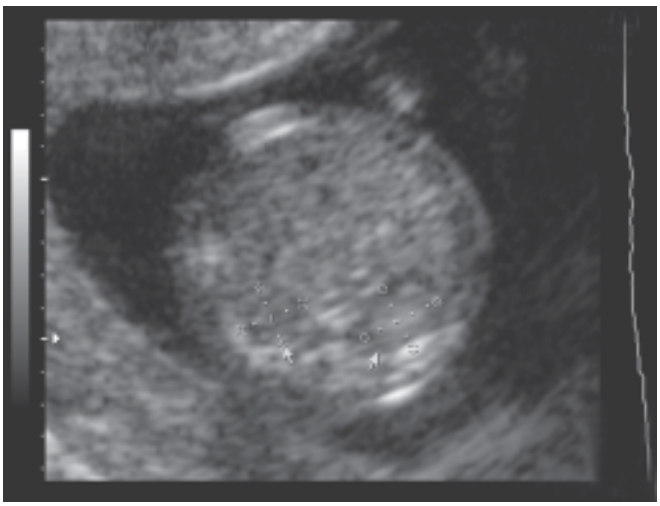

Figure 23.1: Transvaginal sonographic view of fetal kidneys at gestational week 11

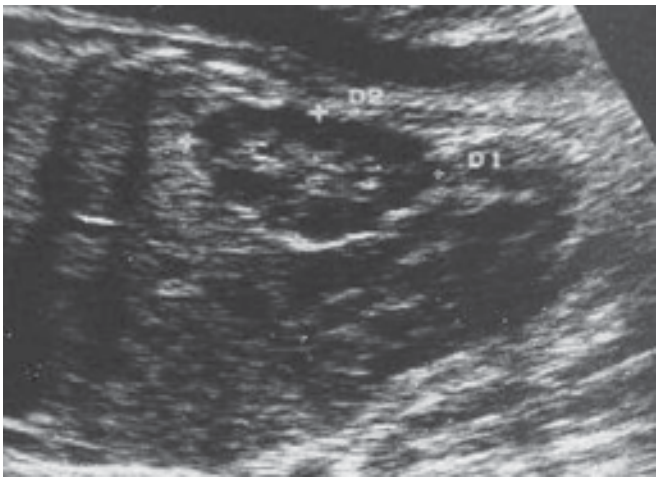

Figure 23.3: The perirenal capsule of the fetal kidney is more echogenic, the medulla is less echogenic, the central echo complex is more echogenic

ULTRASOUND IMAGING OF NORMAL FETAL KIDNEYS AND URINARY TRACT

Fetal kidneys can be recognized sonographically using a transvaginal probe from gestational period of 11 weeks **(Fig. 23.1)** and transabdominally from 12th week onward **(Fig. 23.2)**, aided by their characteristic shape, and echogenic appearance of medullary pyramids and the renal cortex. In the parasagittal plane, kidneys appear next to the lumbar spinal column as elliptic, whereas in the horizontal plane as oval paraspinal organs. The central echogenic pyelon-calyx complex, composed of fat, connective tissue and hilar blood vessels, is surrounded by less echogenic parenchyma and around that there is the echogenic perirenal capsule **(Fig. 23.3)**. There is less than 5 mm of fluid in the pyelon, later the less echogenic medullar and the more echogenic cortical structure can also be differentiated **(Fig. 23.4)**. The size (length, width and depth) of the kidneys keeps on growing constantly during pregnancy. Their circumference, i.e. the renal circumference/abdominal circumference ratio is constant during pregnancy with a value between 0.27 and 0.30. The normal length of a fetal kidney is equal to the height of four to five vertebrae and the renal volume can also be determined using 3D ultrasound technique **(Fig. 23.5)**.

Adrenal glands initially appear as suprarenal hyperechogenic organs and after 30 weeks of gestation,

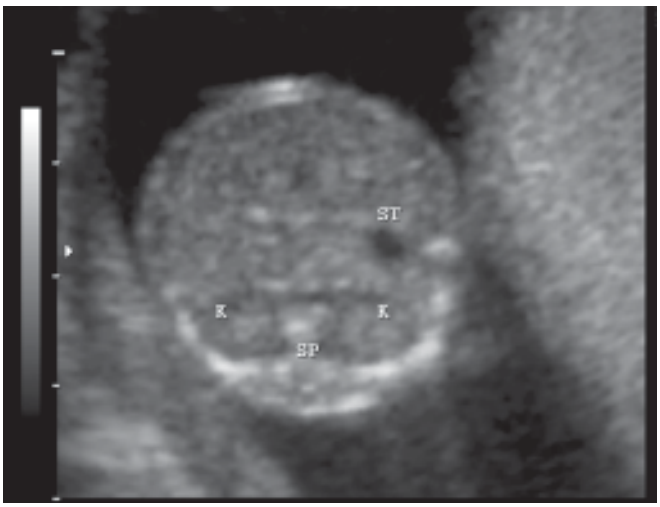

Figure 23.2: Transabdominal sonographic view of fetal kidneys at gestational week 14

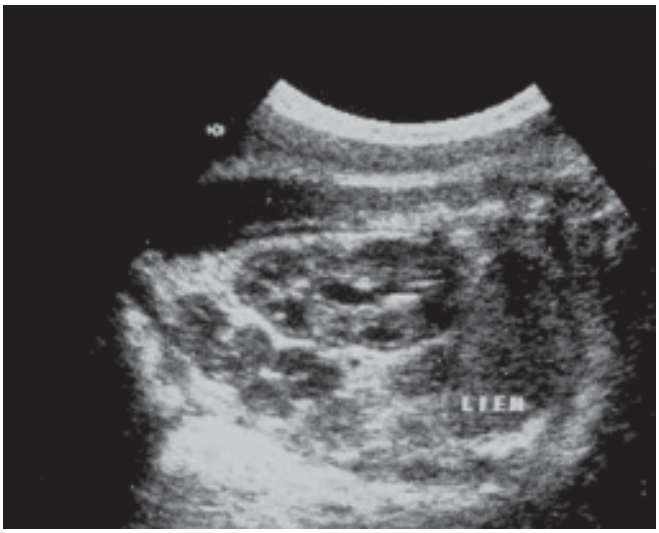

Figure 23.4: Less than 5 mm fluid in the pyelon

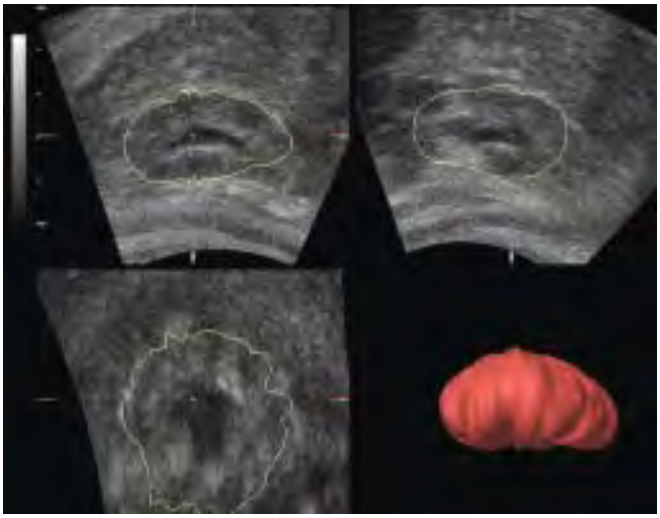

Figure 23.5: Imaging the renal volume using 3D technique

they can be imaged as less echogenic discoid-shaped organs of a size equaling one-third to that of the kidneys **(Figs 23.6A and B)**. Normally developing ureters cannot be imaged by using ultrasound.

The fetal urinary bladder appears as a sonolucent spherical organ between the ischiac and iliac ossification centers in the lesser pelvis. Its size changes constantly over 20–30 minute intervals due to urination **(Figs 23.7 and 23.8)**. On both the sides of the bladder, the intra-abdominal segments of the umbilical arteries can be easily demonstrated using the color-Doppler technique **(Fig. 23.9)**.

Anomalies of the renal kidneys and urinary tract can be diagnosed prenatally by detecting the abnormal amount of amniotic fluid (oligohydramnios, polyhydramnios) and fetal urine, analysis of their components, the absence of the regular filling and emptying of the urinary bladder, the uni- or bilateral dilation of the urinary tract (urethra, urinary bladder, ureters, pyelons, calyces), and the alteration of the size and structure of the kidneys (hyperechogenic, cystic).[6-18]

RENAL AGENESIS

This bilateral abnormality appears almost exclusively in males, with incidence of 1/4000–10000. It is incompatible with life. It's an autosomal dominant form, has incomplete penetrance with unilateral agenesis and hypoplasia, but it can also be autosomal recessive or of multifactorial origin. As a consequence of the resulting oligohydramnios, facial and limb deformities, pulmonary hypoplasia and retardation appear, known as Potter syndrome and deformities resulting from

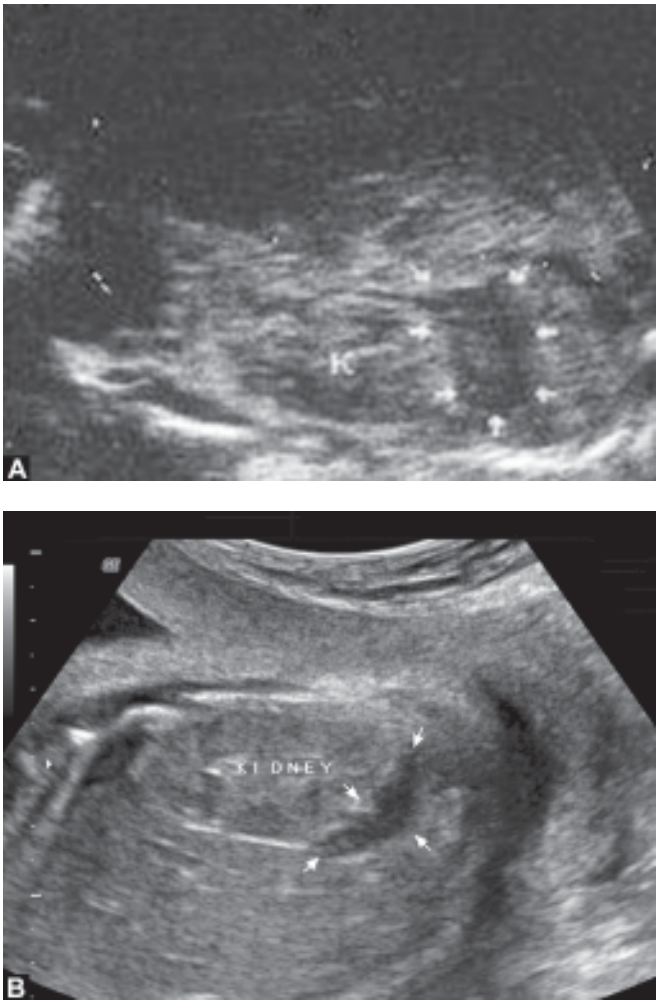

Figures 23.6A and B: The fetal adrenal gland is less echogenic

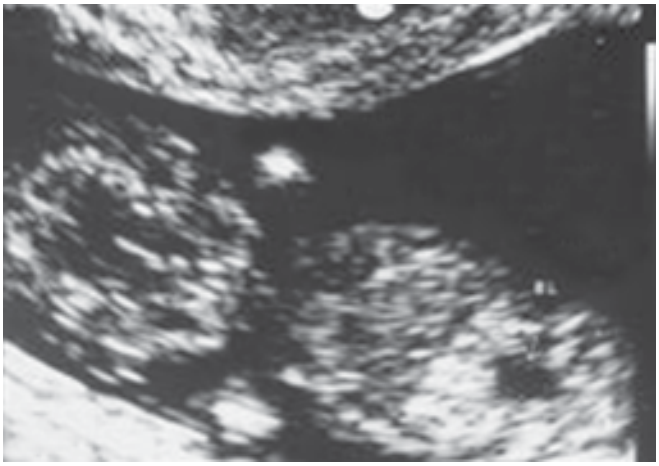

Figure 23.7: The unechogenic region of the bladder in the pelvis minor

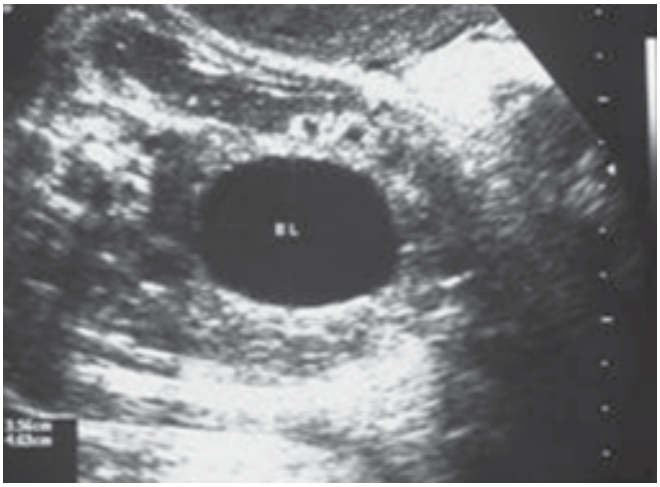

Figure 23.8: The full bladder appears as a round unechogenic organ

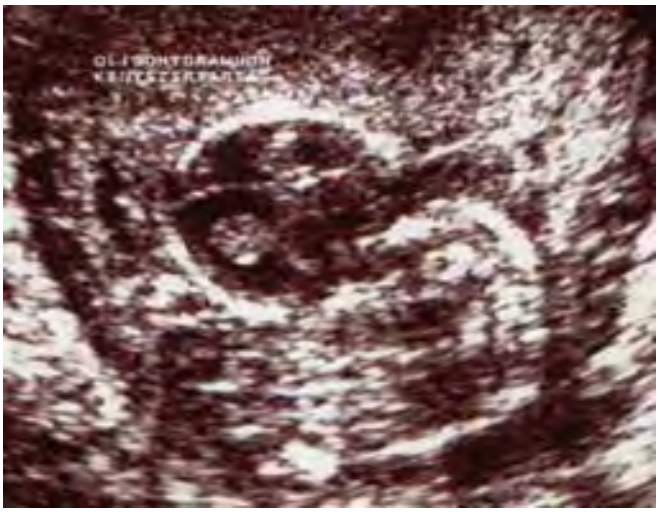

Figure 23.10: Forced position of the fetus due to renal agenesia

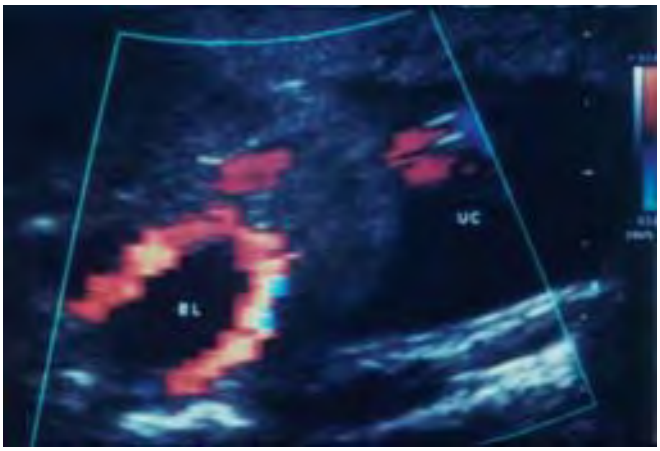

Figure 23.9: The umbilical arteries can be detected next to the wall of the bladder

oligohydramnios of any origin are called Potter sequence or oligohydramnios deformation sequence. In case of bilateral agenesis, ultrasonography reveals severe oligohydramnios, arthrogryposis **(Fig. 23.10)**, growth restriction, the absence of kidneys and absent bladder filling, whereas color-Doppler fails to detect the renal arteries **(Figs 23.11 and 23.12)**. The accompanying central nervous system, cardiovascular, musculoskeletal and gastrointestinal malformations can hardly be imaged due to decreased amount of amniotic fluid under this condition. Adrenal glands that are one-third in size as compared to the size of kidneys, can be misleading, especially in case of unilateral form of renal agenesis that is 4–20 times more common, and is characterized by a urinary bladder of normal volume and a normal amount of amniotic fluid.[6-9,12-16,19]

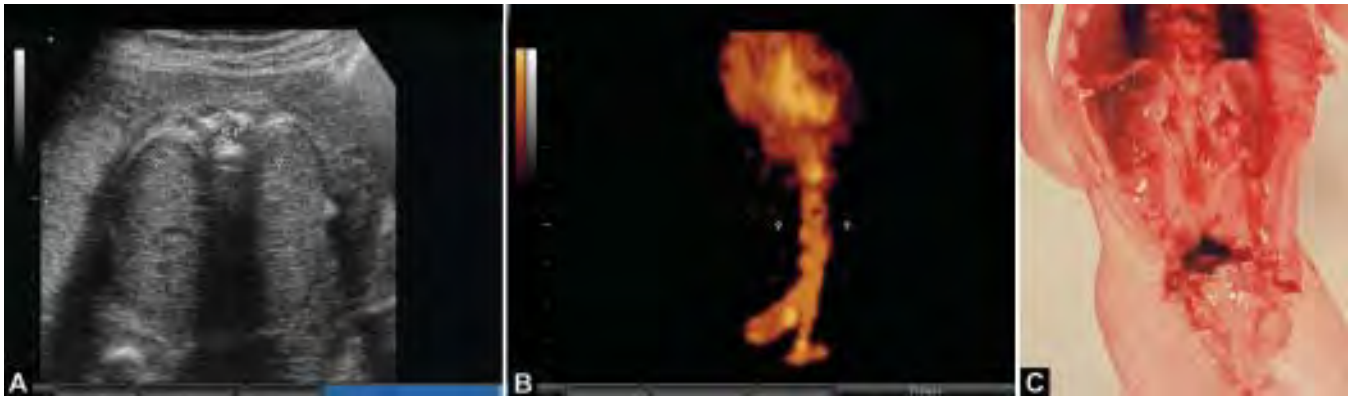

Figures 23.11A to C: Bilateral renal agenesia: (A) No kidneys; (B and C) No renal arteries

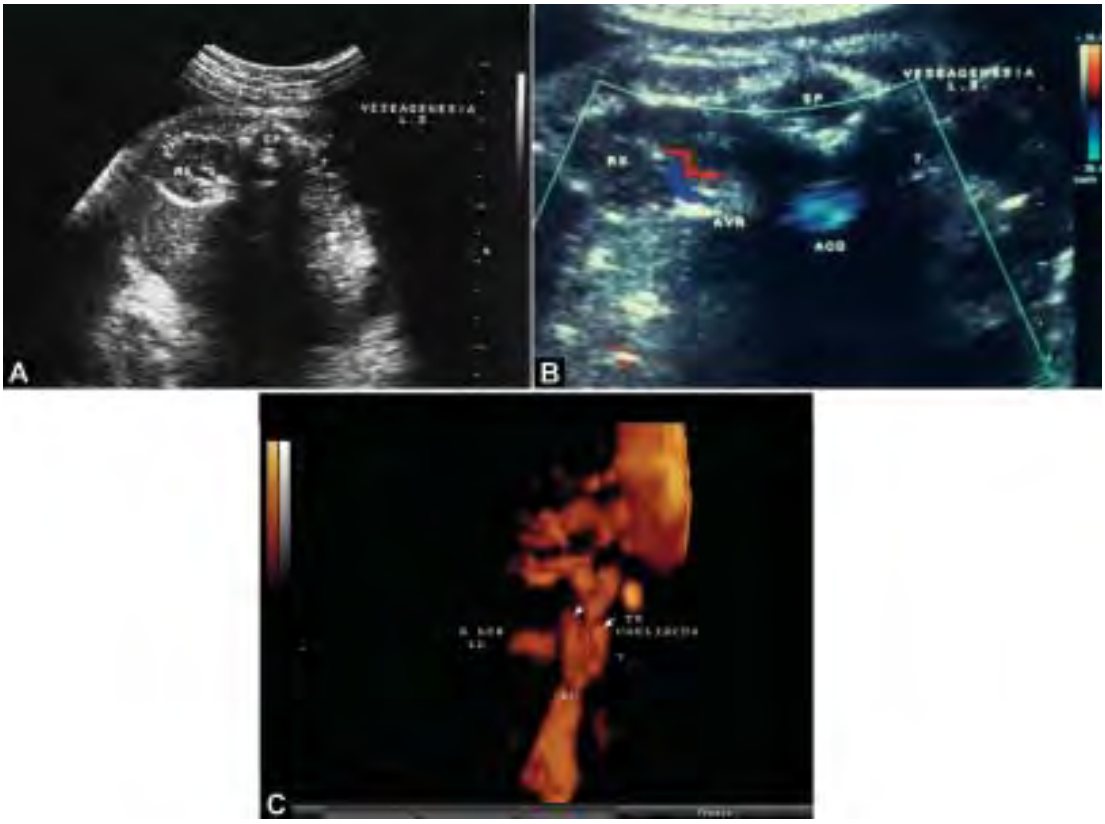

Figures 23.12A to C: (A) Unilateral renal agenesia: only one normal kidney and (B and C) One renal artery

CYSTIC RENAL DYSPLASIA

Cystic renal dysplasia refers to a group of congenital renal parenchymal malformations of different origins. Their etiology, manifestation and clinical course cover a wide range.

Autosomal Recessive (Infantile) Polycystic Renal Dysplasia

The incidence of the disease is 1/40,000, the recurrence risk is 25%, the localization of the gene responsible for the disease is as yet unknown. The development of ureters, pyelons, calyces and papillas are regular, the number of nephrons is normal, but in the medulla collecting ducts form 1–2 mm small cysts, which cause the kidneys to be enlarged and lobular **(Figs 23.13A to D)**. The affected kidneys do not produce urine, thus the bilateral disease results in oligohydramnios and anuria. The liver is also cystically degenerated, which is accompanied by periportal and intralobular fibrosis, bile duct proliferation (biliary dysgenesis), and polycystic pulmonary malformation also appear. Based on the different degree of involvement of the kidneys and the liver, and based on the course of the disease, fetal, neonatal, infantile and juvenile types are differentiated. The fetal and neonatal forms lead to death after birth due to the absence of renal function.

The small (1–2 mm) cysts cannot be detected separately during sonography. At the beginning, kidneys appear moderately enlarged and later they get significantly enlarged. As a result of reverberation of echos, the medullary segment appears hyperechogenic and the central echo complex cannot be differentiated. Later as the pregnancy progresses, the cortex appears less echogenic. As urine production is missing, urinary bladder filling can not be detected, the oligohydramnios forces the fetus in an arthrogrypotic position. Calculating the renal/abdominal circumference ratio can help to detect the enlargement of the kidneys at an early stage. Depending on the extent of the abnormality of the kidney, the characteristic ultrasonographic image might be recognized only in the second trimester. The prenatally diagnosed autosomal recessive polycystic kidney disease is incompatible with life and thus the pregnancy can be terminated upon the request of the parents.[6-9,12-15,20]

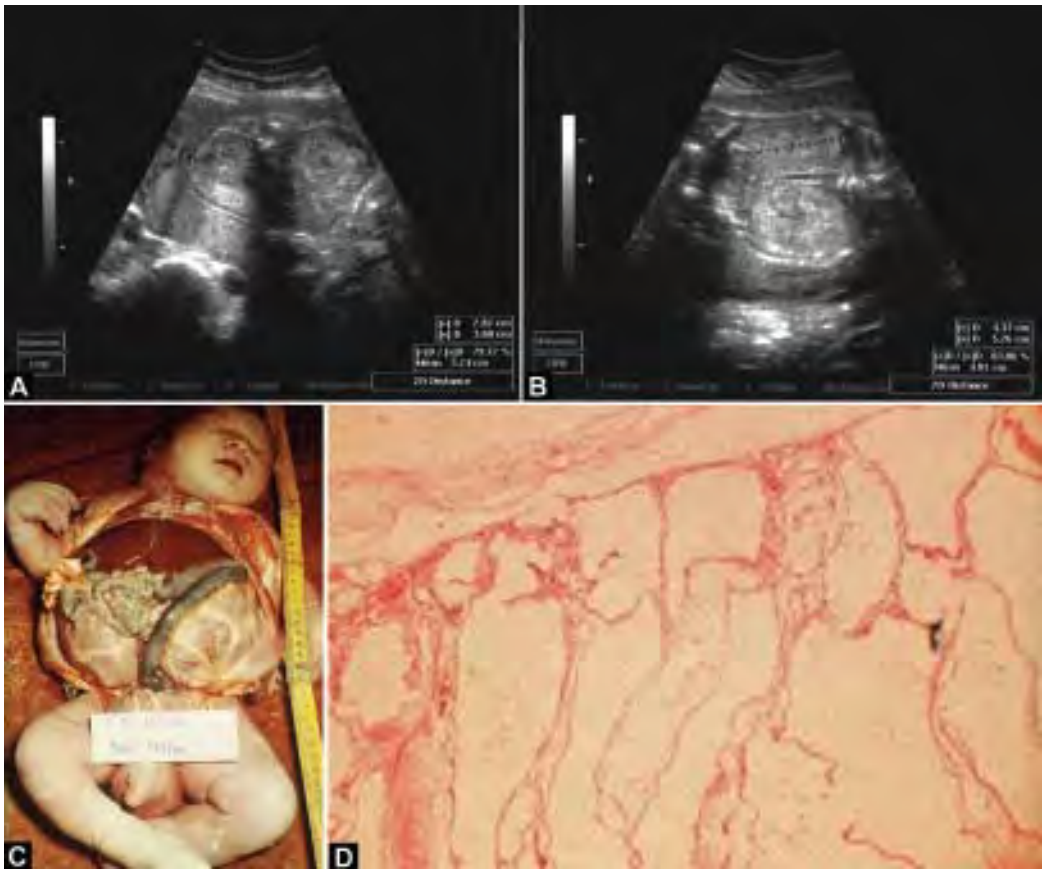

Figures 23.13A to D: (A and B) Infantile polycystic renal dysplasia, enlarged kidneys in horizontal and longitudinal planes; (C) At autopsy typically enlarged, lobular kidneys are seen; (D) The histologic section shows small cysts only

Autosomal Dominant (Adult) Polycystic Renal Dysplasia

The incidence of the disease is 1/15,000. Its recurrence is 50% and the gene responsible for the disease is localized on the short arm of chromosome 16. The expressivity of the disease is variable, it manifests in fetuses, infants or young children, but occasionally it causes no symptoms until around 40 years of age, when hypertensive disease, hematuria and constantly deteriorating renal function reveal it. Some nephrons and loops of Henle turn into cysts with thin walls, collecting ducts form thick-walled cysts, but normally functioning tubules and nephrons are also present, therefore renal dysfunction is less severe. Cysts can also be present in the liver, pancreas and lungs, but hepatic fibrosis and dysfunction are not common. The bilateral manifestation of the disease does not lead to the inability to produce urine, thus urinary bladder filling is present and it does not result in an oligohydramnios.

In case of adult polycystic renal dysplasia manifesting in fetal life, ultrasonography reveals hyperechogenic, more or less enlarged kidneys. Macrocysts can be seen only in severe cases, but the central echo complex can be recognized **(Figs 23.14A to C)**. As urine is produced, urinary bladder filling is present and oligohydramnios complicates some severe cases only. Following the sonographic imaging of the fetus, it is also necessary to examine the kidneys of the parents as well, with respect to the hereditary nature of the disease. In uncertain situations, molecular genetic analysis of the family members may be helpful in differentiating between the autosomal recessive and autosomal dominant forms of the disease.[6-9,12-15,20,21]

Multicystic Renal Dysplasia

The incidence of the disease is 1/10,000, it is more common in males and its etiology is unclear. Activity of the ampullae at the end of the collecting tubules are

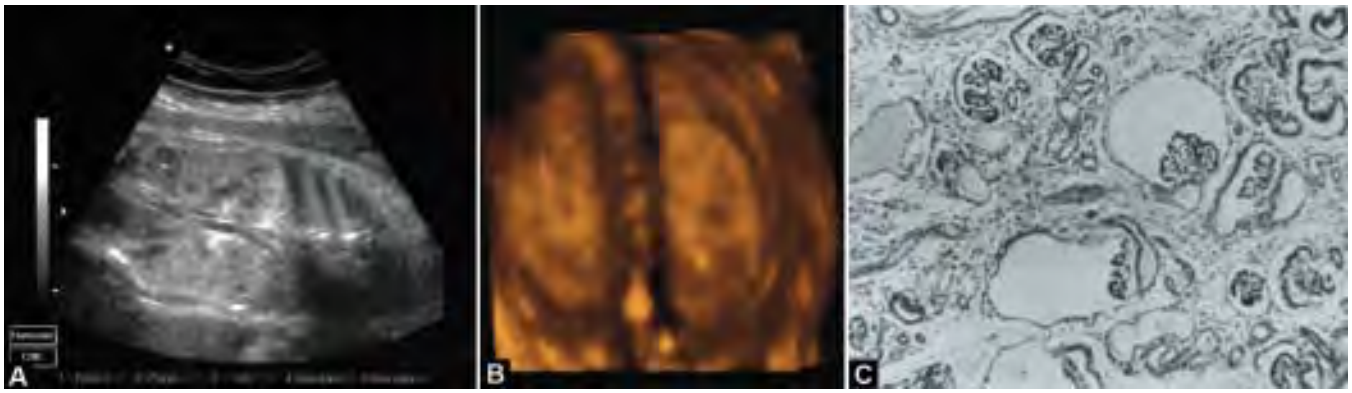

Figures 23.14A to C: (A and B) Enlarged adult polycystic kidneys with central echo complex; (C) Histology: small cysts between glomeruli

inhibited, branching of the collecting tubules decreases and the induction of nephrons is reduced. Collecting tubules form cysts with thick-walls, nephrons turn into thin-walled cysts and in between of which lie loose connective tissues. The kidneys become enlarged, normal renal parenchyma and urine production are missing. In two-third of the cases, abnormality is unilateral, in one-third it is bilateral and rarely it is segmental. Unilateral multicystic renal dysplasia is often accompanied by other urogenital or chromosomal aberrations. Bilateral multicystic renal dysplasia is not accompanied by the cystic dysplasia of other organs. It causes Potter sequence and is incompatible with life. In its isolated form, it cannot be inherited, but as part of a syndrome, such as Meckel-Gruber syndrome or Zellweger syndrome, it can show autosomal recessive inheritance.

Ultrasonographic imaging reveals cysts of diverse sizes in the expected position of the kidneys, but renal parenchyma or central echo complex cannot be identified **(Figs 23.15A to E).** If the disease is unilateral, urinary bladder filling cannot be detected and oligohydramnios is present. In unilaterally-manifesting cases, normal bladder filling and amniotic fluid amount can be seen. Sometimes, even the compensatory hypertrophy of the contralateral kidney and a resulting moderate polyhydramnios can be detected. It is important to differentiate it from dilated and tortuous ureters caused by ureterovesical obstruction, and dilated calyces seen in mild hydronephrosis.[6-9,12-15,20-24]

Obstructive Cystic Renal Dysplasia

Obstruction of the urinary tract at any level (ureteropelvical, ureterovesical or urethral) will cause cystic dysplasia due to increased intraluminar pressure. Morphology of obstruction depends on the place and time of obstruction during nephrogenesis.

Early obstruction causes cystic dysplasia at the end of the primitive mesonephric duct and the ampullae of the collecting tubules leading to multicystic kidney disease.

Increased pressure, beginning later in development will be transferred to the collecting tubules and causes parenchymal disorganization, cystic dilation of the capsule of Bowman, forming of subcapsular cysts[25] and fibrosis at the other end of the collecting ducts.

Starting even later, increased pressure will lead to the degeneration of the parenchyma and as a result, a hydronephrotic kidney appears.

Early obstruction at the upper segment of the ureter results in the appearance of a multicystic kidney. Obstruction at lower parts of the ureter during the second trimester, as well as obstruction at the level of the urethra, can later result in an increased urinary tract pressure, causing formation of subcapsular cysts and hydronephrosis. Early deviation of urine decreases the intraluminal pressure and thus cystic dysplasia can be prevented.

Ultrasound imaging after 20 weeks of gestation shows the dilatation of the pyelon and calyces of the affected kidney, the increased echogenicity due to the small subcapsular cysts, and later the growing subcapsular cysts **(Fig. 23.16)**.[6-9,12-15,20]

OBSTRUCTIVE UROPATHY

Strictures and blockages at different levels of the urinary tract cause urinary retention and increased intraluminal pressure, and thus can lead to different degrees of dilatation not only in the renal parenchyma, but also in the urinary tract. Depending on the place and duration of the blockage, the upper segment of the urethra, the bladder, the ureter, the pyelon and the calyces can be dilated **(Figs 23.17A to D)**. The final result can be

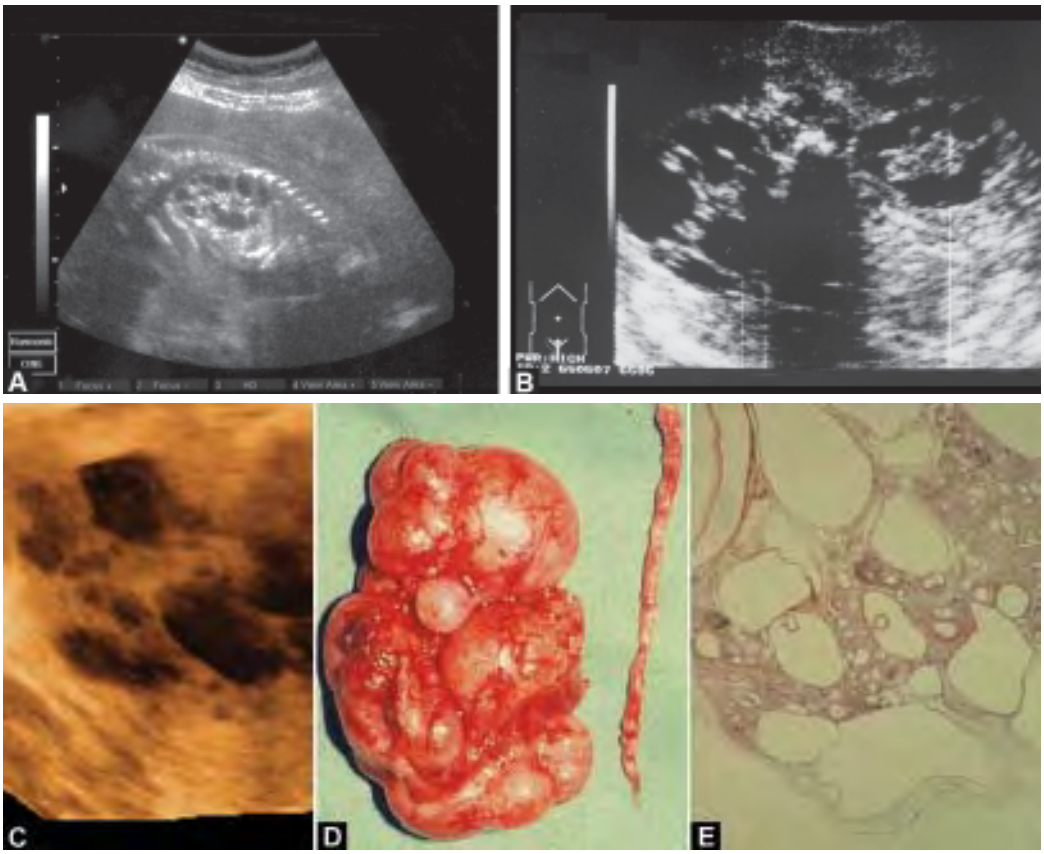

Figures 23.15A to E: Multicystic renal dysplasia: there are 10–20 mm cysts in the kidneys, no central echo complex is present. (A) Unilateral; (B and C) Bilateral; (D) The kidney is made up of various size cysts; (E) Histology: cysts with thin and thick walls

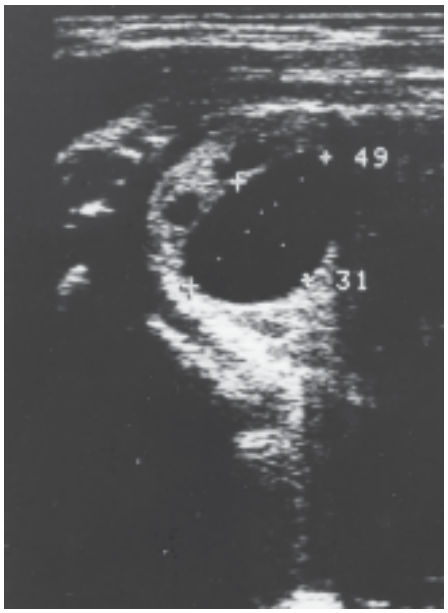

Figure 23.16: Subcapsular cyst in a hydronephrotic kidney

hydronephrosis with the degeneration of renal parenchyma. There are five different degrees of anteroposterior dilation of the renal pelvis and dilation above 10 mm or exceeding 50% of the anteroposterior size of the kidney is considered hydronephrosis.[6,7,13,14,17,26-34]

Obstruction of the Ureteropelvic Junction

Urine passage can be blocked by the abnormal shape of the pyeloureteral junction, adhesion of the lumen, folding of the mucosa, ureteral valve or absence of longitudinal muscle fibers, leading to hydronephrosis. It is twice as common in males as in females, it is sporadic and inheritance is uncommon. In 70% of the cases, it is unilateral with a left side predominance, but in these cases the abnormality of the other kidney (renal agenesis, multicystic dysplasia or ectopic kidney) can also be detected. In the bilateral manifestation (30% of cases), the extent of renal damage on the two sides is different. It is rare and is accompanied by abnormalities of other organs. In 80% cases, it will not produce any

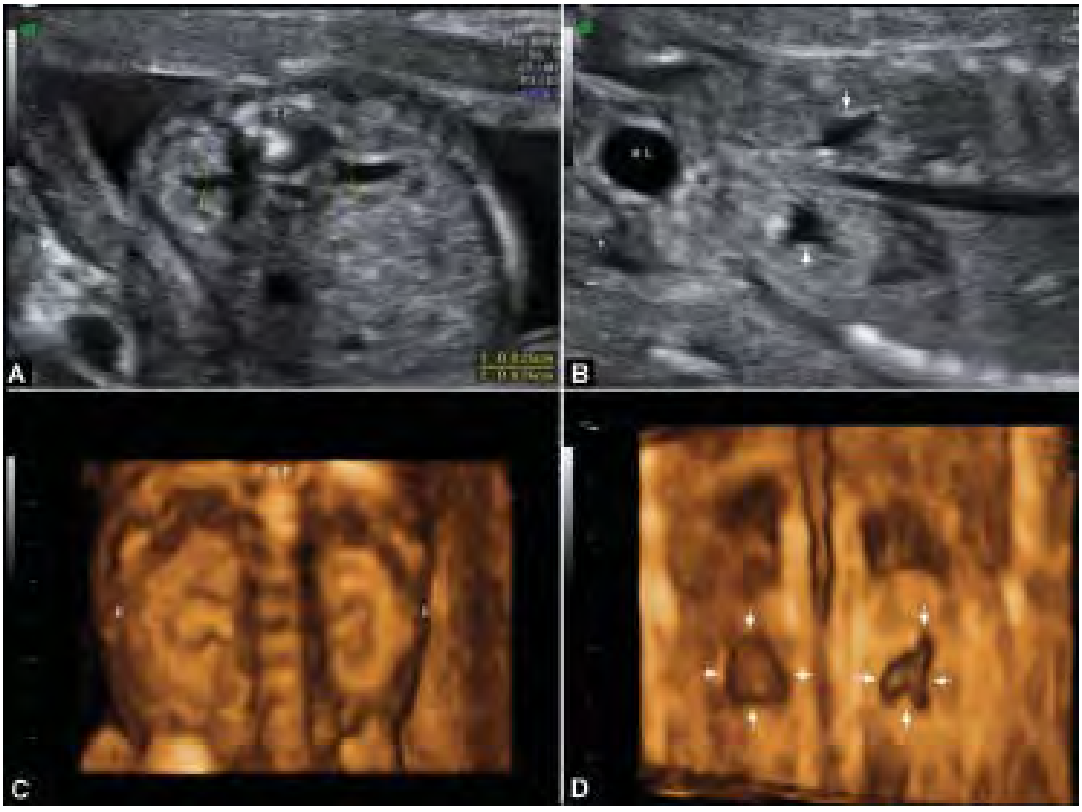

Figures 23.17A to D: The pyelon and calyces are dilated

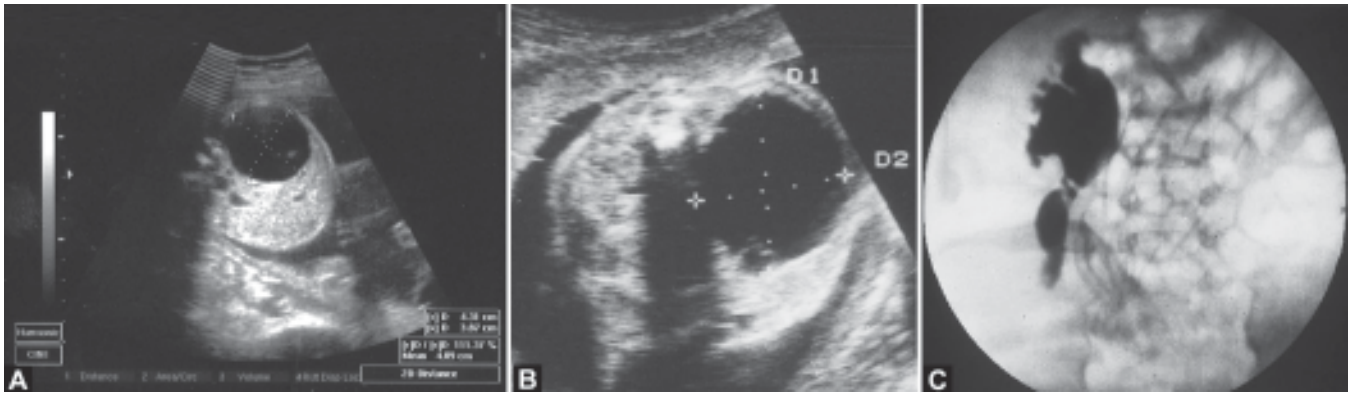

Figures 23.18A to C: (A and B) Extremely dilated hydronephrotic kidney and (C) Its X-ray image

symptoms after delivery. About 10% cases will regress spontaneously and in 90% of cases conservative or surgical treatment becomes necessary.

Ultrasonography shows a certain degree of pyelectasia in the affected kidney **(Figs 23.18A to C)** and at the ureteropelvic junction the renal cortex becomes thinner. Below the block, ureters are not dilated and thus are invisible. If the disease is unilateral, bladder filling is present and the amount of the amniotic fluid is normal, but when an incomplete manifestation is encountered, polyhydramnios can also be found. If the kidney is severely damaged or the contralateral kidney does not function either, bladder filling is missing and the amount of the amniotic fluid is minimal.[6,7,14]

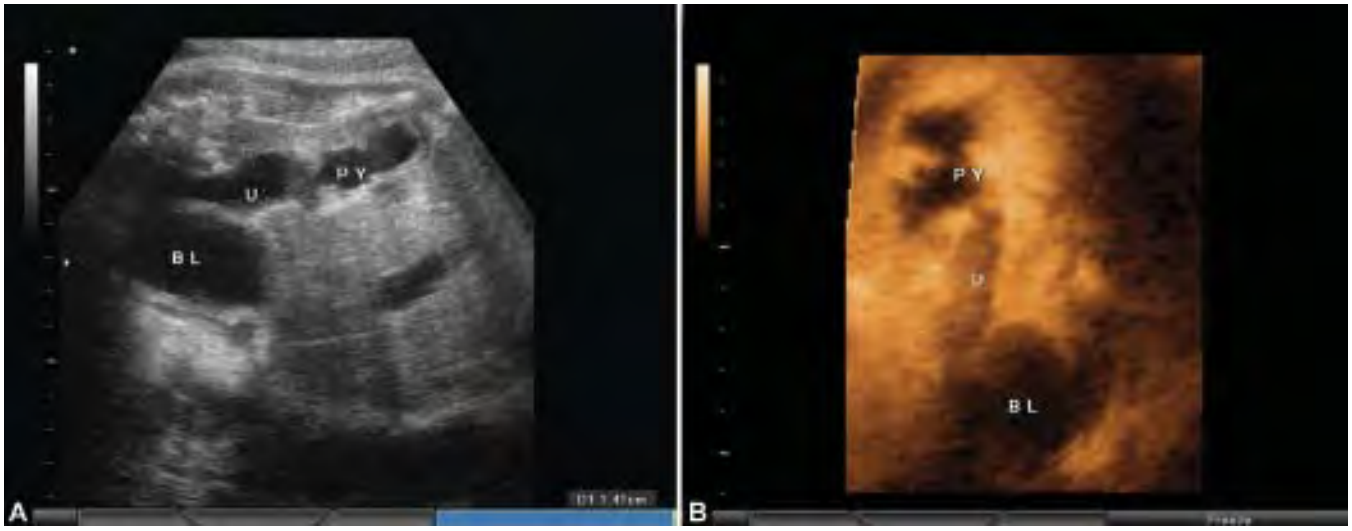

Figures 23.19A and B: (A) Behind the bladder (BL), dilated ureter (U) and dilated pyelon (PY) in a 2D and (B) 3D image

Stricture or Valve of the Ureter

A circular or semicircular mucosal fold or valve containing muscle bands can appear at any level of the ureter and may lead to blockage of urine flow.

Sonography shows the segment of the ureter above the valve as being dilated and having active peristalsis, whereas the segment below the blockage cannot be visualized.

Obstruction of the Ureterovesical Junction: Megaureter

Pathologic dilation of the ureter is four times more common in males, two to three times more frequent on the left side and in 20% of the cases it can be bilateral. It is sporadic, but inherited forms have also been reported. Stenosis, fibrosis, abnormal muscular layer, segmental absence of peristalsis or absence of the antireflux mechanism at the ureterovesical junction lead to primary megaureter, and consecutive hydronephrosis. Blockage at a lower segment of the urinary bladder and consecutive reflux leads to secondary megaureter. Megaureter can be accompanied by renal agenesis, incomplete or complete duplication, contralateral cystic renal dysplasia or Hirschsprung's disease.

Ultrasonography reveals pyelectasis, and a dilated (sometimes even 1–2 cm wide), sonolucent, peristaltic and tortuous ureter that can be followed down to the bladder **(Figs 23.19A and B)**. Double renal pelvis and dilation of the upper part can indicate ureter duplex with the dilation of only one of the two ureters.[6,7,13,14,35,36]

Vesicoureteral Reflux

The ureterovesical junction is positioned higher and more laterally, therefore the submucosal part of the ureter is shorter and thus urine can regurgitate from the bladder into the ureter more easily.[37] The abnormality can be uni- or bilateral, if there is double ureter present, it belongs to the lower one and can lead to mild or moderate hydronephrosis **(Figs 23.20A and B)**. It is considered to be a multifactorial disease, but autosomal recessive and X chromosome linked cases have also been reported.

Ultrasonography reveals mild, nonprogressive and sometimes only intermittently appearing hydronephrosis. A dilated ureter showing no peristalsis and normal amount of amniotic fluid.[6,7,38,39]

Ureterocele

It is four times more common in males and usually appears on the left side, although in 15% of the cases it is bilateral. Simple ureterocele means that the thin membrane of the lower segment of the ureter fails to disappear and it appears in the urinary bladder as a cyst with a thin wall. It hinders urinary flow and leads to hydroureter and hydronephrosis. If ureteral duplication is present, the ectopic ureterovesical junction can result in ectopic ureterocele. The ectopic junction can be at the neck of the bladder or even the urethra, and the ureterocele may block the ipsilateral or contralateral ureteral orifice or the neck of the bladder. The renal segment connected to the ectopic ureterocele is often

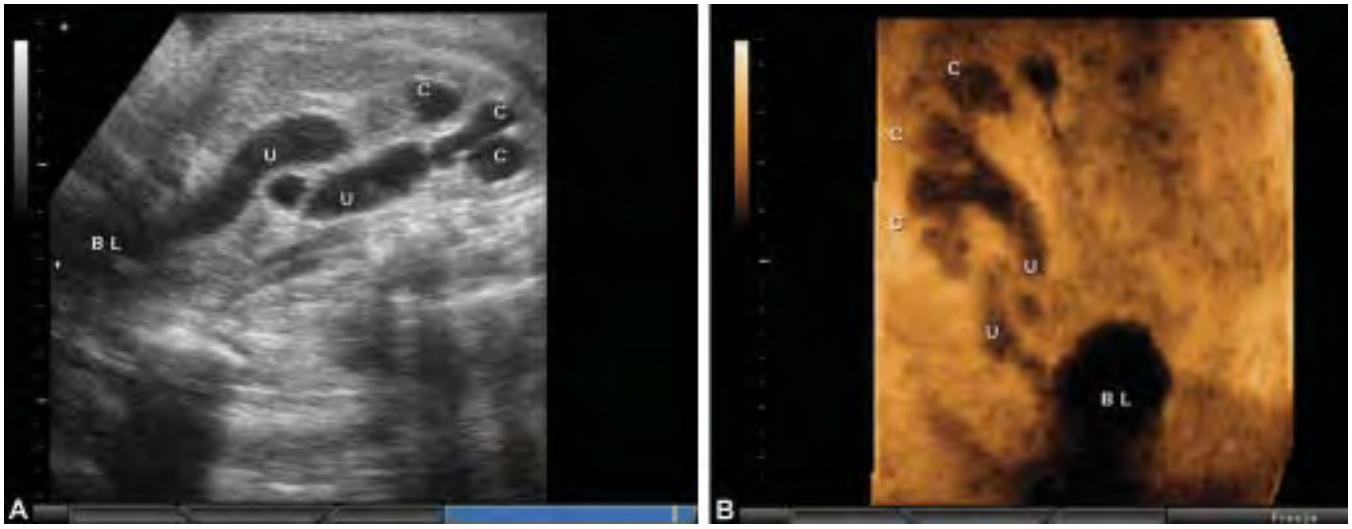

Figures 23.20A and B: Double kidney and ureter, with a ureter connected to the dilated lower pole of the kidney

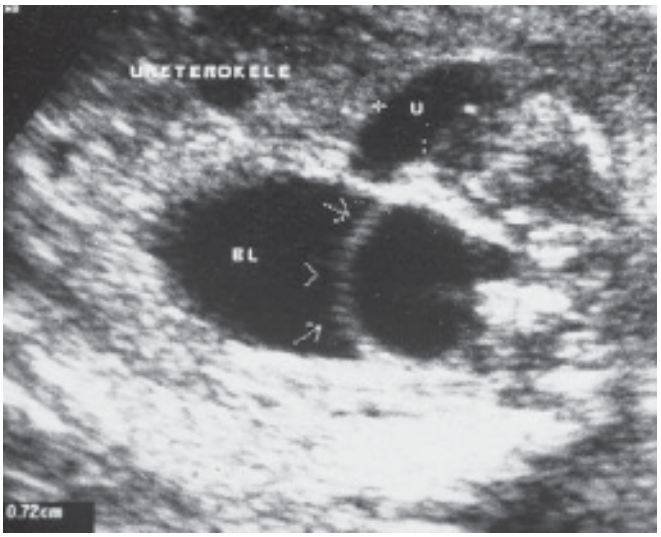

Figures 23.21: Cystic protrusion of ureterocele into the bladder (BL), above the bladder the dilated ureter (U) can also be seen

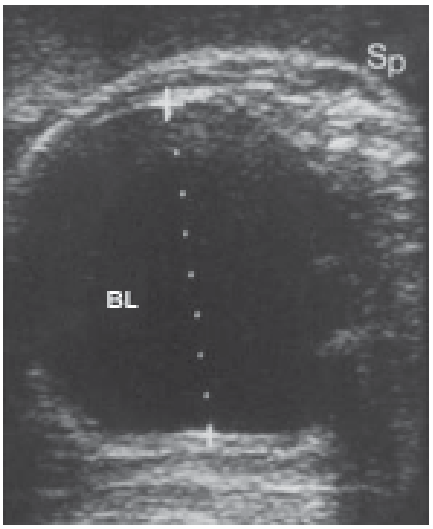

Figure 23.22: Megacystis-microcolon-intestinalis hypoperistalsis syndrome: the wall of the dilated bladder (BL) is thin

found to be abnormal (hypoplasia, dysplasia or hydronephrotic atrophy) and with deteriorated function.

Ultrasonography shows the ureterocele as a cyst with a thin wall inside the bladder **(Fig. 23.21)** and the dilated hydroureter.[7,15]

Megacystis, Microcolon and Intestinal Hypoperistalsis Syndrome

The disease is most probably of multifactorial origin, more common in females and sometimes seems to be hereditary. The affected organs display neurodysplasia, indicating some innervation disorder, which leads to the dilation of the bladder without obstruction (megacystis), small intestines are shorter and dilated, the colon is narrower (microcolon) and intestinal peristalsis is weak or missing. Unable to empty, the distended bladder pushes the abdominal wall forward, the increased pressure affects the both ureters and the kidneys, resulting in dilation. Intestinal dysfunction leads to polyhydramnios.

Ultrasonography reveals polyhydramnios, an extremely dilated bladder **(Fig. 23.22)** with a thin wall, megaureter and hydronephrosis.[13,14]

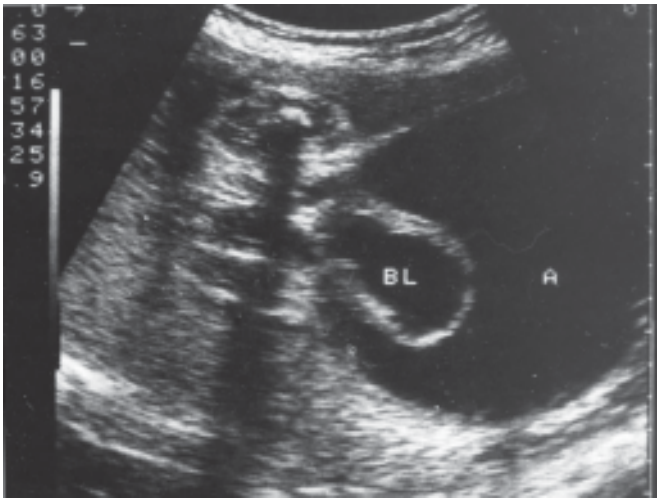

Figure 23.23: Urine ascites: dilated bladder with thick wall (BL) appears in the ascites (A)

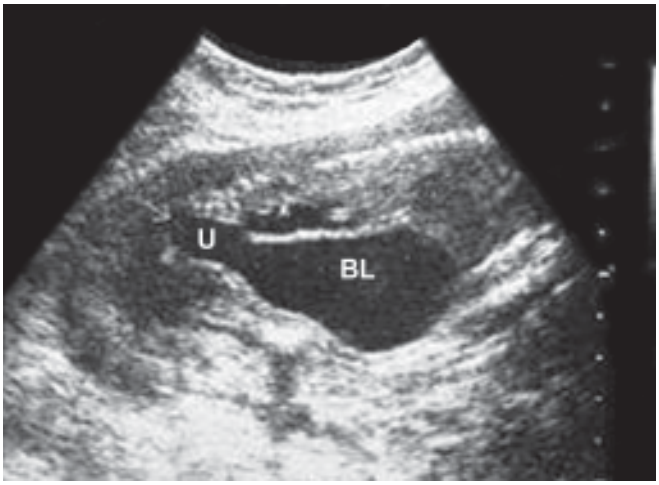

Figure 23.24: Urethral obstruction: the first part of the urethra and the neck of the bladder show funnel-shaped dilation

Urethra Obstruction

The incidence of the disease at birth is between 1/35,000 and 1/50,000. It has a multifactorial etiology, sometimes it is hereditary. The partial or complete blockage of the urethra leads to urine retention, bladder dilation, bilateral hydroureter, hydronephrosis, cystic renal dysplasia, consecutive oligohydramnios, pulmonary hypoplasia, facial and limb deformity (urethral obstruction sequence), cryptorchidism in males, rectus diastasis of the abdominal wall, and a dilated abdominal wall (prune-belly syndrome).[40] The posterior urethral valve is found almost exclusively in males, whereas the rare urethra agenesis is seen in females. The ejaculatory duct evolving from the distal part of the mesonephric duct has an abnormal junction formation, resulting in the appearance of the posterior urethral valve and the dilation of the urinary tract. Increased intraluminal pressure may also lead to a subcortical perinephric urinoma and in case it ruptures, urine ascites can result **(Fig. 23.23)**. The disease is accompanied by urogenital, other organ or chromosomal (chromosomes 13 and 18) abnormalities.

Ultrasonography reveals oligohydramnios (in 50% of the cases), dilated bladder with a thick wall, the funnel-shaped dilation of the neck of the bladder and the first part of the urethra **(Figs 23.24 and 23.25)**, bilateral hydroureter, bilateral hydronephrosis, the damaged renal parenchyma, subcapsular cysts or sometimes urinomas.[6,7,14,41-43]

Persistent Cloaca

If the urorectal septum fails to develop, a persistent cloaca is the result. This sandglass-shaped sinus is the terminal collecting cavity of the urogenital and the gastrointestinal tracts. This common sinus surrounded by the abdominal wall is filled with urine and bowel content, the increased pressure leads to the dilation of the ureters and pyelons. Due to intact cloaca membrane, urine will not pass into the amniotic space, therefore oligohydramnios will be present.

Ultrasonography shows oligohydramnios, the fetal abdomen is pushed forward and inside of it an unusually shaped cystic region can be seen, sometimes containing septa **(Figs 23.26A and B)**. In the horizontal plane, this region extends into the space next to the spinal column.[3,6,7]

Cloaca Exstrophy

The incidence of the malformation is 1/2,00,000 and can be seen in both sexes. During embryogenesis, the urorectal septum dividing the cloaca fails to reach the cloaca membrane and the fusion of the mesodermal crests that normally leads to the closure of the abdominal wall as well as the caudal retraction of the membrane do not take place. After the membrane dissolves, the bladder and the rectum is placed externally, resulting in cloaca exstrophy.[3]

Urinary Bladder Exstrophy

The incidence of the malformation is 1/40,000 births, it is more common in males. The cloaca is divided by the cloaca membrane, but the retraction of the cloaca membrane is abnormal and the posterior wall of the bladder is externalized. The defect of the lower abdominal wall and the absence of the anterior wall of the bladder results in the extra-abdominal position of

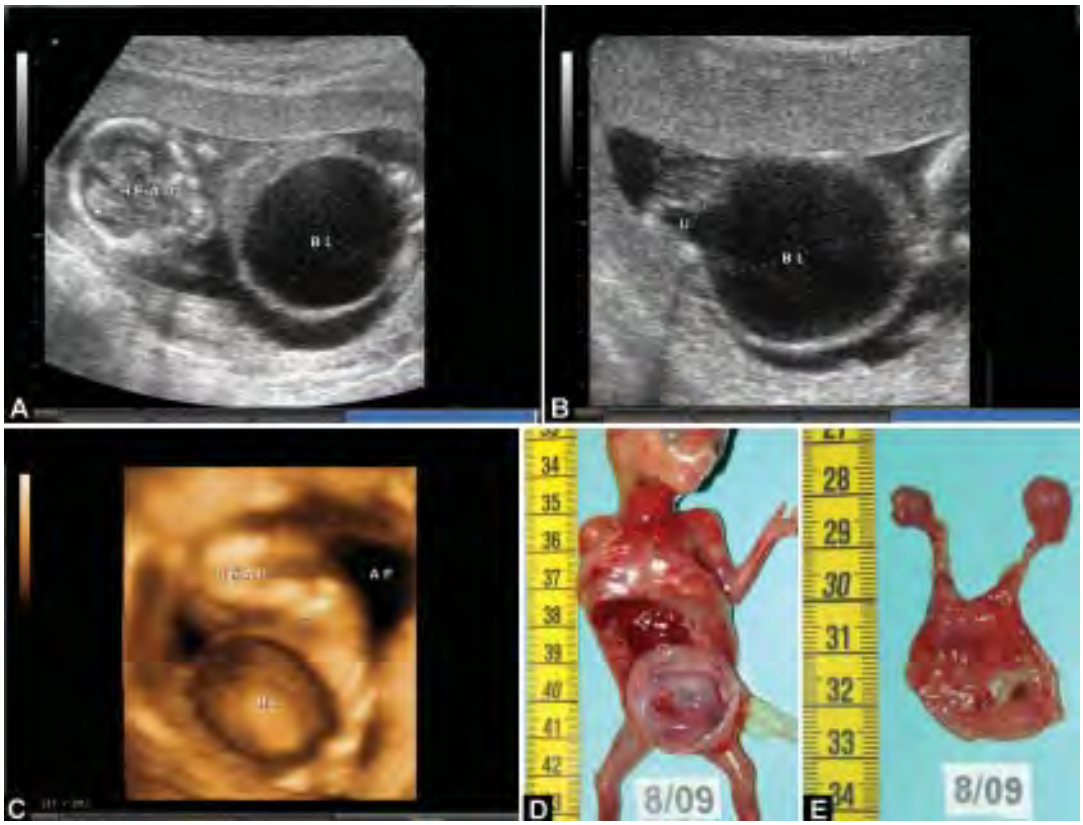

Figures 23.25A to E: Urethra obstruction diagnosed at gestational period of 14 weeks. (A and B) 2D sonographic images; (C) 3D sonographic images; (D and E) Autopsy photographs

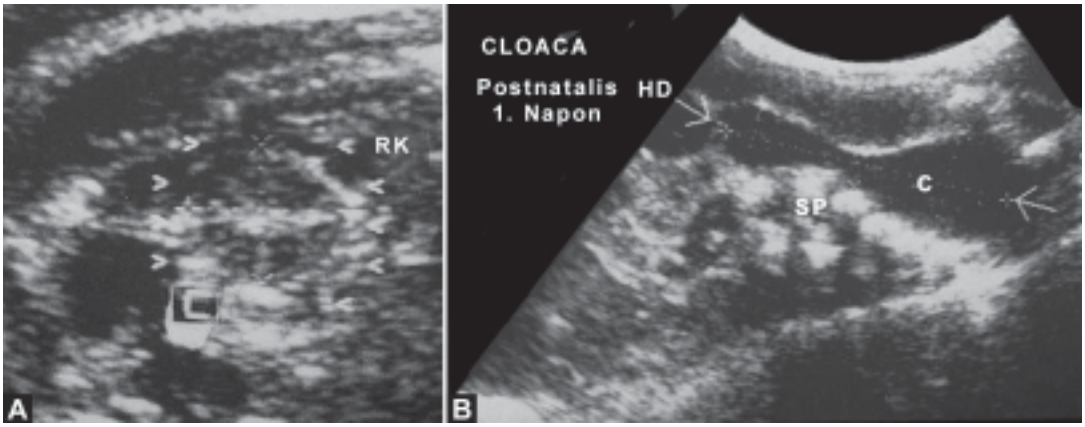

Figures 23.26A and B: (A) Prenatal and (B) Postnatal ultrasound image of persistent cloaca, appearing as an unusual cystic region in the abdomen

the bladder. In a mild case, the divergence of the rectus abdominis muscle and the symphysis is minimal. In common and moderate cases, besides the bladder exstrophy, abdominal wall and symphysis joint get split. In most severe situation, all the above mentioned abnormalities, accompanied by umbilical and inguinal hernia, a ventrally positioned anus with a relaxed sphincter and intermittent rectal prolapse are present. Ultrasonography reveals absence of bladder filling. At the abdominal wall below the umbilicus, sometimes cystic structure or extra soft tissue can be demonstrated. The umbilical arteries can be visualized using color-

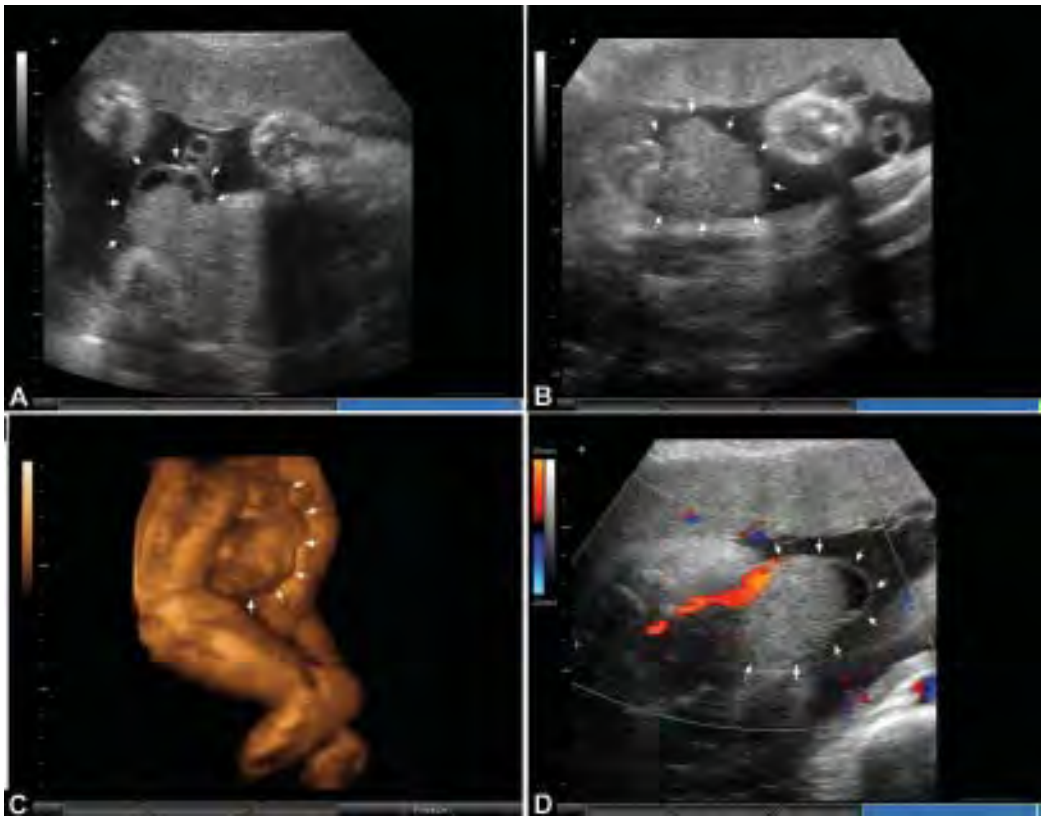

Figures 23.27A to D: (A and B) Urinary bladder exstrophy: in the subumbilical region of the abdominal wall, small, protruding, cystic tissue or; (C) Soft tissue surplus is seen; (D) Umbilical arteries are found outside the abdominal wall using color-Doppler imaging

Doppler outside the abdominal wall **(Figs 23.27A to D)**. Deformity of the pubic bone can be suspected only in severe cases. Accompanying genital or renal malformations can hardly be visualized due to the oligohydramnios.[44]

RENAL TUMORS

Mesoblastic Nephroma

It is a leiomyomatous renal hamartoma containing connective, adipose, smooth muscle tissues and tubular epithelial cells. Clinically it is a benign tumor, histologically dominated by the presence of mesenchymal tissue.

Ultrasonography shows a large, mainly solid bulk in the region of one of the kidneys, it can have cystically degenerated parts and renal capsule is blurred. The other kidney has a normal structure. It almost always produces polyhydramnios.[7,45]

Wilms' Tumor

It is a multifocal, often bilateral tumor, composed mainly of epithelial tissues. It has a more malignant clinical course.

Prenatal ultrasonography shows a bilateral solid bulk, indicating Wilms' tumor. This, however, does not allow determining the exact diagnosis, but it gives information to arrange the necessary postnatal examinations and treatment.

DETERMINATION OF FETAL RENAL FUNCTION

Following the prenatal diagnosis of kidney and urinary tract anomalies, it is important to determine renal function of the fetus. Following points need to be taken care of in determining the renal function of the fetus:

- The amount of amniotic fluid is an indirect indicator of renal function. Early oligohydramnios indicates renal agenesis or severe problems with renal

function. Normal or excessive amount of amniotic fluid requires at least one functioning kidney.[46-48]

- Urinary bladder filling indicates at least one functioning kidney. Absence of filling raises the possibility of renal agenesis, bilateral ureteral obstruction or kidney damage. Distension of the bladder indicates conduction problems at the level of the urethra.
- Ureteral dilation can be observed due to obstruction of the lower segments. There is only a weak correlation between the severity of the dilation and renal impairment.
- Echogenicity of the renal parenchyma and visualization of subcapsular cysts are not suitable for determining precise renal function.[7,26]
- Examination of the circulation of renal arteries can prove to be a useful tool, which helps determine kidney functional impairment in case retrograde pressure increases.[15]
- Biochemical analysis of fetal urine consists of examination of urine acquired from the dilated urinary bladder or the dilated calyces through transabdominal puncture. Urinary $Na^+ < 100$ mmol/l, $Cl^- < 90$ mmol/l, osmolarity < 210 mOsmol/l and creatinine < 150 umol/l indicate good prognosis. Elevated levels and the appearance of proteins smaller than 70,000 dalton molecular weight indicate probable renal functional impairment.[6,7,15]

TREATMENT OF PRENATALLY DIAGNOSED RENAL AND URINARY TRACT ANOMALIES

In cases of bilateral, severe renal impairment incompatible with postnatal life (renal agenesis, infant polycystic kidney, multicystic renal dysplasia, hydronephrotic kidneys, unilateral multicystic and contralateral nonfunctioning kidney, early abnormalities with severe oligohydramnios and pulmonal hypoplasia) termination of pregnancy can be offered to the parents.

In cases of a unilateral, severe anomalies (agenesis, multicystic renal dysplasia, severe hydronephrosis) accompanied by other severe concomitant malformation(s) and termination of the pregnancy can be offered before 24 weeks of gestation. Unilateral malformations without severe concomitant abnormalities and a normal amount of amniotic fluid require regular control and multidisciplinary (obstetrical, neonatological, surgical and urological) counseling.[49]

Urethric obstruction can be solved by a vesico-amniotic shunt prepared before 24 weeks of gestation. So far open fetal surgical techniques have been carried out with poor outcomes.

Dilation of the renal pelvis requires follow-up by repeated ultrasound examinations. Prenatally diagnosed pyelectasy and hydronephrosis are best controlled by 3–7 days after birth, when physiologic postnatal dehydration passes. Cases showing spontaneous regression should be examined by ultrasound again after 2 weeks. In case of an abnormal finding, a detailed examination of the neonate is necessary, including urography (IV), voiding cystography, nuclear renography, laboratory examinations, etc.

Early prenatal diagnosis, timely interventions and thorough postnatal examinations create the possibility to significantly decrease the morbidity and mortality of neonates suffering[50] from kidney and urinary tract anomalies, and to minimize the number of future dialyses.

REFERENCES

1. Potter EL. Normal and abnormal development of the kidney. Medical Publishers: Chicago; 1972.
2. Gersh I. The correlation of structure and function in the developing mesonephros and metanephros. Contrib Embryol. 1937;26:35-9.
3. Tank ES. Urologic complications of imperforate anus and cloacal dysgenesis. In: Campbell S (Ed). Urology, 4th edition. Philadelphia: WB Saunders Co;1986. pp. 1889-2000.
4. McCrory WW. Embryonic development and prenatal maturation of the kidney. In: Edelmann CM (Ed). Pediatric kidney disease. Boston: Little Brown;1978. pp. 3-25.
5. McCrory WW. Embryologic development of the kidney. Developmental nephrology. Cambridge: Harward University Press; 1972.
6. Callen PW (Ed). Ultrasonography in obstetrics and gynecology, 4th edition. Philadelphia, London, New York, St Louis, Sydney, Tokyo: WB Saunders Co; 2000.
7. Filly RA, Feldstein VA. Fetal genitourinary tract. In: Callen PW (Ed). Ultrasonography in obstetrics and gynecology, 4th edition. Philadelphia, London, New York, St Louis, Sydney, Tokyo: WB Saunders Co;2000. pp. 517-50.
8. Grannum PA. The genitourinary tract. In: Nyberg DA, Mahony BS, Pretorius DH (Eds). Diagnostic Ultrasound of Fetal Anomalies: Text and Atlas. St Louis: Mosby Year Book; 1990. pp. 433-91.
9. Kurjak A, Chervenak FA (Eds). Donald School Textbook of ultrasound in obstetrics and gynecology. New Delhi: Jaypee Brothers Medical Publishers Ltd; 2004.
10. Kurjak A, Kupesic S. Color Doppler and 3D ultrasound in gynecology, infertility and obstetrics. New Delhi: Jaypee Brothers Medical Publishers Ltd; 2003.
11. Khurana A, Dahiya N. 3D and 4D ultrasound. A text and atlas. Tunbridge Wells Kent, UK: Anshan Ltd; 2004.
12. Latin V, Kos M, Marton U. Urinary tract malformations. In: Kurjak A (Ed).Textbook of perinatal medicine. London, New York: Parthenon Publishing; 1998. pp. 325-34.
13. Sanders RC. Ultrasonic assessment of genitourinary anomalies in utero. In: Sanders RC, James AE (Eds). The

principles and practice of ultrasonography in obstetrics and gynecology, 3rd edition. Norwalk, Connecticut: Appleton Century Crofts; 1985. pp. 195-209.
14. Papp Z (Ed). Atlas of Fetal Diagnosis. Amsterdam, London, New York, Tokyo: Elsevier; 1992.
15. Luque JMT, Rodriguez MTC. Fetal genitourinary tract: prenatal diagnosis and assessment of nephrouropathies. In: Kurjak A, Chervenak FA (Eds). Donald School textbook of ultrasound in obstetrics and gynecology. New Delhi: Jaypee Brothers; 2004. pp. 298-319.
16. Isaksen CV, Eik-Nes SH, Blaas H-G, et al. Fetuses and infants with congenital urinary system anomalies: correlation between prenatal ultrasound and postmortem findings. Ultrasound Obstet Gynecol. 2000;15:177-85.
17. Grignon A, Filion R, Filiatrault D, et al. Urinary tract dilatation in utero: classification and clinical applications. Radiology. 1986;160:645-7.
18. Roume J, Ville Y. Prenatal diagnosis of genetic renal diseases: breaking the code. Ultrasound Obstet Gynecol. 2004;24:10-8.
19. Kovács T, Csécsei K, Tóth Z, et al. Familial occurrence of bilateral renal agenesis. Acta Paediat Hung. 1991;31:13-21.
20. Tóth Z, Török O, Csécsei K, et al. Cystic kidney diseases diagnosed prenatally by ultrasound. In: Tankó A, Berbik I, Petri E, et al (Eds). Practical Aspects of Gynaecourology. Budapest; 1986; pp. 439-46.
21. Brun M, Maugey-Laulom B, Eurin D, et al. Prenatal sonographic patterns in autosomal dominant polycystic kidney disease: a multicenter study. Ultrasound Obstet Gynecol. 2004;24:55-61.
22. van Eijk L, Cohen-Overbeek TE, den Hollander NS, et al. Unilateral multicystic dysplastic kidney: a combined pre- and postnatal assessment. Ultrasound Obstet Gynecol. 2002;19:180-3.
23. Csécsei K, Szeifert Gy, Tóth Z, et al. Prenatal detection and morphology of dysplastic kidneys in Meckel syndrome. In: Tankó A, Berbik I, Petri E, et al (Eds). Practical Aspects of Gynaecourology. Budapest; 1986. pp. 425-30.
24. Damen-Elias HAM, De Jong TPVM, Stigter RH, et al. Congenital renal tract anomalies: outcome and follow-up of 402 cases detected antenatally between 1986 and 2001. Ultrasound Obstet Gynecol. 2005;25:134-43.
25. Gorincour G, Rypens F, Toiviainen-Salo S, et al. Fetal urinoma: two new cases and a review of the literature. Ultrasound Obstet Gynecol. 2006;28:848-52.
26. Chaumoitre K, Brun M, Cassart M, et al. Differential diagnosis of fetal hyperechogenic cystic kidneys unrelated to renal tract anomalies: a multicenter study. Ultrasound Obstet Gynecol. 2006;28:911-7.
27. Török O, Tóth Z, Csécsei K, et al. Obstructive uropathies diagnosed prenatally by ultrasound. In: Tankó A, Berbik I, Petri E, Kiadó A (Eds). Practical Aspects of Gynaeco-urology. Budapest; 1986. pp. 431-7.
28. Bronhstein M, Yoffe N, Brandes JM, et al. 1st and early 2nd trimester diagnosis of fetal urinary-tract anomalies using transvaginal sonography. Prenat Diagn. 1990;10:653-66.
29. Bouzada MCF, Oliveira EA, Pereira AK, et al. Diagnostic accuracy of fetal renal pelvis anteroposterior diameter as a predictor of uropathy: a prospective study. Ultrasound Obstet Gynecol. 2004;24:745-9.
30. Chudleigh TM, Chitty LS. The postnatal significance of mild fetal pyelectasis. Ultrasound Obstet Gynecol. 2001;18: F63.
31. Cohen-Overbeek TE, Wijngaard-Boom P, Ursem NTC, et al. Mild renal pyelectasis in the second trimester: determination of cut-off levels for postnatal referral. Ultrasound Obstet Gynecol. 2005;25:378-83.
32. Kilby MD, Somerset DA, Khan KS. Potential for correction of fetal obstructive uropathy: time for a randomized, controlled trial? Ultrasound Obstet Gynecol. 2004;23:527-30.
33. Sairam S, Al-Habib A, Sasson S, et al. Natural history of fetal hydronephrosis diagnosed on mid-trimester ultrasound. Ultrasound Obstet Gynecol. 2001;17:191-6.
34. Wollenberg A, Neubaus TJ, Willi UV, et al. Outcome of fetal renal pelvic dilatation diagnosed during the third trimester. Ultrasound Obstet Gynecol. 2005;25:483-8.
35. Abuhamad AZ, Horton CE, Horton SH, et al. Renal duplication anomalies in the fetus: clues for prenatal diagnosis. Ultrasound Obstet Gynecol. 1996;7:174-7.
36. Yang JM, Yang SH, Hsu HC, et al. Transvaginal sonography in the morphological and functional assessment of segmental dilation of the distal ureter. Ultrasound Obstet Gynecol. 2006;27:449-51.
37. Chen CP, Liu YP, Huang JP, et al. Prenatal evaluation with magnetic resonance imaging of a giant blind ectopic ureter associated with a duplex kidney. Ultrasound Obstet Gynecol. 2008;31:360-2.
38. van Eerde AM, Meutgeert MH, de Jong TPVM, et al. Vesico-ureteral reflux in children with prenatally detected hydronephrosis: a systematic review. Ultrasound Obstet Gynecol. 2007;29:463-9.
39. Whitten SM, McHoney M, Wilcox DT, et al. Accuracy of antenatal fetal ultrasound in the diagnosis of duplex kidneys. Ultrasound Obstet Gynecol. 2003;21:342-6.
40. Hoshino T, Ihara Y, Shirane H, et al. Prenatal diagnosis of prune belly syndrome at 12 weeks of pregnancy: case report and review of the literature. Ultrasound Obstet Gynecol. 1998;12:362-6.
41. Carroll SGM, Soothill PW, Tizard J, et al. Vesicocentesis at 10–14 weeks of gestation for treatment of fetal megacystis. Ultrasound Obstet Gynecol. 2001;18:366-70.
42. Kim SK, Won HS, Shim JY, et al. Successful vesicoamniotic shunting of posterior urethral valves in the first trimester of pregnancy. Ultrasound Obstet Gynecol. 2005;26:666-8.
43. Rohyr R, Benachi A, Daikha-Dahmane F, et al. Correlation between ultrasound and anatomical findings in fetus with lower urinary tract obstruction in the first half of pregnancy. Ultrasound Obstet Gynecol. 2005;25:478-82.
44. Lee EH, Shim JY. New sonographic finding for the prenatal diagnosis of bladder exstrophy: a case report. Ultrasound Obstet Gynecol. 2005;21:498-500.
45. Schwärzler P, Bernard JP, Senat MV, et al. Prenatal diagnosis of fetal adrenal masses: differentiation between hemorrhage and solid tumor by color Doppler sonography. Ultrasound Obstet Gynecol. 1999;13:351-5.

46. Gramellini D, Delle Chiaie L, Piantelli G, et al. Sonographic assessment of amniotic fluid volume between 11 and 24 weeks of gestation: construction of reference intervals related to gestational age. Ultrasound Obstet Gynecol. 2001;17:410-5.
47. Lee SM, Jun JK, Lee EJ, et al. Measurement of fetal urine production to differentiate causes of increased amniotic fluid volume. Ultrasound Obstet Gynecol. 2010;36:191-5.
48. Lee SM, Park SK, Shim SS, et al. Measurement of fetal urine production by three-dimensional ultrasonography in normal pregnancy. Ultrasound Obstet Gynecol. 2007;30: 281-6.
49. Bhide A, Sairam S, Farrugia M-K, et al. The sensitivity of antenatal ultrasound for predicting renal tract surgery in early childhood. Ultrasound Obstet Gynecol. 2005;25: 489-92.
50. Carrera JM, Torrents M, Mortera C, et al. Routine prenatal ultrasound screening for fetal abnormalities: 22 years' experience. Ultrasound Obstet Gynecol. 1995;5: 174-9.

CHAPTER 24

The Fetal Musculoskeletal System

Rodó C, Carreras E, Toran N, Castagno R, Higueras T, Arévalo S, Cabero LI

INTRODUCTION

Fetal Musculoskeletal Abnormalities

- Osteochondrodysplasias
  - Thanatophoric dysplasia
  - Osteogenesis imperfecta
  - Achondroplasia
  - Achondrogenesis
  - Others
- Reductional defects
  - Terminal defects
  - Constriction band sequence
  - Phocomelia
  - Proximal femoral focal deficiency (PFFD)
  - Split-hand and split-foot malformation (SHFM), Ectrodactyly
  - Hand and foot deformities
- Polydactyly
- Syndactyly
- Hemivertebrae
- Fetal akinesia deformation syndrome (FADS)
- Other skeletal defects: Patellar anterior luxation; Teratogenic effects: Misoprostol.

NORMAL ULTRASOUND APPEARANCE OF FETAL SKELETON

A systematic fetal musculoskeletal evaluation requires the inspection of all four extremities. Fetal head, thorax **(Fig. 24.1)** and spine must also be assessed.

A standardized approach to sonographic evaluation must include:

- All three portions of the limb (proximal, middle and distal) **(Figs 24.2 to 24.11)**
- Bone characteristics [Long bone measurements, degree of mineralization **(Fig. 24.12)**, presence of bone fractures and bowing] are helpful in categorizing skeletal dysplasias[1]
- Fetal posture and movement
- Hand (metacarpals and phalanges) **(Figs 24.13 to 24.15)** and foot (metatarsals and phalanges) configuration **(Figs 24.16 to 24.18)**
- Fetal head, spine and thorax **(Fig. 24.19)** should be evaluated for abnormal configuration and

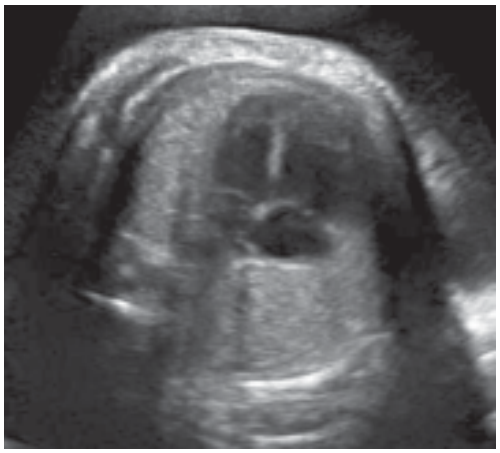

Figure 24.1: Transverse view of a normal fetal thorax. Thoracic shape is correct. There is no thoracic hypoplasia and hence no pulmonary compromise at birth

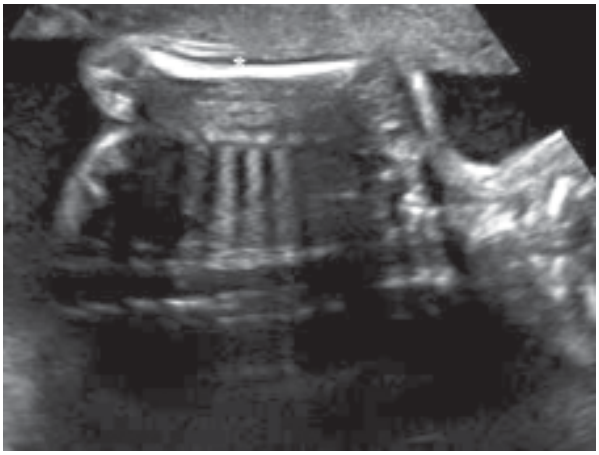

Figure 24.4: Humerus (*). Long bone length is the measurement of the ossification center of bone diaphysis

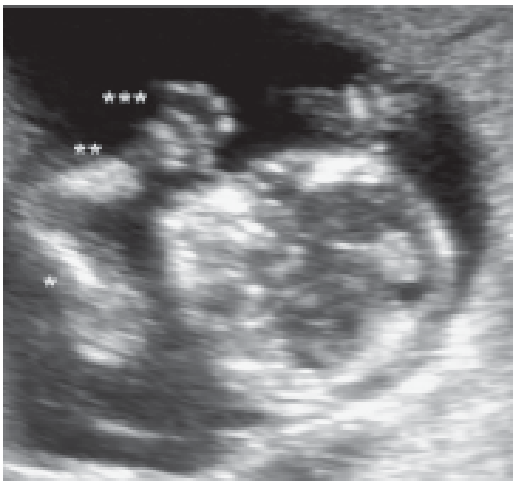

Figure 24.2: 12 weeks embryo. All three portions of the upper limb must be distinguished proximal (humerus *), middle (cubitus and radio **) and distal (hand ***), with five fingers

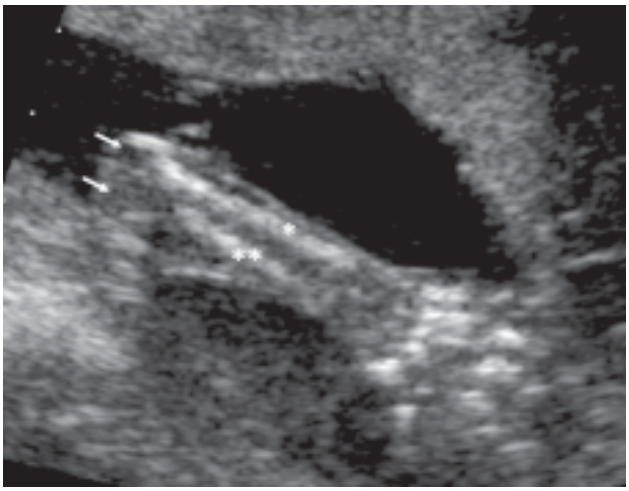

Figure 24.5: Cubitus (*) and radius (**). Cubital diaphysis is longer than radial one. Proximal noncalcified epiphyses may be assessed, as round anechogenic structures (arrows)

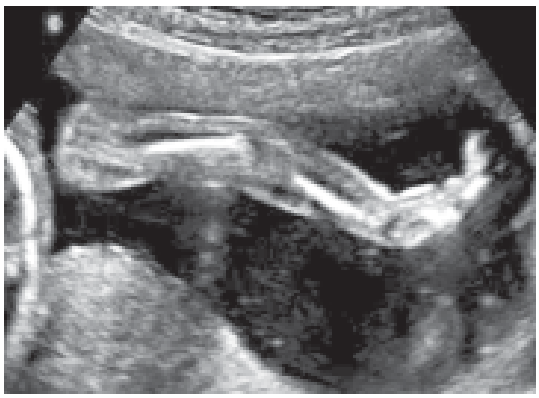

Figure 24.3: Upper limb. For a correct ultrasonographic assessment, all three portions of fetal limbs must be visualized (proximal, middle and distal) aligned following the same axis. Fetal posture and shoulder, elbow and wrist movement must be assessed

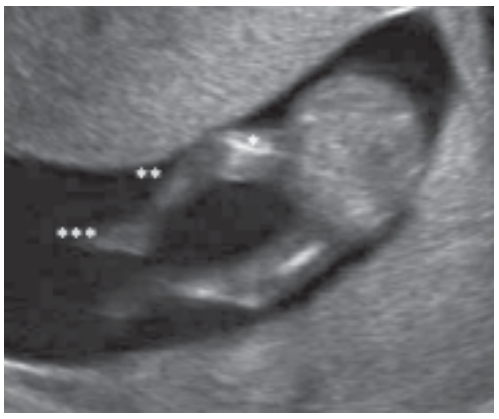

Figure 24.6: 12 weeks embryo. All three portions of the lower limb must be distinguished: proximal (femur *), middle (tibia and perone **) and distal (foot ***)

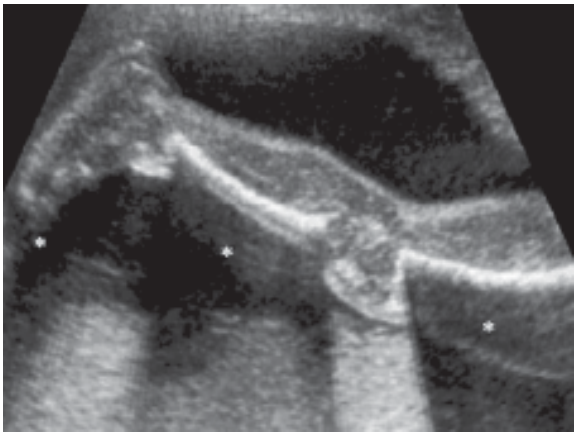

Figure 24.7: Lower limb showing all three portions. All of them responsible of a posterior shadow effect (*). One must assess the femur, tibia and foot normally aligned and the hip, knees and elbows motility

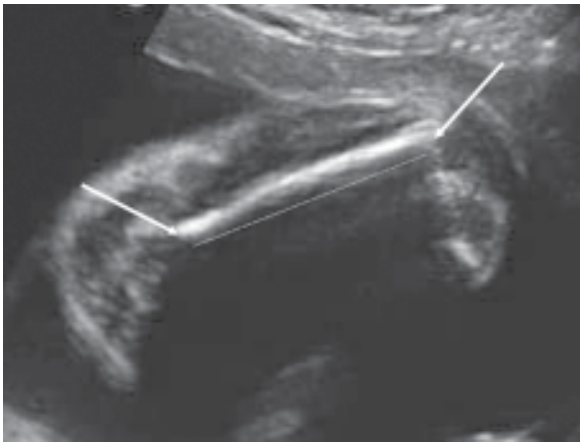

Figure 24.8: Femoral diaphysis. A normal degree of mineralization is indirectly assessed by the appearance of a posterior shadow (arrows) that enables a clear visualization of all diaphyseal thickness (discontinued line). For this reason bone appear thinner than soft tissues that surround it

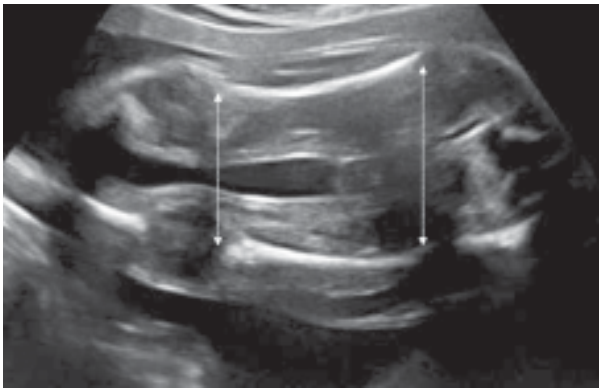

Figure 24.9: Even if you only measure one of them, it is important to assess that both femurs have the same length (arrows)

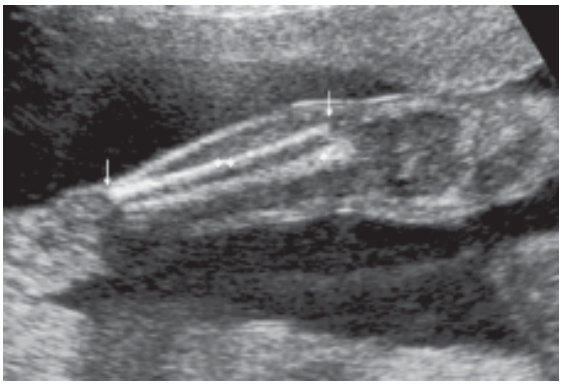

Figure 24.10: Tibia (*) and fibula (**). Tibial diaphysis is longer and thicker than peroneal diaphysis. Nonmineralized peroneal epiphysis (arrows)

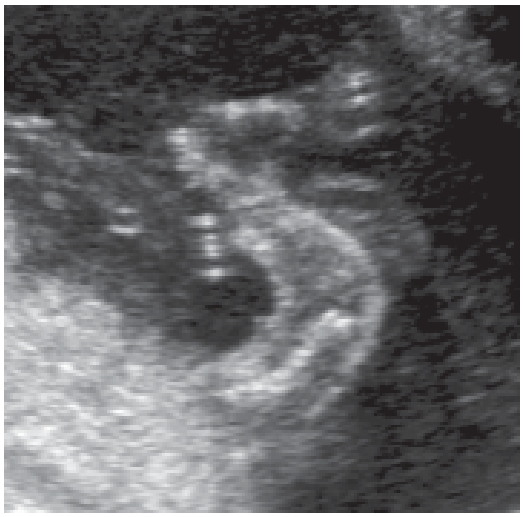

Figure 24.11: Upper limb showing all three portions. They are well aligned on their axes

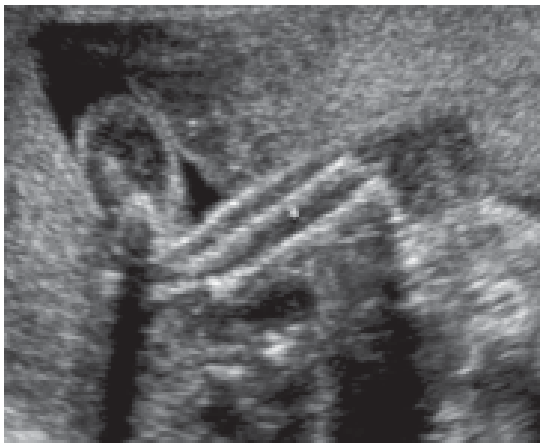

Figure 24.12: Lower extremity uniformly shortened, with a correct degree of mineralization and no angulations or fractures (*)

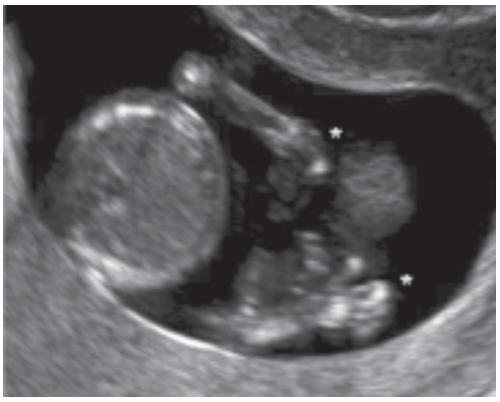

Figure 24.13: 12 weeks embryo. Both upper limbs can be assessed simultaneously (*). A common pitfall is to assess the same limb twice. To avoid this, one should try to visualize simultaneously both hands. It is the ideal gestational age to perform this

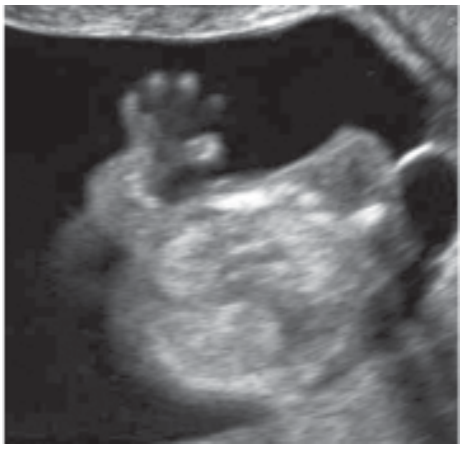

Figure 24.14: 12 weeks embryo. Hands are best assessed when they are opened so one can confirm the integrity of all the phalanges and the normal separation of fingers

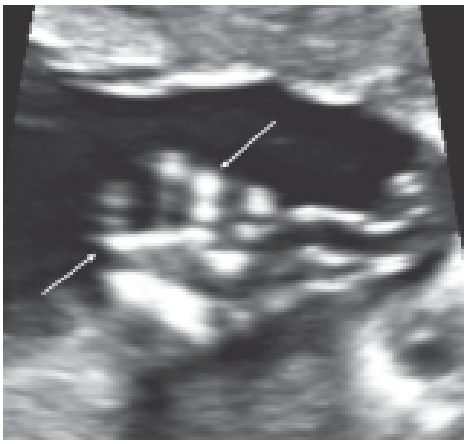

Figure 24.15: 15 weeks fetal hand. Arrows showing phalanges and metacarpals

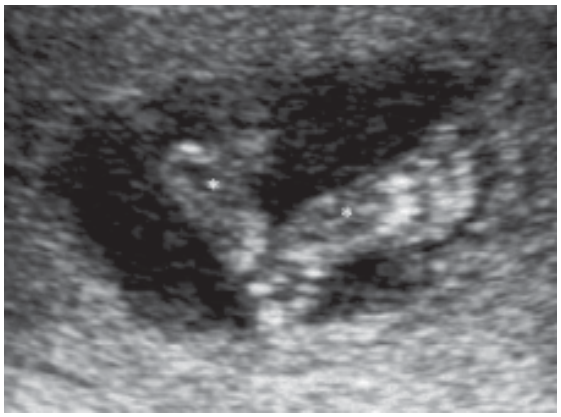

Figure 24.16: 12 weeks embryo. Both feet are simultaneously assessed (*) in order to avoid exploring the same limb twice

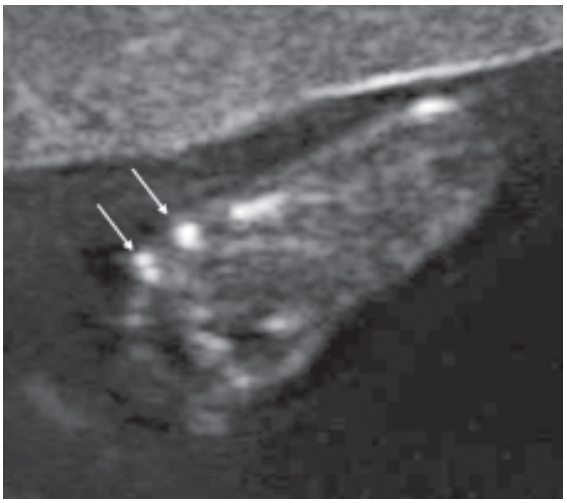

Figure 24 17: Forefoot. Arrows showing metatarsal and phalanges. Fetal tarsus completes its calcification process at 26 weeks of gestation

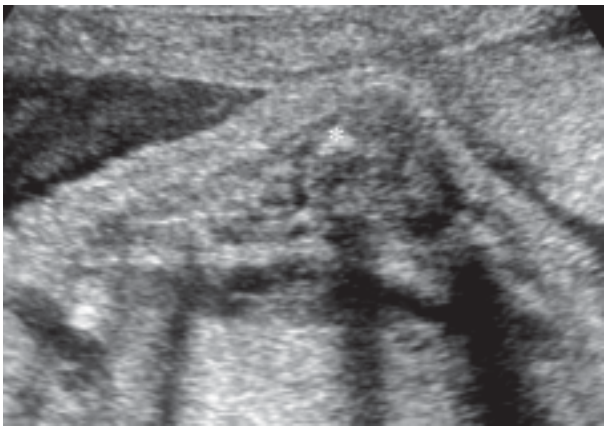

Figure 24.18: Foot in a 28 weeks fetus. By 26 weeks, one can visualize the tarsal ossification centers (*) showing a posterior shadow

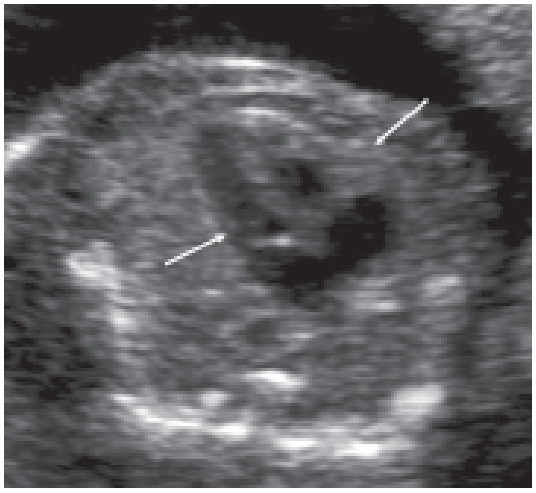

Figure 24.19: Transverse section of fetal thorax. The cardiac circumference is greater than 60% of the thoracic circumference (relative cardiomegaly) (arrows) indicating a hypoplastic thorax

echogenicity or degree of mineralization. Many of the skeletal disorders may have a familial component, so it is important to ask the parents about the findings and relate to them if it is possible.

OSTEOCHONDRODYSPLASIAS

Osteochondrodysplasias or skeletal dysplasias[1] **(Fig. 24.20)** are a genetically heterogeneous group of over 350 distinct disorders. They are traditionally classified in terms of which portions of the limbs[2] are shortened:

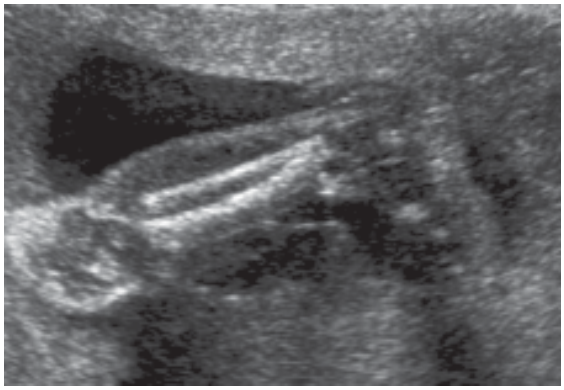

Figure 24.20: Lower extremity showing a correct configuration but with shortened long bones. It may represent an osteochondrodysplasia, but also a normal variant. Parental phenotype must be assessed. Standard obstetrical management is not altered. In postnatal period the growing pattern must be followed up, because the diagnosis cannot be confirmed nor excluded prenatally

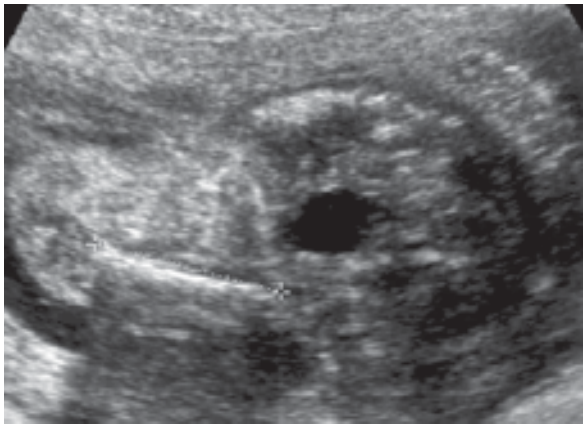

Figure 24.21: 22 weeks fetus that shows a shortened femur but with normal appearance

Rhizomelia denotes shortening of the proximal limb, namely the humerus and femur **(Fig. 24.21).**

Mesomelia indicates shortening of the middle portion of the limb: the forearm or lower leg bone.

Acromelia is shortening of the hand and foot bones.

Micromelia technically means severe shortening of all portions of a limb, but the term is also used to indicate shortening of a limb without a specific reference of the particular portion that is shortened **(Figs 24.22 to 24.27)**.

Many of the skeletal dysplasias can be assessed by ultrasound.[3] However, the most common skeletal dysplasias have more accurate diagnosis by ultrasound[4] than the less common ones.

The osteochondrodysplasias most commonly assessed by ultrasound[5] are:

- Thanatophoric dysplasia
- Osteogenesis imperfecta

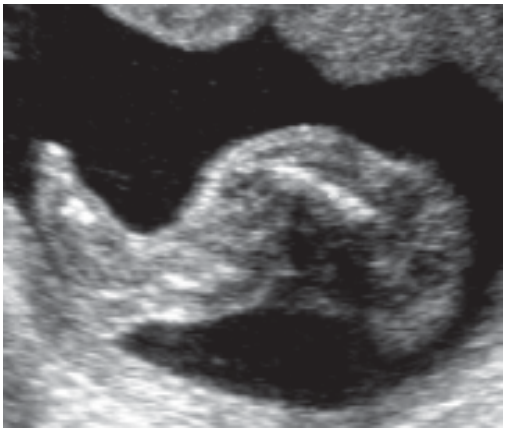

Figure 24.22: Three portions of a lower extremity. The limb is very shortened (micromelia). One can compare femur (*) and foot length

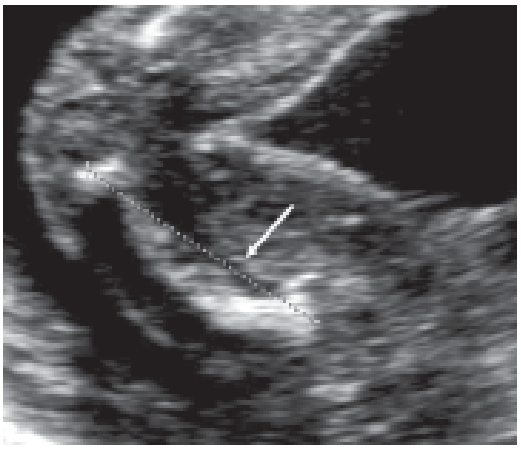

Figure 24.23: Very short lower limbs (micromelia) but without axial deviation of the three portions. A curved femur showing the classical "telephone receiver" configuration (arrow). There are no fractures, and the degree of bone mineralization is normal

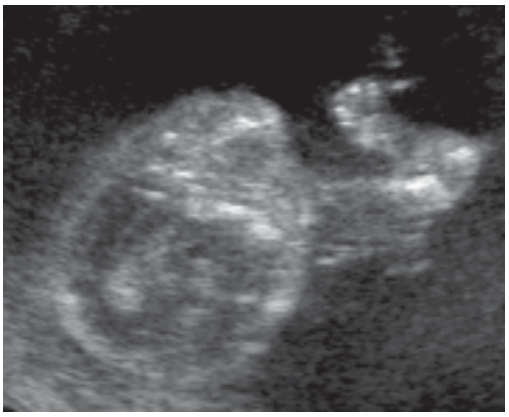

Figure 24.24: Extremely short upper limb (micromelia), showing all three portions

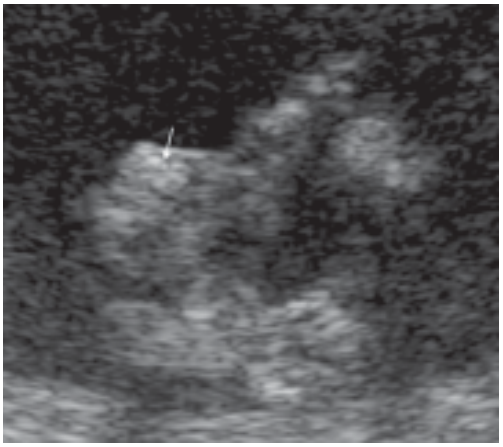

Figure 24.25: Extremely short upper limb (micromelia). The arrow shows multiple irregularities in tibial diaphysis secondary to postfracture callous tissue formation

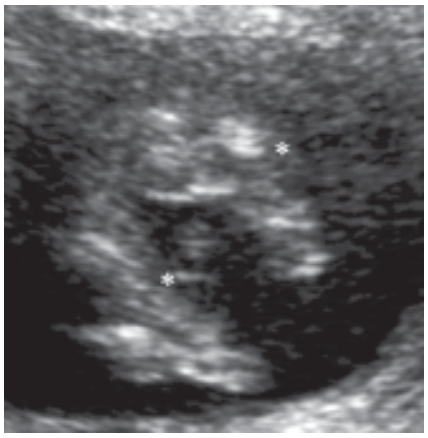

Figure 24.26: Sonogram demonstrating severe micromelia of both lower extremities (*) showing a good degree of mineralization

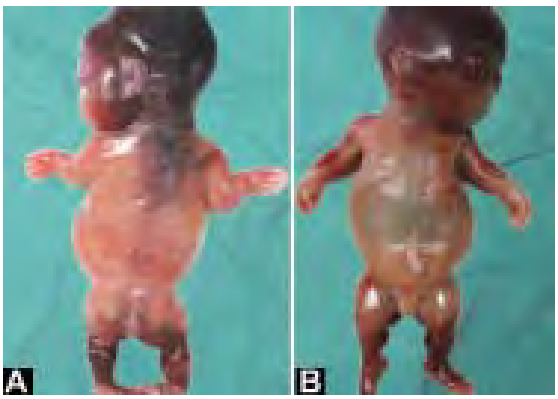

Figures 24.27A and B: Hydropic fetus showing extremely short extremities (severe micromelia). Macrocrania. Very shortened long bones

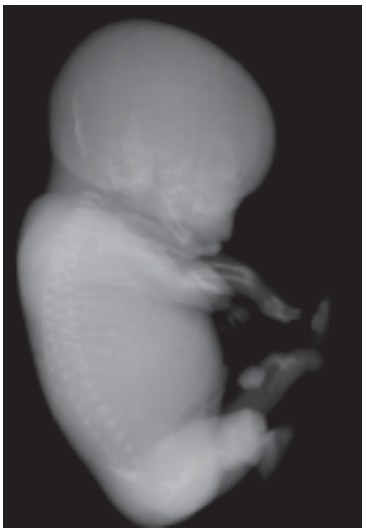

Figure 24.28: Campomelic dwarfism. Postmortem fetography showing short neck and evident long bones anterior bowing

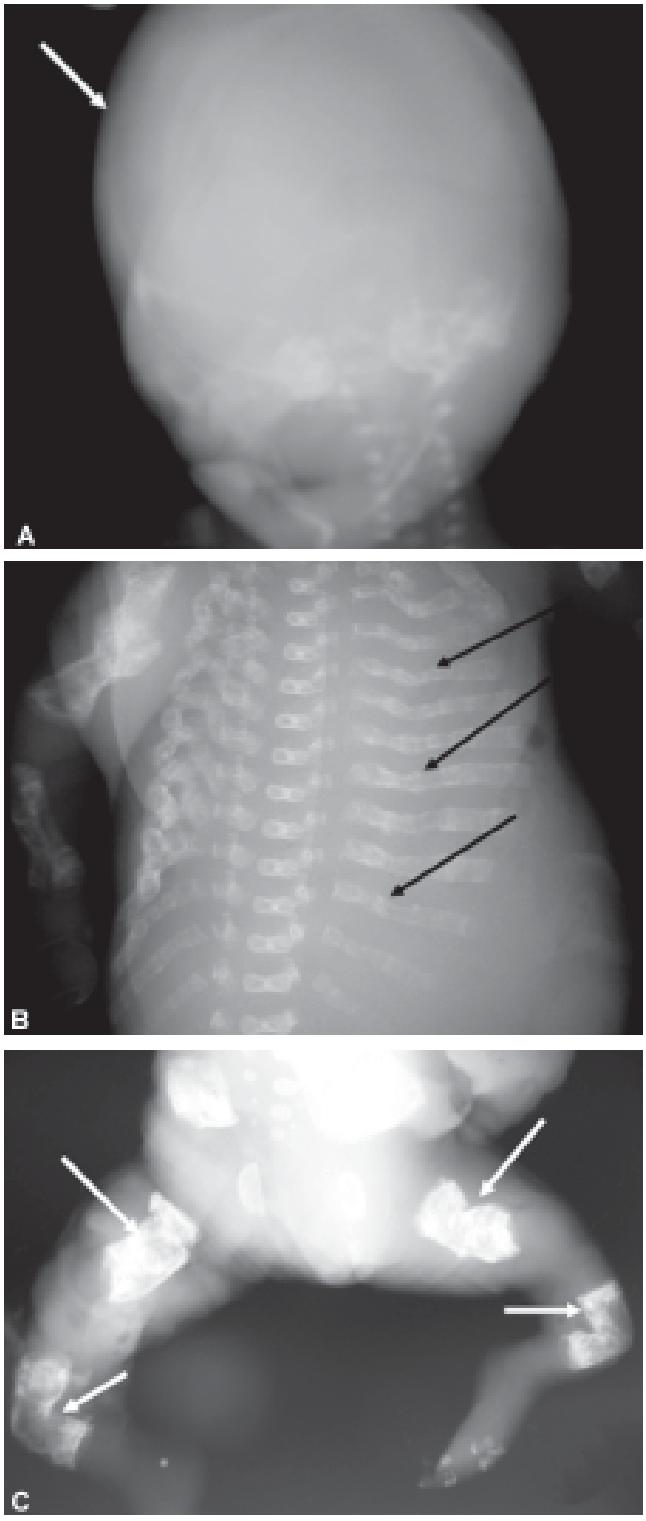

Figures 24.29A to C: Postmortem fetographies. (A) Demineralization of the fetal skull (arrow); (B) Narrow chest caused by multiple fractures of the ribs (arrows); (C) Long bone shortening and angulation due to multiple fractures (arrows)

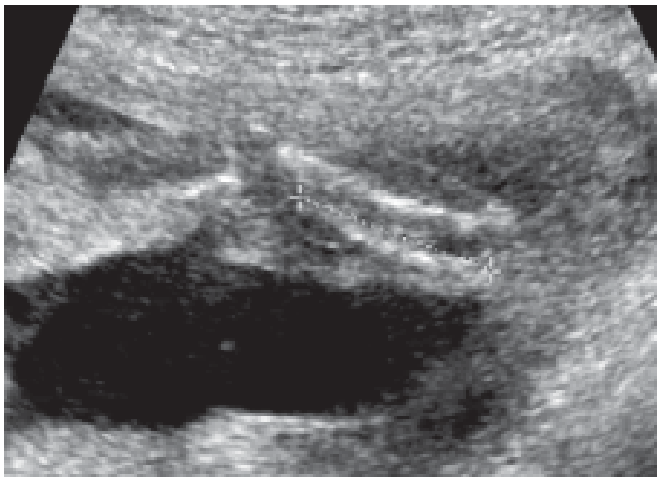

Figure 24.30: One must assess all fetal biometrics. In some cases of early severe IUGR all of them are below the normality

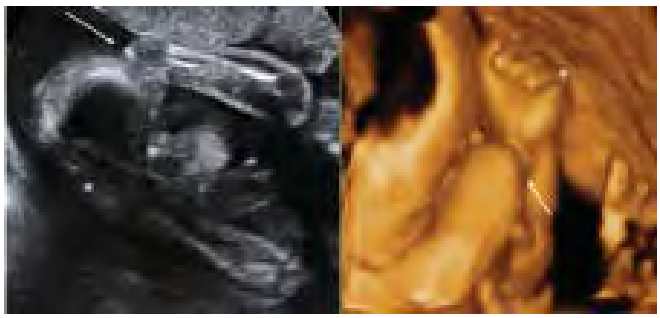

Figure 24.31: Both hands are simultaneously assessed. One can visualize a normal hand (*) and agenesia of the contralateral one (arrow). Assessing simultaneously both hands prevents the error of visualizing twice the same structure

- Achondroplasia
- Achondrogenesis
- Campomelic dysplasia **(Fig. 24.28)**
- Spondylothoracic dysplasia
- Atelosteogenesis
- Others.

The prevalence of skeletal dysplasias **(Figs 24.29A to C)** in newborn is 3–4/10,000 and the frequency of them among perinatal deaths is about 9/1000. Skeletal dysplasias have a variety of phenotypic expressions. Not every case can be assigned a specific diagnosis and other entities may mimic skeletal dysplasias including dysmorphic syndromes and intrauterine growth restriction (IUGR) **(Fig. 24.30)**. The suspicion of a skeletal dysplasia involves systematic imaging of the long bones, thorax, hands **(Fig. 24.31)** and feet, skull **(Figs 24.32 to 24.35)**, spine **(Fig. 24.36)** and pelvis. In the last years,

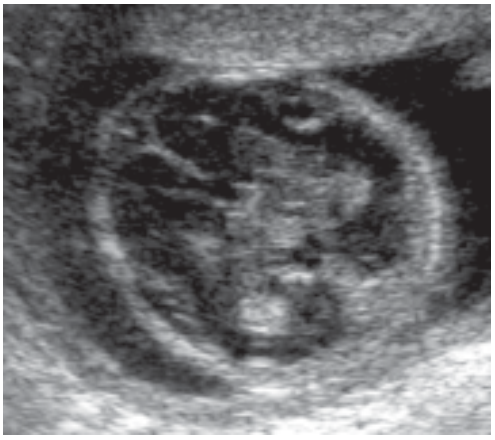

Figure 24.32: The skull demonstrates markedly decreased echogenicity. Normally the distal cortical is shadowed out by the proximal, but not in the severe demineralization of osteogenesis imperfecta. It permits an easy visualization of intracranial structures

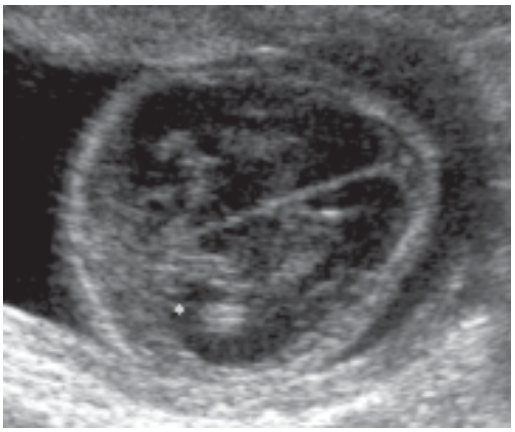

Figure 24.33: Due to the markedly decreased skull mineralization, the encephalic structures may seem abnormal. Note that both atrial shape and measure (*) are normal. The weight of the US probe may deform the head

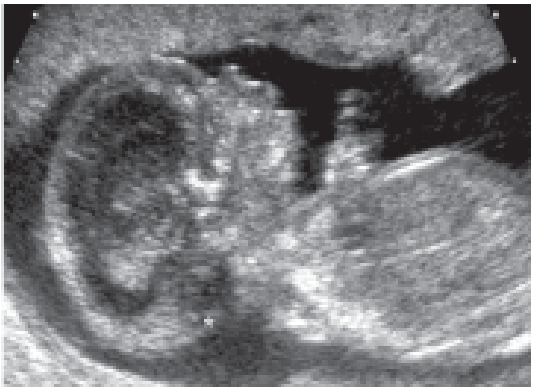

Figure 24.34: Middle sagittal section of the fetal profile assessing the skull demineralization. The distal cortical is only shadowed out in a small occipital zone as shown (*)

Figure 24.35: Demineralized fetal skull. Encephalic tissues can be assessed through the dura mater

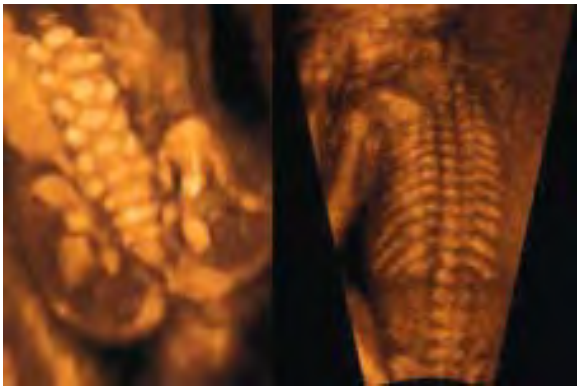

Figure 24.36: Normal fetal 3D spine

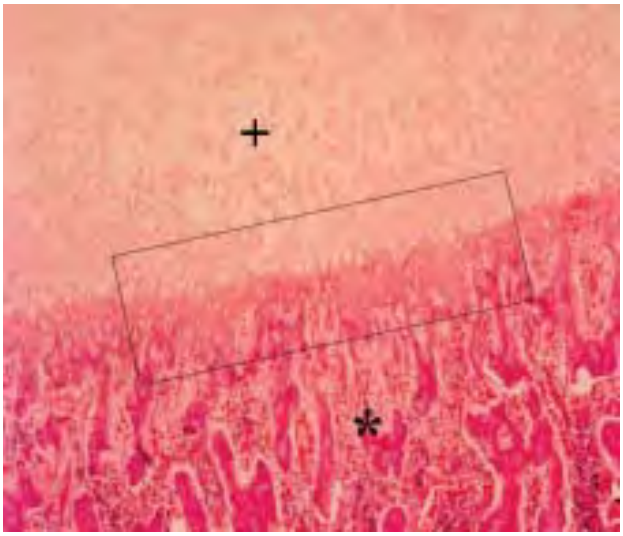

Figure 24.37: Normal enchondral ossification line. Metaphyseal growing region shows a regular aspect (box). One can distinguish the cartilaginous epiphyseal portion (+) and the trabecular bone diaphyseal portion (*)

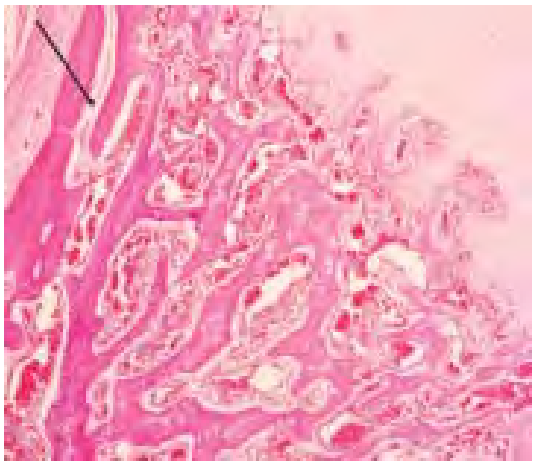

Figure 24.38: Long bones enchondral ossification line showing a severe disruption secondary to vascular invasion (arrow) extending from the metaphyseal ossification zone to the chondrocyte region

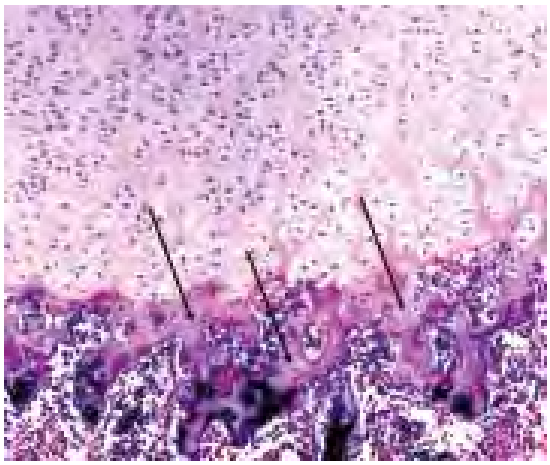

Figure 24.39: Enchondral ossification line of long bones metaphysis showing thick osseous trabeculae that run parallel to the line (arrows)

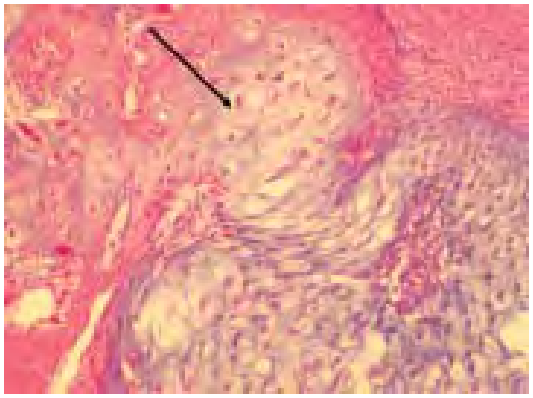

Figure 24.40: Detail of the box shown in Figure 24.37. Note the severe distortion of the enchondral ossification line showing giant anomalous chondrocytes disposed concentrically (arrow)

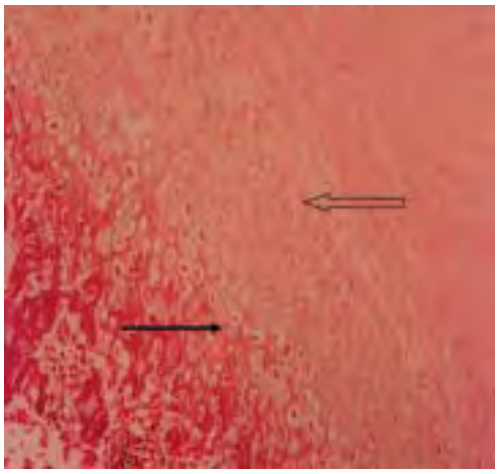

Figure 24.41: Regular enchondral ossification line (arrow). Note the incurvation of epiphyseal region chondrocytes (opened arrow)

3D ultrasound, fetal MRI and fetal CT have been introduced in order to improve diagnostic accuracy. The precise diagnosis is attempted by anatomopathological study, assessing the characteristics of enchondral ossification **(Figs 24.37 to 24.41)** line or ideally by DNA assessment, by identifying mutations responsible for the anatomic alteration.[6] Being able to differentiate lethal disorders from nonlethal disorders, providing differential diagnoses before delivery and determining postpartum management may improve patients' care and postnatal counseling for future pregnancies.

Thanatophoric Dysplasia

It is the most common lethal skeletal dysplasia.[7,8] There are two types, both caused by a gene mutation with an autosomal dominant inheritance. Thanatophoric dysplasia is a severe rhyzomelic micromelia [affecting all portions of a limb **(Figs 24.42A and B)**] with bowing **(Figs 24.43 to 24.45)**. The extremities are very short but the trunk length is normal **(Fig. 24.46)**. Bones are well mineralized and there are no fractures in long bones. The thorax is bell-shaped and the ribs are shortened **(Figs 24.47 to 24.50)**. The platyspondyly (flattened vertebral shape) of the spine is typical **(Figs 24.51 and 24.53)**. There is usually macrocrania **(Fig. 24.53)**, frontal bossing, and a depressed nasal bridge **(Fig. 24.54)**. Approximately 15% of all cases are type II in which the skull is markedly cloverleaf in configuration **(Fig. 24.55)**, with a trilobed appearance in the coronal view, due to the premature closure of cranial sutures. It may associate renal, heart and CNS anomalies **(Fig. 24.56)**. Polyhydramnios occurs in almost 50% of cases. The name is derived from the Greek word thanatophoras

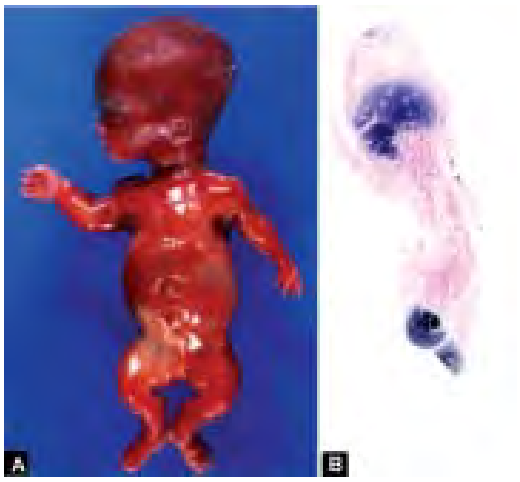

Figures 24.42A and B: (A) Thanatophoric dysplasia. Prominent skull, hypoplastic thorax, severe micromelia. Short and curved thighs; (B) Femur showing the classical telephone receiver configuration, short and curved

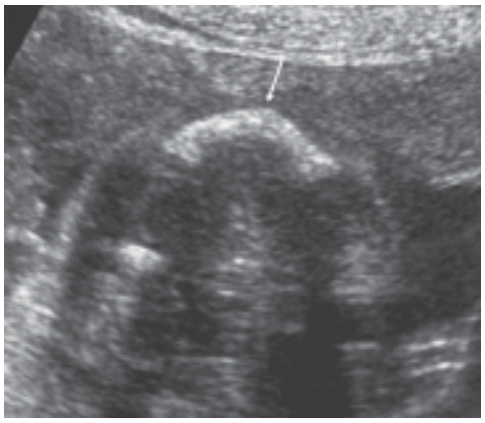

Figure 24.43: Characteristic bowing of the femur (arrow). The classical "bent" bone on ultrasound may mimic a fracture as a result of the acute angulation

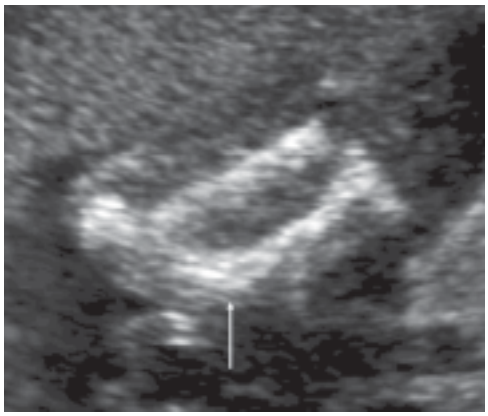

Figure 24.44: Middle portion of lower extremity showing long bone bowing (arrow) but no fractures are seen

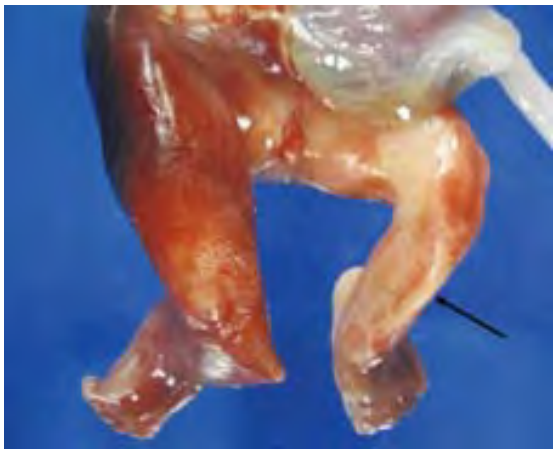

Figure 24.45: Macroscopically one can assess a flattened aspect of the lower limbs tibial bowing (arrow)

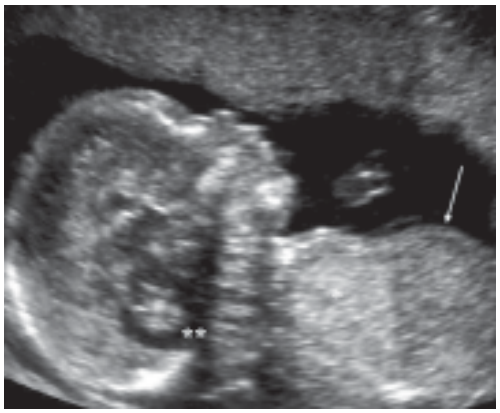

Figure 24.46: Sagittal view of the trunk. A normal abdomen that appears falsely protuberant (arrow) compared to the hypoplastic thorax (*). Bones show a correct mineralization as demonstrated by the posterior shadow behind the jaw (**)

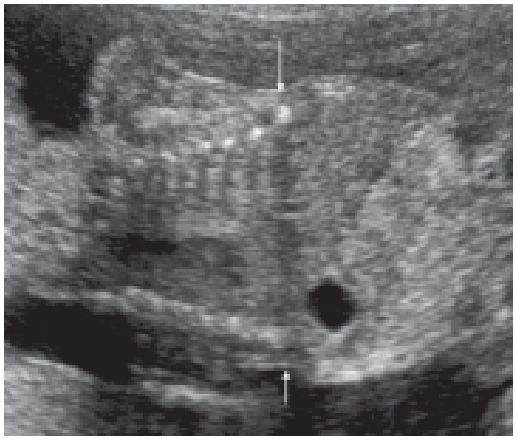

Figure 24.47: Coronal view of the trunk. The thorax is bell-shaped, and the ribs are shortened (but normally mineralized). A normal abdomen appears protuberant compared to the small thorax (arrows)

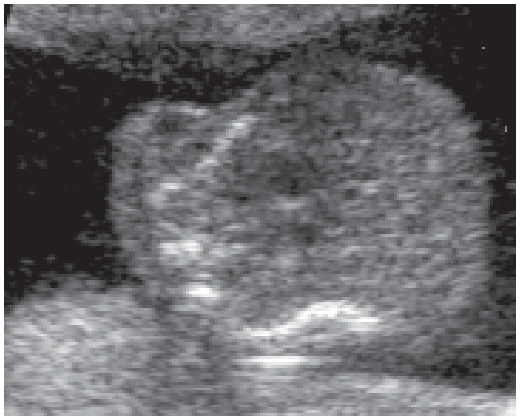

Figure 24.48: Oblique section of the fetal thorax and abdomen. A narrow and bell-shaped thorax can be assessed. The abdomen is normal. Note the anomalous appearance of the ribs (*)

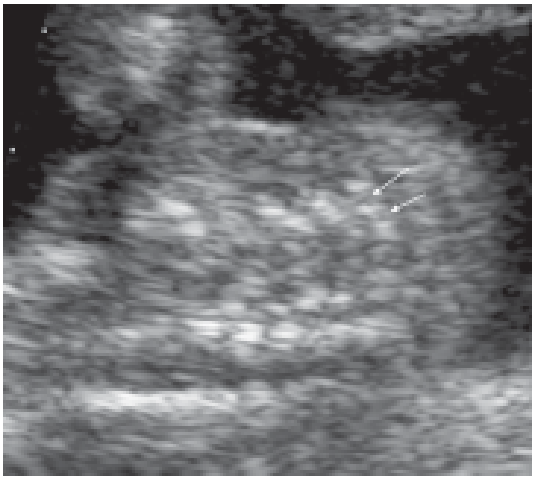

Figure 24.49: Fetal thorax oblique section. Rib shortening, with a wrinkled appearance and angulation caused by multiple fractures (arrows)

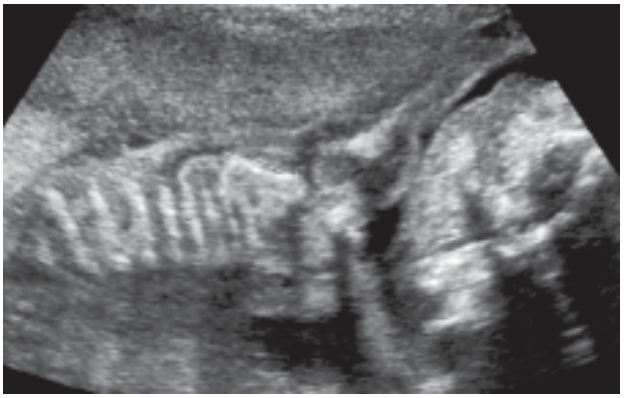

Figure 24.50: Oblique view of fetal thorax. Note the absence of posterior shadow effect behind the scapulae (crosses). Short and bell-shaped thorax

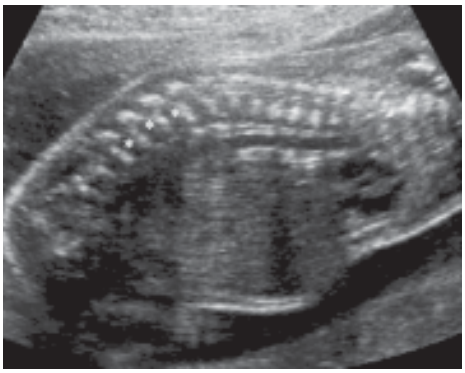

Figure 24.51: Sagittal section of the trunk. Platyspondyly (*) is severe; the vertebral ratio is the smallest of the skeletal dysplasias

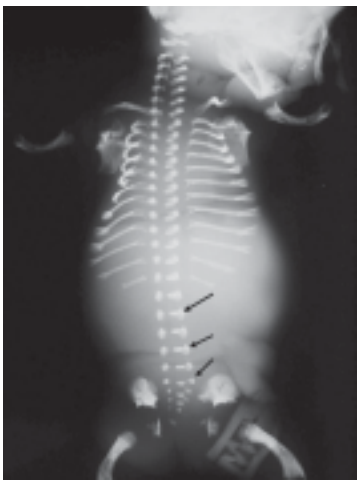

Figure 24.52: Severe platyspondyly (arrows), as shown in this postmortem fetography

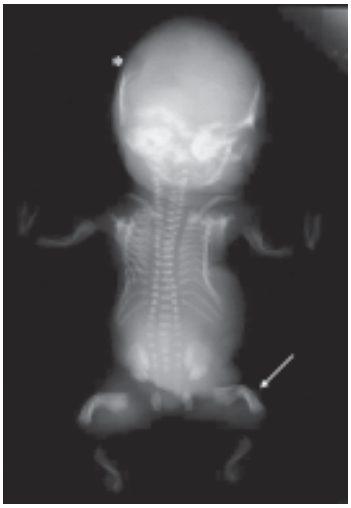

Figure 24.53: Postmortem fetography of a fetus with thanatophoric dysplasia. Macrocrania, normal skull mineralization (*), hypoplastic thorax, micromelic limbs. Femur showing the classical telephone receiver configuration (arrow)

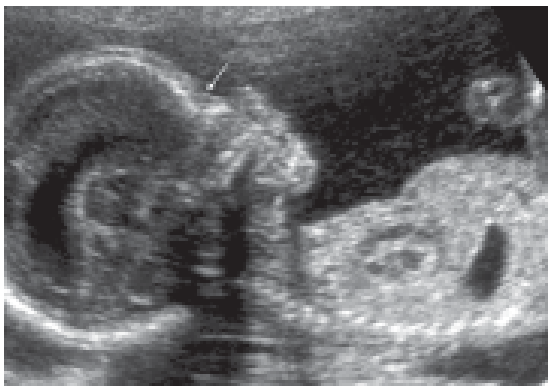

Figure 24.54: Sagittal view. Macrocrania, frontal bossing and depressed nasal bridge. The thorax is hypoplastic and responsible for the classical pulmonary hypoplasia that determinates its ominous prognosis. There are no associated visceral anomalies

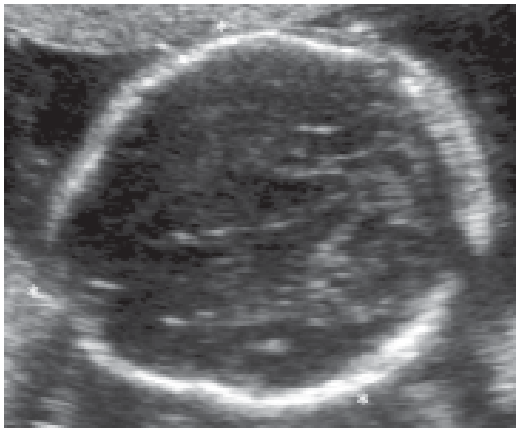

Figure 24.55: Transverse view of fetal skull. Initial form of a cloverleaf skull (*). This sign in association with a severe micromelia is pathognomonic of thanatophoric dysplasia. The encephalic structures are usually normal. Other abnormalities that may be seen include gyration disorders

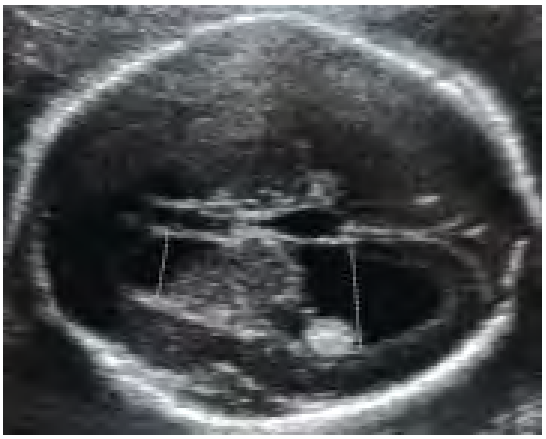

Figure 24.56: Ventriculomegaly (between calipers) secondary to a reduced magnum foramen. When no CNS anomalies are prenatally detected, psychomotor development is normal

meaning "death bearing" because of the uniformly lethal outcome of this dysplasia in the perinatal period, mainly due to pulmonary hypoplasia secondary to thoracic hypoplasia.[9]

Osteogenesis Imperfecta

Heterogeneous group of genetic disorders[10] that affect the type I collagen. It is characterized by severe bone fragility, blue sclera and prenatal growth deficiency. It is caused generally by a new gene mutation with an autosomal dominant inheritance. They are classically divided in four types. Type II (Vrolich type) is the most severe form and the most frequently diagnosed by antenatal ultrasonography. Osteogenesis imperfecta type II presents as a severe global osteochondrodysplasia affecting all segments (micromelic type). It is characterized by severe bone fragility, leading to abnormal ossification **(Fig. 24.57)** and multiple fractures **(Fig. 24.58)** and bone angulations **(Fig. 24.59)**. There are

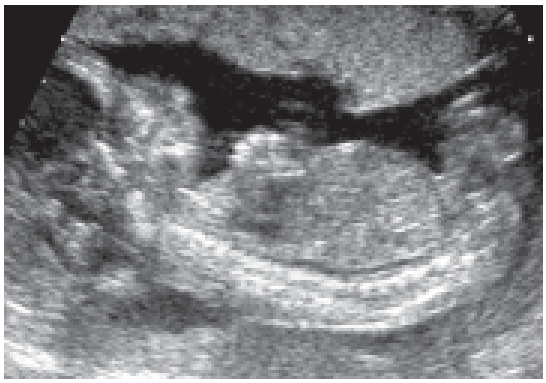

Figure 24.57: Sagittal section. Abnormal ossification of the fetal skull as shown by the absence of posterior shadowing

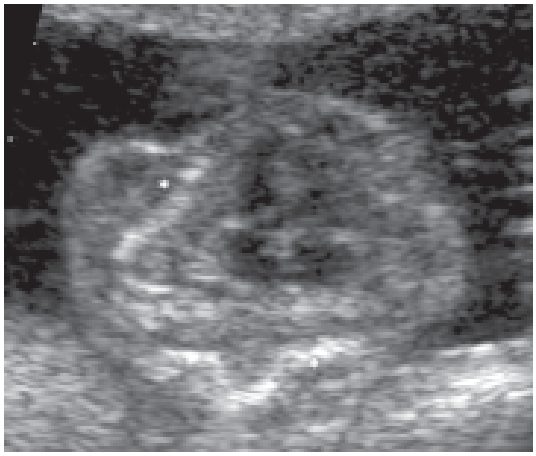

Figure 24.58: The four-chambers view. Narrow chest caused by fractures of the ribs and wrinkling of the surface of the bones due to multiple fractures (*)

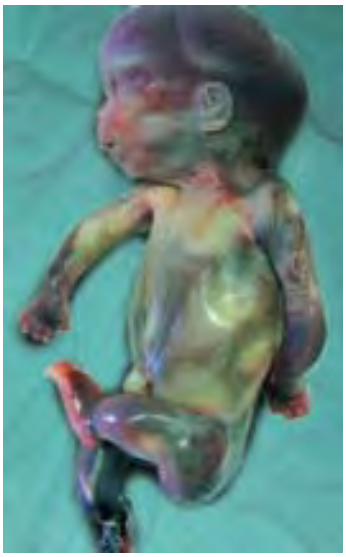

Figure 24.59: Osteogenesis imperfecta type II. Long bone shortening and angulation due to multiple fractures

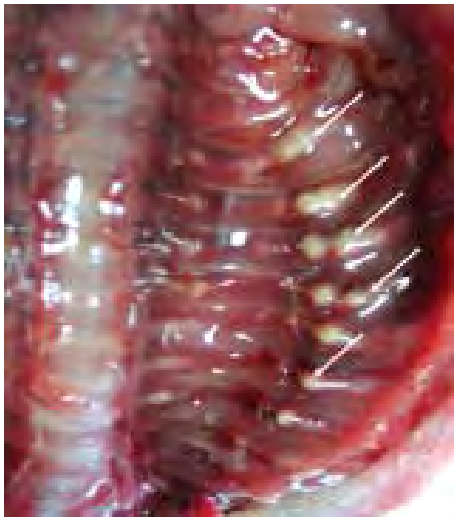

Figure 24.60: Osteogenesis imperfecta type II. Multiple fractures of the ribs. The callous formation may be assessed microscopically (arrows)

no associated visceral malformations and fetal movements may be reduced. Type II osteogenesis imperfecta is uniformly lethal and the most frequent causes are respiratory failure due to pulmonary hypoplasia secondary to thoracic hypoplasia as a consequence of multiple rib fractures **(Fig. 24.60)** and cerebral hemorrhage.

Achondroplasia

Osteochondrodysplasia is characterized by a rhyzomelic (affecting humerus and femur) micromelia. Bone

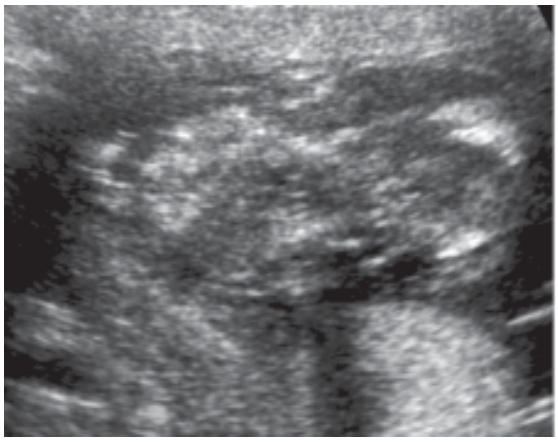

Figure 24.61: Coronal view of a fetus with achondroplasia. Note the hypoplastic and short chest and the characteristic macrocrania. Poorly mineralized fetal spine

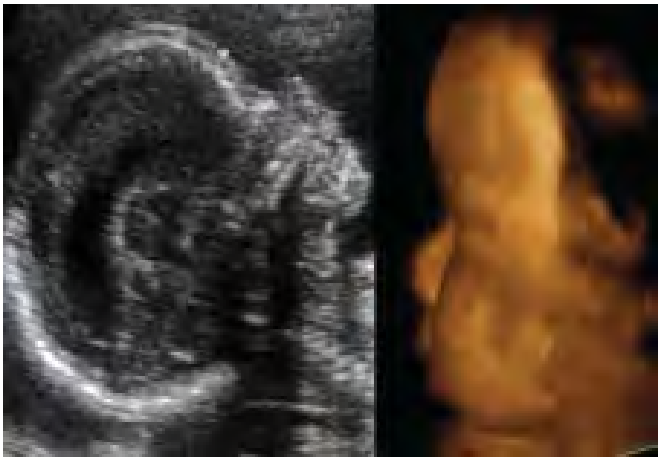

Figure 24.62: Fetal profile. Frontal bossing, depressed nasal bridge. Features are not evident until the third trimester. Usually prenatal detection of this condition cannot be established before 20 weeks

mineralization is normal and there are no long bone fractures. Thoracic shape is normal. A macrocrania **(Fig. 24.54)**, frontal bossing and depressed nasal bridge **(Figs 24.61 and 24.62)** can also be recognized. The trident hand (an increased interspace between the third and fourth digit) **(Fig. 24.64)** or the lack of widening of the lumbar canal can also be identified **(Fig. 24.63)**. Prenatal detection is usually established at late second or third trimester because in most cases osseous **(Fig. 24.65)** lengths are normal up to 25 or 26 weeks of gestation, at this moment the growing pattern reaches a plateau. Homozygous achondroplasia is uniformly lethal. But the most frequent form, the heterozygous type, has a good global and intellectual prognosis.

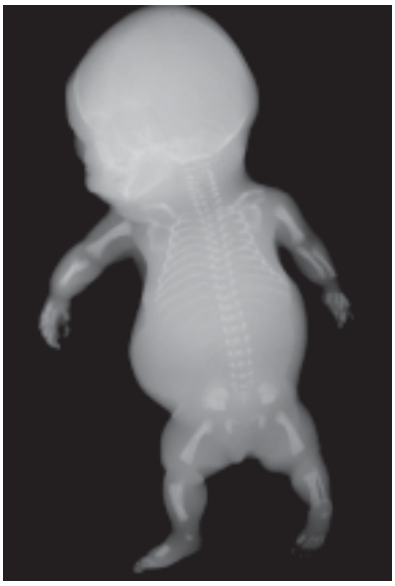

Figure 24.63: Postmortem photography of an achondroplasic fetus showing frontal bossing, depressed nasal bridge and rhizomelia

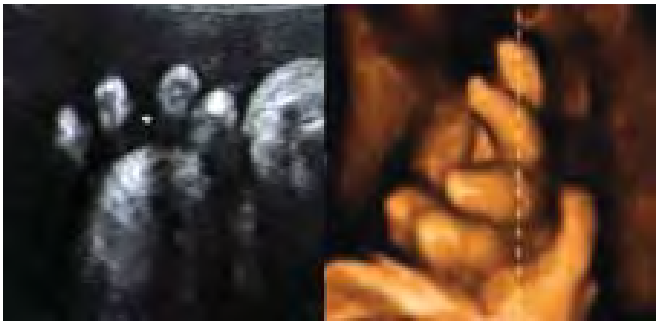

Figure 24.64: 2D and 3D views. A trident hand. The four fingers have the same length. Note the increased interspaces between the third and fourth digit (*). Hand articular motility is still normal

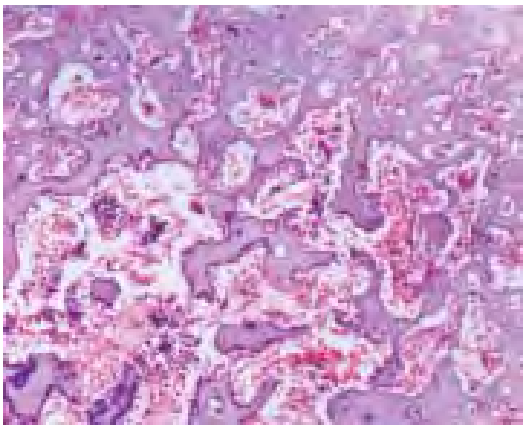

Figure 24.65: Chondrocostal ossification abnormality showing a reduced chondrocyte component. Thick and disorganized osseous trabeculae

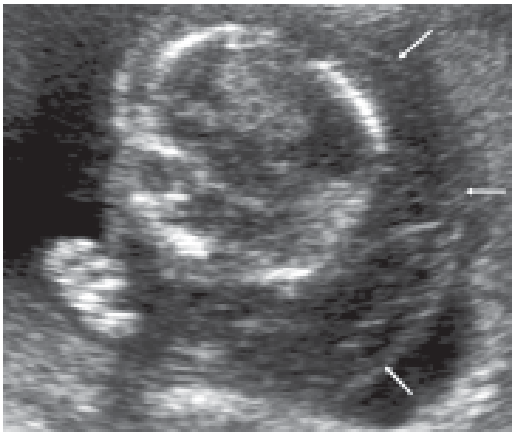

Figure 24.66: View of the head. Note the double contour of the skull (arrows) that suggests a generalized lymphatic drainage defect. The skull is compressible by the transducer, which permits a good visualization of the intracranial structures

Achondrogenesis

Lethal osteochondrodysplasia characterized by bone hypoplasia, resulting in marked global limb shortening (severe micromelia) and associated with severe pulmonary hypoplasia. There is a poor skull and vertebral ossification with macrocrania. It may have gastrointestinal abnormalities. Polyhydramnios is common, as is marked redundancy of the subcutaneous tissues (pseudohydrops) and generalized subcutaneous edema due to lymphatic ectasia **(Fig. 24.66)**. There are two types:

1. Type I involves a lack of ossification of the skull and the spine, with short bones and rib fractures
2. Type II: the skull ossification is relatively normal, without rib fractures. The outcome is fatal, although type II may survive for short periods in the neonatal period.

Campomelic Dysplasia

Campomelic dysplasia is a congenital disorder characterized by development of abnormal curvatures of long bones, particularly from lower extremities such as femur and tibiae **(Fig. 24.67)**. Other sonographic features that are commonly present include bell-shaped narrow chest, eleven pairs of ribs and hypoplasia of the midthoracic vertebral bodies, fibula and scapula **(Fig. 24.68)**. Even if karyotypic sex ratio is approximately M2:F13, the vast majority show a female phenotype with ambiguous genitalia. It may associate heart anomalies, hydronephrosis and hydrocephalus. Almost all result in neonatal or infant death due to respiratory complications secondary to tracheobronchomalacia.

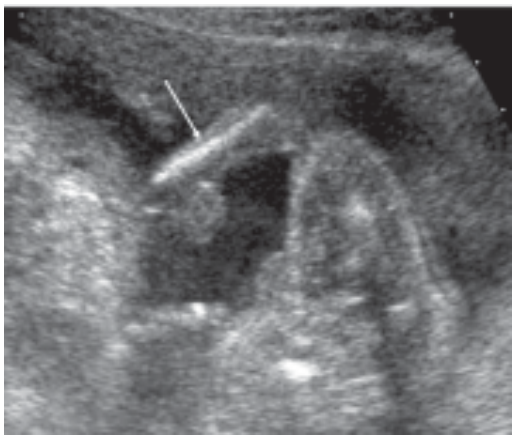

Figure 24.67: Lower extremity showing a single bone (arrow), probably the fibula. It may be isolated or part of a femur-fibula-cubitus complex (that shows sporadic presentation)

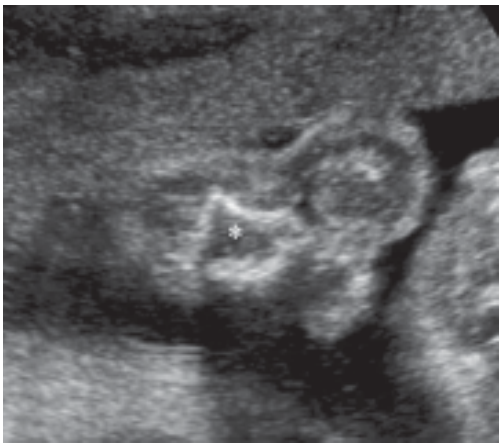

Figure 24.68: Coronal view of the scapula showing its poor mineralization

Spondylothoracic Dysplasia (Jarcho-Levin Syndrome)

The spondylothoracic dysplasia is actually a group of disorders[10] characterized by delayed ossification and deformity of the spine and ribs **(Fig. 24.69)**. The prognosis is variable, with some lethal forms and other types that can reach the adult life. It is important to establish the differential diagnosis with other osteochondrodysplasias such as asphyxiating thoracic dysplasia (Jeune thoracic dystrophy), short ribs-polydactyly syndrome, etc.

Atelosteogenesis

It is also known as spondylohumerofemoral dysplasia. It is characterized by a "bent" tibia **(Fig. 24.70)** showing a "boomerang" configuration **(Figs 24.71 and 24.72)** and the absence of fibula, with shortened long bones.

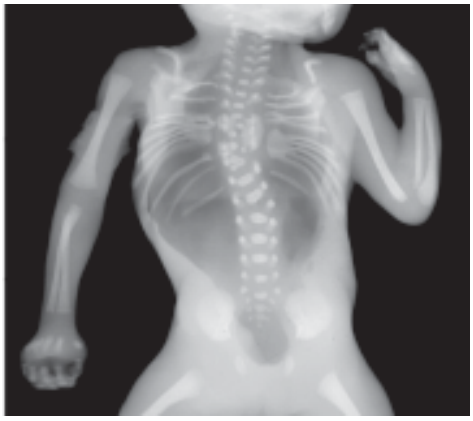

Figure 24.69: Postmortem fetography of a fetus with spondylothoracic dysplasia type Jarcho-Levin, showing hemivertebrae and vertebral fusion. Fused dorsal vertebrae and ribs

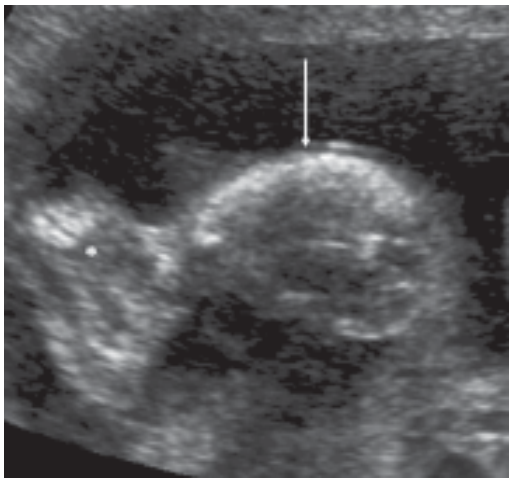

Figure 24.70: Tibia is "bent". Compare tibia (arrow) and forefoot (*) lengths

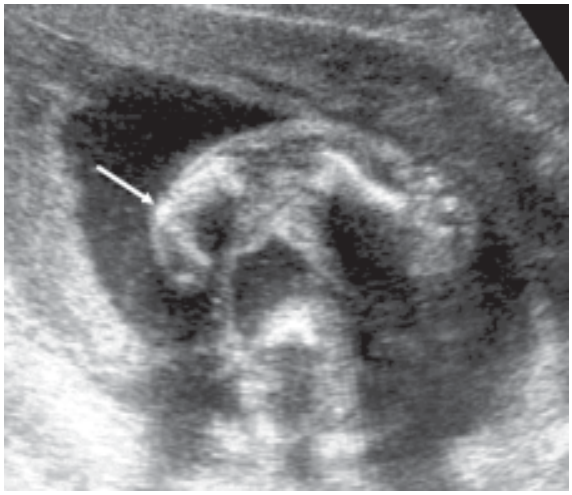

Figure 24.71: Bowing of the tibiae showing the "boomerang" configuration (arrow). The fibula cannot be assessed

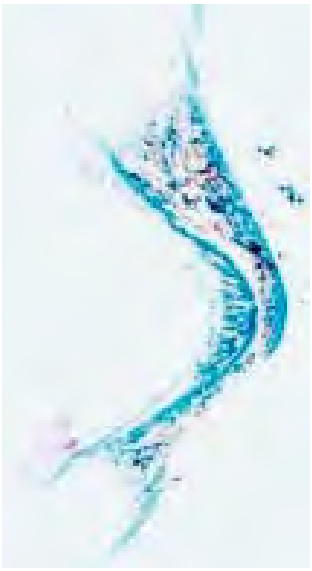

Figure 24.72: Tibial diaphysis bowing showing the classical "boomerang" configuration

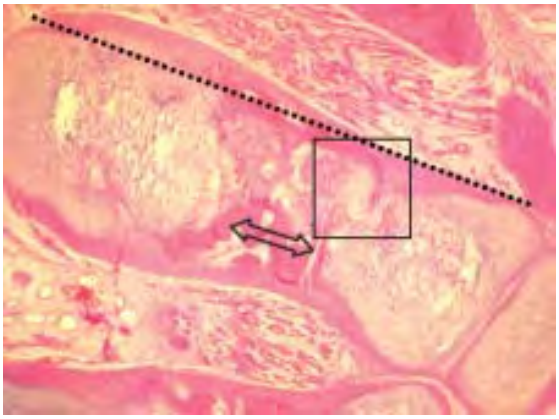

Figure 24.73: Very shortened long bones. Microscopic view of the radius (dot line). Diaphyseal minimal length (double arrow) in a 15 weeks fetus

Other Osteochondrodysplasias

Occasionally long bones have a normal appearance but they are shortened **(Fig. 24.73)**. The differential diagnosis between some conditions, such as an authentic osteochodrodysplasia, a normal variant or an IUGR **(Fig. 24.74)**, must be considered. One must follow up bone growing pattern. Standard obstetrical management is not altered. In the newborn period and during infancy the growing process must be strictly controlled.

Reductional Defects

Heterogeneous group of diseases characterized by the absence of any portion of a limb. Actually the term

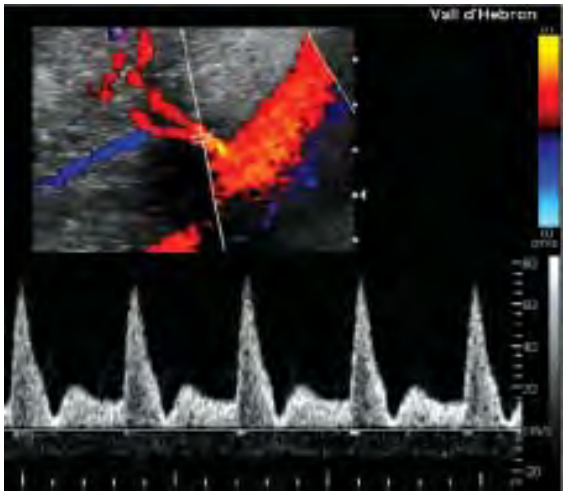

Figure 24.74: Uterine artery Doppler waveform is clearly pathological, orienting the differential diagnosis to an IUGR of vascular etiology excluding in almost all cases the presumption of osteochondrodysplasia

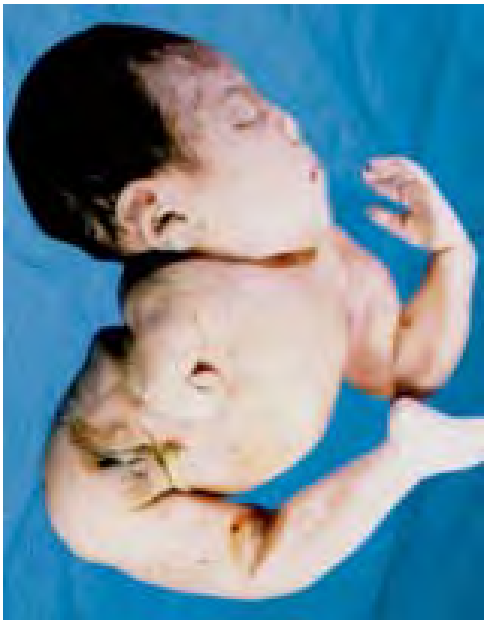

Figure 24.75: Limb reductional defects secondary to constriction in a right lower limb. Amputation of the forearm and hand probably secondary to constriction of the developing limb during fetal life

amputation **(Fig. 24.75)** has been substituted because in the vast majority of cases the defect is due to a development alteration **(Fig. 24.76).** It includes:

- Terminal defects
- Phocomelias
- Proximal focal femoral deficiency
- Split-hand and split-foot syndromes.

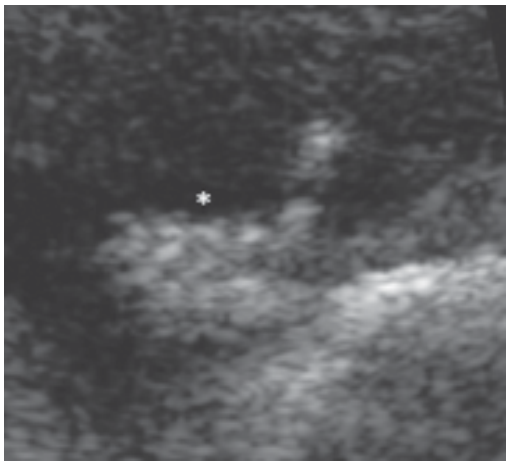

Figure 24.76: Fetal hand showing a reductional defect. Oligodactyly. Absent phalanges of third, fourth and fifth digits (*). To evaluate fetal phalanges the hand must be opened. A closed hand must not be misinterpreted as an adactyly

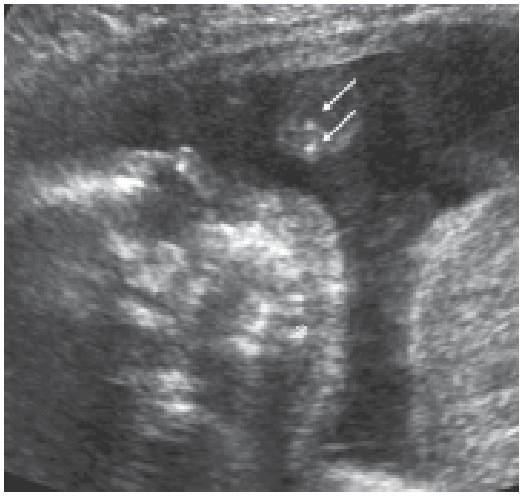

Figure 24.77: Arrows showing hypoplastic ulna and radius as typically seen in reductional defect cases. One must assess facial structures (*) in order to find cleft lips, tongue defects or microretrognathia that may be associated with constituting a genetic syndrome

They are often (50% of cases) isolated defects and usually affect only one extremity. Twenty five percent may affect more than one limb and 25% may be associated with other structural defects or are features of a genetic syndrome **(Fig. 24.77)**. The outcome depends on the degree of compromise and the possibility of a correct postnatal orthopedic surgical repair.The term *amelia* means the complete absence of the limb and *meromelia* is used with the partial absence of a limb **(Fig. 24.78)**. **Figure 24.79** shows fetal arm with elbow pterygium. Various other lower extremity defects are shown in **Figures 24.80 and 24.81**.

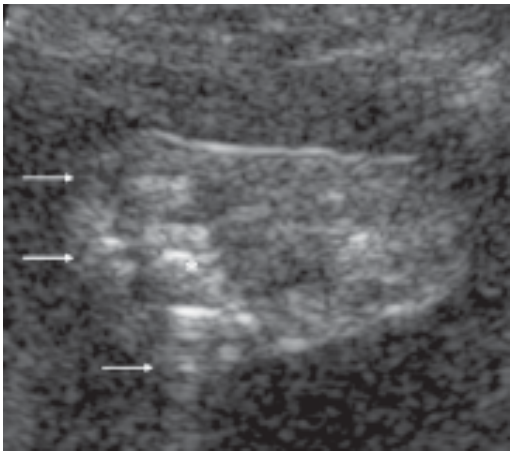

Figure 24.78: Fetal foot showing a reductional defect. One can assess in the forefoot view a normal metatarsal (*) but hypoplastic digits, without any osseous component (arrows)

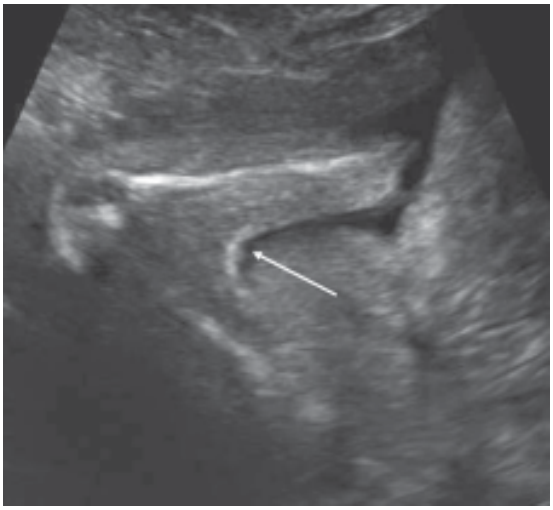

Figure 24.79: Fetal arm with elbow pterygium (arrow)

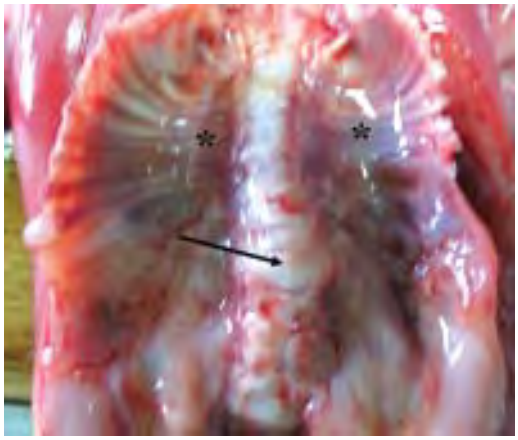

Figure 24.80: Radial disposition of ribs (*) and protrusion of vertebral bodies (arrow)

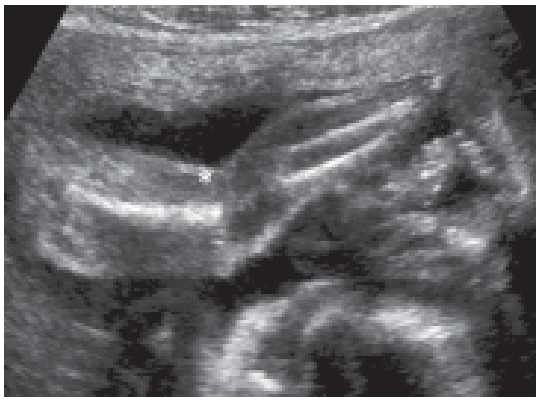

Figure 24.81: Lower extremity showing a normal appearance but very shortened (below 5 centile) (*)

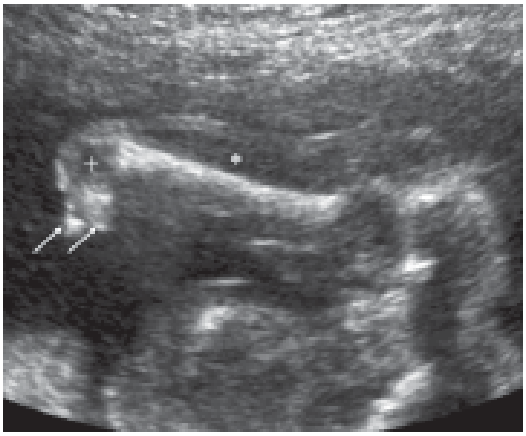

Figure 24.82: Upper extremity showing a terminal defect. Normal humerus (*) with a hypoplastic cubitus and ulna (arrows) and absence of almost all forearm and hand. The articulation below the humerus usually remains unaffected (+)

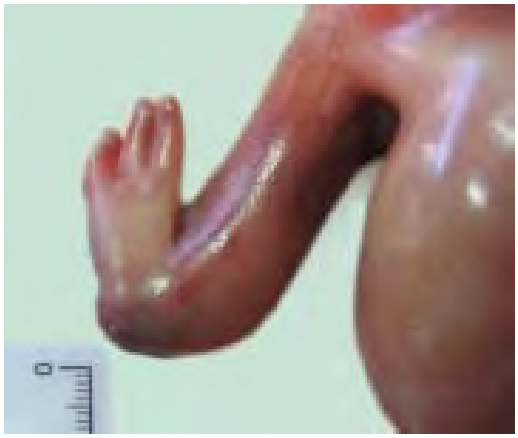

Figure 24.83: Upper extremity showing a terminal defect. Normal humerus with a hypoplastic ulna and radius and absence of almost all forearm and hand. The articulation is usually unaffected

Terminal Defects

Usually affecting upper extremities **(Figs 24.82 and 24.83)**. Seventy five percent under arm articulation and more frequently left sided. They may be associated with other structural defects as features of a genetic syndrome. They can be found in association with facial defects (microretrognathia) as part of genetic syndromes.

Constriction Band Sequence

Sporadic entity, that causes asymmetric amputations of the limbs. Amniotic bands may cause limb reductional defects **(Figs 24.84 to 24.89)**, constrictions or other anomalies due to vascular compromise or interference in the normal development of fetal extremities **(Fig. 24.90)**. They must be distinguished from placental septation that is a septum that crosses the uterine cavity **(Fig. 24.91)** without affecting the fetus.

Phocomelia

The name is derived from the "seal" aspect of the fetuses **(Fig. 24.92)**. The terminal and middle portion of the limbs are aplastic or hypoplastic. Feet and hands are directly articulated to the ankle or shoulder and they may be normal or abnormal. Phocomelia can occur sporadically (for example, related to thalidomide drug) although it can be seen in many genetic syndromes and conditions such as Holt-Oram syndrome, Thrombocytopenia absent radius (TAR) syndrome **(Fig. 24.93)** and Robert's syndrome (characterized by midface and limb anomalies; which are usually severe with microcefalia and growth restriction).

Proximal Femoral Focal Deficiency

It is a rare anomaly varying in severity from a marginally short femur **(Fig. 24.94)** to a complete absence of femur in severe cases **(Figs 24.95 to 24.97)**. It may be a unilateral defect (usually right sided) or bilateral in 10–15% of cases. The PFFD is almost always an isolated occurrence except for associated ipsilateral fibular hemimelia (sporadic) or ulnar hemimelia (genetic).

Split-hand and Split-foot Malformation (Ectrodactyly)

The SHFM is a limb malformation[9] **(Figs 24.98 and 24.99)** involving the central rays of the autopod (the distal division of the limb such as hands or feet) and presenting with syndactyly, median clefts of the hands and feet, and aplasia and/or hypoplasia of the phalanges, metacarpals and metatarsals. The two typical manifestations are:

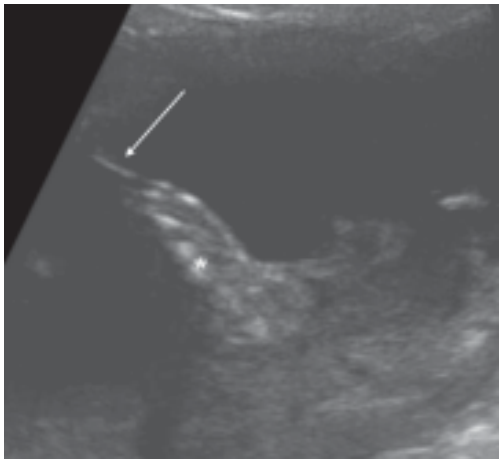

Figure 24.84: Amniotic band (arrow) connecting amnios and foot (*)

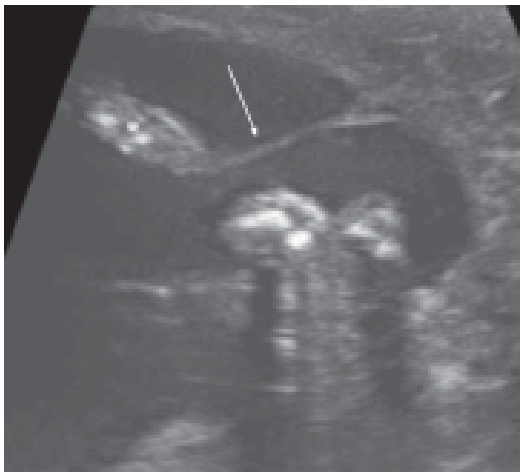

Figure 24.85: Amniotic band (arrow) connecting amnios and hand (*)

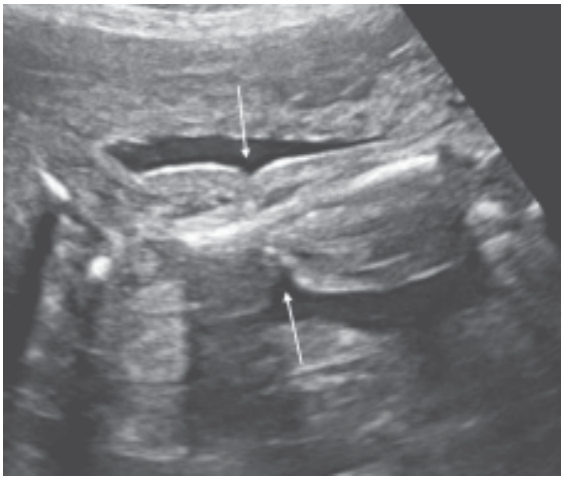

Figure 24.86: Constriction band in a low extremity (arrows). Note the lymphedema secondary to vascular constriction

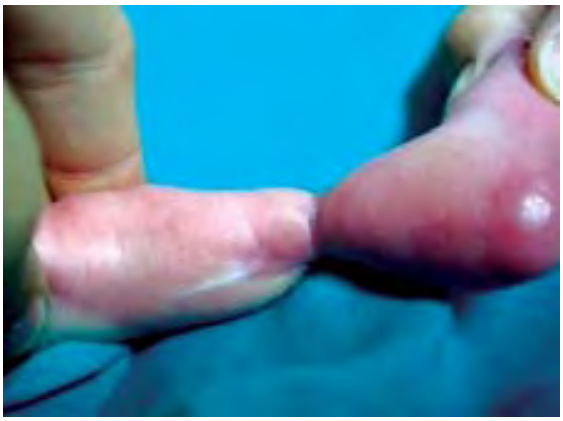

Figure 24.87: 28 weeks newborn with a constriction band in a low extremity

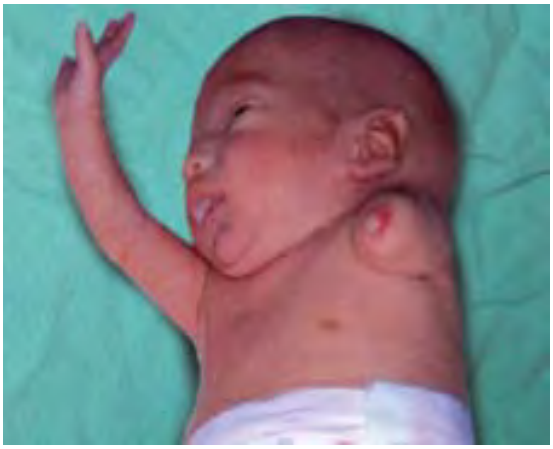

Figure 24.88: Newborn with a reductional defect due to an amniotic band. The articulation remains unaffected. Contralateral upper extremity showing a normal appearance

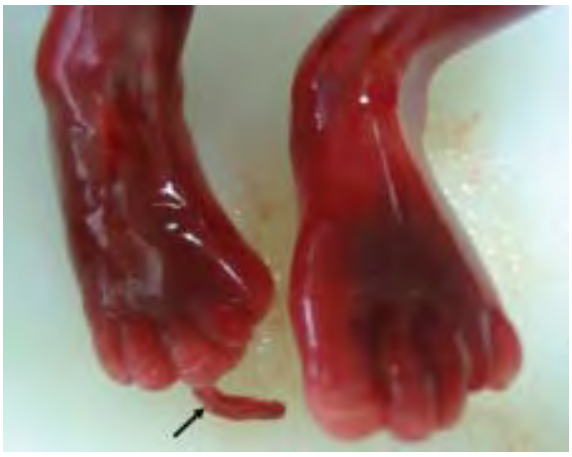

Figure 24.89: Shorter digits of the right foot secondary to amniotic bands (arrows)

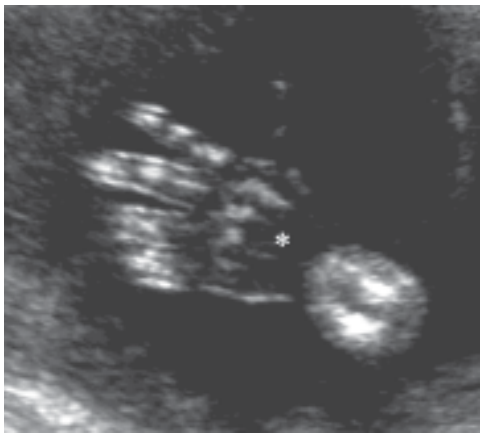

Figure 24.90: Contralateral normal arm and hand (*). In 50% of cases the compromise is isolated and the contralateral limb is unaffected. The US assessment of fetal extremities must be meticulous and must include visualization of both extremities independently

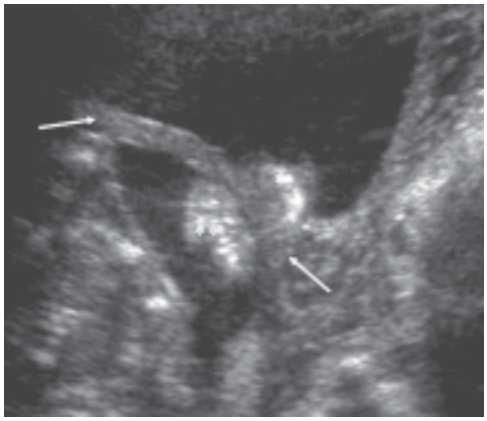

Figure 24.91: Placental septation that does not affect the fetus. It crosses the uterine cavity. Arrows show its myometrial insertions. Fetus with his opened mouth surrounding the septation (upper maxilla*, lower maxilla**). Finding a placental septation is relatively frequent and does not require a special follow-up

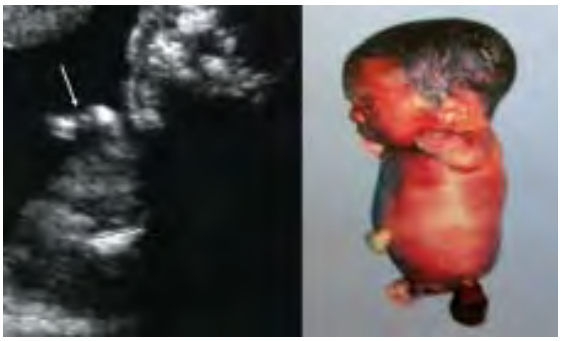

Figure 24.92: Phocomelia of upper fetal extremity. Anomalous hand (between callipers) directly inserted in the trunk without evidence of middle or proximal portions of the upper limb (arrow)

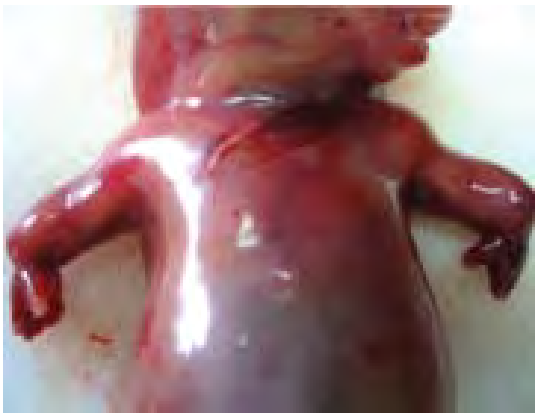

Figure 24.93: TAR (thrombocytopenia-absent radius) syndrome. Note that fetal thumb is present

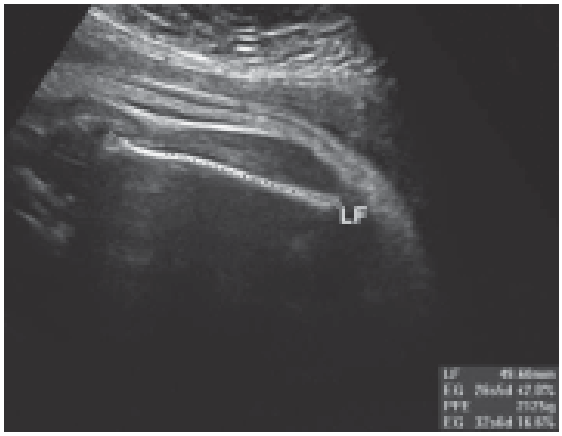

Figure 24.94: Sonogram of a fetal femur that shows a normal configuration but extremely shortened (< 5 percentile). The humerus is also affected. Note the difference between the real gestational age (EG) and the corresponding to the femur measurement on the legend of the picture

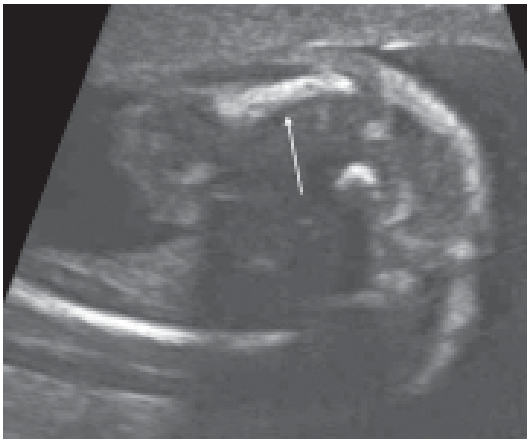

Figure 24.95: The femur appears shorter than the contralateral one (arrow). Even if one measures only one femur, diaphysis of both bones must be visualized in order to exclude any long bone asymmetry

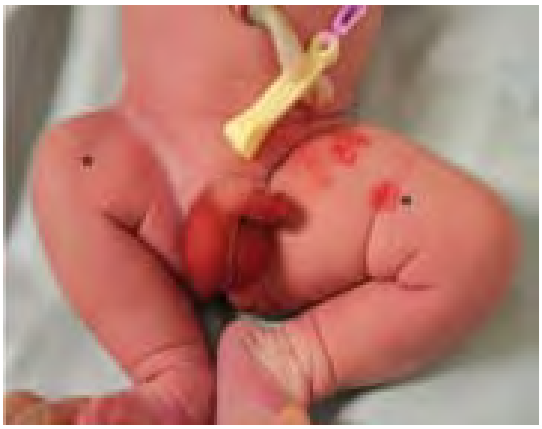

Figure 24.96: Femoral focal deficiency in a newborn. Note the significant difference in the length between the proximal part of the lower extremities (*)

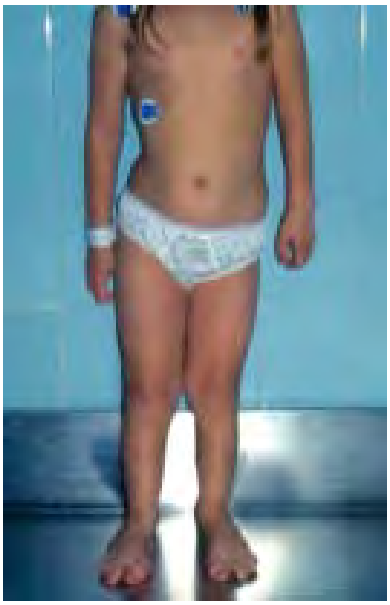

Figure 24.97: Proximal femoral focal deficiency. Asymmetrical shortening of lower extremities

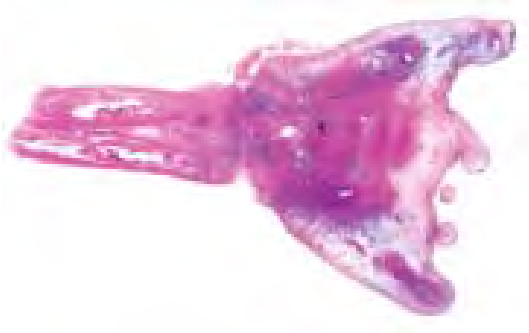

Figure 24.98: Macro-microscopic image (histological specimen) of a characteristic ectrodactyly

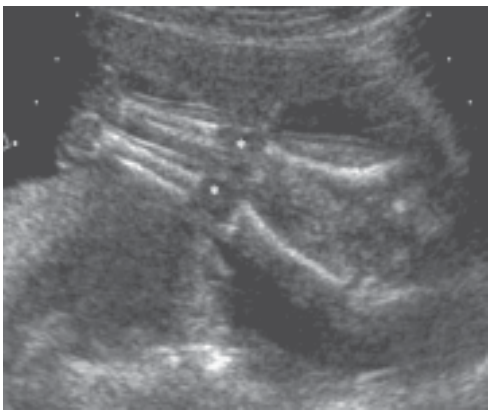

Figure 24.99: Lower limbs extended in a rigid position. The knee joint is rigid (*)

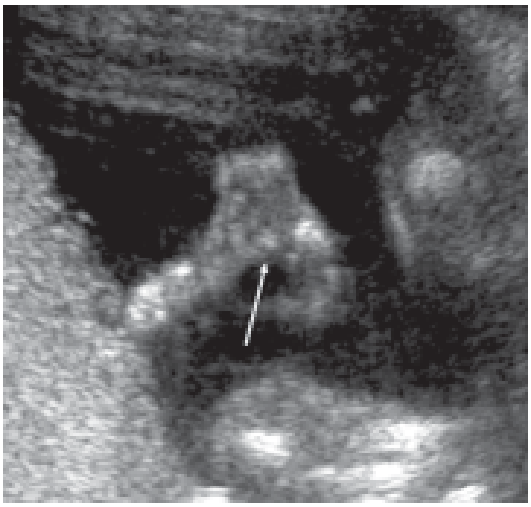

Figure 24.100: Deep fetal hand cleft showing a "V" configuration (arrow). Absence of differentiation of metacarpals and phalanges

1. The typical isolated case, affecting all four limbs in a "V" configuration and showing a familial presentation **(Figs 24.100 to 24.102)**.
2. The atypical isolated case, affecting only one extremity (usually the upper limbs), in a "U" configuration **(Figs 24.103 and 24.104)**.

SHFM may be associated with other structural defects as in the cleft hand and absent tibia syndrome or absent cubitus syndrome.

It may also be associated with the EEC (electrodactyly-ectrodermal dysplasia—cleft lip or palate) syndrome **(Figs 24.105 to 24.107)**.

The differential diagnosis includes constrictive amniotic bands.

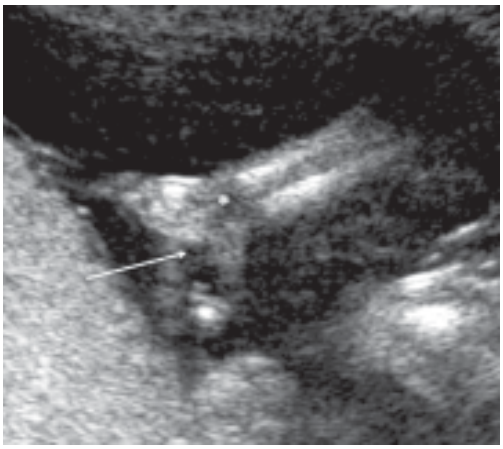

Figure 24.101: Deep cleft in fetal hand, demonstrating a "V" configuration (arrow). The ulna, radius and wrist joint show a normal aspect

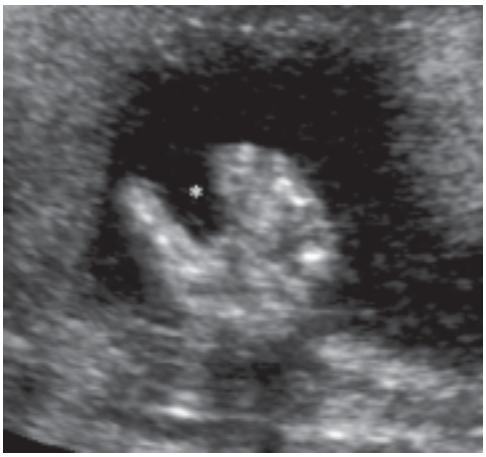

Figure 24.104: "U" configuration of a fetal hand (arrow) demonstrating poorly differentiated fingers

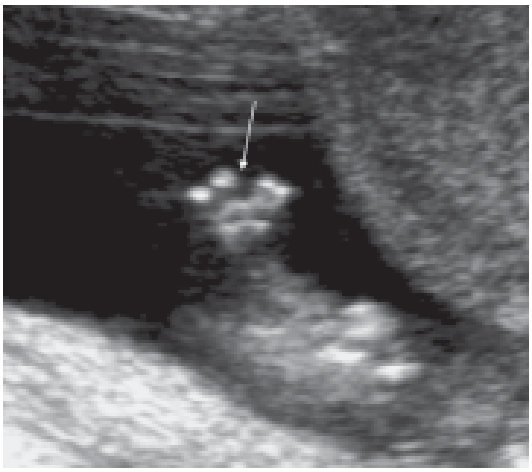

Figure 24.102: 12 weeks fetus showing a "V" configuration hand cleft. The diagnosis is confirmed. Both hands must be assessed in the first trimester sonographic examination

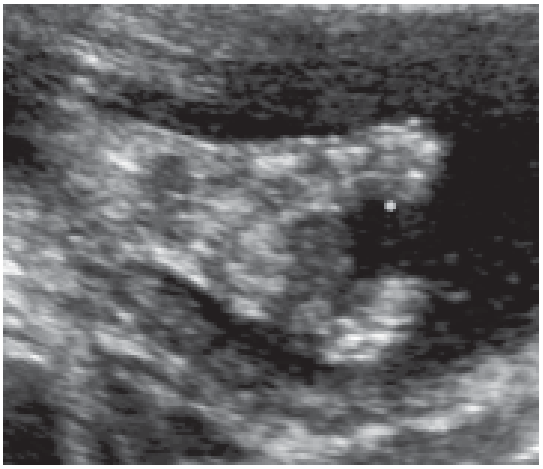

Figure 24.105: View of the sole of a foot showing a deep central cleft with a "U" configuration (*) and syndactyly

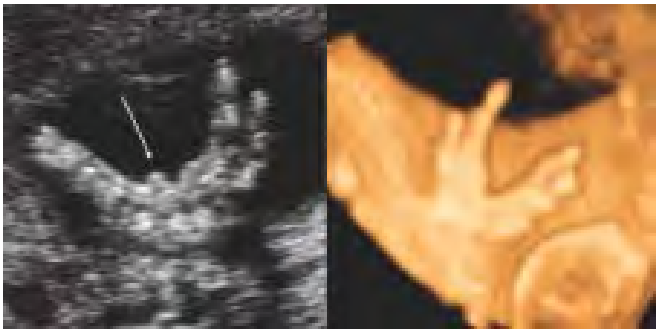

Figure 24.103: "U" configuration hand cleft (arrow). Only three digits can be identified showing a normal differentiation of metacarpals and phalanges. As it constitutes a sporadic event one must strictly explore all four limbs

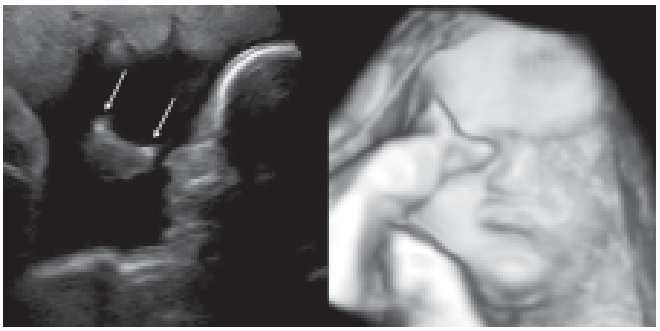

Figure 24.106: Ectrodactyly. Split "V" shaped hand. The arrows show the two fingers. If it is isolated, the prognosis is good

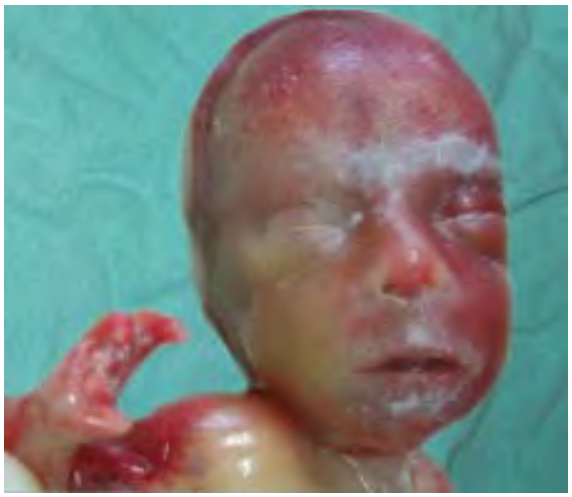

Figure 24.107: Oligodactyly with central cleft and fusion of the second and third digits and the fourth and fifth fingers

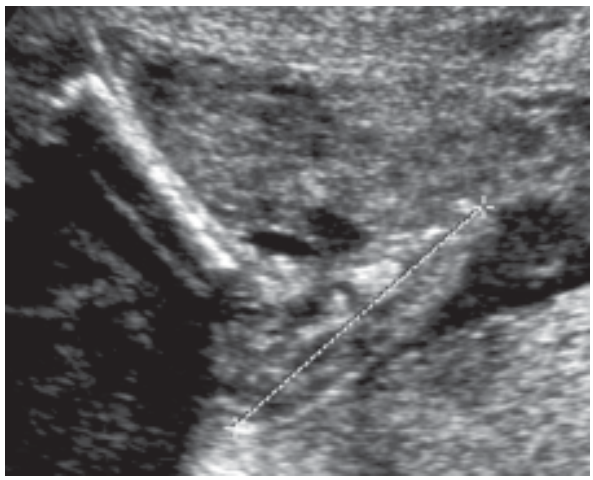

Figure 24.108: Forefoot appears much longer than femur, with a normal position of the foot. Usually femur is longer than the sole of the foot

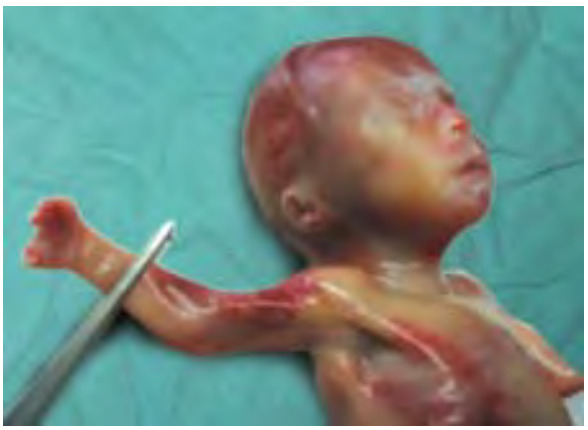

Figure 24.109: Absence of digits: Oligodactyly

Hand and Foot Deformities

Various hand and foot deformities shown in **Figures 24.108 to 24.123**.

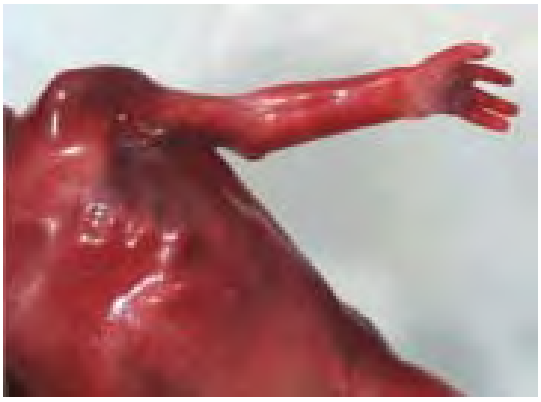

Figure 24.110: Oligodactyly with normal palmar configuration

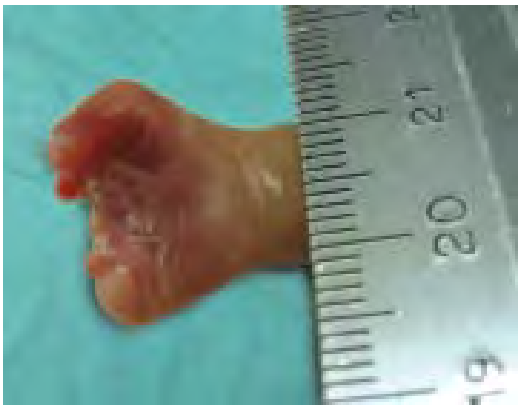

Figure 24.111: Detail of an oligodactyly

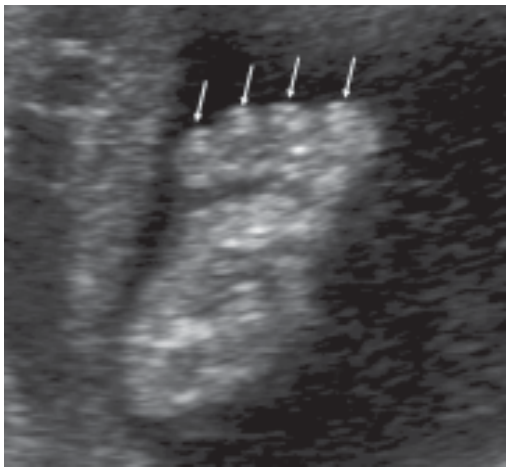

Figure 24.112: Absence of foot digits: Oligodactyly. In the forefoot view only four phalanges can be visualized (arrows)

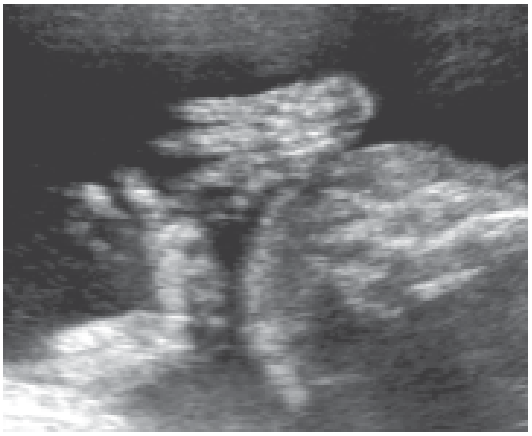

Figure 24.113: Bilateral radial deviation of fetal hands. Thumb is present

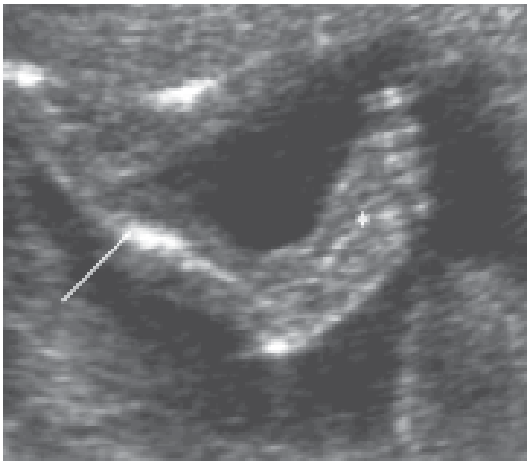

Figure 24.114: Malpositioned foot (*). Fetal leg showing a single bone (arrow), probably the fibula. This defect may be isolated or part of the femur-tibia-radius complex (classically with familial presentation)

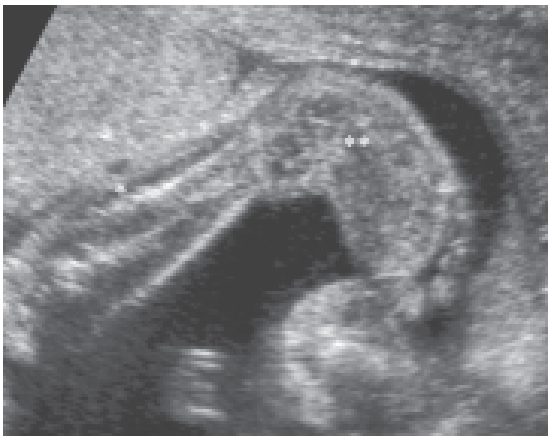

Figure 24.115: Malpositioned fetal foot. One can assess on the same view the whole tibia, fibula (*) and the sole of the foot (**). In normal conditions, in this view one must assess foot profile and not the sole of the foot

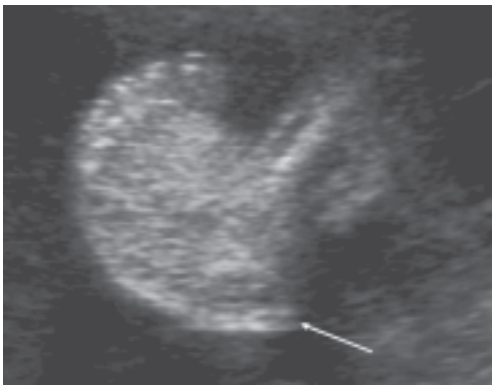

Figure 24.116: Talipes equinovarus foot. The heel cannot be assessed. Forefoot is oriented in the same plane as the lower leg with loss of heel angle (arrow). Even if the knee joint movement is normal, the foot joint is fixed and the foot is permanently malpositioned

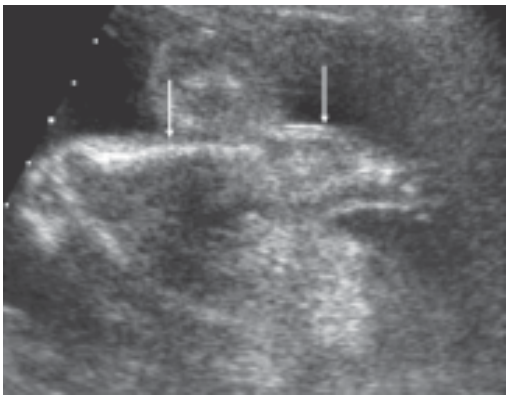

Figure 24.117: Talipes equinovarus with a marked equinus component (permanent plantar flexion). The lower leg's bone is practically aligned with the hindfoot (arrows)

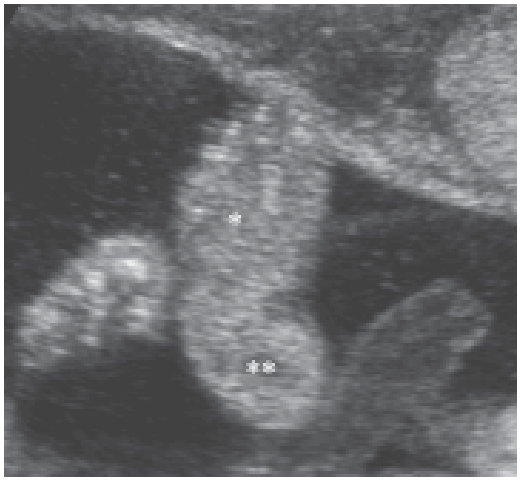

Figure 24.118: Talipes equinovarus with marked varus component. Note the prominent metatarsal adduction (*) with respect to heel (**)

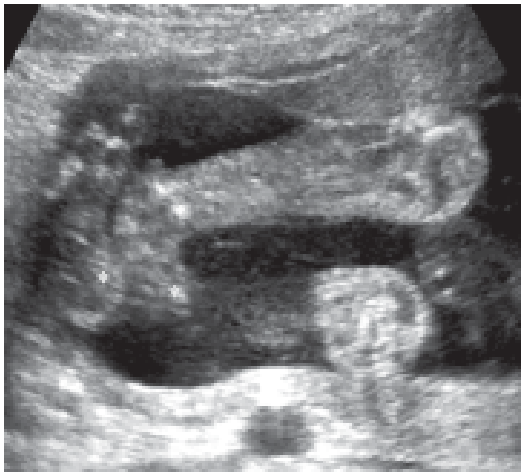

Figure 24.119: Bilateral talipes equinovarus (*). Forefeet are oriented in the same plane as the lower leg with loss of calcaneous angulation

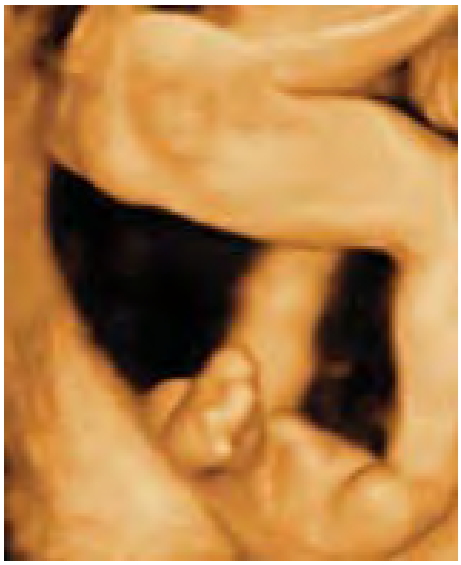

Figure 24.120: Bilateral talipes equinovarus. 3D view

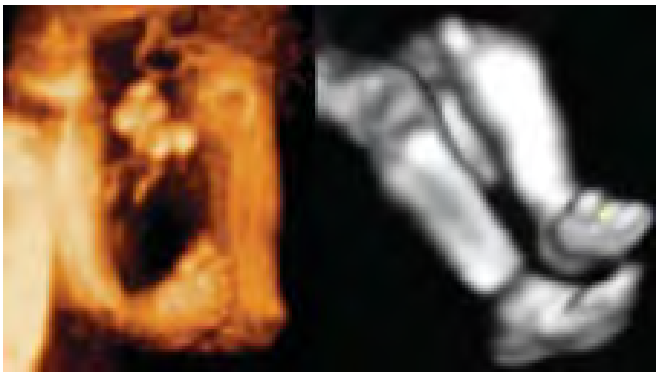

Figure 24.121: 3D ultrasound of fetal feet malposition

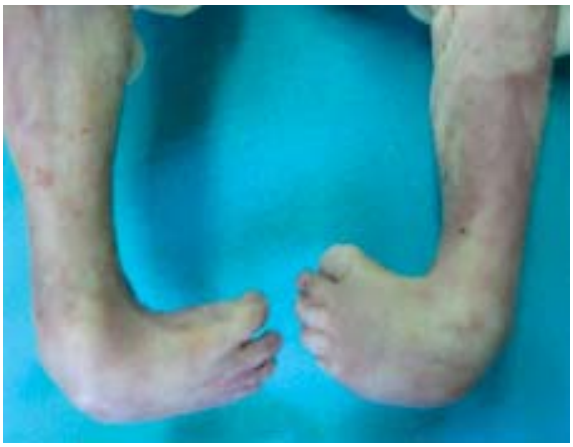

Figure 24.122: Neonatal photograph demonstrating that the angle formed by the lower leg and hindfoot may be rounded laterally in talipes equinovarus deformity

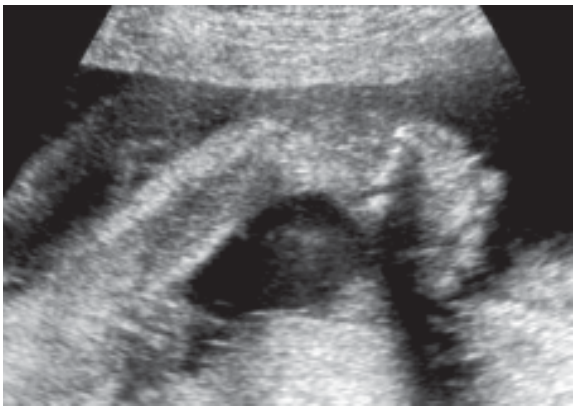

Figure 24.123: Fetal foot showing a 90 degrees angle with the forefoot. The foot is in a fixed position throughout the duration of the sonographic examination

Malpositioned Hands[11]

Malpositioned hands are shown in **Figures 24.124 to 24.126**.

May be cubitals: rare, isolated

Radials: usually associated with an absent or hypoplastic **(Fig. 24.127)** thumb, radial aplasia or hypoplasia, genetic syndromes, chromosome anomalies (t18), hematological disorder (Fanconi pancytopenia), cardiac disorders (Holt-Oram syndrome) or scoliosis **(Fig. 24.128)**.

Malpositioned Feet

May be isolated (with a certain familial predisposition) or associated with chromosome defects (t18) and skeletal dysplasias **(Fig. 24.129)**. Malpositioned fetal foot is shown in **Figures 24.130 to 24.132**.

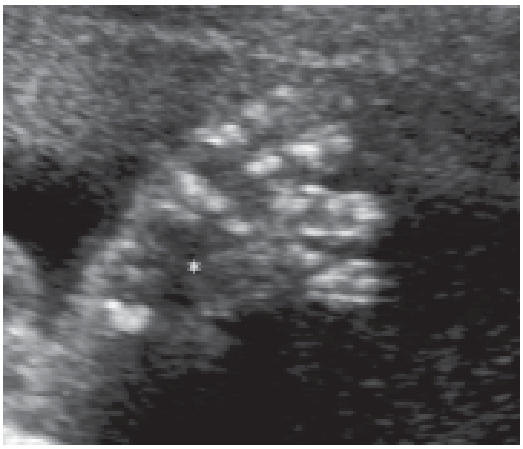

Figure 24.124: Fetal hand (*) showing a classical aspect with thick fingers that appear longer than middle and proximal portions

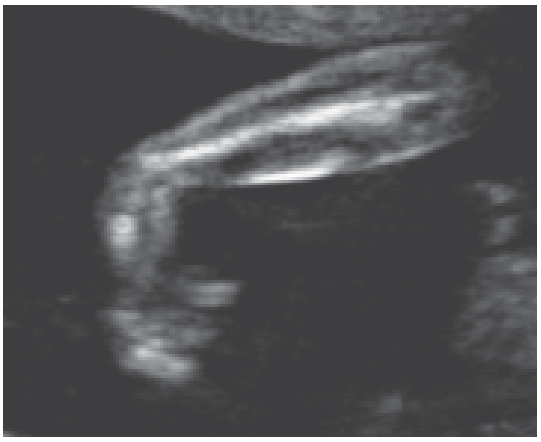

Figure 24.125: Malpositioned fetal hand. They persist in a fixed malposition throughout the exploration. It may be associated with polyhydramnios

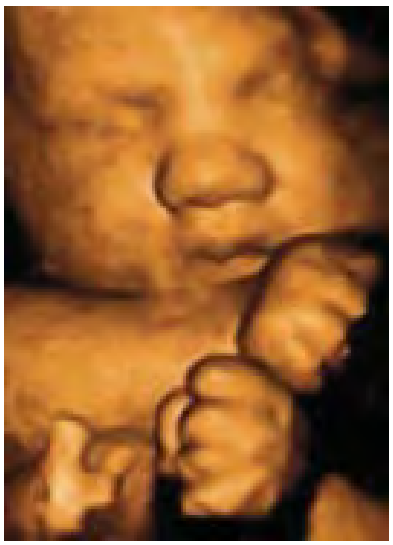

Figure 24.126: Permanently closed hands. 3D ultrasound

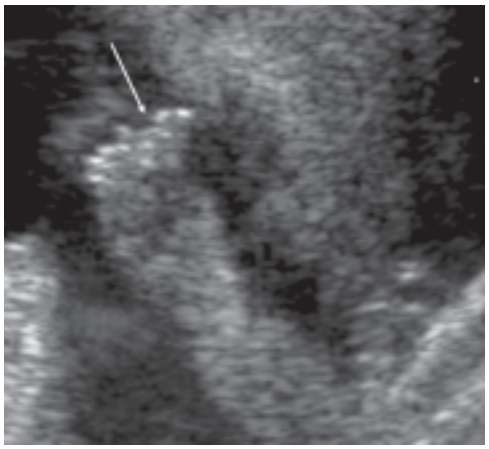

Figure 24.127: Absence of digits (arrow). One can assess hypoplastic digits demonstrating the absence of bone

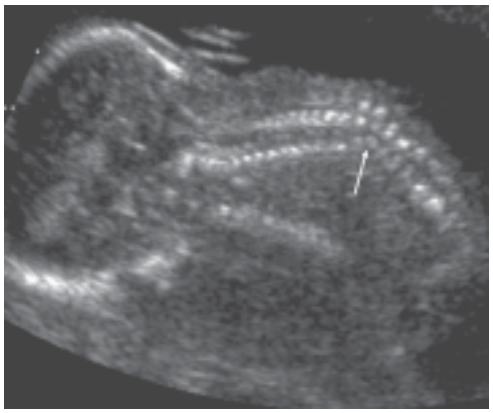

Figure 24.128: Severe fetal scoliosis. Longitudinal view of the spine demonstrating a persistent angulation of the spine. The paired neural arch ossification centers appear disordered or mismatched. It was not associated with a neural tube defect

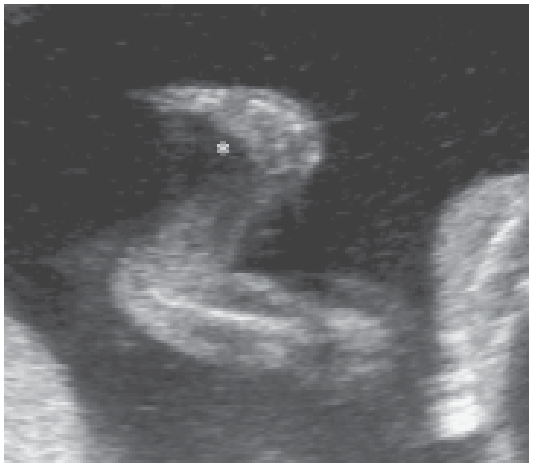

Figure 24.129: The hand is malpositioned, describing a 90º angle with the forearm (*). The deviation is sustained even when articular movements of shoulder and elbow are normal. A transient cubital or radial deviation is considered normal, but if it is fixed, a postural defect must be suspected

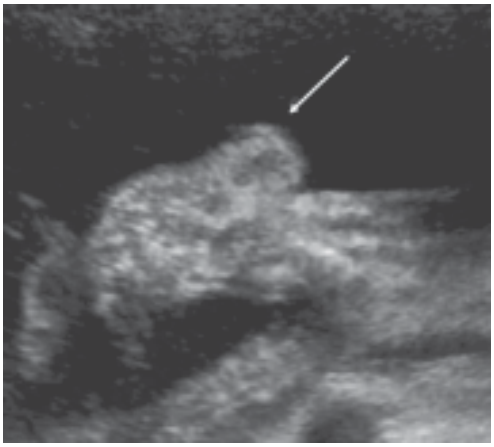

Figure 24.130: Malpositioned calcaneous valgus foot. Prominent calcaneous (arrow). As in talipes equinovarus the forefoot is oriented in the same plane as the lower leg. The foot is fixed in this abnormal position

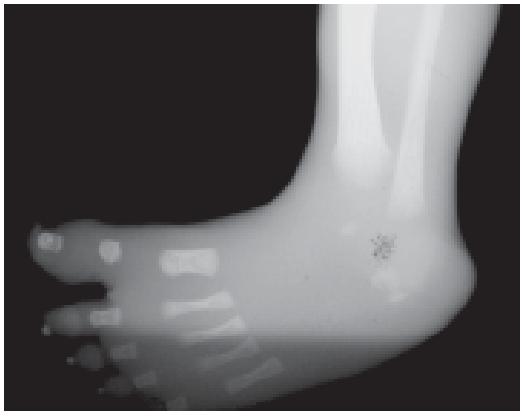

Figure 24.131: Postmortem fetography showing a prominent calcaneous typical of the calcaneous valgus deformity

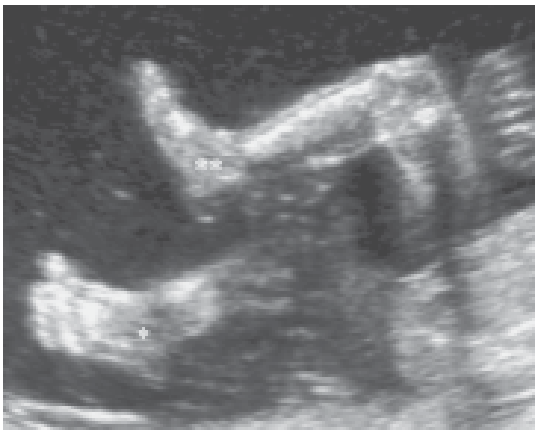

Figure 24.132: The normal fetal foot however can achieve startling degrees of dorsiflexion or plantar flexion. One can assess fetal movements and transient correction of the suspected malposition (with dorsal flexion). In this case shows a better prognosis and best orthopedic results

Polydactyly

Polydactyly is the most common hand anomaly **(Fig. 24.133)**. Prenatal detection is made by finding more than the normal number of digits in the fetal hand, foot or in both **(Figs 24.134 and 24.135)**. It may be a unilateral or bilateral defect. Extra digits may consist solely of soft tissue elements or may contain bone.

They may be isolated defects (showing dominant inheritance pattern) or may occur with a number of associations.

There are three types:

1. Preaxial polydactyly involves the radial aspect of the hand or foot **(Fig. 24.136)**.
2. Postaxial polydactyly involves the ulnar aspect of fetal hand or foot **(Figs 24.137 to 24.141)**.
3. Central polydactyly—when the three central digits are affected.

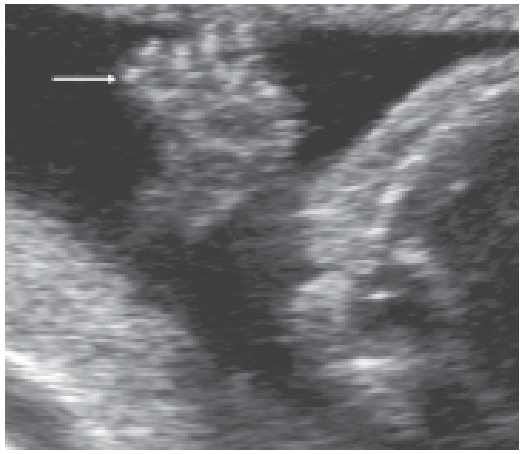

Figure 24.133: Sometimes the first sign is a thicker than normal hand and when we count we find an extra finger (arrow)

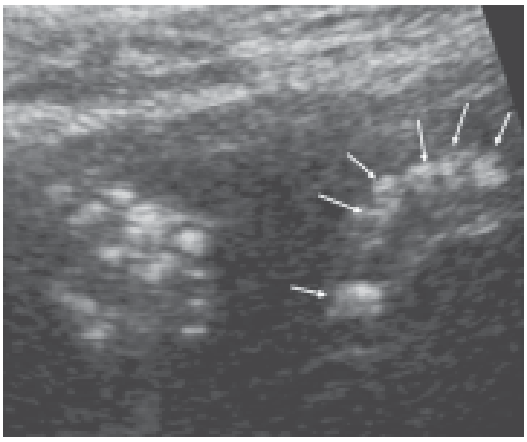

Figure 24.134: Polydactyly is better assessed in the opened hand. Nevertheless one can identify it in a closed hand (arrows)

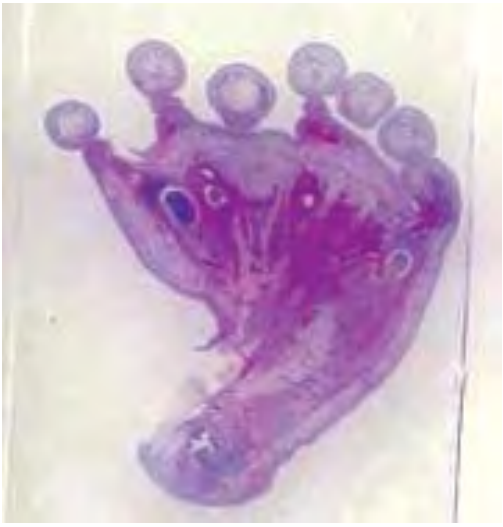

Figure 24.135: Macro-micro photograph (histological specimen) of a foot polydactyly

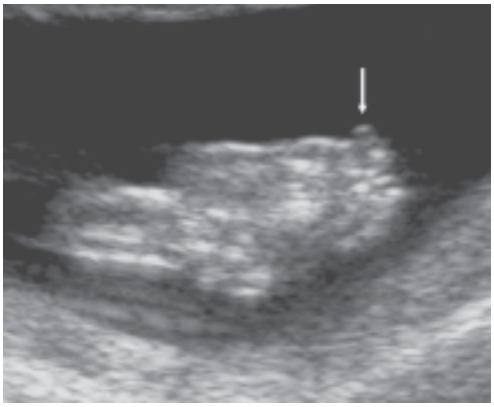

Figure 24.136: View of the sole of the foot. Fetal foot preaxial polydactyly (arrow).The accessory digit contains solely soft tissue elements

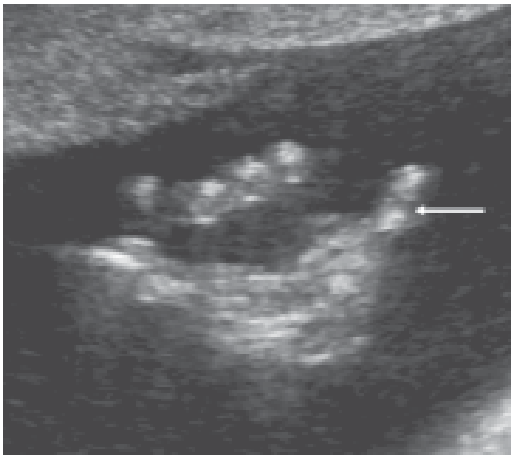

Figure 24.137: Fetal hand with postaxial polydactyly. The accessory digit contains bone (arrow)

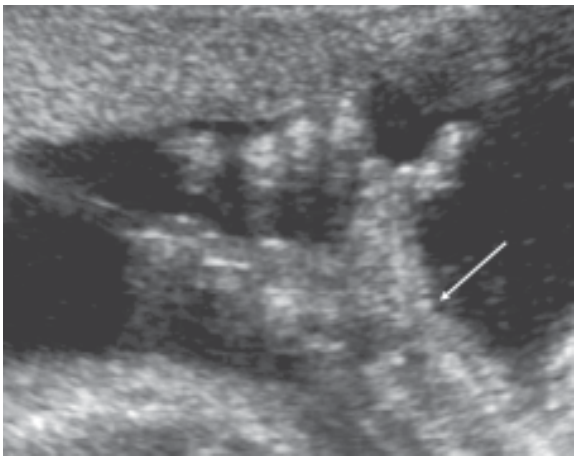

Figure 24.138: Postaxial polydactyly of a hand (arrow). Note the normal forearm position and motility

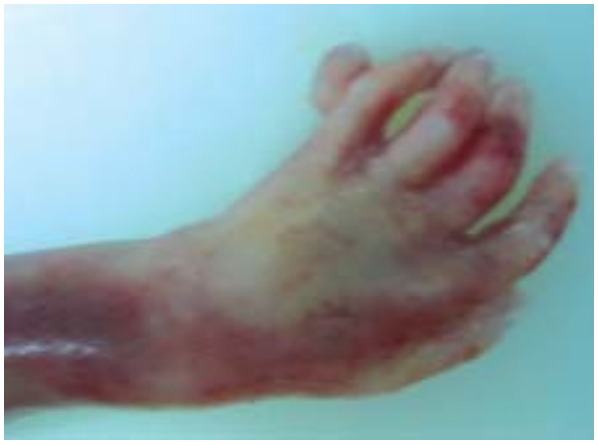

Figure 24.139: Postaxial polydactyly of the left hand

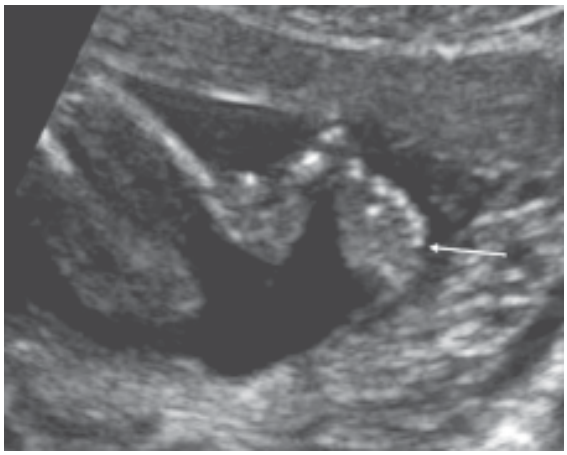

Figure 24.140: Fetal foot postaxial polydactyly (arrow). The accessory digit contains bone

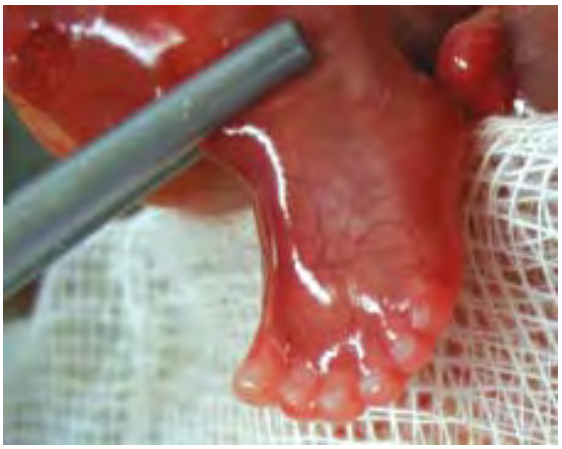

Figure 24.141: Postaxial polydactyly of the fifth digit of the left foot

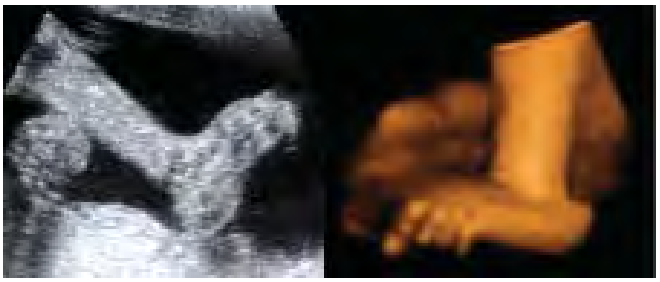

Figure 24.142: Malpositioned fetal foot (*). The foot is in a fixed position throughout the duration of the sonographic examination

The postaxial polydactyly is the most frequent and it is normally isolated and with good prognosis. Preaxial and central polydactyly usually involve a syndromic association.

Foot polydactyly is shown in **Figure 24.142**.

Syndactyly

It is an abnormal fusion between digits. This fusion can involve only soft tissues (simple) or include bones (complex). The complex syndactyly is easier to diagnose *in utero* because the affected fingers are deformed. The syndactyly **(Figs 24.143 and 24.144)** can be complete (involving the whole digit), or incomplete (when spares the distal part).

Any number of fingers can be linked. When more than two fingers are involved, the hand takes a strange appearance (spoon hand or mitten hand). It can be sporadic with a familial tendency, or associated with other anomalies (syndromes or constriction band sequence).

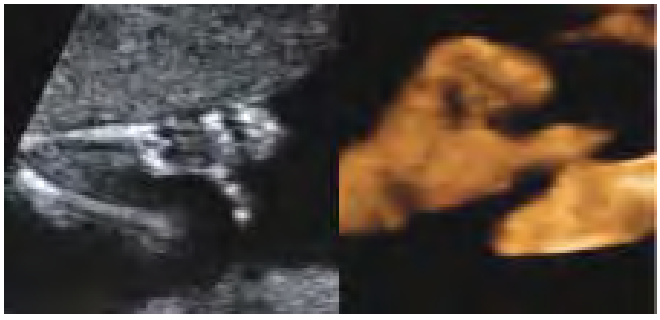

Figure 24.143: Fetal hand syndactyly. 2D and 3D ultrasound

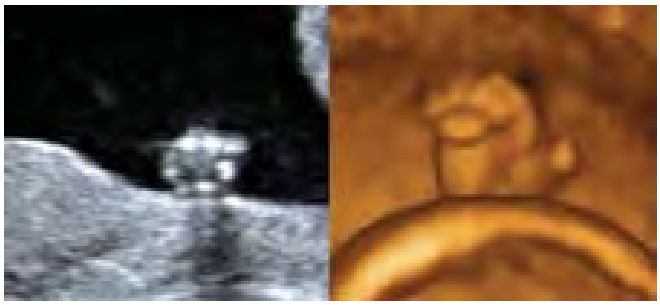

Figure 24.144: Fetal hand syndactyly. 2D and 3D views

Hemivertebrae

Abnormal curvature of the spine is due to a failure in formation of vertebral bodies. Any segment of the spine may be involved; the thoracolumbar **(Fig. 24.145)** is the most frequent and it has the worst prognosis. Mild spinal curvature may be an isolated finding without any associated defect. However, the association with other structural abnormalities is common. If it is isolated, the prognosis is good. Spinal curvature may be part of some genetic syndromes (as Klippel-Feil, characterized by fusion of cervical vertebrae with short neck aspect). **Figure 24.146** shows sagittal view of fetal spine having multiple fusion defects with marked posterior shadowing without any visible intervertebral space.

Fetal Akinesia Deformation Sequence

Deformative sequence secondary to fetal akinesia **(Figs 24.147 and 24.148)** due to intrauterine contractures **(Figs 24.149A to D)** with neurological, muscular, connective or skeletal origin. The term arthrogryposis has been abandoned. Typical features include bilateral feet malposition, heel, knee and elbow deformities (in flexion or extension). The compromise is usually symmetric, affecting all the extremities. It may be found in association with polyhydramnios, thoracic hypoplasia, micrognathia and thick nuchal trans-

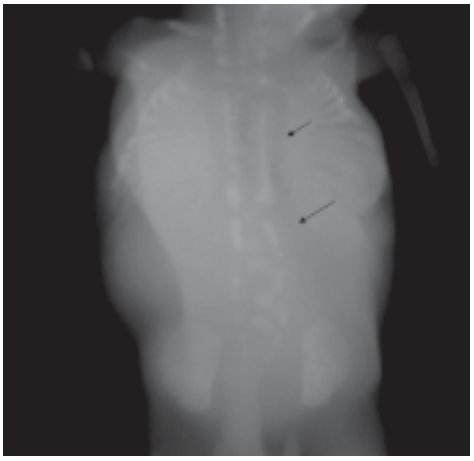

Figure 24.145: Multiple hemivertebrae (arrows) in thoracolumbar spine

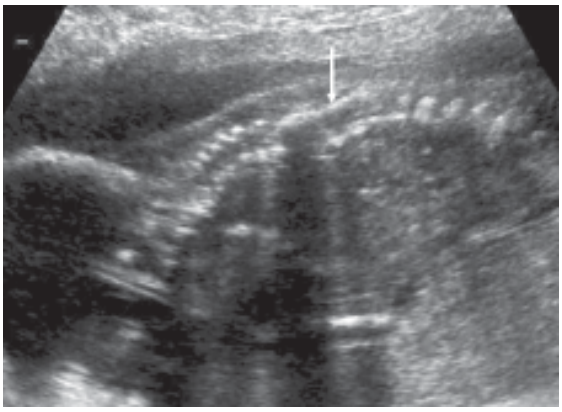

Figure 24.146: Sagittal view of fetal spine. One can assess multiple vertebral fusion (arrow) with marked posterior shadowing, without any visible intervertebral space

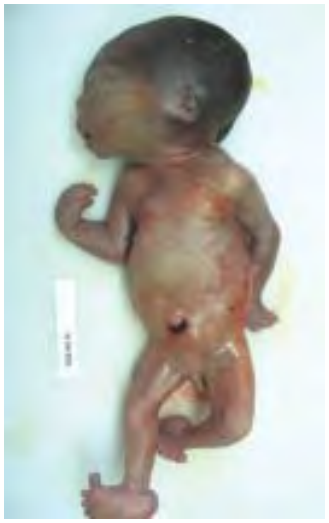

Figure 24.147: Malpositioned fetal extremities with deformation and hyperflexion secondary to fetal akinesia

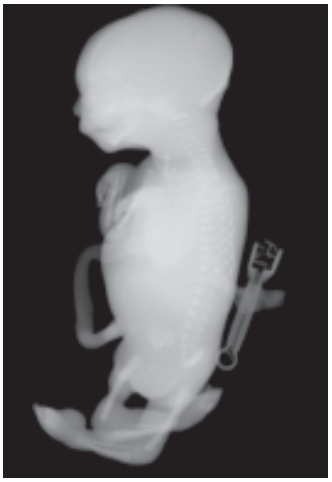

Figure 24.148: Fetography of a fetus with fetal akinesia deformation sequence

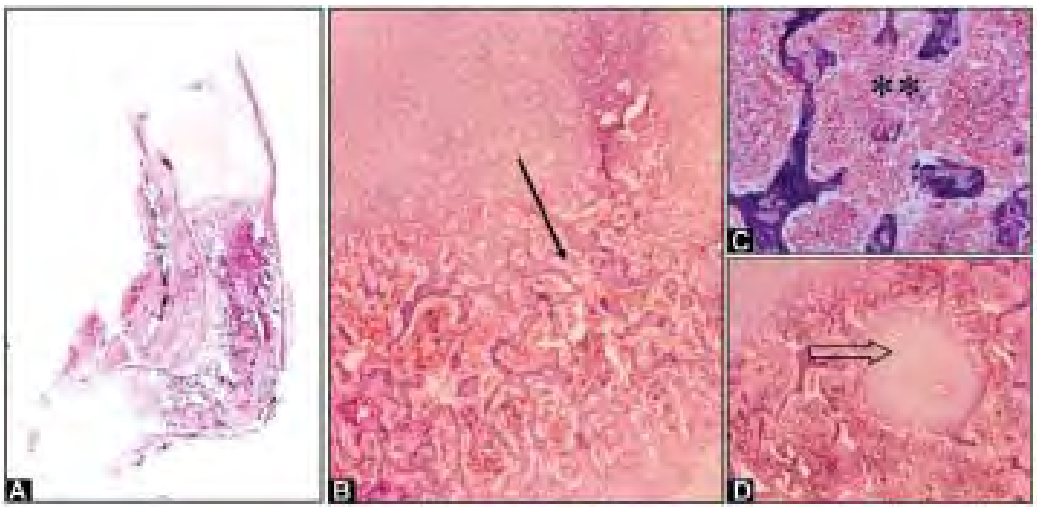

Figures 24.149A to D: Short and angulated long bones due to multiple intrauterine fractures (*): at metaphyseal level conditioning bone shortness (arrow) at diaphyseal level (**) responsible for trabecular destruction and callus formation (open arrow) and pseudoarticulation creation

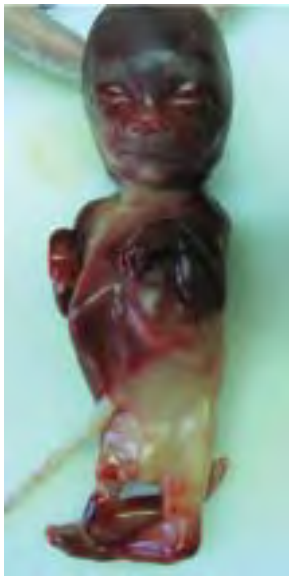

Figure 24.150: Fetus with lethal multiple pterygium. Upper extremities demonstrating a severe degree of refraction. Lower limbs with marked hyperflexion

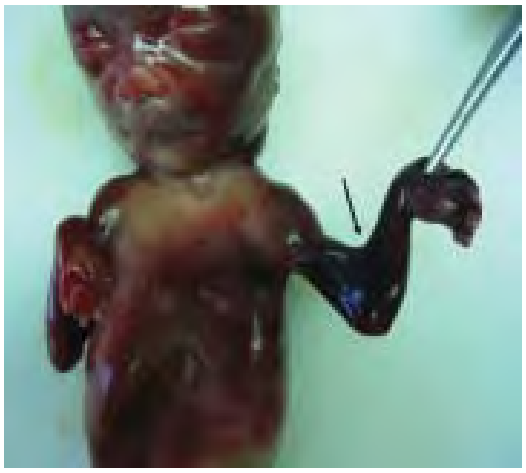

Figure 24.151: Pterygium in detail. Cutaneous membrane joining the forearm and hand

lucency. The generalized FADS is usually lethal due to lung hypoplasia. Some features may be present in other syndromes such as multiple lethal arthrogryposis, multiple pterygium **(Figs 24.150 and 24.151)** syndrome and Pena-Shokeir syndrome. The differential diagnosis includes trisomy 18 and hypokinesia secondary to severe oligohydramnios or to uterine malformation.[12]

Other Skeletal Defects[13]

Patellar Anterior Luxation

Anterior flexion of the knee joint is secondary to a patellar abnormality **(Figs 24.152 to 24.154)**.

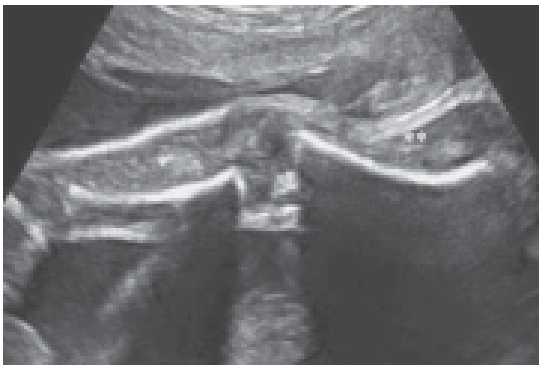

Figure 24.152: Congenital patellar luxation. The middle portion of lower extremity is malpositioned (*) compared to the proximal portion of the extremity (**)

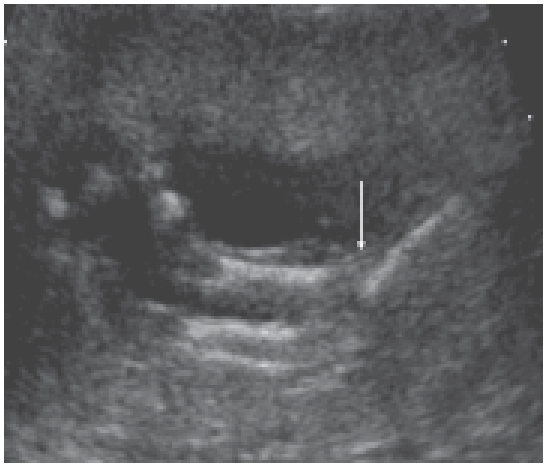

Figure 24.153: Congenital knee luxation. Anterior knee flexion (arrow) due to a patellar anomaly. Other fetal joints seem normal

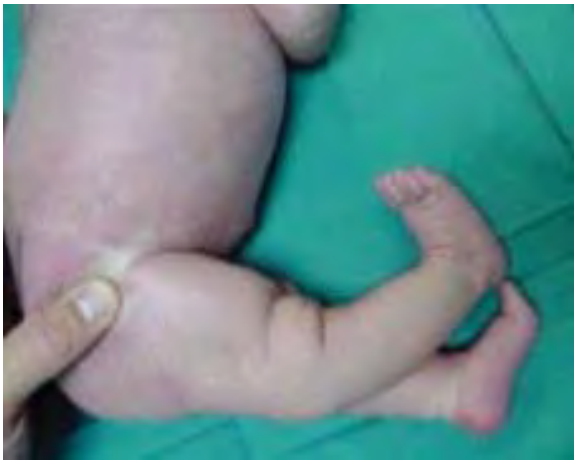

Figure 24.154: Newborn demonstrating a congenital knee luxation

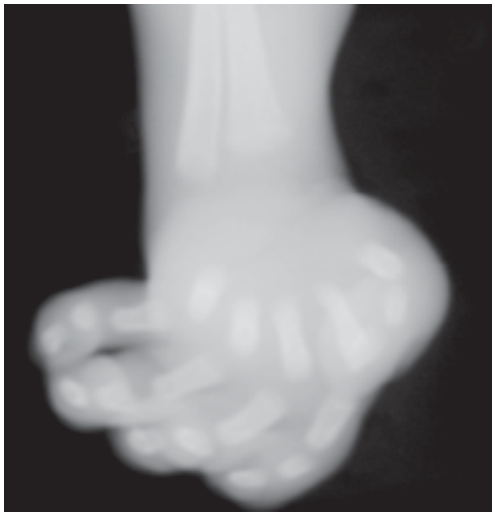

Figure 24.155: Fetography showing malpositioned, disorganized phalanges due to cutaneous compression probably secondary to misoprostol use

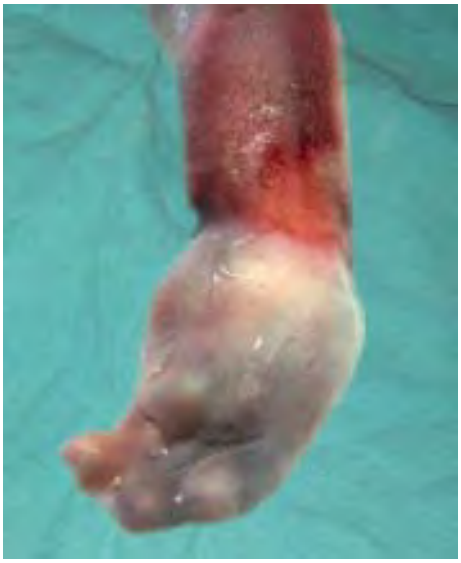

Figure 24.156: Photograph of a dysmorphic hand. Digits are fused and disorganized. It may be associated with misoprostol use

Teratogenic Effects: Misoprostol

The use of misoprostol in the first trimester of pregnancy has been associated with limb distal anomalies **(Figs 24.155 and 24.156)**.

REFERENCES

1. Ruano R, Molho M, Roume J, et al. Prenatal diagnosis of fetal skeletal dysplasias by combining two-dimensional and three-dimensional ultrasound and intrauterine three dimensional helical computer tomography. Ultrasound Obstet Gynecol. 2004;24(2):134-40.
2. Kos M, Hafner T, Funduk-Kurjak B, et al. Limb deformities and three dimensional ultrasound. J Perinat Med. 2002; 30(1):40-7.
3. Garjian KV, Pretorius DH, Budorick NE, et al. Fetal skeletal dysplasia: three-dimensional US initial experience. Radiology. 2000;214(3):717-23.
4. Krakow D, Williams III J, Poehl M, et al. Use of three-dimensional ultrasound imaging in the diagnosis of prenatal-onset skeletal dysplasias. Ultrasound Obstet Gynecol. 2003;21(5):467-72.
5. Kennelly MM, Moran P. A clinical algorithm of prenatal diagnosis of radial ray defects with two and three dimensional ultrasound. Prenat Diagn. 2007;27(8):730-37.
6. Cassart M, Massez A, Cos T, et al. Contribution on three-dimensional computed tomography in the assessment of fetal dysplasia. Ultrasound Obstet Gynecol. 2007;29(5):537-43.
7. Dighe M, Fligner C, Cheng E, et al. Fetal skeletal dysplasia: an approach to diagnosis with illustrative cases. Radiographics. 2008;28:1061-77.
8. Krakow D, Lachman RS, Rimoin DL. Guidelines for the prenatal diagnosis of fetal skeletal dysplasias. Genet Med. 2009;11(2):127-33.
9. Cassart M. Suspected fetal skeletal malformations or bone diseases: how to explore. Pediatr Radiol. 2010;40:1046-51.
10. Hall CM. International nosology and classification of constitutional disorders of bone (2001). Am J Med Genet. 2002;113:65-77.
11. Rypens F, Dubois J, Garel L, et al. Obstetric US: watch the fetal hands. Radiographics. 2006;26:811-32.
12. Atlas de malformaciones fetales congénitas. Carreras E, Toran N. Ediciones Mayo.
13. European Skeletal Dysplasia Network.[online] available from www.esdn.org.

CHAPTER 25

Sonographic Assessment of the Umbilical Cord

Edoardo Di Naro, Luigi Raio, Antonella Cromi, Alessandra Giocolano

INTRODUCTION

For several decades, the morphological and morphometric aspects of the umbilical cord have been studied and retrospectively correlated with the perinatal outcome by pathologists after delivery. The advent of ultrasound has increased our knowledge and added a dynamic form of information in particular on the development of the fetus and its supporting structures such as the placenta and the umbilical cord. However, at the beginning, the umbilical cord has received only little interest mainly due to the limited resolution of the initial ultrasound machines. Indeed, the prenatal sonographic morphologic investigation of the umbilical cord has for long time been limited to the assessment of the number of vessels and later to the evaluation of the impedance to blood flow by Doppler waveform analysis.

However, an increasing body of clinical and experimental evidences show that both prenatal morphology and morphometry of the umbilical cord and its vessels may help in understanding the physiology of development as well as adaptive processes of the fetoplacental unit to pathologic insults. Moreover, studying the umbilical cord may in some circumstances help in the prediction of adverse pregnancy outcome. In the last decade, a considerable amount of scientific work has been published on this topic. We have learned that the umbilical cord is not an inert structure which is suspended between the fetus and placenta but is actively involved in important processes such as fetal growth restriction, preeclampsia, diabetes, stillbirth and chromosomal defect or genetic syndromes.[1-5] The aim of this chapter is to evaluate the role of the sonographic assessment of the umbilical cord during fetal life.

MORPHOLOGY

A normal umbilical cord at term is about 50–60 cm long and its surface is covered by a single layer of amniotic epithelium. The ground substance, in which three vessels—two arteries and one vein—are embedded, is called Wharton's jelly. The characteristic structure of the umbilical cord is determined by the helical course of the arteries around the vein. Between the fetal umbilical ring and the placental insertion, the vessels fulfill usually 10–11 coils. This structure is very dynamic, as its morphology is influenced by a number of factors including gestational age, amount of amniotic fluid and its composition, fetoplacental hemodynamics as well as maternal complications during pregnancy. The evaluation of the umbilical cord can be accomplished either from the long-axis view or from a cross-sectional view. Probably the latter method is more appropriate because it allows quantification not only of the umbilical vessels' size but also of the amount of the Wharton's jelly.

What can be observed in an umbilical cord? How can we read each sign?

Basically, the morphology and morphometry of the umbilical cord is influenced by external factors and/or by factors which are inherent to the cord itself.

Nomograms for the diameter of the umbilical vessels have been reported by Weissman and Raio,[6,7] showing that the diameter of the umbilical arteries increases from 1.2 ± 0.4 mm at 16 weeks to 4.2 ± 0.4 mm at term of gestation and the umbilical vein diameter varies from 2.0 ± 0.6 mm at 16 weeks of gestation to 8.2 ± 0.8 mm at the term of gestation. These nomograms have showed that the diameter increases as a function of gestational age, progressively up to 32 weeks of gestation followed then by a plateau towards the end of the pregnancy due to a reduction of water content of the Wharton's jelly. Moreover, a significant relationship between umbilical cord diameter and cross-sectional area and fetal anthropometric parameters (biparietal diameter, femur length, abdominal circumference) has been described. Experimental and clinical evidence suggest that Wharton's jelly plays a metabolically active role throughout pregnancy; Vizza et al.[8] reported that the collagen fibrillar network of the Wharton's jelly, studied by scanning electron microscopy, shows the presence of a wide system of interconnected cavities consisting of canalicular-like structures as well as cavernous and perivascular spaces. Considering that the Wharton's jelly lack of a proper vasculature, this system of cavities may have an important role facilitating a bidirectional transfer of water and metabolites between amniotic fluid and umbilical cord vessels through the Wharton's jelly. Moreover, Wharton's jelly cushions umbilical blood vessels, preventing disruption of flow due to compression or bending caused by fetal movements and uterine contraction, i.e. at delivery. Modifications in the amount and composition of Wharton's jelly of three-vessel cords have been described in a number of pathological conditions, usually associated with a modification of the amniotic fluid volume and composition, occurring in pregnancy (i.e. hypertensive disorders, gestational diabetes). The reduction of the amount of Wharton's jelly may be the consequence of either an extracellular dehydration or a reduction in extracellular matrix component.

The sonographic cross-sectional area of Wharton's jelly can be computed by subtracting the vessels area from the cross-sectional area of umbilical cord. The umbilical vein and arteries areas are to be computed at the maximal magnification using the software of the ultrasound machine. A reference range for the total vascular area has been generated by Weissman and colleagues.[6]

The umbilical cord can be defined as:

- LEAN, if it's sonographic cross-sectional area is below the 10th percentile for gestational age **(Fig. 25.1)**, and
- LARGE if it's sonographic cross-sectional area is above the 90th percentile for gestational age.

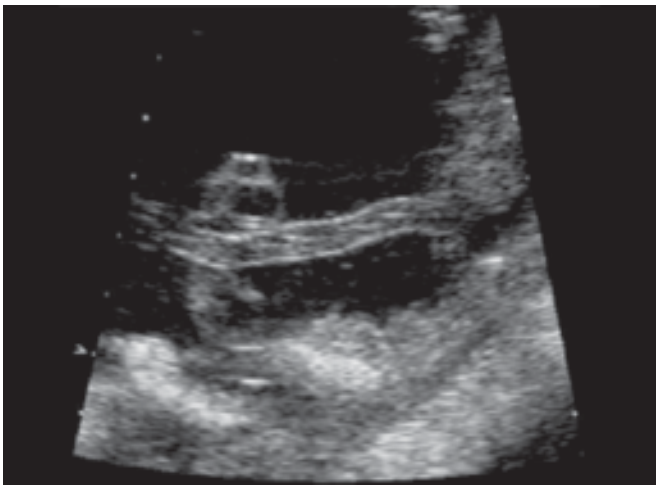

Figure 25.1: Lean cord

"LEAN" UMBILICAL CORD

Just over 40 years ago, observing two cases of macroscopically thin umbilical cord (UC) associated with stillbirth and fetal distress, Hall stated that "*The thin cord is a dangerous cord and a fat cord is a safe cord, all other factors being equal*".[9]

Pathologic studies and case reports demonstrated that a lean umbilical cord is associated with adverse pregnancy outcome, oligohydramnios and fetal distress.[10,11] Raio et al. found an association between the presence of a "lean" umbilical cord and the delivery of a small-for-gestational-age infant. Patients with a "lean" UC after 20 weeks of gestation had a 4.4-fold higher risk (95% confidence interval, 2.16–8.85) of having an SGA infant than those with a normal umbilical cord. Wharton's jelly appears to serve the function of adventitia, which the UC lacks, binding and encasing the umbilical vessels. It has been speculated that the cells of Wharton's jelly appear to possess contractility comparable to that of smooth muscle cells and participate in the regulation of umbilical blood flow and that, at least in some cases, the reduction in fetal growth could be the consequence of Wharton's jelly decrease leading to hypoplasia of the umbilical vessels. In fact, a reduction of wall thickness of umbilical cord arteries and vein has been found in intrauterine growth retardation (IUGR) infants with abnormal umbilical artery flow when compared to IUGR infants without increased umbilical artery resistance. Cumulative evidence suggests that an umbilical cord less than 10th

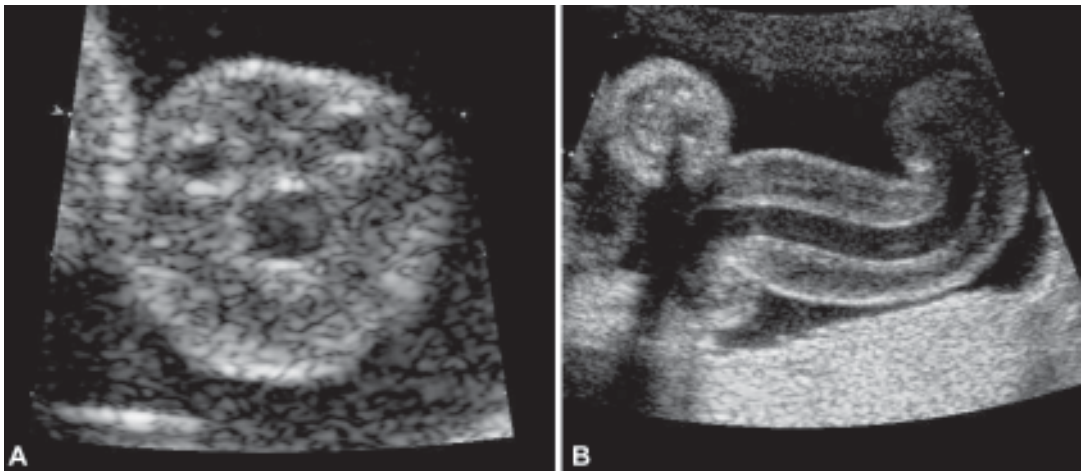

Figures 25.2A and B: Giant UC

centile for gestational age is a simple and early marker SGA infant and the occurrence of intrapartum complication.[11-14] Moreover, a lean UC is frequently associated with signs of fetal distress at the time of delivery (oligohydramnios, low Apgar score and meconium-stained amniotic fluid).

LARGE UMBILICAL CORD

Several reports in the literature have described a large UC associated with other fetal structural anomalies such as umbilical cord tumor, urachal cysts, umbilical cord mucoid degeneration and omphalomesenteric cyst.[15-17] Generally, in these conditions, the morphology is altered in a limited portion of the umbilical cord **(Figs 25.2A and B)**.

However, a consistent association between an ultrasonographic large UC and the presence of a gestational diabetes mellitus has been reported. A large UC can be considered as an additional parameter useful to identify fetuses of a mother with some kind of glucose intolerance during pregnancy. Fetuses of patients with gestational diabetes have a larger UC and this is mainly due to a higher content of Wharton's jelly. Weissman and Jakobi found an alteration in the distribution of Wharton's jelly fibers with large empty spaces among them and speculated that this could be caused by an abnormal accumulation of fluid and plasma proteins within the Wharton's jelly, resulting in an increased surface area and in an increased permeability and hemorrhages due to an increased oncotic pressure in the interstitial spaces of the Wharton's jelly[18,19] **(Figs 25.3A and B)**. This modification can be observed at 24 gestational weeks, suggesting that the involvement of

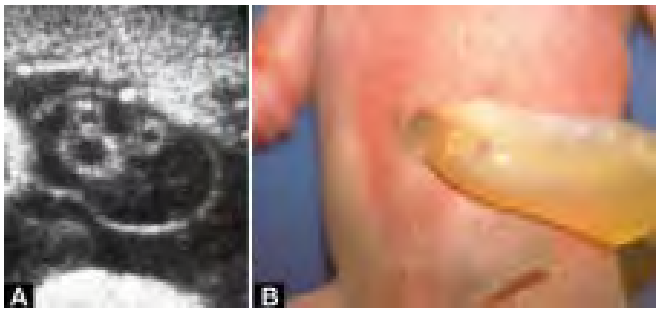

Figures 25.3A and B: Hydropic Wharton's jelly in a syndromic fetus

the umbilical cord in fetuses of diabetic mothers is a phenomenon that occurs early in pregnancy.

In addition, it has been shown that sonographic assessment of umbilical cord area may improve the prediction of fetal macrosomia; although ultrasound remains imprecise in the recognition of fetal macrosomia, obstetrician should not shun the use of biometric methodology to assist in the management of suspected macrosomia, but rather should look forward to further improvements that will enhance its accuracy as a diagnostic tool. Umbilical cord area is an easily obtained sonographic measurement, with highly reliable intraobserver and interobserver reproducibility. The time required to obtain an adequate and satisfactory image of cross-section of UC is about 2 minutes. A large cross-sectional area of the UC performs poorly by itself as a predictor of fetal macrosomia. A sonographic large UC can be used in addition to estimated fetal weight (EFW) as a further marker that may facilitate the detection of fetal overgrowth, potentially improving the performance of ultrasound-based policies for the management of suspected macrosomia.[5]

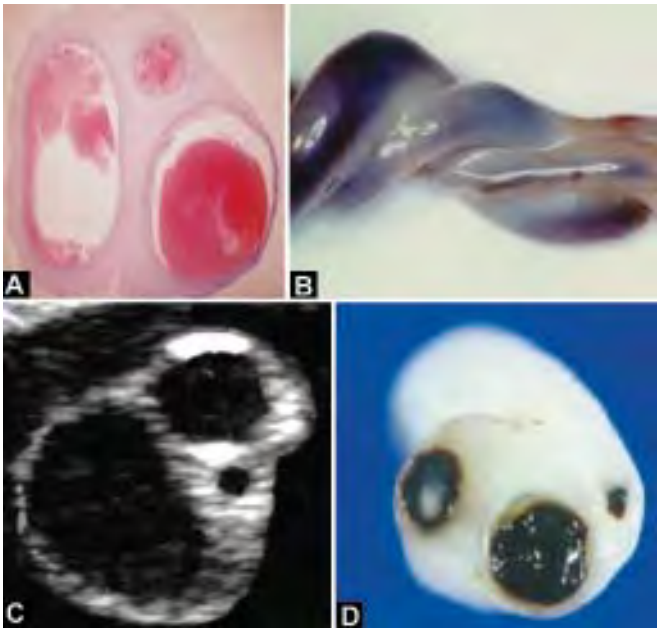

Figures 25.4A to D: Discordant umbilical arteries

DISCORDANT UMBILICAL ARTERY

Discordance between the umbilical arteries is considered to be present when the difference between the diameter of the two arteries is at least 1 mm in three different portions of the UC in both transverse and longitudinal section[20,21] **(Figs 25.4A to D).**

Moreover, these arteries are also characterized by differences in the impedance to blood flow measured by Doppler flow methods with usually a higher resistance index measured in the smaller artery.[21]

Therefore, the information provided by Doppler velocimetry of the smaller umbilical artery should be taken with caution, because the significance of high-resistance patterns observed in other populations seems to represent a more benign condition in patients with discordant umbilical arteries. Therefore, from a clinical point of view, the presence of discordant umbilical artery seems to be a benign condition that does not affect the development of the fetus.

However, cases with discordant arteries are associated with a higher incidence of morphologic placental alterations (placenta bipartite, placenta succenturiata, absence of Hyrtl anastomosis) and anomalous placental insertion (marginal, velamentous). These placental anomalies are similar to those frequently seen in cases of single umbilical artery (SUA) supporting the theory that the presence of a single artery represents the greatest expression of umbilical artery discordance.[22,23] The presence of the Hyrtl anastomosis is a common feature of the vascular system in the human placenta, present in at least 95% of all placentae. This anastomosis is the only vessel that connects the umbilical arteries or their branches on the placental surface, close to the site of cord insertion, playing an active role in equalizing the blood pressure between the territories supplied by each umbilical artery; in fact, although the areas supplied by each of the umbilical arteries may show great discrepancy, the corresponding UC arteries are usually of equal caliber **(Fig. 25.5)**. This equalizing effect might be of utmost importance in particular during uterine contractions when the blood pressure and resistance in the corresponding portion of the intervillous space and cotyledons may differ in

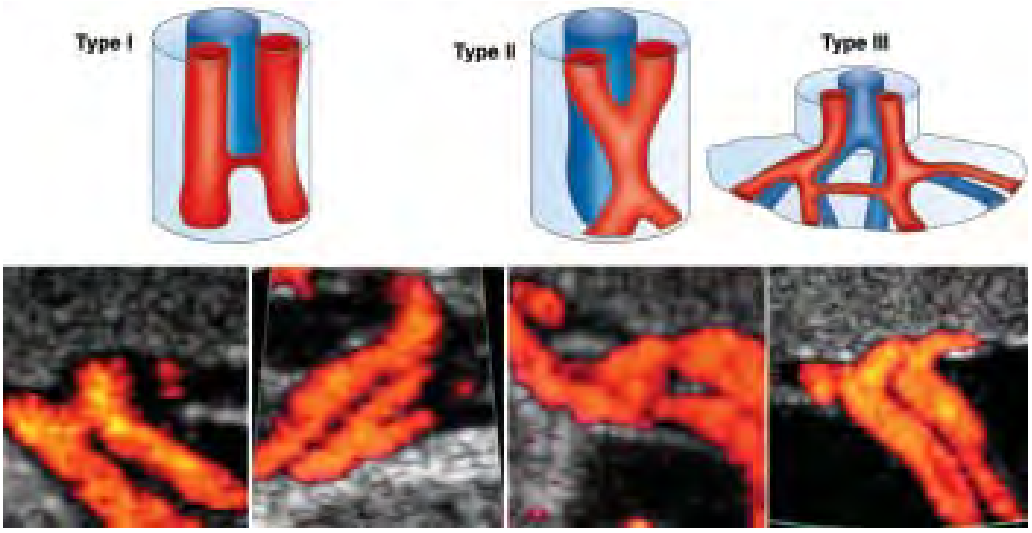

Figure 25.5: Doppler ultrasound demonstration of Hyrtl anastomosis

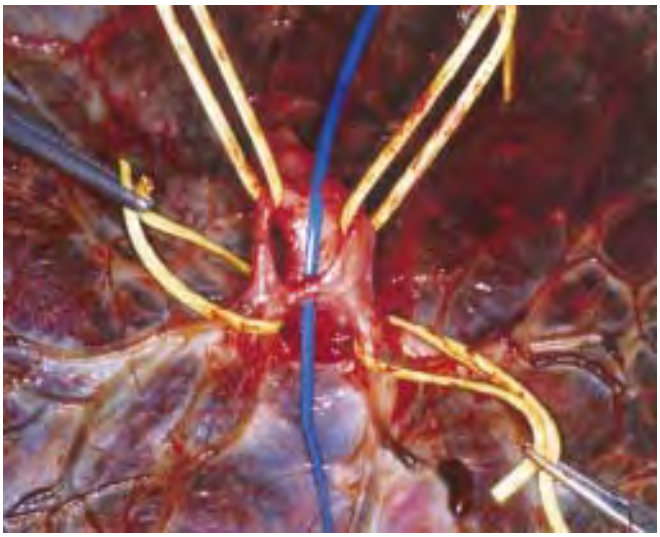

Figure 25.6: Hyrtl anastomosis

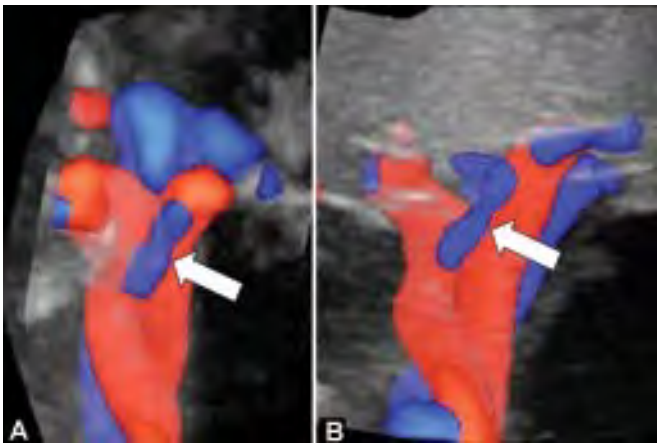

Figures 25.7A and B: 3D view of Hyrtl anastomosis

different part of the placenta **(Figs 25.6 and 25.7)**. Discordance in calibers of the umbilical arteries has been postulated to be the consequence of a failure of the Hyrtl anastomosis to develop anatomically or to function fully. With the advent of more sophisticated ultrasound equipment, the morphologic and functional evaluation of this vessel has now become possible. The absence of a Hyrtl anastomosis has recently been associated with the presence of discordant umbilical arteries; similarly, abnormal umbilical cord insertion such as marginal or velamentous cord insertion has also been associated with a missing Hyrtl anastomosis and discordant umbilical cord arteries.[24,25]

SINGLE UMBILICAL ARTERY (SUA)

The incidence of SUA is reported to be 0.5–2.5% in uncomplicated neonates, but is higher in aborted

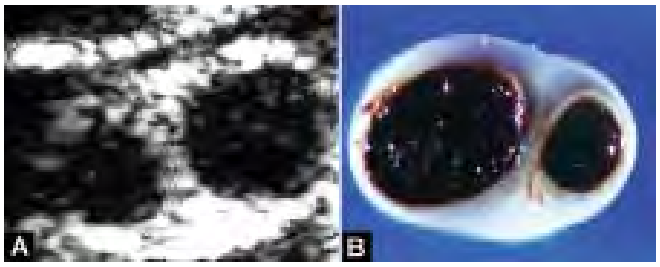

Figures 25.8A and B: Single umbilical arteries

(1.5–7%) and aneuploid fetuses (9–11%). Multiple gestations have a three to seven-fold increased risk of SUA. Fetuses whose umbilical cord has a single artery are at increased risk of intrauterine and intrapartum death, regardless of the presence or not of congenital or chromosomal malformations. Most cases of SUA are diagnosed in the late second trimester **(Figs 25.8A and B)**. Despite the apparently easy recognition of SUA, a low sensitivity of ultrasound is reported. Color Doppler imaging allows earlier and more confident diagnosis of SUA, but its apparent efficacy has to be proven. The patent artery is usually larger than normal and it may approximate to the vein diameter. It has been estimated that the risk of anomalies is seven times greater than in infant with three-vessels cord. The list of anomalies identified to be associated with SUA is long. Persutte and Hobbins[22] divided the reported abnormalities into three groups:

1. To be identified with prenatal ultrasonography
2. To be difficult to be identified prenatally
3. To be unidentifiable prenatally.

Using these criteria, they conclude that prenatal ultrasonography can consistently identify only 37% of fetal anomalies associated with SUA. This low accuracy should well be kept in mind when counseling a patient with a fetus affected by SUA. The prognosis of SUA infants is mainly related to be associated fetal structural or chromosomal anomalies and the frequently present intrauterine growth retardation. The lower amount of Wharton's jelly present in two-vessels cord could be responsible of a higher vulnerability of the UC during the third trimester of pregnancy and during labor. The elevated incidence of stillbirth at the end of pregnancy in patients with a SUA may be in part explained by the cumulative effect of the relative Wharton's jelly reduction that occurs physiologically in the third trimester of pregnancy, acting on a constitutional deficiency of jelly in umbilical cord with a single artery.[26] It is likely that the amount of Wharton's jelly at earlier stages of pregnancy exerts a sufficient protection to the vessels without affecting blood flow

and therefore fetal growth. The SUA fetuses have a lack of the safety warranted by the presence of Hyrtl's anastomosis, a safety valve and this fact partially explains the increased rate of unexplained intrauterine fetal demise in the third trimester of gestation and during labor.

UMBILICAL CORD ANGIOARCHITECTURE

Although the origin and significance of the umbilical cord angioarchitecure has been the subject of extensive research, the developmental process and functional importance of this vascular coiling are not fully understood.

Regardless of its origin, data from both pathologic and ultrasonographic investigations suggest that umbilical coiling is well established as early as 8 weeks of gestation, and the total number of coils at the end of the first trimester is similar to that observed in fully term cords. Moreover, the direction of twist is not randomly determined, since several investigators have found a clear prevalence of left-twisted umbilical cords.

Color flow mapping could be used to enhance the definition of the umbilical cord vascular architecture. The sonographic assessment of the coiling pattern is performed in different UC segments in order to exclude segmental morphologic anomalies (i.e. false knots, varices). The length of one complete umbilical vascular coil (distance between the right outer surface of consecutive arterial coils) is measured in a longitudinal midsection of the UC and a mean of three measurements is used for analysis. The sonographic umbilical coiling index (UCI) is defined as the reciprocal value of that measurement and it represents the number of vascular coils in a given cord. According to the umbilical coiling pattern the UC can be classified as:

- Normal
- Uncoiled (two straight umbilical arteries with an umbilical coiling angle equal to zero)
- Hypocoiled, if the UCI is below the 10th percentile for gestational age
- Hypercoiled, if the UCI is above the 90th percentile for gestational age
- Atypical Coiling **(Figs 25.9A to D)**:
  - *Uncoordinated coiling or bizarre, or aperiodic coiling pattern*, if there is an atypical coiling, in which the absence of a repetitive pattern doesn't allow the measurement of the UCI
  - *Supercoiling*, in the presence of a spring spatial configuration of the UC **(Figs 25.10 to 25.12)**

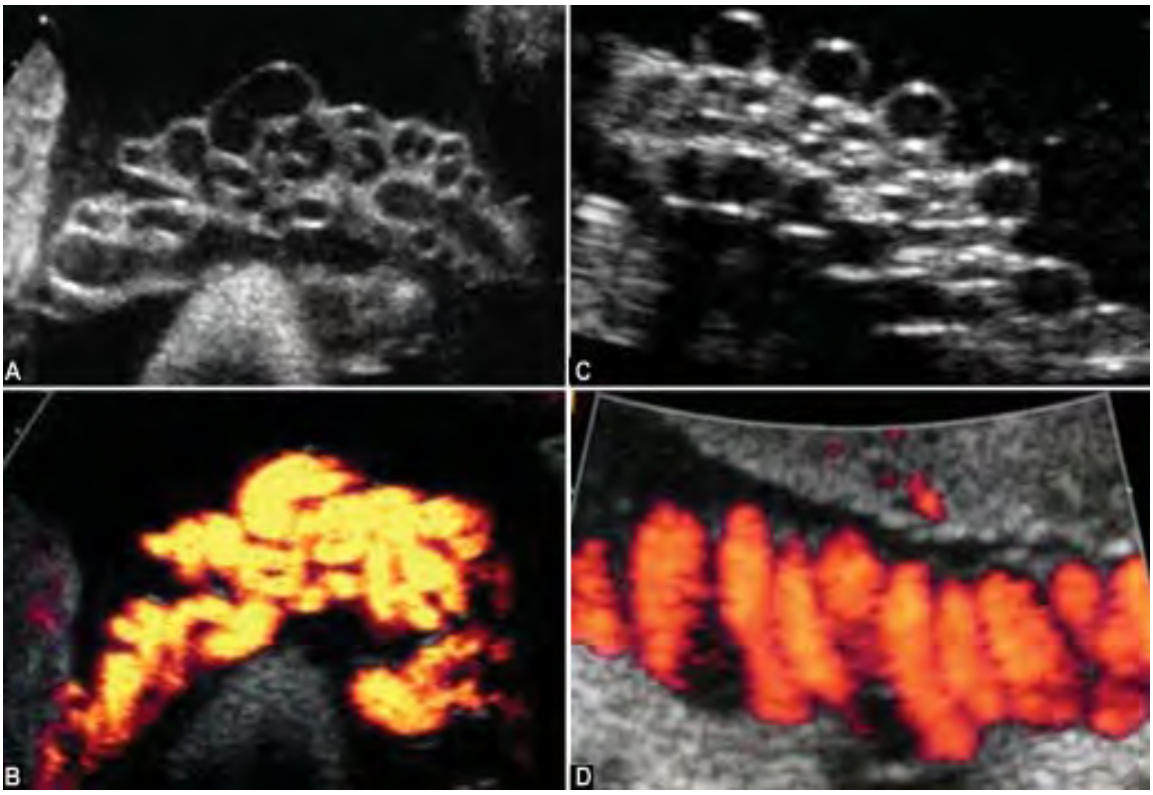

Figures 25.9A to D: Atypical coiling. (A and B) Uncoordinated coiling; (C and D) Supercoiling

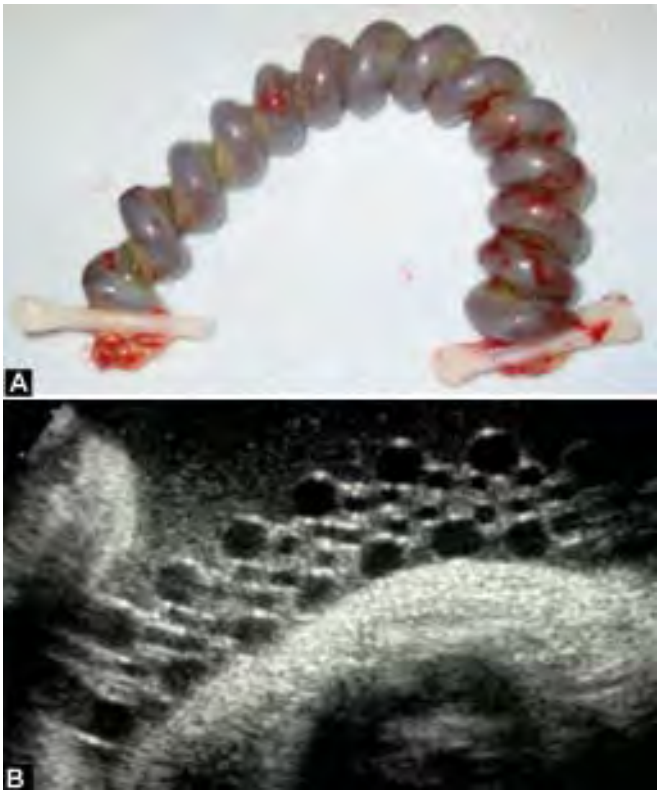

Figures 25.10A and B: Supercoiling postnatal VS ultrasound aspect

The only reference in the pathologic literature on anomalous helical patterns dates back to Hyrtl and Malpas and Symonds,[27,28] which described in their postnatal series some "complicated" cords with different directions of twists, occurring in different segments or a combination of coiled and uncoiled portions.

Compelling evidence has demonstrated a correlation between abnormal umbilical coiling pattern and suboptimal pregnancy outcome in singleton pregnancy.

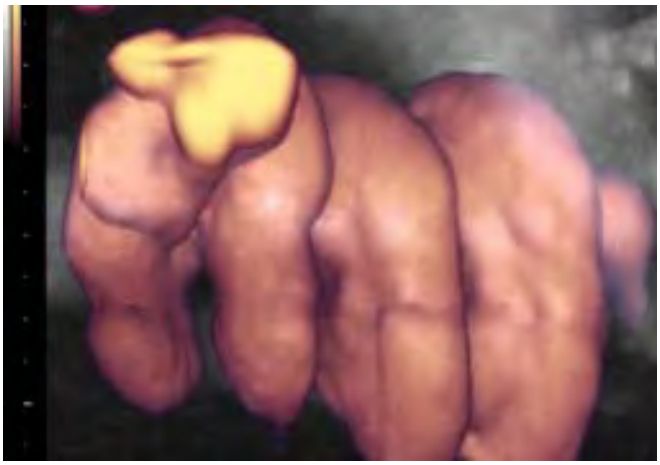

Figure 25.11: Supercoiling cord 3D power flow view

The mechanisms leading to the coiling of the UC are largely unknown and whether it represents a genetically determined or an acquired phenomenon is still the subject of debate. Since the etiology of the vascular coil in normal UC is still an enigma, it is even more intriguing to find a plausible pathophysiologic explanation for an abnormal umbilical cord angioarchitecture. A variety of hypotheses have been advanced to explain the origin of umbilical vascular coiling, including fetal movements,[29] unequal umbilical vascular growth rate (Roach), fetal hemodynamic forces, umbilical vascular wall mechanism and genetics factors. Since the helical course of umbilical vessels is established by 9 weeks of gestation, a hemodynamic imbalance leading to unequal cord morphology is supposed to occur very early in gestation. As this typical repetitive vascular pattern of the umbilical cord is fully established at the end of the first trimester, uncoordinated coiling may be the result of an abnormal coiling process, which takes place during early pregnancy **(Figs 25.13A and B)**. It has been

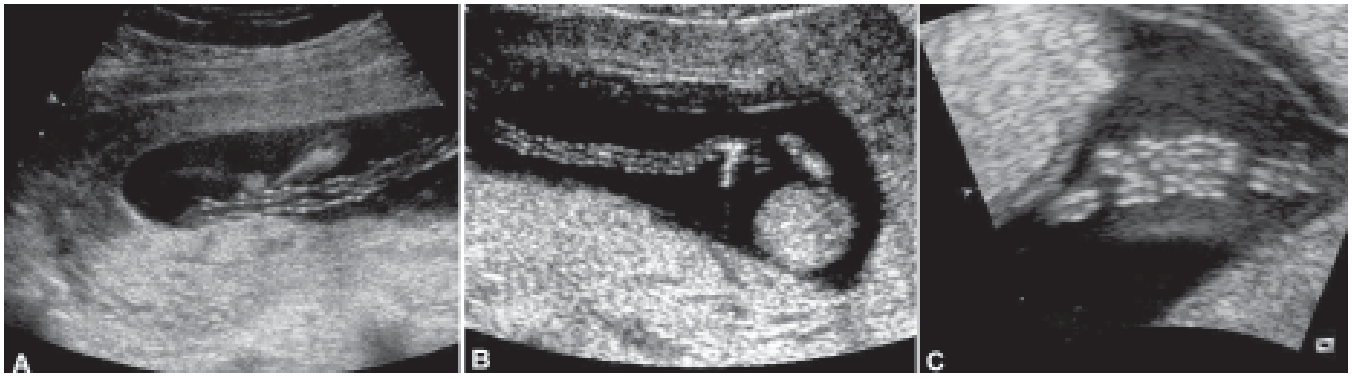

Figures 25.12A to C: First trimester (A) normal; (B) hypercoiled and (C) supercoiled cord

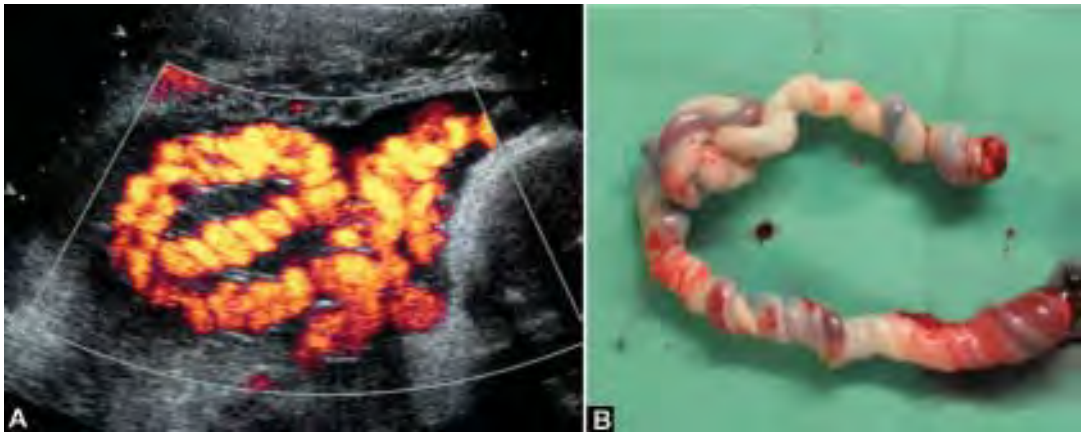

Figures 25.13A and B: Hypercoiling in SUA with UC knot

postulated that coiling is determined by an interaction between the intrinsic properties of the fibers in the umbilical cord vessels wall and hemodynamic forces acting on it during development.

Data from clinical and experimental studies show that the umbilical cord is a dynamic structure where both hemodynamic factors and gestational age influence the vascular umbilical cord pattern.[30-32] Before the fetal kidneys start the excretion of significant amount of urine, fetal membranes are involved in fetal fluid accumulation and regulation by transmembranous mechanism.[33] In early gestation, the fluid exchange between umbilical vessels and amniotic fluid is facilitated by the limited amount of Wharton's jelly wrapped around the umbilical cord vessels.

Reynolds et al. postulated that the UC is a pistonless pulsometer pumping system acting as a cardiac assist pump to sustain the venous return from the placenta.[34] The fetal blood flows through the umbilical vein pumped by slight but definite decreases and increases in venous pressure that are generated from the force of the rising limb of the arterial pressure pulse. The presence of arterial coils that surround the vein along the length of the cord provide multiple variations in an additive fashion; the presence of vascular coils plays a central role in determining the blood flow from the placenta to the fetus. This mechanism is of utmost importance in early gestation when the placental resistance to blood flow is particularly elevated. Therefore, a reduced number of coils in lean umbilical cords could be responsible for a reduced umbilical blood flow which in turn leads to a fetal growth impairment.

Reynolds' hypothesis, according to which the umbilical coils serve as a peristaltic pump mechanism enhancing the venous return to the fetus, has been advocated by several authors to explain how an abnormal coiling could influence the perinatal outcome.

Alterations in morphology and ultrastructure of UC components have been described in pregnancy complications that affect fetoplacental hemodynamics **(Figs 25.14A to D)**. In particular, a high frequency of uncoiled and hypocoiled cords has been reported in intrauterine growth restriction and maternal hypertensive disorders. According to Poiseuille's law, the three factors that might influence blood flow are the caliber of the vessel, the blood flow velocity and the viscosity of the blood. Di Naro stated that the vein blood flow is lower in fetuses with an umbilical cord cross-sectional area below the 10th centile than in those with an umbilical cord of normal caliber and the risk to have an IUGR is very high. The alterations of vein blood flow can be detected earlier than arteries. The umbilical vein area and the umbilical vein blood flow are significantly reduced in growth restricted fetuses compared to normally grown fetuses.[35] The discrepancy in the umbilical vein size might represent an adaptive response to venous overload on the one hand and chronic hypovolemia on the other hand.[36] Supercoiling can be associated with pathologic fetal intraabdominal process and may be explained by a relative increase in resistance at the level of the umbilical ring, which in turn induces a venous congestion of the extraabdominal umbilical vein **(Fig. 25.15).** Kilavuz and Skulstad[37,38] were able to show that blood velocity in the umbilical vein at the abdominal wall is higher than that in the extraabdominal portion of the umbilical cord and that this increase in velocity is due to a progressive tightening of the fetal umbilical ring starting after that the physiologic midgut herniation is completed at 12 weeks of gestation.

Thereafter, umbilical vein constriction is a common finding and does not change during the second half of gestation. As Skulstad stated, the exact role of the fetal umbilical ring remains to be elucidated, and whether extreme degrees of constriction could affect placental

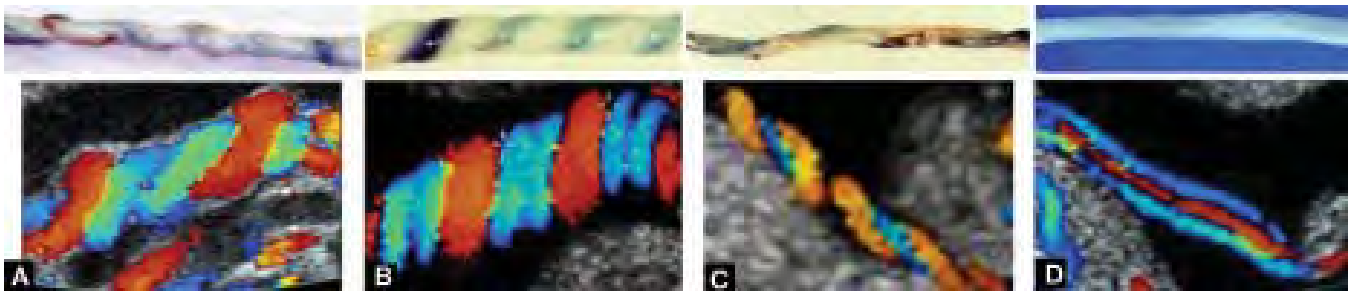

Figures 25.14A to D: Adverse perinatal outcome and coiling. (A) Normal cord; (B) Hypercoiling; (C) Hypocoiling; (D) Uncoiled cord

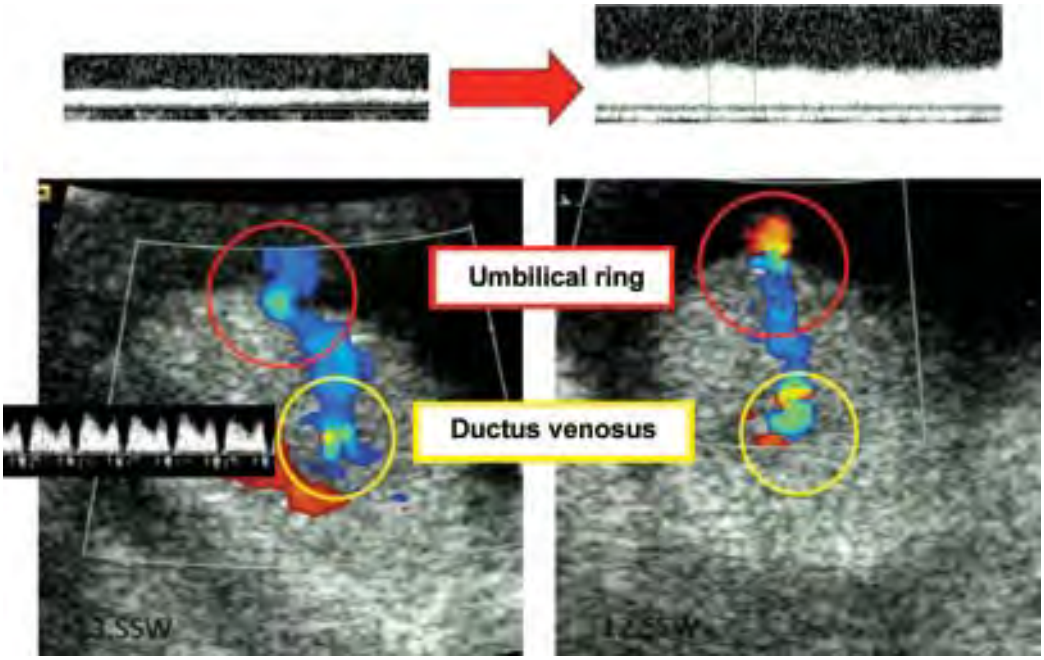

Figure 25.15: Umbilical ring

circulation and are associated with any type of pregnancy complication is unknown.

UMBILICAL CORD AND ANEUPLOIDIES

A number of studies have reported a higher incidence of umbilical cords with decreased coiling index or even absence of coils in fetuses with aneuploidy.[39-41] The UC extracellular matrix is a tissue composed by a high amount of glycosaminoglycans. The Wharton's jelly is composed of an insoluble fibrillar network of different collagen types within which soluble open-coil polysaccharides are held. Hyaluronan, the most represented glycosaminoglycan in the Wharton's Jelly, is known to influence cell behavior and to play a crucial role in angiogenesis, morphogenesis and tissue remodeling especially during embryogenesis. Hyaluronic acid can entrap large amount of water. A smaller part of the Wharton's jelly extracellular matrix is formed by sulfated glycosaminoglycans, which, in turn, are linked to proteins to form proteoglycans.[42] An alteration of the extracellular matrix has been indicated as one of the possible causes of increased nuchal translucency in trisomy 21 human fetuses. The variation in the amount of hyaluronan found in the skin of trisomy 21 fetuses may be present in the extracellular matrix of umbilical cords influencing their macroscopic appearance. There is evidence that fibroblast synthesis of hyaluronic acid

is not different between healthy and trisomy 21 fetuses. Fibroblast of fetuses with trisomy 21 overexpress collagen type VI and experimental evidence has been provided that an inverse correlation exists between collagen synthesis and hyaluronan degradation.[43,44] An increase in collagen type VI may contribute to hyaluronan accumulation. There is evidence that a reduced turnover of hyaluronan could also influence the growth of the umbilical cord vessels and coiling formation.

CONCLUSION

The antenatal measurement of umbilical cord area is probably a better parameter than determination of umbilical cord diameter to identify fetuses at risk of being small for gestational age at delivery or of having distress in labor, or to identify macrosomic fetuses born diabetic mothers. Since the UC area is easy to measure and nomograms are available, its measurement should be part of a routine scan and should prompt a careful and thorough evaluation whenever there is a discrepancy between the observed and the normal values.

REFERENCES

1. Raio L, Ghezzi F, Di Naro E, et al. Sonographic measurement of the umbilical cord and fetal anthropometric parameters. J Obstet Gynecol Reprod Biol. 1999;83(2):131-5.
2. Di Naro E, Ghezzi F, Raio L, et al. Umbilical cord morphology and pregnancy outcome. Eur J Obstet Gynecol Reprod Biol. 2001;96(2):150-7.
3. Todros T, Adamson SL, Guiot C, et al. Umbilical cord and fetal growth—a workshop report. Placenta. 2002;23 Suppl A:S130-2.
4. Raio L, Ghezzi F, Di Naro E, et al. Altered sonographic umbilical cord morphometry in early-onset preeclampsia. Obstet Gynecol. 2002;100(2):311-6.
5. Cromi A, Ghezzi F, Di Naro E, Siesto G, Bergamini V, Raio L. Large cross-sectional area of the umbilical cord as a predictor of fetal macrosomia.Ultrasound Obstet Gynecol. 2007;30(6):861-6.
6. Weissman A, Jakobi P, Bronshtein H, et al. Sonographic measurements of the umbilical cord and vessels during normal pregnancies. J Ultrasound Med. 1994;13(1):11-4.
7. Raio L, Ghezzi F, Di Naro E, et al. Sonographic measurement of the umbilical cord and fetal anthropometric parameters. Eur J Obstet Gynecol Reprod Biol. 1999;83(2): 131-5.
8. Vizza E, Correr S, Goranova V, et al. The collagen skeleton of the human umbilical cord at term. A scanning electron microscopy study after 2N-NaOH maceration. Reprod Fertil Dev. 1996;8(5):885-94.
9. Hall SP. The thin cord syndrome. A review with a report of two cases. Obstet Gynecol. 1961;18:507-9.
10. Raio L, Ghezzi F, Di Naro E, et al. Prenatal diagnosis of a lean umbilical cord: a simple marker for the fetus at risk of being small for gestational age at birth. Ultrasound Obstet Gynecol. 1999;13(3):176-80.
11. Silver RK, Dooley SL,Tamura RK, et al. Umbilical cord size and amniotic fluid volume in prolonged pregnancy. Am J Obstet Gynecol. 1987;157(3):716-20.
12. Bruch JF, Sibony O, Benali K, et al. Computerized microscope morphometry of umbilical vessels from pregnancies with intrauterine growth retardation and abnormal umbilical artery Doppler. Hum Pathol. 1997;28(10):1139-45.
13. Ghezzi F, Raio L, Günter Duwe D, et al. Sonographic umbilical vessel morphometry and perinatal outcome of fetuses with a lean umbilical cord. J Clin Ultrasound. 2005;33(1):18-23.
14. Goodlin RC. Fetal dysmaturity, "lean cord," and fetal distress. Am J Obstet Gynecol. 1987;156(5):1357.
15. Benirschke K, Kaufmann P. Pathology of the human placenta. 3rd edition. New York: Springer; 1995.
16. Chantler C, Baum JD, Wigglesworth JS, et al. Giant umbilical cord associated with a patent urachus and fused umbilical arteries. J Obstet Gynaecol Br Commonw. 1969;76(3):273-4.
17. Iaccarino M, Baldi F, Persico O, et al. Ultrasonographic and pathologic study of mucoid degeneration of umbilical cord. J Clin Ultrasound. 1986;14(2):127-9.
18. Weissman A, Jakobi P. Sonographic measurements of the umbilical cord in pregnancies complicated by gestational diabetes.. J Ultrasound Med. 1997;16(10):691-4.
19. Singh SD. Gestational diabetes and its effect on the umbilical cord. Early Hum Dev. 1986;14(2):89-98.
20. Dolkart LA, Reimers FT, Kuonen CA. Discordant umbilical arteries: ultrasonographic and Doppler analysis. Obstet Gynecol. 1992;79(1):59-63.
21. Raio L, Ghezzi F, Di Naro E, et al. The clinical significance of antenatal detection of discordant umbilical arteries. Obstet Gynecol. 1998;91(1):86-91.
22. Persutte WH, Hobbins J. Single umbilical artery: a clinical enigma in modern prenatal diagnosis. Ultrasound Obstet Gynecol. 1995;6(3):216-29.
23. Heifetz SA. Single umbilical artery. A statistical analysis of 237 autopsy cases and review of the literature. Perspect Pediatr Pathol. 1984;8(4):345-78.
24. Raio L, Ghezzi F, Di Naro E, et al. Prenatal assessment of the Hyrtl anastomosis and evaluation of its function: case report. Hum Reprod. 1999;14(7):1890-3.
25. Raio L, Ghezzi F, di Naro E, et al. In-utero characterization of the blood flow in the Hyrtl anastomosis. Placenta. 2001;22(6):597-600.
26. Raio L, Ghezzi F, Di Naro E, et al. Prenatal assessment of Wharton's jelly in umbilical cords with single artery. Ultrasound Obstet Gynecol. 1999;14(1):42-6.
27. Hyrtl J. Die Blutgefasse der menshlichen nachgeburt in normalen und abnormen Veuhatmissen. Wien: Wilhelem Beamüller; 1870.
28. Malpas P, Symonds EM. Observations on the structures of the human umbilical cord. Surg Gynecol Obstet. 1966;123(4): 746-50.
29. Lacro RV, Jones KL, Benirschke K. The umbilical cord twist: origin, direction, and relevance. Am J Obstet Gynecol. 1987;157(4 Pt 1):833-8.

30. Di Naro E, Ghezzi F, Raio L, et al. Umbilical vein blood flow in fetuses with normal and lean umbilical cord. Ultrasound Obstet Gynecol. 2001;17(3):224-8.
31. Degani S, Lewinsky RM, Berger H, et al. Sonographic estimation of umbilical coiling index and correlation with Doppler flow characteristics. Obstet Gynecol. 1995;86(6): 990-3.
32. Langille BL. Remodeling of developing and mature arteries: endothelium, smooth muscle, and matrix. J Cardiovasc Pharmacol. 1993;21 Suppl 1:S11-7.
33. Gilbert WM, Brace RA. Amniotic fluid volume and normal flows to and from the amniotic cavity. Semin Perinatol. 1993;17(3):150-7.
34. Reynolds RR. Mechanisms of placentofetal blood flow. Ostet Gynecol. 1978;51(2):245-9.
35. Di Naro E, Ghezzi F, Raio L, et al. Umbilical vein blood flow in fetuses with normal and lean umbilical cord. Ultrasound Obstet Gynecol. 2001:17:224-8.
36. Di Naro E, Raio L, Ghezzi F, et al. Longitudinal umbilical vein blood flow changes in normal and growth-retarded fetuses. Acta Obstet Gynecol Scand. 2002;81(6):527-33.
37. Kilavuz O, Vetter K. The umbilical ring—the first rapid in the fetoplacental venous system. J Perinat Med. 1998;26(2): 120-2.
38. Skulstad SM, Rasmussen S, Iversen OE, et al. The development of high venous velocity at the fetal umbilical ring during gestational weeks 11-19. BJOG. 2001; 108(3):248-53.
39. Strong TH, Elliott JP, Radin TG. Non-coiled umbilical blood vessels: a new marker for the fetus at risk. Obstet Gynecol. 1993;81(3):409-11.
40. Qin Y, Lau TK, Rogers MS. Second-trimester ultrasonographic assessment of the umbilical coiling index. Ultrasound Obstet Gynecol. 2002;20(5):458-63.
41. Ghezzi F, Raio L, Di Naro E, et al. First-trimester sonographic umbilical cord diameter and the growth of the human embryo. Ultrasound Obstet Gynecol. 2001;18(4):348-51.
42. Sobolewski K, Bańkowski E, Chyczewski L, et al. Collagen and glycosaminoglycans of Wharton's jelly. Biol Neonate. 1997;71(1):11-21.
43. von Kaisenberg CS, Brand-Saberi B, Christ B, et al. Collagen type VI gene expression in the skin of trisomy 21 fetuses. Obstet Gynecol. 1998;91(3):319-23.
44. Rooney P, Kumar S. Inverse relationship between hyaluronan and collagens in development and angiogenesis. Differentiation. 1993;54(1):1-9.

26
CHAPTER

Clinical Aspects of Ultrasound Evaluation of the Placenta

Ashok Khurana

INTRODUCTION

Ultrasound is currently the finest tool for assessing the placenta. Interestingly, however, some of the oddest appearing placentas on ultrasound have no clinical abnormalities. On the other hand, placental abruption and morbid placental invasion—clinically the most dreaded of placental conditions, are often not evident on ultrasound scans. This chapter highlights the clinical significance of ultrasound findings of the placenta and also presents recent advances in imaging that have reduced the gap between negative ultrasound examinations and critical placental disease.

EMBRYOLOGICAL CONSIDERATIONS IN UNDERSTANDING PLACENTAL DISEASE

Five to six days after fertilization, the blastocyst attaches and invades the endometrium. The outermost layer of the blastocyst transforms into the cytotrophoblast, which is the stem cell of the placenta and membranes. Outermost cytotrophoblast cells fuse to form a multinucleated cell mass called the syncytiotrophoblast. At the point where chorionic villi make contact with decidual stromal external extracellular matrix, the cytotrophoblast layer differentiates to form another type of trophoblast—the junctional trophoblast, which ensures the attachment of the placenta to the uterus. A third type of trophoblast differentiates into an invasive variety which moves outwards and remote from the trophoblastic cell mass—the invasive intermediate trophoblast.

After 3–4 weeks of implantation, the invasive intermediate trophoblast commences to progressively invade maternal spiral arteries.[1] This invasion results in disruption of extracellular matrix as well as replacement of maternal endothelium by cells of trophoblastic origin leading to the development of a low impedance and large capacitance vascular bed that will cater to the increased requirement of blood flow in pregnancy.[2] There is a decrease in resistance to uterine arterial blood flow from early gestation to term.[3] This decrease is rapid up to 12 weeks of gestation, less rapid up to about 22 weeks and minimal from 22 weeks to term.

Failure to convert maternal spiral arteries into low resistance vessels may not only compromise fetal requirements, but also induce the placenta to secrete vasoactive substances that induce maternal hypertension. Abnormalities of trophoblastic invasion have been demonstrated in pathological evaluation of the placenta in early and midtrimester pregnancy loss, pregnancy induced hypertension, preeclampsia, and fetal growth restriction.[4,5] Inadequate trophoblastic invasion is not only a consequence of a primary defect in invasive trophoblasts, but a regulated interplay of maternal and fetal factors. These include endocrine, immunological and inflammatory phenomena. These factors are not yet completely elucidated and consequently the understanding of placental disease remains partly clouded. These gaps in knowledge have resulted in the ongoing use of several empirical treatment protocols that would

perhaps be either logically proven or conclusively excluded from clinical use in the future.

Within two weeks of ovulation, lacunae appear in the trophoblastic mass. These are wide channels that will evolve to constitute the intervillous space. These contain maternal plasma and are the site of nutrition, waste and gas exchanges between the maternal and fetal circulations. Maternal blood flow into these spaces happens only after 12 weeks of gestation thus making the human placenta truly hemochorial[5] only at the end of the first trimester. In fact, the first trimester embryo prefers a low oxygen requirement[6] and many pregnancies destined for first and second trimester abortion, and fetal growth restriction, irrespective of the cause, demonstrate increased blood flow in the intervillous space.[6,7]

The functional unit of the placenta is the chorionic villus. This consists of vascular ramifications of the trophoblast. Each villus has a core of fetal capillaries in a matrix of tissue that contains fibroblasts and macrophages. Two distinct trophoblastic layers, an inner cytotrophoblast and an outer syncytiotrophoblast surround this mesenchymal core. The barrier formed by the cytotrophoblast and syncytiotrophoblast prevents the fetus from immunological and other biochemical "attacks" from the maternal circulation. Maternal circulation is essentially an open system with maternal spiral arteries pouring maternal blood into the intervillous space. This intervillous blood returns to the maternal circulation via drain-like uterine veins. Normal fetal circulation in the placenta, unlike the maternal circulation, is a closed system. Blood enters from terminal ramifications of the umbilical arteries, flows through the capillaries of the chorionic villi and returns to the fetus via the umbilical vein and its tributaries. At the point of their entrance into the placenta, umbilical arteries divide into numerous branches and form units called cotyledons. These are like upside-down trees and constitute anatomical units of the placenta.

By five weeks of menstrual age, villi located opposite the implantation site atrophy and form the chorion laeve. The remaining villi constitute the chorion frondosum. This can be visualized by ultrasound between 8 weeks and 10 weeks of gestation **(Fig. 26.1)**.[8,9] This chorion frondosum will ultimately develop into a placenta.

Placental Size and Thickness

The placenta is a fetal organ and its size is a reflection of the size and health of the fetus.[9] During the course of ultrasound examination, assessment of the size of the placenta is usually subjective.[10] Volume estimations

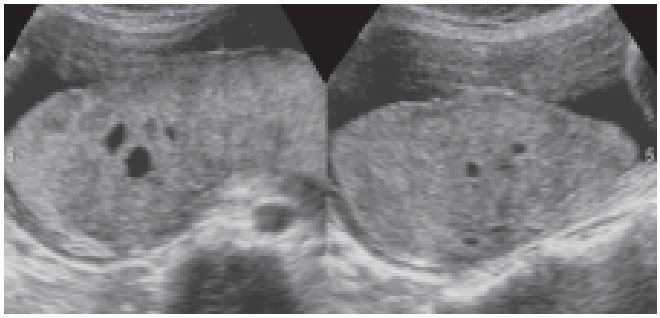

Figure 26.1: Large, thick placenta with globular anechoic spaces. Histopathology showed cystic changes in the villi and no disordered proliferation confirming a mesenchymal dysplasia, excluding a molar change. The fetus showed macrosomia in late pregnancy and a Beckwith-Wiedemann syndrome

using 2D evaluation[11,12] and various mathematical formulae for calculating the volume of an irregularly shaped structure such as the placenta are cumbersome, time-consuming and inaccurate. A 3D evaluation is more accurate,[13] with an error of only 5% compared to the 2D error of 15%. The 3D method has not yet found its way into routine practice. A 3D evaluation of volume is currently undergoing extensive research and is being used along with 3D power Doppler evaluation of placental vascularity and these are discussed in later sections.

During routine 2D evaluation of the placenta, it is important to remember that the estimation of the size of the placenta is based on its thickness and extent. Placentas with a narrower base are often thicker and those with a larger extent are usually thinner. As a convenient "rule" placental thickness in millimeter is usually equal to the gestational age in weeks +/- 10 mm.[9] This is measured at the level of the maximum thickness and is usually the point of cord insertion as well.

The finding of a small placenta should initiate a clinical and if necessary, laboratory evaluation for intrauterine infections in a chronic phase, preconceptional and first-trimester glucose intolerance or diabetes mellitus, some chromosomal abnormalities, and fetal growth restriction of any cause. Severe polyamnios may compress the placenta and give an erroneous impression of thinning.

A large placenta may be seen in fetal hydrops, acute infections, maternal anemia, placental mesenchymal dysplasia, some aneuploidies, triploidy, placental hemorrhage and molar pregnancy.

Placental mesenchymal dysplasia will be elucidated here because its main manifestation is a large and thick

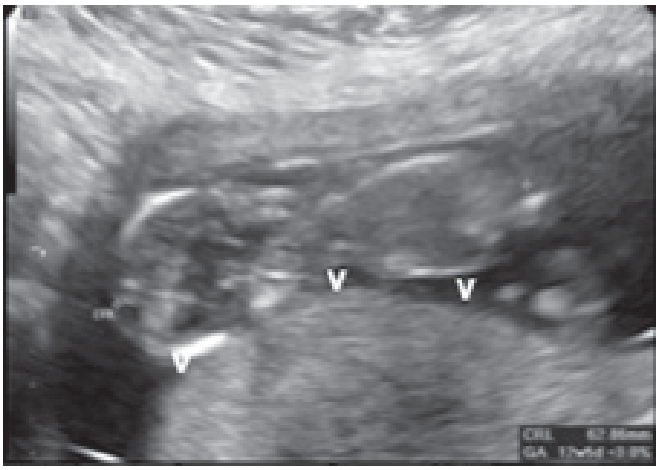

Figure 26.2: Grannum grade 0 placenta. Note the homogeneity, smooth chorionic aspect, lack of indentations of the chorionic plate and absence of cotyledon delineation, and calcification

placenta. This is a rare placental disorder characterized on histopathology by cystic changes in stem villi.[4] On ultrasound, anechoic spaces may be evident similar to a molar change. There is, however, no trophoblastic proliferation on histopathology. Mesenchymal dysplasia has been described in association with abnormal karyotypes and with Beckwith-Wiedemann syndrome.[14-16] Beckwith-Wiedemann syndrome is characterized by macrosomia, macroglossia, visceromegaly and increased susceptibility to childhood tumors. Cases without Beckwith-Wiedemann syndrome have a high incidence of growth restriction and fetal demise.[17]

Placental Texture

The echogenicity of the placenta changes with gestational age. A system of placental "grading" based on echotexture[18,19] was extensively used for several years. Grade 0 referred to a homogeneous placenta **(Fig. 26.2)**, which is the usual appearance seen up to the early second trimester. The grade advanced with the appearance of indentations in the chorionic plate (grade 1) **(Fig. 26.3)**, basal stippling (grade 2) **(Fig. 26.4)** and calcification (grade 3) **(Fig. 26.5)**. Indentations of the chorionic plate delineate placental cotyledons as pregnancy advances. Clinical correlation of placental grade has undergone a major change of understanding in the past decade.[20-22] Calcification is no longer regarded as consistently associated with growth restriction, fetal distress in labor, pregnancy induced hypertension, diabetes and lung maturity. It is, however, more frequently seen in smokers[23] and in patients who are on aspirin and heparin prophylaxis.[9] It is, therefore,

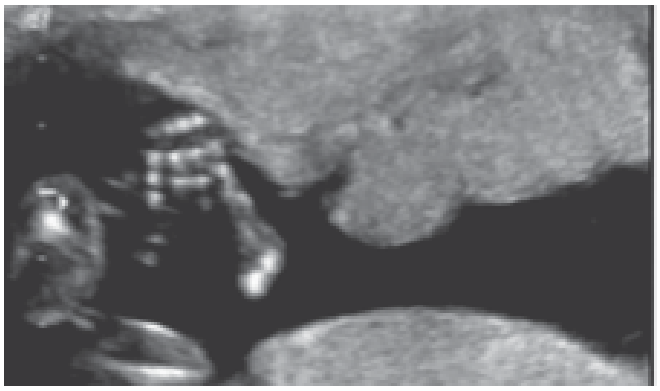

Figure 26.3: Grannum grade 1 placenta. Lobulations of the surface are evident. Chorionic indentations do not extend to the basilar plate. Cotyledons are not delineated and no hyperechogenicities or calcification is evident

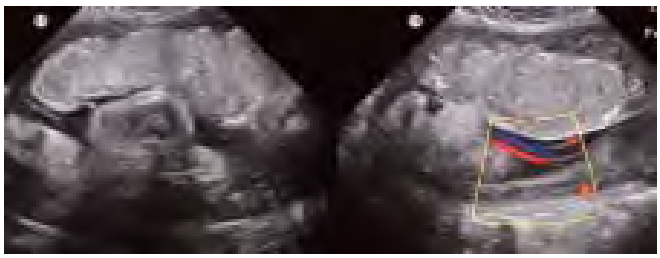

Figure 26.4: Grannum grade 2 placenta. There are chorionic indentations extending to the basilar plate and echogenic marginal delineation of placental cotyledons. No calcification is evident

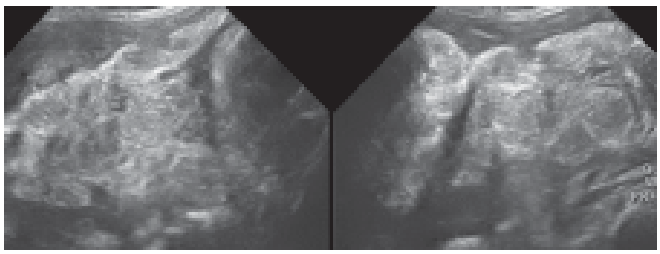

Figure 26.5: Grannum grade 3 placenta. Extensive calcification is evident

currently reasonable to state that placental grading is no longer necessary in reporting ultrasound scans but that extensive calcification must be noted during the course of an ultrasound examination.

Cystic or hypoechoic lesions are almost universal in the placenta after 25 weeks of gestation. Perivillous fibrin deposition is consequent to pooling of blood in the perivillous space.[5] These contain fibrotic villi surrounded by nonlaminated fibrin or blood and are located in the periphery of the placenta **(Figs 26.6A and B)**. They

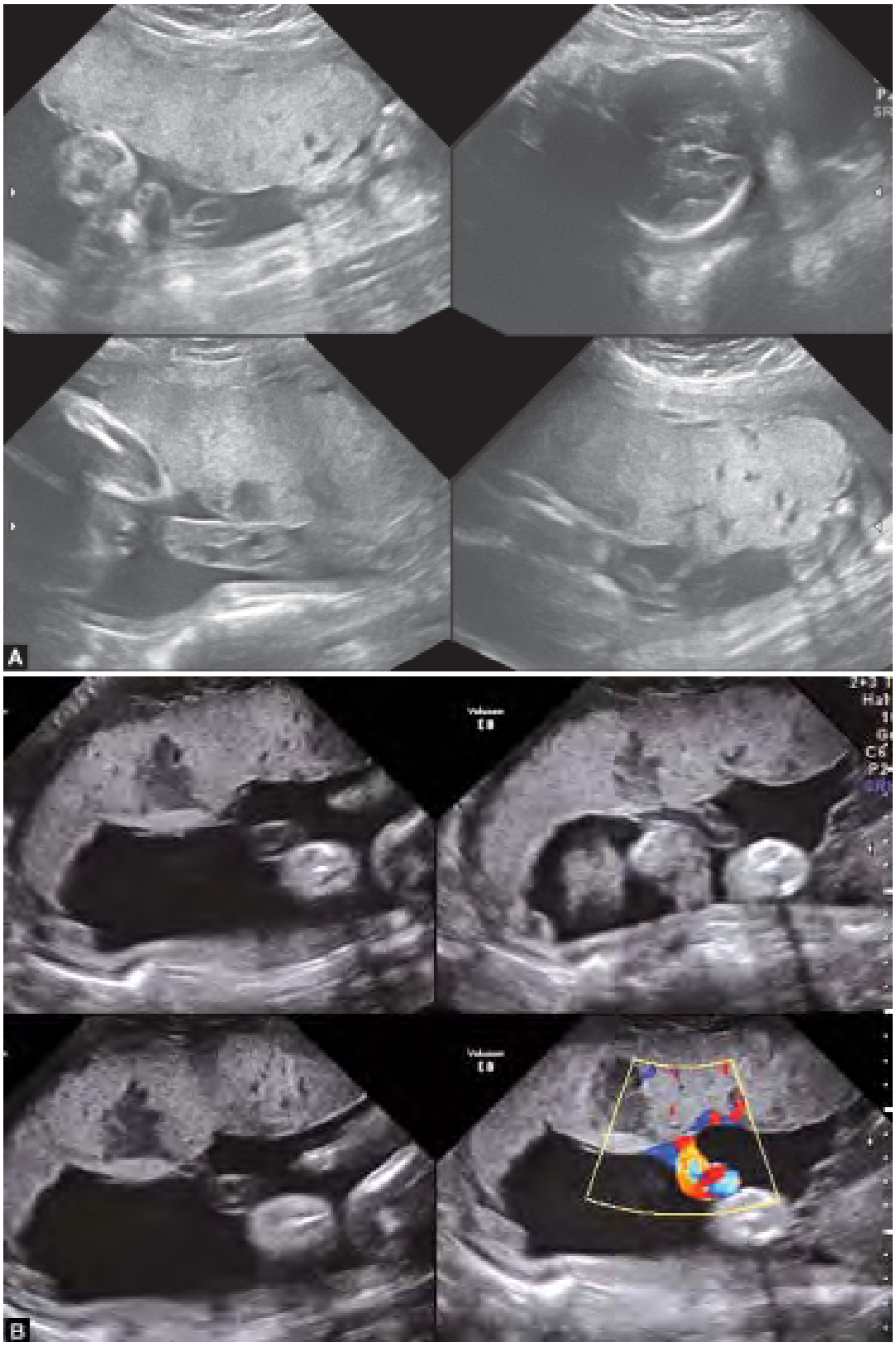

Figures 26.6A and B: Two cases of perivillous fibrin deposition. Anechoic and hypoechoic spaces are seen in the periphery of the placenta. These are of no consequence and are seen in almost all placentas in the third trimester. The larger space in "B" is also perivillous fibrin deposit

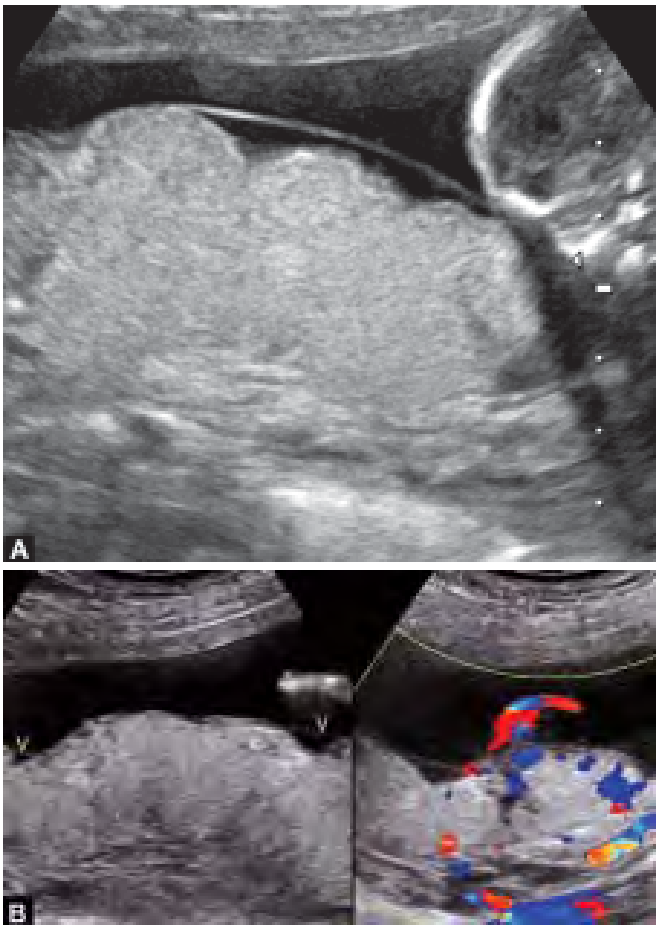

Figures 26.7A and B: Subchorionic fibrin deposit. Note the anechoic subchorionic space in these two cases

are of no clinical significance. Subchorionic fibrin deposition represents pooling of blood in the subchorionic space **(Figs 26.7A and B)**. These pools contain laminated subchorionic fibrin and occasionally fresh blood. These have an ultrasound appearance of triangular or rectangular hypoechoic spaces, often with convex borders. These have no clinical significance.[8] Intervillous thrombosis results from fetal hemorrhage into the intervillous space.[24] Since these represent fetomaternal hemorrhage, they may be of significance in Rh isoimmunization.[5,8,9] Precursors of perivillous and intervillous thrombosis are not uncommon, and may contain flow. These are called maternal "lakes" and are of no clinical significance.[8] Placental cysts are rare and are also called septal cysts, since these arise in the apex of placental septa. Septa are folds of the basal plate that contain decidua. These divide the placenta into 15–20 lobules. These cysts are not of clinical significance, although some large cysts greater than 45 mm across have been associated with growth restriction and fetal demise.[25,26]

Septal cysts, perivillous fibrin deposition and intervillous fibrin deposition are not distinguishable from each other on ultrasound.[8]

Infarcts result from retroplacental hematomas or by thrombotic occlusions of fetal arteries.[5] Small infarcts have no clinical significance.[27] When infarction involves large areas of the placenta, growth restriction and fetal demise have been described.[28] Infarcts are echogenic when fresh and anechoic later. Some placental infarcts may calcify.[27,28] Most infarcts are, however, not evident on ultrasound examinations.

ABNORMALITIES OF PLACENTAL SHAPE

Disordered villous regression in the chorion results in abnormalities of placental shape. Placenta membranacea is a rare anomaly[29] in which the entire chorion is covered by villi. Some of this placenta will, therefore, always span across the internal os.[29,30] A large part of this type of placenta is often dysfunctional from a maternofetal exchange perspective[10] and fetal growth restriction may ensue. About one-third of these placentas also show abnormal adherence.[31] Consequently this type of placenta is associated with recurrent antepartum hemorrhage, growth restriction and postpartum hemorrhage. Very occasionally a partial placenta membranacea[31] has been described. Annular[5] or ring-shaped placentas and horse-shoe[10] shaped placentas have also been described. These are consequent to aberrant villous atrophy.

A circumvallate placenta is one in which the chorion plate is smaller than the basal plate. The membranes, therefore, insert not at the edge of the placenta but towards the center. This region is evident as a thickened, rolled and ridge of membranes **(Fig. 26.8)** with an uplifted placental shelf.[9] Lucent areas representing hemorrhage[9] and fibrin deposits[10] are often seen in the "extrachorial" extent of the placenta. Circumvallation may be complete or partial. The partial variety is clinically insignificant. The complete variety is associated with placental abruption, growth restriction, perinatal mortality and fetal growth restriction. Recognition of this variant of placental shape is therefore important.[32,33]

THE CONCEPT OF PLACENTAL TROPHOTROPISM

Trophotropism is the term used to describe preferential proliferation of trophoblastic villi in regions of better

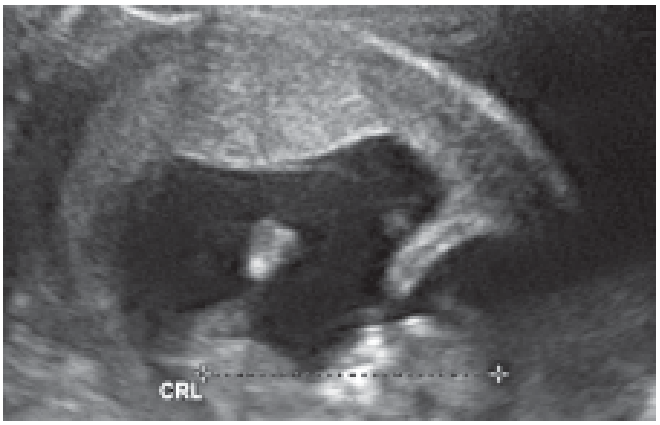

Figure 26.8: Complete circumvallate placenta. Note the associated shelf at the edge of the placenta. This is a commonly associated finding in circumvallate placentas

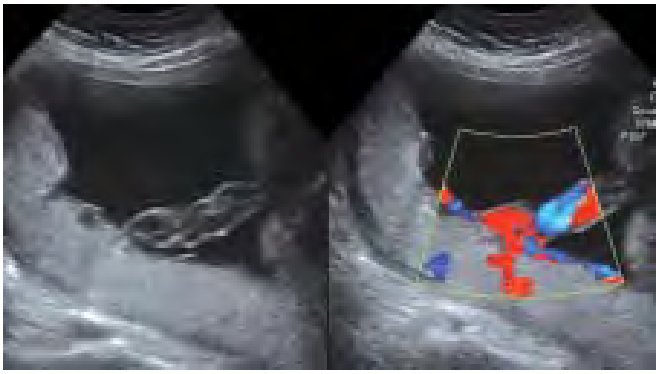

Figure 26.9: Central cord insertion

endometrial supply along with atrophy of villi in areas with a poorer blood supply.[34,35] Placental position and shape can therefore change as pregnancy progresses. Trophotropism explains resolution of placenta previa, increase in pathologic extent of placenta previa, the development of succenturiate lobes or a bilobed placenta, odd shaped placentas and abnormal cord insertions. During early development, the placenta is a rounded disk with the cord insertion at its center **(Fig. 26.9)**. Trophotropism can produce a placenta with an eccentrically located insertion **(Fig. 26.10)**, a marginal insertion at the edge of the cord **(Fig. 26.11)** or a cord insertion into membranes distant from the cord, with fetal vessels running in the membranes unprotected by Wharton's jelly. This last variety is known as velamentous insertion of the cord **(Fig. 26.12)**.

Succenturiate lobes are accessory placental lobes that are located at a distance from the main placenta **(Fig. 26.13)**. It is theorized that these are also consequent to trophotropism. Fetal vessels commence from these

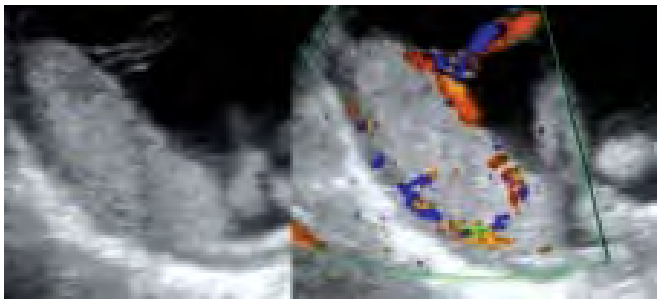

Figure 26.10: Eccentric cord insertion. The placenta must be scanned across its entire extent to ensure that this appearance is not a cross sectional impression. A small region of placental tissue is seen extending beyond the cord insertion excluding a marginal insertion

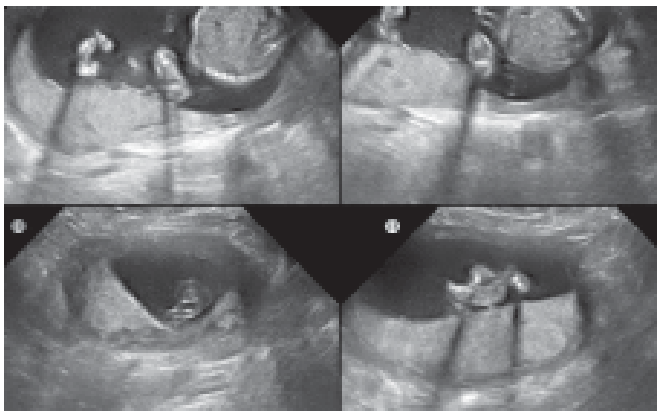

Figure 26.11: Marginal cord insertion. Note the absence of any placental tissue beyond the region of cord insertion

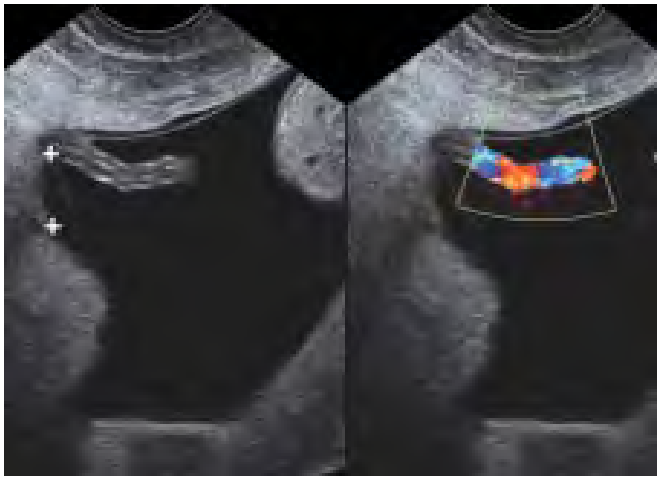

Figure 26.12: Velamentous insertion of the cord. Note the distance of the cord insertion from the placental margin (++)

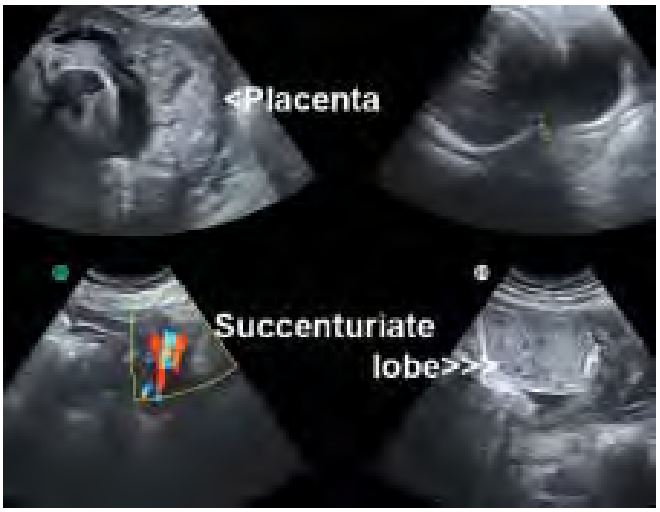

Figure 26.13: Succenturiate lobe in the fundal area. The bulk of the placenta is on the anterior wall in the midcorpus

lobes to merge with the main placenta or participate in the formation of the umbilical cord. Succenturiate lobes are associated with fetal demise in labor consequent to rupture of vessels during rupture of membranes and in scenarios of retained placenta, and postpartum hemorrhage.[36]

Competition for available endometrial surface explains the high frequency of marginal and velamentous insertions in multifetal pregnancies.[34]

In pregnancies with succenturiate lobes, in placentas with velamentous cord insertions and in low-lying placentas with marginal cord insertions, fetal vessels may cross the internal os. This is known as vasa previa. Vasa previa are at an increased risk of rupture[34] and rapid fetal exsanguination. Such variations should, therefore, be looked for during all scans in pregnancy. The overall sensitivity of ultrasound for the detection of vasa previa is low.[34] Color Doppler makes it easier to identify and confirm this condition. Only fetal vessels overlying the internal os are referred to as vasa previa. Occasionally, maternal marginal placental veins also known as the marginal sinus may be positioned over the internal os. These behave like a placenta previa and not like a vasa previa.

PLACENTA ACCRETA

The term placenta accreta is the generic term for abnormal adherence of the placenta to the uterus. It is consequential to a defect in the fibrinoid (Nitabuch's) layer of the decidua[37] underlying the placenta. The term

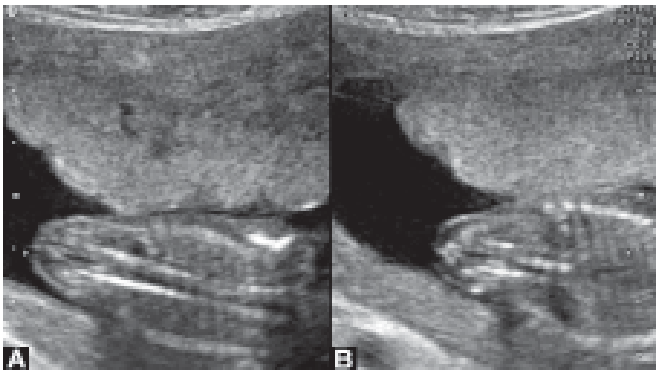

Figures 26.14A and B: Placenta accreta. Note the extensively obscured interface that should have been seen as a hypoechoic zone between the basal extent of the placenta and the subplacental myometrium

placenta accreta vera is used when the placenta is adherent to the myometrium but does not invade it **(Figs 26.14A and B)**. The term placenta increta is used when myometrial invasion takes place **(Figs 26.15A and B)**. Placenta percreta refers to the situation where invasion extends beyond the uterine serosa and into the urinary bladder **(Fig. 26.16)** or rectum. The placenta does not separate after delivery and can result in a situation of retained placenta, life-threatening hemorrhage or uterine rupture, not infrequently requiring an emergency hysterectomy. Risk factors include previous cesarean section, previous curettage, previous morbid adherence, a low lying placenta, advanced maternal age, submucous fibroids and anomalies of uterine structure such as uterine horns.[10,37-39] A multislice ultrasound evaluation[37,40,41] enhances the accuracy of detecting the diagnosis, although these are by no means very sensitive. The normal retroplacental complex is thinned out (2 mm or less) or obliterated. The retroplacental complex refers to the hypoechoic space behind the placenta that is normally 10–20 mm thick. There is loss of the normal decidual interface between the placenta and the myometrium. Multiple hypoechoic or anechoic lacunae are often evident in the placenta **(Fig. 26.17)**. These may give it a Swiss-cheese appearance. Invasion of the bladder or rectum may be evident. Three-dimensional power Doppler studies have helped to identify a new reliable sign.[42] Normal placentas show vessels that run parallel to the long axis of the uterus. Invasive placentas show branches that run perpendicular to these main vessels and show a course running through the myometrium **(Figs 26.18A to D)**. Magnetic resonance imaging (MRI) reports, although initially encouraging, are still undergoing critical evaluation.[43]

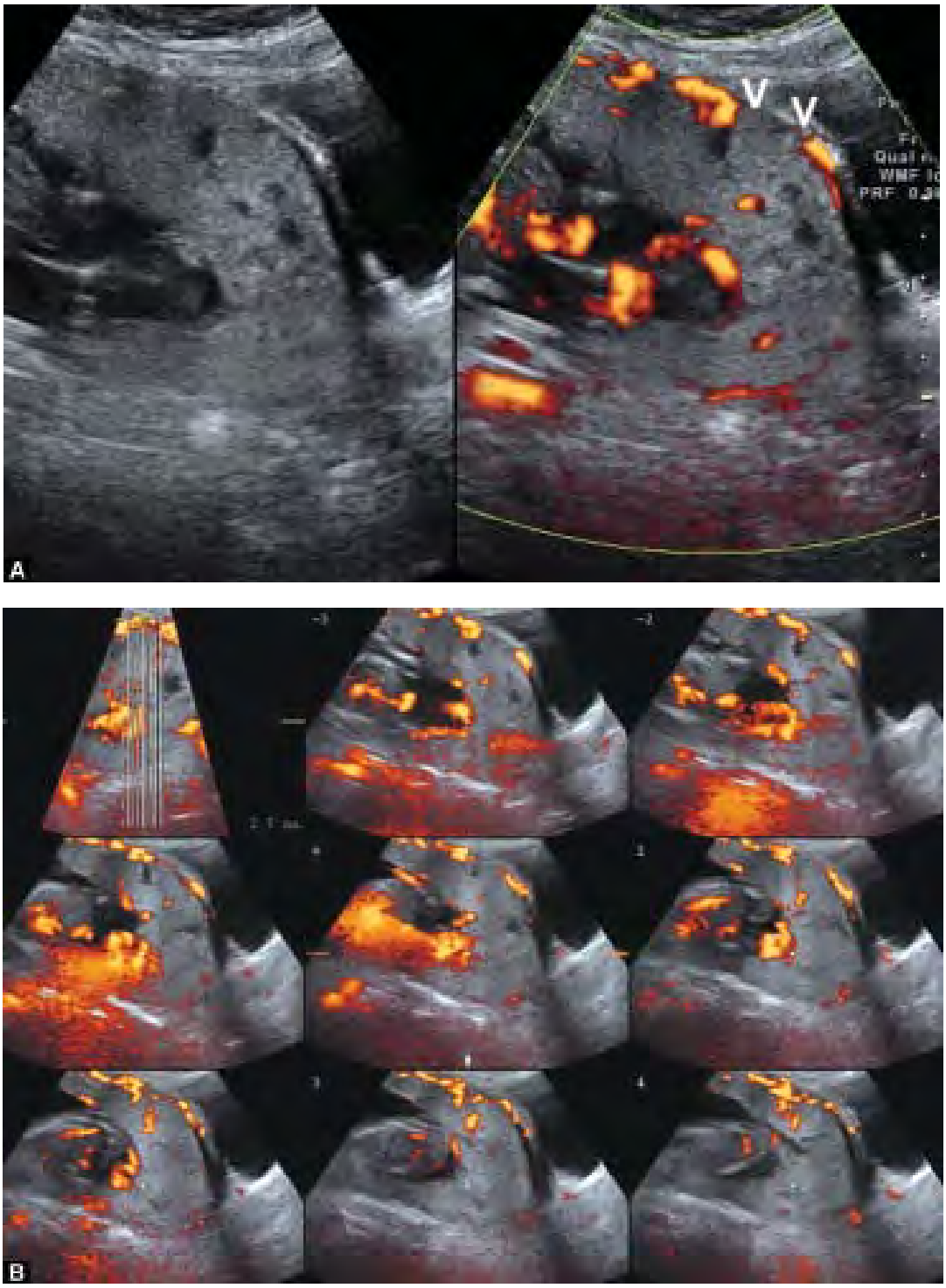

Figures 26.15A and B: Placenta increta. 2D and power Doppler studies demonstrate an area of extensive myometrial invasion. The serosal aspect of the uterus is not invaded. The 3D multislice image (tomographic ultrasound imaging) aids in assessing the entire extent of the placenta. This low-lying placenta has invaded the posterior uterine wall as well (++)

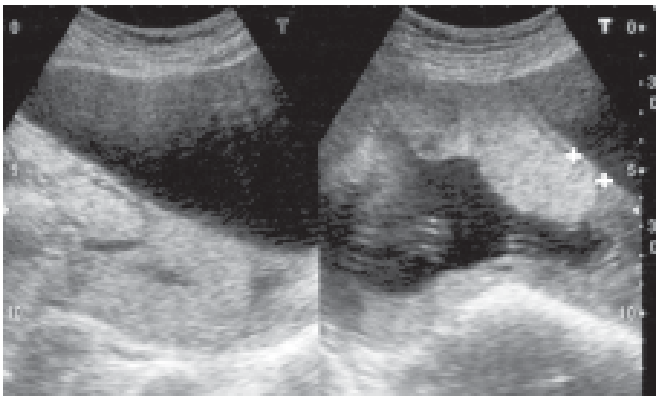

Figure 26.16: Low-lying placenta with invasion through the entire myometrium and into the wall of the urinary bladder

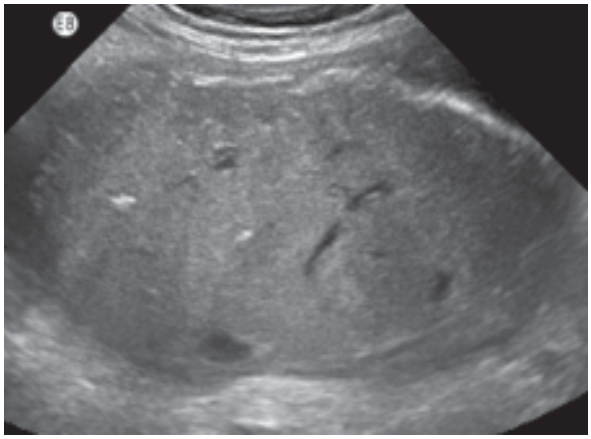

Figure 26.17: Multiple anechoic spaces are often evident in an invasive placenta. These can enlarge and be more extensive giving it a Swiss-cheese appearance. Note the extensively obscured retroplacental decidual stripe and the extension of the placenta up to the wall of the urinary bladder

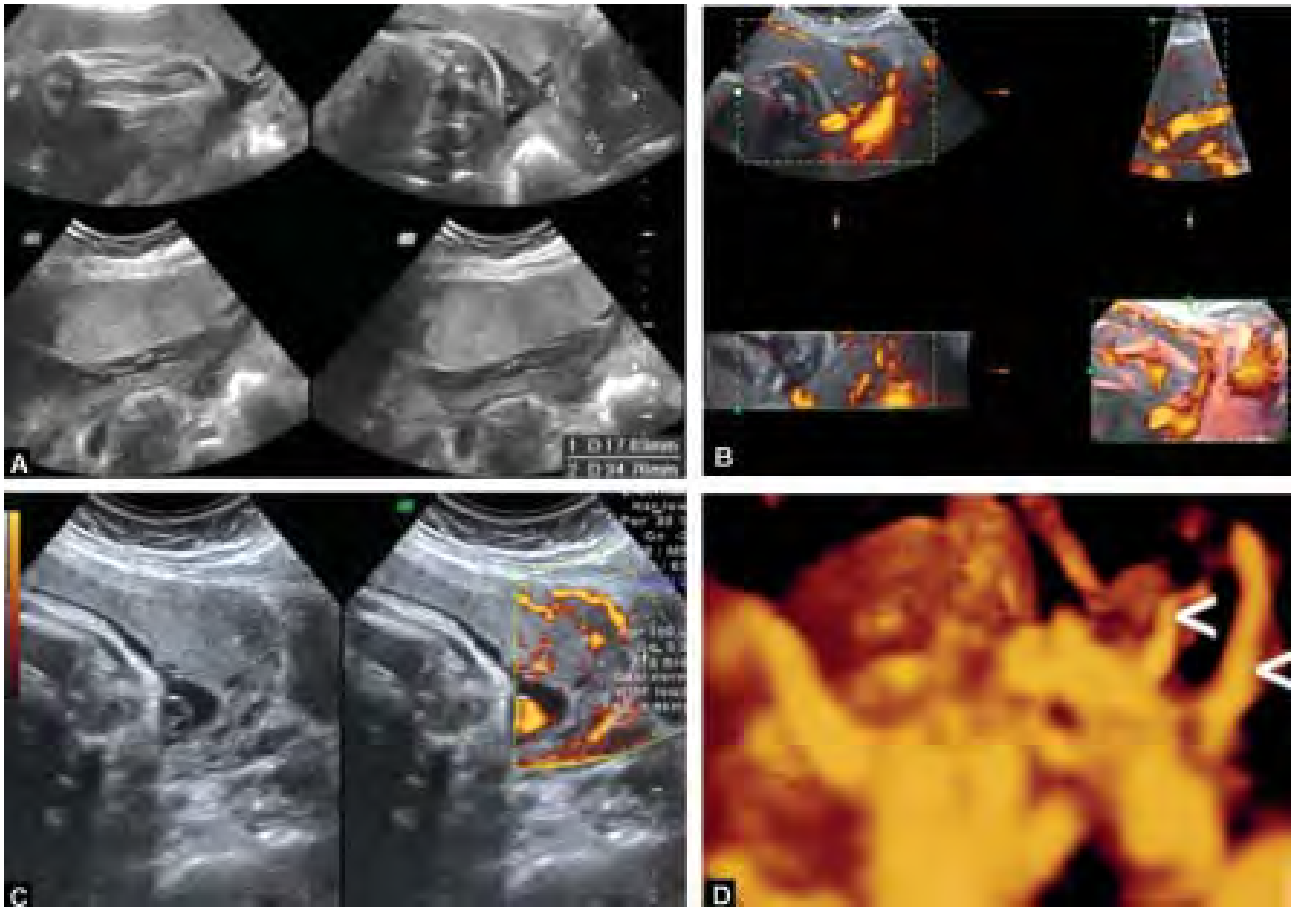

Figures 26.18A to D: 3D power Doppler of the placenta. The multislice format confirms multiple areas of invasive placenta. 3D acquisitions and subsequent rendering formats ensure that the placenta is evaluated throughout its extent. Note the multiple vessels arising radially from the placental vessels in the 3D angio-mode rendering (<)

THE RETROPLACENTAL SPACE, PLACENTAL HEMATOMAS AND PLACENTAL ABRUPTION

Evaluation of the retroplacental area should form an essential part of every ultrasound examination. This facilitates increased accuracy of identifying retroplacental clots and abnormal placental adherence. Retroplacental myometrium and decidua appear hypoechoic when compared to the placenta. Draining veins and spiral arterioles course through this area and can be better identified with color Doppler.

Myometrial contractions are frequent and are not felt by the mother. These mimic retroplacental myomas and hematomas. These are best confirmed by a repeated evaluation 20–60 minutes later. They can distort the lower part of the uterine corpus and result in a false positive for a low placenta.

Retroplacental myomas are well circumscribed, usually hypoechoic, variably vascular lesions. As mentioned earlier, these are difficult to differentiate from myometrial contractions and need to be confirmed after a time interval. They may increase or decrease in size in pregnancy.

Intraplacental, retroplacental and preplacental hematomas are frequently seen during ultrasound examinations. There is considerable confusion in the nomenclature of these lesions. This has arisen because the placenta is often thought of as the chorion.[10] This needs to be clarified, understood and remembered because the location of collections has a bearing on prognosis.[44-46] Retrochorionic should refer to the space between chorionic membrane overlying the placenta and the fetal aspect of the placenta (the villous chorion) and not the retroplacental space. The retrochorionic location is also referred to as the preplacental or subchorionic location. Retrochorionic hematomas are lesions that denote the collection of maternal blood accumulation between the chorionic membrane and the fetal aspect of the placenta **(Fig. 26.19)**. They are generally of little clinical signicance, except if accompanied by clinical symptoms, such as vaginal bleeding or uterine contractions when they can be markers of later complications, such as abortion, intrauterine growth restriction (IUGR), preterm labor, placental abruption and fetal distress.[10,46-48] The occurrence of subamniotic hematomas has added to the confusion in nomenclature. This is an entity where blood is found near the umbilical cord insertion (usually resulting from pulling on the cord during delivery and, therefore, not an ultrasound entity). These are situated between the amniotic and chorionic membrane and result from rupture of chorionic vessels near the cord insertion. Occasional

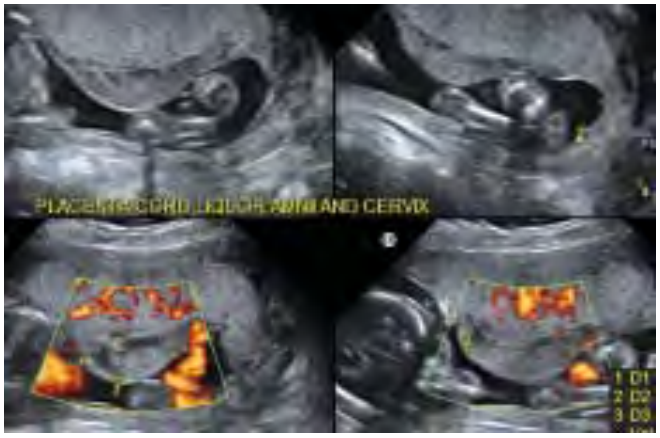

Figure 26.19: Large, variably echoic retrochorionic hematoma near the site of cord insertion. The pregnancy, delivery and puerperium were uneventful

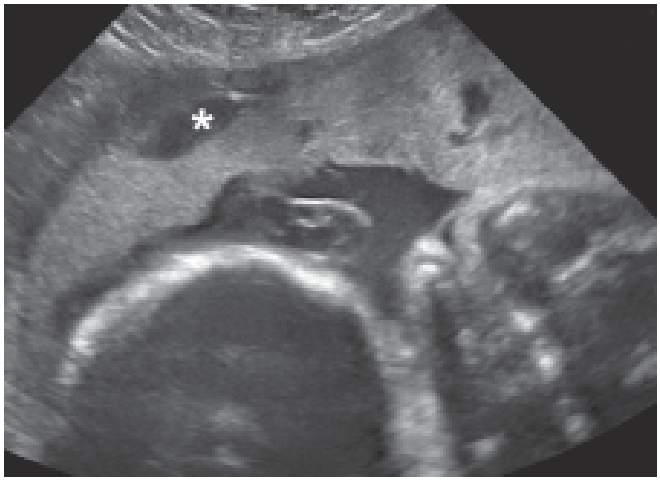

Figure 26.20: Retroplacental hematoma. Note the hypoechoic morphology. Fresh hematomas may be isoechoic with the placenta and missed on an initial scan. Hematomas almost always bulge towards the fetal side

antenatal reports exist[44] and these suggest a minimal clinical significance. Breus mole[49] is a rare form of subamniotic hematoma. This term refers to as a massive subamniotic hematoma associated with growth restriction or fetal demise. The 2D findings can be confused with a chorioangioma. Color Doppler, however, confirms an avascular lesion.[50] Retroplacental hematomas are located between the placental basal plate and the uterine wall **(Fig. 26.20)**. These result from bleeding from spiral arteries and arterioles. These usually bulge towards the fetal side and have been associated with perinatal complications, particularly preterm labor, perhaps as a result of uterine irritation, secondary to the presence of blood.[46] These are often

treated with tocolysis, progesterone and bed rest in early pregnancy, although evidences in the literature are equivocal.[10] Retroplacental hematomas often lead to villous infarction and are associated with maternal hypertension, preeclampsia, anticardiolipin antibodies, blunt trauma, cigarette smoking and cocaine abuse. Clinical significance is related to the size of hematoma and gestational age.[9] A smaller hematoma usually has an impact, only if they occur before 20 weeks of gestation. Larger hematomas must strip away 30–40% of the placenta from the myometrium to cause significant infarction and consequent growth restriction, oligoamnios and abnormal Doppler findings.[9] Fresh hematomas tend to be isoechoic with the placenta and may be missed on initial examination. Older hematomas tend to be hypoechoic. All hematomas are avascular. Placental abruption refers to a sudden retroplacental bleed. This presents as severe abdominal pain, bleeding or both and many patients move straight to an urgent cesarean section and are not scanned. In a subacute situation, the findings are identical with a retroplacental hematoma.

NONTROPHOBLASTIC PLACENTAL TUMORS

These consist of gestational trophoblastic tumors, nontrophoblastic tumors and metastases from cancers in other parts of the body.

Most benign nontrophoblastic tumors of the placenta are chorioangiomas. Small lesions are not uncommon in pathological examinations of the placenta. These are usually asymptomatic and minimally vascular. Larger lesions usually greater than 50 mm across are often symptomatic and present as nonimmune hydrops, fetal cardiomegaly, polyamnios or growth restriction. The lesion itself is well circumscribed, hypoechoic, closer to the fetal aspect of the placenta **(Figs 26.21A and B)** and often close to the umbilical cord.[51,52] These masses are variably vascular on color Doppler evaluation[53,54] and vascularity, and 3D power Doppler[53-57] studies are a pointer for fetal morbidity and mortality.

Placental teratomas are rare lesions.[58] These are cystic cum solid, variably vascular and are almost always located on the surface of the placenta. Some authors believe that these are not true neoplastic lesions and represent an unsuccessful twin pregnancy.

Metastases to the placenta are rare. These include melanomas, lymphomas, leukemias and breast lesions.[59,60] Very rarely, a fetal tumor may metastasize to the placenta.

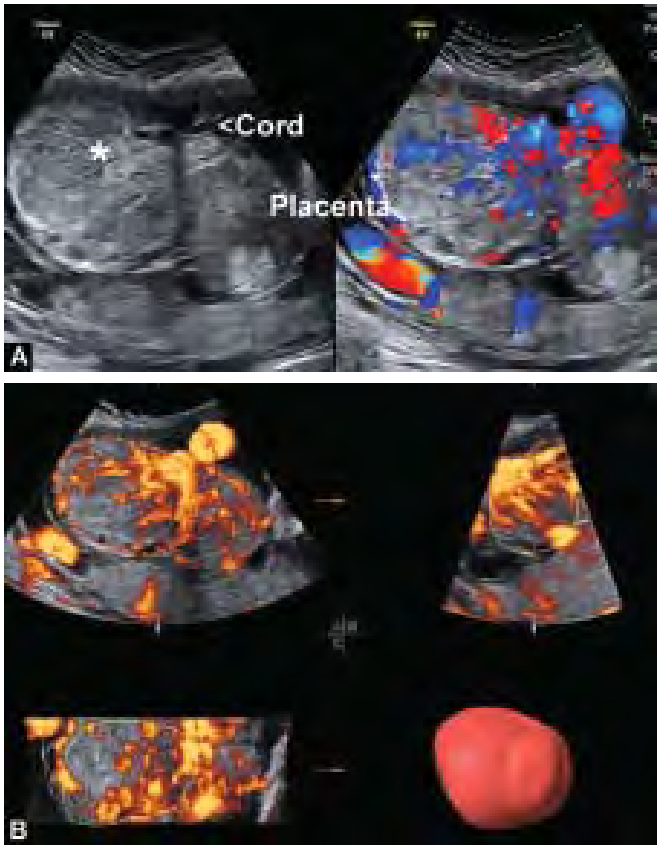

Figures 26.21A and B: Large, vascular chorioangioma adjacent to the fetal surface of the placenta and to the umbilical cord as well. (A) Shows 2D and color Doppler findings; (B) A 3D volume calculation (VOCAL) which indicates the volume and can be used to assess 3D vascular indices

GESTATIONAL TROPHOBLASTIC DISEASE

Gestational trophoblastic disease refers to a spectrum of conditions that includes partial hydatidiform mole, complete hydatidiform mole, invasive mole, choriocarcinoma and placental site trophoblastic tumor. A wide consensus of classification is currently not available. All but partial moles may metastasize and should not be left untreated. Risk factors include Asian ethnicity, advanced maternal age and a previous history of gestational trophoblastic disease. With clinical surveillance of early pregnancy becoming widespread, the presentation has moved from the well known picture of an enlarged uterus with a snowstorm appearance, bleeding per vaginum, passage of vesicles per vaginum, hyperemesis gravidarum and theca lutein cysts, to a presentation of abnormal ultrasound findings,

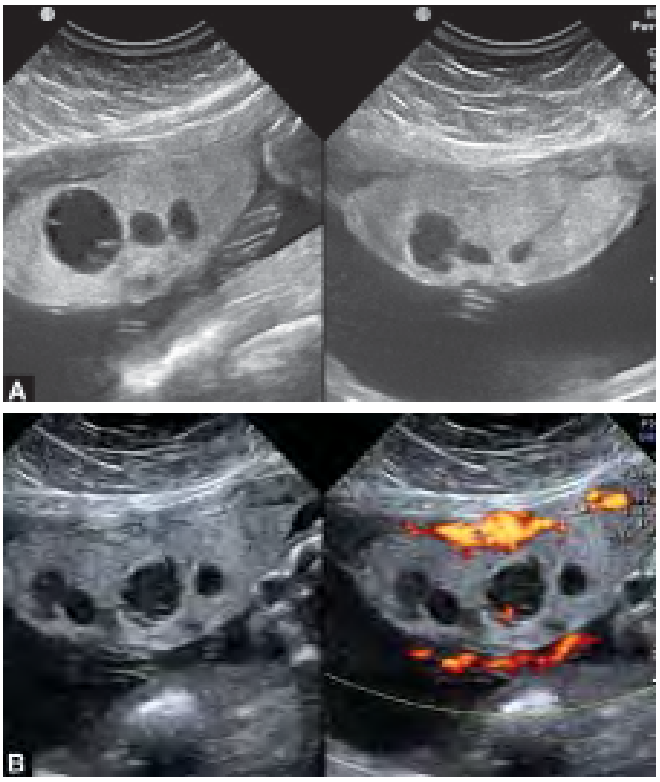

Figures 26.22A and B: Anechoic and hypoechoic, minimally vascular spaces in a bulky placenta. Histopathology confirmed partial mole

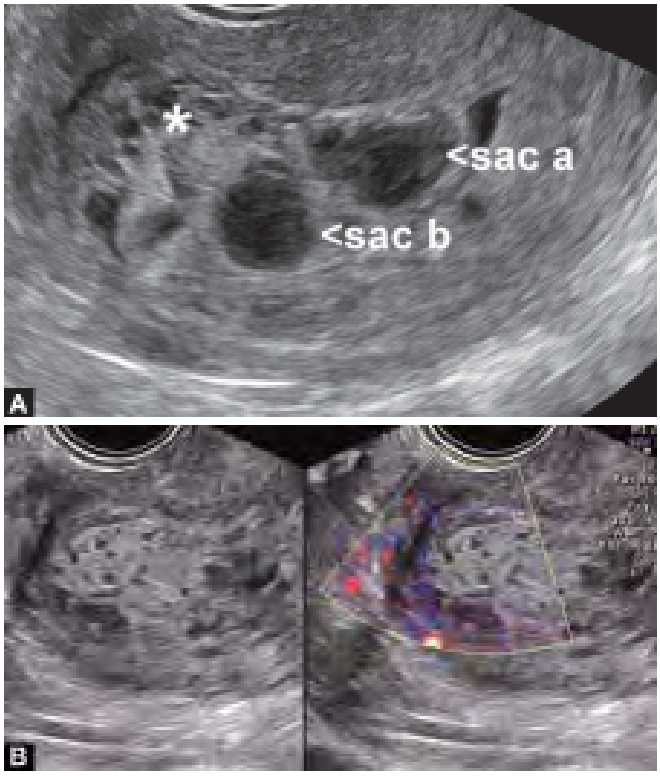

Figures 26.23A and B: Twin nonviable sacs with hydatidiform mole. Note the echogenic appearance of the molar tissue with occasional cystic areas and minimal neovascularity. Early diagnosis has made the classical morphology of a snowstorm appearance a rarity

abnormal histopathology of curettage products and an elevated serum human chorionic gonadotrophin.[61-64] Partial moles present as a small uterus with an incomplete abortion, a missed abortion **(Figs 26.22A and B)** or an ongoing fetus with severe growth restriction usually accompanied by multiple anomalies, oligoamnios and abnormal Doppler.[10,61,62] Partial moles are most commonly due to a fertilization error in which an abnormal ovum is fertilized by two spermatozoa, resulting in a triploid 69XXY karyotype.[10] In 90% of complete moles there are paternally derived chromosomes with a 46XX karyotype.[10,65] These present on ultrasound as incomplete abortions, abundant high level cavity echoes, the classical snowstorm appearance **(Figs 26.23A and B)** and abundant maternal lakes that may show flow on color, and power Doppler.[61-63] Invasive mole, choriocarcinoma and placental site trophoblastic tumors are referred to as gestational trophoblastic tumors, and on ultrasound may present with a variety of appearances including bulky trophoblast, variable myometrial invasion, an echogenic myometrial mass **(Figs 26.24A and B)**, ascites, pleural effusion and metastases.[61,66] Vascularity is variable, includes maternal lakes and arterial signals.[61,62,66]

PLACENTAL LOCATION

The confusion that existed in the "classification" and nomenclature of placental location has undergone significant clarification over the past decade, and a clinically relevant understanding of placental location is now apparent. Terms such as low-lying placenta, marginal placenta previa, partial and total placenta previa, all refer to an abnormally low placenta. A total placenta previa completely spans across the internal os **(Fig. 26.25)**. A partial placenta previa partially spans across the internal os **(Fig. 26.26)**. A marginal placenta extends down to the internal os but does not span across it **(Fig. 26.27)**. It is appropriate to specify the distance between the lower margin of the placenta and the internal os.[67] A placenta that extends down to the internal os is 0 mm away from the internal os. The amount of placenta that overlaps the internal os should also be measured and the distance reported in millimeters.[67] It is also now clear that changes in placental location occur throughout gestation and are consequent to two phenomena: (1) Formation of the lower uterine segment

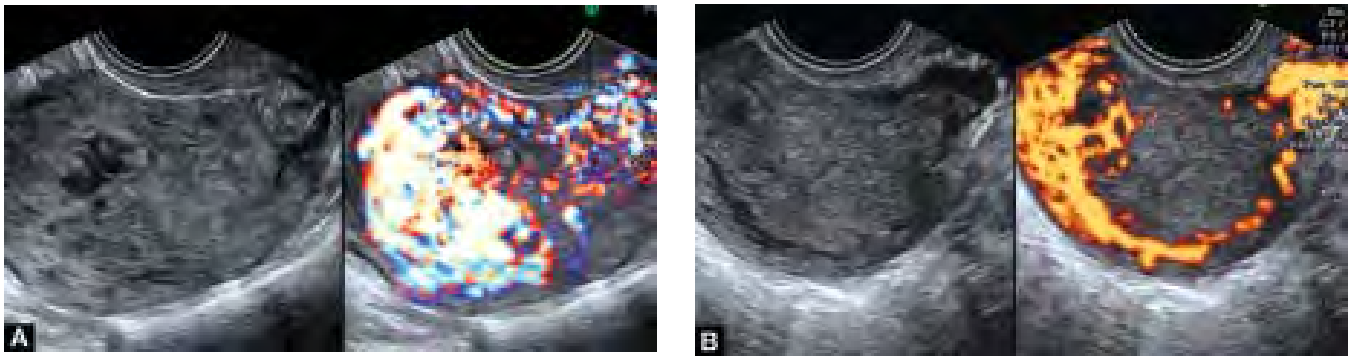

Figures 26.24A and B: (A) Poorly marginated, heteroechoic, intensely vascular myometrial lesion in a patient with rapidly rising serum hCG levels after a missed abortion. Histopathology confirmed a choriocarcinoma; (B) Isoechoic myometrial lesion with obliterated cavity echoes. The lesion is avascular and largely delineated only by intense hyperemia in the rest of the myometrium. Histopathology and follow-up confirmed an invasive mole. Note the nonspecific findings in this case and in "A". Clinical perspective and histopathology are necessary for a diagnosis

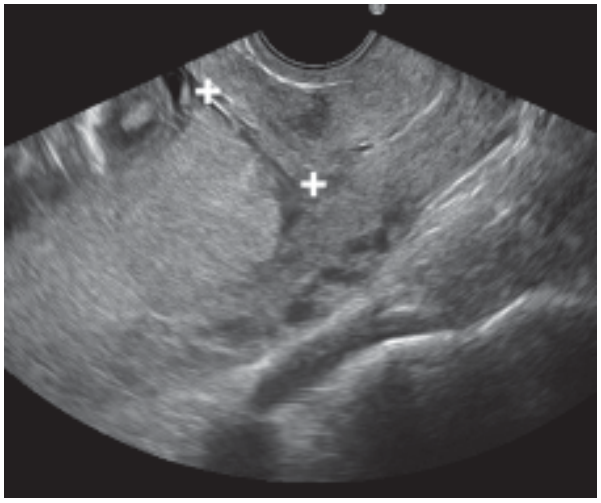

Figure 26.25: Complete placenta previa. Transvaginal image shows a posterior wall placenta spanning across the internal os and extending onto the anterior uterine wall. The ++ calipers measure the extent of the placenta beyond the internal os. This measurement is clinically relevant because the greater the extent beyond the os the smaller the chance of "resolution" of a placenta previa

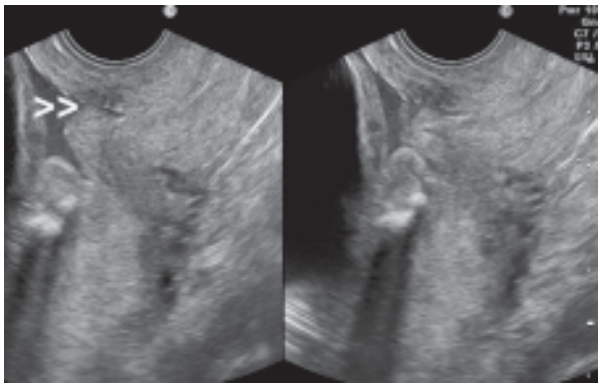

Figure 26.26: Partial placenta previa. The lower limit of this low-lying placenta extends down to the internal os, partially spans across it, but does not extend beyond the os

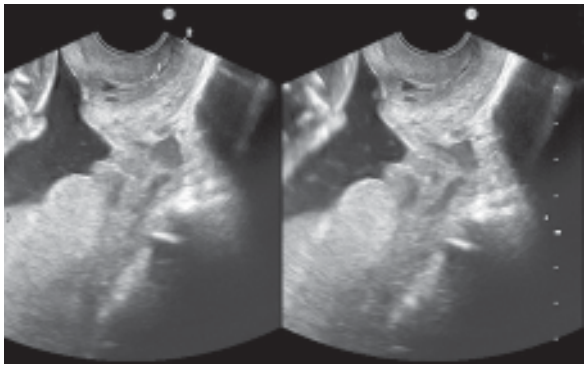

Figure 26.27: Marginal placenta previa. This low-lying placenta extends down to the internal os but does not span across it

and (2) Placental trophotropism.[34,35,68] Over 90% of placentas that are low lying at 20 weeks of gestation will achieve a normal position at term.[68] Transvaginal evaluation is superior to transabdominal evaluation.[40,69,70] The safety of transvaginal scans is also not in doubt[71,72] and the technique, in spite of initial skepticism, now has widespread acceptance.[67] The clinical presentation of placenta previa has changed over the years and most low-lying placentas are now diagnosed during the second-trimester anomalies scan. Predisposing factors for placenta previa include previous cesarean section, previous cavitary surgery, previous vigorous curettage, multiparity and advanced maternal age.[34,73,74] Transvaginal scanning has greatly reduced the incidence of placenta previa[75,76] because of its better delineation of the internal os and inferior placental margin.

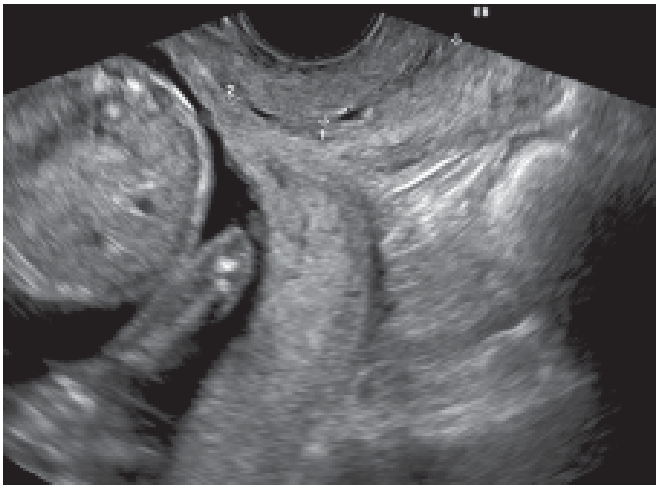

Figure 26.28: Marginal placenta previa with a thin beak-like lower edge. The morphology of the inferior edge has a bearing on clinical outcome. Placentas with a rounded lower edge (Fig. 26.25) are more likely to resolve at term unlike this one, which is likely to persist till term. The cervix should be measured in all low placentas. The chances of bleeding are higher with a short cervix

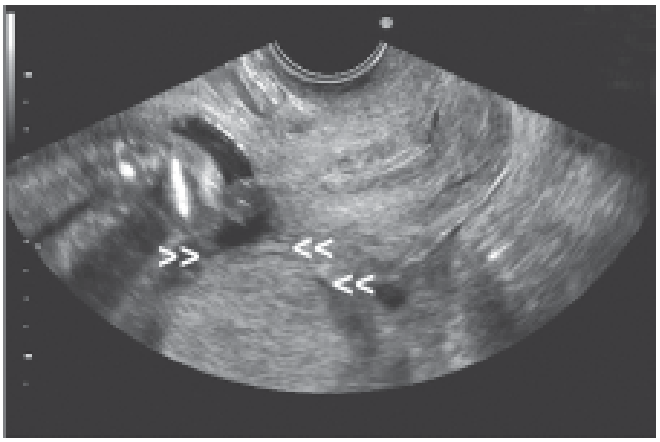

Figure 26.29: Low placenta with a round lower edge. This type is more likely to migrate away from the internal os as pregnancy progresses to term

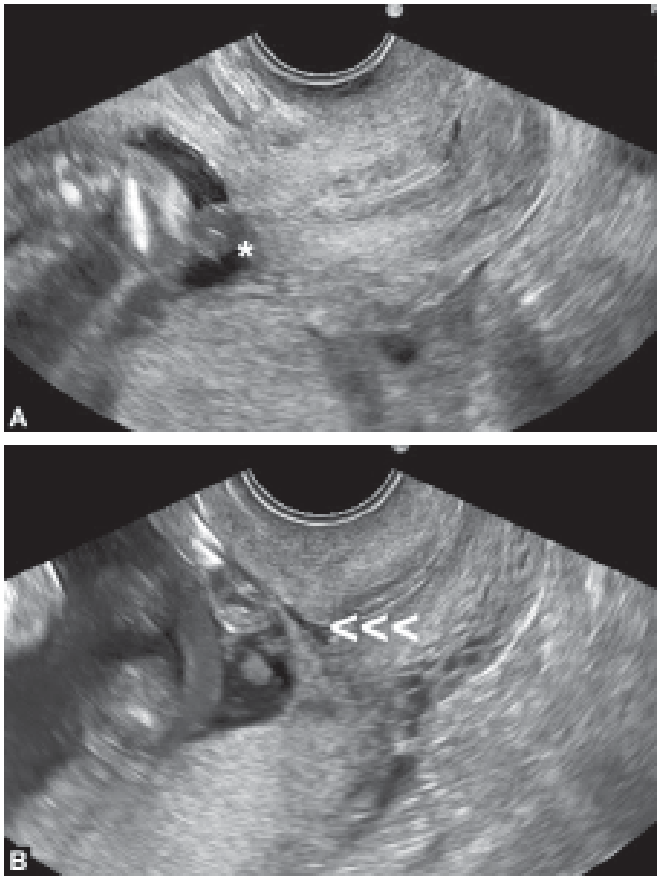

Figures 26.30A and B: Two cases of placenta previa. Note the echo-free fluid space between the placenta and the internal os. Placentas with such a morphology are more likely to bleed

Serial evaluation demonstrates placental migration[77] and it is possible to predict which cases will persist to term.[75,76,78-82] A review of these studies indicates that placentas that overlap the cervix by a distance greater than 10–15 mm in the second trimester are likely to be persistently low at term. Most placentas that do not overlap the internal os are likely to "resolve" at term. Vaginal delivery is generally possible once the placenta is 20 mm superior to the internal os. A significant number of pregnancies with placentas between 10 mm and 20 mm can also be delivered vaginally. Another ultrasound feature that also influences placental migration is the morphology of the inferior edge of the placenta.[83] Placentas with a thin inferior edge **(Fig. 26.28)** are more likely to persist in a low position compared to those with a thick lower edge **(Fig. 26.29)**.

The risk of bleeding from a placenta previa depends on several factors. Irrespective of the distance of a low placenta from the internal os, most patients who do have antepartum bleeding, will not have episodes which are life-threatening or require premature delivery.[67] It must be emphasized, however, that pregnancies with a placenta that is within 40 mm of the internal os do have a higher risk of postpartum hemorrhage.[67] The distance of a low-lying placenta from the internal os does not seem to influence the risk of antepartum bleeding. This is more influenced by cervical length[84] and the presence of an echo-free space **(Figs 26.30A and B)** in the lower edge of the placenta overlying the internal os.[85] Both these factors increase the possibility of the need for an emergency delivery prior to 34 weeks of gestation. Most

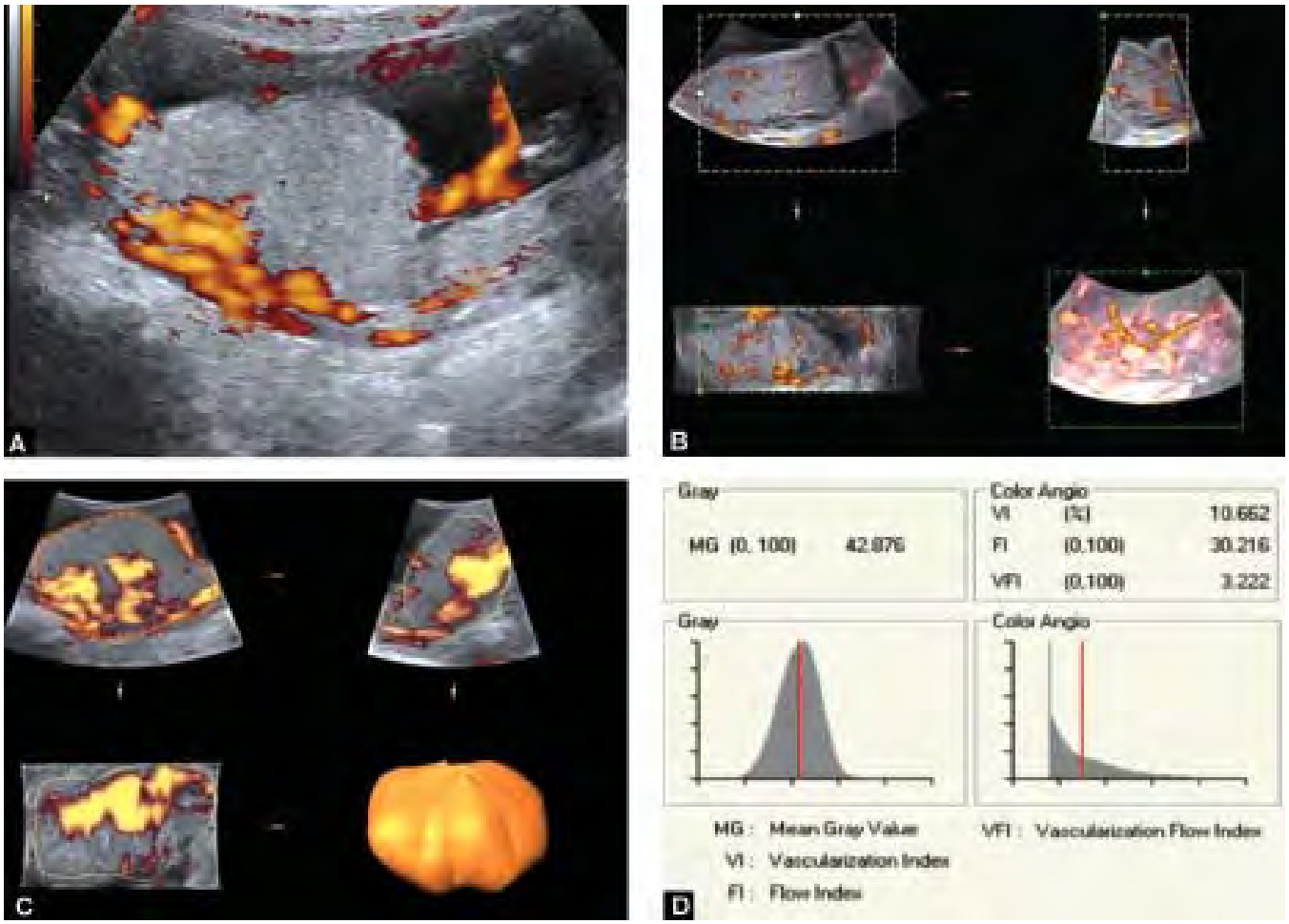

Figures 26.31A to D: A 3D power Doppler of the placenta. The steps involved in this evaluation are: (A) Choosing the entire placenta in a 3D power Doppler window as a region of interest; (B) Acquiring the region in a glass body 3D mode; (C) Performing a VOCAL of the placenta; (D) Activating the volume histogram button

patients without these two features can be managed expectantly without hospitalization.[86-89] Cervical cerclage for a short cervix with a low placenta is not justified.[67,89,90] Placenta accreta and vasa previa are intimately associated with placenta previa.[40,91] In this situation, timed operative delivery[92,93] in an appropriate setting greatly improves perinatal outcomes. Evidence of placenta previa, should therefore, prompt a careful ultrasound evaluation for placenta accreta and vasa previa.[67]

THREE DIMENSIONAL POWER DOPPLER (3DPD) OF THE PLACENTA

Placental disease underlies a wide spectrum of abnormal pregnancy outcomes.[13] Improvements in transducer and software technology have made it possible to accurately evaluate placental volume and placental vascularization **(Figs 26.31A to D)**.[94-104] Doppler parameters derived from 3D interrogation are different from those using conventional ultrasound and include the vascularization index (VI), flow index (FI) and vascularization-flow index (VFI). The VI is an index of the number of vessels in the volume and the ratio of the color voxels inside the volume of interest. It reflects the number of vessels in the volume being studied. Flow index is the ratio of the sum of color intensities to the number of color voxels inside the volume of interest. It reflects the amount of blood flow. The VFI is the ratio of the sum of color intensities to the total number of voxels inside the volume of interest. This represents vessel presence and blood flow. These indices have been

reliably and reproducibly measured in the placenta.[13,100] Abnormal 3D vascular indices are seen in placentas with a low PAPP-A that have growth-restricted fetuses and these changes precede changes evident by conventional Doppler indices.[104] Obliteration of the vascular tree may be extensive before umbilical indices change. Intraplacental blood flow decrease often precedes umbilical resistance increase and, therefore, serves as a reliable early marker for growth restriction and preeclampsia.[103] Although routine 3D power Doppler evaluation is not yet recommended in the protocol for the 11–13 weeks 6 days nuchal translucency scan or the 18–22 weeks anomalies scan, ease of software utilization is likely to foster its routine inclusion in future protocols to identify a subset of patients that would benefit from increased surveillance in pregnancy.

CONCLUSION

Several placental abnormalities evident on systematic ultrasound imaging have a profound effect on pregnancy outcomes. Methodical evaluation should be followed to identify these features to ensure appropriate modifications of treatment protocols and avoid the far-reaching consequences of these abnormalities.[10] Current standard protocol should include placental location, texture, shape, thickness, size, the retroplacental space and cord insertion.

REFERENCES

1. Kliman HJ. Trophoblast infiltration. Reproductive Medicine Review. 1994;3:137-57.
2. Kliman HJ. The placenta revealed. Am J Pathol. 1993;143(2):332-6.
3. Yu CK, Smith GC, Papageorghiou AT, et al. Fetal Medicine Foundation Second Trimester Screening Group. An integrated model for the prediction of preeclampsia using maternal factors and uterine artery Doppler velocimetry in unselected low-risk women. Am J Obstet Gynecol. 2005;193(2):429-36.
4. Sebire NJ, Sepulveda W. Correlation of placental pathology with prenatal ultrasound findings. Clin Pathol. 2008;61(12):1276-84.
5. Fox H. The development and structure of the placenta. In: Fox H (Ed.). Pathology of the placenta. Philadelphia: WB Saunders; 1997. pp. 1-16.
6. Jaffe R, Jauniaux E, Hustin J. Maternal circulation in the first-trimester human placenta-myth or reality? Am J Obstet Gynecol. 1997;176(3):695-705.
7. Burton GJ, Jauniaux E. Placental oxidative stress: from miscarriage to preeclampsia. J Soc Gynecol Invest. 2004;11:342-52.
8. Spirt BA, Gordon LP. Placenta and cervix. In: McGahan JP, Goldberg BB (Eds). Diagnostic ultrasound-A logical approach, 1st edition. Philadelphia: Lippincott-Raven Publishers; 1998. pp. 181-200.
9. Harris RD, Alexander RD. Ultrasound of the placenta and umbilical cord. In: Callen PW (Ed). Ultrasonography in Obstetrics and Gynecology, 4th edition. Philadelphia: WB Saunders Co; 2000. pp. 597-625.
10. Abramowicz JS, Sheiner E. Ultrasound of the placenta: a systematic approach. Part I: Imaging. Placenta. 2008;29(3):225-40.
11. Wolf H, Oosting H, Treffers P. Second trimester placental volume measurement by ultrasound: Prediction of fetal outcome. Am J Obstet Gynecol. 1989;160(1):121-6.
12. Thame M, Osmond C, Wilks R, et al. Second-trimester placental volume and infant size at birth. Obstet Gynecol. 2001;98(2):279-83.
13. Huster KM, Haas K, Schoenborn J, et al. Reproducibility of placental volume and vasculature indices obtained by 3-dimensional power Doppler sonography. J Ultrasound Med. 2010;29(6):911-6.
14. Jauniaux E, Nicolaides KH, Hustin J. Perinatal features associated with placental mesenchymal dysplasia. Placenta. 1997;18(8):701-6.
15. Parveen Z, Tongson-Ignacio JE, Fraser CR, et al. Placental mesenchymal dysplasia. Arch Pathol Lab Med. 2007;131(1):131-7.
16. Cohen MC, Roper EC, Sebire NJ, et al. Placental mesenchymal dysplasia associated with fetal aneuploidy. Prenat Diagn. 2005;25(3):187-92.
17. Pham T, Steele J, Stayboldt C, et al. Placental mesenchymal dysplasia is associated with high rates of intrauterine growth restriction and fetal demise: a report of 11 new cases and a review of the literature. Am J Clin Pathol. 2006;126(1):67-78.
18. Petrucha RA, Platt LD. Relationship of placental grade to gestational age. Am J Obstet Gynecol. 1982;144(6):733-5.
19. Grannum PA, Berkowitz RL, Hobbins JC. The ultrasonic changes in the maturing placenta and their relation to fetal pulmonic maturity. Am J Obstet Gynecol. 1979;133(8):915-22.
20. Sau A, Seed P, Langford K. Intraobserver and interobserver variation in the sonographic grading of placental maturity. Ultrasound Obstet Gynecol. 2004;23(4):374-7.
21. Crawford DC, Fenton DW, Price WI. Ultrasonic tissue characterization of the placenta: is it of clinical value? J Clin Ultrasound. 1985;13(8):533-7.
22. McKenna D, Tharmaratnam S, Mahsud S, et al. Ultrasonic evidence of placental calcication at 36 weeks' gestation: maternal and fetal outcomes. Acta Obstet Gynecol Scand. 2005;84(1):7-10.
23. Brown HL, Miller JM, Khawli O, et al. Premature placental calcification in maternal cigarette smokers. Obstet Gynecol. 1988;71(6 Pt 1):914-7.
24. Salaa CM, Minior VK, Pezzullo JC, et al. Intrauterine growth restriction in infants of less than thirty-two weeks' gestation: associated placental pathologic features. Am J Obstet Gynecol. 1995;173(4):1049-57.

25. Brown DL, DiSalvo DN, Frates MC, et al. Placental surface cysts detected on sonography: histologic and clinical correlation. J Ultrasound Med. 2002;21(6):641-6.
26. Hong SC, Yoo SW, Kim T, et al. Prenatal diagnosis of a large subchorionic placental cyst with intracystic hematomas. A case report. Fetal Diagn Ther. 2007;22(4):259-63.
27. Jauniaux E, Campbell S. Antenatal diagnosis of placental infarcts by ultrasonography. J Clin Ultrasound. 1991;19:58-61.
28. Barclay D, Evans K, Fox R. Ultrasound diagnosed placental infarction in a woman with recurrent fetal growth restriction. J Obstet Gynaecol. 2005;25:200-1.
29. Greenberg JA, Sorem KA, Shifren JL, et al. Placenta membranacea with placenta increta: a case report and literature review. Obstet Gynecol. 1991;78(3 Pt 2):512-4.
30. Dinh TV, Bedi DG, Salinas J. Placenta membranacea, previa and accreta. A case report. J Reprod Med. 1992;37(1):97-9.
31. Wilkins BS, Batcup G, Vinall PS. Partial placenta membranacea. Br J Obstet Gynaecol. 1991;98(7):675-9.
32. McCarthy J, Thurmond AS, Jones MK, et al. Circumvallate placenta: sonographic diagnosis. J Ultrasound Med. 1995;14(1):21-6.
33. Harris RD, Wells WA, Black WC, et al. Accuracy of prenatal sonography for detecting circumvallate placenta. AJR Am J Roentgenol. 1997;168(6):1603-8.
34. Finberg HJ. Umbilical cord and amniotic membranes. In: McGahan JP, Goldberg BB (Eds). Diagnostic ultrasound-A logical approach, 1st edition. Philadelphia: Lippincott-Raven Publishers; 1998.pp.201-29.
35. Predanic M, Perni SC, Baergen RN, et al. A sonographic assessment of different patterns of placenta previa "migration" in the third trimester of pregnancy. J Ultrasound Med. 2005;24(6):773-80.
36. Hata K, Hata T, Aoki S, et al. Succenturiate placenta diagnosed by ultrasound. Gynecol Obstet Invest. 1988; 25(4):273-6.
37. Mazouni C, Gorincour G, Juhan V, et al. Placenta accreta: a review of current advances in prenatal diagnosis. Placenta. 2006;28(7):599-603.
38. Wu S, Kocherginsky M, Hibbard JU. Abnormal placentation: twenty-year analysis. Am J Obstet Gynecol. 2005;192(5):1458-61.
39. Gielchinsky Y, Rojansky N, Fasouliotis SJ, et al. Placenta accretae- summary of 10 years: a survey of 310 cases. Placenta. 2002;23(2-3):210-4.
40. Oyelese KO, Smulian JC. Placenta previa, placenta accreta, and vasa previa. Obstet Gynecol. 2006;107:927-41.
41. Comstock CH. Antenatal diagnosis of placenta accreta: a review. Ultrasound Obstet Gynecol. 2005;26(1):89-96.
42. Shih JC, Palacios Jaraquemada JM, Su YN, et al. Role of three-dimensional power Doppler in the antenatal diagnosis of placenta accreta: comparison with gray-scale and color Doppler techniques. Ultrasound Obstet Gynecol. 2009;33(2):193-203.
43. Lax A, Prince MR, Mennitt KW, et al. The value of specific MRI features in the evaluation of suspected placental invasion. Magn Reson Imaging. 2007;25(1):87-93.
44. Deans A, Jauniaux E. Prenatal diagnosis and outcome of subamniotic hematomas. Ultrasound Obstet Gynecol. 1998;11(5):319-23.
45. Kurjak A, Schulman H, Zudenigo D, et al. Subchorionic hematomas in early pregnancy: clinical outcome and blood flow patterns. J Matern Fetal Med. 1996;5(1):41-4.
46. Nagy S, Bush M, Stone J, et al. Clinical significance of subchorionic and retroplacental hematomas detected in the first trimester of pregnancy. Obstet Gynecol. 2003;102:94-100.
47. Richards DS, Bennett BB. Prenatal ultrasound diagnosis of massive subchorionic thrombohematoma. Ultrasound Obstet Gynecol. 1998;11(5):364-6.
48. Fisteag-Kiprono L, Foster K, McKenna D, et al. Antenatal sonographic diagnosis of massive subchorionic hematoma: a case report. J Reprod Med. 2005;50(3):219-21.
49. Bromley B, Benacerraf BR. Solid masses on the fetal surface of the placenta: differential diagnosis and clinical outcome. J Ultrasound Med. 1994;13(11):883-6.
50. Sepulveda W, Aviles G, Carstens E, et al. Prenatal diagnosis of solid placental masses: the value of color PR imaging. Ultrasound Obstet Gynecol. 2000;16(6):554-8.
51. Zalel Y, Weisz B, Gamzu R, et al. Chorioangiomas of the placenta: sonographic and Doppler flow characteristics. J Ultrasound Med. 2002;21(8):909-13.
52. Sepulveda W, Aviles G, Carstens E, et al. Placental chorioangioma. Ultrasound Obstet Gynecol. 2000;16(6):597-8.
53. Prapas N, Liang RI, Hunter D, et al. Color Doppler imaging of placental masses: differential diagnosis and fetal outcome. Ultrasound Obstet Gynecol. 2000;16(6):559-63.
54. Zalel Y, Gamzu R, Weiss Y, et al. Role of color Doppler imaging in diagnosing and managing pregnancies complicated by placental chorioangioma. J Clin Ultrasound. 2002;30(5):264-9.
55. Shih JC, Ko TL, Lin MC, et al. Quantitative three-dimensional power Doppler ultrasound predicts the outcome of placental chorioangioma. Ultrasound Obstet Gynecol. 2004;24(2):202-6.
56. Hata T, Kanenishi K, Inubashiri E, et al. Three-dimensional sonographic features of placental abnormalities. Gynecol Obstet Invest. 2004;57(2):61-5.
57. Hata T, Inubashiri E, Kanenishi K, et al. Three-dimensional power Doppler angiographic features of placental chorioangioma. J Ultrasound Med. 2004;23(11):1517-20.
58. Ahmed N, Kale V, Thakkar H, et al. Sonographic diagnosis of placental teratoma. J Clin Ultrasound. 2004;32(2):98-101.
59. Altman JF, Lowe L, Redman B, et al. Placental metastasis of maternal melanoma. J Am Acad Dermatol. 2003;49(6): 1150-4.
60. Al-Adnani M, Kiho L, Scheimberg I. Maternal pancreatic carcinoma metastatic to the placenta: a case report and literature review. Pediatr Dev Pathol. 2007;10(1):61-5.
61. Jain KA. Gestational trophoblastic disease: pictorial review. Ultrasound Q. 2005;21(4):245-53.
62. Zhou Q, Lei XY, Xie Q, et al. Sonographic and Doppler imaging in the diagnosis and treatment of gestational trophoblastic disease: a 12-year experience. J Ultrasound Med. 2005;24(1):15-24.

63. Gungor T, Ekin M, Dumanli H, et al. Color Doppler ultrasonography in the earlier differentiation of benign mole hydatidiforms from malignant gestational trophoblastic disease. Acta Obstet Gynecol Scand. 1998;77(8):860-2.
64. Jauniaux E, Nicolaides KH. Early ultrasound diagnosis and follow-up of molar pregnancies. Ultrasound Obstet Gynecol. 1997;9(1):17-21.
65. Berkowitz RS, Goldstein DP. Chorionic tumours. N Engl J Med. 1996;335(23):1740-8.
66. Betel C, Atri M, Arenson AM, et al. Sonographic diagnosis of gestational trophoblastic disease and comparison with retained products of conception. J Ultrasound Med. 2006;25(8):985-93.
67. Oppenheimer L. Society of Obstetricians and Gynaecologists of Canada. Diagnosis and management of placenta previa. J Obstet Gynaecol Can. 2007;29(3):261-73.
68. Oyelese Y. Placenta previa: the evolving role of ultrasound. Ultrasound Obstet Gynecol. 2009;34(2):123-6.
69. Bhide A, Thilaganathan B. Recent advances in the management of placenta previa. Curr Opin Obstet Gynecol. 2004;16:447-51.
70. Timor-Tritsch IE, Monteagudo A. Diagnosis of placenta previa by transvaginal sonography. Ann Med. 1993;25:279-83.
71. Farine D, Fox HE, Jakobson S, et al. Vaginal ultrasound for diagnosis of placenta previa. Am J Obstet Gynecol. 1988;159:566-9.
72. Edlestone DI. Placental localization by ultrasound. Clin Obstet Gynecol. 1977;20:285-7.
73. Yang Q, Wen SW, Oppenheimer L, et al. Association of caesarean delivery for first birth with placenta praevia and placental abruption in second pregnancy. BJOG. 2007;114(5):609-13.
74. Krasznai I, Rigo J, Boze T, et al. Uncommon type of placentation after previous cesarean deliveries. Obstet Gynecol. 2003;102(3):549-51.
75. Smith RS, Lauria MR, Comstock CH, et al. Transvaginal ultrasonography for all placentas that appear to be low-lying or over the internal cervical os. Ultrasound Obstet Gynecol. 1997;9(1):22-4.
76. Hill LM, DiNofrio DM, Chenevey P. Transvaginal sonographic evaluation of first-trimester placenta previa. Ultrasound Obstet Gynecol. 1995;5(5):301-3.
77. Kurjak A, Barsic B. Changes of placental site diagnosed by repeated ultrasonic examination. Acta Obstet Gynecol Scand. 1977;56(3):161-5.
78. Lauria MR, Smith RS, Treadwell MC, et al. The use of second-trimester transvaginal sonography to predict placenta previa. Ultrasound Obstet Gynecol 1996;8(5):337-40.
79. Becker RH, Vonk R, Mende BC, et al. The relevance of placental location at 20–23 gestational weeks for prediction of placenta previa at delivery: evaluation of 8650 cases. Ultrasound Obstet Gynecol. 2001;17(6):496-501.
80. Mustafa SA, Brizot ML, Carvalho MHB, et al. Transvaginal ultrasonography in predicting placenta previa at delivery: a longitudinal study. Ultrasound Obstet Gynecol. 2002;20:356-9.
81. Taipale P. Hiilesmaa V, Ylostalo P. Transvaginal ultrasonography at 18-23 weeks in predicting placenta previa at delivery. Ultrasound Obstet Gynecol. 1998;12(6):422-5.
82. Oppenheimer L, Holmes P, Simpson N, et al. Diagnosis of low-lying placenta: can migration in the third trimester predict outcome? Ultrasound Obstet Gynecol. 2001;18(2):100-2.
83. Ghourab S. Third-trimester transvaginal ultrasonography in placenta previa: does the shape of the lower placental edge predict clinical outcome? Ultrasound Obstet Gynecol. 2001;18(2):103-8.
84. Ghi T, Contro E, Martina T, et al. Cervical length and risk of antepartum bleeding in women with complete placenta previa. Ultrasound Obstet Gynecol. 2009;33(2):209-12.
85. Saitoh M, Ishihara K, Sekiya T, et al. Anticipation of uterine bleeding in placenta previa based on vaginal sonographic evaluation. Gynecol Obstet Invest. 2002;54(1):37-42.
86. Droste S, Keil K. Expectant management of placenta praevia: cost benefit analysis of outpatient treatment. Am J Obstet Gynecol. 1994;170(5 Pt 1):1254-7.
87. Mouer JR. Placenta praevia: antepartum conservative management, inpatient versus outpatient. Am J Obstet Gynecol. 1994;170(6):1683-6.
88. Dola CP, Garite TJ, Dowling DD, et al. Placenta previa: does its type affect pregnancy outcome? Am J Perinatol. 2003;20(7):353-60.
89. Nelson JP. Interventions for suspected placenta praevia (Cochrane review). The Cochrane Library, Issue 2. Oxford: Update software; 2004.
90. Arias F. Cervical cerclage for the temporary treatment of patients with placenta previa. Obstet Gynecol 1988;71(4):545-8.
91. Finberg H, Williams J. Placenta accreta: prospective sonographic diagnosis in patients with placenta previa and prior cesarean section. J Ultrasound Med. 1992;11(7):333-43.
92. O'Brien JM, Barton JR, Donaldson ES. The management of placenta percreta: conservative and operative strategies. Am J Obstet Gynecol. 1996;175(6):1632-8.
93. Ouellet A, Sallout B, Oppenheimer LW. Outcomes of surgical versus conservative management of placenta accreta-percreta: systematic review of literature and case series. Am J Obstet Gynecol. 2003:189(6):S130.
94. Hafner E, Philipp T, Schuchter K, et al. Second-trimester measurements of placental volume by three-dimensional ultrasound to predict small-for-gestational-age infants. Ultrasound Obstet Gynecol. 1998;12(2):97-102.
95. Pairleitner H, Steiner H, Hasenoehrl G, et al. Three-dimensional power Doppler sonography: imaging and quantifying blood flow and vascularization. Ultrasound Obstet Gynecol. 1999;14(2):139-43.
96. Hafner T, Kurjak A, Funduk-Kurjak B, et al. Assessment of early chorionic circulation by three-dimensional power Doppler. J Perinat Med 2002;30(1):33-9.
97. Matijevic R, Kurjak A. The assessment of placental blood vessels by three-dimensional power Doppler ultrasound. J Perinat Med. 2002;30(1):26-32.
98. Pretorius DH, Nelson TR, Baergen RN, et al. Imaging of placental vasculature using three-dimensional ultrasound

and color power Doppler: a preliminary study. Ultrasound Obstet Gynecol. 1998;12(1):45-9.
99. Guimarães Filho HA, da Costa LL, Araújo Júnior E, et al. Placenta: angiogenesis and vascular assessment through three-dimensional power Doppler ultrasonography. Arch Gynecol Obstet. 2008;277(3):195-200.
100. Deurloo K, Spreeuwenberg M, Rekoert-Hollander M, et al. Reproducibility of 3-dimensional sonographic measurements of fetal and placental volumes at gestational ages 11–18 weeks. J Clin Ultrasound. 2007;35(3):125-32.
101. Noguchi J, Hata K, Tanaka H, et al. Placental vascular sonobiopsy using three-dimensional power Doppler ultrasound in normal and growth restricted fetuses. Placenta. 2009;30(5):391-7.
102. Alcázar JL. Three-dimensional power Doppler derived vascular indices: what are we measuring and how are we doing it? Ultrasound Obstet Gynecol. 2008;32(4): 485-7.
103. Guiot C, Gaglioti P, Oberto M, et al. Is three-dimensional power Doppler ultrasound useful in the assessment of placental perfusion in normal and growth-restricted pregnancies? Ultrasound Obstet Gynecol. 2008;31(2):171-6.
104. Rizzo G, Capponi A, Pietrolucci ME, et al. First-trimester placental volume and vascularization measured by 3-dimensional power Doppler sonography in pregnancies with low serum pregnancy-associated plasma protein A levels. J Ultrasound Med. 2009;28(12):1615-22.

CHAPTER 27

Measurement of Cervical Length

O Vasilj, B Miskovic

INTRODUCTION

Preterm birth (PB) is one of the greatest challenges in modern perinatal medicine. Despite of the improvements in perinatal management over the last two decades the rate of PB has not declined and it is still a major cause of perinatal morbidity and mortality.[1] One of the reasons behind this is the fact that the complex underlying ethiopathogenic causes of PB are not fully understood as yet. The role of uterine cervix in PB is undisputed.

GENERAL FACTS ABOUT UTERINE CERVIX

The uterine cervix is a unique organ composed predominately of extracellular matrix, proteins, collagen, elastin and glycosaminoglycans. Among all biological processes, the phenomenal connective tissue remodeling that occurs in the cervix during and after parturition is unparalleled in scope and magnitude. During the pregnancy, cervix undergoes changes that have to be understood prior to transvaginal ultrasonography (TVU) assessment. It changes from a closed and rigid structure before pregnancy to a soft and distensible organ proximate to parturition. Cervical remodeling begins soon after conception and continues throughout pregnancy and the puerperium. It consists of four overlapping phases:

1. Softening alone
2. Ripening (softening with effacement, dilation and change in position)
3. Dilation in response to contractions
4. Postpartum repair.[2]

Dynamic changes and shortening of the cervix during pregnancy differs from one pregnant woman to another. Mean reduction in cervical length in mid-second trimester of pregnancy is around 1.1 mm, but it may be as high as 2.7 mm weekly.[3] This data may be used only for primiparous patients as multiparous patients have different dynamics of cervical shortening.[3,4] According to studies the 50th percentiles for cervical length before 20 weeks of gestation is 40 mm and at 22–32 weeks of gestation is 35 mm.[5]

What is Cervical Insufficiency?

Cervical insufficiency (CI) is defined as asymptomatic cervical dilatation in second and third trimester of pregnancy.[6] The causes of CI may be congenital or acquired. The congenital causes include biological variations in cervical length and collagen or uterine anomalies. All of these can affect the functioning of cervix during pregnancy.[7] Acquired factors that are most commonly attributed to CI are different mechanical or operative procedures on cervix (pregnancy termination with dilatation, hysteroscopy, cervical biopsy, laser ablation, loop excision or cold knife conization).[7] It is unclear whether the increase is due to procedure-related structural injury leading to CI, adverse effects of the underlying cervical disease on cervical function or another mechanism such as subclinical upper genital tract infection.[7] It has been shown that processes that lead to both term and preterm

spontaneous labor resemble an inflammatory reaction. Upregulation of inflammatory cytokines and prostaglandins that occurs over a period of several weeks leads to cervical ripening and membrane rupture.[1] This will again lead to myometrial contractility and labor.[1] The cervix acts as a barrier to this stimulus maintaining the distance from the vagina and retaining the cervical mucus plug as an additional barrier. Women with a short cervix or CI will be at much greater risk of this cervical barrier being breached.

Diagnosis of Cervical Insufficiency

Detection of CI in the first pregnancy is difficult because the symptoms are usually dismissed as normal pregnancy effects, so that cervical effacement and dilatation often progress to a clinical presentation of a bulging amniotic sac or ruptured membranes. The diagnosis of CI is based on a combination of past and present pregnancy history, physical examination and ultrasound findings.

The main goal of physical examination is digital palpation and visualization of the cervix using a speculum. The physical examination is a subjective method and is not ideal for assessment and prediction of PB. This was clearly shown in our study, where the physical examination was compared with ultrasonographic examination of the cervix in the low risk population regarding the prediction of PB.[6]

Transvaginal ultrasonography is the gold standard for the assessment of cervix in pregnancy. Transabdominal and transperineal ultrasound of the cervix can be used but are more difficult and less precise than TVU.[8] If screening of cervical changes in pregnancy is employed to predict PB, this should be done with TVU and not with physical exam or a different ultrasound technique. The TVU cervical measurement is a well described method with intra- and interobserver variations that are acceptable for clinical use.[9]

Transvaginal Ultrasonographic Cervical Assessment and Recommendations for Clinical Application

Measurement of cervical length by TVU examination is a technique that can be learnt rapidly. About 23 supervised ultrasound scans appear necessary for an operator with no experience in TVU.[10] Substantially fewer are required for an operator already familiar with this approach for other indications.[10] For an adequate exam, the maternal bladder has to be emptied. Ultrasound gel is placed on a transvaginal probe before covering it with a condom or specialized cover and then more ultrasound gel is placed on the cover. If the membranes are ruptured, sterile materials should be used. The transducer should be placed in the anterior fornix until the cervix is visualized. The image is enlarged to fill at least one-half of the ultrasound screen. The appropriate sagittal view for measuring cervical length includes the V-shaped notch at the internal os, the triangular area of echo density at the external os, and the endocervical canal, which appears as a faint line of echo density or echolucency between the two. Cervical length is the linear distance between calipers placed at the internal and external os and should only be determined from images when the anterior and posterior lips of the cervix are of equal thickness **(Fig. 27.1)**. When three measurements have been obtained that satisfy measurement criteria the shortest is chosen and recorded as the "shortest best." If the cervix is curved there is no need to measure it in several points or by using a tracer since in these cases the cervical length is usually very long and no additional clinical information is obtained by these procedures.

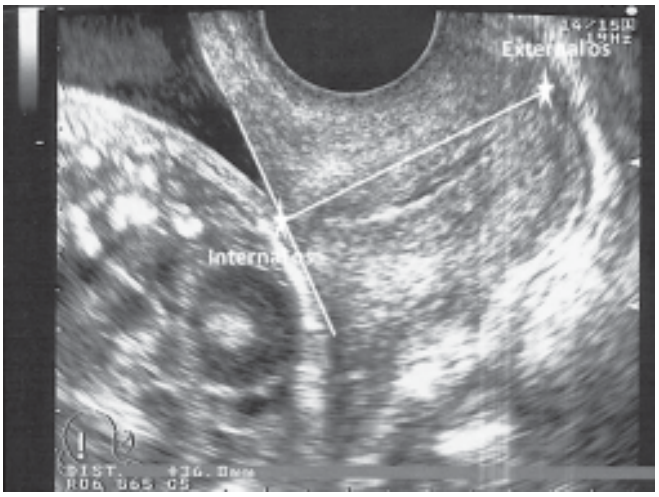

Figure 27.1: The ultrasound assessment of the cervix in pregnancy. A normal "T" shape of the cervix. The linear measurement of cervical length between internal and external os is presented

Two ultrasound based criteria are found to be related to CI. These are the length of the closed part of the cervical canal and the shape of the internal cervical os "T" **(Fig. 27.1)**, "V" **(Fig. 27.2)**, "Y" **(Fig. 27.3)** and "U" so called "funneling" **(Fig. 27.4.)**.[11] Funneling is defined in percentages according to the ratio of the funnel length to the total cervical length (funnel length + remaining closed cervix). The presence or absence of a funnel and its length should be recorded but it is believed that funneling is not clinically important. If funneling is

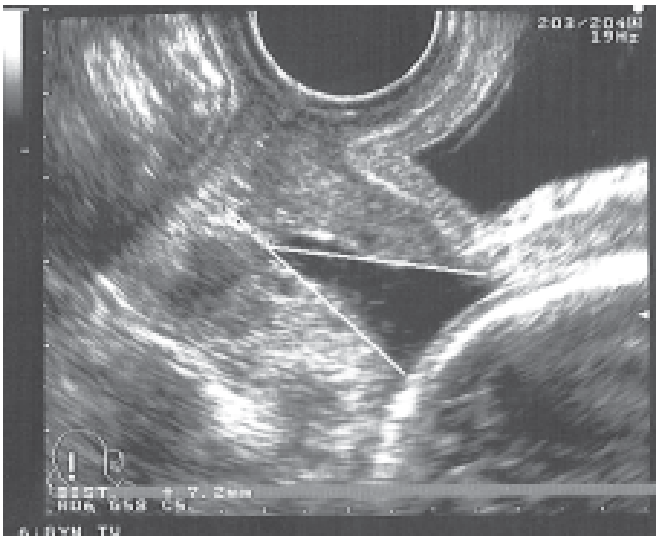

Figure 27.2: A "V" shape of the cervix

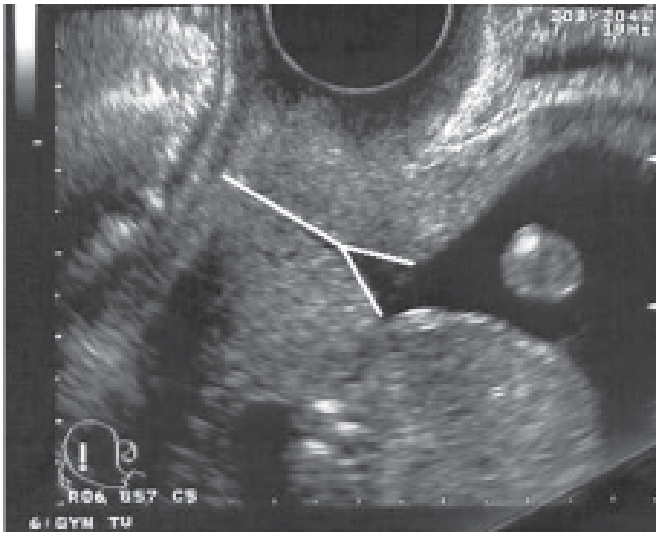

Figure 27.3: A "Y" shape of the cervix

present, the length of the residual closed portion of the cervix is recorded as the true length of the cervix. The length of the funnel is often uncertain because landmarks, such as the shoulder of the internal os, may not be distinct. Dynamic spontaneous funneling seen occasionally above a normal length cervix has little prognostic value.[12]

Intra-amniotic debris ('sludge') refers to the sonographic finding of hyperechoic matter in the amniotic fluid close to the internal cervical os. The composition of the debris is unclear; it may be blood clot, meconium, vernix, or cellular material related to infection/inflammation. Some studies, but not all, have reported

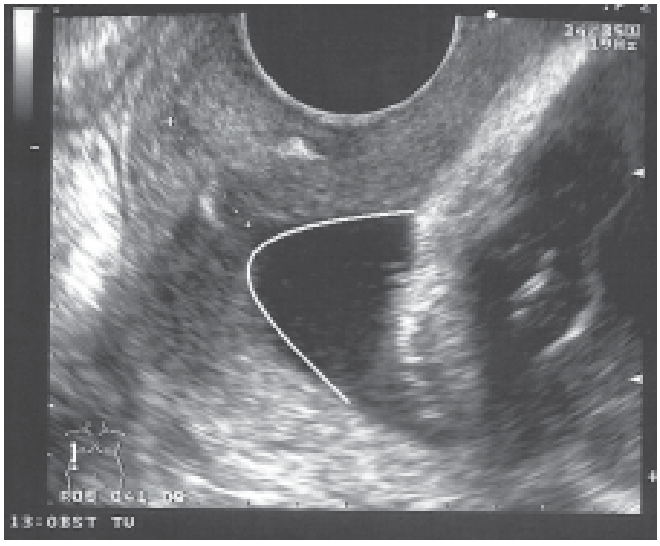

Figure 27.4: Funneling or "U" shape cervix suspicious of CI

an association between the presence of intra-amniotic debris and preterm delivery and other pregnancy complications.[13,14]

The most common mistake during TVU of the cervix is the excess pressure on the anterior cervical lip with the artificial elongation of cervical canal. This can be avoided by withdrawing the probe when the internal and external os are visualized until slight blurring occurs, and then the probe is inserted slightly until a clear image returns.

With well known cervical length and shape in recent years, a new ultrasound-based parameter of CI was presented. The presence of cervical glands and cervical mucus were introduced as additional parameters used in order to define CI.[15,16] The hypoechogenic translucency of cervical mucus area in the middle of the endocervical canal was measured by area trace.[16] Hypo- or hyperechogenic translucencies surrounding the canal that probably corresponds to the histological cervical gland area was measured under a 90° angle from the endocervical canal, as the linear distance from the outer boundary of the deepest invasion of cervical glands.[16] The sonographic images of cervical glands and cervical mucus are shown in **Figures 27.5 and 27.6**. In our study it was shown that absence or diminishment of glandular area of the cervix could be one of the early signs of PB.[16] We defined a new term Qualitative Glandular Cervical Score (QGCS).[16] As a potential screening test for PB low QGCS had sensitivity 83.3% (≤ 34 weeks) and 55.5% (34–37 weeks) with positive predictive value (PPV) 31.2% (≤ 34 and 34–37 weeks). Shortened CL had sensitivity 66.6% (≤ 34 weeks) and 22.2% (34–37 weeks)

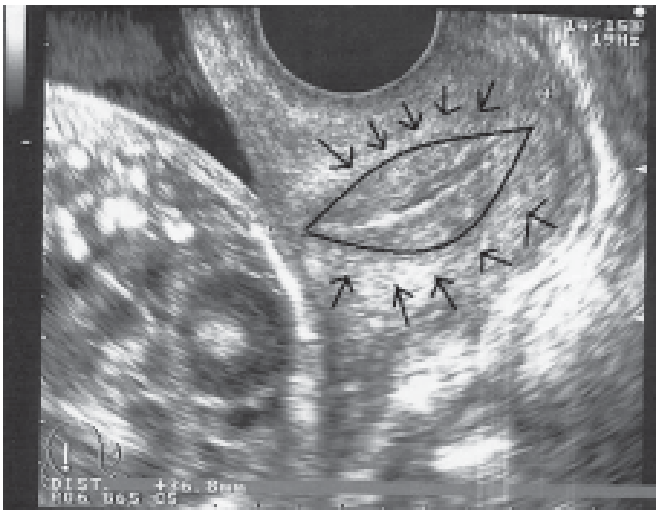

Figure 27.5: The presence of cervical glands as a normal finding

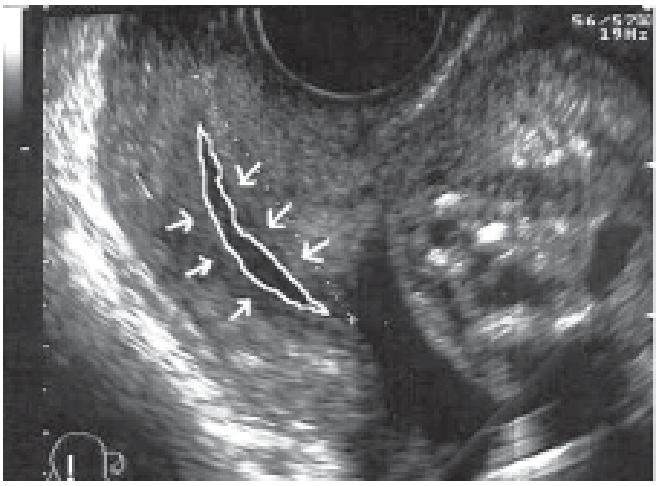

Figure 27.6: Cervical mucus anechoic translucency inside the cervical canal measured with area trace

with PPV 23.5% (≤ 34 weeks) and 11.7% (34–37 weeks). The diagnostic accuracy of this test in prediction of risk for PB was the same if not better than the sole measurement of the closed part of the cervical canal.[16]

In recent years a three-dimensional ultrasound was introduced in the screening program for detection of CI. It was not found to be significantly better regarding the measurements of the cervical length but it introduced the new term of cervical volumetry that may be of help in the further assessment programs.[17]

Numerous studies evaluating the use of TVU cervical measurement for prediction of PB in asymptomatic and symptomatic high risk and low risk women were performed. The following is a summary of recommendations for the use of TVU cervical assessment in prediction of PB:

- Transvaginal ultrasound does not differentiate between CI and other causes of short cervix. It identifies women who are at higher risk of PB regardless of the etiology and one of those etiologies may be CI. The risk of PB is highest for cervical length below the 10th percentile (about 25 mm between 22 and 30 weeks of gestation), there is no threshold value and not all patients with a short cervix will have PB.[18]
- In asymptomatic women with a history of spontaneous PB measurement of cervical length in the second trimester predicted risk of recurrence.[1]
- The low sensitivity and low PPV of cervical length screening limit the usefulness of this test in low-risk asymptomatic obstetric populations. Thus, the use of sonographic measurement of cervical length to screen low-risk populations to determine risk of PB is not recommended.[19]
- In symptomatic women the use of TVU may be useful for distinguishing women with false preterm labor. A high negative predictive value was shown for a 30 mm threshold, but there is no threshold of cervical length that establishes diagnosis.[20]

Is Cerclage Needed?

Cochrane database of systematic reviews assessed effectiveness and safety of prophylactic and therapeutic cerclage in six trials with a total of 2175 women were analyzed. Prophylactic cerclage was compared with no cerclage in four trials. There was no overall reduction in pregnancy loss and preterm delivery rates.

Cervical cerclage was associated with mild pyrexia, increased use of tocolytic therapy and hospital admissions but no serious morbidity. Two trials examined the role of therapeutic cerclage when ultrasound examination revealed short cervix. Pooled results failed to show a reduction in total pregnancy loss, early pregnancy loss or preterm delivery before 28 and 34 weeks in women assigned to cervical cerclage.

The authors concluded that cerclage should not be offered to women at low or medium risk of midtrimester loss, regardless of cervical length by ultrasound. The role of cervical cerclage for women who have short cervix on ultrasound remains uncertain as the numbers of randomized women are too few to draw firm conclusions.[21]

REFERENCES

1. Crane JM, Hutchens D. Transvaginal sonographic measurement of cervical length to predict preterm birth in asymptomatic women at increased risk: a systematic review Ultrasound Obstet Gynecol. 2008;31(5):579-87.
2. Word RA, Li XH, Hnat, M, et al. Dynamics of cervical remodeling during pregnancy and parturition: mechanisms and current concepts. Semin Reprod Med. 2007;25(1):69-79.
3. Bergelin I, Valentin L. Patterns of normal change in cervical length and width during pregnancy in nulliparous women: a prospective, longitudinal ultrasound study. Ultrasound Obstet Gynecol. 2001;18(3):217-22.
4. Bergelin I, Valentin L. Normal cervical changes in parous women during the second half of pregnancy: a prospective, longitudinal ultrasound study. Acta Obstet Gynecol Scand. 2002;81(1):31-8.
5. Hibbard JU, Tart M, Moawad AH. Cervical length at 16–22 weeks' gestation and risk for preterm delivery. Obstet Gynecol. 2000;96(6):972-8.
6. Matijevic R, Grgc O, Vasilj O. Is sonograpic assessment of the cervical length better than digital examination in screening for preterm delivery in a low risk population? Acta Obstet Gynecol Scand. 2006;85(11):1342-7.
7. Vyas NA, Vink JS, Ghidini A, et al. Risk factors for cervical insufficiency after term delivery. Am J Obstet Gynecol. 2006;195(3):787-91.
8. Meijer-Hoogeveen M, Stoutenbeek P, Visser GH. Transperineal versus transvaginal sonographic cervical length measurement in second and third trimester pregnancies. Ultrasound Obstet Gynecol. 2008;32(5):657-62.
9. Valentin L. Bergelin I. Intra- and interobserver reproducibility of ultrasound measurements of cervical length and width in the second and third trimesters of pregnancy. Ultrasound Obstet Gynecol. 2002;20(3):256-62.
10. Vayssière C, Morinière C, Camus E, et al. Measuring cervical length with ultrasound: evaluation of the procedures and duration of a learning method. Ultrasound Obstet Gynecol. 2002;20(6):575-9.
11. Rozenberg P, Gillet A, Ville Y. Transvaginal sonographic examination of the cervix in asymptomatic pregnant women: review of the literature. Ultrasound Obstet Gynecol. 2002;19(3):302-11.
12. Crane JM, Hutchens D. Transvaginal sonographic measurement of cervical length to predict preterm birth in asymptomatic women at increased risk: a systematic review. Ultrasound Obstet Gynecol. 2008;31(5):579-87.
13. Kusanovic JP, Espinoza J, Romero R, et al. Clinical significance of the presence of amniotic fluid 'sludge' in asymptomatic patients at high risk for spontaneous preterm delivery. Ultrasound Obstet Gynecol. 2007;30(5):706-14.
14. Gorski LA, Huang WH, Iriye BK, et al. Clinical implication of intra-amniotic sludge on ultrasound in patients with cervical cerclage. Ultrasound Obstet Gynecol. 2010;36(4):482-5.
15. Yoshimatsu K, Sekiya T, Ishihara K, et al. Detection of the cervical gland area in threatened preterm labor using transvaginal sonography in the assessment of cervical maturation and the outcome of pregnancy. Gynecol Obstet Invest. 2002;53(3):149-56.
16. Grgic O, Matijevic R, Vasilj O. Qualitative glandular cervical score as a potential new sonomorphological parameter in screening for preterm delivery. Ultrasound Med Bio. 2006;32(3):333-8.
17. Severi FM, Bocchi C, Florio P, et al. Comparison of two-dimensional and three-dimensional ultrasound in the assessment of the cervix to predict preterm delivery. Ultrasound Med Biol. 2003;29(9):1261-5.
18. Iams JD, Goldenberg RL, Mercer BM, et al. The preterm prediction study: can low-risk women destined for spontaneous preterm birth be identified? Am J Obstet Gynecol. 2001;184(4):652-5.
19. ACOG Practice Bulletin. Cervical insufficiency. Obstet Gynecol. 2003;102(5 Pt 1):1091-9.
20. Sotiriadis A, Papatheodorou S, Kavvadias A, et al. Transvaginal cervical length measurement for prediction of preterm birth in women with threatened preterm labor: a meta-analysis. Ultrasound Obstet Gynecol. 2010;35(1):54-64.
21. Drakeley AJ, Roberts D, Alfirevic Z. Cervical stitch (cerclage) for preventing pregnancy loss in women (Cochrane Review). Cochrane Database of Systematic Reviews. 2010;(2):CD003253.

CHAPTER 28

Monochorionicity: Unveiling the Black Box

Alexandra Matias, Nuno Montenegro, Isaac Blickstein

Alice´s Adventures in Wonderland
Carroll L

And The Lord said to Rebecca: "Two nations are in thy womb, and two manners of people shall be separated; and the one people shall be stronger than the other people; and the elder shall serve the younger"

And when her days will be over twins were born. And the first came out red.

Genesis 36;25

INTRODUCTION

Monochorionicity: We Need to Know Better and More

Multiple pregnancy represents about 1.2% of all pregnancies. About 30% of these pregnancies are iatrogenic (in a hypothetical obstetric population of 10,000 newborns, 140 spontaneous twins versus 36 are resulting from assisted reproduction will be expected), from which 84 twins would be spontaneously monozygotic (MZ) and four iatrogenic. In fact, an "epidemic" of multiple pregnancies is being observed in the world, as a consequence of the increase in the reproductive age of pregnant women[1] and due to the widespread use of ovulation-induction and assisted reproduction techniques (ART).[2-4]

It is thoroughly known that ART is contributing to the increase in the rate of twins and reshuffled all aspects of multiple pregnancies. Namely in the USA, an increase of 30% in the prevalence of twins was observed since the beginning of the 1990s and of 65% since the 1980s. The ART techniques, naturally associated with multiple ovulation and polyzygotic twins, show a twin rate 20 times higher than the spontaneous conceptions and a dizygotic (DZ) twin rate even higher than the MZ twin rate (10:1). However, mostly unexpected, the rate of MZ twinning consequent to ART seems to be increased as well mainly in association with the transfer of blastocysts (when compared with the transfer of embryos on the third day) and seems not to be affected by the zona pelucida manipulation.[5-8] In a study that included 15,644 cycles and the transfer of a single embryo in 7832 cases of *in vitro fertilization* (IVF), the monozygosity rate was 2.3%, a figure 6 times higher than the 0.4% described in the literature (Blickstein et al. 2003).[8] In contrast, the frequency of MZ twins recorded after ovulation induction (6.4%) was 14 times higher than the rate of spontaneous twins and more than twice the rate of MZ twins after IVF.

The growing concern with multiple pregnancies is mainly related to the higher mortality and greater incidence of adverse perinatal outcome when compared to singleton pregnancies due to the duplication of risk for structural defects and to the higher risk of chromosomal anomalies.[9-15] Although multiple pregnancies represent 1.2% of the population, they heavily contribute to 12.6% of the perinatal mortality. In a particular case of monochorionic twin pregnancies, the known perinatal morbidity and mortality are even more dramatic and should prompt a more differentiated and specialized surveillance.[12,16]

THE MONOZYGOSITY PHENOMENON

The human female was programed by evolution to ovulate once in every menstrual cycle, leading to monofetal pregnancies and to nurturing one infant at a time. Therefore, in about 99% of spontaneous pregnancies, a unique fetus derives from a single zygote. As a consequence of a reproductive disorder, which occurs in 0.8% of spontaneous conceptions, more than one oocyte is produced and fertilized in each cycle, resulting in polyzygotic multiple pregnancies. In another 0.4% of spontaneous pregnancies, as a result of a reproductive anomaly, a single ovum normally destined to produce a single embryo, split to form MZ multiples.

The MZ twinning is a form of "vegetative" reproduction whereby more than one individual results from a single zygote. Monozygotic twins at birth, weigh somewhat less than twice the birth weight of singletons of corresponding gestational age. Hence, a single fertilized egg is capable of producing much more somatic and placental mass than a singleton pregnancy, though the mechanisms of overgrowth in MZ twinning are not fully understood. We can consider the existence of extramitotic cycles and/or reduced apoptosis, but it is a tribute to the plasticity of early embryogenesis that anatomically and well-grown normal MZ twins, triplets or higher order multiples can be produced from a single fertilized egg.

The prevalence of MZ twinning is fairly constant worldwide strongly suggesting that MZ twinning derives from an intrinsic "anomalous" property of human zygotes. Based on the stability of twins' reality, Weinberg´s law was established and allows the accurate prediction of zygosity based on the frequency assessment of twin pairs of different sexes. In spontaneous conceptions, the rate of MZ twins represents about a third of all twin pregnancies, i.e. about 4:1000 births, and about two-thirds of MZ twin pregnancies will develop a monochorionic (MC) placentation, i.e. 2–3:1000 births. In iatrogenic pregnancies the ratio is altered and the MZ twin pregnancies are more prevalent (1:15–20 instead of 1:3). In certain cases a familial tendency to MZ twinning was disclosed, probably due to molecular mechanisms that cause postzygotic cells to disaggregate more easily than usual, forming two or more internal masses.

It is awkward to consider MZ twins "genetically identical", based in equal numbers of multipotential "founder" cells exposed to the same intrauterine milieu. Basically these assumptions are untrue and they are more inaccurate in some fetuses than in others. The complexity and variety of the initial development of MZ twins lend a degree of sophistication and fascination to the understanding of MZ twinning, introducing biases in twin studies. A lot of them do not take into consideration the possibility of discordance at birth that can exist, which is caused by different environmental,

genetic, postzygotic and epigenetic factors of prenatal occurrence.[17]

Why does the division of a single zygote occur? Although scientific evidence does not exist, different hypothesis have been proposed, but all are at present speculative. Presently, four theories are available to explain the mechanism of zygotic splitting: (1) The so-called "repulsion hypothesis" (Hall, 1996)[18]—cells in the developing zygote express genetic differences that translate in repulsive forces and leads to the splitting of the zygote; (2) The existence of codominant axes (Baldwin, 1994)[14]—the continuous "presence of a codominant axis" will cause the zygote to split; (3) Depressed calcium levels in the early embryo (Steinman and Valderrama, 2001) and (4) The blastomere herniation hypothesis—the integrity of the zona pellucida is breached during embryonic development, thereby losing its sequestering and protective role and permitting herniation of pluripotent cells through a gap in the zona pellucida.[8,19] All these theories are, however, not convincingly clear to explain the origin of MZ triplets and quadruplets and do not clarify the higher rate of MZ twins related to ART techniques (with or without manipulation of the zona pelucida). This particular difficulty is due to the inexistence of animal models of monozygosity, in which, with the exception of the human race and the Armadillo *(Dasypus novemcinctus)*, in no other mammals this process is expected to occur. More recently, another hypothesis suggests that human fertilized oocytes that are more splitting-prone, are able to undergo one or two successive binary fissions, or various combinations offered by subsequent secondary fissions, just as the case for the nine-banded armadillo, and give rise to a variety of combinations of MZ pregnancies (zona pellucida assisted binary fission theory).[20] This latter theory would be able to explain MZ triplets and quadruplets, "mirror-image" characteristics as well as some midline asymmetries in MZ twins.[21,22]

The true frequency of zygotic division is not exactly known, but inferred when the number of fetuses exceeds the number of transferred embryos. Clearly, this estimation is poorly reliable. If we consider that after the transfer of two embryos, one is lost and the other originates a MZ pregnancy with dichorionic (DC) placentation, no excess of fetuses will be reckoned. Moreover, it is not clinically possible to differentiate between dichorionic-dizygotic twins of same sex from MZ twins with MC placentation. Finally, Weinberg´s law is based on proportions observed in spontaneous conceptions that are not necessarily reproducible in ART pregnancies.

In a hypothetical model, we can calculate the risk of iatrogenic twins per 1000 births: natural conceptions comprise 1.2% twins including 0.4% MZs, whereas ART conceptions comprise 25% twins, of which 2.5% are MZs. In a department with 10% deliveries after ART, it is predictable 6 MZ twins for every 1000 deliveries as compared with 4 MZs after spontaneous conception. An increase of 1% in iatrogenic conceptions will translate in an increase of monozygosity by 6.25% as compared to 50% increase when 10% of the conceptions are iatrogenic. It can be concluded that the number of MZs increases as a linear function of iatrogenic pregnancies and the overall increase in iatrogenic multiples will significantly increase the total number of MZs in any given population.[3]

Still addressing the issue of iatrogenic pregnancies, it was noticed that the early spontaneous embryonic/fetal loss was slightly superior in the pregnancies resulting from ART than in spontaneous pregnancies. But whenever the end result of ART was a twin pregnancy, this early loss rate appeared importantly reduced. Thus, multiple pregnancy may be faced as a marker of reproductive advantage. A sensible explanation for this advantage of twins over singletons would be that the higher levels of placental hormones produced by a larger placental mass in twin gestations would improve the implantation capacity of the egg. Several studies support this evidence,[23-30] showing loss rates of 24% for singleton pregnancies versus 3–11% in twin pregnancies, i.e. the early fetal loss rate associated with ART is two to five times higher in singleton pregnancies.

Time Matters in Monozygosity: Sharing Levels and a Model of Placentation

The timing of MZ twinning events can be inferred from the type of placentation, X chromosome-inactivation in female MZ twins, asymmetric language function in the cerebral hemispheres and asymmetric dermatoglyphics. Thus, the type of membranes and placentation is assumed to represent the time of splitting, according to Corner´s hypothesis which was never proven, since no evidence of such a split exists in observations from *in vitro* fertilization.

The DZ twins, fraternal or nonidentical, result from the fertilization of two ova by different spermatozoids, showing a different genetic content. The type of placenta resulting from this process of fertilization, in which the trophoblast formation precedes the egg implantation has two chorions and two amniotic sacs, defining a DC-DA pregnancy.

Monozygotic twins comprise one-third of all twin pregnancies. These identical or uniovular twins result from the early division of a single egg (originating from the fertilization of an oocyte and a single spermatozoid) in two cell mass more or less identical, that contain the same genotype (exception: heterokaryotypic monozygotes). This cleavage will occur between the fertilization and the gastrulation period. Individual variations are the result of postzygotic mutations and arbitrary division of mitochondrial-DNA. The placentation inherent to these twins is more complex, depending on the very moment in which the separation occurs.

Dichorionic diamniotic MZ twins (18–36%) have separate membranes and placentas and result from abnormal splitting at the two-cell stage to morula (day 0–3). Consequently, each twin receives trophoblastic and somatic stem cells into their cell masses. Therefore, twinning must have happened before the differentiation and physical separation of somatic, and trophoblastic cells into the outer and inner cell masses, respectively in the cavitated blastocyst at about three days postconception. Dichorionic diamniotic placentas are derived from the splitting of about eight blastomers.

Splitting at any time thereafter results in a single MC placenta that continues even in the face of subsequent MZ twinning in the inner cell mass. Monochorionic diamniotic (MC-DA) twins (~80%) separate at the inner cell mass, after the chorion has formed (day 4–7). Consequently, two fetuses will develop with the same genome, with a single placenta and two amniotic cavities, considering the fact that the amniotic cavity will be formed after the eighth day after conception. The sharing of a single placenta is in itself an anomaly, creating unequal vascular territories for each twin and the eccentric location of the umbilical cords. Eventually, 5–15% will develop a twin-to-twin transfusion syndrome and a late discrepancy in fetal growth can be a frequent finding.

If the division occurs between the 9th and 12th day, at the late blastocyst stage, a single placenta and a unique amniotic cavity will be formed, i.e. all placental structures will be shared, resulting in a monochorionic monoamniotic (MC-MA) twin pregnancy (1%).

The highest level of sharing occurs very rarely when the division happens circa, the 13th day, resulting in the incomplete division of the embryonic disk, originating conjoined twins (estimated prevalence of 1 in 100,000). After that time the undivided egg will maintain the expected course to produce a singleton pregnancy.

If MZ twinning events would take place at a constant rate during the first 12 days postconception, proportions of DC, MC-DA and MC-MA twins would vary from those observed. The underrepresentation at birth of MC-MA and conjoined twins is explained by the higher intrauterine lethality. The relative excess of dichorionic monozygotic (DC-MZ) twins may be the result of their having less placental complications. Considering the level of sharing, this level is inversely proportional to the incidence of twins that result from this sharing [the incidence of MZ twins is about 1:250; the incidence of MC twins is two-third of the MZ pregnancies (1:350–400 births); the incidence of MC-MA twins is 1:2500 liveborns and the one from conjoined twins is less than 1:40,000 liveborns]. On the other hand, perinatal mortality and morbidity are related directly with the level of sharing, i.e. the greater the level of sharing the greater the risk of pregnancy adverse outcome. Whereas, MZ with DC placentation and DZ twins present pregnancies with similar risks; those with MC placentation have an important increase in worse outcome, mainly if the shared circulation is unbalanced or if we are dealing with monoamniotic or conjoined twins.

HOW MUCH IDENTICAL ARE MONOZYGOTIC TWINS?

Phenomena of Genetic and Epigenetic Discordance

Unexpectedly MZ twins may be of a different chromosomal composition (heterokaryotypic twins). Heterokaryotypic twins may be explained by two mechanisms: (1) When the mitotic error occurs before the twinning event, the mosaic will be present in both fetuses with different distribution of the two cell lines between the twins; (2) When the mitotic error occurs after the twinning event, the mosaic will be present in only one twin (Schmid et al. 2000). All possible combinations of karyotypes observed in twins can be attributed to the unequal allocation of the abnormal cells to each twin: abnormal/normal, mosaic/mosaic, abnormal/mosaic and normal/mosaic.[31]

Adding to the complexity of the situation we must consider the timing of the event (responsible for the presence of the mitotic error in somatic regions of one twin) and the placental status of the chromosomes (Machin et al. 1996).

The MZ twins with chromosomal anomalies and discordant phenotypes have been reported, including discordant sex phenotype with mosaicism 46XY/45X, Turner's syndrome in female twins with mosaicism 46XX/45X (Nieuwint et al.1999; Schmid et al. 2000; Zech

et al. 2008), trisomy 21 (Nieuwint et al. 1999) and trisomy 13 (Heydanus et al. 1993). There are a few case reports of MZ twins with discordant phenotype and rare partial chromosomal anomalies including 22q11 deletion (Lu et al. 2001), 7q syndrome (Tsukamoto et al. 1993), monosomy 21 (Cheng et al. 2006)[32] and partial trisomy 1 (Tsukamoto et al. 1993). Trisomy 11p has already been reported (Bourthoumieu et al. 2005)[31] either associated with a nonspecific clinical pattern or with the Beckwith-Wiedemann syndrome (BWS) when the additional region causes paternal disomy.[31] MZ pairs discordant for 45X emerging from 47XXY, 47XXX, 46XY and 46XX zygotes have been reported.[33]

Therefore, various postzygotic events determine a discordant phenotype for MZ twins, that are not so identical as would be expected.

Concordant or Reciprocal X Chromosome-Inactivation (or Lyonization)

This refers to an inactivation of one of the X chromosomes in females to achieve dosage compensation of X-linked genes with males.

Several studies link random inactivation of X chromosome of maternal or paternal inheritance to subtypes and timing of MZ twins, and also indicate that allocation of cells to the twins is not always equal. Despite the female excess in MC twinning, it is not clear that X-inactivation is a major stimulus to MZ twinning per se. The discordance in the inactivated X may justify the phenotypic discordance for aspects linked to chromosome X, such as Duchenne muscular dystrophy. This inactivation precedes the MC placentation and confirms that the production of a monoamniotic sac is a late event in the MC placentation.

An excess of females over males has been observed in surviving MZ twins, mainly with MC placentation, suggesting a relationship with the time of twinning. Discordance for several X-linked recessive conditions has been reported in monozygotic fraternal (MZF) twins, suggesting and often demonstrating nonrandom X-inactivation.[19]

Finally, the highly similar patterns of X chromosome inactivation among MC twins may indicate that X chromosome inactivation occurs before the twinning event in this subgroup of MZ twins.

Chromosomal Mosaicism

The presence of two or more cell lines derived from the same zygote having different chromosomal constitutions (secondary to postzygotic events) is well recognized in aneuploid singletons. Depending on the relative timing of the twinning and chromosomal events, the two or more cell lines may be distributed largely or exclusively in somatic cells of one twin or the other. Blood mosaicism might also be present in normal twins, as a result of interfetal anastomoses, and therefore, karyotyping in MZ twins that are discordant for some fetal abnormality should be performed in amniocytes rather than in fetal blood (Schmid et al. 2000).

This mosaicism is particularly problematic for those fetuses initially 46XY with loss of a Y chromosome, that will result in a male fetus and a mosaic 46XY/45XO reared as a female. This female fetus may suffer masculinization due to the fetal passage of testosterone produced by the 46XY co-twin through the vascular anastomoses.

Whether derived from a 46XX or 46XY zygote, the MZ twin with a predominant or total 45XO constitution is likely to develop fetal-jugulolymphatic obstruction, endangering the life of the co-twin.

Imprinted Genes

Genomic imprinting is a phenomenon in which one of two alleles, from maternal or paternal origin, is inactivated by DNA methylation (Kato et al. 2005).

Imprinting is initiated during gametogenesis and transmitted to embryos via mature male and female gametes. Appropriate imprinting of the two gametes is critical and implicated in prenatal growth, development and differentiation, behavior and human disease (Singh et al. 2002).

Discordance between MZ twins has been reported for several diseases where genomic imprinting is suspected or implicated, such as BWS. The BWS has a higher prevalence than expected between MZ female twins and they are mostly discordant.[19] Although MZ twin concordance for BWS has been described, most MZ male twins are discordant for BWS (Leonard et al. 1996). May well be that unequal splitting of the inner cell mass results in differential methylation between the two cell masses. These parent-of-origin effects, together with the finding of paternal uniparental disomy of chromosome 11p15 in 20% of BWS cases, suggests that abnormal genomic imprinting might play an important role in the etiology of BWS. Discordance for hyperinsulinemic hypoglycemia (Santer et al. 2005) and Russell-Silver syndrome (Blakely et al. 2004) has also been reported and although these are likely to be heterogeneous conditions, it is possible that imprinted genes play nonetheless an important role.[19]

Discordance in MZ twin pairs is well recognized for diseases thought to result from abnormal imprinting of

genes. Beckwith-Wiedemann syndrome is caused by abnormal imprinting of one or more of a cluster of genes in the p15 region chromosome-11. It is not clear how the abnormal imprinting relates to the MZ twinning process, through unequal splitting, postzygotic chromosomal rearrangements or abnormal imprinting at the crucial moment of twinning.

Trinucleotide Repeat Sequence

Several progressive neurological disorders are characterized by phenotypic expression only when a threshold of trinucleotide repeat sequence number is exceeded, such as fragile X syndrome. Discordance has been found in some MZ twin pairs. A more severely affected twin had a complete mutation, whereas his less severely affected sibling has "mosaic" for premutation and full mutation. Therefore, there may be some difficulty in offering predictive tests for these kind of diseases to MZ twins.

Epigenetics

Epigenetic phenomena are characterized by ''modifications in gene expressions that are controlled by heritable but potentially reversible changes in DNA methylation and/or chromatin structure'' (Haque et al. 2009). Epigenetic modifications consist of methylation of cytosines, as well as modifications of histones by methylation, acetylation, phosphorylation and ubiquitination (Kaminsky et al. 2008).

The DNA methylation may occur more frequently in MZ twins and may influence susceptibility to bipolar disorder and schizophrenia. MZ twins discordant for schizophrenia have been more frequently reported. Different DNA methylation patterns have been implied in the discordance for schizophrenia in relation to specific schizophrenia candidate genes. Other studies also focused on the role of epigenetics in twin discordance, implying different methylation patterns in age related diseases, risk-taking behavior and caudal duplication anomaly (Oates et al. 2006, Poulsen et al. 2007, Kaminsky et al. 2008).

More recently, Bianchi and coworkers (2010) pointed out to alternative methods for evaluating *in vivo* genetic differences in MZ twins, such as cell-free fetal DNA (ffDNA) in maternal blood, mRNA in amniotic fluid and RNA single nucleotide polymorphism (SNP) allelic ratio analysis. Therefore, prenatal gene expression investigation *in vivo* may open a new field for prenatal twin research.[34]

Phenotypic Discordance for a Single Gene Mutation

It would be expected that MZ twins affected by an autosomal dominant disorder such as type 1 neurofibromatosis might show different somatic patterns of distribution of discrete lesions because of somatic mosaicism. However, major somatic differences may be attributed to a postzygotic discordance for the causative point mutation.

Phenotypic Discordance with Same Genetic Predisposition

Monozygotic twins are usually discordant for the extent and severity of congenital heart diseases when they have the microdeletion 22q1.1, probably due to a second epigenetic effect on the phenotype.

Discordance for Major Malformation

The prevalence of structural defects in a DZ twin pregnancy is the same as in a singleton pregnancy whereas in MZ twins it will be 2–3 times higher.[14] The concordant defects (both fetuses are affected) are rare, occurring in 10% of DC twin pregnancies and 20% of MC twin pregnancies.[35]

The discordance in DZ twins is due to a genetic predisposition. In the MZ pregnancy this discordance is more prevalent and may be explained by:

- Variable gene expression (postzygotic mutation, asymmetrical X inactivation)
- Asymmetric splitting of the cellular mass
- Splitting after laterality gradients have been established (midline defects and cardiac)
- Hemodynamic factors, in MC gestations with twin-to-twin transfusion syndrome (TTTS) (putatively responsible for disruptions).

The MZ are usually discordant for malformations such as cardiac and urinary tract defects, omphalocele and neural tube defects, but on the contrary, are usually concordant for malformations such as cloacal dysgenesis and omphalocele-exstrophy-imperforate anus-spinal defects syndrome.

Pseudoconcordance of malformations may occur in MZ twins. Although, they are frequently discordant for thyroid dysgenesis, both may only be mildly ill. Due to interfetal connections, the affected fetus may be protected from hypothyroidism by the transplacental transfusion of thyroxin from the thyroid of the unaffected co-twin and present almost normal thyroxin levels at birth.

Another example of pseudoconcordance of phenotype exists for monoamniotic twins with urinary tract malformations, in which the anuric fetus is protected from pulmonary hypoplasia and deformities by the urine output from the other fetus.

Disruptions in MZ twins including limb reduction defects, hemifacial microsomia, and amyoplasia, which may be the result of shared placental circulation leading to secondary disruptions and sometimes to single intrauterine fetal death.

Finally, clubfeet dislocated hips and cranial synostosis are more frequent malformations, which are apparently related to limited space *in utero* for the bearing of two fetuses.

"Mirroring" in Monozygotic Twins

In about 25% of MZ twins, the development of normal lateralization may be impaired by the twinning process itself in such a way that for some of the asymmetrical features, the resulting twins would not be duplicated, but mirror-images (Sommer et al. 1999).

The concept of mirror-image MZ twins is based on inverse laterality. This may suggest that the event that originated the twins began after the cells of the embryonic plate were beginning to lateralize but before formation of the primitive streak.

Later MZ twinning could be occurring when the molecular determinants of left/right asymmetry are beginning to be expressed with lateral discordance. Opposite-handness is more prevalent among both DZ and MZ twin pairs.

"Fine-Tuning": Detailed Peripheral Patterning

Monozygotic twins are not concordant for dermatoglyphics, this being one of the examples by which MZ twins are not "identical". The extent of discordance in dermatoglyphic patterns varies with chorionicity and MC twins show more within-pair variability than DC-MZ twins. There is also evidence of an effect from placental crowding: MZ twins with DC placentation show greater variability than those with separate placentas. This effect was also noted in like-sexed DC twin pairs.

Unequal Placental Territoriality

The unequal allocation of stem cells/blastomeres to the twins can determine the existence of unequal placental masses or the differential sharing of placental territory in MZ twins. As a consequence, discrepant fetal growth and different phenotype can occur in MZ twins.

THE LIMITS OF ZYGOSITY TESTING: POSTNATAL IMPORTANCE

The estimation of MZ twins is frequently based on the number of MC twins observed in obstetric ultrasound. Although all MC placentas correspond to MZ twins and all twin pairs of different sex are DZ, the majority of like-sexed twins with DC placentation is blind to their zygosity. The recognition of zygosity in dichorionic MZ twins is based on physical similarities, but even the most experienced practitioner may misclassify zygosity in about 6% of cases.[18,36] In liked-sex dichorionic twins, we are blind to zygosity in about 44% of the twins. Biochemical characteristics such as blood type, enzyme polymorphisms and HLA types have also been used to classify zygosity. However, the "gold standard" for the determination of zygosity should be based on several genetic markers (including "DNA fingerprinting") in buccal swabs or blood sampling, applied to like-sexed DC twin pregnancies. Although this determination would have more scientific than clinical justification, in particular cases it can be life-saving as in solid organ transplantation. This may be, however, a somewhat misleading approach as all MZ twins share vascular placental connections and might have exchanged DNA (chimerism).

In reality, the final diagnosis of zygosity cannot be accomplished in about 43% of cases without DNA evaluation.[37] In daily practice, the estimation of MZ twins is based roughly on chorionicity and fetal sex, leaving about one-third of MZ twins unconsidered. Therefore, whatever method used will underestimate the real incidence of MZ twins.

Considering the data from the East Flanders Prospective Twin Survey, in which zygosity was studied in all like-sexed DC twins, the frequency of MZ twins after ART was 4.5% (10x superior to the 0.45% MZ rate found in twins after spontaneous conception). The frequency of MZ twins after IVF was 2.6% (6x the rate of spontaneous conceptions).[37]

Chorionicity: A (Re) Definition of Perinatal Prognosis

Clearly, it is chorionicity rather than zygosity that determines several aspects of antenatal management and perinatal outcome. Thus, the routine assignment of chorionicity and the earliest possible diagnosis of MC twinning are highly desirable, although seldom achieved in practice.

Zygosity refers to the type of conception whereas chorionicity denotes the type of placentation. The type

of placentation depends on the time of splitting of the fertilized ova. One study suggests the possibility of determining zygosity, by means of ultrasound, in the beginning of the first trimester by counting the number of yolk sacs,[38] however, a unique placental mass and the same fetal sex suggest but do not prove monozygosity. It is not possible to determine zygosity in about 45% of cases because dizygotic twins of the same sex (about half of the DZ twins) and MZ-DC twins (a one-third of all MZ twins) cannot be differentiated unless molecular tests are used.

Caution should be taken when using the number of chorionic sacs and the number of yolk sacs alone to determine the number of embryos. Shortly after the sixth postmenstrual week, embryonic heartbeats are visible and one can confidently count the number of embryos by the number of beating hearts. By that time, to determine the number of amnions in a MC twin pregnancy, in which two embryos are seen within the chorionic sac, it is wise to wait until the eighth postmenstrual week to ascertain amnionicity. The amniotic membrane is so thin that it may remain inconspicuous until 8–9 weeks, leading to the incorrect consideration of a MC-MA gestation.

After that gestational age it becomes clear that no amniotic membrane is present between the embryos and only one yolk sac is visualized. When two embryos or fetuses assume a parallel, head-to-head position, conjoined twins should be suspected. A jerk with the probe should be inflicted to induce movement between the two fetuses, away from each other or close together when conjoined twins are in question. From then on, it is important to look for sonographic signs of cord entanglement, potentially depicted as early as 12 weeks, with the help of color Doppler.

At 10–14 weeks, the gold standard "window" for chorionicity definition, the chorion frondosum is sufficiently thick to be identified between the two layers of amnion as a wedge-shaped structure in a DC twin pregnancy (not obligatorily a DZ twin pregnancy), yielding the fully diagnostic "twin peak" or "lambda" or "delta" sign (Sepulveda et al. 1996; Wood et al. 1996).[39,40] However, the number of "twin-peak" signs is no secure indication of how many chorionic sacs exist within a given pregnancy. If two fused layers of amnion, without any chorion interposed, are found in the scan creating a T-shaped "take-off" (T sign), showing a very thin membrane with strictly two layers, a MC twin pregnancy can be diagnosed with a 100% certainty (Fisk and Bennett, 1995) **(Figs 28.1A and B)**.

After 16 weeks, physiologically the chorion frondosum regresses and chorionicity becomes a more confounding issue (in the second trimester a false characterization of chorionicity can occur in about 10% cases).[40,41] The delta sign disappears and, if sexes are alike, monochorionicity can be wrongly inferred.[42-45] It is the conjugation of several sonographic criteria that approaches the correct diagnosis of chorionicity, the most and ultimate determinant of perinatal prognosis. Therefore, an adequate first-trimester scan of a multifetal pregnancy makes the subsequent second- and third-trimester evaluation much more meaningful, simpler and faster.

Identifying a single placenta with a paper-thin, reflective hair-like septum without chorion between the two amnions, with a very thin septum with less than 2 mm and like-sex twins, placentation will most probably be MC. In contrast, if one finds two separate placentas of different location, or two fetuses of a different sex or a thick interfetal membrane greater than 2 mm with more than two layers, dichorionicity is strongly suggested. Note that to identify the interfetal membranes, a right-angled orientation of the probe in relation to the membranes should be obtained to take

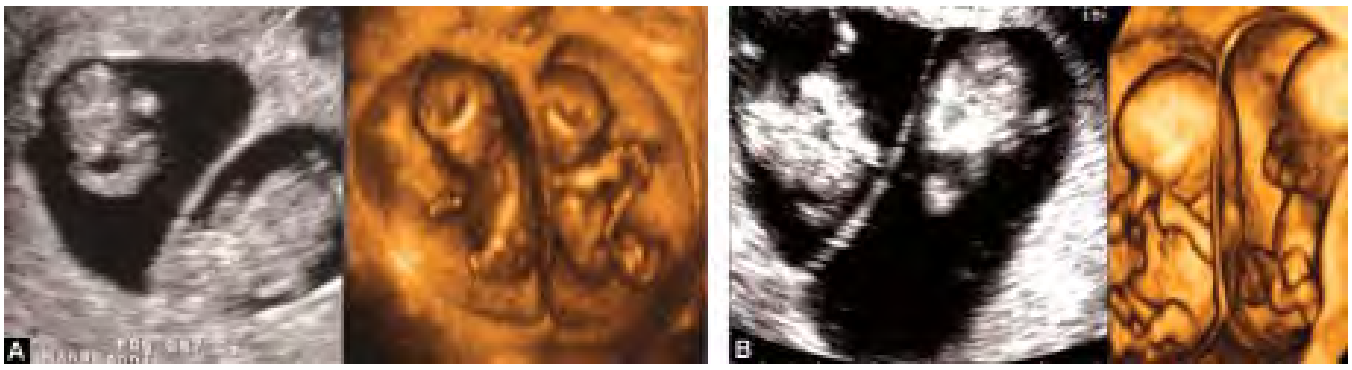

Figures 28.1A and B: Diagnosis of chorionicity at 10–14 weeks of gestation. (A) Lambda sign (dichorionic placentation); (B) T-sign (monochorionic placentation)

advantage of the axial over the lateral resolution. In order to count the number of layers one must "zoom in". In contrast, a membrane placed parallel to the ultrasonic beam will appear thinner and poorly imaged, rendering it impossible to be sure about the number of layers of the intertwin membrane.

The confirmation of a MC placentation by the detailed examination of the placenta is the most reliable proof of monozygosity. Not only is it possible to identify the pathological aspects that interfere with placental function but also the relationship between chorion and fetal membranes (chorionicity), and the pattern and the type of anastomoses of the chorionic vessels. This examination includes the careful macroscopic examination of the placenta with consideration of aspects such as the fusion of the chorion and amnion; thickness and translucency of the septum and the vascular pattern of the fetal surface. The histological evaluation includes cord fragments, membranes and placental parenchyma, and fragments of the transitional zone. To study the vascular anastomoses, the placenta should not be fixed and the amnion should be removed.

When chorionicity is established, stratification of risk is possible, anticipating the complications characteristic of each type of placenta. In fact, complications of MC twin pregnancies are by far more common, such as preterm delivery (in Portugal, out of 7551 newborns of very low birth weight born between 1996 and 2003, 25.6% resulted from multiple gestations), fetal malformations, twin-to-twin transfusion syndrome, intrauterine death of one fetus and cerebral palsy.

Prenatal Screening and Diagnosis: Does Chorionicity Matters?

Twins present unique and problematic issues in prenatal diagnosis. The performance of screening tests designed for singleton pregnancies is altered. Having established correctly the chorionicity, specific aspects of prenatal screening and diagnosis can be adequately programed in multiple pregnancies, since chromosomal abnormalities in twin pregnancies arise serious clinical, ethical and moral problems that need to be addressed.[46] These are as follows:

- Effective methods of screening, such as maternal serum biochemistry, are not applicable and have lower detection rates
- In the presence of a "screen-positive" result, there is no feature to suggest which fetus may be affected
- Invasive testing techniques are more demanding in twins and it may be difficult to ensure that fetal tissue is obtained from each fetus.
- Increased risk of miscarriage of an invasive test in twins
- Which invasive test to offer
- The paucity of data in abnormally affected pregnancies when the fetuses are either concordant or discordant for an abnormality
- The difficulties of clinical management of fetal reduction and the potential increased risk to the unaffected co-twin.

The overall probability that a multiple gestation contains an aneuploid fetus is directly related to its zygosity. In DZ pregnancies, each fetus has an independent risk of aneuploidy, thus, the maternal age-related risk for chromosomal abnormalities for each twin may be the same as in singleton pregnancies, but the chance that at least one fetus will be affected by a chromosomal defect is twice as high as in singleton pregnancies **(Fig. 28.2).**[47a-b] This means that for DZ twin

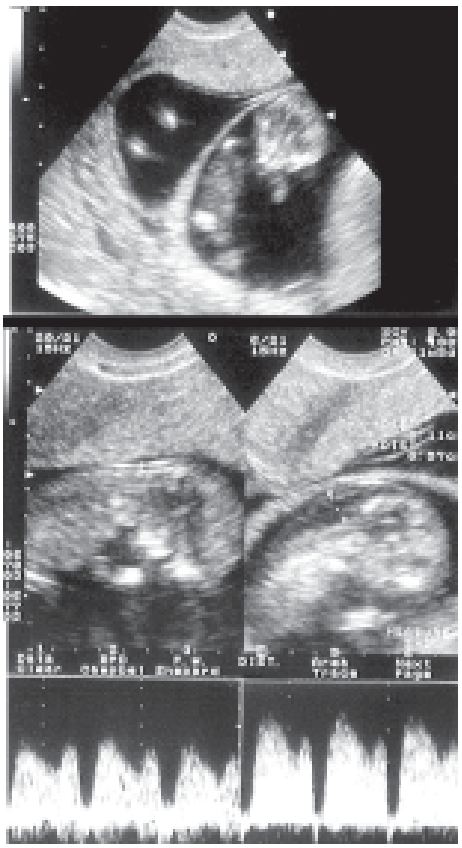

Figure 28.2: Screening for trisomy 21 in dichorionic twins (summing method): the lambda sign is evident at 10–14 weeks. We can observe discrepant nuchal translucencies (NT= 1.1 and 5.7 mm). Ductus venosus Doppler blood flow is abnormal in the fetus with increased NT that eventually revealed to be a fetus affected by trisomy 21

pregnancies, the pregnancy-specific risk is calculated by summing the individual risk estimates for each fetus. Furthermore, since the rate of DZ twinning increases with maternal age, the proportion of twin pregnancies with chromosomal defects is higher than in singleton pregnancies. The 10% of DC twin pregnancies that are MZ will incorrectly have their risks calculated by the summing rather than the averaging method. However, the ultimate effect on screening performance and clinical meaning will be a negligible one.

In MZ twins, the risk of an affected fetus is similar to the maternal age risk of a singleton pregnancy and in the vast majority of cases, the risk for one fetus is, in expectation, the same as the risk for the other (Matias et al. 2005).[47a-b] There is no reason to attribute different risks to the two fetuses because, presumably, both will be affected or both will be unaffected. The most reliable and reproducible method of screening is nuchal translucency (NT) and it is therefore appropriate to take the average of the two NT measurements, so that a single risk estimate can be calculated (averaging method).

This ignores the small possibility of heterokaryotypic MZ twins resulting from a mitotic nondisjunction after the zygote splits. There are occasional reports of MZ twins discordant for abnormalities of autosomes or sex chromosomes, most commonly with one fetus presenting a Turner syndrome and other either a normal male or female phenotype, but usually with a mosaic karyotype or a Klinefelter syndrome.

The relative proportion of spontaneous DZ to MZ is about 2:1 and therefore, the prevalence of chromosomal abnormalities affecting at least one fetus in a twin pregnancy would be expected to be about 1.6 times that in singletons.

If zygosity is unknown, the risk of at least one aneuploid fetus can be approximated as five-thirds that of the singleton risk. This is based on the assumption that a third of all twin pairs are MZ.[15] Counseling based on chorionicity, clinically more feasible than zygosity, results that in MC twins both fetuses can be affected equally. If the pregnancy is DC, then the parents should be counseled that the risk of discordance for a chromosomal abnormality is about twice that in singleton pregnancies, whereas the risk that both fetuses would be affected is a much rarer event, corresponding to the singleton risk squared. However, with higher risk conditions, such as autosomal recessive disorders, this could be as high as one in 16. For example, in a 40-year-old pregnant woman with a risk for trisomy of about 1 in 100 based on maternal age, in a DZ twin pregnancy the risk that one fetus would be affected would be 1 in 50 (1 in 100 plus 1 in 100), whereas the risk that both fetuses would be affected is 1 in 10,000 (1 in 100 x 1 in 100). This is, however, an oversimplification since, unlike all MC pregnancies that are always MZ, only about 90% of DC pregnancies are DZ.

When calculating the risk of higher order multiples, estimates can be made multiplying the singleton risk by the number of fetuses (Jenkins and Wapner, 2000). This method assumes unique chorionicity for each fetus, though monozygosity can occur more frequently than usually thought at higher rates in ART multiple gestations (Wenstrom et al. 1993; Blickstein et al. 1999).[5,6]

The possibility of deriving a risk for trisomy 21 from NT assessment in the first trimester of pregnancy shifted the consideration of a pregnancy-specific risk to a fetus-specific risk.[48] This assumption was based on the observation that the distribution of NT measurements in twin fetuses with trisomy 21 was similar to that in singletons (Pandya et al. 1995; Sebire et al. 1996a-b). The higher rate of false positives for NT among MC twins (8.4%) should be ascribed to the possibility of early hemodynamic imbalance (the risk of developing TTTS if NT is increased is augmented 3–5 fold).[9a-b,49]

Although assessing nasal bones in multiple pregnancies can be more demanding due to the more difficult acquisition of adequate fetal face planes, whenever they are assessed they can be combined with NT and biochemical screening for calculating first-trimester risks. With the addition of nasal bone evaluation, sensitivity for trisomy 21 screening increased from 79–89%, for the same false positive rate of 5%.[50-54]

In contrast, though biochemical screening in twins was the first alternative to age derived risk, it can still be a source of confusion and clearly has a lower detection rate for fetal aneuploidies (50%) and higher rates of false positives.[55-57] This kind of screening only permits the calculation of a pregnancy and not a fetus-specific risk. In twin pregnancies, the levels of maternal serum markers are, on average, expected to be about twice as high in unaffected twin pregnancies as in unaffected singleton pregnancies (Cuckle, 1998),[58] that is, proportional to the number of fetoplacental units. However, as biochemical screening in twins is still investigational and far less powerful than in singletons, it should not be recommended in general practice without extensive counseling.[59,60]

MONOCHORIONIC PREGNANCY AS A HIGH RISK PREGNANCY: TWIN-TO-TWIN TRANSFUSION SYNDROME AS A PARADIGM TO TREAT

Over the last decade, perinatal mortality in singleton pregnancies has fallen due to advances in fetal medicine and improvement in perinatal care. Similar reduction has not been observed in multiple pregnancies in which perinatal loss still remains six times higher than in singleton pregnancies. Even more striking is the perinatal mortality of MC twins (260 per 1000) which remains 3–5 fold higher than in DC pregnancies (90 per 1000): the rate of perinatal loss before 24 weeks in MC compared with DC pregnancies is 12.2% versus 1.8%.[9a-b]

The MC twin placenta is designed and built for a singleton fetus, hence, attempts to cater for the needs of twin fetuses can often be suboptimal. Twin fetal circulations are seldom separate and several intertwin vascular communications of various kinds may be present and quite often there is an unequal sharing of placental parenchyma. An example of a complication almost unique to MZ twinning is twin-to-twin transfusion syndrome (TTTS). By way of intertwin vascular connections, blood is transfused from the donor, who becomes growth-restricted and develops high output cardiac insufficiency and oligohydramnios (depleted-donor twin), to the recipient, who develops circulatory overload with congestive heart failure and polyhydramnios (volume and an overfilled recipient twin). Therefore, TTTS reflects primarily a pathological form of circulatory imbalance that develops chronically between hemodynamically connected MC twin fetuses.

Twin-to-twin transfusion syndrome affects about 5–15% of MC twin pregnancies (1:400 pregnancies) and thus occurs in 1 in 1600 deliveries. This syndrome accounts for 17% of perinatal mortality, nearly 12% of neonatal deaths and 8.4% of infant deaths in twins. This is 3–10 times higher than that attributed to singletons.

This syndrome was always recognized as a devastating complication of "identical" twins, but it took roughly 400 years to understand the way it works. Although clinically identifiable, this condition is still far from being effectively anticipated and treated. The TTTS presents unique characteristics and greatest therapeutic challenges in perinatal medicine which are as follows:

- It affects two babies, not one
- It affects structurally normal babies
- Its basis resides in the placenta, not in the babies
- It is associated with important perinatal morbidity and mortality
- It is amenable to curative therapy.

Vascular anastomoses are found invariably in almost all MC placentas. Thus, interfetal transfusion is a normal event in MC twin pregnancies. When intertwin transfusion in MC twins is balanced, clinical manifestations of TTTS are not expected to occur.

More than a century ago Schatz et al. (1890) suggested that TTTS is due to discordant hemodynamics secondary to transfusional imbalance.[61] Later Bajoria and coworkers (1995)[62] related TTTS with unbalanced intertwin transfusion mediated by one or more arteriovenous (AV) anastomoses in association with absent bidirectional superficial anastomoses, those affected by TTTS had fewer arterioarterial (AA) anastomoses present in 24% versus 84% of MC twins without TTTS (Denbow et al. 2000). Seventy eight percent of MC pregnancies in this series with one or more AV anastomoses and no AA anastomoses developed TTTS (Denbow et al. 2000). When an AA anastomosis is found, the risk of developing TTTS is reduced nine-folds.

Therefore, due to a particular vascular anatomy of the placenta, some MC twins are unable to compensate for the unidirectional flow in a "causative" AV anastomosis. MC twins have a continuous spectrum of severity in the imbalance between their fetoplacental circulations, depending on an angioarchitectural basis, hemodynamic and hormonal factors. The progressive nature of TTTS *in utero* is thought to be due to one twin (the donor) slowly pumping blood to the other (the recipient) through these anastomoses.

Net result of transfusion between twins depends on:

- *Vascular anastomoses*: Combination of type of connections (number, type and diameter) and direction of connections. In some cases, the normal transfusion from the donor´s arterial to the recipient´s venous circulation is not adequately compensated by oppositely directed flow by other deep or superficial anastomoses.[62]
- *Placental sharing*: Unequal placental sharing, both by discrepant size of placental territory or by velamentous insertion of umbilical cord, may further impair growth in TTTS fetuses.[63]
- *Asymmetry* in the progressive reduction of an initially large number of bidirectional AV connections formed during the embryonic unification of placental and fetal vessels.
- *Unbalanced renin-angiotensin system* (RAS): Upregulation of RAS (donor) and downregulation of RAS (recipient) with transfer of angiotensin II may cause or contribute to the development of TTTS.[64]
- *Incomplete remodeling* and defective trophoblastic invasion of maternal spiral arteries.

The pathophysiology of TTTS is poorly understood and although transfusion has been confirmed *in vivo*, the pathophysiology of TTTS includes more than shunting of blood from donor to recipient. A vicious cycle of hypervolemia-polyuria-hyperosmolality is established, leading in about one-third of the cases to the development of acute polyhydramnios/oligohydramnios sequence in the second trimester of pregnancy.

Diagnosis of Twin-to-Twin Transfusion Syndrome

In the past, diagnosis of the syndrome was made only after delivery of the affected twin pair and careful examination of the placenta. The standard neonatal criteria comprised:

- A difference in cord hemoglobin concentrations of 5 gm/dl or more (false positives should be considered whenever there is untimely umbilical cord clamping of either donor or recipient or reversed intrapartum shunts).
- A difference in birth weights of 20% or more (this criterion is not necessarily present in the acute form of fetofetal transfusion syndrome that occurs in labor, and hydroptic fetuses may obscure the real intertwin size disparity).

Danskin and Neilson (1989), revisiting the neonatal criteria for diagnosis of TTTS found that an intertwin hemoglobin disparity of 5 gm/dl or more and birth weight differences of more than 20% were found both in MC and DC twins at similar rates.[65] Wenstrom et al. (1992) concordantly found that weight and hemoglobin level discordance were relatively common among MC twins. Therefore, a definitive diagnosis of TTTS solely based on neonatal criteria seemed insufficient.[66]

Considering the many pitfalls of neonatal findings in TTTS and the more consistent sonographic antenatal criteria,[67-69] the emphasis of screening and diagnosis of TTTS is being pushed backwards in pregnancy. In the early 1980s, the contribution of antenatal ultrasound for redefining the diagnostic criteria of TTTS was recognized by Wittmann and Brennan. Wittmann et al. proposed as discriminating findings in TTTS the discrepancy in the sizes of twins and the polyhydramnios surrounding the larger twin. Brennan and colleagues added to the former criteria, disparity in size of the vessels in the umbilical cords, same sex, single placenta showing different echogenicity of the cotyledons supplying the two cords, and evidence of hydrops in either twin or congestive heart failure in the recipient. More recently, more useful sonographic criteria are adopted:

1. Discordance in Amniotic Fluid Volume (Oligohydramnios Sequence)

In 1988, Chescheir and Seeds disclosed a powerful clue based on the fact that six out of seven twin pregnancies with MC placentas and TTTS had concurrent polyhydramnios and oligohydramnios.[70] This is not surprising when we understand TTTS as a manifestation of a hemodynamic imbalance. Fetal renal perfusion is asymmetric: the congestive heart failure in the recipient will overperfuse the kidneys with consequent polyuria and excess of amniotic fluid; hypovolemia in the donor causes inadequate perfusion of the kidneys with decrease in urinary output and oligohydramnios.

More uniform criteria for the oligohydramnios sequence have been proposed for a quantitative definition: deepest vertical pool in the donor sac less than 2 cm and greater than 8 cm in the recipient´s sac. Not infrequently, anhydramnios in the donor sac results in it becoming "stuck", shrowded by the intertwin membrane, while the recipient´s sac becomes severely polyhydramniotic.

One should bear in mind that sonographic pitfalls may exist in the presence of discordant anomalies in twins that imply differences in amniotic fluid volume, such as one twin with esophageal atresia and consequent polyhydramnios or with renal agenesis, with consequent olygohydramnios/anhydramnios.

Other related confirmatory features include a small or nonvisible bladder due to hipovolemia and renal hypoperfusion in the donor, along with a distended urinary bladder with resulting excessive micturition in the recipient.

2. Discordance in Fetal Size

Discordant growth is a common complication of twin pregnancies. The need for stricter sonographic criteria to define growth has changed gold standards over time. Abdominal circumference rather than head measurements of twins was proposed as the most reproducible and meaningful one. Besides, considering that fetal weight estimations based on singleton growth charts may be inadequate for twins, the abdominal circumference criterion should be definitely used for the sonographic diagnosis of divergent twin growth. A cut-off value of 20 mm for the difference in abdominal circumference between twins indicated growth discordance of more than 20%.

3. Abnormal Doppler Findings

Alterations in cardiac hemodynamics are indirectly put on evidence by alterations in venous blood flow

waveforms. The receptor presents with pulsatility in the umbilical vein and absent or reverse flow in the ductus venosus (Hecher et al. 1995)[71] as signs of congestive heart failure due to hypervolemia and increased preload from placental vascular anastomotic transfusion.

4. Fetal Echocardiography

Both donor and recipient twins have dynamic changes in volume/pressure loading during cardiovascular development constituting a hostile intrauterine environment. Considering the hemodynamic imbalance between the circulations of the twins involving some excess of blood flowing from the donor to the recipient fetus, cardiac involvement is logically expected. Echocardiography is a well-established tool for antenatal assessment of structural and functional heart disease, turning it possible in TTTS to assess cardiovascular adaptation to intertwin transfusion, early recognition of deterioration and evaluation of antenatal management.

Zosmer et al. (1994) showed that some surviving twins of TTTS had a persistent right ventricular hypertrophic cardiomyopathy and proposed that cardiac dysfunction could be induced *in utero* by sustained strain upon the heart by TTTS, predominantly affecting the right ventricle. The right ventricle is stiffer and more afterload-sensitive than the left ventricle, mostly due to the redistribution of blood in the cerebral arteries which decreases the left ventricular afterload.[72] Additionally, recipients remain at increased risk of pulmonary artery stenosis and maintain a slightly reduced early diastolic ventricular filling as compared to donors (diastolic dysfunction).[73]

In contrast, the significant reduction of blood flow velocity in umbilical artery recorded in the "donor" is consistent with hypovolemia and increased placental resistance, increasing cardiac afterload and decreasing umbilical venous return. This is in good agreement with some studies which show that the donor twin has a trend towards a lower Tei-index than in the normal population. Finally, there have been speculations about an increased incidence of aortic coarctation in donors due to a lower venous return from the placenta and hence a decreased loading of the left ventricular outflow tract (Lewi et al. 2011).

In the study from Fesslova et al. (1998), all recipient fetuses showed cardiac hypertrophy and dilatation, well-known compensatory mechanisms of blood volume overload and high cardiac output (Frank-Starling mechanism).[74]

After birth about half of the recipients showed biventricular hypertrophy, with prevalent left ventricular hypertrophic cardiomyopathy.[72-75] A smaller subgroup will develop right ventricular tract obstruction (functional pulmonary stenosis) and pulmonary hypertension in the neonatal period, which may be aggravated by systolic right ventricular dysfunction. Recently diastolic abnormalities were described in the right ventricle, with abnormal filling patterns, prolonged isovolumic relaxation time and abnormal flow patterns in the inferior vena cava and ductus venosus. In addition to hemodynamic remodeling, it is well recognized the role of increased endothelin-1 in the recipient, mainly in the hydropic recipient, as a mitogenic factor to smooth muscle cell in systemic and pulmonary vasculature and for ventricular myocyte proliferation.

More recently, abnormalities of vascular distensibility were described in survivors of TTTS in infancy.[75] The donor fetus shows evidence of chronic hypovolemia resulting in activation of the renin-angiotensin system. This upregulation initially attempts to correct volume depletion and transfusion of increased concentrations of angiotensin II will probably cause increased vascular stiffness in the surviving donor in childhood.

5. Signs of Hydrops in the Recipient Twin

In an advanced stage of TTTS, the recipient twin affected by congestive heart failure may present signs of serosa effusions, such as ascites, pleural effusion and subcutaneous edema.

6. Other Ultrasonographic Findings

- *Identification of cord insertion:* Velamentous insertion of the cord is a frequent finding.
- *Funipuncture:* Theoretically, it may allow the antenatal assessment of intertwin hemoglobin difference, the degree of fetal anemia in the donor twin and the twins' zygosity through blood group studies. However, the possible benefit of this procedure seems to be very poor in clinical grounds and the risks importantly outweigh the informative gain.
- *Difference in color of the placentas:* Due to blood transfusion from one twin to the other, the placenta of the donor twin tends to be whitish (pale) and the placenta of the recipient, of a denser color (excess of blood).

Prediction of TTTS

While accounting for only 1.2% of the population, twins are responsible for 12.6% of the perinatal mortality. In the particular case of MC twinning the fetal loss rate is even more relevant and there is an increased risk of

adverse perinatal outcome. Therefore, targeted surveillance of MC twins at earlier stages of gestation could anticipate and provide timely management of the pregnancies at risk of one of the most devastating type-specific complications, i.e. TTTS.[76]

Nuchal Translucency

Data gathered from the literature show that increased nuchal translucency thickness (NT) at 10–14 weeks of gestation was found twice as much as in MC than in singleton pregnancies and the likelihood ratio of developing TTTS in those twins with increased NT was 3.5.[9a-b,77] Considering that MC pregnancies do not show a higher prevalence of chromosomal abnormalities, the higher prevalence of increased NT in those twins could be ascribed to cardiac dysfunction. With advancing gestation, this transient heart failure eventually resolves with increased diuresis and ventricular compliance. More recently, it was observed that whenever the discrepancy of NT values was above 20%, the detection rate for early fetal death was 63% and for severe TTTS of 52%.[78] In a recent study Lewi et al. (2008) showed that significant predictors in the first trimester were the difference in crown-rump length (odds ratio = 11) and discordant amniotic fluid (OR= 10).[79] Later in pregnancy, at 16 weeks, significant predictors were the difference in abdominal circumference (OR = 29), discordant amniotic fluid (OR = 7), and discordant cord insertions (OR = 3). Risk assessment in the first trimester and at 16 weeks detected 29%, and 48% of cases with a complicated fetal outcome, with a false-positive rate of 3% and 6%, respectively. Combined first-trimester and 16 week assessment identified 58% of fetal complications, with a false-positive rate of 8%.[79]

Ductus Venosus Flowmetry

Can the characteristic circulatory imbalance of TTTS, fully expressed later in pregnancy, disclose indirect signs of cardiac dysfunction in earlier stages of gestation? In recent studies of vascular hemodynamics in fetuses with increased NT at 10–14 weeks, the abnormal flow in DV more frequently recorded in fetuses with chromosomopathies, with or without cardiac defects, was related to heart strain.[80-82] These findings are in good agreement with the overt hemodynamic alterations found in TTTS later in pregnancy. Therefore, strong evidence suggests that increased NT along with abnormal flow in the DV, even in the presence of a normal karyotype, may be early signs of cardiac impairment or defect.

In a study from our unit, nuchal translucency and Doppler blood flow waveforms in the DV were recorded in both twins between 11 weeks and 14 weeks of gestation.[47a-b] The TTTS was recorded in those fetuses which combined increased NT and abnormal flow in the DV. Whenever NT were discrepant but with normal flow in the DV, no cases of TTTS were found **(Figs 28.3A and B)**.[47a-b,83]

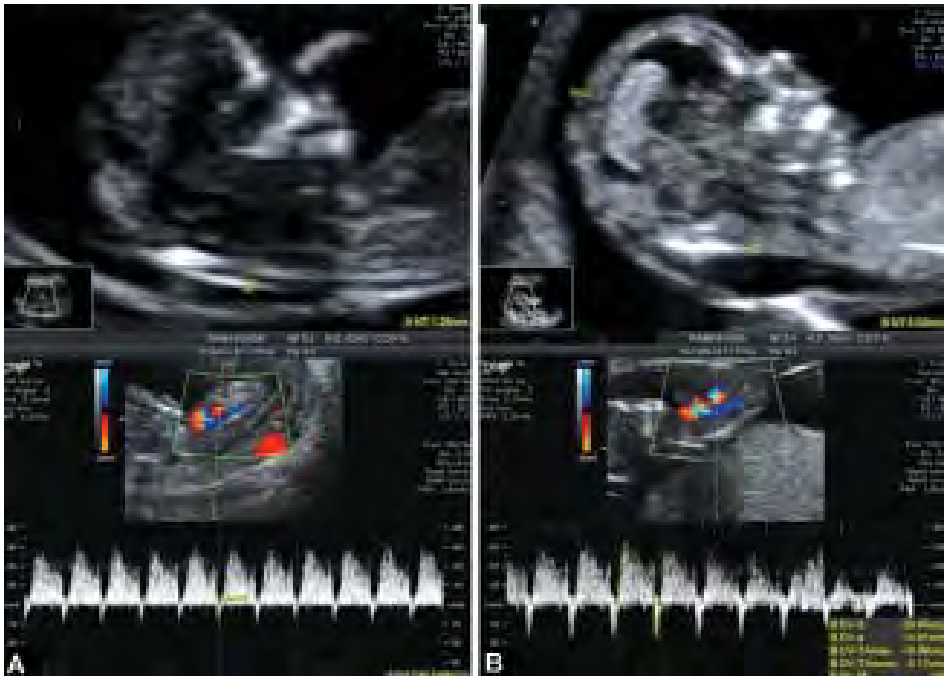

Figures 28.3A and B: Screening for trisomy 21 in monochorionic twins (averaging method). We can observe discrepant nuchal translucencies (NT= 1.25 and 5.02 mm). Ductus venosus Doppler blood flow is abnormal in the fetus with increased NT. This pair of twins was chromosomally normal and developed a twin-to-twin transfusion syndrome at 16 weeks

More recently, in a more inclusive study, we showed that discrepant values for NT over 0.6 mm had a sensitivity of 45.5% and a specificity of 86.9%. The presence of at least one abnormal blood flow waveform in the DV translated in a relative risk for developing TTTS of 11.86 (3.05–57.45) with a sensitivity of 72.7% and a specificity of 91.7%. The combination of abnormal DV blood flow with discrepant NT > 0.6 mm, yielded a relative risk for the development of TTTS, 21 times higher (IC 95% 5.47–98.33).[84]

Therefore, both increased nuchal translucency and abnormal flow in the ductus venosus in MC twins may translate early manifestations of hemodynamic imbalance between donor and recipient. In these pregnancies, in addition to NT measurement at 11–14 weeks, the Doppler assessment of DV blood flow relevantly increases the performance of screening for those at risk of developing TTTS.

Arterioarterial Anastomoses

The search of AA anastomoses in the placental plate of MC placentas by color Doppler has until now mainly provided a negative value: only 5% of MC twins will develop TTTS, if AA anastomoses are present and if absent, 58% will develop TTTS. In the studies of Taylor and coworkers, the sensitivity and positive predictive value for absent AA anastomoses in predicting TTTS was 74% and 61%, respectively.[85] The major limitation to the use of absent AA anastomoses in predicting TTTS is the difficulty in being sure that an AA anastomosis is really absent or simply not yet seen, as it frequently happens before 18 weeks.

Intertwin Membrane Folding

At 15–17 weeks of gestation, the disparity in amniotic fluid volume between the two amniotic sacs seems to cause membrane folding: if present, 28% of cases developed severe TTTS and 72% developed mild TTTS. If membrane folding was absent, no cases of TTTS were recorded.

DISCORDANCE OF FETAL GROWTH: WHAT IS ADAPTATION, PROMOTION AND GROWTH RESTRICTION IN MULTIPLES?

The restriction of intrauterine fetal growth is more frequently found in multiple pregnancies: about 52% of twins and 92% of triplets present low birth weight (< 2500 gm) compared to 6% of singletons, whereas 10% of twins and 32% of triplets are born with very low birth weight (< 1000 gm), when compared to 1% of singletons. This has not been scrutinized in depth because of three limitations, when we define intrauterine growth restriction (IUGR) growth curves of fetuses with comparable growth potentials should be adopted. At present, it is believed that multiples do not have the same growth potential as singletons and there are serious doubts concerning the appropriateness of singleton standards for multiples. Second, the growth pattern of late pregnancy are practically unknown because preterm birth (by singleton standards) is the rule than the exception in multiple gestations (before 37 weeks, about 50% of twins and 91% of triplets were already born in comparison with 9% of singletons). Finally, there are few longitudinal studies and most of our knowledge is derived from birth weight by gestational age relationships (growth curves).

If we monitor fetal growth in multiple pregnancies by singleton standards, more than 50% of triplets are considered small for gestational age (SGA) at 35 weeks and more than 50% of twins are considered SGA at 38 weeks. The average birth weight at 39 weeks is 3357 gm; at 35 weeks 2389 gm and at 32 weeks 1735 gm, for singletons, twins and triplets, respectively. Although many authors classify twin infants as IUGR by using a gender and a gestational age-specific birth weight below the 10th centile,[86,87] the truth is that a biological phenomenon with a frequency of over 50% reluctantly will be considered a pathological event. The re-evaluation of the median birth weight centile of twins and triplets compared to the 10th centile for singletons showed that the average multiple is not "SGA" and weighs more than the 10th birth weight percentile for singletons until 35 weeks in triplets and 38 weeks in twins.[88]

The common growth curves show that deviations from singleton standards occur after 28 weeks.[88] The uterine milieu, comprising uteroplacental, maternal and fetal components, limits physiologically the growth potential of the individual fetus in a multiple pregnancy. This concept implies that most multiples delivered after 28 weeks are growth restricted compared to singletons, as a result of an adaptative process. The total twin and total triplet birth weights exceed that of the 90th birth weight centile for singletons as early as 25 weeks´ gestation (data derived from 3.6 millions singletons from Matria database). The uterine potential adaptation to a multiple pregnancy is also appreciated by realizing that the average singleton birth weight at 40 weeks is reached as early as 32 weeks in twins and as early as 29 weeks in triplets.

Consequently, the individual multiple is relatively growth restricted compared to singletons, whereas the entire pregnancy is growth promoted.[89] This physio-

logical restriction (reduction in fetal size) is a way to promote a more advanced gestation as long as possible, to overcome the tremendous increase in volume, the uterine overdistention and the higher frequency of preterm delivery in multiples.[88] The variables that most strongly influence uterine adaptation are parity (less in nuliparas), maternal age, maternal height and weight gain.

Discordant growth is another potential way to reduce uterine volume in order to promote an advanced gestational age at birth. The problem is to distinguish between natural variation and pathological growth restriction. Differences as large as 15% may be normal, whereas 15–25% discordance may denote adaptation and differences of more than 25% reveal the inability to maintain growth.[90] This latter group presents the best correlation with adverse outcome, namely neonatal mortality and morbidity and intensive care admission.[91]

The risk of occurring a fetal growth restriction in a multiple pregnancy is 10 times greater than in a singleton pregnancy,[92] being even greater in a MC (34%) compared to a DC pregnancy (23%).[9a] More recently, our group put in evidence that in uncomplicated MC twin pregnancies, abnormal DV flow in at least one of the fetuses seems to be associated with a higher discordance in birth weight than in those with normal flow in both fetuses.[93] In fact, in pregnancies with abnormal DV flow in at least one of the fetuses the median discordance in birth weight was higher than in those with normal DV flow in both twins (13.2% vs 7.8%, $p = 0.006$).

Hence, the meaning of a fetal growth discordance in multiples depends on chorionicity. The abdominal circumference is the most reliable sonographic criterion for the establishment of growth discrepancy. A difference of 20 mm translates in a birth weight discrepancy of 20% or more. In a DC twin pregnancy (DZ in 90%) may be ascribed to a different genetic constitution of the twins or to an unequal placental function. In a MC pregnancy, as the genetic content is the same, the growth discordance may be due to an unequal division of the cellular mass (unequal sharing of the placenta), velamentous insertion of the cord, vasa previa or to the unbalanced transfusion of blood through the vascular anastomoses.

By using data from the matched multiple birth data set from the National Center for Health Statistics it was noticed that 10.683 pairs showed a discordance greater than 25% (8.2% of the entire population of twins). This population was subdivided in three groups according to the birth weight of the smaller twin (less than 10th centile, 10–50th centile or greater than 50th centile). These subgroups correspond to severely discordant twin pairs who are growth restricted, growth adapted or growth promoted, respectively. The frequencies of each subgroup were unaltered through the third trimester: 6668 (62.4%), 3514 (32.9%) and 501 (4.7%) severely discordant sets.[91] Neonatal mortality was significantly higher (29.1%) when the smaller twin weighed less than the 10th centile for gestational age, compared with other subgroups (11.2% and 11%). The data prove that even among severely discordant pairs, 40% are appropriately grown twins, of which 6% are in fact growth promoted.

MULTIPLES AND CEREBRAL PALSY: THE EFFECT OF PREMATURITY OR MORE?

In 1897, Sigmund Freud suggested that multiple pregnancy was the most important cause of cerebral palsy more relevant than perinatal asphyxia or preterm birth. A century later, this postulate remains valid, the risk of one of the fetuses being affected by cerebral palsy is 1.5% in twins, 8% in triplets and 43% in quadruplets (Yokoyama et al. 1995).[94-98] In reality, there is an exponential relationship between the number of fetuses in a pregnancy and the rate of cerebral palsy. There is a preponderance of brain damage in MC and like-sex twins than in DC pregnancies, namely when the death of the co-twin occurs: the incidence of the lesions of the white matter after the death of the co-twin in a MC pregnancy is 25% in contrast with 3% in the survivor of a DC twin pregnancy.[99] Prematurity and low birth weight are the most relevant risk factors for long-term neurological morbidity. Factors such as zygosity, intrauterine growth restriction, fetal weight discordance and type of birth are less powerfully correlated with the risk of cerebral palsy in multiple pregnancies.[100]

In a population-based retrospective cohort study comparing neurological problems in Swedish children born after IVF with matched controls, the former were 70% more likely to need rehabilitation. The risk of cerebral palsy was four-fold increased in children born after IVF. The data confirm a model that suggested a significantly lower estimated cerebral palsy rate (2.7/1000 neonates) after spontaneous pregnancies as compared with transfer of three embryos (OR = 6.3), two embryos (OR = 3.3) and transfer of three embryos in which all triplets have been reduced to twins (OR = 3.8). Similar estimations suggested that iatrogenic multiples contribute 8% to the annual number of cerebral palsy cases in the USA.

In the specific case of TTTS, Lopriore and coworkers (2003)[101] presented important data concerning the

psychomotor development of survivors from TTTS evaluated until school entry. From a total of 29 children affected *in utero* by TTTS and evaluated during 8 years, 41% presented cerebral anomalies disclosed by ultrasound and about 21% had cerebral palsy.[101] This figure rose to 50% in the cases of TTTS complicated by intrauterine fetal demise of the co-twin, whereas rates of 14% of cerebral palsy were found in the cases in which both twins survived.

In order to anticipate the neurologic risk in cases of TTTS complicated with death of the co-twin, Senat and coworkers (2003)[102] proposed the sequential evaluation of the fetal middle cerebral artery peak systolic velocity to predict fetal anemia within 24 hours of the death of one MC twin and to monitor hemoglobin concentration in the surviving fetus at risk for acute anemia.[102] This method was found to be a reliable noninvasive diagnostic tool and may be helpful in counseling and planning invasive testing.

CONCLUSION

In clinical terms, the assignment of chorionicity is more relevant than zygosity determination, provided that chorionicity, dependent on the type of placentation, is the one that will dramatically influence perinatal outcome. In fact, about 30% of MC twin pregnancies are complicated by TTTS, isolated discordant growth, twin anemia-polycythemia sequence, congenital defects or intrauterine demise. About 15% will be eligible for invasive fetal therapy. Combining several sonographic markers, ultrasound examination in the first and early second trimester can differentiate the MC twins at high risk for adverse outcome from those likely to be uneventful, which may be useful for patient counseling and planning of care. Therefore, the determination of chorionicity should be mandatory, preferably between 11–14 weeks, since later on it is mostly inaccurate. In doing so, the obstetrician can contribute to the stratification of risk and to the clarification of different aspects of multiple pregnancies such as prenatal screening and diagnosis, discordance of congenital anomalies, complications specific of multiple pregnancies, fetal growth discordance and perinatal mortality and morbidity.

REFERENCES

1. Tromp M, Ravelli AC, Reitsma JB, et al. Increasing maternal age at first pregnancy planning: health outcomes and associated costs. J Epidemiol Community Health; 2010.
2. Blickstein I. The worldwide impact of iatrogenic pregnancy. Int J Gynecol Obstet. 2003;82:307-17.
3. Blickstein I, Keith LG. The decreased rates of triplet births: temporal trends and biologic speculations. Am J Obstet Gynecol. 2005;193:327-31.
4. de Mouzon J, Goossens V, Bhattacharya S, et al. European IVF-monitoring (EIM) Consortium, for the European Society of Human Reproduction and Embryology (ESHRE). Assisted reproductive technology in Europe, 2006: results generated from European registers by ESHRE. Hum Reprod. 2010;25(8):1851-62.
5. Wenstrom KD, Syrop CH, Hammitt DG, et al. Increased risk of monochorionic twinning associated with assisted reproduction. Fert Steril. 1993;60:510-4.
6. Blickstein I, Verhoeven HC, Keith LG. Zygotic splitting following assisted reproduction. N Eng J Med. 1999;340: 738-9.
7. Blickstein I, Jones C, Keith LG. Zygotic splitting rates following single embryo transfers in in-vitro fertilization: a population-based study. N Eng J Med. 2003;348:2366-7.
8. Blickstein I. Estimation of iatrogenic monozygotic twinning rate following assisted reproduction: pitfalls and caveats. Am J Obstet Gynecol. 2005;192:365-8.

9a. Sebire NJ, Snijders RJM, Hughes K, et al. The hidden mortality of monochorionic twin pregnancies. Br J Obstet Gynecol. 1997;104:1203-7.

9b. Sebire NJ, D' Ercole C, Hughes K, et al. Increased nuchal translucency thickness at 10-14 weeks of gestation as predictor of severe twin-to-twin transfusion syndrome. Ultrasound Obstet Gynecol. 1997;10:86-9.

10. Sperling L, Kiil C, Larsen LU, et al. Naturally conceived twins with monochorionic placentation have the highest risk of fetal loss. Ultrasound Obstet Gynecol. 2006;28:644-52.
11. Dudenhausen JW, Maier RF. Perinatal problems in multiple births. Dtsch Arztebl Int. 2010;107(38):663-8.
12. Blickstein I, Arabin B, Lewi L, et al. A template for defining the perinatal care of monochorionic twins: the Istanbul international ad hoc committee. J Perinat Med. 2010;38(2): 107-10.
13. Myrianthopoulos NC. Congenital malformations: the contribution of twin studies. Birth Defects Orig Artic Ser. 1978;14:151-65.
14. Baldwin VJ. Anomalous development of twins. In: Baldwin VJ (Ed). Pathology of Multiple Pregnancy. New York: Springer-Verlag; 1994. pp. 169-97.
15. Rodis JF, Egan JF, Craffey A, et al. Calculated risk of chromosomal abnormalities in twin gestations. Obstet Gynecol. 1990;76:1037-41.
16. Hack KE, Derks JB, Elias SG, et al. Increased perinatal mortality and morbidity in monochorionic versus dichorionic twin pregnancies: clinical implications of a large Dutch cohort study. BJOG. 2008;115(1):58-67.
17. Silva S, Martins Y, Matias A, et al. Why are monozygotic twins different? J Perinat Med. 2011;39(2):195-202.
18. Hall JG. Twinning: mechanisms and genetic implications. Curr Opin Genet Dev. 1996;6(3):343-7.
19. Hall JG. Twinning. Lancet. 2003;62(9385):735-43.

20. Blickstein I, Keith LG. On the possible cause of monozygotic twinning: lessons from the 9-banded armadillo and from assisted reproduction. Twin Res Hum Genetics. 2007;10(2):394-9.
21. Teplica D, Peekna K. The mirror phenomenon in monozygotc twins. In: Blickstein I, Keith LG (Eds). Multiple pregnancy, 2nd edition. London, UK: Taylor and Francis; 2005. pp. 277-88.
22. Blokage CE. Embryogenesis of chimeras, twins and anterior midlines asymmetries. Human Reprod. 2006;21:579-91.
23. Oliviennes F. Avoiding multiple pregnancies in ART double trouble: yes a twin pregnancy is an adverse outcome. Hum Rep. 2000;15:1663-5.
24. Tummers P, De Sutter P, Dhont M. Risk of spontaneous abortion in singleton and twin pregnancies after IVF/ICSI. Hum Reprod. 2003;18:1720-3.
25. Zegers-Hochschild F, Bravo M, Fernandez E, et al. Multiple gestation as a marker of reproductive efficacy: learning from assisted reproductive technologies. Reprod Biomed Online. 2003;8:125-9.
26. La Sala GB, Nicoli A, Villani MT, et al. Spontaneous embryonic loss rates in twin and singleton pregnancies after transfer of top- versus intermediate-quality embryos. Fertil Steril. 2005;84:1602-5.
27. Matias A, Montenegro N, Blickstein I. Sonographic evaluation of multiple pregnancies. In: Kurjak A, Chevernak F (Eds). Textbook of Perinatal Medicine, 2nd edition. New York: Informa Healthcare; 2006. pp. 1591-3.
28. Matias A, Oliveira C, da Silva JT, et al. The effect of ICSI, maternal age, and embryonic stage on early clinical loss rate of twin versus singleton pregnancies. Eur J Obstet Gynecol Reprod Biol. 2006;130:212-5.
29. Matias A, La Sala G, Blickstein I. Early loss rates of the entire pregnancy are lower in singleton pregnancies following assisted reproduction. Fert Steril. 2007;88:1452-4.
30. Lambers MJ, Mager E, Goutbeek J, et al. Factors determining early pregnancy loss in singleton and multiple implantations. Hum Reprod. 2006;22(1):275-9.
31. Bourthoumieu S, Yardin C, Terro F, et al. Monozygotic twins concordant for blood karyotype, but phenotypically discordant: a case of "mosaic chimerism". Am J Med Genet A. 2005;135(2):190-4.
32. Cheng PJ, Shaw SW, Shih JC, et al. Monozygotic twins discordant for monosomy 21 detected by first-trimester nuchal translucency screening. Obstet Gynecol. 2006;107(2 Pt 2):538-41.
33. Hamasaki S, Shirabe S, Tsuda R, et al. Discordant Gerstmann-Straussler-Scheinker disease in monozygotic twins. Lancet. 1998;24:1358-9.
34. Bianchi DW. Prenatal diagnosis: past, present, and future. Prenat Diagn. 2010;30(7):601-4.
35. Machado AP, Ramalho C, Portugal R, et al. Concordance for bilateral congenital diaphragmatic hernia in a monozygotic dichorionic twin pair - first clinical report. Fetal Diagn Ther. 2010;27(2):106-9.
36. Gringras P, Chen W. Mechanisms for differences in monozygous twins. Early Hum Dev. 2001;64(2):105-17.
37. Derom C, Derom R. The East Flanders Prospective Twin Survey. In: Blicktein I, Keith LG (Eds). Multiple Pregnancy, 2nd edition. London, UK: Taylor and Francis; 2005. pp. 39-47.
38. Tong S, Vollenhoven B, Megher S. Determining zygosity in early pregnancy by ultrasound. Ultrasound Obstet Gynecol. 2004;23:36-7.
39. Sepulveda W, Sebire N, Hughes K, et al. The lambda sign at 10-14 weeks of gestation as a predictor of chorionicity in twin pregnancies. Ultrasound Obstet Gynecol. 1996;7: 421-3.
40. Wood SL, St Onge R, Connors G, et al. Evaluation of the twin peak sign in determining chorionicity in multiple pregnancy. Obstet Gynecol. 1996;88:6-9.
41. Pretorious D, Budorick N, Sciosia A, et al. Twin pregnancies in the second trimester in an α-fetoprotein screening program: sonographic evaluation and outcome. Am J Roentgenol. 1993;161:1007-13.
42. Senat MV, Quarello E, Levaillant JM, et al. Determining chorionicity in twin gestations: three-dimensional (3D) multiplanar sonographic measurement of intra-amniotic membrane thickness. Ultrasound Obstet Gynecol. 2006; 28(5):665-9.
43. Blickstein I. The twin-twin transfusion syndrome. Obstet Gynecol. 1990;76:714-22.
44. Sepulveda W, Sebire N, Hughes K, et al. Evolution of the lambda or twin-chorionic peak sign in dichorionic twin pregnancies. Obstet Gynecol. 1997;89:439-41.
45. Blickstein I. Monochorionicity in perspective. Ultrasound Obstet Gynecol. 2006;27:235-8.
46. Linskens IH, Spreeuwenberg MD, Blankenstein MA, et al. Early first-trimester free beta-hCG and PAPP-A serum distributions in monochorionic and dichorionic twins. Prenat Diagn. 2009;29(1):74-8.
47a. Matias A, Ramalho C, Montenegro N. Search for hemodynamic compromise at 11-14 weeks in monochorionic twin pregnancy: is abnormal flow in the ductus venosus predictive of twin-twin transfusion syndrome? J Matern Fetal Neonatal Med. 2005;18(2):79-86.
47b. Matias A, Montenegro N. Down´s syndrome screening in multiple pregnancies. Obst Gynecol Clin North Am. 2005;32(1):81-96.
48. Sebire NJ, Snidjers RJM, Hughes K, et al. Screening for trisomy 21 in twin pregnancies by maternal age and fetal nuchal translucency thickness at 10-14 weeks of gestation. Br J Obstet Gynecol. 1996;103:999-1003.
49. Cheng PJ, Huang SY, Shaw SW, et al. Difference in nuchal translucency between monozygotic and dizygotic spontaneously conceived twins. Prenat Diagn. 2010;30(3):247-50.
50. Cleary-Goldman J, Rebarber A, Krantz D, et al. First-trimester screening with nasal bone in twins. Am J Obstet Gynecol. 2008;199(3):283.e1-3.
51. Sepulveda W, Wong AE, Casasbuenas A. Nuchal translucency and nasal bone in first-trimester ultrasound screening for aneuploidy in multiple pregnancies. Ultrasound Obstet Gynecol. 2009;33(2):152-6.
52. Bush MC, Malone FD. Down syndrome screening in twins. Clin Perinatol. 2005;32(2):373-86.
53. Maymon R, Jauniaux E. Down's syndrome screening in pregnancies after assisted reproductive techniques: an update. Reprod Biomed Online. 2002;4(3):285-93.

54. Gjerris AC, Loft A, Pinborg A, et al. The effect of a 'vanishing twin' on biochemical and ultrasound first trimester screening markers for Down's syndrome in pregnancies conceived by assisted reproductive technology. Hum Reprod. 2009;24(1):55-62.
55. Goncé A, Borrell A, Fortuny A, et al. First-trimester screening for trisomy 21 in twin pregnancy: does the addition of biochemistry make an improvement? Prenat Diagn. 2005;25(12):1156-61.
56. Spencer K, Salonen R, Muller F. Down's syndrome screening in multiple pregnancies using alpha-fetoprotein and free beta hCG. Prenat Diagn. 1994;14: 537-42.
57. Spencer K, Kagan KO, Nicolaides KH. Screening for trisomy 21 in twin pregnancies in the first trimester: an update of the impact of chorionicity on maternal serum markers. Prenat Diagn. 2008;28(1):49-52.
58. Wald NJ, Rish S, Hackshaw AK. Combining nuchal translucency and serum markers in prenatal screening for Down syndrome in twin pregnancies. Prenat Diagn. 2003;23(7):588-92.
59. Nicolaides KH, Spencer K, Avgidou K, et al. Multicenter study of first-trimester screening for trisomy 21 in 75 821 pregnancies: results and estimation of the potential impact of individual risk-orientated two-stage first-trimester screening. Ultrasound Obstet Gynecol. 2005;25(3):221-6.
60. Madsen H, Ball S, Wright D, et al. A re-assessment of biochemical marker distributions in T21 affected and unaffected twin pregnancies in the first trimester. Ultrasound Obstet Gynecol. 2010;37(1):38-47.
61. Schatz F. Clinical for the Physiology of the Fetus. Berlin: Hirschwald; 1890.
62. Bajoria R, Wigglesworth J, Fish NM. Angioarchitecture of monochorionic placentas in relation to twin-to-twin transfusion syndrome. Am J Obstet Gynecol. 1995;172:856-63.
63. Lewi L, Cannie M, Blickstein I, et al. Placental sharing, birthweight discordance, and vascular anastomoses in monochorionic diamniotic twin placentas. Am J Obstet Gynecol. 2007;197(6):587e.1-8.
64. Mahieu-Caputo D, Muller F, Joly D, et al. Pathogenesis of twin-twin transfusion syndrome: the renin-angiotensin system hypothesis. Fetal Diagn Ther. 2001;16(4):241-4.
65. Danskin FH, Neilson JP. Twin-to-twin transfusion syndrome: what are appropriate diagnostic criteria? Am J Obstet Gynecol. 1989;161:365-9.
66. Wenstrom KD, Tessen JA, Zlatnik FJ, et al. Frequency, distribution and theoretical mechanisms of hematologic and weight discordance in MC twins. Obstet Gynecol. 1992;80:257-61.
67. Wittmann BK, Baldwin VJ, Nichold B. Antenatal diagnosis of twin-to-twin transfusion syndrome by ultrasound. Obstet Gynecol. 1981;58:123-7.
68. Brennan JN, Diwan RV, Rosen MG, et al. Fetofetal transfusion syndrome: prenatal ultrasonographic diagnosis. Radiology. 1982;143:535-6.
69. Storlazzi E, Vintzileos AM, Campbell WA, et al. Ultrasonic diagnosis of discordant fetal growth in twin gestations. Obstet Gynecol. 1987;69:363-7.
70. Chescheir NC, Seeds JW. Polyhydramnios and olygohydramnios in twin gestations. Obstet Gynecol. 1988;71:882-4.
71. Hecher K, Ville Y, Snijders R, et al. Doppler studies of the fetal circulation in twin-to-twin transfusion syndrome. Ultrasound Obstet Gynecol. 1995;5:318-24.
72. Zosmer N, Bajoria R, Weiner E, et al. Clinical and echographic features of in utero cardiac dysfunction in the recipient twin-to-twin transfusion syndrome. Br Heart J. 1994;72:74-9.
73. Van Mieghem T, Lewi L, Gucciardo L, et al. The Fetal Heart in Twin-to-Twin Transfusion Syndrome, 2010.
74. Fesslova V, Villa L, Nava S, et al. Fetal and neonatal echocardiographic findings in twin-twin transfusion syndrome. Am J Obstet Gynecol. 1998;179:1056-62.
75. Gardiner HM, Taylor MJ, Karatza A, et al. Twin-twin transfusion syndrome: the influence of intrauterine laser photocoagulation on arterial distensibility in childhood. Circulation. 2003;107:1-6.
76. Saunders NJ, Snijders RJ, Nicolaides KH. Therapeutic amniocentesis in twin-twin transfusion syndrome appearing in the second trimester of pregnancy. Am J Obstet Gynecol. 1992;166:820-4.
77. Sebire NJ, Souka A, Skentou H, et al. Early prediction of severe twin-to-twin transfusion syndrome. Human Reprod. 2000;15:2008-10.
78. Kagan O, Gazzoni A, Sepulveda-Gonzalez G, et al. Discordance in nuchal translucency thickness in the prediction of severe twin-to-twin transfusion syndrome. Ultrasound Obstet Gynecol (in press).
79. Lewi L, Lewi P, Diemert A, et al. The role of ultrasound examination in the first trimester and at 16 weeks' gestation to predict fetal complications in monochorionic diamniotic twin pregnancies. Am J Obstet Gynecol. 2008;199(5):493.e1-7.
80. Montenegro N, Matias A, Areias JC, et al. Increased nuchal translucency: possible involvement of early cardiac failure. Ultrasound Obstet Gynecol. 1997;10:265-8.
81a. Matias A, Montenegro N, Areias JC, et al. Anomalous venous return associated with major chromosomopathies in the late first trimester of pregnancy. Ultrasound Obstet Gynecol. 1998;11:209-13.
81b. Matias A, Gomes C, Flack N, et al. Screening of chromosomal defects at 11-14 weeks: the role of ductus venosus blood flow. Ultrasound Obstet Gynecol. 1998;12:380-4.
82. Matias A, Huggon I, Areias JC, et al. Cardiac defects in chromosomally normal fetuses with abnormal ductus venosus blood flow at 10-14 weeks. Ultrasound Obstet Gynecol. 1999;14:307-10.
83. Matias A, Montenegro N, Areias JC. Anticipating twin-twin transfusion syndrome in monochorionic twin pregnancy. Is there a role for nuchal translucency and ductus venosus blood flow evaluation at 11-14 weeks? Twin Res. 2000; 3(2):65-70.
84. Matias A, Montenegro N, Loureiro T, et al. Screening for twin-twin transfusion syndrome at 11-14 weeks of pregnancy: the key role of ductus venosus blood flow assessment. Ultrasound Obstet Gynecol. 2010;35(2):142-8.

85. Taylor MJ, Denbow ML, Tanawattanacharoen S, et al. Doppler detection of arterio-arterial anastomoses in monochorionic twins: feasibility and clinical application. Hum Reprod. 2000;15:1632-6.
86. Luke B, Minogue J, Witter FR. The role of fetal growth restriction and gestational age on length of hospital stay in twin infants. Obstet Gynecol. 1993;81:949-53.
87. Fraser D, PIcard R, Picard E, et al. Birth weight discordance, intrauterine growth retardation and perinatal outcomes in twins. J Reprod Med. 1994;39:504-8.
88. Blickstein I. Normal and abnormal growth of multiples. Semin Neonatol. 2002;7:177-85.
89. Blickstein I. Is it normal for multiples to be smaller than singletons? Best Pract Res Clin Obstet Gynecol. 2004;18:613-23.
90. Blickstein I. Growth aberration in multiple pregnancy. Obstet Gynecol. 2005;32:39-54.
91. Blicsktein I, Keith LG. Neonatal mortality rates among growth-discordant twins, classified according to the birth weight of the smaller twin. Am J Obstet Gynecol. 2004;190:170-4.
92. Luke B, Keith LG. The contribution of singletons, twins and triplets to low birth weight, infant mortality and handicap in the United States. J Reprod Med. 1992;37:661-6.
93. Matias A, Maiz N, Montenegro N, et al. Ductus venosus flow at 11-13 weeks in the prediction of birthweight discordance in monochorionic twins. J Perinat Med, 2011 (in press).
94. Pharoah P. Neurological outcome in twins. Semin Neonatol. 2002;7:223-30.
95a. Pharoah P. Risk of cerebral palsy in multiple pregnancies. Clin Perinatol. 2006a;33(2):301-13.
95b. Pharoah P. Twins and locomotor disorder in children. J Bone Joint Surg Br. 2006b;88(3):295-7.
96. Blickstein I. Do multiple gestations raise the risk of cerebral palsy? Clin Perinatol. 2004;31:395-408.
97. Topp M, Huusom LD, Langhoff-Roos J, et al. Multiple birth and cerebral palsy in Europe: a multicenter study. Acta Obstet Gynecol Scand. 2004;83:548-53.
98. Yokoyama Y, Shimizu T, Haykawa K. Prevalence of cerebral palsy in twins, triplets and quadruplets. Int J Epidemiol. 1995;24;24:943-8.
99. Bejar R, Vigliocco G, Gramajo H, et al. Antenatal origin of neurologic damage in newborn infants: multiple gestations. Am J Obstet Gynecol. 1990;162:1230-6.
100. Malone FD. Monochorionic pregnancy – Where have we been? Where are we going? Am J Obstet Gynecol. 2003;189:1308-9.
101. Lopriore E, Nagel HT, Vandenbussche FP, et al. Longterm neurodevelopmental outcome in twin-to-twin transfusion syndrome. Am J Obstet Gynecol. 2003;189:1313-8.
102. Senat MV, Loizeau S, Cooudere S, et al. The value of middle cerebral artery peak systolic velocity in the diagnosis of fetal anemia after intrauterine death of one monochorionic twin. Am J Obstet Gynecol. 2003;189:1319-23.

29
CHAPTER

Ultrasonography and Birth Defects

Narendra Malhotra, Jaideep Malhotra, Sakshi Tomar, Neharika Malhotra, JP Rao

INTRODUCTION

"Care Is Absolute, Prevention Is Ideal"

Ultrasound has revolutionized obstetric practice all over the world and there is no doubt about it. With good resolution machines, Color Doppler, 3D and 4D scanning it is now possible to make a prenatal diagnosis of many structural anomalies, which are lethal, life threatening and debilitating.

All pregnancies are at risk of producing fetal malformations or birth defects. Some pregnant women are at a greater risk. The world consensus on whether all pregnancies should be screened by ultrasound for anomalies and when, is still divided.

Birth defect is a global problem. Birth defect is one of the leading causes of perinatal mortality and morbidity, accounting for 2–3% of all live-births.[1]

Presence of anomalies and their undesirable consequences for the affected neonate, family and medical fraternity is a very convincing argument by many experts on universal screening.

Regardless of whether a woman is in low risk (majority cases) or high risk category (genetic, diabetes, etc.) the risk of fetal malformation is always there and because there are no symptoms and these pregnancies may be uneventful.

It is estimated that every year 7.9 million children are born with a serious birth defects of genetic or partly genetic origin. A further 1 million are born with serious birth defects of postconception origin which result from environmental teratogens such as alcohol, rubella, syphilis and iodine deficiency which can either cause death or lifelong disability.[1]

While this problem has been addressed in the West, it is yet to be addressed in developing countries where 94% of those born with birth defects reside and where 95% of the children who die from birth defects are born.[1]

The prevalence of fetal malformations is 65% though only 2–2.5% are potentially life threatening, lethal or represent a major cosmetic defect[1] **(Fig. 29.1)**. It is seen that incidence of aneuploidy (Trisomy 21) screen with maternal age **(Fig. 29.2)**.

Ultrasound routine screening is a very valuable tool for detecting birth defects.[2]

In India, due to its high birth rate, population and consanguinity in certain communities, the burden of birth defects is significant. This has been reported by the Federation of Obstetric and Gynecological Societies of India (FOGSI) birth defects registry (unpublished data).

An estimated 495,000 infants with congenital malformations are born every year.[2] In addition, 21,400 with Down's syndrome, 9,000 with thalassemia, 5,200 with sickle cell anemia, 390,000 with G6PD deficiency and 9,760 with amino acid disorders are born every year.[3]

Diagnosis is generally late or ineffective and the infrastructure for management and rehabilitation of the families is not easily accessible. This makes the burden of genetic diseases and birth defects particularly severe as compared to the western countries.

Social stigma, discrimination, lost hopes and lack of opportunities add to the emotional and financial burdens. To reduce the impact of birth defects, national health policy makers need to first recognize the prevalence, disability and burden of the disease.

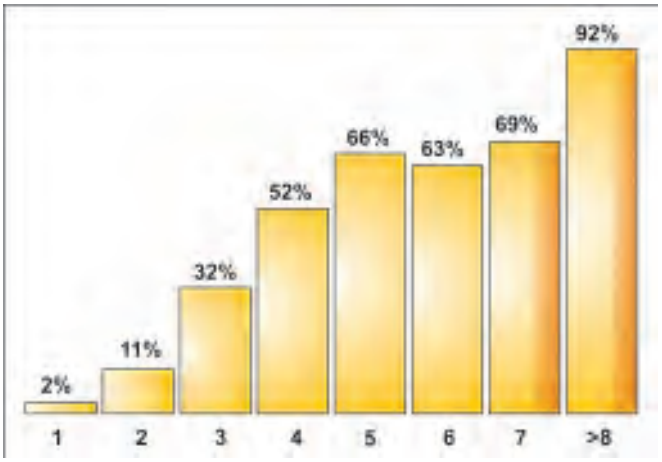

Figure 29.1: Frequency of aneuploidies vs. number of anomalies

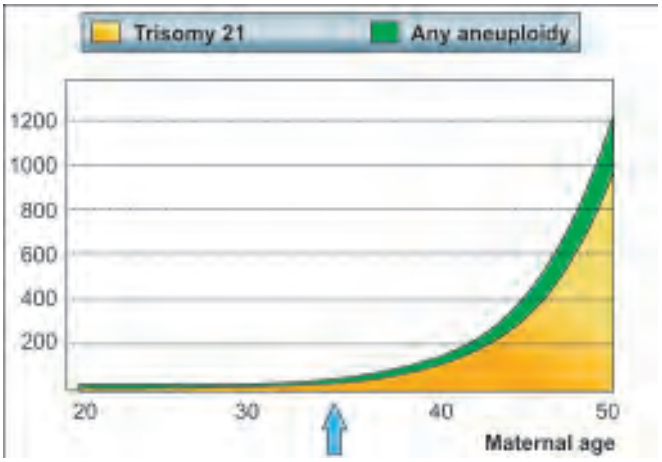

Figure 29.2: Incidence of aneuploidy (Trisomy 21) screen with maternal age

CAUSES

The incidence of birth defects in USA is one out of 33 and may be much more in developing countries and the countries where no formal and structured registry exists.

There are three major categories of causes:

1. Genetic
2. Environmental
3. Complex genetic/unknown.

Genetic Causes

Chromosomal or single-gene disorders are known to account for about 25–30% of all birth defects. Chromosomal abnormalities are seen in about 0.5% of live newborns. Recently, use of 'telomeric probes' has increased this incidence further as about 5–7% of mentally challenged children have a cryptic translocation that cannot be detected by traditional cytogenetic methods. A 'mutation' in the genetic locus can give rise of 'single gene disorder'. Not all mutant genes manifest at birth or lead to structural problems.

Some birth defects are caused by errors in genes or chromosomes. Those caused by genes can be inherited—passed by parents to their children. Some inherited disorders are more common in certain ethnic groups, such as sickle cell disease, cystic fibrosis, and Tay–Sachs disease.

Chromosomal defects are caused by missing, damaged or extra chromosomes. These defects are often the result of an error that occurred when the egg and sperm were joining. Common chromosomal disorders are Down syndrome and trisomy 18. Generally, the risk of having a baby with Down syndrome, trisomy 18, and other chromosomal disorders increases with advancing maternal age.[3]

Environmental Causes

These causes account for 5–10% of birth defects. These include nutritional deficiencies, maternal illnesses, teratogenic drugs or radiation and infectious agents. However, the extent of the damage depends upon the timing of exposure and the individual's genetic susceptibility.

Other birth defects result from the fetus being exposed to harmful agents, such as medications, chemicals, and infections. Whether a woman or her baby is harmed depends on how much of the agent they have been exposed to, when during her pregnancy a woman is exposed to the agent and for how long.

Complex Genetic/Unknown Causes

These comprise of about 65–70% of birth defects. This may be caused by defects in more than one gene or a complex interaction of the environment and genes.

TABLE 29.1
Clinical markers of high-risk pregnancy

1. Advanced maternal age
2. Previous birth of a malformed fetus
3. Family history of a malformed fetus
4. Consanguinity
5. Exposure to drugs/radiation
6. Maternal diabetes mellitus
7. Bad obstetric history
8. Bleeding in early pregnancy

Sometimes, a mixture of factors is the cause. For many birth defects, the exact cause is not known.

Thorough screening of all pregnant patients is impossible in the current scenario, but we can and should offer ultrasound to all possible pregnant women as a prenatal diagnostic test.[4]

Most of the birth defects can be identified and diagnosed *in utero*. A careful history, proper biochemical screening and ultrasound added with invasive testing wherever required can pick up structural, chromosomal, metabolic abnormalities in the unborn. An early diagnosis leads to good counseling and informed choice to the parents with option of termination.

Clinically high risk groups for a detailed anomalies scan are shown in **Table 29.1**.

The sonographic findings which are indications for a detailed anomalies scan are listed in **Tables 29.2 and 29.3**.

Nonsonographic laboratory investigations which can warrant a detailed anomalies scan are listed in **Table 29.4**.

TABLE 29.2
Sonographic findings: *First trimester*

1. Oligoamniotic sac
2. Embryonic bradycardia
3. Abnormal yolk sac
4. Increased nuchal translucency
5. One identified anomaly
6. Dates size discrepancy at 9–12 weeks

TABLE 29.3
Sonographic findings: *Second and third trimester*

1. Increased nuchal translucency
2. Symmetric IUGR
3. Polyhydramnios
4. Oligohydramnios
5. Breech Presentation
6. Twins
7. One identified anomaly

TABLE 29.4
Non-sonographic findings

1. Abnormal results from a CVS/amniocentesis
2. Abnormal immunoglobulin profile
3. Abnormal triple test/increased alfa fetoprotein/Abnormal pregnancy associated plasma protein (PAPP)
4. Abnormal first-trimester Dual Marker test

ULTRASOUND FOR CONGENITAL DEFECTS

First Trimester

Nuchal Translucency

This prenatal test also called the NT or nuchal fold scan. It assesses the baby's risk of having Down's syndrome (DS) and some other chromosomal abnormalities as well as major congenital heart problems. The NT test uses ultrasound to measure the clear (translucent) space in the tissue at the back of developing baby's neck. Babies with abnormalities tend to accumulate more fluid at the back of their neck during the first trimester, causing this clear space to be larger than average. The NT scan is done between 11 and 13 weeks. It is offered along with blood test in what is known as first-trimester combined screening[5] **(Figs 29.3A to E).**

Pitfalls in measuring the nuchal translucency include the presence of an encephalocele, a nuchal cord, an amniotic band or a loose amnion that can be mistaken for the nuchal skin edge.[5] It is therefore imperative to magnify the image. It is sometimes helpful to wait for spontaneous fetal activity.

A cut off of 3 mm was used in many studies as a threshold for an abnormal nuchal translucency, although recently it has become apparent that normal nuchal translucency thickens with increasing gestational age.

Other First-Trimester Signs of Aneuploidy

Growth patterns of the crown-rump length have been evaluated to determine whether growth abnormalities could be utilized as signs of aneuploidy.[6] Growth rates are significantly reduced among fetuses with trisomies 13,18 and with triploidy **(Fig. 29.4)**.

Other sonographic method for detecting aneuploid fetus include abnormal fetal heart rate at 10–14 weeks, absent nasal bone, faccio maxillary angle, intracranial translucency, umbilical cord thickness and wide iliac angle.

By combining maternal age, nuchal translucency and heart rate, 83% fetuses with trisomy 21 were detected[7] **(Figs 29.5A and B)**.

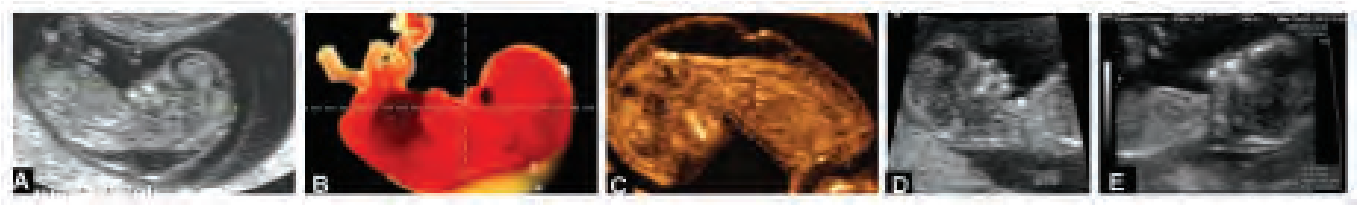

Figures 29.3A to E: Measurement of nuchal translucency in the first trimester

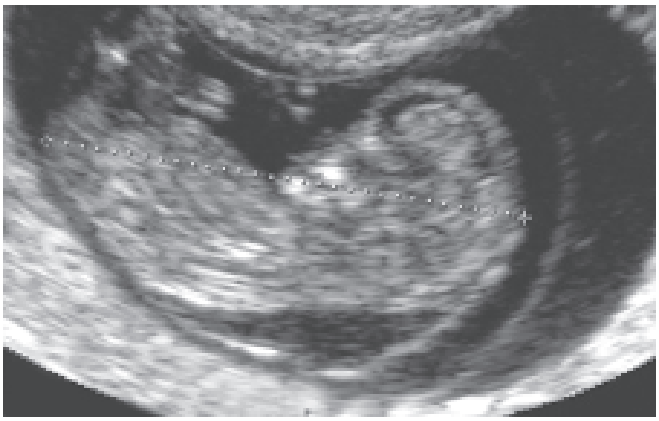

Figure 29.4: Measurement of crown-rump length

Second Trimester

Nuchal Fold

Excessive soft tissue in the back of the neck is known to be a feature of newborns with Down's syndrome. Callen and colleagues[8] described the use of thickened nuchal fold as a sonographic marker for Down's syndrome in 1985. They showed that 2 out of 6 fetuses with Down's syndrome had a nuchal thickness of equal to or greater than 6 mm. This measurement is done using the transverse section of the fetal head angled posteriorly to include the cerebellum and the occipital bone. The measurement is made outside the occipital bone to the outer skin edge. This measurement has remained the most sensitive and specific single marker for the mid trimester detection of Down's syndrome.

Major Anomalies

Infants with trisomy 21 have a 50% incidence of heart defects, most commonly ventricular septal defects and common atrioventricular canal.

Other major anomalies include ventriculomegaly, cerebellar hypoplasia, duodenal atresia, hydrops, omphalocele and limb anomalies.[8]

Femur length: Individuals with trisomy 21 are of short stature and have small femur and humerus.[8]

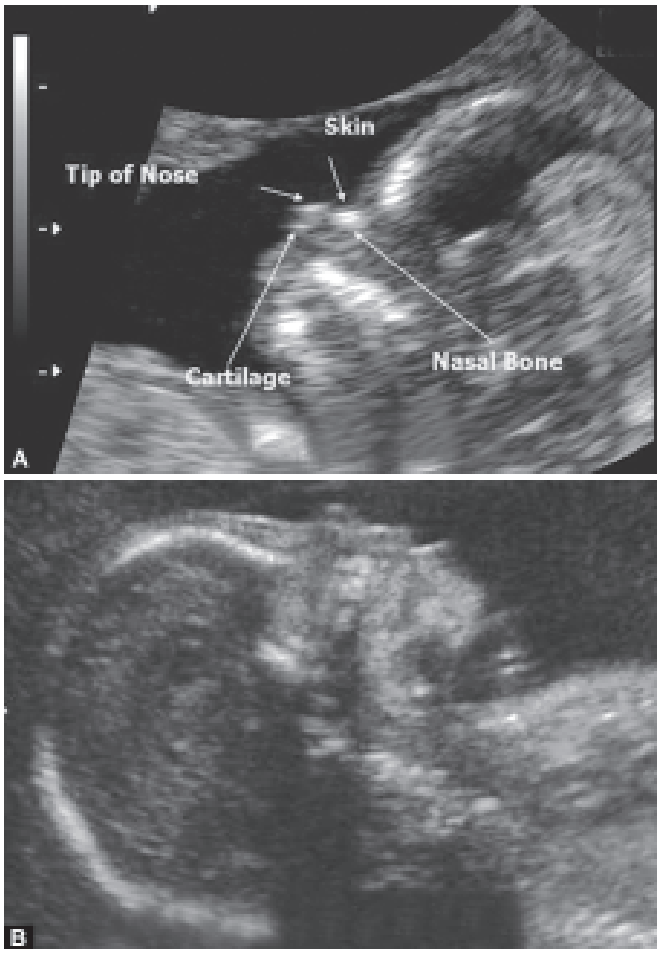

Figures 29.5A and B: (A) Nasal bone; (B) Absent nasal bone

Absent nasal bone: Fetuses with absent nasal bone **(Figs 29.5A and B)** are associated with an increased risk of Down's syndrome.

Mild fetal pyelectasis **(Fig. 29.6)** was associated with an increased risk of Down's syndome. Crane and Gray defined pyelectasis as an anteroposterior diameter of the renal pelvis equal to or greater than 4 mm.[9]

Nyberg and colleagues were the first to demonstrate that hyperechoic bowel **(Fig. 29.7)** is associated with

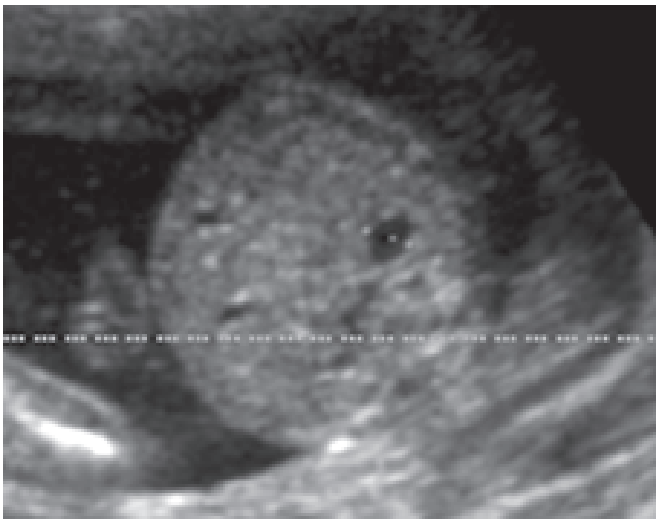

Figure 29.6: Fetal pyelectasis

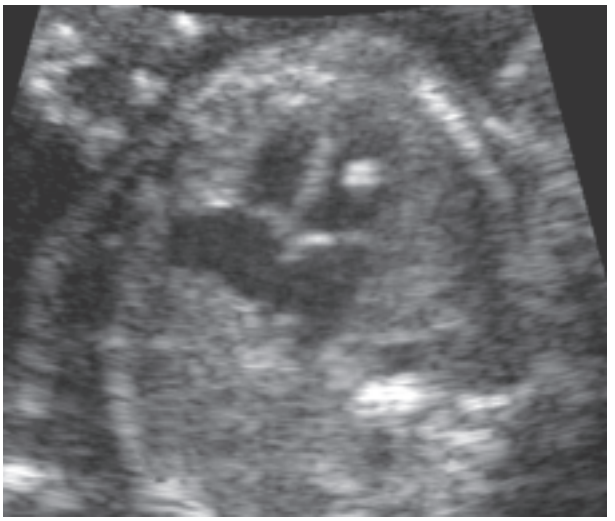

Figure 29.8: Echogenic intracardiac focus

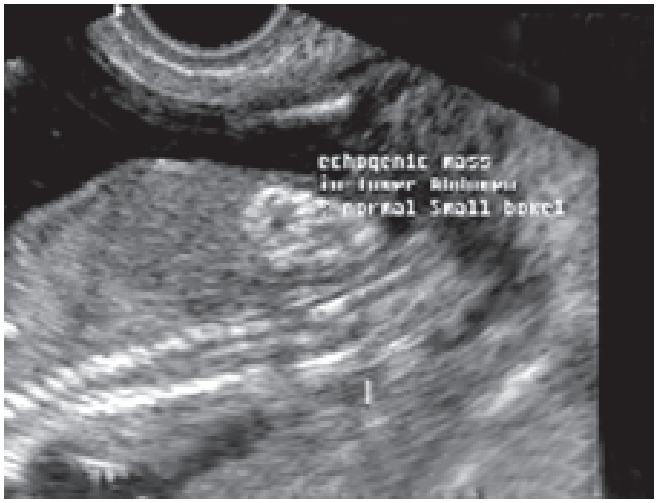

Figure 29.7: Echogenic mass in the small bowel

Down's syndrome. There is also an increased risk of cystic fibrosis among fetuses with this sonographic finding, and parental allele testing for cystic fibrosis carrier status is recommended to evaluate this risk.[10]

The echogenic intracardiac focus (EIF) **(Fig. 29.8)** has been seen among normal fetuses for many years and was considered a normal variant till 1994. Brown, Roberts and Miller in a case report showed that mineralization of the papillary muscle was associated with trisomy 21 in one of three fetuses.[11]

Lehman and colleagues were the first to report the association of EIF with trisomy 13.

Several investigators have suggested that the association between an EIF and chromosomal abnormalities is low enough that, in the absence of other findings in an otherwise low-risk patient, fetal karyotyping is unwarranted.

Minor Markers

Anomalies of the pelvic bones, particularly the iliac wings is associated with Down's syndrome. Children with Down's syndrome have a wider lateral span of the iliac wing than do normal children.

It is known among pediatricians and geneticists that infants with Down's syndrome have brachycephaly and frontal lobe shortening. An attempt is made to evaluate the use of this feature in detecting second-trimester fetuses with Down's syndrome.

The transverse cerebellar diameter was evaluated as a possible marker for Down's syndrome.

Other possible markers for the prenatal detection of Down's syndrome have been put forth, including abnormal fetal heart rate patterns, abnormally shortened ear length, flat facies, clinodactyly, sandal gap great toe and the simian crease of the palm.

Trisomy 13 (Pateau syndrome): The incidence of trisomy 13 is 1 in 5,000 births and it is the most severe of the three autosomal trisomies that can lead to live-born infants. The fetal anomalies most commonly seen with these fetuses include abnormalities of the brain, face, extremities and heart. In particular holoprosencephaly is a common finding that is invariably associated with severe midline facial defects, including hypotelorism, cyclopia, midline clefts, microophthalmia and absence of the nose. Other intracranial anomalies that can be seen with trisomy 13 include microcephaly, abnormal posterior fossa, agenesis of corpus callosum and ventriculomegaly. In addition, approximately 40% fetuses

with trisomy 13 have echogenic intracardiac focus. More than 90% of these fetuses have cardiac defects. Abnormalities of the limbs include polydactyly and radial aplasia. Other major defects include neural tube defects and anterior wall abdominal defects. Thirty percent of affected fetuses have enlarged echogenic kidneys, similar to polycystic kidneys. Placental abnormalities such as partial mole also have been described with trisomy 13.[12,13]

Triploidy: Triploidy is a syndrome that results from three sets of chromosomes yielding 69 chromosomes. Most triploid conceptions end in spontaneous abortion. When the extra set of chromosome arises from the maternal side, the placenta is small and senescent, and there is severe early intrauterine growth restriction. When the extra set of chromosome arises from the paternal side, the placenta is large, full of echolucency and often associated with a partial mole.[14]

Usually the fetuses with triploidy have multiple congenital abnormalities of particularly every organ system. Characteristically, they also have first trimester onset intrauterine growth restriction. They also give rise to an unusual appearance of a very thin body with almost an normal sized head.

Fetal malformations associated with triploidy include early onset intrauterine growth retardation, facial anomalies such as hypertelorism, micrognathia and microphthalmia, brain anomalies such as ventriculomegaly, Dandy-Walker malformation, agenesis of corpus callosum, holoprosencephaly and meningomyelocele. Affected fetuses also have thickened nuchal lucency/cystic hygroma, heart defects, renal anomalies, clubbed feet, single umbilical artery and oligohydramnios. Most helpful of all in the specific diagnosis of triploidy is the syndactyly of the third and fourth digit of the hand, recognizable sonographically.

Turner's syndrome: Turner's syndrome is a chromosomal anomaly due to the loss of one sex chromosome, resulting in a 45X karyotype. The missing chromosome is usually paternal and the syndrome is not related with maternal age. In most cases conceptions with Turner's syndrome are spontaneously aborted, some fetuses may persist into the second trimester with severe lymphatic abnormalities. These fetuses have large cystic hygromas that are typically septated but clear.

Hydrops, pleural effusion, ascites and edema of all body parts is seen.

Mosaicism for Turner's syndrome is more likely to result in live births and these individuals are often not diagnosed until puberty. They suffer from sexual infantilism and short stature.

In general, half of fetuses with Turner's syndrome have cardiac anomalies and 19% have renal anomalies.[15]

Trisomy 18 (Edward's syndrome): Trisomy 18 have an incidence of 3 out of 10,000 live births and is associated with multiple severe structural abnormalities that mostly involve the heart, extremities, face and brain. Affected fetuses are often miscarried or die *in utero*.[16] Structural abnormalities associated with trisomy 18 involve abnormal cisterna magna and Dandy-Walker syndrome. Affected fetuses can also have myelomeningoceles and ventriculomegaly. Limb abnormalities include preaxial upper limb reduction and clenched hands with overlapping index fingers. Second-trimester fetuses with trisomy 18 tend to have strawberry shaped skull, cerebellar deviation beyond two standard deviation below the mean, rocker bottom feet, clubbed feet, single umbilical artery and renal anomalies such as hydronephrosis. Gastrointestinal tract anomalies include omphalocele and diaphragmatic hernia. The triad of polyhydramnios, growth restriction and abnormal hand posturing is highly predictive of trisomy 18 in third trimester.

Umbilical cord cysts have also been associated with an increased incidence of trisomy 18.

Choroid plexus cysts are present in approximately one-third of fetuses with trisomy 18.

USG EXTRA FETAL EVALUATION

Liquor Amnii

Quantity

- The measurement of the amniotic fluid can be done either by a single pocket measurement or the four quadrant approach amniotic fluid index (AFI). The AFI is easily reproducible and more accurate **(Table 29.3)**.
- Fetal swallowing and urinary flow are the primary regulators of amniotic fluid. So abnormalities of these systems cause oligohydramnios (decreased liquor amnii) **(Table 29.4)** or polyhydramnios (increased liquor amnii), which can be indirect signs for detecting anomalies.

Amniotic bands

- Whenever it is seen that the amniotic bands in the uterine cavity are traversing the gestational sac, one should be careful of evaluating whether any fetal part is impinged upon by these bands causing limb reduction defects or any other external anomaly of

the cranium, face, anterior abdominal wall or spine **(Fig. 29.8)**.

Umbilical Cord

Number of Vessels

- There should be two arteries and one vein in the umbilical cord
- Whenever a single umbilical artery is diagnosed, a careful search for anomalies should be done especially of chromosomal abnormalities, major cardiac defects, holoprosencephaly, anterior abdominal wall defects and skeletal deformities. With no other anomaly detected, continuation of pregnancy can be thought of
- In a 2D ultrasound look for the rail-track appearance **(Fig. 29.9)** to assess for number of vessels
- On color flow mapping it is easy to see for two arteries and one vein but whenever in doubt always look for the hypogastric arteries adjacent to the urinary bladder to evaluate whether there are two arteries or not.

Origin and Insertion

- Origin in respect to anomalies is important to differentiate between omphalocele and gastroschisis.

ULTRASONOGRAPHY FOR FETAL MORPHOLOGY EVALUATION

Choroid Plexus

This is evaluated for the following abnormalities **(Fig. 29.9)**:

- Cysts
- Hydrocephalus

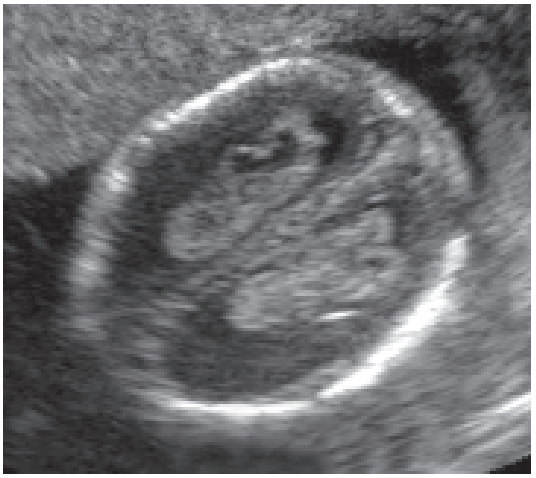

Figure 29.9: Gray scale appearance of the umbilical cord

- Isolated ventricular dilatation
- Tumors.

Cerebellum

This is evaluated for following parameters:

- Cerebellar transverse diameter
- Superior and inferior cerebellar vermis
- Communication between fourth ventricle and cisterna magna.

Cisterna Magna

This is evaluated for following parameters:

- Posterior fossa cyst
- Depth.

Nuchal Skin

This is observed for following parameters:

- Thickness
- Septation
- Generalized hydrops.

Fetal Orbits and Face

The following parameters are observed:

- Hypo or hypertelorism
- Lens
- Lips
- Nostrils
- Ears.

Fetal Spine

This is observed for following parameters:

- Soft tissues
- Longitudinal
- Coronal
- Axial
- Ossification centers.

Fetal Thorax

In this following parameters are observed:

- Ribs
- Diaphragm
- Echotexture of lung
- Lung length
- Masses
- Cardiothoracic ratio.

Fetal Heart

The parameters observed for are as under:

- Situs

- Size
- Rate
- Rhythm
- Configuration
- Connections
- Tumors.

Fetal Abdomen

Gastrointestinal

- Stomach
- Duodenum
- Small bowel
- Large bowel
- Omentum
- Mesentery.

Pancreas

Spleen

Hepatobiliary

- Liver
- Gall bladder.

Genitourinary

- Kidneys
- Urinary bladder
- Genitalia.

Fetal Skeleton

The skeleton is observed for following parameters:

- Cranium
- Mandible
- Clavicle
- Spine
- Extremities.

Fetal Biometry

Following parameters are observed in fetal biometry:

- Biparietal diameter
- Occipitofrontal distance
- Head perimeter
- Abdominal perimeter
- Femoral length
- Humeral length
- Nuchal skin
- Cerebellar transverse diameter
- Cisterna magna depth
- Width of body of lateral ventricle
- Ocular diameter
- Interocular distance
- Binocular distance
- Foot length.

ULTRASOUND TECHNOLOGY AND ADVANCEMENT IN SCREENING

Is Routine Screening Justified?

Screening to be justified should fulfill many criteria; the procedure should be safe, reliable, reproducible, easily available and cost effective. For a population which is at risk an ultrasound scan is justified but in developing countries like India where still almost half of our pregnant women have no access to a proper antenatal care, a routine ultrasound currently may not be practically feasible test for screening even though its utility and efficacy are beyond doubt.[2]

Is Incidence of Fetal Malformation High Enough to Merit Screening?

According to Heinonen (1977) approximately 150,000 children are born with malformations annually in USA where almost 100% pregnant women have antenatal care and institutional deliveries.[1] In developing countries the incidence is higher due to inability for detection, screening and more exposure to teratogens.

Is Outcome of Undetected Congenital Malformations Detrimental Enough to Warrant a Routine Screening?

Out of an incidence of around 6% congenital malformations almost half (2.5%) are lethal, life threatening and have a major cosmetic defect.[17]

Major congenital defect mostly manifest in fetal intrauterine life (ultrasound detectable), sometimes in fetal life (ultrasound suspicion) and occasionally in childhood (ultrasound undetectable). Some experts question the need of routine prenatal ultrasound screening for this reason.[18]

Fetal medicine is still not advanced to treat potential life-threatening conditions like open neural tube defects and cardiac defects where death is the expected outcome after delivery. Occasionally, these defective babies survive and are severely handicapped. Diagnosis of such conditions during pregnancy can give the couple an option of termination. Current technology enables detection of over 60% fetal malformations.[19,20]

Can a Prenatal Diagnosis of Anomalies Ease Emotional Pain?

An antenatal diagnosis of congenital anomaly whether lethal, life threatening or even less serious can still help couples and doctors to prepare themselves for the challenge to come.[21] There is a definite benefit of screening for both patients and physicians. Usually a normal ultrasound scan is good news for the expecting parents because of the relative low prevalence of anomalies in general population and also relative low incidence of false-positive results by ultrasound.[22]

If the ultrasound screening is positive for anomaly then the counseling and discussion of all options can be done and choice left open to the expecting parents.[23]

Is Prenatal Ultrasound Screening Cost Effective?

It is difficult to assess cost-effectiveness of screening and there are only a few studies on this. Certain costs like purchase, maintenance of equipments, salary of well trained technicians and doctors can be assessed and is expensive.[24] Emotional costs of family disorganization and suffering cannot be calculated. Because of the many options for handling anomalies available from termination to major plastic surgery it is again difficult to assess whether it is cost effective to detect an anomaly. Helsinki ultrasound trial (1996)[25] has shown that second-trimester screening for anomalies by ultrasound is cost effective.

How Does Prenatal Anomaly Scan for Screening Influence Infant Health?

Ultrasound screening is not primary prevention because it cannot prevent the anomaly. It can only detect the problem and if the anomaly is lethal, it gives the expecting parents an option to terminate pregnancy—secondary prevention. Also in many cases, severe but curable defects (cardiac) can be managed by treating newborn without delay, if the pediatric surgery unit is prepared. Expertly performed prenatal ultrasound screening and autopsy reports correlate and provide accurate information.[26]

What are the Options After Diagnosis of Congenital Malformations?

The options for managing congenital malformation pregnancy have to be discussed with the expecting parents and the final choice lies with the parents. A team of specialists should provide all information and counseling. This team should consist of obstetrician, sonologist, geneticist, neonatologist, pediatric surgeon and a psychologist.

Options selected depend on severity of the anomaly and can be as mentioned below:

- Termination of pregnancy
- Intrauterine treatment
- Maternal transport to tertiary care center
- Premature delivery
- Immediate specialized neonatal care
- Additional diagnostic tests
- Extensive monitoring.

Alternatives or Adjuncts to Ultrasound?

There are various blood tests like maternal serum alpha fetoprotein (MSAFP), triple test, quadruple tests and many interventional procedures like chorionic villus sampling (CVS) and amniocentesis, cordocentesis and fetal biopsy which can help in direct karyotyping and chromosomal analysis of the fetus. These procedures and techniques are expensive, not easily available and also carry a procedure related risk of miscarriage.

Noninvasive magnetic resonance imaging (MRI) is definitely not a cost-effective method for screening.

Ultrasound advances have made this technology for screening an ideal test because it is:

- Relatively low cost
- Ease to perform
- Real-time display
- Acceptable to all
- Widely available
- Accurate
- Safe
- Reproducible
- Available as office investigation
- Can now be applied from late first trimester also.[27]

How Long Does it Take?

A primary screening ultrasound examination is a systemic analysis of fetal growth and fetal morphology system and will take 10–20 minutes to scan. The screening will stop if everything appears normal in all significant organs and structures.

Depending on image quality, maternal obesity, gestational age, type of anomaly, color Doppler or 3D scan still the total scan duration rarely exceeds 30 minutes. For subtle defects or solitary markers or inexperienced sonologists a second opinion scan might be required by an expert which will take another 30 minutes.

What Does a Prenatal Ultrasound Scan Show?

Depending on the gestational age the defects can be seen and identified, e.g. nuchal translucency in first trimester, duodenal atresia, gastrointestinal defects, neural tube defects and some cardiac defects in second trimester.[28]

When we don't see the expected image of the fetus we suspect a defect. Sometimes, we have to look for soft markers and signs of chromosomal anomalies, e.g. banana sign, lemon sign, etc.

Ultrasound can also pick up functional abnormalities and abnormal fetal biophysical profile and abnormal fetal behaviors.

Abnormal Fetal Activity

- Rapid uncoordinated fetal movements
- Fetal arrhythmia
- Fetal vomiting
- Fetal GI stenosis.

When Should a Screening Prenatal Scan be Done?

Nicolaides has suggested a 11–14 weeks scan for screening for chromosomal anomalies, trisomy 21 by looking at the nuchal translucency and nasal bone ossification.[28] Other workers have suggested addition of biochemical markers.[29] The detection rate for trisomies varies from 80–89% with a false-positive rate of 5% by using multiple markers study in first trimester scan (11–14 weeks).

A second-trimester anomaly scan should be done between 18–22 weeks and a detailed fetal echocardiography and color Doppler uterine artery and ductus venosus should be done.

Third-trimester screening should not be delayed more than 32 weeks gestation and is mainly done for growth and color Doppler studies for hypoxia detection. Late anomaly screening for GI and urinary tract anomaly is usually done at 32 weeks.

Ideal time for ultrasound screening for each and every gravida should be a monthly ultrasound but as this is not practical and feasible, at least each pregnancy should have two scans one 11–14 weeks scan and one second-trimester scan.[30,31]

Ultrasound: How Sensitive it is for Malformation Detection?

In a major study on 500,000 cases about 11,000 (2.2%) were found to be malformed fetus with a range of sensitivity from 14–80% (mean 45.5%).

In another study on 170,000 pregnant women, 4,000 malformed fetus were detected with a sensitivity of 61%.[31]

What Counts as Success in Genetic Counseling?

Whenever anomaly is detected for some people, the abortion and termination of pregnancy is a matter of course response and no ethical dilemma arises. However, among certain religions groups objections to termination pose an ethical dilemma.

Advances in Fetal Surgery

This option is still a research tool and there is an ethical aspect that many of these fetal surgical procedures are still experimental and of uncertain value and to give or not to give this option to couples carrying a malformed pregnancy is a dilemma.

Are 3D and 4D Scans for Screening Useful or Gimmicks?

There is now an increasing availability of 3D ultrasound. The benefits of 3D and 4D ultrasound techniques are now a matter of debate. The 3D and 4D screening help in maternal fetal bondage and also help in recognition and better confirmation of certain anomalies like cleft lips, polydactyly, micrognathia, malformed ears, club foot, vertebral malformations and other exterior surface anomalies. Development of transvaginal scanning (TVS) 3D probes have further enhanced its value in early diagnosis of malformations.

Reassurance Scans—How Reassuring?

It was proposed by Prof Stuart Campbell that a 3D routine scan is to reassure the parents and to rule out anomalies, but also criticized these as entertainment scans used and marketed for unprecedented profit particularly after 4D ultrasound.

SCREENING METHODS AND TESTS

Maternal and Fetal Screening Tests

Noninvasive and Invasive

Introduction: There are many screening tests conducted on the mother or directly on the fetus/pregnancy products, which may be invasive or noninvasive. These tests vary in their effectiveness, i.e. the detection rate or the sensitivity and specificity of the test. The best

way to assess which is the best screening test would be to fix the false-positive rate and compare the detection rate of various tests.

Noninvasive Tests: These tests are performed on maternal blood (serum screening) and by an ultrasound scan. Detection of any abnormal level of hormones in maternal blood or abnormal measurement of fetal parameters increases the relative risk for the fetus to have a chromosomal defect. The 'detection rate' of any test depends upon following the highest standards of practice in both, scanning and as well as in the laboratories. Hence, the 'efficacy' of the test largely depends upon the laboratory performing the blood tests and the operator performing the fetal scan.

Invasive Tests: These tests are largely done to confirm a suspected diagnosis of genetic disease and in a few cases for fetal infections. Test samples are taken from the placenta (chorionic villous sampling, CVS), amniotic fluid (amniocentesis) or fetal blood (cordocentesis). These tests involve inserting a needle into the pregnancy sac to retrieve the sample. This requires a high level of expertise as it carries a risk of miscarriage of the entire pregnancy, which largely depends upon the operator skills.

Screening Tests Versus Diagnostic Tests

It is important to know and understand the difference between screening test and a diagnostic test.

- Screening tests help to evaluate the risk for certain birth defects, but they cannot diagnose a birth defect. Screening tests are noninvasive and pose no risk to mother or baby.

  Diagnostic tests, such as aminocentesis, cordocentesis and chorionic villus sampling (CVS), are highly accurate at diagnosing or ruling out birth defect. However, these tests are invasive and may pose a very small risk of miscarriage.

Application of Various Maternal and Fetal Screening Tests to Pregnant Women

Screening test such as an ultrasound can be performed at any stage of the pregnancy. However, most screening tests, particularly blood tests are not performed after 22 weeks; firstly because the efficacy of the tests declines steeply after that period and secondly in most countries late termination of pregnancy is restricted. The best detection rate for the tests can be obtained when performed in the particular window period of gestations. The following tests are the most widely performed.

CONCLUSION

With improved technology, in particular the development of high frequency transvaginal ultrasound probes and its increased acceptance with the patients, it has become possible to examine the detailed fetal anatomy even in the late first trimester and early second trimester.

The new panorama of normal embryological development is possible with 3D ultrasound and with computers handling the pre- and postprocessing of the ultrasound images gives us a future insight into the future of technology being applied to achieve a better understanding of early human developments and its defects.

ACKNOWLEDGMENTS

The authors are grateful to Prof Asim Kurjak, Dr Ashok Khurana, Dr JP Shah, Dr Kuldeep Singh and Dr P Radha Krishna for their inputs.

REFERENCES

1. Heinonen OP, Sloane D, Shapiro S. Birth defects and drugs in pregnancy. Littleton MA: PSG Publishing; 1977. pp. 410-1.
2. Hill LM, Breckle R, Gehrking WC. The prenatal detection of congenital malformations by ultrasonography. Mayo Clin Proc. 1983;58(12):805-26.
3. Benacerraf Beryl R. Ultrasound of fetal syndromes. Philadelphia: Churchill Livingston; 1998. p. 328.
4. Callen PW, et al. Ultrasonography in Obstet and Gynecol, 4th edition. Philadelphia, PA: WB Saunders; 2000. pp. 38-67.
5. Pandya PP, Santiago C, Sjniders RJM, et al. First Trimester fetal nuchal translucency. Curr Opin Obstet Gynecol. 1995;7(2):95-102.
6. Schemmer G, Wapener RJ, Johnson A, et al. First trimester growth patterns of aneuploid fetuses. Prenat Diag. 1997;17(2):155-9.
7. Hyett JA, Noble PL, Snijders RJM, et al. Fetal heart rate in trisomy 21 and other chromosomal abnormalities at 10–14 weeks of gestation. Ultrasound Obstet Gynecol. 1996;7(4): 239-44.
8. Rotmensch S, Liberati M, Bronstein M, et al. Prenatal sonographic findings in 187 fetuses with Down's syndrome. Prenat Diag. 1997;17(11):1001-9.
9. Rotmensch S, Mandell J, Estroff JA, et al. Fetal Pyelectasis: a possible association with Down syndrome. Obstet Gynecol. 1992;79(5 Pt 1):770-2.
10. Nyberg DA, Resta RG, Mahony BS, et al. Fetal hyperechogenic bowel and Down's syndrome. Ultrasound Obstet and Gynecol. 1993;3:330-3.

11. Brown DL, Roberts DJ, Miller WA. Left ventricular echogenic focus in the fetal heart: pathologic correlation. J Ultrasound Med. 1994;13(8):613-6.
12. Jones KL. Smith's recognizable patterns of human malformations, 5th edition. Philadelphia: WB Saunders; 1997. p. 30.
13. Lehman CD, Nyberg DA, Winter TC III, et al. Trisomy 13 Syndrome: prenatal US findings in a review of 33 cases. Radiology. 1995;194(1):217-22.
14. Rubenstein JB, Swayne LC, Dise CA, et al. Placental changes in fetal triploidy syndrome. J Ultrasound Med. 1986;5:545-50.
15. Shepard J, Bean C, Bove B, et al. Long term survival in a 69 XXY triploid male. Am J Med Genet. 1986;25(2):307-12.
16. Droste S, FitzSimmons J, Pascoe-Mason J, et al. Growth of linear parameters in trisomy 18 fetuses. Am J Obstet Gynecol. 1990;163(1 Pt 1):158-61.
17. Snijders RJM, Nicolaides KH. Ultrasound markers for fetal chromosomal defects. New York, NY:Parthenon Publishing Group;1996. pp. 63-120.
18. Grandjean H, Larroque D, Levi S, et al. The performance of routine ultrasonographic screening of pregnancies in the Eurofetus study. Am J Obstet Gynecol. 1999;181(2):446-54.
19. Levi S. Cost effectiveness of antenatal screening for fetal malformation by ultrasound: an evaluation of antenatal mass screening by ultrasound for the diagnosis of birth defects (1990-1993). Report to the European Commission, European Union, contract MR4*-0225-B;1995.
20. McNeil TF, Torstensson G, Nimby G. Psychological aspects of screening. In: Kurjak S (Ed). Textbook of perinatal medicine. London, England: Parthenon Publishing; 1998. pp. 717-29.
21. Levi S. Screening for congenital malformations by ultrasound. In: Kurjak S (Ed). Textbook of perinatal medicine. London, England: Parthenon Publishing; 1998. pp. 587-609.
22. Reed KL. Why (not) do obstetric ultrasound? An observation on uncertainty. Ultrasound Obstet Gynecol. 1996;8(1):1-2.
23. Leivo T, Tuominen R, Saari-Kemppainen A, et al. Cost-effectiveness of one-stage ultrasound screening in pregnancy: a report from the Helsinki ultrasound Trial. Ultrasound Obstet Gynecol. 1996;7(5):309-14.
24. Cheschire NC, Reitnauer PJ. A comparative study of prenatal diagnosis and perinatal autopsy. J Ultrasound Med. 1994;13(6):451-6.
25. Salvesen KA, Eik-Nes SH. Is ultrasound unsound? A review of epidemiological studies of human exposure to ultrasound. Ultrasound Obstet Gynecol. 1995;6(4):293-8.
26. Rosendahl H, Kivinen S. Antenatal detection of congenital malformations by routine ultrasonography. Obstet Gynecol. 1989;73(6):947-51.
27. Nicolaides KH, Azar G, Byrne D, et al. Fetal nuchal translucency: ultrasound screening for chromosomal defects in 1st trimester of pregnancy. BMJ. 1992;304(6831):867-9.
28. Spencer K, Souter V, Tul N, et al. A screening program for trisomy 21 at 10–14 weeks using fetal nuchal translucency, maternal serum free beta-human chorionic gonadotropin and pregnancy associated plasma protein-A. Ultrasound Obstet Gynecol. 1999;13(4):231-7.
29. Levi S, Montenegro N. Eurofetus: an evaluation of routine ultrasound screening for the detection of fetal defects: aims and method. In: Chervenak F, Levi S (Eds). Ann NY Acad Sci. 1998;847:103-17.
30. Clarke A. What counts as success in genetic counseling. J Med. Ethics. 1993;19(1):47-9.
31. Langham MR, E Reiger KM. Advances in fetal surgery. Surgery Annual. 1994;26:193-226.

30
CHAPTER

Ultrasound in the Management of the Alloimmunized Pregnancy

Daniel W Skupski

INTRODUCTION

Due to the advent of ultrasound imaging, the diagnosis and treatment of red blood cell (RBC) alloimmunization is arguably the quintessential success story in obstetrics. The pathophysiology is well described, the diagnosis is easily and reliably established and life-saving treatment for the fetus and newborn is available both *in utero* and after delivery with a high degree of success. Ultrasound has been used for diagnosis and as an adjunct for the treatment of RBC alloimmunization for several decades, and the applications for ultrasound are continuing to expand. This chapter will outline the current uses of ultrasound in the setting of the alloimmunized pregnancy.

HISTORY

Sir Richard Liley began the modern era of fetal therapy with the introduction of amniocentesis for testing of the amniotic fluid for bilirubin levels by spectrophotometry.[1] The degree of change in the optical density at a wavelength of 450 nm (delta OD450) of light during spectrophotometry of amniotic fluid correlates with the level of bilirubin in the fluid due to the preferential absorption of light at this wavelength by bilirubin. High levels of bilirubin in amniotic fluid correlate with the severity of RBC alloimmunization and have been used to guide therapy. Beginning around 1961, treatment for severe RBC alloimmunization consisted of either percutaneous intraperitoneal fetal transfusion (IPT) or early delivery.[2] At that time, imaging to guide the needle placement for IPT was in the form of amniography (placement of radio-opaque dye into the amniotic cavity) followed by fluoroscopy, using radiation, to outline the fetus and guide needle placement into the fetal abdominal cavity. Real-time ultrasound subsequently replaced amniography as the imaging study of choice.

Real-time ultrasound allowed the development of percutaneous intravascular blood transfusion to the fetus. This first occurred by fetoscopy and later by cordocentesis, also known as funipuncture or percutaneous umbilical blood sampling (PUBS). PUBS is an ultrasound-guided procedure.[3,4] Percutaneous umbilical blood sampling allows more accurate diagnosis of fetal anemia and the need for intrauterine therapy, by directly testing the fetal hematocrit. Due to improved imaging with ultrasound, this procedure has become technically easier. As a result of advances in image quality, intrauterine transfusion (IUT) can now be performed in the early second trimester for the rare cases that present with severe fetal anemia very early in gestation.

During the decade of the 1990s, the Collaborative Group for Doppler Assessment of the Blood Velocity in Anemic Fetuses studied numerous blood vessels in an effort to find a way to reliably diagnose severe fetal anemia (that would require invasive treatment). They were successful with the middle cerebral artery and their results were published in the year 2000.[5] This has paved the way to a noninvasive method for diagnosing

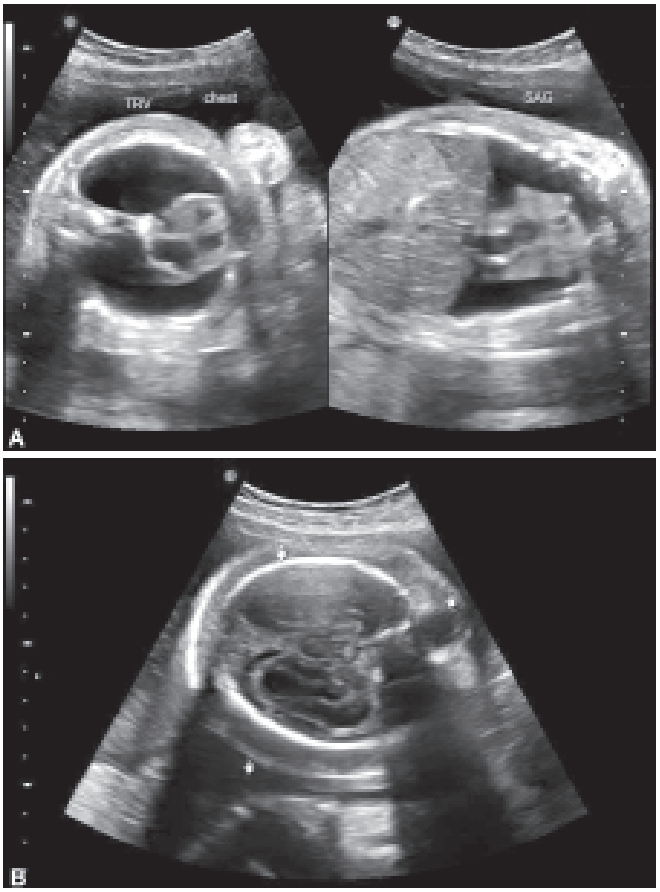

Figures 30.1A and B: Ultrasound image of hydrops fetalis. (A) The left image is a transverse or axial image of the fetal chest showing bilateral large pleural effusions surrounding the fetal heart. The right image is a longitudinal or coronal scan of the fetal thorax (towards the right of the image) and abdomen (towards the left of the image) showing bilateral large pleural effusions above the diaphragm; (B) Axial scan of the fetal head in the same patient showing skin edema (arrows)

fetal anemia, which has led to a decrease in morbidity from invasive procedures.

DIAGNOSIS

The identification of antibodies in maternal serum is the key to finding the alloimmunized pregnancy. Ultrasound has traditionally been used after a pregnancy is known to have RBC alloimunization in order to identify hydrops fetalis **(Figs 30.1A and B)**. Severe fetal anemia can lead to hydrops fetalis and this is probably produced by a combination of pathophysiologic factors, including hypoalbuminemia and hepatic damage from extramedullary hematopoiesis.[6] The fetal

TABLE 30.1

Diagnosis of hydrops fetalis*

- Polyhydramnios
- Thickened placenta (> 6 cm)
- Pericardial effusion
- Ascites
- Skin edema
- Pleural effusion

*Findings are listed in the order of usual progression of disease

hematocrit is usually below 15% when hydrops is present. When immune hydrops fetalis is present, IUT is lifesaving, and usually needs to be performed within 1–7 days. Hydrops fetalis is present when two or more factors listed in **Table 30.1** are present. When only one factor is present, this may be an early sign of hydrops, particularly in the alloimmunized pregnancy.

When fetal anemia becomes severe, there can also be changes in fetal behavior, due to the restriction of oxygen delivery to fetal tissues. The fetus may then conserve energy by limiting its movements. The biophysical profile is an assessment of the character and frequency of fetal movements along with an assessment of the volume of amniotic fluid. The biophysical profile can possibly identify the fetus who is decompensating, but may not be reliable for this purpose. The biophysical profile does not distinguish between severe acidemia, severe anemia, advanced fetal sepsis and severe central nervous system anomaly, nor does it determine the cause of the fetal decompensation.

Ultrasound is commonly used to guide the diagnostic procedure of cordocentesis or PUBS **(Figs 30.2A to C)**. First, ultrasound is used to identify the umbilical cord insertion into the placenta, then a 20 or 22 gauge needle is placed percutaneously through the maternal abdomen into the fetal umbilical vein at the level of the placental cord insertion. An alternative site is the fetal intrahepatic portion of the umbilical vein, which may be chosen if the placenta is posterior and the position of the fetus limits accessibility to the placental cord insertion site. The placental cord insertion is generally chosen because the cord is anchored at this point, allowing the needle to easily puncture the cord.[7] Free loops of umbilical cord have rarely been used as the access point to the umbilical vein because their mobility limits the success of puncture. The vein is chosen because it has a larger caliber and usually allows a shorter procedure time. It is also thought that puncture of an arterial vessel is more likely to produce fetal bradycardia.

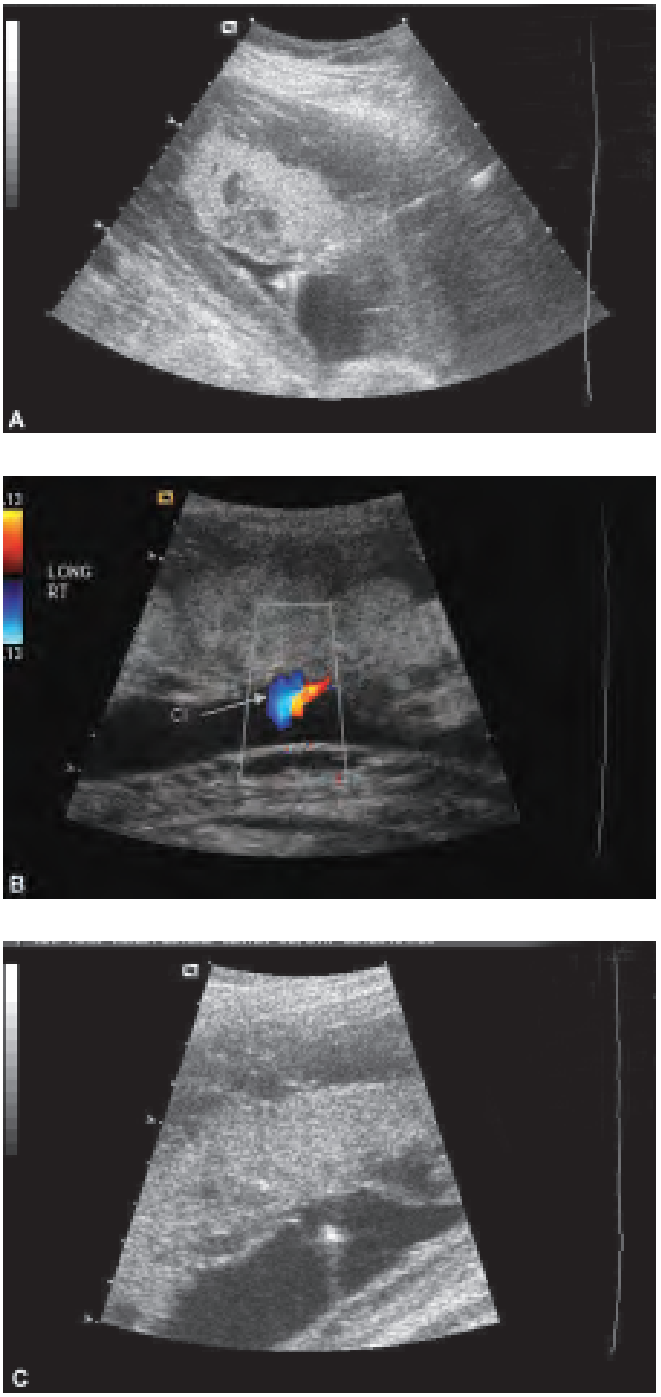

Figures 30.2A to C: Percutaneous umbilical blood sampling or cordocentesis for intrauterine fetal transfusion. (A) Ultrasound image of a needle being placed through the maternal abdominal wall and placenta into the umbilical vein at the placental cord insertion in a pregnancy with an anterior placental attachment; (B) High resolution image of the placental cord insertion using color Doppler; (C) High resolution image of the needle tip in the umbilical vein (color Doppler turned off)

Noninvasive Diagnosis

During the past two decades many fetal vessels and morphologic findings have been evaluated for ultrasound or Doppler findings that would allow a specific diagnosis of severe fetal anemia prior to the development of hydrops fetalis. An excellent review of this experience is available.[8] The optimal time for diagnosis of severe anemia is prior to the development of hydrops fetalis because the mortality increases once hydrops has occurred.[9] A group of investigators working consistently during the decade of the 1990s has now identified that the fetal middle cerebral artery peak systolic velocity (MCA-PSV) reliably predicts fetal anemia and can be performed by sonographers consistently with technical accuracy.[5,10-13] The viscosity of blood is inversely correlated with the speed of blood flow in vessels. Assuming the same pumping force is applied, the lower the viscosity of blood in vessels, the higher the velocity. When fetal anemia becomes severe, the viscosity of blood is markedly decreased, and this leads to a markedly increased peak systolic velocity. The angle of incidence at which the ultrasound beam intersects the blood flowing in a vessel affects the results of many Doppler measurements. Due to this limitation, most Doppler indices include angle correction as a feature of the software that performs the calculations. For optimal accuracy, i.e. low intraobserver and interobserver variability—the measurement of peak systolic velocity of blood in a vessel requires that no angle correction be performed.[10] With a 0° angle of incidence no angle correction is needed and the measurement of peak systolic velocity is then very accurate.

The specific technique for performing MCA-PSV measurements includes magnifying the image on the screen, using color Doppler to visualize the middle cerebral artery of the fetus and adjusting the transducer on the maternal abdomen so that the angle of incidence of the beam to the artery is 0°, i.e. the direction of blood flow in the vessel should be aimed directly at the transducer or directly away from the transducer **(Fig. 30.3)**. Measurements should be taken when there is an absence of marked fetal body and breathing movements. Several measurements should be obtained at each visit. The highest MCA-PSV should be reported and used for management decisions.

The Collaborative Group for Doppler Assessment of the Blood Velocity in Anemic Fetuses has reported the results of a large number of patients with fetuses at risk for anemia who have undergone fetal MCA-PSV testing.[5,12] In their first report, they studied 110 consecutive pregnant women carrying 111 fetuses at risk for fetal anemia due to RBC alloimmunization evaluated

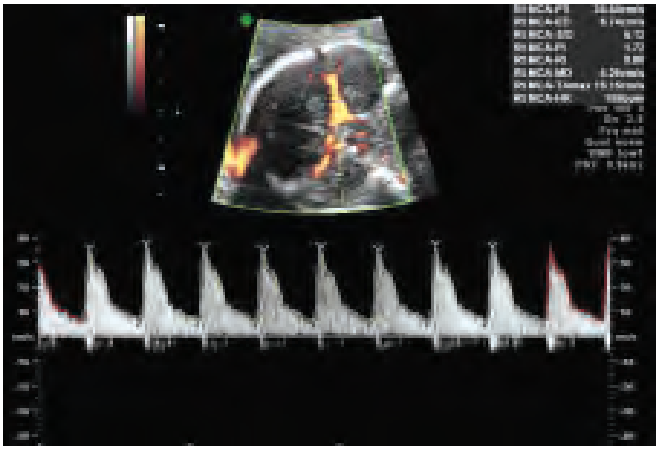

Figure 30.3: Power and pulsed wave Doppler measurement of the peak systolic velocity of the fetal middle cerebral artery (MCA). The peak systolic velocity (PS) of 34.54 centimeter per second is seen in the box in the upper right. Note the orientation of the MCA is as close to 0° as possible to that of the ultrasound beam

between 15 and 36 weeks of gestation.[5] They performed MCA-PSV measurements at the time of initial referral and every two weeks thereafter, including immediately prior to cordocentesis. Since hemoglobin concentration in fetuses increases with gestational age, they developed nomograms for hemoglobin concentration from 265 fetuses undergoing cordocentesis for other reasons (suspicion of fetal infection, alloimmune thrombocytopenia, immune thrombocytopenia purpura and chromosomal anomalies) who did not have anemia. The expected values for MCA-PSV were based on nomograms produced previously.[10] The results from cordocentesis showed that 41 of 111 fetuses at risk for anemia did not have anemia, 35 had mild anemia, 4 had moderate anemia and 31 had severe anemia. Of the 31 fetuses with severe anemia, 12 had hydrops fetalis. The sensitivity of MCA-PSV in detecting moderate or severe anemia was 100% (35/35) and the 95% confidence intervals were 86–100%. Receiver-operator characteristic curves for the MCA-PSV showed that a level of 1.5 multiples of the median (MOM) or greater allowed a sensitivity of 100% while only producing a false-positive rate of 12% (4/35). They concluded that, in fetuses at risk of anemia due to RBC alloimmunization, moderate and severe anemia can be reliably detected by noninvasive Doppler assessment using the middle cerebral artery peak systolic velocity.

In a follow-up prospective multicenter trial with intent-to-treat, MCA-PSV was found to be highly predictive of moderate-to-severe anemia at delivery, with a sensitivity of 88%, specificity of 87%, positive predictive value of 53% and negative predictive value of 98%.[13] The diagnosis of severe anemia was missed in one fetus, but the final outcome was good. They concluded that MCA-PSV will minimize fetal complications associated with invasive testing in pregnancies affected by RBC alloimmunization and recommended a Doppler testing within an interval of seven days.[13]

The same investigators also assessed the ability of MCA-PSV in determining severe anemia longitudinally in 34 fetuses, where measurements were performed serially. They calculated the slope of the MCA-PSV in each fetus over time and determined the average rate of change as a function of gestational age in three groups of fetuses: normal, mildly anemic and severely anemic. The estimated average slope increased significantly in the severely anemic fetuses. This demonstrated that the MCA-PSV can be used to follow fetuses at risk for severe anemia over the course of the pregnancy.[12]

The current status of MCA-PSV as a reliable method for the noninvasive determination of fetal anemia has also been confirmed by meta-analysis.[14] This study showed that the likelihood ratio for a positive test was 8.45 and for a negative test was 0.02. These results are consistent with both clinical and statistical significance.

In a prospective multicenter study, including 164 women with alloimmunized pregnancies, fetal MCA-PSV measurements were demonstrated to be superior to delta OD450 in amniotic fluid for the prediction of severe fetal anemia.[15] These women had Rh(D), Rh(c), Rh(E) and Fy(a) antibodies, had antibody titers $\geq$1:64 and antigen positive fetuses. When clinical findings necessitated invasive assessment in this study, fetal MCA-PSV was performed first, followed by the amniocentesis. Cordocentesis was performed if one or both tests suggested severe fetal anemia (MCA-PSV above 1.5 MOM or Liley upper zone II). Seventy-four fetuses were diagnosed as severely anemic, defined as a hemoglobin five standard deviations below the mean for gestational age. Fetal MCA-PSV was significantly more sensitive than amniotic fluid delta OD 450 measurements using the Liley curve (88% versus 76%, difference in sensitivity 12%, 95% CI 0.3–24.0), but was not more specific (82% versus 77%).

MANAGEMENT

Ultrasound has progressed from a useful adjunct to an indispensable diagnostic tool in the evaluation and treatment of the alloimmunized pregnancy. A management scheme that is significantly less invasive than previous schemes is now possible. The author's

algorithm for management is shown in **Flow chart 30.1**. This management scheme includes the primary use of fetal MCA-PSV measurements rather than amniocentesis as the preferred choice for monitoring for severe fetal anemia. There are times when the fetal MCA-PSV measurement may not be reliable and resort to amniocentesis or cordocentesis may be necessary. Still, there are significantly fewer invasive procedures for these women as a whole than in years past, providing for less procedural complications and less likelihood of iatrogenic premature delivery.

Deoxyribonucleic acid (DNA) testing for the Rhesus D (RhD) locus is a highly reliable diagnostic test and with its use those fetuses who are truly at risk are able to be identified. DNA testing for the RhD locus allows us to separate the fetuses who are antigen negative from antigen positive.[16] This can occur whenever fetal DNA can be obtained at any time in gestation and is irrespective of the paternal zygosity status. The RhD DNA testing by polymerase chain reaction (PCR) is reliable even if paternity is unknown. Fetal tissue can be obtained by amniocentesis or chorionic villus sampling (CVS) in early gestation and further invasive procedures can be avoided in those fetuses who are antigen negative and are thus not at risk for severe anemia.[16] For fathers who are heterozygous for the offending antigen, this includes 50% of fetuses. Ultrasound guidance is an essential component of the diagnostic procedures of amniocentesis and CVS.

When the woman has no prior pregnancy history of severe fetal anemia and the fetus is antigen positive, the patient can be followed with serial ultrasound to detect hydrops fetalis and an MCA-PSV measurement performed every one or two weeks beginning at 18 weeks of gestation to detect severe fetal anemia. If the MCA-PSV is greater than 1.5 MOM for the gestational age at which it is performed, this indicates a severe fetal anemia and is an indication for cordocentesis and possibly IUT. If hydrops fetalis is identified, cordocentesis for IUT would also be chosen.

Management can be tailored based on prior pregnancy history for those fetuses that are antigen positive. Invasive testing in a subsequent pregnancy begins before the time in gestation when the fetus was

Flow chart 30.1: Management of the alloimmunized pregnancy

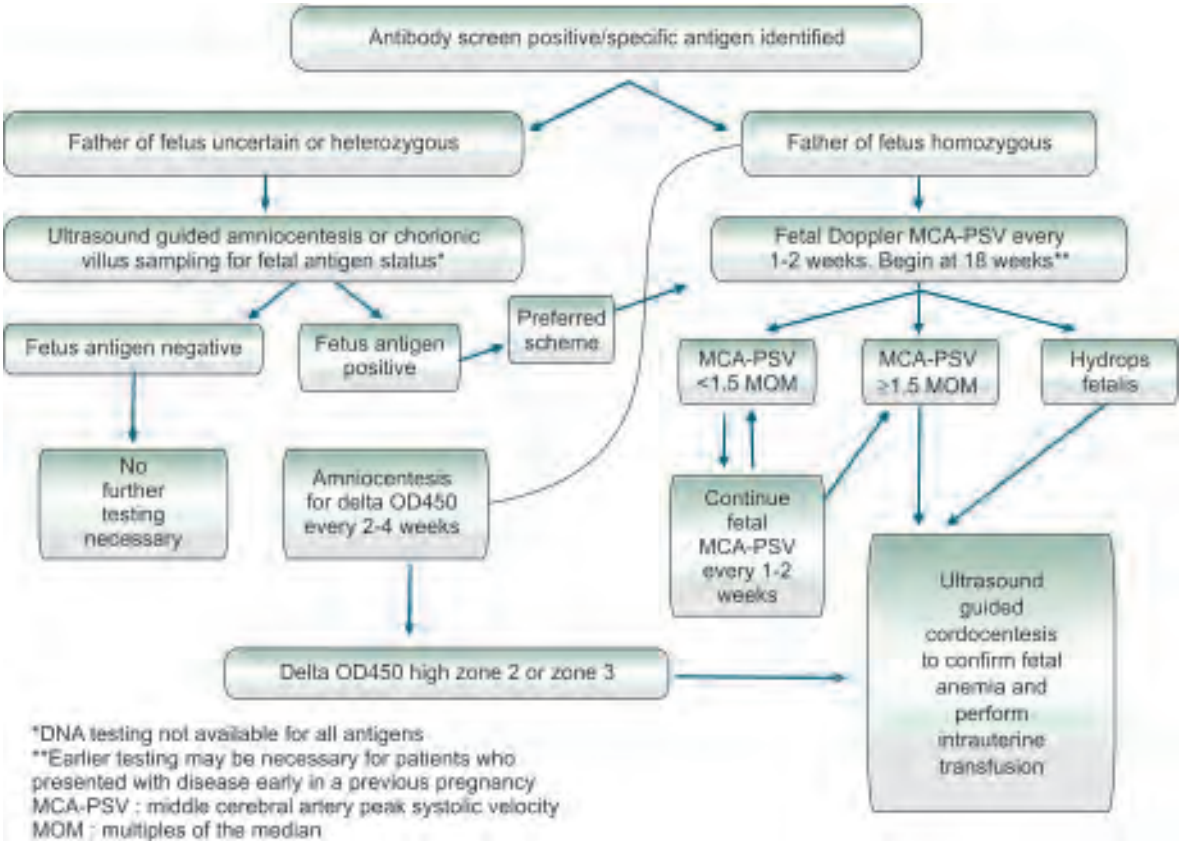

deemed to be affected in a prior pregnancy. For example, if amniocentesis showed delta OD450 in Liley zone 3 at 28 weeks of gestation (or cordocentesis showed severe fetal anemia) in one pregnancy, then invasive testing would be recommended at 20–26 weeks of gestation in the next pregnancy in previous schemes of management. Using the MCA-PSV, earlier testing would not be required (because all patients would begin testing at 18 weeks of gestation) unless an earlier pregnancy was affected prior to 18 weeks. An excellent review of the current state of treatment for RBC alloimmunization is available.[17]

ALLOIMMUNE THROMBOCYTOPENIA

Fetal and neonatal alloimmune thrombocytopenia is the platelet corollary to RBC alloimmunization. The natural history of the disease shows that each subsequent pregnancy is generally more severely affected, including antenatal intracranial hemorrhage and fetal demise.[18] Lifesaving fetal treatment is available in the form of intravenous immune globulin (IVIG) given to the mother on a weekly or twice weekly basis, which is believed to act in part by limiting the placental transfer of antiplatelet IgG antibody that attaches to fetal platelets.[19-21] Antiplatelet IgG that is transferred from maternal plasma to the fetus is thought to coat fetal platelets and enhance the rapid elimination of fetal platelets by the fetal reticuloendothelial system. The ultrasound guided procedure of cordocentesis is used to diagnose the most severely affected cases. Cordocentesis allows fetal blood to be obtained so that a severely low fetal platelet count can be discovered and prenatal treatment can be instituted. Review articles of the diagnosis and treatment of alloimmune thrombocytopenia are available.[22,23]

SUMMARY

From its beginnings as a research tool to its current indispensable status as both a diagnostic tool and an adjunct to therapy, ultrasound is a cornerstone in the fight against alloimmunization. Ultrasound has advanced our knowledge of the pathophysiology and the fetal effects of disease and our ability to manage the alloimmunized pregnancy. The Doppler MCA-PSV measurement is a major advance in our ability to diagnose fetal anemia and thus manage the alloimmunized pregnancy. Advances in ultrasound imaging quality and in our knowledge of the uses of ultrasound in the near future should further refine our ability to diagnose and treat the alloimmunized pregnancy.

REFERENCES

1. Liley AW. Liquor amnii analysis in the management of pregnancy complicated by rhesus immunization. Am J Obstet Gynecol. 1961;82:1359-66.
2. Liley AW. Intrauterine transfusion of foetus in haemolytic disease. Br Med J. 1963;2(5365):1107-13.
3. Rodeck CH, Kemp JR, Holman CA, et al. Direct intravascular fetal blood transfusion by fetoscopy in severe thesus isoimmunization. Lancet. 1981;1(8221):625-7.
4. Rodeck CH, Nicolaides KH, Warsof SL, et al. The management of severe rhesus isoimmunization by fetoscopic intravascular transfusions. Am J Obstet Gynecol. 1984; 150(6):769-74.
5. Mari G, Deter RL, Carpenter RL, et al. Noninvasive diagnosis by Doppler ultrasonography of fetal anemia due to maternal red cell alloimmunization for the Collaborative Group for Doppler Assessment of the Blood Velocity in Anemic Fetuses. N Engl J Med. 2000;342(1):9-14.
6. Bowman JM. Hemolytic disease (erythroblastosis fetalis). In: Creasy RK, Resnik R (Eds). Maternal-Fetal Medicine: Principles and Practice. Philadelphia: WB Saunders Company;1994. p. 719.
7. Grannum PA, Copel JA, Plaxe SC, et al. In utero exchange transfusion by direct intravascular injection in severe erythroblastosis fetalis. N Engl J Med. 1986;314(22):1431-4.
8. Whitecar PW, Moise KJ. Sonographic methods to detect fetal anemia in red blood cell alloimmunization. Obstet Gynecol Survey. 2000;55(4):240-50.
9. Schumacher B, Moise KJ. Fetal transfusion for red blood cell alloimmunization in pregnancy. Obstet Gynecol. 1996;88(1):137-50.
10. Mari G, Adrignolo A, Abuhamad AZ, et al. Diagnosis of fetal anemia with Doppler ultrasound in the pregnancy complicated by maternal blood group immunization. Ultrasound Obstet Gynecol. 1995;5(6):400-5.
11. Mari G, Rahman F, Ologsson P, et al. Increase of fetal hematocrit decreases the middle cerebral artery peak systolic velocity in pregnancies complicated by rhesus alloimmunization. J Matern Fetal Med. 1997;6(4):206-8.
12. Detti L, Mari G, Akiyama M, et al. Longitudinal assessment of the middle cerebral artery peak systolic velocity in healthy fetuses and in fetuses at risk for anemia. Am J Obstet Gynecol. 2002;187(4):937-9.
13. Zimmerman R, Carpenter RJ, Durig P, et al. Longitudinal measurement of peak systolic velocity in the fetal middle cerebral artery for monitoring pregnancies complicated by red cell alloimmunisation: a prospective multicentre trial with intention-to-treat. BJOG. 2002;109(7):746-52.
14. Divakaran TG, Waugh J, Clark TJ, et al. Noninvasive techniques to detect fetal anemia due to red blood cell alloimmunization: a systematic review. Obstet Gynecol. 2001;98(3):509-17.
15. Oepkes D, Seaward PG, Vandenbussche FP, et al. Doppler ultrasonography versus amniocentesis to predict fetal anemia. N Engl J Med. 2006;355(2):156-64.
16. Bennett PR, Le Van Kim C, Colin Y, et al. Prenatal determination of fetal RhD type by DNA amplification. N Engl J Med. 1993;329(9):607-10.

17. Moise KJ. Management of rhesus alloimmunization in pregnancy. Obstet Gynecol. 2002;100(3):600-11.
18. Bussel JB, Zabusky MR, Berkowitz RL, et al. Fetal alloimmune thrombocytopenia. N Engl J Med. 1997;337(1):22-6.
19. Lynch L, Bussel JB, McFarland JG, et al. Antenatal treatment of alloimmune thrombocytopenia. Obstet Gynecol. 1992;80(1):67-71.
20. Bussel JB, Berkowitz RL, Lynch L, et al. Antenatal management of alloimmune thrombocytopenia with intravenous gamma-globulin: a randomized trial of the addition of low-dose steroid to intravenous gamma-globulin. Am J Obstet Gynecol. 1996;174(5):1414-23.
21. Urbaniak SJ, Duncan JI, Armstrong-Fisher SS, et al. Transfer of anti-D antibodies across the isolated perfused human placental lobule and inhibition by high-dose intravenous immunoglobulin: a possible mechanism of action. Br J Haematol. 1997;96(1):186-93.
22. Skupski DW, Bussel JB. Alloimmune thrombocytopenia. Clin Obstet Gynecol. 1999;42(2):335-48.
23. Bussel J. Diagnosis and management of the fetus and neonate with alloimmune thrombocytopenia. J Thromb Haemost. 2009;7 Suppl 1:253-7.

CHAPTER 31

Doppler Sonography in Obstetrics

A Kubilay Ertan, H Alper Tanriverdi

INTRODUCTION

Doppler sonographic applications in pregnancy are the widely accepted functional methods of evaluating fetal wellbeing. Flow velocity waveforms provide important information from the early stages of pregnancy to term. As applications proliferate, awareness of the complexity of fetal and placental circulations, in normal pregnancy and in sequential responses to compromise, has also grown.[1] One of the main aims of routine antenatal care is to identify the "at risk" fetus in order to apply clinical interventions which could result in reduced perinatal morbidity and mortality.

Doppler ultrasound is a noninvasive technique whereby the movement of blood is studied by detecting the change in frequency of reflected sound. Doppler ultrasound has been used in obstetrics since 1977 to study the fetoplacental (umbilical) circulation,[2] and since the 1980s to study the uteroplacental (uterine) circulation[3] and fetal circulation.[4] Recently, this method became an important tool for qualifying pregnancies in risk.

Information obtained with Doppler sonography helps obstetricians managing patients in situations like pregnancies complicated by intrauterine growth restriction (IUGR), Rhesus alloimmunization, multiple pregnancies and anamnestic risk factors. Examination of the uteroplacental and fetomaternal circulation by Doppler sonography in the early second trimester helps predicting pregnancy complications like preeclampsia, IUGR and perinatal death.[5-13]

This chapter aims to introduce Doppler sonographic examinations in modern obstetrics. Doppler blood flow velocity waveforms (FVWs) of the fetal arterial side (umbilical arteries, descending aorta and middle cerebral arteries) and maternal side (uterine arteries) are discussed and nomograms for routine obstetric practice are presented.

THE SAFETY OF DOPPLER ULTRASOUND IN OBSTETRICS

The data available suggests that diagnostic ultrasound has no adverse effects on embryogenesis or fetal growth. In addition, ultrasonographic scanning has no long-term effects on cognitive function or change visual or hearing functions. According to the available clinical trials, there is a weak association between exposure to ultrasonography and non-right handedness in boys (odds ratio 1.26; 95% CI, 1.03–1.54).[14] However, although B and M mode scans are safe during pregnancy, color, power and pulsed Doppler procedures should be performed with caution, especially in the early stages of pregnancy, due to possible thermal effects. Studies concerned with the safety of ultrasound included mostly exposures before 1995, when the acoustic potency of the equipment used was lower than in modern machines. Over the years, there has been a continuous trend of increasing acoustic output, and the findings of the previous studies necessarily apply to currently used equipment. Because of weak regulation of ultrasound equipment output, fetal exposure using current equipment can be almost eight times greater than that used previously, regardless

of whether gray-scale imaging, the three-dimensional technique, color Doppler or duplex Doppler is employed. A short acquisition time of any kind of diagnostic ultrasonic wave may decrease exposure and thus unknown effects on fetal development.[15]

In particular, the use of pulsed Doppler involves the use of higher intensities compared to diagnostic ultrasound, and hence may cause significant tissue heating and thermal effects. However, these thermal effects depend on the presence of a tissue/air interface and may therefore not be clinically significant in obstetric ultrasound examinations.[16] The principle known as ALARA (as low as reasonably achievable) is generally supported and encourages the balance between the necessary medical information, minimal settings and exam time.[17]

In a randomized controlled prospective study, considering the long-term effect of ultrasound examinations on childhood outcome up to 8 years of age, it was shown that exposure to multiple prenatal ultrasound examinations from 18 weeks' gestation onwards might be associated with a small effect on fetal growth, but is followed in childhood by growth and measures of developmental outcome similar to those in children who had received a single prenatal scan.[18]

DEPENDENCY OF DOPPLER FLOW VELOCITY WAVEFORMS ON GESTATIONAL AGE

The amount of perfusion in trophoblastic tissue is related to gestational age. For this reason, in interpreting the Doppler sonographic findings, gestational age must be taken into account. That is, nomograms for Doppler sonographic measurements should be standardized according to gestational age. In the routine use of ultrasound in practice, the accepted time for starting Doppler sonographic examinations is the beginning of the second trimester. This is the right time that allows modifications in antenatal care in a high risk pregnancy. For specific conditions, earlier timing of measurements may be considered.[19]

The main objective in constituting fetomaternal Doppler sonographic nomograms is to improve perinatal outcome in high risk pregnancies. Curves presented below depict normal fetal and maternal Doppler sonographic values, and can be used in routine practice.

Indices

Blood flow velocity in the fetal circulating system depends on the type of vessel: The arteries always have a pulsatile pattern, whereas veins have either a pulsatile or continuous pattern.

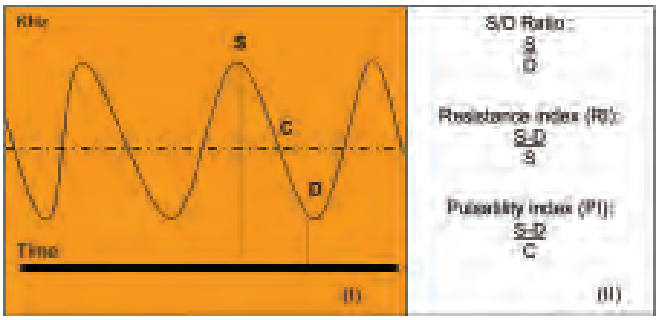

Figure 31.1: Scheme of the Doppler curve (I). S= systolic, D= diastolic, C= temporal average of maximum frequency. Calculation formulas of the main Doppler sonographic indices (II)

Analysis of Doppler sonographic FVWs quantitatively, is more difficult than analyzing qualitatively. Qualitative analysis also overcomes erroneous measurements in small vessels. There are plenty of indices for qualitative analysis.

Following are the most frequently used indices:

- Systolic/Diastolic ratio (S/D ratio, Stuart 1980)
- Resistance index (RI, Pourcelot 1974)
- Pulsatility index (PI, Gosling and King 1977).

In analyzing sonographic results and calculating indices, following characters are used:

S = Temporal peak of maximum frequency
D = End-diastolic maximum frequency
C = Temporal average of maximum frequency, F_{mean}
I = Instantaneous spatial average frequency
E = Temporal average of spatial average frequency

Calculations of formulas are as follows **(Fig. 31.1)**:

S/D ratio = S/D
RI = (S–D)/S
PI = (S–D)/C

While calculating PI values, in some sonographic devices, E values are used instead of C values. As a result PI values increase slightly.

The above presented indices overcome also a very serious problem involved with the angle between the ultrasound beam and the direction of blood flow (insonation angle). These indices are relatively angle independent and are therefore easily applied in clinical practice.

In practice, none of the indices is superior to the other[20-22] and any index may be used. Although the S/D ratio is easily calculated, RI is the easiest to interpret. Resistance index values approach to zero if the resistance decreases and approach to one if resistance increases. If end-diastolic flow is absent, PI is the only index making evaluation of blood flow possible, because

in this situation S/D will equal to infinite and RI to one. The PI is more complex because it requires the calculation of the mean velocity, but modern Doppler sonographic devices provide those values in real time.

Doppler sonographic nomograms are used for the differentiation of normal and abnormal blood FVWs, which helps to determine pregnancies at risk. By taking threshold values of pathologic pregnancies into consideration, nomograms are capable to differentiate between normal and abnormal. The nomograms are presented for meeting this target.[23] While confronting with these nomograms, it must always kept in mind that the values on these nomograms should not be taken as mathematical equations, and that limitations of sensitivity and specificity exist.

Using Nomograms in Practice

Just like the defense mechanism of peripheral vasoconstriction in an adult in the face of hemorrhagic shock, the "brain sparing" mechanism (brain-sparing effect) becomes active in a fetus with hypoxia or chronic placental insufficiency. As a result of the brain sparing effect, resistance either in the umbilical artery (UA) and fetal descending aorta (FDA) increases. As a consequence Doppler indices related to these vessels increase. The end-diastolic blood flow increases in middle cerebral arteries (MCA) by the same effect. Doppler indices for this vessel decreases consequently.

Some points should be considered while using Doppler sonographic nomograms:

- Among the measurements performed on the UA and FDA, values between 90–95th percentiles should be considered as borderline and repeat follow-ups should be planned. Values exceeding the 95th percentile are considered abnormal.
- Doppler values between 5–10th percentiles in MCA should be considered as borderline and repeat follow-ups should be planned. Values below the 5th percentile are considered abnormal.
- Measurements taken after 24 weeks' gestation from uterine arteries are more valuable. The early diastolic notching, and values exceeding the 95th percentile are considered as abnormal. One point to remember is that notching predicts an increased risk of preeclampsia.

CHANGES IN DOPPLER SONOGRAPHIC RESULTS DURING THE COURSE OF PREGNANCY AND COMPLICATED PREGNANCIES

During the course of pregnancy and in some specific pregnancy complications, Doppler sonographic results of fetomaternal vessels display changing values.

Umbilical Artery (UA)

It has been shown in a longitudinal observational study that Doppler ultrasound of the UA is more helpful than other tests of fetal wellbeing (e.g. heart rate variability and biophysical profile score) in distinguishing between the normal small fetus and the "sick" small fetus.[24] However, its exact role in optimizing management, particularly timing of delivery, remains unclear, and is currently being investigated by many study groups. The optimal timing of delivery in pregnancies complicated by highly pathological Doppler flow findings is still an issue to be resolved. To resolve this question and to improve the perinatal morbidity and mortality some multicenter clinical trials[25] have been undertaken. Gestational age, Doppler waveforms, antenatal testing, and maternal status should all be taken into consideration to guide optimal timing of delivery to minimize extreme prematurity, but also to prevent intrauterine injury, in the case of the compromised fetus.

Blood flow velocity in the UA increases with the advancing gestation. As a result impedance to blood flow continuously decreases due to increasing arterial blood flow in the systole and diastole. End-diastolic velocity is often absent in the first trimester[2,26] and the diastolic component increases with advancing gestation[27] **(Fig. 31.2)**. With advancing gestational age, end-diastolic flow becomes evident during the whole heart cycle **(Fig. 31.3)**, proven with previous longitudinal studies of Fogarty et al[22] and Hünecke et al,[28] as with many cross-sectional studies.[27,29]

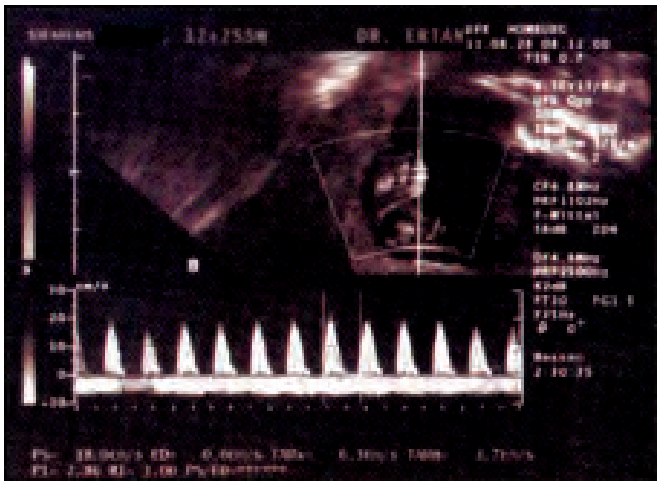

Figure 31.2: Absent end-diastolic flow of the umbilical artery in the first trimester (physiologic) with pulsations of the umbilical vein (physiologic)

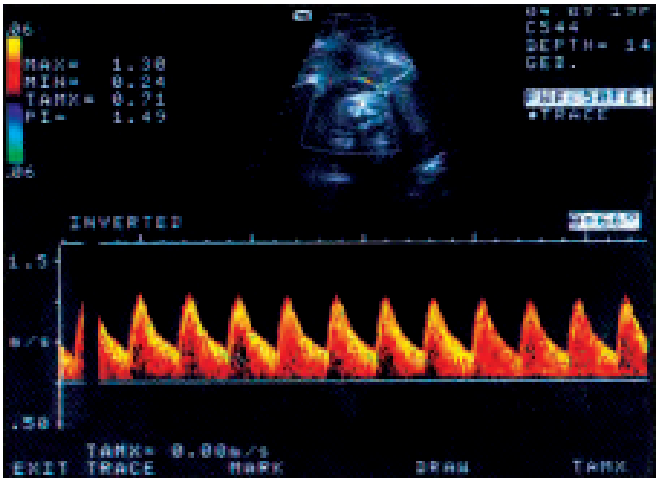

Figure 31.3: Normal flow velocity waveforms of the umbilical artery in the third trimester

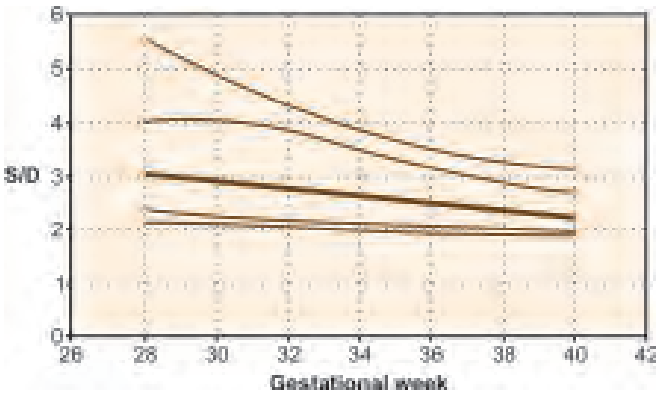

Figure 31.4: Umbilical artery systolic/diastolic (S/D) ratio nomogram

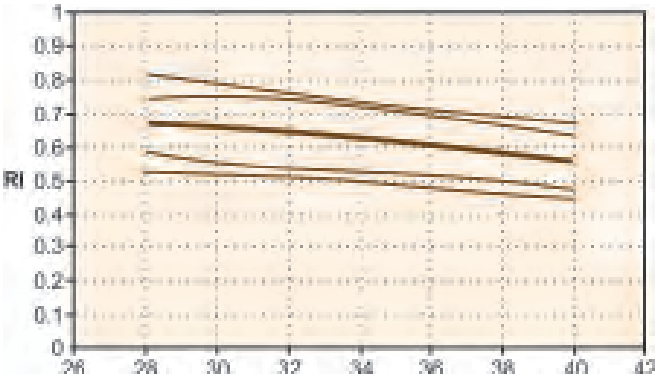

Figure 31.5: Umbilical artery resistance index (RI) nomogram

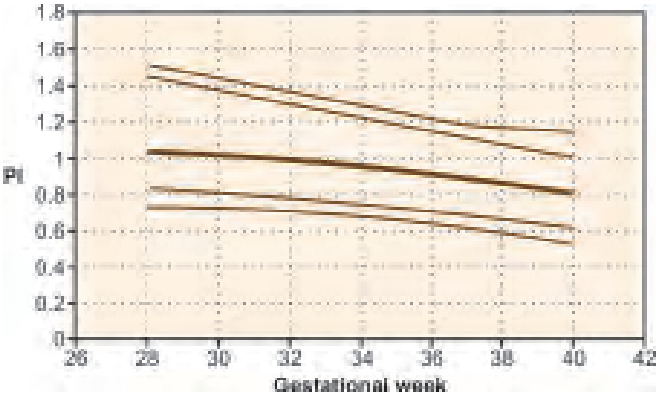

Figure 31.6: Umbilical artery pulsatility index (PI) nomogram

Trudinger et al.[30] explained this phenomenon with the following mechanisms:

- Continuous maturation in placental villi
- Continuous widening of placental vessels cause a continuous decrease in vascular resistance
- Continuous increase in fetal cardiac output
- Continuous changes in the vessel compliance
- Continuous increase in fetal blood pressure.

Especially in the third trimester of pregnancy, depending on the above factors normal values become scattered on nomograms **(Fig. 31.4)**. This scattering is more prominent in the S/D ratio than the PI. Resistance index is not affected by above factors after 28 weeks' gestation **(Figs 31.4 to 31.6)**.

Flow velocity waveforms of the UA are slightly different at the abdominal wall and the placental site, with indices higher at the fetal abdominal wall than the placental insertion.[31] The difference, however, is minimal, and therefore in clinical practice it is not important to obtain the FVWs always at the same level. Flow velocity waveforms must always be obtained during fetal apnea periods because fetal breathing affects the waveforms.

In case of an abnormal test, clinical experience and randomized controlled trials showed significant association with an adverse perinatal outcome.

Intrauterine Growth Restriction

The IUGR fetus is a fetus that does not reach its potential growth. Environmental factors responsible for IUGR may be due to maternal, uteroplacental and fetal factors **(Table 31.1)**. Many authors have reported on the association between an abnormal UA Doppler FVW and IUGR.

Differentiating the fetus with pathologic growth restriction that is at risk for perinatal complications from the constitutionally small but healthy fetus has been an ongoing challenge in obstetrics. Not all infants whose

TABLE 31.1

Factors responsible for intrauterine growth restriction
Maternal factors
• Cardiorespiratory diseases
• Renal disease
• Anemia
• Drugs (Antineoplastic agents, narcotics)
• Smoking
• Alcohol abuse
Uteroplacental factors
• Impaired uteroplacental blood flow
• Chronic hypertension
• Preeclampsia
• Gestational diabetes
• Collagen vascular disease
• Uterine anomalies
• Leiomyomatosis
Placental factors
• Abruptio placentae
• Placenta previa
• Placental infarction
• Placentitis, vasculitis
• Placental cysts, tumors (chorioangioma)
Fetal factors
• Infections
• Cardiac disease
• Anomalies
Chromosomal anomalies

birth weight is below the 10th percentile have been exposed to a pathologic process *in utero*; in fact, most small newborns are constitutionally small and healthy. Doppler sonography has become the most important investigation method to differentiate between these fetuses.

Pathophysiology of abnormal FVWs in placental insufficiency:[32] In the presence of placental insufficiency, there is greater placental resistance, which is reflected in a decreased end-diastolic component of the UA FVWs.[33-37] An abnormal UA FVW has a S/D ratio above the normal range. As the placental insufficiency worsens, the end-diastolic velocity decreases **(Fig. 31.7)**, then become absent **(Fig. 31.8)** and finally it is reversed **(Fig. 31.9)**. Some fetuses have decreased end-diastolic velocity that remains constant with advancing gestation and never become absent or reversed, which may be due to a milder form of placental insufficiency. Pitfalls can be caused due to a high selected wall filter or fetal breathing **(Fig. 31.10)**.

Abnormal UA Doppler studies, but not normal results were found to be associated with lower arterial and venous pH values, an increased likelihood of intrapartum fetal distress, more admissions to the

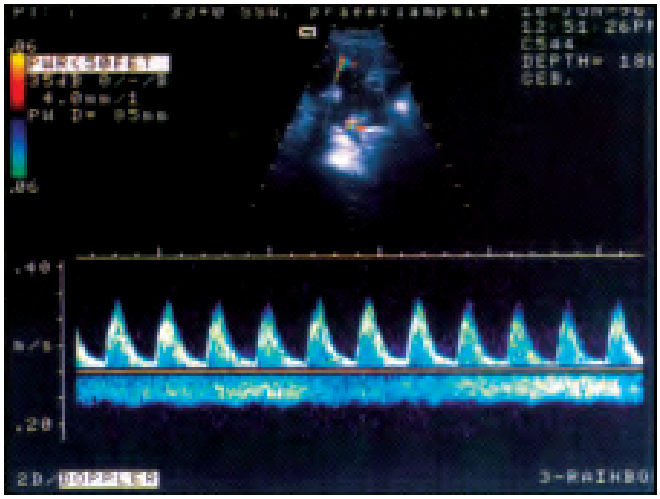

Figure 31.7: Abnormal flow velocity waveforms of the umbilical artery in the third trimester (high resistance index)

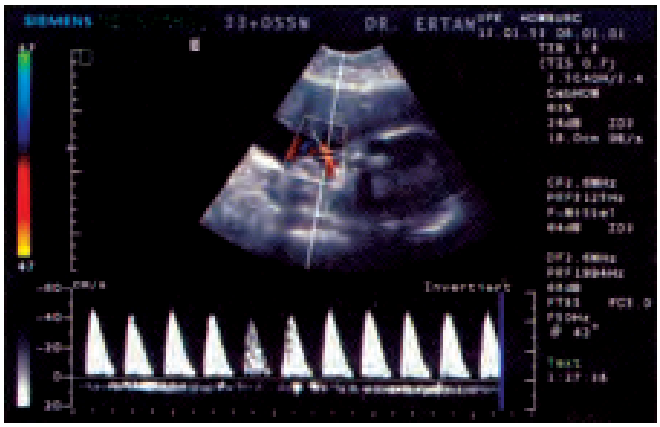

Figure 31.8: Absent end-diastolic flow (AEDF) of the umbilical artery in the third trimester

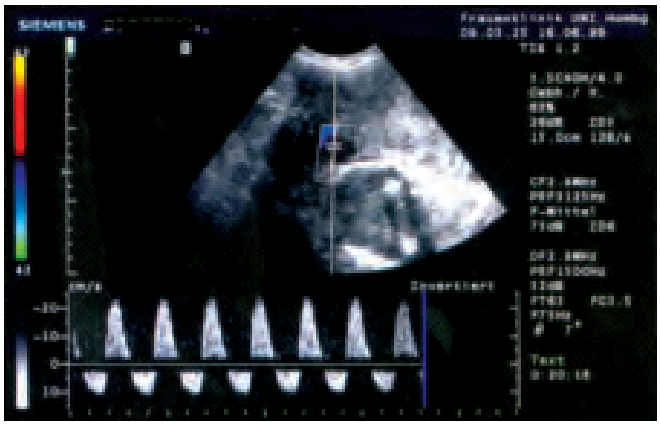

Figure 31.9: Reverse flow (RF) of the umbilical artery

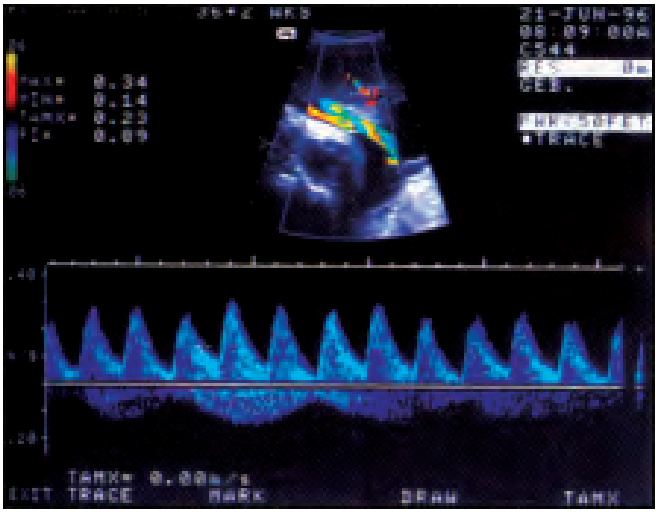

Figure 31.10: Pitfalls in umbilical artery Doppler velocimetry (fetal breathing)

neonatal intensive care unit (NICU), and a higher incidence of respiratory distress in IUGR fetuses.[38] Therefore, intensive antenatal surveillance in fetuses with suspected IUGR with a normal UA Doppler FVW was not recommended by the authors. Conflicting data were presented by McCowan et al;[39] they confirmed that abnormal UA Doppler studies are associated with a poor perinatal outcome in IUGR fetuses but also concluded that the perinatal outcome in small for gestational age fetuses with normal UA Doppler studies is not always benign (i.e. low ponderal index, postnatal hypoglycemia, admission to the NICU). Recently, our study group[40] suggested that reversed flow should be seen as a particular clinical entity with the higher incidences of severe IUGR, perinatal and overall mortality compared to absent end diastolic flow **(Figs 31.8 and 31.9)**.

In our clinical experience, when an IUGR fetus is suspected, the UA, FDA and MCA are the first fetal vessels to be assessed. The ductus venosus (DV), umbilical vein, inferior vena cava Doppler examinations are secondary vessels to be examined, only when an abnormal FVW is detected on the arterial vessels. Adding serial Doppler evaluation of the UA, MCA and DV to IUGR surveillance will enhance the performance of the biophysical score in the detection of fetal compromise and therefore optimizing the timing of intervention.[41]

Chromosomal Abnormalities

It was shown that absent end-diastolic flow in the UA is associated with chromosomal abnormalities like trisomies, triploidies or chromosomal deletions.[42] Setting out from the point that structural anomalies are more frequent in fetuses with chromosomal aberrations, a rapid acquisition of a karyotype in fetuses with congenital anomalies and an absent end-diastolic flow in the UA is recommended.[43]

Impact on Perinatal Consequences

Abnormal UA FVWs are associated in IUGR fetuses with one of the following outcomes: early delivery, reduced birth weight, oligohydramnios, NICU admission, and prolonged hospital stay.[32,44] In a meta-analysis, it was shown that the use of UA Doppler sonography in pregnancies complicated by IUGR reduces perinatal mortality up to 38% and improves perinatal outcome.[45] A review consisting of 7,000 high-risk pregnancies[46] found that Doppler ultrasound was associated with a trend toward reduction in perinatal death especially in pregnancies complicated with preeclampsia or IUGR. The Doppler ultrasound use was also associated with fewer inductions of labor and fewer hospital admissions, without reports of adverse perinatal effects. The reviewers concluded that the use of Doppler ultrasound in high-risk pregnancies is likely to reduce perinatal mortality.

Neonatal Intraventricular Hemorrhage

Fetal status as well as neonatal complications of prematurity in IUGR both contribute to adverse perinatal outcome and increase the risk for the development of intraventricular hemorrhage (IVH). Data suggest that absent and reversed end-diastolic flow in the UA early in gestation carries a high risk of subsequent neonatal IVH.[47] However, this observation is not independent of other perinatal variables: prematurity and difficult births remain the most important determinants of this complication.

Neuromotoric Outcome

Valcomonico et al.[44] evaluated the association of UA Doppler velocimetry with long-term neuromotoric outcome in IUGR fetuses with normal (n=17), reduced (n=23) and absent or reversed (n=31) UA end-diastolic flow. The infants who survived the neonatal period were observed for a mean of 18 months. Their postural, sensorial and cognitive functions were evaluated at 3, 6, 9, 12 and 18 months of age. Although, due to small number of cases, the results did not reach statistical significance, the incidence of permanent neurological sequelae increased as the UA end-diastolic flow decreased (35% with absent or reversed flow, 12% with reduced flow, and 0% with normal flow). Recently, in

another study[48] 23 IUGR fetuses with absent or reversed UA end-diastolic flow were matched with fetuses with appropriate growth. All children were followed for 6 years and intellectual and neuromotor development was significantly diminished in fetuses with abnormal FVWs. Only social development was not impaired in fetuses with abnormal UA FVWs. Similar results were previously published by our working group, too.[49,50]

Intrapartum Studies

A review of intrapartum UA Doppler velocimetry for adverse perinatal outcome gave disappointing results.[51] Out of 2,700 pregnancies, which were evaluated for the intrapartum use of Doppler velocimetry showed that it is a poor predictor for measures like low Apgar scores, intrapartum fetal heart rate abnormalities, umbilical arterial acidosis and cesarean section for fetal distress.

Umbilical Artery Doppler Ultrasound in Unselected Patients

Theoretically, the use of routine UA Doppler ultrasound in unselected or low risk pregnancies would be to detect those pregnancies in which there has been failure to establish or maintain the normal low-resistance umbilical and uterine circulations (a pathological process leading to placental dysfunction and associated with intrauterine growth retardation and preeclampsia), before there is clinical evidence of fetal compromise. In practice, observational and longitudinal studies of Doppler ultrasound in unselected or low-risk pregnancies have raised doubts about its application as a routine screening test, and authors have cautioned against its introduction into obstetric practice without supportive evidence from randomized trials.[52-54] The relatively low incidence of significant, poor perinatal outcomes in low risk and unselected populations presents a challenge in evaluating the clinical effectiveness of routine UA Doppler ultrasound, as large numbers are required to test the hypothesis.

Multiple Gestation

The S/D ratio of twins at the UA are in agreement with singleton pregnancies in the third trimester.[55] Twins with an abnormal UA FVW tend to be born earlier, have a higher perinatal mortality and morbidity, and have more frequent structural anomalies than fetuses without abnormal Doppler results.[56]

Discordant growth between the twins may occur in the cases of twin-twin transfusion syndrome, a poor placental implantation site or chromosomal anomalies. Discordant growth is a very high-risk situation, with a high perinatal mortality and morbidity. The diagnosis is made mainly by ultrasound biometry. The best predictor for the diagnosis of discordant twins appears to be the presence either a difference in the UA S/D ratio greater than 15% or a different estimated fetal weight greater than 15%.[57] Recently it has been reported that abnormal UA FVW can be observed in small twins more often in monochorionic than dichorionic twins.[58] Doppler ultrasound abnormalities of the UA in either twin are associated with poor perinatal outcome in twin-twin transfusion syndrome.

The Biophysical Profile and Multivessel Doppler Ultrasound in IUGR

Biophysical profile scoring (BPS) and Doppler surveillance are the primary methods for fetal assessment in IUGR. As placental insufficiency worsens, the fetus adapts by progressive compensation. Previously, it has been suggested that the sequential changes in arterial and venous flow occur before some biophysical parameters (fetal tonus, movement, breathing, amniotic fluid volume and nonstress test)) decline.[59,60] Baschat et al.[41] evaluated whether multivessel Doppler parameters (UA, UV, MCA, DV and inferior vena cava) precede biophysical fetal parameters in fetuses with severe IUGR. They found that combining multivessel Doppler and composite BPS will provide significant early warning and a definitive indication for action in the management of severe IUGR, and suggested that delivery timing may be based on this new standard. In the preterm growth-restricted fetus, timing of delivery should be critically determined by the balance of fetal versus neonatal risks.[61]

Fetal Descending Aorta (FDA)

Beside the UA, routine Doppler sonographic examination at the descending fetal aorta is possible. Flow velocity waveforms of the FDA are usually recorded at the level of the diaphragm. Infact, FVWs at the level of the diaphragm and distally to the origin of the renal arteries are different.[62] Normal blood FVWs in the FDA is highly pulsatile, with a minimal diastolic component **(Fig. 31.11)**. The descending part of the aorta provides perfusion to the fetal abdominal organs, umbilical-placental circulation and lower extremities. The FVW of the FDA shows a continuous forward stream during the whole heart cycle, but when compared to the FVW of the UA, the end-diastolic flow is less than the systolic component. Due to this reason the S/D ratio in the fetal aorta goes far than the S/D

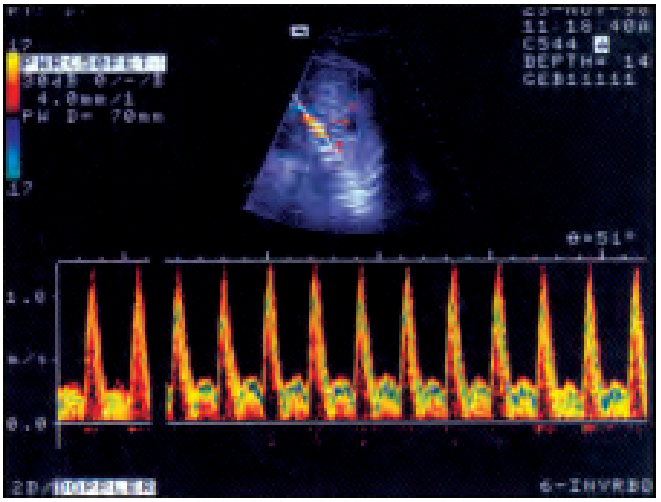

Figure 31.11: Normal flow velocity waveforms of the fetal descending aorta in the third trimester

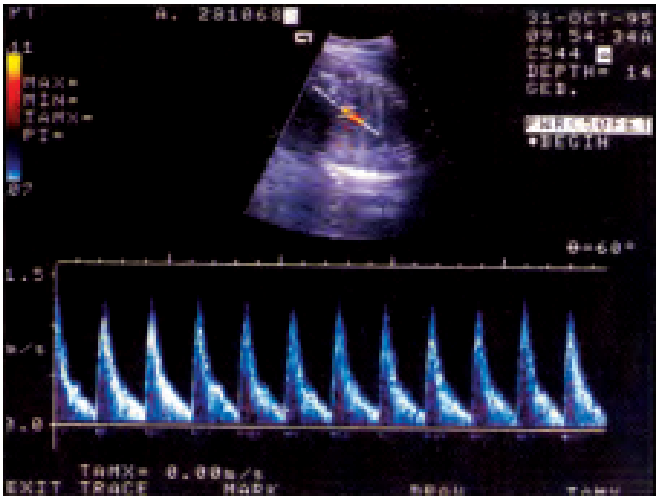

Figure 31.12: Abnormal flow velocity waveforms of the fetal descending aorta in the third trimester (high resistance index)

ratio in the UA. As pregnancy advances, the fetal aortic diameter gets wider, which decreases peripheral resistance and increases diastolic flow component. Nevertheless, this does not cause a significant S/D ratio decrease in the FDA.[63] Resistance and pulsatility indices in the last trimester are also not affected significantly, and show a similar course as in the UA.

Increased placental impedance combined with redistribution of blood flow from nonvital to vital organs may result in changes in the aortic FVWs. An elevated S/D ratio, RI and PI **(Figs 31.12 to 31.15)** is associated with both IUGR and adverse perinatal outcomes, such as severe growth restriction, necrotizing enterocolitis, fetal distress and perinatal mortality.[64-71]

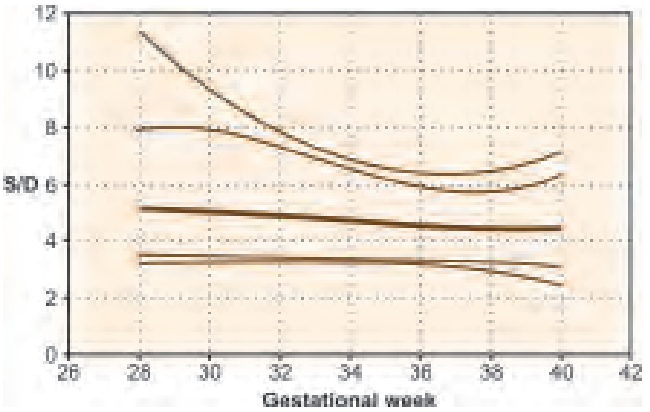

Figure 31.13: Descending fetal aorta S/D ratio nomogram

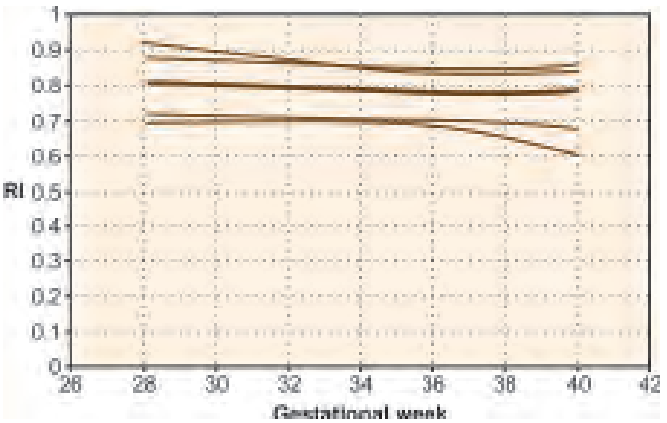

Figure 31.14: Descending fetal aorta RI nomogram

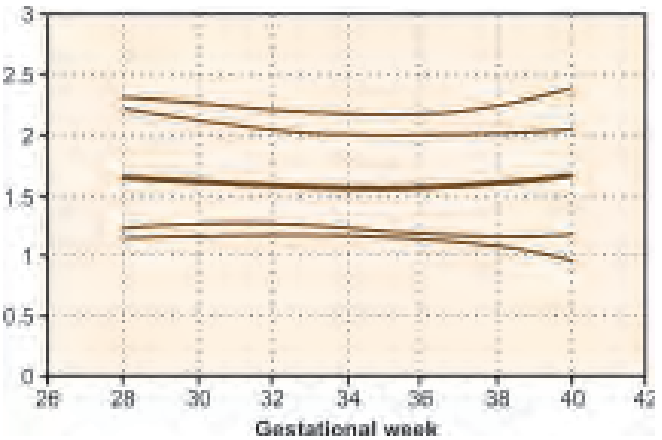

Figure 31.15: Descending fetal aorta PI nomogram

Absent end-diastolic flow at the FDA is also a predictor of fetal heart rate abnormalities **(Fig. 31.16)**. It was shown that absent flow in the FDA were detected 8 days

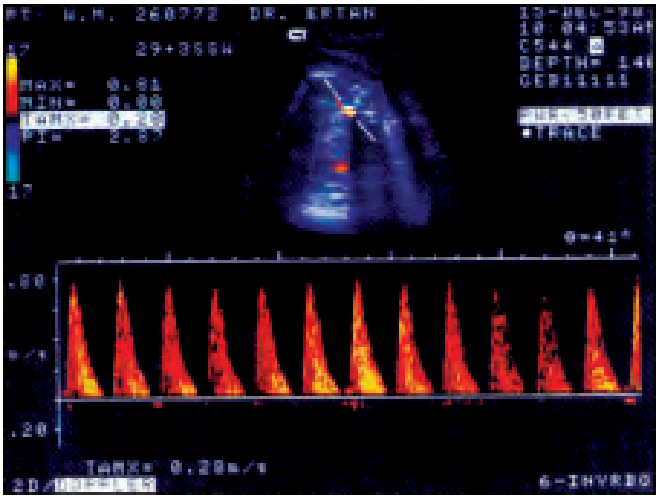

Figure 31.16: Absent end-diastolic flow (AEDF) of the fetal descending aorta (FDA) in the third trimester

prior to the onset of decelerations at fetal heart rate monitoring.[68] The sensitivity and specificity of absent end-diastolic flow in the FDA for prediction of IUGR with fetal heart rate abnormalities are 85% and 80%, respectively.[70,71]

Abnormal FVWs of the FDA were also evaluated for intellectual function, and minor neurological dysfunction.[49,50,72,73] At 7 years of age, verbal and global performances as well as neurological examination were significantly better in the fetuses with normal aortic FVWs. The association found between abnormal fetal aortic velocity waveforms and adverse outcome in terms of minor neurological dysfunction suggests that hemodynamic evaluation of the fetus has a predictive value regarding postnatal neurological development.[72]

Albeit, most of the studies showed Doppler velocimetry abnormalities of the FDA is a predictive test for the onset of decomposition due to placental insufficiency in the IUGR fetuses **(Figs 31.16 and 31.17)**, it cannot be recommended as a screening or diagnostic test for IUGR in an unselected obstetric population.[74]

Middle Cerebral Artery (MCA)

The circle of Willis is composed anteriorly of the anterior cerebral arteries (branches of the internal carotid artery that are interconnected by the anterior communicating artery) and posteriorly of the two posterior cerebral arteries (Branches of the basilar artery that are interconnected on either side with internal carotid artery by the posterior communicating artery).[75] These two trunks and the MCA, another branch of the internal carotid artery, supply the hemispheres on each side **(Fig. 31.18)**. All of the defined arteries have different FVWs, therefore, it is important to know which artery is being examined during clinical practice.[76]

The most favorably positioned vessel for Doppler sonographic examination of fetal brain perfusion is the MCA. As the pregnancy advances, the vascular resistance in the MCA decreases **(Fig. 31.19)** and the Doppler indices change **(Figs 31.20 to 31.22)**.[77] During the early stages of pregnancy, end-diastolic flow velocities in cerebral vessels are small or absent, but velocities increase towards the end of gestation. In the normal developing fetus, the brain is an area of low vascular impedance and receives continuous forward flow throughout the cardiac cycle. Intrauterine growth restriction due to placental insufficiency is likely to be caused by redistribution of fetal blood flow in favor of the fetal brain and "stress organs", at the expense of less essential organs such as subcutaneous tissue, kidneys and liver. Finally, the already low resistance to blood flow in the brain drops further to enhance brain

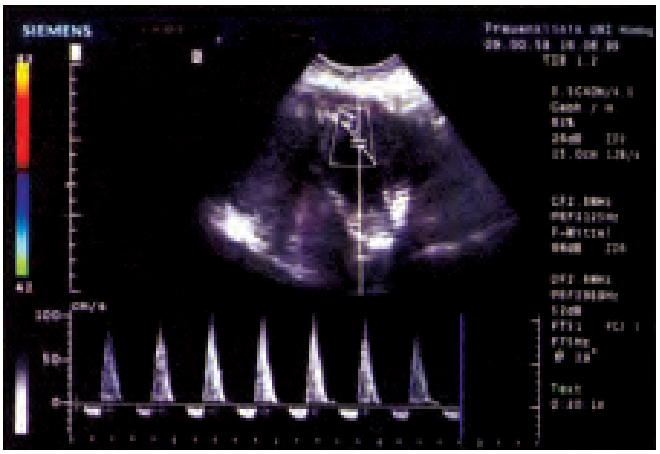

Figure 31.17: Reverse flow (RF) in the fetal descending aorta

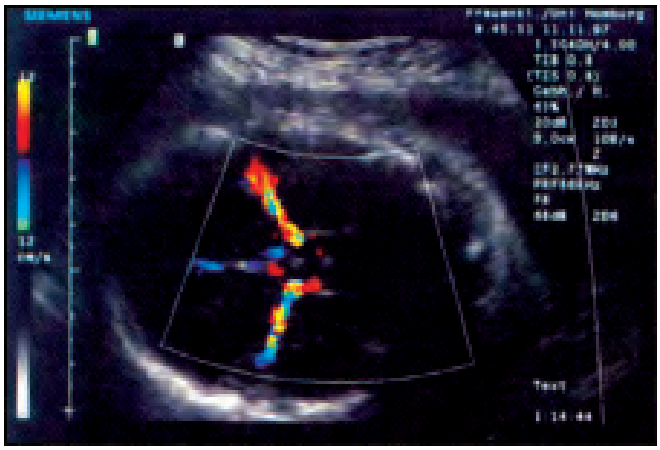

Figure 31.18: Circle of Willis and middle cerebral artery visualized with color Doppler

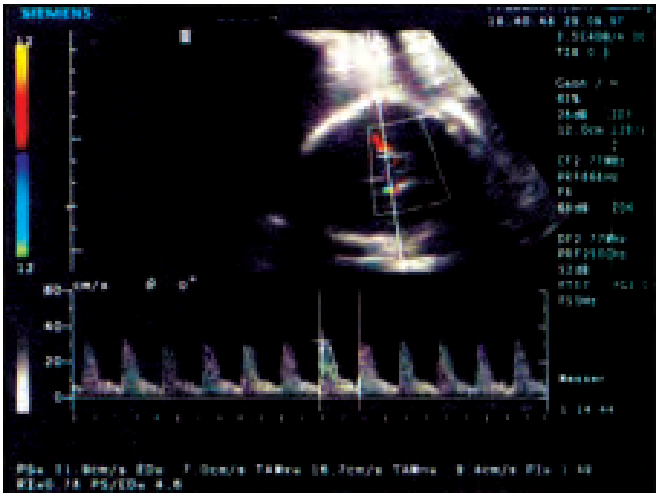

Figure 31.19: Normal flow velocity waveforms of the middle cerebral artery in the third trimester

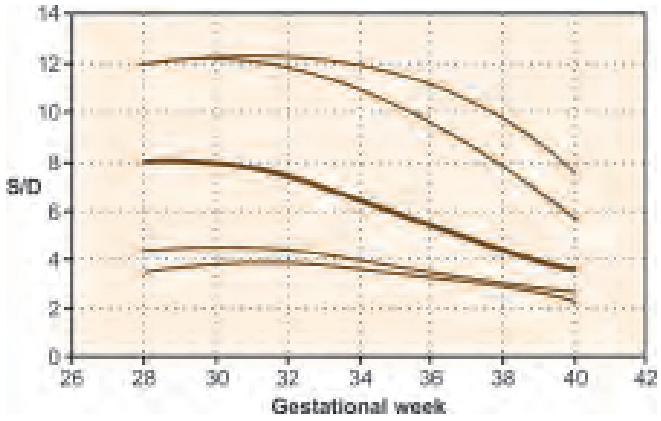

Figure 31.20: Middle cerebral artery S/D ratio nomogram

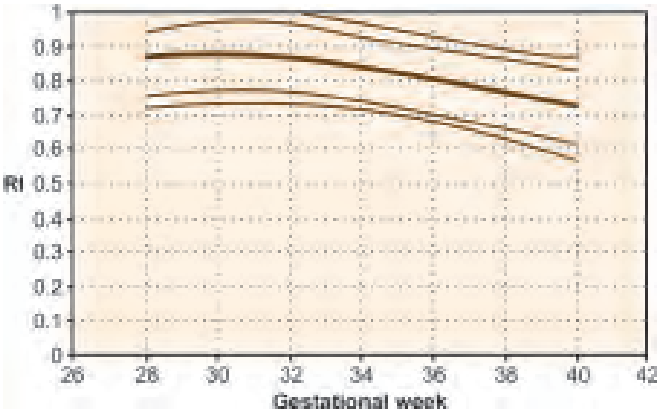

Figure 31.21: Middle cerebral artery RI nomogram

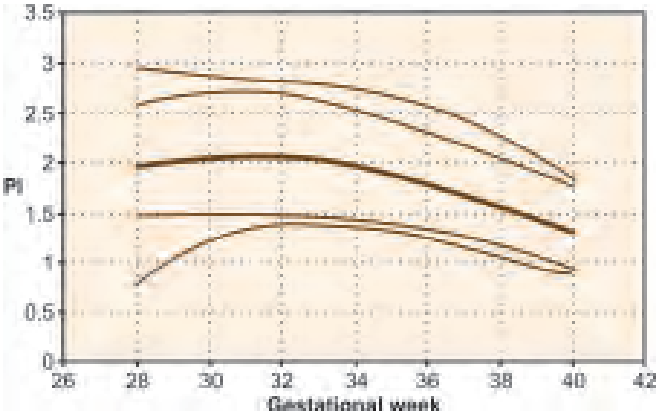

Figure 31.22: Middle cerebral artery PI nomogram

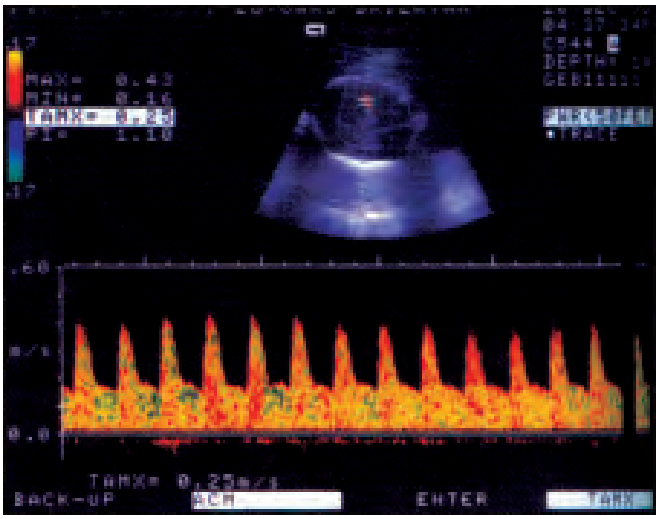

Figure 31.23: Abnormal flow velocity waveforms of the middle cerebral artery in the third trimester (brain sparing effect)

circulation **(Fig. 31.23)**. This results with increased end-diastolic velocities, and a decrease in the S/D ratio of the MCA (Brain sparing effect).[78]

Abnormalities of the UA flow correlated with fetal compromise better than intracerebral artery blood flow impairment. This suggests that high placental impedance precedes the onset of the "brain sparing effect". In a study, in which 576 high risk pregnancies were evaluated for the UA and MCA velocimetry, neither test was able to predict adverse perinatal outcome in the normal growing fetus.[79] Results showed that simultaneous assessment of UA and MCA velocimetry in IUGR fetuses did not improve the perinatal outcome. When the UA velocimetry was normal, the MCA velocimetry did not improve the prediction of IUGR or adverse perinatal outcome.

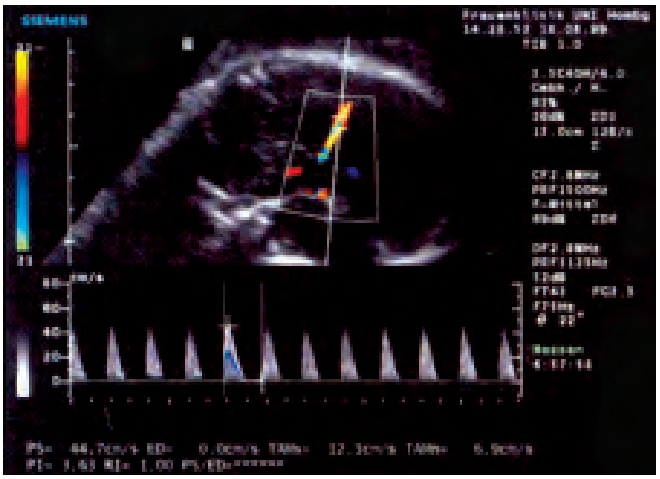

Figure 31.24: Absent end-diastolic flow after the brain sparing effect (de-centralization) this presumably reflects the prefinal stage due to development of brain edema

However, when both arteries velocimetric values were abnormal, the risk of being growth restricted and having an adverse perinatal outcome was doubled.

It has been reported that the MCA PI is below the normal range when pO_2 is reduced.[80] Maximum reduction in PI is reached when the fetal pO_2 is 2–4 standard deviations below normal for gestation. When the oxygen deficit becomes greater, there is a tendency for the MCA PI to rise; this presumably reflects the pre-final stage due to development of brain edema **(Fig. 31.24)**.

Hyperactivity of fetus, increase of intrauterine pressure (e.g. polyhydramnios), and external pressure to the fetal head (e.g. by the probe) might erroneously increase end-diastolic flow velocities in the MCA.[81] Different investigators have undertaken studies — utilizing data obtained from the UA and MC — to develop indices for evaluation of intrauterine risk.[75]

Prediction of Fetal Hemoglobin in Red Cell Alloimmunization

Fetal anemia caused by red cell alloimmunization can be detected noninvasively by Doppler ultrasound on the basis of an increase in the peak systolic velocity in the MCA.[82,83] Although there is not a strong correlation between these two parameters when the fetus is nonanemic, the correlation becomes stronger as the hemoglobin levels decrease.[83] Prospective evaluation of the MCA peak systolic velocity to detect fetuses at risk for anemia in red cell alloimmunization showed that 90 of the 125 anticipated invasive procedures could be avoided.[84]

In anemic fetuses, changes in hematocrit lead to a corresponding alteration in blood viscosity and to an impaired release of oxygen to the tissues. Increased cardiac output and vasodilatation are the main mechanisms by which the fetus attempts to maintain the oxygen and metabolic equilibrium in various organs. It is likely that when the fetus is nonanemic or mildly anemic, there are only minor or insignificant hemodynamic changes. Therefore, the blood velocity does not change. When the fetus becomes more anemic, various mechanisms compensate to maintain the oxygen and metabolic equilibrium in the various organs. The MCA peak systolic velocity changes proportionally to the hemoglobin deficiency.

Doppler measurements appear to be valuable for estimating hemoglobin concentration in fetuses at risk for anemia. Doppler sonography of the MCA has the potential to decrease the need for invasive testing (amniocentesis, cordocentesis) and its potential risks.[85,86]

FETAL VENOUS CIRCULATION

In recent years research on the fetomaternal circulation has focused more on the venous side of the fetal circulation. Physiologically, blood flow velocities in the umbilical vein (UV) and the portal circulation are steady and non-pulsatile. However, it has been shown that both fetal body and breathing movements can interrupt these venous FVWs. In a recent review, it was concluded that several pathologic conditions such as nonimmune hydrops, severe IUGR, and cardiac arrhythmias also result in an abnormal, pulsatile venous blood flow.[87] However, the relationship between fetal venous blood flow patterns and imminent fetal asphyxia or fetal death is still unknown. Many studies on venous circulation in the fetal brain[88] and pulmonary venous circulation in the diagnosis of pulmonary hypoplasia were performed.[89] Recent findings promote the use of venous Doppler to aid in timing delivery of severely growth-restricted fetuses. Whereas initially it appeared that abnormalities in ductus venosus waveform were the endpoint for pregnancies afflicted with intrauterine growth restriction, newer data suggest that these abnormalities may plateau prior to further fetal deterioration as witnessed by changes in the biophysical profile.[90]

Umbilical Vein (UV)

Oxygenated blood returning from the placenta runs from the UV through DV and inferior vena cava. Approximately 20–30% of the blood in the UV goes through the DV and the remaining well oxygenated blood perfused the left lobe of the liver[91] **(Figs 31.25 to 31.27)**. Normally after 15 weeks' gestation the umbilical

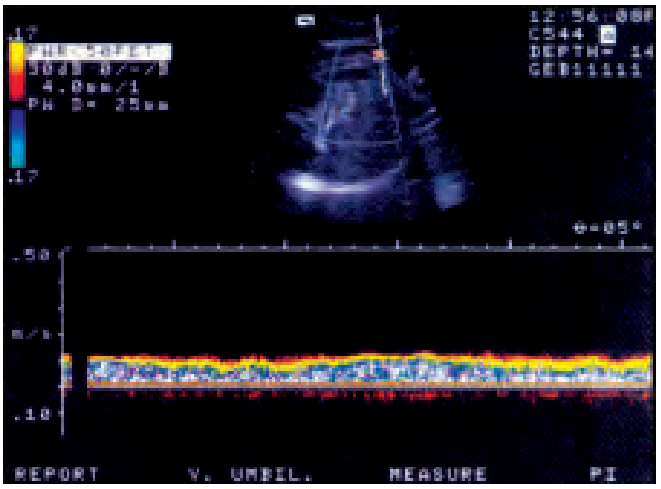

Figure 31.25: Normal flow in the umbilical vein in the third trimester (without pulsations)

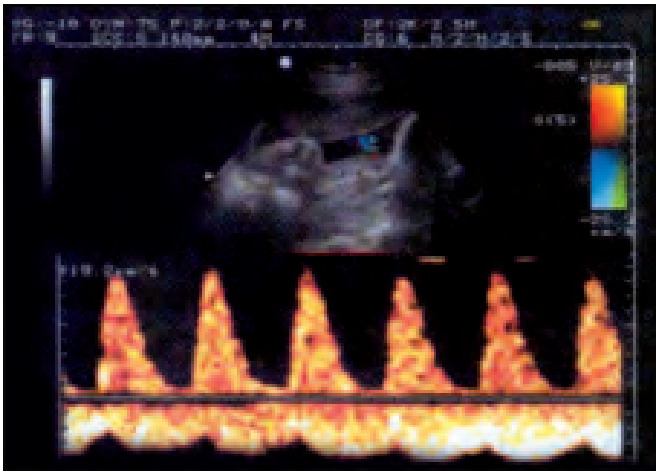

Figure 31.26: Abnormal flow in the umbilical vein (single pulsating pattern during the heart cycle)

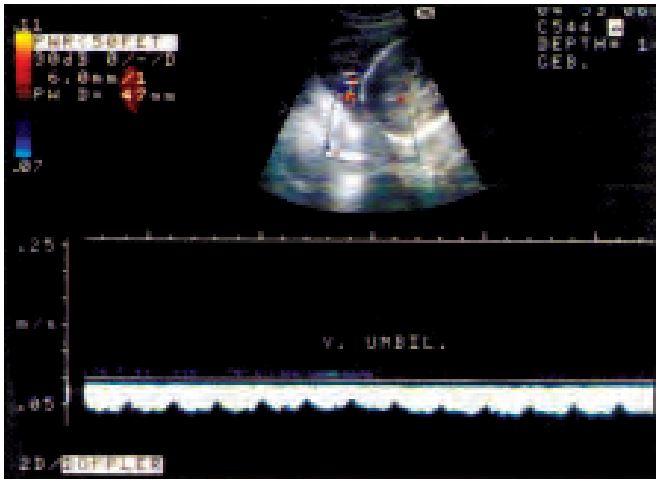

Figure 31.27: Highly pathological flow velocity waveforms of the umbilical vein (double pulsating pattern during the heart cycle)

vein has continuous forward blood flow.[90] The presence of UV FVW pulsatility has been associated with increased perinatal morbidity and mortality.[92,93] In an animal model, Reed et al. evaluated the UV Doppler flow patterns and concluded that pulsations of the UV velocity reflect atrial pressure changes that are transmitted in a retrograde fashion.[94] In some studies, it was also observed that UV pulsations are detected in fetuses with abnormal UA FVWs and/or fetal heart rate abnormalities.[93] More recently, Ferrazzi et al.[95] showed that UV blood flow is reduced in IUGR fetuses and suggested that long-term studies be performed to evaluate the clinical implications of their finding. Umbilical vein pulsations were also reported in pregnancies with nonimmune hydrops fetalis.[96] In this study, all the fetuses without venous pulsations survived, but only 4 of the 14 fetuses with pulsations survived. Fetuses with pulsation in the UV in late gestation have a higher morbidity and mortality, even in the setting of normal UA blood flow.[97] When UV pulsations are found in an IUGR fetus, it is often accompanied by reversal of the umbilical artery end-diastolic flow and reversal of the atrial "kick" on ductus venosus waveform, which is an ominous sign.[90]

Inferior Vena Cava

The flow profile within this vessel is complex: it consists of two phases of forward flow (Systolic and early diastolic), followed by a component of reversed flow in late diastole[87] **(Figs 31.28 and 31.29)**. Like other venous flow patterns, the FVWs are affected by fetal body and breathing movements. The FVW can be used for diagnosis of fetal arrhythmias, by comparing it with the FVW of the fetal aorta due to its proximity.[98] In IUGR fetuses, the FVW is characterized by an increased reversed flow during atrial contraction.[99] The mecha-

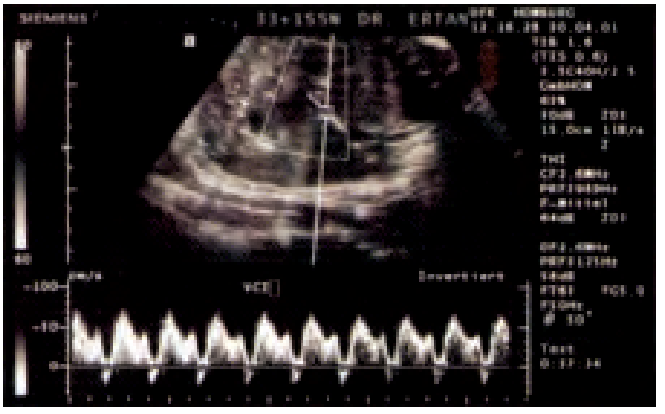

Figure 31.28: Normal flow velocity waveforms of the inferior vena cava (with reverse flow during the end-diastole)

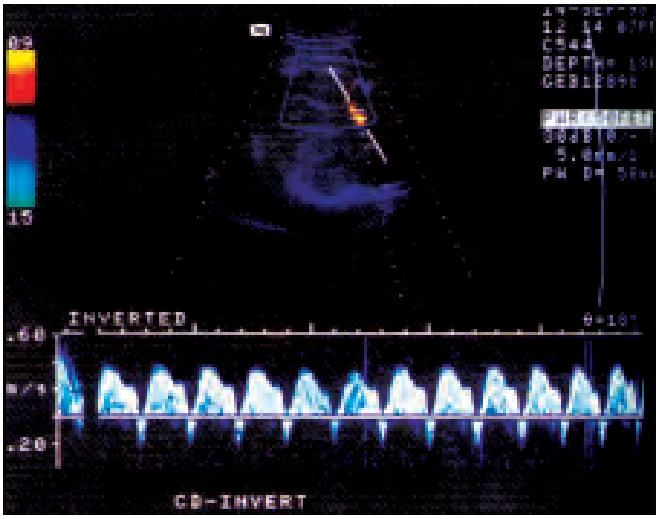

Figure 31.29: Abnormal flow velocity waveforms of the inferior vena cava (with increasing reversed flow during end-diastole)

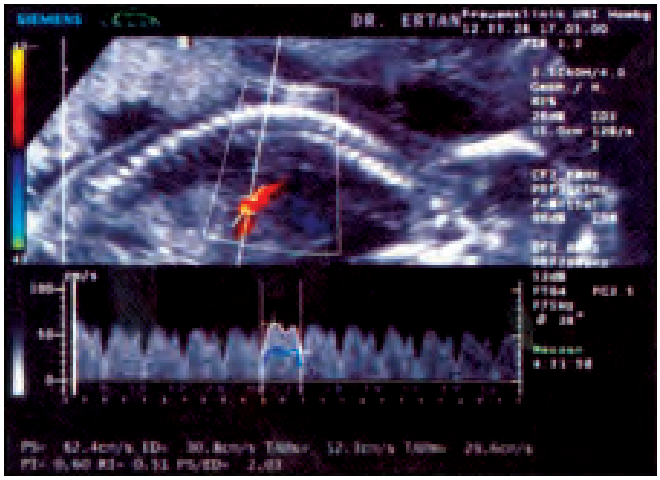

Figure 31.30: Visualization of the ductus venosus with color Doppler and normal flow velocity waveforms (with forward flow during diastole and A-wave: corresponding to atrial contraction during the late diastole)

nism of this increase is attributed to abnormal ventricular filling characteristics, an abnormal ventricular wall compliance, or abnormal end-diastolic pressure.

Ductus Venosus (DV)

The DV transports oxygenated blood from the UV directly through right atrium and foramen ovale to the left atrium and ventricle, and then to the myocardium and brain.[100-106] The ductus venosus carries the most rapidly moving blood in the venous system, and thus is easily identifiable by the aliasing seen on Doppler ultrasound. The DV originates from the portal sinus. Thus, the frequently expressed concept that the DV originates from the left portal vein or UV is anatomically inaccurate.[107] No anatomical continuity between the UV and DV exists, as incorrectly described, in recent Doppler ultrasound studies.[108] It is well accepted that the DV plays a major role in the regulation of fetal circulation by modifying the volume of its flow depending on the pressure gradient between the UV and the heart.[91]

In normal fetuses, color Doppler demonstrates the DV as a vessel bridging the left portal vein and the inferior vena cava with an obvious gradient in velocity compared with the left portal vein.[91] A common error is the sampling of the left hepatic vein rather than the DV.[75] Physiologically, this FVW shows continuous forward flow during the heart cycle, mimicking the pattern of the inferior vena cava **(Figs 31.30 and 31.31)**. The high pressure gradient between the UV and the DV results in high blood flow velocities within this vessel. In contrast to other venous FVWs, reversed flow

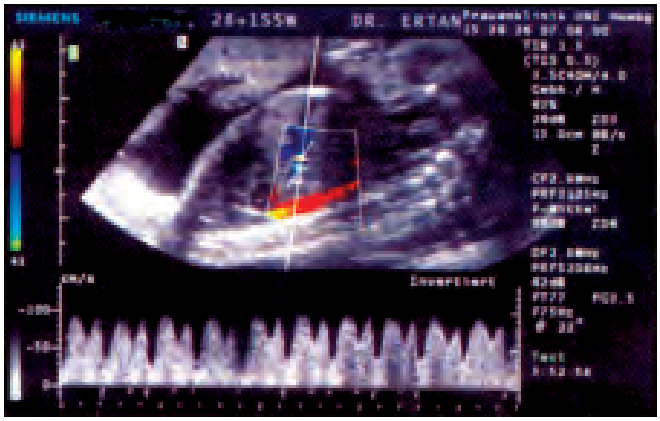

Figure 31.31: Normal flow velocity waveforms in the ductus venosus (with forward flow during diastole and A-wave)

in the DV is an abnormal finding, except for the first trimester due to the immaturity of the sphincter of ductus venosus. However, abnormal FVWs of the DV between 11–14 weeks' gestation was suggested to be a screening test of fetal chromosomal abnormalities and/or cardiac defects.[109] Abnormal ductus venosus FVW (retrograde atrial-wave) is a strong predictor of fetal cardiac abnormality, may enhance the detection of Down syndrome, is a good predictor of diverse causes of fetal hydrops and may be a distant precursor of severe placenta-based IUGR.[1]

In IUGR fetuses, reversed flow in the DV is an ominous sign **(Figs 31.32 to 31.35)**. Reversed flow in the ductus venosus results from a decline and subsequent reversal in forward blood flow velocity

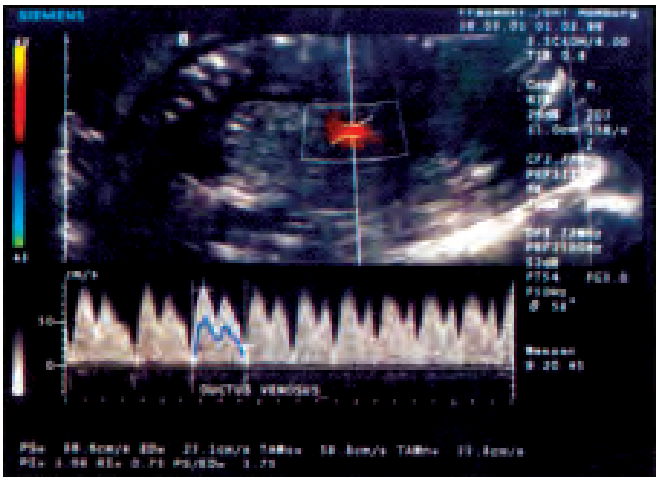

Figure 31.32: Initial pathological flow velocity waveforms of the ductus venosus (with forward flow and decreasing A-wave)

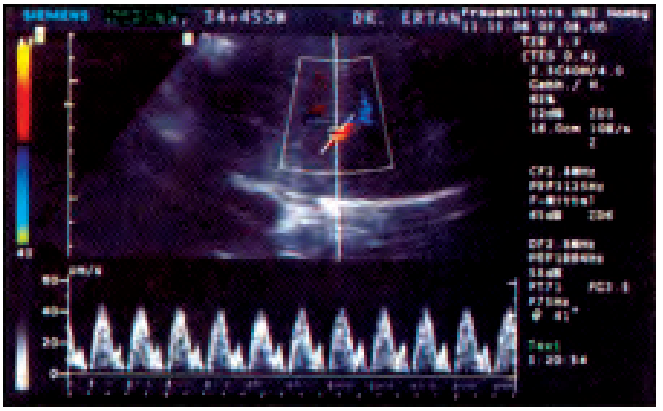

Figure 31.33: Abnormal flow velocity waveforms of the ductus venosus (absent A-wave)

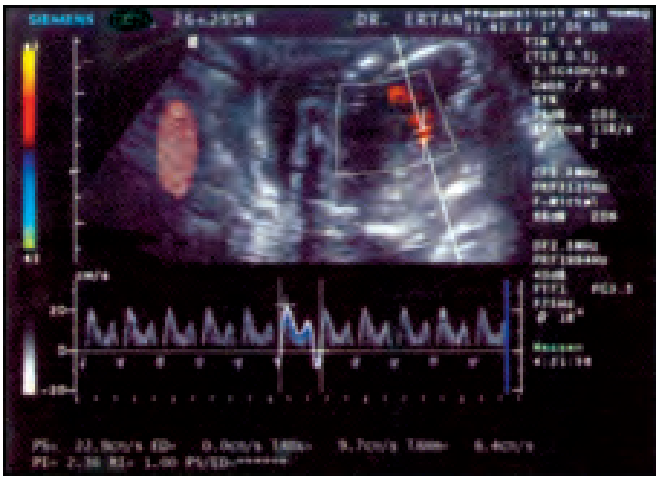

Figure 31.34: Highly pathological flow velocity waveforms of the ductus venosus (reversed A-wave)

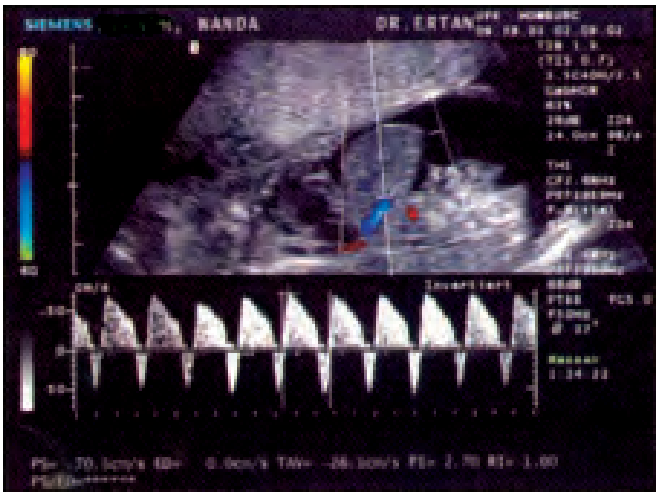

Figure 31.35: Highly pathological flow velocity waveforms of the ductus venosus (pre-final situation)

during atrial systole. The abnormality in forward cardiac function may be related to worsening placental disease, impaired cardiac function due to metabolic compromise, redistribution of hepatoportal blood flow through the liver or a combination of these. It was reported that reverse flow patterns of the DV in IUGR fetuses is the only significant parameter associated with perinatal death.[110]

It has been suggested that changes in DV blood flow pattern precede the appearance of abnormal fetal heart rate patterns in pregnancies complicated with placental insufficiency.[59,111] One should bear in mind, however, that these studies are technically difficult and that blood flow patterns within the DV are also modulated by fetal behavioral states, breathing movements and cardiac anomalies/arrhythmias.[74,112,113]

Timing of Delivery in Pregnancies Complicated with IUGR

The optimal timing of delivery in pregnancies complicated by IUGR is still an issue to be resolved. Clinicians have to balance the risks of prematurity against the risks of prolonged fetal exposure to hypoxemia and acidemia, possibly resulting in fetal damage or death. In a cross-sectional Doppler study of the fetal circulation, the appearance of significant changes in venous Doppler FVWs from the DV, inferior vena cava and hepatic veins was observed after fetal arterial blood flow redistribution from the FDA to the MCA was established.[59] Furthermore, the changes in the venous circulation seemed to be closely related to the onset of abnormal fetal heart rate patterns. Reduced fetal heart rate variation and occurrence of fetal heart rate decelerations

have been associated with fetal hypoxemia,[114] whereas extremely low values of short-term variation were found to be a reliable predictor of metabolic acidemia at delivery or fetal death.[115] In a longitudinal study,[116] the DV pulsatility index and short-term variation of fetal-heart rate were found to be important indicators for the optimal timing of delivery before 32 weeks' gestation, and delivery was advised if one of these parameters becomes persistently abnormal.

In another study[117] to determine time for delivery, the changes in the hepatic vein, DV and UV were investigated. Results of this study suggested that adding venous Doppler ultrasound to the arsenal of fetal surveillance in IUGR fetuses might assist in timing of delivery with less morbidity and mortality. The venous indices of the right hepatic vein and the DV, and double UV pulsations were found to be the most useful tools for this condition. Finally it was stated that venous Doppler evaluation could give valuable clinical information for surveillance in high-risk pregnancies.

In the recently published Growth Restriction Intervention Trial study (GRIT: multicentered randomized controlled trial) it was evaluated and compared if the expectant management of the IUGR cases was superior to the early delivery method.[118] The main outcome was death or disability at or beyond 2 years of age. Overall rate of death or severe disability at 2 years was 55 (19%) of 290 immediate births and 44 (16%) of 283 delayed births. With adjustment for gestational age and umbilical-artery Doppler category, the odds ratio (95% CI) was 1.1 (0.7–1.8). Also the results of this study guided clinicians minimally in constructing guidelines for timing delivery in IUGR cases.

UTEROPLACENTAL PERFUSION

In order to evaluate uteroplacental perfusion, examinations performed at uterine arteries (UtA) give more accurate information than the arcuate arteries.[22] Velocities obtained from UtA are higher than from arcuate arteries **(Fig. 31.36)**. This is important in interpreting Doppler study results, and it should always be paid attention on which vessel examinations were performed.

In the nonpregnant uterus, the UtA FVWs are characterized by high impedance blood flow, and almost always early diastolic notches. Kurjak et al reported the average UtA RI at the proliferative phase to be 0.88 ± 0.04 (2SD).[119] A high resistance to flow during the midluteal phase of the cycle (day 21) has been associated with infertility.[120] In women undergoing in vitro fertilization, those with a higher PI on the day of follicular aspiration have a lower probability of successful pregnancy.[121] Such findings suggest a potential value for UtA Doppler velocimetry in identifying endometrial receptivity in infertile patients.

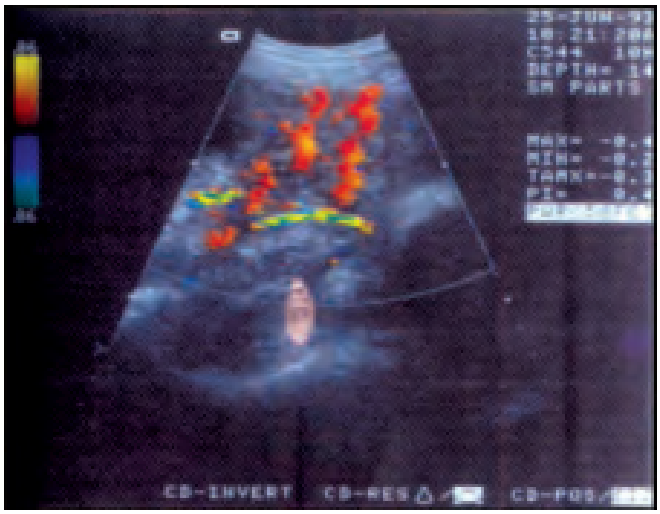

Figure 31.36: Uterine and arcuate arteries, visualized with color Doppler

In the first trimester, the intervillous maternal circulation is established at 7 to 8 weeks.[122] The impedance to blood flow within the intervillous space significantly decreases towards the mid-pregnancy and then remains stable. Blood flow velocities are reaching a plateau between 16 and 22 weeks of gestation, then after these parameters remain almost constant until the 36th gestational week.

From 6 to 12 weeks, FVWs obtained from the UtA are characterized by a high systolic and low diastolic component (elevated S/D ratio), and the presence of a notch in the early diastolic period **(Fig. 31.37)**. Flow velocity waveforms of the arcuate arteries also show notching, but with a higher diastolic component.[123] In the second and third trimester of pregnancy, the UtA diameter enlarge,[124] the systolic peak velocity and volume flow rates increase,[125,126] and a progressive fall in impedance to blood flow can be detected.[127] The early diastolic notch and the difference between S/D ratios of the placental versus nonplacental sites should disappear after 24–26 weeks' gestation.[125,128] Absence of this transition from high to low impedance, and of similar bilateral FVWs is associated with a higher incidence of hypertensive disease, abruption, intrauterine fetal demise, preterm birth and IUGR.

Blood flow velocities in uterine arteries depend on the localization of placenta and gestational age.[129] If the placenta is laterally located, blood flow velocities in the ipsilateral uterine artery are more important than the

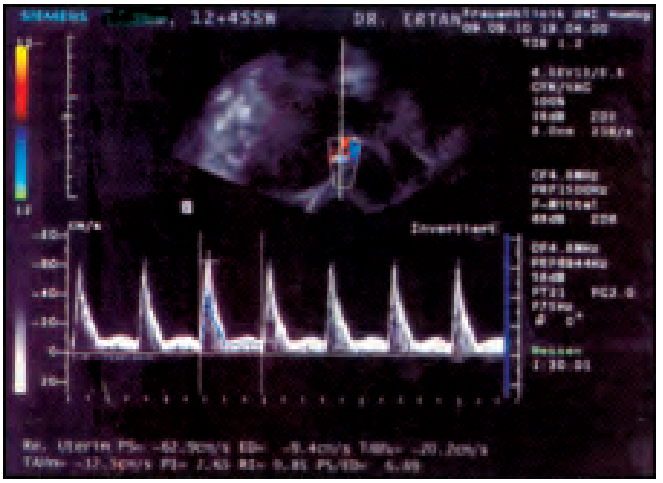

Figure 31.37: Normal flow velocity waveform of the uterine artery in the first trimester (high resistance with an early diastolic notch)

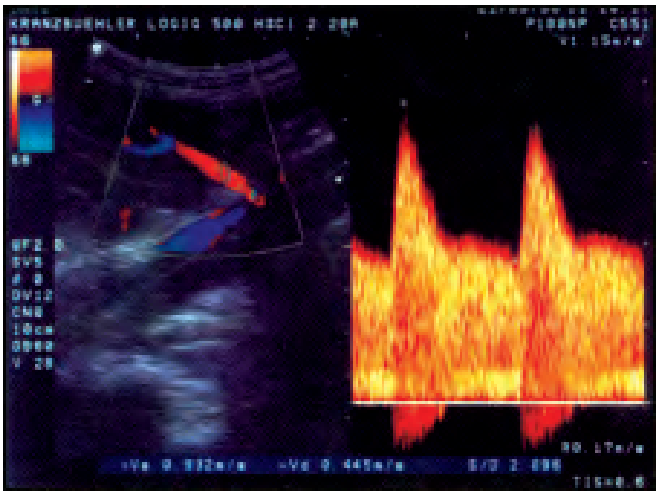

Figure 31.38: Normal flow velocity waveform in the uterine artery in the third trimester (high end-diastolic flow, without notching)

flow velocities of the contralateral vessel. Differences between flow velocities of the right and left uterine artery are evident at the early stages of pregnancy. But in the third trimester, the difference between the S/D ratio of the vessels decrease to a minimum[22] **(Fig. 31.38)**. If an abnormal flow pattern is observed in the uterine arteries, this most probably indicates the defective perfusion of fetoplacental unit, which predicts a high probability for developing preeclampsia, resulting with intrauterine growth retardation[5] **(Fig. 31.39)**.

At the early stages of pregnancy, end-diastolic flow velocities in placental arteries are low, but systolic flow is evident.[22] With trophoblastic invasion and maturation

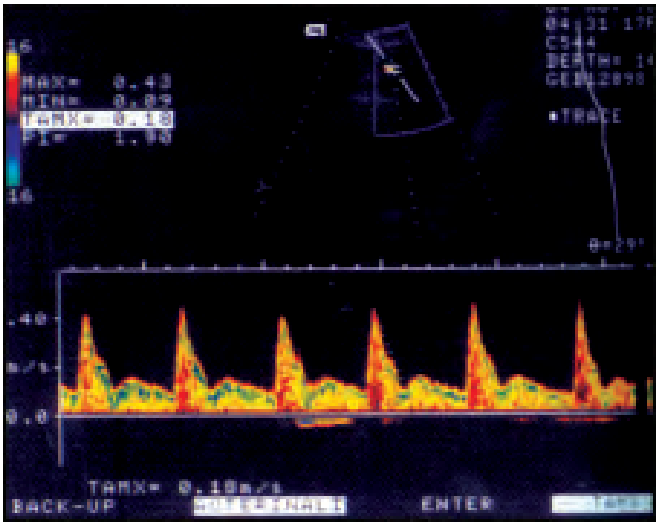

Figure 31.39: Abnormal flow velocity waveform in the uterine artery in the third trimester (low end-diastolic flow, with an early diastolic notch)

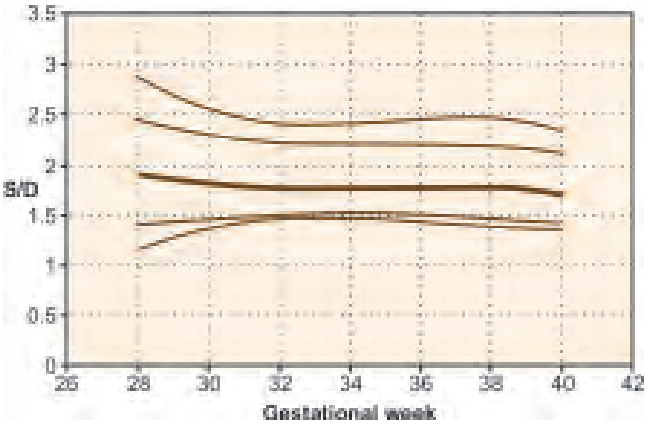

Figure 31.40: Uterine arteries S/D ratio nomogram

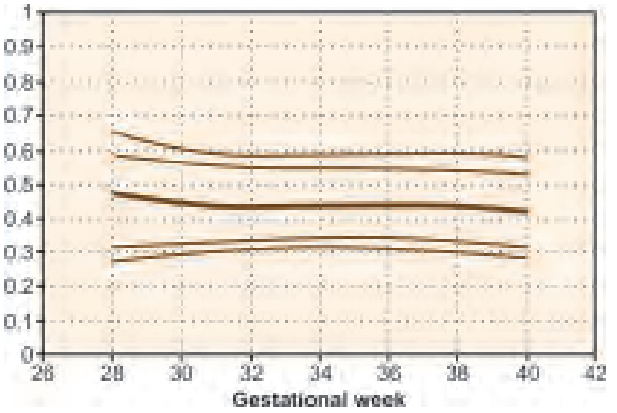

Figure 31.41: Uterine arteries RI nomogram

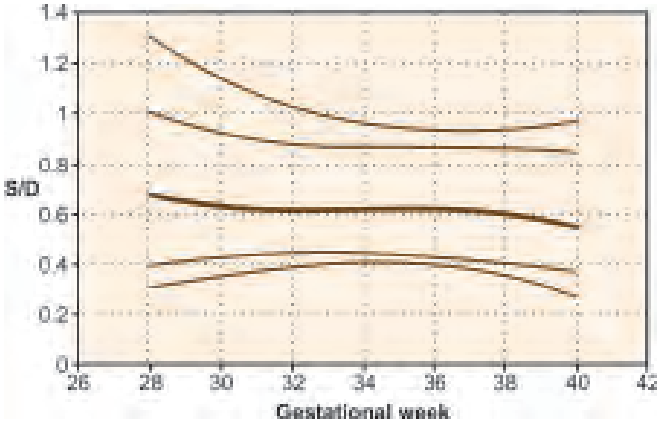

Figure 31.42: Uterine arteries PI nomogram

of the uteroplacental vessels, beyond the second trimester the high pressure system is converted to a low pressure system, and vascular resistance declines.[130] The biologic variability after 20–24 weeks' gestation becomes almost stable **(Figs 31.40 to 31.42)**.

Before 24 weeks' gestation, early diastolic notching due to the immature uteroplacental vascular system is normally observed. Beyond this gestational age, persistent early diastolic notching is associated with preeclampsia.[7,10,12] Elevated RI, PI or S/D ratios and the presence of a diastolic notch are considered as abnormal UtA FVWs.

Prediction of Complicated Pregnancies with Uteroplacental Doppler Velocimetry

Pregnancies complicated with preeclampsia and IUGR show evidence of impaired trophoblastic invasion and maturation.[131] A scoring system was proposed to predict the chance of adverse outcomes (preeclampsia, IUGR, preterm delivery, or fetal demise) using UtA Doppler. This score awarded 1 point for a notch and 1 point for a low end-diastolic flow in each waveform, bilaterally. In example, a score of 4 would indicate bilaterally high S/D ratios with bilateral notches. Those with a score of 4 had an 83% rate of adverse perinatal outcomes, 48% with a score of 3, 31% for a score of 2, and little increased risk for a score of less than 2.[132] Another group proposed a two stage screening protocol for preeclampsia with UtA Doppler at 18-22 weeks and when abnormal re-evaluation at 24 weeks.[5] In that study, 59% of the re-examined patients showed normal UtA Doppler FVWs.[133] Persistence of an abnormal FVW increased the relative risk for developing preeclampsia by 24-fold. Persistent notch in the early diastolic component of the FVW increased the predictive value (from 4.3% to 28%) and was associated with a 68-fold risk for developing preeclampsia.

There were also some studies suggesting Doppler assessment of the UtA can be carried out at 11–14 weeks' gestation and that screening at this early gestation can also identify pregnancies at the risk of developing complications associated with impaired placentation.[134] Chromosomal defects are associated with IUGR,[135] and in the case of trisomy 18 and 13, but not in trisomy 21, the IUGR is evident from the first trimester of pregnancy.[136,137] In a study, in which UtA Doppler between 11–14 weeks of gestation was performed to examine whether the high lethality and IUGR is associated with chromosomal abnormalities, the authors showed that UtA impedance is not associated with chromosomal anomalies,[138] and suggested that the placental histological changes may be responsible for increased impedance in the UA, but not in the UtA.

The relationship between abnormal uterine artery Doppler velocimetry and preeclampsia, IUGR and adverse perinatal outcomes are well established. Some paradoxical findings are attributed to differences in patient selection, gestational ages for screening, type of equipment, multiple definitions of FVWs, different vessels examined and heterogeneous outcome criteria.[139] The sensitivity of the UtA examination improves as the gestational age approaches to 26 weeks and when persistent diastolic notch is one of the criteria for analysis.[140] However, whether its use as a routine screening test ultimately results in a decrease in maternal and perinatal morbidity and mortality remains questionable. Current data do not support the use of Doppler ultrasonography for routine screening of patients for preeclampsia. However several studies show that the combination of the measurement of uterine perfusion in the second trimester and analysis of angiogenic markers have a high detection rate, especially for early onset preeclampsia.[141] Among high-risk patients with a previous preeclampsia, UtA Doppler has an excellent negative predictive value, thus it is an important tool in patient management and care which is of paramount benefit for patients with preeclampsia in a previous pregnancy. A recently published systematic review[142] assessed the use of Doppler ultrasonography in case of preeclampsia. A total of 74 studies (69 cohort studies, 3 randomized controlled trials and 2 case-control studies) with a total number of 79,547 patients, of whom 2,498 developed preeclampsia, were included. The authors showed that UtA Doppler was less accurate in the first trimester, than in the second trimester. The combined data showed that the pulsatility index, alone or in combination with a persistent

notching after 24 weeks of gestation is the most predictive parameter of Doppler ultrasonography to predict preeclampsia.

Although, considering the use of antiplatelet agent prophylaxis during pregnancy, the results of some multicenter randomized trials (Collaborative Low-Dose Aspirin Study-CLASP[143] and ECPPA[144]) were not encouraging, a moderate but consistent reduction in the relative risk of preeclampsia, of birth before 34 weeks' gestation, and of having a pregnancy with a serious adverse outcome.[145] There is good evidence that antiplatelet agents (principally low dose aspirin) prevent preeclampsia. A Cochrane Review[146] identified moderate, but clinically important, reductions in the relative risks of preeclampsia (19%), preterm birth (7%) and perinatal mortality (16%) in women receiving antiplatelet agents. These effects are much smaller than had initially been hoped for but, nevertheless, potentially they have considerable public health importance.

SUMMARY

Doppler ultrasound is a noninvasive technique that is commonly used to evaluate maternal and fetal hemodynamics. Examination of fetomaternal vessels using Doppler sonography has been subject of intensive investigation in recent years. To date, randomized controlled trials were able to establish important clinical value of Doppler velocimetry in obstetrics to improve perinatal outcome in high risk situations. Umbilical artery, fetal descending aorta and middle cerebral artery Doppler velocimetric studies are acceptable tools in the diagnosis and management of intrauterine growth restricted fetuses, and in the reduction of perinatal mortality in high risk pregnancies. But there is no evidence that routine umbilical Doppler in a general or low-risk population leads to any improvement in the health of women or their infants. Although other trials are needed before asserting a definite lack of benefit, umbilical Doppler examinations cannot be recommended as a routine test in low-risk pregnancies.

The majority of severely compromised fetuses also show pathological venous velocimetry, which might give valuable clinical information for surveillance in high-risk pregnancies *and their optimal perinatal management.* In addition, Doppler sonography might have a role in predicting long-term neuromotoric outcome. Large scale randomized controlled trials are needed to establish the clinical utility of Doppler ultrasound in obstetrics.

REFERENCES

1. Harman CR, Baschat AA. Comprehensive assessment of fetal wellbeing: which Doppler tests should be performed? Curr Opin Obstet Gynecol. 2003;15(2):147-57.
2. Fitzgerald DE, Drumm JE. Non-invasive measurement of human fetal circulation using ultrasound: a new method. Br Med J. 1977;2(6100):1450-1.
3. Campbell S, Diaz-Recasens J, Griffin DR, et al. New Doppler technique for assessing uteroplacental blood flow. Lancet. 1983;1(8326 Pt 1):675-7.
4. Eik-Nes SH, Marsal K, Brubakk AO, et al. Ultrasonic measurement of human fetal blood flow. J Biomed Eng. 1982;4(1):28-36.
5. Bower S, Schuchter K, Campbell S. Doppler ultrasound screening as part of routine antenatal scanning: prediction of pre-eclampsia and intrauterine growth retardation. Br J Obstet Gynaecol. 1993;100(11):989-94.
6. Caforio L, Testa AC, Mastromarino C, et al. Predictive value of uterine artery velocimetry at midgestation in low- and high-risk populations: a new perspective. Fetal Diagn Ther. 1999;14(4):201-5.
7. Campbell S, Pearce JM, Hackett G, et al. Qualitative assessment of uteroplacental blood flow: early screening test for high-risk pregnancies. Obstet Gynecol. 1986;68(5):649-53.
8. Harrington K, Cooper D, Lees C, et al. Doppler ultrasound of the uterine arteries: the importance of bilateral notching in the prediction of pre-eclampsia, placental abruption or delivery of a small-for-gestational-age baby. Ultrasound Obstet Gynecol. 1996;7(3):182-8.
9. Harrington K, Goldfrad C, Carpenter RG, et al. Transvaginal uterine and umbilical artery Doppler examination of 12-16 weeks and the subsequent development of pre-eclampsia and intrauterine growth retardation. Ultrasound Obstet Gynecol. 1997;9(2):94-100.
10. Hoffmann H, Chaoui R, Bollmann R, et al. [Potential clinical application of Doppler ultrasound in obstetrics]. Zentralbl Gynakol. 1989;111(19):1277-84.
11. Irion O, Massé J, Forest JC, et al. Prediction of pre-eclampsia, low birthweight for gestation and prematurity by uterine artery blood flow velocity waveforms analysis in low risk nulliparous women. Br J Obstet Gynaecol. 1998;105(4):422-9.
12. Trudinger BJ, Giles WB, Cook CM. Uteroplacental blood flow velocity-time waveforms in normal and complicated pregnancy. Br J Obstet Gynaecol. 1985;92(1):39-45.
13. Zimmermann P, Eiriö V, Koskinen J, et al. D Doppler assessment of the uterine and uteroplacental circulation in the second trimester in pregnancies at high risk for pre-eclampsia and/or intrauterine growth retardation: comparison and correlation between different Doppler parameters. Ultrasound Obstet Gynecol. 1997;9(5):330-8.
14. Torloni MR, Vedmedovska N, Merialdi M, et al. Safety of ultrasonography in pregnancy: WHO systematic review of the literature and meta-analysis. Ultrasound Obstet Gynecol. 2009;33(5):599-608.

15. Hershkovitz R, Sheiner E, Mazor M. Ultrasound in obstetrics: a review of safety. Eur J Obstet Gynecol Reprod Biol. 2002;101(1):15-8.
16. Barnett SB, Kossoff G, Edwards MJ. Is diagnostic ultrasound safe? Current international consensus on the thermal mechanism. Med J Aust. 1994;160(1):33-7.
17. Houston LE, Odibo AO, Macones GA. The safety of obstetrical ultrasound: a review. Prenat Diagn. 2009;29(13): 1204-12.
18. Newnham JP, Doherty DA, Kendall GE, et al. Effects of repeated prenatal ultrasound examinations on childhood outcome up to 8 years of age: follow-up of a randomised controlled trial. Lancet. 2004;364(9450):2038-44.
19. Mires GJ, Christie AD, Leslie J, et al. Are 'notched' uterine arterial waveforms of prognostic value for hypertensive and growth disorders of pregnancy? Fetal Diagn Ther. 1995;10(2):111-8.
20. Deutinger J. [Physiology of Doppler blood flow in maternal blood vessels in pregnancy]. Gynakologe. 1992;25(5):284-91.
21. Fendel H, Fendel M, Pauen A, et al. [Doppler studies of arterial blood flow in the uterus during labor]. Z Geburtshilfe Perinatol. 1984;188(2):64-7.
22. Fogarty P, Beattie B, Harper A, et al. Continuous wave Doppler flow velocity waveforms from the umbilical artery in normal pregnancy. J Perinat Med. 1990;18(1):51-7.
23. Ertan AK, Hendrik HJ, Tanriverdi HA, et al. Fetomaternal Doppler sonography nomograms. Clin Exp Obstet Gynecol. 2003;30(4):211-6.
24. Soothill PW, Ajayi RA, Campbell S, et al. Prediction of morbidity in small and normally grown fetuses by fetal heart rate variability, biophysical profile score and umbilical artery Doppler studies.. Br J Obstet Gynaecol. 1993;100(8):742-5.
25. Romero R, Kalache KD, Kadar N. Timing the delivery of the preterm severely growth-restricted fetus: venous Doppler, cardiotocography or the biophysical profile? Ultrasound Obstet Gynecol. 2002;19(2):118-21.
26. Stuart B, Drumm J, Fitzgerald DE, et al. Fetal blood velocity waveforms in normal pregnancy. Br J Obstet Gynaecol. 1980;87(9):780-5.
27. Thompson RS, Trudinger BJ, Cook CM. Doppler ultrasound waveform indices: A/B ratio, pulsatility index and Pourcelot ratio. Br J Obstet Gynaecol. 1988;95(6):581-8.
28. Huneke B, Holst A, Schroder HJ, et al. [Normal values for relative Doppler indices. A/B ratio, resistance index and pulsatility index of the uterine artery and umbilical artery in normal pregnancy. A longitudinal study]. Geburtshilfe Frauenheilkd. 1995;55(11):616-22.
29. Schulman H, Fleischer A, Stern W, et al. Umbilical velocity wave ratios in human pregnancy. Am J Obstet Gynecol. 1984;148(7):985-90.
30. Trudinger BJ, Giles WB, Cook CM, et al. Fetal umbilical artery flow velocity waveforms and placental resistance: clinical significance. Br J Obstet Gynaecol. 1985;92(1):23-30.
31. Maulik D, Yarlagadda AP, Youngblood JP, et al. Components of variability of umbilical arterial Doppler velocimetry—a prospective analysis. Am J Obstet Gynecol. 1989;160(6):1406-9.
32. Ertan AK, Hendrik HJ, Schmidt W. Perinatologische Auffälligkeiten Bei Hochpathologischen Doppler-Flow-Befunden (Chapter 12). In: Schmidt W, Kurjak A (Eds). Farbdopplersonographie In Gynäkologie Und Geburtshilfe. 1st edition. Stuttgart: Thieme Verlag; 2000. pp. 177-87.
33. Fleischer A, Schulman H, Farmakides G, et al. Umbilical artery velocity waveforms and intrauterine growth retardation. Am J Obstet Gynecol. 1985;151(4):502-5.
34. Devoe LD, Gardner P, Dear C, et al. The significance of increasing umbilical artery systolic-diastolic ratios in third-trimester pregnancy. Obstet Gynecol. 1992;80(4):684-7.
35. Rochelson B, Schulman H, Farmakides G, et al. The significance of absent end-diastolic velocity in umbilical artery velocity waveforms. Am J Obstet Gynecol. 1987;156(5):1213-8.
36. Trudinger BJ, Cook CM, Giles WB, et al. Fetal umbilical artery velocity waveforms and subsequent neonatal outcome. Br J Obstet Gynaecol. 1991;98(4):378-84.
37. Gudmundsson S, Marsal K. Umbilical and uteroplacental blood flow velocity waveforms in pregnancies with fetal growth retardation. Eur J Obstet Gynecol Reprod Biol. 1988;27(3):187-96.
38. Baschat AA, Weiner CP. Umbilical artery doppler screening for detection of the small fetus in need of antepartum surveillance. Am J Obstet Gynecol. 2000;182(1 Pt 1):154-8.
39. Mccowan LM, Harding JE, Stewart AW. Umbilical artery doppler studies in small for gestational age babies reflect disease severity. BJOG. 2000;107(7):916-25.
40. Ertan AK, He JP, Tanriverdi HA, et al. Comparison of perinatal outcome in fetuses with reverse or absent enddiastolic flow in the umbilical artery / fetal descending aorta. J Perinat Med. 2003;31(4):307-12.
41. Baschat AA, Gembruch U, Harman CR. The Sequence of changes in Doppler and biophysical parameters as severe fetal growth restriction worsens. Ultrasound Obstet Gynecol. 2001;18(6):571-7.
42. Rizzo G, Pietropolli A, Capponi A, et al. Chromosomal abnormalities in fetuses with absent end-diastolic velocity in umbilical artery: analysis of risk factors for an abnormal karyotype. Am J Obstet Gynecol. 1994;171(3):827-31.
43. Ertan AK, He JP, Hendrik HJ, et al. Perinatal events of cases with severely abnormal Doppler flow measurements. J Perinat Med. 2003; In Press.
44. Valcamonico A, Danti L, Frusca T, et al. Absent end-diastolic velocity in umbilical artery: risk of neonatal morbidity and brain damage. Am J Obstet Gynecol. 1994;170(3):796-801.
45. Alfirevic Z, Neilson JP. Doppler ultrasonography in high-risk pregnancies: systematic review with meta-analysis. Am J Obstet Gynecol. 1995;172(5):1379-87.
46. Neilson JP, Alfirevic Z. Doppler ultrasound for fetal assessment in high risk pregnancies. Cochrane Database Syst Rev. 2000;(2):CD000073.
47. Baschat AA, Gembruch U, Viscardi RM, et al. Antenatal prediction of intraventricular hemorrhage in fetal growth restriction: what is the role of Doppler? Ultrasound Obstet Gynecol. 2002;19(4):334-9.
48. Wienerroither H, Steiner H, Tomaselli J, et al. Intrauterine blood flow and long-term intellectual, neurologic, and social development. Obstet Gynecol. 2001;97(3):449-53.

49. Ertan AK, Jost W, Hendrik HJ, et al. Perinatal events and neuromotoric development of children with zero flow in the fetal vessels during the last trimester. In: Cosmi E, Di Renzo GC (Eds). 2nd World Congress of Perinatal Medicine. 1st edition. Milano: Monduzzi Editore; 1993. pp. 1049-52.
50. Ertan AK, Jost W, Mink D, et al. Neuromotoric development of children after AED-flow during pregnancy. In: Kurjak A, Latin V, Rippmann E (Eds). Advances On The Pathophysiology Of Pregnancy. 1st edition. Milano: CIC Edizioni Internazionali; 1995. pp. 55-62.
51. Farrell T, Chien PF, Gordon A. Intrapartum umbilical artery doppler velocimetry as a predictor of adverse perinatal outcome: a systematic review. Br J Obstet Gynaecol. 1999;106(8):783-92.
52. Sijmons EA, Reuwer PJ, Van Beek E, et al. The validity of screening for small-for-gestational-age and low-weight-for-length infants by Doppler ultrasound. Br J Obstet Gynaecol. 1989;96(5):557-61.
53. Beattie RB, Dornan JC. Antenatal screening for intrauterine growth retardation with umbilical artery Doppler ultrasonography. BMJ. 1989;298(6674):631-5.
54. Goffinet F, Paris-Llado J, Nisand I, et al. Umbilical artery Doppler velocimetry in unselected and low risk pregnancies: a review of randomised controlled trials. Br J Obstet Gynaecol. 1997;104(4):425-30.
55. Giles WB, Trudinger BJ, Cook CM, et al. Umbilical artery flow velocity waveforms and twin pregnancy outcome. Obstet Gynecol. 1988;72(6):894-7.
56. Gaziano EP, Knox H, Ferrera B, et al. Is it time to reassess the risk for the growth-retarded fetus with normal doppler velocimetry of the umbilical artery? Am J Obstet Gynecol. 1994;170(6):1734-41.
57. Divon MY, Girz BA, Sklar A, et al. Discordant twins—a prospective study of the diagnostic value of real-time ultrasonography combined with umbilical artery velocimetry. Am J Obstet Gynecol. 1989;161(3):757-60.
58. Gaziano E, Gaziano C, Brandt D. Doppler velocimetry determined redistribution of fetal blood flow: correlation with growth restriction in diamniotic monochorionic and dizygotic twins. Am J Obstet Gynecol. 1998;178(6):1359-67.
59. Hecher K, Campbell S, Doyle P, et al. Assessment of fetal compromise by Doppler ultrasound investigation of the fetal circulation. Arterial, intracardiac, and venous blood flow velocity studies. Circulation. 1995;91(1):129-38.
60. Senat MV, Schwarzler P, Alcais A, et al. Longitudinal changes in the ductus venosus, cerebral transverse sinus and cardiotocogram in fetal growth restriction. Ultrasound Obstet Gynecol. 2000;16(1):19-24.
61. Turan S, Miller J, Baschat AA. Integrated testing and management in fetal growth restriction. Semin Perinatol. 2008;32(3):194-200.
62. Lingman G, Marsál K. Fetal central blood circulation in the third trimester of normal pregnancy—a longitudinal study. I. Aortic and umbilical blood flow. Early Hum Dev. 1986;13(2):137-50.
63. Hecher K, Spernol R, Szalay S, et al. [Reference values for the pulsatility index and the resistance index of blood flow curves of the umbilical artery and fetal aorta in the 3d trimester]. Ultraschall Med. 1989;10(4):226-9.
64. Soothill PW, Nicolaides KH, Bilardo K, et al. Uteroplacental blood velocity resistance index and umbilical venous pO2, pCO2, pH, lactate and erythroblast count in growth-retarded fetuses. Fetal Ther. 1986;1(4):176-9.
65. Jouppila P, Kirkinen P. Blood velocity waveforms of the fetal aorta in normal and hypertensive pregnancies. Obstet Gynecol. 1986;67(6):856-60.
66. Laurin J, Lingman G, Marsal K, et al. Fetal blood flow in pregnancies complicated by intrauterine growth retardation. Obstet Gynecol. 1987;69(6):895-902.
67. Hackett GA, Campbell S, Gamsu H, et al. Doppler studies in the growth retarded fetus and prediction of neonatal necrotising enterocolitis, haemorrhage, and neonatal morbidity. Br Med J (Clin Res Ed). 1987;294(6563):13-6.
68. Arabin B, Siebert M, Jimenez E, et al. Obstetrical characteristics of a loss of end-diastolic velocities in the fetal aorta and/or umbilical artery using Doppler ultrasound. Gynecol Obstet Invest. 1988;25(3):173-80.
69. Tonge HM, Wladimiroff JW, Noordam MJ, et al. Blood flow velocity waveforms in the descending fetal aorta: comparison between normal and growth-retarded pregnancies. Obstet Gynecol. 1986;67(6):851-5.
70. Bonatz G, Schulz V, Weisner D, et al. Fetal Heart rate (fhr) pathology in labor related to preceeding Doppler sonographic results of the umbilical artery and fetal aorta in appropriate and small for gestational age babies. A Longitudinal Analysis. J Perinat Med. 1997;25(5):440-6.
71. Marsal K, Laurin J, Lindblad A, et al. Blood flow in the fetal descending aorta. Semin Perinatol. 1987;11(4):322-34.
72. Ley D, Laurin J, Bjerre M, et al. Abnormal fetal aortic velocity waveform and minor neurological dysfunction at 7 years of age. Ultrasound Obstet Gynecol. 1996;8(3):152-9.
73. Ley D, Tideman E, Laurin J. Abnormal fetal aortic velocity waveform and intellectual function at 7 years of age. Ultrasound Obstet Gynecol. 1996;8(3):160-5.
74. Divon MY, Ferber A. Doppler Evaluation of the fetus. Clin Obstet Gynecol. 2002;45(4):1015-25.
75. Mari G, Detti L. Doppler ultrasound application to fetal medicine (Chapter 12). In: Fleischer A, Manning F, Jeanty P, Romero R (Eds). Sonography in obstetrics and gynecology (Principles and Practice). 6th edition. New York, USA: Mcgraw Hill; 2001. pp. 247-83.
76. Mari G, Moise KJ, Deter RL, et al. Doppler assessment of the pulsatility index in the cerebral circulation of the human fetus. Am J Obstet Gynecol. 1989;160(3):698-703.
77. Vetter K. [The significance of Doppler blood flow measurement in recognizing placental insufficiency]. Arch Gynecol Obstet. 1988;244 Suppl:S12-S18.
78. Arabin B, Bergmann PL, Saling E. Simultaneous assessment of blood flow velocity waveforms in uteroplacental vessels, the umbilical artery, the fetal aorta and the fetal common carotid artery. Fetal Ther. 1987;2:17-26.
79. Strigini FA, De Luca G, Lencioni G, et al. Middle cerebral artery velocimetry: different clinical relevance depending on umbilical velocimetry. Obstet Gynecol. 1997;90(6):953-7.

80. Sepulveda W, Shennan AH, Peek MJ. Reverse end-diastolic flow in the middle cerebral artery: an agonal pattern in the human fetus. Am J Obstet Gynecol. 1996;174(5):1645-7.
81. Vyas S, Nicolaides KH, Bower S, et al. Middle cerebral artery flow velocity waveforms in fetal hypoxaemia. Br J Obstet Gynaecol. 1990;97(9):797-803.
82. Mari G, Adrignolo A, Abuhamad AZ, et al. Diagnosis of fetal anemia with Doppler ultrasound in the pregnancy complicated by maternal blood group immunization. Ultrasound Obstet Gynecol. 1995;5(6):400-5.
83. Mari G, Deter RL, Carpenter RL, et al. Noninvasive diagnosis by Doppler ultrasonography of fetal anemia due to maternal red-cell alloimmunization. Collaborative Group for Doppler Assessment of the Blood Velocity in Anemic Fetuses. N Engl J Med. 2000;342(1):9-14.
84. Zimmerman R, Carpenter RJ, Durig P, et al. Longitudinal measurement of peak systolic velocity in the fetal middle cerebral artery for monitoring pregnancies complicated by red cell alloimmunisation: a prospective multicentre trial with intention-to-treat. BJOG. 2002;109(7):746-52.
85. Moise KJ. The usefulness of middle cerebral artery Doppler assessment in the treatment of the fetus at risk for anemia. Am J Obstet Gynecol. 2008;198(2):161-4.
86. Mari G, Detti L, Oz U, et al. Accurate prediction of fetal hemoglobin by Doppler ultrasonography. Obstet Gynecol. 2002;99(4):589-93.
87. Huisman TW. Doppler assessment of the fetal venous system. Semin Perinatol. 2001;5(1):21-31.
88. Laurichesse-Delmas H, Grimaud O, Moscoso G, et al. Color Doppler study of the venous circulation in the fetal brain and hemodynamic study of the cerebral transverse sinus. Ultrasound Obstet Gynecol. 1999;13(1):34-42.
89. Yoshimura S, Masuzaki H, Miura K, et al. Diagnosis of fetal pulmonary hypoplasia by measurement of blood flow velocity waveforms of pulmonary arteries with Doppler ultrasonography. Am J Obstet Gynecol. 1999;180(2 Pt 1):441-6.
90. Hoffman C, Galan HL. Assessing the 'at-risk' fetus: Doppler ultrasound. Curr Opin Obstet Gynecol. 2009;21(2):161-6.
91. Contratti G, Banzi C, Ghi T, et al. Absence of the ductus venosus: report of 10 new cases and review of the literature. Ultrasound Obstet Gynecol. 2001;18(6):605-9.
92. Arduini D, Rizzo G, Romanini C. The development of abnormal heart rate patterns after absent end-diastolic velocity in umbilical artery: analysis of risk factors. Am J Obstet Gynecol. 1993;168(1 Pt 1):43-50.
93. Damron DP, Chaffin DG, Anderson CF, et al. Changes in umbilical arterial and venous blood flow velocity waveforms during late decelerations of the fetal heart rate. Obstet Gynecol. 1994;84(6):1038-40.
94. Reed K, Chaffin DG, Anderson CF, et al. Umbilical venous pulsations are related to atrial contraction pressure waveforms in fetal lambs. Obstet Gynecol. 1997;89:953-6.
95. Ferrazzi E, Rigano S, Bozzo M, et al. Umbilical vein blood flow in growth-restricted fetuses. Ultrasound Obstet Gynecol. 2000;16(5):432-8.
96. Gudmundsson S, Huhta JC, Wood DC, et al. Venous Doppler ultrasonography in the fetus with nonimmune hydrops. Am J Obstet Gynecol. 1991;164(1 Pt 1):33-7.
97. Nakai Y, Miyazaki Y, Matsuoka Y. Pulsatile umbilical venous flow and its clinical significance. Br J Obstet Gynaecol. 1992;99(12):977-80.
98. Chan FY, Woo SK, Ghosh A, et al. Prenatal diagnosis of congenital fetal arrhythmias by simultaneous pulsed Doppler velocimetry of the fetal abdominal aorta and inferior vena cava. Obstet Gynecol. 1990;76(2):200-5.
99. Rizzo G, Arduini D, Romanini C. Inferior vena cava flow velocity waveforms in appropriate and small-for gestational age fetsues. Am J Obstet Gynecol. 1992;166:1271-80.
100. Kiserud T, Eik-Nes SH, Blaas HG, et al. Ultrasonographic velocimetry of the fetal ductus venosus. Lancet. 1991;338(8780):1412-4.
101. Kiserud T, Hellevik LR, Eik-Nes SH, et al. Estimation of the pressure gradient across the fetal ductus venosus based on Doppler velocimetry. Ultrasound Med Biol. 1994;20(3):225-32.
102. Kiserud T. In a different vein: the ductus venosus could yield much valuable information. Ultrasound Obstet Gynecol. 1997;9(6):369-72.
103. Kiserud T, Rasmussen S. How repeat measurements affect the mean diameter of the umbilical vein and the ductus venosus. Ultrasound Obstet Gynecol. 1998;11(6):419-25.
104. Kiserud T, Crowe C, Hanson M. Ductus venosus agenesis prevents transmission of central venous pulsations to the umbilical vein in fetal sheep. Ultrasound Obstet Gynecol. 1998;11(3):190-4.
105. Kiserud T. Ductus venosus blood velocity in myeloproliferative disorders. Ultrasound Obstet Gynecol. 2001;18(2):184-5.
106. Kiserud T. The ductus venosus. Semin Perinatol. 2001;25(1):11-20.
107. Mavrides E, Moscoso G, Carvalho JS, et al. The anatomy of the umbilical, portal and hepatic venous systems in the human fetus at 14-19 weeks of gestation. Ultrasound Obstet Gynecol. 2001;18(6):598-604.
108. Bellotti M, Pennati G, De Gasperi C, et al. Role of ductus venosus in distribution of umbilical blood flow in human fetuses during second half of pregnancy. Am J Physiol Heart Circ Physiol. 2000;279(3):H1256-63.
109. Matias A, Montenegro N. Ductus venosus blood flow in chromosomally abnormal fetuses at 11 to 14 weeks of gestation. Semin Perinatol. 2001;25(1):32-7.
110. Ozcan T, Sbracia M, d'Ancona RL, et al. Arterial and venous doppler velocimetry in the severely growth-restricted fetus and associations with adverse perinatal outcome. Ultrasound Obstet Gynecol. 1998;12(1):39-44.
111. Hecher K, Hackeloer BJ. Cardiotocogram compared to Doppler investigation of the fetal circulation in the premature growth-retarded fetus: longitudinal observations. Ultrasound Obstet Gynecol. 1997;9(3):152-61.
112. Kiserud T. Fetal venous circulation—an update on hemodynamics. J Perinat Med. 2000;28:90-6.
113. Kiserud T. Liver length in the small-for-gestational-age fetus and ductus venosus flow. Am J Obstet Gynecol. 2000;182(1 Pt 1):252-3.
114. Ribbert L, Snijders RJ, Nicolaides KH. Relation of fetal blood gases and data from computer assisted analysis of fetal heart rate patterns. Br J Obstet Gynaecol. 1991;98(8):820-3.

115. Dawes GS, Moulden M, Redman C. Short-term fetal heart rate variation, decelerations, and umbilical flow velocity waveforms before labor. Obstet Gynecol. 1992;80(4):673-8.
116. Hecher K, Bilardo CM, Stigter RH, et al. Monitoring of fetuses with intrauterine growth restriction: a longitudinal study. Ultrasound Obstet Gynecol. 2001;18(6):564-70.
117. Hofstaetter C, Gudmundsson S, Hansmann M. Venous Doppler velocimetry in the surveillance of severely compromised fetuses. Ultrasound Obstet Gynecol. 2002; 20(3):233-9.
118. Thornton JG, Hornbuckle J, Vail A, et al; the GRIT study group. Infant wellbeing at 2 years of age in the Growth Restriction Intervention Trial (GRIT): multicentred randomised controlled trial. Lancet. 2004;364(9433):513-20.
119. Kurjak A, Kupesic-Urek S, Schulman H, et al. Transvaginal color flow Doppler in the assessment of ovarian and uterine blood flow in infertile women. Fertil Steril. 1991;56(5):870-3.
120. Deutinger J, Rudelstorfer R, Bernaschek G. Vaginosonographic Doppler velocimetry in both uterine arteries: elevated left-right differences and relationship to fetal haemodynamics and outcome. Early Hum Dev. 1991;25(3): 187-96.
121. Goswamy R, Williams G, Steptoe P. Decreased uterine perfusion—a cause of infertility. Hum Reprod. 1989;3(8):955-9.
122. Kurjak A, Dudenhausen JW, Hafner T, et al. Intervillous circulation in all three trimesters of normal pregnancy assessed by color Doppler. J Perinat Med. 1997;25(4):373-80.
123. Coppens M, Loquet P, Kollen M, et al. Longitudinal evaluation of uteroplacental and umbilical blood flow changes in normal early pregnancy. Ultrasound Obstet Gynecol. 1996;7(2):114-21.
124. Thaler I, Manor D, Itskovitz J, et al. Changes in uterine blood flow during human pregnancy. Am J Obstet Gynecol. 1990;162(1):121-5.
125. Kofinas AD, Espeland MA, Penry M, et al. Uteroplacental Doppler flow velocity waveform indices in normal pregnancy: a statistical exercise and the development of appropriate reference values. Am J Perinatol. 1992;9(2):94-101.
126. Palmer SK, Zamudio S, Coffin C, et al. Quantitative estimation of human uterine artery blood flow and pelvic blood flow redistribution in pregnancy. Obstet Gynecol. 1992;80(6):1000-6.
127. den Ouden M, Cohen-Overbeek TE, Wladimiroff JW. Uterine and fetal umbilical artery flow velocity waveforms in normal first trimester pregnancies. Br J Obstet Gynaecol. 1990;97(8):716-9.
128. Tekay A, Jouppila P. A longitudinal Doppler ultrasonographic assessment of the alterations in peripheral vascular resistance of uterine arteries and ultrasonographic findings of the involuting uterus during the puerperium. Am J Obstet Gynecol. 1993;168(1 Pt 1):190-8.
129. Schneider KT, Loos W. [The 10th anniversary of obstetric Doppler sonography—development and perspectives]. Geburtshilfe Frauenheilkd. 1989;49(5):407-15.
130. Brosens I, Dixon HG, Robertson W. Fetal growth retardation and the arteries of the placental bed. Br J Obstet Gynaecol. 1977;84(9):656-63.
131. Hitschold T, Ulrich S, Kalder M, ET AL. [Blood flow profile in the uterine artery. Correlation with placental morphology and clinico-obstetrical data within the scope of pre-eclampsia]. Z Geburtshilfe Neonatol. 1995;199(1):8-12.
132. Murakoshi T, Sekizuka N, Takakuwa K, et al. Uterine and spiral artery flow velocity waveforms in pregnancy-induced hypertension and/or intrauterine growth retardation. Ultrasound Obstet Gynecol. 1996;7(2):122-8.
133. Bower S, Bewley S, Campbell S. Improved prediction of preeclampsia by two-stage screening of uterine arteries using the early diastolic notch and color Doppler imaging. Obstet Gynecol. 1993;82(1):78-83.
134. Martin AM, Bindra R, Curcio P, Cicero S, Nicolaides KH. Screening for pre-eclampsia and fetal growth restriction by uterine artery Doppler at 11-14 weeks of gestation. Ultrasound Obstet Gynecol. 2001;18(6):583-6.
135. Snijders RJ, Sebire NJ, Cuckle H, et al. Maternal age and gestational age-specific risks for chromosomal defects. Fetal Diagn Ther. 1995;10(6):356-67.
136. Kuhn P, Brizot ML, Pandya PP, et al. Crown-rump length in chromosomally abnormal fetuses at 10 to 13 weeks' gestation. Am J Obstet Gynecol. 1995;172(1 Pt 1):32-5.
137. Schemmer G, Wapner RJ, Johnson A, et al. First trimester growth patterns of aneuploid fetuses. Prenat Diagn. 1997;17(2):155-9.
138. Bindra R, Curcio P, Cicero S, et al. Uterine artery Doppler at 11-14 weeks of gestation in chromosomally abnormal fetuses. Ultrasound Obstet Gynecol. 2001;18(6):587-9.
139. Goncalves LF, Romero R, Gervasi M, et al. Doppler velocimetry of the uteroplacental circulation (Chapter 13). In: Fleischer A, Manning F, Jeanty P, Romero R (Eds). Sonography in Obstetrics and Gynecology (Principles And Practice). 6th edition. New York, USA: Mcgraw Hill; 2001. pp. 285-313.
140. Newnham JP, Patterson LL, James IR, et al. An evaluation of the efficacy of Doppler flow velocity waveform analysis as a screening test in pregnancy. Am J Obstet Gynecol. 1990;162(2):403-10.
141. Grill S, Rusterholz C, Zanetti-Dällenbach R, et al. Potential markers of preeclampsia—a review. Reprod Biol Endocrinol. 2009;7:70.
142. Cnossen JS, Morris RK, ter Riet G, et al. Use of uterine artery Doppler ultrasonography to predict pre-eclampsia and intrauterine growth restriction: a systematic review and bivariable meta-analysis. CMAJ. 2008;178(6):701-11.
143. CLASP: a randomised trial of low-dose aspirin for the prevention and treatment of pre-eclampsia among 9364 pregnant women. CLASP (Collaborative Low-dose Aspirin Study in Pregnancy) Collaborative Group. Lancet. 1994;343(8898):619-29.
144. ECPPA: randomised trial of low dose aspirin for the prevention of maternal and fetal complications in high risk pregnant women. ECPPA (Estudo Colaborativo para Prevenção da Pré-eclampsia com Aspirina) Collaborative Group. Br J Obstet Gynaecol. 1996;103(1):39-47.
145. Askie LM, Duley L, Henderson-Smart DJ, et al. Antiplatelet agents for prevention of pre-eclampsia: a meta-analysis of individual patient data. Lancet. 2007;369(9575):1791-8.
146. Duley L, Henderson-Smart DJ, Knight M, et al. Antiplatelet agents for preventing pre-eclampsia and its complications. Cochrane Database Syst Rev. 2004;(1):CD004659.

32
CHAPTER

Postpartum Ultrasound

Ajlana Mulic-Lutvica

INTRODUCTION

Postpartum period usually includes six subsequent weeks during which normal pregnancy involution occurs and the uterus returns to the nonpregnant state. Our knowledge about postpartum changes in the uterus has mainly been based on clinical examinations as well as from histological studies from the end of the 19th century and the early part of the 20th century when maternal mortality was high.[1] The involution of the uterus, as a main characteristic of the puerperium was previously assessed by palpation of the fundal height.

Since the introduction of ultrasound (USG) in clinical practice by Ian Donald et al.[2] in 1958 the uterus became one of the first organs to be examined.[3-7] However, few studies have focused on USG investigations during the puerperium and results of published studies are not unambiguous.[1-16] In published studies concerning the involution process, the length,[4,6-9,11,12,14] width,[8,9,12] anteroposterior diameter,[3-7,11-13,16] area,[9] thickness of the uterine wall[10] and volume of the uterus and the uterine cavity,[15] have been used as a measure of uterine involution. Majority of the studies described pathological conditions without knowledge about normal findings,[4,5,8] they were restricted to the early puerperium and designs were cross-sectional.[3-7,12] A few studies concerning uterine cavity during normal puerperium have been published.[13-16]

Postpartum complications involving the uterus occur in about 8–10% of cases. Immediate and late postpartum hemorrhage, puerperal sepsis, and septic pelvic thromboembolism are still potentially life-threatening conditions. Abnormal placentation (placenta accreta, increta or percreta) is a rare cause of postpartum hemorrhage that may continue after delivery. Several studies investigated antenatal ultrasound diagnosis of this condition[17-23] but a few papers have focused on postpartum ultrasound monitoring of retained placenta accreta.[24] Ultrasound can help to diagnose vascular lesions, congenital or acquired,[25-31] placental site tumor[32] and choriocarcinoma, which can also cause severe postpartum hemorrhage.

Thus, whenever puerperal complication occurs, the obstetricians should not hesitate to switch on ultrasound machine.

NORMAL PUERPERIUM

A description of normal ultrasound changes of the uterus and uterine cavity during puerperium is a prerequisite for ultrasound diagnosis of pathological conditions. We can follow the physiological involution of the uterus weighing more than 1 kg soon after delivery to an organ weighing about 80 grams at the end of the puerperium by means of ultrasound. The involution changes concerning the size, shape, position and texture of the uterus have been relatively well examined by ultrasound.[3-16] The influence on the involution process of parity,[7,9,11,13,15,16] route of delivery,[11] oxytocin administration during labor[7] breast-feeding[6,7,9, 11-13,15,16] or the infant's weight[11-13] have been studied. Previously published studies involving

Figures 32.1A to C: Three standard ultrasound sections of the puerperal uterus. (A) Longitudinal; (B) Coronal; (C) Transverse

sonographic examination of uterine cavity are not unambiguous.[6,11,13-16]

In the early and middle puerperium (in the first 2 weeks) the transabdominal approach is to be recommended. A relatively short focal length of the vaginal probe limits its use during the early postpartum period, when the uterus is too large and lies near the abdominal wall. In contrast, during the late postpartum period (> 2weeks) a high frequency transvaginal probe, which better distinguishes minor details, should be used. At that time, the uterus is considerably decreased in size and it lies in the true pelvis. The postpartum uterus should be examined in three standard sections: sagittal, transverse and coronal **(Figs 32.1 and 32.2)**. Urinary bladder should be moderately filled. Gentle compression with the probe should be used in order to avoid uterine distortion.

We can differentiate three typical ultrasound images during normal puerperium: in the early, middle and late puerperium **(Figs 32.3 and 32.4)**. The involution of the uterus is a dynamic process that has no parallel process in normal adult life.[1] There are two physiological life-saving processes occurring soon after placenta delivery:

1. Myotamponade (compression of the vessels by myometrial contraction)
2. Thrombotamponade (enhanced blood clotting activity).

The appearance of ultrasound finding *in the early postpartum period* reflects these physiological changes. The uterus has an angulated form **(Fig. 32.4A)**. It lies in a slightly retroflexed position and arches over the sacral promontory. Wachsberg et al.[12] pointed out the impact of uterine angulation on the measurement of uterine length and recommended segmental measurement. This angulated form of the early puerperal uterus is typical only in early puerperium and it is artificial. An extremely great degree of uterine deformability is caused by a heavy uterine corpus, a hypotonic lower

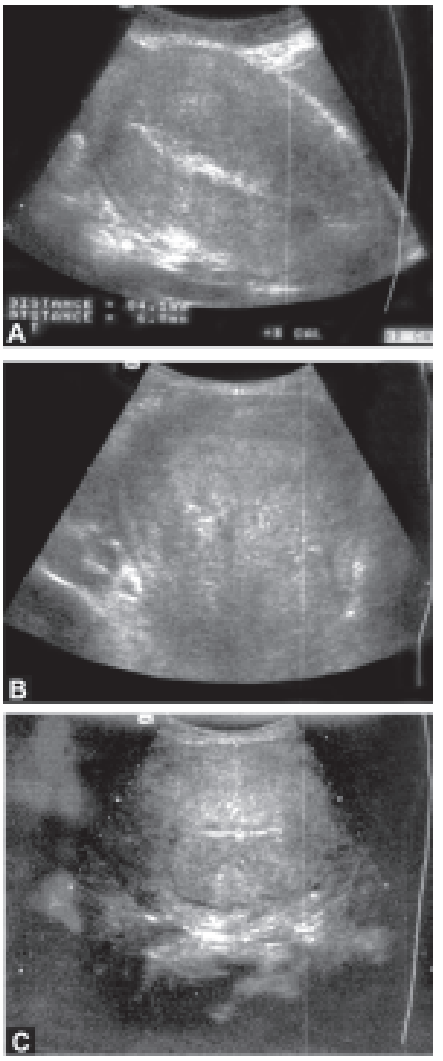

Figures 32.2A to C: Transabdominal ultrasound scans of a normal puerperal uterus on day 1. (A) Longitudinal scan; (B) Coronal scan; (C) Transverse scan

Figures 32.3A to C: The normal ultrasound appearance of the uterus and uterine cavity during the puerperium. (A) Transabdominal approach during the early puerperium; (B) During the middle part of the puerperium; (C) Transvaginal approach during the late puerperium

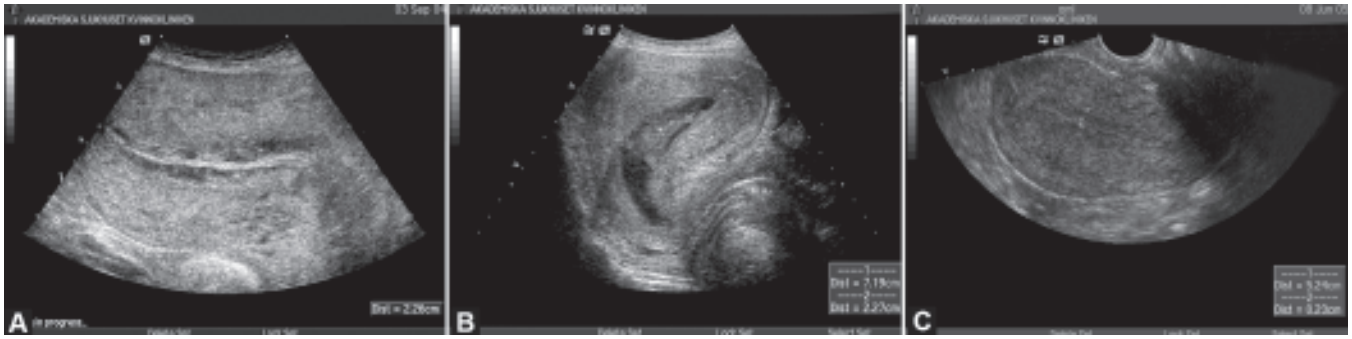

Figures 32.4A to C: Three typical USG images during normal puerperium. (A) In the early puerperium: uterus is retroverted. The cavity is seen as a thin white line; (B) In the middle puerperium: uterus is anteverted. An abundant fluid or mixed echo pattern with echogenic and echo-free area is seen in the whole cavity; (C) In the late puerperium: uterus is considerably decreased in size; the cavity is empty and appears as a thin white line

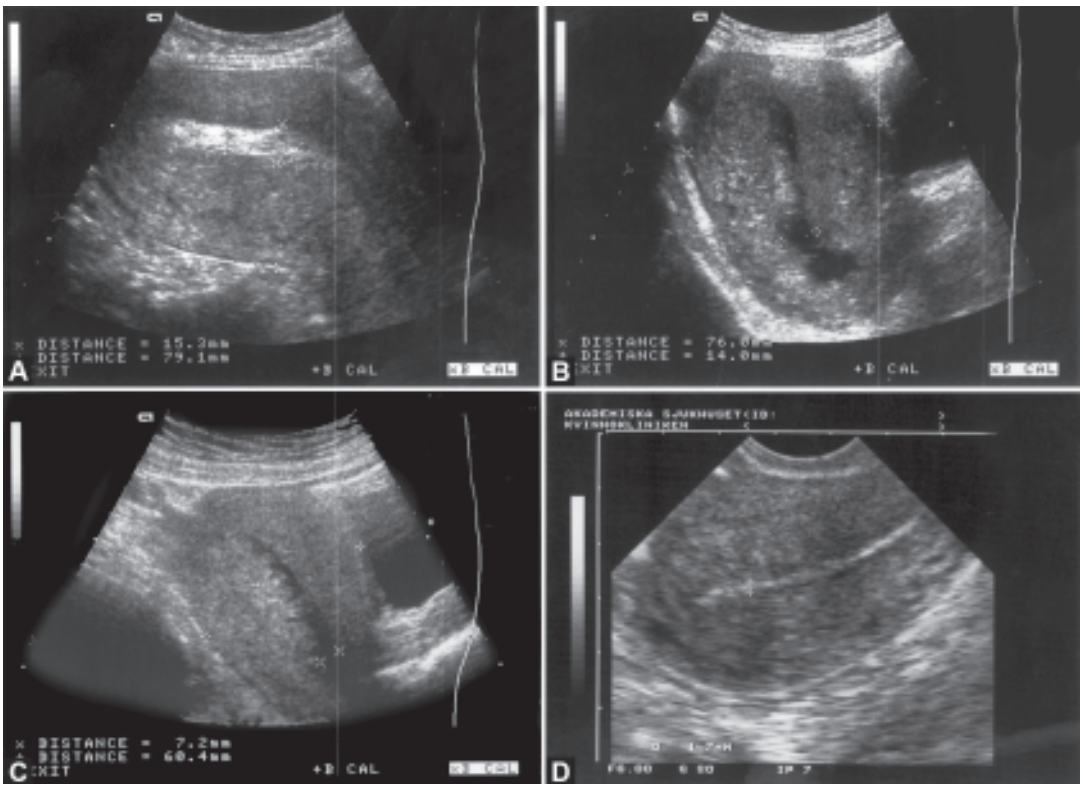

Figures 32.5A to D: Transabdominal, longitudinal scans of the uterus from an uncomplicated puerperium. (A) On day 1; (B) On day 7; (C) On day 14; (D) On day 28

uterine segment and supine position of the examined woman. Lifesaving uterine contraction approaches anterior and posterior uterine walls and just a virtual cavity appears. The uterine cavity is empty and decidua appears as a thin white line from the fundus to the level of the internal cervical os **(Fig. 32.4A)**. Sometimes, this line can be irregular and thicker, which probably depends on the amount of retained decidua **(Fig. 32.5A)**.

The separation of the placenta and membranes generally occurs in the spongy layer; however the level varies. In 1931, Williams wrote concerning the line of separation of the placenta and membranes: *"While separation generally occurs in the spongy layer, the line is very irregular so that in places a thick layer of decidua is retained, in others only a few layers of cells remain, while in still others the muscularis is practically bare."*[33] The variation in

sonographic appearance of the cavity could be seen as a demonstration of these physiological variations in retained decidua. The white thin line seen on ultrasound might possibly represent cases in which only the basal decidual layer is retained or if the muscularis is practically bare **(Fig. 32.4A)**. Whereas the thicker and more irregular lines might represent cases with retention of more amount of spongy decidual layer and perhaps fragments of membranes **(Fig. 32.5A)**.

Fluid or echogenic mass is not common finding in the cavity in the early postpartum period.[13] Small echogenic or echolucent dots in the cavity are harmless physiological findings.[13,34] A heterogeneous mass with fluid and solid components can be seen in the cervical area.[13,14,34,35] This finding has no clinical significance and the mass is usually expelled spontaneously. It probably reflects a collection of blood, blood clots and parts of membranes. On the posterior wall of the uterus the prominent uterine vascular channels are regularly seen.[11] They usually disappear during the 2nd and 3rd postpartum weeks as a result of involution process, which decreases both the size and the amount of uterine vessels. Gas in the cavity is not common finding in the early postpartum period although it can be occasionally seen.[13] Wachsberg detected gas in 19% of normal population during the early postpartum period.[36]

In the middle part of the puerperium (1–2 weeks postpartum) the uterus is diminished, the shape of the uterus is oval. It rotates along its internal cervical os towards an anteflexed position probably due to forming a firm isthmus.[13] The vascular channels are not so prominent. Either pure fluid or mixed echo with fluid and solid components can be seen in the whole cavity not only in the cervical area **(Figs 32.4B and 32.5B and C)**. This finding reflects a normal healing process of the placental site inside uterine cavity, necrotic changes of retained decidua and an abundant shedding of lochia. Echogenic mass or gas is not common finding during middle part of the puerperium. In contrast Edwards, et al.[15] found an echogenic mass in a great proportion of normal puerperal women.

During late puerperium (>2 weeks postpartum), the uterus is considerably diminished **(Figs 32.4C and 32.5D)**. It lies in an anteflexed position in 88% of cases.[13] In 12 % of cases the uterus has a retroflexed position corresponding well to normal prevalence of retroversion of the uterus in general population **(Fig. 32.6A)**. The uterine cavity is again empty. Decidua and necrotic vessel ends are exfoliated, the placental site is recovered and a new endometrium is regenerated from the basal layer of the decidua adjacent to the myometrium. Ultrasonically the cavity in the late puerperium appears as a thin white line **(Figs 32.4C and 32.5D)**. This corresponds to an inactive endometrium and reflects the hypoestrogenic state of the puerperium ("the physiologic menopause"). Sometimes, a small amount of fluid or echogenic dots can be seen (arrow) **(Fig. 32.6B)**.

In 1953, Sharman performed endometrium biopsies and identified fully restored endometrium from the 16th postpartum day.[37] In contrast, a study published in 1986 by Oppenheimer[38] showed that duration of puerperal lochia may be up to 60 days in 13% of women. Similarly in a recently published study,[39] on the duration of postpartum bleeding among 477 breastfeeding women, it was reported that the median duration of lochia was 27 days with a range from 5 to 90 days. Only 15% of the women reported that their lochia had stopped within two weeks postpartum. They also pointed to the fact that bleeding associated with the postpartum healing process commonly stops and starts again. So,

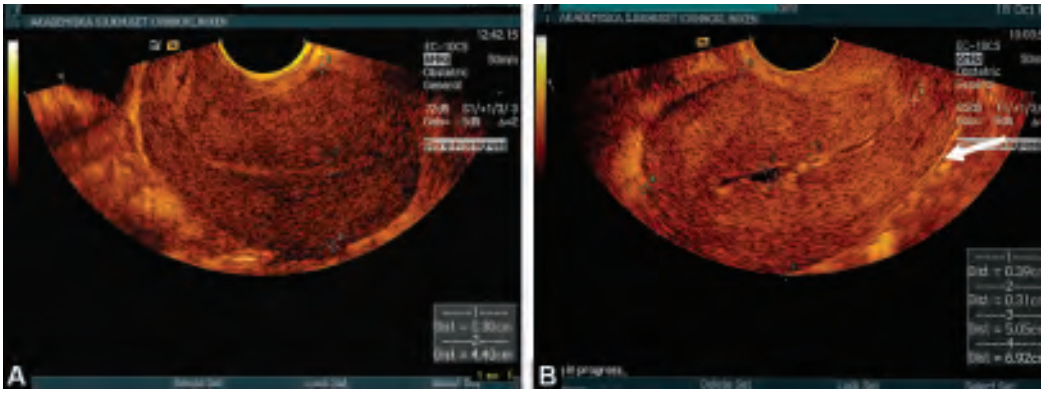

Figures 32.6A and B.: (A) Transvaginal ultrasound image of the uterus on day 28 postpartum shows a retroverted uterus on day 28 postpartum; (B) Transvaginal ultrasound image of the uterus on day 28 postpartum shows a small amount of fluid with echogenic foci in the cavity (white arrow)

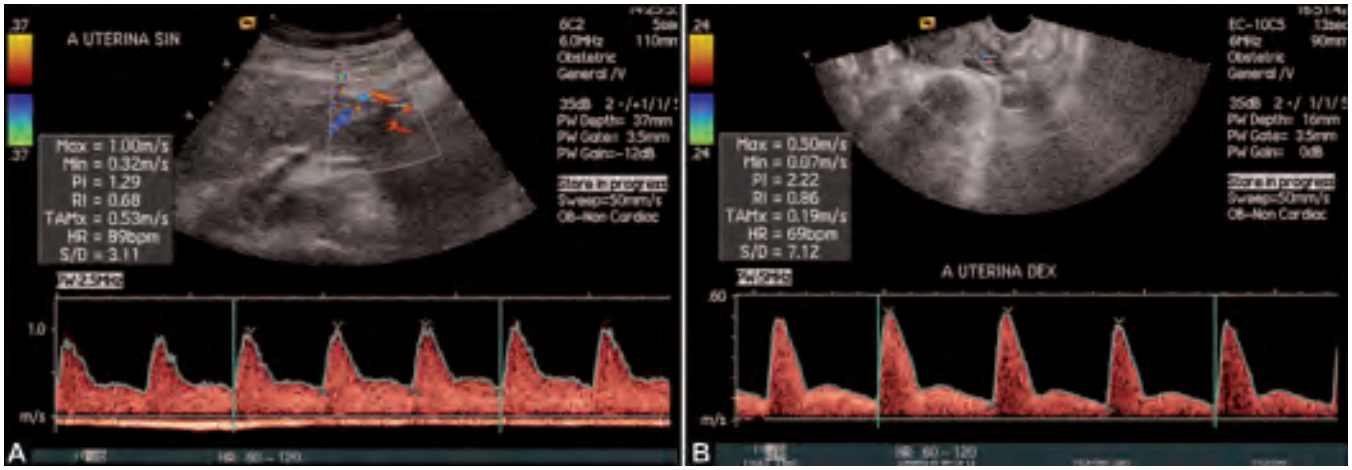

Figures 32.7A and B: (A) Normal flow velocity waveforms of the uterine artery on day 1 (Transabdominal approach) and; (B) 56 (Transvaginal approach) postpartum

the normal physiological time span for the placental site to recover is probably 4–6 weeks and not two weeks as previously considered.

Doppler Ultrasound During Normal Puerperium

Besides conventional ultrasound, Doppler technology is used to study hemodynamic events occurring during the puerperium. Normal pregnancy requires the growth of many new vessels. Consequently, during puerperium dramatically regressive changes must occur. The physiological involution of the uterus involves not only muscle cells and decidua but also the arteries. From histological studies, we know that normal involuted placental bed is characterized by a disappearance of trophoblasts and completely thrombosed spiral arteries.[40-42] High diastolic flow velocities in combination with a disappearance of the early diastolic notch are the main characteristics of the uterine artery Doppler flow pattern from gestational week 20–26 and they reflect the physiological conversion from high (nonpregnant) to low (pregnant) resistance state.[43,44] How fast these physiological changes return to the nonpregnant state is a controversial issue.[45-48] Tekay and Jouppila[14] assessed the peripheral vascular resistance of the uterine arteries in 42 postpartum women and found that the pulsatility index (PI) increased significantly in early puerperium compared to pregnancy, remained unchanged during the next six weeks and then gradually started to increase again. However, nonpregnant values were not reached even three months after delivery. Jaffa et al.,[46] on the other hand, described that PI decreased in the 2nd and remained relatively low until the 4th postpartum week. Similar differences regarding the reappearance of the early diastolic notch have been reported. Tekay and Jouppila[14] noted a reappearance of the early diastolic notch already in early puerperium in 40 of 42 women, while Jaffa et al.[46] found that the early diastolic notch had reappeared in only one of 60 women five weeks postpartum.

According to our findings,[48] in early puerperium the means of Doppler flow resistance indices are higher than those reported in late pregnancy. Thereafter, they do not change markedly until day 28 postpartum. On day 56 postpartum, they are still lower compared to the values reported for nonpregnant women, which speaks for longer duration of physiological vascular return from a pregnant to a nonpregnant state. We observed a diastolic notch in 13% of women on day one and in 90.6% of women on day 56 postpartum **(Figs 32.7A and B)**.

Color and power Doppler ultrasound may detect a localized area of increased vascularity within the myometrium. It may be a common transient ultrasound finding if asymptomatic and it does not require treatment.[47]

THREE-DIMENSIONAL ULTRASOUND POSTPARTUM

Although the volume of the uterus and uterine cavity were previously measured using 2D ultrasound,[15] the volumes assessed by 3D (three-dimensional) ultrasound may provide more accurate measurements than does the conventional ultrasound. 3D ultrasound using VOCAL program (Virtual Organ Computer-aided Analysis) has recently been used to measure the volumes of the uterus and the uterine cavity after normal delivery.[49] It is shown in **Figures 32.8A and B.**

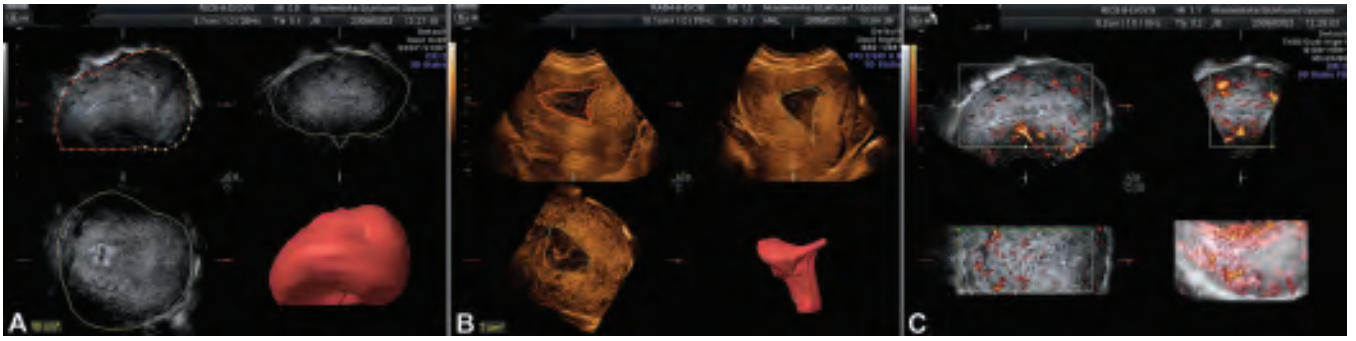

Figures 32.8A to C: (A) Three-dimensional USG of the volume of the uterus on day 28 and; (B) Uterine cavity on Day 7 after normal delivery; (C) With 3D power Doppler a localized area of increased vascularity within the myometrium is seen

3D power Doppler angiography is a new unexplored method for quantifying noninvasively the vascular network of the uterus **(Fig. 32.8C)**.

RETAINED PLACENTAL TISSUE

Both ultrasound diagnosis of RPT (retained placental tissue) and appropriate management for SPH (secondary postpartum hemorrhage) is still a controversial issue. SPH is defined as any abnormal bleeding from the uterus occurring between 24 hours and 12 weeks postpartum[49] and occurs in 1–2% of deliveries.[50,51] In developed countries, half of postpartum women who are admitted to hospital with this condition undergo uterine surgical evacuation.[49-53] In developing countries, it is a major contributor to maternal death.[49] The most common causes of SPH are abnormal involution of the placental site in the uterine cavity that may be idiopathic[42] or it can be caused by RPT[54] or by endometritis.[52] Subinvolution of the placental bed in the absence of RPT or endometritis is a distinctive entity, characterized by widely distended spiral arteries, only partly occluded by thrombi of various ages and invested with extravillous trophoblasts.[40,42] The diagnosis, however, requires histological examination and clinically it is a diagnosis of exclusion. Moreover, placental vascular subinvolution is often underrecognized by general surgical pathologists.[42] Carlan et al.[55] performed manual exploration of the cavity on 131 asymptomatic women, five minutes after placental delivery and within two minutes after an ultrasound examination. They found that 24 of 131(18.8%) women had documented evidence of RPT. This is a surprisingly higher figure compared to Jones et al.[56] who performed manual intrauterine explorations routinely after 1000 births and removed placental fragments or bits of membranes in only 2–4% of cases. Defective decidua, which can be scanty or completely absent in some patients, is a predisposing factor for abnormal attachment of the placenta and for partially RPT.[40] Vascular abnormalities of the uterus have recently been described as possibly more common causes of severe SPH than previously thought.[25-31]

In a Cochrane Review, Alexander et al.[50] identified 45 papers about the management of SPH and concluded that little information is available from randomized trials to guide clinicians in the management of this condition. Since the causes of SPH may be numerous, the best treatment options should be chosen according to the underlying cause of bleeding. However, an essential problem is that the underlying cause of SPH often is unknown and that clinical or ultrasound diagnosis of RPT, which is the indication for surgical treatment, is still a controversial issue.[58-68] The decision whether to perform uterine evacuation for RPT depends on both, clinical finding and the ability to visualize retained placenta by ultrasound.[58-69] Although prompt curettage seems to be necessary, in many cases it usually does not remove identifiable placental tissue. Moreover, it is more likely to traumatize the implantation site and incite more bleeding. Consequently, the complications rate is high. Hoveyda et al. reported in his review regarding secondary postpartum hemorrhage that the frequency of perforation of the uterus was 3% and hysterectomy about 1%.[54] Similar results are reported from an audit of 200 cases concerning puerperal curettage.[70] They showed that 8.5% of patients experienced major morbidity and 7% required a repeat procedure with further morbidity. In addition to immediate complications, late sequelae related to surgical treatment for SPH may influence the reproductive health of women. If curettage damages the endometrium 1–4 weeks postpartum, the endometrium may fail to regenerate, leading to Asherman's syndrome Jensen and Stromme.[71] Westendorp et al.[72] prospectively examined 50 women undergoing either a repeat

removal of placental remnants after delivery or a repeat curettage for incomplete abortion. At a later hysteroscopy, 20 out of 50 (40%) women had intrauterine adhesions. The prevalence of Asherman's syndrome is 2% after manual evacuation of the placenta but, [37] 5% after postpartum curettage.[72] Recently, an update on intrauterine adhesions has been published and the importance of prevention has been emphasized.[73]

First studies concerning RPT performed with old ultrasound equipment showed high rate of false-positive diagnosis.[4,5,8] Similar results have been obtained by modern ultrasound equipment.[58-68] Published studies have demonstrated a variable sensitivity (42–94%) and specificity (62–92%) for ultrasound diagnosis of RPT.[58-68] On the other side, ultrasound appears as a valuable tool to confirm an empty cavity. Lee and Mandrazzo[8] found empty cavity in 20 of 27 patients with late puerperal bleeding. In only one case, RPT was confirmed. The same authors reported that histological confirmation was obtained in eight of nine patients with ultrasound suspected RPT. Although ultrasound technology improved considerably, the diagnosis of RPT is still difficult. Ultrasound finding of RPT may vary depending on many different factors. We cannot expect the same ultrasound image during early **(Figs 32.4A and 32.5A)** and late period of the puerperium **(Figs 32.4C and 32.5D)**. The presence of blood, blood clots, necrotic decidua, membranes or gas can give various ultrasound images and a proper diagnosis is sometimes difficult. Nevertheless, the most common ultrasound finding associated with RPT is an echogenic mass[8,34-35,55,57-68] **(Figs 32.9A to C, 32.10A and B, 32.11A and B, 32.12A, 32.13A to C and 32.14A)**. In contrast, Edwards et al.[15] found in his study an echogenic mass on day 7 in 51% of normal cases, in 21% on day 14 and in 6% on day 21. He questioned ultrasound finding of an echogenic mass in uterine cavity as a sign of RPT. However, the definition of an echogenic mass was not specified and we may hypothesize that others investigators would probably classify many of their "echogenic mass" as "heterogeneous patterns". A heterogeneous pattern is a common and insignificant finding of the involuting uterus[13] **(Figs 32.4B and 32.5C to D)**. It is located in the cervical area in the early puerperium, in the whole uterine cavity in the middle part of the puerperium and it is not common during late postpartum period.[13] Sokol et al.[16]

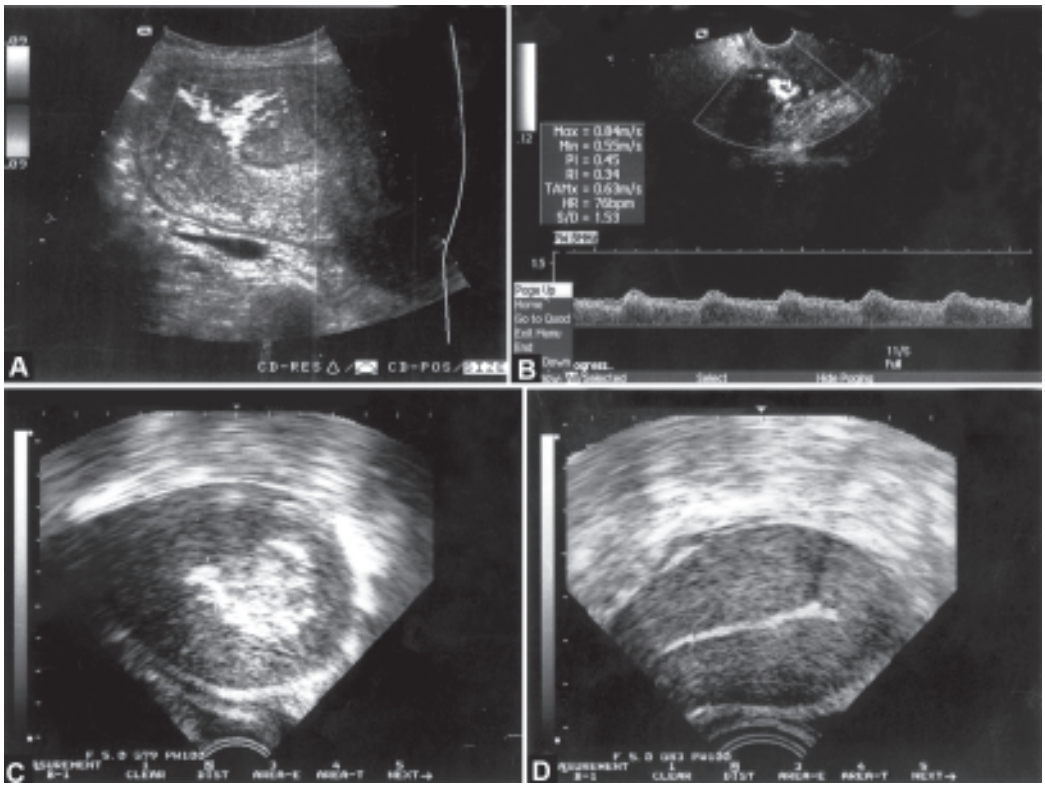

Figures 32.9A to D: Puerperal abnormalities revealed by ultrasound. (A) Retained placental tissue 2 days postpartum; (B) Blood flow in relation to retained placental tissue; (C) Retained placental tissue 6 weeks postpartum; (D) After curettage a thin, echogenic endometrium

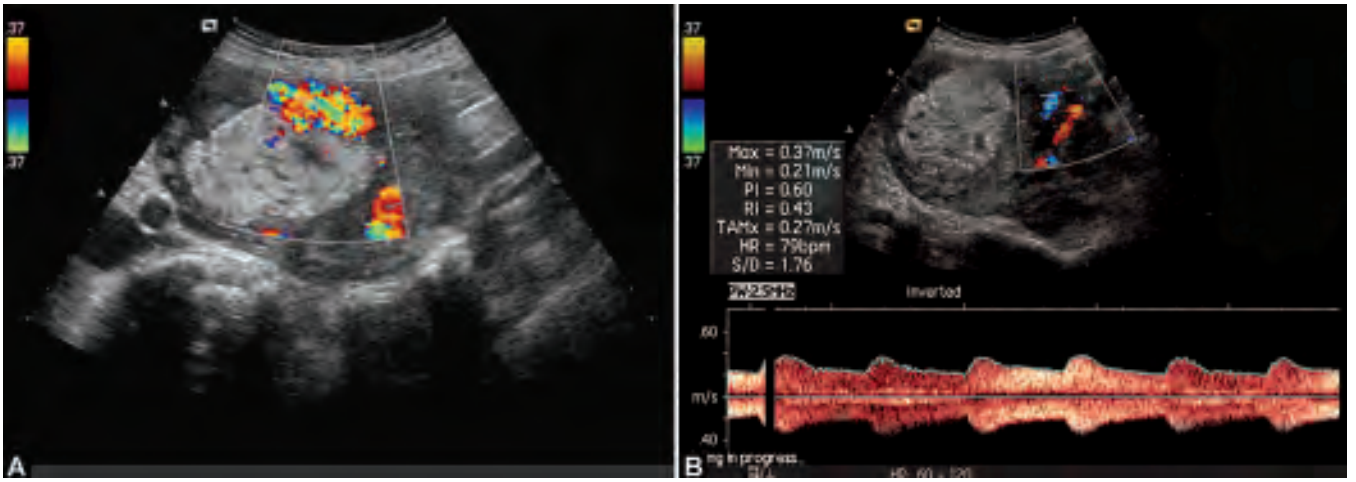

Figures 32.10A and B: Puerperal abnormalities revealed by ultrasound. (A) Transabdominal transverse scan, 9 days postpartum, shows retained placental tissue seen as an echogenic mass; (B) A low resistance blood flow is seen on one side of the echogenic mass

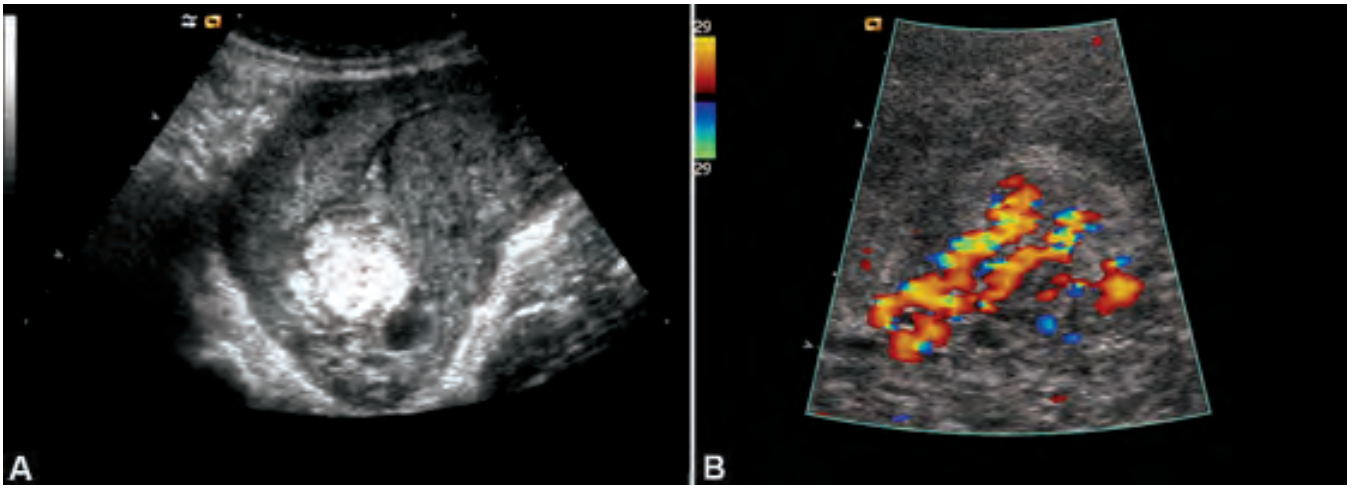

Figures 32.11A and B: (A) Transvaginal longitudinal scan shows retained placental tissue 6 weeks postpartum; (B) By color Doppler, feeding vessels are seen inside the echogenic mass

used the same classification and found "echogenic material" in 40% of women 48 hours after a normal delivery. However, 14 of the 16 cases demonstrated echogenic material in the lower uterine segment, while only two had such findings in the fundus. It is unclear if "echogenic material" is the same as an "echogenic mass" or if it might be a mixed echo pattern. If dysfunctional postpartum bleeding persists for a long time, RPT is highly suspected. Hertzberg et al.[34] described so-called "stippled pattern" of scattered hyperechogenic foci that later on became increasingly generalized echogenic, reflected secondary regressive changes in RPT **(Figs 32.9C and 32.11A)**.

Two studies[61,62] compared the diagnostic accuracy of clinical assessment with transabdominal USG in the management of SPH and concluded that both methods were of limited value. In contrast, recently published studies that assessed diagnostic accuracy of combined clinical and sonographic protocol, concluded that the combined approach was accurate and highly sensitive tool for the diagnosis of retained placental tissue.[66-69]

There are many reasons for discrepancies in the published reports. Factors that might explain the low sensitivity and high false-positive rate include a vague definition of the USG diagnosis of RPT,[58-62] retrospective study design[34,60,64,65] and mixed study populations

including women with bleeding after an abortion and women with postpartum haemorrhage.[8,60,64-66] Three studies often cited in the published literature evaluated asymptomatic women.[55,58] The accuracy of postpartum USG for detection of RPT was calculated either from a small proportion of women who underwent curettage, assuming that women who had an uneventful puerperal course after conservative treatments had no RPT,[34 60-62] or from histological findings among asymptomatic women.[55,58] Finally, the patients and clinicians have not been blinded to the sonographic results in any of the published studies. If ultrasound finding shows an empty cavity with thin white decidua/endometrium during early **(Figs 32.2A and 32.4A)** or late puerperium **(Figs 32.4C, 32.5D and 32.6A)**, pure fluid/heterogeneous content in the cavity during the middle part of the puerperium **(Figs 32.4B and 32.5B and C)**, or only small echolucent or hyperechogenic dots throughout whole postpartum period, a clinically significant amount of retained placental tissue is unlikely.[13,34] Transvaginal ultrasound with high frequency probe as well as transvaginal sonohysterography may better differentiate intrauterine puerperal pathology.[74-77]

Doppler Ultrasound During Pathological Puerperium

A few studies investigated pulsed and color Doppler during puerperium in order to improve diagnostic accuracy of ultrasound regarding RPT.[60,74,75] Some investigators observed low resistance blood flow around intracavitary contents[74-78] **(Figs 32.9A and 32.10A)**. Ashiron et al.[74] measured resistance index (RI) in relation to RPT and found that diagnosis is highly suspected if RI is below 0.35 **(Fig. 32.9B)**. These patients are suitable for invasive treatment. RI above 0.45 should exclude diagnosis. Values between 0.35 and 0.45 form a "gray zone" **(Fig. 32.10B)**. Conservative treatment and repeated ultrasound examinations should be performed.

Power Doppler seems to be a new unexplored modality that could improve our abilities to diagnose clinically significant RPT. Retained placental tissue in the uterine cavity might cause a delay in the normal involution of uterine vessels.[40,41] By color Doppler ultrasound, a localized area of increased vascularity within the myometrium may be detected.[47,78-83] The presence of a hypervascular area in the myometrium, within or close to the echogenic mass, has previously been interpreted alternatively as a common physiological finding,[47] as a finding associated with the presence of RPT[60,74,75,83,84] or with arteriovenous (AV) malformations.[25,78,79] Pulsed Doppler usually demonstrates a low resistance turbulent flow with high systolic velocity, resembling AV malformations. It has recently been suggested that curettage should not be performed on patients who present with SPH and a color Doppler image of a hypervascular area within the myometrium.[78,79] Van den Bosch[80] examined 385 consecutive postpartum women and reported that a hypervascular area in the uterus was relatively common (8.3%) and disappeared either spontaneously or after removal of placental remnants. Mungen[81] has drawn attention to a tendency to overdiagnose true AV malformations. He pointed out that a majority of hypervascular areas in the myometrium probably represented normal "perivillous flow" in the spiral arteries. The regression period may be prolonged in the presence of RPT. Only in very rare instances do they represent true arteriovenous malformations. In our recent work on angiographic embolization for treatment of major postpartum hemorrhage, no true AV malformation was diagnosed among 20 patients but four cases had pseudoaneurysm[85] **(Figs 32.15A and B).**

Our knowledge on uterine artery flow in women with RPT is sparse. It could be that RPT prevents the physiological changes in uterine blood flow during the puerperium. The results of our small study[83] showed the resistance flow indices in uterine artery below the 10th percentile for 8 of 20 (40.0%) women of which seven had histological confirmation of RPT and one did not. There was, however, considerable overlap. No patient had resistance indices above the 90th percentile. In 12 of 20 (60.0%) patients, an early diastolic notch was absent. Early diastolic notches appeared relatively late compared to the findings in normal population. Only one woman had a notch before postpartum day 28. Color Doppler showed a hypervascular area close to the echogenic mass in 12 of 20 (60%) patients, all with histologically confirmed RPT. This figure is slightly higher than that reported by Durfee et al.[60] (55%) and by Zalel et al.[77] (46%). A hypervascular area was absent in eight patients (40%) of which six had an echogenic mass that was histologically confirmed RPT. Our findings that the absence of blood flow does not exclude RPT are in concordance with previously reported results.[60,77]

POSTPARTUM ENDOMETRITIS

Postpartum endometritis is a fairly common clinical condition, affecting 2–5% women following delivery.[86,87] Cesarean section (CS) is the leading predisposing factor.[88] It has been considered that the typical ultra-

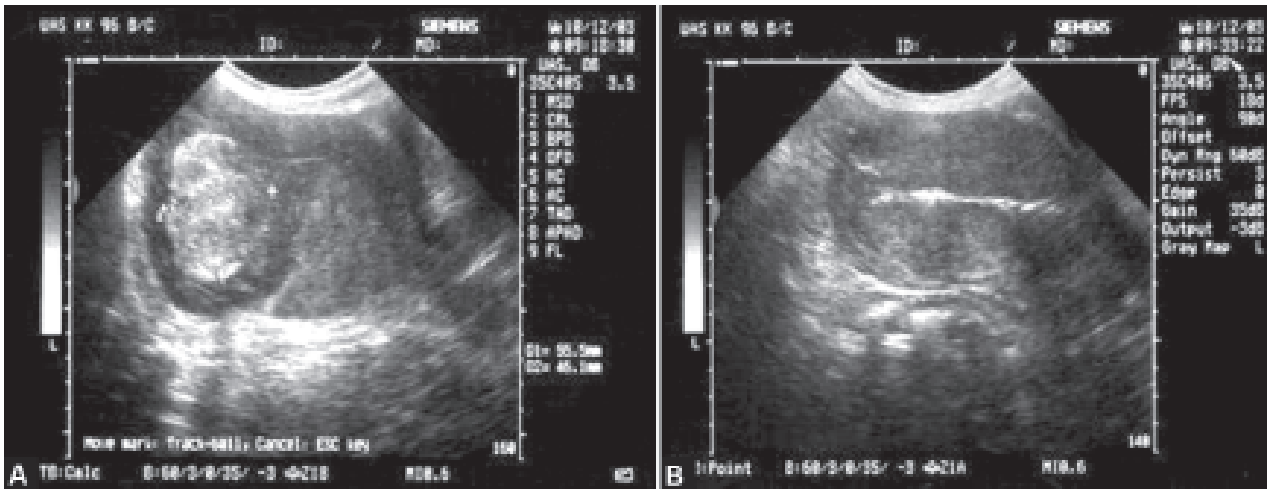

Figures 32.12A and B: (A) Transverse longitudinal scan, 11 days postpartum, shows retained placental tissue seen as an echogenic mass; (B) A thin echogenic endometrium is visible soon after curettage

sound finding in cases of endometritis is the presence of gas in the uterine cavity.[10] Madrazo found gas in uterine cavity in 15% of patients with puerperal endometritis.[10] Nowadays, infections caused by gas-forming organisms *C. perfringens* are very rare and large gas-bubbles are almost never seen. Moreover, Wachsberg and Kurtz[36] detected gas in about 19% of normal cases, which is in accordance with results of a computed tomographic study performed within 24 hours of uncomplicated vaginal delivery (21%). Ultrasound appearance of gas is seen as an intensively hyperechogenic focus equivalent in echogenicity to bowel gas with clean and dirty shadowing or a reverberation artefact.[89] According to our experience, gas is mostly observed following intrauterine manipulations[90] **(Figs 32.12B and 32.16A)** although it is occasionally observed after normal vaginal delivery.[13] The detection of gas within the uterine cavity may be a normal finding during the puerperium and does not necessarily indicate the presence of endometritis or RPT.[13,36] After CS or intrauterine manipulations highly echogenic foci can obscure an existing mass in the uterine cavity or be mistaken for retained placental tissue.[34,90] Thus whenever highly echogenic foci are present in the uterine cavity, the physician who interprets ultrasound finding must be aware of recent uterine manipulations. Gas usually disappears within 1–2 weeks after instrumentation[90] **(Fig. 32.16B)**. Furthermore, it has been claimed that ultrasound image of RPT and endometritis overlap.[8,52] Results from published studies on this issue are inconsistent.[8,41,52-53,62,70,90] Pelage et al.[91] described 14 cases with uncontrollable SPH undergoing selective angiographic embolization. Six of 14 patients had clinical and ultrasound signs of endometritis with RPT. In four cases, histological confirmation was obtained. Two patients had pure endometritis. Conversely, Kong et al.[41] pointed out that endometritis appeared to be an overstated cause of SPH. He found that less than 5% of cases could be ascribed to endometritis. Ben-Ami et al.[62] found that a majority of the patients presenting with

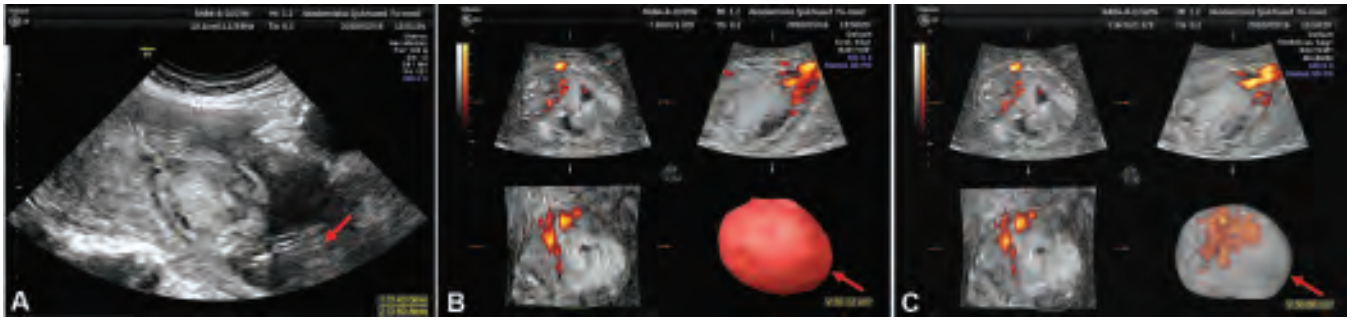

Figures 32.13A to C: (A) Transabdominal longitudinal scan of the uterus on day 17 postpartum. Suspected retained placental tissue seen as an echogenic mass in the uterine cavity (red arrow); (B) 3D USG shows the volume of the suspected retained placental tissue; (C) Power Doppler angiography, glass body mode shows vessels in the placental tissue (red arrow)

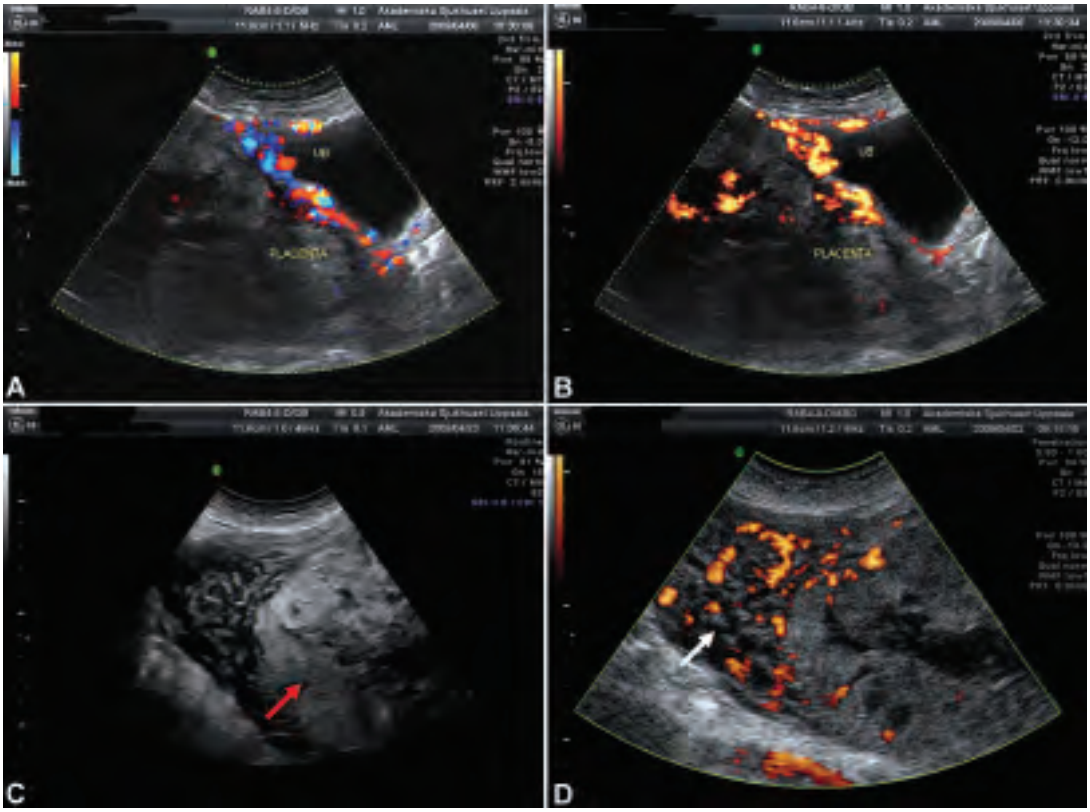

Figures 32.14A to D: Ultrasound image of placenta praevia perccreta left *in situ*. (A) Color Doppler and; (B) Power Doppler show the interface between the uterus and urinary bladder 7 days after cesarean section; (C) Retained placenta occupies the most part of the uterine cavity (arrow); (D) Power Doppler shows increased myometrial vascularity behind the retained placenta (arrow)

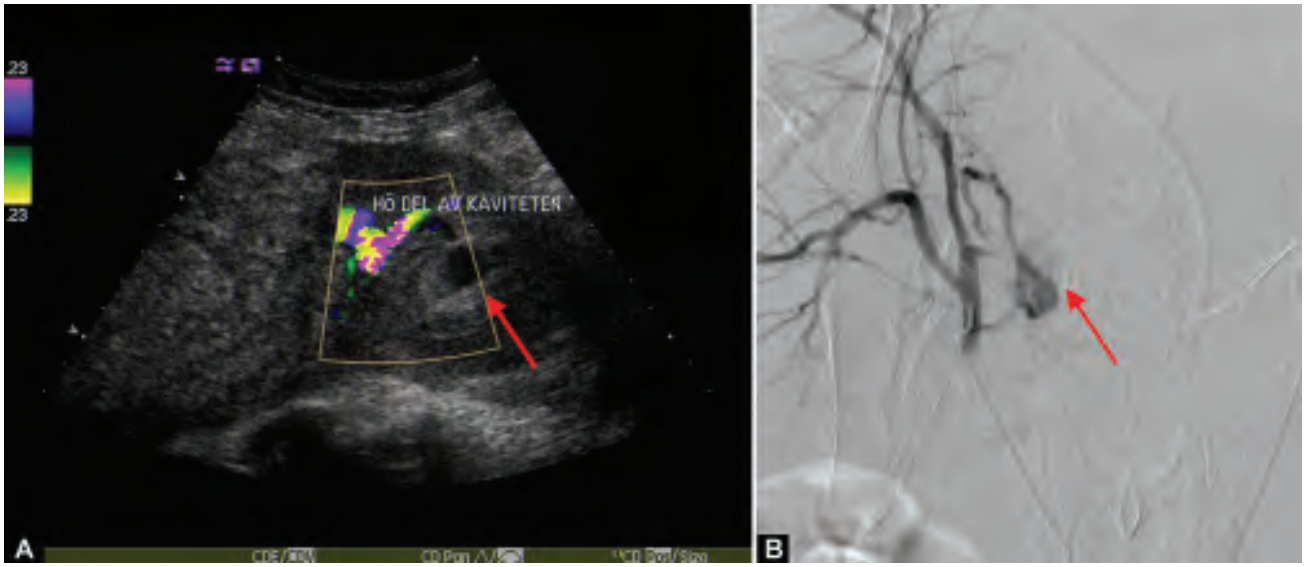

Figures 32.15A and B: (A) Transabdominal scan of the uterus on day 8 postpartum shows a huge defect in the uterus forming a pseudoaneurysm (arrow). Color Doppler reveals a feeding damaged uterine artery; (B) Angiography confirmed the ultrasound finding

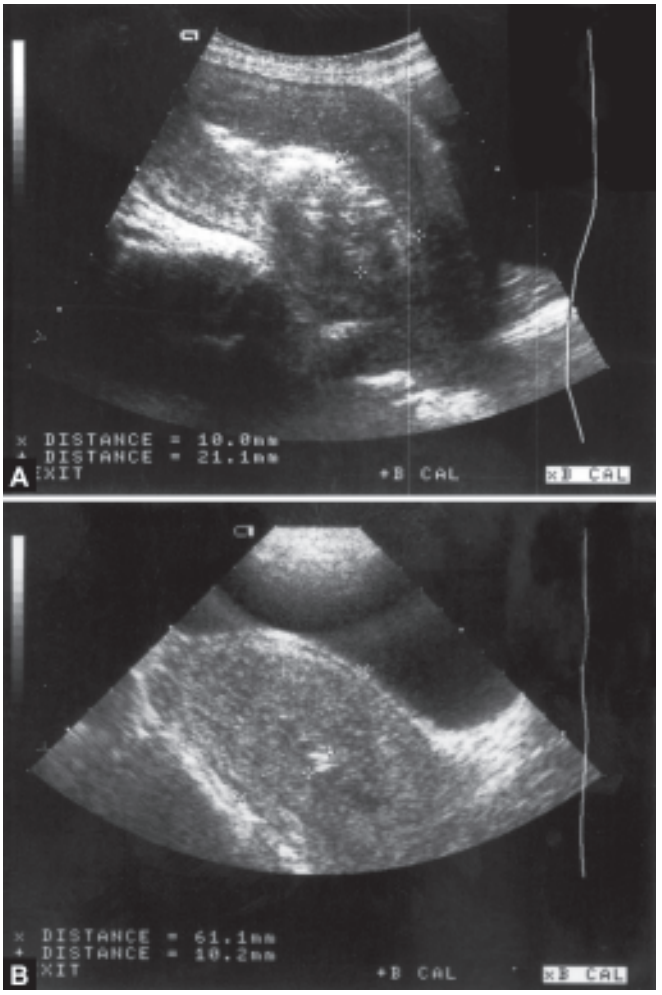

Figures 32.16A and B: (A) Gas in uterine cavity one-day post curettage; (B) Six days post curettage

fever ≥38°C postpartum were falsely diagnosed by ultrasound as having suspected RPT.

The presence of RPT may result in intrauterine infection and in these cases ultrasound examination can help us to select patients suitable for invasive treatment. In the vast majority of cases of isolated endometritis, ultrasound findings are normal and have no pathognomonic ultrasound image.[35,90] Kirkinen et al.[45] found that blood flow to the infected uterus could be different from normal. Deutchman and Hartman described postpartum pyometra as a lucent area within the uterus.[92] They also advocated the usage of Ultrasound to assist in guiding a drainage procedure. Septic pelvic thrombophlebitis, well known as an "enigmatic puerperal fever" is another uncommon complication of the puerperium. It most commonly presents in early postpartum period and antibiotic treatment is usually unsuccessful. Rudoff et al.[93] suggests ultrasound examination in case of clinical suspicion of pelvic thrombophlebitis. Although ultrasound diagnosis of ovarian vein thrombophlebitis is well described,[94-96] the diagnosis is still difficult and an ultrasound expertise is needed. Asymmetric dilatation of the ovarian or other pelvic vein may sometimes be observed.[95] Furthermore a complex or hypoechoic mass near the lower pole of the kidney particularly in clinical setting of an "enigmatic puerperal fever" should suggest thrombophlebitis. An echogenic intracaval mass is considered diagnostic and anticoagulation treatment should be added.[96]

Cesarean Section

Nowadays, when CS rates are continuously rising, higher incidence of all puerperal complications can be expected.[88] The ultrasound image of the uterus following CS usually shows three distinctive patterns:

1. Gas in the cavity
2. A small rounded area at the incision site that reflects tissue reaction due to localized edema and
3. Several echogenic dots at the incision site, which is related to the type of closure and the suture material used[82,90,97] **(Figs 32.17A and B)**. All these characteristics are normal findings and no correlation with

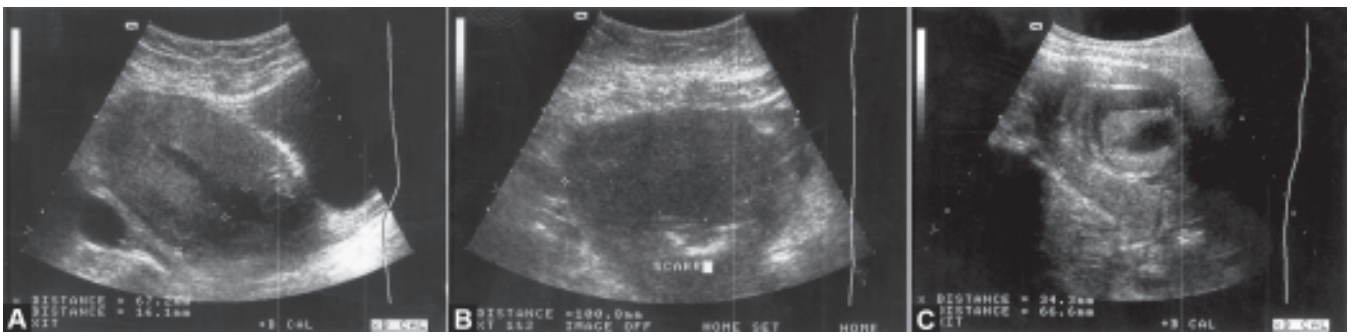

Figures 32.17A to C: (A) The uterus after cesarean section—longitudinal section; (B) Coronal section—hyperechogenic scar in lower uterine segment; (C) Hematometra

pathological conditions is found. The involution rate of the uterus following CS is not markedly different from the involution rate after vaginal delivery.[90,98-100] We observed a few morphological differences between the women delivered by CS and the women who had a vaginal delivery such as the less common; anteverted position of the uterus and the empty uterine cavity in early puerperium, which might reflect slightly delayed uterine involution process.[90] The significant infectious morbidity is associated with CS.[88] Ultrasound may be useful in postpartum women with clinical suspicion of a postoperative complication like phlegmona,[101] abscess, pyometra, hematometra **(Fig. 32.17C)**, wound infection, subfascial hematoma or intra-abdominal postoperative hemorrhage. Baker et al. described bladder flap hematoma after a low uterine transverse CS.[102] A solid or complex mass between the posterior bladder wall and the anterior uterine wall may be observed by ultrasound. An abscess appears as a cystic structure with internal debris surrounded by thicker irregular walls. An infected hematoma initially has similar ultrasound appearance. During the resolution process, it may change and appears more solid. However, the physician must be aware that ultrasound diagnosis is just a complement and clinical condition of the patient should guide the therapeutic approach.

UNCOMMON BUT POTENTIALLY LIFE-THREATENING CAUSES OF POSTPARTUM BLEEDING

There are a few uncommon but potentially life-threatening causes of postpartum bleeding which contribute significantly to maternal mortality and morbidity. These are placenta accreta/increta/percreta,[17-23] vessel's lesions (true AV malformations,[25] pseudoaneurysm[26-31]) placental site tumor[32] and choriocarcinoma.

Placenta Accreta/Increta/Percreta

The incidence of abnormal placentation, placenta accreta/increta/percreta, has increased in recent years, particularly due to the increasing rates of cesarean section. It is the most common factor for uncontrolled postpartum hemorrhage leading to emergency postpartum hysterectomy, which is associated with significant maternal morbidity and mortality.[17] Antenatal diagnosis of severe invasive placentation is feasible with ultrasound. Both, conventional 2D and 3D ultrasound have been used and several reports have been recently published.[18-23] Optimal management strategies for placenta accreta is highly dependent on accurate antenatal diagnosis and it is also associated with decreased maternal morbidity.[103,104] Placenta accreta may be left *in situ*, as the whole or just partly[103] and ultrasound may be of help to monitor spontaneous resorption of the retained tissue. However, the reports about ultrasound findings in these cases are sparse[24] **(Figs 32.14A to D)**.

Uterine Arteriovenous Lesions (True AV malformations, Acquired AV Malformations /Pseudoaneurysm)

True arteriovenous malformations (AV) are a rare errors of morphogenesis, which do not regress spontaneously and they are extremely rare causes of SPH.[25,81] In contrast, acquired AV abnormalities of the uterus are associated with trauma after previous intrauterine procedures, RPT, infection or malignancy and are more common.[26-31] The difference between normal perivillous blood flow increased myometrial flow related to RPT and AV malformations seems to be difficult.[25,47,81] Three typical ultrasound signs of pseudoaneurysm include: a pulsating hypoechoic area connected to feeding artery by a narrow neck on Gray-scale ultrasound, a turbulent flow inside the pseudoaneurysm on color Doppler and a reversed flow on the neck of the pseudoaneurysm on pulse Doppler. During systole, blood enters the pseudoaneurysm and during diastole it reverses back into the uterine artery because of the pressure gradient between the pseudoaneurysm and the feeding artery **(Figs 32.15A and B)**. Curettage should not be performed on patients who present with severe postpartum bleeding and a pseudoaneurysm is suspected on color Doppler scan. Further investigation with pelvic angiography or MRI should be performed.

Placental Site Tumor and Choriocarcinoma

These are rare forms of gestational trophoblastic disease and ultrasound image is difficult to distinguish them from each other as well as from retained placenta accreta and from acquired arteriovenous lesions. MRI findings are more sensitive but not specific. Thus the appropriate diagnosis may be delayed.

Placental site tumor[32] and choriocarcinoma may appear as an irregular mass with both cystic and hyperechoic components in the cavity often involving myometrium **(Figs 32.18A and B)**. With color Doppler, low-resistance flow may be seen.

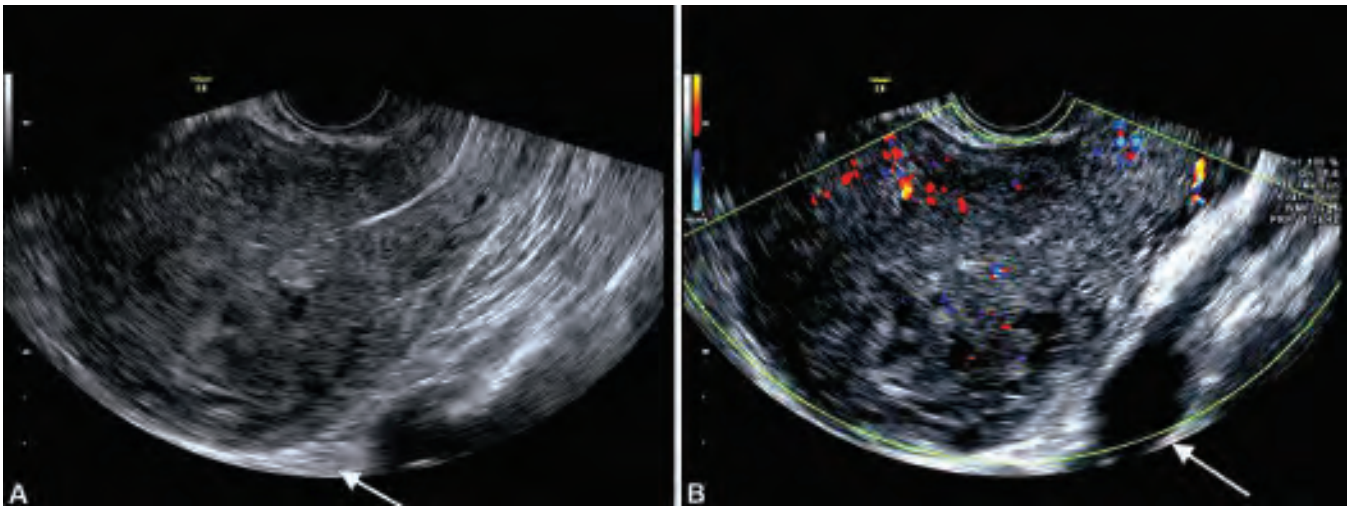

Figures 32.18A and B: (A) Transvaginal, longitudinal scan shows an irregular heterogeneous mass in the cavity involving the myometrium (arrow); (B) By color Doppler moderately increased myometrial vascularity is seen. Histological finding was choriocarcinoma

CONGENITAL UTERINE MALFORMATIONS

The prevalence of the congenital uterine malformations in general population is largely unknown. Failed fusion of the two Mullerian ducts to form the genital organs may cause reproductive, fetal and maternal hazards (infertility, premature labor, abnormal fetal presentations, retained placental tissue and postpartum hemorrhage). It is well known that uterine anomalies may remain undiscovered except when they are associated with reproductive or obstetric problems. Already in 1976, Bennett suggested puerperal ultrasonic hysterography as a screening procedure prior to radiological examination in women whose reproductive performance suggests a diagnosis of congenital malformation of the uterus.[105] Since then, a few studies concerning the issue were published. Szoke and Kiss[106] in 1977, manually examined patients, revealing a uterus differing in shape from normal, the patient had a breach presentation in her previous or present pregnancy and the involution of the uterus was slow. The ultrasound echo technique was applied and uterine anomalies were found in five cases postpartum.[106] In 1984, Land et al. performed ultrasonic hysterography in 104 patients between the 2nd and 5th postpartum day. An unexpectedly high number of women (16%) showed an abnormal uterine configuration.[107]

The coronal section seems to be the most appropriate section in order to reveal uterine cavity anatomy **(Figs 32.19A to C)**.[13,82] It is difficult to obtain the coronal section by abdominal examination in nonpregnant patients. However, the puerperium when the uterus is extremely large makes an exception. The ultrasound examination should perform in the early puerperium

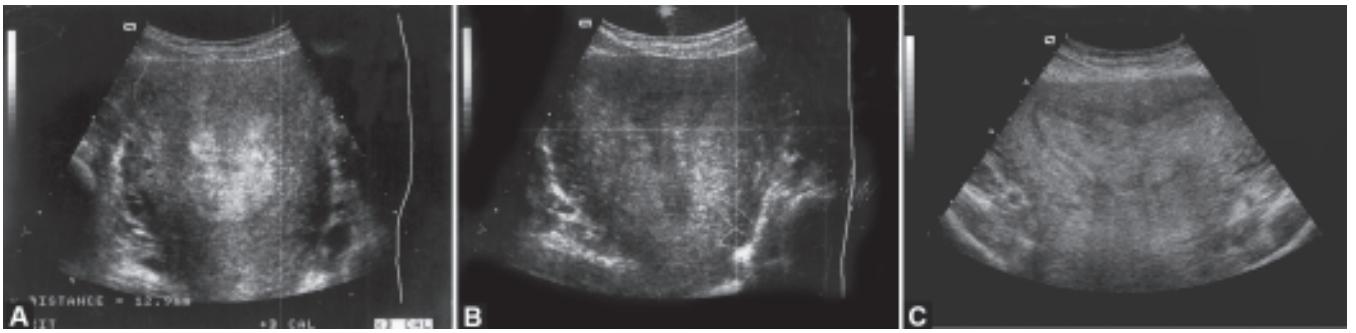

Figures 32.19A to C: (A) A coronal section shows a subseptate uterus one day after manual evacuation of the placenta; (B) The uterus of the same patient 8 days later; (C) A coronal section on day three postpartum shows uterus arcuatus in a woman who had twice breach position and preterm delivery

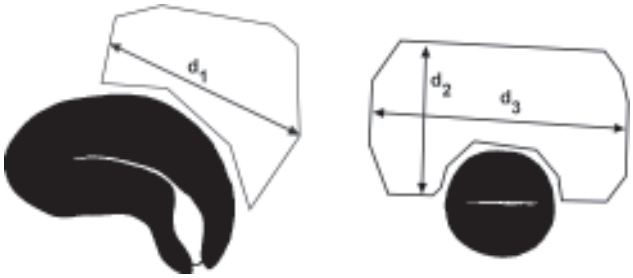

Figure 32.20: Residual urine volume measurement

because a large uterus lies in near proximity to the ultrasound probe and highly echogenic decidua outlines well the shape of the cavity. Puerperal ultrasound might detect uterine developmental abnormality, providing an explanation for complications in labor and the puerperium **(Fig. 32.19C)**.

Postpartum Urinary Retention

Postpartum urinary retention is a relatively common condition and incidence ranges between 1–18%.[108] According to the International Continence Society, 100 ml is considered as the upper limit of residual urine. Ultrasound is the method of choice when assessing urinary bladder and residual urine postpartum. Invasive catheterization with the discomfort and the risk of infection can be avoided. Conventional bladder scanner is not to be recommended during the puerperium. Large uterus may have content of fluid and thus a misinterpretation may be done. Many different techniques for bladder volume measurement are used and the accuracy of the method varies widely. We prefer a method where the longest distance of the maternal bladder (d1) is measured in a longitudinal section, and then two perpendicular diameters (d2 and d3) are measured in the transverse section **(Fig. 32.20)**. The estimated amount of residual urine can be calculated using the formula for approximation of the ellipsoid: Volume (ml) = (d1 × d2 × d3) / 2 **(Fig. 32.13)**.

Puerperal Mastitis and Breast Abscess

Puerperal mastitis is a common complication in lactating women, particularly in primiparous women. Reported incidence varies from 1–24%.[109] If treatment with antibiotics is delayed or inadequate it can progress to more serious complication, breast abscess. Breast tenderness limits clinical assessment and clinical diagnosis may be difficult, particularly if the abscess lies deeply in the breast or if it is too small. Ultrasound with a 7.5–12 MHz probes is being used to differentiate

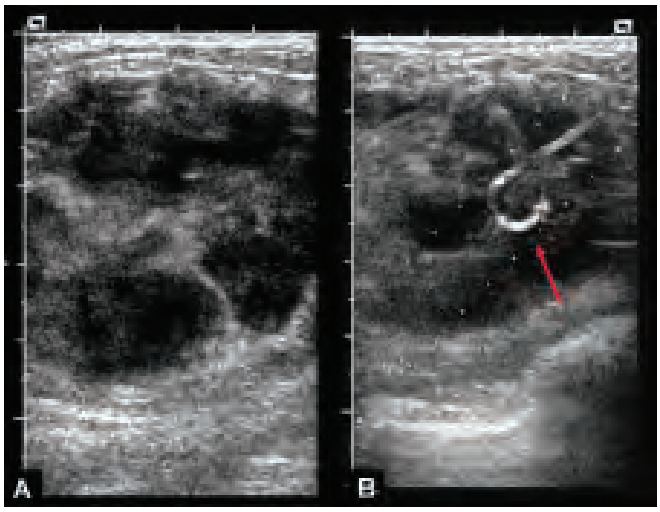

Figures 32.21A and B: (A) Ultrasound image of breast abscess before drainage with pigtail catheter; (B) After drainage with pigtail catheter (arrow)

abscess from puerperal mastitis.[109] Ultrasound findings of mastitis are increased parenchyma/fat echogenicity, skin thickening and increased vascularity by color Doppler. Ultrasound diagnosis of breast abscess, in contrast, is made when a round/oval or irregular hypoechogenic lesion is detected **(Fig. 32.21A)**. Color Doppler detects any vessels. The traditional treatment of breast abscess by surgical incision and drainage requires general anesthesia, major duct may be damaged and it usually makes a poor cosmetic result due to scar formation. More recently USG guided needle aspiration of breast abscess or catheter placement was used instead of surgical treatment. Ulitzsch et al.[109] reported ultrasound treatment of 56 breast abscesses among 43 breastfeeding women and the treatment was successful in all but one woman. In 52% of cases repeat needle aspirations were required. The authors recommended a 21 gauge needle aspiration alone if the abscess diameter < 3 cm. In contrast an abscess ≥ 3 cm should treat with placement of pigtail catheter **(Fig. 32.21B)** which should be removed when ultrasound shows no residual fluid and when only minimal saline can be irrigated into the residual cavity. Breastfeeding is not contraindicated. However, in cases of recurrence, lactation stop with dopamine agonist is to be required.

CONCLUSION

Present ultrasound technology with high image resolution has made ultrasound a valuable diagnostic tool for assessing numerous postpartum clinical conditions.

Suspicion of retained placental tissue, unknown cause of the puerperal sepsis, surgical complications or acute abdominal pain are some of the possible reasons to switch on ultrasound machine. Not only the involution changes of the uterus or pathological changes in uterine cavity but also the other organs like kidneys, urinary bladder, gallbladder, ovaries and abdominal cavity can be easily examined by ultrasound during postpartum period.

Sonohysterography may better differentiate intrauterine pathology by injecting saline under sonographic control and so improve the accuracy of the diagnosis of puerperal pathology.

Color, pulsed and power Doppler have improved our ability to study for the first time the vascular changes of the uterine involution noninvasively. With three-dimensional ultrasound, the possibility to measure volumes of the uterus and the cavity postpartum has been introduced. Uterine vascular network can also be investigated by 3D PD angiography more extensively.

More studies are required in this important area and all these new modalities need further evaluation. Moreover, the knowledge obtained through ultrasound examinations can help us to better understand both the physiology and patophysiology of the puerperium. The usefulness of ultrasound examinations during puerperium is not questioned any more, but ultrasound has become the first imaging modality used whenever puerperal complications are suspected.

REFERENCES

1. Hytten F. The Clinical Physiology of the Puerperium. London, UK: Farrand Press; 1996.
2. Donald I, MacVicar J, Brown TG. Investigation of abdominal masses by pulsed ultrasound. Lancet. 1958;1(7032): 1188-95.
3. Robinson HP. Sonar in the puerperium. A means of diagnosing retained products of conception. Scott Med J. 1972;17(11):364-6.
4. Szoke B, Kiss D. The use of the ultrasonic echo technique in examining the normal and pathological involution in the puerperium. Int J Gynaecol Obstet. 1976;14(6):513-6.
5. Malvern J, Campbell S. Ultrasonic scanning of the puerperal uterus following postpartum haemorrhage. J Obstet Gynaecol Br Commonw. 1973;80(4):320-4.
6. Rodeck CH, Newton JR. Study of the uterine cavity by ultrasound in the early puerperium. Br J Obstet Gynaecol. 1976;83(10):795-801.
7. Defoort P, Benijts G, Thiery M, et al. Ultrasound assessment of puerperal uterine involution. Eur J Obstet Gynaecol. 1978;8(2):95-7.
8. Lee CY, Madrazo B, Drukker BH. Ultrasonic evaluation of the postpartum uterus in the management of postpartum bleeding. Obstet Gynaecol. 1981;58(2):227-32.
9. VanRees D, Bernstine RL, Crawford W. Involution of the postpartum uterus: an ultrasonic study. J Clin Ultrasound. 1981;9(2):55-7.
10. Madrazo BL. Postpartum Sonography. The principle and practice of ultrasonography in obstetrics and gynecology, 3rd edn. East Norwalk:Appleton-Century-Crofts; 1985. pp. 449-56.
11. Lavery JP, Shaw LA. Sonography of the postpartum uterus. J Ultrasound Med. 1989;8:481-6.
12. Wachsberg RH, Kurtz AB, Levine CD, et al. Real-time ultrasonographic analysis of the normal postpartum uterus: technique, variability and measurements. J Ultrasound Med. 1994;13:215-21.
13. Mulic-Lutvica A, Bekuretzion M, Axelsson O, et al. Ultrasonic evaluation of the uterus and uterine cavity after normal, vaginal delivery. Ultrasound Obstet Gynecol. 2001;18:491-8.
14. Tekay A, Jouppila P. A longitudinal Doppler ultrasonographic assessment of the alterations in peripheral vascular resistance of uterine arteries and ultrasonographic findings of the involuting uterus during the puerperium. Am J Obstet Gynecol. 1993; 168(1 Pt 1):190-8.
15. Edwards A, Ellwood DA. Ultrasonographic evaluation of the postpartum uterus. Ultrasound Obstet Gynecol. 2000;16(7):640-3.
16. Sokol ER, Casele H, Haney EI. Ultrasound examination of the postpartum uterus: what is normal? J Maternal Fetal Neonat Med. 2004;15(2):95-9.
17. Rossi AC, Lee RH, Chmait RH. Emergency postpartum hysterectomy for uncontrolled postpartum bleeding: a systematic review. Obstet Gynecol. 2010;115(3):637-44.
18. Chou MM, Ho ESC, Lee YH. Prenatal diagnosis of placenta previa accreta by transabdominal color Doppler ultrasound. Ultrasound Obstet Gynecol. 2000;15(1):28-35.
19. Yang JI, Lim YK, Kim HS, et al. Sonographic findings of placental lacunae and the prediction of adherent placenta in women with placenta previa totalis and prior Cesarean section. Ultrasound Obstet Gynecol. 2006;28(2):178-82.
20. Japaraj RP, Mimin TS, Mukudan K. Antenatal diagnosis of placenta previa acreta in patients with previous cesarean scar. J Obstet Gynaecol Res. 2007,33(4),431-7.
21. Bauer ST, Bonanno C. Abnormal placentation. Semin Perinatol. 2009;33:88-96.
22. Shin JC, Jaraquemada JMP, Su YN, et al. Ultrasound Obstet Gynecol. 2009;33:193-203.
23. Chou M-M, Chen W-C, Tseng J-J, et al. S-C Prenatal detection of bladder wall involvement in invasive placentation with sequential two-dimensional and adjunctive three-dimensional ultrasonography. Taiwan J Obstet Gynecol. 2009;48(1):38-45.
24. Shapiro JL, Sherer DM, Hurley JT, et al. Postpartum ultrasonographic findings associated with placenta accreta. Am J Obstet Gynecol. 1992;167(3):601-2.
25. Kelly SM, Belli AM, Campbell S. Arteriovenous malformation of the uterus associated with secondary postpartum hemorrhage. Ultrasound Obstet Gynecol. 2003;21(6):602-5.
26. Henrich W, Fuchs I, Luttkus A, et al. Pseudoaneurysm of the uterine artery after cesarean delivery: sonographic diagnosis and treatment. J Ultrasound Med. 2002; 21(12):1431-4.

27. Cooper BC, Hocking-Brown M, Sorosky JI, et al. Pseudoaneurysm of the uterine artery requiring bilateral uterine artery embolization. J Perinat. 2004;24(9):560-2.
28. Eason DE, Tank RA. Avoidable morbidity in a patient with pseudoaneurysm of the uterine artery after cesarean section. J Clin Ultrasound. 2006;34(8):407-11.
29. Mammen T, Shanthakumari H, Gopi K, et al. Iatrogenic secondary postpartum haemorrhage: apropos of two uncommon cases. Australas Radiol. 2006;50(4):392-4.
30. McGonegle SJ, Scott Dziedzic T, Thomas J, et al. Pseudoaneurysm of the uterine artery after an uncomplicated spontaneous vaginal delivery. J Ultrasound Med. 2006;25(12):1593-7.
31. Marnela K, Saarelainen S, Palomäki O, et al. Sonographic diagnosis of postpartum pseudoaneurysms of the uterine artery: a report of 2 cases. J Clin Ultrasound. 2010;38(4):205-8.
32. Vaswani K, Vitellas KM, Bennet WF, et al. Sonography case of the day. Am J Roentgenol. 2000;175:895-901.
33. Williams JW. Regeneration of the uterine mucosa after delivery with special reference to the placental site. Am J Obstet Gynecol. 1931;22:640, 664.
34. Hertzberg BS, Bowie JD. Ultrasound of the postpartum uterus, prediction of retained placental tissue. J Ultrasound Med. 1991;10:451-6.
35. Sakki A, Kirkinen P. Ultrasonography of the uterus at early puerperium. Eur J Ultrasound. 1996;4:99-105.
36. Wachsberg RH, Kurtz AB. Gas within the endometrial cavity at postpartum US. A normal finding after spontaneous vaginal delivery. Radiology. 1992;183(2):431-3.
37. Sharman A. Reproductive Physiology of the Postpartum Period. Livingston: Edinburgh E andS; 1966.
38. Oppenheimer LW, Sherriff EA, Goodman JDS, et al. The duration of lochia. Br J Obstet Gynaecol. 1986;93:754-7.
39. Visness CM, Kennedy KI, Ramos R. The duration and character of postpartum bleeding among breast-feeding women. Obstet Gynecol. 1997;89(2):159-63.
40. Andrew AC, Bulmer JN, Wells M, et al. Subinvolution of the uteroplacental arteries in the human placental bed. Histopathology. 1989;15(4):395-405.
41. Khong TY, Khong TK. Delayed postpartum hemorrhage: a morphologic study of causes and their relation to other pregnancy disorders. Obstet Gynecol. 1993;82(1): 17-22.
42. Weydert JA, Benda JA. Subinvolution of the placental site as an anatomic cause of postpartum uterine bleeding. A Review. Arch Pathol Lab Med. 2006;130:1538-42.
43. Campbell S, Diaz-Recasen J, Griffin D, et al. New Doppler technique for assessing uteroplacental blood flow. Lancet. 1983;1(8326 Pt 1):675-7.
44. Bernstein IM, Ziegler WF, Leavitt T, et al. Uterine artery hemodynamic adaptations through the menstrual cycle into early pregnancy. Obstet Gynecol. 2002;99(4):620-4.
45. Kirkinen P, Dudenhausen J, Baumann H, et al. Postpartum blood flow velocity waveforms of the uterine arteries. J Reprod Med. 1988;33(9):745-8.
46. Jaffa AJ, Wolman I, Har-Toov J, et al. Changes in uterine artery resistance to blood flow during puerperium: a longitudinal study. J Matern-Fetal Invest. 1996;6:27-30.
47. Van Schoubroeck D, Van den Bosch T, Scharpe K, et al. Prospective evaluation of blood flow in the myometrium and uterine arteries in the puerperium. Ultrasound Obstet Gynecol. 2004;23(4):378-81.
48. Mulic-Lutvica A, Eurenius K, Axelsson O. Longitudinal study of Doppler flow resistance indices of uterine artery after normal vaginal delivery. Acta Obstet Gynecol Scand. 2007;86(10):1207-14.
49. Belachew J, Mulic-Lutvica A, Eurenius K. Three-dimensional ultrasound of the uterus postpartum. Abstract, Presented as an oral poster at 20th World Congress on ultrasound in Obst and Gynecol in Prag 10-14 October. 2010.
50. Alexander J, Thomas P, Sanhghera J. Treatments for secondary postpartum haemorrhage. The Cochrane Library, Issue 4:2002.
51. Dewhurst C. Secondary postpartum hemorrhage. J Obstet Gynaecol Br Commonwealth. 1966;73:53-8.
52. Rome RM. Secondary postpartum haemorrhage. Br J Obstet Gynaecol. 1975;82(4):289-92.
53. King PA, Duthie SJ, Dong ZG, et al. Secondary postpartum haemorrhage. Aust NZ Obstet Gynaecol. 1989;29(4):394-8.
54. Hoveyda F, MacKenzie IZ. Secondary postpartum haemorrhage: incidence, morbidity and current management. Br J Obstet Gynaecol. 2001;108(9):927-30.
55. Carlan SJ, Scott WT, Pollack R, et al. Appearance of the uterus by ultrasound immediately after placental delivery with pathologic correlation. J Clin Ultrasound. 1997;25(6): 301-8.
56. Jones RF 3rd, Warren BL Jr, Thorton WN Jr. Planned postpartum exploration of uterus, cervix, and vagina. Obstet Gynecol. 1996;27(5):699-702.
57. Shalev J, Royburt M, Fite G, et al. Sonographic evaluation of the puerperal uterus: correlation with manual examination. Gynecol Obstet Invest. 2002;53(1):38-41.
58. Shen O, Rabinowitz R, Eisenberg VH, et al. Transabdominal sonography before uterine exploration as a predictor of retained placental fragments. J Ultrasound Med. 2003;22(6): 561-4.
59. Sadan O, Golan A, Girtler O, et al. Role of sonography in the diagnosis of retained products of conception. J Ultrasound Med. 2004;23(3):371-4.
60. Durfee SM, Frates MC, Luong A, et al. The sonographic and color Doppler features of retained products of conception. J Ultrasound Med. 2005;24(9):1181-6.
61. Neill AMC, Nixon RM, Thornton S. A comparison of clinical assessment with ultrasound in the management of secondary postpartum haemorrhage. Eur J Obstet Gynecol Reprod Biol. 2002;104(2):113-5.
62. Ben-Ami I, Schneider D, Maymon R, et al. Sonographic versus clinical evaluation as predictors of residual trophoblastic tissue. Hum Reprod. 2005;20(4):1107-11.
63. Mulic-Lutvica A, Axelsson O. Ultrasound finding of an echogenic mass in women with secondary postpartum hemorrhage is associated with retained placental tissue. Ultrasound Obstet Gynecol. 2006;28(3):312-9.
64. Rufener SL, Adusumilli S, Weadock WJ, et al. Sonography of uterine abnormalities in postpartum and postabortion

patients. A potential pitfall of interpretation. J Ultrasound Med. 2008;27(3):343-8.
65. Kamaya A, Petrovitch I, Chen B, et al. Retained products of Conception: spectrum of color Doppler Findings. J Ultrasound Med. 2009;28(8):1031-41.
66. Van den Bosch T, Daemen A, Van Schoubroeck D, et al. Occurrence and outcome of residual trophoblastic tissue. J Ultrasound Med. 2008;27(3):357-61.
67. Matijevic R, Knezevic M, Grgic O, et al. Diagnostic accuracy of sonographic and clinical parameters in the prediction of retained products of conception. J Ultrasound Med. 2009;28(3):295-9.
68. Wolman I, Altman E, Faith G, et al. Combined clinical and ultrasonographic work-up for the diagnosis of retained products of conception. Fertil Steril. 2009;92:1162-4.
69. Wolman I, Altman E, Faith G, et al. Evaluating retained products of conception in the setting of an ultrasound unit. Fertil Steril. 2009;91(4):1586-8. Supplement.
70. Pather S, Ford M, Reid R, et al. Postpartum curettage: an audit of 200 cases. Aust N Z J Obstet Gynaecol. 2005;45(5): 368-71.
71. Jensen PA, Stromme WB. Amenorrhhea secondary to puerperal curettage (Asherman's Syndrom). Am J Obstet Gynecol. 1972;113:150-7.
72. Westendorp IC, Ankum WM, Mol BW, et al. Prevalence of Asherman's syndrome after secondary removal of placental remnants or a repeat curettage for incomplete abortion. Hum Reprod. 1998;13(12):3347-50.
73. Al-Inany H. Intrauterine adhesions. An update. Acta Obstet Gynecol Scand. 2001;80:986-93.
74. Achiron R, Goldenberg M, Lipitz S, et al. Transvaginal duplex Doppler Ultrasonography in bleeding patients suspected of having residual trophoblastic tissue. Obstet Gynecol. 1993;81(4):507-11.
75. Alcazar JL, Lopez-Garcia G, Zornoza A. A role of color velocity imaging and pulsed Doppler sonography to detect retained trophoblastic tissue. Ultrasound Obstet Gynecol. 1996;8(Suppl 1):41.
76. Wolman I, Hartoov J, Amster R, et al. Transvaginal sonohysterography for the early detection of residual trophoblastic tissue. Ultrasound Obstet Gynecol. 1986;8:37.
77. Zalel Y, Gamzu R, Lidor A, et al. Color Doppler imaging in the sonohysterographic diagnosis of residual trophoblastic tissue. J Clin Ultrasound. 2002;30(4):222-5.
78. Timmerman D, Van Den Bosch T, Peeraer K, et al. Vascular malformations in the uterus: ultrasonographic diagnosis and conservative management. Eur J Obstet Gynecol Reprod Biol. 2000;92(1):171-8.
79. Timmerman D, Wauters J, Van Calenbergh S, et al. Color Doppler imaging is a valuable tool for the diagnosis and management of uterine vascular malformations. Ultrasound Obstet Gynecol. 2003;21(6):570-7.
80. Van den Bosch T, Van Schoubroeck D, De Brabanter J, et al. Color Doppler and gray- scale ultrasound evaluation of the postpartum uterus. Ultrasound Obstet Gynecol. 2002;20(6):586-91.
81. Müngen E. Vascular abnormalities of the uterus: have we recently over-diagnosed them? Opinion. Ultrasound Obstet Gynecol. 2003;21:529-31.
82. Mulic-Lutvica A, Axelsson O. The chapter " Labor and Puerperium" in the section "Ultrasound in perinatal medicine in the Textbook of Perinatal Medicine, July 2001.
83. Mulic-Lutvica Ajlana, Eurenius K, Axelsson O. Uterine artery Doppler ultrasound in postpartum women with retained placental tissue. Acta Obstet Gynecol Scand. 2009;88(6):724-8.
84. Kido A, Togashi K, Koyama Y, et al. Retained products of conception masquerading as acquired arteriovenous malformation. J Comput Assist Tomogr. 2003;27(1):88-92.
85. Eriksson LG, Mulic-Lutvica A, Jangland L, et al. Massive postpartum hemorrhage treated with transcatheter arterial embolization: long-term effects, implication on fertility and technical considerations. Acta Radiologica. 2007;48:635-42.
86. Stovall TG, Ambrose SE, Ling FW, et al. Short-term course antibiotic therapy for the treatment of chorioamnionitis and postpartum endomyometritis. Am J Obstet Gynecol. 1998;159(2):404-7.
87. Calhoun BC, Brost B. Emergency management of sudden puerperal fever. Obstet Gynecol Clin North Am. 1995;22(2):357-67.
88. Zelop C.Heffner Lj. The downside of caesarean delivery; short-and long-term complications. Clin Obstet Gynecol. 2004;47:386-93.
89. Carson PL. Clean and dirty shadowing at US: a reappraisal. Radiology. 1991;181: 231-6.
90. Mulic-Lutvica A, Axelsson O. Postpartum ultrasound in women with postpartum endometritis, after cesarean section and after manual evacuation of the placenta. Acta Obstet Gynecol Scand. 2007;86:210-7.
91. Pelage JP, Soyer P, Repiquet D, et al. Secondary Postpartum Hemorrhage: treatment with selective arterial embolization. Radiology. 1999;212:385-9.
92. Deutchman ME, Hartmann KJ. Postpartum pyometra: a case report. J Fam Pract. 1993;36:449-52.
93. Rudoff JM, Astranskas LJ, Rudoff JC, et al. Ultrasonographic Diagnosis of Septic Pelvic Thrombophlebitis. J Ultrasound Med. 1988;7:287-91.
94. Warhit JM, Fagelman D, Goldman MA, et al. Ovarian vein thrombophlebitis: diagnosis by ultrasound and CT. J Clin Ultrasound. 1984;12:301.
95. Wilson PC, Lerner RM. Diagnosis of ovarian vein thrombophlebitis by ultrasonography. J Ultrasound Med. 1983;2:187.
96. Sherer DM, Fern S, Mester J, et al. Postpartum ultrasonographic diagnosis of inferior vena cava thrombus associated with ovarian vein thrombosis. Am J Obstet Gynecol. 1997;177(2):474-5.
97. Burger NF, Dararas B, Boes EGM. An echogenic evaluation during the early puerperium of the uterine wound after caesarean section. J Ultrasound Med. 1983;2:18.
98. Meyenburg M, Schulze-Hagen K, Schaller G. Involution of the uterus following vaginal or abdominal delivery. Z Geburtshilfe Perinatol. 1983;187(4):200-2.
99. Negishi H, Kishida T, Yamada H, et al. Changes in uterine size after vaginal delivery and caesarean section determined by vaginal sonography in the puerperium. Arch Gynecol Obstet. 1999;263(1-2):13-6.

100. Koskas M, Nizard J, Salomon LJ, et al. Abdominal and pelvic ultrasound findings within 24 hours following uneventful cesarean section. Ultrasound Obstet Gynecol. 2008;32(4):520-6.
101. Lavery JP, Howell RS, Shaw L. Ultrasonic demonstration of a phlegmona following Caesarean section: case report. J Clin Ultrasound. 1985;13:134-6.
102. Baker ME, Bowie JD, Killan AP. Sonography of postcaesarean-section bladder-flap hematoma. Am J Roentgenol. 1984;144:757-9.
103. Sentilhes L, Ambroselli C, Kayem G, et al. Maternal outcome after conservative treatment of placenta accreta. Obstet Gynecol. 2010;115(3):526-34.
104. Warshak CR, Ramos GA, Eskander R, et al. Effect of predelivery diagnosis in 99 consecutive cases of placenta accreta. Obstet Gynecol. 2010;115(1):65-9.
105. Bennett MJ. Puerperal ultrasonic hysterography in the diagnosis of congenital uterine malformations. Br J Obstet Gynaecol. 1976;83(5):389-92.
106. Szoke B, Kiss D. The use of ultrasonic echo technique in the diagnosis of developmental anomalies of the uterus. Ann Chir gynaecol. 1977;66(1):59-61.
107. Land JA, Stoot JE, Evers JL. Puerperal ultrasonic hysterography. Gynecol Obstet Invest. 1984;18(3):165-8.
108. Weissman A, Grisarn D, Shenhav M, et al. Postpartum surveillance of urinary retention by ultrasonography: the effect of epidural analgesia. Ultrasound obstet Gynecol. 1995;6:130-4.
109. Ulitzsch D, Nyman MKG, Carlson RA. Breast abscess in lactating women: US guided Treatment. Radiology. 2004;232(3):904-9.

33
CHAPTER

Three-Dimensional Sonoembryology

Ritsuko K Pooh, Kohei Shiota, Asim Kurjak

INTRODUCTION

Owing to recent reproductive revolution, the beginning of human life has been marvelously elucidated. Furthermore, in a field of embryology, advanced technologies of experimental magnetic resonance (MR) microscopy of embryos[1,2] and computer graphic[3] have contributed to comprehensive early human development. "Sonoembryology" was first described in 1990[4] after introduction of high-frequency transvaginal transducer in obstetrical field. Combination of transvaginal approach and three-dimensional (3D) ultrasound has been establishing "3D sonoembryology", producing more objective and accurate information of early embryonal and fetal development and natural history of fetal abnormalities.[5] Although 3D sonoembryology has been approaching modern high-tech embryology, it still cannot demonstrate internal organs of embryos as clearly as by embryonal MR microscopy. However, a great advantage in sonoembryology, which human embryology cannot possess, is "demonstration of living embryos with circulation *in vivo*". Human embryology is based on dead embryos, which had been well preserved. Three-dimensional sonoembryology has a remarkable potential to discover new findings of living embryos and fetuses *in utero*. In this chapter, we introduce up-to-date embryology and 3D sonoembryology. The staging and aging of embryos are different in embryology from in obstetrics. Although "gestational age" usually used in obstetrical field based on menstrual period or crown rump length (CRL), has been criticized in the embryological point of view,[6] it is used in this chapter on description of sonograms.

MODERN EMBRYOLOGY BY MAGNETIC RESONANCE MICROSCOPY AND COMPUTER GRAPHICS

Carnegie stages **(Fig. 33.1)**, well-known embryonal staging system till eight weeks after conception, was named after the famous institute, which began collecting and classifying embryos in the early 1900s. An embryo is assigned a Carnegie stage (numbered from 1 to 23) based on its external morphological features. Age and size proves a poor way to organize embryos. It is very difficult to accurately age an embryo and it could shrink a full 50% in the preserving fluids. Therefore, this staging system is neither dependent on the chronological age nor the size of the embryo. The stages are in a sense, arbitrary levels of maturity based on multiple physical features. Embryos that might have different ages or sizes can be assigned the same Carnegie stage based on their external appearance because of the natural variation, which occurs between individuals. **Table 33.1** shows the Carnegie stages from stages 1 to 23.

The recent advance in magnetic resonance (MR) microscopic technology has made it possible to scan and visualize relatively small samples, including mammalian embryos.[1] The MR microscopy demonstrates tomographic imaging of small objects and the digitized data can be manipulated to achieve 3D reconstruction of the samples.[1] Although the resolution and long imaging speed were initial problems in MR microscopy those have been solved by invention of a super-parallel

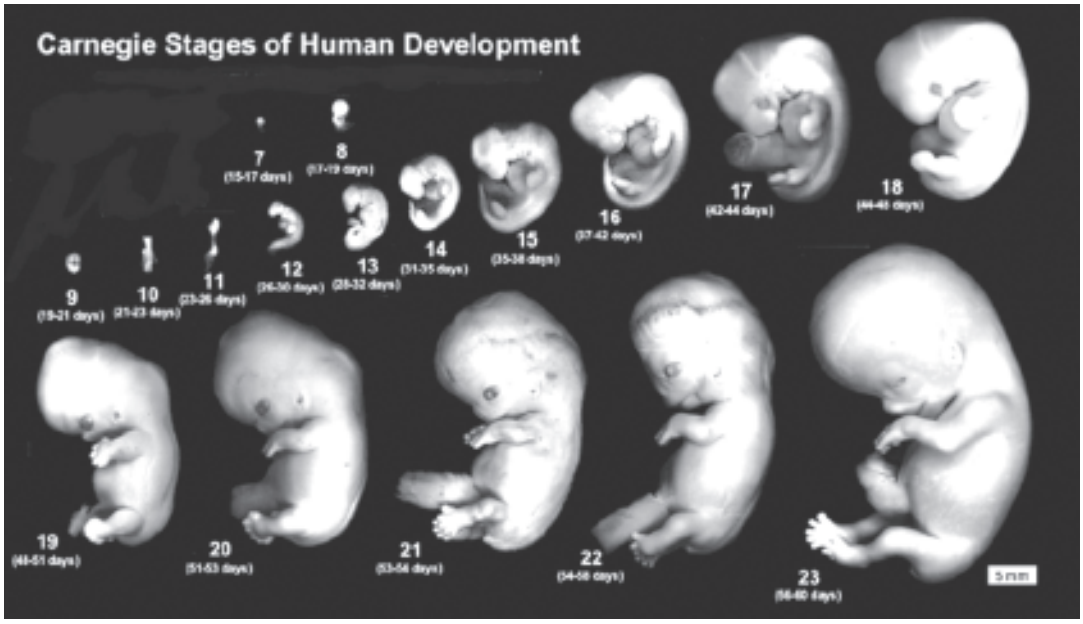

Figure 33.1: Development of human embryos at 4-8 weeks after conception (Kyoto Collection of Human Embryos)

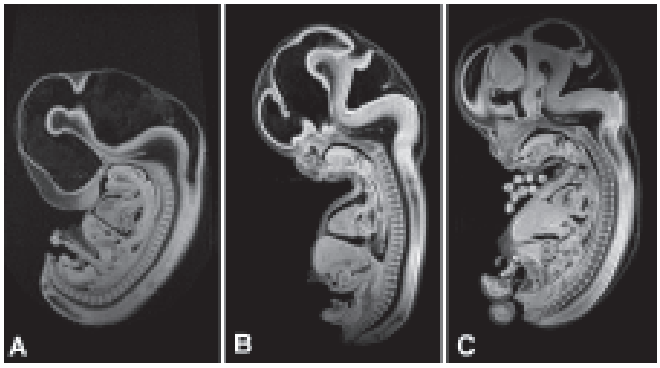

Figures 33.2A to C: Magnetic resonance images of two-dimensional cross sections selected from three-dimensional data sets of fixed human embryos. (A) Carnegie stage (CS)18; (B) CS20; (C) CS23

MR microscope.[2] Additionally, recent advanced computer graphics techniques combined MR microscopy have produced detailed 3D images of human embryos. Yamada and his colleagues[3] successfully constructed a series of 3D images of human embryos, based on the MR microscopy data of human embryo specimens in the Kyoto collection **(Figs 33.2A to C)**, with the aid of CG techniques, to illustrate 3D structures and morphogenetic movements in human embryos **(Figs 33.3 and 33.4)**. In addition, they produced movies using these 3D images, (supplementary movies, which can be viewed at http://www.interscience.wiley.com/jpages/1058-8388/suppmat) to show the entire process of morphogenesis in human embryos from fertilization to the completion of organogenesis.[3]

NORMAL EMBRYO VISUALIZATION BY THREE-DIMENSIONAL SONOEMBRYOLOGY

Since the introduction of high frequency transvaginal transducer, ultrasonographic visualization of embryos and fetuses in early stage has been remarkably progressed and sonoembryology[4] has been established. In addition, the recent introduction of 3D and four-dimensional (4D) ultrasounds combined with the transvaginal approach has produced more objective and accurate information on embryonal and early fetal development.[5,7] **Figures 33.5A and B** show a gestational sac at four weeks of gestation and the yolk sac visualization at five weeks of gestation. Demonstration of small embryo less than 10 mm of greatest length has been difficult and not visualized in detail. **Figures 33.6 and 33.7** show 5.5 mm long-embryo with yolk sac at six weeks of gestation and 18.3 mm CRL embryo at eight weeks of gestation, respectively depicted by using the most up-to-date 3D equipment with high-frequency transvaginal transducer (Voluson® E8 with 12 MHz/256 element vaginal probe, GE Healthcare, Milwaukee, USA). Early neural tube and premature spinal cord are successfully demonstrated in a small embryo. **Figures 33.8A and B** are macrographic images of an aborted specimen taken just after abortion. Premature spinal

TABLE 33.1
Carnegie stages table

Stage	*Days after conception (approx)*	*Size (mm)*	*Events*
1	1 (Week 1)	0.1-0.15	Fertilized oocyte, pronuclei
2	2-3	0.1-0.2	Cell division with reduction in cytoplasmic volume, formation of inner and outer cell mass
3	4-5	0.1-0.2	loss of zona pellucida, free blastocyst
4	5-6	0.1-0.2	Attaching blastocyst
5	7-12 (Week 2)	0.1-0.2	Implantation
6	13-15	0.2	Extraembryonic mesoderm, primitive streak
7	15-17 (Week 3)	0.4	Gastrulation, notochordal process
8	17-19	1.0-1.5	Primitive pit, notochordal canal
9	19-21	1.5-2.5	Somite Number 1-3 neural folds, cardiac primordium, head fold
10	22-23 (Week 4)	2-3.5	Somite Number 4-12 neural fold fuses
11	23-26	2.5-4.5	Somite Number 13-20 rostral neuropore closes
12	26-30	3-5	Somite Number 21-29 caudal neuropore closes
13	28-32 (Week 5)	4-6	Somite Number 30 leg buds, lens placode, pharyngeal arches
14	31-35	5-7	Lens pit, optic cup
15	35-38	7-9	Lens vesicle, nasal pit, hand plate
16	37-42 (Week 6)	8-11	Nasal pits moved ventrally, auricular hillocks, foot plate
17	42-44	11-14	Finger rays
18	44-48 (Week 7)	13-17	Ossification commences
19	48-51	16-18	Straightening of trunk
20	51-53 (Week 8)	18-22	Upper limbs longer and bent at elbow
21	53-54	22-24	Hands and feet turned inward
22	54-56	23-28	Eyelids, external ears
23	56-60	27-31	Rounded head, body and limbs

cord is visualized on the back, which is compatible with 3D image on **Figure 33.7**. **Figure 33.9** shows the development of spinal cord in embryonal size of 5.5 mm, 18.3 mm and 26.3 mm.[7] Thereafter, the vertebral bony structure can be visualized from 11 weeks of gestation and gradual closure of bilateral laminae caudally from the cervical region **(Fig. 33.10).**

The development of the embryonic circulation became visualized by 3D power Doppler imaging technology.[8] **Figures 33.11A to C** illustrate the vascular network of an embryo at nine weeks of gestation. In 1993 and 1994, color Doppler detection and assessment of brain vessels in the early fetus using a transvaginal approach was reported.[9,10] Clear visualization by transvaginal power Doppler of the common carotid arteries, internal and external carotid arteries, middle cerebral arteries at 12 weeks of gestation was reported in 1996.[11] By using 3D power Doppler technology, the vascular anatomy can now be imaged clearly by identification of the common carotid arteries, internal carotid arteries, circle of Willis and middle cerebral arteries **(Figs 33.12A to C).**

The utilization of postprocessing algorithms such as maximum mode can be used to demonstrate the fetal

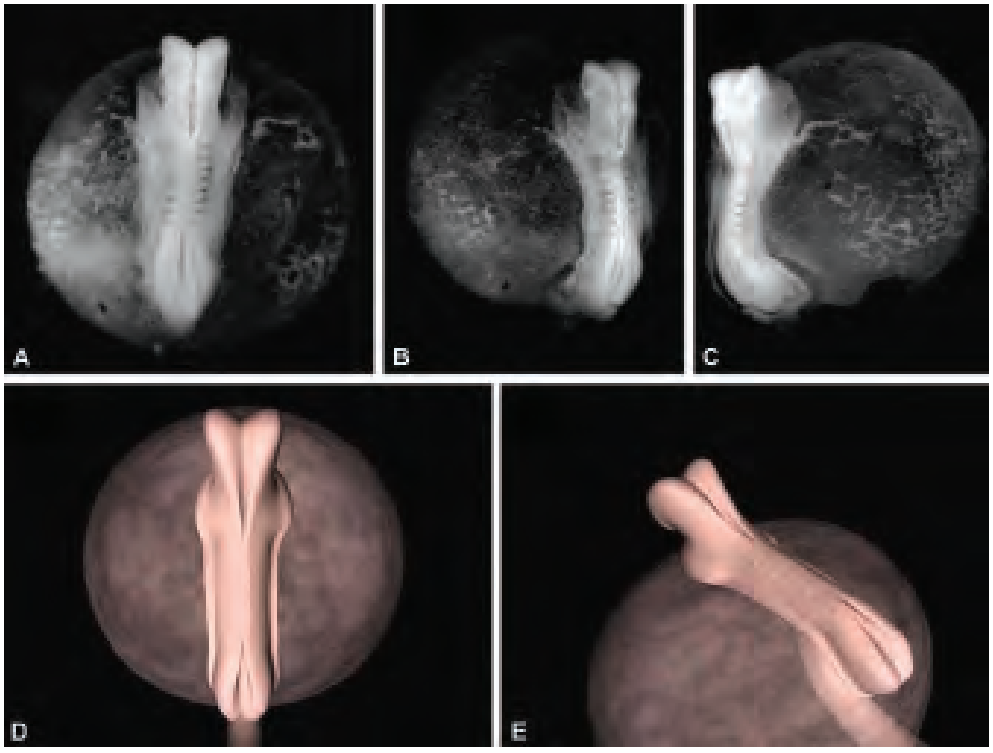

Figures 33.3A to E: A neurulating human embryo (Carnegie stage [CS] 10) and its three-dimensional (3D) computer graphics model. (A to C) Photographs of a CS10 embryo with the closing neural tube. Ten pairs of somites are recognizable. The round ball-like structure on the ventral side of the embryo is the yolk sac; (D and E) A 3D computer graphics model of the embryo shown in A to C. This model was reconstructed based on its gross pictures and histological sections

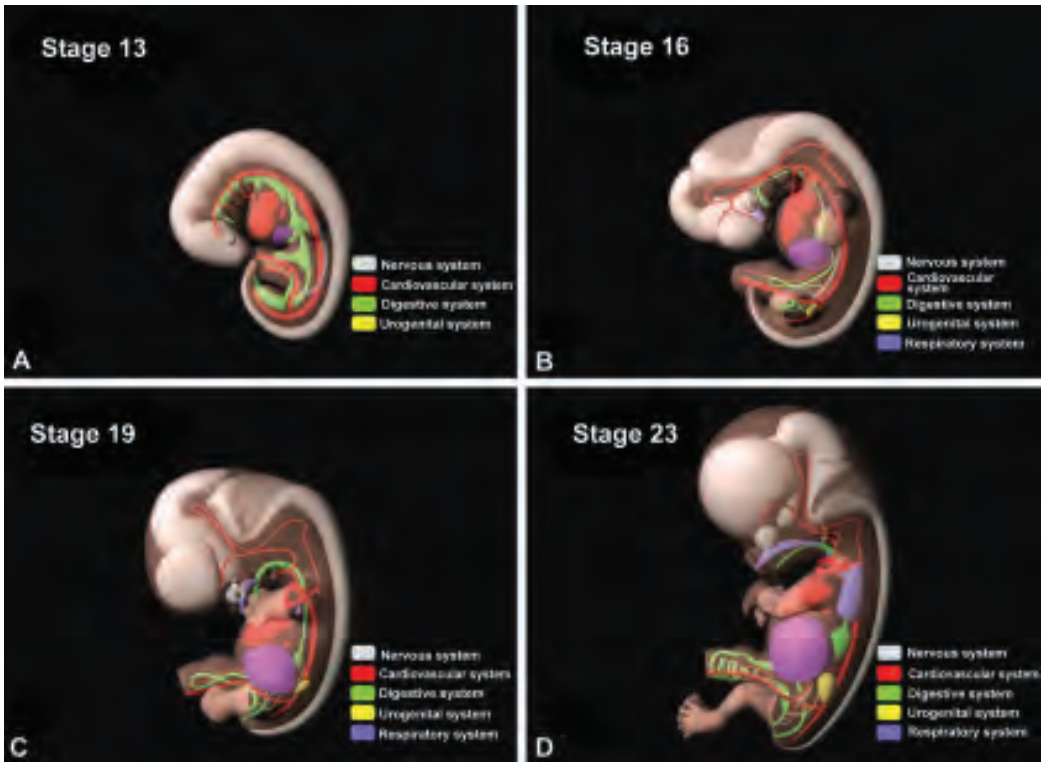

Figures 33.4A to D: Computer graphics model of human embryos showing major internal organs overlapped with the surface contour. The internal organs were reconstructed according to magnetic resonance images, histological sections and textbook illustrations. (A) Carnegie stage (CS) 13; (B) CS16; (C) CS19; (D) CS23

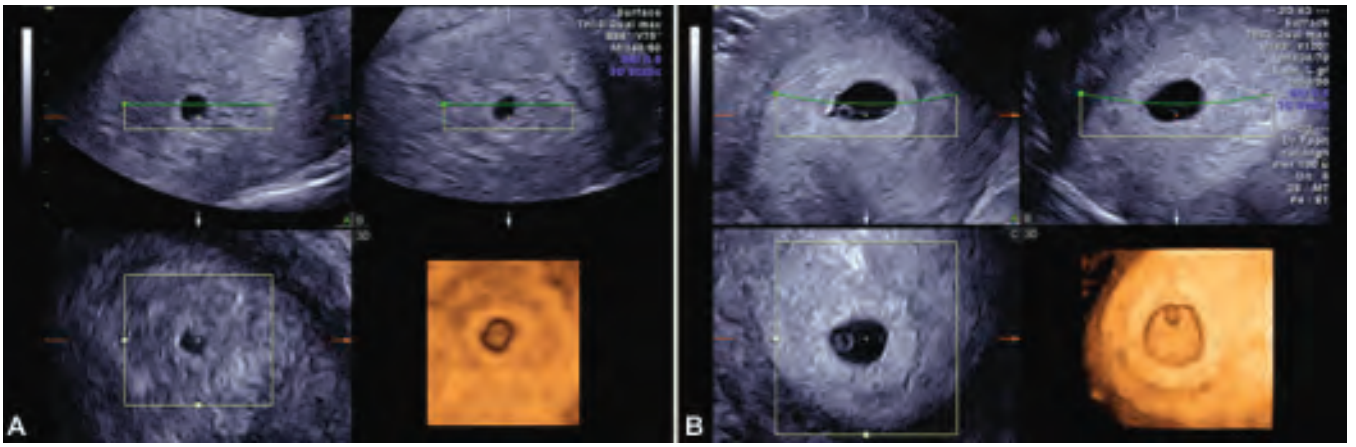

Figures 33.5A and B: Development of gestational sac (4 weeks and 5 weeks of gestation). (A) 4 weeks (2 weeks after conception) of gestation. Three orthogonal view and 3D constructed image demonstrated early gestational sac; (B) The beginning of 5 weeks, yolk sac is detectable inside gestational sac

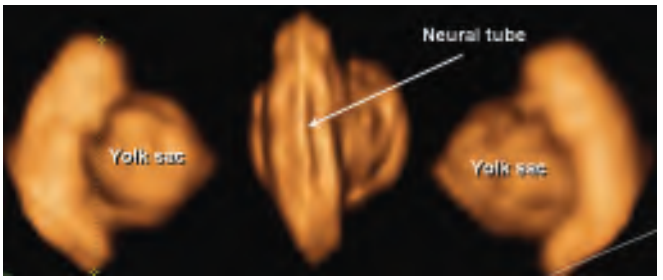

Figure 33.6: Three-dimensional reconstructed image of the yolk sac and 5.5 mm-CRL-embryo (6 weeks of gestation). Normal 6-week-embryo (CRL 5.5 mm) and yolk sac. Occipital view shows the neural tube on the embryonal back

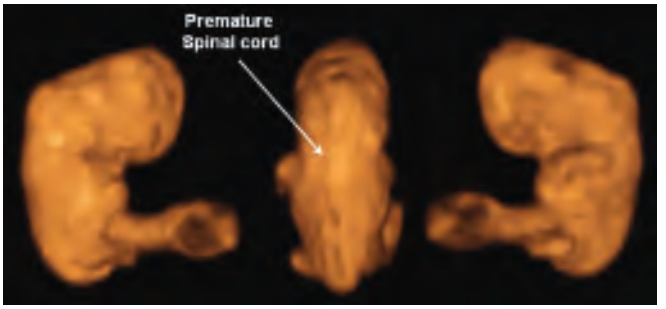

Figure 33.7: Three-dimensional reconstructed image of the embryo (8 weeks of gestation). Normal 8-week-embryo. Occipital view shows the premature spinal cord, which is seen in the Figure 33.4B

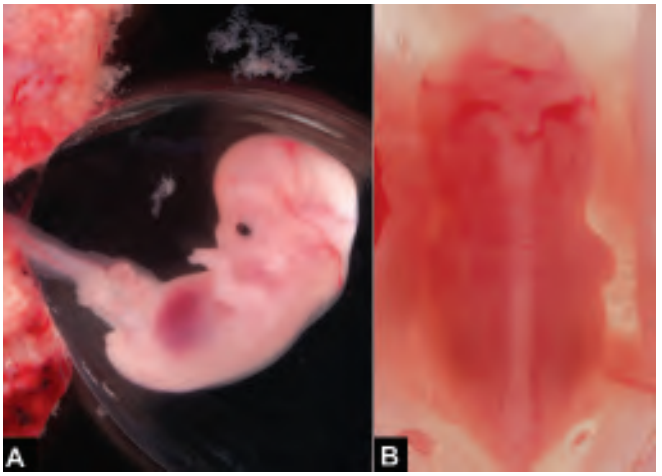

Figures 33.8A and B: Lateral and back view of aborted embryo at 8 weeks of gestation. (A) Lateral view. Physiological umbilical hernia is seen; (B) Backside view. Premature spinal cord is seen. This photo was taken just after abortion before preserving in formalin

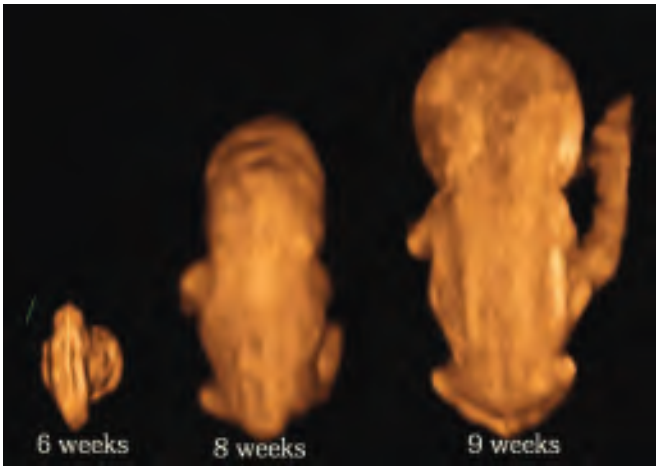

Figure 33.9: Three-dimensional reconstructed image of the embryo (6 to 9 weeks of gestation). Embryonal sizes are 5.5 mm, 18.3 mm and 26.3 mm. At 9 weeks of gestation, the spinal cord is demonstrated as a thin line, compared with that at 8 weeks of gestation

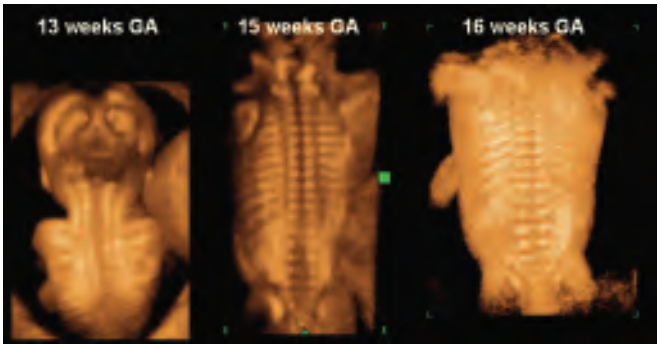

Figure 33.10: Three-dimensional reconstructed image of fetal vertebral development between 13 and 16 weeks of gestation

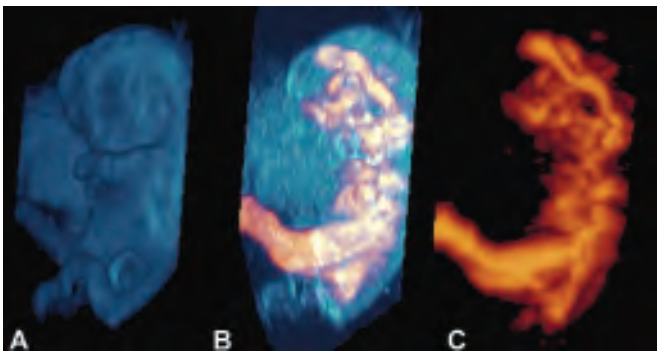

Figures 33.11A to C: Early vascular system at 9 weeks of gestation. (A) Three-dimensional (3D) gray mode; (B) 3D power Doppler with surface appearance; (C) 3D power Doppler image

skeleton. Chaoui et al.[12] reported clear 3D images for the identification of an abnormally wide metopic suture in the second trimester of pregnancy. However, rapid ossification of the craniofacial bones occurs during the first trimester of pregnancy. We demonstrate in this paper the identification of the craniofacial skeleton from 10 weeks of gestation onwards. **Figures 33.13 and 33.14** show early fetal craniofacial bony structures at 11 and 14 weeks, respectively, using the maximum mode algorithm. The difference of frontal bone morphology between 11 and 14 weeks demonstrates membranous ossification of the cranium at this stage. **Figure 33.15** demonstrates the structure of the skull in the occipital region at 13 weeks of gestation.

During the early embryonic period, the central nervous system anatomy rapidly changes in appearance. The MR images **(Fig. 33.2)** shows remarkable change of central nervous system (CNS) appearance in a short period between Carnegie stage 18 and 23. Detailed cerebrospinal structure at Carnegie stage 23 is visualized in **Figure 33.16**.

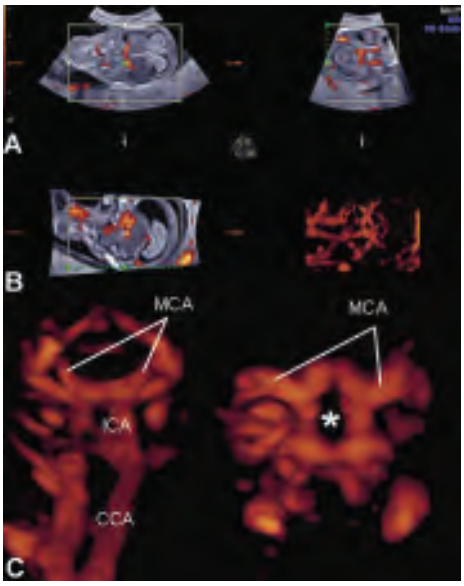

Figures 33.12A to C: Premature vascularity of normal 12-week brain. (A) Three orthogonal view of power Doppler image and three-dimensional (3D) reconstructed image (front-back view of A plane); (B) Front-back image of common carotid arteries (CCA), internal carotid arteries (ICA) and brain basilar arteries, middle cerebral artery (MCA). (C) 3D image from fetal parietal direction. The circle of Willis (asterisk) is clearly visualized

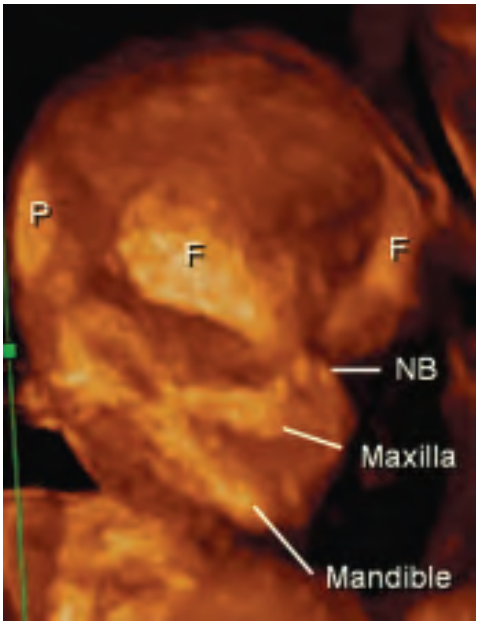

Figure 33.13: Three-dimensional (3D) maximum mode image of normal craniofacial structure at 11 weeks of gestation. Premature bony structure of frontal bone (F), parietal bone (P), nasal bone (NB), maxilla and mandible are recognizable

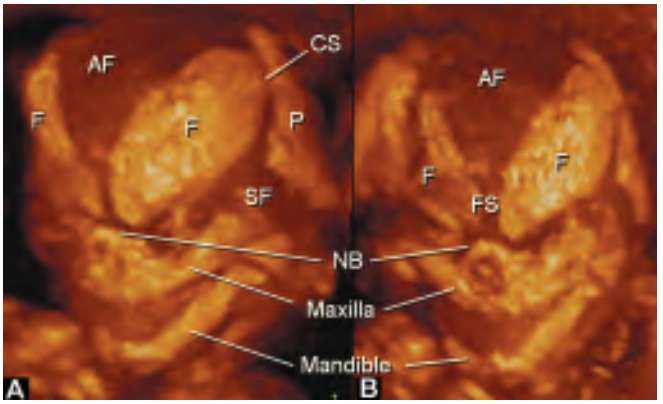

Figures 33.14A and B: Three-dimensional maximum mode image of normal craniofacial structure at 14 weeks of gestation. (A) Oblique view; (B) Frontal view. Anterior fontanelle (AF), sphenoidal fontanelle (SF), frontal suture (FS), coronal suture (CS), nasal bone (NB), maxilla and mandible are gradually formed according to cranial bony development

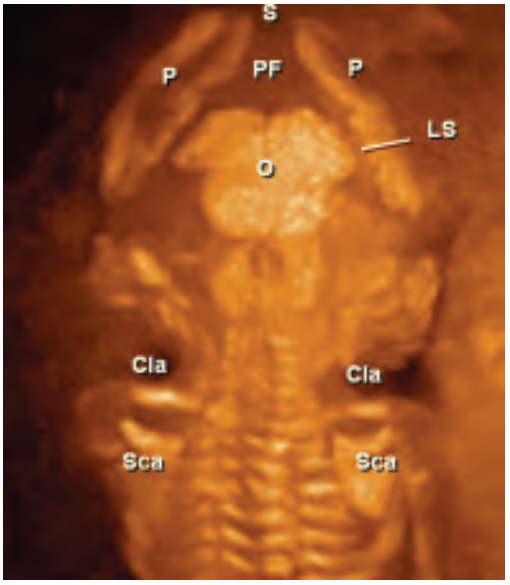

Figure 33.15: 3D maximum mode image of occipital view at 13 weeks of gestation. Note the premature occipital bone appearance. Midline crack is demonstrated. S: Sagittal suture, P: Parietal bone, PF; Posterior fontanelle, O: Occipital bone, Cla: Clavicula, Sca: Scapula, LS: Lambdoid suture

Three-dimensional sonography using transvaginal sonography with high-resolution probes allows imaging of early structures in the embryonic brain. **Figures 33.17 to 33.19** demonstrate fetal brain detailed morphology between the beginning of 8th and 10th week and this can be accomplished through the use of three orthogonal planes, and "tomographic ultrasound imaging". Serial

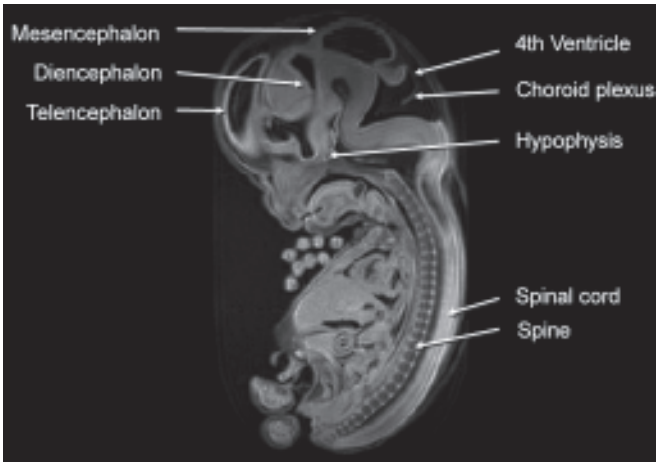

Figure 33.16: Embryo structures visualized by magnetic resonance image (Carnegie stage 23)

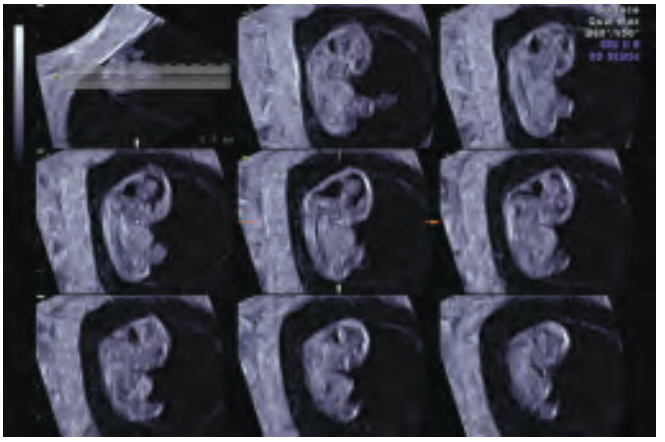

Figure 33.17: Tomographic sagittal imaging of normal fetus at the beginning of 8 weeks of gestation

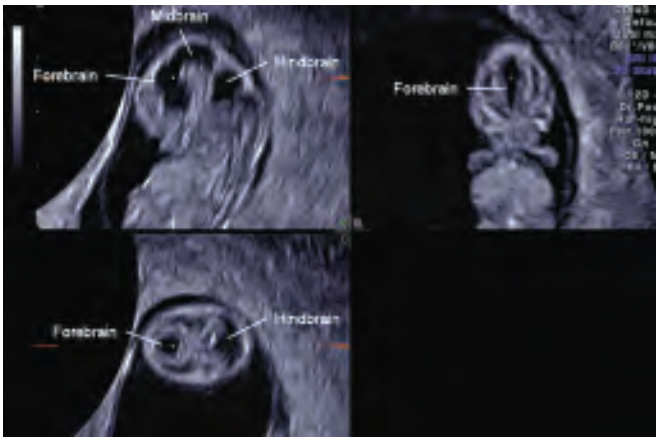

Figure 33.18: Three orthogonal images of normal brain at the end of 8 weeks of gestation. The development of premature ventricular system is seen. Note the different appearance from the beginning of 8 weeks of gestation (Figure 33.17)

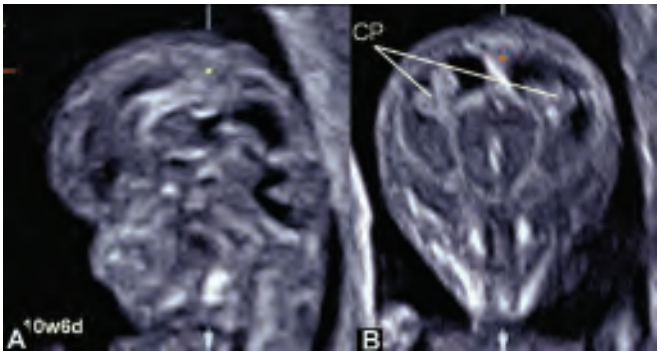

Figures 33.19A and B: (A) Sagittal section; (B) Coronal sections of 10-week-fetus. CP: Choroid plexus of the lateral ventricles

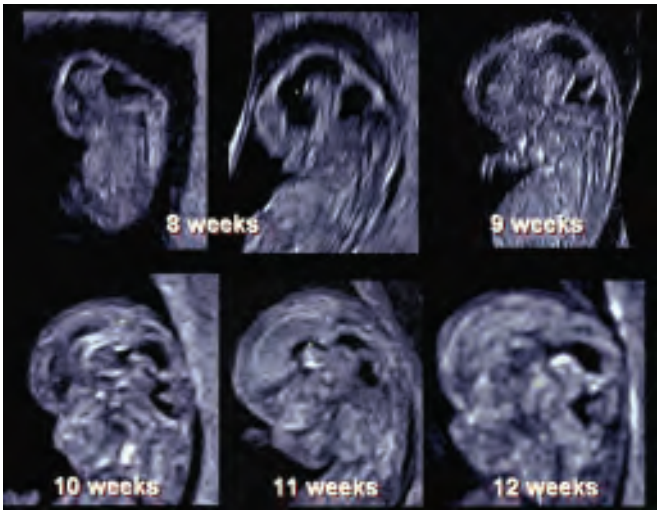

Figure 33.20: Normal brain development by midsagittal three-dimensional ultrasound (3D US) section between 8 and 12 weeks of gestation

examinations allow obtaining similar sections of the fetal brain at different stages of development. Therefore, it is possible to document the changes in central nervous system (CNS) development between 8th and 12th week as demonstrated in **Figure 33.20**. Recent reports published on embryonal ventricular development from 6th or 7th week by the use of 3D inversion-rendering mode, have made sonoembryology more sophisticated and objective.[13,14] It is possible that by developing 3D neurosonoembryology imaging *in utero*, current fetal staging (which uses gestational age based on last menstrual period or CRL measurement) may change into a "morphological staging system", such as the Carnegie staging system, which has been central to embryology.[7]

Thoracoabdominal structures can also be imaged in the first trimester. For example, **Figure 33.21** shows

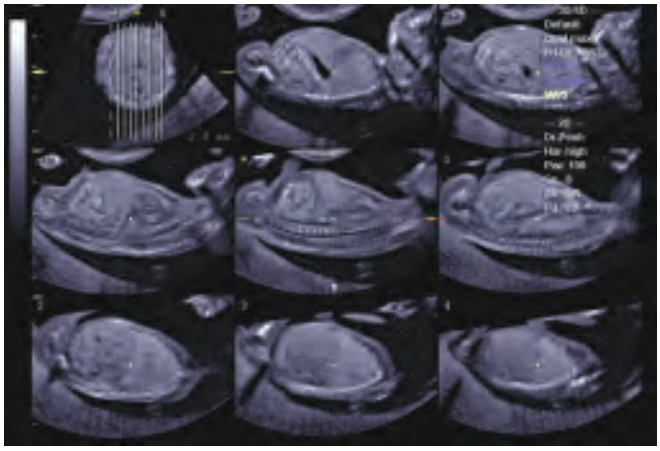

Figure 33.21: Tomographic ultrasound imaging of normal thoracoabdominal structure at 13 weeks of gestation. Parallel sagittal sections are shown. Lung-liver border and intraabdominal organs are clearly visualized

tomographic ultrasound imaging of fetal chest and abdomen at 13 weeks of gestation. Clear visualization of the lung-liver interface can be of value in the early diagnosis of thoracoabdominal abnormalities such as a diaphragmatic hernia.

FETAL ABNORMALITIES IN EARLY GESTATION

Yolk Sac

The yolk sac plays an important role in embryonal hemopoiesis and fetomaternal transportion of nutritive properties before establishment of fetoplacental circulation. The primary yolk sac forms at around 3rd week of the menstrual age, then following the formation of the extraembryonic coelom and the secondary yolk sac is formed. From the 6th week of gestation, it appears as a spherical and cystic structure covered by numerous superficial small vessels merging at the basis of the vitelline duct. This connects the yolk sac to the ventral part of the embryo, the gut and main blood circulation. During the 10th week of gestation, the yolk sac begins to degenerate and rapidly ceases to function.[15]

It has been reported that abnormal size and/or shape of yolk sac may be associated with ominous pregnant outcome.[16] Large yolk sac is defined more than two standard deviations above the mean, which indicates over 5.6 mm of diameter at less than 10 weeks menstrual age.[16,17] Large yolk sac is associated with chromosomal aberration of autosomal trisomy **(Figs 33.22 and 33.23)**. Echogenic yolk sac **(Figs 33.24A and B)** is also related to adverse pregnant outcome with autosomal trisomy.

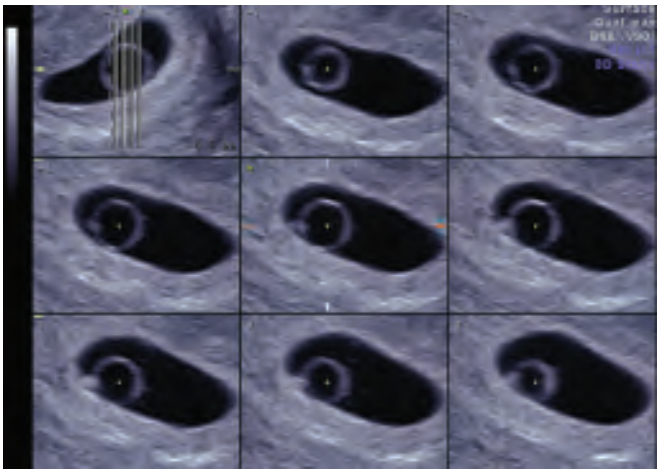

Figure 33.22: Tomographic imaging of large yolk sac at 6 weeks of gestation. Large yolk sac with normal fetal heart beat was observed. Fetal demise was confirmed at 8 weeks. Villous chromosome exam resulted in 47, XY, +22

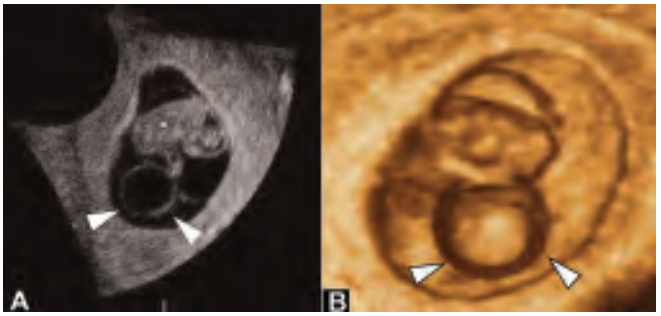

Figures 33.23A and B: Large yolk sac (arrowheads) at 8 weeks of gestation. **(**A) Two-dimensional (2D) sagittal section of the fetus. Normal appearance of 8-week-fetus and amniotic membrane are visible, but large yolk sac with 12 mm of diameter is demonstrated; (B) Three-dimensional (3D) image. Intrauterine fetal demise was confirmed 30 hours later. Villous chromosome exam resulted in doubled trisomy of 48, XY, +15,+21

Prenatal Diagnosis of Anatomical Congenital Anomalies in the Human Embryo

The prenatal diagnosis of congenital anomalies with ultrasound is based upon identification of a substantial departure of normal anatomy. This has been possible in the second and third trimester of pregnancy and this achievement has made the diagnosis of congenital anomalies one of the objectives of modern prenatal care. The definition of the "normal anatomy" of the human embryo provides the basis for the identification of congenital anomalies at the earliest stages of human development. This goes beyond the mere identification

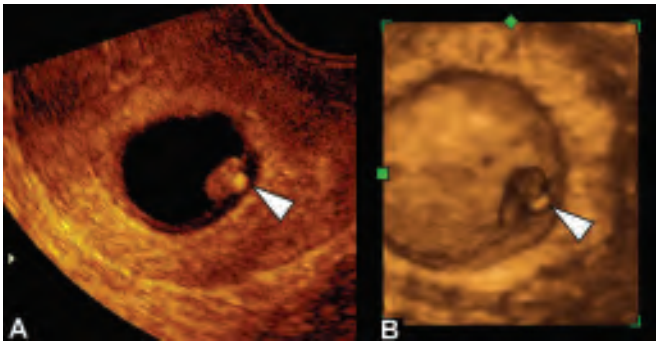

Figures 33.24A and B: High echogenic yolk sac (A) Two-dimensional (2D) ultrasound image of yolk sac (arrowhead) at 9 weeks and 1 day. Small embryo compatible with 7-week-embryo was visible with regular heart beats in the abnormally large amniotic sac; (B) Three-dimensional (3D) ultrasound image. Intrauterine fetal demise was confirmed three days later and villous chromosome was trisomy 15

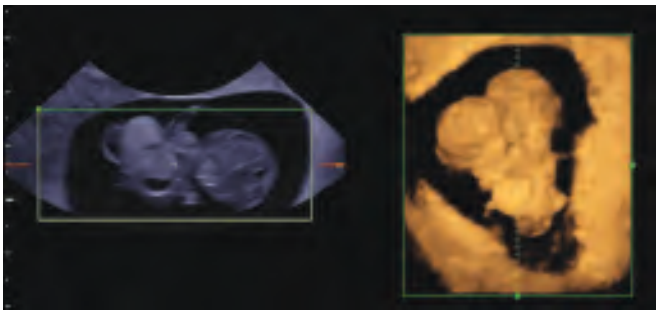

Figure 33.25: Conjoined twins with limb-body-wall complex (LBWC) at 9 weeks of gestation. Two heads and one body are obviously demonstrated. Liver and other abdominal organs were prolapsed

of nuchal translucency because it is now possible to identify anomalies even in the absence of an abnormal nuchal translucency. Therefore, the scope of prenatal diagnosis during embryonic life has been widened by sonoembryology with 3D ultrasound.[7]

Conjoined Twins

Conjoined twins are defined as monochorionic-monoamniotic twins fused at any portion of their body as a result of an incomplete division of the embryonic disk after the 13th day of conception. Pathogenesis of the condition is considered as the result from failure of complete separation. Careful observation in the first trimester can reveal this condition from the early pregnancy. **Figure 33.25** demonstrates conjoined twin with limb-body-wall complex (LBWC) at 9 weeks of gestation. Three-dimensional ultrasound can objectively depict this rare abnormality.

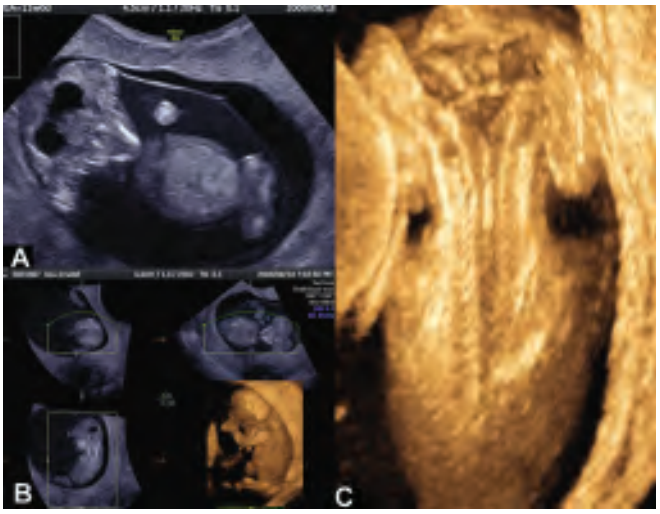

Figures 33.26A to C: Acrania with cervical spina bifida (craniorachischisis) at 11 weeks of gestation. (A) Two-dimensional (2D) image. Note the amniotic fluid is more turbid than chorioamniotic cavity due to floating nerve tissue from destroyed brain; (B) Three orthogonal view and reconstructed image; (C) Three-dimensional (3D) reconstructed image of cerebrospinal region. This fetus is complicated with acrania and cervical spina bifida, so-called craniorachischisis

Central Nervous System (Cranium, Brain, Vertebra and Spinal Cord) Anomalies

Acrania, frequently found by early ultrasound scan, is characterized by a partial or complete absence of the cranium. The cranial shape and appearance vary, according to the extent of brain destruction. **Figures 33.26A to C** show acrania complicated with cervical spina bifida, which is demonstrated by 3D reconstructed imaging. Holoprosencephaly can be detectable by careful observation of the midline and choroid plexus appearance **(Fig. 33.27)**. Occasionally, cephalocele is detectable as shown in **Figure 33.28**.

Spina bifida is the most common congenital spinal cord anomaly. It is often detected during the second and third trimesters. However, the fundamental basis for this anomaly is a failure of the neural tube to close during early embryonic age. Most reports of the diagnosis of spina bifida *in utero* have occurred after 12 weeks of gestation. Blaas et al.[18] reported an early diagnosis using 2D and 3D ultrasound before 10 weeks of gestation. **Figures 33.29A and B** show the early diagnosis of spina bifida in a case of omphalocele, bladder exstrophy, imperforate anus, spina bifida (OEIS) complex at 9 weeks of gestation. Iniencephaly is a rare neural tube defect that combines extreme retroflexion (backward bending) of the head with severe defects of the spine, associated with acrania,

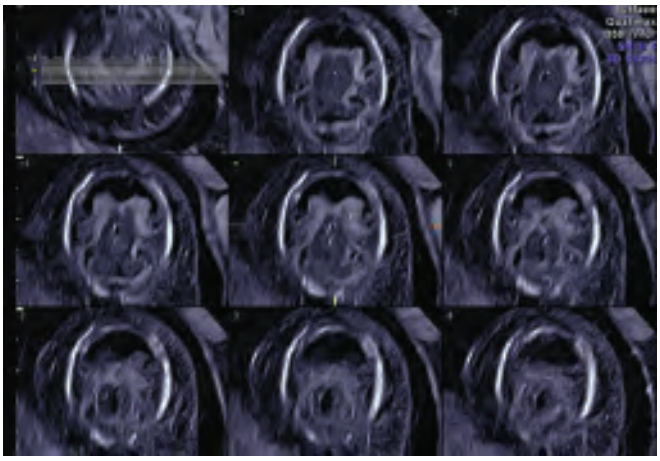

Figure 33.27: Holoprosencephaly at 12 weeks of gestation. Tomographic ultrasound imaging shows a single ventricule due to nonseparated hemispheres

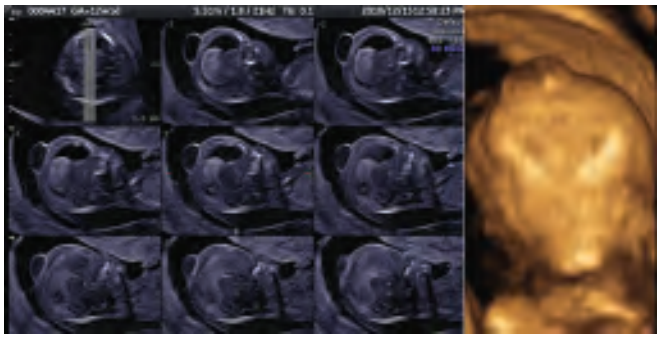

Figure 33.28: Cephalocele at 12 weeks of gestation. Cephalocele containing translucent fluid is seen on the parietal right side of the head. This cyst disappeared two weeks later

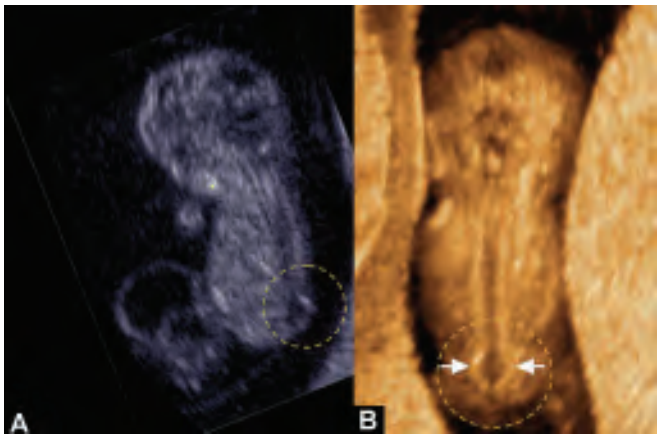

Figures 33.29A and B: Spina bifida at 9 weeks of gestation. (A) Two-dimensional (2D) sagittal image. Cystic formation was seen (white circle) at lumbar part; (B) Three-dimensional (3D) image of neural tube. Clear dilatation of the neural tube is demonstrated (arrows)

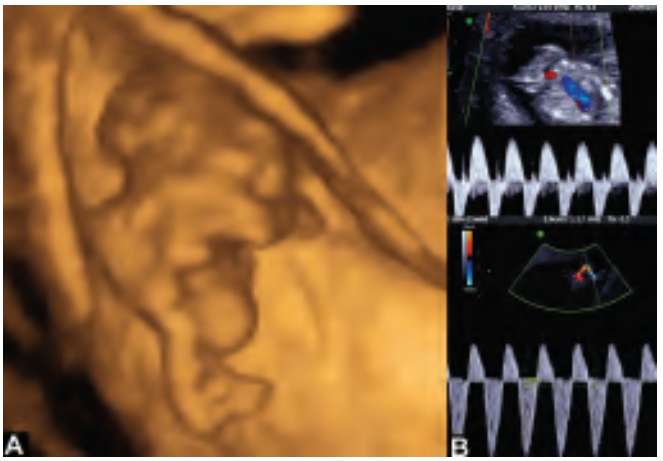

Figures 33.30A and B: Iniencephaly at 12 weeks of gestation. (A) Three-dimensional (3D) reconstructed image. Acrania, short body with dorsiflexion are well demonstrated; (B) This fetus had reverse flows of descending aorta (right upper) and umbilical artery (right lower) and intrauterine fetal demise was confirmed one week later

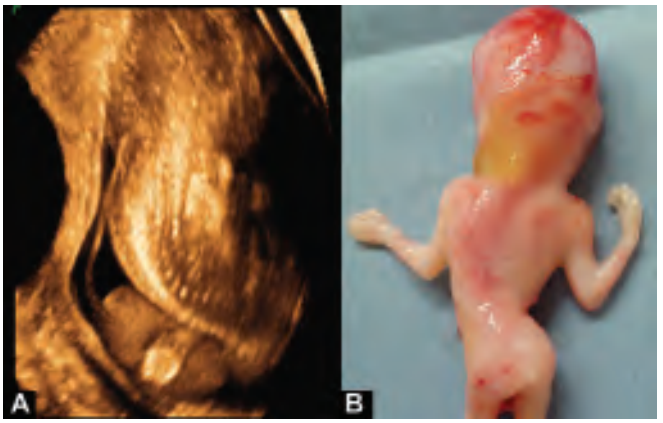

Figures 33.31A and B: Severe scoliosis at 12 weeks of gestation. (A) Three-dimensional (3D) image of fetal back. Severe scoliosis is demonstrated; (B) Back view of aborted fetus. Fetal karyotype was normal

anencephaly and encephalocele. The prognosis for those with iniencephaly is extremely poor. Early detection of iniencephaly is possible **(Figs 33.30A and B).** Scoliosis is often associated with LBWC **(Figs 33.31A and B)** and rarely scoliosis is associated with early vertebral fusion as shown in **Figures 33.32A to C**. Extreme hyperdorsiflexion (backward bending) is a rare finding with unknown clinical significance. **Figures 33.33A to C** demonstrates extreme hyperdorsiflexion seen in a case of trisomy 21.

Facial Abnormalities

A facial anomaly can be associated with a central nervous system anomaly (e.g. holoprosencephaly as

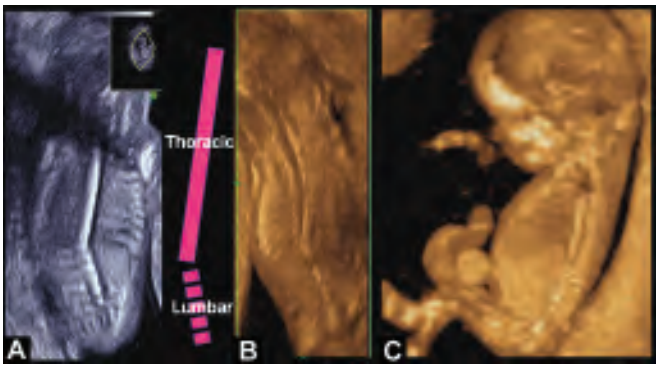

Figures 33.32A to C: Fused thoracic vertebral body with scoliosis at 13 weeks of gestation. (A) Two-dimensional (2D) sagittal image. Thoracic vertebral body is completely fused while lumbar vertebral bodies are apart; (B) Three-dimensional (3D) maximum mode of dorsal view; (C) Three-dimensional (3D) maximum mode of lateral view

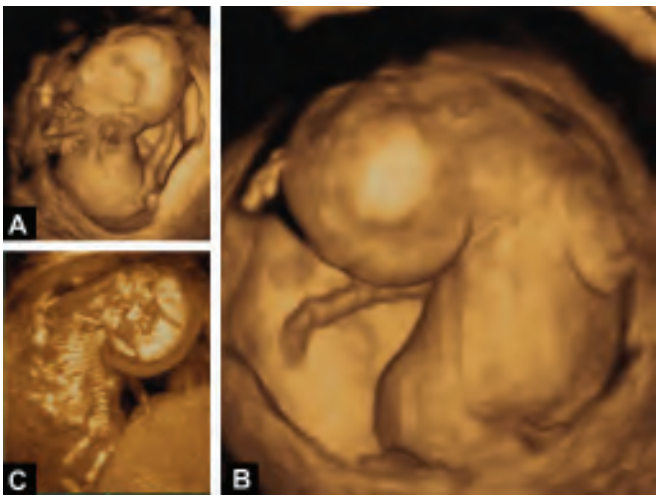

Figures 33.33A to C: Extreme hyperdorsiflexion seen in a case of trisomy 21 at 14 weeks of gestation. (A and B) Three-dimensional (3D) reconstructed oblique anterior and lateral views of the fetus; (C) 3D maximum mode demonstrating bony structure

shown in **Figures 33.34 and 33.35**), be an isolated finding or part of a syndrome. Detection of the presence or absence of a nasal bone has been found to be of value in the assessment of aneuploidy in the first trimester of pregnancy (risk assessment for trisomy 21).[19-23] Cicero and her colleagues reported that the nasal bone was absent in 113 (0.6%) of the 20,165 chromosomally or phenotypically normal fetuses and in 87 (62.1%) of the 140 fetuses with trisomy 21.[23] Three-dimensional sonography allows a midsagittal section of the fetal face to be obtained by utilizing the three orthogonal planes,

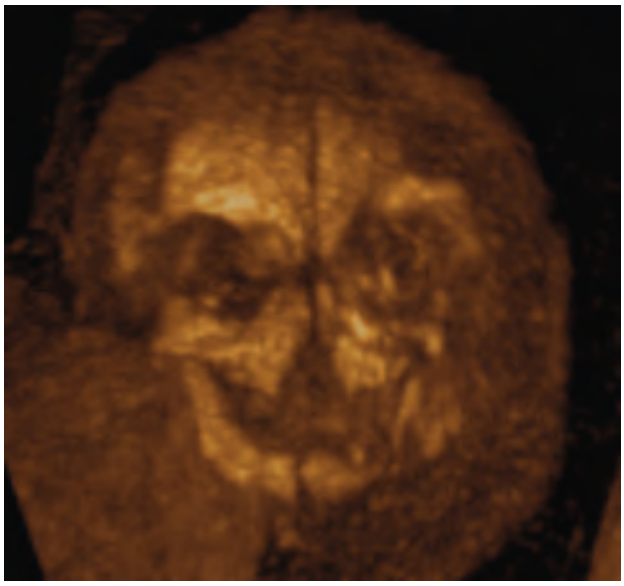

Figure 33.34: Cleft palate associated with holoprosencephaly. 3D maximum mode image demonstrates midline large cleft of maxilla

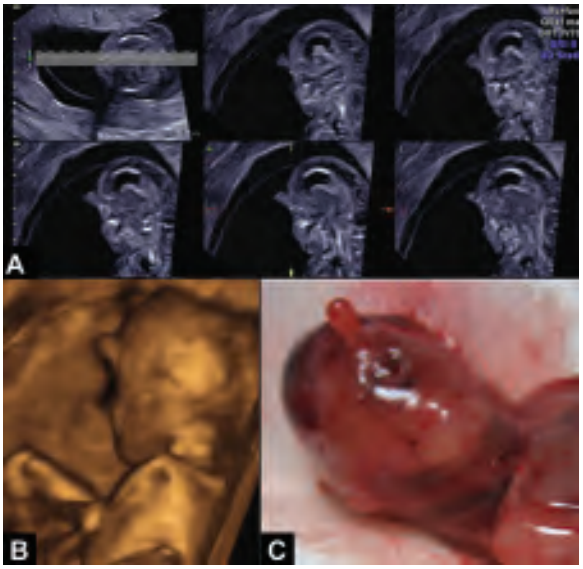

Figures 33.35A to C: Proboscis associated with holoprosencephaly at 12 weeks of gestation. (A) Tomographic facial sagittal imaging of holoprosencephalic fetus; (B) Three-dimensional (3D) reconstructed image of fetal face, lateral view; (C) Macroscopic picture after termination of pregnancy

and avoids the pitfall of obtaining a parasagittal view, which could lead to false negative results. Tomographic ultrasound imaging also allows the demonstration of facial midline structures in detail, by examining close parallel sections **(Fig. 33.36)**. It is important to be aware

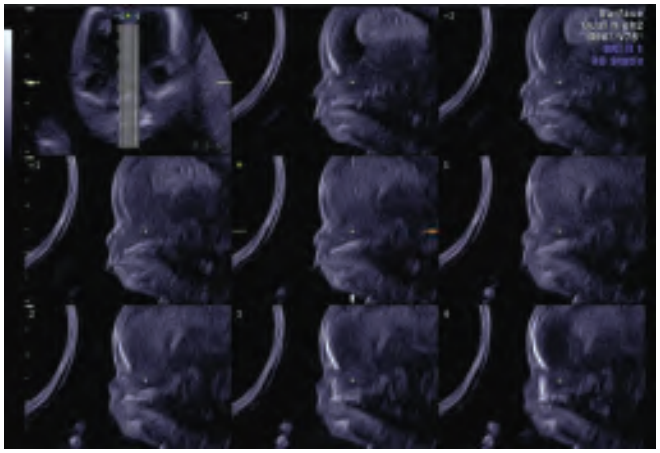

Figure 33.36: Tomographic ultrasound image of fetal profile with hypoplastic nasal bone at the end of 13 weeks of gestation. Thinly sliced parallel cutting section of midsagittal plane shows fetal profile in detail and hypoplastic nasal bone. Trisomy 21 was confirmed by CVS

that the quality of the orthogonal planes or tomographic imaging is strongly dependent upon the original plane of acquisition. Rembouskos et al.[24] described that routine application of 3D scanning for the nasal bone in screening for trisomy 21 is likely to be associated with a very high false-positive rate due to the possible limits of 3D technology. Benoit and Chaoui[25] described the diagnosis of bilateral or unilateral absence or hypoplasia of nasal bones in second trimester screening for Down syndrome by using 3D sonography with maximal mode rendering. **Figures 33.37A to F** shows the midsagittal section of fetal face and craniofacial bony reconstructed image of normal fetus and trisomy 21 fetuses in the first trimester.

A short maxillary length has been associated with trisomy 21.[26] Micrognathia can be detected as an isolated structural anomaly, as one of the features of a chromosomal abnormality, or a syndrome.[27] Congenital micrognathia and the lowest ears are frequently detected together as shown in **Figure 33.38,** in cases with chromosomal aberrations and other syndromic diseases, because mandibula and ears arises from the first pharyngeal (branchial) arch. Assessment of the facial features, chin development and mandibular size by 3D ultrasound in the second and third trimesters has been reported.[28] By using the surface mode and maximum mode **(Figs 33.39A to D)**, the fetal profile and facial bone structure in normal and abnormal fetuses can be described in the first trimester.

Cleft lip and palate is usually demonstrated and diagnosed in the second and third trimesters. However, recent advances of the transvaginal 3D ultrasound have

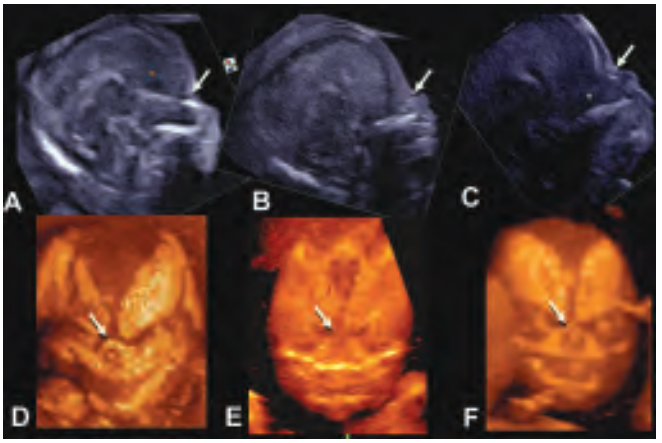

Figures 33.37A to F: (A) Midsagittal two-dimensional (2D) image of fetal profile and craniofacial bony reconstructed image of normal fetus; (B and C) Trisomy 21 fetuses at 13-14 weeks of gestation; (D) Normal fetus. Nasal bone is clearly visualized in both 2D and three-dimensional (3D) images (arrows); (E) Nasal bone defect in a case of trisomy 21. Nasal bone is completely missing in both 2D and 3D; (F) Nasal bone hypoplasia in a case of trisomy 21. Small nasal bone is visualized in both 2D and 3D

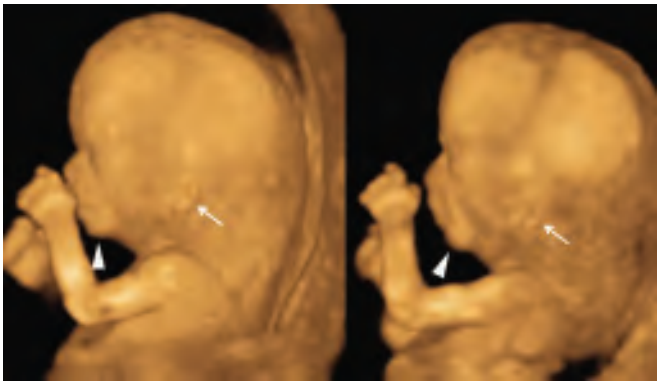

Figure 33.38: Micrognathia and lowset ears at 13 weeks of gestation. Both images are from the same fetus. Micrognathia (arrowheads) and lowset ears (arrows) are clearly demonstrated by three-dimensional (3D) reconstructed images

provided accurate and informative diagnostic images of cleft lip with orientation of left-sided, right-sided or bilateral cleft lip **(Figs 33.40 and 33.41)**. Furthermore, the palate is still created during pregnancy but 3D reconstructed image can demonstrate cleft palate shown in **Figures 33.34 and 33.42.** Up-to-date tomographic ultrasound imaging can provide the precise demonstration of palate shown in **Figure 33.43** and the possibility of early diagnosis of cleft palate.

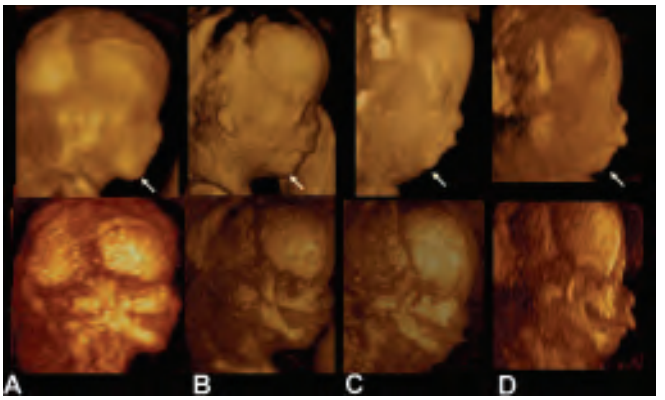

Figures 33.39A to D: Fetal profile and facial bone development in normal fetus (A) and abnormal fetuses (B,C,D) at 12-13 weeks of gestation. (A) Normal fetus; (B) Trisomy 21 fetus; (C) Trisomy 18 fetus; (D) Mild micrognathia with normal chromosome. Lateral views of fetal profile show the difference of chin-angle. Maximum mode images indicate the hypoplastic maxilla and mandible in B to D

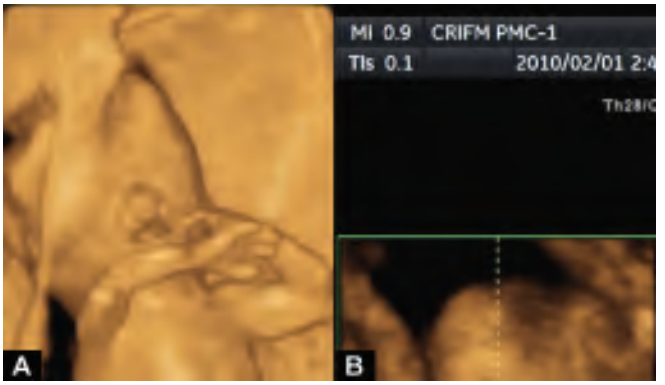

Figures 33.40A and B: Bilateral and unilateral cleft lip seen at 12 weeks of gestation. (A) Three-dimensional (3D) reconstructed images of bilateral cleft lip seen in cases of trisomy 18; (B) 3D reconstructed image of unilateral cleft lip seen as a single finding

Eyeballs and lenses are detectable by ultrasound from the late first trimester. Cataract is defined by the presence of any lens opacity. The incidence of congenital cataract ranges from 1 to 6 newborn infants out of 10,000 births.[29] Cataract development is strongly linked to the embryonic ocular development. The lens differentiates from the surface ectoderm before the 6th week of gestation, explaining the absence of cataract in case of late first trimester fetal infection.[30,31] A genetic cause is responsible for 30% of unilateral cataracts and 50% of bilateral cataracts. Prenatal diagnosis of fetal cataract was reported in the late second and third pregnancy.[32-36]

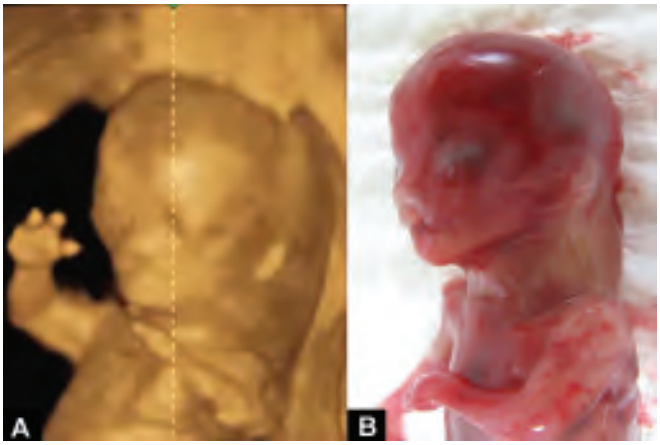

Figures 33.41A and B: Left-sided cleft lip seen at 12 weeks of gestation. (A) Three-dimensional (3D) reconstructed images of bilateral cleft lip seen in cases of trisomy 21; (B) Macroscopic picture of aborted fetus

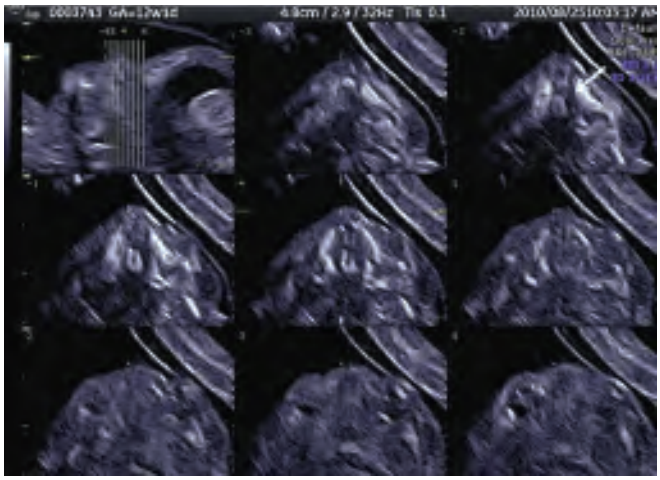

Figure 33.43: Tomographic ultrasound imaging of cleft palate at 12 weeks of gestation. Unilateral cleft palate is demonstrated (arrow)

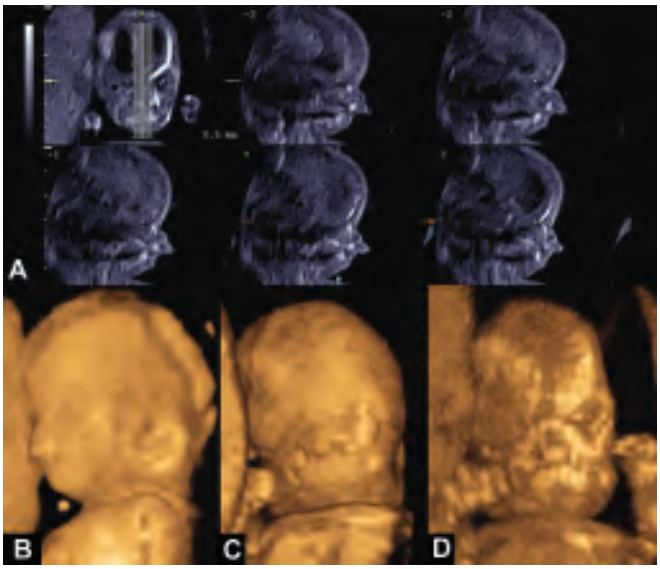

Figures 33.42A to D: Bilateral cleft lip and palate at 13 weeks of gestation. (A) Tomographic sagittal facial imaging of the normal-karyotype anomalous fetus; (B to D) Three-dimensional (3D) reconstructed images; (B) Oblique; (C) Frontal and maximum-mode frontal views. Maximum image shows bilateral cleft of maxillary bone

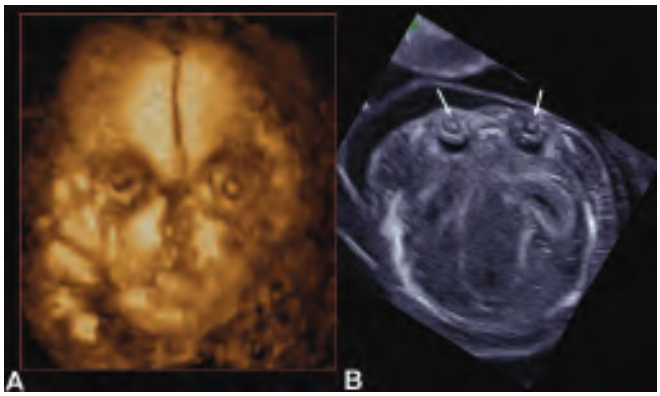

Figures 33.44A and B: Congenital cataract at 14 weeks of gestation. (A) Bilateral congenital cataract with microphthalmia is demonstrated as lens opacity (arrows) in three-dimensional (3D); (B) Two-dimensional (2D) images

Figures 33.44A and B shows fetal bilateral cataract with microphthalmia as early as 14 weeks of gestation.

Limb Abnormalities

Limb abnormalities can occur as isolated findings or as one component of a syndrome or sequence. However, only 5% of congenital hand anomalies occur as a part of a recognized syndrome.[37] Overlapping fingers, wrist contracture **(Figs 33.45A and B)** and forearm deformities

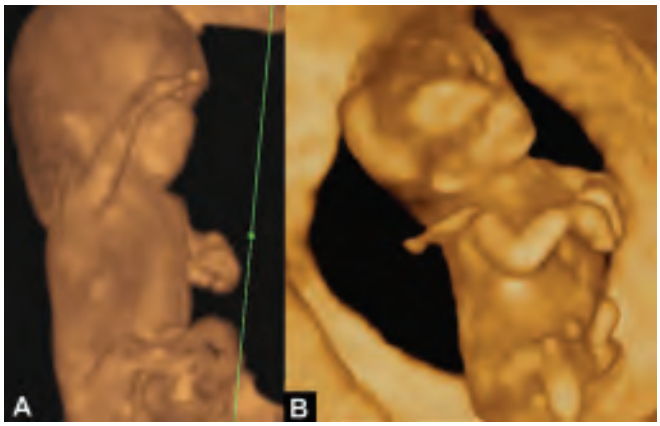

Figures 33.45A and B: Mild-to-moderate wrist contracture seen in cases of trisomy 18 at 12-13 weeks of gestation. (A) Mild wrist contracture is seen; (B) Moderate wrist contracture is seen. Trisomy 18 was confirmed by chorionic villi sampling

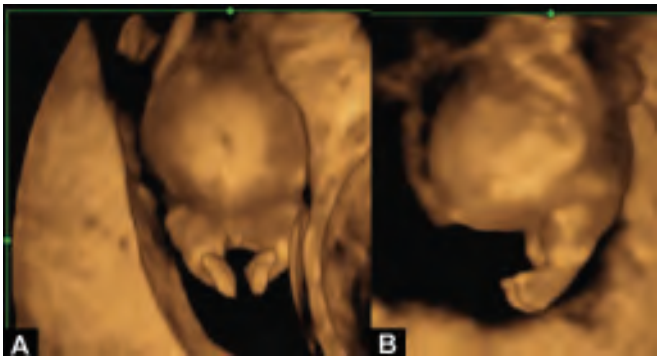

Figures 33.46A and B: Short limb abnormality at 13 weeks of gestation. (A) Short lower extremities with large abdomen is clearly demonstrated in the frontal; and (B) Lateral views

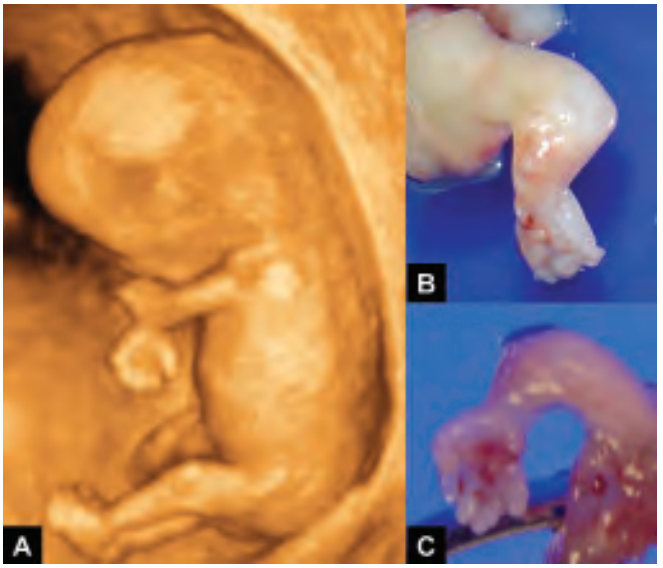

Figures 33.47A to C: Upper limb abnormality at 11 weeks of gestation. **(**A) Three-dimensional (3D) ultrasound revealed contracted elbow joint abnormality; (B and C) Macroscopic appearance of upper limbs of aborted fetus

are often associated with a chromosomal abnormality, such as trisomy 18. Most skeletal anomalies are recognizable in the second trimester. However, several reports on congenital skeletal abnormalities (such as sirenomelia and others) in the first trimester have been documented.[38-42] Short limb abnormality in the first trimester has been shown in **Figures 33.46A and B. Figures 33.47A to C** show an 11 week fetus on 3D sonography with skeletal dysplasia of the bilateral upper extremities and normal lower extremities. Clubfoot as shown in **Figures 33.48A and B** is not so common as club hands in the first trimester. Finger abnormalities, such as polydactyly, oligodactyly and syndactyly, are detectable from the late first trimester.

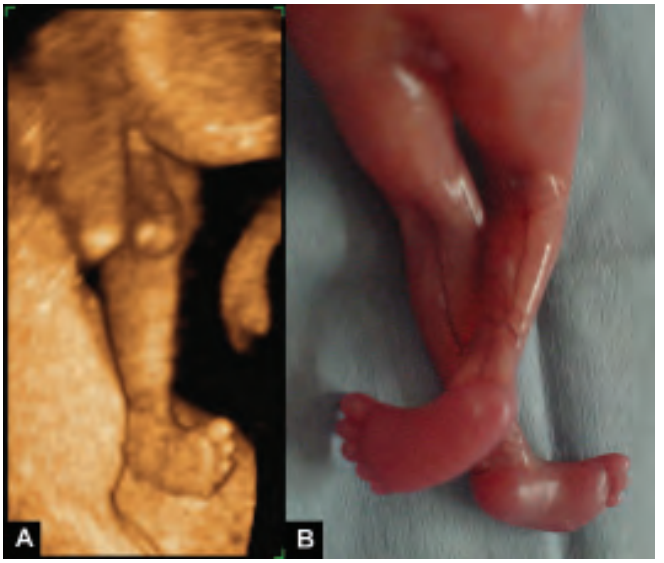

Figures 33.48A and B: Fetal clubfoot at 13 weeks of gestation. (A) Three-dimensional 3D image of fetal leg; (B) Legs of aborted fetus. This case was associated with chromosomal aberration

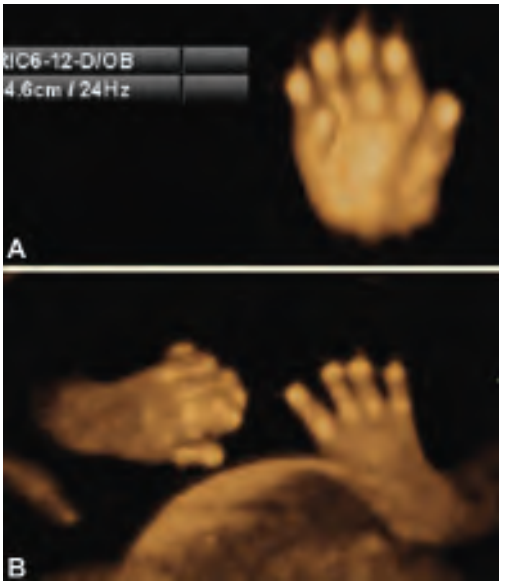

Figures 33.49A and B: Polydactyly and syndactyly at the beginning of 14 weeks of gestation. (A) Three-dimensional (3D) reconstructed ultrasound images clearly depicted bilateral polydactyly; (B) Left poly-/syndactyly (lower). Both cases were associated with holoprosencephaly

In **Figures 33.49A and B**, polydactyly and syndactyly at 14 weeks in the cases of holoprosencephaly are well demonstrated by 3D ultrasound.

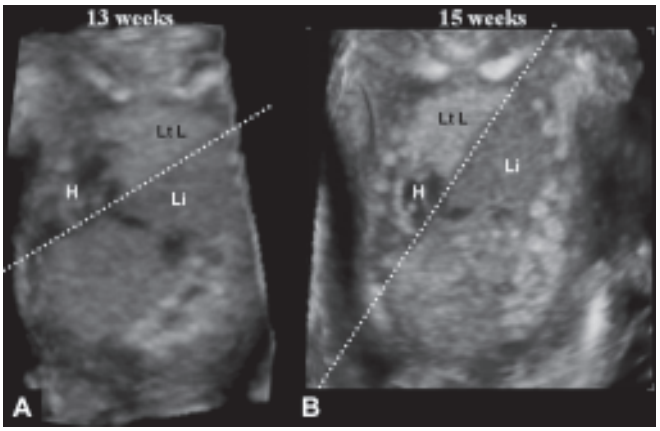

Figures 33.50A and B: Congenital diaphragmatic defect at 13 and 15 weeks of gestation. Referral case due to nuchal translucency of 3 mm at 11 weeks of gestation. (A) Frontal view at 13 weeks. Dextrocardia (H), liver-up (Li) and oppressed left lung (Lt L) are demonstrated; (B) Frontal view at 15 weeks. The line of Lung-liver border indicates acute angle changing in a short period due to progressive liver-up

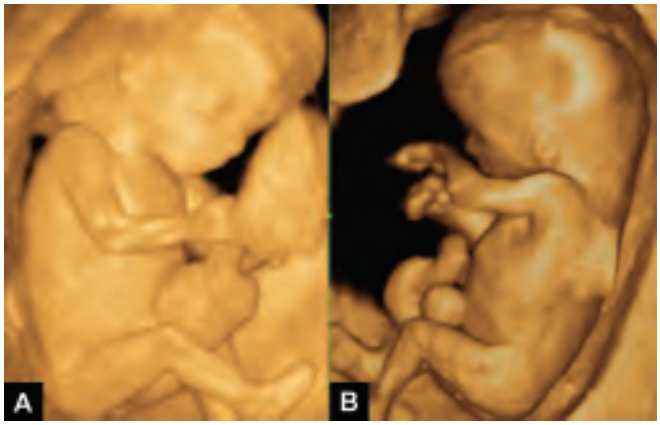

Figures 33.51A and B: Omphalocele at 12 and 13 weeks of gestation. Three-dimensional (3D) reconstructed ultrasound images clearly demonstrates omphalocele. Trisomy 18 was confirmed by chorionic villi sampling in both cases

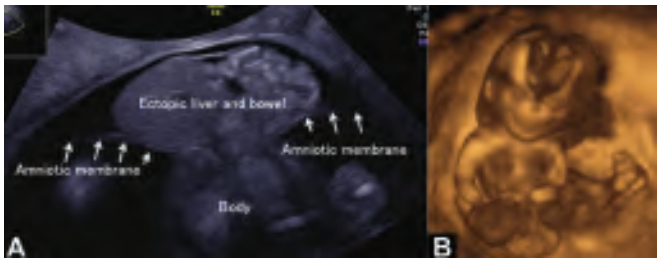

Figures 33.52A and B: Limb-body-wall complex (LBWC) at 13 weeks of gestation. (A) Two-dimensional (2D) image. Note the ectopic liver and bowels are outside amniotic membrane; (B) Three-dimensional reconstructed image. Ectopic abdominal organs and abnormal position of lower limbs are well demonstrated

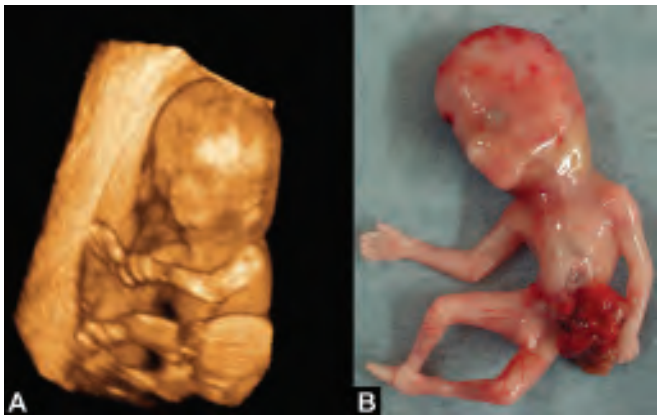

Figures 33.53A and B: Omphalocele at 12 weeks of gestation. (A) 3D ultrasound image at 12 weeks and 5 days; (B) Macroscopic picture of aborted fetus. Hernial sac was ruptured at delivery

Thoracoabdominal Abnormalities

Congenital diaphragmatic hernia (CDH) occurs in 1 of every 2,000–4,000 live births and accounts for 8% of all major congenital anomalies.[43] There are three types of CDH; posterolateral or Bochdalek hernia (occurring at approximately 6 weeks' gestation), the anterior Morgagni hernia and a hiatus hernia. The left-sided Bochdalek hernia occurs in approximately 90% of cases. Left-sided hernias allow herniation of both small and large bowel, as well as intra-abdominal solid organs into the thoracic cavity. Early diagnosis of CDH in the first trimester has been reported.[44] **Figures 33.50A and B** shows the thoracoabdominal area of a fetus with a congenital diaphragmatic defect where the lung-liver border line acutely changes its angle from 13 to 15 weeks, due to progressive liver upward movement into the chest. Early diagnosis of this defect is important.[44]

Omphalocele is often seen from the first trimester. Physiological umbilical hernia is usually observed around 8–10 weeks of gestation, however, umbilical hernia seen after the beginning of 12 weeks is definitely pathological **(Figs 33.51A and B)**. Ectopic abdominal organs outside of amniotic cavity is often associated with short umbilical cord, abnormal limbs and this condition is called as short umbilical cord complex, LBWC or body-stalk anomaly as shown in **Figures 33.52 and 33.53**, different from amniotic band syndrome.

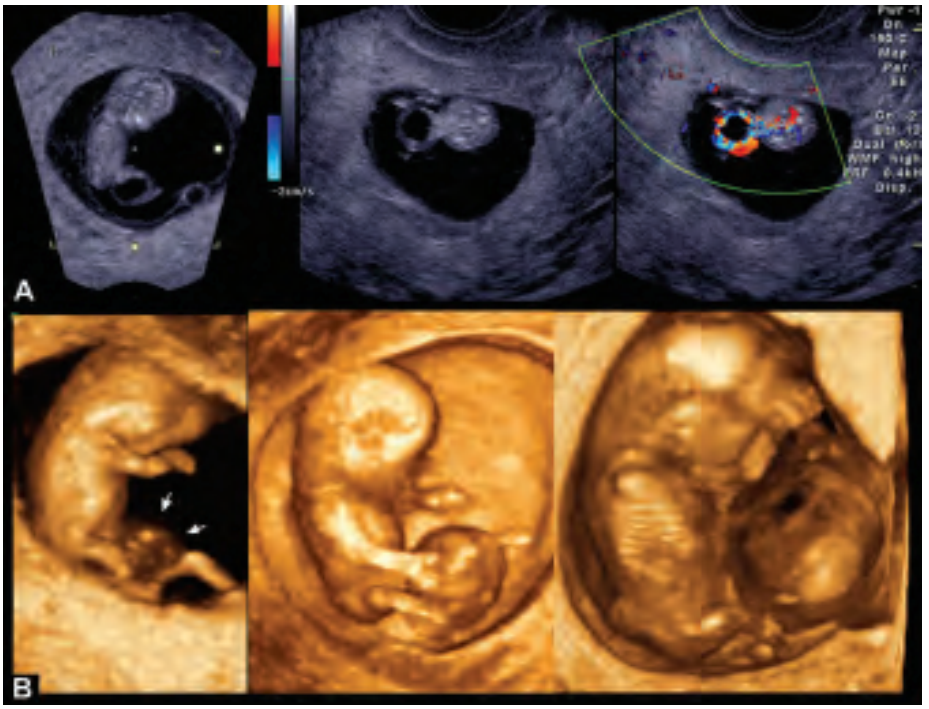

Figures 33.54A and B: Bladder exstrophy in the first trimester. (A) Cystic formation between bilateral umbilical arteries. No bladder is visible inside of the fetus; (B) Three-dimensional (3D) US images at 10, 11 and 12 weeks from the left. Rapid increase in size of external bladder is clearly demonstrated

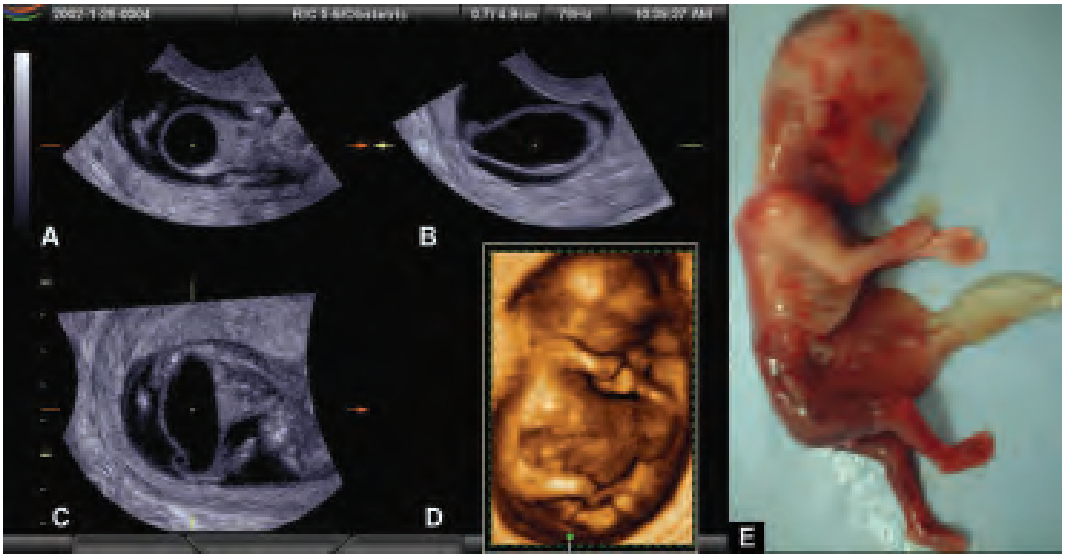

Figures 33.55A to E: Prune-Belly syndrome at 11 weeks of gestation. (A) Three-dimensional (3D) orthogonal views of coronal; (B) Axial; (C) Sagittal sections; (D) Huge bladder of Prune-Belly shape and fragile abdominal wall are visible; (E) Macroscopic picture of aborted fetus

Urinary Tract Abnormality

Bladder extrophy **(Figs 33.54A and B)** is a rare abnormality, which may be associated with cloaca malformation or the OEIS complex. Prune Belly syndrome **(Figs 33.55A to E)** describes the triad of dilation of the urinary tract, a deficiency of the abdominal wall musculature and failure of testicular descent. Hydronephrosis is the most common pathologic finding in the urinary tract on prenatal screening by ultrasonography. Fetal obstructive uropathy has become detectable earlier and fetal therapy of vesicoamniotic shunting (VAS) is the accepted procedure in well-defined cases. It has been reported that the long-term outcomes indicate that VAS at 18–30 weeks may not change the prognosis of renal function and that fetal surgery for obstructive uropathy should be performed only for the carefully selected patient who has severe oligohydramnios and normal-

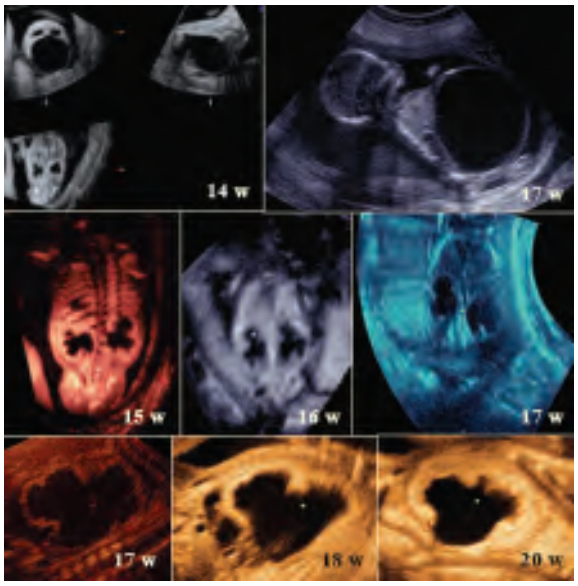

Figure 33.56: Huge bladder before and after vesicoamniotic shunt (VAS) operation. (left upper) 3D orthogonal view at 14 weeks of gestation. Huge bladder and bilateral hydronephrosis are demonstrated. Abdominal wall is not fragile like Prune-Belly syndrome. (right upper) sagittal image at 17 weeks before VAS. Bladder volume is 137.7 ml. (middle figures) Changing appearance of kidneys at 15,16 and 17 weeks from the left. Rapid thinning of renal parenchyma with progressive hydronephrosis is clearly demonstrated. (lower figures) Changing appearance of renal parenchyma (17,18 and 20 weeks from the left) after VAS operation performed at 17 weeks. Renal parenchyma thickness was rapidly recovered after VAS procedure, with improvement of hydronephrosis

appearing kidneys.[45] To preserve renal function, however, earlier VAS may be preferable **(Fig. 33.56).**

CONCLUSION

Recent advances of imaging technologies and computerized technologies have greatly contributed to the fields of both embryology and sonoembryology. In near future, further new findings will be discovered. We must recognize "the embryo as a patient" as well as "the fetus as a patient".

ACKNOWLEDGMENTS

The authors are grateful to the members of the Academic Center for Computing and Media Studies, Kyoto University, for their collaboration in making computer graphics images. We greatly thank Professor Katsumi Kose of the University of Tsukuba for his contributions to MR imaging of human embryo specimens. We also thank members of Global Ultrasound and IT and Women's Healthcare and Specialty in GE Healthcare (Milwaukee, USA) for their technical support and collaboration.

REFERENCES

1. Smith BR, Huff DS, Johnson GA. Magnetic resonance imaging of embryos: an Internet resource for the study of embryonic development. Comput Med Imaging Graph. 1999;23(1):33-40.
2. Matsuda Y, Utsuzawa S, Kurimoto T, et al. Super-parallel MR microscope. Magn Reson Med. 2003;50(1):183-9.
3. Yamada S, Uwabe C, Nakatsu-Komatsu T, et al. Graphic and movie illustrations of human prenatal development and their application to embryological education based on the human embryo specimens in the Kyoto collection. Dev Dyn. 2006;235(2):468-77.
4. Timor-Tritsch IE, Peisner DB, Raju S. Sonoembryology: an organ-oriented approach using a high-frequency vaginal probe. J Clin Ultrasound. 1990;18(4):286-98.
5. Benoit B, Hafner T, Kurjak A, et al. Three-dimensional sonoembryology. J Perinat Med. 2002;30(1):63-73.
6. O'Rahilly R, Muller F. Prenatal ages and stages-measures and errors. Teratology. 2000;61(5):382-4.
7. Pooh RK, Shiota K, Kurjak A. Imaging of the human embryo with magnetic resonance imaging microscopy and high-resolution transvaginal three-dimensional sonography: human embryology in the 21st century. Am J Obstet Gynecol. 2011;204(1):77.e1-16.
8. Kurjak A, Pooh RK, Merce LT, et al. Structural and functional early human development assessed by three-dimensional and four-dimensional sonography. Fertil Steril. 2005;84(5):1285-99.
9. Kurjak A, Zudenigo D, Predanic M, et al. Recent advances in the Doppler study of early fetomaternal circulation. J Perinat Med. 1993;21(6):419-39.
10. Kurjak A, Schulman H, Predanic A, et al. Fetal choroid plexus vascularization assessed by color flow ultrasonography. J Ultrasound Med. 1994;13(11):841-4.
11. Pooh RK, Aono T. Transvaginal power Doppler angiography of the fetal brain. Ultrasound Obstet Gynecol. 1996;8(6):417-21.
12. Chaoui R, Levaillant JM, Benoit B, et al. Three-dimensional sonographic description of abnormal metopic suture in second- and third-trimester fetuses. Ultrasound Obstet Gynecol. 2005;26(7):761-4.
13. Kim MS, Jeanty P, Turner C, et al. Three-dimensional sonographic evaluations of embryonic brain development. J Ultrasound Med. 2008;27(1):119-24.
14. Hata T, Dai SY, Kanenishi K, et al. Three-dimensional volume-rendered imaging of embryonic brain vesicles using inversion mode. J Obstet Gynaecol Res. 2009;35(2):258-61.
15. Jaumiaux E, Gulbis B, Burton GJ. The human first trimester gestational sac limits rather than facilitates oxygen transfer to the fetus-a review. Placenta. 2003;24(17):S86-S93.

16. Kucuk T, Duru NK, Yenen MC, et al. Yolk sac size and shape as predictors of poor pregnancy outcome. J Perinat Med. 1999;27(4):316-20.
17. Lindsay DJ, Lovett IS, Lyons EA, et al. Yolk sac diameter and shape at endovaginal us: predictors of pregnancy outcome in the first trimester. Radiology.1992;183(1):115-8.
18. Blaas HG, Eik-Nes SH, Isaksen CV. The detection of spina bifida before 10 gestational weeks using two- and three-dimensional ultrasound. Ultrasound Obstet Gynecol. 2000;16(1):25-9.
19. Nicolaides KH. Nuchal translucency and other first-trimester sonographic markers of chromosomal abnormalities. Am J Obstet Gynecol. 2004;191(1):45-67.
20. Cicero S, Curcio P, Papageorghiou A, et al. Absence of nasal bone in fetuses with trisomy 21 at 11-14 weeks of gestation: an observational study. Lancet. 2001;358(9294):1665-7.
21. Zoppi MA, Ibba RM, Axiana C, et al. Absence of fetal nasal bone and aneuploidies at first-trimester nuchal translucency screening in unselected pregnancies. Prenat Diagn. 2003;23(6):496-500.
22. Cicero S, Rembouskos G, Vandecruys H, et al. Likelihood ratio for trisomy 21 in fetuses with absent nasal bone at the 11-14-week scan. Ultrasound Obstet Gynecol. 2004;23(3):218-23.
23. Cicero S, Avgidou K, Rembouskos G, et al. Nasal bone in first-trimester screening for trisomy 21. Am J Obstet Gynecol. 2006;195(1):109-14.
24. Rembouskos G, Cicero S, Longo D, et al. Assessment of the fetal nasal bone at 11-14 weeks of gestation by three-dimensional ultrasound. Ultrasound Obstet Gynecol. 2004;23(3):232-6.
25. Benoit B, Chaoui R. Three-dimensional ultrasound with maximal mode rendering: a novel technique for the diagnosis of bilateral or unilateral absence or hypoplasia of nasal bones in second-trimester screening for Down syndrome. Ultrasound Obstet Gynecol. 2005;25:19-24.
26. Cicero S, Curcio P, Rembouskos G, et al. Maxillary length at 11-14 weeks of gestation in fetuses with trisomy 21. Ultrasound Obstet Gynecol. 2004;24(1):19-22.
27. Teoh M, Meagher S. First-trimester diagnosis of micrognathia as a presentation of Pierre Robin syndrome. Ultrasound Obstet Gynecol. 2003;21(6):616-8.
28. Tsai MY, Lan KC, Ou CY, et al. Assessment of the facial features and chin development of fetuses with use of serial three-dimensional sonography and the mandibular size monogram in a Chinese population. Am J Obstet Gynecol. 2004;190(2);541-6.
29. Francis PJ, Berry V, Bhattacharya SS, et al. The genetics of childhood cataract. J Med Genet. 2000;37(7):481-8.
30. Thut CJ, Rountree RB, Hwa M, et al. A large-scale in situ screen provides molecular evidence for the induction of eye anterior segment structures by the developing lens. Dev Biol. 2001;23(1):63-76.
31. Karkinen-Jääskeläinen M, Saxen L, Vaheri A, et al. Rubella cataract in vitro: sen- sitive period of the developing human lens. J Exp Med. 1975;141:1238-48.
32. Romain M, Awoust J, Dugauquier C, et al. Prenatal ultrasound detection of congenital cataract in trisomy 21. Prenat Diagn. 1999;19(8):780-2.
33. Pedreira DA, Diniz EM, Schultz R, et al. Fetal cataract in congenital toxoplasmosis. Ultrasound Obstet Gynecol. 1999;13(4):266-7.
34. Daskalakis G, Anastasakis E, Lyberopoulos E, et al. Prenatal detection of congenital cataract in a fetus with Lowe syndrome. J Obstet Gynaecol. 2010;30(4):409-10.
35. Reches A, Yaron Y, Burdon K, et al. Prenatal detection of congenital bilateral cataract leading to the diagnosis of Nance-Horan syndrome in the extended family. Prenat Diagn. 2007;27(7):662-4.
36. Léonard A, Bernard P, Hiel AL, et al. Prenatal diagnosis of fetal cataract: case report and review of the literature. Fetal Diagn Ther. 2009;26(2):61-7.
37. Bolitho DG. Hand, Congenital hand deformities (online). emedicine 2006. http://www.emedicine.com/plastic/TOPIC298.HTM (Accessed on Feb 2011).
38. Carbillon L, Seince N, Largillière C, et al. First-trimester diagnosis of sirenomelia. A case report. Fetal Diagn Ther. 2001;16(5):284-8.
39. Monteagudo A, Mayberry P, Rebarber A, et al. Sirenomelia sequence: first-trimester diagnosis with both two- and three-dimensional sonography. J Ultrasound Med. 2002;21(8):915-20.
40. Schiesser M, Holzgreve W, Lapaire O, et al. Sirenomelia, the mermaid syndrome—detection in the first trimester. Prenat Diagn. 2003;23(6):493-5.
41. Dugoff L, Thieme G, Hobbins JC. First trimester prenatal diagnosis of chondroectodermal dysplasia (Ellis-van Creveld syndrome) with ultrasound. Ultrasound Obstet Gynecol. 2001;17(1):86-8.
42. Percin EF, Guvenal T, Cetin A, et al. First-trimester diagnosis of Robinow syndrome. Fetal Diagn Ther. 2001;16(5):308-11.
43. Doyle NM, Lally KP. The CDH Study Group and advances in the clinical care of the patient with congenital diaphragmatic hernia. Semin Perinatol. 2004;28:174-84.
44. Daskalakis G, Anastasakis E, Souka A, et al. First trimester ultrasound diagnosis of congenital diaphragmatic hernia. J Obstet Gynaecol Res. 2007;33(6):870-2.
45. Holmes N, Harrison MR, Baskin LS. Fetal surgery for posterior urethral valves: long-term postnatal outcomes. Pediatrics. 2001;108(1):E7.

34
CHAPTER

3D Ultrasound in the Visualization of Fetal Anatomy in the Three Trimesters of Pregnancy

Giovanni Centini, Gabriele Centini, Lucia Rosignoli, Mario Lituania

INTRODUCTION

Biophysical Monitoring Of Pregnancy

Embryo-Fetal Anatomical Study By 3D And 4D Ultrasound

During 1970s, the use of ultrasound in obstetric diagnostics was a driving force for the study of the fetus, revolutionizing the concept of prenatal monitoring. The development of increasingly sophisticated techniques, such as high frequency, real-time computing, echo-Doppler flow imaging, color and power Doppler and the second harmonic, and was followed in the 90s by a period of relative immobility for ultrasound upgrading. However, since the turn of the millennium, volumetric probes that store volume samples, acquiring up to 25 images per second (and multiples of this figure are already in view), have transformed the classical concept of two-dimensional ultrasound, generating enormous interest and a great spurt of research which still has to be translated into scientific knowledge. So it is now widely considered that three- and four-dimensional (3-4D), namely 3D with a fourth dimension, time, offer too many possibilities to be ignored.[1-3] Acquisition of a volume or region of interest is the great novelty of 3D technique and just as exciting is the possibility of studying it in movement during ultrasound examination or afterwards, also by other operators and in an infinite number of section planes that can all be perfectly reproduced. Moreover, the many systems of representing acquired volumes make this technique very similar to computed axial tomography (CAT) and nuclear magnetic resonance (NMR) imaging:

- Multiplanar scan: The image can be visualized and studied in the three classical scan planes—coronal, sagittal and transverse
- Minimum rendering: This is the classical 3D image of external embryo fetal or other anatomical morphology
- Maximum rendering: This highlights deep echoes to visualize skeletal details
- Glass body: This highlights blood vessels in an anatomical part which is rendered transparent like glass
- Vocal: Enabling volumes to be calculated with great accuracy
- Invert: Transformation of liquid into solid parts
- STIC (spatiotemporal imaging correlation): Storage of a moving volume over a time interval with the possibility of representing and studying it later in slow motion and in different planes
- TUI (tomography ultrasound imaging) or Multislice: A field is sectioned in up to 27 scans at predefined distances and in real time (like NMR)
- 4D: 3D represented in time

- VCI-c-plane: Improved tissue contrast resolution in real time (4D), coronal plane imaging (orthogonal plane of the scan plane)
- B-flow: The direct visualization of blood reflectors has made B-mode flow imaging (B-flow) possible without the limitations of Doppler technology, angle independent
- Omni-view: To study the same volume-by-volume contrast imaging (VCI c-plane multiple sections). It is possible to shape the box of observation (linear, curve, etc.) to region of interest (ROI). This possibility is very important because the human anatomy usually has a curve or round shape. By omni-view we can realize more detailed pictures[4]
- SonoAVC: In (sono Automated Volume calculation) there is possibility to detect areas by different colors and to calculate the volume of these areas.

Other possibilities are the electronic scalpel to eliminate parts not of interest and rotation about orthogonal axes or cine calculation to present the volume in different kinds.

Today ultrasound research is so active that new applications have probably been found as these words are being written. One new advance is already available, namely the electronic matrix probe. The possibilities of electronic rather than volumetric probes that combine electronic scans with mechanical movement to cover the area of interest will provide even more sophisticated images and the possibility of obtaining volume samples from hitherto unthinkable angles and perspectives, especially useful in cardiology.[5] These innovations, however, require relatively long development periods before they are applied.

The above raises the question whether 3-4D offers greater certainty in embryo study and detection of fetal and ovarian pathology.[6-8] The scientific community seems unanimous in considering that we cannot yet fully answer this question, but ten years after the finalization of volumetric probe was acquired, many experiences that can make a real contribution to define the role and importance of 3-4D in the study of various embryo-fetal organs and systems.

However, there are already many papers comparing 2D and 3D, and their results define the use of 3-4D complementary to 2D, with the exception for neurosonology and fetal cardiology, where it can offer better possibility to explore physiological and pathological fetal anatomy. This technique has unique applications but it is commonly considered that 3-4D offers an improvement and completion of 2D, of such interest that it cannot be forgone once tried. Hence there are specific situations in which 3D is indispensable, such as when a coronal scan is needed (visualization of the corpus callosum or a fetal profile in anterior occipital position), though a good instrument in the hands of an experienced sonographer can meet all the needs of ultrasound monitoring in pregnancy **(Figs 34.1 and 34.2).** Those with long experience with 2D and subsequently with 3-4D, know the pleasure of working better and obtaining images superior to those obtained by 2D. The possibility of saving a volume and studying it later, discussing it with other operators and visualizing it in an infinite number of planes, superior to those obtained with 2D and perfectly reproducible, is as close as one can imagine to CAT or NMR scans, with the advantage of speed, easy repetition and much lower costs. The old recorded cassette to transmit images of a malformation, for example, cannot compare with volumetric acquisition. It seems certain that in the near future nearly all instruments will be equipped with 3-4D, even if not all sonographers know how to exploit it fully. It is therefore necessary to begin to train experts who think and work directly in 3D without having to make the often difficult transition from 2D. Sonographers of tomorrow working today directly with 3D techniques will certainly obtain better results than those who began with 2D because they will already have in mind the field of interest to explore in 3D.

The aim of this atlas is to provide pictorial documentation of pregnancy monitoring with 3D images, sometimes with the corresponding 2D image, so readers can begin to habituate themselves and hopefully acquire a different and personal key to the 3D image.

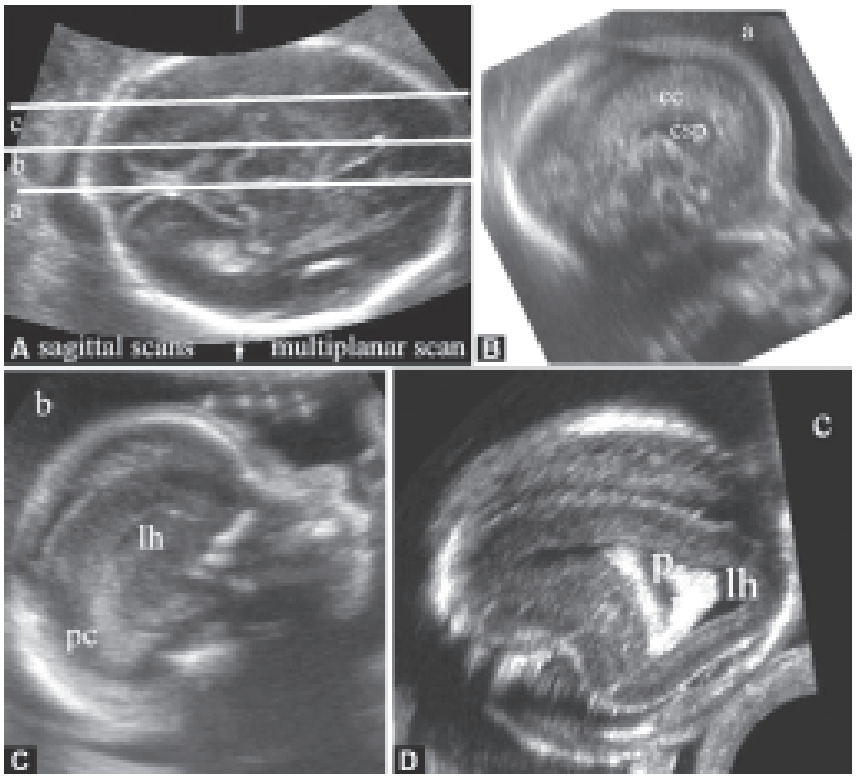

Figures 34.1A to D: Sagittal scans. Image *a* shows the corpus callosum and cavum septi pellucidi perfectly. This section is very difficult to obtain by 2D, but easy by 3D multiplanar scan. The parasagittal scan offers a good view of the lateral horn and the anterior, posterior and subtemporal horns. Cc: corpus callosum; csp: cavum septi pellucidi; lh: lateral horn; p: choroid plexus

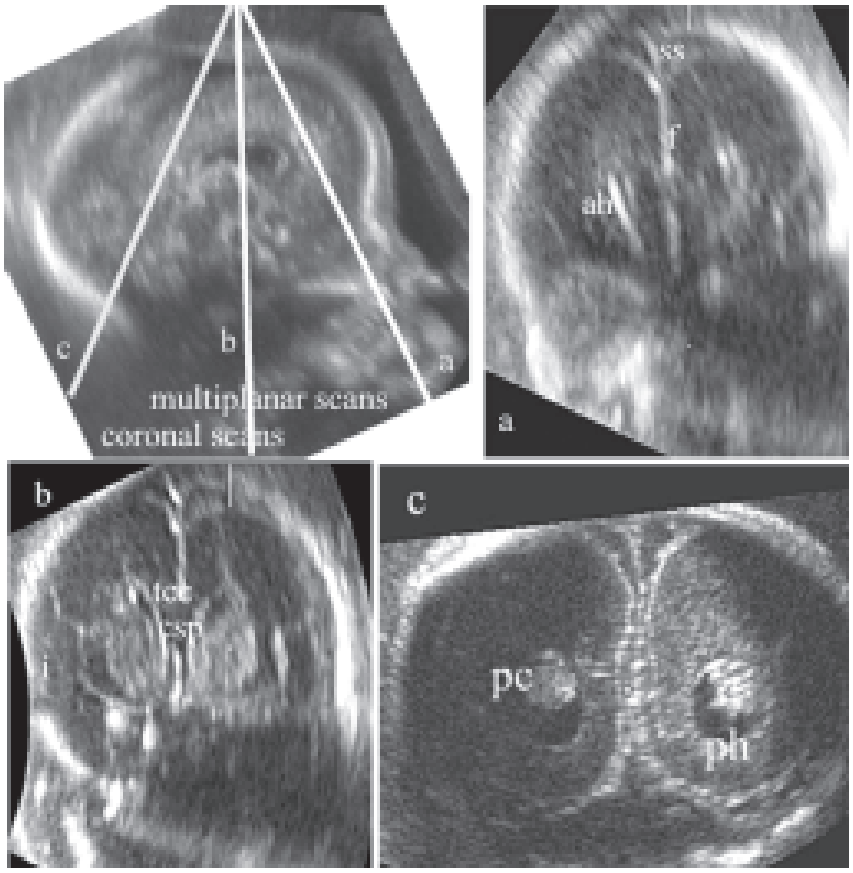

Figure 34.2: Coronal scans. Section *a* is known as oxhead because the anterior horns resemble those of an ox; section *b* shows a good view of the corpus callosum, cavum septi pellucidi and lateral ventricles; section *c* is known as owl eyes because of the contrast between the posterior horn and the white nervous system with eye-like choroid plexi. ah: anterior horn; csp: cavum septi pellucidi; f: falx; i: insula; lv: lateral ventricle; cp: choroid plexus; ph: posterior horn

THE FIRST TRIMESTER OF PREGNANCY

From Conception to Week 10

The sophistication achieved by ultrasound instruments associated with clinical and ultrasound knowledge and know-how, which was unthinkable only ten years ago, enables us to monitor pregnancy from before conception. For fertility control, 2D ultrasound with power or color Doppler makes it possible to determine with sufficient certainty the following aspects on day 12:

- Uterine morphology and myometrial structure; the 3D scan in coronal section is a good instrument comparable to ISG-RNM to explore the uterine cavity and find the anatomical uterine malformation which represents 3–5%:arcuate uterus, didelphys and bicornuate.
- Endometrial echostructure and morphology by detecting a three-line image characteristic of the ovulatory period and myometrial vascularization **(Figs 34.3A to J)**
- Uterine artery flow values which should not have a pulsatility index of less than three
- The dominant follicle measuring 16–18 mm with peak systolic velocity (PSV) of 5–10 cm/sec in neighboring vessels
- About 4–5 antral follicles per ovary with PSV of 6–12 cm/sec in stromal vessels **(Figs 34.4A to E).**

By means of 3-4D or better the 4D VCI-c-plane system it is possible to obtain a correct view of the uterine cavity[9,10] **(Figs 34.5A to G)**. This means that with only one examination, the existence of anatomical and functional conditions for pregnancy can be ascertained. Once conception has occurred, ultrasound monitoring of pregnancy should not necessarily begin in the first weeks of gestation. This type of protocol is usually used for medically assisted conception, however it is possible to follow the progress of pregnancy week by week, acquiring important information on physiological or pathological evolution by monitoring embryo-fetal growth and studying embryo-fetal anatomy. At present, a 3-4D volumetric acquisition provides superior images in terms of definition and visual impact, but with only slight improvements in diagnostic capacity with respect to 2D.

An Ultrasound View of the First Trimester of Pregnancy

In indicating the period of embryo-fetal development, it is correct to distinguish between menstrual age and true gestational age. Menstrual age is counted from the last menstrual period and is unreliable. About 40% of pregnant women, or one in two, have ovulation problems for various reasons. Moreover, even in women with physiological ovulation patterns, conception may occur between day 11 and day 17 of the menstrual cycle. It is therefore essential to date pregnancy by means of ultrasound parameters during the first trimester. Gestational age is counted from when the gametes fuse and is on average 14 days less than the menstrual age used by embryologists.[11] Internationally, in fact, obstetricians now speak of gestational age when they really mean menstrual age. A compromise is the term ultrasound age, namely age established by ultrasound. When it is desired to indicate the effective period of embryo-fetal life, however, this is usually specified.

In order to better understand ultrasound images, especially for early detection of anatomical structures and embryo-fetal morphology, it is useful to refer to embryology, though naturally the anatomical age is earlier. In practice, it is important to be clear about the terms used.

The first trimester of pregnancy is divided into three periods: pre-embryonic, embryonic and fetal.

Pre-embryonic Period

Embryology: days 4–19

- Day 4: Morula
- Days 4–7: Implant of avillous morula in the uterus
- Days 8–12: Implant of blastocyst deep in decidua; presence of amniotic and celomic cavities
- Days 13–19: Presence of chorionic villi, yolk sac (YS) and neural plate.

Ultrasonography: Weeks 3 and 4 of Gestation

Ultrasound detects decidualization of the endometrium and the luteal body but cannot confirm pregnancy. Endometrial flow can be assessed and when absent suggests lack of implantation **(Figs 34.6A and B)**.

Embryonic Period

Embryology: Days 17–49 (seven full weeks)
Ultrasonography: Weeks 5–9 inclusive (up to day 63)

Comparison of tissue, organ and system formation detected and studied anatomically during the embryonic period demonstrates the capacities and limits of ultrasound for monitoring the product of conception. Another small distinction between embryology and ultrasound is that in the former case, reference is made to exact parameters such as crown rump length (CRL) or the presence of tissues, organs and systems, whereas in the latter, gestational age is usually indicated in

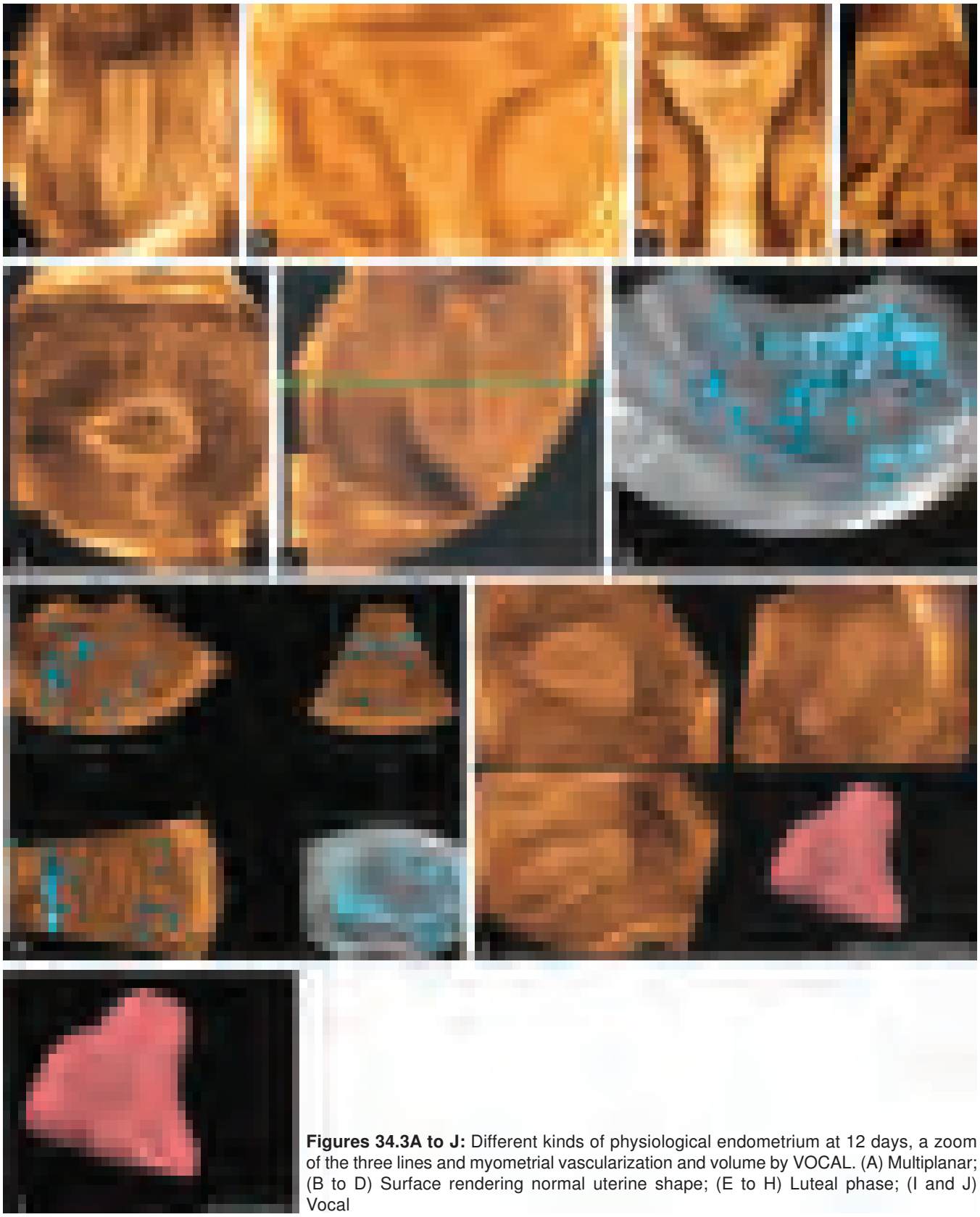

Figures 34.3A to J: Different kinds of physiological endometrium at 12 days, a zoom of the three lines and myometrial vascularization and volume by VOCAL. (A) Multiplanar; (B to D) Surface rendering normal uterine shape; (E to H) Luteal phase; (I and J) Vocal

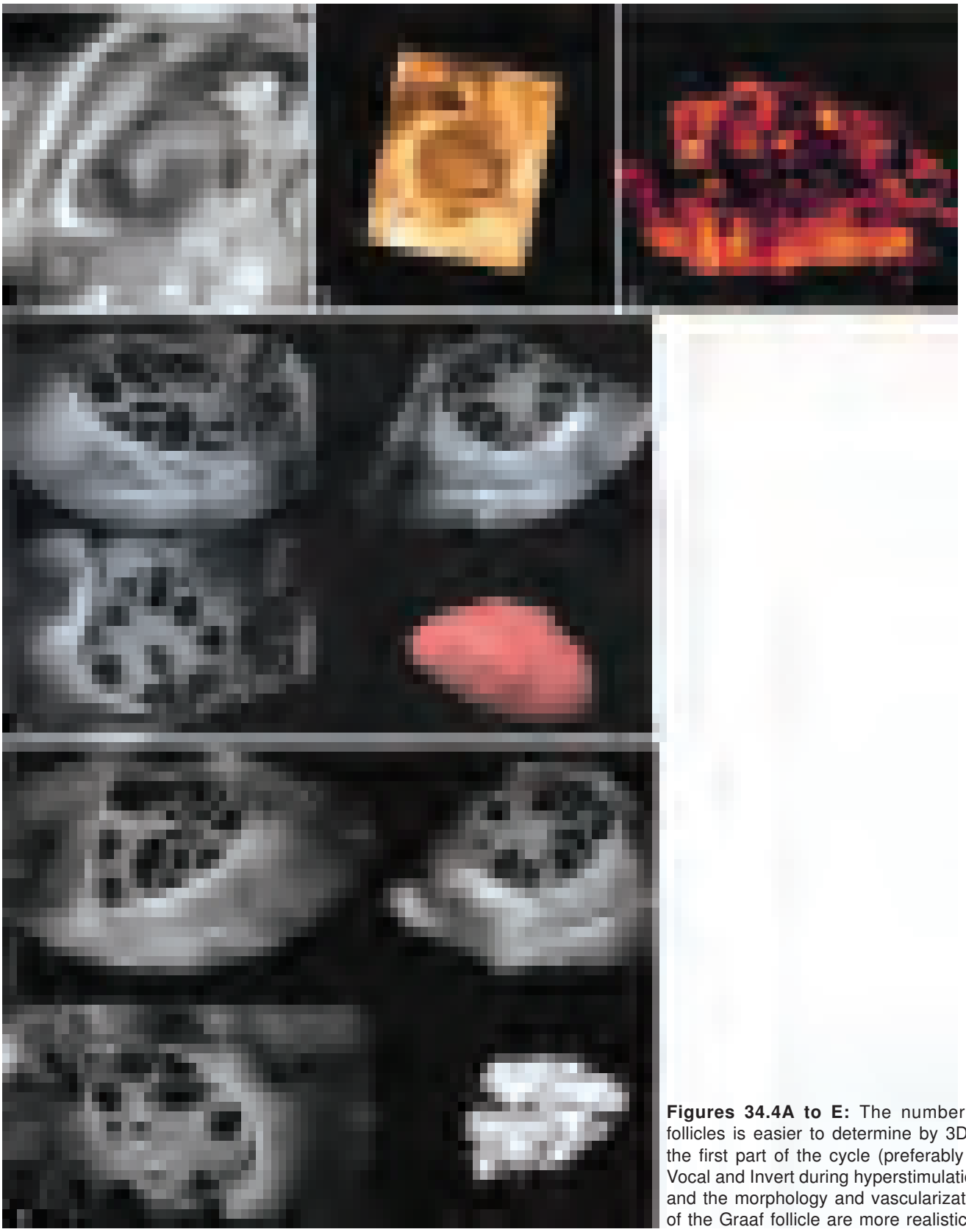

Figures 34.4A to E: The number of follicles is easier to determine by 3D in the first part of the cycle (preferably by Vocal and Invert during hyperstimulation) and the morphology and vascularization of the Graaf follicle are more realistic

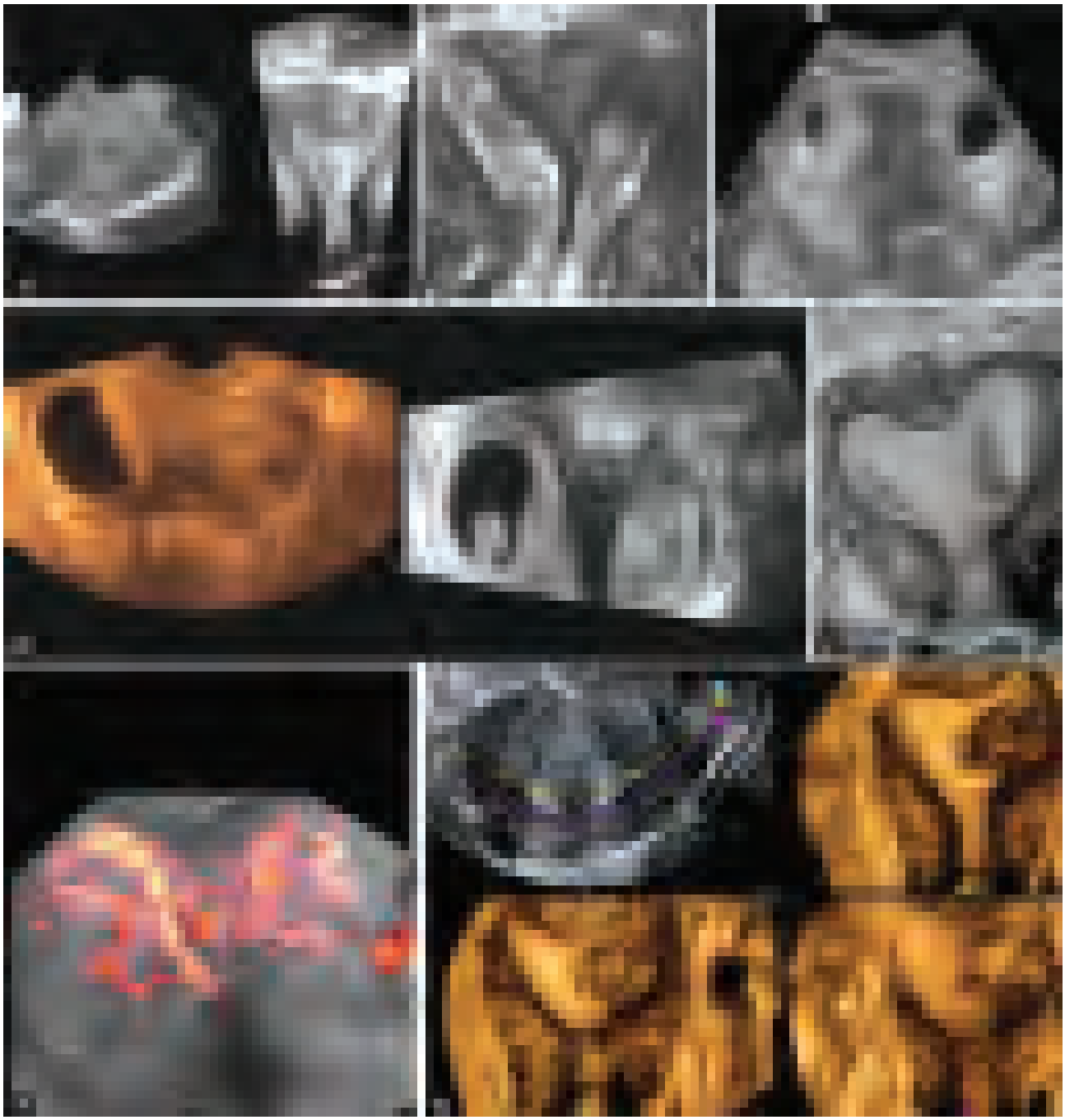

Figures 34.5A to G: 3-4D offers a good view of the endometrium and can enable diagnosis of different kinds of uterine malformation. In early pregnancy (8th week) detection is easier, but for correct diagnosis it is important to see vascularisation of two cornua. (A and B) Utero didelfo; (C and D) Bicornuate uterus with pregnancy at 6th and 8th week; (E and F) Didelfo uterus with vessels; (G) By multiplanar and surface it is easier to define the position of myoma

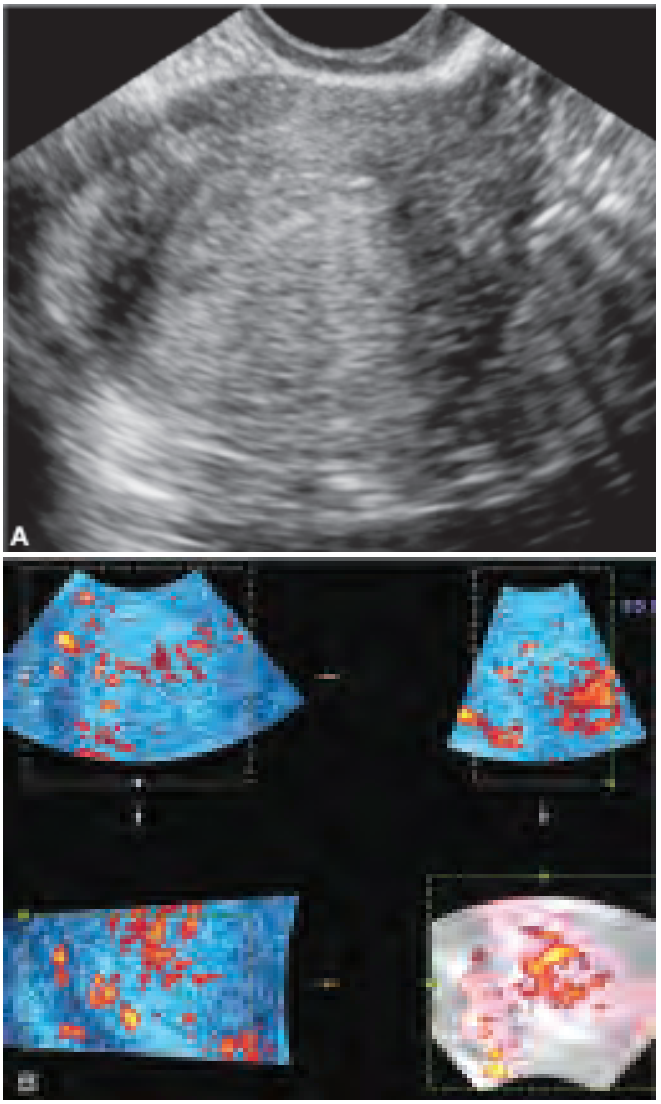

Figures 34.6A and B: Until the end of week 4, it is usually possible to observe transformation of the endometrium into decidua and its vascularization

weeks (the definition of which we have already discussed), with considerable limitations.

Embryology: Days 20–23

CRL = 1.5–2.0 mm;

cloacal membranes and posterior cerebral vesicle (rhombencephalon).

Week 5 (Ultrasonographic)

From 4 weeks + 0 days to 4 weeks + 6 days from the last menstrual period

Week 5 of gestation **(Figs 34.7A to J)**: It is possible to identify the gestation chamber (GC) from 4 weeks + 2–3 days in pregnancies with regular menstrual cycles, and by the end of week 5 this is possible in almost 100% of pregnancies. The number of GCs can also be determined. Spiral circulation around the GC can be detected from week 4. Using multiplanar 3D with surface rendering mode, it is easier to see the yolk sac (YS). Detection of the GC in uterus is an essential condition for excluding ectopic pregnancy and its eccentric position with respect to the uterine cavity. The presence of chorionic villi and consequent peripheral vascularization,[12] combined with hCG monitoring, leave progressively less room for diagnostic uncertainty. It is also possible to visualize vascularization of the myometrium and decidua and check their homogeneous vasculogenesis, though these observations do not yet have clinical implications.

Detection of a GC measuring 2–4 mm in week 5 enables exact dating of pregnancy with an error of only 2–3 days. Visualization of the YS may be possible in the same week and is the first ultrasound-detectable embryonic structure; 2–4 days later it is possible to see the embryo as a double bubble. In the following days and in practice from week 6, the yolk sac moves away from the embryo and the amnios is seen to divide the celomatic from the amniotic cavity. The yolk sac appears as a transonic ring above the cephalic pole of the embryo, growing slowly until weeks 8–9 without exceeding a diameter of 5 mm and then reducing progressively to disappear between weeks 12 and 14. An absent yolk sac or a large, nonspherical, hyperechogenic one with echo-rich internal structure is a condition associated with a poor prognosis for the pregnancy. A GC of mean diameter greater or equal to 20 mm, of lower than expected volume for gestational age, bounded by a thin trophoblast towards the periphery and devoid of embryo suggests blighted ovum syndrome. In such cases, it is advisable to repeat ultrasound examination a week later (for diagnosis at week 7).

Embryology: Days 24–27

CRL = 4.0 mm, head and body distinguishable; formation of prosencephalic cerebral vesicles or anterior brain, mesencephalon or middle brain and rhombencephalon or posterior brain, which subsequently give rise to:

- Prosencephalon
- Median vesicle (diencephalon) that gives rise to third ventricle
- Two lateral vesicles (telencephalon) that give rise to the hemispheres and lateral ventricles
- Formation of optic vesicles
- Formation of falx cerebri
- Formation of limbs, liver, pancreas, lungs, thyroid and mesonephrium tubes.

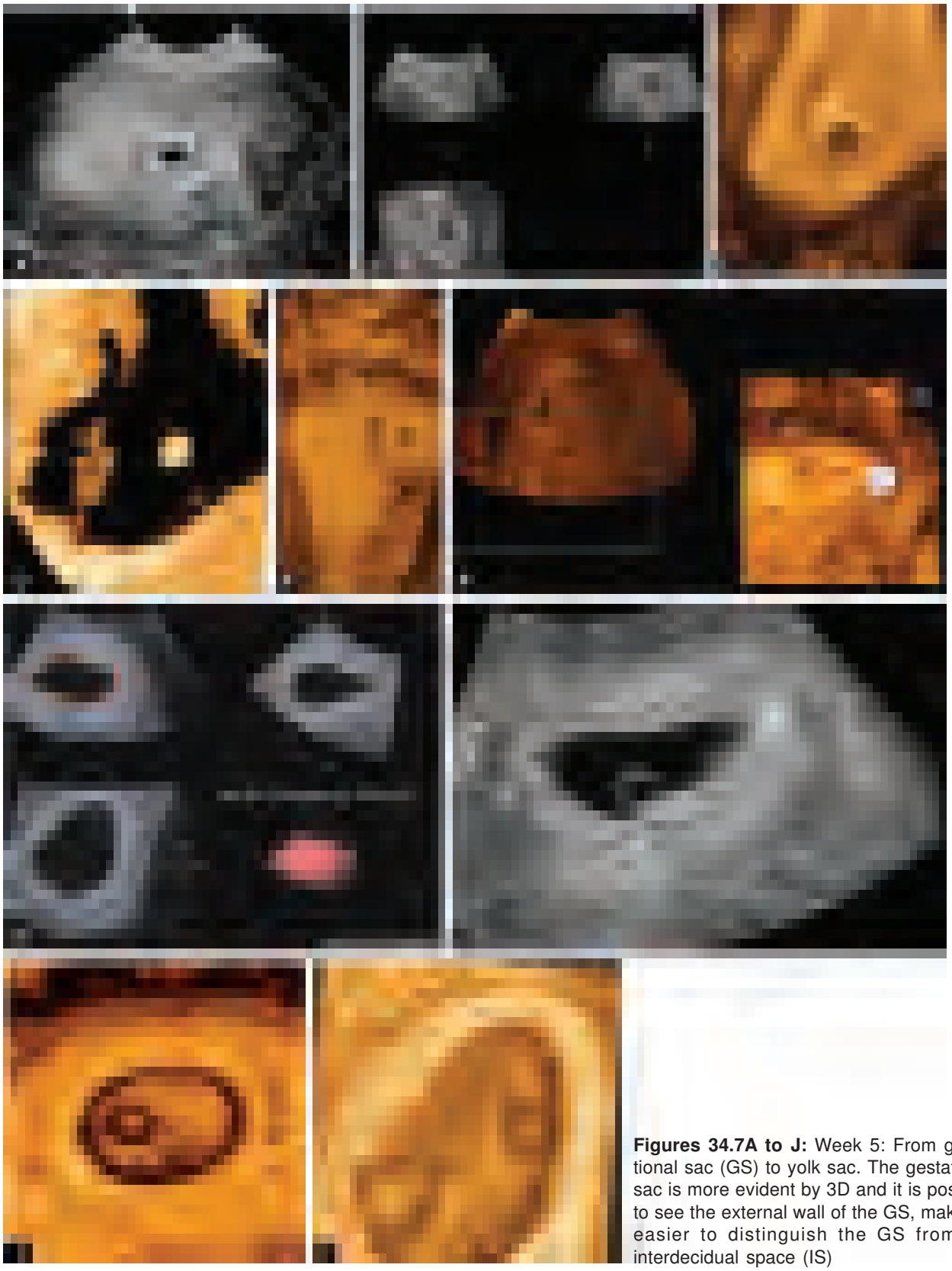

Figures 34.7A to J: Week 5: From gestational sac (GS) to yolk sac. The gestational sac is more evident by 3D and it is possible to see the external wall of the GS, making it easier to distinguish the GS from the interdecidual space (IS)

Fusion of two cardiac tubes along the median line and initiation of heart activity.

Week 6 (Ultrasonographic)

From 5 weeks + 0 days to 5 weeks + 6 days

The ultrasonographic features from 6 weeks onwards are demonstrated in **Figures 34.8A to I.** GC should still be visible; if not, hCG should be assayed and repeated a week later to determine the possibility of delayed conception or ectopic pregnancy. Bi-, tri-, chorionic multiple pregnancies are readily detected. The YS is detected in almost 100% of cases towards the end of the week and the double bubble image is increasingly frequent with a percentage detection of the embryo of about 20–40%. The CRL is 1.5–4.0 mm at the end of week 6 and embryo heart beat (93–106 bpm) is visible. From now until week 12, the CRL is the most reliable biometric value for dating pregnancy; mean error in expert hands is ± 2–3 days.

Embryology: 28–35 days
CRL = 6–9 mm

- Slow heartbeat evident through chest wall
- The hemispheres increase
- Budding of limbs
- Primitive intestine present
- First movement of embryo.

Week 7 (Ultrasonographic)

The sonographic features from 7th weeks onwards are shown in **Figures 34.9A to D**.

From 6 weeks + 0 days to 6 weeks + 6 days

- The amnios is still distinct from the chorion
- The yolk sac is increasingly distant from the embryo, sometimes already compressed between the two membranes
- Prosencephalon and rhombencephalon detectable
- Budding of limbs
- First movements of embryo.

Embryology: 36–42 days
CRL = 11–20 mm

- Formation of olfactory and auditory systems
- Separation of aortic-pulmonary trunk and of right and left atrioventricular canals
- Herniation of midgut in umbilical cord
- Formation of limb extremities (fingers and toes)
- Spine is detectable (in more detail with 3D) **(Figs 34.9A to D)**.

Week 8 (Ultrasonographic)

From 7 weeks + 0 days to 7 weeks + 6 days

- The amnios is still distinct from the chorion and the two membranes constrain and envelop the YS, making it disappear when they fuse, which usually occurs at 14–16 weeks
- Choroid plexuses present **(Figs 34.10A to G)**
- Herniated intestine in umbilical cord which should resume its intra-abdominal position by week 12 (omphalocele differentiation)
- Embryo tachycardia > 110 bpm
- Evident movement of embryo
- Facial features are detectable
- Extremities are detectable.

Embryology: 43-49 days
CRL = 22–30 mm

- Legs form circle with knees turned out and feet in contact (frog attitude)
- Formation of eyebrows and external ear.

Week 9 (Ultrasonographic)

From 8 weeks + 0 days to 8 weeks + 6 days

The embryo is clearly visible through vaginal and abdominal windows and begins to appear human. Its movements are often jumpy and abrupt. More articulated and refined movements are not seen until development of the neopallium in months 6–7. The face is clearly delineated, especially by 3D volumetric scans. In the brain, the hemispheres and ventricles with their posterior (choroid plexuses) and anterior horns are observed developing from the two vesicles of the telencephalon (**Figs 34.11A to N)**. The brainstem is sometimes detectable. The rhombencephalon persists and is dividing to form the fourth ventricle (metencephalon) and the spinal cord (myelencephalon). The spine and ribs are clearly visible. Differentiation process of chorion laeve and chorion frondosum is also seen.

The embryonic period comes to an end after week 9, ushering in the fetal period with its rapid longitudinal (hyperplastic) growth that continues until week 20, with further differentiation with organization of organs and tissues formed in the embryonic period and with acquisition of specific functions **(Figs 34.11A to N)**.

Fetal Period

Anatomy: From day 50–84 (8–12 full weeks)

Ultrasonography: Until day 98 (10–14 full weeks)

Ultrasonographic features between 10 to 14th weeks of gestation are illustrated in **Figures 34.12 to 34.14**. Until week 10, the transvaginal route is universally recognized as the acoustic window for embryo study.

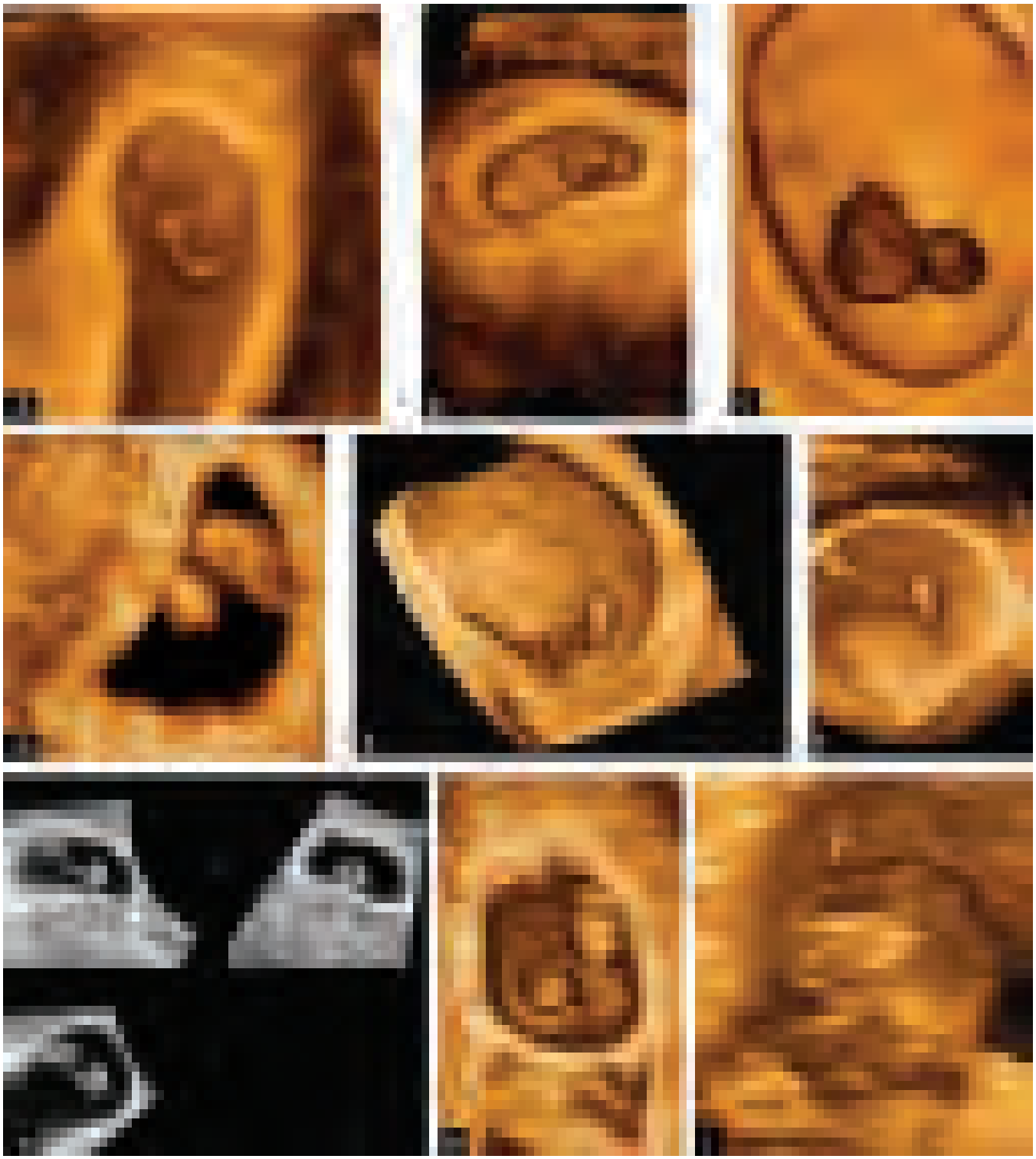

Figures 34.8A to I: (A to H) Week 6: The embryo appears and the double bubble becomes more evident during the week. The embryo moves away from the yolk sac, which remains near the uterine wall and disappears in weeks 12–14; (I) Zoom of embryo head showing prosencephalon (P)

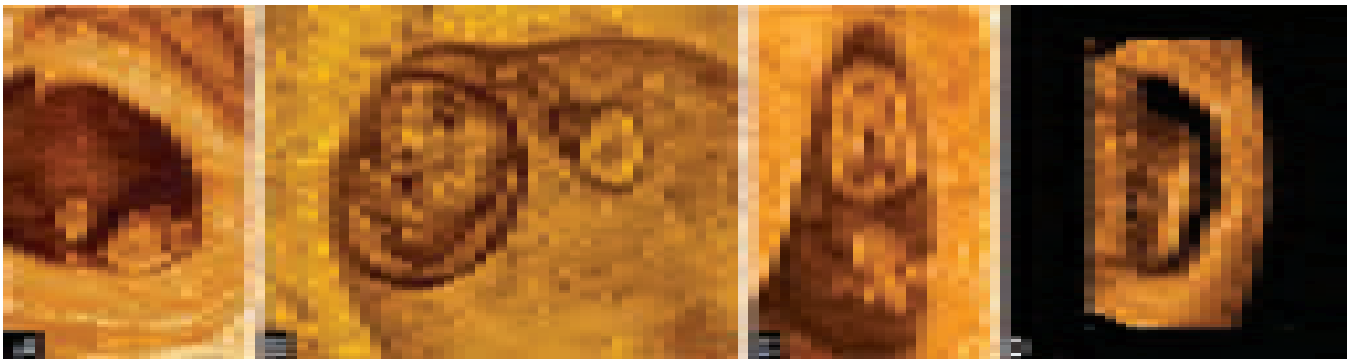

Figures 34.9A to D: Week 7 (6-12 mm): Embryo anatomy is more complex: note promesorhomboencephalon and first image of face. Arms and legs are present, as are the queue and the vertebral column. The amniotic membrane is well formed and divides the amniotic cavity from the celomatic cavity; the yolk sac lies between the amniotic and chorionic membranes

Figures 34.10A to G: Week 8 (22 mm): Head structures are better defined. 4th: fourth ventricle; c: cerebellum; pcf: posterior cranial fossa; cp: choroid plexus; m: mesencephalon

After week 10, the transabdominal route may also be used with good ultrasound instruments in women with normal fat distribution. By week 10, CRL is no longer precise for dating pregnancy, acquiring an error of ± 5 days (due to fetal flexion and extension). From week 11, biparietal diameter (BPD) is therefore preferred, though CRL is still important, for example in measuring nuchal translucency (NT).

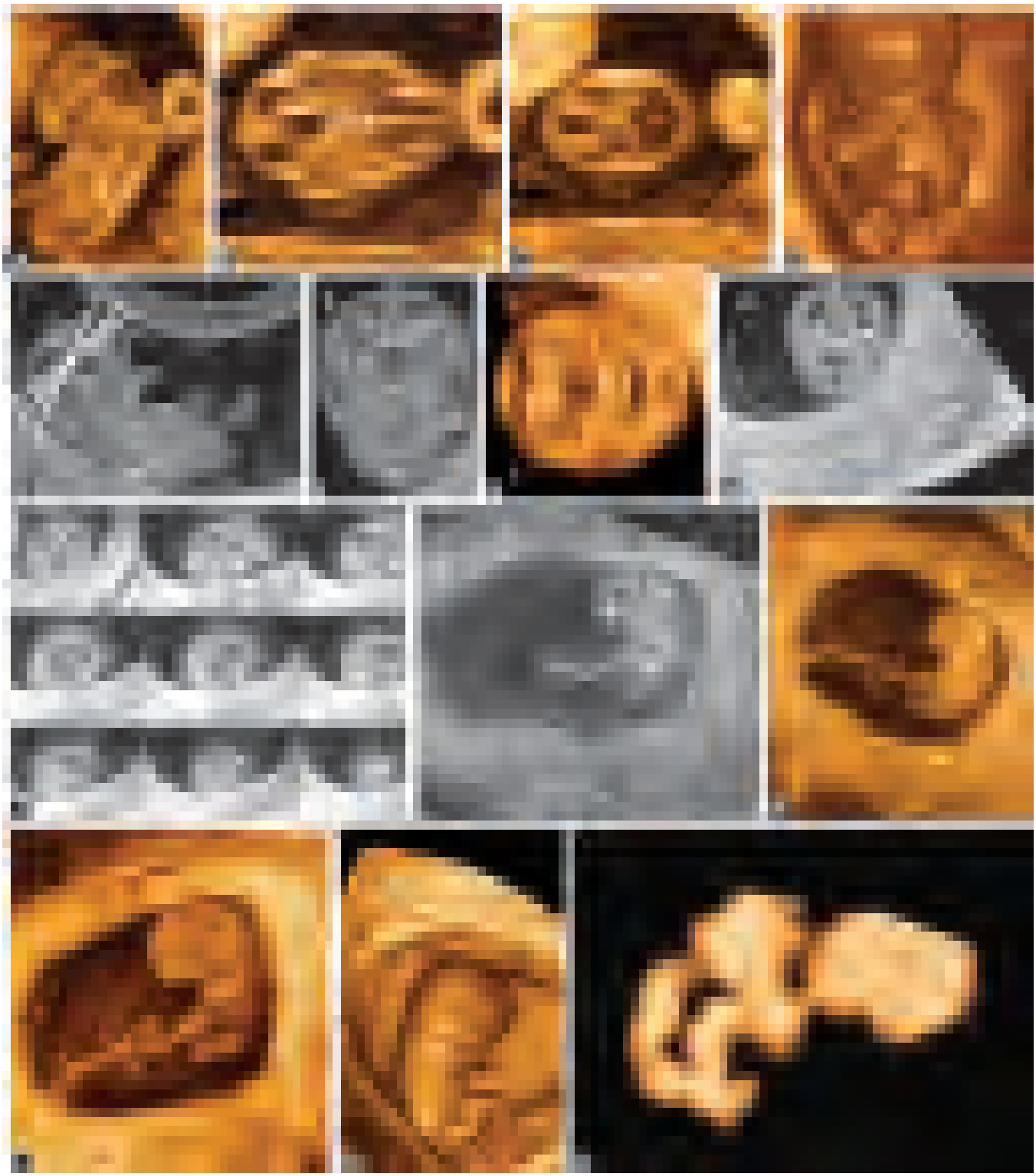

Figures 34.11A to N: Week 9 (29 mm): (A to M) Embryo acquires human features and external morphology is now fixed. Detection of physiological umbilical hernia. Complete view of brain clearer with TUI (tomography ultrasound imaging) which makes ultrasonography similar to NMR (the image can be cut in real time up to 18 times at predetermined distances); (N) Invert mode shows spatial extent of ventricles

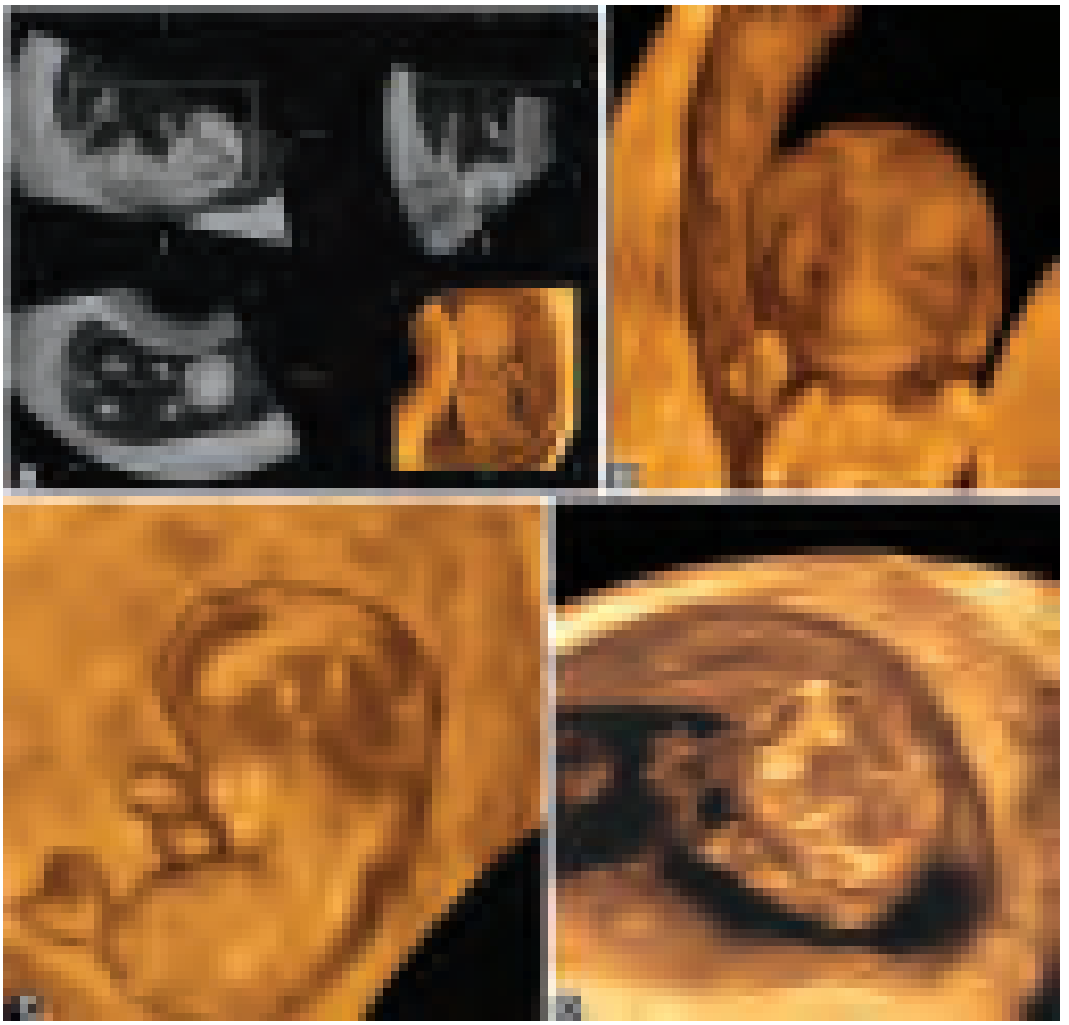

Figures 34.12A to D: Week 10: Beginning of fetal period. Body organs have formed and will grow, and acquire organ functions. Multiplanar view of 34 mm fetus, showing face, ventricles and cerebellum

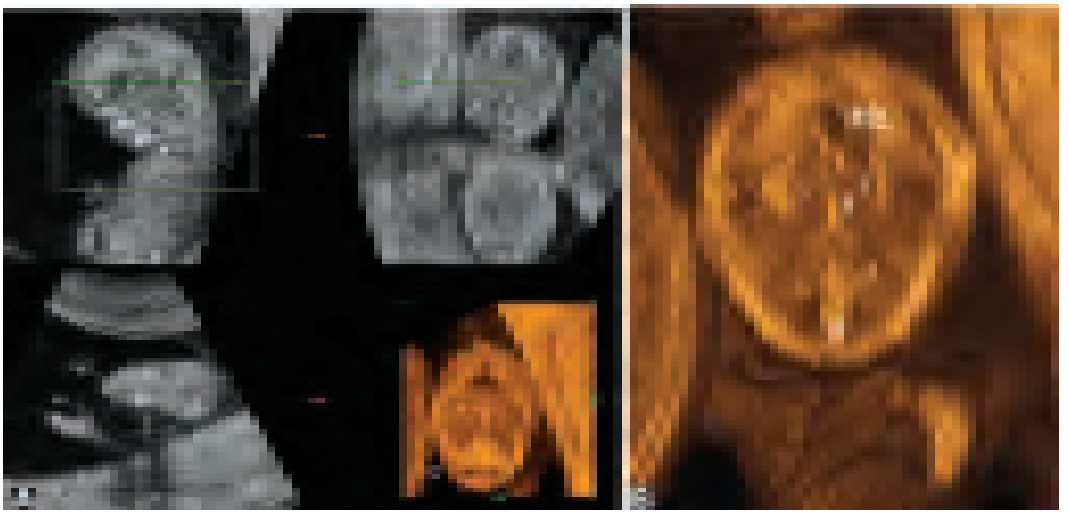

Figures 34.13A and B: Weeks 11–12: Multiplanar view showing brain: 4th: fourth ventricle, f: falx, H: hypothalamus, d: diencephalon, t: telencephalon.

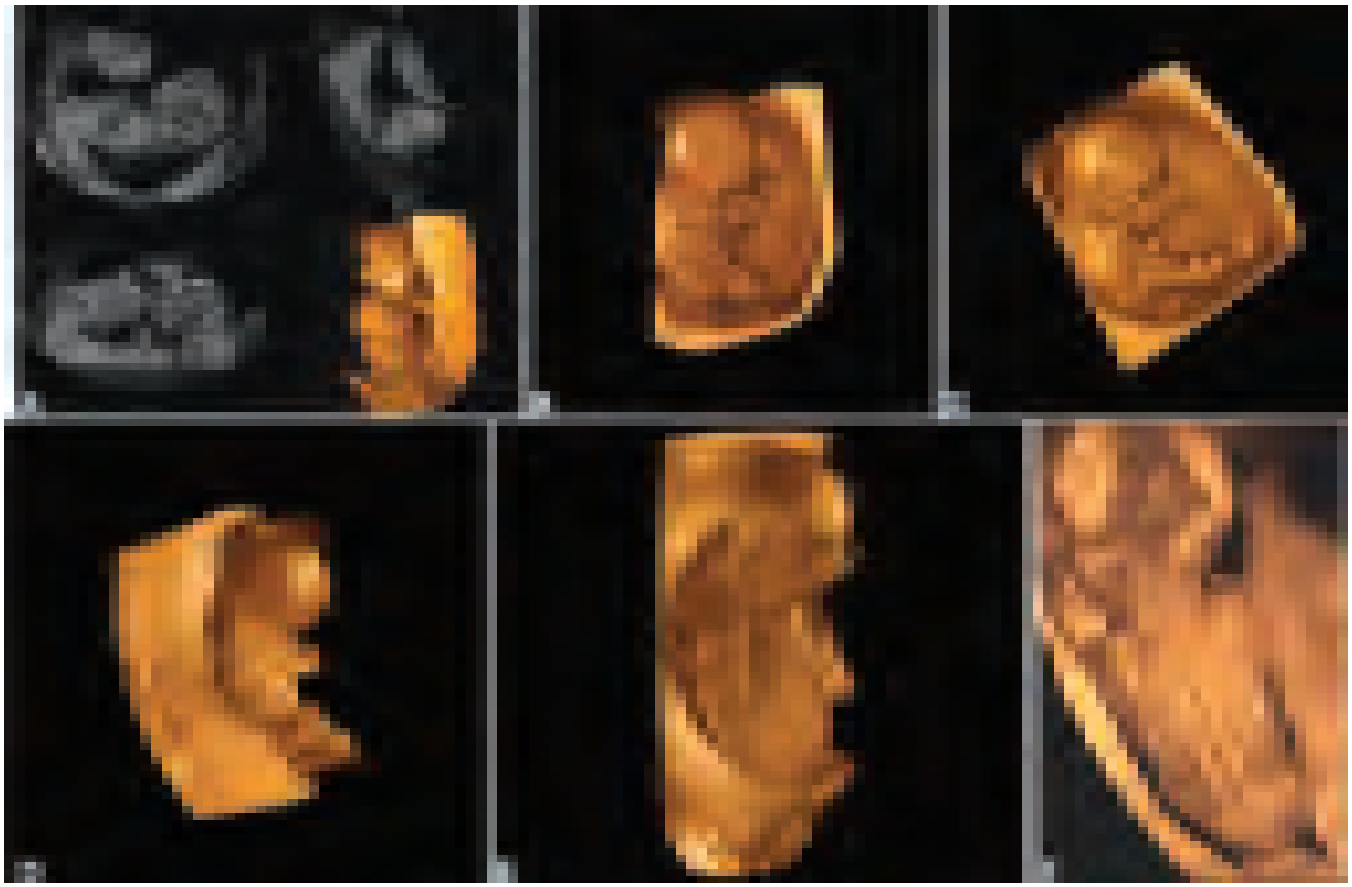

Figures 34.14A to F: Weeks 13–14: Fetal morphology is clear; note details of face, limbs, fingers, toes and neck. Detailed study of spine is possible

By week 10, the fetus acquires definite anatomical characteristics that will persist for the rest of gestation, albeit with changes in size and function. By week 12, umbilical hernia disappears and by week 14 the YS is hardly visible and the two membranes fuse. In the brain, the choroid plexuses that almost filled the cranial cavity, are relegated to the posterior horns. The brainstem is increasingly evident and the posterior cranial fossa is readily detected by week 14.[13] Although the corpus callosum ceases its formation later and is detectable by ultrasound by weeks 20-22, the cavity of the septum pellucidum can be detected. The heart with its four chambers becomes visible from week 12 transvaginally, however not in all cases.[14] The detection percentage increases dramatically by week 14 and indeed more and more centers are delaying transvaginal screening for cardiopathy until weeks 14–16. The fetal face is increasingly human and offers striking images by 3-4D. By week 12, BPD is the most reliable biometric value for dating pregnancy, having a mean error of ± 1 week.

Embryo-Fetal Pathology Detectable by Ultrasound in the First Trimester

The acoustic window of the first trimester of pregnancy (until week 14) offers the possibility of suspecting or diagnosing embryo-fetal malformations, chromosome anomalies and perinatal outcome. The possibilities in the first trimester have been described by Nikolaides and colleagues, who all concentrated their research on the fetus from week 11 to 14, documenting many chromosome pathologies and malformations that could be detected by them. The fact that ultrasonographic diagnosis is becoming possible increasingly early in pregnancy partly attenuates the psychological problem of the mother and her partner when the painful question of whether or not to interrupt pregnancy arises.[15] There have been many examples illustrating the significance of the first trimester for detecting chromosome and/or structural anomalies or at least for selecting populations at risk, whereas the second trimester is more indicated for malformations, for example the heart (for which

there is ample documentation that suspected or actual diagnosis is possible in week 14), spina bifida[16] and Dandy-Walker syndrome.[17] In any case, knowledge of the natural history of malformations is fundamental for understanding missed diagnosis. For example, the partial or total agenesis of the corpus callosum cannot be diagnosed until week 22–24, when the corpus callosum completes its formation. First trimester ultrasonography (weeks 11-14) is increasingly viewed as a time for morphological and structural check-up, similar if not better than second trimester scans, hence increasing use of the term—first trimester sonoembryology, meaning the whole of the first trimester **(Figs 34.15 to 34.26)**.

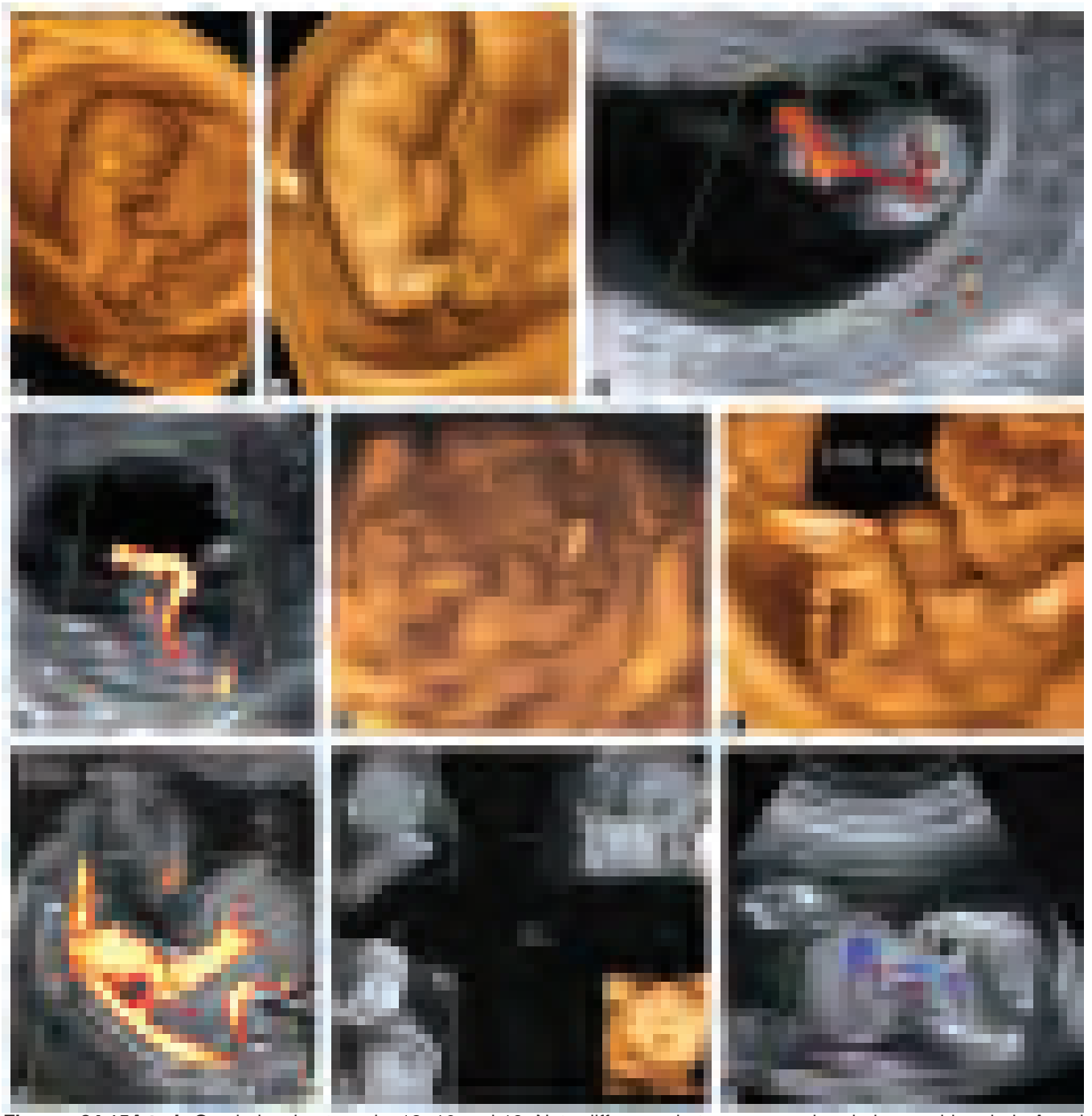

Figures 34.15A to I: Omphalocele at weeks 13, 16 and 18. Note difference between normal and abnormal hernia in A and B: umbilical artery starts from top of hernia (color and power glass body mode). Week 16 and 18 images show homogeneous echogenicity of small intestine and stomach

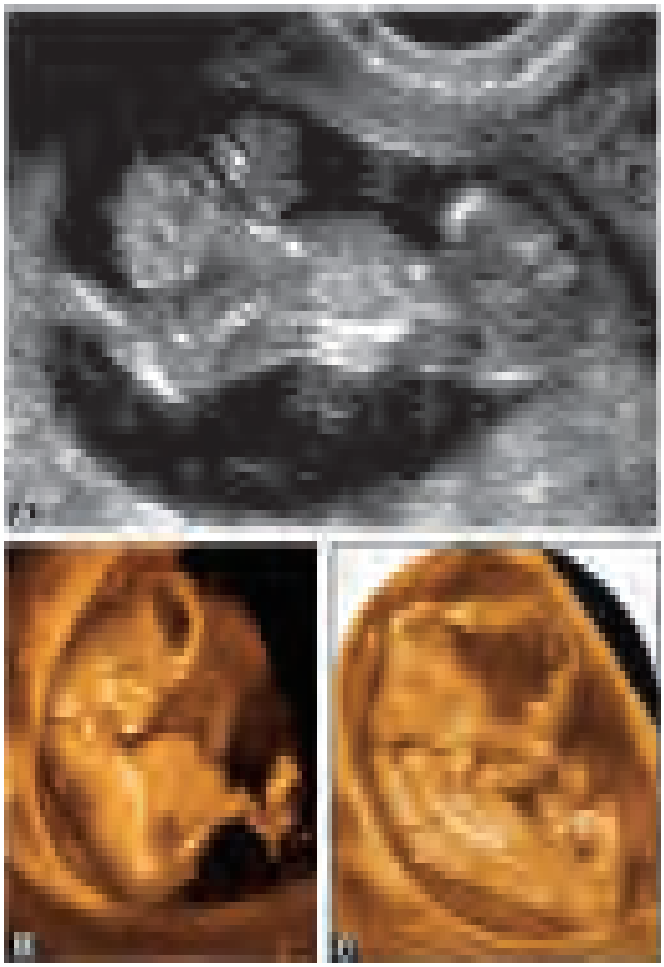

Figures 34.16A to C: Alobar holoprosencephaly associated with omphalocele in a 46,XX fetus at week 12. The 3D provides more information than 2D

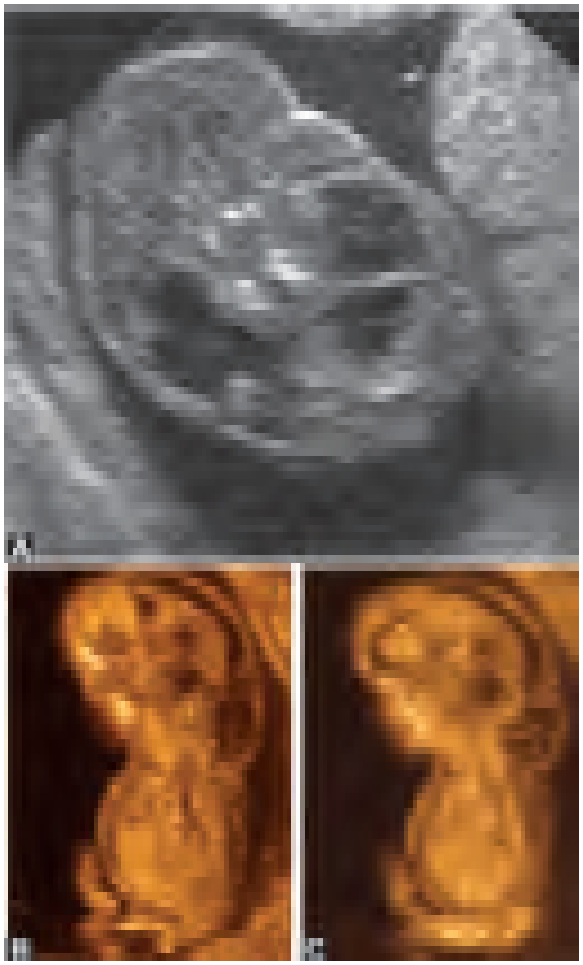

Figures 34.17A to C: Septate cystic hygroma at week 13 as shown by 3D and 2D

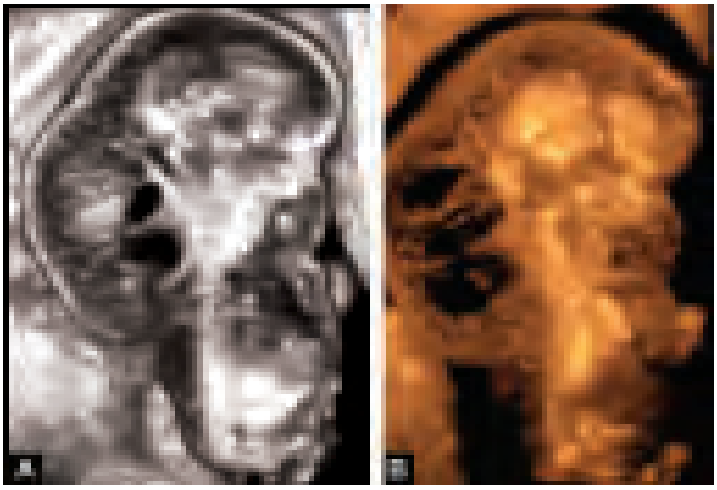

Figures 34.18A and B: Hygroma and fetal hydrops at 16 weeks. The hygroma plurisepimentato extends back to the fetus

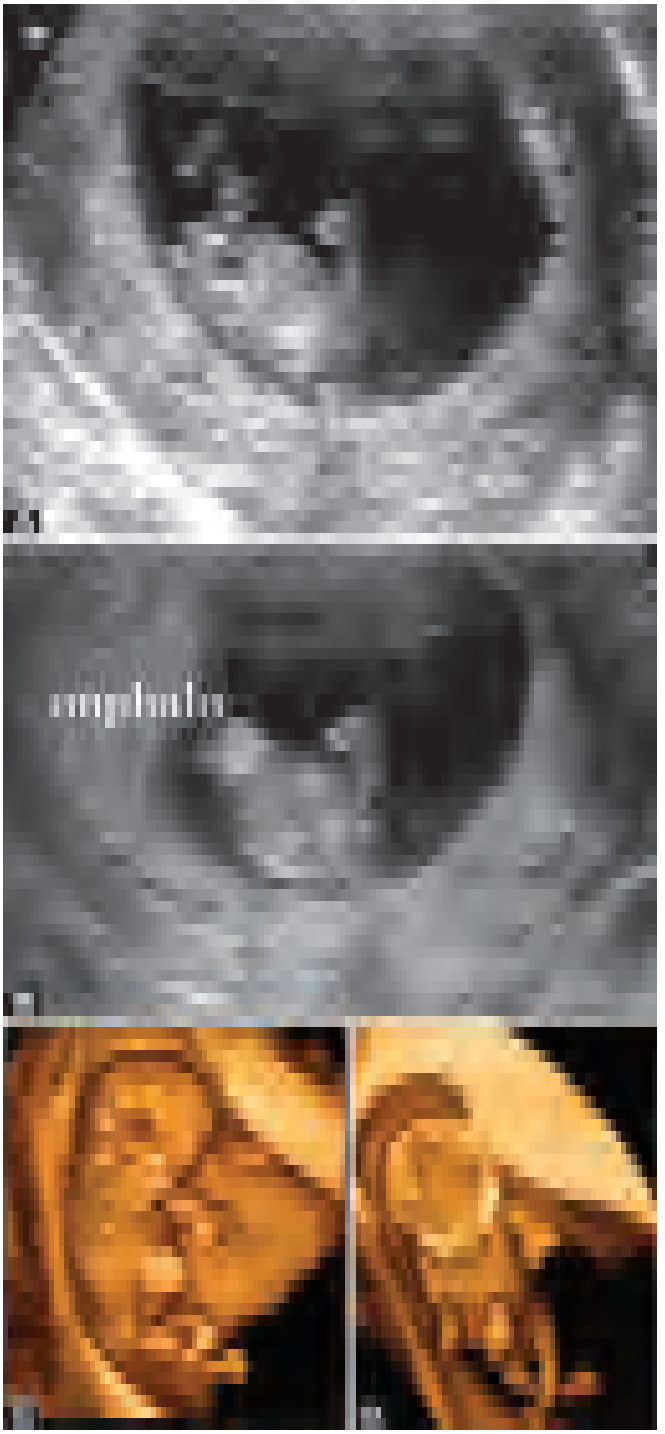

Figures 34.19A to D: Radius-ulnar agenesis with omphalocele in fetus with trisomy 18 at week 10

Figures 34.20A to D: Anencephaly at week 11. The image shows the typical face and the absent skull

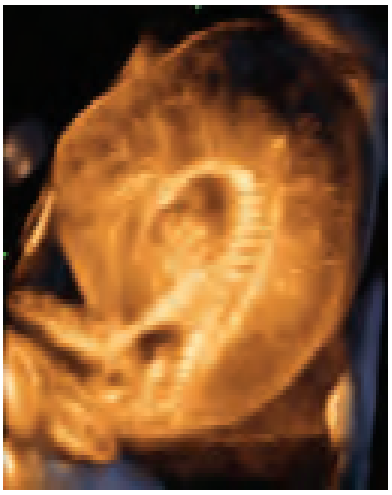

Figure 34.21: Twin reversed arterial perfusion syndrome (TRAP). (A) Acardius acephalus (13 weeks) is characterized by amorphous shape of the cephalic pole, the upper limbs are absent; the lower limbs are present and the intrathoracic and abdominal organs are rudimentary, with diffuse subcutaneous edema

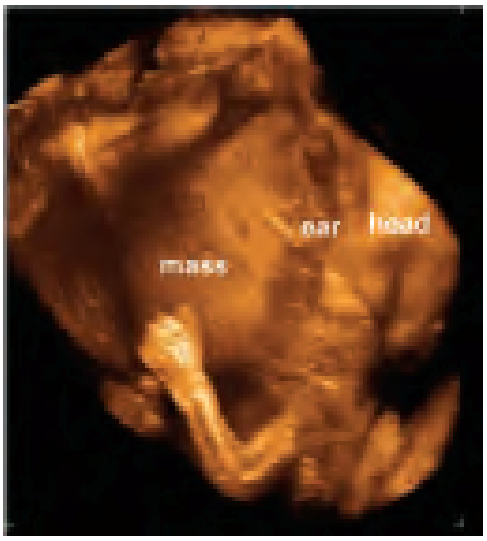

Figure 34.22: Epicanto at 14 weeks. The mass distance morphology of the face

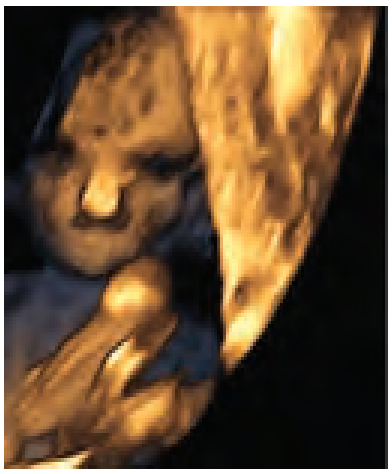

Figure 34.23: Frontal holoprosencephaly. Elephant fetus at 11 weeks

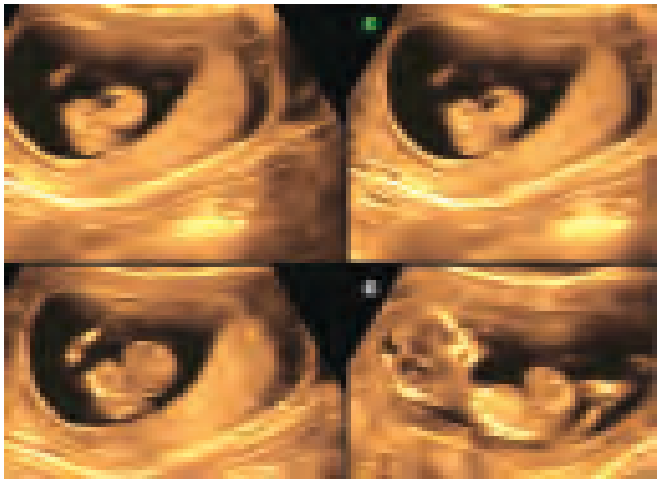

Figure 34.24: Omphalocele at 12 weeks

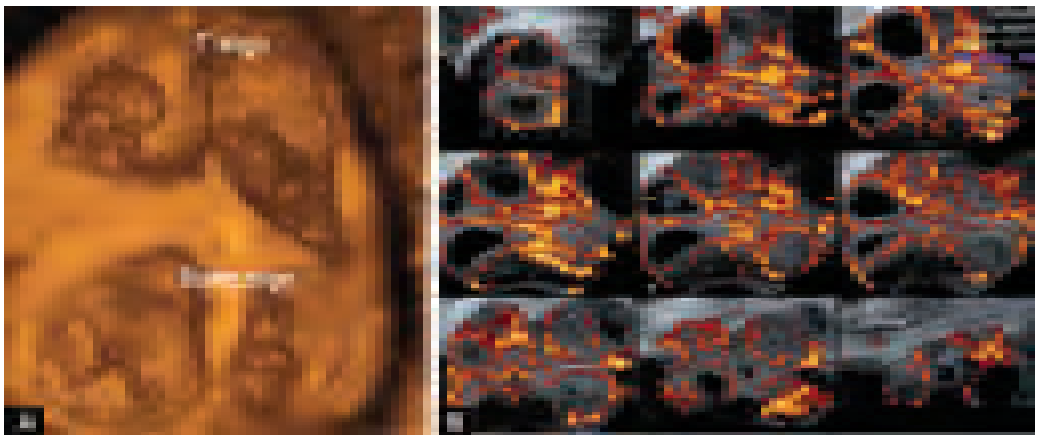

Figures 34.25A and B: Unusual scan of quadrigeminal pregnancy arising from FIVET of three oocytes: two twins are clearly bichorionic-biamniotic (delta sign) and two monochorionic-monoamniotic (T sign) and a distribution of vessels in multiple pregnancy in the first trimester

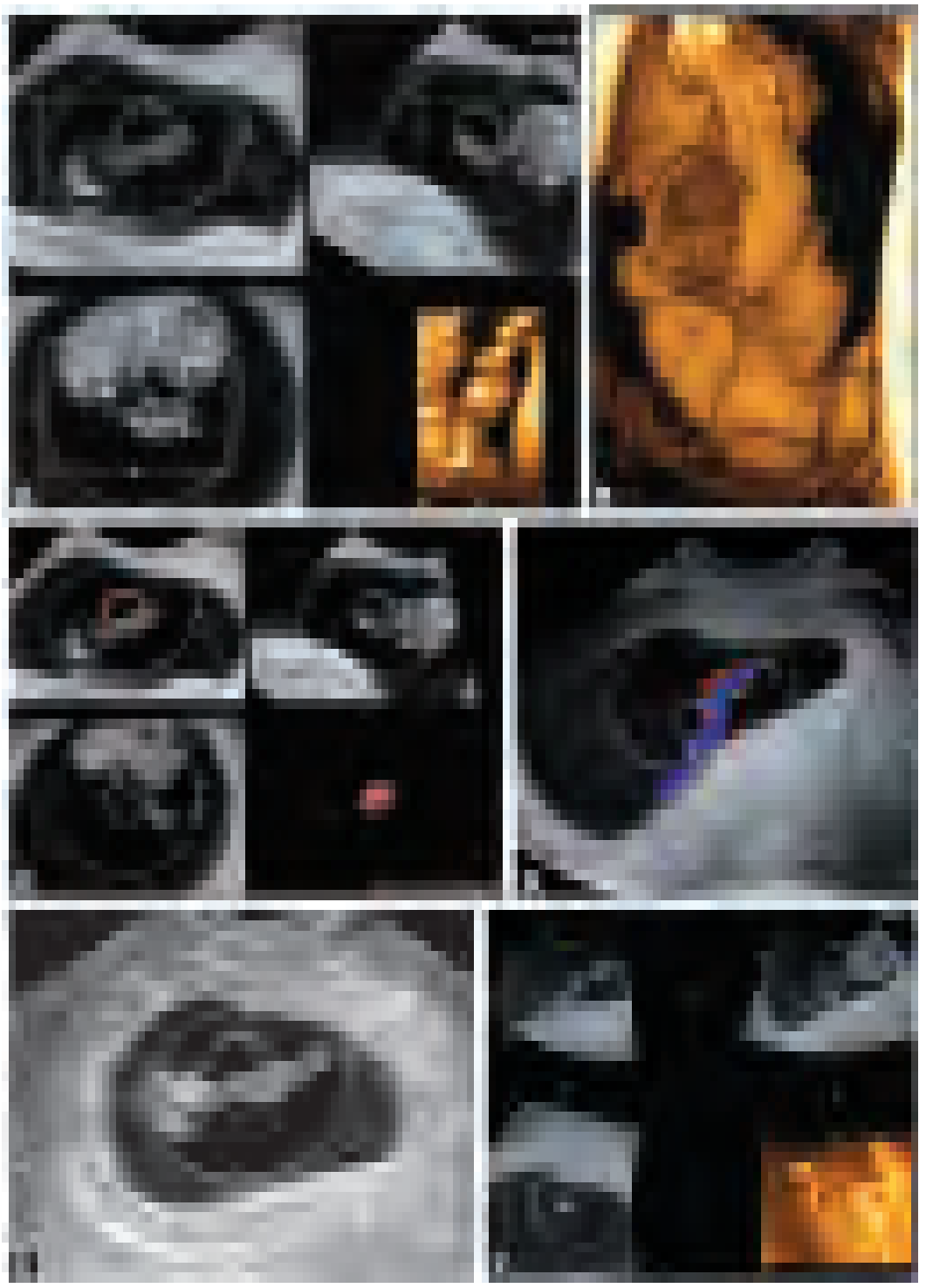

Figures 34.26A to F: Umbilical cord cyst at week 9. This is a transient soft marker of aneuploidy (about 25% sensitivity — present in about 5% of pregnancies)

Signs Predictive of Aneuploidy and Structural Embryo—Fetal Alterations in the First Trimester (Soft Markers)

It is a common practice to obtain verbal or written informed consent before determining nuchal translucency. It also seems reasonable to make a similar contract (implying correct counseling and specific request) for predictive markers of aneuploidy in the first trimester, as is customary in the second trimester (so-called genetic ultrasonography). In my opinion, consent of scanning for structural alterations, the only therapy for which would be an interruption of pregnancy, is also advisable. Today, ultrasonography in pregnancy is a powerful instrument for serenity, but may also create gratuitous anguish. Before carrying it out, it is important to discuss it with the woman, not only specifying the limits of the method and of the operator, but also asking clearly what the woman expects and wants from the scan.

Nuchal Translucency

The problem with screening tests in which nuchal translucency (NT) is a constant component is too complex to discuss in an atlas, however, the detection of this transient sign is easier and quicker with multiplanar than with classical 2D **(Figs 34.27A to F)**. The current scientific findings have shown that one can detect even an intracranial translucency (fourth ventricle) that seems to offer a sensitivity and specificity of nearly 100% in the early detection of spina bifida.[18,19]

At 11–13 weeks' gestation, during the first trimester screening of chromosomal abnormalities in the midsagittal view of the fetal face we can obtain the nuchal translucency thickness and the nasal bone view **(Figs 34.28A to E)**. In this view, the fourth ventricle is visible. In the normal fetuses, the fourth ventricle was always visible and the median anterior-posterior diameter increased from 1.5 mm at a crown-rump length (CRL) of 45 mm to 2.5 mm at a CRL of 84 mm. In the fetuses with spina bifida, the fourth ventricle space was compressed and nothing could be seen, and it can also be used for early detection of open spina bifida.[20]

Pending clinical confirmation, it is important to be able, during a 11–14 week scan, to detect these markers that can be considered as an alarm bell in identifying cases at risk assessment of intracranial translucency (IT) in the detection of spina bifida at the 11–13 week scan **(Figs 34.29A and B)**.

Ductus Venosus

Measurement of NT in the first trimester has become a consolidated method for identifying fetuses at risk for chromosomal abnormality. The high percentage of heart defects **(Figs 34.30A to C)** in fetuses with increased NT, whether isolated or caused by chromosome anomalies, has stimulated considerable interest. The association, together with echo-Doppler modifications of the ductus venosus (DV) in fetuses with increased NT, suggests that altered heart function could play a role in determining an increase in NT.[21,22]

In particular, inverted flow in the DV during heart's contraction (A wave) has been associated with increased NT. The DV is a communicating vessel that carries well oxygenated blood of the umbilical vein into the right atrium, through the oval foramen. This vessel is important for assessing the presence of heart function anomalies. Blood flow in the DV is characterized by high velocity during ventricular systole (S wave) and diastole (D wave) and also by forward flow during atrial contraction (A wave) **(Figs 34.31A to C)**. In heart dysfunction due to heart defects, the A wave is absent or negative.

Assessment of flow in the DV could play a role in secondary screening, permitting further reduction in the percentage of false positives in screening for chromosome anomalies in the first trimester.[23,24] A major association has been demonstrated between chromosome anomalies and abnormal blood flow in the DV at 11–14 weeks of pregnancy in high risk pregnancies.[25,26] The DV flow anomaly associated with heart defects and adverse outcome of pregnancy has also been observed. Some authors suggest that the DV can be an important prognostic factor in fetuses with increased NT and normal karyotype.

In fetuses with chromosome anomalies, whose parents decided to continue the pregnancy, heart dysfunction has been found to be a temporary condition: transitory anomalous flow in the DV, detected by color Doppler, manifested as reversed flow during contraction. This marker is detected early, around week 13, and usually disappears by week 20. The dysfunction that caused it, aggravates retronuchal edema and may culminate in fetal hydrops, which could explain some cases of intrauterine fetal death. At 10–13 weeks + 6 days, the duct anomaly is therefore associated with aneuploidy (80% of Down fetuses versus 5% of euploid fetuses), heart malformations and unfavorable outcome of pregnancy. To study the DV, 3-4D does not offer

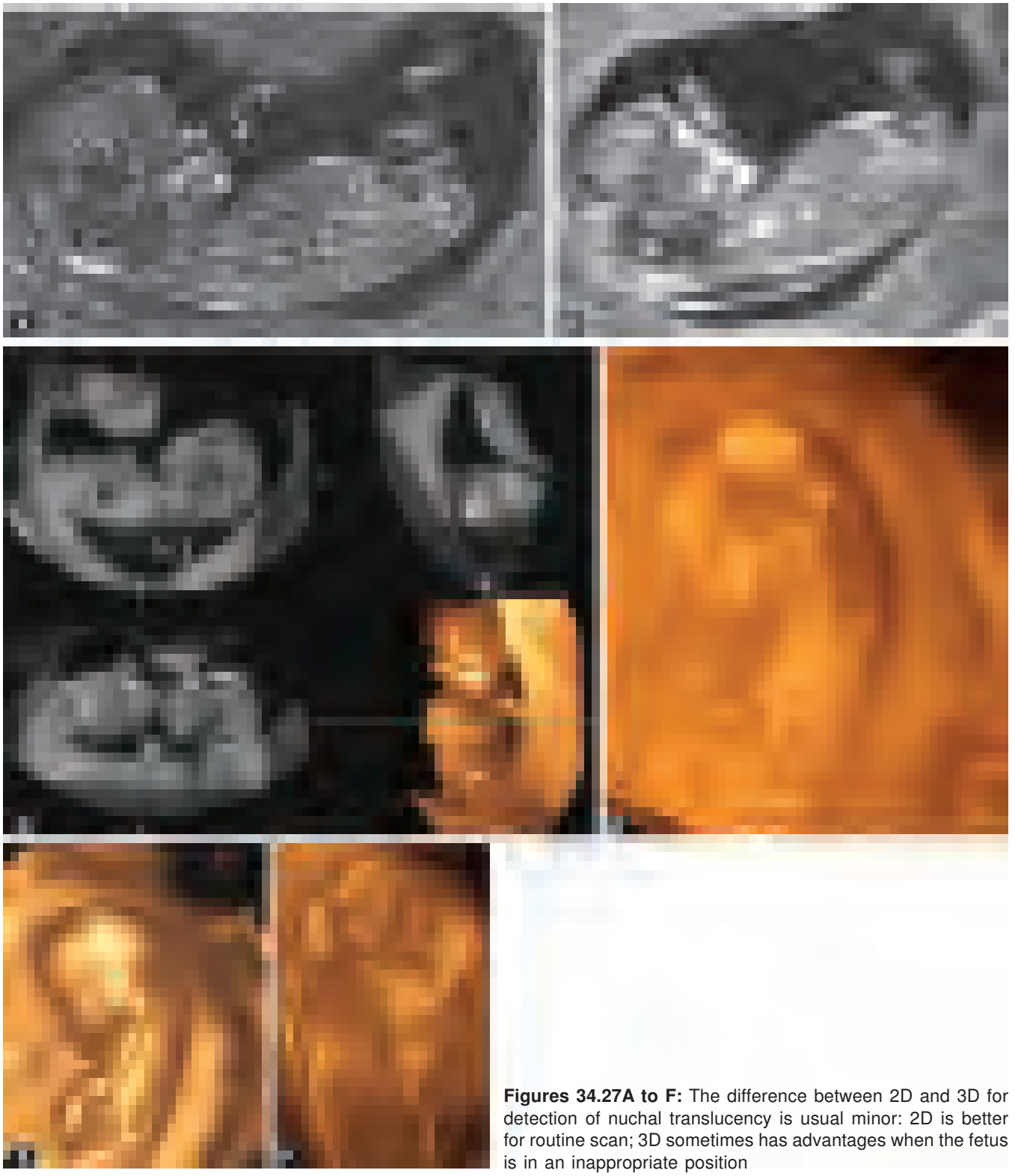

Figures 34.27A to F: The difference between 2D and 3D for detection of nuchal translucency is usual minor: 2D is better for routine scan; 3D sometimes has advantages when the fetus is in an inappropriate position

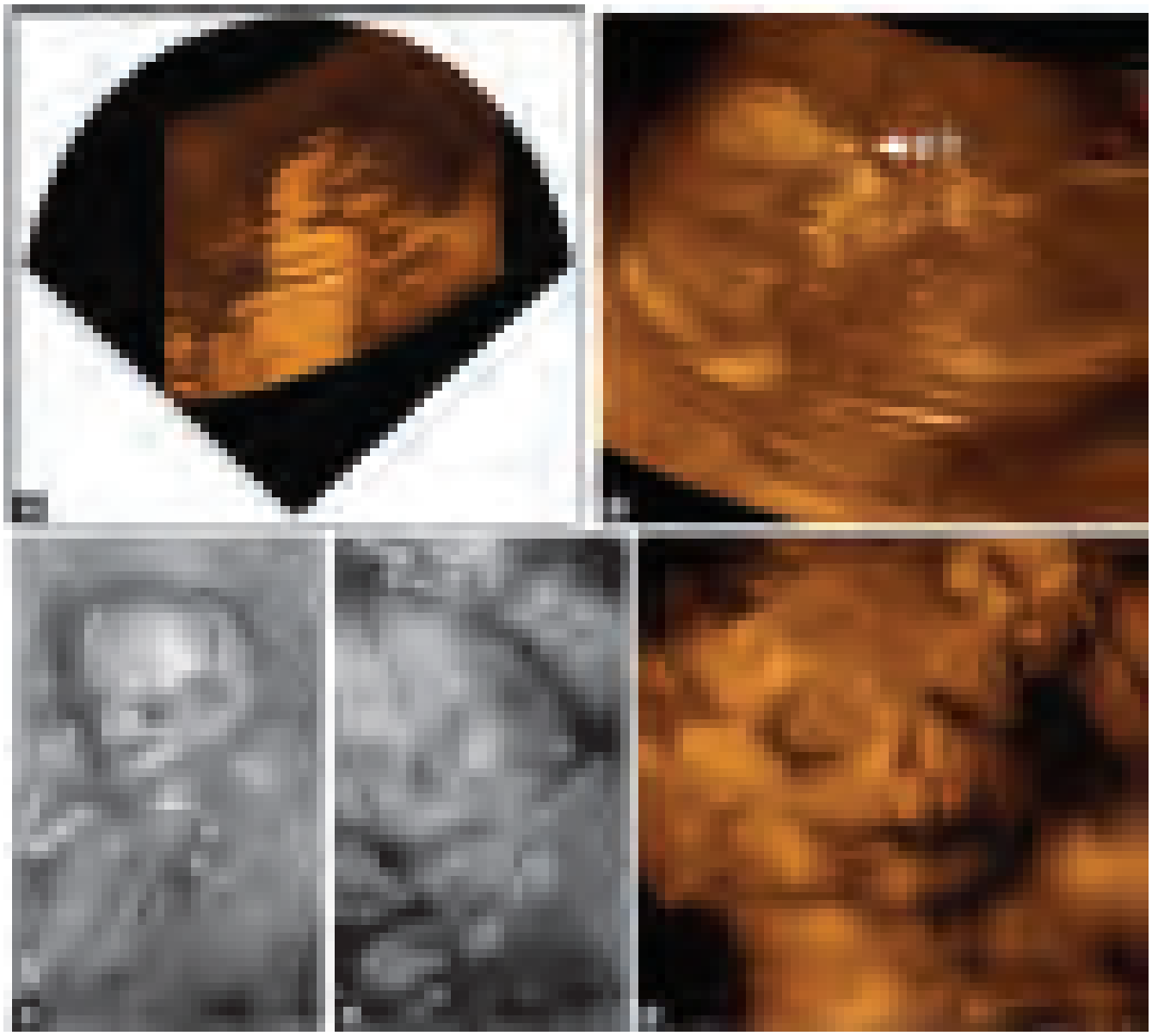

Figures 34.28A to E: Weeks 13 and 20. It is easy to find the nasal bone and to detect both bones by 3D in the first and second trimesters; it is more difficult by 2D. nb; nasal bone, the pictures are at 13th and 20th weeks

particular advantages, whereas 2D is fundamental and exclusive for correct detection.

Cystic Hygroma

Cystic hygroma is a congenital malformation of the lymphatic system characterized by a thin walled cystic structure full of liquid. It is usually situated in the nuchal region, extending from the superior occipital bone, caudally and medially to the sternocleidomastoid muscle. It consists of two symmetrical cavities completely separated by a median nuchal ligament and is distinguished from other craniocervical masses, such as encephalocele, meningocele, teratoma, hemangioma and retronuchal edema.[27,28]

At about 40 days of embryo development, the jugular lymphatic sac forms a connection between the jugular duct and the internal jugular veins which become the terminal portions of the lymphatic and thoracic ducts. According to the theory of obstruction of the jugular lymphatic sac, the connection between the jugular lymphatic sac and the jugular veins does

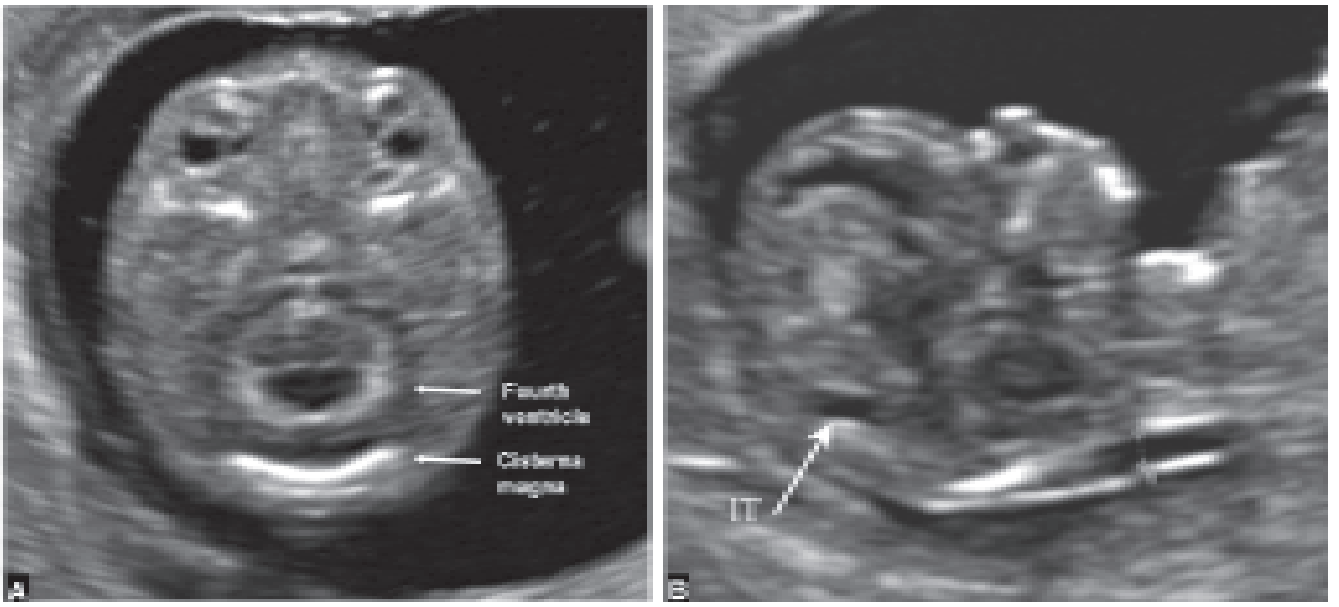

Figures 34.29A and B: Intracranial translucency 2D and 3D. It is easy with a correct scan to find the IT between two hyperechoic lines

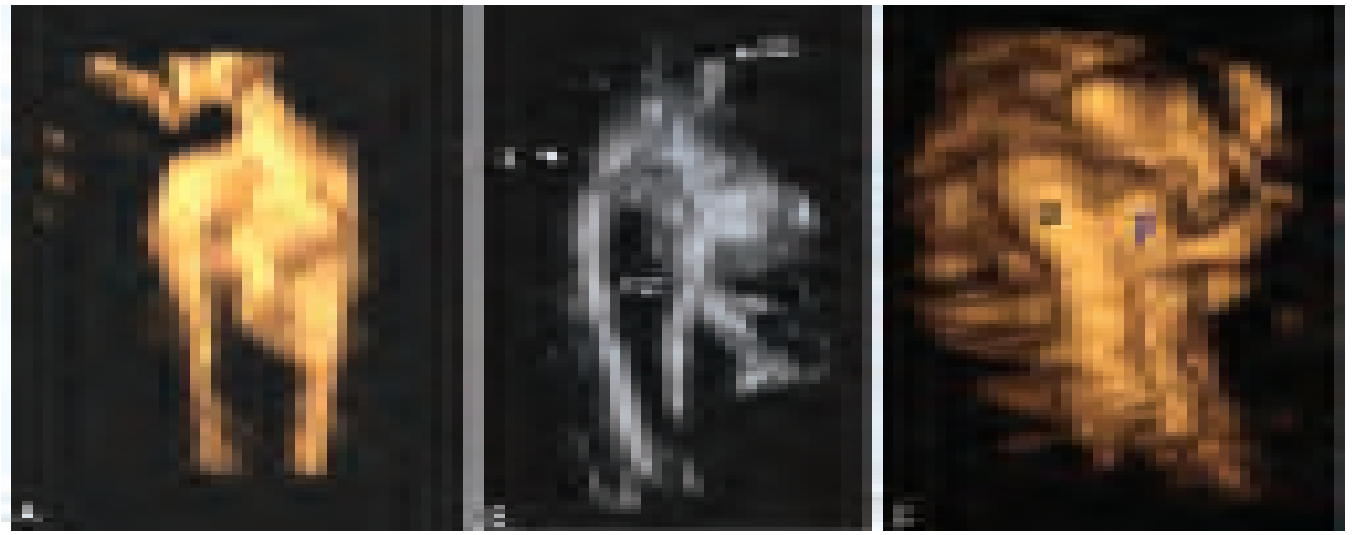

Figures 34.30A to C: An example of great vessels transposition. The b-flow is not an easy technique but improves the heart defects about pulmonary veins. a: aorta; p: pulmonary artery; vci: inferior vena cava; aa) anonymous artery

not form in the case of cystic hygroma and the lymph builds up in tissues around the neck, causing the sac to swell. The cystic hygroma is often detected by prenatal ultrasound, though some cases develop in the postnatal period, with an incidence of about 1%. The defect may regress spontaneously during pregnancy, leaving extra skin in the neck region or progress dramatically towards a form of generalized fetal hydrops.[29]

Fetal cystic hygroma was usually readily diagnosed by transabdominal ultrasound in the second trimester of pregnancy. Today transvaginal ultrasound has increased the percentage of diagnoses in the first trimester.[30] Ultrasound diagnosis of cystic hygroma is based on visualization of a prominent anechogenic or hypoechogenic area (more than 3 mm thick) in the occipital, nuchal or upper thoracic regions, bilaterally. On the

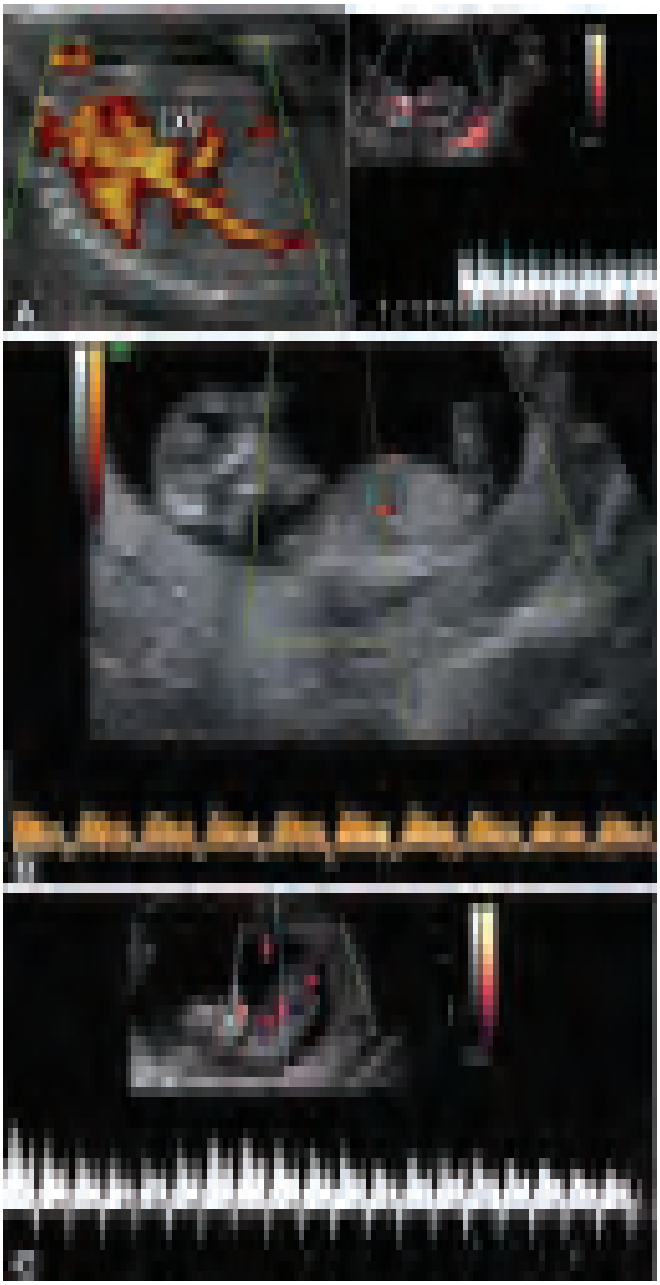

Figures 34.31A to C: Ultrasound flow imaging of the ductus venosus is only feasible by 2D, but 3D provides good images of the vessel. The images show normal A wave in ductus venosus in first trimester and a case of reversed flow. DV; ductus venosus

other hand, physiological build-up of fluid or the nuchal bleb is generally considered normal when it is less than 3 mm thick. These build-ups seem to occur in 40% of embryos before week 10 and disappear at week 11.

Cystic hygroma may be single or consist of multiple cysts and is classified as septate and nonseptate. Though confused for years by various authors, this distinction is important for prognosis, because septate cystic hygroma is strongly associated with aneuploidies.[31]

The presence of cystic hygroma in the first trimester is associated with increased risk of fetal chromosome anomalies. About 50% of fetuses with ultrasound diagnosis of cystic hygroma in the first trimester also have a chromosome anomaly. A high percentage of the cases undergoing cytogenetic analysis show Turner syndrome, often associated with trisomy 21, 18, 13 or other structural anomalies. The risk of this transient anomaly increases with increasing maternal age.

As yet there are no ultrasonographic elements for distinguishing cystic lesions which may regress from those that persist. However, when the nuchal cyst is small and nonseptate and karyotype is normal, it usually resolves spontaneously with good fetal outcome. When septate cystic hygroma is diagnosed early in pregnancy, the risk of chromosome aberrations is much greater and the outcome is therefore worse, also because septate hygroma is often larger and frequently develops into fetal hydrops. Spontaneous regression of cystic hygroma has been reported in chromosomally normal fetuses and in Down, Turner and Robert syndrome fetuses.

Fetuses diagnosed with nonseptate and septate forms, with or without associated malformations, are at high risk of chromosome aneuploidies. The mothers need correct counseling to assess the possibility of cytogenetic tests to determine fetal karyotype, to programme subsequent ultrasound monitoring to exclude morphological anomalies, particularly of the heart and circulatory system, and to evaluate any worsening of edema or its resolution. Fetuses with normal karyotype are usually free of hygroma by weeks 16–17 and many have normal phenotypes at birth. Ultrasound parameters such as hygroma size and the time of its disappearance associated with fetal echocardiography may be useful in identifying pregnancies at risk for dysmorphic conditions such as Noonan syndrome.

Persistent Signs

Nasal Bone

In 1866, Langdon Down noticed that subjects with trisomy 21 had a small nose. An anthropometric study on 105 Down patients confirmed that the nasal bone (NB) was smaller than normal in 49.5% of cases. Recent radiological and ultrasound studies have shown that nasal hypoplasia is already present in the uterus.[32,33] A study of 105 fetuses with trisomy 21, aborted at weeks 12–25, showed lack of ossification of the NB in 32.4%

and hypoplasia in 21.4% of cases. The correlation between absence of NB at weeks 11–14 and increased risk of trisomy 21 was reported for the first time in 2001. Indeed, about 65% of Down fetuses lack or have a small NB.

The nasal bone can be seen by scan from week 11.[34] Many recent studies show a strong association between absence of NB at this gestational age and trisomy 21 and other chromosome anomalies.[35,36] We can therefore say that at 11–13 weeks + 6 days, fetal profile can be examined correctly in more than 95% of cases and that the NB is absent in about 70% of fetuses with trisomy 21 and in about 55% of fetuses with trisomy 13. The incidence of absence of NB in euploid fetuses is less than 1%. Absence of NB is therefore a major marker of trisomy 21. There are some limiting factors in the ultrasonographic assessment of NB.[37,38] Between weeks 11 and 14 from the last menstrual cycle, the probability of visualizing the NB increases with increasing gestational age. The presence of NB is not independent of fetal nuchal thickness, since the possibility of visualizing it seems to decrease with increasing NT. Finally, ultrasound detection of NB at 11–14 weeks requires much technical skill of the operator, unlike later in pregnancy.[39]

Absence of NB has a higher incidence in fetuses of African origin than in Caucasians and decreases with CRL. In calculating individual patient-specific risk of Down syndrome, it is necessary to consider these demographic and ultrasonographic aspects.

If examination of fetal profile to detect NB is associated with NT and maternal serum proteins (free beta hCG and PAPP-A) during first trimester screening for trisomy 21, the detection rate can increase substantially and the false positive rate decrease. For a false positive rate of about 5%, the detection rate increases from about 75% [NT] and 90% [NB + maternal serum proteins] to 93% [NT+NB] and 97% [NT+NB+ maternal serum proteins]. For a false positive rate of 1%, the detection rate could be about 57% for NT, 86% for NT + NB and 93% for NT, NB and maternal serum proteins.

In conclusion, the absence of NB or small NB is more common in fetuses with chromosome anomalies. It is therefore clear that NB is becoming a major marker in the prenatal diagnosis of aneuploidies.

There is a statistically significant difference between detection of NB by 2D and 3D techniques. Traditional scan is about 20% less reliable in detecting presence/absence of NB and also for the number of bones detected. This difference can be as high as 40% when 2D is performed with mediosagittal scan of the fetal face, since detection of the NB requires a longitudinal fetal scan as for detection of NT, but in the case of NB the section is 1–2 mm from the sagittal median. Further studies seem to suggest greater reliability in the second trimester, with a cut-off of 2.5 mm for NB and the presence of both nasal bones. In the second trimester, 3D plays an important role, making detection of the bones simpler and more reliable.[40]

Palate

It is possible to investigate the normality of the secondary palate better than the primary palate because it is very difficult to define a normality of the lips in the first trimester. We can detect the secondary palate by two methods: by the evidence of the retronasal angle with a 100% confidence by the authors, using 2D or 3D multiplanar or omniview and by the Faure method with a coronal/sagittal 3D scan of the fetus's profile and rotation of the picture avoiding the maxillary shadow and maximum or minimum rendering of the palate by axial section (delta sign) **(Figs 34.32 and 34.33).**

Jaw Bone

In a series of 89 Down fetuses compared with a population of 900 euploid fetuses, Cicero in year 2004 found jaw bones shorter by about 0.7 mm (with variations in growth from 4.8 to 8.3 mm from 11-14 weeks) in fetuses with NB and 0.5 mm in fetuses without NB.[41] This characteristic is specific to trisomy 21 and not detectable in other aneuploidies. It is important to assess the jaw correctly by sagittal scan taking the mandibular condyle as reference point.

Single Umbilical Artery

A single umbilical artery in the first trimester of pregnancy is associated with trisomy 21 and especially trisomy 18. Nikolaides and colleagues showed that an umbilical artery is missing in 77% of cases of trisomy 18.[42] Normal localization of umbilical artery is shown in **Figure 34.34A to E**.

The screening tests for Down syndrome in the first trimester with the use of NT and other marker (nasal bone, ductus venosus) have focused the investigator's attention to the first trimester 11–14 week and today it's possible to diagnose about the 50% of structural fetal malformation that we can detect in the second trimester.[43]

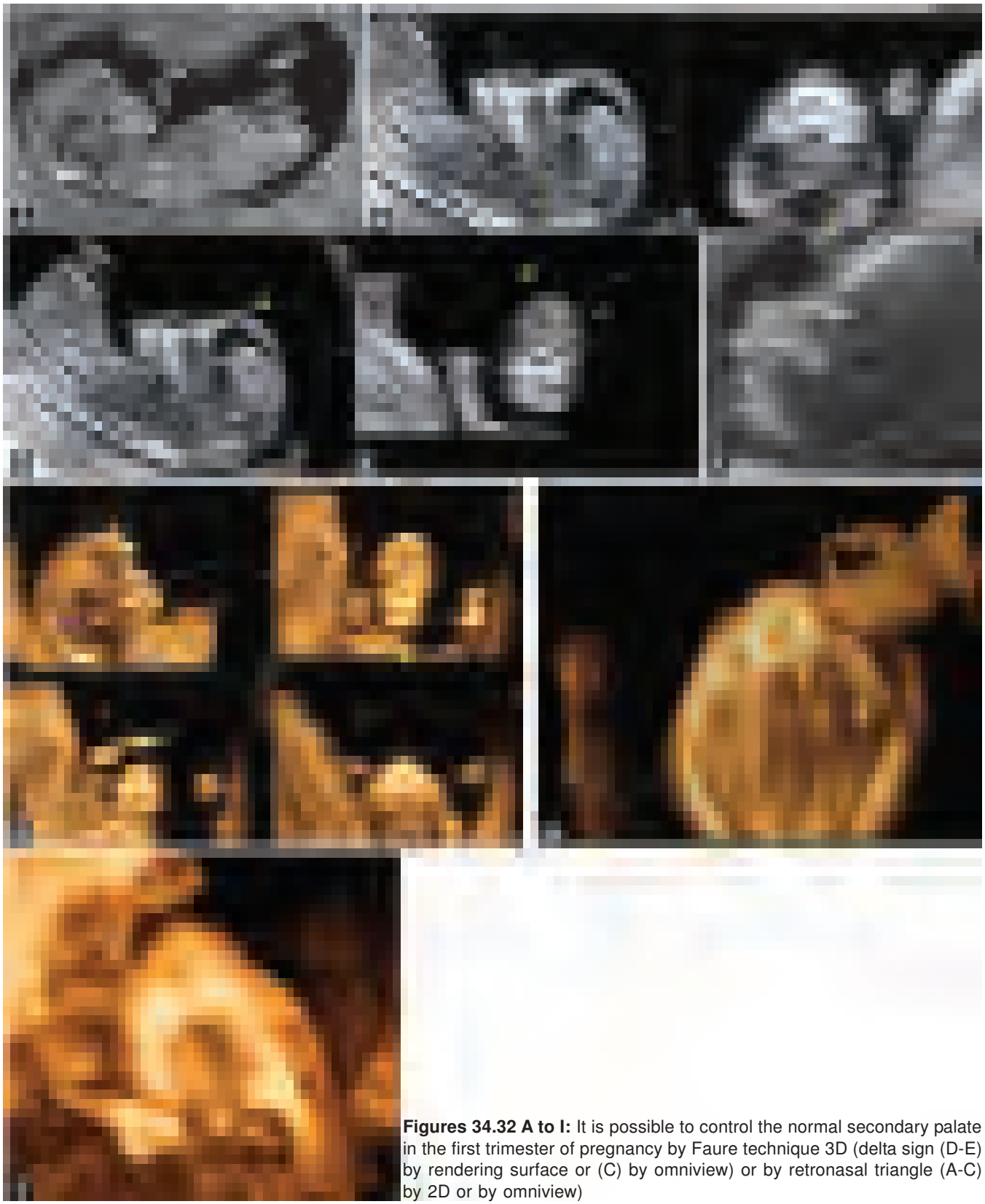

Figures 34.32 A to I: It is possible to control the normal secondary palate in the first trimester of pregnancy by Faure technique 3D (delta sign (D-E) by rendering surface or (C) by omniview) or by retronasal triangle (A-C) by 2D or by omniview)

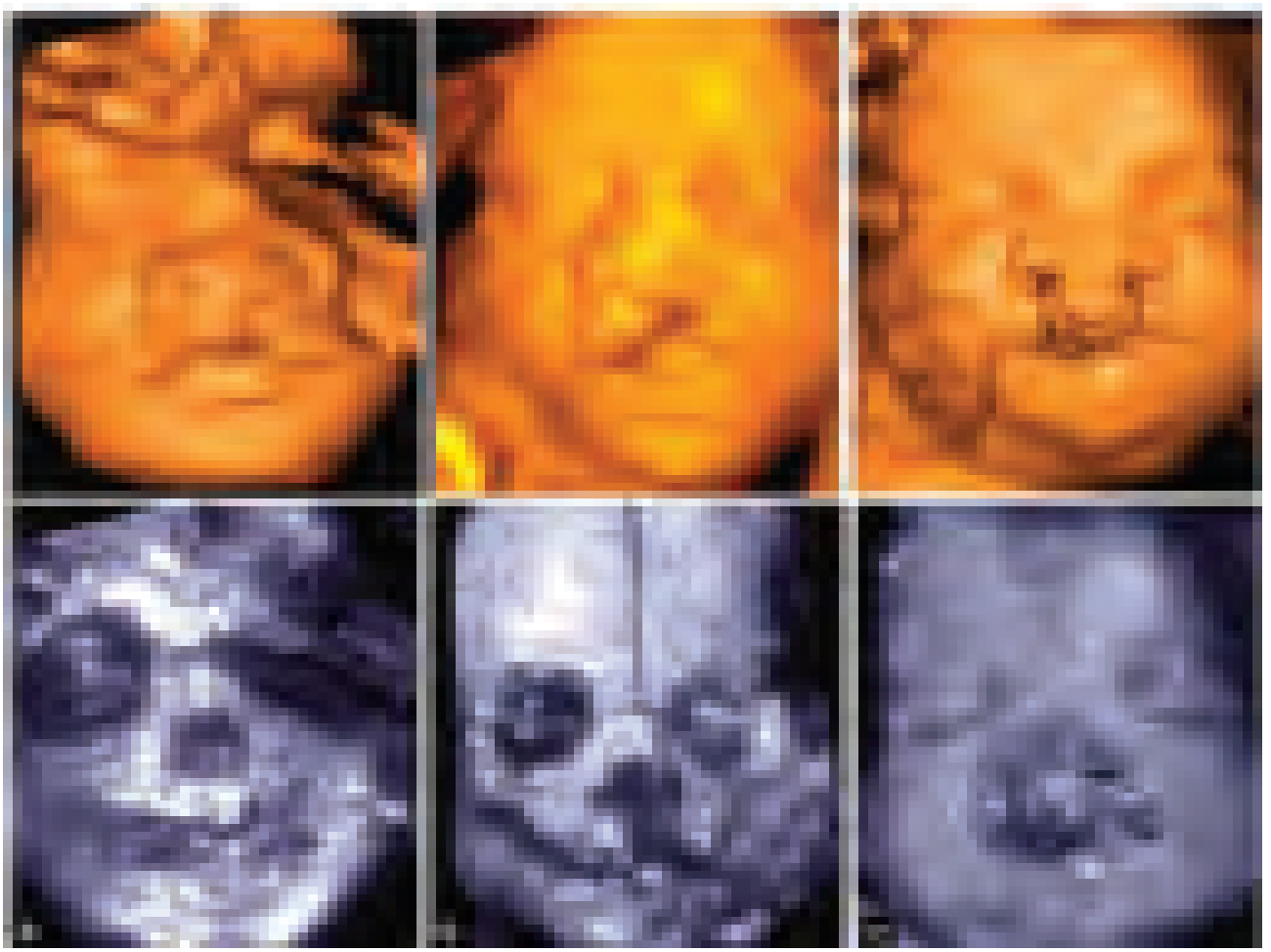

Figures 34.33A to C: Maximum and minimum rendering in three cases of l-p cleft. It is easy to understand the extension of the cleft

THE SECOND AND THIRD TRIMESTERS

The scan performed in the second trimester, usually around week 20 (range week 18-23, depending on the protocol), is used to study fetal anatomy and detect fetal malformations, as well as to evaluate fetal growth by means of biometric parameters.[44] Despite of the high expectations of pregnant women about the diagnostic capacity of ultrasound (presumably due to incorrect information in the media and often also from specialists), the various studies on detection of fetal malformations by standard ultrasound in the second trimester show rates that do not exceed 40–60% of all malformations detected at birth, with a homogeneous mean prevalence of 2.5%. The Eurocat report[45] for example, documents a diagnostic capacity of 62% for 11 major pathologies among 4366 malformations in 1,198,519 babies born in 17 European regions in the period (1995-1999). Variability was high, ranging from 25% in Croatia to 88% in Paris, with enormous regional differences. Moreover, about 30–40% of cases were diagnosed after week 24, for various reasons, not least of which the natural history of malformations. No malformation was diagnosed in all carriers; for example, anencephaly was diagnosed in 94% of cases. It is therefore necessary to be precise and careful when informing women about the intrinsic limits of general ultrasound, as well as individual limits determined by the type of equipment and operator experience. As mentioned for ultrasound in the first trimester, the sophistication of instruments and operator experience also make very accurate and difficult diagnosis possible in the second trimester. Indeed, today the study of fetal anatomy can be much more detailed than in the 1990s. Thus greater experience and attention to areas, such as face, heart and circulatory system, should improve the sensitivity

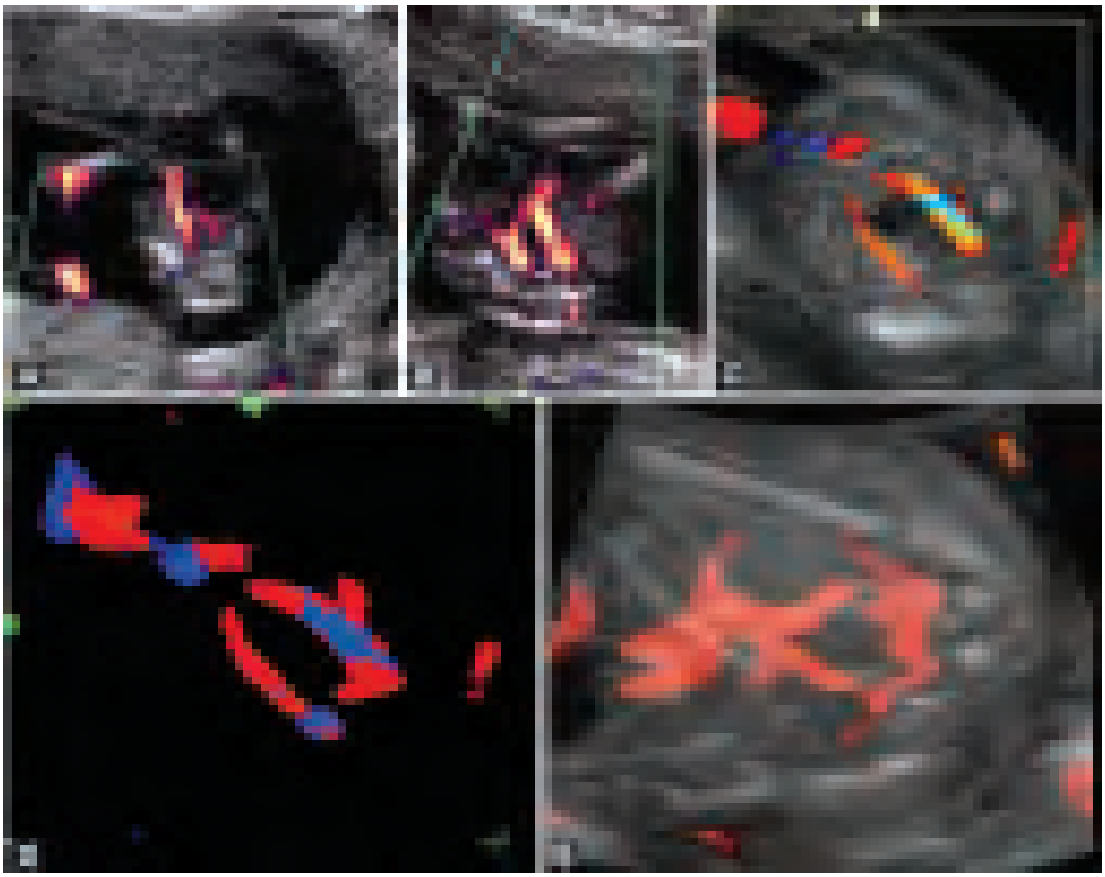

Figures 34.34A to E: In the first and second trimesters it is easy to find both umbilical arteries at bladder level; 3D color, power and glass body modes provide more realistic images

of diagnosis of malformations, though this quite reasonable claim has not yet been demonstrated. Specialists in prenatal diagnosis can also achieve great morphological detail with the aid of sophisticated new instruments with 3-4D technology.[46] For specific use of these instruments, we consider the various systems and organs.

The Head

The head offers the possibility of detailed examination of a series of morphological signs by 3-4D.[47-49] The face is accessible and it is relatively easy to exclude or diagnose cleft lip in this period **(Figs 34.35A and B)**.[50] Note that 3D technology includes 2D as base, so the capacity to visualize the fetal face by 3-4D in the second trimester is certainly much better than with 2D, with due enhancement and limitation related to fetal position, maternal abdominal fat, the placenta and quantity of amniotic fluid **(Figs 34.36A and B)**.[51] Given time (and perhaps more than one session) it is possible to obtain

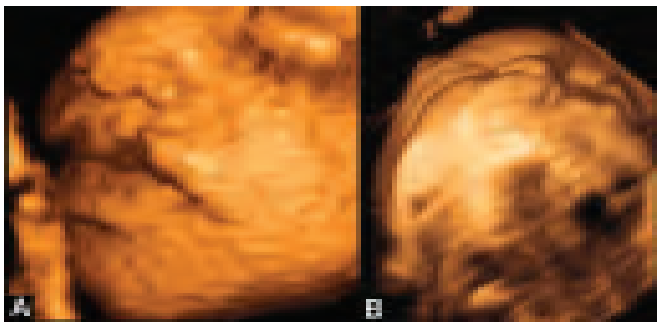

Figures 34.35A and B: Cleft-lip and cleft alveolar ridge by surface rendering front face

a good image of the fetal face in almost all cases in the period 19–23 weeks in 85–90% of cases (our personal percentage for 3540 pregnancies is 92%). In the next period of pregnancy, the possibility of exploring the fetal face decreases as pregnancy proceeds **(Figs 34.37A to R)**. Indeed, in the third trimester, after week 35, the face can only be visualized in 30–50% of cases and

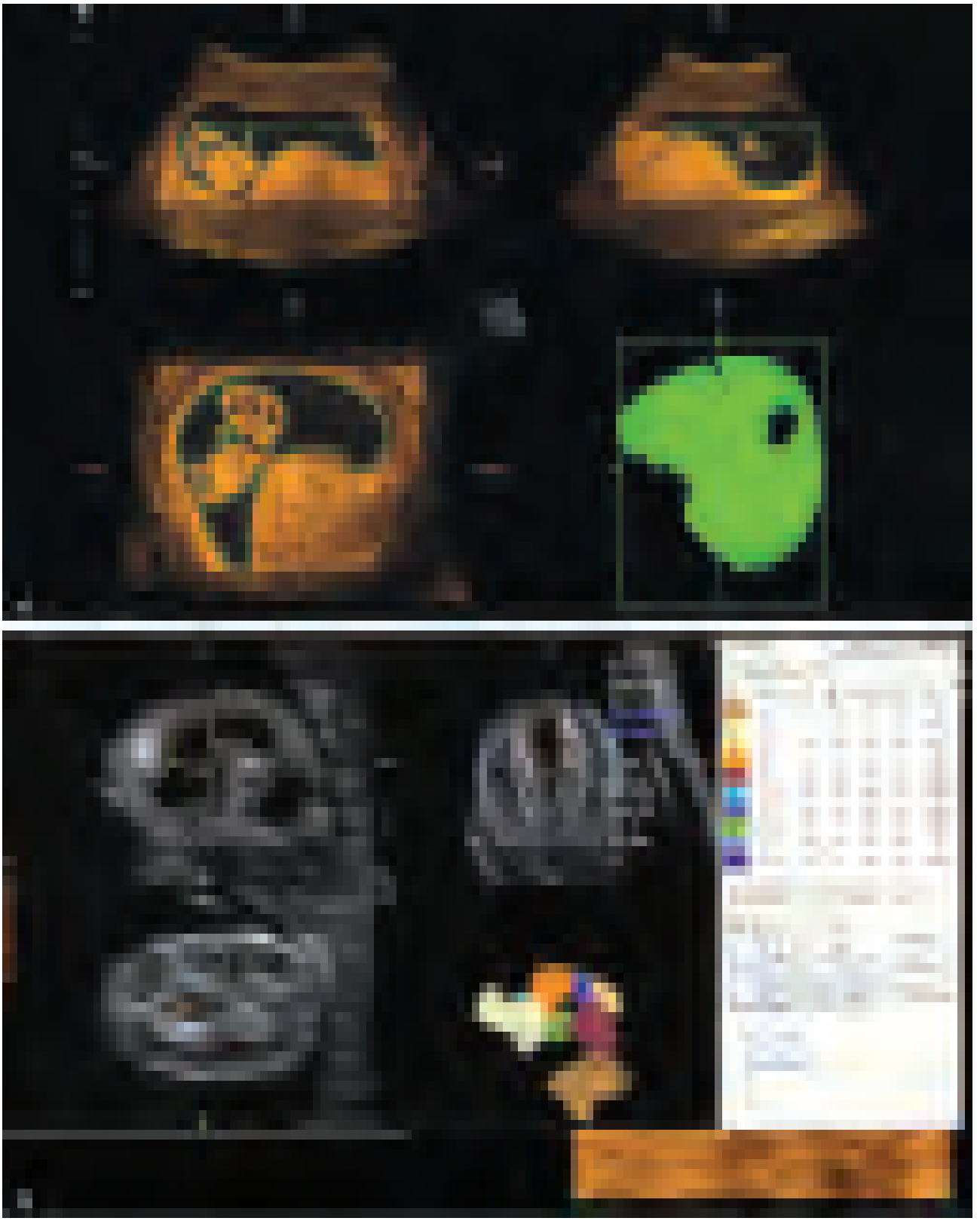

Figures 34.36A and B: The control of volume of amniotic fluid in the first trimester or the dimension of ventricles is possible by sonoAVC

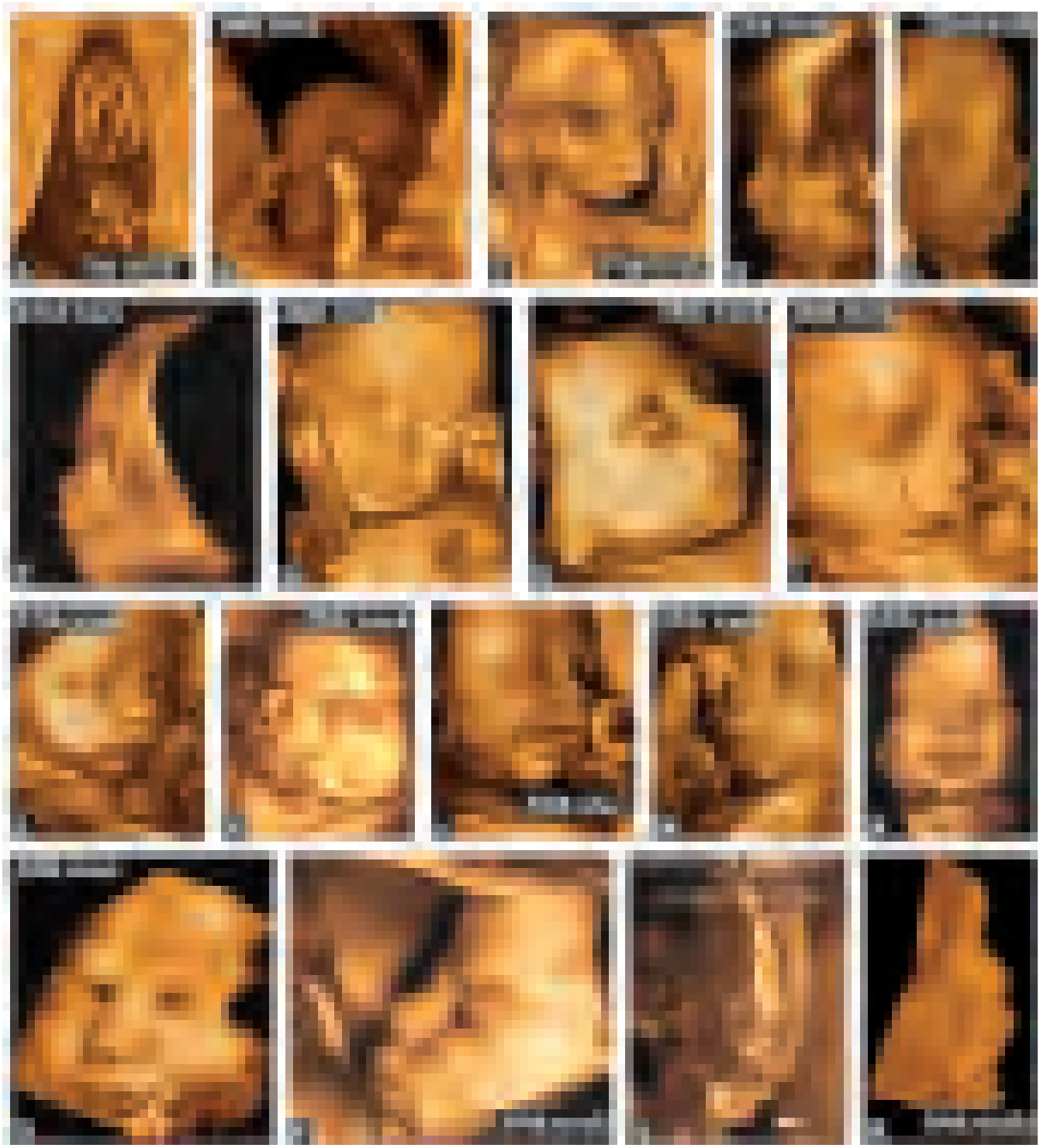

Figures 34.37A to R: The fetal face acquires human features during gestation. The face of the embryo is quite unattractive, whereas in the second trimester it becomes softer and more pleasant and remains thus into the postnatal period. Facial modelling is related to the formation of facial musculature, fat and the thick consistency of skin due to soaking. 3-4D provides completely realistic images, especially with high quality instruments and experienced operators. It is therefore relatively easy to assess facial symmetry and reliably recognize facial dysmorphisms (e.g. mandibular hypoplasia), which may be of genetic disorders and to diagnose cleft lip or palate

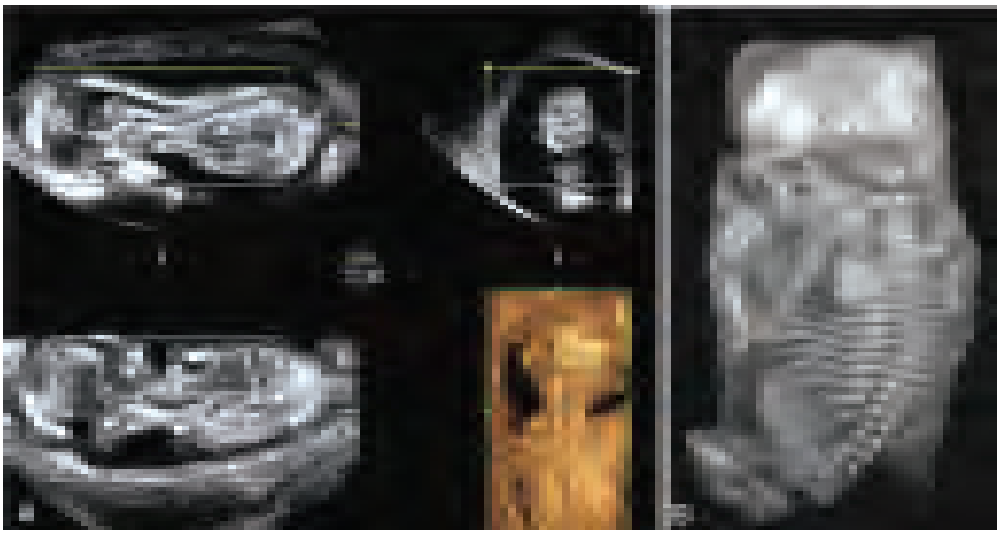

Figures 34.38A and B: It is possible in the first trimester to study the bones of the skull (A) Occipital bone at 12 week) or the total skeleton with the spina; (B) The skeleton at 12th weeks by maximum mode

sometimes requires two or three sessions in the case of suspected diagnosis.

Operator experience is critical. After initial successes, considerable difficulty is often encountered in analyzing a saved volume: to obtain good images, 3D takes time and application as well as interest and predisposition. The 3-4D is much less instinctive than 2D, which gratifies the operator with interpretable images after a few hours of practice (for example, measurement of BPD). The first impression of a face naturally cannot have scientific value, though many facial dysmorphisms depend on genetic syndromes and aneuploidies. Hyper and hypotelorism, a weak chin and low ear position are easily and immediately detectable by 3D and this prompts us to consider the fetus as if it was a newborn. Moreover, with 4D we can observe sucking movements and attitudes, yawning, retroflexion of the tongue and movements of the hands, arms and legs, all characteristic of fetal wellbeing.[52] Maximum mode rendering enables exact views of bones,[53] detailed study of cranial bones and sutures **(Figs 34.38 and 34.39)**, as well as measurement and counting of nasal bones making easier a diagnosis of craniosynostosis.[54-56] Minimum mode surface rendering can show details such as ear lobes which are markers of urinary system pathology. The study of the fetal face is now the less important and significant field of the three-dimensional study of the cephalic extreme. The so called "granny" effect that is achieved by pleasing images of the fetal face to take home is the playful part of the use of ultrasound that has always existed, even when we were only able to hear the heartbeat. The facial dimorphisms are relevant in certain diseases such as achondroplasia **(Figs 34.40A to C)** and in many syndromes, (holoprosencephaly, elephant man) where the face is often one of many markers, though often very impressive. Finally, today the three-dimensional have bought or better earned its place as a complement or as a significant contribution to the two-dimensional ultrasound diagnostic of malformations.

Internal structures of the brain can be explored in more detail **(Figs 34.41 to 34.44)**. A correct view of the corpus callosum and pellucid fossa can be obtained in real time by 3-4D with volume contrast imaging in the C-plane. The posterior horns and the vermis can also be explored and their volume calculated[57,58] foto. The optic chiasma is easily detected and is an important prognostic factor in cases of anterior brain anomalies. Brain vascularization provides much material for future study. The Willis circle and the pericallosa and marginal arteries are easily detected in glass-body mode and angio mode of power or color Doppler, from the first trimester **(Figs 34.45A to I)**.

Detailed study of the jaw and oral cavity is another aspect of the head. We have extensively studied the ears **(Figs 34.46A to F)**, their size, morphology and position (normal or low), prompted by observations of neonatologists who attribute importance to the anatomy of the external ear. Neurosonology represents the area in which the three-dimensional really makes the difference enabling the operator to browse inside the brain structures using multiplanar method; the study

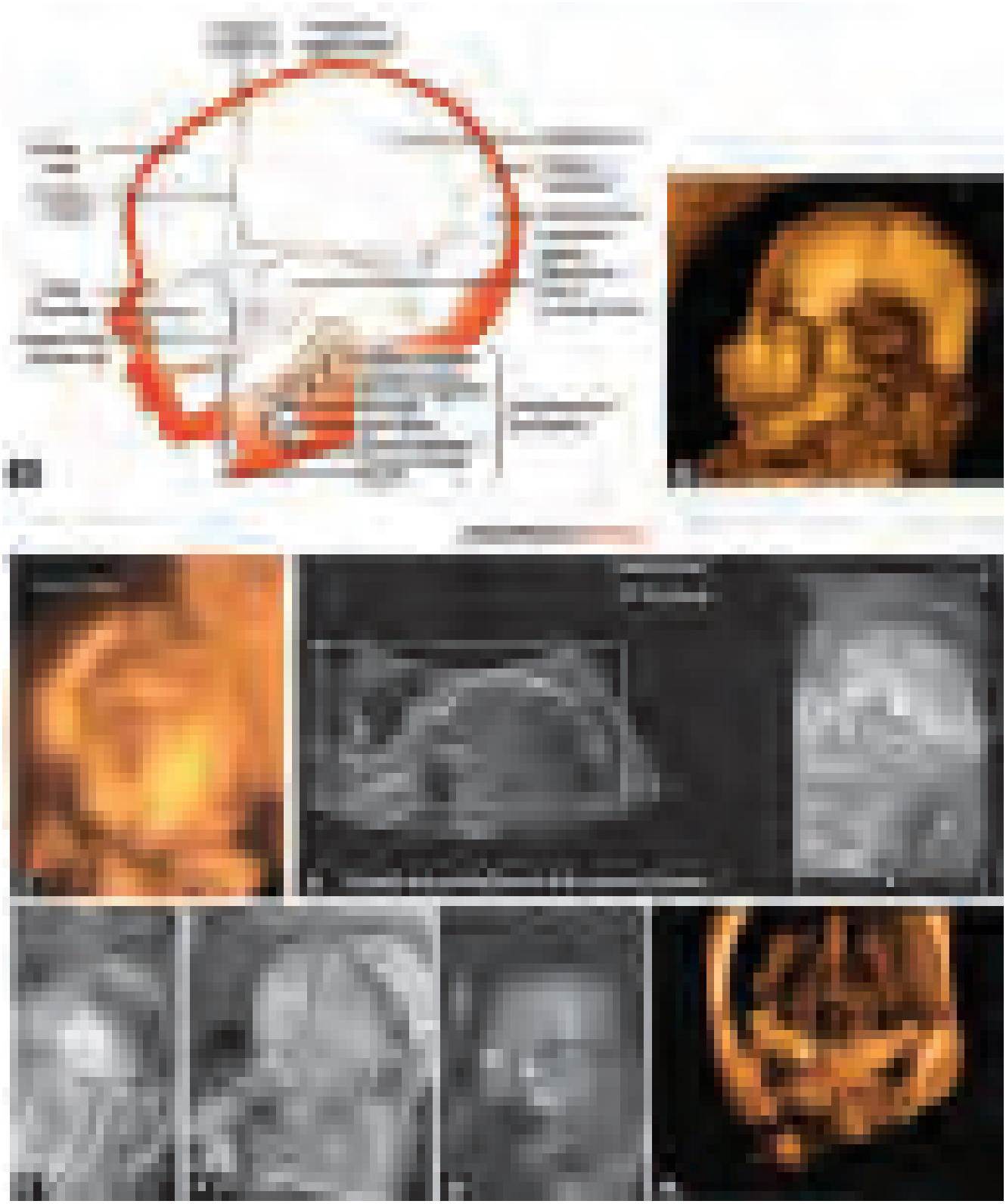

Figures 34.39A to H: (A to C) The maximum mode imaging can detect so many features of the skull than it is possible to compare the image with a design; (D to G) Examination of the skull can detect many malformations: cranial bones and fissures are detectable by 3D, pathology of the bones like craniosinostosis at 20th week detected by maximum mode, or (H) Sphenoid bone

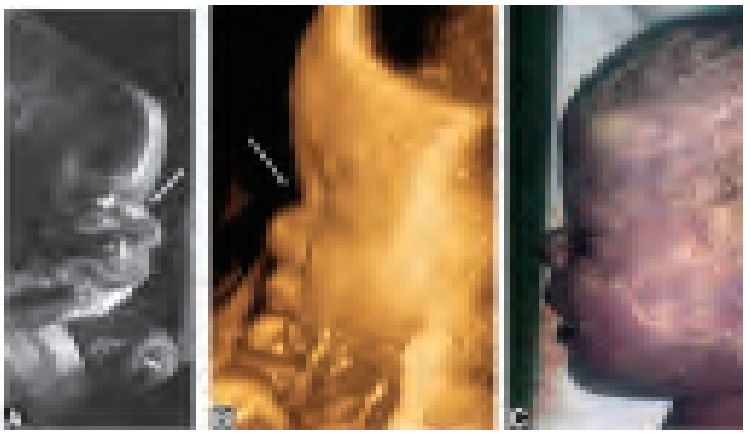

Figures 34.40A to C: Typical face of achondroplasia

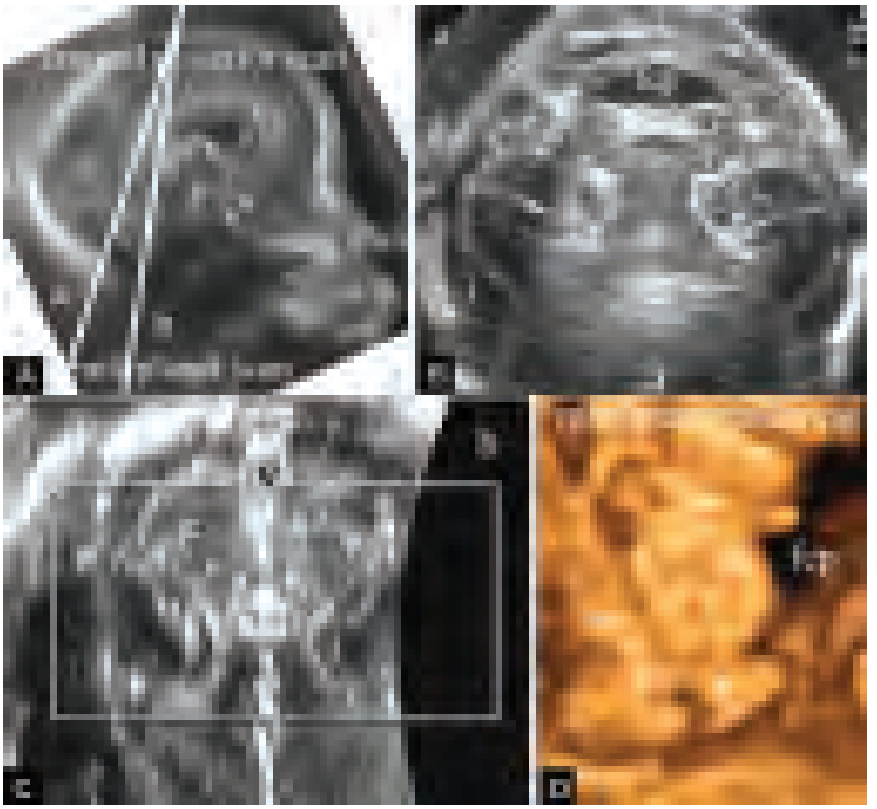

Figures 34.41A to D: Posterior coronal scan. By 3D multiplanar and minimum rendering we can obtain a view of the cerebellum, fourth ventricle, acqueductus silviani and vermis that is difficult to obtain by 2D. as: acqueductus silviani; c: cerebellum; pcf: posterior cranial fossa; i: insula; v: vermis; 4: fourth ventricle

of the corpus callosum has become a reality in almost all cases, with the ability to detect the partial agenesis, while both ventricles and posterior fossa are now easier to explore.

Inside the cranium it is now possible to highlight structure otherwise unimaginable as the optic chiasm or sphenoid bone, although currently there is a lack of clinical utility but it is representative to signify the depth anatomical study allowed by 3-4D. Finally, the study of the palate which today represents a new barrier demolished by ultrasound with a great contribution of the three-dimensional **(Figs 34.47 to 34.64)**.

Renewed interest in the study of primary and secondary palatal morphology has arisen with new ultrasound diagnostic methods in 3-4D[59-61] and the fact that facial cleft accounts for 13% of all congenital malformations.[62] Malformation of the lip and palate may be isolated, associated with other malformations

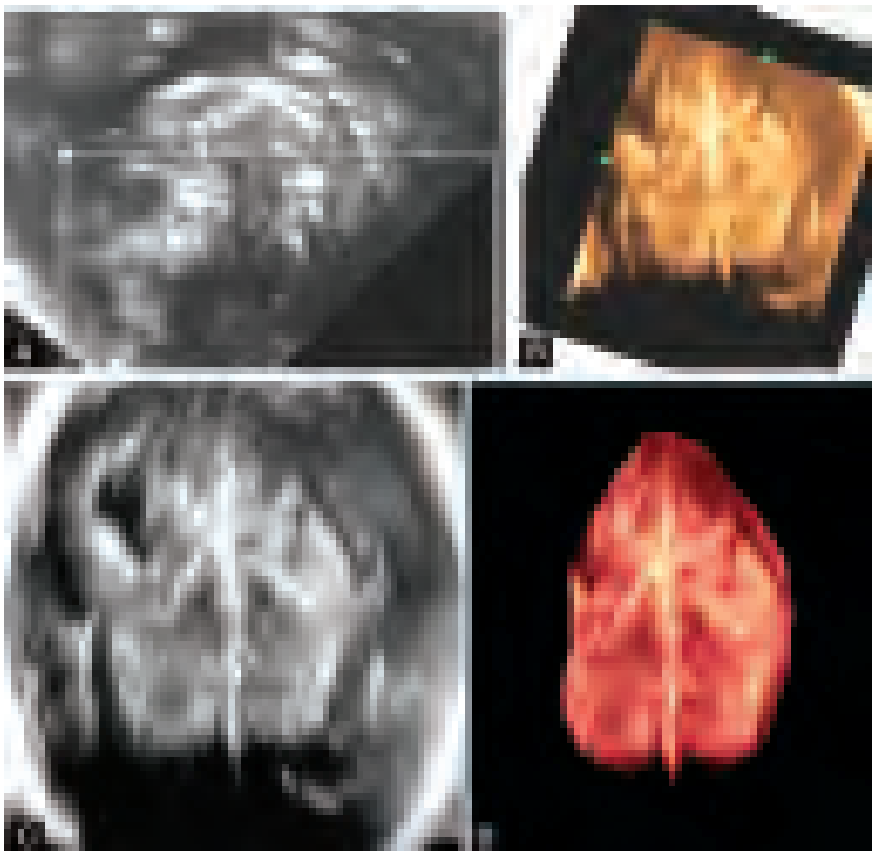

Figures 34.42A to D: Exploration of the brain by 3D multiplanar mode offers a splendid view of the optic chiasma, important in cases of partial agenesis of the corpus callosum

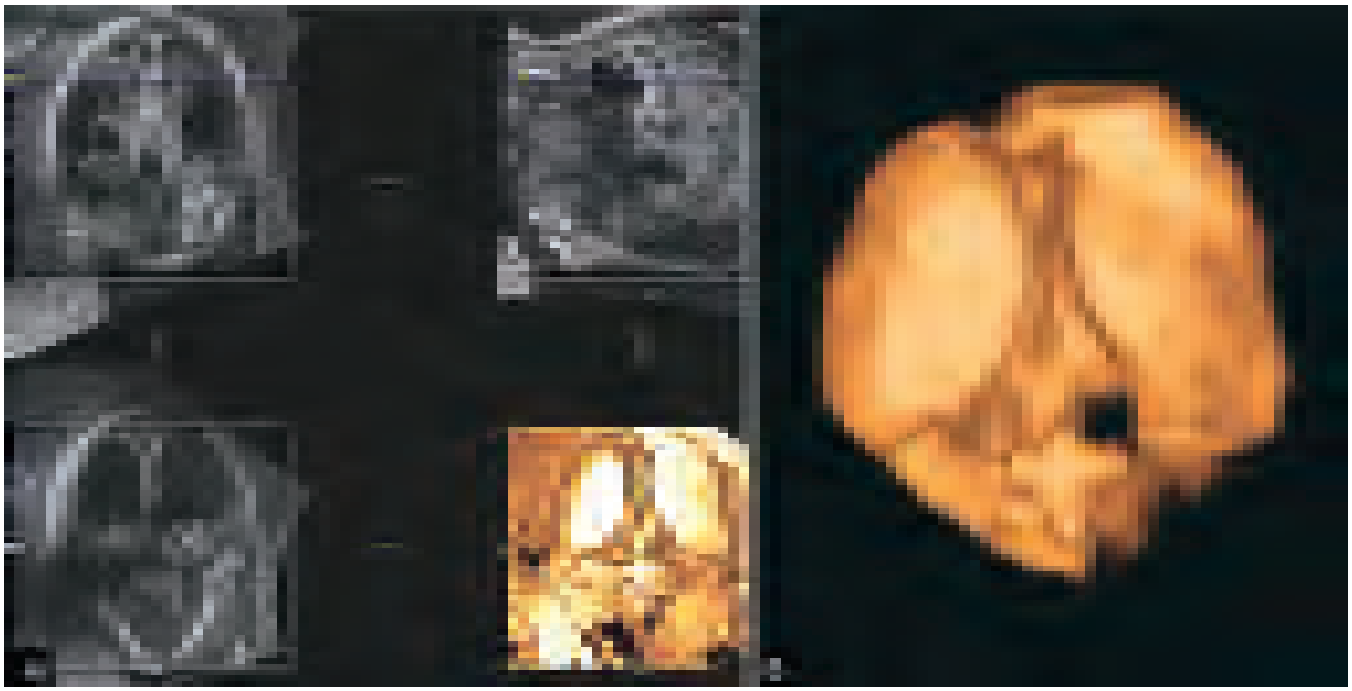

Figures 34.43A and B: Invert and vocal modes are suitable for determining hydrocephaly

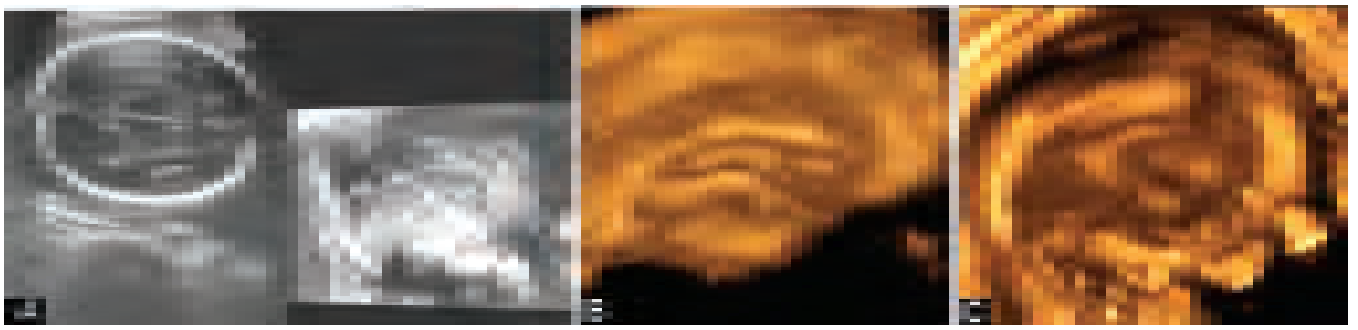

Figures 34.44A to C: Examination of the corpus callosum is easy and quick by 3D and volume contrast imaging in c-plane; by 2D it is very difficult

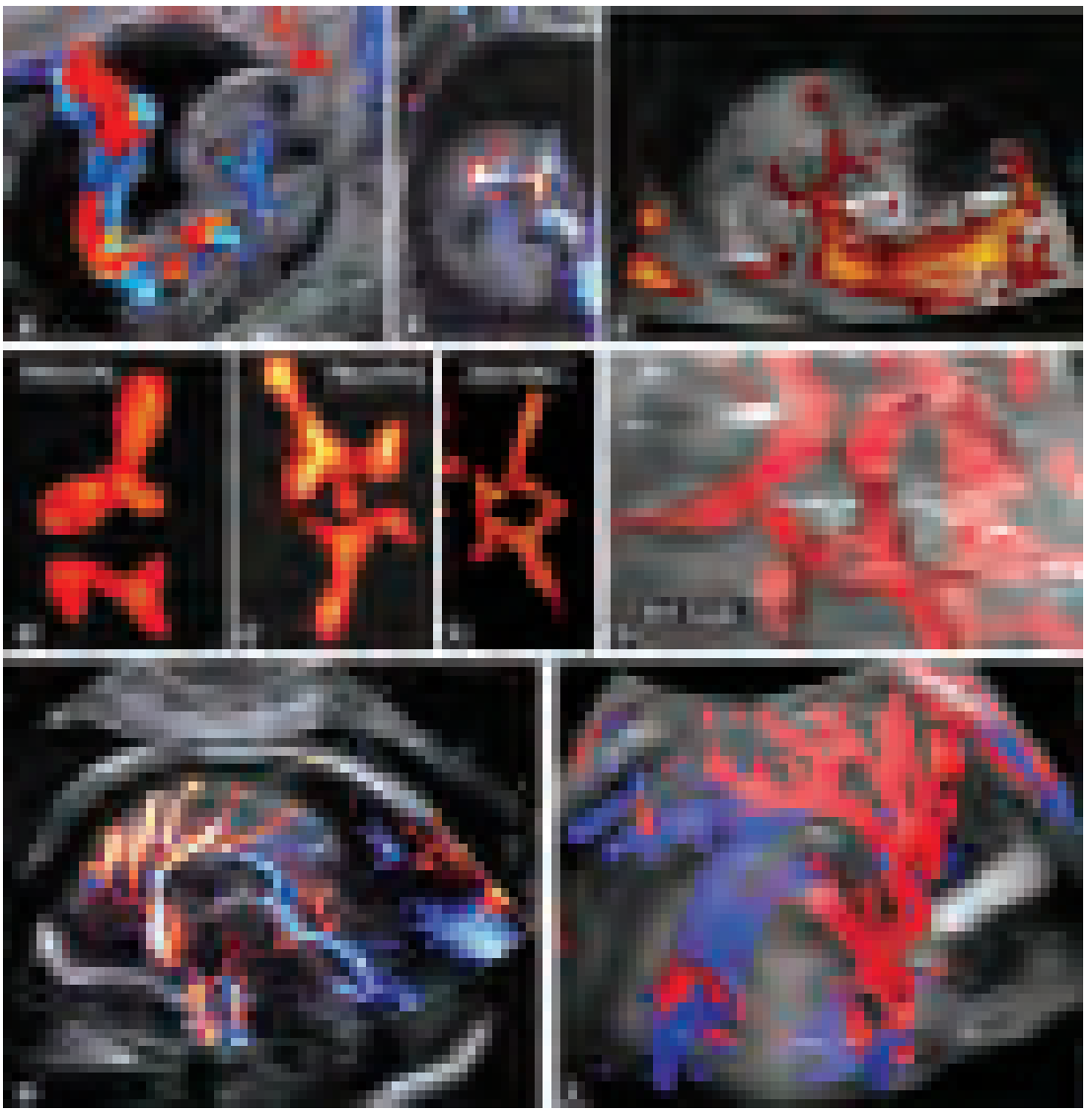

Figures 34.45A to I: Brain circulation starts in the first trimester of pregnancy. The Willis circle and pericallosa artery are readily viewed by power or color glass-body mode

Figures 34.46A to F: By 3D it is possible to detect very small appendix auricularis (an important marker for many other malformations); ear position is important, because low placement or a helix more than 30 degrees out of the skull are a marker of aneuploidy. External ear morphology changes during gestation: until week 20 it is a ring; final morphology is only achieved at about week 29

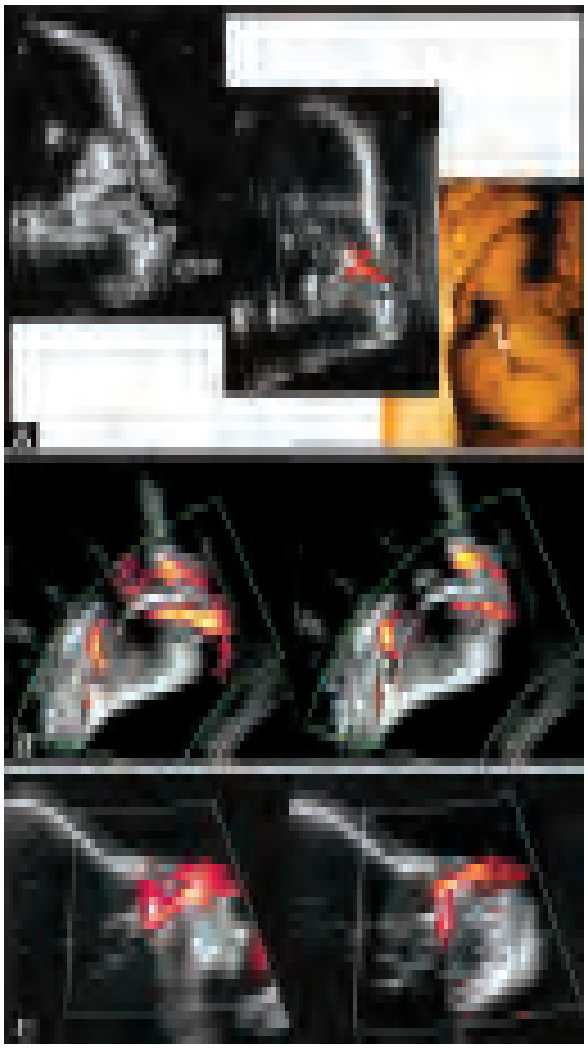

Figure 34.47: (A) The use of 2D, 3D and color Doppler offers a good possibility to diagnose the l-p cleft. It is suggestive of the passage of amniotic fluid directly from oral to nasal choana; (B) Sagittal scan power-color to demonstrate the normality of secondary palate during swallowing; (C) The amniotic fluid crosses through the palate

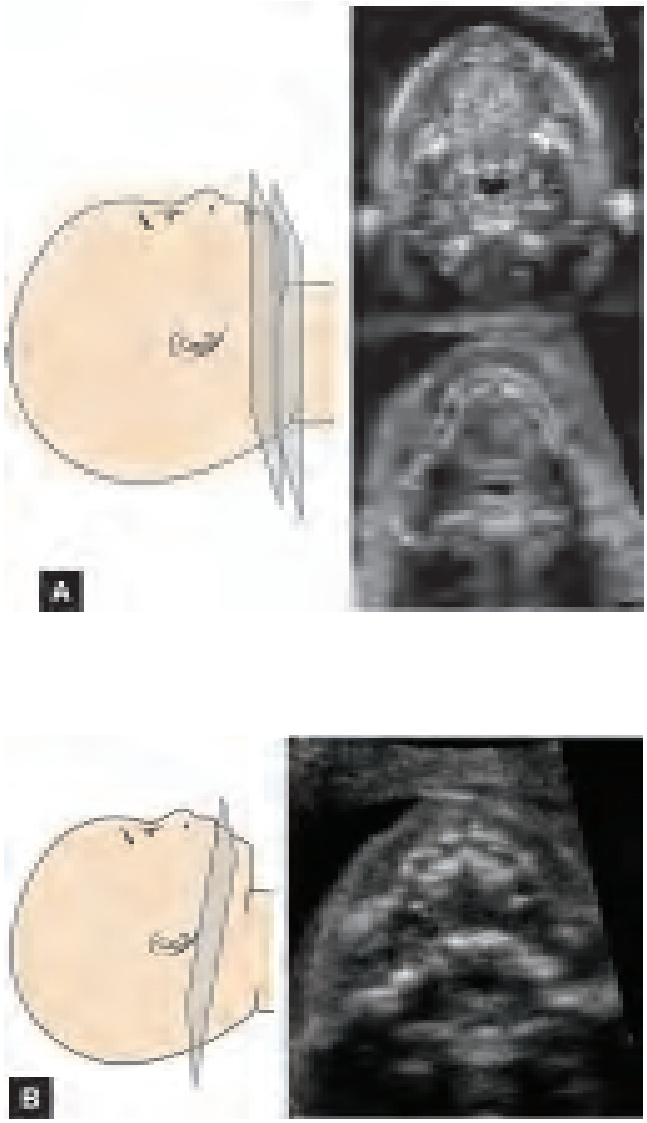

Figures 34.48A and B: Different planes of axial 2D scan for the jaw and the tongue. (A) The maxilla; (B) The proximal part of the maxilla and the eyes

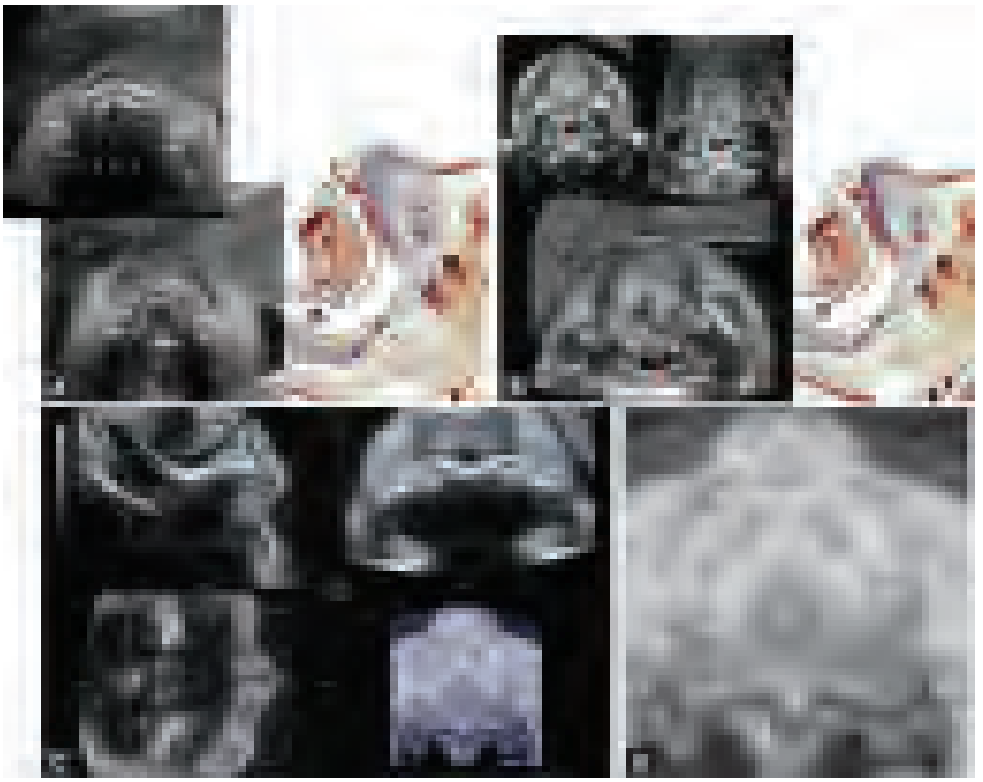

Figures 34.49A to D: (A) A correct axial 2D scan for the maxillary bone; (B) The tongue and the uvula; (C) The secondary palate with the uvula by 3D flipped-face view multiplanar; (D) and surface rendering

Figure 34.50: This picture of Berkowitz (2006) shows the different possibilities of facial cleft. It is important to note that the palate-cleft starts from the uvula until the primary palate

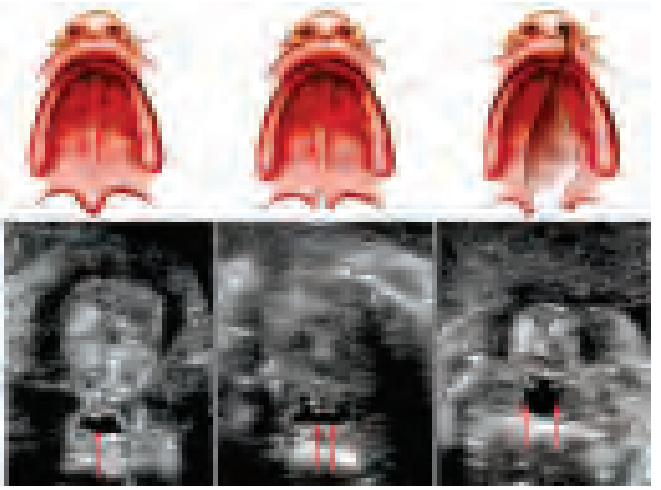

Figure 34.51: Beautiful 2D pictures of uvula-cleft; the uvula-cleft is always associated with palate-cleft

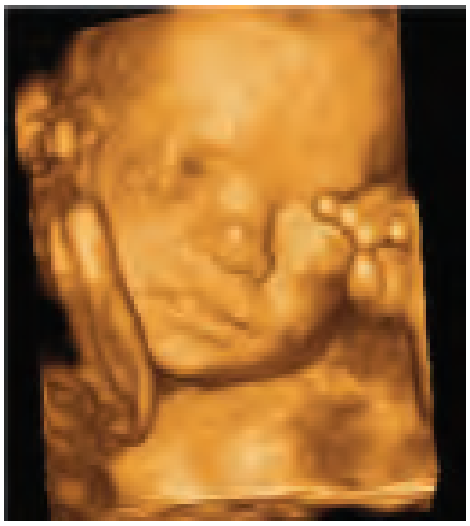

Figure 34.52: The study of the nose and the lips is very easy in the second trimester of pregnancy by 3D

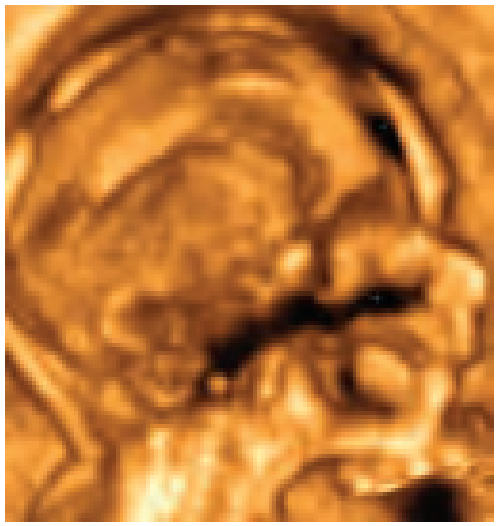

Figure 34.53: The sagittal section of secondary palate shows the two portions of hard and soft palate with the uvula

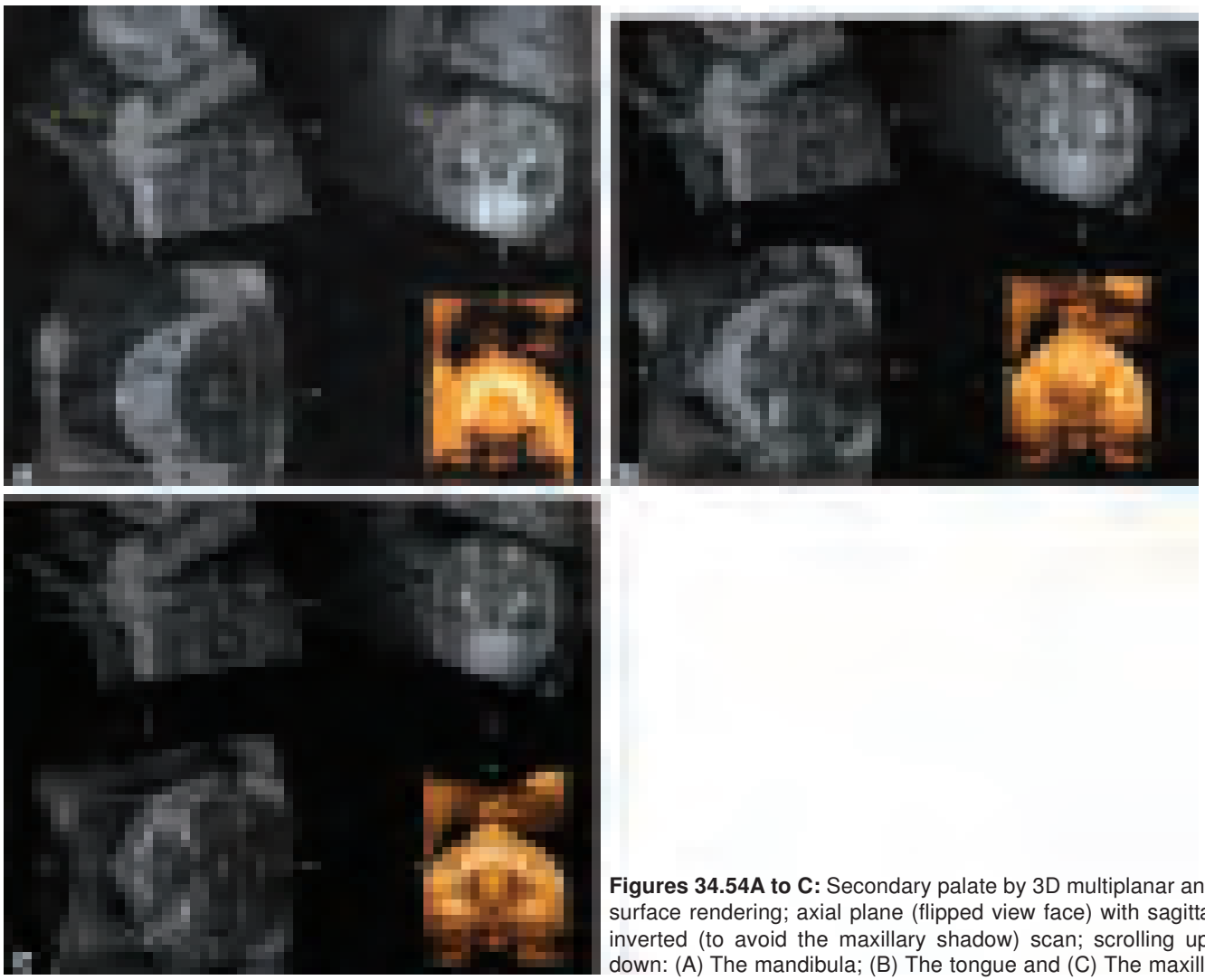

Figures 34.54A to C: Secondary palate by 3D multiplanar and surface rendering; axial plane (flipped view face) with sagittal inverted (to avoid the maxillary shadow) scan; scrolling up-down: (A) The mandibula; (B) The tongue and (C) The maxilla

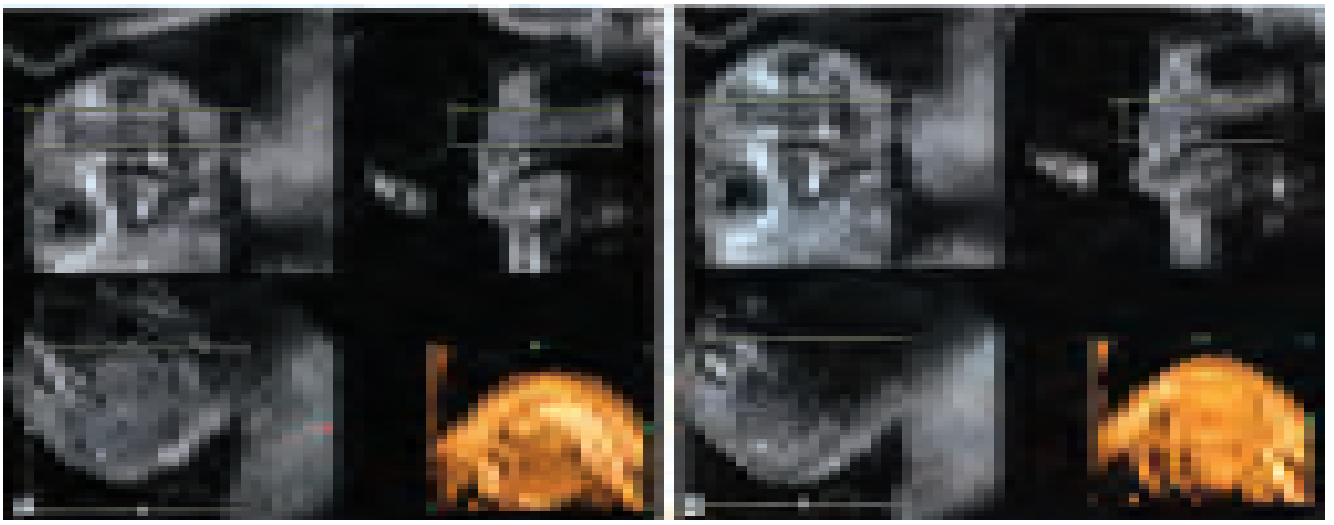

Figures 34.55A and B: Secondary palate by 3D multiplanar and surface rendering: axial plane with coronal inverted (to avoid the maxillary shadow) scan; scrolling up-down: (A) Mandibula; (B) Tongue and maxillary bone

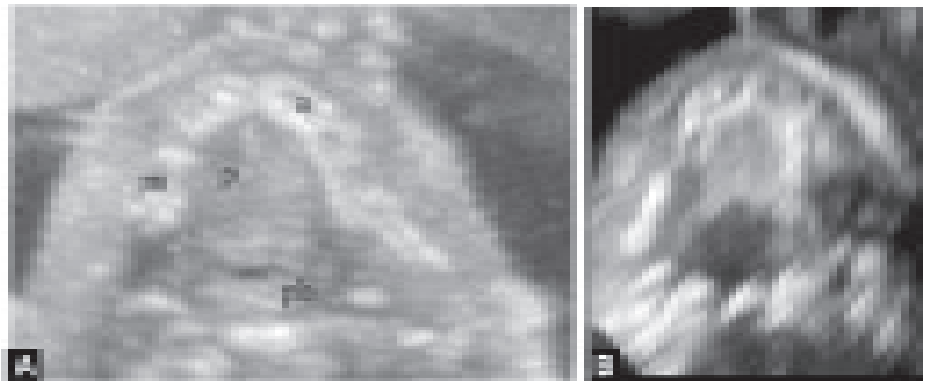

Figures 34.56A and B: Secondary palate by axial 3D plane (A) Maximum mode and (B) Minimum mode

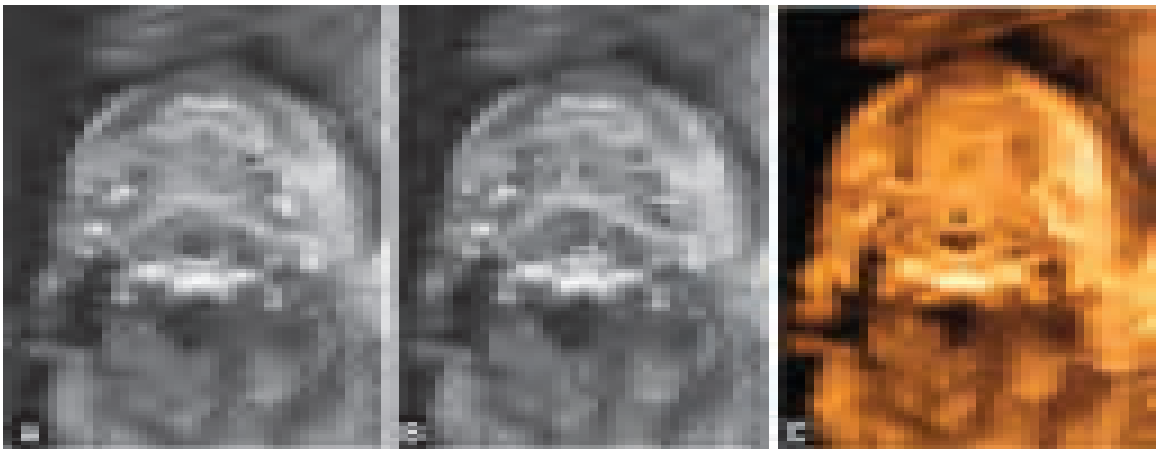

Figures 34.57A to C: Secondary palate by 3D plane minimum mode without and with captions. a: alveolar ridge; m: maxilla; i: interpalatal suture; p: palatine process; pns: posterior nasal spine; pp: pterygoid process; u: uvula

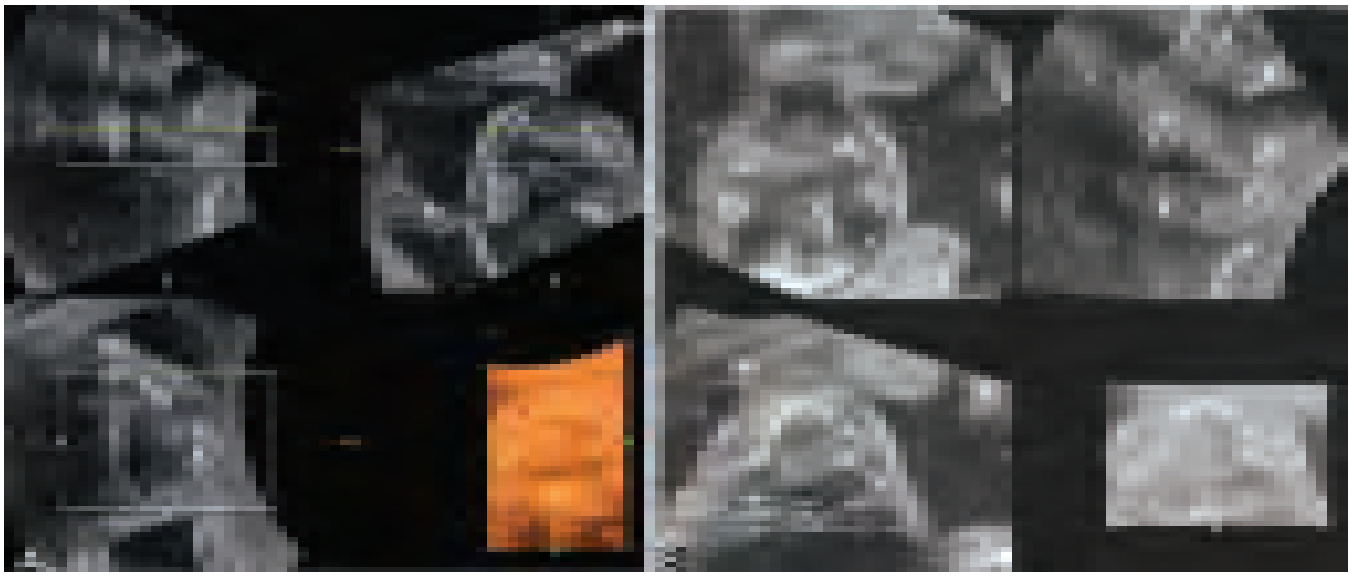

Figures 34.58A and B: By axial 3D plane there is no difference between (A) Sagittal and (B) coronal scan to see the secondary palate

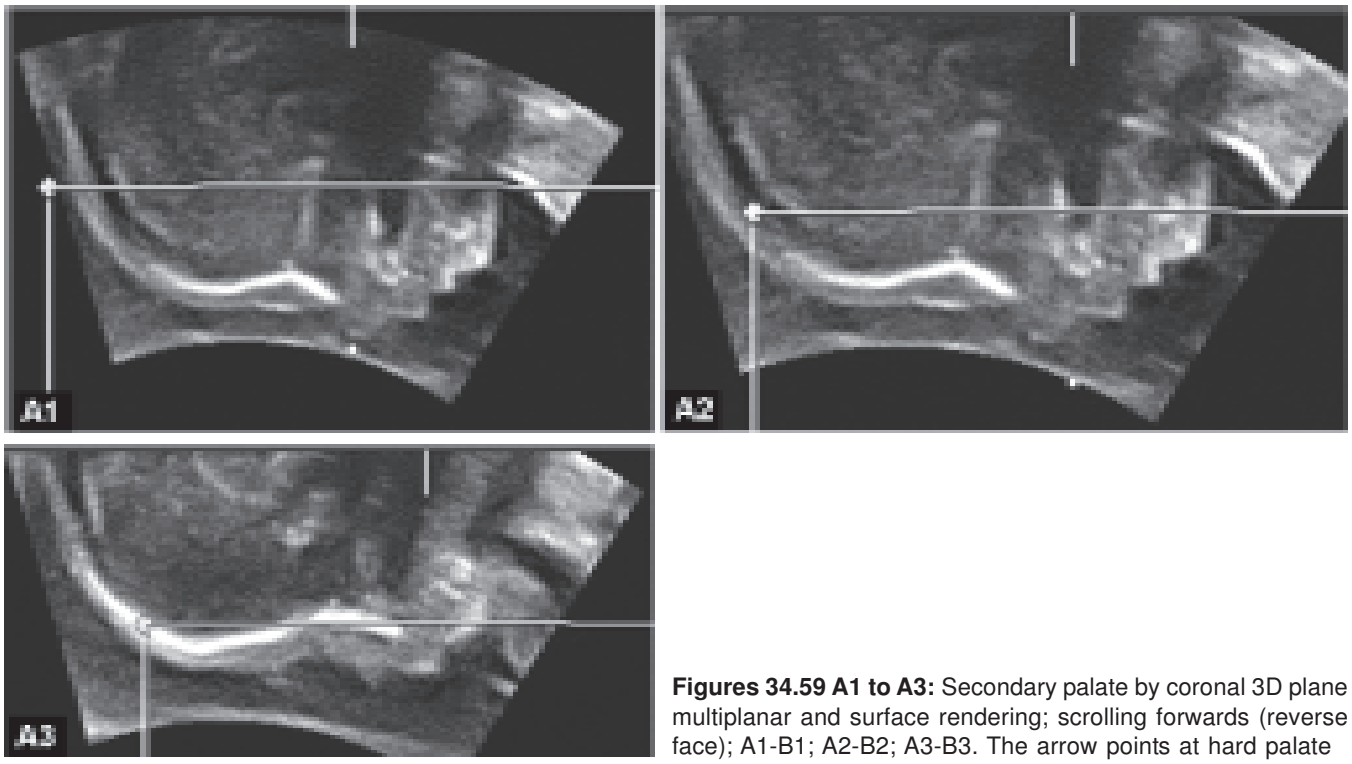

Figures 34.59 A1 to A3: Secondary palate by coronal 3D plane multiplanar and surface rendering; scrolling forwards (reverse face); A1-B1; A2-B2; A3-B3. The arrow points at hard palate

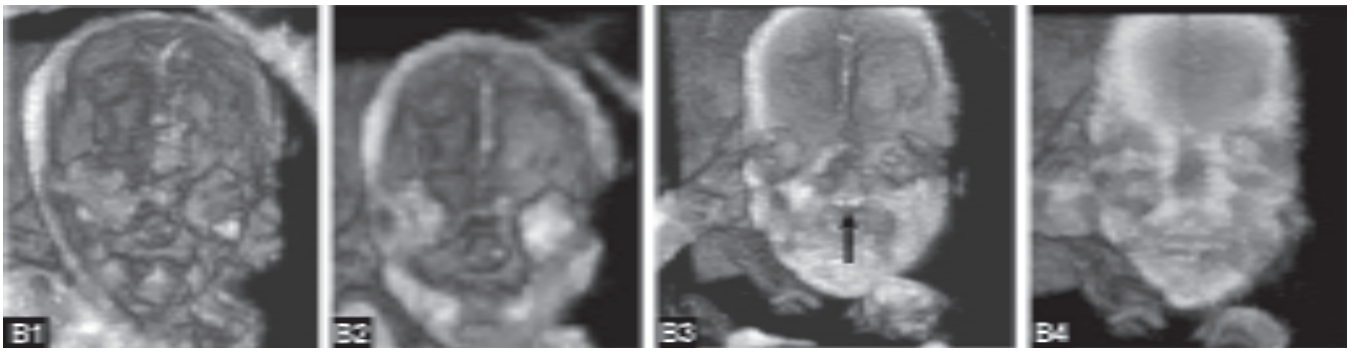

Figures 34.60 B1-4: Secondary palate by coronal 3D plane multiplanar and surface rendering; scrolling forwards (reverse face); A1-B1; A2-B2; A3-B3; A4-B4. The arrow points at hard palate

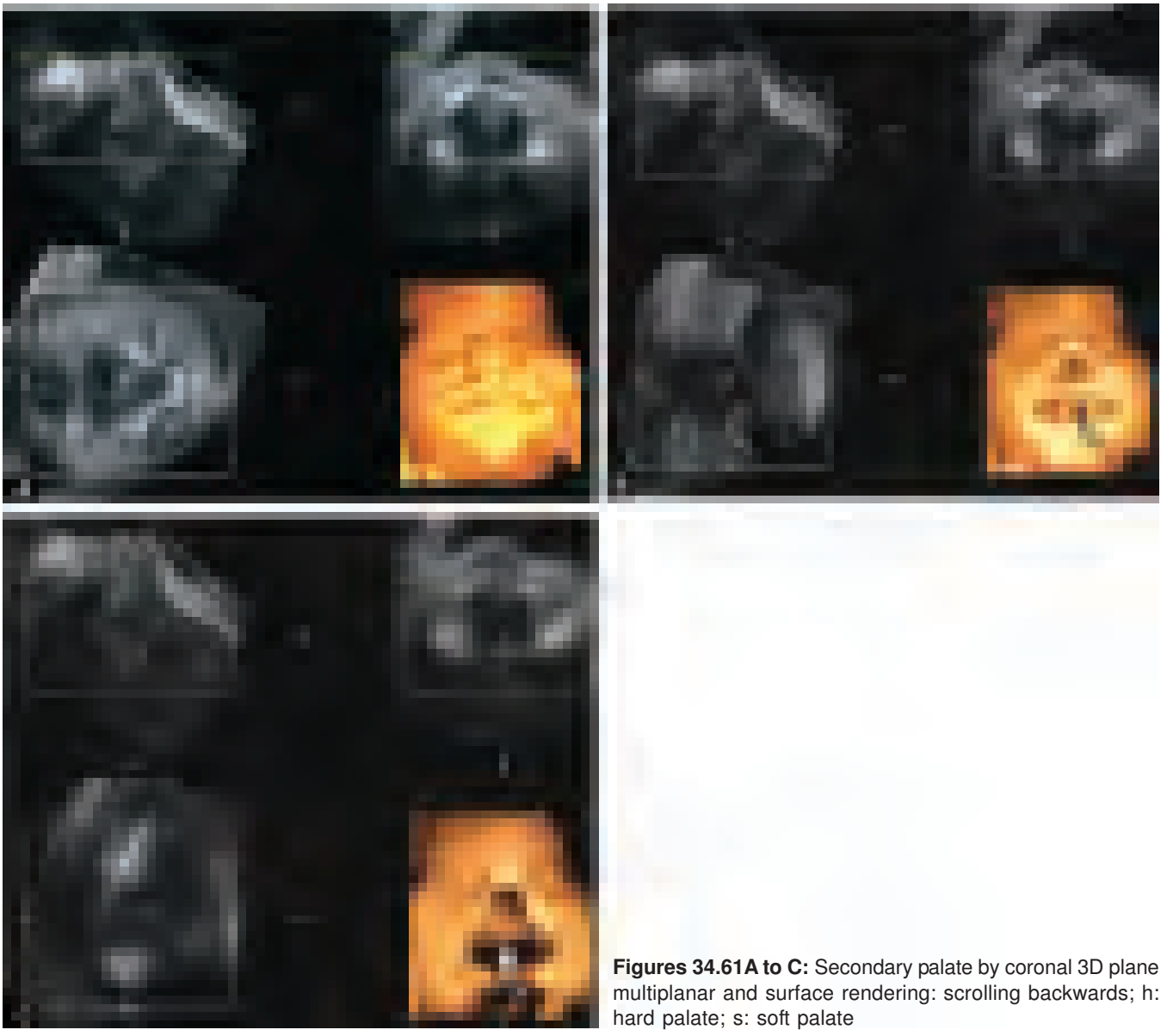

Figures 34.61A to C: Secondary palate by coronal 3D plane multiplanar and surface rendering: scrolling backwards; h: hard palate; s: soft palate

Figures 34.62A to C: (A) TUI (Tomographic Ultrasound Imaging) of the secondary palate in the coronal plane; (B) TUI of the secondary palate in the axial plane; (C) omniview of the secondary palate in the axial plane

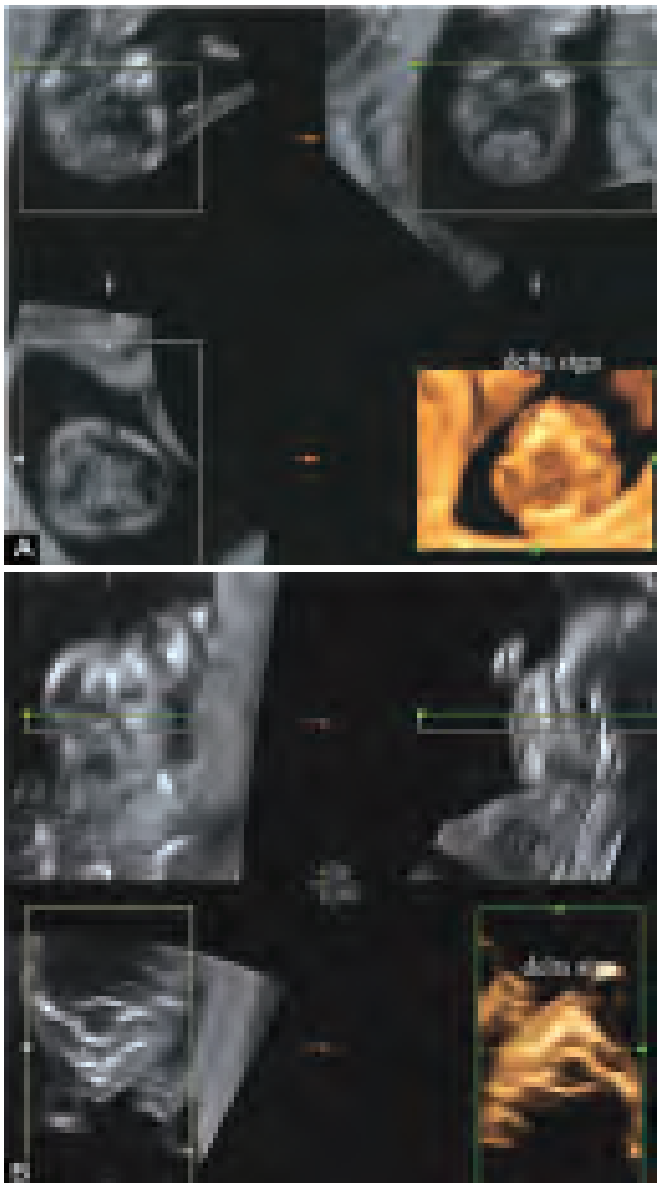

Figures 34.63A and B: Axial 3D plane multiplanar and surface rendering (flipped view) to see the maxilla (delta sign) and hard palate at 12 weeks by (A) sagittal and (B) coronal scan

and/or sequences of malformations, associated with chromosome anomalies or with manifestations of a syndrome. Typical facial cleft, including cleft lip, cleft lip/cleft palate and cleft palate, have a prevalence of 9.1/10,000 and 6.4/10,000 births, respectively. Cleft lip accounts for 36% of all lip and palate malformations and the birth prevalence of isolated orofacial clefts

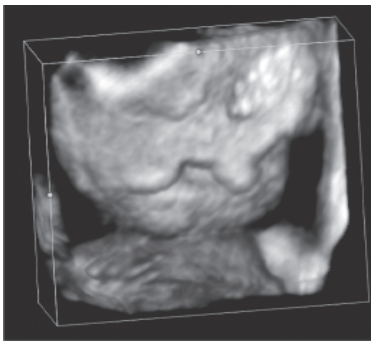

Figure 34.64: A diagnosis at 14 weeks of cleft lip associated to holoprosencephaly by 3D vaginal probe 9-12 Mhz (E8 GE)

accounts for 61.67% of total facial cleft **(Figs 34.65A to C)**.[63] The prevalence is high (about one/1000) and in about two-thirds of cases not only involves the lips but also the palate. Unfortunately in 45–47% of cases the defect affects the palate only.[64] From an epidemiological viewpoint, isolated malformations of the palate are associated with other malformations in about 18% of cases and with syndromes in 27.2%.[65] Cleft lip-cleft palate is isolated in 70–79% of cases and in the other 21–29% it is part of a syndrome or associated with other malformations.[66-68] Chmait in 2006[69] reports 45 cases of cleft lip-cleft palate diagnosed by 2D and 3-4D scan, among which 21.6% of forms diagnosed as isolated revealed malformations not detected by ultrasound at follow-up. The report EUROSCAN (2000)[70] documents a total ultrasound sensitivity of 27% for cleft lip-cleft palate, a sensitivity of 17% for isolated forms and 7% for isolated cleft palate. Other reports indicate a detection rate of up to 73% for cleft lip by 2D scan performed after week 20 of pregnancy ultrasound but there are papers which report sensibility for isolated cleft of palate about 0% **(Figs 34.66 and 34.67)**.[71] The prevalence of this malformation and especially the high incidence of associations with other anatomic and genetic malfor-

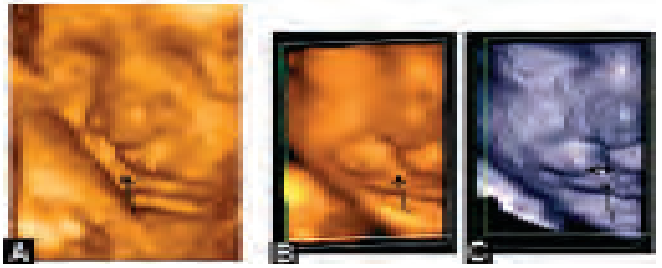

Figures 34.65A to C: Three images of cleft lip

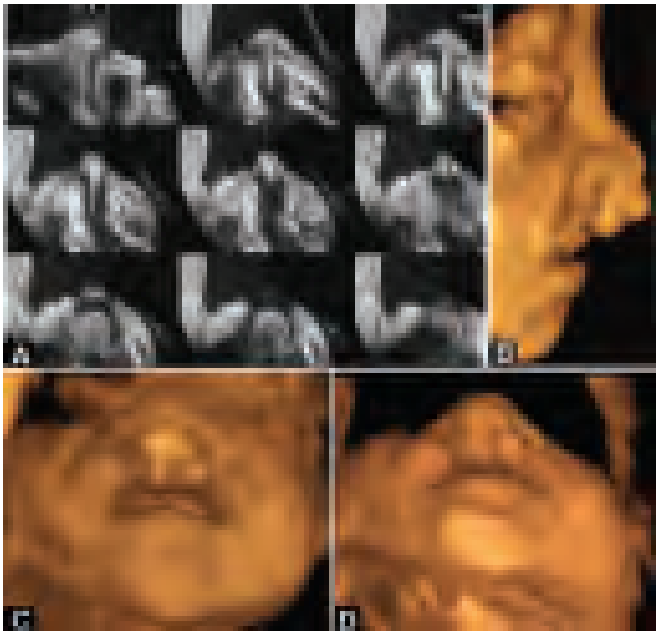

Figures 34.66A to D: Bilateral l-p cleft with TUI and rendering surface

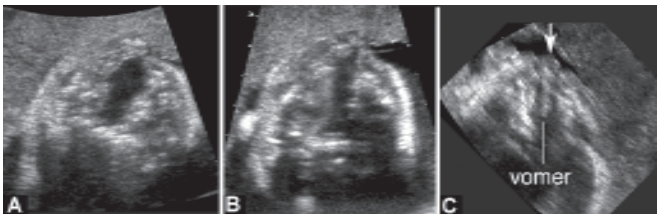

Figures 34.67A to C: Monolateral cleft-lip and cleft-palate by axial 2D scan

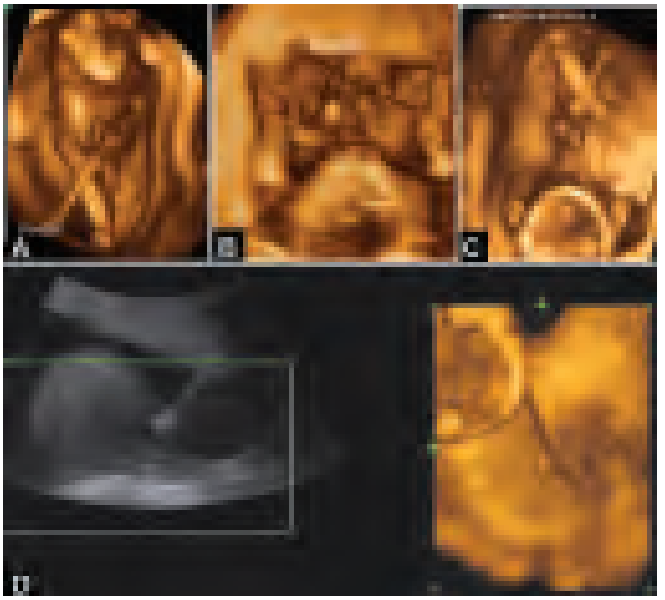

Figures 34.68A to D: (A to C) 3D images of amniocentesis; (D) Gives a good idea of the difference between 2D and 3D

mations has prompted research to improve ultrasound definition of the secondary palate. Usually the amniocentesis for karyotype should be offered in all cases of cleft lip/palate because of the risk of aneuploidy **(Fig. 34.68A to D)**; also the patients should be counseled that ultrasound occult additional anatomic abnormalities might be present with all clefts.[72,73]

Ultrasonographic Detection of the Palate

The primary palate includes the lips and jaw bone to the nose root and is the most easily detected part of the anatomy by 2D scan. Indeed many sustain that it is worthwhile visualizing the lips, jaw bone and nose root with an oblique coronal scan, scrolling upwards during the routine second trimester scan and it is evident to users of 3D that this suggestion is almost superfluous when a scan of the fetal face is part of the routine. The secondary palate consists of a hard palate, which runs posterior and horizontal to the incisive foramen and soft palate or velum, which curves downwards and backwards from the posterior aspect of the hard palate and ends in the uvula. In the fetus, the hard/soft palate is 2.1 and the soft palate has the similar thickness. Usually the cleft of the secondary palate is always midline and results from failure of the palatine processes to elevate and grow. Cleft of the secondary palate starts from uvula and soft palate, but it is possible the cleft of soft palate with an intact hard palate[74]. The severe shadowing of the maxilla made difficult but not impossible the visualization and the diagnosis of clefts of the secondary palate. Sherer and colleagues[75] say that visualization of the secondary palate is not difficult by axial plane 2D scan, but they don't report any cases of defects of secondary palate. In this case, the new volumetric probe 3D multiplanar and surface rendering offers greater possibilities of study of the normality and of diagnosis of the cleft of the primary and secondary palate.[76-78] By 3D it is possible to see the alveolus and maxilla by axial scan and secondary palate by coronal scan by scrolling front-to-back in coronal plane. In this method one faces the problem of maxillary shadow. Campbell[79] overcame this problem by rotating the face through 180° and scrolling from back-to-front. This technique, described as 'reverse face view' eliminates the shadowing of the maxilla, but it offers the possibility to have a good vision of the hard palate but not of the soft palate. Platt and colleagues[80] found a different technique to see also the soft palate by axial 3D plane (multiplanar and surface rendering) with inverted picture to avoid the shadowing of the maxilla and using a little acoustic box scrolling from chin to nose (flipped-face view) **(Fig. 34.69A and B)**. Platt and colleagues[81] used a sagittal scan and by this technique the mandibula, the tongue, the maxilla, the alveolar ridge, the secondary complete palate are systematically seen and offers a good mode to diagnose the clefts of the primary and secondary palate **(Figs 34.70A to C).** Faure and colleagues (13) propose the same technique of Platt by coronal scan, because they were able to obtain the view of the palate in all 100 low-risk cases, all with normal anatomy after delivery, from 17 to 23 weeks. Pilu and Segata[82] describe a new multiplanar approach to study the secondary palate

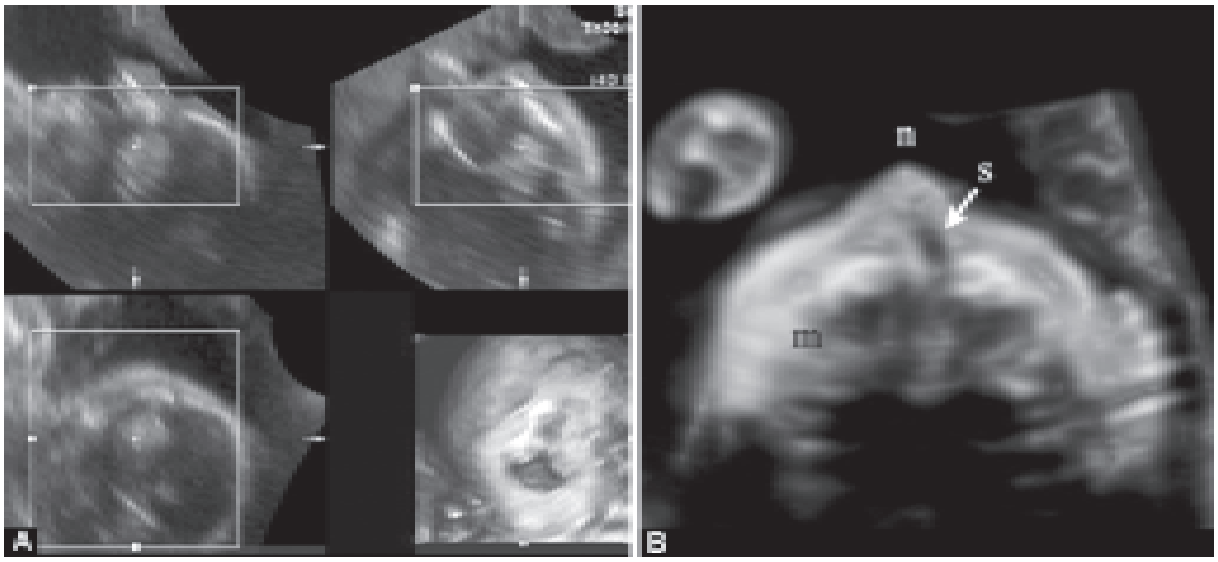

Figures 34.69A and B: The axial 3D plane by multiplanar and surface rendering "flipped view face" to see a cleft-lip cleft alveolar ridge

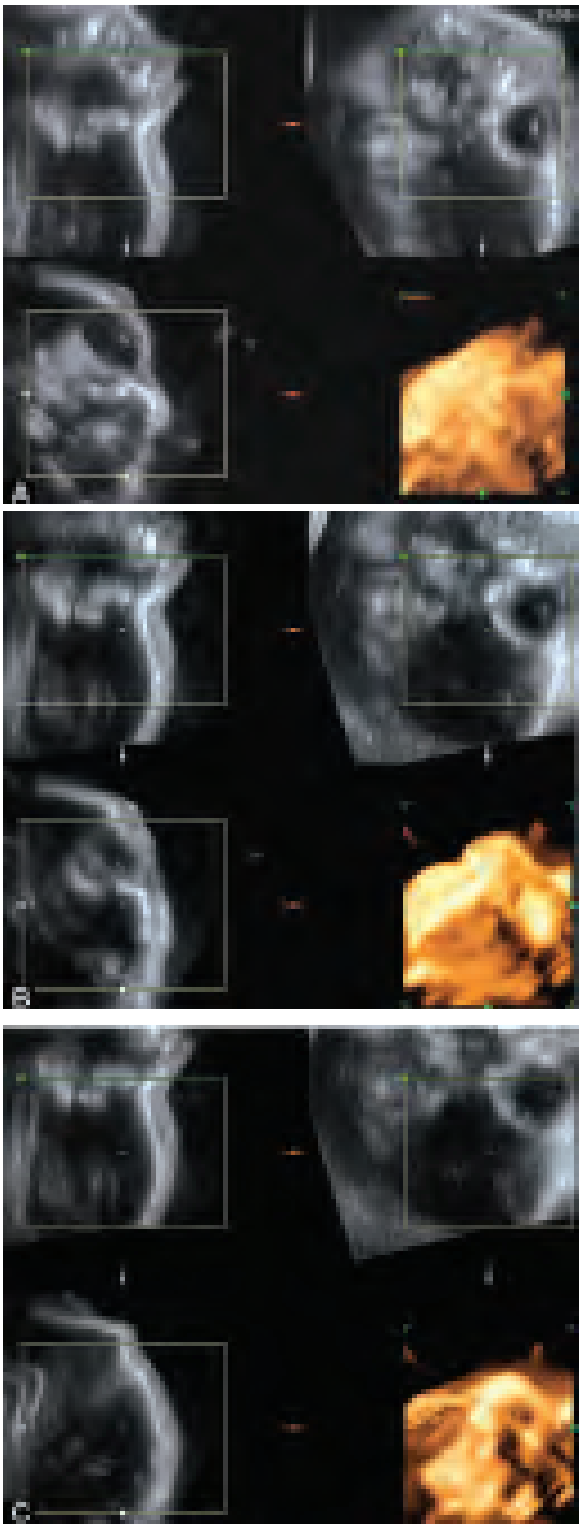

Figures 34.70A to C: Axial 3D plane, inverted image, "flipped view face", sagittal scan: (A) Cleft lip; (B) Cleft alveolar ridge; (C) Cleft palate

using TUI (Tomography Ultrasound Imaging); to avoid the shadowing of the alveolar ridge. The authors used a scan with an angle of 45° and obtained a satisfactory view in 10 of 15 cases between 19–28 weeks. Now, then, we have many possibilities to study systematically the primary and the secondary palate by 2D, but with greater possibilities by 3D[83]. It is reasonable to say that gold standard is to have experience with all techniques, above all in cases of doubt or of diagnosis of facial cleft to define exactly the limit of lesion. By axial 3D plane (sagittal or coronal scan) Campbell[84] proposes a screening of secondary palate in the first trimester. In fact it is easy from 11–14 weeks to see the secondary palate (delta sign) but, if the screening is effective in diagnosing orofacial clefting, it will require further study. (Delta sign). The scan in the second trimester, week 19–22, is associated with a greater possibility of detecting the primary and secondary palate and of diagnosis of facial clefts.

Secondary Palate

The scheme of Berkowitz illustrates that the uvula is always involved in cleft palate and could simplify detection, but in practice it is difficult to detect this small anatomical part with 2D and 3-4D.

Two-dimensional (2D) scans can be used to study the hard and soft parts of the secondary palate and detect the uvula. However, it is necessary that the fetal head be in a favorable position, possibly with the lips slightly apart. Today (Whilelm 2010) a new marker the equal sign **(Figs 34.71A to E)** offers a new easy possibility to detect or suspect an isolated palate cleft. In axial scan (better than coronal, unusual and difficult),with the same scan to measure the BPD **(Figs 34.72A to D)** with a little inclination, is relatively easy to find the pharynx like an anechoic round area with double signs of the uvula. In case of the bifid uvula, it is important to study the secondary palate and the 3D (min-max rendering, Faure method or others, omniview). It became a beautiful tool to investigate.

Three-dimensional (3D) scans have greater possibilities because a volume can be saved and examined later in an infinite number of scanning planes. Various methods have been proposed:

- Axial surface rendering plane with a small box (flipped face view) and inverted scan to avoid maxillary shadow (scrolling upwards) by sagittal or coronal scan
- Coronal surface rendering plane, reverse-face (scrolling forwards) or front face (scrolling backwards) scan **(Fig. 34.73)**

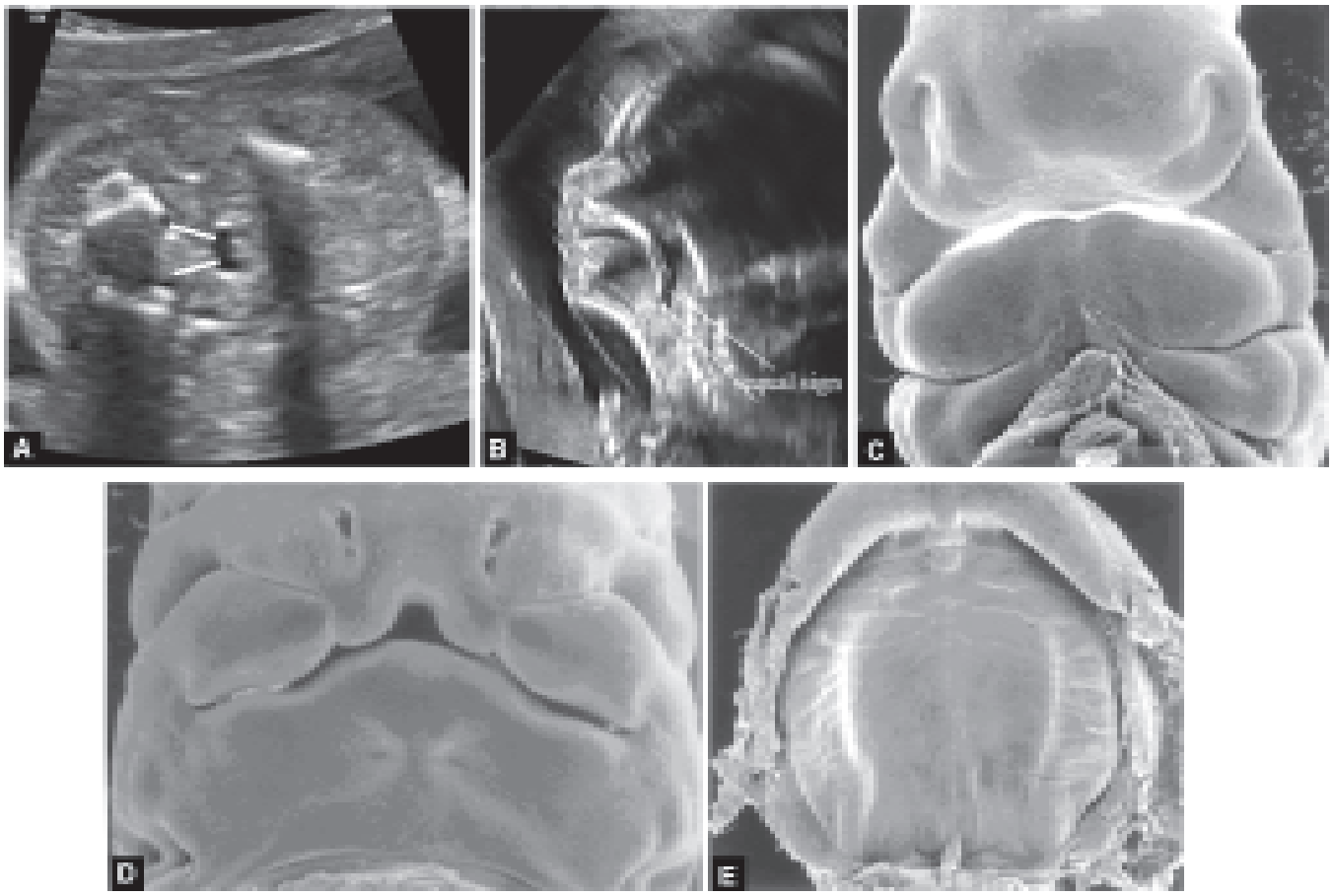

Figures 34.71A to E: (A and B) Sagittal and axial scan offer a good possibility to see the "equal sign". The arrows indicate the two signs; (C) 6-weeks-old embryo: maxillary swellings fuse with medial nasal swellings, which merge with each other. The upper lip is still incompletely formed; (D) 53-day-old embryo: secondary palate: the fusion with primary palate has occurred; (E) 59-days-old embryo: complete fusion of the secondary palate has occurred.
Courtesy: K Sulik, Chapel Hill, Nort Carolina

- TUI tomography ultrasound imaging sagittal scan with angle of 45°.

Ultrasound technicians will be increasingly called upon to check the integrity of the secondary palate due to the high prevalence of facial defects at birth and the high percentage of malformations, syndromes and chromosome anomalies, associated especially with cleft palate. Three-dimensional techniques offer ways of achieving this. Among those described above, the 3D axial plane is the fastest and easiest to apply, and has been reported to detect the secondary palate in almost all cases in 2–3 minutes when echographic conditions do not pose an impediment. Variable fetal position in relation to maternal fat is the only serious obstacle to its correct detection. Today it would seem reasonable to propose study of the hard and soft palate only in cases with suspected or confirmed diagnosis of facial clefting and in cases with a positive family history or after nonvisualization of the equal signs in 2D.[85]

The Chest

The chest contains the heart, an organ fundamental for human life. Study of the heart, efflux and the circulatory system[86] has exploited 3-4D technology and STIC **(Figs 34.74A and B)** mode (spatiotemporal imaging correlation), which being in four dimensions, cannot be illustrated in an atlas. However, fixed, invert, power, color and Doppler 3D images and study in real time by tomography ultrasound imaging (TUI) are striking, interesting, and considerably improve diagnostic

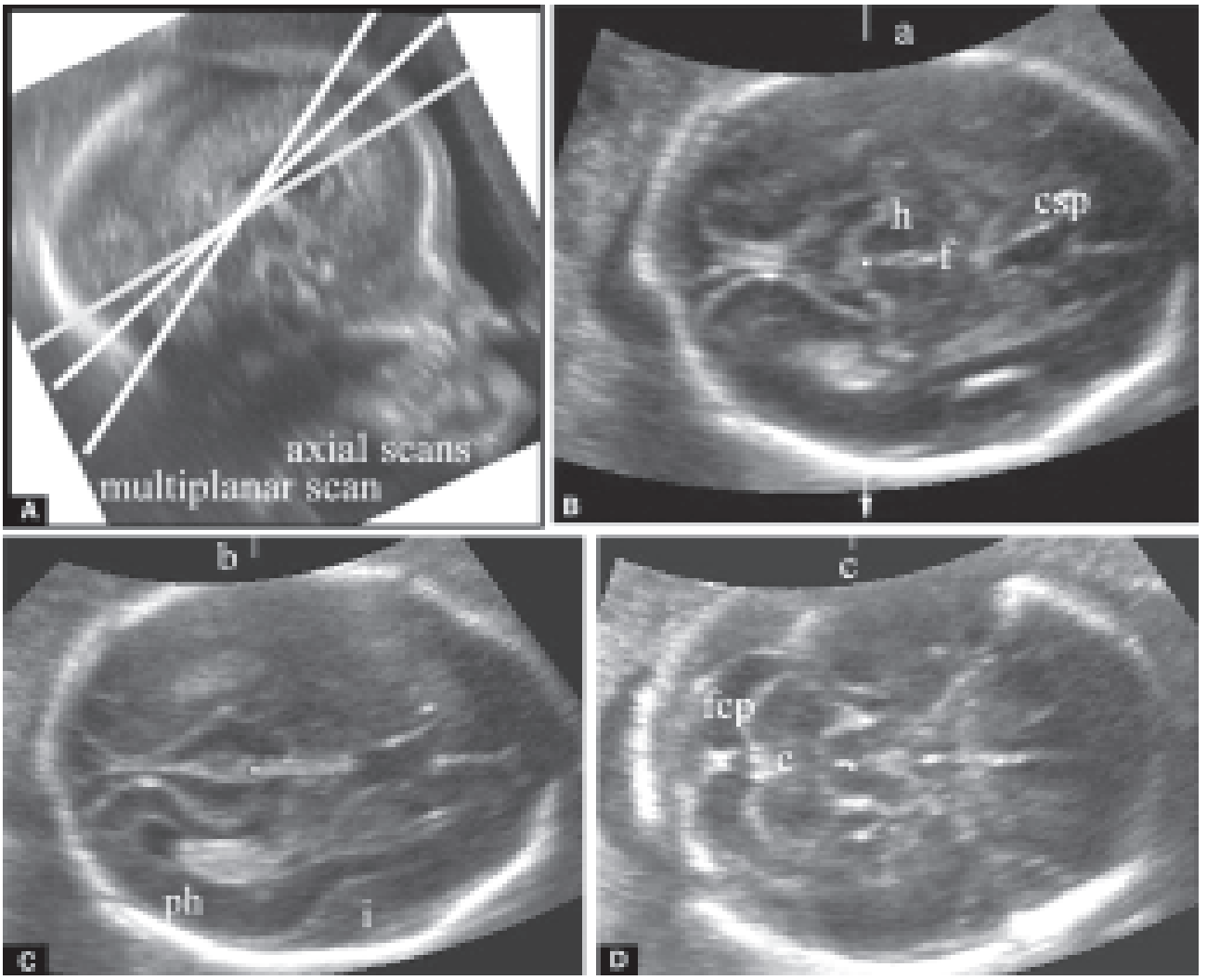

Figures 34.72A to D: Axial scans of fetal head. The three scans are the usual sections to measure BPD, to see the posterior horns and to measure the cerebellum. c: cerebellum; csp: cavum septi pellucidi; f: falx; pcf: posterior cranial fossa; ph: posterior horn; h: hypothalamus

capacity. At this time, the b-flow is the alone possibility to study the vein efflux with low flow and can also become complementary to STIC in heart pathology; but it is not easy to learn the b-flow. Lung volume can be measured by the VOCAL system[87,88] improving the prognosis and outcome of fetuses with diaphragm hernia, and is expected to replace thickness as an indication for therapy *in utero*. With special experience it is possible to correctly visualize the course and morphology of the esophagus. The volume of the thymus, an important fetal organ, can be assessed. The diaphragm is quite evident, reducing diagnostic doubts about hernia. The gall bladder is also easily visualized **(Figs 34.75 and 76)**.

The Abdomen

Visualization of the viscera and stomach are less exciting than the face, though the vascularization of the liver is striking.[89] Regarding the urinary system, it is easier to study the renal arteries and parenchyma vessels, and kidney volume is a better index of development than traditional biometry.

Neural Tube and Limbs

The normal feet are shown in **Figures 34.77A and B.**

The volume acquisition is one of the most important technological achievements of the last decade in diagnostic ultrasound and offers a good possibility to

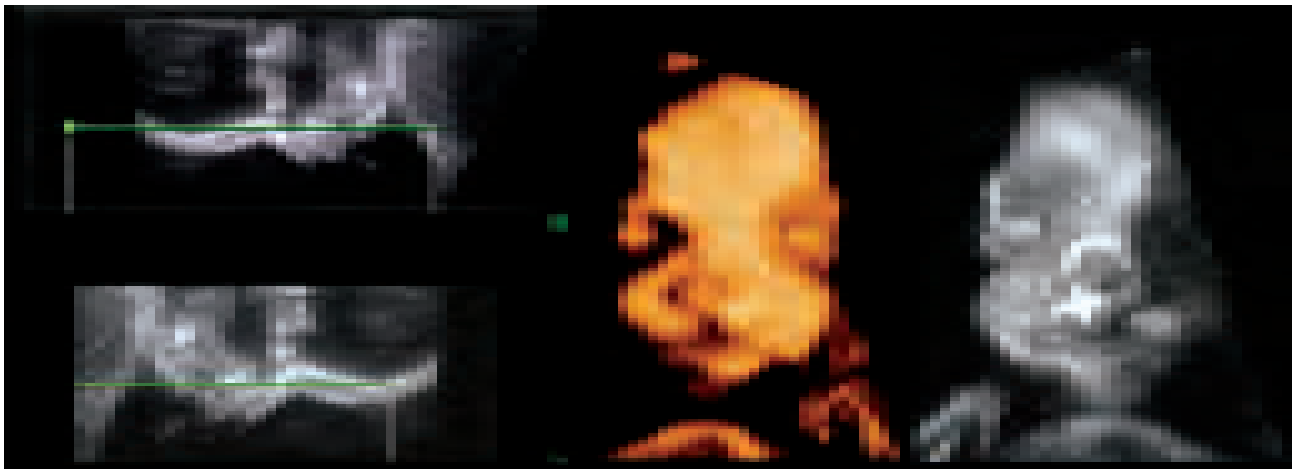

Figure 34.73: Cleft-lip by "reverse face" mode and "front face" in the same case, of course change the position of the cleft

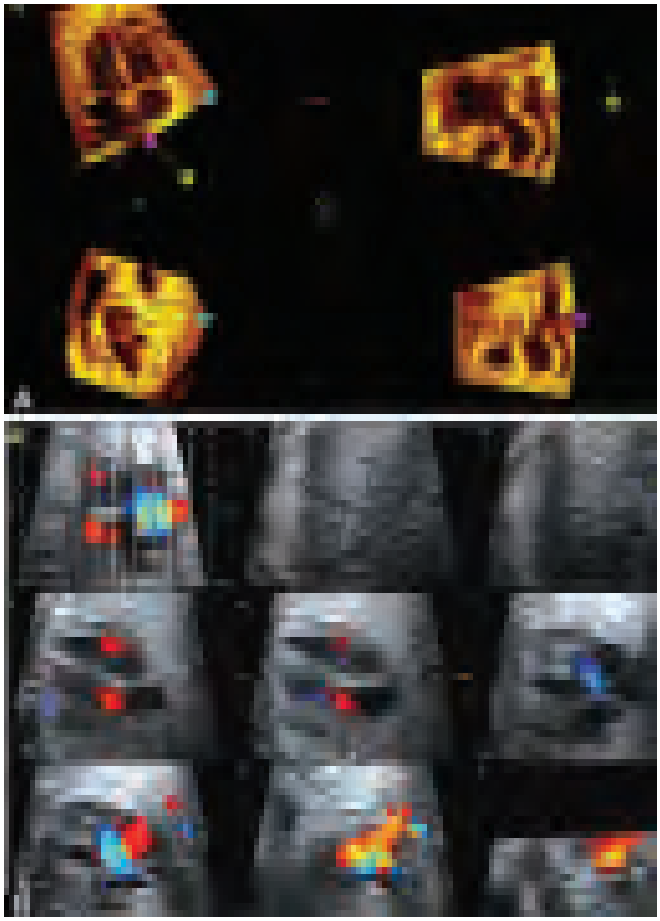

Figures 34.74A and B: The omniview and STIC are good tools to explore the heart

study the spine. In particular, there is the multiplanar which gives the possibility to navigate within a volumetric space through infinite reproducible imaging planes (including the crown), in real time. There is also rendering which has the ability to represent surfaces, as well as the VCI-c plane that makes it possible to dissect an orthogonal plane with ultrasound scanning by integrating multiplanar and rendering.[90] A further step forward is the VCI-OmniView, which has the ability to model the source of 3D insonation by adapting to the structures of the fetal body that are normally represented by curved and straight lines (also the median line at the bottom is an artifact ultrasound).[91] This technique allows direct and relatively simple scans which adapt to the adjustable thickness of the structures corpus studied (20 mm spine). There is no doubt that with a 3D-4D instrument equipped with VCI-c-plane adapted to insonation, can produce virtually overlaping results in terms of detecting anatomical structures in almost all three trimesters, also if with significantly reduced times using the omniview in the second trimester. The VCI-OmniView, sharing the latest technological achievements, allows one to specify the anatomical study of the fetus by choosing the ideal section plane. Regarding the multiple planes, that being in 3D and 4D in the same volume, it can better yet follow the natural curves and angles of the structures, while rotating like a real scanner box that can focus on very small points, which would otherwise be very difficult to explore.

The detailed study is therefore quite superior since it can easily and quickly visualize the structures, which can be sometimes detectable with 3D-4D, only under particular conditions.

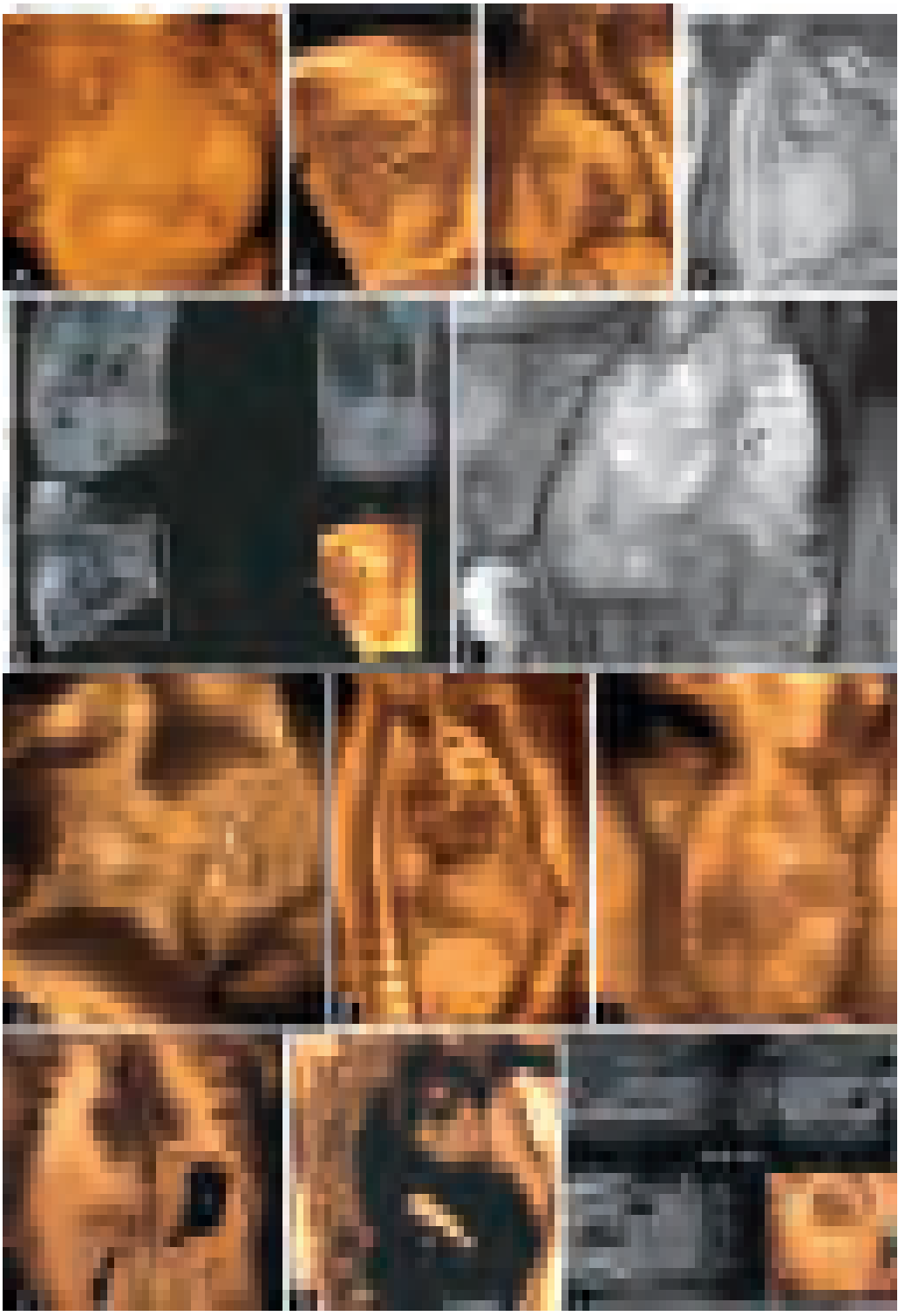

Figures 34.75A to L: The chest and abdomen from the oral cavity to the esophagus are conveniently examined by 3-4D. The esophagus can be viewed from the oral cavity to the stomach by 3D, aiding diagnosis of stenosis-agenesis. All organs (lung, diaphragm, heart, thymus and bowel) are realistically represented by 3D. a: aorta; b: bowel; c: gallbladder; d: diaphragm; e: esophagus; h: heart; t: thymus

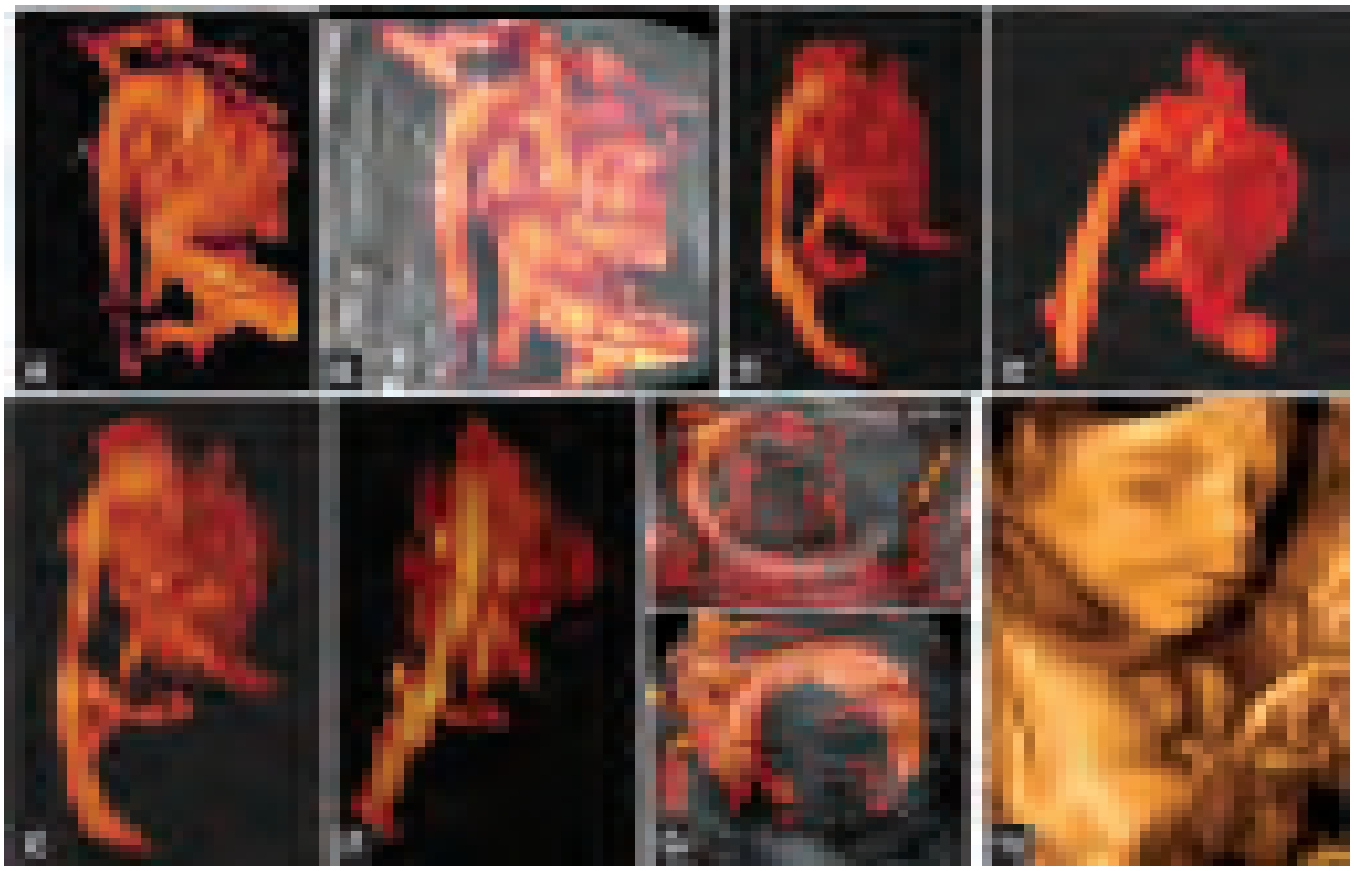

Figures 34.76A to H: The glass body tool enhance the fetal circulation and thoracic conformation (a) aorta; (p) pulmonary artery; (vci) inferior vena cava, (u) umbilical artery

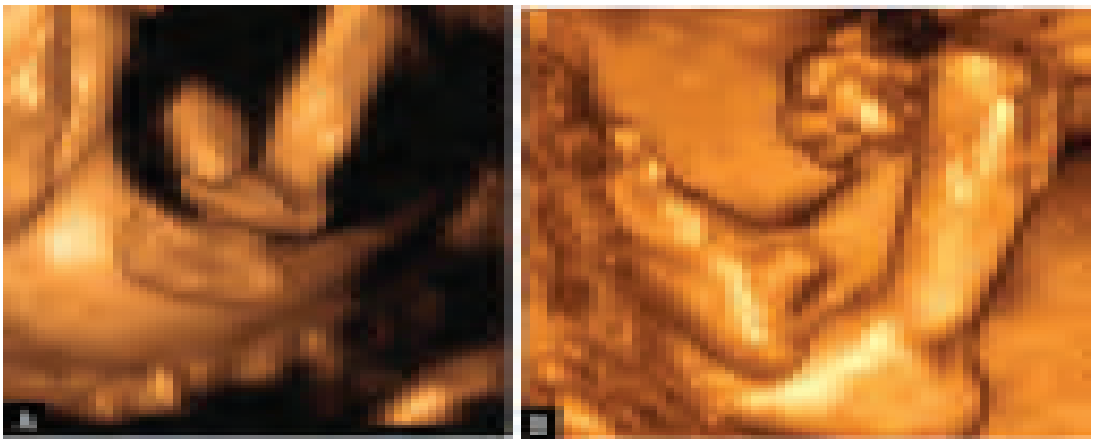

Figures 34.77A and B: The normal feet

Study of the vertebral column and possible anomalies is much more convenient with 3-4D maximum mode which provides easy visualization of all bones including the phalanges, as well as faster identification of any anomalies (platyspondyly, hemivertebrae, kyphosis, scoliosis such as absence (agenesis) or extra elements **(Figs 34.78 and 34.79).** The osteochondrodysplasia have a prevalence of approximately 2.4 per 10,000 births and are represented in about 70% of four conditions: thanatophoric dysplasia, achondroplasia, achondrogenesis, osteogenesis imperfecta (type II). Dysplasia of the nasal bone has been shown in **Figure 34.80.**

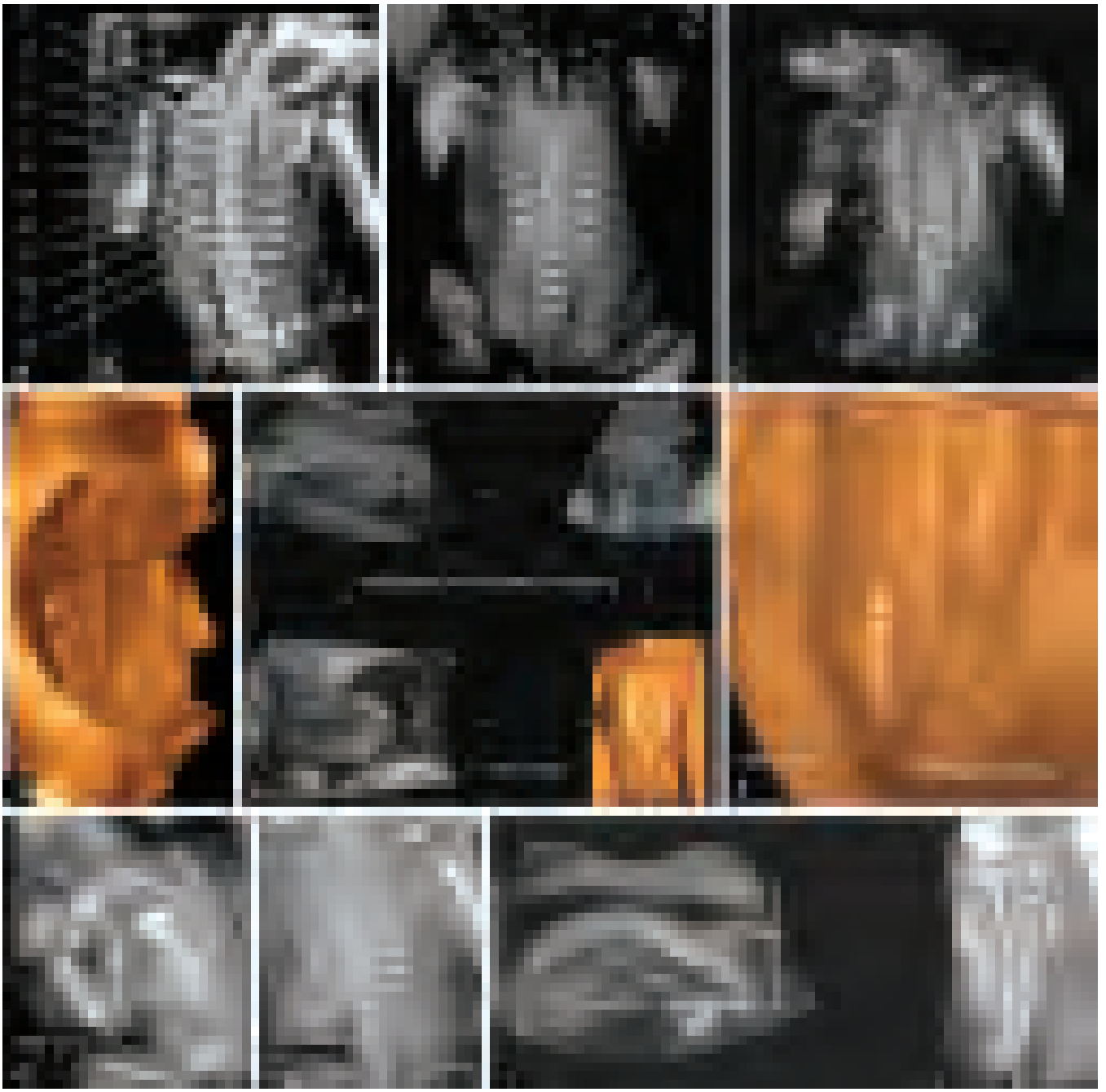

Figures 34.78A to I: The vertebral column and vertebra are a striking field of application of 3-4D. The images are beautiful and enable diagnosis of the exact point of malformation

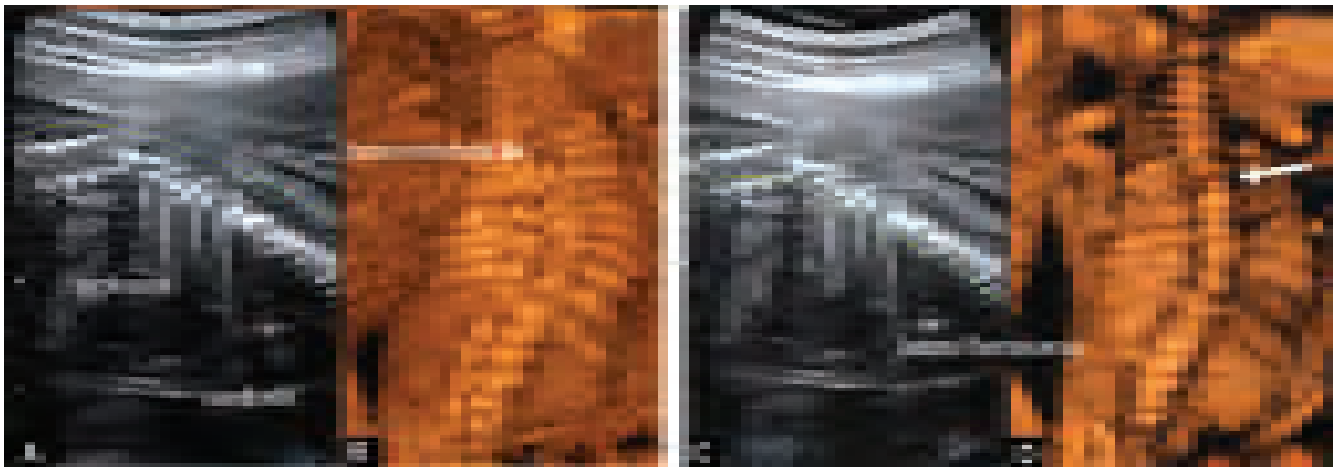

Figures 34.79A to D: By omniview today we can achieve pictures of the spina more detailed and also diagnose or kyphosis with hemivertebra or lateral hemisoma. The 3D improves the ultrasound diagnosis

The use of 3D doesn't offer a better condition to study the long bones, even if it is a good tool to store a volume and to explore by infinitive planes; but the study of dimension of the long bones, for instance the femur and the humerus **(Figs 34.81 and 34.82)** for the suspicion of Down syndrome is the same by 2D or 3D **(Figs 34.82A to E)**. Instead the control of the extremity is a good field of exploration for three-dimensional scan. The club foot **(Figs 34.83A to D)** varus or valgus meet 415 syndromes in London Medical Databases; it is an important malformation because it is often associated with other malformations or in about 2% with aneuploid malformation and in the last decade the detection rate of club foot achieve approximately 80% with about 15% of false-positive rate.[92] It is reasonable to think that the use of 3-4D, by tools maximum mode and omniview, will possibly improve the diagnosis of malformation of the extremity (feet and hands) and decrease the false-positive rate, because three-dimensional scan is better in the study of anatomical detail **(Figs 34.84A to F).**

Genitals

The genitals are a new field of study. It is relatively easy to diagnose sex in the second trimester by 2D and to determine descent of the testicles at 26–28 weeks (third trimester). However, the diagnosis of pathology of the external genitalia, such as hypospadia, is much easier with 3D (tulip sign)[93] **(Figs 34.85A to D)**.

Placenta and Umbilical Cord

Detection of cord pathology (such as cysts), retrocervical position and number of twists is especially easy and reliable with power color glass-body mode **(Figs 34.86A to C)**. Also the study of position and vascularity of the placenta is easier by 3-4D[94,95] **(Figs 34.87A to I)**.

The perfusion of the placenta at different weeks (12th,16th, 20th) are shown in **Figures 34.86A to C**.

The above is not intended as a scientific evaluation of the merits of 3-4D with respect to 2D, however almost all researchers report improved sensitivity and a better detection rate using 3-4D to measure volumes, determine orientation and definition of vessels and more precise definition of malformation, study coronal planes and the fetal face, diagnose heart malformations (by STIC), visualize limbs and fingers and study embryo-fetal anatomy (especially neurosonology). All this does not establish a need for 3D for the structural study of the fetus, but certainly indicates that 3D instruments can improve ultrasound and make examination easier and more pleasant.

Motor Activity and Facial Expression

The structure of the fetal brain is in the process of development and in each phase of intrauterine life, it has a maximum functional level. The first regions to mature are those necessary for life, such as sucking, swallowing and breathing. A first growth spurt is recognized between 10 weeks of gestation and 18 months of neonatal life, with synapse formation and myelination.

Fetal movements can be divided into primary motor patterns and primary automatisms. The former are present in the first half of pregnancy and are genetically determined, whereas the latter depend on interaction

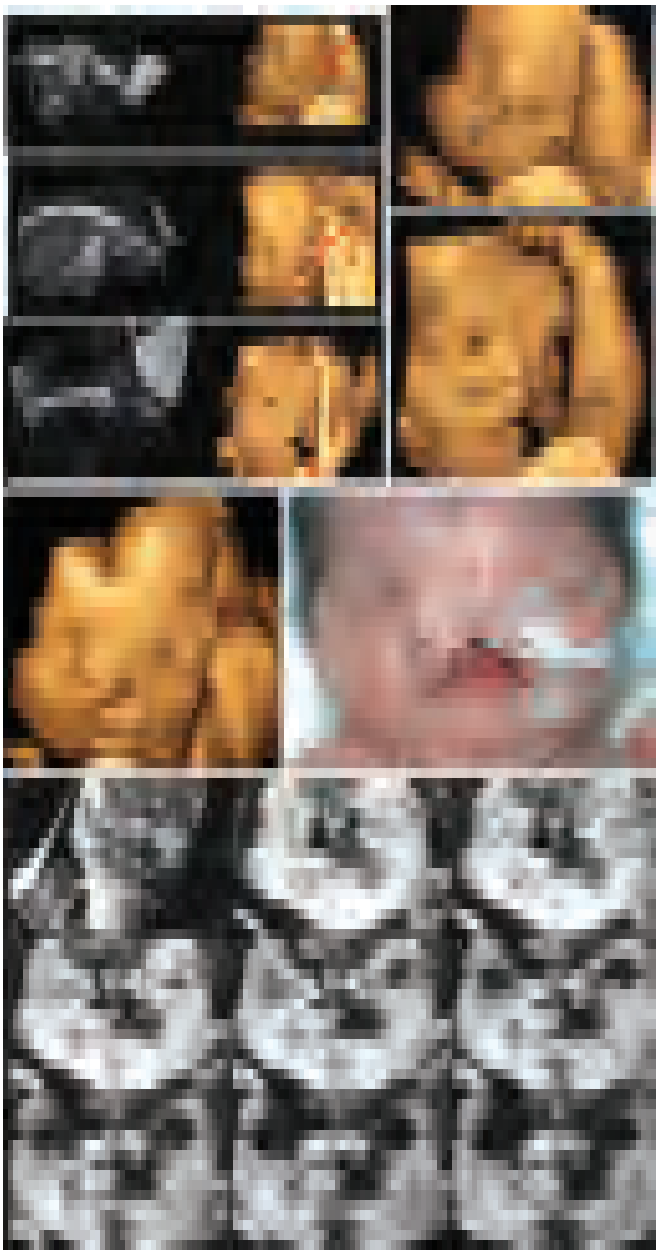

Figure 34.80: Frontonasal dysplasia

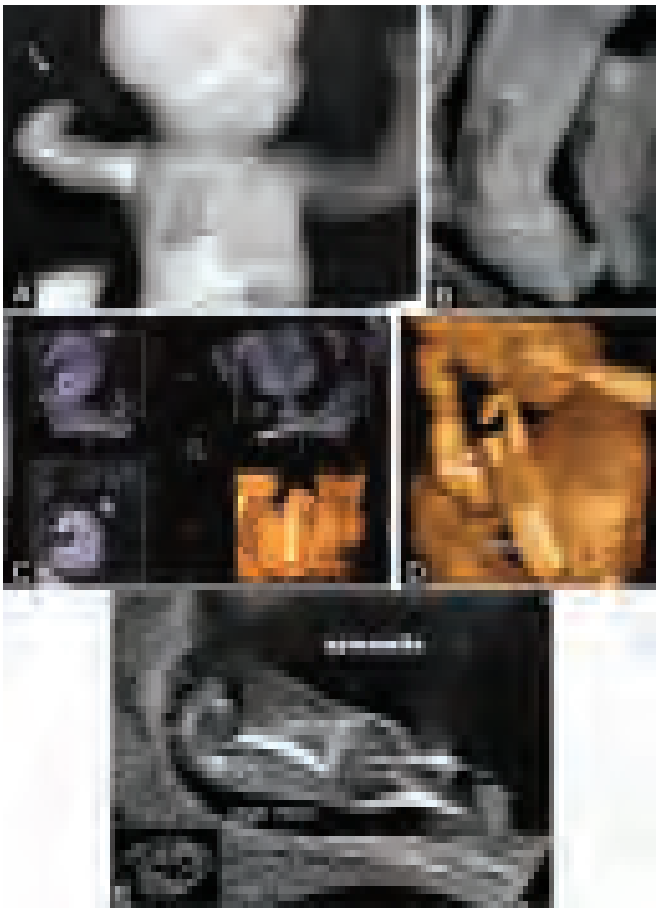

Figures 34.81A to E: Pathology: amputation of the left arm and symmelia

of the fetus with its environment and occur from week 10 of gestation into the first years of extrauterine life. Active fetal movements increase with maturation of the nervous system, reaching a maximum at 32 weeks (after which they begin to decline)[96]; in the term fetus movements are similar to neonatal movements. Fetal circadian rhythm and fetal behavioral states such as quiet sleep, active sleep, quiet waking state, active waking state and crying, are recognized. Alternation of these fetal behaviors in the 24 hour period is a sign of neurological maturation. Ultrasound can assess a fetal biophysical profile composed of fetal movements, muscle tone, respiratory movements, placental maturation and amount of amniotic fluid.

Doppler flow imaging plays a fundamental role in assessing fetal wellbeing, by evaluating alterations in blood flow in the placenta, fetus and mother. Robles de Medina and colleagues sustain that male and female fetuses do not show behavioral differences.[97] Dynamic 3D scan (4D) can be useful together with 2D to study fetal behavior in the second trimester of pregnancy.[98]

Brain Function

Though up to a few years ago, the study of fetal brain function and hence motor activity, attitudes, posture and facial expression were of little interest but now, with 4D techniques that enable more accurate visualization in real time of everything the fetus can do

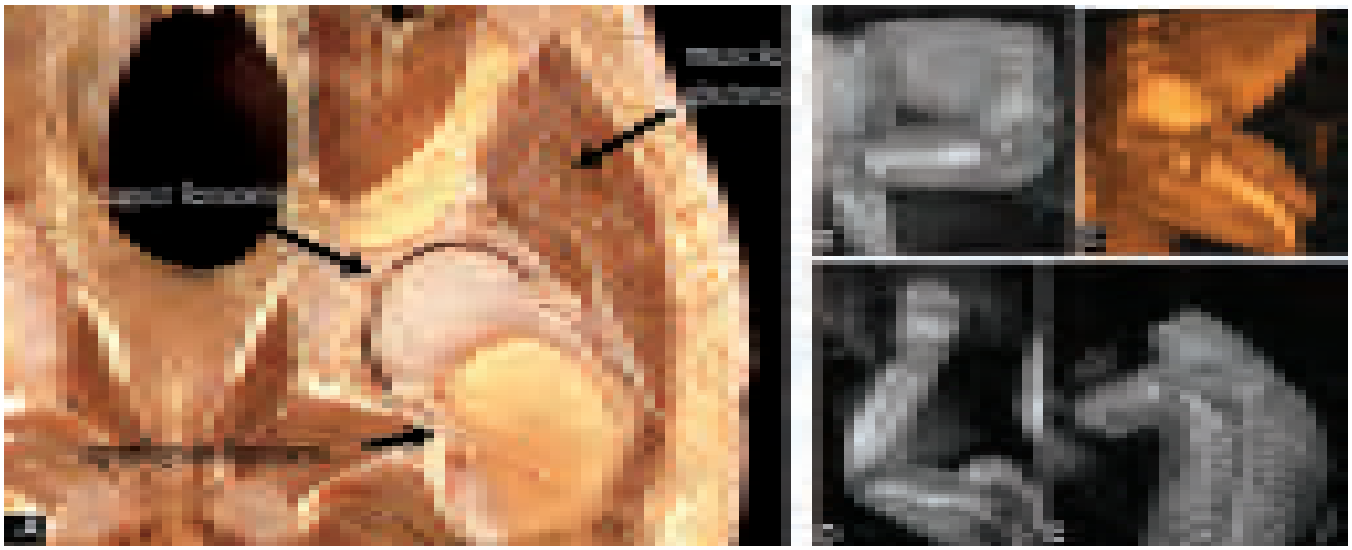

Figures 34.82A to E: By omniview, the study of long bones and their articulations is feasible. Some examples of femur and humerus articulations

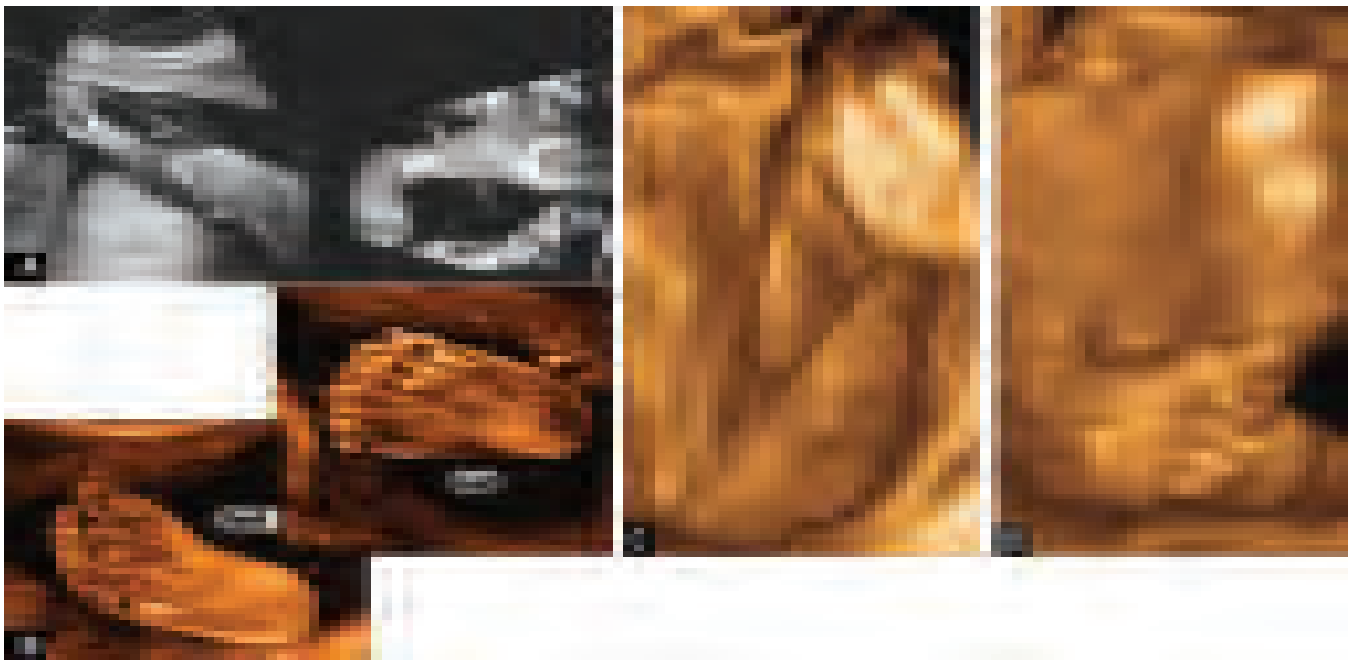

Figures 34.83A to D: Club feet at different weeks by minimum and maximum mode

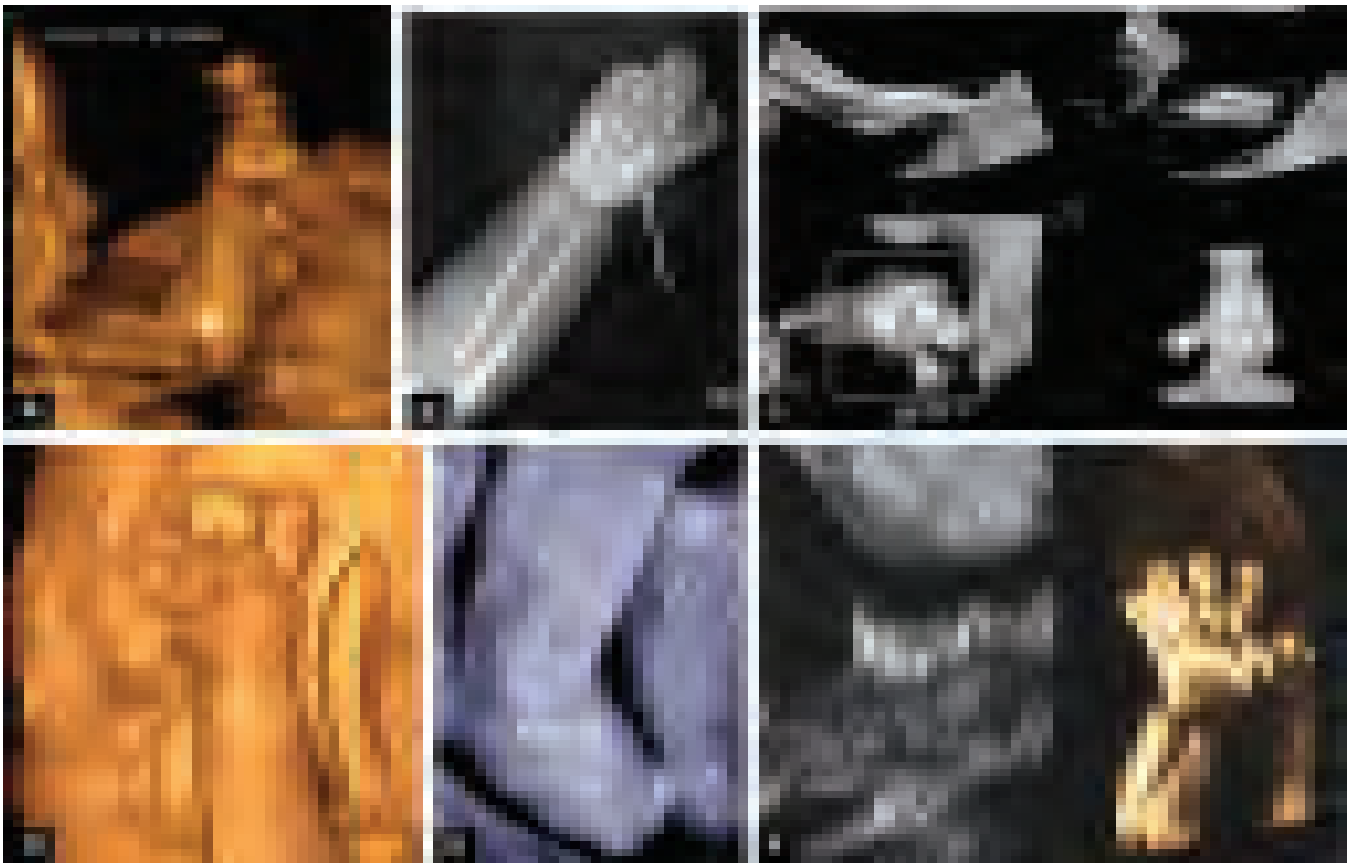

Figures 34.84A to F: Pathology of the hand: agenesis of right hand, syndattilia and fused metacarpal bones (4th-5th), amputation of the forearm, brachidattilia

in utero, studies of fetal activity have become increasingly numerous. These studies are concerned with activity from the point of view of physiology as well as brain pathology.[99] We now know much about fetal cognitive and emotional development from observation of premature babies who now survive from as early as 22–23 weeks of gestation. Clearly, extrauterine life involves stressors that force the premature baby along the path of brain development, often with irremediable delays due to anoxia. Observation of premature babies therefore cannot be taken as validation of the physiological evolutionary milestones of the fetal brain. Renewed interest in this field has been spearheaded by Kurjak, who foresees major clinical benefits for 4D study of fetal behavior. We personally have studied the moment when laterality, the predominance of one hemisphere over the other, is established. Laterality has been the same all over the world for thousands of years. No scientific explanation of the predominance of the left over the right hemisphere has yet been found, if not an ancestral genetic mutation. Today there have been many papers, especially from Scandinavia, associating predominance of the right hemisphere, and hence predominant use of the left side of the body, with a significant increase in mental disorders. The 4D scan enabled us to determine laterality in about 90% of fetuses between weeks 10 and 11.

Behavior, Senses and Response to Stimulation in The Second and Third Trimester

As mentioned, much is now known about fetal behavior at various gestational ages from the study of premature babies. However, the possibility of observing the fetus in its natural habitat in real time by 3-4D has led much research that may help us to assess fetal wellbeing and specifically, the degree of neurological development in physiological situations and in the presence of CNS pathology. It is fairly easy to detect a fetus who yawns, puts out its tongue, touches itself and its surroundings,

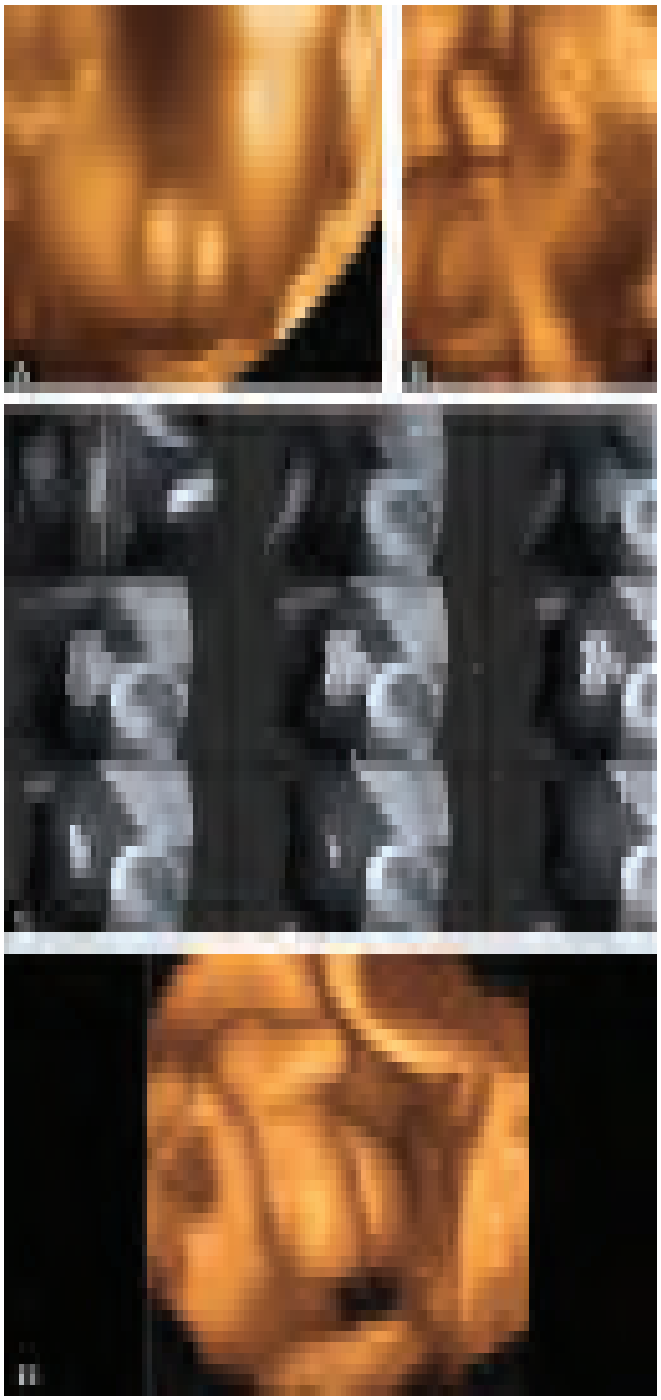

Figures 34.85A to D: By 2D it is easy to see the genitalia in the second and third trimesters but 3-4D (3D and TUI) is more practical for finding tulip sign

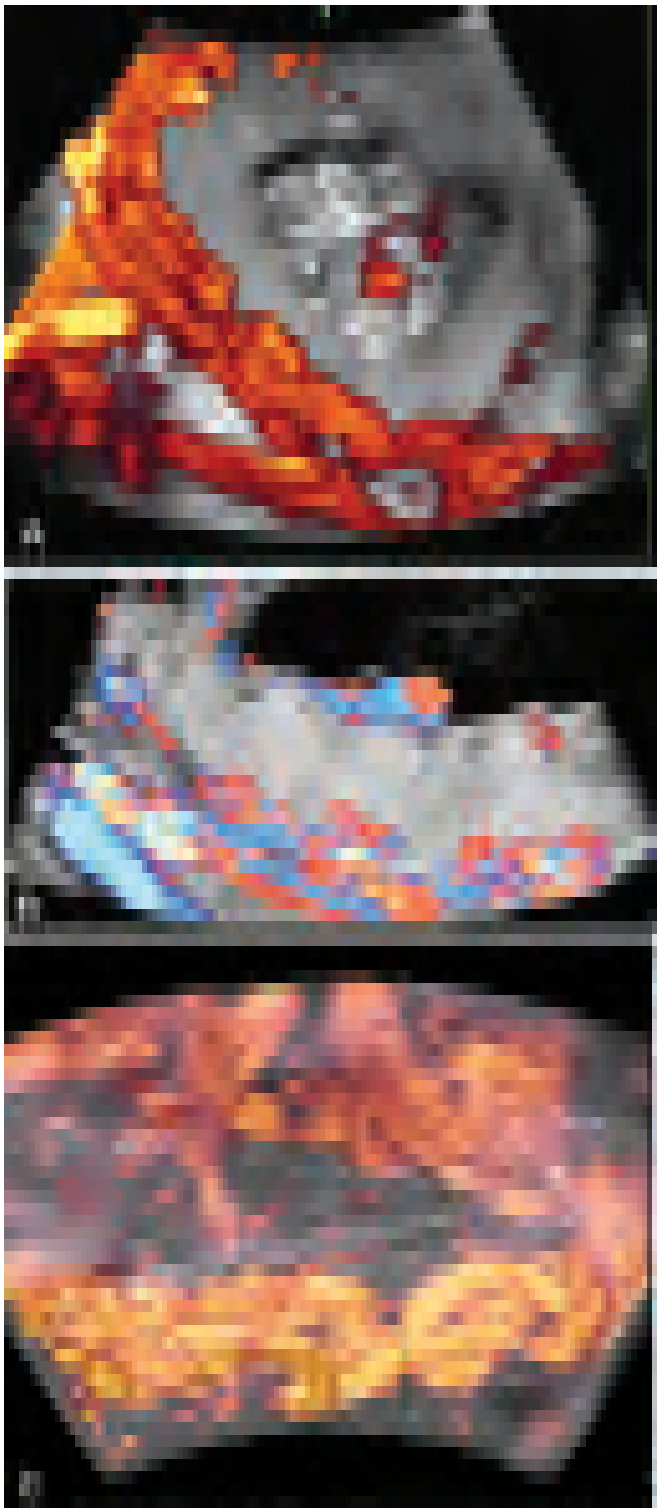

Figures 34.86A to C: The perfusion of the placenta at different weeks (12th,16th, 20th)

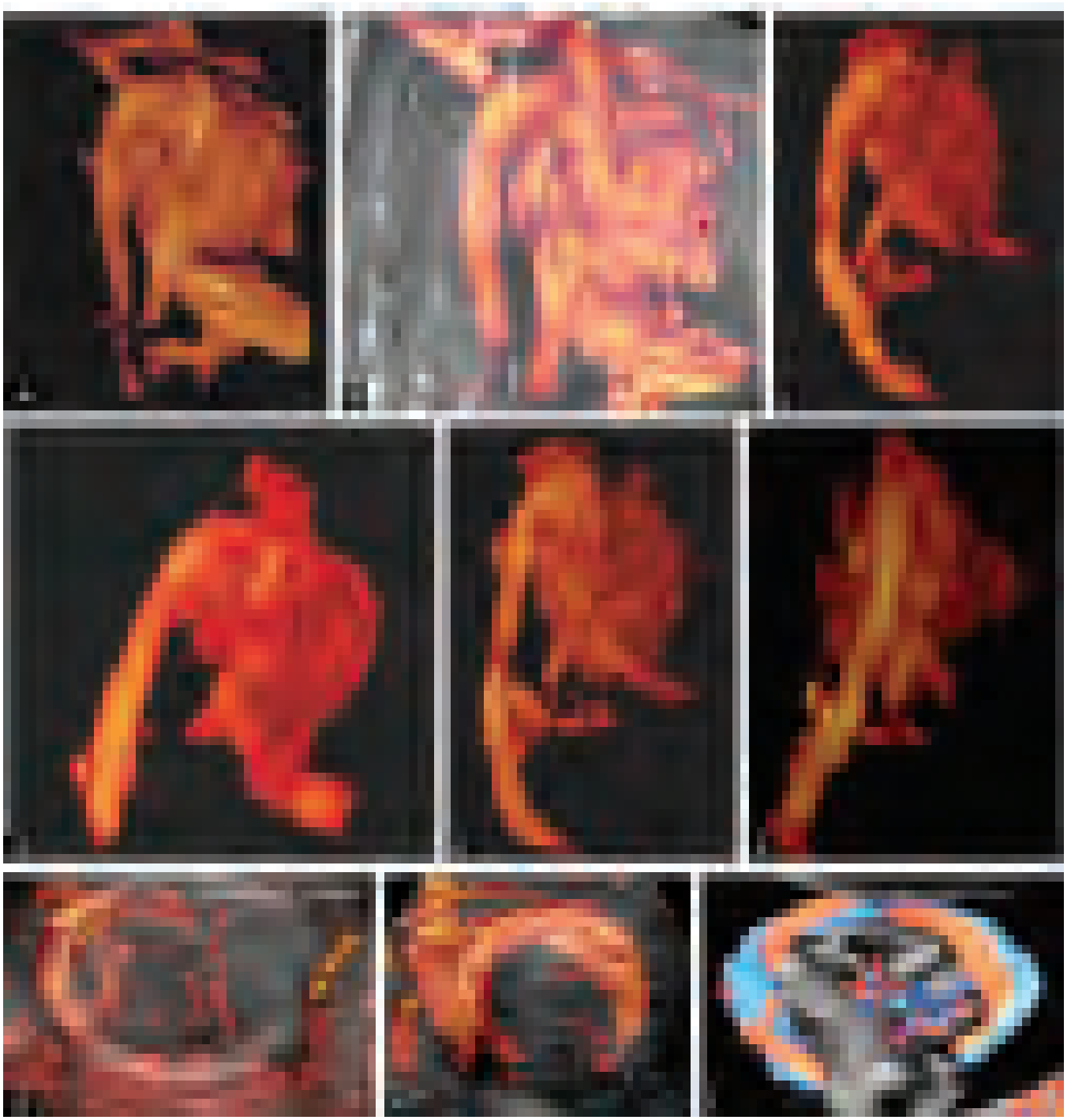

Figures 34.87A to I: Cardiovascular system images are beautiful in 3D. It is even possible to determine the position of the umbilical cord and the number of turns around the neck. a: aorta; p: pulmonary artery; ivc: inferior vena cava; u: umbilical cord or artery

developing its sense of touch, pulls faces after ingesting amniotic fluid (taste), opens its eyes (attempts at seeing?), responds to sounds (hearing), responds to manual stimulation (many sustain that parental stimulation of the fetus by stroking or patting the maternal abdomen leads to faster and more intense development of neuronal function), starts (from weeks 11-12 the fetus can be observed reacting whenever its fingers and toes touch the wall of the uterus), hiccups, smiles, grimaces, frowns and expresses pain or serenity. The fetus therefore sends us many messages through its behavior. Though much progress has been made, no scientifically demonstrated clinical applications of behavior have yet been developed. It is certainly fascinating for parents and specialists to observe a fetus by 4D, and it reinforces the hedonistic aspect of ultrasound examination in pregnancy.

REFERENCES

1. Dyson RL, Pretorius DH, Budorick NE, et al. Three-dimensional ultrasound in the evaluation of fetal anomalies. Ultrasound Obstet Gynecol. 2000;16(4):321-8.
2. Merz E, Bahlmann F, Weber G, et al. Three-dimensional ultrasonography in prenatal diagnosis. J Perinat Med. 1995;23(3):213-22.
3. Merz E, Welter C. 2D and 3D Ultrasound in the evaluation of normal and abnormal fetal anatomy in the second and third trimesters in a level III center. Ultraschall Med. 2005;26(1):9-16.
4. Pilu GL, Ghi T. Preliminary experience with advanced volume contrast imaging (VCI) and OmniView in obstetric and gynecologic ultrasound. GE Healthcare. 2010
5. Forsberg F, Berghella V, Merton DA, et al. Comparing image processing techniques for improved 3-dimensional ultrasound imaging. J Ultrasound Med. 2010;29(4):615-9.
6. Michailidis GD, Papageorgiou P, Economides DL. Assessment of fetal anatomy in the first trimester using two- and three-dimensional ultrasound. Br J Radiol. 2002;75(891):215-9.
7. Xu HX, Zhang QP, Lu MD, et al. Comparison of two-dimensional and three-dimensional sonography in evaluating fetal malformations. J Clin Ultrasound. 2002;30(9):515-25.
8. Downey DB, Fenster A, Williams JC. Clinical utility of three-dimensional US. Radiographics. 2000;20(2):559-71.
9. Campbell S. Doppler and 3D ultrasound in infertility: do they alter the outcome for the patient? Ultrasound Ostet Gynecol. 2003;22(Suppl 1):24-5.
10. Rosignoli L, Periti E, Centini G. 3D Omniview sonography in the pre-assisted reproductive medicine programme. Ultrasound Obstet Gynecol. 2010;36(Suppl.1):52-167.
11. Timor-Tritsch IE, Fuchs KM, Monteagudo A, et al. Performing a fetal anatomy scan at the time of first-trimester screening. Obstet Gynecol. 2009;113(2 Pt 1):402-7.
12. Hafner E, Metzenbauer M, Stümpflen I, et al. First trimester placental and myometrial blood perfusion measured by 3D power Doppler in normal and unfavorable outcome pregnancies. Placenta. 2010;31(9):756-63.
13. Souka AP, Pilalis A, Kavalakis Y, et al. Assessment of fetal anatomy at the 11-14-week ultrasound examination. Ultrasound Obstet Gynecol. 2004;24(7):730-4.
14. Tonni G, Centini G, Taddei F. Can 3D ultrasound and doppler angiography arteries be included in second trimester echocardiographic examination? A prospective study on low-risk pregnancy population. Echocardiography. 2009;26(7):815-22.
15. Centini G, Sollazzi S, Rosignoli L, et al. Capacità diagnostica ecografica dei processi mal formativi nel primo trimestre di gravidanza: è proponibile l'ecografia morfologica dalla 11a alla 14a settimana? Il Ginecologo. 2010;5(1-2):22-9.
16. Merz E. Spina bifida aperta: detection of a shallow defect of the spine by 3D sonography. Ultraschall Med. 2007;28(3):246-7.
17. Tonni G, Centini G. Three dimensional first-trimester diagnosis of alobar holoprosencephaly associated with omphalocele in a 46, xx fetus. Am J perinat. 2006;23(1):67-9.
18. Chaoui R, Nicolaides KH. From nuchal translucency to intracranial translucency: towards the early detection of spina bifida. Ultrasound Obstet Gynecol. 2010;35(2):133-8.
19. Chaoui R, Benoit B, Mitkowska-Wozniak H, et al. Assessment of intracranial translucency (IT) in the detection of spina bifida at 11-13 week scan. Ultrasound Obstet Gynecol. 2009;34(3):249-52.
20. Schramm T, Gloning KP, Minderer S, et al. The 3D ultrasound in fetal spina bifida. Ultraschall Med. 2008;29(5):289-90.
21. Bilardo CM, Muller MA, Zikulnig L, et al. Ductus venosus studies in fetuses at high risk for chromosomal or heart abnormalities: relationship with nuchal translucency measurement and fetal outcome. Ultrasound Obstet Gynecol. 2001;17(4):288-94.
22. Nicolaides KH. Nuchal translucency and other first-trimester sonographic markers of chromosomal abnormalities. Am J Obstet Gynecol. 2004;191(1):45-67.
23. Matias A, Gones C, Flack N, et al. Screening for chromosomal abnormalities at 10-14 weeks: the role of ductus venosus blood flow. Ultrasound Obstet Gynecol. 1998;12(6):380-4.
24. Borrell A, Martinez JM, Serès A, et al. Ductus venosus assessment at the time of nuchal translucency measurement in the detection of fetal aneuploidy. Prenat Diagn. 2003;23(11):921-6.
25. Matias A, Montenegro N. Ductus venosus blood flow in chromosomally abnormal fetuses at 11 to 14 weeks of gestation. Seminars in Perinatology. 2001;25(1):32-7.
26. Toyama JM, Brizot ML, Liao AW, et al. Ductus venosus blood flow assesment at 11 to 14 weeks of gestation and fetal outcome. Ultrasound Obstet Gynecol. 2004;23(4):341-5.
27. Chevernak FA, Isaacson G, Blakemore KJ, et al. Fetal cystic hygroma: cause and natural history. N Engl J Med. 1983;309(14):822-5.

28. Mathias B, Forrester BS, Ruth D, et al. Descriptive epidemiology of cystic hygroma: Hawaii, 1986 to 1999. Southern Medical Journal. 2004;97(7):631-6.
29. Bernstein HS, Filly RA, Goldberg JD, et al. Prognosis of fetuses with a cystic hygroma. Prenat Diagn. 1991;11(6):349-55.
30. Podobnik M, Singer Z, Podobnik-Sarkanji S, et al. First trimester diagnosis of cystic hygromata using transvaginal ultrasound and cytogenetic evaluation. J Perinat Med. 1995;23(4):283-91.
31. Rosati P, Guariglia L. Transvaginal ultrasound detection of septated and non-septated cystic hygroma in early pregnancy. Fetal Diagn Ther. 1997;12(3):132-5.
32. Farkas LG, Katic MJ, Forrest CR, et al. Surface anatomy of the face in Down's syndrome: linear and angular measurements in the craniofacial regions. J Craniofac Surg. 2001;12:373-9.
33. Stempfle N, Huten Y, Fredouille C, et al. Skeletal abnormalities in fetuses with Down's syndrome: a radiographic post-mortem study. Pediatr Radiol. 1999;29(9):682-8.
34. Rosignoli L. An early diagnosis of trisomy 18 by 2-3-4D at 10th week. Ultrasound obstet gynecol London 2006.
35. Sonek J, Nicolaides KH. Prenatal ultrasonographic diagnosis of nasal bone abnormalities in three fetuses with Down syndrome. Am J Obstet Gynecol. 2002;186(1):139-41.
36. Cicero S, Rembouskos G, Vandecruys H, et al. Likelihood ratio for trisomy 21 in fetuses with absent nasal bone at the 11-14 weeks scan. Ultrasound Obstet Gynecol. 2004; 23(3):218-23.
37. Kelekci S, Yazicioglu HF, Oguz S, et al. Nasal bone measurement during the first trimester: is it useful? Gynecol Obstet Invest. 2004;58(2):91-5.
38. Peralta CF, Falcon O, Wesrzyn P, et al. Assessment of the gap between the fetal nasal bone at 11 to 13+6 weeks of gestation by three-dimensional ultrasound. Ultrasound Obstet Gynecol. 2005;25(5):464-7.
39. Cicero S, Binda R, Rembouskos G, et al. Integrated ultrasound and biochemical screening for trisomy 21 at 11 to 14 weeks. Prenat Diagn. 2003;23(4):306-10.
40. Benoit B, Chaoui R. Three dimensional ultrasound with maximal mode rendering: a novel technique for the diagnosis of bilateral or unilateral absence or hypoplasia of nasal bones in second-trimester screening for Down syndrome. Ultrasound Obstet Gynecol.2005;25(1):19-24.
41. Cicero S, Curcio P, Rembouskos G, et al. Maxillary length at 11-14 weeks gestation in fetuses with trisomy 21. Ultrasound Obstet Gynecol. 2004;24(1):19-22.
42. Rembouskos G, Cicero S, Sacchini C, et al. Single umbilical artery at 11-14 weeks of gestation: relation to chromosomal defects. Ultrasound Obstet Gynecol. 2003;22(6):567-70.
43. Sollazzi S, Centini G, Ciani V, et al. First trimester ultrasonography in detection of fetal anomalies. Ultrasound obstet and gynecology. 2010;36(1):119.
44. Guidelines SIEOG 2010.
45. Eurocat Group. Prenatal diagnosis of severe structural congenital malformations in Europe. Ultrasound Obstet Gynecol. 2005;25(1):6-11.
46. Rosignoli L, Tonni G, Centini G. Cranial development in the first trimester: the use of 3D in the study of complex structures. Imaging Med. 2010;2(3):251-7.
47. Rotten D, Levaillant JM. Two- and three-dimensional sonographic assessment of the fetal face. 1. A systematic analysis of the normal face. Ultrasound Obstet Gynecol. 2004 Mar; 23(3):224-31.
48. Rotten D, Levaillant JM. Two- and three-dimensional sonographic assessment of the fetal face. 2. Analysis of cleft lip, alveolus and palate. Ultrasound Obstet Gynecol. 2004;24(4):402-11.
49. Tonni G, De felice C, Centini G. Cervical and oral teratome in the fetus: a systematic review of etiology, pathology, diagnosis, treatment and prognosis. Arch. Gynecol Obstet. 2010;282(4):355-61.
50. Lee W, Kirk JS, Shaheen KW, et al. Fetal cleft lip and palate detection by three-dimensional ultrasonography. Ultrasound Obstet Gynecol. 2000;16(4):299-301.
51. Hata T, Kenenishi K, Akiyama M, et al. Real-time 3-D sonographic observation of fetal facial expression. J Obstet Gynecol Res. 2005;31(4):337-40.
52. Kurjak A, Stanojevic M, Azumendi G, et al. The potential of four-dimensional (4D) ultrasonography in the assessment of fetal awareness. J Perinat Med. 2005;33(1):46-53.
53. Yanagihara T, Hata T. Three-dimensional sonographic visualization of fetal skeleton in the second trimester of pregnancy. Gynecol Obstet Invest. 2000;49(1):12-6.
54. Dikkeboom CM, Roelfsema NM, Van Adrichem LN, et al. The role of three-dimensional ultrasound in visualizing the fetal cranial sutures and fontanels during the second half of pregnancy. Ultrasound Obstet Gynecol. 2004;24(4):412-6.
55. Faro C, Benoit B, Wegrzyn P, et al. Three-dimensional sonographic description of the fetal frontal bones and metopic suture. Ultrasound Obstet Gynecol.2005;26(6):618-21.
56. Chaoui R, Levaillant JM, Benoit B, et al. Three-dimensional sonographic description of abnormal metopic suture in second-and third-trimester fetuses. Ultrasound Obstet Gynecol. 2005;26(7):761-4.
57. Vinals F, Munoz M, Naveas R, et al. The fetal cerebellar vermis: anatomy and biometric assessment using volume contrast imaging in the C-plane (VCI-C). Ultrasound Obstet Gynecol. 2005;26(6):622-7.
58. Chang CH, Chang FM, Yu CH, et al. Assessment of fetal cerebellar volume using three dimensional ultrasound. Ultrasound Med Biol. 2000;26(6):981-8.
59. Benacerraf BR, Sadow PM, Barnewolt CE, et al. Cleft of the secondary palate without cleft lip diagnosed with three-dimensional ultrasound and magnetic resonance imaging in a fetus with Fryns' syndrome. Ultrasound Obstet Gynecol. 2006;27(5):566-70.
60. Tonni G, Panteghini M, Pattacini P, et al. Integrating 3D sonography with targeted MRI in the prenatal diagnosis of posterior cleft lip. Journal of Diagnostic Medical Sonography. 2006;22:367-71.
61. Tonni G, Centini G, Rosignoli L. Prenatal screening for fetal face and clefting in a prospective study on low-risk popu-

lation: can 3-4dimensional ultrasound enhance visualization and detection rate? Oral Pathology. Oral Radiology and Endodontics. 2005;100:420-6.
62. Gorlin RJ, Cervenka J, Pruzansky S. Facial clefting and its syndromes. Birth Defects Orig Artic Ser. 1971;7(7):3-49.
63. Calzolari E, Pierini A, Astolfi G, et al. Associated anomalies in multi-malformed infants with cleft lip and palate: an epidemiologic study of nearly 6 million births in 23 EUROCAT registries. Am J Med Genet A. 2007;143(6):528-37.
64. Stoll C, Alembik Y, Dott B, et al Associated malformations in cases with oral clefts. Cleft Palate Craniofac J. 2000;37(1): 41-7.
65. Calzolari E, Bianchi F, Rubini M, et al. Epidemiology of cleft palate in Europe: implications for genetic research. Cleft Palate Craniofac J. 2004.41(3): 244-9.
66. Milerad J, Larson O, Ph DD, et al. Associated malformations in infants with cleft lip and palate: a prospective, population-based study. Pediatrics. 1997;100(2 Pt 1):180-6.
67. Walker SJ, Ball RH, Babcook CJ, et al. Prevalence of aneuploidy and additional anatomic abnormalities in fetuses and neonates with cleft lip with or without cleft palate: a population-based study in Utah. J Ultrasound Med. 2001;20(11):1175-80.
68. Ghi T, Tani G, Savelli L, et al. Prenatal imaging of facial clefts by magnetic resonance imaging with emphasis on the posterior palate. Prenat Diagn. 2003;23(12):970-5.
69. Chmait R, Pretorius D, Moore T, et al. Prenatal detection of associated anomalies in fetuses diagnosed with cleft lip with or without cleft palate in utero. Ultrasound Obstet Gynecol. 2006;27(2):173-6.
70. Clementi M, Tenconi R, Bianchi F, et al. Evaluation of prenatal diagnosis of cleft lip with or without cleft palate and cleft palate by ultrasound: experience from 20 European registries. EUROSCAN study group. Prenat Diagn. 2000;20(11):870-5.
71. Hanikeri M, Savundra J, Gillett D, et al. Antenatal transabdominal ultrasound detection of cleft lip and palate in western Australia from 1996 to 2003. Cleft Palate Craniofac J. 2006;43(1):61-6.
72. Shannon J Walker, Ball RH, Babcook CJ, et al. Prevalence of aneuploidy and additional anatomic abnormalities in fetuses and neonates with cleft lip with or without cleft palate. L Ultrasound Med. 2001;20:1175-80.
73. Mulliken JB, Benacerraf BR. Prenatal diagnosis of cleft lip: what the sonologist needs to tell the surgeon. J Ultrasound Med. 2001;20(11): 1159-64.
74. Berkowitz S. Cleft lip and palate: Diagnosis and management, 2nd edition. Berlin: Springer-Verlag; 2006. pp.395-404.
75. Sherer DM, Sokolovski M, Santoso PG, et al. Nomograms of sonographic measurements throughout gestation of the fetal hard palate width, length and area. Ultrasound Obstet Gynecol. 2004;24(1):35-41.
76. Shipp TD, Mulliken JB, Bromley B, et al. Three-dimensional prenatal diagnosis of frontonasal malformation and unilateral cleft lip/palate. Ultrasound Obstet Gynecol. 2002;20(3):290-3.
77. Centini G, Rosignoli L, Faldini E, et al. Comparison between three different methods of scan to visualize the secondary foetal palate by three-dimensional ultrasonography. 17th World Congress on Ultrasound in Obstetrics and Gynecology. Florence. ISUOG 2007.
78. Centini G, Rosignoli L, Faldini E. L'ecografia del primo e secondo trimestre in 3D.: 82-104. Vol. Diagnosi Prenatale Ed Paletto. 2006.
79. Campbell S, Lees C, Moscoso G, et al. Ultrasound antenatal diagnosis of cleft palate by a new technique: the 3D "reverse face" view. Ultrasound Obstet Gynecol. 2005;25(1): 12-8.
80. Platt LD, Devore GR, Pretorius DH. Improving cleft palate/cleft lip antenatal diagnosis by 3-dimensional sonography: the "flipped face" view. J Ultrasound Med. 2006;25(11): 1423-30.
81. Faure JM, Captier G, Baumler M, et al. Sonographic assessment of normal fetal palate using three-dimensional imaging: a new technique. Ultrasound Obstet Gynecol. 2007;29(2):159-65.
82. Pilu G, Segata M. A novel technique for visualization of the normal and cleft fetal secondary palate: angled insonation and three-dimensional ultrasound. Ultrasound Obstet Gynecol. 2007;29(2):166-9.
83. Tonni G, Centini G, Inaudi P, et al. Prenatal diagnosis of severe epignathus in a twin: case report and review of the literature. Cleft Palate Craniofac J. 2010;47(4):421-5.
84. Campbell S. Prenatal ultrasound examination of the secondary palate. Ultrasound Obstet Gynecol. 2007;29(2):124-7.
85. Wilhelm L, Borgers H. The 'equals sign': a novel marker in the diagnosis of fetal isolated cleft palate. Ultrasound Obstet Gynecol. 2010;36(4):439-44.
86. Cohen L, Mangers K, Grobman WA, et al. Three-dimensional fast acquisition with sonographically based volume computer-aided analysis for imaging of the fetal heart at 18 to 22 weeks' gestation. J Ultrasound Med. 2010;29(5):751-7.
87. Ruano R, Martinovic J, Dommergues M, Aubry MC, Dumez Y, Benachi A. Accuracy of fetal lung volume assessed by three-dimensional sonography. Ultrasound Obstet Gynecol. 2005;26(7):725-30.
88. Ruano R, Benachi A, Joubin L, et al. Three dimensional ultrasonographic assessment of fetal lung volume as prognostic factor in isolated congenital diaphragmatic hernia. Brit J Obstet Gynaecol. 2004;111(5):423-9.
89. Chang CH, Yu CH, Chang FM, Ko HC, Chen HY. The assessment of normal fetal liver volume by three-dimensional ultrasound. Ultrasound Med Biol. 2003;29(8):1123-9.
90. Rosignoli L, Periti E, Tonni G. VCI-Omniview e studio della colonna vertebrale. XVII Congresso Nazionale Società Italiana Ecografia Ostetrica-Ginecologica. (SIEOG)17-20 Ottobre Sorrento 2010.
91. Pilu GL, Ghi T. Preliminary experience with advanced volume contrast imaging (VCI) and OmniView obstetric and gynecologist ultrasound. GE Healthcare 2010 White book.

92. Lauson S, Alvarez C, Patel MS, et al. Outcome of prenatally diagnosed isolated clubfoot. Ultrasound Obstet Gynecol. 2010;35(6):708-14.
93. Cafici D, Iglesias A. Prenatal diagnosis of severe hypospadias with two-and three-dimensional sonography. J Ultrasound Med. 2002;21(12):1423-6.
94. Costa J, Rice H, Cardwell C, et al. An assessment of vascularity and flow intensity of the placenta in normal pregnancy and preeclampsia using three-dimensional ultrasound. J Matern Fetal Neonatal Med. 2010;23(8):894-9.
95. Huster KM, Haas K, Schoenborn J, et al. Reproducibility of placental volume and vasculature indices obtained by 3-dimensional power Doppler sonography. J Ultrasound Med. 2010;29(6):911-6.
96. D'Elia A, Pighetti M, Moccia G, et al. Spontaneous motor activity in normal fetuses. Early Hum Dev. 2001; 65(2):139-47.
97. Robles de Medina PG, Visser GH, Huizink AC, et al. Fetal behavior does not differ between boys and girls. Early Hum Dev. 2003;73(1-2):17-26.
98. Kuno A, Akiyama M, Yamashiro C, et al. Three-dimensional sonographic assessment of fetal behavior in the early second trimester of pregnancy. J Ultrasound Med. 2001; 20(12):1271-5.
99. Blaas HG, Eik-Nes SH. Sonoembryology and early prenatal diagnosis of neural anomalies. Prenat Diagn. 2009;29(4): 312-25.

35
CHAPTER

3D Ultrasound in Detection of Fetal Anomalies

Ritsuko K Pooh, Asim Kurjak

INTRODUCTION

Recent Advances of Three-Dimensional Ultrasonography

Recent advances of three/four dimensional (3D/4D) sonography have assessed not only the structural but also the early functional human developments.[1]

The 3D images of embryos were generated using the high frequency transvaginal transducer (Voluson ® E8 with 12 MHz/256 element transvaginal transducer, GE Healthcare, Milwaukee, USA). Demonstration of an embryo of less than 10 mm (greatest length) has been difficult in the past and not visualized in detail (*See* the chapter on Three Dimensional Sonoembryology). During the early embryonic period, the anatomy of central nervous system (CNS) changes rapidly in appearance. The 3D sonography using transvaginal sonography with high resolution probes allow imaging of early structures in the embryonic brain. This can be accomplished through the use of three orthogonal planes and "tomographic ultrasound imaging". Serial examinations allow obtaining similar sections of the fetal brain at different stages of development. Therefore, it is possible to document the changes in CNS development from early embryonic period. **Figures 35.1A to C** show dramatical changes of Sylvian fissures between 20 weeks and 31 weeks demonstrating by transvaginal 3D ultrasound. Observation of the brain cortical development should have a great potential to discover migration disorders during pregnancy. Thoracoabdominal structures can also be imaged in the first trimester. For example, **Figure 35.2** shows tomographic ultrasound imaging of fetal chest and abdomen at 13 weeks of gestation. Clear visualization of the lung-liver interface can be of value in the early diagnosis of thoracoabdominal abnormalities, such as a diaphragmatic hernia. The detailed structure of small parts, for instance the lenses of eyeballs **(Fig. 35.3)** can be visualized by 3D orthogonal view. A 3D ultrasound technology will contribute to demonstration of *in utero* pathological changes of congenital diseases arising *in utero*.

Color Doppler detection and assessment of brain vessels in the early fetus using a transvaginal approach was reported[2,3] in 1993 and 1994. Clear visualization by transvaginal power Doppler of the common carotid arteries, internal and external carotid arteries, and middle cerebral arteries at 12 weeks of gestation were reported in 1996.[4] By using 3D power Doppler technology, the vascular anatomy can now be imaged clearly by identification of the common carotid arteries, internal carotid arteries, circle of Willis and middle cerebral arteries. It is important to stress that such images can be obtained at 12 weeks of gestation. Transvaginal high-resolution power Doppler can demonstrate the fine vascular structure of medullary vessels inside the fetal brain **(Figs 35.4A to D)**. The powerful technology of 3D ultrasound will promisingly uncover the veil of unknown etiology of congenital diseases *in vivo.*

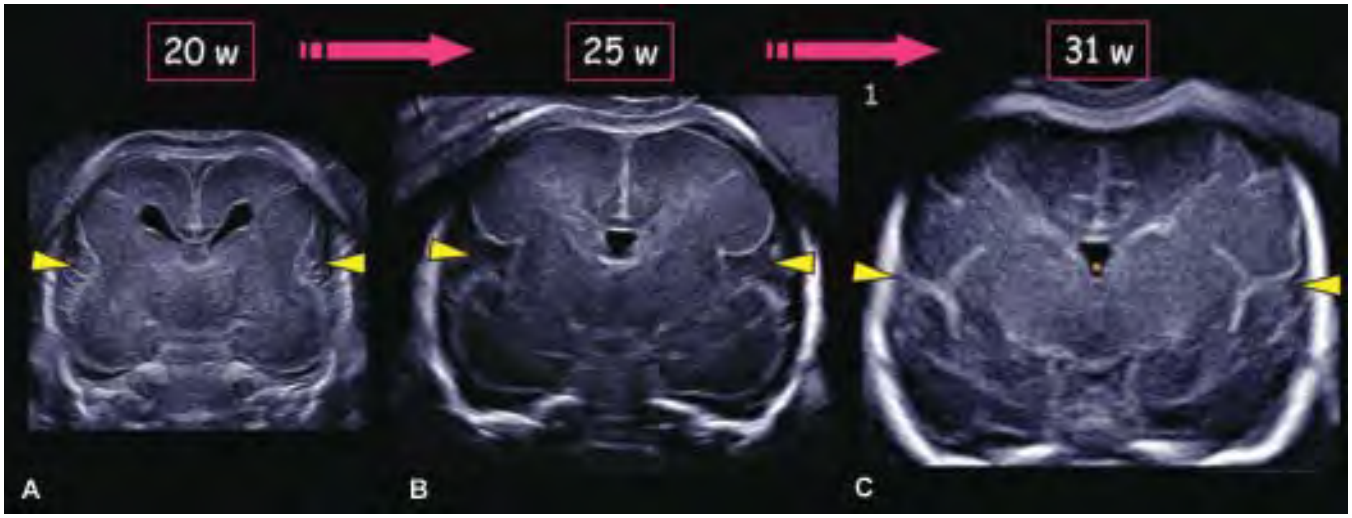

Figures 35.1A to C: Changing appearance of Sylvian fissure in the anterior coronal section by transvaginal 3D sonography. (A) At 20 weeks of gestation, bilateral Sylvian fissures (arrowheads) appear to be indentations; (B) With cortical development, Sylvian fissures are formed during the latter half of second trimester and (C) become as lateral sulci. Sylvian fissure appearance is one of the most reliable ultrasound markers for the assessment of cortical development

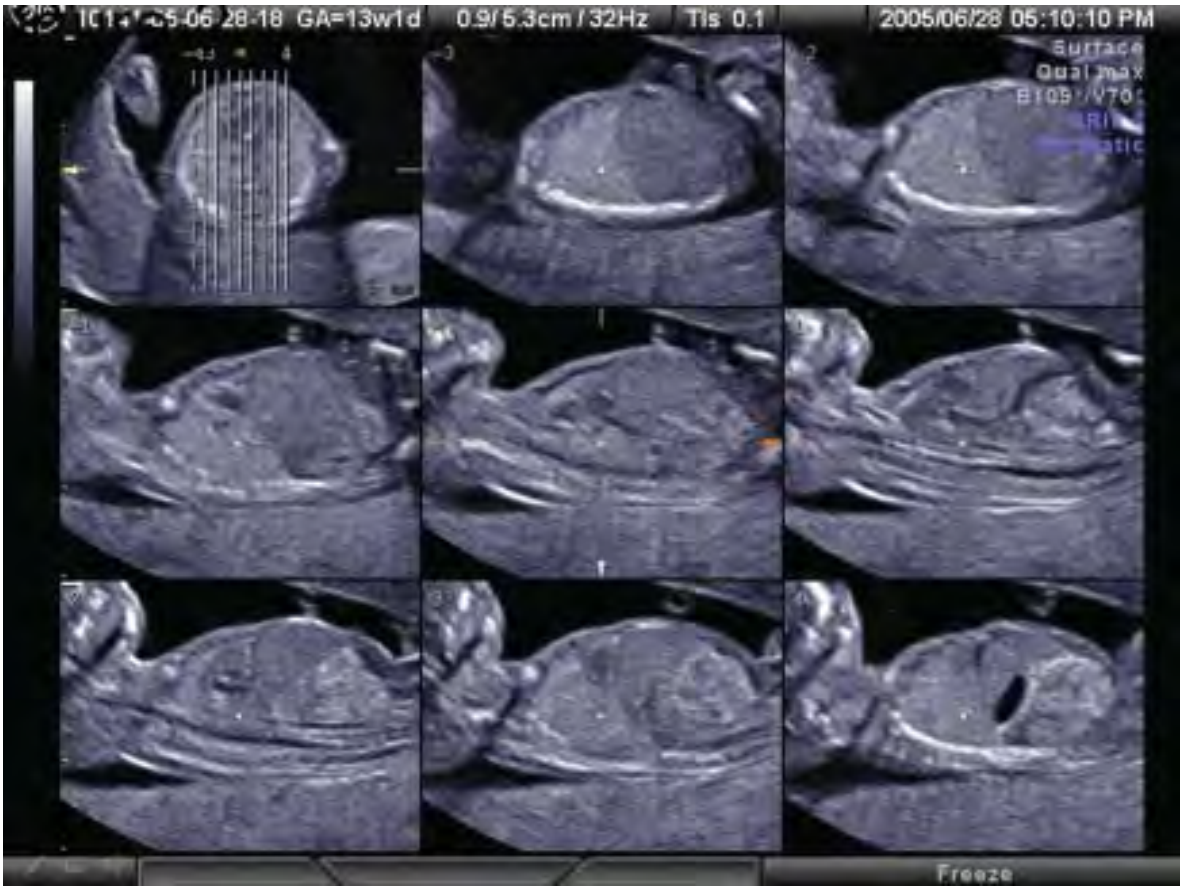

Figure 35.2: Tomographic ultrasound sagittal image of thoracoabdominal structure at 13 weeks. Note clear visualization of the lung-liver border (diaphragmatic line), lung, liver, stomach, bowels, umbilical vein and ductus venosus

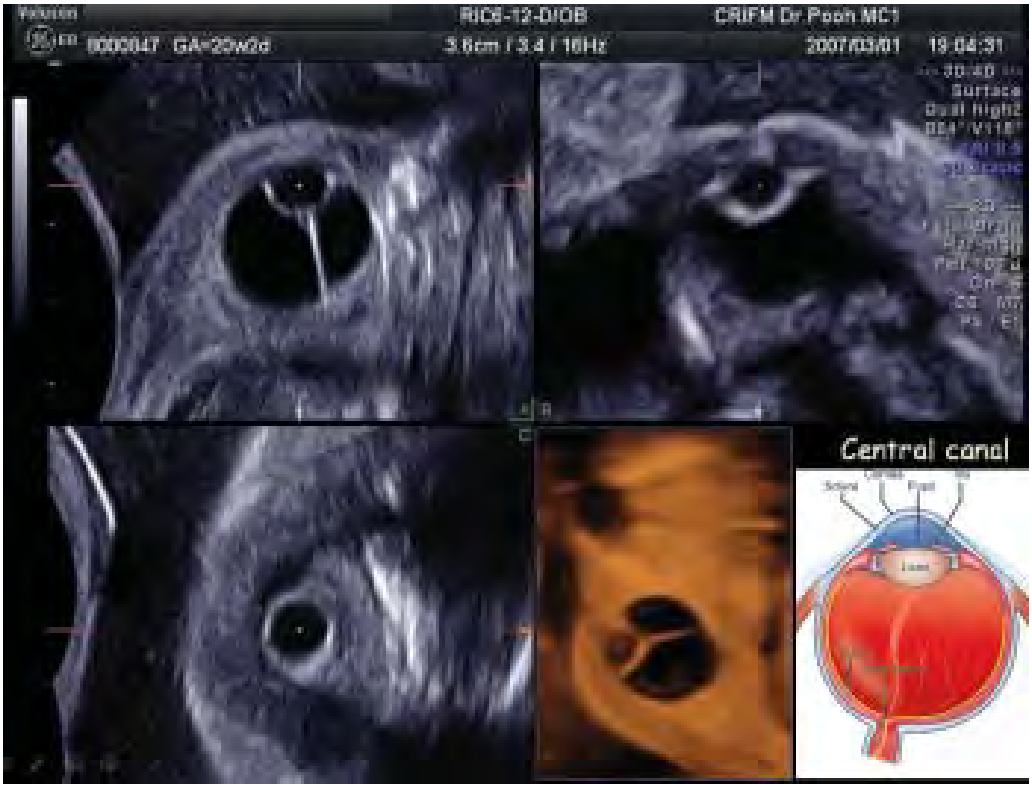

Figure 35.3: Eyeball structure at 20 weeks. Three orthogonal views and reconstructed image of the eyeball. Lens and central canal towards the optic nerve are clearly demonstrated

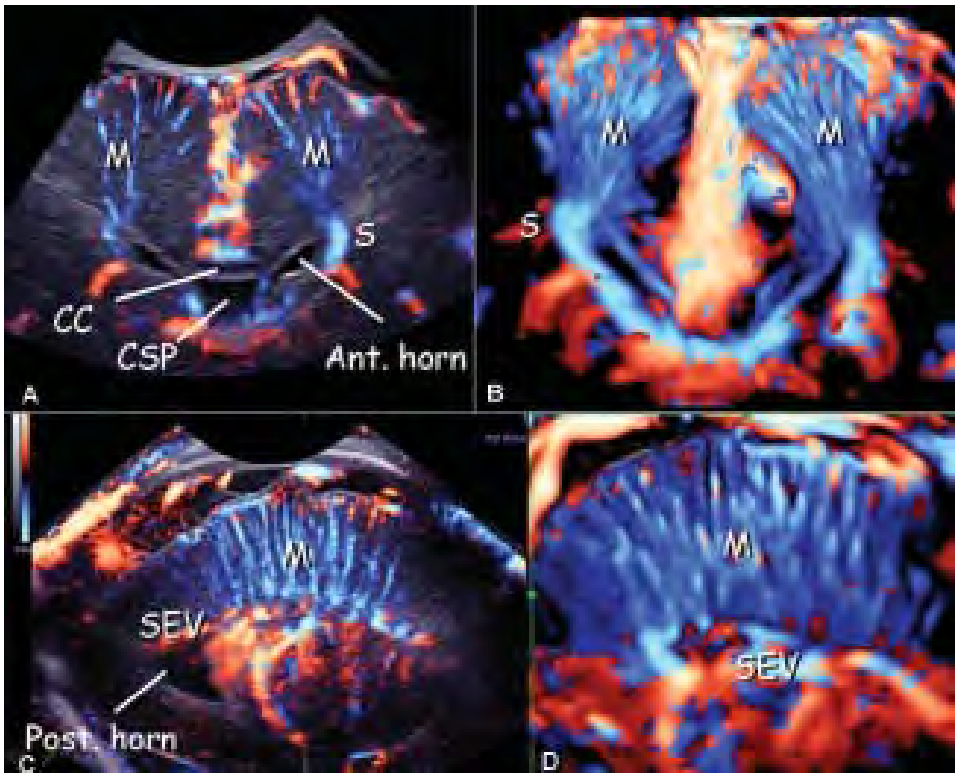

Figures 35.4A to D: Normal medullary vessels visualized by 3D power Doppler at 28 weeks. (A) Anterior coronal section of 2D bidirectional power Doppler image. Medullary vessels (M), longitudinal caudate vein of Schlesinger (S) Corpus callosum (CC), cavum septum pellucid (CSP) and anterior horn of the lateral ventricle (Ant. horn) are well demonstrated; (B) Posteroanterior view of 3D reconstructed image of medullary vessels. Numerous medullary vessels (M) from pia mater towards Schlesinger veins (S) are demonstrated; (C) Parasagittal 2D bidirectional power Doppler image. Cerebral pial vessels are on the surface of cerebrum. Numerous linear vessels run down from the cerebral cortex towards subependymal veins (SEV) are medullary vessels (M); (D) Coronal view of 3D reconstructed image

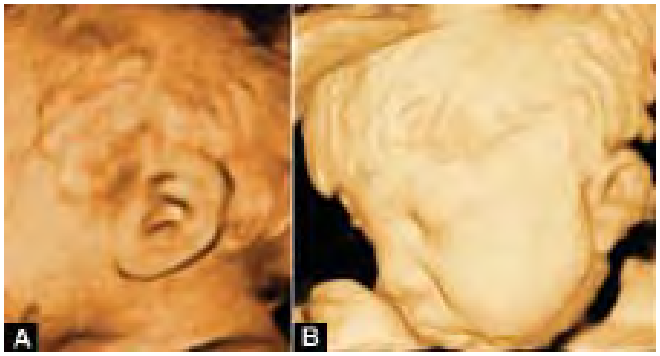

Figures 35.5A and B: Fetal hair in the (A) 35 and (B) 33 weeks of gestation

PRENATAL DIAGNOSIS OF ANATOMICAL CONGENITAL ANOMALIES

The prenatal diagnosis of congenital anomalies with ultrasound is based upon identification of a substantial departure of normal anatomy. This has been possible in the second and third trimester of pregnancy, and this achievement has made the diagnosis of congenital anomalies one of the objectives of modern prenatal care.

Facial Anomalies

Recent advanced 3D imaging has provided the detailed superficial structure including fetal hair (**Figs 35.5A and B)**. A facial anomaly can be associated with a central nervous system anomaly, be an isolated finding or part of a syndrome. Micrognathia **(Figs 35.6A and B)** can be detected as an isolated structural anomaly, as one of the features of a chromosomal abnormality or a syndrome.[5] **Figures 35.7A to C** demonstrate the slow jaw development during pregnancy in a case of Pierre Robin sequence, detected by serial 3D ultrasound scans. Assessment of the facial features, chin development and

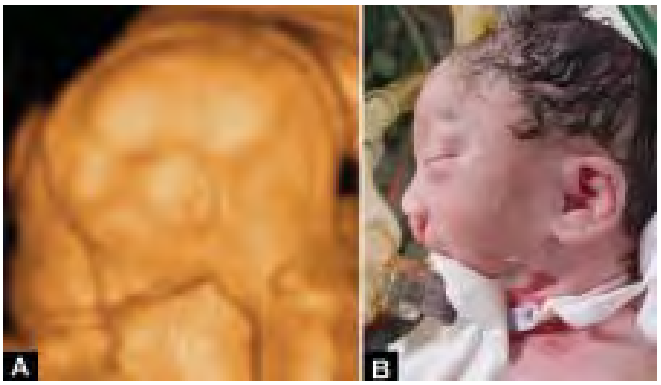

Figures 35.6A and B: Agnathia with cleft lip at 19 weeks. (A) 3D reconstructed lateral image of the fetal face at 19 weeks; (B) Postnatal facial appearance

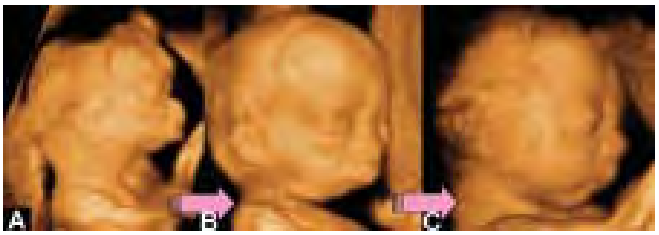

Figures 35.7A to C: Slow jaw development in a case of Pierre Robin sequence during pregnancy. Serial 3D scan clearly reveals slow jaw development (A) at 17 weeks; (B) 20 weeks and (C) 29 weeks associated with Pierre Robin sequence

mandibular size by 3D ultrasound in the second and third trimesters has been reported.[6] Facial abnormalities are often associated with craniosynostosis **(Figs 35.8A to E)** due to deformed cranial structure. Cleft lip and palate is one of common congenital facial anomalies. Cleft lip occurs unilaterally **(Figs 35.9A to C)** or bilaterally **(Figs 35.10A to D)**. Recent 3D tomographic ultrasound can demonstrate anterior maxillary structure, indicating the evidence of alveolar cleft presence **(Figs 35.9A to C)**. Congenital cataract can also be visualized by 3D ultrasound as echogenic structure inside the lenses from as early as 14 weeks of gestation.

Brain Anomalies

The brain structure should be understood as 3D structure.[7,8] A 3D sonographic assessment of premature brain in the early pregnancy was reported from 1995.[9,10] From 2000, fetal brain assessment in the second and third trimesters by 3D ultrasound was reported.[7,8,11-20] Recent advanced 3D ultrasound has enabled to assess detailed brain structure as an understandable organ. The 3D ultrasound abilities, such as tomographic ultrasound imaging and three orthogonal view, greatly contribute to evaluation of fetal brain morphology.[19,20] **Figures 35.11A to C** show transvaginal 3D tomographic coronal, sagittal and axial ultrasound views of intracranial structure in a case of ventriculomegaly at 20 weeks of gestation. Thus, accurate assessment of brain pathology can be done by 3D ultrasound. Furthermore, ventricular appearance can be demonstrated comprehensively by inversion mode, as shown in **Figures 35.12A and B**. Cortical development of fetal brain can also be visualized by 3D surface imaging, demonstrating gyral and sulcal development and migration disorder, which had been difficult to be detected during pregnancy, can be depicted by 3D ultrasound.[21] **Figures 35.13A to C** demonstrate the asymmetrical cortical development due to migration disorder by 2D ultrasound and 3D surface imaging. The

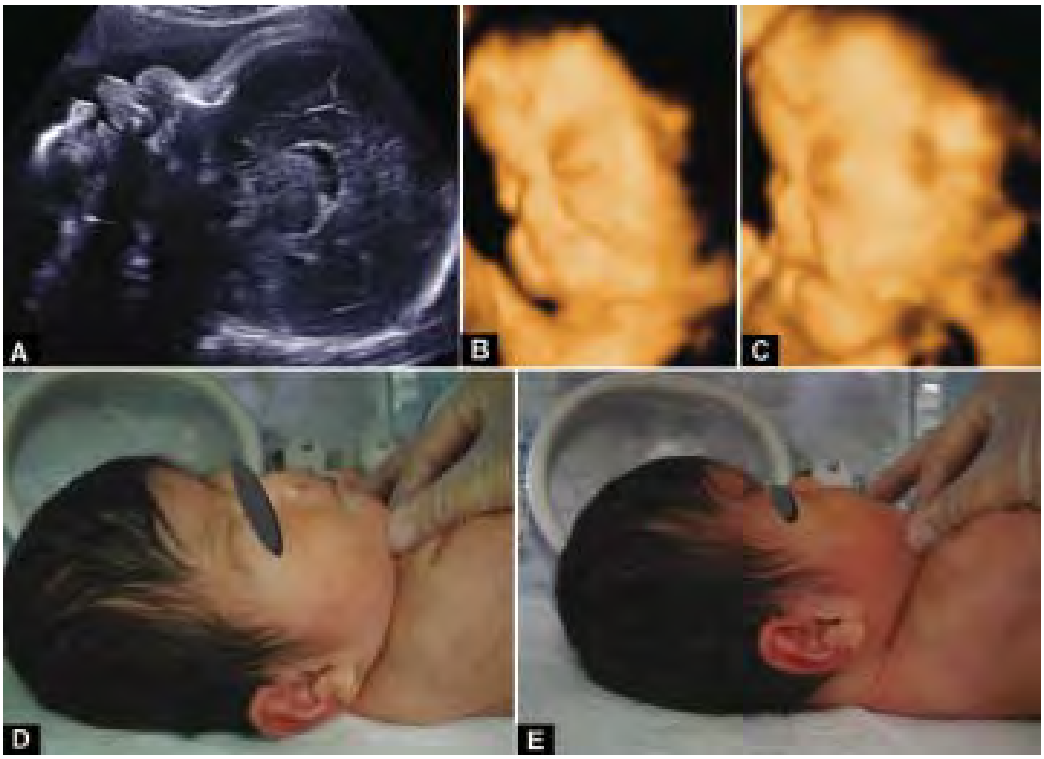

Figures 35.8A to E: Facial abnormality associated with Apert syndrome at 31 weeks. (A) 2D sagittal image of the fetal face. Note the marked frontal bossing and low nasal bridge; (B and C) 3D reconstructed images of fetal face. Exophthalmos is clearly visualized. This facial appearance occurs due to craniosynostosis of coronal sutures seen in a case of Apert syndrome; (D and E) Postnatal facial appearance of the same baby

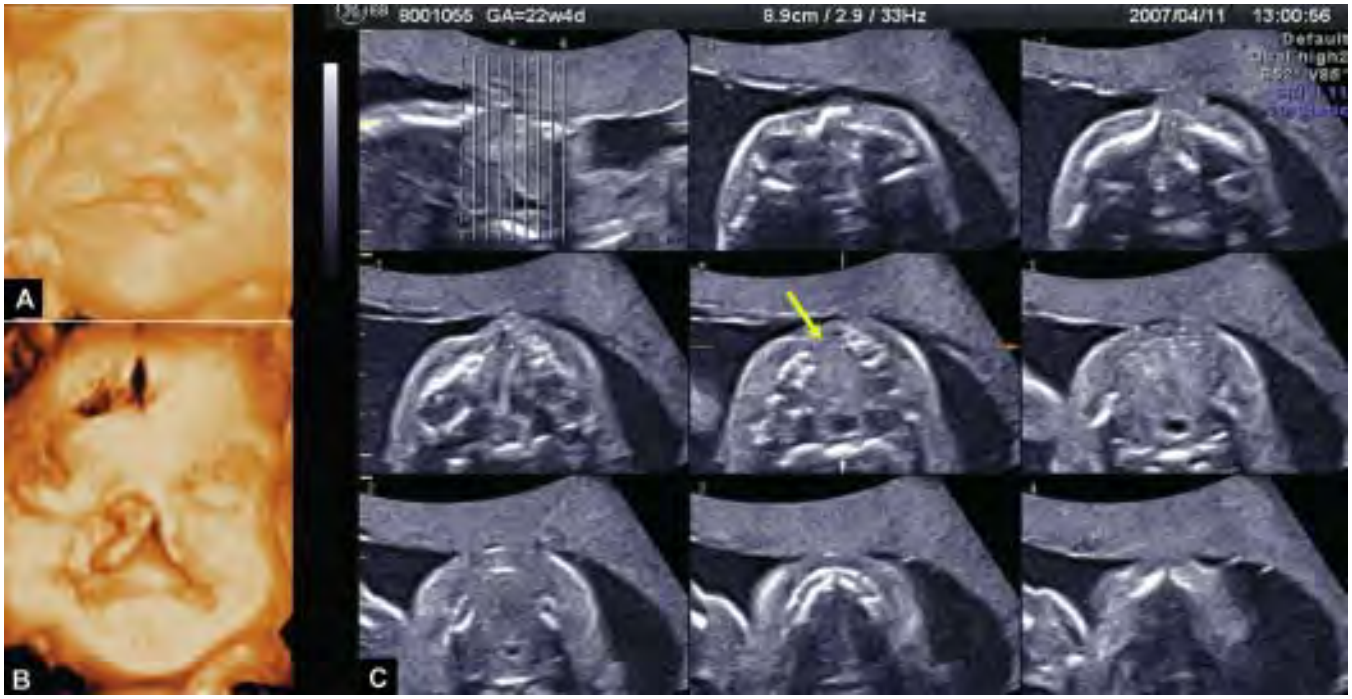

Figures 35.9A to C: Cleft lip and palate at 22 weeks. (A) Surface image of the fetal face. Left sided cleft lip and deformed nasal structure is clearly demonstrated; (B) 3D reconstructed image inside the oral cavity. Cleft palate is visualized; (C) Tomographic ultrasound image of the anterior maxillary structure, indicating the evidence of alveolar cleft presence (arrow)

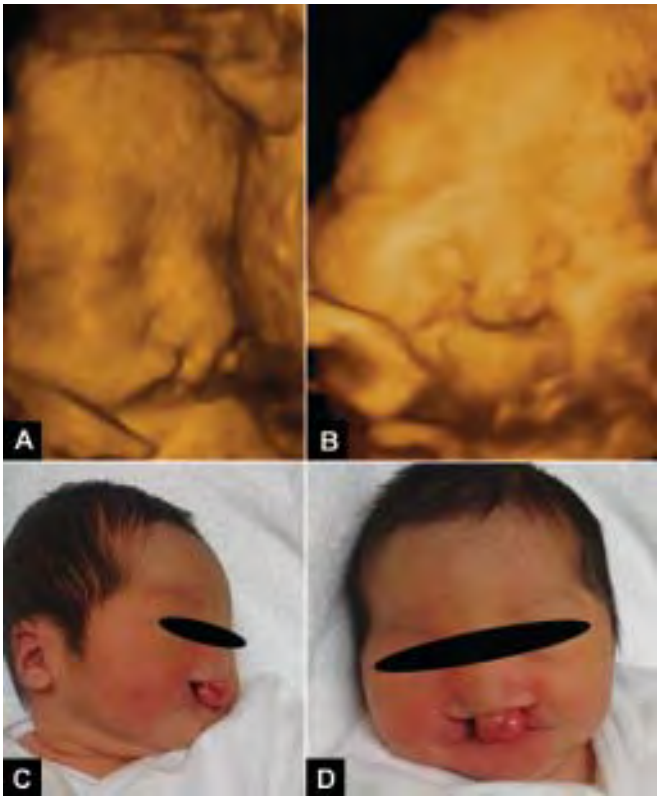

Figures 35.10A to D: Bilateral cleft lip at 35 weeks. Bilateral cleft lip is often overlooked because of its symmetrical facial structure. (A and B) 3D ultrasound shows the clear visualization of the bilateral cleft lip; (C and D) Postnatal facial appearance of the same baby

3D volume contrast imaging demonstrated the cortical development **(Figs 35.14A and B)**. Thus, 3D ultrasound surface imaging is useful in objective assessment of brain surface. The cranial bone abnormality, seen in a case of encephalocele can also be visualized by 3D ultrasound maximum mode imaging as shown in **Figures 35.15A and B**.

Vertebra and Spinal Cord Abnormalities

Spina bifida is the most common anomaly of the CNS. It is often detected during the second and third trimesters. However, the fundamental basis for this anomaly is a failure of the neural tube to close during early embryonic age. Most reports of the diagnosis of spina bifida *in utero* have occurred after 12 weeks of gestation. Blaas et al. reported an early diagnosis using 2D and 3D ultrasound before 10 weeks of gestation.[22] **Figures 35.16A and B** demonstrate myelomeningocele at 20 weeks. The vertebral bony structure can be depicted by 3D ultrasound for better understanding the

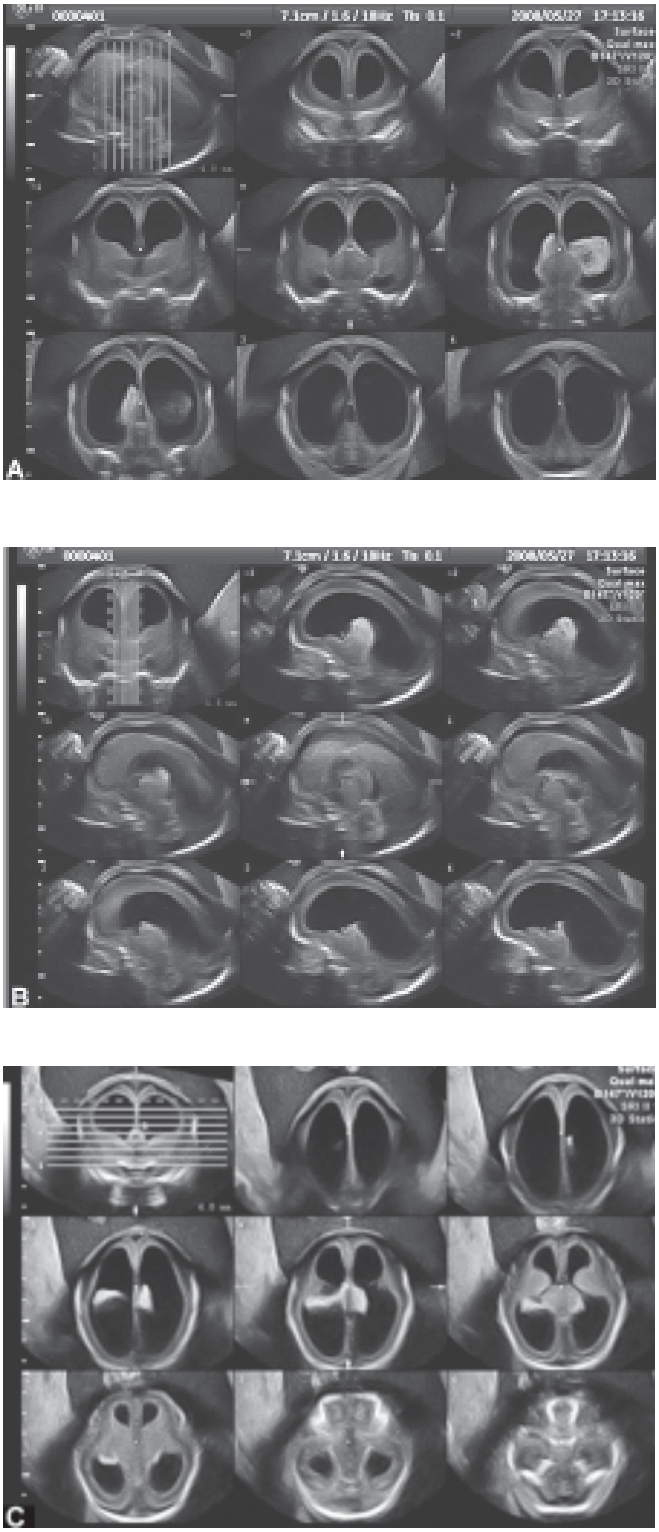

Figures 35.11A to C: Hydrocephalus at 20 weeks. Tomographic ultrasound images of (A) Coronal; (B) Sagittal; (C) Axial views. Clear visualization of intracranial structure is acquired

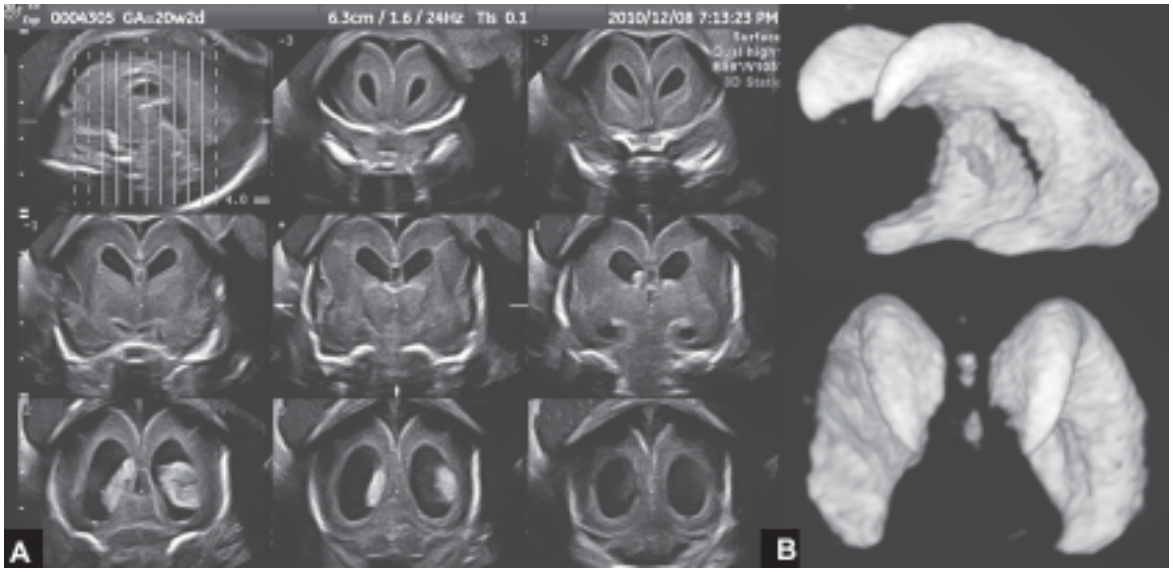

Figures 35.12A and B: Ventriculomegaly at 20 weeks. (A) Tomographic ultrasound image of coronal section; (B) Lateral ventricular appearance by using 3D inversion mode

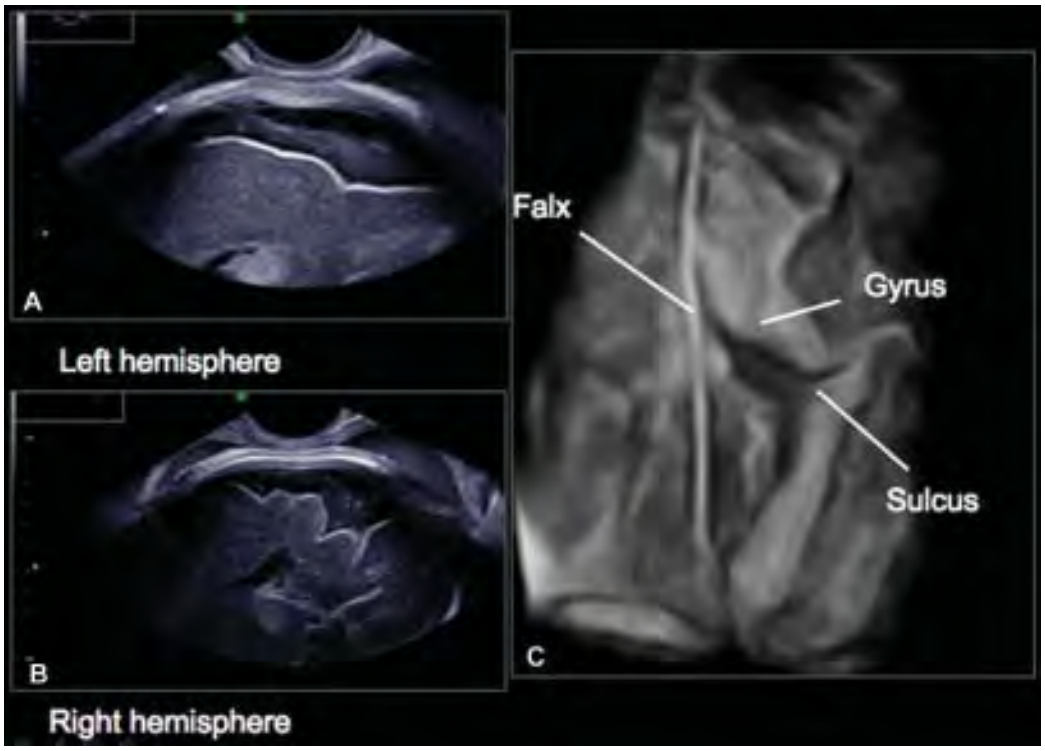

Figures 35.13A to C: Asymmetrical cortical formation at 29 weeks. (A and B) Note the marked difference between left and right cortical appearance; (C) Asymmetrical superficial image of the brain. Clear visualization of the brain surface with asymmetrical gyral/sulcal formation is acquired

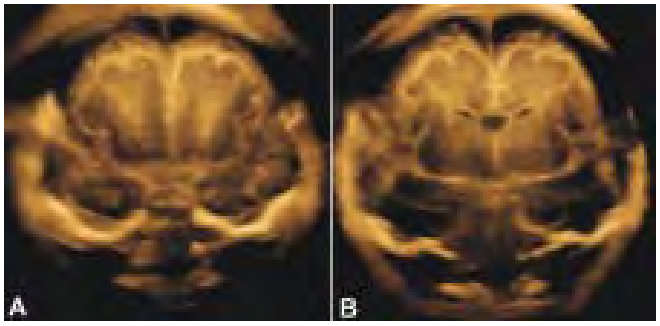

Figures 35.14A and B: Hydrocephalus ex-vacuo at 30 weeks. The 3D volume contrast images demonstrate the cortical development. Note the abnormal large subarachnoid space around the hemispheres

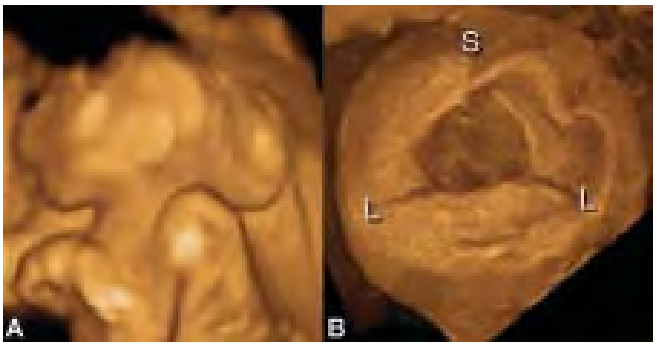

Figures 35.15A and B: Encephalocele at 19 weeks. (A) 3D reconstructed lateral image of the fetus. Microcephaly with encephalocele is clearly demonstrated; (B) The postero-anterior view of the cranial bones. The round shaped bony defect is demonstrated. S: Sagittal suture; L: Lambdoid suture

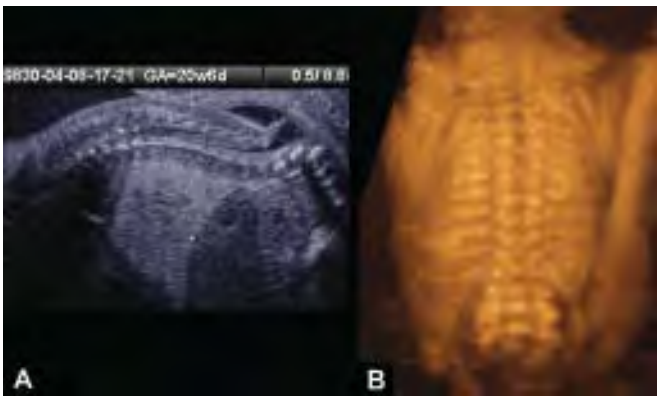

Figures 35.16A and B: Myelomeningocele with kyphosis at 20 weeks. (A) Sagittal image of the fetal trunks from 3D orthogonal view. Severe kyphosis and myelomeningocele is seen; (B) 3D reconstructed image of the fetal back. The huge mass is seen from L1 to S region. The ribs are clearly seen and the level of spina bifida is easily understandable

level of spina bifida. Vertebral scoliosis is often seen in cases of limb body wall complex **(Figs 35.17A to G)** or cases of hemivertebra as shown in **Figures 35.18 and 35.19**. In hemivertebral cases, asymmetrical rib number can also be demonstrated. **Figures 35.20A to C** show the segmental spinal dysgenesis, characterized by focal agenesis or dysgenesis of the lumbar or thoracolumbar spine, with focal abnormality of the underlying spinal cord and nerve roots.[23]

Chest-Abdominal Abnormalities

Congenital diaphragmatic hernia (CDH) occurs in 1 of every 2000–4000 live births and accounts for 8% of all major congenital anomalies.[24] There are three types of CDH:

1. Posterolateral or Bochdalek hernia (occurring at approximately 6 weeks' gestation).
2. Anterior Morgagni hernia.
3. A hiatus hernia.

The left-sided Bochdalek hernia occurs in approximately 90% of cases. Left-sided hernias allow herniation of both small and large bowel as well as intraabdominal solid organs into the thoracic cavity. Early diagnosis of CDH in the first trimester has been reported.[25] **Figure 35.21** shows the tomographic ultrasound imaging of Bochdalek hernia at 16 weeks. Early diagnosis of this defect is important for the option of fetal treatment. Congenital cystic adenomatoid malformation (CCAM), as shown in the **Figures 35.22A and B**, is a benign mass of abnormal lung tissue, located usually on one section of the lung. This condition is caused by overgrowth of abnormal lung tissue that may form fluid filled cysts and has no function of normal lung tissue. Early diagnosis of CCAM by 3D ultrasound was reported.[26] Pleural effusion and ascites **(Fig. 35.23)** can be easily diagnosed by both 2D/3D ultrasound technologies. In cases of pleural effusion, the lung is floated inside the fluid, whereas in cases of pericardiac effusion, the lungs are oppressed to posterior portion of the chest **(Fig. 35.24)**. Umbilical hernia is often associated with chromosomal abnormality or other syndromic diseases. **Figures 35.25A to D** show a huge umbilical hernia at 12 weeks.

Renal and Urinary Abnormalities

Hydronephrosis **(Figs 35.26A and B)** occasionally occurs during pregnancy. The causes are vary, obstruction or stenosis of ureters, posterior urethral valves **(Fig. 35.27)** or others. Multicystic dysplastic kidney (MCDK), as shown in the **Figure 35.28**, is a form of renal dysplasia

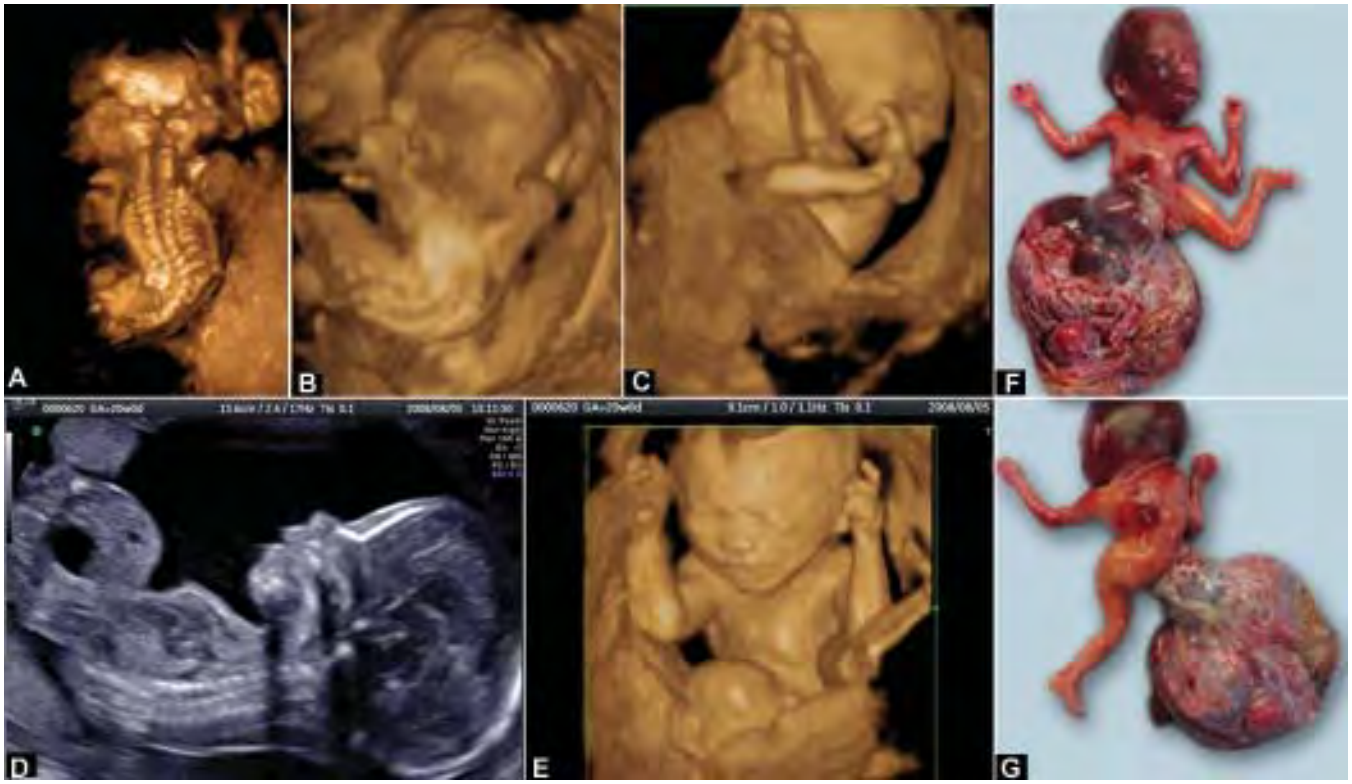

Figures 35.17A to G: Vertebral scoliosis associated with limb body wall complex at 20 weeks. (A to E) Severe vertebral scoliosis, abnormal leg position with one leg missing, Umbilical hernia with short umbilical cord are clearly demonstrated by 2D/3D ultrasound; (F and G) The appearance of the aborted fetus

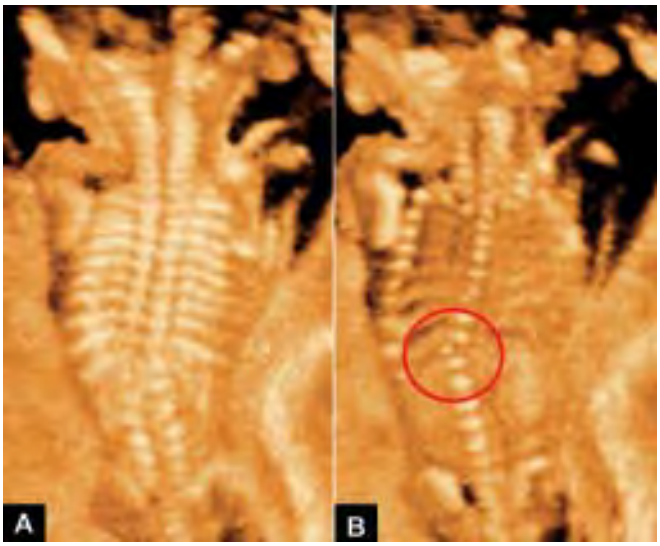

Figures 35.18A and B: Hemivertebra at 19 weeks. (A) 3D maximum mode image of the fetal back. Scoliosis with asymmetrical number of ribs (left; 11 ribs, right; 10 ribs) is clearly demonstrated; (B) 3D image of the vertebral body layer reveals Th12 hemivertebra (red circle) and this hemivertebra should be the cause of scoliosis

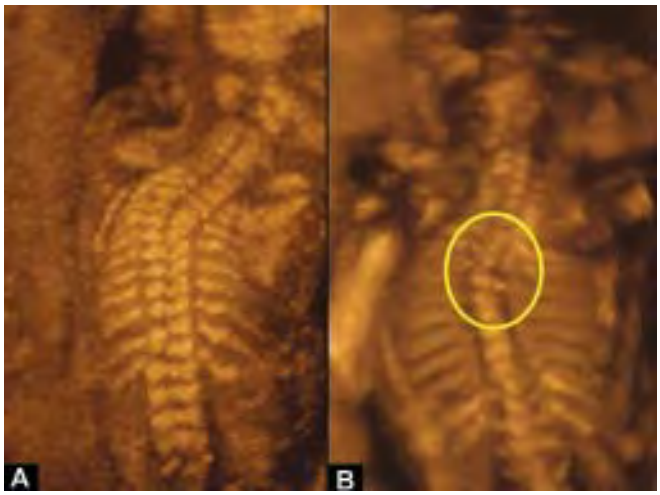

Figures 35.19A and B: Three levels hemivertebra at 20 weeks. (A) 3D maximum mode image of the fetal back. Severe scoliosis with asymmetrical number of ribs (left; 12 ribs, right; 9 ribs) is clearly demonstrated; (B) 3D image of the vertebral body layer reveals three levels hemivertebrae (Th1-Th3, yellow circle)

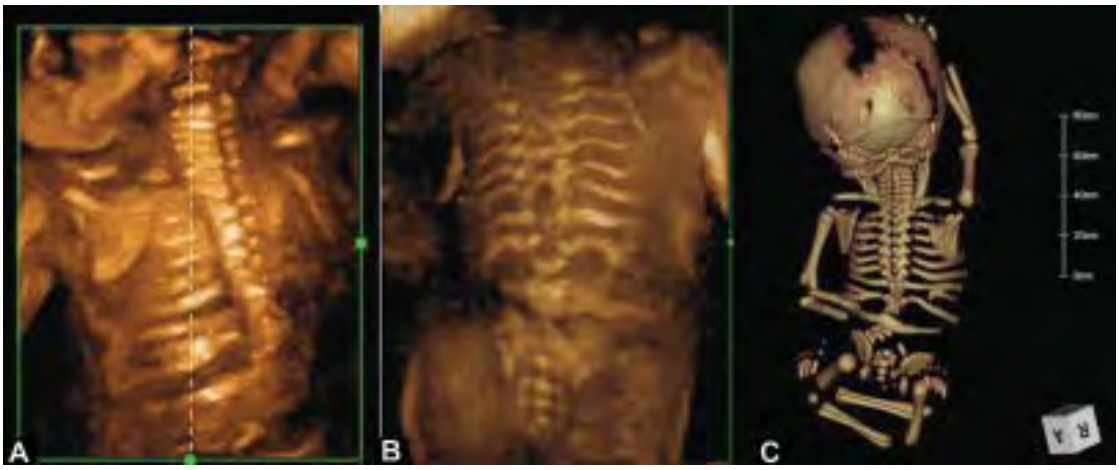

Figures 35.20A to C: Segmental spinal dysgenesis at 27 weeks (3D ultrasound and 3D-CT images). (A and B) 3D US reconstructed images. Note the focal dysgenesis of the thoracolumbar vertebra, with rib abnormality which indicates features of segmental spinal dysgenesis; (C) 3D-CT scan image of the same fetus. Clear visualization of the bony structure is acquired

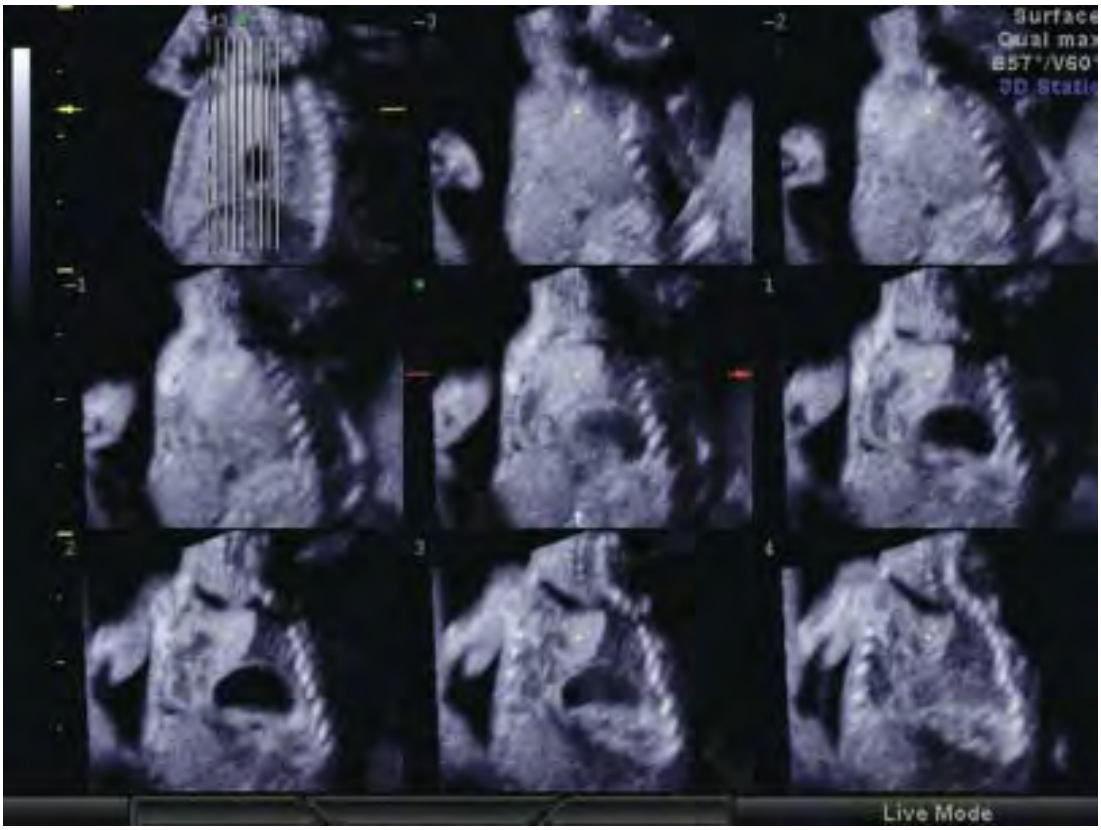

Figure 35.21: Congenital diaphragmatic hernia at 16 weeks. Tomographic ultrasound image. Typical Bochdalec hernia is seen. Tomographic image clearly shows oppressed and hypoplastic left lung, heart replacement to the right, and the stomach inside thoracic space

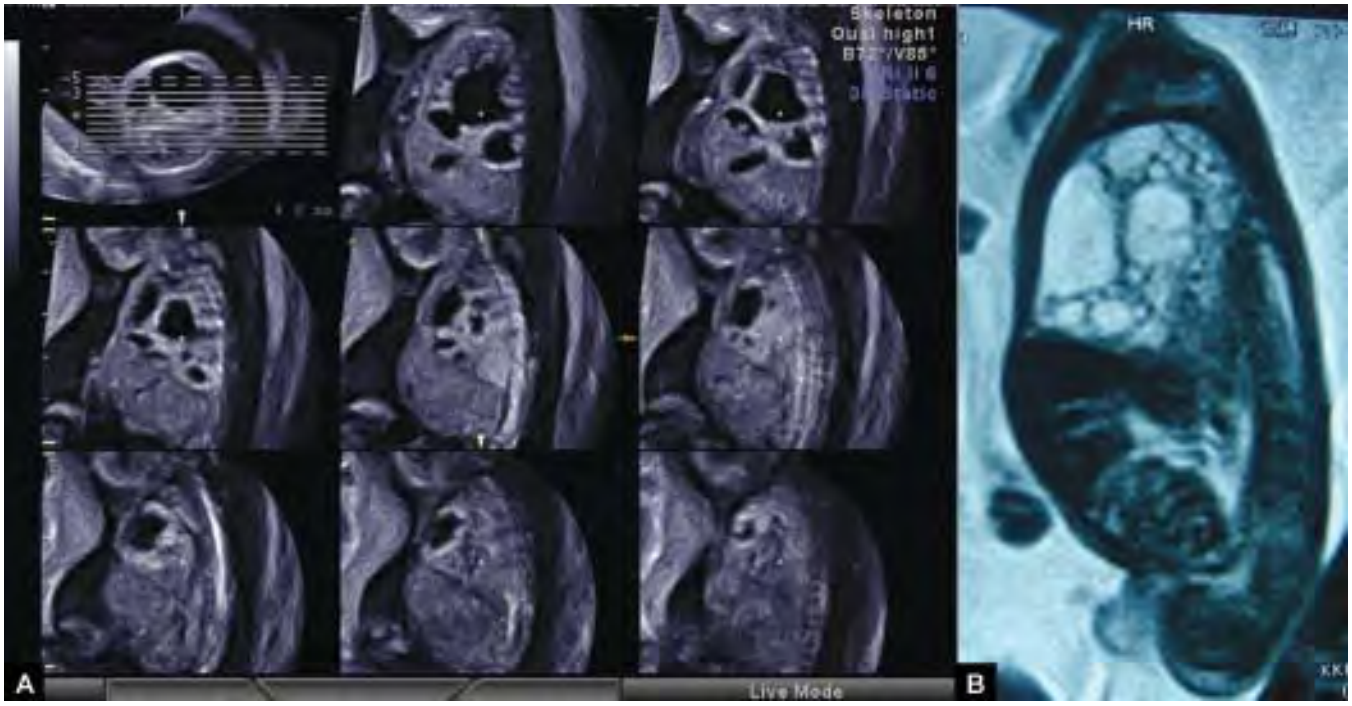

Figures 35.22A and B: Congenital cystic adenomatoid malformation (CCAM) at 24 weeks. (A) Tomographic ultrasound sagittal image of fetal chest. Multiple cysts with different size are seen; (B) MR image of the same fetus

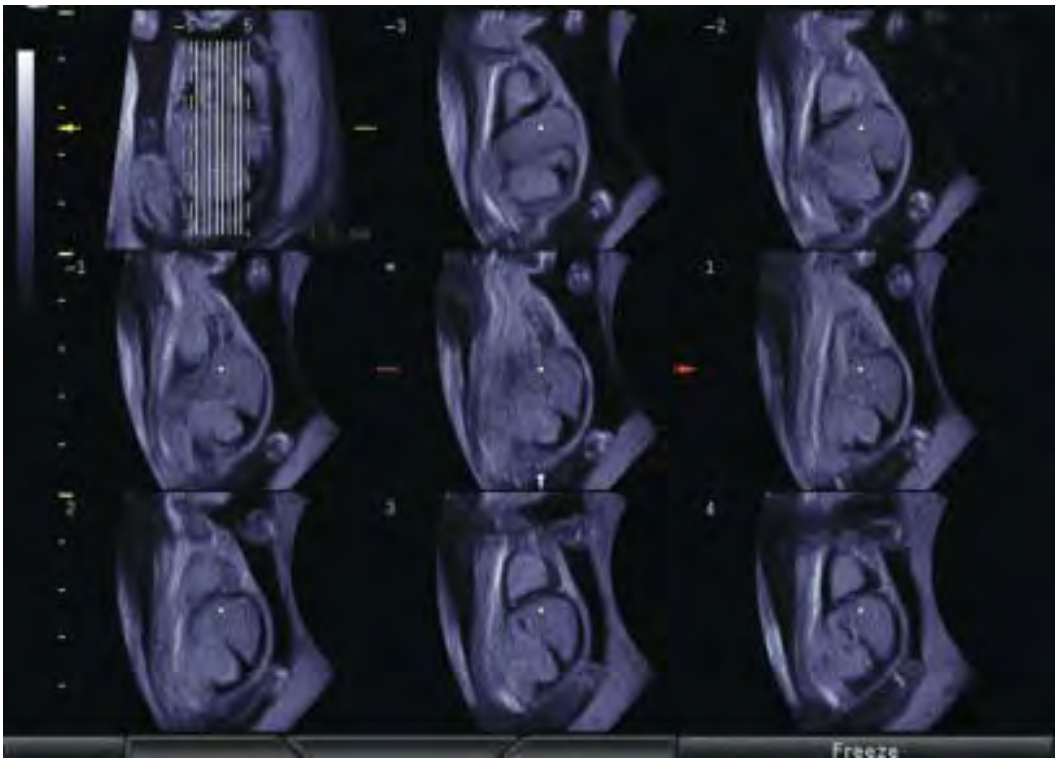

Figure 35.23: Pleural effusion and ascites at 19 weeks. Tomographic ultrasound sagittal image of the fetal trunk. Fluid collection in both chest and abdomen are clearly demonstrated

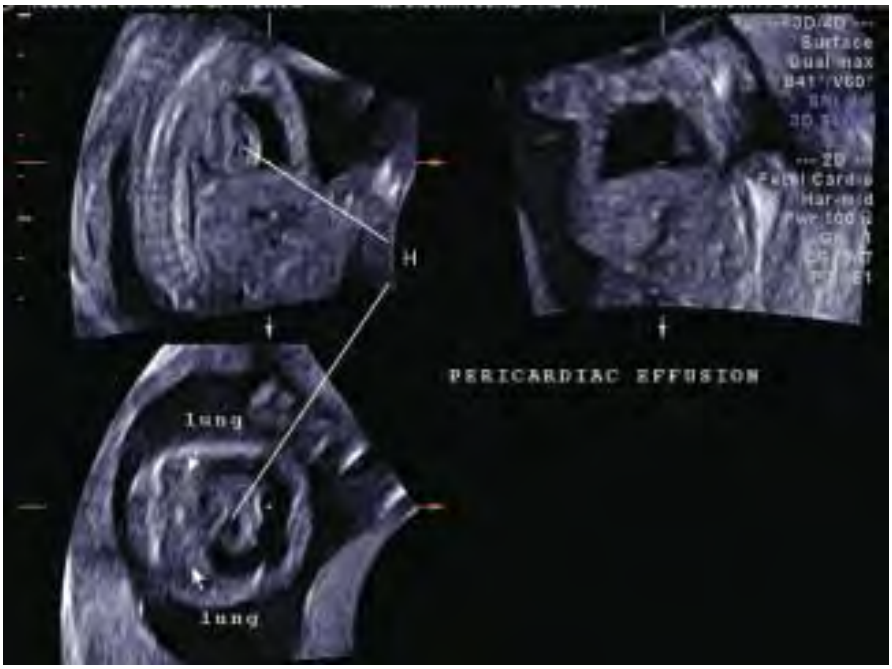

Figure 35.24: Pericardiac effusion at 19 weeks. Three orthogonal view of the fetal chest. Due to fluid collection inside epicardium, the lungs are oppressed to posterior portion of the chest

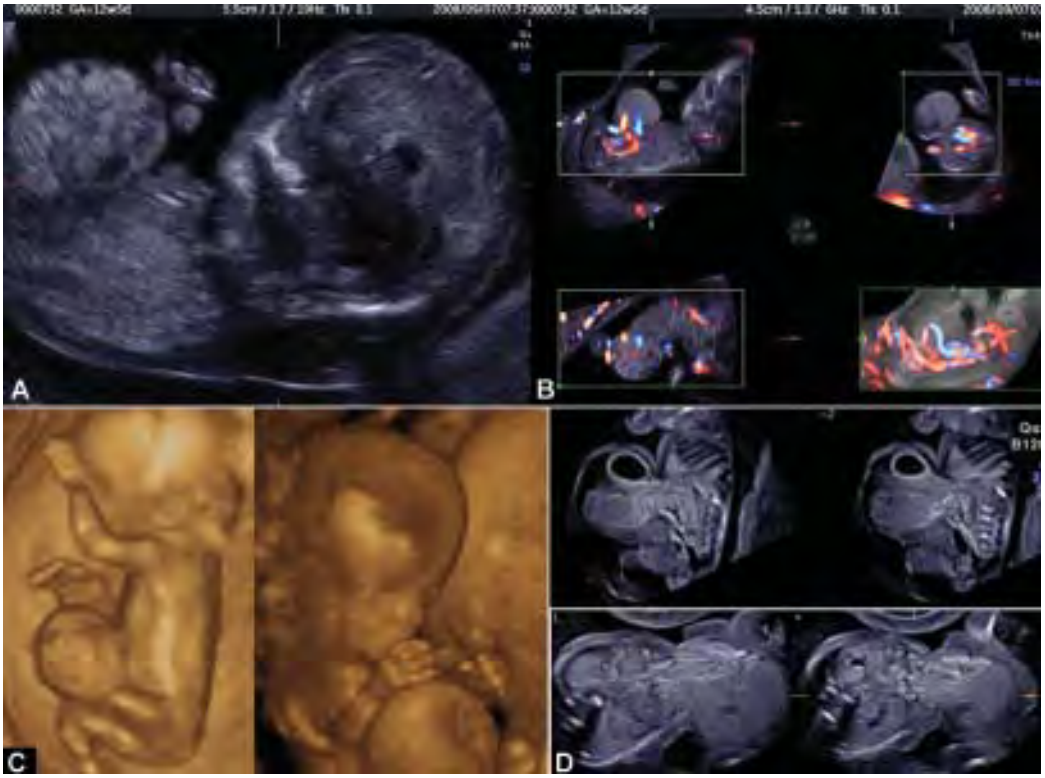

Figures 35.25A to D: Huge omphalocele at 12 weeks. (A) Sagittal image from 3D orthogonal view. Increased nuchal translucency is seen; (B) Three orthogonal view and reconstructed image of the fetal circulation. Because of the ectopic liver, the umbilical vein and ductus venosus run outside the body toward the heart inside the body. The ductus venosus reversed flow was seen in this case; (C) 3D reconstructed images; (D) Four selected images from tomographic ultrasound images, demonstrating the relation of ectopic organs and inside organ. After confirming normal chromosome and no other associated anomalies were confirmed, parents decide to continue pregnancy. Postnatal surgery was successful and postoperative course has been favorable

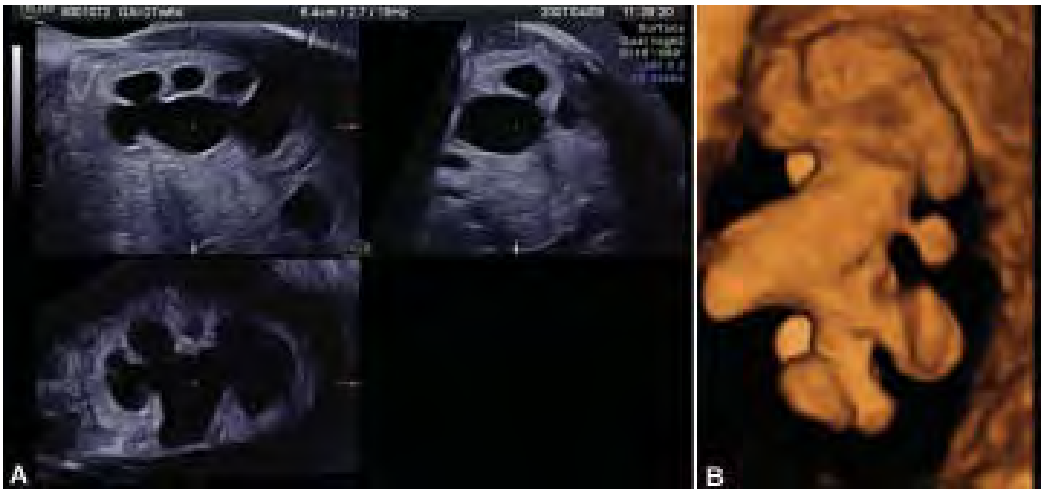

Figures 35.26A and B: Mild hydronephrosis at 27 weeks. (A) Three orthogonal view and (B) 3D reconstructed inverted image of the renal pelvis

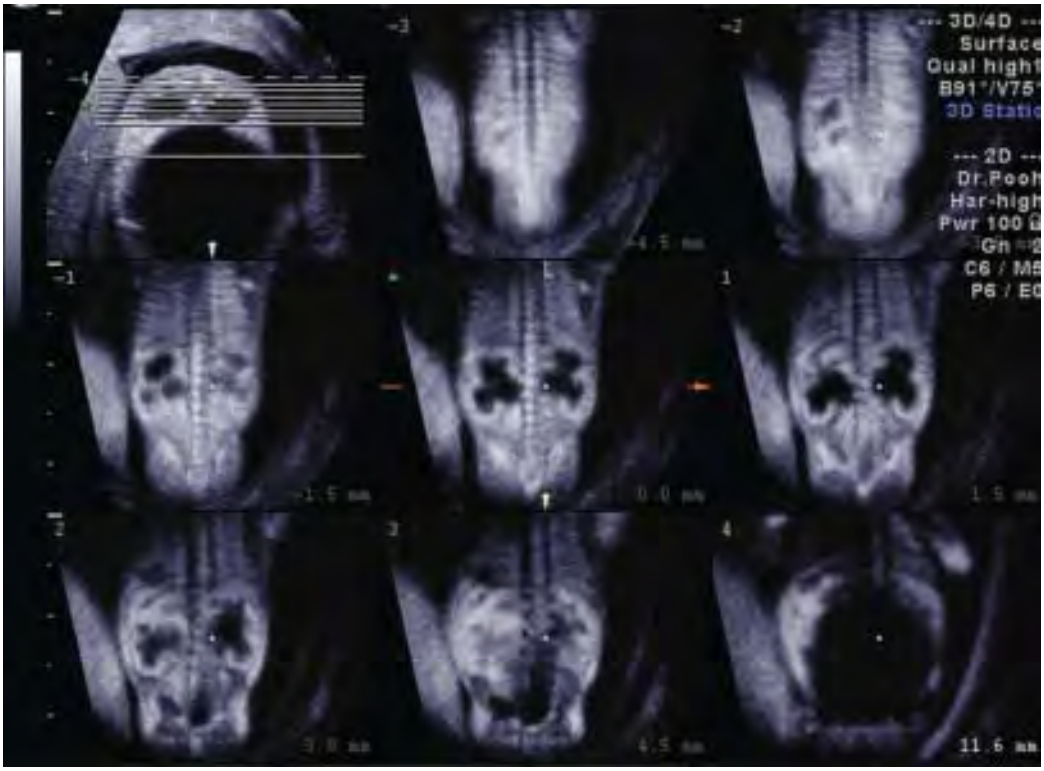

Figure 35.27: Bilateral hydronephrosis due to posterior urethral valve stenosis at 15 weeks. Tomographic ultrasound coronal image of the bilateral kidneys. Bilateral hydronephrosis with huge bladder occurred due to posterior urethral valve stenosis. Vesicoamniotic shunt at 17 weeks was successfully performed in this case and postnatal course was favorable

characterized by the presence of multiple cysts of varying size in the kidney and the absence of a normal pelvocaliceal system. Fetal MCDK occasionally decreased its size during pregnancy and it is reported that MCDK size tends to decrease during the first 30 postnatal months.[27]

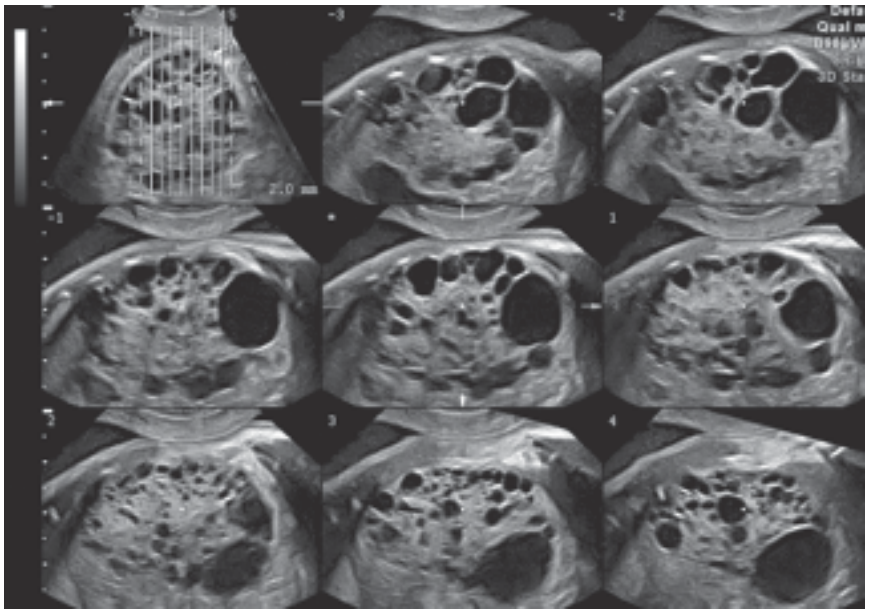

Figure 35.28: Multicystic dysplastic kidney (MCDK) at 22 weeks. Tomographic ultrasound image of unilateral MCDK. Note the numerous intrarenal cysts in different size are demonstrated

Limb Abnormalities

Limb abnormalities can occur as isolated findings or as one component of a syndrome or sequence. However, only 5% of congenital hand anomalies occur as part of a recognized syndrome.[28] **Figures 35.29A to D** show thin limbs with no other abnormalities in a case of triploidy. **Figures 35.30A to G** demonstrate 3D ultrasound images and postmortem pictures in a case of lethal pterygium syndrome. Pterygium is used to describe webbing of the skin across the joint. The term means "wing-like". Limb pterygia, at birth, indicates an abnormal developmental process probably occurring in the first trimester and involving reduced mobility of the webbed limb. Prenatal diagnosis in the first trimester was reported.[29] **Figures 35.31A to C** show unilateral forearm and thumb abnormality with no other abnormalities in case of partial chromosomal abnormality. **Figures 35.32A to H** demonstrate two cases of thanatophoric dysplasia at 19–20 weeks.

Recent high resolutional ultrasound can demonstrate finger/toe abnormality in detail. Polydactyly **(Figs 35.33 and 35.34,** syndactyly **(Figs 35.35 and 35.36)** and cleft hand/toe **(Figs 35.37 to 35.39)** are clearly seen by 3D ultrasound during pregnancy. Thumb abnormality, especially adducted thumb is one of the important signs for assessment of fetal brain development.[30,31] Genetic hydrocephalus or brain abnormalities which is strongly related to L1CAM gene, are associated with adducted thumbs **(Figs 35.40A to C)**.[32,33]

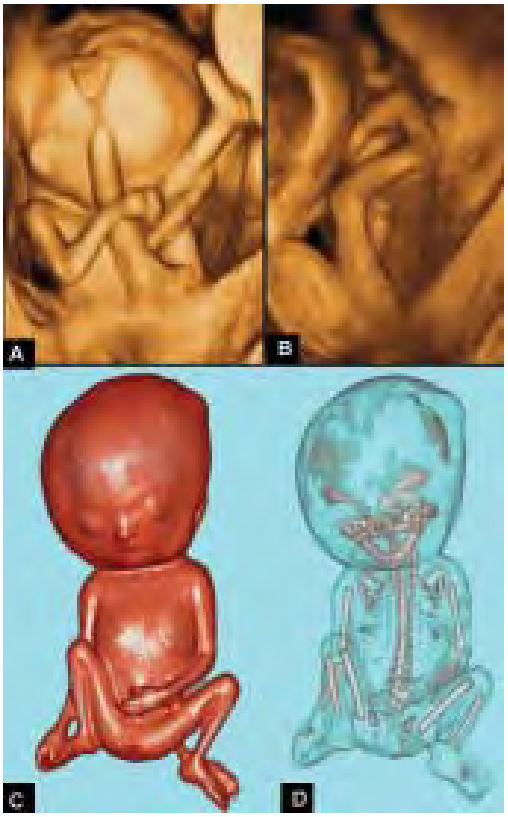

Figures 35.29A to D: Thin limbs in a case of triploidy at 17 weeks. (A and B) 3D US reconstructed images. Small for date baby with abnormal proportion, large head and thin limbs and trunk, is demonstrated. Postmortem 3D-CT scan image of (C) surface anatomy and (D) bony structure of the same baby

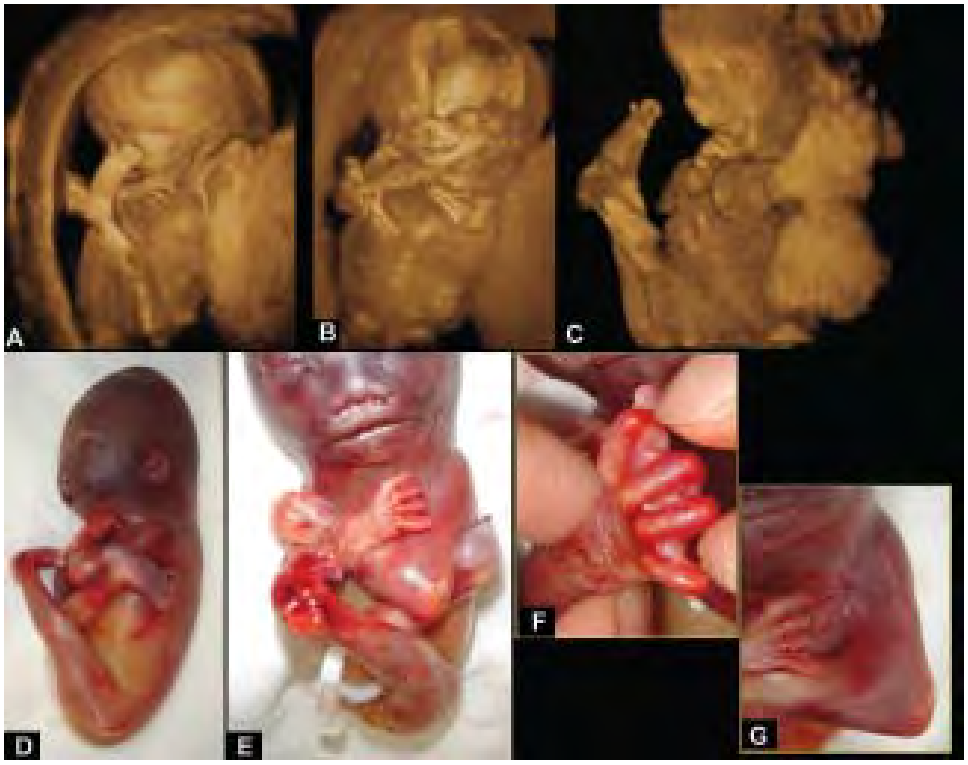

Figures 35.30A to G: Lethal pterygium syndrome detected at 14 weeks. (A to C) 3D reconstructed images. Middle image demonstrated the bony structure by maximum mode. The fetus did not move with the same appearance for weeks; (D to G) Aborted fetus at 20 weeks. The same appearance as prenatal images is seen. The wing-like shoulders and elbows, finger webs are characteristics of this syndrome

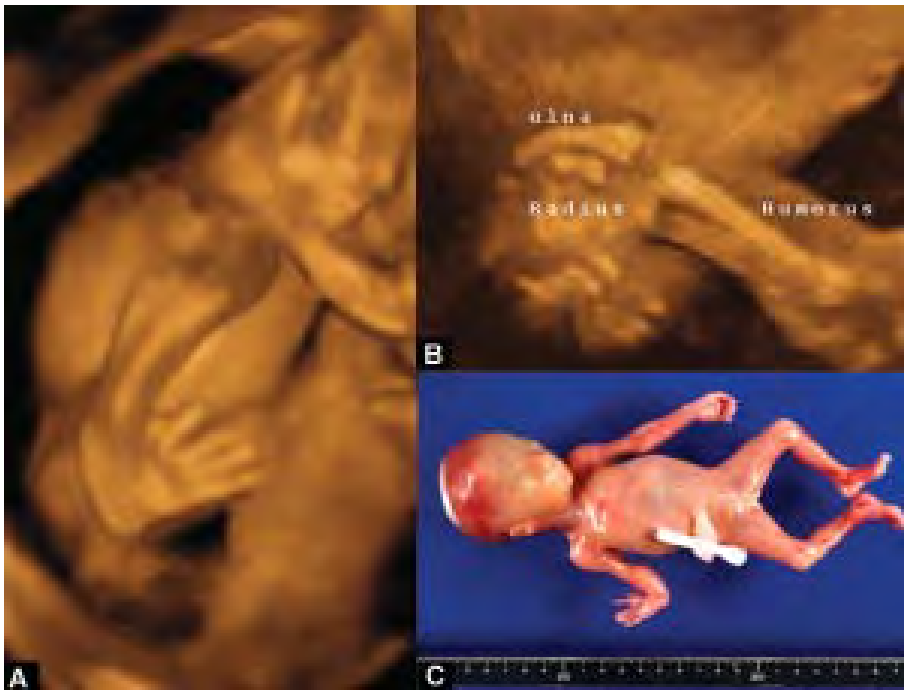

Figures 35.31A to C: Right arm abnormality at 18 weeks. (A) Abnormal appearance of right arm by 3D reconstructed image. Short forearm and thumb abnormality are demonstrated; (B) Maximum mode image of the right arm. Short ulna and extremely short radius are clearly demonstrated; (C) Postmortem appearance of the aborted fetus. Partial chromosomal abnormality was confirmed

Source: Dr Takemura H, Kosaka Women's Hospital, Higashiosaka, Japan.

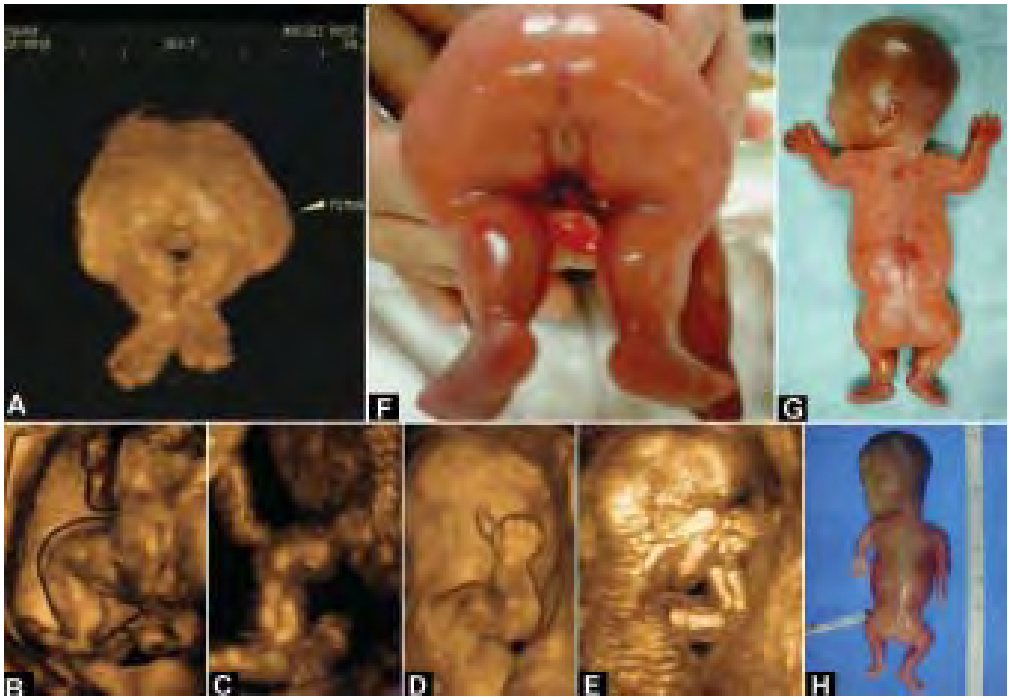

Figures 35.32A to H: Thanatophoric dysplasia at 19 weeks. (A to E) 3D reconstructed images and (F to H) postmortem appearance of two cases with short limbs and abnormally curved femurs, are shown

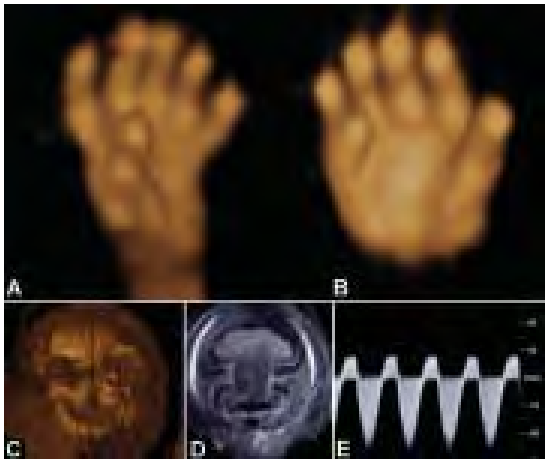

Figures 35.33A to E: Polydactyly at 14 weeks. (A and B) Bilateral polydactyly is clearly demonstrated; (C) This case has cleft palate; (D) holoprosencephaly; (E) umbilical artery reversed flow

Figures 35.34A to C: Polydactyly/syndactyly at 19 weeks. 3D reconstructed images of the right toe. (A and B) The first big toe is demonstrated in the figures; (C) The figure clearly shows six toe bones

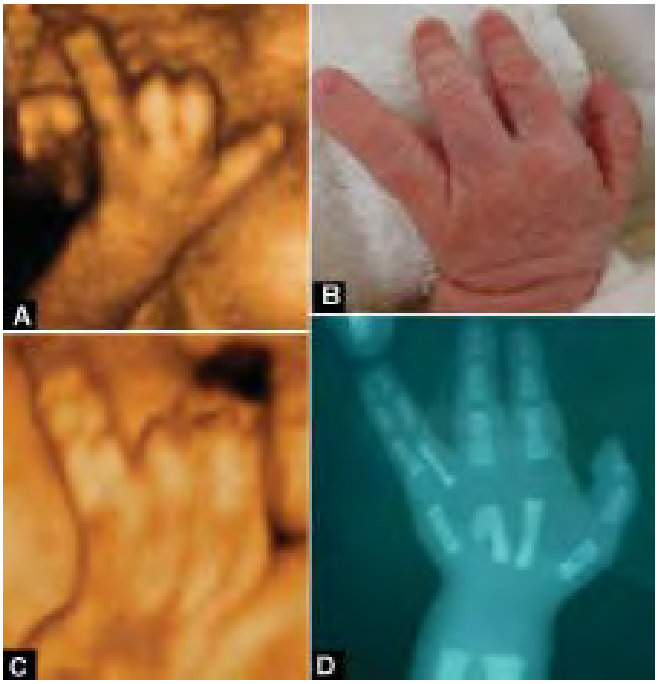

Figures 35.35A to D: Syndactyly (single finding) at 28 weeks. (A and C) 3D reconstructed images of the left hand. The fourth and fifth fingers are almost the same size and abnormally stretched together; (B) Postnatal hand appearance; (D) Postnatal X-ray image

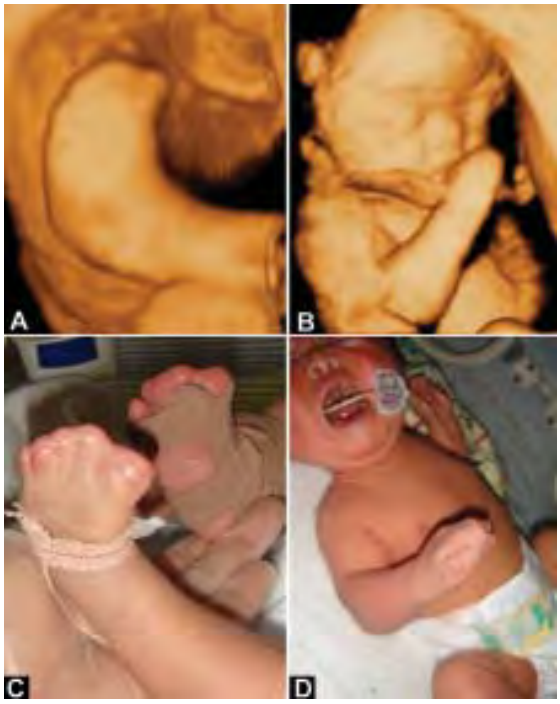

Figures 35.36A to D: Syndactyly in a case of Apert syndrome at 31 weeks. (A and B) 3D reconstructed images of the foot and hand. All of toes and fingers are sticked together; (C and D) Postnatal appearance of foot and hand. The same appearance as prenatal imaging is seen

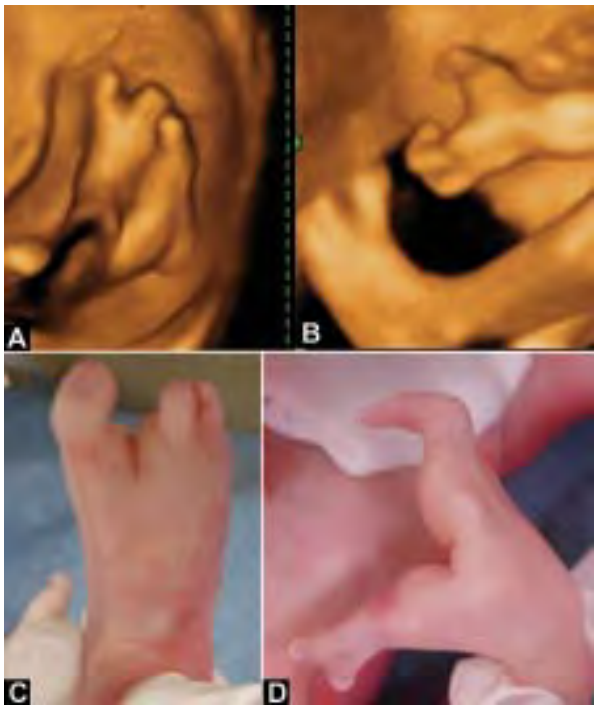

Figures 35.37A to D: Cleft foot and cleft hand, oligodactyly/syndactyly at 28 weeks. (A and B) 3D reconstructed images of the foot and hand; (C and D) Postnatal appearance

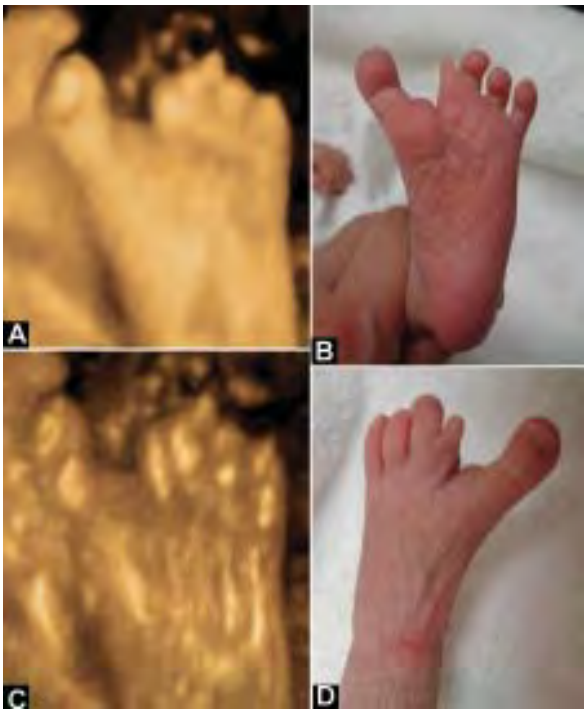

Figure 35.38A to D: Cleft foot with toe dysplasia at 35 weeks. (A) 3D reconstructed image; (C) Maximum mode; (B and D) Postnatal appearance

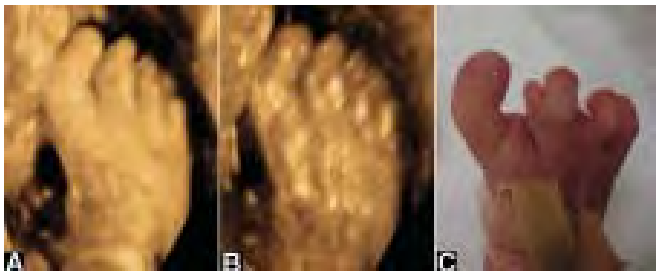

Figures 35.39A to C: Cleft foot with toe dysplasia and first toe contracture at 35 weeks. (A) 3D reconstructed image; (B) Maximum mode; (C) Postnatal appearance

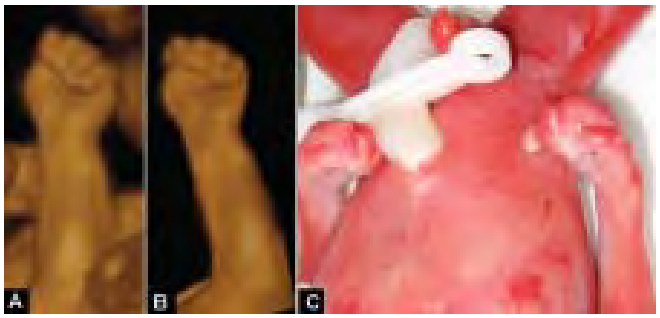

Figures 35.40A to C: Adducted thumbs in a case of genetic hydrocephalus. (A and B) 3D reconstructed images of adducted thumb; (C) Postmortem appearance of clenched hands with adducted thumbs. This case is complicated with hydrocephalus, partial agenesis of the corpus callosum. Postmortem genetic test revealed L1CAM disorder

CONCLUSION

This chapter reviews and illustrates the power of high-resolution 3D ultrasound in defining normal fetal anatomy as well as in the identification of congenital anomalies. The advances of 3D ultrasound in the last decade have been remarkable and contributed to the field of embryology, fetal physiology and pathology. Further researches by 3D ultrasound will bring more accurate and detailed prenatal diagnosis for better prenatal care.

ACKNOWLEDGMENTS

The authors thank members of Global Ultrasound and Information Technologies and Women's Healthcare and Specialty of General Electrics Healthcare (Milwaukee, USA) for their technical support and collaboration in three-dimensional ultrasound technology.

REFERENCES

1. Kurjak A, Pooh RK, Merce LT, et al. Structural and functional early human development assessed by three-dimensional and four-dimensional sonography. Fertil Steril. 2005;84(5):1285-99.
2. Kurjak A, Zudenigo D, Predanic M, et al. Recent advances in the Doppler study of early fetomaternal circulation. J Perinat Med. 1993;21:419-39.
3. Kurjak A, Schulman H, Predanic A, et al. Fetal choroid plexus vascularization assessed by color flow ultrasonography. J Ultrasound Med. 1994;13:841-4.
4. Pooh RK, Aono T. Transvaginal power Doppler angiography of the fetal brain. Ultrasound Obstet Gynecol. 1996;8:417-21.
5. Teoh M, Meagher S. First-trimester diagnosis of micrognathia as a presentation of Pierre Robin syndrome. Ultrasound Obstet Gynecol. 2003;21:616-8.
6. Tsai MY, Lan KC, Ou CY, et al. Assessment of the facial features and chin development of fetuses with use of serial three-dimensional sonography and the mandibular size monogram in a Chinese population. AmJ Obstet Gynecol. 2004;190:541-6.
7. Pooh RK. Three-dimensional ultrasound of the fetal brain. In: Kurjak A (Ed). Clinical application of 3D ultrasonography. Carnforth: Parthenon Publishing; 2000. pp. 176-80.
8. Pooh RK, Pooh KH, Nakagawa Y, et al. Clinical application of three-dimensional ultrasound in fetal brain assessment. Croat Med J. 2000;41:245-51.
9. Blaas HG, Eik-Nes SH, Kiserud T, et al. Three-dimensional imaging of the brain cavities in human embryos. Ultrasound Obstet Gynecol. 1995;5:228-32.
10. Blaas HG, Eik-Nes SH, Berg S, et al. In-vivo three-dimensional ultrasound reconstructions of embryos and early fetuses. Lancet. 1998;352:1182-6.
11. Timor-Tritsch IE, Monteagudo A, Mayberry P. Three-dimensional ultrasound evaluation of the fetal brain: the three horn view. Ultrasound Obstet Gynecol. 2000;16:302-6.
12. Monteagudo A, Timor-Tritsch IE, Mayberry P. Three-dimensional transvaginal neurosonography of the fetal brain: 'navigating' in the volume scan. Ultrasound Obstet Gynecol. 2000;16:307-13.
13. Pooh RK, Nagao Y, Pooh KH. Fetal neuroimaging by transvaginal 3D ultrasound and MRI. Ultrasound Rev Obstet Gynecol. 2006;6:123-34.
14. Pooh RK, Pooh KH. Fetal neuroimaging with new technology. Ultrasound Review Obstet Gynecol. 2002;2:178-81.
15. Pooh RK. Fetal brain assessment by three-dimensional ultrasound. In: Kurjak A, Kupesic S (Eds). Clinical Application of 3D Sonography. Carnforth, UK: Parthenon Publishing; 2000. pp. 171-9.
16. Pooh RK, Pooh KH. Transvaginal 3D and Doppler ultrasonography of the fetal brain. Semin Perinatol. 2001;25:38-43.
17. Pooh RK, Pooh KH. The assessment of fetal brain morphology and circulation by transvaginal 3D sonography and power Doppler. J Perinat Med. 2002;30:48-56.
18. Pooh RK, Pooh KH. Fetal Ventriculomegaly. Donald School J Ultrasound Obstet Gynecol. 2007;2(2):40-6.
19. Pooh RK, Maeda K, Pooh KH. An Atlas of Fetal Central Nervous System Disease. Diagnosis and Management. London, New York: Parthenon CRC Press; 2003.
20. Pooh RK. Neuroscan of congenital brain abnormality. In: Kurjak A (Ed.). Fetal Neurology. New Delhi: Jaypee Brothers Medical Publishers; 2009. pp. 59-139.
21. Pooh RK. Fetal Neuroimaging of Neural Migration Disorder. Ultrasound Clinics: Elsevier. 2008;3(4):541-55.
22. Blaas HG, Eik-Nes SH, Isaksen CV. The detection of spina bifida before 10 gestational weeks using two- and three-dimensional ultrasound. Ultrasound Obstet Gynecol. 2000;16(1):25-9.
23. Scott RM, Wolpert SM, Bartoshesky LE, et al. Segmental spinal dysgenesis. Neurosurgery. 1988;22(4):739-44.
24. Doyle NM, Lally KP. The CDH Study Group and advances in the clinical care of the patient with congenital diaphragmatic hernia. Semin Perinatol. 2004;28(3):174-84.
25. Daskalakis G, Anastasakis E, Souka A, et al. First trimester ultrasound diagnosis of congenital diaphragmatic hernia. J Obstet Gynaecol Res. 2007;33:870-2.
26. Sanz-Cortés M, Raga F, Bonilla-Musoles F. Prenatal diagnosis of congenital cystic adenomatoid malformation using three-dimensional inversion rendering: a case report. J Obstet Gynaecol Res. 2008;34(4 Pt 2):631-4.
27. Siqueira Rabelo EA, Oliveira EA, Silva JM, et al. Ultrasound progression of prenatally detected multicystic dysplastic kidney. Urology. 2006;68(5):1098-102.
28. Bolitho DG (2006). Hand, Congenital hand deformities. [online] emedicine website. Availiable from www.emedicine.medscape.com. Accessed February 2011.
29. Gundogan M, Fong K, Keating S, et al. First trimester ultrasound diagnosis of lethal multiple pterygium syndrome. Fetal Diagn Ther. 2006;21(5):466-70.

30. Kurjak A, Miskovic B, Stanojevic M, et al. New scoring system for fetal neurobehavior assessed by three- and four-dimensional sonography. J Perinat Med. 2008;36(1):73-81.
31. Kurjak A, Tikvica A, Stanojevic M, et al. The assessment of fetal neurobehavior by three-dimensional and four-dimensional ultrasound. J Matern Fetal Neonatal Med. 2008;21(10):675-84.
32. Yamasaki M, Thompson P, Lemmon V. CRASH syndrome: mutations in L1CAM correlate with severity of the disease. Neuropediatrics. 1997;28(3):175-8.
33. Kanemura Y, Takuma Y, Kamiguchi H, et al. First case of L1CAM gene mutation identified in MASA syndrome in Asia. Congenit Anom, Kyoto. 2005;45(2):67-9.

36
CHAPTER

Fetal Behavior

Zehra Nese Kavak, Tevfik Yoldemir

INTRODUCTION

Fetal behavior can be defined as any observable spontaneous movement or reaction (to an external stimulus) by the fetus.[1] Fetal behavior gives information about the maturation of the nervous system and the orderly progression of movement sequences and profiles.[2,3] Descriptive studies of fetal behavior give insight to developmental differences in the frequency and timing of certain functions and the effect by environmental influence. Assessment of behavior is a predictor of neurodevelopmental disability.[4,5] The association between fetal behavior and developmental course during different periods of gestation might show the distinction between normal and abnormal brain development, hence the early diagnosis of various structural or functional abnormalities.[3,4] Fetal behavior may be noted by maternal perception of movement or real-time ultrasound imaging by means of which fetal behavior can be observed.[6,7] Innovations in imaging technology have created the possibility to study fetal behavior *in utero*.[8]

Numerous studies using conventional two-dimensional (2D) ultrasound have shown that normally developing fetuses and fetuses at risk exhibit different patterns of behavior.[9-13] Although fetal facial expressions have been studied using two-dimensional (2D) ultrasonography.[14,15] There are limitations and difficulties of this technique. Anatomical features of the face make it hard to evaluate the complex facial activity. Because of the 2D character of conventional real-time scanning, fetal movements and facial expressions outside the scanning plane cannot be displayed on the monitor screen.[16] Three-dimensional (3D) ultrasonography provides improved visualization of fetal movements as compared with conventional 2D ultrasonographic imaging. However, all conventional 3D ultrasonographic pictures were static images and dynamic or real-time fetal movements could not be evaluated. Only with the development of real-time 3D (4D) ultrasound, fetal behavioral movements and the full range of facial expressions could be observed.[17-25]

Studies of fetal brain function suggest standardized evaluation of fetal behavior.[26-28] If behavioral analysis is to have a role in the routine clinical environment, then normal standard parameters for individual fetal movements need to be validated.[4,20] In the past 30 years, several different diagnostic strategies were introduced in order to identify fetuses at risk for neurological damage. Several different tests were proposed but their concept, complexity and time consuming was not practical for daily use. Kurjak et al. constructed a scoring system for fetal neurobehavior assessed by 3D real time or 4D sonography.[29] They compared this scoring system with the postnatal neurological assessment according to Amiel-Tison (ATNAT).[30] All neonates underwent postnatal neurological assessment according to Amiel-Tison (ATNAT) at the age of 1–3 days. The usefulness of KANET to identify fetuses from high-risk pregnancies at neurological risk was investigated by comparing with postnatal examination of the neonates. After the assessment, infants were assigned as normal, borderline, or abnormal. Infants from the borderline and abnormal groups were assigned to the high-risk group for development of neurological impairment.

TECHNICAL ASPECTS OF 4D ULTRASOUND

A 4D image is produced by first selecting an ideal representative 2D image within the region of interest and then superimposing on it a volume box defined by the examiner.[31] The crystal array of the transducer sweeps mechanically over the defined region of interest through an 85° angle. Most devices are capable of recording up to 40 frames/s depending on the size of region of interest (ROI) window. In clinical practice, 4D scanning is not real time, but rather dynamic, with the frame rate being in the region of 4–6 frames/s depending on the size of the ROI and number of lines employed.[32] At these relatively slow frame rates, the ability to study fetal behavior in the surface-rendered mode, especially long-duration fetal movements, such as gross body, limb and complex limb movements, is satisfactory.[33] However, 4D ultrasound has restrictions to study short-duration fetal movements during the early gestation.

TECHNICAL ASPECTS OF REAL-TIME 3D ULTRASOUND

Real-time 3D ultrasonography captures large volumes of data and processes it while the target is moving.[34] The development of a transducer that can interpret the entire volume of interest as opposed to one 2D slice made this imaging system possible. The transducer has more elements than the conventional 2D transducers.[35] This transducer, which is capable of imaging the fetus in 3D in real-time, has 3,000 crystals incorporated into its head that emit and receive sound. Each crystal is connected to a particular channel. The innovative engineering feature is that all of the boards have been miniaturized and housed within the transducer.[36] This real-time 3D sonographic device is capable of providing continuous 3D images with the frame rate being in the region of 20–28 frames/s. A limitation of this 3D sonographic technique is the narrow defined region of interest through a 201° angle.[37]

IMAGING DURING THE FIRST AND EARLY SECOND TRIMESTERS

The study of fetal movements in the first half of gestation could be achieved with conventional real-time 2D sonographic equipment and the improved resolution adds new information to the study of fetal morphology.[38] However, less of the fetal parts in any single view could be visualized in the sonographic scan plane as pregnancy advanced.[31] The fetal movements can be visualized as a whole by 4D ultrasonography before 20 weeks of gestation. Fetal behavioral assessment using 4D ultrasonography in the first and early second trimesters of pregnancy have been reported.[8,26,31,39-41] The equipment used in all previous studies was a 4D ultrasound device and the frame rate was 0.5 frames/s in most of them. However, the frame rate in conventional 2D ultrasonography was usually about 40 frames/s. Therefore, 4D scans in all previous investigations were dynamic (stop-motion images) and not real-time images. Rapid fetal movements (those lasting less than 2 seconds) or subtle fetal movements (e.g. breathing movements and chest contractions) could not be depicted with 4D machines that had slow acquisition.[31] However, new high end machines allow study of these movements as well. General body, head and limb movements recorded by 2D sonography were notable by 4D sonography between 6 and 14 weeks of gestation. Several movement patterns, such as sideway bending, hiccup, breathing movements, mouth opening and facial movements, could be observed by the 2D sonographic technique and not by 4D ultrasound with slow acquisition. Thus 2D and 4D sonography should be used as complementary methods for the evaluation of fetal movement patterns in early gestation.[33]

We[41] had suggested a tendency towards an increased frequency of fetal movement patterns with increasing gestational age in the first trimester. Only the startle movement pattern seemed to occur stagnantly during the first trimester. In this type of movement there was no significant correlation with gestational age. At the beginning of the second trimester, there was a tendency towards an increase in the frequency of fetal movement patterns.

IMAGING DURING LATE SECOND AND THIRD TRIMESTERS

Fetal behavioral assessment was accomplished in the late second and third trimesters of pregnancy with 4D or real-time 3D ultrasonography.[8,26,37,40-45] Assessment of fetal facial expressions and other body movements, especially of the hands were of main focus. The 4D technology made it possible to image facial as well as hand movements and their co-occurrence. Studying the early coordination of hand-to-mouth activity and the assessment of fetal emotion through the evaluation of facial expressions could be achieved with this imaging feature. It is difficult to evaluate complex facial activity due to the anatomical features of the face and limitations of the 2D character of conventional 2D ultrasonography. However, 4D ultrasonography provides consecutive sculpture-like 3D images of the fetal face in real time.

Rapid fetal facial activities including rapid blinking, subtle lip movement and dynamic lingual movement could not be depicted using these 4D ultrasound devices because the frame rate in most studies was 0.5 frames/s, which translates into 4–6 frames/s and is too slow to obtain a satisfactory image.[33]

The fetal behavior proceeds from rapid, somewhat isolated fetal movements, to a greater proportion of less jerky and smooth wholebody movements later in gestation. The 4D technique is not capable of assessing the subtle and rapid movements. Hence assessing the developmental level across gestation may be compromised in the absence of detecting these short-duration fetal movements. Such movements, sometimes referred to as isolated fetal movements and isolated spikes, represent the immature development of the nervous system and a lack of coordinated behavior.

After approximately 30 weeks of gestation, there is an increase in long-duration fetal movements, referred to as epochs and episodes. However, the frame rate of the real-time 3D ultrasound apparatus is 20–21 frames/s.[37] For this reason, real-time 3D ultrasound should be used in order to resolve the limitations of 4D sonographic fetal imaging. Moreover, distinctions between short and long-duration fetal movements across gestation might be observable.[33] However, the narrow defined region of interest is a limitation associated with real-time 3D ultrasound.

We[41] had reported that mouthing, yawning, tongue expulsion, smiling, sucking and swallowing expressions displayed a peak frequency between the 24th and 32nd gestational weeks. Grimacing and eye blinking expressions displayed peak frequency between the 28th and 36th weeks and after the 32nd week, respectively. In the middle of the third trimester, the fetuses displayed decreasing or stagnant incidence of fetal facial expressions except for eye blinking, which showed increased frequency with increasing gestational age. A statistically significant correlation was found between all head movements and hand-to-body contact patterns during the second and third trimesters except for head anteflexion **(Fig. 36.1)**. While the most frequent facial pattern between the 18th and 27th weeks of gestation was mouthing followed by swallowing and sucking, between the 28th and 36th gestational weeks the most frequent facial expression pattern was found to be grimacing followed by mouthing and eye blinking.

4D ULTRASONOGRAPHIC OBSERVATION OF THE FETAL FACE

For the fetal facial expressions and movements, the Kurjak classification is mostly used, as defined in

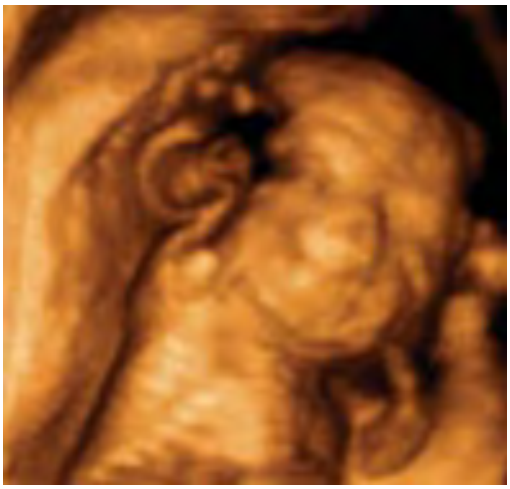

Figure 36.1: Isolated head anteflexion

Table 36.1.[40] Kurjak et al.[40] found that facial activities and different forms of expression could be easily recognized, with 4D ultrasonography in ten healthy fetuses aged from 30 to 33 weeks. Eyelid and mouthing dominated at this gestational age. Kurjak et al.[26] used 4D ultrasonographic examinations to evaluate fetal neurodevelopmental parameters from the 15th to 40th week.[26] All types of facial expression displayed a peak frequency at the end of the second trimester, except for isolated eye blinking, which increased in frequency at the beginning of the 24th week. We[41] also used 4D ultrasonography in the second and third trimesters and found significant changes in tongue expulsion, smiling, grimacing, swallowing and eye blinking, but there were no significant change in mouthing, yawning and sucking. By the middle of the third trimester, the fetuses displayed a decreasing or unchanging incidence of fetal facial expressions except for eye blinking, which showed an increased frequency with increasing gestational age. Yan et al.[45] reported a full range of fetal facial expressions early in the third trimester (from 28 to 34 gestational weeks) using 4D ultrasonographic techniques. Mouthing was found to be the most active facial expression during this gestational period just as in previous reports.[26,40] However, the frequency of eye blinking, which in other studies was thought to be similar to that of mouthing, was lower. Kurjak et al.[26] observed that an increase in facial movement was simultaneously associated with a decrease in the number of general movements (GMs). This observation is considered to reflect the normal neurological development of the fetus.[3,5,6] A full range of fetal facial expressions similar to emotional expression in adults have been detected by 4D ultrasound.[18,19,26] Moreover, different

TABLE 36.1

Classification of facial expression and movement patterns

1. Mouthing movement: consisted of a series of rhythmic movements involving the mandible and tongue, characterized by constant frequency and duration until disappearance
2. Yawning: slow and prolonged wide opening of the jaws followed by quick closure with simultaneous retroflexion of the head and sometimes elevation of the arms of exoration. The duration is about three seconds
3. Tongue expulsion: facial activity characterized by mouth opening with protruding of fetal tongue
4. Smiling: the expression consists of the bilateral elevation of the mouth angle
5. Scowling and grimacing: the expression consists of bilateral contraction of eyebrows and mimic musculature between them
6. Sucking and swallowing: rhythmical bursts of regular jaw opening and closing at a rate of about 1/s may be followed by swallowing, indicating that the fetus is drinking amniotic fluid. Swallowing consists of displacements of the tongue and/or larynx
7. General movements: this category is applicable if the whole body is moved but no distinctive patterning or sequencing of the body parts can be recognized. The complex movements of the limb, trunk and head are clearly visible and cause a shift in fetal position
8. Startle: a startle is a quick generalized movement, always initiated in the limbs and sometimes spreading to the neck and trunk
9. Stretch: a stretch is a complex motor pattern, which is always carried out at a slow speed and consists of the following components: forceful extension of the back, retroflexion of head, and external rotation and elevation of the arms
10. Isolated limb movement: these may be rapid or slow movement, and may involve extension, flexion, external and internal rotation, or abduction and adduction of an extremity, without movements in other body parts
11. Isolated retroflexion of the head: retroflexions of the head are usually carried out slowly, but they can also be fast and jerky. The displacement of the head can be small or large. The latter may cause overextension of the spine of the fetus
12. Isolated anteflexion of the head: anteflexion of the head is carried out only at a slow velocity. The displacement of the head is small. The duration is about one second.

facial expressions and movements might be indices of fetal states.

4D ULTRASONOGRAPHIC OBSERVATION OF THE ENTIRE FETAL BODY

Fetal behavior reflects the activity of the fetal central nervous system.[2,46] Early neuromuscular development is expressed as endogeneous motility and reactions towards stimuli.[47] Local reflexes begin to appear at 7.5 weeks of gestation and the ratio of axosomatic synapses increases rapidly between 11 and 13.5 weeks.[48] Reflexes are elicited only at the proximal part of the body in the presence of simultaneous stimuli applied to differentiate reflexogenic sites by 11.5 weeks of gestation. However, reflexes can be elicited at both distal and proximal sites in fetuses older than 12.5 weeks.[49]

As the fetus advanced in age the reflex response changes from simple lateral head flexion to movements of the upper limbs, trunk, rump and lower limbs.[50,51] Opening of the mouth was seen from 10 weeks of gestation, reflex swallowing from 12 weeks and the gag reflex from 18 weeks.[52] Humphrey[53] suggested that reflex activities demonstrable before 20 weeks of gestation are executed through the mesencephalon, lower brainstem and spinal cord. Shawker et al.[54] showed an orderly developmental progression of fetal activity beginning with the beating of the fetal heart (7 weeks), progressing to fetal trunk movement (8 weeks) and later individual fetal limb movement (9 weeks) with conventional 2D ultrasound. Reinold[55] reported rapid changes of position and posture of the fetus between 9 and 12 weeks, and more prolonged episodes of changes of position, as well as flexion and extension of the limbs from 13 to 16 weeks. Furthermore, fetuses from 17 to 20 weeks made jerky or slow flexion and extension movements of the trunk, sometimes accompanied by movement of a single limb. Boue et al.[56] reported that healthy fetuses at 18–20 weeks performed slow and harmonious movements with isolated leg movements, in contrast to the synchronized movements of the whole body with twitches and kicking, as frequently noted at 12–13 weeks. Moreover, some movement patterns occurred more frequently than others at 7–19 weeks of gestation. Kurjak et al.[39] used 4D ultrasonography to fetuses aged from 6 to 12 weeks and found that body and limb movements can be visualized a week earlier than with 2D ultrasonography. Three types of movements could be visualized in the first trimester:

1. Gross body movements between 7 and 8 weeks
2. Limb movements after 10 weeks
3. Complex limb movements after 11 weeks of gestation.

Kurjak et al.[26] used 4D ultrasonographic examination to evaluate fetal neurodevelopmental parameters from the 7th to 14th week. The measurements of seven parameters (general movements, stretching, isolated arm movements, isolated leg movements, head retroflexion, head rotation and head anteflexion) were correlated with the gestational age. These parameters showed an increasing frequency of fetal movement during the first trimester. However, the frequency of a startle pattern did not correlate with gestation in the first trimester. We[41] also employed 4D ultrasonography to investigate fetuses at 11 and 14 weeks of gestation and noted a tendency towards an increased frequency of fetal movement patterns with increasing gestational age. Only the startle movement pattern frequency seemed to remain unchanged during the first trimester. Moreover, the frequency of fetal movement patterns tended to increase at the beginning of the second trimester. Kuno et al.[31] performed 4D ultrasonographic examinations at 14–18 weeks of gestation. The most active fetal behavior pattern was arm movement, whereas the least was mouth movement. Each fetal movement was synchronized and harmonized with other movements although few movement patterns were found to be generated simultaneously. More short-duration isolated movements constituted more pronounced fetal movements in early gestation, whereas whole-body movements constituted the majority of movements in late gestation.

Andonotopo et al.[8] compared 4D ultrasonography with 2D ultrasonography in the assessment of embryonic and early fetal motor activity at 6 and 14 weeks of gestation. General body, head and limb movements recorded by 2D ultrasonography were notable using the 4D technique. However, sideway bending, hiccup, breathing movements, mouth opening and facial movements could be observed only by employing the 2D ultrasonographic technique in this period of gestation.

COMPARISON OF FETAL BEHAVIOR IN HIGH RISK AND NORMAL PREGNANCIES

Andonotopo and Kurjak[26] compared the frequency of all types of fetal facial expression between 50 normal and 50 growth-restricted fetuses in the third trimester and noted that there were significant differences in isolated eye blinking, mouthing, yawning, tongue expulsion, grimacing and swallowing. Moreover, the correlation reached significance between normal and growth restricted fetuses in the third trimester for head rotation, head anteflexion and head retroflexion. Significant differences were also noted in five qualitative categories of head and hand movement (hand-to-head, hand-to-mouth, hand-to-eye, hand-to-face and hand-to-ear movement). In conclusion, future use of 4D ultrasound for the quantitative and qualitative assessment of fetal behavior should be investigated as possible indicators of the neurological condition in growth-restricted fetuses.

Miskovic B et al.[57] found a significant difference for 8 out of 10 parameters of KANET **(Table 36.2)**: isolated anteflexion of the head, eye blinking **(Fig. 36.3)**, facial expressions (grimacing, tongue expulsion), mouth movements **(Figs 36.4 and 36.5)** (mouthing, yawning, swallowing), isolated hand movement **(Fig. 36.6)**, hand-to-face movement **(Fig. 36.7)**, fist and finger movements **(Fig. 36.8)** and GMs. Moderate correlation between KANET **(Table 36.3)** and Atnat tests was found. The neuropediatrician who examined the newborns with Atnat test confirmed the results of KANET. Sival DA et al. had shown disorder of GM and fetal behavioral states in intrauterine growth restriction (IUGR) fetuses.[58]

The ultimate purpose of evaluating the development of the central nervous system (CNS) by 4D ultrasonography is to determine whether 4D ultrasonography could serve as a prenatal diagnostic method to detect cerebral palsy prior to birth. In addition, 4D ultrasonography may become a method to assess fetal well-being.[58,59] New fetal nervous behaviors were observed in the fetuses of healthy and high-risk gravidas by examining two cranial closure areas by 3D ultrasonography and by scoring facial expression and fetal movement.[60] A postnatal follow-up study was performed and it became the basic research that facilitates detection of anomalies involving the nerves and CNS; however, in cerebral palsy, it is not easy to clearly detect abnormal development of the CNS.[24]

CONCLUSION

In the last three decades, there were several attempts to create a diagnostic test for evaluation for fetal behavior. The tests were different, but none of them were implemented into daily practice.[61-63] The KANET is based on 4D USG and original scoring system. The KANET might be useful in standardization of neurobehavioral assessments. At this stage, it seems that KANET separates serious structural anomalies associated with brain impairment. Furthermore, whether KANET has the potential for antenatal detection of serious neurological problems of other etiologies needs to be evaluated. The

TABLE 36.2
Kurjak's antenatal neurological test (KANET)

		Score		*Sign score*
Sign	*0*	*1*	*2*	
Isolated head anteflexion	Abrupt	Small range (0–3 movements)	Variable in full range, many alternation (43 movements)	
Cranial sutures **(Fig. 36.2)** and head circumference	Overlapping of cranial sutures head circumference below or above the normal limit ((2 SD) according to GA	Normal cranial sutures Normal head circumference	Not present	
Isolated eye blinking		Not fluent (1-5 blinking)	Fluency (> 5 blinking)	
Facial movements (grimace or tongue expulsion)		Not fluent (1-5 blinking)	Fluency (> 5 alternation)	
Mouth opening (yawning or mouthing)		Not fluent (1-3 blinking)	Fluency (>3 alternation)	
Isolated hand movement	Cramped	Poor repertoire	Variable and complex	
Isolated leg movement	Cramped	Poor repertoire	Variable and complex	
Hand-to-face movements	Abrupt	Small range (0-5 movements)	Variable in full range, many alternation (>5 movements)	
Finger movements	Unilateral or bilateral clenched fist, (neurological thumb)	Cramped invariable finger movements	Smooth and complex, variable finger movements	
Gestalt perception of GMs	Definitely abnormal	Borderline	Normal	
			Total score	

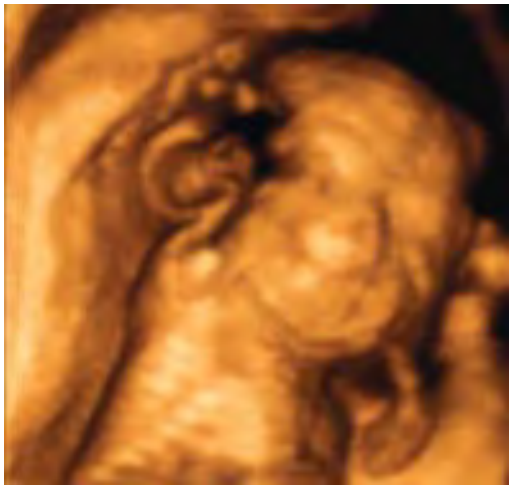

Figure 36.2: Cranial sutures

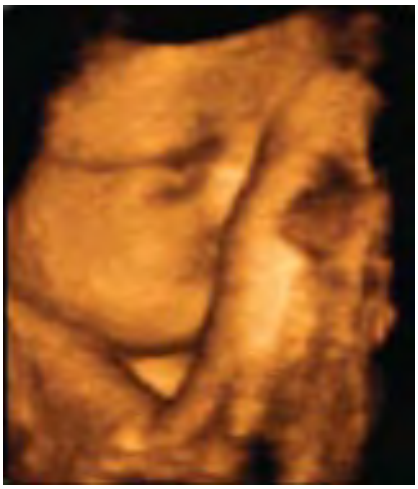

Figure 36.3: Isolated eye blinking

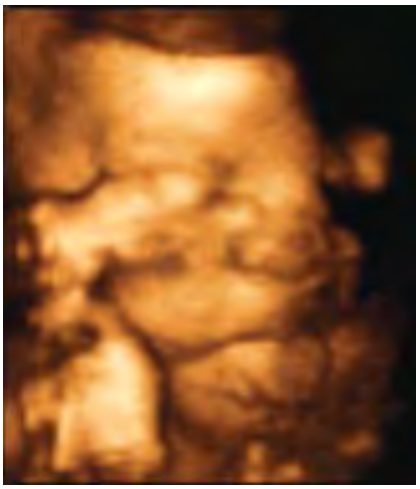

Figure 36.4: Tongue expulsion

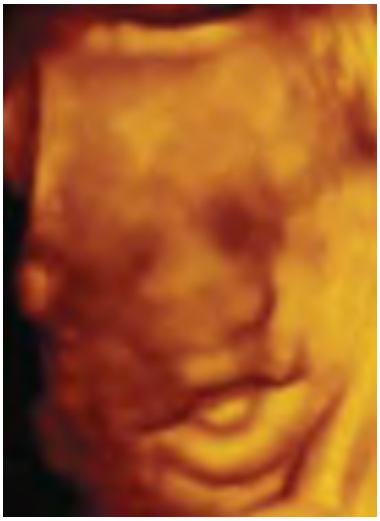

Figure 36.5: Mouth opening

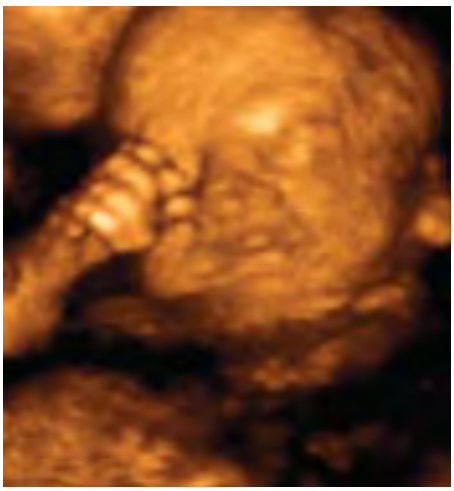

Figure 36.6: Isolated hand movement

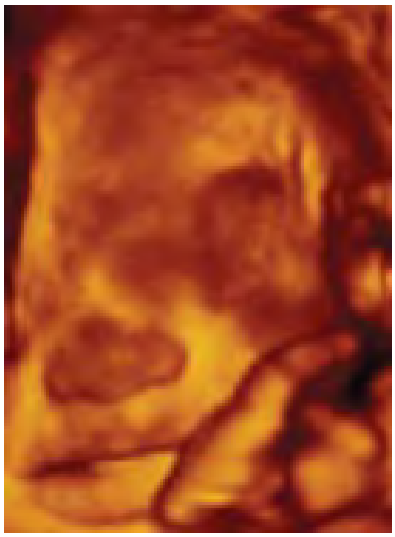

Figure 36.7: Hand-to-face movements

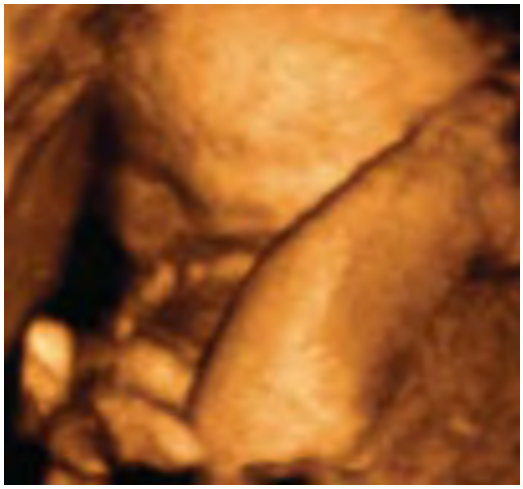

Figure 36.8: Finger movements

TABLE 36.3

Kurjak's antenatal neurological test risk groups

Total score	*Interpretation of fetal behavior*
0-5	Abnormal
6-13	Borderline
14-19	Normal

result of multicenter study are promising, but KANET's concept and diagnostic value still have to be established.[64]

REFERENCES

1. de Vries JI, Visser GH, Prechtl HF. The emergence of fetal behavior. I. Qualitative aspects. Early Hum Dev. 1982;7(4):301-22.
2. Nijhuis JG. Fetal behavior. Neurobiology of Aging. 2003;24(Suppl. 1):S41-46.
3. Prechtl HF. State of the art of a new functional assessment of the young nervous system: an early predictor of cerebral palsy. Early Hum Dev. 1997;50(1):1-11.
4. Kurjak A, Carrera JM, Andonotopo W, et al. The role of 4D sonography in the neurological assessment of early human development. Ultrasound Rev Obstet Gynecol. 2004;4(3):148-52.
5. Prechtl HF. Qualitative changes of spontaneous movements in fetus and preterm infant are a marker of neurological dysfunction. Early Hum Dev. 1990;23(3):151-8.
6. Prechtl HF, Einspieler C. Is neurological assessment of the fetus possible? Eur J Obstet Gynecol Reprod Biol. 1997;75(1):81-4.
7. Prechtl HF. Ultrasound studies of human fetal behavior. Early Hum Dev. 1985;12(2):91-8.
8. Andonotopo W, Medic M, Salihagic-Kadic A, et al. The assessment of fetal behavior in early pregnancy: Comparison between 2D and 4D sonographic scanning. J Perinat Med. 2005;33(5):406-14.
9. Andonotopo W, Kurjak A, Kosuta MI. Behavior of an anencephalic fetus studied by 4D sonography. J Matern. Fetal Neonatal Med. 2005;17(2):165-8.
10. Arabin B, Riedewald S. An attempt to quantify characteristics of behavioral states. Am J Perinatol. 1992;9(2):115-9.
11. Goldstein I, Zimmer EA, Tamir A, et al. Evaluation of normal gestational sac growth: appearance of embryonic heartbeat and embryo body movements using the transvaginal technique. Obstet and Gynecol. 1991;77(6):885-8.
12. Roodenburg PJ, Wladimiroff JW, van Es A, et al. Classification and quantitative aspects of fetal movements during the second half of normal pregnancy. Early Hum. Dev. 1991;25(1):19-35.
13. Sival DA. Studies on fetal motor behavior in normal and complicated pregnancies. Early Hum Dev. 1993;34(1-2):13-20.
14. Petrikovsky B, Kaplan G, Holsten N. Fetal yawning activity in normal and high-risk fetuses: A preliminary observation. Ultrasound in Obstet Gynecol. 1999;13(2):127-30.
15. Petrikovsky B, Kaplan G, Holsten N. Eyelid movements in normal human fetuses. J Clin Ultrasound. 2003;31(6):299-301.
16. Jorgensen NP, Marsal K, Lindstrom K. Quantification of fetal motor activity in early pregnancy. Eur J Obstet Gynecol. Reprod Biol. 1989;30(1):11-8.
17. Amiel-Tison C, Gosselin J, Kurjak A. Neurosonography in the second half of fetal life: a neonatologist's point of view. J Perinat Med. 2006;34(6):437-46.
18. Andonotopo W, Stanojevic M, Kurjak A, et al. Assessment of fetal behavior and general movements by four-dimensional sonography. Ultrasound Rev Obstet Gynecol. 2004;4(2):103-14.
19. Azumendi G, Kurjak A. Three-dimensional and four-dimensional sonography in the study of the fetal face. Ultrasound Rev Obstet Gynecol. 2003;3:160-9.
20. Kurjak A, Carrera JM, Medic M, et al. The antenatal development of fetal behavioral patterns assessed by four-dimensional sonography. J MaternFetal Neonatal Med. 2005;17(6):401-16.
21. Kurjak A, Pooh RK, Merce LT, et al. Structural and functional early human development assessed by three-dimensional and four-dimensional sonography. Fertil Steril. 2005;84(5):1285-99.
22. Kurjak A, Azumendi G, Andonotopo W, et al. Three- and four-dimensional ultrasonography for the structural and functional evaluation of the fetal face. Am J Obstet Gynecol. 2007;196(1):16-28.
23. Pooh RK, Ogura T. Normal and abnormal fetal hand positioning and movement in early pregnancy detected by three- and four-dimensional ultrasound. Ultrasound Rev Obstet Gynecol. 2004;4:46-51.
24. Salihagic-Kadic A, Kurjak A, Medic M, et al. New data about embryonic and fetal neurodevelopment and behavior obtained by 3D and 4D sonography. J PerinatMed. 2005;33(6):478-90.
25. Walusinski O, Kurjak A, Andonotopo W, et al. Fetal yawning assessed by 3D and 4D sonography. Ultrasound Rev Obstet Gynecol. 2005;5(3):210-7.
26. Kurjak A, Andonotopo W, Hafner T, et al. Normal standards for fetal neurobehavioral developments—longitudinal quantification by four-dimensional sonography. J Perinat Med. 2006;34(1):56-65.
27. Salihagic-Kadic A, Medic M, Kurjak A, et al. Four-dimensional sonography in the assessment of fetal functional neurodevelopment and behavioral patterns. Ultrasound Rev Obstet Gynecol. 2005;5(2):1-10.
28. Visser GH. The second trimester. In: Nijhuis JG (Ed). Fetal behavior, developmental and perinatal aspects. Oxford: Oxford University Press; 1992. pp. 17-26.
29. Kurjak A, Miskovic B, Stanojevic M, et al. New scoring system for fetal neurobehavior assessed by three- and four-dimensional sonography. J Perinat Med. 2008;36(1):73-81.
30. Amiel-Tison, C. Update of the Amiel–Tison neurologic assessment for the term neonate or at 40 weeks corrected age. Pediatr Neurol. 2002;27(3):196-212.
31. Kuno A, Akiyama M, Yamashiro C, et al. Three-dimensional sonographic assessment of fetal behavior in the early second trimester of pregnancy. J Ultrasound Med. 2001;20(12):1271-5.
32. Campbell S. 4D, or not 4D: that is the question. Ultrasound in Obstet Gynecol. 2002;19(1):1-4.
33. Hata T, Dai SY, Marumo G. Ultrasound for evaluation of fetal neurobehavioral development:from 2-D to 4-D Ultrasound Inf. Child. Dev. 2010;19:99-118.
34. Ge, S. 3D echocardiography. Clinical application in pediatric cardiology. Pediatric Ultrasound Today. 2002;7: 145-64.
35. Gill EA. Live three-dimensional echo—A major incremental step in the development of cardiac ultrasound. J Cardiovasc Manag. 2003;14(2):13-7.
36. Forrest W, Roberto M, Lange M. D echocardiography closes in on 3D as it turns 50. Medical Imaging. 2003;18:C64210-2.

37. Hata T, Kanenishi K, Akiyama M, et al. Real-time 3-D sonographic observation of fetal facial expression. J Obstet Gynecolo Res. 2005;31(4):337-40.
38. de Vries JIP, Visser GHA, Prechtl HFR. The emergence of fetal behavior. II. Quantitative aspects. Early Hum Dev. 1985;12(2):99-120.
39. Kurjak A, Vecek N, Hafner T, et al. Prenatal diagnosis: what does four-dimensional ultrasound add? J Perinat Med. 2002;30(1):57-62.
40. Kurjak A, Azumendi G, Vecek N, et al. Fetal hand movements and facial expression in normal pregnancy studied by four-dimensional sonography. J Perinat Med. 2003;31(6):496-508.
41. Yigiter AB, Kavak ZN. Normal standards of fetal behavior assessed by four-dimensional sonography. J Matern Fetal Neonatal Med. 2006;19(11):707-21.
42. Andonotopo W, Kurjak A. The assessment of fetal behavior of growth restricted fetuses by 4D sonography. J Perinat Med. 2006;34(6):471-78.
43. Kozuma S, Baba K, Okai T, et al. Dynamic observation of the fetal face by three-dimensional ultrasound. Ultrasound Obstet Gynecol. 1998;13(4):282-4.
44. Kurjak A, Stanojevic M, Azumendi G, et al. The potential of four-dimensional (4D) ultrasonography in the assessment of fetal awareness. J Perinat Med. 2005;33(1):46-53.
45. Yan F, Dai SY, Akther N, et al. Four-dimensional sonographic assessment of fetal facial expression early in the third trimester. Int J Gynecol Obstet. 2006;94(2):108-13.
46. Hepper PG. Fetal behavior: Why so skeptical? Ultrasound Obstet Gynecol. 1996;8:145-8.
47. Arabin B, Bos R, Rijlaarsdam R, et al. The onset of inter-human contacts: longitudinal ultrasound observations in early twin pregnancies. Ultrasound Obstet Gynecol. 1996;8(3):166-73.
48. Okado N. Development of the human cervical spinal cord with reference to synapse formation in the motor nucleus. J Com Neurol. 1980;191(3):495-513.
49. Humphrey T, Hooker D. Double simultaneous stimulation of human fetuses and the anatomical patterns underlying the reflexes elicited. J Com Neurol 1959;112:75-102.
50. Hooker D. The origin of overt behavior. Ann Arbor, MI: University of Michigan; 1944. p. 38.
51. Tuck SM. Ultrasound monitoring of fetal behavior. Ultrasound Med Bio. 1986;12:307-17.
52. Humphrey T. Function of the nervous system during prenatal life. In: U Stave (Ed), Perinatal Physiology. New York: Plenum; 1978. pp. 751-96.
53. Shawker TH, Schuette WH, Whitehouse W, et al. Early fetal movement: A real-time ultrasound study. Obstet Gynecol. 1980;55:194-8.
54. Reinold E. Identification and differentiation of fetal movements. Contrib Gynecol Obstet. 1979;6:29-32.
55. Boue J, Vignal P, Aubrey MC, et al. Ultrasound movement patterns of fetuses with chromosomal anomalies. Prenat Diagnos. 1982;2:61-5.
56. Miskovic B, Vasilj O, Stanojevic M, et al. The comparison of fetal behavior in high risk and normal pregnancies assessed by four-dimensional ultrasound. J Matern Fetal Neonat Med. 2010;23(12):1-7.
57. Sival DA, Visser GH, Prechtl HF. The effect of intrauterine growth retardation on the quality of general movements in the human fetus. Early Hum Dev. 1992;28(2):119-32.
58. Kurjak A, Miskovic B, Andonotopo W, et al. How useful is 3D and 4D ultrasound in perinatal medicine? J Perinat Med. 2007;35(1):10-27.
59. Kurjak A, Miskovic B, Stanojevic M, et al. New scoring system for fetal neurobehavior assessed by three and four-dimensional sonography. J Perinat Med. 2008;36(1):73-81.
60. Kurjak A, Tikvica A, Stanojevic M, et al. The assessment of fetal neurobehavior by three-dimensional and four-dimensional ultrasound. J Matern Fetal Neonatal Med. 2008;21(10):675-84.
61. Horimoto N, Koyanagi T, Maeda H, et al. Can brain impairment be detected by in utero behavioral patterns? Arch Dis Child. 1993;69(1):3-8.
62. Morokuma S, Fukushima K, Yumoto Y, et al. Simplified ultrasound screening for fetal brain function based on behavioral pattern. Early Hum Dev. 2007;83(3):177-81.
63. Prechtl HFR, Einspieler C. Is neurological assessment of the fetus possible? Eur J Obstet Gynecol Reprod Biol. 1997;75(1):81-4.
64. Kurjak A, Abo-Yaqoub S, Stanojevic M, et al. The potential of 4D sonography in the assessment of fetal neurobehavior multicentric study in high-risk pregnancies. J Perinat Med. 2010;38(1):77-82.

37
CHAPTER

Fetal Behavior Assessed by 4D Sonography

Asim Kurjak, Badreldeen Ahmed, Berivoj Miskovic, Maja Predojevic, Aida Salihagic Kadic

INTRODUCTION

The current and evolving challenge for investigators in obstetric ultrasound is to understand fetal neurological function by assessing fetal behavior and to identify fetuses with impaired brain development. The implementation of four-dimensional (4D) ultrasound has provided new opportunities to study fetal movement patterns, opening the new diagnostic window in the area of fetal neurology. There are many functional neurological abnormalities such as cerebral palsy whose causes are poorly understood and whose early diagnosis would represent significant progress in perinatology. Recently, in several journals, data on the assessment of fetal behavior by 4D ultrasound and application of Kurjak antenatal-neurodevelopmental scoring test (KANET) have been published. The purpose of this chapter is to review and analyze the published literature on the use of 4D ultrasound in the assessment of fetal behavior and to describe new neurological test of KANET.

BASIC TECHNOLOGY OF THE 4D SONOGRAPHY IN THE ASSESSMENT OF FETAL BEHAVIOR

Fetal behavior could be described as any fetal action or reaction observed by the mother or more objective method, such as ultrasonography.[1] Although, two-dimensional (2D) sonography enhanced our understanding of fetal neuromuscular development, the real breakthrough in studying fetal behavior was achieved by 4D ultrasound. The rapid development of digital ultrasound systems has allowed three dimensional (3D) image reconstructions. Recently, this technology has been improved with the near-real-time or 4D scanning, which makes possible the inspection of anatomical regions as well as the dynamic-functional analysis of fetal motility. Three-dimensional images are static and do not provide information of movements and dynamic changes of the object of interest.[2] Moreover, fetal movements are the source of significant artifacts and volume scanning should be performed during the fetal inactive phase, which limits the usage of classic 3D ultrasound. The 4D scanning technique overcomes this disadvantage, making it possible to obtain qualitative 3D image, regardless of fetal movements. The only limiting factor for 4D sonography is the quantity of adjacent amniotic fluid. The acquisition of volume datasets is performed by 2D scans with special transducers (linear, convex and transvaginal) designed for 2D scans, 3D and real-time 4D volumes.[3] The real time 4D mode is obtained from simultaneous volume acquisition and computing of 3D images, which is infact a multidimensional ultrasound.[4] The movement of the ultrasound beam over the region of interest (ROI) is automatic and enables simplified 3D and 4D acquisition. Ultrasound probes include a scanning mechanism moved by a built-in electromotor. The processing speed allows continuous acquisition and processing of 4D volumes. The volume acquisition begins with a 2D image and superimposed volume box, and initial 2D

image is the central 2D image of the volume. According to the dimensions of the volume box, the volume-scan sweeps between the margins of the volume box, this is set for framing the ROI. During the 3D and 4D acquisition, sweep time depends on the volume box size, scan quality and adjusted scan parameters such as depth, number of focuses and other parameters, which affect B-mode image frame rate. The smallest element of 2D images is pixel, whereas voxel is the smallest information unit in 3D and 4D imaging. Volume rendering provides visualization of animated voxel-based images on a 2D screen. Development of instant computer technology and fast data transmission, volume acquisition and data processing are accelerated to enable 3D rendering in real time (4D). Fast volume data processing enables calculation of 5–30 volumes per second depending on the system hardware and size of the render box. As 4D imaging is almost a real time, there is always some delay as a result of time needed to reconstruct 3D image from 2D scans. It is always desirable to achieve as many volumes per second (volume rate) as possible. Number of volumes per second is some kind of trade-off between image quality and frame rate. The 3D and 4D image quality mostly depends on 2D image quality. Prior to volume acquisition it is important to achieve the best 2D image quality, as all the 2D image artifacts will also be present on 3D and 4D image reconstruction.[4] The 3D and 4D imaging provide additional dimensions to conventional 2D sonography.

The main advantage of ultrasound in general is dynamic imaging of human body. A 4D imaging follows this tradition permitting visualization of dynamic changes inside body and organs. Further, the ability to study fetal activity in the surface-rendered mode is particularly favorable for fetal movements and it is better in visualization of the fetal face.[5] With 4D ultrasound, it is now feasible to study a full range of facial expressions including smiling, crying, scowling and eyelid movements.[6,7] The observation of facial expression may be of scientific and diagnostic value and such scientific approach opens an entirely new field. Simultaneous imaging of complex facial movements was not possible using real time 2D ultrasound **(Fig. 37.1)**. A 4D ultrasound integrates the advantage of the spatial imaging of the fetal face with the addition of time. This new technology, therefore allows the appearance and duration of each facial movement, and expression to be determined and measured **(Fig. 37.2)**. Furthermore, additional advantage in comparison with 2D ultrasound is the ability to visualize the whole fetus continuously during early pregnancy **(Fig. 37.3)**. The

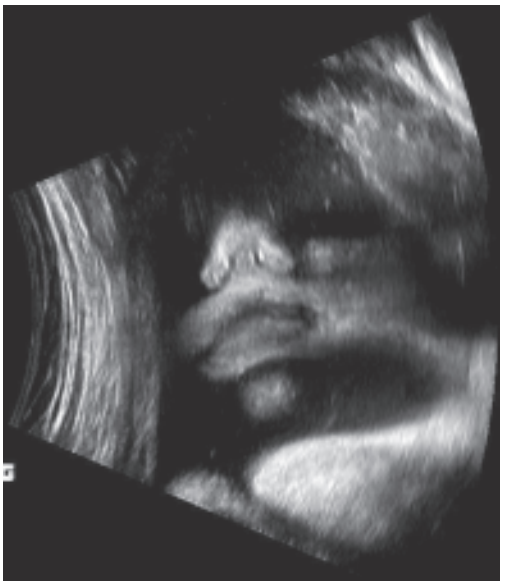

Figure 37.1: A 2D ultrasound image showing part of fetal face, fetal nose and lips

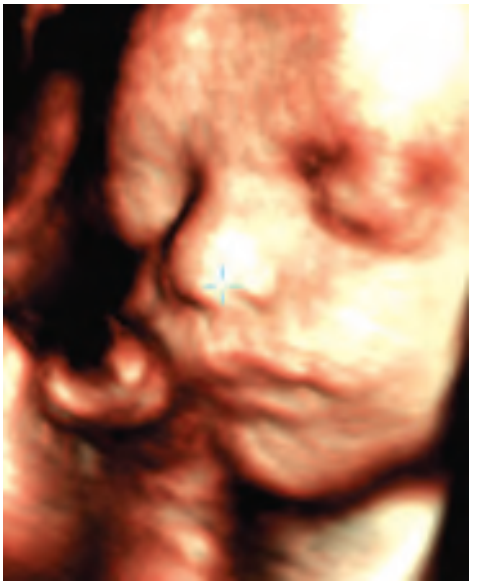

Figure 37.2: A 4D ultrasound image showing fetal face

key benefit of 4D ultrasound lies in providing real-time 3D images of embryonic or fetal movements, previously limited by technological possibilities. The introduction of high-frequency transvaginal tranducers has resulted in remarkable progress in ultrasonographic visualization of early embryos and fetuses, and the development of sonoembryology. For the first time parallel analyses of structural and functional parameters in the first 12 weeks of gestation has become possible. In the early

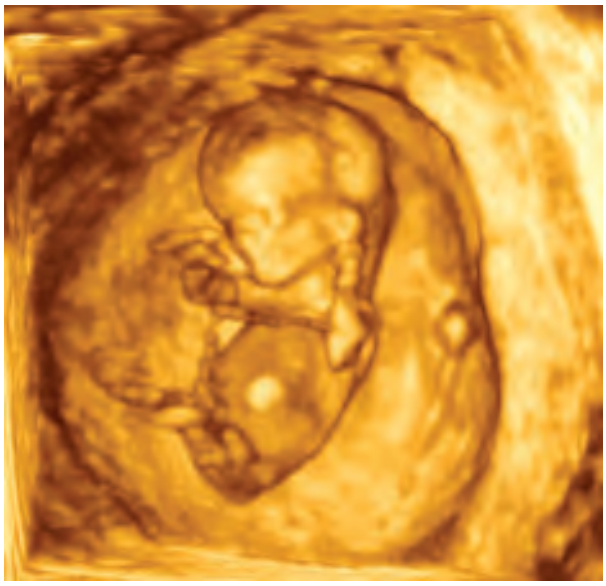

Figure 37.3: A 4D ultrasound image demonstrating the ability of 4D sonography to visualize the whole fetus continuously during early pregnancy

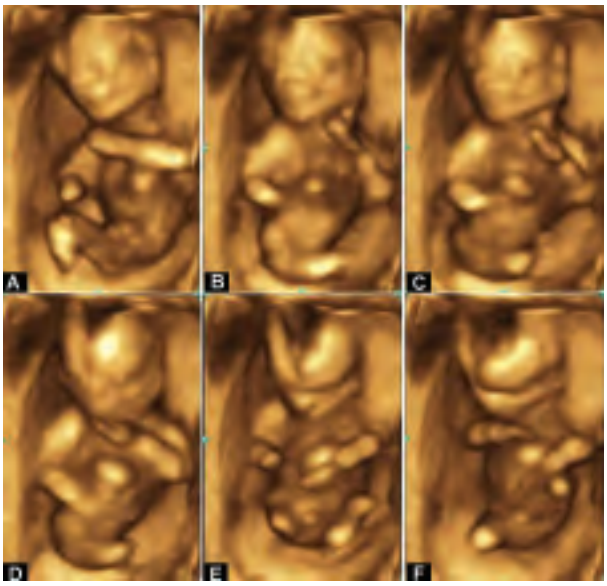

Figures 37.4A to F: Sequence of images of the fetus in the first trimester recorded by 3D/4D sonography showing general movements

second trimester 4D ultrasound provides simultaneous visualization of all four extremities, and enables confident recognition of isolated arm movements and their direction. Due to the limitations of 2D ultrasound only five types of isolated hand movements could be described. These include: 1. hand-to-head; 2. hand-to-trunk; 3. hand-to-foot; 4. hand-to-fluid and 5. hand-to-the uterine wall. If one performs 4D ultrasound hand-to-head movement, it can be differentiated into seven subgroups: 1. hand-to-head; 2. hand-to-mouth; 3. hand-near-mouth; 4. hand-to-face; 5. hand-near-face; 6. hand-to-eye and 7. hand-to-ear.[2] Further, using 4D ultrasound in obstetrics, it is possible for the first time to monitor quality and quantity of fetal movements on 3D real-time reconstructed images. It is our belief that 4D ultrasound should have its place in everyday obstetric practice, combining patient acceptance and sensitivity of diagnosis.

Classification of Movement Patterns

Based on the first analysis of fetal movements by 2D ultrasonography, de Vries classified movements into different patterns as follows:[8,9]

Sideways bending: Started between seventh and eighth gestational weeks, slow and small displacements at one or two poles of the fetus occur, lasting from half a second to two seconds, which usually occur as a single event and disappear through gestation.

Startle: A startle consists of a rapid phase contraction of all limb muscles. It often spreads to the trunk and neck. It occurs frequently in the first trimester from 8 weeks on.

General movements: These movements are complex movements including neck, trunk and limbs that are applicable if the whole body is moved but no distinctive patterning or sequencing of the body parts can be recognized **(Figs 37.4A to F)**. They wax and wane in intensity, force and speed, and they have gradual beginning and end. These movements are performed from eight weeks and on.

Hiccups: These consist of a jerky contraction of the diaphragm. Hiccups appear from nine weeks and on, often in series, for up to several minutes, and isolated arm and leg movements can be observed.

Breathing-like: Fetal breathing-like movements are usually paradoxical in a way that every contraction of the diaphragm (which after birth leads to an inspiration) causes an inward movement of the thorax. The onset of fetal breathing-like is around the 10th week of gestation. Early in pregnancy, they are present continually and are associated with activity in the postural muscles of the neck and limbs.

Isolated arm or leg movement: These movements appear around the 10th week of gestation and they vary in speed and amplitude. They involve extension, flexion,

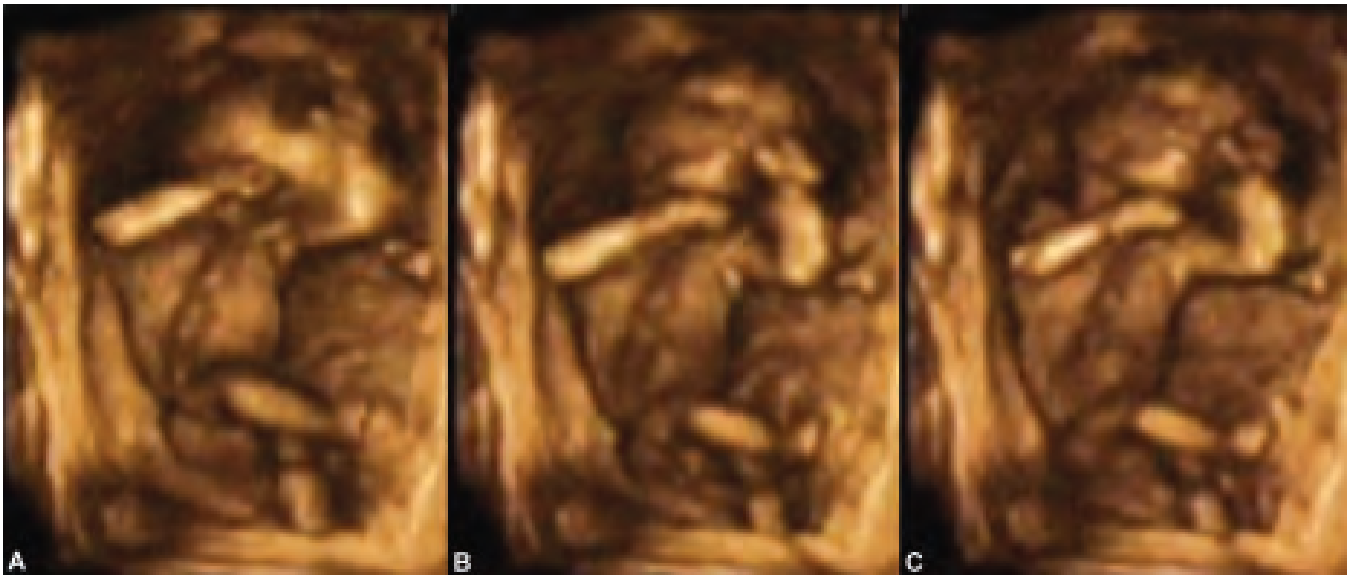

Figures 37.5A to C: A sequence of images of the fetus in the first trimester recorded by 3D/4D sonography showing retroflexion of the head

external and internal rotation, or abduction and adduction of an extremity, without movements in other body parts.

Twitches: Twitches are quick extensions or flexions of a limb, or the neck. They are not generalized or repetitive.

Clonic movements: These are repetitive movements of one or more limbs at a rate of about three per second.

Isolated retroflexion of the head: Retroflexions of the head are usually carried out slowly, but they can also be fast and jerky **(Figs 37.5A to C)**. These movements can be seen around the 10th week of gestation and on.

Isolated rotation of the head ***(Figs 37.6A to C)***: Rotation of the head is carried out at a slow velocity and only exceptionally at a higher speed. The head may turn from a midline position to one side and back.

Isolated anteflexion of the head: Anteflexion of the head is carried out only at a slow velocity. The displacement of the head is small. The duration is about one second.

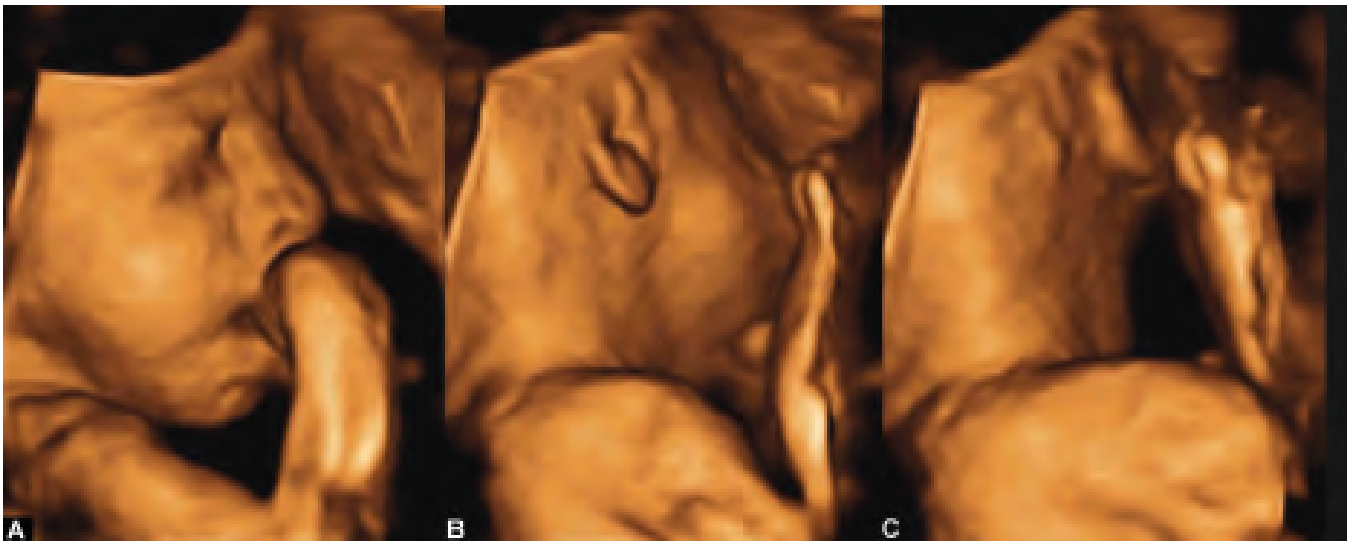

Figures 37.6A to C: A sequence of images of the fetus recorded by 3D/4D sonography showing rotation of the head

Jaw movements: The onset of irregular jaw opening is at 11th week. The opening may be either slow or quick. The duration of opening varies from less than 1–5 second.

Sucking and swallowing: At 13 weeks rhythmical sucking movements, often followed by swallowing, occur in bursts indicating that the fetus is drinking amniotic fluid.

Hand-head contact: In this pattern of movement, the hand slowly touches the face, and the fingers frequently extend and flex. These movements appear from 10th week onwards and at first they usually represent an accidental contact of a hand with the face or mouth. Subgroups of these movements are:

- Hand-to-head: When hand movement ends at contact of fingers with the parieto-occipitotemporal region of the head
- Hand-to-mouth: When hand movement ends at contact of thumb or finger with the mouth, lips or the immediate oral region
- Hand-near-mouth: When movement ends with fingers in fluid between nose and shoulders/nipples or between both shoulders. Hands must be below eyes and within the area defined by the ears, less than a hand away from the mouth
- Hand-to-face: When movement ends with hand in contact with the face (cheeks, chin, forehead)
- Hand-near-face: When movement ends with finger in fluid in front of the face but not in mouth region
- Hand-to-eye: When movement ends with hand or palm or fingers in the eye region
- Hand-to-ear: When movement ends at hand contact with the ear.

Stretching: This movement is a complex motor pattern, which is always carried out at a slow speed and consists of the following components: forceful extension of the back, retroflexion of head, and external rotation and elevation of the arms. It retains an identical movement form into adult life.

Yawning: This motor activity is similar to the yawning observed after birth: prolonged wide opening of the jaws followed by quick closure, often with retroflexion of the head and sometimes elevation of the arms. This movement pattern is nonrepetitive and it appears around 11th week. The anatomical criterion for fetal yawning is retraction of the tongue, whereas yawning in adults is characterized by an extended tongue.

Rotation of the fetus: Rotation of the fetus occurs around the sagittal or transverse axis. A complete change in position around the transverse axis, usually with a backwards somersault, is achieved by a complex general movement, including alternating leg movements, which resemble neonatal stepping.

Onset of Specific Fetal Behavioral Patterns Assessed by Three- or Four-Dimensional Ultrasonography

First Trimester

Ultrasonic studies have revealed that fetal activity occurs far earlier than a mother can register it, in fact as early as the late embryonic period. Although early embryonic development is characterized by the immobility of an embryo, most types of movement pattern will emerge between seven weeks and 15 weeks of gestation.[10] One of the important prerequisites for the motility is the development of the central nervous system (CNS) structures for better understanding of these processes.[11] The introduction of 4D ultrasound brought significant advance in the investigation of fetal behavior by providing the capability of simultaneous spatial imaging of the entire fetus and its movements.[10,12-18]

First spontaneous fetal movements can be observed with conventional 2D ultrasound around the eighth gestational week, while the 4D ultrasound allows the visualization of fetal motility at seven weeks of gestation.[10,12,19-21] Obviously, this new technology enables the visualization of the moving phenomenon approximately one week earlier than 2D ultrasound. At seven weeks of gestation, the dominant embryonic feature is the head, which is strongly flexed anteriorly. Upper and lower limb buds are visible on the lateral aspects of the embryo. However, embryonic movements are not frequent and consist mainly of movements of the head towards the rest of the body. At 8–9 weeks, the head is less flexed and the changes of the position of the head towards the body are clearly visible.[2]

General movements are the first complex fetal movement patterns observable by 2D ultrasound.[9] They can be recognized from 8–9 weeks of pregnancy and continue to be present until 16–20 weeks after birth.[22] According to Prechtl, these are gross movements, involving the whole body.[23] Movements of the limbs, trunk and head are of variable speed, but smooth in appearance. They wax and wane in intensity, force and speed and they have a gradual beginning and ending.[23] The 4D sonography allows the simultaneous visualization of fetal head, trunk and limbs. The majority of sequences of extension and flexion of the legs and arms

is complex, and may be better assessed with 4D ultrasound **(Figs 37.4A to F)**. Furthermore, 4D sonography seems to be the method of choice for detecting subtle changes such as superimposed rotations and changes in direction of the movements. These additional components make the movements fluent and elegant, and create the impression of complexity and variability.

The cited range of first appearance of limb movements is between 8th and 12th weeks concerning.[9,10,12,18-21] With 4D ultrasonography, limb movements at 8–9th weeks were found.[18] The organization of the appearance of the movement pattern occurs with increase in frequency.[16] In addition, the movements in the elbow joint appear at 10 weeks, changes in finger position at the 11th week, and easily recognizable clenching and unclenching of the fist at 12–13 weeks. Finally, at 13–14 weeks, isolated finger movements can be observed, as well as increases in the activity and strength of the hand/finger movements.[24] Using 4D sonography, Kurjak and collaborators have found that from 13 gestational weeks onwards, a "goal orientation" of hand movements appear and a target point can be recognized for each hand movement.[2] According to the spatial orientation, they classified the hand movements into several subtypes: hand-to-head, hand-to-mouth, hand-near-mouth, hand-to-face, hand-near-face, hand-to-eye and hand-to-ear.

Besides the general body movements and isolated limb movements, hiccups, sucking and swallowing movements can be seen from the ninth week of gestation. Further, retroflexion, anteflexion, rotation of the head, breathing-like movements, jaw opening and yawning can be observed during the 10th week of gestation. From 10 weeks onwards, the number and frequency of fetal movements increase, and the repertoire of movements begins to expand as a result of the CNS structures maturation.[11]

A longitudinal study carried out by the authors, which was performed by using the 4D ultrasound in 100 fetuses from all trimesters of normal pregnancies has shown increasing frequency of various movement patterns, such as general movements, isolated arm and leg movements, stretching, as well as head movements, during the first trimester. Only the startle movement pattern seemed to occur stagnantly in this period of gestation.[25] Using 4D sonography, general movements were found to be the most frequent movement pattern between 9 weeks and 14 weeks of gestation.[26]

In the recent 4D sonographic study, Hata et al. showed that the most common movements at 10–11 weeks of gestation were isolated arm movements and at 12–13 weeks are jumping movements.[27] Authors provided possible explanation of the difference between this study and previous investigations in terms of behavior patterns assessed. As stated by Hata et al. "it is important to bear in mind that more short-duration isolated movements might constitute more pronounced fetal movements in early gestation, whereas whole-body movements that are characteristic of the mature fetus may constitute greater movements in late gestation. However, whole-body movements are actually a composite of isolated body movements,"[28] and it may be important to standardize the definition of behavior patterns for future studies. According to authors, another possible explanation is the difference in the frame rates of the machines used in the studies. The frame rate was 0.5 per second in all previous investigations, whereas in this study it was 2.6–4.0 per second. A final potential explanation of the authors was the small number of subjects in studies and conclusion that further researches involving a larger sample are needed to evaluate the exact frequencies of fetal movement in the first trimester of pregnancy.[27]

Second Trimester and Third Trimester

The second trimester of pregnancy begins at 15 weeks of gestation (13 weeks after conception). The brainstem gradually begins to take the control over fetal movements and behavioral patterns during the first trimester and continues its maturation in the second trimester, resulting in expansion and complexity of the behavioral repertoires.[11] From 14 to 19 weeks of gestation, fetuses are highly active and the longest period between movements last only 5–6 minutes.[11] According to Kuno et al. the most active fetal behavior pattern between 14 and 18 weeks of gestation was an arm movement, whereas the least was a mouth movement. Further, the active phase (time with fetal movements) was 59.4% and the resting phase was 40.6% during 60 minutes of recording.[29] In the 15th week, 16 different types of movements can be observed.[11] Further, at 16–18 weeks of gestation the earliest eye movements appear as sporadic movements with a limited frequency.[30,31] Significant trends in fetal eye movement organization can be observed during the second half of pregnancy.[30,31] From 20–22 weeks of gestation, fetal movements, e.g. breathing-like activity and heart rate begin to follow daily cycles called circadian rhythms.[32] The second half of pregnancy is characterized by organization of fetal movement patterns and increase in the complexity of movements. The periods of fetal quiescence begin to increase and the rest-activity cycles become recognizable. Hardly any new movement pattern emerges in this period. The number of general

body movements, which tends to increase from the ninth week onwards, gradually declines during the last 10 weeks of the pregnancy.[33-35] It is very important to point out that general movements are characterized by large variation and complexity in the third trimester.[36] Simultaneously, with the decrease in the number of general movements, an increase in facial movements, including opening/closing of the jaw, swallowing and chewing was observed using 2D sonography between 28 and 38 weeks of gestation. These movements appeared mostly in the periods of absence of generalized movements and such pattern was considered to be a the reflection of normal neurologic development of the fetus.[33] However, a revolutionary improvement in the study of fetal facial movements came with the development of 3D and 4D sonography. Our results confirmed the potential of 3D/4D sonography for the investigation of structural and functional development of the fetal face.[37] The incorporation of 3D ultrasound technology into clinical practice has resulted in remarkable progress in visualization and anatomic examination of the fetal face. Due to its curvature and small anatomic details, the fetal face can be visualized and analyzed only to a limited extent with 2D ultrasound,[38] but 3D ultrasound allows spatial reconstruction of the fetal face and simultaneous visualization of all facial structures such as the fetal nose, eyebrows, mouth and eyelids. Further, 4D ultrasound provided for the first-time an opportunity to evaluate subtle fetal facial expressions. In addition, the application of 4D sonography in the examination of fetal facial movements has revealed the existence of a full range of facial expressions, including smiling **(Figs 37.7A and B)**, crying and eyelid movements.[6,25] similar to emotional expressions in adults, in the second and third trimesters. Other facial movements, such as yawning **(Figs 37.8 and B)**, sucking, swallowing and jaw opening can also be observed in this period by 4D ultrasound. According to Yan et al. mouthing was the most frequent facial movement during early third trimester, whereas the least frequent were scowling and sucking.[39,40] Our longitudinal analysis of the frequencies of different facial movements in the second and third trimester revealed some interesting results. Contrary to the declining trend of head movement and hand movement patterns from the beginning of the second trimester to the end of the third trimester, a constant increase in the frequencies of almost all facial movement patterns was observed during the second trimester. Various types of facial expression patterns displayed a peak frequency at the end of second trimester, except eye blinking pattern (**Figs 37.9A to D)**, which displayed a peak

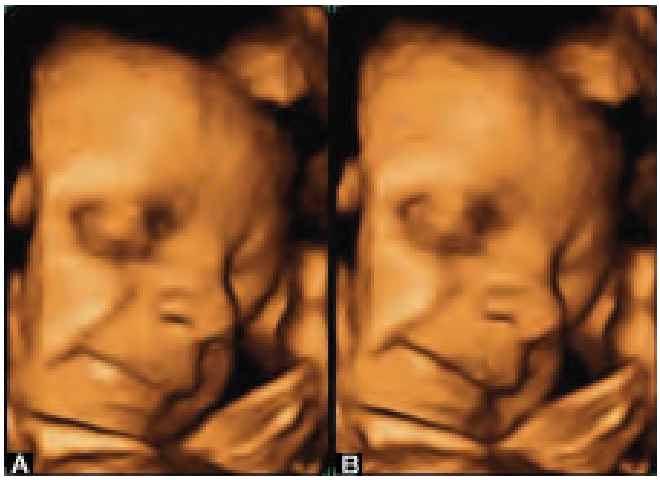

Figures 37.7A and B: A sequence of images of the fetus recorded by 3D/4D sonography showing smiling movement

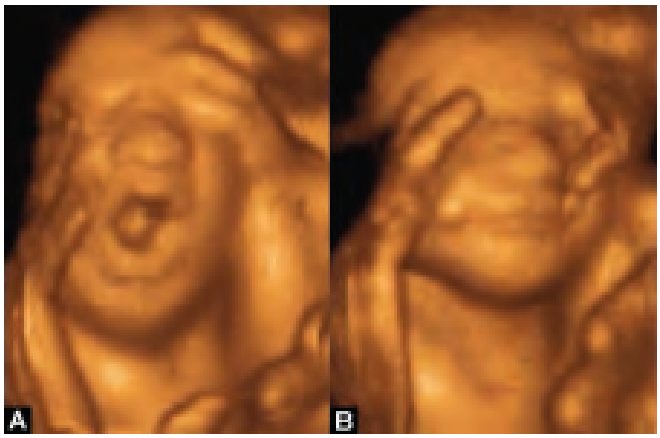

Figures 37.8A and B: A sequence of images of the fetus recorded by 3D/4D sonography showing yawning

frequency at 28 weeks of gestation. During the remainder of pregnancy, decreasing or stagnant incidence of facial expression patterns was noted.[25]

Further, in recent study main challenge was to determine what proportion of fetal movements resembles those seen in preterm and term infants. Fetal movements were recorded by 4D ultrasound in 10 term-pregnancies and after birth, neonatal spontaneous motor activity was recorded. Interestingly, authors found no statistically significant differences in either quality or quantity of fetal hand-to-face movements or fetal facial movements. There were no movements observed in fetal life that were not present in neonatal life, whereas Moro reflex was present only in neonates. This pilot study confirmed the existence of a prenatal-neonatal continuum even in subtle and fine movements such as facial mimics.[16]

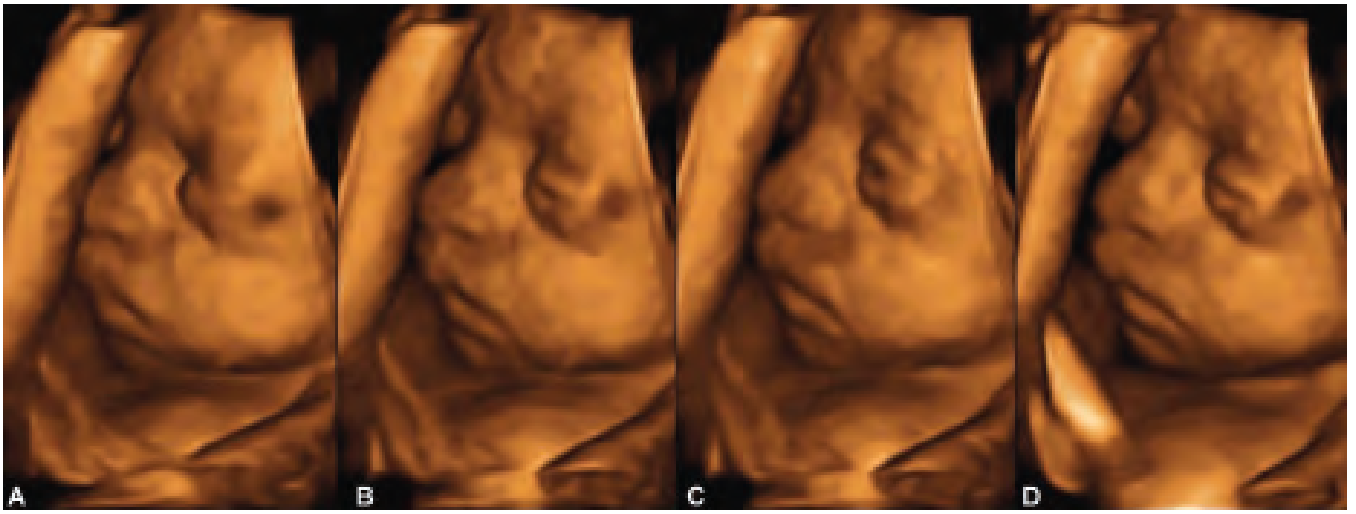

Figures 37.9A to D: A sequence of images of the fetus recorded by 3D/4D sonography showing eye-blinking movement

During the last decade, 4D sonography has stimulated studies on fetal behavior with more convincing imaging and data than those obtained by conventional ultrasonic and nonultrasonic methods.[41] Further, it is well known that fetal behavioral patterns directly reflect developmental and maturational processes of the fetal CNS.[42] Hence, fetal behavior represents the diagnostic window into the brain development. The findings indicate that a good understanding of the relationship between fetal behavior and developmental processes in different periods of gestation might provide an important distinction between normal and abnormal brain development, as well as the tool for early diagnosis of structural or functional abnormalities.[23] Contrary to this obvious fact, the idea of diagnosis *in utero* of some functional neurological disorders was very intriguing.

Fetal Behavior as an Indicator of Disturbed Brain Development

The traditional concept that brain damage is caused during birth or early neonatal period has been challenged, now antenatal and unclassifiable factors are considered to be the most important etiological factors of brain impairment.[43-46] In addition, clinical and epidemiological studies have shown that even cerebral palsy (CP) most frequently results from prenatal rather than perinatal or postnatal causes.[43] Nowadays, as early as possible, neonatologists try to identify neonates at risk of unfavorable neurodevelopmental outcomes. They are fairly reliable in predicting very poor outcomes as well as optimal outcomes, but within these two extremes, the prediction still remains a challenge.[47] Due to a growing pool of evidence that many neurological disorders originate from intrauterine period, efforts have been made to diagnose neurological damage before birth. However, even after the fetal brain anatomy can be visualized by ultrasound and the development of the fetal brain is well understood, not much is known about the functional development of the fetal CNS. In other words, the fetal CNS is not directly accessible. It is possible only to ascertain the output of the CNS, i.e. "fetal behavior." In addition, even after delivery, behavioral patterns frequently provide the most useful indicators of brain function inspite of having extending access to neurological, physiological and pharmacological measures. Prenatal motility is considered to reflect the developing nervous system, but also involves functional and maturational properties of the fetal hemodynamic and muscular systems. The major problem with the study of fetal behavior is that it is very time-consuming. Nevertheless, there is no other possible means of assessing the function of the CNS *in utero* and this is needed for the understanding of hidden information in the neurodevelopmental pathways of the fetal CNS. It is important to notice that only if normal behavior is well understood, it is possible to identify and to perceive abnormal behavior before birth.

Abnormalities in fetal motor activity may consist of a delayed first emergence of specific movements, quantitative changes, an abnormal quality of movements (i.e. changes in the execution of movements patterns) and an abnormal development of fetal

behavioral (or sleep) states.[48] Abnormal movement patterns, indicative of altered brain or muscular development have been described in fetuses with chromosomal anomalies, anencephalic fetuses, fetuses with other cerebral malformations, growth restricted fetuses and in fetuses suffering from prolonged oligohydramnios.[49] Common features in all these cases are the qualitative changes in the execution of movement patterns, which are abrupt and forceful, with large amplitude in the majority of fetuses with a chromosomal or CNS defect and slow, with small amplitude, in the others. Fetal seizures have been described in association with severe brain abnormalities. These movement abnormalities are mainly qualitative and not quantitative in nature, which is in agreement with data on preterm infants with brain lesions.[23,48] In **Table 37.1** review of the literature on the behavior in the high-risk pregnancies for cerebral palsy is presented.

Cerebral Palsy and Neonatal Neurological Assessment

Cerebral palsy (CP) is the most common chronic motor disability of childhood. Cerebral palsy is an ''umbrella term'' for disorders of development, movements and posture, resulting in limitations of activity due to non progressive impairment of developing brain.[45] The motor disorders in CP are often accompanied by disturbances of sensation, cognition, communication, perception, behavior and/or by a seizure disorder.

The worldwide prevalence ranges from 2–2.5 per 1000 live-births and the incidence did not change since 1951, respectively.[74] Improvement of obstetrical and neonatal care did not result in decreasing prevalence rate of CP. On the contrary, the incidence and severity of CP increased due to a better survival rate of very immature and tiny premature infants with significant morbidity, and increased number of risk factors. Further, in preterm infants periventricular white-matter injury is the most common cause of brain injury and the leading cause of chronic neurological morbidity. Cerebral palsy does not result from a single event, but rather from a sequence of interdependent adverse events. This time frame of evolving adverse events should be taken into account when considering the possibility of CP diagnosis in infants.[74]

The diagnosis is retrospective and specificity of the diagnosis improves as the child grows and the nature of the disability evolves.[74] From the pediatric experience it is well known that one should wait until the age of 6 months postnatally to be able to diagnose a severe CP, 12 months for a moderate CP and 24 months for a minor nondisabling CP. This delay for the full clinical expression of functional consequences of a brain damage depends on brain maturation. Standardized methods of clinical neurological assessment from the neonatal period onwards were developed in order to identify three grades of neurological impairment: 1. Severe; 2. Moderate and 3. Mild. The clinical identification of severely affected patients is less problematic than the identification of moderately and mildly affected infants. Cranial ultrasound, magnetic resonance imaging, magnetic resonance spectroscopy and diffusion weighted imaging are helpful in very low birth weight premature and in-term infants with encephalopathy.[46] One crucial question often posed to neonatologists is to determine the exact timing of brain damage, prenatal or intrapartum, in the context of neonatal encephalopathy. In this perspective, repeated neurological assessments over the first days of life allow identification of two profiles. The first, a dynamic profile is associated with signs of CNS depression, are increasing within the first three days and then decreasing gradually with obvious improvement in alertness, motor activity and sucking.[74] This profile is typical of recent insult, most often intrapartum. The second one, a static profile, is disclosed by lack of changes along repeated assessments in the first week of life. This latter profile is typical of a prenatal insult that occurred *in utero* at least several weeks earlier and therefore, already stable at the time of birth. In addition, the identification of three signs already present at birth offers a precious clue to fetal brain damage, when observed in a cluster:

1. High-arched palate (due to insufficient melding forces of a hypoactive tongue)
2. Nonreducible adduction of the thumb in a clenched fist (due to absence of spontaneous motor activity)
3. Cranial ridges over each suture or restricted to the squamous suture (due to severe or moderate impairment of hemispheric growth).[75]

It is very interesting that using 3D or 4D ultrasound, two of these three signs can be very easily diagnosed *in utero*. Further, even sign that was believed as prenatally undetectable became visible by modern technology. Recently, the 3D "reverse face technique" has been described.[76,77] This technique overcomes shadowing of the fetal face by rotating the frontal facial image through 180° along the vertical axis, so that the palate, nasal cavity and orbits become visualized.[76,77]

Mentioned signs of the neurological impairment were described by Amiel Tison. Clinical neurological assessment proposed and practiced by Amiel-Tison is very useful tool in the early detection of newborns at risk. Neurological assessment at-term by Amiel-Tison (ATNAT) is taking into account neurological matura-

TABLE 37.1

Review of the literature on the behavior in the high-risk pregnancies for cerebral palsy

Authors	*Year*	*Main findings*
		Risk factor: Diabetes
Visser et al.	1985	First study on diabetes-related influence on delay emergence of fetal behavioral patterns. The results showed that there is a delay of 1–2 weeks in almost all but one of the movement patterns emerging in the first 12 weeks of gestation. Only fetal breathing-like movements were observed for the first time at the same gestational age as in the control group.[50]
Mulder et al.	1987	Study on diabetes-related influence on delay emergence of fetal behavioral states. According to this study, the development of behavioral states was disturbed in fetuses of nulliparous diabetic women. Further, tight metabolic control, achieved with continuous insulin infusion, did not prevent mentioned disturbances in development.[51]
Visser et al.	1986	Integrated results on diabetes-related influence on fetal behavioral pattern through the gestation.[52]
Mulder et al.	1991	Additional findings on diabetes-related influence on fetal behavioral patterns. It was concluded that delay in motor development does not run completely parallel with the delay in growth which indicates the possible existence of a specific diabetes-related influence on the functional development of the embryonic and fetal nervous system. Further, it was found that before the 9th week of gestation, fetal movements occurred less frequently which was related to the quality of maternal glucose control. After 12 weeks, the overall incidence was higher than in the control group, due to an increase in the incidence of breathing-like movements that was generally slower than in the control group.[53,54]
Mulder et al.	1990	Study on diabetes-related influence on behavioral states in the near-term fetuses. This study showed the continuity of the poor behavioral state regulation from prenatal into postnatal life in the diabetic group which resembled that of more immature fetuses and infants indicating that this cannot be attributed to the instantaneous unfavorable condition, like hyperglycemia before birth.[55]
Mulder et al.	1992	Indicated that diabetic disorders occurring in early life may influence abnormal functional development in later gestation.They found no relationship between the degree of early growth delay and birth weight, while the mean growth delay per fetus in early diabetic pregnancy was negatively correlated with the occurrence of no coincidence between behavioral state parameters at 36 weeks. Those results have shown that disorders occurring in early life may underlie abnormal functional development in later life, whereas (catch up) growth is mainly determined during the second half of pregnancy.[56]
Mulder et al.	1995	Study on fetal breathing-like movements in relation to other parameters of fetal well-being in late diabetic pregnancies. It was concluded that the (neural) mechanism underlying fetal breathing-like movements differs from that in normal pregnancy resulting in breathing-like movements in late diabetic pregnancy being not influenced by Braxton Hicks' contractions and not showing a clear-cut state-dependency.[57]
Reece et al.	1995	Findings on how maternal hypoglycemia affects fetal behavioral parameters. The results showed that mean number of fetal limb and body movements did not change depending on maternal blood glucose levels. In addition, no significant reductions in fetal breathing-like movements or heart rate were observed, although maternal epinephrine and growth hormone levels were significantly increased. These data suggest that fetal well-being remains unaltered in spite of moderate maternal hypoglycemia in diabetic women.[58]
Devoe et al.	1995	Study on diabetes-related influence on fetal biophysical activities in the third-trimester. These results confirmed previously reported results that inspite of good maternal glycemic control fetuses of diabetic women behaved differently from those of no diabetic women.[59]
		Risk factor: IUGR
Van Vliet	1985	Results on relationship between fetal activity and behavioral states in the third-trimester growth-restricted fetuses.[60]
Van Vliet	1985	Showed that the quality and quantity of the growth restricted fetal motility is disturbed. Authors suggest that some aspects of CNS function are disturbed in growth-retarded fetuses, even in the absence of fetal distress.[61]
Arduini	1988	Showed that the quality and quantity of the asymmetrical growth-restricted fetal motility is disturbed.[62]
Rizzo	1987	Findings on the influence of fetal blood flow on the IUGR fetal motility. The results were in accordance with previous findings that growth restricted fetuses showed a delay in the integration of behavioral patterns and a lower coincidence of behavioral states. These findings are particularly evident in the fetuses with a severe increase of peripheral vascular resistance

Contd...

Table 37.1 Contd...

		(absence of end diastolic flow in descending aorta) suggesting that a delay in CNS development is present in asymmetrical growth retarded fetuses and that there is a possible relationship of this delay to the degree of peripheral vascular resistance.[63]
Sival	1992	Findings on the IUGR influence on the fetal general movements. This study showed that in contrast to prenatal period, uncomplicated IUGR had no marked effect on the quality of general movements or on the results of the neurological examination at the age of 1 year.[64,65]
Ribbert et al.	1993	Showed the dynamics of fetal movements and relations to other parameters of fetal well-being in growth restricted fetuses. It was concluded that with progressive deterioration of the fetal condition, abnormal velocity wave form patterns occur first; FHR variation is reduced subsequently while GMs and fetal breathing-like movements are the last to become abnormal.[66]
Vindla et al.	1997	Findings on fetal movements as the predictor of fetal condition. This published report offered the possibility that objective evaluation of fetal behavior could be used in a clinical setting and could provide a more sensitive method of fetal assessment than biophysical profile scores.[67]
Bekedam et al.	1991	The effects of maternal hyperoxia on fetal breathing-like movements, body movements and heart rate variation in IUGR fetuses. It was concluded that in IUGR fetuses the increase in fetal heart rate variation and the increase in the incidence of breathing-like and body movements during maternal hyperoxygenation substantiates the relationship between these variables and the oxygenation status of the fetus.[68]
Andonotopo et al.	2006	4D findings on fetal behavior of growth restricted fetuses. The results showed that the median value of all movement patterns in the normal fetuses differed from fetuses with intrauterine growth restriction (IUGR). Statistical evaluation revealed significant differences in the distribution of the movements between these groups. A tendency that IUGR fetuses have less behavioral activity than normal fetuses was noted in all observed movement patterns. Correlation reached statistical significance between normal and IUGR fetuses in the third trimester in hand-to-head, hand-to-face and head retroflexion. Statistically significant differences could be shown in the distribution of the median values of observation over the five qualitative categories of head and hand movements. These recent data on IUGR fetuses obtained by 4D sonography are stimulating and might result in a more effective strategy to assess development before birth and may encourage future use of 4D ultrasound for quantitative and qualitative assessment of fetal behavior as possible indicators of the neurological condition in IUGR fetuses.[69]
		Risk factor: Maternal infection
Konstantinidou et al.	2007	Case report on the effect of Coxsackievirus B3 on fetal motility. Transplacental infection with coxsackie B3 confirmed by molecular techniques resulted in severe reduction of fetal movements at the 27th week detected by prenatal 2D ultrasound. Late onset of fetal akinesia deformation sequence with mild arthrogryposis was the finding at fetal autopsy following interruption of the pregnancy.[70]
Craig et al.	1996	Study on the effect of *Listeria monocytogenes* on fetal motility. Presentation of the infection include premature labor, an influenza-like illness and reduced fetal movements.[71]
Goldstein et al.	1988	Findings on fetal body and breathing-like movements as predictors of intraamniotic infections. The conclusion was that the breathing-like movements could be used as a predictor of intraamniotic infection.[72]
Del Valle et al.	1992	Findings on fetal body and breathing-like movements as poor predictors of intraamniotic infections. Showed that the biophysical profile with breathing-like movements included and the NST are poor predictors of perinatal infectious complications.[73]

tion, exploring so called lower subcortical system developing earlier from the reticular formation, vestibular nuclei and tectum, and upper cortical system developing from the corticospinal pathways.[78,79] The lower system matures early (beginning at 24 GW) in an ascending wave. Its essential role is to maintain posture against gravity and flexor tone in the limbs. The upper system matures later (beginning at 32 GW) and rapidly for the first two years in a descending wave. Its essential role is to control the lower system, with relaxation of the limbs and control of the antigravity forces, finally allowing erect posture, walking and fine motor skills.[47]

At the corrected age of 40 gestational weeks optimality assessment consists of: head circumference measurement, assessment of cranial sutures, visual pursuit, social interaction, sucking reflex, raise-to-sit and reverse, passive tone in the axis, passive tone in the limbs, fingers and thumbs outside the fist, and autonomic

control during assessment.[79] The ATNAT is increasing accuracy in assessing CNS function in the neonate by using simple scoring system, focusing on the most meaningful items, promoting a clinical synthesis at term, for term and preterm infants.[79] It was recognized that clinicoanatomic correlations using high resolution neuroimaging techniques could be helpful in the neurological assessment of newborns, while the neurological examination and the functional assessment of the developing CNS are bringing a new perspective of CNS status in neonatal period.[80] According to the investigation of very low-birth-weight infants, ATNAT at 40 weeks had a positive predictive value of 33% and negative predictive value of 88%, respectively, with similar results for neurodevelopmental assessment at the age of three months.[81] This means that we still need some other methods to be used in order to predict neuro- developmental outcome of low- and high-risk infants.[82]

Other method for the functional assessment of the developing CNS, initiated by Prechtl is based on observing the quality of general movements. Prechtl and his followers proposed a conception of motor behavior which is understood as " the net result of the activity of complex spinal or brainstem machineries, which are subtly modulated by segmental afferent information and ingeniously controlled by supraspinal networks."[47,83] In other words, the young nervous system generates a variety of motor patterns originating in "neural networks that are able to coordinate autonomously (i.e. without sequential sensory or supraspinal information) the activity of many muscles."[47,83] The observation of pre- and postnatal spontaneous motor behavior drove Prechtl to describe general movements (GMs) as "series of gross movements of variable speed and amplitude, which involve all parts of the body but lack a distinctive sequencing of the participating body parts."[47,83] Due to the timing of neuronal maturation and the occurrence of GMs, this motor pattern is considered as being produced without afferent information. "Remarkably, GMs are among the first movements that the human fetus develops and they emerge prior to isolated limb movements. General movements can already be observed before the completion of the spinal reflex arc, which is accomplished at eight weeks postmenstrual age (PMA)."[47,83] The GMs show age-specific characteristics with increasing variation, movement direction, amplitude, speed and complexity. Prechtl and colleagues propose a sequence in the acquisition of these different GMs [preterm (from ± 28 weeks until 36–38 weeks), writhing (from 36–38 weeks until 46–52 weeks), fidgety (from 46 weeks to 52 weeks until 54–58 weeks) with overlaps].[47] According to Prechtl any fetal brain damage will interfere with the endogenous motor activity.[23,84-87] Therefore, spontaneous movements, as an expression of neural activity could be used as a marker for fetal brain status,[23,86] and indeed, alterations of spontaneous general movements can be observed in preterm and term newborns with cerebral impairment.[11] Their movements seem to lose the characteristic fluency and complexity, and become cramped and unsynchronized. In addition, assessment of GMs at so called fidgety GM age has been found to have the highest predictive value for development of CP, if abnormal.[23,88] Lack of fluency and existence of considerable variation, and complexity are the main characteristics of mildly abnormal GMs.[89] When complexity, variation and fluency are absent, than we are dealing with definitely abnormal GMs.[89] General movements have to be videotaped and then analyzed based on visual ''Gestalt perception,'' which provides an overall impression of GMs with standardized procedures.[87] Development of Prechtl's GM for postnatal neurological evaluation encouraged obstetricians to implement this technique for fetal neurological evaluation using 2D ultrasound.[23,84-87] Qualitative alterations in fetal general movements have been observed in several conditions, including maternal diabetes mellitus, fetal anencephaly and intrauterine growth restriction (IUGR).[11] The fact that the same criteria can be used for the fetus and young infants seemed especially attractive. However, inspite of encouraging results of fetal GMs assessed by 2D ultrasound in the last 25 years, which showed that qualitative assessment of GMs is a good marker of brain dysfunction, the diagnosis of neurological impairment was not shift to the prenatal period. The purposes of early diagnosis of CP would be important from the point of view of the infant, the mother, the family and the gynecologist, who is often accused for clinical negligence.[74] Further, although randomized studies confirming that the early intervention as an effective strategy for treatment of CP is not available, it should be considered as feasible.[75] Development of computer and ultrasound technology enabled evaluation of fetal GM in three dimensions and in real time, and brought new advances in the understanding of fetal behavior.

New Scoring System for Fetal Neurobehavior Assessed by Four-Dimensional Sonography

As mentioned, one of the most promising improvements in the intriguing field of prenatal behavior has been the new 3D/4D sonographic technology. Its advance has been completed in giving visualizations in almost real time, and production of standards for different movement patterns to appear and develop. The 4D study of fetal behavior provided us with a great

possibility of understanding the hidden function of the developmental pathway of the fetal CNS and the potentialities of originating a neurological investigation *in utero*. The remarkable continuity of endogenously generated activity from prenatal to postnatal life may allow identification of those fetuses and infants with evolving neurological impairment.[23,87,90-93] After standardization of valid reference ranges of movements appropriate for the gestational age, the Zagreb group published a new scoring system for fetal neurobehavior based on prenatal assessment by 3D/4D sonography **(Table 37.2)**.[94] This test was developed after discussions and consensus between members of international collaborative project.[25,95]

New scoring system for the assessment of neurological status in fetuses is a combination of the postnatal ATNAT and GM assessments.[23,78,79,90,96,97] Similarity between neonatal optimality test of Amiel-Tison and new scoring system can be observed in assessments of head growth parameters including sutures' status, primary reflexes (restricted to sucking behavior), fingers movements and abduction of thumbs.[75] Some criteria observed in the fetus are only prerequisites for *ex utero* functional achievements: opening of the eyes for visual pursuit and facial expressions for social interaction. Their identification by 4D imaging, in addition to efficient and rhythmic sucking supports the absence of CNS depression.[75] However, analytical criteria of typical passive and active tone in the neonate cannot be elicited in the fetus, viz. head anteflexion versus retroflexion and ventral versus dorsal incurvations in the axis, both are of utmost importance postnatally to confirm CNS optimality. Still, optimality in the fetus should be reflected in typical GMs. Criteria aiming to check autoregulation are slightly different: typical non-stress test (NST) in the fetus and absence of reactions in the neonate.[75]

Selected parameters assessed during application of new test are:[94]

Isolated head anteflexion: This movement is usually carried out slowly, but can also be fast and jerky. Activity of the flexor muscles responsible for this pattern depend on the upper system since 34 GWs. Abnormal movement looks abrupt when marked by sudden changes in subject and sharp transitions. Abnormally rhythmic movements are sometimes related to seizures occurring *in utero*. Absence of active flexion of the head in the 40th GW is one of the major neurological signs.

Overlapping cranial sutures and head circumference (HC): Normally cranial sutures are not overlapping. They are smooth and ridges are not visible. Abnormal cranial ridges over suture or HC below normal limit are related to severe or moderate impairment of hemispheric growth.

Isolated eye blinking ***(Figs 37.9A to D)***: A reflex that closes and opens the eyes rapidly by involuntary normal periodic closing or by voluntary action. Movement looks fluent, smooth and unconstrained. The presence of this movement indicates absence of the CNS depression.

Facial alteration (grimace or tongue expulsion) ***(Figs 37.10A to D)***: The wrinkling of the brows or face in frowning, sometimes characterized by expulsion of the tongue. The presence of this movement indicated the absence of CNS depression. Almost absent mimic of the face or very rare movements (face looks always the same, mask-like face) is abnormal.

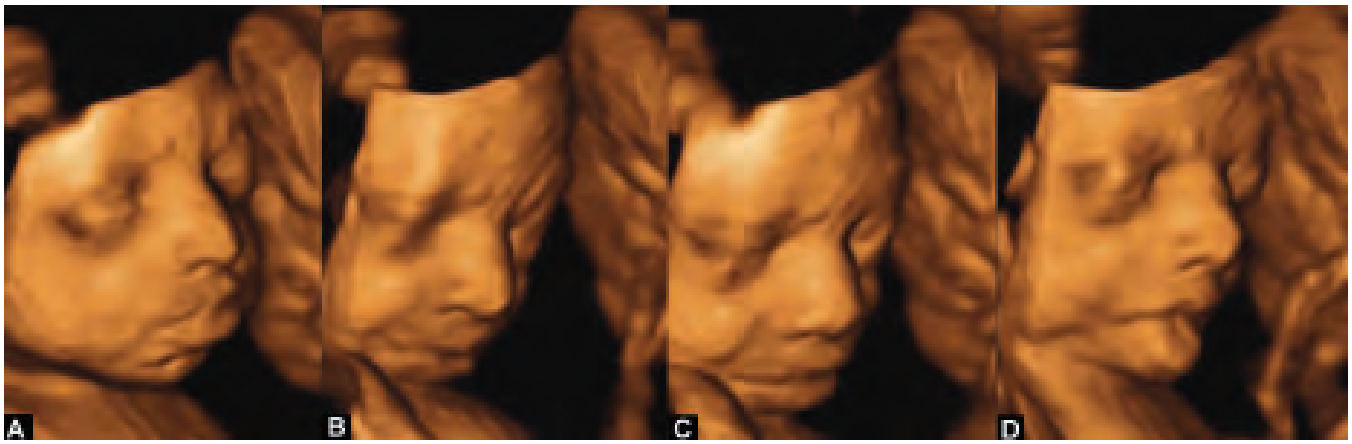

Figures 37.10A to D: A sequence of images of the fetus recorded by 3D/4D sonography showing facial alterations, grimace or tongue expulsion

TABLE 37.2

Antenatal Neurological Screening Test[94]

Sign	*Score* 0	1	2
Isolated head anteflexion 	Abrupt	Small range (0-3 times of movements)	Variable in full range, many alternation (> 3 times of movements)
Cranial sutures and head circumference 	Overlapping of cranial sutures. Head circumference below or above the normal limit (-2SD) according to GA	Normal cranial sutures Normal head circumference	
Isolated eye blinking 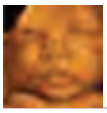	Not present	Not fluent (1-5 times of blinking)	Fluency (> 5 times of blinking)
Facial alternation (grimace or tongue expulsion) 	Not present	Not fluent (1-5 times of alternation)	Fluency (> 5 times of alternation)
Mouth opening (yawning or mouthing) 	Not present	Not fluent (1-3 times of alternation)	Fluency(> 3 times of alternation)
Isolated hand movement 	Cramped	Poor repertoire	Variable and complex
Isolated leg movement 	Cramped	Poor repertoire	Variable and complex
Hand-to-face movements 	Abrupt	Small range (0-5 times of movement)	Variable in full range, many alternation (> 6 times of movements)
Finger movements 	Unilateral or bilateral clenched fist, (neurological thumb)	Cramped invariable finger movements	Smooth and complex, variable finger movements
Gestalt perception of GMs	Definitely abnormal	Borderline	Normal
			Total score

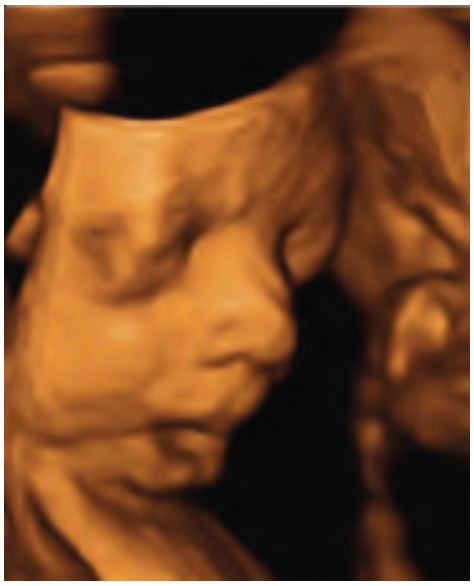

Figure 37.11: Image of the fetus recorded by 3D/4D sonography showing mouth opening

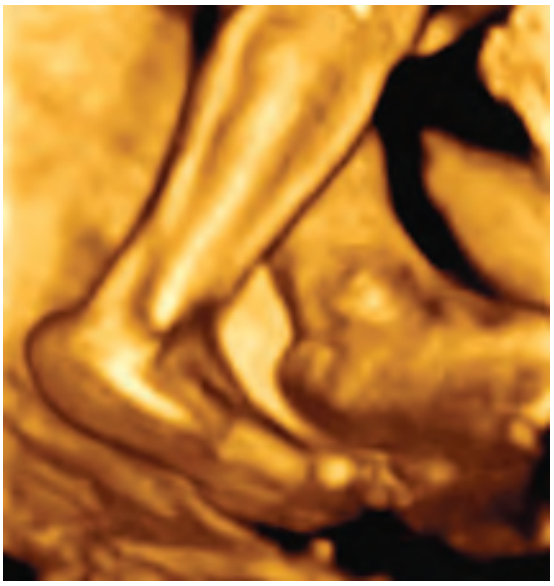

Figure 37.12: Image of the fetus recorded by 3D/4D sonography showing isolated leg movement

Mouth opening (yawning or mouthing) ***(Fig. 37.11)***: Yawning is characterized with prolonged wide opening of the jaws followed by quick closure, retroflexion of the head and elevation of the arms. Mouthing indicates that the fetus is opening the mouth. Sometimes consists of displacements of tongue and/or larynx. The presence of this movement indicated the absence of CNS depression. Absence of movements or very rare movements of the tongue and yawning are abnormal.

Isolated hand and leg movements ***(Fig. 37.12)***: Rapid or slow movements can involve extension, flexion, external and internal rotation, or abduction and adduction of an extremity, without movements in other body parts. Automatic leg movement or walking movement is a precompetent stage, present very early in fetal life and still at birth, then diminishing in the first three months postnatally. Apparently, walking movement are disappearing, but later involved in the automatization of independent walk for the rest of the life. This is a typical example of ''change of power'' from a lower (brainstem) to a higher (cortical) command. Abnormal isolated hand and leg movement during prenatal life is characterized by poor repertoire when the sequence of successive components is monotonous and movements do not occur in the complex manner. Further, the movement characterized by cramped when it looks rigid, with lack of the normal, smooth and fluent character. Abnormally rhythmic movements are sometimes related to seizures occurring *in utero*.

Hand-to-face movements: The hand touches the face parts, sometimes with extension and flexion of the fingers. Abnormal movement looks abrupt when it is marked by sudden changes in subject and sharp transitions. Abnormally rhythmic movements are sometimes related to seizures occurring *in utero.*

Finger movements and thumb position: Normally thumb is outside the fist most of the time and finger movements are present **(Fig. 37.13)**. This motor activity depends on the lower system up to 30–32 GWs and switches to the upper control later on. Neurological sign of the thumb, that indicates brain impairment, is demonstrated when the adduction of the thumb in a clenched fist is non reducible **(Fig. 37.14)**. In addition, disturbance in fingers and thumb movements correlated with absence of spontaneous motor activity. Unilateral side of the clenched fist is a precious orientation in case of infarction of the middle cerebral artery.

Gestalt perception of general movements: This parameter is defined as overall perception of the body and limb movements with their qualitative assessment (fluency, variability and amplitude). Normally movements are synchronized showing fluency and elegance, creating the impression of complexity and variability. Abnormal finding are poor amplitude, variability and fluency of the movements. The identification of the ''CNS depression'' during fetal life is based on quality of GMs.[94]

To produce the new scoring test the Zagreb group identified severely brain damaged infants and those

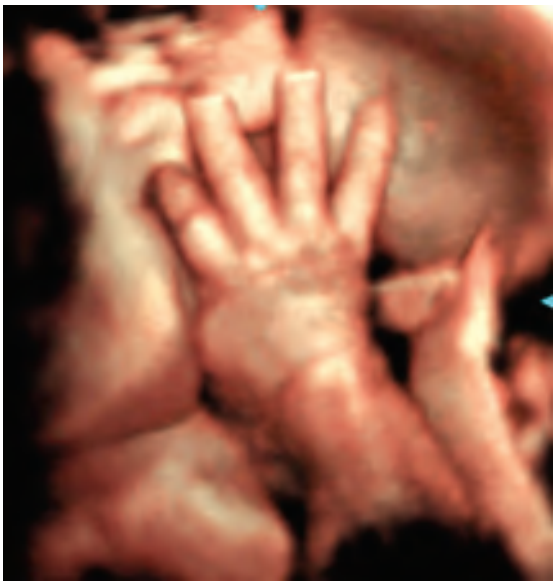

Figure 37.13: Image of the fetus recorded by 3D/4D sonography showing normal position of the fingers. Normally, thumb is outside the fist most of the time, and finger movements are present

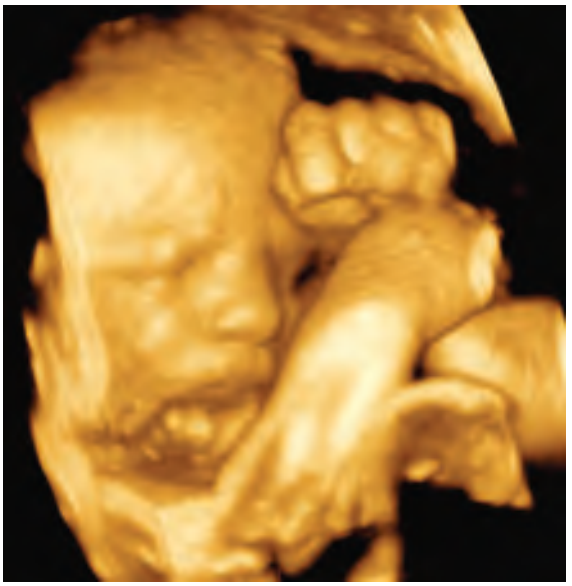

Figure 37.14: Image of the fetus recorded by 3D/4D sonography showing neurological sign of the thumb, the adduction of the thumb in a clenched fist

with optimal neurological findings by comparing fetal with neonatal findings. In the group of 100 low-risk pregnancies they retrospectively applied new scoring system. After delivery, postnatal neurological assessment (ATNAT) was performed and all neonates assessed as normal reached a score between 14 and 20, which was assumed to be a score of optimal neurological development.[94] New scoring system was applied in the group of 120 high-risk pregnancies in which, based on postnatal neurological findings, three subgroups of newborns were found: 1. Normal; 2. Mildly abnormal or 3. Moderately abnormal. Based on this a neurological scoring system has been proposed. All normal fetuses reached a score in the range from 14–20. Ten fetuses who were postnatally described as mildly or moderately abnormal achieved prenatal score of 5–13, while another ten fetuses postnatally assigned as neurologically abnormal had a prenatal score from 0 to 5. Among this group four had alobar holoprosencephally; one had severe hypertensive hydrocephaly; one had tanatophoric dysplasia and four fetuses had multiple malformations.[94]

It was a preliminary study that has been continued in several collaborative centers. The potential of the test was investigated at four university departments and the objective of this multricentric study[98] was to apply the new antenatal scoring system, named Kurjak antenatal neurodevelopmental test (KANET) to the fetuses from high-risk pregnancies for neurological disorders and to verify the results of the test by two neonatal neurological tests: 1. ATNAT and 2. General movements test by Prechtl. About 288 pregnant women meeting the inclusion criteria given in **Table 37.3** were found eligible to be included in the study.[98]

In this study seven fetuses had abnormal KANET scores and 25 fetuses were borderline, which gives all together 32 fetuses at neurological risk. Of seven fetuses with abnormal KANET score, postnatal neurological assessment by Amiel Tison's method (ATNAT) has revealed three newborns (arthrogryposis, vermis aplasia and neonate of the mother with the previous child with

TABLE 37.3

Inclusion criteria for the high-risk pregnancies[98]

Inclusion criteria	*Associated risk*
Family history	Previous child with cerebral palsy
Maternal condition	Diabetes mellitus type I and II, thyroid disease, pre-existent hypertension, drug abuse, thrombophilia, anemia and epilepsy.
Pregnancy related disorders	Gestational diabetes, Rh immunization, threatened preterm labor, preeclampsia, intrauterine infections, viral illness and cholestasis.
Fetal condition	Structural and chromosomal abnormalities, polyhydramnion, intrauterine growth restriction, pathological findings in electrical fetal heart monitoring or Doppler findings.

CP), who were considered as abnormal, while four were considered normal (ventriculomegaly, preeclampsia, thrombophylia and oligohydramnios). Out of 25 borderline KANET fetuses, there were 22 borderline newborns by ATNAT, while three were normal (ventriculomegaly, syndrome of intraamniotic infection and mother's thrombocytopenia). Those who were abnormal prenatally and normal postnatally had following prenatal risk factors: ventriculomegaly, Dandy-Walker syndrome, skeletal dysplasia, polihydramnios, hydrocephaly, diabetes in pregnancy, nonimmune hydrops, syndrome of intraamniotic infection, IUGR, trisomy 21, thrombocytopenia, thrombophylia, preeclampsia, achondroplasia, oligohydramnios, etc. Out of three abnormal neonates after ATNAT assessment, two were definitely having abnormal Prechtl's premature general movements (arthrogryposis and vermis aplasia), and additional six were considered abnormal (neonate of the mother with the previous child with CP, Dandy-Walker syndrome, hydrocephaly, trisomy 21, ventriculomegaly and non immune hydrops). Rest of the 24 children had normal optimal or normal suboptimal GMs.[98]

The three very illustrative cases with abnormal KANET scoring were: 1. Arthrogryposis; 2. Vermis aplasia and 3. Fetus whose previous sibling had verified CP. The fetuses in these three cases had especially reduced facial movements and the faces were like mask during repeated scans. Fetuses with vermis aplasia and arthrogryposis had normal cranial sutures, but the isolated head flexion was small in range for both the cases. Isolated hand movements, hand-to-face and leg movements were poor in repertoire for all three cases. The finger movements were cramped and invariable in all three cases. The Gestalt perception of GMs was abnormal in all three cases.[98]

In this study the behavior of a fetus with acranius was also longitudinally followed.[98] The mother decided not to terminate the pregnancy due to religious reasons. It has been observed that the fetus at 20 weeks of gestation had hypertonic movements with high amplitude and high speed. The movements emerged abruptly with burst-paused patterns and the variability of head movements was missing without changes of facial expressions. As the gestational age advanced and the motor control was shifting from lower to upper control center the movement patterns changed as well. At the gestational age of 32 weeks the fetus had no facial expressions (mask-like face) and hand movement repertoire was very poor. At 36 weeks the absence of both the facial expressions and limb movements was observed.[98] In this fetus, abnormal behavior patterns as a result of lack of the supraspinal centers influence on the motor activity was clearly documented.

Results of this study showed that the new test might be useful in standardization of neurobehavioral assessments.[98] Furthermore, there is a potential for antenatal detection of serious neurological problems. At this stage, test easily separates serious structural anomalies associated with brain impairment (arthrogryposis, vermis aplasia and anencephaly).[98]

Significant difference for 8 out of 10 parameters of KANET: isolated anteflection of the head, eye blinking, facial expressions (grimacing and tongue expulsion), mouth movements (mouthing, yawning and swallowing), isolated hand movement, hand-to-face movement, fist and finger movements, and GMs has been showed. Authors have also confirmed statistically significant and moderate correlation of KANET, and ATNAT tests. In practical sense, it means that the neuropediatrician who examined the newborns with ATNAT test confirmed the results of KANET.[99]

New results regarding the potential of 4D sonography in the assessment of fetal behavior in high-risk pregnancies were recently published.[100] The group in Khartoum applied KANET to large number of fetuses during the period of one year. The aim of the study was to assess the behavior in large sample of fetuses from normal and high-risk pregnancies by application of the KANET scoring test and to compare the scores obtained in low- and high-risk pregnancies.

In this prospective longitudinal cohort study, the KANET was applied in 620 singleton pregnancies, between 26th and 38th week of gestation.[100] Pregnant women were assigned to low- and high-risk group. There were 520 pregnant women in high-risk and 100 pregnant women in low-risk group. Contrary to the previous studies, the fetuses with congenital anomalies and multiple pregnancies were excluded from the study. High-risk group of patients consisted of the following subgroups: threatened preterm delivery with or without preterm premature rupture of membranes (PPROM); previous child diagnosed with CP; hypertension in pregnancy with or without preeclampsia; diabetes before pregnancy or gestational diabetes; intrauterine growth restriction (IUGR); polyhydramnios; Rh isoimmunization; placental bleeding and maternal fever above 39°C. Fetal KANET scores from low-risk and high-risk pregnancies were compared, and the difference was statistically significant.[100] The distribution of fetuses from the subgroups of the high-risk pregnancies according to the KANET score is presented in **Table 37.4**.

The largest incidence of fetuses with abnormal KANET was noticed in the subgroup of participants

TABLE 37.4 (Adapted from reference 100)

The distribution of fetuses from the subgroups of the high-risk pregnancies according to the KANET score

Subgroup of fetuses	*Total N*	*KANET score Normal*	*Borderline*	*Abnormal*
Threatened preterm delivery	74	58	9	7
• With PPROM	10	2	3	5
• Without PPROM	64	56	6	2
Previous child with CP	21	8	8	5
Hypertension	145	129	12	4
• RR < 160/100	107	102	4	1
• RR > 160/100	38	27	8	3
Diabetes	42	36	3	3
• Type I	2	1	0	1
• Type II	12	8	2	2
• Gestational	28	27	1	0
IUGR	47	34	11	2
• With MCA RI changes	11	0	9	2
• Normal MCA RI	36	34	2	0
Placental bleeding	39	20	13	6
• Subchorionic	14	9	4	1
• Subplacental	25	11	9	5
Maternal fever > 39ºC	55	17	31	7
Rh isoimmunization	87	81	5	1
• Without hydrops fetalis	76	76	0	0
• With hydrops fetalis	11	5	5	1
Polyhydramnios	10	8	1	1

N: Number of examinees; PPROM: Preterm premature rupture of membranes; CP: Cerebral palsy; RR: Riva Rocci—blood pressure; IUGR: Intrauterine growth restriction; MCA: Middle cerebral artery; RI: Resistance index (Adapted from 100)

with a previous child diagnosed with CP (23.8%) and the largest incidence of fetuses with borderline KANET was observed in the subgroup of mothers with fever (56.4%). Statistically significant difference was found between KANET scores of the fetuses from the low-risk group compared to the following subgroups of the high-risk group: previous child diagnosed with CP; hypertension (RR > 160/100); threatened preterm delivery; maternal fever; IUGR; Rh isoimmunization and placental bleeding. Furthermore, KANET scores significantly differed comparing threatened preterm delivery with PPROM versus threatened preterm delivery without PPROM; hypertension above 160/100 mm Hg versus hypertension below 160/100 mm Hg; diabetes before pregnancy versus gestational diabetes; IUGR with decreased resistance index (RI) of middle cerebral artery (MCA) versus IUGR without decreased RI of MCA and Rh isoimmunization without hydrops fetalis versus Rh isoimmunization with hydrops fetalis. Comparison of individual KANET parameters between the fetuses from the low-risk and high-risk pregnancies showed statistically significant difference for overlapping cranial sutures and head circumference, isolated eye blinking, facial expressions (grimacing and tongue expulsion), mouth movements (yawning and mouthing), isolated hand movements, isolated leg movements, hand-to-face movement, finger movements, and GM. For isolated head anteflexion, the difference was not statistically significant.[100] These data are in contrast with previously published reports, where isolated head anteflexion showed statistically significant difference between normal and high-risk pregnancies, and overlapping cranial sutures, head circumference and isolated leg movements did not show statistically significant difference between normal and high-risk group.[99] However, previous study and this study had different inclusion and exclusion criteria. In this study, fetuses with any structural anomaly were excluded, while in the mentioned research, there were fetuses with structural anomalies that severely influenced head

circumference by decreasing and/or by increasing it.[99] Further, during this research it was observed that low-KANET scores were predictable either of intrauterine or postnatal death. During this study, two fetuses with KANET scores of 3 and 4 died *in utero*, while one neonate with KANET score of two, died on the 27th postnatal day.[100] Up to now, this was the study with the largest number of fetuses where prenatal KANET test was applied.

The KANET test has the potential to detect and discriminate normal from borderline, and abnormal fetal behavior in normal and in high-risk pregnancies, which means that it could become a valuable diagnostic tool for fetal neurological assessment.[94,98-102] It is important to critically review and improve the test; making it more simple and applicable as the screening tool for prenatal neurological assessment. In order to achieve this ambitious goal, more studies are needed with long-term postnatal follow-up.

CONCLUSION

One of the most promising improvements in the field of ultrasonography has been the new 4D ultrasound technology. Its advance has been completed in giving visualizations in almost real time. The availability of new diagnostic data has in an extraordinary way raised our knowledge about intrauterine life, substantially modifying some earlier interpretations. The 4D study of fetal behavior provided us with a great possibility of understanding the hidden function of the developmental pathway of the fetal CNS and the potentialities of originating a neurological investigation *in utero*. Now, by 4D technology, we might be able to visualize an intrauterine neurological condition that would enable to identify which fetus is at risk and which is not. Behavioral perinatology assessed by 4D sonography should be an interdisciplinary area of research involving concepts and conducting studies of the dynamic interplay between behavioral processes in fetal, neonatal and infant life. The ultimate clinical application of fetal neurobehavioral assessment will be to identify functional characteristics of the fetus that predict a range of subsequent developmental dysfunction. Establishing this link will require demonstration of positive and negative predictability to outcomes significantly beyond the immediate perinatal period. After standardization of valid reference ranges of movements appropriate for the gestational age, attempts have been made to produce a new scoring system for fetal neurobehavior based on prenatal assessment by 3D/4D sonography. This preliminary work might help in detecting fetal brain and neurodevelopmental alterations due to *in utero* brain impairment.

REFERENCES

1. Nijhuis JG. Neurobehavioral Development of the fetal brain. In: Nijhuis JG (Ed). Fetal Behaviour: Developmental and Perinatal Aspects. London: Oxford University Press; 1992. p. 489.
2. Kurjak A, Azumendi G, Vecek N, et al. Fetal hand movements and facial expression in normal pregnancy studied by four-dimensional sonography. J Perinat Med. 2003;31(6):496-508.
3. Hu W, Wu MT, Liu CP, et al. Left ventricular 4D echocardiogram motion and shape analysis. Ultrasonics. 2002;40:949-54.
4. Kossoff G. Basic physics and imaging characteristics of ultrasound. World J Surg. 2000;24:134-42.
5. Lee A. Four-dimensional ultrasound in prenatal diagnosis: leading edge in imaging technology. Ultrasound Rev Obstet Gynecol. 2001;1:194-98.
6. Kozuma S, Baba K, Okai T, et al. Dynamic observation of the fetal face by three-dimensional ultrasound. Ultrasound Obstet Gynecol. 1999;13:283-84.
7. Campbell S. 4D or not 4D: That is the question. Ultrasound Obstet Gynecol. 2002;19:1-4.
8. Kurjak A, Pooh RK, Merce LT, et al. Structural and functional early human development assessed by three-dimensional and four-dimensional sonography. Fertil Steril. 2005;84(5):1285-99.
9. de Vries JIP, Visser GH, Prechtl HF. The emergence of fetal behavior. I. Qualitative aspect. Early Hum Dev. 1982;7: 301-22.
10. Andonotopo W, Stanojevic M, Kurjak A, et al. Assessment of fetal behavior and general movements by four-dimensional sonography. Ultrasound Rev Obstet Gynecol. 2004;4:103.
11. Salihagić Kadić A, Predojević M, Kurjak A. Advances in fetal neurophysology. In: Pooh RK, Kurjak A (Eds). Fetal neurology. New Delhi: Jaypee Brothers Medical Publishers; 2009. pp 161-221.
12. Andonotopo W, Medic M, Salihagic-Kadic A, et al. The assessment of embryonic and fetal neurodevelopment in early pregnancy: comparison between 2D and 4D sonographic scanning. J Perinat Med (In Press).
13. Azumendi G, Kurjak A, Carrera JM, et al. 3D and 4D sonography in the evaluation of normal and abnormal fetal facial expression. In: Kurjak A, Carrera JM (Eds). Atlas of Clinical Application of Ultrasound in Obstetrics and Gynecology. New Delhi: Jaypee Brothers Medical Publishers; 2005 (In Press).
14. Carrera JM. Fetal ultrasonography: the first 40 years. Ultrasound Rev Obstet Gynecol. 2004;4:141-59.
15. Kurjak A, Carrera JM, Andonotopo W, et al. Behavioral perinatology assessed by four.dimensional sonography. In: Kurjak A, Chervenak FA (Eds). Textbook of Perinatal Medicine. London: Taylor and Francis; 2005 (In Press).
16. Kurjak A, Stanojevic M, Andonotopo W, et al. Behavioral pattern continuity from prenatal to postnatal life – a study

by four-dimensional (4D) ultrasonography. J Perinat Med. 2004;32:346-53.
17. Kurjak A, Stanojevic M, Azumendi G, et al. The potential of four-dimensional (4D) ultrasonography in the assessment of fetal awareness. J Perinat Med. 2005;33: 46-53.
18. Kurjak A, Vecek N, Hafner T, et al. Prenatal diagnosis: what does four-dimensional ultrasound add? J Perinat Med. 2002;30:57-66.
19. Andonotopo W, Kurjak A, Azumendi G. Ultrasound studies on early pregnancy. In: Kurjak A, JM Carrera (Eds). Atlas of Clinical Application of Ultrasound in Obstetrics and Gynecology. New Delhi: Jaypee Brothers Medical Publishers; 2005 (In Press).
20. Azumendi G, Arenas JB, Andonotopo W, et al. Three dimensional sonoembriology. In: Kurjak A, Arenas JB (Eds). Textbook of Transvaginal Sonography. London: Taylor and Francis; 2005. p. 407.
21. Kurjak A, Vecek N, Kupesic S, et al. Four dimensional ultrasound: how much does it improve perinatal practice? In: Carrera JM, Chervenak FA, Kurjak A (Eds). Controversies in Perinatal Medicine, Studies on the Fetus as a Patient. New York: Parthenon Publishing; 2003. p. 222.
22. Hopkins B, Prechtl HFR. A qualitative approach to the development of movements during early infancy. In: Prechtl HFR (Ed). Continuity of Neural Functions from Perinatal to Postnatal Life. Oxford: Blackwell Scientific Publications; 1984. pp. 179-97.
23. Prechtl HFR. Qualitative changes of spontaneous movements in fetus and preterm infant are a marker of neurological dysfunction. Early Hum Dev. 1990;23:151-8.
24. Pooh RK, Ogura T. Normal and abnormal fetal hand positioning and movement in early pregnancy detected by three and four-dimensional ultrasound. Ultrasound Rev Obstet Gynecol. 2004;4:46-51.
25. Kurjak A, Andonotopo W, Hafner T, et al. Normal standards for fetal neurobehavioral developments—longitudinal quantification by four-dimensional sonography. J Perinat Med. 2006;34(1):56-65.
26. Andonotopo W, Medic M, Salihagic-Kadic A, et al. The assessment of fetal behavior in early pregnancy: comparison between 2D and 4D sonographic scanning. J Perinat Med. 2005;33(5):406-14.
27. Hata T, Kanenishi K, Sasaki M. Four-dimensional sonographic assessment of fetal movement in the late first trimester. Int J Gynaecol Obstet. 2010;109(3):190-3.
28. Hata T, Dai SY, Marumo G. Ultrasound for evaluation of fetal neurobehavioral development: from 2D to 4D ultrasound. Infant Child Dev. 2010;19(1):99-118.
29. Kuno A, Akiyama M, Yamashiro C, et al. Three-dimensional sonographic assessment of fetal behavior in the early second trimester of pregnancy. J Ultrasound Med. 2001;20(12):1271-5.
30. Awoust J, Levi S. Neurological maturation of the human fetus. Ultrasound Med Biol. 1983;9(2):583-7.
31. Inoue M, Koyanagi T, Nakahara H. Functional development of human eye-movement in utero assessed quantitatively with real-time ultrasound. Am J Obstet Gynecol. 1986;155:170-4.
32. de Vries JIP, Visser GHA, Mulder EJH, et al. Diurnal and other variations in fetal movement and heart rate patterns at 20-22 weeks. Early Hum Dev. 1987;15(6):333-48.
33. D'Elia A, Pighetti M, Moccia G, et al. Spontaneous motor activity in normal fetus. Early Human Dev. 2001;65(2): 139-44.
34. Natale R, Nasello-Paterson C, Turlink R. Longitudinal measurements of fetal breathing, body movements, and heart rate accelerations, and decelerations at 24 and 32 weeks of gestation. Am J Obstet Gynecol. 1985;151:256-63.
35. Eller DP, Stramm SL, Newman RB. The effect of maternal intravenous glucose administration on fetal activity. Am J Obstet Gynecol. 1992;167:1071-4.
36. Haddres-Algra M. Putative neural substrate of normal and abnormal general movements. Neurosci Biobehav Rev. 2007;31(8):1181-90.
37. Kurjak A, Azumendi G, Andonotopo W, et al. Three- and four-dimensional ultrasonography for the structural and functional evaluation of the fetal face. Am J Obstet Gynecol. 2007;196(1):16-28.
38. Azumendi G, A Kurjak. Three-dimensional and four-dimensional sonography in the study of the fetal face. Ultrasound Rev Obstet Gynecol. 2003;3:160-9.
39. Yan F, Dai SY, Akther N, et al. Four-dimensional sonographic assessment of fetal facial expression early in the third trimester. Int J Gynaecol Obstet. 2006;94(2): 108-13.
40. Kurjak A, Stanojevic M, Andonotopo W, et al. Behavioral pattern continuity from prenatal to postnatal life – a study by four-dimensional (4D) ultrasonography. J Perinat Med. 2004;32:346-53.
41. Kurjak A, Miskovic B, Andonotopo W, et al. How useful is 3D and 4D ultrasound in perinatal medicine? J Perinat Med. 2007;35:10-27.
42. Nijhuis JG. Fetal behavior. Neurobiol Aging. 2003;24:41-6.
43. Back SA. Perinatal white matter injury: the changing spectrum of pathology and emerging insights into pathogenetic mechanisms. Ment Retard Dev Disabil Res Rev. 2006;12:129-40.
44. Back SA, Riddle A, McClure MM. Maturation-dependent vulnerability of perinatal white matter in premature birth. Stroke. 2007;38:724-30.
45. Bax M, Goldstein M, Rosenbaum P, et al. Proposed definition and classification of cerebral palsy. Dev Med Child Neurol. 2005;47:571-6.
46. Rosenbaum P, Paneth N, Leviton A, et al. A report: the definition and classification of cerebral palsy. Dev Med Child Neurol. 2007;109:8-14.
47. Amiel-Tison C, Gosselin J. From Neonatal to Fetal Neurology: Some Clues For Interpreting Fetal Findings. In: Pooh RK, Kurjak A (Eds). Fetal neurology. New Delhi: Jaypee Brothers; 2009.
48. Visser GH, Mulder EJ, Tessa Ververs FF. Fetal behavioral teratology. J Matern Fetal Neonatal Med. 2010;23 Suppl 3:14-6.
49. Visser GHA, Mulder EJH. Fetal movement patterns and fetal behavioural states. In: Wladimiroff JW, Eik-Nes S, (Eds). Ultrasound in obstetrics and gynaecology. Philadelphia: Elsevier; 2009. pp. 271-84.

50. Visser GH, Bekedam DJ, Mulder EJ, et al. Delayed emergence of fetal behaviour in type-1 diabetic women. Early Hum Dev. 1985;12(2):167-72.
51. Mulder EJ, Visser GH, Bekedam DJ, et al. Emergence of behavioural states in fetuses of type-1-diabetic women. Early Hum Dev. 1987;15(4):231-51.
52. Visser GH, Mulder EJ, Bekedam DJ, et al. Fetal behaviour in type-1 diabetic women. Eur J Obstet Gynecol Reprod Biol. 1986;21(5-6):315-20.
53. Mulder EJ, Visser GH. Growth and motor development in fetuses of women with type-1 diabetes. II. Emergence of specific movement patterns. Early Hum Dev. 1991;25(2): 107-15.
54. Mulder EJ, Visser GH, Morssink LP, et al. Growth and motor development in fetuses of women with type-1 diabetes. III. First trimester quantity of fetal movement patterns. Early Hum Dev. 1991;25(2):117-33.
55. Mulder EJ, O'Brien MJ, Lems YL, et al. Body and breathing movements in near-term fetuses and newborn infants of type-1 diabetic women. Early Hum Dev. 1990;24(2): 131-52.
56. Mulder EJ, Visser GH. Impact of early growth delay on subsequent fetal growth and functional development: a study on diabetic pregnancy. Early Hum Dev. 1992;31(2):91-5.
57. Mulder EJ, Leiblum DM, Visser GH. Fetal breathing movements in late diabetic pregnancy: relationship to fetal heart rate patterns and Braxton Hicks' contractions. Early Hum Dev. 1995;43(3):225-32.
58. Reece EA, Hagay Z, Roberts AB, et al. Fetal Doppler and behavioral responses during hypoglycemia induced with the insulin clamp technique in pregnant diabetic women. Am J Obstet Gynecol. 1995;172(1 Pt 1):151-5.
59. Devoe LD, Youssef AA, Castillo RA, et al. Fetal biophysical activities in third-trimester pregnancies complicated by diabetes mellitus. Am J Obstet Gynecol. 1994;171(2): 298-303.
60. van Vliet MA, Martin CB, Nijhuis JG, et al. The relationship between fetal activity and behavioral states and fetal breathing movements in normal and growth-retarded fetuses. Am J Obstet Gynecol. 1985;153(5):582-8.
61. Van Vliet MA, Martin CB, Nijhaus JG, et al. Behavioural states in growth-retarded human fetuses. Early Hum Dev. 1985;12:183-97.
62. Arduini D, Rizzo G, Romanini C, et al. Computerized analysis of behavioural states in asymmetrical growth retarded fetuses. J Perinat Med. 1988;16(4):357-63.
63. Rizzo G, Arduini D, Pennestri F, et al. Fetal behaviour in growth retardation: its relationship to fetal blood flow. Prenat Diagn. 1987;7(4):229-38.
64. Sival DA, Visser GH, Prechtl HF. The effect of intrauterine growth retardation on the quality of general movements in the human fetus. Early Hum Dev. 1992;28(2):119-32.
65. Sival DA, Visser GH, Prechtl HF. The relationship between the quantity and quality of prenatal movements in pregnancies complicated by intra-uterine growth retardation and premature rupture of the membranes. Early Hum Dev. 1992;30(3):193-209.
66. Ribbert LS, Visser GH, Mulder EJ, et al. Changes with time in fetal heart rate variation, movement incidences and haemodynamics in intrauterine growth retarded fetuses: a longitudinal approach to the assessment of fetal well being. Early Hum Dev. 1993;31(3):195-208.
67. Vindla S, James DK, Sahota DS, et al. Computerised analysis of behaviour in normal and growth-retarded fetuses. Eur J Obstet Gynecol Reprod Biol. 1997;75(2): 169-75.
68. Bekedam DJ, Mulder EJ, Snijders RJ, et al. The effects of maternal hyperoxia on fetal breathing movements, body movements and heart rate variation in growth retarded fetuses. Early Hum Dev. 1991;27(3):223-32.
69. Andonotopo W, Kurjak A. The assessment of fetal behavior of growth restricted fetuses by 4D sonography. J Perinat Med. 2006;34:471-8.
70. Konstantinidou A, Anninos H, Spanakis N, et al. Transplacental infection of Coxsackievirus B3 pathological findings in the fetus. J Med Virol. 2007;79(6):754-7.
71. Craig S, Permezel M, Doyle L, et al. Perinatal infection with Listeria monocytogenes. Aust N Z J Obstet Gynaecol. 1996;36(3):286-90.
72. Goldstein I, Romero R, Merrill S, et al. Fetal body and breathing movements as predictors of intraamniotic infection in preterm premature rupture of membranes. Am J Obstet Gynecol. 1988;159(2):363-8.
73. Del Valle GO, Joffe GM, Izquierdo LA, et al. The biophysical profile and the nonstress test: poor predictors of chorioamnionitis and fetal infection in prolonged preterm premature rupture of membranes. Obstet Gynecol. 1992;80(1):106-10.
74. Palmer FB. Strategies for the early diagnosis of cerebral palsy. J Pediatr. 2004;145:S8-11.
75. Kurjak A, Pooh RK, Tikvica A, et al. Assessment of Fetal Neurobehavior By 3D/4D Ultrasound. In: Pooh RK, Kurjak A (Eds). Fetal neurology. New Delhi: Jaypee Brothers; 2009. pp. 221-87.
76. Kurjak A, Azumendi G. The Fetus in Three Dimensions. Imaging, Embryology and Fetoscopy. London: Informa Healthcare; 2007.
77. Campbell S, Lees C, Moscoso G, et al. Ultrasound antenatal diagnosis of cleft palate by a new technique the 3D reverse face view. Ultrasound Obstet Gynecol. 2005;25:12-8.
78. Gosselin J, Gahagan S, Amiel-Tison C. The Amiel-Tison neurological assessment at termconceptual and methodological continuity in the course of follow up. Mental Retardation and Developmental Disabilities Research Reviews. 2005;11:34-51.
79. Amiel-Tison C. Update of the Amiel-Tison Neurological assessment for the term neonate or at 4 weeks corrected age. Pediatr Neurol. 2002;27:196-212.
80. Volpe JJ (Ed). Neurological examination Normal and abnormal fetuses. Neurology of the newborn, 4th edition. Philadelphia: WB Saunders; 2001. p. 127.
81. Stahlmann N, Hrtel C, Knopp A, et al. Predictive value of neurodevelopmental assessment versus evaluation of general movements for motor outcome in preterm infants with birth weights <150g. Neuropediatrics. 2007;38:91-9.

82. Stanojevic M, Kurjak A. Continuuity Between Fetal and Neonatal Neurobehavior. In: Pooh RK, Kurjak A (Eds). Fetal neurology. New Delhi: Jaypee Brothers; 2009. pp. 405-29.
83. Hadders-Algra M. General movement during prenatal and early postnatal life. In: Kurjak A, Azumendi G. The Fetus in Three Dimensions Imaging, Embryology, and Fetoscopy. UK: Informa Health Care; 2007.
84. Cioni G, Prechtl HFR, Ferrari F, et al. Which better predicts later outcome in full term infants quality of general movements or neurological examination? Early Hum Dev. 1997;50:71-85.
85. Einspieler C, Prechtl HFR, Bos AF, et al. Prechtl's method on the qualitative assessment of general movements in preterm, term and young infants. London: Mac Keith Press; 2004.
86. Einspieler C, Prechtl HFR. Prechtl's assessment of general movements. A diagnostic tool for the functional assessment of the young nervous system. Ment Retard Dev Disabil Res Rev. 2005;11:6-17.
87. Hadders Algra M. General movements a window for early, identification of children at high risk of developmental disorders. J Pediatr. 2004;145:S128.
88. Einspieler C, Prechtl HFR, Bos AF, et al. Prechtls method on the qualitative assessment of general movements in preterm, term and young infants. Cambridge: Mac Keith Press; 2004.
89. Hadders-Algra M, Klip Van den Niewcendijk WJ, Martijn A, et al. Assessment of general movements towards a better understanding of a sensitive method to evaluate brain function in young infants. Dev Med Child Neurol. 1997;39:89-9.
90. Amiel-Tison A, Gosselin J, Kurjak A. Neurosonography in the second half of fetal life a neonatologists point of view. J Perinat Med. 2006;34:437-46.
91. Groen SE, de Blecourt AC, Postema K, et al. General movements in early infancy predict neuromotor development at 912 years of age. Dev Med Child Neurol. 2005;47:731-8.
92. Hepper PG. Fetal habituation another Pandoras box? Dev Med Child Neurol. 1997;39:27-48.
93. Stanojevic M, Kurjak A, Andonotopo W. Assessment of fetal to neonatal behavioral continuity by 4D ultrasonography. Ultrasound Obstet Gynecol. 2006;28:3-60.
94. Kurjak A, Miskovic B, Stanojevic M, et al. New scoring system for fetal neurobehavior assessed by three- and four-dimensional sonography. J Perinat Med. 2008;36:73-81.
95. Yigiter AB, Kavak ZN. Normal standards of fetal behavior assessed by four-dimensional sonography. J Matern Fetal Neonatal Med. 2006;19:707-21.
96. Amiel-Tison C. Neurological assessment of the neonate revisiteda personal view. Dev Med Child Neurol. 1990;32:1105-13.
97. Amiel-Tison C, Gosselin J. Neurological development from birth to six years. Baltimore: Johns Hopkins University Press; 2001.
98. Kurjak A, Abo-Yaqoub S, Stanojevic M, et al. The potential of 4D sonography in the assessment of fetal neurobehavior multicentric study in high-risk pregnancies. J Perinat Med. 2010;38:77-82.
99. Miskovic B, Vasilj O, Stanojevic M, et al. The comparison of fetal behavior in high risk and normal pregnancies assessed by four dimensional ultrasound. J Matern Fetal Neonatal Med. 2010;23:146114-67.
100. Talic A, Kurjak A, Ahmed B, et al. The potential of 4D sonography in the assessment of fetal behavior in high risk pregnancies. J Matern Fetal Neonatal Med; 2010.
101. Kurjak A, Ahmed B, Abo-Yaguab S, et al. An attempt to introduce neurological test for fetus based on 3D and 4D-sonography. Donald School J Ultrasound Obstet Gynecol. 2008;2:29-44.
102. Kurjak A, Tikvica Luetic A, Stanojevic M, et al. Further experience in the clinical assessment of fetal neurobehavior. Donald School J Ultrasound Obstet Gynecol. 2010;4:59-71.

CHAPTER 38

Ultrasound-Guided Fetal Invasive Procedures

Aris J Antsaklis, George A Partsinevelos

INTRODUCTION

The tremendous advances in fetal diagnosis recorded during the last four decades are undoubtedly attributed to the introduction of ultrasonography in fetal imaging. Development of high resolution ultrasound equipment combined with increasing operator expertise allows early detection and accurate diagnosis of many congenital fetal anomalies. Ultrasound-guided invasive procedures integrate prenatal diagnostic sequel and also serve in *in utero* management of selected cases of fetal malformations.

In this context, amniocentesis, chorionic villus sampling (CVS) and fetal blood sampling (FBS) have been adequately evaluated in both singleton and multiple pregnancies and have long been applied in the clinical practice. The inception of celocentesis a few years ago initially in animal models and later in humans might represent an alternative technique for prenatal diagnosis and potentially a mean for *in utero* gene therapy in immunoincompetent embryos. Ultrasound-guided fetal diagnosis through fetal biopsy and fetal therapy for anemia, thrombocytopenia, obstructive uropathy, pleural effusion, congenital diaphragmatic hernia (CDH), congenital heart defects have also been applied with either acceptable or promising results in selected cases. Finally, interventions in twin-to-twin transfusion syndrome (TTTS), multifetal pregnancy reduction (MFPR) and selective feticide have been successfully accomplished through sonographic guidance.

AMNIOCENTESIS

Introduction

Amniocentesis defined as the transabdominal aspiration of amniotic fluid is traditionally considered the oldest invasive procedure in pregnancy. It was first applied therapeutically to drain excess amniotic fluid in a woman with polyhydramnios at the end of the 19th century.[1] For diagnostic reasons it was first used in 1950s to determine the amniotic composition in cases of rhesus isoimmunization[2] and later in fetal sex diagnosis by the identification of Barr bodies in noncultured amniocytes.[3] However, amniocentesis for genetic diagnosis through fetal karyotype determination in amniotic fluid cell culture was not applied before mid 1960s.[4] In the late 1960s and early 1970s, this procedure was reserved only for the highest risk patients in the tertiary setting.[5,6] Thenceforth, amniocentesis has been increasingly used as an invaluable diagnostic tool in prenatal invasive screening for fetal chromosomal abnormalities and diagnosis of congenital fetal metabolic or enzymatic diseases, evaluation of the severity of hemolytic disease, assessment of fetal lung maturity and diagnosis of endometrial infections. Furthermore, its role in evacuation of hydramnios and infusion of drugs into the amniotic cavity has been validated.

Indications

The main indication for amniocentesis is fetal karyotyping to exclude numerical and structural chromosomal aberrations. Although traditionally

advanced maternal age (≥35 years) suggested genetic screening with amniocentesis, it is currently stated that maternal age itself should no longer be used as a cut-off to discern pregnant women at those who should be offered noninvasive screening tests (ultrasound and maternal serum biochemistry) versus those who should undergo invasive diagnostic tests (amniocentesis or CVS). Currently, it is recommended that all pregnant women, regardless of age, should be offered noninvasive screening for chromosomal abnormalities before 20 weeks of gestation and those identified with increased risk of carrying an abnormal fetus should be referred for invasive genetic screening. However, all pregnant women irrespectively of age should have the option of invasive testing on maternal request.[7] Furthermore, history of previous fetal aneuploidy, parental balanced translocation and an ambiguous result from a previous test, such as placental mosaicism in CVS represent indications for amniocentesis. Fetal karyotype is examined either in cultured amniotic fluid cells or with polymerase chain reaction (PCR) technology. The result of the latter technique however should always be confirmed with cell culture.

Amniocentesis also serves in the diagnosis of genetic diseases in the fetus. Beta-thalassemia, cystic fibrosis and hemophilia can be accurately identified through deoxyribonucleic acid (DNA) analysis using fluorescent labeled in situ hybridization (FISH). In the past, some metabolic diseases and other pathologic conditions, such as cystic fibrosis and congenital adrenal hyperplasia, were diagnosed using determination of relevant enzymes in the amniotic fluid. In the new era, DNA analysis has replaced this approach ensuring accurate detection of gene mutation in fetal cells collected through amniocentesis.

Quantitative and qualitative characteristics of the amniotic fluid can be used in fetal lung maturity assessment. Lecithin: sphingomyelin ratio, phosphatidylglycerol determination, foam stability index, fluorescent polarization test for surfactant: albumin ratio measurement, lamellar bodies detection in the amniotic fluid and other tests may indirectly estimate the risk of respiratory distress syndrome in the neonate. However, amniocentesis is rarely used for fetal pulmonary maturity evaluation nowadays, as advances in neonatal care and accuracy in the determination of gestational age early in pregnancy with ultrasonography have limited its necessity.

Congenital fetal infection with toxoplasma gondii, cytomegalovirus, rubella, etc. can be ruled out in the case of maternal infection accompanied by seroconversion via amniocentesis and application of PCR-based technologies in the amniotic fluid. Moreover, Gram's stain microscopy and culture of the amniotic fluid may help towards identification of the bacterial agent responsible for premature rupture of membranes (PROM) and preterm labor in case of underlying chorioamnionitis.

Several indications for amniocentesis used in the past are not valid nowadays. For example, the severity of fetal hemolytic anemia in the cases of rhesus isoimmunization was traditionally assessed using amniotic fluid spectrophotometry. This practice has been abandoned since middle cerebral artery (MCA) Doppler velocimetry offers a noninvasive alternative approach in the evaluation of fetal hemolysis and anemia.

Finally, fetal therapy can be applied using amniocentesis. Polyhydramnios in singleton pregnancies and twin oligohydramnios-polyhydramnios sequence (TOPS) in monochorionic twin pregnancies complicated by twin-to-twin transfusion syndrome (TTTS) can be treated with serial drainage of excess amniotic fluid (amnioreduction). On the contrary, severe oligohydramnios has been managed with amnioinfusion, although further evaluation of the indications and outcome of this technique is needed. Furthermore, infusion of various drugs in the amniotic cavity, such as thyroxine to treat fetal goitrous hypothyroidism has been achieved.

Technique

Amniocentesis for prenatal screening for chromosomal abnormalities and genetic diagnosis of congenital diseases is ideally performed between 15 and 18 weeks of gestation.[8] Early application at 11 to 14 weeks has been associated with increased risk of fetal loss, amniotic fluid leakage and fetal talipes equinovarus and thus is not recommended.[9]

The procedure is preceded by a detailed ultrasound examination of the pregnancy, which includes the determination of the number of gestational sacs and fetuses, mapping of fetuses and placentas in case of multiple pregnancy, assessment of cardiac function, gestational age, amniotic fluid volume and identification of possible fetal abnormalities. Moreover, the existence of fibroids and adnexal masses are recorded. The site for the entry of the needle is chosen preferably distally from the fetal face, the umbilical cord and the placenta. Antiseptic solution is applied on the skin and a disposable 22 G spinal needle is inserted under direct ultrasound guidance in the selected amniotic fluid pocket. The inner needle is removed and a syringe is attached to the needle hub. The first 1–2 ml of amniotic

fluid aspirated is discarded to avoid contamination with maternal cells, which might render testing inaccurate. A new syringe is attached and approximately 20 ml of amniotic fluid are drained and sent to the cytogenetic laboratory. Repeat ultrasound assessment confirms fetal heart activity and the absence of intraamniotic bleeding. Advice to rest and avoid sexual intercourse for several days and information about signs of potential postprocedure complications, such as persistent uterine cramping, fever, leakage of amniotic fluid or bleeding, are given.

In twins and higher order pregnancies, certain modifications of the technique of amniocentesis have been applied. In particular, three methods of tapping multiple sacs have been described so far. The first one, introduced in 1980, involves two or more needle insertions, one for each sac, also called the technique of double amniocentesis.[10] In particular, two or more 22-G spinal needles are separately and sequentially inserted transabdominally under ultrasound visualization into each sac and approximately 20 ml of amniotic fluid is readily aspirated. Another technique described in 1990 is the single needle insertion technique.[11] The needle entry is made into the proximal sac near the insertion of the dividing membrane and 20 ml of amniotic fluid are retrieved. After the stylet is replaced, the needle is advanced through the second sac under direct ultrasound guidance. In order to avoid contamination the first few milliliters of amniotic fluid are discarded and aspiration of 20 ml from the second sac integrates the procedure. Double simultaneous amniocentesis represents the third approach first applied in 1992.[12] Two needles are inserted separately into the amniotic sacs under ultrasound visualization and following aspiration of the amniotic fluid from the first sac, the needle is left in place indicating the sampled cavity, while the second needle is advanced into the other sac. Each of these techniques has advantages and disadvantages and finally operators' familiarity with the approach might determine the method of choice.

Complications

Amniocentesis has been proven to be a safe technique in fetal diagnosis and therapy. However, as an invasive procedure, it has been linked to a number of complications. Undoubtedly, many of them are directly influenced by the operators' experience.

Fetal loss is considered the major risk of second trimester genetic amniocentesis. It should be noted that in order to assess procedure-related risk of fetal loss, background loss rate associated with maternal age, gestational age, parity, maternal pathologic conditions (uncontrolled diabetes mellitus, severe hypertension related to lupus, etc.) and fetal anomalies (structural aberrations, karyotype abnormalities, etc.) should be taken into account.

Only one randomized controlled trial has compared the risks of amniocentesis to control so far. In this study, which was conducted in Denmark approximately 25 years ago, amniocentesis was performed at 14–20 weeks of gestation, although most procedures were performed between 16 and 18 weeks.[13] The amniocentesis group had a total fetal loss rate 1% higher than the controls (1.7% and 0.7%, respectively). Apparently, this issue cannot be objectively re-tested in this era as such a prospective randomized controlled study is impossible to be repeated due to ethical reasons.

Since then a lot of studies reported amniocentesis-related fetal loss rate between 0.2% and 0.9%.

In a retrospective study conducted in our center involving amniocentesis performed between 1990 and 2006, we found 1.25% pregnancy loss rate in 12,413 women who underwent amniocentesis versus 0.9% in 5,654 women who did not (control group), which corresponds to 0.35% excess rate in the amniocentesis group, though it did not reach statistical significance (Fishers exact test $p<0.214$). Moreover, age specific analysis did not find statistical significance in the fetal loss rate between the two groups (unpublished data). Delivery rate earlier than 24, 28 and 37 weeks in the amniocentesis group was 0.2%, 0.7% and 12.8%, respectively **(Table 38.1)**.

Other complications related to amniocentesis include preterm delivery,[14] fetal injury to the amniocentesis needle,[15] rhesus alloimmunization resulting from fetomaternal hemorrhage,[16-18] neonatal respiratory

TABLE 38.1

Pregnancy outcome after amniocentesis in "Alexandra" Hospital, University of Athens, Medical School (1990-2006)

Pregnancy outcome	*(n=12,413)*
Delivery at <24 weeks	0.2%
Delivery at <28 weeks	0.7%
Delivery at <37 weeks	12.8%
Birth weight <1500 gm	1%
Cesarean section rate	43.4%
Mean gestational age at birth	38.2 week
Mean birth weight	3,370 gm
SCBU admission (>24 hrs)	1.9%

distress syndrome possibly due to postprocedure chronic oligohydramnios,[19-20] orthopedic abnormalities (talipes equinovarus, congenital dislocation and subluxation of the hip) possibly due again to oligohydramnios,[21] and usually self-limited uterine contractions, vaginal spotting (2–3%) and leakage of amniotic fluid (1%).[14]

CHORIONIC VILLUS SAMPLING

Introduction

Chorionic villus sampling performed either transcervically or transabdominally is an alternative invasive procedure for prenatal genetic diagnosis. It was first introduced in 1968 by means of transcervical route under direct visualization and later using a 4 mm hysteroscope.[22-24] Introduction of ultrasonography along with improved systems for trophoblastic tissue culture obtained with CVS, allowed increasing implementation of this technique in the routine practice. In 1983, Brambati in Milan introduced a 1.5 mm polyethylene tube with a soft stainless steel malleable obturator inserted into the 1 mm internal barrel, setting the basis for transcervical CVS till our days.[25,26] One year later, the transabdominal technique using a fine needle for villus aspiration under ultrasound guidance was described in Copenhagen.[27] In 1991, concerns regarding safety of the procedure transiently obscured its popularity. Actually, babies with limb reduction defects were born in an unacceptable high rate following the application of transabdominal CVS at 7–8 weeks of gestation in a single center.[28] Other physicians could not confirm these findings, which were probably attributed to the early gestational age the procedure had been performed in relation to the operator inexperience or the technique employed.[29] Nowadays, it is believed that the risk of limb reduction defect following CVS performed at 10 weeks or more does not exceed the background population risk.[30,31]

Indications

Chorionic villus sampling allows the examination of conception derived tissue, thus offering an alternative to amniocentesis much earlier in pregnancy. Fetal karyotype and DNA analysis for monogenic (thalassemia, cystic fibrosis, hemaophilia, Duchenne/Becker muscular dystrophy, etc.) and metabolic disorders (mucopolysacharidosis, lipidosis, amino acid and carbohydrate metabolism disorders) are the main indications of this technique.

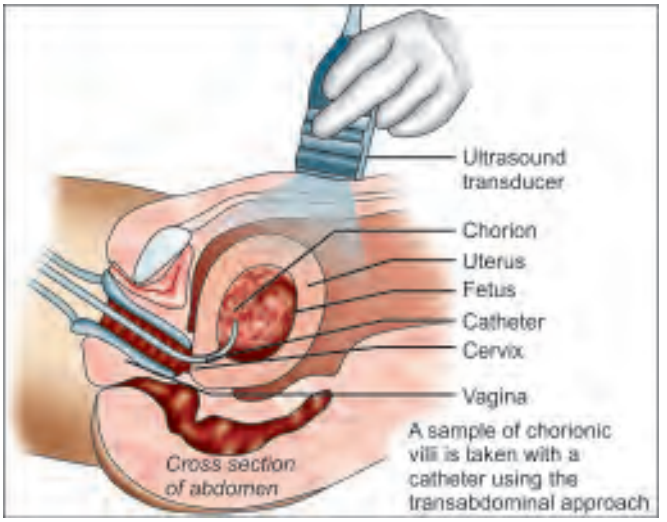

Figure 38.1: Transcervical ultrasound-guided chorionic villus sampling

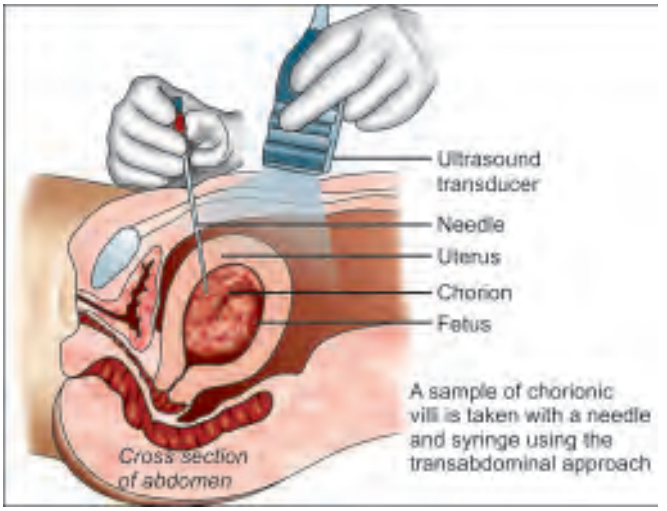

Figure 38.2: Transabdominal ultrasound-guided chorionic villus sampling

Technique

Both transcervical and transabdominal approach **(Figs 38.1 and 38.2)** have been used for CVS so far and certain advantages and disadvantages have been ascribed to each technique. Transcervical CVS is performed either by a 1.55 mm in diameter and 26 cm in length polyethylene catheter **(Fig. 38.3)** or a biopsy forceps under real time ultrasound guidance. With the woman in the lithotomy position local antisepsis is performed and the aspiration catheter or the biopsy forceps is advanced transcervically to obtain the sample. A tenaculum is occasionally required to straighten the cervical canal. A sample of 5–40 mg is considered

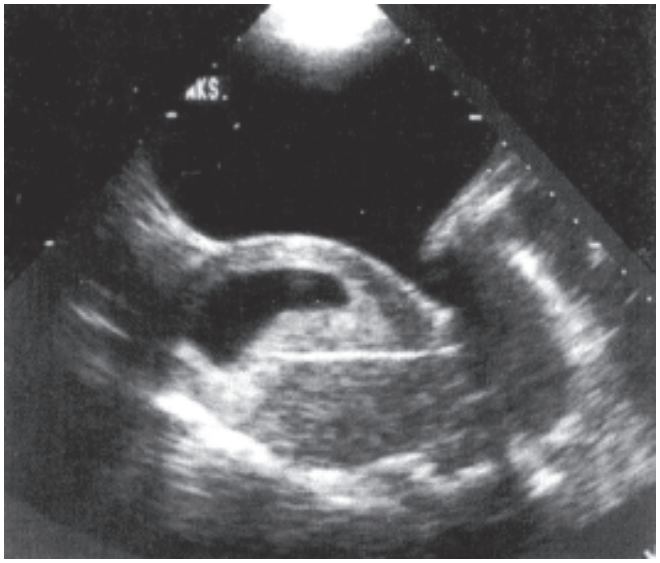

Figure 38.3: Transcervical ultrasound-guided chorionic villus sampling

sufficient for prenatal diagnosis. Technically, transcervical approach is more demanding and the "learning curve" appears to involve many cases.

Transabdominal CVS uses an aspiration needle and can be performed either with the "two-needle" or the "free hand" (or single needle) technique. The mother lies on her back and local antisepsis of the skin is performed. In the two needle technique, a 18-G 15 cm long biopsy needle guide is advanced till the placental limit, followed by a 20-22-G 20 cm long aspiration needle under ultrasound guidance. In the "free hand" technique a 20-G 9-12 cm long spinal needle is inserted percutaneously targeting the placenta. A sample of 5–40 mg is again required for diagnosis. Transabdominal CVS is technically more similar to mid-trimester amniocentesis. Maybe this is the reason for this technique being most widely adopted by physicians. However, besides operator's skill and preferences, certain parameters may dictate the method of choice. For example, posterior placental site, potential bowel adhesions and retroversion-retroflexion of the uterus may render transabdominal CVS difficult and risky, thus indicating transcervical approach.

The CVS allows early diagnosis as genetic results are feasible either within hours by direct preparations of the cytotrophoblast layer or within 3–7 days by tissue culture of chorionic villus mesenchymal core.

In twin or higher order multiple pregnancies, continuous ultrasound localization of the tip of the needle or catheter is required to assure sampling from each chorion. If in doubt, a follow-up procedure should be performed either by an immediate repeat CVS or by second trimester amniocentesis. Moreover, combination of transcervical and transabdominal approach in specific cases[32] along with the increasing experience available today can eliminate the possibility of contamination of one sample by villi belonging to the other chorion. In this context, obtaining samples adjacent to the cord insertion site or alternatively far away from the dividing membrane is reasonably recommended.

Complications

Chorionic villus sampling is currently considered a safe alternative to amniocentesis for early fetal diagnosis. It is best performed between 11 and 13 weeks of gestation. Although fears about fetal limb reduction defects emerged in mid to late 1980s after the first reports of congenital anomalies in fetuses following CVS,[33-34] it was subsequently proven that timed CVS at 10 weeks or later does not increase the background population risk.[30-31]

Fetal loss rate has not been studied through prospective randomized controlled studies so far. Most studies comparing CVS to amniocentesis have shown no statistical significance in procedure-related pregnancy loss rate.[35,36] However, a prospective randomized collaborative trial published in 1991 showed that CVS was associated with a statistical significant 4.6% greater fetal loss rate than amniocentesis.[37] Nevertheless, it is believed that this difference should be attributed to relative operator inexperience. This was confirmed by a recent systematic review, which showed a marginally higher pregnancy loss rate following CVS compared to amniocentesis (2.0% vs 1.9%).[38]

In a retrospective study conducted in our center involving 3,132 CVS performed between 1992 and 2005, we found 3.32% total pregnancy loss rate. When we analyzed CVS performed between 2000 and 2005 we found 1.7% fetal loss rate, suggesting that increasing operator experience renders the procedure safer. However, the potential contribution of technologically advanced ultrasound equipment should not be ignored **(Table 38.2)** (unpublished data).

Several factors have been associated with increased fetal loss following CVS. In 1998, Brambati et al. found a relation with maternal age more than 35 years and earlier than 8 weeks' gestation sampling (RR 2.2). However, no increased risk was shown in case of more than one needle insertions.[39] In our study, we also found an increase in fetal loss in older women (>35 years) and an association with significant per vagina bleeding early in pregnancy (RR 12.8). Nevertheless, more than one needle insertions and history of more than three miscarriages were not related to fetal loss.

TABLE 38.2
Chorionic villus sampling studies assessing procedure-related fetal loss rate

Study	*(n)*	*Maternal age*	*Mean gest. age*	*Fetal loss % (Total)*	*Fetal loss % (weeks)*	*Comments*
Hogge, 1986	1000			3.8		Mosaicism 1.7%
Papp, 2002	1044		15		5.7 2.5 (10 weeks Post-CVS)	TA and TC *† TA
Brun, 2003	4552	36	15	1.9		↑↑ mean gestational age
Caughey, 2006	9886	37.1	9-15		3.12 (at <24/40)	
Philip, 2004	1878	37	11-14		1.4 (at <28/40)	
Akhlaghpoor, 2006	1381	26.2	11+4		1.45	Losses 2 weeks post-CVS
Brambati, 1998	9365	36	10	3.01	2.69 (at <28/40)	
'Alexandra' Hospital, 1992-2005	3132	30	11+1	**3.32**	**2.88** (at <24/40) **1.7%**	1992-2005 2000-2005

* TA: Transabdominal CVS
†TC: Transcervical CVS

Self-limited vaginal bleeding and post CVS infections are also potential complications, which occur infrequently.

FETAL BLOOD SAMPLING

Introduction

Although fetal blood was initially obtained in 1972 using endoscopy during second trimester termination of pregnancy by cesarean section, the first successful transabdominal fetoscopic fetal blood sampling was performed 2 years later under ultrasound guidance.[40,41] However, the origin of the technique currently available for fetal blood sampling using a needle, which is introduced transabdominally under ultrasound visualization, goes back in 1983.[42]

Fetal blood sampling is also known as cordocentesis, omphalocentesis and percutaneous umbilical cord sampling. In the past, a frequent indication was the need for rapid chromosomal diagnosis (rapid karyotyping), inasmuch as results were offered in 2–3 days time. Today, novel molecular techniques allow rapid karyotype determination even earlier.

Currently, amniocentesis and CVS represent first line invasive diagnostic procedures for prenatal diagnosis, thus limiting fetal blood sampling's application considerably. However, the latter is indicated in case of abnormal findings in amniocentesis or CVS, which require confirmation. Moreover, rhesus isoimmunization, hydrops of unknown origin and fetal infections are some of the conditions where fetal blood sampling can be indicated. Finally, cordocentesis can be practiced in order to inject pharmacologic agents into the fetal circulation or even perform blood transfusion for severe fetal anemia.

Technique

Three different approaches for fetal blood sampling have been described so far: cordocentesis, intrahepatic fetal blood sampling and cardiocentesis. The last two are rarely used nowadays because of the higher fetal loss rate associated with them, which is estimated to be 6.2% and 5.6%, respectively.[43-45]

A detailed ultrasound examination of the pregnancy is conducted before the procedure to ensure fetal viability and assess normality of the developing fetus. Furthermore, the location of the placenta and the

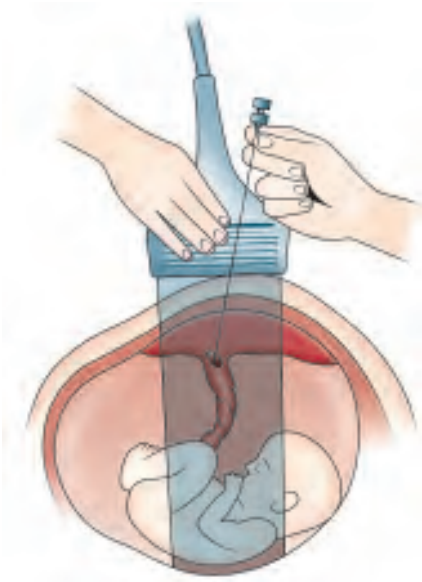

Figure 38.4: Transabdominal ultrasound-guided fetal blood sampling in case of anterior placenta

insertion site of the umbilical cord in the placenta are documented.

A 22-G spinal needle 9–15 cm in length is introduced into the amniotic cavity transabdominally under ultrasound guidance using the freehand technique. The needle-within-needle technique is rarely used nowadays. The needle is advanced towards the insertion of the umbilical cord into the placenta if possible **(Figs 38.4 and 38.5]**. This is facilitated by the anterior

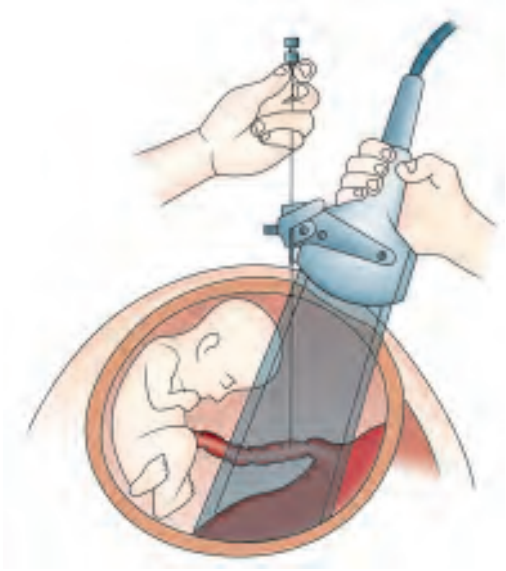

Figure 38.5: Transabdominal ultrasound-guided fetal blood sampling in case of posterior placenta

position of the placenta. No more than 4 ml and 6 ml of fetal blood should be withdrawn during the second and third trimester, respectively. The cord puncture site should be sonographically followed-up for 10 minutes to exclude bleeding or hematoma formation and fetal heart rate should be observed for 30–60 minutes following the procedure.[46]

Complications

The major concern of fetal blood sampling is fetal loss, which has been shown to be higher than other prenatal invasive diagnostic procedures frequently used, such as amniocentesis and CVS.[47] A 0.9–3.2% fetal loss rate has been recorded in previous studies. However, no randomized controlled trials have assessed this risk so far.

Bleeding at the puncture site, umbilical cord hematoma, fetal bradycardia, fetomaternal blood transfusion, preterm labor and chorioamnionitis are all potential complications of fetal blood sampling. Thus, it is prudent to reserve this procedure for cases, where the results of other noninvasive and invasive techniques were inconclusive or cordocentesis is the unique option for fetal therapy.

With regards to twin or higher order pregnancies, fetal blood sampling does not differ technically from that in singletons. In a study conducted in 2003, involving 84 twin pregnancies, mainly screened for hemoglobinopathies, the overall procedure-related fetal loss (up to 2 weeks postprocedurally) was 8.2%, about fourfold higher than the correspondence risk in singletons. However, this technique can be used as an alternative to amniocentesis after 20 weeks' gestation to confirm an abnormal karyotype in a dichorionic twin pregnancy, when selective feticide is considered a few weeks after the initial procedure.[48]

CELOCENTESIS

Introduction

Currently, first trimester screening for fetal aneuploidies and congenital diseases can be performed as early as 10 completed weeks using chorionic villus sampling (CVS). The application of this procedure earlier in pregnancy has been linked with fetal anomalies, such as limb reduction syndrome and oromandibular hypoplasia.

Undoubtedly, the earlier in pregnancy fetal diagnosis is achieved, the better for the couple in terms of earlier reassurance of a healthy pregnancy and decision making in the case of fetal aneuploidy or

congenital anomaly. Termination of pregnancy can be accomplished in first rather than second trimester of pregnancy in this case, when the complication rates are lower. Moreover, in terms of privacy, the earlier an abnormal pregnancy is terminated the lesser the chance of being widely socially recognized. However, a potential drawback is the termination of a pregnancy, which is otherwise destined to end up with a miscarriage.

In this context, celocentesis was introduced to offer diagnosis of fetal abnormalities earlier than 10 weeks of gestation. Although this approach was initially performed between 6 and 10 weeks, later it was restricted to 7–8 weeks of gestation.

Indications

Fetal sex, β-thalassemia, sickle cell anemia, Marfan syndrome detection and paternity testing are some of the initial applications of the procedure. The implementation of the technique for fetal karyotyping has not been proven successful yet and further evaluation of its role is required.[49] Difficulties in culturing celomic cells for conventional cytogenetic analysis obscure its efficacy and hinder the application of celocentesis in the clinical setting.[50]

Technique

Celomic cavity occupies the vast majority of gestational sac until 9th week of gestation **(Fig. 38.6)**. Celocentesis involves the transvaginal insertion of a 20 G needle into the celomic (extra-embryonic) cavity under ultrasound guidance and the aspiration of celomic fluid. The first 0.2 ml of fluid is discarded to avoid contamination with maternal genetic component and a sample of 1–2 ml is subsequently aspirated and sent for biochemical analysis, fetal karyotype or cytogenetic studies.

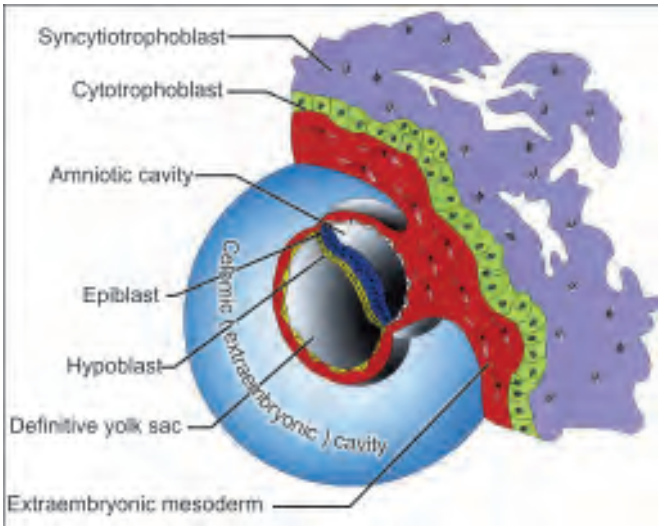

Figure 38.6: Celomic (extraembryonic cavity). The needle is inserted into the celomic (extraembryonic) cavity and 1-2 ml of celomic fluid is aspirated

Complications

A study evaluating short-term safety of celocentesis showed a 2% procedure-related fetal loss rate in women who were subjected to celocentesis 1–3 weeks before termination of pregnancy for social reasons. However, celocentesis was performed at 6–10 weeks of gestation in this study.[51]

In theory, intracelomic hemorrhage may result in fetal hypovolemia and hypoperfusion of the developing fetus. Moreover, postprocedure uterine contractions may lead to hypoxia and vasoactive agents released following intrauterine trauma may have direct action on the heart and the blood vessels.[51] Concerns of potential developmental abnormalities due to these theoretic effects have not been validated so far as no significant hemorrhage or impact in fetal heart has been shown in previous studies.[52,53] However, large scale prospective randomized controlled studies are needed to address the issue of safety of the procedure before it is widely adopted in the clinical practice.

EMBRYOSCOPY- FETOSCOPY

Introduction

Diagnosis of various fetal congenital anomalies and genetic disorders has substantially improved with the advanced resolution in ultrasonography and the guided diagnostic procedures. Sonographic and fetoscopic techniques have been used for detailed imaging studies and direct visualization of the fetus, respectively. Ultrasonoghraphy serves in fetal diagnosis in all trimesters of pregnancy, whereas fetoscopy is applied beyond 12 weeks of gestation. Earlier than 12 weeks embryoscopy can be used instead.

Historically, in late 1970s and early 1980s transabdominal fetoscopy was used during the second trimester of pregnancy for direct visualization of the external anatomy of the fetus and for fetal blood and tissue sampling. Subsequently, high resolution ultrasound imaging rendered second trimester fetoscopy obsolete. Thus, novel techniques for prenatal diagnosis emerged changing the practice in perinatal medicine.

Recent developments in the field of fiberoptics allowed the introduction of progressively smaller visualization equipments. To this end, the introduction

of embryoscopy, which allows direct inspection of the embryo earlier in the first trimester of pregnancy before 12 weeks of gestation, has drawn much interest.

During the past decade, prenatal diagnosis has increasingly moved to the first trimester of pregnancy with the application of transvaginal sonography, chorionic villus sampling, transcervical and transabdominal embryoscopy.

Transabdominal Fetoscopy

The terms embryoscopy and fetoscopy correspond to the gestational age at which pregnancy is endoscopically visualized. Although there has been a tendency to refer to embryoscopy as a synonym for the use of transcervical route and fetoscopy for transabdominal approach, we prefer to use gestational age for this terminology.

Transabdominal route for the endoscopic visualization of the fetus was first used by Mandelbaum in 1967. The endoscope carried only optical fibers and the illumination was provided by a device delivered through a second port.

In this technique, endoscopes of 1.7 mm to 3.5 mm in diameter have been used. The model we used for several years had an outer diameter of 1.7 mm (Needlescope Dyonics Inc. Woiburn USA) with an oval outer sheath of 2.2 × 2.7 mm to accommodate a working channel.

In 1980s, advances in ultrasonography allowed ultrasound-guided invasive techniques, which displaced fetoscopy for the majority of clinical purposes, including anatomic visualizations, cordocentesis and fetal tissue biopsy. Efficacy of ultrasound-guided percutaneous umbilical blood sampling (PUBS) was emphasized, particularly after the Daffos' report (1985) in which "cordocentecis" (a new technique) was performed successfully solely under ultrasound guidance for fetal blood sampling in over 600 pregnancies.[54] However, transabdominal fetoscopy is still a valid invaluable tool with certain indications, such as fetal skin sampling for the diagnosis of certain genodermatoses, liver, kidney or muscle biopsies, and laser photocoagulation of anomalous placental vessel anastomosis in severe cases of TTTS.

Transcervical Embryoscopy

Transcervical endoscopic observation of human fetus was first achieved by Westin in Sweden in 1954.[55] He used a 10 mm rigid hysteroscope to perform transcervical fetoscopy in three patients before termination of pregnancy at 16–20 weeks.

Transcervical endoscopy was first applied for the detection of congenital anomalies in the second trimester of pregnancy by Dubuisson (1979) and Roume (1985), while Gallinot (1978) suggested that the fetus could be best visualized beyond seventh week of gestation. Girardini (1991) pointed out that in order to adequately visualize the embryo, the chorionic membrane needed to be perforated. In his early work presented in Athens in 1988, Dumez (1988) performed successfully transcervical endoscopy in over 50 continuing pregnancies. Initially two pregnancies were lost, however no fetal losses were reported in his subsequent work.[56]

Cullen (1990) used a modification of the Dumez's technique to confirm congenital anomalies suspected by ultrasound during the first trimester of pregnancy.[57] The technique for first trimester transcervical embryoscopy is described as follows: the patient lies in the lithotomy position and a rigid fiberoptic endoscope 30 cm in length with a diameter of 2.0–3.5 mm and a 0° to 30° angle connected to a light source, is passed under ultrasound guidance through the cervical canal and apposed by the fetal membranes. The chorionic membrane is penetrated bluntly by a rapid thrust and the tip of the endoscope enters the celomic cavity leaving the amniotic sac intact. The yolk sac and the placenta are directly visualized. The embryo can be observed through the transparent amniotic membrane and structural defects of the head, neck and limbs are expected to be diagnosable with embryoscopy in early pregnancy. Because of the wide-in-diameter endoscope used, images are very clear and is rarely impossible to obtain a complete anatomic survey of the fetus. In contrast to midtrimester transabdominal fetoscopy, the wide angle lens and the small size of the embryo during embryoscopy often permit visualization of the embryo in total.

Limitations include trauma to fetal membranes as a result of the relatively large bore of the endoscope, bleeding especialy in cases of placenta previa and potential infection. Another drawback is the potential rupture of the amniotic membrane. Finally, severely anteverted or retroverted uterus may be inaccessible to the endoscope. Due to procedure-related limitations, there is no quite eagerness to offer this procedure to patients at risk for congenital anomalies in ongoing pregnancies.

Thus, transcervical embryoscopy was replaced by the less traumatic and more practical transabdominal approach.

Transabdominal Embryoscopy

Considering the limitations of transcervical embryoscopy, in 1993 Quintero developed a transabdominal

endoscopic technique to visualize the embryo in the first trimester of pregnancy with the use of the new submillimetric fiberoptic endoscopes.[58] These endoscopes are of such a small diameter that they can be passed through the lumen of a thin needle.

The endoscope is percutaneously introduced into the amniotic cavity through the uterine wall mimicking amniocentesis' technique. The eyepiece of the endoscope is attached to a video camera and the procedure is watched on a video monitor and recorded for subsequent review. During the procedure, successful visualization of both eyes, nostrils, mouth, ears, anterior chest wall, umbilicus, hands and feet can be achieved.

Thus, abdominal embryoscopy can be performed as early as three conceptional weeks gestation and this technique is useful not only for detecting abnormalities, but also for visualizing normal milestones of embryonic development of the trunk and limbs, including complete closure of the neural tube and fully development of the hand, by the age of seven conceptional weeks.

Transabdominal embryoscopy is considered invaluable in identifying fetal anomalies nonrecognizable by ultrasound early in pregnancy and confirming others already detected ultrasonographically. An additional application of transabdominal embryoscopy is fetal tissue sampling. This application serves as a basis for further studies into diagnosis and treatment of congenital diseases early in pregnancy. If the concept of human gene therapy and stem cell transplantation becomes a reality, embryoscopy will permit accessibility to the human embryos, which are immunologically "naive" and may therefore be receptive to grafts.

Potential Applications

Current applications of the technique include accurate endoscopic description of the embryonic development **(Figs 38.7A to E)**, first trimester diagnosis of congenital anomalies and intraluminal endoscopic description of blood flow within fetal vessels in the second trimester.

Fetal Therapy

The next step in the evolution of transabdominal embryofetoscopy is fetal surgery. Fetoscopic ligation of the umbilical cord in case of TTTS or selective fetal termination has less complications and does not have the recanalization problems associated with percutaneous ultrasound-guided intraarterial injection of either thrombogenic coils or fibrin in the umbilical cord.[59]

It has been suggested that fetal cystoscopy using thin transabdominal embryoscopy is useful in the evaluation and treatment of obstructive defects of the urinary system in uteri.[60,61]

The introduction of transabdominal visualization of the embryo in the first trimester using a thin gauge

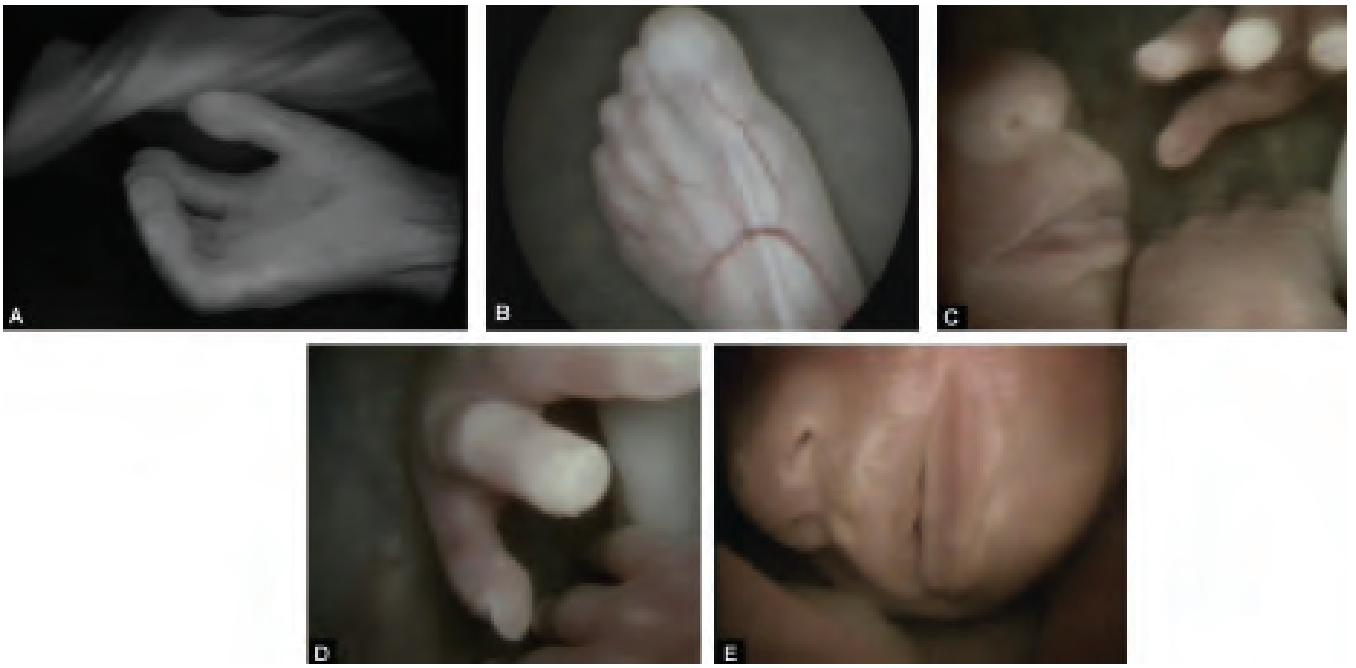

Figures 38.7A to E: Fetal imaging through fetoscopy

embryoscopy allows earlier diagnosis of congenital anomalies currently beyond the resolution of ultrasound.[62] In addition, it has the true potential of providing access to the fetal circulation at an early age, an accomplishment that would have important diagnostic and therapeutic applications. In the first and second trimesters, operative fetoscopy techniques promise to open new frontiers in the diagnosis and management of fetal surgical and medical conditions.

MULTIFETAL PREGNANCY REDUCTION AND SELECTIVE TERMINATION

The significant increase in the incidence of multiple pregnancies recorded during the last four decades is mainly attributed to the dramatic evolutions in reproductive medicine. Presently, the widespread use of ovulation induction and in vitro fertilization (IVF) techniques account for approximately two thirds of the increase in multiple gestations in Sweden, whereas the other one third results from delayed childbearing in increasingly advanced reproductive age.[63] During the last decade, a substantial effort towards reducing the number of transferred embryos in IVF/ICSI cycles has been made and there are rumors that the target of single embryo transfer at least for women with the best chance of success, is not far away. In addition, close monitoring and even cancellation of ovulation induction cycles in case of multifollicular development, serve in reducing twin or higher order multiple pregnancy rate.

There is no doubt that multifetal pregnancies are associated with prematurity and low-birth weight, which result in increased perinatal morbidity and mortality. In fact, it would appear that despite modern prenatal management, prematurity rate in multiple pregnancies has not changed during the last 50 years, although perinatal mortality rates have declined due to improved neonatal care.[64]

Cerebral palsy, a major component of perinatal morbidity, is related to preterm birth, intrauterine growth restriction (IUGR) and intrapartum complications, factors that are more common in multifetal pregnancies. In particular, the risk of cerebral palsy in twins has been estimated to be 5 times that in singletons and in triplets increases up to 17 to 20-fold. Nevertheless, antenatal death of the co-multiple *in utero* has been associated with cerebral palsy in the survived co-multiple.[65-68]

In addition to potential fetal complications, multiple pregnancies increase maternal risks. A woman carrying multiples has a higher risk of developing hypertensive disorders in pregnancy, cardiovascular and respiratory system complications. Placenta previa, placental abruption and postpartum hemorrhage are also increased in these women.[69,70]

Multifetal pregnancy reduction describes the reduction in the number of theoretically normal fetuses mainly in order to lower the likelihood of low-birth weight and premature birth. On the contrary, selective termination refers to the "reduction" of the affected fetus and is also called selective feticide, selective embryocide and selective abortion.

Multifetal Pregnancy Reduction

Introduction

Taking into account increased fetal and maternal risks, pregnant women carrying high order multiples along with their partners should be offered three options: termination of the entire pregnancy, continuation of the high-risk gestation and MFPR. The first option is not usually adopted by the couple, especially in case that the conception has been achieved through reproductive medicine technologies following a long period of infertility. The second option requires informed consent due to the potential pregnancy risks and the third aims to lower these risks and optimize the chance of a successful outcome.[71]

Technique

A meticulous ultrasound examination is considered mandatory before proceeding with MFPR. Fetal viability should be assessed and structural anomalies should be ruled out. Location of the gestational sacs and chorionicity will dictate, which fetus/fetuses should be reduced as well as the appropriate method for reduction.

Both transabdominal and transvaginal approach have been employed for this purpose. Historically, cervical dilatation and transvaginal ultrasound-guided aspiration of the gestational sacs was first used in 1986. Later, transabdominal "freehand" technique for the insertion of a 22-G 9 cm long spinal needle under direct sonographic visualization was applied. The needle targets fetal thorax and 2–3 ml of strong potassium chloride (2 mEq/ml) are injected. If cardiac activity persists for more than 2 minutes, more potassium chloride is added. A new needle insertion is required for each fetus. As a general rule, termination of more than three fetuses should be performed in two sessions one week apart. Finally, one should avoid reducing the fetus lying over the internal cervical os. The patient is followed up for one hour for the signs of uterine contractions, vaginal bleeding and leakage of amniotic

fluid, as well as a repeat ultrasound examination of the nonreduced fetuses is performed to integrate the procedure.

Multifetal pregnancy reduction is usually performed between 11–14 weeks of gestation. The cut-off of 10 weeks was set to make transabdominal accessibility of the gestational sacs and fetal thorax more feasible, to avoid reducing fetuses that are destined to spontaneous fetal loss later in pregnancy and to have the time for nuchal translucency measurement and a limited ultrasound assessment for the signs of fetal anomalies before deciding, which fetus is going to be reduced.[72,73] On the contrary the upper limit of 14 weeks has been applied to reduce the risk of pregnancy loss and premature delivery.

Some physicians recommend first trimester nuchal translucency measurement accompanied by early anomaly scan to evaluate the risk of chromosomal abnormalities in each fetus prior to MFPR. Chorionic villus sampling has been suggested if the calculated risk justifies this invasive diagnostic procedure. An alternative but less popular approach is to perform amniocentesis to the nonreduced fetuses 4 weeks post MFPR, if indicated.

Complications

Perinatal outcome of reduced twins approaches but never reaches that of spontaneous twins.[74,75] The major risk of MFPR is procedure-related pregnancy loss. It is stated that contemporaneous high resolution ultrasound combined with increasing operator experience tends to keep the overall miscarriage to an acceptable low rate.[76,77] To this end, transabdominal MFPR has almost entirely replaced the transvaginal alternative due to the lower pregnancy loss rate associated with the former (5.4% versus 12%).[76,78]

Total pregnancy loss is correlated with the initial and final number of fetuses. In a recent single center study, when more than four fetuses were reduced to twins, there was a 12.1% loss rate. The corresponding features for 4 and 3 fetuses were 5.8% and 4.5%.[77]

On the contrary, maternal complications and risk of congenital anomalies in nonreduced fetuses are not increased.

It is common sense that MFPR using intrathoracic injection of potassium chloride cannot be applied in monochorionic fetuses, as the risk of an adverse event in the nonreduced fetus is possible. Actually, 30–50% risk of death or neurological damage has been reported.[79,80] Only newly developed vasoocclusive techniques available in specific centers could be appropriate in these cases.

Reduction of Triplets to Twins

Although MFPR has been deemed as an effective technique in reducing preterm delivery and perinatal loss in quadruplets and higher order pregnancies, considerable debate exists regarding its efficacy in triplets.[81-83] Increasing knowledge and experience in dealing with multifetal pregnancies along with advances in neonatal care has improved perinatal outcome in triplets.[84,85] Furthermore, there are no randomized control trials questioning the benefit of MFPR in triplet gestations. Based on available evidence, reduction of triplets to twins significantly reduces preterm delivery and low-birth weight rate without any effect on the miscarriage rate. Thus, it is a recommended invasive procedure not only from a medical point of view, but also from an ethical perspective based on individual's autonomy, moral and religious beliefs.[86] However, it should be stressed that expectant management of trichorionic triplet pregnancies has a fairly good perinatal outcome.

Reduction to Singleton

In the vast majority of cases, the goal of MFPR is twin pregnancy. However, there are cases where singleton pregnancy is desired. No data have linked this approach with better perinatal outcome in the absence of underlying maternal cardiac disease, history of cervical incompetence, uterine abnormalities and previous preterm labor. In a recent review, the authors concluded that reduction to a singleton increases the risk of miscarriage, but overall appears to have lowest risk of preterm labor.[87]

In case of nontrichorionic triplets, reduction to singleton using a single intracardiac potassium chloride technique is a feasible option, whereas reducing one of the monchorionic fetuses using modern vasoocclusive methods, such as bipolar cord occlusion or radiofrequency ablation, will lead to a dichorionic twin pregnancy.

Selective Termination for Fetal Anomaly

Introduction

A dilemma arises in case one of the fetuses in a twin or higher order pregnancy is affected by aneuploidy or severe structural anomaly. Prospective parents need to decide the future of the pregnancy among continuing with both normal and abnormal fetuses, terminating the entire pregnancy or selectively terminating the abnormal fetus. The terms selective reduction and selective feticide of the abnormal multiple have alter-

natively been used. In selective reduction, a defective fetus is terminated, whereas a healthy one is protected at the same time.[88,89] The main difference from MFPR is that selective termination is usually performed later in pregnancy following the diagnosis of abnormal fetus.

Technique

The technique of selective termination is similar to that for first trimester MFPR. Transabdominal insertion of the needle into the fetal thorax is performed under ultrasound guidance, but the potassium chloride must be injected directly into the fetal heart. The dose of potassium chloride increases with gestational age, but rarely exceeds 3 ml.[90]

Determination of chorionicity is mandatory before the procedure, as monochorionicity in case of monochorionic twins or nontrichorionic triplets, is a contraindication for intracardiac potassium injection. Possible mechanism of postprocedure death or neurological damage of the nonreduced twin is agonal twin-to-twin blood transfusion through placental vascular anastomosis from the alive twin to the dying one. This results in hypotension and subsequent brain damage in the surviving fetus.[80,91] Vaso-occlusion techniques can be only applied in these cases. Ultrasound-guided bipolar cord occlusion, ultrasound-guided radiofrequency ablation, fetoscopic or ultrasound-guided laser coagulation, fetoscopic cord ligation and ultrasound-guided cord ligation have all been used. Radiofrequency ablation has better results in early to midpregnancy (12–23 weeks) and bipolar cord occlusion in midpregnancy (18–25 weeks). Laser coagulation is not frequently used nowadays and fetoscopic cord ligation has been rather replaced by ultrasound-guided cord ligation in advanced pregnancies (>26 weeks).

It would appear that a rational approach based on chorionicity would be summarized as follows: In dichorionic twins delayed termination of the affected fetus at 32 weeks of gestation would protect the healthy multiple of pregnancy loss. On the contrary, in monochorionic twins the earlier selective feticide takes place the better the prognosis for the unaffected twin.[87]

Complications

Although the aim of selective termination is to reduce the abnormal fetus and protect the healthy one, pregnancy loss is a recognized complication of this procedure. In a recent review of the literature, radiofrequency was associated with the lower pregnancy loss rate (14%). Corresponding features for bipolar cord occlusion, laser cord coagulation and cord ligation were 18%, 28% and 30%. Operator's experience as well as parent's preferences following informed consent should be taken into consideration in decision making.[92]

TWIN-TO-TWIN TRANSFUSION SYNDROME

Introduction

Multiple pregnancies have long been associated with increased perinatal morbidity and mortality.[93] For example, multiple births represent 3% of all deliveries, but account for 15% of preterm birth and 20% of low-weight birth (2,500 gr) neonates born in the United States.[94] Pregnancy risks are 3- to 10-fold higher in monochorionic compared to dichorionic twins[95,96] and some of them are unique for monochorionic gestations. Twin-to-Twin Transfusion Syndrome is one of them complicating 5.5–17.5% of monochorionic pregnancies.[97]

Pathophysiology

Three distinct types of anastomoses between placental vessels have been described in monochorionic placentas: arteriovenous anastomoses (AVA), arterioarterial anastomoses (AAA) and venovenous anastomoses (VVA). Arteriovenous anastomoses are deep and unidirectional **(Fig. 38.8)**. On the contrary, AAA and VVA are superficial and bidirectional, the direction of

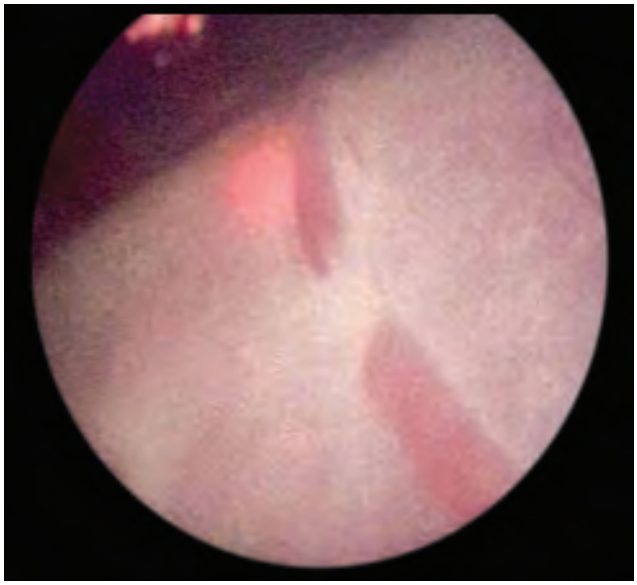

Figure 38.8: Fetoscopic aspect of arteriovenous placental anastomoses in twin-to-twin transfusion syndrome [from High risk pregnancy, management options. D. James (Ed.). 3rd edition. Philadelphia: Elsevier Saunders; 2006]

blood flow determined by the inter-vessel changes in hydrostatic pressure. The presence of AVA has been considered the cause of unbalanced blood transfusion from the "donor" to the "recipient" fetus, which in the absence of adequate AAA and VVA anastomoses can result in TTTS. Thus, AVA appear to be the causative factor, whereas AAA and to a lesser extend VVA play a significant protective role in TTTS development and progression.

Arteriovenous anastomoses are found in almost all monochorionic pregnancies and *ex vivo* placental studies have shown that they are present in all TTTS placentas, but in 84% of nonTTTS monochorionic diamniotic placentas.[98]

Intertwin unbalanced blood flow through AVA leads to hypovolemia and hypoperfusion of the donor twin, which is accompanied by elevation in renin, angiotensin II and aldosterone.[99,100] At the same time, hypervolemia and hyperperfusion of the recipient twin results in an increase in atrial natriuretic peptide (ANP) release as well as decrease in antidiuretic hormone (ADH) secretion. This sequel is responsible for oligohydramnios (stuck twin), intrauterine growth restriction (IUGR) and multiorgan malfunction in the donor, while polyhydramnios, visceromegaly, cardiac, renal failure and hydrops are observed in the recipient.[101]

Complications

Monochorionic pregnancies are considered high-risk pregnancies, mainly due to the risk of developing TTTS, which is currently considered one of the most serious perinatal complications. Actually, it has a 80–100% mortality rate and a 15–50% risk of disability, including brain damage, in survivors if left untreated.[93]

Diagnosis

Taking into account that TTTS complicates only monochorionic pregnancies along with gestational age-related limitations of ultrasound diagnostic efficacy in determining chorionicity in multiples, early ultrasound scan at 10–14 weeks' gestation is recommended in these cases. "Twin peak" or "lambda" sign as opposed to "T" sign for dichorionic and monochorionic diamniotic pregnancy respectively is diagnostic. Alternatively, intertwin membrane thickness with a cut-off of 2 mm, above which a dichorionic pregnancy is suggested, can be used. Finally, discordance in twins' gender can confirm dichorionicity.

The TTTS can develop at different gestational ages. However, it typically develops between 15 and 26 weeks.[102,103]

Sonographic features of TTTS include significant growth discordance (>20%) accompanied by polyhydramnios (maximum vertical pocket of amniotic fluid >8 cm before 20 weeks of gestation and >10 cm after 20 weeks) in the donor and oligohydramnios in recipient (maximum vertical pocket of amniotic fluid <2 cm). The donor has usually signs of IUGR, small or invisible urinary bladder, and abnormal Doppler studies in the umbilical artery. Circulatory redistribution with abnormal MCA and ductus venosus (DV) Doppler flow can be evident.

The recipient is often characterized by visceromegaly, abnormal DV Doppler studies, pulsatile flow in the umbilical vein and tricuspid regurgitation. An advanced sign of the syndrome is hydrops in the recipient.

Quintero's staging system for TTTS severity is widely used nowadays as it allows comparison of the outcome of different treatments, which help in decision making.[104]

Treatment

Amnioreduction

As twin oligohydramnios-polyhydramnios sequence (TOPS) is a common feature of multiple gestations affected by TTTS, serial amnioreduction was traditionally practiced aiming to correct uteroplacental hypoperfusion and relief maternal discomfort.[105]

A 18 G EchoTip needle is usually inserted into the polyhydramnios sac under ultrasound guidance and excess amniotic fluid is drained. Local anesthesia and/or sedation can be applied on center's preferences. A maximum vertical amniotic fluid pocket of 5–6 cm indicates the end of the procedure. Repeat of amnioreduction can be performed in the case of recurrence. Preterm premature rupture of membranes (PPROM), preterm labor, intrauterine infection and placental abruption complicates 15–20% of cases.[106] Retrospective trials have shown that serial amnioreduction results in 66% survival rate of at least one twin at the expense of 15% cerebral palsy rate.[97]

Amniotic Septostomy

This technique, also known as interventional amniotomy, employs a 20–22-G needle to create an opening between the gestational sacs under ultrasound guidance in order to equilibrate intramniotic pressures. The benefits of this approach are not quite clear nowadays. One of the drawbacks is the possibility of converting diamniotic to pseudomonoamniotic twin

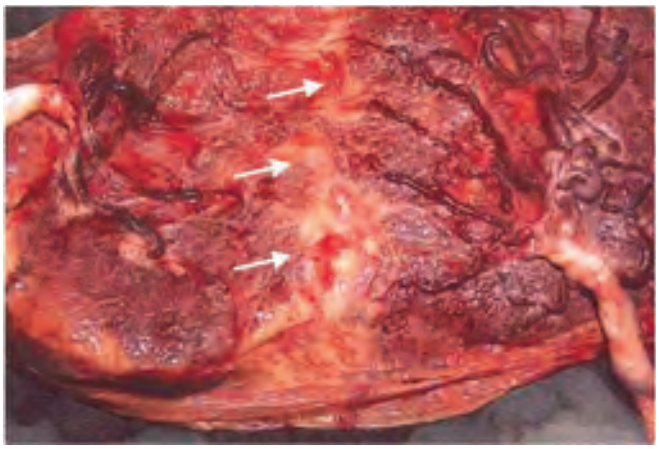

Figure 38.9: Placenta following previous laser ablation. Scars are evident. [from High risk pregnancy, management options. D James (Ed.). 3rd edition. Philadelphia:Elsevier Saunders; 2006]

pregnancy with the accompanied risks for cord entanglement and the formation of the amniotic band syndrome.[107,108] Another problem is the difficulty in assessing the syndrome's effect in the donor's renal function and also the postseptostomy inability to add laser treatment or serial amnioreduction if needed.[109] Compared to amnioreduction, septostomy seems to have similar results in terms of survival rate, although more than one procedure is usually needed with the amnioreduction approach. However, its use is not supported on an etiological basis and many physicians would probably prefer an alternative treatment option today.[110]

Laser Therapy

Pathophysiology of the syndrome justifies laser application to divide communicating vessels on the placental surface. This approach was initially performed through laparotomy and later through ultrasound-guided fetoscopy.[111] Nd:YAG or preferably diode laser can be used to perform selective or nonselective coagulation **(Fig. 38.9)**. In the selective technique only the anastomotic vessels considered responsible for the syndrome are targeted, whereas in the nonselective all superficial placental vessels approaching or crossing the intertwin membrane are ablated **(Fig. 38.10)**. However, in the majority of cases, accurate mapping and characterization of placental anastomosis is not feasible and a combination of selective and nonselective coagulation is usually performed. Subsequent amnioreduction integrates laser treatment. The selective technique has been related to higher survival rates compared to the nonselective approach.

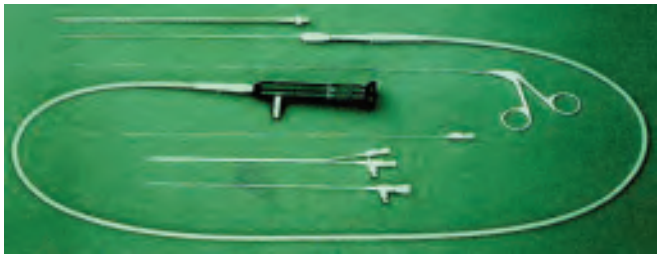

Figure 38.10: Fetoscope [from High risk pregnancy, management options. D James (Ed.). 3rd edition. Philadelphia: Elsevier Saunders; 2006]

Laser coagulation has been linked with at least one surviving fetus in 71–83% of cases[112-114] and also reduced neurological complications ranging from 5–11% compared to amnioreduction and amniotic septostomy.[115]

Selective Feticide

Selective termination of the severely affected twin can be an option to salvage the co-twin in strictly selected cases, as an overall intact survival rate of 70–80% is expected in the co-multiple.[102] Vasoocclusion techniques such as fetoscopic laser cord coagulation before 18–20 weeks or ultrasound-guided bipolar cord coagulation at advanced gestational ages may serve to this end.

Conclusion

Accumulated evidence implies that amnioreduction may suffice for Quintero stage I and II and about 20% of stage II may recede to stage I after initial treatment. For stage III laser treatment and subsequent amnioreduction may represent the best option.

FETAL BIOPSY PROCEDURES IN PRENATAL DIAGNOSIS

Introduction

Prenatal diagnostic techniques implemented in maternal-fetal medicine during the last 40 years have accomplished the detection of an increasing number of fetal anomalies. In addition to noninvasive diagnostic modalities, interventional approaches have been validated as an invaluable component of modern obstetrics. Amniocentesis, CVS and fetal blood sampling are routine prenatal tests nowadays, whereas other invasive diagnostic techniques are applied less frequent. Fetal biopsy procedures are included among them.

Fetoscopy was initially used to access the intrauterine cavity and the fetus. Nevertheless, the introduction of ultrasonography allowed safer approach of the developing embryo for diagnostic purposes. Presently, ultrasound-guided insertion of fetal biopsy needles or forceps is the preferable method for fetal tissue sampling.

Technique

Technical difficulties in accessing fetal organs for biopsy explain the long-learning curve related to this procedure. However, an experienced operator can ensure adequate fetal tissue sampling at an acceptable complication rate.

Fetal skin sampling is deemed as one of the most difficult fetal biopsy procedures in prenatal diagnosis. Kidney, muscle biopsy follows in terms of technical demands and liver sampling seems to be a relatively feasible procedure. With regards to instrumentation, both biopsy forceps and conventional needles with isometric aspiration techniques can be used depending on the tissue targeted. Care to avoid placenta should be taken, if possible. Insertion and thorough advancement of the biopsy instrument should be ultrasound guided preferably via the freehand technique. To avoid fetal movements, which may render the procedure difficult and risky, a rational approach is to enter the fetal tissue abruptly as soon as the puncture point has been determined. Anesthesia may be required only in the cases of lengthy procedures such as paracentesis of fetal pleural or pericardial effusion.[116]

Skin Biopsy

The procedure should be better performed around 20 weeks of gestation. A skin sample of at least 1 mm in thickness and 1 mm in length is recommended in order to eliminate inadequate sampling rate.[117] Both biopsy forceps and conventional needles can be used. The puncture site should be chosen based on the suspected diagnosis and if possible more than one biopsy from different skin areas should be obtained.

Liver Biopsy

Again, this procedure is better performed around 20 weeks of gestation. Liver biopsy is considered one of the most feasible *in utero* biopsy procedures due to the location, the large size and the texture of the organ. It is succeeded using 18-G biopsy needle and isometric vacuum aspiration. The needle puncture is usually performed at the external third of the right lobe for anatomical reasons.

Kidney Biopsy

A tissue sample of fetal kidney is mainly indicated in the cases of obstructive uropathy, which is diagnosed during second trimester ultrasound screening for fetal anomalies. The aim is to assess a potential detrimental effect in renal function and estimate its reversibility following prompt *in utero* intervention.

Renal function can be also assessed through analysis of urine obtained by puncture of the distended urinary tracts. Furthermore, renal biopsy can be performed at the same time.

Muscle Biopsy

Muscle biopsy is mainly indicated for the diagnosis of Duchenne's muscular dystrophy, in case DNA analysis is not adequately informative. Immunofluorescence is employed to determine the presence of dystrophine, which is absent in the disease.[118-121] External face of the thigh can be punctured using conventional 18-G needle or the sure cut method.[122-126]

Complications

Current practice implies the utilization of conventional needles for fetal biopsy procedures as they are associated with minimal risks compared to forceps inserted through trocars into the amniotic cavity.[124] Obviously, procedure-related miscarriage rate does not differ substantially than that linked to amniocentesis.

CONGENITAL DIAPHRAGMATIC HERNIA

Introduction

Embryologically, diaphragm initially appears at approximately 4 weeks of gestation and completes its development at around 8 weeks with the closure of the pleuroperitoneal canals. Failure of the septum transversum to fuse to the structures surrounding the esophagus and to connect to the pleuroperitoneal membranes results in CDH.

Congenital diaphragmatic hernia has an incidence of 1 in 2,000 to 3,000 live births.[127] In the vast majority of cases it is unilateral (95%). Eighty percent of unilateral cases involve the left side, whereas 20% are right sided.[128] In approximately, one-third of cases CDH is not an isolated malformation and co-exist with other fetal anomalies as part of genetic syndromes or chromosomal abnormalities.[129]

The diaphragmatic defect can be repaired in the newborn by primary closure or using a patch. However, the main problem is the associated developmental

deficiency of fetal lungs causing pulmonary hypoplasia and pulmonary hypertension. Therefore, *in utero* interventional procedures have been applied to prevent the consequences of CDH in fetal respiratory system.

Diagnosis

Although the defect exists since the first trimester, CDH is usually detected during second trimester anomaly scan. The severity of the anomaly is assessed using lung-to-head ratio (LHR), which corresponds to the degree of pulmonary hypoplasia. Magnetic resonance imaging has been also employed to confirm the diagnosis of herniated viscera. Fetal karyotype should be always performed in these cases to exclude aneuploidies or genetic syndromes.

Prenatal Intervention

Fetal tracheal occlusion has been shown to reverse CDH-induced pulmonary hypoplasia either by entrapping lung secretions and thereby mechanically stimulating pulmonary development or by the release of growth factors in response to intraalveolar pressure.[130] The procedure was initially performed by open fetal surgery and later endoscopy using tracheal clips.[131] However, in 2004 these techniques were replaced by percutaneous fetoscopic endoluminal tracheal occlusion (FETO) **(Figs 38.11 and 38.12)**.[132,133] An endotracheal balloon is introduced to occlude the respiratory tract fetoscopically through a single port under ultrasound guidance. The procedure is applied between 26–28 weeks of gestation and the balloon can be removed prenatally either by fetoscopy or ultrasound-guided puncture, intrapartum by *ex-utero* intrapartum therapy (EXIT) or postnatally either by tracheoscopy or percutaneous puncture.[134]

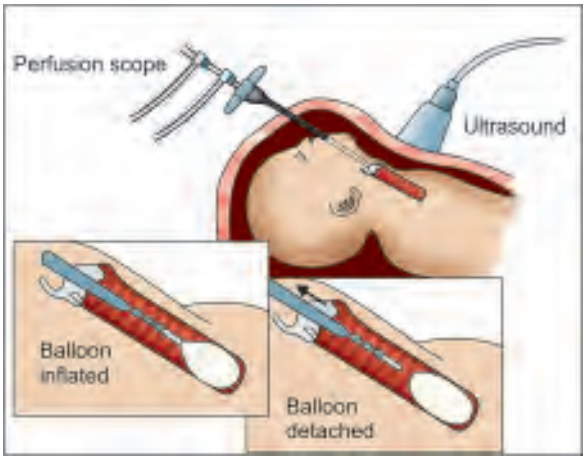

Figure 38.11: Schematically percutaneous fetoscopic endoluminal tracheal occlusion (FETO) for congenital diaphragmatic hernia

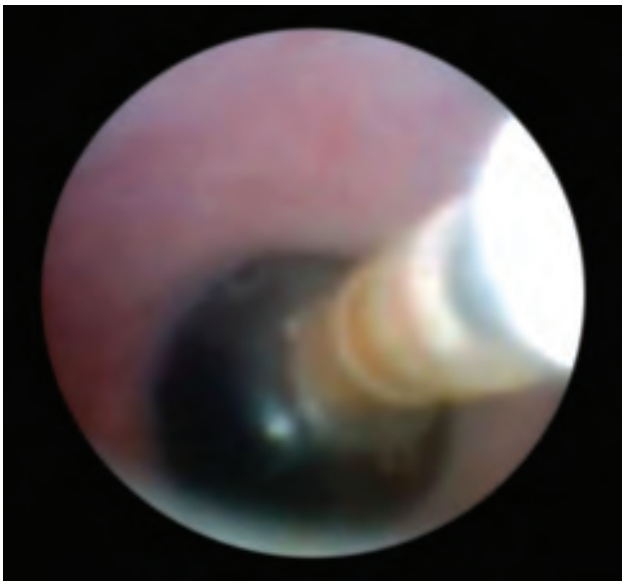

Figure 38.12: Fetoscopic image of percutaneous fetoscopic endoluminal tracheal occlusion (FETO) for congenital diaphragmatic hernia

Complications-Prognosis

Fetoscopic endoluminal tracheal occlusion is associated with the complications of fetoscopy. Concerns regarding the appropriate gestational age at which the procedure should be performed have been raised. In theory, the later FETO is performed, the less the risk of preterm birth. However, the benefit of FETO later in fetal life has not been adequately studied and current evidence dictates that it should be reserved only for milder cases.[135,136]

Although MRI can assess hepatic herniation, which has been related to the severity of the defect, prognosis of CDH is mainly based on sonographically measured lung-to-head ratio (LHR). In case of LHR, less than 15%, no chance of survival is expected, whereas in LHR of 15–25% survival reaches 15%. The LHR above 25% yields survival rates of at least 60%.[137] However, neonatal survival rates in reference centers may be as high as 80–90%.[138]

FETAL PLEURAL EFFUSION

Introduction

Fetal pleural effusion is a rare condition in fetal medicine with an estimated incidence of 1 in 10,000–

15,000 pregnancies.[139] It may be either unilateral or bilateral and according to the causative factor is characterized as primary or secondary. Primary results from lymphatic leakage in the pleural cavity and antenatally is called hydrothorax, whereas postnatally chylothorax. Secondary pleural effusion results from generalized fluid retention associated with immune or nonimmune hydrops.[139,140] In the newborn, primary pleural effusion is much more common than secondary. On the contrary, secondary is much more common in the fetus than in the neonate.

Hydrothorax can resolve or progress during pregnancy. Once progression is observed, the mediastinal shift, cardiac compression, vena cava obstruction sequel occurs and subsequent hydramnios and hydrops develop. Furthermore, pulmonary hypoplasia can result from persistent or progressive pleural effusion.

Diagnosis

Ultrasonography can accomplish prenatal diagnosis of pleural effusion as early as 15 weeks of gestation.[141] In the past, the condition was not diagnosed until the third trimester.[139] However, in more recent series the median gestational age at diagnosis was 20 weeks (range 6–35).[142]

It should be clarified that in order to define a case of pleural effusion as primary, detailed diagnostic approach similar to that for fetal hydrops should be undertaken. Investigations for congenital infections (TORCH), blood type and antibody screen, Kleihauer-Betke test, hemoglobin electrophoresis, MCA Doppler studies and fetal karyotype should be performed.[142-147] In 6–10% of cases fetal aneuploidy is expected,[148] whereas structural malformations are detected in 25% fetuses with pleural effusion.[149] Therefore, anomaly scan, including echocardiography, should focus on potential associated fetal defects.

In Utero Intervention

Expectant management and close follow-up at weekly intervals can be justified in primary small nonhydropic effusions, as spontaneous regression has been reported. However, thoracocentesis or pleuroamniotic shunting can be applied in all other cases to prevent pulmonary hypoplasia and fetal death. Drainage of pleural effusion can result in expansion of fetal lungs and resolve hydramnios and hydrops improving fetal and neonatal survival. In addition, it can allow further investigations in the aspirated fluid.

Thoracocentesis was first applied in 1982 for primary fetal hydrothorax.[150] A 20–22-G needle is introduced transabdominally under ultrasound guidance. Although it has been reported that pleural effusion can be treated with one session of thoracocentesis, which is possible to correct the underlying imbalance in fluid development, usually recurrence of the hydrothorax is expected and repeat thoracocentesis is required.[151] Thus this procedure is reserved for cases where transient decompression is combined with diagnostic evaluation of the aspirated fluid. Furthermore, it can be applied in the immediate prepartum period to facilitate neonatal respiratory function.

Pleuroamniotic shunting was initially described in 1986.[152] It involves the transabdominal introduction of a 3 mm metal trocar with a cannula into the amniotic cavity under direct ultrasound visualization. The mid-axillary line is considered the ideal site for the insertion of the trocar-cannula system into the fetal thorax. The trocar is withdrawn and a double pigtail silastic catheter is inserted into the fetal pleural cavity before the removal of the cannula in order to drain pleural fluid to the amniotic cavity. In bilateral pleural effusion, the operator should avoid double uterine puncture and an attempt to access the contralateral thoracic cavity through the same uterine trocar is recommended.

A novel approach for pleural effusion currently under evaluation is pleurodesis with the injection of the sclerosant substance OK-432 into the pleural space. The initial results are inconclusive and more studies are needed to clarify its role in hydrothorax management.[153-157]

Complications-Prognosis

Although chylothorax in the newborn is associated with mortality rate, which reaches 15%, a 53% mortality rate has been ascribed to prenatally diagnosed hydrothorax.[139] Nevertheless, secondary pleural effusion associated with hydrops has been linked to a mortality rate as high as 95%.[148]

Catheter migration and shunt obstruction are the most frequent complications of pleuroamniotic shunting.[139, 158-160]

Conclusively, in early stages of pleural effusion conservative management is considered a rational approach, as spontaneous regression of the condition is possible, whereas thoracocentesis may be performed predelivery. On the contrary, in advanced pleural effusion with hydrops, mediastinal shift and hydramnios diagnosed earlier than 36 weeks of gestation pleuroamniotic shunting is recommended. In case the diagnosis is made after 35–36 weeks thoracocentesis and prompt delivery should be the appropriate practice.[139, 161]

INTERVENTIONAL FETAL CARDIOLOGY

Introduction

Advances in fetal imaging with the use of high resolution ultrasonography, modern ultrasound techniques and increasing operator experience allows diagnosis of congenital heart defects as early as 12–14 weeks of gestation. Early identification of cardiac anomalies suggests further detailed imaging of the developing fetus in order to exclude co-existent structural defects. Furthermore, prenatal invasive genetic studies (CVS or amniocentesis) for fetal karyotyping and DNA analysis are required in these cases. The parents are informed about the prognosis of the anomaly and potential available intrauterine interventions aiming to alleviate the consequences of the anomaly to flow-dependent cardiac morphogenesis until birth. Postnatal management options of the affected child are also discussed based on current evidence. Finally, they are offered the option of terminating the pregnancy.

Currently, most of these pregnancies are terminated due to the couple's reluctance to adopt the medical, emotional and socioeconomic consequences of a child with congenital heart disease.[162] However, modern fetal echocardiography has encouraged the application of intrauterine therapy in some cardiac diseases during the last decade.[163]

Technique

Till now, intrauterine interventions for fetal cardiac defects have been performed from 20 weeks of gestation onwards.[164-170] For intracardiac stenotic lesions, transabdominal or open abdominal transuterine ultrasonography, accomplishes the introduction of a needle into the amniotic cavity and subsequently into the fetal heart. The needle facilitates the insertion of a floppy-tipped guide wire and a balloon catheter into the stenotic area and the balloon is inflated to correct the defect.

Fetoscopy assisted by concurrent transesophageal or intra-amniotic fetal echocardiography has been also employed for fetal cardiac surgery. Alternatively, open abdominal surgery with direct fetal exposure has been used, but it has been associated with high complication rates rendering this technique unacceptable for fetal cardiac intervention.[164]

Complications

Due to the lack of randomized controlled trials, the outcome of prenatal intrauterine interventions for cardiac anomalies has been assessed through case reports and case series. Uncertainties regarding the efficacy of these procedures along with their potential risks for both the fetus and the mother reserve the application of these techniques in an investigational setting. The progress of the cardiac disease later in pregnancy following successful intrauterine intervention is possible.[171] Moreover, additional postnatal procedures may be required to integrate management of the defect.[172] Conclusively, more data concerning the results of intrauterine interventions for fetal cardiac anomalies are needed before this approach is considered as a realistic option in the clinical practice.

REFERENCES

1. Von Schatz F. Gine besondere art von einseitiger polyhydramnie mit anderseitiger oligohydramnie bie eineiigen zwillingen. Arch Gynaecol. 1882;19:329.
2. Bevis DC. Composition of liquor amnii in haemolytic disease of newborn. Lancet. 1950;2(6631):443.
3. Fuchs F, Riis P. Antenatal sex determination. Nature. 1956; 177(4503):330.
4. Steele MW, Breg WR. Chromosome analysis of human amniotic-fluid cells. Lancet. 1966;1(7434)383-5.
5. Jacobson CB, Barter RH. Intrauterine diagnosis and management of genetic defects. Am J Obstet Gynecol. 1967;99(6):796-807.
6. Nadler HL, Gerbie AB. Role of amniocentesis in the intrauterine detection of genetic disorders. N Engl J Med. 1970;282(11):596-9.
7. ACOG Committee on Practice Bulletins. ACOG Practice Bulletin No. 77: screening for fetal chromosomal abnormalities. Obstet Gynecol. 2007;109(1):217-27.
8. Emery AE. Antenatal diagnosis of genetic disease. Modern Trends Hum Genet. 1970;1:267.
9. Alfirevic Z, Sundberg K, Brigham S. Amniocetesis and chorionic villus sampling for prenatal diagnosis (review) the Cochrane Collaboration. 2005.
10. Elias S, Gerbie AB, Simpson JL, et al. Genetic amniocentesis in twin gestations. Am J Obstet Gynecol. 1980;138(2):169-74.
11. Jeanty P, Shah D, Roussis P. Single-needle insertion in twin amniocentesis. J Ultrasound Med. 1990;9(5):511-7.
12. Bahado-Singh R, Schmitt R, Hobbins JC. New technique for genetic amniocentesis in twins. Obstet Gynecol. 1992;79(2):304-7.
13. Tabor A, Philip J, Madsen M, et al. Randomised controlled trial of genetic amniocentesis in 4606 low-risk women. Lancet. 1986;1(8493):1287-93.
14. Medda E, Donati S, Spinelli A, et al. Genetic amniocentesis: a risk factor for preterm delivery? Eur J Obstet Gynecol Reprod Biol EUROPOP Group CzechRepublic,EUROPOP Group Finland,EUROPOP Group France,EUROPOP Group Germany,EUROPOP Group Greece,EUROPOP Group Italy,EUROPOP Group The Netherlands,EUROPOP Group Slovak Republic,EUROPOP Group Spain,EUROPOP Group Sweden. 2003;110:153-8.

15. Seeds JW. Diagnostic mid trimester amniocentesis: how safe? Am J Obstet Gynecol. 2004;191(2):607-15.
16. Clayton EM, Layton EM, Feldhaus WD, et al. Fetal erythrocytes in the maternal circulation of pregnant women. Obstet Gynecol. 1964;23:915-9.
17. Tabor A, Bang J, NOrgaard-Pedersen B. Feto-maternal haemorrhage associated with genetic amniocentesis: results of a randomized trial. Br J Obstet Gynaecol 1987;94(6):528-34.
18. Murray JC, Karp LE, Williamson RA, et al. Rh isoimmunization related to amniocentesis. Am J Med Genet. 1983;16(4):527-34.
19. Midtrimester Amniocentesis for Prenatal Diagnosis: Safety and Accuracy.The NICHD National Registry for Amniocentesis Study Group 1976. J Am Med Assoc. 236:1471.
20. Hunter AG. Neonatal lung function following mid-trimester amniocentesis. Prenat Diagn. 1987;7(6):433-41.
21. An assessment of the hazards of amniocentesis. Report to the Medical Research Council by their Working Party on Amniocentesis. Br J Obstet Gynaecol. 1978;85 Suppl 2:1-41.
22. Mohr J. Foetal genetic diagnosis: development of techniques for early sampling of foetal cells. Acta Pathol Microbiol Scand. 1968;73(1):73-7.
23. Tietung Hospital on Ansham Iron and Steel Co, Fetal sex prediction by sex chromatin of chorionic villi cells during early pregnancy. Chin Med J. 1975:1117-26.
24. Kazy Z, Rozovsky SI, Bakharev AV. Chorion biopsy in early pregnancy: A method of early prenatal diagnosis for inherited disorders. Prenat Diagn. 1982;2:39-45.
25. Brambati B, Oldrini A, Aladerun SA. Transcervical specimen of chorionic villi in the 1st trimester of pregnancy. Pathologica. 1983;75 Suppl:179-83.
26. Simoni G, Brambati B, Danesino C, et al. Efficient direct chromosome analyses and enzyme determinations from chorionic villi samples in the first trimester of pregnancy. Hum Genet. 1983;63(4):349-57.
27. Smidt-Jensen S, Hahnemann N. Transabdominal fine needle biopsy from chorionic villi in the first trimester. Prenat Diagn. 1984;4(3):163-9.
28. Firth HV, Boyd PA, Chamberlain P, et al. Severe limb abnormalities after chorion villus sampling at 56-66 days' gestation. Lancet. 1991;337(8744):762-3.
29. Evans MI, Andriole S. Chorionic villus sampling and amniocentesis in 2008. Curr Opin Obstet Gynecol. 2008;20(2):164-8.
30. Froster UG, Jackson L. Limb defects and chorionic villus sampling: results from an international registry, 1992-94. Lancet. 1996;347(9000):489-94.
31. Kuliev A, Jackson L, Froster U, et al. Chorionic villus sampling safety. Report of World Health Organization/EURO meeting in association with the Seventh International Conference on Early Prenatal Diagnosis of Genetic Diseases, Tel-Aviv, Israel, May 21, 1994. Am J Obstet Gynecol. 1996;174(3):807-11.
32. Brambati B, Tului L, Lanzani A, et al. First-trimester genetic diagnosis in multiple pregnancy: principles and potential pitfalls. Prenat Diagn. 1991;11(10):767-74.
33. Planteydt HT, van de Vooren MJ, Verweij H. Amniotic bands and malformations in child born after pregnancy screened by chorionic villus biopsy. Lancet. 1986;2(8509):756-7.
34. Christiaens GC, Van Baarlen J, Huber J, et al. Fetal limb constriction: a possible complication of CVS. Prenat Diagn. 1989;9(1):67-71.
35. Multicentre randomised clinical trial of chorion villus sampling and amniocentesis. First report. Canadian Collaborative CVS-Amniocentesis Clinical Trial Group. Lancet. 1989;1(8628):1-6.
36. Smidt-Jensen S, Permin M, Philip J, et al. Randomised comparison of amniocentesis and transabdominal and transcervical chorionic villus sampling. Lancet. 1992;340(8830):1237-44.
37. Medical Research Council European trial of chorion villus sampling. MRC working party on the evaluation of chorion villus sampling. Lancet. 1991;337(8756):1491-9.
38. Mujezinovic F, Alfirevic Z. Procedure-related complications of amniocentesis and chorionic villous sampling: a systematic review. Obstet Gynecol. 2007;110(3):687-94.
39. Brambati B, Tului L, Cislaghi C, et al. First 10,000 chorionic villus samplings performed on singleton pregnancies by a single operator. Prenat Diagn. 1998;18(3):255-66.
40. Valenti C. Antenatal detection of hemoglobinopathies. A preliminary report. Am J Obstet Gynecol. 1973;115(6):851-3.
41. Chang H, Hobbins JC, Cividalli G, et al. In utero diagnosis of hemoglobinopathies. Hemoglobin synthesis in fetal red cells. N Engl J Med. 1974;290(19):1067-8.
42. Daffos F, Capella-Pavlovsky M, Forestier F. A new procedure for fetal blood sampling in utero: preliminary results of fifty-three cases. Am J Obstet Gynecol. 1983;146(8):985-7.
43. Nicolini U, Santolaya J, Ojo OE, et al. The fetal intrahepatic umbilical vein as an alternative to cord needling for prenatal diagnosis and therapy. Prenat Diagn. 1998;8(9):665-71.
44. Nicolini U, Nicolaidis P, Fisk NM, et al. Fetal blood sampling from the intrahepatic vein: analysis of safety and clinical experience with 214 procedures. Obstet Gynecol 1990;76(1):47-53.
45. Antsaklis AI, Papantoniou NE, Mesogitis SA, et al. Cardiocentesis: an alternative method of fetal blood sampling for the prenatal diagnosis of hemoglobinopathies. Obstet Gynecol. 1992;79(4):630-3.
46. Papantoniou N. Fetal Blood Sampling. In: Antsaklis AJ, Troyano JM (Eds). Donald School Textbook of Interventional Ultrasound. New Delhi: Jaypee Brothers Medical Publishers (P) LTD; 2008. pp. 86-99.
47. Antsaklis A, Daskalakis G, Papantoniou N, et al. Fetal blood sampling—indication-related losses. Prenat Diagn. 1998;18(9):934-40.
48. Antsaklis A, Gougoulakis A, Mesogitis S, et al. Invasive techniques for fetal diagnosis in multiple pregnancy. Int J Gynaecol Obstet. 1991;34(4):309-14.
49. Jurkovic D, Jauniaux E, Campbell S, et al. Coelocentesis: a new technique for early prenatal diagnosis. Lancet. 1993;341(8861):1623-4.

50. Makrydimas G. Celocentesis: An Alternative Technique for prenatal Diagnosis. In: Antsaklis AJ, Troyano JM (Eds). Donald School Textbook of Interventional Ultrasound New Delhi: Jaypee Brothers Medical Publishers (P) LTD; 2008. pp. 57-63.
51. Makrydimas G, Kaponis A, Skentou C, et al. Short-term safety of celocentesis for the mother and the fetus. Ultrasound Obstet Gynecol. 2002;19:243-5.
52. Lau TK, Fung TY, Wong YF, et al. A study of fetal sex determination in coelomic fluid. Gynecol Obstet Invest. 1998;45(1):16-8.
53. Lestou VS, Desilets V, Lomax BL, et al. Comparative genomic hybridization: a new approach to screening for intrauterine complete or mosaic aneuploidy. Am J Med Genet. 2000;92:281-4.
54. Daffos F, Capella-Pavlovsky M, Forestier F. Fetal blood sampling during pregnancy with use of a needle guided by ultrasound: a study of 606 consecutive cases. Am J Obstet Gynecol. 1985;153(6):655-60.
55. Westin B. Hysteroscopy in early pregnancy. Lancet. 1954;264:872.
56. Dumez Y, Oury J, Duchetel F. Embryoscopy and congenital malformations. In Proceedings of the International Conference on Chorionic Villus Sampling and early Prenatal Diagnosis Athens, Greece 1988.
57. Cullen MT, Reece EA, Whetham J, et al. Embryoscopy: description and utility of a new technique. Am J Obstet Gynecol. 1990;162(1):82-6.
58. Jeffcoate TN, Fliegner JR, Russell SH, et al. Diagnosis of the adrenogenital syndrome before birth. Lancet. 1965; 2(7412):553-5.
59. De Lia JE, Kuhlmann RS, Harstad TW, et al. Fetoscopic laser ablation of placental vessels in severe previable twin-twin transfusion syndrome. Am J Obstet Gynecol. 1995;172(4 Pt 1):1208-11.
60. Quintero RA, Hume R, Smith C, et al. Percutaneous fetal cystoscopy and endoscopic fulguration of posterior urethral valves. Am J Obstet Gynecol. 1995;172(1 Pt 1):206-9.
61. Quintero RA, Johnson MP, Romero R, et al. In-utero percutaneous cystoscopy in the management of fetal lower obstructive uropathy. Lancet. 1995;346(8974):537-40.
62. Reece EA, Homko CJ, Wiznitzer A, et al. Needle embryofetoscopy and early prenatal diagnosis. Fetal Diagn Ther. 1995;10(2):81-2.
63. Bergh T, Ericson A, Hillensjö T, et al. Deliveries and children born after in-vitro fertilisation in Sweden 1982-95: a retrospective cohort study. Lancet. 1999;354(9190):1579-85.
64. Kiely JL, Kleinman JC, Kiely M. Triplets and higher-order multiple births. Time trends and infant mortality. Am J Dis Child. 1992;146(7):862-8.
65. Pharoah PO, Cooke T. Cerebral palsy and multiple births. Arch Dis Child Fetal Neonatal Ed. 1996;75(3):F174-7.
66. Yokoyama Y, Shimizu T, Hayakawa K. Prevalence of cerebral palsy in twins, triplets and quadruplets. Int J Epidemiol. 1995;24(5):943-8.
67. Nelson KB, Ellenberg JH. Childhood neurological disorders in twins. Paediatr Perinat Epidemiol. 1995;9(2):135-45.
68. Petterson B, Nelson KB, Watson L, et al. Twins, triplets, and cerebral palsy in births in Western Australia in the 1980s. BMJ. 1993;307(6914):1239-43.
69. Lynch L, Bercowitz R. Multifetal pregnancy reduction. Ultrasonography in reproductive medicine. 1991;2:771-81.
70. Klein VR. Maternal complications associated with triplet pregnancies in triplet pregnancies and their consequences. In: Eeith L, Blickstein I (Eds). The Parthenon Publ Group; 2002.
71. Berkowitz RL, Lynch L, Chitkara U, et al. Selective reduction of multifetal pregnancies in the first trimester. N Engl J Med. 1988;318(16):1043-7.
72. Landy HJ, Keith LG. The vanishing twin: a review. Hum Reprod Update. 1998;4(2):177-83.
73. Lipitz S, Shulman A, Achiron R, et al. A comparative study of multifetal pregnancy reduction from triplets to twins in the first versus early second trimesters after detailed fetal screening. Ultrasound Obstet Gynecol. 2001;18:35-8.
74. Cheang CU, Huang LS, Lee TH, et al. A comparison of the outcomes between twin and reduced twin pregnancies produced through assisted reproduction. Fertil Steril. 2007;88:47-52.
75. Lipitz S, Uval J, Achiron R, et al. Outcome of twin pregnancies reduced from triplets compared with nonreduced twin gestations. Obstet Gynecol. 1996;87:511-4.
76. Evans MI, Berkowitz RL, RJ W, et al. Improvement in outcomes of multifetal pregnancy reduction with increased experience. Am J Obstet Gynecol. 2001;184:97-103.
77. Stone J, Ferrara L, Kamrath J, et al. Contemporary outcomes with the latest 1000 cases of multifetal pregnancy reduction (MPR). Am J Obstet Gynecol. 2008;199:406.e1-4.
78. Melgar CA, Rosenfeld DL, Rawlinson K, et al. Perinatal outcome after multifetal reduction to twins compared with nonreduced multiple gestations. Obstet Gynecol. 1991;78:763-7.
79. Pharoah PO, Adi Y. Consequences of in-utero death in a twin pregnancy. Lancet. 2000;355:1597-602.
80. Ong SS, Zamora J, Khan KS, et al. Prognosis for the cotwin following single-twin death: a systematic review. BJOG. 2006;113:992-8.
81. Evans MI, Krivchenia EL, SE G, et al. Selective reduction. Clin Perinatol. 2003;30:103-11.
82. Stone J, Eddleman K, Lynch L, et al. A single center experience with 1000 consecutive cases of multifetal pregnancy reduction. Am J Obstet Gynecol. 2002;187:1163-7.
83. Boulot P, Vignal J, Vergnes C, et al. Multifetal reduction of triplets to twins: a prospective comparison of pregnancy outcome. Hum Reprod Update. 2000;15:1619-23.
84. Lipitz S, Reichman B, Uval J, et al. A prospective comparison of the outcome of triplet pregnancies managed expectantly or by multifetal reduction to twins. Am J Obstet Gynecol. 1994;170:874-9.
85. Albrecht JL, Tomich PG. The maternal and neonatal outcome of triplet gestations. Am J Obstet Gynecol. 1996;174:1551-6.
86. Yaron Y, Bryant-Greenwood PK, Dave N, et al. Multifetal pregnancy reductions of triplets to twins: Comparison with nonreduced triplets and twins. Am J Obstet Gynecol. 1999;180:1268-71.
87. Wimalasundera RC. Selective reduction and termination of multiple pregnancies. Semin Fetal Neonatal Med. 2010;15:327-35.
88. Antsaklis A, Politis J, Karagiannopoulos C, et al. Selective survival of only the healthy fetus following prenatal

diagnosis of thalassaemia major in binovular twin gestation. Prenat Diagn. 1984;4:289-96.
89. Boulot P, Hedon B, Pelliccia G, et al. Obstetrical results after embryonic reductions performed on 34 multiple pregnancies. Hum Reprod Update. 1990;5:1009-13.
90. Evans MI, Littmann L, King M, et al. Multiple gestation: the role of multifetal pregnancy reduction and selective termination. Clin Perinatol. 1992;19:345-57.
91. Benirschke K. Intrauterine death of a twin: mechanisms, implications for surviving twin, and placental pathology. Semin Diagn Pathol. 1993;10:222-31.
92. Rossi AC, D'Addario V. Umbilical cord occlusion for selective feticide in complicated monochorionic twins: a systematic review of literature. Am J Obstet Gynecol. 2009;200:123-9.
93. Martin JA, Hamilton BE, Sutton PD, et al. Births: final data for 2003. Natl Vital Stat Rep. 2005;54:1-116.
94. Goodnight W, Newman R. Optimal nutrition for improved twin pregnancy outcome. Obstet Gynecol. 2009;114:1121-34.
95. Burn J, Corney G. Zygosity determination and the types of twinning. In: MacGillivray I, Campbell D, Thompson B (Eds). Twinning and twins. Chichester, UK: John Wiley; 1988. pp. 7-25.
96. Pasquini L, Wimalasundera RC, Fisk NM. Management of other complications specific to monochorionic twin pregnancies. Best Pract Res Clin Obstet Gynaecol. 2004;18:577-99.
97. Quintero RA. Twin-twin transfusion syndrome. Clin Perinatol. 2003;30:591-600.
98. Denbow ML, Cox P, Taylor M, et al. Placental angioarchitecture in monochorionic twin pregnancies: relationship to fetal growth, fetofetal transfusion syndrome, and pregnancy outcome. Am J Obstet Gynecol. 2000;182:417-26.
99. Van Peborgh P, Morineau G, Bussières L, et al. Twin-to-twin transfusion syndrome: polyhydramnios-associated changes in maternal plasma volume and maternal plasma aldosterone concentrations. A preliminary study. Fetal Diagn Ther. 1998;13:184-6.
100. De Paepe ME, Stopa E, Huang C, et al. Renal tubular apoptosis in twin-to-twin transfusion syndrome. Pediatr Dev Pathol. 2003;6:215-25.
101. Bajoria R, Ward S, Sooranna SR. Atrial natriuretic peptide mediated polyuria: pathogenesis of polyhydramnios in the recipient twin of twin-twin transfusion syndrome. Placenta. 2001;22:716-24.
102. El Kateb A, Ville Y. Update on twin-to-twin transfusion syndrome. Best Pract Res Clin Obstet Gynaecol. 2008;22:63-75.
103. Bebbington M. Twin-to-twin transfusion syndrome:current understanding of pathophysiology,in utero therapy and impact for future development. Seminars in Fetal and Neonatal Medicine. 2010;15:15-20.
104. Quintero RA, Morales WJ, Allen MH, et al. Staging of Twin-Twin Transfusion Syndrome. J Perinatol. 1999;19:550-5.
105. Saunders NJ, Snijders RJ, Nicolaides KH. Therapeutic amniocentesis in twin-twin transfusion syndrome appearing in the second trimester of pregnancy. Am J Obstet Gynecol. 1992;166:820-4.
106. Mari G, Roberts A, Detti L, et al. Perinatal morbidity and mortality rates in severe twin-twin transfusion syndrome: results of the International Amnioreduction Registry. Am J Obstet Gynecol. 2001;185:708-15.
107. Gilbert WM, Davis SE, Kaplan C, et al. Morbidity associated with prenatal disruption of the dividing membrane in twin gestations. Obstet Gynecol. 1991;78:623-30.
108. Gilbert WM, Davis SE, Kaplan C, et al. Morbidity associated with prenatal disruption of the dividing membrane in twin gestations. Obstet Gynecol. 1991;78:623-30.
109. Trevett T, Johnson A. Monochorionic twin pregnancies. Clin Perinatol. 2005;32:475-94.
110. Quintero R, Quintero L, Morales W, et al. Amniotic fluid pressures in severe twin-to-twin transfusion syndrome. Prenat Neonatal Med. 1998;3:607-10.
111. De Lia JE, Cruikshank DP, Keye WR. Fetoscopic neodymium:YAG laser occlusion of placental vessels in severe twin-twin transfusion syndrome. Obstet Gynecol. 1990;75:1046-53.
112. Ville Y, Hyett J, Hecher K, et al. Preliminary experience with endoscopic laser surgery for severe twin-twin transfusion syndrome. N Engl J Med. 1995;332:224-7.
113. Ville Y, Hecher K, Gagnon A, et al. Endoscopic laser coagulation in the management of severe twin-to-twin transfusion syndrome. Br J Obstet Gynaecol. 1998;105:446-53.
114. Quintero RA, Morales WJ, Mendoza G, et al. Selective photocoagulation of placental vessels in twin-twin transfusion syndrome: evolution of a surgical technique. Obstet Gynecol Surv. 1998;53:97-103.
115. Papantoniou N. Twin to twin transfusion syndrome. In: Antsaklis AJ, Troyano JM (Eds). Donald School Textbook of Interventional Ultrasound. New Delhi: Jaypee Brothers Medical Publishers (P) LTD; 2008. pp. 100-12.
116. Troyano JM, Alvarez de la Rosa, Martinez-Wallin MI. Fetal Biopsy Procedures in Prenatal Diagnosis. In: Antsaklis AJ, Troyano JM (Eds). Donald School Textbook of Interventional Ultrasound. New Delhi: Jaypee Brothers Medical Publishers (P) LTD; 2008:72-85.
117. Elias S, Emerson DS, Simpson JL, et al. Ultrasound-guided fetal skin sampling for prenatal diagnosis of genodermatoses. Obstet Gynecol. 1994;83:337-41.
118. Evans MI, Farrell SA, Greb A, et al. In utero fetal muscle biopsy for the diagnosis of Duchenne muscular dystrophy in a female fetus "suddenly at risk". Am J Med Genet. 1993;46:309-12.
119. Kuller JA, Hoffman EP, Fries MH, et al. Prenatal diagnosis of Duchenne muscular dystrophy by fetal muscle biopsy. Hum Genet. 1992;90:34-40.
120. Fanin M, Pegoraro E, Angelini C. Absence of dystrophin and spectrin in regenerating muscle fibers from Becker dystrophy patients. J Neurol Sci. 1994;123:88-94.
121. Lindahl M, Bäckman E, Henriksson KG, et al. Phospholipase A2 activity in dystrophinopathies. Neuromuscul Disord. 1995;5:193-9.
122. Benzie RJ, Ray P, ThompsonD, et al. Prenatal exclusion of Duchenne muscular dystrophy by fetal muscle biopsy. Prenat Diagn. 1994;14:235.
123. Evans MI, Hoffman EP, Cadrin C, et al. Fetal muscle biopsy: collaborative experience with varied indications. Obstet Gynecol. 1994;84:913-7.

124. Evans MI, Krivchenia EL, Johnson MP, et al. In utero fetal muscle biopsy alters diagnosis and carrier risks in Duchenne and Becker muscular dystrophy. Fetal Diagn Ther. 1995;10:71-5.
125. Evans MI, Quintero RA, King M, et al. Endoscopically assisted, ultrasound-guided fetal muscle biopsy. Fetal Diagn Ther. 1995;10:167-72.
126. Troyano JM, Padron E, Clavijo M. Fetal biopsy and puncture.Actual status. In: Balkan Ohrid's School of Ultrasound. Ohrid,Macedonia: Dobri S.Filipche; 1996. pp. 51-61.
127. Langham MR, Kays DW, Ledbetter DJ, et al. Congenital diaphragmatic hernia. Epidemiology and outcome. Clin Perinatol. 1996;23:671-88.
128. Torfs CP, Curry CJ, Bateson TF, et al. A population-based study of congenital diaphragmatic hernia. Teratology. 1992;46:555-65.
129. Witters I, Legius E, Moerman P, et al. Associated malformations and chromosomal anomalies in 42 cases of prenatally diagnosed diaphragmatic hernia. Am J Med Genet. 2001;103:278-82.
130. Gratacos E. Congenital Diaphragmatic Hermia. In: Antsaklis AJ, Troyano JM (Eds). Donald School Textbook of Interventional Ultrasound. New Delhi: Jaypee Brothers Medical Publishers (P) LTD; 2008. pp. 33-41.
131. Sydorak RM, Harrison MR. Congenital diaphragmatic hernia: advances in prenatal therapy. World J Surg. 2003;27:68-76.
132. Deprest J, Gratacos E, Nicolaides KH, et al. Fetoscopic tracheal occlusion (FETO) for severe congenital diaphragmatic hernia: evolution of a technique and preliminary results. Ultrasound Obstet Gynecol. 2004;24:121-6.
133. Gucciardo L, Deprest J, Doné E, et al. Prediction of outcome in isolated congenital diaphragmatic hernia and its consequences for fetal therapy. Best Pract Res Clin Obstet Gynaecol. 2008;22:123-38.
134. Jani JC, Nicolaides KH, Gratacós E, et al. Severe diaphragmatic hernia treated by fetal endoscopic tracheal occlusion. Ultrasound Obstet Gynecol. 2009;34:304-10.
135. Cannie MM, Jani JC, De Keyzer F, et al. Evidence and patterns in lung response after fetal tracheal occlusion: clinical controlled study. Radiology. 2009;252:526-33.
136. Deprest J, Jani J, Gratacos E, et al. Deliberately delayed and shortened fetoscopic tracheal occlusion-a different strategy after prenatal diagnosis of lifethreatening congenital diaphragmatic hernias-Repy. J Pediatr Surg. 2006;41:1345-6.
137. Deprest JA, Flemmer AW, Gratacos E, et al. Antenatal prediction of lung volume and in-utero treatment by fetal endoscopic tracheal occlusion in severe isolated congenital diaphragmatic hernia. Semin Fetal Neonatal Med. 2009;14:8-13.
138. Javid PJ, Jaksic T, Skarsgard ED, et al. Survival rate in congenital diaphragmatic hernia: the experience of the Canadian Neonatal Network. J Pediatr Surg. 2004;39:657-60.
139. Longaker MT, Laberge JM, Dansereau J, et al. Primary fetal hydrothorax: natural history and management. J Pediatr Surg. 1989;24:573-6.
140. Estoff JA, Parad RB, Frigoletto FJ, et al. The natural history of isolated fetal hydrothorax. Ultrasound Obstet Gynecol. 1992;2:162.
141. Weber AM, Philipson EH. Fetal pleural effusion: a review and meta-analysis for prognostic indicators. Obstet Gynecol. 1992;79:281-6.
142. Smith RP, Illanes S, Denbow ML, et al. Outcome of fetal pleural effusions treated by thoracoamniotic shunting. Ultrasound Obstet Gynecol. 2005;26:63-6.
143. Barron SD, Pass RF. Infectious causes of hydrops fetalis. Semin Perinatol. 1995;19:493-501.
144. Dupre AR, Morrison JC, Martin JN, et al. Clinical application of the Kleihauer-Betke test. J Reprod Med. 1993;38:621-4.
145. Achiron R, Weissman A, Lipitz S, et al. Fetal pleural effusion: the risk of fetal trisomy. Gynecol Obstet Invest. 1995;39:153-6.
146. Klam S, Bigras JL, Hudon L. Predicting outcome in primary fetal hydrothorax. Fetal Diagn Ther. 2005;20:366-70.
147. Waller K, Chaithongwongwatthana S, Yamasmit W, et al. Chromosomal abnormalities among 246 fetuses with pleural effusions detected on prenatal ultrasound examination: factors associated with an increased risk of aneuploidy. Genet Med. 2005;7:17-421.
148. Castagno R, Carreras Moratonas E, Toran N, et al. Fetal Pleural Effusion. In: Antsaklis AJ, Troyano JM (Eds). Donald School Textbook of Interventional Ultrasound. New Delhi: Jaypee Brothers Medical Publishers (P) LTD; 2008. pp. 113-25.
149. Klam S, Bigras JL, Hudon L. Predicting outcome in primary fetal hydrothorax. Fetal Diagn Ther. 2005;20:366-70.
150. Petres RE, Redwine FO, Cruikshank DP. Congenital Bilateral Chylothorax: Antepartum Diagnosis and Successful Intrauterine Surgical Management. JAMA. 1982;248:1360-1.
151. Benacerraf BR, Frigoletto FD, Wilson M. Successful midtrimester thoracentesis with analysis of the lymphocyte population in the pleural effusion. Am J Obstet Gynecol. 1986;155:398-9.
152. Seeds JW, Bowes WA. Results of treatment of severe fetal hydrothorax with bilateral pleuroamniotic catheters. Obstet Gynecol. 1996;68:57-580.
153. Okawa T, Takano Y, Fujimori K, et al. A new fetal therapy for chylothorax: pleurodesis with OK-432. Ultrasound Obstet Gynecol. 2001;18:376-7.
154. Tanemura M, Nishikawa N, Kojima K, et al. A case of successful fetal therapy for congenital chylothorax by intrapleural injection of OK-432. Ultrasound Obstet Gynecol. 2001;18:371-5.
155. Jorgensen C, Brocks V, Bang J, et al. Treatment of severe fetal chylothorax associated with pronounced hydrops with intrapleural injection of OK-432. Ultrasound Obstet Gynecol. 2003;21:66-9.
156. Chen M, Shih JC, Wang BT, et al. Fetal OK-432 pleurodesis: complete or incomplete? Ultrasound Obstet Gyneco. 2005;26:791-3.
157. Nygaard U, Sundberg K, Nielsen HS, et al. New treatment of early fetal chylothorax. Obstet Gynecol. 2007;109:1088-92.

158. Nicolaides KH, Azar GB. Thoraco-amniotic shunting. Fetal Diagn Ther. 1990;5:153-64.
159. Rodeck CH, Fisk NM, Fraser DI, et al. Long-term in utero drainage of fetal hydrothorax. N Engl J Med. 1988;319: 1135-8.
160. Weiner C, Varner M, Pringle K, et al. Antenatal diagnosis and palliative treatment of nonimmune hydrops fetalis secondary to pulmonary extralobar sequestration. Obstet Gynecol. 1986;68:275-80.
161. Cardwell MS. Aspiration of fetal pleural effusions or ascites may improve neonatal resuscitation. South Med J. 1996; 89:177-8.
162. Galindo A, Guttierrez-Larraya F, Velasco J, et al. Interventional fetal cardiology. In: Antsaklis AJ, Troyano JM (Eds). Donald School Textbook of Interventional Ultrasound. New Delhi: Jaypee Brothers Medical Publishers (P) LTD; 2008. pp. 15-34.
163. Galindo A, Guttierrez-Larraya F, de la Fuente P. Congenital heart defects in fetal life:an overview. Ultrasound Obstet Gynecol. 2004;4:194-207.
164. Kohl T. Fetal echocardiography: new grounds to explore during fetal cardiac intervention. Pediatr Cardiol. 2002;23: 334-46.
165. Kohl T, Sharland G, Allan LD, et al. World experience of percutaneous ultrasound-guided balloon valvuloplasty in human fetuses with severe aortic valve obstruction. Am J Cardiol. 2000;85:1230-3.
166. Marshall AC, van der Velde ME, Tworetzky W, et al. Creation of an atrial septal defect in utero for fetuses with hypoplastic left heart syndrome and intact or highly restrictive atrial septum. 2004;110:253-8.
167. Tworetzky W, Wilkins-Haug L, Jennings RW, et al. Balloon dilation of severe aortic stenosis in the fetus: potential for prevention of hypoplastic left heart syndrome: candidate selection, technique, and results of successful intervention. Circulation. 2004;110:2125-31.
168. Tulzer G, Arzt W, Franklin RC, et al. Fetal pulmonary valvuloplasty for critical pulmonary stenosis or atresia with intact septum. Lancet. 2002;360:1567-8.
169. Galindo A, Gutiérrez-Larraya F, Velasco JM, et al. Pulmonary balloon valvuloplasty in a fetus with critical pulmonary stenosis/atresia with intact ventricular septum and heart failure. Fetal Diagn Ther. 2006;21:100-4.
170. Quintero RA, Huhta J, Suh E, et al. In utero cardiac fetal surgery: laser atrial septotomy in the treatment of hypoplastic left heart syndrome with intact atrial septum. Am J Obstet Gynecol. 2005;193:1424-8.
171. Jouannic JM, Boudjemline Y, Benifla JL, et al. Re: in-utero intervention for hypoplastic left heart syndrome: for which fetus and for what? Ultrasound Obstet Gynecol. 2006;27:101.
172. Allen HD, Beekman RH, Garson A, et al. Pediatric therapeutic cardiac catheterization: a statement for health-care professionals from the Council on Cardiovascular Disease in the Young, American Heart Association. Circulation. 1998;97:609-25.

39
CHAPTER

Chorionic Villus Sampling

Cihat Sen

INTRODUCTION

It is now more than 40 years since amniocentesis was introduced as a diagnostic invasive procedure in the second trimester of pregnancy.[1] The chromosomal results of amniocentesis tend to be available after 18–19 weeks of gestation, making termination of pregnancy, in case of an abnormal result, very stressful. Chorionic villus sampling (CVS) can be performed as a first-trimester alternative. Traditionally, the indications for both tests have been very similar. In some European countries, more than 10% of the pregnant population undergoes invasive prenatal testing.[2] However, the combination of ultrasound and biochemical markers has changed the paradigm of antenatal screening for Down's syndrome. The proportion of pregnant women having an invasive test has been steadily declining[3] with the shift towards earlier testing and to earlier invasive test of CVS. The risk assessment may be available as early as 11–12 weeks of gestation underlining the importance of early and safe invasive tests.

Advanced maternal age, usually defined as 35 years or more, used to be the most common indication for invasive prenatal diagnosis. But since many years in various countries, this indication has been replaced by an individualized risk assessment for Down's syndrome based on maternal age, gestational age and a combination of ultrasonic and biochemical markers. Maternal age proved to be a poor indicator of invasive diagnostic testing as only about 30% of Down's syndrome fetuses were detected by offering amniocentesis or CVS. An individualized risk assessment for Down's syndrome requires a set-up capable of offering screening to all pregnant women with an invasive procedure when the estimated risk is above a certain and non-acceptable cut-off for patients. First-trimester risk assessment using the biochemical test [pregnancy-associated plasma protein A (PAPP-A) and free beta-human chorionic gonadotropin (free beta-hCG)] and nuchal translucency thickness in combination with maternal age has been shown to be very efficient with a detection rate of 90 for a 5% false-positive rate.[4] It has been possible to incorporate this policy at a national level, while maintaining detection and false-positive rates.[3]

Risk assessment for Down's syndrome has been continuously evolving and new markers, such as nasal bone, ductus venosus, tricuspid regurgitation, facial angle, minor markers for Down's syndrome in first trimester are investigated and may be incorporated into the screening algorithm.[4] Also other indications include a previous pregnancy with a chromosomal abnormality, a parent with a chromosomal abnormality or carrier of an autosomal recessive disorder and a structural fetal abnormality by ultrasound.

In multiple pregnancies, the risk of having at least one fetus with a chromosome abnormality is higher than in singleton pregnancies of the same maternal age. Before undergoing invasive testing, the pregnant woman and her partner should be informed about the option of selective termination. Data from a large collaborative study including 345 selective terminations in twins showed that the miscarriage rate of the whole pregnancy before 24 weeks was 7.0%.[5] Selective terminations before 15 weeks seemed associated with a lower risk than if the procedure were performed later in pregnancy. Therefore, CVS is an invasive procedure of choice

in twin pregnancies. If monochorionic, the figure is completely different from dichorionic in the terms of counseling for prenatal diagnosis and perinatal morbidity-mortality.

Chorionic villus sampling as a prenatal diagnostic test was first reported from China in 1975. This procedure was performed by inserting the catheter blindly into cervical canal and aspirating villi.[6] Later on, the techniques evolved into transcervically ultrasound-guided procedure. Following the transcervical approach, transabdominal ultrasound-guided technique has been introduced and has been widely being used because of the higher risk for infections and bleeding complications in transcervical sampling.[7]

Chorionic villus sampling has been mainly used to perform first-trimester prenatal diagnosis. The technique of sampling procedure is well documented. In experienced hands, CVS is safe and can be utilized as a primary prenatal diagnostic tool. Due to more technically demanding aspects of sampling, CVS has still not replaced amniocentesis in many centers. In experienced hands and well-established centers, there is a tendency of deviation from amniocentesis to CVS due to widely used first-trimester screening program for Down's syndrome and having the karyotype results earlier than amniocentesis.[3]

Prior to performing the procedure, a detailed scanning is performed to assess fetal anatomy, viability, and gestational age and to identify the location of the chorion. The presence of twins as well as other pregnancy-related pathology such as a subchorionic hematoma or coexisting anembryonic pregnancy should be identified since they could potentially change the interpretation. Preferably, the procedure should be performed after the 11th–12th weeks of gestation because some major fetal defects can be identified after this period. At the time of this examination, a detailed genetic counseling is given and the procedure is explained to the parents and discussed with them.

TECHNICAL ASPECTS OF THE PROCEDURE

Transabdominal CVS is performed like amniocentesis. After a detailed scanning and locating the chorion, the insertion site on the skin and the course of the needle to enter into chorionic tissue is defined and planned **(Figs 39.1 to 39.3)**. The skin surface is treated with antiseptic solution and a local anesthetic is injected. Trajectory of the needle should be chosen as much as parallel to the long axis of the trophoblast. The needle (20-gauge needle) is inserted into the chorionic villi (single needle technique). In some centers, double needle technique is used. With this technique, 18-gauge needle is inserted into chorionic villi and the stylet is removed. Then a smaller needle (20-gauge) with the aspirating syringe is inserted through this needle in order to obtain a sample and moderate suction is applied. Therefore, if the sample is not adequate, sampling procedure with this smaller needle, through 18-gauge needle, can be repeated if necessary. Most centers use the single needle technique. With single needle technique, a sampling path is chosen so that the tip of the needle should pass within the chorion frondosum parallel to the chorionic membrane. The tip of needle is inserted into the myometrium and then advanced into the frondosum. The needle is then redirected so that the tip will course parallel to the membrane through as much as villus tissue as possible. Insertion of the needle into the decidua or myometrium, rather than the frondosum, will result in a "gripping" feeling and in this case, adjustment of the tip back into the frondosum should be made. After placement of the tip of the needle in the chronic villi, the stylet is removed and a 20-ml syringe containing 2–3 ml of media is attached and negative pressure is applied. The needle is moved up and down four or five times in the frondosum parallel to the chorionic plate, and after that it is removed. Some operators use a biopsy guide with

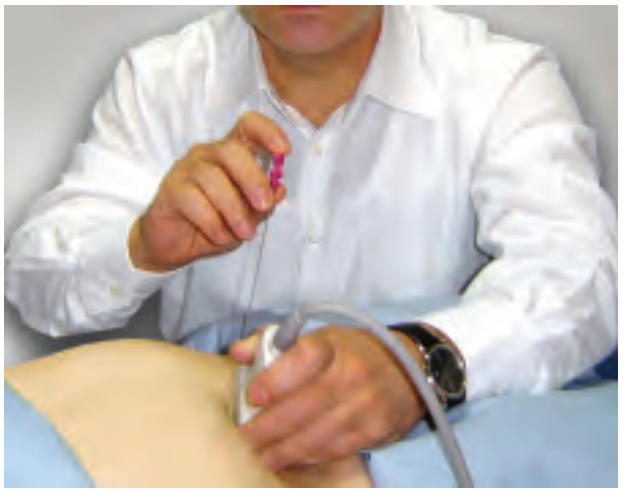

Figure 39.1: Single needle and free-hand technique

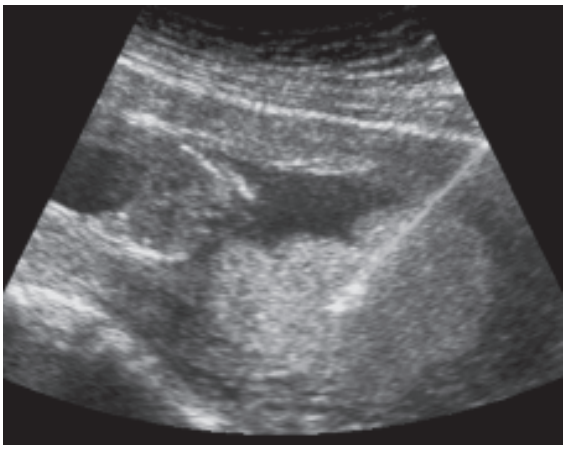

Fig. 39.2: CVS needle in the chorion frondosum

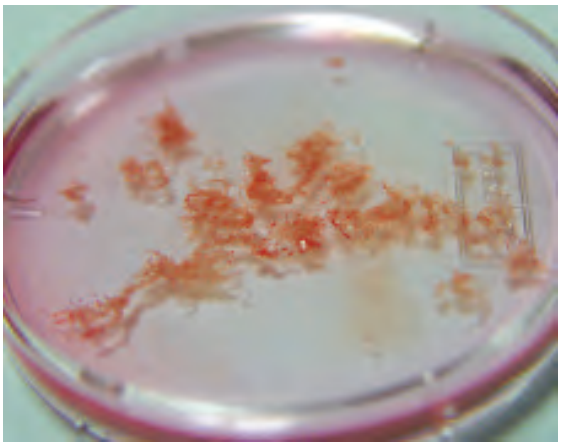

Fig. 39.3: Chorionic villi after separation

a computer-generated needle path. It is quite helpful in determining the anticipated biopsy path and in assuring correct initial needle placement. However, once the needle is within the frondosum, the guide apparatus becomes cumbersome and restricts the motion required to retrieve an adequate sample. Therefore, we do choose to use one operator-single needle technique, which is so easy and flexible technique in the experienced hand.

Both transabdominal single and double-needle techniques appear to be equally safe. The double-needle technique is theoretically less traumatic since the outer trocar remains still during sampling. It also has the advantage of allowing the operator to obtain additional villi by reinserting the sampling needle without requiring a second puncture and needling. During the learning period of operator, double-needle technique is most appropriate approach to make the sampling procedure easy and less traumatic. On the other hand, the single-needle approach is quicker, less uncomfortable, and able to retrieve adequate tissue with minimal insertions on an experienced hand.

After aspiration, the chorionic villi retrieved can be easily identified in the syringe by holding it up to a light or by putting the media in a petri dish. Operator should confirm the presence of adequate villus tissue by visual inspection. If insufficient villi are obtained on the first attempt, a second pass should be made. Pregnancy loss rates increase significantly when more than two insertions are required, and may be as high as 10% if three attempts are made.[8] Prior to performing the procedure, the patient should be evaluated carefully, the correct placental location should be confirmed and interfering contractions should be identified. Experience is important in determining which approach is preferred for an individual patient. An anteverted or midposition uterus with a posterior or anterior placenta is most easily sampled. Moreover, a retroverted uterus with an anterior placenta is also easily sampled. However, sampling of a retroverted uterus with posterior placenta is difficult. If the placenta is located on posterolateral position, CVS can be performed easily by redirection of the tip of the needle in the myometrium by the double-needle technique in experienced hand. In these difficult cases, the double-needle technique is so helpful and makes the procedure safer and quicker. In some retroverted and very rare cases, the procedure could not be possible and in this case the CVS procedure is postponed to one-week later to allow the uterus move up and the chorionic tissue grow and therefore the procedure would be possible.

Performing an atraumatic procedure can minimize the incidence of fetal loss. Operator should attempt to avoid the areas of venous lakes or slow venous flow. Direct perforation of these will frequently lead to significant postprocedure hemorrhage and hematoma formation.

Decreasing the number of needling improves pregnancy outcome. If there is a local contraction that makes the correct direction and the movement of the needle difficult, it should be waited. Passing needle parallel to the chorionic plate increases sample size by maximizing the amount of chorion frondosum sampled. Insertion perpendicular to the membrane may only result in membrane injury and also will frequently limit the amount of tissue. Accurate demarcation of the placental boundaries is mandatory. Inserting the needle too lateral to the bulk of the villus tissue will lead to sampling failure. Scanning in a transverse plane in addition to the routine sagittal plane is quite helpful in avoiding this problem. Inadvertent injury of the membranes can be avoided by continuous monitoring

of the needle tip. It should be cautioned that the tip of the needle must be imaged rather than a portion of the shaft. The operator, carefully observing the scan as the catheter is advanced, can make this differentiation. A correct view is assured if the ultrasound image of the tip moves when the catheter is advanced.

After sampling, the separation process is immediately carried out as it is very important. The chorionic villi should be carefully separated from clots, decidual or any other maternal cells and tissues if available. Villi are free-floating, white tissues with finger-like branches. Contaminating decidual tissue is more amorphous in shape, lacks branches and is usually easily differentiated from villi on gross inspection. Chorionic villus samples consist of a mixture of placental villi and maternal decidual cells and blood. Although washed and dissected, some maternal cells may remain and grow in culture but not in direct preparation. A careful dissection and use of enzymatic digestion prior to culture is required to reduce it. Then the sample is transferred to the transfer media.

In some conditions such as posterior low lying placenta and retroflexed uterus, transcervical approach can be preferred. However, after 11 weeks of gestation, chorionic tissue is reachable by transabdominal approach in experienced hand. On the other hand, delaying until this gestational age will avoid the high spontaneous miscarriage rate in earlier pregnancy.

For transcervical CVS, the patient is put in lithotomic position. After exposing the cervix, the vagina and the cervix are prepared with an iodine solution. Tenaculum is not usually necessary. A polyethylene catheter (approximately 16-gauge) with an obturator (malleable stainless steel) is directed to the trophoblastic area under ultrasound guidance. Operator should pay more attention to avoid the tip of the catheter close to the fetal membranes because of the possibility that it can rupture the membrane and the decidua, which can cause bleeding and making the procedure difficult. During this insertion procedure, the patient can feel a cramp-like pain, but anesthesia is usually not necessary. After removing the obturator, a 20-ml syringe is attached to the catheter, negative pressure is applied and then the catheter is withdrawn slowly. The sample taken is transferred into transport media and the separation process is performed, which is very important step.

COMPLICATIONS, PREGNANCY LOSS AND SAFETY

Post-procedure complications following CVS are rare. Vaginal bleeding is the most common complication, occurring in 7–10% of transcervical cases but less frequently following transabdominal CVS.[9] In up to 4% of cases, a small hematoma may be identified at the sampling site immediately following procedure.[10] Other complications such as infection and oligohydramnios occur only rarely. Infection following CVS occurs very rarely unless hematoma forms or significant tissue trauma occurs.

The procedure-related risk of pregnancy loss following chorionic villus sampling appears to be the same as midtrimester amniocentesis when performed in experienced centers. The Canadian collaborative experience (a prospective, randomized study comparing CVS to second-trimester amniocentesis), published in 1989, showed no significant increase in fetal loss following CVS when compared to midtrimester amniocentesis.[11] There were 7.6% fetal losses (spontaneous abortions, induced abortions and late losses) in the CVS group and 7.0% in the amniocentesis group. Thus an excess loss rate of 0.6% for CVS over amniocentesis was obtained; this difference was not statistically significant.

Shortly thereafter, American collaborative study showed no significant difference in loss between CVS and amniocentesis.[12] This was a prospective, non-randomized trial of over 2,200 women who chose either transcervical CVS or second-trimester amniocentesis. An excess pregnancy loss rate of 0.8% referable to CVS over amniocentesis was seen, which again was neither clinically nor statistically significant.

In contrast, a collaborative European Trial (a prospective, randomized comparison of over 3,200 pregnancies sponsored by the European MRC Working Party on the Evaluation of CVS) reported a 4.6% increased loss rate following CVS as compared to midtrimester amniocentesis.[9] This difference reflected more spontaneous deaths before 28 weeks' gestation (2.9%), more terminations of pregnancy for chromosomal anomalies (1.0%), and more neonatal deaths (0.3%) in the CVS group. After examining studies, it appears that MRC study was performed at a greater number of centers and with more practitioners than the other studies. In addition, each practitioner performed fewer procedures. Thus, it has been suggested that the relative lack of experience might have contributed to the increased loss rate in the MRC study. While the American trial consisted of 7 centers and the Canadian trial 11 centers, the European trial included 31 sampling sites. There were, on average, 325 cases per center in the United States study, 106 in the Canadian study, and only 52 in the European trial. While no significant change in pregnancy loss rate was demonstrated during the course of the European trial, the learning curve for

both transcervical and transabdominal CVS exceeds 400 or more cases.[13] Operators who have performed fewer than 100 cases may have two or three times pregnancy loss rate of operators who have performed more than 1,000 procedures.

Chorionic villus sampling was compared to early amniocentesis (prior to 14 weeks' gestation). Nicolaides and colleagues compared transabdominal CVS to amniocentesis performed between 10 and 13 weeks' gestation. In this prospective comparison, the pregnancy loss rate was significantly higher after early amniocentesis (5.3%) than after CVS (2.3%).[14] Recently, Cederholm reported their comparison of transabdominal CVS and early amniocentesis.[13,15] Spontaneous fetal loss occurred in 6.8% of the early amniocentesis and in 1.7% of the CVS group ($p < 0.05$). Nineteen per cent of the early amniocentesis patients required a second procedure due to culture and sample failure, while 5.2% of the CVS group was resampled because of ambiguous results. Present information seems to indicate that CVS is the preferred prenatal diagnostic procedure under 14 weeks' gestation.

Smidt-Jensen, one of the pioneers of transabdominal CVS, have added additional information to the safety of the procedures.[16] In a prospective, randomized study they found no difference in pregnancy loss between transabdominal CVS and second-trimester amniocentesis, but did demonstrate an increased risk for transcervical CVS.

Since last 10 years, early CVS less than 10–11 weeks of gestation is not being used due to increased risk for limb reduction.[17,18] Chorionic villus sampling has been linked to limb reduction defects. The first report identified five infants with severe limb malformations among 539 pregnancies having undergone CVS before 66 days of gestation.[17] After 10 weeks, there was no increased risk of limb reduction defects, while the evidence below 10 weeks of gestation is less substantial. Chrionic villus sampling is best avoided before 10 weeks. In exceptional circumstances, patients should be informed about a 1% or higher risk of limb reduction defects.

There has been much discussion in the literature regarding the association of CVS and fetal limb reduction following the report by Firth in 1991 of five infants born with limb reduction defects following CVS in a series of 539 women.[17] Four of the infants had the oromandibular-limb hypogenesis syndrome and one had a terminal transverse limb reduction defect. All of the CVS procedures in the affected infants were between 55 and 66 days of gestation and done by transabdominal sampling. Oromandibular-limb hypogenesis syndrome is hypothesized to be secondary to fetal vascular disruption providing a possible etiological link to CVS.

Using the Italian multicenter birth defects registry, Mastroiacovo and colleagues reported a case-control study with an odds ratio of 11:3 for transverse limb abnormalities following first-trimester CVS.[19] The cases, which were sampled prior to 70 days, had a 19.7-fold increased risk of transverse limb reduction defects, while patients sampled later did not demonstrate a significantly increased risk. Brambati and colleagues, an extremely experienced group with no increased risk of limb defects in patients sampled beyond 9 weeks, had a 1.6% incidence of severe limb reduction defects in patients sampled at 6 and 7 weeks.[10] This rate decreased to 0.1% for sampling at 8–9 weeks. Many other small series have also reported an increased incidence of limb reduction defects following CVS. The most common association seems to be with procedures performed prior to 70 days of gestation.[20]

In the cohort study published by Hsieh et al. they surveyed 78,842 deliveries in Taiwan during 1991 (one quarter of the total annual births). The incidence of severe limb defects in the general population was only 0.26 per 10,000 but was 22 per 10,000 after CVS ($P<0.001$). There are some reports in the literature in which the question continues to be debated of whether CVS sampling after 10 weeks of gestation has the potential of causing more subtle defects, such as shortening of the distal phalanx or nail hypoplasia.[21,22] On the contrary, most experienced centers performing CVS after 10 weeks have not seen an increase in limb defects of any type. Recently a review of the almost 140,000 CVS procedures reported to the World Health Organization registry demonstrated no increase in the overall incidence of limb reduction defects following CVS nor in any specific type or pattern of defects between 9 and 12 weeks of gestation.[23] In one study that was consisted of the period of 1985–1991 reported that there was not any difference between the group of transcervical CVS performed at the 10th week of gestation and the group of amniocentesis performed at the 16th week of gestation in terms of short- and long-term outcomes including limb defects and many other.[24] In another study for the period of 1986–1998 with the cases of more than 2,700 CVS procedure after 11 weeks of gestation, there were not any significant differences between the group of patients at the 11–12 weeks, 13–14 weeks and 15–20 weeks of gestation in the terms of feasibility, effectiveness and risk of prenatal diagnosis.[25] The fetal loss rates were 1.02%, 0.86% and 0.46% respectively. Thus it appears that procedures performed after 10 weeks of gestation in

experienced hands carry no increased risk of limb reduction defects.

Over 15 years of practice, Papp et al. reported their experience on CVS. They performed transcervical CVS between 1984 and 1993 and transabdominal CVS thereafter until 1999 in 1,149 cases between the 10th and 32nd gestational week. The fetal loss rate of 4.8% in the period of 1984–1993, occurring within three weeks from the date of sampling, dropped to 1.7% in the period of 1994–1999. Premature births (6.4%) and stillbirth rates (1.1%) did not exceed normal rates observed in the general population. They concluded that transabdominal CVS is a real alternative method of mid-trimester amniocentesis and it is recommended for use at any stage of the pregnancy.[26]

Transabdominal CVS should be regarded as the procedure of first choice when testing is done before 15 weeks of gestation. Alternatively second-trimester amniocentesis is safer than early amniocentesis or transcervical CVS, and is the procedure of choice for second-trimester testing.[27]

The total pregnancy loss after invasive prenatal diagnostic procedures consists of a procedure-related loss, which should be added to the background loss rates. On the other hand, the spontaneous fetal loss rate has been difficult to estimate, as large populations have not been followed from early pregnancy. Previously published attempts to ascertain spontaneous fetal losses may have been biased because of different definitions of fetal loss and follow-up, different methods to confirm the viability of pregnancy and different intervals between the ultrasound scan showing a live fetus and fetal demise.[28] The background loss rate in women in whom invasive testing may be indicated is related to maternal age, gestational age and the indication for the procedure. The risk will therefore be different for a unit serving to general population than a referral center serving a high-risk population. The background loss rate thus depends on the unit. In a randomized trial, comparing amniocentesis with ultrasonography only in the control group, the procedure-related fetal loss due to amniocentesis performed at a mean gestational age of 16 weeks was estimated to be 1.0%.[29] A number of more recently published case-control or uncontrolled studies in women at increased risk for Down's syndrome did not show an increased risk of pregnancy loss associated with second-trimester amniocentesis, but those studies often lacked sufficient power to identify small differences.[30-32] The very low procedure-related risk of 1 in 1,600 attributable to amniocentesis suggested by a study derived from the FASTER trial[33] may be due to the use of a nonrandomized control group with a source of considerable bias.[34]

The fetal loss rate following CVS has not been compared with no invasive testing in randomized studies, but was found to be comparable to the fetal loss rate after amniocentesis.[9,11,12] A Cochrane review of amniocentesis and CVS concluded that the total pregnancy loss of transabdominal CVS is comparable to that of second-trimester amniocentesis (OR: 0.90), while transcervical CVS is likely to be associated with a significantly higher risk of miscarriage (OR: 1.40).[27] Early amniocentesis performed between 9 and 14 weeks, on the other hand, was shown to carry a significantly higher risk of fetal loss than either CVS or amniocentesis performed in week 16 or later.[14,35] The most recent systematic review of the procedure-related complications of amniocentesis and CVS included 29 observational studies published after 1995 on amniocentesis and 16 studies on CVS.[34] In this review, the pregnancy loss before 24 weeks was 0.9% following amniocentesis and 1.3% following CVS with a wide variation between studies.

In the randomized trial of amniocentesis, the control group had a 0.7% rate of fetal loss from week 16, and the same rate was found in a French study of 3,472 women having amniocentesis compared to 47,004 controls.[36] The spontaneous miscarriage rate is higher following CVS than following amniocentesis, given that CVS is performed at around 12 weeks of gestation and amniocentesis at 16 weeks. Therefore, the estimated pregnancy loss rates from the systematic review[34] suggest that the procedure-related loss rate may be lower than the 1% found in the randomized trials. In a Danish national register-based cohort study, the post-procedural fetal loss rate before 24 weeks, was assessed among singleton pregnant women who had an amniocentesis (n = 32,852) or CVS (n =31,355) between 1996 and 2006.[37] The miscarriage rate after amniocentesis was 1.4% and 1.9% after CVS before 24 completed weeks. The differences between fetal loss rates following amniocentesis and CVS may be explained by the difference of background miscarriage rate in gestational age at the time of the procedures.[38] Furthermore, there does not seem to be any major difference in fetal loss rate between the two procedures.

In a study of national registry from Denmark, the postprocedural loss rate for both procedures did not change during the 11-year study period, and was not correlated with maternal age. The number of procedures for each department had a significant effect on the risk of miscarriage. In departments performing fewer than 500 amniocenteses, the odds ratio for fetal loss was 2.2 (95% CI, 1.6–3.1) when compared to departments performing more than 1,500 procedures during the 11-year period. For CVS, the risk of miscarriage was

40% greater in departments performing 500–1,000 and 1,001–1,500 as compared to the departments performing more than 1,500 procedures.

Also after the introduction of first-trimester risk assessment in Denmark during the period 2004–2006 has resulted in a shift towards CVS as a diagnostic test.[3] Restricting invasive tests to women at an increased risk changed the proportion of invasive test from 10.6 to 4.9% and has increased the number of Down's syndrome diagnosed prenatally. Despite decreasing the number of invasive test and increasing the number of Down's syndrome, the proportion of CVS has been preferred as 69% of invasive tests.

It may thus be concluded that data from randomized controlled trials as well as from systematic reviews and a large national registry study are consistent with a procedure-related miscarriage rate of 0.5–1.0% for amniocentesis as well as for CVS. In single-center studies performance may be remarkably good due to very skilled operators,[31,39] but these figures cannot be used for general counseling.

Multiple Pregnancy

The prevalence of twin pregnancy increases with maternal age and increased by assisted reproductive techniques. There has not been a screening method for chromosomal abnormalities in multiple pregnancies other than maternal age that has been used as a screening method such as older than 35 years old, until the nuchal screening was introduced as a screening method for chromosomal abnormalities in multiple pregnancies.[40] It has been possible to calculate the risk of trisomy-21 for each fetus in multiple pregnancies by using this screening method. Also by this policy, the fetal anatomy and some major fetal anomalies can be evaluated and diagnosed in first trimester that can make this pregnancy at risk for chromosomal abnormalities. Therefore, the CVS makes early prenatal diagnosis possible in multiple pregnancies as earlier. But one should remember that the fetal loss rate after CVS in twin pregnancy is high compared to amniocentesis (single entry to sample both sites at the same attempt) and about 2%. If one uses two entry and needling technique to sample in both CVS and amniocentesis, the fetal loss rate is about the same.[25,41] Therefore, the proper genetic counseling should be given to the family according to the procedure-related fetal loss rate and the risk of trisomy-21 in twin pregnancy, and then the family can make a decision based on the information available. In twin pregnancy, CVS in the first trimester in a patient at risk for chromosomal abnormality (by nuchal screening) gives an opportunity to make selective feticide earlier if there is chromosomal abnormality in the fetus. One of the benefits of an earlier result from CVS allowing for earlier selective feticide is a lesser risk of miscarriage against the higher risk of the CVS procedure in comparison to amniocentesis.

Chorionic villus sampling has been demonstrated to be both safe and effective method for sampling twin gestation and has the advantage of an earlier diagnosis than amniocentesis.[42] Initial scanning identifies the locations of the individual chorion frondosum sites, confirms viability and gestational age, and the location and characteristics of the dividing membrane and chorionicity (monochorionic or dichorionic). Sampling of each gestation is performed by needling each distinct frondosum. To assure sampling of each frondosum, continuous ultrasound localization of the needle tip is required. A combination of both sagittal and transverse views is utilized to confirm that individual samples are being retrieved. If the chorions are fused and the borders of the chorion frondosum are indistinct, sampling near to cord insertion sites is suggested. If there is a doubt, a follow-up procedure should be performed as a repeat CVS performed immediately, or a second-trimester amniocentesis. However, the need for a second procedure in experienced hand is rare.[43] Contamination of one sample with villi from the second occurs most frequently when sampling is performed close to the dividing membrane. Twin-twin contamination can also occur if a needle is dragged through one frondosum while attempting to sample another. In two twin series,[42,43] fetal karyotype abnormalities occurred in 2.0% and 3.1% of fetuses. Therefore, documentation of the location of the fetuses is important. If later there is doubt as to the location of the affected fetus a repeat placental biopsy can be performed prior to selective termination and a direct villous preparation or FISH technique utilized to confirm correct fetal location. As with amniocentesis, there is the possibility of one fetus having an abnormal result. This discrepancy may occur somewhat more frequently with CVS than following amniocentesis since chromosomal abnormalities are more common in earlier gestations.

Laboratory Work-up

Until recent years, the karyotyping was carried out by the method of short-term culture in cytotrophoblast cells obtained by chorionic villus sampling, but this karyotyping method was abandoned due to false-positive results in this technique. In some studies, it was reported that QF-PCR or rapid FISH analysis could be used for confirmation or quick result for Tr-21, 18, 13 and XY.[44] In a certain manner, the chorionic villi should

be processed for long-term culture for karyotyping. Reported false-negative findings in the latter series of over 62,000 chorionic villus samples were extremely rare (0.03%) and most occurred with only one exception, after direct preparation alone.[45,46]

The tissue obtained from chorionic villus sampling can also be used for a variety of biochemical and DNA diagnoses (such as hemoglobinopathies, hemophilia, Duchenne dystrophy, cystic fibrosis, etc.). The quantity of tissue is usually sufficient to allow an analysis without the need for tissue culture. In this type of analysis, there is the concern of maternal cell contamination. This can be minimized by careful initial separation of the tissue by a technician experienced in handling chorionic villi.

Placental Confined Mosaicism

Mosaicism is detected in approximately 1% of CVS samples, i.e. 10 times more frequently than in amniotic fluid samples. When placental mosaicism is detected, amniocentesis is often performed to assess whether the fetus is affected, which is the case in 10–20% of these cases.[47]

The chorionic villi obtained are composed of three cell types, syncytiotrophoblast, cytotrophoblast and a central mesenchymal core. The mesenchymal core is grown out in a long-term culture and produces a fibroblast-like cell type that is similar to amniocytes. On the other hand, the trophoblast cells are divided very quickly and actively, and may be analyzed for karyotyping after 24 to 48 hours culture (short-term culture). Although this short-term culture gives a rapid result, there have been discrepancies with the true fetal karyotype. If we do use short-term culture, we should make long-term culture to make the results sure in any case. Most centers are not using the short-term culture technique anymore because now they rely on the long-term culture result.

When mosaicism is limited to the direct preparation, amniocentesis seems to correlate well with fetal genotype. In cases of tissue culture mosaicism, false-positive as well as false-negative results have been found in the amniocentesis sample.[48] In this case, fetal blood sampling can be taken into account.

The major source of diagnostic error in CVS is placental-confined mosaicism that is caused by the result of nondisjunction occurring during embryogenesis, presence of aneuploid cells in the extraembryonic tissue but not in the fetus. Most common type of placental confined mosaicism (PCM) involves the mosaicism in the direct preparation but normal results in culture and the fetus (postzygotic nondisjunction in trophoblast cell line). Rare type PCM involves mosaicism in the culture but not in the direct preparation and the fetus (postzygotic nondisjunction in the inner cell mass that will migrate into the villi). Very rare type involves PCM in the direct preparation and the culture but not in the fetus (mixed type of nondisjunction).

In the case of placental mosaicism, we need to perform amniocentesis or fetal blood sampling to define the karyotype of the fetus. The effect of confined placental mosaicism on the developing embryo is somewhat controversial, although some studies have shown an increased incidence of intrauterine growth restriction and perinatal death.[49] Follow-up ultrasound evaluation may be helpful in assessing this condition.

Acceptance

Prenatal diagnosis in the first trimester has rapidly gained approval for a number of reasons. Most important is the advantage of an earlier procedure. This approach not only provides earlier reassurance when results are normal but also allows an easier and more private pregnancy termination when necessary. Additionally, early diagnosis is essential when *in utero* gene or stem cell therapy is contemplated to correct a genetic defect. First-trimester procedures lowered maternal anxiety levels earlier and more consistently than traditional midtrimester amniocentesis. In a study, women undergoing CVS reported greater attachment to the pregnancy than women undergoing amniocentesis. These authors concluded that the benefits afforded by CVS confirmed earlier reports demonstrating a patient preference for CVS.[50] Also the gestational at the time of result is earlier in CVS than in amniocentesis. Earliest time for having the chromosome result is the 14th week with CVS and the 18th–19th week with amniocentesis.

CONCLUSION

Chorionic villus sampling has been demonstrated to be a safe and effective technique that is capable of providing information and diagnosis to couples at genetic risk about their pregnancy. In most cases, the genetic results are reassuring but when abnormal, the medical and psychological complications of second-trimester pregnancy termination can be avoided.

Despite these advantages, utilization of CVS has failed to become widely available. This lack of complete acceptance has been primarily due to exaggerated reports of the risks of pregnancy loss and possible

congenital abnormalities. The etiology of most of these problems can be directly attributed to inexperience with the procedure. Performing CVS is technically demanding, as demonstrated, the relatively long learning curve. As first-trimester screening for chromosomal abnormality with the detection rate of 97% by maternal age, nuchal thickness, nasal bone, ductus venosus, tricuspid regurgitation, facial angle, minors markers in first trimester and free-beta-hCG and PAPP-A became a reality, we do perform more early prenatal diagnosis. Recent developments in laboratory techniques, we can give early result of rapid FISH or QF-PCR evaluation even for limited chromosomes on the same day and then complete result within 14–20 days. That makes CVS a requested method of early prenatal diagnosis. Studies suggest that CVS is the procedure of choice resulting in the need for additional centers with expertise in this procedure.

The procedure-related miscarriage rate is same about 0.5–1.0% for both CVS and amniocentesis.

Chorionic villus sampling should not be performed before 11 weeks due to the risk of limb reduction defects, amniocentesis not before 15 weeks due to an increased miscarriage rate and more talipes in the newborns.

Experienced operators have a higher success rate and a lower complication rate. Decreasing number of prenatal invasive procedures with increasing number of chromosomally abnormal cases following the introduction of first- or second-trimester risk assessment calls for quality assurance and monitoring of operators' performance.

REFERENCES

1. Jacobson CB, Barter RH. Intrauterine diagnosis and management of genetic defects. Am J Obstet Gynecol. 1967;99(6):796-807.
2. Boyd PA, DeVigan C, Khoshnood B, et al. EUROCAT Working Group. Survey of prenatal screening policies in Europe for structural malformations and chromosome anomalies, and their impact on detection and termination rates for neural tube defects and Down's syndrome. BJOG. 2008;115(6):689-96.
3. Ekelund CK, Jørgensen FS, Petersen OB, et al. Danish Fetal Medicine Research Group. Impact of a new national screening policy for Down's syndrome in Denmark: population based cohort study. BMJ. 2008;337:a2547.
4. Nicolaides KH. First-trimester screening for chromosomal abnormalities. Semin Perinatol. 2005; 29(4):190-4.
5. Evans MI, Goldberg JD, Horenstein J, et al. Selective termination for structural, chromosomal, and Mendelian anomalies: international experience. Am J Obstet Gynecol. 1999;181(4):893-7.
6. Fetal sex prediction by sex chromatin of chorionic. Department of Obstetrics and Gynecology, Tietung Hospital, Anahan, China. Chinese Medical Journal. 1975;1:117-26.
7. RJ, Wapner. Chorionic villus sampling. Obstetr Gynecol Clin North Am. 1997;24:83-110.
8. Jackson LG, Wapner RJ. Risks of chorionic villus sampling. Clin Obstet Gynecol. 1987;1:513-31.
9. Council, MRC Working Group Party on the evaluation of chorionic villus sampling. Medical Research. European trial of chorionic villus sampling. Lancet. 1991;337:1491-9.
10. Brambati B, Oldrini A, Ferrazzi E, et al. Chorionic villus sampling: an analysis of the obstetric experience of 1000 cases. Prenat Diagn. 1987;7:157-69.
11. Canadian Collaborative CVS-Amniocentesis Clinical Trial Group. Multicentre randomized clinical trial of chorion villus sampling and amniocentesis. Lancet. 1989;1:1-6.
12. Rhoads GG, Jackson LG, Schlesseslman SE, et al. The safety and efficacy of chorionic villus sampling for early prenatal diagnosis of cytogenetic abnormalities. N Eng J Med. 1989;320:609-17.
13. Saura R, Gauthier, Taine L, et al. Operator experiences and fetal loss rate in transabdominal CVS. Prenat Diagn. 1994;14:70-1.
14. Nicolaides KH, Brizot M, Patel F, et al. Comparison of chorionic villus sampling and amniocentesis for fetal karyotyping at 10-13 weeks' gestation. Lancet. 1994;344: 435-40.
15. Cederholm M, Axelsson O. A prospective comparative study on transabdominal chorionic villus sampling and amniocentesis performed at 10-13 weeks' gestation. Prenat Diagn. 1997;17:311-17.
16. Smidt-Jensen S, Permin M, Philip J. Sampling success and risk by transabdominal chorionic villus sampling, transcervical chorionic villus sampling and amniocentesis: a randomized study. Ultrasound Obstet Gynecol. 1991;1: 86-90.
17. Firth HV, Boyd PA, Chamberlain P, et al. Severe limb abnormalities after chorion villus sampling at 56-66 days' gestation(see comments). 1991:762-763.
18. Brambati B, Simoni G, Travi M, et al. Genetic diagnosis by chorionic villus sampling before 8 weeks: efficiency, reliability, and risks on 317 completed pregnancies. 1992;12:789-9.
19. Mastroiacovo P, Botto LD, Cavalcanti DP. Limb anomalies following chorionic villus sampling: a registry based case control study. Am J Med Genet. 1992;44:856-63.
20. Hsieh FJ, Shyu MK, Sheu BC, et al. Limb defects after chorionic villus sampling. Obstet Gynecol. 1995;85:84-8.
21. Burton BK, Schultz CJ, Burd LI. Spectrum of limb disruption defects associated with chorionic villus sampling. Pediatrics. 1993;91:989-93.
22. OlneyS, Khoury MJ, Alo CJ, et al. Increased risk for tranverse digital deficiency after chorionic villus sampling:results of the United States Multistate Case-Control Study, 1988-1991. Teratology. 1995;51:20-9.
23. Kuliev A, Jackson L, Froster U, et al. Chorionic villus sampling safety. Report of World Health Organization/ EURO meeting in association with the Seventh International

Conference on Early Prenatal Diagnosis of Genetic Diseases. Am J Obstet Gynecol. 1996;174:807-11.
24. Schaap AHP, van der Pol HG, Boer K, et al. Long-term follow-up of infants after transcervical chorionic villus sampling and after amniocentesis to compare congenital abnormalities and health status. Prenat Diagn. 2002;22: 598-4.
25. Brambat Bi, Tului L, Camurri L, et al. Early second trimester (13 to 20 weeks) transabdominal chorionic villus sampling (TA-CVS): a safe and alternative method for both high and low risk populations. Prenat Diagn. 2002;22:907-13.
26. Papp C, Beke A, Mezei G, et al. Chorionic villus sampling:a 15-year experience. Fetal Diagn Ther. 2002;17:218-27.
27. Alfirevic Z, Mujezinovic F, Sundberg K. Amniocentesis and chorionic villus sampling for prenatal diagnosis (Review). Cochrane Database of Systematic Reviews. 2003;3:Art. No.: CD003252. DOI: 10.1002/14651858.CD003252. 2003 (Updated 28 June 2008 and republished in the Issue 2, 2009), 3.
28. Hoesli IM, Walter-Goebel I, Tercanli S, et al. Spontaneous fetal loss rates in a non-selected population. Am J Med Genet. 2001;100:106-9.
29. Tabor A, Madsen M, Obel E, et al. Randomised controlled trial of genetic amniocentesis in 4606 low-risk women. Lancet. 1986;i:1287-93.
30. Caughey AB, Hopkins LM, Norton ME. Chorionic villus sampling compared with amniocentesis and the difference in the rate of pregnancy loss. Obstet Gynecol. 2006;108: 612-6.
31. Odibo AO, Gray DL, Dicke JM, et al. Revisiting the fetal loss rate after second-trimester genetic amniocentesis: a single center's 16-year experience. Obstet Gynecol. 2008;111:589-95.
32. Tongsong T, Wanapirak C, Sirivatanapa P, et al. Amniocentesis-related fetal loss: a cohort study. Obstet Gynecol. 1998;92:64-7.
33. Eddleman KA, Malone FD, Sullivan L, et al. Pregnancy loss rates after midtrimester amniocentesi. Obstet Gynecol. 2006;108:1067-72.
34. Mujezinovic F, Alfirevic Z. Procedure-related complications of amniocentesis and chorionic villus sampling. Obstet Gynecol. 2007;110:687-94.
35. Canadian early and mid-trimester amniocentesis trial (CEMAT) group. Randomised safety and fetal outcome of early and midtrimester amniocentesis. 1998;351:242-7.
36. Muller F, Thibaud D, Poloce F, et al. Risk of amniocentesis in women screened positive for Down syndrome with second trimester maternal serum markers. Prenat Diagn. 2002;22:1036-9.
37. Tabor A, Vestergaard CHF and Lidegaard Ø. Fetal loss rate after chorionic villus sampling and amniocentesis: an 11-year national registry study. 2009;34:19-24.
38. Snijders RJ, Sundberg K, Holzgreve W, et al. Maternal age- and gestation-specific risk for trisomy 21. Ultrasound Obstet Gynecol. 1999;13:167-70.
39. Odibo AO, Dicke JM, Gray DL, et al. Evaluating the rate and risk factors for fetal loss after chorionic villus sampling. Obstet Gynecol. 2008;112:813-9.
40. Sebire NJ, Snijders RJM, Hughes K, et al. Screening for trisomy in twin pregnancies by maternal age and fetal nuchal translucency thickness at 10-14 weeks of gestation. Br J Obstet Gynecol. 1996;103:999-3.
41. Antsaklis A, Souka AP, Daskalakis G, et al. Second-trimester amniocentesis vs. chorionic villus sampling for prenatal diagnosis in multiple gestations. Ultrasound Obstet Gynecol. 2002;20:476-81.
42. Pergament E, Schulman J, Copeland K, et al. The risk of and efficacy of chorionic villus sampling in multiple gestations. Prenat Diagn. 1992;12:377-84.
43. Wapner RJ, Johnson A, Davis G. Prenatal diagnosis in twin gestations: a comparison between second trimester amniocentesis and first trimester chorionic villus sampling. Obstet Gynecol. 1993;82:49-56.
44. Schuring-Blom GH, Hoovers JMN, van Lith JMM, et al. FISH analysis of fetal nucleated red cells from CVS washings in cases of aneuploidy. Prenat Diagn. 2001;21: 864-7.
45. Schuring-Blom GH, Boer K, Knegt AC, et al. Trisomy 13 or 18 (mosaicism) in first trimester cytotrophoblast cells: false-positive results in 11 out of 51 cases. Eur J Obstet Gynecol and Rep Bio. 2002;101:161-8.
46. Hahnemann JM, Vejerslev LO. Accuracy of cytogenetic findings on chorionic villus sampling (CVS)-diagnostic consequences of CVS mosaicism and non-mosaic discrepancy in centres contributing to EUCROMIC 1986-1992. Prenat Diagn. 1997;17:801-20.
47. Goldberg JD, Wohlferd MM. Incidence and outcome of chromosomal mosaicism found at the time of chorionic villus sampling. Am J Obstet Gynecol. 1997;176:1349-53.
48. Eisenberg B, Wapner RJ. Clinical procedures in prenatal diagnosis. Clin Obstet Gynecol. 2002;16: 611-27.
49. Johnson A, Wapner RJ. Mosaicism:Implications for postnatal outcome. Curr Opin Obstet Gynecol. 1997;9:126-35.
50. McGovern MM, Goldberg JD, Desnick RJ. Acceptability of chorionic villi sampling for prenatal diagnosis. Am J Obstet Gynecol. 1996;155:25-9.

CHAPTER 40

Amniocentesis and Fetal Blood Sampling

Aris J Antsaklis, George A Partsinevelos

INTRODUCTION

The introduction of ultrasonography in fetal medicine has been uniformly recognized as the milestone in prenatal screening for chromosomal abnormalities and congenital fetal malformations. High resolution ultrasound equipment currently available allows detailed fetal imaging. These facilities combined with increasing operator experience accomplish accurate noninvasive prenatal diagnosis. Nevertheless, invasive diagnostic procedures are required to establish diagnosis in case of suspected aneuploidy or genetic disease. The vast majority of these tests are performed under ultrasound guidance and aim to obtain fetal samples, such as amniotic fluid (amniocentesis), chorionic villi (chorionic villus sampling) and fetal blood (fetal blood sampling) for fetal karyotyping and/or DNA analysis. Unavoidably, each of them is linked to certain potential complications and procedure-related risks, while fetal loss represents the worst scenario in these cases. Gestational age, suspected underlying fetal anomaly and mainly physician's experience should be taken into consideration in deciding the method of choice.

AMNIOCENTESIS

Introduction

Traditionally considered as the oldest invasive procedure in pregnancy, amniocentesis is defined as the transabdominal aspiration of amniotic fluid. At the end of 19th century, it was therapeutically applied for the first time to drain excess amniotic fluid in a women having polyhydramnios.[1] For diagnostic reasons, it was first used in 1950s to assess the severity of cases of Rhesus (Rh) isoimmunization through spectrophotometric analysis of the amniotic fluid[2] and later in fetal sex diagnosis by the identification of Barr bodies in the noncultured amniocytes.[3] Before mid 1960s, amniocentesis for genetic diagnosis through fetal karyotype determination in amniotic cell culture was never applied.[4] In the late 1960s and early 1970s, this procedure was reserved only for the highest risk patients in the tertiary setting.[5,6] Since then, amniocentesis has been increasingly used as an invaluable method in prenatal invasive screening for fetal chromosomal abnormalities and diagnosis of congenital fetal metabolic or enzymatic diseases, evaluation of the severity of hemolytic disease, assessment of fetal lung maturity and diagnosis of endometrial infections. Furthermore, its role in evaluation of hydramnios and infusion of drugs into the amniotic cavity has been validated.

Indications

Main indication for amniocentesis is fetal karyotyping. It is done to exclude numerical and structural fetal chromosomal abnormalities. Traditionally genetic screening with amniocentesis is suggested due to advanced maternal age (greater than or equal to 35 years), but current statement is that the maternal age itself

should no longer be used as a cut-off to discern pregnant women at those who should be offered noninvasive screening tests (ultrasound and maternal serum biochemistry) versus those who should undergo invasive diagnostic tests [amniocentesis or chorionic villus sampling (CVS)]. Present recommendation for all pregnant women, regardless of age is that before 20 weeks of gestation, they should be offered noninvasive screening for chromosomal abnormalities and invasive genetic screening should be advised to females having increased risk of varying abnormal fetus. An option of invasive testing on maternal request should be open for all women irrespective of their age.[7] Other indications for amniocentesis are:

- History of previous fetal aneuploidy
- Parental balanced translocation
- An ambiguous result from a previous test, such as placental mosaicism in CVS.

Fetal karyotype examination is done either in cultured amniotic fluid cells or with polymerase chain reaction (PCR) technology. Cell culture must be done to confirm the result of latter technique.

Amniocentesis also serves in the diagnosis of genetic diseases in the fetus. DNA analysis using fluorescent labeled in situ hybridization (FISH), can help in accurately identifying beta-thalassemia, cystic fibrosis and hemophilia. In the past, some metabolic diseases and other pathologic conditions, such as cystic fibrosis and congenital adrenal hyperplasia, were diagnosed using determination of relevant enzymes in the amniotic fluid. In the new era, DNA analysis has replaced this approach ensuring accurate detection of gene mutation in fetal cells collected through amniocentesis.

Quantitative and qualitative characteristics of the amniotic fluid can be used in fetal lung maturity assessment. Lecithin-sphingomyelin ratio, phosphatidylglycerol determination, foam stability index, fluorescent polarization test for surfactant-albumin ratio measurement, lamellar body detection in the amniotic fluid and other tests may indirectly estimate the risk of respiratory distress syndrome (RDS) in the neonate. However, amniocentesis is rarely used for fetal pulmonary maturity evaluation nowadays, as advances in neonatal care and accuracy in determination of gestational age early in pregnancy with ultrasonography have restricted its necessity.

Congenital fetal infection with *Toxoplasma gondii*, *Cytomegalovirus* (CMV), *Rubella virus*, etc. can be ruled out in case of maternal infection accompanied by seroconversion via amniocentesis and use of PCR based technologies in the amniotic fluid. Bacterial agent responsible for premature rupture of membranes (PROM) and preterm labor in case of underlying chorioamnionitis can be identified by Gram's stain microscopy and culture of the amniotic fluid.

Many indications of amniocentesis that were useful in past are discarded nowadays. For example, the severity of fetal hemolytic anemia in cases of Rh isoimmunization was traditionally assessed using amniotic fluid spectrophotometry. After the advent of middle cerebral artery (MCA) Doppler velocimetry, this practice has been abandoned, as MCA offers a noninvasive alternative approach in the evaluation of fetal hemolysis and anemia.

Finally, fetal therapy can be accomplished in several cases using amniocentesis. Polyhydramnios in singleton pregnancies and twin oligohydramnios-polyhydramnios sequence (TOPS) in monochorionic twin pregnancies complicated by twin-to-twin transfusion syndrome (TTTS) can be treated with serial drainage of excess amniotic fluid (amnioreduction). On the contrary, severe oligohydramnios has been managed with amnioinfusion, although further evaluation of the indications and outcome of this technique is needed. Furthermore, infusion of various drugs in the amniotic cavity, such as thyroxine to treat fetal goitrous hypothyroidism has been applied.

Technique

Ideally, amniocentesis for prenatal screening of chromosomal aberrations and genetic diagnosis of congenital diseases is performed between 15-18 weeks of gestation.[8] If early application is done. i.e. in 11-14 weeks, an increaseed risk of fetal loss, amniotic fluid leakage and fetal talipes equinovarus may be associated. Thus, this practice is not recommended.[9]

Genetic counseling based on family history, parents' medical history, maternal age, first and/or second trimester prenatal screening with ultrasonography, and/or maternal serum biochemistry, should initially be offered. Counseling is imperative to include efficacy and shortcomings of the technique including procedure-related risks and also expectations from testing. Available options in case of abnormal results should be also discussed.

The procedure is preceded by a detailed ultrasound examination of the pregnancy, which includes determination of the number of gestational sacs and fetuses, mapping of fetuses and placentas in case of multiple pregnancy, assessment of cardiac function, gestational age, amniotic fluid quantity and identification of possible fetal abnormalities. Moreover, the existence of fibroids and adnexal masses are recorded.

The site for the entry of the needle is chosen preferably distally from the fetal face, the umbilical cord and the placenta. The anterior placenta rarely covers the entire anterior uterine wall, thus a window for lateral approach is almost always available. Antiseptic solution is applied on the skin and the free hand "Single operator's technique" (one hand holds the needle and the other the ultrasound transducer) is usually employed to insert a disposable 22-G spinal needle in the selected amniotic fluid pocket. The inner needle is removed and a syringe is attached to the needle hub. The first 1–2 ml of amniotic fluid is discarded to avoid contamination with maternal cells which might render results inaccurate (1/600 pregnancies). A new syringe is attached and approximately 20 ml of amniotic fluid is drained and sent to the cytogenetic laboratory. In case that amniotic fluid cannot be aspirated, juxtaposes of the needle to the membrane and rotation to 180º may solve the problem. If not, reinserting of the stylet and advancing the needle under ultrasound guidance may help. Selection of a new insertion site should be reserved as the last resort.

When blood or blood stained amniotic fluid is drawn, the needle tip should be rechecked and slightly moved as it may have not completely transversed the uterine wall. However, the dark or brown color of amniotic fluid indicates the presence of old blood into the amniotic cavity and this is associated with an earlier vaginal bleeding or a previous unsuccessful amniocentesis. This is more often associated with failure of amniotic fluid cells culture.

Repeat ultrasound assessment confirms fetal heart activity and the absence of intraamniotic bleeding. Advice to rest and avoid sexual intercourse for several days and information about signs of potential post-procedure complications, such as persistent uterine cramping, fever, leakage of amniotic fluid or bleeding, are given.

Certain modifications of the technique of amniocentesis have been applied in twins and higher order pregnancies. So far, three methods of tapping multiple sacs has been described. First one was introduced in 1980, which involved two or more needle insertions, one for each sac. It is also known as technique of double amniocentesis.[10] In a twin or higher-order multiple pregnancy, two or more 22-G spinal needles are separately and sequentially inserted transabdominally under ultrasound visualization into each sac and approximately 20 ml of amniotic fluid is readily aspirated. Another technique described in 1990 is the single needle insertion technique.[11] The needle entry is made into the proximal sac near the insertion of the dividing membrane and 20 ml of amniotic fluid is retrieved. After the stylet is replaced, the needle is advanced through the second sac under direct ultrasound guidance.[12] In order to avoid contamination and subsequent false negative results, the first few milliliters of amniotic fluid are discarded and aspiration of 20 ml from the second sac integrates the procedure. Double simultaneous amniocentesis represents the third approach first applied in 1992.[12] Two needles are inserted separately into the amniotic sacs under ultrasound visualization and following aspiration of the amniotic fluid from the first sac, the needle is left in place indicating the sampled cavity while the second needle is advanced into the other sac. Each of these techniques has advantages and disadvantages and finally operator's familiarity with the approach might determine his option.

Complications

In fetal diagnosis and therapy, amniocentesis has proven to be a safe technique. But numerous complications are also linked to it due to its invasive nature. Undoubtedly, many of them are directly influenced by operators' experience.

Fetal loss is considered as the major risk of second trimester genetic amniocentesis. It should be noted that in order to assess procedure-related risk of fetal loss, background loss rate associated with maternal age, gestational age, parity, maternal pathologic conditions (uncontrolled diabetes mellitus, severe hypertension related to lupus, etc.) and fetal anomalies (structural aberrations, karyotype abnormalities, etc.) should be taken into account.

Advanced maternal age is associated with increased background fetal loss rate. On the contrary, gestational age at the procedure is inversely related to fetal loss rate. In fact, the earlier the pregnancy the higher the background risk of miscarriage. In 1988, it was demonstrated that 2% of clinical pregnancies diagnosed sonographically in women younger than 35 years resulted in miscarriage at 9–11 weeks of gestation. The risk of miscarriage was 4.5% among women aged 35–39 years and estimations for a lower background fetal loss rate later in pregnancy were made.[13]

Only one randomized trial has compared the risks of amniocentesis to control so far. In this study, which was conducted in Denmark approximately 25 years ago, amniocentesis was performed at 14–20 weeks of gestation, although most procedures were performed between 16 and 18 weeks.[14] The amniocentesis group had a total fetal loss rate 1% higher than the controls (1.7% and 0.7% respectively). In the original paper it

was stated that amniocenteses were carried out with a 18-G needle. However, the authors subsequently retracted this statement and indicated that a smaller needle was in fact used. Apparently, this issue cannot be objectively retested in this era, as such a prospective randomized control study is impossible to be repeated due to ethical reasons.

Thenceforth, a lot of studies reported amniocentesis related fetal loss rate between 0.2% and 0.9%. The difficulties in evaluating the post-procedure miscarriage rate have been clearly shown by the controversial results of several multicenter trials. In 1978 the National Institute of Child Health and Human Development (NICHD) evaluating the safety and accuracy of midtrimester amniocentesis for prenatal diagnosis, reported a fetal loss rate of 3.5% in the amniocentesis group and 3.2% in the controls.[15] The same year, the Medical Research Council[16] reported an amniocentesis related fetal loss rate between 1–1.5% and a small, but significant association with neonatal respiratory distress syndrome. It was suggested that these complications could be the result of oligohydramnios following leakage of amniotic fluid. This British study also found an increase in postural deformities, such as talipes and congenital dislocation of the hip.[16] The possible mechanism of this deformity is compression due to oligohydramnios or tissue injury from the amniocentesis needle. However, the study was later criticized for significant selection biases. In 1996 Brumfield[17] reported a total fetal loss of 0.2% following amniocentesis at 16–19 weeks' gestation. In the Canadian early and midtrimester amniocentesis collaborative study a total pregnancy loss of 3.2% was reported, but there were no controls.[18] In 1999, Roper et al. reported a 0.9% risk for miscarriage after midtrimester amniocentesis.[19] A systematic review published early this decade showed a procedure-related pregnancy loss of 0.6%.[20] In 2006, patients who participated in the Fisrt and Second Trimester Evaluation of Risk for Aneuploidy (FASTER) trial were analysed and the total spontaneous fetal loss rate earlier than 24 weeks of gestation in the study group was 1.0% and was statistically significant different from the background 0.94% rate seen in the control group.[21] A recent systematic review of complications related to amniocenetesis and CVS showed a pooled pregnancy loss within 14 days after amniocentesis of 0.6% and the figure reached 0.9% for pregnancy loss before 24 weeks of gestation.[22]

In a retrospective study conducted in our center involving amniocentesis performed between 1990 and 2006, we found 1.25% pregnancy loss rate in 12,413 women who underwent amniocentesis versus 0.9% in 5,654 women who did not (control group), which corresponds to 0.35% excess rate in the amniocentesis group, though it did not reach statistical significance (Fishers exact test p<0.214). Moreover, age specific analysis did not find statistical significance in the fetal loss rate between the two groups [unpublished data]. Delivery rate earlier than 24, 28 and 37 weeks in the amniocentesis group was 0.2%, 0.7% and 12.8% respectively **(Table 40.1)**.

TABLE 40.1

Pregnancy outcome after amniocentesis in "Alexandra" Hospital, University of Athens, Medical School (1990–2006)

Pregnancy outcome	*(n=12,413)*
Delivery at <24 weeks	0.2%
Delivery at <28 weeks	0.7%
Delivery at <37 weeks	12.8%
Birth weight <1500 gms	1%
Cesarean section rate	43.4%
Mean gestational age at birth	38.2 week
Mean birth weight	3,370 gr
SCBU admission (>24 hrs)	1.9%

Gestational age at amniocentesis has an impact on fetal loss rate. Estimations of fetal loss rate of less than 0.5%, 1% and 3% following amniocentesis at 15, 14 and 13 weeks of gestation respectively have been made. Blood stained amniotic fluid and amniotic fluid leakage were strong predictors for fetal loss. Transplacental needle insertion was initially linked with increased fetal loss, however, several studies concluded, that transplacental needle insertion does not influence the risk of pregnancy loss.[14,23] With regards to the number of needle insertions, literature yields contradictory results. In particular, no increased risk for pregnancy loss after multiple needle insertions have been reported in some studies, whereas an increased risk has been documented in some others.[15,23] A possible association between history of bleeding and increased risk of pregnancy loss postamniocentesis (+0.6%) has been reported in a previous study conducted by our team.[24] Other factors associated with increased fetal loss following amniocentesis are more than three terminations of pregnancy and/or miscarriages, thyroid disease, elevated maternal serum α-fetoprotein (MSAFP) and usage of needle with diameter larger than 18-G.

In our retrospective study, we found an increased risk of fetal loss with advanced maternal age 34 years (OR 2.19), history of more than three terminations of pregnancy and/or miscarriages (OR 3.9), mild bleeding in early pregnancy (OR 2.53), severe bleeding in early pregnancy (OR 5.6), blood stained amniotic fluid (OR 3.82) and the presence of uterine fibroids (OR 2.52).

Other complications related to amniocentesis include preterm delivery,[25] fetal injury ascribed to the amniocentesis needle,[20] Rh alloimmunization resulting from fetomaternal hemorrhage,[26-28] neonatal respiratory distress syndrome possibly due to postprocedure chronic oligohydramnios,[29,30] orthopedic abnormalities (talipes equinovarus congenital dislocation and subluxation of the hip) possibly due again to oligohydramnios,[31] and usually self-limited uterine contractions and vaginal spotting (2-3%) and leakage of amniotic fluid (1%).[25]

FETAL BLOOD SAMPLING

Introduction

Although fetal blood was initially obtained in 1972 endoscopically during second trimester termination of pregnancy by cesarean section, the first successful transabdominal fetoscopic fetal blood sampling was performed two years later under ultrasound guidance.[32,33] However, the origin of the technique currently available for fetal blood sampling using a needle, which is introduced transabdominally under ultrasound visualization, goes back in 1983.[34]

Fetal blood sampling is also known as cordocentesis, omphalocentesis and percutaneous umbilical blood sampling (PUBS) and involves ultrasound-guided puncture of the umbilical vein. However, the intrahepatic portion of the umbilical vein and the left portal vein as well as the right heart ventricle has also been used to obtain fetal blood sample.[35]

In the past, a frequent indication was the need for rapid diagnosis of chromosomal abnormalities (rapid karyotyping), inasmuch as results were offered in 2–3 days-time. Today, novel molecular techniques allow rapid karyotype determination even earlier.

Currently, amniocentesis and CVS represent first line invasive diagnostic procedures for prenatal diagnosis, thus limiting fetal blood sampling's application considerably. However, the latter is indicated in case of abnormal findings in amniocentesis or CVS, which require confirmation. Moreover, Rh isoimmunization, hydrops of unknown origin and fetal infections are some of the conditions where fetal blood sampling can be indicated. Finally, cordocentesis can be practiced in order to inject pharmacologic agents into the fetal circulation or even perform blood transfusion in severe fetal anemia.

Technique

There are three different approaches for fetal blood sampling, which have been described so far as: cordocentesis, intrahepatic fetal blood sampling and cardiocentesis. The last two are rarely used nowadays because of the higher fetal loss rate associated with them, which is estimated to be 6.2% and 5.6% respectively.[35-37]

A detailed ultrasound examination of the pregnancy is conducted before the procedure to ensure fetal viability and assess normality of the developing fetus. Furthermore, amniotic fluid volume, location of the placenta and the insertion site of the umbilical cord in the placenta are documented. To this end, color Doppler can be used as it provides useful information regarding blood flow and facilitates identification of the umbilical vein.

Once the insertion site of the needle has been determined, the skin is cleansed with antiseptic solution and local anesthetic is injected.

Transabdominal ultrasound-guided free-hand technique is usually opted. A 22-G spinal needle 9–15 cm in length is introduced either trans-placentally in case of anterior placenta or through the amniotic cavity in case of posterior placenta targeting the umbilical vein proximal to the insertion of the umbilical cord into the placenta (around 1 cm distance) **(Figs 40.1 and 40.2)**. The needle-within-needle technique is rarely used nowadays. Puncturing free loops of the umbilical cord is much more difficult and often turns out unsuccessful. No more than 4 ml and 6 ml of fetal blood should be withdrawn during the second and third trimester respectively. The cord puncture site should be

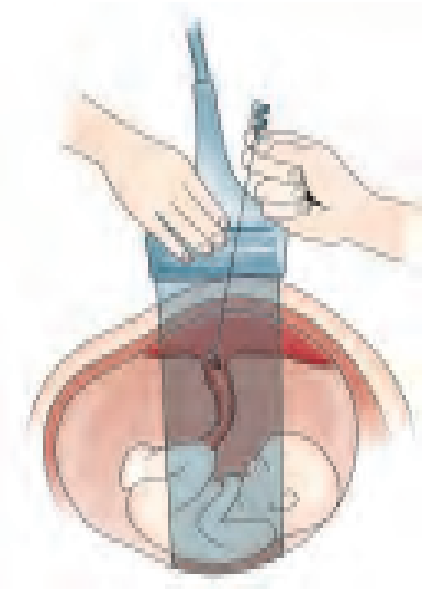

Figure 40.1: Transabdominal ultrasound-guided fetal blood sampling in case of anterior placenta

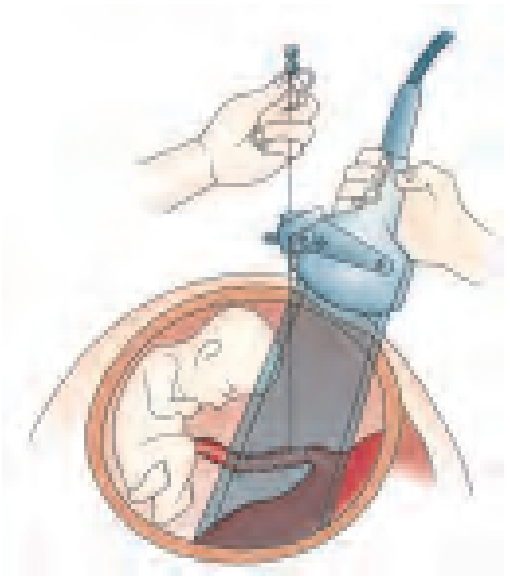

Figure 40.2: Transabdominal ultrasound-guided fetal blood sampling in case of posterior placenta

sonographically followed-up for 10 minutes for bleeding or hematoma formation and fetal heart rate for 30–60 minutes following the procedure.[37]

Complications

The major concern of fetal blood sampling is fetal loss which has been shown to be higher than other prenatal invasive diagnostic procedures frequently used, such as amniocentesis and CVS.[38] A 0.9–3.2% fetal loss rate has been recorded in previous studies. However, no randomized controlled trials have assessed this risk so far.[34,39] Notwithstanding, the relatively increased background pregnancy loss rate associated with pregnancies selected to undergo fetal blood sampling should be always taken into account in assessing adverse pregnancy outcome related with the procedure.

Bleeding at the puncture site has been shown to accompany 41–53% of cases with a mean duration of 35 sec,[40] although a longer duration of bleeding is expected in cases where the umbilical artery has been punctured.[41] However, it is considered the most common usually benign complication of fetal blood sampling.

Umbilical cord hematoma (17%),[42] transient fetal bradycardia (3–12%),[41] fetomaternal blood transfusion (65.6% in anterior placenta versus 16.6% in posterior placenta),[43] uterine contractions (7%)[44] and chorioamnionitis due to *Staphylococcus aureus* or bowel bacteria[37] are all potential complications of fetal blood sampling. Thus, it is prudent to reserve this procedure for cases where the results of other noninvasive and invasive techniques were inconclusive or cordocentesis is the unique option for fetal diagnosis and therapy.

With regards to twin or higher order pregnancies, fetal blood sampling does not differ technically from that in singletons. In a study conducted in 2003, involving 84 twin pregnancies, mainly screened for hemoglobinopathies, the overall procedure-related fetal loss (up to 2 weeks post-procedurally) was 8.2%, about four-fold higher than the correspondence risk in singletons. However, this technique can be used as an alternative to amniocentesis after 20 weeks' gestation to confirm an abnormal karyotype in a dichorionic twin pregnancy, when selective feticide is considered a few weeks after the initial procedure.[45]

REFERENCES

1. Von Schatz F. Gine besondere art von einseitiger polyhydramnie mit anderseitiger oligohydramnie bie eineiigen zwillingen. Arch Gynaecol. 1882;19:329.
2. Bevis DC. Composition of liquor amnii in haemolytic disease of newborn. Lancet. 1950;2(6631):443.
3. Fuchs F, Riis P. Antenatal sex determination. Nature. 1956;177(4503):330.
4. Steele MW, Breg WR Jr. Chromosome analysis of human amniotic-fluid cells. Lancet. 1966;1(7434):383-5.
5. Jacobson CB, Barter RH. Intrauterine diagnosis and management of genetic defects. Am J Obstet Gynecol. 1967;99(6):796-807.
6. Nadler HL, Gerbie AB. Role of amniocentesis in the intrauterine detection of genetic disorders. N Engl J Med. 1970;282(11):596-9.
7. American College of Obstetricians and Gynecologists. ACOG practice bulletin-Screening for fetal chromosomal anomalies. Obstet Gynecol. 2007:217-26.
8. Emery AE. Antenatal diagnosis of genetic disease. Modern Trends Hum Genet. 1970;1:267.
9. Alfirevic Z, Sundberg K, Brigham S. Amniocetesis and chorionic villus sampling for prenatal diagnosis (review) the Cochrane Collaboration. 2005.
10. Elias S, Gerbie AB, Simpson JL, et al. Genetic amniocentesis in twin gestations. Am J Obstet Gynecol. 1980;138(2):169-74.
11. Jeanty P, Shah D, Roussis P. Single-needle insertion in twin amniocentesis. J Ultrasound Med. 1990;9(9):511-7.
12. Bahado-Singh R, Schmitt R, Hobbins JC. New technique for genetic amniocentesis in twins. Obstet Gynecol. 1992;79(2):304-7.
13. Mackenzie WE, Holmes DS, Newton JR. Spontaneous abortion rate in ultrasonographically viable pregnancies. Obstet Gynecol. 1988;71(1):81-3.
14. Tabor A, Philip J, Madsen M, et al. Randomised controlled trial of genetic amniocentesis in 4606 low-risk women. Lancet. 1986;1(8493):1287-93.

15. Stone J, Ferrara L, Kamrath J, et al. Contemporary outcomes with the latest 1000 cases of multifetal pregnancy reduction (MPR). Am J Obstet Gynecol. 2008;199(4):406.e1-4.
16. Pharoah PO, Adi Y. Consequences of in-utero death in a twin pregnancy. Lancet. 2000;355(9215):1597-602.
17. Brumfield CG, Lin S, Conner W, et al. Pregnancy outcome following genetic amniocentesis at 11-14 versus 16-19 weeks' gestation. Obstet Gynecol. 1996;88(1):114-8.
18. Simpson NE, Dallaire L, Miller JR, et al. Prenatal diagnosis of genetic disease in Canada: report of a collaborative study. Can Med Assoc J. 1976;115(8):739-48.
19. Wimalasundera RC. Selective reduction and termination of multiple pregnancies. Semin Fetal Neonatal Med. 2010;15(6):327-35.
20. Seeds JW. Diagnostic mid trimester amniocentesis: how safe? Am J Obstet Gynecol. 2004;191(2):607-15.
21. Eddleman KA, Malone FD, Sullivan L, et al. Pregnancy loss rates after midtrimester amniocentesis. Obstet Gynecol. 2006;108(5):1067-72.
22. Mujezinovic F, Alfirevic Z. Procedure-related complications of amniocentesis and chorionic villous sampling: a systematic review. Obstet Gynecol. 2007;110(3):687-94.
23. Marthin T, Liedgren S, Hammar M. Transplacental needle passage and other risk-factors associated with second trimester amniocentesis. Acta Obstet Gynecol Scand. 1997;76(8):728-32.
24. Antsaklis A, Papantoniou N, Xygakis A, et al. Genetic amniocentesis in women 20-34 years old: associated risks. Prenat Diagn. 2000;20(3):247-50.
25. Medda E, Donati S, Spinelli A, et al. Genetic amniocentesis: a risk factor for preterm delivery? Eur J Obstet Gynecol Reprod Biol EUROPOP Group CzechRepublic, EUROPOP Group Finland, EUROPOP Group France, EUROPOP Group Germany, EUROPOP Group Greece, EUROPOP Group Italy, EUROPOP Group The Netherlands, EUROPOP Group Slovak Republic, EUROPOP Group Spain, EUROPOP Group Sweden. 2003;110:153-8.
26. Clayton EM Jr, Layton EM Jr, Feldhaus WD, et al. Fetal erythrocytes in the maternal circulation of pregnant women. Obstet Gynecol. 1964;23:915-9.
27. Tabor A, Bang J, NOrgaard-Pedersen B. Feto-maternal haemorrhage associated with genetic amniocentesis: results of a randomized trial. Br J Obstet Gynaecol. 1987;94(6):528-34.
28. Murray JC, Karp LE, Williamson RA, et al. Rh isoimmunization related to amniocentesis. Am J Med Genet. 1983; 16(4):527-34.
29. Midtrimester Amniocentesis for Prenatal Diagnosis: Safety and Accuracy. The NICHD National Registry for Amniocentesis Study Group 1976. JAMA. 1976;236:1471-6.
30. Hunter AG. Neonatal lung function following mid-trimester amniocentesis. Prenat Diagn. 1987;7(6):433-41.
31. An assessment of the hazards of amniocentesis. Report to the Medical Research Council by their Working Party on Amniocentesis. Br J Obstet Gynaecol. 1978;85 Suppl 2:1-41.
32. Valenti C. Antenatal detection of hemoglobinopathies. A preliminary report. Am J Obstet Gynecol. 1973;115(6):851-3.
33. Chang H, Hobbins JC, Cividalli G, et al. In utero diagnosis of: hemoglobinopathies. Hemoglobin synthesis in fetal red cells. N Engl J Med. 1974;290(19):1067-8.
34. Daffos F, Capella-Pavlovsky M, Forestier F. A new procedure for fetal blood sampling in utero: preliminary results of fifty-three cases. Am J Obstet Gynecol. 1983; 146(8):985-7.
35. Antsaklis AI, Papantoniou NE, Mesogitis SA, et al. Cardiocentesis: an alternative method of fetal blood sampling for the prenatal diagnosis of hemoglobinopathies. Obstet Gynecol. 1992;79(4):630-3.
36. Nicolini U, Nicolaidis P, Fisk NM, et al. Fetal blood sampling from the intrahepatic vein: analysis of safety and clinical experience with 214 procedures. Obstet Gynecol. 1990;76(1):47-53.
37. Papantoniou N. Fetal Blood Sampling. In: Antsaklis AJ, Troyano JM. (Eds). Donald School Textbook of Interventional Ultrasound. New Delhi: Jaypee Brothers Medical Publishers (P) LTD; 2008. pp. 86-99.
38. Antsaklis A, Daskalakis G, Papantoniou N, et al. Fetal blood sampling—indication-related losses. Prenat Diagn. 1998;18(9):934-40.
39. Weiner CP, Okamura K. Diagnostic fetal blood sampling-technique related losses. Fetal Diagn Ther. 1996;11(3):169-75.
40. Hogge WA, Thiagarajah S, Brenbridge AN, et al. Fetal evaluation by percutaneous blood sampling. Am J Obstet Gynecol. 1988;158(1):132-6.
41. Weiner CP, Wenstrom KD, Sipes SL, et al. Risk factors for cordocentesis and fetal intravascular transfusion. Am J Obstet Gynecol. 1991;165(4 Pt 1):1020-5.
42. Jauniaux E, Donner C, Simon P, et al. Pathologic aspects of the umbilical cord after percutaneous umbilical blood sampling. Obstet Gynecol. 1989;73(2):215-8.
43. Nicolini U, Kochenour NK, Greco P, et al. Consequences of fetomaternal haemorrhage after intrauterine transfusion. BMJ. 1988;297(6660):1379-81.
44. Ghidini A, Sepulveda W, Lockwood CJ, et al. Complications of fetal blood sampling. Am J Obstet Gynecol. 1993;168(5):1339-44.
45. Antsaklis A, Gougoulakis A, Mesogitis S, et al. Invasive techniques for fetal diagnosis in multiple pregnancy. Int J Gynaecol Obstet. 1991;34(4):309-14.

CHAPTER 41

Invasive Genetic Studies in Multiple Pregnancy

Aris J Antsaklis, George A Partsinevelos

INTRODUCTION

Multiple pregnancies including twin and higher order pregnancies *a priori*, are considered high-risk pregnancies. They are mainly associated with prematurity and low birth weight, which undoubtedly increase perinatal morbidity and mortality. In fact, it would appear that despite modern prenatal management, prematurity rate in multiple pregnancies has not changed during the last 50 years. However, perinatal mortality rates have declined due to improved neonatal care.[1]

The risk of complications is not only related to the number of fetuses, but also strongly influenced by chorionicity. Chorionicity refers to placentation, whereas zygosity implies the genetic profile of the pregnancy and therefore determines the degree of risk and whether or not the fetuses may be concordant or discordant for chromosomal abnormalities, and genetic diseases. In terms of physiology, zygosity is associated with the number of fertilized oocytes, which resulted in multiples and chorionicity, reflects the exact postconception day when the early embryonic splitting took place. Epidemiologic studies have shown that more than 30% of twin pregnancies are monozygotic (MZ) and nearly 70% are dizygotic (DZ).

Monozygotic twins originate from the division of a single fertilized ovum with an incidence rate of about 2.3–4/1000 pregnancies. The rate of spontaneous MZ twin pregnancies is constant contrary to the increased incidence of MZ twin pregnancies derived from infertility treatment techniques. Monozygotic twins may be dichorionic (DC) or monochorionic (MC), the chorionicity is determined by the period of embryonic development when zygotic division takes place. In about 20–30% of cases, splitting occurs within 3 days of fertilization resulting in separate fetuses with independent placental circulations, therefore being dichorionic-diamniotic (DC-DA), even if placentas may seem to be in continuity or fused. In the majority of cases (about 70%) splitting within the first week but later than the third day results in a single MC plate and two distinct amniotic sacs, hence monochorionic-diamniotic (MC-DA) twins are generated. Delayed zygotic splitting leads to monochorionic-monoamniotic (MC-MA) twins, accounting for 1% of MZ twins, though later than 13th day is extremely rare, resulting in the formation of the abnormal conjoined (Siamese) twins.

Dizygotic twins result from the fertilization of two distinct ova, thus may be of the same or different sex. The incidence rate varies significantly, influenced by race (higher in blacks, lower in Asians), heredity, maternal age (peak between 35–40 years of age), history of previous DZ twin pregnancy, nutrition habitus and anthropometric features (height and weight) of the woman.

INCIDENCE OF STRUCTURAL FETAL ANOMALIES IN MULTIPLES

The rising rate of multiple pregnancies recorded nowadays is mainly attributed to the widespread use of infertility treatment modalities. *In vitro* fertilization and ovulation induction with or without intrauterine insemination account for approximately two-thirds increase in multiple gestations, whereas the other one-third results from delayed childbearing in increasingly advanced reproductive age.[2]

Advanced maternal age has been associated with higher rate of aneuploidies. Assisted conception has been claimed to result in an increased rate of MZ twins to greater than 10-fold, the latter being at high-risk of functional and structural abnormalities, affecting 10–15% of these twins.[3-5] In particular, neural tube defects, anencephaly, holoprosencephaly, sirenomelia complex, cloacal exstrophy and abnormalities that fit into the expanded VATER/VACTERAL associations are more common in MZ twins. Abnormalities unique to the MZ multiple conception include conjoined twinning, fetus in feto, acardia and fetus papyraceous. A plausible explanation for the increased incidence of abnormalities in MZ twins, involve the role of hemodynamic imbalance between MC twins through placental vascular anastomoses. Hence, the frequency of malformations in MZ twins is two-three times higher than singletons, whereas in DZ twins is thought to be similar to that of singletons (2–3%).

It has been stressed that the risk of fetal abnormalities in twins may be biased because multiple pregnancies are intensively scanned, increasing the chances of detecting underlying anomalies. Moreover, twinning is much more common in women of advanced age, in whom prenatal screening is more likely to yield the diagnosis of fetal defects as far as maternal aging is associated with increased risk for fetal abnormalities.

Conclusively, available data confirm that twin pregnancies *per se* are at increased risk for fetal chromosomal abnormalities than singletons.[6-7] Hence, the increasing incidence of multiple pregnancies highlights a concomitant increase in the need for invasive diagnostic procedures in these pregnancies.

RISK OF ANEUPLOIDY IN MULTIPLES

Contrary to the constant frequency of MZ twinning all over the world, which is independent of the age of the woman, DZ twin rate is strongly related to maternal age possibly attributed to changes in follicle stimulating hormone production to the higher side.

Zygosity represents the genetic make-up of the developing entities, thus determination of this parameter is considered a prerequisite in multiple pregnancy prenatal screening for aneuploidies.

Taking into consideration the incidence of MZ-DC-DA (20–30% of MZ twins, the latter accounting for 30% of all twin pregnancies) and DZ pregnancies, which are always DC-DA (70% of all twin pregnancies), once dichorionicity is diagnosed, the pregnancy is most likely DZ (around 10% chance of monozygosity). Therefore, chorionicity roughly corresponds to zygosity in these cases.[8]

Accurate diagnosis of chorionicity in multiples is limited to the first trimester of pregnancy. To this end, sonographic measurement of the thickness of the intertwin membrane and recognization of "lambda" or "twin peak" sign have been used. A cut-off value of 2 mm for intertwin membrane thickness may discern MC versus DC twinning, though a high inter- and intra-observer variability has been reported. Sonographic detection of the "lambda" or "twin peak" sign is reported as a more reliable indicator of DC placentation with an accuracy of 100% in 10–14 weeks gestation.[9] Delayed in the second-trimester ultrasound assessment is associated with a 10–12% chorionicity misinterpretation rate,[10,11] while after 20 weeks of gestation the determination may be impossible.

In the absence of the "lambda" or "twin peak" sign in a DA twin pregnancy, single placentation and monozygosity is concluded. However, when a single amniotic sac is detected, monochorionicity is indisputable.

Monozygoyic twins are of the same sex and genetically identical. Therefore, the risk for chromosomal abnormalities does not differ from that in singletons. Very infrequently, mutations can cause genetic discordance between MZ siblings, involving mosaicism, skewed-X-inactivation, differential gene imprinting and small scale mutation.[12] Heterokaryotypia, is used to define the rare karyotypic discordance, most commonly expressed by one fetus affected by Turner syndrome, whereas the other presents either a normal male or normal female karyotype.[13-15] Monozygotic discordance for trisomy 21, Klinefelter syndrome, Pateau syndrome, trisomy 1 and 22q11 deletion syndrome have also been described.[15-19] However, these unusual discrepancies are not taken into consideration when calculating aneuploid risk, though it should always be assumed when invasive prenatal diagnosis is performed dictating sampling from both sacs.

In DZ twins, each embryo has an independent risk for aneuploidy and therefore the risk that at least one fetus being affected will be almost twice the maternal

age risk for a singleton. The probability of both fetuses being involved is minimal.[20] In cases with uncertain chorionicity and thus zygocity, aneuploidy risk assessment requires an estimation of the most likely zygocity, which may vary according to maternal age and race. In general, given that one-third of all twin pairs are monozygotic, the risk for one twin being aneuploid in case of unknown zygosity is calculated to five-thirds that of the singleton risk.[8,10] Based on these estimations, a 33-year-old woman bearing twins has a risk for at least one aneuploid offspring, comparable to the risk of a 35-year-old woman bearing a singleton. On this assumption, such women should be offered prenatal testing.[21] However, despite these aspects, reported series show a lower risk for fetal chromosomal abnormalities in live-born twins.

INDICATIONS FOR PRENATAL DIAGNOSIS

In fetal medicine, it is common practice to extrapolate the data derived from singletons to multiples. Currently, all pregnancies singletons and multiples should undergo prenatal screening for chromosomal and structural abnormalities. Furthermore, advanced maternal age, a previous conceptus with chromosomal abnormality, a parent with a structural chromosome rearrangement and the presence of gene associated inborn errors of metabolism draw more attention and render prenatal screening imperative. Screening strategies have been extensively studied in singletons. Nuchal translucency (NT) measurement along with maternal serum biochemistry determination have been widely adopted in first trimester risk assessment for fetal aneuploides, whereas additional sonographic markers, such as absent nasal bone, abnormal Doppler waveform in the ductus venosus and tricuspid regurgitation have been recently validated. In order to apply these screening tests in multiple pregnancies, cautious interpretation of the results is needed to minimize possible erroneous high false positive rate and subsequent high rate of undue invasive procedures. Fortunately, as non-invasive early pregnancy risk assessment is rapidly gaining popularity, invasive procedures such as chorionic villus sampling (CVS) and amniocentesis are gradually restricted in cases where rationale exists.

In fact, first trimester utrasound screening for chromosomal abnormalities in DC multiple pregnancies has yielded comparable results to singletons in terms of detection rate as well as false positive rate.[22] However, in MC twins, a cautious interpretation of increased NT thickness should be adopted in respect to the possibility of an underlying early twin-to-twin transfusion syndrome. A rational approach would be to use the average of NT measurement of both fetuses in risk assessment.[23]

On the other hand, first trimester maternal serum biochemistry, including β-hCG and PAPPA has been blamed for low sensitivity and specificity in multiple gestations due to the innability to determine the degree to which each fetus contributes to the overall maternal biochemistry level. A reasonable model of "pseudo risk" approach has been proposed based on the utilization of the quotient derived from the division of the biomarkers' level as multiples of the median (MoM) by the corresponding medians for normal twins.[24-26] However, no adequate data has validated this approach so far.

With regards to maternal serum alpha-fetoprotein (MSAFP) level in the second trimester, in twin pregnancy it is measuring twice as high as in a singleton and 40% of twins are associated with MSAFP levels of more than a 2.5 MoM at 16 weeks.[27] Obviously, elevation of this serum marker may be attributed to the existence of more than one fetuses in multiple pregnancies. However, the possibility of an open neural tube defect in one or more fetuses should always be beared in mind. Thereby, amniocentesis performed in twins where MSAFP exceeds 4.5 MoM is probably justified.[28]

Since the implementation of maternal biochemistry in risk assessment for aneuploides in twin or higher-order multiple gestations remains arguable, ultrasound scan has been proven of greater value for early determination of chorionicity and subsequent standardized NT measurement as well as genetic sonogram, targeting to identify possible sonographic markers of fetal aneuploidy.

INVASIVE PROCEDURES FOR PRENATAL DIAGNOSIS

Amniocentesis

As alluded to earlier, twin or higher order multiple pregnancies are at increased risk of aneuploides and fetal structural defects compared with singletons. Estimations of a maternal age older than 35 years at which invasive genetic studies would be justified in these pregnancies have been made.

Amniocentesis, performed in the second trimester of pregnancy later than 15 weeks has been proven a safe and efficient procedure for sampling fetuses of a multiple gestation. Ideally, it is performed between 15–18 weeks of gestation.[29] Application of the procedure

earlier in pregnancy has been associated with increased risk of fetal loss, amniotic fluid leakage and fetal talipes equinovarous, and therefore is not recommended.[10,30,31]

A detailed ultrasound evaluation of the multiple pregnancy should be performed before amniocentesis to determine chorionicity, amnionicity, and location of the placenta(s), the size, anatomy and position of each fetus. Furthermore, "labeling" of the multiples should be encouraged to ensure correct sampling from each sac. Recently, the role of amniotic fluid alpha-fetoprotein (AFAFP) level was evaluated in confirmation of both the sacs in a DC pregnancy being sampled.[32]

To date, three different approaches for tapping multiple sacs have been described. All of them use a needle to aspirate amniotic fluid transabdominally under ultrasound guidance. The first one, initially described by Elias et al. in 1980, is called the technique of double amniocentesis.[33] It involves two or more separate and sequential needle insertions, one for each sac. In particular, a 22G 3.5 inch spinal needle is inserted into each sac transabdominally under ultrasound visualization, and about 20 ml of amniotic fluid is readily aspirated and sent for cytogenetic evaluation or fetal karyotyping. The possibility of sampling twice the same amniotic sac is probably the major drawback of this technique. Although, the instillation of a foreign substance into the amniotic cavity is of concern, marking the sampled sac with a dye following aspiration to avoid reinsertion into it and thereby erroneous sampling, has been practiced. In this context, indigo carmine has been successfully used without any adverse event,[34] although a mild vasoconstrictive effect following intravenous injection has been reported. However, indigo carmine tends to concentrate at the bottom of the sac following instillation and takes some time before the stained fluid surrounds the fetus. Methylene blue used as a marker dye in the past has been linked to certain toxic manifestations such as fetal hemolysis, fetal small bowel atresias and fetal death.[35-40] Presently, technologic advances combined with increasing operator experience render the high-resolution ultrasound equipment in expertise hands as an invaluable tool for safer and accurate sampling from each sac,[41,42] reserving the installation of dye for cases of amniotic volume discordance where detection of the septum is uncertain or high-order pregnancies, where preprocedure sonographic mapping and "labeling" of sacs is not feasible.[43]

An alternative approach is the single-needle insertion technique. It was first described by Jeanty et al. in 1990.[44] The needle entry is made into the proximal sac near the insertion of the dividing membrane and 20 ml of amniotic fluid are retrieved. Following replacement of the stylet, the needle is advanced through the second sac under direct ultrasound guidance. In order to avoid contamination, the first few milliliters of amniotic fluid are discarded and aspiration of 20 ml from the second sac integrates the procedure. Many advantages linked to this technique have been reported: requiring only one needle insertion, and being swifter and shorter reduces woman's discomfort as well as the risk of postprocedural complications. Moreover, advancing the needle through the septum between the two sacs under ultrasound guidance provides positive proof of tapping both of them, diminishing the need for dye insertion. However, potential disadvantages render this approach less popular. Possible contamination of the second sample with amniotic fluid and fetal cells from the first one may lead to an incorrect diagnosis of mosaicism in the second fetus. This complication can be avoided by strictly adhering to the technique by replacing the stylet prior to intertwin membrane penetration and by discarding the first few milliliters from the second sac. Besides, the possibility of converting DA to pseudo-MA twin preganancy with the corresponding risks for cord entanglement and the formation of the amniotic band syndrome cannot be precluded.[45] In addition, a technical difficulty in penetrating a "tenting" dividing membrane has been reported.

In 1992, a novel approach for amniocentesis was introduced by Bahado-Singh et al. It was described as the double simultaneous amniocentesis technique.[46] Basically, two needles are inserted separately into the amniotic sacs under ultrasound visualization like in the technique of double amniocentesis. The difference is that after aspiration of the amniotic fluid from the first sac, the needle is left in place indicating the sampled cavity and the second insertion is made into the other sac. The main advantage seems to be the documentation of correct sampling from each sac. However, it is not widely used mainly because it is more time consuming and thereby the experience with this approach is limited. Procedure-related fetal loss rate in multiple pregnancies has been assessed in various studies. Early reports suggested a higher fetal loss rate in twin pregnancies than in singletons.[47-49] However, these studies did not take into account the possibility that the increased fetal wastage might be attributed to the twin pregnancy itself rather than the invasive procedure. Subsequently, it was reported that the maternal history of twins *per se* carries a pregnancy loss rate up to 24 weeks of about 6.3% and severe prematurity (24–28 weeks) rate of about 8%.[50] Most series of pregnancy outcome following second trimester amniocentesis report loss rates before 20

weeks' gestation of between 1% and 2.5% and a much higher loss rate before 28 weeks. In a multicenter European study, the pregnancy loss rate was estimated to be 2.3% and 3.7% before 20 and 28 weeks' gestation respectively.[51] In a case-control study, a similar fetal loss rate was reported between sampled twins and unsampled matched twin controls (3.5% vs 3.2%).[52]

In conclusion, amniocentesis in twin pregnancies has been shown to be a safe and accurate diagnostic tool, providing that sampling involve both the sacs regardless of the zygocity and chorionicity.

Chorionic Villus Sampling

Chorionic villus sampling is a standard first trimester invasive approach for genetic studies in case of suspected aneuploidy or congenital genetic disease. It is considered a safe alternative invasive procedure to amniocentesis for prenatal diagnosis in singletons, whenever early diagnosis is needed. Furthermore, CVS has been shown to be safe and effective for sampling twin gestations as well.[53-55]

Chorionic villus sampling is best performed between 11 weeks and 13 weeks of gestation. Genetic results are available either within hours by direct preparations of the cytotrophoblast layer or within 3–7 days by tissue culture of chorionic villus mesenchymal core. Thus, early diagnosis is reached in case that routine first trimester prenatal screening for chromosomal abnormalities yields a high risk for one of the fetuses or in case that an increased risk of a genetic disease such as beta-thalassemia, cystic fibrosis, hemophilia and congenital adrenal hyperplasia are estimated due to the carrier status of one or both the prospective parents. Undoubtedly, early diagnosis provides earlier reassurance of fetal well-being and thereby eliminates both maternal anxiety and uncertainty regarding the present gestation. On the other hand, the diagnosis of one or both abnormal fetuses allows subsequent selective reduction of the affected fetus or termination of the total pregnancy as early as in the first trimester, where complication rates are lower. Moreover, fetal reduction performed earlier in pregnancy is associated with a higher survival rate of the unaffected twin.[56] In terms of privacy and maternal psychology, the earlier an abnormal pregnancy is terminated, the lesser the chance of being widely recognized.

Two different approaches have been used so far for first trimester CVS in multiple gestations, depending on physician's experience and location of the placenta: transabdominal and transcervical. Several pros and cons have been linked to each of them, but it is postulated that irrespective of the route adopted, first trimester CVS is technically more challenging than second trimester amniocentesis. Transcervical CVS is performed either with an aspiration catheter or using biopsy forceps under ultrasound guidance. Technical difficulties and a "learning curve" that involves many patients characterize this approach. Transabdominal technique uses an aspiration needle and is technically more similar to mid-trimester amniocentesis. Subsequently, this technique is more familiar to specialists in fetal medicine and thus more widely adopted by many centers.

Since no marker is available to assure sampling from each chorion, continuous ultrasound localization of the tip of the needle or catheter is required. If in doubt, a follow-up procedure should be performed either by an immediate repeat CVS or by second trimester amniocentesis. A serious drawback of CVS is a potential contamination of one sample by villi belonging to the other chorion leading to a confusing or even misleading diagnosis. Although, early studies suggested a contamination rate as high as 4%, more recent studies report a much lower rate, almost nullified.[57,58] Still, Weisz and Rodeck suggest that it would be prudent to counsel patients that about 2–3% of twin pregnancies having CVS will need resampling because of uncertainty of results.[43] A tip to eliminate this unfortunate possibility is to obtain samples adjacent to the cord insertion site far away from the dividing membrane.

In case that chorions are not readily accessible transcervically, the combined transabdominal-transcervical route can be opted.

Diagnosis of aneuploidy or severe genetic disease in one of the multiples is usually indicative of selective termination of the affected fetus. In such cases, detailed documentation and "labeling" of the fetuses, and the chorions is as equally important with CVS as with amniocentesis in order to diminish the possibility of unintentional erroneous termination of the healthy co-multiple. Although, the position of sacs will remain unchanged during the 2–3 weeks time following sampling, it is standard practice to reconfirm the original diagnosis in both fetal and chorionic tissues before selective termination of the affected twin. Of note, CVS does not increase pregnancy loss rate before multifetal pregnancy reduction.[59]

The estimated risk of CVS associated fetal loss in singletons varies widely (1.3–4.3%). Two or more samplings during one procedure have been linked to increased risk of post-procedural miscarriage,[60,61] implying that the risk may be higher in twin sampling. Overall an estimated risk of 2–4% in twin pregnancies has been reported. However, available data demonstrate significant variations. In a study, the risk of CVS asso-

ciated fetal loss before 28 weeks' gestation did not seem to differ between twin and singleton pregnancies (4.9 vs 4%).[53] When only chromosomal normal pregnancies are considered, the overall loss rate found in a study of 202 twin pregnancies that underwent CVS became 3.7%, a figure that is considerably less than that of amniocentesis.[53] In another study, the pregnancy loss rate before 20 weeks following CVS was found 3.3% comparable to 2.8% in a control group of twin pregnancies undergone amniocentesis. Hence, it may be claimed that in experienced centers, CVS is as safe as amniocentesis for sampling twins.

The ideal method for prenatal invasive genetic screening in multiple pregnancies is still a matter of debate. Available data confirm that amniocentesis and CVS share the same safety, and efficacy profile in expertise hands. However, amniocentesis is technically easier and widely adopted, whereas CVS results are available about one month earlier, thus therapeutic as well as selective termination is safer. Hence, none of them can be considered superior than the other, if the characteristics of the pregnancy are not taken into account. By all odds, each case should be individualized and the ultimate choice should be based on several factors, such as gestational age at referral date, placental location, operator's experience and the likelihood of selective feticide. It should be emphasized that if the center is not skilled and experienced in CVS, amniocentesis should be preferred. A rational approach may be as follows: the choice of invasive technique should be based on individual risk calculated from the combination of maternal age and fetal NT thickness measured in the first trimester. When the risk for a chromosomal defect, in at least one of the fetuses is greater than one in 50, it may be preferable to perform CVS. For pregnancies with a lower risk, amniocentesis after 15 weeks may be more appropriate.

FETAL BLOOD SAMPLING

The main principles of fetal blood sampling in twins and higher order multiple pregnancies do not differ substantially from those in singletons. However, from a technical point of view, the procedure in multiples is much more challenging.

Traditionally, fetal blood sampling was mainly indicated in cases that amniocentesis or CVS yielded uncertain or equivocal results, necessitating confirmation or clarification respectively. Another indication was the need for a rapid chromosomal diagnosis (rapid karyotyping), in as much as the results are available in 2–3 days time. Nowadays, novel molecular techniques allow rapid karyotype determination using amniocentesis specimen, thereby reserving fetal blood sampling in cases where rationale exists. The main indications today are rhesus isoimmunization, hydrops of unknown origin and fetal infections. From a therepeutic aspect, cordocentesis can serve in injecting pharmacologic agents into the fetal circulation or even blood transfusion in severe fetal anemia.

Similarly to singletons, a meticulous ultrasound examination should precede fetal blood sampling in multiples. In addition to fetal growth, anatomy and position of each fetus, chorionicity, amnionicity, location of the placenta(s), and umbilical cord insertion should be determined. Furthermore, "labeling" of the multiples is needed to assure correct sampling from each fetus.

In a study conducted in 2003, involving 84 twin pregnancies, mainly screened for hemoglobinopathies, the overall procedure-related fetal loss (up to 2 weeks post-procedurally) was 8.2%, about four-fold higher than the correspondence risk in singletons. However, this technique can be used as an alternative to amniocentesis after 20 weeks of gestation to confirm an abnormal karyotype in a DC pregnancy, when selective feticide is considered a few weeks after the initial procedure.[62]

CONCLUSION

Nowadays, there is an increasing demand for invasive genetic studies in multiple pregnancies due to the rising rate of multiple conceptions, the latter mainly attributed to infertility treatment modalities. Diagnosis of fetal aneuploidies and genetic defects can be accomplished either by first trimester CVS or by second trimester amniocentesis, whereas it is claimed that they are equally safe in expertise hands. Hence, the experience of the center performing the procedure should be emphasized in decision making with regards to the procedure opted. The indications of fetal blood sampling are currently limited and progressively replaced by novel molecular techniques implemented in CVS or amniocentesis specimen. High resolution ultrasound equipment available today, together with increasing operator experience gained throughout the years, results in more accurate and effective invasive prenatal diagnosis in twin or higher-order pregnancies, minimizing post-procedural fetal loss risk.

REFERENCES

1. Kiely JL, Kleinman JC, Kiely M. Triplets and higher-order multiple births.Time trends and infant mortality. Am J Dis Child. 1992;146:862-8.

2. Bergh T, Ericson A, Hillensjö T, et al. Deliveries and children born after in-vitro fertilisation in Sweden 1982-95: a retrospective cohort study. Lancet. 1999;354:1579-85.
3. Derom C, Vlietinck R, Derom R, et al. Increased monozygotic twinning rate after ovulation induction. Lancet. 1987;1:1236-8.
4. Wenstrom KD, Syrop CH, Hammitt DG, et al. Increased risk of monochorionic twinning associated with assisted reproduction. Fertil Steril. 1993;60:510-4.
5. Blickstein I. Estimation of iatrogenic monozygotic twinning rate following assisted reproduction: Pitfalls and caveats. Am J Obstet Gynecol. 2005;192:365-8.
6. Kohl SG, Casey G. Twin gestation. Mt Sinai J Med. 1975;42: 523-39.
7. Nicolaides KH, Sebire NJ, Snjiders RJM. The 11-14 Week Scan. The Diagnosis of Fetal Abnormalities. In: Nicolaides K, Sebire NJ, Snjiders RJM (Eds). New York: Parthenon Publishing; 1999.
8. Matias A, MontenegroN, Blickstein I. Down syndrome screening in multiple pregnancies. Obstet Gynecol Clin North Am. 2005;32:81-96.
9. Sepulveda W, Sebire NJ, Hughes K, et al. Evolution of the lambda or twin-chorionic peak sign in dichorionic twin pregnancies. Obstet Gynecol. 1997;89:439-41.
10. Jenkins TM, Wapner RJ. The challenge of prenatal diagnosis in twin pregnancies. Curr Opin Obstet Gynecol. 2000;12:87-92.
11. Wood SL, St Onge R, Connors G, et al. Evaluation of the twin peak or lambda sign in determining chorionicity in multiple pregnancy. Obstet Gynecol. 1996;88:6-9.
12. Machin GA. Some causes of genotypic and phenotypic discordance in monozygotic twin pairs. Am J Med Genet. 1996;61:216-28.
13. Rogers JG, Voullaire L, Gold H. Monozygotic twins discordant for trisomy 21. Am J Med Genet. 1982;11:143-6.
14. Dallapiccola B, Stomeo C, Ferranti G, et al. Discordant sex in one of three monozygotic triplets. J Med Genet. 1985;22:11.
15. Perlman EJ, Stetten G, Tuck-Müller CM, et al. Sexual discordance in monozygotic twins. Am J Med Genet. 1990;37:551-7.
16. Schmid O, Trautmann U, Ashour H, et al. Prenatal diagnosis of heterokaryotypic mosaic twins discordant for fetal sex. Prenat Diagn. 2000;20:999-1003.
17. Wachtel SS, Somkuti SG, Schinfeld JS. Monozygotic twins of opposite sex. Cytogenet Cell Genet. 2000;91:293-5.
18. Lespinasse J, Gicquel C, Robert M, et al. Phenotypic and genotypic variability in monozygotic triplets with Turner syndrome. Clin Genet. 1998;54:56-9.
19. Nieuwint A, Van Zalen-Sprock R, Hummel P, et al. Identical' twins with discordant karyotypes. Prenat Diagn. 1999;19:72-6.
20. RodisJ.F, EganJ.F, Craffey A, et al. Calculated risk of chromosomal abnormalities in twin gestations. Obstet Gynecol. 1990;76:1037-41.
21. Weinblatt V, Wapner RJ. Chorionic villus sampling and amniocentesis in multiple pregnancy. In: Creasy RK, Resnik R (Eds). Maternal-Fetal Medicine Principles and Practice, 4th edition. Philadelphia: WB Saunders; 1999. pp. 201-11.
22. Sebire NJ, Snijders RJ, Hughes K, et al. Screening for trisomy 21 in twin pregnancies by maternal age and fetal nuchal translucency thickness at 10-14 weeks of gestation. Br J Obstet Gynaecol. 1996;103:999-1003.
23. Vandecruys H, Faiola S, Auer M, et al. Screening for trisomy 21 in monochorionic twins by measurement of fetal nuchal translucency thickness. Ultrasound Obstet Gynecol. 2005;25:551-3.
24. Spencer K, Salonen R, Muller F. Down's syndrome screening in multiple pregnancies using alpha-fetoprotein and free beta hCG. Prenat Diagn. 1994;14:537-42.
25. Muller F, Dreux S, Dupoizat H, et al. Second-trimester Down syndrome maternal serum screening in twin pregnancies: impact of chorionicity. Prenat Diagn. 2003;23:331-5.
26. Wald NJ, Rish S. Prenatal screening for Down syndrome and neural tube defects in twin pregnancies. Prenat Diagn. 2005;25:740-5.
27. Gardner S, Burton BK, Johnson AM. Maternal serum alpha-fetoprotein screening: a report of the Forsyth County project. Am J Obstet Gynecol. 1981;140:250-3.
28. Wapner RJ. Genetic diagnosis in multiple pregnancies. Semin Perinatol. 1995;19:351-62.
29. Emery AE. Antenatal diagnosis of genetic disease. Modern Trends Hum Genet. 1970;1:267.
30. Jenkins TM, Wapner RJ. First trimester prenatal diagnosis: chorionic villus sampling. Semin Perinatol. 1999;23:403-13.
31. Cleary-Goldman J, D'Alton ME, Berkowitz RL. Prenatal diagnosis and multiple pregnancy. Semin Perinatol. 2005;29:312-20.
32. Delisle MF, Brosseuk L, Wilson RD. Amniocentesis for twin pregnancies: is alpha-fetoprotein useful in confirming that the two sacs were sampled? Fetal Diagn Ther. 2007;22:221-5.
33. Elias S, Gerbie AB, Simpson JL, et al. Genetic amniocentesis in twin gestations. Am J Obstet Gynecol. 1980;138:169-74.
34. Cragan JD, Martin ML, Khoury MJ, et al. Dye use during amniocentesis and birth defects. Lancet. 1993;341(8856): 1352.
35. Nicolini U, Monni G. Intestinal obstruction in babies exposed in utero to methylene blue. Lancet. 1990;336:1258-9.
36. Kidd SA, Lancaster PA, Anderson JC, et al. Fetal death after exposure to methylene blue dye during mid-trimester amniocentesis in twin pregnancy. Prenat Diagn. 1996;16:39-47.
37. McEnerney JK, McEnerney LN. Unfavorable neonatal outcome after intra-amniotic injection of methylene blue. Obstet Gynecol. 1983;61:35S-7S.
38. McFadyen I. The dangers of intra-amniotic methylene blue. Br J Obstet Gynaecol. 1992;99:89-90.
39. van der Pol JG, Wolf H, Boer K, et al. Jejunal atresia related to the use of methylene blue in genetic amniocentesis in twins. Br J Obstet Gynaecol. 1992;99:141-3.
40. Vincer MJ, Allen AC, Evans JR, et al. Methylene-blue-induced hemolytic anemia in a neonate. CMAJ. 1987;136: 503-4.
41. Antsaklis A, Souka AP, Daskalakis G, et al. Second-trimester amniocentesis vs. chorionic villus sampling for

prenatal diagnosis in multiple gestations. Ultrasound Obstet Gynecol. 2002;20:476-81.
42. Taylor MJ, Fisk NM. Prenatal diagnosis in multiple pregnancy. Baillieres Best Pract Res Clin Obstet Gynaecol. 2000;14:663-75.
43. Weisz B, Rodeck CH. Invasive diagnostic procedures in twin pregnancies. Prenat Diagn. 2005;25:751-8.
44. Jeanty P, Shah D, Roussis P. Single-needle insertion in twin amniocentesis. J Ultrasound Med. 1990;9:511-7.
45. Megory E, Weiner E, Shalev E, et al. Pseudomonoamniotic twins with cord entanglement following genetic funipuncture. Obstet Gynecol. 1991;78:915-7.
46. Bahado-Singh R, Schmitt R, Hobbins JC. New technique for genetic amniocentesis in twins. Obstet Gynecol. 1992;79: 304-7.
47. Palle C, AndersenJ.W, Tabor A, et al. Increased risk of abortion after genetic amniocentesis in twin pregnancies. Prenat Diagn. 1983;3:83-9.
48. Pijpers L, Jahoda MG, Vosters RP, et al. Genetic amniocentesis in twin pregnancies. Br J Obstet Gynaecol. 1988;323-326:4.
49. Anderson RL, Goldberg JD, Golbus MS. Prenatal diagnosis in multiple gestation: 20 years' experience with amniocentesis. Prenat Diagn. 1991;11:263-70.
50. Yaron Y, Bryant-Greenwood PK, Dave N, et al. Multifetal pregnancy reductions of triplets to twins: comparison with nonreduced triplets and twins. Am J Obstet Gynecol. 1999;180:1268-71.
51. Pruggmayer MR, Jahoda MG, Van der Pol JG, et al. Genetic amniocentesis in twin pregnancies: results of a multicenter study of 529 cases. Ultrasound Obstet Gynecol. 1992;2:6-10.
52. Ghidini A, Lynch L, Hicks C, et al. The risk of second-trimester amniocentesis in twin gestations: a case-control study. Am J Obstet Gynecol. 1993;169:1013-6.
53. Pergament E, Schulman JD, Copeland K, et al. The risk and efficacy of chorionic villus sampling in multiple gestations. Prenat Diagn. 1992;12:377-84.
54. Brambati B, Tului L, Lanzani A, et al. First-trimester genetic diagnosis in multiple pregnancy: principles and potential pitfalls. Prenat Diagn. 1991;11:767-74.
55. Wapner RJ, Barr MA, Heeger S, et al. Chorionic villus sampling: a 10-year over 13,000 consecutive case experience. In: Orlando FL (Ed). American College of Medical Genetics, First Annual Meeting; 1994.
56. Evans MI, Goldberg JD, Horenstein J, et al. Selective termination for structural, chromosomal, and Mendelian anomalies: international experience. Am J Obstet Gynecol. 1999;181:893-7.
57. De Catte L, Liebaers I, Foulon W. Outcome of twin gestations after first trimester chorionic villus sampling. Obstet Gynecol. 2000;96:714-20.
58. Brambati B, Tului L, Guercilena S, et al. Outcome of first-trimester chorionic villus sampling for genetic investigation in multiple pregnancy. Ultrasound Obstet Gynecol. 2001;17:209-16.
59. Ferrara L, Gandhi M, Litton C, et al. Chorionic villus sampling and the risk of adverse outcome in patients undergoing multifetal pregnancy reduction. Am J Obstet Gynecol. 2008;199:408.e1-4.
60. Rhoads GG, Jackson LG, Schlesselman SE, et al. The safety and efficacy of chorionic villus sampling for early prenatal diagnosis of cytogenetic abnormalities. N Engl J Med. 1989;320:609-17.
61. Kuliev A, Jackson L, Froster U, et al. Chorionic villus sampling safety. Report of World Health Organization/ EURO meeting in association with the Seventh International Conference on Early Prenatal Diagnosis of Genetic Diseases, Tel-Aviv, Israel, May 21, 1994. Am J Obstet Gynecol. 1996;174:807-11.
62. Antsaklis A, Gougoulakis A, Mesogitis S, et al. Invasive techniques for fetal diagnosis in multiple pregnancy. Int J Gynaecol Obstet. 1991;34:309-14.

42
CHAPTER

Magnetic Resonance Imaging: How to Use it During Pregnancy?

Ichiro Kawabata, Yuichiro Takahashi, Shigenori Iwagaki

INTRODUCTION

It has became possible to get easily and safely various kinds of information about the mother and fetus during pregnancy by using ultrasonography (USG). However, unsatisfactory results are obtained in some cases due to maternal fat tissue, fetal position or some other reasons. Magnetic resonance imaging (MRI), an imaging tool that has been rapidly spreading in medicine can provide clear images from multiple angles without X-ray exposure. We of course well understand the usefulness of USG, but believe that it is also important to evaluate the usefulness of MRI and how to use it during pregnancy.

SAFETY OF MRI

It is generally understood that X-ray exposure should be avoided during pregnancy. In contrast, MRI seems to be safe for the fetus, as indicated by the fact that there are no reported harmful effects from its use, including any mutagenic effects.[1] One potential problem of magnetic power is that it may lead to an elevation of the temperature especially in a packed cavity like the pregnant uterus. **Figure 42.1** shows our experimental values of intrauterine temperature measured during MRI procedure using a pregnant rabbit. This experiment revealed there was almost no temperature changing in the uterine cavity during exposure to magnetic power of 2.0 teslas which is higher than that used clinically. Thus, with respect to temperature, MRI seems to be safe for the fetus.

We have been administered contrast medium to the mother for MRI in some special cases. Harada reported data from animal experiments in which contrast medium was administered during the first trimester and concluded that these agents had made no bad effects on the fetus.[2]

Absolute safety of such agents cannot be assured until much larger studies are available for outcome analysis. Though the National Radiological Protection Board in The United States advises against imaging during the first trimester unless termination of pregnancy is probable; MRI is at least safer than X-ray procedures.

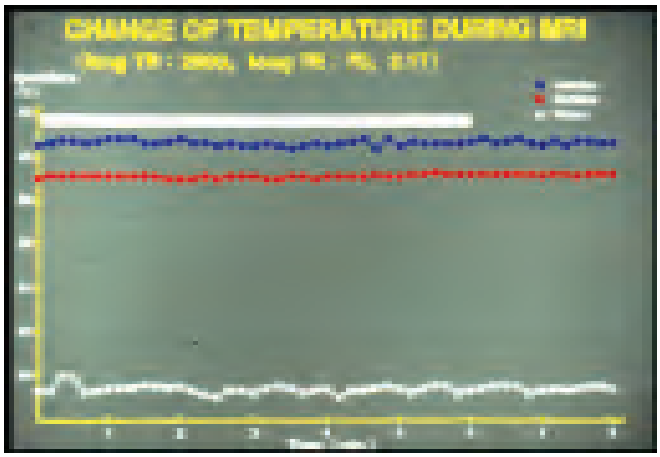

Figure 42.1: Measurement of intrauterine temperature. Results of an animal experiment using a pregnant rabbit. The intrauterine temperature was quite stable during the magnetic resonance imaging procedure

INDICATION AND PROCEDURES FOR MRI DURING PREGNANCY

First of all, MRI is not suitable for screening for fetal anomalies. However, there have been many reports of prenatal diagnoses of malformed cases based on MRI.[3] Based on our experience, we can divide the indications for MRI into the following categories:

- Pelvimetry
- Fetal anomalies
- Maternal tumors
- Examinations of the placenta
- Examinations of the umbilical cord.

We have performed 588 MRI procedures during pregnancy according to the above indications. The equipment we used was either a *signa advantage* or a *signa horizon* (1.5 T, GE medical systems, Milwaukee, WI) and *magnetom symphony* (1.5 T siemens medical solution erlangen). No drug was administered to the mother or fetus to control fetal movement because it was not necessary. We sometimes requested mothers to walk around for 15–20 minutes just before the MRI procedure to reduce fetal movement. Because of recent advances in MRI techniques that allow us to obtain a fetal image in a few seconds, it is not necessary to do anything to reduce the fetal movement. If the mother suffers from supine hypotension, the decubitus position is recommended.

Most MRI specialists might consider that thin-slice imaging should be performed, especially in cases of fetal anomaly, to get images from small fetuses. We disagree that thin-slice imaging is optimal in such cases because thin slices result in poorer image quality, especially from the point of image resolution. Even when the fetus is small, we recommend 10 mm imaging slices. After evaluation by such thick-slice imaging, if necessary or if possible, thin-slice imaging should be performed in cases in which it might yield useful information.

Pelvimetry

Maternal pelvic size and shape has in the past been evaluated by X-ray pelvimetry despite the fact that X-ray exposure should be avoided during pregnancy because there was no other way of evaluation. Several trials of MRI pelvimetry have been reported.[4,5] The MRI can be used to delineate pelvic size and shape clearly by obtaining images like the Guthmann and Martius images obtained in X-ray pelvimetry **(Figs 42.2 and 42.3)**. Furthermore, the pelvic size can be measured without any calculation such as that necessary in X-ray pelvimetry. **Figure 42.4** shows a T1-weighted image of

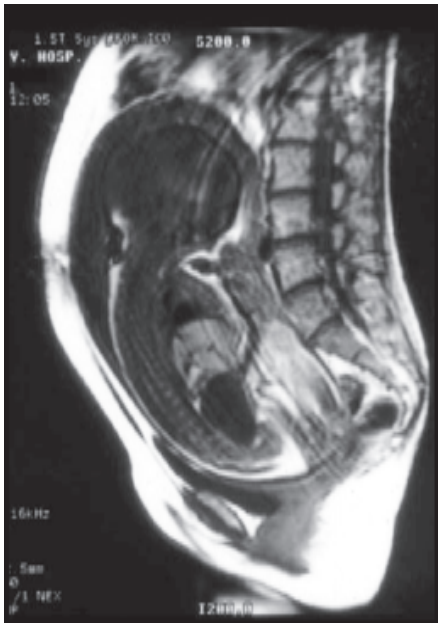

Figure 42.2: Magnetic resonance imaging pelvimetry, Guthmann's image. This image can be obtained by determining the maternal sagittal image. It is possible to measure the pelvic diameter directly without any calculation

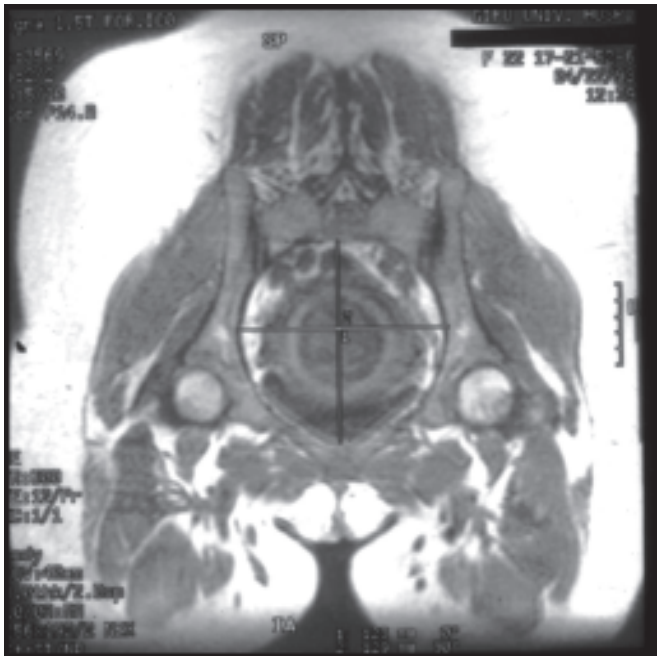

Figure 42.3: Magnetic resonance imaging pelvimetry, Martius image. The maternal pelvic shape is delineated clearly. We can obtain this image from the maternal sagittal image, which provides a theoretically better method of pelvimetry than X-ray pelvimetry

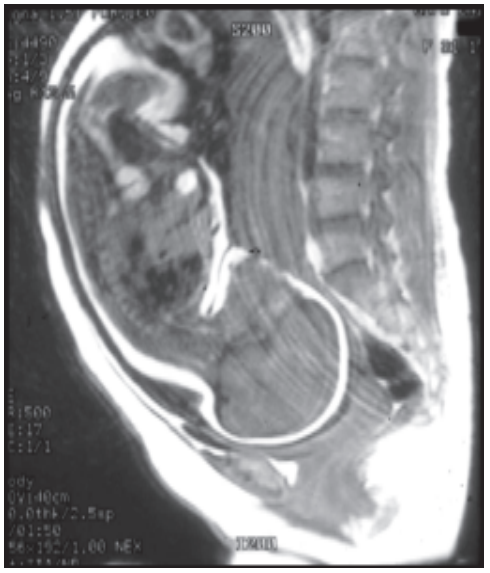

Figure 42.4: Diabetic macrosomia. The macrosomic fetus is rich in fat tissue especially in cases complicated with a maternal diabetic condition. Magnetic resonance imaging detects fetal subcutaneous fat tissue as high-intensity substance in T1-weighted images. This image makes it possible to evaluate relative fetal-pelvic disproportion, including disproportion of fetal soft tissue, unlike X-ray evaluation

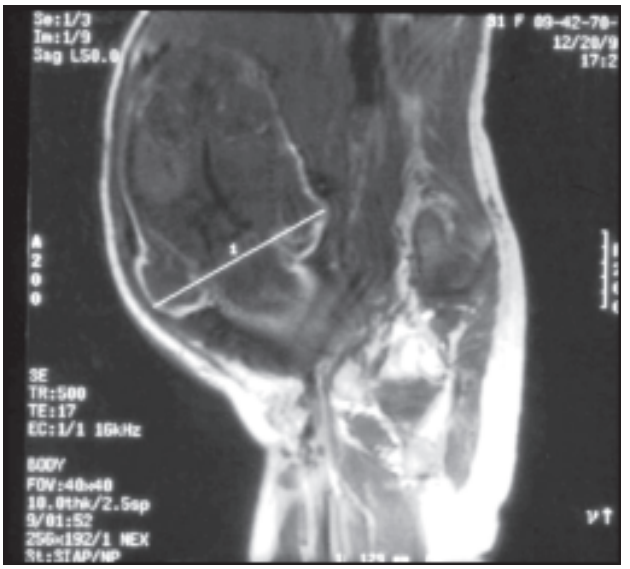

Figure 42.5: Shoulder size evaluation. Magnetic resonance imaging can image the fetus from multiple angles and thus allows us to measure the fetal shoulder size. Although the fetal shoulder size is flexible, it is an additional potentially important kind of information about the fetus

a diabetic macrosomic fetus. In this method of imaging, fat tissue is delineated as a high-intensity, white color. This image revealed that the fetal subcutaneous fat tissue was markedly thickened compared with that of a nondiabetic fetus like that in **Figure 42.2**. Thus MRI pelvimetry makes it possible to make a precise detection of relative cephalopelvic disproportion based on the ability to delineate fetal subcutaneous fat tissue as a high-intensity substance. This ability also makes it possible to measure fetal shoulder size **(Fig. 42.5)**. We can detect fetal malrotation clearly and precisely by MRI because it can delineate the whole fetal body in one image even just before onset of labor pain **(Fig. 42.6)**.

Maternal Tumors

Maternal tumors are not related to pregnancy but may occur and can be diagnosed during pregnancy. Similarly, luteinizing ovarian cysts related to pregnancy may occur. When a malignant tumor is suspected, the appropriate diagnostic tests should be performed on the mother. The MRI must be performed carefully in the first trimester of pregnancy. It is preferred to perform MRI first rather than X-ray imaging after the initial detection by USG because MRI is safer than X-ray imaging.

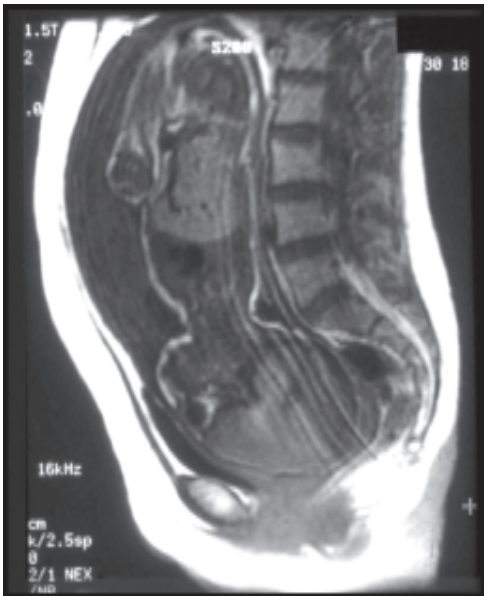

Figure 42.6: Malrotation of fetus. Fetal rotation can be evaluated by X-ray pelvimetry. However, magnetic resonance imaging provides information about this condition that is easier to understand

During pregnancy, obstetricians tend to image the fetus only to evaluate the fetal heartbeat, size, and so on. This tendency sometimes leads to missing the chance to detect maternal tumors in the early phase of pregnancy. With the advance of gestational age,

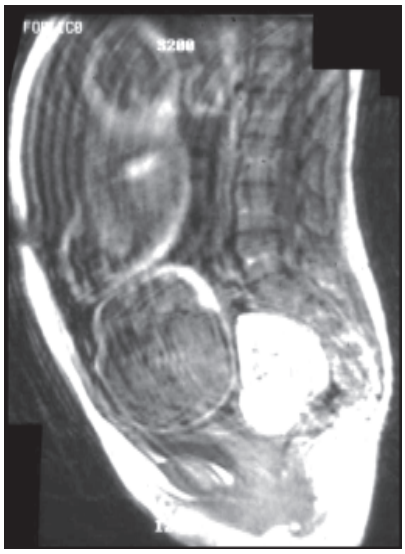

Figure 42.7: Maternal ovarian tumor. Because of the increased size of the uterus, maternal ovarian tumors are sometimes difficult to detect by ultrasonography. Magnetic resonance imaging can demonstrate such tumors even in the late phase of pregnancy

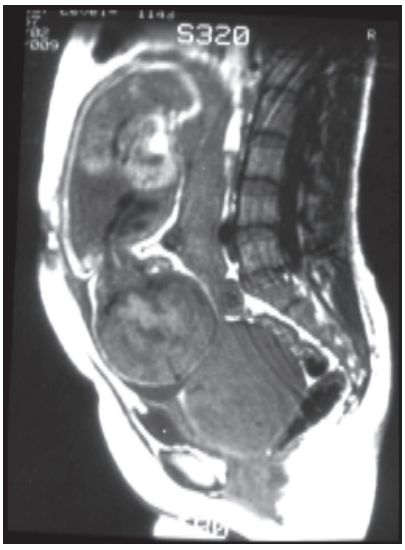

Figure 42.8: Maternal cervical myoma. It is difficult to differentiate between ovarian tumors and cervical myoma in advanced pregnancy. Magnetic resonance imaging provides a clear image of the cervical myoma

maternal tumors become difficult to diagnose because of the enlarged uterus. It may become difficult to distinguish between uterine tumors and ovarian tumors, especially when the tumor is located in the Douglas cavity. In such cases, MRI can provide critical information for a precise diagnosis **(Figs 42.7 and 42.8)**.

Fetal Anomalies

There have been many reports about prenatal diagnosis of various fetal anomalies that were detected by USG. The USG is convenient and easy to perform and it is the most popular tool for fetal diagnosis. However, this wonderful imaging tool is unfortunately not always perfect. Because of maternal fat tissue or fetal position, one sometimes gets unsatisfactory images that are not adequate for making a precise prenatal diagnosis. In such situations, it is necessary to use some other imaging tool to obtain important information about fetal problems.

The MRI is an imaging diagnostic tool that provides clear soft tissue images using magnetic power rather than X-rays. Thus, MRI can be performed during pregnancy. In the past, fetal MRI was performed while controlling fetal movement with sedatives or muscle relaxants, which in some cases were injected directly into the fetal circulation.[6] This procedure makes fetal MRI an invasive method. Although it is essential to control fetal movement to get a clear image of the fetus, we believe that MRI must ideally be a completely safe and drug-free examination for the pregnant woman and fetus. Accordingly the best way of perform fetal MRI is under condition of "spontaneously controlled fetal movement". When the mother walks around for 15 minutes just before the MRI procedure, the fetal movement markedly decreases. We cannot explain the reason for this decrease of fetal activity, but regular and rhythmic movement of the mother such as occurs in normal walking may produce an effect similar to rocking the baby in a cradle.

Another interference in fetal MRI is maternal breathing. With the advance of gestational age, the maternal breathing style changes to abdominal breathing. The maternal abdomen moves conspicuously, especially in the supine position. For these two reasons, the decubitus position may be recommended for fetal MRI procedures.

Figure 42.9 shows the success rate of fetal MRI using various imaging protocols through our experience. Obtaining superior-quality images of the fetus depends on the imaging time, with better images obtained during shorter times. Recently, MRI imaging techniques have rapidly advanced.[7] It takes only a few seconds to get an image using the latest method for imaging, which is called single shot fast spin echo or half fourier acquisition single shot turbo spin echo (HASTE).[8] Using such an ultra-high-speed imaging method, it is not necessary to control the fetal movement. Using this method of imaging, we could successfully obtain fetal images in all cases.

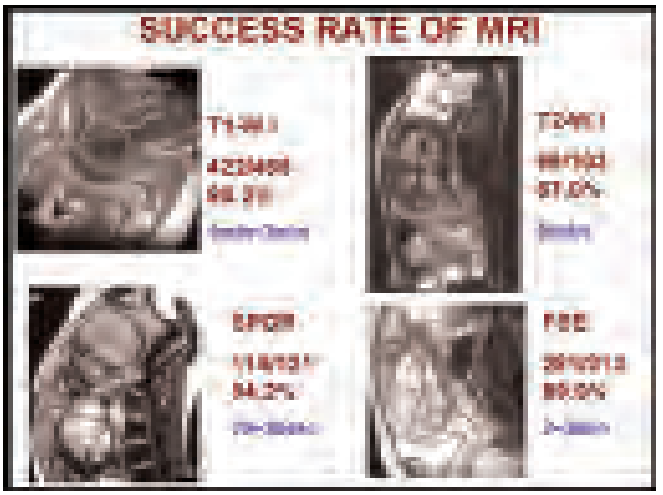

Figure 42.9: Success rate of fetal magnetic resonance imaging. We performed fetal magnetic resonance imaging without any drug use in the mother or fetus. The success rate of fetal magnetic resonance imaging depended on the imaging time

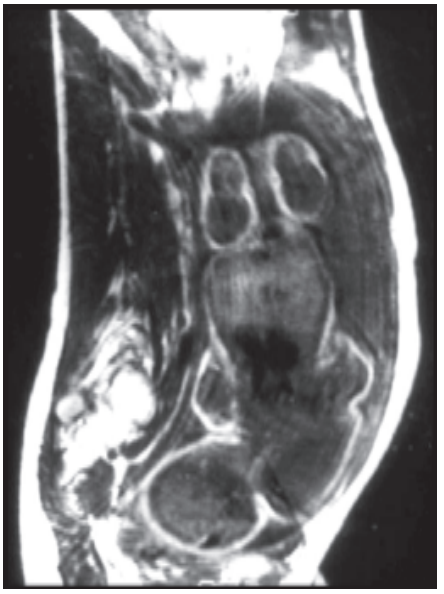

Figure 42.10: Cystic hygroma, T1-weighted image. From below the fetal ear to the shoulder, a huge tumor was delineated in low intensity. We measured the maximum fetal diameter, including the tumor

Figure 42.10 shows the MRI image of a cystic hygroma. It clearly reveals that a huge cystic tumor exists from below the ear to the shoulder, because MRI can delineate the fetal whole body in one image even in the late phase of pregnancy, which is one of the advantages of MRI. From this image, the origin of the tumor was clear and MRI made it possible to measure

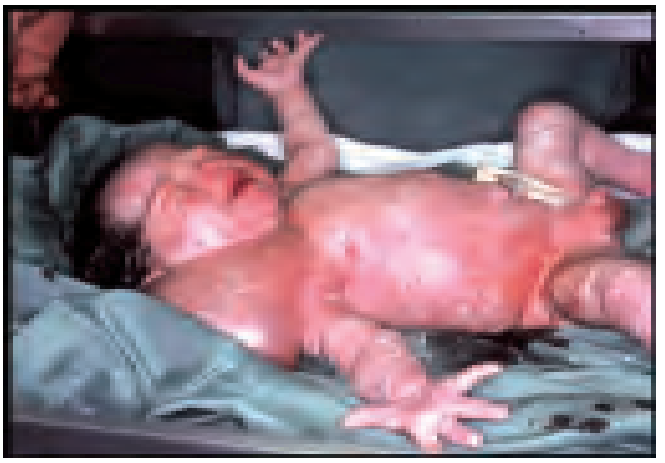

Figure 42.11: Cystic hygroma at birth. Macroscopic findings of the baby at birth. It is easy to see how good the information provided by magnetic resonance imaging was

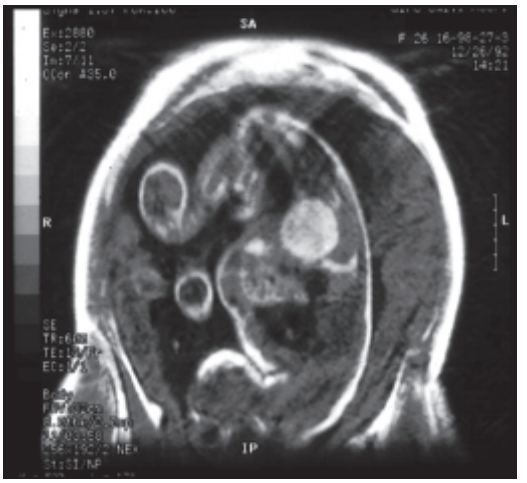

Figure 42.12: Fetal ovarian tumor, T1-weighted image. Fetal ovarian tumors are usually delineated with low intensity because they are serous tumors arising due to hormonal stimulation from the mother. However, this tumor shows high intensity

the maximum diameter of the fetus, including the cystic tumor. This information was useful in deciding how to perform the delivery and choosing the shape of the uterine incision at cesarean delivery. The quality and usefulness of MRI is clear from the findings of the baby at birth **(Fig. 42.11)**.

The usefulness of MRI for imaging fetal structural anomalies is easily demonstrated. However, MRI also has the ability, unlike USG, to characterize tissues based on the differences of signal intensity that depend on the macromolecules in the tissue under various pulse sequences.[9] **Figure 42.12** shows a case of fetal ovarian tumor. Usually fetal ovarian tumors result from maternal

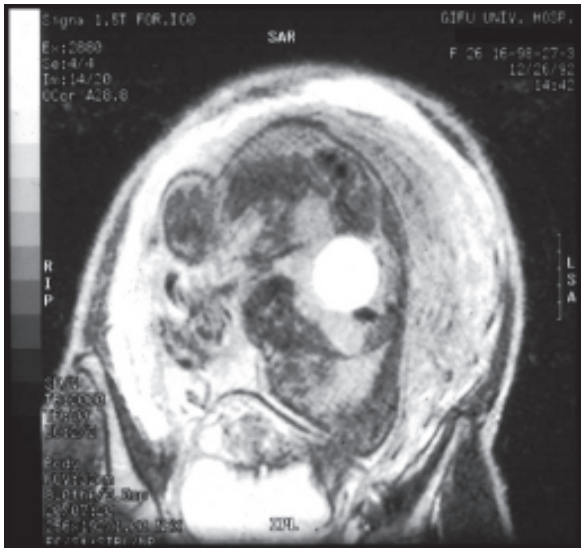

Figure 42.13: Fetal ovarian tumor, T2-weighted image. The tumor is delineated with remarkably high intensity. In this figure and in Figure 42.10, the contents of tumor must be fat or blood

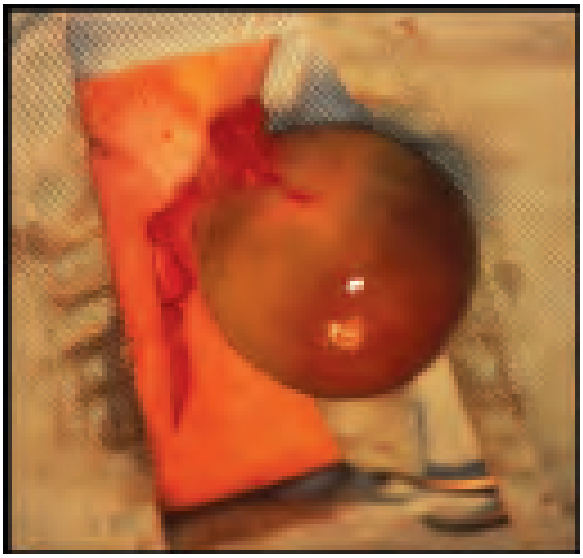

Figure 42.15: Macroscopic findings of the tumor. The macroscopic findings of this tumor during surgery revealed that it contained 12 ml of degenerated blood

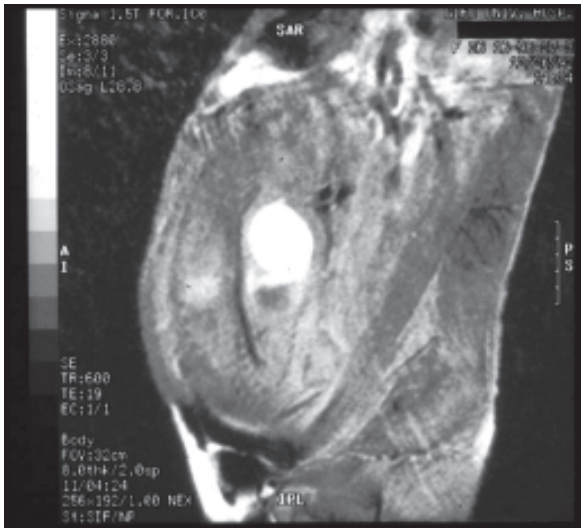

Figure 42.14: Fetal ovarian tumor, fat-suppressed T1-weighted image. While the color of the maternal and fetal skin was changed from white to black, the tumor was still delineated in high intensity. We, therefore, concluded that this tumor was a hematoma

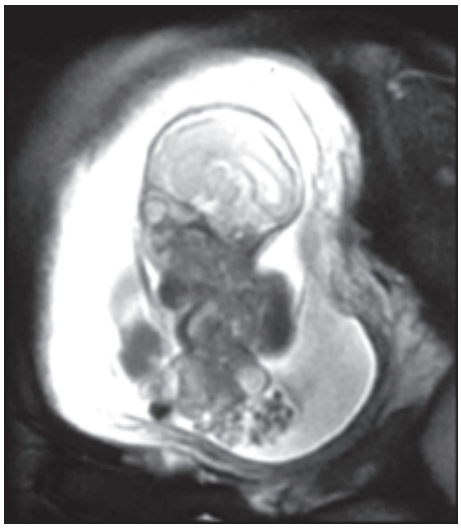

Figure 42.16: Body-stalk anomaly, half Fourier acquisition single shot turbo spin echo. Severe fetal condition is demonstrated on this image

hormonal stimulation. Such tumor must be a simple serous cystic tumor. However, this MRI showed high-intensity and low-intensity parts in the center of the tumor on the T1-weighted image. The tumor also showed high-intensity on the T2-weighted image **(Fig. 42.13)**. These findings are quite different from those of serous cystic tumors and indicated that the contents of the tumor might be fat or blood. We then determined the fat-suppressed T1-weighted image which could eliminate the signal from fat tissue **(Fig. 42.14)**.[10] The tumor was still delineated with remarkably high intensity, which was consistent with subacute bleeding in the tumor and suggested that there was torsion in the tumor. Operative findings after birth revealed 12 ml of dark-colored blood in the ovarian tumor **(Fig. 42.15)**.

Figure 42.16 shows an HASTE image of a malformed fetus diagnosed with body stalk anomaly. The problem

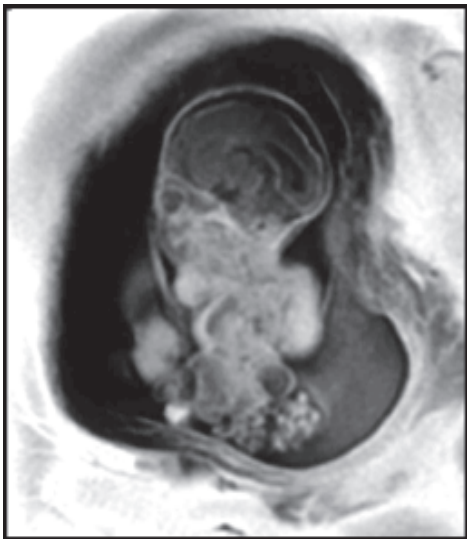

Figure 42.17: Body-stalk anomaly, color-inverted single shot fast spin echo (SSFSE). By the technique of color inversion, the color of the amnion was changed from white to black. This image is similar to that obtained by ultrasonography, which is more easier to perform for evaluating problems of malformed fetuses

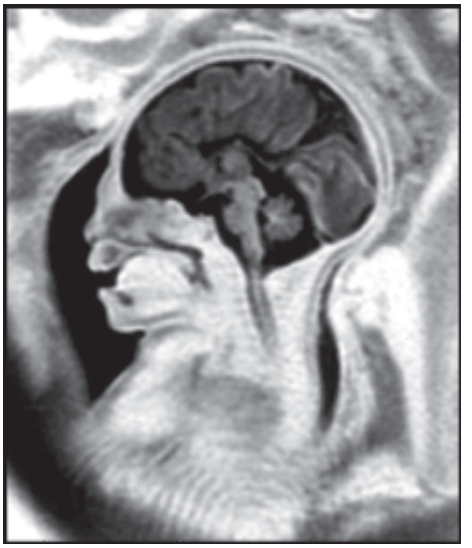

Figure 42.18: Fetal brain, color-inverted SSFSE. The color inversion technique makes clear the findings of the fetal brain. Magnetic resonance imaging provides high quality image of brainstem which is not easy to detect by ultrasonography

of this fetus can be clearly determined from this image. Since MRI is computerized imaging, color inversion can be performed, and we recommend it, as in MRI hydrography, because it makes it much easier to understand what is wrong in cases such as this case, because the signal of the amnion changes from white to black upon color inversion **(Fig. 42.17)**.[11] This image is basically the same as that obtained by USG. The fetal brain is one of the most suitable organs for analysis by MRI.[12] Using the color inversion technique, MRI reveals the fetal brain structure much more clearly than USG, especially for evaluation of the brainstem **(Fig. 42.18).**

Diaphragmatic herniation is a severe fetal problem because it requires immediate respiratory management after birth. This fetal problem is first suspected based on USG findings. We show MRI findings of this malformation in **Figure 42.19**. This image clearly reveals that the fetal intestine is herniated into the thoracic cavity. **Figure 42.20** also shows a case of suspected diaphragmatic herniation. However, the lower margin of the left lung is sharply delineated and the small intestine remains in the abdominal cavity. We concluded that this case was a diaphragmatic problem, but eventration rather than herniation. These images also revealed differences of the findings of the right lung. The right lung in **Figure 42.20** was far smaller than that in **Figure 42.19**. Actually, the outcomes of these two fetuses was opposite, survival and death before surgical

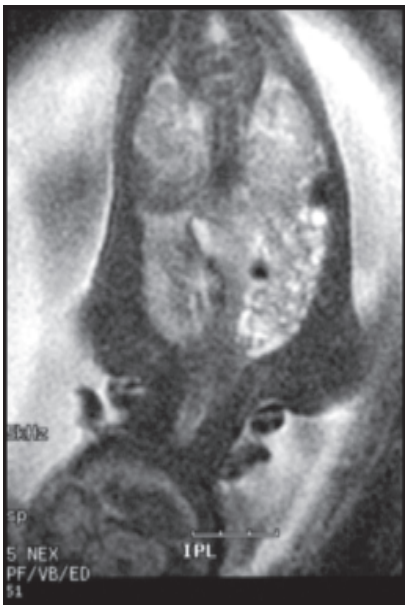

Figure 42.19: Diaphragmatic herniation, SSFSE. Magnetic resonance imaging revealed the fetal intestine herniated into the thoracic cavity. It also clearly revealed the size and shape of the fetal right lung

treatment in the cases **Figures 42.19 and 42.20**, respectively. We speculate that the size of the lung may be a marker of lung hypoplasia. In any case, it seems possible to make differential diagnosis between diaphragmatic herniation and diaphragmatic eventration by MRI.

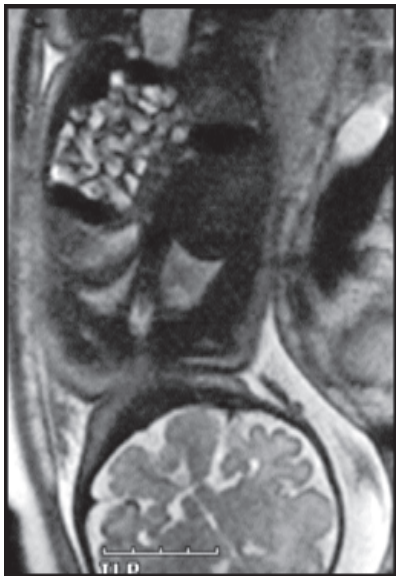

Figure 42.20: Diaphragmatic eventration, SSFSE. The small intestine remained in the abdominal cavity, and the lower margin of the left lung was seen sharply and clearly. These findings are quite different from those of diaphragmatic herniation. We concluded that this was a case of diaphragmatic eventration

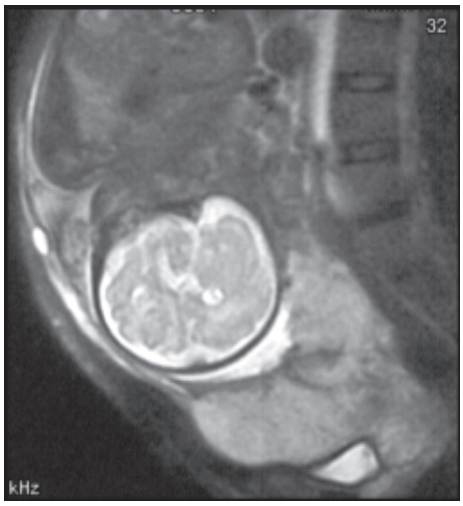

Figure 42.21: Usefulness of magnetic resonance imaging (MRI), based on our data. In almost half of the cases, MRI was not necessary. On the other hand, the diagnosis of 12.9% of fetal anomalies required MRI. Thus, there are limited but definite indications for the use of MRI to diagnose fetal anomalies

In our experience, almost half of fetal anomalies could be diagnosed using only USG and the indications for MRI for prenatal diagnosis are limited. However, it is important to note that 12.9% of such cases required MRI **(Fig. 42.21)**.

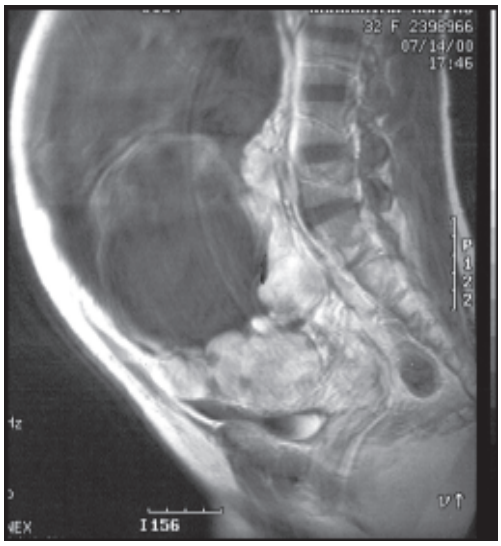

Figure 42.22: Placenta percreta, SSFSE. Deformity of the lower segment of the uterus and discontinuity of the uterine wall are revealed

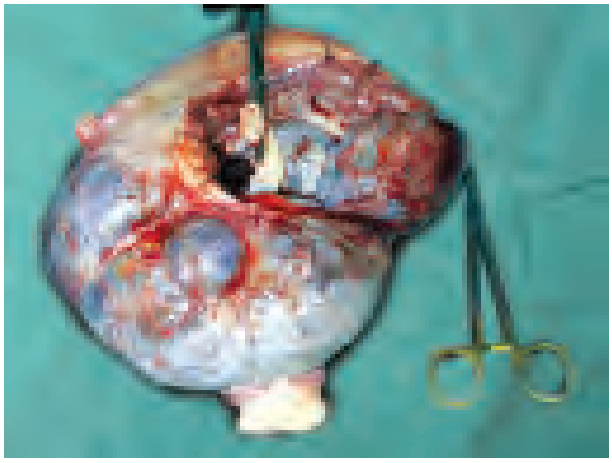

Figure 42.23: Placenta percreta, enhanced T1-weighted image. By administrating contrast medium, it became clear that part of the cervix was also invaded by the placenta

Placenta

The most common reason for imaging of the placenta is to detect its location, namely placenta previa. However, transvaginal USG is much more convenient than MRI. It simply detects the location of the placenta.

Placenta percreta is a rare but terrible placental problem.[13] **Figure 42.22** shows the MRI findings of placenta percreta. It clearly revealed important findings, including deformity of the lower segment of the uterus and discontinuity of the uterine wall. We also obtained enhanced images **(Fig. 42.23)**. They showed deformity of the uterine cervix and revealed that the placenta

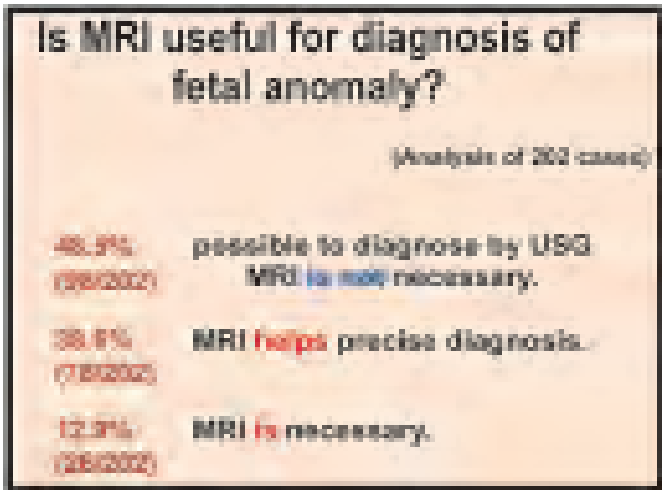

Figure 42.24: Macroscopic findings of placenta percreta. We performed hysterectomy immediately after cesarean delivery. The lower segment of the uterus and the cervix were displaced due to invasion by the placenta

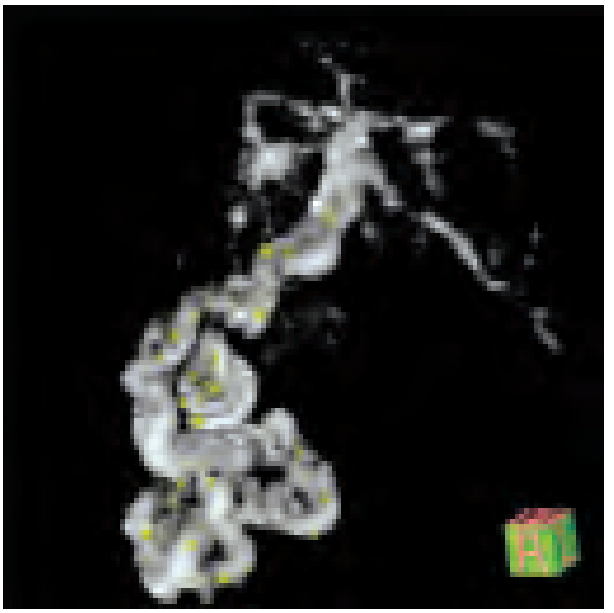

Figure 42.25: Umbilical cord by three-dimensional magnetic resonance imaging (3D MRI) angiography. By 3D MRI angiography, whole shape of umbilical cord is delineated clearly. We can measure its length from this image

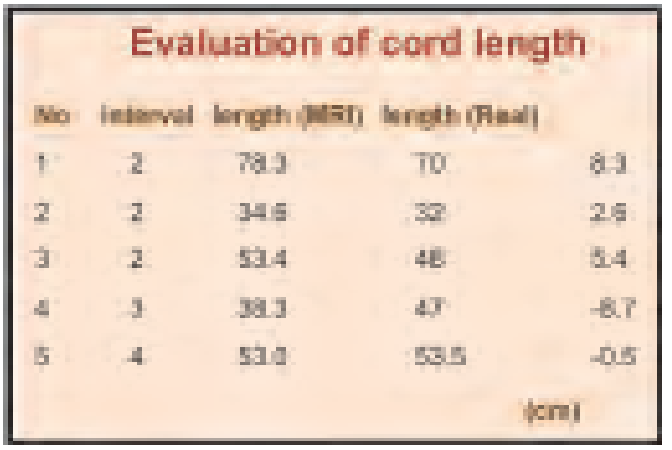

Figure 42.26: Result of the measurement of umbilical cord. The difference between real length is within 10 cm. It will be possible to measure more precisely

invaded into the uterine muscle. We had to perform a hysterectomy immediately after cesarean delivery. The macroscopic finding presented on **Figure 42.24**. It will be important that how to detect mild cases not such severe one.

Umbilical Cord

It may easy to detect umbilical cord by USG. On the other hand, it is impossible to image whole length of it especially in late phase of pregnancy by USG. The most common cause of unexpected intrapartum problem must be based on the cord trouble. If we can detect its position and measure the whole length of umbilical cord in term of pregnancy, it contributes intrapartum management absolutely.

Figure 42.25 is three-dimensional (3D) image of umbilical cord by MRI. From placenta to fetus, the whole length of umbilical cord is delineated clearly. We tried various latest angiographic imaging tool to get this image. But through our trial, we finally reached the way called "time of flight" or "phase contrast" which is one of the most conventional tool of 3D MRI angiography. By this procedure, umbilical cord became possible to delineate clearly even just before onset of labor pain.

The result of our cord length measurement by MRI is demonstrated on **Figure 42.26**. We could measure it precisely, difference between real length was within 10 cm. We believe that we will be able to detect its length more precisely. To make this procedure much easier, further experience should be necessary.

To measure umbilical cord means possible to detect the location of it in the pregnant uterus. **Figure 42.27** is the MRI angiography, suspected of umbilical cord coiling around fetal body. This image revealed that umbilical cord is coiling three times around fetal abdomen, further, fetal heart and great vessels also delineated clearly. Because of frequent variable deceleration, we performed cesarean section for this case. **Figure 42.28** is finding of

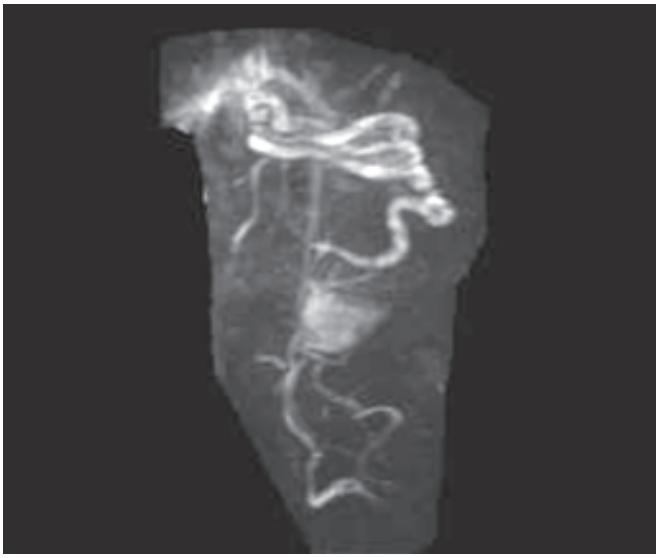

Figure 42.27: Umbilical cord and fetal vessels by magnetic resonance imaging angiography. Fetal heart and great vessels are delineated clearly. This image reveals that cord coiled three times around fetal abdomen

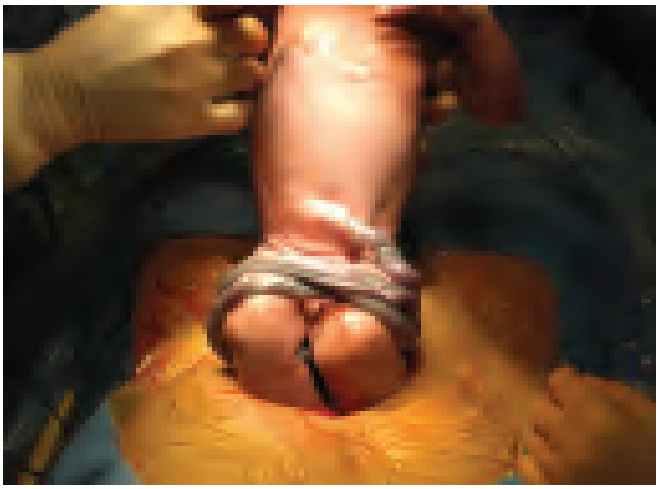

Figure 42.28: Macroscopic finding during cesarean section. Umbilical cord coiled three times same as a finding of magnetic resonance imaging angiography

umbilical cord during operation. It coiled three times as finding of MRI.

CONCLUSION

The USG or MRI: which is better for the diagnosis of mother or fetus? This is a very common question.[14] Nobody can deny the usefulness of USG during pregnancy, but this excellent imaging technique is not perfect. When we cannot get useful information about the mother or fetus using USG, we really need some tool not subject to the weak points of USG in order to obtain information vital for the health of the mother and fetus. As we mentioned above, MRI has the ability unlike USG to provide information different from that obtained using USG and useful for diagnosis of anomalies during pregnancy. Of course, MRI is not always superior to USG: indications for MRI during pregnancy are limited but definite. The MRI is in general useful as a tool for further evaluation of problems that are first detected by USG. When MRI is performed in such cases, we must consider the purpose of the MRI and accordingly determine the appropriate procedure that would provide the most precise and useful diagnostic information.

REFERENCES

1. Geard CR, Osmak RS, Hall EJ, et al. Magnetic resonance imaging and ionizing radiation: a comparative evaluation in vitro of oncogenic and genotoxic potential. Radiology. 1984;152(1):199-202.
2. Harada S, Itabashi M. Intravenous teratology study of DV-7572 in rats-additional investigation. Jpn Pharmacol Ther. 1983;21(3):123-42.
3. Garel C, Brisse H, Sebag G, et al. Magnetic resonance imaging of the fetus. Pediatr Radiol. 1998;28(4):201-11.
4. Michel SC, Rake A, Treiber K, et al. MR obstetric pelvimetry: effect of birthing position on pelvic bony demension. Am J Roentogenol. 2002;179(4):1063-67.
5. Sporri S, Thoney HC, Raio L, et al. MR imaging pelvimetry: a useful adjunct in the treatment of women at risk for dystocia? Am J Roentgenol. 2002;179(1):137-44.
6. Moise KJ. The use of fetal neuro-muscular blockade during intrauterine procedure. Am J Obstet Gynecol. 1987;157 (4 Pt 1):874-8.
7. Ferrucci JT. Advance in abdominal MR imaging. Radiographics. 1998;18(6):1569-86.
8. Chung HW, Chen CY, Zimmerman RA, et al. T2-weighted fast MR imaging with true FISP versus HASTE: comparative efficacy in the evaluation of normal fetal brain maturation. Am J Roentgenol. 2000;175(5):1375-80.
9. Kawabata I, Imai A, Tamaya T. Antenatal subdural hemorrhage causing fetal death before labor. J Gynecol Obstet. 1993;43:57-61.
10. Adamek HE, Weitz M, Breer H, et al. Value of magnetic-resonance cholangio-pancreatography (MRCP) after unsuccessful endoscopic-retrograde cholangio-pancreatography (ERCP). Endoscopy. 1997;29(8):741-4.
11. Jara H, Barish MA, Yucel EK, et al. MR hydrography: theory and practice of static fluid imaging. Am J Roentgenol. 1998;170(4):873-82.
12. Merzoug V, Ferey S, Andre Ch, et al. Magnetic resonance imaging of the fetal brain. J Neuroradiol. 2002;29(2):76-90.
13. Lam G, Kuller J, McMahon M. Use of magnetic resonance imaging and ultrasound in the antenatal diagnosis of placenta accreta. J Soc Gynecol Investig. 2002;9(1):37-40.
14. Elias P, Zizka J, Balicel P. Current triad: S and MRI diagnosis in the fetus and mother. Perinat Diagn. 2002;22(11):1005-10.

43
CHAPTER

3D Sonography in the Evaluation of Normal and Abnormal Fetal Face

Guillermo Azumendi, Asim Kurjak

INTRODUCTION

The face is the anatomical structure that clearly demonstrates the utility and advantages of three-dimensional (3D) and four-dimensional (4D) ultrasound. It is difficult to find a book on ultrasound published in the last few years that does not include a 3D picture of a fetal face on its cover. Even in a text dedicated to gynecological ultrasound, it is usual to find a 3D picture of a fetal face helping illustrate the potential of such a new technology.

Practically all the pioneering studies on 3D ultrasound provide an example of 3D fetal face reconstruction.[1-29] We have all taken our first steps in 3D ultrasound by exploring the fetal face and our main aim has always been to obtain good pictures of this anatomic structure. It is, therefore, a good opportunity to elaborate on the role of 3D and 4D ultrasound of the fetal face **(Figs 43.1 to 43.118)**.

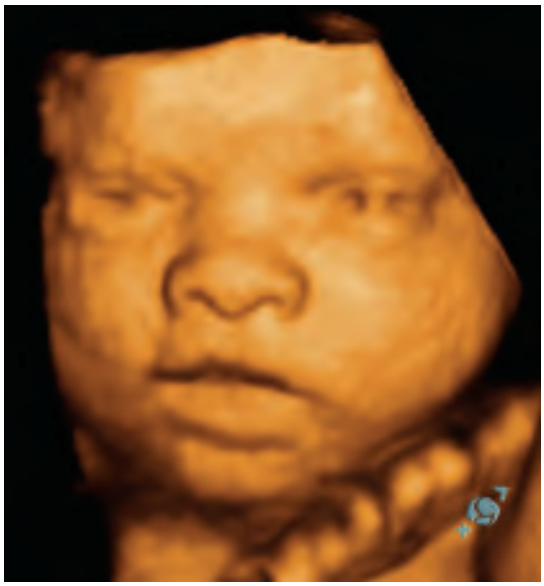

Figure 43.1: 3D scan of a fetus showing complete face profile at 33rd week of gestation. Eyelids are open and surface of facial features are discernible

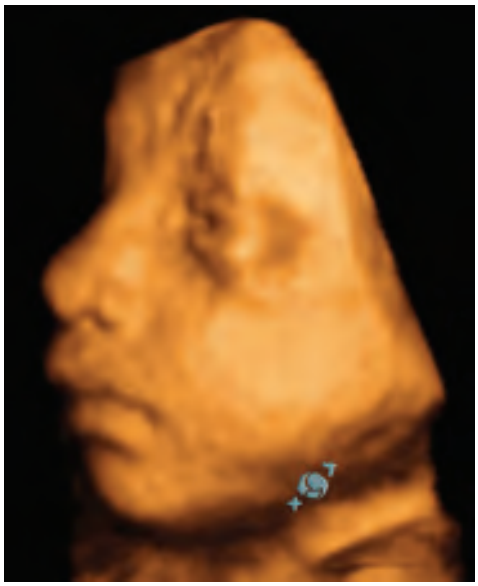

Figure 43.2: 3D scan of a fetal semiprofile showing facial contours of the facial muscle

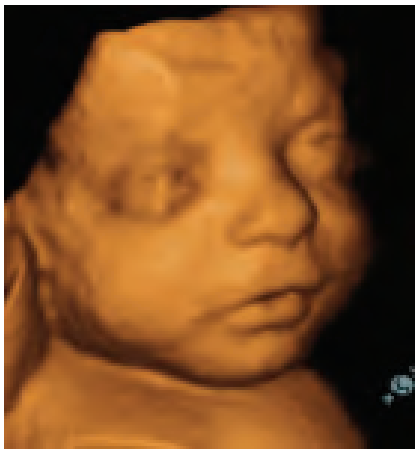

Figure 43.3: 3D scan of a fetus with semiprofile position showing contours of both eyelids and surrounding soft tissue structures such as nose and cheeks

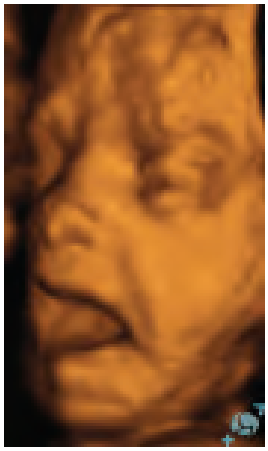

Figure 43.4: 3D image shows alteration of the facial expression of the fetus. The fetus seems to be glumness

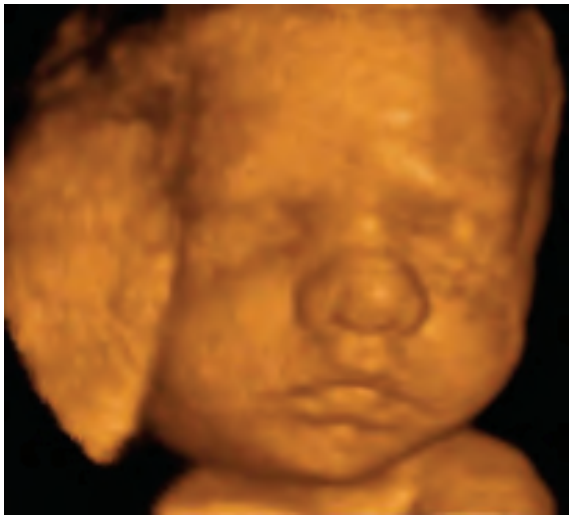

Figure 43.5: This image shows alteration of the facial expression. The movements of the facial musculature show as if the fetus is sleeping

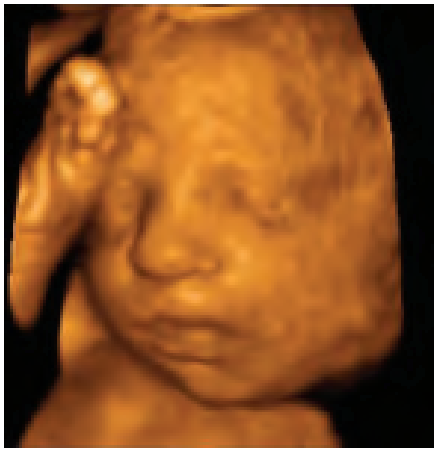

Figure 43.6: Sleeping expression of the fetus is clearly visible

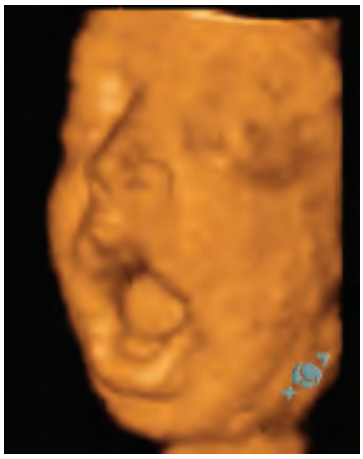

Figure 43.7: Other facial expression of the fetus showing mouth opening

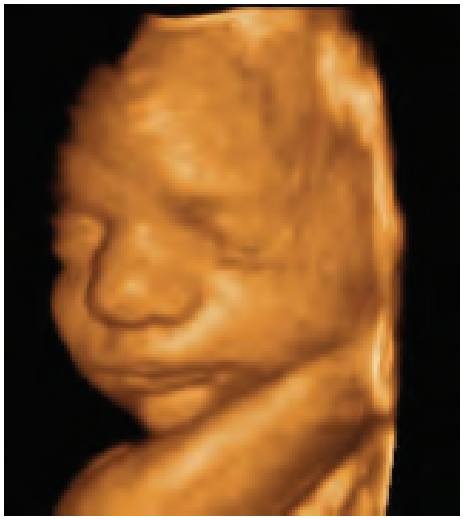

Figure 43.8: Surface rendering by 3D demonstrates the facial contours of the lips and nose. The fetus seems to be sleeping

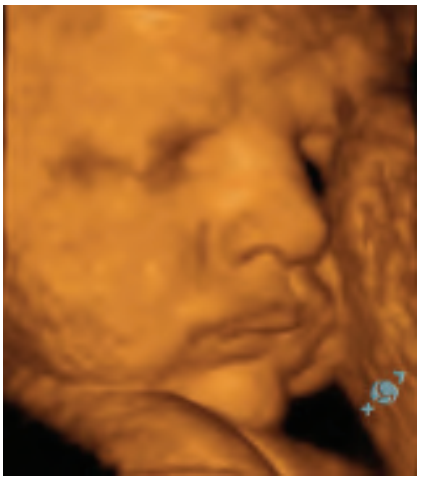

Figure 43.9: Facial expression showing distortion of the facial muscles. The fetus seems to be angry

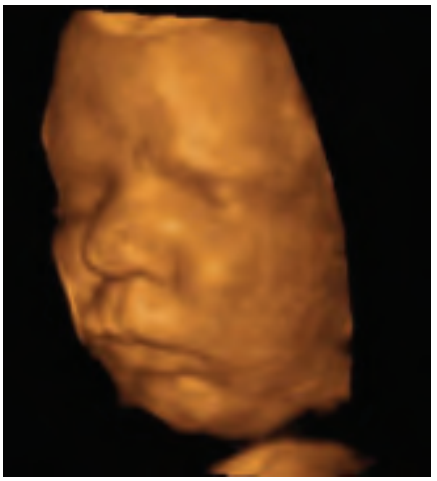

Figure 43.10: Semiprofile expression of the facial contour

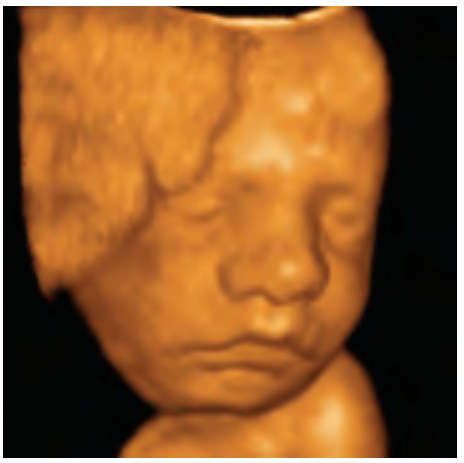

Figure 43.11: Semiprofile surface rendering showing the contours of the fetal face, eyelids and nose

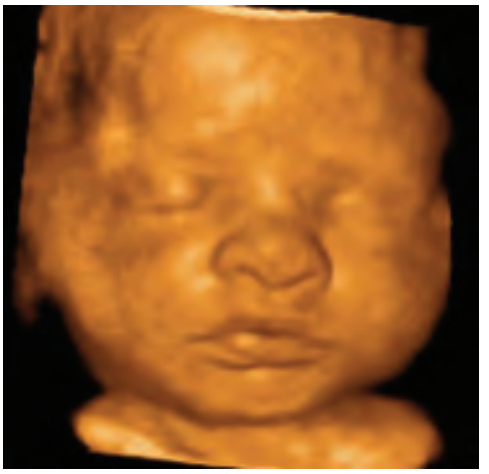

Figure 43.12: Complete profile of surface rendering showing movements of the bilateral part of eyebrows is clearly visible

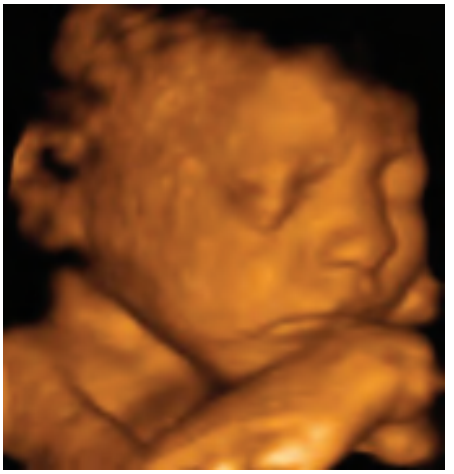

Figure 43.13: The entire face is discernible, with clear visualization of nostrils, right ear and eyelids. The fetal hand is positioned in front of the mouth

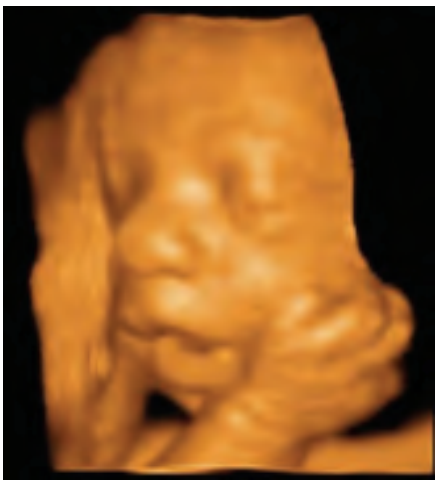

Figure 43.14: 3D surface rendering showing opening of the mouth and movements of the eyebrows

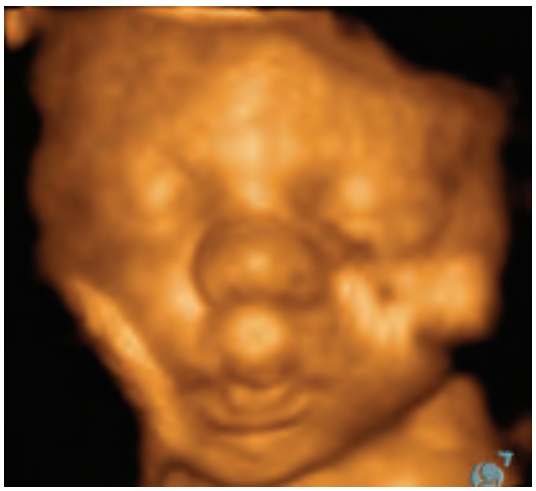

Figure 43.15: Surface rendering of the facial contour showing expression of the sleeping fetus

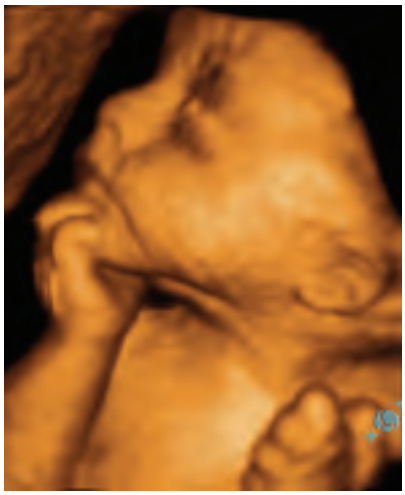

Figure 43.16: Semiprofile position of the fetus showing eyelids opening and all facial features

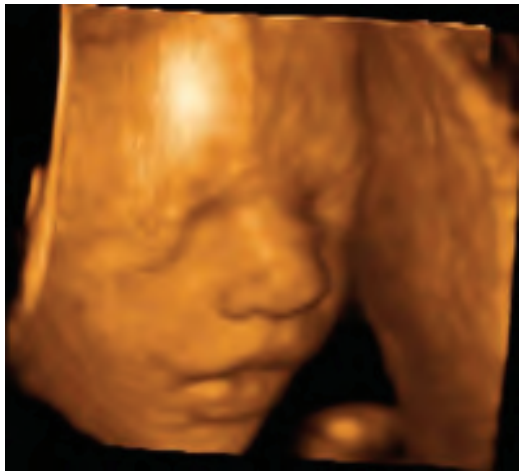

Figure 43.17: Semiprofile position showing facial contour of the fetal lips which leads to the change in facial expression

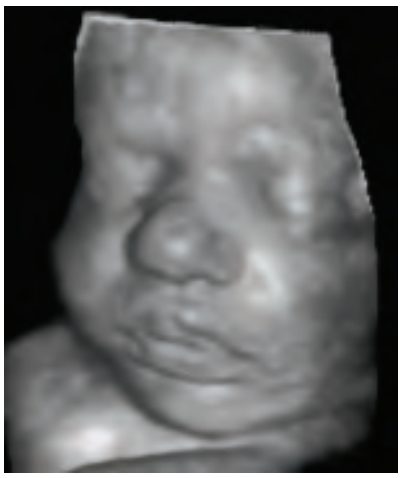

Figure 43.18: Surface rendering demonstrates clear visualization of facial anatomical structures

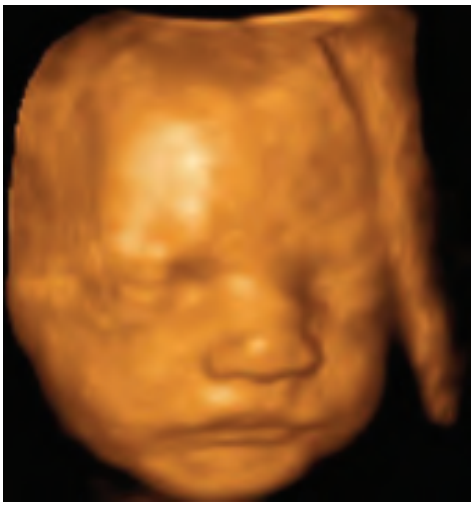

Figure 43.19: 3D surface rendering of complete profile showing discernible contour of facial musculatures

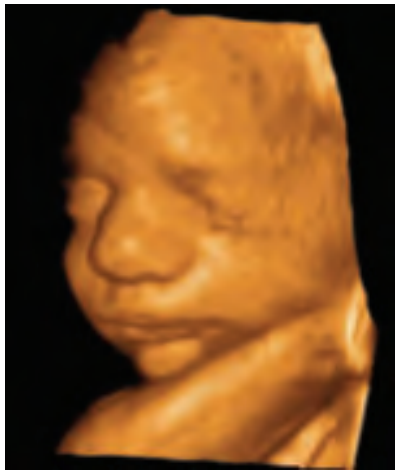

Figure 43.20: Semiprofile surface rendering showing sleeping expression of the fetus

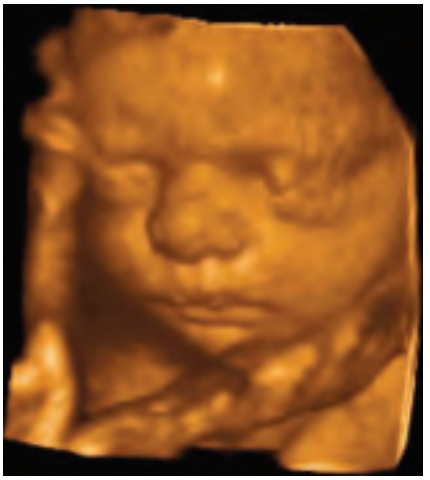

Figure 43.21: Complete profile of the fetus showing the facial contour. Even the umbilical cord is observable surrounding the fetal neck

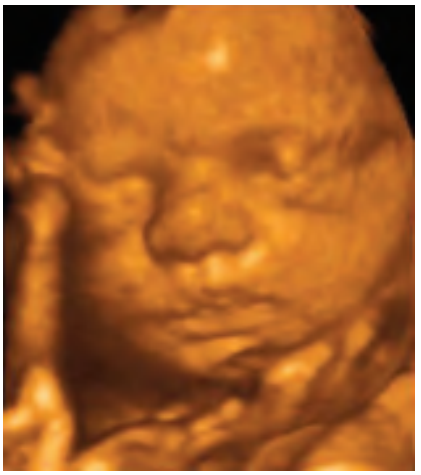

Figure 43.22: 3D surface rendering shows sleeping expression of the fetus. Note the nuchal cord around the neck is clearly visible

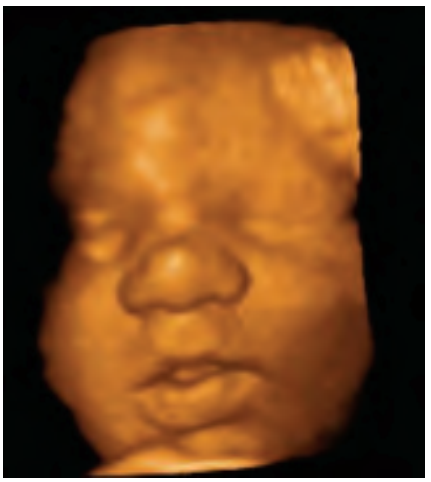

Figure 43.23: Asymmetry of the facial expression caused by changing in lateral parts of the cheek

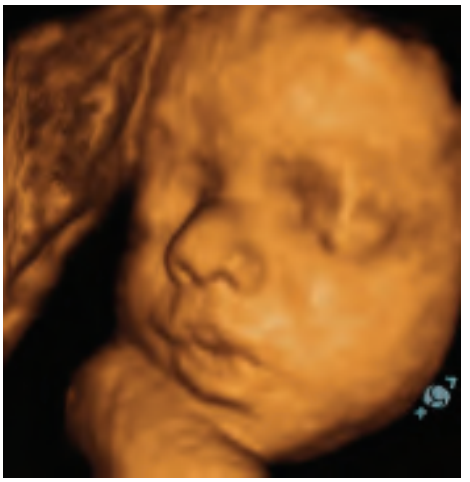

Figure 43.24: Changing of the facial expression due to the movements of the bilateral parts of the eyebrows

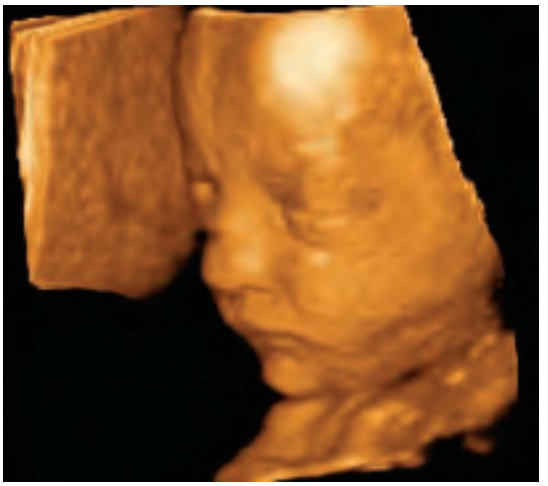

Figure 43.25: Fetal profile by 3D surface rendering showing the facial texture

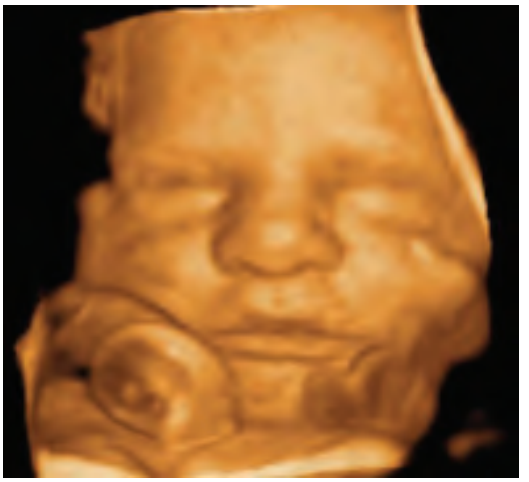

Figure 43.26: Surface rendering demonstrates the beginning of opening of the right fetal eyelids

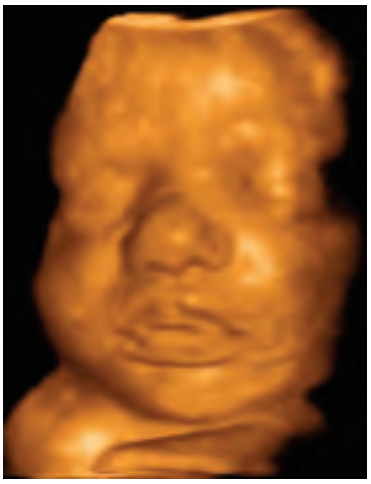

Figure 43.27: Surface rendering of complete profile of the facial contour

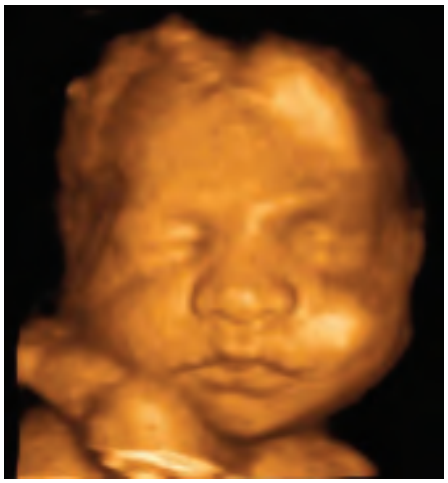

Figure 43.28: Sleeping expression is clearly visible on this image

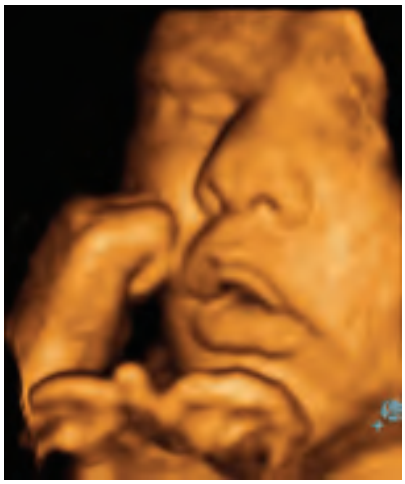

Figure 43.29: 3D scan of the fetus in complete profile showing opening of the mouth. Note clear demonstration of the fetal lips

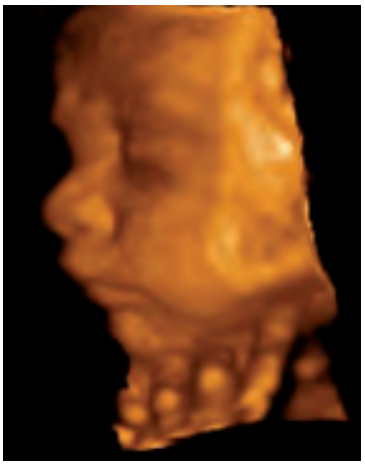

Figure 43.30: Profile of the fetus by 3D surface rendering, with clear visualization of small anatomical features from the fingers

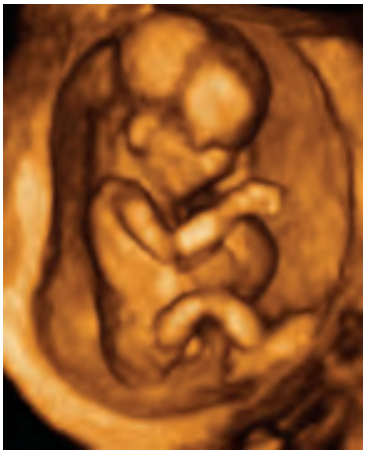

Figure 43.31: 3D surface rendering of the facial contour in early pregnancy. Facial structures have reached an adequate degree of development in order to start studying them for diagnostic purposes

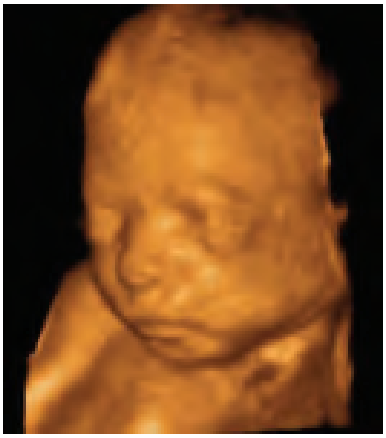

Figure 43.32: High quality of fetal facial image could be obtained in the surface rendering mode, when other structures are not shadowing the fetal face

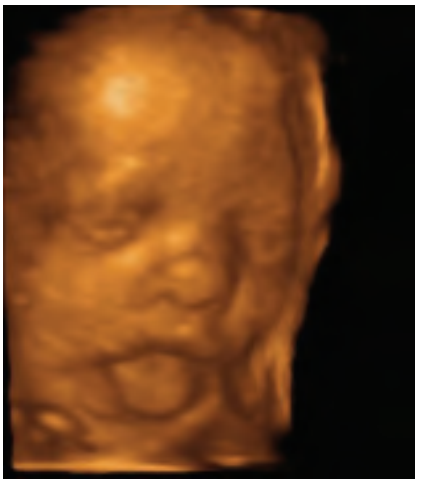

Figure 43.33: 3D scan of the fetus in semiprofile position showing expulsion of the tongue

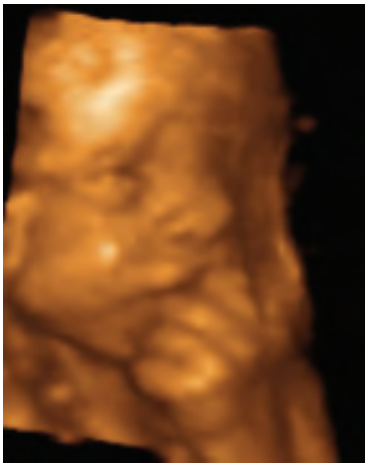

Figure 43.34: 3D scan of the fetus in semiprofile position, the eyelids are opened and the surfaces of all visible facial features are discernible. The fetus seems to be observing the surrounding environment

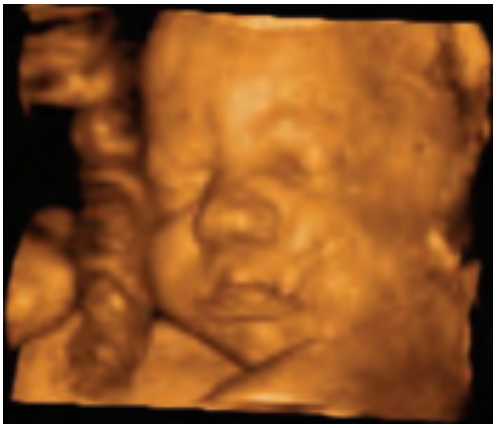

Figure 43.35: 3D ultrasound of the fetus in the third trimester of gestation. Note clear demonstration of surrounding structure such as umbilical cord

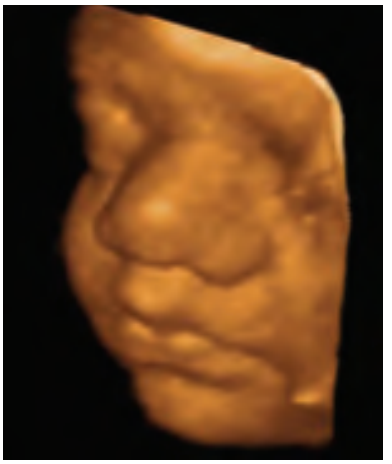

Figure 43.36: 3D scan of the fetus in semiprofile position demonstrates clearly facial anatomy such as nose, mouth and eyelids

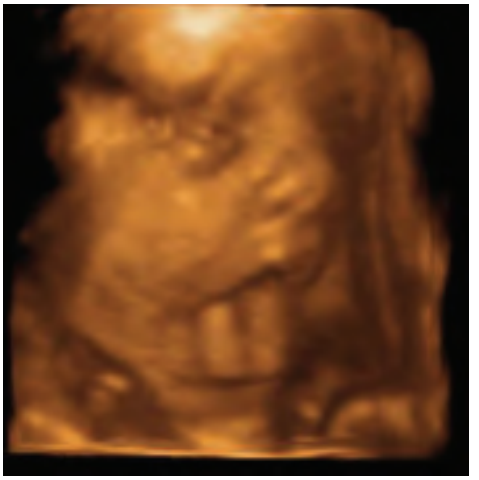

Figure 43.37: 3D surface rendering shows the expulsion of the tongue and change of the facial expression due to eyelids opening

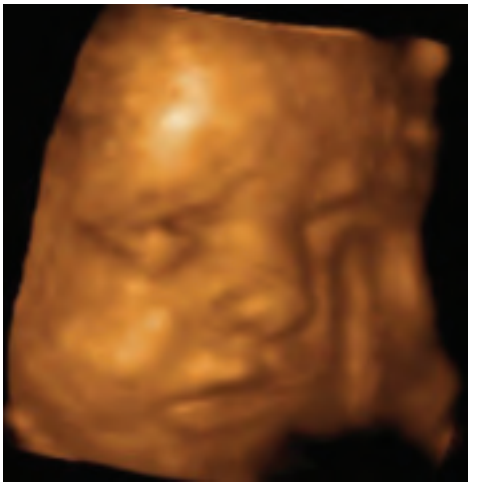

Figure 43.38: Eyelids opening and clearly observable anatomy of the eyes such as the eyeballs

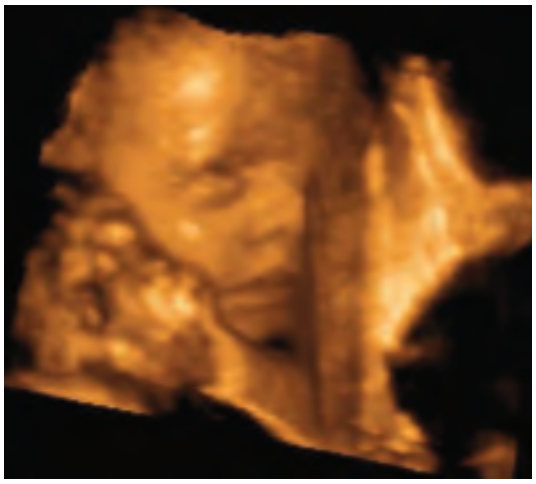

Figure 43.39: The fetal hand is positioned on the right side of the fetal cheek and the entire face is discernible, with clear visualization of the eyeballs

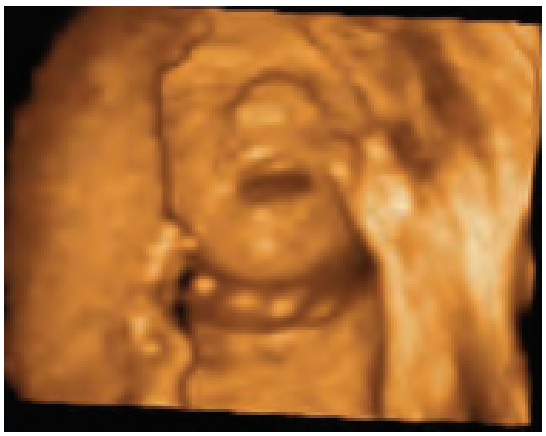

Figure 43.40: Nuchal cord image around the fetal neck is obtained by 3D surface rendering

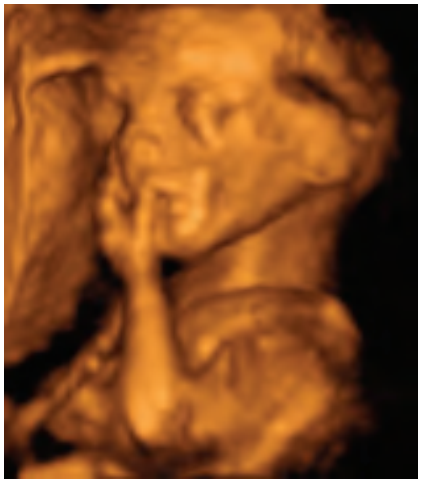

Figure 43.41: Change in fetal expressions together with hand to mouth movement

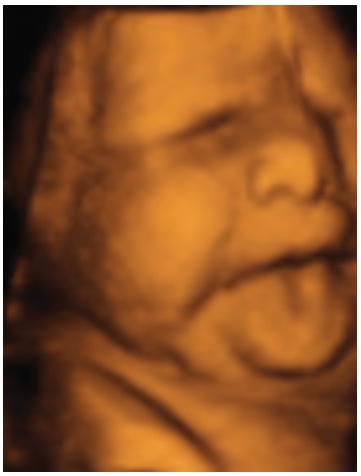

Figure 43.42: Change in fetal expression due to expulsion of the tongue

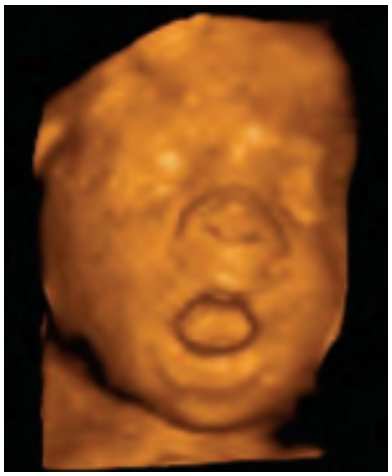

Figure 43.43: Opening of the mouth is clearly visible

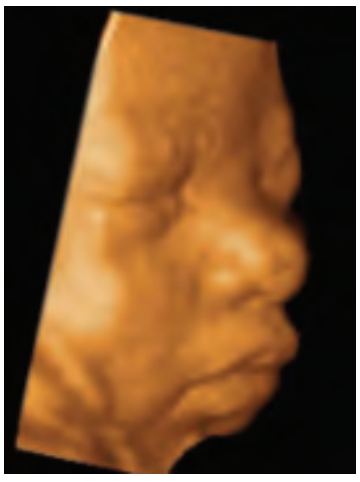

Figure 43.44: High quality of semiprofile facial contour demonstrate the lips, nostrils and forehead

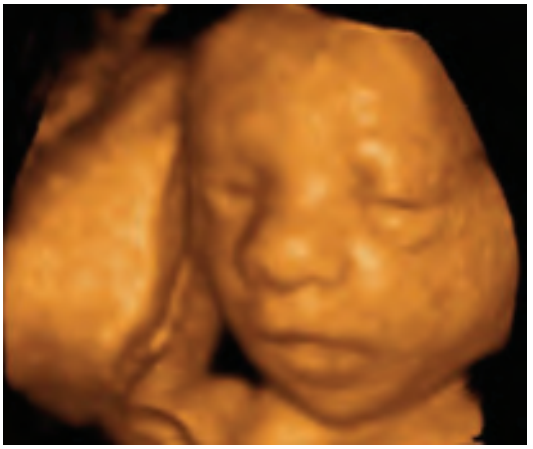

Figure 43.45: Surface rendering demonstrates the beginning of opening of the eyelids. Note the fetus seems to be observing something in the left side

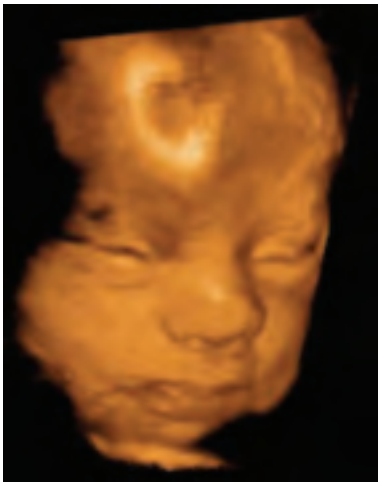

Figure 43.46: 3D image shows the beginning of opening of the eyelids

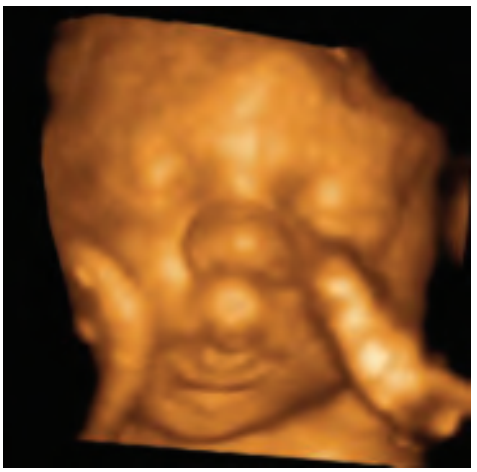

Figure 43.47: Alteration of the facial expression is clearly visible on this image which illustrates the surrounding influence, altering the facial expression on one side

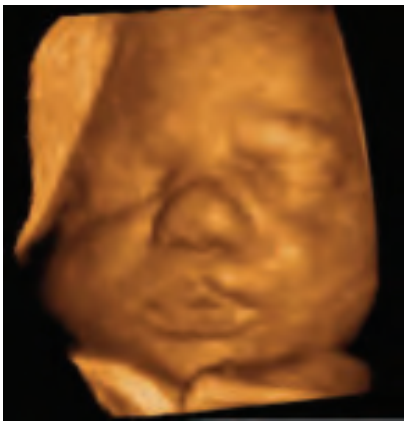

Figure 43.48: 3D surface rendering of the fetal face shows alteration of the facial expression. Movement of the lateral side of facial musculature causes transient and slight asymmetry. However, it should be differentiated from pathological features such as unilateral paresis

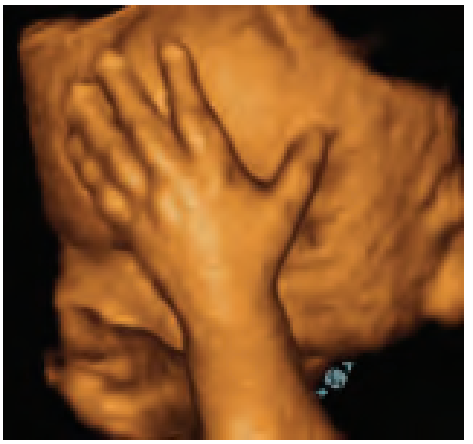

Figure 43.49: The subtle alteration of the facial expression is clearly visible on this image with illustrates influence of the fetal hand

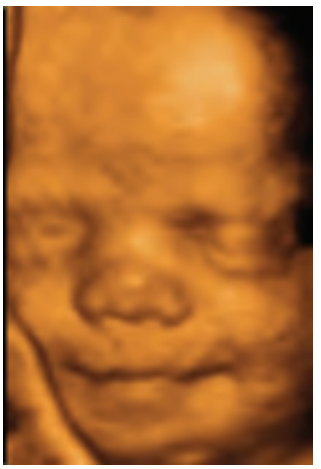

Figure 43.50: The change of the facial expression due to turning up the corners of the mouth. The fetus appears to be smiling

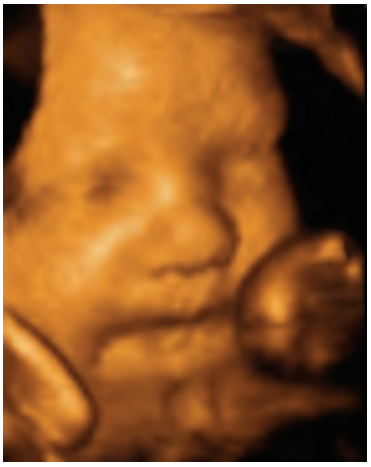

Figure 43.51: A facial expression characterized by turning up the corners of the mouth. The fetus seems to be smiling

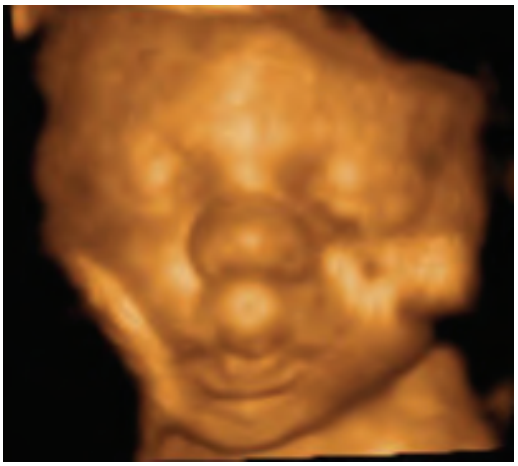

Figure 43.52: A facial expression characterized by mouthing expression. This is most common in fetus and it may develop into a persistent, stereotyped behavior pattern

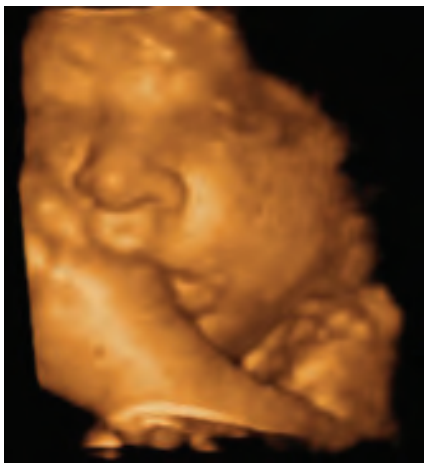

Figure 43.53: The fetus is placing the finger or thumb on the roof of the mouth behind the teeth and sucking with lips closed. Thumb sucking is a very frequent fetal behavioral pattern

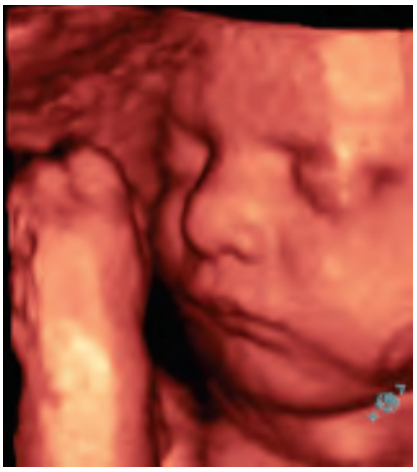

Figure 43.54: The entire face is discernible, with clear visualization of the left hand positioned in front of the face

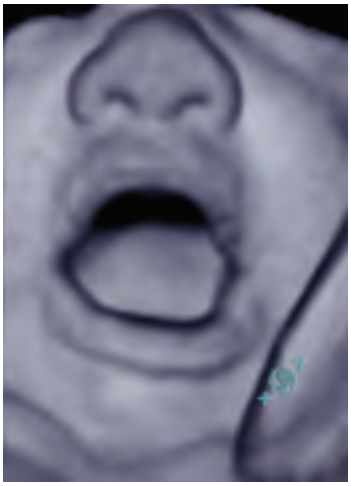

Figure 43.55: Yawn expression is defined as an involuntary wide opening of the mouth, with maximal widening of the jaws followed by quick closure

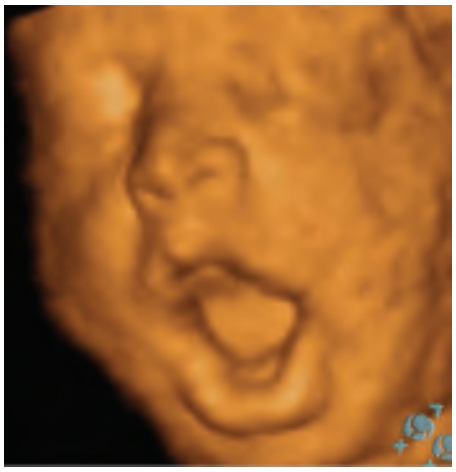

Figure 43.56: 3D surface rendering of fetal yawning. This movement is often followed by retroflexion of the head and sometimes elevation of the arms

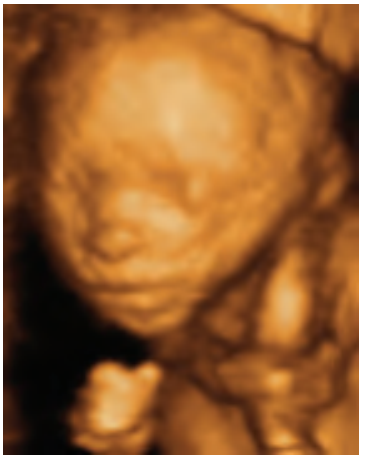

Figure 43.57: 3D scan of facial expression in the second trimester of gestation is adequate enough for diagnostic purpose

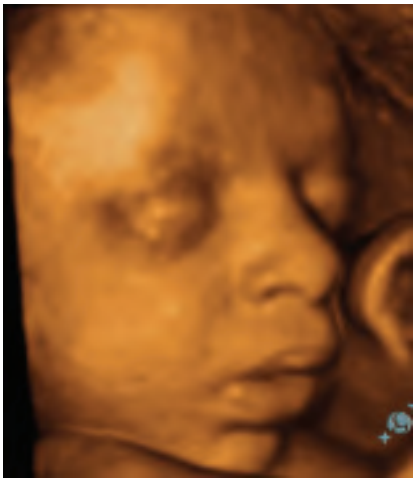

Figure 43.58: Semiprofile of the fetal face showing distinct contour of facial musculature

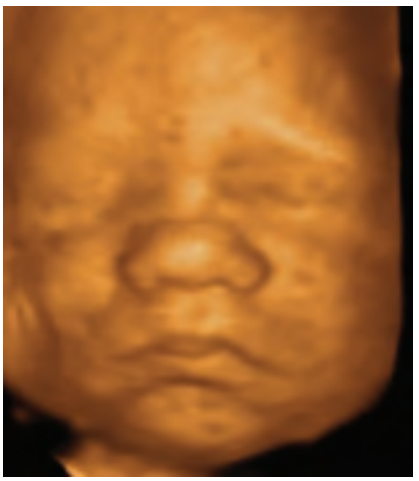

Figure 43.59: Both of the eyes and the mouth are closed and the fetus appears calm

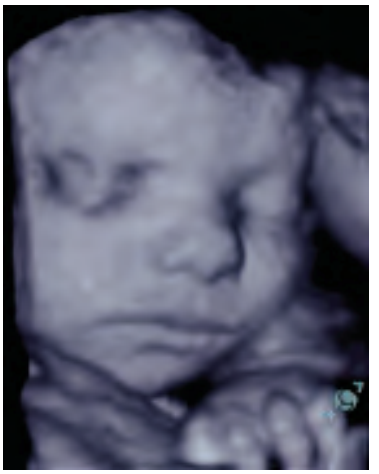

Figure 43.60: Calm and tranquil expression of the fetus obtained by 3D technique

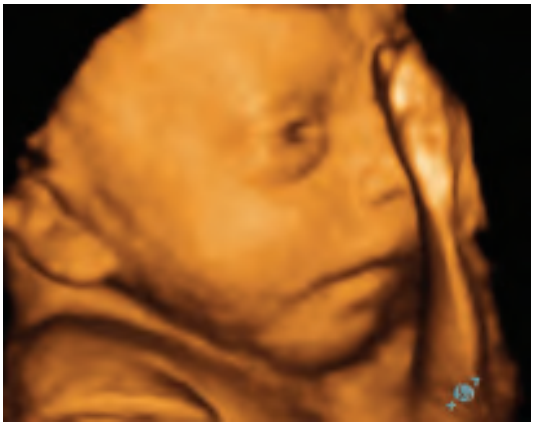

Figure 43.61: 3D scan of the fetus in semiprofile image. The eyelids are opened and the surfaces of all visible facial features are distinctly clear

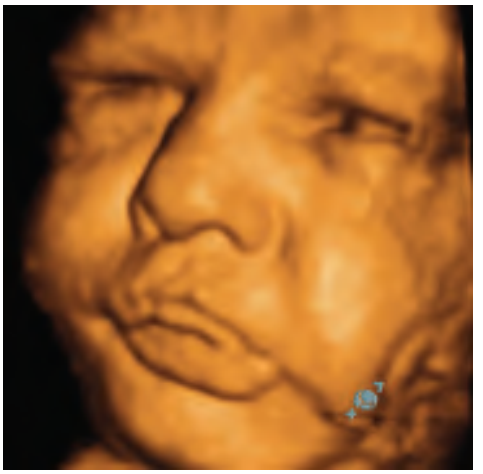

Figure 43.62: Surface rendering shows the beginning of eyelids opening. Note clear demonstration of the facial contour of the fetal lips

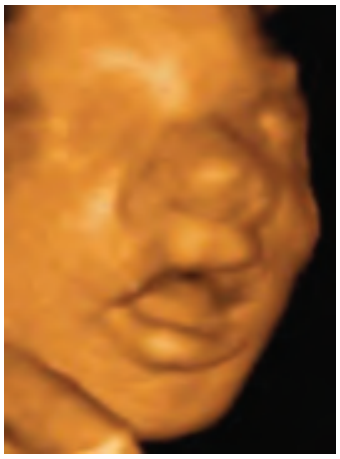

Figure 43.63: The beginning of opening of the fetal mouth

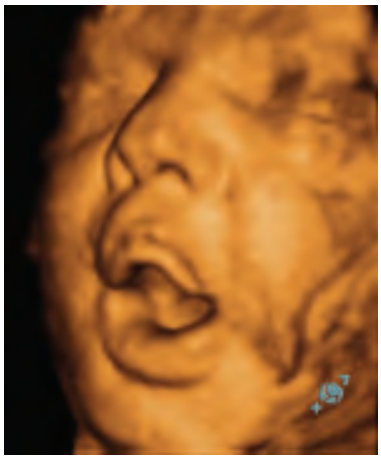

Figure 43.64: The ending of maximal opening of the mouth

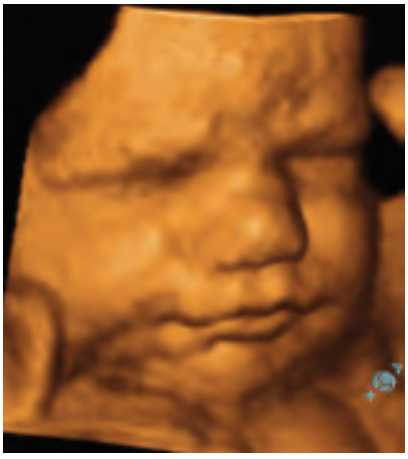

Figure 43.65: The change of the facial expression due to movements of the lateral parts of the eyebrows and the facial musculature between them is clearly visible

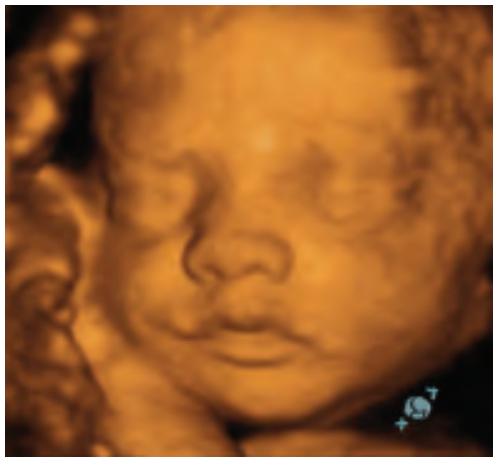

Figure 43.66: Calm expression of the fetus is obtained by 3D surface rendering

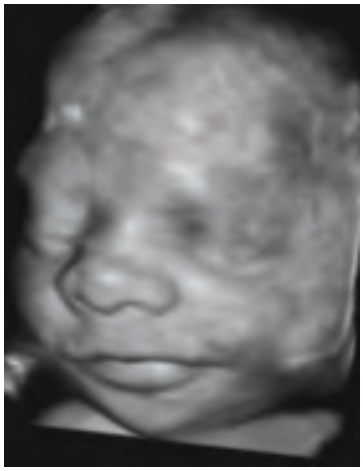

Figure 43.67: Smiling expression of the fetus. Both of the lateral side of the mouth is turning up

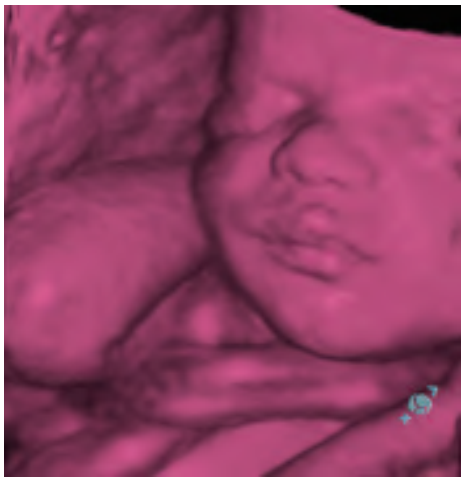

Figure 43.68: The fetus appears to be calm in this 3D image

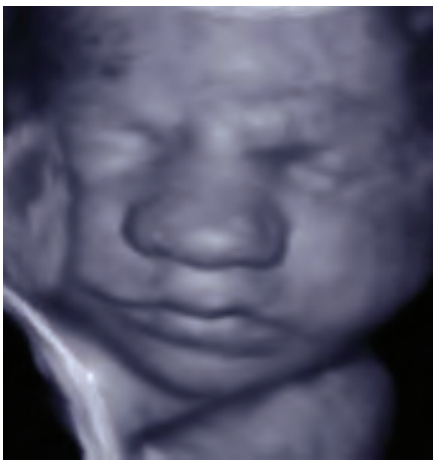

Figure 43.69: Grimacing expression demonstrated by 3D surface rendering

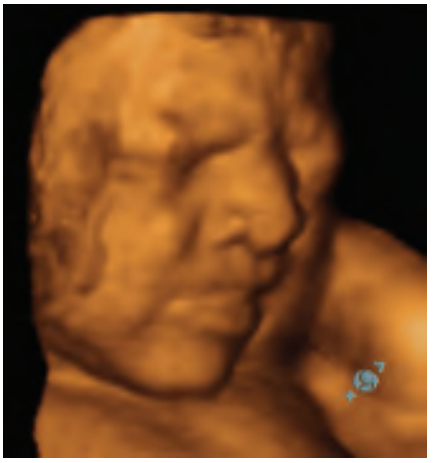

Figure 43.70: The frontalis muscle also can be responsible for the appearance of grimacing. However, the main agent responsible for the appearance of scowling is the corrugator muscle. The fetus seems to be sad

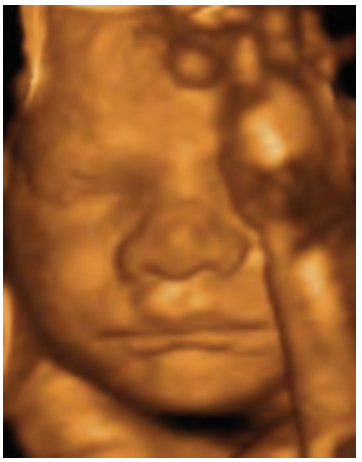

Figure 43.71: Both of the mouth and eyes are closed and fetus appears tranquil

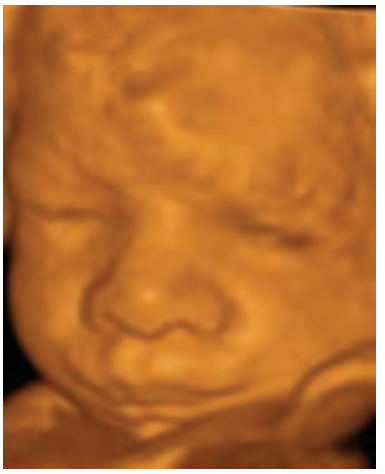

Figure 43.72: The fetus seems trying to manipulate something with mouth in this 3D image

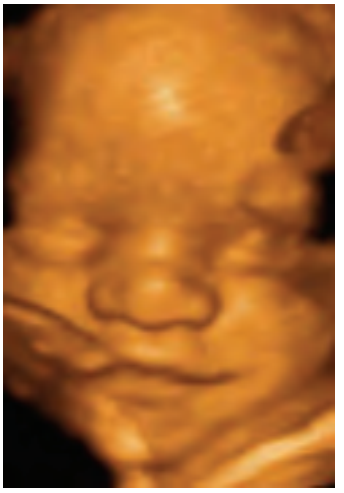

Figure 43.73: Smiling expression is obtained by 3D surface technique

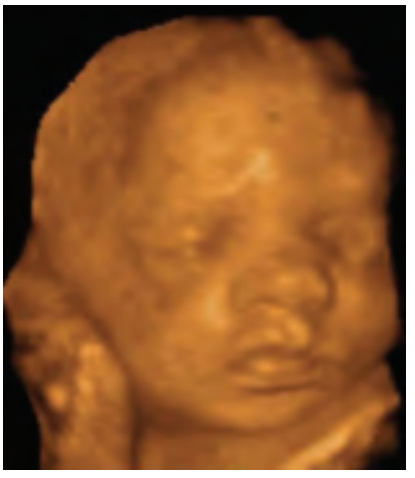

Figure 43.74: High quality of full profile of the fetal expression shows sleeping expression

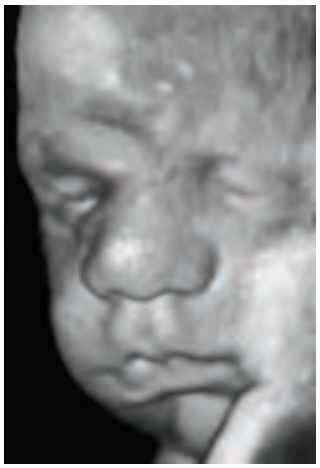

Figure 43.75: Asymmetry of the facial expression due to movement of lateral side of the fetal facial musculature

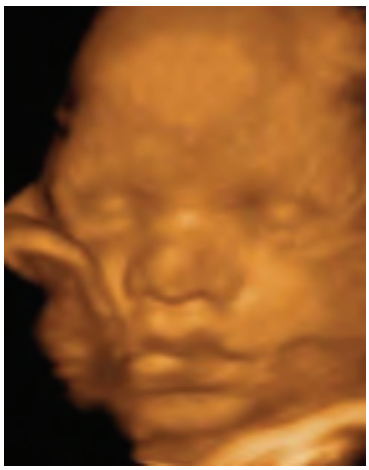

Figure 43.76: Sleeping expression is clearly depicted

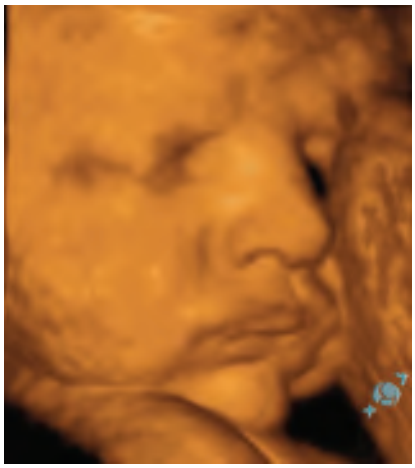

Figure 43.77: Grimacing expression is obtained by surface rendering technique

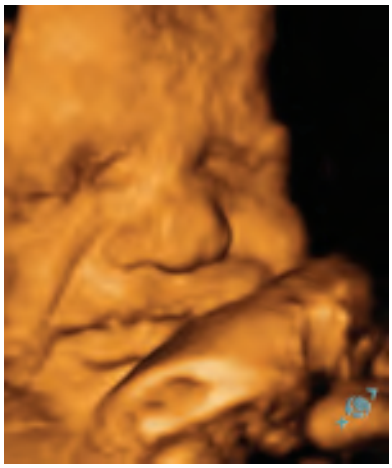

Figure 43.78: The fetus in this 3D image seems to be displeasure

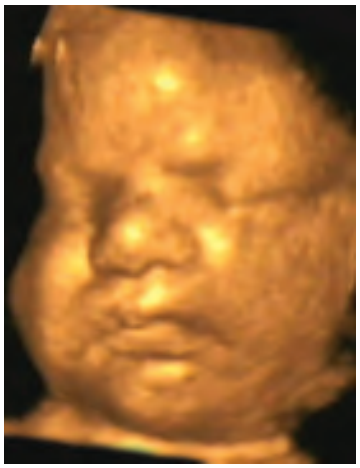

Figure 43.79: 3D surface rendering demonstrates grimacing expression

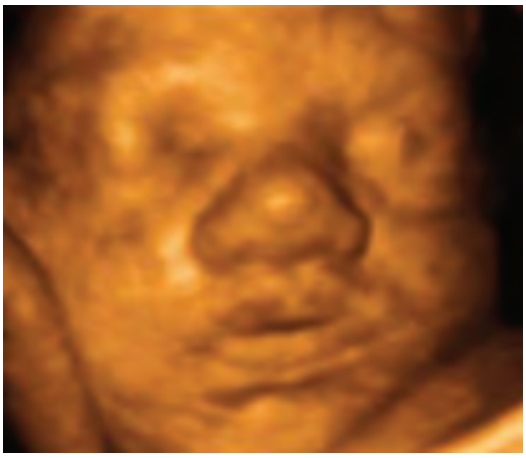

Figure 43.80: 3D surface rendering shows contour of fetal face clearly

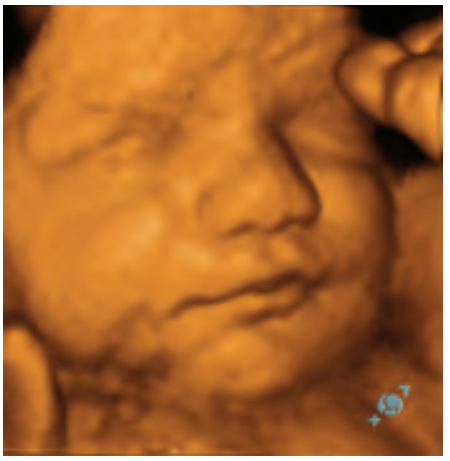

Figure 43.81: 3D ultrasound of the fetus shows alteration of the facial expression. This kind of asymmetry, however, should be differentiated from pathological features such as unilateral facial paresis

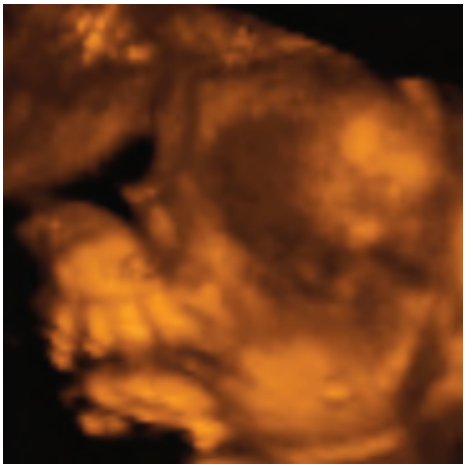

Figure 43.84: Facial expression and hand movement of the fetus with trisomy 18

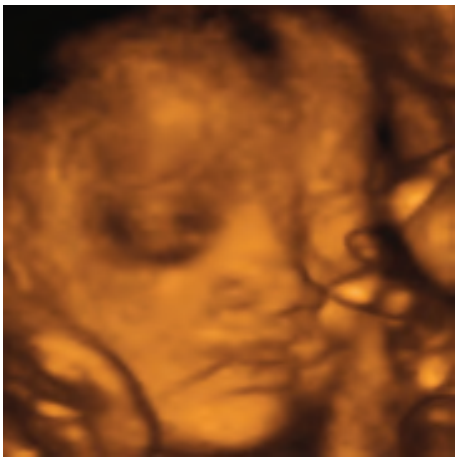

Figure 43.82: 3D surface rendering of the fetus with trisomy 18 shows the round face

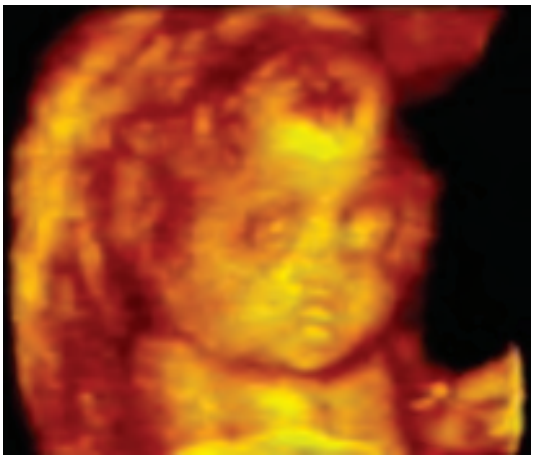

Figure 43.85: 3D surface rendering of the fetus with thanatophoric dysplasia

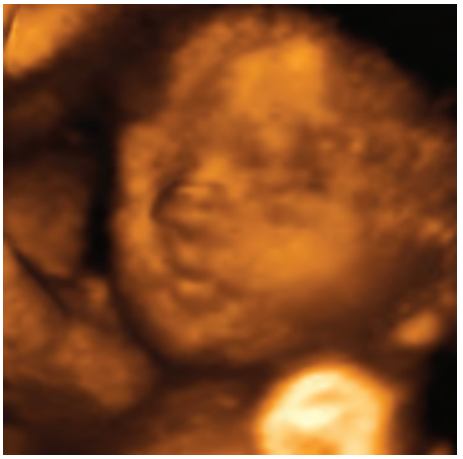

Figure 43.83: 3D surface rendering of the fetus with trisomy 18

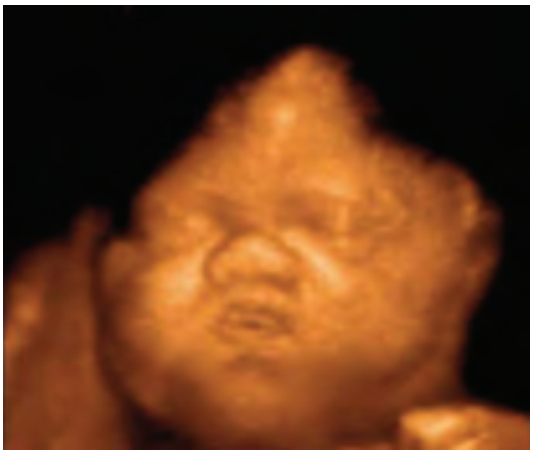

Figure 43.86: 3D image of the fetus with thanatophoric dysplasia

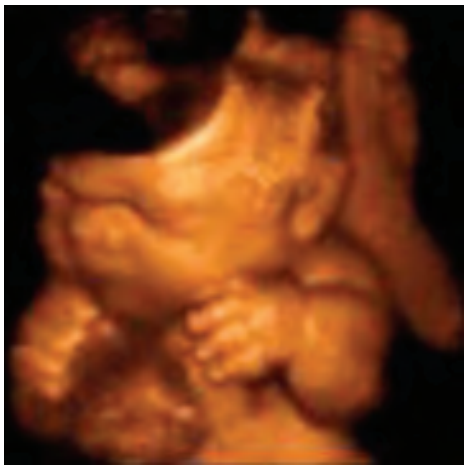

Figure 43.87: 3D surface rendering of the fetus with osteochondrosis dysplasia

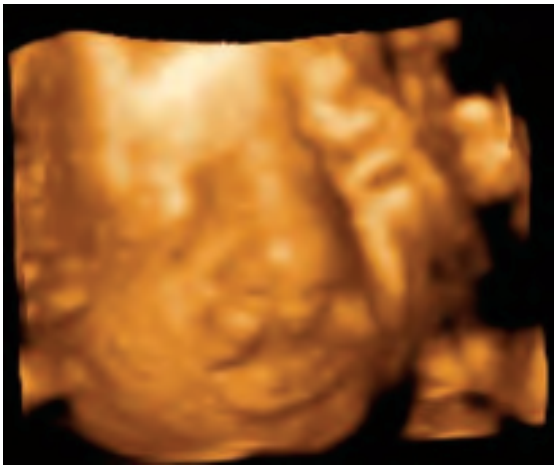

Figure 43.90: 3D ultrasound of a fetus with bilateral cleft lip

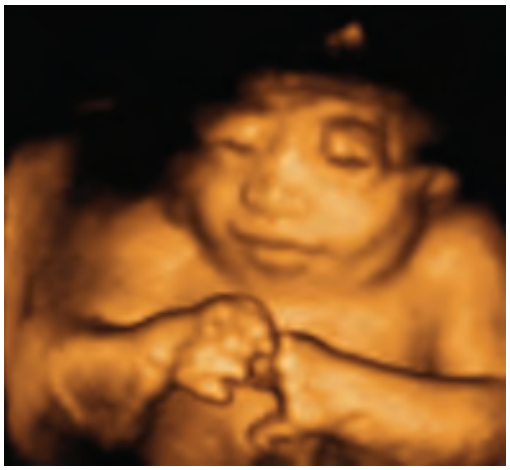

Figure 43.88: 3D surface rendering of the fetus with anencephaly

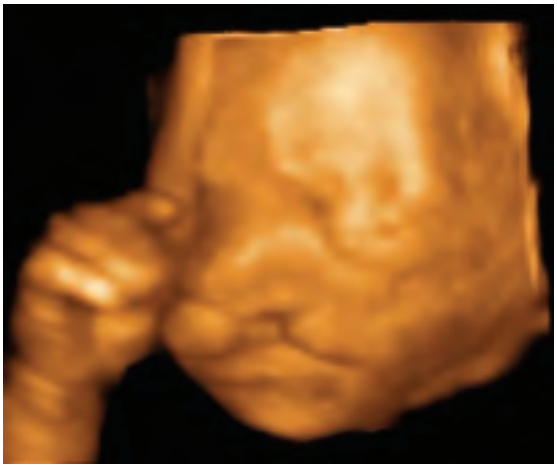

Figure 43.91: Cleft lip is clearly visible by 3D surface rendering. The exact location and surrounding affected structure are visible

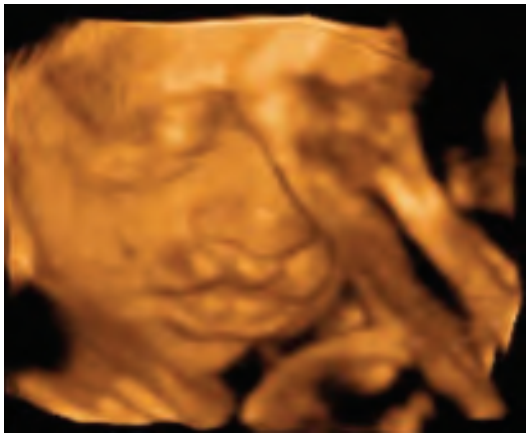

Figure 43.89: 3D ultrasound image of a fetal face in the fetus with bilateral cleft lip

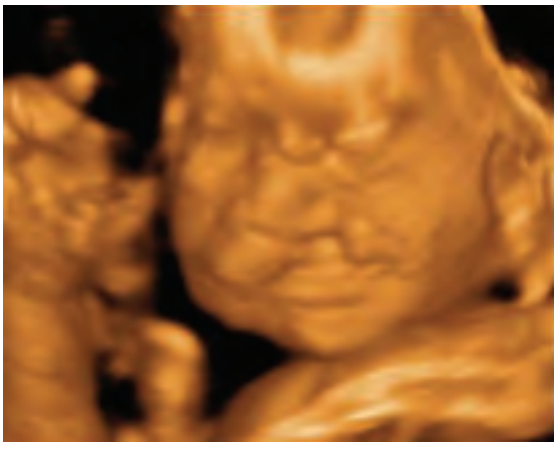

Figure 43.92: 3D surface rendering of a fetus with unilateral cleft lip

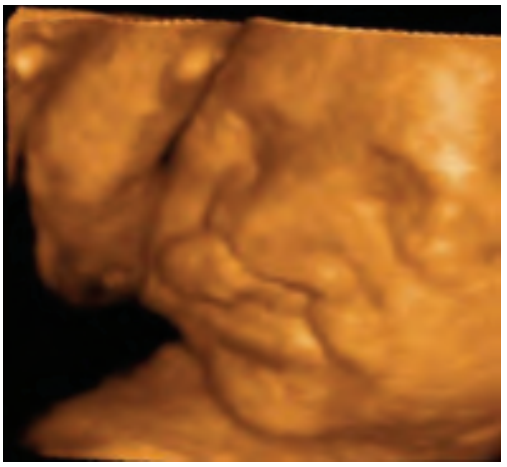

Figure 43.93: 3D scan of a fetus with a unilateral cleft lips

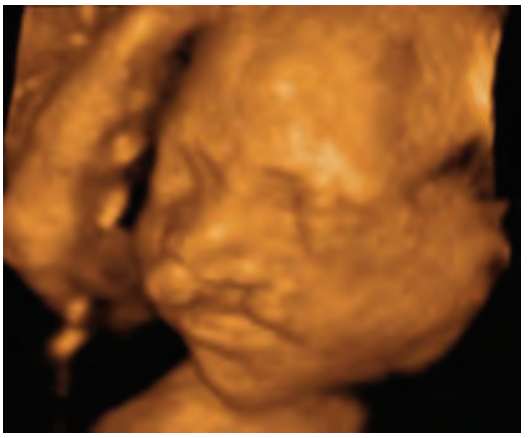

Figure 43.94: 3D surface rendering of facial expression of the fetus with unilateral cleft lip

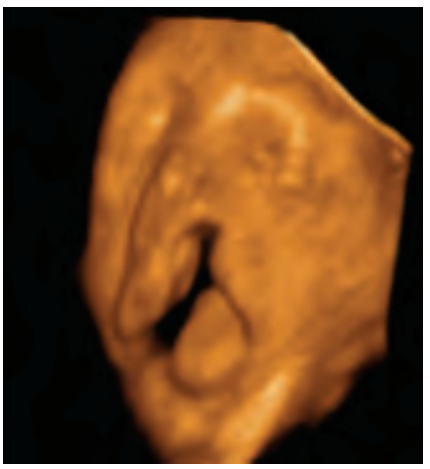

Figure 43.95: 3D surface rendering demonstrates fetus with labiopalatoschisi

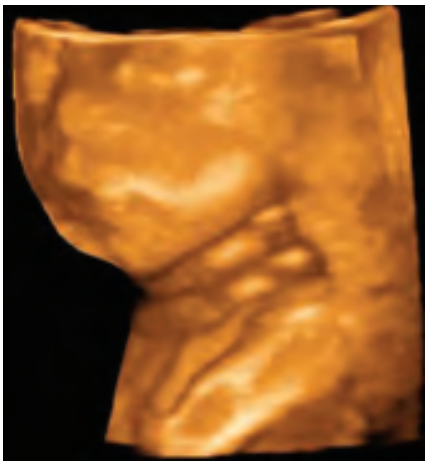

Figure 43.96: 3D surface rendering of the nuchal cord

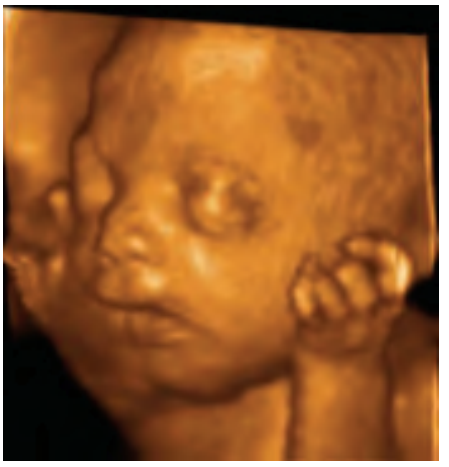

Figure 43.97: 3D surface rendering shows the facial expression of the fetus with arthrogryposis

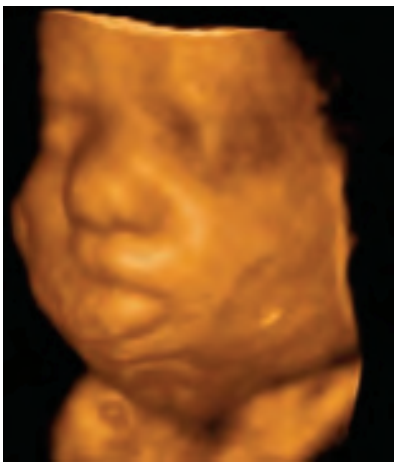

Figure 43.98: 3D surface rendering of the fetus with macroglossia

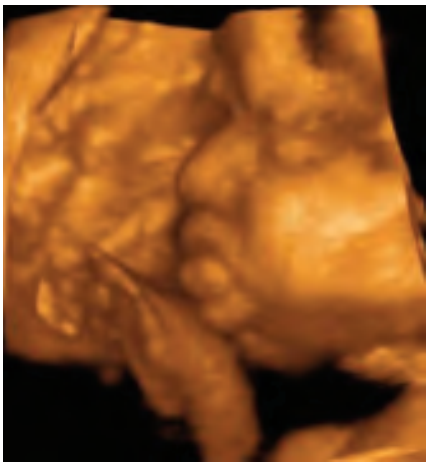

Figure 43.99: 3D surface imaging showing fetus with macroglossia

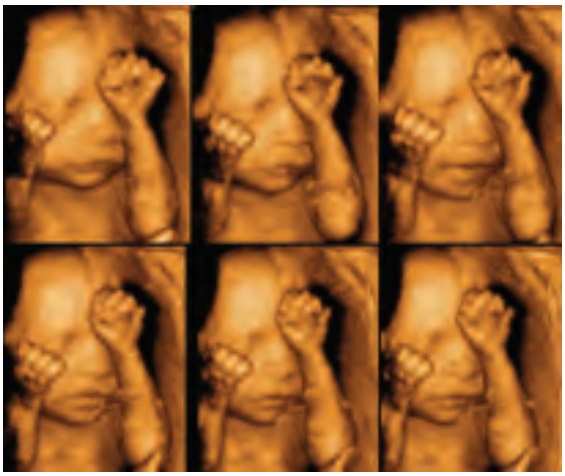

Figure 43.100: 4D sequence demonstrates alteration in facial expression and movement of the hands beside the head

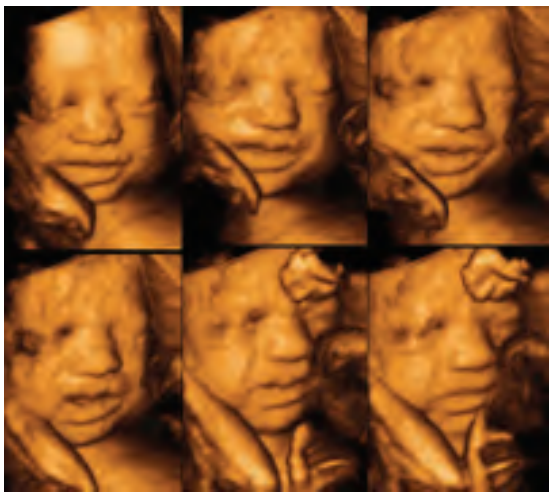

Figure 43.101: 4D sequence demonstrates grimacing expression of the fetus

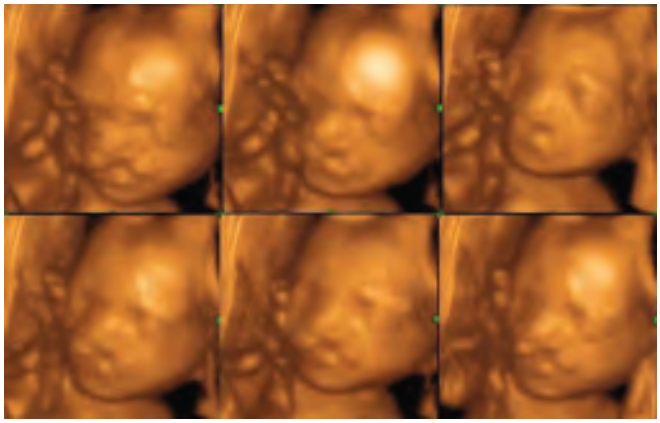

Figure 43.102: 4D sequence shows changing in the facial expression in the fetus with unilateral cleft lip

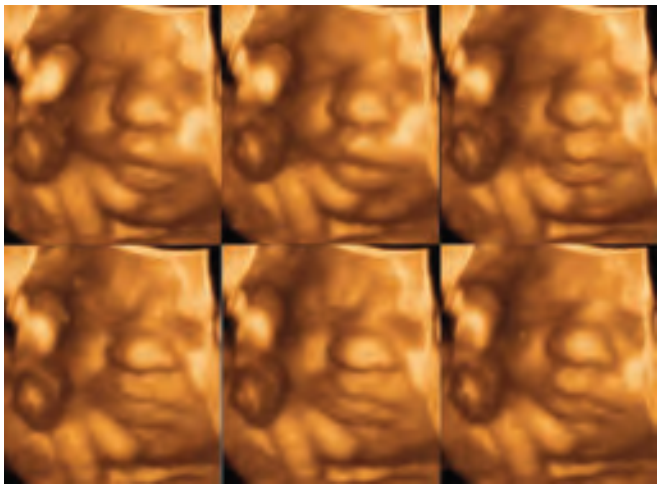

Figure 43.103: Grimacing expression of the fetus shows the wrinkling of the brows or face

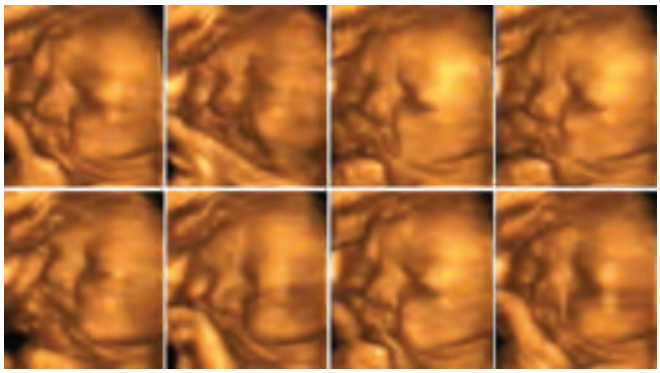

Figure 43.104: The fetus seem to express displeasure in this 4D sequence

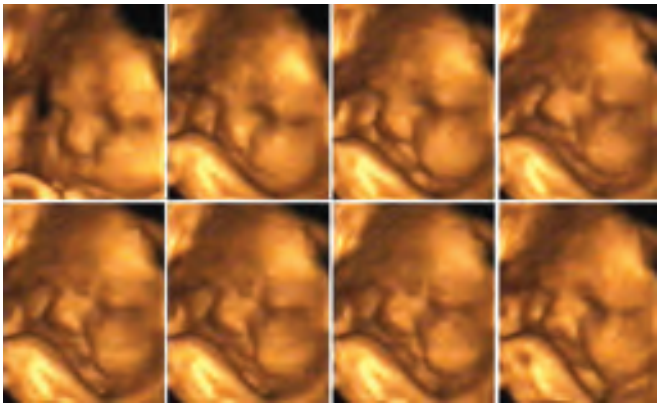

Figure 43.105: 4D sequence shows wrinkling of the brows or the face

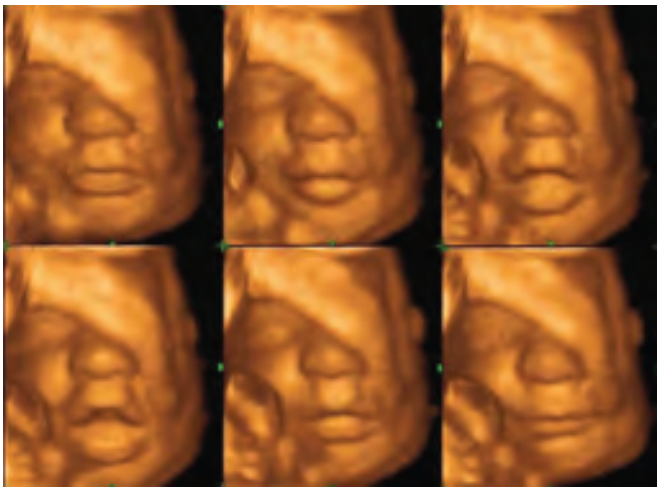

Figure 43.106: Mouthing expression is obtained by 4D technique

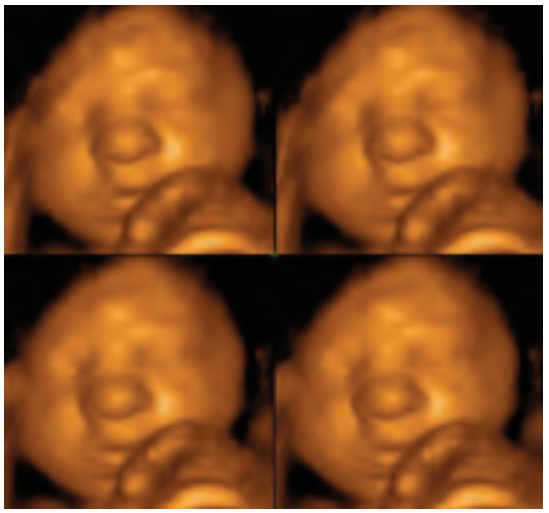

Figure 43.107: 4D sequence shows mouthing expression

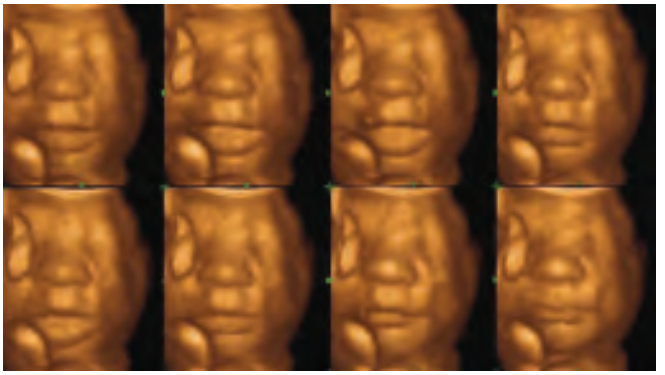

Figure 43.108: A facial expression characterized by mouthing expression

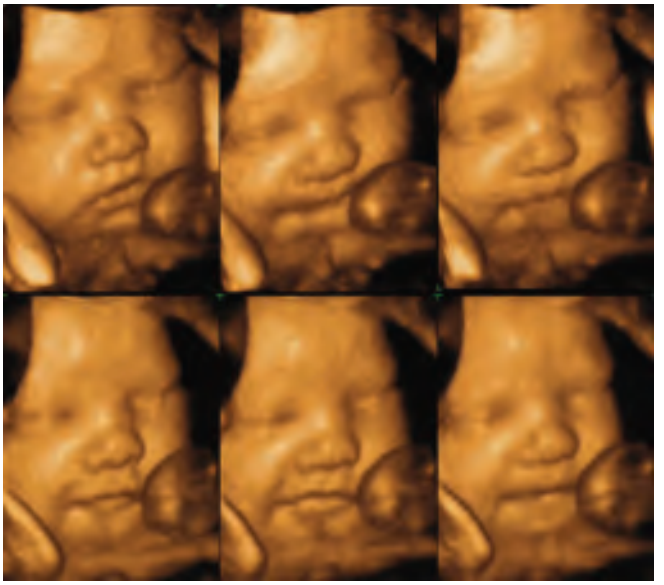

Figure 43.109: This image is showing change in the lateral side of the mouth which results in smiling expression

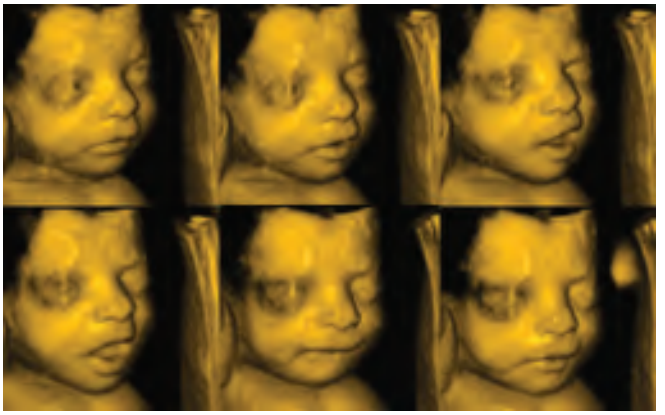

Figure 43.110: 4D images show a brief closing of the eyelids by involuntary normal periodic closing

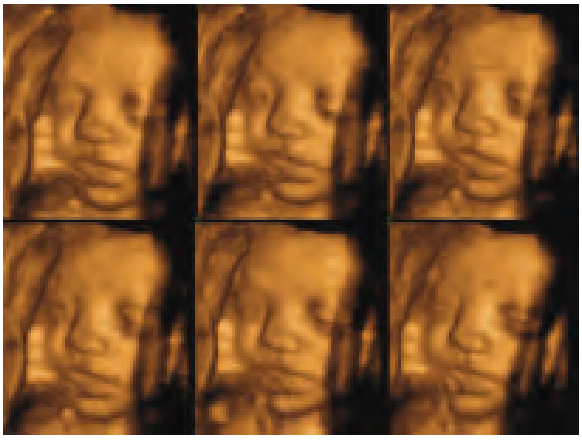

Figure 43.111: 4D sequence showing a reflex that closes and opens the eyes rapidly

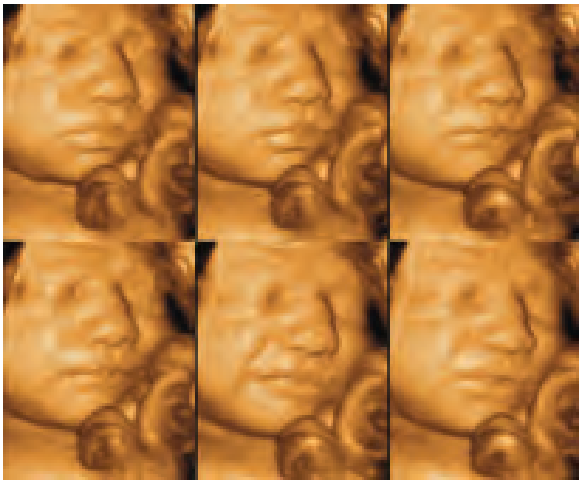

Figure 43.112: 4D sequence characterized by mouthing expression

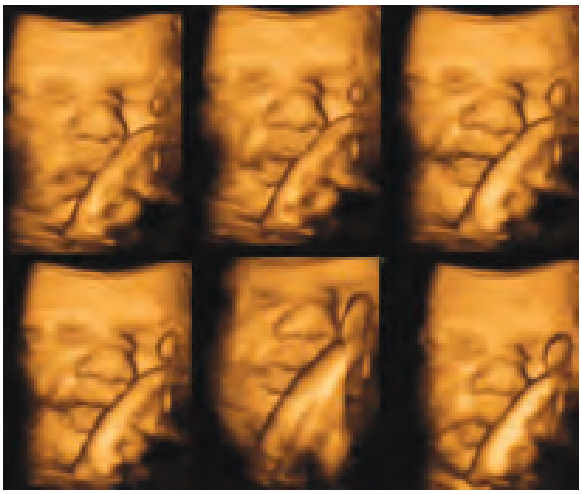

Figure 43.113: 4D imaging characterized by turning up the corners of the mouth. The fetus seems to be smiling

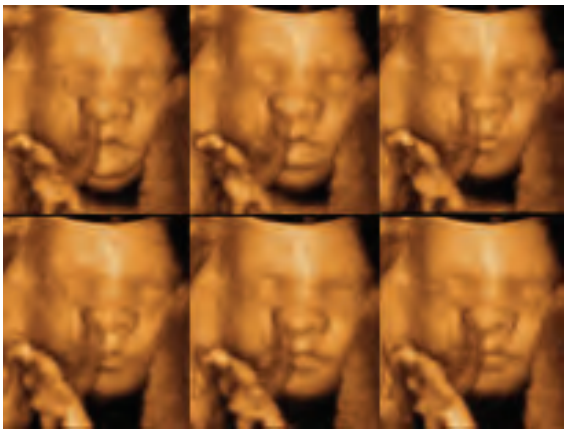

Figure 43.114: 4D sequence characterized by mouth manipulation to investigate an object. Mouthing is most common in fetus and it may develop into a persistent, stereotyped behavior pattern

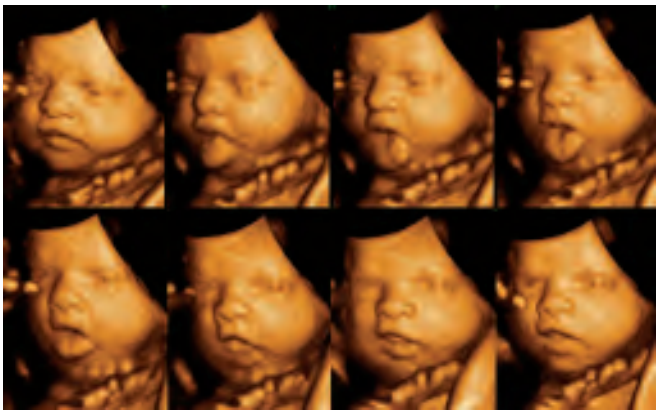

Figure 43.115: 4D sequence demonstrates the beginning and the ending of tongue expulsion

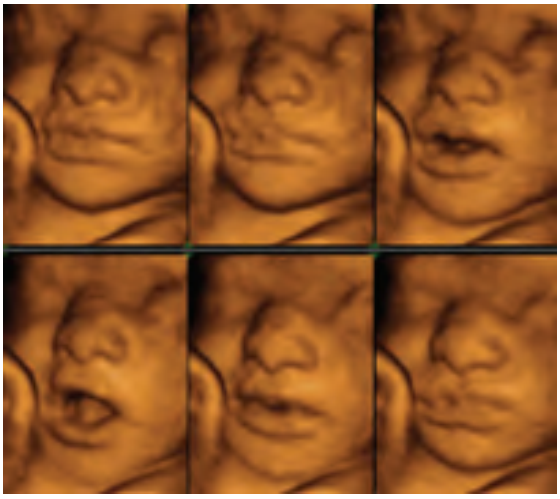

Figure 43.116: 4D sequence shows mouth opening. The fetus demonstrates drinking and swallowing of the amniotic fluid

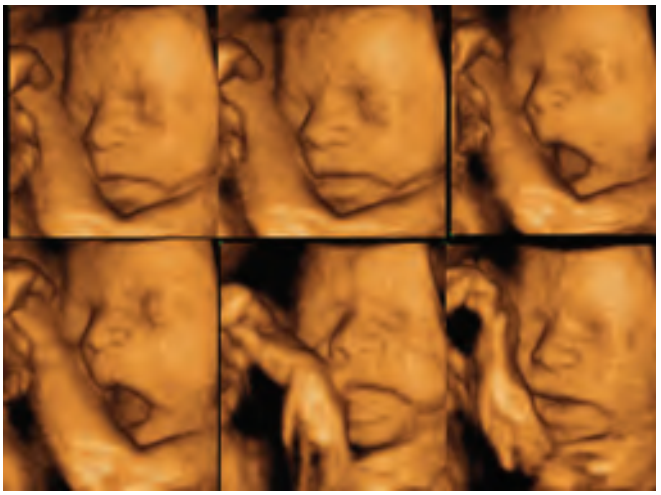

Figure 43.117: 4D sequence demonstrates mouth opening and hand movement of both the hands beside the head in the yawning expression

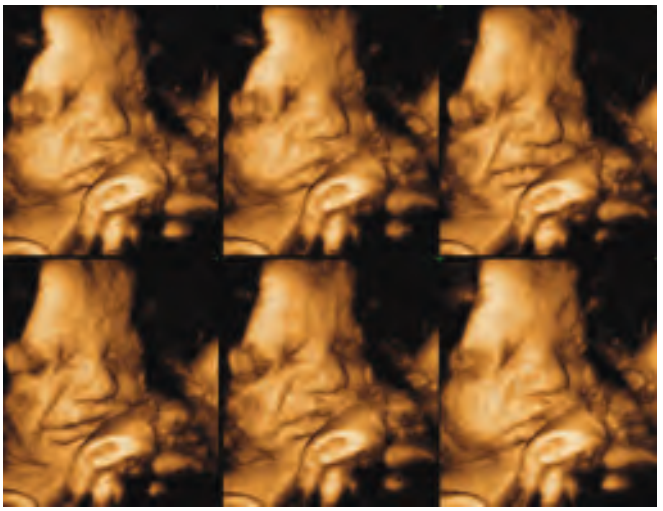

Figure 43.118: 4D sonography sequence demonstrates changing in the facial expression. The fetus seems to be angry

ADVANTAGES AND LIMITATIONS OF 3D ULTRASOUND

The study of the fetal face is of great importance in prenatal medicine because some facial and encephalic structures share the same embryologic origin. This is why every malformation detected at the facial level must necessitate the corresponding study at encephalic level.[30,31] We all recognize the thought of De Meyer and colleagues, who said, "The face predicts the brain".[32] In the ever-increasing body of knowledge on this topic, there are papers that demonstrate some advantages of 3D ultrasound compared with the use of 2D ultrasound in perinatal medicine, mainly in the study of the fetal face.[18,19,32,33] Three-dimensional ultrasound shows perspectives that cannot be obtained with 2D ultrasound and depicts the anatomy in the most appropriate and comprehensive position.[34] This standardized display of images helps us to obtain a better understanding of the fetal anatomy for both the parents and less-experienced doctors. Because of its curvature and small anatomical details, the fetal face can be visualized and analyzed only to a limited extent with 2D sonography.[35,36] The entire face cannot be seen on a single image. Three-dimensional ultrasound provides a spatial reconstruction of the fetal face and simultaneous visualization of all facial structures such as the fetal nose, eyebrows, mouth, jaws, dental germs and eyelids **(Figs 43.11 and 43.12)**.[28,33-37]

Advantages

Improved Maternal-fetal Bonding

Ji and colleagues have stated that, for many parents, the image taken by 2D ultrasound is abstract, whilst with 3D ultrasound the features of the baby are instantly recognized, regardless of whether they are normal or not, which allows parental bonding with the baby.[38] This is one of the unquestionable benefits of 3D ultrasound over 2D.[18,22,39,40] In a few papers in which no other real benefits are found with the use of 3D, the reinforcement of the affective bonding is unchallengeable.[40] Three-dimensional images give the mother more security and a deeper vision of the psychological aspects of ongoing pregnancy.[41] It has also been noted that these positive and close affective bonds between the mother and the fetus can help her to stop smoking or end any other potentially harmful habits[42] **(Figs 43.1 to 43.80)**.

Improvement in Identifying Anomalies

The improvement in the identification of anomalies by the performance of images in perspectives and planes that cannot be obtained with 2D ultrasound has proved vital. It is precisely stated that most fetal face deformations have been diagnosed with 3D ultrasound whilst they had gone unnoticed with 2D ultrasound. Ultrasound cases of micrognathia, cleft lip **(Figs 43.88 to 43.93)**, midfacial hypoplasia, orbitary hypoplasia, facial dysmorphea, defects in the cranium ossification and auricular dysplasia have been picked up.[18,22,31,32] Some of these abnormalities have been diagnosed in the 3D presentations and some others in the planes not available with conventional 2D ultrasound. By allowing evaluation of the volume millimeter by millimeter and

in three perspectives, it is possible to study the upper lip in coronal and axial images and the palate in the axial plane. Three-dimensional ultrasound assists by visualizing the facial profile in the correct axis, which is not always obtainable on a 2D image.[43] Merz and colleagues analyzed the effect of 3D facial profile reconstruction on 125 fetuses.[22] They found that 30.4% of the profiles were turned 3–20 degrees from the real one. Therefore, in only 69.6% of the cases was the true profile obtained with 2D ultrasound. The magnitude of this discovery cannot be disputed, since previously those anomalies could not be detected or were overdiagnosed. Several papers state the clear superiority of 3D ultrasound for the study of the fetal face in both normal and abnormal conditions,[1-7,9-15,17-20,22-29,44,45] although some authors do not find these differences so significant.[40]

Improved Assessment of Extent and Location of Fetal Anomalies

Assessment of the extent and location of fetal anomalies can be improved by using 3D ultrasound **(Figs 43.81 to 43.97)**.[18,28,32,46] A cleft lip and/or a cleft palate are often difficult to diagnose with 2D ultrasound, or at least it has been difficult to precisely evaluate their extent, especially if the operator has little experience or lacks anatomic references with the appropriate image plane. In the Routine Antenatal Diagnostic Imaging with Ultrasound Study (RADIUS) study, 7,685 low-risk fetuses were studied and only three out of nine cleft lips were prenatally identified.[47] Using 3D ultrasound, the operator can evaluate the front alveolar ledge or the primary palate in the appropriate axial plane, using the correct reconstruction or the sagittal planar image as a reference, and can then move on to the parallel axial images. This possibility for studying axial or frontal parallel planes of the fetal face' is not obtained with 2D ultrasound. It is extremely useful to show the anomaly to both relatives and trainee doctors in order to assist their decision regarding future diagnostic and therapeutic options.[18,22,23,28,33,48]

Four-dimensional Ultrasound

Four-dimensional ultrasound has some additional advantages such as the ability to study fetal activity in the surface-rendered mode, and is particularly superior for fast fetal movements.[49] With 2D ultrasound, fetal movements such as yawning, swallowing and eyelid movements cannot be displayed simultaneously, whilst, with 4D sonography, the simultaneous facial movements can be clearly depicted.[50] There are several types of jaw movement patterns, such as isolated jaw movement, sucking and swallowing, which can be observed by 2D ultrasound.[51] The variable amplitudes of jaw opening and speed characterize isolated jaw movements **(Fig. 43.3)**. Yawning can be observed as a movement pattern identical to that seen in infants, children and adults: slow opening, prolonged wide opening of the jaws followed by quick closure, with simultaneous retroflexion of the head. With 4D ultrasound, it is now feasible to study a full range of facial expressions including smiling, crying, scowling and eyelid movement.[50,52]

The observation of the facial expression may be of scientific and diagnostic value and this scientific approach opens an entirely new field. There are many unanswered questions. When do facial expressions start? Which expression dominates and at what gestational age do they occur? An important diagnostic aim of the observation of facial expression is prenatal diagnosis of facial paresis. The criterion for the diagnosis is asymmetrical facial movement and detection of the movements limited to only one side of the face. Unfortunately during the relaxed phase, it is not possible to evaluate the status of the facial nerve.

Therefore, during the active phase, the fetus should be scanned by 4D ultrasound. Since the origin of the facial expression can be external, the sonographer should be aware of this pitfall. For example, force of the fetal hand can alter the facial expression on one side of the face, causing asymmetry **(Fig. 43.80)**. This kind of asymmetry, however, should be differentiated from pathological features such as unilateral facial paresis **(Fig. 43.6)**. We believe that the largest challenges for 4D ultrasound are in the unexplored areas of parental and fetal behavior.[53-55] Two-dimensional realtime ultrasound and 4D sonography are complementary methods used for evaluation of fetal movements. It is clear that the quality of each fetal movement can be visualized and evaluated more reliably by 4D ultrasound. It appears that there are still not enough prospective studies that may clarify or prove real benefits of 3D ultrasound in daily practice and there is an urgent need for randomized control studies.[40] Our group have been evaluating fetal behavioral patterns in the third trimester between 30th to 33rd week of gestation in 10 gravidas.[56] The continuity between fetal and neonatal behavior have been published recently from Zagreb, Barcelona and Malaga groups[57] **(Figs 43.81 to 43.102).**

Limitations

As with any new technique, there are some limitations. Failure rates are reported in obtaining high-quality

images in surface mode under certain circumstances such as oligohydramnios or the shadowing by hands, feet, umbilical cord or placenta **(Fig. 43.34)**. Under these circumstances, it is advisable to re-examine the reconstructions together with the planar data of the same volume, in order to evaluate the direction of the ultrasound beam that is more visible on planar images than on those reconstructed. One report described how a totally normal fetal face appeared to have a cleft lip due to the shadow of the umbilical cord adjacent to the upper lip on the multiplanar images.[46] Sometimes, we have difficulties in identifying other surface features such as fingers and toes because they are frequently opposed to the wall of the uterus. An additional limitation of 4D ultrasound, at least for the moment, is the inability to display fetal movements that are too quick (within 1–2 sec) and subtle fetal movements such as those of breathing. However, many of these limitations may disappear in the near future as more powerful equipment is developed and appears on the market.

ASSESSMENT OF FETAL FACIAL EXPRESSION

Classification of Facial Patterns

We had classified several facial expressions in at least eight different activities, which are as follows:

1. Yawning: This movement is similar to the yawn observed after birth. An involuntary wide opening of the mouth, with maximal widening of the jaws followed by quick closure often with retroflexion of the head and sometimes elevation of the arms. This movement pattern is nonrepetitive **(Figs 43.54 and 43.55)**.
2. Swallowing: Indicating that the fetus is drinking amniotic fluid. Swallowing consists of displacements of tongue and/or larynx. Swallowing activity develops earlier than sucking in the course of fetal development **(Fig. 43.115)**.
3. Sucking: Rhythmical bursts of regular jaw opening and closing at a rate of about one per second. Placing the finger or thumb on the roof of the mouth behind the teeth and sucking with lips closed. Thumb sucking is a very frequent fetal behavioral pattern **(Fig. 43.52)**.
4. Smiling: A facial expression characterized by turning up the corners of the mouth **(Fig. 43.50)**.
5. Tongue expulsion: A facial expression characterized by expulsion of the tongue **(Fig. 43.33).**
6. Grimacing: The wrinkling of the brows or face in frowning to express displeasure **(Figs 43.103 and 43.104)**.
7. Mouthing: A facial expression characterized by mouth manipulation to investigate an object. Mouthing is most common in fetus and it may develop into a persistent, stereotyped behavior pattern **(Fig. 43.112)**.
8. Isolated eye blinking: A reflex that closes and opens the eyes rapidly. Brief closing of the eyelids by involuntary normal periodic closing, as a protective measure, or by voluntary action **(Figs 43.103 to 43.118)**.

OPTIMUM CONDITIONS FOR 3D SCANNING OF THE FETAL FACE

For 3D visualization of the fetal face, the surface mode is generally used. This normally needs a shorter training period with acceptable results in a relatively limited period of time. It must be said, however, that the achievement of appropriate images requires a set of previous conditions without which our results would probably be discouraging. It is clear that one of the great advantages of 3D ultrasound is that the information remains captured as a volume and it is possible to reconstruct the recorded image and modify all the adjustments as if the patient is still present. This enables us to manipulate the image, re-rotate it three-dimensionally and achieve another 3D reconstruction from the data already taken. There are also electronic scalpels, which assist by cutting off and eliminating all parts that can hide or distort the area we wish to study. With these facilities, we can improve the 3D reconstruction made from an image that is less than favorable.

Appropriate Gestational Age to Visualize the Fetal Face

The appropriate gestational age is neither too early (as the facial structures are not sufficiently developed) nor too late (the relative lack of space available during the last gestational weeks might hinder an appropriate visualization of the fetal face, due to its immediate closeness to the uterine wall, the placenta or the fetal extremities). From week 13, facial structures acquire an adequate degree of development so that studying them for diagnostic purposes can be started. At this stage, it may still be too early to show the mother any images if we support the contribution of the scan to reinforce the affective bonds between the fetus and the future parents. Our experience shows that it is counterproductive to show the 3D image of the fetal face to the parents during the first trimester. For most parents, the image appears to be strange and it can create a distorted image of their child, which will not reinforce the affective

bonds. It could indeed create anxiety. From weeks 18–19, we can obtain 3D reconstruction of the fetal face which is starting to show clear facial features[58] and these can be shown to the parents. From this moment and until week 35 or 36, we can obtain 3D reconstructions of the facial surface in a high percentage of mothers. Experience and much patience are needed to wait for the fetus to adopt an appropriate position for this type of scanning.[59] We think that the most favorable age for 3D scanning of the fetal face is from weeks 23 until 30. During this period of gestation, we have succeeded in visualizing the face three-dimensionally in a high percentage of the cases (higher than 70%) without extending the length of the prenatal 2D ultrasound scan.

Favorable Fetal Position

To obtain the best images, the probe has to be moved so that the face of the fetus is facing the probe surface. In addition, it is very important for the fetal face not to be in contact with other structures such as the uterine wall, the placenta or fetal extremities. Sometimes, it will be of much assistance to stimulate the fetus using the free hand over the abdominal wall. The fetus may then change position and move away from the structures that prevent correct visualization. Once the correct position is obtained, the capture box is placed over the reference line in the closest possible way to the fetal face. We will have to wait for the baby to keep still, if we seek a static 3D reconstruction, or to make facial movements (yawning, suctioning, lids opening) if we seek a 4D scanning.

Postprocessing of the Image

In addition to these previous requirements, one should not forget that, after capturing the image, there are many adjustment possibilities. Amongst all the tools we have at the moment, the most useful one is the electronic scalpel, which allows us to eliminate all areas that are of no interest and also those which disturb the demonstration of the structure that we wish to visualize. This tool can be used in both multiplanar and 3D images. The control of all these adjustments, possibilities and tools does take time, but the final achievement of images shown will surely compensate for all our efforts.

Once we have acquired this experience, we can verify that, while all the procedures stated here are very complicated and complex, with time they become relatively easy and in fact, require only a few seconds to adjust the equipment and just a few minutes to retouch the 3D reconstruction. Usually, we start the conventional scanning and, when we acquire a favorable position of the fetal face, we interrupt the 2D exploration and capture the image for 3D reconstruction, following which 2D ultrasound study is then continued. With this procedure, we can achieve 3D visualization of the fetal face without adding more than 3 or 4 minutes to the complete length of the usual ultrasound scanning.

CONCLUSION

Three-dimensional ultrasound offers the possibility of studying the fetal face in a more global way than conventional two-dimensional ultrasound. In normal cases, the images obtained help to transmit a feeling of calmness to the parents and reinforce the affective bond with their child. In pathological cases, 3D ultrasound can help parents and other doctors involved to take a more realistic view of the problem. It is expected that the use of this novel technology will provide parents with the knowledge to have a better judgement whilst taking decisions. Four-dimensional ultrasound has enormous potential in perinatal research. This technique is still in its infancy but there is much scope for investigation of fetal anatomy as well as fetal behavior. This technique should assist us in the better understanding of both the somatic and functional development of the early embryo and the fetus.

References

1. Baba K, Okai T, Kozuma S. Real-time processable three-dimensional fetal ultrasound. Lancet. 1996;348:1307.
2. Baba K, Satoh K, Sakamoto S, et al. Development of an ultrasonic system for three-dimensional reconstruction of the foetus. J Perinat Med. 1989;17:24.
3. Baba K, Okai T, Kozuma S, et al. Real-time processable three-dimensional US in obstetrics. Radiology. 1997;203: 571-4.
4. Bonilla-Musoles F, Raga F, Osborne N, et al. Ecografia tridimensional en Obstetricia y Ginecologia. Obstet Ginecol Espan. 1994;3:233-50.
5. Bonilla-Musoles F, Raga F, Blanes J, et al. Three-dimensional ultrasound in reproductive medicine: preliminary report. Hum Reprod Update. 1995,1:4 item 21 CDRom.
6. Bonilla-Musoles F, Machado L. Ultrasonidos y Reproduction. Cuadernos de Medicina Reproductiva, No 2. Madrid: Panamericana; 1999. p. 6.
7. Devonald KJ, Ellwood D, Cnffiths K, et al. Volume imaging: three-dimensional appreciation of the fetal head and face. J Ultrasound Med; 1995. pp.919-26.
8. Hull AD, Pretorius DH. Fetal face: what we can see using two-dimensional and three-dimensional ultrasound. Semin Roentgeno. 1998;33:369-74.
9. Hata T, Yonehara T, Aoki S, et al. Three-dimensional sonographic visualization, of the fetal face. Am J Roentgenol. 1998;170:481-3.
10. Kelly IMC, Cardener JE, Lees WR. Three-dimensional fetal ultrasound. Lancet. 1991;339:1062-4.

11. Kelly IMC, Cardener JE, Brett AD, et al. Three-dimensional US of the fetus. Work in progress. Radiology. 1994;192:253-9.
12. Kratochwil A. Versuch der 3-dimensionalen Darstellung in der Ceburtshilfe. Ultraschall Med. 1992;13:183-6.
13. Kuo HC, Chang FM, Wu CH, et al. The primary application of three-dimensional ultrasonography in obstetrics. Am J Obstet Gynecol. 1992;166:880-6.
14. Lee A, Deutinger J, Bernaschek C. Three-dimensional ultrasound: abnormalities of the fetal face in surface and volume rendering mode. Br J Obstet Gynaecol. 1995;102:302-6.
15. Levaillant JM, Benoit B, Bady J, et al. Echographie tridimensionelle apport technique et clinique en echographie obstetricale. Reprod Humaine Hormone. 1995;3: 341-7.
16. Ludomirski A, Khandelwal M, Uerpairojkit B, et al. Three-dimensional ultrasound' evaluation of fetal facial and spinal anatomy. Am J Obstets Gynecol. 1996;174(Suppl): 318.
17. Manabe A, Hata T, Aoki S, et al. Three-dimensional sonographic visualization of fetal facial anomaly. Acta Obstet Gynecol Scand. 1999;78:917-8.
18. Merz E, Bahlmann F, Weber C. Volume scanning in the evaluation of fetal malformations: a new dimension in prenatal diagnosis. Ultrasound Obstet Gynecol. 1995;5:222-7.
19. Merz E, Bahlmann F, Weber C, et al. Three-dimensional ultrasonography in prenatal diagnosis. J Perinat Med. 1995:23:213-22.
20. Merz E. Einsatz der 3D-Ultraschalltechnik in der pranatalen Diagnostik. Ultraschall Med. 1995;16:154-61.
21. Merz E. Three-dimensional ultrasound in the evaluation of fetal anatomy and fetal malformations. In: Chervenak FA, Kurjak A. (Eds). Current Perspectives on the Fetus as a Patient. London: Parthenon Publishing; 1996. pp. 75-87.
22. Merz E, Weber C, Bahlmann F, et al. Application of transvaginal and abdominal three-dimensional ultrasound for the detection or exclusion of malformations of the fetal face. Ultrasound Obstet Gynecol. 1997;9:237-43.
23. Mueller CM, Weiner CE, Yankowitz J. Three-dimensional ultrasound in the evaluation of fetal head and spine anomalies. Obstet Gynecol. 1996,88:372-8.
24. Nelson TR, Pretonus DH. Three-dimensional ultrasound of fetal surface features. Ultrasound Obstet Gynecol. 1992;2:166-74.
25. Pretorius DH, Nelson TR, Jaffe JS. Three-dimensional US of the fetus. Radiology. 1990;177:194.
26. Pretorius DH, Nelson TR. Three-dimensional ultrasound imaging in patient diagnosis and management: the future. Ultrasound Obstet Gynecol. 1991;1:381-3.
27. Pretorius DH, Nelson TR. Prenatal visualization of cranial sutures and fontanelles with three-dimensional ultrasonography. J Ultrasound Med. 1994;13:871-6.
28. Pretonus DH, Johnson DD, Budonck NE, et al. Three-dimensional ultrasound of the fetal lip and palate. Radiology. 1997;205(Suppl):245.
29. Steiner H, Merz E, Staudach A. Three-dimensional fetal facing. Hum Reprod Update. 1995;1:item 6.
30. Hegge FN, Prescott CH, Watson PT. Fetal tadal abnormalities identified during sonography. J Ultrasound Med. 1986;5:679-88.
31. De Meyer V, Zeman W, Palmer CC. The face predicts the brain: diagnostic significance of medial facial anomalies for holoprosencephaly (archinencephaly). Pediatrics. 1964,34:256-8.
32. Hamper UM, Trapanotto V, Sheth S, et al. Three-dimensional US: preliminary clinical expenence. Radiology. 1994,191:397.
33. Pretorius DH, House M, Nelson TR, et al. Evaluation of normal and abnormal lips in fetuses: comparison between three-and two-dimensional sonography. Am J Roentgenol. 1995;165:1233-7.
34. Nelson TR, Downey DB, Pretorius DH, et al. Ecografia 3D en Obstetrida en Ecografia 3D. Madrid: Marban, 2000.
35. Hepper PC, Shannon FA, Dornan JC. Sex differences in fetal mouth movements. Lancet. 1997;350:1820.
36. Kozuma S, Okai T, Ryo F, et al. Differential developmental process of respective behavioral states in human fetuses. Am J Perinatol. 1998;15:203-8.
37. Ulm MR, Kratochwil A, Ulm B, et al. Three-dimensional ultrasound evaluation of fetal tooth germs. Ultrasound Obstet Gynecol. 1998;12:240-3.
38. Ji EK, Pretorius DH, Newton R, et al. Effects of ultrasound on maternal-fetal bonding: a comparison of two- and three-dimensional imaging. Ultrasound Obstet Gynecol. 2005;25:473-7.
39. Merz E, Weber G, Bahlmann AF, et al. Transvaginale 3D-Sonographie in der Gynaekologie. Gynaekologe. 1995;28: 270-5.
40. Schart A, Chazwiny MF, Steinbom A, et al. Evaluation of two-dimensional versus three-dimensional ultrasound in obstetric diagnostics: a prospective study. Fetal Diagn Ther. 2001;16:333-41.
41. Maier B, Steiner II, Wienerroither H, et al. The psychological impact of three-dimensional fetal imaging on the fetomaternal relationship. In: Baba K, Jurkovic D (Eds): Three-dimensional Ultrasound in Obstetrics and Cynecology. Lancaster: Parthenon Publishing; 1997. p. 67-74.
42. Pretonus DH. Maternal smoking habit modification via fetal visualization. University of California Tobacco Related Disease Research Program. Annual Report to the California State Legislature, 1996.pp.76.
43. Merz E. 3-D Ultrasound in Obstetrics and Gynecology. Philadelphia: Lippincott Williams & Wilkins, 1998.
44. Lees WR, Gardener JE, Gilliams A. Three-dimensional US of the fetus. Radiology. 1991;181:131-2.
45. Ludomirski A, Ucrpairojkit B, Whiteman VE, et al. New technology in three-dimensional obstetrical ultrasonography: technique, advantages and limitations. Am J Obstet Gynecol. 1996;174(Suppl):328.
46. Pretonus DH, Richards RD, Budorick NE, et al. Three-dimensional ultrasound in the evaluation of fetal anomalies. Radiology. 1997;205(P)(Suppl):245.
47. Crane JP, LeFevre ML, Winbom RC, et al. A randomized trial of prenatal ultrasonographic screening: impact on the detection, management, and outcome of anomalous fetuses. Am J Obstet Gynecol. 1994;171:392-9.
48. Pretorius DH, Nelson TR. Fetal face visualization using three-dimensional ultrasonography. J Ultrasound Med. 1995;349-56.

49. Lee A. Four-dimensional ultrasound in prenatal diagnosis; leading edge in imaging technology. Ultrasound Rev Obstet Gynecol. 2001;1:194-8.
50. Kozuma S, Baba K, Okai T, et al. Dynamic observation of the fetal face by three-dimensional ultrasound. Ultrasound Obstet Gynecol. 1999;13:283-4.
51. Roodenburg PJ, Vladimiroff IW, van Es A, et al. Classification and quantitative aspect of fetal movements during the second half of normal pregnancy. Early Hum Dev. 1991;25:19-35.
52. Campbell S. 4D or not 4D: that is the question. Ultrasound Obstet Gynecol. 2002;19:1-4.
53. Kurjak A, Vecek N, Kupesic S, et al. Four-dimensional sonography: how much does it improve perinatal practice. In: Carrera JM, Kurjak A, Chervenak FA. (Eds). Controversies in Perinatal Medicine. London: Parthenon Publishing; 2003.
54. Kurjak A, Vecek N, Hafner T, et al. Prenatal diagnosis: what does four-dimensional ultrasound add. J Perinat Med. 2002;30:57-62.
55. Kuno A, Akiyama M, Yamashiro C, et al. Three-dimensional sonographic assessment ot fetal behavior in the early second trimester of pregnancy. J Ultrasound Med. 2001;20:1271-5.
56. Kurjak A, Azumendi G, Vecek N, et al. Fetal hand movements and facial expression in normal pregnancy studied by four-dimensional sonography. J Perinat Med. 2003;31:496-508.
57. Kurjak A, Stanojevic M, Andonotopo W, et al. Behavioral pattern continuity from prenatal to postnatal life: a study by four-dimensional (4D) ultrasonography. J Perinat Med. 2004;32:346-53.
58. Hohlteld J. Le diagnostic prenatal des feintes labio-palatines. Med Foct Echographie Gynecol. 1995;22:4-15.
59. Bonilla-Musoles F, Machado LE, Osborne NC. Ecograha tridimensional en Obstetricia en el nuevo milemo. Madrid: Marco Crafico; 2000.

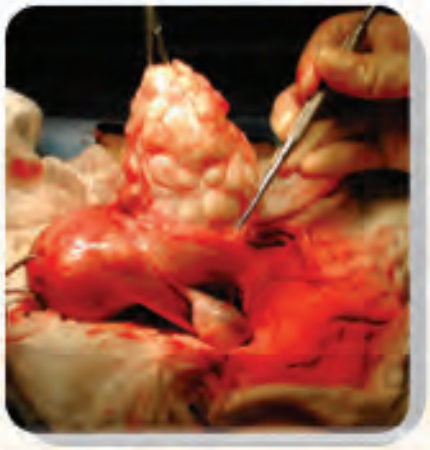

Gynecology

Section Three

44
CHAPTER

Normal Female Reproductive Anatomy

Sanja Kupesic Plavsic, Bhargavi Patham, Ulrich Honemeyer, Asim Kurjak

INTRODUCTION

Transvaginal ultrasound is superior to transabdominal ultrasound in female gynecologic examination due to (i) use of high-frequency transvaginal transducer with better spatial resolution and (ii) no need to fill the urinary bladder. Because of these characteristics, transvaginal ultrasonography became essential in gynecologic ultrasound examination.

Two-dimensional (2D) ultrasound imaging is limited by the movement of the transvaginal transducer in the narrow space of vagina allowing biplanar display (sagittal and transverse). In stark contrast, three-dimensional (3D) sonography permits multiplanar display (coronal, sagittal and transverse). The (3D) sonography measures the volume of the studied organ and evaluate it more accurately, stores of the data without degradation of the image quality and allows retrospective analysis and application of teleconsultation in telemedicine.

Color Doppler capability of the transvaginal probes allows visualization of small intraovarian and endometrial vessels, enabling depiction of normal and pathological changes in reproductive organs.

Three-dimensional color histogram measures the color percentage and flow amplitudes in the volume of interest. Therefore, histogram enables quantification of the vascularization and blood flow within a tissue block, in contrast to 2D color histogram measurements, where only single planes can be investigated. Here, three-dimensional tissue block is swept through with a volume probe to get the 3D information and after that, to border the volume of interest, which contains the color, information resulting in an automatic delineation called “shell imaging”.

UTERUS

Various parameters regarding uterus are described as under:

Position

In the female pelvis, uterus is considered to be a reliable landmark because of its central location, relatively large size and the well-known pear-shape.[1] The cervix is less mobile than the uterine body due to uterosacral ligaments that position the cervix in the midline of the pelvis.

Anteverted uterus projects from the anterior fornix of the vagina and extends anterosuperiorly to the uterine fundus. Retroverted uterus projects from the posterior fornix of the vagina to its posterosuperior extension. Anteflexion of the uterus describes its position when the uterine body is angled forward concerning the axis of the cervix, while retroversion describes backward angulation.

Difficulties in demonstrating the uterine fundus exists if the uterus is retroverted and retroflexed behind the interposed cervix on transabdominal ultrasound. Some rare positions of the uterus include its anteverted and retroflexed or retroverted and anteflexed position.

On transvaginal sonography, transducer is pressed on the flexed cervical-corporeal junction, oriented at the superior apex of the screen. The fundus of the anteverted uterus is often placed on the left side of the ultrasound screen and anteflexed position is imaged as concave upward. Fundus of the retroverted uterus is placed to the right, with retroflexion concave upward. Transvaginal scanning might be limited when the uterus is in the same axis as the cervix and vagina, because the ultrasound beam and uterine position are not perpendicular.

Commonly, uterus can be slightly deviated to the right or left side, but larger deviations might exist due to pelvic masses or peritoneal adhesions. The position of the uterus is an important factor during the various invasive procedures (curettage, hysteroscopy, insertion of an intrauterine contraceptive device and embryo transfer). Transitory change of uterine position and deviation can be caused by bladder and rectal fullness, patient's posture or external manual pressure.

Size, Shape and Echo Texture

The normal size, shape, the length ratio of body and cervix of the uterus and appearance of the endometrium depend on the patient's age and parity.

The dimensions of the uterus can be accurately measured with transabdominal and transvaginal ultrasound. Uterine volume measured using the conventional formula for ellipsoid is less informative because the uterine shape does not approximate an ellipsoid.

Uterus consists of the body and the cervix, having a 2:1 length ratio. Dimensions of the body are approximately 7.5–9 cm length × 4.5–6 cm width × 2.5–4 cm thickness. Multiparity increases dimensions by 1–2 cm in all directions. Dimensions of the cervix are 2.5 cm length and 2.5 cm diameter.

In sagittal section, the endometrial cavity is slit-like, with touching anterior and posterior surface. In coronal section or anteroposteriorly on hysterosalpingography, the endometrial cavity appears triangular (cervical canal opens up to the lateral angles of the cavity containing uterotubal junctions).

The myometrium is by far the thickest part of the uterine wall. Normal echo texture of the myometrium is homogeneously echodense. The inner layer of the myometrium can be a little less echogenic, but the junction zone with endometrium is very well demarcated and smooth.

The outer layers of myometrium may contain small circular hypoechoic spaces, calcified with age, which correspond to arcuate arteries in cross-section **(Fig. 44.1)**. On color Doppler, they are represented with slow laminar blood flow signals in color. The development of the endometrium, its thickness and echo texture are highly influenced by ovarian hormones, estrogen and progesterone.

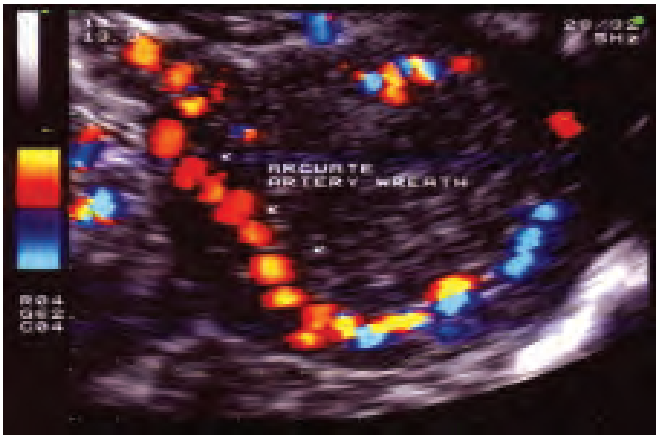

Figure 44.1: Transvaginal color Doppler ultrasound of the uterus demonstrating arcuate arteries wreath

Newborn and Prepubertal Uterus

The newborn uterus is tubular in shape with body to cervix length ratio 1:1, and is poorly differentiated. Neonatal uterus can be 0.5–1 cm larger than the uterus in infants due to the influence of pregnancy hormones. Prepubescent dimensions of the uterus are approximately 3 cm length × 2 cm width × 2 cm thickness, tubular shaped with the same length ratio as in newborns. During puberty, period shape of the uterus changes to pear shape and the corpus enlarges.

Adult Uterus

Dimensions of the adult nulliparous uterus are 7.5 × 5 × 2.5 cm, and its position depends on bladder and rectal fullness. Normal uterine size varies with parity, but after postpartum involution it stabilizes at approximately 1.5 cm.[2] During the reproductive period, the pelvic organs (their size and echogenicity) are influenced with cyclic changes controlled by the ovaries. These changes are especially evident in the uterus duration the normal menstrual cycle which is 28 days, with about equal time for the preovulatory (follicular) and postovulatory (luteal) phase. In women with normal fertility, duration of the menstrual cycle can vary with the range between 25 and 36 days. While the follicular phase (proliferative phase of the endometrium) may vary, the luteal phase (secretory phase of the endometrium) remains 14 days.

Approaching the menopause, the follicular phase becomes shorter, shortening the whole menstrual cycle and bringing the time of ovulation sooner.

Proliferative Phase

Uterine endometrium consists of two layers: the inner stratum functionalis—subjected to the changes during menstrual cycle, peeled off with menstruation, and the outer stratum basalis—permanent layer not influenced by cyclic changes, contains glandular buds from which glands develop.

As menstruation ceases, the functional layer of the endometrium responds to small amounts of estrogens secreted by the ovary. Parallel with follicular development and rising estrogen production, the endometrial glands in basal layer proliferate, elongate and become tortuous. The endometrium is best depicted on transvaginal sonography in the sagittal plane. In the sagittal plane, the endocervical canal is seen continuing into the endometrial echo. For the most patients who do not have significant amount of intraluminal fluid, the endometrium is measured in a bilayer thickness from the proximal myometrial-endometrial junction to the distal myometrial-endometrial junction. If intraluminal fluid is present, each endometrial thickness should be measured separately and the combined endometrial thickness should be expressed as a sum of the two layers. In the early proliferative phase endometrium is imaged as a thin echogenic line, measuring 1–3 mm. With the progression of proliferative phase the endometrium becomes less echogenic than the surrounding myometrium **(Fig. 44.2)**. The most characteristic sign of the late proliferative phase is the triple-line endometrium. The central echogenic line represents

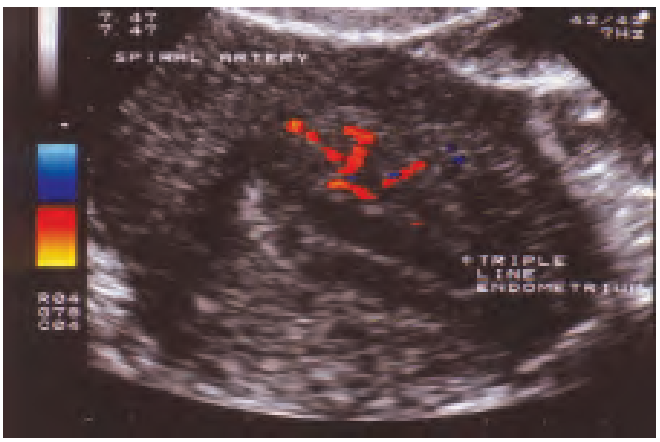

Figure 44.2: Transvaginal scan of the uterus in the late proliferative phase of the menstrual cycle. The endometrium is sonolucent compared with myometrium. Note an echo demarcating the endometrium from the junctional layer, and a third line representing the point of the contact between front and back mucosal surfaces. Color Doppler delineates subendometrial vessels

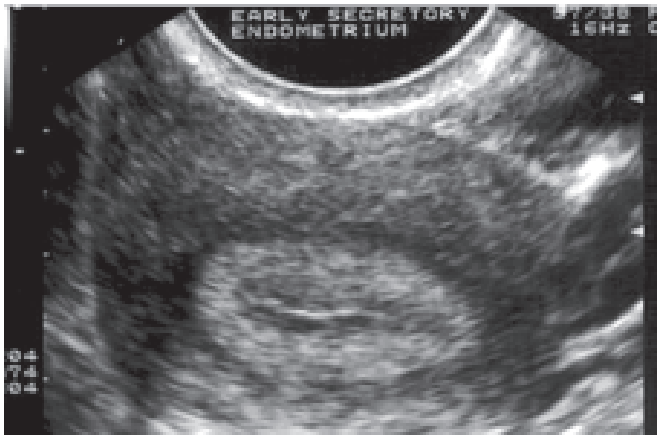

Figure 44.3: Transvaginal scan of the uterus with echogenic endometrial lining during the early luteal phase of the menstrual cycle

touching of the anterior and posterior endometrial layers. The two outer hyperechogenic lines represent endometrial-myometrial junction or echo of the basal layer. The endometrial tissue (functional layer) between the two lines becomes hypoechoic and thick during the proliferative phase, continuing to widen basal echogenic line toward uterine cavity and central echogenic zone **(Fig. 44.2)**.

The thickness and echogenicity of the endometrium can be used for prediction of the probability of implantation. To achieve a good implantation rate, the endometrium has to be thicker than 7 mm and show a triple-line pattern.[2]

Secretory Phase

Progesterone surge, seen in postovulatory luteal phase ceases epithelial and stromal proliferation of the endometrium and differentiates endometrial glands for secreting glycoproteins, evidenced as blurring of the three lines ultrasonographically in the late proliferative endometrium. The endometrium appears as homogeneous and hyperechogenic layer measuring 7–14 mm **(Fig. 44.3)**. Color Doppler reveals subendometrial and intraendometrial vessels of the secretory transformed endometrium **(Fig. 44.4)**.

Secretion of endometrial glands is fully developed seven days after ovulation. Despite the manifestation of stromal edema and predecidual reaction, there is no further change of the ultrasound appearance of the endometrium. If pregnancy occurs, echogenicity and thickness are maintained as decidual reaction to implantation starts to progress. In absence of a pregnancy, endometrium starts to regress in thickness, but not in echogenicity.

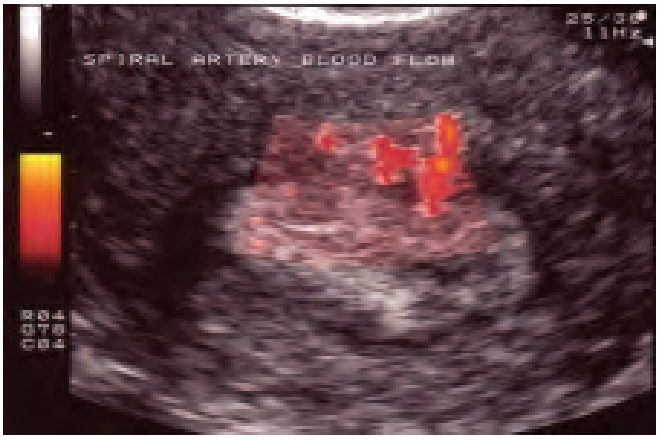

Figure 44.4: Color Doppler imaging of the endometrial vessels during the luteal phase of the menstrual cycle

Menstrual Phase

Menstruation begins when circulating levels of estrogen and progesterone decrease at the end of the ovarian cycle, causing break down of the functional endometrial layer. Ultrasound image varies depending on the amount of blood clots and endometrial fragments which can be seen as echogenic debris. Basal layers are imaged as thin, irregular and hyperechogenic lines.

Postmenopausal State

The size of the cervix and the body of the uterus decreases gradually after menopause from approximately 6.5–3.5 cm.

Due to quiescent ovaries in postmenopausal women, the endometrium is thin and atrophic not subjected to cyclic changes. The mean endometrial thickness is 2.3±1.8 mm.[3] In postmenopausal state ovaries do not secrete estrogens, but still produce androgen, which together with androgens derived from the adrenal glands are converted to estrogens in peripheral adipose cells. Production of estrogens at that way may be responsible for endometrial thickening and proliferation changes showed as hyperplasia or neoplasm. An endometrial thickness cut-off level of less than 5 mm in a symptomatic patient seems to have a high negative predictive value for the presence of endometrial cancer.[4] Once the endometrial thickness is greater than 8 mm in asymptomatic postmenopausal women not taking hormonal replacement therapy (HRT) an outpatient biopsy is required to exclude endometrial hyperplasia or malignancy. Women taking HRT have an increased endometrial thickness, which changes according to the phase of the cyclical therapy. In continuous combined regimens the endometrium is likely to be relatively thin.

Subendometrial Myometrial Waves

Contractions of the hypoechoic junction zone of the myometrium adjacent to the endometrium are very well documented with real-time transvaginal ultrasound and video playback. These contractions have a possible role in propelling sperm to the fallopian tubes before ovulation as well as in positioning the pre-embryo for proper implantation.[5] The frequency, amplitude and direction of myometrial waves require estrogens, while progesterone decreases its motility. Subendometrial myometrial peristalsis during menstrual bleeding is directed from the fundus towards the cervix.

Cervix

Cervix of the uterus is oval-conic shaped canal measuring approximately 2.5 cm in length, entering the vagina vertically. It consists of the supravaginal and vaginal part or endocervix (cervical canal) and ectocervix (seen clearly in the specula). The ectocervix can be visualized on ultrasound better if the fluid surrounds the vaginal fornices. The site where the uterine body turns away from the cervix marks the internal cervical os. This point is clearly seen on ultrasound examination of the anteflexed uterus as indentation in the anterior wall. Ovarian hormonal changes do not influence on the epithelium of the endocervical canal, neither histologically nor sonographically. The mucus in the endocervical canal is viscous and echogenic, except at the time of ovulation, when it is diluted and seen as an echolucent area on ultrasound examination. Nabothian cysts are retention cysts of the cervical glands within the ectocervix undergoing metaplasia from columnar to stratified squamous epithelium. They measure approximately 10 mm in diameter with thin walls and spherical shape containing echolucent fluid. Nabothian cysts have no clinical value even when they are multiple and large in size.

Vagina

The vagina is thin-walled tubular structure, located anteroinferiorly from the uterine cervix to the perineum, posterior to the bladder and urethra, and anterior to the rectum. It can be visualized by transabdominal ultrasound, with transducer directed caudally, while transvaginal ultrasound is less efficient to demonstrate this structure. Ultrasound determination of the vaginal length is not reliable because of the variable degree of bladder distension. During the menstruation, blood can pool in the vagina and can be visualized as anechoic fluid collection. Similar appearance can be obtained in postmenopausal patients with incontinence, who lie in

the supine position, due to the collection of the urine in the vagina.

FALLOPIAN TUBE

The Fallopian tubes are approximately 10–12 cm long and a few millimeters wide. They spread from the lateral uterine angles towards the corresponding ovary. Anatomically, the fallopian tubes are divided into: (i) Intramural part—within the uterine wall (1 cm long, less than 1 mm wide); (ii) Isthmic part (2 cm long); (iii) Ampular part (5 cm long, meandering with thin walls, varying in diameter); (iv) Fimbriae and (v) Infundibulum. Fallopian tubes can be only occasionally seen on ultrasound, when distended with fluid (hydrosalpinx), transfused with an echogenic contrast or cannula, or when peritoneal fluid is present surrounding the adnexa. Demonstration of oblique sagittal view during ultrasound scanning enables visualization of the origin of the fallopian tubes at the lateral uterine angles.

OVARIES

Although both transabdominal and transvaginal ultrasound are able to identify ovaries properly, better resolution, closer focusing and avoiding the need for a full bladder make transvaginal ultrasound much preferable for scanning the ovaries.

Position

Localization of the ovaries is on each side of the cervix, close to the lateral wall of the pelvis in Waldeyer's fossa. Iliac vessels are a reliable landmark for their visualization. Due to mobility of the ovaries and transducer pressure, position of the ovaries is often varying, for example: in the cul-de-sac, in front of the uterus, above the uterus or in the abdominal cavity. Sometimes, previous inflammatory disease or surgical interventions might cause origination of pelvic adhesions that fix the position of the ovaries, commonly close to the lateral fornices of the vagina.

Size, Shape and Echo Texture

Normal ovaries are ellipsoid, with dimensions approximately 3 × 2 × 2 cm. Ovarian volume estimated using the ellipse formula (volume = length × width × depth × 0.523) is between 6 and 10 cm^3 (maximum volume 14–16 cm^3).[6]

Ovaries are imaged as homogeneous, hypoechogenic ovoid structures with slightly echogenic central part.

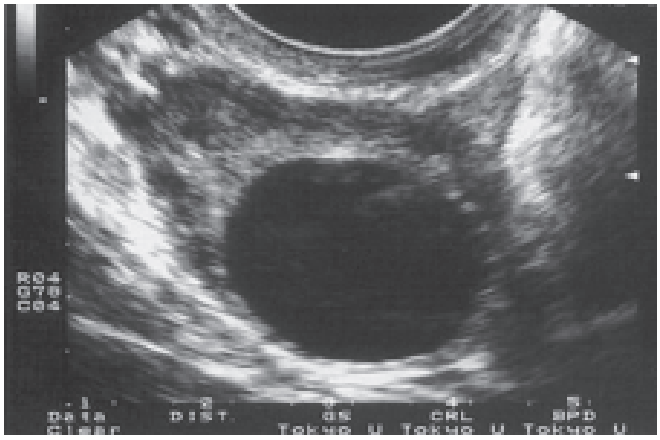

Figure 44.5: Transvaginal image of the preovulatory follicle

Ovarian follicles facilitate the identification of the ovaries containing echolucent fluid and varying in size from 2–25 mm in diameter **(Fig. 44.5)**. In postmenopausal women, the detection of ovaries is difficult due to lack of follicles and small size of the ovaries.

Ovarian Cycle

About 7 million follicles containing oocytes are present in a female fetus at about 20 weeks gestation.[7] These follicles, called primordial, are microscopic in size and metabolically quiescent. Later in childhood, reproductive age or during oral contraceptive therapy, they grow from primordial to primary, secondary and tertiary follicles (microscopic in size) forming a fluid-filled antrum. In adequate hormonal conditions (increased local follicle stimulating hormone-FSH levels) follicles continue to grow until they become sonographically detectable. If endocrine conditions do not support the growth, atresia and permanent loss of the oocytes from the follicular oocyte pool takes place. Only 100 to 1,000 follicles are left until the menopausal period, the majority of which will go through the process of atresia and only a little fraction will ovulate **(Fig. 44.6)**.

Follicular Phase

The small and transient rise in FSH serum levels at the end of each ovarian cycle affects the small antral follicles reaching a size of 1–2 mm. These follicles have a potential to grow further instead to become atretic. During the early follicular phase of the ovarian cycle, hypophyseal FSH affects follicular cells to secrete estrogen, estradiol and the peptide hormone inhibin (reduces FSH production as the follicular phase progresses). The smaller follicles go to regression with the drop in FSH levels, while the larger ones grow

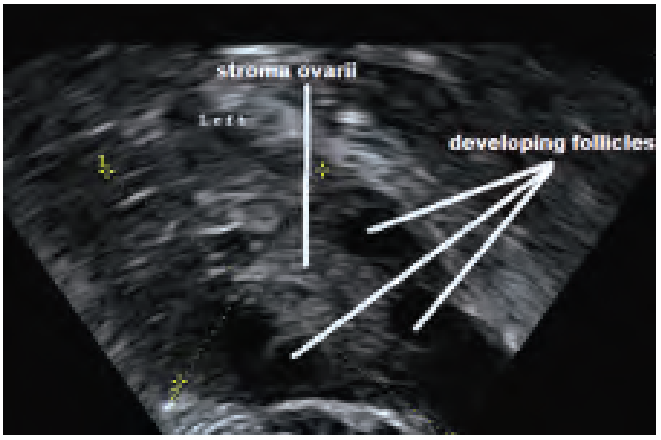

Figure 44.6: Normal ovary in a reproductive age patient. Note multiple follicles measuring between 2 and 5 mm

regardless. One or sometimes two follicles become dominant, producing the substantial amounts of estradiol as they grow, while the others become atretic. This turnover happens by the end of the first week of the follicular phase. Atretic follicles can still be visible and can grow, especially in the dominant side, although they are undergoing atresia.

The dominant follicle, also called Graafian follicle, increases in size at a rate of 2.5 mm/day until it reaches about 2 cm in size **(Fig. 44.6)**, after that it decelerates to 1.3 mm/day.[8] Follicles grow due to increased number of follicle cells and accumulation of fluid inside the antrum. Cumulus oophorus, consisting of the oocyte and surrounding follicle cells, protrudes as a small papillary projection from the follicular wall **(Fig. 44.7)**. The side of ovulation in the present and previous ovarian cycle does not have to be the same.

Dominant follicular development is not always sustained by ovulation, especially in early reproductive age when ovulation does not occur and hence follicular phase and consequently the entire menstrual cycle becomes longer and irregular (oligomenorrhea or amenorrhea).

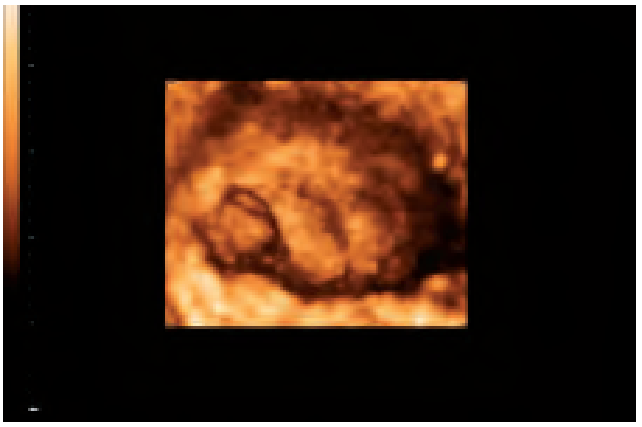

Figure 44.7: A 3D ultrasound of preovulatory cumulus oophorus

The multifollicular appearance of the ovaries means persistence of variable sized developing follicles, some of them functioning and some atretic. Difference from polycystic ovaries is the relative lack of hyperechogenic ovarian stroma and central and peripheral location of the follicles. Multifollicular appearance can be normal during adolescence and recovery from weight loss, but in older women is associated with significant ovulation disorder of primarily ovarian origin and/or beginning of the ovarian failure.

Ovulation

Ovulation occurs with segmental/partial dissolution of the follicle wall, liberation of the oocyte and escape of the follicular fluid into the peritoneal cavity. It takes place about 38 hours after the luteinizing hormone (LH) surge begins, as a consequence of pituitary response to high circulating estrogen levels. At that time, the dominant follicle is 2.1 cm in diameter with range from 1.6–3.3 cm, and sometimes contains a triangular structure representing mucus-like cumulus oophorus surrounding the preovulatory oocyte[9] **(Fig. 44.7)**. The preovulatory follicle luteinizes and begins to secrete progesterone with formation of new blood vessels around the follicle, visible on color Doppler ultrasound examination. High estrogen levels affect on fallopian tube fluid secretion, and transudation through the follicle, resulting on ultrasonically recognizable accumulation of free peritoneal fluid. Besides the free fluid imaged on ultrasound, ovulation is presented as sudden disappearance of the echolucent dominant follicle and after several days, with formation of the corpus luteum. Corpus luteum maturation into a solid-cystic steroid-producing "organ" reflects on the rise of the progesterone level in serum.

In cases when ovulation does not take place, the follicle continues to grow and becomes a follicular cyst. On ultrasound scanning it is demonstrated as a thin-walled cystic lesion filled with lucent fluid and very well demarcated from the rest of the ovary. The size of the follicular cyst ranges between 3–6 cm in diameter and it usually regresses spontaneously. Sometimes it continues to produce estrogens resulting in endometrial proliferation.

Luteal Phase

Post-ovulatory changes include: collapse of (Graafian) follicle wall; secretion of progesterone by follicular/

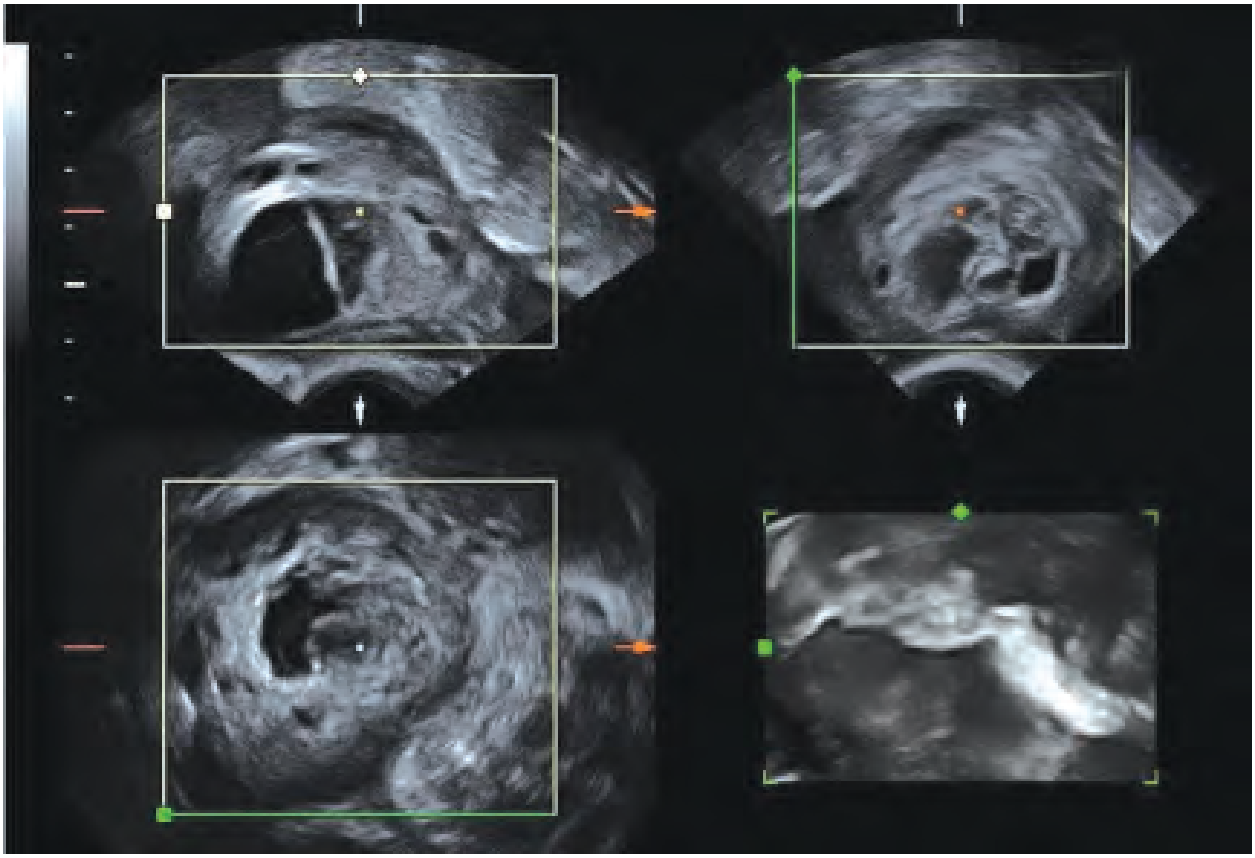

Figure 44.8A: Transvaginal three-dimensional ultrasound image of an early corpus luteum. Blood filled cavity of the former follicle is clearly visualized on three orthogonal planes

granulosa cells and neovascularization for future corpus luteum. Proliferating capillaries invading theca interna and granulosa layer are fragile and start to transudate serum or blood. In majority of the ovulatory patients corpus luteum is visualized as a blood filled cavity of the ruptured follicle **(Figs 44.8A and B)**. Capillaries invade the blood filled cavity of the corpus luteum and give rise to the corpus luteum angiogenesis **(Figs 44.8C and D)**.

Sometimes, corpus luteum can be hardly seen on transvaginal ultrasound due to variety of echoes in the ovary **(Fig. 44.9)**. Commonly it is visualized as a structure containing thick hyperechogenic walls enclosing the hypoechoic center. Neovascularization starts about 24 hours after the LH surge and continues to be detectable by the means of transvaginal color Doppler through the entire functional life of the corpus luteum **(Figs 44.10 and 44.11)**.

Sometimes after follicle ruptures, corpus luteum or hemorrhagic cyst may be formed. It can be even 5–6 cm in diameter, and due to its clot component can be

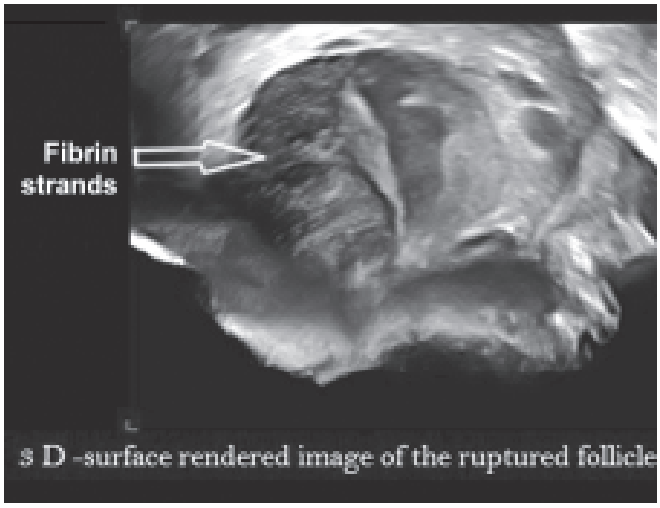

Figure 44.8B: Three-dimensional ultrasound of an early corpus luteum

mistaken for endometrioma **(Figs 44.12A to D)**. If the corpus luteum is filled with serous fluid and persists

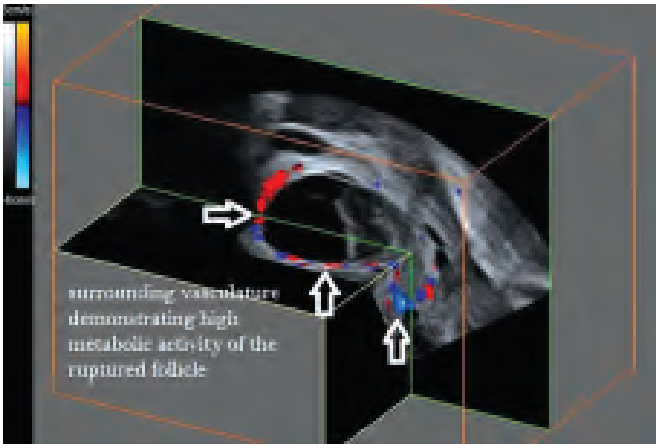

Figure 44.8C: Three-dimensional color Doppler ultrasound. Using niche image, capillaries invading the blood filled cavity of the follicle are clearly visualized

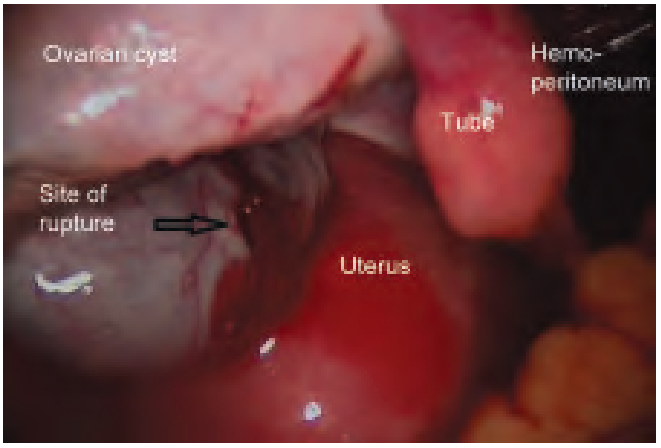

Figure 44.8D: Laparoscopy image of the same patient

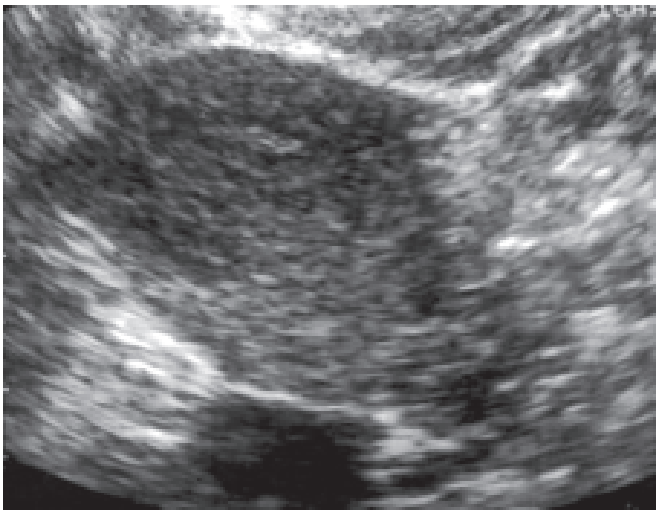

Figure 44.9: Transvaginal scan of the ovary during the luteal phase of the menstrual cycle. Corpus luteum is hardly visible among the stromal ovarian tissue

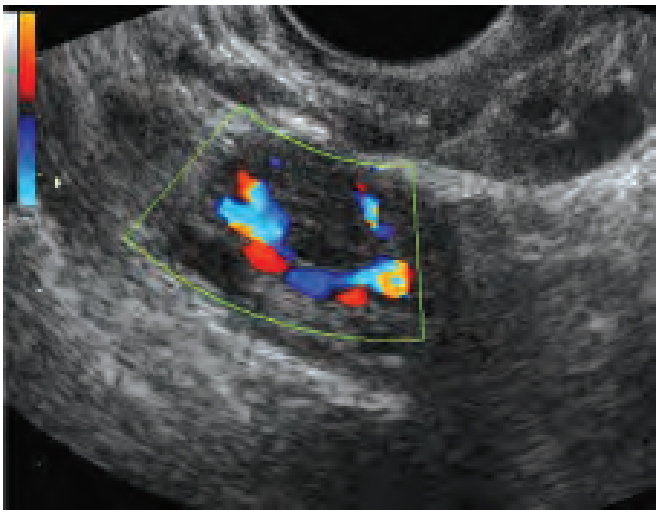

Figure 44.10: Transvaginal color Doppler scan of the corpus luteum, visualized as a ring of angiogenesis within the ovary

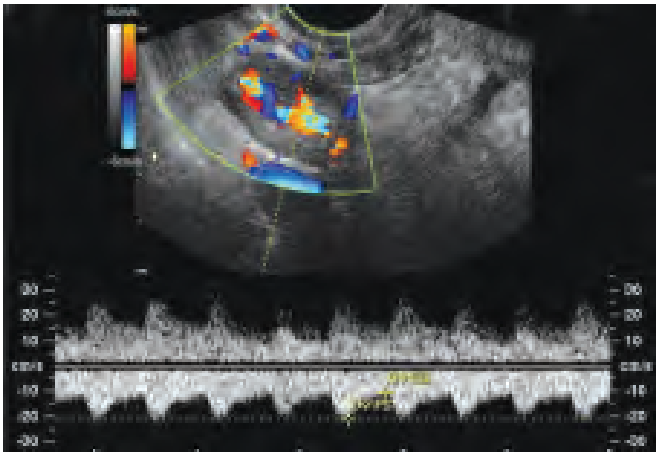

Figure 44.11: The same patient as in Figure 44.10. Angiogenesis signals typical of corpus luteum formation are easily displayed by color Doppler ultrasound

more than two weeks, it is called corpus luteum cyst. Cysts persist more than a month or two in the absence of pregnancy does are termed "functional" or "dysfunctional" cysts. While luteal cysts have thicker walls than follicular cysts, it can be very hard to differentiate them. In that case previous record of ultrasound or hormonal studies of ovulation may help. In general, luteal cysts are more painful than follicular cysts. This is especially true if pregnancy occurs due to chorionic gonadotropin stimulation. Luteal and follicular cysts, which do not resolve with time, require hormonal treatment.[10]

The ultrasound and color Doppler evaluation of ovarian lesions and cysts is best done during the follicular phase of the menstrual cycle due to diagnostic

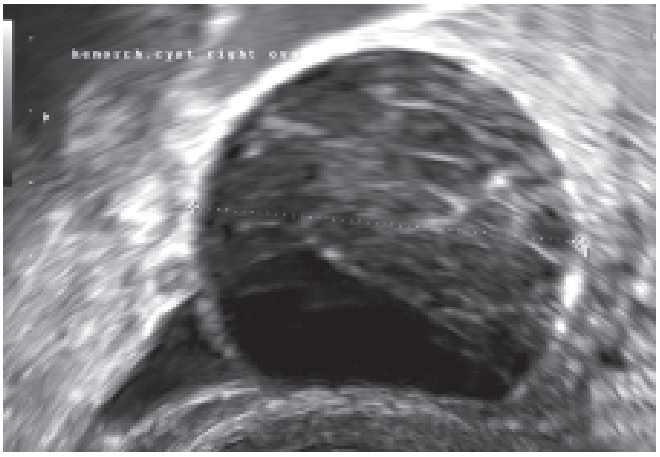

Figure 44.12A: Hemorrhagic cyst of the ovary. Note intracystic appearance of a retracting clot and free fluid in the cul-de-sac

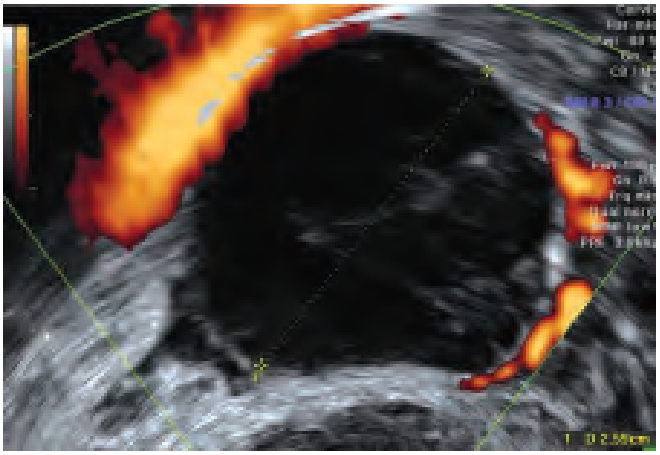

Figure 44.12B: Power Doppler ultrasound demonstrates ring of angiogenesis surrounding the hemorrhagic cyst

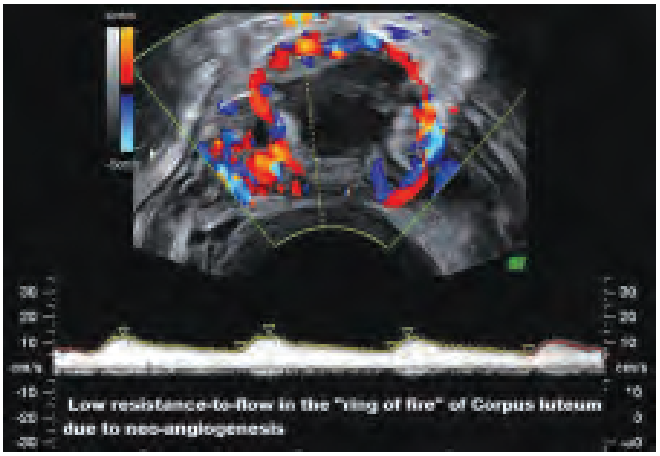

Figure 44.12C: Low impedance blood flow signals (RI = 0.48) are isolated from the ring of angiogenesis encircling the hemorrhagic cyst

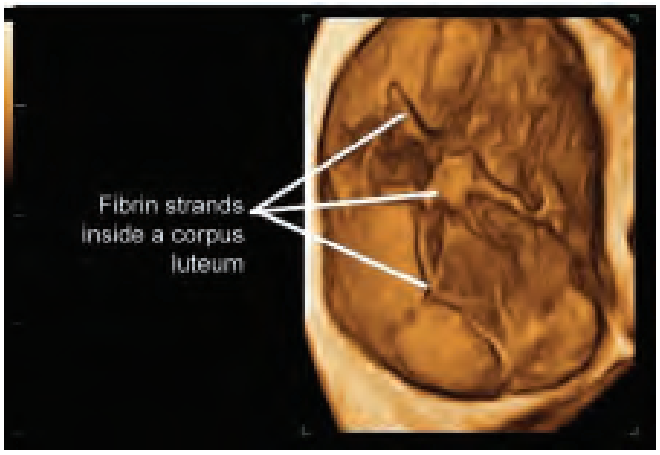

Figure 44.12D: Intracystic fibrin strands within the hemorrhagic cyst are better visualized using surface rendering by three-dimensional ultrasound

confusion that can be caused by the different appearances of a corpus luteum **(Figs 44.13A to D)**.

If the dominant follicle does not release follicular fluid and the oocyte, but luteinization takes place, and growing continues toward a diameter of about 3 cm with echogenic or lucent contents, the structure is called luteinized unruptured follicle (LUF syndrome). Luteinized unruptured follicles occur in about 5% of normal menstrual cycles and in a higher rate of abnormal cycles. Progesterone production in LUF syndrome is less than in a normal luteal phase that is usually shorter than normal.

Newborn

In the newborns, the ovaries can be difficult to demonstrate with ultrasound due to their small size, a need for transabdominal scanning and difficulty to obtain a full bladder to move the intestines. Developing follicles remain small and invisible to ultrasound resolution. The ovaries continue to decrease in size for the first two years of childhood. Cohen and colleagues,[11] demonstrated that the mean ovarian volume was 1.2 cm^3 among the girls up to 3 months old; 1.1 cm^3 among the girls 4–12 months old; and 0.7 cm^3 among the girls 13–24 months old. In conclusion, failure to demonstrate the ovaries in newborns does not imply ovarian dysgenesis.

Childhood

The ovaries grow slowly through the childhood, increasing in the mean ovarian volume from 0.5 cm^3 at the age of 3–2.8 cm^3 at the age of 18 years.[12] We can

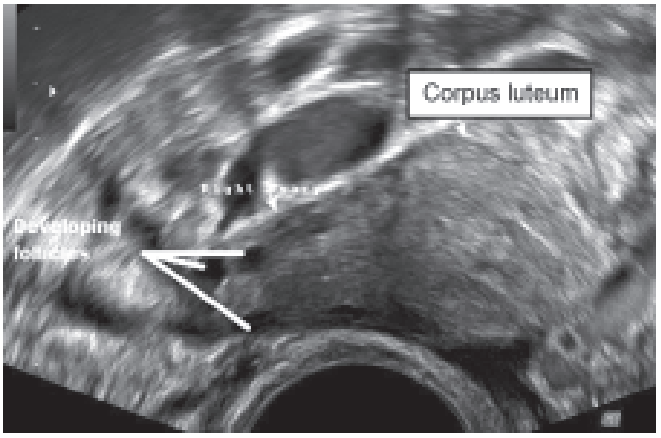

Figure 44.13A: Sometimes corpus luteum may have solid appearance

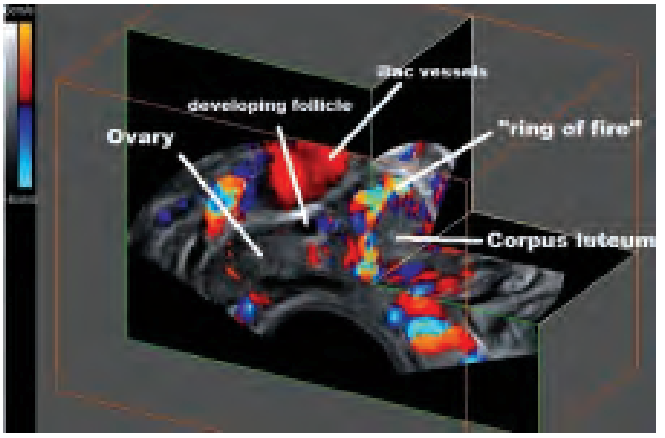

Figure 44.13C: A 3D color Doppler image demonstrating open cut view to the angiogenesis of the corpus luteum

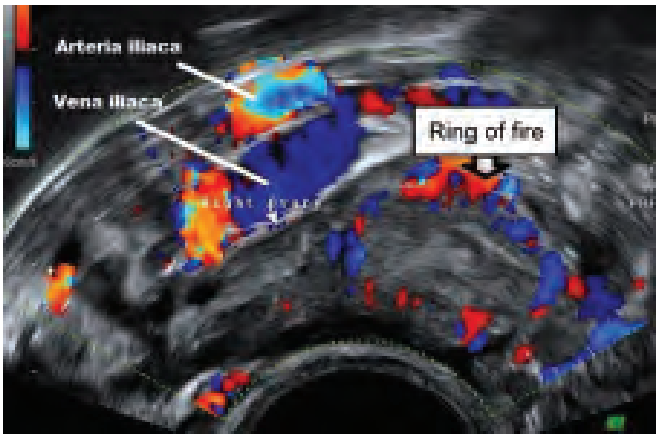

Figure 44.13B: Color Doppler image demonstrating "ring of fire" encircling the corpus luteum

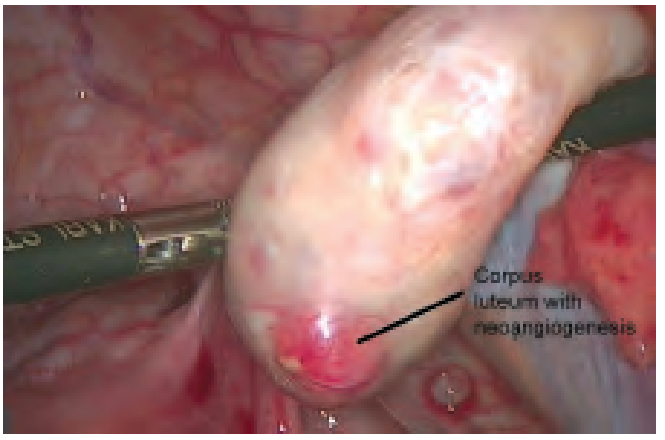

Figure 44.13D: Laparoscopy image of the corpus luteum neoangiogenesis

distinguish two periods of the rapid growth: at around 8 years of age during the time of adrenarche and gradually rising levels of FSH; and before and during puberty. It is documented that taller girls have larger ovaries.[2]

Adolescence and Adulthood

This period is characterized with the appearance of the ovary changes through the ovarian cycle. The interruption of normal ovulatory cycle can cause in both the early and late reproductive age functional or dysfunctional follicular or luteal cysts affecting menstrual irregularities.

The number of follicular "recruits" visible on ultrasound is proportional to the number of primordial follicles present in the ovaries and is inversely proportional to the woman's age.

Perimenopausal and Postmenopausal State

Perimenopausal state is characterized by: (i) ovarian follicular depletion, (ii) diminishing antral follicles for recruitment, (iii) lower production of follicular inhibin, and (iv) early rise of FSH levels (during the late luteal phase) causing premature start of follicular development of such recruits (before menstruation takes place). As menopause approaches, the follicular phase and menstrual cycle get shorter. During the perimenopausal years, it is common to have functional cysts and/or multifollicular appearance of the ovaries.

In postmenopausal state, estrogens and inhibin production falls, but FSH levels increase. The ovaries become small and homogeneous with true depletion of follicles.

The addition of color Doppler capabilities to transabdominal and transvaginal probes permits

visualization of uterine and ovarian vessels. Recent advances in three-dimensional ultrasound have made accurate non-invasive measurements of the ovarian, follicular and endometrial volumes feasible.[12] Storage capacities, reconstruction of the volume images and simultaneous viewing of all three orthogonal planes are main advantages of this method in gynecology.

REFERENCES

1. Ramsay PA, Jansen RPS. Ultrasonography of the normal female pelvis. In: Anderson JC (Ed). Gynecologic imaging. London: Churchill Livingstone; 1999. pp. 61-80.
2. Abdalla HI, Brooks AA, Johnson MR, et al. Endometrial thickness: a predictor of implantation in ovum recipients. Hum Reprod. 1994;9(2):363-5.
3. Kurjak A, Kupesic S. Ovarian senescence and its significance on uterine and ovarian perfusion. Fertil Steril. 1995;64:532-8.
4. Wikland M, Granberg S. Endometrial changes as imaged by transvaginal sonography in fertile and infertile women. In: Fleischer A, Kurjak A, Granberg S (Eds). Ultrasound and endometrium. New York: Parthenon Publishing, London; 1996. pp. 17-23.
5. Brosens JJ, de Souza NM, Braker FG. Uterine junctional zone: function and disease. Lancet. 1995;346(8974):558-60.
6. Higgins RV, Van Nagell JR, Woods CH, et al. Interobserver variation in ovarian measurements using transvaginal sonography. Gynecol Oncol. 1990;39(1):69-71.
7. Faddy MJ, Gosden RG, Gougeon A, et al. Accelerated disappearance of ovarian follicles in mid-life: implications for forecasting menopause. Hum Reprod. 1992;7(10): 1342-6.
8. Nugent D, Smith J, Balen AH. Ultrasound and the ovary. In: Kupesic S, de Ziegler D (Eds). Ultrasound in Infertility. London: Parthenon Publishing; 2000. pp. 23-43.
9. Hamilton CJ, Evers JL, Tan FE, et al. The reliability of ovulation prediction by a single ultrasonographic follicle measurement. Hum Reprod. 1987;2(2):103-7.
10. Kupesic S, Kurjak A, Bjelos D. Three- and four-dimensional ultrasound in human reproduction. In: Kurjak A, Jackson D (Eds). An Atlas of three-and four-dimensional sonography in Obstetrics and Gynecology. London, New York: Taylor and Francis; 2004. pp. 19–39.
11. Cohen HL, Shapiro MA, Mandel FS, et al. Normal ovaries in neonates and infants: a sonographic study of 77 patients 1 day to 24 months old. Am J Roentgenol. 1993;160:583-6.
12. Bridges NA, Cooke A, Healy MJR, et al. Standards for ovarian volume in childhood and puberty. Fertil Steril. 1993;60(3):456-60.

45
CHAPTER

Uterine Lesions: Advances in Ultrasound Diagnosis

Sanja Kupesic Plavsic, Bhargavi Patham, Ulrich Honemeyer, Asim Kurjak

INTRODUCTION

The aim of this chapter is to investigate the role of color Doppler and three-dimensional (3D) ultrasound in the evaluation of the uterine lesions. Morphological and vascular criteria assessed by different forms of ultrasound are listed for each type of the uterine lesions.

The uterus lies in the middle of the pelvis with its long axis perpendicular to the ultrasound probe. Two-dimensional (2D) ultrasound gives an inadequate view of the uterus and uterine pathology as the examination of the uterine lesions is limited to transverse and sagittal planes. The 3D ultrasound provides a simultaneous display of coronal, sagittal and transverse planes **(Fig. 45.1)**. Volume data can be viewed using a standard anatomic orientation demonstrating entire volume and continuity of curved structures in a single image. More accurate evaluation of numerous sections through the studied organ becomes possible due to unlimited numbers and the orientations of reformatted planes. When three perpendicular axes are simultaneously displayed on the screen, the sagittal plane is chosen for volume measurements whereas the other two planes are used for pathological determinations. Surface rendering mode allows exploration of the outer or inner contour of the lesion, while "niche aspect" presents detection and analysis of the selected sections of the uterine lesion. The 3D ultrasound offers improved visualization of the lesions, more accurate volume estimation, retrospective review of stored data and assessment of tumor invasion. Additionally, rendered image can accurately identify location of abnormalities eventually requiring surgical intervention.

The 3D saline infusion sonography (SIS) is very useful in the evaluation of the uterine cavity and is more useful than hysterosonography by 2D transvaginal ultrasound in cases of submucous myomas and polyps.

The 3D power Doppler system improves the information available on normal and abnormal (tumoral) vascularity, enabling visualization of overlapping vessels and assessment of their relationship to other vessels or surrounding tissue. Power Doppler ultrasound, compared to standard color Doppler, has the advantage of more sensitivity-to-low velocity flow overcoming the angle dependence and aliasing. Using contrast agents it is possible to enhance the 3D power Doppler examination rate of small vessels.

In this chapter findings of uterine lesions with conventional B-mode will be compared with those by transvaginal color Doppler ultrasound and 3D and power Doppler ultrasound.

NORMAL UTERUS

Use of 2D ultrasound imaging of the uterus is limited due to the movement of the transducer allowing sagittal and transverse planes through the uterus. The 3D sonography permits multiplanar display of all three perpendicular sections: coronal, sagittal, and transverse plane **(Fig. 45.1)**. The coronal plane of the uterus enables simultaneous visualization of endometrial horns and cervix. The normal uterus is usually presented by a

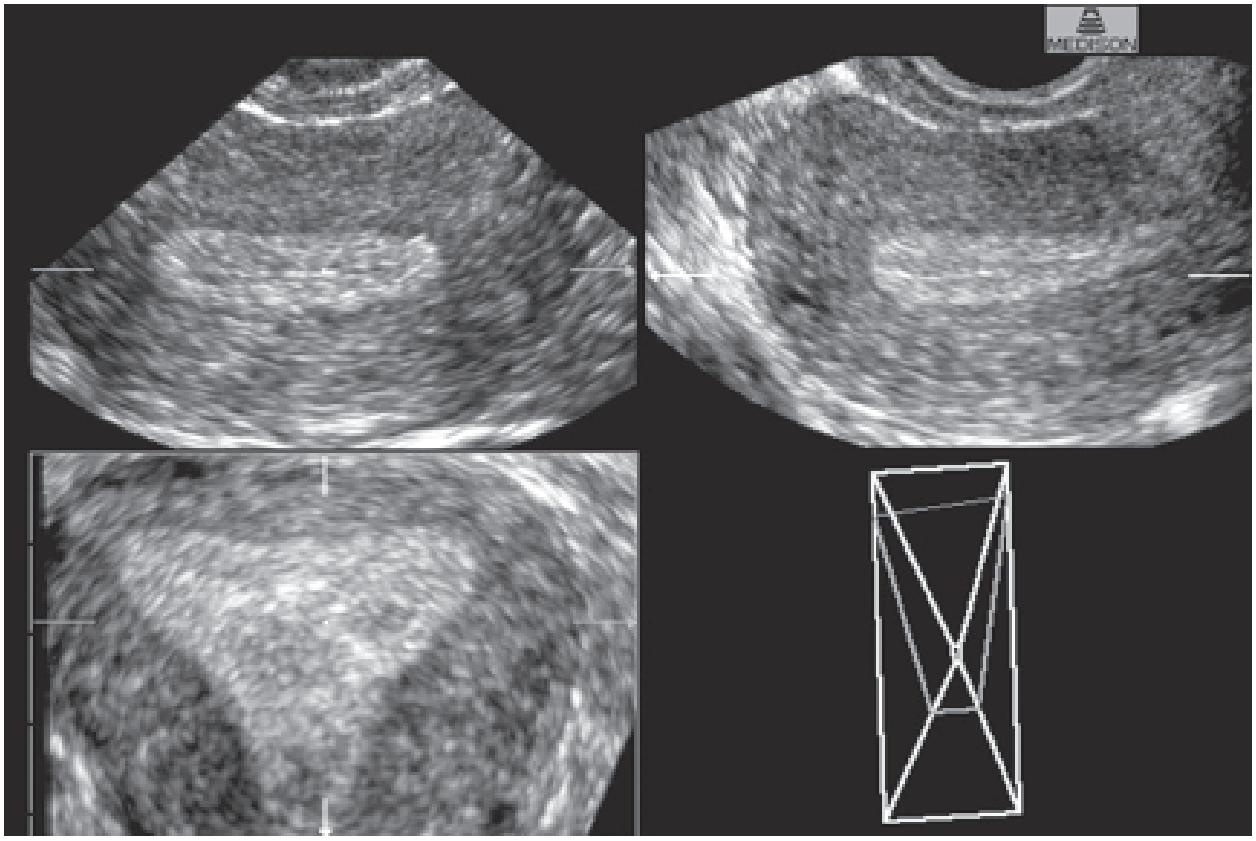

Figure 45.1: Three-dimensional ultrasound of the normal uterine cavity. Note secretory appearance of the endometrium and triangular shape of the uterine cavity in frontal reformatted section (low left image)

convex shape of the endometrium and myometrium in the fundus. Blood vessels of the uterus and endometrium can be detected by color and power Doppler ultrasound where endometrium and myometrium constitute an anatomical and functional unit **(Fig. 45.2)**. Uterine arteries branch off the internal iliac arteries. Ultrasonically, they look like hyperechoic structures running along the cervix and the isthmic part of the uterus. Arcuate arteries are tortuotic anechoic structures that spread through myometrium. Radial arteries penetrate vertically through the myometrial layers of smooth muscle cells. Spiral arteries supply to the stratum functionale of the endometrium. Shape and size of this layer of endometrium changes during the menstrual cycle and it sheds during menstruation along with glandular tissue. During pregnancy, these arteries become uteroplacental decidual arteries. Basal arterioles supply to the endometrial stratum basale, which remains unchanged during menstruation. Color Doppler research has identified unique waveform from each blood vessel. These waveforms are influenced by several factors including hormones, ischemia and

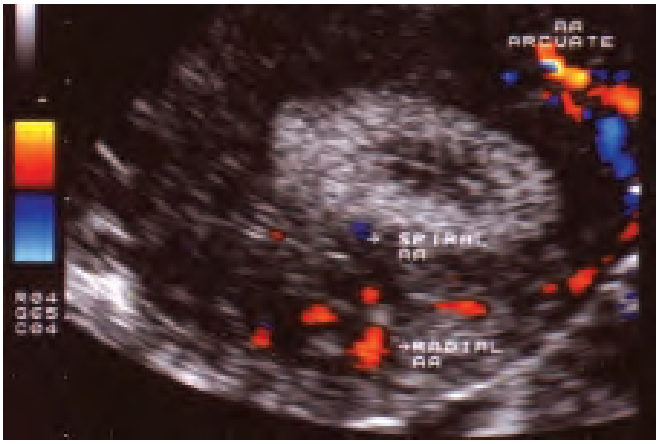

Figure 45.2: Transvaginal color Doppler scan of the secretory transformed endometrium. Note spiral arteries (at the periphery of the endometrium), radial arteries (within the myometrial portion of the uterus) and arcuate arteries (within the outer portion of the myometrium, close to serosa)

internal or external vasoactive factors. The vessels in genital tract undergo cyclic changes dictated by the

hormonal cycle. During the menstrual phase, due to hormonal deprivation and alterations in the spiral arteriolar system, spiral arteries undergo increased coiling and cause a circulatory stasis that leads to tissue ischemia. Vasoconstriction of the spiral arterioles and necrosis of their walls results in bleeding. Visualization of anechoic areas indicate endometrial breakdown. Subsequently, mixed appearance of anechoic area (indicating blood) and hyperechoic parts (exfoliated endometrium and clots) can be observed. During the late menstrual phase, the endometrium appears sonographically as a thin, single-line, slightly irregular echogenic interface. In this phase, the uterine artery shows high resistance index (RI). In the early follicular phase, the endometrium is imaged as a hyperechoic line with endometrial thickness of less than 5 mm and visualization of the endometrial-myometrial junction is difficult. As ovulation approaches, glands become numerous and the expected endometrial thickness is about 10 mm. A triple-line endometrium is typical of the periovulatory phase. The hyperechoic echo that represents the endometrial-myometrial junction becomes more prominent and does not produce posterior enhancement. The central echogenic interface probably represents refluxed mucus. Doppler velocimetry of the spiral arteries shows progressive diminution of resistance indices. Secretory phase is characterized by hyperechoic and homogeneous endometrium with a loss of the triple-line morphology and surrounding anechoic halo. During this phase of the cycle the ultrasonographic image of the endometrium shows increased echogenicity with respect to the myometrium. The interface of the myometrium with the endometrium is still visible as a hypoechoic zone. Maximum echogenicity is seen in the mid-luteal phase when the endometrium appears homogenously hyperechoic. Posterior enhancement is a sonographic characteristic of this phase. Doppler velocimetry demonstrates further decrease of the vascular resistance in uterine and spiral arteries being the lowest in the mid-luteal phase.

Since changes in the texture and volume of the endometrium can be precisely observed using 3D ultrasound, and retrospectively reviewed by experts, this method may become a method of choice for scanning endometrial pathology in multitude of clinical conditions.

ENDOMETRIAL POLYPS

Endometrial polyps develop as solitary or multiple, sessile or pedunculated soft tumors containing

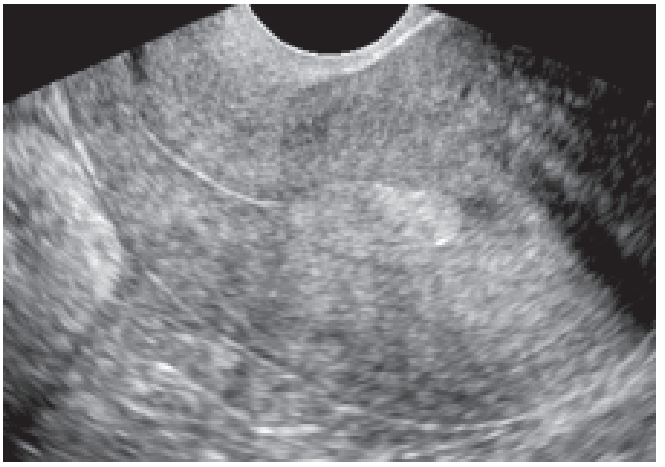

Figure 45.3: Focal endometrial lesion by transvaginal ultrasound

hyperplastic endometrium.[1,2] Patients with endometrial polyps maybe clinically asymptomatic or may present with abnormal genital tract bleeding, infertility, or pain. Ultrasonographic appearance of endometrial polyps is best imaged during the early proliferative phase of the menstrual cycle or during the secretory phase after injection of a negative contrast medium into the uterine cavity **(Fig. 45.3)**. The vascularization of polyps is supported by already existing vessels originating from terminal branches of the uterine arteries assessed by transvaginal color Doppler ultrasound **(Fig. 45.4)**. It is possible to identify flow in regularly separated vessels and analyze the velocity of blood flow through them. The RI is moderate, usually higher than 0.45[1,3] **(Figs 45.5 and 45.6)**. Infection or necrosis of polyps may lower the impedance to blood flow (RI_{MIN} = 0.37). The importance of endometrial polyps lies in the fact that marked reduction in blood flow impedance noted on the periphery and/or within the endometrial polyps

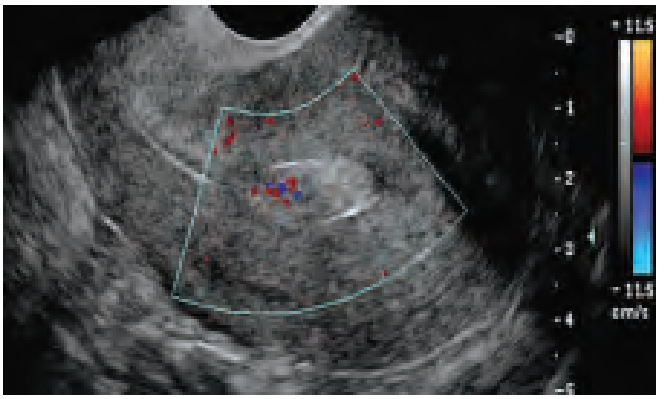

Figure 45.4: Color Doppler scan of an endometrial polyp demonstrating stalk vessels

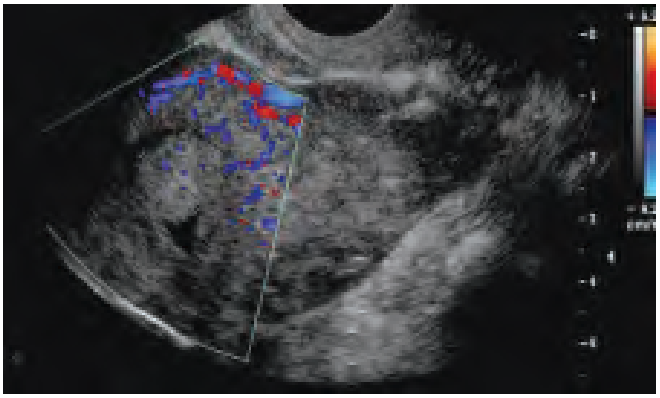

Figure 45.5: Focal endometrial thickening demonstrated by color Doppler ultrasound

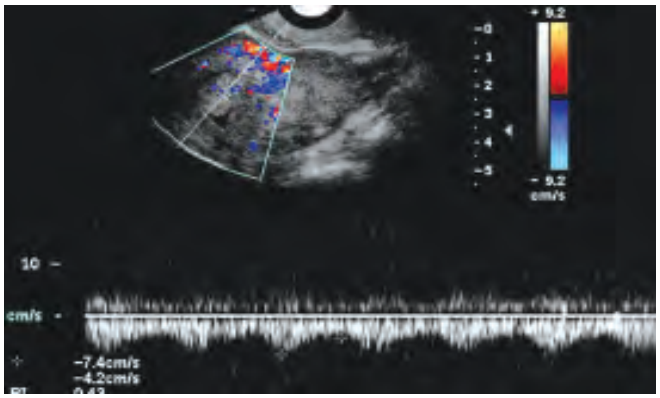

Figure 45.6: Pulsed Doppler waveform analysis demonstrates low-to-moderate vascular impedance blood flow signals (RI of 0.43) isolated from the endometrial polyp. Secondary degenerative changes were diagnosed by histology

may lead an inexperienced ultrasonographer to a false-positive diagnosis of endometrial malignancy.

Tamoxifen is a nonsteroidal anti-estrogen that is widely used in the hormonal therapy of breast cancer. However, the weak estrogen-like effect that tamoxifen has on the endometrium is a cause of great concern. Patients using tamoxifen should, therefore, be monitored at regular intervals, since several studies have described cases of endometrial cancer associated with this therapy. A wide spectrum of pathological uterine findings has been described in association with long-term tamoxifen therapy at a dose of 20 mg/day.[4] These findings include epithelial metaplasia, simple and atypical hyperplasia, endometrial polyps and endometrial carcinoma.[5] Endometrial changes are characterized sonographically by abnormal endometrial thickening and nonhomogeneous hyperechogenicity, with multiple, small cystic structures. At least three studies indicate that tamoxifen treatment in postmenopausal breast cancer patients is associated with a high incidence of endometrial polyps.[6–8] Achiron and colleagues[7] found that a peculiar endometrial honeycomb appearance, manifested on gray-scale transvaginal sonography, occurred in 44% of this population and was associated with the same high incidence (40%) of endometrial polyps. The effect of tamoxifen on endometrial blood flow has not been extensively evaluated. Achiron and his group described blood flow changes in the endometrial and subendometrial regions. In asymptomatic postmenopausal patients receiving tamoxifen whose endometrial thickness was less than 5 mm, increased endometrial blood flow with significant reduction of the RI compared to untreated, control menopausal women was reported. Another study by the same authors[5] found that women with thick endometrium and particularly those with endometrial polyps, presented a significantly lower RI, compared to those with thin endometrium (mean RI of 0.39 vs 0.79). The RI values returned to normal following resection of the endometrial polyps, thus supporting a benign transitory effect of long-term tamoxifen therapy on the endometrium.

The data from Goldstein et al.[9] suggest that the objective assessment of blood flow impedance [RI, pulsatility index (PI)] in endometrial polyps and the size of these polyps cannot replace surgical removal and pathologic evaluation to predict histologic type. Patients with nonfunctional polyps were older and less likely to have vaginal bleeding.

Perez-Medina et al.[10] evaluated the efficacy of color Doppler exploration for assessing atypia inside endometrial polyps (polyp stalk). Thirty five polyps (out of 106) with sonographic indications of atypia were pathologically confirmed. Sonographic indications of atypia inside 16 polyps were not confirmed. Three nonquestionable endometrial polyps had atypia inside them. They concluded that low Doppler resistance (RI < 0.50) is highly predictive of atypia inside endometrial polyps.

The 3D SIS offers a better visualization of the uterine cavity and the endometrial thickness as compared to transvaginal sonography, 2D SIS, transvaginal color Doppler or hysteroscopy according to Bonilla-Musoles et al.[11] Multiplanar views in 3D SIS can be used to visualize polypoid structures allowing optimal plane to present their pedicle. Surface rendering mode can suppress undesirable echoes offering further clarity in visualization of polypoid structure in continuity with the endometrial lining.[12]

Gruboeck et al.[13] performed the measurements of endometrial thickness assessed by conventional 2D

ultrasound and endometrial volume assessed with 3D ultrasound in symptomatic postmenopausal patients and compared the results. The volume measurement is performed using longitudinal plane delineating the whole of the uterine cavity in a number of parallel longitudinal sections 1–2 mm apart. Endometrial volume is then calculated using VOCAL software. The endometrial thickness was similar in patients with endometrial hyperplasia and polyps, but the endometrial volume in hyperplasia was significantly higher than the volume in patients with polyps. Polyps, localized thickenings of the endometrium, do not affect the entire uterine cavity and thus have a smaller volume albeit having similar thickness to that of hyperplasia. In conclusion, differences between endometrial hyperplasia and polyps cannot be detected by sole measurement of endometrial thickness but can be clearly identified based on 3D volume measurement.

INTRAUTERINE SYNECHIAE (ADHESIONS)

Destruction of the basal layer of the endometrium may result in development of bands of scar tissue (synechiae) in the uterine cavity. This damage of endometrium may occur as a result of vigorous curettage of an advanced pregnancy. Infection with tuberculosis may also cause uterine adhesions. Menstrual pattern is characterized by amenorrhea or hypomenorrhea. Ultrasound scan of a patient with Asherman's syndrome shows a mixed picture: in some parts of uterine cavity no endometrium is visualized; whereas in other parts there is appearance of a normal endometrium. Adhesions in the uterine cavity are visualized as hyperechoic bridges. Intrauterine adhesions do not display increased vascularity on color Doppler examination **(Fig. 45.7)**. They are better visualized during menstruation when intracavitary fluid outlines them. An alternative is SIS (Saline Infusion Sonography).

The SIS with 3D ultrasound has several advantages over that with conventional 2D ultrasound. It gives more accurate information about the location of abnormalities which is very important for preoperative assessment and distinguishing pathologies. Furthermore in SIS, compared to 2D exams, the uterus is distended for a shorter time translating to better patients' acceptance. However, according to Momtaz et al.[14] in cases of intrauterine adhesions, the use of echogenic contrast media (e.g. Echovist, Schering) is more accurate than 3D SIS. Intrauterine synechiae can be accurately visualized on both multiplanar and rendered imaging traversing the uterine cavity.[12] Weinraub et al.[12] concluded that surface rendering in cases of equivocal

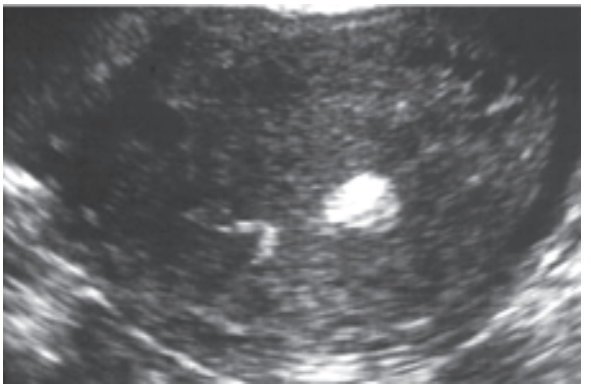

Figure 45.7: Irregular hyperechogenic bridges visualized within the central part of the uterine cavity in a patient with secondary amenorrhea following dilatation and curettage

signals confirmed their presence, appearance, actual size, volume, and relationship to the surrounding structures.

The 3D ultrasound is helpful in delineation of intracavitary adhesions and determination of their location which assists in surgical planning. In the cases of bridging adhesions, the degree of cavity obliteration is accurately assessed. Similarly, this technique is beneficial for differentiation between small polyps and adhesions.

ADENOMYOSIS

Adenomyosis of the uterus is a condition in which clusters of endometrial tissue grows into the myometrium. It may be localized close to endometrium, or may extend through the myometrium and serosa. Adenomyosis affects 20% of women, mainly multiparous. The uterus can be normal-sized or enlarged with symptoms such as dysmenorrhea, pelvic pain and menometrorrhagia.

The 2D ultrasound findings include "Swiss cheese" appearance of the myometrium due to areas of hemorrhage and clots within the muscle **(Figs 45.8 and 45.9)**. Disordered echogenicity of the middle layer of the myometrium is usually present in severe cases. Sometimes the uterus is generally hypoechoic, with the large cysts rarely seen. On SIS or hysterosalpingography, contrast medium penetrates the myometrium. Color Doppler characteristics present increased vascularity by moderate vascular resistance within the myometrium (RI = 0.56 ± 0.12), while the RI of the uterine arteries show a decreased value compared to controls **(Figs 45.10 and 45.11)**.[15] Statistically significant differences exist between adenomyosis and uterine

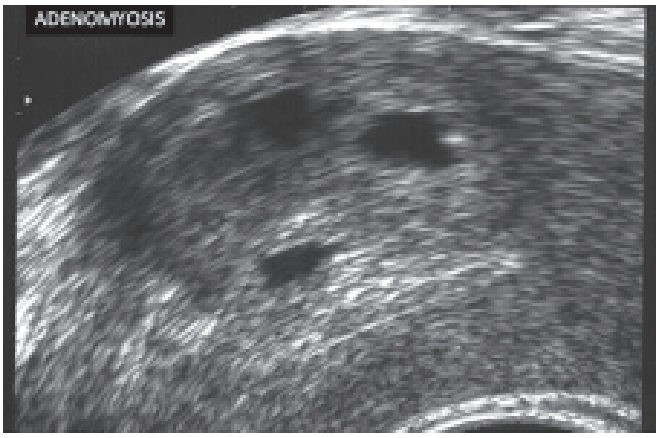

Figure 45.8: Multiple cystic structures within all three layers of the myometrium are typical of severe adenomyosis

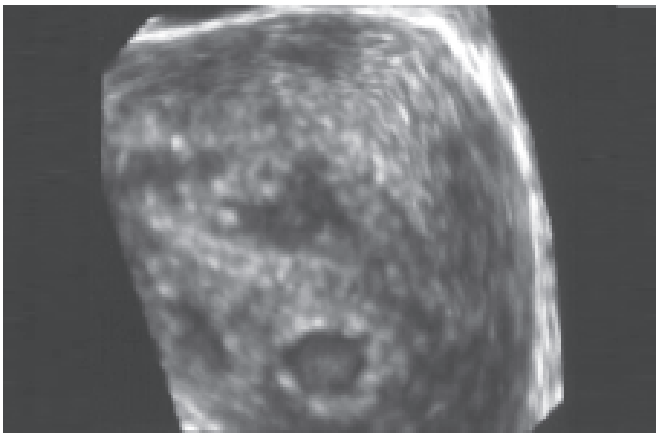

Figure 45.9: "Swiss cheese" appearance of the myometrium on three-dimensional ultrasound is typical of deep adenomyosis. Cystic lesions are visualized within the myometrial layer of the uterus

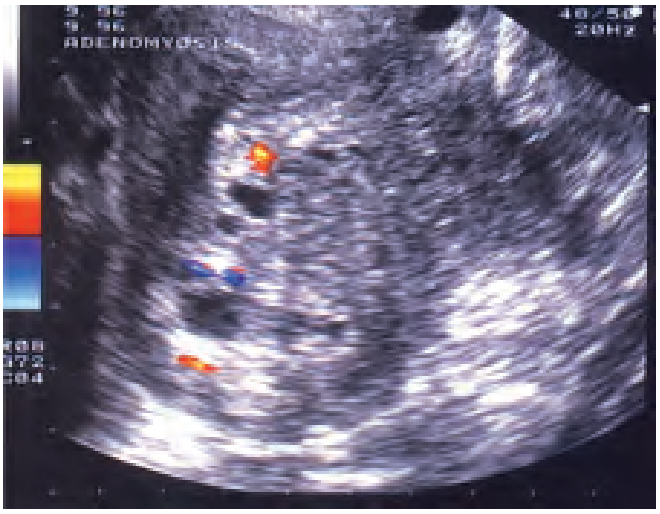

Figure 45.10: Transvaginal color Doppler scan of severe adenomyosis

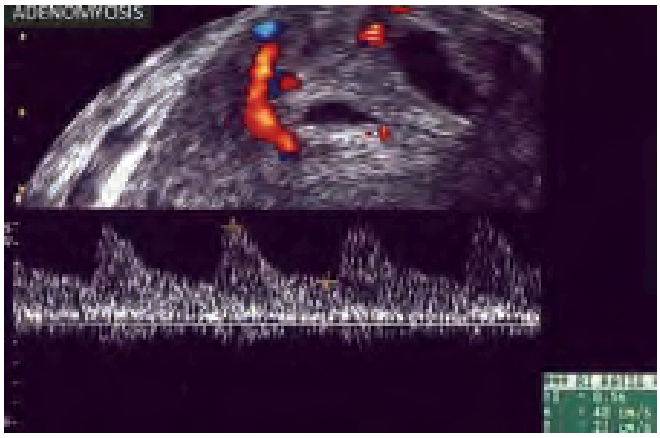

Figure 45.11: Moderate-to-high vascular impedance blood flow signals (RI of 0.56) are detected at the periphery of adenomyotic lesions

malignancies in both RI and maximum velocity. However, no significant difference was noted between adenomyosis and myoma in RI but slight differences were observed in maximum velocity.[16]

In some cases, transonic areas may not represent adenomyosis, but prominent vessels, or other conditions which give rise to hyperemia. Lee et al.[17] performed the study which confirmed the superiority of 3D power Doppler sonography compared to transvaginal color Doppler ultrasound in the detection of flow in the areas of adenomyosis. Women with a provisional diagnosis of adenomyosis listed for hysterectomy were studied. Gray scale ultrasound was first used to screen for the presence of adenomyosis using predetermined ultrasound criteria. Then 3D power Doppler sonography of adenomyotic areas was then performed. Ultrasound findings such as distribution of vessels and pattern of flow in adenomyotic foci were compared with histological results. The same method was used for tracing regular vessels' course in this abnormality. Using 3D power Doppler sonography, authors were not only able to demonstrate perfusion in adenomyotic foci but also the vessels' distribution and branching pattern.

ENDOMETRIAL HYPERPLASIA

The endometrial thickness in postmenopausal women is no more than a thin line of 1–3 mm. Abnormal endometrial thickness may be detected in some benign uterine conditions, as well as in the endometrial malignancy. Endometrial thickness greater than 14 mm in premenopausal and greater than 5 mm in postmenopausal women should be further investigated.[1] B-mode transvaginal sonography by itself is insufficient

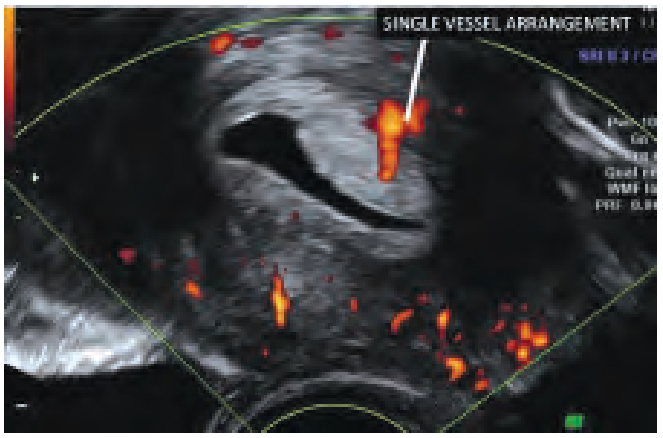

Figure 45.12: Single vessel arrangement obtained by power Doppler ultrasound in a patient with endometrial hyperplasia

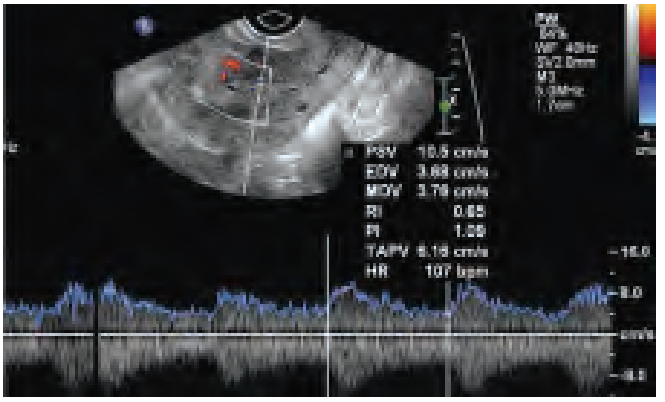

Figure 45.14: Pulsed Doppler waveform analysis of endometrial hyperplasia. Note moderate vascular impedance blood flow signals with RI of 0.65

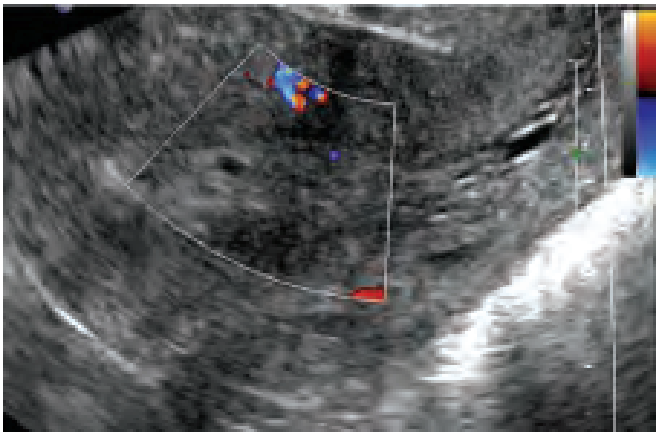

Figure 45.13: Color Doppler ultrasound of endometrial hyperplasia

to distinguish between endometrial hyperplasia and carcinoma. More accurate diagnosis of endometrial pathology can be obtained by color and pulsed Doppler sonography[2,3] **(Fig. 45.12)**. Color Doppler findings characteristically for endometrial hyperplasia include peripheral distribution of the regularly separated vessels with RI significantly higher (mean RI = 0.55 ± 0.05) **(Figs 45.13 and 45.14)** than in carcinoma (mean RI = 0.42 ± 0.02).[18] However, reliable differentiation between endometrial hyperplasia and carcinoma is not possible due to an overlap in the endometrial thickness measurements, as well as because of the controversial results of blood flow measurements assessed by transvaginal color Doppler ultrasound. There is a positive correlation between arterial blood flow impedance and number of years from menopause.[19] Hence, one can presume that the risk of uterine malignancy is increased for postmenopausal patients with decreased uterine artery vascular resistance.

Emoto et al.[20] examined the usefulness of transvaginal color Doppler ultrasound in differentiating between endometrial hyperplasia and endometrial carcinoma and in predicting tumor spread in patients with carcinoma. No significant difference was found in the mean value of endometrial thickness between patients with hyperplasia (n = 18 patients; 16.2 mm +/- 15.9 mm) and patients with carcinoma (n = 53 patients; 18.7 mm +/- 17.1 mm). Intratumoral blood flow was detected in significant numbers of patients who had endometrial carcinoma (71.7%, 38 of 53 patients) compared with patients who had endometrial hyperplasia (5.6%; 1 of 18 patients; $P < 0.0001$). This study implies that transvaginal color Doppler may be more useful in differentiating between endometrial hyperplasia and carcinoma than measuring endometrial thickness by transvaginal gray-scale sonography. For patients with carcinoma, the detection of intratumoral blood flow may be helpful in distinguishing between low-grade and high-grade tumors and predicting myometrial invasion. However, intratumoral blood flow analysis using RI, PI, or peak systolic velocity (PSV) may not be useful for predicting tumor spread before surgery.

Jarvela et al.[21] evaluated uterine blood flow changes in using transvaginal color Doppler ultrasonography after thermal balloon endometrial ablation therapy. Thermal balloon endometrial ablation induces a rise in uterine blood flow impedance, but not until 6 months after the treatment. The rise in impedance may be due to fibrosis in the uterine cavity which has been attributed to the thermal balloon therapy.

More recently, 3D ultrasound has been successfully used for endometrial volume measurements. According to Gruboeck et al,[13] endometrial volume was measured in 94.2% of patients, while in others the presence of

anterior uterine wall myomas caused acoustic shadowing on 3D records. The volume of the endometrium was measured by delineating the uterine cavity on parallel longitudinal sections 1–2 mm apart. The sections were added together using in-built software to calculate the volume. The endometrial volume was significantly lower in patients with benign pathology such as hyperplasia (mean 8.0 ml, SD 7.81 ml) than in patients with endometrial carcinoma (mean 39.0 ml, SD 34.16 ml). Normal endometrial volume in this study was 0.9 ml (SD 1.72 ml).

Kupesic et al.[18] reported on the use of 3D power Doppler sonography in patients with endometrial hyperplasia. They were able to demonstrate regularly separated vessels at the periphery of the examined endometrium.

Bonilla-Musoles et al. suggest that in patients on hormone replacement therapy or tamoxifen, 3D SIS allowed for differentiation of normal proliferative from hyperplastic endometrium.[11]

ENDOMETRIAL CARCINOMA

Endometrial carcinoma is the most common gynecological malignancy in many countries with the reported incidence of about 10% in postmenopausal patients presenting uterine bleeding. Early transabdominal sonographic investigations have demonstrated that increased endometrial thickness is associated with endometrial neoplasms in postmenopausal women, but the quality of transabdominal sonographic images is affected by obesity, retroversion of the uterus, and an unfilled bladder, factors that do not influence transvaginal sonographic visualization of the endometrium. Ultrasound findings assessed by conventional B-mode sonography include increased endometrial thickness greater than 5 mm in postmenopausal women or greater than 8 mm in perimenopausal women, hyperechoic endometrium, free fluid in the cul-de-sac, intrauterine fluid or possible invasion in patients with disrupted endometrial-subendometrial layer. In addition, color and pulsed Doppler improves diagnostic accuracy, because the endometrial carcinoma shows abnormal blood flow due to tumor angiogenesis.[22] Endometrial blood flow is absent in normal, atrophic and most cases of endometrial hyperplasia, while, according to Kupesic's investigation[18] in 91% of the cases of endometrial carcinoma areas of neovascularization were demonstrated as intratumoral or peritumoral **(Fig. 45.15)**. Neovascular signals from the central parts of the lesion demonstrate low vascular resistance (RI = 0.42 ± 0.02), while increased vascularity signals

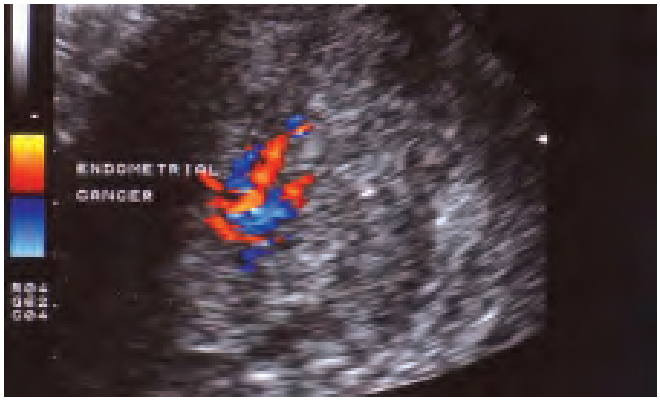

Figure 45.15: Thick heterogeneous endometrium with peripheral and intratumoral neovascularization demonstrated by color Doppler imaging

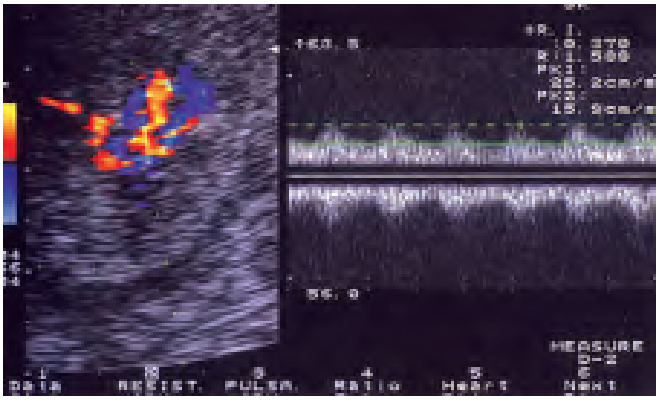

Figure 45.16: Color Doppler analysis shows low vascular resistance (RI of 0.37). Endometrial malignancy was confirmed by histology

surrounding the lesion indicate tumor invasion. If the myometrial vessels are invaded, low vascular resistance is detected due to incomplete or absent membrane and leaky structure **(Figs 45.16 to 45.19)**.

Conventional 2D ultrasound measurements of endometrial thickness have disadvantages in distinguishing patients with benign and malignant endometrial pathology due to varying thickness, and interference of other pathology like polyps or hypoplasia.

In distinguishing cancer from benign pathology endometrial volume measurements assessed by 3D ultrasound seems to be more helpful. Gruboeck et al[13] compared endometrial thickness and volume in patients with postmenopausal bleeding and examined the value of each parameter in differentiating between benign and malignant endometrial pathology. Each patient underwent 3D ultrasonography for the measurement of endometrial thickness and volume. The results were

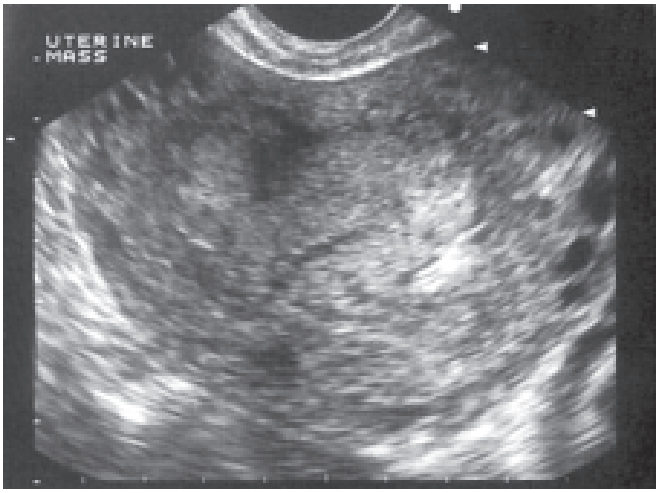

Figure 45.17: Transvaginal scan of a postmenopausal patient with enlarged and heterogeneous uterus. Using transvaginal ultrasound it was impossible to delineate an endometrial lining

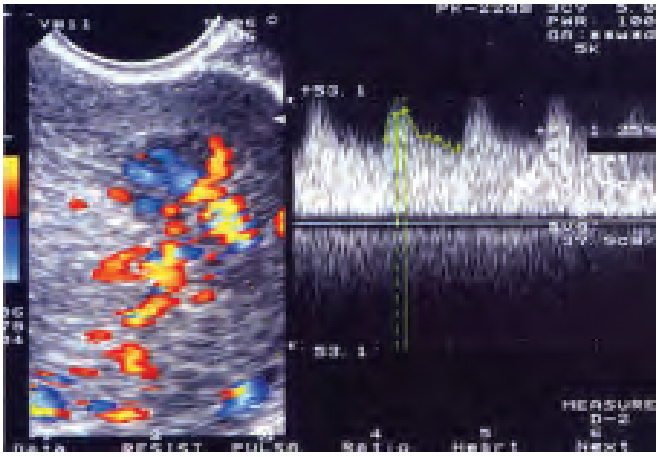

Figure 45.19: Low vascular impedance (RI of 0.35) and high velocity of the blood flow (47.7 cm/s) suggest neovascularization within the deep myometrial layer. Histopathology revealed deep myometrial invasion

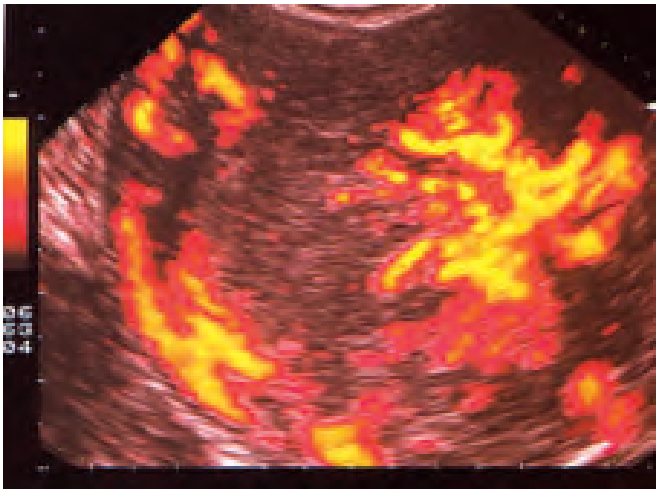

Figure 45.18: Power Doppler imaging demonstrates neovascular areas within the myometrium. Such a finding suggests deep myometrial invasion of an endometrial carcinoma

compared to the histological diagnosis after endometrial biopsy or dilatation and curettage. The mean endometrial thickness in patients with endometrial cancer was 29.5 mm (SD 12.59) and the mean volume was 39.0 ml (SD 34.16). The optimal cut-off value of endometrial thickness for the diagnosis of cancer was 15 mm, with the test sensitivity of 83.3% and positive predictive value (PPV) of 54.4%. With a cut-off level of 13 ml, the diagnosis of cancer was made with the sensitivity of 100%. One false-positive result in a patient with hyperplasia gave a specificity of 98.8% and PPV of 91.7%. According to these authors[13] the endometrial volume was significantly higher in patients with carcinoma than those with benign lesions. The measurements of endometrial volume were superior to endometrial thickness as a diagnostic test for the detection of endometrial cancer in symptomatic postmenopausal women. Increased volume size is associated with the severity or higher grade of the endometrial carcinoma and progressive myometrial invasion. The depth of myometrial invasion showed a positive correlation with both the endometrial thickness and the endometrial volume. Only patients with tumor volume larger than 25 ml had evidence of pelvic node involvement at operation.

Bonilla et al.[11] suggest that 3D hysterosonography allowed for better visualization of myometrial invasion, which may have a significant role in malignant tumors staging. Using simultaneous display of the transverse plane with 3D ultrasound it is possible to detect infiltration of cervical or endometrial carcinoma into the bladder or rectum.

Apart from endometrial volume, Kupesic et al.[23] used 3D power Doppler sonographic criteria for diagnosis of endometrial malignancy together with the assessment of subendometrial hallo, endometrial irregularity, presence of intracavitary fluid, chaotic vessel's architecture and branching pattern **(Table 45.1)**. In patients with endometrial carcinoma, mean endometrial volume was 37.0 ± 31.8 ml **(Table 45.2)**. The endometrial volume in hyperplasia had the mean value of 7.82 ± 7.60 ml and was significantly higher than the volume in patients with polyps (mean 2.63 ± 2.12 ml). In patients with normal or atrophic endometrium the

TABLE 45.1

Three-dimensional sonographic and power Doppler criteria for the diagnosis of endometrial malignancy (from reference 23, with permission)

The 3D sonographic and power Doppler criteria		*Score*
Endometrial volume	< 13 ml	0
	≥ 13 ml	2
Subendometrial hallo	Regular	0
	Disturbed	2
Intracavitary fluid	Absent	0
	Present	1
Vessel's architecture	Linear vessel arrangement	0
	Chaotic vessel arrangement	2
Branching pattern	Simple	0
	Complex	2
TOTAL SCORE		

Total score = sum of individual scores
Cut-off score = greater than or equal to 4 is associated with a high risk of endometrial malignancy

mean volume was 0.8 ± 1.51 ml. Subendometrial hallo was regular in all patients with benign endometrial pathology, whereas 8 out of 12 patients with endometrial carcinoma had irregular endometrial-myometrial border. Intracavitary fluid was present in four patients with benign endometrial lesions and five patients with endometrial malignancy. Dichotomous branching and randomly dispersed vessels were detected in 91.67% of the patients with endometrial carcinoma, while single vessel arrangement and regular branching were typical for benign lesions. The 3D power Doppler sonography accurately detected structural abnormalities of malignant tumor vessels such as microaneurysms, arteriovenous shunts, tumoral lakes, elongation and coiling. Combining morphological and power Doppler criteria, the diagnosis of endometrial carcinoma had a sensitivity of 91.67%. One false positive result was obtained in a patient with endometrial hyperplasia and one false negative in a patient with endometrial carcinoma receiving tamoxifen therapy. In this case endometrial lesion demonstrated regularly separated peripheral vessels, and was falsely interpreted as hyperplasia.

Kupesic et al.[24] performed staging of endometrial carcinoma by 3D power Doppler sonography. The objective of their study was to evaluate the accuracy of 3D power Doppler sonography in determining the depth of myometrial invasion in patients in whom the adenocarcinoma of the endometrium has been proven. Sonographic results were compared relative to the amount of myometrial invasion measured by histology **(Table 45.3)**. Thirty four patients with histologically proven adenocarcinoma of the endometrium were analyzed. Deep myometrial invasion (> 50%) was present at postoperative histology in 22.73% (5/22) women, while superficial was reported in 77.23% (17/22) women. The 3D power Doppler sonography demonstrated a sensitivity of 100% (5/5) and a specificity of 94.44% (17/18) for deep invasion, with a PPV of 83.33% (5/6) and a negative predictive value (NPV) of 100% (17/17). In only one patient with adenomyosis, invasion was overestimated by 3D power Doppler. Data showed acceptable accuracy in determining the depth of myometrial invasion in patients with adenocarcinoma. Thus 3D power Doppler sonography can potentially detect lesions that require aggressive intervention and thus direct to proper treatment.

Lee et al.[25] evaluated the relationship between blood flow in the tumor assessed by color Doppler ultrasound, microvessel density immunohistochemically and

TABLE 45.2

Volume and vascularity of the endometrial lesions (N = 57) obtained by three-dimensional power Doppler sonography (from reference 23, with permission)

Histopathology	*N*	*V (SD) ml*	*Regular endometrial hallo (%)*	*Intracavitary fluid (%)*	*Neovascular signals (%)*
Normal and/or atrophic endometrium	10	0.8 (1.51)	100	20.00	0
Endometrial hyperplasia	27	7.82 (7.60)	100	37.00	0
Endometrial polyp	28	2.63 (2.12)	100	35.71	3.57
Endometrial carcinoma	12	37.0 (31.8)	66.67	41.67	100

TABLE 45.3
Invasion of endometrial carcinoma assessed with the aid of three-dimensional power Doppler sonography. (from reference 24, with permission)

Invasion	*3D Power Doppler*	*Pathohistology*
Superficial*	17	18
Deep**	5	4

* Invasion into less than a half of the total myometrial thickness
** Invasion into more than a half of the myometrial thickness

vascular endothelial growth factor levels in endometrial carcinoma. Significantly lower RIs were noted in tumors of stage II or greater (0.37 compared with 0.50, $P < 0.001$), of high histologic grade (grade 3) (0.34 compared with 0.49, $P = 0.004$), with deep myometrial invasion (one-half depth or greater) (0.39 compared with 0.49, $P = 0.002$), with lymphovascular emboli (0.38 compared with 0.49, $P < 0.001$), or with lymph node metastasis (0.30 compared with 0.49, $P < 0.001$) compared with stage I tumors and tumors of histologic grade 1 or 2, with superficial myometrial invasion, without lymphovascular emboli, or with no lymph node metastasis. Increased vascular endothelial growth factor levels and microvessel density also were detected in tumors of stage II or greater, with lymphovascular emboli, or with lymph node metastasis. The RI, microvessel density, and vascular endothelial growth factor levels in the tumor showed linear correlations. Blood flow assessed by color Doppler ultrasound has histologic and biologic correlations with angiogenesis and vascular endothelial growth factor levels and may play an important role in predicting tumor progression and metastasis in patients with endometrial carcinoma. Alcazar et al.[26] correlated intratumoral blood flow as assessed by transvaginal color Doppler ultrasound (RI and PSV) with tumor histopathologic characteristics, tumoral stage, and risk for recurrence in endometrial carcinoma. Significantly lower RI was found in tumors with the following characteristics:

- Infiltrative growth pattern
- Grade 3 tumors
- Infiltrating greater than or equal to 50% of the myometrium
- Cervical involvement
- Lymph-vascular space invasion
- Lymph-node metastasis
- Stage greater than or equal to IC
- High-risk for recurrence.

Significantly higher PSV was found in tumors with the following characteristics:

- Grade 3 tumors
- Tumors which infiltrated more or equal to 50% of the myometrium
- Tumor stages greater or equal to IC
- Tumors with a high risk for recurrence.

Their data indicate that a correlation between intratumoral blood flow features and histopathological characteristics, tumor stage, and risk for recurrence exists in endometrial cancer.

Yaman et al.[27] evaluated the reproducibility of transvaginal 3D endometrial volume measurement in patients with postmenopausal bleeding and compared the reproducibility of this technique to that of 2D endometrial thickness measurement. Endometrial volume measurement by 3D ultrasound showed better reproducibility than endometrial thickness measurements by 2D ultrasound.

LEIOMYOMA

Leiomyomas are the most common tumors of the female pelvis and occur in 20–25% of women of reproductive age. Leiomyomas mostly arise from the smooth muscle and soft tissue of the uterine fundus and corpus **(Fig. 45.20)**, while a small fraction originate from the cervix.[28] Myomas are usually multiple and of various sizes **(Fig. 45.21)**. Intramural tumors are the most common **(Figs 45.22 and 45.23)**, while the submucosal are the least common **(Figs 45.24 to 45.26)**. If they extend outward, they become either pedunculated or subserosal[29] **(Figs 45.27 to 45.29)**. Symptoms of submucosal leiomyomas include metrorrhagia, pelvic pain or infertility, whereas most subserosal leiomyomas are asymptomatic.

On the gray-scale ultrasound the uterine leiomyomas may be represented with uterine enlargement, distortion of the uterine contour and varying echogenicity depending on the amount of connective or smooth muscle tissue **(Fig. 45.20)**.

Transvaginal color Doppler sonography demonstrates vascularization on the periphery of the leiomyoma of uterine origin, with the RI of 0.54 ± 0.08, allowing better delineation of the tumor **(Figs 45.22 and 45.23)**. Blood vessels in the central part of the myoma in case of necrosis, inflammation or other degenerative changes demonstrate lower RI. Uterine arteries present lower impedance to blood flow in patients with myomas ($RI = 0.74 \pm 0.09$) compared to normal ($RI = 0.84 \pm 0.09$) **(Figs 45.30 to 45.34)**.[30]

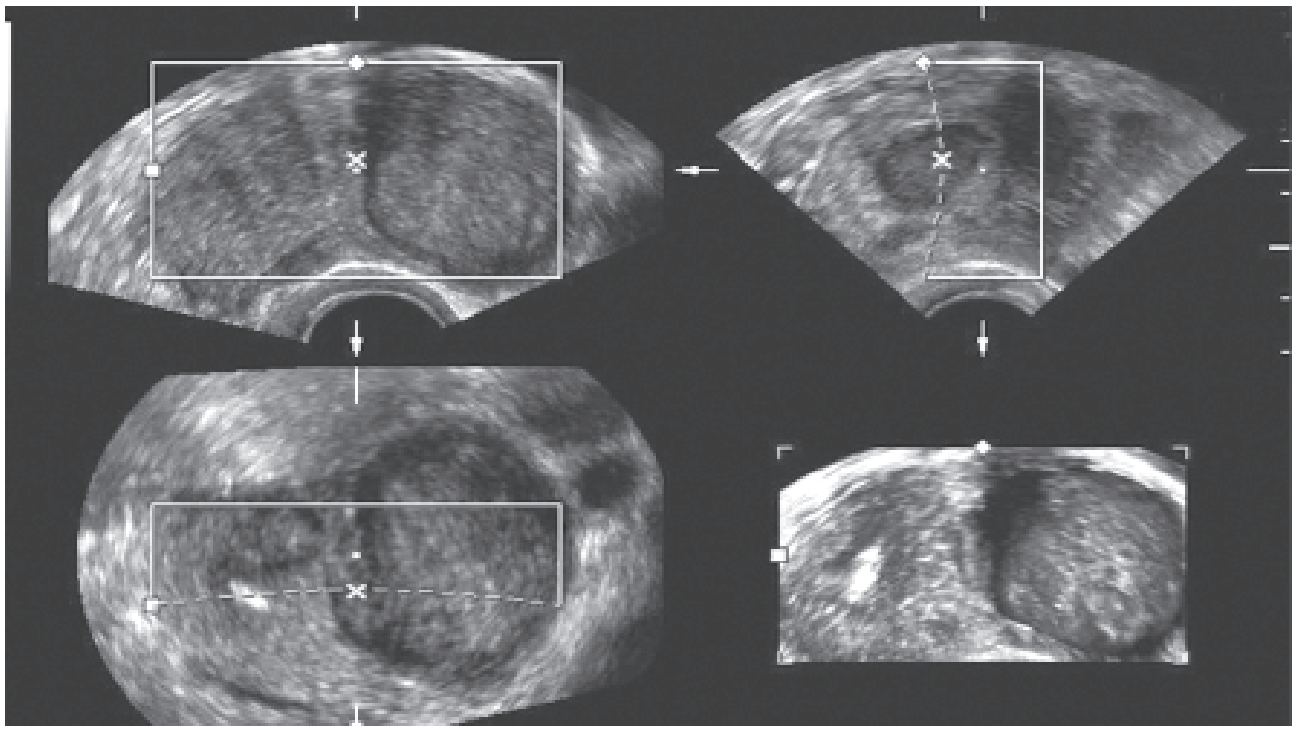

Figure 45.20: Three-dimensional ultrasound image of a subserosal uterine fibroid

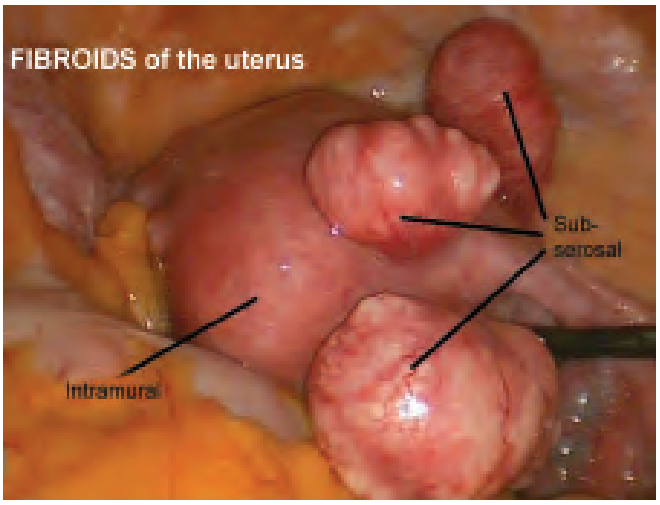

Figure 45.21: Laparoscopic image of the uterine fibroids

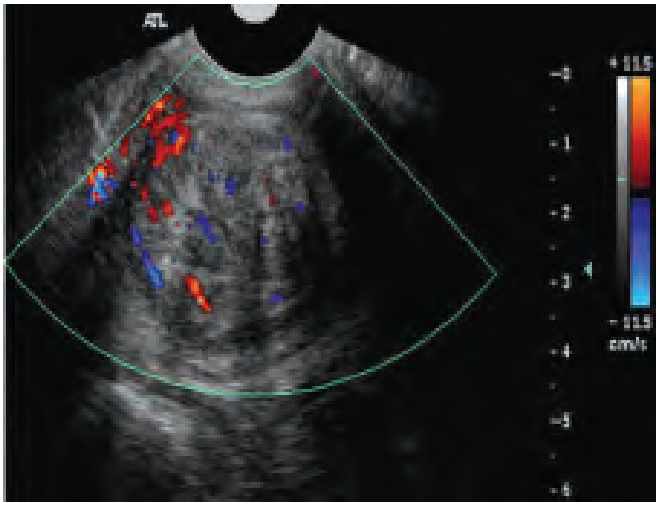

Figure 45.22: Color Doppler scan of an intramural fibroid

Simultaneous display of three perpendicular planes in 3D ultrasound demonstrates accurate location and size of leiomyomas, and its relationship to the endometrium that is very important in therapy planning. Patients receiving medical therapy such as gonadotropin-releasing hormone may be followed with serial 3D ultrasound scans to estimate myoma size and effectiveness of the therapy. The SIS by 3D ultrasound is valuable in obtaining submucosal myomas **(Fig. 45.25)**.[11,12,31,32] Balen et al.[31] found that 3D ultrasound and SIS was useful in demonstrating the position of submucosal myomas. They studied both saline and a positive ultrasound contrast agent (Echovist) and found the positive contrast to be superior when visualizing the cavity wall. Weinraub et al.[12] found that the negative contrast was better for accurately evaluating the contents of the uterine cavity delineating of the outer surface of lesions,

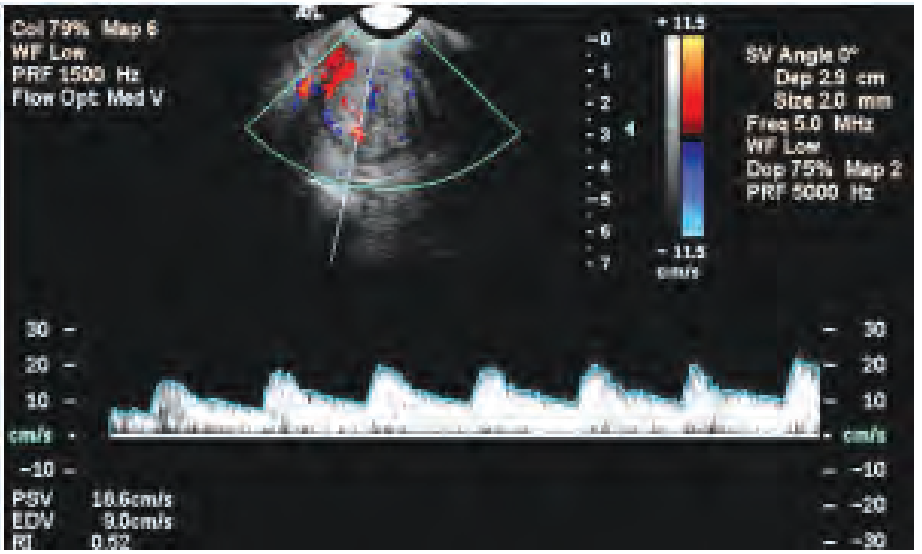

Figure 45.23: Pulsed Doppler waveform analysis demonstrated moderate vascular impedance blood flow signals at the periphery of the uterine fibroid, typical of a benign uterine lesion

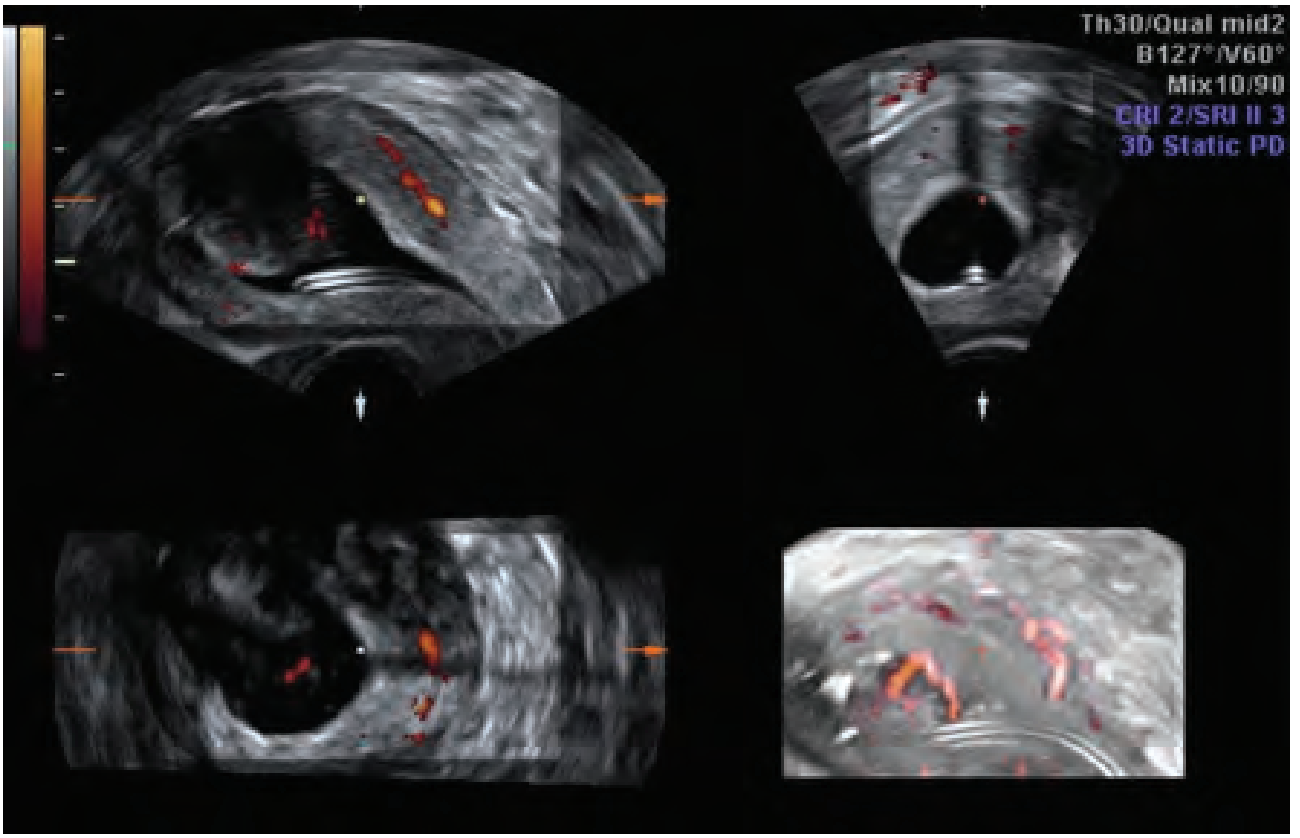

Figure 45.24: The three dimensional saline infusion sonography of submucosal fibroid

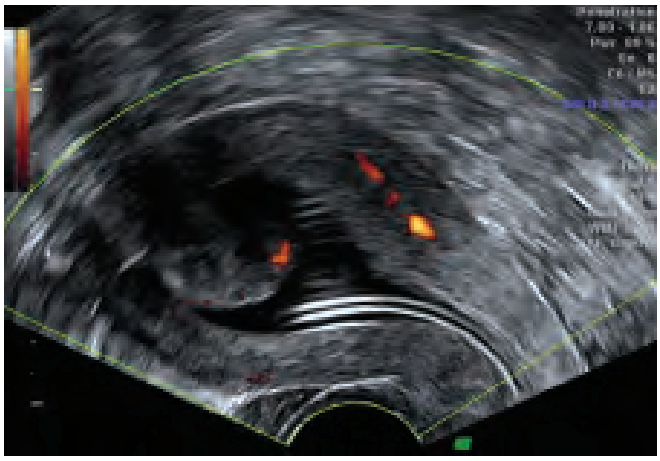

Figure 45.25: The two dimensional saline infusion sonography of submucosal fibroid

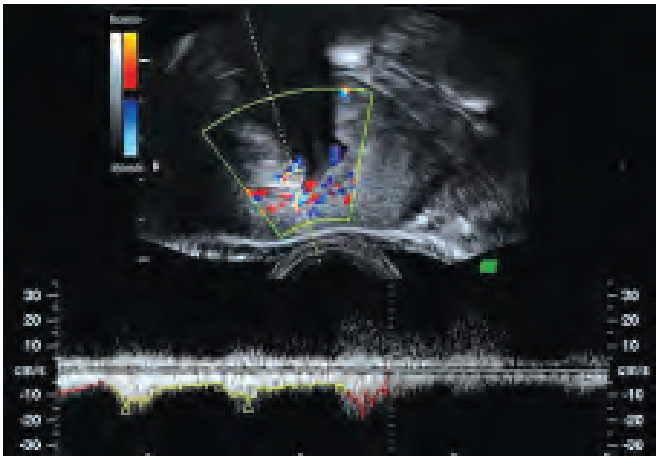

Figure 45.26: Color Doppler following saline infusion sonography. Note moderate vascular impedance

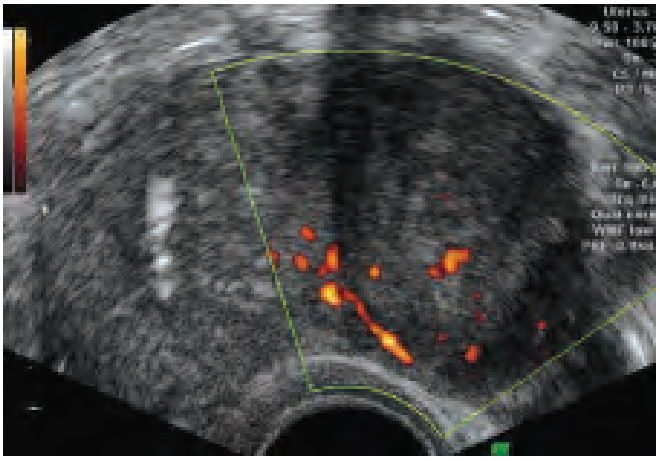

Figure 45.27: The two-dimensional color Doppler of the uterine artery branches supplying the subserosal fibroid

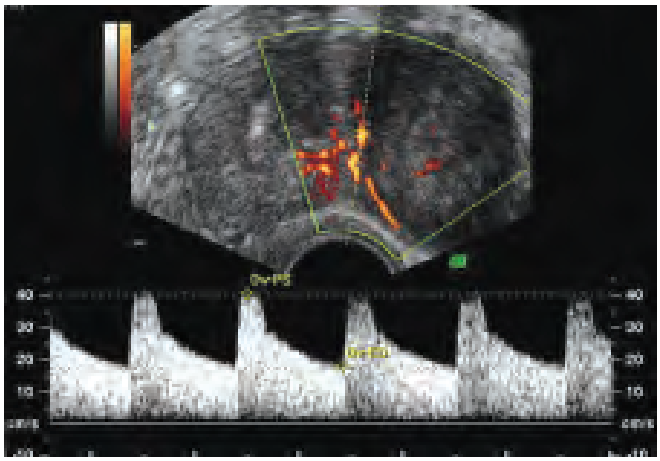

Figure 45.28: Moderate vascular impedance blood flow signals are isolated from the fibroid vessels using pulsed Doppler waveform analysis

whereas positive contrast only created a cast of the cavity.

One limitation of scanning the uterus with myomas by 3D or 2D ultrasound is significant shadowing due to calcification.

Kurjak and Kupesic[23] evaluated myometrial lesions, morphology, volume, and vascularization with 3D ultrasound and power Doppler sonography. The mean volume of the leiomyomas undergoing surgery was 78.52 ± 51.8 ml. In 84.38%, 3D power Doppler detected regular vascularity at the periphery, while in cases of secondary degenerative lesions the findings were suggestive of neovascularity, irregular branching and chaotic vascular arrangement, because necrosis, inflammation and degeneration altered the leiomyoma vasculature **(Fig. 45.35)**. The authors concluded that because of the low PPV of 16.67% this method should not be used for the evaluation of myometrial pathology, both benign and malignant.

LEIOMYOSARCOMA

Uterine leiomyosarcoma is a rare tumor, accounting for only 1–3% of all genital tract tumors and 3–7.4% of malignant tumors of the corpus uteri,[33] characterized by early dissemination and poor prognosis for survival. Through the years, several questions regarding these tumors have remained unanswered, and a method for its early and correct diagnosis is still unknown. Furthermore, uterine sarcoma is expected to be more common in the near future, as gynecologists more commonly use the conservative treatment of uterine leiomyomas. Abnormal vaginal bleeding is the most common presenting symptom in patients with uterine sarcoma.

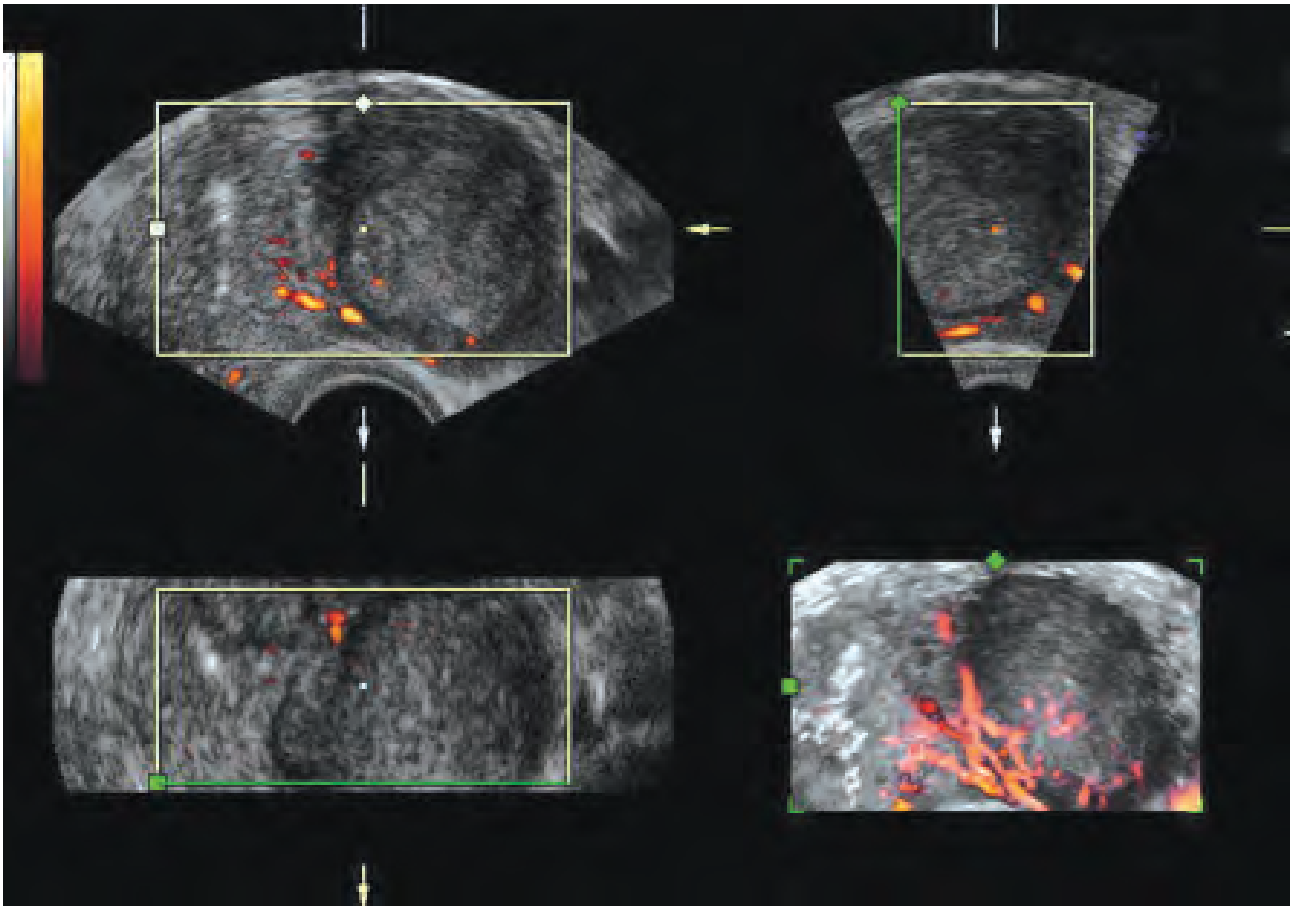

Figure 45.29: The three dimensional power Doppler ultrasound of the subserosal fibroid

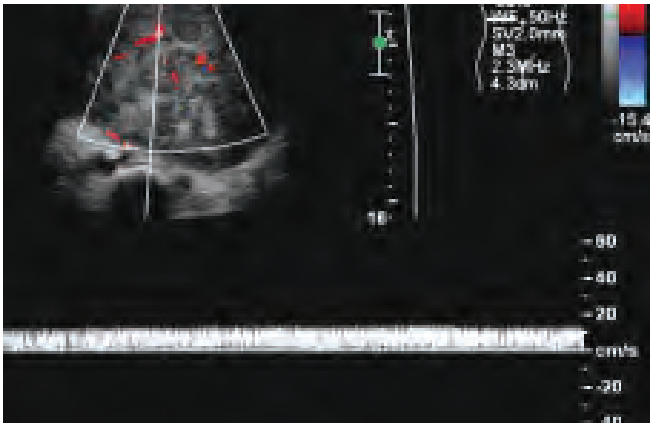

Figure 45.30: Pulsed Doppler ultrasound of a patient with degenerative fibroid. Note venous type of the blood flow signals obtained from the central portion of a degenerative fibroid

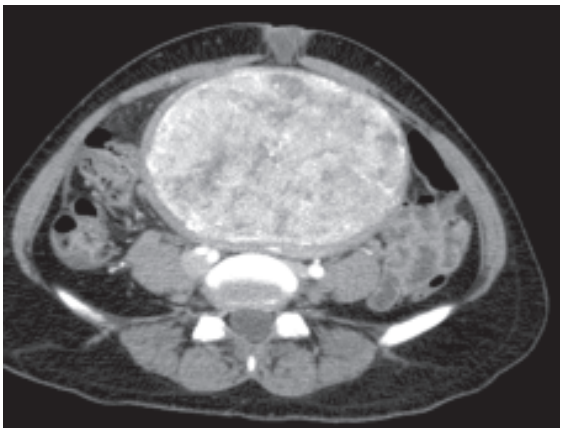

Figure 45.31: Computerized tomography scan of a large degenerative fibroid

Lower abdominal pain or pressure and a palpable abdominal mass are additional findings. An enlarged bulky uterus is palpated, and/or the tumor may be seen protruding through the cervix. Dilatation and curettage may be helpful in distinguishing benign from malignant pathology only if the tumor is submucosal. Clinically, a rapid increase in the size of a uterine tumor after the menopause arouses suspicion of sarcoma.

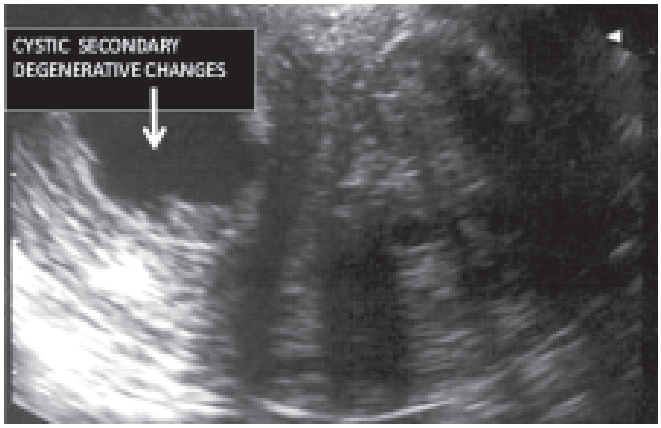

Figure 45.32: Cystic degenerative changes (dark area) in a patient with intramural uterine fibroid

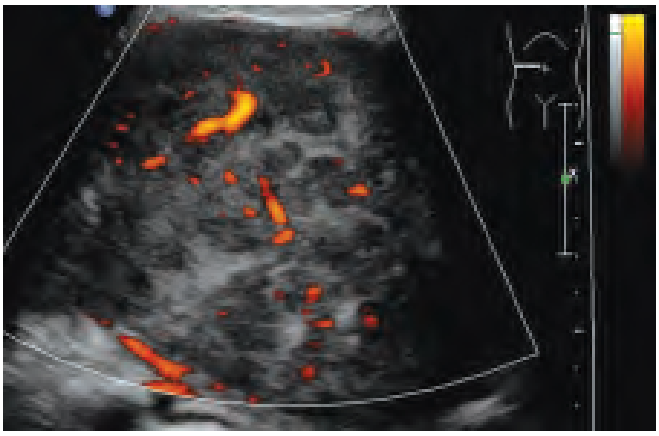

Figure 45.35: Uterine fibroid with secondary degenerative changes. Power Doppler ultrasound displays prominent color/power signals within the central portion of the fibroid

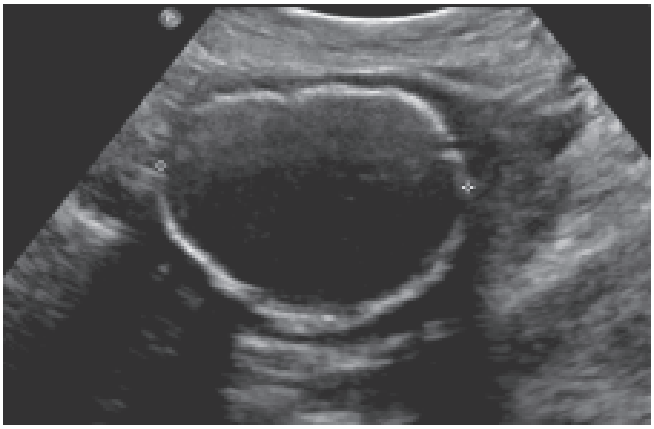

Figure 45.33: Transvaginal ultrasound scan of a calcified uterine fibroid

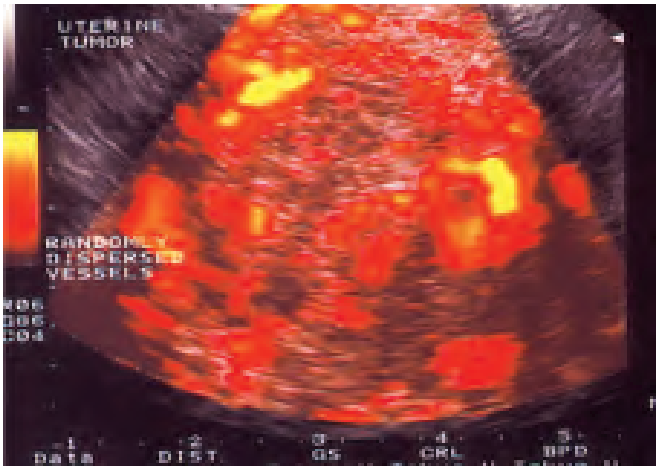

Figure 45.36: Power Doppler facilitates detection of numerous, small, randomly dispersed vessels, typical of uterine malignancy

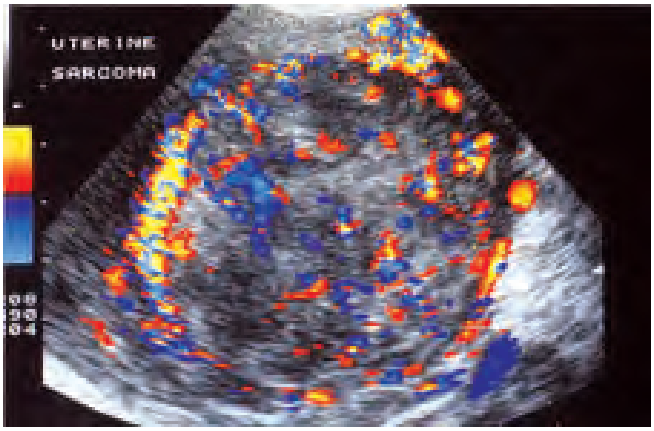

Figure 45.34: Uterine tumor showing highly vascularized area; the tumor proved to be uterine sarcoma

On ultrasound, leiomyosarcoma presents as solid or solid-cystic structure, altering echogenicity of the myometrium. On transvaginal color Doppler, neovascularization of leiomyosarcoma is detected at the border or in the center of the tumor **(Figs 45.34 and 45.36)** with high blood flow velocity and low impedance to blood flow (RI = 0.37 ± 0.03), with irregular, thin, randomly dispersed vessels **(Fig. 45.37)**. When cut-off value for RI of less than 0.40 was used, this method reached the sensitivity of 90.91%, specificity 99.82%, PPV of 71.43% and NPV of 99.96%.[34] Because of their rarity, uterine sarcomas are not suitable for screening. Transvaginal ultrasound can detect differences in myometrial tissue density, and therefore can be used for detection of

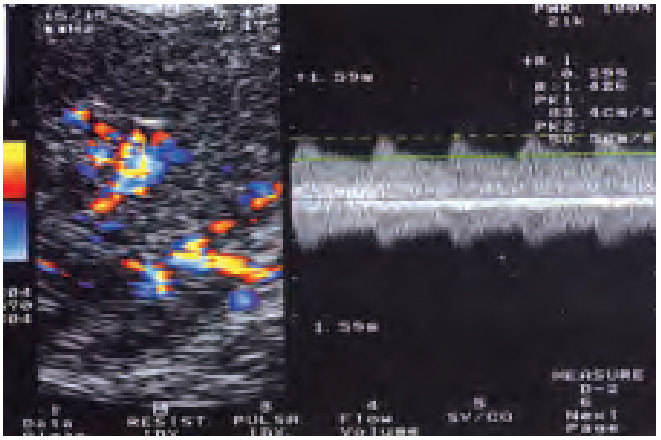

Figure 45.37: Pulsed Doppler waveform analysis demonstrates prominent flow with small systolic-to-diastolic variation and low vascular resistance (RI of 0.42), indicative of uterine malignancy. Uterine sarcoma was confirmed by histopathology

uterine sarcoma, but because of low specificity this method is not appropriate as a screening procedure.

Szabo et al.[35] investigated uterine vascularity by color and pulsed Doppler in cases of uterine leiomyomas and uterine sarcomas, and determined the efficiency of uterine blood flow analysis in differentiating between them. The mean intratumoral RI and PI were significantly lower and the intratumoral PSV was significantly higher in patients with sarcomas than in patients with uterine leiomyomas. Marked reduction of RI and PI, and increased PSV could be found in the leiomyoma cases which showed necrotic, degenerative and inflammatory changes. When a cut-off value of 0.5 for the RI was considered, the detection rate for uterine leiomyosarcoma was 67% and the false-positive rate was 11.8%. These results suggest that the intratumoral RI detected by color and pulsed Doppler ultrasonography cannot be used for preoperative differentiation from uterine leiomyosarcoma.

In our study,[23] one patient with uterine leiomyosarcoma was examined with 3D and power Doppler ultrasound. Enlarged volume of the tumor (97.2 ml) and irregular randomly vessels dispersed both in the central and peripheral parts of the tumor were obtained using this method. The diameters of these vessels were "uneven", with numerous microaneurysms and stenosis.

CONCLUSION

Transvaginal sonography allows for detailed analysis of the endometrial thickness and texture. Blood flow studies can be efficiently used to monitor endometrial development and distinguish between benign and malignant uterine cavity lesions. Use of color Doppler minimizes the need for invasive procedures such as dilatation and curettage or hysteroscopy for detection of the uterine cavity lesions.

Implementation of these techniques could lower potential risks and economic costs. Transvaginal color and pulsed Doppler sonography represents a noninvasive diagnostic tool that can be used repeatedly for assessing vascularity in endometrial lesions. The application of transvaginal color Doppler to the postmenopausal population for the screening of endometrial carcinoma may be a viable option if combined with ovarian screening. In this way, capital costs would be shared and oncological preventive medicine for women could be initiated. Assessment of vascularization of uterine tumors, if used together with analysis of morphology and size, can increase our accuracy in differentiating between uterine leiomyosarcoma and leiomyoma. However, it is unrealistic to expect Doppler studies to clarify confounding histological findings. It seems that the multiparameter sonographic approach, which includes morphology and size depicted by transvaginal ultrasonography and color flow imaging with pulsed Doppler analysis of neovascular signals, can help in the diagnosis of uterine leiomyosarcoma in high-risk groups such as postmenopausal patients with a rapidly enlarging uterus. Therefore, serial measurements are recommended for evaluation of myometrial density, follow-up of the tumoral growth and detection of the impedance to blood flow. Only such complex observations can lead to proper diagnosis of these rare tumors, which have an unpredictable prognosis.

The 3D and power Doppler ultrasound is a new diagnostic technique and its role in the assessment of uterine lesions has yet to be investigated. The 3D ultrasound offers improved visualization of uterine lesions providing simultaneous display of coronal, sagittal, and transverse planes. It displays the entire volume demonstrating continuity of curved structures in a single image, offers more accurate volume estimation using a standard anatomic orientation, retrospective review of data, more complete viewing of pathology using rendered images identifying the location of abnormalities, and assessment of tumor invasion. The 3D SIS demonstrates the exact location of intrauterine pathology. The 3D power Doppler sonography provides a better understanding of malignant tumor angiogenesis. Interactive rotation of power Doppler rendered images improves visualization of the tumor vasculature. This method permits the ultrasonographer to view structures in three dimensions interactively, rather than having to assemble the sectional images in his/her mind. Contrast agents are another possibility for enhancing the 3D power Doppler examination by increasing the detection rate of small vessels.

REFERENCES

1. Kurjak A, Kupesic S, Zalud I, et al. Transvaginal color Doppler. In: Dodson MG (Ed). Transvaginal Ultrasound. New York: Churchill Livingstone; 1995. pp. 325-39.
2. Fleischer AC, Kepple DM, Entman SS. Transvaginal sonography of uterine disorders. In: TimorTritsch IE, Rottem S (Eds). Transvaginal Sonography, 2nd edition. New York: Elsevier; 1991. pp. 109-30.
3. Kurjak A, Kupesic S. Transvaginal color Doppler and pelvic tumor vascularity: lessons learned and future challenges. Ultrasound Obstet Gynecol. 1995;6(2):1-15.
4. Ismail SM. Pathology of the endometrium treated with tamoxifen. J Clin Path. 1994;47(9):827-33.
5. Achiron R, Grisaru D, Golan PN. Tamoxifen and the uterus: an old drug tested by new modalities. Ultrasound Obstet Gynecol. 1996;7(5):374-8.
6. Lahti E, Blanco G, Kauppila A. Endometrial changes in postmenopausal breast cancer patients receiving tamoxifen. Obstet Gynecol. 1993;81(5):660-4.
7. Achiron R, Lipitz S, Sivan E. Changes mimicking endometrial neoplasia in postmenopausal, tamoxifen-treated women with breast cancer: a transvaginal Doppler study. Ultrasound Obstet Gynecol. 1995;6(2):116-20.
8. Exacoustos E, Zupi E, Cangi B. Endometrial evaluation in postmenopausal breast cancer patients receiving tamoxifen: an ultrasound, color flow Doppler hysteroscopic and histological study. Ultrasound Obstet Gynecol. 1995;6(6):435-42.
9. Goldstein SR, Monteagudo A, Popiolek D, et al. Evaluation of endometrial polyps. Am J Obstet Gynecol. 2002; 186(4): 669-74.
10. Perez MT, Bajo J, Huertas MA, et al. Predicting atypia inside endometrial polyps. Journal Ultrasound Med. 2002;21(2):125-8.
11. Bonilla MF, Raga F, Osborne N, et al. Three-dimensional hysterosonography for the study of endometrial tumors: comparison with conventional transvaginal sonography, hysterosalpingography, and hysteroscopy. Gynecol Oncol. 1997;65(2):245-52.
12. Weinraub Z, Maymon R, Shulman A, et al. Three-dimensional saline contrast hysterosonography and surface rendering of uterine cavity pathology. Ultrasound Obstet Gynecol. 1996;8(4):277-82.
13. Gruboeck K, Jurkovic D, Lawton F, et al. The diagnostic value of endometrial thickness and volume measurements by three-dimensional ultrasound in patients with post-menopausal bleeding. Ultrasound Obstet Gynecol. 1996;8(4):272-6.
14. Momtaz M, Ebrashi AE. 3D sonohysterography in the evaluation of the uterine cavity. Syllabus. Las Vegas: 1999.
15. Fedele I, Bianchi S, Dorta M, et al. Transvaginal ultrasonography in the diagnosis of diffuse adenomyosis. Fertil Steril .1992;58(1):94.
16. Hirai M, Shibata K, Sagai H, et al. Transvaginal pulsed and color Doppler sonography for the evaluation of adenomyosis. J Ultrasound Med. 1995;14(7):529-32.
17. Lee SL, Busmanis I, Tan A. 3D–Angio of Adenomyotic Uteri. Syllabus. Las Vegas: 1999.
18. Kupesic US, Shalan H, Kurjak A. Early detection of endometrial cancer by transvaginal color Doppler. EUROBS. 1993;49(1-2):46-9.
19. Kurjak A, Kupesic S. Ovarian senescence and its significance on uterine and ovarian perfusion. Fertil Steril. 1995; 64(3):532-7.
20. Emoto M, Tamura R, Shirota K, et al. Clinical usefulness of color Doppler ultrasound in patients with endometrial hyperplasia and carcinoma. Cancer. 2002;94(3):700-6.
21. Jarvela I, Tekay A, Santala M, et al. Thermal balloon endometrial ablation therapy induces a rise in uterine blood flow impedance: a randomized prospective color Doppler study. Ultrasound Obstet Gynecol. 2001;17(1):65-70.
22. Folkman J, Cole D, Becker F. Growth and metastasis of tumor in organ culture. Tumor Res. 1963;16:453-67.
23. Kurjak A, Kupesic S. Three-Dimensional ultrasound and power Doppler in assessment of uterine and ovarian angiogenesis: a prospective study. Croatian Medical J. 1999;40(3):51-8.
24. Kupesic S, Kurjak A, Zodan T. Staging of endometrial carcinoma by 3-D power Doppler. Gynecol Perinatol. 1999;8(1):1-5.
25. Lee CN, Cheng WF, Chen CA, et al. Angiogenesis of endometrial carcinomas assessed by measurement of intratumoral blood flow, microvessel density, and vascular endothelial growth factor levels. Obstet Gynecol. 2000;96(4):615-21.
26. Alcazar JL, Galan JM, Jurado M, et al. Intratumoral blood flow analysis in endometrial carcinoma: correlation with tumor characteristics and risk for recurrence. Gynecol Oncol. 2002;84(2):258-62.
27. Yaman C, Ebner T, Jesacher K, et al. Reproducibility of three-dimensional ultrasound endometrial volume measurements in patients with postmenopausal bleeding. Ultrasound Obstet Gynecol. 2002;19(3):282-6.
28. Kurjak A, Zalud I. Uterine masses. In: Kurjak A (Ed). Transvaginal Color Doppler. Carnforth, UK: Parthenon Publishing; 1991. p. 123.
29. Fleischer AC, Entman SS, Porrath SA, et al. Sonographic evaluation of uterine malformations and disorders. In: Sanders RC (Ed). The Principles and Practice of Ultrasonography in Obstetrics and Gynecology. Norwalk: Appleton Century Crofts; 1985. p. 531.
30. Kurjak A, Kupesic US, Miric D. The assessment of benign uterine tumor vascularization by transvaginal color Doppler. Ultrasound Med Biol. 1992;18(6-7):645-8.
31. Balen FG, Allen CM, Gardener JE, et al. 3-Dimensional reconstruction of ultrasound images of the uterine cavity. Br J Radiol. 1993;66(787):588-91.
32. LevToaff AS, Rawool NM, Kurtz AB, et al. Three-dimensional sonography and 3D transvaginal US: a problem solving tool in complex gynecological cases. Radiology. 1996;201(P):384.
33. Olah KS, Gee H, Blunt S, et al. Retrospective analysis of 318 cases of uterine sarcoma. Eur J Cancer. 1991;27(9):1095-9.
34. Kurjak A, Kupesic S, Shalan H, et al. Uterine sarcoma: a report of 10 cases studied by transvaginal color and pulsed Doppler sonography. Gynecol Oncol. 1995;59(3):342-6.
35. Szabo I, Szantho A, Csabay L, et al. Color Doppler ultrasonography in the differentiation of uterine sarcomas from uterine leiomyomas. E J Gynaecol Oncol. 2002;23(1):29-34.

46
CHAPTER

Ultrasound and Uterine Fibroid

Aleksandar Ljubic, Tatjana Bozanovic, Srboljub Milicevic

INTRODUCTION

Definition

Uterine fibroids are referred to as fibroid, leiomyoma, leiomyomata and fibromyoma. They are benign (non cancerous) tumors that grow within the muscle tissue of the uterus. Depending on the prevailing type of tissues, i.e. parenchyma or interstitial, they are called differently as myoma, fibroma, fibromyoma, etc. As they are developed mainly from muscle cells, the most correct terminology is considered to be myoma (leiomyoma).

Incidence

The incidence of fibroids in women of reproductive age is reported to be between 20% and 40%.[1] Uterine fibroid is the most common pelvic tumor and they are diagnosed in up to 15–20% of women in pubertal period.[1] Their presence could cause failure to conceive, but no scientific evidence supports improvement after the surgical removal of the fibroid. This was recently highlighted in a review, reporting a pregnancy rate after myomectomy in infertile women varying between 10% and 80%. While many women do not experience any problems, symptoms can be severe enough to require treatment.

Although fibroid (uterine fibroids) is generally considered to be a slowly growing tumor, in 20–40% of women at the age of 35 and more, uterine fibroids of significant sizes with severe clinical symptoms are commonly seen. Moreover, fibroid can be relapsed in 7–28% of patients after surgical treatments and in certain cases it may even turn into malignant tumor.

Etiology and Pathophysiology

Although, the exact etiology of fibroid is not known yet, the growth of uterine fibroid is featured as a benign, hormone sensitive diffuse or nodulus hyperplasia of myometrium, and is characterized by having multiple factors of pathogenesis and systemic changes **(Figs 46.1A and B)**.

Uterine fibroid is developed on the background of hyperestrogens, progesterone deficits and hypergonadotropins. The majority of the researchers consider that the growth of fibroid depends on concentration of cytosolic receptors to the sexual hormones and their interactions with the endogenous or exogenous hormones. In accordance to clinical observations, it can be admitted that both growth and regression of fibroid are estrogen-dependant; the tumor size gets increased during pregnancy and is regressed after menopause.

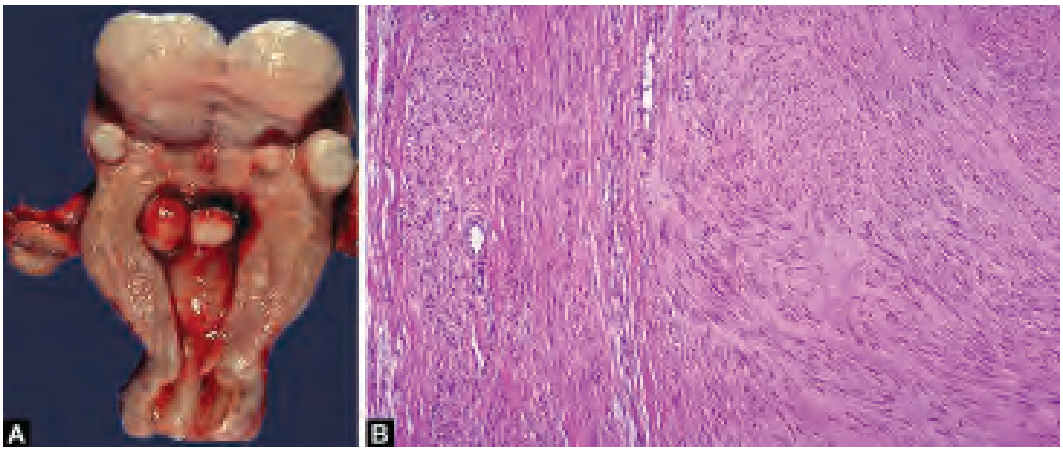

Figures 46.1A and B: (A) Various types of fibroid and (B) histopathological picture. Proliferation of muscle tissue surrounded by pseudocapsule can be seen

Possible Causes of Fibroids

***Genetics*:** About 40% of fibroids contain alterations in genes that code for uterine muscle cells. Patients with hereditary leiomyomatosis and renal cell carcinoma (HLRCC cutaneous and uterine leiomyoma) are at risk for papillary renal cell carcinoma (the incidence in women is greater than in men). They also have mutation in fumarate hydratase gene. The chromosomal anomaly (12q13–15) is quite common in myomatous cells. In fact, in 30–40% cases, the predisposition to uterine fibroid is passed down from mothers to daughters on hereditary line. A form of fibroid so called "family type" is present where uterine fibroid are seen in all the family line, i.e. in grandmother, mother, aunts and sisters.

***Heredity*:** If a mother or sister had fibroids, then there is an increased risk of developing them.

***Race*:** Black women are more likely to have fibroids than are women of other racial groups. Also, black women have fibroids at younger age and they are more likely to have more or larger fibroids.

***Hormonal imbalance*:** Estrogen and progesterone appear to promote the growth of fibroids. Fibroids contain more estrogen and estrogen receptors than do normal uterine muscle cells. Other chemicals that help the body maintain tissues, such as insulin-like growth factor, may also affect fibroid growth.

***Obesity*:** Overweight women have a greater risk of developing fibroids.

Fibroids rarely have malignant potential (leiomyosarcoma) **(Figs 46.2A and B)**.

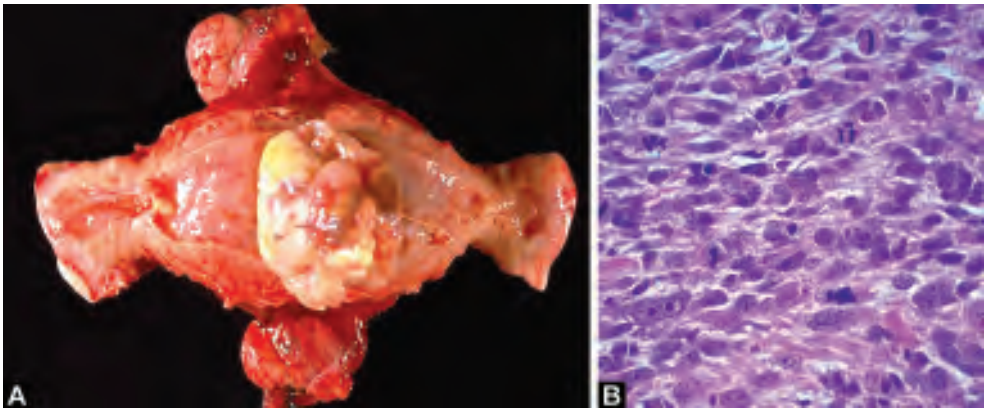

Figures 46.2A and B: (A) Leiomyosarcoma with (B) histopathological picture

Localization

Fibroid may be located in the external, middle or inner layers of uterus (subserous, interstitial and submucous). Nodules can be located in the isthmus (5%) or in the uterine body (95%) **(Fig. 46.3)**.

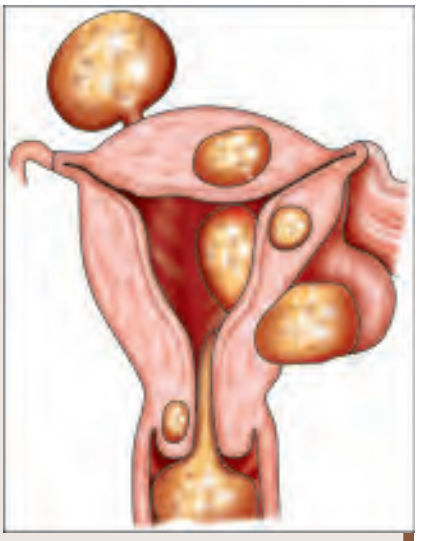

Figure 46.3: Different fibroids and their orientation to the uterine wall

Types of Fibroids

***Intramural*:** Fibroids embedded within the myometrium. This is the most common type of fibroid. These develop within the uterine wall and expand, making the uterus feel larger than normal (which may cause "bulk symptoms").

***Subserosa*:** Fibroids that bulge on the outside. These fibroids develop in the outer portion of the uterus and continue to grow outward.

***Submucosal*:** Fibroids that grow into the inner cavity. These fibroids develop just under the lining of the uterine cavity. These are the fibroids that have the most effect on heavy menstrual bleeding and the ones that can cause problems with infertility, and miscarriage.

***Pedunculated*:** Fibroids that hang from a stalk inside or outside of the uterus. Fibroids that grow on a small stalk that connects them to the inner or outer wall of the uterus.

Symptoms

Women with fibroids can be asymptomatic (in 50–60% of cases) or may present with menorrhagia (30%), pelvic pain with or without dysmenorrhea or pressure symptoms (34%), infertility (27%), and recurrent pregnancy loss (3%).[1] Much of the data describing the relationship between the presence of fibroids and symptoms are based on uncontrolled studies that have assessed the effect of myomectomy on the presenting symptoms.[2] The prevalence of fibroids in infertile women can be as high as 13%, but no direct causal relationship between fibroids and infertility has been established.[3]

Main fibroid symptoms are bleeding, pressure, pain as well as infertility and pregnancy complications, such as cesarean delivery, breech presentation, malposition, preterm delivery, placenta previa and severe postpartum hemorrhage occur in half of the patients.

Symptoms depend on location, size, growth rate and relation with surrounding organs. Ultrasound is the most important diagnostic tool in determining all previous facts.

Diagnosis

While making an ultrasound diagnosis, it is important to determine size, shape, echogenicity and clear edge with the surrounding tissues. For that purpose we can use two-dimensional (2D) **(Fig. 46.4)**, three-dimensional (3D) and four-dimensional (4D) ultrasound. In order to assess the vascularization of the fibroids, color doppler is used **(Figs 46.5A and B)**.

Endometrial and subendometrial blood flow measured by 3D power Doppler ultrasound in patients with small intramural uterine fibroids during *in vitro* fertilization (IVF) treatment, can be a predictor of a treatment success.[6]

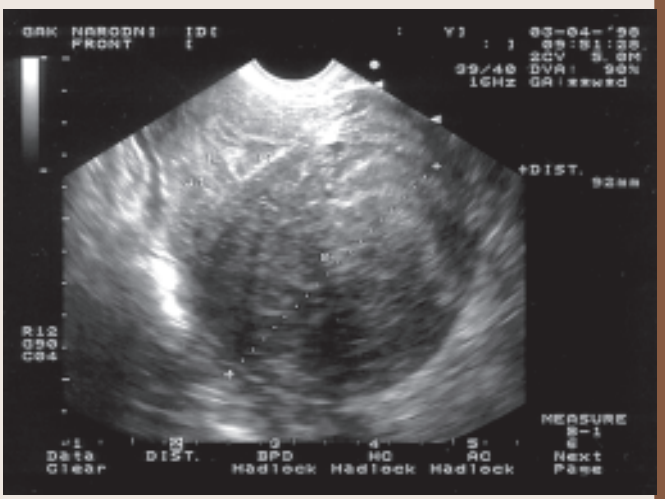

Figure 46.4: Two-dimensional ultrasound of intramural fibroid. Possible predictor of the uterine growth is fibroid circulation, which can be assessed by color Doppler examination[4]

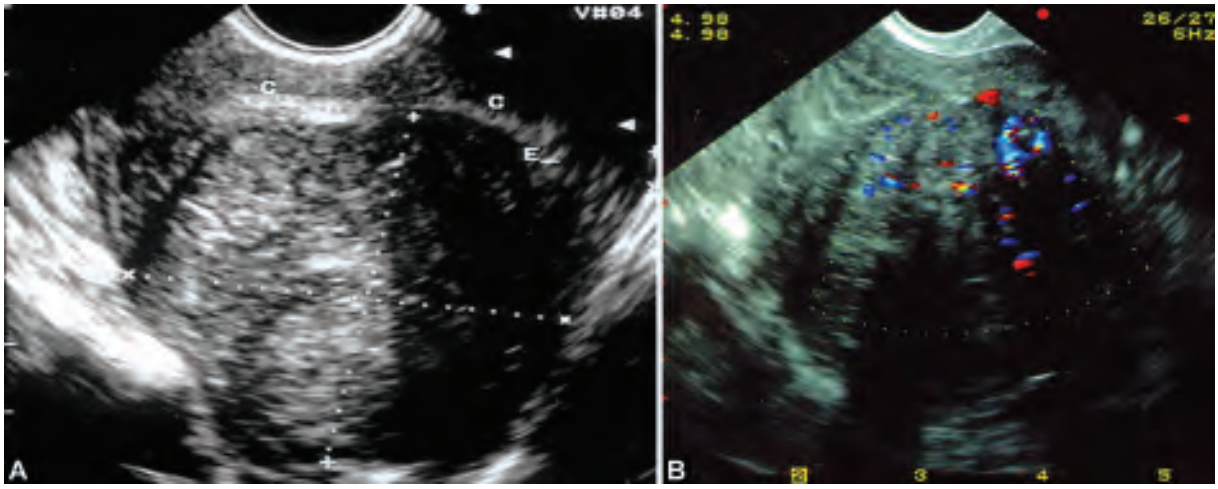

Figures 46.5A and B: Examination of the fibroid circulation

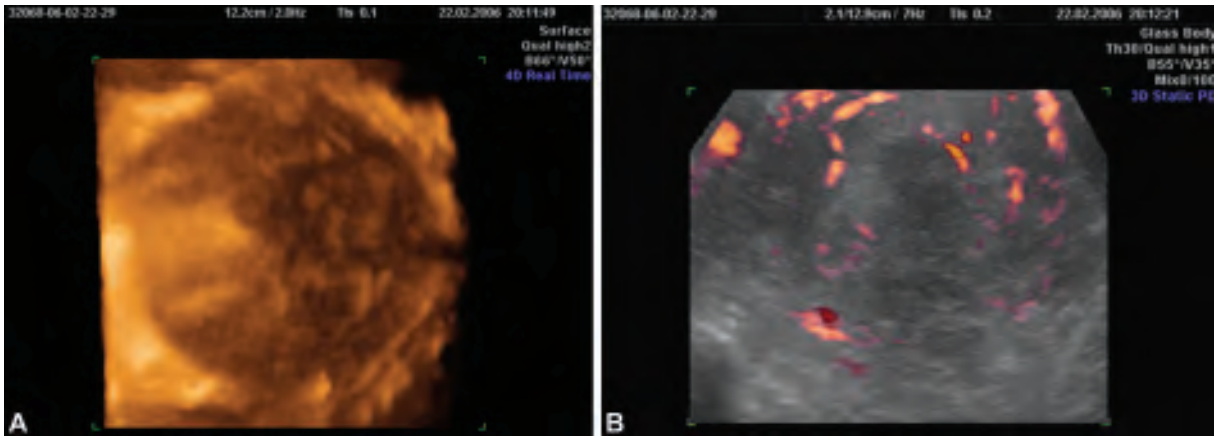

Figures 46.6A and B: (A) Three-dimensional and (B) glass body picture of the uterine fibroid

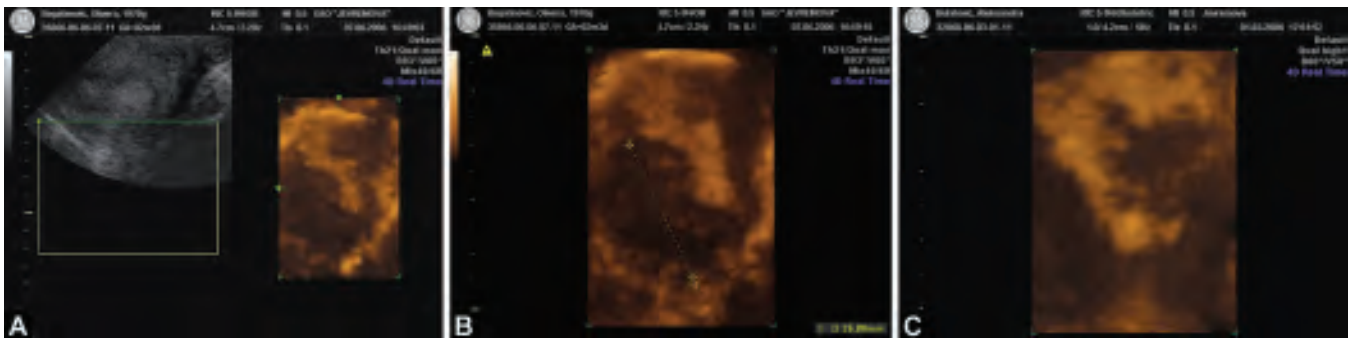

Figures 46.7A to C: Three-dimensional ultrasound pictures of the uterine fibroid

The circulation can be even better assessed using new 3D technologies such as glass body rendering. Using of 3D and 4D ultrasound enable us in better delineating the fibroid **(Figs 46.6 and 46.7)**.

ELASTOGRAPHY

Elastography is a non-invasive method in which stiffness or strain images of soft tissue are used to detect or classify tumors. A tumor or a suspicious cancerous growth is normally 5–28 times stiffer than the background of normal soft tissue. When a mechanical compression or vibration is applied, the tumor deforms less than the surrounding tissue, i.e. the strain in the tumor is less than the surrounding tissue.

Ultrasonic imaging is the most common medical imaging technique for producing elastograms. Some research has been conducted using magnetic resonance elastography (MRE) and computed tomography. However, using ultrasound has the advantages of being cheaper, faster and more portable than other techniques.

Benefits of Elastoscan

Elastoscan can help gynecologist to find fibroid more easily **(Figs 46.8A and B)**.

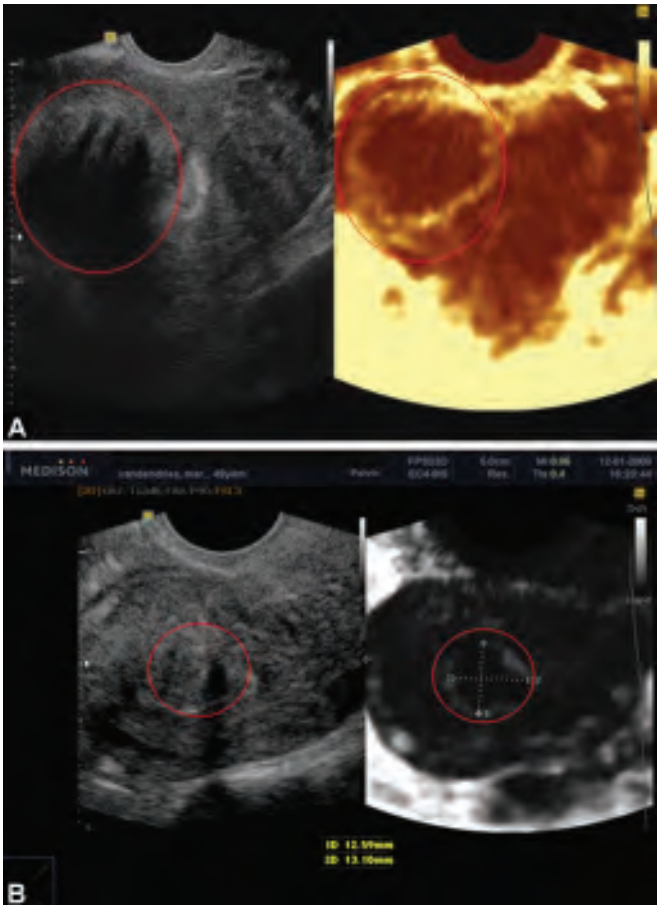

Figures 46.8A and B: Fibroid elastoscans

Uterine fibroids are composed of the same smooth muscle fibers as the uterine wall. They are many times denser than the normal myometrium. This characteristic is frequently responsible for the poor visualization of fibroids on transvaginal ultrasonography, due to strong acoustic shadowing.

As the distribution of fibroids can be difficult to determine on conventional B-mode ultrasonography, their number and size can be underestimated.[6] Three-dimensional ultrasound, computed tomography and magnetic resonance imaging have all been used for better fibroid visualization. However, a new easy-to-use ultrasound tool, real time transvaginal elastography[7] has been suggested as a new method for evaluating fibroids.[8,9]

With conventional ultrasound, the ultrasound beam is often strongly attenuated by the fibroid. As a result, with low gain, the posterior wall of the uterine fibroid is poorly visualized, but as the gain is increased, noise or artifactual echoes appear inside the mass, obscuring the image of the fibroid.[6] Real time elastosonography provides an instantaneous color map that precisely delineates the fibroids, thus overcoming the limitations of conventional ultrasound.

The principle of the ultrasonographic technique is based on slight external tissue compression on the structures examined, which produces strain (displacement) within the tissue, with subsequent calculation of the strain profile along the axis of compression algorithm to produce the elastographic image. The strain profile is converted into an elastic modules image, i.e. the tissue elasticity distribution, called an elastogram. The calculated elasticity values are then color-coded and superimposed on the translucent, corresponding B-mode scan image **(Fig. 46.9)**. The stiffness of the tissue is displayed in a range of color from red (components with the greatest strain, i.e. the softest components) to blue (components with no strain, i.e. the hardest components). The components with average are displayed as green.

All fibroids were seen easily on the color display in elastography mode and their extent was easier to define than it was in conventional B-mode. The distance between the fibroid and the endometrial cavity or uterine serosa could also be measured easily in each case **(Fig. 46.10)**.[10]

Endovaginal ultrasonography is safe, accessible and inexpensive, and remains the primary imaging method for gynecological evaluation. Real time elastosonography offers complementary diagnostic and mapping information. It is easy to perform and the procedure requires only a few seconds of manipulation.

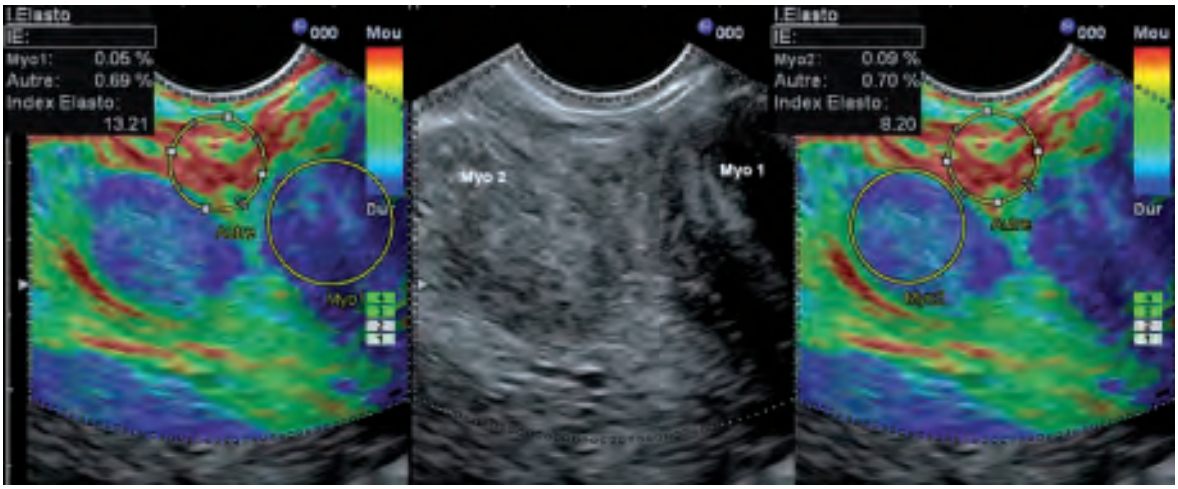

Figure 46.9: A real-time elastosonographic images of the two fibroids. The strain ratio is evaluated by comparing the mean strain in a region of interest centered on the fibroid, with the mean strain in a region of interest in the surrounding myometrium close to the probe[10]

Source: Ami O, Lamazou F, Mabille M, et al. Real-time transvaginal elastosonography of uterine fibroids. Ultrasound Obstet Gynecol. 2009;34:486-8

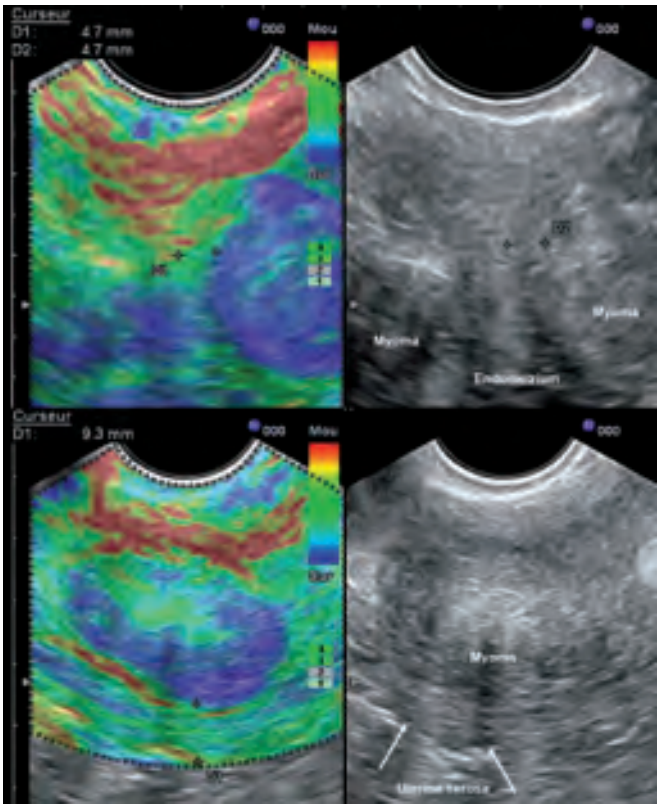

Figure 46.10: Color mapping of uterine strain allows precise determination of the so-called "security wall" between the fibroids and the endometrium or uterine serosa before surgical resection with laparoscopy or hysteroscopy respectively

Source: Ami O, Lamazou F, Mabille M, et al. Real-time transvaginal elastosonography of uterine fibroids. Ultrasound Obstet Gynecol. 2009;34:486-8

Tables 46.1 and 46.2 show the characteristics of different tests in examining uterine changes.[11]

Predictive characteristics of hysteroscopy in the diagnosis of submucosal fibroids comparing to other pathology is given in **Table 46.3**.[12]

Submucosal fibroids grow into the inner cavity. Ultrasound is of great value in assessing the operability of submucosal fibroids. Contrast ultrasound is of greater efficacy in better diagnosis of submucosal fibroids.[12,13]

Comparison between 3D contrast sonography and diagnostic hysteroscopy in the diagnosis of different types of submucosal fibroids is presented in **Table 46.4** and **Figures 46.11A and B**.[8]

There was agreement between the two methods in 11/12 cases of type 0 fibroids (92%), 34/37 (92%) of type I fibroids and 9/12 (75%) of type II fibroids. The overall level of agreement was good with a kappa value of 0.80.

In differential diagnosis, it is most important not to miss diseases, such as gestational trophoblastic neoplasm or endometrial carcinoma **(Figs 46.12A and B)**.

TREATMENT

The uterine fibroid by itself is not an indication for operative method of treatment. Mainly it depends upon the patients' overall health condition, severities of the clinical symptoms and the sizes of the tumor. The major indications for the operative methods of treatment are severe pain, fast growth rate of the nodules, arising suspicions about the malignancy of fibroid,

TABLE 46.1

Ultrasound and hysteroscopy: test characteristics

Features	*Transvaginal ultrasound*	*Saline infusion sonography*	*Outpatient hysteroscopy*	*Evidence and prevailing clinical opinion*
Safety	✓✓✓	✓✓✓	✓✓✓	All safe, with very low rates of adverse effects reported
Acceptability	✓✓✓	✓✓	✓✓	All acceptable, ultrasound least painful and invasive. Instrumentation and distension of the uterine cavity more painful
Feasibility	✓✓✓	✓✓	✓✓	Typical failure rates higher in procedures requiring uterine instrumentation—saline infusion sonography (7%) higher than hysteroscopy (4%)
Other	Provides extracavity/ pelvic information	Facilitates diagnosis of intracavity lesions/ provides extra-cavity information	Directed endometrial biopsies and removal of focal pathology possible	Advances in the technology and application of ultrasound (three-dimensional color Doppler) techniques give this modality the greatest future potential in diagnosis. Hysteroscopy has greater therapeutic potential

TABLE 46.2

Ultrasound and hysteroscopy: test accuracy in abnormal uterine bleeding

		Accuracy (likelihood ratio[a])		
		Positive test	*Negative test*	
Endometrial diseases	*Test*	*[Pooled estimate (95% CI) if available or range if not]*		*Systematic review*
Cancer	TVS (< 5 mm)[b]	2.0 (1.9-2.2)	0.08 (0.04-0.14)	Smith-Bindman (1998)[c]
		2.0 (1.6-2.4)	0.08 (0.03-0.17)	Gupta (2002)[c]
	SIS	–	–	–
	Hysteroscopy	60.9 (51.2-72.5)	0.15 (0.13-0.18)	Clark (2002)
Cancer and/or hyperplasia	TVS (<5 mm)[b]	2.9(2.7-3.2)	0.13 (0.10-0.16)	Smith-Bindman (1998)[c]
		2.2 (1.7-2.7)	0.07 (0.04-0.11)	Gupta (2002)[c]
	TVS (8-14 mm)	2.6-679	0.04-1.0	Farquhar (2003)[d]
	SIS	1.6-70.4	0.14-0.88	Farquhar (2003)[d]
	Hysteroscopy	10.4 (9.7-11.1)	0.24 (0.22-0.25)	Clark (2002)
Polyps	TVS	–	–	–
	SIS	5.2 (4.0-6.9)	0.12 (–0.08-0.17)	de kroon (2003)
	Hysteroscopy	–	–	–
Submucous fibroids	TVS	1.6-62.3	0.03-0.8	Farquhar (2003)[d]
	SIS	29.6 (17.8-49.6)	0.06-0.47	Farquhar (2003)[d]
		11.0 (6.9-17.6)	0.07 (0.03-0.11)	de Kroon (2003)
	Hysteroscopy	29.4 (13.3-65.3)	0.08-0.48	Farquhar (2003)[d]

TVS—transveginal ultrasound; SIS—saline infusion sonography.

[a]The likelihood ratio (LR) is the ratio of the probability of a positive (or negative) test result in women with disease, to the probability of the same test result in women without disease. The desirable size of a positive likelihood ratio (LR+) is over 10 and of a negative likelihood ratio (LR–) less than 0.1. This is because a test is deemed clinically useful (i.e. substantially increases or lowers the pretest probability, hence ruling in or excluding disease, respectively) at these levels. Likelihood ratios below these levels are at best moderately informative (LR + 5–10 and LR– 0.1 – 0.5) and at worst useless (LR+ <5 and LR –> 0.5.

[b]Data from TVS systematic review by Tabor et al not presented as not stratified by endometrial thickness.

[c]Postmenopausal women only.

[d]Premenopausal women only.

TABLE 46.3

Predictive characteristics of hysteroscopy in the diagnosis of various conditions in a series of 770 consecutive women with menorrhagia

Condition	*Sensitivity (%)*	*Specificity (%)*	*Positive predictive value (%)*	*Negative predictive value (%)*
Submucous myomas	95	81	85	93
Endometrial polyps	86	94	91	90
Endometrial hyperplasia	45	99	38	94

TABLE 46.4

Comparison between three-dimensional saline infusion sonohysterography (3D SIS) and diagnostic hysteroscopy for classification of submucous fibroids

Hysteroscopy	*3D SIS*			*Total*
	Type 0	*Type I*	*Type II*	
Type 0	11	1	0	12
Type I	0	34	3	37
Type II	0	3	9	12
Total	11	38	12	61

Type 0: fibroid polyp.
Type I: < 50% contained within the myometrium.
Type II: > 50% contained within the myometrium.

inflammatory changes in the tumor nodules and dysfunction of closely lying organs (urinary bladder, intestines, etc.) and infertility (when all other reasons are already excluded).

It is necessary to watch the dynamic changes of fibroid (ultrasound examination with vaginal probe), which in most cases gives sufficient information and neither operations nor other therapies are required. First line of therapy is medical therapy which might include the use of non steroidal anti-inflammatory drugs, birth control pills or hormone therapy, i.e. GnRH analogues (reduced blood flow with decreasing the size).

Surgical Treatment: Myomectomy

Myomectomy is a surgical procedure that removes visible fibroids from the uterine wall. It leaves the uterus in place and may, therefore, preserve the woman's ability to have children. There are several ways to perform myomectomy, including hysteroscopic myomectomy **(Figs 46.13A to C)**, laparoscopic myomectomy and abdominal myomectomy.

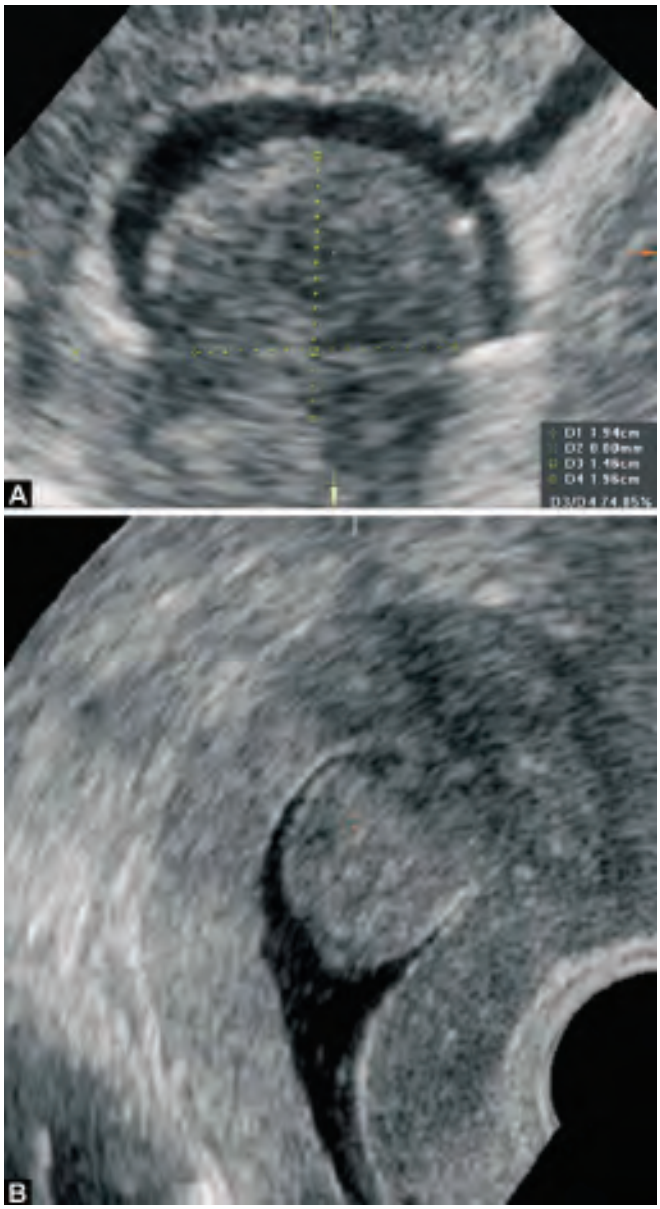

Figures 46.11A and B: (A and B) Contrast sonography in diagnosis of submucosal fibroids

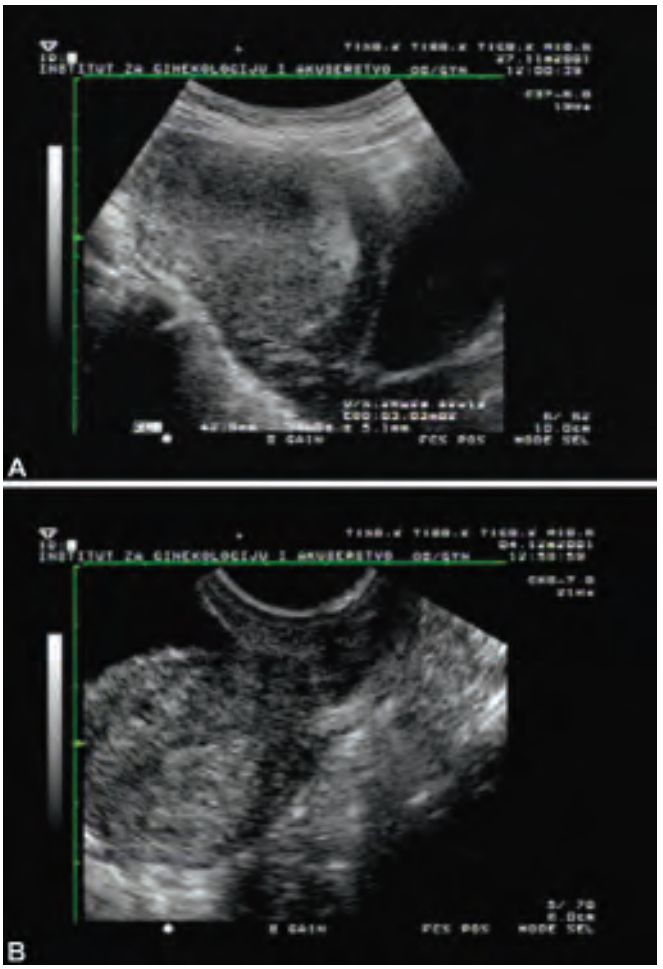

Figures 46.12A and B: (A) Gestational trophoblastic neoplasm; (B) Endometrial cancer

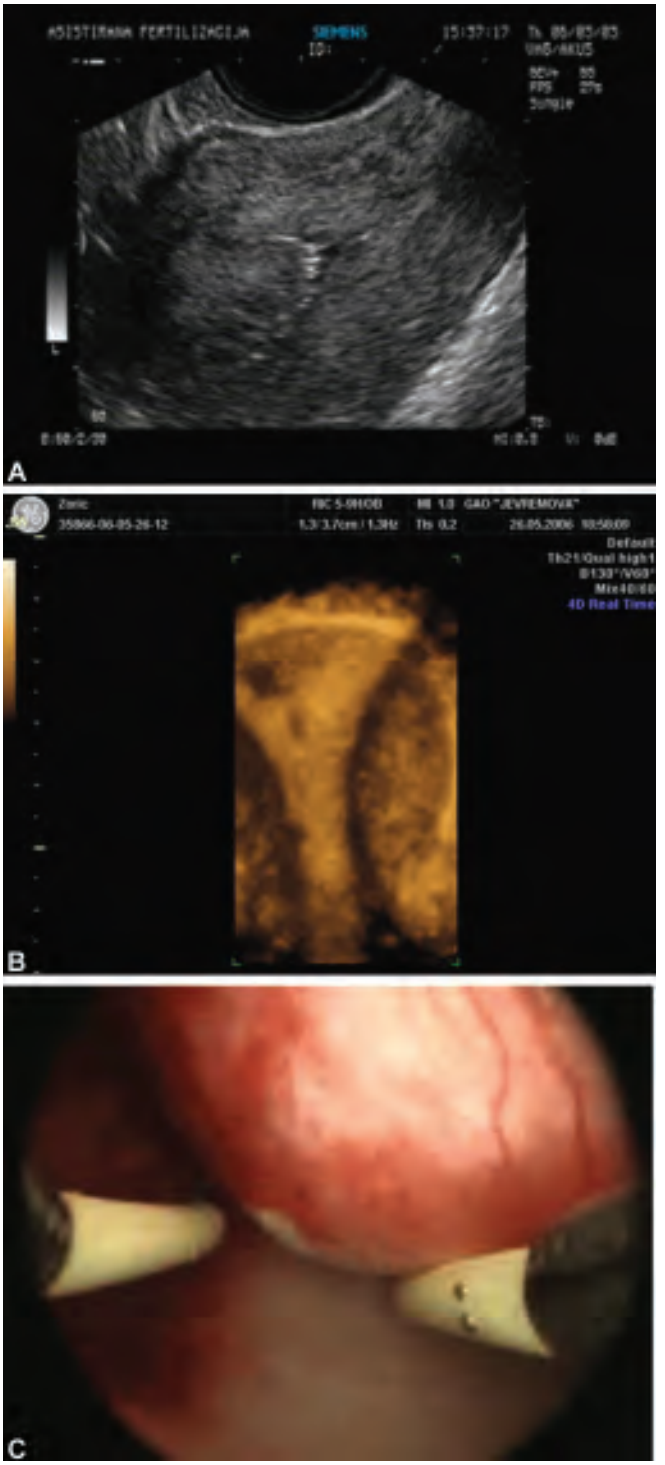

Figures 46.13A to C: Contrast 2D, 3D and hysteroscopic view of submucosal fibroid

Hysteroscopic Myomectomy

Hysteroscopic myomectomy is used only for fibroids that are just under the lining of the uterus and that protrude into the uterine cavity.

Laparoscopic Myomectomy

Laparoscopic myomectomy may be used if the fibroid is on the outside of the uterus **(Figs 46.14A and B)**.

Abdominal Myomectomy

Abdominal myomectomy is a surgical procedure, in which an incision is made in the abdomen to access the uterus and another incision is made in the uterus to remove the tumor. Once the fibroids are removed, the uterus is stitched closed. The patient is given general anesthesia and is not conscious for this procedure, which

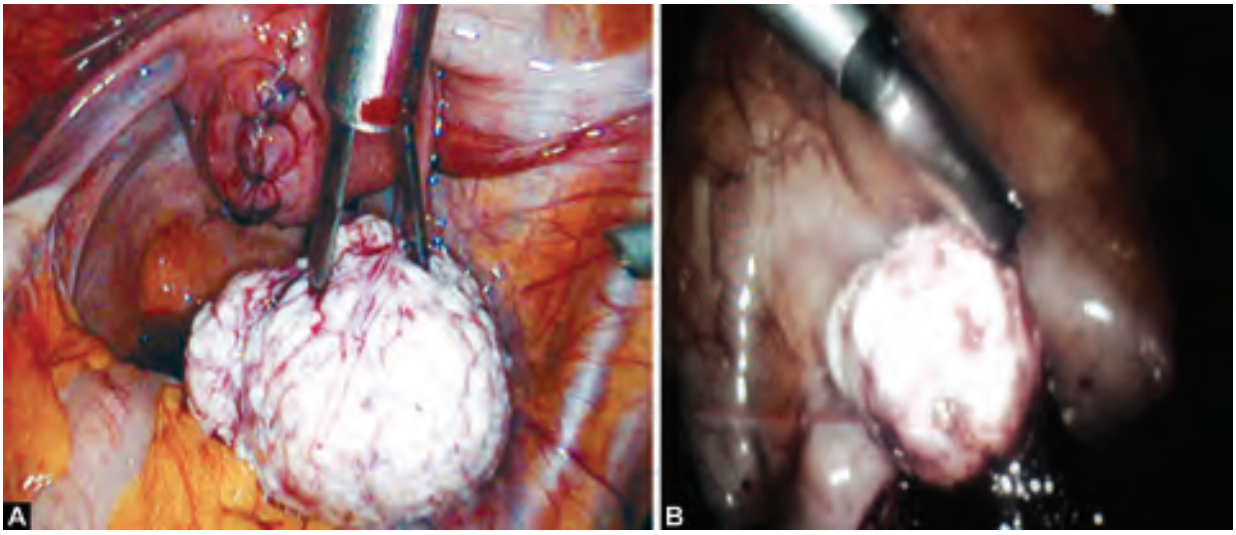

Figures 46.14A and B: Laparoscopic myomectomy

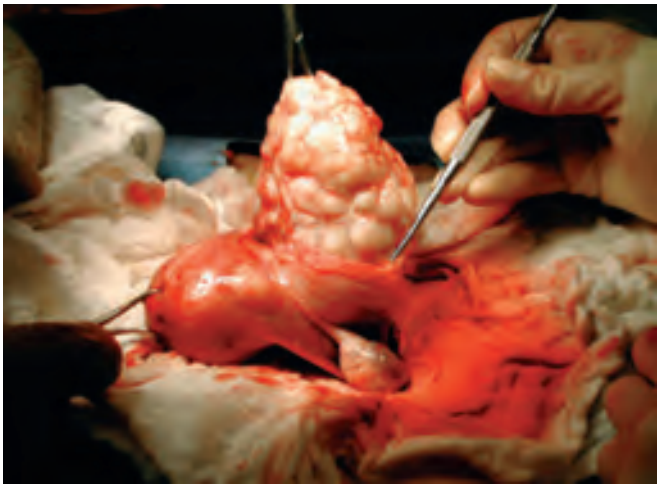

Figure 46.15: Abdominal myomectomy

requires a several-day hospital stay. Typical recovery is 4–6 weeks **(Fig. 46.15)**.

Hysterectomy

In a hysterectomy, the uterus is removed in an open surgical procedure. Hysterectomy is the most common current therapy for women who have fibroids. It is typically performed in women who have completed their childbearing years.

A generation ago, doctors almost uniformly recommended a hysterectomy—removal of the uterus for the treatment of uterine fibroids. This operation remains the only proven permanent solution for this condition **(Fig. 46.15)**. Nearly 600,000 women have such surgery each year in the United States and more than one-third of these operations are performed to treat fibroids.

Uterine Fibroid Embolization

Uterine fibroid embolization (UFE) also called uterine artery embolization (UAE) is a minimally invasive surgical procedure used to treat uterine fibroids. This surgery uses a technique called embolization, which blocks the flow of blood through the vessels around the fibroids depriving them of the oxygen they need to grow. The oxygen deprivation results in the fibroids shrinking. Although, a relatively new treatment for fibroids, UFE has been used for years to control heavy bleeding after childbirth. Fibroid embolization is performed by an interventional radiologist who works in consultation with gynecologist. UFE is not recommended for women who are planning future pregnancies because its effects on fertility are not conclusively known. It is the minimally invasive procedure with no need for general anesthesia; treats all fibroids simultaneously; has a short recovery period (1–2 weeks); no abdominal scars and minimal blood loss; infrequent complications and preserved uterus with normal menstrual cycles usually resume after the procedure **(Figs 46.16A and B)**.

The disadvantages of UFE are:

- Moderate to severe pain and cramping in the first several hours or days following the procedure
- Postembolization syndrome causing nausea and fever

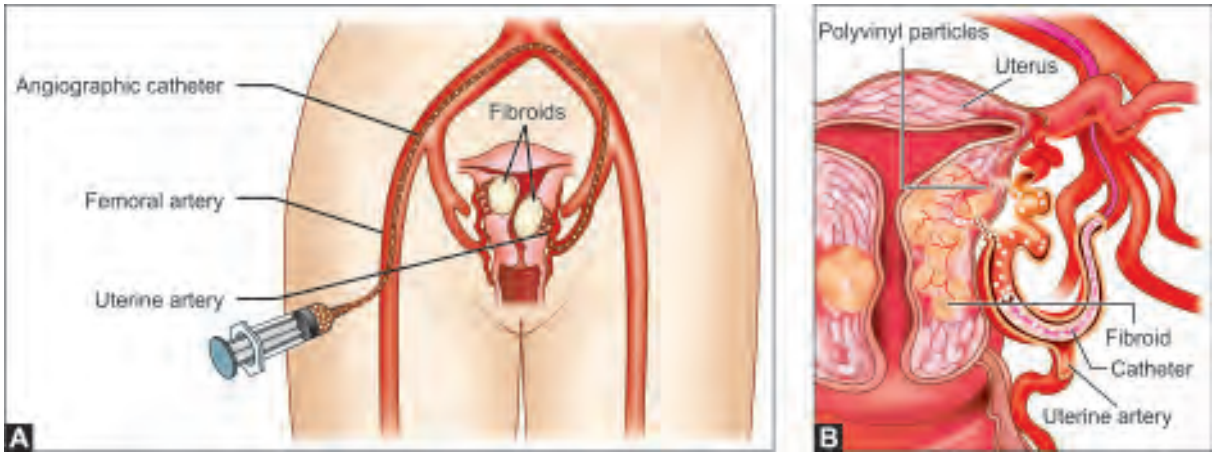

Figures 46.16A and B: Schematic representation of uterine fibroid embolization

- Up to 2% technically unsuccessful procedures, 10–15% of procedures do not respond despite technical success and no tissue obtained for pathologic diagnosis
- The risks of UFE are a 1% chance of injury to the uterus, potentially leading to hysterectomy, damage to blood vessels, infection, early-onset menopause (1–5% of women) and allergy to X-ray contrast material (iodine).[14,15]

Magnetic Resonance Guided Focused Ultrasound

Magnetic resonance guided focused ultrasound (MRGFU) is a noninvasive outpatient procedure that uses high intensity focused ultrasound waves to ablate (destroy) the fibroid tissue. During the procedure, an interventional radiologist uses magnetic resonance imaging (MRI) to see inside the body to deliver the treatment directly to the fibroid. The procedure is FDA approved for treating uterine fibroids. Magnetic resonance imaging scans identify the tissue in the body to treat and are used to plan each patient's procedure. It provides a 3D view of the targeted tissue, allowing for precise focusing and delivery of the ultrasound energy. It also enables the physician to monitor tissue temperature in real time, to ensure adequate but safe heating of the target. Immediate imaging of the treated area following MRGFU helps the physician determine if the treatment was successful.[16]

The ultrasound energy used in MRGFU can pass through skin, muscle, fat and other soft tissues. High intensity ultrasound energy that is directed to the fibroid heats up the tissue and destroys it. This method of tissue destruction is called thermal ablation **(Figs 46.17A and B).**

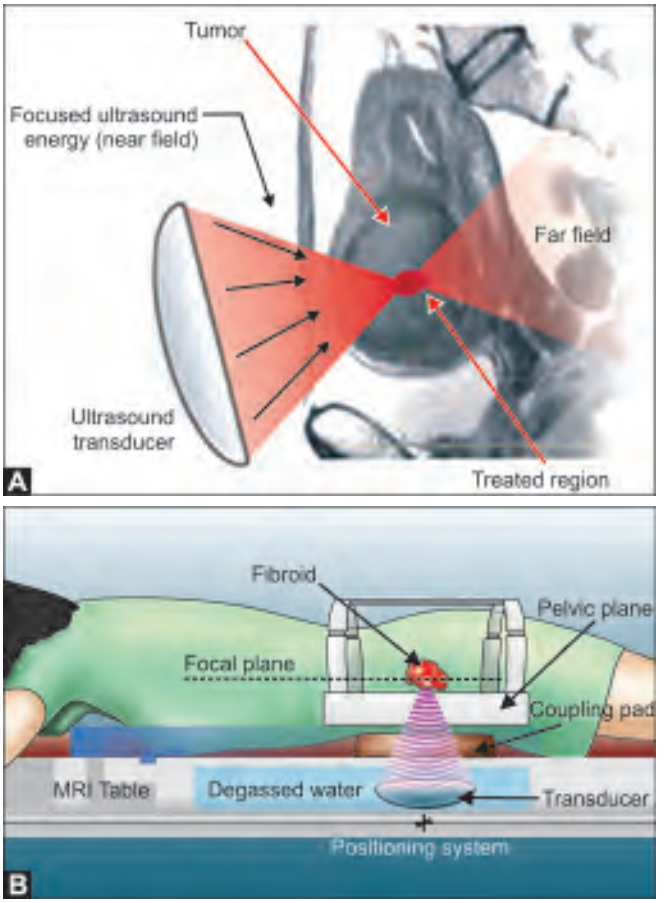

Figures 46.17A and B: Schematic representation of a focused ultrasound surgery

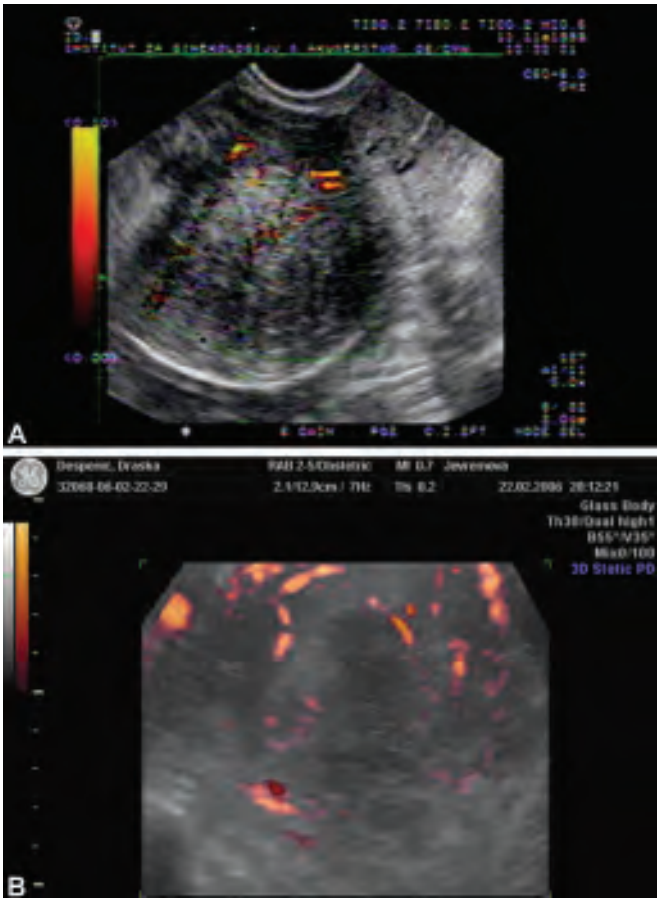

Figures 46.18A and B: (A) Vascularization mapping of fibroid; (B) Glass mode with vascular mapping of fibroid

Ultrasound Guided Fibroid Sclerosation

Several years ago, authors presented a new method of fibroid therapy: sonographically guided vascular sclerosation. Sclerosation was performed under color doppler sonographic visualization, generally after circulation mapping. Sclerosation was performed with 96% alcohol and aetoxisclerol (5–15 ml depending on the fibroid volume). There was no difference in age, size, location, vascularization and degeneration of uterine fibroids. Indication for treatment (bleeding, pain and pressure) showed no difference. Sclerosation was intravascular in 15% and perivascular in 85% of patients. During procedure, pain was present in 20%, burning in 85% and bleeding in 15% **(Figs 46.18A and B)**.

Procedure had to be repeated in 30% and it was done three times in 15% of patients. There was decrease in vascularization (in 85%) and in size (in 95% of patients) after vascular sclerosation. After sclerosation decrease in bleeding occurred in 75% of patients, 65% had less pain and 80% had decreased pelvic pressure. Hospitalization was significantly shorter: 1.5 days and 6.3 days, ICU treatment 0 and 1.5 days, and time to return to work are 3 days and 33 days, in the two groups respectively. Authors have concluded that sonographically-guided vascular sclerosation was safe and effective fibroid treatment. It has less complications and shorter recovery time.[17]

Ultrasound is of great use in making a diagnosis of the uterine fibroids, assessing the circulation, making a treatment choice and monitor the therapy effects.

UTERINE FIBROID AND PREGNANCY

Effects of Pregnancy

Normal rapid uterine expansion that occurs during pregnancy is likely a more complex mechanism mediated in part by estrogen, progesterone, various growth factors especially platelet-derived growth factor and an increase in cells with Ki-67 antigen.[18,19]

These observations support the concept that the same or similar hormonal and growth factors that normally cause uterine growth during pregnancy also stimulate growth of fibroid early in pregnancy. This may serve to explain the paradoxical observations that large fibroids remain unchanged or increase in size late in pregnancy. It is likely that during pregnancy, fibroid estrogen receptors are down regulated due to massive amounts of estrogen. Without effective estrogen receptors and thus estrogen action in the fibroids, epidermal growth factor binding is also decreased.

Effects of Fibroid Size, Location and Number of Pregnancy

Several investigators have attempted to assess the effects of fibroid size, location and number of pregnancy **(Tables 46.5 and 46.6)**.

During the first trimester, fibroids of all sizes either remained unchanged or increased in size (early response due to increased estrogen). During the second trimester, smaller fibroids (2–6 cm) usually remained unchanged or increased in size, whereas larger fibroids become smaller (start of downregulation of estrogen receptors). Regardless of initial fibroid size, during the third trimester, fibroids usually remained unchanged or decreased in size (estrogen receptors downregulated) **(Fig. 46.19)**. The importance of these observations is that an accurate prediction of fibroid growth in pregnancy

TABLE 46.5

Ultrasonically measured changes in fibroids during pregnancy

	Small fibroids[a] (n = 111)			*Large fibroids[b] (n = 51)*		
Trimester	*No change Number (%)*	*Increase Number (%)*	*Decrease Number (%)*	*No change Number (%)*	*Increase Number (%)*	*Decrease Number (%)*
First	7 (58)	5 (42)	0 (0)	1 (20)	4 (80)	0 (0)
Second	42 (55)	23 (30)	11 (15)	11 (38)	4 (14)	14 (48)
Third	14 (61)	1 (4)	8 (35)	5 (29)	2 (12)	10 (59)

[a] Small fibroids = 2.0–5.9 cm
[b] Large fibroids = 6.0–11.9 cm
Modified from Lev-Toaff and coworkers (1987)

TABLE 46.6

Pregnancy complications and relationships of fibroid to placenta

Study	*Complication*	*Fibroid (%)*	
		No contact with placenta	*Contact with placenta*
Winer-Muram et al. (1984)	Bleeding and pain	5/54 (9)	8/35 (23)
	Major complications		
	Abortion	1/54 (2)	9/35 (26)
	Preterm labor	0	5/35 (14)
	Postpartum hemorrhage	0	4/35 (11)
Rice et al. (1989)	Major complications		
	Preterm labor	19/79 (24)	1/14 (7)
	Abruption	2/79 (3)	8/14 (57)
Total	·	48/133 (36)	35/49 (71)

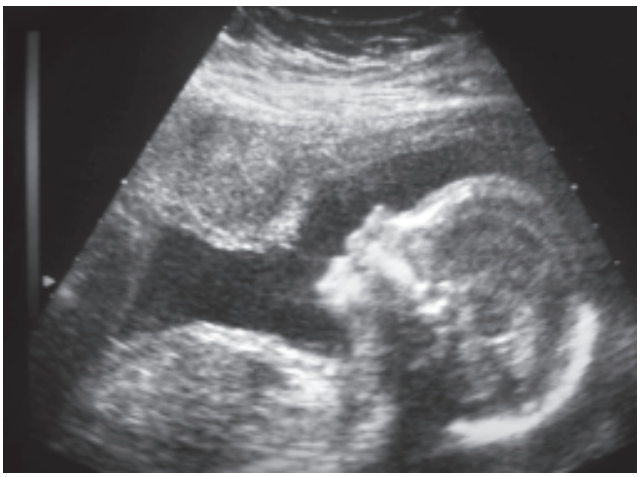

Figure 46.19: Anterior wall fibroid and pregnancy

cannot be made.[20-24] Pregnancy complications associated with uterine fibroids and relationships of fibroid to placenta are elaborated in **Tables 46.6 and 46.7**.

Several conclusions can be delivered:

- Growth of fibroids during pregnancy cannot be predicted
- Placental implantation over or in contact with a fibroid increases the likelihood of placental abruption, abortion, preterm labor and postpartum hemorrhage
- Multiple fibroids are associated with an increased incidence of fetal malposition and preterm labor
- Degeneration of fibroids may be associated with a characteristic sonographic pattern
- The incidence of cesarean delivery is increased.

TABLE 46.7
Pregnancy complications associated with uterine fibroids

Study	*Complications (%)*									
	Antepartum pain and/or bleeding	*Placental abruption*	*Preterm ruptured membranes*	*Preterm labor*	*Abortion*	*Fetal malpresentation*	*Postpartum hemorrhage*	*Obstructed labor*	*Cesarean delivery*	
									Indicated	*Elective*
Winer-Muram et al. (1984)	Table 46.6[a]	NS	NS	5/79 (6)	10/89 (11)	NS	Table 46.6[a]	NS	11/79 (14)	–
Lev-Toaf et al. (1987)										
Uterine corpus	NS	NS	0/68	NS	6/68 (9)	NS	NS	1/68 (2)	11/68 (16)	10/68 (15)
Lower uterine segment	NS	NS	0/68	NS	0/68	NS	NS	8/45 (18)	15/45 (33)	9/45 (20)
Rice et al. (1989)[a]	Table 46.6[a]	10/93 (11)	NS	20/93 (22)	NS	11/93 (12)	NS	NS	26/39 (38)	–
Katz et al. (1989)	Increased	0/28	6/24 (25)	2/24 (8)	2/24 (8)	4/24 (17)	NS	NS	9/24 (38)	–
Hasan et al. (1990)	NS	NS	NS	16/60 (27)	NS	22/60 (37)	10/60 (17)	9/60 (21)	24/60 (40)	20/60 (33)
Davis et al. (1990)	NS	NS	6/85 (7)	15/85 (18)	NS	NS	NS	NS	NS	NS

NS = not started
[a]Additional data presented in Table 46.3

REFERENCES

1. Buttram VC, Reiter RC. Uterine leiomyomata: etiology, symptomatology and management. Fertil Steril. 1981;6:433-45.
2. Lumsden MA, Wallace EM. Clinical presentation of uterine fibroids. Baillieres Clin Obstet Gynaecol. 1998;12:177-95.
3. Valle RF. Hysteroscopy in the evaluation of female infertility. Am J Obstet Gynecol. 1980;137:425-31.
4. Weston GC, Cattrall F, Lederman F, et al. Differences between the pre-menopausal and post-menopausal uterine fibroid vasculature. Maturitas. 2005;51(4):343-8.
5. Ng EH, Chan CC, Tang OS, et al. Endometrial and subendometrial blood flow measured by three-dimensional power Doppler ultrasound in patients with small intramural uterine fibroids during IVF treatment. Hum Reprod. 2005;20(2):501-6.
6. Vitiello D, McCarthy S. Diagnostic imaging of fibroids. Obstet Gynecol Clin North Am. 2006;33:85-95.
7. Janssen J. [(E)US elastography: current status and perspectives]. Z Gastroenterol. 2008;46:572-9.
8. Hobson MA, Kiss MZ, Varghese T, et al. In vitro uterine strain imaging: preliminary results. J Ultrasound Med. 2007;26:899-908.
9. Kiss MZ, Hobson MA, Varghese T, et al. Frequency-dependent complex modulus of the uterus: preliminary results. Phys Med Biol. 2006;51:3683-95.
10. Ami O, Lamazou F, Mabille M, et al. Real time transvaginal elastosonography of uterine fibroids. Ultrasount Obstet Gynecol. 2009;34:486-8.
11. Clark TJ. Outpatient hysteroscopy and ultrasonography in the management of endometrial disease. Current opinion in Obstetrics and Gynecology. 2004;16:305-11.
12. Vercellini P, Cortesi I, Oldani S, et al. The role of transvaginal ultrasonography and outpatient diagnostic hysteroscopy in the evaluation of patients with menorrhagia. Human Reproduction. 2006;12:1768-71.
13. Salim R, Lee C, Davies A, et al. A comparative study of three-dimensional saline infusion sonohysterography and diagnostic hysteroscopy for the classification of submucous fibroids. Human Reproduction. 2005;20(1):253-7.
14. Spies JB, Scialli AR, Jha RC, et al. Initial results from uterine fibroid embolization for symptomatic leiomyomata. Journal of Vascular and Interventional Radiology. 1999;10(9):1149-57.
15. McLucas B, Goodwin S, Adler L, et al. Pregnancy following uterine fibroid embolization. Int J Gynaecol Obstet. 2001;74(1):1-7.

16. Smart OC, Hindley JT, Regan L, et al. Magnetic resonance guided focused ultrasound surgery of uterine fibroids—The tissue effects of GnRH agonist pre-treatment. European Journal of Radiology. 2006;59(2):163-7.
17. Ljubić A, Šulović V. Sonographically guided vascular sclerosation: new method of myoma treatment. Glas SANU. 2002;47:169-79.
18. Mendoza AE, Young R, et al. Increqsed platelet-derived growth factor A-chain expression in human uterine smooth muscle cells during the physiologic hypertrophy of pregnancy. Proc Natl Acad Sci USA. 1990;87(6):2177-81.
19. Kawaguchi K, Fujii S, Konishi I, et al. Immunohistochemical analysis of oestrogen receptors, progesterone receptors and Ki-67 in leiomyomata and myometrium during the menstrual cycle and pregnancy. Virchows Arch A Pathol Anat Histopathol. 1991;419(4):309-15.
20. Lev-Toaff AS, Coleman BG, Arger PH, et al. Leiomyomas in pregnancy: sonographic study. Radiology. 1987;164(2):375-80.
21. Winer-Muram HT, Muram D, Gellieson MS, et al. Uterine myomas in pregnancy. J Assoc Can Radiol. 1984;35:168-70.
22. Davis JL, Ray-Mazumder S, Hobel CJ, et al. Uterine leiomyomas in pregnancy: A prospective study. Obstet Gynecol. 1990;75:41-4.
23. Hasan F, Arumugam K, Sivanesaratnam V. Uterine leiomyomata in pregnancy. Int J Gynaecol Obstet. 1990;34:45-8.
24. Rice JP, Kay HH, Mahony MJ. The clinical significance of uterine leiomyomas in pregnancy. Am J Obstet Gynecol. 1989;160:1212-6.
25. Katz Z, Ben-Arie A, Lurie S. Beneficial effect of hysteroscopic metroplasty on the reproductive outcome in a "T-shaped" uterus. Gynecol Obstet Invest. 1996;41:41-3.

47
CHAPTER

Three-Dimensional Static Ultrasound and 3D Power Doppler in Gynecologic Pelvic Tumors

Juan Luis Alcázar

INTRODUCTION

Pelvis tumors from gynecologic origin are common disorders in clinical practice. Ultrasound has been used largely for the differential diagnosis of pelvic tumors, such as endometrial, myometrial and adnexal pathologies.

In the case of endometrial cancer, the measurement of endometrial thickness has been proved to be an effective method to exclude malignancy.[1] However, a thickened endometrium is a nonspecific finding. The use of pulsed Doppler remains controversial[2,3] and for this reason some authors have advocated the use of color mapping for differentiating endometrial cancer from other benign conditions.[4] However, this approach is only reproducible in experienced hands.[5]

Uterine myomas are a very common benign disease. The diagnosis use to be easy by ultrasound[6] and there is evidence that uterine blood flow is increased in the presence of fibroids.[7] Some authors have stated that the use of color Doppler may discriminate benign fibroids from uterine sarcomas.[8] However, other authors have challenged this concept.[9,10]

Cervical cancer has been largely obviated from the assessment by ultrasound. However, recently the assessment of tumor vascularization in cancer of the uterine cervix has gained attention from researches, because some studies have shown that it may be possible to predict therapeutic response to neoadjuvant chemotherapy or chemoradiation.[11,12]

Adnexal masses are probably one of the most frequent problems in gynecology. Patients with questionable adnexal tumors should be referred to a gynecologic oncologist specialist[13] whereas benign tumors should be treated by laparoscopic surgery by general gynecologist[14] or even managed expectantly.[15] Morphological ultrasound assessment of adnexal masses can be considered as the primary imaging modality to be used because of its high sensitivity. However, false-positive rate remains high.[16] The role of pulsed Doppler is still controversial.[17]

Some authors have proposed a simpler approach by just looking tumor blood flow mapping with encouraging results.[18]

In the last years, three-dimensional ultrasound (3D USG) has become available in clinical practice, opening a formidable research area.[19]

The objective of the present chapter is to review current evidence of the use of 3D USG and three-dimensional power Doppler ultrasound (3D PD-USG) in the evaluation of pelvic gynecologic tumors.

ENDOMETRIAL CANCER

Few studies have evaluated the role of 3D ultrasound in the diagnosis and assessment of endometrial cancer.

Three-dimensional ultrasound allows the assessment of endometrial volume **(Figs 47.1 and 47.2)**. In our experience, this measurement is highly reproducible.[20] The intraobserver intraclass correlation coefficient (ICC) is 0.97 and the interobserver ICC is 0.70.

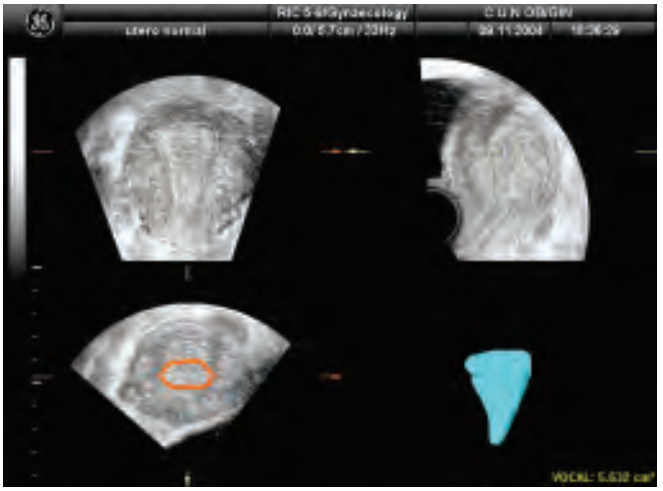

Figure 47.1: Endometrial volume calculation by using the VOCAL rotational method

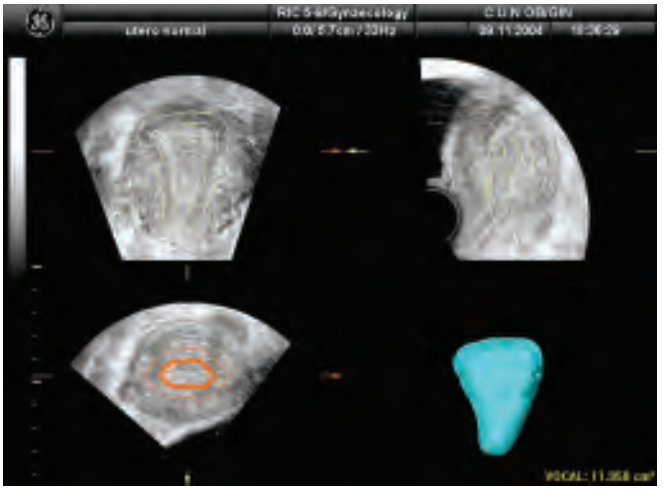

Figure 47.2: Subendometrial area volume calculation by using the VOCAL rotational method

Gruboeck compared the diagnostic performance of endometrial thickness and endometrial volume in a series of 103 women with postmenopausal bleeding.[21] They found that both mean endometrial thickness (29.5 mm versus 15.6 mm) and endometrial volume (39.0 ml versus 5.5 ml) were significantly higher in women with endometrial cancer as compared with those with benign conditions. Using a cutoff of 15 mm for endometrial thickness and 13 ml for endometrial volume, this parameter was more sensitive (100% versus 83%) and had a higher positive predictive value (91.7% versus 54.5%).

Kurjak et al.[22] evaluating a series of 41 women with suspected endometrial pathology obtained similar results. They reported that endometrial volume as well as endometrial thickness was significantly higher in women with endometrial cancer as compared with those patients with benign conditions such as polyps, endometrial hyperplasia or cystic atrophy.

More than one decade later, Mansour et al. reached the same conclusions than Gruboeck et al. comparing endometrial volume and thickness in a series of 170 women with postmenopausal bleeding.[23] However, these authors reported that the best cutoff for endometrial volume was 1.35 ml with a sensitivity of 100% and a false-positive rate of 29%, much higher than that reported by Gruboeck. An explanation for that is that Mansour's study included patients with "endometrial atypia" in the group of endometrial cancer.

However, Yaman et al. found that endometrial volume was more specific than endometrial thickness in a series of 213 women, 42 with endometrial cancer.[24] With a cutoff of 2.7 ml, sensitivity was 100% and specificity was 69%. Odeh et al.[25] and Merce et al.[26] have reported similar findings.

Opolskiene et al. did not find differences between endometrial volume and thickness in the terms of sensitivity and specificity for diagnosing endometrial cancer.[27]

In our experience,[28] in a series of women with postmenopausal bleeding and thickened endometrium (≥ 5 mm) we also found that endometrial volume was significantly higher in endometrial cancer as compared with polyps or hyperplasia **(Fig. 47.3)**. In agreement with previous authors endometrial volume is more specific than endometrial thickness **(Fig. 47.4)**.

These studies are summarized in **Table 47.1**.

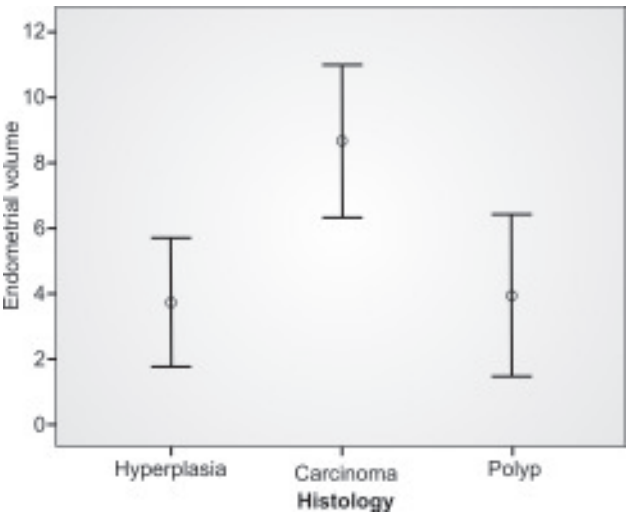

Figure 47.3: Mean endometrial volume with 95% CIs in endometrial cancer, hyperplasia and polyps

TABLE 47.1

Endometrial volume compared with endometrial thickness for diagnosing endometrial cancer in women with postmenopausal bleeding

Author	*N*	*EC prevalence*	*Cutoff*	*Endometrial thickness*		*Endometrial volume*	
				Sensitivity	*Specificity*	*Sensitivity*	*Specificity*
Gruboeck [21]	97	11%	ET 15.0 mm EV 13 cc	83%	88%	100%	99%
Mansour [23]	170	16%	EV 1.35 mL			100%	71%
Yaman [24]	213	20%	ET 7.0 mm EV 2.70 mL	100%	43%	100%	69%
Odeh [25]*	56	20%	ET 5.5 mm EV 3.56 mL	97%	12%	93%	36%
Merce [26]†	84	65%	ET 12.1mm EV 6.86 mL	69%	55%	63%	69%
Alcazar [28]‡	99	44%	ET 7.6 mm EV 2.30 mL	90%	36%	93%	62%
Opolskiene [27]‡	62	20%	ET 11.8 mm EV 5.30 mL	85%	71%	69%	88%

EC: Endometrial cancer. ET: endometrial thickness. EV: endometrial volume
* Endometrial hyperplasia and cancer included in the same "pathologic" group
† Retrospective study assessing only women with endometrial hyperplasia and cancer.
‡ Prospective study including only women with thickened endometrium

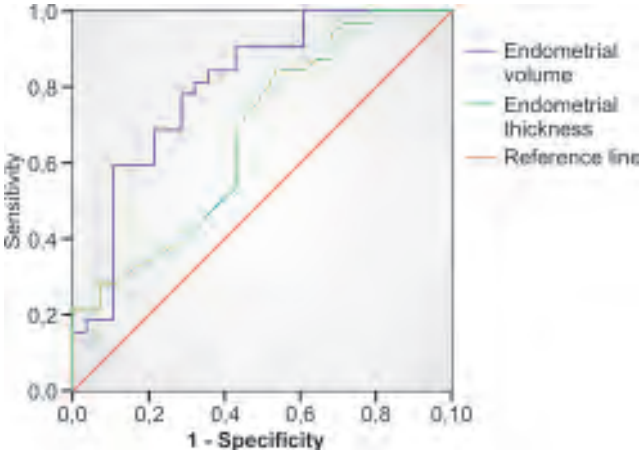

Figure 47.4: Receiver-operating characteristics (ROC) curves for endometrial thickness and endometrial volume for detecting endometrial cancer in women with postmenopausal bleeding

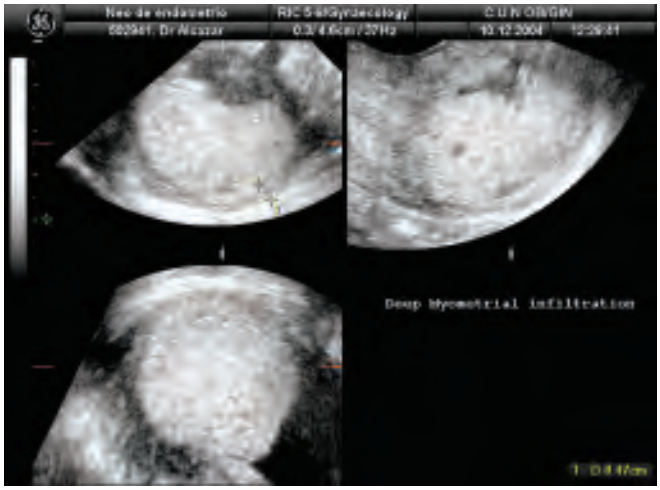

Figure 47.5: Estimation of myometrial invasion in endometrial cancer by using 3D multiplanar navigation. In this case infiltration is considered as deep

The use of 3D ultrasound has been also found to be effective to assess myometrial invasion in endometrial cancer by analyzing the myometrial-endometrial interface and to estimate the maximum penetration of the tumor within the myometrium[29,30] **(Figs 47.5 and 47.6)**. Our group described and analyzed the diagnostic performance of a new method for assessing myometrial infiltration preoperatively based on 3D ultrasound.[31] This new approach was based on a 3D virtual navigation through the uterus for detecting the deepest point

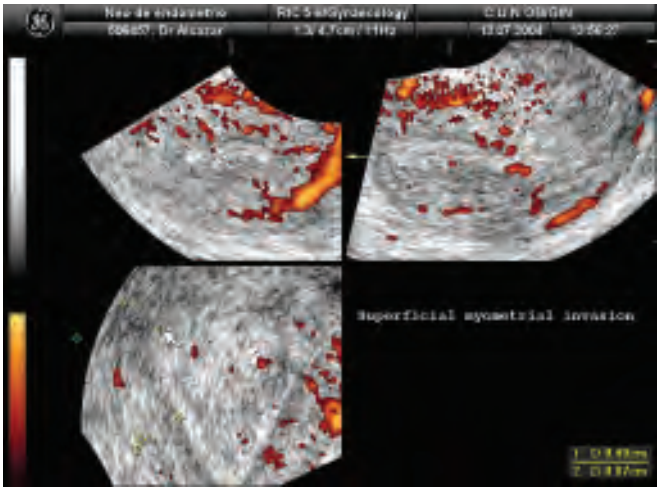

Figure 47.6: Estimation of myometrial invasion in endometrial cancer by using 3D multiplanar navigation. In this case infiltration is considered as superficial

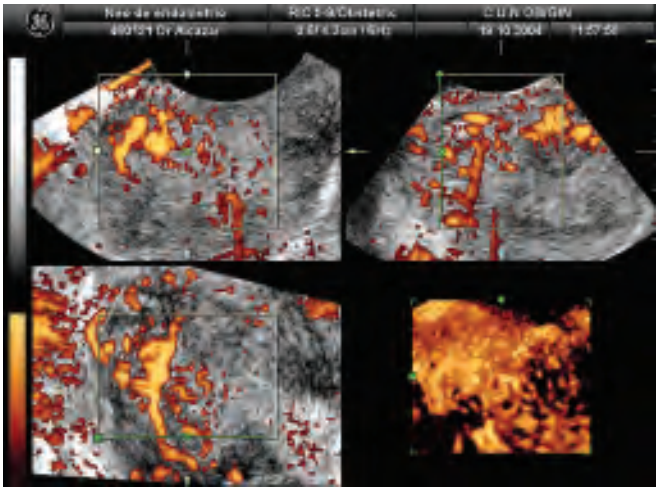

Figure 47.7: Three-dimensional power Doppler depiction of vascular architecture in a case of endometrial cancer. Chaotic pattern is clearly seen

of myometrial infiltration in a series of 96 women with endometrial cancer. Sixty-nine women had < 50% myometrial infiltration on histologic analysis and 27 had ≥ 50% myometrial infiltration. The most interesting finding from this study was the negative predictive value reported (100%) using this approach. The false-positive rate reported was 39%. The reproducibility of the method was good.

Another possibility for 3D ultrasound is the assessment of tumor vascularity by 3D PD.[32] This technique allows the depiction of vascular network in endometrial lesions as well as the estimation of three vascular indexes (VI, FI and VFI) by the VOCAL™ rotational method. Vascular network in malignant tumor used to be irregular with chaotic branching, changes in vessels caliber, pseudoaneurysms **(Figs 47.7 and 47.8)**. On the other hand, these features used to be absent in benign conditions such as polyp **(Fig. 47.9)** or hyperplasia **(Fig. 47.10)**.

Kupesic et al. reported that assessing the vascular network by 3D PD they were able to determine correctly the depth of myometrial invasion in 21 out of 22 women with endometrial cancer.[33] They assessed the presence of chaotic vessels in the endometrial-myometrial interface. Depending on whether more than half or less than half of the myometrium was involved by these chaotic vessel, patients were considered as having deep or superficial myometrial invasion **(Fig. 47.11)**.

The use of vascular indexes **(Figs 47.12A to C)** has not been extensively assessed. Odeh et al. reported that all three 3D PD indexes were significantly higher in women with endometrial cancer as compared with those

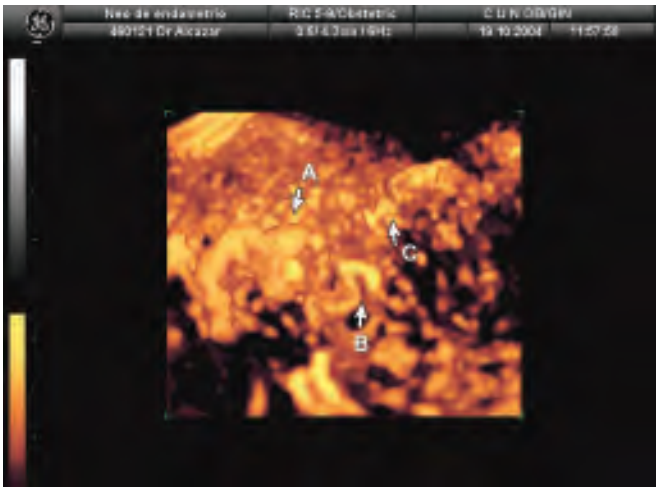

Figure 47.8: Same as Figure 47.7. Different vessel caliber (A), abnormal branching (B) and mycroaneurysms (C) are seen

with benign pathology.[25] However, they did not compare with conventional 2D PD and the specificity reported was low. Mercé et al. found that 3D PD indexes were significantly higher in women with endometrial cancer as compared with those with endometrial hyperplasia.[26] Alcázar et al. also found that 3D PD indexes were significantly higher in women with endometrial cancer as compared with those with benign pathology,[28] but this study included only women with endometrial thickness above 5 mm and did not compare 3D results with conventional 2D color Doppler. Opolskiene et al. reported data in a series of women

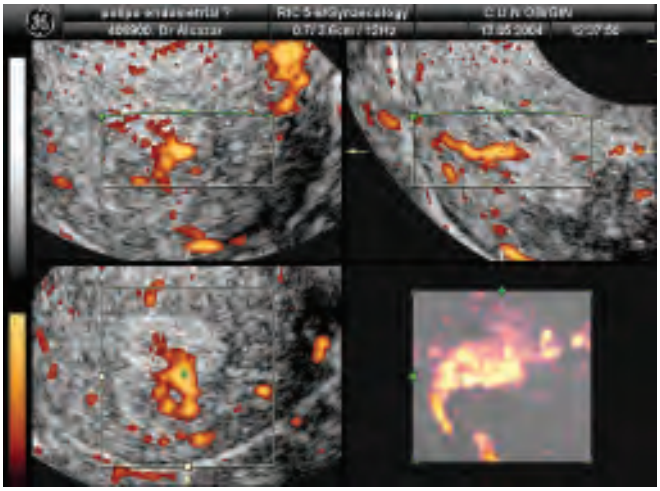

Figure 47.9: Vascular pattern for an endometrial polyp. A single predominant vessel is seen within the lesion

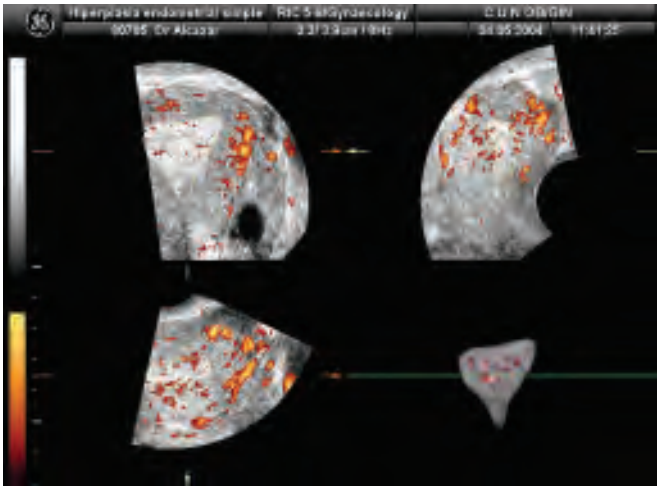

Figure 47.10: Vascular pattern for endometrial hyperplasia. Scattered vessels can be seen within the endometrium

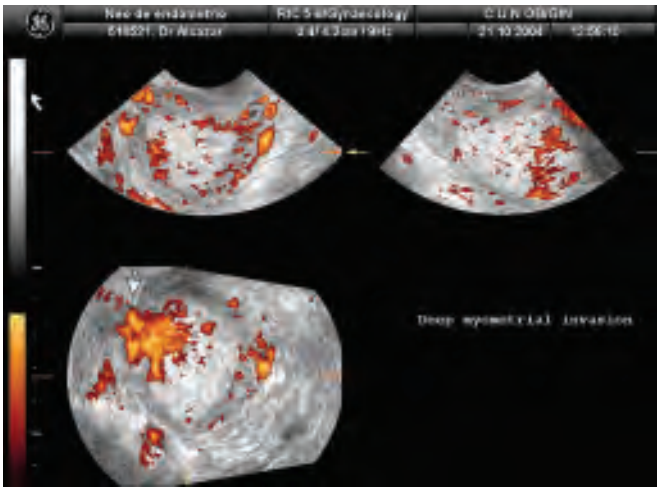

Figure 47.11: Assessment of myometrial invasion by three-dimensional power Doppler. In this case, deep myometrial infiltration was considered at the level of the right uterine cornu

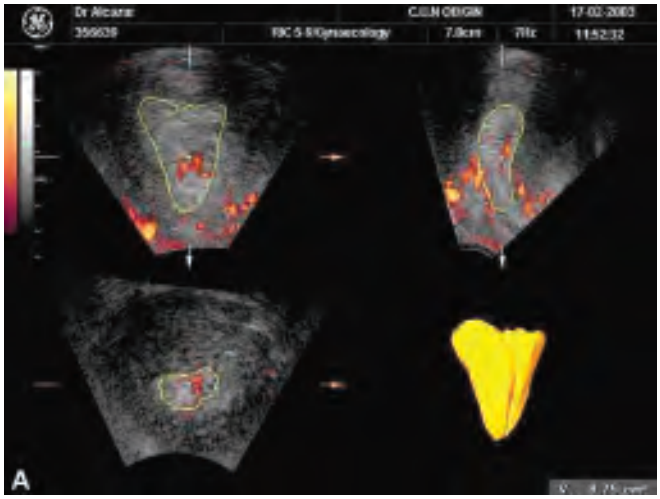

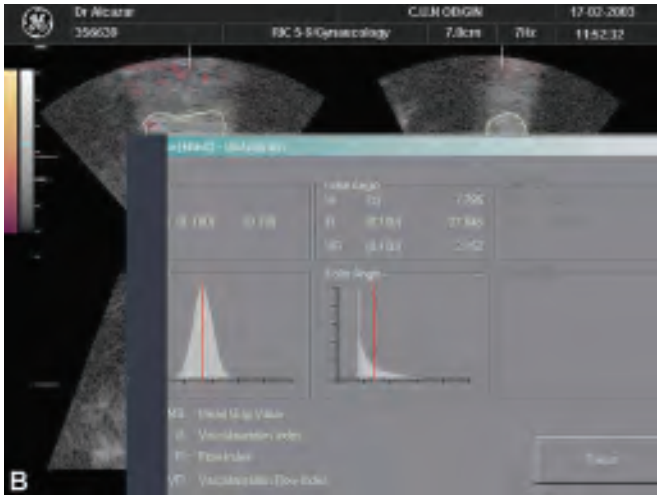

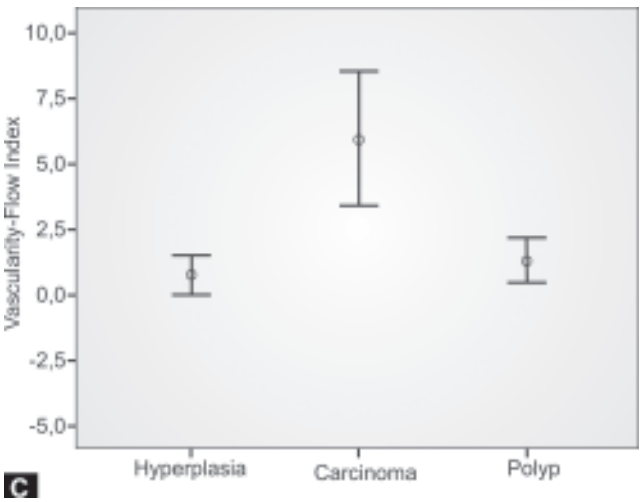

Figures 47.12A to C: Three-dimensional power Doppler volume and indices calculated in a case of endometrial cancer

with postmenopausal bleeding and endometrial thickness ≥ 4.5 mm.[27] They concluded that although 3D PD indexes were significantly higher in women with endometrial cancer as compared with those with benign pathology, this technique adds little information to endometrial thickness or volume. Lieng et al. analyzed a small series of women with endometrial polyps (n = 17) and endometrial cancer (n = 17) comparing 3D PD indexes within the lesions before and after contrast-enhanced examination.[29] They did not find differences between groups in 3D PD indexes.

Galvan et al. assessed the correlation between intratumoral 3D PD indexes and several histological tumor characteristics in a series of 99 women with endometrial cancer.[34] In their analysis endometrial volume and vascularization index were independently associated with myometrial infiltration and tumor stage, vascularization index was independently associated with tumor grade and endometrial volume correlated with lymph node metastases.

In conclusion, endometrial volume seems to be a better predictor for endometrial cancer than endometrial thickness in women with postmenopausal bleeding. Three-dimensional power Doppler assessment of endometrial vascularity is reproducible and seems to be useful for differentiating endometrial cancer than benign endometrial conditions. Its performance seems to be better than endometrial volume. This technique also seems to be useful to predict some histological features of endometrial cancers, especially myometrial invasion.

UTERINE LEIOMYOMAS AND SARCOMAS

Uterine fibroids are the most common pelvic tumors of women in reproductive age. The sonographic appearance of uterine leiomyomas use to be a hypoechoic rounded or oval well-defined lesion arising from the myometrium. Sometimes, some secondary changes may occur with a wide spectrum of ultrasonic images.

The use of 3D ultrasound in the assessment of uterine fibroids has been evaluated in few studies.

Salim and coworkers found that 3D sonohysterography is very useful to classify submucous myomas and the agreement with the hysteroscopic classification is high (Kappa index = 0.81) **(Fig. 47.13)**.[35]

We also have found that 3D multiplanar display of submucous myomas is very useful to determine the myometrial safety margin prior to hysteroscopic resection **(Fig. 47.14)**.

The assessment of leiomyoma vascularity by 3D PD ultrasound allows the assessment of its vascular network. This assessment clearly shows that typical vascular network of uterine fibroids has a "nest" appearance **(Fig. 47.15)**. Their findings are in agreement with those studies based on corrosion analysis of vascular network.[36]

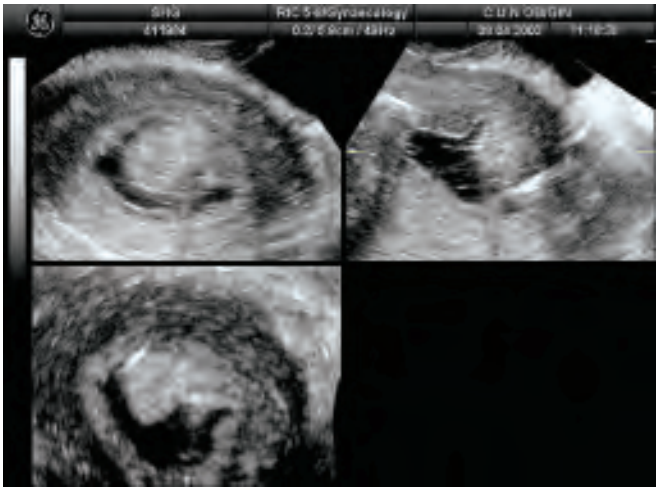

Figure 47.13: Three-dimensional sonohysterography in a case of submucous myoma

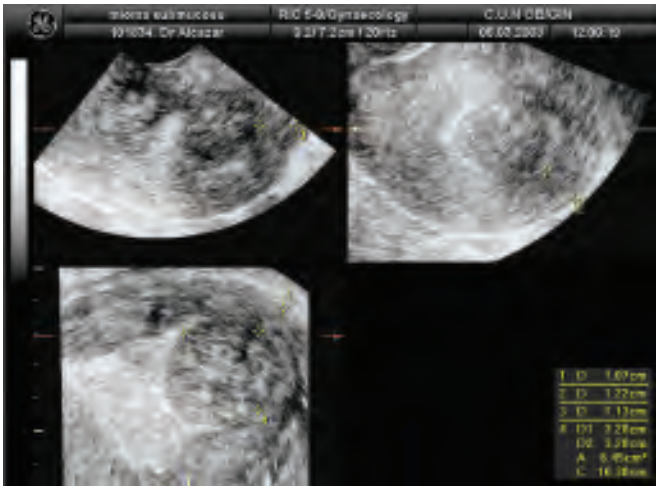

Figure 47.14: Estimation of safety margin for hysteroscopic resection in a case of submucous myoma using 3D multiplanar navigation

One possible clinical application of this technique is its use for predicting response to medical treatment. Muñiz et al. assessed 15 women with uterine fibroids prior to uterine artery embolization by 3D PD USG[37] and concluded that this technique can reveal collateral blood flow not detected by uterine artery arteriography and could predict response to treatment.

Exacoustos evaluated and compared the role of 2D and 3D ultrasound before, during and after laparoscopic

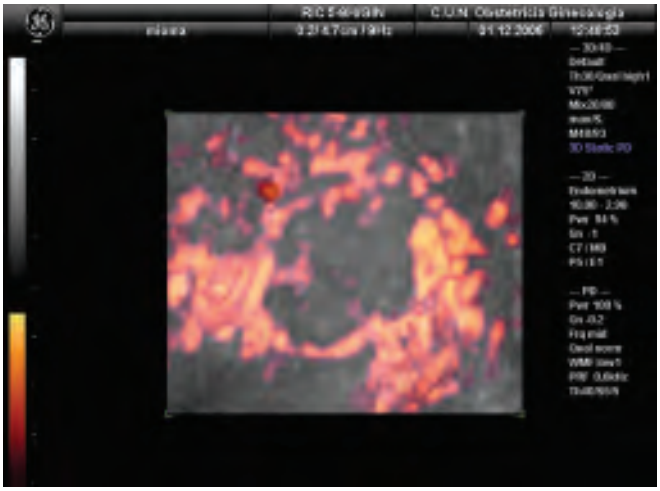

Figure 47.15: "Nest" appearance of the vascular network of uterine fibroid by 3D PD

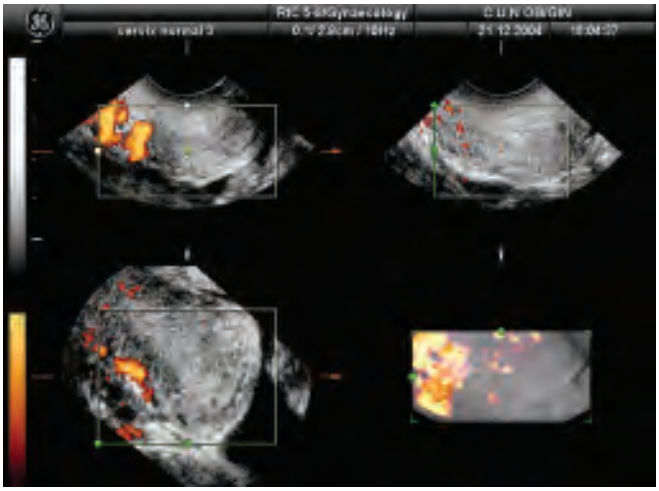

Figure 47.17: Three-dimensional power Doppler appearance of cervical vascularity in a case of uterine cervix without pathology

cryomyolysis in 10 women with uterine fibroid.[38] The authors used a semi-quantitative assessment of blood flow at the level of the fibroid capsule and inside the tumor. This study found that both, 2D and 3D power Doppler ultrasound was useful to assess fibroid vascularization but 3D power Doppler were best to evaluate such an evaluation.

The preoperative diagnosis of uterine sarcoma remains a formidable clinical challenge. Attempts have been made for such diagnosis using 3D PD USG. Kupesic et al. reported that typical vascularization of uterine sarcoma was characterized by irregular vessels that were randomly dispersed both in central parts of the tumor.[39] However, this findings can also be found in growing large benign fibroids **(Fig. 47.16)**.

In conclusion, 3D PD USG seems to be a potential tool for predicting response to medical treatment of uterine fibroids and to assess their growth potential. Its role in the diagnosis of uterine sarcoma remains to be established.

CERVICAL CANCER

Suren and co-workers were the first to report the assessment of intracervical vascularization by 3D PD USG.[40] They found that the typical finding in cases of cervical cancer a chaotic network with tortuous vessels as compared with benign conditions in which the course of vessels has a regular structure **(Figs 47.17 and 47.18)**.

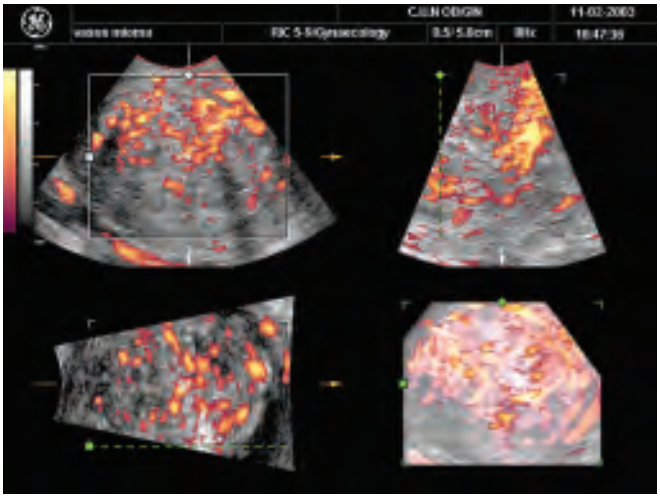

Figure 47.16: Chaotic vascular network in a fast growing uterine fibroid

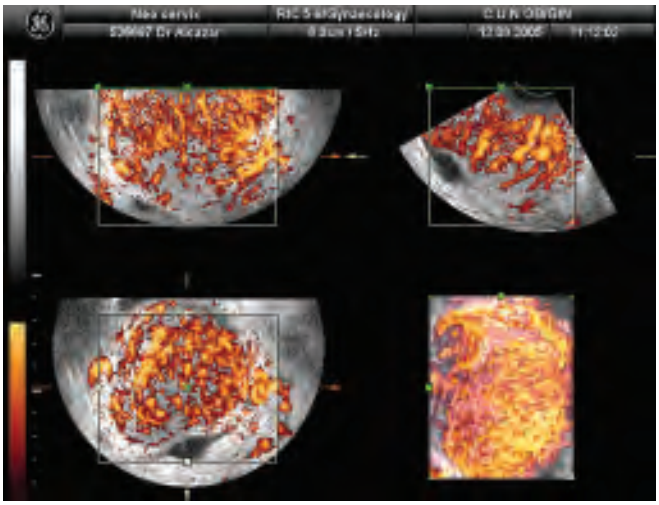

Figure 47.18: Three-dimensional power Doppler appearance of cervical vascularity in a case of uterine cervical cancer

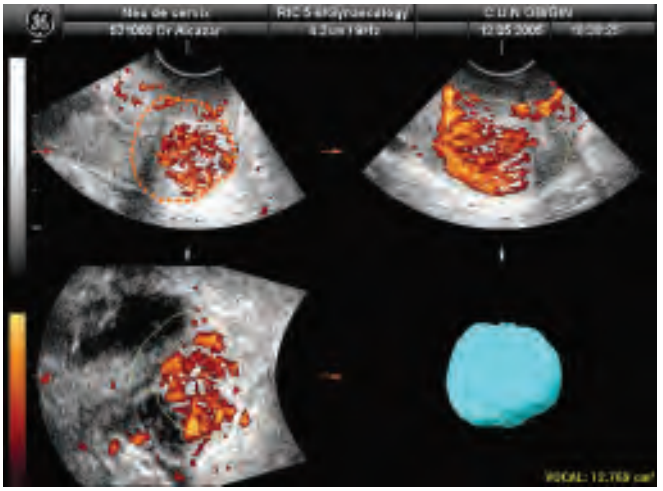

Figure 47.19: Tumor volume calculation in cervical cancer by using the VOCAL rotational method

Figure 47.20: Three-dimensional power Doppler indices calculated in a case of cervical cancer

This technique can assess precisely tumor volume and vascularization **(Figs 47.19 and 47.20)**.

Hsu et al.[41] analyzed 141 women with early stage cervical cancer. They described four types of intratumoral vascularity patterns, which were not correlated with vascularization index (VI), vascularization flow index (VFI) and flow index (FI) values: localized, peripheral, scattered and single-vessels types. Tumor volume was related to FI ($r = 0.373$, $p < 0.001$), but not with VI or VFI. They concluded that this technique was a useful tool to investigate intratumoral vascularization.

However, Testa et al.[42] did not find differences in 3D power Doppler blood flow parameters in cervical cancer according to tumor diameter, tumor grade and histological type. They found a marginal statistical significant according to tumor stage, being III/IV stages more vascularized than I/II stages tumors.

In our experience, a progressive increase in VI, VFI and FI exists in patients with no cervical pathology, intraepithelial neoplasia and invasive cervical cancer.[43] We reported data on 56 women with cervical cancer.[44] No correlation was found between tumor volume and 3D-PDA indexes with histologic type, lymphovascular space invasion (LVSI) and lymph node metastases. Moderately and poorly differentiated tumors and advanced stage tumors had larger volume and higher 3D-PDA indexes.

Although the clinical value of 3D-PDA assessment of tumor vascularization in cervical cancer still needs to be established all these studies pointed out that the noninvasive assessment of tumor vascularity prior to treatment could be useful to identify high-risk patients for recurrence. In fact, some preliminary data show that it may be useful for assessing tumor response to chemoradiation in advanced cancer.[45]

One study described a novel technique using 3D ultrasound for local staging of cervical carcinoma.[46] This method was based on the multiplanar display and was used in 14 women. The concordance of 3D ultrasound and pathology for assessing parametrial, rectum and bladder involvement was 93%, 93% and 100%, respectively.

Adnexal Tumors

Three-dimensional ultrasonography overcomes some limitations of conventional 2D ultrasound allowing a more detailed assessment of morphologic features of the object studied, with no restriction to the number and orientation of the scanning planes.

Among the advantages of 3D ultrasound are the possibilities of obtaining images from all spatial planes and eliminate echoes by using the "threshold" function. The first allows a more detailed assessment of intracystic structures and the second allows eliminating internal echoes mimicking solid tissue, such as clots, debris and fatty and mucinous plugs **(Fig. 47.21)**. In our experience, surface rendering was the most useful mode for 3D TVS evaluation **(Fig. 47.22)**. The "niche mode" may be also helpful in some instances **(Figs 47.23A and B)**. However, some pitfalls when using 3D transvaginal ultrasound (TVS) might be born in mind. By using the surface rendering mode alone some daughter cysts may be interpreted as solid areas. On the other hand, threshold function works similarly to gain in conventional 2D ultrasound. An excessive gain adjusting may eliminate some true solid areas, leading to reclassify as benign an actually malignant lesion.

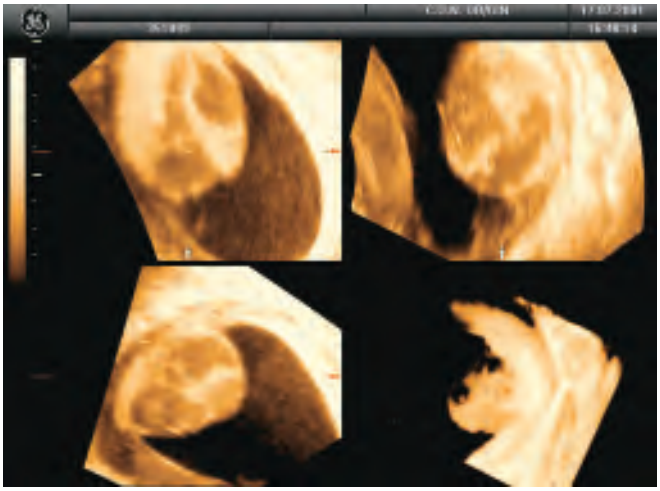

Figure 47.21: The use of the "threshold" function allows eliminating some internal echoes in a case of cystic dermoid tumor

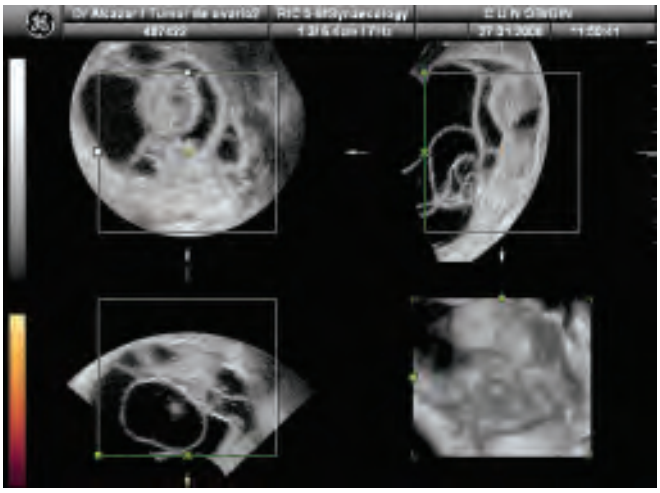

Figure 47.22: Three-dimensional surface rendering of the internal appearance in an ovarian multilocular cyst with solid components

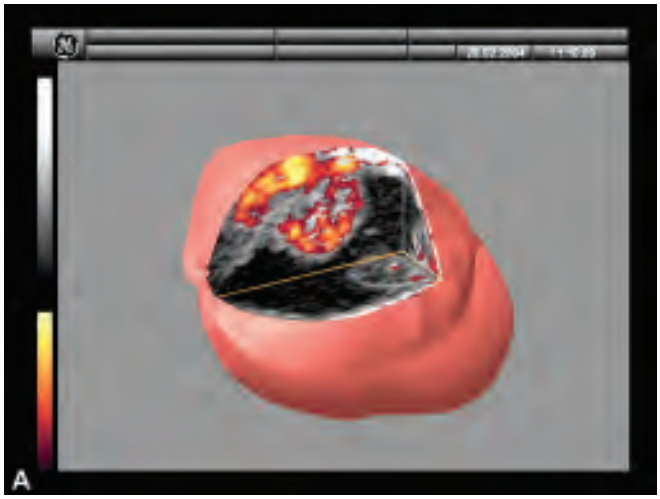

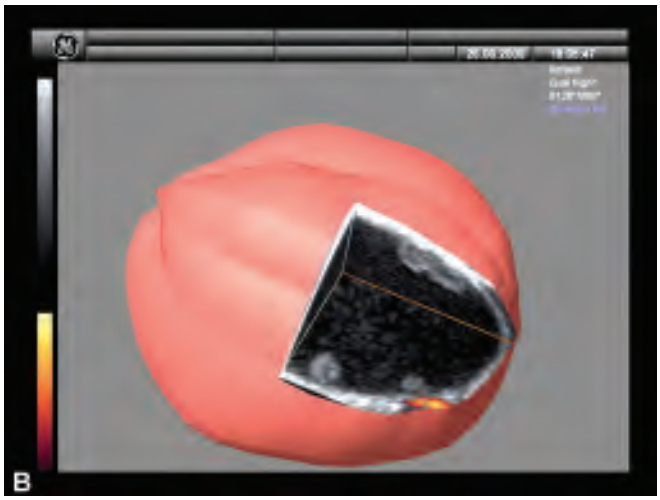

Figures 47.23A and B: Two cases of ovarian cyst with a gross papillary projection. In case A "niche" mode allows confirming that vessels coming from the cyst wall enter the papillary projection. In case B, it can be seen how no vessels appear within the papillary projection. (*Courtesy:* Dr MA Pascual)

A new image display modality is the "inversion mode," which can be depicted as "solid," the cystic components of the tumor. This could be helpful in predominantly cystic complex lesions such as hydrosalpinx **(Fig. 47.24)**.

Studies evaluating the role of 3D TVS in assessing adnexal masses are scanty and reported controversial results **(Table 47.2)**.

Bonilla-Musoles and colleagues evaluated by 2D and 3D ultrasonography, 76 women diagnosed as having an adnexal mass. They concluded that 3D TVS was more sensitive than 2D TVS.[47]

Hata and co-workers compared 3D TVS with 2D TVS in 20 patients with adnexal masses. They found that 3D TVS was more specific than 2D TVS.[48]

More recently, Kurjak reported the results of a study comparing five different sonographic techniques in a series of 251 adnexal tumors. They found 3D TVS more sensitive than 2D TVS with similar specificity.[22]

We found that 3D ultrasonography had not statistically better diagnostic performance than 2D in a series of 44 selected complex adnexal masses.[49] We found 3D TVS useful to reinforce initial diagnostic impression. In a second series, we found similar results

TABLE 47.2

Three-dimensional versus two-dimensional ultrasound for diagnosing ovarian cancer

Author	*N*	*OC prevalence*	*Sensitivity*		*Specificity*		*P value*
			3D	*2D*	*3D*	*2D*	
Bonilla [47]	76	7%	100%	80%	100%	99%	< 0.05
Hata [48]	20	25%	100%	100%	92%	38%	< 0.05
Alcazar [49]	49	48%	100%	90%	78%	61%	NS
Alcazar [50]	82	33%	93%	89%	98%	94%	NS

OC: Ovarian cancer 2D: Two-dimensional ultrasound. 3D: Three-dimensional ultrasound. N.S: statistically non-significant

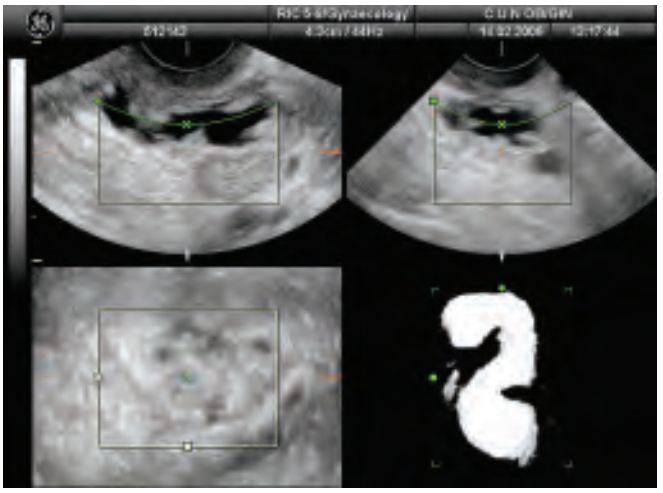

Figure 47.24: Three-dimensional reconstruction of a hydrosalpinx by using the "inversion mode". The shape of the tube is clearly shown

to the previous one.[50] In this second study, we showed that 3D USG had a good intra- and interobserver reproducibility for assessing adnexal masses.[50]

These controversial results might be explained by the fact that in the first two studies the number of malignant tumors was small and probably because all of them, except ours, included many not complex tumors. On the other hand, the sonographic criteria for malignant suspicion on 3D USG were the same than in 2D USG.

With the advent of 3D USG, 3D PD imaging has also become available for clinical practice. This technique allows tumor vascularization assessment, both quantitatively by means of 3D PD USG-derived vascular indexes and qualitatively by depicting three-dimensionally the tumor vascular network.

Kurjak et al. in two different studies on 120 and 90 adnexal masses, respectively, concluded that 3D PD was superior to conventional color Doppler by increasing the sensitivity.[51,52] This same group found that the use on sonographic contrast agents would improve even more the performance of 3D Power Doppler.[53] They compared a scoring system that included some morphological features and 3D PD evaluation of tumor vessels characteristics, such as vessels arrangement and branching pattern, with another scoring system that included the same morphological features with pulsed Doppler velocimetric parameters (RI ≤ 0.42 or > 0.42). They based their diagnostic criteria for malignancy suspicion on vessel architecture as depicted by 3D such as branching pattern, vessel caliber and presence of microaneurysms or vascular lakes **(Figs 47.25 and 47.26)**. This was based on the chaos theory,[54] which establish that vascular architecture of a vascular network of newly formed vessels in malignant tumors is built following a chaotic distribution but not in a predetermined fashion. Although, this has been demonstrated in corrosion studies,[55] the reproducibility of this approach is just moderate.[56]

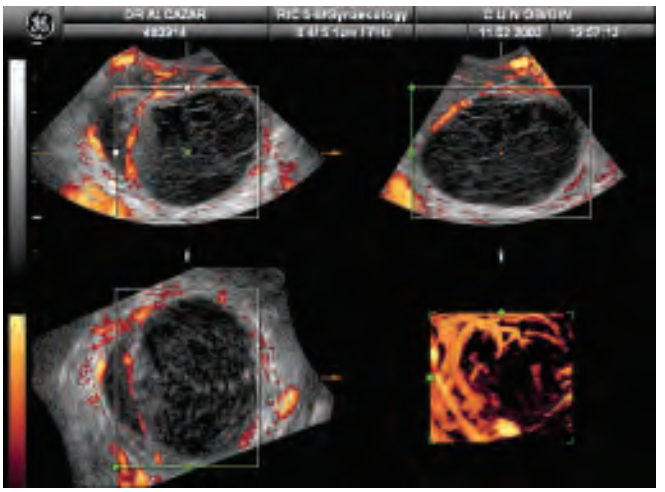

Figure 47.25: Three-dimensional power Doppler depiction of the vascular network from a benign ovarian cystic tumor

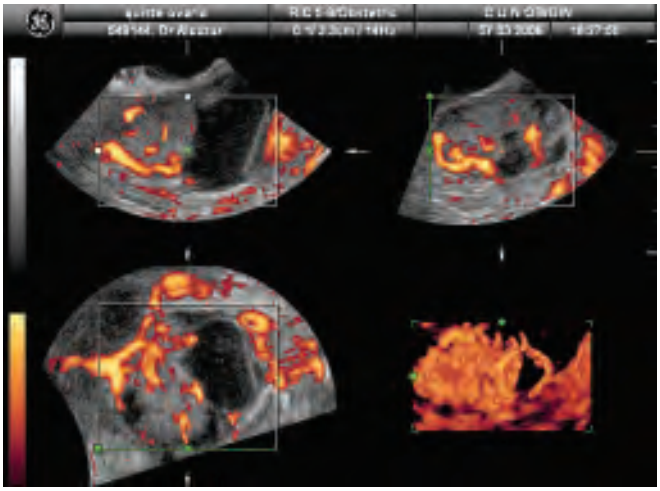

Figure 47.26: Three-dimensional power Doppler depiction of the vascular network from a malignant ovarian tumor

Several subsequent studies, using all of them similar criteria for malignancy suspicion, reported similar findings: 3D PD vascular tree assessment adds little to conventional ultrasound.[57-60] These studies are summarized in **Table 47.3**.

Cohen et al. evaluated the role of 3D PD in a series of 71 complex adnexal masses on 2D TVS.[61] They did not use 2D conventional color Doppler nor 2D PD. In their approach, they combined 2D and 3D morphological features with 3D PD evaluation of blood flow tumor location, considering a tumor as malignant in the presence of complex morphological pattern and central (in papillary projections and/or septations) blood flow location. They concluded that the addition of 3D PD improved the specificity of 2D TVS (75% versus 54%), without decreasing the sensitivity. Similar results have been recently reported by Geomini et al.[62] These results are not surprising and can be achieved also by using a simpler technique such as color Doppler.[18]

We found that the diagnostic performance of 3D PD was not statistically better than that of 2D PD in a series of 69 complex adnexal masses, presenting both techniques similar sensitivity (97.8% for both techniques) and specificity (87% versus 79%).[63] We compared the 2D PD diagnostic criteria proposed by Guerriero et al.[18] with the 3D PD diagnostic criteria proposed by Kurjak et al.[22]

However, when a complex mass with detectable blood flow within solid areas or thick papillary projections is found, it should be categorized mass as "malignant" or "highly suspicious". However, a considerable number of benign tumors may exhibit this appearance, for example, cystadenofibroma, tubo-ovarian abscess or solid benign ovarian tumor.

Using conventional 2D color or power Doppler we have no means to differentiate these benign entities from true malignant tumors. Three-dimensional Power Doppler ultrasound provides a new approach to assess tumor vascularization. We have termed this new approach "3D PD vascular sampling".[64] It consists of assessing the vascularization of a given suspicious area in a given tumor by calculating 3D PD-derived indexes within these areas **(Figs 47.27 and 47.28)**. In a series of 49 vascularized complex adnexal masses, we found that 3D PD-derived indexes were significantly higher in

TABLE 47.3

Three-dimensional power Doppler tumor vascular tree assessment for diagnosing ovarian cancer

Author	*N*	*OC prevalence*	*Sensitivity*		*Specificity*		*P value*
			3D PD	*2D*	*3D PD*	*2D*	
Kurjak [51]†	120	9%	100%	91%	99%	97%	N.S.
Kurjak [52]†	90	10%	100%	89%	99%	37%	N.S
Laban [57]†*	50	62%	100%	100%	74%	74%	N.S
Sladkevicius [58]‡	104	26%	96%	100%	96%	90%	N.S
Alcazar [56]§	39	51%	90%	95%	74%	74%	N.S.
Dai [59]§*	36	83%	77%	97%	50%	50%	< 0.05
Mansour [60]§	400	62%	88%	94%	89%	73%	N.S

OC: Ovarian cancer. 2D: Two-dimensional ultrasound. 3D PD: Three-dimensional power Doppler. N.S: statistically non-significant
† Criteria for malignancy suspicion: Scoring system combining morphology and 3D PD features
‡ Criteria for malignancy suspicion: Logistic model combining morphology and 3D PD features
§ Criteria for malignancy suspicion: only 3D PD features
* Only "complex" masses included in the study

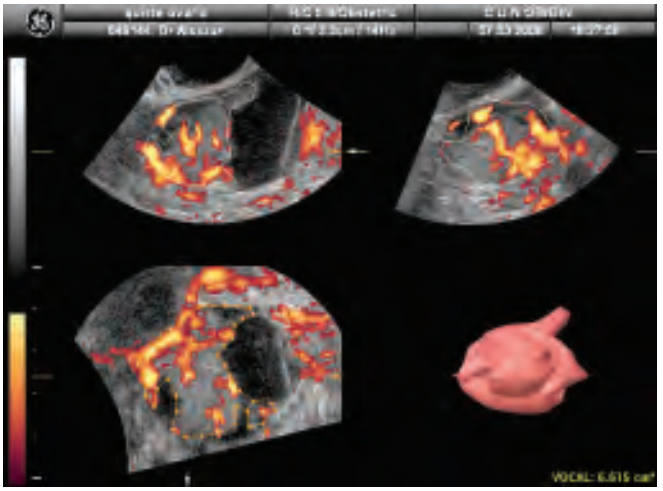

Figure 47.27: Volume calculation from the solid portion from a cystic-solid ovarian tumor

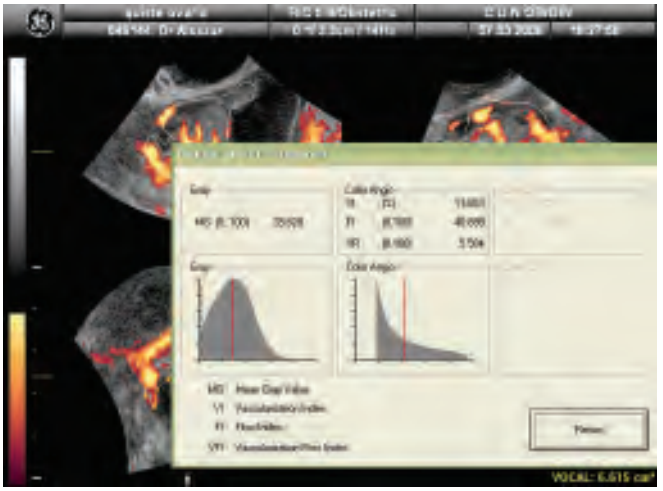

Figure 47.28: Three-dimensional power Doppler derived vascular indices from the solid component (vascular sampling) from the case of the previous figure

malignant tumors as compared with benign ones. Pulsed Doppler indexes were not helpful. Almost simultaneously to our study, Testa et al. published a study on 24 solid pelvic masses with basically identical results to ours.[65]

After these pioneering reports, Geomini et al. reported data from a series of 181 women with adnexal masses using the method proposed by Alcazar.[62] This group included any kind of mass diagnosed at TVS and performed the vascular assessment from the whole tumor. They found that FI, but not VI and VFI, was significantly higher in ovarian cancer.

Jokubkiene et al. proposed a modified approach based on the use of a virtual 5-cc spherical sampling from the most vascularized area from the tumor. They also found that 3D PD vascular indexes were higher in ovarian cancer as compared with benign tumors.[66] Similar results were reported by Kudla et al. but using a 1 cc spherical sampling.[67]

The only study that has not shown differences in 3D PD indexes between benign and malignant ovarian tumors was reported by Ohel et al.[68] However, the series was too small (only 17 cases) and the methods used were not fully explained.

Alcazar and Prka compared manual and spherical sampling and concluded that both methods are comparable and that spherical sampling is faster to perform but cannot be used in some small tumors.[69] This may be solved using 1 cc sphere.[67]

Several studies have shown that, whatever the approach used, manual or spherical sampling, reproducibility is high between observers.[69-71]

Regarding to the contribution to diagnosis of ovarian cancer, Geomini et al. reported a multicenter prospective study concluding that the use of 3D ultrasound significantly improves the prediction of malignancy as compared to 2D ultrasonography.[72] Alcazar et al.[73] and Kudla et al.[74] have shown that 3D PD may decrease false-positive rate of 2D PD in solid and cystic-solid adnexal masses. However, Joubkiene et al. concluded that 3D PD does not add more information to gray-scale imaging than that provided by subjective quantification by 2D PD.[67] Guerriero et al. found that the use of 3D PD increased the specificity of ultrasound in suspicious masses but also decreased significantly the sensitivity.[75] These studies are summarized in **Table 47.4**.

Furthermore, we have recently demonstrated that vascularization, as assessed by 3D PD vascular indexes, is higher in advanced stage and metastatic ovarian cancers than in early stage ovarian cancer.[76] These preliminary results may be valuable for future research. It would be worth exploring if 3D PD-derived vascular indexes in ovarian cancer could be used as prognostic factor in ovarian cancer.

Other Applications

Three-dimensional ultrasound has been proposed as a means for monitoring the response to treatment in gynecologic malignancies.

Yaman and Fridrik reported on one case of cervical cancer and one case of ovarian cancer evaluated by 3D power Doppler ultrasound before and after treatment with radio- and /or chemotherapy. They observed a reduction of tumor volume, VI, FI and VFI in both cases after treatment.[77]

TABLE 47.4
Three-dimensional power Doppler vascular sampling for diagnosing ovarian cancer

Author	*N*	*OC prevalence*	*Sensitivity*		*Specificity*		*P value*
			3D PD	*2D*	*3D PD*	*2D*	
Geomini [62]†	181	20%	57%	91%	85%	63%	< 0.05
Jokubkiene [66]†	106	25%	100%	100%	92%	90%	< 0.05
Alcazar [73]*§	143	74%	95%	100%	33%	0%	< 0.05
Kudla [74]*§	138	82%	91%	100%	77%	0%	< 0.05
Guerriero [75]*§	35	71%	68%	100%	40%	0%	< 0.05

OC: Ovarian cancer. 2D. Two-dimensional ultrasound. 3D-PD: Three-dimensional power Doppler.
† Criteria for malignancy suspicion: Logistic system combining morphology and 3D PD indexes
§ Criteria for malignancy suspicion: only 3D PD indexes
* Only "complex" masses included in the study

Su et al. reported on one case of primary papillary serous carcinoma of the peritoneum evaluated by 3D PD USG before and after treatment with chemotherapy. They also reported that tumor volume and 3D PD indices decreased progressively during treatment.[78]

REFERENCES

1. Smith-Bindman R, Kerlikowske K, Feldstein VA, et al. Endovaginal ultrasound to exclude endometrial cancer and other endometrial abnormalities. JAMA. 1998;280:1510-7.
2. Kurjak A, Shalan H, Sosic A, et al. Endometrial carcinoma in postmenopausal women: evaluation by transvaginal color Doppler ultrasonography. Am J Obstet Gynecol. 1993;169:1597-603.
3. Sladkevicius P, Valentin L, Marsal K. Endometrial thickness and Doppler velocimetry of the uterine arteries as discriminators of endometrial status in women with postmenopausal bleeding: a comparative study. Am J Obstet Gynecol. 1994;171:722-8.
4. Alcazar JL, Castillo G, Minguez JA, et al. JEndometrial blood flow mapping using transvaginal power Doppler sonography in women with postmenopausal bleeding and thickened endometrium. Ultrasound Obstet Gynecol. 2003;21:583-8.
5. Alcazar JL, Ajossa S, Floris S, et al. Reproducibility of endometrial vascular patterns in endometrial disease as assessed by transvaginal power Doppler sonography in women with postmenopausal bleeding. J Ultrasound Med. 2006;25:159-63.
6. Aleen F, Predanic M. Uterine leiomyoma: transvaginal color Doppler studies and new aspects of management. In: Osmers R, Kurjak A (Eds). Ultrasound and the uterus. London: Parthenon Publishing Group. 1995. pp. 61-70.
7. Alcázar JL, Griffioen M, Jurado M. Uterine artery blood flow in women with uterine myomas. Eur J Ultrasound. 1997;5:165-9.
8. Kurjak A, Kupesic S, Shalan H, et al. Uterine sarcoma: a report of 10 cases studied by transvaginal color and pulsed Doppler sonography. Gynecol Oncol. 1995;59:342-6.
9. Szabo I, Szantho A, Csabay L, et al. Color Doppler ultrasonography in the differentiation of uterine sarcomas from uterine leiomyomas. Eur J Gynaecol Oncol. 2002;23:29-34.
10. Aviram R, Ochshorn Y, Markovitch O, et al. Uterine sarcomas versus leiomyomas: gray-scale and Doppler sonographic findings. J Clin Ultrasound. 2005;33:10-3.
11. Alcázar JL, Castillo G, Jurado M, et al. Intratumoral blood flow in cervical cancer as assessed by transvaginal color Doppler ultrasonography: correlation with tumor features. Int J Gynecol Cancer. 2003;13:510-4.
12. Alcázar JL, Jurado M. Transvaginal colour Doppler for predicting pathological response to preoperative chemoradiation in locally advanced cervical carcinoma: a preliminary study. Ultrasound Med Biol. 1999;25:1041-5.
13. Engelen MJ, Kos HE, Willemse PH, et al. Surgery by consultant gynecologic oncologists improves survival in patients with ovarian carcinoma. Cancer. 2006;106:589-98.
14. Canis M, Rabischong B, Houlle C, et al. Laparoscopic management of adnexal masses: a gold standard? Curr Opin Obstet Gynecol. 2002;14:423-8.
15. Alcázar JL, Castillo G, Jurado M, et al. Expectant management of sonographically benign ovarian cysts in asymptomatic premenopausal women. Human Reprod. 2005;20:3231-4.
16. Kinkel K, Hricak H, Lu Y, et al. US characterization of ovarian masses: a meta-analysis. Radiology. 2000;217:803-11.
17. Tekay A, Jouppila P. Controversies in assessment of ovarian tumors with transvaginal color Doppler ultrasound. Acta Obstet Gynecol Scand.1996; 75:316-29.
18. Guerriero S, Alcázar JL, Coccia ME, et al. Complex pelvic mass as a target of evaluation of vessel distribution by color Doppler for the diagnosis of adnexal malignancies: results of a multicenter European study. J Ultrasound Med. 2002;21:1105-11.

19. Alcázar JL. Three-dimensional ultrasound in Gynecology: Current status and future perspectives. Curr Women's Health Rev. 2005;1:1-14.
20. Alcázar JL, Mercé LT, García-Manero M, et al. Endometrial volume and vascularity measurements by transvaginal three-dimensional ultrasonography and power Doppler angiography in stimulated and tumoral endometria: an inter-observer reproducibility study. J Ultrasound Med. 2005;24:1091-8.
21. Gruboeck K, Jurkovic D, Lawton F, et al. The diagnostic value of endometrial thickness and volume measurements by three-dimensional ultrasound in patients with postmenopausal bleeding. Ultrasound Obstet Gynecol. 1996;8:272-6.
22. Kurjak A, Kupesic S, Sparac V, et al. Preoperative evaluation of pelvic tumors by Doppler and three-dimensional sonography. J Ultrasound Med. 2001;20:829-40.
23. Mansour GM, El-Lamie IK, El-Kady MA, et al. Endometrial volume as predictor of malignancy in women with postmenopausal bleeding. Int J Gynaecol Obstet. 2007;99:206-10.
24. Yaman C, Habelsberger A, Tews G, et al. The role of three-dimensional volume measurement in diagnosing endometrial cancer in patients with postmenopausal bleeding. Gynecol Oncol. 2008;110:390-5.
25. Odeh M, Vainerovsky I, Grinin V, et al. Three-dimensional endometrial volume and 3-dimensional power Doppler analysis in predicting endometrial carcinoma and hyperplasia. Gynecol Oncol. 2007;106:348-53.
26. Mercé LT, Alcázar JL, López C, et al. Clinical usefulness of three-dimensional sonography and power Doppler angiography for diagnosis of endometrial carcinoma. J Ultrasound Med. 2007;26:1279-87.
27. Opolskiene G, Sladkevicius P, Jokubkiene L, et al. Three-dimensional ultrasound imaging for discrimination between benign and malignant endometrium in women with postmenopausal bleeding and sonographic endometrial thickness of at least 4.5 mm. Ultrasound Obstet Gynecol. 2010;35:94-102.
28. Alcazar JL, Galvan R. Three-dimensional power Doppler ultrasound scanning for the prediction of endometrial cancer in women with postmenopausal bleeding and thickened endometrium. Am J Obstet Gynecol. 2009;200: 44.e1-6.
29. Bonilla-Musoles F, Raga F, Osborne NG, et al. Three-dimensional hysterosonography for the study of endometrial tumors: comparison with conventional transvaginal sonography, hysterosalpingography, and hysteroscopy. Gynecol Oncol. 1997;65:245-52.
30. Su MT, Su RM, Yue CT, et al. Three-dimensional transvaginal ultrasound provides clearer delineation of myometrial invasion in a patient with endometrial cancer and uterine leiomyoma. Ultrasound Obstet Gynecol. 2003;22:434-6.
31. Alcázar JL, Galván R, Albela S, et al. Assessing myometrial infiltration by endometrial cancer: uterine virtual navigation with three-dimensional US. Radiology. 2009;250:776-83.
32. Pairleitner H, Steiner H, Hasenoehrl G, et al. Three dimensional power Doppler sonography: imaging and quantifying blood flow and vascularization. Ultrasound Obstet Gynecol. 1999;14:139-43.
33. Kupesic S, Kurjak A, Zodan T. Staging of the endometrial carcinoma by three-dimensional power Doppler ultrasound. Gyneacol Perinatol. 1999;8:1-7.
34. Galván R, Mercé L, Jurado M, et al. Three-dimensional power Doppler angiography in endometrial cancer: correlation with tumor characteristics. Ultrasound Obstet Gynecol. 2010;35:723-9.
35. Salim R, Lee C, Davies A, et al. A comparative study of three-dimensional saline infusion sonohysterography and diagnostic hysteroscopy for the classification of submucous fibroids. Hum Reprod. 2005;20:253-7.
36. Walocha JA, Litwin JA, Miodonski AJ. Vascular system of intramural leiomyomata revealed by corrosion casting and scanning electron microscopy. Hum Reprod. 2003;18:1088-93.
37. Muniz CJ, Fleischer AC, Donnelly EF, et al. Three-dimensional color Doppler sonography and uterine artery arteriography of fibroids: assessment of changes in vascularity before and after embolization. J Ultrasound Med. 2002;21:129-33.
38. Exacoustos C, Zupi E, Marconi D, et al. Ultrasound-assisted laparoscopic cryomyolysis: two- and three-dimensional findings before, during and after treatment. Ultrasound Obstet Gynecol. 2005;25:393-400.
39. Kupesic S, Kurjak A. Three-dimensional power Doppler ultrasound examination of uterine lesions. In: Kurjak A (Ed.) Three-dimensional Power-Doppler in Obstetrics and Gynecology. London: Parthenon Publishing Group. 2000. pp. 39-52
40. Suren A, Osmers R, Kuhn W. 3D Color Power Angio imaging: a new method to assess intracervical vascularization in benign and pathological conditions. Ultrasound Obstet Gynecol. 1998;11:133-7.
41. Hsu KF, Su JM, Huang SC, et al. Three-dimensional power Doppler imaging of early-stage cervical cancer. Ultrasound Obstet Gynecol. 2004;24:664-71.
42. Testa AC, Ferrandina G, Distefano M, et al. Color Doppler velocimetry and three-dimensional color power angiography of cervical carcinoma. Ultrasound Obstet Gynecol. 2004;24:445-52.
43. Alcázar JL. Transvaginal color Doppler in the assessment of cervical carcinoma. Cancer Ther. 2005;3:139-46.
44. Alcázar JL, Jurado M, López-García G. Tumor vascularization in cervical cancer by 3-dimensional power Doppler angiography: correlation with tumor characteristics. Int J Gynecol Cancer. 2010;20:393-7.
45. Tanaka K, Umesaki N. Impact of three-dimensional (3D) ultrasonography and power Doppler angiography in the management of cervical cancer. Eur J Gynaecol Oncol. 2010;31:10-7.
46. Ghi T, Giunchi S, Kuleva M, et al. Three-dimensional transvaginal sonography in local staging of cervical carcinoma: description of a novel technique.
47. Bonilla-Musoles F, Raga F, Osborne NG. Three-dimensional ultrasound evaluation of ovarian masses. Gynecol Oncol. 1995;59:129-35.
48. Hata T, Yanagihara T, Hayashi K, et al. Three-dimensional ultrasonographic evaluation of ovarian tumours: a preliminary study. Hum Reprod. 1999;14:858-61.

49. Alcázar JL, Galán MJ, García-Manero M, et al. Three-dimensional ultrasound morphologic assessment in complex adnexal masses a preliminary experience. J Ultrasound Med. 2003;22:249-54.
50. Alcázar JL, García-Manero M, Galván R. Three-dimensional sonographic morphologic assessment of adnexal masses: a reproducibility study. J Ultrasound Med. 2007;26:1007-11.
51. Kurjak A, Kupesic S, Sparac V, et al. Three-dimensional ultrasonographic and power Doppler characterization of ovarian lesions. Ultrasound Obstet Gynecol. 2000;16:365-71.
52. Kurjak A, Kupesic S, Anic T, et al. Three-dimensional ultrasound and power Doppler improve the diagnosis of ovarian lesions. Gynecol Oncol. 2000;76:28-32.
53. Kupesic S, Kurjak A. Contrast-enhanced three-dimensional power Doppler sonography for differentiation of adnexal masses. Obstet Gynecol. 2000;96:452-8.
54. Breyer B, Kurjak A. Tumor vascularization, Doppler measurements and chaos: what to do? Ultrasound Obstet Gynecol. 1995;5:209-10.
55. Konerding MA, Miodonski AJ, Lametschwandtner A. Microvascular corrosion casting in the study of tumor vascularity: a review. Scanning Microsc. 1995;9:1233-43.
56. Alcázar JL, Cabrera C, Galván R, et al. Three-dimensional power Doppler vascular network assessment of adnexal masses: intraobserver and interobserver agreement analysis. J Ultrasound Med. 2008;27:997-1001.
57. Laban M, Metawee H, Elyan A, et al. Three-dimensional ultrasound and three-dimensional power Doppler in the assessment of ovarian tumors. Int J Gynaecol Obstet. 2007;99:201-5.
58. Sladkevicius P, Jokubkiene L, Valentin L. Contribution of morphological assessment of the vessel tree by three-dimensional ultrasound to a correct diagnosis of malignancy in ovarian masses. Ultrasound Obstet Gynecol. 2007;30:874-82.
59. Dai SY, Hata K, Inubashiri E, et al. Does three-dimensional power Doppler ultrasound improve the diagnostic accuracy for the prediction of adnexal malignancy? J Obstet Gynaecol Res. 2008;34:364-70.
60. Mansour GM, El-Lamie IK, El-Sayed HM, et al. Adnexal mass vascularity assessed by 3-dimensional power Doppler: does it add to the risk of malignancy index in prediction of ovarian malignancy?: four hundred-case study. Int J Gynecol Cancer. 2009;19:867-72.
61. Cohen LS, Escobar PF, Scharm C, et al. Three-dimensional ultrasound power Doppler improves the diagnostic accuracy for ovarian cancer prediction. Gynecol Oncol. 2001;82:40-8.
62. Geomini PM, Kluivers KB, Moret E, et al. Evaluation of adnexal masses with three-dimensional ultrasonography. Obstet Gynecol. 2006;108:1167-75.
63. Alcázar JL, Castillo G. Comparison of 2-dimensional and 3-dimensional Power-Doppler imaging in complex adnexal masses for the prediction of ovarian cancer. Am J Obstet Gynecol. 2005;192:807-12.
64. Alcazar JL, Merce LT, Garcia Manero M. Three-dimensional power Doppler vascular sampling: a new method for predicting ovarian cancer in vascularized complex adnexal masses. J Ultrasound Med. 2005;24:689-96.
65. Testa AC, Ajossa S, Ferrandina G, et al. Does quantitative analysis of three-dimensional power Doppler angiography have a role in the diagnosis of malignant pelvic solid tumors? A preliminary study. Ultrasound Obstet Gynecol. 2005; 26:67-72.
66. Jokubkiene L, Sladkevicius P, Valentin L. Does three-dimensional power Doppler ultrasound help in discrimination between benign and malignant ovarian masses? Ultrasound Obstet Gynecol. 2007;29:215-25.
67. Kudla MJ, Timor-Tritsch IE, Hope JM, et al. Spherical tissue sampling in 3-dimensional power Doppler angiography: a new approach for evaluation of ovarian tumors. J Ultrasound Med. 2008;27:425-33.
68. Ohel I, Sheiner E, Aricha-Tamir B, et al. Three-dimensional power Doppler ultrasound in ovarian cancer and its correlation with histology. Arch Gynecol Obstet. 2010;281:919-25.
69. Alcázar JL, Prka M. Evaluation of two different methods for vascular sampling by three-dimensional power Doppler angiography in solid and cystic-solid adnexal masses. Ultrasound Obstet Gynecol. 2009;33:349-54.
70. Kudla M, Alcázar JL. Does the size of three-dimensional power Doppler spherical sampling affect the interobserver reproducibility of measurements of vascular indices in adnexal masses? Ultrasound Obstet Gynecol. 2009;34:732-4.
71. Alcázar JL, Rodriguez D, Royo P, et al. Intraobserver and interobserver reproducibility of 3-dimensional power Doppler vascular indices in assessment of solid and cystic-solid adnexal masses. J Ultrasound Med. 2008;27:1-6.
72. Geomini PM, Coppus SF, Kluivers KB, et al. Is three-dimensional ultrasonography of additional value in the assessment of adnexal masses? Gynecol Oncol. 2007;106:153-9.
73. Alcázar JL, Rodriguez D. Three-dimensional power Doppler vascular sonographic sampling for predicting ovarian cancer in cystic-solid and solid vascularized masses. J Ultrasound Med. 2009;28:275-81.
74. Kudla MJ, Alcázar JL. Does sphere volume affect the performance of three-dimensional power Doppler virtual vascular sampling for predicting malignancy in vascularized solid or cystic-solid adnexal masses? Ultrasound Obstet Gynecol. 2010;35:602-8.
75. Guerriero S, Ajossa S, Piras S, et al. Three-dimensional quantification of tumor vascularity as a tertiary test after B-mode and power Doppler evaluation for detection of ovarian cancer. J Ultrasound Med. 2007;26:1271-8.
76. Alcázar JL. Tumor angiogenesis assessed by three-dimensional power Doppler ultrasound in early, advanced and metastatic ovarian cancer: a preliminary study. Ultrasound Obstet Gynecol. 2006;28:325-9.
77. Yaman C, Fridrik M. Three-dimensional ultrasound to assess the response to treatment in gynecological malignancies. Gynecol Oncol. 2005;97:665-8.
78. Su JM, Huang YF, Chen HHC, Gheng YM, Chou CY. Three-dimensional power Doppler ultrasound is useful to monitor the response to treatment in a patient with primary papillary serous carcinoma of the peritoneum. Ultrasound Med Biol. 2006;32:623-6.

48
CHAPTER

Ultrasound in Human Reproduction

Veljko Vlaisavljevic, Marko Dosen

INTRODUCTION

Since the introduction of ultrasound imaging in medicine, the indications and the scope of application of this visualization technique in the field of gynecology and obstetrics have been constantly widening. Indeed, transvaginal ultrasonography has become invaluable non-invasive tool for assessment of normal and abnormal pelvic anatomy.[1] Evaluation of follicular growth pattern, the structure of perifollicular vascular network and endometrium allows us to closely monitor and predict the success of in vitro fertilization (IVF) cycles. A modification of the standard sonographic technique with the vaginal probe known as hysterosalpingo-contrast sonography (HyCoSy) gives us even further possibility to assess changes of structures which usually occult during standard pelvic ultrasonography. However, because this procedure requires additional education of already experienced operator, its description is beyond the scope of this chapter.[2]

FOLLICULOGENESIS

Folliculogenesis is a constant process, which starts in the embryonic period and ends with the disappearance of the last functional follicle when woman enters menopause. Ovarian life cycle is a synonym for broader meaning of folliculogenesis and encompasses all phases a primordial germ cell has to pass to become the mature healthy oocyte which is subsequently fertilized and produces new organism and new ovary in females.[3-6]

Histological studies of Gougeon and Lefèvre on primate and human ovarian tissues have established the useful morphological classification of follicles and have given a more detailed insight into the dynamics of follicle growth.[7-10] According to morphometric criteria set by these authors, any given follicle can be classified into one of the eight classes and/or two major developmental phases.

During the course of sequential dramatic cellular proliferation and differentiation, the primordial follicles of approximately 60 μm in diameter differentiate into intermediate, then primary and eventually mature secondary but still preantral follicles of 120 μm in diameter, through the process called the slow growth phase. The development of a primordial into a full-grown secondary follicle requires approximately 290 days or about 10 regular menstrual cycles.[11]

The smallest early growing follicles lack an independent blood supply, but secondary follicles 80–100 μm in diameter are served by one or two arterioles, terminating in an anastomotic network just outside the basal lamina.[12] After the introduction of color and power Doppler ultrasonography it became possible to indirectly assess processes of angiogenesis, vessel maturation and vessel regression, which seemed to be of key importance for selection of the dominant follicle, ovulation and corpus luteum formation and function.[13-15] The development of an independent blood supply exposes the follicle directly to substances circulating in the blood. Secondary preantral follicles with a diameter of approximately 120 μm have multiple layers of granulosa cells (GCs) which are coupled by

gap junctions, thus forming the functional syncytium concerned with metabolic functions and chemical and electrical messaging pathways, thereby compensating for the otherwise avascular intrafollicular environment.[11]

At this point of development, the follicle begins to change into the antral follicle and after an 85-day journey becomes a follicle of preovulatory size. This antral phase of follicle development is typically divided into four stages. After the formation of the antrum (~0.4 mm in diameter), the rate of follicular growth accelerates and follicle development enters the so-called accelerated growth phase.[10,11]

Healthy antral follicles measuring 2–9 mm which are present during the late luteal phase constitute the cohort of follicles from which the one destined to ovulate during the subsequent cycle will be selected. These follicles are commonly called "recruited follicles" and the term recruitment is employed to indicate the process of constant follicle growth through which these follicles are provided. Their number in the late luteal phase is between 3 and 11 per ovary in women aged 24–33 years[16] (this number decreases with age). The process of follicular selection represents the final winnowing of the maturing follicular cohort, by the process of atresia, down to a number of dominant follicles characteristic for given species (ovulatory quota).

In our species, follicular selection is presumed to occur during the first five days of the cycle,[11] at a time when the diameter of a leading follicle is 5–10 mm.[11] The follicle destined to ovulate is the dominant follicle and the term dominance refers to its status in comparison with other follicles recruited in the same cycle. It is presumed that the dominant follicle itself has the key role in regulating the size of the ovulatory quota. Generally, in humans one of the selected follicles becomes dominant about a week before ovulation, as early as days 5–7 of the cycle, at the time when the follicular diameter is approximately 10 mm in size. After attaining dominance, the follicle grows with an almost uniform rate of 2–3 mm per day, until it reaches a mean diameter, ranging from 17 to 27 mm just prior to ovulation.[10,17]

The main pathway of blood supply to the mature follicle is through vascular network around the inner border of the theca interna. From there, the transport of nutrients, oxygen, precursors of steroidogenesis and waste products continues through the avascular granulosa layer to the oocyte by diffusion. Introduction of color and power Doppler techniques made research of perifollicular blood flow of the given preovulatory follicle possible. Investigations of correlation between Doppler indices of dominant follicle and the quality of its oocyte might improve our possibility to predict cycle outcome in the IVF program.

Under the influence of the midcycle luteinizing hormone surge, the dominant follicle undergoes dramatic morphological transformation, its oocyte further matures and finally the follicle ruptures. Mechanically, ovulation consists of a rapid enlargement of follicle and its protrusion from the ovarian surface. Finally, follicular rupture results in the expulsion of an oocyte-cumulus complex into the abdominal cavity. Endoscopic visualization of the ovary during ovulation has revealed that it is a gentle, rather than explosive process.[5]

After ovulation, rapid morphological transformation of the dominant follicle continues. Capillaries and fibroblasts from the surrounding stroma proliferate and penetrate the basal lamina. At the same time mural granulosa cells undergo morphological changes collectively referred to as luteinization. Thus, luteinized granulosa cells (GCs), surrounding theca-interstitial cells and invading vasculature, intermingle to give rise to the corpus luteum, which is a highly vascularized temporarily endocrine gland and a major source of sex steroids in the postovulatory phase of the cycle. If pregnancy does not occur, the corpus luteum spontaneously regresses after 14 ± 2 days through a process called luteolysis. At least five cycles later it is replaced by an avascular scar (corpus albicans). If pregnancy does occur, hCG secreted by the trophoblast maintains the life span of corpus luteum and its ability to produce progesterone for at least 8 additional weeks.

However, not all cycles are ovulatory. Nonovulatory cycles could be classified into three types as described under:

1. The cycle without dominant follicle development (a cohort of selectable follicles starts developing, but the dominant follicle does not emerge)
2. The cycle with atretic dominant follicle (the dominant follicle develops, but becomes irregular, continues to grow until midcycle and then disorganizes without ovulation)
3. The cycle with luteinized unruptured follicle (the dominant follicle grows till midcycle, does not ovulate, oocyte degenerates, luteal transformation of follicular wall occures).

Ultrasound and Follicular Growth

The ovary is a relatively small, paired organ with a complex, mosaic-like, constantly changing structure.[18] It has a central role in reproduction as the only source of oocytes and the main site of sex steroid hormone production in females. Despite of the fact that

ultrasonography has been introduced in clinical practice since 1970s, the first USG study of follicular growth dynamics started much later.[19-21] Technological advancements of ultrasound devices and adequate computer processing had made this possible.[22]

From the aspect of assisted reproduction, ability to evaluate antral follicle count, monitor follicular growth, predict the time and/or confirm ovulation and identify clinically applicable parameters of follicle quality is of critical importance.[23-25]

Antral follicles of different size could be found in both ovaries during all phases of menstrual cycle.[26] The fashion of appearance of antral follicles is random and it is not restricted to a particular location within the ovary. This represents a developmental advantage that is if follicles were formed in one particular part of the ovarian cortex only, they would be more easily compromised by pathological processes.[23]

For the purpose of reproducible and reliable data collection, it is common to take a diameter equal to or greater than 2 mm as the lower visible limit for a follicle. So, secondary antral follicles are the first follicular structures that may be visualized and investigated by USG device.[27]

Various visible characteristics of antral follicles[19-21] which may be used for the prediction of the ultimate fate of a follicle are described as under:

- Size (the largest diameter of the follicle)
- Shape (round, oval, rectangular, triangular)
- Echogenicity (high, medium, low)
- Antral edge quality (smooth, intermediate, rough).

In natural cycles, throughout follicular phase antral follicle which will gain dominance usually have more regular shape and antral edge and bigger size than follicles which will undergo atresia. Dominant follicle has echogenicity in the middle range, follicles destined to become atretic have more pronounced echogenicity and the follicle which will not rupture but will become luteinized has very low echogenicity.[21] Also, early angiographic studies in natural cycles showed that the main characteristics of blood flow in perifollicular tissue of nondominant growing antral follicles were of lower velocity and higher resistance in comparison to perifollicular flow of the dominant follicle.[28]

Dominant follicle regulates its own growth and the growth of other follicles from the same cohort secreting various paracrine regulators. This phenomenon was clearly demonstrated by day-by-day ultrasonographic observation and mapping of the follicles using 3D model. Reduction of antral follicles is most pronounced around the middle luteal phase; thereafter their number rapidly increases. Selection of the dominant follicle occurs before the 5th day of the cycle. Its occurrence becomes apparent till the 7th day of the cycle by its characteristic growth rate.[23]

Dominant follicle undergoes great changes during last seven days of its development. There is a marked increase in number and size of granulosa cells and increase of perifollicular flow in vessels of the theca layer. These changes can be assessed by ultrasound as an increase in diameter and volume of the follicle. Thickness of granulosa layer is directly correlated with health of the follicle. A thin follicular wall is a characteristic of atretic follicle.[29]

The growth rate of dominant follicle measures 1.4–2.2 mm per day till the luteinizing hormone (LH) peak;[23] after the LH surge it is even higher. In natural cycles, at the time of ovulation, the mean diameter of dominant follicle is 17–22 mm.[23]

In stimulated cycles, the diameter of leading follicle is the main parameter which is used to determine the right timing of hCG or gonadotropin releasing hormone (GnRH) antagonist administration. In GnRH agonist cycles, where stimulation is achieved by human menopausal gonadotropin the mean diameter of the leading follicle at the time of hCG administration should be 18–19 mm.[30] If recombinant follicle stimulating hormone (FSH) is used, hCG should be administered at slightly lower mean diameter of leading follicle (17–18 mm). In flexible protocols, GnRH antagonists should be administered at the moment when leading follicle reaches the mean diameter of 12–14 mm; the criteria for hCG or agonist administration for final maturation of oocyte are the same as for GnRH agonist cycles.[29,31]

Mean diameter of the dominant follicle is also an important parameter for proper timing of hCG administration in unstimulated IVF/ICSI cycles, but only in relation with serum estradiol levels. Acceptable pregnancy rate could be achieved if hCG is administered when serum E_2 is greater than 0.49 nmol/L and mean follicle diameter is at least 15 mm.[32]

Ultrasound and Ovulation

At the time of ovulation, dominant follicle reaches its maximal size, ruptures and shortly after that luteogenesis begins.[33] Several sonographic parameters as mentioned below have been investigated as potential markers of ovulation:[34]

- Disappearance of dominant follicle or sudden decrease in its size (the most reliable sign of ovulation)
- Increase of intrafollicular echogenicity (less reliable sign, because gradual increase of intrafollicular echogenicity may start as far as 3 days before

ovulation, usually with the most pronounced increase during the first day after ovulation)
- Loss of follicular wall regularity.

Accumulation of free fluid in the pouch of Douglas (it could be seen in during follicular phase also, but only in 3–11% of the cycles).[35]

During the late follicular phase, the ovary with dominant follicle has larger volume and increased perifollicular blood flow than the other one, but there is no significant difference in the values of sonographic indices of blood flow. The observation is the consequence of the definition of these indices, which take into account both volume and flow.[36]

With the introduction of advanced ultrasound devices it has become possible to investigate blood flow not only at the level of ovaries, but also at the level of a single follicle. Doppler studies of dominant follicles in natural cycles have showed a marked increase of blood flow velocity in perifollicular vessels around the time of ovulation. This increase starts approximately 29 hours before and continues for at least 72 hours after ovulation.[13,37-39] Not all parts of the follicular wall are equally perfused at the time of ovulation. There is a marked decrease in blood flow at the apex of the follicle. Described differences in perifollicular blood flow may be of crucial importance for normal release of the mature oocyte.[38]

Hypothetically, Doppler indices of perifollicular flow could be used as markers of outcome in IVF/ICSI cycles.[40] Unfortunately, investigating blood flow characteristics of the dominant follicle in unstimulated IVF/ICSI cycles, researches have found no statistically significant differences in pulsed and power Doppler indices of dominant follicles among groups with various cycle outcome as mentioned below:
- Group A: No oocyte was retrieved
- Group B: No fertilization occurred
- Group C: No implantation occurred
- Group D: Pregnancy occurred.[41]

Ultrasound as the Tool for Prediction of Outcome and for Monitoring of IVF/ICSI Cycles

Identification of factors that may predict outcome of IVF/ICSI cycles could improve the pregnancy rate. The strongest predictive factors for IVF/ICSI cycle outcome are maternal age, ovarian reserve and past reproductive history. Also, prognostic values of several sonographic parameters have been investigated, namely mean follicular diameter, growth rate of dominant follicle and follicular wall thickness.

Attention has also been focused on sonographic studies of perifollicular blood flow characteristics as parameters that may influence oocyte quality and indirectly cycle outcome. Various independent lines of evidence support the conduction of these studies. Also, insufficient perifollicular vascular network could result in hyporia of the growing and/or preovulatory follicle.[45] This may have deleterious effects on the organization and stability of the meiotic spindle. Knowing the fact that more than 25% of normal-appearing oocytes obtained for IVF are affected by lethal chromosomal abnormalies,[43,44] is another strong reason for conducting the studies of correlation between perifollicular blood flow and the quality of oocyte.[45]

Sonographic parameters with predictive value on cycle outcome have been tested mostly in stimulated cycles and only few studies are focused exclusively on natural cycles.

Ultrasound Monitoring in Stimulated Cycles

The age of the patient is the single most useful non-sonographic parameter for prediction of ovarian response, followed by the early follicular phase serum FSH levels.[46-49] Clinical importance of many sonographic parameters were investigated. The most important sonographic predictors of ovarian response in stimulated cycles are ovarian volume, antral follicle number and ovarian stromal blood flow.

Ovarian volume is the parameter most easily assessed compared to the others. Using transvaginal sonography, it was showed that ovarian volume has predictive importance for ovarian response to ovulation induction.[50] Later, a strong association between ovarian volume and ovarian reserve was recognized and investigators recommended that this parameter should be measured in all patients prior to IVF.[51] These results showed that small ovaries were associated with poor response to human menopausal gonadotropin and with a high cancellation rate during IVF. In another study, where investigators used 3D ultrasound technology there was not a statistically significant difference in ovarian volume between low responders and controls on day three of the cycle.[52] In the study of the influence of ageing on morphometric parameters of the ovary and FSH levels in infertile women a statistically significant correlation between age and FSH levels, and between FSH levels and the number of antral follicles, was found, but the correlation between age and ovarian volume or between FSH levels and ovarian volume was not detected.[53] In one later study, the same authors observed that in a group of IVF women with small ovarian volumes ($< 3\ cm^3$) the implantation and pregnancy rates

could be comparable to those with larger ovarian volumes if they were treated with higher doses of gonadotropins.[54] Other team of researchers showed that the number of retrieved oocytes and the conception rate were higher in patients with a greater ovarian volume and a greater ovarian vascularity, but ovarian volume and vascularity were not independent predictors and their measurement was more complicated in comparison to total antral follicle number (independent predictor of cycle outcome which can be easily measured).[55] Despite of its promising predictive importance at the beginning, it is nowadays accepted that ovarian volume has a limited predictive value, because it is not an independent factor in the prediction of cycle outcome.

Ovarian volume and stromal area are parameters which could be used for differentiation between multifollicular and polycystic ovaries.[56] The polycystic ovary (PCO) has a typical visual appearance and can be recognized as an almost spherical ovary with more than 10 follicles (with mean diameter less than 9 mm) grouped along its surface ("necklace sign"). The ovarian stromal area is increased ("sandstorm sign"), which usually makes the ovary larger than normal, but not always. The multifollicular ovary is of normal size, or slightly enlarged and it has six or more follicles of various sizes. The stromal area is not increased and the follicles are not located along the ovarian surface, but are dispersed within the ovary.[57] The ovarian stromal blood flow was proven to be significantly higher in polycystic ovaries, so it has been suggested that this parameter could be used as a possible marker for polycystic ovaries.[58] It should be emphasized that polycystic ovary is just a sign and not a pathognomonic marker of polycystic ovary syndrome (PCOS). Not all women with PCOS have polycystic appearing ovaries. However, ovaries with polycystic appearance are an independent risk factor for ovarian hyperstimulation syndrome.[59]

On the other hand, the number of antral follicles was found to be quite useful in everyday clinical practice. This sonographic criterion is a better predictor of ovarian response to ovarian induction and controlled ovarian hyperstimulation than ovarian volume or age alone.[60] If antral follicle count is less than three, there is a significantly higher chance for cycle cancellation, detection of lower E_2 levels and use of higher doses of gonadotropins.[61] In another study on a group of women with proven natural fertility, strong correlation between number of antral follicles and age of the patient was shown.[50] There was a mean annual decline in the number of antral follicles of near 5% before the age of 37, with the sharp increase of annual follicle loss thereafter.[50] In patients with normal basal serum FSH levels, the total antral follicle number was the most important predictor of ovarian response and IVF outcome.[62]

With the introduction of Doppler techniques, clinical importance of parameters of ovarian stromal blood flow was thoroughly investigated. Commonly used parameters were (PSV), pulsatility index (PI), resistance index (RI) and lately, vascularization index (VI), FI, VFI.[58,63-69]

Ovarian stromal vessels are thin and torturous and it is impossible to obtain the angle between the ultrasound beam and the intraovarian vessel accurately. This represents the potential limitation of PSV as the predictor of cycle outcome, because it leads to more subjective measurements and depends on the experience of the examiner, who should search for the highest velocity in the intraovarian vessels. Before the new generation of more powerful ultrasound devices was introduced in clinical practice, working hypothesis that at least one vessel in the vascular bed at the appropriate angle for accurate measurement of PSV would be located during examination was acceptable.[37,68,69]

Nowdays, it is recognized that using PSV as a predictive parameter has too many shortcomings. PSV has been replaced with new sonographic parameters of blood flow (FI and VFI), which are more objective and easier to measure. In the study using 3D ultrasound device, it was recognized that mean ovarian stromal FI was the second most important predictor of ovarian response to controlled stimulation (only antral follicle count was had better predictive power).[62] The same authors also concluded that 3D ultrasound enabled more objective assessment of ovarian morphology and ovarian stromal blood flow, shortened the time of examination and increased the patient's comfort during examination.[62]

In another study VI, FI and VFI were measured in patients after pituitary down-regulation and stimulation with gonadotropins, in order to evaluate whether 3D power Doppler could predict ovarian response. Despite of the fact all three indices of vascularity were significantly increased during gonadotropin stimulation in the group of normal responders compared to the low ovarian reserve group, the number of retrieved oocytes correlated only with the antral follicle number and ovarian volume, but not with VI, FI and VFI.[70,71]

Ultrasound Monitoring in Unstimulated Cycles

The term "natural cycle" is used to describe spontaneous, unstimulated cycles from which oocytes are recovered for IVF/ICSI after human chorionic gonadotropin (hCG) administration.[72] IVF/ICSI in natural

cycles is an accepted method for treatment of infertility in selected patients.[73-76] Monitoring of these cycles has greatly extended our knowledge of human reproductive physiology. These cycles have several advantages in comparison with stimulated ones, but the failure rate is high at each step and delivery rate per recovered oocyte remains unacceptably low.[77] These are the main reasons why unstimulated cycles are not widely used in IVF/ICSI programs.[78]

For evaluation of follicular maturity in unstimulated cycles, serum E2 levels and sonographic monitoring are used. According to one study, the right time to apply hCG is when the mean follicle diameter reaches 18 mm and serum estradiol is more than 0.66 nmol/L. Consensus on optimal E2 level as a criterion for hCG applications has not been reached. Proposed cut-off levels of E2 for oocyte maturity in unstimulated cycles are for example, 1.1 nmol/L,[77] 0.73-1.1 nmol/L,[78] 0.88 nmol/L,[79] 0.50 nmol/L[80] and 0.40 nmol/L.[81]

In natural IVF/ICSI cycles which were monitored by ultrasound only, the main problem was unpredicted and unwanted spontaneous LH surge. Even when folliculometry was repeated every second day until the follicle reached a diameter of 16 mm and then carried out daily, at the time when the mean diameter of the dominant follicle was 18 mm, spontaneous LH surge had been already occurred in 40% patients or ovulation was observed at the time of oocyte pick up.[73]

In another approach to monitoring natural IVF/ICSI cycles, ultrasound monitoring of follicle development was started on day 3 of the menstrual cycle. Folliculometry was then carried out every second day[82]. Three follicle diameters were measured and the mean value was taken into consideration. When the follicle reached the average diameter of 16 mm, folliculometry was done daily. At this time, the determination of the estradiol level and the presence of LH in urine also started. Decisions regarding the application of hCG were made on the basis of criteria which were a combination of serum estradiol levels and mean follicle diameter. On the day when mean follicle reached a mean diameter of 18 mm and serum E2 a level of 0.91 nmol/L was measured, the injection of hCG was given. In cases where the E2 level did not reach 0.91 nmol/L while the mean follicle diameter reached 20 mm, hCG was given when E2 reached 0.73 nmol/L at least. In cases where E2 reached higher values than 1.1 nmol/L before the follicle diameter reached 18 mm, hCG was administered only in cases when follicle diameter was 16 mm at least. Even with such a flexible approach to monitoring, spontaneous ovulation was not completely eliminated.[71]

Other investigators showed that comparable fertilization and implantation rate could be achieved if smaller follicles were aspirated. The hCG was given when the follicle had mean diameter of 15 mm and serum E2 was at least 0.49 nmol/L. Aspirated oocytes were suitable for IVF/ICSI and fertilization and implantation rate were satisfactory. Spontaneous LH surge or ovulation before OPU was detected in less than 10% of cases.[32]

Several studies on perifollicular blood flow indices as parameters which could be used for monitoring in natural IVF/ICSI cycles were conducted.[36,40,67,76,83,84] None of the investigated parameters (PSV, PI, RI or VFS-the percentage of blood volume showing a volume flow signal) was a suitable monitoring tool inside a 5 mm capsule of perifollicular tissue was not a suitable monitoring tool. The only conclusion was that in cycles which ended with implantation there was a more uniform vascular network in the capsule of the dominant follicle, but this difference only reached borderline statistical significance.[41] At this stage of our knowledge, we may conclude that quantitative Doppler measurement of perifollicular blood flow is of limited value as a parameter for decision making in unstimulated IVF/ICSI cycles.

Ultrasound as the Only Monitoring Tool

Ultrasound is the primary tool in monitoring stimulated IVF/ICSI cycles. At the beginning of controlled ovarian hyperstimulation, information about the presence of ovarian cyst can modify our clinical approach or lead to cycle cancellation. Sonographic evaluation of follicle growth and number influence gonadotropin dosage regime—we increase or decrease the dose or cancel the cycle if there is too weak or too strong ovarian response.

Maturity of the oocyte is closely associated with the size of the follicles and the serum estradiol levels. Commonly, we determine serum estradiol level for the first time at day 3–5 of the cycle. Afterwards, transvaginal USG scans are performed every 1–3 days (interval between measurements depends upon clinical findings). At the same time, serum levels of E2 could be measured. The goal is to obtain at least two follicles measuring 17–18 mm in mean diameter, optimally accompanied by a few others with mean diameter of 14–16 mm, accompanied by the serum estradiol levels which are consistent with the overall size and maturity of the cohort of follicles (serum E2 of at least 200 pg/ml per follicle measuring ≥ 14 mm). These thresholds are just a rough guideline, because interobserver and

intraobserver variability during follicular measurement is present. Also, serum E2 levels are not completely reliable monitoring tool, so each IVF institution has to empirically establish its own monitoring protocols.

The growing follicle matures and secretes increasing levels of estradiol (E_2). E_2 affects the target organs and promotes proliferation of the endometrium, increasing its thickness. Clear associations between the diameter of the dominant follicle and the levels of E_2 and between the levels of E_2 and endometrial thickness inspired some authors to try to use ultrasound as the only monitoring tool for IVF cycles. Another important reasons that made this approach attractive were its noninvasiveness and the cost-benefit ratio.

In 1985 it was suggested that ultrasound alone is sufficient to estimate follicular maturity.[85,86] Other researchers also advocated a simplification of cycle monitoring.[87,88] Simplification had to be weighed against possible reduction of the pregnancy rate and increase of incidence of ovarian hyperstimulation syndrome (OHSS).

The OHSS is a potentially life-threatening condition. Risk factors for OHSS are young age, lean posture, PCOS, the need for high doses of gonadotropins for optimal stimulation, high absolute (exceeding 2,500 pg/mL) or rapidly rising serum estradiol levels and previous episodes of OHSS. Caution is indicated when more than 20 follicles are growing simultaneously.[88]

The OHSS is the main reason why some authors recommend intensive monitoring of stimulated cycles with both serial serum E_2 levels and ultrasound scanning. However, emphasizing the nature of OHSS which makes us incapable to prevent this condition completely, other authors think that intensive monitoring (E2 plus folliculometry) is only justified in cases where risk factors are present.[89] In one retrospective study, the intensive monitoring protocol was compared to ultrasound scanning as the only monitoring tool. There was no difference in the duration of stimulation, the amount of gonadotropins used, the number of oocytes retrieved, fertilization rates and clinical pregnancy rates. Most importantly, the incidence of OHSS in the two approaches did not differ significantly.[90]

At present, data that would help us accept one and abandon the other approach are insufficient. There is a clear need for additional investigation of this issue.

The Role of Sonographic Evaluation of Endometrium

For any ART procedure, optimally primed endometrium is *conditio sine qua non,* successful implantation. Morphological characteristics of endometrium depend on the circulating levels of estrogen and progesterone. Interface between myometrium and endometrial lining could be easily recognized in all phases of the menstrual cycle. At the end of menstrual phase, the endometrium appears as a thin, hyperechogenic line. During proliferative phase, it becomes thicker (double layer endometrial thickness is normally 5–12 mm) and less echogenic. As early as day six and as late as one day before the LH peak, the sonographic picture of endometrium starts to change three stripe pattern appears. At the time of ovulation endometrium is 10–16 mm thick.[17,91] After ovulation, characteristic three stripes pattern disappears as the consequence of progesterone influence. Endometrium becomes homogenous and hyperechogenic. This is the secretory phase of the cycle. Thickness of endometrium increases only slightly. As a contrast to hyperechogenicity of endometrium, observer could also identify a hypoechoic band at the interface with myometrium.[92]

Technically speaking, endometrial thickness is defined as the distance between the anterior and posterior stratum basalis layers.[93] Its measurement should be performed in the sagittal plane. During a normal menstrual cycle spontaneous uterine contractions may occur and this may influence the accuracy of measurement.[94] It was proposed that the endometrium should be measured before, during and after this wave-like contractions and the mean value should be used as the definitive one.[95]

Also, in the luteal phase of the unstimulated cycle endometrium does seem to be thicker in conception compared to non-conception cycles and in normal pregnancy compared to abnormal pregnancy. However, at present there is no enough data to confirm that endometrial volume measurement will be a powerful tool in differential diagnosis of early normal and abnormal pregnancy.[96]

Endometrial thickness measurement is an essential part of evaluation of patient with fertility problems.[97] Although multiple studies examined the predictive value of endometrial thickness and sonographic appearance in IVF cycles, conclusions remain controversial. Typical trilaminar appearance and thickness of at least 8 mm are considered as sound markers of endometrial receptivity. On the other hand, thickness of 7 mm or less, homogenous appearance of endometrium on the day of hCG administration and uterine artery pulsatility index less than three were connected with poor results of stimulated IVF/ICSI cycle.[98-103] While some investigators suggested that excessive endometrial growth (greater than 14 mm) was also shown to be poor prognostic indicator,[104] others refuted this conclusion.[105,106]

The importance of Doppler angiographic indices as tools for evaluation of endometrium has also been studied. Cycle-dependent changes in uterine artery blood flow (velocity and pulsatility index of uterine artery) are evident, but their predictive value is hard to interpret because of diurnal variations and difference between the two uterine arteries (ipsilateral or contralateral to the dominant follicle). Clinical relevance of these parameters is of limited value.[98-103]

Despite of the controversies about prognostic value of the endometrial thickness and echo texture, some investigators proposed therapeutic strategies for improving endometrial and uterine blood flow (enhancing endometrial growth on that way) to the patients who were ultrasonographically identified as having reduced endometrial receptivity based on previously described criteria. One interesting approach was the treatment of such patients with vaginal sildenafil with good results.[106] Researchers in another report concluded that low-dose aspirin treatment improves ovarian responsiveness, uterine and ovarian blood flow velocity and implantation and pregnancy rates in IVF patients.[107]

Although measurements of endometrial growth are routine, their objective importance and prognostic value remain uncertain and the decisions to change stimulation regimen or to cancel the cycle based on these parameters are difficult to justify.[108] It is very likely that key determinants of successful implantation are detectable on molecular level only. Until such determinants are discovered and made clinically applicable and reliable, treatment decisions based on endometrial ultrasonographic parameters should be made with caution.

REFERENCES

1. Matijevic R, Grgic O. Predictive values of ultrasound monitoring of the menstrual cycle. Curr opin Obstetri Gynecol. 2005;17(4):405-10.
2. Ekerhovd E, Fried G, Granberg S. An ultrasound-based approach to the assessment of infertility, including the evaluation of tubal patency. Best Pract Res Clin Obstet Gynaecol. 2004;18(1):13-28.
3. Gourgeon A. Initiation of ovarian follicular growth: few facts and many hypothesis. In: Filicori M, Flamingi C (Eds). The Ovary; Regulation,Dysfunction and Treatment. Amsterdam: Excerpta Medica ICS; 1996. pp. 3-12.
4. Fortune JE, Cushman RA, Wahl CM, et al. The primordial to primary follicle transition. Mol Cell Endocrinol. 2000;163(1-2):53-60.
5. Erickson GF. Ovulation: evolving scientific and clinical concepts, 1st edition. New York: Springer-Verlag; 2000. pp. 31-48.
6. Erickson GF, Shimasaki S. The role of the oocyte in folliculogenosis. Trends Endocrinol Metab. 2000;163:61-6.
7. Gougeon A, Lefèvre B. Evolution of diameters of the largest healthy and atretic follicles during the human menstrual cycle. J Reprod Fertil. 1983;69(2):497-502.
8. Gougeon A, Chainy GB. Morphometric studies of small follicles in ovaries of women at different ages. J Reprod Fertil. 1987 81(2):433-42.
9. Balakier H, Stronell RD. Color doppler assessment of folliculogenesis in in vitro fertilization patients. Fertil Steril. 1994;62(6):1211-6.
10. Gougeon A. Regulation of ovarian follicular development in primates: facts and hypotheses. Endocr Rev. 1996;17(2): 121-55.
11. Suh CS, Sonntag B, Erickson GF. The ovarian life cycle: a contemporary view. Rev Endocr Metab Disord. 2002;3(1):5-12.
12. Bassett DL. The changes in the vascular pattern of the ovary of the albino rat during the estrous cycle. Am J Anat. 1943;73:252-92.
13. Sladkevicius P, Valentin L, Marsal K. Blood flow velocity in the uterine and ovarian arteries during the normal menstrual cycle. Ultrasound Obstet Gynecol. 1993;3(3):199-208.
14. Van Blerkom J, Antczak M, Schrader R. The developmental potential of the human oocyte is related to the dissolved oxygen content of follicular fluid: association with vascular endothelial growth factor levels and perifollicular blood flow characteristics. Human Reprod. 1997;12:1047-55.
15. Abulafia O, Sherer DM. Angiogenesis of the ovary. Am J Obstet Gynecol. 2000;182(1 Pt 1):240-6.
16. Pache TD, Wladimiroff JW, de Jong FH, et al. Growth patterns of non dominant ovarian follicles during the normal menstrual cycle. Fertil Steril. 1990;54(4):638-42.
17. Bakos O, Lundkvist O, Wide L, et al. Ultrasonographical and hormonal description of the normal ovulatory menstrual cycle. Acta Obstet Gynecol Scand.1994;73(10):790-6.
18. Kratochwil A, Urban G, Fridrich F. Ultrasonic tomography of the ovary. Ann Chir Gynecol Fenn. 1972;61(4):211-4.
19. Fleisher AC, Darnell JF, Rodier J, et al. Sonographic monitoring of ovarian follicular development. J Clin Ultrasound. 1981;9(6):275-80.
20. O'Herlihy C, de Crespigny LCH, Robinson HP. Monitoring ovarian follicular development with real-time ultrasound. Br J Obstet Gynecol. 1980;87:613-8.
21. Gore MA, Nayudu PL, Vlaisavljevic V, et al. Prediction of ovarian cycle outcome by follicular characteristics, stage 1. Hum Reprod. 1995;10(9):2313-9.
22. Gore MA, Nayudu PL, Vlaisavljević V. Attending dominance in vivo: distinguishing dominant from challenger follicles in humans. Human Reprod. 1997; 12(12):2741-7.
23. Pashe TD, Wladimiroff JD, de Jong FH, et al. Growth patterns of non-dominant ovarian follicles during normal menstrual cycle. Fertile Steril. 1990;54(4):638-42.

24. Nayudu P. Relationship of constructed follicle growth patterns in stimulated cycles to outcome after IVF. Human Reprod. 1991;6:465-71.
25. Vlaisavljević V. Analysis of follicular growth in conceivers and nonconceivers after intrauterine insemination. Gynecol Perinatol. 1995;4:49-451.
26. Chikazawa K, Araki S, Tamada T. Morphological and endocrinological studies on follicular development during the human menstrual cycle. J Clin Endocrinol Metab. 1986;62(2):305-13.
27. Bomsel-Helmreich O, Al-Mufti W. Ultrasonography of normal and abnormal follicular development. In: Jaffe R, Pierson RA, Abramowicz JS, (Eds). Imaging in infertility and reproductive endocrinology. 1st edition. Philadelphia: JB Lippincott; 1994. pp. 117-28.
28. Bourne TH, Jurkovic D, Waterstone J, et al. Intrafollicular blood flow during human ovulation. Ultrasound Obstet Gynecol. 1991;5:53-9.
29. Ecochard R, Marret H, Rabilloud, et al. Sensitivity and specificity of ultrasound indices of ovulation in spontaneous cycles. Eur J Obstet Gynecol Reprod Biol. 2000;91(1): 59-64.
30. Hackelöer BJ, Nitche-Debelstein S, Daume E, et al. Ultraschalldarstellung von Ovarveränderungen bei Gonadotropin Stimulierung. Geburtshilfe Frauenheild. 1977;37:185.
31. Vlaisavljević V, Reljiè M, Lovrec Gavrić V, et al. Comparable effectiveness using flexible single-dose GnRH antagonist (cetrorelix) and single-dose long acting GnRH agonist (goserelin) protocol for IVF cycles – a prospective, randomized study. Reprod Biomed Online. 2003;7(3):301-8.
32. Vlaisavljević V, Kovaèiè B, Reljiè M, et al. Three protocols for monitoring follicle development in 587 unstimulated cycles of in vitro fertilization and intracytoplasmic sperm injection. A comparison. J Reprod Med. 2001:46(10):892-8.
33. Assey RJ, Hyttel P, Greve T, et al. Oocyte morphology in dominant and subordinate follicles. Mol Reprod Dev. 1994;37(3):335-44.
34. Quenan JT, O'Brein GD, Bains LM, et al. Ultrasound scanning of ovaries to detect ovulation in women. Fertil Steril. 1980;34(2):99-105.
35. Pearlstone AC, Surrey ES. The temporal relation between the urine LH surge and sonographic evidence of ovulation: determinants and clinical significance. Obstet Gynecol. 1994;83:184-7.
36. Jarvela IY, Sladkevicius P, Kelly S, et al. Three-dimensional sonographic and power Doppler characterization of ovaries in late follicular phase. Ultrasound Obstet Gynecol. 2002;20(3):281-5.
37. Campbell S, Bourne T, Waterstone J, et al. Transvaginal color blood flow imaging of the preovulatory follicle. Fertil Steril. 1993;60(3):433-8.
38. Kupesic S, Kurjak A. Uterine and ovarian perfusion during the periovulatory period assessed by transvaginal color doppler. Fertil Steril. 1993;60(3):439-43.
39. Vlaisavljevic V, Borko E, Radaković B, et al. Changes in perifollicular vascularity after administration of human chorionic gonadotropin measured by quantitative three-dimensional power Doppler ultrasound. Wien Klin Wochenschr. 2010;(Suppl 2):1-6.
40. Brannstrorm M, Zackrisson U, Hagstroom HG, et al. Blood flow indices as measured by color doppler ultrasonography in different regions of the human periovulatory follicle. Fertil Steril. 1998;69(3):435-42.
41. Vlaisavljevic V, Reljic M, Gavric Lovrec V, et al. Measurement of perifollicular blood flow of the dominant preovulatory follicle using three-dimensional power Doppler. Ultrasound Obstet Gynecol. 2003;22(5):520-6.
42. Zeleznik AJ, Schuler HM, Reichert LE. Gonadotropin-binding sites in the Rhesus monkey ovary: role of the vasculature in the selective distribution of human chorionic gonadotropin to the preovulatory follicle. Endocrinology. 1981; 109(2):356-62.
43. Kranzfelder D, Maurer-Schultze B. Development of the perifollicular network. Autoradiographic and morphometric studies in the rabbit ovary. Eur J Obstet Gynecol. 1989;30:163-71.
44. Plachot M, Veiga A, Montagut J. Are clinical and biological parameters correlated with chromosomal disorder in early life: a multicenter study. Hum Reprod. 1988;3(5):627-35.
45. Gaulden M. Maternal age effect: the enigma of Down syndrome and other trisomic conditions. Mutat Res. 1992;296(1-2):69-88.
46. Padilla SL, Garcia JE. Effect of maternal age and number of in vitro fertilization procedures on pregnancy outcome. Fertil Steril. 1989;52(2):270-3.
47. Toner JP, Philput CB, Jones GS, et al. Basal follicle-stimulating hormone level is a better predictor of in vitro fertilization performance than age. Fertil Steril. 1991;55(4):784-91.
48. Tan SL, Rayston P, Campbell S, et al. Cumulative conception and livebirth rates after in vitro fertilisation. Lancet. 1992;339(8806):1390-4.
49. Check JH, Lurie D, Callan C, et al. Comparison of the cumulative probability of pregnancy after in vitro fertilization-embryo transfer by infertility factor and age. Fertil Steril. 1994;61(2):257-61.
50. Syrop CH, Willhoite A, Voorhis BJ. Ovarian volume: a novel outcome predictor for assisted reproduction. Fertil Steril. 1995;64(6):1167-71.
51. Lass A, Skull J, McVeigh E, et al. Measurement of ovarian volume by transvaginal sonography before ovulation induction with human menopausal gonadotropin for in vitro fertilization can predict poor response. Hum Reprod. 1997;12(2):294-7.
52. Pellicer A, Ardiles G, Neuspiller F, et al. Evaluation of ovarian reserve in young low responders with normal basal levels of follicle-stimulating hormone using three-dimensional ultrasonography. Fertil Steril. 1998;70(4):671-5.
53. Sharara FI, McClarmrock HD. The effect of aging on ovarian volume measurements in infertile women. Obstet Gynecol. 1999;94(1):57-60.
54. Sharara FI, McClarmrock HD. Use of microdose GnRH agonist protocol in women with low ovarian volumes undergoing IVF. Hum Reprod. 2001;16(3):500-3.
55. Kupesic S, Kurjak A, Bjelos D, et al. Three-dimensional ultrasonographic ovarian measurements and in vitro fertilization outcome are related to age. Fertil Steril. 2003;79(1):190-7.
56. Wu MH, Tang HH, Hsu CC, et al. The role of three-dimensional ultrasonographic images in ovarian measurements. Fertil Steril. 1998;69(6):1152-5.
57. Adams J, Franks S, Polson DW, et al. Multifollicular ovaries: clinical and endocrine features and response to pulsatile

gonadotropin releasing hormone. Lancet. 1985;2(8469-70):1375-9.
58. Zaidi J, Campbell S, Pitroff R, et al. Ovarian stromal blood flow in women with polycystic ovaries - a possible new marker for diagnosis? Hum Reprod. 1995;6:191-8.
59. The Rotterdam ESHRE/ASRM-sponsored PCOS consensus workshop group. Revised 2003 consensus on diagnostic criteria and long term health risk related to polycystic ovary syndrome (PCOS). Human Reprod. 2004;19:41-7.
60. Ng EH, Tang OS, Ho PC. The significance of the number of antral follicles prior to stimulation in predicting ovarian response in an IVF programme. Hum Reprod. 2000;15(9):1937-42.
61. Chang MY, Chiang CH, Hsieh TT, et al. Use of antral follicle count to predict the outcome of assisted reproduction technologies. Fertil Steril. 1998;69(3):505-10.
62. Kupesic S, Kurjak A. Predictors of IVF outcome by three-dimensional ultrasound. Hum Reprod. 2002;17(4):950-5.
63. Engmann L, Sladkevicius P, Agrawal R, et al. Value of stromal blood flow velocity measurement after pituitary suppression in the prediction of ovarian responsiveness and outcome of in vitro fertilization treatment. Fertil Steril. 1999;71(1):22-9.
64. Nagrund G, Bourne T, Doyle P, et al. Associations between ultrasound indices of follicular blood flow, oocyte recovery and preimplantation embryo quality. Hum Reprod. 1996;11(1):109-13.
65. Balakier H, Stronell RD. Color Doppler assessment of folliculogenesis in in vitro fertilization patients. Fertil Steril. 1994;62(6):1211-6.
66. Tekay A, Martikainen H, Jouppila P. Blood flow changes in uterine and ovarian vasculature and predictive value of transvaginal pulsed colour Doppler ultrasonography in an in vitro fertilization programme. Hum Reprod. 1995;10(3): 688-93.
67. Coulam CB, Goodman C, Rinehart JS. Colour indices of follicular blood flow as predictors of pregnancy after in vitro fertilization and embryo transfer. Hum Reprod. 1999;14(8):1979-82.
68. Collins W, Jurkovic D, Bourne T, et al. Ovarian morphology, endocrine function and intrafollicular blood flow during the periovulatory period. Hum Reprod. 1991;6(3):319-24.
69. Zaidi J, Collins W, Campbell S, et al. Blood flow changes in the intraovarian arteries during the preovulatory period: relationship to the time of the day. Ultrasound Obstet Gynecol. 1996;7(2):135-40.
70. Järvelä IY, Sladkevicius P, Kelly S, et al. Quantification of ovarian power Dopppler signal with three-dimensional ultrasonography to predict response during in vitro fertilization. Obstet Gynecol. 2003;102(4):816-22.
71. Paulson RJ. Natural cycle in vitro fertilization. Infertil Reprod Med Clin North Am. 1993;4:653-65.
72. Fahy UM, Cahill DJ, Wardle PG, et al. In vitro fertilization in completely natural cycles. Hum Reprod. 1995;10(3):572-5.
73. Vlaisavljevic V, Gavric V, Kovacic B. In vitro fertilization in natural cycles: Maribor experience. The world congress on in vitro fertilization and assisted reproduction held in Vienna, Austria, 1995 April 3-7. Aburumich A, Bernat E, Dohr G, Feichtinger W, Fischl F, Huber J, Mueller E, Szalay S, Urdl W, Zech H, Eds). Bologna: Monduzzi Editore; 1995. pp. 573-5.
74. Vlaisavljević V, Kovaèiè B, Reljiè M, et al. Is there any benefit from the culture of a single oocyte to a blastocyst-stage embryo in unstimulated cycles? Hum Reprod. 2001;16:101-5.
75. Lenton EA, Woodward B. Controversies in assisted reproduction. Natural versus. stimulated cycles in IVF: is there a role for IVF in natural cycle? J Assist Reprod Genet. 1993;10(6):406-8.
76. Foulot H, Ranoux C, Dobuisson JB, et al. In vitro fertilization without ovarian stimulation: a simplified protocol applied in 80 cycles. Fertil Steril. 1989;52(4):617-21.
77. Ramsewak SS, Cooke ID, Li TC, et al. Are factors that influence oocyte fertilization also predictive? An assessment of 148 cycles of in vitro fertilization without gonadotropin stimulation. Fertil Steril. 1990;54(3):470-4.
78. Paulson R, Sauer M, Francis M, et al. In vitro fertilization in unstimulated cycles: the University of Southern California experience. Fertil Steril. 1992;57(2):290-3.
79. Paulson RJ, Sauer MV, Francis M, et al. Factors affecting pregnancy success of human in vitro fertilization in unstimulated cycles. Hum Reprod. 1994;9(8):1571-5.
80. Reljiè M, Vlaisavljević V. The preovulatory serum estradiol pattern in natural IVF/ICSI cycles. J Assist Reprod Genet. 1999;16(10):535-9.
81. Toma•eviè T, Geršak K, Meden-Vrtovec H, et al. Clinical parameters to predict the success of in vitro fertilization-embryo transfer in the natural cycle. Assisted Reproduction. 1999;9:149-56.
82. Tan SL, Zaidi J, Campbell S, et al. Blood flow changes in the ovarian and uterine arteries during normal menstrual cycle. Am J Obstet Gynecol. 1996;175(3):625-31.
83. Gavrić Lovrec VG, Vlaisavljevic V, Reljic M. Dependence of the in-vitro fertilization capacity of the oocyte on peri-follicular flow in the preovulatory period of unstimulated cycles. Wien Klin Wochenschr. 2001;113(Suppl 3):21-6.
84. Nilsson L, Wikland M, Hamburger L, et al. Simplification of the method of in vitro fertilization: sonographic measurements of follicular diameter as a sole index of follicular maturity. J In Vitro Fert Embryo Transf. 1985;2(1):17-22.
85. Vlaisavljević V, Kovaèiè B, Gavrić V. In vitro fertilization program based on programmed cycles monitored by ultrasound only. Int J Gynecol obstet. 1992;39(3):227-31.
86. Vlaisavljeviæ V, Kovaèiè B, Gavriæ Lovrec V, et al. Simplification of the clinical phase of IVF and ICSI treatment in programmed cycles. Int J Gynecol Obstet. 2000;69(2):135-42.
87. Practice Committee of American Society for Reproductive Medicine, Birmingham, Alabama, USA. Ovarian hyperstimulation syndrome. Fertil Steril.2003;80(5):1309.
88. Braude P, Rowell P. Assisted conception. III-problems with assisted conception. BMJ 2003;327(7420):920-3.
89. Ben-Shlomo I, Geslevich J, Shalev E. Can we abandon routine evaluation of serum estradiol levels during controlled ovarian hyperstimulation for assisted reproduction? Fertil Steril. 2001;76(2):300-3.
90. Toma•eviè T, Meden Vrtovec H. Early timed follicular aspiration prevents severe ovarian hyperstimulation syndrome. J Assist Reprod Genet. 1996;13(4):282-6.

91. Quigley MM. In vitro fertilization: a new procedures and new questions. Investigative Radiology. 1986;21(6):503-10.
92. Persadie R. Ultrasonographic assessment of the endometrial thickness: a review. J Obstet Gynecol Can. 2002;24:131-6.
93. De Vries K, Lyons EA, Ballard G, et al. Contractions of the inner third of the myometrium. Am J Obstet Gynecol. 1990;162(3):679-82.
94. Dastidar KG, Dastidar SG. Dynamics of endometrial thickness over time: a reappraisal to standardize ultrasonographic measurements in an infertility program. Fertil Steril. 2003;80(1):213-5.
95. Dmitrovic R, Simunic V. Will endometrial volume measurements add something new to the diagnosis of early pregnancy? Current Women's Health Reviews. 2009;5:24-8.
96. Friedler S, Schenker JG, Herman A, et al. The role of ultrasonography in the evaluation of endometrial receptivity following assisted reproductive treatments: a critical review. Human Reproduction Update. 1996;2(4):323-35.
97. Steer CV, Campbell S, Tan SL, et al. The use of transvaginal color flow imaging after in vitro fertilization to identify optimum uterine conditions before embryo transfer. Fertility and Sterility. 1992;57:371-6.
98. Steer CV, Tan SL, Dillon D, et al. Vaginal color Doppler assessment of uterine artery impedance correlates with immunohistochemical markers of endometrial receptivity for the implantation of an embryo. Fertility and Sterility. 1995;63(1):101-8.
99. Ueno J, Oehninger S, Bryzski RG, et al. Ultrasonographic appearance of the endometrium in natural and stimulated in vitro fertilization cycles and its correlation with outcome. Hum Reprod. 1991;6(7):901-4.
100. Check JH, Nowroozi K, Choe J, et al. The effect of endometrial thickness and echo pattern on in vitro fertilization outcome in donor oocyte-embryo transfer cycle. Fertil Steril. 1993;59(1):72.
101. Oliveira JB, Baruffi RL, Mauri AL, et al. Endometrial ultrasonography as a predictor of pregnancy in an in vitro fertilization programme after ovarian stimulation and gonadotropin-releasing hormone and gonadotropins. Hum Reprod. 1997;12(11):2515-8.
102. Fanchin R, Righini C, Ayoubi JM, et al. New look at endometrial echogenicity objective computer-assisted measurements predict endometrial receptivity in in vitro fertilization-embryo transfer. Fertil Steril. 2000;74(2):274-81.
103. Weissman A, Gotlieb L, Casper RF. The detrimental effect of increased endometrial thickness on implantation and pregnancy rates and outcome in an in vitro fertilization program. Fertil Steril. 1999;71(1):147-9.
104. Dietterich C, Check JH, Choe JK, et al. Increased endometrial thickness on the day of human chorionic gonadotropin injection does not adversely affect pregnancy or implantation rates following in vitro fertilization-embryotransfer. Fertil Steril. 2002;77(4):781-6.
105. Yakin K, Akarsu C, Kahraman S. Cycle lumping or-sampling a witches' brew? Fertil Steril. 2000;73(1):175.
106. Sher G, Fisch JD. Effect of vaginal sildenafil on the outcome of in vitro fertilization (IVF) after multiple IVF failures attributed to poor endometrial development. Fertil Steril. 2002;78(5):1073-6.
107. Rubinstein M, Marazzi A, Polak de Fried E. Low-dose aspirin treatment improves ovarian responsiveness, uterine and ovarian blood flow velocity, implantation and pregnancy rates in patients undergoing in vitro fertilization: a prospective, randomized, double-blind placebo-controlled assay. Fertil Steril. 1999;71(5):825-9.
108. De Geyter C, Schmitter M, De Geyter M, et al. Prospective evaluation of ultrasound appearance of the endometrium in a cohort of 1,186 infertile women. Fertil Steril. 2000;73(1):106-13.

CHAPTER 49

New Insights into the Fallopian Tube Ultrasound

Sanja Kupesic, Bhargavi Patham, Ulrich Honemeyer, Asim Kurjak

INTRODUCTION

The fallopian tubes (oviducts) are embryologically derived from the müllerian ducts. Anatomically, they arise from the cornual end of the uterus. They act as a conveyer and meeting ground for the oocytes and the sperms. The fallopian tubes are about 9–11 cm long and are covered by peritoneum, which duplicates to form one of its loose attachments (mesosalpinx), to the broad ligament.

The arterial blood supply to the oviducts is derived from the terminal branches of the uterine and the ovarian arteries. The branches of the uterine arteries supply the medial two-thirds of each tube. The ovarian arteries supply the lateral one-third of the tube. The venous drainage parallels the arterial supply.

The ultrasonic scanning and evaluation of the fallopian tube present a true challenge to even the best sonographers. The normal fallopian tube can be imaged only if fluid surrounds it and creates a sonic interface to outline its boundaries.[1] The most proximal part of it can also be imaged in the normal state, since it is held steady by the uterus, which in this case serves as a landmark for finding the proximal part of the tube.

In certain instances, some sonolucent fluid is present in the pelvis, which acts as a contrast medium to highlight the normal fallopian tube:

- At times, a certain amount of pelvic fluid is present and this may be enough to highlight portions of the fallopian tube
- At midcycle, after the release of follicular fluid, at the time of ovulation or immediately after it, parts of the tube may be detectable
- Blood may be present in the pelvis for various reasons, such as rupture of the corpus luteum, or rupture of an ectopic pregnancy. Such larger amounts of fluid in the pelvis may increase the chance to detect one or both fallopian tubes
- Ascites present in the pelvis arising from ovarian hyperstimulation or other conditions, may serve as an excellent contrast medium around the fallopian tube and the fimbriae in order to highlight them
- Fluid originating from infectious processes may also enable us to outline the fallopian tubes.

In absence of fluid, placing the patient into an antitrendelenburg position may increase the pooling of fluid and therefore, create the acoustic interface for imaging the tube.[2,3]

PELVIC INFLAMMATORY DISEASE

Pelvic inflammatory disease (PID) is defined as "the acute clinical syndrome associated with ascending spread of microorganisms (unrelated to pregnancy or surgery) from the vagina or cervix to the endometrium, fallopian tubes and/or contiguous structures."[4] Very rarely, PID can develop as a result of surgical intervention. The PID causes more morbidity than necessary for three major reasons:

1. Women are not hospitalized when they should be
2. Many women receive inadequate or inappropriate antibiotic therapy and
3. The male sex partner is not treated or is treated inadequately.

The origin of PID is mostly considered ascending and polymicrobial. Rarely, the infection is hematogenous or spreads directly from another abdominal organs (diverticulitis and appendicitis). Among the sexually transmitted pathogens, *Neisseria gonorrhoeae* and *Chlamydia trachomatis* are most commonly identified.

Over half of women suffering from PID develop tubal damage without any symptoms of the disease, Chlamydia being the most frequent cause of this infection. Because of this observation, PID was classified into four major groups:

1. Silent (asymptomatic) PID (tubal scarring occurs without patient's knowledge)
2. Atypical PID (patients have only minimal symptoms)
3. Acute PID (this form is most commonly seen in patients presenting to emergency rooms) and
4. PID residual syndrome (patients suffer from chronic pelvic pain, infertility and scar tissue formation).[5]

Chronologically, PID can be divided into:

- Acute PID with formation of pyosalpinx and tubo-ovarian abscess and
- PID-residual syndrome with hydrosalpinx and scar tissue formation.

ULTRASOUND FINDINGS

Fallopian tube pathology is discerned by evaluating the wall of the tube, the luminal content, the tubal motility, as well as its relation with the surrounding pelvic structures.

Early in the course of the acute inflammation, pelvic sonography may be entirely normal. As the process of inflammation progresses, the endometrium becomes hyperechogenic and hyperperfused **(Figs 49.1A and B)**, and the tubes become thick-walled and irregular **(Figs 49.1A to F)**. The associated pelvic exudate allows better delineation of the gynecologic structures **(Fig. 49.1G)**. The inflamed tubes are represented by one of the following pictures:[6]

- A dilated tubular structure **(Fig. 49.2)**
- Echogenic tubal wall which reflects the inflammatory process of the mucosal lining
- The presence of internal echoes within the dilated tubes indicates pyosalpinx **(Figs 49.1C to F)**. Sonography-guided aspiration of the pus could be helpful for diagnostic purposes and for determining the optimal antibiotic therapy.

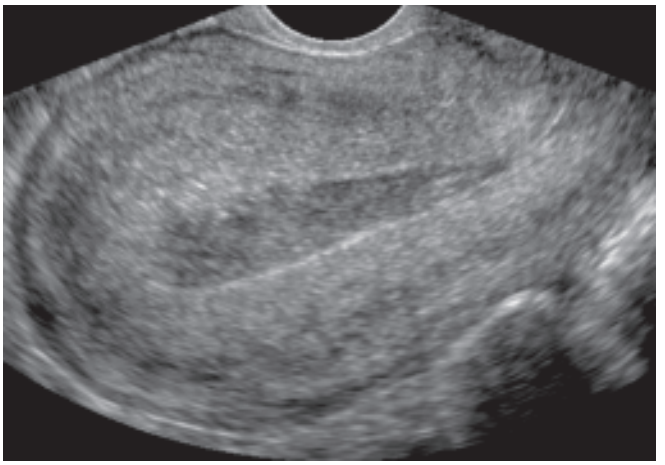

Figure 49.1A: Transvaginal ultrasound image of endometritis. Note hyperechogenic endometrium and intracavitary fluid

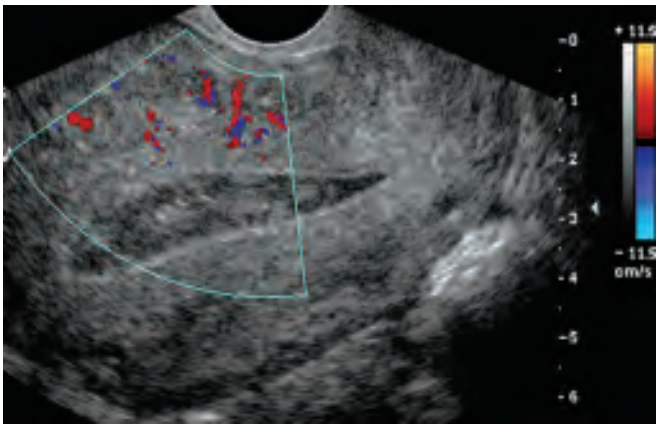

Figure 49.1B: The same patient as in previous figure. Color Doppler demonstrates vascularized endometrium

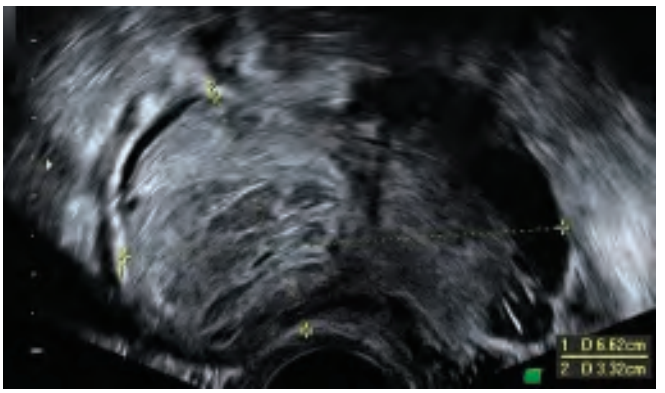

Figure 49.1C: Transvaginal ultrasound of a thickened tube filled with echogenic fluid (pus)

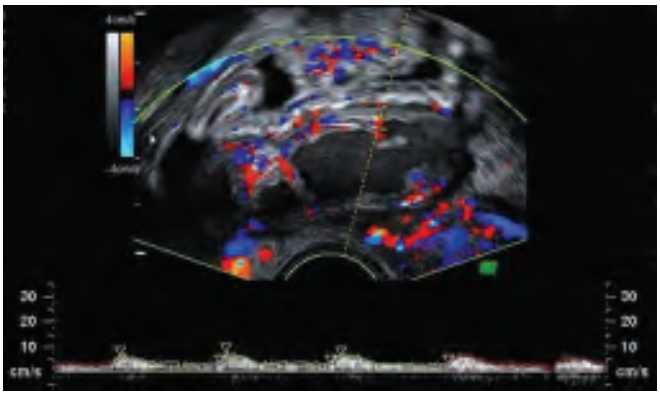

Figure 49.1D: Transvaginal color Doppler of the same patient. Note prominent vascularization of thickened tubal walls

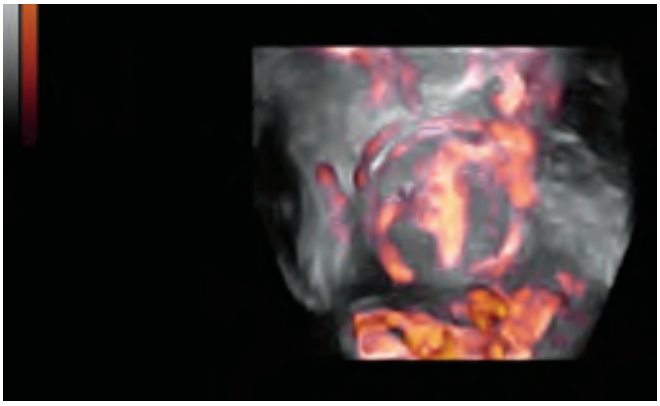

Figure 49.1E: Three-dimensional power Doppler image illustrating tubal angiogenesis secondary to inflammation

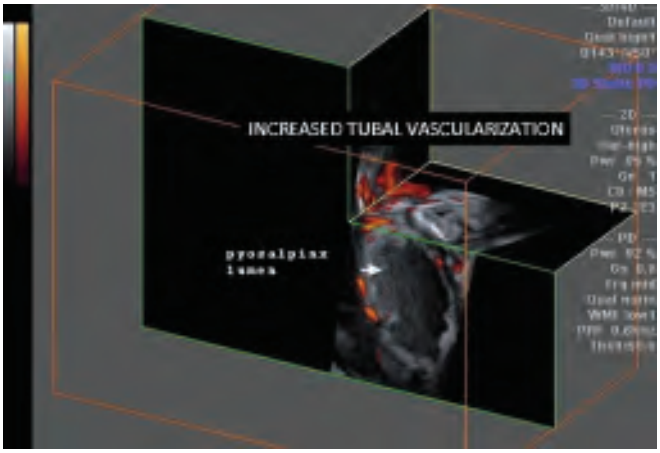

Figure 49.1F: Niche mode of an acute PID. Open cut view enables visualization of the tubal lumen and increased vascularization within the tubal wall

- A complex adnexal mass with thickening of the ovarian capsule and loculated fluid collections in the adnexal cul-de-sac represents the tubo-ovarian abscess **(Fig. 49.3)**.

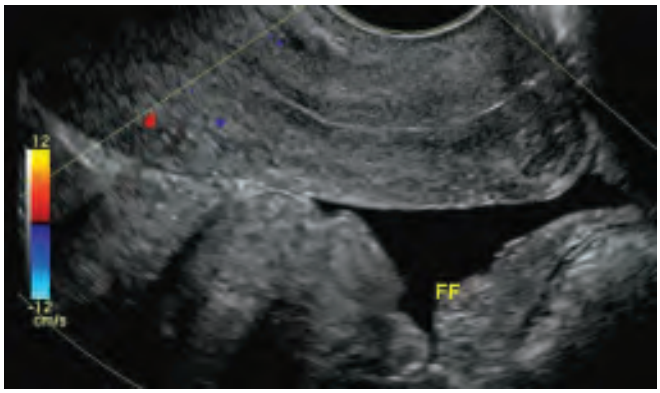

Figure 49.1G: Free fluid in the posterior cul-de-sac secondary to peritonitis

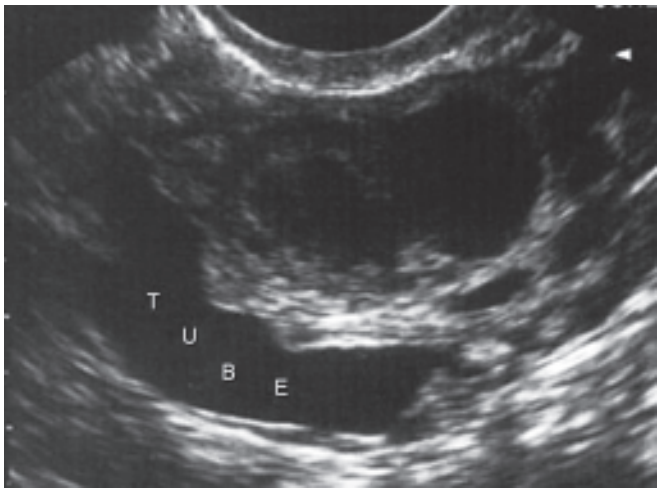

Figure 49.2: Complex adnexal mass occupying the pouch of Douglas in a patient with acute pelvic inflammation. Tubal diameter is increased, tubal mucosa is thickened and anechoic fluid fills the tubal lumen. Note enlarged ovary filled with inflamed follicles on the right

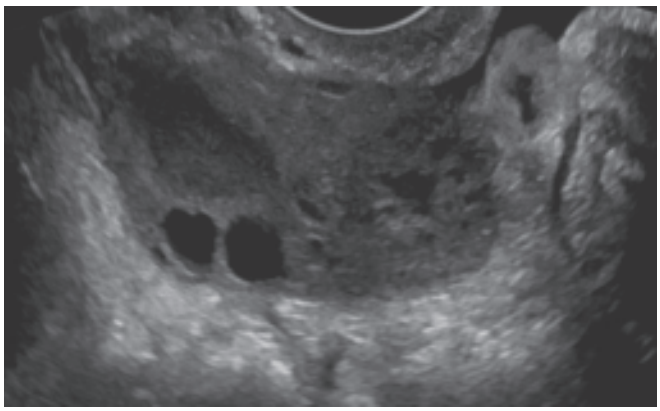

Figure 49.3: A complex adnexal mass with thickening of the ovarian capsule and fluid collection are typical features of tubo-ovarian abscess

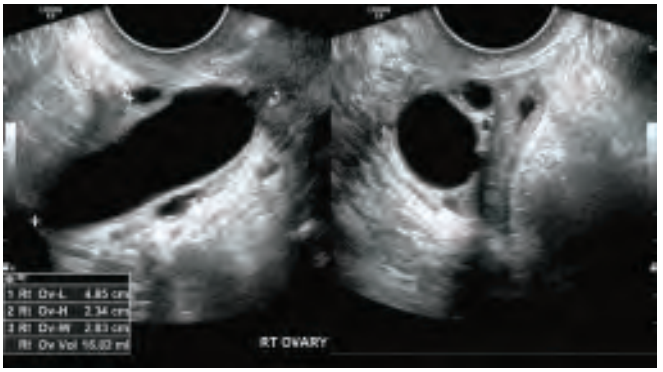

Figure 49.4: Transvaginal sonogram of a patient with hydrosalpinx in two different planes. Note the importance of performing different planes, because hydrosalpinx may sometimes be misinterpreted as ovarian or paraovarian cyst

Sonographic appearance of hydrosalpinx differs depending on the stage of the disease. During the acute phase, the tubal wall is thick and tender to the probe touch **(Figs 49.1 to 49.3)**. In the chronic phase, hydrosalpinx shows a typically thin wall, which is not tender. Chronic hydrosalpinx is usually discovered accidentally, on a routine transvaginal scan or during an infertility procedure **(Fig. 49.4)**. Patients are often unaware of their pelvic pathology, but can recall one or few episodes of pelvic pain and vaginal discharge.

Transvaginal sonography seems to be accurate in identification of fallopian tube pathology by evaluating the structure of the tubal wall and luminal contents. However, it is difficult to differentiate tubal from ovarian pathology when complex masses are found. During the acute stage of pelvic inflammatory disease, the tortuous and dilated fluid-filled tube "embraces" the adjacent ovary. At this time the ovary could not be well delineated, although visualization of the ovarian follicles enables localization of the ovarian component of the mass. During the chronic stage of PID the thin-walled hydrosalpinx is the main sonographic hallmark. Hydrosalpinx produces the typical image of a homogeneous, elongated fluid-filled mass adjacent and medial to the ovary. Incomplete and thin tubal septa are clearly distinguished from the distended tubal wall. However, when hydrosalpinx is presented as a complex lesion with thick walls, septa, suspicious papillary projections and mixed echogenic structures, incorrect diagnosis of an ovarian malignancy could be drawn.

Color Doppler Findings

Introduction of the color Doppler imaging has dramatically changed transvaginal ultrasound imaging. Color Doppler can depict blood flow within the pelvic structures and tell us more about the vessel quality in a particular organ or structure. The same modality can also depict movement of the liquid component, such as in the case in hydrosalpinx, when tubal content moves and changes the position compressed by vaginal probe or sliding over bowels during peristalsis. Furthermore, color Doppler is very useful in making a differential diagnosis between hydrosalpinx and pelvic congestion syndrome. When color is turned on, pelvic congestion syndrome lights up magnificently on the screen. Contrastingly, hydrosalpinx remains black and white, with specs of color only during peristalsis or deliberate probe movements.

Kupesic et al.[7] evaluated 102 women with laparoscopically proven PID. Seventy-two had acute symptoms, 11 presented with chronic pelvic pain and 19 were infertility cases suspected of tubal etiology. The mean resistance index (RI) in patients with acute symptoms was 0.53 ± 0.09. It significantly differed from those obtained in patients with chronic stage (RI = 0.71 ± 0.07) and infertility cases (RI = 0.73 ± 0.09). Therefore, the bizarre morphology during both the chronic and acute stages of PID if evaluated by color and pulsed Doppler should not cause an overlap with adnexal malignancy, since vascular resistance demonstrates significantly higher values.

Many studies have been undertaken to assess blood flow-related functional changes in the ovaries since our team first introduced the technique.[8] Significant changes have been demonstrated during the menstrual cycle in the active ovary and most of them were attributed to angiogenesis in the follicle and subsequently, the corpus luteum.[9,10] Transvaginal color Doppler has proved to be an extremely valuable tool in infertility evaluation and management, as well as in the assessment of adnexal masses and early detection of ovarian cancer.[11-14]

Kupesic et al.[7] assumed that an inflammatory process within the pelvis might affect ovarian blood flow. The ovary is in a close proximity to the tube, which is the primary focus of infection and it shares a significant part of its blood supply with the ipsilateral tube. Therefore, it can be expected that the ovarian blood flow is altered according to the changes in inflammatory process. Indeed, our study[7] demonstrated the correlation of intraovarian blood flow changes with pathophysiological changes. Findings obtained in the acute stage demonstrated rapidly changing patterns. The ongoing vasodilatation mediated by the local products of inflammation causes the decrease in RI **(Figs 49.5A to C)**, while the subsequent edema of the ovarian parenchyma causes the increase in the RI

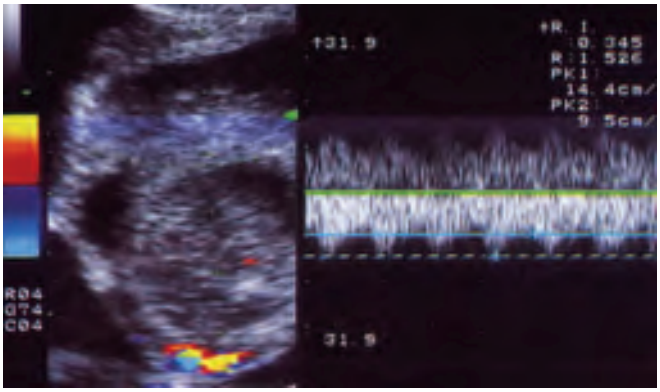

Figure 49.5A: Transvaginal color Doppler scan of acute pelvic inflammatory disease. Note hyperechogenic tubal walls and low impedance blood flow signals (RI=0.35) obtained from tiny tubal arteries

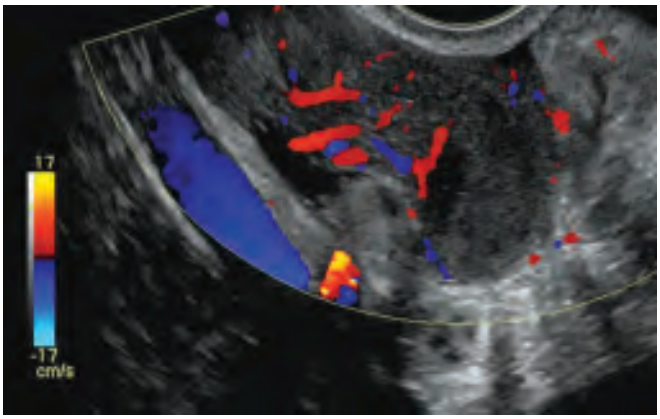

Figure 49.5B: Color Doppler ultrasound of a patient with acute PID. Note complex adnexal mass (usually multilocular cystic structure with echogenic fluid and thick septations) and free fluid in the cul-de-sac. Dilated vessels indicate increased angiogenesis

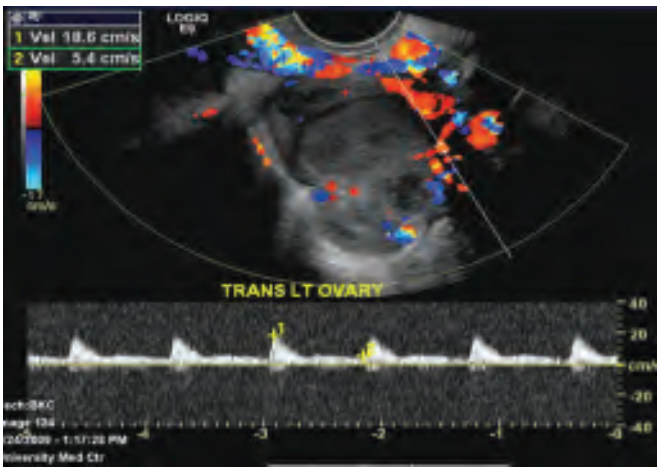

Figure 49.5C: The same patient as in previous figure. Pulsed Doppler waveform analysis demonstrates moderate to high vascular impedance blood flow signals

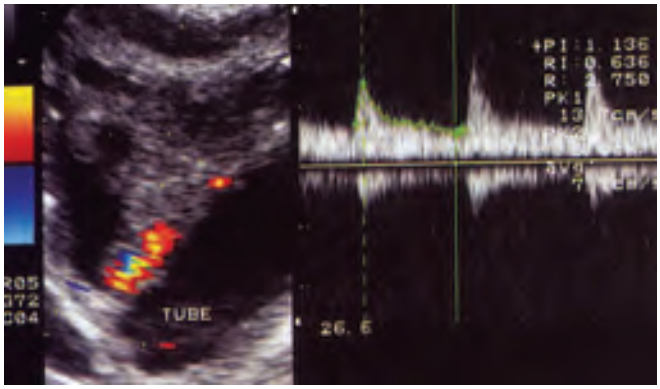

Figure 49.6A: Complex adnexal mass containing fluid filled distended tube and pseudopapillomatous vascularized structure protruding into the tubal lumen. Moderate-to-high resistance blood flow signals (RI:0.64) are obtained from a pseudopapillomatous lesion. This finding suggests subacute PID. Elevation of the vascular impedance is secondary to edema of the ovarian parenchyma

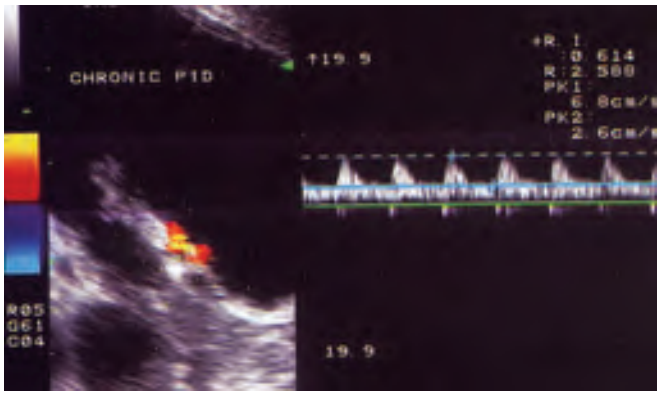

Figure 49.6B: Another case of chronic PID. Moderate to high vascular impedance signals (RI: 0.61) are clearly displayed from the pseudopapillomatous protrusion

(Figs 49.6A and B). As the ovarian capsule may vary in its rigidity, the intraovarian pressure differs from case to case. It affects the intensity of the intraovarian blood flow, which is reflected by variable values of RI. Furthermore, fluid collection within the tubes may influence the blood flow characteristics by compressing the vessels' wall. As the process advances, the proliferation of the fibroblasts and scarring tissue formation leads towards reduction of the local blood flow, which is demonstrated by the progressive increase in RI **(Fig 49.7)**. Very similar results were obtained by other authors, but on small series of patients.[15,5] Clearly, transvaginal color Doppler imaging can be used as an additional tool in evaluating the patients with suspected PID. Furthermore, we noticed that flow indices returned

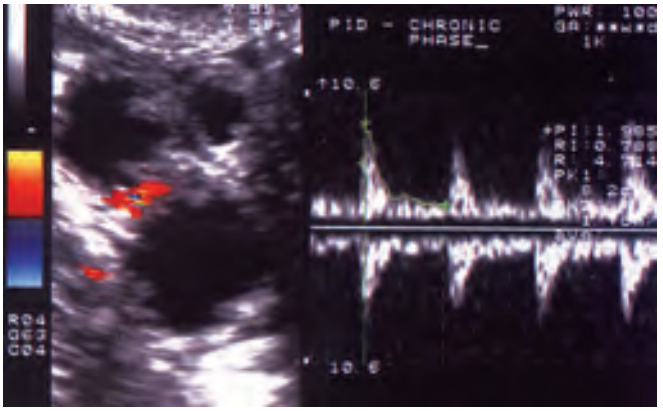

Figure 49.7: "Cogwheel" sign produced by hyperechogenic knots and pseudopapillomatous structures is typical of chronic phase of PID. Color Doppler helps to differentiate suspicious morphology

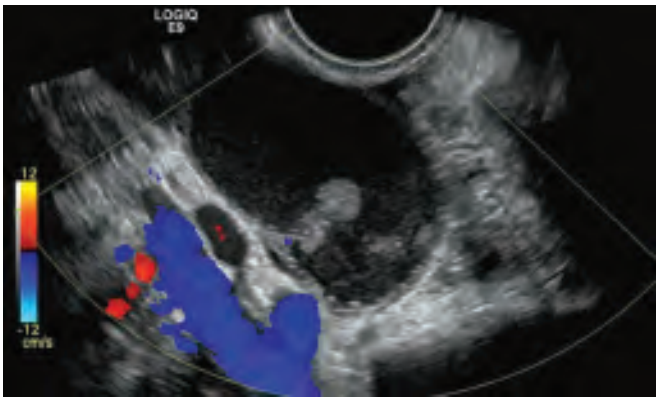

Figure 49.8A: Complex adnexal mass in a patient with chronic pelvic inflammatory disease. Hypovascularized papillary protrusion represents tubal mucosal fold

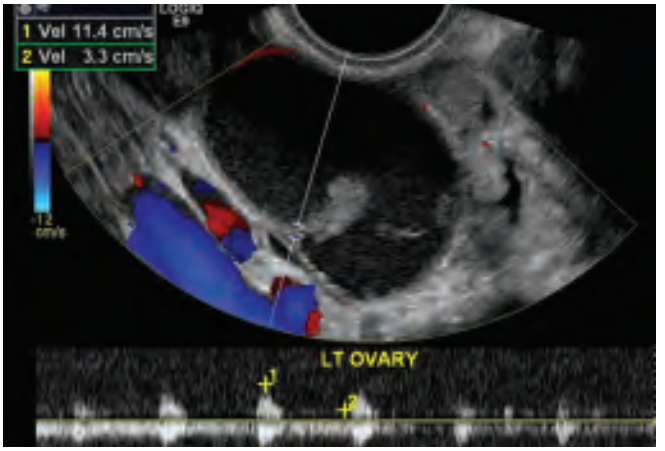

Figure 49.8B: The same patient as in previous figure. Moderate to high vascular impedance blood flow signals are obtained from the base of the papillary-like structure. Laparoscopy confirmed hydrosalpinx (tubal cause of infertility)

to normal values after the treatment in 36 (48.65%) patients.

The same method was useful in differentiating pyosalpinx from hematosalpinx in ectopic pregnancy cases. Ectopic pregnancies are characterized with high velocity and low impedance (RI <0.42) blood flow signals which indicate peritrophoblastic flow.[16,10]

As the inflammation may mimic a wide variety of findings and sometimes even suggest malignancy, serial assessment by color Doppler ultrasound is recommended, always with respect to the patient's age and the phase of the menstrual cycle. Serial examination may demonstrate morphological changes as well as variations in blood flow intensity according to the stage of the disease. Doppler studies are particularly useful in the chronic stage of PID, when pseudopapillomatous structures protruding into the cystic counterpart may morphologically suggest malignancy **(Figs 49.7 and 49.8A and B)**. Absence of blood flow, typical for this stage, helps differentiating it from adnexal malignancy. In the acute stage, low resistance to blood flow, suggestive of malignancy may be demonstrated. In those patients, it is useful to do some additional tests (e.g. erythrocyte sedimentation rate, total and differential cells counts, CA-125) that may help in reaching the final diagnosis. Serial ultrasound examination in these cases reveals the changes that correlate with the pathophysiological stage of the process **(Figs 49.9A and B)**. However, there is no single parameter that is sufficiently reliable for the adnexal mass characterization.[17]

In patients with tubo-ovarian abscess, abscess drainage under transvaginal sonographic guidance can hasten the recovery process and improve the efficacy of the antibiotic therapy.[18] Addition of the color Doppler facilities enables visualization of the large pelvic vessels and thereby may reduce the complication rate of the interventional procedure **(Figs 49.10A to C)**. However, a careful clinical examination, transvaginal ultrasound evaluation and blood tests are required before performing the procedure to avoid infection propagation.

Three-Dimensional Ultrasound

Three-dimensional ultrasound helps in spatial delineation of the inflammatory conglomerates. Any scanned volume can be rotated in all dimensions and thus it is possible to observe borders of tissues and organs. By conventional B-mode ultrasound hydrosalpinx can be mistaken for a multilocular cyst, but when 3D is applied the true, spatial position and shape of hydrosalpinx is clearly visible **(Fig. 49.11A)**. By using three-dimensional

Figure 49.9A: Transvaginal ultrasound demonstrates significant reduction of the adnexal mass following the antibiotic therapy

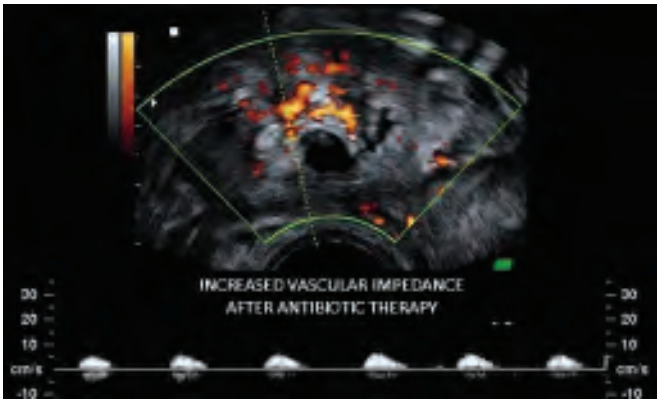

Figure 49.9B: Simultaneously with morphologic changes there was an increased RI of the tubal arteries after introduction of the antibiotic therapy

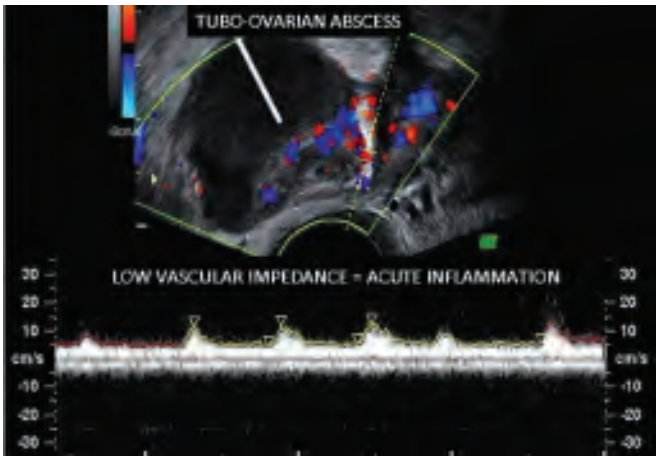

Figure 49.10A: Transvaginal color Doppler scan of a tubo-ovarian abscess. Note prominent vascularization and low impedance blood flow signals obtained from the tubal walls and incomplete septations

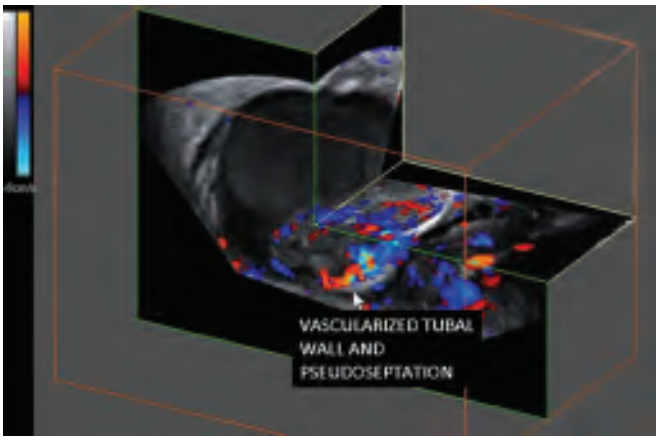

Figure 49.10B: The same patient as in previous figure. Niche mode enables better visualization of the vascularized tubal wall and pseudoseptation

volume sections it is possible to visualize the tortuous structure and contiguous spread of hydrosalpinx. The 3D ultrasound enables accurate visualization of three perpendicular planes simultaneously and by moving the cursor, sonographer "sees through" the slices of the hydrosalpinx. Another useful mode in this clinical situation is the so-called "niche" mode that enables the "cut-into" view of a certain tissue **(Figs 49.1F and 49.10B)**. With the use of this mode we can show the spatial spreading of hydrosalpinx and at the same time, visualize the lumen. Furthermore, pseudopapillomatous structures within the tubal lumen can be better assessed. The surface of such papillary protrusions can be thoroughly scanned by surface mode and its subtype "X-ray mode." When applying this mode, the spaces that appeared anechoic on the conventional ultrasound scan are even darker, while the echoic tissues are shown

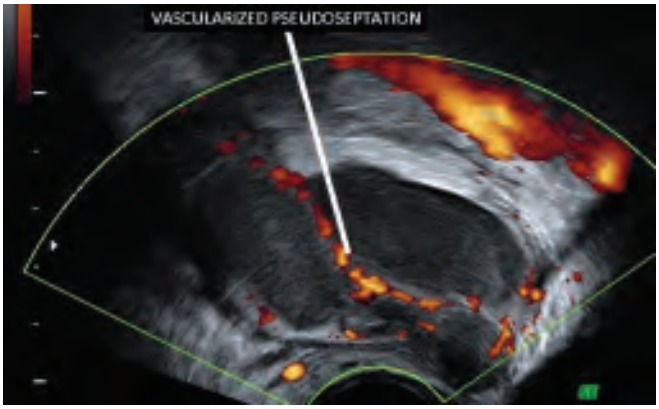

Figure 49.10C: Transvaginal power Doppler scan demonstrates tubal and ovarian angiogenesis. Simultaneous visualization of the neighboring pelvic vessels may reduce the complication rate of the ultrasound-guided interventional procedure

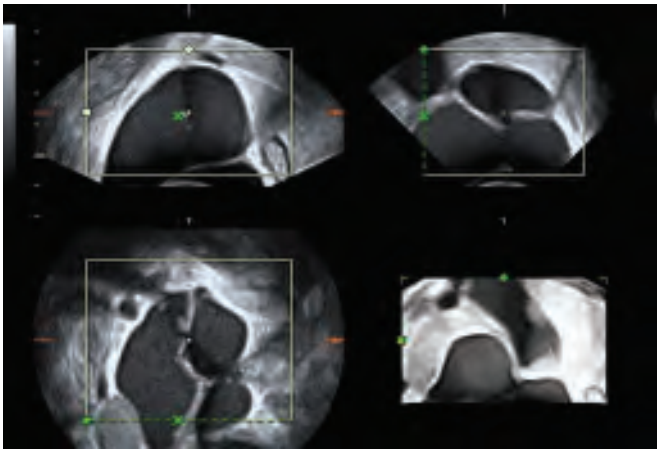

Figure 49.11A: Three-dimensional ultrasound of a pelvic inflammatory conglomerate. By conventional B-mode ultrasound hydrosalpinx can be mistaken for a multilocular cyst, but when 3D is applied the true, spatial position and shape of hydrosalpinx is clearly visible

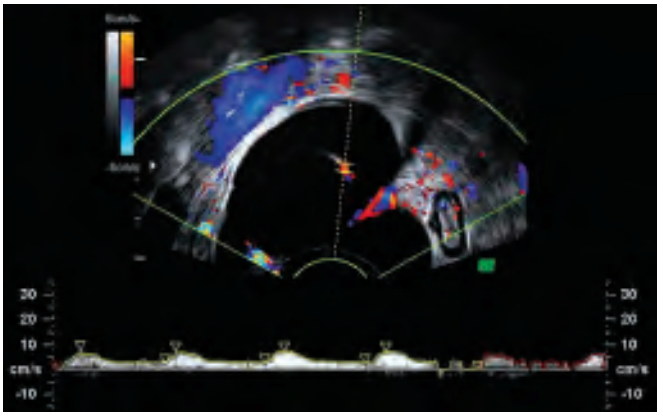

Figure 49.11B: Transvaginal color Doppler ultrasound of the same patient as in previous figure. Moderate vascular impedance blood flow signals (RI=0.67) are isolated from the incomplete tubal septation

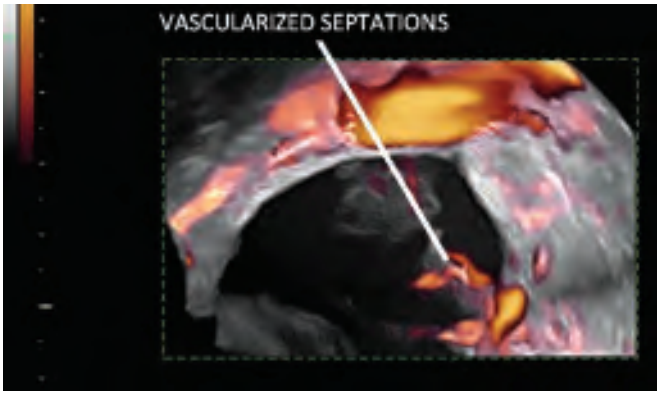

Figure 49.11C: The same patient as in figures 49.11A and B. Three-dimensional power Doppler ultrasound demonstrates intense vascularization within the tubal pseudoseptation

lighter allowing better sharpness and contrast of the entire image.

Various inflammatory conglomerates sometimes pose a problem to the ultrasonographer. They may form a part of tubo-ovarian abscess or stay encapsulated by two sheets of peritoneum in the retrouterine space. Because of echogenicity and low vascular resistance such structures may be mistaken for malignant tumors. Various forms of 3D ultrasound can define more clearly the spatial relations of such a lesion and its connection to surrounding structures.

The vascularity of the fallopian tube can be assessed using superimposed color and/or power Doppler **(Figs 49.11B and C)**. By the use of this modality it is possible to visualize vascular pattern and to study the branching and shape of the vascular structures. The interesting future possibility for the use of 3D power Doppler in the field of PID stems from work on 3D color Doppler histograms and vascularity index (VI) measurements counting on the number of color voxels in the cube of the tissue, which represent the evolved vessels. Flow index (FI), a mean color value of all blood flow or induced flow intensities, represents the intensity of flow at the time of the three-dimensional sweep. With these indices it would be easier to quantify the flow and conclude on the phase of the inflammatory process. The changes caused by vasodilatation or those caused by scar tissue formation could be better understood.

Clearly, 3D ultrasound enables better assessment of the anatomic relationship in patients with chronic PID **(Figs 49.12A and B)**.

Senoh et al.[19] reported on a laparoscopy-assisted intrapelvic sonography with a high-frequency, real-time miniature transducer in the assessment of the fallopian tubes. They developed a special 20 MHz flexible catheter-based high-resolution, real-time miniature (2.4 mm outer diameter) ultrasound transducer and tested it in the population of infertile patients. A total of 21 women (20 infertile, one with unilateral hydrosalpinx and one tubal pregnancy) were studied with pelvic saline effusion under laparoscopy. The presented technique seems to be useful in the assessment of tubal texture and functional evaluation in tubal disorders, possibly in infertility practice.

BENIGN TUMORS OF THE FALLOPIAN TUBE

Although the muscles of the fallopian tube and the uterus are of the same embryological origin (Müllerian ducts), leiomyoma of the fallopian tube are exceptionally rare. Leiomyomas of the fallopian tube are commonly incidental findings, as they are asymptomatic

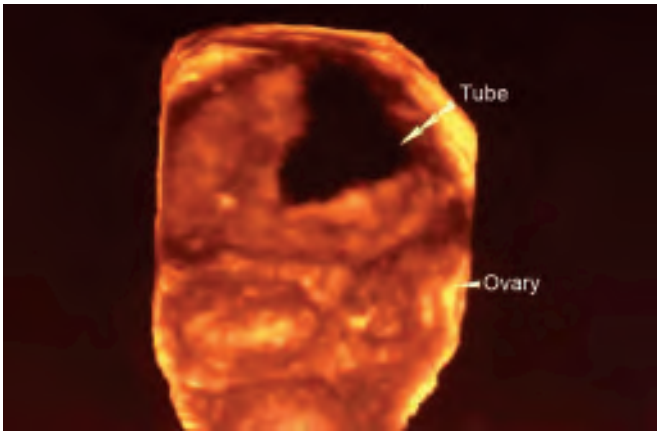

Figure 49.12A: Three-dimensional ultrasound of a fluid-filled fallopian tube and ovary in a patient with secondary infertility due to pelvic inflammatory disease

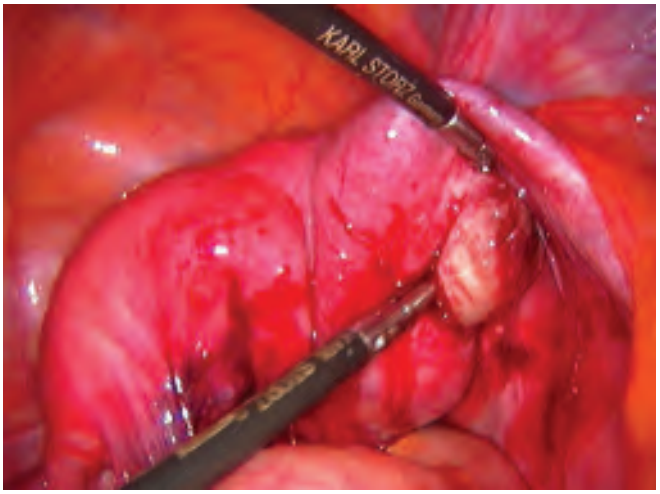

Figure 49.12B: Laparoscopic image of the same patient

and small. However, there are reported cases of large tubal myomas associated with acute abdomen consequent to its torsion.[20]

Tubal pregnancy associated with tubal leiomyomas, in which the tubal myoma was the obstructing factor have also been reported.[1,20,21] Kobayashi et al.[22] reported on a case of a 28-year-old woman presented with secondary infertility in which pelvic ultrasound showed a multicystic septated mass extending to the umbilicus. At laparotomy, a 25 × 14 × 4 cm mass originating from the left fallopian tube and the tube was excised. Pathologic examination confirmed an angiomyofibroblastoma of the fallopian tube. Although, angiomyofibroblastoma is a rare tumor that occurs most commonly in the vulva and vagina, this case shows that it can occur in the fallopian tube and should be differentiated from more aggressive angiomyoma.

Conventional B-mode sonography reveals little of the nature of a benign tubal tumor. A smaller papilla can resemble a chronic PID remnant while a bigger mass in the oviduct can be mistaken for an inflammatory conglomerate. Because of its limited imaging possibilities, 2D ultrasound cannot always define the borders of the lesion and delineate it from the surrounding tissue.

Color Doppler can be used for the assessment of vascularity. As any other benign tissues, the oviduct leiomyomas would have a moderate-to-high resistance index. If they undergo necrosis of inflammation, they can present a true complication in the diagnostic process, caused by a significant reduction of the vascular indices.

Three-dimensional ultrasound can help in diagnosis of benign ovarian lesions by its possibility to precisely delineate and spatially define a certain tumor. With the use of 3D power Doppler it is possible to visualize regular branching of benign intratubal structures and distinguish them from uterine and ovarian vascular network.

MALIGNANT TUMORS OF THE FALLOPIAN TUBE

Although rare, tubal malignancy must be considered in the differential diagnosis of an adnexal mass. Of all gynecological cancers, malignancy of the fallopian tube is the most rare. The triad of pain, bleeding and leucorrhea are considered pathognomonic of tubal carcinoma. Sedlis[23] defined parameters for better differentiation between ovarian and tubal malignancies. He postulated that the tumor is of fallopian origin if:

- It derives from the fallopian tube
- Has the same histological structure as fallopian tube mucosa
- There is a clear transition zone between benign and malignant epithelium and
- There is no endometrial or ovarian carcinoma.

Ultrasound Findings

The sonographic findings in all reported cases of fallopian tube carcinoma were complex, predominantly cystic adnexal masses and/or sausage-shaped structures apparently separated from the uterus.[24-37]

Table 49.1 reviews data from the literature on B-mode diagnosis of primary fallopian tube carcinoma.

In a remarkable review of 376 cases of tubal carcinoma, Mc Goldrick et al. found only one diagnosed

TABLE 49.1

Review of literature on B-mode diagnosis of primary fallopian tube carcinoma

Reference	*No. of cases*	*Histopathology*
Subramayon et al.[30]	3	Papillary cystadeno-carcinoma
Meyer et al.[31]	1	Adenocarcinoma
Kol et al.[47]	1	Adenocarcinoma
Ajjimakorn et al.[32]	4	Papillary cystadeno-carcinoma
Granberg and Jansson [33]	1	Adenocarcinoma
Chang et al. [28]	1	Mixed Muellerian tumor
Chiou et al.[27]	1	Mixed Muellerian tumor
Slanetz et al.[34]	9	Adenocarcinoma and mixed Muellerian tumor
Ong [35]	1	Adenocarcinoma

preoperatively.[38] Recently, Eddy et al. analyzed the data of 74 patients regarding tubal malignancies and only two cases of tubal carcinoma were correctly diagnosed before surgery.[39]

Ayah et al. reported a study of eight cases of primary fallopian tube carcinoma.[24] Dava et al. described six adenocarcinomas of the fallopian tube that resembled the female adnexal tumor of probable Wolffian origin.[25] Microscopically, the tumors were characterized by a predominant pattern of small, closely packed cells punctured by numerous glandular spaces, which were typically small but occasionally were cystically dilated. Soundara et al. published a review of fallopian tube carcinoma over 20 years.[26] Nine cases of tubal carcinoma were found among approximately 9000 gynecological malignancies.

Based on the data from the literature[26,38,39] more than 80% of patients have had pelvic mass detected before surgery. However, cervical cytology, X-ray of the pelvis, computed tomography or hysterosalpingography are usually no more specific than the pelvic examination. Conventional transvaginal sonography is one of the most important tools in preoperative diagnosis, but the efficacy of morphologic scoring systems alone is hampered by the degree of overlap between benign and malignant appearing adnexal masses.[40-42]

Color Doppler Findings

Kurjak et al. was first to publish a case of primary adenocarcinoma of the fallopian tube (stage I FIGO)

TABLE 49.2

Review of literature on transvaginal color Doppler diagnosis of primary fallopian tube carcinoma

Reference	*No. of cases*	*RI*	*Histopathology*
Shalan et al.[43]	1	0.35	Adenocarcinoma
Kurjak et al.[45]	8	0.29–0.40	Adenocarcinoma and papillary cystadeno-carcinoma
Podobnik et al.[44]	1	0.34	Clear-cell carcinoma

preoperatively diagnosed by color and pulsed Doppler ultrasound.[43] Podobnik et al. published the case of a 69-year-old woman with a history of right-sided lower abdominal pain accompanied by profuse watery vaginal discharge for the past three months.[44] Six years after the initial report Kurjak et al.[45] reported on the series of eight cases of preoperatively diagnosed fallopian tube malignancy. Probably the most illustrative case of successful preoperative diagnosis of the primary fallopian tube carcinoma in his series was a 45-year-old woman treated because of infertility problems. During the routine transvaginal ultrasound examination a pendular myoma and a complex bilateral adnexal mass were discovered. In the left adnexal region a sausage-shaped cystic structure, 3.4 x 4.8 x 3.4 cm in size was present. In the upper part of the cyst, a solid papillary protrusion less than 1 cm, richly perfused with the lowest RI of 0.38 was detected **(Figs 49.13 A and B)**. In the right adnexal region a hydrosalpinx 3.0x1.6 cm was delineated from the ovary. Moderate vascular resistance (RI=0.55) was obtained from the fallopian tube with chronic inflammatory changes. According to the visualization of the area of neovascularization and low vascular impedance, the authors suspected tubal carcinoma of the left side. Frozen section pathological examination reported papillary fallopian tube carcinoma. **Table 49.2** reviews data from the literature on color Doppler diagnosis of primary fallopian tube carcinoma.

Tubal malignancy displays angiogenesis that can be detected by color and pulsed Doppler. Reports from the literature demonstrate the potential of transvaginal color Doppler to depict tumor neovascularization and low resistance indices (below 0.42) typical of tubal malignancy.[46-48] Similar color Doppler results were obtained by Gojnic et al.[49] who reported on preoperative diagnosis of two fallopian tube carcinomas in a group of 78 postmenopausal women with adnexal

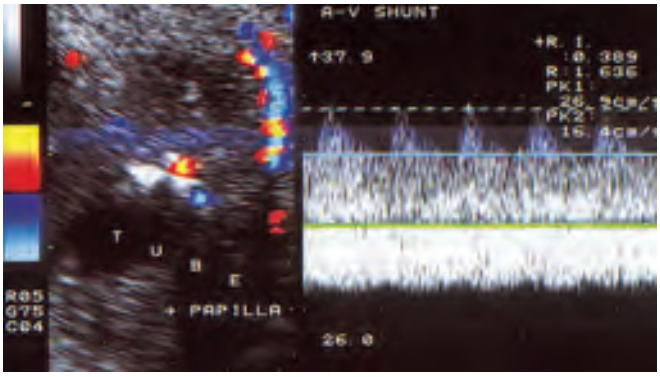

Figure 49.13A: Fallopian tube carcinoma as seen by color Doppler ultrasound. Note vascularized papillomatous projection protruding into the distended tube in a postmenopausal patient. Low vascular resistance (RI=0.38) and arteriovenous shunt indicate tubal malignancy, which was confirmed by histopathology

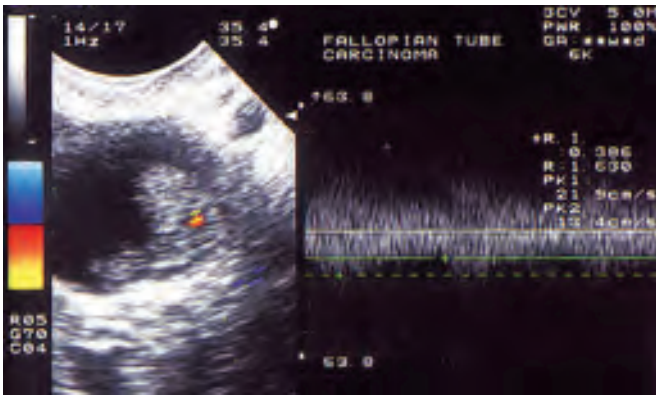

Figure 49.13B: The same patient as in previous figure. Cross section through the fallopian tube reveals vascularized carcinoma

masses. Resistance index ranged between 0.20 and 0.30, and CA 125 was not remarkably elevated.

Three-Dimensional Ultrasound

A new progress in diagnostic procedures was made when 3D and power Doppler ultrasound was introduced. Transvaginal 3D ultrasound enables the clinician to perceive the true, spatial relations and thus easily distinguish the origin of an adnexal mass, while 3D power Doppler allows detailed analysis of the neovascularization. Kurjak et al.[46] were the first to report on preoperative diagnosis of the primary fallopian tube carcinoma by 3D power Doppler ultrasound. Three-dimensional ultrasound was used to evaluate 520 adnexal masses prior to elective surgery during a two-year-period. These lesions were originally detected with conventional transvaginal sonography and/or transvaginal color Doppler. Patients with suspicious morphology and/or Doppler findings underwent a second assessment at the referral center by the investigator performing 3D ultrasound that was unaware of the previous ultrasound examinations. Three-dimensional transvaginal ultrasound was performed using either 5 or 7.5 MHz transvaginal transducers (Voluson 530, Kretztechnik, Austria). Once the region of the interest was identified, a volume box was superimposed to scan the image. The patient was asked to lie still on the examination bed, while the ultrasound probe was kept steady in the vagina. Depending on the size of the volume box the scanning procedure lasted between 5 and 13 seconds. The ability to store 3D ultrasound data on a hard disk drive allowed the investigator to keep the examination time short (between 2 and 4 minutes). Detailed analysis of the adnexal tumor was performed after the patient had gone and lasted between 10 and 20 minutes. Rotation and translation of the stored volumes allowed evaluation of different tumor sections in many planes. The "niche mode" enabled meticulous study through selected sections of the adnexal tumor and was found especially useful in evaluation of the sausage-shaped complex masses. The "surface reconstruction" allowed plastic image of the inner and outer wall of the tumor **(Fig. 49.14A)**. Demonstration of the complex adnexal mass and/or sausage-shaped cystic lesions with papillary projections was the morphological criteria for detection of the tubal malignancy.

After B-mode analysis, power Doppler imaging was switched on together with the volume mode. In order to reduce the acquisition time the volume of the color box and sweep angle were reduced. The color frame rate was adjusted as follows: both color density and color quality were as low as necessary to obtain a good color image, while pulse repetition frequency was as high as possible in order to enable the display of targeted flow velocity. The spatial peak temporal average (SPTA) intensity was approximately 80 mW/cm^2. Wall filters (50 Hz) were used to eliminate low-frequency signals. The patient examination time by 3D power Doppler was 3 minutes. Using the fast line density, the average acquisition time was 48 s (range 25–88 s). At the end of each examination combined color and gray rendering mode was used, allowing simultaneous analysis of the morphology, texture and vascularization. The subsequent analysis of the power Doppler reformatted sections lasted between 5 and 10 minutes. Demonstration of the chaotic, randomly dispersed vessels with irregular branching within the papillary protrusions and/or solid parts was suggestive of tubal malignancy. Other structural abnormalities of the malignant tumor vessels were demonstration of the

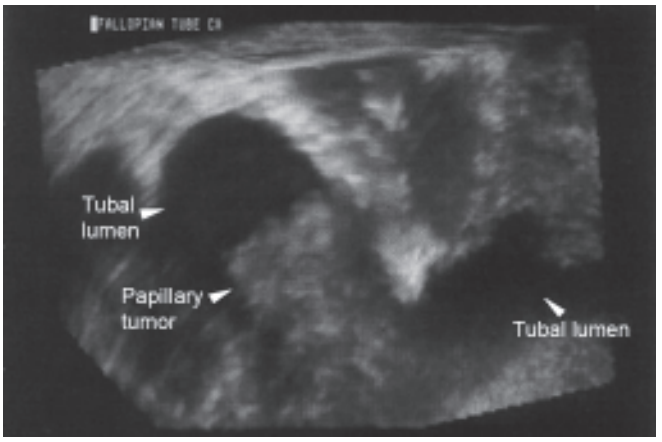

Figure 49.14A: Three-dimensional ultrasound image of primary fallopian tube carcinoma. Papillary protrusions suggestive of fallopian tube malignancy are clearly seen within the distended tubal wall

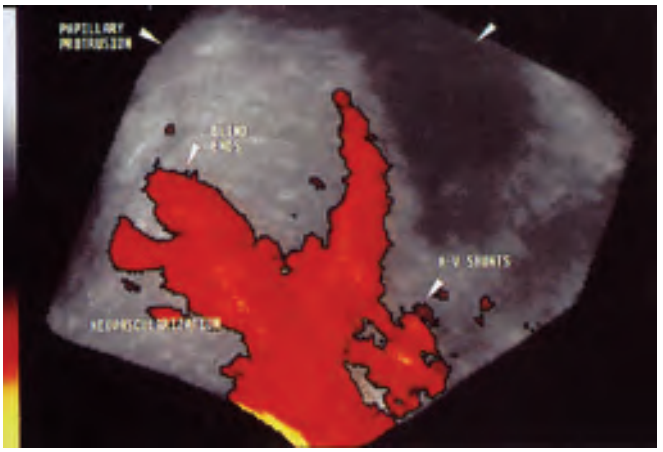

Figure 49.14B: Three-dimensional power Doppler imaging enables evaluation of vascular geometry of the newly formed vessels in a case of fallopian tube carcinoma. Note irregular branching of the vessels, blind-ended lakes and disproportional calibration all indicative for tumoral neovascularization

microaneurysms, arteriovenous shunts, tumoral lakes, disproportional calibration, coiling and dichotomous branching **(Fig. 49.14B)**. Using the above-mentioned criteria, five cases of the fallopian tube carcinoma were successfully identified prior to surgery. They all presented nonpathognomonic appearance by B-mode ultrasound: the image was usually similar to that of pyosalpinx or a fluid-filled tube with a significant solid component adjacent to the tube. Three-dimensional transvaginal ultrasound allowed more precise distinction of the tubal mass from that of the ovary, cervix and uterus. Furthermore, the change in shape and size of the mass and passage of free fluid from tubal mass through the uterine cavity can be documented dynamically. The three perpendicular planes displayed simultaneously on the screen provided the opportunity to obtain multiple sections of the tortuous adnexal lesion by the capacity of rotation and translation in any planes. The ability to reconstruct 3D plastic images improved the recognition of the adnexal lesion anatomy, characterization of the surface features and determination of the extent of tumor infiltration through the capsule.

The "niche" aspect of 3D ultrasound revealed intratumoral structures in selected sections, which was mandatory for evaluation of the tubal pathology. Multiple sections of the tumor, rotation, translation and reconstruction allowed prediction of the tumor spread to the uterus and/or the ovary, or other surrounding structures. Shortened scanning time and detailed analysis of the stored data by trained and experienced ultrasonographer were additional advantages of 3D over 2D sonography.

Malignant tumor vessels that are usually randomly dispersed within the central and peripheral parts demonstrate irregular course, complicated branching and disproportional calibration, features that can be recognized using three-dimensional power Doppler technology. Improved detection and classification of tumor architecture might contribute to better preoperative diagnostics for fallopian tube carcinoma.

CONCLUSION

Transvaginal ultrasound with color Doppler facilities is expedient not only for accurate assessment of the regional blood flow, but also for differentiating benign adnexal conditions from malignant. Based on Color Doppler assessment acute pelvic inflammatory disease can be distinguished from the chronic one. The introduction of 3D ultrasound enables spatial delineation of examined structures giving the information whether the pathologic structure is of the ovarian or tubal origin. It is expected that wide application of this novel technique will enable early detection of fallopian tube tumors, thus enabling early intervention and increased survival rates.

REFERENCES

1. Timor-Tritsch IE, Rottem S. Transvaginal ultrasonographic study of the fallopian tube. Obstet Gynecol. 1987;70 (3 Pt.1):424-8.
2. Timor-Tritsch IE, Bar-Yam Y, Elgali S, et al. The technique of transvaginal sonography with use of a 6.5 MHz probe. Am J Obstet Gynecol. 1988;158(5):1019-24.
3. Timor-Tritsch IE, Rottem S, Lewit N. The Fallopian tubes. In: Timor-Tritsch I.E, Rottem S. (Eds). Transvaginal Sonography, 2nd edition. New York: Elsevier; 1991.pp.131-44.
4. Westroem L, Wolner-Hanssen P. Pathogenesis of pelvic inflammatory disease. Genitourinary Medicine. 1993;69:9-17.

5. Toth M, Chervenak FA. Color Doppler ultrasound in the diagnosis of pelvic inflammatory disease. In: Kurjak A. (Ed). An Atlas of Transvaginal Color Doppler, Parthenon Publishing Group; 1994. pp.215-21.
6. Patten RM, Vincent LM, Wolner-Hanssen P, et al. Pelvic inflammatory disease: endovaginal sonography with laparoscopic correlation. J Ultrasound Med. 1990;9(12):681-9.
7. Kupesic S, Kurjak A, Pasalic L, et al. The value of transvaginal color Doppler in the assessment of pelvic inflammatory disease. Ultrasound Med Biol. 1995;21(6):733-8.
8. Kurjak A, Zalud I, Jurkovic D, et al. Transvaginal color Doppler for the assessment of the pelvic circulation. Acta Obstet Gynecol Scand. 1989;68(2):131-5.
9. Collins W, Jurkovic D, Kurjak A, et al. Ovarian morphology, endocrine function and intrafollicular blood flow during the periovulatory period. Hum Reprod. 1991;6:319-9.
10. Kurjak A, Kupesic S, Schulman H, et al. Transvaginal color Doppler in the assessment of the ovarian and uterine blood flow in infertile women. Fertil Steril. 1991;56(5):870-3.
11. Bourne T. Transvaginal colour Doppler in gynaecology. Ultrasound Obstet Gynecol. 1992;80:359-73.
12. Kurjak A, Zalud I, Alfirevic Z. Evaluation of adnexal masses with transvaginal color ultrasound. J Ultrasound Med. 1991;10(6):295-7.
13. Kurjak A, Zalud I, Schulman H. Ectopic pregnancy: transvaginal color Doppler study of trophoblastic flow in questionable adnexa. J Ultrasound Med. 1991;10(12):685-9.
14. Kurjak A, Predanic M, Kupesic S, et al. Transvaginal color Doppler for the assessment of adnexal tumor vascularity. Gynecol Oncol. 1993;50(1):3-9.
15. Tinkannen H, Kujansuu E. Doppler ultrasound findings in tubo-ovarian infectious complex. J Clin Ultrasound. 1993;21(3):175-8.
16. Jurkovic D, Bourne TH, Jauniaux E, et al. Transvaginal color Doppler study of blood flow in ectopic pregnancies. Fertil Steril. 1992;57(1):68-73.
17. Kurjak A, Predanic M. New scoring system for prediction of ovarian malignancy based on transvaginal color Doppler sonography. J Ultrasound Med. 1992;11(12):631-8.
18. Teisala K, Heinonen PK, Punnonen JR. Transvaginal ultrasound in the diagnosis and treatment of tubo-ovarian abscess. Br J Obstet Gynaecol. 1990;97(2):178-80.
19. Senoh D, Yanagihara T, Akiyama M, et al. Laparoscopy-assisted intrapelvic sonography with a high-frequency, real-time miniature transducer for assessment of the Fallopian tube: a preliminary report. Hum Reprod. 1999;14(3): 704-6.
20. Woodruff JD,Pauerstein CJ. The fallopian tube. Baltimore: Williams & Wilkins; 1969.
21. Mroueh J, Margono F, Feinkind L. Tubal pregnancy associated with ampullary tubal leiomyoma. Obstet Gynecol. 1993;81(5 Pt.2):880-2.
22. Kobayashi T, Suzuki K, Arai T, et al. Angiomyofibroblastoma arising from the fallopian tube. Obstet Gynecol. 1999;94(5 Pt. 2):833-4.
23. Sedlis A. Carcinoma of the fallopian tube. Surg Clinic N Am. 1978;58:121.
24. Ayhan A, Deren D, Yuce K, et al. Primary carcinoma of the Fallopian tube: a study of 8 cases. Eur J Gynecol Oncol. 1994;15(2):147-51.
25. Dava D, Young RH, Scully RE. Endometrioid carcinoma of the Fallopian tube resembling and adnexal tumor of probable Wolffian origin: a report of six cases. Int J Gynecol Pathol. 1992;11(2):122-30.
26. Soundara RS, Ramdas CP, Reddi RP, et al. A review of fallopian tube carcinoma over 20 years (1971-90) in Pondicherry. Indian J Cancer. 1991;28(4):188-95.
27. Chiou YK, Su IJ, Chen CA, et al. Malignant mixed Muellerian tumor of the fallopian tube. J Formos Med Associ. 1991;90(8):793-5.
28. Chang HC, Hsueh S and Soong YK. Malignant mixed Muellerian tumor of the fallopian tube. Case report and review of literature. Chang Keng I Hsueh. 1991;14 (4): 259-63.
29. Tokunaga T, Miyazaki K, Okamura H. Pathology of the Fallopian tube. Curr Opin Obstet Gynecol. 1991;3(4): 574-9.
30. Subramayon BR, Raghavendra BN, Whalen CA, et al. Ultrasonic features of Fallopian tube carcinoma. J Ultrasound Med. 1984;3(9):391-3.
31. Meyer JS, Kim CS, Price HM, et al. Ultrasound presentation of primary carcinoma of the fallopian tube. J Clin Ultrasound. 1987;15(2):132-4.
32. Ajjimakorn S, Bhamarapravati Y. Transvaginal ultrasound and the diagnosis of fallopian tubal carcinoma. J Clin Ultrasound. 1991;19(12):116-19.
33. Granberg S, Jansson I. Early detection of primary carcinoma of the fallopian tube by endovaginal ultrasound. Acta Obstet Gynecol Scand. 1990;69(7-8):667-8.
34. Slanetz PJ, Whitman GJ, Halpern EF, et al. Imaging of the fallopian tube tumors. Am J Roentgenol. 1997;169(5):1321-4.
35. Ong C.L. Fallopian tube carcinoma with multiple tumor nodules seen on transvaginal sonography. J Ultrasound Med. 1998;17(1):71-3.
36. Hinton A, Bea C, Winfield AC, et al. Carcinoma of the fallopian tube. Krol Radiol. 1988;10:113-5.
37. Ekici E, Vicdan K, Danisman N, et al. Ultrasonographic Appearance of fallopian-Tube Carcinoma. Int J Gynecol Obstet. 1992;49:325-9.
38. McGoldrick JL, Strauss H, Rao J. Primary carcinoma of the fallopian tube. Am J Surg. 1943;59:559-63.
39. Eddy GL, Schlaerth JB, Nalick RH, et al. Fallopian tube carcinoma. Obstet Gynecol. 1984;64:546-51.
40. Lerner JP, Timor-Tritsch IE, Federmann A, et al. Transvaginal ultrasonographic characterization of ovarian masses with an improved weighted scoring system. Am J Obstet Gynecol. 1994;170(1 Pt. 1):81-5.
41. Bourne TH, Campbell S, Steer C, et al. Transvaginal color flow imaging a possible new screening technique for ovarian cancer. Br Med J. 1994;299(6712):1367-70.
42. Kawai M, Kano T, Kikkawa F, et al. Transvaginal Doppler ultrasound with color flow imaging in the diagnosis of ovarian cancer. Obstet. Gynecol. 1992;79(2):163-7.
43. Shalan H, Sosic A, Kurjak A. Fallopian tube carcinoma: recent diagnostic approach by color Doppler imaging. Ultrasound Obstet Gynecol. 1992;2(4):297-9.
44. Podobnik M, Singer Z, Ciglar S, et al. Preoperative diagnosis of primary fallopian tube carcinoma by transvaginal ultrasound, cytological finding and CA-125. Ultrasound Med Biol. 1993;19(7):587-91.

45. Kurjak A, Kupesic S, Ilijas M, et al. Preoperative diagnosis of primary fallopian tube carcinoma. Gynecol. Oncol. 1998;68(1);29-34.
46. Kurjak A, Kupesic S,Jacobs I. Preoperative diagnosis of the primary fallopian tube carcinoma by three-dimensional static and power Doppler sonography. Ultrasound Obstet. Gynecol. 1999;15(3):246-51.
47. Kol S, Gal D, Friedman M,et al. Preoperative diagnosis of primary fallopian tube carcinoma by transvaginal sonography and CA 125. Gynecol. Oncol. 1990;37(1):129-37.
48. Kurjak A, Kupesic S, Breyer B, et al. The assessment of ovarian tumor angiogenesis: what does three-dimensional power Doppler add? Ultrasound Obstet Gynecol. 1998; 12(2):136-46.
49. Gojnic M, Pervulov M, Petkovic S, et al. The significance of Doppler flow and anamnesis in the diagnosis of fallopian tube cancer. Eur J Gynaecol Oncol. 2005;26(3): 309-10.

50
CHAPTER

The Use of Sonographic Imaging with Infertility Patients

Sanja Kupesic Plavsic, Nadah Zafar, Guillermo Azumendi

INTRODUCTION

Infertility is defined as the failure to conceive a desired pregnancy after 12 months of unprotected intercourse, and affects 10% of married couples. With recent technological advances and the proper use of medically-assisted reproduction techniques, one half of these couples are able to conceive successfully.

More than any other new modality, ultrasound has made significant improvements in the modern management of the infertile female patient. Transvaginal sonography provides the reproductive endocrinologist with a tool that cannot only evaluate normal and stimulated cycles, but also assists in follicle aspiration and subsequent transfer of the embryo. The addition of color Doppler capabilities to transvaginal probes permits visualization of small intraovarian and endometrial vessels, allowing depiction of normal and abnormal physiologic changes in the ovary and uterus. It may help to predict ovulation and detection of certain ovulatory disorders such as the luteal phase defect (LPD). Doppler investigation of ovarian blood flow may improve the early diagnosis of ovarian hyperstimulation syndrome (OHSS) in patients with ovulation induction. Numerous studies conducted during the last decade have confirmed the initial impressions about the usefulness of blood flow studies in infertile patients. This chapter reviews the assessment of ovarian, uterine and tubal causes of infertility, and the current and future role of color Doppler and three-dimensional (3D) ultrasound in the field of reproductive endocrinology.

UTERINE CAUSES OF INFERTILITY

The uterine cavity must provide an environment for successful sperm migration from the cervix to the fallopian tube. It is necessary for the uterus to have a normal mucous lining, glandular secretion, and vascularity in order to support implantation and placentation. Uterine anomalies, polyps, leiomyomas, neoplasia, infections and intrauterine scar tissue can lead to poor reproductive performance. Attempts have been made to correlate the sonographic parameters (such as thickness and reflectivity) with the endometrial receptivity.

Perfusion in Infertile Patients

Transvaginal color and pulsed Doppler sonography has been established as an additional tool in the management of infertile patients. In anovulatory cycles, a continuous increase of the uterine artery resistance index (RI) has been detected **(Graph 50.1)**.[1,2] Moreover, in some infertile patients, an end-diastolic flow is absent.[3] The results of some research indicate that absent diastolic flow might be associated with infertility and poor reproductive performance. Therefore, the uterine artery blood flow can potentially be used to predict a hostile uterine environment prior to embryo transfer (ET) **(Fig. 50.1)**. Steer and coworkers[4] calculated the

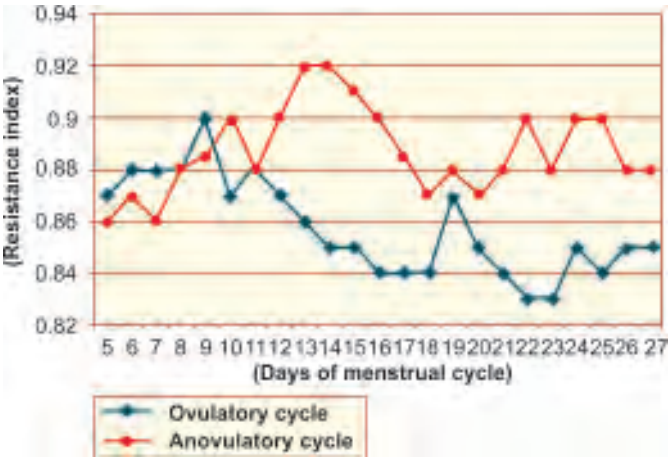

Graph 50.1: Changes in the uterine artery blood flow in ovulatory and anovulatory cycles

Source: Kurjak A, Kupesic-Urek S, Schulman H, et al. Transvaginal color Doppler in the assessment of ovarian and uterine blood flow in infertile women. Fertil Steril. 1991;56(5):870-3. (with permission)

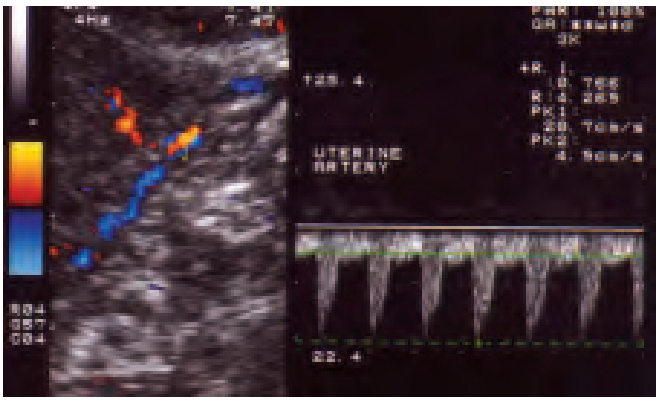

Figure 50.1: Uterine artery demonstrated laterally to the cervix at the level of the cervicocorporeal junction (left). The blood flow velocity form the uterine artery in the secretory phase is characterized by increased end-diastolic velocity and decreased resistance index (RI=0.76)

probability of pregnancy by using pulsatility index (PI) values obtained from the uterine artery on the day of ET. With the use of these measurements, the highest probability of becoming pregnant was obtained in those patients having medium values of PI for uterine arteries. A mean PI of more than 3.0 before the transfer can predict up to 35% of pregnancy failures. Tsai and colleagues[5] evaluated the prognostic value of uterine perfusion on the day of human chorionic gonadotropin (hCG) administration in patients who were undergoing intrauterine insemination. They calculated PI of the ascending branch of the uterine arteries on the day of administration of hCG and compared the uterine artery

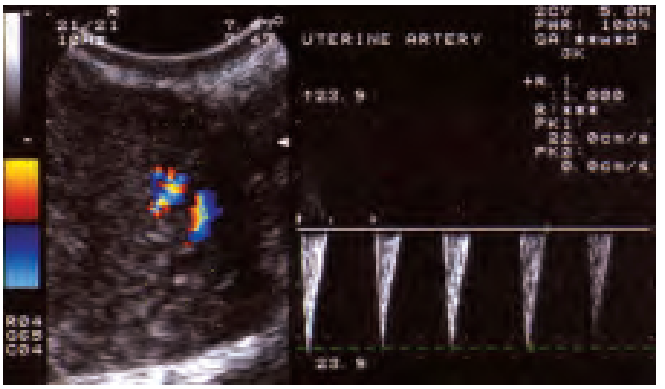

Figure 50.2: Absent diastolic flow of the uterine artery may be associated with infertility or poor reproductive performance

vascular resistance to the outcome of intrauterine insemination. Pregnancy did not occur when the PI of the ascending branch of the uterine arteries was more than three **(Fig. 50.2)**. The fecundity rate was 18% when the PI was less than 2% and 19.8% when the PI was between 2 and 3. Their data suggest that the measurement of uterine perfusion on the day of hCG administration may have a predictive value regarding fertility in patients undergoing intrauterine insemination.

In infertile women, the uterine artery PI measured in the midluteal phase of an unstimulated cycles correlates inversely with the endometrial thickness[6] suggesting a direct effect of uterine perfusion on endometrial growth.[7] Furthermore, the PI correlates directly with the age of patients,[3] suggesting a detrimental effect of age on uterine perfusion. Cacciatore et al.[8] did not find any correlation between uterine artery PI measured at the time of ET and endometrial thickness or the age of the patients. These findings could be explained by the hormonal environment of the superovulated cycles, where the high E_2 levels achieved in almost all subjects are likely to reduce differences between individuals.

A high prevalence of increased uterine artery impedance among infertile patients with the diagnosis of endometriosis has been reported by Steer and coworkers.[6] In this study, women with a history of endometriosis have significantly higher PI and RI values than the others even after hormonal stimulation. This evidence, although gained in different settings, seem to suggest an adverse effect of endometriosis on uterine perfusion. This is another way, where endometriosis can compromise a woman's fertility potential. Whether this is due to mechanical effects on the pelvic vessels as a result of adhesions or is mediated by production of agents with vasoactive properties remains to be explained.

Endometrial Thickness, Volume and Vascularity

The question of a correlation between endometrial thickness and the likelihood of implantation, in the context of assisted reproduction, remains a contentious issue. However, a very thin endometrium (below 7 mm) seems to be an accepted reliable sign of suboptimal implantation potential.

Recently, Freidler and colleagues[9] reviewed 2665 assisted reproduction cycles from 25 reports. Eight reports found that the difference in the mean endometrial thickness of conception and nonconception cycles was statistically significant, while 17 reports found no significant difference. They concluded that the results from the various trials are conflicting and that insufficient data exists describing a linear correlation between endometrial thickness and the probability of implantation. The main advantage of measuring endometrial thickness lies in its high negative predictive value in cases where there is minimal endometrial thickness. Gonen and colleagues[10] reported an absence of pregnancies in donor insemination cycles when the endometrial thickness did not reach at least 6 mm. Similarly, in a group of oocyte recipients, no pregnancies were reported in women who had an endometrial thickness of less than 5 mm, whereas several pregnancies occurred in patients with an endometrial thickness between greater than 5 mm and 7.5 mm.[11] Finally, in case of *in vitro* fertilization (IVF) cycles, Khalifa and colleagues reported a minimal endometrial thickness of 7 mm to be compatible with pregnancy.[12] Endometrial pattern is defined as the relative echogenicity of the endometrium and the adjacent myometrium as demonstrated on a longitudinal ultrasound scan **(Fig. 50.3)**.

In a prospective study, Serafini and colleagues[13] found the multilayered pattern to be more predictive

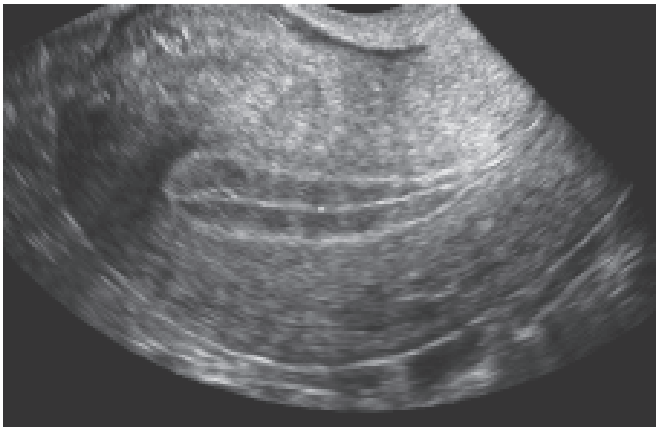

Figure 50.3: Multilayered pattern of the endometrium assessed in a longitudinal ultrasound scan

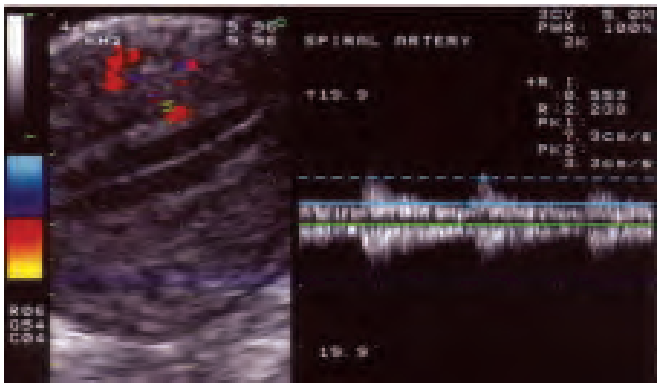

Figure 50.4: Blood flow velocity waveforms of the spiral arteries during the periovulatory phase. Note the triple-line endometrium (left) and the moderate resistance index (RI=0.55) (right) obtained from spiral arteries

of implantation than any other parameter measured. Sher and colleagues[14] correlated a nonmultilayered echo pattern of the endometrium with advanced maternal age and the presence of uterine abnormalities. In the literature of the 13 studies that examined the value of the endometrial pattern in predicting pregnancy, only four failed to confirm its predictive value. The endometrial pattern does not appear to be influenced by the type of ovarian stimulation and it is of prognostic value for both fresh IVF, as well as frozen ET cycles.

Zaidi et al.[15] reported that if subendometrial blood flow is detectable, the endometrial morphology may be less important than previously described and it may be that the absence of blood flow is more significant.

The authors evaluated 96 women undergoing in IVF treatment on the day of hCG administration. They assessed endometrial thickness, endometrial morphology, presence or absence of subendometrial or intraendometrial color flow, intraendometrial vascular penetration and subendometrial blood flow velocimetry on the day of hCG administration and related the results to pregnancy rates **(Fig. 50.4)**. The overall pregnancy rate was 32.3% (31/96) and there was no significant difference between the pregnant and nonpregnant groups with regard to endometrial thickness, subendometrial peak systolic blood flow velocity (V_{max}) or subendometrial PI. The pregnancy rates based on endometrial morphology were not significantly different, being 17.6% (3/17), 33.3% (2/6) and 35.6% (26/73) for types A (hyperechoic), B (isoechoic) and C (triple-line) endometria respectively. In eight (8.3%) patients, subendometrial color flow and intraendometrial vascularization were not detected. This absence of blood flow was associated with failure of implantation ($p< 0.05$). The pregnancy rates related to the zones

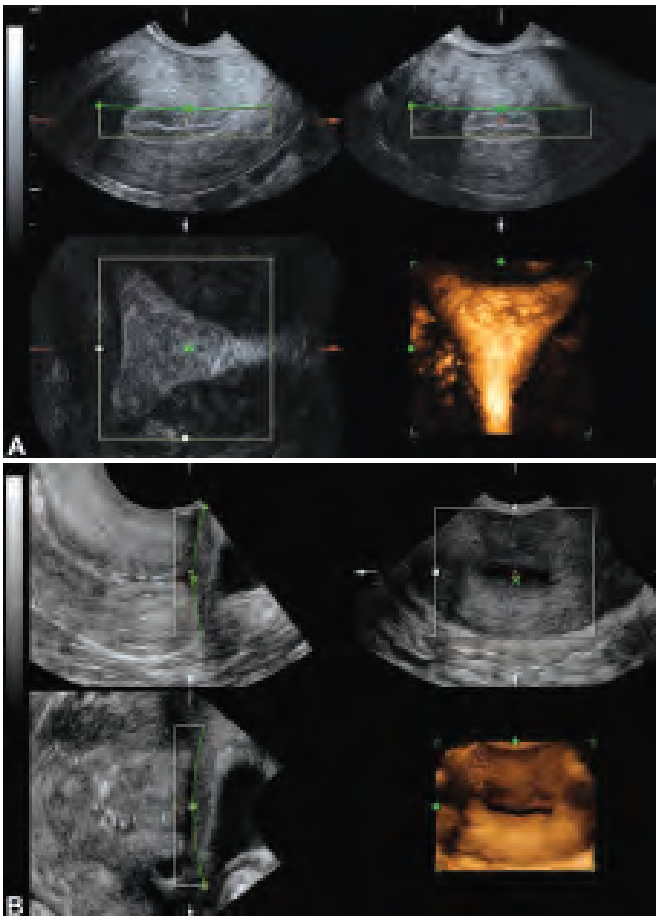

Figures 50.5A and B: (A) Three-dimensional ultrasound of normal uterus. Triangular appearance of the endometrium is clearly visualized in coronal and surface rendering images; (B) The same modality can be used for visualization of the cervix and assessment of its mucus

of vascular penetration into the subendometrial and endometrial regions were: 26.7% (4/15) for zone 1 (subendometrial zone), 36.4% (16/44) for zone 2 (outer hyperechogenic zone) and 37.9% (11/29) for zone 3 (inner hypoechogenic zone), and these were not significantly different.

Endometrial thickness obtained by two-dimensional (2D) sonography is considered the most important parameter of endometrial growth. However, this parameter does not include the total volume of the endometrium. It is useful to have certain diagnostic parameters concerning the endometrium, one of which is the endometrial volume measurement **(Fig. 50.5A)**. Furthermore, retarded endometrial development can be associated with primary infertility. In addition to endometrial volume and echogenicity the sonographer can evaluate the shape and length of the cervix, as well as determine the presence of the cervical mucus **(Fig. 50.5B)**. The ability to quantify the volume of the endometrium using 3D ultrasound may help to correlate cycle outcome with a quantitative parameter rather than endometrial thickness, which is prone to greater subjective variation in measurement.[16] By stepping through the volume in plane mode, the outer limits of endometrium are traced and in addition, volume calculations can be performed immediately The accurateness of this method has already been described.[17,18] To obtain the best results, stepping through the volume should be performed in small units. In each new plane the area tracing has to be corrected to its new extent. Low contrast in ultrasound data can increase the error of volume estimation. In general, the endometrium shows a good contrast to the surrounding myometrial tissue and therefore in most cases volume estimation can be performed. Measurements can best be reproduced in longitudinal and transverse viewing planes. Other sources of measuring error may derive from the low contrast of the caudal end of the endometrium and the uterus. Endometrial fluid may also increase measuring error because the fluid volume may be too small to be measured accurately by 3D ultrasound.

Lee et al.[19] were first to demonstrate volume estimation of the endometrium by 3D ultrasound. Using the same method Kyei-Mensah et al.[20] assessed the reliability of 3D ultrasound in measuring endometrial volume on 20 patients undergoing ovarian stimulation. Endometrial volumes of these patients were obtained on the day of hCG administration. The intraobserver and interobserver coefficient of variation were 8% and 11% respectively. Repeatability within and between investigators was also expressed as the intra-class correlation coefficient and inter-class correlation coefficient (intra-CC and inter-CC). The coefficients describe the proportion of variation in a measurement, which is caused by true biological subject differences. For a single measurement of endometrial volume, the intra-CC was 0.90 and inter-CC was 0.82. These results clearly demonstrate that 3D ultrasound volume measurements are highly reliable, with a small measurement error. However, one could expect higher interobserver differences in the ability to accurately locate the internal os and endometrial margins. This may explain the greater interobserver variability for endometrial volume than for ovarian volume. Since it is applied in the same manner as 2D vaginal ultrasound, it does not cause additional discomfort.

It is expected that 3D endometrial volumetry studies will increase diagnostic potential and give additional

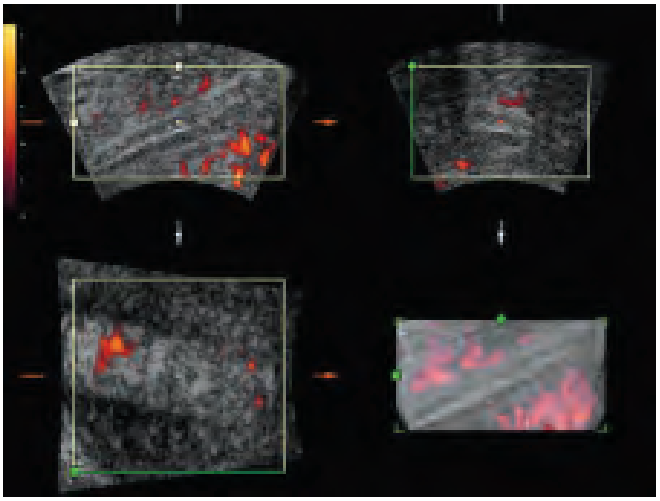

Figure 50.6: Three-dimensional power Doppler of the endometrium. Subendometrial flow reflects the degree of endometrial perfusion and may be used as a noninvasive assay of uterine receptivity

information to 2D ultrasound. Furthermore, quantification of endometrial volume by 3D ultrasound in combination with blood flow studies may be the best way to predict pregnancy rates.

Kupesic et al.[21] investigated the usefulness of transvaginal color Doppler and 3D power Doppler ultrasonography for the assessment of endometrial receptivity in patients undergoing IVF procedures **(Fig. 50.6)**. The patients were evaluated for endometrial thickness and volume, endometrial morphology and subendometrial perfusion on the day of ET. Neither the volume nor the thickness of the endometrium on the day of ET had a predictive value for implantation during IVF cycles. Patients who became pregnant were characterized by a significantly lower RI (0.53+/-0.04 vs 0.64+/-0.04), obtained from subendometrial vessels by transvaginal color Doppler ultrasonography and a significantly higher flow index (13.2+/-2.2 vs 11.9+/-2.4), as measured by a 3D power Doppler histogram. No differences were found in the predictive value of scoring systems analyzing endometrial thickness and volume, endometrial morphology and subendometrial perfusion by color Doppler and 3D power Doppler ultrasonography. The high degree of endometrial perfusion shown by both techniques on the day of ET can indicate a more favorable endometrial milieu for successful IVF.

Congenital Anomalies

Congenital uterine malformations are variable in frequency and are usually estimated to represent 3–4% of the general population, although less than half have clinical symptoms.[22-24]

The respective frequency of symptomatic malformations is dominated by the septate uterus.[24,25] During the first trimester of pregnancy, the risk of spontaneous abortion in this group is between 28 and 45%, while during the second trimester the frequency of late spontaneous abortions is approximately 5%.[24] Premature deliveries, abnormal fetal presentations, irregular uterine activity and dystocia at delivery are likely to prevail in cases of septate uterus.[26] Poor vascularization of the septum was proposed as a potential cause of miscarriages.[25] Electron microscopy study conducted by Fedele et al.[27] indicate a decreased sensitivity of the endometrium covering the septa of malformed uteri to preovulatory changes. This could play a role in the pathogenesis of primary infertility in patients with septate uterus.

It is clear that unfavorable obstetric prognosis can be transformed by surgical correction of the intrauterine septum. Hysteroscopic treatment was currently proposed as the procedure of choice for the management of these disorders. This simple and effective treatment has an obvious advantage. The uterus is not weakened by a myometrial scar. Cararach et al.[28] and Goldenberg et al.[29] reported 75% and 88.7% pregnancy rates respectively after operative hysteroscopy.

The clear simplicity and effectiveness of hysteroscopy makes it necessary for the clinician to arrive at an early and correct diagnosis of uterine anomalies. When used as a screening test for detection of congenital uterine anomalies, transvaginal ultrasound had a sensitivity of almost 100%.[30,31] However, clear distinction between different types of abnormalities was impossible and operator dependent.[32,33]

X-ray hysterosalpingography (X-ray HSG) is an invasive test, which requires the use of contrast medium and exposure to radiation. Although HSG provides a good outline of the uterine cavity, the visualization of minor anomalies and clear distinction between different types of lateral fusion disorders is sometimes impossible to visualize. Fifteen years ago, hysterosonography was introduced.[34] This method utilizes the transvaginal ultrasound after distension of the uterine cavity by instillation of a saline solution. This simple and minimally invasive approach allows anatomical images of the endometrium and myometrium, an accurate depiction of the septate uterus, and even the measurement of the thickness and height of the septum.[35]

Although some reports have indicated a high diagnostic accuracy of magnetic resonance imaging[36,37] in the diagnosis of congenital uterine anomalies, this

technique is rarely routinely used for this pathology. More recently, a 3D ultrasound has been shown to have a high diagnostic accuracy in detection of a septate uterus[38] suggesting that invasive procedures such as CO_2 diagnostic hysteroscopy are not necessary in patients scheduled for corrective surgery.[39]

Kupesic and Kurjak attempted to evaluate the combined use of transvaginal ultrasound, transvaginal color and pulsed Doppler sonography, hysterosonography and 3D ultrasound in the preoperative diagnosis of a septate uterus.[40]

A total of 420 infertile patients undergoing operative hysteroscopy were included in this study. With the use of B-mode transvaginal sonography, the morphology of uterus was carefully explored with emphasis on the endometrial lining in both sagittal and transverse sections. The septum was visualized as an echogenic portion separating the uterine cavity into two parts. Once an experienced sonographer completed the B-mode examination, another skilled operator who was unaware of the previous finding performed the transvaginal color Doppler examination.

Color and pulsed Doppler was superimposed to visualize intraseptal and myometrial vascularity. Flow velocity waveforms were obtained from all the interrogated vessels. For each recording, at least five waveform signals of good quality were obtained. During each procedure the RI was automatically calculated. The RI was calculated from the maximum frequency envelope and consisted of: peak systolic velocity (PSV) minus end-diastolic velocity divided by PSV. Instillation of isotonic saline (hysterosonography) was carried out on a gynecological examination table. Transverse and sagittal sections were carefully explored and the septum was visualized as an echogenic portion separating the uterine cavity into two parts.

Eighty six women undergoing hysteroscopy were examined by 3D ultrasound. When the patients were evaluated using 3D ultrasound, three perpendicular planes of the uterus were simultaneously displayed on the screen, allowing a detailed analysis of the uterine morphology **(Fig. 50.7)**. The frontal reformatted sections and tomographic ultrasound imaging (TUI) were particularly useful for detection of the uterine abnormalities **(Fig. 50.8)**. Major advantages of 3D ultrasound is a simultaneous visualization of the uterine cavity **(Fig. 50.9A)** and assessment of the fundal shape **(Fig. 50.9B)**. Diagnosis of a septate uterus is based on visualization of the "V" or "Y" shape of the uterine cavity and convex or planar uterine fundus.

Table 50.1 summarizes the sensitivity, specificity, positive and negative predictive values of the transvaginal sonography, transvaginal color and pulsed Doppler ultrasound, HSG, and 3D ultrasound for the diagnosis of a septate uterus. The sensitivity of transvaginal sonography in the diagnosis of septate uteri was 95.21%. Transvaginal color and pulsed Doppler enabled the diagnosis of a septate uterus in 276 cases, reaching a sensitivity of 99.29%. In one patient with an endometrial polyp and one with intrauterine synechiae, a septate uterus was not correctly diagnosed. Therefore, the reliability of color and pulsed Doppler examination was reduced if other intracavitary structures (such as endometrial polyp or submucous leiomyoma) were present.

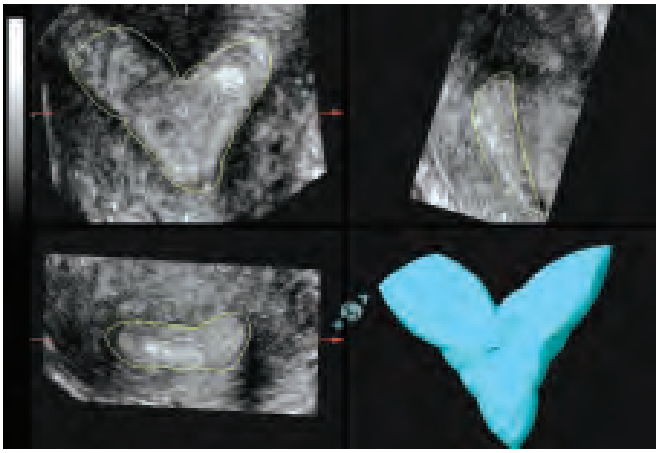

Figure 50.7: Three-dimensional ultrasound of a septate uterus. Note partial division of the uterine cavity and "Y" shape of the uterine cavity. Hysteroscopy confirmed subseptate uterus

TABLE 50.1

Sensitivity, specificity, positive (PPV) and negative predictive (NPV) values of various imaging modalities for the diagnosis of septate uterus in 420 patients with history of infertility and recurrent abortions

Imaging modality	*Sensitivity (%)*	*Specificity (%)*	*PPV (%)*	*NPV (%)*
Transvaginal sonography	95.21	92.21	95.86	91.03
Transvaginal color Doppler	99.29	97.93	98.03	98.61
Hysterosonography	98.18	100.00	100.00	95.45
Three dimensional ultrasound	98.38	100.00	100.00	96.00

Source: Kupesic S, Kurjak A. Septate uterus: detection and prediction of obstetrical complications by different forms of ultrasonography. J Ultrasound Med. 1998;17:631-6.

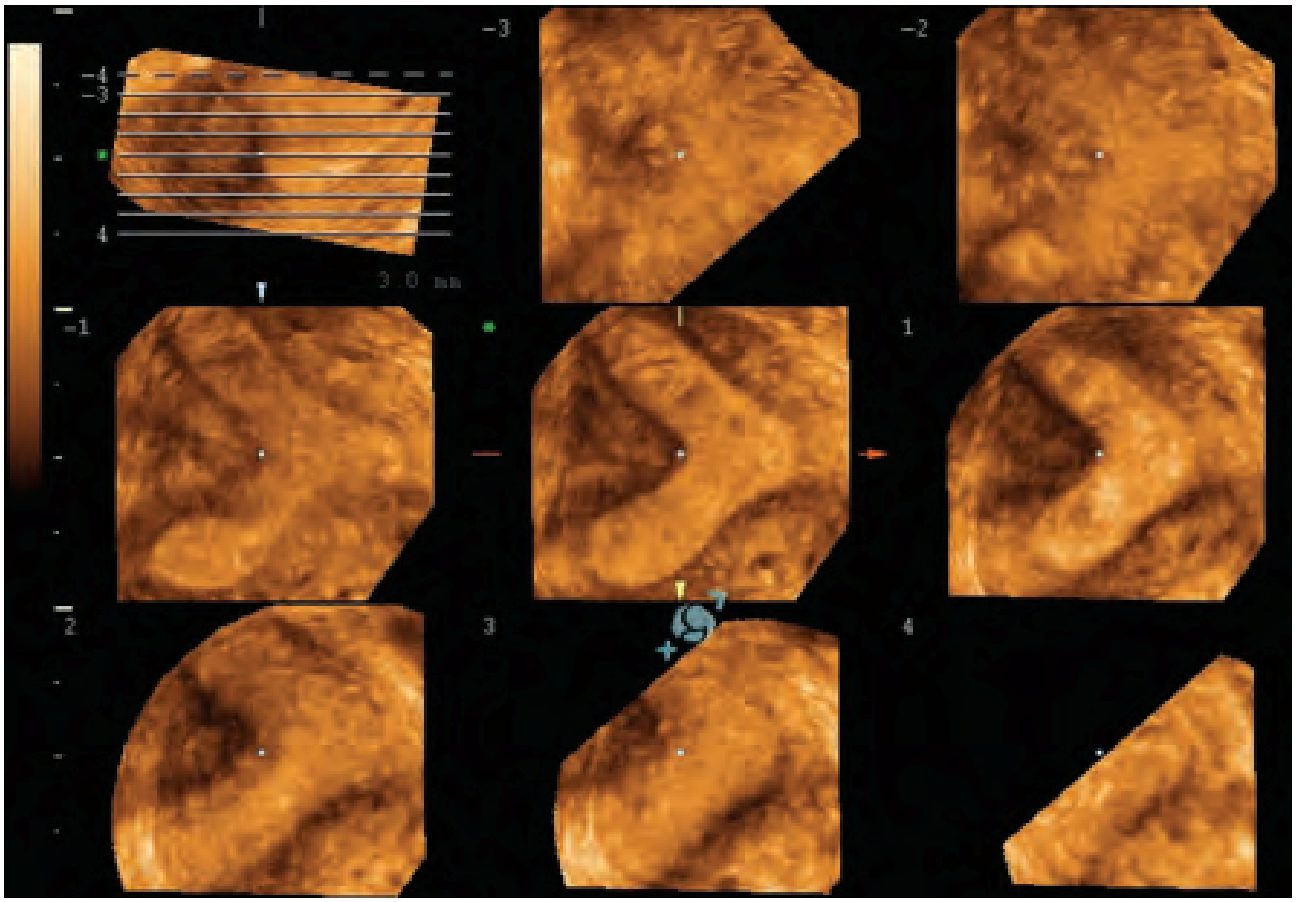

Figure 50.8: Frontal reformatted section and tomographic ultrasound images (TUI) of a septate uterus

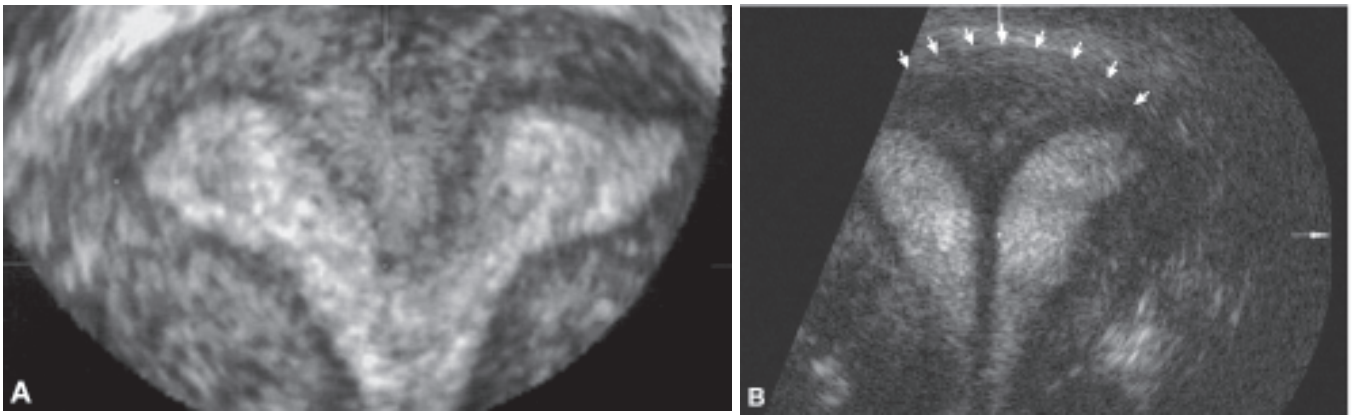

Figures 50.9A and B: (A) Frontal reformatted section of a septate uterus. Note clear division of the uterine cavity in the upper half of the uterine cavity and convex shape of the uterine fundus; (B) Another case of a septate uterus. Note a complete division of the uterine cavity and convex shape of the uterine fundus

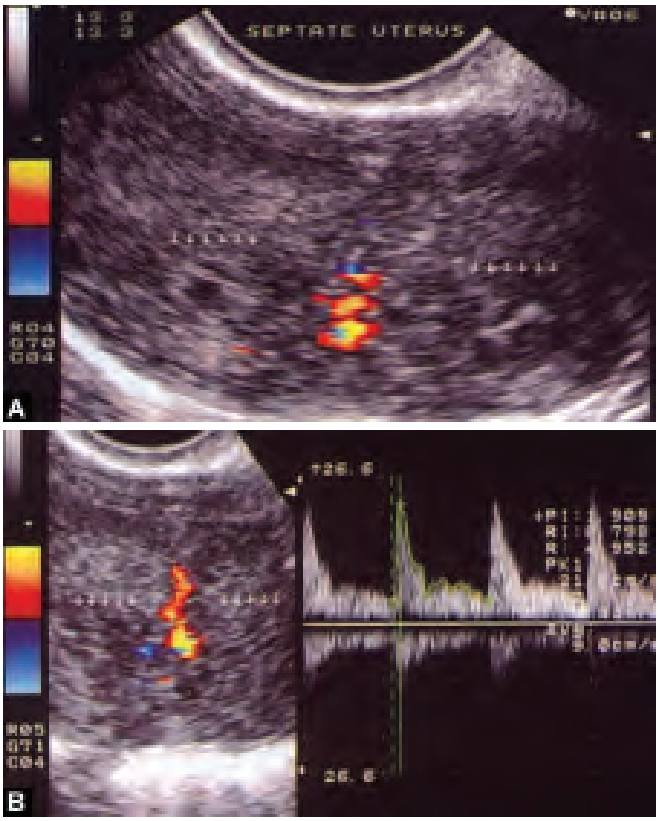

Figures 50.10A and B: (A) Septate uterus demonstrated by color Doppler imaging. Vascularity within the septal area is easily observed by this technique; (B) Pulsed Doppler waveform analysis (right) reveals moderate to high vascular resistance (RI=0.79) of the vessels involved in the septum

Color and pulsed Doppler studies of the septal area revealed vascularity in 198 (71.22%) patients. The RI values obtained from the septum ranged from 0.68–1.0 (mean RI=0.84 ± 0.16) **(Figs 50.10A and B).** Hysterosonography reached both a 100% specificity and positive predictive value. In one patient with extensive intrauterine synechiae and hysterosonography did not detect an intrauterine septum.

The sensitivity and specificity of 3D ultrasonography were 98.38% and 100% respectively. A false-negative result in one patient was caused by a fundal fibroid distorting the uterine cavity. Interestingly, in our study the septate uterus was not mistaken for a bicornuate uterus.

In our study, a transvaginal color Doppler sonography, a hysterosonography and a 3D ultrasonography were performed. However, in one patient with a bicornuate uterus the transvaginal sonogram was misinterpreted as a septate uterus.

One hundred eighty eight patients underwent X-ray HSG within 12 months prior to our examination. The sensitivity of X-ray HSG for the diagnosis of septate uteri was only 26.06%.

Fedele et al.[27] recently indicated that an intrauterine septum may be a cause of primary infertility. The ultrastructural morphological alterations of the septal area were indicative of irregular differentiation and estrogenic maturation of septal endometrial mucosa. Since the hormonal levels of the patients enrolled in this study were normal for the cycle phase, the most

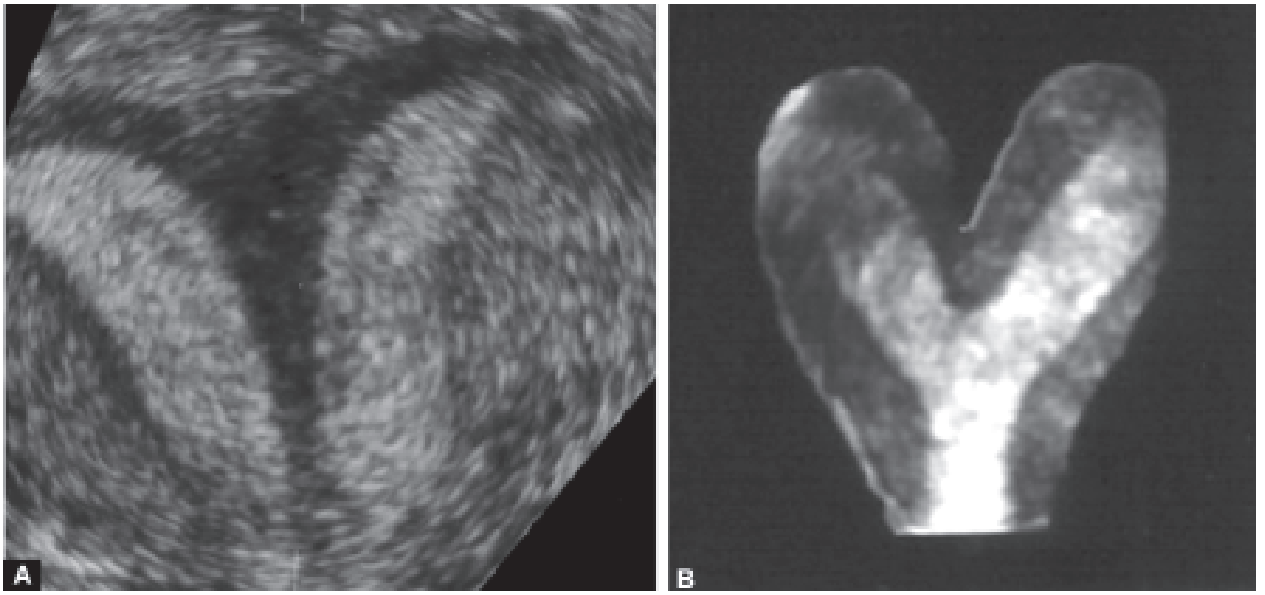

Figures 50.11A and B: (A) Frontal reformatted section; (B) Surface rendering of a bicornuate uterus. Note division of the uterine cavity and fundal cleft exceeding 1 cm. Bicornuate uterus was confirmed by hysterolaparoscopic procedure

convincing hypothesis was that the endometrial mucosa covering the septum was poorly responsive to estrogens probably due to scanty vascularization of septal connective tissue.

Dabirashrafi et al.[41] performed a histologic study of the uterine septa from 16 patients undergoing abdominal metroplasty. Statistical analysis confirmed less connective tissue in the septum compared to the amount of muscle tissue, amount of muscle interlacing and vessels with a muscle wall, which was contradictory to the classic view about the histologic features of the uterine septum. Less connective tissue in the septum can be a reason for poor decidualization and placentation in the area of implantation.[35] Increased amounts of muscle tissue and muscle interlacing in the septum can cause an abortion by a higher and uncoordinated contractility of these muscles.

Ultrasound and Doppler studies found no correlation between septal height and thickness, and occurrence of obstetrical complications ($p > 0.05$).[40] Pregnancy loss correlated significantly with septal vascularity. Patients with vascularized septa had significantly higher incidence of early pregnancy failure and late pregnancy complications than those with avascularized septa ($p < 0.05$).

A 3D ultrasound enables planar reformatted sections through the uterus, which allows a precise evaluation of the fundal indentation and uterine cavity **(Figs 50.7 to 50.14)**. This approach allows precise assessment of different types of the uterine anomalies such as arcuate, septate, dydelphic **(Figs 50.12 and 50.13)** and unicornuate uterus **(Fig. 50.14)**. Based on our experience, this technique may give a mistaken impression of an arcuate uterus in patients who have a fundal location of a leiomyoma. In these cases the uterine cavity has a concave shape, while the fundal indentation is shallower. Furthermore, shadowing caused by the uterine fibroids, irregular endometrial lining and decreased volume of the uterine cavity (in cases of intrauterine adhesions) are obvious limitations of the 3D ultrasound. More recently 3D power Doppler was used to detect vascularization of the uterine septa in a combined angio and gray rendering mode. This approach allows simultaneous analysis of the morphology, texture and vascularization of the endometrium.

Balen et al.[42] described a technique of 3D reconstruction of the uterine cavity using a positive contrast medium (Echovist). The main problem encountered with Echovist was an acoustic shadowing artifact owing to its highly reflective properties. Despite this, Echovist proved to be superior to saline as an intrauterine contrast agent for 3D reconstruction while testing 10 patients with both methods.

Weinraub et al.[43] used 3D saline contrast hysterosonography on 32 volunteers ranging from 22–65 years of age, all in good health and with no evidence of active infections or disease.

Contrast 3D hysterosonography offers a more comprehensive overview of the uterine cavity and surrounding myometrium, and gives access to planes unobtainable by conventional 2D ultrasound examination. Further research is required to document whether contrast instillation contributes to better diagnosis of uterine cavity pathology when compared to unenhanced frontal reformatted section.

Kupesic et al.[44] studied the incidence of surgically correctable uterine abnormalities (congenital uterine anomalies, submucous leiomyoma, endometrial polyps and intrauterine synechiae) in the infertile population attending a tertiary infertility clinic. All of the infertile patients enrolled in the study were evaluated by 3D ultrasound. An additional objective was to assess pregnancy rates before and after operative hysteroscopy in patients affected by uterine causes of infertility. They found the incidence of a uterine septum in their infertile population to be 17.9%. Uterine septum was the most common uterine abnormality accounting for 77.1% of the intrauterine lesions. Out of 310 patients that were followed, 225 (72.6%) patients achieved pregnancy after hysteroscopic metroplasty for an intrauterine septum.

Endometrial Polyp

An endometrial polyp is an anatomic defect, which is implicated in the etiology of a recurrent pregnancy loss and infertility. Polyps appear as diffuse or focal thickening of the endometrium **(Fig. 50.15A)**. Using sonohysterography an intracavitary polyp is seen surrounded by anechoic fluid at the point of the attachment. If the examination is performed in the follicular phase, the use of a distending medium is not necessary to detect abnormal endometrial thickening. However, during the periovulatory and secretory phase, polyps are better visualized when outlined by fluid.

By using transvaginal color and pulsed Doppler we can study minor arteries supplying the growth of an endometrial polyp **(Fig. 50.15B).** Three-dimensional ultrasound allows a detailed analysis of the uterine cavity in frontal reformatted sections, which enables clear demarcation of the polyps **(Figs 50.15C and D)**.

Submucosal Leiomyomas

The diagnosis of a submucosal leiomyoma is based on distortion of the uterine contour, uterine enlargement and textural changes. Since leiomyomas have a varying amount of smooth muscle and connective tissue, these

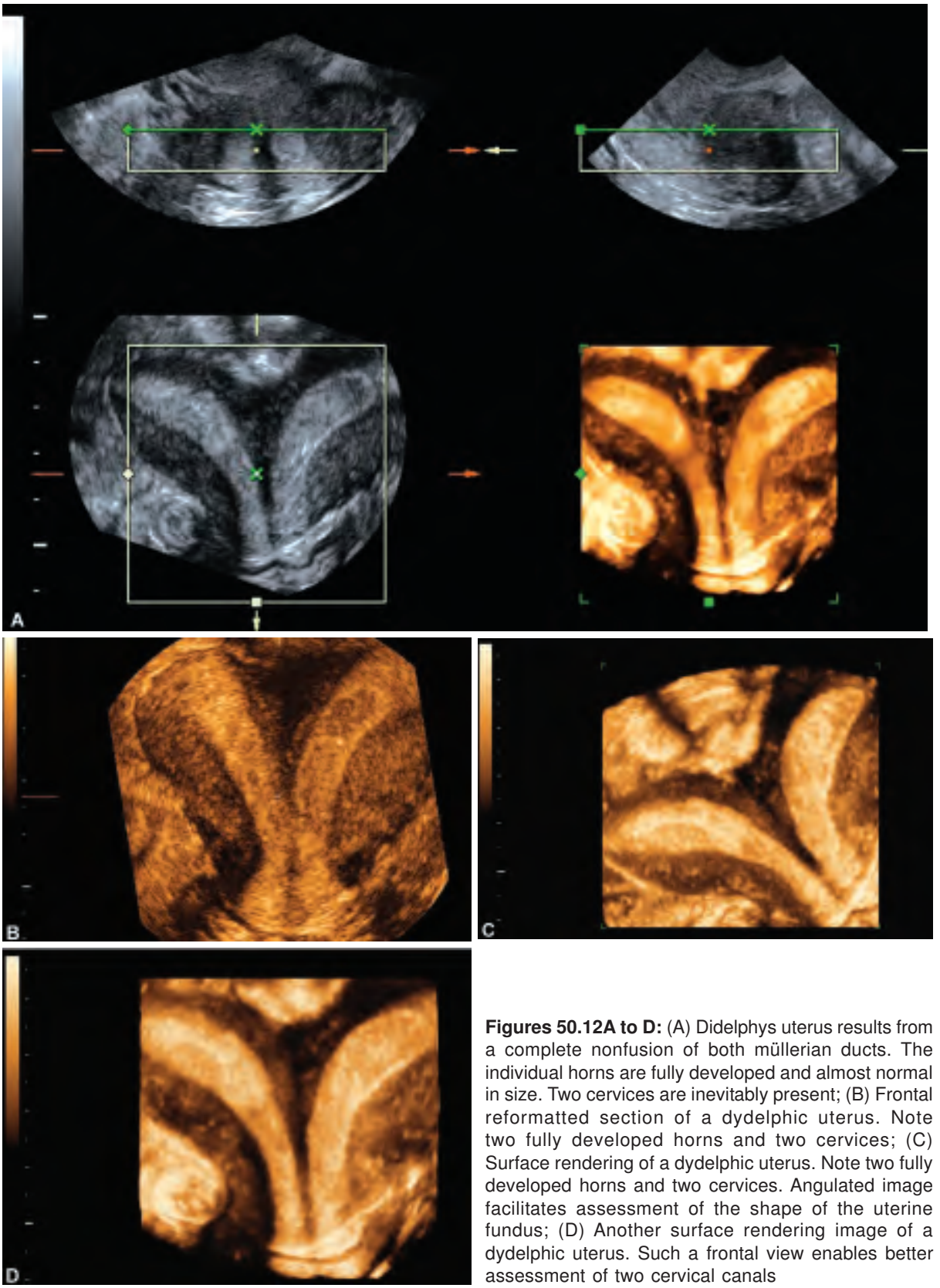

Figures 50.12A to D: (A) Didelphys uterus results from a complete nonfusion of both müllerian ducts. The individual horns are fully developed and almost normal in size. Two cervices are inevitably present; (B) Frontal reformatted section of a dydelphic uterus. Note two fully developed horns and two cervices; (C) Surface rendering of a dydelphic uterus. Note two fully developed horns and two cervices. Angulated image facilitates assessment of the shape of the uterine fundus; (D) Another surface rendering image of a dydelphic uterus. Such a frontal view enables better assessment of two cervical canals

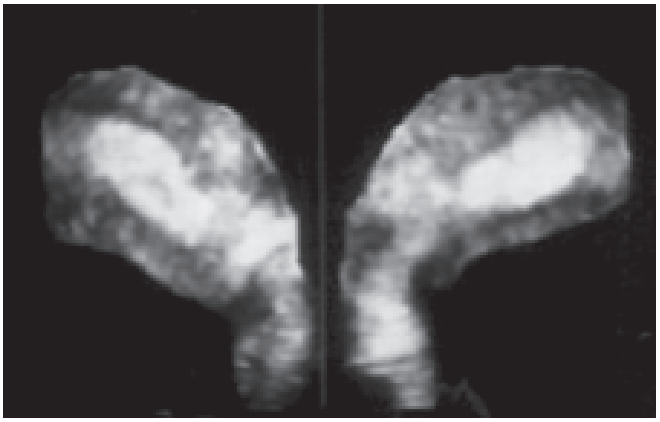

Figure 50.13: Three-dimensional ultrasound image of a didelphys uterus. Duplication of the cervix and the vagina is clearly visualized

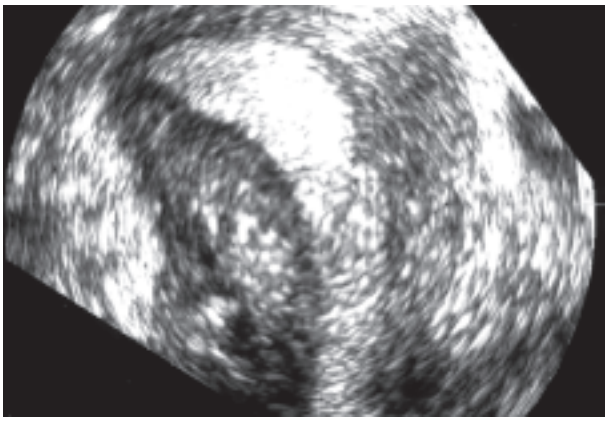

Figure 50.14: Three-dimensional ultrasound of a unicornuate uterus

benign tumors also have a variety of sonographic features. The sonographic texture ranges from hypoechoic to echogenic, depending on the amount of smooth muscle and connective tissue. Central ischemia, which is a consequence of tumor enlargement and inadequate blood supply, is usually followed by various stages of degeneration. The most common cause of calcification within the uterus is calcific degeneration within a fibroid. Other types of degeneration include cystic, myxomatous and hyaline degeneration. Sometimes because of the variety of appearances, submucosal leiomyomas may be mistaken for endometrial polyps, endometrial carcinoma, blood or mucus. Patients with submucosal fibroids have a uterine environment which is not conducive to nidation of a fertilized ovum. In addition the blood supply might be inadequate. Leiomyomas grow centripetally as proliferation of smooth muscle cells and fibrous connective tissue, creating a pseudocapsule of compressed muscle fibers. Therefore, color Doppler demonstrates most of the myometrial blood vessels at its periphery **(Figs 50.16A and B)**. Presence of blood vessels in the central portion of the leiomyomas is usually correlated with necrotic, degenerative and inflammatory changes. These vessels display lower RI values than peripherally located vessels and sometimes can be misinterpreted for malignant neovascular pulsed Doppler signal.[45] Vascular impedance to blood flow in the myometrial supplying vessels depends not only on size but location within the uterus. A significant difference was shown in the blood flow characteristics for the leiomyoma supplying vessels between entirely subserosal versus intramural and submucosal leiomyomas. Lower impedance value for subserosal leiomyomas can be explained by the fact that these leiomyomas are supplied with blood vessels through a very small contact area. These blood vessels are surrounded by loose connective tissue and therefore dilated with a very low vascular impedance to blood flow. In contrast, submucosal leiomyomas and those located within the myometrium are supplied by blood vessels with higher vascular impedance. A high basal tone of myometrial tissue surrounding intramural or submucosal leiomyomas can cause a difference in hemodynamic parameters. A 3D ultrasound precisely estimates the relationship between the submucosal leiomyoma and the uterine cavity.

Kurjak et al.[45] performed transvaginal color flow evaluation in 101 patients with palpable uterine fibroids and 60 healthy volunteers. The mean RI from the periphery of leiomyoma covered the value of 0.54. Mean PI value was 0.89. The pathohistological finding was benign uterine tumor in all the cases, even when RI was very low. Lowered RI were present in cases with necrosis, and secondary degenerative and inflammatory changes within the fibroid. Increased blood flow velocity and decreased RI (mean RI = 0.74) in both uterine arteries occurred in patients with uterine fibroids. Three-dimensional power Doppler ultrasound opens new avenues in evaluation of the patients with uterine fibroids **(Figs 50.16C and D)**.

Adenomyosis

Adenomyosis is characterized by the ingrowing of the endometrium into the myometrium. It is usually asymptomatic, but may present as uterine bleeding, pain and infertility. A diffusely enlarged uterus without discrete fibroids, an intact endometrium and multiple small cysts in the myometrium have been reported as a

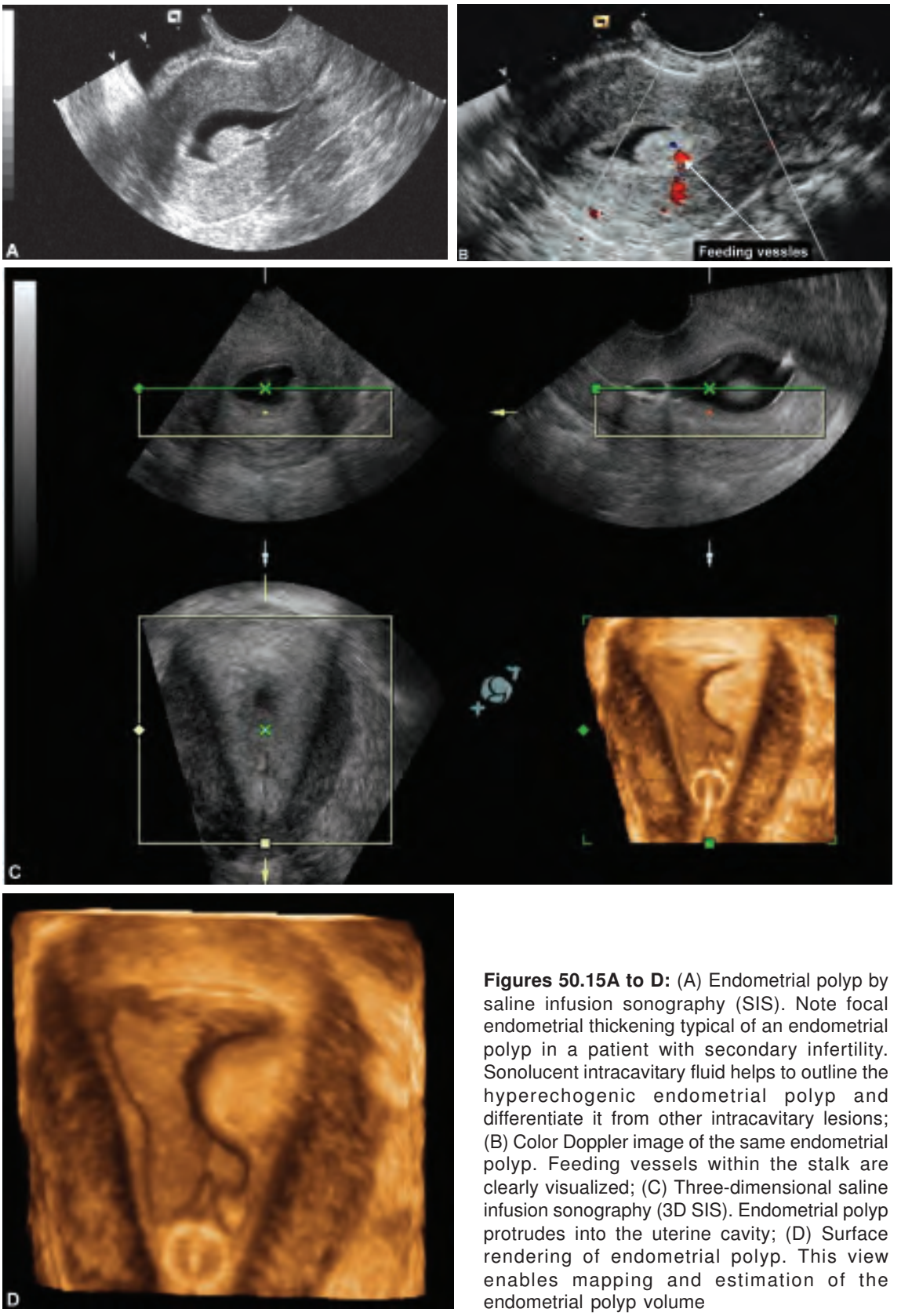

Figures 50.15A to D: (A) Endometrial polyp by saline infusion sonography (SIS). Note focal endometrial thickening typical of an endometrial polyp in a patient with secondary infertility. Sonolucent intracavitary fluid helps to outline the hyperechogenic endometrial polyp and differentiate it from other intracavitary lesions; (B) Color Doppler image of the same endometrial polyp. Feeding vessels within the stalk are clearly visualized; (C) Three-dimensional saline infusion sonography (3D SIS). Endometrial polyp protrudes into the uterine cavity; (D) Surface rendering of endometrial polyp. This view enables mapping and estimation of the endometrial polyp volume

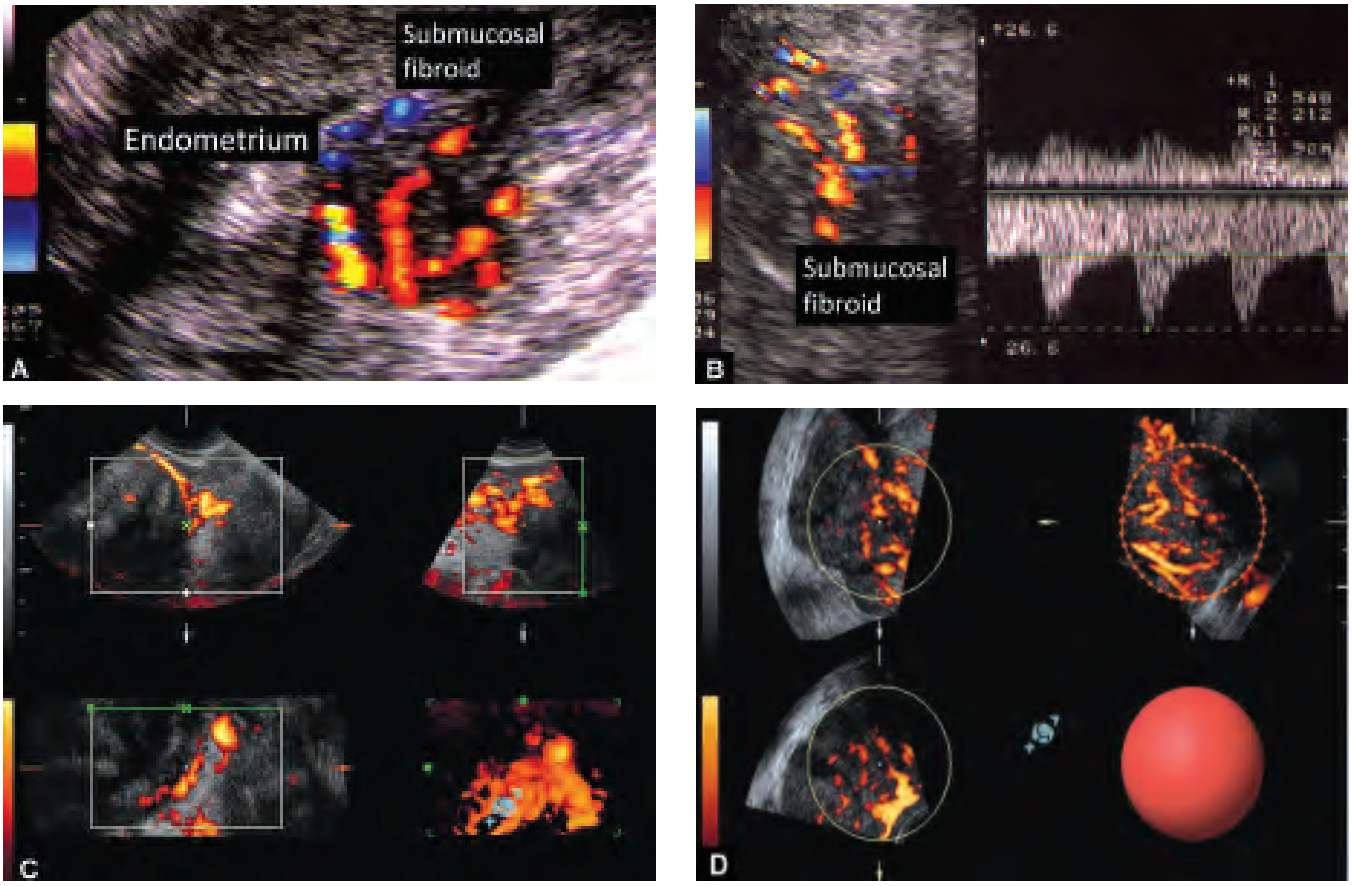

Figures 50.16A to D: (A) Color Doppler ultrasound of submucosal fibroid in a patient with menorrhagia and primary infertility; (B) Pulsed Doppler waveform analysis of the fibroid feeding vessels. Moderate vascular impedance blood flow signals and resistance index of 0.55 are isolated from the vessels within the capsule of the fibroid; (C) Three-dimensional power Doppler ultrasound outlines uterine fibroid feeding vessels within the capsule; (D) Three-dimensional power Doppler ultrasound of the same patient. In addition to vascularity assessment, VOCAL software enables determination of the leiomyoma volume

suggestive appearance of adenomyosis **(Fig. 50.17).**[46] Disordered echogenicity of the middle layer of the myometrium is present in some severe cases. Reported sensitivity and specificity of transvaginal ultrasound in detection of this benign entity is 86% and 50% respectively.[46] Color Doppler may reveal increased vascularity mainly characterized with moderate vascular resistance.

Endometritis

Chronic endometritis is characterized by increased echogenicity, thickness and vascularity of the endometrium. The most common cause of a chronic endometrial infection is *Mycobacterium tuberculosis*. During the active infective stage, a pregnancy often terminates ectopically or as an abortion. The transvaginal sonographic findings may include calcified pelvic

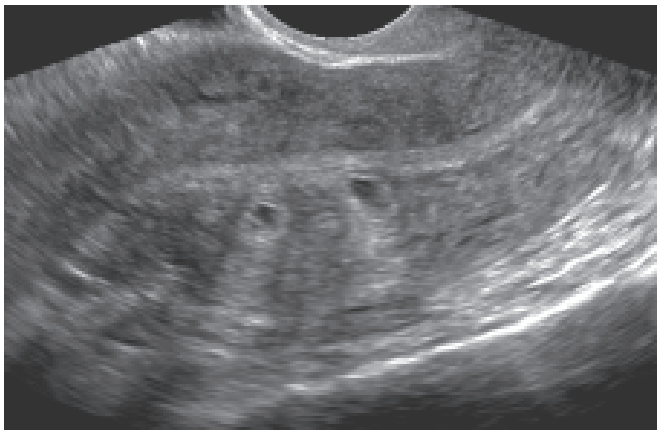

Figure 50.17: Longitudinal plane of the uterus in a patient with superficial adenomyosis. Two adenomyotic implants are visualized within the superficial posterior myometrial layer

lymph nodes or smaller irregular calcifications in the adnexa and deformity of the endometrial cavity suggestive of adhesions in the absence of a history of prior curettage or abortion. In the acute stage of the endometritis, low to moderate impedance blood flow signals are easily obtained on the periphery of the endometrium, as opposed to cases with irreversible tissue damage where blood flow is usually absent. Transvaginal sonography allows elucidation of the abnormal endometrial morphology, after which appropriate cultures should be taken and broad spectrum antibiotic therapy administered. In order to prevent the development of intrauterine adhesions, especially after dilatation and curettage (D and C) administration of conjugated estrogen for 1–2 months is recommended. This therapy allows for the regeneration of a healthy endometrium, which is paralleled by a sharp increase in the end-diastolic velocities of the spiral arteries at the time of color flow and pulsed Doppler analysis.

Asherman's Syndrome

Destruction of the endometrium may result in scarring and the development of bands of scar tissue or synechiae within the uterine cavity. This destruction may occur as a result of a vigorous curettage of the uterus following an abortion or more often, after curettage of an advanced pregnancy. Tuberculosis may also cause uterine synechiae, but only in rare cases. This may result in formation of adhesive bands of different sizes, which leads to a subsequent partial or total obliteration of the endometrial cavity. Amenorrhea or hypomenorrhea characterizes the menstrual patterns.

Patients with endometrial adhesions, such as Asherman's syndrome may have a distorted endometrial pattern consisting of areas where no endometrium can be imaged, mixed with areas that appear normal. Adhesions are observed as endometrial irregularities or hyperechoic bridges within the endometrial cavity.

Schlaff and Hurst[47] analyzed seven amenorrhoic patients with severe Asherman's syndrome. Transvaginal sonography demonstrated a well developed endometrial stripe in three of the seven women, while three others had virtually no endometrium seen **(Figs 50.18A and B)**. All the patients with a well developed endometrium who were found to have adhesions after undergoing a hysteroscopy for the intrauterine adhesions, who had a normally functioning endometrium had resumption of normal menses and normalization of the uterine cavity. The women with a minimal endometrium had no cavity identified and thus derived no benefit from surgery. The conclusion of that study was that the endometrial pattern

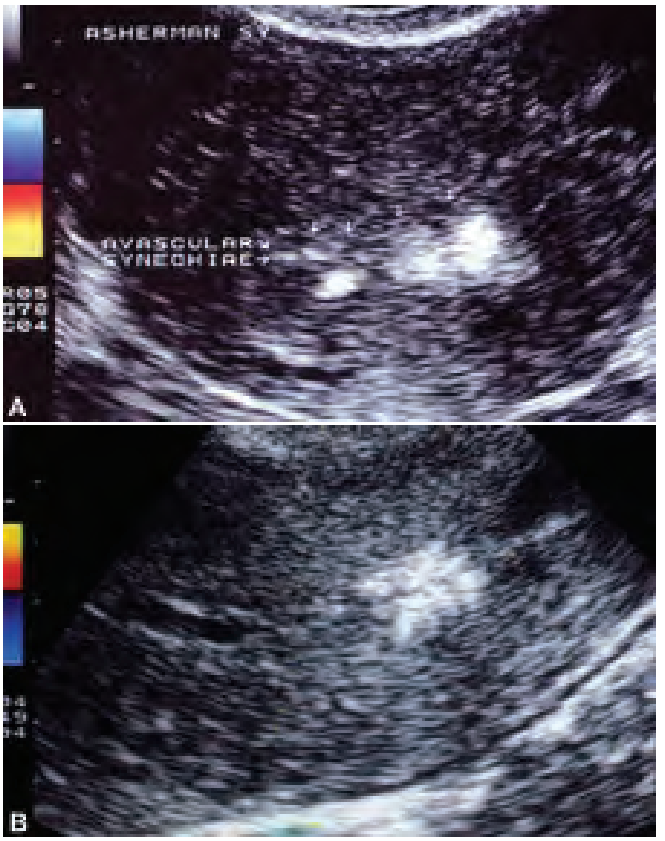

Figures 50.18A and B: (A) Irregular hyperechogenic bridges visualized within the central part of the uterine cavity in a patient with secondary amenorrhea following dilatation and curettage. Color Doppler does not reveal any blood flow signals from the irregular hyperechogenic bridges within the uterine cavity. Hysteroscopy detected intrauterine adhesions (Asherman's syndrome); (B) Hyperechogenic bridges cranially from the internal cervical os are suggestive of intrauterine adhesions

visualized using transvaginal sonography is highly predictive of both surgical and clinical outcomes in patients with severe Asherman's syndrome who are characterized by a complete obstruction of the cavity by a hysterosalpingogram.

Intrauterine synechiae do not present with increased vascularity on color Doppler examination. They are better visualized during menstruation when the intracavitary fluid outlines them or following a hysterosonography. A 3D ultrasound demonstrates a significant reduction of the endometrial cavity volume in all reformatted sections.

OVARIAN CAUSES OF INFERTILITY

The transvaginal sonogram is considered the most reliable method for monitoring follicular growth. It

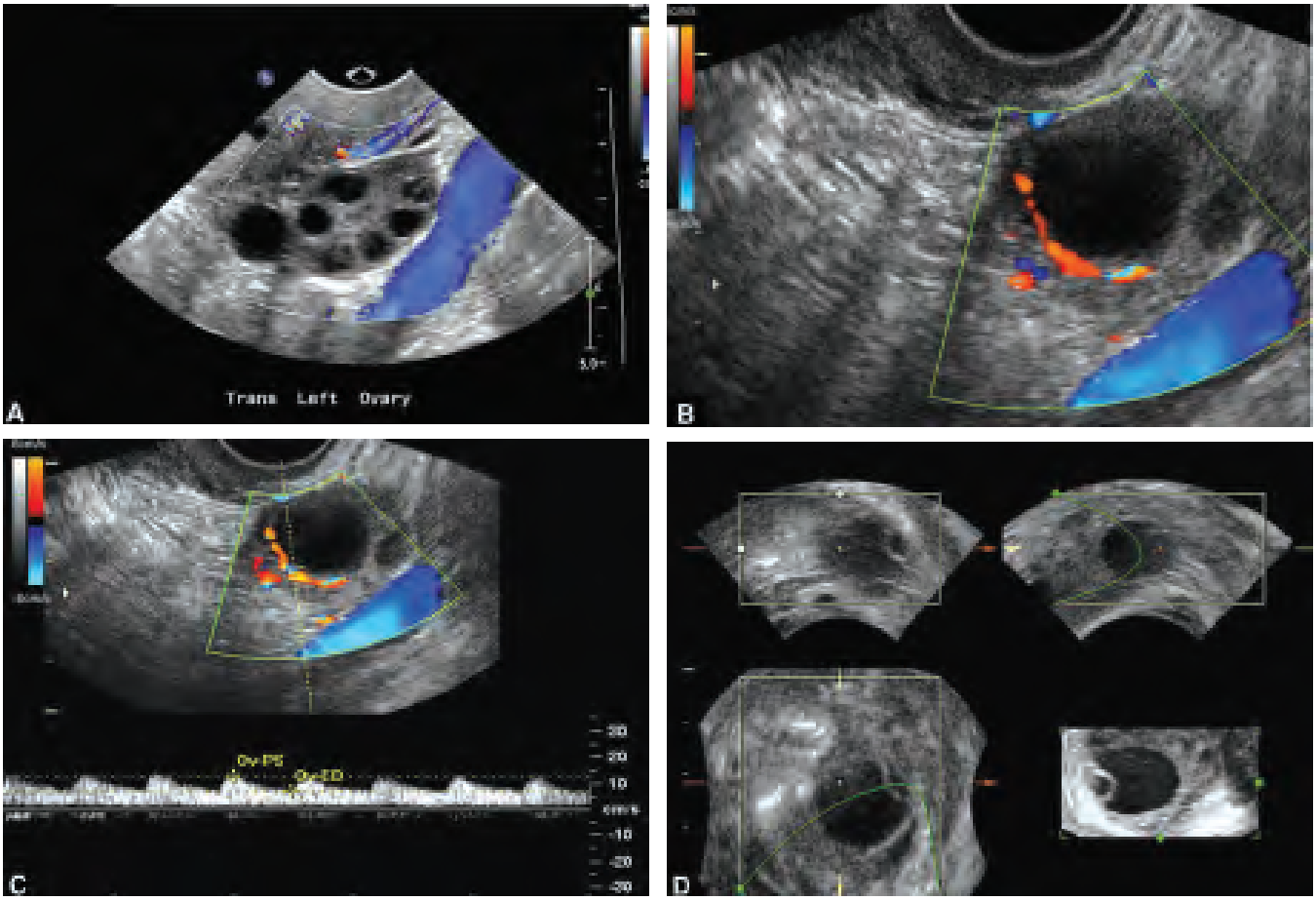

Figures 50.19A to D: (A)Transvaginal color Doppler ultrasound of an ovary containing a dominant follicle on day 10 of the menstrual cycle. Iliac vein is visualized in adjacent to the ovary; (B) Transvaginal color Doppler scan demonstrating a dominant follicle with ring of angiogenesis; (C) Transvaginal color Doppler scan of a dominant follicle. The pulsed Doppler waveform analysis of the follicular vessels shows a resistance index of 0.45. Note that there is a decrease in vascular resistance as ovulation approaches; (D) Three-dimensional ultrasound of a preovulatory follicle. Careful exploration of its inner wall depicts a cumulus oophorus

enables an accurate prediction of ovulation and detection of ovulation abnormalities **(Figs 50.19 and 50.20)**.

The success of IVF treatment is dependent on the ability of the ovary to respond to controlled stimulation by gonadotropins and to develop a reasonable number of mature follicles, and oocytes simultaneously. Failure to respond is associated with cancellation of the cycle or poor outcome of treatment. Prior prediction of the likelihood of optimal ovarian response is therefore essential in identifying patients who are most likely to benefit from IVF treatment.

Zaidi et al.[48] were the first to show that there was a relation between ovarian stromal blood flow velocity and ovarian follicular response. They measured the ovarian stromal PSV in the early follicular phase and showed that poor responders had a low ovarian blood flow PSV. Increased ovarian stromal blood flow velocity was detected in patients with polycystic ovaries, in combination with a relatively unchanged impedance to blood flow. This may reflect an increased intraovarian perfusion and thus a greater delivery of gonadotropins to the granulosa-thecal cell complex with a resultant greater than normal number of follicles being produced **(Figs 50.19B and C)**. This mechanism may help to explain why patients with polycystic ovaries tend to respond excessively to the administration of gonadotropins, and may possibly explain their increased risk of OHSS.

Documentation of ovarian stromal vascularity at an initial baseline scan may be important and may provide useful information for assisted reproduction techniques.

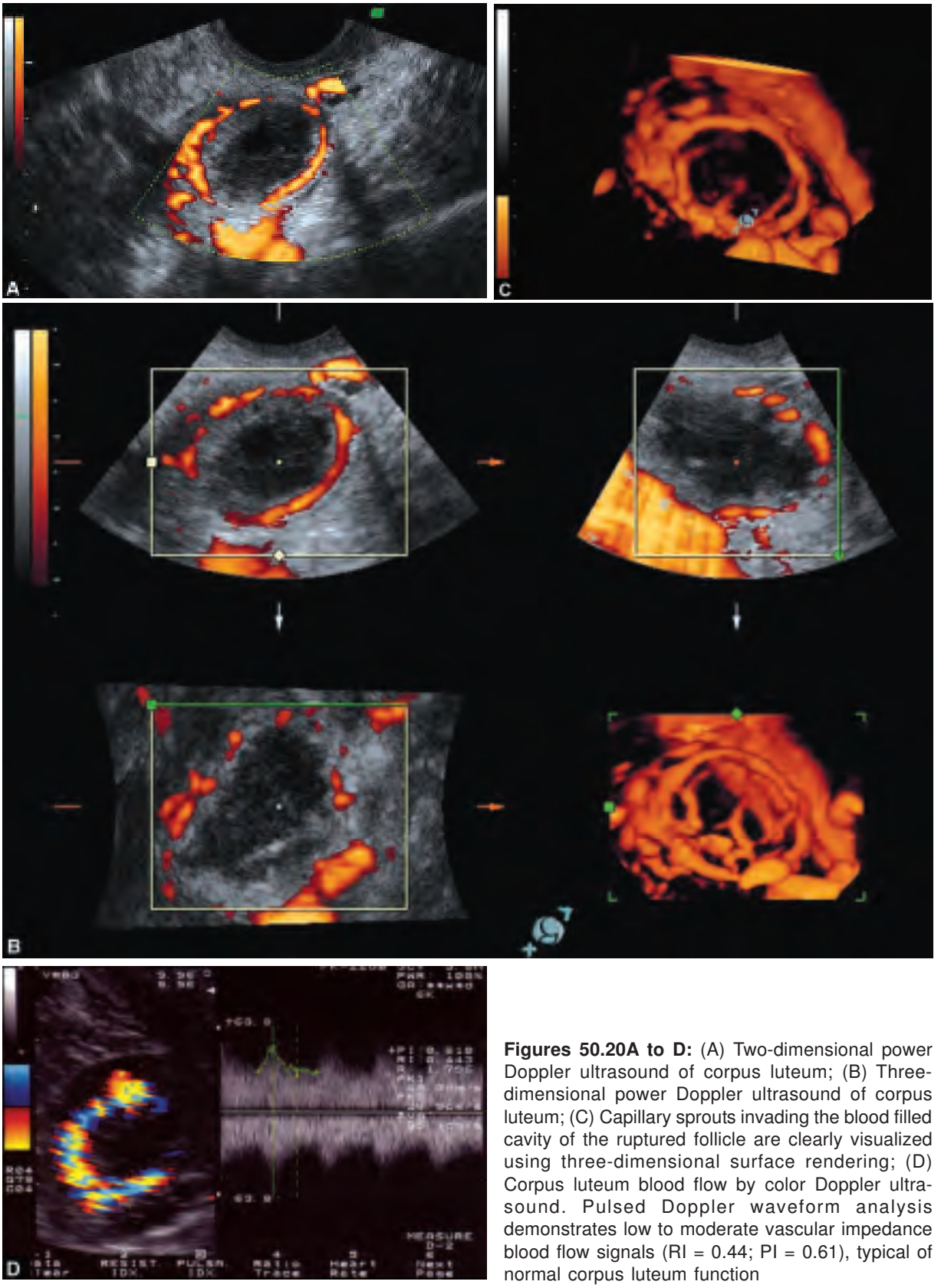

Figures 50.20A to D: (A) Two-dimensional power Doppler ultrasound of corpus luteum; (B) Three-dimensional power Doppler ultrasound of corpus luteum; (C) Capillary sprouts invading the blood filled cavity of the ruptured follicle are clearly visualized using three-dimensional surface rendering; (D) Corpus luteum blood flow by color Doppler ultrasound. Pulsed Doppler waveform analysis demonstrates low to moderate vascular impedance blood flow signals (RI = 0.44; PI = 0.61), typical of normal corpus luteum function

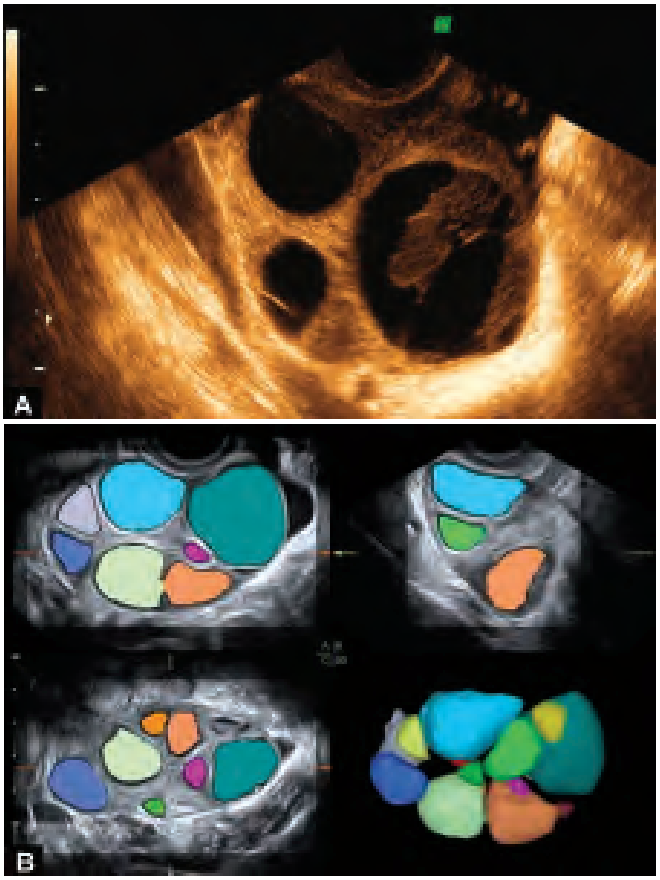

Figures 50.21A and B: (A) Two-dimensional ultrasound of hyperstimulated ovary. Note synchronous growth of the follicles and early corpus luteum formation on the right; (B) Three-dimensional ultrasound of the hyperstimulated ovary after ovulation induction. The ovary is enlarged and filled with numerous follicles that are coded in different colors

Furthermore, it seems that measurement of ovarian stromal blood flow in the early follicular phase is related to subsequent ovarian responsiveness in IVF treatment.[48] This is particularly useful since the ability to predict ovarian response to stimulation by exogenous gonadotropins is still central to success in any IVF program. Most programs determine the dose of gonadotropins used for the first attempt based on the chronological age of the patient, with adjustments being made in subsequent attempts depending on their initial response. Unfortunately the ovarian age (capacity of the ovary to produce fertilizable oocytes), and chronological age are not always synchronous, leading to a degree of unpredictability in the number of developing follicles and collected oocytes. Certainly, if an inadequate dose of gonadotropins is used then there may be a relatively poor response, which reduces the number of oocytes retrieved, whereas if an excessive dose is used, there may be an increased risk of OHSS **(Figs 50.21A and B)**.

Engman et al.[49] speculated that the ovarian stromal blood flow velocity after 2–3 weeks of pituitary suppression is a true representative of baseline ovarian blood flow because the ovaries are in a quiescent state. The primordial follicles in the ovary have no independent capillary network, lying simply among vessels of the stroma, and therefore depend on their proximity to the stromal vessels for the delivery of nutrients and hormones. The subsequent growth of primary follicles leads to the acquisition of a vascular sheath through the process of angiogenesis. The administration of a GnRH agonist suppresses follicular activity and consequently the ovaries become inactive; ovarian stromal blood flow at this time might be at its lowest and may truly reflect the baseline ovarian blood flow.

Therefore, ovarian stromal blood flow velocity after pituitary suppression is predictive of ovarian responsiveness and the outcome of IVF treatment.

One might speculate that by improving the ovarian stromal blood flow velocity, the delivery of gonadotropins to the follicles will be improved and as a result, the number and quality of mature oocytes produced, and the implantation rate will improve.

The accuracy of diagnosis and monitoring of infertility treatments such as ovulation induction has increased greatly because of the availability of sophisticated ultrasound technology and equipment.[20] Accurate follicular assessment is essential for a safe and effective infertility treatment. In IVF-ET cycles, follicles with a mean follicular diameter of 12–24 mm are associated with optimal rates of oocyte recovery, fertilization and cleavage.[50] This corresponds to follicular volumes between 3 mL and 7 mL. In the hands of experienced operators, ultrasound alone suffices for cycle monitoring, without the necessity of additional hormonal estimations.[51-53]

The basic structural information provided by conventional scans in the longitudinal and transverse plan can now be augmented by the new 3D ultrasound systems that provide additional views of the coronal or C-plane, which is parallel to the transducer face.[20] The computer-generated scan is displayed in three perpendicular planes. Translation or rotation can be carried out in one plane, while maintaining the perpendicular orientation of all three so that serial translation will result in an ultrasound tomogram from which volumetric data can be captured.[54] Kyei-Mensah et al.[20] evaluated the accuracy of 3D ultrasound measurement of follicular volume compared with current standard techniques. They compared the volume of individual

follicles estimated by both methods with the corresponding follicular aspirates. The volume of follicular fluid aspirated was compared with the corresponding volume of the follicle measured by 3D ultrasound and with the conventional 2D ultrasound volume measurement calculated by using the formula 0.52 × ($D_1 \times D_2 \times D_3$). Limits of agreement and 95% confidence intervals were calculated and systematic bias between the methods was analyzed. The limits of agreement between the volume of follicular aspirate and follicular volume determined by ultrasound were + 0.96 to -0.43 mL for 3D measurements and +3.47 to -2.42 mL for 2D measurements. The high accuracy of 3D measurement of follicular volume is demonstrated clearly in this study by the limits of agreement, which are within 1 mL of the true volume. These limits encompass 95% of the volume measurements. On the other hand, the 2D method produced limits of agreement that was up to 3.5 mL above or 2.5 mL below the true volume of clinical range.

Therefore, the shape and numbers of the follicles influence the reliability of the standard 2D ultrasound technique for follicular volume measurement. There may be technical difficulty in measuring the diameters of a follicle when its shape is distorted because of compression by adjacent follicles. Penzias et al.[55] showed that the mean follicular diameter accurately predicts volume in round and polygonal follicles but not in ellipsoid shaped follicles. Rounded follicles were most prevalent in patients with the fewest follicles. The patients selected for this study had produced fewer follicles than normal and therefore represent the group in which the conventional technique was likely to be most accurate. Kyei-Mensah et al.[20] found that the 3D assessment of follicular volume produced a more accurate reflection of the true volume. This is because the 3D measurement is not affected by follicular shape, since the changing contours are outlined serially to obtain the specific volume measurement. The disparity in accuracy between 3D assessment of follicular volume and the conventional approach therefore is likely to increase significantly, if there is a florid multifollicular ovarian response because the conventional formula is less precise with ellipsoid follicles, which are likely to predominate in these cases **(Fig. 50.21B)**. One limitation of 3D volume assessment is that follicles with a mean diameter less than 10 mm cannot be assessed accurately because the limits of agreement are too wide in this range.

Feichtinger et al.[56] found that 3D ultrasound may be useful for the distinction of ovarian cysts from ovarian follicles. Since both the ovarian cysts and the follicles demonstrate an elevation of the serum estradiol levels, it is difficult to distinguish them by E2 assay alone. For the purpose of the prospective observational study, the authors evaluated 50 IVF patients after ovulation induction. Three-dimensional ultrasound was used to search for the presence of cumuli in follicles greater than 15 mm **(Fig. 50.19D)**. Only cumuli demonstrable in all three planes by multiplanar imaging predicted mature oocyte recovery. Follicles without visualization of the cumulus in all three planes were not likely to contain mature fertilizable oocytes.

Lass et al.[57] tested the hypothesis that small ovaries measured on transvaginal sonography are associated with a poor response to ovulation induction by human menopausal gonadotropin for IVF. A total of 140 infertile patients with morphologically normal ovaries undergoing IVF were studied and represented. The mean ovarian volume of each patient was measured on transvaginal sonography before starting HMG. Subsequent routine IVF management was conducted without the knowledge of the transvaginal sonography results. The mean ovarian volume was 6.3 cm^3 (ranges 0.5–18.9, SD=3.1). Patients (n=17; group A) with small ovaries of equal to 3 cm^3 represented group B. Both groups were of similar age (mean 35.8 vs 34.4 years). Early basal follicle stimulating hormone concentrations were increased in group A (9.5 vs 7.0 mIU/ml, P=0.025). The cycle was abandoned before planned oocyte recovery in nine patients (52.8%) from group A and in 11 patients (8.9%) from group B because of poor response to ovulation induction.

Oyesanya et al.[58] measured the total ovarian volumes before the administration of hCG in 42 women undergoing treatment for infertility by IVF and ET and considered to have an exaggerated response to stimulation (> 20 follicles). Seven women who subsequently developed moderate or severe OHSS (n=7; group 1) were compared with 35 matched controls (five matched controls per case; n=35; group 2) of similar age, number of follicles and duration of infertility who underwent follicular stimulation, oocyte recovery, IVF and ET during the same period but did not develop moderate or severe OHSS. The mean age, duration of infertility and total number of follicles were similar, but the mean total ovarian volume was significantly higher in the group of women who developed moderate or severe OHSS compared with controls (271.00 ± 87.00 mlvs 157.30 ± 54.20 mL).

Kupesic and Kurjak[59] designed a study to evaluate whether ovarian antral follicle number, ovarian volume, stromal area and ovarian stromal blood flow are predictive of ovarian response and IVF outcome. Total

ovarian antral follicle number, total ovarian volume, total stromal area and mean flow index (FI) of the ovarian stromal blood flow were determined by 3D and power Doppler ultrasound after pituitary suppression. Pretreatment 3D ultrasound ovarian measurements were compared with subsequent ovulation induction parameters (peak estradiol on hCG administration day and number of oocytes) and cycle outcome (fertilization and pregnancy rates). The total number of antral follicles achieved the best predictive value for favorable IVF outcome, followed by ovarian stromal FI, total ovarian stromal area and total ovarian volume.

A recent study by Kupesic et al. evaluated whether ovarian antral follicle number, ovarian volume and ovarian stromal blood flow changes with a woman's age, if they are predictive of ovarian response and IVF outcome. Total ovarian antral follicle number, total ovarian volume and mean FI of the ovarian stromal blood flow were determined by 3D and power Doppler ultrasound after pituitary suppression. Patients were separated into three groups based upon age and in each group median values of 3D ultrasound parameters (total ovarian antral follicle number, total ovarian volume and mean ovarian stromal vascularity) were measured and presented. Pretreatment 3D ultrasound ovarian measurements were compared with subsequent ovulation induction parameter (number of oocytes) and cycle outcome (fertilization and pregnancy rate). Increasing age is associated with poor ovarian response, smaller ovarian volume, lower antral follicle count and poor stromal vascularity.

Clearly, there is a place for 3D ultrasound in the assessment of the ovaries prior to ovulation induction and medically assisted reproduction.

POLYCYSTIC OVARIAN SYNDROME

Polycystic ovarian syndrome (PCOS) is a major cause of anovulation and oligomenorrhea. In its classic form it is characterized by infertility, oligo- and amenorrhea, hirsutism, acne or seborrhea, and obesity. In 1986 Adams et al. defined the criteria for the ultrasonographic diagnosis of polycystic ovaries: multiple (n > 10), small (2–8 mm) peripheral cysts surrounding a dense core of stroma in enlarged (≥ 8 ml) ovaries.[60] However, ovaries which are normal in volume can be polycystic, as demonstrated by histological and biochemical studies. Anatomical structure of the ovaries cannot adequately be assessed with the transabdominal approach in about 42% of cases. Underlying causes are obesity, limited resolution of low-frequency transducers, a full bladder distorting pelvic anatomy and bowel loops covering the adjacent ovary. More recently, the transvaginal approach for ultrasound scanning of pelvic organs has been used. The high frequency of the transvaginal probe avoids the need for a full bladder and bypasses the problems of attenuation and, artifacts associated with obesity. Furthermore, transvaginal ultrasonography has the advantage of improved resolution, better visualization of pelvic organs and greater acceptance among patients.

The number of follicles necessary to establish the diagnosis of polycystic ovaries by ultrasonography has been reported to vary between five and fifteen. However, in many reports the highest number of atretic follicles obtained in normal control patients was five per ovary, so it may be established that in polycystic ovaries the number of atretic follicles per ovary would be at least six. Matsunaga and colleagues identified two types of polycystic ovaries on the basis of ultrasonographic follicular distribution: the peripheral cystic pattern (PCP) and the general cystic pattern (GCP).[61] In the PCP, small cysts are distributed in the subcapsular region of the ovary, whereas in the GCP they are scattered throughout the entire ovarian parenchyma. Recently, Takahashi and colleagues have shown that these two different ovarian morphologies reflect histopathological differences, and that the PCP and GCP appearances reflect specific endocrine PCOS patterns.[62]

Another parameter considered in the diagnosis of polycystic ovaries is the ovarian volume. However, the wide volume overlap between normal patients and those with PCOS suggests that the discriminative capacity of ovarian volume alone is not sufficient for the ultrasound diagnosis of PCOS.[63] Although the role of the hyperechogenic ovarian stroma has been emphasized, appraisal of the ovarian stroma echodensity,[64] comparable with computerized quantification,[65] is absolutely subjective and may be interpreted differently by different operators.

Color doppler studies have shown that in patients with PCOS important changes in ovarian vascularization occur at the level of the intraovarian arteries **(Fig. 50.22A)**. Although intraovarian arteries are usually not seen before day 8–10 of the 28 day cycle,[66] Battaglia and colleagues have detected distinct arteries with characteristic low vascular impedance as early as cycle day 3–5.[67] In the studied population the results were associated with typical PCOS hormonal parameters and were inversely correlated with the luteinizing hormone to follicle stimulating hormone (LH/FSH) ratio. Tonic hypersecretion of LH during the follicular phase of the menstrual cycle occurs in PCOS and is associated with thecal cell and stromal hyperplasia with resultant

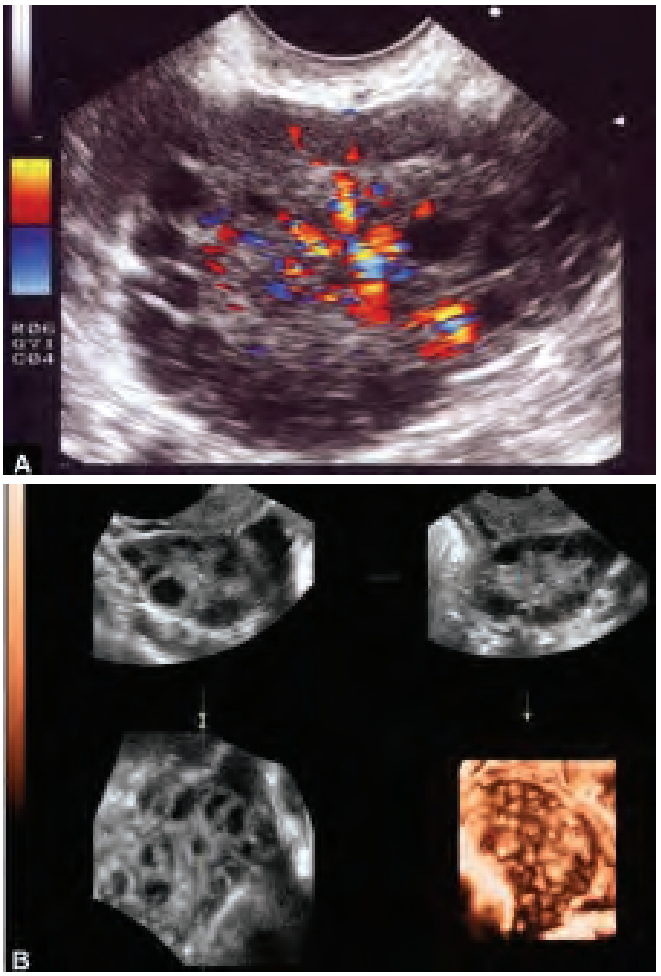

Figures 50.22A and B: (A) Transvaginal color Doppler scan of polycystic ovary. A large number of small cystic structures are crowded together and stand out from the enlarged ovarian stroma. Stromal vessels are easily visualized by color Doppler imaging; (B) Three-dimensional ultrasound image of a polycystic ovary

androgen overproduction.[67] Elevated LH levels may be responsible for increased stromal vascularization by different mechanisms that may act individually or in a cumulative way such as neoangiogenesis, catecholaminergic stimulation and leukocyte, and cytokine activation. In the same study the PCOS patients showed a higher uterine PI values than non-hirsute normal menstruating women. This finding was correlated with androstenedione levels, confirming a possible direct androgen vasoconstrictive effect due to activation of specific receptors present in the arterial vessel walls and collagen, and elastin deposition in smooth muscle cells. The above condition by reducing the uterine perfusion has been the theoretical cause that prevents blastocyst implantation, increasing the incidence of miscarriages in PCOS patients. Zaidi and colleagues[48,68] and Aleem and Predanic,[69] also having confirmed that the doppler analysis of stromal arteries in PCOS may be useful in improving the diagnosis, and providing further information about the pathophysiology and evolution of the syndrome obtained similar results.

The doppler evaluation showed that PCP patients, in comparison with GCP patients, present with significantly lower RI values at the level of the ovarian stromal arteries. In addition, in 22% of GCP patients, the intraovarian vessels are not recognized[70] and that the GCP appearance of the ovary is more common in the early phase of the disease,[61,62] during the peripubertal period. Thus, the ovarian morphology may evolve from a normal multicystic to polycystic PCP pattern, passing through an ovarian GCP phase. If left untreated PCOS may be regarded as a progressive syndrome. Furthermore, it has recently been shown by comparing oligo versus amenorrheic PCOS patients that the amenorrheic patients are older and present with higher PI values in the uterine arteries, and lower RI values in intraovarian vessels than oligomenorrheic patients.[71] This finding is associated with a higher plasma LH and androstenedione levels, and with a more elevated LH/FSH ratio. Furthermore, significantly higher ovarian volumes and subcapsular small-sized follicles are observed in amenorrheic PCOS patients. This data shows that as the number of ovarian microcysts increases, ovarian volume enlarges and Doppler indices worsen. The clinical and endocrine abnormalities become more remarkable, and the menstrual disturbances become more severe.[70]

Recently, it has been demonstrated that obese PCOS women show a higher PI values within the uterine arteries than do lean patients.[72] This is associated with higher hematocrit values, hyperinsulinemia, higher triglyceride levels and lower high-density lipid concentrations.

In overweight patients, hyperinsulinemia may be proposed as the uniting factor between increased vascular resistance, obesity, lipid abnormalities and cardiovascular disease.[72,73] Thus, assuming that PCOS patients are at increased risk for cardiovascular disease, it is possible to affirm that obesity may further increase the risk. Unopposed estrogen stimulation is an important contributing factor of endometrial carcinoma and this helps to explain the increased risk in patients with obesity and chronic anovulation.

Recent advances in 3D ultrasound have made accurate non-invasive assessment of the pelvic organs feasible. The ability to visualize the oblique or coronal

plane allows accurate volume measurements, especially of irregularly shaped objects.[17,20] Due to the enhanced ability to accurately track an individual's variations in structure during the measurement process, the measurements are considered reliable and highly reproducible.[16]

Wu et al.[74] studied 44 women who presented with a history of irregular menstrual periods; most of whom had been diagnosed with PCOD. The diagnosis of PCOD was based on the clinical symptoms (e.g. menstrual problems, obesity, acne, hirsutism), endocrinologic data (all with reversed serum LH/FSH ratio) and ultrasonographic features (increased ovarian stroma and volume, subcapsular cysts and thickened capsule). Another 22 women with regular ovulatory cycles were recruited as normal controls. There was no statistically significant difference in age (range 17–35 years) between these two groups. Three-dimensional ultrasonography was performed to store and document whole volumes of the ovaries for evaluation. Three perpendicular planes of bilateral ovaries were rotated to obtain the largest dimensions. The 3D volume was measured using the trapezoid formula. The ovaries of the patients with PCOD were larger in size, area and volume than those of normal controls. The mean ovarian volumes (three dimensions; mean ± SD) were 11.3 ± 3.5 cm^3 in patients with PCOD and 5.5 ± 1.4 cm^3 in the normal controls ($P< 0.0001$). The volumes of the right ovary were 12.2 ± 4.7 cm^3 and 5.3 ± 2.0 cm^3, and the left ones were 10.5 ± 3.6 cm^3 and 5.7 ± 1.6 cm^3 in the PCOD and normal groups respectively. The right ovary demonstrated a larger volume than the left ovary in women with PCOD ($P< 0.0001$); however, the left ovary was significantly larger than the right one in the normal controls ($P< 0.0001$).

The ovaries in PCOD were significantly increased in size, stroma and volume ($P< 0.0001$) compared with those of the normal controls. Cut-off values for the ovarian area, stroma and volume in PCOD were 5.2 cm^2 (sensitivity 93%, specificity 91%), 4.6 cm^2 (sensitivity 91%, specificity 86%) and 6.6 cm^3 (sensitivity 91%, specificity 91%) respectively. The stroma, total ovarian areas and volume detected by careful rotation and outlining of the longitudinal ovarian cut were increased in 84% (37 of 44), 89% (39 of 44) and 80% (35 of 44) of the patients with PCOD respectively, in comparison with normal controls. The total ovarian area was highly correlated with the stromal area ($r^2= 0.66$).

Undoubtedly, 3D ultrasonography facilitates non-invasive retrospective evaluation and volume calculation. The examination time is short, without increasing the patient discomfort. Three maximal dimensions of the ovaries can be measured easily once the digital volume is documented from either transvaginal or transabdominal 3D ultrasonography and a superior volume determination can be obtained from the 3D images. The volume measurement in 3D ultrasonography is accurate and highly reproducible **(Fig. 50.22B)**. The volume of the follicles can be determined precisely and the volume of the ovary from 3D sonography correlates better with direct measurement of the surgical specimen than that from 2D ultrasonography.[20] The ability of reconstruction increases the diagnostic potential for determining PCOD. The ovaries in PCOD are usually enlarged bilaterally, but they may be about normal size (up to 20% in our study). The stroma areas in PCOD are hypertrophic and provide yet another subjective ultrasonographic criterion that could differentiate PCOD from the multifollicular ovary. The multifollicular ovary demonstrates a normal or slightly increased size, but an increased number of follicles are noted without an increased amount of stroma. However, the results are usually subjective and not quantitative. Using the computerized quantification measurement, an increased total ovarian area of greater than 5.5 cm^2 highly correlates with increased ovarian stroma at a strict longitudinal ovarian section in the diagnosis of PCOD.[65]

Three-dimensional ultrasonography allows careful and objective evaluation of the ovaries and can repeatedly follow the outline of the ovarian area even after the examination. The value of ovarian stroma can be obtained after subtracting the sum area of ovarian cysts from the total area. The 3D scanning can obtain a more accurate volume data by outlining the contour of the target organ, which is better than traditional 2D ultrasonographic scanning calculated by the ellipsoid formula (height × width × thickness x 0.523).

In conclusion, 3D ultrasonography can complement 2D ultrasonography for the diagnosis of PCOD. It allows excellent spatial evaluation of PCOD with direct quantitative computations from the data.

Apart from morphological and volume measurements assessment of ovarian and uterine vessels can be added to the traditional endocrinologic and ultrasonographic parameters clinically used for the diagnosis of PCOD.

Patients with PCOD undergoing ovulation induction for IVF are more likely to develop a greater number of follicles and generate more oocytes compared with women with normal ovaries even though they require less gonadotropin stimulation.[75] Furthermore, since they develop more follicles of all sizes and in particular small and medium sized follicles, women with PCOD are at greater risk for OHSS.[76] This suggests that the PCOD is

more sensitive to gonadotropin stimulation. The exact mechanism is unknown although it is possible that the increased ovarian stromal blood flow velocity, in combination with a relatively unchanged impedance to blood flow may reflect an increased intraovarian perfusion and thus a greater delivery of gonadotropins to the granulosa cells of the developing follicles. This theory may help to explain the greater likelihood of a multifollicular response. In conclusion, women with PCOD have a significantly greater stromal blood flow velocity as detected by transvaginal color Doppler ultrasound. The implication of this in ovulation induction treatment is unknown but may help to explain the excessive response often seen in women with PCOD when they are administered gonadotropins. The presence of an increased stromal blood flow velocity in both the PCOD and PCOS groups compared to women with normal ovaries supports the notion that the PCOD is a primary disorder of the ovary. The detection of increased ovarian stromal blood flow velocity by color and pulsed Doppler ultrasound may be a marker in the diagnosis of PCOD. It seems that evaluation of the ovarian stromal vascularity by 3D power Doppler will further increase our knowledge on this enigmatic syndrome.

Luteinized Unruptured Follicle Syndrome

Luteinized unruptured follicle syndrome (LUF Sy) is characterized by regular menses and presumptive ovulation as suggested by a cyclic hormonal profile, similar to that seen in normal ovulatory women but without the release of the ovum. Although, LUF was first diagnosed at laparoscopy by the absence of an ovulation stigma and the demonstration of lower concentrations of estradiol and progesterone in peritoneal fluid compared with normal ovulatory cycles, diagnosis is most commonly made on ultrasound examination, in which there is persistence of the ovarian follicle with progressive loss of its typical echo-free cystic appearance and accumulation of internal echogenicity. The precise etiology of LUF remains uncertain, but impairment of the mid-cycle LH surge, the absence of the preovulatory progesterone rise, abnormalities of prostaglandin synthesis and a primary abnormality of the oocyte has all been suggested as possible causes. There is a possible association between LUF syndrome and unexplained infertility, chronic pelvic infection and endometriosis. The estimated frequency of this syndrome is between 6% and 47%.

Kupesic and coworkers[77] tried to evaluate intraovarian RI in 47 healthy volunteers with ovulatory cycles and compare them to 28 patients with LPD and four patients with LUF Sy. Serial sonography allowed daily measurement of the mean follicular diameter and observation of LUF Sy development which include the follicular collapse, demarcation of the hypoechoic structure with an irregular wall, formation of solid or complex structure representing the corpus luteum and the extraovarian signs, such as the thickened endometrium, and the lack of the free fluid in the cul-de-sac. All these findings were suggestive of ovulation. Doubtful cases (nonvisualization of the corpus luteum and/or lack of the serial measurement) were excluded from the current study. The LUF Sy was documented by daily ultrasound observations and endocrinological measurement. During the period of expected ovulation, the follicle remained of the same size and maintained a tense appearance. Luteinization of the unruptured follicle was seen as a progressive accumulation of the strong echoes located at its periphery.

In the group with regular ovulatory cycles, moderate to high RI (0.56+/-0.06) was obtained at the rim of the follicle. Significant decline of the RI occurred on the day of LH peak (RI 0.44+/-0.04). The lowest RI values were obtained during the mid-luteal phase (RI 0.42+/-0.06), with a return to higher vascular resistance of 0.50+/-0.04 during the late luteal phase. In 15 patients, endometrial biopsy was performed and normal endometrial dating was detected. In the patients with LUF Sy, there was no difference in terms of intraovarian RI which was obtained after the LH peak. Similar RI values were obtained during the follicular and luteal phase (0.55+/-0.04 vs 0.54+/-0.06). Furthermore, there was no difference between the sides in terms of intraovarian vascular resistance. The mean progesterone value in this group was 14.1 ± 6.2 ng/ml and normal endometrial data was obtained in all patients with LUF Sy.

Similar results were reported by Merce and colleagues,[78] who did not observe any drop in perifollicular intraovarian resistance after the LH peak. Interestingly, the so called "luteal conversion" did not take place, indicating that the intraovarian and perifollicular neovascularization were either not produced or were altered in LUF, probably because the follicle failed to rupture.

Indeed, the rise in perifollicular blood flow during the periovulatory period appears to be primarily regulated by LH. Zaidi et al.[68] reported a decreased blood flow velocity of the peripheral vessels in a patient with LUF Sy after the LH surge to values comparable with those seen in the early follicular phase of the cycle. The reduction in perifollicular blood flow velocity has also been reported in a patient with drug-associated LUF.[79]

Extensive Doppler measurement, biochemical research and 3D ultrasound studies still have to be done to further clarify the causes and consequences of this syndrome.

Luteal Phase Defect

The formation of corpus luteum is an important event in reproductive cycle and one of the crucial factors in early pregnancy support. After ovulation, blood vessels of the theca layer invade the cavity of the ruptured follicle starting the formation of the corpus luteum.

Small luteal cells produce more and more LH receptors, and thus amplify the production of progesterone. This chain reaction goes on till the so called mid-luteal phase which is characterized by peak values of blood LH, progesterone and the lowest RI in corpus luteum blood vessels as proven by transvaginal color and pulsed Doppler by Kupesic et al.[80] Consequently progesterone suppresses the secretion of the gonadotropin, LH and progesterone levels decrease and RI in the vessels of corpus luteum increases. Whether because of "intrinsic error of mechanism" or because of the interference with external factors (e.g. strenuous exercise, ovulation stimulating drugs), a condition called LPD occurs. Various names have been assigned to the disorder: short luteal phase, luteal insufficiency, inadequate luteal phase, luteal defect and luteal phase deficiency. All these names describe the same condition: lack of progesterone, a luteal phase of the cycle shorter than 11 days and when related to the endometrium, an out-of-phase endometrium by two or more days. The new method to detect a corpus luteum abnormality is by ultrasonography. For a better visualization of the corpus luteum a transvaginal approach is used. As an addition to B-mode and real time image, sophisticated ultrasound equipment includes color and pulsed Doppler sonography. The research into the corpus luteum, LPD, early pregnancy and early pregnancy failures has already taken a whole new direction. Until recently, research in this field was carried out mainly using B-mode and real time imaging. Glock et al[81] tried to determine whether the ultrasound appearance size or change in size of the corpus luteum of early pregnancy correlated with serum progesterone, estradiol E2 or 17-hydroxyprogesterone or were even predictive of pregnancy outcome. Their hypothesis stated: corpus luteum volumes of early human pregnancy would correlate with the serum concentration of steroids produced in the corpus luteum; appearance of the corpus luteum, based on the amount of cystic component, would correlate with serum hormone concentration or pregnancy outcome and a decrease in corpus luteum volume would be associated with pregnancy loss. Disappointingly, the acquired data showed a lack of correlation between corpus luteum size and steroid products, and no correlation between changes in volume and changes in steroid products in early human pregnancy. However, a decreasing corpus luteum volume before 8 weeks' gestation is associated with a higher probability of pregnancy loss. Color flow pulsed Doppler was only used to determine the dominant ovary with corpus luteum and the contralateral one. The dominant ovary showed a low impedance waveform with RI 0.39–0.49, which is characteristic of the blood flow in early pregnancy. The contralateral ovary in each patient demonstrated a high impedance flow RI 0.69–1.0, characteristic of a nondominant ovary. One patient had an RI value of 0.74 in the ovary identified as having a corpus luteum and RI of 0.79 in the opposite ovary; this high RI in both ovaries was associated with a nonviable outcome.

Kupesic et al.[80] tried to evaluate the intraovarian RI in 47 healthy fertile volunteers with ovulatory cycles and compare them to 28 patients with LPD, and four patients with LUF Sy. Serial sonography allowed a daily measurement of the mean follicular diameter, visualization of the follicular collapse and demarcation of the hypoechoic structure with an irregular wall, solid or complex structure representing the corpus luteum, as well as observation of the thickened endometrium and presence of the free fluid in the cul-de-sac. All these findings were suggestive of ovulation. Doubtful cases (non-visualization of the corpus luteum and/or lack of the serial measurements) were excluded from the current study. The LPD was diagnosed by measuring the progesterone levels and performing the endometrial biopsy during the midluteal phase of the menstrual cycle. Sonographic and Doppler findings were correlated to hormonal and histopathological data.

In the group with regular ovulatory cycles (n=47) different ovarian RI values had been observed. During the stage of the follicular growth and development, moderate to high RI (mean 0.56 ± 0.06) was obtained at the rim of the follicle. Significant decline of the RI occurred for the day of LH peak (RI 0.44 ± 0.04). The lowest RI values were obtained during the mid-luteal phase (RI 0.42 ± 0.06), with a return to higher vascular resistance of 0.50 ± 0.04 during the late luteal phase. In the LPD group (n=28) no difference was obtained in terms of intraovarian RI during the follicular phase. However, the mean RI throughout the luteal phase (RI 0.56 ± 0.04) was significantly higher compared to the normals. Furthermore, it did not show any difference between the early, middle and late luteal phase in LPD group.

In the control group, both follicular and luteal RI was significantly lower on the dominant side. However, in the LPD group no difference occurred in terms of intraovarian RI between the sides. The mean progesterone levels were significantly lower in the LPD group (6.9 ± 2.3 ng/ml) than in the controls (24.1 ± 11.4 ng/ml), while histopathology revealed delayed endometrial pattern in all the patients with LPD. The correlation was observed between progesterone and RI during the mid-luteal phase.

Merce et al.[78] elaborated on all aspects of transvaginal color and pulsed Doppler ultrasonography: its advantages, disadvantages, current possibilities and future directions. In their study of luteal ovarian blood flow they introduced the term "luteal conversion" to describe the Doppler findings during the luteal phase. These Doppler findings include easily obtained Doppler signals, increase in intensity of frequency spectrum, increase in turbulence of the blood flow with extensive dispersion of the maximum frequencies and superposition of multiple waveforms presenting variable maximum systolic velocities, and finally an increase in the surface and intensity that the color signal occupies in the ovary. The same authors, in their study of LPD, observed that the RI of the dominant ovary drops during the luteal phase with respect to the follicular phase, which also occurs in normal cycles and that there were no differences noted regarding this aspect when compared with any phase of the normal cycle. No significant correlation was demonstrated between the index values and serum progesterone levels either.

Glock and Brumsted[82] correlated ovarian blood flow to values of progesterone throughout the cycle. Mean progesterone levels were significantly lower for LPD patients than for normal women throughout the luteal phase. Mean RI in LPD patients was significantly higher compared with normal women throughout the follicular and luteal phases. Although systolic and diastolic velocities were observed to be lower in LPD patients compared with normal women, these differences were not statistically different. High correlations were observed between progesterone and RI within each of the luteal time points, achieving its highest value during the mid-luteal phase. The mean RI in the dominant ovary was significantly lower than in the nondominant ovary throughout the cycle in normal women (0.50 vs 0.65), but not in those with LPD (0.60 vs 0.66 P=0.37). In one patient with an anovulatory cycle, the intraovarian RI values remained high (mean 0.76, range 0.70–0.82).

This study[82] showed a clear correlation between the RI of the corpus luteum blood flow and the plasma progesterone in a natural cycle. The strongest correlation was seen in the mid-luteal phase, the period that corresponds to a peak neovascularization of the corpus luteum. Consistent with this finding, the authors have shown an increase in blood flow impedance in the late luteal phase, the period associated with the onset of the corpus luteum regression. These findings suggest the possibility of using the RI of the corpus luteum blood flow as an adjunct to plasma progesterone assay and as an index of luteal function.

Tinkanen,[83] on the other hand found no difference between the blood flow in the corpus luteum in controls with normal luteal phase and infertility patients with an abnormal luteal phase. A short luteal phase claims the author is not due to premature vascular regression of the corpus luteum as evaluated by measurement of the vascular resistance.

Strigini et al.[84] observed the change of impedance during the luteal phase of FSH-treated cycles. The uterine PI during stimulated cycles, both before and after ovulation was significantly reduced compared with spontaneous cycles. That was explained by an increase of plasma E2. Furthermore, Strigini advocates administration of exogenous progesterone as a supplementation to FSH treated cycles, stating that the uterine PI after administration of progesterone drops even more than in spontaneous or only with FSH treated cycles.

Kupesic et al.[80] correlated Doppler velocimetry, histological and hormonal markers. They presumed that when the ultrasound results are combined together, the measurement of hormone values and an endometrial biopsy could explain more about LPD. They found out that the mean progesterone levels were significantly lower in the group with LPD (10.2 ± 4.3 ng/ml) than in controls (21 ± 4.2 ng/ml). The FSH/LH ratio was significantly lower in the group with a delayed endometrial pattern compared to normal subjects during follicular and periovulatory phases (0.70 vs 1.24; 0.58 vs 0.75 respectively). There was a close correlation between estradiol levels and the mean diameter of the dominant follicle from days -5 to -1 relative to the days of sonographically observed ovulation. An increase in follicular diameter and endometrial thickness was noted for both normal and LPD groups.

Intraovarian blood flow resistance showed no difference between the groups during the proliferative phase. A significant decline of the RI occurred in the control group for the day of the LH peak (RI=0.45 ± 0.04), with a return to the follicular phase level of 0.49 ± 0.02 during the second phase of the menstrual cycle **(Fig. 50.23A)**. The mean intraovarian RI for the LPD

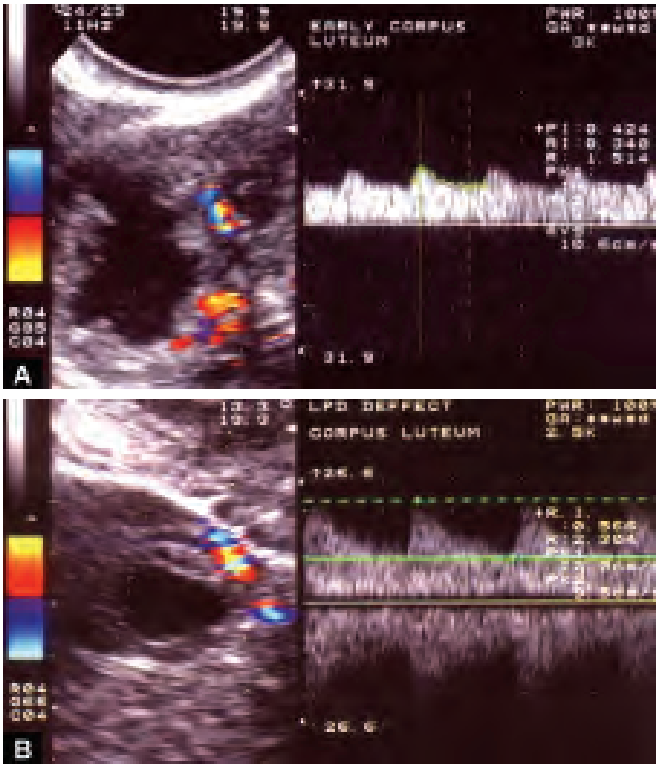

Figures 50.23A and B: (A) Color Doppler ultrasound of a normal corpus luteum. Pulsed Doppler waveform analysis shows high velocity and low resistance index (RI = 0.34), both indicative of a normal corpus luteum function; (B) Color Doppler ultrasound illustrating LPD. The increased intraovarian resistance index (RI = 0.56) obtained during the midluteal phase indicates LPD

group (RI=0.58 ± 0.04) was significantly higher than in the control group throughout the luteal phase **(Fig. 50.23B)**. Patients in the control group had a significantly lower RI in the dominant than in the nondominant ovary, whereas LPD patients had almost the same RI in both the ovaries. The authors measured blood flow in the spiral arteries as well. The spiral arteries in the control group demonstrated an RI of 0.53 ± 0.04 during the periovulatory phase, and RI values of 0.50 ± 0.02 and 0.51 ± 0.04 were obtained during the mid-luteal and late luteal phase respectively. Higher impedance values were obtained from the spiral arteries in the LPD group during the periovulatory phase (RI=0.70 ± 0.06, p< 0.001), mid-luteal phase (RI=0.72 ± 0.06, p< 0.001) and late luteal phase (RI=0.72 ± 0.04, p< 0.001). A close correlation has been found between plasma levels of estradiol and the mean diameter of the follicle. This study clearly demonstrated that patients with normal endometrial development show a similar trend of regression for uterine, radial and spiral artery impedance from the follicular to the luteal phase. In contrast, patients with a delayed endometrial pattern are characterized by an increased uterine vascular resistance during the luteal phase. Since the most significant difference in terms of RI is obtained for spiral arteries, it might be expected that the endometrial blood flow changes could be used to predict the development of the endometrium and likelihood of pregnancy.

Salim et al.[85] correlated luteal blood in normal pregnancies to the flow in abnormal pregnancies. Their study proved the hypothesis that an absence of luteal flow cannot coexist with a normal pregnancy. The impedance to intraovarian blood flow was significantly higher in patients with an abnormal early pregnancy (missed, incomplete and threatened abortion) than in women with a normal pregnancy. However, this was not confirmed in patients with a blighted ovum, molar and an ectopic pregnancy. The impedance to luteal blood flow was almost the same as in normal pregnancy. This difference amongst the subgroups of an abnormal early pregnancy may relate to a different natural history of the disease. Missed and incomplete abortions are manifested as failed early pregnancy with no prospects for further development. A threatened abortion is a potentially similar condition. Whether a decreased corpus luteum blood flow is a potential cause or a consequence of the disease remains unclear. Anembryonic pregnancies, molar or ectopic pregnancies are somewhat different. These pathologic conditions usually are progressive and not self-limited. This can explain why impedance to luteal blood flow in these women is similar to those women with a normally progressing pregnancy.

Alcazar et al.[86] agree only partially with the results obtained by Salim et al.[85] Alcazar's group found that the mean RI in a missed abortion was higher than in controls. This increased vascular resistance could be explained by the fact that a missed abortion consists of a failure of an early pregnancy to develop, in which the production of hCG is impaired, which in turn could have a negative effect on the luteal function. On the other hand, they found no statistically significant difference in RI of patients with a threatened abortion.

TUBAL CAUSES OF INFERTILITY

The tubal mucosa responds to the hormonal changes during the menstrual cycle in order to facilitate the transport of sperm and fertilized ova in the process of fertilization. During the luteal phase, decreased tube secretion and more prominent ciliary activity propel the

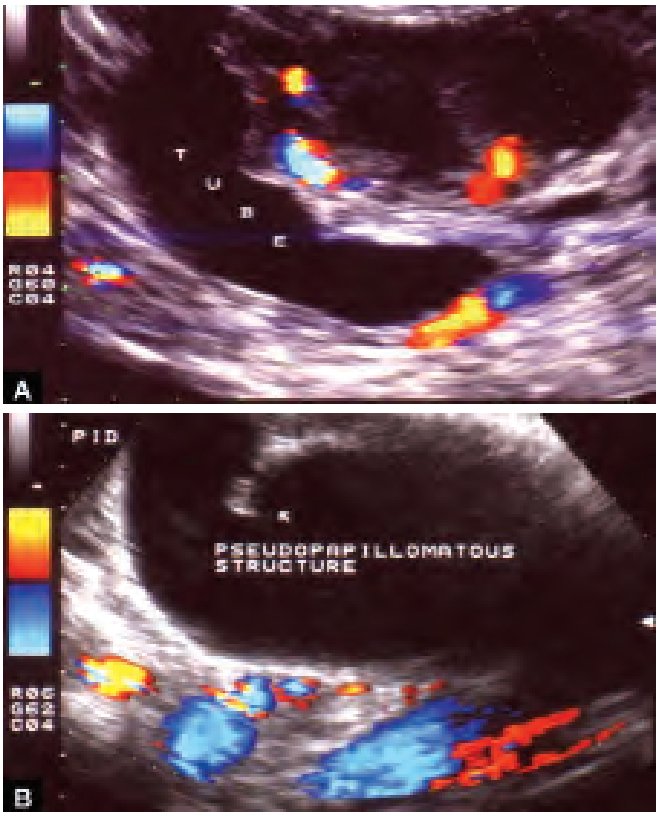

Figures 50.24A and B: (A) Transvaginal color Doppler image of a dilated and fluid filled tube in an infertile patient with tubal cause of infertility; (B) Dilated and fluid filled tube with incomplete septation in an infertile patient, caused by a previous pelvic infection

ova into the uterine fundus. If conception does not occur, the secretory and ciliary cells are significantly reduced in number due to withdrawal of endocrine support.

The normal fallopian tubes are narrow and usually not seen by transabdominal or transvaginal ultrasound unless they contain fluid within their lumina or are surrounded by fluid. The motility and transport function of the oviducts are impaired during all stages of pelvic inflammatory disease. First, during the acute phase, the tube becomes thickened and edematous, and contains a large amount of purulent exudate within its lumen **(Fig. 50.24A)**. Later, the inflammatory process may organize to form a tubo-ovarian abscess, which will in most cases lead to scarring and occlusion of the tube. Chronic hydrosalpinx is the ultimate remnant of PID: the tube is occluded, thin-walled and filled with fluid **(Fig. 50.24B)**.

Infertility caused by tubal dysfunction is found in approximately 35% of patients. A history of pelvic inflammatory disease, septic abortion, intrauterine contraceptive device, ruptured appendix, tubal surgery or ectopic pregnancy should alert the physician to the possibility of tubal damage. Amorphous acellular plugs have been identified as the probable cause of obstruction in the proximal tube in nearly 50% of women whose tubes did not opacify on HSG. The improved pregnancy rate after uterotubal insufflation and HSG suggests that their therapeutic effect may partially result from dislodgment of fallopian tube debris. Reversed spasm at the uterotubal junction is another cause of apparent obstruction on a conventional hysterosalpingogram. In 100 patients with nonfilling on the initial hysterosalpingogram, Lang[87] found that only 39 had persistent occlusion after pharmacologic manipulation and selective tubal salpingography. In the remaining 61 patients the apparent cause of tubal nonfilling was spasm and debris in 49 patients, submucous fibroids in six, synechiae in three, salpingitis isthmica nodosa in two, and a septated uterus in one.

Until a few years ago the assessment of the uterine cavity and the fallopian tube lumen relied on complicated, painful and invasive procedures. The major problem was how to visualize the hollow space within these organs and how to describe the contours of uterine, and oviduct walls. The functions of the uterus and the fallopian tubes depend on their cavities: a uterus filled with endometrial polyp or distorted by a myoma is an obstacle to implantation, while a tortuous and narrow tube with the PID changes does not permit oocytes to descend.

Hysterosalpingography, using radio-opaque dye for X-ray assessment of tubal and uterine anatomy, has been the standard form of investigation for several decades. The disadvantage of this type of investigation is that the ionizing radiation presents a risk to the oocyte: if the conception takes place in the investigation cycle, congenital fetal anomalies may occur. Furthermore, iodine-containing dyes used in X-ray HSG can cause an allergic reaction.

In the last two decades, laparoscopy has been the usual procedure for the assessment of tubal status. However, it requires general anesthesia and carries the risk of the anesthetic and of potential surgical complications, such as bowel or vascular injury, false pneumoperitoneum and postoperative discomfort.

Together with the development of ultrasound techniques, a totally new concept of diagnostic procedures has been initiated.[88,89] We have already described in the chapter on hysterosonosalpingography the benefits and limitations of the sonographic evaluation of the tubal patency.

CONCLUSION

Transvaginal sonography, color Doppler and 3D ultrasound with power Doppler facilities have made a significant improvement in the assessment of infertility. They may help in the prediction of ovulation and detection of ovulatory disorders.[90] Measurements of uterine perfusion have a predictive value regarding fecundity in patients undergoing different methods of medically assisted reproduction. Absent subendometrial and intraendometrial vascularization on the day of hCG administration appears to be a useful predictor of failure of implantation in IVF cycles, irrespective of the morphological appearance of the endometrium. Studies on spiral artery perfusion might produce a non-invasive assay of uterine receptivity, giving us more information about the pathophysiology of infertility, especially in the group of patients with unexplained causes.[91,92]

REFERENCES

1. Kurjak A, Kupesic-Urek S, Schulman H, et al. Transvaginal color Doppler in the assessment of ovarian and uterine blood flow in infertile women. Fertil Steril. 1991;56(5):870-3.
2. Kurjak A, Kupesic-Urek S. Normal and abnormal uterine perfusion. In: Jaffe R, Warsof LS (Eds). Color Doppler Imaging in Obstetrics and Gynecology. New York: McGraw Hill; 1992. pp. 255-63.
3. Goswamy RK, Silliams G, Steptoe PC, et al. Decreased uterine perfusion a cause of infertility. Hum Reprod. 1988;3:955-8.
4. Steer CV, Mills CV, Campbell S. Vaginal color Doppler assessment on the day of embryo transfer (ET) accurately predicts patients in an in vitro fertilization programme with suboptimal uterine perfusion who fail to become pregnant. Ultrasound Obstet Gynaecol. 1991;1:79-82.
5. Tsai YC, Chang JC, Tai MJ, et al. Relationship of uterine perfusion to outcome of intrauterine insemination. J Ultrasound Med. 1996;15:633-6.
6. Steer CV, Tan SL, Mason BA, et al. Midluteal phase vaginal color Doppler assessment of uterine artery impedance in a subfertile population. Fertil Steril. 1994;61:53-8.
7. Kupesic S. The first three weeks assessed by transvaginal color Doppler. J Perinat Med. 1996;24:301-17.
8. Cacciatore B, Simberg N, Fusaro P, et al. Transvaginal Doppler study of uterine artery blood flow in in vitro fertilization - embryo transfer cycles. Fertil Steril. 1996;66(1):130-4.
9. Freidler S, Schenker JG, Herman A, et al. The role of ultrasonography in the evaluation of endometrial receptivity following assisted reproductive treatments: a critical review. Hum Reprod Update. 1996;2:323-35.
10. Gonen Y, Calderon M, Direnfeld M, et al. The impact of sonographic assessment of the endometrium and meticulous hormonal monitoring during natural cycles in patients with failed donor artificial insemination. Ultrasound Obstet Gynecol. 1991;1:122-6.
11. Abdalla HI, Brooks AA, Johnson MR, et al. Endometrial thickness: a predictor of implantation in ovum recipients? Hum Reprod. 1994;9:363-5.
12. Khalifa E, Brzyski RG, Oehninger S, et al. Sonographic appearance of the endometrium: the predictive value for the outcome of in vitro fertilization in stimulated cycles. Hum. Reprod. 1992;7:677-80.
13. Serafini P, Batzofin J, Nelson J, et al. Sonographic uterine predictors of pregnancy in women undergoing ovulation induction for assisted reproductive treatments. Fertil Steril. 1994;62:815-22.
14. Sher G, Herbert C, Maassarani G, et al. Assessment of the late proliferative phase endometrium by ultrasonography in patients undergoing in vitro fertilization and embryo transfer (IVF/ET). Hum Reprod. 1991;6:232-7.
15. Zaidi J, Campbell S, Pitroff R, et al. Endometrial thickness, morphology, vascular penetration and velocimetry in predicting implantation in an in vitro fertilization program. Ultrasound Obstet Gynecol. 1995;6:191-8.
16. Kyei-Mensah A, Maconochie N, Zaidi J, et al. Transvaginal three-dimensional ultrasound: reproducibility of ovarian and endometrial volume measurements. Fertil Steril. 1996;66:718-22.
17. Riccabona M, Nelson TR, Pretorius DH. Three-dimensional ultrasound: accuracy of distance and volume measurements. Ultrasound Obstet Gynecol. 1996;4:29-34.
18. Gilja OH, Smievoll I, Thune N, et al. In vivo comparison of 3D ultrasonography and magnetic resonance imaging in volume estimation of human kidney. Ultrasound Med Biol. 1995;21:25-32.
19. Lee A, Sator M, Kratochwil A, et al. Endometrial volume change during spontaneous menstrual cycles: volumetry by transvaginal three-dimensional ultrasound. Fertil Steril. 1997;68:831-5.
20. Kyei-Mensah A, Zaidi J, Pittrof R, et al. Transvaginal three-dimensional ultrasound: accuracy of follicular volume measurements. Fertil Steril. 1996;65:371-6.
21. Kupesic S, Bekavac I, Bjelos D, et al. Assessment of endometrial receptivity by transvaginal color Doppler and three-dimensional power Doppler ultrasonography in patients undergoing in vitro fertilization procedures. J Ultrasound Med. 2001;20:125-34.
22. Ashton D, Amin HK, Richart RM, et al. The incidence of asymptomatic uterine anomalies in women undergoing transcervical tubal sterilization. Obstet Gynecol. 1988;72:28-30.
23. Sorensen S. Estimated prevalence of mulerian anomalies. Acta Obstet Gynecol Scand. 1988;67:441-5.
24. Gaucherand P, Awada A, Rudigoz RC, et al. Obstetrical prognosis of septate uterus: a plea for treatment of the septum. Eur J Obstet Gynecol Reprod Biol. 1994;54:109-12.
25. Fedele L, Arcaini L, Parazzini F, et al. Metroplastic hysteroscopy and fertility. Fertil Steril. 1993;59:768-70.
26. Heinonen PK, Saarikoski S, Pystynen P. Reproductive performance of women with uterine anomalies. An evaluation of 182 cases. Acta Obstet Gynecol Scand. 1982;61:157-62.

27. Fedele L, Bianchi S, Marchini M, et al. Ultrastructural aspects of endometrium in infertile women with septate uterus. Fertil Steril. 1996;65:750-2.
28. Cararach M, Penella J, Ubeda J, et al. Hysteroscopic incision of the septate uterus: scissors versus resectoscope. Hum Reprod. 1994;9:87-9.
29. Goldenberg M, Sivan E, Sharabi Z. Reproductive outcome following hysteroscopic management of intrauterine septum and adhesions. Hum Reprod. 1995;10:2663-5.
30. Valdes C, Malini S, Malinak LR. Ultrasound evaluation of female genital tract anomalies: a review of 64 cases. Am J Obstet Gynecol. 1995;149:285-90.
31. Nicolini U, Bellotti B, Bonazzi D, et al. Can ultrasound be used to screen uterine malformation? Fertil Steril. 1987;47:89-93.
32. Reuter KL, Daly DC, Cohen SM. Septate versus bicornuate uteri: errors in imaging diagnosis. Radiology. 1989;172:749-52.
33. Randolph J, Ying Y, Maier D, et al. Comparison of real time ultrasonography, hysterosalpingography, and laparoscopy/hysteroscopy in the evaluation of uterine abnormalities and tubal patency. Fertil Steril. 1986;5:828-32.
34. Richman TS, Viscomi GN, Cherney AD, et al. Fallopian tubal patency assessment by ultrasound following fluid injection. Radiology. 1984;152:507-10.
35. Salle B, Sergeant P, Galcherand P, et al. Transvaginal hysterosonographic evaluation of septate uteri: a preliminary report. Hum Reprod. 1996;11:1004-7.
36. Marshall C, Mintz DI, Thickman D, et al. MR evaluation of uterine anomalies. Radiology. 1987;148:287-9.
37. Carrington BM, Hricak M, Naruddin RN. Mullerian duct anomalies: MR evaluation. Radiology. 1990;170:715-20.
38. Jurkovic D, Giepel A, Gurboeck K, et al. Three dimensional ultrasound for the assessment of uterine anatomy and detection of congenital anomalies: a comparison with hysterosalpingography and two-dimensional sonography. Ultrasound Obstet Gynecol. 1995;5:233-7.
39. Taylor PJ, Cumming DC. Hysteroscopy in 100 patients. Fertil Steril. 1979;31:301-4.
40. Kupesic S, Kurjak A. Septate uterus: detection and prediction of obstetrical complications by different forms of ultrasonography. J Ultrasound Med. 1998;17:631-6.
41. Dabrashrafi H, Bahadori M, Mohammad K, et al. Septate uterus: new idea on the histologic features of the septum in this abnormal uterus. Am J Obstet Gynecol. 1995;172:105-7.
42. Balen FG, Allen CM, Gardener JE, et al. 3-dimensional reconstruction of ultrasound images of the uterine cavity. The British Journal of Radiology. 1993;66:588-91.
43. Weinraub Z, Maymon R, Shulman A, et al. Three-dimensional saline contrast rendering of uterine cavity pathology. Ultrasound Obstet Gynecol. 1996;8:277-82.
44. Kupesic S, Kurjak A, Skenderovic S, et al. Screening for uterine abnormalities by three-dimensional ultrasound improves perinatal outcome. J Perinat Med. 2002;30:9-17.
45. Kurjak A, Kupesic S, Miric D. The assessment of benign uterine tumor vascularization by transvaginal color Doppler. Ultrasound Med Biol. 1992;18:645-9.
46. Brosens JJ, deSouza NM, Barker FG, et al. Endovaginal ultrasonography in the diagnosis of adenomyosis uteri: identifying the predictive characteristics. Br J Obstet Gynaecol. 1995;102(6):471.
47. Schlaff WD, Hurst BS. Preoperative sonographic measurement of endometrial pattern predicts outcome of surgical repair in patients with severe Asherman's syndrome. Fertil Steril. 1995;63:410-3.
48. Zaidi J, Barber J, Kyei-Mensah A, et al. Relationship of ovarian stromal blood flow at baseline ultrasound to subsequent follicular response in an in vitro fertilization program. Obstet Gynecol. 1996;88:779-84.
49. Engmann L, Sladkevicius P, Agrawal R, et al. Value of ovarian stromal blood flow velocity measurement after pituitary suppression in the prediction of ovarian responsiveness and outcome of in vitro fertilization treatment. Fertil Steril. 1999;71(1):22-29.
50. Wittmack FM, Kreger DO, Blasco L, et al. Effect of follicular size on oocyte retrieval, fertilization, cleavage, and embryo quality in vitro fertilization cycles: a 6-year data collection. Fertil Steril. 1994;62:1205-10.
51. Golan A, Herman A, Soffer Y, et al. Ultrasonic control without hormone determination for ovulation induction in in-vitro fertilization/embryo-transfer with gonadotrophin-releasing hormone analogue and human menopausal gonadotrophin. Hum Reprod. 1994;9:1631-3.
52. Shoham Z, DiCarlo C, Pater A, et al. Is it possible to run a successful ovulation induction program based solely on ultrasound monitoring? The importance of endometrial measurements. Fertil Steril. 1991;56:836-41.
53. Tan SL. Simplification of IVF therapy. Curr Opin Obstet Gynecol. 1994;6:111-4.
54. Steiner H, Staudach A, Spitzer D, et al. Three-dimensional US in obstetrics and gynaecology: technique, possibilities and limitations. Hum Reprod. 1994;9:1773-8.
55. Penzias AS, Emmi AM, Dubey AK, et al. Ultrasound prediction of follicle volume: is the mean diameter reflective? Fertil Steril. 1994;62:1274-6.
56. Feichtinger W. Transvaginal three-dimensional imaging for evaluation and treatment of infertility. In: Merz E (Ed.). 3-D Ultrasound in Obstetrics and Gynecology. Philadelphia: Lippincott Williams and Wilkins; 1998. pp. 37-43.
57. Lass A, Skull J, McVeigh E, et al. Measurement of ovarian volume by transvaginal sonography before ovulation induction with human menopausal gonadotrophin for in-vitro fertilization can predict poor response. Hum Reprod. 1997;12:294-7.
58. Oyesanya OA, Parsons JH, Collins WP, et al. Total ovarian volume before human chorionic gonadotrophin administration for ovulation induction may predict the hyperstimulation syndrome. Hum Reprod. 1995;10:3211-2.
59. Kupesic S, Kurjak A. Predictors of in vitro fertilization outcome by three-dimensional ultrasound. Hum Reprod. 2002;17(4):950-55.
60. Adams J, Franks S, Polson DW, et al. Multifollicular ovaries: clinical and endocrine features and response to pulsatile gonadotropin-releasing hormone. Lancet. 1985;2:1375-8.
61. Matsunaga I, Hata T, Kitao M. Ultrasonographic identification of polycystic ovary. Asia-Oceania J Obstet Gynecol. 1985;11:227-32.
62. Takahashi K, Ozaki T, Okada M, et al. Relationship between ultrasonography and histopathological changes in

polycystic ovarian syndrome. Hum Reprod. 1994;9:2255-8.
63. Battaglia C, Artini PG, D'Ambrogio G, et al. Uterine and ovarian blood flow measurement. Does the full bladder modify the flow resistance? Acta Obstet Gynecol Scand. 1994;73:716-8.
64. Ardaens Y, Robert Y, Lemaitre L, et al. Polycystic ovarian disease: contribution of vaginal endosonography and reassessment of ultrasonic diagnosis. Fertil Steril. 1991;55: 1062-8.
65. Robert Y, Dubrulle F, Gaillandre L, et al. Ultrasound assessment of ovarian stroma hypertrophy in hyperandrogenism and ovulation disorders: visual analysis versus computerized quantification. Fertil Steril. 1995;64:307-12.
66. Merce LT, Garces D, Barco MJ, et al. Intraovarian Doppler velocimetry in ovulatory, dysovulatory and anovulatory cycles. Ultrasound Obstet Gynecol. 1992;2:197-202.
67. Battaglia C, Artini PG, D'Ambrogio G, et al. The role of color Doppler imaging in the diagnosis of polycystic ovary syndrome. Am J Obstet Gynecol. 1992;172:108-13.
68. Zaidi J, Campbell S, Pittrof R, et al. Ovarian stromal blood flow in women with polycystic ovaries - a possible new marker for diagnosis? Hum Reprod. 1995;10:1992-5.
69. Aleem FA, Predanic M. Transvaginal color Doppler determination of the ovarian and uterine blood flow characteristics in polycystic ovary disease. Fertil Steril. 1996;65:510-16.
70. Battaglia C, Artini PG, Salvatori M, et al. Ultrasonographic patterns of polycystic ovaries; color Doppler and hormonal correlations. Ultrasound Obstet Gynecol. 1998;11:332-6.
71. Battaglia C, Artini PG, Genazzani AD, et al. Color Doppler analysis in oligo- and amenorrheic women with polycystic ovary syndrome. Gynecol Endocrinol. 1997;11:105-10.
72. Battaglia C, Artini PG, Genazzani AD, et al. Color Doppler analysis in lean and obese women with polycystic ovary syndrome. Ultrasound Obstet Gynecol. 1996;7:342-6.
73. Wild RA, Van Nort JJ, Grubb B, et al. Clinical signs of androgen excess as risk factors for coronary artery disease. Fertil Steril. 1990;54:255-9.
74. Wu MH, Tang HH, Hsu CC, et al. The role of three-dimensional ultrasonographic images in ovarian measurement. Fertil Steril. 1998;69:1152-5.
75. MacDougall MJ, Tan SL, Balen A, et al. A controlled study comparing patients with and without polycystic ovaries undergoing in-vitro fertilization. Hum Reprod. 1993;8:233-7.
76. MacDougall MJ, Tan SL, Jacobs HS. In-vitro fertilization and the ovarian hyperstimulation syndrome. Hum Reprod. 1992;7:597-600.
77. Kupesic S, Kurjak A. The assessment of normal and abnormal luteal function by transvaginal color Doppler sonography. Eur J Obstet Gynecol Reprod Biol. 1997;72:83-7.
78. Merce LT, Garces D, De la Fuente F. Conversion lutea de la onda de velocidad de fluio ovarica: nuevo parametro ecografico de ovulacion y funcion lutea. Acta Obstet Gynecol Scand. 1989;(ed. esp.)2:113-4.
79. Bourne TH, Reynolds K, Waterstone J, et al. Paracetamol-associated luteinized unruptured follicle syndrome: effect on intrafollicular blood flow. Ultrasound Obstet Gynecol. 1991;1:420-5.
80. Kupesic S, Kurjak A, Vujisic S, et al. Luteal phase defect: comparison between Doppler velocimetry, histological and hormonal markers. Ultrasound Obstet Gynaecol. 1997;9:1-8.
81. Glock JL, Blackman JA, Badger GJ, et al. Prognostic significance of morphologic changes of the corpus luteum by transvaginal ultrasound in early pregnancy monitoring. Obstet Gynecol. 1995;85:37-41.
82. Glock JL, Brumsted JR. Color flow pulsed Doppler ultrasound in diagnosing luteal phase defect. Fertil Steril. 1995;64:500-4.
83. Tinkanen H. The role of vascularization of the corpus luteum in the short luteal phase studied by Doppler ultrasound. Acta Obstet Gynecol Scand. 1994;73:321-3.
84. Strigini FAL, Scida PAM, Parri C, et al. Modifications in uterine and intraovarian artery impedance in cycles of treatment with exogenous gonadotropins: effects of luteal phase support. Fertil Steril. 1995;64:76-80.
85. Salim A, •alud I, Farmakides G, et al. Corpus luteum blood flow in normal and abnormal early pregnancy: Evaluation with transvaginal color and pulsed Doppler sonography. J Ultrasound Med. 1994;13:971-5.
86. Alcazar JL, Laparte C, Lopez-Garcia G. Corpus luteum blood flow in abnormal early pregnancy. J Ultrasound Med. 1996;15:645-9.
87. Lang EK. Organic vs. functional obstruction of the fallopian tubes: differentiation with prostaglandin antagonist-and B2-mediated hysterosalpingography and selective ostial salpingography. AJR. 1991;157:77-80.
88. Kupesic S, Plavsic MB. 2D and 3D hysterosalpingo-contrast-sonography in the assessment of uterine cavity and tubal patency. Eur J Obstet Gynecol Reprod Biol. 2007;133(1):64-9.
89. Tur-Kaspa I, Gal M, Hartman M, et al. A prospective evaluation of uterine abnormalities by saline infusion sonohysterography in 1,009 women with infertility or abnormal uterine bleeding. Fertil Steril. 2006;86(6):1731-5.
90. Sun W, Stegmann BJ, Henne M, et al. A new approach to ovarian reserve testing. Fertil Steril. 2008;90(6):2196-202.
91. Kupesic S. Three-dimensional ultrasound in reproductive medicine. Ultrasound Obstet Gynecol. 2005;5:304-15.
92. Zohav E, Bar Hava I, Meltcer S, et al. Early endometrial changes following successful implantation. 2and 3D ultrasound study. Clin Exp Obstet Gynecol. 1991;35:255-6.

CHAPTER 51

Newer Developments in Ultrasound in Infertility

Radu Vladareanu, Cristian Andrei, Mona Zvanca

INTRODUCTION

The standard definition of infertility is failure to conceive after 12 months of unprotected regular intercourse. Statistically, it affects almost 10% of the couples, with 40% of the cases related to female pathology.[1] Male infertility is involved in a similar percentage and in 20% of the situations, the etiologies are intricate. With an increasing incidence, with deep social and psychological implications, it may be related to any kind of cervical, uterine/endometrial, tubal and peritoneal infertility, and finally, ovarian anomalies.

The ability to diagnose and then decide on appropriate treatment is invaluable in helping women achieve better fertility outcomes where identified pathology is detrimental, but also in improving patient well-being where this may be more serious. With the technical development, ultrasound tends to overpass its limits and to become the main investigation tool even for situations when it was traditionally considered "second best". Diagnosing gross pathology is the main purpose of ultrasound, but lately great accent is put on depicting subtle deviations from the physiological processes that may explain cases of so called "idiopathic infertility", one of the most frustrating diagnostics both for clinician and for the couple.

After the development of the new technologies and rendering modes, it became possible to acquire valuable diagnostic images of the female genital organs. There appears to be few differences in the diagnostic accuracy of standard two-dimensional (2D) versus three-dimensional (3D) images in detecting pelvic pathology, but 3D scanning can improve efficiency by reducing scanning time and therefore improving patient throughout. Furthermore, 3D ultrasound is able to rapidly acquire and store ultrasonographic data that can later be retrospectively analyzed with the little loss of information. The most important advantage was the visualization of the coronal plane. It is therefore likely that the application of 3D ultrasound scanning will increase in the future for diagnostic purposes, particularly when the purchase cost of ultrasound equipment falls.

UTERINE/ENDOMETRIAL FACTORS OF INFERTILITY

The uterus is the implantation site and growth for developing pregnancy. Any distortion of the uterine cavity or any change in the blood supply may result in infertility or miscarriage. The normal mucosa lining, glandular secretion and vascularity are necessary to support implantation and placentation. Uterine anomalies, polyps, leiomyoma, adenomyosis can lead to poor reproductive performance.

Endometrium

Recognition of relationship between endometrial characteristics visualized by ultrasound (USG) and ability to become pregnant in assisted reproductive technology (ART), ovulation induction and even spontaneous cycles is one of the important advances in infertility treatment during the last 20 years. Ultrasound measurement of the endometrium is now an indispensable part of ovulation induction monitoring and assisted reproductive technologies. It also has a role in evaluation of unexplained infertility.

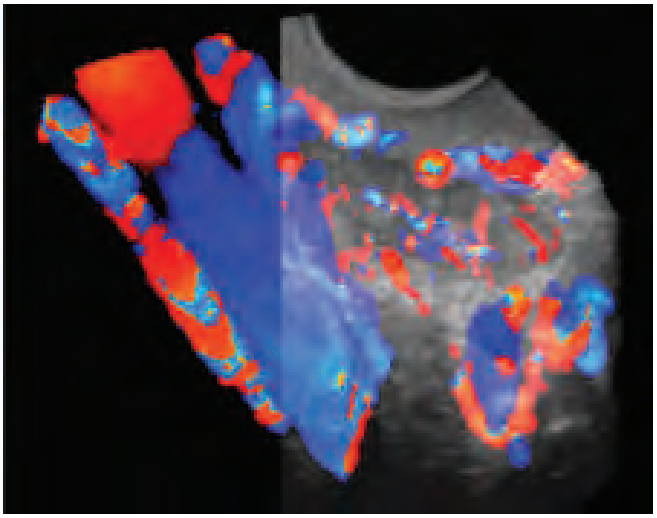

Figure 51.1: Three-dimensional angiography of the iliac artery and the uterine artery origin

Endometrial thickness is measured from the echogenic interface at the junction of endometrium and myometrium at the level of the maximum anteroposterior diameter in the sagittal plane. For standardization and accuracy, the measurement should be taken between the two endometrial-myometrial interfaces within 5–10 mm from the fundus of the uterine cavity.

The clinical significance of the endometrial sonographic changes during menstrual cycle, the relation between endometrial thickness and echogenicity and pregnancy outcome, is still unclear and subject to debate.

More recent studies, however, brought two new elements: uterine and endometrial vascularization. The human endometrium undergoes intense angiogenesis during menstrual cycle and angiogenesis is a key process for successful embryo implantation and development.

The uterine artery may be detected in virtually all premenopausal women[2] with color or power Doppler anywhere along its trajectory, but the measurement is recommended to be performed as close as possible to its origin from the internal iliac artery **(Fig. 51.1)**. The characteristic waveform presents a high velocity/high resistance pattern in nonpregnant women. The uterine flow is dependent on the estrogen level.[3] Within the reproductive age group, the resistivity index (RI) varies with the menstrual phase. It is statistically lower during the luteal phase (0.84 +/- 0.06) than during the proliferative phase (0.86 +/- 0.06).[4] The RI starts to decrease 1–2 days before midcycle, reaches a nadir 48 hours after ovulation, then it remains at the same level for the rest of the cycle. These changes do not occur in anovulatory cycles. There is no significant difference between left and right uterine arteries, related to the site of ovulation. Also, a good implantation prognosis is related to a uterine pulsatility index (PI) between 2 and 3 in both arteries. The pregnancy chances decrease significantly with a value over 3 or when there is absent diastolic flow.[5] Flow changes regard also the radial and endometrial arteries. Generally, they follow the same pattern, with a decrease in vessel resistance during the second half of an ovulatory cycle. The human endometrium undergoes intense angiogenesis during menstrual cycle, a key process for successful embryo implantation and development. Power Doppler combined with 3D USG is a noninvasive way to study the layers of the whole endometrium using perfusion analysis. The spiral arteries are responsible for the endometrial vascularization with a very high impact on early embryonic development. Doppler mapping of the subendometrial flow[6] depicted four types of endometrial flow during early luteal phase, as folllows: Type 0: Vascularization far from subendometrial region; Type 1: Peripheral – vessels reaching the outer echogenic layer of the endometrium; Type 2: Intermediate – flow within the middle hypoechogenic layer; Type 3: Central– blood flow on the entire endometrial thickness.

The evaluation should be performed with power Doppler in order to visualize even low flow vessels and to avoid loss of signal with increasing insonation angle **(Fig. 51.2)**. The vascularity type may be predictor of ovulation and implantation, therefore, it is important to be assessed in infertile patients. Usually, there is a poor vascularity in anovulatory cycles. Each type correlates with a different implantation prognosis, which varies from 0% for type 0 to 37.9% for type 3.

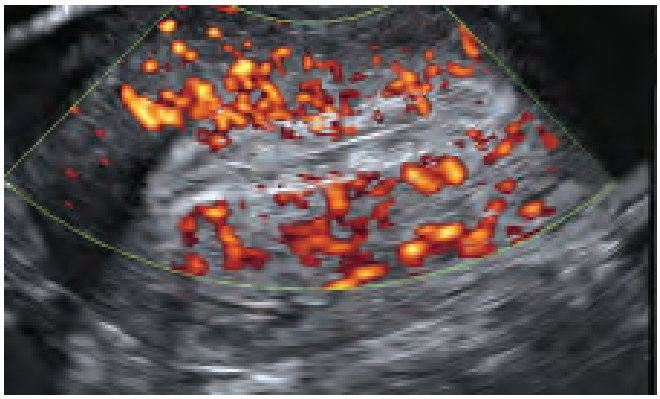

Figure 51.2: Endometrial vascularization in midcycle – the radial and spiral arteries. Power Doppler is used to visualize the low velocity flow in small vessels penetrating the endometrium. In this case the flow reaches the inner half of the endometrium (type III)

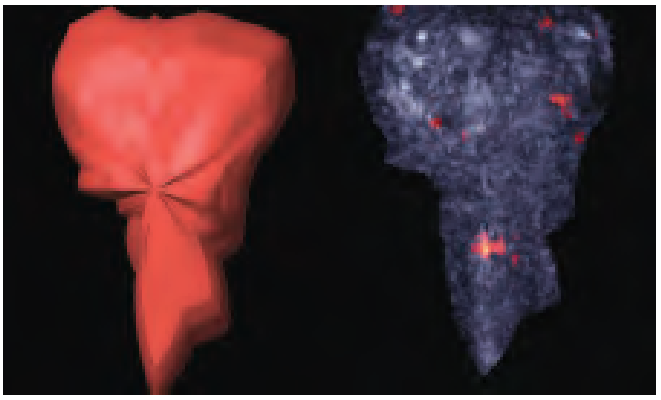

Figure 51.3: A digitally reconstructed image of the endometrium, including a periendometrial region (shell), using VOCAL software, useful for vascularity indices calculations

Using the three-dimensional techniques, endometrial vascularization may be quantified in a semiautomatic manner. The VOCAL (Volume Organ Computer-aided Analysis) provided three indices:

1. Vascularization index (VI) represents total number of color voxels or total number of voxels from region of interest and reflects the number of vessels in the tissue.
2. Flow index (FI) represents total intensity of color voxels or total number of color voxels in the volume and reflects the total blood volume.
3. Vascularization/flow index (VFI) represents total intensity of color voxels or total number of voxels (color + gray) in the volume and combines information about the quality and quantity of vascularization.

It also offers a general view of both subendometrial and endometrial blood flow, along with the measurement of endometrial volume **(Fig. 51.3)**.

Changes in endometrial and subendometrial flow were investigated in 27 healthy, fertile volunteers with regular menstrual periods, using 3D power Doppler (3D PD) on alternate days, starting on cycle day 3 until ovulation and then every 4 days afterward until initiation of menses.[7] With the use of the VOCAL, the vascular indexes were calculated for each time point. For the subendometrial vascular index, an arbitrary limit of 5 mm was established and the inner third of the endometrium and the area irrigated by the radial arteries. Both endometrial and subendometrial vascular flow increased to a maximum 3 days prior to ovulation, then decreased until postovulatory day 5 and finally begun a gradual increase during the rest of the luteal phase. The proliferative phase increment was related to estradiol levels and its vasodilating effects, while the luteal phase increase was related to serum progesterone. Interestingly, the flow indexes continued to increase during menstruation regardless of a drastic drop in progesterone levels; this might be explained by the high endometrial vascular density due to progressive compaction of the spiral arteries. The reduction in the postovulatory vascular indexes is explained by vasodilatation of the subepithelial capillary plexus, which induces the required stromal edema to allow embryo implantation. Another study found that the lowest vascularization index occurred two days after ovulation and progressively increased during the luteal phase.[8]

Thus, 3D USG is a reliable technique for investigating cyclic, physiological changes in endometrial vascularization, showing that there are maximum values 2–3 days prior to ovulation, decreasing to minimal values 2–5 days postovulation and increasing thereafter. Vascular flow is delicately orchestrated in order to provide human embryos a favorable microenvironment for implantation, although the amount of oxygen the embryo needs from the endometrium during the implantation process is still controversial. More studies are needed to definitively establish the role of endometrial/subendometrial vascular oscillations in embryo implantation.

The question is at this moment, when there are so many sonographic tools, which one is better and more predictive in evaluating endometrial receptivity and a potential pregnancy outcome. The most reproducible measurement seems to be the endometrial volume, but in similar stimulated cycles the 2D and 3D endometrial parameters are similar.[9]

A recent study[10] evaluating the predictive value of power Doppler angiography and 3D endometrial parameters for endometrial receptivity in *in vitro* fertilization (IVF) cycles, found a very good correlation between endometrial volume, VI, FI and VFI and pregnancy outcome. Moreover, the indices are even better predictive when one grade I embryo or no grade one embryo are transferred, with an important role in the management of single embryo transfer politics. On the other hand, endometrial pattern ("triple line" aspect) and endometrial thickness were of less predictive value.

Subendometrial contractions are also important in evaluation of infertile women. They are seen on prolonged examinations, in the late proliferative phase and periovulatory. In periovulatory phase, there are approximately three contractions per minute, which progress from cervix towards uterine fundus, with important role in sperm transport. They are seen on ultrasound as deformation of the subendometrial area with hypoechoic halo.

Endometrium in Infertile Women

Three-dimensional ultrasound facilitates noninvasive evaluation of the endometrium and identifies some organic problems that can negatively influence the implantation process in infertile women.[11] Specifically, endometrial volume determination and evaluation of endometrial angiogenesis using vascularization indexes can easily and accurately be performed using 3D USG.

The vascularization indexes are different in fertile women than in patients with unexplained infertility; the latter show a dramatic decrease in both endometrial and subendometrial vascularization indexes that are unrelated to both estradiol or progesterone levels and to endometrial thickness and volume. This suggests that vascular dysfunction may compromise embryo implantation.[12] Similarly, vascular changes that take place during natural menstrual cycles have been compared with those occur in stimulated cycles and appeared a 35% decrease in endometrial and subendometrial vascularization in stimulated cycles.[13]

Endometrial Studies in Women Undergoing ART

Only 30% of embryos transferred into the uterine cavity after ART successfully implant. In many cases, this may be due to the embryo, but in all cases, endometrial receptivity may also be impaired. Prognostic endometrial receptivity markers are still needed to identify patients with a good, fair or poor prognosis. Patients with a good prognosis might benefit from single embryo transfer, whereas patients with a poor prognosis may be advised to have embryo frozen and transferred at a later stage in a natural cycle.

Throughout the years, multiple variables relating cycle outcome with endometrial thickness and pattern have been identified based on 2D USG assessment of endometrial perfusion at uterine, arcuate, radial and spiral arteries. Endometrial/subendometrial mapping with color Doppler and power Doppler has also been used.[14] Some have reported a positive correlation between endometrial thickness, volume and/or texture and IVF cycle outcome;[15] others have not observed this positive correlation.[16] Two reports concluded that pregnancy cannot result if the endometrial volume is less than 1–2 ml.[17]

Initially, pulsed Doppler studies of uterine arteries appeared extremely promising in the terms of determining a cutoff value for predicting pregnancy, but subsequent studies failed to confirm this link. This may be due to the lack of correlation between the uterine artery pulsatility index and endometrial vascularization.

Three-dimensional USG allows prompt, integrated evaluation of all known receptivity markers by measuring endometrial thickness, texture, pattern, volume and global perfusion. Endometrial/subendometrial perfusion provides a more direct estimate of endometrial receptivity. It has been evaluated in different phases of the stimulated ART cycle: on the day of hCG administration,[17] the day of egg retrieval,[18] and the day of embryo transfer.[19] Generally, there is no consensus about the area that should be studied for adequate assessment of subendometrial vascularization. While some groups consider 1 mm outside the endometrium adequate,[20] others postulate that a 5 mm[7] or 10 mm margin[18] should be used. The choice of a smaller margin (i.e. 1 mm) is based on the fact that cyclic changes in vascularization occur in that region in response to sex steroid secretion throughout the cycle. A wider margin may inadvertently include leiomyomas, which could interfere with the accuracy of indexes. Not unexpectedly, the results of these studies have been variable. Some authors found a direct relationship between pregnancy rates and subendometrial vascularization (VI, FI, VFI) on the day of hCG administration[21] or on the day of embryo transfer,[22] whereas others found no correlation with the day of hCG,[20] or even found the opposite (a higher pregnancy rate when endometrial/subendometrial flow was absent). Although no differences were found in patients with a good prognosis, cycle outcome seemed improved in patients with poor embryo quality but with better endometrial vascularization (VI, FI, VFI). This was true for in vitro fertilization as well as for cryopreserved embryo transfers.

Endometrial/subendometrial vascularization may also serve as a prognostic marker of ongoing pregnancy as lower perfusion correlates with miscarriages. None of the other study parameters – endometrial thickness, volume or texture – had any predictive value in terms of pregnancy evolution. This finding may be helpful in order to appropriately counsel patients with a high chance of miscarriage and also as a guideline for implementing early preventive measures.

Endometrial Polyp

Polyps are common cavity lesions, well-defined within the endometrial cavity, that originate from endometrial tissue. Benign endometrial polyps are found in up to 30% of women. They range in size from 5 to 30 mm in diameter and are usually sited at the fundus. Polyps are associated with abnormal intermenstrual bleeding, pre-menstrual spotting and occasionally abdominal pain and dysmenorrhea, but are often asymptomatic and

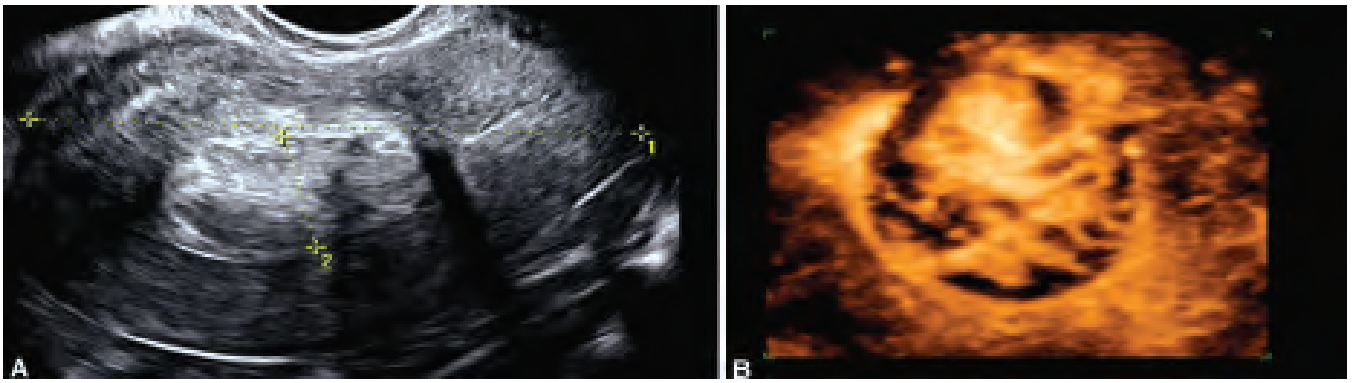

Figures 51.4A and B: Large endometrial polyp. (A) conventional transvaginal sagittal scan; (B) 3D image in the coronal plane

detected at the time of an ultrasound for another indication, typically assessment of infertility. The mechanisms of infertility in the case of endometrial polyps are mass effect, fallopian tube occlusion, altered implantation process, miscarriage, cervical occlusion and interference with sperm transport towards tubes.

They typically assume a slightly higher echogenicity that the endometrium itself, with a single feeding vessel. They induce an unequal thickening of the endometrium **(Figs 51.4A and B)**. Large polyps may appear as diffuse endometrial thickening, being difficult to differentiate from simple hyperplasia. A differential diagnosis for an endometrial polyp is a submucosal fibroid. Because the polyp is echogenic, it is more easily identified within the proliferative phase of the cycle, whereas a small submucosal fibroid would be more easily seen in the secretory phase. The shape, the dimensions, the origin and the impact on the endometrial cavity are clearly visualized, guiding the therapeutic procedure. Color Doppler is a useful tool for distinguishing between a polyp **(Fig. 51.5)** and a submucosal fibroid and can be used to visualize feeding vessels to the polyp (the "pedicle sign") and improve the detection rate to a level comparable with hysteroscopy with studies suggesting a sensitivity and specificity for color Doppler ultrasound of 95% and 80%, respectively. Endometrial polyp has a moderate vascular resistance (RI = 0.48 ± 0.06). Infection or necrosis lowers the impedance to blood flow.

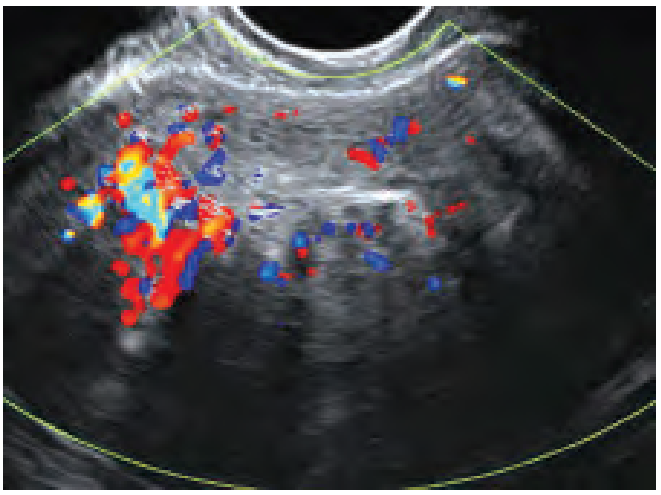

Figure 51.5: Feeding vessel of the endometrial polyp using color Doppler scan

Three-dimensional sonography may facilitate diagnosis, using static acquisition **(Fig. 51.4)**, direct or inversion mode during saline infusion sonography (SIS) and also help differentiate between endometrial polyp and submucosal fibroid. The extraordinary capacity of the multiplanar mode to study the whole endometrium simplifies identification of polyps, which can hamper embryo implantation if they are larger than 10 mm.

Saline infusion sonography may also be used to improve the detection rate and reduce the number of false positives. It often helps define the position and size of the polyp **(Figs 51.6A to C)**, which can allow the surgeon to modify their approach and resect the larger, more broad-based polyps rather than list them for simple polypectomy.

The tomographic ultrasound imaging mode provides tomographic sections of the uterus, permitting global evaluation of the uterus.

Leiomyomas

Leiomyomas are benign smooth-muscle growth of the uterus that can occur as a single lesion, though it more often presents as multiple lesions. Together with endometrial polyps, are the most frequent benign uterine pathologies and both can interfere with the reproductive process. Uterine myomas may be

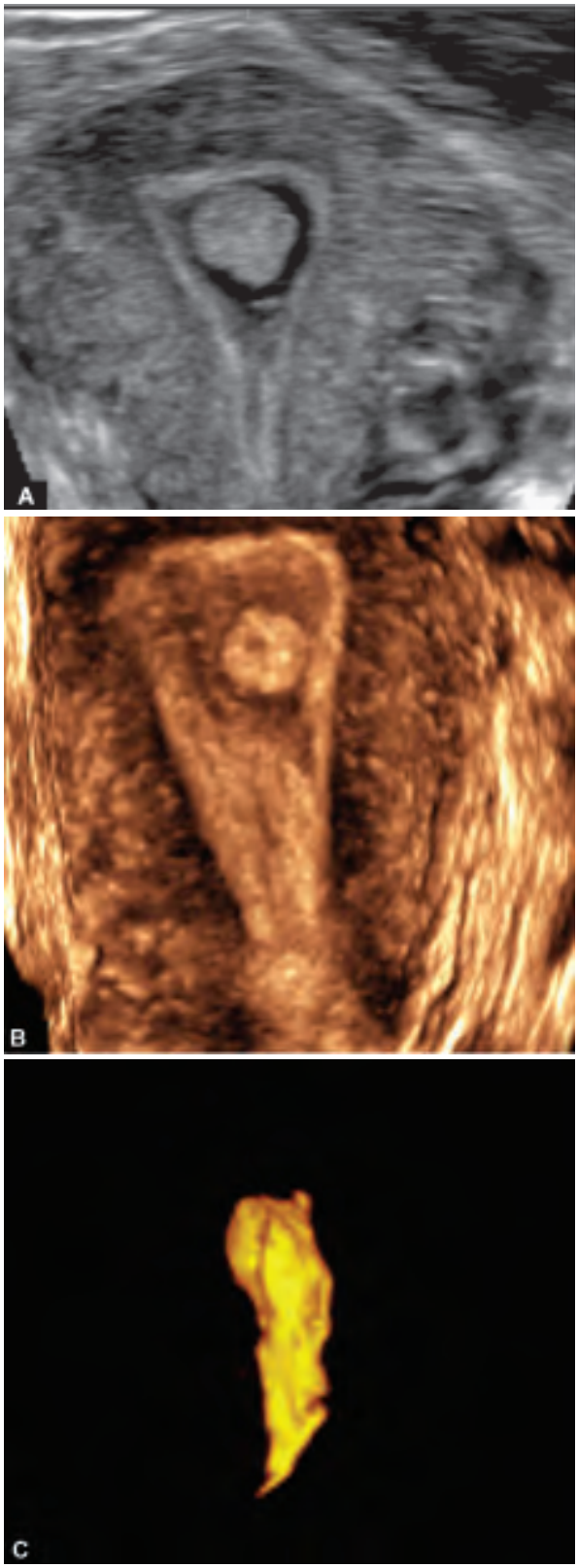

Figures 51.6A to C: Endometrial polyp during SIS. (A) Conventional acquisition; (B) 3D static render; (C) Inversion mode

generators of infertility by obstructing the fallopian tubes, distorting the endometrial cavity and causing subendometrial ischemia, thus interfering with gamete transport and implantation.[23] The effects on fertility depends on the location and size of the fibroid, with large myomas indenting the endometrium having greater impact on fertility performance and pregnancy outcome.

The relationship of the fibroids to the uterine cavity is better examined by transvaginal ultrasound (TVS). A fibroid outline is usually well visualized by TVS, even in the very small lesion, because of the pseudocapsule. Fibroids may be identified by disruption of either the uniform myometrial reflectivity or the smooth uterine outline.

Sonographically, they present as focal enlargements of the uterus, with a texture similar to the myometrium and posterior shadowing. The appearance greatly depends upon the presence of calcification or necrosis. Fibroids are commonly hypoechoic compared to adjacent myometrium, but they can also be isoechoic or even hyperechoic. Very large fibroids are best seen with transabdominal (TAS) as they often extend beyond the effective range of transvaginal probe. Doppler ultrasound visualizes circular surface vessels, sometimes detecting the main feeding vessel. The resistance index is always relatively high with an average of 0.55.[24] Color or power Doppler can be useful in the assessment of the fibroid blood supply. It is particularly useful in identifying the pedicle connecting a pedunculated fibroid to the uterus when there is uncertainty about the etiology of a fibroid lying within the pelvis. It can also be used to help distinguish between an endometrial polyp and submucosal fibroid. The polyp vessels typically have a central feeder vessel branching into smaller vessels, whereas the blood vessels to the fibroid are identified at its periphery. Color Doppler has also been used for treatment planning and post-treatment follow-up for radiologic treatment of fibroids such as uterine artery embolization.

The exact position, the impact on the ostium tubae and the uterine cavity may be difficult to assess by conventional ultrasound. A very easy solution in many cases is offered by a static 3D acquisition or static VCI – C, which can show the fibroid in the coronal plane **(Figs 51.7A and B)**. The increased echogenicity of the endometrium improves the visualization of the uterine cavity contour, but sometimes, especially in large myomas located on the anterior wall, this may be extremely difficult. It can be used to precisely establish the size, vascularization and location of myomas and can determine their relation to the endometrial cavity.

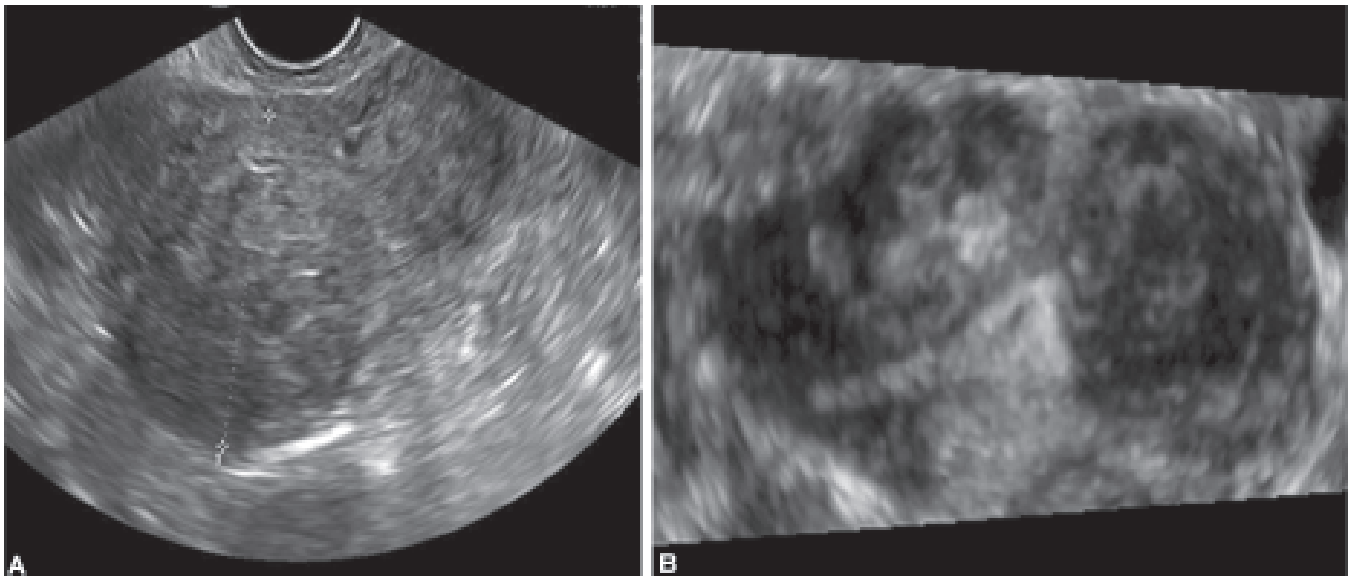

Figures 51.7A and B: Uterine fundal leiomyoma distorting the uterine cavity. (A) 2D scan; (B) VCI-C rendering

Saline infusion sonohysterography has become a vital tool in the assessment of the cavity distortion caused by fibroids. Instillation of saline enhances contrast and delineates the uterine myoma. By distending the cavity with saline, it is usually possible to view clearly both the separated cavity surfaces for significant cavity wall distortion or irregularity and the potential cavity for space-occupying lesions **(Fig. 51.8)**.

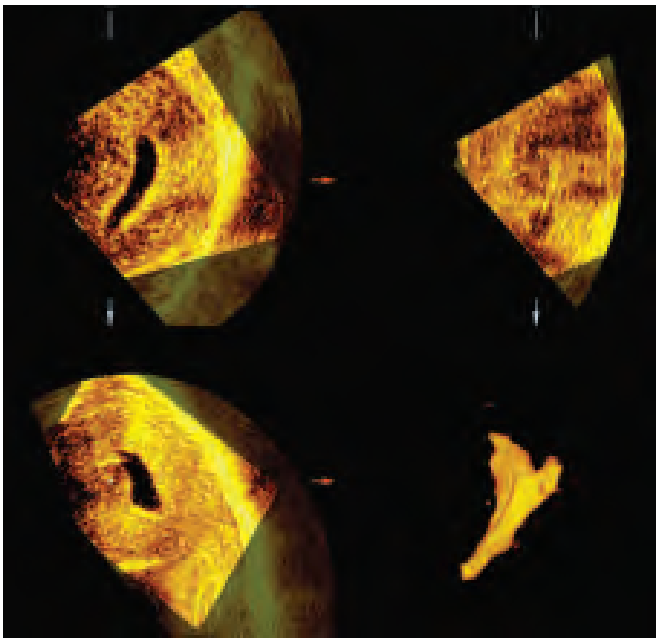

Figure 51.8: Submucous small myoma distorting the uterine cavity. SIS inversion mode

If a fibroid impinges on the cavity then assessment is made of what percentage of the lesion projects into cavity and its degree of extension into the myometrium. It can be categorized as a Type 0, I or II (Wamsteker and de Blok classification) to help plan the mode of surgical treatment. Three-dimensional scanning can be performed in conjunction with SIS to provide the additional coronal plane for further diagnostic accuracy, and with reconstruction of the volume creates a very good hysterographic image, without supplementary investigations. Inversion mode and rotation of the image may offer exact data regarding the dimension, position of the tumor and degree of distortion of the cavity. In the same procedure it is possible to assess tubal patency, by direct view of the fluid spillage through the fallopian tubes under Doppler control, or indirectly, by the easy depletion of the uterine cavity with fluid accumulation in the Douglas pouch. If a fibroid is situated close to the ostia, a hysterosalpingo contrast sonography (Hy-Co-Sy) test may help to clarify whether the fibroid is causing an ostial obstruction, as indicated by an absence of cornual exit of contrast. Echovist (the contrast for Hy-Co-Sy) also provides a positive contrast for clearly outlining submucosal fibroids.

Three-dimensional scanning guides the therapeutic procedure in cases deferred to hysteroscopic resection, by evaluating the degree of protrusion in the uterine cavity. In the same manner, it also selects the cases to benefit from laparoscopic or classic myomectomy.

It is recommended to remove myomas that distort the endometrial cavity, so 3D USG is a valuable tool

when surgery is being discussed. Similarly, 3D USG provides a more reliable postsurgical evaluation of the uterine cavity.

Müllerian Anomalies

Congenital uterine abnormalities (müllerian anomalies) are associated with infertility, recurrent miscarriage, preterm labor and malpresentations.

The exact incidence of congenital uterine anomalies is difficult to determine since many women with such anomalies are not diagnosed, especially if they are asymptomatic, but it seems to be around 2–4% of live births and accordingly to various studies range from 1% to 26% in infertile females.[25] The most common type of müllerian anomalies are uterine anomalies, with a distribution as follows: septate/arcuate uterus (90%), bicornuate uterus (5%) and didelphic uterus (5%).

The uterus develops from fusion of the paramesonephric ducts, which join in the midline at about the 10th week of gestation to form the unified body of the uterus. Abnormalities in resorption of the fused midline tissues occur by the 20th week and can result in the formation of septa of variable length and position. The various müllerian anomalies are the consequences of four major disturbances:

1. Failure of one or more müllerian duct to develop (agenesis, unicornuate uterus without rudimentary horn)
2. Failure of the ducts to canalize (unicornuate uterus with rudimentary horn without proper cavities)
3. Failure to fuse or abnormal fusion of the ducts (uterus didelphys, bicornuate uterus)
4. Failure of resorption of the midline uterine septum (septate uterus, arcuate uterus)

Among all types of congenital uterine anomalies, the septate uterus presents the highest rate of miscarriage.[26] Clinically, this is of greatest importance, as septate uterus is considered a "mild" anomaly and the differential diagnosis with bicornuate uterus, anomaly with a better fertility prognosis, is difficult.

An accurate diagnosis in all cases implies a very good visualization of the uterine cavity, with focus on the fundus, and a delineation of the uterine external contour. So far, the most commonly used diagnostic method was hysterosalpingography (HSG). It provides excellent view of the uterine cavity and cervical canal as well as, information related to tubal patency, but no data regarding the fundal shape. Magnetic resonance imaging (MRI) may be employed in certain cases, with very good results, but at high costs.

Transvaginal 2D USG is a good screening test with high sensitivity for detection of müllerian uterine anomalies. However, 2D USG has a limited ability to distinguish different types of uterine abnormalities and is operator dependent.[27] Consequently, 3D USG is now used extensively. Transvaginal 3D USG has the ability to generate accurate images of both the endometrial cavity and the external contour of the uterus. A major advantage of 3D USG is the multiplanar capability, the ability to image the three orthogonal planes of the uterus, of which the coronal view of the uterus and the cervix are the most important. Coronal view is essential for assessing the external uterine contour and viewing the fundus, shows the relationship between the endometrium and the myometrium at the uterine fundus, delineates the entire cervical canal, and depicts the corneal angles. Also shows the whole length of the uterus down to the cervix – and consequently for determining the exact type of uterine anomaly. This enables the operator to measure the depth of the uterine septum or depth of the fundal cleft and the distance between the apex of the septum and the internal os. In addition, the use of 3D enables us to diagnose new types of the uterine septum, such as unequal sides. Three-dimensional USG is more accurate than HSG when estimating the depth of the septum accuracy 98%.[28] Using 3D power Doppler, vascularization of the septum can also be determined. Furthermore, 3D USG can differentiate between arcuate uterus and a short, incomplete septum, which is not always possible with hysteroscopy. It can therefore differentiate different müllerian anomalies with good reported sensitivity and specificity.[29]

Three-dimensional USG has become a key tool for diagnosing uterine malformations, because is non-invasive, reproducible, relatively inexpensive and well tolerated compared with techniques such as laparoscopy/hysteroscopy, MRI or HSG. The main sources of error are uterine leiomyomas, synechiae or other distorting process within the cavity.

Assessment of cervical length in this specific group of patients is of importance due to their higher incidence of preterm labor; it was found that a short cervical length on transvaginal ultrasonography in women with uterine anomalies had a 13-fold risk for preterm birth. Of all müllerian anomalies, unicornuate uterus had the highest rate of cervical shortening and preterm delivery.[30] A further advantage of ultrasound is that allows for the simultaneous screening for urinary tract abnormalities commonly associated with uterine abnormalities (20–30% of women).

Optimal imaging of the endometrium and myometrium may require distension of the uterine cavity with saline to separate the walls of the uterus to make clear the outline of the endometrial contour, and to detect endoluminal lesions, i.e. lesions protruding into the uterine cavity or uterine septum. The procedure is SIS, which is thought to have almost 100% sensitivity and specificity when compared with the gold standard of surgery and has the same diagnostic accuracy as the gold standard for polypoid lesions and endometrial hyperplasia. The consensus by the experts in the area of ultrasonography of uterine cavity disorders is that SIS and HSG are highly sensitive in the diagnosing of major uterine malformations. However, SIS is not sufficiently sensitive in the diagnosis of minor uterine abnormalities.[31] A recent report suggests the use of a very small volume of viscous gel, with impressive results. Sonohysterography performs better in the diagnosis of müllerian anomalies than HSG and, with TVS, has no false-positive diagnoses.[32]

Also with 3D USG, a volume of ultrasonographic data is rapidly stored and made available for later analysis and is a reproducible method in diagnosing uterine congenital malformations. This is particularly helpful in the case of SIS, the amount of time during which the uterine cavity must remain distended decreases. Three-dimensional USG permits an unlimited number of scan planes to be obtained from the original data set, an advantage that should significantly reduce operator-dependent bias. Additional findings not initially detected during the real-time examination can be made by scrolling through the volume data without inconveniencing the patient by prolonged or repeated vaginal scanning. Combining SIS with 3D USG can add to the accuracy of both procedures.

One limitation of 3D USG is shadowing caused by uterine fibroids, irregular endometrial lining or thickened endometrial lining (as seen during the periovulatory period), as well as the decreased volume of the uterine cavity (in cases of intrauterine adhesions). When the uterus is retroverted in position some difficulty is encountered in making the diagnosis of subtle uterine septum or arcuate uterus by 3D USG.

Three-dimensional USG has been reported to have sensitivity and specificity of 100% in diagnosing arcuate uteri compared with 67% and 94%, respectively, for transvaginal 2D USG. Interestingly, in diagnosing major müllerian anomalies, while the sensitivity and specificity of transvaginal 3D USG are both 100% compared with 100% sensitivity and 95% specificity for transvaginal 2D USG, the positive predictive value is 100% for 3D USG but only 50% for 2D USG. Because of the higher accuracy of the 3D USG in diagnosing müllerian disorders, higher prevalence (6%) was reported when 3D USG was applied for detecting those disorders. Compared with HSG, 3D USG has a higher accuracy.

Use of 3D USG to examine patients with recurrent miscarriage as compared with normal controls showed no difference in the relative proportions of congenital uterine anomalies in the two groups of women; arcuate and septate uterus were the most common anomalies prevalent (90%). The measurement of depth of the uterine septum and residual cavity depth showed that in both arcuate and subseptate uteri the length of remaining uterine cavity was significantly shorter ($P<0.01$) and the distortion ratio was significantly higher ($P<0.01$) in patients with recurrent miscarriages.[33]

Arcuate/Septate Uterus

Müllerian ducts can develop into two distinct types of tissue: the smooth muscle tissue of the uterus and the fibrous tissue of the cervix. This could explain the various structural subtypes of uterine septum containing different proportions of fibrous and muscle structure. Such structural disparity might be a cause in the mechanism of reproductive failure associated with uterine septum.

The septate/arcuate uterus develops from a defect in canalization or resorption of the midline septum between the two müllerian ducts. The classification of uterine anomalies divides the uterine septum into complete (septate) or partial (subseptate) groups according, respectively, to whether the septum approaches the internal os or does not. The complete septum that divides both the uterine cavity and the endocervical canal may be associated with a longitudinal vaginal septum. The presence or absence of a complete or partial vaginal septum is not relevant to the classification.

A septate or arcuate uterus has a normal external surface, but two endometrial cavities, in contrast to a bicornuate uterus, which has an indented fundus and two endometrial cavities. The distinction between arcuate and septate uterus is rather difficult and up to some point, subjective. It is accepted that the arcuate uterus has a slight midline septum with a broad, fundal basis and normal external surface, while the septate uterus presents a more important septum and sometimes may have a small indentation that does not exceed 10 mm depth. Septate uterus is the most common müllerian anomaly and is known to result in adverse obstetric outcomes; it is therefore of great importance to differentiate septate from bicornuate uterus, which is much less common, so that hysteroscopic septum

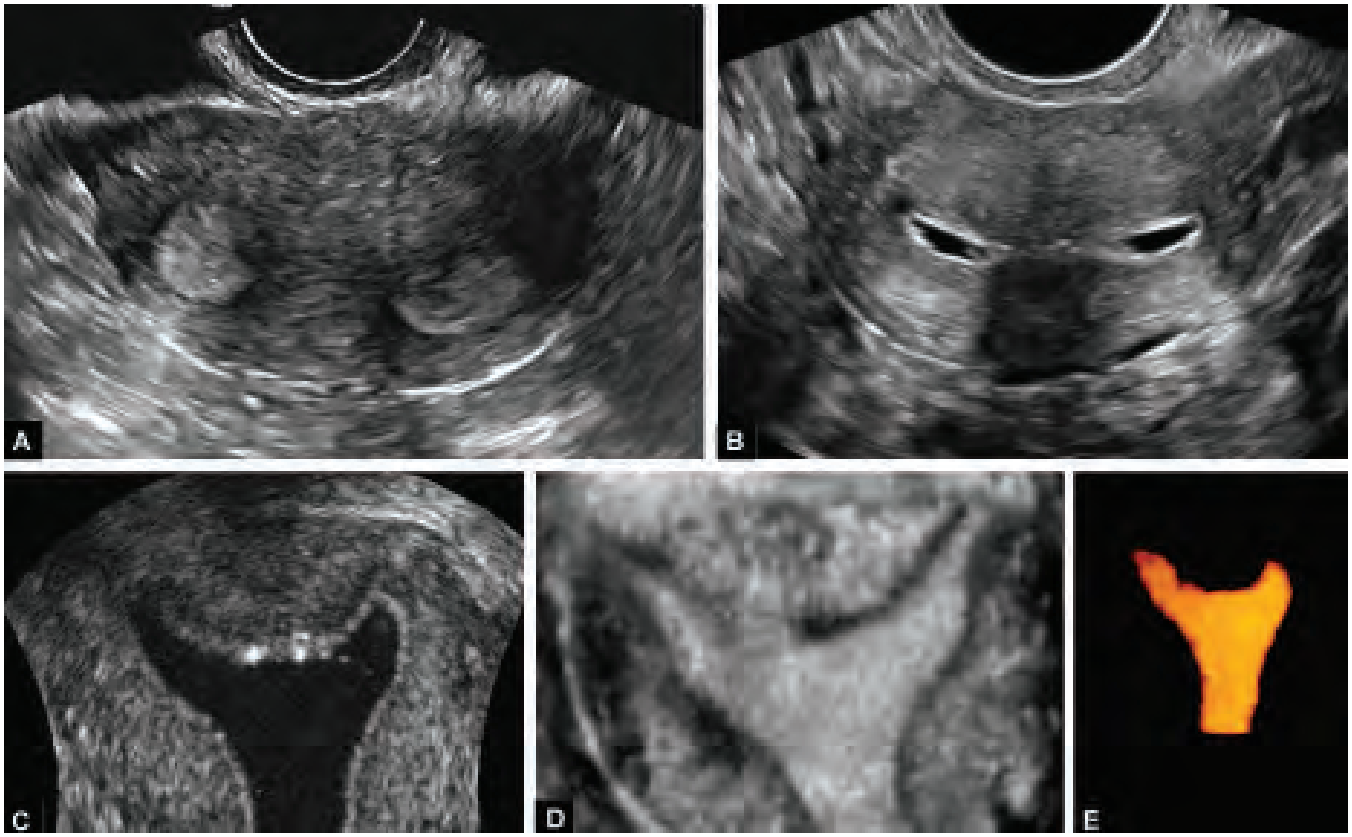

Figures 51.9A to E: (A) Arcuate uterus seen on 2D scan; (B) SIS; (C) 3D reconstructed coronal plane during SIS; (D) 3D VCI-C rendering; (E) 3D inversion mode

excision can be performed.[34] Surgery has reportedly improved pregnancy rate from 3–20 to 70–90%.

Sonographically, in case of arcuate uterus, the two uterine cavities are seen as split endometrial echoes, best visualized during secretory phase **(Figs 51.9A to E)**. With anteroposterior/transverse diameter < 0.6, the width is larger than height on axial (transverse) section. Arcuate uteri are less obvious and have a subtle indentation at the fundus.

The typical ultrasound appearance of a septate uterus is a convex, flat or mildly concave, but notch < 10 mm, minimally indented fundal contour with an echogenic mass dividing the cavity. Proximally, the septum has the echogenic appearance of myometrium, distally the mass consists of hypoechoic fibrous tissue **(Figs 51.10A to C)**. The septum is partial or complete.

The degree of septation may be assessed by conventional scan or, much better, by 3D sonography, thick slice or VCI-C. The coronal plane offers a very good diagnostic image of the endometrial cavity as well as the fundal contour. In unclear cases, saline infusion gives a perfect image of the uterine cavity. Three-dimensional acquisition with inversion mode creates a hysterogram sometimes of better quality than the radiological image.

Various studies confirm that the sensitivity and specificity of sonohysterography are the same as for hysteroscopy,[35] but SIS, because it is an easy and cheap technique, it should be the first used in infertile patients. Three-dimensional sonohysterography is advantageous compared with 2D sonohysterography, with the coronal plane being the most important in providing information. Addition of sonohysterography to 3D imaging allows precise recognition and localization of the lesion.

Evaluation of the vascularity of the septum by Doppler USG provides important information about structure and the risk of reproductive problems. Color and pulsed Doppler, sonohysterography and 3D USG are superior to 2D USG in diagnosing septate uterus.[36] Patients with vascularized septa have significantly higher prevalence of early and late pregnancy complications than those with avascular septa and this may reflect an increased amount of muscle in the septum, producing local uncoordinated myometrial contractility that resulted in adverse obstetric outcomes.

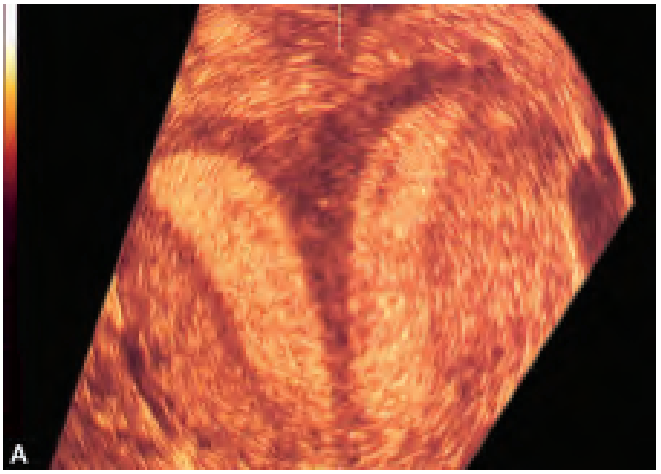

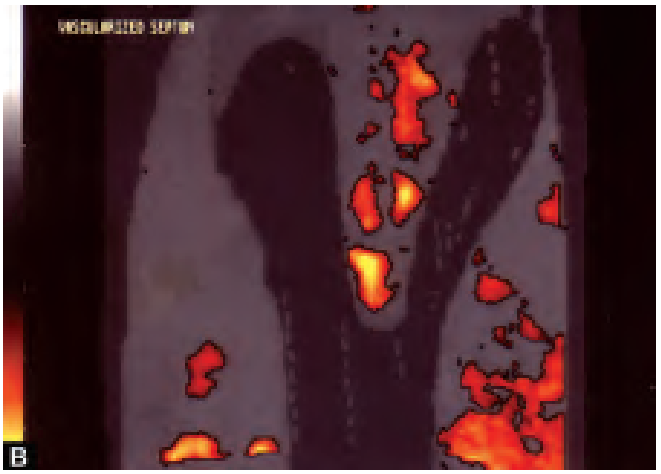

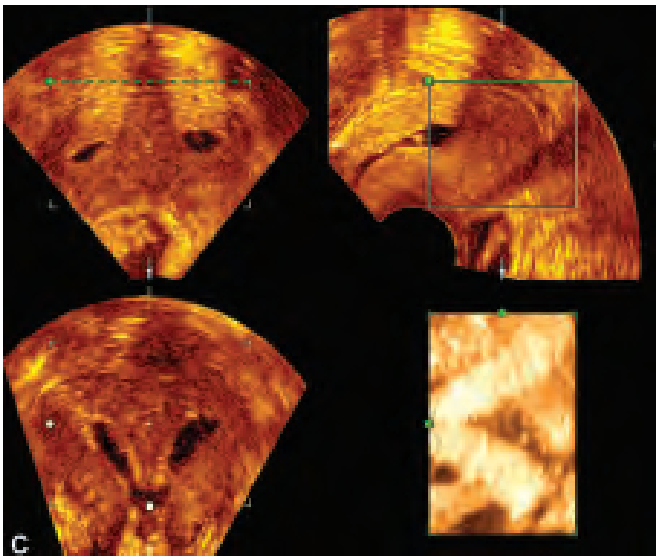

Figures 51.10A to C: (A) Septate uterus seen on 3D VCI-C; (B) Septal vessels on 3D power Doppler; (C) 3D SIS with coronal plane

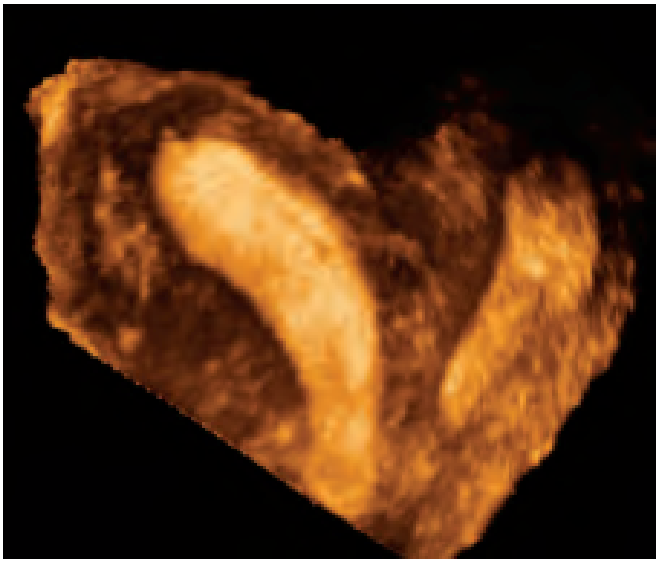

Figure 51.11: Bicornuate uterus on 3D US. Visible notch in coronal plane, two cavities

Bicornuate Uterus

A bicornuate uterus refers to a uterus in which the fundus is indented (arbitrarily defined as >1 cm)—incomplete fusion of the fundus. The vagina is generally normal.[37] This anomaly results from only partial fusion of the müllerian ducts. This leads to a variable degree of separation of the uterine horns that can be complete or partial. Characteristically, there is only one cervix. Thus, the diagnosis depends on the very good visualization of the two endometrial cavities and the cervix. Sonographically, there are two separate uterine horns with a variable depth of the fundal cleft, more than 10 mm (18 +/– 12 mm) and anteroposterior/transverse diameter ratio of < 0.7 suggests bicornuate or septate uterus. From a theoretical point of view, it is easy to obtain a good coronal plane, but, sometimes, it may turn out to be quite difficult, due to some degree of uterine rotation. Saline infusion remains a very good method of clearing up a diagnosis, when necessary **(Fig. 51.11)**.

Didelphic Uterus

Uterus didelphys, or double uterus, occurs when the two müllerian ducts fail to fuse, thus producing duplication of the reproductive tract. Generally, the duplication is limited to the uterus and cervix (uterus didelphys and bicollis-two cervices) although duplication of the vulva, bladder, urethra, vagina and anus may also occur. A complete vaginal septum, generating an obstructed hemivagina may be associated with ipsilateral renal agenesis.

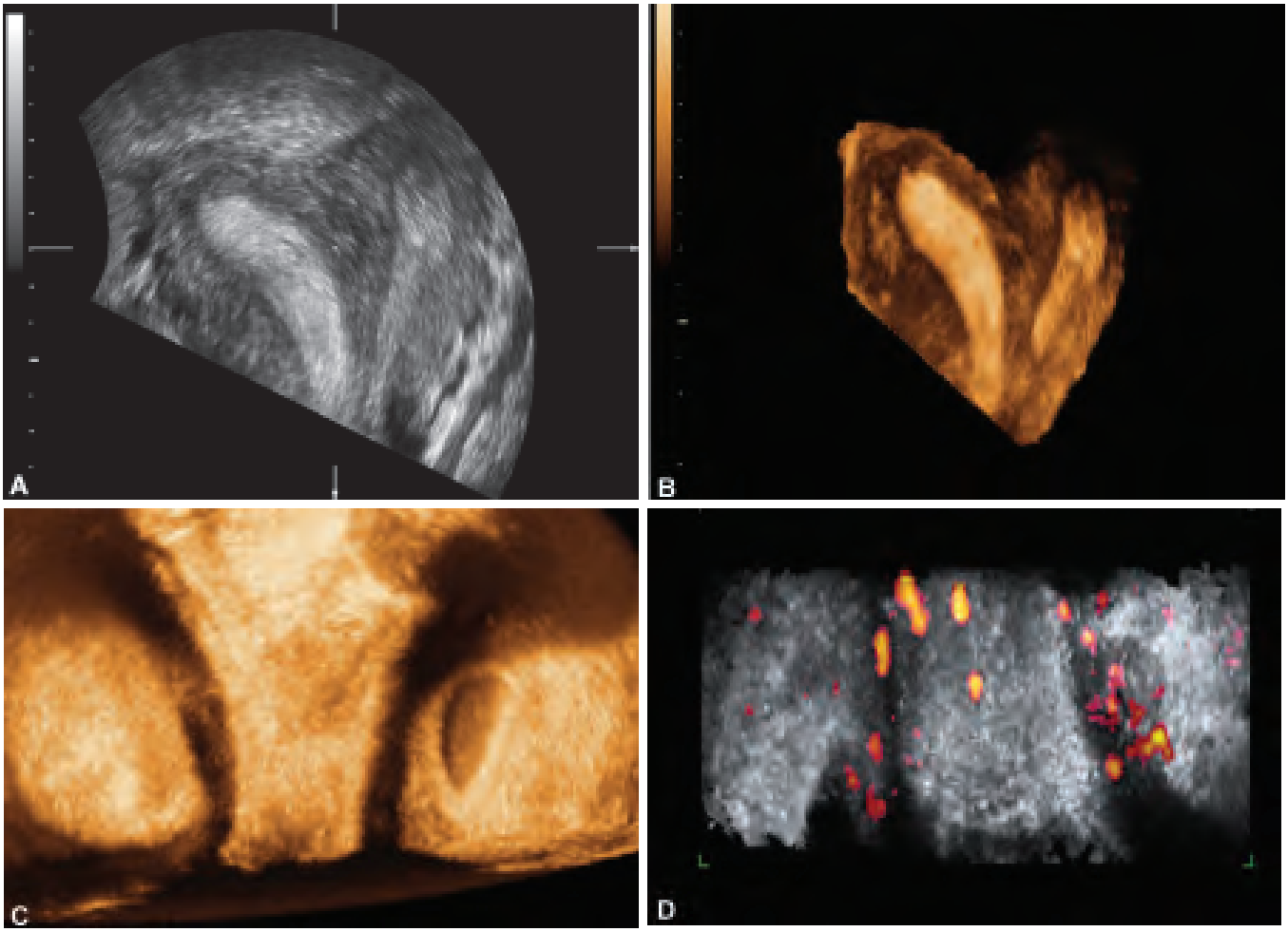

Figures 51.12A to D: (A and B) Didelphic uterus on 3d VCI-C scan; (C and D) With early pregnancy in one hemiuterus

Sonographically, the features are: deep fundal cleft (average 32 mm), two separate endometrial cavities and two cervices. A septated vagina occurs in 75% of cases and may cause difficulty with sexual intercourse or vaginal delivery.[38]

A correct diagnosis was stated in both cases using 3D ultrasound, with the remark that sonography cannot evaluate vaginal septum **(Figs 51.12A to D)**. Women with a didelphic uterus and bicollis often have good reproductive outcomes.

Adenomyosis

Adenomyosis is a benign disease of the uterus characterized by the presence of ectopic endometrial glands and stroma within the myometrium with adjacent smooth muscle hyperplasia producing diffuse uterine enlargement. Frequently under diagnosed, is evident in 40% of hysterectomy specimens. It is associated with menorrhagia, dysmenorrhea and chronic pelvic pain. The relationship with infertility is unclear but most women with adenomyosis are multiparous suggesting it does not reduce fecundity. Generalized adenomyosis typically involves the inner two thirds of the myometrium and is often found at the fundus. In 75% patients, moderate symmetrical uterine enlargement is present, the uterus appearing smooth in outline with a normal myometrial and endometrial echo texture. Multiple shadowing in the myometrium, described as a "rain-in-the-forest" picture, may occur. Occasionally, small cystic areas are seen measuring 2–4 mm representing distended endometrial glands containing menstrual blood. The myometrium is divided structurally into an outer myometrial layer and an inner subendometrial layer or junctional zone. Adenomyosis causes disruption of the myometrial-endometrial border and an irregular thickened junctional zone. This can be demonstrated

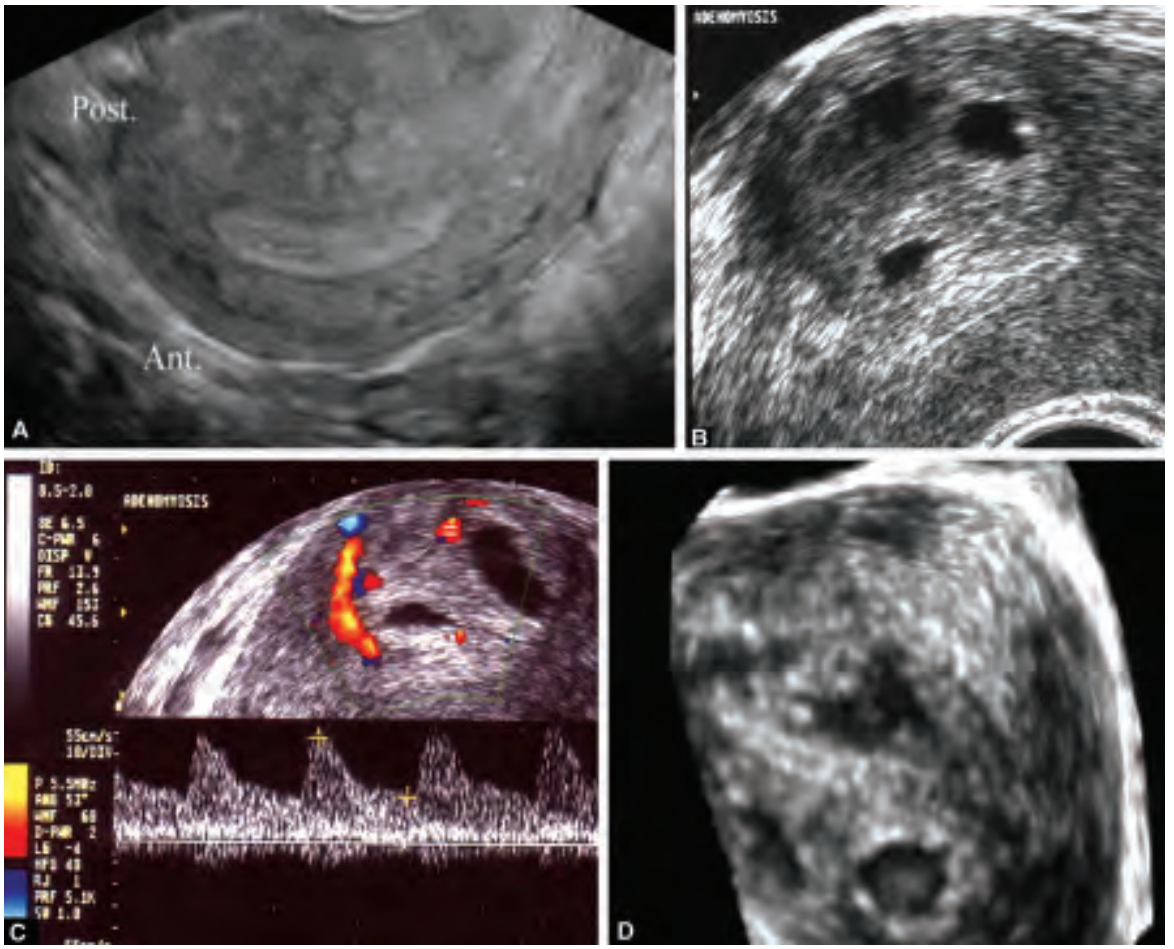

Figures 51.13A to D: (A) Adenomyosis with diffuse, asymmetrical thickening of the myometrium on 2D USG; (B) Mottled gray scale appearance with small, numerous focal lesions. Disturbed echogenicity of the middle myometrial layer with multiple small cysts within; (C) Myometrium with increased vascularity, moderate vascular resistance and uterine artery with lower RI values; (D) 3D image of adenomyosis

with MRI or 3D USG. Traditionally, the gold standard for the diagnosis of adenomyosis has been histopathological but noninvasive methods are increasingly providing reliable alternatives. Transvaginal ultrasound is reported to have a sensitivity of 53–70% and specificity of 65–97% with a positive predictive value (PPV) and negative predictive value (NPV) of 42–92% and 85–96%, respectively. Magnetic resonance imaging has a sensitivity of 70–82% and a specificity of 84–92% with a PPV and NPV of 58–83% and 86–95%, respectively.

A number of specific ultrasound features seems to be collectively indicative of uterine endometriosis **(Figs 51.13A to D)**:

- Diffuse, asymmetrical thickening of the uterine wall
- Textural (mottled) irregularities of the myometrium
- Formation of focal lesions (adenomyomas)
- Prominent development of myometrial glands
- Poor differentiation of the endometrial-myometrial interface
- Increased developments and contractile movements of the endometrium
- Developments and growth of endometrial polyps, fibroids, etc.
- Increased myometrial vascularity.

The level of gray scale imaging currently available and, in particular, color Doppler sensitivity has significantly increased the accuracy of ultrasound in predicting the likelihood of adenomyosis. There is a distorted pattern of contractility in adenomyosis where the contraction wave begins at mid-cycle at the cervix but then travels into the middle layer of the myometrium at the site of adenomyosis rather than extending up to the fundus and then down the fallopian

tube. An interruption of the contraction waves should therefore have an adverse effect on sperm travel and their success in fertilization.

Ongoing studies involve patients presenting with a history of pelvic pain, dysmenorrhea, etc. who have been scanned prior to laparoscopic investigation. Results to date indicate over 90% of those cases where pelvic endometriosis (Grade I–IV) was found at surgery, preoperative TVS + color Doppler (blood perfusion studies) assessments confirmed increased myometrial vascularity. Detailed examination of myometrial changes, to include both vascular as well as textural features, not only indicates the presence of adenomyosis but also the likelihood of pelvic endometriosis even in early stages of the disease. The ability to diagnose changes associated with very early stages of the disease has considerable implications in terms of the clinical management of endometriosis.

ENDOMETRIOSIS

Ultrasound scanning had in the past a limited to confirm the presence of the disease in some cases only on the basis of identifying the formation of endometriotic cysts. This did not necessarily reflect the extent of the disease nor the level of clinical symptoms. Recent advances in ultrasound have considerably increased the ability to detect endometriosis at a much earlier stage and gauge its spread within the pelvic-abdominal tissues with far greater diagnostic confidence.

Significant progress in TVS gray-scale (G-S) imaging have been achieved as a result of developments in both transducer design and performance. The introduction of the latest processing algorithms and functions such as harmonic imaging (HI), speckle reduction imaging (SRI) and cross-beam focusing (resolution) imaging (CRI) have further increased the quality of G-S ultrasound. The detection of extremely small lesions of the ovary as well as the subtle textural changes within stromal tissue often found to be associated with early ovarian endometriosis can now be visualized.

In addition, textural changes and the formation of localized focal lesions within the myometrium are frequently found in the cases of adenomyosis. Improved G-S (TVS and TRS) imaging is able to demonstrate infiltrations of the disease into the deep pelvic tissues and in particular the rectovaginal septum and utero-sacral ligaments, etc. as well as the intestine and urinary bladder.

Increased sensitivity of conventional color Doppler (CDI) systems and power Doppler (PD), and certainly the recent development of "high-definition" (directional) power Doppler (HDI), has greatly enhanced the role of ultrasound in virtually all aspects of gynecology. Hyperemic changes within the myometrium and extrauterine pelvic tissues are increasingly recognized in significant numbers of cases presenting with endometriosis. This includes those with a history of chronic, severe pelvic pain in particular. The frequent formation of persistent, hemorrhagic functional cysts of the ovary and their increased levels of activity indicated by peripheral angiogenesis, are readily demonstrated by combined TVS-CDI scanning.

Three-dimensional ultrasound imaging has had considerable impact in the assessment of severe endometriosis, by multiplanar reconstruction (MPR). Tomographic ultrasound imaging (TUI) produces anatomical slices or sections at varying depths within a given anatomical plane **(Fig. 51.14)**. The combination of MPR/TUI provides far greater detail indicating the extent of the disease and involvement of other pelvic structures. The MPR/TUI clearly delineates ovarian lesions as well as accurately assessing the nature and extent of preserved functional tissue remaining within the ovary, particularly in cases of large endometriomas. The extent and nature of adhesions are demonstrated with more confidence particularly with utilization of 4D facilities.

The combined use of 3D TVS-PD technology provides quantitative measurement of fine, capillary blood flow through a given volume of tissue as part of blood perfusion studies (BPS). Again, current work utilizing BPS techniques appear to confirm increased myometrial vascularity associated with adenomyosis. It also highlights the relationship between pelvic hypervascularity and increasing levels of pelvic pain particularly in the presence of more extensive endometriosis. Transvaginal scanning (TVS) is now fully established as the principal mode for imaging of the pelvic organs and is essential in the investigation of endometriosis. Nevertheless, TAS scanning still has an important role in this respect. Dense pelvic adhesion can cause localized constriction of the lower ureters resulting in secondary changes within the kidneys. Ultrasound of the renal tract is therefore strongly indicated in cases of moderate-severe endometriosis.

Improved TAS imaging enables bowel adhesions and infiltration of abdominal/pelvic tissues to be detected. Visualization of adherent ("high," superficial) ovaries again requires a TAS approach. Transrectal (TRS) scanning provides a more suitable alternative to TVS in the studies of the deep pelvis. Increased access to relevant structures allows more detailed assessment of the uterosacral ligaments, rectovaginal septum, etc. and associated spread of the disease.

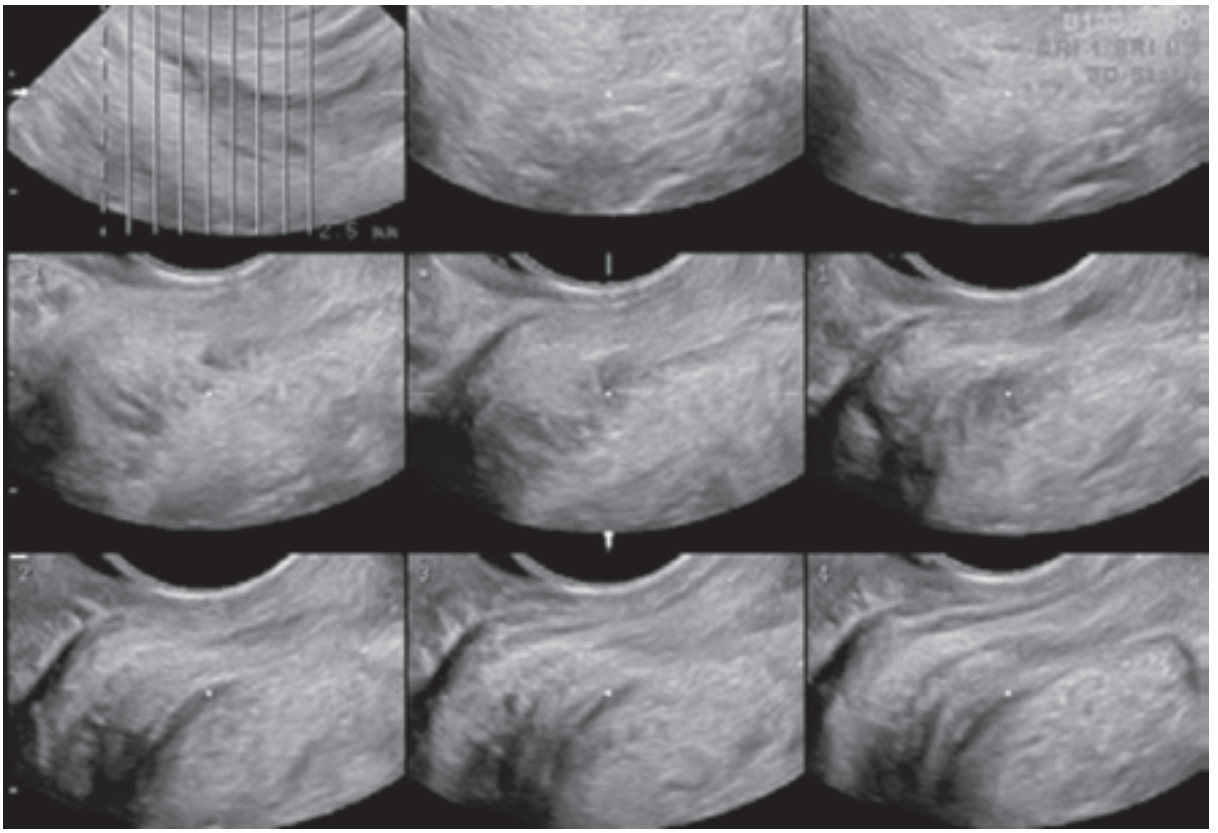

Figure 51.14: Active endometriosis. Precise post-scan interrogation utilizing parasagittal TUI imaging identifies dense recto-vaginal adhesions. Image sections "+2" – "+4" demonstrate a clear interface between the vagina ("V") and rectum ("R"); this interface is completely lost as we scroll from image sections "+1" – "–3" with adhesions delineated with good clarity

Ovarian Endometriosis

The ability to delineate extremely small endometriotic lesions (< 1 cm size) as a result of high-quality TVS G-S imaging now allows very early evidence of the disease to be identified. Smaller lesions tend to be uniform in their G-S appearances at all stages of the menstrual cycle and somewhat hyperechoic compared to surrounding stromal tissue. Subtle changes within the ovarian stroma can now be recognized in addition to early focal lesions. Larger endometriotic cysts (>> 1 cm size) are normally diagnosed as a result of their characteristic, uniform (homogenous) gray scale appearances. They can nevertheless present with higher or lower echogenicity compared to the surrounding stromal tissue. In addition, textural changes can vary according to the stage of the menstrual/ovulatory cycle and certainly reflect ovarian activity or exposure to exogenous hormonal influences, etc. Internal (menstrual) bleeding can lead to "loculated" appearances. This is the result of a well-defined interface or series of interfaces, forming between areas of differential clotting involving fresh and old blood within the lesions. Typical, "textbook" appearances are normally restored by cycle days 6–10.

Very little peripheral bloodflow, confirmed by HDI, plus the absence of internal vascularity within endometriotic cysts, reliably exclude "high risk" malignant changes certainly when cyclical variations as described above are demonstrated. Torsion of larger endometriotic cysts remain of clinical concern and can usually be confirmed by changes in the outline of the lesion, differential internal bleeding outside of menstruation and reduced vascularity as shown by HDI within normally functional ovarian tissue. Rupture of endometriotic cysts result in the formation of subcapsular hemorrhage within the ovary as well as spill, bleeding, etc. from the collapsed lesion into the pelvic cavity.

Anatomical changes associated with endometriotic cysts are readily confirmed by 3D ultrasound. Three-dimensional technology (MPR + TUI) remain important in confirming the preservation of normal functioning stroma and follicle activity in ovaries significantly

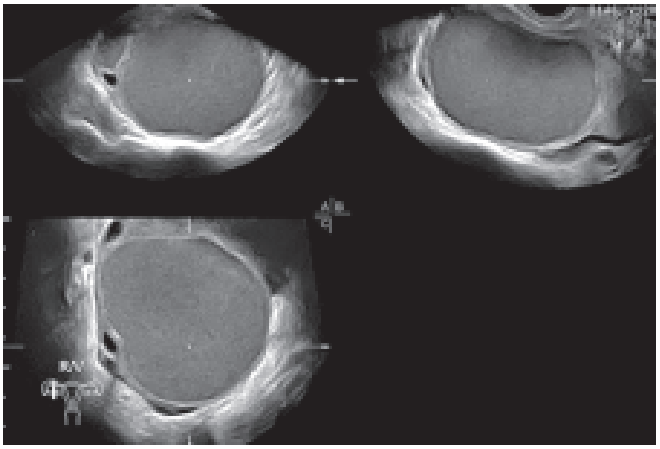

Figure 51.15: 3D multiplanar reconstruction of an endometriotic cyst

enlarged by single or multiple lesions **(Fig. 51.15)**. Postscan analysis of ovarian volumes promote careful, unpressurised assessment of the number and sizes of endometriotic lesions. Three-dimensional "single sweep technology" and the facility to retrieve 3D (volumetric) data for postscan analysis improves diagnoses and is of tremendous benefit as part of clinical and presurgical planning. Differential diagnosis between endometriotic cysts and other ovarian lesions presenting with similar ultrasound (G-S) appearances, such as hemorrhagic luteal cysts, dermoid cysts, mucinous cystadenomas, etc. can be difficult on the basis of a single scan examination. Serial scanning has a crucial role and a single postmenses follow-up study considerably enhances diagnostic effectiveness in this respect. Endometriotic cysts usually increase in size following each menstrual period with corresponding internal changes as previously described.

Dermoids or mucinous cyst adenomas, for example, might mimic the ultrasound appearance of an endometrioma but would show no change either side of menstruation. The vast majority of ovulatory-related, functional cysts of the ovary will collapse during or following menstruation—if they remain intact, there will nevertheless be a likely (CDI) alteration in the level of peripheral vascularity shown as well as associated endometrial change. Recent work has increasingly shown an association between endometriosis and changes in ovarian morphology, namely follicle-stromal patterns. There appears to be a tendency for multifollicular development with definite increase in stromal thickening and vascularity. Ovarian changes very often involve cyclical formation of very active hemorrhagic luteal cysts and increased endometrial development and which, unsurprisingly, very often present with menstrual issues.

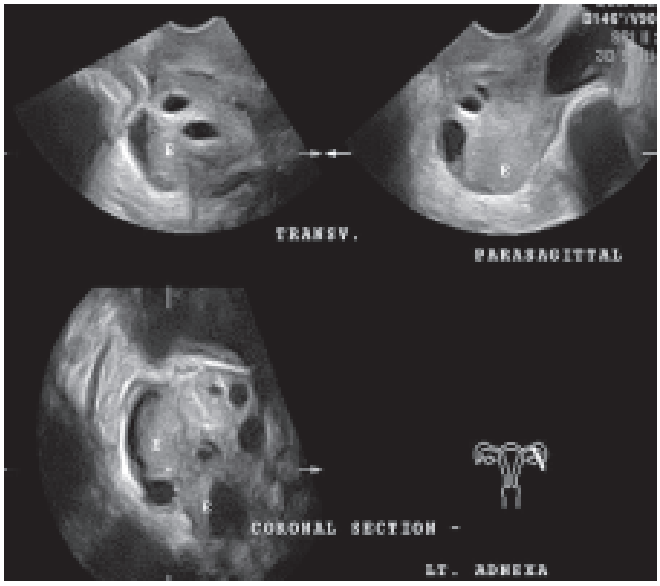

Figure 51.16: Multiplanar reconstruction of adherent ovary containing a small endometriotic cyst with pelvic adhesions and loculated fluid

There is certainly an increasing impression that discomfort associated with mild-moderate stages of endometriosis arise as a result of changes in ovarian activity and its (hormonal) effects on other tissues, such as the bowel, urinary bladder, breast, etc.

Pelvic/Abdominal Endometriosis

Thickening of pelvic tissues, increased localized vascularity and the early formation of nodules are more readily identified on ultrasound today and indicate the spread of the disease within the pelvis. Detailed ultrasound of the deep pelvic structures, i.e. uterosacral ligaments, rectovaginal septum and rectosigmoid colon in particular, as well as the urinary bladder, kidneys and ureters, small and large intestine, etc. require a flexible approach to scanning to include TVS, TRS and TAS applications. Three-dimensional scanning has proven to be an essential part of evaluating the formation of adhesions and widespread involvement of pelvic organs **(Fig. 51.16)**.

Studies have shown that TVS alone will detect over 80% of cases of deep pelvic infiltrative disease although the patient groups were probably highly selective. Nevertheless the importance of TRS assessments in these cases has been well recognized particularly in the assessment of the rectosigmoid junction and rectovaginal septal areas. The TAS remains essential in the terms of general examination of the small and large bowel, surgical scars, umbilical region and urinary tract, etc.

OVARIAN FACTOR IN INFERTILITY

Evaluation of the Ovarian Reserve (OR)

Assessment of the OR is a key point in aging infertile women. First of all, "OR" refers to the number of antral follicle able to follow the last steps of folliculogenesis and, potentially, ovulate. Additionally, in a different approach, the number of follicles able to be productively stimulated. With advancing age, thousands and thousands of follicles per year are lost due to atresia.[39]

It relies both on detailed endocrine tests and ultrasound. Biochemical markers [follicle-stimulating hormone (FSH), estradiol E2, inhibin B, antimullerian hormone, FSH/LH—luteinizing hormone ratio] on day 3 of the menstrual cycle offers a good image over ovarian endocrine function and ovarian ultrasonographic morphometric markers that are assessed in the early follicular phase (basal) of the menstrual cycle.[40]

Four morphological markers have been commonly used:

1. Ultrasonographic assessment of antral follicle count
2. Measurement of ovarian volume
3. Measurement of mean ovarian diameter size
4. Assessment of ovarian blood flow of the stroma.

Antral Follicle Count (AFC)

This represents a start point for ovarian stimulation, a rough prediction of the ovarian response. On cycle day 1, menstruation arrives and a new cycle begins. During the follicular phase an orderly sequence of events takes place that ensures that the proper number of follicles is ready for ovulation. Folliculogenesis is a process that is initiated well prior to the arrival of menstruation. Once a primary follicle leaves the resting state it will take 85 days, or three complete menstrual cycles, to reach the point of ovulation. The follicle destined to ovulate is recruited in the first few days of the third cycle. It will measure 1–2 mm on cycle day 1. Folliculogenesis is thought to occur in four phases. Recruitment takes place during cycle days 2, 3 and 4, when a cohort of quasi-synchronous follicles has entered a gonadotropin-dependent rapid growth phase. By cycle day 5, both menstrual flow and follicular recruitment end. Selection refers to the reduction of the cohort size down to the species-specific ovulatory quota. Fluid accumulates amid the granulosa cell mass. The antrum is formed as the oocyte is displaced to one side by this process. Follicles at this stage measure 4–6 mm. By day 6, the follicle destined to become dominant secrets the greatest amount of estradiol, which in turn, increases the density of FSH receptors on the granulosa cell membrane. The nondominant follicles cease development and then become atretic.[40]

Antral follicles are responsive to gonadotropin stimulation and the measure of OR can be defined as the total number of follicles that can be stimulated to grow under maximal stimulation. The AFC is defined as the number of follicles smaller than 10 mm in diameter detected by transvaginal ultrasound in the early follicular phase. Ultrasound measurement of the ovarian AFC is a reproducible test with low interobserver variability and can predict response to gonadotropin stimulation.

Transvaginal sonography is the best means for the assessment of total AFC. To determine the diameter of the follicle, the mean of measurements in two perpendicular directions should be taken. The number of follicles in both ovaries should be added for the total antral follicle count. The follicles visualized and counted by TVS in the early follicle phase should be 2–10 mm in size. Normal AFC in one ovary range from 5 to 10. The scan may be performed up to day 7.

The AFC is an ultrasound marker of ovarian aging. In the ART literature, a lower AFC has been associated with poor ovarian response. Various cutoff points for a low AFC, most often less than 4 or 6, have been described in predicting poor ovarian response.

The AFC correlates negatively with age and positively with the total number of follicles and E2 on hCG day and with the number of oocytes. The AFC has predictive value for ovarian response in an IVF cycle, with a cutoff value of seven follicles, above which there are more chances of normal response. Its predictive value is higher than that of basal FSH. The value of AFC in predicting pregnancy is lower. However, patients with eight or more follicles may achieve statistically significantly higher pregnancy rates.[41]

A great advantage of AFC over any test is its potential usefulness in its ability to concomitantly predict low and high responders. The cutoff level of >14 could lead to the decision to adjust the gonadotropin dose in trying to prevent a hyper-response leading to ovarian hyperstimualtion syndrome (OHSS).[6] The cutoff level of less than 6 antral follicles correctly predicted poor response to stimulation in an IVF treatment in 75% positive predictive value.[42]

If an AFC is performed, only follicles sized 2–6 mm could be counted and used for the interpretation of the outcome.

The AFC may be a useful tool for predicting pregnancy loss in IVF pregnancies. Women with AFC of less than 7.5 on day 3 of stimulation were 4.2 times more likely to have an abortion and 5.5 times more likely

to have a biochemical pregnancy loss following an IVF pregnancy, compared to those who had more than 7.5 antral follicles. Women with diminished OR have significantly higher rates of pregnancy loss than do patients with normal OR.

Ovarian Volume

Ovarian volume decreases significantly in each 10-year period of woman's fertile life and is not related to parity. Transvaginal sonography is a reasonably accurate tool for measuring ovarian volume by measuring three organ diameters, applying the formula for an ellipsoid: (D1×D2×D3×π/6) or using the semiautomatic VOCAL program, when available **(Figs 51.17A and B)**. The volumes of both ovaries are added for the total basal ovarian volume. It is assumed that the number of ovarian follicles correlates with ovarian size, based on the fact that aging and menopausal women have small, atrophic ovaries.

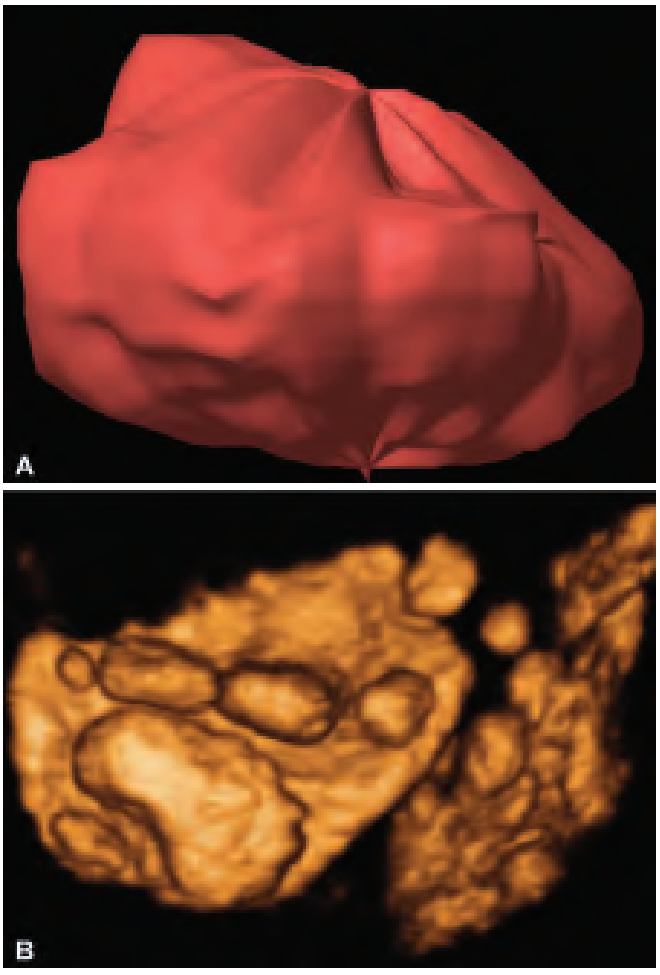

Figures 51.17A and B: (A) A stimulated ovary. Volume calculation using VOCAL; (B) Three-dimensional reconstruction with inversion mode

The ovaries should be visualized and measured in the early follicular phase.[42] Only measurement of ovaries not containing cysts or large follicles will achieve an accurate net ovarian volume. In most studies, only ovaries with follicles of less than 10–15 mm were included.

A mean volume of less than 3 cm^3 is associated with an increased risk of cancellation and of poor response to IVF. Ovarian volume may be a clinically important predictor of reproductive success being superior to cycle day 3 FSH or estradiol concentrations as an assessment of OR. Total volume of the ovaries detected by TVS is correlated with the outcome parameters but not better than the count of antral follicles.

Measuring ovarian volume in the early follicular phase does not appear to be a test of choice for OR assessment in IVF-indicated patients. Ovarian volume will remain rather stable across the third and fourth decades of female life but starts to decline after the age of 36 years. The performance of ovarian volume in the prediction of poor ovarian response after IVF is clearly lower than that of AFC. In the prediction of nonpregnancy, the performance of ovarian volume and the AFC is equally poor. Therefore, AFC is the test of first choice in the assessment of diminished OR.[43] The AFC has the lowest intercycle variability.

In a comparison between the accuracy of 3D techniques for AFC, the inversion mode and multiplanar rendering, to classic 2D measurement, the inversion mode.[44] The inversion mode showed a higher, but statistically insignificant, correlation with the number of retrieved oocytes than did comparable measurements made with the conventional method (r = 0.665) and 3D multiplanar (r = 0.687) techniques.

Mean Ovarian Diameter/Size

Using the largest cross-sectional sagittal view of the ovary, the mean ovarian diameter could be calculated from the measurement of two perpendicular diameters with the formula (D1+D2)/2.[45] A mean ovarian diameter of less than 20 mm on cycle day 3 predicts higher cancellation rates during ART cycles, but in patients who continued and underwent oocyte retrieval, no difference in the pregnancy or delivery rates was apparent.

The mean ovarian diameter significantly correlated with age, day 3 FSH, LH, and estradiol and with mean ovarian volume. Ovarian diameters correlates well with OR and stimulation parameters,[46] so we can more effectively assess OR during baseline ultrasound

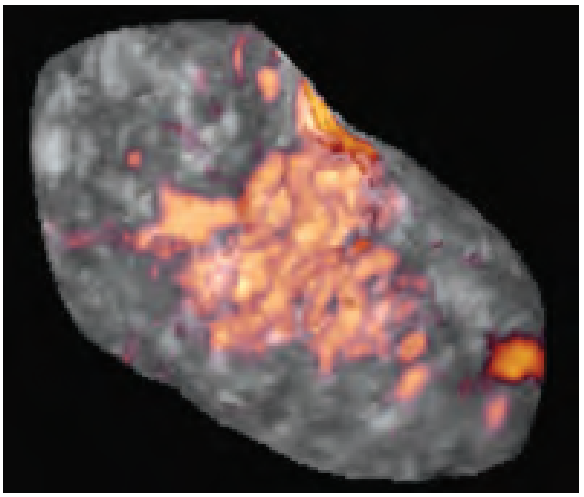

Figure 51.18: Stromal ovarian vascularization by 3D angiography

examination and thus change the patient's stimulation protocol to optimize results.[45]

Ovarian Stromal Blood Flow

The physiological significance of basal ovarian stromal blood flow was investigated with pulsed color Doppler for the assessment of OR **(Fig. 51.18)**. Undetectable basal ovarian stromal blood flow in at least one ovary is related to low OR in infertile women undergoing IVF embryo transfer, linked to the pathophysiology of ovarian aging. This goes to low pregnancy rate.

Poor responders have ovarian arterial flow that is altered in early follicular phase, in spontaneous cycles and after pituitary inhibition. Ovarian stromal peak systolic velocity (PSV) was the most important single independent predictor of ovarian response in patients with a normal basal serum FSH level. Patients with high PSV (greater than or equal to 10 cm/s) had a significantly higher median number of mature oocytes retrieved and a higher clinical pregnancy rate (35.3% versus 11.3%) than patients with low PSV (less than 10 cm/s), even after controlling for age.[47]

Three-dimensional Ultrasonography

In a stimulated cycle, pretreatment AFC measurement using methods specific to 3D USG **(Figs 51.19A and B)** offers minimal additional information over that derived from conventional 2D USG in the prediction of the number of follicles measuring 10 mm or more that will be evident on the day of hCG, the actual number of oocytes that will be retrieved thereafter and the incidence of nonconception. Furthermore, measurements made with the inversion mode take significantly

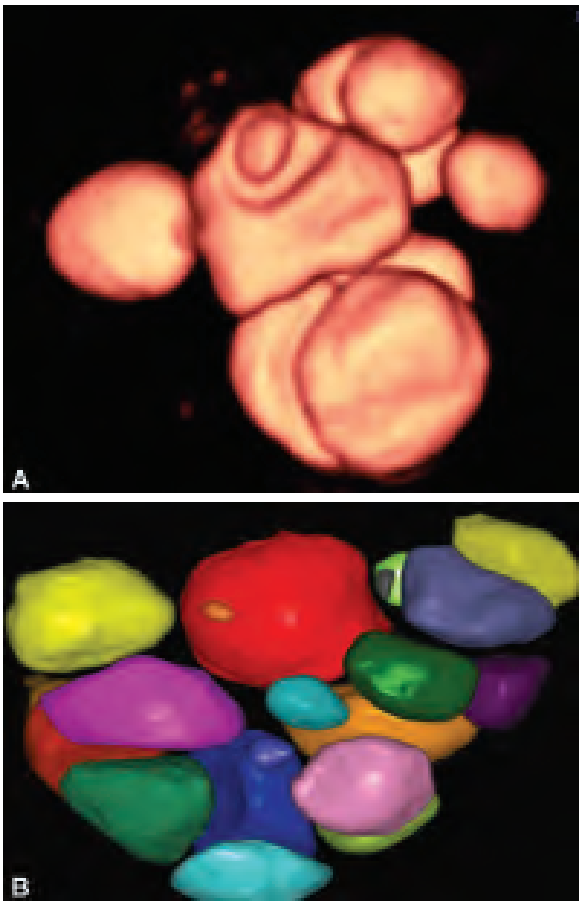

Figures 51.19A and B: Antral follicle count by inversion mode

longer than those made with the 2D equivalent and 3D multiplanar-view techniques.[44]

Ovulation

Assessing the follicle growth and ovulation is a well-known ultrasound use, which is far better than basal body temperature or urinary LH tests. Apart from documenting the ovulation, estimating the interval to that point is important, especially in stimulated cycles. This prediction is based on the fact that follicles grow approximately 1.6 mm per day in natural cycles and 1.8 mm per day in stimulated cycles. Also, the mean diameter at ovulation is 21.7 mm, without significant differences between the two types.

Similar to the endometrium, vascularity changes also affect the ovary. During the follicular phase the ovarian medullary vessels are difficult to visualize, with the highest resistivity index on the first day of the menstrual cycle. With the follicle growth, the rise in estradiol and FSH levels, the impedance to flow decreases, reaching the lowest value on the LH peak day. Vascularity

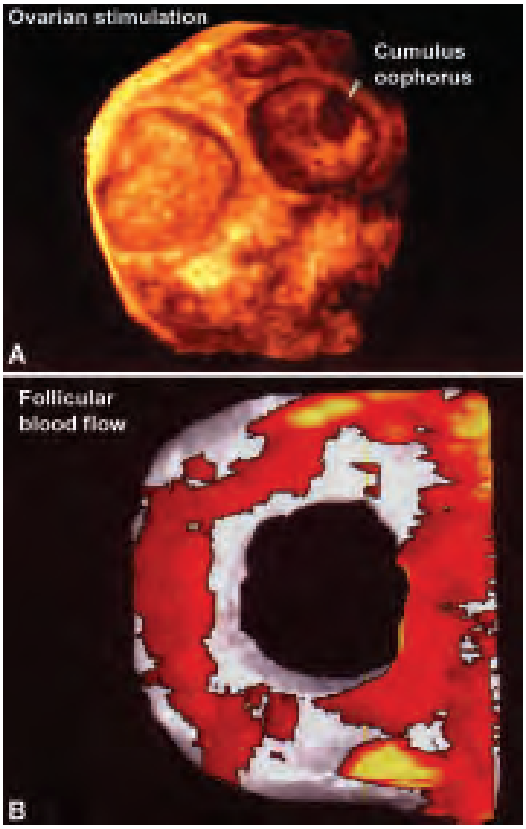

Figures 51.20A and B: (A) Three-dimensional image of the ovary with a follicle with cumulus oophorus; (B) Perifollicular vascularization on 3D power Doppler scanning

changes are uneven, affecting dominantly the ovulatory ovary. Moreover, the vascularity increases with the follicular diameter. Both of the aspects may be evaluated with conventional serial ultrasound or with 3D techniques **(Figs 51.20A and B)**. Several recent studies discovered a strong correlation between oocyte quality and pregnancy outcome, on one hand, and the level of perifollicular vascularity, on the other hand. Thus, the parameter seems to be of real clinical value, used to determine the appropriate time for hCG administration in stimulated cycles.[48]

Recently, using extensive serial scans, the actual process of follicle rupture was observed. Evacuation of follicular fluid and cumulus oophorus—oocyte complex, followed by the creation of the corpus luteum is a process that takes anywhere between 1–20 minutes, with an average of 10 minutes.[49]

The luteinized unruptured follicle may be seen as a preovulatory size follicle that undergoes all the changes to the corpus luteum, without elimination of the cumulus oophorus complex. The typical appearance is a thick-walled, fluid filled structure with homogenous

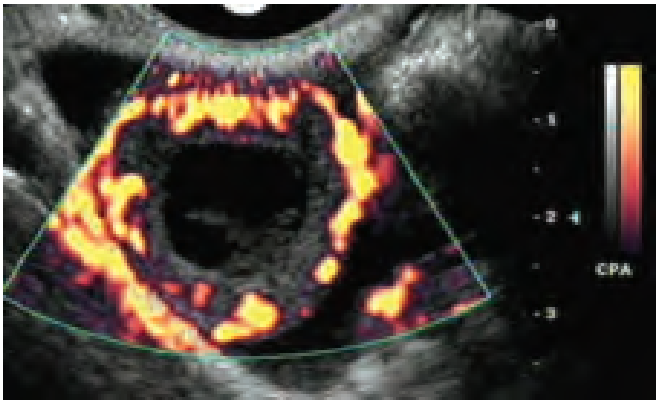

Figure 51.21: Peripheral blood flow in a corpus luteum with typical aspect of "ring of fire"

hypoechoic aspect and good peripheral vascularity. Ovulation failure may present as an overgrown follicle that persists throughout the luteal phase and into the next menstrual cycle. Sometimes the follicular wall is fenestrated by vessels and it becomes a hemorrhagic anovulatory follicle. The luteinization does not occur and the progesterone levels are low.

The Corpus Luteum

The corpus luteum is generally easy to detect, even though is present in a wide variety of forms. But one aspect remains constant: the rich peripheral vascularity, the "ring of fire" seen with power Doppler, as a result of decreased blood flow impedance and neoangiogenesis **(Fig. 51.21)**. The vascular parameters are maintained throughout the first half of the luteal phase than slowly regain the high values. For simplification, there are two morphological types of corpora lutea: with and without a central fluid-filled cavity. The fluid does not represent remnants of the follicular fluid, but blood leakage from the surrounding vessels. This explains the subsequent aspect in most of the corpora lutea. Disseminated thin hyperechoic strands, homogenous echoic texture, "snow flakes" image, echogenic structures protruding within the cavity, all are a result of fibrin formation and physiological changes of a clot. In some cases even fluid-filled structures may evolve to apparently solid aspects, thus being difficult to distinguish. So far seems to be a clear relation between the aspect of peripheral vascularization and the circulating level of progesterone and estrogen. The color flow mapping shows increased vascularization at the middle of the luteal phase, when progesterone levels are the highest, which progressively decreases in the following days. Persistence of an increased flow may be an indicative of incipient pregnancy. The luteal

resistance index remains low until the seventh week of gestation and increases afterwards, accompanying corpus luteum regression.[50] In luteal phase defects, the resistance index shows higher values during the midluteal phase. This seems to be a promising area of research, with regard to early recognition of pregnancy and embryonic loss.

Polycystic Ovarian Syndrome

Polycystic ovary syndrome (PCOS) is the most common endocrine disorder, first described by Stein and Leventhal in 1935, affecting 5–10% of women of reproductive age. The PCOS signs and symptoms include hyperandrogenism, anovulation and oligomenorrhea, but the phenotypic expression of the syndrome is quite variable. Diagnostic criteria for PCOS:

- National Institute of Health (NIH) criteria (1990): Hyperandrogenism (clinical or biochemical), oligoovulation, exclusion of disorders such as Cushing syndrome, hyperprolactinemia, and congenital adrenal hyperplasia. A fourth criterion, polycystic ovary on ultrasound, was not included in the diagnostic criteria since it was considered controversial.
- Rotterdam Criteria (2003): A diagnosis of PCOS is to be made when at least two of three elements are present—chronic anovulation, clinical or biochemical hyperandrogenism, and clearly defined PCOS on ultrasound. There is exclusion of other androgenic and anovulatory disorders prior to the diagnosis of PCOS.

Polycystic ovaries are detected by TVS in only approximately 75% of women with a clinical diagnosis of PCOS and 25% of women with PCOS do not have characteristic findings on ultrasound. The false-positive rate is relatively high.

Diagnosis of polycystic ovaries can be established when at least one ovary demonstrates an ovarian volume of greater than 10 cm^3 (10 ml) and/or 12 or more follicles measuring 2–9 mm in diameter.[51] Women with oligoamenorrhea and polycystic-appearing ovaries on ultrasonography, but no evidence of hyperandrogenism, do not have PCOS.

Currently, ultrasound is the most widely used noninvasive means of evaluating ovarian morphology in women with suspected PCOS. Technical recommendations for ultrasound assessment of polycystic ovaries (PCO) from the 2003 Rotterdam PCOS consensus:

- State-of-the-art equipment operated by appropriately trained personnel
- Whenever possible, the transvaginal approach should be used
- Regularly menstruating women should be scanned in the early follicular phase (days 3–5). Oligo/amenorrheic women should be scanned either at random or between days 3–5 after a progestin-induced withdrawal bleeding
- Calculation of ovarian volume is performed using the simplified formula for a prolate ellipsoid (0.5×length×width×thickness)
- Follicle number should be estimated both in longitudinal and anteroposterior cross-sections of the ovaries. The size of follicles less than 10 mm should be expressed as the mean of the diameters measured on the two sections.

Three-dimensional ultrasound facilitates the quantitative assessment of follicle count, measurement of total ovarian and stromal echogenicity and assessment of volume and quantitative assessment of the vascularity within a defined volume of tissue in a way that has not been possible with 2D USG.[52] Also provides a more objective tool to examine stromal echogenicity through the assessment of the mean grayness of the ovary. The mean echogenicity of the gray voxels represents the mean tissue density or echogenicity in the region of interest and provides a new measure that can be objectively quantified. Ovarian volumes of images can be analyzed with the patient off the examination table. However, the criteria for the diagnosis of PCO by 3D USG need to be defined and tested prospectively alongside 2D USG parameters before it can be used in routine clinical care. Although the diagnostic criteria of PCOS do not include 3D imaging, the diagnostic threshold of mean 20 follicles per ovary using 3D USG may be appropriate to minimize false-positive diagnoses of PCO.

Ultrasound Criteria for Diagnosing PCOS

Antral Follicle Count

The Rotterdam criteria for the diagnosis of PCOS include the presence of 12 or more follicles in each ovary measuring 2–9 mm in diameter and/or increased ovarian volume (greater than 10 ml). Typically, PCO has follicles measuring 2–9 mm arranged peripherally around a dense core of stroma or scattered throughout the increased ovarian stroma. Each ovary should be scanned from the inner to outer margins, in the longitudinal plane for determination of follicle count. The orthogonal plane should be used to estimate the size and distribution of follicles. The mean diameter of each follicle should be based on two orthogonal measurements. The evaluation of the follicular distribution was omitted from the definition of PCO. The presence of a

single PCO is sufficient to meet the ovarian morphology criterion for diagnosis of PCOS.

The PCO should be differentiated from the multifollicular ovary (MFO), which is defined as 6 or more follicles 4–10 mm in size with normal stroma and caused by normal early follicular phase, puberty, hypothalamic amenorrhea and hyperprolactinemia.[53] An excess of 2–5 mm follicles seen at ultrasonography has been associated with follicular arrest in PCOS.

Total Ovarian Volume

Ovaries of PCOS patients are often enlarged, more spherical than ovoid. Ovarian volume is used as a surrogate for stromal hypertrophy. The Rotterdam criterion for diagnosis of PCO is an ovarian volume of greater than 10 ml. The most commonly used formula for ovarian volume is the prolate ellipsoid: length × width × height or thickness × 0.5. The use of 3D USG makes calculation of ovarian volume easier. Ovarian area can be used as a surrogate for ovarian volume in difficult cases.

Stromal Area and Ovarian Area

Stromal hypertrophy is a specific feature of ovarian androgenic dysfunction. The most severe form is referred to as hyperthecosis. Ultrasound examination shows bilateral enlarged, solid-appearing ovaries with no antral follicles. In these women, the whole ovary is replaced by ovarian stroma. Although an increase in stromal volume represents one of the most specific features of PCO, assessment of stromal volume is not practical in routine clinical practice, and therefore ovarian volume has been used as a good surrogate. Dewailly et al. proposed the presence of ovarian hypertrophy (an ovarian area >5.5 cm^2 unilaterally or bilaterally) as a morphological indicator for PCOS.[54] The stromal area is measured by "outlining with the caliper the peripheral profile of the stroma, identified by a central area slightly hyperechoic with respect to the other ovarian area." The ovarian area is calculated by outlining with the caliper the external limits of the ovary in the maximum plane section. The average of the parameters for both ovaries is used to determine mean ovarian area and stromal area and then calculate the stromal area to ovarian area ratio (S/A ratio), who has the strongest correlation with serum androgens when compared with total ovarian area, stromal area, ovarian volume and AFC.

Stromal Echogenicity

Increased ovarian stroma is an important marker for the presence of PCOS. Using 2D TVS and newly advanced software, the brightness, or echogenicity, of the ovarian stroma was determined objectively and showed that the mean stromal echogenicity was similar between PCOS and normal ovaries. The total echogenicity of PCOS was shown to be significantly less than the total echogenicity of control ovaries and this can be explained by the presence of many hypoechoic cysts in PCOS. Stromal index (stromal echogenicity/total ovarian echogenicity) was significantly higher in PCOS than in control ovaries. The subjective appearance of brighter stroma in PCOS patients in previous studies was due to the difference between the echogenicity of the stroma and total ovarian echogenicity and not due to a difference between the stroma of PCO and normal ovaries.

Vascularity

Stromal blood flow was shown to be most elevated in lean, hirsute women as compared with obese and normoandorgenic women. This findings suggest that ovarian stroma plays an important role in the development of hyperandrogenism. It also may explain why patients with PCOS are hyperresponsive to gonadotropins and thus prone to developing ovarian hyperstimualtion syndrome (OHSS). Three-dimensional ultrasound **(Fig. 51.22)** is especially useful in the quantitative assessment of the vascularity within a defined volume of tissue.[52] The total vascularized volume of the ovary can be expressed in volume units and quantification of vascularization using histogram software. Frequency-based color Doppler analyzes the frequency shift of blood velocity, whereas power Doppler uses the amplitude component of the signals received to present the number of blood cells moving. The total vascularized volume in the ovary (in ml) was obtained by multiplying VI by the volume of

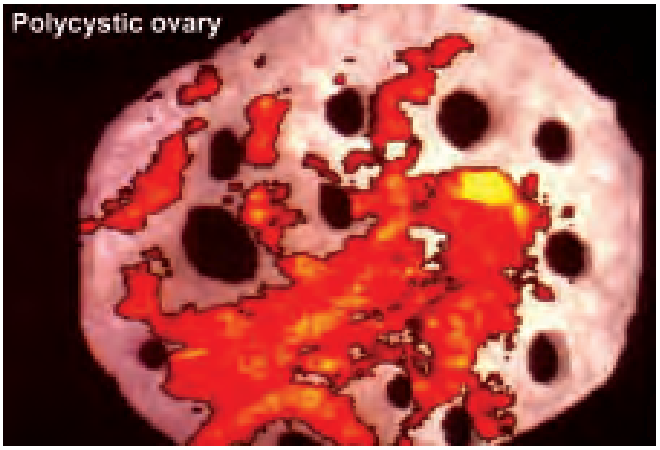

Figure 51.22: 3D power Doppler in polycystic ovary

the ovary. Although some authors reported higher VI, FI and VFI values than the normal ovaries in PCO after FSH stimulation,[56] others did not find any difference in the vascularization of polycystic ovarian stroma compared with normal ovarian stroma.[56]

Ultrasound Evaluation of the Endometrium

When patients are seen at the initial visit, it is important to establish the endometrial thickness. In women with amenorrhea greater than 6 months with a thickened endometrial complex, an endometrial biopsy may be indicated to exclude endometrial hyperplasia, which is common in PCOS due to unopposed estrogenic activity.

TUBAL FACTOR OF INFERTILITY

Evaluating the tubal patency represents a key step in the assessment of the infertile couple, especially in situations with risk factors for tubal damage.

Over the past 20 years there has been a shift in the causes of infertility, passing from the ovarian and uterine anomalies, to tubal and male infertility factors. Obstruction and damage of the fallopian tubes are accounting for almost 35% of all infertility cases.[57] Normally, the fallopian tubes are not accessible to ultrasound evaluation, unless their diameter is increased by a pathological process, such as hydrosalpinx, pyosalpinx, ectopic pregnancy, tubal carcinoma or torsion. The diagnosis of tubal patency has changed very little during time, laparoscopy with chromo per tubation being still considered the "gold standard", as it was 20 years ago, along with radiological HSG. Even though it is not possible in all situations 3D USG may represent a very good diagnostic tool, in cases with dilated tubes and a good image of the female pelvis. The most representative rendering mode is inversion mode, very spectacular and easy to handle, especially in patients with an amount of fluid in Douglas pouch. A special remark has to be made regarding the evaluation of tubal patency in patients with nondilated salpingae.

Even though very little related to 3D ultrasound, SIS may beneficiate from its techniques. A variable amount of saline solution is injected in pulses, under continuous vaginal scan. Power Doppler permits a good image of the tubal passage **(Fig. 51.23)** and it may be combined with 3D acquisition, creating a graphic representation of the fallopian tube. In some cases during the saline passage the tube is dilated such as a static acquisition with inversion mode is possible, but this is rather accidental, as it requires a long saline pulse and an important tubal diameter.

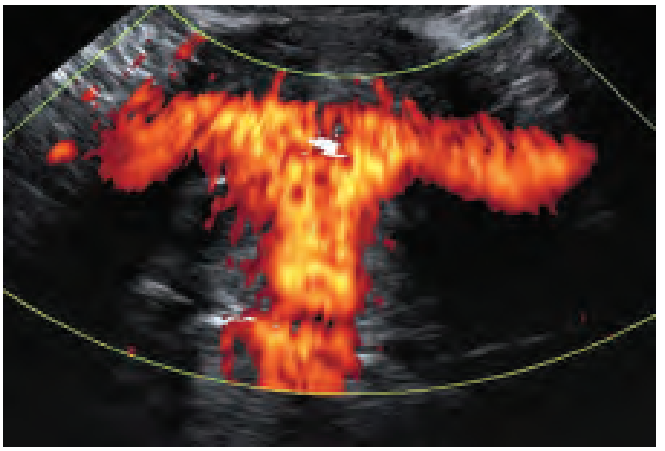

Figure 51.23: Saline infusion hysterosalpingography under power Doppler control shows easy passage of the fluid through both fallopian tubes

With all its disadvantages (case-to-case variability, time consuming technique and high rate of false positive results) the ultrasound evaluation of the fallopian tubes still represents the main developing direction for future tubal investigation.

SONOHYSTEROGRAPHY

Sonohysterography is the instillation of fluid into the uterine cavity to act as a negative contrast agent. Saline infusion sonohysterography is a minimally invasive office technique designed to maximize investigation of the female genital tract. The TVS is performed while sterile saline is simultaneously infused into the uterus to distend the endometrial cavity. The fluid contrast enhances ultrasound visualization by outlining intracavitary defects or growths. The result is a simple screening method for pelvic anomalies with major advantages over imaging modalities and without the invasive risks or expense of surgical evaluation.

Preparation of the patient for SIS is more or less similar to that for HSG, i.e. ensure that the patient is not pregnant and there is no evidence of active pelvic infection or other less likely contraindications to the procedure such as allergy to the ultrasound contrast medium. In addition, conventional TVS examination should be done before SIS to assess the appearance of the uterus before instillation of fluid into the uterine cavity and to determine the orientation of the uterus to facilitate insertion of a catheter into the cervical canal for instillation of the saline or the ultrasound contrast medium. Performing the procedure during the follicular phase has the advantage of avoiding the risk of

disturbing an early pregnancy. It is preferable to use a balloon-bearing catheter to occlude the internal os so as to allow adequate distension of the uterine cavity, with the disadvantages of being more uncomfortable for the patient and the fact that its shadow might obscure lesions present in the lower uterine segment or the cervical canal. In the majority of cases, an adequate distension of the uterine cavity can be achieved without the need to inflate a balloon, with the use of balloon-free catheters such as those used for intrauterine insemination.

Although SIS provides an indirect look inside the uterus, its ability to accurately diagnose intracavitary filling defects, such as myomas and polyps and adhesions (intrauterine synechia) and congenital uterine anomalies, matches that of the gold "standard" hysteroscopy. SIS adds more information than TVS alone; in addition its performance is consistently much more sensitive and specific than that of HSG, without exposing the patient to either ionizing radiation or contrast allergy. This procedure images far more in the female pelvis than simply the uterine cavity; yet, it is relatively simple to learn and perform, and it can easily be provided by those gynecology practices already offering TVS.

Three-Dimensional Saline Infusion Sonohysterography

The ability to rapidly acquire and store a set of volume data about the entire uterus has some potential advantages:

- The volume data can be evaluated in any plane desired, retrospectively, possibly reducing the usual amount of time necessary during two-dimensional SIS for uterine distension and multiple still images
- The true "C-plane", or coronal view, of the uterus maximizes the information about the endometrial cavity, the myometrium, and the fundal contour to potentially improve diagnostic accuracy in the setting of congenital uterine anomalies **(Figs 51.24 and 51.25)**. Its value in assessing intrauterine adhesions is limited. Also, TUI can be used **(Fig. 51.26)**.

Gel Infusion Sonohysterography (GIS)

Gel instillation (viscous gel containing hydroxyethyl cellulose and glycerine) is an alternative for saline infusion and can be used effectively and safely for sonohysterography. The GIS offers a more stable filling of the uterine cavity allowing better detailed 3D-examination without inconveniences and discomfort

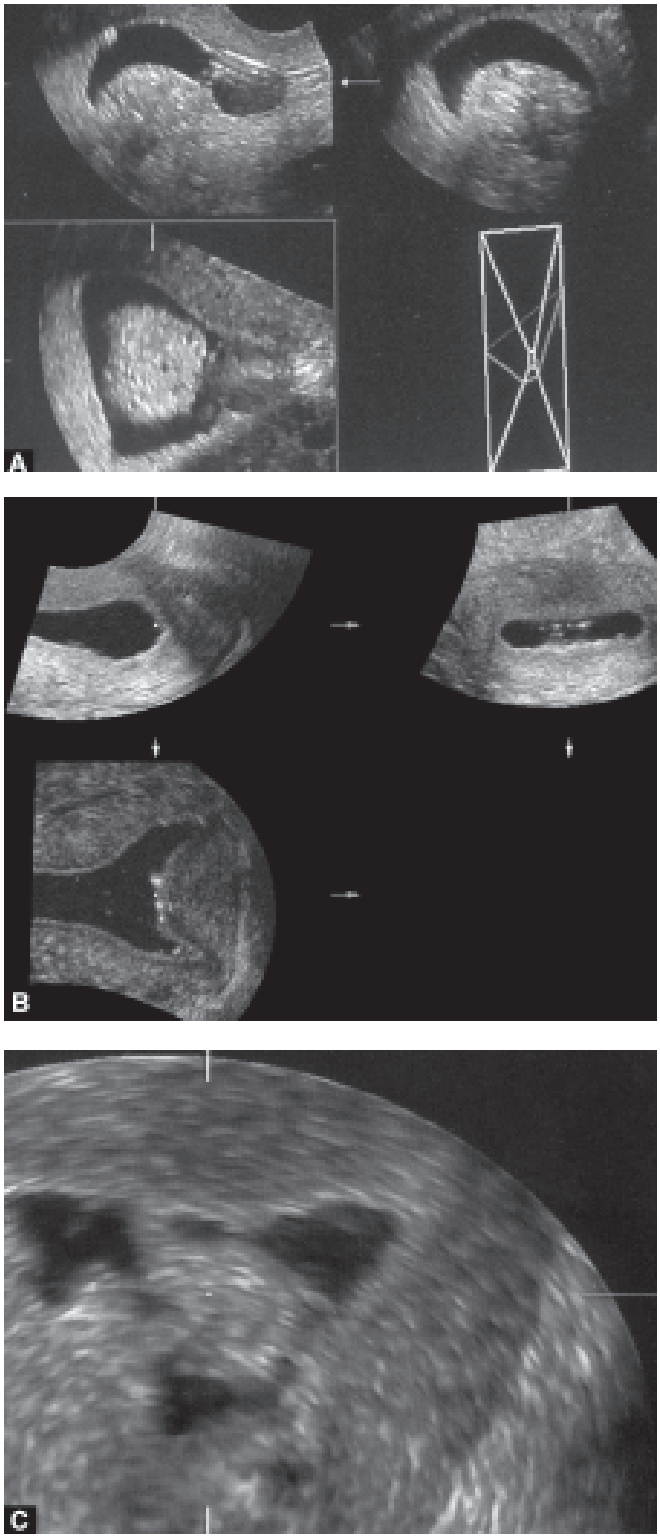

Figures 51.24A to C: (A) Three-dimensional multiplanar acquisition showing endometrial polyp; (B) Arcuate uterus; (C) Asherman syndrome with hyperechogenic avascular bridges within the uterine cavity

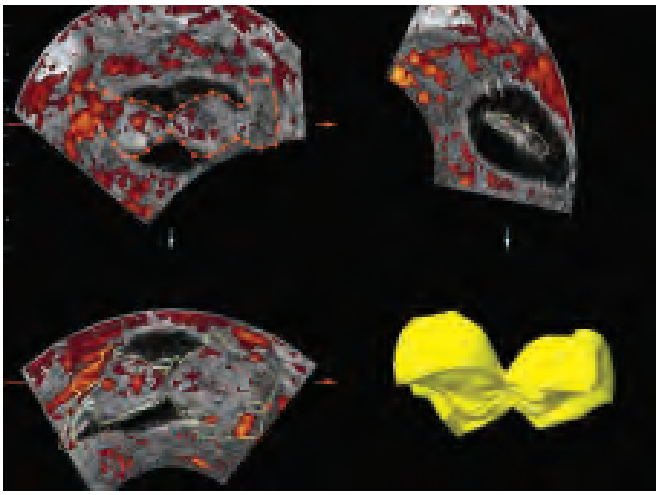

Figure 51.25: Two endometrial polyps in SIS 3D multiplanar acquisition with power Doppler and inversion mode

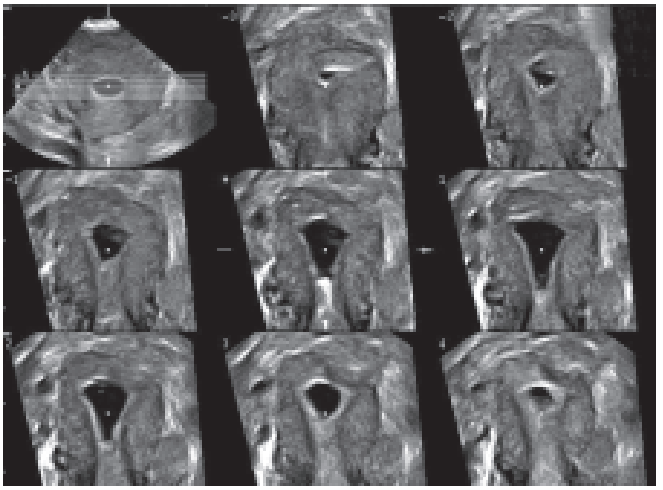

Figure 51.26: Tomographic image rendering (TUI) during SIS

due to fluid leakage and pain for both patient and ultrasonographer.[58]

Hysterosalpingo-contrast-salpingography

This procedure uses a technique similar to SIS to evaluate tubal obstruction in infertility patients. It's effective as first-step examination in the evaluation of infertile women. Involves the introduction of a fluid into the uterine cavity and the fallopian tubes. Sterile saline is used as an echo-free (negative) contrast medium for the assessment of the uterine cavity. For the examination of the fallopian tubes, a positive contrast medium is used, such as air, albumin with microbubbles or galactose with micro air bubbles. These positive contrast agents outline the fallopian tubes, giving a hyperechoic

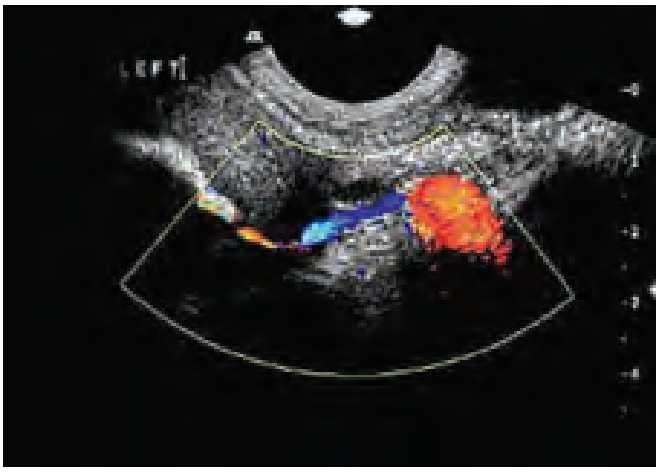

Figure 51.27: Color Doppler imaging of the fallopian tube during Hy-Co-Sy

appearance. The advantage of this low acoustic pressure technique is that the bubbles are not immediately destroyed but can be detected for several minutes. This permits an easier evaluation of tubal patency even by inexperienced sonographer. Hy-Co-Sy proved to be as effective as HSG in diagnosing tubal patency, and the detection rate for tubal obstruction was 80%.[59] Complete visualization of the entire fallopian tube using B-mode and Echovist may not always be possible. Pulsed-wave Doppler is recommended as a supplement to gray scale imaging in cases of suspected tubal occlusion or if there is intratubal flow demonstrable only over a short distance.[60] The color Doppler gate is placed over the presumed mural portion of the tube and movement of contrast medium is registered. In this way, a pulsed Doppler range gate can be used to obtain a flow velocity waveform, diagnostic of tubal patency. Characteristic Doppler spectra can be generated, representing patent, partially occluded, and completely occluded tubes. Adding color and pulsed Doppler to 2D Hy-Co-Sy **(Fig. 51.27)** and power Doppler to 3D Hy-Co-Sy contribute to an increase in the diagnostic precision in detection of tubal patency **(Fig. 51.28)**.

Since the surrounding bowel and the fimbrial ends have similar echogenicity, is not easy to visualize spillage of the saline-air mix at the distal portion of the tubes. Recently, evolved 3D Hy-Co-Sy with coded contrast imaging technology with many advantages:

- The imaging of the tube is produced only by contrast microbubbles and the broadband ultrasonic signals from surrounding tissue are filtered out completely.
- The clarity with which spillage is seen, when there is tubal patency, of the hyperechoic contrast media in a completely anechoic pelvic cavity, make this

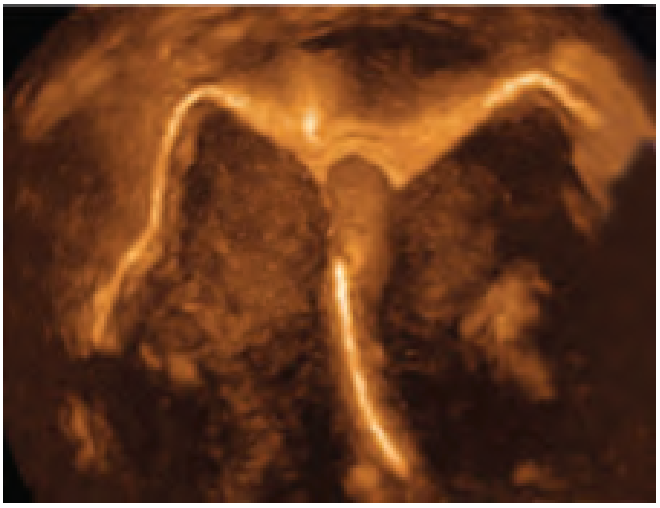

Figure 51.28: 3D Hy-Co-Sy showing the coronal plane

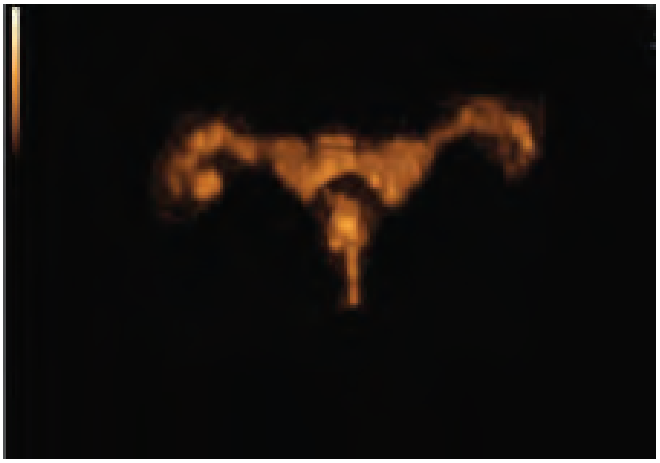

Figure 51.29: Fallopian tube during Hy-Co-Sy with coded contrast imaging technology

diagnostic method easier for even an inexperienced sonographer.

- The visualization for few minutes of the contrast media makes possible the use of 3D examination showing the tubal course in different planes and in the space[61] **(Fig. 51.29)**.

Insonation of echo-enhancing contrast agents with high acoustic power produces disintegration of microbubbles, resulting in a phenomenon called stimulated acoustic emission (SAE). The SAE techniques were successfully applied to Hy-Co-Sy and allowed the visualization of the free spill of contrast agent into the peritoneal cavity in the majority of cases. The SAE-Hy-Co-Sy showed good agreement with HSG.[62]

CONCLUSION

Today, sonography plays a central role in the diagnosis and treatment of fertility disorders. Ultrasonography in infertility investigations has proven to be as accurate and effective as the traditional alternatives, and in many cases even superior to HSG, hysteroscopy and laparoscopy. In addition is a quick procedure that in majority of cases causes little or no pain. Color Doppler and 3D USG with power Doppler has significantly improved diagnostic accuracy, not only for evaluating infertility but also for ART and follow-up of early pregnancy. With 3D USG, we can assess infertile women in three different volumes (uterus, right and left adnexa). Once the data stored, the investigation can be continued without the presence of the patient, so the total examination time for the patient is considerably reduced. The use of 3D TVS after injection of saline solution or/and echo enhancing contrast medium allows us the visualization of the uterine cavity, especially the portion close to tubal ostia with great accuracy. Quantification of endometrial volume in combination with blood flow studies assess the endometrial receptivity and can predict pregnancy rates in ART. An ultrasound-based approach appears to be more cost-effective than traditional comprehensive infertility investigation protocols. In the next years, 3D USG will become even more useful both for performing common simple procedures and for furthering advanced, clinically oriented research.

REFERENCES

1. Hill ML. Infertility and reproductive assistance. In: Neiberg DA, Hill LM, Bohm-Velez M (Eds). Transvaginal Ultrasound. St. Louis: Mosby Year Book; 1992.
2. Kurjak A, Zalud I. Normal pelvic blood flow. In: Kurjak A (Ed.). Transvaginal Color Doppler. Park Ridge, NJ: Parthenon; 1991. pp. 25.
3. Kurjak A, Kupesic S. Ovarian senescence and its significance on uterine and ovarian perfusion. Fertil Steril. 1995;64(3):532-7.
4. Kupesic S, Kurjak A. Uterine and ovarian perfusion during the periovulatory period assessed by transvaginal color Doppler. Fertil Steril. 1993;60(3):439-43.
5. Deichert U, Albrand-Thielman C, van de Sandt M. Doppler sonographic pelvic blood flow measurements and their prognostic value in terms of luteal phase and implantation. Hum Reprod. 1996;11(8):1591-3.
6. Yuval Y, Lipitz S, Dor J, et al. The relationships between endometrial thickness, and blood flow and pregnancy rates in in-vitro fertilization. Hum Reprod. 1999;14(4):1067-71.
7. Raine-Fenning NJ, Campbell BK, Kendall NR, et al. Quantifying the changes in endometrial vascularity

throughout the normal cycle with three-dimensional power Doppler angiography. Hum Reprod. 2004; 19:330-8.
8. Jokubkiene L, Sladkevicius P, Rovas L, et al. Assessment of changes in endometrial and subendometrial volume and vascularity during the normal menstrual cycle using three-dimensional power Doppler ultrasound. Ultrasound Obstet Gynecol. 2006;27:672-9.
9. Ng EH, Chan CC, Tang OS, et al. Comparison of 2-dimensional, 3-dimensional and vascular ultrasonographic parameters for endometrial receptivity between 2 consecutive stimulated in vitro fertilization cycles. J Ultrasound Med. 2007;26(7):931-9.
10. Mercé LT, Barco MJ, Bau S, et al. Are endometrial parameters by three-dimensional ultrasound and power Doppler angiography related to in vitro fertilization/embryo transfer outcome? Fertil Steril. 2008;89(1):111-7.
11. Linhard A, Ravn V, Bentin-Ley U, et al. Ultrasound characteristics and histological dating of the endometrium in a natural cycle in infertile women compared with fertile controls. Fertil Steril. 2006;86:1344-55.
12. Raine-Fenning NJ, Campbell BK, Kendall NR, et al. Endometrial and subendometrial perfusion are impaired in women with unexplained subfertility. Hum Reprod. 2004;19:2605-14.
13. Ng EH, Chan CC, Tang OS, et al. Comparison of endometrial and subendometrial blood flow measured by three-dimensional power Doppler ultrasound between stimulated and natural cycles in the same patients. Hum Reprod. 2004;19:2385-90.
14. Pierson RA. Imaging the endometrium: are there predictors of uterine receptivity? J Obstet Gynaecol Can. 2003;25:360-8.
15. Richter KS, Bugge KR, Bromer JG, et al. Relationship between endometrial thickness and embryo implantation, based on 1,294 cycles of in vitro fertilization with transfer of two blastocyst-stage embryos. Fertil Steril. 2007;87:53-9.
16. Puerto B, Creus M, Carmona F, et al. Ultrasonography as a predictor of embryo implantation after in vitro fertilization: a controlled study. Fertil Steril. 2003;79:1015-22.
17. Yaman C, Ebner T, Sommergruber M, et al. Role of three-dimensional ultrasonographic measurement of endometrium volume as a predictor of pregnancy outcome in an IVF-ET program: a preliminary study. Fertil Steril. 2000;74:797-801.
18. Jarvela IY, Sladkevicius P, Kelly S, et al. Evaluation of endometrial receptivity during in-vitro fertilization using three-dimensional power Doppler ultrasound. Ultrasound Obstet Gynecol. 2005;26:765-76.
19. Kupesic S, Bekavac I, Bjelos D, et al. Assessment of endometrial receptivity by transvaginal color Doppler and three-dimensional power Doppler ultrasonography in patients undergoing in vitro fertilization procedures. J Ultrasound Med. 2001;20:125-34.
20. Ng EH, Chan CC, Tang OS, et al. The role of endometrial and subendometrial blood flows measured by three-dimensional power Doppler ultrasound in the prediction of pregnancy during IVF treatment. Hum Reprod. 2006;21:164-70.
21. Merce LT, Barco MJ, Bau S, et al. Are endometrial parameters by three-dimensional ultrasound and power Doppler angiography related to in vitro fertilization/embryo transfer outcome? Fertil Steril. 2008;89:111-17.
22. Kupesic S, Kurjak A, Bjelos D, et al. Three-dimensional ultrasonographic ovarian measurements and in vitro fertilization outcome are related to age. Fertil Steril. 2003;79:190-7.
23. Oliveira FG, Abdelmassih VG, Diamond MP, et al. Impact of subserosal and intramural uterine fibroids that do not distort the endometrial cavity on the outcome of in vitro fertilization-intracytoplasmic sperm injection. Fertil Steril. 2004;81:582.
24. Kurjak A, Kupesic-Urek S, Miric D. The assessment of benign uterine tumor vascularization by transvaginal color Doppler. Ultrasound Med Biol. 1992;18:645-9.
25. Grimbizis GF, Camus M, Tarlatzis BC, et al. Clinical implications of uterine malformations and hysteroscopic treatment results. Hum Reprod Update. 2001;7:161-6.
26. Acien P. Incidence of Mullerian defects in fertile and infertile women. Hum Reprod. 1997;12:1372-5.
27. Nicolini U, Bellotti M, Bonazzi B, et al. Can ultrasound be used to screen uterine malformations? Fertil Steril. 1987;47:89-93.
28. Kupesic S. Three-dimensional ultrasound in reproductive medicine. Ultrasound Rev Obstetr Gynecol. 2005;5:304-15.
29. Wu MH, Hsu CC, Huang KE. Detection of congenital mullerian duct anomalies using three-dimensional ultrasound. J Clin Ultrasound. 1997;25:487-92.
30. Airoldi J, Berghella V, Sehdev H, et al. Transvaginal ultrasonography of the cervix to predict preterm birth in women with uterine anomalies. Obstet Gynecol. 2005;106(3):553-6.
31. Kupesic S. Clinical implications of sonographic detection of uterine anomalies for reproductive outcome. Ultrasound Obstet Gynecol. 2001;18:387-400.
32. Exalto N, Stappers C, van Raamsdonk LA, et al. Gel instillation sonohysterography: first experience with a new technique. Fertil Steril. 2007;87:152-5.
33. Salim R, Woelfer B, Backost M. Reproductibility of three-dimensional ultrasound diagnosis of congenital uterine anomalies. Ultrasound Obstet Gynecol. 2003;21:578-82.
34. Alborzi S, Dehbashi S, Parsanezhad ME. Differential diagnosis of septate and bicornuate uterus by sonohysterography eliminates the need for laparoscopy. Fertil Steril. 2002;78:176-8.
35. Valenzano MM, Mistrangelo E, Lijoi D. Transvaginal sonohysterographic evaluation of uterine malformations. Eur J Obstet Gynecol Reprod Biol. 2006;124(2):246-9.
36. Kupesic S, Kurjak A. Septate uterus: Detection and prediction of obstetrical complications by different forms of ultrasonography. J Ultrasound Med. 1998;17:631-6.
37. Troiano RN, McCarthy SM. Mullerian duct anomalies: imaging and clinical issues. Radiology. 2004;233:19-23.
38. Kurjak A, Kupesic-Urek S, Schulman H, et al. Transvaginal color flow Doppler in the assessment of ovarian and uterine blood flow in infertile women. Fertil Steril. 1991;56:870-4.
39. Bowen S, Norian J, Santoro N, et al. Simple tools for assessment of ovarian reserve (OR): individual ovarian dimensions are reliable predictors of PR. Fertil Steril. 2007;88(2):390-5.
40. Quenan J. The menstrual cycle. In: Lewis V (Ed.). Reproductive Endocrinologyand Infertility. Austin, TX: Landes Bioscience; 2007. pp. 3-10.

41. Soldevila PN, Carreras O, Tur R, et al. Sonographic assessment of ovarian reserve. Its correlation with outcome of in vitro fertilization cycles. Gynecol Endocrinol. 2007;23(4): 206-12.
42. Kwee J, Elting ME, Schats R, et al. Ovarian volume and antral follicle count for the prediction of low and hyper responders with in vitro fertilization. Reprod Biol Endocrinol. 2007;5:9.
43. Hendricks DJ, Kwee J, Mol BW, et al. Ultrasonography as a tool for the prediction of outcome in IVF patients: a meta-analysis of ovarian volume and antral follicle count. Fertil Steril. 2007;87(4):764-75.
44. Jayaprakasan K, Hilwah N, Kendall NR, et al. Does 3D ultrasound offer any advantage in the pretreatment assessment of ovarian reserve and prediction of outcome after assisted reproduction treatment? Hum Reprod. 2007; 22(7):1932-41.
45. Frattarelli JL, Levi AJ, Miller BT. A prospective novel method of determining ovarian size during in vitro fertilization cycles. J Assist Reprod Genet. 2002;19(1):39-41.
46. Hendricks DJ, Mol BW, Bancsi LF, et al. Antral follicle count in the prediction of poor ovarian response and pregnancy after in vitro fertilization: a meta-analysis and comparison with basal follicle-stimulating hormone. Fertil Steril. 2005;83(2):291-301.
47. Engmann L, Sladkevicius P, Agrawal R, et al. Value of ovarian stromal blood flow velocity measurement after pituitary suppression in the prediction of ovarian responsiveness and outcome of in vitro fertilization treatment. Fertil Steril. 1999;71(1):22-9.
48. Shrestha SM, Costello MF, Sjoblom P. Longitudinal assessment of ovarian perifollicular and endometrial vascularity by power Doppler ultrasound in pregnant and non-pregnant cycles in IVF settings. J Assist Reprod Genet. 2004;21:387
49. Baerwald AR, Adams GP, Pierson RA. Form and function of the corpus luteum during the human menstrual cycle. Ultrasound Obstet Gynecol. 2005;25:498.
50. Guerriero S, Ajossa S, Melis GB. Luteal dynamics during the human menstrual cycle: new insight from imaging. Ultrasound Obstet Gynecol. 2005;25:425.
51. The Rotterdam ESHRE/ASRM-sponsored PCOS consensus workshop group. Revised 2003 consensus on diagnostic criteria and long-term health risks related to polycystic ovary syndrome (PCOS). Hum Reprod. 2004;19:41-7.
52. Lam PM, Johnson IR, Raine-Fenning NJ. Three-dimensional ultrasound features of the polycystic ovary and the effect of different phenotypic expressions on these parameters. Hum Reprod. 2007;22:3116-23.
53. Brown MA, Chang RJ. Polycystic ovary syndrome: clinical and imaging features. Ultrasound Q. 2007;23:233-8.
54. Dewailly D, Robert Y, Helin Y, et al. Ovarian stromal hypertrophy in hyperandrogenic women. Clin Endocrinol (Oxf). 1994;41:557-62.
55. Jarvela IY, Sladkevicius P, Kelly S, et al. Comparison of follicular vascularization in normal versus polycystic ovaries during in vitro fertilization as measured using 3-dimensional power Doppler ultrasonography. Fertil Steril. 2004;82(5):1358-63.
56. Jarvela IY, Mason HD, Sladkevicius R, et al. Characterization of normal and polycystic uvaries using three-dimensional power Doppler ultrasonography. J Asist Reprod Genet. 2002;19:582-90.
57. Hill ML. Infertility and reproductive assistance. In: Neiberg DA, Hill LM, Bohm-Velez M, Mendelson EB (Eds). Transvaginal Ultrasound. St. Louis: Mosby Year Book; 1992.
58. Emanuel MH, Exalto N, van Raamsdonk, et al. Gel Instillation, a new technique for Sonohysterography (GIS). Ultrasound in Obstetrics and Gynecology. 2006;28:359-411.
59. Exacoustos C, Zupi E, Carusotti C, et al. Hysterosalpingo-contrast sonography compared with hysterosalpingography and laparoscopic dye perturbation to evaluate tubal patency. J Am Assoc Gynecol Laparosc. 2003;10(3):367-72.
60. Kupesic S, Plavsic B. 2D and 3D hysterosalpingo-contrast-sonography in the assessment of uterine cavity and tubal patency. Eur J Obstet Gynecol Reprod Biol. 2007;133:64-9.
61. C Exacoustos, E Zupi, ME Romanini, et al. Three-dimensional Coded Contrast Imaging: a newultrasound approach to evaluate tubal patency. Ultrasound Obstet Gynecol. 2008;32:308-97.
62. Prefumo F, Serafini G, Martinoli C, et al. The sonographic evaluation of tubal patency with stimulatedacoustic emission imagin. Ultrasound Obstet Gynecol. 2002;20:386-9.

52
CHAPTER

2D and 3D Saline Infusion Sonography and Hystero-Contrast-Salpingography

Sanja Kupesic Plavsic, Branko M Plavsic

INTRODUCTION

Evaluation of uterine anatomy and tubal status is on one of the initial steps in the diagnostic workup of infertile patients. Saline infusion sonography (SIS) and hystero-contrast-sonography (Hy-Co-Sy) are currently performed as a part of the infertility workup to rule out uterine abnormalities and assess the tubal patency, respectively.

The number of cases of tubal sterility is increasing and tubal factors, such as tubal dysfunction or obstruction, account for approximately 35% of the causes of infertility.[1,2] A history of pelvic inflammatory disease (PID), septic abortion, intrauterine contraception device use, ruptured appendix, tubal surgery, or ectopic pregnancy should alter the physician to the possibility of tubal damage. One aspect of the infertility investigation which has changed little over the last 20 years is that of the assessment of fallopian tube patency. Until now, the most frequently used procedures to demonstrate tubal patency have been X-ray hysterosalpingography (HSG) and chromopertubation during laparoscopy.[3]

Hysteroscopy is a technique, which complements hysterosalpingography. It can accurately differentiate between endometrial polyps and submucous leiomyomas and can be used for their treatment. The same method is useful in establishing the definitive diagnosis and treatment of intrauterine adhesions and congenital anomalies of the uterus. Risk factors include perforation of the uterus, hemorrhage, infection and eventually anesthetic risk if anesthesia is required.

Hysteroscopy-directed falloposcopy can detect obstruction of the tubal ostium and can be utilized to examine the entire length of the tubal lumen.[4] Treatment of the proximal tubal obstruction can immediately follow the diagnosis. Transcervical tubal cannulation or balloon tuboplasty performed by hysteroscopic approach are the methods of choice.[5]

During the last three decades laparoscopy was used as a gold standard for investigation of the tubal status, but it requires a general anesthesia and carries a risk of surgical complications, such as bowel or vascular injury, hemorrhage, infection, anesthetic risk, and postoperative discomfort. With a Jarcho-type of cannula placed in the uterine cavity, one can manipulate the uterus and by instilling indigo-carmine saline, or other tinted saline, can test for tubal competence. Using laparoscopy, physician can explore pelvic anatomy and upper abdominal cavity. This approach is useful for evaluation of the ovarian disease, genital anomalies and assessment of tubal patency. Furthermore, it is a valuable tool for staging of endometriosis. Laparoscopy is also used for the assessment of patients with chronic pelvic pain, evaluation and staging of pelvic neoplasia, as well as for a prognostic review of the previous infertility surgical procedure. It has also been helpful in obtaining peritoneal washings and cultures in patients with positive history of PID.

Ultrasound imaging of female pelvis has significantly improved with the use of high-frequency vaginal ultrasound probes. Normal fallopian tubes are usually not seen by vaginal sonography unless some fluid surrounds them. The contrasting fluid may be one of the following:

- Normal serous fluid
- Follicular fluid during or after ovulation
- Blood, ascitic fluid
- Products of an exudative or an infectious process.

If the fallopian tube is not filled with fluid its lumen cannot be detected.

The SIS of the uterine cavity and Hy-Co-Sy are informative variations of X-ray HSG, a standard radiographic technique for studying the uterine cavity and fallopian tubes following transcervical infusion of the iodinated contrast under fluoroscopic observation. When sonographic evaluation of the uterine lumen with contrast is combined with evaluation of the tubes, this procedure is called Hy-Co-Sy, sonohysterosalpingography, or sono-HSG. Sonohysterography has also been called hysterosonography and saline infusion sonohysterography. The Hy-Co-Sy is based on introduction of a sonographic enhancing positive contrast medium into the uterine cavity and the fallopian tubes. This positive contrast medium is usually used following the instillation of the negative contrast media into the uterine cavity. The advantage of sonolucent fluid is that it better delineates hyperechogenic surface of the endometrium. Positive contrast agents outline the course of the fallopian tubes, producing their hyperechogenic appearance. Microparticles of galactose, micro air bubbles and albumin have been extensively studied.[6-9] The most affordable option is to use saline solution with air.

Benefits of Hy-Co-Sy procedure are the following:

- Avoidance of the ionization and/or idiosyncrasy to contrast media
- Easy repeatability
- Intraprocedural active participation of the patient (increases her knowledge of tubal status).

The course of this dynamic analysis of tubal patency and motility can be stored, reviewed, analyzed and interpreted to the infertile couple using CINE mode.

According to Peters, Volpi and their colleagues,[6,7] the accuracy of Hy-Co-Sy compared to X-ray HSG varies from 70.37 to 92.20% **(Table 52.1)**. The accuracy of Hy-Co-Sy compared to chromopertubation varies from 81.82 and 91.48% respectively[8,9] to 100% **(Table 52.2)**.[10]

TABLE 52.1

The accuracy of Hystero-Contrast-Salpingography (Hy-Co-Sy) compared to X-ray HSG

Authors (Year)	*Total number*	*Accuracy N (%)*	*Sensitivity (%)*	*Specificity (%)*
Richman et al. (1984)[13]	36		100%	96%
Peters and Coulam (1991)[6]	27	19 (70,37)	–	–
Volpi et al. (1991)[7]	21	19 (92,20)	–	–
Stern et al. (1992)[8]	89	72 (80,90)		
Battaglia et al. (1996)[31]	60	52 (86,66)		

TABLE 52.2

The accuracy of Hy-Co-Sy compared to laparoscopic chromopertubation

Authors (year)	*Total number*	*Accuracy (%)*
Allahbadia et al. (1993)[33]	27	25 (92,59)
Tüfekci et al. (1992)[20]	38	37 (97,37)
Peters and Coulam (1991)[6]	58	50 (86,20)
Kupesic et al. (1994)[9]	47	43 (91,48)
Stern et al. (1992)[8]	121	99 (81,82)
Deichert et al. (1992)[10]	16	16 (100,00)
Volpi et al. (1996)[7]	29	24 (82.7)
Battaglia (1996)[31]	60	56 (93,33)
Raga (1996)[36*]	42	39 (92)
Sladkevicius (2000)[39*]	67	–
Jeanty (2000)[30]	115	91 (79.4)
Kiyokawa (2000)[42*]	25	–

* three-dimensional Hy-Co-Sy

ULTRASOUND ASSESSMENT OF THE UTERUS AND THE FALLOPIAN TUBES

In 1954, Rubin was the first to assess fallopian tubes by insufflation.[11] Ultrasound visualization of the internal

genital tract using exogenous contrast media was first described by Nanini, Richman, Randolph and their colleagues,[12-14] who performed abdominal sonography after intracervical injection of the fluid.

Randolph and colleagues[14] used transabdominal ultrasound for observation of the cul-de-sac after injection of 200 ml isotonic saline through the Rubin catheter. Presence of retrouterine fluid was accepted as a criterion for patency of one or both tubes. Tubal patency was deduced indirectly from the presence of increasing fluid amount in the pouch of Douglas, without differentiation of the sides.

Lesions projecting into the uterine cavity could not be clearly delineated following the instillation of the echogenic contrast media, e.g. dextran. Therefore, for visualization of the uterine cavity abnormalities injection of a small amount of sonolucent fluid contributes to better evaluation of the intracavitary lesions. After evaluation of the uterine cavity following saline infusion sonography, sonographer continues with instillation of highly echogenic contrast to visualize the lumen of fallopian tubes.[13,15-18] Deichert and colleagues were the first to analyze tubal patency following transcervical injection of an echogenic and ultrasonic contrast fluid SHU 454 (Echovist; Schering, Berlin, Germany). The method was named transvaginal hystero-contrast-salpingography (Hy-Co-Sy).[19]

Tüfekci and colleagues[20] developed transvaginal sonosalpingography, a technique consisting of intrauterine injection of isotonic saline. This method performed without anesthesia was safe, cost-effective, non-invasive and more convenient when compared with other conventional methods. Due to the use of saline, there is no idiosyncrasy to the contrast agents.

Ultrasound Contrast Agents

Contrast media are divided into two groups:
1. Hypoechogenic, and
2. Hyperechogenic media.

Isotonic saline, ringer or dextran solutions belong to the hypoechogenic group. Instillation of these media facilitates the detection of echogenic border surfaces. The main disadvantage is that it is not possible to visualize the phenomena of motion and flow.

Hyperechogenic contrast media enhance echo signals and allow detection of the flow by both B-mode and Doppler ultrasound. Gramiak and Shah[21] found that small gas bubbles effectively reflect ultrasonic waves. Therefore, all the commercial echo contrast media contain microbubbles. Commercial products Echovist and Levovist (Schering AG, Berlin) represent suspension of microbubbles made of special galactose microparticles. Galactose microparticle granules are suspended either in galactose solution (Echovist) or sterile water (Levovist).[21]

Echovist (SHU 454) is an ultrasound contrast medium consisting of a suspension of monosaccharide microparticles (50% galactose, diameter 2 mm) in a 20% aqueous solution of galactose (w/v). The echogenic suspension is reconstituted immediately before the use from granules and a vehicle solution (200 mg microparticles in 1 ml of suspension).[22] This contrast medium is licensed for gynecological applications and is available on the market since 1995. In addition to galactose, Levovist (SHU 508) microparticle granules contain a very low concentration of physiological palmitic acid.

A few minutes before use, the granules have to be shaken vigorously for 5–10 seconds to be dissolved by an appropriate volume of aqueous galactose solution (Echovist) or sterile water (Levovist). A milky suspension of galactose microparticles in a solution is created after disaggregation of the microparticle "snowball". The suspension of Echovist is stable for about 5 minutes after preparation. Due to its extended stability, Levovist may be administered up to 10 minutes after the suspension procedure. Depending on the indication and the imaging modality (B-mode or Doppler), clinically adequate suspension of Echovist has concentrations of 200 and 300 mg/ml. For Levovist, the maximum concentration is about 400 mg/ml. The predominant limitation at concentrations lower than 200 mg/ml is the decreasing suspension stability. Concentrations exceeding 400 mg/ml are limited by a rapid increase of viscosity.

After intrauterine administration and emergence of Echovist from the fimbriae into the pelvis, the galactose microparticles dissolve. Warming to body temperature and dilution by the peritoneal fluid facilitates this process. *In vitro*, a rise in temperature of the Echovist suspension to 37° C leads to complete dissolution within 30 minutes. The dissolved galactose is subsequently absorbed and metabolized.

Numerous clinical studies in the field of echocardiography, venous vascular system analysis and HSG showed no evidence of serious side effects. Absolute contraindication for instillation of these contrast media is galactosemia (autosomal recessive disease in which, due to deficiency of galactose-1-phosphate uridyltransferase, galactose cannot be metabolized into glucose).

A second-generation contrast agent, such as SonoVue, provides a substantial harmonic response at a low acoustic pressure. Primarily it is used intravenously to study microcirculation of the liver, breast lesions and various gynecological lesions and it has also

been studied extensively in the assessment of myocardial perfusion.[23] Recently, it was introduced for sonographic tubal patency evaluation.[24]

Hy-Co-Sy Requirements

A detailed case history should be obtained from a woman considered for Hy-Co-Sy, to rule out the possibility of the rare condition of galactosemia, which is the only absolute contraindication, apart from acute inflammatory disease of the genital organs. A gynecological and ultrasound examination prior to the procedure is necessary to define the uterine position and anomalies if present. Before any intervention, a pregnancy test should be performed for legal reasons. The possibility of local or systemic infections is excluded by clinical examination (normal body temperature), inspection of the genital tract and assessment of cervical smears. The procedure should never be performed on patients with active pelvic infections, and antibiotic prophylaxis (doxycycline and metronidazole) should be used in patients with a history of PID. Hy-Co-Sy should always be performed during the early follicular phase of the menstrual cycle, after complete cessation of menses. This avoids dispersion of menstrual debris into the peritoneal cavity. Procedures performed during this period allow absorption of the media prior to ovulation, thus avoiding the presence of a foreign substance around the time of an imminent corpus luteum. This decreases any theoretic effect the media may have on tubal transport. Hysterosalpingography performed during the immediate premenstrual phase of the cycle has been advocated to rule out cervical incompetence, as that is the point in the cycle with maximum uterine contractions. Therefore, in order to maximize the information obtained, the indication for the study has influence on timing.

Patients are informed about the benefits and the possible risks of the procedure, and the procedure itself is described to them in detail. Anesthesia is generally not required for Hy-Co-Sy, and the patient can follow the course of the examination on the monitor. If Hy-Co-Sy is performed without anesthesia, patients occasionally report discomfort, especially if the tubes are occluded. The degree of discomfort depends on the individual response of the patient. Premedication or sedation is routinely used (5–10 mg of diazepam intravenously) especially in anxious patients. Pain signifies the obstruction and potential intravasation or tubal rupture, and should not be masked by anesthesia. However, tubal spasm may occur if Hy-Co-Sy is performed without anesthesia and may mimic tubal occlusion. Pretreatment with atropine (0.5 mg) may prevent this complication. Parenteral administration of 1 mg glucagon relieves the spasm and allows the flow of the contrast.

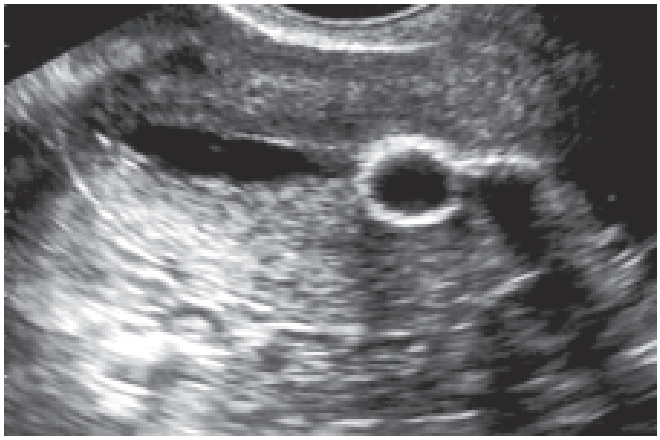

Figure 52.1: Transvaginal ultrasound of the uterus following injection of the isotonic saline solution. The balloon fixed at the level of the internal cervical os prevents the reflux of the intrauterine contrast

Hy-Co-Sy Procedure

The patient voids and is positioned supine on the gynecological table. With the patient's legs flexed, a speculum is inserted into the vagina and positioned such that the entire cervix is visualized and the os is easily accessible. The cervix and the vagina are then thoroughly scrubbed with Betadine solution. A tenaculum is placed on the anterior lip of the cervix, and the cannula is gently guided into the endocervical canal. Application of the contrast medium is performed via a small and very thin uterine catheter fitted with a balloon for stabilization and occlusion of the internal cervical os. The first observation to be made is of the uterine cavity, with verification of the catheter placement **(Fig. 52.1)**. After removal of the tenaculum, the transvaginal probe is gently introduced into the posterior fornix of the vagina. The contrast (sterile saline) is then injected slowly, under control of the ultrasound. Usually, no more than 5–10 ml of contrast is instilled into the uterine cavity. At this stage one can observe the morphology of the uterus and its endometrial lining **(Figs 52.2 and 52.3)** and detect duplication anomalies of the uterus **(Fig. 52.4)** or existence of endometrial polyps **(Figs 52.5 and 52.6)** or submucosal fibroids that are protruding into the uterine cavity **(Fig. 52.7)**.

If used by a trained physician, Hy-Co-Sy is a well-tolerated and rapid procedure that enables a reliable assessment of tubal patency. In addition, it avoids exposure to X-rays and shows tubal patency to the

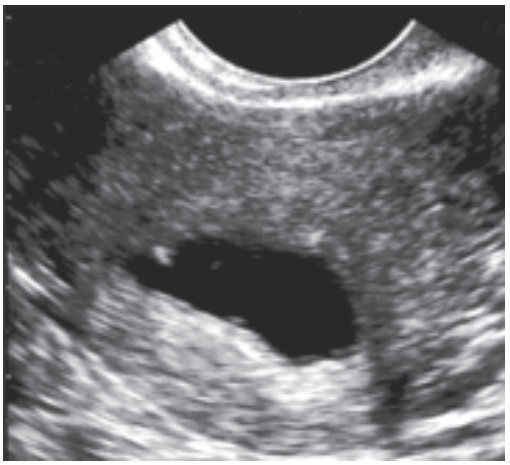

Figure 52.2: Triangular shape of the uterine cavity is visualized in transverse section, and indicates normal anatomy of the uterine cavity

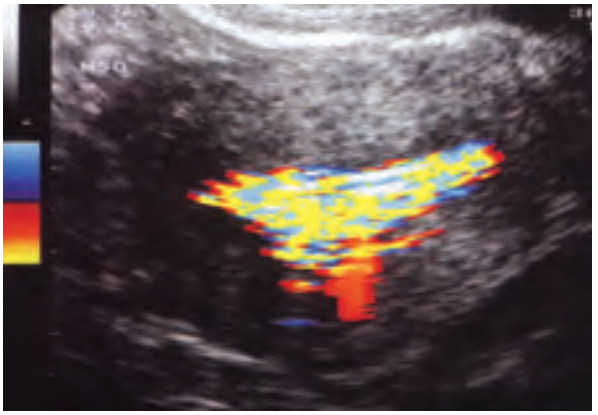

Figure 52.3: Saline infusion sonography by color Doppler ultrasound. Note a triangular shape of the uterine cavity

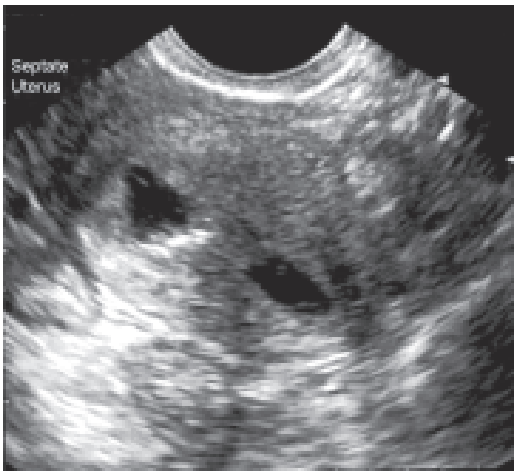

Figure 52.4: Saline infusion sonography demonstrates a division of the uterine cavity. Convex shape of the uterine fundus and hypoechogenic separation indicate septate uterus

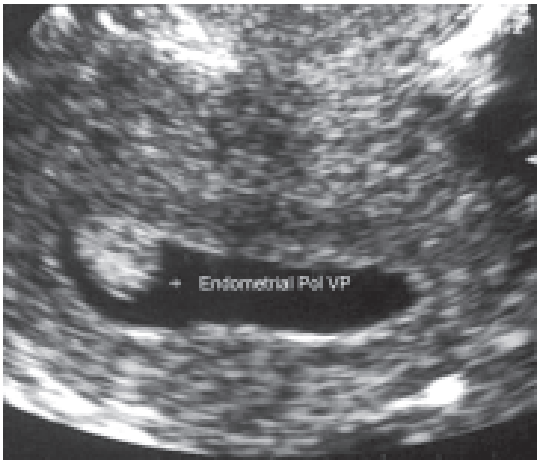

Figure 52.5: Saline infusion sonography enables precise detection of the focal endometrial thickening. Note endometrial polyp protruding into the uterine cavity after injection of isotonic saline

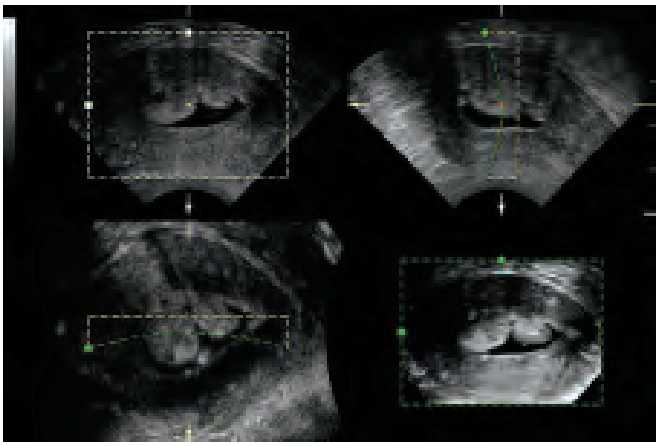

Figure 52.6: Three-dimensional saline infusion sonography in an infertile patient with two endometrial polyps

patient in "real time". Since it is performed without anesthesia, it can be performed as an outpatient procedure. Tubal spasm may sometimes lead to misdiagnosis of tubal occlusion and tubal flow in the proximal part of hydrosalpinx may occasionally give a false impression of tubal patency. To gain familiarity and technical competence, physician has to perform between 10 and 20 investigations.

Benefits and limitations of hystero-contrast-salpingography are listed in **Table 52.3**.

Gray-Scale (B-Mode) Hy-Co-Sy

Deichert and colleagues[10,25] described transvaginal Hy-Co-Sy for the assessment of tubal patency with gray-scale imaging (B-mode). The uterine cavity, which in most cases will still be dilated by the Ringer's solution

TABLE 52.3
Benefits and limitations of Hy-Co-Sy

Benefits	*Limitations*
• Reproducible and reliable assessment of tubal patency if used by a trained physician	• Tubal spasm may lead to misdiagnosis of tubal occlusion (spasm also seen with other methods)
• Avoids exposure to X-rays	• In hydrosalpinx, tubal flow may give a false impression of tubal patency
• Avoids allergic reactions	• Cannot visualize pelvic and bowel pathology
• Avoids general anesthesia	• Requires a degree of technical competence (10-20 investigations are needed to acquire this technique)
• Can be performed as outpatient procedure	
• Rapid	
• Well tolerated: little discomfort and few adverse events	
• Shows tubal patency in "real time"	

instilled previously, is slowly filled with the echogenic ultrasound contrast medium. If the tube is patent, constant flow in a pattern resembling a point, spot or streak is seen. Further intermittent injections of 1–2 ml of contrast, given slowly and continuously, with further lateral sweeps of the US probe, allow visualization of intraluminal or intratubal flow. For the diagnosis of tubal patency, two or three observation phases per tube are needed, with an observation period of continuous flow of about 10 seconds (during which the contrast medium is slowly injected). Although visualization of a longer segment of the tube beyond the pars intramuralis confirms tubal patency, sonographer should carefully examine the adnexal regions for filling of the distal segments of the tube to exclude sactosalpinx. Examination of the pouch of Douglas for any increase in retrouterine fluid should be compared with the finding at the beginning of the examination.

Pulsed Doppler Analysis of Tubal Patency

Deichert has proposed that B-mode findings should be confirmed by the use of pulsed wave Doppler ultrasound. Every patient with finding suggestive of tubal occlusion should undergo pulsed Doppler analysis of tubal patency.[10,25] After the Doppler gate has been positioned over the area to be examined, the gate width is reduced to measure only the flow noise from the perturbation (not the vascular or any other noise). Tubes are analyzed following brief injections of the contrast medium lasting about 5 seconds. A long drawn-out and initially hissing sound, with the simultaneous visualization of a broad noise band on the monitor, which slowly decreases after injection, indicate that the tube is patent. Thus, unobstructed flow is characterized by a short filling phase with a rapid, steep increase in Doppler shift and a slow, uniform fall in Doppler shift along the time axis, indicates unobstructed free distal outflow. The absence of these acoustic signals or optical tracings indicates obstruction of tubal flow or tubal occlusion. In this case there is only a short, steep Doppler shift with no subsequent noise signals. This indicates an absence of outflow of the contrast medium distal to the Doppler gate. A sonographic finding of unobstructed tubes on the basis of noise band in pulsed wave Doppler sonography is more impressive than that of a shorter segment of tube in standing B-mode.

Deichert and colleagues evaluated 17 patients with infertility.[10] Each patient had Hy-Co-Sy by gray-scale ultrasound and pulsed wave Doppler, and follow-up chromolaparoscopy (n = 16) or X-ray HSG (n = 1). The diagnostic efficacies of gray-scale and pulsed wave Doppler were compared with each other and with a conventional control procedure (chromolaparoscopy or X-ray HSG). The gray-scale findings were confirmed by pulsed wave Doppler in five cases on one side; pulsed wave Doppler in seven cases on both sides; corrected by pulsed wave Doppler in one case on one side, and confirmed on the other side by pulsed wave Doppler. In all 17 cases, tubal findings detected by pulsed Doppler waveform analysis were confirmed by chromolaparoscopy or X-ray HSG. The additional use of pulsed wave Doppler in Hy-Co-Sy is recommended as a supplement to gray-scale imaging in cases of suspected tubal occlusion, and in the event of intratubal flow demonstrable only over a short distance.

In more recent study Deichert assessed tubal patency using Hy-Co-Sy, conventional X-ray HSG and laparoscopy with dye in 76 women and 152 Fallopian tubes.[25] Hy-Co-Sy showed 87.5% concordance with other techniques, predicted 100% of tubal occlusions and detected 86% of patent tubes.

According to Ayida and colleagues,[26] when saline infusion sonography (SIS) is used as a screening test for evaluation of the uterine cavity, and results are compared to hysteroscopy findings, SIS has 87.5% sensitivity, 100% specificity, 100% positive predictive value and 91.6% negative predictive value for detection of uterine abnormalities.

Color Doppler Hy-Co-Sy

Transvaginal color Doppler Hy-Co-Sy is a safe and efficacious method for evaluation of fallopian tube patency without exposure to radiation or iodine based contrast dyes. The cost of this outpatient procedure is significantly lower than for X-ray HSG and does not require collaboration with radiology department. It is advisable that all the scans are recorded on video-recorder, DVD and/or polaroid films. Similar to X-ray HSG abnormal uterine bleeding, pregnancy and presence of adnexal masses on pelvic or ultrasound examination are contraindications for color Doppler Hy-Co-Sy.

Equipment needed to perform color Doppler Hy-Co-Sy is identical to the equipment needed to perform B mode Hy-Co-Sy. The only difference is that the monitoring of the procedure is performed using an ultrasound unit with color Doppler capability. The intrauterine cannula is placed into the uterus. One balloon is placed on the level of the internal cervical os, while another one is fixed in the external cervical os. Approximately two to five ml of sterile saline is instilled into the uterine cavity **(Fig. 52.3)**. Sonographer should provide representative images of intracavitary findings **(Figs 52.4 to 52.7)**. After careful observation of the morphology of the uterus end endometrial lining color Doppler is directed to the cornual region. Color signals passing through the fallopian tubes indicate tubal patency **(Fig. 52.8)**, while the absence of color signals is interpreted as tubal occlusion.[6,27] Accumulation of the fluid in the cul-de-sac on the side of injection controlled by transvaginal color and pulsed Doppler is an accurate indicator of the ipsilateral tubal patency **(Fig. 52.9)**. Selective tubal injection using tubal catheter with metal end increases the accuracy of the procedure and appropriateness of the interpretation. In this case, the procedure should be repeated for the contralateral side.

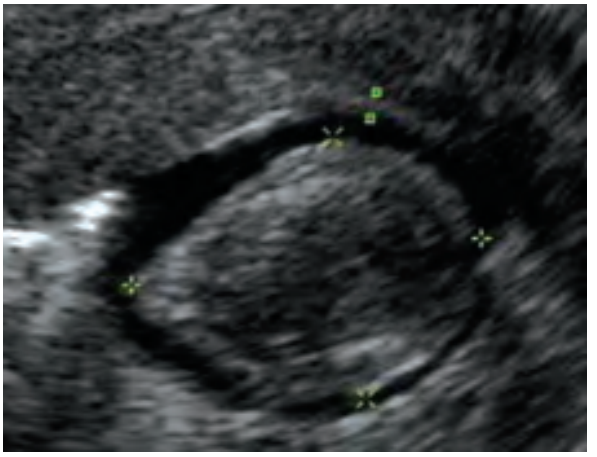

Figure 52.7: Saline infusion sonography enables visualization of the intracavitary fibroid

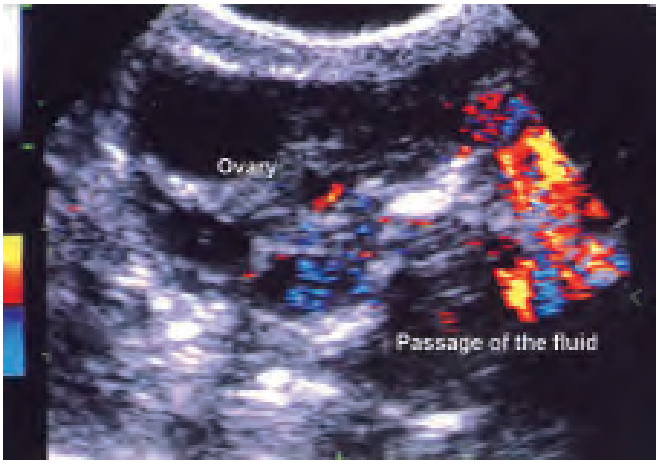

Figure 52.8: Transvaginal color Doppler Hy-Co-Sy demonstrates regular tubal patency. Note color flow signals passing through the right tube and simultaneous accumulation of the anechoic fluid in the cul-de-sac

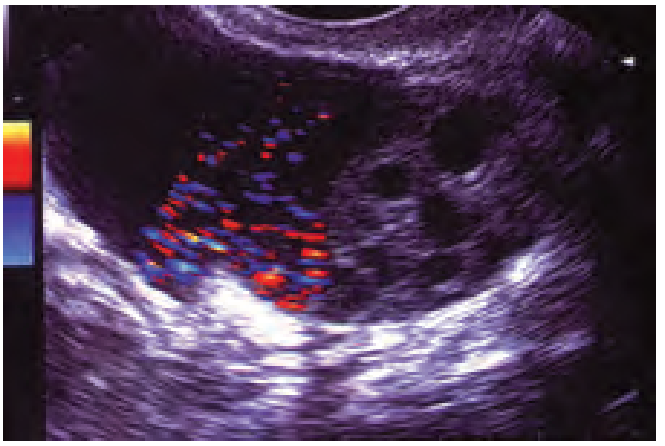

Figure 52.9: Color Doppler imaging of the ovary and retrouterine space after injection of the anechoic contrast medium. Color coded signals indicate contrast spillage into the cul-de-sac

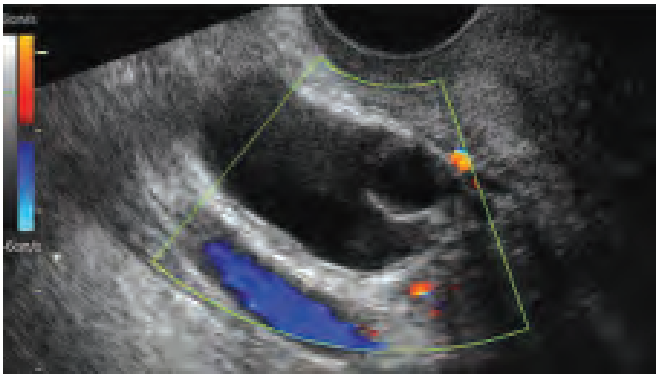

Figure 52.10: Transvaginal color Doppler imaging of the distally occluded tube following of the injection of the anechoic contrast medium

Difficulty in making the diagnosis of tubal occlusion arises in those patients with dilated fallopian tubes (hydrosalpinx), because the flow through the dilated fallopian tube may stimulate spillage in the cul-de-sac **(Fig. 52.10)**. To avoid this error, careful observation of both adnexa and cul-de-sac should be performed before everyHy-Co-Sy procedure. Since the tubal architecture is not demonstrated with color Doppler or B-mode Hy-Co-Sy, this method is not useful in preoperative salpingoplasty procedures.[28]

Using our modified technique, we compared the findings of color Doppler Hy-Co-Sy from 47 patients with those of chromopertubation at the time of laparoscopy.[9] Forty-three out of 47 (91.48%) color Doppler Hy-Co-Sy findings agreed with observations at laparoscopic chromopertubation. In only one patient, in whom no patency was seen in both tubes under color Doppler evaluation, indirect diagnosis of tubal patency was performed by observation of the accumulation of free fluid in the cul-de-sac. The increased incidence of conception during the three months after the procedure (in our study, two patients) may be an effect of a mechanical lavage of the uterus by dislodging the mucous plugs, breakdown of the peritoneal adhesions, or a stimulatory effect on the tubal cilia. No serious side effects were observed during and after the transvaginal color Doppler Hy-Co-Sy procedure. Eighteen patients complained of a pain that continued for 2–10 minutes after the procedure. No medication was required for these cases. The shortest time taken for the transvaginal color Doppler Hy-Co-Sy was 5 minutes, while the longest time was 14 minutes. After removing the instruments, the cervix should always be inspected for hemostasis and pressure applied to the tenaculum site whenever necessary.

To assess the accuracy of the diagnosis of tubal occlusion with the use of color Doppler flow ultrasonography and HSG, Peters and Coulam[6] studied 129 infertile women. When results of Hy-Co-Sy were compared with those of X-ray HSG and/or chromopertubation, 69 of 85 (81%) studies showed agreement, and 50 out of 58 (86%) Hy-Co-Sy findings agreed with observations at chromopertubation. The frequency of comparable findings between X-ray HSG and chromopertubation was 75%.

Richman and colleagues[13] evaluated tubal patency in 36 infertile women. They compared Hy-Co-Sy findings with conventional hysterosalpingograms, which had been obtained subsequently. Ultrasound demonstrated bilateral occlusion with a sensitivity of 100%, and showed tubal patency with a specificity of 96%.

Tüfekci and colleagues[20] studied 38 women with infertility complaints. The results obtained by transvaginal Hy-Co-Sy and subsequent laparoscopy were completely consistent for 29 cases (76.32%), and partially consistent for eight cases (21.05%). Only one case showed inconsistent result. Complete consistence means that the passage through both fallopian tubes is identical by both methods. Partial consistence indicated identical results for only either the left or the right tube. Transvaginal Hy-Co-Sy correctly indicated tubal patency or non-patency in 37 of 38 cases.

Heikkinen and colleagues[29] evaluated the advantages and accuracy of transvaginal Hy-Co-Sy in the assessment of tubal patency with regards to laparoscopic chromopertubation. Sixty-one fallopian tubes were examined by both techniques, resulting in concordance of 85%. By transvaginal Hy-Co-Sy, 45 tubes were found to be patent and 16 occluded. In chromopertubation, 50 tubes were patent and 11 were occluded. Bilateral tubal patency was detected by transvaginal Hy-Co-Sy in 17 cases, and by laparoscopy in 22 cases. Bilateral occlusion was found in three cases using either technique. Based on their results, the authors concluded that transvaginal Hy-Co-Sy with the combination of air and saline is a low-cost, reliable, safe and comfortable examination method that can be used for the primary investigation of infertility on an outpatient basis.

Jeanty and colleagues[30] assessed the use of air as a sonographic contrast agent in the investigation of tubal patency by Hy-Co-Sy. They examined 115 women assessed for infertility. After saline infusion sonography, a small amount of air was insufflated and the tubal passage of bubbles was monitored. Air-sonohysterography and laparoscopy with chromopertubation showed agreement in 79.4%. In 17.2% of patients, the

tubes were not visualized by air-sonohysterography when they were patent, which lead to the sensitivity of 85.7% and specificity of 77.2%. In conclusion, air assisted Hy-Co-Sy is a comfortable, simple and inexpensive first line of tubal patency investigation. Similarly, Battaglia and colleagues[31] confirmed the correlation between color Doppler Hy-Co-Sy and X-ray HSG with chromolaparoscopy for 86% versus 93% of patients studied, respectively.

Boudghene and colleagues[32] compared the efficiency of air-filled albumin microspheres (Infoson) with saline solution in determining fallopian tube patency during Hy-Co-Sy. The Hy-Co-Sy was performed with a 7-MHz transvaginal probe using both B-mode and color Doppler ultrasound, and tubal patency was demonstrated by the appearance of contrast agent in the peritoneal cavity near the ovaries. Infoson enhanced Hy-Co-Sy provided a significantly larger number of correct diagnoses (20 out of 22 fallopian tubes) than did saline Hy-Co-Sy (12 out of 24 fallopian tubes), and the same number of patients as by X-ray HSG. A positive ultrasound contrast agent appears to be more efficient than saline solution at determining fallopian tube patency in infertile women by means of Hy-Co-Sy, and as efficient as an iodinated contrast agent in the same population explored by X-ray HSG.

Stern and colleagues[8] administered saline transcervically during transvaginal color Doppler sonography in 238 women. Traditional X-ray HSG was performed in 89 women, while laparoscopy with chromopertubation was performed in 121 women. Forty-nine women had all three procedures performed. Correlation between color Doppler Hy-Co-Sy and X-ray findings with chromopertubation occurred in 81% versus 60% ($p = 0.0008$) of all women studied. In forty-nine patients who had all three procedures performed, color Doppler Hy-Co-Sy results correlated with chromopertubation more often than X-ray HSG (82% versus 57%, $p = 0.0152$). In their previous report,[6] discrepancies between color ultrasound Hy-Co-Sy and chromopertubation findings involved a diagnosis of unilateral patency. Based on their observation, these authors recommend repeating color ultrasound Hy-Co-Sy before making a diagnosis of unilateral occlusion.

Allahbadia[33] reported a 92.6% agreement between color Doppler Hy-Co-Sy compared with X-ray HSG and laparoscopy. The same author described the so-called Sion procedure or hydrogynecography. This procedure takes about 15 minutes as compared to the 5–6 minutes for Hy-Co-Sy. After accomplishing the first part of the procedure, sterile normal saline is injected until approximately 350 ml have flooded the pelvis. With the adnexa and uterus submerged in a fluid medium, the rescanning of the pelvis is repeated. If there is a bilateral tubal block and reflux of the saline is seen in the stem of the Foley's catheter, filling up the pelvis by alternative means is applied. The saline fills up the pelvis and delineates all sorts of adhesions. All the patients undergoing this procedure are given prophylactic antibiotics.

Contrary to optimistic results of different ultrasound techniques for evaluation of tubal patency, Balen and colleagues[34] found Hy-Co-Sy using both sterile saline and Echovist contrast media insufficiently accurate and inferior to conventional X-ray HSG. False-positive rates in the range of 9% and false-negative rates in the range of 20% have been reported in the diagnosis of tubal obstruction by color Doppler Hy-Co-Sy.[8] Therefore, all abnormal hysterosalpingogram studies deserve laparoscopic or hysteroscopic follow-up.

Also, normal X-ray or color Doppler Hy-Co-Sy do not rule out the need for diagnostic laparoscopy. While X-ray HSG is the most accurate method of diagnosing intramural or intraluminal abnormalities of the fallopian tube, color Doppler Hy-Co-Sy is the only available noninvasive method for evaluation of the tubal patency and motility.

To obtain maximum information, a well-trained physician who is familiar with the color Doppler investigation and who is capable of manipulating the instruments, the patient's reproductive tract and the rate of injection should perform the procedure.

Sueoka and colleagues[35] report on the use of the linear everting (LE) catheter to safely guide a falloposcope into the entire length of fallopian tube in order to observe the tubal lumen. This catheter may also be useful therapeutically for the recanalization of occluded tubes. On the basis of tubes attempted, the LE catheter successfully accessed 85.3% (87 out of 102) of the tubes. A follow-up hysterosalpingogram was completed 1–3 months following the falloposcopic tuboplasty (FT) procedure, which revealed an overall patency rate of 79.4% (81 out of 102). In this study, FT was found to be a highly useful, less invasive and novel treatment for tubal infertility.

THREE-DIMENSIONAL HY-CO-SY

Information provided by 2D ultrasound conventional scans in the longitudinal and transverse planes can now be augmented using 3D ultrasound that provides an additional view of the coronal plane, parallel to the transducer face, and surface rendering[36,37] **(Fig. 52.11)**. The computer generated scan is automatically displayed in three perpendicular planes. Presentation of three

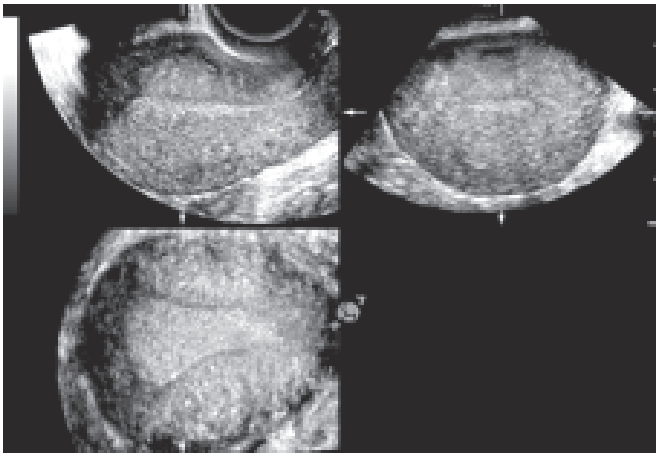

Figure 52.11: Three-dimensional ultrasound image of normal uterine cavity

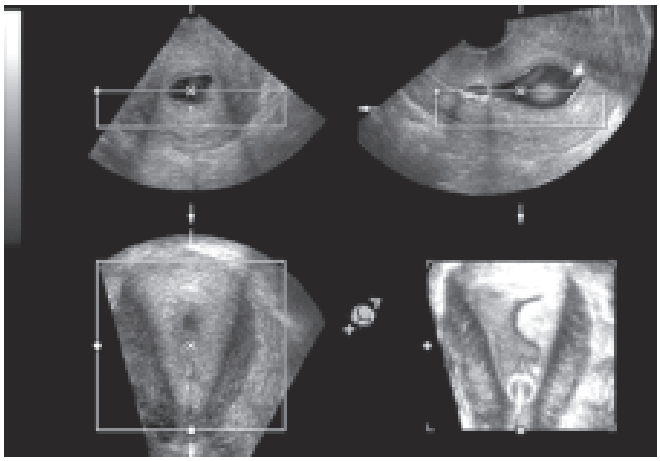

Figure 52.12: Three-dimensional saline infusion sonography of an endometrial polyp protruding into the uterine cavity (lower right image)

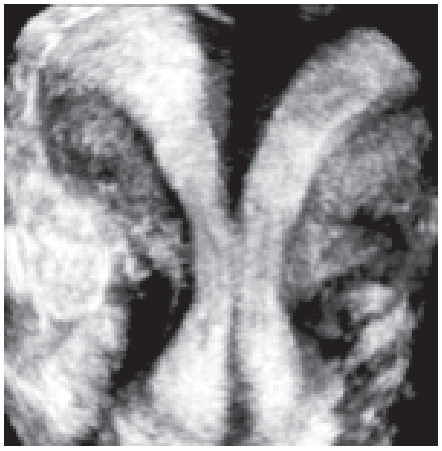

Figure 52.13: Duplication anomaly of the uterus demonstrated in frontal reformatted section

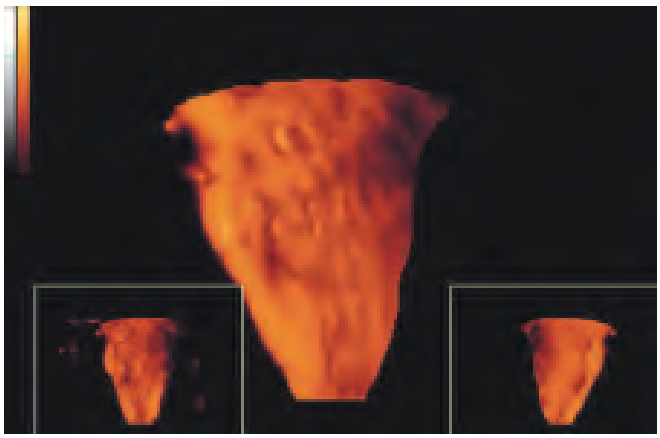

Figure 52.14: Three-dimensional power Doppler image of normal uterine cavity following injection of echogenic contrast medium. This modality facilitates visualization of the normal uterine cavity shape in frontal plane and by surface rendering

orthogonal planes on a screen allows free scrolling of an endless amount of frames through the volume of interest. The coronal or "c" plane view allows more detailed analysis of the uterus and, for the first time, the endometrial cavity between the uterine angles can be visualized. Translation or rotation can be carried out in one plane while maintaining the perpendicular orientation of all three. The images produced by transvaginal ultrasound are superior to those produced by transabdominal ultrasound because vaginal transducers are in closer proximity to the tissues.[37] Because of that, higher frequencies are used and artifactual echoes caused by multiple reflections from intervening tissues are minimized.

Demonstration of the coronal plane is mandatory for the diagnosis of uterine pathology, such as endometrial polyps **(Fig. 52.12)** or duplication anomalies of the uterus **(Fig. 52.13)**. Also, this plane provides the most exact measurement of the endometrial width when transected in a mid perpendicular manner. During 3D saline infusion sonography the typical triangulated uterine cavity appears in its full shape[38] **(Fig. 52.14)**. Surface rendering and maximal/minimal or X-ray renderings provide even more information on the uterine findings, such as mapping of the fibroids and localization of the endometrial polyp(s) **(Fig. 52.12)**. There are two techniques to accomplish this goal: "native" approach, and the use of echogenic contrast medium that is especially useful for demonstration of the uterine cavity shape. Due to its dual consistency the uterus is an excellent ultrasonic medium. Endometrium and myometrium have different acoustic impedance, which permits visualization of the size and shape of the uterus and its cavity. However, contrast medium may be mandatory in cases where a thin

endometrium or pathologic content of the uterine cavity precludes its visualization.

Similarly to B-mode and color Doppler Hy-Co-Sy, the negative contrast medium (normal saline), is used for demonstration of the entire uterine cavity, its shape, pathology, and the frame of the myometrial mantel, whereas for demonstrating the permeability of the fallopian tubes a positive contrast medium (Echovist) is used.

Weinraub and Herman[38] were the first to report on the uterine cavity assessment by 3D saline infusion sonography. Using three perpendicular planes on one screen, where the left upper plane is coronal and is termed "a", the right upper plane is sagittal and is termed "b", and the left lower plane is transverse and is termed "c" one can detect numerous causes of infertility. Looking at the fundal region in "a" it is very important not to overlook a small indentation, typical of arcuate uterus. The maximal endometrial width could be easily measured in sagittal plane. Clear concavity in the middle of the uterine fundus indicates a bicornuate uterus.

The same method is very useful for evaluation of the intracavitary pathologies, such as adhesions, submucosal and intracavitary leiomyomas, endometrial polyps, endometrial carcinoma or location of intrauterine devices (IUDs). Saline infusion sonography with 3D surface rendering is particularly useful in evaluation of the patients with abnormal endomentrial thickening and submucosal fibroids.[38]

There are numerous technical difficulties in visualization of the fallopian tubes by 2D Hy-Co-Sy.[37]. Due to its tortuosity, tubes are rarely seen completely in a single scanning plane and the echo-contrast medium is, therefore, observed in small sections. The position of the tube is very variable and distended bowel may prevent the visualization of the distal parts of the tubes. In most patients only the tubal ostia and proximal parts of the tubes are visualized by gray-scale 2D ultrasound imaging. Free spread of the dye is frequently difficult to visualize because of the surrounding bowel, which also produces strong echogenic signals. Instead of visualizing the echo contrast with gray-scale ultrasound Sladkevicius and colleagues[39] used 3D power Doppler technology sensitive to slow flow. The aim of their study was to evaluate the feasibility of three-dimensional power Doppler imaging (3D-PDI) in the assessment of the patency of the fallopian tubes during Hy-Co-Sy procedure. Hy-Co-Sy using contrast medium Echovist was performed on 67 women, and findings on the 2D gray-scale scanning and 3D PDI were compared. The first technique was used to visualize the positive

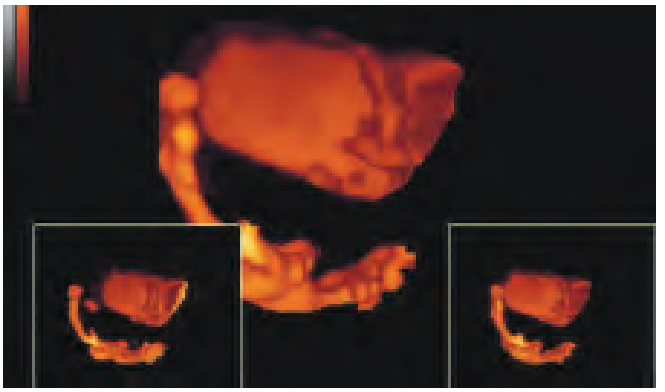

Figure 52.15: Three-dimensional power Doppler Hy-Co-Sy enables simultaneous analysis of the uterine cavity and tubal patency

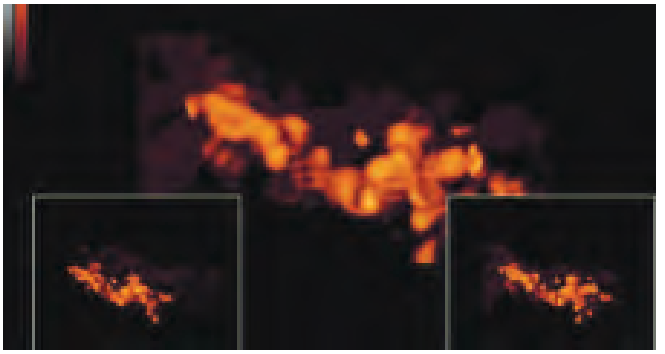

Figure 52.16: Three-dimensional power Doppler image of the entire tubal length and spillage of the contrast medium through the fimbrial end as demonstrated by echo-enhanced 3D power Doppler Hy-Co-Sy

contrast in the fallopian tube, while the second demonstrated flow of medium through the tube. Using 3D-PDI patent tubes were demonstrated as prominent color coded signals **(Figs 52.15 and 52.16)**. Using this technique, free spill from the fimbrial end of the fallopian tubes was demonstrated in 114 (91%) tubes, and in 58 (46%) of the tubes using conventional (2D) Hy-Co-Sy. The mean duration of the imaging procedure was significantly decreased for 3D-PDI, but the operator time, which included post-procedural analysis of the stored information, was similar. A significantly lower volume of contrast medium (5.9 +/- 0.6 mL) was used for 3D-PDI Hy-Co-Sy in comparison with conventional 2D HyCoSy (11.2 +/- 1.9 mL). The authors concluded that color-coded 3D-PDI with surface rendering allows visualization of the flow of the contrast medium through the entire tubal length. Using the same technique in majority of cases, the operator can assess the free spillage of the contrast into the cul-de-sac. The 3D-PDI Hy-Co-Sy appeared to have advantages over the

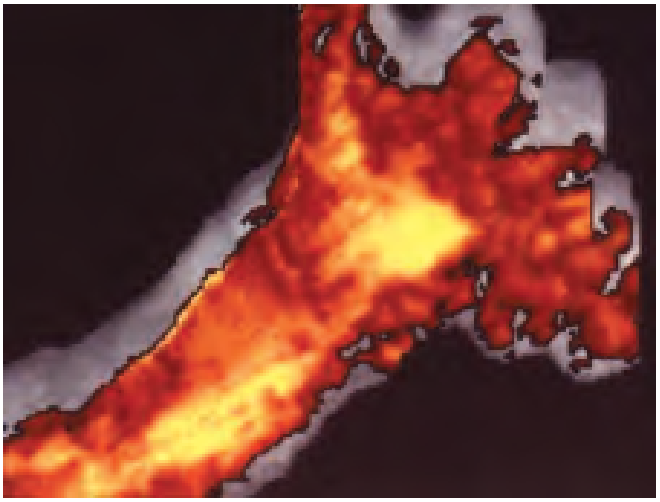

Figure 52.17: Regular spillage of the contrast medium following 3D power Doppler Hy-Co-Sy

conventional technique, especially in terms of visualization of the free spill from the distal end of the tube, which was achieved twice as often with the 3D ultrasound modality **(Fig. 52.17)**. Although the design of the investigation did not allow the side effects of the two techniques to be compared, the shorter duration of the imaging and lower volume of the contrast medium used suggested that the 3D-PDI Hy-Co-Sy may have a better side-effect profile. Also, the 3D-PDI Hy-Co-Sy allowed better storage of the information for re-analysis and archiving than conventional 2D method.

Ayida and colleagues[40] compared conventional 2D and 3D ultrasound scanning of the uterine cavity with and without saline contrast medium. Two dimensional ultrasound scanning suggested cavity abnormalities in 4 of 10 women (three fibroids and one hyperechoic thick endometrium). The 3D scanning confirmed these and revealed one additional abnormality suggestive of a uterine septum. The 2D scanning with saline injection diagnosed abnormalities in 5 of 10 patients (one uterine septum, three fibroids and one endometrial polyp). In this study, 3D contrast scanning with saline did not add any further information to 2D contrast scanning with saline. Weinraub and colleagues[41] have demonstrated the feasibility of combined 3D ultrasound and saline contrast hysterosonography. Since volume sampling has a short pick-up time of a few seconds, the examination is over almost immediately after the uterus is reasonably distended. In such an uncomfortable examination this type of advantage should not be underestimated. Evaluation of the uterine cavity at a later time allows the operator to manipulate the data at leisure and scrutinize findings in desired planes, which were not available during the initial examination. Simultaneous display of the three perpendicular planes offers a more comprehensive overview of the examined area and gives access to planes unobtainable by conventional 2D examination. Surface rendering may confirm the presence of pathological findings in equivocal cases and characterize their appearance, size, volume and relationship to the surrounding structures. Surface rendering of the polypoid structures shows echogenic masses on a pedicle protruding into the uterine cavity. Submucosal fibroids appear as mixed echogenic sites bulging into the cavity. Intrauterine synechiae appear as bands of varying thickness traversing the uterine cavity. This can be useful when deciding on treatment options, such as conservative management versus surgery and can be a valuable tool in surgical procedures carried out under ultrasonographic guidance.

Kiyokava and colleagues[42] evaluated 25 unselected infertile patients for tubal patency and uterine cavity morphology by 3D Hy-Co-Sy with saline as a contrast medium. The efficacy of the procedure was compared with X-ray HSG as a reference. The positive predictive value, negative predictive value, sensitivity and specificity of predicting tubal patency by 3D Hy-Co-Sy were 100%, 33.3%, 84.4% and 100% respectively. Using 3D Hy-Co-Sy, the full contour of the uterine cavity was depicted in 96% of cases and 64% by X-ray HSG ($P < 0.005$). The uterine cavity area measured by 3D Hy-Co-Sy correlated well with the volume of contrast medium required on HSG. Also, 3D Hy-Co-Sy allowed better assessment of the uterine cavity and tubal patency. In addition, reduced examination time and better tolerance by the patients minimized the need for sedation or anesthesia. Thus, a 3D Hy-Co-Sy with saline as a contrast medium is feasible and could comprise a routine outpatient procedure in the initial evaluation of infertile patients.

Unterweger and colleagues[43] introduced a new method, three-dimensional dynamic magnetic resonance – hysterosonosalpingography (3D dMR-HSG) for imaging of the uterine cavity and fallopian tube patency. The authors used MR imaging to assess the visualization of the fallopian tubes following injection of a higher viscosity contrast solution, 20 ml of gadolinium-polyvidone. Three-dimensional dynamic magnetic-resonance –HSG may represent a new and promising imaging approach to female infertility patients, primarily because of the avoidance of the ovarian exposure to ionizing radiation. Use of a higher viscosity MR-contrast agent allowed clear visualization of the uterine cavity and fallopian tube patency and morphology.

During the course of last five years 3D ultrasound became more and more utilized for evaluation of tubal patency. Report by Chan and colleagues[44] quotes the sensitivity, specificity, positive and negative predictive values of 3D Hy-Co-Sy in detecting tubal patency of 100%, 67%, 89% and 100%. In their recent study Kupesic and Plavsic[45] analyzed 152 women by 2D B-mode, color and pulsed Doppler Hy-Co-Sy and 116 other women using 3D B-mode and power Doppler Hy-Co-Sy. The diagnostic performance (sensitivity, specificity, PPV and NPV) of 2D and 3D Hy-Co-Sy were assessed and compared to hysteroscopy, and laparoscopy and dye test in the assessment of uterine abnormalities and tubal patency. The sensitivity, specificity, PPV and NPV of 2D hysterosonography compared to hysteroscopy were 93.6%, 97.3%, 98.2% and 97.3% respectively. The sensitivity, specificity, PPV and NPV of 3D hysterosonography compared to hysteroscopy were 97.9%, 100%, 97.9% and 100 % respectively. Addition of color and pulsed Doppler to 2D Hy-Co-Sy and power Doppler to 3D Hy-Co-Sy contributed to diagnostic precision in detection of tubal patency. The sensitivity, specificity, PPV and NPV of 3D power Doppler Hy-Co-Sy in detection of tubal patency compared to laparoscopy and dye intubation were 100%, 99.1%, 99.2% and 100% respectively.[45] The authors concluded that 3D Hy-Co-Sy was less time consuming than 2D Hy-Co-Sy, since measurements, reconstruction of planes of interest and surface rendering could be performed off-line. Furthermore, half a dose of the contrast medium was needed for 3D B-mode and power Doppler Hy-Co-Sy. By shortening the procedure and using less contrast medium the discomfort to the patients was significantly reduced. Clearly, smaller contrast volume and slower injection rate have reduced the intraluminal pressure and pain due to the cornual and tubal spasm. The 2D and 3D Hy-Co-Sy significantly decreased the cost in comparison with laparoscopy, since it can be done on an outpatient basis. Clearly, Hy-Co-Sy performed by 3D US is a superior screening method for evaluation of infertile patients.[46] Screening positives should be directed to operative hysteroscopy and/or laparoscopy.

A new automated 3D coded contrast imaging software (3D CCI by GE may aid to diagnostic accuracy of 3D Hy-Co-Sy.[47] This special ultrasound technology that emits an ultrasound beam of a selected frequency and receives a narrow band of harmonic signal avoids the overlap between the tissue and contrast response. The CCI software optimizes the use of ultrasound contrast medium by means of low acoustic pressure.

CONCLUSION

Color Doppler and 3D Hy-Co-Sy are safe and efficacious methods for evaluation of fallopian tube patency without exposure to contrast dyes or radiation. Three-dimensional technique offers the possibility of simultaneous presentation of the uterine cavity and the corresponding tube. Transvaginal 3D ultrasound examination time is not less than that needed for 2D sonography, but some parts of the examination, like measurements, reconstruction of the planes of interest and surface rendering can be performed off-line. The acquired volumes of the most appropriate planes of interest can be stored on removable hard disk for additional re-evaluation and documentation. Ultrasonic tomography can be performed using one panel control, producing parallel sections in increments of less than 1 mm. The ability of 3D ultrasound systems to produce serial scans that can be stored for subsequent analysis, 3D reconstruction, accurate assessment of volume, and coronal plane with more detailed analysis of the uterus and endometrial cavity between uterine angles is superior to conventional 2D ultrasound.

In conclusion, Hy-Co-Sy performed either by 2D or 3D US is superior screening method for evaluation of the infertile patients. Screening positives should be directed to operative hysteroscopy and/or laparoscopy.

REFERENCES

1. Hill ML. Infertility and reproductive assistance. In Neiberg DA, Hill LM, Bohm-Velez M, Mendelson EB (eds.) Transvaginal Ultrasound. St. Louis: Mosby Year Book; 1992. pp. 43-6.
2. Arronet GM, Aduljie SY, O'Brien IR. A 9-year survey of Fallopian tube dysfunction in human infertility: diagnosis and therapy. Fertil Steril. 1969 20, 903-18.
3. Page H. Estimation of the prevalence and incidence of infertility in a population: a pilot study. Fertil Steril. 1989;71:571-4.
4. Kerin JF, Williams DB, San Roman GA, et al. Falloposcopic classification and treatment of Fallopian tube disease. Fertil Steril. 1992;57:731-5.
5. Thurmond AS, Rosch J. Non-surgical Fallopian tube recanalization for treatment of infertility. Radiology. 1990;174:371-4
6. Peters JA, Coulam CB. Hysterosalpingography with color Doppler ultrasonography. Am.J.Obstet.Gynecol. 1991;164: 1530-2.
7. Volpi E, Zuccaro A, Patriarca S, et al. Transvaginal sonographic tubal patency testing air and saline solution as contrast media in a routine infertility clinic setting. Ultrasound Obstet.Gynecol. 1996;7:43-8.

8. Stern J, Peters AJ, Coulam CB. Color Doppler ultrasonography assessment of tubal patency: a comparison study with traditional technique. Fertil Steril. 1992;58:897-900.
9. Kupesic S. and Kurjak, A. (1994). Gynecological vaginal sonographic interventional procedures – what does color add? Gynecol.Perinatol., 3, 57-60
10. Deichert U, Schlief R, van de Sandt M, et al. Transvaginal hysterosalpingo-contrast sonography for the assessment of tubal patency with gray scale imaging and the additional use of pulsed wave Doppler. Fertil.Steril. 1992;57:62-7.
11. Rubin I. Differences between the uterus and tubes as a cause of oscillations recorded during uterotubal insufflation. Fertil Steril. 1954;5:147-53.
12. Nannini R, Chelo E, Branconi F, et al. Dynamyc Echohysteroscopy. A new diagnostic technique in the study of female infertility. Acta Europ.Fertil. 1981;12:165-71.
13. Richman TS, Viscomi GN, deCherney A, et al. Fallopian tubal patency assessed by ultrasound fluid injection. Radiology. 1984;152:507-10.
14. Randolph JR, Ying YK, Maier DB, et al. Comparison of real-time ultrasonography, hysterosalpingography and laparoscopy/hysteroscopy. Fertil Steril. 1986;46:828-32.
15. Davison GB, Leeton J. A case of female infertility investigated by contrast-enhanced echogynecography. J.Clin.Ultrasound. 1988;16:44-7.
16. Allahbadia GN. Fallopian tubes and ultrasonography. The Sion experience. Fertil Steril. 1992;58:901-7.
17. Broer KH, Turanli R. Überprüfung des Tubenfaktors mitels Vaginalsonographie. Ultraschall Klin.Prax. 1992;7:50-3.
18. Bonilla-Musoles F, Simón C, Sampaio M, et al. An assessment of Hysterosalpingosonography (HSSG) as a diagnostic tool for uterine cavity defects and tubal patency. J.Clin.Ultrasound. 1992;20:175-81.
19. Deichert U, Schlief R, van de Sandt M, et al. Transvaginal hysterosalpingo-contrast sonography (Hy-Co-Sy) compared with conventional tubal diagnostics. Hum.Reprod. 1989;4:418-22.
20. Tüfekci EC, Girit S, Bayirli MD, et al. Evaluation of tubal patency by transvaginal sonosalpingography. Fertil Steril. 1992;57, 336-40.
21. Gramiak R, Shah PM. Echocardiography of the aortic root. Invest.Radiol. 1968;3:356-66.
22. Testa AC, Ferrandina G, Fruscella E, et al. The use of contrasted transvaginal sonography in the diagnosis of gynecologic diseases: a preliminary study. J Ultrasound Med. 2005;24:1267-78.
23. Lanzani C, Savasi V, Leone FPG, et al. Two-dimensional HyCoSy with contrast tuned imaging technology and a second generation contrast media for the assessment of tubal patency in a infertility program. Fertil Steril. 2009;92: 1158-61.
24. Schlief R. Ultrasound contrast agents. Radiology. 1991;3: 198-207.
25. Deichert U, van de Sandt M. Transvaginal hysterosalpingo-contrast sonography (Hy-Co-Sy). The assessment of tubal patency and uterine abnormalities by contrast enhanced sonography. Advances in Echo-Contrast. 1993;2:55-8.
26. Ayida G, Chamberlain P, Barlow D, et al. Uterine cavity assessment prior to in vitro fertilization: comparison of transvaginal scanning, saline contrast hysterosonography and hysteroscopy. Ultrasound Obstet. Gynecol. 1997;10: 59-62.
27. Peters JA, Stern JJ, Coulam CB. Color Doppler hysterosalpingography. In Jaffe R, Warsof SL (Eds). Color Doppler in Obstetrics and Gynecology. New York: McGraw Hill; 1992. pp.283-8.
28. Groff TR, Edelstein JA, Schenken RS. Hysterosalpingography in the preoperative evaluation of tubal anastomosis candidates. Fertil Steril. 1990;53:417-20.
29. Heikkinen H, Tekay A, Volpi E, et al. Transvaginal salpingosonography for the assessment of tubal patency in infertile women: methodological and clinical experiences. Fertil Steril. 1995;64:293-8.
30. Jeanty P, Besnard S, Arnold A, et al. Air contrast sonohysterography as a first step assessment of tubal patency. J Ultrasound Med. 2000;19(8):519-27.
31. Battaglia C, Artini PG, D'Ambrogio G, et al. Color Doppler hysterosalpingography in the diagnosis of tubal patency. Fertil Steril. 1996;65:317-22.
32. Boudghene FP, Bazot M, Robert Y, et al. Assessment of Fallopian tube patency by HyCoSy: comparison of a positive contrast agent with saline solution. Ultrasound. Obstet. Gynecol. 2001;18(5):525-30.
33. Allahbadia GN. Fallopian tube patency using color Doppler. Int.J.Gynecol.Obstet. 1993;40:241-4.
34. Balen FG, Allen CM, Siddle NC, et al. Ultrasound contrast hysterosalpingography – evaluation as an outpatient procedure. Br.J.Radiol. 1993;66:592-9.
35. Sueoka K, Asada H, Tsuchiya S, et al. Falloposcopic tuboplasty for bilateral tubal occlusion. A novel infertility treatment as an alternative for in-vitro fertilization? Hum. Reprod. 1998;13:71-4.
36. Raga F, Bonilla-Musoles F, Blanes J, et al. Congenital Müllerian anomalies: diagnostic accuracy of three-dimensional ultrasound. Fertil Steril. 1996;65:523-8.
37. Kyei-Mensah A, Zaidi J, Pittrof R, et al. Transvaginal three-dimensional ultrasound: accuracy of follicular volume measurements. Fertil Steril. 1996;65:371-6.
38. Weinraub Z, Herman A. Three-Dimensional Hysterosalpingography. In Merz E (Ed). 3-D Ultrasonography in Obstetrics and Gynecology. Philadelphia: Lippincott Williams and Wilkins; 1998. pp.57-64.
39. Sladkevicius P, Ojha K, Campbell S, et al. Three-dimensional power Doppler imaging in the assessment of fallopian tube patency. Ultrasound Obstet Gynecol. 2000;16(7):644-7.
40. Ayida G, Kennedy S, Barlow D, et al. Conventional sonography for uterine cavity assessment: a comparison of conventional two-dimensional with three-dimensional transvaginal ultrasound; a pilot study. Fertil Steril. 1996;66:848-50.
41. Weinraub Z, Maymon R, Shulman A, et al. Three-dimensional saline contrast hysterosonography and surface rendering of uterine cavity pathology. Ultrasound Obstet.Gynecol. 1996;8(4):277-82.
42. Kiyokawa K, Masuda H, Fuyuki T, et al. Three-dimensional hysterosalpingo-contrast sonography (3D-HyCoSy) as an outpatient procedure to assess infertile women: a pilot study. Ultrasound. Obstet. Gynecol. 2000;16(7):648-54.

43. Unterweger M, De Geyter C, Fröhlich JM, et al. Three-dimensional dynamic MR-hysterosalpingography; a new, low invasive, radiation-free and less painful radiologic approach to female infertility. Hum Reprod. 2002;17(12): 3138-41.
44. Chan CC, Ng EH, Tang OS, et al. Comparison of 3-D hysterosalpingo-contrast-sonography and diagnostic laparoscopy in the assessment of tubal patency for the investigation of subfertility. Acta Obstet Scand. 2005;84: 909-13.
45. Kupesic S, Plavsic MB. 2D and 3D hysterosalpingo-contrast-sonography in the assessment of uterine cavity and tubal patency. Eur J Obstet Gynecol Reprod Biol. 2007;133(1):64-9.
46. Watermann D, Denschlag D, Hanjalic Beck A, et al. Hysterosalpingo-contrast-sonography with 3-D ultrasound — a pilot study. Ultraschall Med. 2004;25:367-72.
47. Exacoustos C, Zupi E, Szabolcs B, et al. Contrast tuned imaging and second generation contrast agent Sono-Vue: a new Ultrasound approach to evaluate Tubal Patency J Minim Invasive Gynecol. 2009;16:437-44.

53
CHAPTER

Guided Procedures Using Transvaginal Sonography

Sanja Kupesic Plavsic, Nadah Zafar, Asim Kurjak

INTRODUCTION

With the recent advances in transvaginal ultrasonographic equipment, settings and techniques, guided procedures using transvaginal sonography, in many cases have replaced invasive abdominal procedures.

In 1974, Smith and Bartrum first to use ultrasound-guided invasive procedures for both diagnostic and therapeutic goals.[1] They performed percutaneous aspiration of intrabdominal abscesses. Gerzof et al. used sonography to place an abdominal catheter in order to drain purulent collections.[2,3] The advantages of these procedures over surgery include ease of procedural performance, accurate needle placement, rare injury to adjacent organs and low cost, shorter time of the procedure, portability and patient comfort. The complications although rare include: bleeding, infection, unintentional organ puncture and in the case of a fetal reductions, miscarriage.

When puncture procedures are performed abdominally, one of two techniques is employed: guided needle or free hand. When puncture procedures are performed transvaginally, mobility of the probe is limited making the free hand approach more difficult. A fixed needle guide attached to the probe shaft facilitates easier visualization of the entire length of the needle within the scanning plane and better control for the exact placement of the needle. Recently developed automated puncture devices attached to the shaft of the vaginal probe, provides extreme accuracy and precision. While its high velocity release makes the procedure virtually painless thus no anesthesia or analgesia is required. This technique was first used for ovum retrieval during assisted reproductive technology programs, but it was quickly abandoned secondary to the need for reloading and reshooting for each new follicle aspirated. The automated puncture device is crucial when extreme accuracy is needed for any needle placement that is controlled and guided by a transvaginal probe. A manual needle introduction is less accurate and more painful because of the slower forward motion of the needle displacing mobile targets rather than penetrating them.

The punctures are usually performed with the guidance of a 5.0–7.5 MHz vaginal transducer probe through a needle guide that is attached to the shaft of the probe. A software-generated fixed “biopsy guided line” is displayed on the ultrasound monitor screen, which marks the path of the entering needle. Needle gauges ranging from 14–21 are employed. Depending on the nature of the procedure, the narrowest possible needle able to perform the desired task should be used. For better imaging, the “zoom” feature of the equipment should be used as frequently as possible. After the initial withdrawal of the needle, the pelvic structures and cul-de-sac must be observed sonographically for approximately ten minutes and rescanned after a two to three hour period of observation to check for internal bleeding or previously undetected complications.

TRANSVAGINAL PUNCTURE PROCEDURES

This chapter will be describing the more commonly performed transvaginally directed punctures such as:

- Transvaginal oocyte retrieval
- Ovarian cyst aspiration
- Drainage of pelvic abscesses
- Multiembryo reduction
- Culdocentesis
- Obstetrical implications
- Treatment of ectopic pregnancy.

Transvaginal Oocyte Retrieval

For this procedure, experience has shown that the transvaginal technique using a needle guided transvaginal probe is superior to all other ultrasound-guided techniques.[4]

The proximity of the transducer to the pelvic organs makes possible the use of a high frequency probe, thereby enhancing the resolution and clinical efficiency. The elastic vault of vagina allows for better proximity to the ovaries by the increased pressure on the tip of the probe. Since, there is no need for full a urinary bladder, the pelvic anatomy is undistorted and the ovaries are kept beyond the focal zone of the transducer. Obesity or adhesions do not significantly inhibit the visualization of the follicles and are not contraindications for this technique.

Standardized programmed stimulation is monitored by transvaginal sonography.[5] Additional information may be obtained by hormonal estimation and color Doppler studies[6-8] of the ovarian and uterine circulation.

The entire treatment is carried out in an outpatient setting. The patient is placed on a gynecological table in the lithotomy position. Although, anesthesia and sedative agents are not being utilized in approximately 50% of *in vitro* fertilization (IVF) programs,[9] sedative medication, such as Flunitrazepam, Droperidol and Pentazocine, may still be used. Since the mean duration of oocyte retrieval is ten minutes, most of the patients easily tolerate the procedure. However, the operator should be aware of possible changes in vital signs and discomfort experienced by some patients. Before inserting the probe into the cover, the operator should apply the ultrasonic coupling gel. The cover which is either a sterile condom, surgical rubber glove or specially produced rubber cover is stretched over the gel to expel the air from the tip of the probe. This better prevents artifacts during the procedure. The gel or lubricant should not be used while inserting the probe because of spermicidal action and reported embryotoxicity[10] of the gel. Instead, one can use physiologic saline or a culture medium. Sterile needle guides are used for the transvaginal puncture of the follicles. A sterile cover is applied on to the keyboard of the ultrasound machine, which enables the operator to make any readjustments under sterile conditions. The patient's legs and perigenital area are then covered using the sterile drapes. The vaginal probe is inserted into the vagina after cleaning the vagina with isotonic saline or a cultured medium.

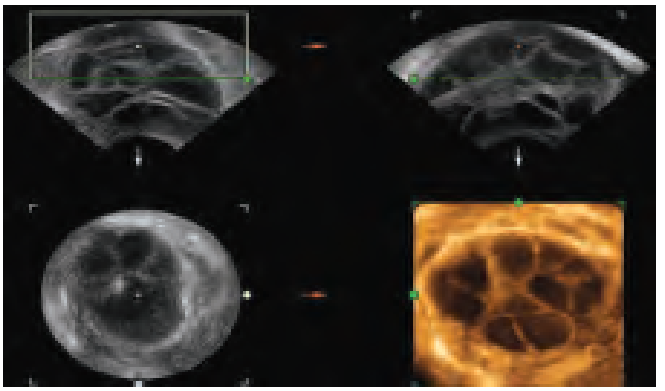

Figure 53.1: Transvaginal three-dimensional ultrasound scan of a hyperstimulated ovary at the time of guided aspiration of the oocytes. Note the tip of the needle within the follicle in C plane

An automatic puncturing device has been developed in order prevent potential risks of puncture procedures. This device contains a mobile metal tube, a needle carrier into which the aspiration needle is inserted and locked into place by a twisting movement.[4] Before inserting the probe into the vagina with a puncture device, the device should be loaded and secured. After insertion, a detailed ultrasound examination is performed to locate the uterus and the ovaries. The probe is directed to allow the biopsy vector to be placed to the central part of the nearest follicle indicating the direction of the needle **(Fig. 53.1)**. The operator calculates the distance of the biopsy vector on the screen and "shoots" the follicle either automatically using a depth limiting screw on "shooting device" or manually. After the needle is rapidly advanced into the follicle, the operator begins to suction the tubing connected with the suction pump. As the follicular fluid is aspirated, one can see the follicle collapsing, while the follicular fluid is pulled into the collecting chamber.[4] A flushing procedure may be employed to improve the retrieval rate of the aspirated oocytes. The flushing medium which contains heparin is injected through the tubing or by using an automated flushing system. All the follicles along the same line are aspirated without withdrawing the needle. Feichtinger et al.[11] reported a low incidence of

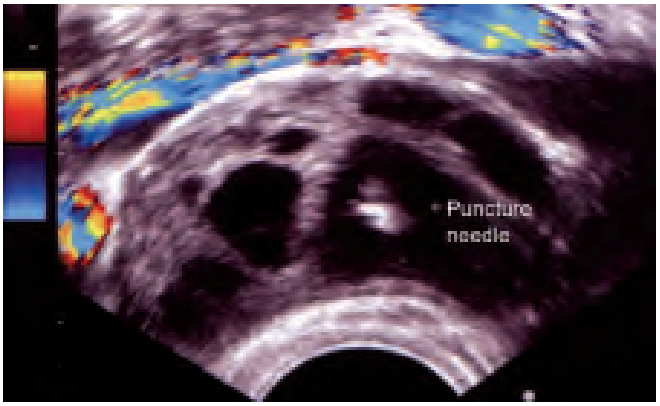

Figure 53.2: Transvaginal color Doppler scan of the ovary during an aspiration procedure. The tip of the needle is advanced into the proximal follicle. The iliac vessels are clearly displayed using color Doppler facility

complications while using the transvaginal technique for oocyte recovery. In 2.4 % of patients iliac veins were confused for a follicle and were mistakenly punctured. In all cases, bleeding into the pouch of Douglas was detected on the ultrasound screen and stopped spontaneously. One observation made was that a full bladder may exert pressure on the site and therefore, stop the bleeding. Color Doppler can easily prevent such a complication, since the iliac vessels are easily visualized using this technique **(Fig. 53.2)**.

The bleeding from the vaginal vault is easily detectable and can be stopped by compression. Pelvic inflammatory disease (PID) is a rare complication of a transvaginal follicle aspiration and is reported in 0.14% of the patients.[9] The disease was mostly caused by infected semen and occurred in patients with a positive history of PID.

Damario[12] reported a case of 26-year-old patient with Müllerian agenesis who underwent a controlled ovarian hyperstimulation, a transabdominal-transperitoneal ultrasound-guided oocyte retrieval and an embryo transfer of two cleavage-stage embryos to the gestational carrier (a 44-year-old woman) resulting in a twin pregnancy. For various reasons, patients with Müllerian agenesis may not be candidates for standard transvaginal ultrasound-guided oocyte retrieval. Although, laparoscopic oocyte retrieval has been frequently used in this setting, the approach of transabdominal-transperitoneal ultrasound-guided oocyte retrieval may offer further advantages in selected cases.

Feichtinger[13] evaluated the possibility of performing follicle puncturing procedures under three-dimensional ultrasound control close to real time using a new commercially available system **(Fig. 53.1)**. He has performed a transvaginal needle-guided aspiration of ten follicles using a newly developed ultrasound machine with a built-in rapid and powerful calculation software program for three-dimensional interactive volume and flow translation during operation. The interactive three-dimensional imaging was carried out during the aspiration of each follicle. Oocyte recovery was successful for all of the follicles. There was a mean delay of 5.00+/–1.22 seconds form coasting to resuming real-time ultrasound scanning during the interactive volume calculation and the search for the needle tip in the three-dimensional mode. This did not delay the procedure remarkably but enabled the precise localization of both the needle and its tip after each penetration. The integration of flow signals allowed an impressive color-coded demonstration of the needle within the tissue, but the delay was significantly longer for color-coded volume acquisition (18.40+/–4.56 seconds). This technique seems to be potentially useful in fetal medicine, oncology and surgery.

Intrauterine transfer of fertilized oocytes is not always performed as a sonographically guided procedure but transabdominal or transvaginal sonography is occasionally used for directing embryo transfers. A new technique of embryo transfer based on an ultrasound-guided transmyometrial puncture has been performed in 104 cases and described by Kato, et al.[14] The use of this technique is proposed to overcome problems of difficult transfers because of cervical abnormalities. Thirty-eight patients conceived with a clinical pregnancy rate of 36.5% per attempt. No serious complications were observed. Tubal catheterization is a diagnostic and therapeutic technique of diagnosing tubal patency via injecting and observing fluid passage into the pelvis. The fallopian tubes can be reached using a transvaginally guided catheter introduced into the cervix. In the same way, fertilized ova may be carried into the ampullary portion of the tube.

Ovarian Cyst Aspiration

Transvaginal guidance permits direct visualization and aspiration of persistent follicular cysts[11] **(Fig. 53.3)**. Such cysts may impair folliculogenesis due to release of hormones or as a result of a decreased perfusion by parenchymal compression. In the puncture of an ovarian or paraovarian cyst, the center of the cyst is targeted and the needle is inserted. Such a procedure is highly debated in the literature. The concern of cell spillage from a potentially malignant ovarian cyst into the abdominal cavity prevents many from using it more frequently. Although the aspirated fluid is submitted for a cytologic evaluation, a negative cytologic result

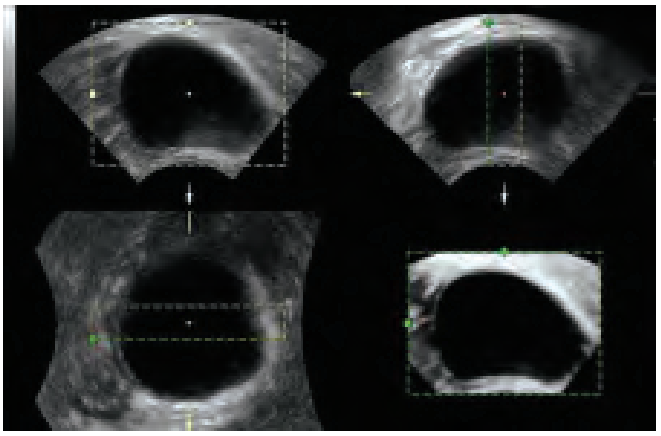

Figure 53.3: Three-dimensional ultrasound image of a simple ovarian cyst. Only cysts without papillary protrusions and septa can be treated by transvaginal ultrasound-guided aspiration

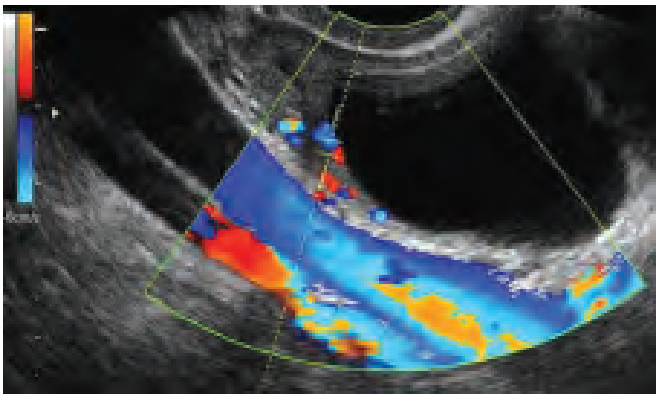

Figure 53.4: Simple ovarian cyst as seen by color Doppler ultrasound. Note the smooth surface of the cyst and extraovarian vessels, while no vascularity is detected within the cystic wall. Color Doppler may help to avoid penetration of the surrounding vessels

may sometimes represent a false negative result. The high sensitivity and specificity of the transvaginal color Doppler in differentiating between a benign and a malignant adnexal lesion seems to increase the reliability in decision-making process as to which cysts should be aspirated **(Fig. 53.4)**.

Bret et al.[15,16] published two papers describing their experience using transvaginal sonography in the aspiration of ovarian cysts. They reported a 48% recurrence rate after cyst aspiration in premenopausal patients and an 80% recurrence rate in postmenopausal women. This group attempted to prevent cyst recurrence by injecting alcohol immediately after cyst aspiration, but this procedure was successful in only four out of seven patients.[16]

The aspiration of an endometrioma is considered to be relatively contraindicated. Aboulghar et al.[17] studied 21 patients in which transvaginal sonographically guided aspiration of pelvic and endometriotic cysts was performed. Reaccumulation occurred in only six cases during a 12 months follow-up. Certainly, the aspiration of endometriotic cysts is technically simple, however, its overall benefit and safety are still inconclusive due to the lack of experience obtained by evaluating a larger series.[18] In infertility program Vaegemaekers et al.[19] aspirated 32 unilocular anechoic cysts with an average diameter of 45 mm transvaginally. The authors concluded that puncture and aspiration of ovarian cysts in the early follicular phase could diminish the cancellation rate of *in vitro* fertilization cycles.

Drainage of Pelvic Abscesses

Infertility attributed to tubal obstruction or dysfunction is seen in 30–40% of patients. It is well known that a tubal occlusion is common sequelae of PID. Since recurrent episodes of PID are frequent, one should expect a high incidence of this entity in the infertile population. In patients with a tubo-ovarian abscess, abscess drainage with sonographic guidance can hasten the recovery process and improve the efficacy of antibiotic therapy. Once the needle is placed into the abscess cavity, the fluid can be aspirated and the needle withdrawn. In addition, an indwelling drainage catheter can be left in place.[11] Teisala et al.[20] used the transvaginal ultrasound guided aspiration technique to drain 10 tubo-ovarian abscesses on patients receiving antimicrobial treatment. Only light sedation was required and the procedure was well tolerated by the patients. This technique is accepted as an alternative to open laparoscopy for treating a tubo-ovarian abscess.

Fetal Reduction

During the past 15 years, with the increased use of ovulation inducing drugs as well as the increased number of medically assisted reproduction procedures, have resulted in a large number of multiple gestations. Multiple pregnancies are associated with high mortality and morbidity rates. In addition, probability of achieving a term pregnancy with healthy neonates is inversely proportional to the number of the fetuses. Therefore, fetal reduction seeks to reduce the number of fetuses to improve survival for the remaining ones.[21] Women with four or more fetuses may be offered selective reduction, with the number of fetuses usually reduced to two.[11] The procedure is normally delayed till eight weeks, after which the spontaneous loss is relatively low. The transabdominal ultrasound guided

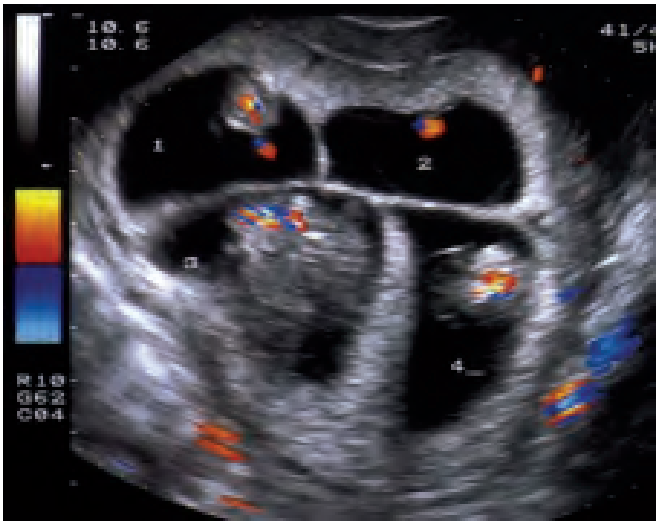

Figure 53.5: Transvaginal color Doppler scan of quadruplet pregnancy. Color Doppler enables visualization and monitoring of heart activity during the procedure of fetal reduction

technique was first presented by a French group[22] and adopted by others.[23,24] With the developing use of transvaginal sonography this approach was attempted and successfully applied in fetal reduction, as well. Advantages of this technique are shorter puncture route and a more precise needle placement which reduces the risk of inadvertent injury to the adjacent gestational sacs and or other pelvic structures. Color Doppler may aid in monitoring fetal heart activity during this interventional procedure **(Fig. 53.5)**. The brief explanation of the technique for transvaginal fetal reduction is as follows:

- Baseline mapping procedure of the chorionic sacs, detailed evaluation of the heartbeats of the targeted fetus
- Placement of the needle with 0.5–1 ml of 2 mEq/ml KCl solution.

The heartbeat of each injected fetus is observed for five to ten minutes to confirm cessation. The patients should be rescanned three hours later and then one week after the procedure. The disadvantage of a transvaginal fetal reduction is that at an early gestational age the final number of fetuses is not yet established.[18]

Coffler et al.[25] reported on their experience with 90 women who underwent early (mean 7.5 weeks gestation, range 7.0–8.0 weeks) intracardiac insertion of KCl injected into a selected fetal heart in the vicinity of a non-selected fetal heart for fetal reduction using the transvaginal sonographic approach. The procedure was associated with a total pregnancy loss rate of 11.7%. Early transvaginal fetal aspiration is a simple and relatively safe method for pregnancy reduction. The overall pregnancy loss rate associated with an early fetal aspiration is similar to that of procedures performed at a later gestational age, but is significantly lower when the initial number of fetuses is four or greater. Iberico et al.[26] reported on early transvaginal intracardiac embryo puncture until a systole is verified without the injection of any substances as an effective and safe technique. The baby take-home rate was 89.5% for twins and 80.0% for singletons.

Diagnostic Culdocentesis

The introduction of transvaginal sonography has limited the need for diagnostic culdocentesis. The presence or absence of fluid in the pelvic cavity is easily established by a vaginal approach, but it may be necessary to differentiate between different biological fluids (clear fluid, blood or pus). The wide availability of transvaginal color Doppler sonography to distinguish the dominant pelvic pathology in the presence of pelvic fluid on the basis of different vascularity patterns is very helpful in routine investigations. There are times when the clinician still requires information provided by culdocentesis despite having the knowledge acquired by the history and physical examination, the transvaginal color Doppler and the rapid β-human chorionic gonadotropin (β-hCG) test. Inserting a needle in the cul-de-sac is a simple technique that can be performed safely and accurately with transvaginal ultrasound guidance.[27] High quality β-mode transvaginal sonography with superimposed color Doppler flow allows accurate and simultaneous identification of the main pelvic vessels, physiological angiogenesis (corpus luteum) and ectopic peritrophoblastic blood flow. The color Doppler will help in the accurate placement of the needle, diminishing the risk of injury to adjacent vessels, especially in women who have had previous inflammatory disease of the pelvis with an obliterated cul-de-sac.

Obstetrical Procedures

The high frequency transvaginal probe enables a detailed analysis of embryonic, extraembryonic and early fetal structures. By this method, screening for structural anomalies can be initiated during the first and early second trimester. Recent advances in tissue culture technology have established chorionic villous sampling and early amniocentesis as early invasive diagnostic modalities. Color Doppler imaging has added important information on the functional integrity of the maternal-

fetal circulation. The main advantages of the application of color Doppler imaging is in the following invasive transvaginal diagnostic techniques such as:

Chorionic Villous Sampling

The diagnostic accuracy and safety of chorionic villous sampling are nearly the same as those of amniocentesis. Chorionic villous sampling is generally performed with transabdominal ultrasound guidance, with either a catheter placed through the cervix or a needle placed percutaneously through the abdominal wall. The transvaginal route, in which the needle is placed through the vaginal and uterine wall, is usually performed at a gestational age of 8–12 weeks. The ultrasound-guided transmural puncturing procedure promises to be the most accurate and the least traumatic and painful method. The small depth of penetration under high-resolution ultrasound guidance is the most striking advantage of this method. Color Doppler allows precise sonographic imaging of the placental site by visualization of the umbilical cord and its insertion.

Early Amniocentesis

Using a transvaginal approach and directed needle it is possible to aspirate the amniotic fluid as early as nine weeks of gestation. The advantages of early amniocentesis are clear images, patient preference for early amniocentesis over chorionic villous sampling and availability of chromosome analysis and amniotic α-fetoprotein[28] measurement. The main complications during this procedure include fetal demise, rupture of the membranes, bleeding and infection. It seems that color Doppler could decrease the fetal loss rate by a more precise identification of the placental localization and visualization of the umbilical cord.

CONSERVATIVE MANAGEMENT OF AN ECTOPIC PREGNANCY

In the past, the diagnosis of ectopic pregnancy was made at the time of laparotomy and very often in the presence of a hemodynamically unstable patient. The physician was often left with little choice but to perform a salpingectomy, salpingo-oophorectomy or segmental resection of the fallopian tube. At that time, the physician's main concern was to save the patient's life and the potential preservation of the affected fallopian tube was a secondary concern. More recently, by using sensitive pregnancy tests and transvaginal and/or abdominal ultrasonography, it has become possible to diagnose an ectopic pregnancy at such an early stage that currently less radical surgical therapies in addition to medical therapies are being used as the preferred treatment.

The use of a needle, which is inserted into a tubal pregnancy under transvaginal ultrasound guidance, can save a patient from a more invasive procedure. Feichtinger was the first to describe the use of transvaginally guided needle puncture to treat the ectopic tubal gestation.[29] Since then several centers have used this modality as an additional tool in treatment of patients with an ectopic pregnancy.[28,30-33] One complication that may occur is concurrent or delayed hemorrhaging. Fortunately, this is a very uncommon event and generally occurs during the first one or two days post procedure in approximately 15% of patients.[28] Other complications include a persistence of the trophoblastic tissue within the fallopian tube and a persistent elevation of the hCG levels following the procedure. Many of these cases can be treated in a non-surgical fashion, using the systemic administration of methotrexate.[34] Systemic use of methotrexate has been documented to be safe, effective and well tolerated.[34,35] Preliminary evidence suggests that the fertility potential after such a treatment is comparable to that following conservative surgery.[34-36]

Since the introduction of transvaginal sonography with color flow imaging within a high frequency probe, a more accurate and faster diagnosis of ectopic pregnancy is feasible. Color Doppler appears to be useful for the positive diagnosis of ectopic pregnancy with ultrasonography when no adnexal gestational sac is observed.[37] Peritrophoblastic flow is prominent, randomly dispersed inside the solid part of an adnexal mass and clearly separated from the ovarian tissue. A low impedance signal and a resistance index, usually less than 0.45 extracted from the color-coded area indicates an invasive trophoblast. The clinical impression of probable tubal abortion is seen in patients when with no color flow or an increased vascular resistance of the peritrophoblastic flow and a β-hCG level less than 1000 IU/ml. Using Doppler, it is possible to identify the vitality and invasiveness of the trophoblast. These are the most important characteristics to consider when planning the management of an ectopic pregnancy.

At our department 11 patients with an unruptured ectopic pregnancy of less than 3 cm in diameter were treated locally with methotrexate. After the patient received slight sedation, the tubal pathology ("tubal ring" containing the ectopic embryo or solid part of the complex adnexal mass) was imaged. Color flow was superimposed on the anatomical structure and a pulsed Doppler waveform analysis showed low impedance (resistance index cut-off value of 0.45 or less) and a high

velocity. Using the equipment's software-generated puncture path line, the needle was introduced in the area of the maximal color signal. We administered methotrexate using the dose of 1 mg/kg of body weight, into the area of active trophoblastic flow. Determination of serum β-hCG levels and transvaginal sonography were performed every second day, until the β-hCG levels reached non-pregnant levels. Color flow imaging, with its excellent potential for tissue characterization, was used for serial determinations of blood flow from the questionable adnexa. In patients with successful salpingocentesis, serially analyzed serum levels of β-hCG returned to non-pregnant levels (n=9), while pulsed Doppler waveform analysis showed increasing values of impedance to flow. Changes in the vascularity could be correlated with the effect of the medication on the vitality and invasiveness of active ectopic trophoblastic tissue.

Based on our own experience, with regards to an ectopic pregnancy, a transvaginal color Doppler has both a diagnostic and therapeutic potential. By comparing color Doppler findings to declining β-hCG levels, it is possible to follow patients undergoing conservative treatments, safely. Serial β-hCG determinations demonstrated that in patients who underwent successful salpingocentesis, serum levels of β-hCG returned to a non-pregnant levels after 10–22 days. With the use of color flow imaging, it becomes possible to avoid puncturing through a highly vascular area hence bleeding during or immediately following the procedure is significantly reduced. In suspicious cases of tubal pregnancy in which color flow within the tube was absent and β-hCG levels were less than 1000 mIU/ml, local administration of methotrexate could not be advised.

There is still much to be learned about the diagnosis and management of an ectopic pregnancy. The transvaginal color Doppler represents an important addition in selection of patients for conservative treatment, as well as in defining the individual therapeutic strategy.

In a patient with a history of a previous cervical pregnancy who currently had a cervical pregnancy and a simultaneous intrauterine pregnancy Monteagudo et al.[38] reported a successful transvaginal ultrasound-guided puncture and injection. They treated the cervical pregnancy by selective reduction using an injection of potassium chloride guided by transvaginal sonography. A cesarean section was performed to deliver the intrauterine gestation at 34 weeks. Timor-Tritsch et al.[39] described a proposed transvaginal ultrasound-guided puncture route to be performed on a cornual ectopic pregnancy by leading the needle into the cornual ectopic pregnancy. To accomplish this procedure the needle would first be traversing the myometrium while simultaneously approaching the gestational sac from the medial aspect. The probe was rotated into a position that enables the software-generated directional puncture lines to "transect" the thick uterine myometrium before reaching the gestational sac. This line approaches the ectopic cornual pregnancy form the medial aspect and avoids the puncture of a stretched out thin myometrium. Only cornual pregnancies with positive heartbeats were considered for puncture. With the use of an automated puncture device, a 21-gauge needle was then introduced into the chorionic sac and the embryo. There was no need for analgesia because the automated spring-loaded puncture device advances the needle with a high-speed, thus making it virtually a painless procedure. The embryo is injected with methotrexate (25 or 50 mg in 1 or 2 ml solvent, respectively) or, in the case of a live heterotopic pregnancy, with potassium chloride. Half of the amount is injected into the embryo to stop the heartbeats and if possible, the balance into the placental site when the needle is extracted. After completing the procedure the puncture area is observed for approximately 5–10 minutes to detect any moderate post-procedure bleeding. The puncture injection of a cornual pregnancy is a relatively new treatment modality which seems promising because the patient may avoid surgery and the potential outcomes and risks of surgery, such as a future Cesarean section, uterine scar and a cornual rupture, during a desired future pregnancy. Approaching the cornual pregnancy with its chorionic sac, embryo and placenta form the medial aspect and traversing the thicker myometrium creates a significant and protective safety layer, through which rupture or bleeding are less likely to occur.

OTHER APPLICATIONS

Zanetta et al.[40] reported on the use of transvaginal ultrasound-guided fine needle sampling of deep cancer recurrences in the pelvis. For aspirates and biopsies, the sensitivity was 76 and 91% respectively, while the accuracy was 83 and 91% respectively. This technique is a safe procedure with limited invasiveness and extremely high specificity even when performed on small targets (the median diameter in this study was 30 mm). Whenever possible, biopsies are preferred. A negative fine needle biopsies obtained from a clinically suspicious lesion requires a repeat sampling.

A recent study by Hammoud et al.[41] reported that a ultrasound-guided endometrial biopsy is a viable option for endometrial sampling in patients with a stenotic

cervix. Under control of transvaginal sonography, in two postmenopausal patients with vaginal bleeding and a failed endometrial biopsy due to a stenotic cervix, a 20-gauge needle was inserted through the vaginal vault and anterior uterine wall into the endometrium. The endometrium was aspirated and the specimens were submitted for cytology. One patient had an endometrial adenocarcinoma and underwent a staging procedure, while the other patient had a benign cytology and was followed clinically.

Another already reported application of transvaginal ultrasound-guided procedures is aspiration of tubo-ovarian abscesses. Gjelland et al.[42] evaluated 449 transvaginal aspiration performed on 302 women. A total of 282 (93.4%) were successfully treated by transvaginal aspiration of the purulent fluid, together with antibiotic therapy. In the remaining 20 patients, surgery was performed. The main indications for surgery were diagnostic or therapeutic uncertainty such as suspected residual tubo-ovarian abscess or pain. Sudakoff et al.[43] evaluated the techniques, patient selection, pre and post-procedural care and monitoring aspects of tranrectal and transvaginal ultrasound-guided drainage of the infected pelvic collections. A transrectal ultrasound-guided biopsy of a pelvic mass is also a feasible method of establishing a pathological diagnosis.[44]

CONCLUSION

Although ultrasound guided procedures are most commonly used in the field of reproductive assistance, it is clear that similar techniques can be applied to other clinical situations as well. The extreme accuracy and high patient tolerance have initiated the widespread use of transvaginally performed puncture procedures. The use of transabdominal and transvaginal sonography has improved the accuracy of embryo placement into the uterine cavity or via the uterus, into the fallopian tube and guidance of fallopian tube catheterization. Other ultrasound-guided procedures analyzed in this chapter are aspiration of the ovarian cysts, drainage of pelvic collections and abscesses and selective reduction of multiple pregnancies. The advantages of ultrasound-guided procedures are their performance under real-time imaging, relative simplicity and low procedure-related complication rate.

REFERENCES

1. Smith EH, Bartrum RJ. Ultrasonically guided percutaneous aspiration of abscesses. Am J Roentgenol Radium Ther Nucl Med. 1974;122(2):308-12.
2. Gerzof SG, Johnson WC, Robbins AH. Expanded criteria for percutaneous abscess drainage. Arch Surg. 1985;120(2): 227-32.
3. Gerzof SG, Johnson WC. Radiologic aspects of diagnosis and treatment of abdominal abscesses. Surg Clin North Am. 1984;64(1):53-65.
4. Feichtinger W. Transvaginal oocyte retrieval. In: Chervenak FA, Isaacson GC, Campbell S (Eds). Ultrasound in obstetrics and gynecology, London: Little Brown and Company; 1993.pp.1397-406.
5. Kemeter P, Feichtinger W. Experience with a new fixed-stimulation protocol without hormone determinations for programmed oocyte retrieval for in-vitro fertilization. Hum Reprod. 1989;4(8 suppl.):53-8.
6. Kurjak A, Kupesic S, Schulman H, Zalud I. Transvaginal color Doppler in the assessment of ovarian and uterine blood flow in infertile women. Fertil Steril. 1991;56(5): 870-3.
7. Kupesic S, Kurjak A. Uterine and ovarian perfusion during the periovulatory phase assessed by transvaginal color Doppler. Fertil Steril. 1993;60(3):439-43.
8. Kurjak A, Kupesic S. Ovarian senescence and its significance on uterine and ovarian perfusion. Fertil Steril. 1995;64(3):532-7.
9. Feichtinger W, Putz M, Kemeter P. New aspects of vaginal ultrasound in an in vitro fertilization program. Ann N Y Acad Sci. 1988;541:125-33.
10. Schwimer SR, Rothman CM, Lebovic J, et al. The effect of ultrasound coupling gels on sperm motility in vitro. Fertil Steril. 1984;42(6):946-50.
11. Hill ML, Nyberg DA. Transvaginal sonography guided procedures. In: Nyberg DA, Hill LM, Bohm-Velez M, Mendelson EB (Eds). Transvaginal Ultrasound, St. Louis: Mosby Year Book; 1992.pp. 319-29.
12. Damario MA. Transabdominal-transperitoneal ultrasound-guided oocyte retrieval in a patient with Müllerian agenesis. Fertil Steril. 2002;78(1):189-91.
13. Feichtinger W. Follicle aspiration with interactive three-dimensional digital imaging (Voluson): a step toward real-time puncturing under three-dimensional ultrasound control. Fertil Steril. 1998;70(2):374-7.
14. Kato O, Takatsuka R, Asch RH. Transvaginal-transmyometrial embryo transfer: the towako method: experiences of 104 cases. Fertil Steril. 1993;59(1):51-3.
15. Bret PM, Guibaud L, Atri M. Transvaginal US-guided aspiration of ovarian cysts and solid pelvic masses. Radiology. 1992;185(2):377-80.
16. Bret PM, Atri M, Guibaud L. Ovarian cysts in postmenopausal women: preliminary results with transvaginal alcohol sclerosis. Radiology. 1992;184(3):661-3.
17. Aboulghar MA, Mansour RT, Serour GI, et al. Ultrasonic transvaginal aspiration of endometriotic cysts: an optional line of treatment in selected cases of endometriosis. Hum. Reprod. 1991;6(10):1408-10.
18. Lerner JP, Monteagudo A. Vaginal sonographic puncture procedures. In: Goldstein SR, Timor-Tritsch, IE (Eds). Ultrasound in Gynecology, New York: Churchill Livingstone; 1995.pp.223-38.
19. Waegemaekers CT, Berg-Helder A, Blankhart A, et al. Transvaginal ovarian cyst puncture in the early follicular

phase of an IVF cycle, indications and results. Hum. Reprod. 1988;3;(1 suppl):80.
20. Teisala K, Heinonen PK, Punnonen R. Transvaginal ultrasound in the diagnosis and treatment of tuboovarian abscess. Br J Obstet Gynaecol. 1990;97(2):178-80.
21. Berkowitz RI, Lynch L. Selective reduction: an unfortunate misnomer. Obstet Gynecol. 1990;75(5):873-4.
22. Dumez Y, Oury JF. Method for first trimester selective abortion in multiple pregnancy. Contrib Gynecol Obstet. 1986;15:50-3.
23. Birnholz JC, Dmowski WP, Binor Z, et al. Selective continuation in gonadotropin-induced multiple pregnancy. Fertil Steril. 1987;48(5):873-6.
24. Brandes JM, Itskovitz J, Timor-Tritsch IE. Reduction of the number of embryos in multiple pregnancy. Fertil Steril. 1987;48(2):326-7.
25. Coffler MS, Kol S, Drugan A, et al. Early transvaginal embryo aspiration: a safe method for selective reduction in high order multiple gestations. Hum. Reprod. 1999;14(7): 1875-8.
26. Iberico G, Navarro J, Blasco L, et al. Embryo reduction of multifetal pregnancies following assisted reproduction treatment: a modification of the transvaginal ultrasound-guided technique. Hum. Reprod. 2000;15(10):2228-33.
27. Fleischer AC, Pennel RG, McKee MS, et al. Ectopic pregnancy: features and transvaginal sonography. Radiology. 1990;174(2):375-8.
28. Timor-Tritsch IE, Peisner DB, Monteagudo A. Vaginal sonographic puncture procedures. In: Timor-Tritsch IE, Rottem S (Eds). Transvaginal Sonography, New York: Elsevier; 1991.p.427.
29. Feichtinger W, Kemeter P. Conservative treatment of ectopic pregnancy by transvaginal aspiration under sonographic control and methotrexate injection. Lancet. 1987;1(8529):381-2.
30. Menard A, Crequat J, Mandelbroat L, et al. Treatment of unruptured tubal pregnancy by local injection of methotrexate under transvaginal sonographic control. Fertil Steril. 1990;54(1):47-8.
31. Egarter, C. Methotrexate treatment of ectopic gestation and reproductive outcome. Am J Obstet Gynecol. 1990;62: 406-9.
32. Brown DL, Felker RE, Stowall TG, et al. Serial endovaginal sonography of ectopic pregnancies treated by methotrexate. Obstet Gynecol. 1991;77(3):406-8.
33. Mottla GL, Rulin MC, Guzick DS. Lack of resolution of ectopic pregnancy by intratubal injection of methotrexate. Fertil Steril. 1992;57(3):685-7.
34. Stowall TG, Ling FW, Gray LA. Single dose methotrexate for treatment of ectopic pregnancy. Obstet Gynecol. 1991;77(5):754-7.
35. Fernandez H, Baton C, Lelaidier C, et al. Conservative management of ectopic pregnancy: prospective randomized clinical trial of methotrexate versus prostaglandin sulprostone by combined transvaginal and systemic administration. Fertil Steril. 1991;55:746.
36. Ory SL. Chemotherapy for ectopic pregnancy. Obstet Gynecol Clin N Am. 1991;18(1):123-4.
37. Kurjak A, Zalud I, Schulman H. Ectopic pregnancy: transvaginal color Doppler of trophoblastic flow in questionable adnexa. J Ultrasound Med. 1991;10(12):685-9.
38. Monteagudo A, Tarricone NJ, Timor-Tritsch IE, et al. Successful transvaginal ultrasound-guided puncture and injection of a cervical pregnancy in a patient with simultaneous intrauterine pregnancy and a history of a previous cervical pregnancy. Ultrasound Obstet Gynecol. 1996;8(6): 381-6.
39. Timor-Tritsch IE, Monteagudo A, Lerner JP. A "potentially safer" route for puncture and injection of cornual ectopic pregnancies. Ultrasound Obstet Gynecol. 1996;7(5):353-5.
40. Zanetta G, Brenna A, Pittelli M, et al. Transvaginal ultrasound-guided fine needle sampling of deep cancer recurrences in the pelvis: usefulness and limitations. Gynecol Oncol. 1994;54(1):59-63.
41. Hammound AO, Deppe G, Eikhechen SS, et al. Ultrasonography-guided transvaginal endometrial biopsy: a useful technique in patients with cervical stenosis. Obstet Gynecol. 2006;107(2 Pt. 2):518-20.
42. Gjelland K, Ekerhovd E, Granberg S. Transvaginal ultrasound-guided aspiration for treatment of tubo-ovarian abscess: a study of 302 cases. Am J Obstet Gynecol. 2005;193(4):1323-30.
43. Sudakoff GS, Lundeen SJ, Otterson MF. Transrectal and transvaginal sonographic intervention of infected pelvic fluid collections: a complete approach. Ultrasound Q. 2005;21(3):175-85.
44. Giede C, Toi A, Chapman W, et al. The use of transrectal ultrasound to biopsy pelvic masses in women. Gynecol Oncol. 2004;95(3):552-6.

54
CHAPTER

Ultrasound in the Postmenopause

Martina Ujevic, Biserka FundukKurjak, Boris Ujevic

INTRODUCTION

The menopause occurs because the ovary has no longer any follicles to respond to hypothalamic/pituitary stimulation. At menarche, there are some 250,000–300,000 oocytes present, which are gradually used up in the succession of menstrual cycle from menarche until around 50 years of age, which is the average age for the menopause in Europe and the United States.[1]

Climacteric defines a more prolonged period of estrogen withdrawal, starting first with the decrease in frequency of ovulation and ending in atrophy of secondary sexual characteristics. A single point in that curve, when insufficient follicle maturity results in inadequate estrogen and no menses is the menopause.[1] The postmenopausal period begins with the last menstrual bleeding (LMB).

Prior to menopause, the remaining follicles begin to perform less well. Release of the hypothalamic and the pituitary gland hormones from inhibition resulted in raised gonadotropins levels, which is a characteristic of the menopause and their level is well above those seen in the menstrual cycle at times other than the luteinizing hormone (LH) surge. Eventually, there is a 10–20 fold increase in follicle stimulating hormone (FSH) and approximately a three-fold increase in LH, reaching a maximal level 1–3 years after menopause, after which there is a gradual, but slight decline in both gonadotropins.[1]

Estrogen production by the ovaries does not continue beyond the menopause, however, estrogen levels in postmenopausal women can be significant, principally due to the extraglandular conversion of androstenedion and testosterone, produced by the adrenal gland and the postmenopausal ovary respectively. The clinical impact of this estrogen will vary from one postmenopausal woman to another, depending upon the degree of extraglandular production, modified by variety of factors, such as body weight, age and stress.[1]

According to that degree, wide ranges of clinical diversity and symptomatology can be seen in practice.

The genital organs undergo general atrophic changes. The ovaries become shrunken and fibrous. The uterus and tubes shrink, and in the case of uterus the body shrinks to a greater extent than the cervix so that the ratio of the body to cervix becomes 1:1 or even 1:2. The vaginal epithelium shrinks markedly, glycogen disappears from the cells, lactic acid is no longer produced and the environment of the vagina becomes alkaline.[1]

A series of menopausal symptoms arise in many patients. Some concerned directly with hormone deficiency, some possibly concerned with aging and other are emotionally related. Those directly concerned with estrogen lack are vasomotor symptoms and urogenital atrophic changes, which can lead to dyspareunia and incontinence. Demineralization of bone leads to postmenopausal osteoporosis. Cardiovascular changes are evident too. Premenopausal women appear to have some immunity from coronary thrombosis and anginal attacks, which may be causally related to their different lipid background when compared with men. After the menopause, all lipid levels rise and there is an increase in low-density lipid (LDL) cholesterol with little change in high-density lipid (HDL) cholesterol.

CHALLENGES OF THE POSTMENOPAUSE

For a female, life expectancy in the developed world approaching 80 years. A woman may, on an average expect to spend some 30 years or 40% of her active life in the postmenopausal era.[1]

It is probably true that today women have greater expectations of high-quality life than previous generations. Therefore, it seems likely that climacteric and postmenopausal women will continue to place increasing demands on health care resources for many years to come. The gynecological care of the fertile female population has already been well established in most countries. In the not too distant future, postmenopausal women will constitute the major proportion of the gynecological patient population. Preventive medicine and care for elderly will be an essential part of the general gynecological practice. In parallel with the demands "climacteric and postmenopausal clinics" are being established world-wide with the active participation of gynecologists, cardiologists, rheumatologists, etc.

With better nutrition, health care and living conditions, more women are living long enough to develop ovarian and endometrial cancers, which are known to be more common after the menopause. Undoubtedly, the care of postmenopausal population must include the early detection of ovarian and endometrial cancers, just as the access to the benefits of hormone replacement therapy (HRT).

Estimating the potential individual benefits and monitoring, the HRT poses further challenges in the medical care of the postmenopausal women.

Vaginosonographic examination has become an examination technique that is very well accepted by postmenopausal women. Recent advantages of transvaginal color Doppler and three-dimensional ultrasound enables the more experienced examiner to visualize even the smallest vessels and investigate blood flow characteristics in the poorly perfused small pelvis in the postmenopause, which helps to differentiate between the normal, suspicious and pathologic variations of the structures or detect, and follow the effects of the HRT on the perfusion of genital tract. In this chapter we will discuss the role of ultrasound in the management of the postmenopausal women.

INSTRUMENTATION

There are variety of configuration of transvaginal probes, including various number of sizes and shapes. Examining a woman in the postmenopause, the ovaries and the endometrium must be the special field of interest. In general, the curved linear multielement transducers afford the best density and overall field-of-view for imaging.

In elderly women the stenosis of the upper part of the vagina or adhesions of the vaginal walls can occur in addition to the atrophic changes of the epithelia. One must take special care when introducing the probe into the vagina of a woman in the senescence. Transvaginal sonography (TVS) can induce unnecessary bleeding and pain. Using thinner transducers and lubricant gels could help to avoid the unnecessary injuries. The same caution applies to women who have vaginal adhesions secondary to previous surgery for whom the vaginal examination may be painful.

It is advisable to have an additional medical person being present during any kind of vaginal procedure.

SCANNING IN THE POSTMENOPAUSE

The first and perhaps the most important condition for TVS should be a thorough emptying of the urinary bladder. This is the condition, which makes the TVS more comfortable for the significant group of incontinent postmenopausal patients; comparing to the transabdominal ultrasonography, which requires full bladder. On the other hand, some elderly patients who are unable to empty their bladder completely may need catheterization for better visualization.

Once the probe is covered with condom, it should be inserted into the introitus with slight downward pressure on the perineum, while gently separating the labia majora with the fingers of the other hand. A small amount of gel applied outside the condom can act as lubricating interface. If the patient desires she can insert the probe herself.

Inserting the probe into the midvagina, the anteflexed uterus can be normally imaged in its sagittal (long-axis) plane. However, in the postmenopause with the loss of the strength of uterine ligaments and the pelvic support, the uterus will frequently alter its position in the female pelvis. With the advanced age, it is usually situated in the midline in a straighten position and can be imaged only after inserting the probe into the fornix. Additionally, a descended, even a prolapsed uterus let the examiner to be able to orientate only after re-establishing the near normal situation by pushing the uterus upwards manually and then holding it there with the help of a probe.

In the long axis, one can appreciate the different interfaces of the endometrium, beginning with the interface of the cervical canal. As the echogen cervical

mucus is very poor and the endometrium can be very thin, and atrophied in the postmenopause, visualization of the endometrium can be difficult; it usually appears in the form of a thin and echopoor line in the midline of the sagittal plane of the uterus.

After adequate image in the long axis is obtained, the probe can be moved 90° to image the uterus in a horizontal (semicoronal, semiaxial) plane.

Once the endometrium is adequately depicted in its long and short axes, the probe is withdrawn into the midvagina and images of the cervix can be obtained.

The ovaries usually located lateral to the uterus, above and medial to the hypogastric vessels, lying in the area called "Waldeyer's fossa." Their size, morphology and locations are altered by the age, previous diseases, surgeries and other factors in the postmenopause. During the reproductive year the follicles serve as "sonographic markers" of the ovaries. After the menopause, it is hard to find them because these "markers" are not present, the ovaries themselves atrophied and there is less pelvic fluid to provide an acoustic interface. Their detection becomes more difficult with advancing age. Beside negative bimanual pelvic examination, non visualization of the ovaries can be accepted without serious concern about ovarian pathology. With the introduction of color-coded Doppler flow imaging, by finding the color-coded flow of the ovarian artery or vein, one can better detect the otherwise "sonographically non detectable" ovaries. Using the other hand can be very useful for manipulating the ovaries into the "scanning sight" of the probe by pushing them slightly downward through the lower abdominal wall into the direction of the tip of the probe.

Detecting some free fluid in the cul-de-sac doesn't necessarily means pathological finding, but in its presence ovarian pathology must be searched with special care. The same goes for any palpated or visualized solid structure in the cul-de-sac. The vascularization of these gynecological findings must be examined intentionally by color and pulsed Doppler.

When a large amount of fluid is present, such as in ascites, first questions is whether the pathological condition arises from an ovarian tumor or is related to a non gynecological disorder. Fluid clearly outline the boundaries of the structures and ovarian pathology may be revealed. If the ovaries appear normal, one may consider other reasons leading to ascites.

Constipation is not rare in postmenopausal patients. Scybalous should not be confused with pelvic masses. Excluding the vascularization of a structure by the color Doppler helps in differentiating normal to abnormal.

Solid pelvic masses must also be differentiated from the intestines. In real time mode the motion of the bowels help to distinguish the peristalting intestines from the fixed structures. In the postmenopause, the peristalsis is frequently inert, which requires proper patience from the examiner. In case of a vascularized mass color and pulsed Doppler again offers a quick possibility.

From all of the above mentioned techniques, it follows that the sonographer get to know the finding of bimanual pelvic examination, which should therefore precede the transvaginal ultrasound examination. It strengthens the recommendation that the person, who performs the transvaginal ultrasound examination in a postmenopausal patient should perform a bimanual pelvic examination before, thus orienteering the anatomical situation and obtaining previous information to decide what are the adequate ways for ultrasonography, or whether there were any suspicious structures palpated. In case of uncertainty of the origin of the palpated or visualized structure transrectal examination or enema might become necessary.

THE POSTMENOPAUSAL OVARY

Visualization

In the reproductive years, the normal ovary is relatively easy to detect by TVS. The characteristic small sonolucencies, representing follicles or corpus luteum are missing in the postmenopause. Ovarian volume and diameter decrease with age. The normal atretic ovaries become more difficult to image, but even in the senescence, the small but normal ovaries are sometimes imaged.[2]

The postmenopausal ovaries appear small, uniform and hypoechoic ellipsoidal structures with a smooth outline located above and medial to the hypogastric vessels.[3] A small amount of pelvic fluid, which is less frequent in the postmenopause than in the fertile period, may also help to delineate the ovaries. Larger amount of fluid (ascites) makes them easily outlined.

In significant number of patients, the ovaries may not be detected, even after considerable time spent searching for them.

Eventually, the ovary becomes an inert residue that consist of connective tissue and it clings to the posterior leaf of the broad ligament. Postmenopause, loosing the strength of the ligaments and the support of the pelvic floor the uterus might descent, while the ovaries remain in their position, fixed to the pelvic wall by the atrophic infundibulopelvic ligaments. In this situation, their

distance from the fornices increase, thus their transvaginal visualization becomes more difficult and sometimes impossible. This can be the reason that Granberg and Wikland[4] found TVS to be slightly less accurate (23%) than abdominal ultrasound (34%) in visualizing the postmenopausal ovary. The above mentioned use of the abdominal hand might help in directing them into the scanning sight of the transvaginal probe and distinguish them from the bowel.

Previous surgery or the presence of adhesions as the consequences of previous pelvic inflammatory diseases can also fix the ovaries in abnormal locations.

Hall et al.[5] visualized both ovaries in two third of postmenopausal patients and atleast one ovary in three fourth of patients. Campbell et al.[6] identified both ovaries in 84% of postmenopausal patients by transabdominal sonography. Rodrigez et al.[7] imaged 84% of the postmenopausal ovaries by transvaginal ultrasound. In a study of Fleischer et al.[8] on postmenopausal patients at least one ovary was detected 80% of the time and both ovaries were imaged 60% of the time by transvaginal approach. Healy et al. identified both ovaries by TVS in 71% of women. The right ovary was visualized in 86.3% of women and the left ovary was visualized in 78%.[3]

According to the published data the introduction of the TVS did not result in improvement in the visualization rate of the postmenopausal ovary. However, much clearer images can be obtained using the transvaginal approach when the ovaries are localized. When both the transvaginal and the transabdominal approach were used, the visualization rate came close to 100%.[4] Therefore, in case of any difficulty in detecting the postmenopausal ovary, the techniques of transabdominal and transvaginal ultrasound may be used to supplement each other.[9] In some cases the significantly enlarged ovary can be situated out of the pelvis and out of the range of the transvaginal probe.

There is no consistent view as to whether the inability to visualize the postmenopausal ovary assures a lack of pathology. The general consensus seems to favor the view that lack of visualization of postmenopausal ovaries and a negative bimanual examination suggests ovarian atrophy and lack of disease.[2] In a study Rodrigez et al.[7] were not able to visualize 19 of 104 ovaries preoperatively and during the subsequent histological evaluation all were found to be atrophied without any sign of disease.

Inability to visualize the postmenopausal ovary by experienced examiner can be accepted as normal finding.

Morphology and Biometry

The menopausal ovary tends to atrophied and shrink when the Graafian follicles and ovary disappear. The tunica albuginea becomes dense, and causes the surface of the ovary to become scarred and shrunken. The cortex is marked with increasing thinning as well as numerous corpora fibrosa and corpora albuginea with areas of dense fibrosis, and hyalinization.[10]

The ovarian weight decreases from an average of 14 g in the fourth decade to approximately 5 g in the postmenopausal state. Whereas the normal ovary measures 3.5 x 2.0 x 1.5 cm after the menopause it shrinks to 2.0 x 1.5 x 0.5 cm and in some instances it may be even smaller. At this point, it can be palpated very rarely.

Several sonographic studies have attempted to define normal ovarian size and the general conclusion is that it should not exceed 2 x 3 x 4 cm.[2,8,11-15] According to the measurements of Fleischer[8] the mean size of the normal sonographically imaged postmenopausal ovary was 2.2 x 1.2 x 1.1 cm. Others measured postmenopausal ovarian volume rather than size (ovarian volume = d1 x d2 x d3 x 0.523 where d1, d2, d3 are the maximal transverse, anterioposterior and longitudinal parameters), the mean figure of this parameter was 4.33 cm^3 in the pioneer work of Campbell.[6] In the paper of Goswamy[12] the mean ovarian volume was reported to measure 3.6 ml after examining 2246 postmenopausal women by transabdominal ultrasound. Granberg and Wikland[4] found it less smaller (1.4 +/– 1.0 cm^3) in a different age group. In the series of Hall et al.[5] all the ovarian volumes were equal or less than 2.5 cm^3. Pavlik examined 13,963 women and found that mean ovarian volume is 2.2 cm^3.[16]

Despite the difference in the size reported for the normal ovary, there is a close correlation between the size of the left and the right ovaries. In the above mentioned work on a large population Goswamy et al.[12] found 0.01 ml difference between the means of the volumes of the left and the right ovaries. Difference in size is particularly important, since each serves to some extent as a normal control for its sister.[9] Campbell et al.[6] recommends that an ovary twice than the size of its pair should be regarded a suspicious finding.

Multiparous women have ovaries that are approximately 12% larger. There seems to be no additional effect of parity if the woman had more than two children. History of breast cancer was associated with an increase in mean ovarian volume of approximately 11%.[12]

Hormone replacement therapy does not seem to influence neither the size nor the perfusion of the postmenopausal ovaries.[17-19]

Ovarian Malignancy in the Postmenopause

Although the ovary becomes too old to function, it is never too old to form a cancer.[10] Visualization and measurement of ovarian volume in the postmenopausal patient are sometimes difficult, but potentially afford early detection of cancer or neoplasm. Ovarian cancer is the fourth leading cause of cancer-death in women both in the United States and the UK.[20,21] The incidence increases over the age of 40 and the peak age for the appearance of common epithelial ovarian cancer is age 56–67 years.[10] The importance of early detection of ovarian cancer is evidenced by the fact that five-year survival rates for stage I disease are 50–70%, whereas these figures for stage III and IV disease are 13% and 4% respectively. The five-year survival rate for women with ovarian cancer has not changed significantly over the past 30 years.[20] The ovarian cancer is asymptomatic until it has reached an advanced stage and mostly it is not diagnosed until the advanced stage. Several attempts were made by different investigators to establish an ultrasound-based safe and cost-effective screening system for ovarian malignancy, including morphological criteria, color and pulsed Doppler, and scoring systems.

Despite of these efforts, currently there are no fully accepted screening methods to detect ovarian cancer at an early stage. On the other hand, ultrasonography offers the capability of detecting even small increases in ovarian size and at least the potential for early diagnosis of ovarian malignancy. It is the responsibility of the examiner to take a chance and search for the ovaries very thoroughly, and measuring them precisely when examining a postmenopausal patient. In case of any suspicious finding, deviation from the normal ovarian morphology or enlargement of the ovarian diameters or volume and change in ovarian volume at repeat scan,[3] the patients must immediately be directed to the higher center and examined in detail according to the established ovarian cancer detecting protocols.

Postmenopausal Palpable Ovary Syndrome (PMPO)

Enlargement of the ovaries in elderly women was considered pathological by Barber et al. who called this the "postmenopausal palpable ovary syndrome" (PMPO).[22] For years, surgical exploration and oophorectomy were recommended when PMPO was detected, i.e. the ovary continued to demonstrate the size and consistency of a premenopausal ovary.[23,24]

According to the approach of Barber, in the PMPO, the finding which is interpreted as a normal-sized ovary in the premenopausal patient represents an ovarian tumor in the patient, atleast five years after the menopause. This statement doesn't mean that anything that is palpated in the adnexa is abnormal. It only refers to the size and consistency of the ovary.[10,25,26]

Cautious examination of the ovaries by transvaginal color and pulsed Doppler is strongly recommended in PMPO syndrome to resolve the doubts. Mostly ultrasound examination found simple ovarian cyst, which shouldn't necessarily be considered abnormal. For management of simple ovarian cyst see further.

Unilocular (Simple) Ovarian Cysts in the Postmenopause

The spreading use of the TVS and improved resolution of the equipment led to the detection of more unilocular, simple ovarian cysts in the postmenopausal women than detected by earlier known techniques. The question is what is the risk of a completely anechoic unilocular tumor being malignant and whether the risk of a simple cystic tumor being malignant increases with age and size?[27]

Only the cysts without any septation and papillary formations can be regarded unilocular.[28] Many reports presented on unilocular and anechoic ovarian cysts in the postmenopause diagnosed by ultrasound.[27,29-41] The values in these studies indicate that anechoic unilocular ovarian cysts in postmenopausal women carry a low-risk of malignancy.

Andolf et al. reported 30 simple postmenopausal adnexal cysts (2–8 cm).[31] After the surgical treatment of 15 of them no malignancy was revealed, while the following of another 15 by transvaginal ultrasound, six disappeared after one month and altogether 12 disappeared after seven months. After two years, only two cases with 2 cm cysts remained. In their next work[32] they confirmed on a larger number that small anechoic lesions are seldom, if ever, malignant in elderly women. However, among their 33 patients having totally anechoic cysts greater than 5 cm they found three malignancies.

Upon the histological examination of 28 unilocular postmenopausal cysts less than 5 cm, Goldstein et al.[33] also reported 0% incidence of malignancy. Another 14 patients were followed from 10–73 months without any change in size or character of the cyst.

Parker et al.[34] reported 25 unilocular cyst (3–9 cm, mean 5 cm) diagnosed by transabdominal sonography in postmenopausal women, who later underwent cystectomy by laparoscopy or laparotomy. None of the cysts were malignant.

In their studies Granberg et al.[28,30] examined 140 postmenopausal unilocular cysts, 60 of them were less than 5 cm in diameter, 51 measured 5–10 cm and 29 cyst was greater than 10 cm. Only one malignant tumor was found among them, this measured greater than 5 cm in diameter. The sensitivity and specificity for excluding malignancy in an ovarian cyst in postmenopausal women by transvaginal ultrasound was 100%.[27]

Valentin and Akrawi[35] followed 134 postmenopausal women found to have an adnexal cyst are judged to be benign and not causing any symptoms. Transvaginal ultrasound examination were performed at 3 months, 6 months and 12 months time-interval and thereafter every 12 months interval. Median follow-up time was three years. In majority of women the cysts disappeared or remained unchanged. With advancing age chance for regression of cyst is declining.

Valentin et al.[36] examined 52 women which died from causes other than gynecological cancer or intraperitoneal cancer of extragenital origin. They found 36 simple cyst. All cysts were benign.

Modesitt et al.[37] examined 15,106 women atleast 50-year-old, 2763 women (18%) were diagnosed with 3259 unilocular ovarian cysts. A total of 2261 (69.4%) of these cysts resolved spontaneously, 537 (16.5%) developed a septum, 189 (5.8%) developed a solid area and 220 (6.8%) persisted as a unilocular lesion. During this time, 27 women received a diagnosis of ovarian cancer and ten had been previously diagnosed with simple ovarian cysts. All ten of these women, however, developed another morphologic abnormality, experienced resolution of the cyst before developing cancer or developed cancer in the contralateral ovary. No woman with an isolated unilocular cystic ovarian tumor has developed ovarian cancer in this population. The authors concluded that the risk of malignancy in unilocular ovarian cystic tumors of less than 10 cm in diameter in women 50-year-old or older, is extremely low.

Nardo et al.[38] followed-up 226 women with simple cysts for five years. The CA-125 is also measured and found that 54 cysts increase in size. They were removed and two carcinomas were found. Both carcinomas had increased CA-125 levels.

Castillo et al.[39] examined 8794 asymptomatic postmenopausal women by transvaginal ultrasound. Two hundred and twenty-three simple adnexal cysts in 215 women were found out (prevalence: 2.5%). Annual incidence did not change significantly. One hundred and forty-nine patients with 153 cysts were entered ultimately in the study. Forty-five (30%) underwent surgery (34 after initial diagnosis and 11 during follow-up). A total of 49 cysts were removed. The most frequent histological diagnosis was serous cystadenoma (84%). There was a case of a stage IA ovarian carcinoma (2% of the cysts removed, 0.6% of all the cysts included in the study). One hundred and four patients with 104 cysts underwent conservative follow-up throughout the study period. Forty-six (44%) of these cysts were resolved spontaneously (74% of them within 2 years). In 14 (30%) of these women, a new cyst was diagnosed when follow-up went on. In 58 patients, cysts persisted during all study period (median follow-up: 48 months, range: 6–90 months), 69.6% of them remained unchanged, 17.2% increased and 17.2% decreased. Patients in whom cysts resolved spontaneously had a shorter menopausal time (P=0.001) and tend to be younger (P=0.06). No differences were found regarding cyst features.

Dorum et al.[40] examined 234 woman, died from non gynecological causes. They found 36 simple benign cysts.

In a paper from Greenlee et al.[41] simple cysts were ascertained among a cohort of 15,735 women from the intervention arm of the prostate, lung, colorectal and ovarian cancer screening trial through four years of transvaginal ultrasound screening. Simple cysts were seen in 14% of women, the first time that their ovaries were visualized. The one year incidence of new simple cysts was 8%. Among ovaries with one simple cyst at the first screen, 54% retained one simple cyst and 32% had no cyst one-year later. Simple cysts did not increase risk of subsequent invasive ovarian cancer.

Due to the physics of ultrasound, structures which are further from probe tip can be easily missed out. The risk of missing papillary formation increases with diameter of the cyst. Most of the authors agree that cyst which is larger than 5 cm cannot be properly examined and therefore should not be consider simple.

The cytological evaluation of the cyst content proved to be very limited value for identifying malignancy even after the irrigation of the cystic tumor and the combination of it with transvaginal ultrasound did not increase the diagnostic accuracy as compared with ultrasound alone.[29,42-44]

Once again, only unilateral cyst smaller than 5 cm, filled with clear anechoic fluid, with entirely smooth and thin walls (up to 3 mm), without any septation and papillary formations can be regarded as unilocular simple cyst.

Royal College of Obstetricians and Gynaecologists recommendation for such cyst is ultrasound and CA-125 follow-up in four months intervals for a year. If there is no change in cyst morphology and size (or cyst

size decrease) and/or CA-125 levels, further follow-up is not necessary.[45] Any change in cyst morphology or increased cyst size or blood flow, or increased CA-125 warranted removing of ovaries.

With its widespread utilization in the near future transvaginal color Doppler will make it possible to increase the reality of ultrasound diagnosis of unilocular cystic ovarian lesions. In their paper of 18 stage I ovarian cancers, Kurjak et al.[46] reported that ovarian cancer stage I was also discovered in two simple unilocular ovarian cysts using transvaginal color Doppler as well as in two morphologically normal ovaries which would have been missed if the morphology alone was considered. This finding would have an important clinical implication as these simple cysts are not always innocent and color Doppler is, therefore, mandatory to rule-out the malignant revascularization.

Color Doppler Velocimetry of the Postmenopausal Ovary

The ovarian blood flow is significantly affected by ageing and the postmenopausal ovary shows varying degree of avascularity.

The ovarian artery is a tributary of the upper aorta and reaches the lateral aspect of the ovary through the infundibulopelvic ligament. Color Doppler enables visualization of the ovarian artery at the lateral edge of the ovary. In some patients, especially in the postmenopausal, these vessels are not clearly visualized and the sample volume should be moved across the ligament and then through the ovary until the arterial signal is identified. Signals from the ovarian artery are characterized by low Doppler shifts of a small artery with low velocity.

The first published data from direct and non-invasive measurement of normal ovarian and uterine perfusion in the postmenopause are from Kurjak et al.[47] Unlike in the presence of unilateral folliculogenesis and corpus luteum formation during the normal menstrual periods, there is no difference in the vascular impedance between the left and right ovaries in the postmenopause.[48,49] Significantly, increased ovarian blood flow impedance can be demonstrated already during the climacterium, when compared to that of the "dominant" ovary in a normal menstrual cycle. The mean RI increasing further in the next years of the postmenopause reaching the value of one after ten years. The absence of the diastolic flow is already common in the early postmenopausal period and constantly found in patients with more than 11 years of postmenopause.

Even with the latest advanced equipment seems to be not possible to detect velocity waveform signals from the ovarian parenchyma in normal postmenopausal patients. This can be the result of the relative increase of the amount of the connective tissue. Therefore, any color flow obtained from a postmenopausal ovary should generate a high index of suspicion for abnormal revascularization and requires detailed pulsed waveform Doppler analysis.[47,50]

In a previous study, Kurjak et al. examined 1000 postmenopausal women with transvaginal color and pulsed Doppler sonography.[50] A total of 74% were asymptomatic; the others were referred or self referred for symptoms. There were 83 women with findings that resulted in surgery. Separation of the groups into benign and malignant cases did not reveal significant differences in age, duration of the menopause or symptomatology. A total of 29 tumors were malignant, prevalence rates were 36% in the group underwent surgery and 3% in the total postmenopausal group underwent examination. An ultrasound score was used to analyze the morphology of the tumors. The score was successful in separating benign from malignant tumors with all indices of normality >=90%. Color flow was identified in 27 of 29 malignant tumors and 35% of benign masses. A cut-off value in the Doppler RI is 0.40, in the feeder vessels, it had a sensitivity and specificity of 96% and 95% for separating benign tumors from malignant tumors respectively. Positive and negative predictive values were 96% and 95%.

In their next retrospective study on this topic already mentioned above, 18 patients with ovarian carcinoma stage I were studied to evaluate the efficiency of transvaginal color Doppler sonography.[46] Four of these patients were asymptomatic and self-referred for their annual check-up. Another four asymptomatic women, two with morphologically normal ovaries and two with simple unilocular cysts were picked up during the screening program. Ovarian carcinoma stage I was detected in two normal-sized ovaries from only color and pulsed color signals, which represented tumor angiogenesis and low impedance to blood flow (RI <0.40).

Fleischer et al. published data of nine stage I ovarian carcinomas where three of them had benign appearance but suspicious blood flow characteristics.[51]

Crade et al. calculated that a postmenopausal women with a mass greater than 5 cm and an RI below 0.50 had a malignancy risk of 66%, while a mass having an RI value higher than 0.60 had only a risk of 2.4%.[52]

If further investigations by other researchers also confirm these results, transvaginal color Doppler ultrasonography may provide a valuable tool for monitoring the ovarian involution in the postmenopause and

objective aid for choosing between the conservative, laparoscopic or radical management of pelvic masses found in postmenopausal patients.

THE POSTMENOPAUSAL UTERUS

Morphology

The uterus can be imaged in three major scanning planes with TVS. There is generally a homogenous echo pattern in the postmenopause, and the uterine cavity is not frequently imaged.[53] The uterine wall is smooth and clearly outlined against its surroundings. In the myometrium, towards its periphery and often protruding can found echoless vessels. In the postmenopause the arteries can calcify in this region. These calcifications appear as small, bright reflections and regularly spreaded in the uterine wall. They can evoke shadowing, which may impair the assessment of structures lying beyond, e.g. the endometrium.[54] Unlike in all phases of the menstrual cycles, undulatory motions, i.e. uterine contractions[55] cannot be observed in the postmenopause.

Biometry

As in the case of all genital organs in the female, the development, the maintenance of the fertile size and shape, and the postmenopausal physiologic involution of the uterus are highly dependent on the actual serum level of the estrogen.

Measurement of the uterus in the sagittal plane can be carried out either by determination of the portio-fundus distance or in postmenopause, the separate measurement of the cervix and corpus uteri can also be used. It was already mentioned in the introduction that the corpus-cervix ratio of the postmenopausal uterus shows remarkable changes in favor of the cervix, with advanced ages it can even fall below one and can reach a ratio of 1:2, like in childhood.

The sagittal measurement is supplemented by the determination of the largest anteroposterior diameter of the corpus uteri and of the largest transverse diameter of the corpus. The size of the corpus decreases markedly in the postmenopause, shrinking to average size of 4.5 x 1.5 x 2.5, with the cervix predominantly over the corpus in the sense of the elongation of the cervix.[53] The mean length of the postmenopausal uterus was shown to be 59 +/– 11 mm by Andolf et al.[56] The upper size limit of the postmenopausal uterus has been suggested to be 3 cm in the anterior-posterior diameter, with a cervical-fundal length of 8 cm. The patient who is only 1–3 years postmenopausal when still has significant endogenous estrogen production by the ovaries or who has significant endogenous estrogen production by fat from adrenal precursors will have larger uterus than the patient who is over ten years postmenopausal. Clinical judgment is needed in interpreting normality of uterine size in postmenopausal uterine size in the postmenopausal patient.[9]

Uterine involution is a slow process. Myometrial thickness is changed as the years of the postmenopause progresses.

The Uterus under HRT

Comparing myometrial thickness between groups of postmenopausal with and without HRT, Zalud et al.[57] did not demonstrated statistical difference, though slight difference were found in favor of women, who received HRT for more than five years. These data are not surprising in the mirror of the findings of the same group, namely, that the myometrial involution could not been statistically expressed over the years throughout the postmenopause too. The involutional process of the myometrium is very slow and other factors than estrogen can also influence, as the sizes of the uteruses of fertile women can show greater variability too.

Color Doppler Velocimetry in the Postmenopausal Uterus

The vascular supply of the uterus is provided by a complex network of arteries originating from the uterine artery, which is a branch of the hypogastric artery. The color Doppler signal from the main uterine vessels can be seen lateral to the cervix at the level of the cervicicorporal junction of the uterus.[58] Flow velocity waveforms from the radial arteries can be obtained within the myometrial fibers, while spiral arteries are visualized at the level of endometrial-myometrial junction.[48]

Visualization of both uterine artery by transvaginal color Doppler can be achieved even in the advanced years of the postmenopause. In contrary, visualization rate of the myometrial and endometrial vessels are highly dependent on the length of the postmenopausal period.

The aging process affects the uterine perfusion. In general high impedance and high velocity is characteristic for the uterine arteries, though the uterine perfusion is largely dependent on age, phase of menstrual cycle, other conditions (e.g. pregnancy, tumor)[59] and there are complex relationships between the concentration of the ovarian hormones in the serum and uterine artery blood flow parameters.[60-62]

Additionally, there might also be a relationship between the serum gonadotropin levels and uterine perfusion. Examining normal postmenopausal patient and premenopausal patients treated with GnRH analogues Luzi et al. found that the pulsatility index of the uterine artery in spontaneous menopausal women is significantly higher than in artificial menopausal women. This phenomenon may be due to a different hormonal pattern which exists in the two groups, i.e. the gonadotropin levels increased in the former and decreased in the latter. The vascular compliance in artificially-induced menopause is higher than that observed in spontaneous menopause, as shown by a higher diastolic flow and a less deep notch. The decrease of the vascular compliance in postmenopause can be caused by progressive sclerosis of the vessel walls.[63]

Resistance to blood flow increases in both the main uterine and the radial arteries as the years of postmenopause progress, though the increase of ovarian blood flow impedance is more pronounced. The fact that uterine artery RI does not change significantly in the first year of menopause, strongly support the thesis that ageing process initially affects the uterus less than the ovary.

The diastolic flow decreases in postmenopause and the systolic peak increases.[63] The RI in the main uterine arteries continuously increases with the number of the postmenopausal ages, but unlike in the case of the ovarian artery, it doesn't reach the maximum in all women even at advanced ages.

Absent diastolic flow in uterine arteries was found in 15% of women with 1–5 years duration of menopause, while clear interruption of diastolic blood flow was observed in the uterine artery of one third of the women in the next five years of the postmenopausal period. More than half of the women has this finding with 11–15 years lasting postmenopause and finally, 80% of women whom LMB occurred more than 16 years ago demonstrated absent diastolic blood flow signal indicative of high vascular impedance.

The changes in flow velocity patterns of the radial arteries in postmenopausal patients parallel the blood flow dynamics of the uterine arteries.

Visualization of clear Doppler signals from the spiral artery is possible only in less than one-third of postmenopausal women, in whom LMB occurred 1–5 years previously. The impedance is significantly increased in these vessels too, when comparing to the premenopausal levels. In normal postmenopausal women already six years after the LMB, no blood flow signals can be expected from the inner-third of myometrium and the area of the myometrioendometrial junction.[62]

Myomas and Malignant Potential after the Menopause

Uterine fibroids of 0.5 cm can be detected by TVS and their relationship to the endometrial cavity can be precisely defined (e.g. submucosus, intramural, subserosus). They appear with TVS as rounded, well-defined space occupying structures.[64]

Growth of myomas is known to be estrogen-dependent. The management of the myoma around the menopause is highly conservative, since after the menopause they supposed to regress in the lack of the hormonal support. Myomas with good vascularization can be seen less frequently after the menopause. They show more hypoechogenic structure, compared to the normal uterine tissue, while homogenous and hyperechogenic myoma have often undergone regressive changes, and have a large amount of connective tissue. Other regressive changes such as necrosis, caseous and cystic degeneration can be recognized by the presence of hypoechogenic regions or regions without echogenicity in the myoma. Such a necrotic myoma can be confounded with an ovarian cyst or a colliquated endometrial carcinoma depending on its localization. Hyalinization and calcifications of the myoma responsible for bright reflections can be seen frequently in the postmenopause.[53]

Transvaginal color Doppler can be used to assess leiomyoma vascularity, as well as the physiological and pathophysiological characteristics of uterine arterial blood flow.[65,66] The vascularization of leiomyomas is supported by pre-existing myometrial vessels originating from terminal branches of uterine arteries. Since the leiomyoma grows centripetally as proliferation of smooth muscle cells and fibrous connective tissue, the color Doppler demonstrates most of the leiomyometrial blood vessels at its periphery. While their visualization rate is high in the premenopausal period (58–70%),[67-69] it decreases after the menopause with the decreased blood supply of the uterus.[47]

The growing inclination of the myoma is in correlation with the increased blood flow in the uterine network, the latter is thought to be a result of large concentration of estrogen receptors and estrogens.[70-72] Whether the regression of the myoma after the menopause is resulted directly by the fallen estrogen levels or it is only a secondary consequence of the decreased perfusion, which is still not known. Though Doppler studies on the perfusion of the uterine fibroids in the postmenopause are not available yet, it can be anticipated from the Doppler studies on myomas under treatment with GnRH analogs[69,73] that with the decreasing estrogen levels the previously decreased

impedance of the uterine artery and the supplying myometrial vessels are increasing to the level of a normal postmenopausal uterus leading to the involution of the myoma.

It must be emphasized that in case of necrotic and degenerative changes in the myoma, the presence of blood vessels in the central portion is usual and the impedance of them can be so low that it might be misinterpreted as malignant neovascularization.

One can use TVS as a means of monitoring the size and the ability for growth of the leiomyomas around, and after the menopause. If there is evidence of rapid growth of a predescribed myoma in a postmenopausal women and in ultrasound an increase of echoless areas as a sign of necrosis, laparotomy should be performed because of a suspected malignant transformation.

Though the sarcomas accounted for only 1–3% of the malignant tumors of the uterus (including the endometrium), their early diagnosis can greatly depend on an occasional but accurate ultrasound examination, since there are scarcely any symptoms of an early process.[74]

Nevertheless, there are, similar to macroscopic aspects, sonographic indications for the existence of sarcoma. Primary sarcomas in ultrasound examinations appear as poorly outlined masses, partly hyperechogenic, partly irregularly limited and hypoechogenic or without echogenicity. Morphological differentiation from myoma can be facilitated by the absence of any systematic structure (onion-skin or whirlpool pattern). Differential diagnosis of inhomogenous, myometrial masses can be myomas undergoing carneous degeneration, with a pool of liquid or bleeding into the myoma.[53]

Application of the color and pulsed Doppler may confirm or preclude the *in vivo* diagnosis of uterine sarcoma. The presence of irregular, thin and randomly dispersed vessels in the peripheral and/or central area of tumor, with very low impedance shunts characterizes intratumoral neovascularization and is in favor of the malignant transformation. In benign uterine lesions, even if intratumoral vascularization can be detected, the resistance to blood flow was found significantly higher. Furthermore, in the case of the uterine sarcoma, both uterine arteries shows a low impedance in comparison with that of normal, even the postmenopausal or myomatosus uteri.[75,76]

Unfortunately, as a result of the wide range of the biological variations and the vascular characteristics of tumors, an overlap exists between the blood flow patterns of benign and malignant uterine tumors.[76] At the moment the realistic approach is to consider the above mentioned guidelines only in general, but one has to take the decreased intratumoral impedance and increased vascularity into serious consideration, especially it is accompanied with rapid growth of the tumor during the serial examination.

Leiomyomas under HRT

Leiomyomas are the most common pelvic tumors in women of the reproductive age; 20 to 25% of women have uterine myomas.[77] Higher concentrations of estrogens[70] and estrogen receptors[71] within leiomyomas than in adjacent myometrium were taken as evidence of the hormone-dependence of their growth.

Though they tend to regress after menopause with the decreasing serum level of the promoter estrogen, it is questionable, whether the introduction of the HRT promotes the growing process again. The data are confronting, in some papers myoma growing, in some there is no difference in size and in some there is even decrease in size[78-82] However, even if there are increase in myoma size, this does not appear to cause clinical symptoms.

In practice, uterine and fibroid size can be closely monitored by ultrasound, and HRT can be easily discontinued if the fibroid enlarges.

THE POSTMENOPAUSAL ENDOMETRIUM

Visualization and Morphology

After the menopause, decrease of ovarian estrogen production leads to atrophy of the endometrium. In consequence the endometrium of a postmenopausal women is typically thin when examined by TVS, which corresponds to the stratum basale adjacent to the myometrium.[83] Its sonographic feature is very similar to that of the endometrium in the early follicular phase.[84] The endometrial band is sonographically narrowed and the echogenic line of the uterine cavity often cannot be visualized.[54] In the study of Andolf[56] the endometrium could not be localized in 7% of postmenopausal women without bleeding disorder. Granberg et al. could not visualize 10% of the histologically atrophic postmenopausal endometrium.[85] In addition, shadowing arising from myomas or arteriosclerosis make visualization more difficult.

Echotexture of the endometrium is usually more echogenic than the surrounding myometrium. In the above mentioned study by Andolf, 85% of the assessable endometrium were less echogenic than the myometrium in asymptomatic postmenopausal women.

The poorly echogenic myometrial zone, the subendometrial halo round the endometrium is frequently absent in the postmenopause.[54] However, the interrupted subendometrial halo was reported as a common sign of the myometrial invasion of the endometrial carcinoma.[86]

The Postmenopausal Endometrial Thickness

Contrary to earlier methods of measurement of the thickness of the endometrium, today according to general agreement, measurement should be carried out as follows: the uterus is viewed vaginosonographically in the longitudinal section and the total thickness of the endometrium is measured in the largest diameter (double layer). In case of any kind of intrauterine fluid collection, the thickness of the fluid pool in the uterine cavity is subtracted from the total thickness.[84]

It is very important to know that transvaginal ultrasound cannot differentiate between focal and symmetrical thickness.[87]

The postmenopausal endometrial thickness is 2–4 mm, with a considerable scatter range of 0–10 mm and consequently, there are different limiting values for the normal state in the literature.

There is a correlation between the endometrial thickness and the body weight. Women with pure estrogen replacement therapy frequently have endometrial thickness exceeding that of postmenopausal women without it.[88]

Suspect Postmenopausal Endometrium

Endometrial carcinoma is the most common invasive gynecological malignancy in the United States and Europe today. The incidence of the disease increases considerably during the fifth decade of life and the average age at diagnosis is 59 years. In the more cosmopolitan, higher income population the rate has overcome the 40 cases per 100,000 related to increased longevity, increased cholesterol in diet and exogenous estrogen supplementation or substances with an estrogen-like effect.[89,90] The five-year survival rate is related to myometrial invasion, ranging from 93.7% when no invasion is present to 36.2%, if the invasion is deep.[91] When the first clinical sign, vaginal bleeding occurs, the myometrial infiltration depth is already 10 mm on average.[83]

Of endometrial carcinomas 80–90% present with atypical bleeding demonstrating the ineffectiveness of exfoliative cervical cytology and the need for early recognition of this most frequent genital malignancy.[83,92] Until now curettage and histologic evaluation is the accepted method to assess the background of the atypical bleeding. However, less than 10% of women with postmenopausal bleeding have endometrial cancer.[85,93] Therefore, a new non-invasive screening method must fulfill atleast double requirements: it should be able to recognize the abnormal endometrial process at an earlier stage, when bleeding occurs and it should reduce the number of the "unnecessary" curettage, when postmenopausal bleeding occurs.

Several publications have reported that endosonographically measured endometrial thickness correlates closely with the presence or absence of endometrial cancer in asymptomatic postmenopausal women.[94,95] An endometrium that measures greater than 8 mm from one myometrial-endometrial interface to another in postmenopausal woman without HRT, is highly likely to be associated with significant endometrium pathology. Approximately, 10% of asymptomatic postmenopausal women have endometrium exceeding this cut-off level and 1–3% of them can be expected to have endometrial carcinoma.[96,97] There is, however, a significant false-positive rate. Cut-off level of 8 mm has a very high sensitivity, but a low specificity.[83] The only way to increase the specificity would be to adjust the cut-off value to a higher level, but in this case the sensitivity of the screening would decrease and more positive cases might be overlooked.

Another possible approach to reduce the number of false-positive findings could be the use of color Doppler.

Up to now, there are no sonomorphologic criteria to differentiate between benign and malignant endometrial neoplasm. Therefore, there is no accepted screening method for endometrial cancer.

Postmenopausal Bleeding and Transvaginal Sonography (Transvaginal Sonography Versus Dilatation and Curettage)

In atypical bleeding in the postmenopause, besides clinical and cytological examination, careful sonographic assessment should be made of the ovaries and the cervix uteri.[84]

Transvaginal ultrasound has become an important tool for diagnosing endometrial pathology in women with postmenopausal bleeding too. In patients with postmenopausal bleeding, the endometrium are considerably thicker than in asymptomatic women.[98]

Several studies have been investigated the effectiveness of the endometrial thickness measurement in detecting malignancy in patients with postmenopausal bleeding, using different cut-off levels.[83,99-105] Summarizing the results of the published works in none of the case was endometrial carcinoma found below 4 mm.

Measuring an endometrium less than 4 mm is safe enough to exclude the possibility of endometrial carcinoma in case of postmenopausal bleeding. Nevertheless, if this method is to be used for identifying those women who will not have a dilatation and curettage (D and C) performed, based on the findings on the endometrium, training is needed to minimize the error. Karlsson et al. found considerable differences, when compared the measurements of experienced and inexperienced examiners.[106]

If endometrial thickness is more than 4 mm (regardless woman is bleeding or not), it should be differentiated between focal and symmetrical thickness. As is mentioned before ultrasound itself cannot differentiate.

A great help to this is hysterosonography which can easily differentiate between focal thickness (polyp) and symmetrical thickness.[104] Symmetrical thickness should be further investigate with pipelle biopsy.[107] If there is a polypus structure in the uterus, hysteroscopy is recommended. Blind curettage is not recommended.[108]

In office setting alternative method to sonography or hysterosonography is office hysteroscopy.

Postmenopausal Intrauterine Fluid Collection

Occasionally, a small amount of intraluminal fluid may be detected in the postmenopausal uterus, the detection rate of it can reach 16% in asymptomatic postmenopausal women.[84]

We can only speculate as to the pathophysiology of fluid accumulation in the uterine cavity. Senile cervical stenosis can prevent drainage of possibly minimal endometrial secretion leading to small intrauterine pools. This, however, speculative as some degree of cervical stenosis is ubiquitous in postmenopausal women, whereas intrauterine fluid is a rare finding. Patients with ascites are more likely to have intrauterine fluid.[109] The possibility of the tubal cancer is rather theoretical than practical, although, one case reported by Carlson,[110] cancer of the cervix may obstruct the cervical canal and can cause intrauterine fluid accumulation. However, the main suspected reason must remain the endometrial malignancy.

Although the presence of intrauterine fluid has been considered ominous and related to malignancy by some authors,[111,112] most authors today disagree on this.

In their series of twenty postmenopausal women with intrauterine fluid collection Pardo et al.[113] revealed three cases of endometrial carcinoma, though it must be emphasized that in all of these positive cases, the endometrial thickness was more than 4 mm.

Carlson et al. also reported 20 cases of endometrial fluid collection in the postmenopause, of which five proved to be the results of some kind of genital malignancy (two ovarian, one tubal, one endometrial and one cervical).[110]

However, examining the fluid pools in the uterine cavity Osmers et al. did not find association with pathological changes in narrow endometrium.[84]

For Smith and colleagues[114] endometrial fluid by itself, without assessment of the endometrium does not indicate the requirement for additional histological clarification. As diagnostics, authors especially suggested the endometrial morphology a better choice.

Bar-Hava et al.[115] examined 1175 asymptomatic postmenopausal women. They found 166 women with intrauterine fluid accumulation. Of the 166 women with intrauterine fluid accumulation, 91 had an endometrial biopsy, of which 70% were insufficient for evaluation and 30% were normal on histology. They concluded that postmenopausal intrauterine fluid accumulation is a common and mostly benign phenomenon that typically occurs in the late postmenopausal age subgroups.

The extensive use of sonography will lead to an eventual increase in the number of postmenopausal patients diagnosed with intrauterine fluid. In every case, careful scanning is recommended to rule-out ovarian and tubal pathology. Certainly, cytological evaluation of the cervix, with special regard to the cervical canal is essential. Obviously, the endometrium must be submitted to serious examination by transvaginal ultrasound. Polyploid growths and irregularity of the endometrial surface are particularly well seen when surrounded by intraluminal fluid. In that case hysteroscopy is recommended. When thin endometrium surrounds fluid endometrial, sampling is not necessary.[114,115]

Undoubtedly, color Doppler offers an additional help in getting closer to the proper management, as it is able to assess the vascularization around this questionable ultrasound finding of postmenopausal intrauterine fluid collection.

Color Doppler Velocimetry and the Postmenopausal Endometrium

The visualization rate of the postmenopausal endometrial vessels are very low. The visualization rate of the endometrial vessels are in accordance with decreasing endometrial thickness with the postmenopausal years.[62] As it was already mentioned, vascularization of the inner third of the myometrium and the endometrio-myometrial junction is possible only in about or

less than one-third out those of normal postmenopausal patient, who had the LMB not more than five years previously.[47] No flow can be detected in the normal and atrophic endometrium in the postmenopause.[86]

Although a thick endometrium may be a sign of pathological processes, no morphological features that are unique to malignant disease have been identified.[96] Transvaginal color and pulsed Doppler have shown that the presence of intratumoral vascularization with a low impedance to blood flow can be used as an end point in screening programs for some gynecological malignancies.[93,116,117]

Bourne et al. reported the impedance to blood flow in the uterine arteries and the endometrial thickness in women with postmenopausal bleeding with or without cancer.[90] In the women with postmenopausal bleeding who did not have endometrial cancer and in those without postmenopausal bleeding were similar. Conversely, the highest PI in the group with cancer (1.49) was below the lowest value in the group without cancer (1.95). Data from this study suggest that in the presence of malignant tissue, the impedance to blood flow within the uterine artery is reduced significantly when compared to control groups. This observation was later confirmed by others.[118] If color Doppler is used to interrogate the endometrium in such cases, angiogenesis can be demonstrated as areas of color superimposed on the B-mode gray-scale image and the sensitivity of the technique is enhanced.[93]

Hata et al. found a feeder artery in patients of endometrial cancer and in seven out of nine endometrial cancers even venous blood flow in the endometrium could be detected, while no flow was detected around and within the endometrium in noncancer patients.[119] These findings were confirmed by pelvic angiography.

In the work of Kurjak et al. visualization rate of the abnormal blood flow within the endometrium was 100% in the cases of endometrial carcinoma.[86] Of the cases with detected endometrial carcinoma, 90 had endometrial (tumoral) thickness greater than 10 mm, which is already a suspect sonographic sign alone. However, 10% of these endometrial carcinomas with endometrial thickness 5–10 mm would have been missed without color Doppler.

It was also suggested in the same work that color Doppler should help in distinguishing between cancerous and hyperplastic thickened endometrium. Flow could be detected only in 92% of cases of endometrial hyperplasia. Blood flow patterns was characterized with a low RI near or less than 0.40, which constituted statistically significant difference compared with that of endometrial hyperplasia, if any flow is detected.[86]

By using color Doppler and measurement of the endometrium thickness together whilst maintaining the sensitivity, the false-positive rate of the ultrasound-based test is reduced.[90] If further data confirm, superimposing the color Doppler onto the endometrium at a questionable thickness (5–10 mm) and searching for vascularization in or around the endometrium might help to determine the further management of the patient and can lead a further reduction of the number of D and C in the postmenopause.

Endometrium under Hormone Replacement Therapy

It is now well established that unopposed exogenous estrogen increases a woman's risk for endometrial hyperplasia and thus has an etiologic role in endometrial carcinoma,[120,121] and that this effect is both dose- and duration-dependent.[122] Stimulating normal menstrual cycles by the use of progestogens have been found to effectively reduce estrogen-induced breakthrough bleeding, and lower the risk of endometrial hyperplasia and carcinoma.[98,122] Development of a hyperplasia can be prevented and a pre-existing glandular-cystic or adenomatosus hyperplasia can be eliminated by regular administration of gestagens.[84]

Some of the most common adverse effects of postmenopausal estrogen treatment are bleeding disturbances, regardless of whether therapy is sequential or continuous estrogen/progestogen.[123] In those women, who receives exogenous hormones continuously, the delicate task of balancing appropriate dosages of estrogen and progestogen may lead to breakthrough bleeding even more often. Since uterovaginal bleeding is the cardinal symptom of endometrial cancer, a disease which has been found to occur more frequently during unopposed estrogen therapy, it is not a surprise that rising estrogen consumption resulted in a need for appropriate invasive examinations to be carried out more frequently. Jensen et al. found that the frequency of D and C and endometrial biopsies in sequentially-treated women as compared with untreated women was 3.1 times higher in the 55–59 age group.[123]

Since TVS has been progressively used as an alternative recourse of monitoring the endometrium both in the pre- and postmenopause, detailed in the previous chapters, it is also suggested that it may be a useful method of monitoring the effects of HRT on the endometrium.[84,124,125] Vaginosonography as a screening method enables us to survey the postmenopausal endometrium, but sonographic assessment of endometrium is a completely different manner. It is therefore desirable to correlate hormone replacement regimens with the

sonographic appearance of the endometrium. Establishment of the normal range of endometrial widths for each hormone regimen would help limit unnecessary invasive procedures for suspected endometrial hyperplasia.[88]

Women which are receiving continuous hormone replacement are in favorable position. It is now well established that the kind of therapy is protective for endometrium. There are less cases of endometrial cancer in continuous regime group than in postmenopausal woman without any therapy.[126]

In women receiving sequential hormone replacement, endometrial thickness would be expected to vary throughout the cycle, depending on whether the endometrium was undergoing proliferative or secretory transformation due to estrogenic or progestational stimulation respectively. For this purpose, the examiner should have the knowledge of the type of HRT and the day of the menstrual cycle, in order to distinguish pathological endometrial findings. It seems to be the best time of examination in the early postmenstrual period.

Contrary, in woman receiving continuous hormone replacement, endometrial thickness should be always the same (thin).

On the basis of the current literature the following approach can be regarded as guidelines when examining the endometrium of an asymptomatic postmenopausal woman by vaginosonography. The recommendations are only for woman on sequential therapy. Woman on continuous therapy should be regarded and followed as postmenopausal woman without therapy.

- The endometrium of all postmenopausal women should be assessed vaginosonographically before the onset of HRT, whereas the guidelines for assessing the postmenopausal endometrium detailed in the previous chapter should be taken into consideration
- All patients on HRT are advised to have yearly sonographic checks of the endometrium. They shoud be examined after completion of the progestational phase of the cycle (days 1–2)
- Endometrial thickness up to 8 mm is regarded as normal finding
- Endometrial thickness of 9 mm and more is regarded suspicious. After administration of an oral gestagen, subsequent to the withdrawal bleeding, a second sonography is performed. If the endometrium still measures more than 8 mm, hysterosonography is recommended. With endometrial thickness of less than 8 mm, control sonography in three months time is recommended.

REFERENCES

1. Shifren JL, Shiff I. Menopause. In: Berek JS (Ed.). Berek & Novak's Gynecology, 14th edition. Philadelphia: Lippincott, Williams & Wilkins; 2007. pp. 1323-42.
2. Lerner JP, Timor-Tritsch IE. Morphological evaluation of the ovary using transvaginal sonography. In: Kurjak A (Ed.). Ultrasound and the Ovary. London, New York: Parthenon Publishing; 1994. pp. 115-28.
3. Healy DL, Bell R, Robertson DM, et al. Ovarian status in healthy postmenopausal women. Menopause. 2008;15: 1109-14.
4. Granberg S, Wikland M. Comparison between endovaginal and transabdominal transducers for measuring ovarian volume. J Ultrasound Med. 1987;6:649-56.
5. Hall DA, McCarthy KA, Kopans DB. Sonographic visualization of the normal postmenopausal ovary. J Ultrasound Med. 1986;5:9-15.
6. Campbell S, Goswamy R, Goessens L, et al. Real-time ultrasonography for determination of ovarian morphology and volume: a possible early screening test for ovarian cancer? Lancet. 1982;1:425-9.
7. Rodrigez H, Platt L, Medearis A, et al. The use of transvaginal sonography of evaluation of postmenopausal ovarian size and morphology. Am J Obstet Gynecol. 1988;159:810-4.
8. Fleischer A, McKee M, Gordon A, et al. Transvaginal sonography of postmenopausal ovaries with pathological correlation. J Ultrasound Med. 1990;9:637-44.
9. Kurjak A, Prka M, Pascual MA, et al. Assessment of normal and abnormal ovaries by transvaginal songraphy. In: Kurjak A, Arenas JB (Eds). Donald School Textbook of Ultrasound in Obstetrics and Gynecology. New Delhi: Jaypee Brothers Medical Publishers; 2005. pp. 446-64.
10. Barber HRK. The postmenopausal ovary. In: Kurjak A (Ed.). Ultrasound and the Ovary. London, New York: Parthenon Publishing;1994. pp. 231-4.
11. Andolf E, Jorgensen C, Svelaneius E, et al. Ultrasound measurement of ovarian volume. Acta Obstet Gynecol Scand. 1987;66:387-9.
12. Goswamy R, Campbell S, Royston J, et al. Ovarian size in postmenopausal women. Br J Obstet Gynaecol. 1988;95:795-801.
13. Wehba S, Fernandes CE, Ferreira JA, et al. Transvaginal ultrasonography assessment of ovarian volumes in postmenopausal women. Rev Paulista de Med. 1996;114: 1152-5.
14. Merz E, Miric-Tesanic D, Bahlmann, et al. Sonographic size of uterus and ovaries in pre- and perimenopausal women. Ultrasound Obstet Gynecol. 1996;7:38-42.
15. Tepper R, Zalel Y, Markov S, et al. Ovarina volume in postmenopausal women — suggestions to an ovarian size normogram for menopausal age. Acta Obstet Gynecol Scand. 1995;74:208-11.
16. Pavlik EJ, DePriest PD, Gallion HH, et al. Ovarian volume related to age. Gynecol Oncol. 2000;77:410-2.
17. Bakos O, Smith P, Heimer G, et al. Transvaginal sonography of the internal genital organs in postmenopausal

women on low-dose estrogen treatment. Ultrasound Obstet Gynecol. 1994;4:326-9.
18. Bar-Hava I, Perri T, Zahavi Z, et al. Influence of hormone replacement therapy on postmenopausal pelvic organs. Climacteric. 2001;4:160-5.
19. Manonai J, Chittacharoen A, Theppisai U. Transvaginal color Doppler sonographic assessment of uterus and ovaries in postmenopausal women: the effect of local estrogen treatment. Eur J Obstet Gynecol Reprod Biol. 2006;127:222-6.
20. Davis AP, Oram D. Screening for ovarian cancer. In: Kurjak A (Ed.). Ultrasound and the Ovary. London, New York: Parthenon Publishing; 1994. pp. 235-53.
21. Goozner M. Personalizing ovarian cancer screening. J Natl Cancer Inst. 2010;102:1112-3.
22. Barber HRK, Graber EA. The PMPO syndrome. Obstet Gynecol. 1971;38:921-3.
23. Kase NG, Weingold AB. Principles and practice of clinical gynecology. New York: John Wiley and Sons; 1983. p. 579.
24. Barber HRK. Ovarian cancer: Diagnosis and management. Am J Obstet Gynecol. 1984;150:910-5.
25. Barber HRK. The postmenopausal palpable ovary syndrome. Compr Ther. 1979;5:58.
26. Barber HRK. Editorial: A second look at the postmenopausal palpable ovary. Fem Patient. 1988;13:13-4.
27. Granberg S, Wikland M. Endovaginal Ultrasound in the diagnosis of unilocular ovarian cysts in postmenopausal women. Ultrasound Quarterly. 1992;10:1-13.
28. Granberg S, Wikland M, Jansson I. Macroscopic Characterization of ovarian cancer and relation to the histological diagnosis: criteria to be used for ultrasound evaluation. Gynecol Oncol. 1989;35:139-44.
29. Granberg S, Norström A, Wikland M. Endovaginal ultrasound and cytological evaluation of cystic ovarian tumors, a comparison. J Ultrasound Med. 1991;10:9-14.
30. Granberg S, Norström A, Wikland M. Tumours in lower pelvis imaged by vaginal ultrasound. Gynecol Oncol. 1989;37:224-9.
31. Andolf E, Jörgensen C. Simple adnexal cysts diagnosed by ultrasound in postmenopausal women. J Clin Ultrasound. 1988;16:301-3.
32. Andolf E, Jörgensen C. Cystic lesions in elderly women, diagnosed by ultrasound. Br J Obstet Gynaecol. 1989;96:1076-9.
33. Goldstein SR, Subramanyam B, Snyder JR, et al. The postmenopausal cystic adnexal mass: The potential role of ultrasound in conservative management. Obstet Gynecol. 1989;73:8-10.
34. Parker WH, Berek JS. Management of selected cystic adnexal masses in postmenopausal women by operative laparoscopy: a pilot study. Am J Obstet Gynecol. 1990;163:1574-7.
35. Valentin L, Akrawi D. The natural history of adnexal cysts incidentally detected at transvaginal ultrasound examination in postmenopausal women. Ultrasound Obstet Gynecol. 2002;20:174-80.
36. Valentin L, Skoog L, Epstein E. Frequency and type of adnexal lesions in autopsy material from postmenopausal women: ultrasound study with histological correlation. Ultrasound Obstet Gynecol. 2003;22:284-9.
37. Modesitt SC, Pavlik EJ, Ueland FR, et al. Risk of malignancy in unilocular ovarian cystic tumors less than 10 centimeters in diameter. Obstet Gynecol. 2003;102:594-9.
38. Nardo LG, Kroon ND, Reginald PW. Persistent unilocular ovarian cysts in a general population of postmenopausal women: is there a place for expectant management? Obstet Gynecol. 2003;102:589-93.
39. Castillo G, Alcazar JL, Jurado M. Natural history of sonographically detected simple unilocular adnexal cysts in asymptomatic postmenopausal women. Gynecol Oncol. 2004;92:965-9.
40. Dorum A, Blom GP, Ekerhovd E, et al. Prevalence and histologic diagnosis of adnexal cysts in postmenopausal women: an autopsy study. Am J Obstet Gynecol. 2005;192:48-54.
41. Greenlee RT, Kessel B, Williams CR, et al. Prevalence, incidence, and natural history of simple ovarian cysts among women >55 years old in a large cancer screening trial. Am J Obstet Gynecol. 2010;202:373.e1-9.
42. Dietrich M, Osmers RG, Grobe G, et al. Limitations of the evaluation of adnexal masses by its macroscopic aspects, cytology and biopsy. Eur J Obstet Gynecol Reprod Biol. 1999;82:57-62.
43. Tahir Z, Yusuf NW, Ashraf M, et al. Fine needle aspiration of unilocular ovarian cysts—a cytohistological correlation. J Pak Med Assoc. 2004;54:266-9.
44. Papathanasiou K, Giannoulis C, Dovas D, et al. Fine needle aspiration cytology of the ovary: is it reliable? Clin Exp Obstet Gynecol. 2004;31:191-3.
45. RCOG. Ovarian Cysts in Postmenopausal Women: RCOG guideline No. 34. London: RCOG Press; 2003. pp. 1-8.
46. Kurjak A, Shalan H, Matijevic R, et al. Stage I ovarian cancer by transvaginal color Doppler sonography: a report of 18 cases. Ultrasound Obstet Gynecol. 1993;3:195-8.
47. Kurjak A, Kupesic S. Ovarian senescence and its significance on uterine and ovarian perfusion. Fertil Steril. 1995;3:532-7.
48. Kurjak A, Kupesic-Urek S, Schulman H, et al. Transvaginal color Doppler in the assessment of ovarian and uterine blood flow in infertile women. Fertil Steril. 1992;56:870-3.
49. Scholtes MCW, Wladimiroff J, Rijen HJM, et al. Uterine and ovarian flow velocity waveforms in the normal menstrual cycle; a transvaginal color Doppler study. Fertil Steril. 1989;52:981-5.
50. Kurjak A, Schulman H, Sosic A, et al. Transvaginal ultrasound, color flow, and Doppler waveform of the postmenopausal adnexal mass. Obstet Gynecol. 1992;80:917-21.
51. Fleischer AC, Rodgers WH, Kepple DM, et al. Color Doppler sonography of ovarian masses: a multiparameter analysis. J Ultrasound Med. 1993;12:41-8.
52. Crade M, Patel J, Yiu-Chiu V. Evaluation of 103 pelvic masses: correlation of surgical diagnosis with transvaginal ultrasound size, complexity scores and resistive index values. Ultrasound Obstet Gynecol. 1993;3:23.
53. Kulenkampff D, Puchta J, Osmers R. Sonographic appearance of the myometrium. In: Osmers R, Kurjak A

(Eds). Ultrasound and the Uterus. Carnforth, New York: Parthenon Publishing; 1995. pp. 53-9.
54. Rempen A. Normal sonographic features of the uterus. In: Osmers R, Kurjak A (Eds). Ultrasound and the uterus. Carnforth, New York: Parthenon Publishing; 1995. pp. 1-12.
55. deVries K, Lyons KEA, Ballard G, et al. Contractions of the inner third of the myometrium. Am J Obstet Gynecol. 1990;162:679-82.
56. Andolf E, Dahlander K, Aspenberg P. Ultrasonic thickness of the endometrium correlated to body weight in asymptomatic postmenopausal women. Obstet Gynecol. 1993;82:936-40.
57. Zalud I, Conway C, Schulman H, et al. Endometrial and myometrial thickness and uterine blood flow in postmenopausal women: the influence of hormonal replacement therapy and age. J Ultrasound Med. 1993;12:737-41.
58. Kurjak A, Kupesic-Urek S. Normal and abnormal uterine perfusion. In: Jaffe R, Warsof LS (Eds). Color Doppler imaging on Obstetrics and Gynecology. New York: McGraw Hill; 1992. pp.255-63.
59. Long MG, Boultbee JE, Hanson ME, et al. Doppler time velocity waveform studies of the uterine artery and the uterus. Br J Obstet Gynaecol. 1989;96:588-93.
60. Goswamy RK, Steptoe PC. Doppler ultrasound studies of the uterine artery in spontaneous ovarian cycles. Hum Reprod. 1988;3:721-3.
61. Goswamy RK, Williams G, Steptoe PC. Decreased uterine perfusion a cause of infertility. Hum Reprod. 1988;3:955-8.
62. Kupesic S, Kurjak A. Uterine perfusion. In: Osmers R, Kurjak A (Eds). Ultrasound and the Uterus. Carnforth, New York: Parthenon Publishing; 1995. pp. 87-90.
63. Luzi G, Coata G, Cucchia GC, et al. Doopler studies of uterine arteries in spontaneous and artificially induced menopausal women. Ultrasound Obstet Gynecol. 1993;3:354-6.
64. Lewit N, Thaler I, Rottem S. The uterus: a new look with transvaginal sonography. J Clin Ultrasound. 1990;18:331-6.
65. Kurjak A, Shalan H, Kupesic S, et al. Transvaginal color Doppler assessment in the pelvic tumor vascularity. Ultrasound Obstet Gynecol. 1993;3:137-54.
66. Hata T, Hata K, Senoh D, et al. Doppler ultrasound assessment of tumor vascularity in gynecologic disorders. J Ultrasound Med. 1989;8:309-14.
67. Kurjak A, Zalud I. The characterization of uterine tumors by transvaginal color Doppler. Ultrasound Obstet Gynecol. 1991;1:50-2.
68. Kurjak A, Kupesic-Urek S, Miric D. The assessment of benign uterine tumor vascularisation by transvaginal color Doppler. Ultrasound Med Biol 1992;18:645-9.
69. Matta WHM, Stabile I, Shaw RW, et al. Doppler assessment of uterine blood flow changes in patients with fibroids receiving the gonadotropin-releasing hormone agonist Buserelin. Fertil Steril. 1988;49:1083-5.
70. Wilson EA, Yang F, Rees ED. Estradiol and progesterone binding in uterine leiomyomata and in normal uterine tissues. Obstet Gynecol. 1980;55:20-4.
71. Solues MR, McCarthy KS. Leiomyomas: steroid receptor content. Variations within normal menstrual cycle. Am J Obstet Gynecol. 1982;143:6-11.
72. Filicori M, Hall DA, Loughlin JS, et al. A conservative approach to the management of uterine leiomyoma: pituitary desensitization by a luteinizing hormone-releasing analogue. Am J Obste Gynecol. 1983;147:726-7.
73. Aleem F, Predanić M. Uterine leiomyomata: transvaginal color Doppler studies and new aspects of management. In: Osmers R, Kurjak A (Eds). Uterus and Ultrasound. Carnforth: Parthenon Publishing; 1995. pp. 61-70.
74. Meyer WR, Meyer AR, Diamond MP. Unsuspected leiomyosarcoma: treatment with gonadotropin-releasing hormone analogue. Obstet Gynecol. 1990;75:529-34.
75. Kurjak A, Kupesic S, Shalan H, et al. Uterine sarcoma: a report of 10 cases studied by transvaginal color and pulsed Doppler sonography. Gynecol Oncol. 1995;59:342-6.
76. Szabó I, Szánthó A, Csabay L, et al. Color Doppler ultrasonography in the differentiation of uterine sarcomas from uterine leiomyomas. Eur J Gynaecol Oncol. 2002;23:29-34.
77. Vollenhoven BJ, Lawrence AS, Healy DL. Uterine fibroids: a clinical review. Br J Obstet Gynaecol. 1990;97:285-98.
78. Jirapinyo M, Theppisai U, Leelapatana P, et al. Sonographic findings of uterus and ovaries in normal pre- and post-menopausal women. J Med Assoc Thai. 1998;81:527-31.
79. Fedele L, Bianchi S, Raffaelli R, et al. A randomized study of the effects of tibolone and transdermal estrogen replacement therapy in postmenopausal women with uterine myomas. Eur J Obstet Gynecol Reprod Biol. 2000;88:91-4.
80. Colacurci N, De Francis P, Cobellis L, et al. Effects of hormone replacement therapy on postmenopausal uterine myoma. Maturitas. 2000;35:167-73.
81. Polatti F, Viazzo F, Colleoni R, et al. Uterine myoma in postmenopause: a comparison between two therapeutic schedules of HRT. Maturitas. 2000;37:27-32.
82. Simsek T, Karakus C, Trak B. Impact of different hormone replacement therapy regimens on the size of myoma uteri in postmenopausal period. Tibolone versus transdermal hormonal replacement system. Maturitas. 2002;42:243-6.
83. Osmers R, Kuhn W. Endometrial cancer screening. Current Opinion Obstet Gynecol 1994;6:75-9.
84. Osmers R, Puchta J, Suren A. Pathological findings of the postmenopausal endometrium. In: Osmers R, Kurjak A (Eds). Ultrasound and the Uterus. Carnforth, New York: Parthenon Publishing. 1995:31-44.
85. Granberg S, Wikland M, Karlsson B, et al. Endometrial thickness as measured by endovaginal ultrasound for identifying endometrial abnormality. Am J Obstet Gynecol. 1991;164:47-52.
86. Kurjak A, Shalan H, Sosic A, et al. Endometrial carcinoma in postmenopausal women: evaluation by transvaginal Color Doppler. Am J Obstet Gynecol. 1993;169:1597-603.
87. Kamel HS, Darwish AM, Mohamed SA. Comparison of transvaginal ultrasonography and vaginal sonohysterography in the detection of endometrial polyps. Acta Obstet Gynecol Scand. 2000;79:60-4.

88. Lin MC, Gosin BB, Wolf SI, et al. Endometrial thickness after the menopause: effect of the hormone replacement. Radiology. 1991;180:427-32.
89. Lurain JR. Uterine cancer. In: Berek JS (Ed.). Berek & Novak's Gynecology, 14th edition. Philadelphia: Lippincott, Williams & Wilkins; 2007. pp. 1343-402.
90. Bourne TH, Campbell S, Whitehead MI, et al. Detection of endometrial cancer in postmenopausal women by transvaginal ultrasonography and colour flow imaging. Br Med J. 1990;301(6748):369.
91. Lehtovirta P, Cacciatore B, Wahlstrom T, et al. Ultrasonic assessment of endometrial cancer invasion. J Clin Ultrasound. 1987;15:519-24.
92. Osmers R. Transvaginal sonography in endometrial cancer. Ultrasound Obstet Gynecol. 1992;2:2-3.
93. Bourne TH. Transvaginal color Doppler in Gynecology. Ultrasound Obstet Gynecol. 1991;1:359-73.
94. Osmers R, Völksen M, Rath W, et al. Vaginosonographic detection of endometrial cancer in postmenopausal women. Int J Gynecol Obstet. 1990;32:35-7.
95. Wikland M, Granberg S, Karlsson B. Assessment of the endometrium in the postmenopausal woman by vaginal sonography. Ultrasound Quarterly. 1992;10:15-27.
96. Osmers R, Volksen M, Schauer A. Vaginosonography for early detection of endometrial carcinoma. Lancet. 1990;1:1569-71.
97. Gambacciani M, Monteleone P, Ciaponi M, et al. Clinical usefulness of endometrial screening by ultrasound in asymptomatic postmenopausal women. Maturitas. 2004;48:421-4.
98. Flowers CE, Wilborn WH, Hyde BM. Mechanisms of uterine bleeding in postmenopausal patients receiving estrogen alone or with a progestin. Obstet Gynecol. 1983;61:135-43.
99. Goldstein SR, Nachtigall M, Snyder JR, et al. Endometrial assessment by vaginal ultrasonography before endometrial sampling in patients with postmenopausal bleeding. Am J Obset Gynecol. 1990;163:119-23.
100. Varner RE, Sparks JM, Cameron CD, et al. Transvaginal sonography of the endometrium in postmenopausal women. Obstet Gynecol. 1991;78:195-9.
101. Botsis D, Kassanos D, Pyrgiotis E, et al. Vaginal sonography of the endometrium in postmenopausal women. Clin Exp Obstet Gynecol. 1992;19:189-92.
102. Dorum A, Kristensen GB, Langebrekke A, et al. Evaluation of endometrial thickness measured by endovaginal ultrasound in women with postmenopausal bleeding. Acta Obstet Gynecol Scand. 1993;72:116-9.
103. Bakos O, Smith P, Heimer G. Transvaginal ultrasonography for identifying endometrial pathology in postmenopausal women. Maturitas. 1995;20:181-9.
104. Epstein E, Ramirez A, Skoog L, et al. Transvaginal sonography, saline contrast sonohysterography and hysteroscopy for the investigation of women with postmenopausal bleeding and endometrium >5 mm. Ultrasound Obstet Gynecol. 2001;18:157-62.
105. Moodley M, Roberts C. Clinical pathway for the evaluation of postmenopausal bleeding with an emphasis on endometrial cancer detection. J Obstet Gynaecol. 2004;24:736-41.
106. Karlsson B, Granberg S, Ridell B, et al. Endometrial thickness as measured by transvaginal sonography: interobserver variation. Ultrasound Obstet Gynecol. 1994;4:320-5.
107. Machado F, Moreno J, Carazo M, et al. Accuracy of endometrial biopsy with the Cornier pipelle for diagnosis of endometrial cancer and atypical hyperplasia. Eur J Gynaecol Oncol. 2003;24:279-81.
108. Epstein E, Ramirez A, Skoog L, et al. Dilatation and curettage fail to detect most focal lesions in the uterine cavity in women with postmenopausal bleeding. Acta Obstet Gynecol Scand. 2001;80:1131-6.
109. Fleischer AC, Kepple DM, Entman SS. Transvaginal sonography of uterine disorders. In: Timor-Tritsch IE, Rottem S (Eds). Transvaginal sonography, 2nd edition. New York: Elsevier Science Publishing; 1993. pp. 109-30.
110. Carlson JA, Arger P, Thompson S, et al. Clinical and pathologic correlation of endometrial cavity fluid detected by ultrasound in the postmenopausal women. Obstet Gynecol. 1991;77:119-23.
111. Brechenridge JW, Kurtz AB, Ritchie WGM, et al. Postmenopausal uterine fluid collection: indicator of carcinoma. Am J Radiol. 1982;139:529-34.
112. McCarthy KA, Hall DA, Kopans DB, et al. Postmenopausal endometrial fluid collections: always of indicator of malignancy? J Ultrasound Med. 1986;5:647-9.
113. Pardo J, Kapan B, Nitke S, et al. Postmenopausal intrauterine fluid collection: correlation between ultrasound and hysteroscopy. Ultrasound Obstet Gynecol. 1994;4:224-6.
114. Schmidt T, Nawroth F, Breidenbach M, et al. Differential indication for histological evaluation of endometrial fluid in postmenopause. Maturitas. 2005;50:177-81.
115. Bar-Hava I, Orvieto R, Ferber A, et al. Asymptomatic postmenopausal intrauterine fluid accumulation: characterization and significance. Climacteric. 1998;1:279-83.
116. Kurjak A, Zalud I, Jurkovic D, et al. Transvaginal color flow Doppler for the assessment of pelvic circulation. Acte Obstet Gynecol Scand. 1989;68:131-5.
117. Kurjak A, Shalan H, Kupesic S, et al. An attempt to screen asymptomatic women for ovarian and endometrial cancer with transvaginal color and pulsed Doppler sonography. J Ultrasound Med. 1994;13:295-301.
118. Kupesic-Urek S, Shalan H, Kurjak A. Early detection of endometrial cancer by transvaginal color Doppler. Eur J Obstet Gynecol Reprod Biol. 1993;49:46-9.
119. Hata K, Hata T, Manabe A, et al. New pelvic sonography for detection of endometrial carcinoma: a preliminary report. Gynecol Oncol. 1992;45:179-84.
120. Smith DC, Prentice R, Thompson DJ, et al. Association of exogenous estrogen and endometrial carcinoma. N Engl J Med. 1975;293:1164-7.
121. Ziel HK, Finkle WD. Increased risk of endometrial carcinoma among users of conjugated estrogens. N Engl J Med. 1975;293:1167-70.

122. Whitehead MI, Townsend PT, Pryse-Davies J, et al. Effects of various types and dosages of progestogens on the postmenopausal endometrium. J Reprod Med. 1982;27:539-48.
123. Jensen LC, Obel EB, Linhard E, et al. Frequency of curettage in middle-aged women treated with sequential preparations versus untreated women. Maturitas. 1992;15:61-9.
124. Castelo-Branco C, Puerto B, Durán M, et al. Transvaginal sonography of the endometrium in postmenopausal women: monitoring the effect of hormone replacement therapy. Maturitas. 1994;19:59-65.
125. Meuwissen JHJM, van Langen H, Moret E, et al. Monitoring of oestrogen replacement therapy by vaginosonography of the endometrium. Maturitas. 1992;15:33-7.
126. Archer DF, Pickar JH. Hormone replacement therapy: effect of progestin dose and time since menopause on endometrial bleeding. Obstet Gynecol. 2000;96:899-905.

55
CHAPTER

The Use of Ultrasound as an Adjunct to the Physical Examination for the Evaluation of Gynecologic and Obstetric Causes of Acute Pelvic Pain

Sanja Kupesic Plavsic, Nadah Zafar, Ulrich Honemeyer, Branko M Plavsic

INTRODUCTION

Acute pelvic pain may be the manifestation of various gynecologic and nongynecologic disorders ranging from a less alarming rupture of a follicular cyst to life-threatening conditions such as rupture of an ectopic pregnancy or perforation of an inflamed appendix.

Pelvic inflammatory disease presents with many ultrasonographic signs such as thickening of the tubal wall, incomplete septa within the dilated tube, demonstration of hyperechoic mural nodules, free fluid in the "cul-de-sac," etc. Other pathologies, such as hemorrhagic ovarian cysts, present with a variety of ultrasound findings since intracystic echoes depend upon the quality and quantity of the blood clots. The color Doppler investigation demonstrates a moderate-to-low vascular resistance typical of luteal flow. Another example that demonstrates another use of ultrasound as an aid in diagnosis is endometriosis. The classic symptom of endometriosis is chronic pelvic pain, in some patients acute pelvic pain does occur. Most of these patients demonstrate an endometrioma or "chocolate" cyst containing diffuse carpet-like echoes. One should be aware that the detection of a pericystic and/or hilar type of an ovarian endometrioma vascularization by color Doppler ultrasound facilitates correct recognition of this entity. Pelvic congestion syndrome is another condition that can cause an attack of acute pelvic pain. It usually occurs as a consequence of dilatation of venous plexuses, arteries or both systems. By switching to color Doppler, gynecologist can differentiate pelvic congestion syndrome from multilocular cysts, pelvic inflammatory disease or adenomyosis. Acute pelvic pain may occur even in normal intrauterine pregnancy. This may be explained by hormonal changes, rapid growth of the uterus and increased blood flow. Ultrasound is mandatory for distinguishing normal intrauterine pregnancy from a threatened or spontaneous abortion, ectopic pregnancy and/or other complications that may occur in patients with a positive pregnancy test.

Detection of uterine dehiscence and rupture in patients with history of prior surgical intervention on uterine wall relies exclusively on correct ultrasound diagnosis. In patients with placental abruption the sonographer can detect a hypoechoic complex, which may represent a retroplacental hematoma, a subchorionic hematoma or a subamniotic hemorrhage.

In conclusion, the ultrasound has already become an important and easily available tool, which can efficiently recognize patients with a variety of threatening conditions.

GYNECOLOGIC ETIOLOGIES OF ACUTE PELVIC PAIN

Acute pelvic pain may be the manifestation of various gynecologic and nongynecologic disorders ranging from life-threatening conditions such rupture of an ectopic pregnancy or the perforation of an inflamed appendix to the less the alarming setting of a rupture of a periovulatory follicle. The astute clinician must bear in mind all of the possibilities when evaluating patients

presenting with acute pelvic pain.[1,2] Localizing the site of pain in combination with an ultrasound examination of the affected area leads to prompt and accurate clinical diagnosis. Ultrasound has become a valuable tool in evaluating the patient presenting with acute pelvic pain of both gynecological and nongynecological in origin such as appendicitis or urinary stones.[3] It would be advisable to offer some type of an algorithm for the differential diagnosis that could guide physicians through the management of such a problem.

A ruptured ectopic pregnancy, salpingitis and hemorrhagic ovarian cysts are the three most commonly diagnosed gynecologic conditions presenting with an acute abdomen. Degenerating leiomyomas and adnexal torsion occur less frequently.[4] In order to have a systematic approach, gynecologic causes of acute pelvic pain can be further divided into two categories those with a negative pregnancy test and those with a positive pregnancy test.

Acute Pelvic Pain with a Negative Pregnancy Test

Pelvic inflammatory disease: Pelvic inflammatory disease (PID) is defined as the acute clinical syndrome associated with the spread of microorganisms (unrelated to pregnancy or surgery) from the vagina or cervix to the endometrium.[5] fallopian tubes and/or the contiguous structures.[6] This disease can lead to infertility, ectopic pregnancy and chronic pelvic pain.[7,8] Sexually active adolescents are at the greatest risk for PID. Other risk factors include multiple sexual partners, a high number of sexual partners throughout an individual's lifespan, the use of an intrauterine device (IUD), an untreated infected male sex partner (s), a history of previous PID, presence of Neisseria gonorrhoeae or Chlamydia trachomatis in the reproductive tract and frequent vaginal douching.[7] PID causes more morbidity than necessary for three reasons: women are not hospitalized when they should be, many women receive inadequate antibiotic therapy and the male partner was not treated or is treated inappropriately.[9] The PID may manifest itself by various clinical presentations: silent (asymptomatic), atypical, acute and chronic. The patient with acute PID complains mainly of low abdominal tenderness. Some of them may have an increased body temperature, but it is not unusual to have patients with a normal temperature. Laboratory findings show an increased sedimentation rate and white blood cell count. The next step is to evaluate the pelvis ultrasonographically keeping in mind that the sonographic findings may be normal in the early course of the disease.[10] Acute PID is usually presents with:

1. Thickening of the tube wall of greater than or equal to 5 mm.
2. Incomplete septa correlating with the mucosal folds in the dilated tube that is sonolucent or contain low-level echoes. (This finding does not discriminate between acute and chronic cases).
3. "Beads-on-a-string" sign, which defines hyperechoic mural nodules measuring about 2–3 mm, visualized on the cross-section of a fluid filled distended tube.
4. Formation of the tubo-ovarian complex (the ovary cannot be separated from the tube by pushing it with the vaginal probe).
5. Fluid in the Cul-de-sac.
6. Low-to-moderate resistance index (RI = 0.53 ± 0.09) obtained from the adnexal region.

Figures 55.1A to C demonstrate complex adnexal mass in a patient with acute PID.

Chronic PID can develop either as the consequence of an acute, symptomatic infection or as a consequence of a silent asymptomatic disease in patients without any clinical evidence of salpingitis. The most common ultrasound appearance is the hydrosalpinx, formed when the fimbrial part of the tube is closed because of pelvic adhesions causing the accumulation of tubal mucus. Chronic hydrosalpinx is usually discovered accidentally on a routine transvaginal ultrasound scan or during the assessment of infertile patients **(Table 55.1)**.

Hemorrhagic Ovarian Cysts

Cyclic causes of pelvic pain include crampy abdominal pain due to normal menstruation and development of the corpus luteum cyst. Corpus luteum cyst may be painful either due to the large size of the cyst or due to the hemorrhage within the cyst. Patients with a hemorrhagic ovarian cyst may experience abrupt onset of low abdominal or pelvic pain and in this case the complete blood count may demonstrate a low hematocrit value. Cyst rupture with hemorrhage into the peritoneum is a rare cause of pelvic pain. Functional cysts other than corpus luteum can also be complicated by hemorrhage and rupture. Hemorrhage is excellent evidence that an ovarian mass is benign. Of the hemorrhagic cysts reported in the sonographic literature 98% were non-neoplastic and the remaining 2% were benign tumors.[11-13] The ultrasonographic appearance of the hemorrhagic cysts has different characteristics due to the retracting blood clots. They can look solid or have

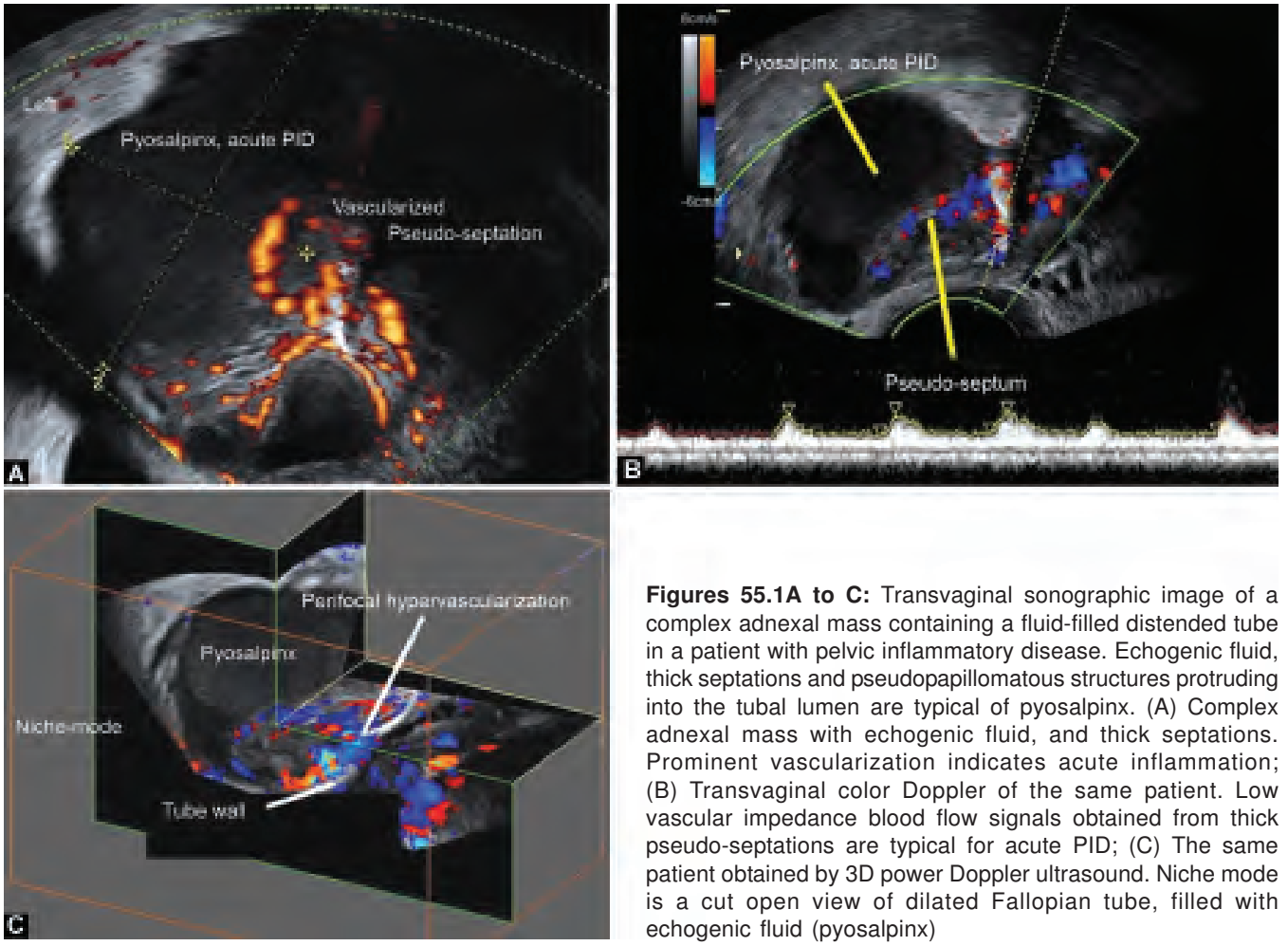

Figures 55.1A to C: Transvaginal sonographic image of a complex adnexal mass containing a fluid-filled distended tube in a patient with pelvic inflammatory disease. Echogenic fluid, thick septations and pseudopapillomatous structures protruding into the tubal lumen are typical of pyosalpinx. (A) Complex adnexal mass with echogenic fluid, and thick septations. Prominent vascularization indicates acute inflammation; (B) Transvaginal color Doppler of the same patient. Low vascular impedance blood flow signals obtained from thick pseudo-septations are typical for acute PID; (C) The same patient obtained by 3D power Doppler ultrasound. Niche mode is a cut open view of dilated Fallopian tube, filled with echogenic fluid (pyosalpinx)

TABLE 55.1

A suggested algorithm for the diagnosis of pelvic inflammatory disease

Diagnosis	*Clinical signs*	*Ultrasound findings*	*Color Doppler findings*
Acute salpingitis	Low abdominal tenderness Increased/normal body temperature ↑ SE, ↑ L	Tubes filled with inflammatory secretions Retort-shaped tubes	Low to moderate resistance index (RI = 0.53 ± 0.09)
Tubo-ovarian abscess	Severe pain in the lower abdomen High fever↑ SE, ↑ L	Multilocular or unilocular fluid-filled structure Air bubbles in case of gas-producing bacterial infection	Low vascular resistance signals obtained from the septa or periphery of the lesion (RI = 0.40 ± 0.08)
Chronic salpingitis	Mild or absent symptoms Infertility	"Cogwheel sign" Distended tubes with incomplete septa Hyperechogenic knots may be visualized every few millimeters in a transverse section	High vascular resistance (RI = 0.71 ± 0.09) Absence of diastolic flow, indicating irreversible scarification (RI = 1.0)

SE—erythrocyte sedimentation rate; L—white blood cell count

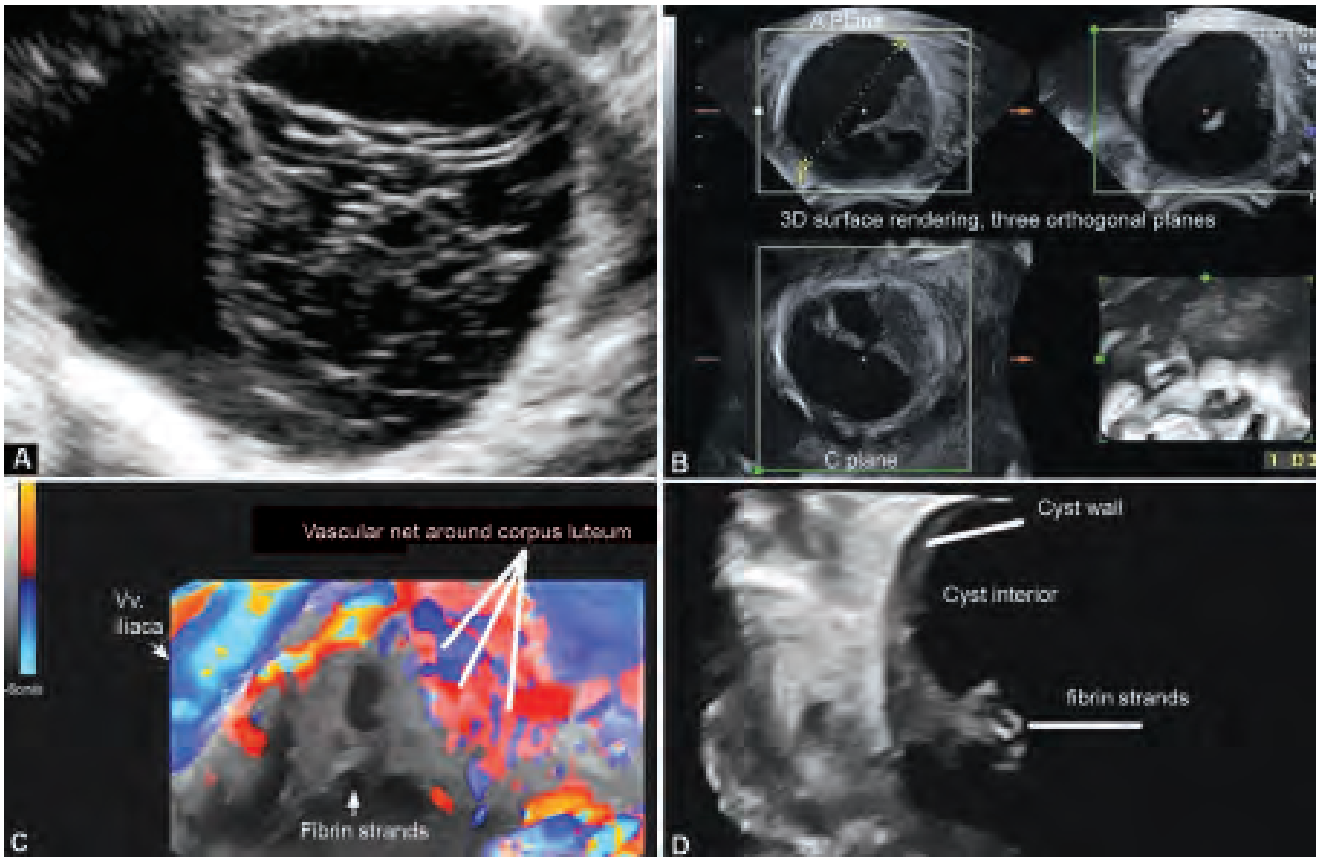

Figures 55.2A to D: Transvaginal ultrasound of a hemorrhagic ovarian cyst. Echogenic content represents a retracting clot within the blood-filled cavity of the former follicle. (A) Corpus luteum hemorrhagic cyst obtained by 2D ultrasound. Internal echoes represent retracting clot; (B) Three-dimensional ultrasound of a hemorrhagic cyst. Three orthogonal planes (a, b and c) and surface rendering (right lower image) demonstrate a complex cystic lesion; (C) Color Doppler image of the same patient. Prominent blood flow signals visualized at the periphery of the cystic lesion indicate corpus luteum angiogenesis; (D) Three-dimensional ultrasound of the same patient. Note fibrin strands protruding from the wall of the cystic structure

focal thickening of the walls with a fluid level sometimes resembling an endometrioma. Some hemorrhagic ovarian cysts can mimic sonographic features of solid ovarian masses, such as a teratoma. In most cases, the degree of through transmission is greater than in truly solid masses, and the mass regresses in size over a 2–3 week period. On sonography, the most common appearance is a complex mass with internal echoes, in addition there is enhanced through transmission **(Figs 55.2A to D).** Although the fibrinolized clot is typically hypoechoic, an acute intraparenchymal hemorrhage frequently appears as an irregular echogenic area. The cyst wall may be irregular in contour due to a clot that is adherent to it. Occasionally, a mildly echogenic interface can be seen within a hemorrhagic cyst, most likely representing a partially solid clot.[12,13] Hemorrhagic cysts show moderate-to-low vascular resistance (RI = 0.50 ± 0.08) and are usually detected at the periphery, while the solid component representing a blood clot remains avascular.

Degenerating Leiomyomas

Leiomyomas are the most common tumors of female pelvis and occur in 20–25% of women of reproductive age. Clinically, symptoms such as metrorrhagia, pelvic pain and infertility are usually present in patients with submucosal leiomyomas, whereas subserosal leiomyomas are mainly asymptomatic. Subserosal leiomyomas may cause lumbar pain and urinary or bowel symptoms due to compression.[14] Acute symptoms are usually seen in leiomyomas undergoing torsion or necrosis.[15] The ultrasound appearance of leiomyomas depends on its size, site and age of the tumor. They are usually spherical in shape and sharply demarked from the myometrium unlike adenomyosis. Sonographic texture of leiomyomas ranges from hypoechoic to echogenic,

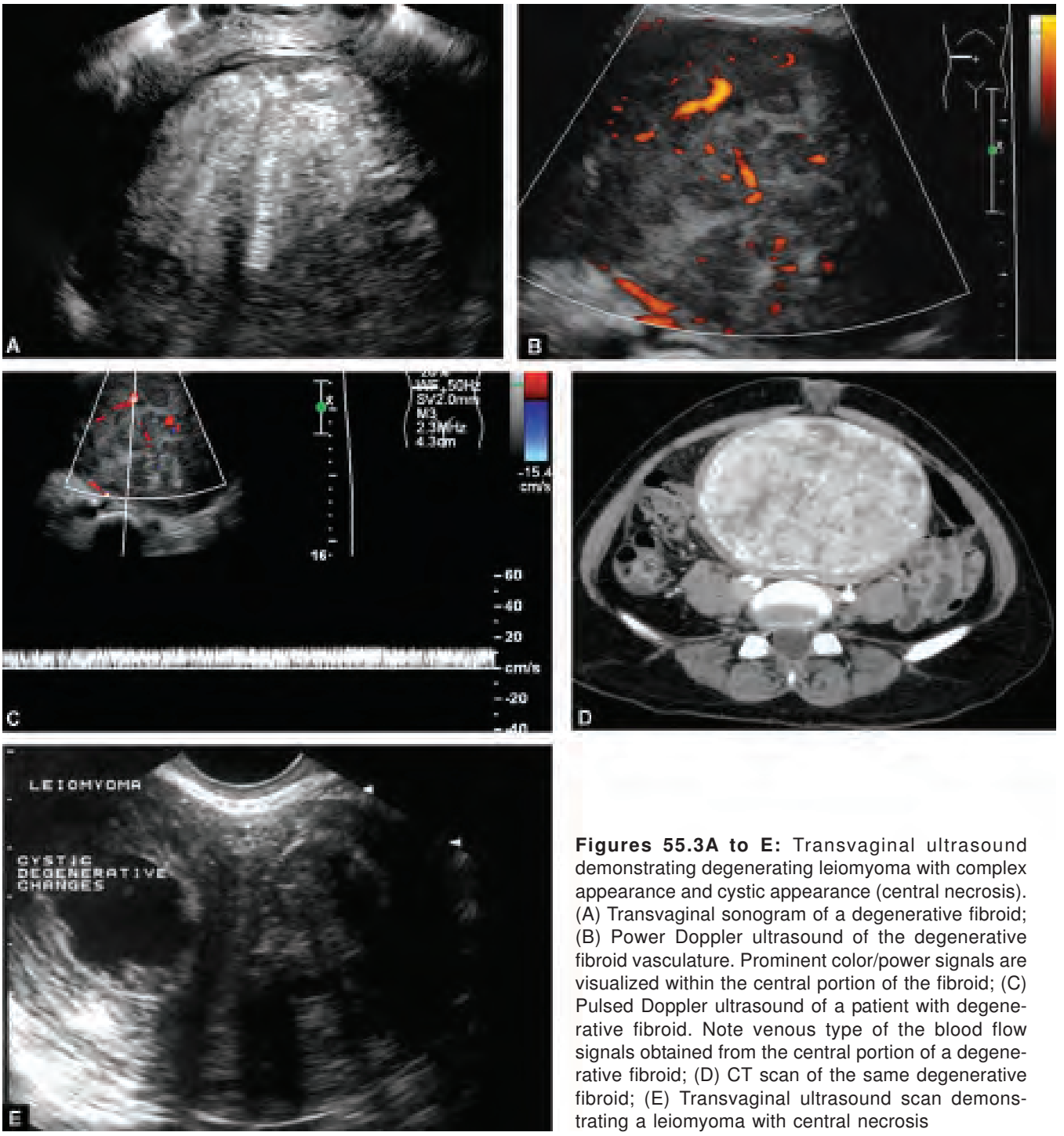

Figures 55.3A to E: Transvaginal ultrasound demonstrating degenerating leiomyoma with complex appearance and cystic appearance (central necrosis). (A) Transvaginal sonogram of a degenerative fibroid; (B) Power Doppler ultrasound of the degenerative fibroid vasculature. Prominent color/power signals are visualized within the central portion of the fibroid; (C) Pulsed Doppler ultrasound of a patient with degenerative fibroid. Note venous type of the blood flow signals obtained from the central portion of a degenerative fibroid; (D) CT scan of the same degenerative fibroid; (E) Transvaginal ultrasound scan demonstrating a leiomyoma with central necrosis

depending on the amount of smooth muscle and connective tissue. If present, secondary changes such as necrosis, hemorrhage, degeneration and or calcification are represented by a wide spectrum of ultrasonic images. A leiomyoma undergoing cystic degeneration (hemorrhagic or proteolytic) presents as a complex or anechoic uterine mass **(Figs 55.3A to E)**, which demonstrates far acoustic enhancement. There might be highly echogenic portions and an associated acoustic shadowing from areas of calcification, varying from small focal deposits to extensive calcifications, usually seen in older women.[16] Color flow detects the myoma's

feeder vessels that arise from the myometrial vasculature and form a regular ring of angiogenesis and central vessels that develop as a response to the angiogenic activity of the tumor cells, perhaps due to a necrotic or inflammatory process. Resistance index of the myometrial blood flow in the patients with leiomyoma is 0.54 ± 0.12. Very low resistance indices are usually present in cases with secondary degenerative or inflammatory changes within the leiomyoma. In such cases it is essential to differentiate this benign condition from a uterine sarcoma that shows rapid increase in size and lower RI of the tumoral blood flow (RI = 0.37 ± 0.03) and RI of the uterine artery (RI = 0.62 ± 0.07, in comparison to the RI of the uterine artery in myomatous uterus that shows a RI of 0.74 ± 0.09)[17] or normal a uterus (RI = 0.84 ± 0.09).[18] The difference in vascular signatures noted in this study may have a predictive value in the growth rate evaluation of these benign uterine masses.

Adnexal Torsion

Torsion of the ovary and the Fallopian tube is a gynecological emergency that manifests itself with acute pelvic pain.[19] It mostly occurs in patients with adnexal lesions measuring 4–8 cm in diameter. Masses which measure smaller than this do not typically cause torsion. While larger masses are not mobile enough to cause torsion.[20] The recent literature has reported the occurrence of tubal torsion following tubal ligation and laparoscopic tubal cauterization.[21] Adnexal torsion is associated with massive edema and/or hemorrhage within the ovary. The Doppler features relate to the grade and chronicity of the torsion.[22-24] In the initial stage of the torsion, venous blood flow is reduced while arterial signals demonstrate high-impedance blood flow signals indicating that venous and lymphatic occlusion occur first. It is useful to bear in mind that ovarian flow, both venous and arterial may be present in the setting of an ovarian torsion. This is due either to partial torsion of the vascular pedicle or to the dual blood supply of the ovary (from the adnexal branch of the uterine artery and the ovarian artery). In extreme cases, reverse diastolic flow of the intraovarian arteries can be detected.[25] At a later stage when the occlusion is total and involves the arterial circulation, no adnexal blood flow is seen **(Figs 55.4A to C)**. Expeditious and early diagnosis of adnexal torsion is highly dependent on the operator's experience. Color Doppler allows prompt and early diagnosis of adnexal torsion before irreversible ischemic changes occur, leading to necrosis and gangrene of the involved organs. This may contribute to conservative treatment by minimally

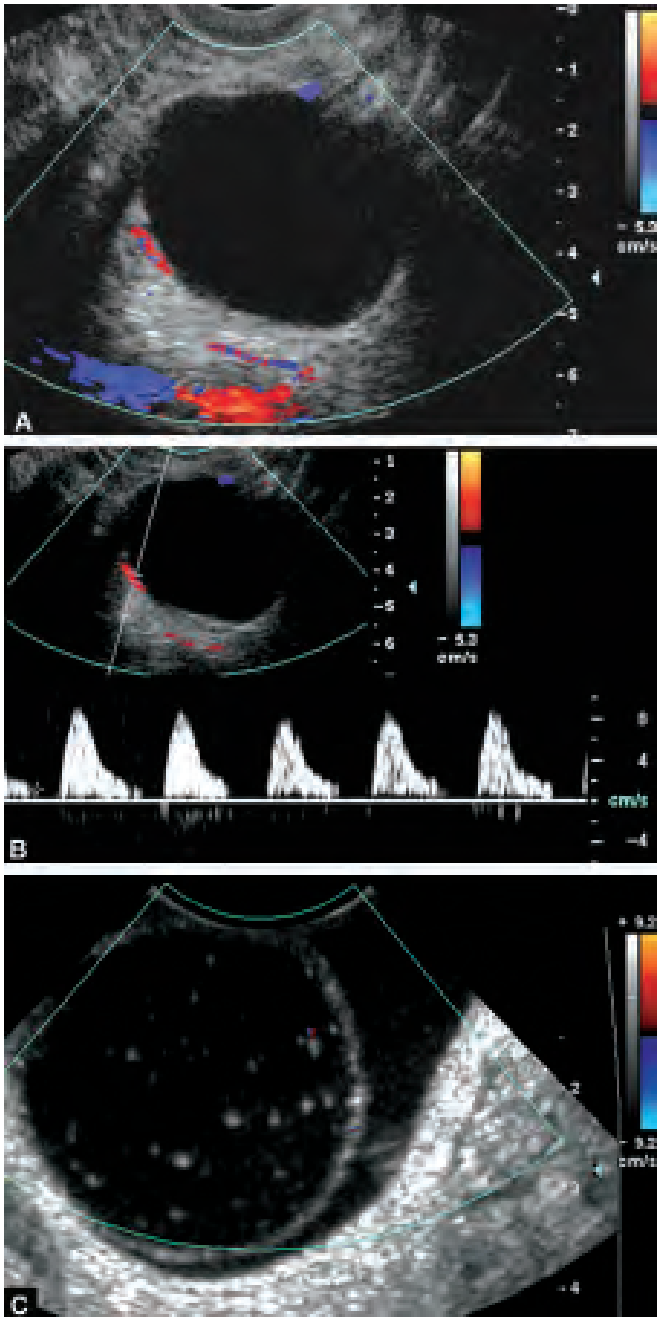

Figures 55.4A to C: Transvaginal color Doppler images of adnexal torsion. (A) Partial adnexal torsion of a simple ovarian cyst in a patient presenting with pelvic pain. Discrete blood flow signals are detected at the periphery of the ovarian cyst; (B) The same patient as in previous figure. Pulsed Doppler waveform analysis demonstrates arterial type of blood flow signals with absence of diastolic flow. Sonographic and Doppler findings are suggestive of partial adnexal torsion. Venous type of blood flow signals were also obtained; (C) Color Doppler scan of a complete adnexal torsion. Note the absence of both the venous and arterial blood flow signals

invasive surgery and may prevent surgical removal of the affected structures.[26]

Endometriosis

It is defined as a condition resulting from the ectopic location of the endometrial tissue outside the uterine cavity (peritoneal cavity, abdominal and pelvic organs and pelvic ligaments).[27] The precise etiology of this disease is still to be determined. Many theories, some of them more probable than the others have been proposed to explain the pathogenesis of endometriosis. The metastatic theory postulates the importance of the transportation of the viable endometrial cells regurgitated through the fallopian tubes at the time of menstruation. The metaplasia theory explains the origin of endometriosis by metaplastic differentiation of the original celomic membrane with prolonged irritation and/or estrogen stimulation of the endometrium-like tissue. It is proposed that the adult cells undergo de-differentiation back to their primitive origin and then transform into endometrial cells. The third theory, which is the genetic theory, postulates that there may be a genetic component in the pathogenesis of endometriosis. This is because it has been shown that there is a statistically higher incidence of endometriosis in first-degree relatives of patients with this disorder.[28] The classic symptom of endometriosis is chronic pain associated with menstruation and or the immediate premenstrual phase or persistent pain without the cyclicity.[29] Even though the classic symptom of endometriosis is chronic pain, in 21% of the cases it manifests itself with acute pelvic pain.[30] Other symptoms associated with this condition frequently noted are dysmenorrhea, dyspareunia, atypical bleeding, premenstrual spotting, menometrorrhagia, while rectal bleeding or hematuria although pathognomonic are rarely encountered. An endometrioma (so called "chocolate cyst") has a variety of ultrasonographic appearances ranging from an anechoic cyst, cyst containing diffuse low-level echoes with or without solid components, to a solid-appearing mass **(Figs 55.5A to C)**. "Carpet-like" echoes or "grinded glass appearance" are found in 82% of endometriomas.[31] Sometimes it is difficult to differentiate an endometrioma from a hemorrhagic ovarian cyst or corpus luteum cyst but the sonographer should always bear in mind the typical morphological features of endometrioma, which are thick walls, homogenicity of the echogenic content, bilaterality and multiplicity of the lesions.[32] In order to facilitate recognition of endometriosis, Kurjak and Kupesic[33] developed a new noninvasive scoring system using clinical symptoms, CA-125 level, sonographic

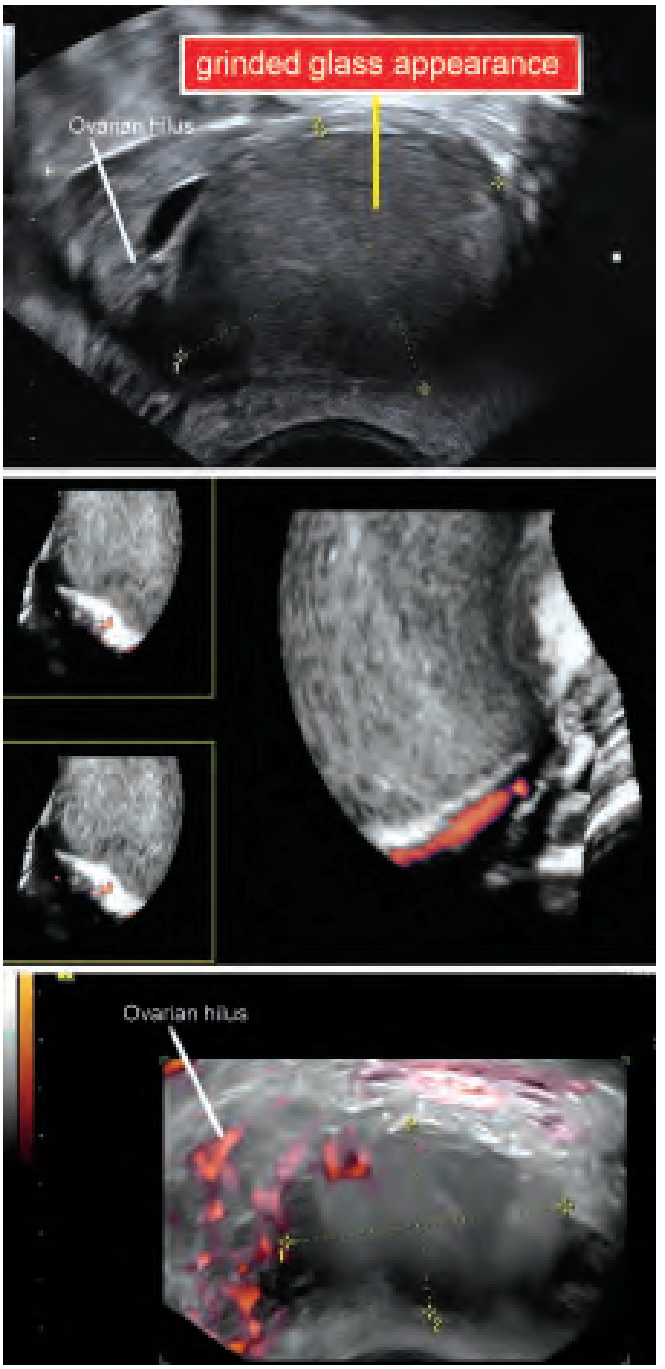

Figures 55.5A to C: Two, three-dimensional and color Doppler ultrasound images of ovarian endometrioma. Note the parenchymatous texture of the cystic content and single vessel arrangement at the periphery of the ovarian lesion. (A) Transvaginal ultrasound scan of ovarian endometrioma. Grinded glass appearance of cystic content is typical for ovarian endometrioma; (B) Color and/or power Doppler identifies peripheral vessels; (C) Another vascular pattern commonly seen in patients with ovarian endometrioma is vascularization within the ovarian hilus

TABLE 55.2
The combined scoring system for an ovarian endometrioma (from ref. 33).

Parameters	*Score*
Reproductive age	2
Chronic pain (premenstrual or menstrual)	1
Infertility	1
B-mode sonography	
Position	2
Multiplicity	1
Serial sonography positive	2
Thick walls	2
Homogeneous echogenicity	2
Clear demarcation from surrounding structures	1
Transvaginal color Doppler sonography	
Vascularization	2
Pericystic/hilar location	2
Regularly separated vessels	2
Existence of notching	1
Resistance index <0.40 (menstrual phase)	2
Resistance index 0.40 – 0.60 (late follicular/ corpus luteum phase)	2
CA-125 range 35–65 IU/ml	2

findings and transvaginal color and pulsed Doppler parameters **(Table 55.2)**.

Pelvic Congestion Syndrome

Pelvic congestion syndrome is a condition characterized by formation of pelvic varicosities with concomitant vascular stasis and congestion. There are three possible mechanisms of pelvic congestion. Varicose veins are thought to result from the effects of gravity and defective valves. Worsening of pelvic pain in the erect position in women with pelvic pain syndrome and improvement of the pain upon lying down supports this concept. The second possibility is that an abnormal increase in blood flow through a region with many arteriovenous connections could lead to a state of chronic pelvic venous dilation. The third possibility is that pelvic varicosities may occur as a result of relaxation of the smooth muscle in the walls of the pelvic veins caused by some vasoactive substance as yet unidentified.[34] Pelvic congestion syndrome's clinical presentation is that of abdominal pain in the small pelvis. It is more common in the right iliac fossa, although some patients complain of left-sided pain with movement of the pain from one side to the other. Arterial type of congestion causes predominantly acute symptoms, while venous congestion presents mainly with chronic pain.[35] Changes in position or abdominal pressure alter the symptomatology.[36] This syndrome tends to be accompanied by a polysymptomatic picture in which backache and headache occur together with leukorrhea, dysmenorrhea and functional bleeding like changes in frequency, amount and duration of bleeding or intermenstrual bleeding (result of a minute hemorrhage from the excessively congested endometrium or endocervix which is not hormone conditioned). A leukorrhoic discharge is characterized by clear mucus due to hypersecretion uncomplicated by infection. Many methods have been employed to diagnose this condition such as contrast-enhanced computed tomography, nuclear magnetic resonance,[37] angiography,[38] ultrasound and color Doppler sonography.[39,40] However, laparoscopy remains an essential component when investigating pelvic pain.[41] The sonographic findings of pelvic congestion syndrome include multiple serpentine, anechoic structures within the pelvis.[39] Although real time sonography depicts this feature, the findings of multiple cystic lesions in the pelvis suggest the occurrence of other entities as well, including hydrosalpinx, multilocular ovarian cysts, or fluid filled loops of bowel. Transvaginal color Doppler was shown as the safest and most definitive diagnostic technique within the gynecologist's reach **(Figs 55.6A to C)**. Its use has allowed a demonstration of the existence of vascular dilatation that affects not only the veins but also the arterial system.[35] The venous plexuses are more thick and in most of cases, observable with vaginal sonography. This is not true for the arteries, which are thinner and have a tendency to show their dilatation in intraparenchymatous locations usually visible only after switching color Doppler. Sometimes both systems are affected, with the vascular disturbance being more intense and more widespread because of the involvement of myometrial vessels as well. Therefore, cross-sections of the dilated intramyometrial vessels may be misinterpreted as a "Swiss cheese" appearance of the myometrium as in the case of adenomyosis.

Ovarian Vein Thrombosis

This uncommon and potentially fatal disorder occurs most often in the postpartum period, but it has been reported after surgical intervention of the pelvis, trauma of the pelvis or PID.[42] Pelvic vein thrombosis may occur in nonpuerperal patients with hypercoagulable blood and has significant sequelae.[43] Ovarian vein thrombosis affects the right side in 80–90% of cases even though it has been described on the left side and bilaterally.[44-46] Right-sided predominance is explained by dextrotorsion

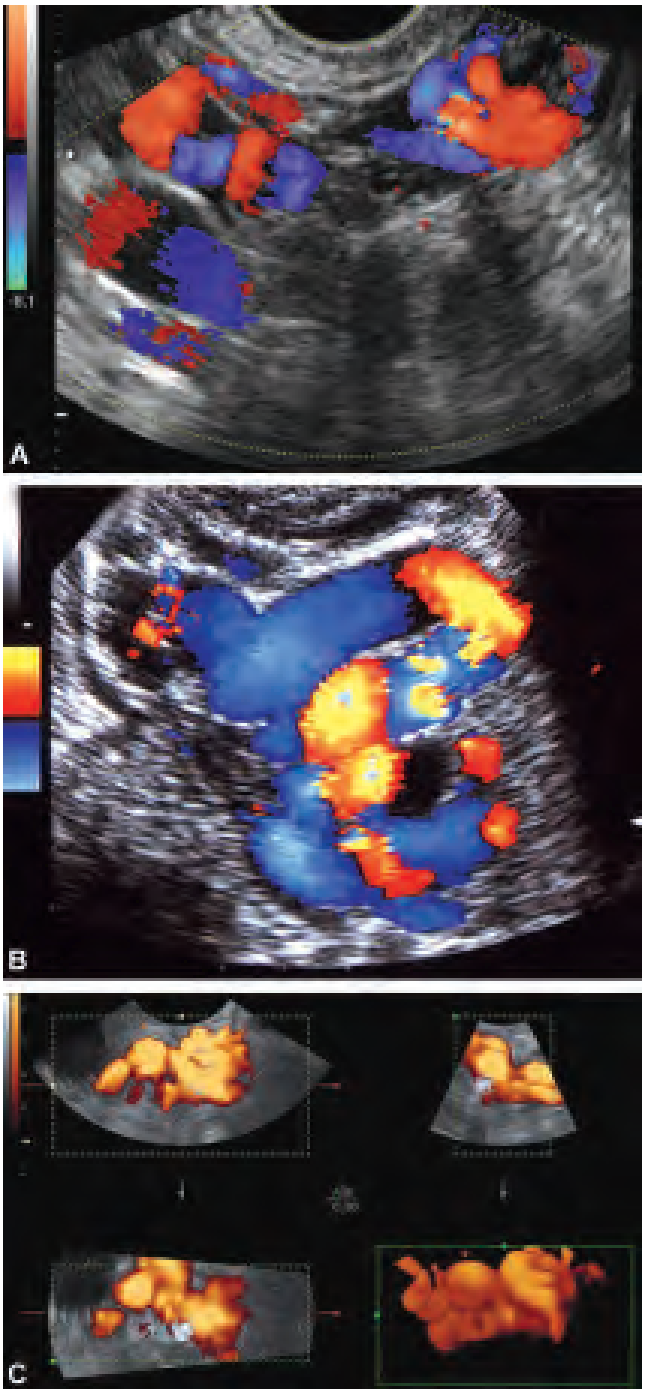

Figures 55.6A to C: 2D and 3D color Doppler and power Doppler images of pelvic congestion syndrome Bright color signals extracted from a bizarre adnexal mass represent pelvic congestion syndrome. (A) Color Doppler ultrasound of dilated periovarian and periuterine veins in a patient with pelvic congestion syndrome; (B) Tortuous and dilated pelvic venous plexuses may mimic complex adnexal mass; (C) Three dimensional power Doppler ultrasound of pelvic varicosities in a patient with chronic pelvic pain

of the gravid uterus compressing the right ovarian vein and retrograde flow in the left ovarian vein.[47,48] Most cases occur during the first week after delivery, however, rare antepartum and delayed postpartum cases have also been reported.[45] During a full-term pregnancy, ovarian veins reach the three times their normal diameter. Immediate collapse of the dilated veins observed after delivery results in low-pressure state and combined with hypercoagulability increases the risk of ovarian vein thrombosis.[49] Infection and stasis associated with the hypercoagulable state in pregnancy have been cited as additional etiologic factors,[44,49] as well as coexisting endometritis.[50] Whether thrombosis follows or precedes infection is unknown.

Acute Pelvic Pain with a Positive Pregnancy Test

Normal Intrauterine Pregnancy

It is probably the most common cause of pelvic pain in the first trimester. Crampy pelvic pain is due to hormonal changes, rapid growth of the uterus and increased blood flow. Besides clinical and laboratory signs (β-hCG), the transvaginal ultrasound examination may give additional information on the presence, location and development of the pregnancy.

Spontaneous Abortion

Threatened and spontaneous abortion is the most common complications of early pregnancy. Thirty to forty percent of pregnancies fail after implantation and only 10–15% manifest with clinical symptoms.[51-53] Patients with a spontaneous abortion usually present to a clinic/healthcare facility with symptoms of vaginal bleeding and abdominal pain, with or without the expulsion of the products of conception 8–10 weeks from their last menstrual period.[54] The decreased diameter of the gestational sac and/or its irregular shape and early intrauterine growth retardation registered on the basis of decreased crown-rump length (CRL) values are indicative for making the diagnosis of early pregnancy failure. Absences of clear visualization of the embryonic parts as well as absent embryonic heart activity are clear signs of a nonviable gestation. There are two specific manifestations of early pregnancy failure, which is important to describe, an anembryonic pregnancy (blighted ovum) and a missed abortion. An anembryonic pregnancy is defined as a gestational sac in which an embryo either failed to develop or died at the stage too early to be visualized. The diagnosis of an anembryonic pregnancy is based on the absence of embryonic echoes within the gestational sac large

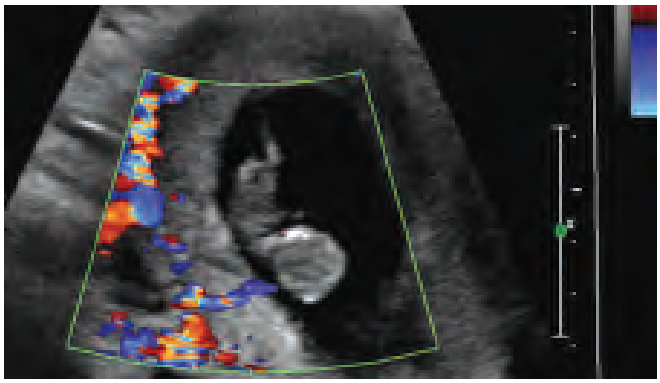

Figure 55.7: Transvaginal power Doppler scan of a missed abortion at 8 weeks' gestation. The flow pattern reveals blood flow within the maternal vessels and absence of the flow in fetal vessels. Ultrasound findings should always be correlated with the patient's symptoms, gestational age, and β-hCG values

enough for the embryonic structures to be visible, independent of the clinical data or the menstrual cycle.[55] In these patients, the gestational sac represents only an empty chorionic cavity. The studies conducted regarding the intervillous circulation demonstrated a lower PI values (0.54 ± 0.04) of the artery-like signals in patients with blighted ovum when compared to those with normal pregnancies (0.80 ± 0.04) and missed abortion (0.75 ± 0.04).[56,57] A lower PI value from the intervillous space of the anembryonic pregnancy group may reflect changes in the placental stroma, where the individual villi are prone to edema. The diagnosis of missed abortion is characterized by the identification of the fetus, which does not demonstrate any heart activity[58] **(Fig. 55.7)**. It is also described as a type of spontaneous abortion when after fetal demise, spontaneous expulsion of the conceptus outside the uterus does not occur.[59] Ultrasound findings can differentiate changes that occur in the gestational sac as time passes from the incident that caused the fetal demise and circulation break. The gestational sac image differs from a normal shape (a recent fetal demise) to a collapsed and altered shape and size (in later stages of fetal demise).The basic ultrasound finding is an embryo without heart activity and dynamics. If the event occurred recently the morphology might be preserved, but with time the embryo morphology is altered (completely amorphous or fragmented) and the size gets smaller. Another characteristic ultrasound finding of this condition is changes of trophoblast tissue. Such changes include an inhomogeneous, degenerative (hydropic or calcified) trophoblast tissue, with the presence of intrauterine hematomas and separation of membranes.

It is relatively easy to make this diagnosis by means of the transvaginal color Doppler facilities. The main parameter is the absence of the heart activity and the lack of color flow signals at expected position of the embryonic/fetal heart after the sixth gestational week.[60] However, one should be aware that the length of the time elapsing between arrest of embryonic development and clinical presentation determines the sonographic image and therefore is open for interpretation.

Ectopic Pregnancy

An ectopic pregnancy occurs when the fertilized ovum implants itself in places other than the uterine cavity. Although an ectopic pregnancy is most often localized in the fallopian tube (95%), a zygote implantation may also occur in abdominal, ovarian, intraligamentous, cornual, intramural or cervical sites.[60-64] An ectopic pregnancy is called "the great masquerader" since its clinical presentation can vary from light vaginal spotting to vasomotor shock and hemoperitoneum. The classic triad of delayed menses, irregular vaginal bleeding and abdominal pain is often not encountered. Patients presenting with acute symptoms (frequently in emergency departments) are usually at a more advanced gestational age compared to the asymptomatic infertility patients who are closely followed because of their increased risk for an ectopic pregnancy. Physical examination reveals abdominal tenderness or peritoneal irritation in the presence (or sometimes the absence) of a palpable adnexal mass. The astute clinicians should consider all presenting signs and symptoms as a possible ectopic pregnancy case until an intrauterine pregnancy or an ectopic pregnancy is diagnosed.[62]

The absolute value of the β-hCG levels in circulation are much lower than the levels of the same hormone present in a normal intrauterine pregnancies of the same gestational age. The dynamics of the titer show a slower increase of circulating concentrations which prolongs the doubling time values.

The most important use of the quantitative β-hCG determination in conjunction with ultrasonography is in understanding the value of the β-hCG "discriminatory zone." The discriminatory zone represents that level of β-hCG above which all normal intrauterine chorionic sacs will be detected by ultrasound. Now, there is almost a universal consensus as to the discriminatory zone level to be between 1000–1500 mIU/ml with the use of transvaginal probe of at least 5 MHz.[65-68] Ultrasonography, more precisely, transvaginal sonography has become the "gold standard" laboratory modality for the effective and fast diagnosis of an ectopic pregnancy.

The ultrasonographic criteria for an ectopic pregnancy can be divided into uterine and extrauterine signs (keeping in mind that all of them can be suggestive or diagnostic).[69]

The most common sign of ectopic pregnancy is the empty uterus, with or without increased endometrial thickness. A central hypoechoic area or a sac like structure inside the uterine cavity is the so-called pseudogestational sac. In some cases, a concurrent intrauterine pregnancy can be found together with an ectopic pregnancy, but this is extremely rare. It usually occurs in patients undergoing some form of an assisted reproduction technique.

Adnexal sonographic findings in women with an ectopic pregnancy are variable. A gestational sac in the adnexal region with a clear embryonic echo and heart activity directly proves an ectopic pregnancy. This is only seen in 15–28% of the cases **(Figs 55.8A to C).** A gestational sac with or without an embryonic echo can be detected in the adnexal region in 46–71% of reported cases, if the tube is unruptured. The tubal ring is generally 1–3 cm in diameter, consisting of a concentric ring of echogenic tissue measuring 2–4 mm surrounding the hypoechoic center. Very often an unspecific adnexal tumor can be visualized. In 40–83% of ectopic pregnancies cases free fluid is detected in the retrouterine space. The color Doppler is an excellent and rapid guide for identification of the peritrophoblastic tissue in patients with an ectopic pregnancy. The color flow pattern usually presents as randomly dispersed multiple small vessels showing high velocity and low-resistance signals. The sensitivity of transvaginal color and pulsed Doppler ranges from 73–96% and the specificity ranges from 87–100%.[70] Demonstration of a "hot flow pattern" shortens the diagnostic procedure and enables an earlier clinical decision to be reached for the treatment of an ectopic pregnancy. Ultrasound may aid in triage of the patient who may benefit from medical treatment, and detection of those who need immediate surgery **(Figs 55.9A and B)**.

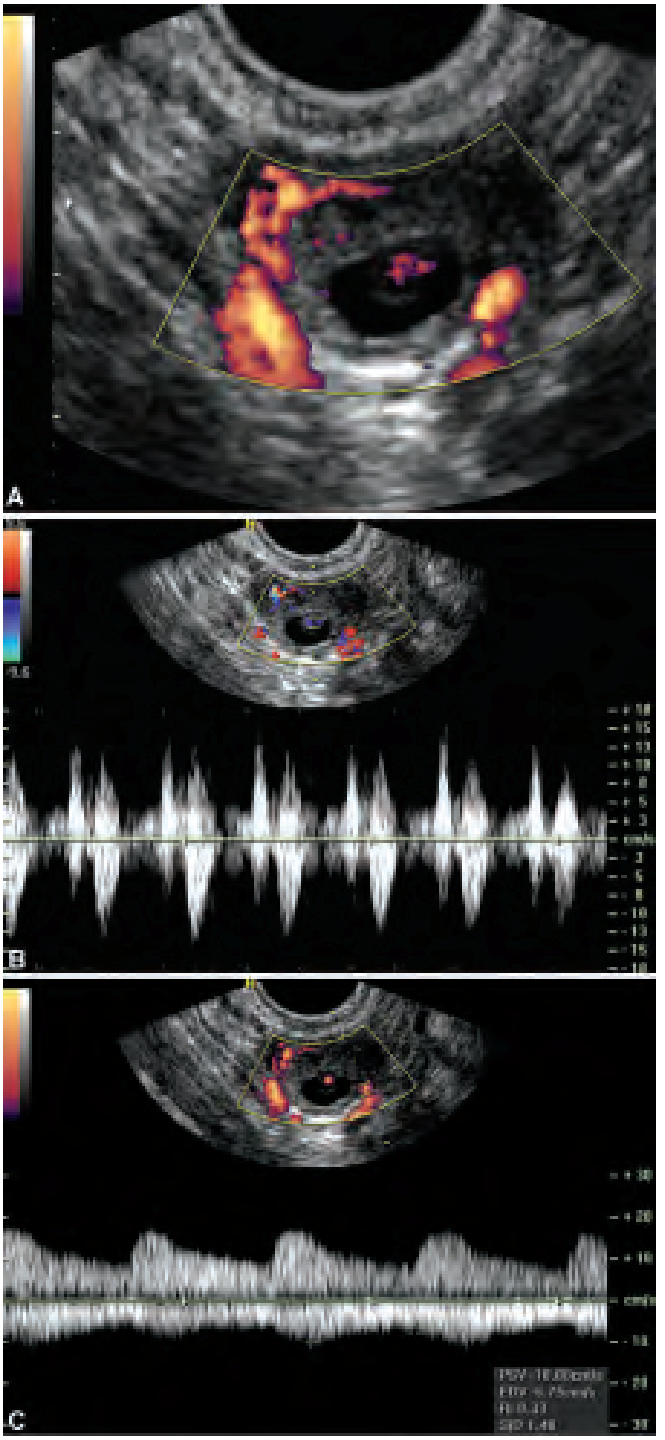

Figures 55.8A to C: Transvaginal color, power and pulsed Doppler images of ectopic pregnancy. (A) Prominent blood flow signals derived from ectopic gestational sac indicate invasive trophoblast; (B) The same patient as in Figure A. Pulsed Doppler waveform analysis obtained from the living embryo demonstrates rhythmic heart activity; (C) The same patient as in Figures A and B. Pulsed Doppler waveform analysis demonstrates low resistance index (RI = 0.33)

Corpus Luteum Cysts

Pelvic pain during pregnancy is usually attributed to the adnexal masses and the most common cause considered is a corpus luteum cyst. Pain is typically lateralized and may be either due to the size of the cyst, hemorrhage within the cyst or torsion. Ultrasound characteristics of corpus luteum cyst are described above. A corpus luteum cyst usually resolves by the second trimester.

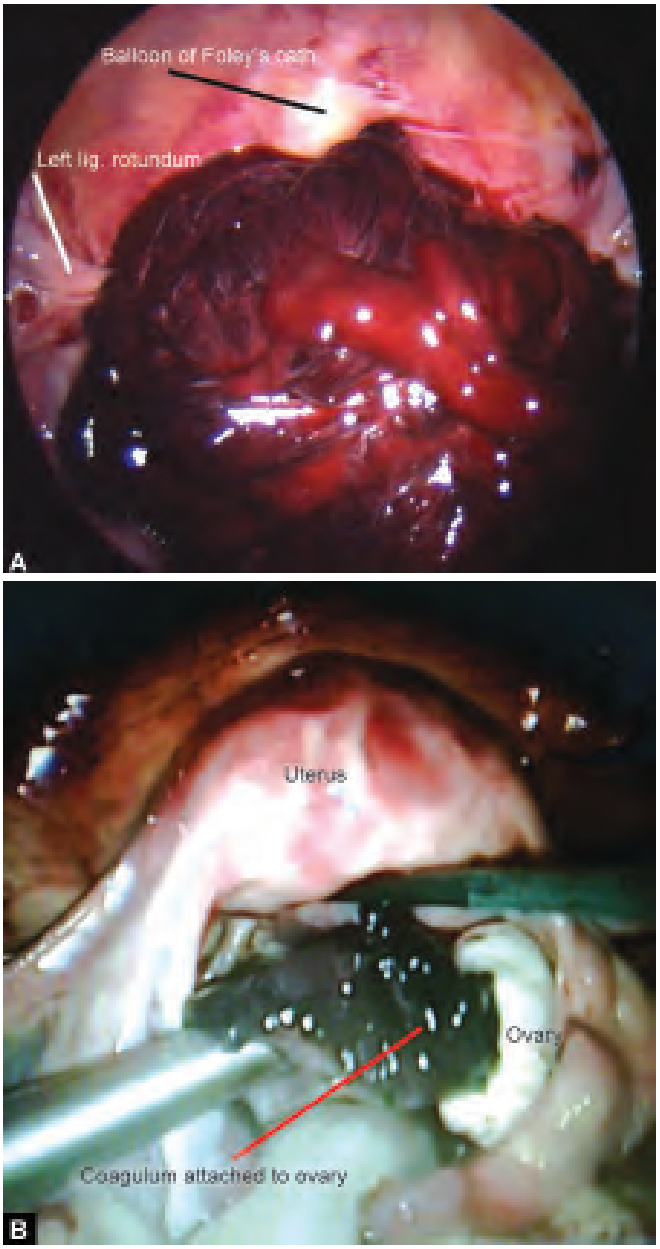

Figures 55.9A and B: Laparoscopy images of ectopic pregnancy. (A) Laparoscopy image of a large ectopic pregnancy complicated by bleeding; (B) Coagulum containing ectopic gestational sac in the left adnexal region

Leiomyoma

Because leiomyomas are hormonally responsive they usually grow and change their echotexture during early pregnancy.[71] Their rapid growth with degeneration can lead to pelvic pain localized to the site of the leiomyoma. Leiomyomas have a variable sonographic appearance ranging from hypoechoic to hyperechoic and complex, depending on their composition and the degree of degeneration. The size of leiomyoma increases with the gestational age, mainly due to pregnancy hormones. Leiomyomas also cause some blood flow changes in the uteroplacental circulation during pregnancy. Our study[72] showed an increase of the flow velocity in radial arteries supplying the uterine leiomyoma ($p < 0.01$) from the 10th to 13th gestational week. This finding is most likely a consequence of higher levels of the estriol hormone that is metabolized in placenta. All these changes however do not influence the blood flow in spiral and uterine arteries.[72]

Uterine Dehiscence and Rupture

Uterine dehiscence and rupture are uncommon obstetric complications with potentially devastating outcome for both the mother and the baby. The term rupture describes a complete separation of the uterine wall (endometrium, myometrium and serosa),[73] while dehiscence represents separation that involves only a portion of the uterine scar.[74] Patients at high risk for uterine dehiscence and rupture have a history of prior surgical intervention on the uterine wall leading to a thinning of the myometrium. In a uterine dehiscence, the scar most likely stretches to the point of translucency, but does not rip. This condition does not necessarily cause a problem. A uterine rupture represents a splitting of the uterus, exposing the fetus to the hostile environment of the intrabdominal cavity and consequently to oxygen deprivation. Oxygen deprivation greater than seven minutes results in irreversible brain damage, with outcomes ranging from learning disabilities, cerebral palsy, permanent vegetative state, to death. On the maternal side, a uterine rupture can cause internal hemorrhage, which, if not rapidly diagnosed, leads to death in minutes.

Many obstetric and nonobstetric conditions may mimic the symptoms and signs of uterine rupture or dehiscence, especially during the third trimester of pregnancy. Sonography may be useful in the diagnosis of these cases.[75] Diagnosis of this life-threatening condition is based upon extrusion of the uterine contents into the abdominopelvic cavity.

Placental Abruption

Placental abruption is a condition caused by the acute separation of the placenta accompanied by vaginal bleeding, pain, uterine tenderness and hypovolemic shock. Placental abruption should always be considered if the retroplacental hypoechoic complex mass (composed of uteroplacental vessels-predominantly veins) measurement exceeds 1–2 cm in thickness **(Fig. 55.10)**. Uterine contraction may create focal thickening of this

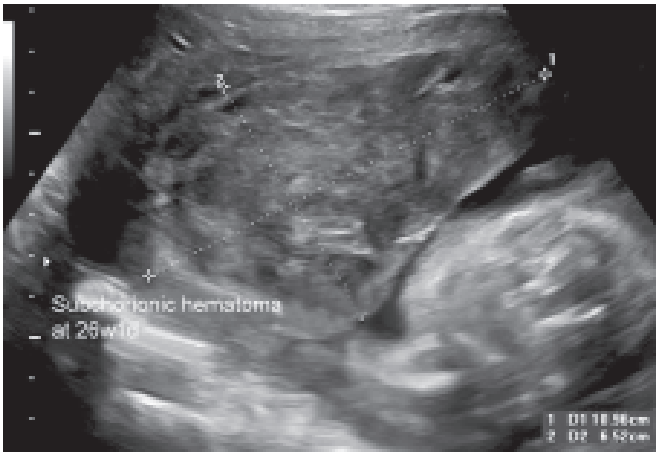

Figure 55.10: Ultrasound image of subcorionic hematoma in a patient presenting with vaginal bleeding, abrupt pain and hypovolemic shock. Note subchorionic hematoma measuring 10.9 x 6.5 cm at 26 weeks gestation. Finding indicates placental abruption

area. Differentiation from placental abruption may be made on the basis of a transient nature of the contraction and by switching on the color Doppler. Uterine leiomyomas can also be mistaken for the retroplacental hemorrhage, but are generally more rounded in shape and demonstrate greater vascularity on color Doppler.

Patient with conditions, such as maternal hypertension, preeclampsia, abdominal trauma, cocaine abuse, cigarette smoking, advanced maternal age, multiparity, twin pregnancy, diabetes, previous history of placental abruption and male fetuses (intriguing but unexplained phenomenon) are at increased risk of this complication.[76,77] The ultrasound presentation of a placental hemorrhage depends on the gestational age, location and patient's hematocrit. We can differentiate three types of abruption considering the location of the separation:

1. Retroplacental hematoma
2. Subchorionic (marginal) hematoma
3. Subamniotic hemorrhage

A retroplacental hematoma is caused by hemorrhage from the spiral arteries, and leads to separation of the basal lamina from uterine/retroplacental hematoma and is caused by hypertension or overdose of anticoagulants. A subchorionic hematoma is caused by hemorrhage from marginal the veins, and leads to a separation of the chorionic membrane from the decidua at the edge of the placenta, while a subamnionic hemorrhage is caused by hemorrhage from the fetal blood vessels at the fetal surface of the placenta. It is useful to perform a nonstress test to check the baby's heart rate and look for signs of fetal distress. Placental abruption may have various effects on the baby such as increased risk of stillbirth, premature delivery and low-birth weight among infants born to mothers who experience separation of the placenta before delivery.[78] If a large amount of the placenta separates from the uterus, the baby will probably be in distress until delivery. The baby may be premature and need to be placed in the newborn intensive care unit. If the fetus is in distress in the uterus, the newborn baby may have a low blood pressure or a low blood count. If the separation is severe enough, the baby could suffer brain damage or die before or shortly after birth.[79]

CONCLUSION

Acute pelvic pain as a clinical presentation can be a consequence of various pathological conditions. A prudent approach is to select the best imaging modalities, which can depict a particular subset of clinical conditions to help narrow the differential diagnosis. The advantages of ultrasound are its low cost and widespread use, while the main disadvantage is the subjectivity and limited number of trained radiologist, gynecologist and sonographers.[80,81] The perceptive clinician must consider all possible causes of acute pelvic pain in order to submit the patients to the proper diagnostic and therapeutic procedures.[82] The combined use of the clinical examination and the ultrasound as an adjunct to the physical examination along with laboratory tests increases the sensitivity and specificity in arriving at the correct diagnosis in patients presenting with gynecologic and/or obstetric causes of acute pelvic pain.[81]

REFERENCES

1. Baines PA, Allen GM. Pelvic pain and menstrual related illnesses. Emerg Med Clin North Am. 2001;19:763-80.
2. Hewitt GD, Brown RT. Acute and chronic pelvic pain in female adolescents. Med Clin North Am. 2000;84:1009-25.
3. Bau A, Atri M. Acute female pelvic pain: ultrasound evaluation. Semin Ultrasound CT MR 2000;21:78-93.
4. Bennett GL, Slywotzky CM, Giovannello G. Gynecologic causes of acute pelvic pain. Radiogrphics 2002;22:785-801.
5. Kupesic S, Kurjak A, Zodan T. Color Doppler ultrasound in the diagnosis of pelvic inflammatory disease. In: Kurjak A (Ed.). An Atlas of Transvaginal Color Doppler. The London-New York: Parthenon Publishing Group. 2000. pp.127-35.
6. Westroem L, Wolner Hanssen P. Pathogenesis of pelvic inflammatory disease. Genitourin Med. 1993;69:9-17.
7. Expert Committee on Pelvic Inflammatory Disease. Research directions for the 1990s. Sex Trans Dis. 1991;18:46-64.

8. Gales W, Wasserheit JN. Genital chlamydial infections: epidemiology and reproduction sequelae. Am J Obstet Gynecol. 1991;164:1771-81.
9. Toth M, Chervenak FA. Infection as the cause of infertility. In: Kupesic S, De Ziegler D (Eds). Ultrasound and Infertility. Carnforth, UK: Parthenon Publishing; 2002. pp.205-14.
10. Patten RM, Vincent LM, Wolner-Hanssen P. Pelvic inflammatory disease: Endovaginal sonography with laparoscopic correlation. J Ultrasound Med. 1990;9:861-5.
11. Reynolds T, Hill MC, Glassman LM. Sonography of hemorrhagic ovarian cyst. J Clin Ultrasound. 1986;14:449-53.
12. Baltrarowich OH, Kurtz AB, Pasto ME. The spectrum of sonographic findings in hemorrhagic ovarian cyst. Am J Roentgenol. 1987;148:901-5.
13. Bass IS, Haller JO, Freidman AP. The sonographic appearance of the hemorrhagic ovarian cyst in adolescents. J Ultrasound Med. 1984;3:509-14.
14. Kupesic S, Kurjak A. Color Dopler assessment of uterine leiomyoma and sarcoma. In: Kurjak A (Ed.). An Atlas of Transvaginal Color Doppler. London-New York: The Parthenon Publishing Group; 2000. pp. 179-86.
15. Siskin GP, Bonn J, Worthington-Kirsch RL. Uterine fibroid embolization:pain management. Tech Vasc Interv Radiol. 2002;5:35-43.
16. Richengerg J, Cooperberg P. Ultrasound of the Uterus. In: Callen P (Ed.). Ultrasound in obstetrics and gynecology. Philadelphia: W B Saunders Company; 2000. pp. 814-46.
17. Kurjak A, Kupesic S, Shalan H, et al. Uterine sarcoma: a case report of 10 cases studied by transvaginal color and pulsed Doppler sonography. Gynecol Oncol. 1995;59: 342-6.
18. Kurjak A, Kupesic-Urek S, Miric D. The assessment of benign uterine tumor vascularization by transvaginal color Doppler. Ultrasound Med Biol. 1992;18:645-8.
19. Kupesic S, Kurjak A. Color Doppler assessment of patients with pelvic pain. In: Kurjak A (Ed.). An Atlas of Transvaginal Color Doppler. London-New York: The Parthenon Publishing Group; 2000. pp. 241-4.
20. Worthington-Kirsch RL, Raftopoulos V, Cohen IT. Sequential bilateral torsion of normal ovaries in a child. J Ultrasound Med. 1986;5:663-4.
21. Sozen I, Kadako R, Fleischman S, et al. Diagnosis and laparoscopic management of a fallopian tube torsion following Irving tubal sterilization: a case report. Surg Endosc. 2002;16:217-21.
22. Fleischer A, Stein S, Cullinan J, et al. Color Doppler sonography of adnexal torsion. J Ultrasound Med. 1995;14:523-8.
23. Rosado WM, Trambert MA, Gosnik BB, et al. Adnexal torsion: diagnosis by using Doppler sonography. Am J Roentgenol. 1992;159:1251-3.
24. Van Voorhis BJ, Schwaiger J, Syrop CH, et al. Early diagnosis of ovarian torsion by color Doppler ultrasonography. Fertil Steril. 1992;58:215-7.
25. Lineberry TD, Rodriguez H. Isolated torsion of the fallopian tube in an adolescent: a case report. J Pediatr Adolesc Gynecol. 2000;13:135-7.
26. Kupesic S, Plavsic BM. Adnexal torsion: color Doppler and three-dimensional ultrasound. Abdominal Imaging. 2010;35:602-6.
27. Kurjak A, Kupesic S. Benign ovarian lesions assessed by color and pulsed Doppler. In: Kurjak A (Ed.). An Atlas of Transvaginal Color Doppler. London-New York: The Parthenon Publishing Group; 2000. pp. 191-202.
28. Simpton JL, Elias S, Malinak LR, et al. Heritable aspects of endometriosis I: genetic studies. Am J Obstet Gynecol. 1980;137:327-31.
29. Barlow D, Kennedy H. Endometriosis: clinical presentation and diagnosis. In: Shaw RW (Ed). Endometriosis. Carnforth, UK: Parthenon Publishing; 1989. pp. 1-10.
30. Bai SW, Cho HJ, Kim JY, et al. Endometriosis in an adolescent population: the severance hospital in Korean experience. Yonsei Med J. 2002;43:48-52.
31. Kupfer MC, Schwimer RS, Lebovic J. Transvaginal sonographic appearance of endometriomata: spectrum of findings. J Ultrasound Med. 1992;11:129-32.
32. Atri M, Nazarnia S, Bret P. Endovaginal sonographic appearance of benign ovarian masses. Radiographics. 1996;14:747-9.
33. Kurjak A, Kupesic S. Scoring system for prediction of ovarian endometriosis based on transvaginal color and pulsed Doppler sonography. Fertil Steril. 1994;62:81-8.
34. Beard RW, Highman JH, Pearce S, et al. Diagnosis of pelvic varicosities in women with chronic pelvic pain. Lancet. 1985;2:956-9.
35. Kurjak A, Kupesic S. Congestion syndrome of the uterus. In: Osmers R, Kurjak A (Eds). Ultrasound and the Uterus . Carnforth, UK: Parthenon Publishing; 1995. pp. 115-8.
36. Bonilla-Musoles F, Ballesteros MJ. Transvaginal color Doppler in the diagnosis of pelvic congestion syndrome. In: Kurjak A (Ed.). An Atlas of Transvaginal Color Doppler. Carnforth, UK: Parthenon Publishing; 1994. pp. 207-15.
37. Fakhri A, Fisherman EK, Mitchel SE, et al. The role of CT in the management of pelvic arteriovenous malformations. Cardiovasc Intervent Radiol. 1987;10:96-9.
38. Bottomley JP, Whitehouse GH. Congenital arteriovenous malformations of the uterus demonstrated by angiography. Acta Radiol. 1975;16:43-8.
39. Diwan RV, Brennan JN, Selim MA. Sonographic diagnosis of arteriovenous malformations of the uterus and pelvis. J Clin Ultrasound. 1983;11:295-8.
40. Juhasz B, Kurjak A, Lampe LG. Pelvic varices simulating bilateral adnexal masses: differential diagnosis by vaginal color Doppler. J Clin Ultrasound. 1992;20:81-4.
41. Promecene PA. Laparoscopy in gynecologic emergencies. Semin Laparosc Surg. 2002;9:64-75.
42. Kurman RJ. Blaustein's Pathology of the Female Genital Tract, 4th edition. New York: Springer-Verlag. 1994:532-5.
43. Visaria SD, Davis JD. Pelvic vein thrombosis as a cause of acute pelvic pain. Obstet Gynecol. 2002;99:897-9.
44. Munisck RA, Gillanders LA. A review of the syndrome of puerperal ovarian vein thrombophlebitis. Obstet Gynecol Surv. 1981;36:57-61.
45. Simons GR, Piwnica Worms DR, Goldhaber SZ. Ovarian vein thrombosis. Am Heart J. 1993;136:641-3.

46. Khurana BK, Rao J, Friedman SA. Computed tomographic features of puerperal ovarian vein thrombosis. Am J Obstet Gynecol. 1998;159:905-7.
47. Cranston PE, Hamrick-Turner J, Morano JU. Pseudothrombosis of the right ovarian vein: Pitfall of abdominal spiral CT. Clin Imaging. 1995;19:176-9.
48. Dure-Smith P. Ovarian syndrome: Is it a myth? Urology. 1995;13:355-8.
49. Toland KC, Pelamder WM, Mohr SJ. Postpartum ovarian vein thrombosis presenting as urethral obstruction: a case report and review of literature. J Urol. 1993;149:1538-42.
50. Savader SJ, Otero RR, Savader BL. Puerperal ovarian vein thrombosis: evaluation with CT, US and MR imaging. Radiology. 1988;167:637-9.
51. Hakim RB, Gray RH, Zacur H. Infertility and early pregnancy loss. Am J Obstet Gynecol. 1995;172:1510-7.
52. Wilcox AJ, Weinbert C, O'Connor JF. Incidence of early loss in pregnancy. N Engl J Med. 1988;319:159-64.
53. Alberman E. The epidemiology of repeated abortion. In: Beard RW, Bishop F (Eds). Early pregnancy loss: mechanism and treatment. New York: Springer-Verlag; 1988. pp. 9-17.
54. Cetin A, Cetin M. Diagnostic and therapeutical decision-making with transvaginal sonography for first trimester spontaneous abortion, clinically thought to be complete or incomplete. Contraception. 1998;57:393-7.
55. Kurjak A, Kupesic S. Blood flow studies in normal and abnormal pregnancy. In: Kurjak A, Kupesic S (Eds.) An Atlas of Transvaginal Color Doppler. London-New York: Parthenon Publishing Group; 2000. pp. 41-51.
56. Kurjak A, Kupesic S. Doppler assessment of intervillous blood flow in normal and abnormal early pregnancy. Obstet Gynecol. 1997;89:252-6.
57. Kurjak A, Kupesic S. Parallel Doppler assessment of yolk sac and intervillous circulation in normal pregnancy and missed abortion. Placenta. 1998;19:619-23.
58. Jaffe R, Warsof SL. Color Doppler imaging in the assessment of uteroplacental blood flow in abnormal first trimester intrauterine pregnancies: and attempt to define etiologic mechanism. J Ultrasound Med. 1992;11:41-4.
59. Kos M, Kupesic S, Latin V. Diagnostics of spontaneous abortion. In: Kurjak A (Ed.). Ultrasound in Gynecology and Obstetrics. Zagreb: Art Studio Azinovic. 2000;314-21.
60. Szulman AE. The natural history of early human spontaneous abortion. In: Barnea ER, Check JH, Grudzinkas JG, (Eds). Implantation and early pregnancy in humans. Carnforth UK: Parthenon Publishing. 1993:309-21.
61. Ectopic pregnancy. In: Speroff L, Glass RH, Kase NG (Eds). Clinical Gynecologic Endocrinology and Infertility. London: Williams & Wilkins. 1999:1149-67.
62. Timor-Tristch IE, Monteagudo A. Ectopic pregnancy. In: Kupesic S, de Ziegler D (Eds). Ultrasound and infertility. London-New York: Parthenon Publishing Group. 2000;215-39.
63. Kurjak A, Kupesic S. Ectopic pregnancy. In: Kurjak A (Ed.). Ultrasound in Obstetrics and Gynecology. Boston: CRC Press. 1990;225-35.
64. Kupesic S, Kurjak A. Color Doppler assessment of ectopic pregnancy. In: Kurjak A, Kupesic S (Eds). An Atlas of Transvaginal Color Doppler. London-New York: Parthenon Publishing Group. 2000;137-47.
65. Timor-Tristch IE, Rottem S, Thale I. Review of transvaginal ultrasonography: description with clinical application. Ultrasound. 1988;6:1-32.
66. Peisner DB, Timor-Tritsch IE. The discriminatory zone of beta hCG for vaginal probes. J Clin Ultrasound. 18:280-5.
67. Fossum GT, Dvajan V, Kletzky DA. Early detection of pregnancy with transvaginal ultrasound. Fertil Steril. 1988;49:788-91.
68. Bernascheck G, Euaelstorfer R, Csaicsich P. Vaginal sonography versus serum human chorionic gonadotropin in early detection of pregnancy. Am J Obstet. 1988;158:608-12.
69. Kurjak A, Zalud I, Volpe G. Conventional B-mode and transvaginal color Doppler on ultrasound assessment of ectopic pregnancy. Acta Med. 1990;44:91-103.
70. Kupesic S, Kurjak A. Color Doppler assessment of ectopic pregnancy. In: An atlas of transvaginal Color Doppler. Kurjak Kupesic S (Eds). The Parthenon Publishing Group. 2000. pp. 137-47.
71. Rosati P, Bellatti U, Exacoustos C. Uterine myoma in pregnancy: ultrasound study. Int J Gynecol Obstet. 1989; 28:109-17.
72. Kurjak A, Predanic M, Kupesic S, et al. Transvaginal color Doppler in the study of early cornual pregnancies and pregnancies associated with fibroids. J Matern Fetal Invest. 1992;2:81-5.
73. Depp R. Cesarian delivery. Obstetrics: Normal and Problem Pregnancies. Gabbe SG, Niebyl JR, Simpson JL (Eds). New York: Churchil Livingstone, Inc, 3rd edition; 1986. pp. 606-7.
74. Cunningham FG, MacDonald PC, Gant NF. Obstetrical Hemorrhage. Williams Obstetrics. Stamford Conn, Appleton and Lange, 20th edition; 1997. pp. 772-8.
75. Huang WC, Yang JM. Sonographic Findings of Uterine Dehiscence in the Early Third Trimester: Report of a Case. J Med Ultrasound. 2000;8:116-9.
76. Annath CV, Savitz DA, Luther ER. Maternal cigarette smoking as a risk factor for placental abruption, placenta previa and uterine bleeding in pregnancy. Am J Epidemiol. 1996;144:881-5.
77. Kramer M, Usher R, Pollack R. Etiologic deteminants of abruptio placentae. Obstet Gynecol. 1997;89:211-5.
78. Ananth CV, Johnson RW. Placental abruption increases risk of stillbirth and preterm delivery. JAMA. 1999;282:1646-51.
79. Brown HL. Trauma in pregnancy. Obstet Gynecol. 2009; 114(1):147-60.
80. Kupesic S, Aksamija A, Vucic N, et al. Ultrasonic assessment of acute pelvic pain. Acta Medica Croatica. 2002;56: 171-80.
81. Kupesic S, Aksamija A. Sonographic evaluation of gynecological and obstetric causes of acute pelvic pain. Ultrasound Rev Obstet Gynecol. 2003;5:192-202.
82. Neis KJ, Neis F. Chronic pelvic pain: cause, diagnosis and therapy from a gynaecologist's and an endoscopist's point of view. Gynecol Endocrinol. 2009;25(11):757-61.

56
CHAPTER

Three-Dimensional and Four-Dimensional Sonography in Gynecological Patients

Ashok Khurana

INTRODUCTION

The relevance of newer imaging techniques in improving patient outcomes needs to be periodically reassessed. An audit of this nature needs to be done in the perspective of cost-effectiveness, cost containment and health priorities, since the cost of health is ultimately to be borne by each member of a community or nation, irrespective of whether the health provider is reimbursed by the state, by an insurance arrangement or directly by a patient.

This paper discusses the state of the art and science of three-dimensional (3D) and four-dimensional (4D) ultrasound techniques in gynecology.

TECHNOLOGICAL ADVANCES

Two technical advances have greatly influenced the widespread use of ultrasound in gynecological disease in the last decade. These include variable and high frequency transvaginal transducers and the utilization of 3D power Doppler technology.

Higher transducer frequencies improve resolution. However, the trade-off is the decreased depth of penetration. Newer transducers combine frequencies as high as 12 MHz with a multi-frequency option of low (about 5 MHz) and mid-frequency, thereby allowing combinations of high resolution and depth penetration by using keys and knobs on the console. Increased 2D resolution implies sharper and more accurate images in 3D and 4D as well.

The second technological advance is the combination of power Doppler with 3D. About a decade and a half ago, several groups reported a newer Doppler technique now widely called power Doppler. Unlike conventional color Doppler, where flow information represents flow direction, mean velocity and range of velocities, the power Doppler is a technique that assesses amplitude or energy. Information displayed represents reflected (scatter) information from clumps of red blood cells within the sampled vessel. The greater the clump density, the higher is the amplitude of the signal, and therefore the brighter is the color coding. The technique is known by several names, including power Doppler, power angiography, color Doppler energy, color amplitude imaging and amplitude-mode color Doppler ultrasound. Mathematically speaking, the signal represents the area under the power spectral curve. The technique, by its very nature, enhances low flow sensitivity and this makes it an excellent method for detecting slow flow vessels and the areas of omni-directional vessels. A gain of 10–15 dB is achieved without interference by noise. Since power Doppler is less angle dependent, tortuous vessels are more completely demonstrated. This method of detecting flow information has consequently emerged as the method of choice for studying parenchymal flow in normal and pathological areas in the pelvis. Although the information display initially lacked color-coded direction information, directional information could be obtained from any image by a spectral Doppler

waveform study. Currently, high definition power Doppler carries with it the added technological marvel of direction color-coding as well to enable rapid analysis.

Data Acquisition and Display

Automated devices to acquire volume data for 3D evaluation have largely replaced freehand devices. In the freehand method the transducer was manually moved through the region of interest and a position sensor registered the slice in space and time, or alternatively, image based software was built into the 3D package. The freehand method could be used online where the ultrasound unit managed all functions or can be used also offline where the analog video output was fed into a workstation. The transducer and attachments in the free-hand system were bulky and awkward to use, particularly in the vagina. Most units currently in use, therefore, are automated 3D probes. These are unit specific, more accurate and easy to use. When these units are employed, an area of interest is chosen in the real time 2D image and the size and depth are outlined. A speed of acquisition is then selected and the acquisition activated. The transducer elements automatically sweep through the chosen volume box. It is pertinent to note that the slower the speed of acquisition, the higher is the resolution. Resolution is highest in the plane of acquisition. Additionally, the closer the plane of acquisition to the plane of study the better is the resolution. The machine automatically receives and stores data from the region of interest and displays it in an orthogonal format **(Fig. 56.1)**. Images may then be rendered by various algorithms, which rely on the difference between acoustic impedances at tissue interfaces and have been variably named by various manufacturers **(Figs 56.2 and 56.3)**.

In a conventional ultrasound, the uterus is visualized as a variably thick, linear or ovoid structure in longitudinal, transverse and oblique plane. The shape of the cavity is difficult to assess, as is the coronal plane. With 3D, the entire extent of the endometrium and myometrium can be shown, including the corpus, fundus, cervix and cornual areas. Coronal, sagittal and transverse planes can be simultaneously displayed to permit more exhaustive viewing **(Figs 56.4A to C)**. The images may be automatically zoomed in or out **(Fig. 56.5)**. Once acquired, the volume data can be reviewed by first rotating the planes to obtain standard anatomic orientations and then scrolling through the entire data to locate and characterize lesions, both focal and diffuse. Newer software permits multi sections to be obtained in curvilinear, non-orthogonal planes and this has revolutionized data manipulation **(Figs 56.6A to D)**. Multi planar orthogonal and non-orthogonal viewing offers virtually unlimited numbers of planes, and time constraints should not impede the endeavor

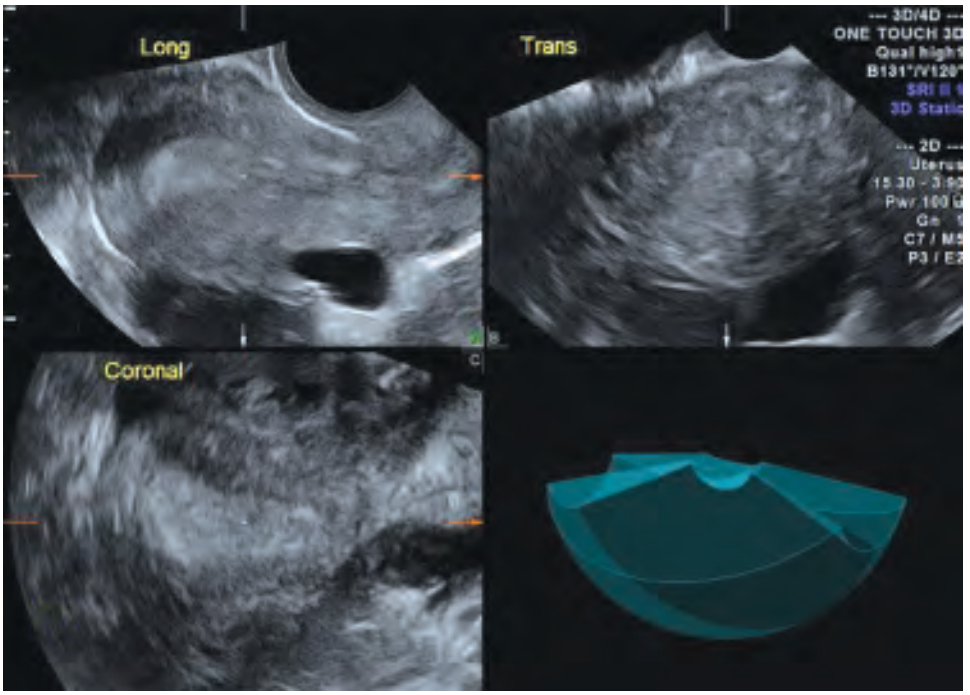

Figure 56.1: 3D units sweep through the region of interest and store the entire information in computer memory. Knobs on the keyboard are employed to reconstruct any desired plane. One of the most useful and commonly employed display formats is the display in three orthogonal planes: longitudinal, transverse and coronal. The coronal view is difficult to obtain on 2D scans and remarkably easy to visualize with 3D

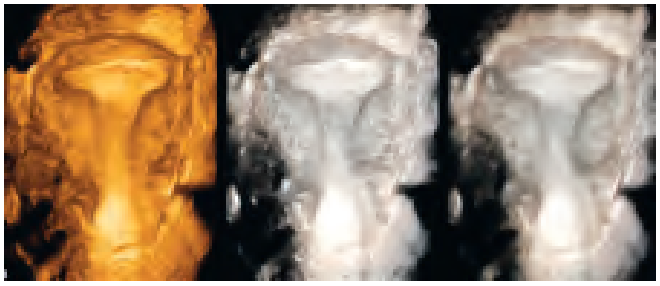

Figure 56.2: Various rendering modes enable textural differentiation between the endometrium and the myometrium as well as textural variation within the endometrium and myometrium. These may be selected by choices on the console. The three displays shown here are labeled by this vendor as gradient light, skin texture and skin smooth

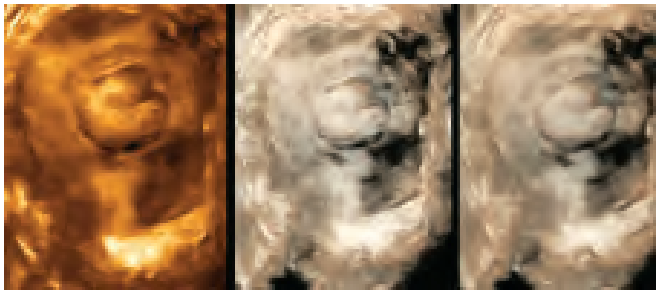

Figure 56.3: Render modes as mentioned in Figure 56.2 highlight various aspects of this fibroid differently in different render modes

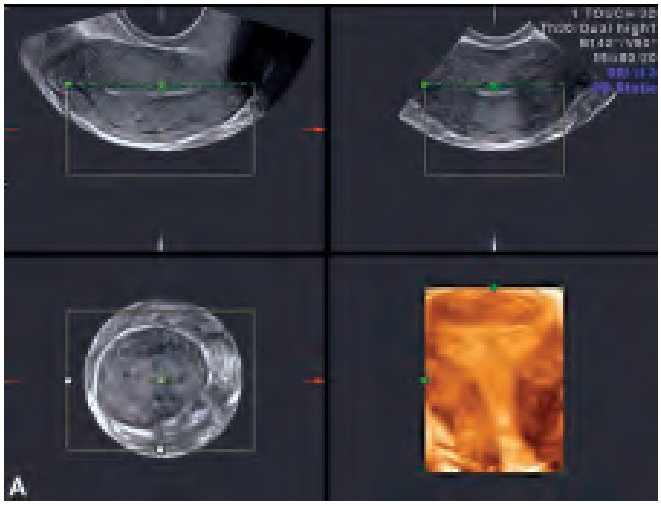

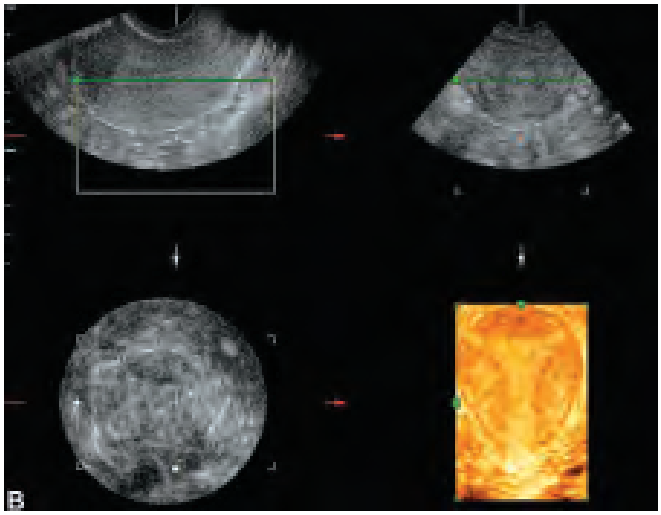

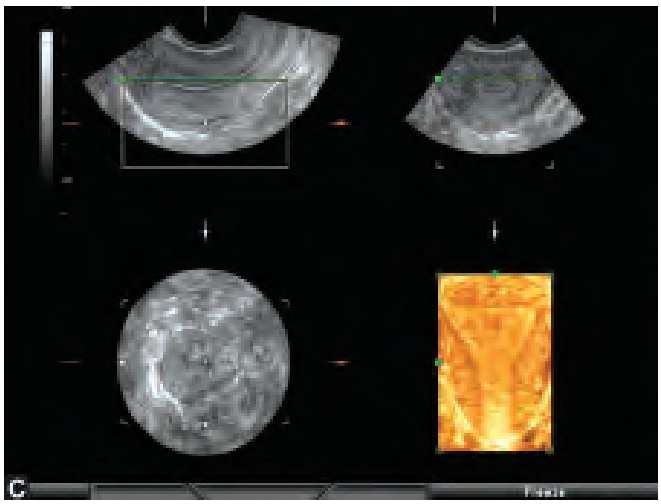

Figures 56.4A to C: (A and B) 3D rendered displays show the entire configuration of the cavity including the tubal ostia, corpus and cervix. Note the convex contour of the uterine cavity and the subtle concavity of the fundal aspect of the cavity. These features exclude any uterine duality or septations. The hypoechoic zone around the cavity is a normal feature and is important to delineate because it loses definition in adenomyosis, endometritis and neoplastic conditions. All three rendered images show a normal uterus. Note how the triangular configuration can differ within the normal population. Rendered images can be obtained even in a thin endometrium; (C) While rotating orthogonal planes to render the endometrium in the region of the ostia, the cavity may show hypoechoic artifacts (<<) which represents areas of myometrium. This can be confirmed by referring to the orientation of the plane of interest in the selected plane of imaging (the longitudinal selected plane in this case) and should not be mistaken for focal endometrial lesions

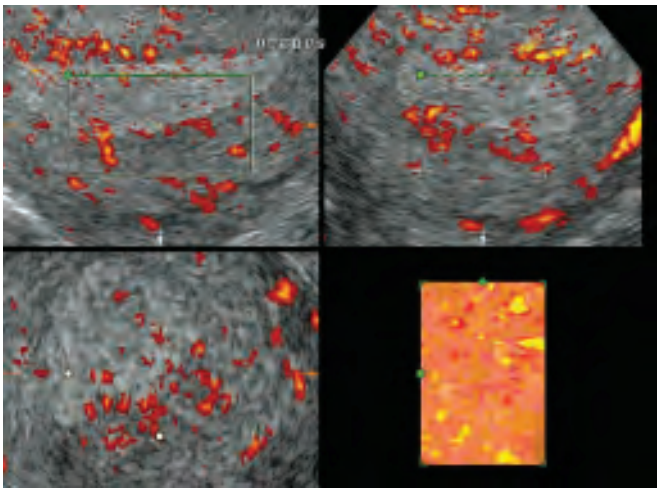

Figure 56.5: 3D acquisition can be obtained simultaneously in gray scale and color Doppler/power Doppler modes. These may be zoomed in for better visualization

to obtain information. In fact, the additional time spent on a 3D gynecologic scan is far less than on 3D obstetric scan because this time is spent not so much on data acquisition but in exploring the data obtained. The time factor would, of course, depend on the complexity of a case and on operator expertise. In experienced hands the exercise takes no more than three to ten minutes. Once identified in any one plane, the lesion can be marked by a center point, and this center point is automatically displayed in all planes. All or part of the studied volume can be automatically rendered and displayed as a single image or along with the orthogonal planes. The evaluation can be enhanced by using volume measurements, niche mode studies (**Fig. 56.7**), power Doppler studies **(Fig. 56.8)**, translational cine studies **(Figs 56.9A to D)** or a retrospective review of stored data. Unlike obstetric 3D, surface rendering is infrequently required in gynecologic 3D studies except

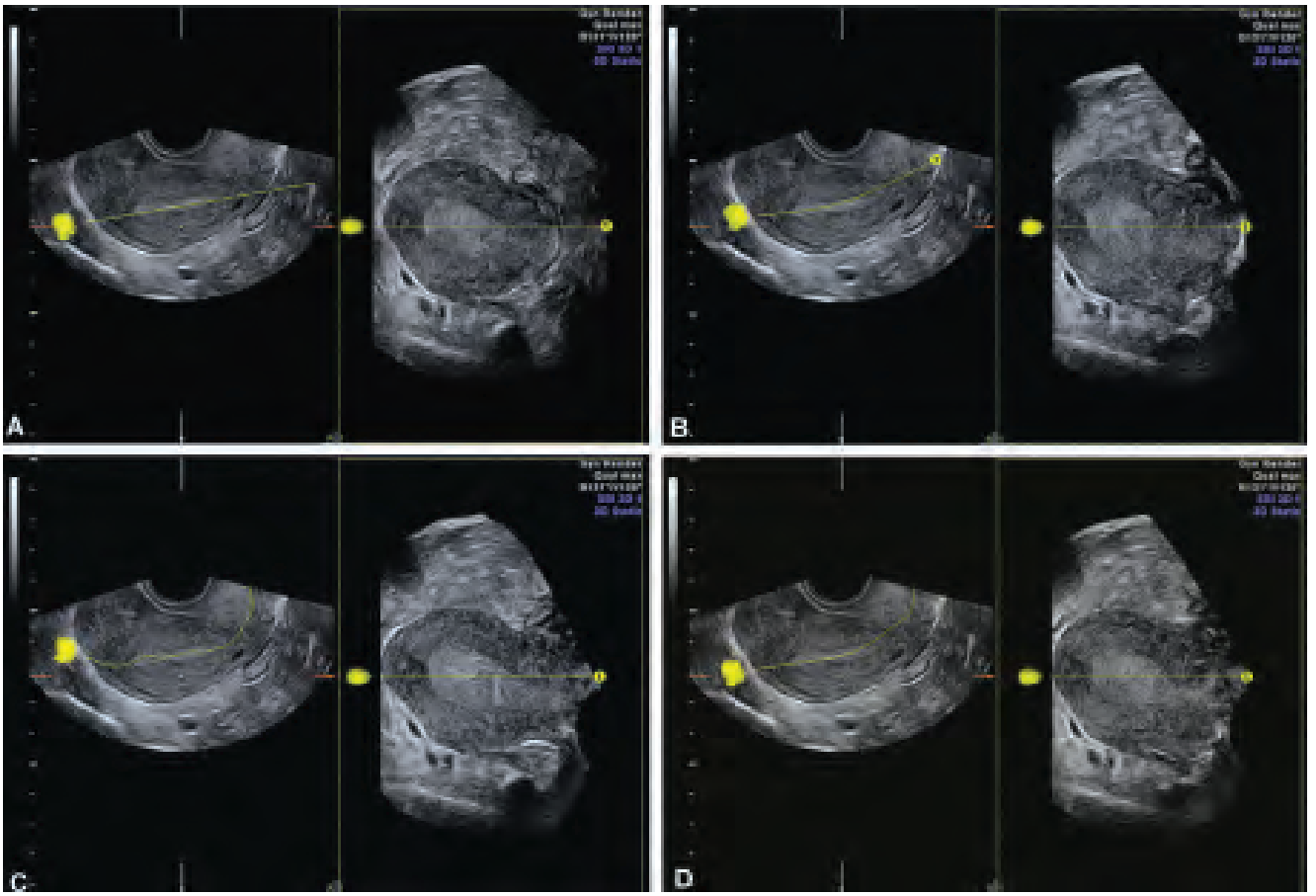

Figures 56.6A to D: (A and B) Conventional orthogonal planes as studied by 3D originally consisted of linear planes only. One such plane is shown in Figure 56.6A. The rendering line through the longitudinal plane of this uterus is a straight line, and since the endometrium and the uterus are curved structures, the cavity is largely not represented. The curved line of acquisition and rendering, improved on this but was unable to demonstrate any structure that was not along a geometrical arc. This is shown in Figure 56.6B. Newer software commits curvilinear planes that offer reconstructions through any imaginable trace including a zigzag, variable curves and straight sections, singly or in combination at the same time; (C and D) Demonstrate this. Note how this "anatomical" trace can give an excellent display of the cavity, the uterine contour and the cervix

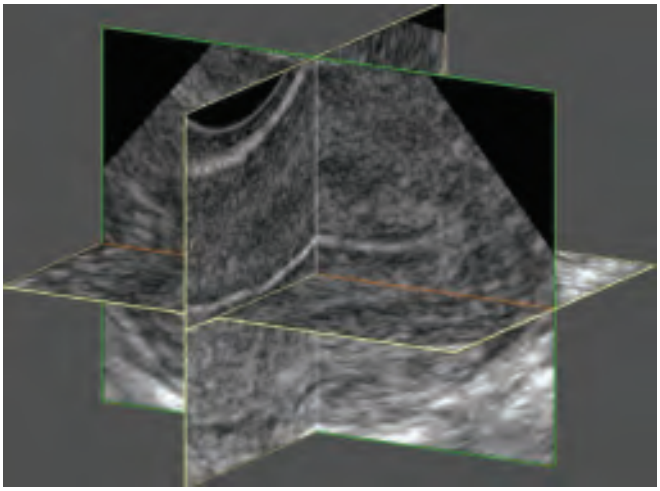

Figure 56.7: Niche mode studies permit a biplanar scrolling through acquired data. These are useful for enhancing accuracy of identifying and localizing lesions

in saline infusion sonohysterography where it often adds diagnostic information. The entire acquired data can be transmitted electronically to obtain second opinions, facilitate remote conferencing with experts, and also can be efficiently stored for review and recall. The sagittal plane is selected for volume measurements and the other two planes for ensuring that the entire pathology is included in the measured area. Surface rendering permits contoural evaluation. Niche mode and translational cine studies permit a virtual tour of the entire lesion and surrounding tissue along including an evaluation of vascular morphology wherever necessary, by a manual and automatic mode respectively. The 3D power Doppler permits an unsurpassed view of vascularity and permits quantification of neovascularization. The 3D saline infusion sonohysterography enhances the sensitivity in select situations. The 4D studies are useful in saline infusion sonohysterography

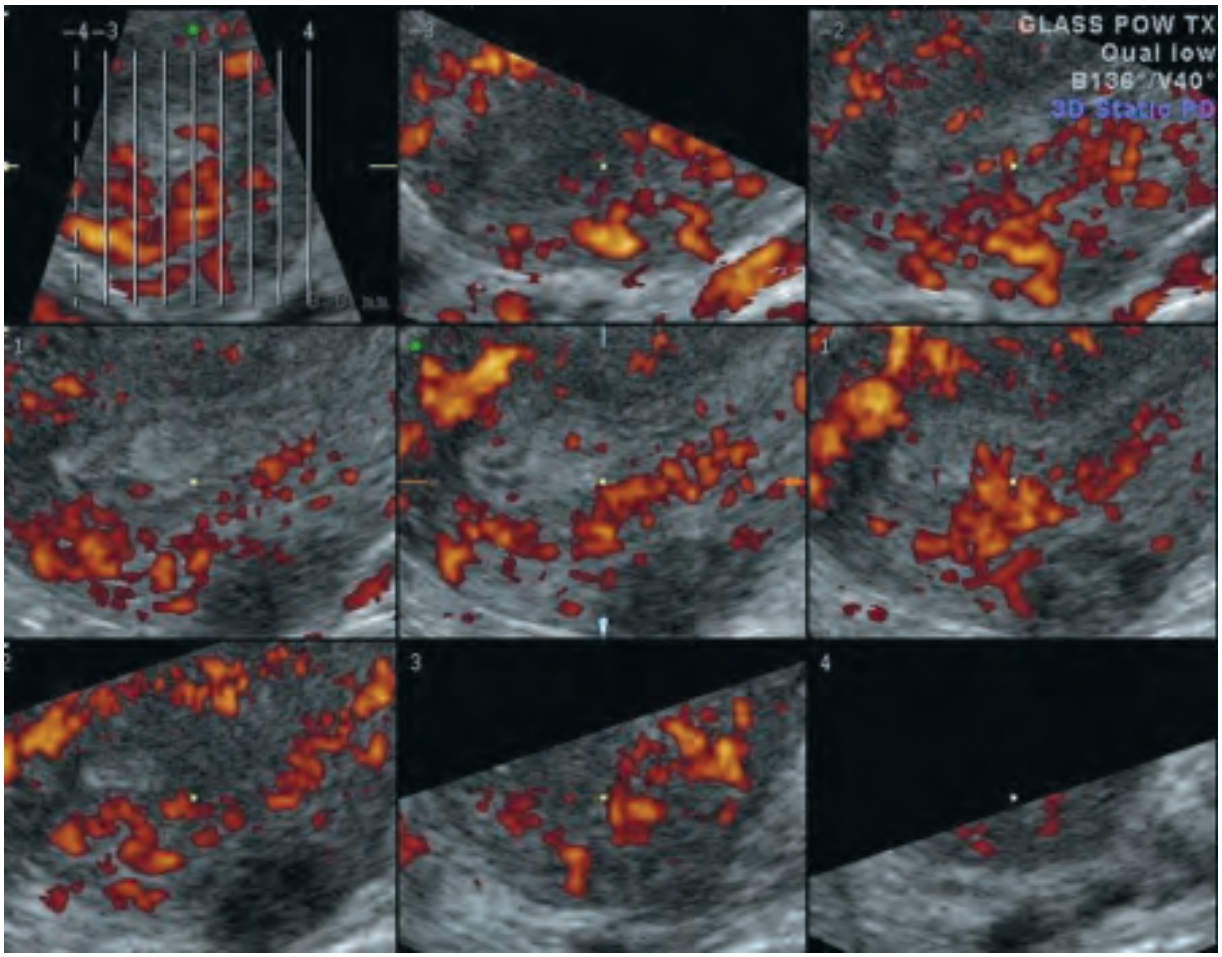

Figure 56.8: Gray scale and power Doppler 3D acquisitions may be displayed in a tomographic sectional format akin to CT and MR. This format permits excellent localization and identification of pathological lesions and vascular signals

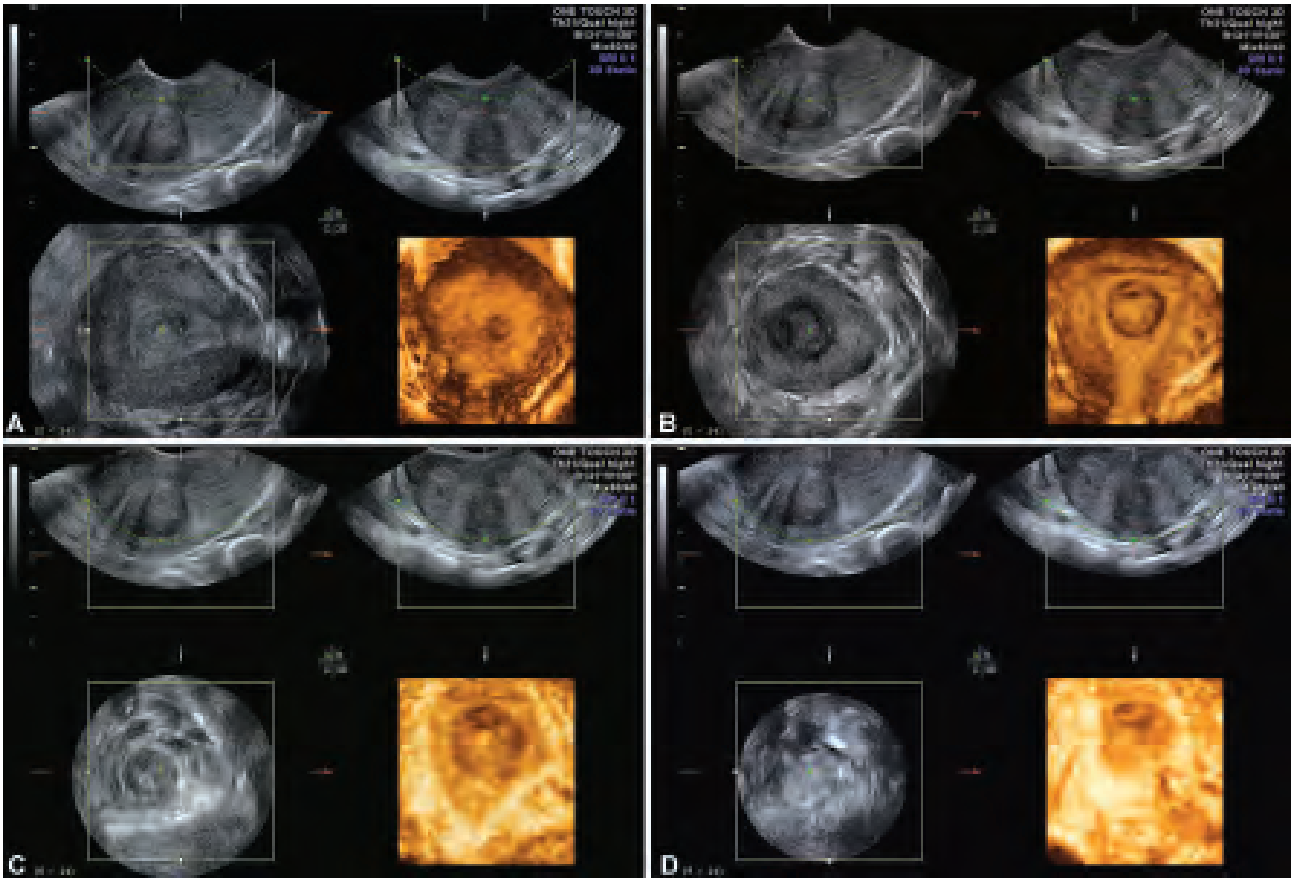

Figures 56.9A to D: Translation cine scrolls automatically through a chosen volume of interest yielding cine sections through the block. The figures show stills from a translation cine sequence from the anterior to the posterior aspect of a uterus with a posterior wall fibroid. Careful translational studies reveal that this fibroid extends from the cavity to the surface and is not just interstitial as would be presumed from the 2D and 3D rendered images

for storing data sets, excluding the need for re-instillation, permitting multiplanar analysis and allowing magnification of stored data during re-evaluation.

In patients who have not been sexually active, 3D data acquisition via the rectum, using an intracavitary transducer, can greatly enhance delineation of pelvic lesions and developmental abnormalities when compared to transabdominal 3D studies.

The 3D data is basically a sum total of 2D data sets, and as a logical consequence, a 3D study does not replace a 2D study. It in fact, extends the wealth of information obtainable from an ultrasound scan.

Müllerian Anomalies

Anomalous Mullerian development is estimated to occur in 3–4% of women[1] and about half of these are associated with clinical disease.[2-4] The clinical significance lies in the associated infertility, implantation failures,[5] miscarriages,[6] premature labor, malpresentations, uterine irritability, fetal growth and dystocia.[4,7] Correction of these anomalies by hysteroscopy and other minimally invasive surgical procedures greatly improves reproductive outcomes.[8,9] Precise delineation of the type and extent of the anomaly is important to assess the need for surgical correction and the technique of correction.[6,9-11]

The 2D transvaginal scanning is a sensitive screening tool[12,13] for developmental uterine malformations, but lacks specificity and is markedly operator dependent.[14,15] Often a minimal and usually clinically innocuous duality, such as an arcuate uterus, may display two endometrial stripes in an axial section through the fundus.[16] This results in a false positive diagnosis with embarassing situations at operative hysteroscopy! The markers for

uterine duality in conventional ultrasound include a double endometrial echo complex, a wide transverse uterine diameter and rarely, a distinctive complete uterine duality.[17] For several decades, X-ray contrast hysterosalpingography has been the standard technique for evaluation of uterine malformations. Although the technique is reasonably safe, it involves radiation exposure and lacks specificity in detailing lateral fusion anomalies.[18] The outline of the cavity can be displayed in accurate detail. However, and understandably, the surface contour of the uterus cannot be evaluated. Since the differentiation of a septate from a bicornuate uterus is based on the morphology of the fundal contour and not the morphology of the cavity, hysterosalpingography is an inadequate method for complete delineation. For some years now, saline infusion sonohysterography has evolved as an adjunct to transvaginal 2D sonography.[15,17,19] However, the procedure fails to differentiate the septate uterus from the bicornuate uterus because the surface contour of the uterus and fundus cannot be delineated by this technique either. In fact, a hysteroscopy alone also fails to make this distinction and a concurrent laparoscopy needs to be carried out to make a complete diagnosis. This is important because the repair is so distinctively different in the two diagnoses. Magnetic Resonance Imaging can delineate these malformations since it images the cavity and the fundal surface contour together. However, the method is expensive and the software is cumbersome and coarse.[20,21] The 3D ultrasound with its inherent ability to demonstrate the entire endometrium and the myometrium is emerging as a sensitive and remarkably specific modality for mapping the anomalous uterus.[12,22,23] It is becoming increasingly apparent that precise anatomical information can be obtained without the need for radiation, contrast material or surgical intervention.[16,18]

The unique ability of 3D ultrasound to display the coronal plane and the immense possibilities of multiplanar display consequent to interactive manipulation of acquired data sets, has placed this modality as the optimal method for evaluating the structurally anomalous uterus.

Similar to the technique used to evaluate the uterus for acquired pathologic processes, the method for obtaining 3D data remains the transvaginal imaging with an automated and dedicated transducer. These units are specific, more accurate and easy to use. The data obtained by these units is easy to manipulate and has far fewer artifacts especially for the relatively uninitiated observer. The 3D window should include the entire uterine contour seen on an appropriately zoomed in 2D image. The transducer elements automatically sweep through the chosen volume box. For enhanced resolution, a slow sweep speed and a longitudinal sweep are selected. In patients who have not been sexually active, data may be obtained by a transrectal scan. Once acquired, the data can be reviewed, stored, retrieved, brainstormed, transmitted by phone lines or satellite and networked. It is imperative to obtain one 3D data set in the power Doppler mode in order to display a vascular guide map to the congenitally malformed uterus as this has a bearing on management protocols[24-26] **(Figs 56.10A and B)**. In a uterine duality where the horns have a largely horizontal orientation, an additional acquisition in the coronal plane may be useful. Very rarely in such uteri, it may not be possible to obtain both horns and the entire cervix in a single rendered image. Surface rendering may be required in some cases to assess the fundal contour.[22] The 3D acquisition of Saline Infusion Sonohysterography (SISH) yields excellent details of global uterine anatomy. However, it is being realized

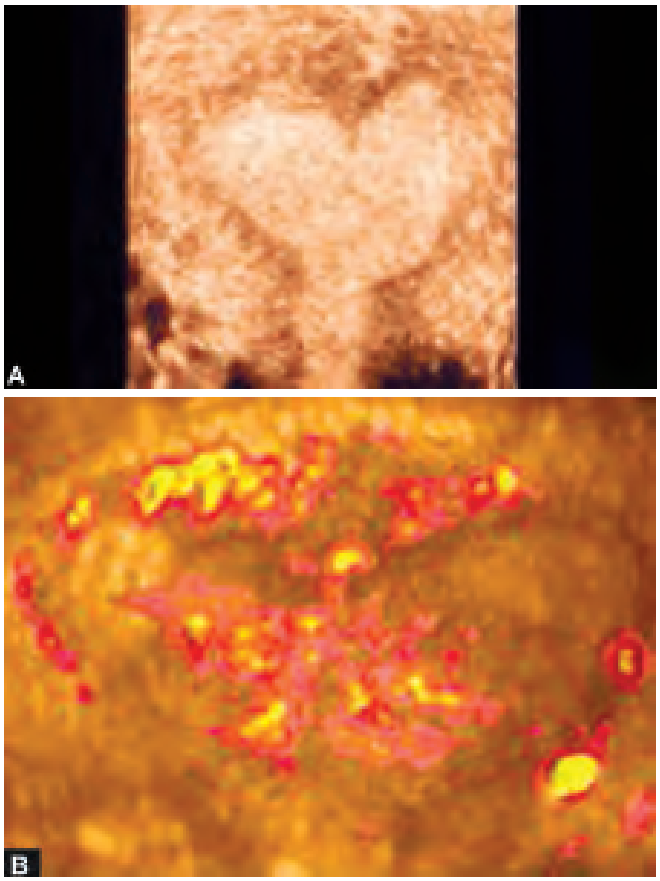

Figures 56.10A and B: (A) 3D rendering of a subseptate uterus; (B) 3D power Doppler rendering reveals an extensively vascular septum. This is associated with a poor prognosis

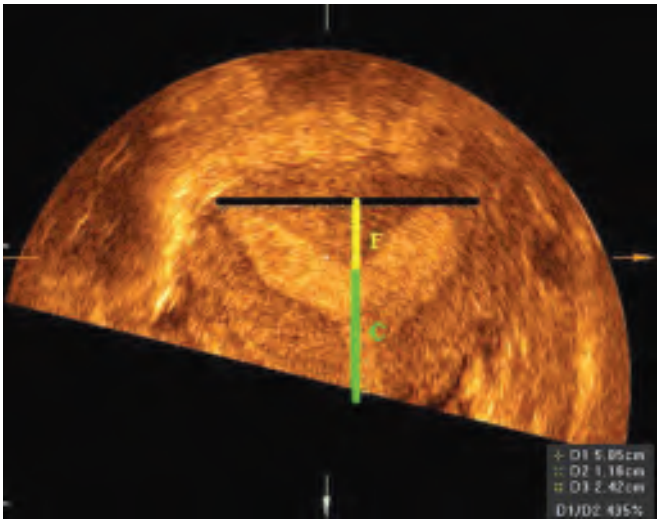

Figure 56.11: Mullerian anomalies can be quantified. A horizontal line is drawn between the two ostia. F represents distance of the depth of the septum from this line. C represents the vertical extent of the residual cavity and has a bearing on prognosis

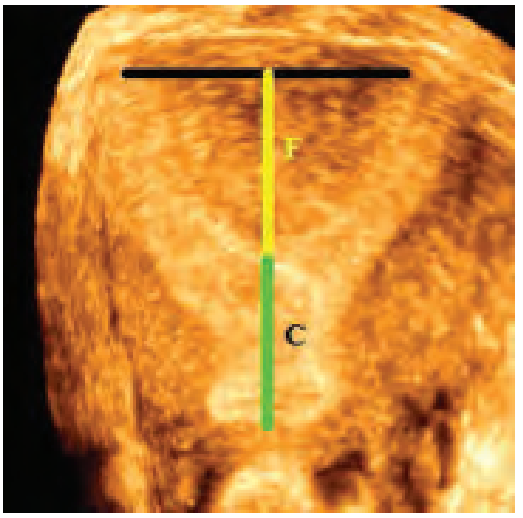

Figure 56.12: 3D rendered coronal image of a subseptate uterus. The length of the septum is considerably longer than the length of the residual cavity and indicates relatively poor prognosis

that the superb contrast resolution of 3D techniques is rapidly reducing the need of these studies in evaluating Müllerian anomalies. In the presence of concurrent uterine pathology such as fibroids and polyps in the anomalous uterus, however, the 3D sonohysterography is a useful problem solving modality.[27] Positive contrast sonohysterography was described for better cavity delineation in the past but currently it is rarely employed.[28] Quantification of developmental uterine anomalies is possible[29] **(Fig. 56.11).** The tubal ostia are delineated in the coronal plane and a line drawn through them. The midpoint of this line is extended to the inferior most point of indentation of the uterine cavity or the extent of the septum (distance F). The other measurement taken is the vertical extent of the uterine cavity (distance C). These distances are reliably reproducible[30] and the ratio F/F+C can be obtained. In women who have recurrent pregnancy losses, the length of the indentation or the length of the septum is not as important. It is the vertical height of the residual uterine cavity, which is considerably shorter, and the degree of distortion that is considerably greater in women with recurrent pregnancy losses **(Fig. 56.12)**.

Paired Müllerian ducts appear in the embryo at six weeks of gestation. Soon thereafter, these fuse in the midline in their caudal extent. This is known as lateral fusion. A septum representing the fused segments gradually breaks down, resulting in one uterine cavity. The fused portions form the uterus, cervix and upper two thirds of the vagina. The cranial portions of the Müllerian ducts remain unfused and form the fallopian tubes. Developmental malformations are consequent to truncation of normal development, abnormal fusion or disordered resorption.[1] Failure of development of both Müllerian ducts results in agenesis of the uterus or in a hypoplastic uterus. Unilateral failure results in a unicornuate uterus. Failure of lateral fusion results in a didelphys uterus or a bicornuate uterus. Failure of resorption of the septum results in a septate or arcuate uterus.

The nomenclature of developmental anomalies of the uterus remained confusing for several years. The American Fertility Society[10] (AFS) Classification Scheme based on embryological derangements, has put these in an appropriate perspective and facilitates a precise diagnosis which can then be managed by proven protocols that improve obstetric outcomes. The AFS classification is described as under:

- The AFS Class I includes uterine agenesis and hypoplasia. The 3D studies are useful for calculating uterine size and assessing canalization.
- The AFS Class II is a unicornuate uterus. A true unicornuate uterus is the result of complete unilateral arrest of Müllerian development. In case of partial arrest of development, as is more usual, a rudimentary horn with or without functioning endometrium is present. The 2D ultrasound is frequently unable to identify the subtle findings of a unicornuate uterus. The 3D rendered images reveal a banana shaped relatively narrow uterus with or without a

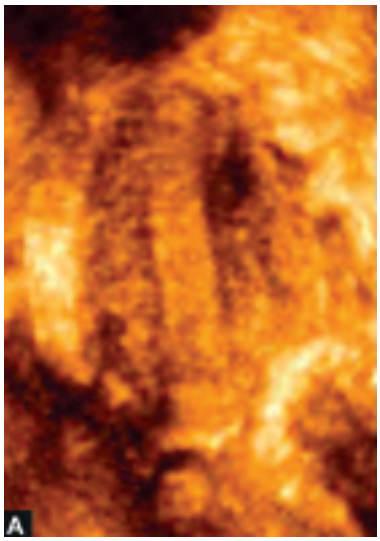

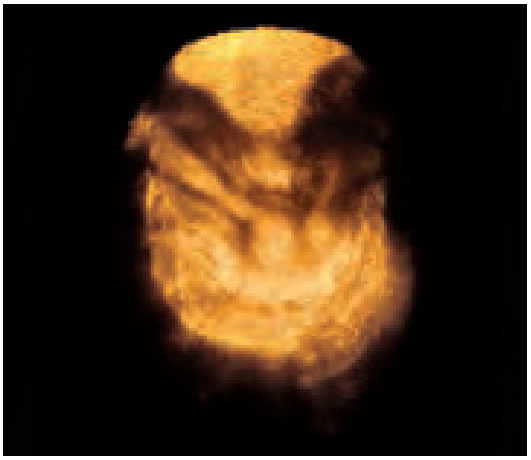

Figure 56.14: 3D rendered coronal image of a uterus didelphys. The two horns and two cervices are clearly evident

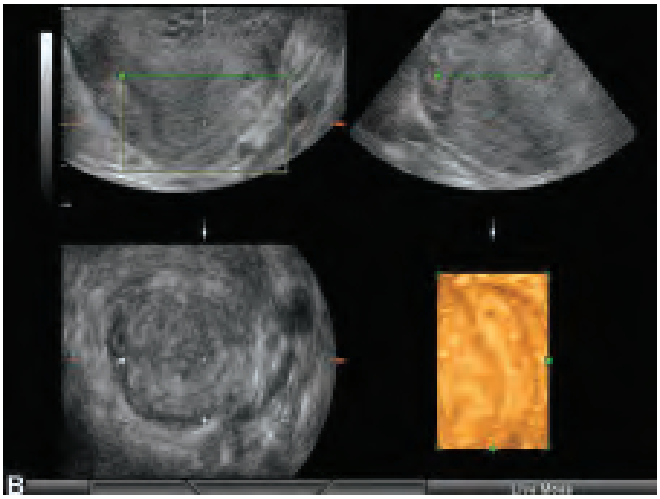

Figures 56.13A and B: Elongated narrow uterus with no cornual angle: unicornuate uterus

rudimentary horn **(Figs 56.13A and B)**. Multiplanar imaging helps to confirm a single cornual angle.[16]

- The AFS Class III refers to a didelphys uterus, which is a result of complete non-fusion of the Müllerian ducts. The two horns are usually fully developed and two cervices are present **(Figs 56.14 and 56.15)**. There may be an associated transverse vaginal septum **(Figs 56.16A to D)**. All these features can be evaluated with ease and accuracy with 3D techniques. The cervices are very close to each other but the canals are distinct.
- The AFS Class IV is a bicornuate uterus. This results from partial non-fusion of the Müllerian ducts. The central myometrium may extend to the internal os (bicornuate unicollis) **(Figs 56.17A and B)** or the external os (bicornuate bicollis) **(Fig. 56.18)**. The horns are typically low normal or small in size. A

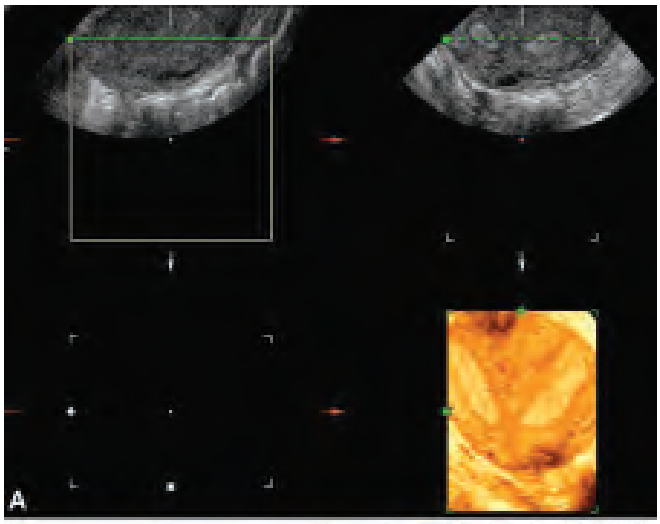

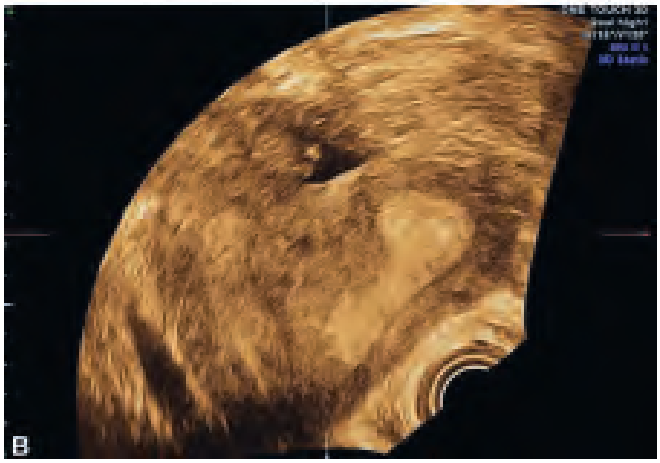

Figures 56.15A and B: Uterus didelphys. The uterine cavity is well defined on either side. The cervices were poorly defined even on 3D scans. Examination under anesthesia and cervical dilatation confirmed a narrow spiral cervix on either side

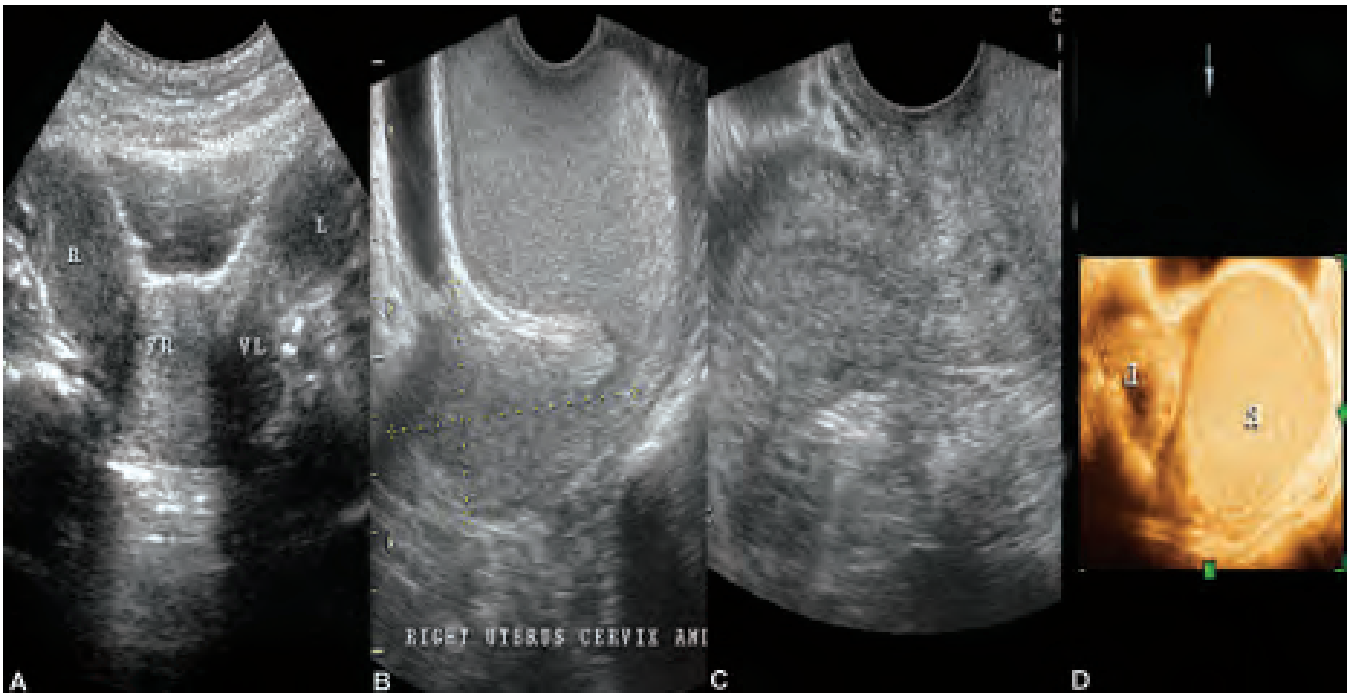

Figures 56.16A to D: Evaluation of a patient of primary amenorrhea who has never been sexually active. (A)The transabdominal scan reveals a didelphys uterus with possibly two vaginas; (B) There is a right hematocolpos seen on a transrectal scan; (C) This also reveals a normal left horn, cervix and vagina; (D) 3D rendering confirms a dual vagina with a right hematocolpos

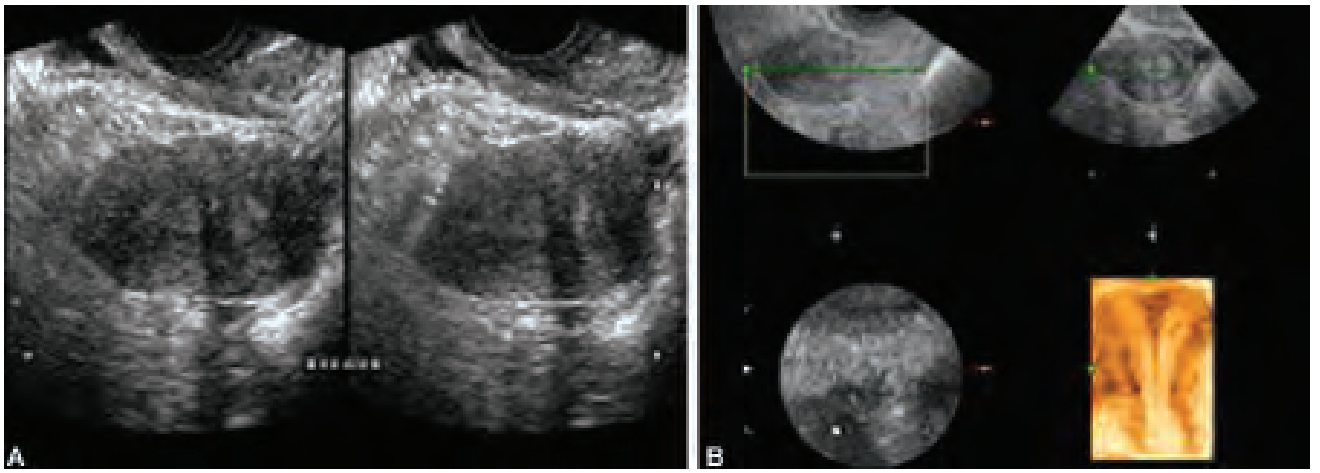

Figures 56.17A and B: (A) 2D transvaginal scan showing two uterine cavities; (B) 3D coronal rendering reveals a bicornuate uterus with a single cervix

3D orthogonal plane study with coronal reformatting is the method of choice for evaluating these uteri. A midsagittal indentation of 10 mm or more is evident in the bicornuate uterus **(Fig. 56.19).**

- The AFS Class V is a septate uterus. This results from a failure of resorption of the septum between the fused Müllerian ducts. The septum may be shallow (subseptate) **(Fig. 56.20)** or extensive (down to the external os) **(Fig. 56.21)**, fibrous, muscular or mixed. The septate uterus may be associated with a septate cervix, a septate vagina or both. Coronal plane analysis is necessary for assessing this condition and

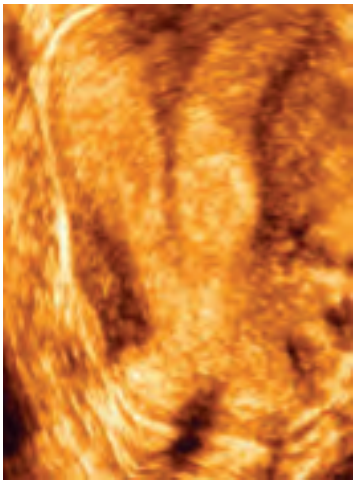

Figure 56.18: 3D rendered image of a bicornuate uterus with two cervices

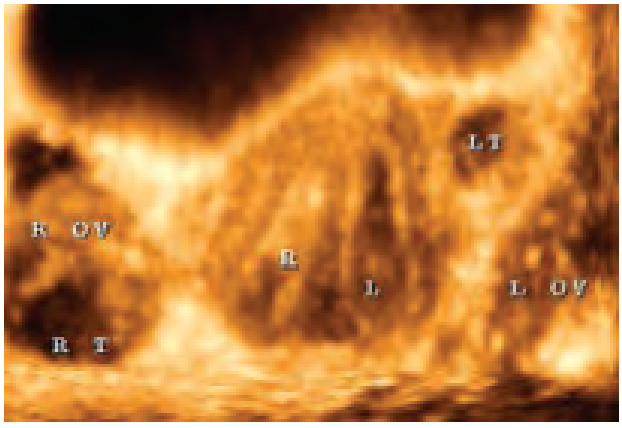

Figure 56.19: 3D rendered image of a bicornuate uterus with a bilateral hematometra and bilateral hydrosalpinx

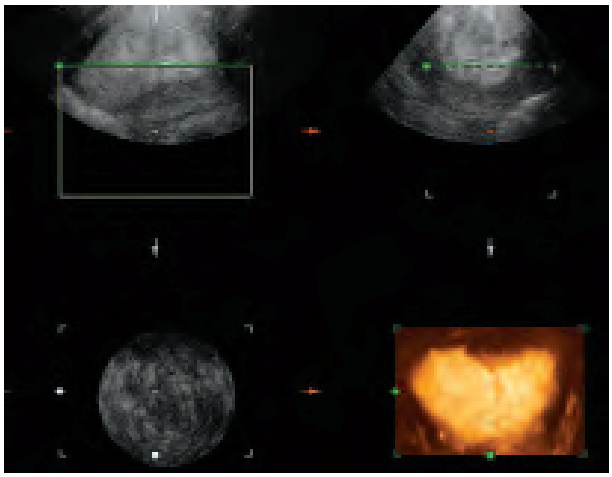

Figure 56.20: 3D rendered image in the coronal plane revealing a shallow fundal muscular septum and a longer fibrous septum

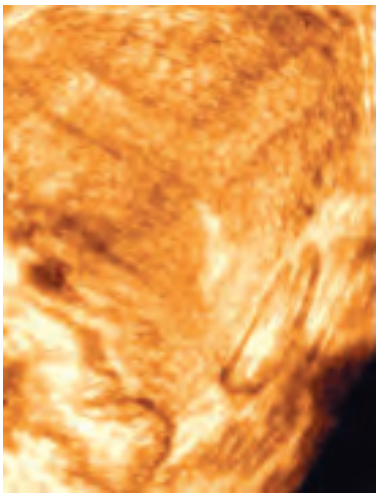

Figure 56.21: 3D rendered image showing a subseptate uterus with an extensive separation of the two horns

differentiating it from a bicornuate uterus. Recognition of this condition is imperative because obstetric outcomes greatly improve with hysteroscopic metroplasty in appropriately selected cases. With bicornuate and didelphys uteri, the approach has to be an abdominal one. In recent years, 3D criteria have helped greatly in patient selection.[26,29] The muscular septum lacks supporting connective tissue[25] and shows poor preovulatory changes and poor decidualization with consequently poor placentation. Additionally, a vascular septum shows enhanced irritability.[31] Most of the septa show poor vascularization responses in the pregnant state. Although the incidence of septate uteri is similar in patients with recurrent pregnancy losses compared to women with normal obstetric outcomes, there is no doubt that the height of the residual uterine cavity and the degree of distortion are related to poor outcomes. The degree of indentation and the height of the septum do not correlate with poor outcomes. It has been traditional obstetric practice not to treat a subseptate uterus until two pregnancy losses have occurred. Poor obstetric outcomes and the accurate information obtained by 3D now justify septal resection by a hysteroscopic method as soon as they are diagnosed.

- The AFS class VI is an arcuate uterus. The cavity is single but demonstrates a convexity towards the cavity. This is less than 10 mm in height from an imaginary line between the cornua. The serous contour of the fundus is convex or flat. The arcuate uterus is rarely associated with pregnancy failures. The pathophysiology for poor reproductive

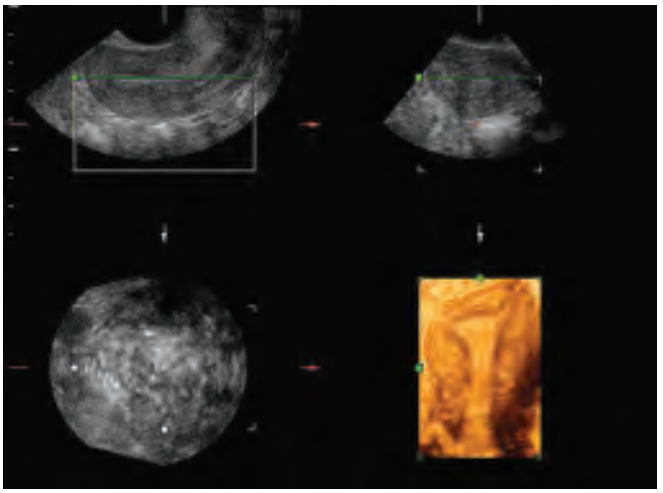

Figure 56.22: 3D rendered image of a T-shaped uterus. The vertical limb of the cavity is remarkably long

outcomes in these uteri is not known. Hysteroscopic fundal repair does not improve outcomes and the only treatment suggested is a cervical cerclage to prevent premature labor and delivery.

- The AFS Class VII of the classification refers to the T-shaped uterine cavity **(Fig. 56.22)** of the type seen in children of mothers who have been on diethylstilboestrol. The T-shaped uterus has now been observed in some patients who have had no intrauterine exposure to diethylstilboestrol. Patients are likely to benefit from a hysteroscopic lateral metroplasty.

Focal Endometrial Lesions

Although 2D studies can identify a large number of focal lesions in the endometrium, SISH enhances the sensitivity of identifying polyps. The 3D techniques with their inherent increased contrast resolution have reduced the need for sonohysterography. SISH can be combined with 3D to increase the sensitivity of both techniques.[27,32] The 3D technique also increases the possibility of identifying multiple polyps and multiple endometrial lesions **(Figs 56.23A and B)**. Power Doppler studies are useful to assess the origin and vascular pattern of polyps.[32] The 3D power Doppler can help to differentiate fibroid polyps from endometrial polyps and adenomyomatous polyps. Endometrial polyps typically show a solitary feeding vessel **(Figs 56.24A to D)**. Fibroid polyps often show only peripheral flow **(Fig. 56.25)**. Central flow in fibroid polyps is secondary to degeneration, inflammation and very rarely consequent to a sarcomatous change. Adenomyomatous polyps show a typical spoke-wheel appearance with a central large vessel and radiating smaller vessels

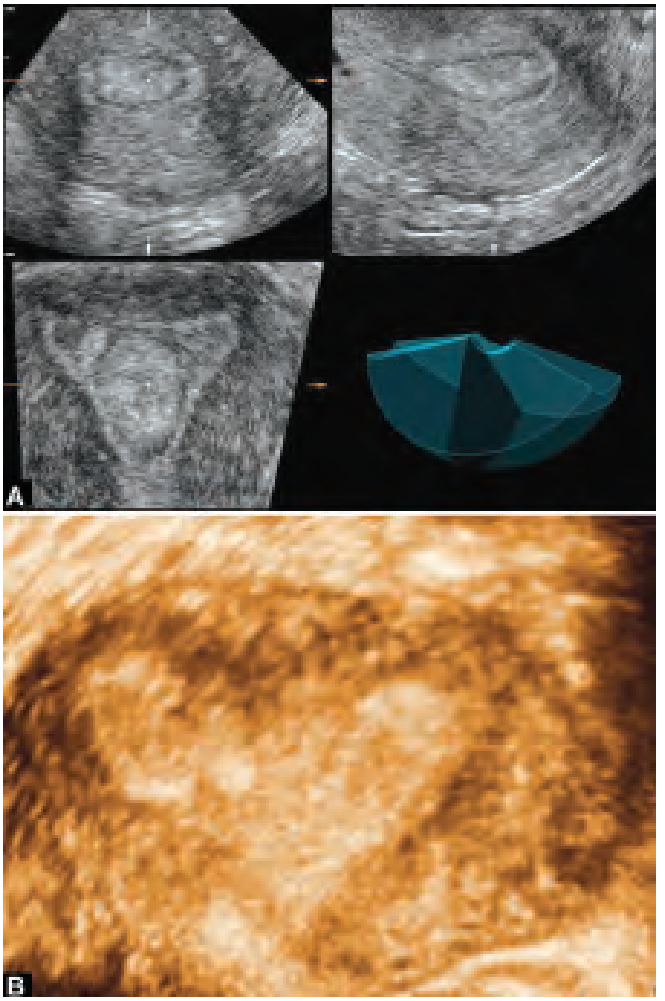

Figures 56.23A and B: (A) 3D orthogonal displays help to identify multiplicity of polyps; (B) When lesions in the endometrium are concurrent such as polyps, congenital uterine malformations and fibroids, the ultrasound image may be dramatic or confused. MR is useful in such situations. This 3D rendering shows a subseptate uterus with submucous fibroids and polyps

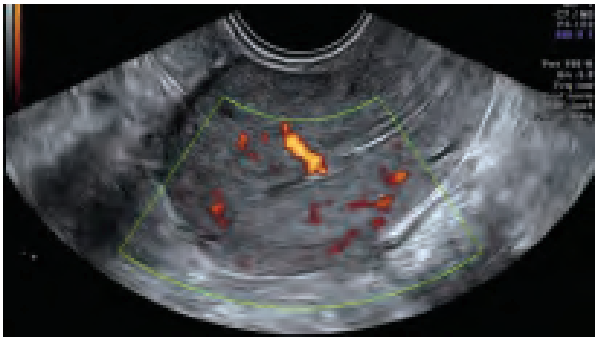

Figure 56.24A: Endometrial polyps typically show a solitary feeding vessel. This usually shows no branching and becomes smaller and smaller as it reaches the center of the lesion

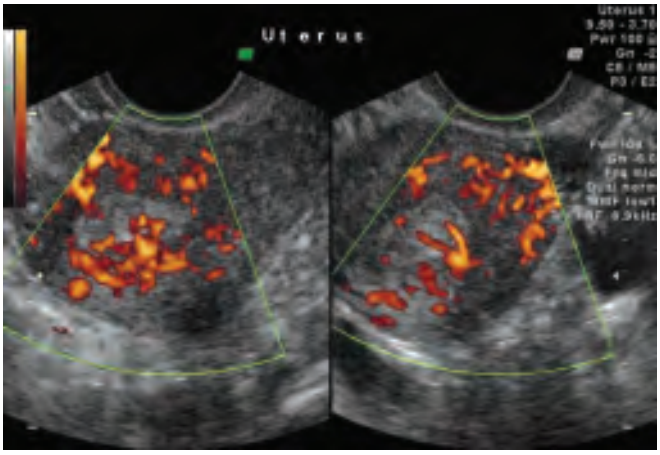

Figure 56.24B: Dichotomous branching of a feeder vessel should raise a strong suspicion for a malignant histopathology

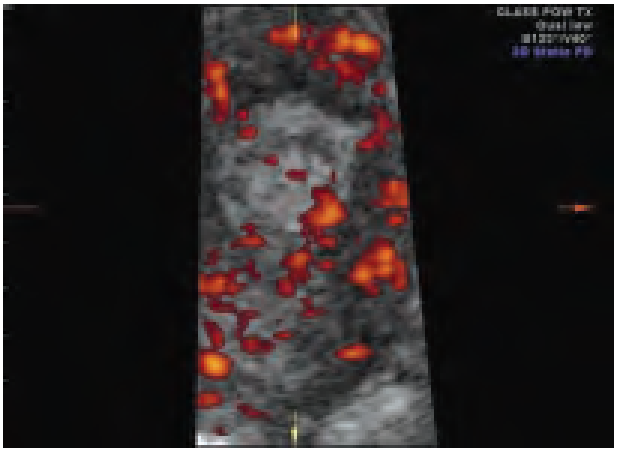

Figure 56.24C: Coronal reconstructed images are useful to identify feeding vessels

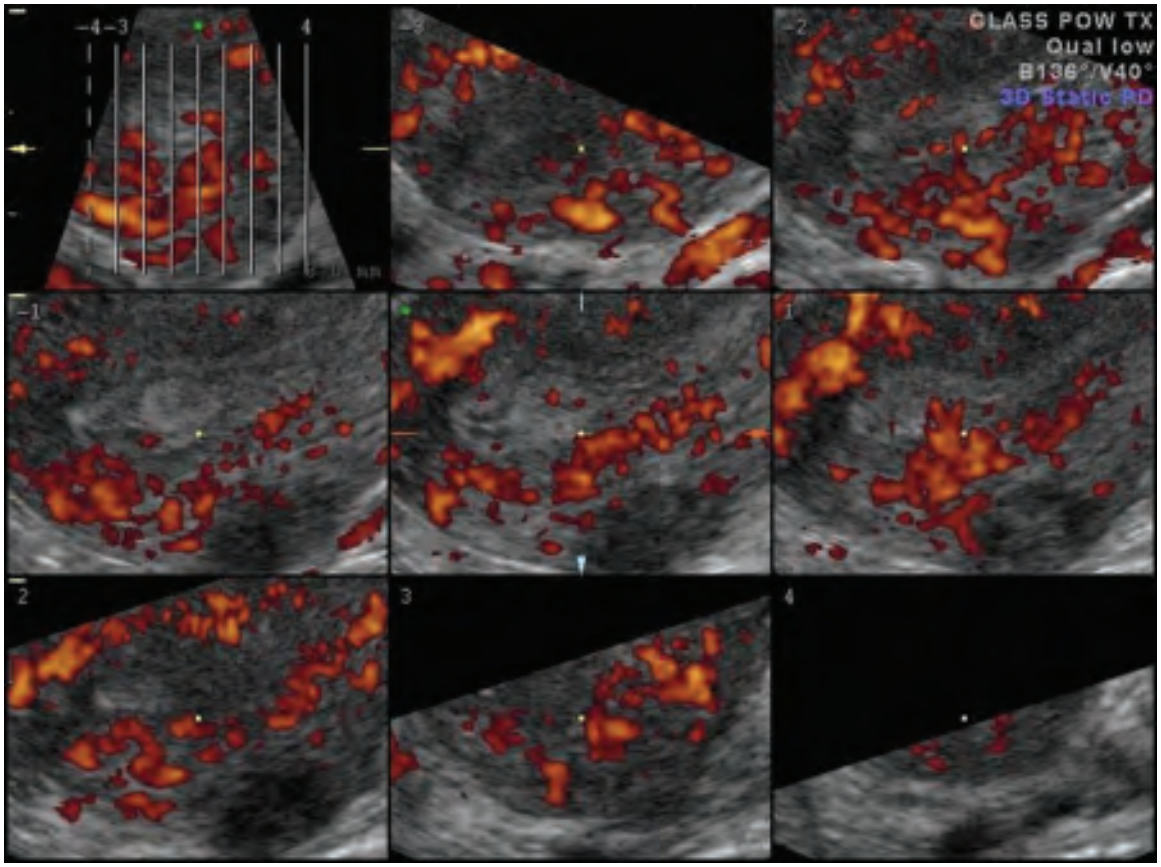

Figure 56.24D: Tomographic ultrasound imaging is a 3D technique that permits sectional imaging in parallel planes. This is useful for identifying the number and location of polyps. Gray scale and power Doppler intensities can be displayed simultaneously

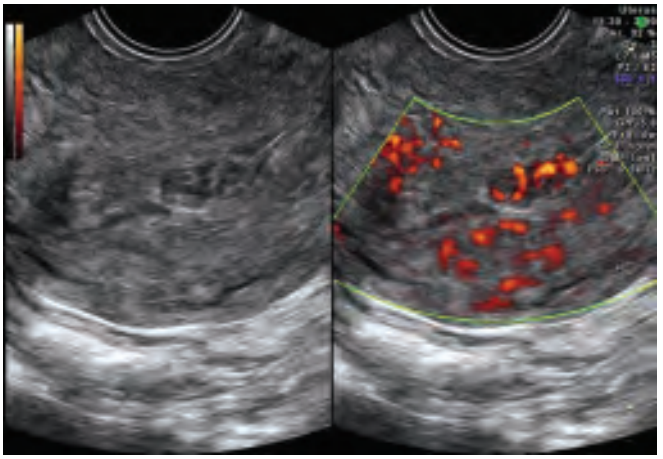

Figure 56.25: Fibroid polyps often show only peripheral flow. Central flow secondary to degeneration, inflammation or sarcomatous change may also be evident

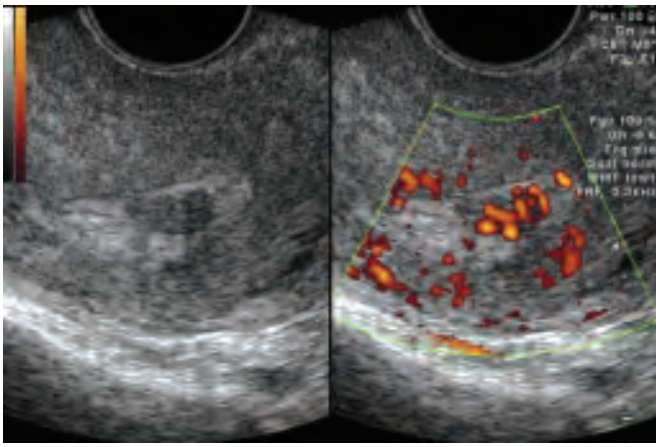

Figure 56.26A: Adenomyomatous polyps show a typical spoke-wheel appearance with a central large vessel and radiating smaller vessels

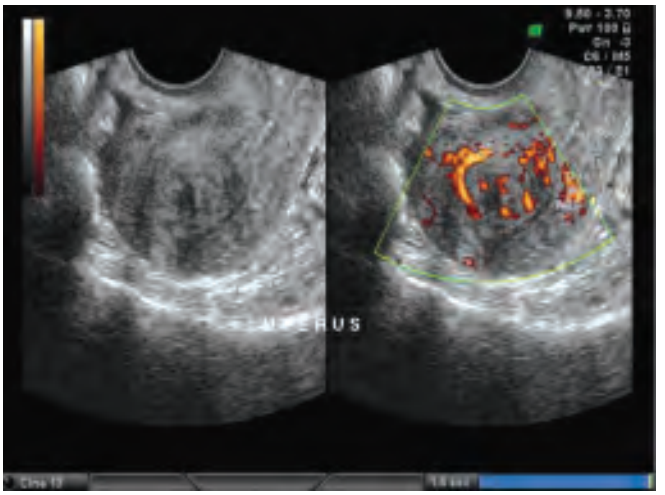

Figure 56.26B: Central flow in adenomyomatous polyps of the endometrium may not always have a spoke-wheel appearance. In these situations central vessels are randomly distributed and have no specific pattern

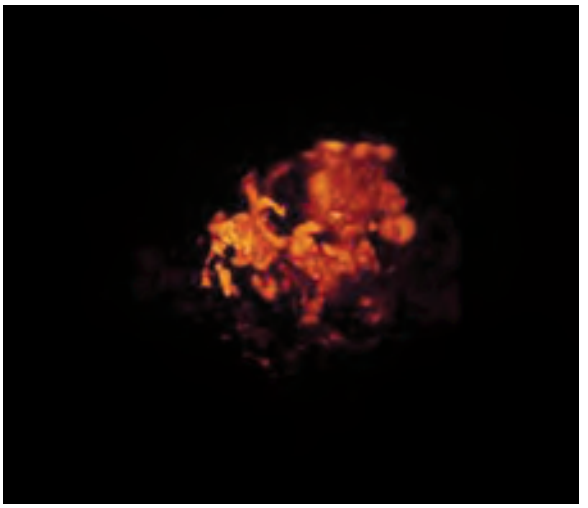

Figure 56.26C: In adenomyomatous polyps can sometimes radiate from two areas within the lesions. This is not necessary a sign of a malignant change

(Figs 56.26A to C). Quantification of indices, such as peak systolic velocity, diastolic velocity, systolic diastolic ratios, resistive index, pulsatility index, time to peak velocity and 3D vascular indices, are not reliable predictors of the histopathology of these focal endometrial lesions.

Malignant endometrial lesions in the endometrium are difficult to characterize when they are small. Larger lesions are poorly marginated, variably vascular and when invasive, obscure the endometrial-myometrial interface. Focal increased echogenicity, diffuse increased echogenicity and diffuse inhomogeneity on 2D studies increase the predictability of pathologic findings.[33-40] In addition, these findings, even in an endometrium which is thinner, the cutoff values of normal postmenopausal endometrium are indicators for inclusion in the group for invasive endometrial sampling. Aggressive evaluation for a malignancy must be made if there is a focal increased echogenecity or a diffuse inhomogeneity even in a thin endometrium.[41] The 3D endometrial volume, although initially promising,[32] is no longer regarded as a significant solitary parameter for discerning endometrial malignancy from benign lesions[38,40] and needs to be assessed in the perspective

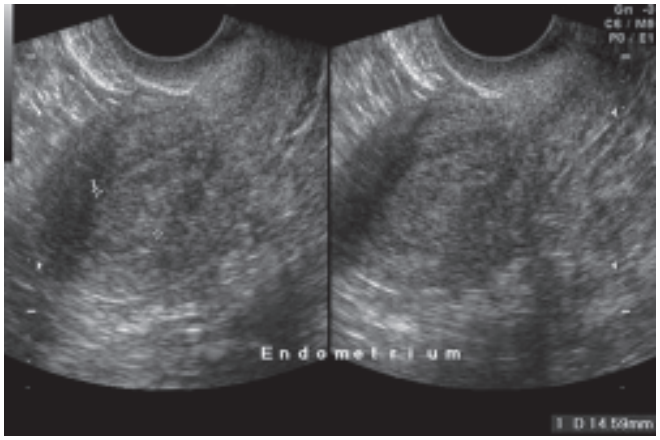

Figure 56.27A: A 15 mm thick, inhomogeneous endometrium with a poorly differentiated endometrial/myometrial interface of the posterior wall suggesting a strong possibility of an endometrial cancer

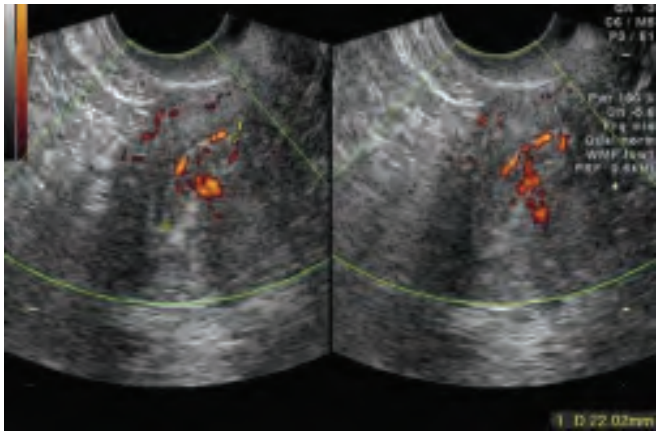

Figure 56.27B: Same case as in Figure 56.27A showing dilated and tortuous feeder vessels

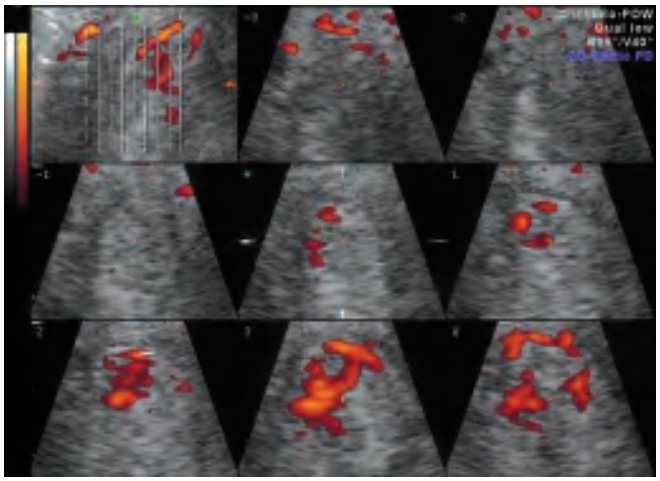

Figure 56.27C: Same patient as in Figure 56.27A and B showing markedly abnormal caliber vessels when analyzed with 3D Tomographic Ultrasound Imaging studies. Histopathology confirmed a poorly differentiated endometrial carcinoma

of echo texture and vascularity. The 3D power Doppler demonstration of dichotomous branching of a feeder vessel is a strong marker of a malignant mass **(Figs 56.27A to C)**. Other markers for endometrial malignancy include dilated, saccular, tortuous vessels and arteriovenous anastamoses. The shaggy surface of malignant masses is easier to identify in the presence of endometrial fluid collections with 3D techniques **(Figs 56.28A and B)** and with saline infusion sonohysterography.

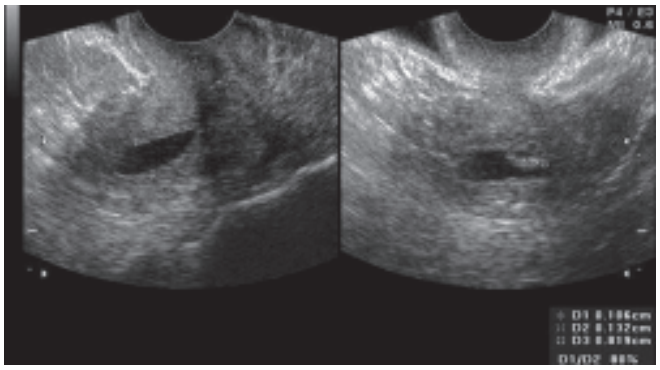

Figure 56.28A: Transvaginal scan showing an endometrial fluid collection with echogenic areas within it. It is difficult to differentiate whether this corresponds to debris or a mass

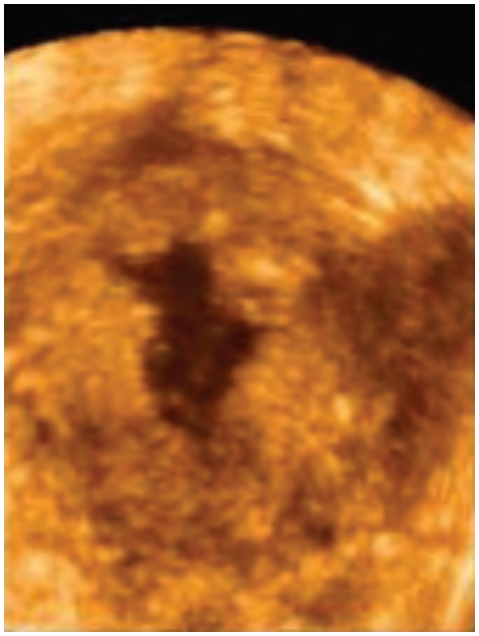

Figure 56.28B: A 3D rendering of the endometrium in the same patient as Figure 56.28A. Note the thick lobulated endometrium. Hysteroscopy confirmed a malignancy confined to the endometrium

Intrauterine Devices

Intrauterine devices (IUDs) are normally located in the cavity in the fundus and upper part of the uterine corpus. Migration into the myometrium is associated with lost threads, pain and abnormal vaginal bleeding. A low location is associated with a higher rate of contraceptive failure. The type of device can often be identified only by 3D rendering **(Figs 56.29A to C)**. This technique also improves delineation of abnormal migration of a device.[42] Medicated devices are often less echogenic than copper loaded devices and the inherent higher contrast resolution of 3D software coupled with the ability of demonstrating distal acoustic shadowing from the device, make 3D the method of choice in assessing these devices. The 3D studies have demonstrated that patients with embedded IUDs have a smaller fundal endometrial cavity diameter compared to those with normally placed IUDs.[43] This preliminary work suggests that pre-procedural quantitative 3D ultrasound for women who are IUD candidates needs further study followed by clinical consideration. It must be remembered that once a device has migrated beyond the myometrium and into the peritoneum or bowel, it is very difficult to identify with ultrasound. In this situation, conventional abdominal X-Ray imaging remains the modality of choice to identify or exclude the presence of the device in the abdomen or pelvis.

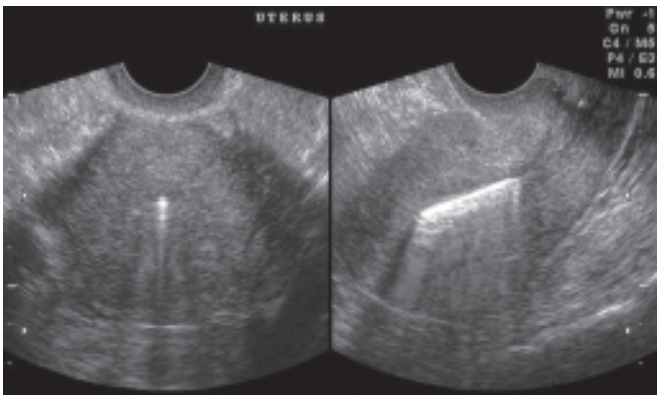

Figure 56.29A: Intrauterine device in the uterine cavity in a patient with lost threads. The device is confirmed to lie within the cavity

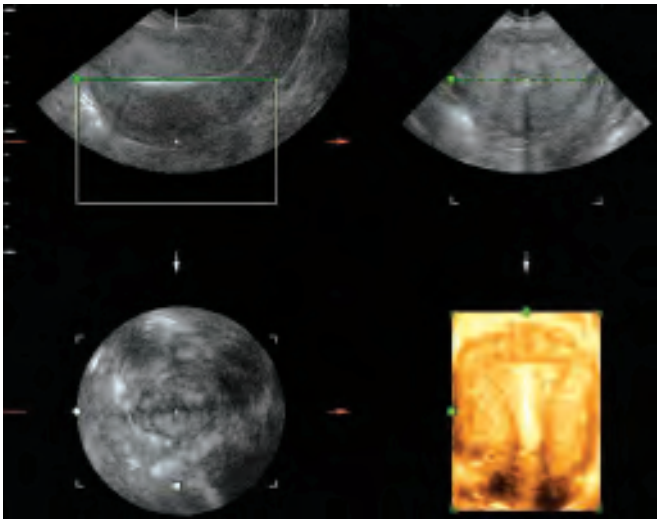

Figure 56.29B: A 3D reconstruction of the same patient as in Figure 56.29A. The 3D confirms the normal location of the device

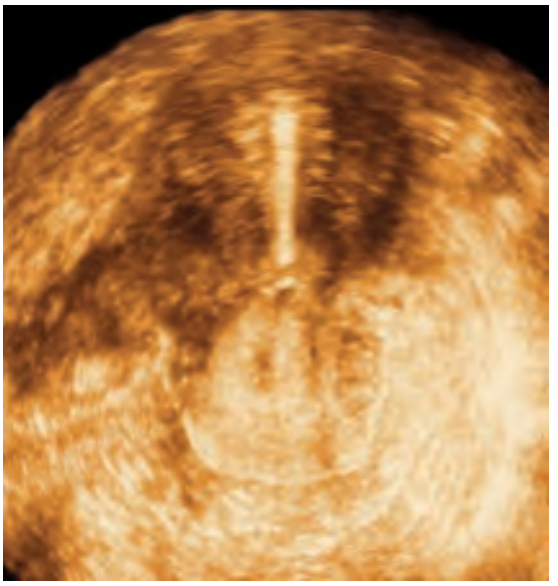

Figure 56.29C: The 3D permits recognition of various types of intrauterine devices. This rendering shows a multiload device in the uterine cavity

Endometrial Fluid Collections

Free fluid collections in the endometrial cavity are physiological in the immediate post menstrual phase and in menopause. These are thin-walled and clear. Any focal thickening or vascularization of the endometrium associated with free fluid in the cavity warrants histopathological sampling. The presence of echoes inside the fluid contained in the uterine cavity can be consequent to a large number of causes including menstrual debris, inflammatory debris, blood or pus. Only a gross examination and microscopy can reveal the pathological basis in these situations. Adhesive bands can be seen as echogenic, laminar, variably thick structures that traverse the uterine cavity. These are largely missed on routine 2D scans but well delineated with 3D SISH **(Figs 56.30A to G)**. Failure to sharply delineate the

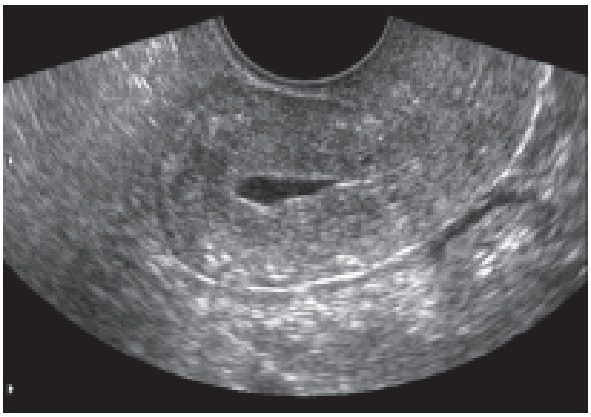

Figure 56.30A: Saline infusion sonohysterography excludes synechial bands within this endometrium

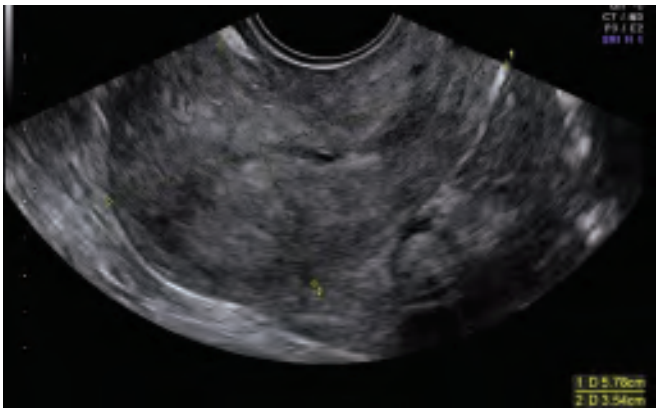

Figure 56.30D: 2D evaluation of an endometrium in a patient with secondary amenorrhea. No abnormality is evident

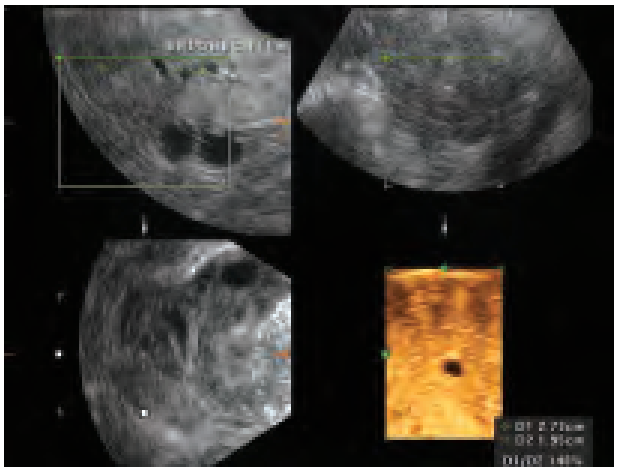

Figure 56.30B: 3D rendering of an endometrium showing multiple fluid loculi confirming adhesive bands in a chronic inflammation of the endometrium

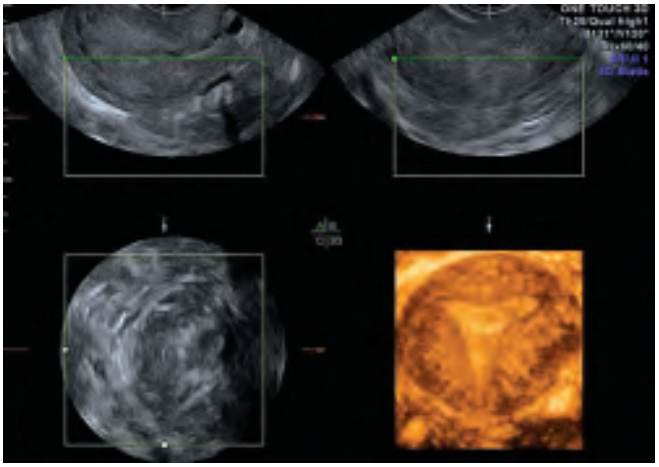

Figure 56.30E: 3D rendering and orthogonal plane evaluation suggesting synechial bands in the endometrium

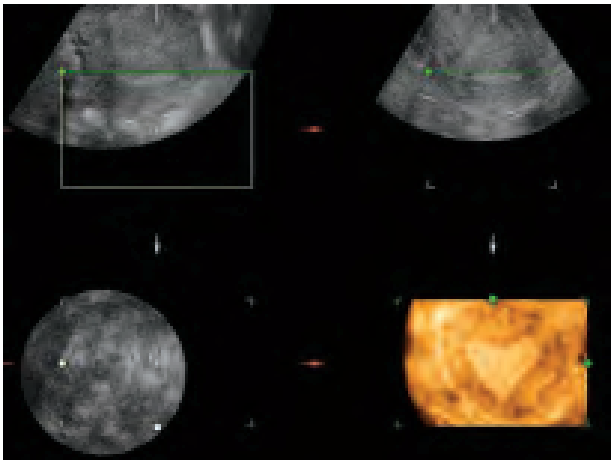

Figure 56.30C: 3D rendering of an endometrium that showed no abnormality on 2D studies. Amputation of the endometrium is evident at the left cornu. Histopathology confirmed tubercular synechial bands

endometrial contour should raise the suspicion for adhesive bands. Sensitivity for detecting adhesions is best in the secretory phase of the menstrual cycle.

Endometrial Receptivity

Currently available ultrasound techniques of evaluation for endometrial receptivity include gray-scale sonography using high frequency transvaginal scans, conventional color Doppler studies, power Doppler, 3D and real time 3D, i.e. 4D studies and tomographic ultrasound imaging.

The parameters that have been studied over the past two decades, more so the last four years, include endometrial thickness, endometrial volume, endometrial ultrasound morphology, subendometrial peristalsis, endometrial and subendometrial vascularization, subendometrial vascularization, myometrial echogenecity, myometrial power Doppler, spectral analysis

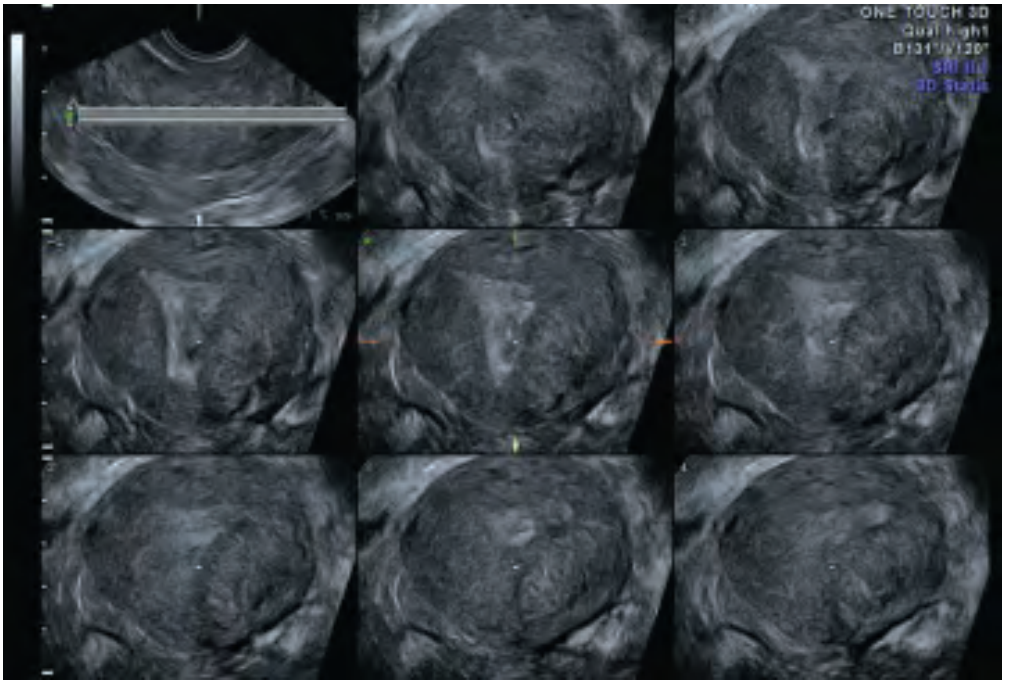

Figure 56.30F: 3D Tomographic Ultrasound Imaging studies in the same case as in Figure 56.30E reveal a markedly interrupted endometrium confirming extensive synechiae in the cavity

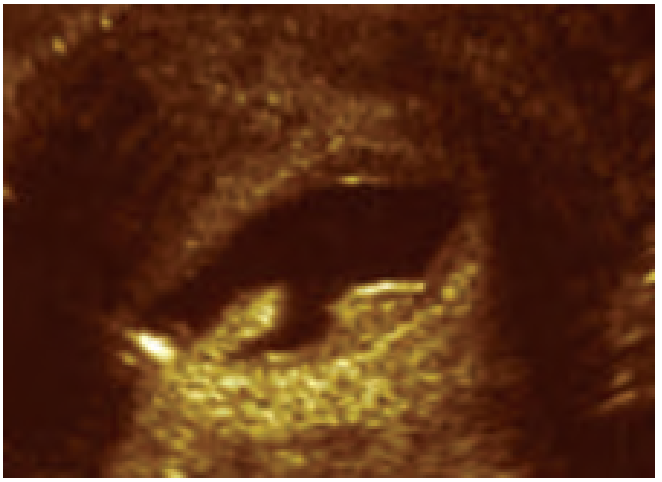

Figure 56.30G: 3D rendering of polypoid endometrial lesions. Visualization is enhanced by the presence of fluid within the cavity

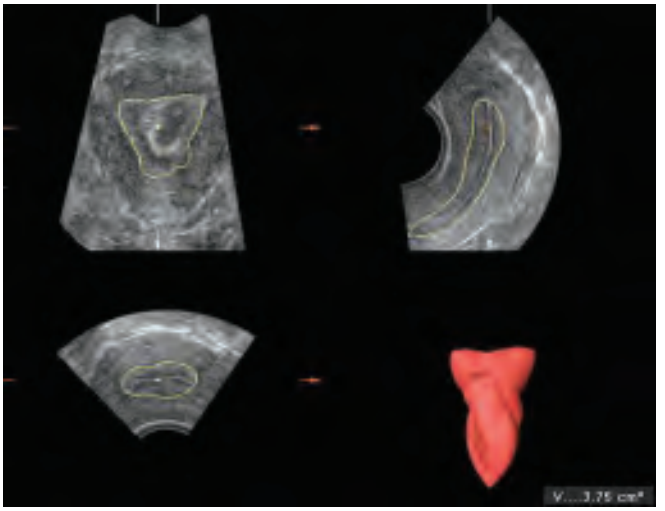

Figure 56.31: Three-dimensional volume measurement of the endometrium. Using branded software called Virtual Organ Computer Aided Analysis (VOCAL) the outline of the endometrium is traced through an acquired volume. The machine automatically calculates endometrial volume and displays it as shown in the bottom right hand picture. The other three frames show an orthogonal multiplanar display of the endometrium. The minimum volume associated with implantation is 1.59 ml

of uterine artery flow velocity waveforms and perifollicular vascularization.

Endometrial thickness below 6–8 mm is rarely associated with conception.[44-47] Increase in endometrial thickness above this level, however, does not enhance implantation rates and there is no difference in the mean endometrial thickness in patients who become pregnant and those who do not become pregnant in ART cycles.[48] The minimum endometrial volume **(Fig. 56.31)** associated with pregnancy is 1.59 ml as calculated by 3D.[46] This is calculated using a manual or

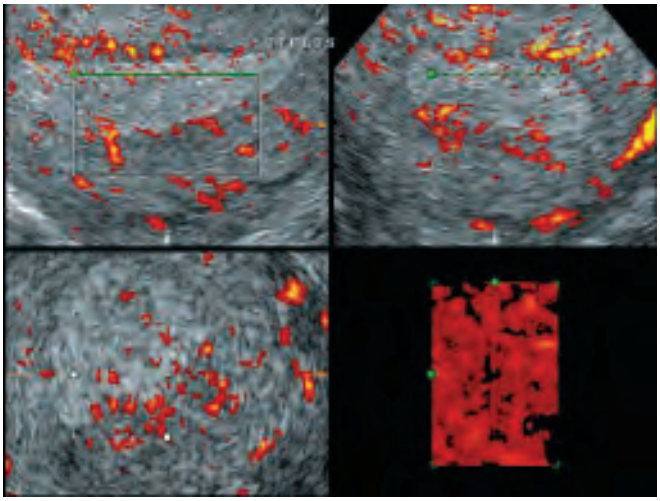

Figure 56.32: Proliferation of spiral arteries and their subsequent growth into the endometrium is reflected as morphologic and quantitative increases in endometrial vascularity when imaged by power Doppler. This is seen in the late proliferative and periovulatory phases. The deeper the vascularization into the endometrium, the better is the endometrial receptivity. 3D multiplanar studies with appropriate rendering afford an accurate delineation and quantification of angiogenesis in the endometrium. The illustration shows endometrial neovascularization in the longitudinal, axial and coronal planes along with the morphological rendering of endometrial vessels

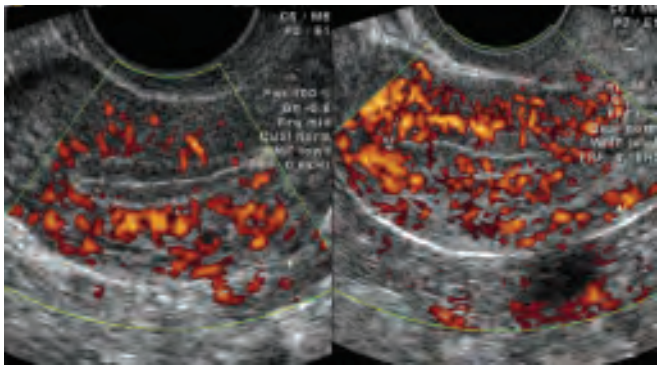

Figure 56.33: Frame (A) shows vascularization into the midzone of the endometrium demonstrated by 2D power Doppler. Frame (B) shows extensive endometrial vascularization up to the cavity

semi-automated planimetry and automated software called VOCAL (Virtual Organ Computer Aided Analysis).

By far the best correlation with implantation rates are being observed with power Doppler[45] and 3D power Doppler studies **(Fig. 56.32)**.[49-51] Ultrasound delineation and quantification of endometrial and subendometrial angiogenesis is emerging as a reliable and reproducible indicator of endometrial receptivity.[52,53] Basic static 3D, VOCAL and 3D shell imaging have been used to assess and quantify endometrial and subendometrial vascularization.[49-51] The vascularization index (VI), flow index (FI) and vascularization flow index of endometrial and subendometrial vessels increases during the proliferative phase, peaks 3 days prior to ovulation and decreases to a nadir 5 days post ovulation.[51] The VI is the ratio of color voxels to the total number of voxels inside the volume of interest and reflects the number of vessels in the volume being studied. The FI is the flow index and is the ratio of the sum of color intensities to the number of color voxels inside the volume being interrogated. It reflects the amount of blood flow. The VFI is the vascularization/flow index and is the ratio of the sum of color intensities to the total number of voxels inside the volume of interest. This reflects vessel presence and blood flow. Endometrial and subendometrial VI/FI/VFI is significantly lower in stimulated cycles than in natural cycles.[50] Smoking is associated with significantly lower VI and VFI. Patients who become pregnant have a significantly lower Resistive Index (RI) of subendometrial vessels: 0.53 compared to 0.64 +/– 0.04 in pregnant and non pregnant patients respectively.[49] Undetectable subendometrial artery flow is not associated with a lower implantation rate.[46]

Inner zone vascularization **(Fig. 56.33)** of the endometrium observed on the day of hCG administration or on the day of embryo transfer is associated with higher pregnancy rates. This can be assessed subjectively by direct observation but may be more objectively evaluated by quantification. Quantification can be done using the power Doppler area technique which measures the vascularized area in anyone endometrial plane or with VOCAL which involves a 3D acquisition followed by semi-automated planimetry **(Figs 56.34A and B)**. Pre retrieval hCG does not enhance endometrial PI although more embryos are generated.[54] Interestingly, impedance in the uterine and spiral arteries does not show any significant difference between normal pregnancies, missed abortions and anembryonic pregnancies.[55]

Ovarian antral follicle number, ovarian volume **(Fig. 56.35)** and ovarian stromal blood flow 3D quantification **(Fig. 56.36)** and 2D perifollicular vascularization **(Fig. 56.37)** correlate well with embryo quality and fertilization rates but do not have a direct correlation with endometrial receptivity.[50-52]

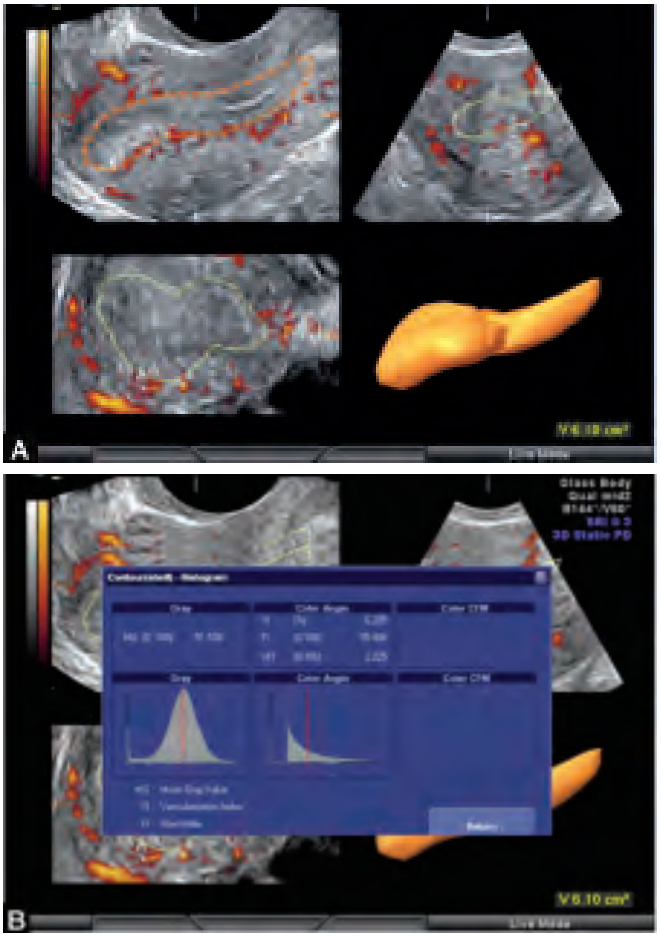

Figures 56.34A and B: 3D automated volume calculation (VOCAL) of the endometrium with calculation of 3D vascular indices

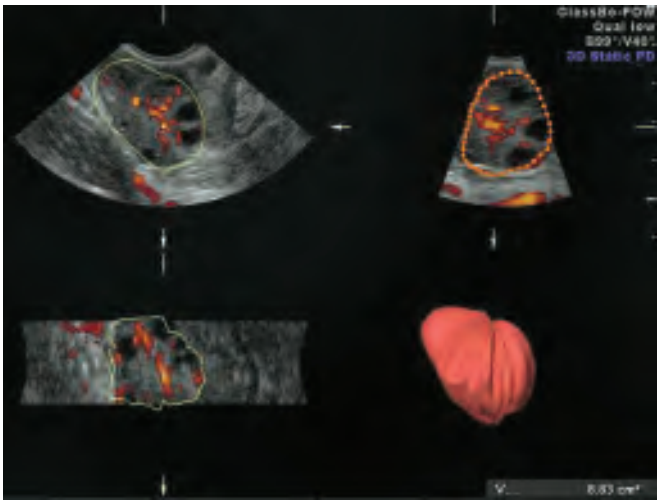

Figure 56.35: Ovarian volume using three-dimensional acquisition techniques and three-dimensional quantification software is more accurate than 2D methods. However, volumes correlate well with embryo quality and fertilization rates but not with endometrial receptivity

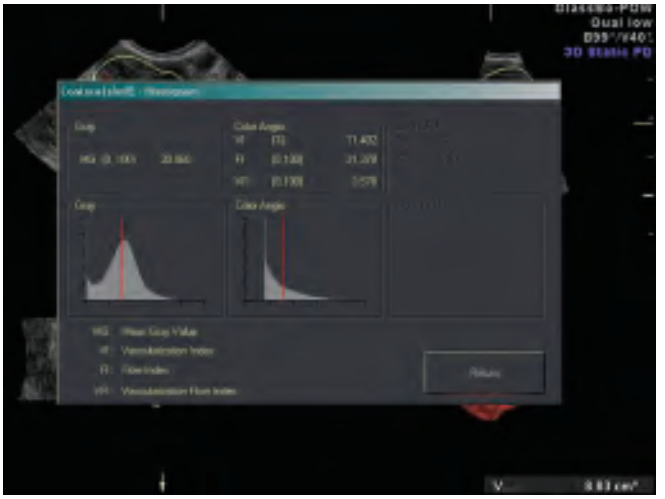

Figure 56.36: Gray scale and power Doppler acquisition of ovarian morphological data and stromal blood flow can be quantified using 3D software. Stromal blood flow correlates well with oocyte yield and embryo quality but not with implantation rates

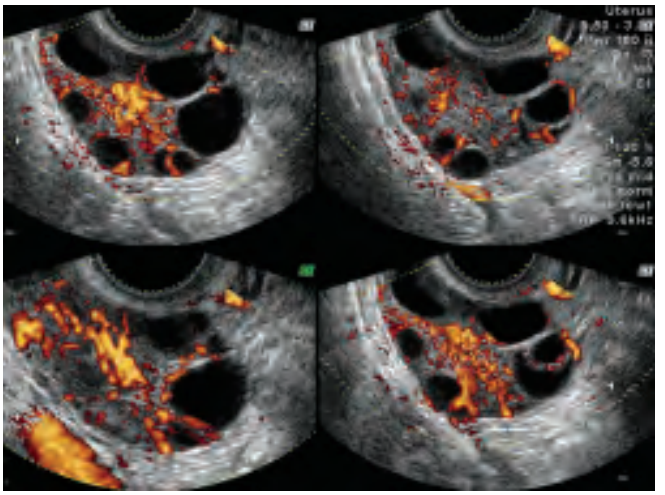

Figure 56.37: Follicular maturation is accompanied by perifollicular neovascularization. This can be recognized by the appearance of occasional perifollicular vascular signals when the follicle reaches 12–14 mm in size, which then progress to 50–100% of perifollicular vascularization as the cycle progresses. This phenomenon correlates well with parameters of oocyte quality such as the levels of follicular fluid estradiol, pH, follicular fluid pO2 and absence of oocyte aneuploidy. This neoangiogenesis, however, does not correlate well with endometrial receptivity

Fibroids

Fibroids are the most frequently encountered pathological finding on ultrasound. The number and location of fibroids is best assessed with 3D studies **(Figs 56.38 to 56.40)**. Fibroids are frequently multiple. Not

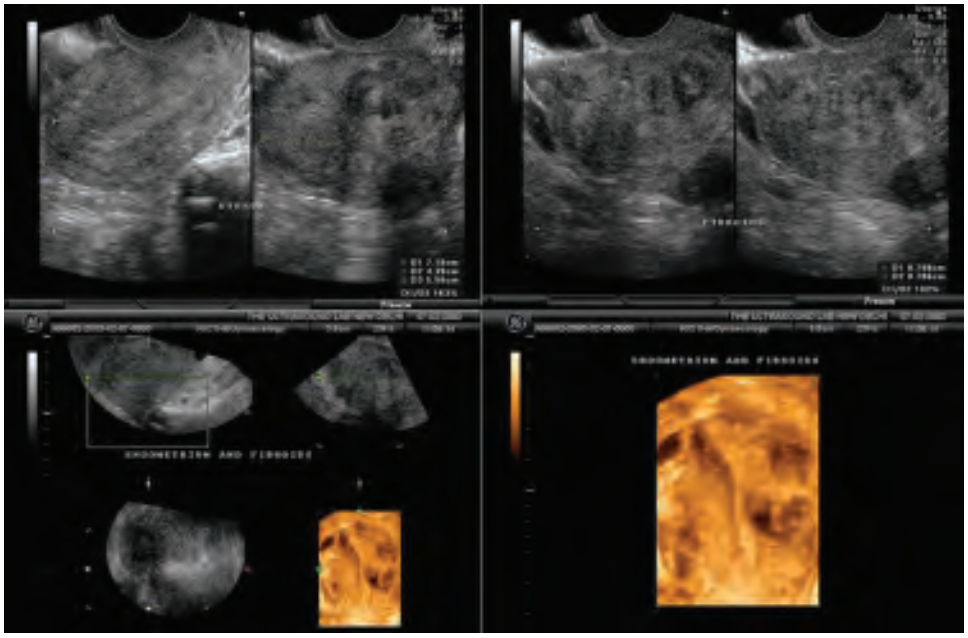

Figure 56.38: Multiple fibroids are often difficult to localize on 2D transabdominal and transvaginal scans. 3D rendering demonstrates with great clarity the exact location of these fibroids and the extent of cavity components

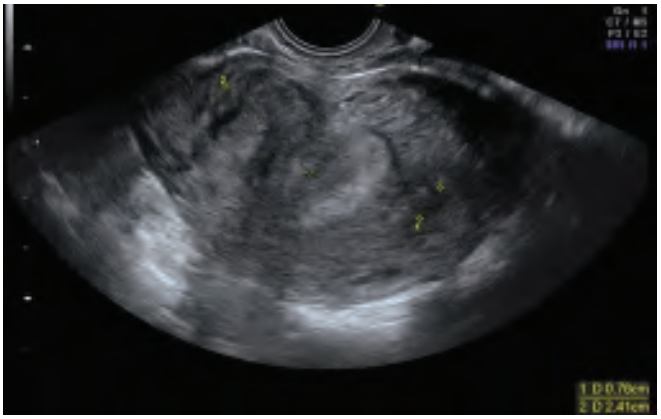

Figure 56.39A: Interstitial fibroids with a possible submucous component. 3D rendering clarifies the location as shown in Figure 56.39B

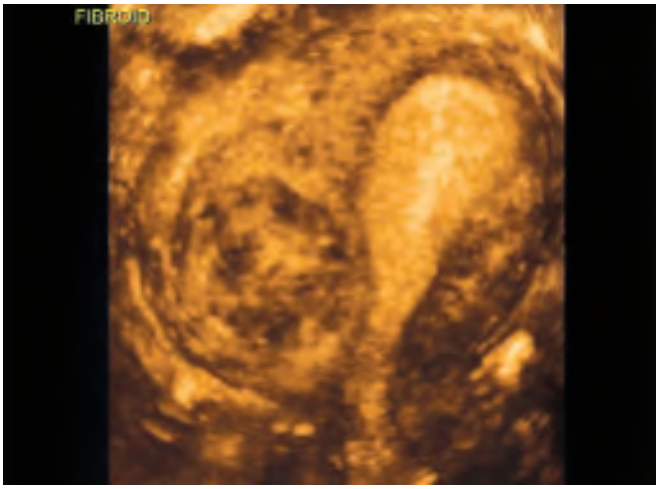

Figure 56.39B: Same patient as in Figure 56.39A. 3D rendering shows a largely interstitial fibroid with a minimal submucous component. The other fibroid is not evident in this plane

infrequently, fibroids are large and a transabdominal and transvaginal approach may be necessary for adequate delineation. Magnetic resonance imaging may be useful in delineating very large fibroids from normal portions of the uterus and the ovaries.

Adenomyosis

Ectopic endometrial tissue in the myometrium is referred to as adenomyosis. The most frequent presenting symptom is heavy, painful periods with clots. Other manifestations include backache and infertility. Occasionally, the process may be clinically silent. The findings on 2D ultrasound are variable and numerous. These include focal or generalized myometrial thickening, diffuse or focal speckling, myometrial cysts and an obscured endometrial-myometrial junction. Myometrial thickening may be diffuse and present as an enlarged, globular uterus with a markedly increased transverse diameter or a differential thickening of the posterior wall and occasionally a differential thickening of the anterior wall. Sometimes, the process is focal and presents as a globular myometrial mass mimicking a

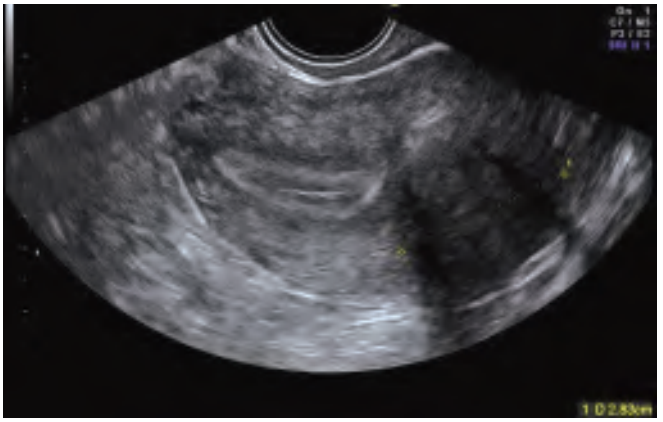

Figure 56.40A: Interstitial fibroid with a doubtful cavity component. 3D studies showed a better delineation and are shown in Figures 56.40B and C

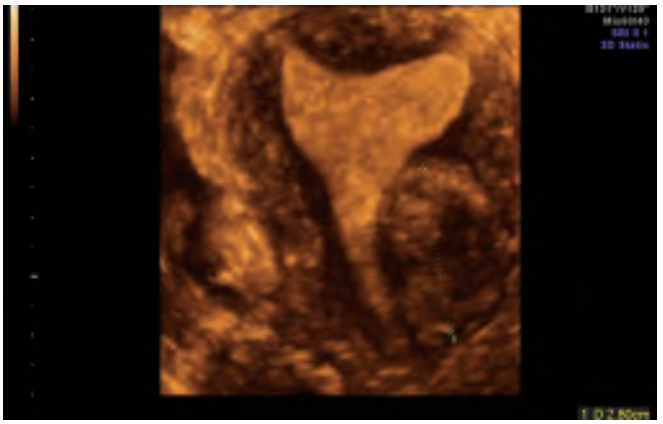

Figure 56.40B: 3D rendering shows the same fibroid as in Figure 56.40A. The cavity is mildly displaced but the fibroid has no cavity component

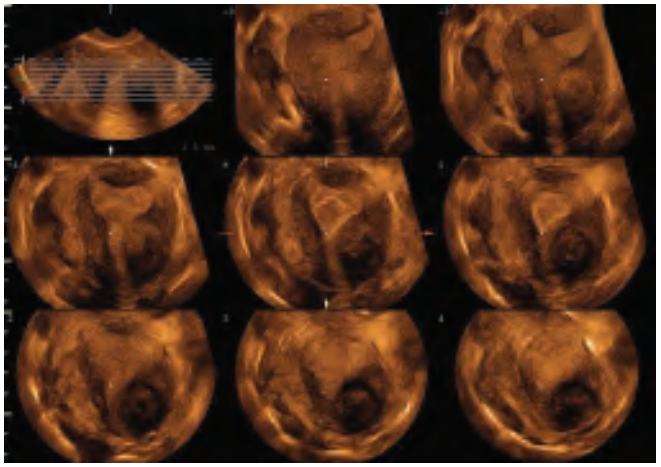

Figure 56.40C: Tomographic Ultrasound Imaging demonstrates a lesion in multiple parallel planes. This makes it a useful modality for a more accurate delineation of the location of fibroids as shown in this entirely interstitial fibroid

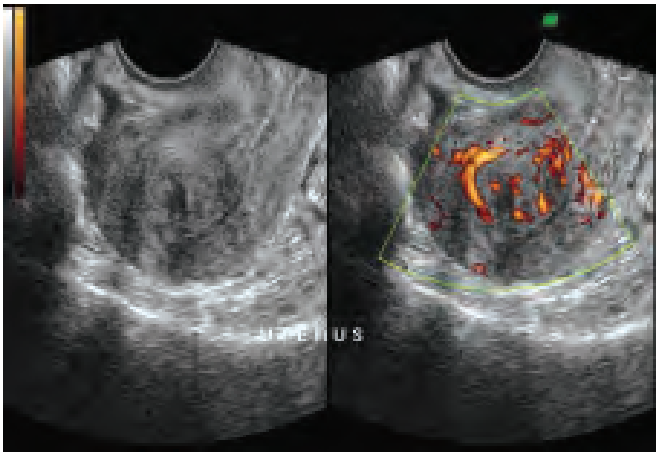

Figure 56.41A: Focal subendometrial lesion. Differentiating this adenomyoma from a fibroid is possible with power Doppler studies. These reveal central vascularity with a spoke wheel radial pattern characteristic of an adenomyoma. Fibroids usually show only peripheral flow. Central flow in a fibroid is usually secondary to degeneration

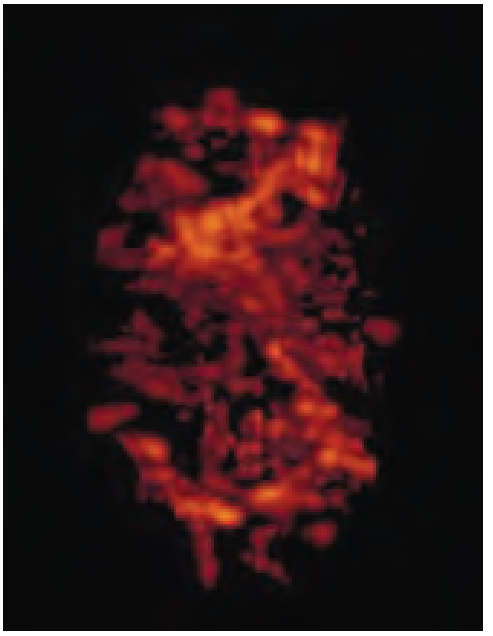

Figure 56.41B: Power Doppler mapping reveals spoke-wheel pattern vascularity in the adenomyoma

fibroid. Differentiation is possible with the use of 3D power Doppler which demonstrates the classical spoke wheel pattern of an adenomyoma **(Figs 56.41A and B)**. This consists of a central vascular pool with radiating vessels and rim vascularization. Differentiation between fibroids and adenomyomas is important because management differs remarkably. Fibroids are handled

with focal resection whereas adenomyomas do better with medical management or myolysis. Both lesions respond to GnRH analogues as a depot preparation.

The Fallopian Tubes

Healthy tubes are not visualized with 2D or 3D transvaginal scans. The interstitial part of the tubes is evident as an echogenic line extending towards the cornu from the cavity. Dilated tubes may be visualized depending on the extent, echogenicity and status of surrounding structures. Free fluid in the pelvis permits complete visualization of the tubes. These are seen as echogenic curvilinear structures engulfing the ovaries and are seen equally well on 2D and 3D scans. 3D scans are particularly useful for delineating adnexal organ relationships **(Figs 56.42A to C)** and for differentiating the tubal and ovarian components of the clinical tubo-ovarian mass **(Figs 56.43A to E).**

The Pelvic Peritoneum

The peritoneum serves as a useful window for systemic disease, for clues to pelvic pathology and for unusual diagnosis.

Hypoechoic fluid loculi of variable sizes are frequently seen in endometriosis. These may also be evident in non-specific pelvic inflammatory disease. Deep pelvic endometriosis is well visualized on 3D ultrasound but has to be specifically looked for.

Functional Ovarian Cysts

Cyclical changes in the ovary are prone to go into disarray and form cystic areas in the ovaries. Although referred to as functional cysts, these lesions are truly "dysfunctional" cysts. The clinical features are abnormal vaginal bleeding or pain, although some are entirely coincidental findings on an ultrasound examination. On ultrasound these are thin-walled and unilocular. Internal echoes and peripheral vascularity may be evident. The 3D images, although dramatic, rarely

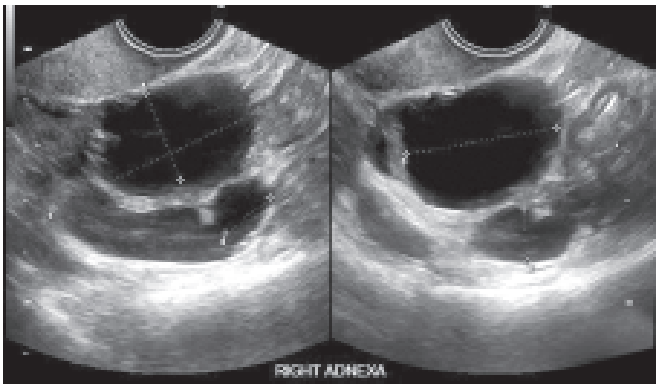

Figure 56.42A: A classical tubo-ovarian mass consists of a fluid ovary surrounded by a fluid filled tube. Scan shows a lobulated fluid lesion in the ovary draped by a hydrosalpinx which is thin-walled and clear

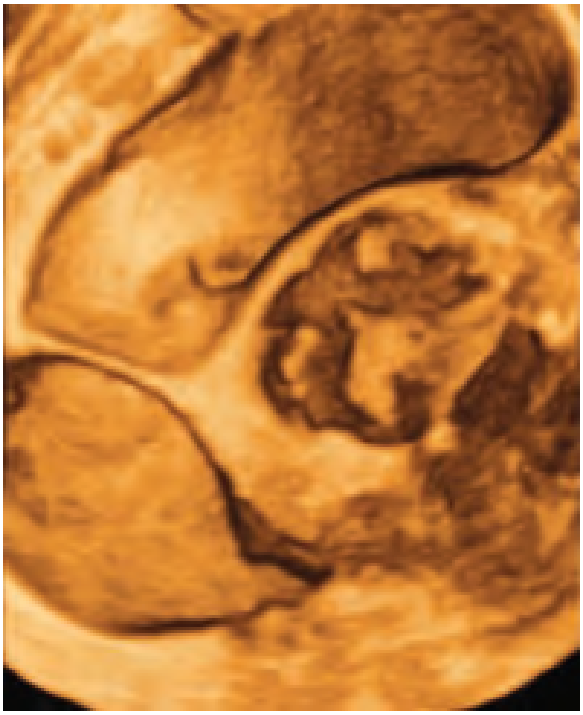

Figure 56.42B: Same patient as in Figure 56.42A. The 3D rendering reveals a variably echogenic ovary surrounded by a multilocular hydrosalpinx. The texture of the walls of these lesions is best studied by 3D

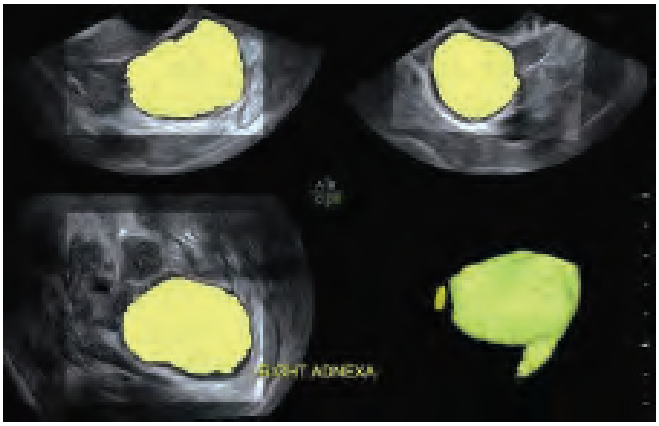

Figure 56.42C: The SonoAVC software provided by one vendor automatically delineates fluid loculi with a color signal. This helps to highlight fluid collections anywhere in the body and can be used to delineate a hydrosalpinx as well

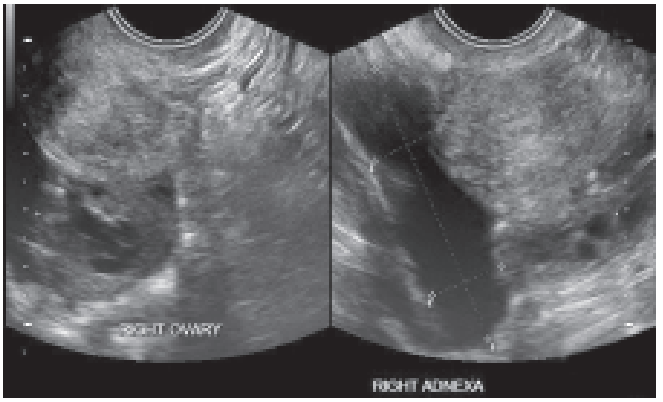

Figure 56.43A: Transvaginal scan showing a hypoechoic right ovary and a tubular fluid loculus in the right adnexal. Further evaluation using 3D studies yielded information as shown in Figures 56.43B and C

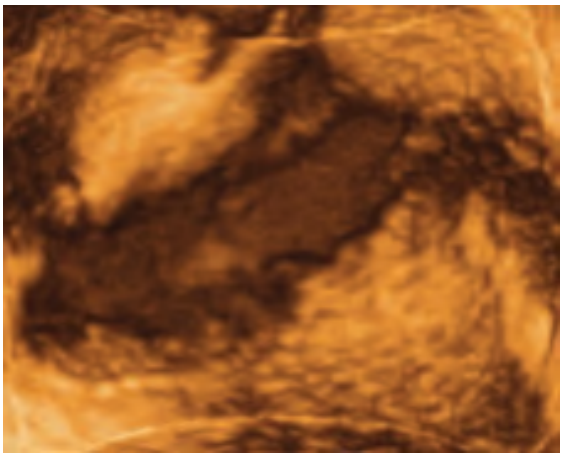

Figure 56.43B: A 3D reconstruction of the same patient as in Figure 56.43A, the tubular structure is suggestive of a shaggy hydrosalpinx enveloping a corrugated ovarian surface

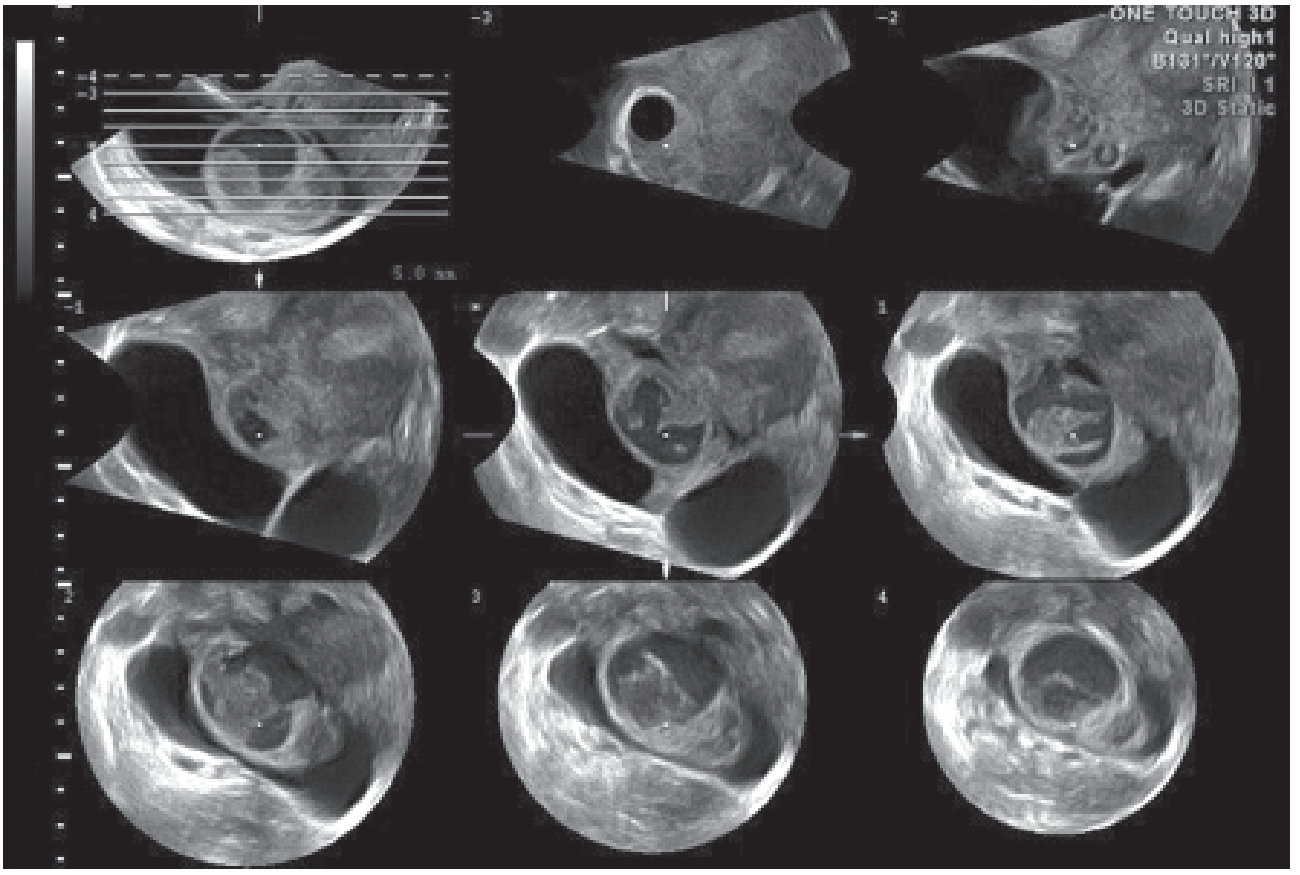

Figure 56.43C: A 3D Tomographic ultrasound imaging of the same patient as in Figures 56.43A and B. Sequential sections show a distinct hydrosalpinx enveloping an ovary, one edge of which shows echogenic debris, confirming acute salpingo-oophoritis

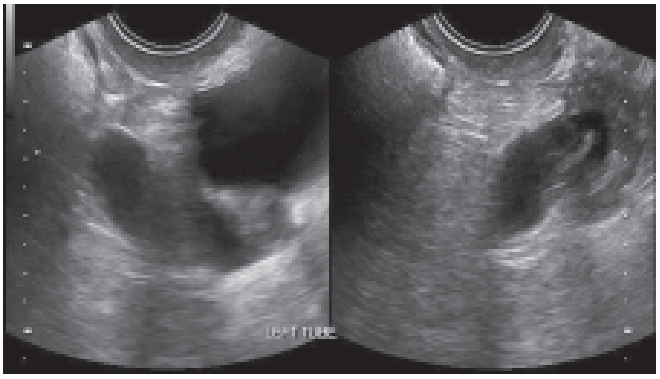

Figure 56.43D: Transvaginal scan showing multiple hypoechoic and clear fluid loculation in the left adnexa. It is not possible to delineate the ovary from the tube

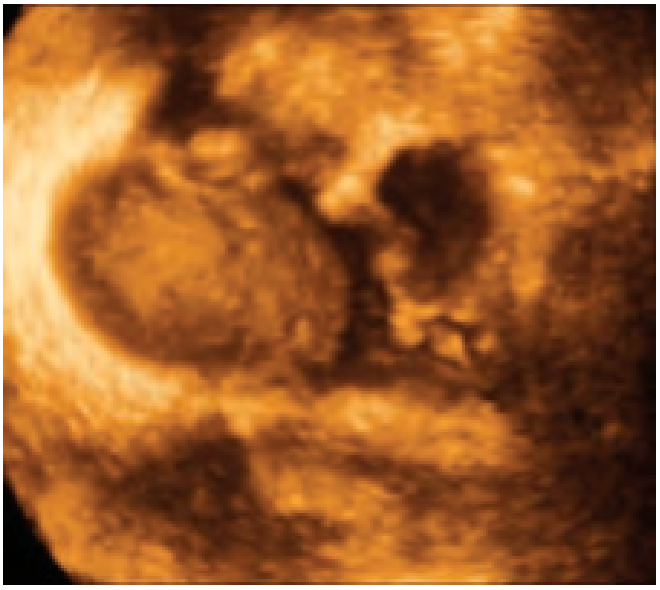

Figure 56.43E: 3D reconstruction showing a distinct hydrosalpinx enveloping a globular ovary

add diagnostic information to 2D observations. Care should be taken to differentiate between cysts of ovarian and paraovarian origin during transvaginal scanning and 3D is particularly useful for this.

Polycystic Ovaries

The Rotterdam ultrasound criteria for diagnosis of polycystic ovaries include at least one of the following:

- An ovarian volume of greater than 10 cm^3
- Demonstration of 12 or more follicles with size of 2–9 mm across **(Figs 56.44A to D)**.

If even one of the follicles exceeds 10 mm the study is to be repeated when the ovaries are quiescent. The introduction of 3D "inversion mode" and "SonoAVC"

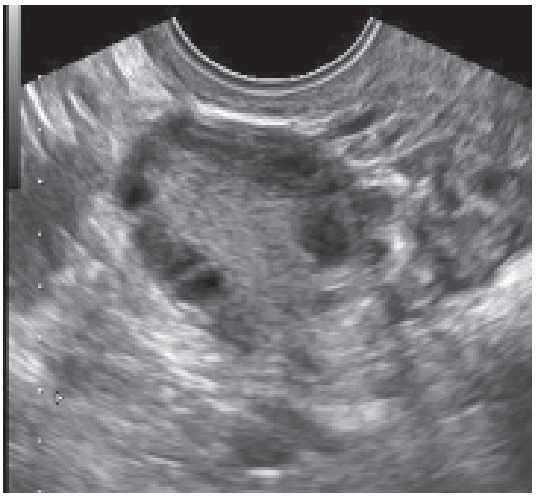

Figure 56.44A: Polycystic ovaries are classically those which show a volume exceeding 10 cm^3 and 12 or more follicles 2–9 mm across. These strict criteria will exclude a large number of polycystic ovaries because the condition is influenced by associated endocrine disorders, treatment status and equipment resolution

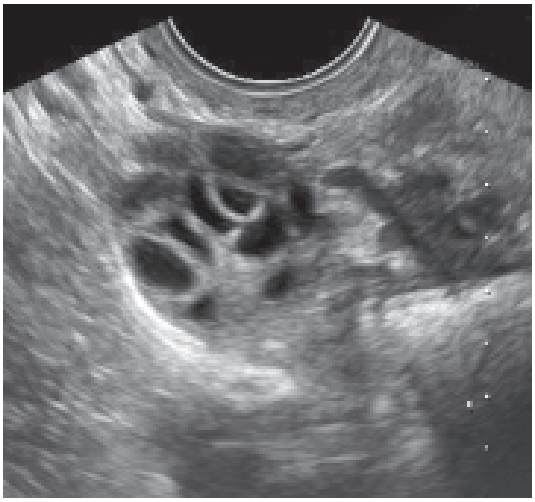

Figure 56.44B: Polycystic ovary showing a peripheral and central distribution of follicles. The older criterion for only peripheral distribution of follicles is no longer followed

software has revolutionized the objective evaluation of cystic spaces in the ovary. This finds widespread application in polycystic ovaries (PCO) assessment and in follicle monitoring. Data is acquired in the inversion mode, which reverses the gray scale and renders fluid as dark/colored and solid areas as voids. Activation of the SonoAVC function then tracks each cystic space and assesses diameters, volumes, location and total number of cysts/follicles **(Figs 56.45A to E)**.

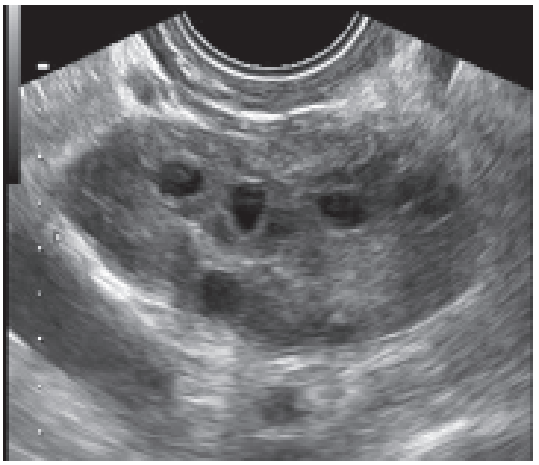

Figure 56.44C: Polycystic ovary showing the variant of largely central location of numerous follicles

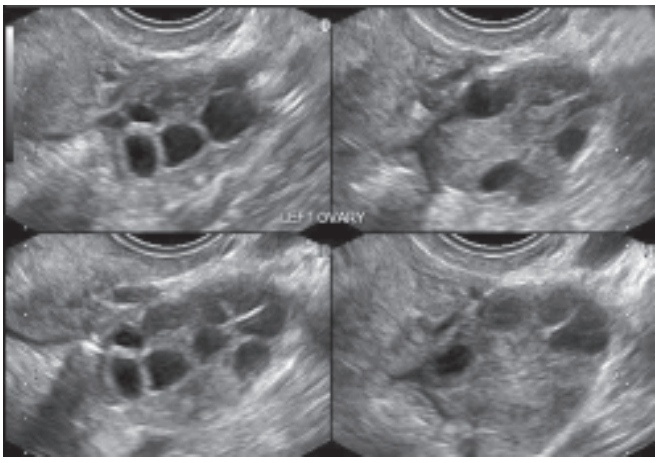

Figure 56.44D: Scanning technique is important for delineating polycystic ovaries. Four views of the same ovary are shown in this Figure. Failure to scan the ovary from left to right and superior to inferior results in a suboptimal display of follicular number and distribution

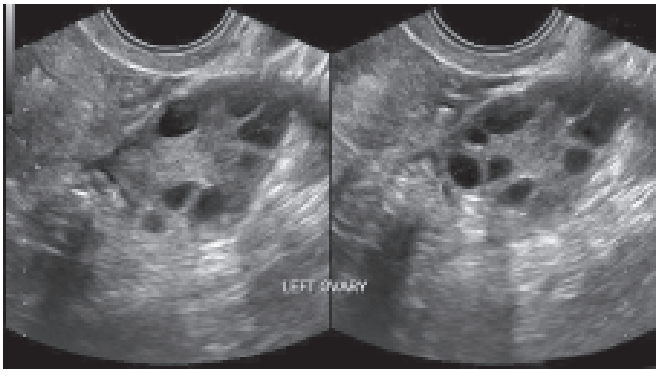

Figure 56.45A: Polycystic ovary showing multiple peripherally located abundant follicles and excessive stroma. Figures 56.45B to E show further evaluation of this ovary

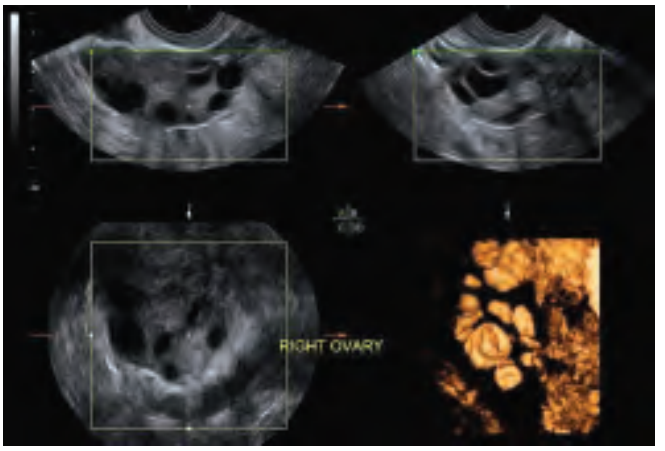

Figure 56.45B: Same case as in Figure 56.45A. A 3D acquisition has been made of the entire ovary and displayed in three orthogonal planes. Frame D shows a 3D inversion mode rendering. Using this method, follicles are highlighted and the stroma blacked out. This improves the appreciation of the number and distribution of follicles

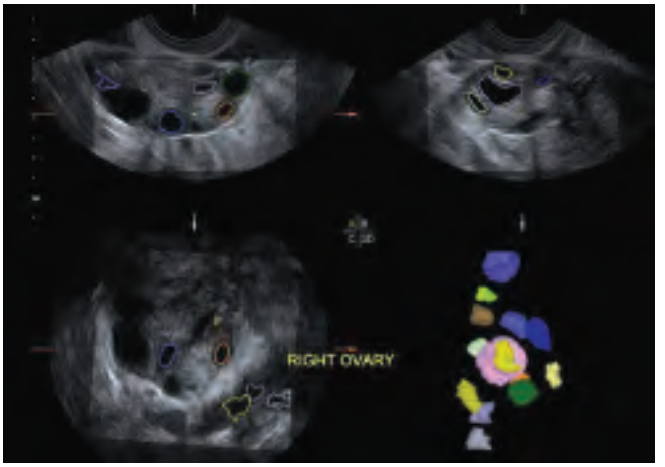

Figure 56.45C: The calculation of follicle number can be automated using proprietary 3D software. In this technique, the ovary is chosen as the region of interest and the appropriate software choice key is activated on the equipment console. The software automatically assesses the size and number of follicles and allots a different color to each follicle. Frame D shows a color coded display of the polycystic ovary shown in section planes A, B and C

Strict application of the Rotterdam criteria in day-to-day practice would miss a large number of polycystic ovaries. This is because the ultrasound morphology is influenced by several factors including transducer resolution, patient habitus, treatment status, associated hypothyroidism, hyperprolactinemia and incipient coexistent premature ovarian failure. The expanded ultrasound criteria in literature include stromal hyperplasia assessed subjectively and by 3D, increased

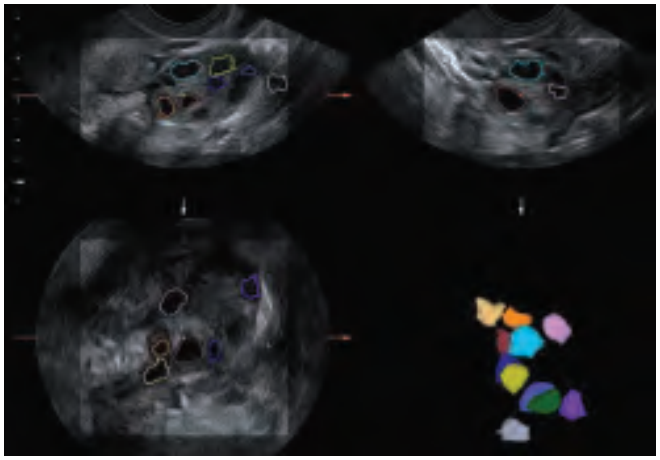

Figure 56.45D: Same patient as in Figure 56.45A showing a 3D graphic display of the contralateral ovary

Figure 56.45E: Automated report of follicular size and number of the same patient as in Figure 56.45A. The report shows color coding of each follicle, the three dimensions of each follicle and the mean diameter of each follicle

stromal echogenicity assessed subjectively, stromal hyperemia assessed with 3D power Doppler studies and peripheral, central or random distribution of excessive number of follicles. The 2D and 3D power Doppler indices correlate well with fertility outcomes but are not consistent diagnostic criteria.[52]

Ovarian Hyperstimulation

Ovulation induction with gonadotropins and occasionally even with clomiphene citrate can result in enlarged ovaries with multiple follicles, multiple corpora lutea and varying severity of increased capillary permeability manifesting as ascites and pleural effusion. The 3D SonoAVC function is very useful to quantify the size and number of cysts.

Premature Ovarian Failure

Although premature ovarian failure is essentially a diagnosis made by serum follicle stimulating hormone (FSH) estimations, ultrasound is useful for guiding the diagnosis and assessing ovarian reserve in patients desirous of beating the body clock. The ovaries shrink in volume to less than 3.0 ml and there is a paucity of antral follicles. The antral follicle count which is a good predictor of in vitro fertilization treatment outcomes can be extrapolated for the diagnosis of ovarian failure. Transvaginal scans done on day 3, 4 or 5 of the cycle reveal less than 4 antral follicles in the ovaries. The 3D evaluation with inversion mode and the SonoAVC function is superior to a subjective 2D sweep.

Neoplastic Ovarian Masses

One of the main aims of gynecological ultrasound is early identification of malignant ovarian masses in order to improve outcomes. Early detection improves 5 year survival rates from 30–35% in stage III and stage IV disease to 80–85% in stage I disease. Neoplastic ovarian masses have a wide pathological spectrum and vary in appearance from simple, thin walled, unilocular, avascular cysts to completely solid masses. Advances in transducer technology, color Doppler, power Doppler and 3D studies have greatly enhanced the accuracy of histological prediction of benign and malignant adnexal lesions.[56,57] The criteria for a diagnosis of a malignant mass include grey scale observations of a solid mass, a cystic mass with solid areas, focal or diffusely thick walls or septations, mural nodules and heterogeneous internal echoes. Pelvic and paraaortic lymph nodes enlargement, ascites, suprarenal and liver metastases and pleural effusions can be elucidated by trans-abdominal ultrasound. Color flow and 3D vascular reconstruction criteria include abnormal calibration of vessels, dichotomous branches, elongation, coiling, aneurysms, vascular lakes, arterio-venous anastomosis and veno-venous anastomosis **(Figs 56.46 to 56.53)**. Low resistive and pulsatility indices are inadequately a wide-range to be reliable. Serial evaluation using 3D power Doppler quantification is also proving useful for following up patients on treatment, particularly those on anti-neoangiogenesis agents.

Miscellaneous Adnexal Lesions

Several extra-ovarian adnexal lesions are found on transvaginal scans and many of these are of no clinical

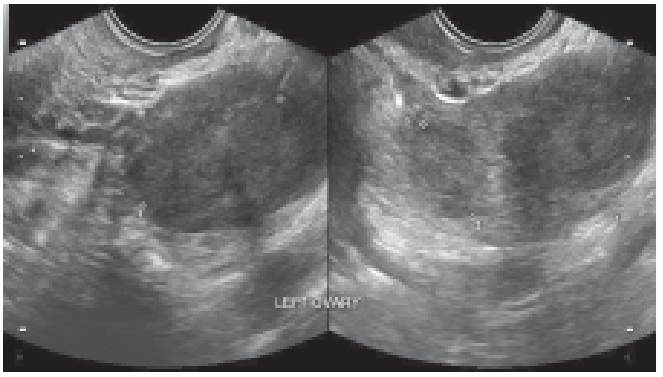

Figure 56.46: Solid ovarian lesions as seen in this ovary are not necessarily malignant and the 2D morphology needs to be supplemented with color and 3D color criteria for histologic characterization as shown in Figures 56.52 and 56.53

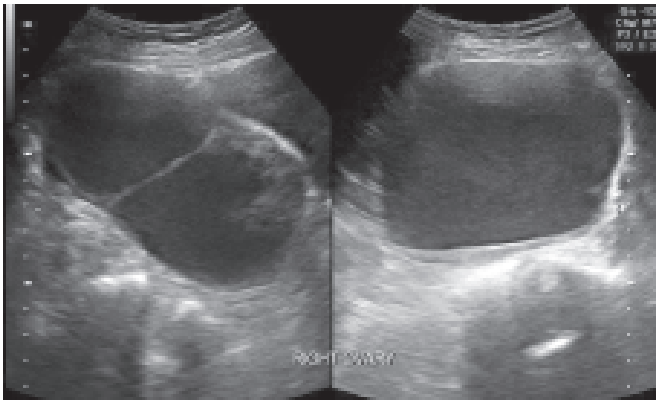

Figure 56.47: Echogenic cystic lesions with thin septations are usually benign hemorrhagic lesions. Occasionally, however, these may be pathologic surprises and should be assessed with power and color Doppler to confirm a benign pattern as shown in Figure 56.53

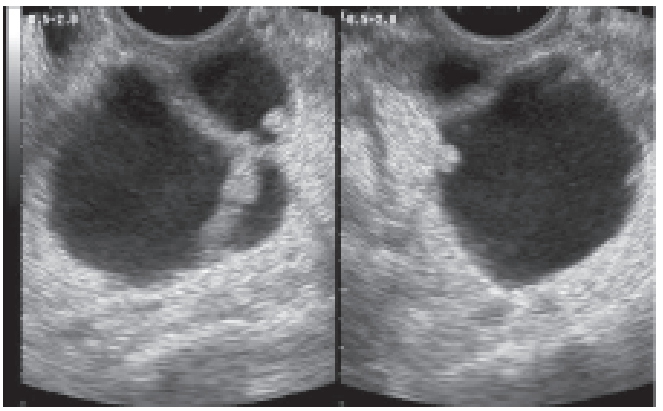

Figure 56.48: Cystic lesions with thick septations and mural nodules are highly suspicious for malignancy on 2D criteria alone

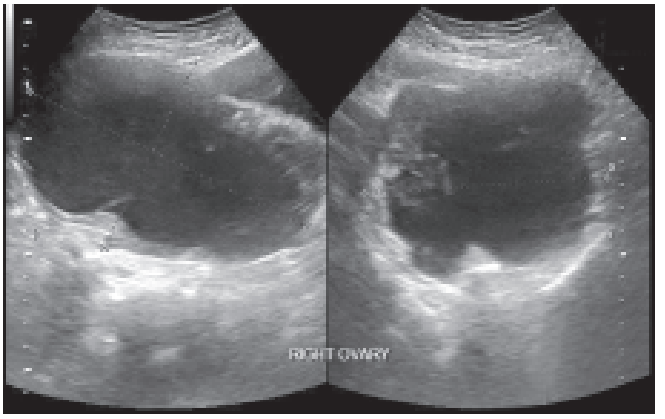

Figure 56.49: Shaggy lesions with echogenic fluid contents usually indicate old benign hemorrhagic lesions or mucinous neoplasm. The latter are often avascular and difficult to characterize. Magnetic Resonance Imaging is sensitive to iron content of lesions and helps to differentiate hemorrhagic lesions from those that do not contain blood

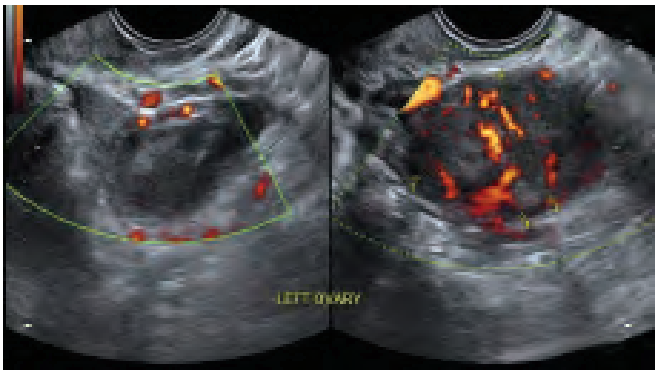

Figure 56.50: All solid lesions should be assessed with power Doppler. The presence of vascularity within a solid lesion confirms the presence of tissue and excludes fluid. This is a useful criterion for a neoplastic lesion. Occasionally, benign granulation tissue such as within an abscess may mimic this finding. A clinical perspective is therefore useful in the interpretation of these findings

consequence. Paraovarian cysts are thin-walled, clear, avascular cystic lesions. These may be unilocular or multilocular **(Figs 56.54A and B)**. The 3D enhances the detection of para-ovarian and extra-ovarian location of adnexal cysts. Other thin-walled cystic lesions include paratubal cysts, fimbrial cysts and cysts of Morgagni. Pelvic kidneys may masquerade as solid pelvic lesions. Subserous fibroids may be indistinguishable from solid adnexal lesions. Inflammatory bowel lesions such as diverticulitis, appendicitis and focal enteritis may masquerade as gynecological lesions.

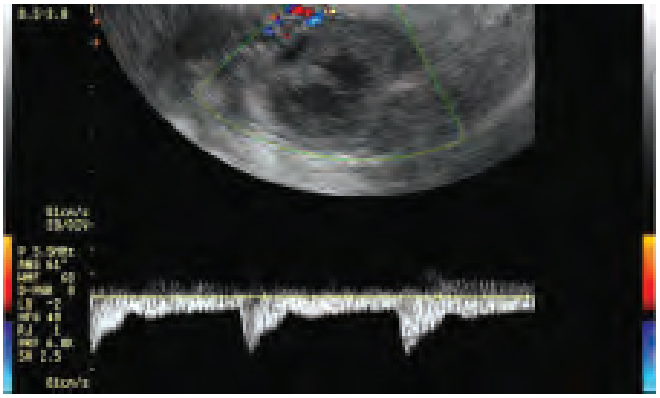

Figure 56.51A: Spectral Doppler is often misleading in characterizing adnexal lesions. This is so because vessels in the periphery of the lesion are usually host vessels and may not show low impedance characteristics. Intratumoral vessels are low impedance circuits because tumor neoangiogenesis usually gives rise to vessels that lack muscle in their walls

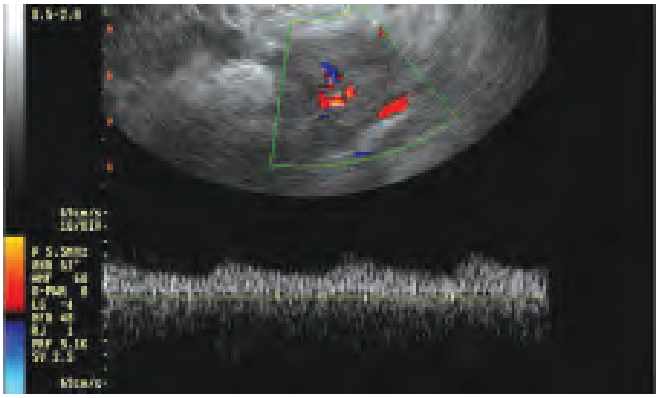

Figure 56.51B: Classical low impedance flow in the center of a malignant mass. Some workers quantify cut-offs at a resistive index of 0.40 and others at 0.33. Specific Figures should be disregarded and emphasis laid on morphology as detailed in the text.

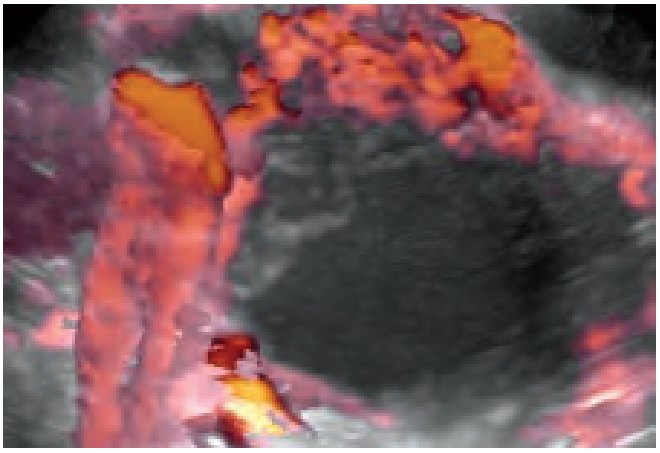

Figure 56.52A: Markedly tortuous vessels with extensive coiling in a mucinous cystadenocarcinoma

Figure 56.52B: Tortuous vessels with abnormal caliber in a malignant mass. In a benign lesion, larger vessels give rise to narrower vessels. In malignant lesions, second, third and higher-order branches are often wider than the parent vessels. Note also that several also larger vessels are giving rise to multiple branches at a single point. This type of branching is a characteristic of malignant lesion. Benign lesions show a single branch at a time

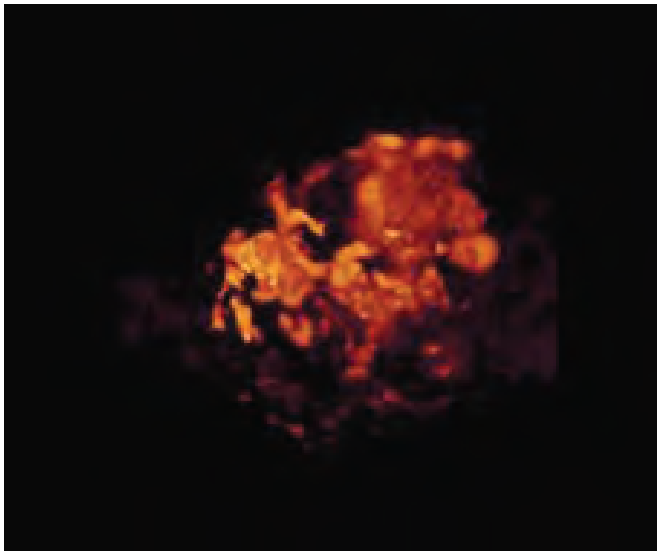

Figure 56.52C: Same lesion as in Figure 56.51B. Note the aneurysmal dilatation of vessels and the vascular lakes characteristic of malignant lesions

Ultrasound in Urogynecology

Recent years have seen ultrasound images replace conventional radiology as the modality of choice for imaging the female patient with a voiding dysfunction. This is consequent to remarkable technological advances combined with innovative techniques of obtaining relevant morphological and dynamic information. Transabdominal ultrasound has now been complemented by a wide variety of ultrasound techniques which

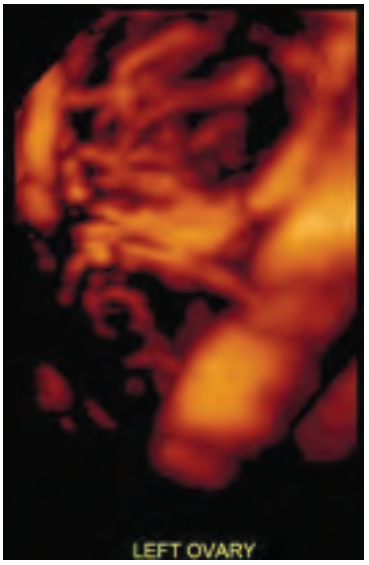

Figure 56.52D: Cluster of abnormal vessels showing bizarre sizes. These features indicate a malignant lesion

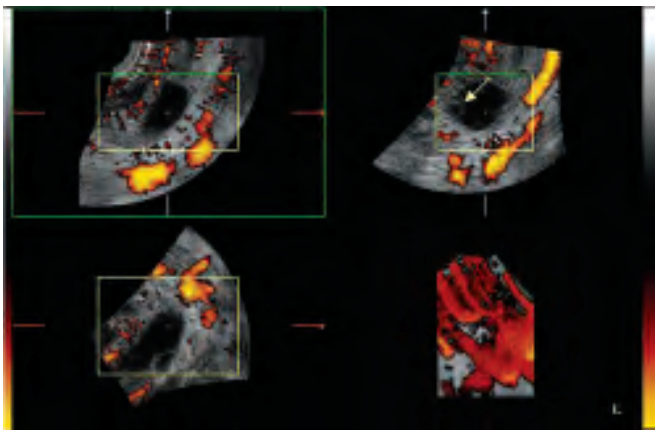

Figure 56.52E: Small cystic lesions throwing up a surprise on 3D power Doppler. The 3D rendering shows a bizarre branching pattern suggesting malignancy which was confirmed after surgery

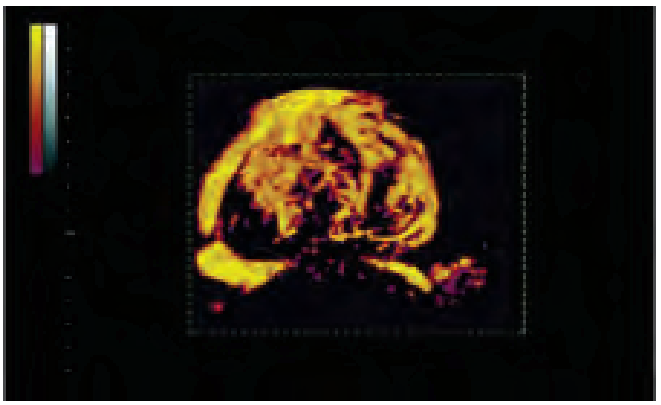

Figure 56.52F: Central spoke-wheel pattern in a solid adnexal mass seen on 3D rendered studies. Surgical pathology confirmed a malignant fibroma

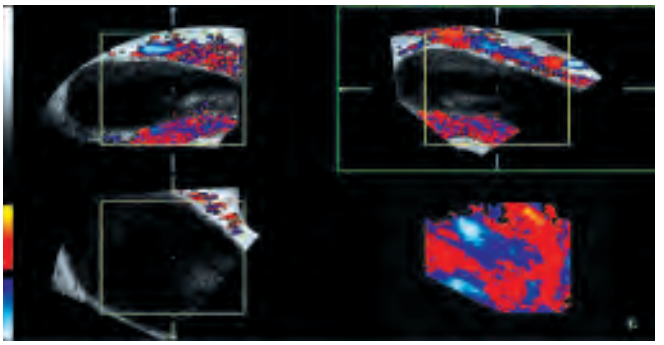

Figure 56.52G: Unilocular cystic lesions showing a thick vascular wall on 3D studies. The 3D rendering shows arteriovenous anastomoses. Surgery confirmed a serous cystadenocarcinoma

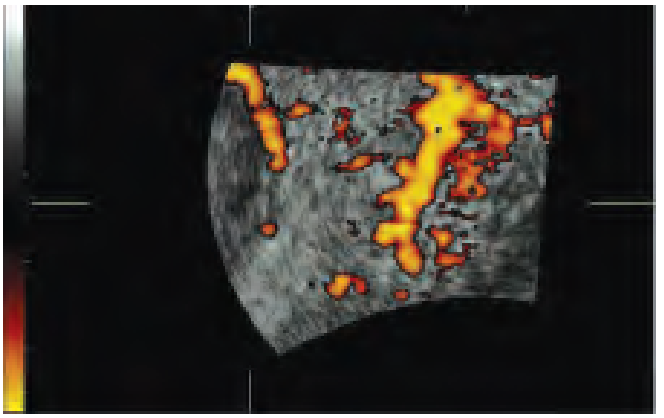

Figure 56.53: Benign vessel showing one branch at a time. Note the regular decrease in the size of this feeder vessel as it goes towards the center of the solid lesion. Surgery confirmed a benign fibroma

include transurethral ultrasound, introital ultrasound, perineal ultrasound, endoanal and transectal scanning, power Doppler information and 3D and 4D technology.

Transvaginal, introital and perineal ultrasound can all be performed with the same transducer. This should be an end-firing intracavitary transducer with an emission angle of at least 90°. The availability of higher frequencies up to 12 MHz will permit better resolution of superficial structures and the use of lower frequencies such as 5 MHz will allow a better assessment of large pelvic masses and a very large uterus.

Whereas, (MRI) has been the modality for visualizing the endopelvic fascia, in recent years 3D ultrasound sectional images are replacing MRI **(Fig. 56.55)** because of an equivalent resolution **(Figs 56.56 and 56.57)** and the added advantage of ease of utility and the ability for vascular display. Anatomical atrophy of the endopelvic fascia, change in the configuration of the

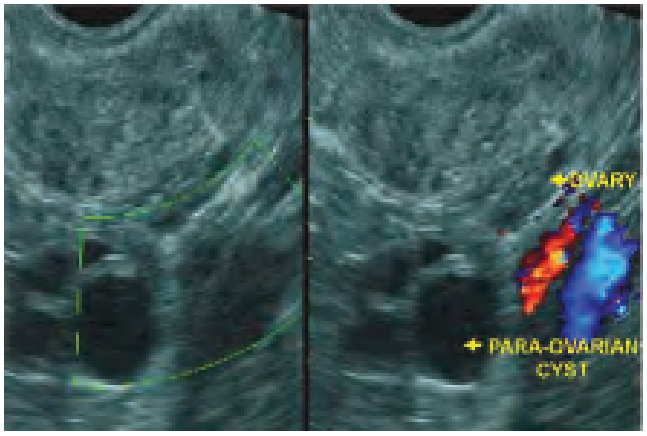

Figure 56.54A: Para-ovarian cysts are best characterized by demonstrating the ovary separate from them

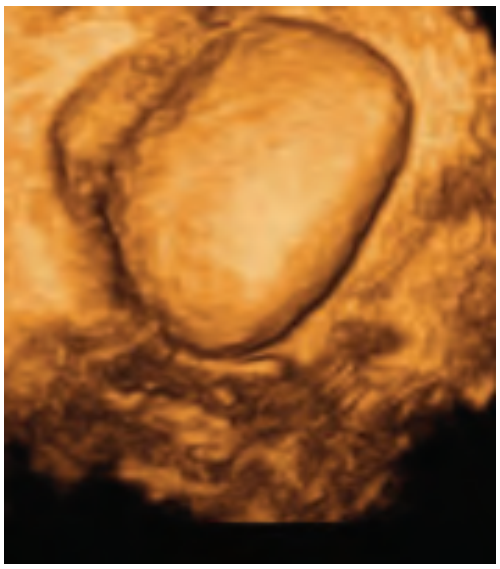

Figure 56.54B: 3D reconstructions are particularly useful for demonstrating the spatial relationships of adnexal structures. Figure shows a normal ovary with an adjacent large para-ovarian cyst

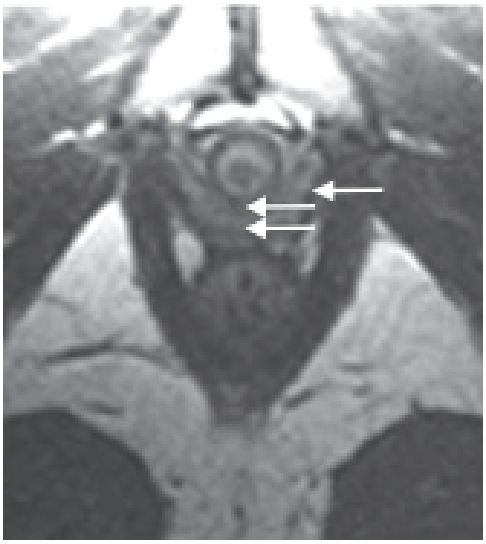

Figure 56.55: Magnetic Resonance Image (MRI) of the pelvis showing in the midline, the urethra anteriorly, the pubocervical ligament (two arrows), the levator ani (single arrow), the vagina and rectum

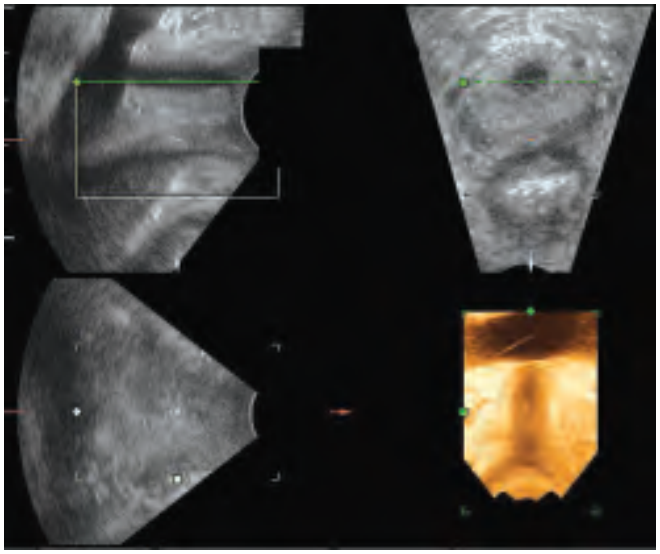

Figure 56.56: Three-Dimensional (3D) images of the endopelvic fascia showing the region in three orthogonal planes and one rendered plane. The top left image shows (from top to bottom) the urethra, vagina and rectum in the midline and the fibromuscular tissue laterally. The rendered image (bottom right) shows the urethra flanked by the endopelvic fascia

vagina **(Fig. 56.58)** and paucity of vasculature **(Fig. 56.59)** can be documented with amazing clarity and reproducibility. Vascular response to perineal exercises and local estrogen application **(Fig. 56.60)** can be demonstrated by serial scans done 6 weeks to 12 weeks apart. Transanal and transrectal side-firing linear transducers now offer detailed delineation of the anal and urethral sphincters and sphincter mechanisms and in the future are likely to find increased application. 3D provides objective evaluation of outcomes from urethral bulking agent therapy using collagen injections[58] and helps in assessing failure and the need for re-injection. Tension free vaginal tape slings are highly echogenic and can be assessed by 3D ultrasound.[59] Tape movement occurs in an arc around the posterior aspect of the posterior symphysis which serves as the fulcrum. Mechanical compression of the urethra

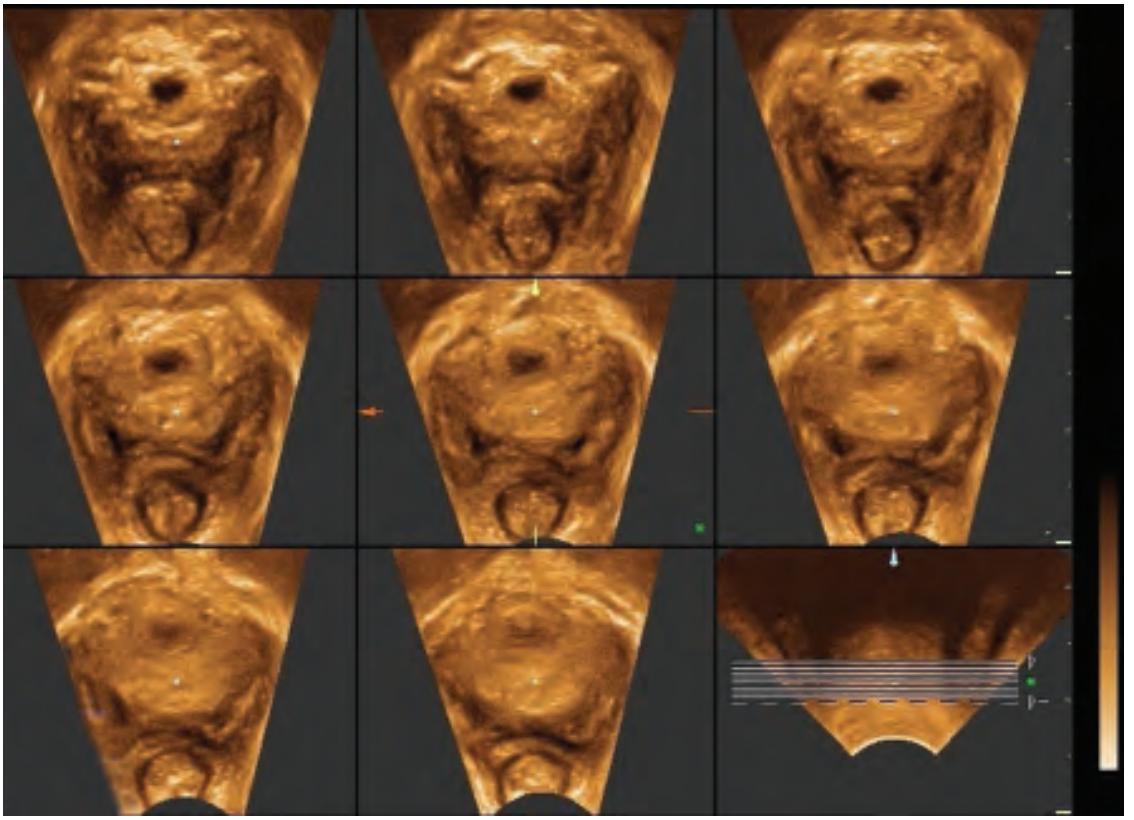

Figure 56.57: 3D Tomographic Ultrasound Imaging (TUI). Currently available 3D transducers acquire information in sweeps across the region of interest. Each signal thus acquired can be rendered in an infinite number of planes. TUI allows a choice of plane direction and thickness in much the same format as CT or MRI. Note the exquisite soft tissue detail of the urethra, vagina, rectum and endopelvic fascia. The vagina has an H-shaped configuration as evident in sections 1–4

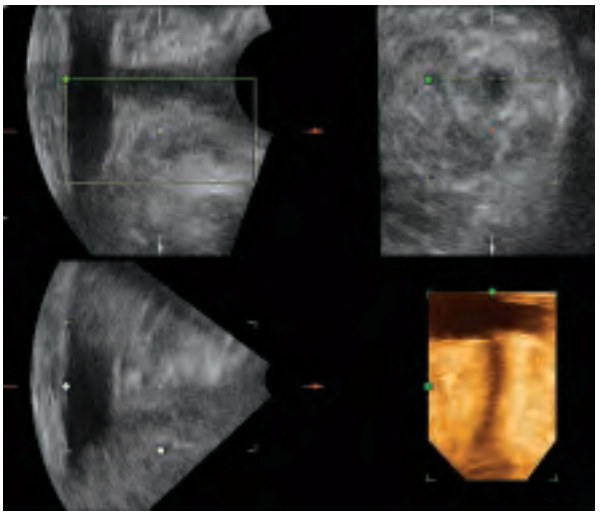

Figure 56.58: Complete loss of anatomical delineation of the vagina, rectum and endopelvic fascia in post-menopausal atrophy in a patient with incontinence. The difference is striking when the plane displayed in the top right area is compared with its counterpart in Figure 56.56

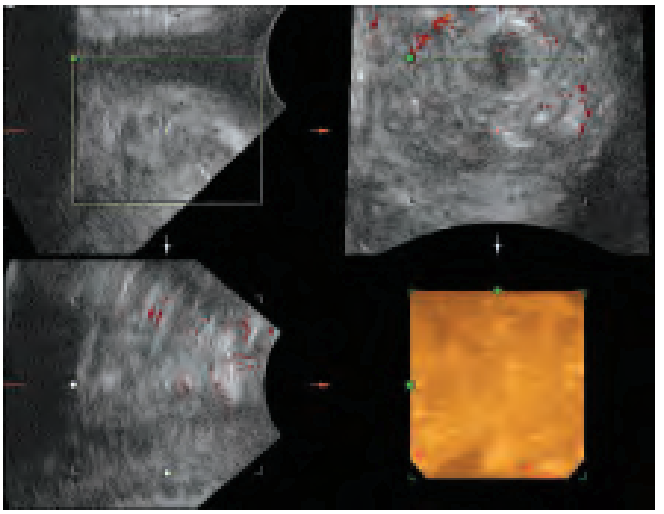

Figure 56.59: 3D Tomographic Ultrasound Imaging with gray scale and power Doppler information. Note the scanty vascular signals seen in the top right image and the complete absence of vascular signals in the other orthogonal planes

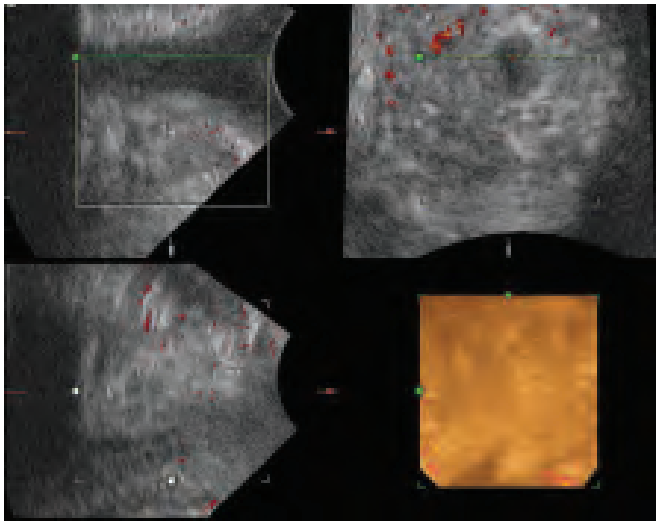

Figure 56.60: 3D Tomographic Ultrasound Imaging with 2D and power Doppler information in a patient on perineal exercises and local estrogen cream application. Note the increased vascular signals in the top right frame when compared with Figure 56.58

by the tape is evident as a reduction in the gap between the tape and the symphysis pubis.

CONCLUSION

Until less than a decade ago, reports of 3D and 4D ultrasound techniques were fraught with inconsistencies of outcomes, inconsistencies of method, personal bias and skeptical overtones. There was also a dramatic but often unrecognizable lack of declaration of the degree of technical sophistication of the equipment used. As a consequence, the utility of the technique as a component of good clinical practice remained unacknowledged. The scenario today has changed completely. The techniques are established as a yardstick of morbid anatomy and pathophysiology.

REFERENCES

1. Kupesic S, Kurjak A, Bjelos D. Sonographic imaging in infertility. In Kurjak A, Chervenak FA (Eds). Donald school textbook of ultrasound in Obstetrics and Gynecology, 1st edition. New Delhi: Jaypee Brothers Medical Publishers; 2003. pp. 658-90.
2. Ashton D, Amin HK, Richart RM, et al. The incidence of asymptomatic uterine anomalies in women undergoing transcervical tubal sterilization. Obstet Gynecol. 1988;72: 28-30.
3. Sorenson S. Estimated prevalence of mullerian anomalies. Acta Obstet Gynecol Scand. 1988;67:441-5.
4. Heinonen PK, Saarikoski S, Pystynen P. Reproductive performance of women with uterine anomalies. An evaluation of 182 cases. Acta Obstet Gynecol Scand. 1982;61:157-62.
5. Fedele L, Bianchi S, Marchini M, et al. Ultrastructural aspects of endometrium in infertile women with septate uterus. Fertil Steril. 1996;65:750-2.
6. Fedele L, Arcaini L, Parazzini F, et al. Metroplastic hysteroscopy and fertility. Fertil Steril. 1993;59:768-70.
7. Valdes C, Malini S, Malinak LR. Ultrasound evaluation of female genital tract anomalies: a review of 64 cases. Am J Obstet Gynecol. 1984;149:285-90.
8. Cararach M, Penella J, Ubeda J, et al. Hysteroscopic incision of the septate uterus: scissors versus resectoscope. Hum Reprod. 1994;9:87-9.
9. Goldenberg M, Sivan E, Sharabi Z. Reproductive outcome following hysteroscopic management of intrauterine septum and adhesions. Hum Reprod. 1995;10:2663-5.
10. The American Fertility Society. The American Fertility Society classifications of adnexal adhesions, distal tubal occlusion, tubal occlusion secondary to tubal ligation, tubal pregnancies, mullerian anomalies and intrauterine adhesions. Fertil Steril. 1988;49(6):944-55.
11. Homer HA, Li TC, Cooke ID. The septate uterus: a review of management and reproductive outcome. Fertil Steril. 2000;73:1-4.
12. La Torre R, Prosperi Porta R, Franco C, et al. Three-dimensional sonography and hysterosalpingosonography in the diagnosis of uterine anomalies. Clin Exp Obstet Gynecol. 2003;30(4):190-2.
13. Nicolini U, Belloti M, Bonazzi B, et al. Can ultrasound be used screen uterine malformations? Fertil Steril. 1987;47: 89-93.
14. Reuter KL, Daly DC, Cohen SM. Septate versus bicornuate uteri: errors in imaging diagnosis. Radiology. 1989;172: 749-52.
15. Randolph J, Ying Y, Maier D, et al. Comparison of real time ultrasonography and laparoscopy/hysteroscopy in the evaluation of uterine abnormalities and tubal patency. Fertil Steril. 1986;5:828-32.
16. Bega G, Lev-Toaff AS, O'Kane P, et al. Three-dimensional ultrasonography in gynecology: technical aspects and clinical applications. J Ultrasound Med. 2003;22(11):1249-69.
17. Salle B, Sergeant P, Galcherand P, et al. Transvaginal hysterosonographic evaluation of septate uteri: a preliminary report. Hum Reprod. 1996;11:1004-7.
18. Kupesic S, Kurjak A. Septate uterus: detection and prediction of obstetrical complications by different forms of ultrasonography. J Ultrasound Med. 1998;17:631-6.
19. Richman TS, Viscomi GN, Cherney AD, et al. Fallopian tubal patency assessment by ultrasound following fluid injection. Radiology. 1984;152:507-10.
20. Marshall C, Mintz DI, Thickman D, et al. MR evaluation of uterine anomalies. Radiology. 1987;148:287-9.
21. Carrington BM, Hricak M, Naruddin RN. Mullerian duct anomalies: MR evaluation. Radiology. 1990;170:715-20.

22. Raga F, Bonilla-Musoles F, Blanes J, et al. Congenital Mullerian anomalies: diagnostic accuracy of three-dimensional ultrasound. Fertil Steril. 1996;65(3):523-8.
23. Wu MH, Hsu CC, Huang KE. Detection of congenital mullerian duct anomalies using three-dimensional ultrasound. J Clin Ultrasound. 1997;25:487-92.
24. Jurkovic D, Giepel A, Gurboeck K, et al. Three-dimensional ultrasound for the assessment of uterine anatomy and detection of congenital anomalies: a comparison with hysterosalpingography and two-dimensional sonography. Ultrasound Obstet Gynecol. 1995;5:233-7.
25. Dabrashrafi H, Bahadori M, Mohammad K, et al. Septate uterus: new idea on the histologic features of the septum in this abnormal uterus. Am J Obstet Gynecol. 1995;172:105-7.
26. Kupesic S, Kurjak A, Skenderovic S, et al. Screening for uterine abnormalities by three-dimensional ultrasound improves perinatal outcome. J Perinat Med. 2002;30:9-17.
27. Weinraub Z, Maymon R, Shulman A, et al. Three-dimensional saline contrast rendering of uterine cavity pathology. Ultrasound Obstet Gynecol. 1996;8(4):277-82.
28. Balen FG, Allen CM, Gardener JE, et al. Three-dimensional reconstruction of ultrasound images of the uterine cavity. The British journal of radiology. 1993;66(787):588-91.
29. Salim R, Regan L, Woelfer B, et al. A comparative study of the morphology of congenital uterine anomalies in women with and without a history of recurrent first trimester miscarriage. Human Reproduction. 2003;18(1):162-6.
30. Salim R, Woelfer B, Backos M, et al. Reproducibility of three-dimensional ultrasound diagnosis of congenital uterine anomalies. Ultrasound Obstet Gynecol. 2003;21(6):578-82.
31. Kupesic S, Kurjak A. Three-dimensional ultrasound and power Doppler assessment of the septate uterus. In Kurjak A (Ed). Three dimensional power Doppler in Obstetrics and Gynecology, 1st edition. New York: Parthenon Publishing; 2000. pp. 85-91.
32. Khurana A. The endometrium. In Khurana A, Dahiya N (Eds). 3D and 4D ultrasound: a text and atlas, 1st edition. New Delhi: Jaypee Brothers Medical Publishers; 2004. pp. 166-98.
33. Delisle M-F, Villeneuve M, Boulvain M. Measurement of endometrial thickness with transvaginal ultrasonography: is it reproducible? J Ultrasound Med. 1998;17:481-4.
34. Buyuk E, Durmusoglu F, Erenus M, et al. Endometrial disease diagnosed by transvaginal ultrasound and dilatation and curettage. Acta Obstet Gynecol. 1999;79:419-22.
35. Jorizzo JR, Riccio GJ, Chen MYM, et al. Sonohysterography: the next step in the evaluation of the abnormal endometrium. RadioGraphics. 1999;119:S117-30.
36. Weigel M, Friese K, Strittmatter HJ, et al. Measuring the thickness is that all we have to do for sonographic assessment of endometrium in postmenopausal women. Ultrasound Obstet Gynecol. 1995;6(2):97-102.
37. Sousa R, Silvestre M, Almeida e Sousa L, et al. Transvaginal ultrasonography and hysteroscopy in postmenopausal bleeding: a prospective study. Acta Obstet Gynecol Scan. 2001;80(9):856-62.
38. Goldstein RB, Bree RL, Benson CB, et al. Evaluation of the woman with postmenopausal bleeding. Society of radiologists in ultrasound-sponsored consensus conference statement. J Ultrasound Med. 2001;20(10):1025-36.
39. Epstein E, Valentin L. Rebleeding and endometrial growth in women with postmenopausal bleeding and endometrial thickness more than 5 mm managed by dilatation and curettage or ultrasound follow-up: a randomized controlled study. Ultrasound Obstet Gynecol. 2001;18(5):499-504.
40. Randelzhofer B, Prompeler HJ, Sauerbrei W, et al. Value of sonomorphological criteria of the endometrium in women with postmenopausal bleeding: a multivariate analysis. Ultrasound Obstet Gynecol. 2002;19(1):62-8.
41. Sheikh M, Sawhney S, Khurana A, et al. Alteration of sonographic texture of the endometrium in postmenopausal bleeding: a guide to further management. Acta Obstet Gynecol Scand. 2000;79:1006-10.
42. Benacerraf BR, Shipp TD, Bromley B. Three-dimensional ultrasound detection of abnormally located intrauterine contraceptive devices which are a source of pelvic pain and abnormal bleeding. Ultrasound Obstet Gynecol. 2009;34(1):110-5.
43. Benacerraf BR, Bromley B, Shipp TD. The width of the uterine cavity is narrower in patients with an embedded intrauterine device (IUD) compared to a normally positioned IUD. J Ultrasound Med. 2010;29:1453-6.
44. Pierson RA. Imaging the endometrium: are there predictors of uterine receptivity? J Obstet Gynaecol Can. 2003;25(5):360-8.
45. Baruffi RL, Contart P, Mauri AL, et al. A uterine ultrasonographic scoring system as a method for the prognosis of embryo implantation. J Assist Reprod Genet. 2002;19(3):99-102.
46. Schild RL, Knobloch C, Dorn C, et al. Endometrial receptivity in an in vitro fertilization program as assessed by spiral artery blood flow, endometrial thickness, endometrial volume, and uterine artery blood flow. Fertil Steril. 2001;75(2):361-6.
47. Ardaens Y, Gougeon A, Lefebvre C, et al. Contribution of ovarian and uterine color Doppler in medically assisted reproduction techniques (ART). Gynecol Obstet Fertil. 2002;30(9):663-72.
48. Chien LW, Lee WS, Au HK, et al. Assessment of changes in utero-ovarian arterial impedance during the peri-implantation period by Doppler sonography in women undergoing assisted reproduction. Ultrasound Obstet Gynecol. 2004;23(5):496-500.
49. Kupesic S, Bekavac I, Bjelos D, Kurjak A. Assessment of endometrial receptivity by transvaginal color Doppler and three-dimensional power Doppler ultrasonography in patients undergoing in vitro fertilization procedures. J Ultrasound Med. 2001;20(2):125-34.
50. Ng EHY, Chan CCW, Tang OS, et al. Comparison of endometrial and subendometrial blood flow measured by three-dimensional power Doppler ultrasound between stimulated and natural cycles in the same patients. Hum Reprod. 2004;19(10):2385-90.
51. Raine-Fenning NJ, Campbell BK, Kendall NR, et al. Quantifying the changes in endometrial vascularity

throughout the normal menstrual cycle with three-dimensional power Doppler angiography. Hum Reprod. 2004; 19(2):330-8.
52. Yokota A, Nakai A, Oya A, et al. Changes in uterine and ovarian arterial impedance during the periovulatory period in conception and nonconception cycles. J Obstet Gynaecol Res. 2000;26(6):435-40.
53. Kupesic S. Three-dimensional ultrasonographic uterine vascularization and embryo implantation. J Gynecol Obstet Biol Reprod. 2004;33(1 Pt 2):S18-20.
54. Buckett WM, Chian RC, Tan SL. Human chorionic gonadotropin for in vitro oocytes maturation: does it improve the endometrium or implantation? J Reprod Med. 2004;49(2): 93-8.
55. Carbillon L, Perrot N, Uzan M, et al. Doppler ultrasonography and implantation: a critical review. Fetal Diagn Ther. 2001;16(6):327-32.
56. Alcazar JL, Garcia-Manero M, Galvan R. Three-dimensional sonographic morphologic assessment of adnexal masses: a reproducibility study. J Ultrasound Med. 2007;26 (8): 1007-11.
57. Alcazar JL, Merce LT, Garcia-Manero M. Three-dimensional power Doppler vascular sampling: a new method for predicting ovarian cancer in vascularized complex adnexal masses. J Ultrasound Med. 2005;24(5):689-96.
58. Poon CI, Zimmern PE. Role of three-dimensional ultrasound in assessment of women undergoing urethral bulking agent therapy. Curr Opin Obstet Gynecol. 2004;16(5): 411-7.
59. Dietz HP, Wilson PD. The 'iris effect': how two-dimensional and three-dimensional ultrasound can help us understand anti-incontinence procedures. Ultrasound Obstet Gynecol. 2004;23(3):267-71.

CHAPTER 57

Ultrasound in Urogynecology

Ashok Khurana

INTRODUCTION

Ultrasound images have replaced conventional radiology as the modality of choice for imaging the female patient with a voiding dysfunction. This is consequent to remarkable technological advances combined with innovative techniques of obtaining relevant morphological and dynamic information. Transabdominal ultrasound has now been complemented by a wide variety of ultrasound techniques which include transurethral ultrasound, introital ultrasound, perineal ultrasound, endoanal and transrectal scanning, power Doppler information and 3D and 4D technology. This chapter reviews basic concepts and newer developments in the context of their applications in routine and specialized practice and attempts to put the plethora of presentations in recent literature in clinical perspective.

CLINICAL CONSIDERATIONS

Urogynecological problems that need investigation include recurrent lower urinary tract infections, persistent dysuria, urgency and frequency, urinary incontinence and genitourinary prolapse. These problems, particularly in the aging female, need appropriate management because of their social and economic impact, not only from direct costs related to matters, such as absorbent pads, diapers, medication, surgery and fractures, from falls as a result of nocturnal urgency, but also indirect costs and intangible costs. Examples of indirect costs include loss of productivity at home and at work and time spent on elaborate clinical investigations and clinic visits. Intangible factors include suffering from illness, deterioration of lifestyle, reduced sexual activity, low self-esteem, depression and social isolation consequent to desperation for restrooms and a urinary body odor.

Clinical history can often in itself be conclusive as in the diagnosis of stress urinary incontinence. In most cases, of course, it is useful to enumerate symptoms with duration and intensity and patient perception of distress. Other important information includes assessing fluid intake (e.g. caffeine), voiding difficulty, previous treatment, obstetric history, pelvic and abdominal surgery, drug therapy, pelvic organ prolapse and concomitant fecal incontinence.[1] A voiding diary is an excellent method of guiding further investigation and treatment regimens in patients with incontinence.

Physical examination is aimed at evaluating concomitant pathology, such as atrophic changes, vulvovaginitis, organ prolapse and pelvic masses, as also neurologic disease and general debility. Stress urinary incontinence can be observed on a cough stress test. The tone and strength of the pelvic floor muscles should be assessed. This can be done by inspection (drawing up of the anus, lifting of the posterior wall of the vagina and narrowing of the vaginal introitus), digital palpation (e.g. the Oxford score) or more advanced techniques such as perineometry and electromyography.[1]

Investigations

Urinalysis is usually the first investigation in most patients and offers pointers to the diagnosis by identifying hematuria, glycosuria, pyuria and bacteriuria.

Ultrasound scans reveal anatomical details of the kidneys, ureters, urinary bladder, postmicturition residual urine, uterus and adnexae.

Urodynamic studies are not recommended as part of the initial work-up of urogynecological problems except if there is a significant postmicturition residue or if incontinence is so severe that surgical methods are considered as a first-line option. Uroflometry can detect obstructed voiding. The technique is a nonimaging, noninvasive method which measures urinary flow rate and volume voided per second. Urethral pressure profilometry is a graphic observation method that can provide information on urethral function and can often be useful, even though it is not always reproducible. Videocystourethrography is the gold standard investigation. In the filling phase, increases in detrusor pressure associated with urgency are indicative of detrusor overactivity. Urinary bladder volumes at which first, strong and urge sensations are noted, help in diagnosis. Incontinence can be recorded during stress maneuvers. During voiding, poor contractility of the detrusor muscle can be assessed. This helps in differentiating poor detrusor function which is a low pressure/low flow state from outlet obstruction which shows high pressure and low flow. It is of note that all these studies are markedly operator dependent.

Specialized ultrasound studies are considered before or after urodynamic evaluation and will be discussed further. Magnetic Resonance Imaging (MRI) with its capabilities of soft tissue delineation is currently being evaluated against information from three-dimensional (3D) and real-time four-dimensional (4D) ultrasound and will be discussed as well.

TECHNICAL CONCEPTS, NORMS AND ANATOMICAL CONSIDERATIONS

The utility of transabdominal ultrasound in assessing the bladder and urethra in women with incontinence was described as far back as 1980.[2] Standardized protocols were published much later[3] and incorporated newer techniques such as introital and perineal ultrasound scans.

Transvaginal, introital and perineal ultrasound can all be performed with the same transducer. This should be an end-firing intracavitary transducer with an emission angle of at least 90°. The availability of higher frequencies up to 12 MHz will permit better resolution of superficial structures and the use of lower frequencies, such as 5 MHz will allow a better assessment of large pelvic masses and a very large uterus. The transducer is prepared as with standard transvaginal

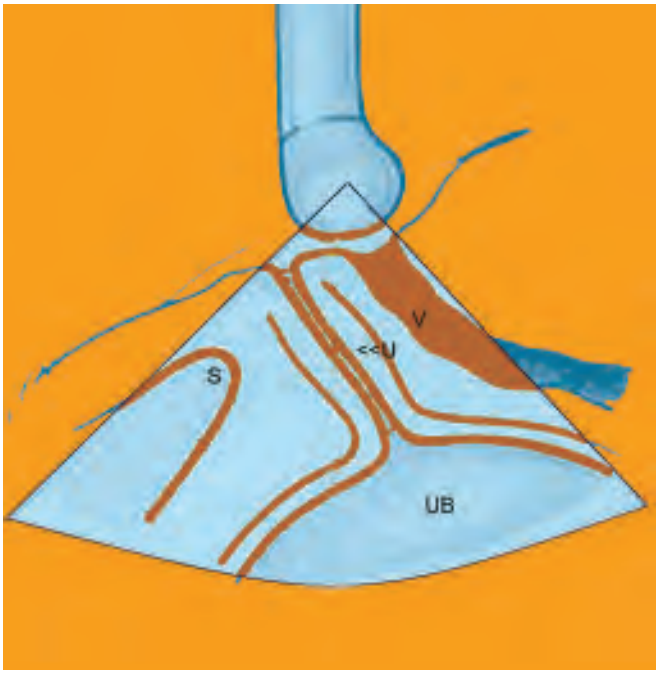

Figure 57.1: Graphic representation of introital scanning showing transducer position and the structures to be included in an ideal view. Note that the beam includes the inferior extent of the symphysis pubis (S), the urethra along its long axis (U), the urinary bladder (UB) and its neck and the vagina (V). Posterior angulation would help to include the rectum when necessary

scanning. Warm gel prevents tightening of the perineal musculature by the patient. The examination is best performed in a semi-reclining position because in a completely supine position the patient may not be able to press adequately when asked to and because in a standing position the transducer is difficult to place and maintain in position.[4] There is no significant difference in the dynamic assessment of the bladder neck in the semi-reclining and standing position.[5] For introital scans the transducer is placed over the external urethral orifice with the long axis of the transducer along the long axis of the body **(Fig. 57.1)**. After orientation, the transducer can be angulated and also moved vertically, horizontally and obliquely to assess the urethra, urinary bladder, periurethral tissues, the entire endopelvic fascia, vagina and rectum **(Figs 57.2 and 57.3)**. Studies are done at rest, with contractions, while coughing, with pressure and with a Valsalva maneuver. For introital scans the transducer has to be held gently because excessive pressure can displace the bladder neck. Recommended bladder filling to ensure reliability and reproducibility of obtained data is about 300 ml.[3,6] In clinical practice, a significant number of patients may become incontinent

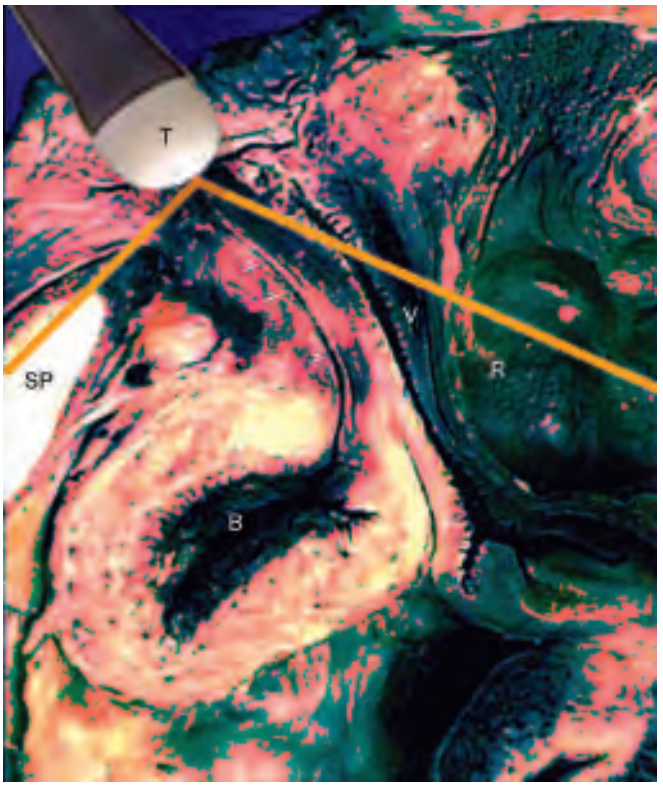

Figure 57.2: Long axis through the midline in a cadaver pelvis to show the orientation of the pelvic viscera and transducer position. The transducer (T) is placed as shown and the beam insonates the symphysis pubis (SP), the urethra (>>U), urinary bladder (UB), vagina (V) and rectum (R)

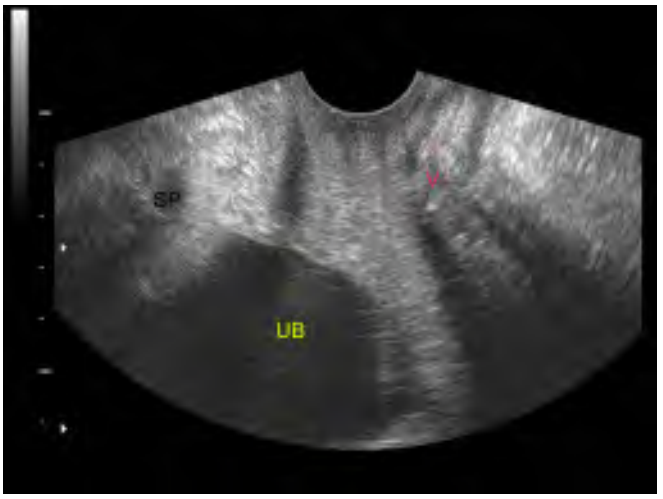

Figure 57.3: Ultrasound image as obtained with an ideal transducer placement. Note the hypoechoic symphysis pubis (SP) with an echogenic inferior margin, the urinary bladder (UB) and the vagina (V). The normal urethra is seen as a markedly hypoechoic, long structure and the bladder neck is closed

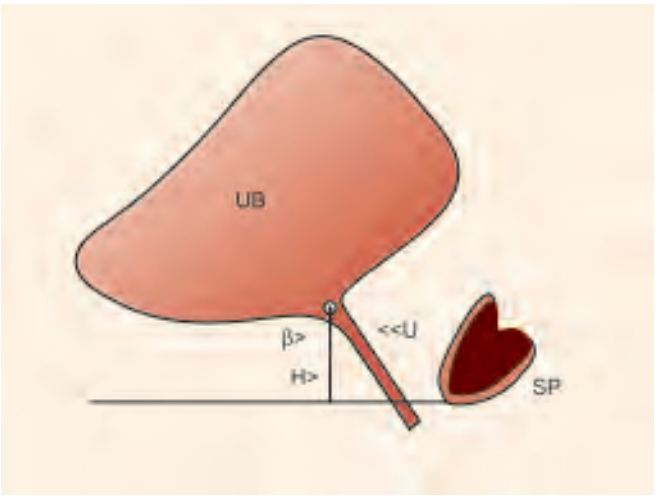

Figure 57.4: Graphic representation of quantification of the orientation and length of the urethra. The scan should necessarily include the symphysis pubis (SP), urethra (<<U) and urinary bladder (UB). A horizontal line is drawn at the level of the inferior extent of the symphysis pubis and the vertical height (not the oblique extent) H is calculated as the length of the perpendicular extending upwards from the horizontal line to the bladder neck. The angle beta is the angle between the line H and the bladder neck

before achieving this volume and this standard may need to be compromised. Urethral funneling is more pronounced in an appropriately filled bladder.[7] Prolapse is less apparent when pressing with a full bladder than with a partially full bladder.[7] In perineal ultrasound the transducer is placed just over the labia. In this technique there is a complete visualization of the symphysis pubis from its upper to its lower end whereas in introital ultrasound only the lower edge is seen. Both are equally good in depicting the cystourethral junction. Several studies[8-11] have compared introital and perineal ultrasound with conventional lateral chain cystourethrography and colpocystourethrography and confirmed its reliability.

Quantification of imaging findings **(Fig. 57.4)** involves measuring the height H which is the distance between the bladder neck and a line through the lower edge of the pubic symphysis and measuring the posterior urethrovesical angle β which is the angle between the urethral long axis and bladder floor. These are determined at rest and during contraction, coughing and pressing.[3] Changes in these parameters during contraction and pressing and in particular, visual real-time ultrasound assessment serves to evaluate the reactivity of the pelvic floor muscles and the adequacy of the connective tissue supportive structures of the

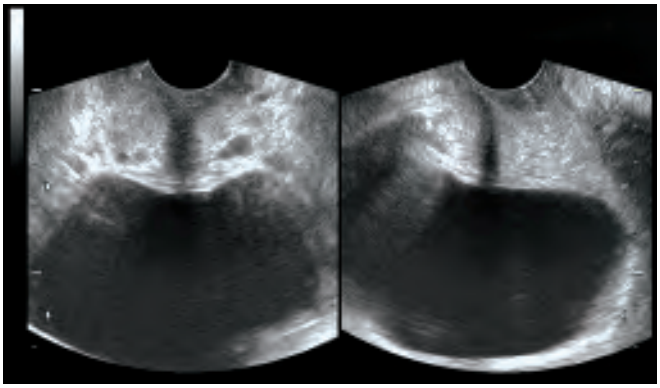

Figure 57.5: Anteroposterior (left) and long axis (right) views of a normal urethra with a normal bladder neck. The long hypoechoic area represents the anterior and posterior walls and the urethral lumen. The bladder neck is closed and normal

urogenital organs.[4] In women without stress urinary incontinence and prolapse, the posterior urethrovesical angle is 96.8° at rest and 108.1° during pressing, with a distance H between the bladder neck and lower edge of the pubic symphysis of 20.6 mm and 14.0 mm, respectively.[3,12-14] There are no significant age-related changes in these normal values.[5]

Normal mobility of the bladder neck is influenced by body habitus, pregnancy and delivery. Racial differences in bladder neck mobility between white and black nulliparous continent women have been identified.[15] In volunteers, pelvic floor awareness education alone can significantly reduce bladder neck mobility in nulliparous women.[16,17] Vaginal and instrumental deliveries are associated with a hypermobility of the bladder neck.[18-20]

Bladder wall thickness is best measured after micturition in a lithotomy position with a transvaginal image.[21] These measurements are taken at the thickest part of the trigone, dome and anterior wall of the urinary bladder.

The bladder neck is closed at rest and funneling is not evident in normal individuals **(Fig. 57.5)**. The anterior and posterior urethral walls appear as a hypoechoic zone. The morphological layers of the urethra cannot be differentiated in the midsagittal plane due to artifacts. In most cases the mucosa and submucosa are uniformly depicted as a hypoechoic structure and may mimic an open lumen if the gain settings are inappropriate. Failure to demonstrate funneling of the urethra in patients with incontinence is usually a reflection of poor examination technique such as studies in a recumbent position, insufficient force during Valsalva or an empty bladder.[4]

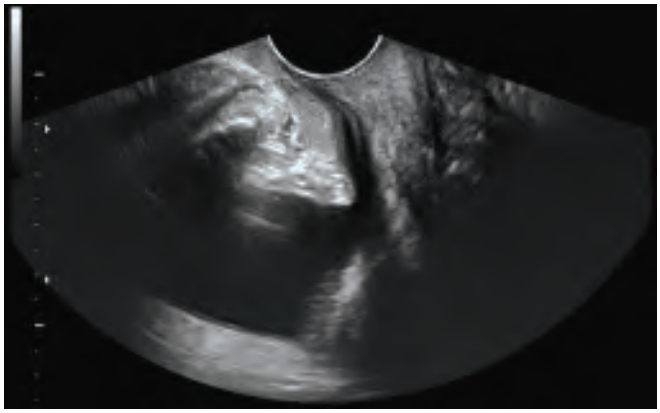

Figure 57.6: Longitudinal midline section showing an abnormal bladder neck with funneling. The bladder neck is open in this patient at rest, and, there is urine in the urethra. If this opening of the bladder neck and filling of the urethra and incontinence coincide with straining or Valsalva maneuver, a diagnosis of genuine stress incontinence may be made. If the bladder neck opens at rest, further investigation is warranted to differentiate urge and mixed incontinence

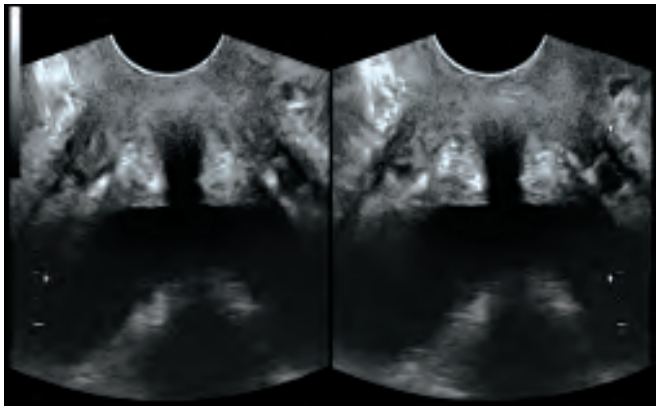

Figure 57.7: Anteroposterior view of an open bladder neck

Bladder neck hypermobility and funneling of the urethra[22-24] **(Figs 57. 6 and 57.7)** are typical findings in incontinence but do not always correlate with urodynamic parameters.[25] Mobility of the bladder neck is of two varieties. One of these is a rotational posteroinferior descent[26,27] with the inferior limit of the symphysis pubis as a pivot **(Fig. 57.8)**. The other is a vertical descent along the urethral axis[28] **(Fig. 57.9)**. A vector-based assessment of the magnitude and direction of the bladder neck has been assessed.[29] The results of bladder neck and pubic-point movement were as follows (extent in mm +/– SD): strain and bladder neck 16.9 +/– 6.1, pubic point 4.8 +/– 3.9, cough bladder neck 10.2 +/– 5.4, pubic point 2.9 +/– 3.4 and Kaegel's exercise bladder neck 7.0 +/– 3.6 and pubic point 7.0 +/– 1.4.[30]

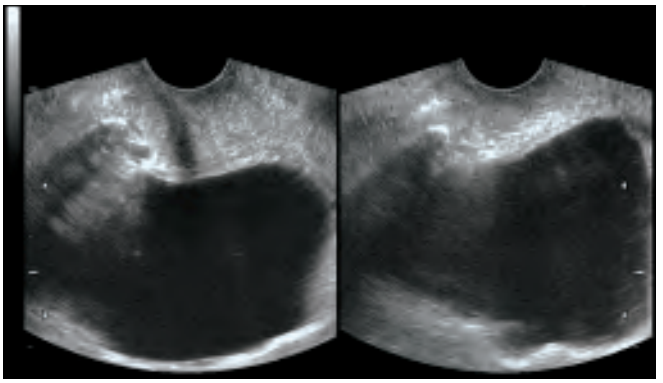

Figure 57.8: Rotational hypermobility of the bladder neck is commonly evident in incontinent patients. The scan shows posteroinferior descent of the bladder neck and bladder base to a level below that of the symphysis pubis. The frame on the left is taken at rest and the one on the right is taken during straining, Valsalva or observed incontinence. The inferior limit of the symphysis pubis is seen as an echogenic rim capping the anechoic pubic bone

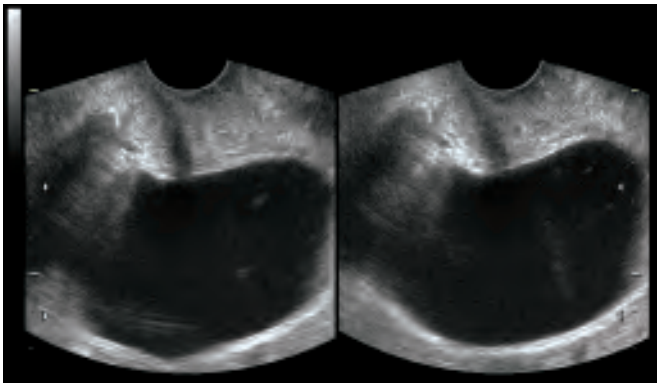

Figure 57.9: Vertical descent of the bladder neck can be observed in incontinent patients. The finding is convincingly evident when a scan at rest (left) is compared side-by-side with an image during straining or coughing (right)

Urinary continence in the female is consequent to several factors.[30] The endopelvic fascia and the anterior vaginal wall form a supportive layer upon which the urethra courses across.[31,32] When intra-abdominal pressure is increased the urethra is compressed against this layer and incontinence is prevented. The endopelvic fascia consists of smooth muscle and fibrous connective tissue and inserts into the fascial coverings of the obturator internus and levator ani muscles. The part of the fascia that lies between the vagina and the urinary bladder and supports the bladder is called the pubocervical fascia. Interruption of the support mechanism results in a prolapse, genuine stress incontinence, incontinence cystocele, urethrocele or both. Knowledge of anatomy, physiology and a detailed ultrasound

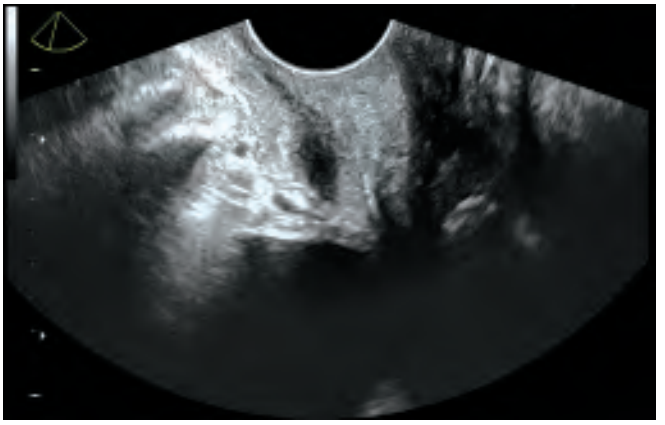

Figure 57.10: Assessment of levator ani reactivity. Image at rest for comparison with Figure 57.11

evaluation can distinguish between these defects.[30] Unilateral or bilateral separation of the pubocervical fascia from the arcus tendineus fascia covering the obturator internus and levator ani muscles is often accompanied by stress urinary incontinence and cystourethrocele.[33-35] Paravaginal defect repair operations and Burch colposuspension restore position and normal mobility of the urethrovesical junction and correct the cystourethrocele and the posterior urethrovesical angle.[30] Differentiation of a lateral defect from a central defect of the anterior compartment is important to decide whether a colposuspension or a tension-free vaginal tape would relieve stress urinary incontinence.[22] Reactivity of the pelvic floor can be assessed by observing the height of the bladder neck relative to a line through the lower edge of the symphysis pubis at rest and during voluntary contractions of the pelvic floor muscles. An increased distance **(Figs 57.10 and 57.11)**

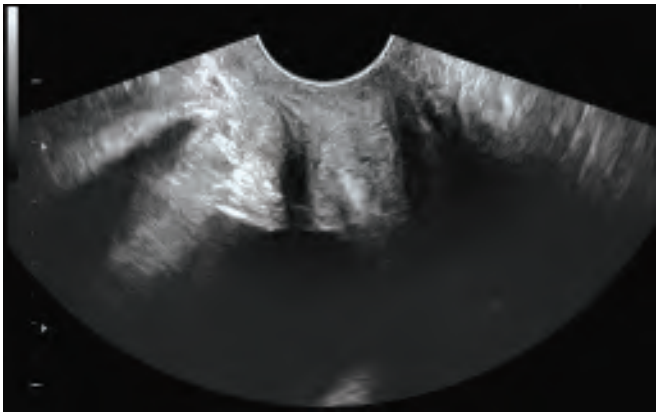

Figure 57.11: Increased distance of the bladder neck from the symphysis pubis in a patient with good levator ani reactivity. Image obtained during voluntary contractions of the pelvic floor. For comparison with Figure 57.10

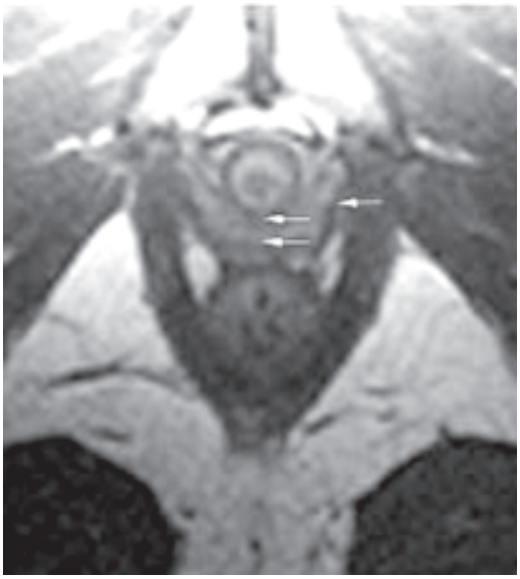

Figure 57.12: Magnetic resonance image (MRI) of the pelvis showing in the midline, the urethra anteriorly, the pubocervical ligament (two arrows), the levator ani (single arrow), the vagina and rectum

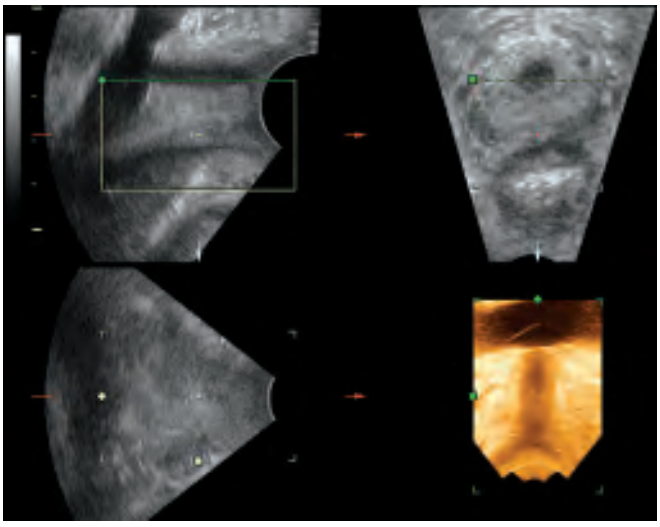

Figure 57.13: Three-Dimensional (3D) images of the endopelvic fascia showing the region in three orthogonal planes and one rendered plane. The top left image shows (from top to bottom) the urethra, vagina and rectum in the midline and the fibromuscular tissue laterally. The rendered image (bottom right) shows the urethra flanked by the endopelvic fascia

reflects good levator ani reactivity.[36] Intraoperative ultrasound can help prevent the development of *de novo* incontinence by optimizing surgical elevation of the bladder neck during open colposuspension.[37]

Whereas, magnetic resonance imaging (MRI) has been the modality for visualizing the endopelvic fascia, in recent years 3D ultrasound sectional images are replacing MRI **(Fig. 57.12)** because of an equivalent resolution **(Figs 57.13 and 57.14)** and the added advantage of ease of utility,[38] dynamic display[39] and vascular display. Anatomical atrophy of the endopelvic fascia, change in the configuration of the vagina **(Fig. 57.15)** and paucity of vasculature **(Fig. 57.16)** can be documented with amazing clarity and reproducibility. The deep muscles of the pelvic floor are referred to as the levator ani or the pelvic diaphragm. The muscles that comprise the levator ani include the pubococcygeus, puborectalis and iliococcygeus. These muscles span the space between the obturator internus muscle laterally, the pubis symphysis anteriorly and the coccyx posteriorly. The superficial muscles of the pelvic floor make up the urogenital diaphragm and include the ischiocavernosus, bulbospongiosus and the transverses perinea superficialis.[40] The levator hiatus is a space between the various muscle groups that form the levator ani through which the urethra, vagina, and anal canal and pass.[41] The puborectalis is the inferior most muscle of the pelvic floor and is composed of two limbs attached to the two pubic rami anteriorly; they merge posterior to the anal canal.[42] The important role of the pelvic floor musculature is to perform voluntary contractions as well as involuntary, or reflex, contractions preceding or at the time of increased abdominal pressure. These types of contractions preserve fecal and urinary continence. In response to increased abdominal pressures, the superficial pelvic muscles, such as the anal and urethral sphincters, resist these pressures and the levator ani muscles support the pelvic floor and counteract these pressures by contracting and creating a circular closing of the levator hiatus and an upward movement of the pelvic floor and perineum.[43-46] The puborectalis provides pelvic floor support and ensures continence. When it contracts, the length of its limbs is reduced and this change lifts the anal canal anteriorly, compressing the structures within the levator hiatus against each other as well as the back of the pubic symphysis.[47] Three-dimensional ultrasound can also visualize anatomic defects of the individual components of the anal sphincter.[48] Patients with anatomical defects of the puborectalis have longer anterior-posterior lengths of the pelvic floor hiatus compared with controls.[39] Other measurements that can be obtained with three-dimensional ultrasound include the muscular component of the levator hiatus (the length of the suprapubic arch subtracted from the hiatal circumference) and the muscle strain on contraction (hiatal

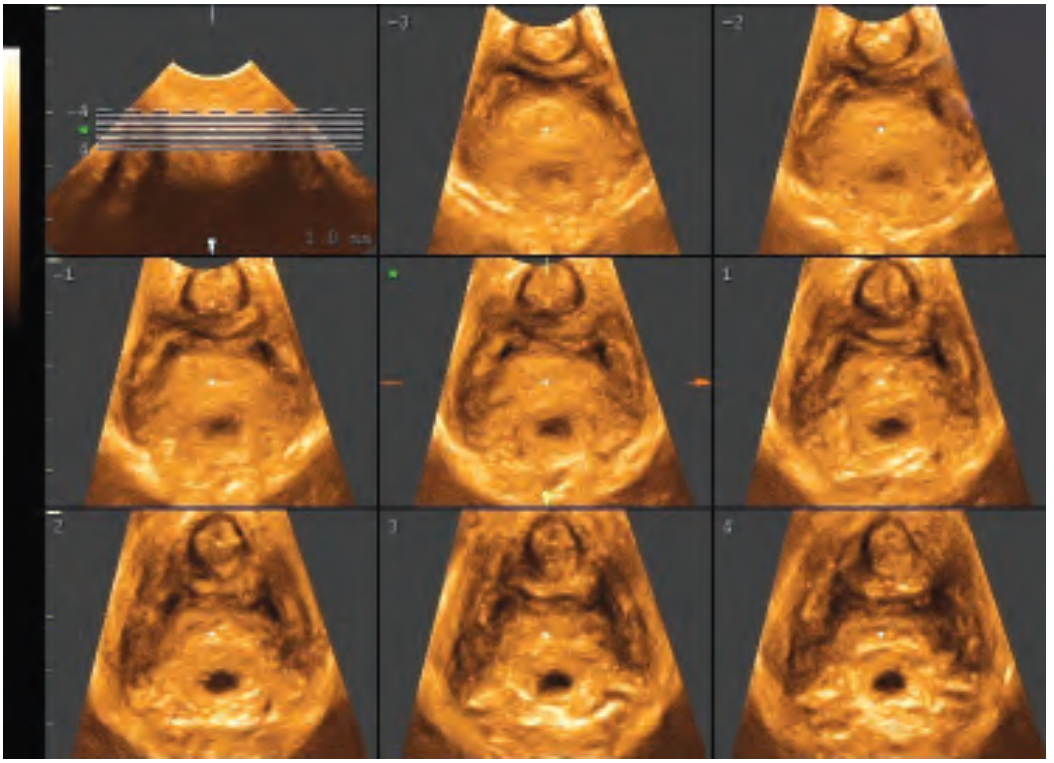

Figure 57.14: 3D Tomographic ultrasound imaging (TUI). Currently available 3D transducers acquire information in sweeps across the region of interest. Each signal thus acquired can be rendered in an infinite number of planes. TUI allows a choice of plane direction and thickness in much the same format as CT or MRI. Note the exquisite soft tissue detail of the urethra, vagina, rectum and endopelvic fascia. The vagina has an H-shaped configuration as evident in sections 1–4

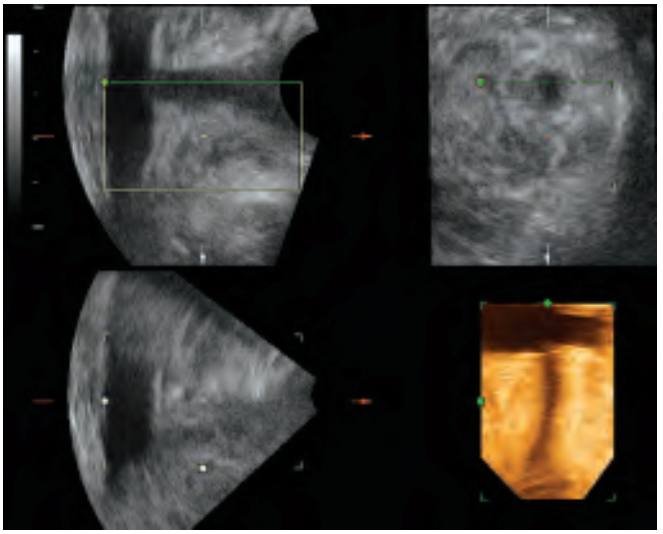

Figure 57.15: Complete loss of anatomical delineation of the vagina, rectum and endopelvic fascia in postmenopausal atrophy in a patient with incontinence. The difference is striking when the plane displayed in the top right area is compared with its counterpart in Figure 57.13

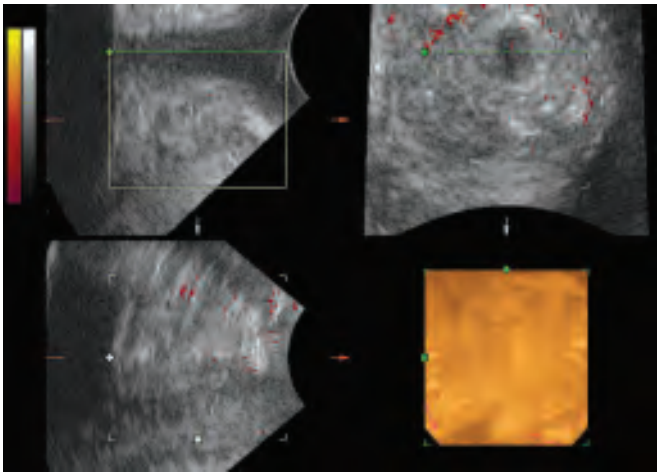

Figure 57.16: 3D Tomographic ultrasound imaging with gray scale and power Doppler information. Note the scanty vascular signals seen in the top right image and the complete absence of vascular signals in the other orthogonal planes

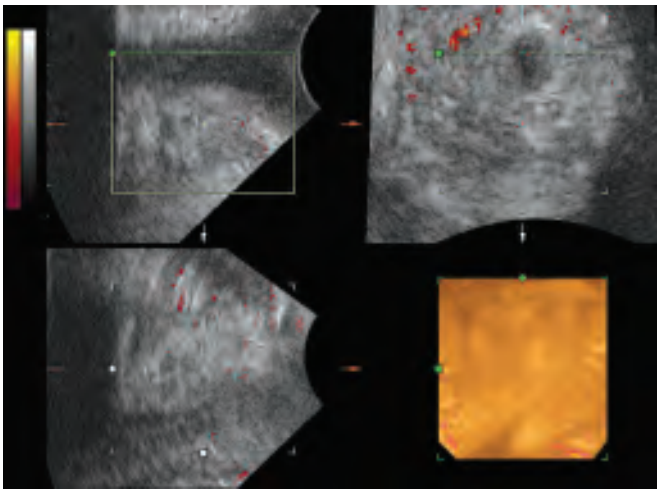

Figure 57.17: 3D tomographic ultrasound imaging with 2D and power Doppler information in a patient on perineal exercises and local estrogen cream application. Note the increased vascular signals in the top right frame when compared with Figure 57.15

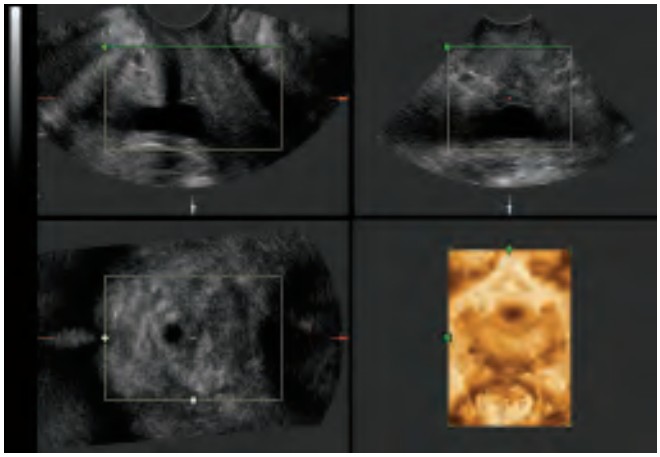

Figure 57.18: 3D Tomographic imaging with a display of three orthogonal planes and one rendered (bottom right) image. Note the complete distortion of vaginal echoes best evident in the rendered image in this patient with atrophy

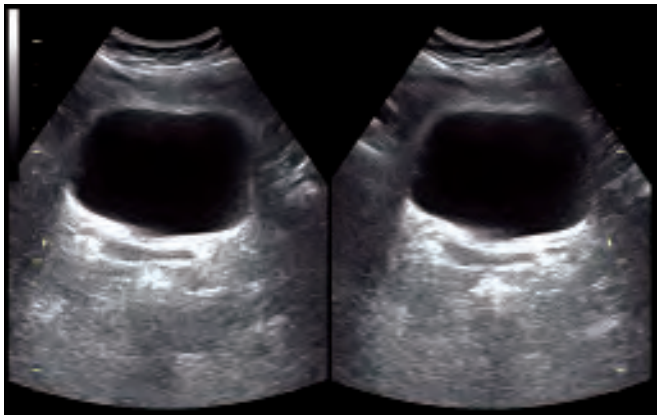

Figure 57.19: Significant postmicturition residue in a patient with recurrent urinary tract infection. The upper limit of normal postmicturition residue is 15 ml

circumference subtracted from the hiatal circumference at rest). These images offer an excellent display of avulsion injuries, which appear as abnormal insertion or interruptions of the puborectalis.[48] Vascular response to perineal exercises and local estrogen application **(Fig. 57.17)** can be demonstrated by serial scans done 6–12 weeks apart. Transanal and transrectal side-firing linear transducers now offer detailed delineation of the anal and urethral sphincters and sphincter mechanisms and in the future are likely to find increased application. Three-dimensional method provides objective evaluation of outcomes from urethral bulking agent therapy using collagen injections[49] and helps in assessing failure and the need for re-injection. Tension-free vaginal tape slings are highly echogenic and can be assessed by 3D ultrasound.[50] Tape movement occurs in an arc around the posterior aspect of the posterior symphysis which serves as the fulcrum. Mechanical compression of the urethra by the tape is evident as a reduction in the gap between the tape and the symphysis pubis.

Ultrasound Findings in Urogynecological Conditions

Most disorders of voiding dysfunction are characterized by a group of ultrasound findings that not only confirm clinical suspicion but also facilitate treatment decision options.

Recurrent lower urinary tract infections are marked by atrophied endopelvic fascia **(Fig. 57.18)** and increased residual urine **(Fig. 57.19)** consequent to a distension cystocele or surgical overcorrection of the urethra. Occasionally, bladder diverticuli, urethral diverticuli, intravesical calculi, foreign bodies or an abnormally located intrauterine device may be in evidence.

Patients with urgency and frequency may show periurethral or intravesical masses, bladder and urethral diverticuli, anterior uterine fibroids and a discordant funneling of the proximal urethra **(Fig. 57.20)**.

In patients with dysuria and dyspareunia, urethral diverticuli, periurethral masses and migrating old intrauterine contraceptive devices may be in evidence. Urge incontinence is marked by a thickened bladder wall **(Fig. 57.21)**.

Stress urinary incontinence shows either a fixed or a hypermobile urethra **(Fig. 57.22)**, reduced or absent

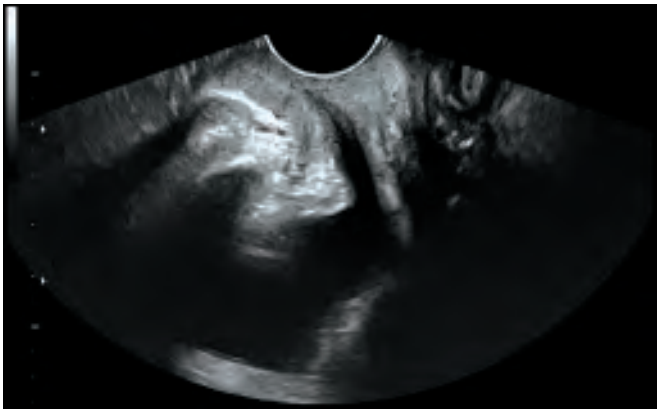

Figure 57.20: Funneling of the urethra in a patient with severe genuine stress incontinence

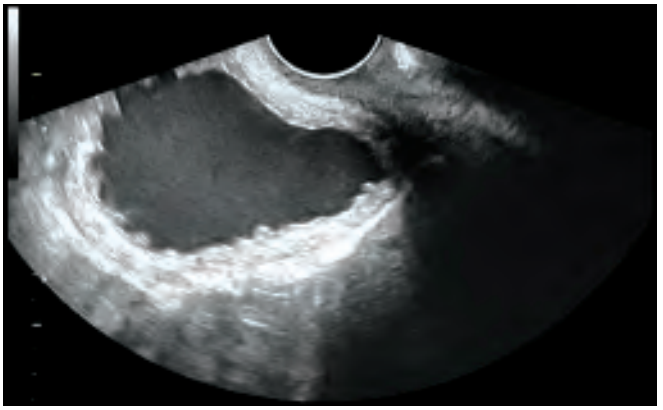

Figure 57.21: Markedly thickened wall of the urinary bladder. The normal thickness of the wall is 01–03 mm. Patient of postviral asthenia

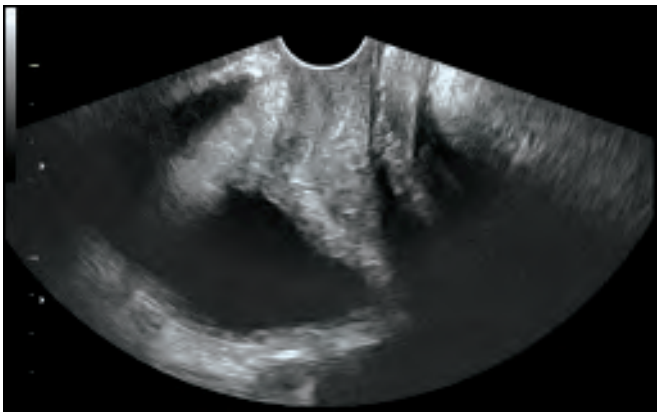

Figure 57.22: Incontinent patient showing findings at rest, for comparison with Figure 57.23. The bladder neck is closed

pelvic floor reactivity or a cystocele and a funneling of the urethra during stress **(Fig. 57.23)**.

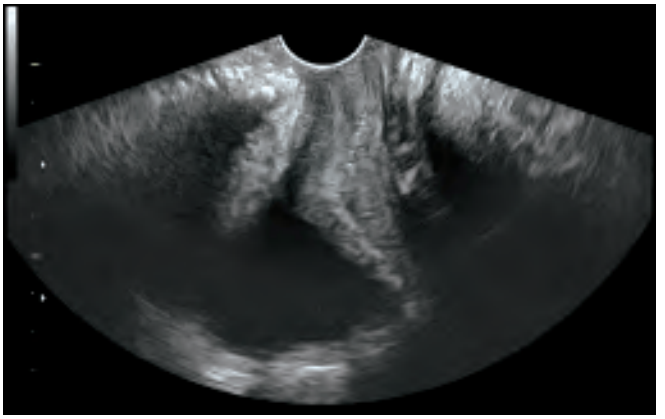

Figure 57.23: Same patient as in Figure 57.22 showing funneling of the bladder neck, hypermobile urethra and absent pelvic floor reactivity

CONCLUSION

Several years after its introduction, technical advances and remarkably reproducible objective parameters, have put ultrasound and in particular 3D evaluation in a unique position for clinical support. Enhanced tissue contrast and proven safety have thrown open numerous imaging protocols which are being perfected rapidly.

REFERENCES

1. Pantazis K, Freeman RM. Investigation and treatment of urinary incontinence. Current Obstet Gynecol. 2006;16(6): 344-52.
2. White RD, McQuown D, McCarthy TA, et al. Real-time ultrasonography in the evaluation of urinary stress incontinence. Am J Obstet Gynecol. 1980;138(2):235-7.
3. Schaer G, Koelbl H, Voigt R, et al. Recommendations of the German Association of Urogynecology on functional sonography of the lower female urinary tract. Int Urogynecol J Pelvic Floor Dysfunct. 1996;7(2):105-8.
4. Tunn R, Petri E. Introital and transvaginal ultrasound as the main tool in the assessment of urogenital and pelvic floor dysfunction: an imaging panel and practical approach. Ultrasound Obstet Gynecol. 2003;22(2):205-13.
5. Bader W, Degenhardt F, Kauffels W, et al. Ultrasound morphologic parameters of female stress incontinence. Ultraschall Med. 1995;16(4):180-5.
6. Schaer GN, Koechli OR, Schuessler B, et al. Perineal ultrasound: determination of reliable examination procedures. Ultrasound Obstet Gynecol. 1996;7(5):347-52.
7. Dietz HP, Wilson PD. The influence of bladder volume on the position and mobility of the urethrovesical junction. Int Urogynecol J Pelvic Floor Dysfunct. 1999;10(1):3-6.
8. Kohorn EI, Scioscia AL, Jeanty P, et al. Ultrasound cystourethrography by perineal scanning for the assessment of female stress urinary incontinence. Obstet Gynecol. 1986;68(2):269-72.

9. Koelbl H, Bernaschek G, Wolf G. A comparative study of perineal ultrasound scanning and urethrocystography in patients with genuine stress incontinence. Arch Obstet Gynecol. 1988;244:39-45.
10. Gordon D, Pearce M, Norton P, et al. Comparison of ultrasound and lateral chain urethrocystography in the determination of bladder neck descent. Am J Obstet Gynecol. 1989;160(1):182-5.
11. Mouritsen L, Strandberg C. Vaginal ultrasonography versus colpo-cystourethrography in the evaluation of female urinary incontinence. Acta Obstet Gynecol Scand. 1994;73(4):338-42.
12. Weber AM, Abrams P, Brubaker L, et al. The standardization of terminology for researchers in female pelvic floor disorders. Int Urogynecol J Pelvic Floor Dysfunct. 2001;12(3):178-86.
13. Khullar V, Cardozo LD, Salvatore S, et al. Ultrasound: a noninvasive screening test for detrusor instability. Br J Obstet Gynaecol. 1996;103(9):904-8.
14. Schaer GN, Koechli OR, Schuessler B, et al. Perineal ultrasound for evaluating the bladder neck in urinary stress incontinence. Obstet Gynecol. 1995;85(2):220-4.
15. Howard D, Delancey JO, Tunn R, et al. Racial differences in the structure and function of the stress urinary continence mechanism. Obstet Gynecol. 2000;95(5):713-7.
16. Peschers UM, Vodusek DB, Fanger G, et al. Pelvic muscle activity in nulliparous volunteers. Neurourol Urodyn. 2001;20(3):269-75.
17. Miller JM, Perucchini D, Carchidi LT, et al. Pelvic floor muscle contraction during a cough and decreased vesical neck mobility. Obstet Gynecol. 2001;97(2):255-60.
18. Peschers U, Schaer G, Anthuber C, et al. Changes in vesical neck mobility following vaginal delivery. Obstet Gynecol. 1996;88(6):1001-6.
19. Wijma J, Weis Potters AE, de Wolf BT, et al. Anatomical and functional changes in the lower urinary tract during pregnancy. Br J Obstet Gynaecol. 2001;108(7):726-32.
20. King JK, Freeman RM. Is antenatal bladder neck mobility a risk factor for postpartum stress incontinence? Br J Obstet Gynaecol. 1998;105(12):1300-7.
21. Khullar V, Salvatore S, Cardozo L, et al. A novel technique for measuring bladder wall thickness in women using transvaginal ultrasound. Ultrasound Obstet Gynecol. 1994;4(3):220-3.
22. Tunn R, Perucchini D. Morphologic assessment for diagnosing urogynaecologic disorders. Zentralbl Gynakol. 2001;123(12):672-9.
23. Schaer GN, Perucchini D, Munz E, et al. Sonographic evaluation of the bladder neck in continent and stress-incontinent women. Obstet Gynecol. 1999;93(3):412-6.
24. Schaer GN, Koechli OR, Schuessler B, et al. Improvement of perineal sonographic bladder neck imaging with ultrasound contrast medium. Obstet Gynecol. 1995;86(6):950-4.
25. Dietz HP, Clarke B. The urethral pressure profile and ultrasound imaging of the lower urinary tract. Int Urogynecol J Pelvic Floor Dysfunct. 2001;12(1):38-41.
26. Petri E, Koelbl H, Schaer G. What is the place of ultrasound in urogynecology? A written panel. Int Urogynecol J Pelvic Floor Dysfunct. 1999;10(4):262-73.
27. Yang JM, Huang WC. Discrimination of bladder disorders in female lower urinary tract symptoms on ultrasonographic cystourethrography. J Ultrasound Med. 2002;21(11):1249-55.
28. Yang JM, Yang SH, Huang WC. Dynamic morphological changes in the anterior vaginal wall before and after laparoscopic Burch colposuspension in primary urodynamic stress incontinence. Ultrasound Obstet Gynecol. 2005;25(3):289-95.
29. Reddy AP, DeLancey JO, Zwica OM, et al. On-screen vector-based ultrasound assessment of vesical neck movement. Am J Obstet Gynecol. 2001;185(1):65-70.
30. Martan A, Massata J, Halaska M, et al. Ultrasound Imaging of paravaginal defects in women with stress incontinence before and after paravaginal defect repair. Ultrasound Obstet Gynecol. 2002;19:496-500.
31. DeLancy JOL. Structural support of the urethra as it relates to stress urinary incontinence: the hammock hypothesis. Am J Obstet Gynecol. 1994;170:1713-20.
32. DeLancy JOL. Stress urinary incontinence: Where are we now, where should we go? Am J Obstet Gynecol. 1996;175:311-9.
33. Gosling JA. The structure of the bladder neck, urethra and pelvic floor in relation to female urinary continence. Int Urogynecol J. 1996;7(4):177-8.
34. Monga A. Fascia—defects and repair. Curr Opin Obstet Gynecol. 1996;8(5):366-71.
35. Martan A, Masata M, Halaska M, et al. Ultrasound imaging of the urethral sphincter. Ceska Gynekol. 1997;62(6):330-2.
36. Dietz HP, Wilson PD, Clarke B. The use of perineal ultrasound to quantify levator activity and teach pelvic floor muscle exercises. Int Urogynecol J Pelvic Floor Dysfunct. 2001;12(3):166-8.
37. Viereck V, Bader W, Skala C, et al. Determination of bladder neck position by intraoperative introital ultrasound in colposuspension: outcome at 6-month follow-up. Ultrasound Obstet Gynecol. 2004;24(2):186-91.
38. Umek WH, Laml T, Stutterecker D, et al. The urethra during pelvic floor contraction: observations on three-dimensional ultrasound. Obstet Gynecol. 2002;100(4):796-800.
39. Dietz HP, Shek C, Clarke B. Biometry of the pubovisceral muscle and levator hiatus by three-dimensional pelvic floor ultrasound. Ultrasound Obstet Gynecol. 2005;25(6):580-5.
40. Unger CA, Weinstein MM, Pretorius DH. Pelvic Floor Imaging. Ultrasound Clinics. 2010;5(2):313-30.
41. Kruger JA, Heap SW, Murphy BA, et al. Pelvic floor function in nulliparous women using three-dimensional ultrasound and magnetic resonance imaging. Obstet Gynecol. 2008;111(3):631-8.
42. Weinstein MM, Jung SA, Pretorius DH, et al. The reliability of puborectalis muscle measurements with 3-dimensional ultrasound imaging. Am J Obstet Gynecol. 2007;197(1):68.e1-6.
43. Deindl FM, Vodusek DB, Hesse U, et al. Activity patterns of pubococcygeal muscles in nulliparous continent women. Br J Urol. 1993;72(1):46-51.
44. Peschers UM, Vodusek DB, Fanger G, et al. Pelvic muscle activity in nulliparous volunteers. Neurourol Urodyn. 2001;20(3):269-75.

45. Yang JM, Yang SH, Huang WC. Biometry of the pubovisceral muscle and levator hiatus in nulliparous Chinese women. Ultrasound Obstet Gynecol. 2006;28(5):710-6.
46. Sapsford RR, Hodges PW, Richardson CA, et al. Coactivation of the abdominal and pelvic floor muscles during voluntary exercises. Neurourol Urodyn. 2001;20(1):31-42.
47. Jung SA, Pretorius DH, Padda BS, et al. Vaginal high-pressure zone assessed by dynamic 3 dimensional ultrasound images of the pelvic floor. Am J Obstet Gynecol. 2007;197(1):52.e1-7.
48. Abdool Z, Shek KL, Dietz HP. The effect of levator avulsion on hiatal dimension and function. Am J Obstet Gynecol. 2009;201(1):89.e1-5.
49. Poon CI, Zimmern PE. Role of three-dimensional ultrasound in assessment of women undergoing urethral bulking agent therapy. Curr Opin Obstet Gynecol. 2004;16(5):411-7.
50. Dietz HP, Wilson PD. The 'iris effect': how two-dimensional and three-dimensional ultrasound can help us understand anti-incontinence procedures. Ultrasound Obstet Gynecol. 2004;23(3):267-71.

58
CHAPTER

USG Role in Perinatal Infection

Alaa Ebrashy

INTRODUCTION

There are two situations where the obstetricians might need to know the role of ultrasound in perinatal infection. The first situation is that when the pregnant lady reports to her doctor that she has a rash, she is exposed to infection by getting near to a diseased person, she did some investigations raising the suspicion of being attracted infection during pregnancy, etc. In all these conditions the main question is: How could she know that her baby is safe, Can ultrasonography (USG) give a clue to this question?

The second situation is that during a routine fetal USG examination, doctor is encountered with some fetal abnormalities that could be related or not to intrauterine infection.

In order to be ready in both situations you should:

- First, know a brief knowledge about each organism that cause intrauterine infection and how could it be detected by USG
- Second, what are the USG signs that should arouse your suspicion for intrauterine infection.

How to detect, when to detect, modalities of diagnosis, with major emphasis on ultrasound is what will be covered in this chapter.

First, we start with the general ultrasound features of perinatal infection, the role of invasive tests in their diagnosis.

Second, we shall discuss in brief each organism separately together with its USG signs that could be present in case of infection

ULTRASOUND FEATURES IN CONGENITAL INFECTION

Intrauterine infection can present with a wide spectrum of USG markers and lesions depending on the type of the organism and the age of pregnancy at which the mother contracted the disease and above all the time between acquiring infection and USG examination.

Characteristic ultrasound markers in a mother with a positive TORCH (Toxoplasmosis, other agents, Rubella, CMV, Herpes simplex) screening test have a high predictive value for congenital infection and may have prognostic significance.

Among these markers we can mention early pregnancy loss, nonimmune hydrops fetalis (NIHF), intrauterine growth restriction, cranial lesions, cardiothoracic lesions, gastrointestinal lesions and other lesions.

Early Pregnancy Loss

Defined as a miscarriage within the first 12 weeks of pregnancy. Infection is considered a rare cause of early pregnancy loss.[1] Among these organisms are *toxoplasmosis gondii*, *cytomegalovirus* (*CMV)* and *parvovirus B19* (PVB19). The USG suggestive of the occurrence of early pregnancy loss include fetal bradycardia, discrepancy between the gestational age and crown-rump length.

Definite diagnosis depends on the demonstration of an empty sac of more than 15 mm by transvaginal sonography (TVS) and embryo with no pulsations documented by Doppler.[2] There is no any recent evidence suggesting that infection could be related to repeated abortion.

Nonimmune Hydrops Fetalis

Hydrops fetalis represents a specific condition characterized by an increase of total body water content. In such a condition, the excess fluid collects by ultra filtration in body cavities (pleural, pericardial and peritoneal effusions) and/or in the subcutaneous tissue. Placental edema and polyhydramnios are frequently associated (30–70%). By definition, the term NIHF refers to fluid collections in at least two body cavities or to one fluid collection plus diffuse subcutaneous edema.

ETIOLOGY AND PATHOGENESIS IN INTRAUTERINE INFECTION

The NIHF is a nonspecific sign of various infections vertically transmitted from mother to fetus, including both viral and nonviral infections.

Severe hemolytic anemia or aplastic anemia that can precipitate heart failure is often the primary cause.[3]

In the case of viral infections, the etiology is probably due to different and synchronous mechanisms: inflammation, myocarditis with pump deficit as in *Coxsackievirus B* or a major cardiac structural defect secondary to a rubella infection during the first trimester. Toxoplasmosis may cause NIHF possibly due to excessive extramedullary hematopoiesis with portal hypertension secondary to liver congestion.

PVB19 is tropic to rapidly diving cells in particular the bone marrow red cell precursors causing hemolysis and aplasia of the bone marrow.[4]

The pathophysiology of NIHF in cases of *CMV* or *T.pallidum* is less clear and could be due to combined effect of anemia and hepatic dysfunction resulting in hypoprotinemia and portal hypertension. The viruses most frequently associated with fetal hydrops are *PVB19, Coxsackievirus*, *Herpes virus* (*Varicella*), CMV, *adenovirus* and *influenza virus type B*. Among the nonviral infections, the most common are *syphilis*, *listeriosis* and *toxoplasmosis*.

The final result of the various conditions mentioned above is a breakdown of equilibrium between intracapillary and extracapillary pressures, with consequent fluid ultra filtration in the interstitial space.

The NIHF due to fetal infection can occur anytime in pregnancy but more common in second- and third-trimester. The fluid collections in the abdomen, pleura or pericardium appear as sonolucent areas with different shapes characteristic of the different locations. Subcutaneous edema appears as a moderately hyperechoic thickening of the soft tissue of the fetal face, trunk and sometimes limbs, the fluid collection may be limited to one or two sites and therefore its diagnosis needs dedicated planes. Axial views of the head, neck and thorax may allow assessment of the extent and severity of the effusions and the subcutaneous edema. With regards to the ascites, it should be noted that initially the fluid collects in the pelvis only and therefore it should be sought in this region and not at the level of the liver.

Intrauterine Growth Restriction

It is also a nonspecific feature of most congenital infections. It is a more common in *Rubella*, *CMV* and *T. pallidum*.[5] It also has some relationship with varicella-zoster, HIV and Malaria. The IUGR in cases of intrauterine infection may be explained on the ground of capillary endothelial damage during organogenesis, which in turn induces a decrease in the number of cells having a cytoplasmic mass within the normal range together with a cytopathic effect. When the infection is transmitted to the fetus in the first trimester, the IUGR will be a manifestation of the second trimester USG usually severe symmetrical pattern and associated with oligohydramnios in most cases hence the fetal anatomy could not be well appreciated. In any case showing symmetrical IUGR early in the second trimester, infection should be always considered and TORCH test is therefore always be performed.[6]

Cranial Lesions

The most common cranial lesions secondary to fetal infection is seen by are cerebral echogenic foci (calcifications), ventriculomegaly **(Fig. 58.1)**, microcephaly and hydrancephaly. A fetal infection should be suspected when ventriculomegaly is associated with hyperechogenic foci and periventricular cysts.

These lesions are both inflammatory (Gliosis) and destructive lesions. The most common organism that causes cerebral lesions is CMV and less commonly *T. Gondii*. The ventriculomegaly that may be seen in such cases is the consequence of aqueductal obstruction. Hydrancephaly observed in cases of congenital infections, such as Toxoplasma and CMV can be explained on the basis of causing necrotizing vasculitis with consequent destruction of the cerebral tissue.[7]

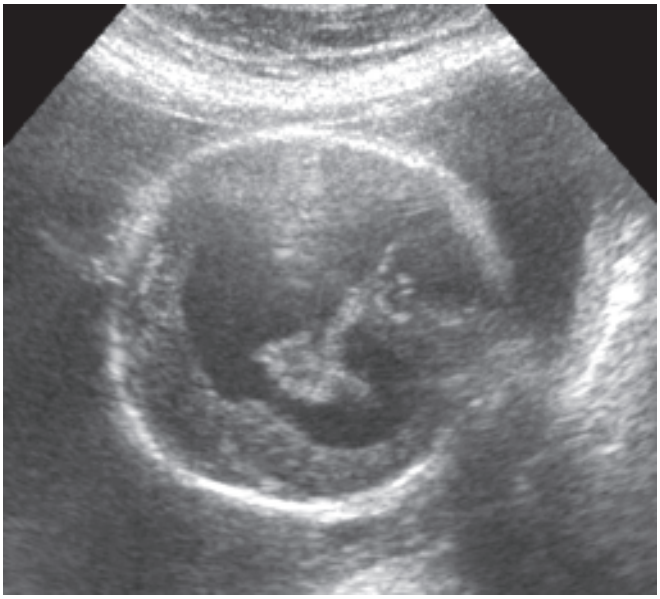

Figure 58.1: Ventriculomegaly

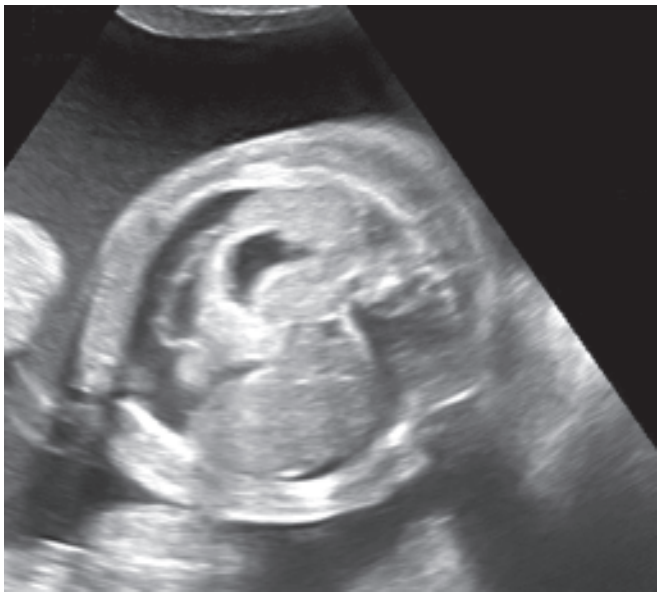

Figure 58.2: Hydrops hepatosplenomegaly

The addition of magnetic resonance imaging (MRI) increases the positive predictive value for diagnosis of fetal brain abnormalities with CMV.[8]

Eye Lesions

Eye lesions seen in congenital infection include congenital cataract, micro-ophthalmia and chorioretinitis. They are observed mainly with congenital rubella and congenital toxoplasmosis.[9]

Cardiothoracic Lesions

Congenital heart defects mainly as pulmonary valvular stenosis and ventricular septal defect are among the clinical features of congenital rubella syndrome. Similar defects have occasionally been observed following first trimester congenital CMV or toxoplasmosis infection. Cardiomyopathies, such as endocardial fibroelastosis (interstitial myocarditis) have been linked to *Coxsackievirus B* and to *adenovirus* and *PVB19*.[10] Major heart anomalies are usually complicated by NIHF. Pleural effusion may represent an early stage of NIHF and may be associated with a major fetal infection usually the heart. Isolated pleural effusion is rarer and has only been observed in one case of *adenovirus* infection[11] and one case of *PVB19* infection.[12]

Gastrointestinal Lesions

Most congenital infections show abnormal features of the liver, spleen and bowel on USG. The most common sonographically detected markers are peritoneal hyperechogenicities and/or hyperechogenic bowel which have been described mainly within the context of congenital *CMV*, *HSV*, *VZV* and *PVB19*.[13] True parenchymal liver or splenic hyperechogenicities are far less common and have occasionally been related to congenital infection.[14] The pathophysiology of these echogenicities is unclear. Focal lesions are probably secondary to localized ischemia or inflammatory reaction with calcification of the tissue, diffuse bowel hyperechogenicity could be due to thickened meconium. Congenital infections due to *PVB19*, *CMV*, *T. pallidum* or toxoplasmosis may be associated with ascitis and hepatosplenomegaly **(Fig. 58.2)**. These anomalies are secondary to direct infection of the fetal liver parenchyma with secondary enlargement and progressive alteration of liver function.[15] Ascitis can be detected by USG even there is less than 50 ml of intraperitoneal fluid and can be the first presenting sign of congenital infection. Small amounts of ascitis are best visualized at the edge of the liver and may be seen to gradually outline the liver. In severe cases USG picture of the fetal abdomen show free floating or compressed bowel loops. Ascitis is often is early manifestation of serous fluid accumulation in fetuses who later develop full blown hydrops. Intrauterine fetal infections are among the most common causes of hepatomegaly, *CMV* infection, when severe is commonly associated with hepatosplenomegaly **(Fig. 58.3)**. Fetal infections are also the primary cause of splenomegaly with or without hepatomegaly. In particular, *CMV* infection, when severe is typically associated with splenomegaly, as well

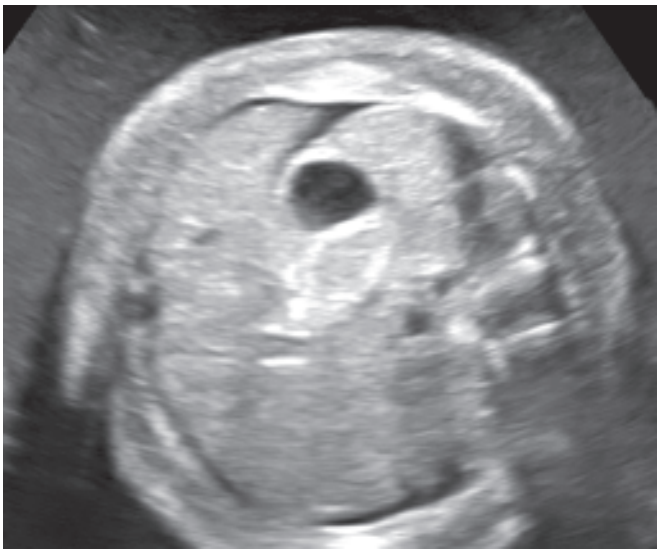

Figure 58.3: Hydrops splenomegaly hepatomegaly

as hepatomegaly and ascites. If the enlargement of the spleen and/or liver is severe, the diagnosis of these conditions is straightforward, the two organs occupying most of the abdomen. The recognition of hepatomegaly and splenomegaly is made even simpler if ascites, which acts as an intra-abdominal contrast medium, is associated. If hepatomegaly is very pronounced, the prominence of the liver pushes the anterior abdominal wall, causing a dip at the thoracoabdominal junction, similarly to what happens in cases of severe thoracic hypoplasia, although in this case it is the abdomen that is enlarged rather than the thorax that is hypoplastic. Nomograms of the maximum diameters of the liver and the spleen have been published. Then 3D ultrasound also have recently been used for estimation of liver and spleen volumes versus gestational age.[16]

Other Lesions

Placental edema and enlargement is commonly found specially in cases of NIHF as in *CMV* and *Toxoplasmosis*.[16] Urogenital tract lesions have occasionally been reported in cases of *CMV* and toxoplasmosis. Limb defects have been rarely observed in congenital *VZV*.

What is the Role of Invasive Procedures in the Diagnosis of Intrauterine Infection

There are three modalities of invasive procedures for the diagnosis of fetal infection namely amniocentesis, chorionic villus sampling (CVS) and cordocentesis.

The CVS can be done after 11 weeks and have been used in particular for first trimester rubella. Its main disadvantage is early diagnosis which may be useful when there is maternal serological evidence of infection early in pregnancy however this method poses a theoretical risk to the fetus as it damages the placental barrier, which may result in an increased transfer of viral particles or parasites to the fetus.[17]

Cordocentesis is played a key role in the diagnosis of most common congenital infections in the 1980s and early 1990s. No fetus with a documented infection has a completely normal hematological profile [5] white blood count total and differential, TORCH specific IgM, fetal liver enzymes measurement, all can be assessed in cases of infection. However, with the development of polymerase chain reaction (PCR) analysis on the amniotic fluid, its role in this context is fading.[5]

The only advantage of cordocentesis is in cases of *PVB19* infection in which the fetal hematological profile is crucial in the management of these cases.

We left with the amniocentesis which is now the most common invasive procedure used for diagnosis of fetal infection.[17] The PCR is now the preferred method for analysis of the amniotic fluid in cases of fetal infection. The development of quantitative PCR analysis has optimized the specificity of this assay, preventing the false-positive results that were seen with the earlier qualitative PCR analysis. Current studies in case of *CMV* are now trying to correlate viral load and degree of fetal damage.[18] An essential point to be mentioned here is the timing for amniocentesis to avoid false-negative PCR results delays of more than 5–6 weeks between the serological diagnosis of maternal *CMV* and toxoplasmosis infection and the invasive procedure are recommended to increase the sensitivity of prenatal diagnosis.[19]

PRENATAL MANAGEMENT OF SPECIFIC CONGENITAL INFECTIONS USING ULTRASOUND MARKERS AND INVASIVE PROCEDURES

Cytomegalovirus

Cytomegalovirus is found universally throughout locations and is species specific. Seroconversion occurs in approximately 1% of pregnant women in UK, more than 2% in other European countries and the USA.[20]

Primary CMV carries a high mother to fetus transmission rate ranging from 25–40% regardless of the stage of pregnancy.[21] In secondary recurrent infection, the transmission rate is much lower almost 5%.[19] Overall congenital *CMV* infection is asymptomatic at birth in 90% of infants infected *in utero*.

The classic triad of blood dyscrasia (petechiae and thrombocytopenia), IUGR and chorioretinitis is

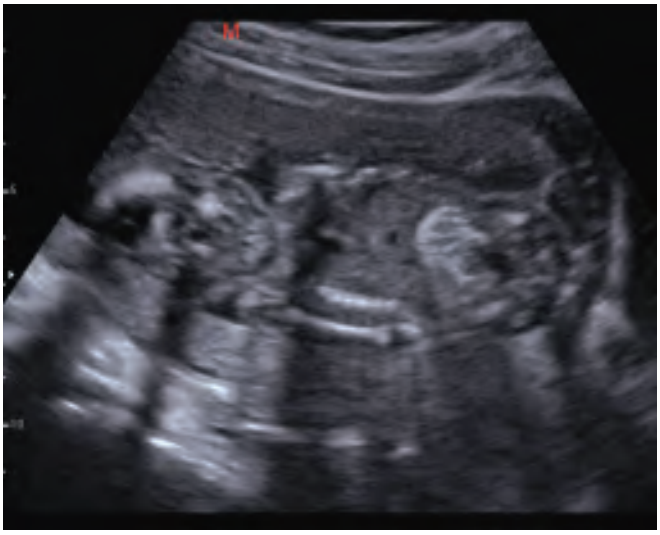

Figure 58.4: Echogenic bowel

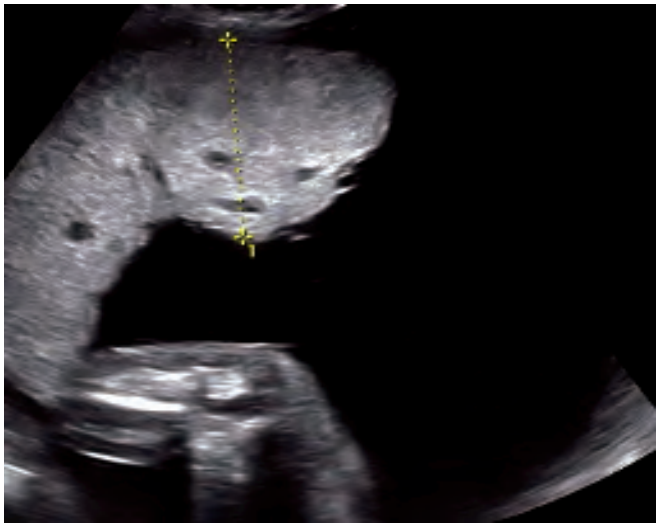

Figure 58.6: Placentomegaly

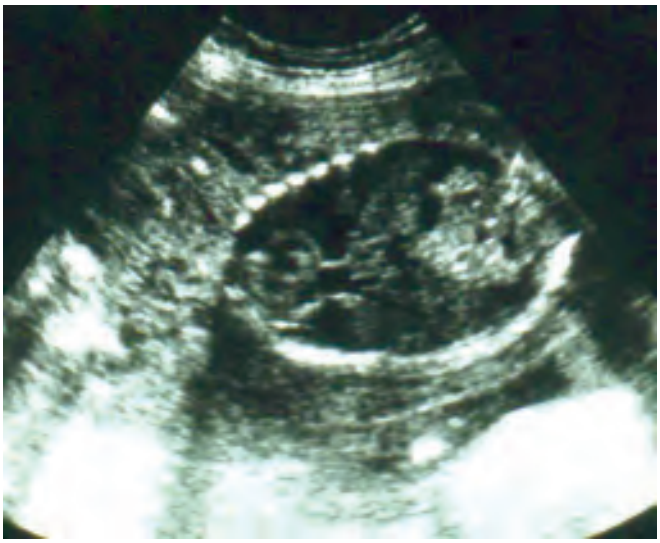

Figure 58.5: Hydrops e-bowel

uncommon less than 10% *in utero* or at birth. Among the ultrasound markers for *CMV* infection that could be detected are cranial calcification periventricular in position without shadowing, ventriculomegaly, echogenic bowel **(Figs 58.4 and 58.5)**, enlarged liver and spleen, focal calcification in the liver and mild ascitis, severe IUGR. Placentomegaly **(Fig. 58.6)** is noted in 32% of the time. Those cases showing cerebral manifestations and/or severe IUGR are more prone to develop neurological sequel.[22,23]

The mere detection of positive IgM and IgG is not indicative of active infection unless we obtain a rising titer within 2 weeks since the IgM could persist in the circulation for more than 18 months from last infection.[23] Differentiating between primary or secondary infection is somewhat important for assessing the possibility of fetal infection as mentioned earlier. The CMV IgG avidity test is very useful in this domain.[24]

Intrauterine infection diagnosis could be achieved through amniocentesis and isolation of the *CMV* DNA by PCR with a sensitivity of 80–99% of cases.[17] It should be noted that it takes 5–7 weeks after fetal infection for viral replication in the fetal kidneys to be present in sufficient quantity to be secreted into amniotic fluid, also the PCR testing is unreliable prior to the 21st weeks of pregnancy. This means that amniocentesis for *CMV* detected by PCR should not be performed before the 21st weeks and with an elapse of at least 5 weeks from the time of maternal infection.[19]

Treatment of CMV Infection

There is currently no approved treatment for congenital infection. Gangciclovir being effective treatment for *CMV* however not safe in the first trimester.[22] Valaciclovir is showing some promise for use however with limited research till now.[25] Hyperimmunoglobulin appears to be an effective drug for fetal however also with limited data.[22]

Toxoplasma

Mode of Infection

It is caused by the protozoon, *Toxoplasma gondii*. The definitive host is the cat and the intermediate hosts

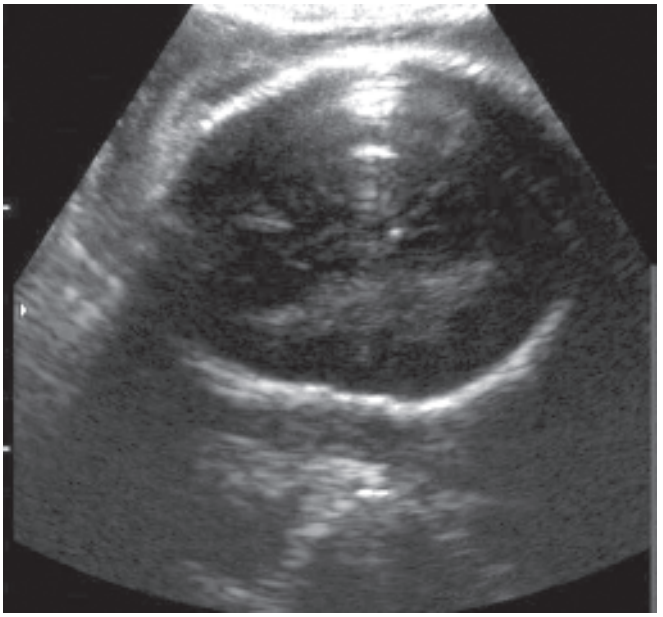

Figure 58.7: Cranial calcification

include humans, numerous mammals and birds which acquire the infection from the oocysts contained in cat feces and thus seronegatives are urged to avoid contact with cats, wash fruits and vegetables thoroughly and avoid raw meat.[26]

Transmission

The rate of mother to fetus transmission depends on the gestational age and the time of the initial infection. It is around 15%, 30%, 60–70%, in the first, second and third trimesters respectively. However, the reverse is the situation for the severity of infection, being highest in first trimester and almost nil in the third trimester.[27]

Ultrasound Signs

The main ultrasound sign of prenatal toxoplasmosis infection is ventriculomegaly, intracranial calcification **(Fig. 58.7)**. Choroidoretinitis is among the sequelae detected postnatal. Other ultrasound markers include hepatosplenomegaly, ascitis.[15]

Testing

If the serologic testing shows that the woman has contracted toxoplasmosis during pregnancy by a positive IgG and IgM with a rising titer, detecting *T. gondii* in the amniotic fluid by PCR through amniocentesis is the preferred methods for assessing fetal infection with a sensitivity more than 80% and specificity of 96%.[28,29]

Treatment

Spiramycin can decrease the risk of congenital toxoplasmosis by around one half. It is taken as 1g every 8 hourly and is continued until delivery.[30]

This drug does not cross the placenta, so in the evidence of fetal infection by amniocentesis and PCR, treatment should be in favor of other drugs that are effective and also cross the placenta.[30] This include both Pyrimethamine and Sulfadiazine. Different regimens are used however in all of them folic acid is added as both of them are folic acid antagonist.

Examples are: Pyrimethamine 50 mg/day + Sulfadiazine 1 g tid + folinic acid 10–25 mg/day for 3 weeks alternating with 3 weeks of Spiramycin 1 g tid. This regimen is continued until term.[30,31]

Parvovirus B19 Infection

It is caused by the human *Parvovirus B19* which belongs to the Parvoviruses group a single DNA strand.[32] The viruses affect the function of the hematopoietic organs through the infection and lysis of erythropoid cells. The disease is very mild for the mother and carries a 33% placental transmission rate following maternal seroconversion at any stage of pregnancy. The virus can cause severe destruction of erythroid progenitor cells in the fetus with the risk of developing fetal anemia, hydrops and intrauterine death.[32]

Transmission

It would lead to fetal anemia in 7–17% of affected cases. It is not associated with a clinically significant risk of malformations.[32]

Ultrasound Signs

The hallmark of this infection is fetal hydrops which may be severe in very low hemoglobin levels. It accounts for 10–15% of nonimmune fetal hydrops NIHF.[33,34]

Testing

Nonimmune hydrops should call for a *Parvovirus B19* IgG and IgM antibody testing in the maternal serum. In 80% of the cases, the virus can be detected in the fetal blood by PCR. In case of NIHF the evaluation of middle cerebral artery peak systolic velocity is an important tool to diagnose and follow-up fetal anemia.[35,36] This should be followed by cordocentesis and intrauterine blood transfusion which is the only way for fetal survival, more than 80% of the fetuses transfused *in utero* will survive.

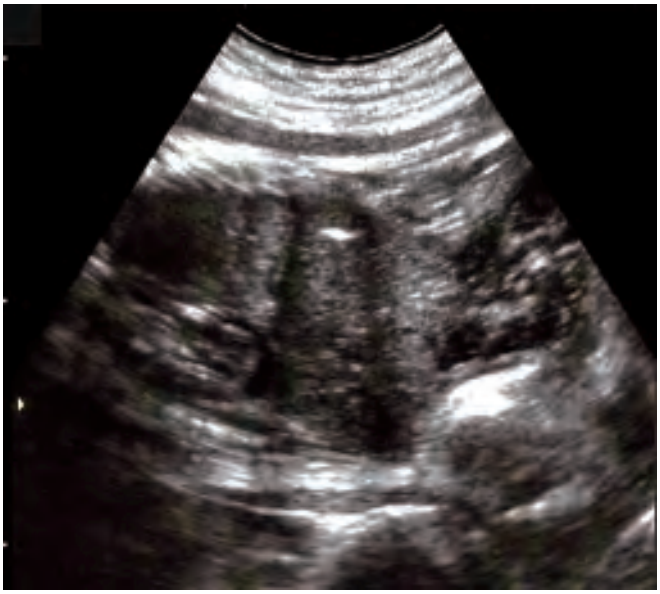

Figure 58.8: Liver calcification

Varicella Zoster

DNA virus of the Herpes family responsible for chicken pox (varicella), the primary infection and Herpes Zoster shingles, a reactivation of the virus occurring at any age but with an increasing incidence in adulthood transmission via droplet infection and infection is followed by long lasting immunity.

Both maternal and fetal infection is important and serious. Pregnancy increases the risk of disease associated complications particularly in late pregnancy. Pneumonia occurs in up to 10% of cases and could be so severe that it necessitates mechanical ventilation.[37] Fetal varicella syndrome occurs when the fetus is infected during maternal viremia in the first 20 weeks of gestation. The risk of fetal varicella syndrome is estimated to be 0.4% in the first 12 weeks of pregnancy, 2% between 13–20 weeks of gestation, the syndrome does not occur if maternal infection occurs after 20 weeks.[37]

Prenatal diagnosis of fetal varicella syndrome depend on serial USG examination 5 weeks or later after primary infection among the signs are polyhydramnios, microcephaly, liver calcification **(Fig. 58.8)**, NIHF, limb hypoplasia. Varicella embryopathy is the term used for infants contracted the infection intrauterine.[37] It comprises cutaneous scars, denuded skin, limb hypoplasia, muscle atrophy and rudimentary digits, other more frequent abnormalities are microcephaly, intracranial calcification cortical atrophy, cataract, chorioretinitis, micro-ophthalmia and psychomotor retardation.

MANAGEMENT

Exposure Before 20 Weeks

If the mother is not immune: I. globuline 1000 gm IM may be given. If she develops chicken pox, council her for the possibilities of fetal infection and follow-up by serial USG.

Exposure After 20 Weeks

There is no fetal infection in these cases, however the mother may develop some complications mainly Pneumonitis, thus if she is presented within 24 hours of chicken pox rash. She may be given oral acyclovir 800 mg 5 times daily for 7 days to reduce the severity and duration of illness. If presented after 24 hours, the acyclovir is of no effect and just follow-up the disease progression.[38,39] In Herpes Zoster, the fetus is unaffected by maternal Herpes Zoster unless mother is immunosuppressed.

Rubella

Mode of Infection

It is caused by a small RNA togavirus, the rubella virus.

Transmission

Direct contact with infected droplets. If the infection is contracted in the first 6 weeks of gestation, two-thirds of the fetuses will develop a rubella syndrome. Infections in later weeks are associated with lower risks, 25% between 7 and 9 weeks, 20% between 10–12 weeks and 10% between 13–17 weeks.[40]

Ultrasound Signs

The anomaly typically found in rubella embryopathy is ventricular septal defect (VSD) or tetralogy of Fallot. Additional signs include growth retardation and microcephaly. The triad of cataract, cardiac anomalies and deafness (Gregg syndrome) is a classic embryopathy caused by the infection.[15]

Testing

A normal ultrasound scan cannot exclude fetal rubella infection, thus in cases of primary rubella infection, it is possible to detect the virus in chorionic villi or amniotic fluid. Cordocentesis has reasonable accuracy but should not be performed earlier than 22 weeks since the IgM production may still be too low before 21 weeks. A good strategy in earlier cases is to start with CVS or

amniocentesis and if negative, confirm the result by cordocentesis at 22 weeks.[41]

CONCLUSION

- Ultrasound markers of a congenital infection include echogenic bowel, hepatosplenomegaly, NIHF, cranial anomalies mainly hydrocephalus and cranial calcifications and early symmetrical IUGR
- Maternal screen for TORCH and TORCH-like infections is recommended in these cases
- Serial ultrasound should be performed every two weeks in pregnancies at risk for congenital infection as in case of exposure to infection or maternal seroconversion
- Amniocentesis is considered the standard invasive test for the diagnosis of most intrauterine infection where isolation of the virus is done by PCR with a sensitivity now approaching 100%
- Intrauterine infection are not a cause for recurrent pregnancy loss, so TORCH is not indicated in these cases.

REFERENCES

1. Simposon JL, Mills JL, Kim H, et al. Infections processes: an infrequent cause of first trimester spontaneous abortions. Hum Reprod. 1996;11(3):668-72.
2. Jauniaux E, Gavril P, Nickolaides KH. Ultrasongraphic assessment of early pregnancy. In: Jurkovic D,Jauniaux E (Eds). Ultrasound and Early pregnancy. Carnforth UK:Parthenon publishing; 1995. pp.53-64.
3. Iskaros J, Jauniaux E, Rodeck C. Outcome of non immune hydrops fetalis diagnosed during the first half of pregnancy. Obstet Gynecol. 1997;90:321-5.
4. McCoy MC, Katz VL, Gould N, et al. Non Immune hydrops after 20 weeks gestation, review of 10 years experience with suggestions for management. Obstet Gynecol. 1995;85:578-82.
5. Weiner CP, Grose CF, Naides SJ. Diagnosis of fetal infection in a patient with an ultrasongraphically detected abnormality but a negative clinical history. Am J Obstet Gynecol. 1993;168:6-11.
6. Kilby M, Hodgett S. Perinatal viral infections cause of intrauterine growth restriction. In: Kingdom J, Baker P (Eds). Intrauterine Growth Restriction: Aetiology and Management, London:SpringerVerlag; 2000. pp. 29-49.
7. Holliman RE. Clinical sequelae of chronic maternal toxoplasmosis. Rev Med Microbiol. 1994;5:47-55.
8. Benoist G, Salomon L, Mohlo M, et al. Cytomegalovirus related fetal brain lesions: comparison between targeted ultrasound examination and magnetic resonance imaging. Ultrasound Obstet Gynecol. 2008;32(7):900-5.
9. Hall SM. Congenital toxoplasmosis. Br Med J. 1992; 305(6848):291-7.
10. Ranucci Weiss D, Uerpairojkit B, Bowles N, et al. Intrauterine adenovirus infection associated with non immune hydrops. Prenat Diagn. 1998;18(2):182-5.
11. Lambot MA, Noel JC, PenyMO, et al. Fetal parvovirus B19 infection associated with myocardial necrosis. Prenat Diagn. 1998;18:182-5.
12. Parilla BV, Tamura RK, Ginsberg NA. Association of parvovirus infection with isolated fetal effusions. Am J Perinatol. 1997;14(6):357-8.
13. Muller F, Dommergues M, Aubry MC, et al. Hyperechogenic fetal bowel: an ultrasonographioc marker for adverse fetal and neonatal outcome. Am J Obstet Gynecol. 1995;173(2):508-13.
14. Mac Gregor SN, Trmura R, Sabbagha R, et al. Isolated Hyperechoic Fetal Bowel: Significance and implications for management. Am J. Obstet Gynecol. 1995;173(4):1254-8.
15. Yaron Y, Hassan S, Geva E, et al. Evaluation of fetal echogenic bowel in the second trimester. Fetal Diagn Ther. 1999;14(3):176-80.
16. Degani S. Sonographic finding in fetal viral infection: A systematic review. Obstet Gynecol Surv. 2006;61(5):329-36.
17. Jauniaux E. A comparison of Chorionic villus sampling and amniocenetsis for prenatal diagnosis in early pregnancy. In: Grudzinskas JG,Ward RHT (Eds). Screening for Down Syndrome in the First Trimester. London: RCOG press; 1997. pp. 259-69.
18. Guerra B, Lazzarotto T, Quarta S, et al. Prenatal diagnosis of symptomatic congenital cytomegalovirus infection. Am J Obstet Gynecol. 2000;183(2):476-82.
19. Nigro G, Mazzocco M, Anceschi M, et al. Prenatal diagnosis of fetal cytomegalovirus infection after primary or recurrent maternal infection. Obstet Gynecol. 1999;94(6):909-14.
20. Malm G, Engman ML. Congenital cytomegalovirus infections. Semin Fetal Neonatal Med. 2007;12(3):154-59.
21. Stagno S, Pass R, Cloud G. Primary cytomegalovirus infection in pregnancy. Incidence, transmission to fetus, and clinical outcome. JAMA. 1986;256(14):1904-8.
22. Nigro G. Maternal fetal cytomegalovirus infection: From diagnosis to therapy. J matern. Fetal Neonatal Med. 2009; 22(2):169-74.
23. Omoy A, Diav-Citrin O. Fetal effects of primary and secondary cytomegalovirus infection in pregnancy. Reprod Toxicol. 2006;21(4):399-409.
24. Evaluation of the new architect cytomegalovirus immunoglobulin M (IgM), IgG and IgG avidity assays. J Clin Microbiol. 2009;47(6):1695-9.
25. Jacquemard F, Yamamoto M, Costa J, et al. Maternal administration of valaciclovir in symptomatic intrauterine cytomegalovirus infection. Br J Obstet Gynaecol. 2007; 114(9):1113-21.
26. Joynson DHM, Payne R. Screening for toxoplasmosis in pregnancy. Lancet. 1988;2(8614):795-6.
27. Gilbert R, Gras L. European multicentre study on congenital toxoplasmosis. Effect of timing and type of treatment on the risk of mother to child transmission of Toxoplasma gondii. Br J Obstet Gynaecol. 2003;110(2):112-20.
28. Gras L, Gilbert RE, Wallon M, et al. Duration of the IgM response in women acquiring *Toxoplasma gondii* during pregnancy: implications for clinical practice and cross-sectional incidence studies. Epidemiol Infect. 2004;132(3): 541–8.

29. Foulon W, Pinon JM, Stray-Pedersen B, et al. Prenatal diagnosis of congenital toxoplasmosis: multicenter evaluation of different diagnostic parameters. Am J Obstet Gynecol. 1999;181(4):843-7.
30. Wallon M, Liou C, Garner P, et al. Congenital toxoplasmosis: systematic review of evidence of efficacy of treatment in pregnancy. Br Med J. 1999;318(7197):1511–4.
31. Foulon W, Villena I, Stray-Pedersen B, et al. Treatment of toxoplasmosis during pregnancy: a multicenter study of impact on fetal transmission and children sequelae at age 1 year. Am J Obstet Gynecol. 1999:180(2 Pt. 1):410-5.
32. Hedrick J. The effects of human parvovirus B19 and cytomegalovirus during pregnancy. J Perinat Neonatal Nurs. 1996;10(2):30–9.
33. Chisaka H, Morita E, Yaegashi N, et al. Parvovirus B19 and the pathogenesis of anaemia. Rev Med Virol. 2003; 13:347–59.
34. Al Khan A, Caliguri A, Apuzio J. Parvovirus B19 infection during pregnancy. Infect Dis Obstet Gynecol. 2003;11(3): 175-9.
35. Cosmi E, Mari G, Chiaie LD, et al. Noninvasive diagnosis by Doppler ultrasonography of fetal anemia resulting from parvovirus infection. Am J Obstet Gynecol. 2002;187(5): 1290–3.
36. Hernandez-Andrade E, Scheler M, Dezerga V, et al. Fetal Middle cerebral artery peak systolic velocity in the investigation of non immune hydrops. Ultrasound Obstet Gynecol. 2004;23(5):442-5.
37. Pretorius DH, Hayward I, Jones Kl, et al. Sonographic evaluation of pregnancies with maternal varicella infection. J Ultrasound Med. 1992;11(9):459-63.
38. AL Levy M, Schick B, et al. Outcome after maternal varicella infection in the first 20 weeks of pregnancy. N Engl J Med. 1994;330(13):901-5.
39. Smego RA, Asperilla MO. Use of acyclovir for varicella pneumonia during pregnancy. Obstet Gynecol. 1991;78: 1112-6.
40. Banatvala J, Brown DWG. Rubella. Lancet. 2004;363(9415): 1127-37.
41. Sever JL, South MA, Shaver KA. Delayed Manifestations of Congenital Rubella. Rev Infect Dis. 1985;7:(Supp. 1) S164-9.

INDEX

B

C

D

E

F

N

O

P

R

S

T

U

V

W

X

Y

Z